

# PROCEEDINGS



## ASNR 50<sup>th</sup> Annual Meeting

Hilton New York • New York, NY • April 21-26, 2012



**ASNR 50<sup>th</sup>  
ANNIVERSARY**  
1962-2012  
**ANNUAL MEETING**  
NEW YORK, NY

**Dear ASNR Members, Visitors, and Neuroscience Colleagues:**

I am happy to invite you to the American Society of Neuroradiology 50th Anniversary Meeting. For this special event the Society is returning to its birthplace in New York City. The Meeting will be held April 21-26 at the Hilton New York, in the heart of Manhattan. President-Elect and Program Chair, Pamela Schaefer, MD, and the Program Committee have planned an exciting symposium and scientific program, along with special celebrations recognizing our milestone 50th Annual Meeting.

The Foundation of the ASNR Symposium 2012 ***“Acute Ischemic Stroke Imaging,”*** is at the heart of neuroradiology and will feature speakers with expertise across the range of adult and pediatric brain ischemia. We will continue to offer a Saturday morning session in collaboration with the International Society of Magnetic Resonance in Medicine (ISMRM). This mini symposium on ***“Advanced MR Imaging of Acute Ischemic Stroke”*** will feature new techniques and emerging new technologies that increasingly are applied to stroke.

The 50<sup>th</sup> Annual Meeting will provide informative updates on general neuroradiology and showcase subspecialty programming from the ***ASFNR, ASHNR, ASPNR, ASSR, and SNIS***. As always, the heart of the meeting will be the **invited lectures, original presentations, scientific posters, and educational exhibits**. After a record number of abstract submissions, I can promise you more new and exciting material than ever before.

There will be approximately 50 hours of continuing medical education credit available including size (6) ***Self-Assessment Module (SAM)*** sessions, ***Maintenance of Certification (MOC)*** interactive audience response technology case reviews, and new Expert: ***“How I Do It”*** sessions with practical clinical approaches to common imaging challenges. We will again feature valuable non-CME ***“How To Sessions”*** sponsored by our commercial partners, updating you on the capabilities and use of their hardware and software. Our ***Synaptic Junction*** this year will feature talks on practical issues in neuroradiology, including **MR Safety for Patients with Implants, DTI for Dummies, Dose Extraction** (for monitoring patient exposure), **and a lively session on Communicating Results Directly to Patients**. In response to rapid changes in the economic and health care environments, we will continue to feature programming on socioeconomic issues facing neuroradiology and practice quality improvement. We will expand our programming specific to **fellows, residents, medical students and neuroradiologists in their first three years in practice**.

In celebration of our 50th Anniversary we have planned some outstanding special events including reviews of the history of the field and the Society, where we are headed in the future, recognition of our founders and early members, a Keynote Address from one of our notable leaders in Neuroradiology, and an unforgettable **50th Anniversary Reception at The Museum of Modern Art (MoMA)**.

Among its most valuable functions, the Annual Meeting will be the ideal opportunity to stay connected with friends and colleagues and get the latest in brain, spine, and head and neck imaging. As befits a golden anniversary, this will be a truly unique event. I look forward to seeing you there!



**David B. Hackney, MD, FACR**  
ASNR President



**David B. Hackney, MD, FACR**  
ASNR President





THE CITY OF NEW YORK  
OFFICE OF THE MAYOR  
NEW YORK, NY 10007

April 21, 2012

Dear Friends:

It is a great pleasure to welcome everyone to the American Society of Neuroradiology's 50<sup>th</sup> Annual Meeting and The Foundation of the ASNR Symposium 2012.

New York City is focused on helping all our residents enjoy the benefits of lifelong good health. Thanks to innovative public policies and our world-class medical institutions, we have made amazing gains over the past decade, and our residents are living longer than ever before as a result. That is why we are proud to applaud the ASNR's thousands of neuroradiology professionals for their outstanding commitment to their patients. And as ASNR celebrates its 50<sup>th</sup> Anniversary right here in New York where it was founded, we look forward to the latest research initiatives and advances in care making a lasting difference for people across the five boroughs and beyond.

On behalf of all New Yorkers, I offer my best wishes for a productive meeting and symposium, a wonderful stay in our great City, and continued success in your vital mission.

Sincerely,

A handwritten signature in black ink, reading "Michael R. Bloomberg".

Michael R. Bloomberg  
Mayor



# ASNR ANNUAL MEETING HAS GONE MOBILE!

Scan to download!



Schedule, Maps, Twitter and more on your  
mobile device - completely free.

Download **Guidebook** on the Apple App  
Store or Android Marketplace or visit  
[guidebook.com/getit](http://guidebook.com/getit)

Search for the 'ASNR' guide under the "download guides" section of the application.

**guidebook**

[guidebook.com](http://guidebook.com)



# Table of Contents

II.....	2011 - 2012 ASNR Executive Committee
II-III .....	2011 - 2012 ASNR Annual Meeting Arrangements Committees
IV .....	AJNR/ASNR Staff
V-VI.....	General Information
VII.....	Important Information for Young Professionals
VIII.....	Social Programs
IX.....	Past Annual Meetings of the ASNR
X.....	ASNR Past Presidents & Founders
XI.....	2012 ASNR Gold Medal Award Recipient & Past Recipients
XII .....	2012 ASNR Honorary Member & Past Honorary Members
XIII.....	2012 The Foundation of the ASNR Award for Outstanding Contributions in Research Award & Past Recipients
XIII-XIV .....	2012 ASNR Cornelius G. Dyke Memorial Award Recipient & Past Recipients
XV .....	ASNR 2011 Outstanding Presentation Awards
XV .....	2011/2012 Specialty/Regional Society Awards
XVI-XVII .....	The Foundation of the ASNR Basic Science Research Award Past Recipients
XVIII.....	2012 The Foundation of the ASNR Scholar Award in Neuroradiology Research & Past Recipients
XIX .....	2012 The Foundation of the ASNR Research Scientist Award & Past Recipients
XIX .....	2012 The Foundation of the ASNR Comparative Effectiveness Award & Past Recipients
XIX .....	The Foundation of the ASNR Award in Cerebrovascular Disease Past Recipients
XX.....	Continuing Medical Education (CME), Accreditation Statement, Credit Designation Statement and Target Audience
XXI.....	ASNR 50th Annual Meeting Educational Objectives
XXII.....	Synaptic Junction Lectures
XXIII .....	How-To Sessions
XXIV .....	Technical Exhibition Floor Plan
XXV .....	Technical Exhibition Roster
XXVI - XXVII.....	ASNR 50th Annual Meeting Invited Speakers
XXVIII - XXXI.....	Scientific Program Overview
XXXII.....	ASNR Future Annual Meetings
Page 1-97 .....	Monday Sessions
Page 98-183.....	Tuesday Sessions
Page 184-231 .....	Wednesday Sessions
Page 232-322.....	Thursday Sessions
Page 322-391 .....	Electronic Excerpta Extraordinaire (EE)
Page 391-466.....	Scientific Posters (P) Printed
Page 466-660.....	Electronic Scientific Posters (eP)
Page 660-716.....	Education Exhibits (EdE) Printed
Page 716-796.....	Electronic Education Exhibits (eEdE)
Page 797-824.....	Index of Program Participants



# 2011-2012 ASNR Executive Committee

David B. Hackney, MD, FACR  
President

Pamela W. Schaefer, MD  
President-Elect/Program Chair

Mauricio Castillo, MD, FACR  
Vice President/AJNR Editor

Laurie A. Loevner, MD  
Treasurer

David J. Seidenwurm, MD  
Secretary

Pratik Mukherjee, MD, PhD  
Research Committee Co-Chair

Pina C. Sanelli, MD, MPH  
Research Committee Co-Chair &  
Evidence Based Medicine Chair

Joseph A. Maldjian, MD  
Functional Representative

Suresh K. Mukherji, MD, FACR  
Fellowship Director Chair & Head  
and Neck Representative

Joshua A. Hirsch, MD, FACR  
Neurointerventional Surgery  
Representative

Caroline D. Robson, MB, ChB  
Pediatric Representative

Walter S. Bartynski, MD  
Spine Representative

Carolyn Cidis Meltzer, MD, FACR  
1st Past President & ACR Neuro  
Committee Liaison

John R. Hesselink, MD, FACR  
2nd Past President

Robert D. Zimmerman, MD, FACR  
3rd Past President & 2nd ABR Trustee

Robert M. Barr, MD  
Member-at-Large &  
Clinical Practice Chair  
& ACR Councilor

Barton F. Branstetter IV, MD  
Education Committee Chair

Vincent P. Mathews, MD  
Rules Committee Chair  
& ABR 1st Trustee

Tina Young Poussaint, MD  
Publication Committee Chair

Clifford J. Belden, MD  
Membership Committee Chair

Steven Falcone, MD  
Delegate to the AMA

Jacqueline A. Bello, MD  
AMA Alternate, ACR Alternate  
Delegate and ACR Neuro Committee  
Representative

James B. Gantenberg, FACHE  
ASNR Executive Director/CEO  
Commercial Relations Chair

Peter B. Barker, D.Phil.  
Research Scientist Chair  
& Physicist Advisor

Michael Tyszka, PhD  
Physicist Advisor

Nafi Aygun, MD  
Physicist Advisor

Howard A. Rowley, MD  
The Foundation of the ASNR Chair

# 2011-2012 ASNR Meeting Arrangements Committees

## Scientific Program Committee

Pamela W. Schaefer, MD  
President-Elect/Program Chair

Konstantinos Arfanakis, PhD

Daniel P. Barboriak, MD

Peter B. Barker, D.Phil.

Robert M. Barr, MD

Walter S. Bartynski, MD

Barton F. Branstetter IV, MD

Mauricio Castillo, MD, FACR

Colin P. Derdeyn, MD

John L. Go, MD

David B. Hackney, MD, FACR

Ellen G. Hoeffner, MD

Nickoleta L. Hoefling, MD

Jerry G. Jarvik, MD

Walter Kucharczyk, MD, FRCP(C)

Christopher J. Moran, MD

Jeffrey R. Petrella, MD

C. Douglas Phillips, MD, FACR

Whitney B. Pope, MD, PhD

James M. Provenzale, MD

Timothy P. L. Roberts, PhD

Caroline D. Robson, MB, ChB

Pina C. Sanelli, MD, MPH

Erin Simon Schwartz, MD

David J. Seidenwurm, MD

Dikoma C. Shungu, PhD

A. Gregory Sorensen, MD

Max Wintermark, MD

## Technical Exhibits Committee

A. Orlando Ortiz, MD, MBA, FACR  
Chair

Alan L. Williams, MD, FACR, MBA  
Consultant

Todd Abruzzo, MD

William G. Bradley, MD, PhD, FACR

Joseph P. Comunale, Jr., MD

Thomas S. Dina, MD

Steven Falcone, MD

John L. Go, MD

Meng Law, MD

Gregg H. Zoarski, MD



# 2011-2012 ASNR Meeting Arrangements Committees

## Audio Visual Committee

Edward A. Michals, MD  
**Chair**  
Richard M. Berger, MD  
Andrew G. Bleicher, MD  
James Y. Chen, MD  
Steven W. Hetts, MD  
Jenny K. Hoang, MBBS  
Lucien M. Levy, MD, PhD  
Mark E. Mullins, MD, PhD  
Hemant A. Parmar, MD  
Stuart R. Pomerantz, MD  
Erin Simon Schwartz, MD  
Frank C. Tong, MD  
Achala S. Vagal, MD  
Richard H. Wiggins, III, MD, CIIP  
Max Wintermark, MD

## Education Exhibits Committee (Formerly Scientific Exhibits Committee)

Dheeraj Gandhi, MD  
**Chair**  
Stephen Gebarski, MD  
**Consultant**  
Ellen G. Hoeffner, MD  
**Consultant**  
Ashley H. Aiken, MD  
Sameer A. Ansari, MD, PhD  
Nafi Aygun, MD  
Kathleen A. Barry, MD  
Mary E. Cunnane, MD  
Lawrence E. Ginsberg, MD  
Ajay Gupta, MD  
Blaine L. Hart, MD  
Daniel P. Hsu, MD  
Peter A. Janick, MD  
Carl E. Johnson, MD  
Michele H. Johnson, MD  
Bernadette L. Koch, MD  
Susan Palasis, MD  
Gregory W. Petermann, MD  
Jay J. Pillai, MD  
Jordan M. Prager, MD  
Stein Erik Rafto, MD  
Otto Rapalino, MD  
Amit M. Saindane, MD  
Haris Sair, MD  
Gaurang V. Shah, MD  
James G. Smirniotopoulos, MD  
Ashok Srinivasan, MD  
Bruce A. Wasserman, MD  
Christopher P. Wood, MD  
Geoffrey Young, MD  
Robert J. Young, MD

## Education Committee

Barton F. Branstetter IV, MD  
**Chair**  
Ashley H. Aiken, MD  
Nafi Aygun, MD  
Peter B. Barker, D.Phil.  
Richard M. Berger, MD  
Eric C. Bourekas, MD  
Jerrold Boxerman, MD  
Dale A. Charletta, MD  
Rebecca S. Cornelius, MD  
H. Christian Davidson, MD  
Richard K. Downs, Sr., MD  
Edward J. Escott, MD  
Nikdokht Farid, MD  
Adam E. Flanders, MD  
Melanie B. Fukui, MD  
John L. Go, MD  
David B. Hackney, MD, FACR  
Joshua A. Hirsch, MD, FACR, FSIR  
Jenny K. Hoang, MBBS  
Steven G. Imbesi, MD  
Andrew Ku, MD  
Meng Law, MD  
Laurie A. Loevner, MD  
Joseph A. Maldjian, MD  
David S. Martin, MD  
Carolyn Cidis Meltzer, MD, FACR  
Gary M. Miller, MD  
Gul Moonis, MB, BS  
Toshio Moritani, MD, PhD  
Suresh K. Mukherji, MD, FACR  
Mark E. Mullins, MD, PhD  
Gerard J. Muro, MD  
Gregory W. Petermann, MD  
C. Douglas Phillips, MD, FACR  
Tina Young Poussaint, MD  
Edward P. Quigley, III, MD, PhD  
Caroline D. Robson, MB,ChB  
Karen L. Salzman, MD  
Pina C. Sanelli, MD, MPH  
Pamela W. Schaefer, MD  
David J. Seidenwurm, MD, FACR  
James G. Smirniotopoulos, MD  
Jay Starkey, MD  
Apostolos John Tsiouris, MD  
Achala S. Vagal, MD  
Daniel B. Vigneron, PhD  
Richard H. Wiggins, III, MD, CIIP  
Christopher P. Wood, MD  
Robert D. Zimmerman, MD, FACR

## AJNR Staff

### American Journal of Neuroradiology Headquarters Office

2210 Midwest Road, Suite 205

Oak Brook, IL 60523-8205

**Telephone:** 630-574-1487

**Fax:** 630-786-6251

**Internet:** <http://www.ajnr.org>

---

#### **Karen Halm**

*Managing Editor*

Ext. 238, [khalm@asnr.org](mailto:khalm@asnr.org)

#### **Jason Gantenberg**

*Editorial Assistant*

Ext. 240, [jason@asnr.org](mailto:jason@asnr.org)

#### **Mary Harder**

*Editorial Assistant*

Ext. 239, [mharder@asnr.org](mailto:mharder@asnr.org)

## Additional Email Addresses

---

### **Clinical Practice**

[cpc@asnr.org](mailto:cpc@asnr.org)

### **Communications**

[communications@asnr.org](mailto:communications@asnr.org)

### **Executive**

[executive@asnr.org](mailto:executive@asnr.org)

### **Finance**

[finance@asnr.org](mailto:finance@asnr.org)

### **Foundation**

[foundation@asnr.org](mailto:foundation@asnr.org)

### **Meetings**

[meetings@asnr.org](mailto:meetings@asnr.org)

### **Membership**

[membership@asnr.org](mailto:membership@asnr.org)

## ASNR Staff

### American Society of Neuroradiology Headquarters Office

2210 Midwest Road, Suite 207

Oak Brook, IL 60523-8205

**Telephone:** 630-574-0220

**Fax:** 630-574-0661/630-574-1740

**Internet:** <http://www.asnr.org>

---

#### **James B. Gantenberg, FACHE**

*Executive Director/CEO*

Ext. 224, [jgantenberg@asnr.org](mailto:jgantenberg@asnr.org)

#### **Arthur An**

*Educational Technologist*

Ext. 241, [aan@asnr.org](mailto:aan@asnr.org)

#### **Angelo Artemakis**

*Director of Communications and Media Management*

Ext. 227, [aartemakis@asnr.org](mailto:aartemakis@asnr.org)

#### **Kenneth Cammarata**

*Director of Specialty Societies and Member Services*

Ext. 226, [kcammarata@asnr.org](mailto:kcammarata@asnr.org)

#### **Tina Cheng, CPA**

*Director of Finance and Information Systems*

Ext. 225, [tcheng@asnr.org](mailto:tcheng@asnr.org)

#### **Michelle Davies**

*Meetings & Logistics Assistant*

Ext. 232, [mdavies@asnr.org](mailto:mdavies@asnr.org)

#### **Pat Galle-Bingham**

*Staff Accountant*

Ext. 222, [pat@asnr.org](mailto:pat@asnr.org)

#### **Valerie Geisendorfer, CMP**

*Senior Manager of Scientific Meetings*

Ext. 228, [vgeisendorfer@asnr.org](mailto:vgeisendorfer@asnr.org)

#### **Bonnie Mack**

*Membership/Society Coordinator*

Ext. 234, [bmack@asnr.org](mailto:bmack@asnr.org)

#### **Karen Mansfield**

*Office Manager/Executive Assistant*

Ext. 221, [kmansfield@asnr.org](mailto:kmansfield@asnr.org)

#### **Kelsey Pliner**

*Meetings Registrar*

Ext. 231, [kpliner@asnr.org](mailto:kpliner@asnr.org)

#### **Lora Di Padova-Tannehill, CMP**

*Director of Scientific Meetings*

Ext. 229, [ltannehill@asnr.org](mailto:ltannehill@asnr.org)

#### **Stephanie Walsh, MBA**

*Director of Development*

Ext. 235, [swalsh@asnr.org](mailto:swalsh@asnr.org)



# General Information (as of 3/21/12)

## Meeting Location

Hilton New York  
1335 Avenue of the Americas  
New York, NY 10019  
(212) 315-1374

## Meeting Registration

Registration is located on the 2<sup>nd</sup> Floor Promenade of the Hilton New York. The registration desk will be open during the following hours:

Friday, April 20 .....	3:00 pm - 8:00 pm
Saturday, April 21 .....	6:30 am - 6:00 pm
Sunday, April 22 .....	6:30 am - 6:00 pm
Monday, April 23 .....	6:30 am - 6:00 pm
Tuesday, April 24 .....	6:30 am - 6:00 pm
Wednesday, April 25 .....	6:30 am - 6:00 pm
Thursday, April 26 .....	6:30 am - 6:00 pm

## Speaker Ready Room Location & Hours

### Hilton New York - Bryant (2nd Floor)

Friday, April 20 .....	3:00 pm - 8:00 pm
Saturday, April 21 through Thursday, April 26 .....	6:00 am - 6:00 pm

## Name Badges

Please wear name badges at all times while you are attending the scientific sessions, social programs, and technical exhibits. Badge colors are identified as follows:

ASNR Members, ASNR Members-In-Training & ASNR Subspecialty Societies (ASFNR, ASHNR, ASPNR, ASSR & SNIS) .....	Blue
Non-Member .....	Green
Other Professional .....	Yellow
Guest .....	Peach
Exhibitor .....	Gold
Staff .....	Purple

## Committee/Specialty/Regional Society Meetings

Please refer to the Daily Postings on the Meetings & Announcements Board located on the 2<sup>nd</sup> Floor Promenade at the Hilton New York.

## Meetings & Announcements Board

The Meetings & Announcements Board is located on the 2<sup>nd</sup> Floor Promenade at the Hilton New York. Please refer to the Daily Postings on the Meetings & Announcements Board for information on committee meetings.

## CME Pavilion/Message Center/ Alternate SAM Response Area

Located in Gibson (2<sup>nd</sup> Floor) the CME Pavilion computer terminals will be available to registered attendees that can be used to evaluate attended sessions, print CME certificates and to check E-mail.

### Hilton New York - Gibson

Saturday, April 21 .....	7:00 am - 9:00 pm
Sunday, April 22 through Thursday, April 26 .....	6:30 am - 9:00 pm

## Coat Check

### 2<sup>nd</sup> Floor Promenade at the Hilton New York

#### Hours of Operation:

Saturday, April 21 .....	6:30am - 6:00pm
Sunday, April 22 .....	6:00am - 6:00pm
Monday, April 23 and Tuesday, April 24 .....	6:00am - 7:00pm
Wednesday, April 25 .....	6:00am - 8:00pm
Thursday, April 26 .....	6:00am - 7:00pm

## Concierge Desk

### Lobby Level of the Hilton New York

Friday, April 20 through Friday, April 27 .....	7:00am - 11:59pm
---	------------------

## Local Hospital

Roosevelt Hospital - St. Luke's • (212) 523-4000  
1000 Tenth Avenue  
New York, NY 10019

## Emergency Service Procedure

The Hilton New York is fully prepared to handle different types of situations to assist our guests. The following is information on The Hilton New York's emergency procedures:

***Do not call 9-1-1 from your cellular phone. Calling 9-1-1 delays the response to the emergency by the first responders.***

- Locate the nearest Hilton New York **HOTEL PHONE** and dial our Security Control at extension **5747** or "66" for a life emergency.
- If you are calling from a cellular phone, the number is **212-261-5747** or **the hotel general number at 212-586-7000**.
- Notify the Security Control of the location of the person requiring medical attention, along with a description of the person and their injury. The Security Control will contact your contracted medical service provider.
- Return to the individual.
- The hotel has an emergency response team 24 hours a day. In the event of an emergency, calling the emergency number 66 will initiate the appropriate response.
- Paramedics, Fire Department, and the Police Department are all located within minutes from the hotel.
- The Hilton New York's Security Department, as well as a small number of other employees, are trained in CPR and First Aid.
- Emergency evacuation routes and procedures are located on the inside of all guest room doors.

## Remote Access Features Continues in 2012!

**A link will be provided so that you can evaluate for CME credits from your personal devices (phone/laptop/PDA) at any time.**

**In addition you will be able to participate in SAM sessions remotely through Sunday, May 6.**

# General Information (continued) (as of 3/21/12)

## Food Service

**Monday through Thursday:** ASNR will provide Continental Breakfast, Morning & Afternoon Beverage Breaks. Lunch on own.

Please refer to the schedule below.

## Continental Breakfast

Monday, April 23 through Thursday, April 26.....3<sup>rd</sup> Floor Promenade

## Continuous Coffee Service

Tuesday, April 24 through Thursday, April 26 ..... Americas Hall I

## Morning Beverage Breaks

Saturday, April 21 through Monday, April 23.....3<sup>rd</sup> Floor Promenade

Tuesday, April 24 through Thursday, April 26 ..... Americas Hall I

## Afternoon Beverage Breaks

Saturday, April 21 through Monday, April 23.....3<sup>rd</sup> Floor Promenade

Tuesday, April 24 through Thursday, April 26 ..... Americas Hall I

## ASNR Publications Booth 3rd Floor Promenade

All attendees are invited to stop by the booth any time to tour the *AJNR* and *Neurographics* Web sites and *AJNR* Blog and app.

## Meet *AJNR*'s Editor-in-Chief

Dr. Mauricio Castillo, *AJNR*'s Editor-in-Chief, will be present at the Journal's booth Monday - Thursday from 11:00 am until noon to answer questions regarding the Journal's online features, listen to suggestions, talk about projects with prospective authors, and advise fellows regarding their future contributions to *AJNR*.

## Neurographics

*Neurographics* is ASNR's quarterly online educational journal, featuring peer-reviewed scientific exhibits and select case reports. *Neurographics* is available free online [www.neurographics.org](http://www.neurographics.org). *Neurographics* Editor Dr. Barton Branstetter IV will be available in the ASNR Publications booth Monday through Thursday from 11:00 am to noon to answer questions.

## Booth Schedule

### Hilton New York - 3rd Floor Promenade

Saturday, April 21 through Sunday, April 22 ..... 7:30 am - 5:00 pm

Monday, April 23 through Thursday, April 26..... 8:30 am - 5:00 pm

## How-To Sessions

Grand Ballroom Suite (3rd Floor)

## Focus/Scientific Paper Sessions

Grand Ballroom Suite, Trianon Ballroom, Beekman/Sutton North, Sutton Center/South, Murray Hill

## Synaptic Junction Lectures

Murray Hill, Beekman/Sutton North

## EXHIBITS

## Education Exhibits & Electronic Education Exhibits

Rhineland (2nd Floor)

## Scientific Posters, Electronic Scientific Posters and Electronic Excerpta Extraordinaire

Americas Hall II

## Technical Exhibits

Americas Hall I

## MISCELLANEOUS

## American Board of Radiology (ABR) Information Desk

2<sup>nd</sup> Floor Promenade

## Young Professionals Lounge (Fellows, Residents, Medical Students and Neuroradiologists in their first three years in practice)

Regent (2nd Floor)

## Headquarters Office

Nassau West (2nd Floor)

## VIP/The Foundation of the ASNR Lounge

Hudson (4th Floor)



# Important Information for Young Professionals

## Young Professionals Lounge - Regent (2<sup>nd</sup> Floor) (Fellows, Residents, Medical Students and Neuroradiologists in their first three years in practice)

Visit the Fellows, Residents & Medical Students Lounge in the Regent (2<sup>nd</sup> Floor) open from 6:30am – 6:00pm daily from Saturday, April 21 - Thursday, April 26. This will provide a “home base” for Young Professionals to network and share knowledge and experiences throughout the meeting.

### Young Professionals Luncheon

Tuesday, April 24 • 12:00pm - 1:00pm

Gramercy West (2<sup>nd</sup> Floor)

Fellows, Residents, Medical Students and Neuroradiologists in their first three years in practice – join ASNR Leaders for Lunch, at 12:00pm on Tuesday, April 24, 2012 in the Gramercy West (2<sup>nd</sup> Floor).

### Young Professionals Sessions

Fellows, Residents, Medical Students and Neuroradiologists in their first three years in practice, the ASNR has designed specific program topics for learning during the ASNR Annual Meeting. You won't want to miss the following session presentations:

#### Tuesday, April 24

##### Entering And Thriving In Private Practice

8:30am - 10:00am • Murray Hill

Welcome to the Real World

*John E. Jordan, MD*

Understanding the Food Chain

*Robert M. Barr, MD*

The Corporate Environment

*Stephen T. Sweriduk, MD*

The HMO Environment

*D. Christian Sonne, MD*

Making the Transition

*David J. Seidenwurm, MD, FACR*

Questions and Answers

##### Academic Session

1:00pm - 2:30pm • Murray Hill

Getting Your First Job

*Carolyn C. Meltzer, MD, FACR*

Building a Research Program

*Soonmee Cha, MD*

The Different Component of Academic Radiology

*Suresh K. Mukherji, MD, FACR*

Getting Promoted: The Different  
Promotion Tracks

*David M. Yousem, MD, MBA*

Discussion



## Social Programs

### **“ASNR Welcome Reception”**

**Monday, April 23**

**7:00 pm - 10:00 pm**

**Off-site Location:**

**The Museum of Modern Art (MoMA)**

Join us at The Museum of Modern Art to celebrate ASNR's 50th Anniversary. MoMA is often identified as the most influential museum of modern art in the world. Art enthusiasts and novices alike are often awestruck by the masterpieces before them, including Monet's Water Lilies, Picasso's Les Femmes d'Alger, and van Gogh's Starry Night. The museum's collection offers an unparalleled overview of modern and contemporary art, including works of architecture and design, drawings, painting, sculpture, photography, prints, illustrated books and artist's books, film and electronic media. In addition to the artwork, one of the main draws of MoMA is the building itself. The main entrance is a 110 foot atrium and inside a maze of glass walkways permits art viewing from many angles. Also of interest is the Abby Aldrich Rockefeller Sculpture Garden. A glass wall lets visitors look directly into the surrounding galleries from the garden, where there's also a reflecting pool and trees. You don't want to miss this special experience. We look forward to welcoming you to The Museum of Modern Art.

- Includes access to the 5th floor gallery, sculpture garden (weather permitting), dinner buffet and three (3) hour open bar.
- FREE for those who register for the meeting.
- Guest Ticket is \$75.00.

### **“Closing Reception with Technical Exhibitors”**

**Wednesday, April 25**

**6:30 pm - 7:30 pm**

**Hilton New York Hotel in Americas Hall I**

We look forward to closing the social events with a pre-dinner reception of New York's culinary favorites. The reception, located in Americas Hall I offers attendees the perfect opportunity to see this year's Technical Exhibition, the ASNR's annual showcase for the newest products and services for the field of Neuroradiology. Enjoy complimentary pre-dinner hors d'oeuvres and beverages while you network with exhibitor representatives and fellow colleagues. The ASNR Technical Exhibition is the place where advanced technology, diagnostic and interventional Neuroradiological excellence come together.

- Includes pre dinner buffet and one (1) hour open bar.
- FREE for those who register for the meeting.
- Guest Ticket is \$40.00.

### **2012 Education Exhibits Tour**

**Rhineland (2<sup>nd</sup> Floor)**

Monday, April 23 .....12:00pm - 1:00pm

Wednesday, April 25.....12:00pm - 1:00pm

***NEW in 2012! You will receive CME credits for participating in the Education Exhibits Tour!***

Review Education Exhibits, visual presentation/educational displays designed to further the understanding of Neuroradiology by featuring cutting-edge material or by offering an instructional review of a particular topic. The session will allow for review of visually-oriented educational displays that demonstrate novel and innovative applications for computers in Neuroradiology clinical practice, training and research. Share this educational opportunity with your colleagues and primary Exhibit presenters and exchange in a lively Questions & Answers Session.

***Another unique feature not to be missed at the ASNR...See you on the tour!***

### **“Case of the Day”**

**Monday, April 23 through**

**Wednesday, April 25**

**Rhineland (2<sup>nd</sup> Floor)**

***New Program Feature at the ASNR 50th Annual Meeting!***

A new addition to the ASNR program for the ASNR 50th Annual Meeting is the Case of the Day (COD) program. Led by Drs. Mark Mullins and Char Branstetter, COD is scheduled from Monday, April 23, through Wednesday, April 25.

Cases will be presented in Rhineland at the Hilton New York and will be available in printed poster format as well as on a video loop at a nearby monitor. There will be 6 categories: brain, functional, head & neck, pediatric, spine and vascular/interventional, each with 1 case per day. Answers will be presented on the day following their respective questions.

An online system will be available for submission of preferred diagnoses. Be sure to participate in this new interactive programming feature with a limited number of prizes awarded to those participants with highest daily correct responses.

***No CME credit is available for this activity.***

# Past Annual Meetings

## **Organizational Meeting**

May 19, 1962 - New York

**Keene's English Chophouse**

## **Second Business Meeting**

October 5, 1962 - Washington, DC

**Shoreham Hotel**

## **First Annual Meeting**

October 7, 1963 - Montreal

**Queen Elizabeth Hotel**

## **Second Annual Meeting**

September 23, 1964 - New York

**Waldorf Astoria**

## **Third Annual Meeting**

June 11, 1965 - Atlantic City

**Dennis Hotel**

## **Fourth Annual Meeting**

June 15-16, 1966 - Washington, DC

**Sheraton-Park Hotel**

## **Fifth Annual Meeting**

May 15, 1967 - New York

**Columbia University**

## **Sixth Annual Meeting**

September 27-28, 1968 - New Orleans

**Jung Hotel**

## **Seventh Annual Meeting**

May 13-19, 1969 - Cleveland

Joint Meeting with American  
Association of Neurological Surgeons

**Sheraton-Cleveland Hotel**

## **Eighth Annual Meeting**

February 12-13, 1970 - Washington, DC

**Washington Hilton**

## **Ninth Annual Meeting**

May 27-29, 1971 - San Francisco

**Fairmont Hotel**

## **Tenth Annual Meeting**

February 21-24, 1972 - Mexico City

**Maria-Isabel Sheraton**

## **Eleventh Annual Meeting**

May 26-28, 1973 - Boston

**Statler Hilton**

## **Twelfth Annual Meeting**

March 14, 1974 - Punta del Este, Uruguay

(In conjunction with X Symposium  
Neuroradiologicum)

**Punta del Este, Uruguay**

## **Thirteenth Annual Meeting**

June 3-7, 1975 - Vancouver

**Bayshore Inn**

## **Fourteenth Annual Meeting**

May 18-22, 1976 - Atlanta

**Peachtree Plaza**

## **Fifteenth Annual Meeting**

March 27-31, 1977 - Bermuda

**Hamilton Princess Hotel**

## **Sixteenth Annual Meeting**

February 26-March 2, 1978 - New Orleans

**Hyatt Regency**

## **Seventeenth Annual Meeting**

May 20-24, 1979 - Toronto

**Hotel Toronto**

## **Eighteenth Annual Meeting**

March 16-21, 1980 - Los Angeles

**Century Plaza**

## **Nineteenth Annual Meeting**

May 5-9, 1981 - Chicago

**Marriott Hotel**

## **Twentieth Annual Meeting**

October 10-16, 1982 - Washington, DC  
(In conjunction with XII Symposium  
Neuroradiologicum)

**Washington Hilton**

## **Twenty-First Annual Meeting**

June 5-9, 1983 - San Francisco

**St. Francis Hotel**

## **Twenty-Second Annual Meeting**

June 2-7, 1984 - Boston

**Westin Copley Place Hotel**

## **Twenty-Third Annual Meeting**

February 18-23, 1985 - New Orleans

**Marriott Hotel**

## **Twenty-Fourth Annual Meeting**

January 19-23, 1986 - San Diego

**Sheraton Harbor Island  
Hotel**

## **Twenty-Fifth Annual Meeting**

(Silver Anniversary)

May 10-15, 1987 - New York

**Hilton New York**

## **Twenty Sixth Annual Meeting**

May 15-20, 1988 - Chicago

**Chicago Hilton & Towers**

## **Twenty-Seventh Annual Meeting**

March 19-24, 1989 - Orlando

**The Peabody Orlando**

## **Twenty-Eighth Annual Meeting**

March 19-23, 1990 - Los Angeles

**Century Plaza Hotel & Tower**

## **Twenty-Ninth Annual Meeting**

June 9-14, 1991 - Washington, DC

**The Washington Hilton and  
Towers**

## **Thirtieth Annual Meeting**

May 31-June 5, 1992 - St. Louis

**Adam's Mark**

## **Thirty-First Annual Meeting**

May 17-20, 1993 - Vancouver

**Vancouver Trade and  
Convention Center**

## **Thirty-Second Annual Meeting**

May 3-7, 1994 - Nashville

**Opryland Hotel and  
Conference Center**

## **Thirty-Third Annual Meeting**

May 23-27, 1995 - Chicago

**Sheraton Chicago Hotel and  
Towers**

## **Thirty-Fourth Annual Meeting**

June 23-27, 1996 - Seattle

**Washington State  
Convention  
and Trade Center**

## **Thirty-Fifth Annual Meeting**

May 18-22, 1997 - Toronto

**Metro Toronto Convention  
Center**

## **Thirty-Sixth Annual Meeting**

May 17-21, 1998 - Philadelphia

(In conjunction with XVI Symposium  
Neuroradiologicum)

**Pennsylvania Convention  
Center**

## **Thirty-Seventh Annual Meeting**

May 23-28, 1999 - San Diego

**San Diego Convention  
Center**

## **Thirty-Eighth Annual Meeting**

April 4-8, 2000 - Atlanta

**Hyatt Regency Atlanta**

## **Thirty-Ninth Annual Meeting**

April 23-27, 2001 - Boston

**Hynes Convention Center**

## **Fortieth Annual Meeting**

May 13-17, 2002 - Vancouver

**Vancouver Convention  
& Exhibition Center**

## **Forty-First Annual Meeting**

April 28 - May 2, 2003 - Washington, DC

**Marriott Wardman Park  
Hotel**

## **Forty-Second Annual Meeting**

June 7-11, 2004 - Seattle

**Washington State  
Convention and Trade Center**

## **Forty-Third Annual Meeting**

May 21-27, 2005 - Toronto

**Metro Toronto Convention  
Center**

## **Forty-Fourth Annual Meeting**

April 29-May 5, 2006 - San Diego

**San Diego Convention  
Center**

## **Forty-Fifth Annual Meeting**

June 9-14, 2007 - Chicago

**Hyatt Regency Chicago**

## **Forty-Sixth Annual Meeting**

May 30-June 5, 2008 - New Orleans

**Ernest N. Morial Convention  
Center**

## **Forty-Seventh Annual Meeting**

May 16-21, 2009 - Vancouver

**Vancouver Convention and  
Exhibition Centre**

## **Forty-Eighth Annual Meeting**

May 15-20, 2010 - Boston

**Hynes Convention Center**

## **Forty-Ninth Annual Meeting**

June 4-9, 2011 - Seattle

**Washington State  
Convention Center**

# ASNR Past Presidents and Founders

## 1962-64

Juan M. Taveras, MD\*

## 1964-65

Mannie M. Schechter, MD\*

## 1965-66

Donald L. McRae, MD\*

## 1966-67

Ernest H. Wood, MD\*

## 1967-68

Harold O. Peterson, MD\*

## 1968-69

Colin B. Holman, MD\*

## 1969-70

Giovanni Di Chiro, MD\*

## 1970-71

D. Gordon Potts, MD

## 1971-72

Norman E. Chase, MD

## 1972-73

Fred J. Hodges, III, MD\*

## 1973-74

T. Hans Newton, MD\*

## 1974-75

Hillier L. Baker, Jr., MD\*

## 1975-76

Irvin I. Kricheff, MD

## 1976-77

Norman E. Leeds, MD

## 1977-78

Sadek K. Hilal, MD\*

## 1978-79

Stephen A. Kieffer, MD

## 1979-80

David O. Davis, MD

## 1980-81

George Wortzman, MD

## 1981-82

Gabriel H. Wilson, MD\*

## 1982-83

Arthur E. Rosenbaum, MD

## 1983-84

O. Wayne Houser, MD

## 1984-85

Samuel M. Wolpert, MD

## 1985-86

R. Thomas Bergeron, MD

## 1986-87

Derek C. Harwood-Nash, MD\*

## 1987-88

Michael S. Huckman, MD

## 1988-89

Anne G. Osborn, MD

## 1989-90

Joseph F. Sackett, MD

## 1990-91

Anton N. Hasso, MD, FACR

## 1991-92

R. Nick Bryan, MD, PhD, FACR

## 1992-93

David Norman, MD

## 1993-94

Glenn S. Forbes, MD

## 1994-95

Robert M. Quencer, MD

## 1995-96

Robert R. Lukin, MD

## 1996-97

Burton P. Drayer, MD

## 1997-98

Richard E. Latchaw, MD

## 1998-99

A. James Barkovich, MD

## 1999-00

Eric J. Russell, MD, FACR

## 2000-01

William S. Ball, Jr., MD

## 2001-02

William P. Dillon, MD

## 2002-03

Patrick A. Turski, MD

## 2003-04

Charles M. Strother, MD

## 2004-05

Victor M. Haughton, MD

## 2005-06

Patricia A. Hudgins, MD

## 2006-07

Robert I. Grossman, MD

## 2007-08

David M. Yousem, MD, MBA

## 2008-09

Robert D. Zimmerman, MD, FACR

## 2009-10

John R. Hesselink, MD, FACR

## 2010-11

Carolyn C. Meltzer, MD, FACR

## Founding Members

Norman E. Chase, MD

Giovanni Di Chiro, MD\*

William N. Hanafee, MD

Fred J. Hodges, III, MD\*

Colin B. Holman, MD\*

Norman E. Leeds, MD

Eugene V. Leslie, MD\*

Donald L. McRae, MD\*

Thomas H. Newton, MD\*

Harold O. Peterson, MD\*

D. Gordon Potts, MD

Mannie M. Schechter, MD\*

Juan M. Taveras, MD\*

Ernest H. Wood, MD\*

\*deceased





# Awards and Honors

## 2012 ASNR Gold Medal Award



The Gold Medal fosters the highest standards of the American Society of Neuroradiology, based on exceptional quality, service, and excellence, and not necessarily on fame. It emphasizes both professional and personal attributes... individuals who are superb neuroradiologists, clinicians, or scientists, and truly outstanding. The recipients are individuals who have extended themselves beyond furthering their own careers through contributions at all levels of professional strata, with an accent on consistency and duration of these outstanding contributions.

### 2012 Gold Medal Recipient

**A. James Barkovich, MD**

*University of California, San Francisco*

Anthony James Barkovich, M.D. is Professor of Radiology and Biomedical Imaging, Neurology, Pediatrics, and Neurosurgery and Chief of Pediatric Neuroradiology at the University of California, San Francisco. His undergraduate education was at the University of California at Davis, he pursued graduate studies in Chemistry at the University of California at Berkeley, and he received his medical education at the George Washington University. He completed his internship and Radiology residency at the Letterman Army Medical Center in San Francisco, CA and then a neuroradiology fellowship at the Walter Reed Army Medical Center in Washington, D.C. During his fellowship, he spent time at Johns Hopkins Hospital, Children's National Medical Center in Washington, D.C., and the Hospital for Sick Children in Toronto. After serving 3½ years in the U.S. Army as the neuroradiologist at Letterman Army Medical Center in San Francisco, Dr. Barkovich joined the faculty of the University of California, San Francisco in 1989, where he has remained for more than 22 years.

Dr. Barkovich is fascinated by normal development of the central nervous system and the results of perturbations of that process. He recognized early that MRI was a potentially groundbreaking tool for the study of normal and abnormal brain development, so he focused upon optimizing techniques for the evaluation of small brains. This pursuit involved conceptualizing and aiding in designing and building MRI compatible incubators and high resolution

imaging coils, and adapting imaging sequences to maximize the information gained from these studies. Combining embryology, genetics, molecular biology and basic physical and biological science, he collaborated with fellow researchers to better understand and classify steps in brain development and determine at what steps normal development became perturbed. This work led to a series of grants funded by the NIH, which have supported much of the work since 1993. This work gained him recognition in many fields including metabolic disease, medical genetics and epilepsy. His ideas in these areas were published in many peer-reviewed papers and a series of books that he single-authored, co-authored, or co-edited.

Dr. Barkovich has served the ASNR and other radiology organizations for many years, serving as Secretary, Vice-President, and President-Elect of the ASNR before ascending to the Presidency in 1998. He was the Chairman of The Foundation of the ASNR (formerly the Neuroradiology Education and Research Foundation) from 2001-2007. He served as Secretary-General of the World Federation of Neuroradiological Societies from 2002-2006. Dr. Barkovich's contributions have been recognized by multiple awards, including the Goldenson Technology Award from the United Cerebral Palsy R&E Foundation, the Peter Emil Becker Award from the German-Swiss-Austrian Society of Child Neurology for Outstanding Contributions to Pediatric Neurology and Neuroradiology, honorary membership in the European Society of Neuroradiology, and the initial Gold Medal of the American Society of Pediatric Neuroradiology.

## Awards and Honors

### ASNR Gold Medal Award Past Recipients

<b>1995</b> Juan M. Taveras, MD* T. Hans Newton, MD*	<b>1999</b> Grant B. Hieshima, MD Michael S. Huckman, MD	<b>2003</b> Norman E. Leeds, MD, FACR Anne G. Osborn, MD, FACR	<b>2007</b> Robert M. Quencer, MD
<b>1996</b> Sadek K. Hilal, MD* Giovanni Di Chiro, MD*	<b>2000</b> Hillier L. "Bud" Baker, Jr., MD*	<b>2004</b> Ralph Heinz, MD, FACR Stephen A. Kieffer, MD, FACR	<b>2008</b> Robert R. Lukin, MD
<b>1997</b> Derek C. Harwood-Nash, MB, ChB., DSc, FRCPC, FACR, RCRAD(SA)*	<b>2001</b> O. Wayne Houser, MD J. Arliss Pollock, MD*	<b>2005</b> Samuel M. Wolpert, MD	<b>2009</b> Glenn S. Forbes, MD, FACR
<b>1998</b> Irvin I. Kricheff, MD D. Gordon Potts, MD	<b>2002</b> R. Thomas Bergeron, MD David O. Davis, MD	<b>2006</b> R. Nick Bryan, MD, PhD, FACR Charles W. Kerber, MD	<b>2010</b> Anton N. Hasso, MD, FACR
			<b>2011</b> Burton P. Drayer, MD, FACR, FAAN

\*deceased

# Awards and Honors

## 2012 ASNR Honorary Member



The Gold Medal fosters the highest standards of the American Society of Neuroradiology, based on exceptional quality, service, and excellence, and not necessarily on fame. It emphasizes both professional and personal attributes... individuals who are superb neuroradiologists, clinicians, or scientists, and truly outstanding. The recipients are individuals who have extended themselves beyond furthering their own careers through contributions at all levels of professional strata, with an accent on consistency and duration of these outstanding contributions.

### 2012 ASNR Honorary Member Recipient:

**Francis O. Brunelle, MD**

*Hospital Necker-Enfants Malades, Paris, France*

Professor Francis Brunelle graduated from Cochin Medical School in Paris in 1972. He served as a volunteer in Africa (Togo) as a military surgeon and, during his stay, he created the first nursing school in Togo. During his residency, he trained as a paediatrician, neonatologist, and finally as a radiologist. Prof. Brunelle received a master's degree in biochemistry during his residency. Afterwards, he spent a year as a visiting fellow in Alex Margulis' department, where he trained with Harry Genant and Roy Filly, as well as with Hans Newton and David Norman in neuroradiology.

Back in France he became an associate professor of radiology in Dr. Chaumont's department in Bicetre Hospital. The presence of Professor Daniel Alagille, a world specialist of liver diseases in children, led him to develop diagnostic and interventional radiology in liver diseases in children. Most of the abdominal interventional techniques were developed during this time.

During this period, in 1981, he spent four months in Derek Harwood-Nash's department, where he trained in paediatric neuroradiology, writing a paper entitled, "Brain vascular malformations in children."

In 1985, he became full professor of radiology at Necker Enfants-Malades Hospital, which was the turning point of his career. The presence at Necker of Professor Hirsch, a pioneer of paediatric neurosurgery, and Doctor Jean Aicardi, one of the leading people in paediatric neurology, led him to develop

the diagnostic and interventional neuroradiology techniques in children. He created the first paediatric neuroradiology course in France, which rapidly became the European Course of Paediatric Neuroradiology, held in conjunction with the European Society of Paediatric Radiology and the European Society of Neuroradiology. In addition, he also created the first European course of Paediatric Radiology in 1992.

The presence of a very active department of genetics allowed the development of research in neurogenetics diseases in children. The creation of a research unit made possible the development of research in this field, mainly in autism. The department was a pioneer in foetal imaging with MRI, the first foetal MRI being performed in 1987.

Prof. Brunelle wrote 322 peer-reviewed papers and 3 books, among them *Imaging Children* (with Carty, Stringer and Kao). He is a former President of the Medical Board in Necker; Editor of *Paediatric Radiology*; Secretary of the French College of Radiologists (CERF); and Counsellor of the Minister of Health (2004-2007). He served as President (co-president Janet Strife) of the International Paediatric Radiology (IPR) meeting in Paris in 2001, and Director and Chairman of the Imaging Department at Necker. He is one of the founders of the renovation plan for Necker Hospital, whose new building is to be opened in July 2012. Prof. Brunelle is one of the three authors of the redaction of the medical strategy of the Necker Hospital. He is also one of the two founders of a university diploma, "Management for Doctors."

Prof. Brunelle and his wife Anne, an architect, are the parents of six children.

### Past ASNR Honorary Members

Torsten Almen, MD

Mitchel S. Berger, MD

James W. Bull, MD\*

Graeme M. Bydder, MD, ChB

M. Paul Capp, MD

Sten Cronqvist, MD\*

B. G. Ziedses des Plantes, MD\*

George du Boulay, MD\*

Richard R. Ernst, MD

Torgny V. B. Greitz, MD

Godfrey N. Hounsfield, PhD\*

Yun Peng Huang, MD

Ian Isherwood, MD

Pierre Lasjaunias, MD, PhD

Paul C. Lauterbur, PhD\*

Dennis LeBihan, MD, PhD

Marco Leonardi, MD

Erik Lindgren, MD\*

Claude H. Manelfe, MD

Professor Luc Picard

Michel Ter Pogossian, MD\*

Joseph Ransohoff, MD\*

Jesus Rodriguez-Carbajal, MD

Lee F. Rogers, MD

Prof. Lucy Balian Rorke

Michael Radford Sage, MD,

FRANZCR, FRCR, FRCPC

(Lon), FRCPC (Ed), FHKCR (Hon)

Georges Salamon, MD

George Schuyler

S. I. Seldinger, MD

Fjodor Serbinenko, MD

Mutsumasa Takahashi, MD

E. Turgut Tali, MD

Galdino E. Valvassori, MD

Marjo S. van der Knaap, MD

Prof. Jacqueline Vignaud

M. Gazi Yasargil, MD

Ian R. Young, BSc, PhD

\*deceased



# Awards and Honors

## The Foundation of the ASNR Award for Outstanding Contributions in Research



THE FOUNDATION OF THE ASNR

This award, created in 2004 in recognition of consistent excellence and lifelong accomplishment in basic or clinical neuroscience research, is given to an ASNR senior member over the age of 50 recognized in the neuroradiology field for distinguished long term achievement in basic or clinical research.

### The recipient of the 2012 award is:

**Robert A. Zimmerman, MD**

*Children's Hospital of Philadelphia, Pennsylvania*

Dr. Robert A. Zimmerman graduated from Temple University in Philadelphia, Pennsylvania, and from Georgetown University School of Medicine in Washington, D.C., Summa Cum Laude. He completed a Residency in Radiology and a Fellowship in Special Procedures at the Hospital of the University of Pennsylvania in Philadelphia. In 1969, Dr. Zimmerman left for Europe, where he served three years as a radiologist in the U.S. Army. After his tour of duty, he returned to the Hospital of the University of Pennsylvania and advanced through the ranks from Assistant to Associate to Full Professor of Radiology and Radiology in Neurosurgery at the University of Pennsylvania School of Medicine. In 1989, Dr. Zimmerman moved his full-time practice from the Hospital of the University of Pennsylvania to the Children's Hospital of Philadelphia, where he became the Division Chief and the Director of the Neuroradiology Fellowship Program. Dr. Zimmerman also served as Vice-Chief of Radiology at The Children's Hospital from 2000-2004, and in 2007, Dr. Zimmerman received The Children's Hospital of Philadelphia Endowed Chair in Pediatric Neuroradiology.

Dr. Zimmerman was the Co-Principal Investigator on the first NIH grant for the CT evaluation of cerebral trauma. He authored many papers that described, for the first time, CT findings in non-accidental trauma of children and infants, cerebral brain swelling in trauma, shearing injuries, active bleeding in epidural hematoma and evolution of hematomas on CT. Dr. Zimmerman also used the first clinical spiral CT. He worked with GE on the development of the first high field (1.5T) MRI and published the first high field images done clinically and the first MRS performed in a clinical MRI. He described,

often for the first time, characteristics of pediatric brain tumors and showed the correlation of pathology with imaging findings.

Dr. Zimmerman has authored over 400 manuscripts in peer-reviewed journals and has contributed over 80 chapters to medical texts and reviews, as well as co-editing two Neuroradiology textbooks. For his work, Dr. Zimmerman has received the Gold Medal Award from the American Society of Pediatric Neuroradiology (2002), and has been awarded Honorary Membership in the European Society of Neuroradiology (2001). He served as the USA Editor-in-Chief of Neuroradiology from 1989 through 2005. His current research interests include the use of diffusion imaging, and proton spectroscopy and ASL in brain tumors. His interests also include fetal MR imaging, neuroimaging of pediatric stroke, imaging of pediatric trauma and hypoxic/ischemic brain injury in neonates.

With his wife, Dianne, Dr. Zimmerman enjoys traveling, gardening, and spending time with his two grandchildren.

### Past Award Recipients:

**2011** Thomas P. Naidich, MD

**2010** Victor M. Haughton, MD

**2009** R. Gilberto Gonzalez, MD, PhD

**2008** A. James Barkovich, MD

**2007** Clifford R. Jack, Jr., MD

**2006** No Award Given

**2005** Dixon M. Moody, MD

**2004** Robert I. Grossman, MD

## 2012 ASNR Cornelius G. Dyke Memorial Award

This award was established to honor Cornelius G. Dyke, one of the pioneers in neuroradiology, and is given to a trainee or junior faculty member in neuroradiology for excellence as demonstrated in a paper, which represents original, unpublished research in some aspect of neuroradiology.

### The recipient of the 2012 award is:

**Rahul S. Desikan, MD, PhD**

*University of California, San Diego*

*"Phospho-tau not APOE ε4 Modulates Amyloid-β Associated Neurodegeneration Cognitively Normal Older Individuals"*

Dr. Rahul S. Desikan is a first year research-track radiology resident at the University of California, San Diego (UCSD), and a research fellow in the laboratory of Dr. Anders Dale, also at UCSD. He completed his undergraduate studies in Classics, Biology and Neuroscience at Boston University in 1999, and his MD and PhD degrees also at Boston University in 2009. During his third and fourth years of the medical school, Rahul simultaneously served as a postdoctoral fellow in the laboratory of Dr. Bruce Fischl at the Athinoula A. Martinos Center at Massachusetts General Hospital. His graduate research

involved developing an automated, structural MRI-based technique for automatically parcellating the human cerebral cortex into gyral-based regions, and applying this methodology for the early detection of Alzheimer's disease. His current research involves elucidating the genetic, cellular and neuroimaging characteristics of Alzheimer's disease. He is the recipient of a Junior Investigator Award from the American Foundation for Aging Research-General Electric Healthcare, and a Young Scholar's Award from the Alzheimer's Association San Diego-Imperial Chapter.

Presentation Time: Monday, April 23, 3:48pm

Location: Beekman/Sutton North



# Awards and Honors

## ASNR Cornelius G. Dyke Memorial Award Past Recipients

**1972**

**George M. McCord, MD**

"The Venous Drainage to The Inferior Sagittal Sinus"

**1973**

**Barton Lane, MD**

"Cerebrospinal Fluid Pulsations at Myelography: A Video-Densitometric Study"

**1974**

**Jacques Theron, MD**

"Anatomical-Radiological Correlates of the Anterior Choroidal Artery"

**1975**

**Thomas P. Naidich, MD**

"The Normal Anterior Inferior Cerebellar Artery"

**1976 - No Award**

**1977**

**Burton P. Drayer, MD**

"The Capacity for CT Diagnosis of Cerebral Infarction. An Experimental Study in the Non-Human Primate"

**1978**

**Joseph A. Horton, MD**

"The Grain in the Stone: A Computer Search for Hidden CT Patterns"

**1979**

**Dieter R. Enzmann, MD**

"Experimental Brain Abscess Evolution Studied with the CT Scan and Neuropathological Correlation"

**1980 - No Award**

**1981**

**A. Ronald Cowley, MD**

"The Influence of Fiber Tracts on the CT Appearance of Cerebral Edema: An Anatomical Pathological Correlation"

**1982**

**B. Ludwig, MD**

"Postmortem CT and Autopsy in Perinatal Intracranial Hemorrhage"

**1983 - No Award**

**1984**

**Val M. Runge, MD**

"Contrast Enhanced Magnetic Resonance Evaluation of a Brain Abscess Model"

**1985 - No Award**

**1986**

**Jeremy B. Rubin, MD**

"Part 1 Imaging Spinal CSF Pulsation by 2DFT Magnetic Resonance: Significance During Clinical Imaging"  
"Part 2 Harmonic Modulation of Proton MR Precessional Phase by Pulsatile Motion Origin of Spinal CSF Flow Phenomenon"

**1987 - No Award**

**1988**

**Vincent P. Mathews, MD**

"Gadolinium Enhanced MR Imaging of Experimental Bacterial Meningitis: Evaluation and Comparison of CT"

**1989**

**Allen D. Elster, MD**

"Europium-DTPA: Development and Testing of a Gadolinium Analogue Traceable by Fluorescence Microscopy"

**1990**

**Marvin D. Nelson, Jr., MD**

"The Search for Human Telencephalic Ventriculofungal Arteries"

**1991**

**Udo P. Schmiedl, MD**

"Quantitation of Pathological Blood-Brain Barrier Permeability in an Astrocytic Glioma Using Contrast Enhanced MR"

**1992**

**R. Gilberto Gonzalez, MD**

"Quantitative In Vivo Human Brain Lithium Magnetic Resonance Spectroscopy"

**Frank J. Lexa, VII, MD**

"Wallerian Degeneration in the Feline Visual System: Characterization by Magnetization Transfer Rate with Histopathologic Correlation"

**1993**

**Marc Jouandet, MD**

"Mapping the Human Cerebral Cortex with Brainprints"

**1994**

**A. Gregory Sorensen, MD**

"Functional Magnetic Resonance Imaging of Brain Activity and Perfusion in Patients with Chronic Cortical Stroke A"

**1995**

**John L. Ulmer, MD**

"Magnetization Transfer or Spin-Lock? An Investigation of Off-Resonance Saturation Pulse Imaging Using Varying Frequency Offsets"

**1996**

**John C. Strainer, MD**

"fMRI of Primary Auditory Cortex: An Analysis of Pure Tone Activation and Tone Discrimination"

**1997**

**Stephen G. Imbesi, MD**

"Why Do Ulcerated Atherosclerotic Carotid Artery Plaques Embolize? A Flow Dynamics Study"

**David F. Kallmes, MD**

"Guglielmi Detachable Coil Embolization for Unruptured Aneurysms in Neurosurgical Candidates: A Cost Effectiveness Exploration"

**1998 - No Award**

**1999**

**Aquilla S. Turk, DO**

"Definition of Aneurysm Ostium (Neck) and Morphology Using Intravascular Ultrasound: An Experimental Study in Canines"

**2000**

**William F. Marx, MD**

"Endovascular Treatment of Experimental Aneurysms Using Biologically Modified Embolic Devices: Coil-Mediated Intra-Aneurysmal Delivery of Fibroblast Tissue Allografts"

**2001 - No Award**

**2002**

**Mehmet Kocak, MD**

"Functional MR Imaging of the Motor Homunculus: Towards Optimizing Paradigms for Clinical Scenarios"

**2003 - No Award**

**2004**

**Eric D. Schwartz, MD**

"Apparent Diffusion Coefficients Within Spinal Cord Transplants and Surrounding White Matter Correlate With Degree of Axonal Dieback Following Injury"

**2005 - No Award**

**2006**

**Ashok Panigrahy, MD**

"Quantitative Short Echo Time 1H Magnetic Resonance Spectroscopy of Untreated Pediatric Brain Tumors: Pre-operative Diagnosis and Characterization"

**2007**

**Yulin Ge, MD**

"Quantitative Assessment of Iron Accumulations in the Deep Gray Matter of Multiple Sclerosis by Magnetic Field Correlation Imaging"

**2008 - No Award**

**2009**

**Josser E Delgado Almandoz, MD**

"Diagnostic Accuracy and Yield of Multi-Detector CT Angiography in the Evaluation of Spontaneous Intraparenchymal Cerebral Hemorrhage"

**2010**

**Elysa Widjaja, MD**

"Alteration of Human Fetal Subplate Layer and Intermediate Zone During Normal Development on MR and Diffusion Tensor Imaging"

**2011 - No Award**



# Awards and Honors

## ASNR 2011 Outstanding Presentation Awards

ASNR is pleased to announce the winners of the Outstanding Presentation Awards. The overall quality of the paper and poster presentations at the Seattle meeting was excellent, and the winners should be commended for their outstanding work. A \$1,000 award will be given to the primary author of each winning presentation.

Seven awards were presented in Six categories: in *Adult Brain/General Neuroradiology* (two awards, one awarded by the ASNR, and another awarded by The Foundation of the ASNR), *Functional Neuroradiology*, *Head and*

*Neck, Interventional* (The Michael Brothers Memorial Award), *Pediatrics* (The Derek Harwood-Nash Award), and *Spine*. Both awards in Adult Brain/General Neuroradiology were selected by a panel of ASNR members under the direction of the Education Committee. The five subspecialty awards were judged by panels selected from each of the specialty societies, including ASFNR, ASHNR, ASPNR, ASSR, and SNIS. We would like to thank all of the judges for their tremendous effort in evaluating the presentations. Congratulations to the winners!

### General Neuroradiology

(on behalf of the ASNR)

**PAPER 217: Comparison of Arterial Spin Labeling and Bolus Perfusion-Weighted Imaging for Detecting Mismatch in Acute Stroke**

Elmogy, I.S.<sup>1</sup> • Zaharchuk, G.<sup>2</sup> • Fischbein, N.J.<sup>2</sup> • Albers, G.W.<sup>2</sup>

(<sup>1</sup>Mansoura Advanced Radiology Center, Mansoura, EGYPT, <sup>2</sup>Stanford University, Stanford, CA)

### General Neuroradiology

(on behalf of The Foundation of the ASNR)

**PAPER 248: Diffusion Kurtosis Imaging of Normal Pressure Hydrocephalus**

Pawar, R.V.<sup>1</sup> • Kong, S.E.<sup>2</sup> • Jenson, J.H.<sup>3</sup> • Golomb, J.B.<sup>1</sup> • Babb, J.S.<sup>1</sup> • George, A.E.<sup>1</sup>

(<sup>1</sup>New York University Langone Medical Center, New York, NY, <sup>2</sup>New York Medical College, Valhalla, NY, <sup>3</sup>New York University School of Medicine, New York, NY)

### Functional Neuroradiology

**PAPER 87: Resting Brain for Neurosurgical Planning**

Stufflebeam, S.M.<sup>1</sup> • Liu, H.<sup>1</sup> • Buckner, R.<sup>1</sup> • Tanaka, N.<sup>1</sup> • Grant, P.<sup>2</sup>

(<sup>1</sup>Massachusetts General Hospital Martinos Center, Charlestown, MA, <sup>2</sup>Children's Hospital Boston, Charlestown, MA)

### Head and Neck Radiology

**Paper 429: Peripheral Nerve Tractography in Brachial Plexus Lesions**

Kasprian, G.J. • Breitenscher, J. • Mallouhi, A. • Czerny, C. • Prayer, D.

(University of Vienna, Vienna, AUSTRIA)

### Interventional Neuroradiology

(The Michael Brothers Memorial Award)

**Paper 117: Intra-Arterial Chemotherapy (Chemosurgery) in the Treatment of Retinoblastoma: 4-Year Experience**

Gobin, Y.<sup>1</sup> • Abramson, D.<sup>2</sup> • Marr, B.<sup>2</sup> • Brodie, S.<sup>3</sup> • Dunkel, I.<sup>2</sup>

(<sup>1</sup>Weill Cornell Medical College, New York, NY, <sup>2</sup>Memorial Sloan-Kettering Cancer Center, New York, NY, <sup>3</sup>Mount Sinai College of Medicine, New York, NY)

### Pediatric Neuroradiology

(The Derek Harwood-Nash Award)

**PAPER 225: Application of Diffusion Tensor Imaging as a Surrogate for Neurologic Deficit of Spinal Cord Injury**

Schopf, V. • Kasprian, G. • Mitter, C. • Brugger, P.C. • Prayer, D.

(Medical University of Vienna, Vienna, AUSTRIA)

### Spine

**PAPER 33: Diffusion Tensor Imaging and Tractography of Traumatic Brachial Plexus Palsies: Preliminary Experience**

Zohrabian, V.<sup>1</sup> • Zussman, B.<sup>1</sup> • Frangos, A.<sup>1</sup> • iMatthews, J.<sup>1</sup> • Lackey, J.<sup>1</sup> • Dresner, M.A.<sup>2</sup> • Lai, S.<sup>1</sup> • i Marino, R.<sup>1</sup> • iGorniak, R.<sup>1</sup> • Flanders, A.E.<sup>1</sup>

(<sup>1</sup>Thomas Jefferson University Hospital, Philadelphia, PA, <sup>2</sup>Philips Medical Systems, Cleveland, OH)

## 2011/2012 Specialty/Regional Society Awards

The American Society of Neuroradiology is pleased to announce the recipients of the 2011/2012 Special/Regional Society Awards. These individuals were selected by the respective societies as having the best presentation at each society's most recent Annual Meeting.

### American Society of Spine Radiology (ASSR)

(Mentor Award)

"Improved Outcomes with Percutaneous Image-Guided Lumbar Synovial Cyst Treatment: Novel Approaches and Techniques"

**Leena Tekchandani, MD**

Winthrop-University Hospital, Mineola, NY

### Eastern Neuroradiological Society (ENRS)

(The Norman E. Leeds Award)

"Dynamic Susceptibility Contrast MRI Perfusion May Not Predict Progressive Disease in Patients with Recurrent Glioblastoma Receiving Bevacizumab."

**Andrew D. Schweitzer, MD**

Memorial Sloan-Kettering Cancer Center, New York

### Southeastern Neuroradiological Society (SENRS)

"Morphologic Approach to White Matter Disease"

**Jeff L. Creasy, MD**

Vanderbilt University Medical Center, Nashville

### Western Neuroradiological Society (WNRS)

(The Gabriel H. Wilson Award)

"Adult Cystic Fibrosis Sinonasal CT Findings"

**Sarah Elizabeth Stilwill, MD**

University of Utah, Salt Lake City



# Awards and Honors

## The Foundation of the ASNR Basic Science Research Award Past Recipients

### 1986-87

**Jeremy B. Rubin, MD**  
**Stanford University Medical Center**

*"New Methods Using MRI to Assess Ventricular Shunt Function and Measure Intravenous Pressure Non-invasively in Patients with Ventricular Shunt Catheters"*

### 1987-88

No Award

### 1988-89

**Apichai Jarenwattananon, MD**  
**University of Wisconsin Medical Center**

*"In-Vivo Sodium MRI (Na-MRI) in Canine Model of Status Epilepticus"*

**Warren A. Stringer, MD**  
**Loma Linda University Medical Center**

*"Evaluation of the Relationships Between Cerebral Perfusion, Ventilation, and Intracranial Pressure by Xenon-enhanced Computed Tomography in Children with Cerebral Edema"*

### 1989-90

**Todd Lempert, MD**  
**University of California at San Francisco**

*"Evaluation of the Healing Response to Thrombogenic Coil Occlusion of Experimental Aneurysms"*

### 1990-91

**Lori L. Baker, MD**  
**Stanford University Medical Center**

*"Evaluation of MR Diffusion Imaging Versus Magnetic Susceptibility Enhanced Mapping of Perfusion Pool in Regional Cerebral Ischemia"*

**Lee H. Monsein, MD**  
**The Johns Hopkins University School of Medicine**

*"Primate Model of Reversible Regional Cerebral Ischemia"*

### 1991-92

**Steven N. Breiter, MD**  
**The Johns Hopkins Hospital**

*"Proton MRS in the Determination of Lactic Acid Concentration in Seizures, Both Human and Animal"*

**Frank J. Lexa, VII, MD**  
**University of Pennsylvania**

*"MRI Demonstration of Axonal Transport in the Mammalian CNS"*

### 1992-93

**Michael A. Kraut, MD, PhD**  
**The Johns Hopkins Hospital**

*"Lactate Production and Metabolism in Cerebral Activation"*

**Brian W. Chong, MD**  
**University of California at San Diego**

*"A Search for Hidden MRI Flow Patterns in Human Cranial Vessels"*

### 1993-94

**Thomas E. Conturo, MD, PhD**  
**The Johns Hopkins Hospital and Johns Hopkins University**

*"Mechanisms of the Phase Enhancement Effects of Bolus-Injected Paramagnetic Contrast Agents and Applications in Quantitative Cerebral Blood Volume and Flow Imaging"*

**John P. Karis, MD**  
**Barrow Neurological Institute**

*"Epilepsy Localization: Advanced High Resolution MRI-PET FDG Correlation"*

### 1994-95

**Jerry Burke, MD**  
**Bowman Gray School of Medicine**

*"Serial Positron Emission Tomography and Functional MR Imaging of Stroke"*

**Robert Fulbright, MD**  
**Yale University School of Medicine**

*"Functional MR Imaging of the Spine"*

### 1995-96

**Norman J. Beauchamp, MD**  
**The Johns Hopkins Hospital**

*"The Natural History of 'Areas of Risk of Infarction' as Defined by Perfusion MRI and MR Spectroscopy"*

**Anthony Masaryk, MD**  
**University of Wisconsin-Madison**

*"Analysis of Aneurysm Hemodynamics Using MRI/MRA Morphology and Flow Measurements Correlated with Hemodynamic Numerical Analysis and Simulation"*

### 1996-97

**Joseph T. Lurito, MD, PhD**  
**The Johns Hopkins Hospital**

*"Functional MRI and Electrophysiologic Correlates of Sub-modality Specific Somatosensory Activation"*

**Jeffrey L. Sunshine, MD**  
**University Hospitals of Cleveland**

*"Early Identification of Ischemic Penumbra by Diffusion and Perfusion MR in Acute Stroke"*

### 1997-98

**Huy M. Do, MD**  
**University of Virginia Health Sciences Center**

*"The Neuroprotective Effect of Intraarterial Nerve Growth Factor (HGF) in a Rabbit Embolic Stroke Model"*

### 1998-99

**William F. Marx, MD**  
**University of Virginia**

*"Endovascular Treatment of Experimental Aneurysms Using Biologically Modified Embolic Coils: Promotion of Permanent Occlusion via Intra-aneurysmal Fibroblast Delivery"*



THE FOUNDATION OF THE ASNR



# Awards and Honors

## The Foundation of The ASNR Basic Science Research Award Past Recipients (continued)

### 1999-00

**Kevin R. Moore, MD**  
**University of Utah Center for Advanced Medical Technology**

*"Meg-Constrained High-Resolution Surface-Coil MR Imaging and MR Spectroscopy for Evaluating Medically Refractory Epilepsy"*

**John G. Short, MD**  
**University of Virginia**

*"Induction of Spinal Interbody Fusion Using Gene Therapy Tissue Engineering Techniques"*

### 2000-01

**John Port, MD, PhD**  
**The Johns Hopkins Medical Institution**

*"Imaging Selective Attention Mechanisms"*

**Eric Schwartz, MD**  
**Hospital of the University of Pennsylvania**

*"Diffusion-based MR Imaging in a Rat Spinal Cord Following Injury and Transplantation"*

### 2001-02

**Pratik Mukherjee, MD, PhD**  
**Mallinckrodt Institute of Radiology, Washington University School of Medicine**

*"Comparison of Magnetic Resonance Imaging and Positron Emission Tomography in the Study of Cerebral Hemodynamics"*

### 2002-03

**John G. Dalle, DO**  
**University of Utah School of Medicine**

*"Polymer-Chelate Conjugates for Diagnostic Cancer Imaging"*

**Christopher Lascola, MD, PhD**  
**Duke University Medical Center**

*"Magnetic Resonance Imaging of Spreading Depression-Induced Reactive Gliosis in Mice"*

### 2003-04

**Dheeraj Gandhi, MD**  
**University of Michigan Health System**

*"Can the Choline/Creatine Ratio Predict Early Treatment Response of Head and Neck Squamous Cell Carcinoma Treated with Radiation Therapy in an Animal Model: A Prospective Study"*

**Susan M. Kealey, MD**  
**Duke University Medical Center**

*"Correlation of MR Permeability Measurements with Histologic Markers of Angiogenesis in Rodent High-Grade Brain Tumors Before and After Treatment with Antiangiogenesis Agent PTK 787"*

### 2004-05

**Tuong Huu Le, MD, PhD**  
**University of California, San Francisco**

*"Structural and Functional Correlates of Axonal Shearing in Traumatic Brain Injury: A Combined DTI, fMRI and MSI Study"*

**Whitney B. Pope, MD, PhD**  
**David Geffen School of Medicine at University of California, Los Angeles**

*"Identification of Unstable Atherosclerotic Plaque at the Carotid Bifurcation Using High-Resolution CT-PET Imaging: Correlation to Histopathology and Patient Symptoms"*

### 2005-06

**Srinivasan Mukundan, Jr., PhD, MD**  
**Duke University Medical Center**

*"Toward the Development of a Nanoscale, Target-Specific Liposomal Platform Technology for Computed Tomography Based Molecular Imaging"*

**Max Wintermark, MD**  
**University of California, San Francisco**

*"Morphometric and Functional Characterization of Atherosclerotic Carotid Disease by Multidetector-Row CT-Angiography: A Comparative Study with Ex Vivo Histology and Imaging"*

### 2006-07

**Michelle S. Bradbury, MD, PhD**  
**Memorial Sloan Kettering Cancer Center**

*"In Vivo Monitoring of Human Embryonic Stem Cell-derived Grafts in the Central Nervous System of Living Animals Using Optical Imaging Technologies"*

**Edwin Wang, MD**  
**New York University School of Medicine**

*"In Vivo Imaging of the Epidermal Growth Factor Receptor with a Bimodal MRI/Optical Contrast Agent"*

### 2007-08

**Myria Petrou, MA, MBChB**  
**University of Michigan, Ann Arbor, MI**

*"Investigation of Axonal Loss, Demyelination and Response to Treatment in a Mouse Model of Multiple Sclerosis Using Diffusion Tensor Imaging"*

**Elysa Widjaja, MD**  
**Hospital for Sick Children, Toronto, Canada**

*"Determining the Extent of Diffusion Tensor Abnormalities in Focal Cortical Dysplasia"*

### 2008-09

**Bradley Foerster, MD**  
**Johns Hopkins Hospital, Baltimore, Maryland**

*"MR Molecular Imaging of Glutamate Carboxypeptidase II (GCP II) Modulation in an Experimental Model of Stroke"*

**Noriko Salamon, MD**  
**David Geffen School of Medicine at the University of California at Los Angeles, Los Angeles, California**

*"Diffusion Tensor Imaging in the Identification of the Extra-Hippocampal Abnormality in the Patients with Mesial Temporal Lobe Epilepsy with Hippocampal Sclerosis"*

### 2009-10

**Christopher T. Whitlow, MD, PhD**  
**Wake Forest University School of Medicine, Chapel Hill, NC**

*"Evolving Patterns of Functional Connectivity in the Developing Brain: An Arterial Spin Labeling Perfusion MRI and Computational Network Analytical Investigation"*

### 2010-11

**Stephen E. Jones, MD, PhD**  
**Cleveland Clinic**

*"Validation of Probabilistic DTI Algorithms Using Direct Stimulation Data from Stereotactic EEG Electrodes in Humans"*

### 2011-12

**Rivka R. Colen, MD**  
**Brigham and Women's Hospital, Boston, MA**

*"Targeted Drug Delivery of Bortezomib using 'Microbubble' Enhanced MR-guided Focused Ultrasound (MRgFUS): A Glioma Rat Model of Concept Study"*



# Awards and Honors

## 2012 The Foundation of the ASNR Scholar Award in Neuroradiology Research

Since 1995, The Foundation of the ASNR has been in the process of raising funds to support neuroradiology research. This is one of the most important goals of the The Foundation of the ASNR, and of the ASNR as the premier organization for neuroradiology. This award was created for young investigators in the early stages of their careers, to enhance their competency in areas important to the future of neuroradiology, including health services research, physiological imaging and interventional neuroradiology. It also affords the Foundation the opportunity to begin to develop leadership in these areas.



THE FOUNDATION OF THE ASNR

### The recipient of the 2012 award is:

**Seena Dehkharghani, MD**  
**Emory University, Atlanta, GA**

*"Investigating the Utility of MR Thermometry and Perfusion in the Evaluation of Cerebrovascular Ischemia: Applications to the Ischemic Penumbra Model of Neurovascular Injury"*

## The Foundation of the ASNR Scholar Award in Neuroradiology Research Past Recipients

### 1999

**L. Santiago Medina, MD, MPH**  
**Children's Hospital Medical Center, Cincinnati, OH**

*"The Role and Cost-Effectiveness of Imaging in Newborns with Suspected Occult Spinal Dysraphism"*

### 2000

**Melanie B. Fukui, MD**  
**University of Pittsburgh Medical Center, Pittsburgh, PA**

*"Carotid Stenosis Evaluation: Cost-Effectiveness of Computed Tomographic Angiography vs. Magnetic Resonance Angiography"*

### 2001

**Soonmee Cha, MD**  
**New York University Medical Center, New York, NY**

*"Dynamic Contrast Enhanced T2\*-weighted MRI and Histopathological Assessment of Experimental Glioma"*

### 2002

**James D. Eastwood, MD**  
**Duke University Medical Center, Durham, NC**

*"CT Perfusion Imaging in Subarachnoid Hemorrhage Related Vasospasm"*

### 2003

**Steven G. Imbesi, MD**  
**University of California, San Diego Medical Center, San Diego, CA**

*"Alteration of Intracranial Aneurysm Flow Dynamics: Development and Evaluation of Potential Neurointerventional Endovascular Treatment Regimens of Wide Necked Aneurysms"*

### 2004

**Pratik Mukherjee, MD, PhD**  
**University of California San Francisco, San Francisco, CA**

*"Diffusion Tensor MR Imaging and Quantitative Tractography of Brain Development in Premature Newborns"*

### 2005

**Donna R. Roberts, MD**  
**University of California, San Francisco, CA**

*"The Assessment of Image-guided Transcranial Magnetic Stimulation as an Adjuvant to Extradural Cortical Stimulation for the Treatment of Chronic Facial Pain"*

**Steven G. Imbesi, MD**  
**University of California Medical Center, San Diego, CA**

*"Alteration of Intracranial Aneurysm Flow Dynamics: Development and Evaluation of Potential Neurointerventional Endovascular Treatment Regimens for Wide Necked Aneurysms"*

### 2006

**Erin Simon Schwartz, MD**  
**Children's Hospital of Philadelphia, Philadelphia, PA**

*"A Comprehensive MR Assessment of Fetal Physiologic Well-Being"*

### 2007

**Pina C. Sanelli, MD**  
**Weill Medical College of Cornell University, New York, NY**

*"Assessing the Value of CT Perfusion in Improving Clinical Outcomes in Aneurysmal Subarachnoid Hemorrhage Using a Decision Analytic Model"*

### 2008

**Tammie L. S. Benzinger, MD, PhD**  
**Washington University School of Medicine, St. Louis, MO**

*"Childhood Leukodystrophy with Neuromuscular Disability: Translational Use of MRI Directional Diffusivity as a Tool for Prognosis and Response to Therapy"*

**Vivek Prabhakaran, MD, PhD**  
**Johns Hopkins Hospital, Baltimore, MD**

*"Characterizing the Neural Substrates of Stroke Recovery Utilizing fMRI and Perfusion Imaging"*

### 2009

**Greg Zaharchuk, M.D., PhD**  
**Stanford University Medical Center, Stanford, CA**

*"Optimizing Arterial Spin Label MRI for the Visualization of Collateral Flow in Moyamoya Disease"*

### 2010

**Steven W. Hetts, MD**  
**University of California, San Francisco**

*"Endovascular Catheter for Magnetic Navigation under MRI Guidance: Evaluation of Healing In Vivo at 1.5T"*

**Danel Mandell, MD**  
**Hospital for Sick Children**

*"Evolution of Individual White Matter Lesions in Leukodystrophy: A Serial MRI Study"*

### 2011

**Michael J. Paldino, MD**  
**Children's Hospital Boston**

*"Abnormal Structural and Functional Connectivity in Pediatric Patients with Focal Cortical Dysplasia"*



# Awards and Honors

## 2012 The Foundation of The ASNR Research Scientist Award



THE FOUNDATION OF THE ASNR

The Foundation of the ASNR and Partner Organizations have established the Research Scientist Award to provide research opportunities for PhD investigators to advance the science of Neuroradiology. Scientific research is the foundation upon which the clinical practice of Neuroradiology is built. Research scientists in partnership with radiologists have traditionally led the development of new imaging technologies and image-guided procedures. The directive of these awards is to assist young scientists in their transition to becoming independent investigators in neuroradiology research, as well as to help established investigators initiate new projects with relevance to neuroradiology.

**2011**

**Jaime F Mata, PhD**  
**University of Virginia, Charlottesville, VA**

*"Non-Invasive Targeted Delivery and In-vivo Evaluation of Brain Therapy Using MR Guided Focused Ultrasound"*

### The recipient of the 2012 award is:

**Jeffrey I. Berman, PhD**  
**Children's Hospital of Philadelphia, Philadelphia, PA**

*"Diffusion MR Assessment of the Auditory Radiation in Autism"*

## 2012 The Foundation of the ASNR Comparative Effectiveness Research Award

The Foundation of the ASNR has established the Comparative Effectiveness Research Award to support investigators in the generation and synthesis of evidence that compares the benefits and harms of diagnostic imaging methods or interventions to prevent, diagnose, treat, and monitor a clinical condition or to improve the delivery of care. Comparative effectiveness research (CER) is valuable to clinicians, patients, purchasers, and policy makers in making informed decision that will improve health care at both the individual and population levels. Neuroradiologists have an important role in the development of new imaging technologies and image-guided procedures, as well as in the assessment of these techniques in the clinical care of patients.

**2011**

**Ajay Gupta, MD**  
**New York Presbyterian Hospital**

*"Comparison of CT Perfusion and Digital Subtraction Angiography in the Evaluation of Delayed Cerebral Ischemia Using Bayesian Analysis"*

### The recipient of the 2012 award is:

**Ari M. Blitz, MD**  
**Johns Hopkins Hospital**

*"Comparative Effectiveness of High Resolution 3D vs. Standard 2D Protocol Pituitary MRI for Cushing's Disease"*

## The Foundation of the ASNR Award in Cerebrovascular Disease Research Award Past Recipients

**2003-04**

**Joshua Shimony, MD, PhD**  
**Washington University School of Medicine, St. Louis, MO**  
*"Improved MR Methods for Evaluation of Brain Perfusion in Patients with Carotid Stenosis"*

**2004-05**

**Timothy J. Kaufmann, MD**  
**Mayo Clinic and Foundation, Rochester, MN**  
*"A Prospective Clinical Trial of 3.0T MR Angiography in the Follow-up of Intracranial Aneurysms Treated with Endovascular Coils"*

**2005-06**

**Donna Hoghooghi, MD**  
**University of California, San Francisco, CA**  
*"Extent and Effectiveness of Embolization and Determination of Vascular Supply in Meningiomas Using a Combined Interventional X-ray/MR Fluoroscopy Suite"*

**2006-07**

**Albert Yoo, MD**  
**Massachusetts General Hospital, Boston, MA**  
*"Predicting Clinical Outcomes of Intra-arterial Thrombolysis in Acute Stroke Using Diffusion/Perfusion MRI"*

**2007-08**

**Todd Abruzzo, MD**  
**University of Cincinnati Medical Center, Cincinnati, OH**  
*"Modeling Modes of Intracranial Aneurysm Recurrence After Coil Embolization: Mechanisms of Coil Compaction and Aneurysm Re-Growth"*

**2008-09**

**Humberto Morales, MD**  
**University of Cincinnati, Cincinnati, OH**  
*"Safety of Iodinated Contrast Material in a Middle Cerebral Artery Occlusion/Reperfusion Model"*



# Continuing Medical Education (CME)

## Take Your Official Continuing Medical Education (CME) Certificate Home With You!

An enhancement of the Continuing Medical Education online evaluation system allows for attendees to print out their official CME certificate for the number of hours claimed during The Foundation of the ASNR Symposium 2012 and ASNR 50th Annual Meeting and take it with them when they leave. Go to any terminal in the CME Pavilion and follow the simple directions for printing out an official The Foundation of the ASNR Symposium 2012 and ASNR 50th Annual Meeting CME Certificate.

Following the meeting, the ASNR 2012 CME certificate site will be available online by mid-July for 90 days for attendees to print out their CME certificates.

**Please Note:** Due to the availability of CME certificates online, certificates will not be mailed to attendees.

### Letter of Attendance

If you wish to obtain a Letter of Attendance, please request one at the Registration Desk located on the 2<sup>nd</sup> Floor Promenade of the Hilton New York.

### Continuing this year!

- Evaluations available online with remote access 24/7 through the meeting!
- Streamlined format!
- Open throughout the meeting until Sunday, May 6, 2012

### CME Pavilion - Gibson (2<sup>nd</sup> Floor)

To access the CME evaluation program, scan the barcode on the front of your badge at the reader at one of the terminals and follow the simple directions for selecting and evaluating the sessions you have attended. The CME credit hours awarded to a session will automatically be recorded in your record when the evaluation for a session is completed. Evaluations can be completed at the end of a session, during breaks, at the end of the day or the end of the week, as well as on your personal device. You will be able to view a record of the sessions you have evaluated and the number of CME credit hours earned throughout the program. It will also be possible to print your certificate and transcript to take home with you.

*Please Note: To receive CME credit for sessions attended at The Foundation of the ASNR Symposium 2012 and ASNR 50th Annual Meeting, all evaluations must be entered by Sunday, May 6, 2012.*

### Scientific Program and Meeting Evaluation

The 2012 Continuing Medical Education (CME) Pavilion allows online recording of CME credits via the Internet. The improvements have created a faster and more user-friendly system for evaluating sessions and speakers and recording CME hours electronically.

The CME Pavilion is easily accessible in the Gibson at the Hilton New York. Please complete the evaluations for each session to assist in planning future meetings and to help us maintain accreditation of future programs.

## Accreditation Statement

The American Society of Neuroradiology is accredited by the Accreditation Council for Continuing Medical Education (ACCME) to provide continuing medical education for physicians. The American Society of Neuroradiology takes responsibility for the content, quality, and scientific integrity of the CME activity.

## Credit Designation Statement

The American Society of Neuroradiology designates this live activity for a maximum of 33.75 AMA PRA Category 1 Credit(s)<sup>TM</sup>. Physicians should claim only credit commensurate with the extent of their participation in the activity.

## Target Audience

The 50th Annual Meeting is the premier Neuroradiology meeting in the world. It is designed for general radiologists who read Neuroradiology studies, dedicated neuroradiologists who strive to better integrate advanced imaging and image-guided diagnostic and therapeutic strategies into daily practice, and scientists who seek better understanding of the current state of these technologies and how they are applied to evaluate the brain, spine, and head and neck. All participants will benefit from exchange of ideas with colleagues from around the world. Programming will include invited talks and original presentations of new results in imaging methods and techniques such as MR diffusion and perfusion weighted imaging, susceptibility weighted imaging, magnetic resonance spectroscopy, functional magnetic resonance imaging, MR angiography, CT perfusion, CT angiography, CT iterative reconstruction techniques, dual energy CT, catheter-based angiography and associated therapies, image-guided spine interventions, molecular imaging and positron emission tomography. Sessions dealing with pediatric neuroradiology, head and neck imaging, diagnostic imaging of the spine and spinal therapeutic interventions, vascular imaging and interventions, functional and molecular imaging, and adult neuroradiology will be offered. There will also be sessions on multiple relevant socioeconomic and practice management issues.



# ASNR 50th Overall Annual Meeting Educational Objectives

## After attending the 50th Annual Meeting, you will be able to:

- Analyze the clinical spectrum and imaging finding associated with cerebellar disorders, craniofacial malformations, epilepsy and prematurity in children
- Review in Maintenance of Certification (MOC) and Self-Assessment Module (SAM) programming with sessions highlighting Pediatric Neuroradiology, Head and Neck Imaging, Cerebrovascular Diseases, and Spine Imaging and Intervention.
- Identify major health policy and socioeconomic factors likely to affect the future of Neuroradiology, including changes in payment systems, evolution of health care reform, comparative effectiveness research, and evidence based medicine.
- Analyze the indications for, imaging findings, and outcomes related to diagnosis and endovascular therapy of venous disease, dural arteriovenous fistulae, carotid disease and aneurysms.
- Describe imaging findings associated with sinonasal, skull base and temporal bone pathology as well as head and neck cancer.
- Identify abnormalities of and perform interventional procedures on the spine, disk, pelvis and sacro-iliac joint.
- Apply conventional and advanced imaging methods to the diagnosis and treatment planning of psychiatric diseases, dementias, acute stroke and other vascular diseases, traumatic brain injury, white matter diseases, infections and intracranial neoplasms.
- Define and analyze new developments in molecular imaging, positron emission tomography imaging, functional MRI, diffusion imaging, brain perfusion imaging, and MR spectroscopy.
- Analyze new developments in computed tomography including iterative reconstruction, dual energy CT, and 4D CT.
- Evaluate leadership and management approaches to optimizing performance of radiology practice.



# Synaptic Junction Programming (as of 3/21/12)

The ASNR Synaptic Junction provides the opportunity for connecting your practice to the future through offerings focused on enhancing workflow, efficiency, standardization of interpretation and reporting, and improvements in revenue cycle, particularly those that involve software, hardware and informatics-based solutions.

## Monday, April 23

8:30am - 10:00am • Murray Hill  
**MR Safety for Patients with Implants**

*Emanuel Kanal, MD*

*Alex Mamourian, MD*

*Harold I. Litt, MD, PhD*

## Tuesday, April 24

8:30am - 10:00am • Beekman/Sutton North

**DTI For Dummies**

**Diffusion Tensor Imaging/Physics**

*Michael L. Lipton, MD, PhD*

**Current Applications**

*Vikas Agarwal, MD*

**Current Research and Future Innovations**

*Andrew G. Bleicher, MD*

4:45pm - 6:15pm • Murray Hill

**Point/Counterpoint: Communicating Results Directly to Patients**

*Annette J. Johnson, MD, MS*

*Barton F. Branstetter IV, MD*

## Wednesday, April 25

1:00pm - 2:30pm • Murray Hill

**Dose Extraction**

*Tessa Cook, MD*



# SYNAPTIC JUNCTION

connecting your practice

## Lecture Programming Only in 2012

## 2011-2012 Education Subcommittee: Synaptic Junction

*John L. Go, MD*

*Chair*

*Barton F. Branstetter IV, MD*

*Falgun Chokshi, MD*

*Nikdokht Farid, MD*

*Adam E. Flanders, MD*

*Andrew Ku, MD*

*Laurie A. Loevner, MD*

*Gul Moonis, MB, BS*

*Mark E. Mullins, MD*

*C. Douglas Phillips, MD, FACR*

*Edward P. Quigley, III, MD, PhD*

*Pina C. Sanelli, MD, MPH*



How-To Sessions (As of 3/21/12)

HOW-TO SESSIONS

The leadership of the ASNR is pleased to present more instructional How-To Sessions. These one hour sessions, presented by major corporate contributors, deal with advances in imaging and procedures, as well as principles in Neuroradiology and image information management. The How-To Sessions are scheduled throughout the week. The How-To Sessions offer a unique opportunity for neuroradiologists to discuss techniques, procedures and products with their colleagues as well as with technical specialists from the imaging industry. The sessions may include

a brief didactic presentation and demonstration, all with a strong practical emphasis. A significant portion of each session is devoted to questions and answers. As problems and solutions relating to the imaging techniques will be addressed with previous years sessions addressing clinical CT Imaging, Practical Neuro CTA and advances in MR Imaging. Please note: Due to the direct financial support from companies to conduct these sessions, CME credit hours will not be granted for any How-To Sessions.

How-To Session Programming in the Grand Ballroom Suite.

Sunday, April 22 ..... 6:50am - 7:50am



Medtronic

Monday, April 23 ..... 6:20am - 7:20am



LIFE FROM INSIDE

Tuesday, April 24 ..... 6:20am - 7:20am

PHILIPS

Tuesday, April 24 ..... 6:30pm - 7:30pm



ALZHEIMER'S  
IMMUNOTHERAPY PROGRAM  
INNOVATION TO REMEMBER™



Wednesday, April 25 ..... 6:20am - 7:20am

TOSHIBA  
Leading Innovation >>>

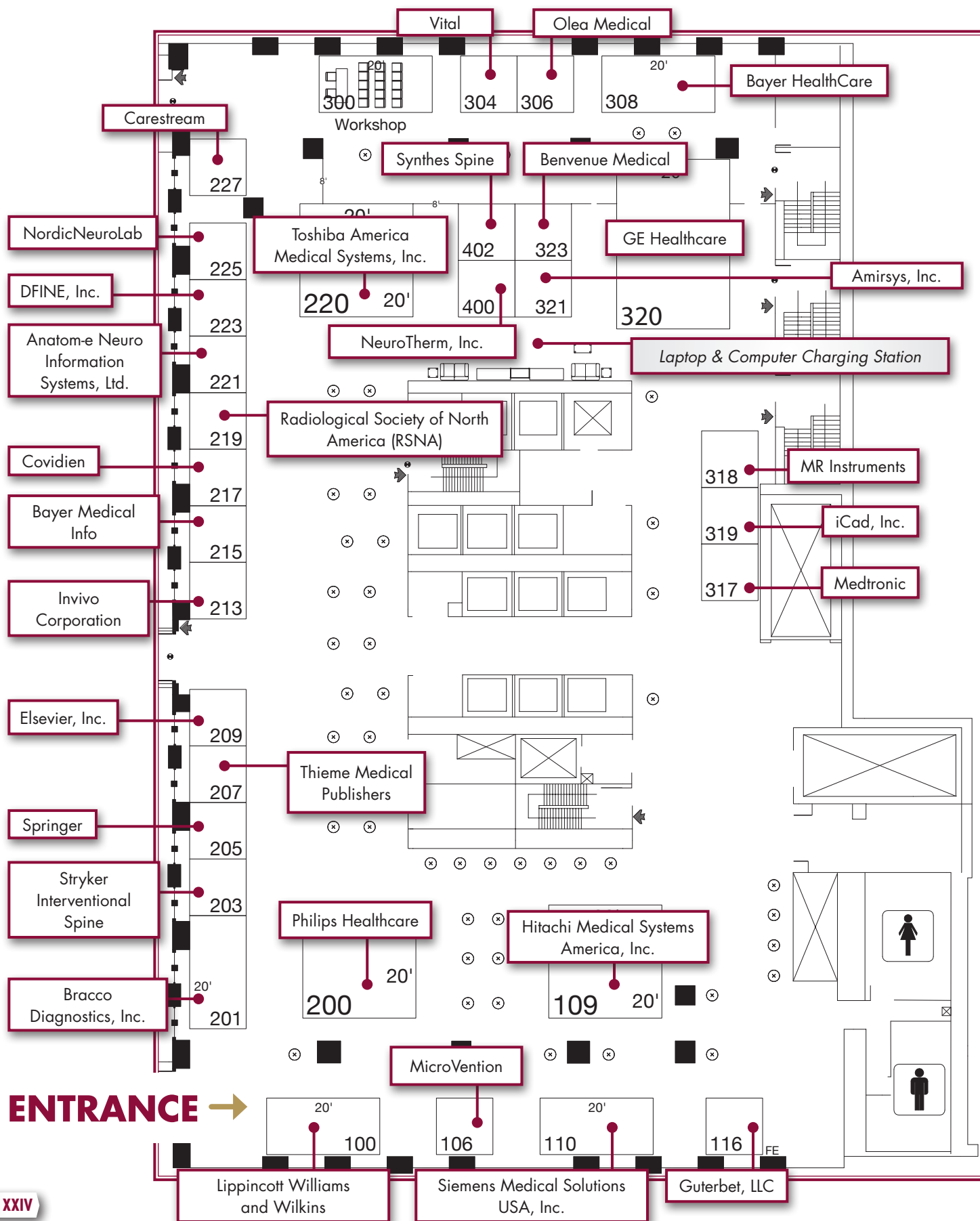
Thursday, April 26 ..... 6:20am - 7:20am

SIEMENS

# Technical Exhibition Hall - Americas Hall I (as of 3/21/12)

## Exhibit Hours

Tuesday, April 24 through Thursday, April 26 ..... 10:00am – 4:00pm



# Technical Exhibits Roster (as of 3/21/12)

## Hilton New York - America Hall I

Tuesday, April 24..... 10:00 am – 4:00 pm  
 Wednesday, April 25..... 10:00 am – 4:00 pm  
 Thursday, April 26 ..... 10:00 am – 4:00 pm

Amirsys, Inc ..... Booth #321  
 2180 South 1300 East, Suite 570  
 Salt Lake City, UT 84106

Anatom-e Neuro Information Systems, Ltd..... Booth #221  
 2047 University Boulevard  
 Houston, TX 77030

Bayer HealthCare ..... Booth #308  
 6 West Belt  
 Wayne, NJ 07470

Bayer Medical Info ..... Booth #215  
 6 West Belt  
 Wayne, NJ 07470

Benvenue Medical ..... Booth #323  
 3052 Bunker Hill Lane, Suite 120  
 Santa Clara, CA 95054

Bracco Diagnostics Inc. .... Booth #201  
 107 College Road East  
 Princeton, NJ 08540

Carestream ..... Booth #227  
 150 Verona Street  
 Rochester, NY 14608

Covidien ..... Booth #217  
 9775 Toledo Way  
 Irvine, CA 92618

DFINE, Inc. .... Booth #223  
 3047 Orchard Parkway  
 San Jose, CA 95134

Elsevier Inc..... Booth #209  
 1600 John F. Kennedy Boulevard, Suite 1800  
 Philadelphia, PA 19103

GE Healthcare..... Booth #320  
 9900 West Innovation Drive  
 Wauwatosa, WI 53226

Guerbet LLC..... Booth #116  
 1185 West 2nd Street  
 Bloomington, IN 47403

Hitachi Medical Systems America, Inc. .... Booth #109  
 1959 Summit Commerce Park  
 Twinsburg, OH 44087

iCad, Inc. .... Booth #319  
 98 Spit Brook Road, Suite 100  
 Nashua, NH 03062

Invivo Corporation ..... Booth #213  
 N27 W 23676 Paul Road  
 Pewaukee, WI 53072

Lippincott Williams and Wilkins ..... Booth #100  
 New York, NY

Medtronic ..... Booth #317  
 2600 Sofamor Danek Drive  
 Memphis, TN 38132

MicroVenton..... Booth #106  
 1311 Valencia Avenue  
 Tustin, CA 92780

MR Instruments..... Booth #318  
 5610 Rowland Road, Suite 145  
 Minneapolis, MN 55343

NeuroTherm, Inc. .... Booth #400  
 30 Upton Drive, Suite 2  
 Wilmington, MA 01887

NordicNeuroLab ..... Booth #225  
 234 West Florida Street, Suite 210  
 Milwaukee, WI 53204

Olea Medical..... Booth #306  
 533 A Putnam Avenue  
 Cambridge, MA 02139

Philips Healthcare ..... Booth #200  
 22100 Bothell Everett Highway  
 Bothell, WA 98021

Radiological Society of North America (RSNA) ..... Booth #219  
 820 Jorie Boulevard  
 Oak Brook, IL 60523

Siemens Medical Solutions USA, Inc..... Booth #110  
 51 Valley Stream Parkway  
 Malvern, PA 19355

Spinger ..... Booth #205  
 233 Spring Street  
 New York, NY 10013

Stryker Interventional Spine..... Booth #203  
 4100 East Milham Avenue  
 Kalamazoo, MI 49001

Synthes Spine ..... Booth #402  
 1302 Wrights Lane East  
 West Chester, PA 19380

Thieme Medical Publishers ..... Booth #207  
 333 Seventh Avenue  
 New York, NY 10001

Toshiba America Medical Systems, Inc ..... Booth #220  
 2441 Michelle Drive  
 Tustin, CA 92780

Vital ..... Booth #304  
 5850 Opus Parkway, Suite 300  
 Minnetonka, MN 55343



# ASNR 50th Annual Meeting Invited Speakers (as of 3/21/12)

- Vikas Agarwal, MD  
*University of Pittsburgh Medical Center*
- Frederica Agosta, MD  
*San Raffaele Scientific Institute and Vita-Salute University, Italy*
- Andres Arbelaez, MD  
*Corbic Cardioneurovascular / Hospital Pablo Tobon Uribe, Columbia*
- Krystal Archer-Aarroyo, MD  
*University of Maryland School of Medicine*
- Roland Bammer, PhD  
*Stanford University*
- Peter B. Barker, D.Phil.  
*Johns Hopkins University School of Medicine*
- Frederik Barkhof, MD  
*Vrije Universiteit Medical Centre, Netherlands*
- A. James Barkovich, MD  
*University of California, San Francisco Medical Center*
- Robert M. Barr, MD  
*Mecklenburg Radiology Associates, P.A.*
- Walter S. Bartynski, MD  
*Presbyterian University Hospital*
- Tracy T. Batchelor, MD, MPH  
*Massachusetts General Hospital / Harvard Medical School*
- Jacqueline A. Bello, MD  
*Montefiore Medical Center*
- Alex Berenstein, MD  
*Roosevelt Hospital*
- Rafeeqe A. Bhadelia, MD  
*Beth Israel Deaconess Medical Center*
- Erin D. Bigler, PhD  
*Brigham Young University*
- Susan I. Blaser, MD  
*Hospital for Sick Children, Canada*
- Andrew G. Bleicher, MD  
*University of Pittsburgh Medical Center*
- Timothy N. Booth, MD  
*Children's Medical Center of Dallas / University of Texas at Southwestern*
- Craig A. Branch, PhD  
*Albert Einstein College of Medicine*
- Barton F. Branstetter IV, MD  
*University of Pittsburgh Medical Center*
- Allan L. Brook, MD  
*Montefiore Medical Center*
- Francis Brunelle, MD  
*Hopital Necker-Enfants Malades, France*
- R. Nick Bryan, MD, PhD  
*University of Pennsylvania Health System*
- Soonmee Cha, MD  
*University of California, San Francisco Medical Center*
- Tessa Cook, MD  
*University of Pennsylvania*
- DeWitte T. Cross III, MD  
*Washington University School of Medical*
- Mary E. Cunnane, MD  
*Massachusetts Eye and Ear Infirmary*
- Anders M. Dale, PhD  
*University of California, San Diego*
- Colin P. Derdeyn, MD  
*Mallinckrodt Institute*
- William D. Donovan, MD, MPH, FACR  
*The William W. Backus Hospital*
- Howard L. Dorne, MD  
*Vascular and Interventional Specialists of Orange County*
- Paul Dreyfuss, MD  
*University of Washington*
- Clifford J. Eskey, MD, PhD  
*Dartmouth-Hitchcock Medical Center*
- Zahi A. Fayad, PhD, FAHA, FACC  
*Mount Sinai School of Medicine*
- David J. Fiorella, MD, PhD  
*Stony Brook University Medical Center*
- Donald F. Frei, Jr., MD  
*Radiology Imaging Associates*
- William C. Gaetz, PhD  
*University of Pennsylvania School of Medicine*
- Emerson L. Gasparetto, MD, PhD  
*University Federal of Rio De Janeiro and DASA, Brazil*
- Lawrence E. Ginsberg, MD  
*MD Anderson Cancer Center*
- Christine M. Glastonbury, MBBS  
*University of California, San Francisco*
- R. Gilberto Gonzalez, MD, PhD  
*Massachusetts General Hospital*
- P. Ellen Grant, MD  
*Children's Hospital Boston*
- Robert I. Grossman, MD  
*NYU Langone Medical Center*
- Rajiv Gupta, MD, PhD  
*Massachusetts General Hospital*
- David B. Hackney, MD, FACR  
*Beth Israel Deaconess Medical Center*
- Daniel K. Hallam, MD, MSc  
*University of Washington, Harborview Medical Center*
- H. Ric Harnsberger, MD  
*University of Utah School of Medicine*
- Donald V. Heck, MD  
*Forsyth Radiology Associates*
- Jeroen Hendrikse, MD, PhD  
*University Medical Center-Utrecht, Netherlands*
- Alan S. Hilibrand, MD  
*Jefferson Medical College / The Rothman Institute*
- Andrei I. Holodny, MD  
*Memorial Sloan-Kettering Cancer Center / Weill Medical College of Cornell University*
- Michael S. Huckman, MD  
*Rush University Medical Center*
- Patricia A. Hudgins, MD  
*Emory University School of Medicine*
- Jeffrey G. Jarvik, MD  
*University of Washington*
- Mahesh V. Jayaraman, MD  
*Warren Alpert School of Medicine at Brown University / Rhode Island Hospital*
- Annette J. Johnson, MD, MS  
*Wake Forest University School of Medicine*
- Crystal A. Jones  
*University of Michigan Health System*
- John E. Jordan, MD  
*Advanced Imaging of South Bay*
- Emanuel Kanal, MD  
*University of Pittsburgh Medical Center*
- Marc D. Keshishian, MD  
*Blue Care Network*
- Elizabeth A. Krupinski, PhD  
*The University of Arizona*
- David A. Kumpe, MD, FACR  
*University of Colorado Hospital*
- John I. Lane, MD  
*Mayo Clinic Rochester, MN*
- Meng Law, MD  
*Keck Medical Center of USC*
- Frank J. Lexa, VII, MD  
*The Wharton School of The University of Pennsylvania*
- Catherine Limperopoulos, PhD  
*Children's National Medical Center / George Washington University School of Medicine and Health Science*
- Michael L. Lipton, MD, PhD  
*Albert Einstein College of Medicine*
- Andrew W. Litt, MD  
*Dell Healthcare and Life Sciences*
- Harold I. Litt, MD, PhD  
*Perelman School of Medicine at The University of Pennsylvania*
- Laurie A. Loevner, MD  
*University of Pennsylvania Medical Center*
- Jeffrey C. Lotz, PhD  
*University of California, San Francisco*
- Hanzhang Lu, PhD  
*University of Texas Southwestern Medical Center*
- Joseph A. Maldjian, MD  
*Wake Forest University School of Medicine*
- Alex Mamourian, MD  
*University of Pennsylvania*
- Graeme F. Mason, PhD  
*Yale School of Medicine*
- Chester A. Mathis, PhD  
*University of Pittsburgh School of Medicine*
- Sean Meagher, MD  
*Central Illinois Radiological Associates, Ltd.*
- Carolyn C. Meltzer, MD, FACR  
*Emory University School of Medicine*
- Michelle A. Michel, MD  
*Medical College of Wisconsin / Froedtert Hospital*
- David J. Mikulis, MD  
*Toronto Western Hospital, Canada*
- Michael T. Modic, MD  
*Cleveland Clinic Foundation*
- Andrew J. Molyneux, MD  
*Neurovascular Research Nuffield Surgery*
- Gul Moonis, MD, BS  
*Beth Israel Deaconess Medical Center*
- Christopher J. Moran, MD  
*Washington University School of Medicine*

# ASNR 50th Annual Meeting Invited Speakers (as of 3/21/12)

Pratik Mukherjee, MD, PhD <i>University of California, San Francisco</i>	Richard L. Robertson, MD <i>Children's Hospital Boston</i>	Hyunsuk Shim, PhD <i>Emory University</i>	Richard H. Wiggins, III, MD, CIIP <i>University of Utah, Health Sciences Center</i>
Suresh K. Mukherji, MD, FACR <i>University of Michigan Health System</i>	Caroline D. Robson, MB, ChB <i>Children's Hospital Boston</i>	Daniel K. Sodickson, MD, PhD <i>NYU Langone Medical Center</i>	Daniel W. Williams, III, MD <i>Wake Forest University School of Medicine</i>
Srini Mukundan, Jr., MD, PhD <i>Brigham and Women's Hospital</i>	Howard E. Rockette, PhD <i>University of Pittsburgh</i>	D. Christian Sonne, MD <i>Kaiser Permanente Oakland Medical Center</i>	Dean F. Wong, MD, PhD <i>Johns Hopkins Medical Institutions</i>
Cameron G. McDougall, MD <i>Barrow Neurological Associates</i>	Gary F. Rogers, MD <i>Children's National Medical Center</i>	Michael G. Stewart, MD, MPH <i>Weill Medical College of Cornell University</i>	Wade H.M. Wong, DO <i>University of California San Diego Medical Center</i>
Geraldine McGinty, MD, MBA <i>NRAD Medical Services</i>	Bruce R. Rosen, MD, PhD <i>Boston Massachusetts General Hospital</i>	Jeffrey A. Stone, MD <i>Mayo Clinic Florida</i>	David M. Yousem, MD, MBA <i>Johns Hopkins Medical Institution</i>
Thomas P. Naidich, MD <i>Mount Sinai Medical Center</i>	Jeffrey S. Ross, MD <i>Barrow Neurological Institute, St. Joseph's Hospital</i>	Pia Maly Sundgren, MD, PhD <i>Institution of Clinical Sciences Lund University, Sweden</i>	Gregory G. Zaharchuk, MD, PhD <i>Lucille Packard Children's Hospital at Stanford</i>
Edward A. Neuwelt, MD <i>Oregon Health &amp; Science University</i>	Andrea Rossi, MD <i>G. Gaslini Children's Hospital, Italy</i>	Joel D. Swartz, MD <i>Germantown Imaging Associates</i>	Gregory J. Zipfel, MD <i>Washington University in St. Louis, School of Medicine</i>
Darren B. Orbach, MD, PhD <i>Children's Hospital Boston</i>	Alex Rovira, MD <i>Hospital Vall d'Hebron University, Spain</i>	Rick Swartz, MD, PhD <i>Sunnybrook Health Sciences Centre, Toronto</i>	
Anne G. Osborn, MD <i>University of Utah Medical Center</i>	Laura M. Rowland, PhD <i>University of Maryland School of Medicine/Maryland Psychiatric Research Center</i>	Stephen T. Sweriduk, MD <i>Shields Healthcare Group</i>	
Enrique Palacios, MD, FACR <i>Tulane University</i>	Howard A. Rowley, MD <i>University of Wisconsin</i>	E. Turgut Tali, MD <i>Gazi University School of Medicine, Turkey</i>	
Susan Palasis, MD <i>Children's Healthcare of Atlanta</i>	Zoran Rumboldt, MD, PhD <i>Medical University of South Carolina</i>	Majda M. Thurnher, MD <i>Medical University of Vienna, Austria</i>	
Michael J. Paldino, MD <i>Children's Hospital Boston</i>	Haris Sair, MD <i>Johns Hopkins Medicine</i>	Frank C. Tong, MD <i>Emory University School of Medicine</i>	
Jeffrey R. Petrella, MD <i>Duke University Medical Center</i>	Stephen Salloway, MD, MS <i>The Warren Alpert Medical School of Brown University</i>	Johan W. Van Goethem, MD, PhD <i>University Hospital of Antwerp, Belgium</i>	
C. Douglas Phillips, MD, FACR <i>Weill Medical College of Cornell University / New York Presbyterian Hospital</i>	Pina C. Sanelli, MD, MPH <i>New York Presbyterian Hospital/ Cornell University</i>	Gilbert Vezina, MD <i>Children's National Medical Center</i>	
Stuart R. Pomerantz, MD <i>Massachusetts General Hospital</i>	Pamela W. Schaefer, MD <i>Massachusetts General Hospital</i>	Fernando Vinuela, MD <i>UCLA Medical Center</i>	
Whitney B. Pope, MD, PhD <i>David Geffen School of Medicine at University of California, Los Angeles</i>	Ilona M. Schmalfuss, MD <i>NF/SG Veterans Administration/ University of Florida</i>	Katie D. Vo, MD <i>Mallinckrodt Institute of Radiology / Washington University Medical Center</i>	
John D. Port, MD, PhD <i>Mayo Clinic, Rochester MN</i>	David J. Seidenwurm, MD, FACR <i>Radiological Associates</i>	Ajay K. Wakhloo, MD, PhD <i>University of Massachusetts</i>	
Judith M. Donovan Post, MD, FACR <i>Miller School of Medicine at The University of Miami</i>	Aseem Sharma, MD <i>Washington University School of Medicine/ Mallinckrodt Institute of Radiology</i>	Bruce A. Wasserman, MD <i>Johns Hopkins University</i>	
James M. Provenzale, MD, FACR <i>Duke Medical Center</i>	Rahul Sharma, MD, MBA, FACEP <i>Weill Cornell Medical College</i>	Alyssa T. Watanabe, MD <i>Voxel Imaging, Inc. / University of Southern California School of Medicine</i>	
Robert M. Quencer, MD <i>Miller School of Medicine at The University of Miami</i>	Deborah R. Shatzkes, MD <i>Lenox Hill Hospital</i>	Patrick Y. Wen, MD <i>Dana-Farber / Brigham &amp; Women's Cancer Center</i>	
Perry F. Renshaw, MD, PhD, MBA <i>The University of Utah</i>	Martha E. Shenton, PhD <i>Harvard Medical School / Brigham and Women's Hospital</i>	Christopher T. Whitlow, MD, PhD <i>Wake Forest University School of Medicine</i>	
Timothy P.L. Roberts, PhD <i>The Children's Hospital of Philadelphia</i>			

# ASNR 50th Annual Meeting

## Scientific Program Overview (as of 3/21/12)

**Monday through Thursday:** ASNR will provide Breakfast, Morning & Afternoon Beverage Breaks. Lunch on own.  
**Tuesday through Thursday:** ASNR will provide Continuous Coffee Service in the Technical Exhibit Hall Americas Hall I

### Monday April 23, 2012

#### 6:00am - 7:55am Continental Breakfast

- 6:20am - 7:20am How-To Session - Bracco Diagnostics Inc.
- 7:25am - 7:30am (1) Opening Remarks  
p. 1
- 7:30am - 8:30am (2) Maintenance of Certification (MOC) - Review  
Session (AR) Pediatrics  
p. 1
- 8:30am - 10:00am (3) Collaboration with Society For Neuro  
Oncology (SNO): Assessment of Tumor  
Recurrence In The Modern Era  
p. 1
- 8:30am - 10:00am (4) ASPNR Programming: Fetal And Neonatal  
Imaging  
p. 2
- 8:30am - 10:00am (5) Synaptic Junction Programming: MR Safety  
For Patients With Implants  
p. 3
- 8:30am - 10:00am (6) Advanced CT Imaging  
p. 4
- 8:30am - 10:00am (7) Cutting Edge Research Support By The  
Foundation of The ASNR  
p. 4

#### 10:00am - 10:30am Morning Beverage Break

- 10:30am - 12:00pm (8) Parallel Scientific Paper Sessions  
Session 8a Adult Brain - Cerebrovascular I  
p. 5  
Session 8b Adult Brain - New Techniques/Post  
Processing - I  
p. 13  
Session 8c Pediatrics: New Techniques  
p. 21  
Session 8d Adult Brain: Trauma  
p. 28  
Session 8e Anatomy & Applications of Advanced  
Imaging  
p. 36

#### 12:00pm - 1:00pm Lunch On Own

- 12:00pm - 1:00pm (9) Education Exhibits Tour
- 1:00pm - 2:30pm (10) ASFNR Programming Implementing  
Functional Imaging In The Clinical Setting  
(SAM # 1) (AR)  
p. 43

1:00pm - 2:30pm

(11) ASPNR Programming: Advanced Pediatric  
Neuroimaging Techniques  
p. 45

1:00pm - 2:30pm

(12) Socioeconomic Programming: Healthcare/  
Payment Methodology/Health Services  
p. 46

1:00pm - 2:30pm

(13) General Programming: CNS Infections  
p. 46

1:00pm - 2:30pm

(14) An Expert: How I Do It  
p. 48

#### 2:30pm - 3:00pm

#### Afternoon Beverage Break

3:00pm - 4:30pm

- (15) Parallel Scientific Paper Sessions  
Session 15a Adult Brain: Neoplasms I  
p. 49  
Session 15b Adult Brain: New Techniques/Post  
Processing - II  
p. 57  
Session 15c Adult Brain: Degenerative/  
Demyelinating/Metabolic Diseases  
p. 65  
Session 15d Pediatrics: Developmental/Congenital  
Malformations  
p. 72  
Session 15e Intracranial Manifestation and Rare  
Diseases/Miscellaneous  
p. 79  
(16) ASPNR Programming: Pediatric Head and  
Neck (SAM #2) (AR)  
p. 86  
(17) ASFNR Programming: Advanced Imaging In  
Psychiatric Disease: Opportunities And Trends  
p. 87  
(18) Advanced Imaging Seminar: Molecular  
Imaging Update  
p. 88  
(19) Appropriate Utilization of Cervical Spine  
Imaging in Trauma  
p. 89  
(20) Parallel Session: Pediatric: Miscellaneous  
P. 90

4:45pm - 6:15pm

4:45pm - 6:15pm

4:45pm - 6:15pm

4:45pm - 6:15pm

4:45pm - 6:15pm

#### 7:00pm - 10:00pm

**Welcome Reception At The Museum of Modern  
Art (MoMA) (Off Site)**

\*AR = Audience Response Session

\*\*Session Programming qualified by the American Board of Radiology (ABR) in meeting the criteria for self-assessment toward the purpose of fulfilling requirements in the ABR Maintenance of Certification Program. 3/12. To obtain current SAM credit information, visit [www.asnr.org](http://www.asnr.org)



# Scientific Program Overview (as of 3/21/12)

## Tuesday April 24, 2012

**6:00am - 7:55am**

### Continental Breakfast

6:20am - 7:20am

How - To Session - Philips Healthcare

7:30am - 8:30am

(21) Maintenance of Certification (MOC) - Review Session (AR) Head And Neck  
p. 98

8:30am - 10:00am

(22) General Programming: Collaboration with Society The SILAN Session  
In Honor of Dr. Juan Taveras  
p. 98

8:30am - 10:00am

(23) General Programming: Alzheimer's Dementia  
p. 100

8:30am - 10:00am

(24) Synaptic Junction Programming: DTI For Dummies  
p. 102

8:30am - 10:00am

(25) An Expert: How I Do It  
p. 102

8:30am - 10:00am

(26) Young Professional Programming: Entering And Thriving In Community Practice  
p. 104

**10:00am - 10:30am**

### Morning Beverage Break

10:30am - 12:00pm

(27) Parallel Scientific Paper Sessions  
Session 27a Adult Brain: Neoplasms II  
p. 105  
Session 27b Functional Imaging I  
p. 114  
Session 27c Adult Brain: Vascular, Intracranial  
p. 122  
Session 27d Head & Neck: Anatomy, Face, Orbit and Congenital  
p. 129  
Session 27e Pediatric: Functional Imaging & Neonatal Imaging  
p. 135

**12:00pm - 1:00pm**

### Lunch On Own

**12:00pm - 1:00pm**

### Young Professionals Luncheon

12:00pm - 1:00pm

(28) American Society of Pediatric Neuroradiology (ASPNR) Business Meeting (for members only) (with lunch provided)

1:00pm - 2:30pm

(29) ASPNR Programming: 2012 ASPNR Interesting Case Session  
p. 142

1:00pm - 2:30pm

(30) ASFNR Programming: Emerging Techniques In Functional Neuroradiology  
p. 143

1:00pm - 2:30pm

(31) ASHNR Programming: Skull Base  
p. 144

1:00pm - 2:30pm

(32) General Programming: Vessel Wall Imaging  
p. 145

1:00pm - 2:30pm

(33) Young Professionals Programming: Academic Session  
p. 146

**2:30pm - 3:00pm**

### Afternoon Beverage Break

3:00pm - 4:30pm

(34) Parallel Scientific Paper Sessions  
Session 34a Adult Brain: Neoplasms III  
p. 147  
Session 34b Pediatric: Other  
p. 154  
Session 34c Interventional: Arteriovenous Malformations, Fistulae & Other Vascular Lesions  
p. 161  
Session 34d Head & Neck: Pharynx, Larynx, Soft Tissue Neck, Sinonasal and Temporal Bone  
p. 169  
(35) Grant Writing Seminar  
p. 177  
(36) ASHNR Programming: Sinus / Orbit  
p. 177  
(37) General Programming: Aneurysms  
p. 179  
(38) What Is Quality? ...Perspectives From Patient, The Payers And (Least Importantly) Us? (SAM #3) (AR)  
p. 179

3:00pm - 4:30pm

4:45pm - 6:15pm

4:45pm - 6:15pm

4:45pm - 6:15pm

4:45pm - 6:15pm

4:45pm - 6:15pm

6:30pm - 7:30pm

How-To Session  
-Janssen Alzheimer Immunotherapy/Pfizer Inc.

\*AR = Audience Response Session

\*\*Session Programming qualified by the American Board of Radiology (ABR) in meeting the criteria for self-assessment toward the purpose of fulfilling requirements in the ABR Maintenance of Certification Program. 3/12. To obtain current SAM credit information, visit [www.asnr.org](http://www.asnr.org)

# Scientific Program Overview (as of 3/21/12)

**Wednesday April 25, 2012**

<b>6:00am - 7:55am</b>	<b>Continental Breakfast</b>	<b>2:30pm - 3:00pm</b>	<b>Afternoon Beverage Break</b>
6:20am - 7:20am	How - To Session –Toshiba Medical Systems America, Inc.	3:00pm - 4:30pm	(53) Parallel Scientific Paper Sessions
7:30am - 8:30am	(41) Maintenance of Certification (MOC) - Review Session (AR) Cerebrovascular p. 814		Session 53a Adult Brain: Vascular, Extracranial & Intracranial p. 190
8:30am - 10:00am	(42) General Session: Luminary Session: Past, Present And Future p. 184		Session 53b Spine: Other p. 197
<b>10:00am - 10:30am</b>	<b>Morning Beverage Break</b>		Session 53c Interventional: Aneurysms I p. 206
10:30am - 11:00am	(43) Keynote Speaker p. 185		Session 53d Head & Neck: Other, New Techniques & Temporal Bone p. 212
11:00am - 11:15am	(44) ASNR Presidential Address p. 186		Session 53e Socioeconomics p. 219
11:15am - 11:30am	(45) ASNR Award Announcements -Gold Medal Award -Honorary Member Award -2012 The Foundation of the ASNR Outstanding Contribution in Research Award -2012 The Foundation of the ASNR Scholar Award in Neuroradiology Research -2012 The Foundation of the ASNR Research Scientist Award -2012 The Foundation of the ASNR Comparative Effectiveness Research Award -2012 Women in Neuro Award -Cornelius G. Dyke Memorial Award -2011 Trainee Award -2011 Outstanding Presentation Awards	4:45pm - 6:15pm	(54) ASSR Programming: Epidemiology Basics For Spine Imaging And Interventions p. 226
		4:45pm - 6:15pm	(55) Socioeconomics Programming: The Nuts & Bolts of Health Care Payment And Reform: What You Need To Know! p. 227
		4:45pm - 6:15pm	(56) SNIS Programming: Dural Arteriovenous Fistulae p. 229
		4:45pm - 6:15pm	(57) ASHNR Programming: Temporal Bone p. 229
		4:45pm - 6:15pm	(58) Advanced Imaging Seminar: Faster And Faster p. 231
		<b>6:30pm - 7:30pm</b>	<b>Closing Reception with Technical Exhibitors</b>
11:30am - 12:00pm	(46) American Society Of Neuroradiology (ASNR) Annual Business Meeting (Members Only)		<b>Americas Hall I, Hilton New York</b>
12:00pm - 1:00pm	(47) Education Exhibits Tour		
<b>12:00pm - 1:00pm</b>	<b>Lunch On Own</b>		
1:00pm - 2:30pm	(48) ASHNR Programming: Head And Neck Cancer (SAM # 4) (AR) p. 186		
1:00pm - 2:30pm	(49) SNIS Programming: Venous Disease p. 187		
1:00pm - 2:30pm	(50) ASSR Programming: Advanced Imaging of The Spine And Disk p. 188		
1:00pm - 2:30pm	(51) Synaptic Junction Programming: Dose Extraction p. 189		
1:00pm - 2:30pm	(52) An Expert: How I Do It p. 190		

\*AR = Audience Response Session

**XXX** \*\*Session Programming qualified by the American Board of Radiology (ABR) in meeting the criteria for self-assessment toward the purpose of fulfilling requirements in the ABR Maintenance of Certification Program. 3/12. To obtain current SAM credit information, visit [www.asnr.org](http://www.asnr.org)



# Scientific Program Overview (as of 3/21/12)

## Thursday April 26, 2012

<b>6:00am - 7:55am</b>	<b>Continental Breakfast</b>	<b>2:30pm - 3:00pm</b>	<b>Afternoon Beverage Break</b>
6:20am - 7:20am	How - To Session - Siemens Medical Solutions USA, Inc.	3:00pm - 4:30pm	(67) SNIS Programming: Carotid Disease (SAM #6) (AR) p. 313
7:30am - 8:30am	(59) Maintenance of Certification (MOC) - Review Session (AR) Spine p. 232	3:00pm - 4:30pm	(68) General Programming: Mild Traumatic Brain Injury p. 314
8:30am - 10:00am	(60) ASSR Programming: The Sacroiliac Joint and Pelvis: Imaging and Interventions (SAM #5) (AR) p. 232	3:00pm - 4:30pm	(69) ASSR Programming: Spine Potpourri p. 315
8:30am - 10:00am	(61) Collaboration With European Society Of Neuroradiology (ESNR): White Matter Diseases p. 234	3:00pm - 4:30pm	(70) Parallel Session: Interventional and Spine: Miscellaneous p. 316
8:30am - 10:00am	(62) Socioeconomic Programming: Current Issues In Stroke Imaging And Treatment: What Is The Evidence? p. 236	4:30pm - 4:45pm	(72) Closing Remarks p. 322
8:30am - 10:00am	(63) Parallel Session: Interventional and Spine: Miscellaneous p. 237		
<b>10:00am - 10:30am</b>	<b>Morning Beverage Break</b>		
10:30am - 12:00pm	(65) Parallel Scientific Paper Sessions Session 65a Adult Brain: Degenerative/ Demyelinating/Metabolic Diseases II p. 242 Session 65b Interventional: Aneurysms II p. 249 Session 65c Spine Intervention p. 256 Session 65d Epilepsy & Other p. 263 Session 65e Neoplasms - Spine and Brain p. 267		
<b>12:00pm - 1:00pm</b>	<b>Lunch On Own</b>		
1:00pm - 2:30pm	(66) Parallel Scientific Paper Sessions Session 66A Adult Brain: Cerebrovascular II p. 276 Session 66b Interventional: Thrombolysis/Stroke p. 285 Session 66c Interventional: New Devices & Techniques p. 293 Session 66d Spine: New Techniques & Degenerative p. 299 Session 66e Adult Brain: Functional Imaging II p. 306		

\*AR = Audience Response Session

\*\*Session Programming qualified by the American Board of Radiology (ABR) in meeting the criteria for self-assessment toward the purpose of fulfilling requirements in the ABR Maintenance of Certification Program. 3/12. To obtain current SAM credit information, visit [www.asnr.org](http://www.asnr.org)

# American Society of Neuroradiology (ASNR) Future Annual Meetings



## ASNR 2013

NEURORADIOLOGY FOR THE 21<sup>ST</sup> CENTURY

ASFNr ASHNR ASPNR ASSR SNIS

51<sup>st</sup> Annual Meeting | May 18 - 23

*San Diego Convention Center, San Diego, California*

## SAN DIEGO 2013

52<sup>nd</sup> Annual Meeting | May 17 - 22

*Palais des Congrès de Montreal, Montreal, Quebec, Canada*

## MONTREAL 2014







## **Simplify** the MOC Process



## **Manage** your CME Credits Online

**CMEgateway.org**

### **Available to Members of Participating Societies**

American Board of Radiology (ABR)  
American College of Radiology (ACR)  
American Roentgen Ray Society (ARRS)  
American Society of Neuroradiology (ASNR)  
Commission on Accreditation of Medical  
Physics Educational Programs, Inc. (CAMPEP)  
Radiological Society of North America (RSNA)  
Society of Interventional Radiology (SIR)  
SNM  
The Society for Pediatric Radiology (SPR)

### **It's Easy and Free!**

Log on to CME Gateway to:

- View or print reports of your CME credits from multiple societies from a single access point.
- Print an aggregated report or certificate from each participating organization.
- Link to SAMs and other tools to help with maintenance of certification.

### **American Board of Radiology (ABR) participation!**

By activating ABR in your organizational profile, your MOC-fulfilling CME and SAM credits can be transferred to your own personalized database on the ABR Web site.

### **Sign Up Today!**

go to [CMEgateway.org](http://CMEgateway.org)

## Platinum Level



Bayer HealthCare

- An educational grant in support of The Foundation of the ASNR Symposium 2012: Acute Ischemic Stroke Imaging
- Annual educational grant in support of the Maintenance of Certification (MOC) and Self Assessment Modules (SAM)\* programming live and as an internet activity on the ASNR website
- Performance and Quality Improvement (PQI) Initiative

## Gold Level



**ALZHEIMER'S  
IMMUNOTHERAPY PROGRAM**  
INNOVATION TO REMEMBER™



**PHILIPS**

**TOSHIBA**  
Leading Innovation >>>

## Silver Level

**SIEMENS**



**Medtronic**



imagination at work

## Bronze Level

**V i T A L**

A Toshiba Medical Systems Group Company

PROGRAM CONTRIBUTORS

\* Session Programming qualified by the American Board of Radiology (ABR) in meeting the criteria for self-assessment toward the purpose of fulfilling requirements in the ABR Maintenance of Certification Program. 3/12. To obtain current SAM credit information, visit [www.asnr.org](http://www.asnr.org)



## Monday Morning

**7:25 AM - 7:30 AM**  
**Grand Ballroom Suite**

(1) Opening Remarks

**O-1** **7:25 AM - 7:30 AM**

### Opening Remarks

David B. Hackney, MD, FACR

Radiology, Beth Israel Deaconess  
 Boston, MA, USA

## Monday Morning

**7:30 AM - 8:30 AM**  
**Grand Ballroom Suite**

(2) MAINTENANCE OF  
 CERTIFICATION (MOC) - REVIEW  
 SESSION (AR) PEDIATRICS

**O-2** **7:30 AM - 8:00 AM**

### Pediatrics

Gilbert Vezina, MD

Children's Nat'l Med Ctr.  
 Washington, DC, USA

Unknown cases with pertinent multiple choice questions will be presented. Illustrative cases of congenital and acquired disorders of the pediatric brain will be used; the difficulty level will be that expected within the fund of knowledge possessed by neuroradiologists.

**O-3** **8:00 AM - 8:30 AM**

### Pediatrics

Timothy N. Booth, MD

Radiology, Children's Medical Center of Dallas  
 Dallas, TX, USA

Unknown cases with pertinent multiple choice questions will be presented with related cases presented. Illustrative cases of congenital and acquired disorders of the pediatric head and neck will be used; the difficulty level will be that expected within the fund of knowledge possessed by neuroradiologists.

## Monday Morning

**8:30 AM - 10:00 AM**  
**Grand Ballroom Suite**

(3) COLLABORATION WITH  
 SOCIETY FOR NEURO ONCOLOGY  
 (SNO): ASSESSMENT OF TUMOR  
 RECURRENCE IN THE MODERN  
 ERA

**O-4** **8:30 AM - 8:50 AM**

### Advanced Neuroimaging of Response and of Progression Following Anti-Angiogenic Therapy

Pia Maly Sundgren, MD, PhD

Center for Medical Imaging Physiology, Lund University  
 Lund, Sweden

Glioblastoma is the most common primary brain tumor and is a highly angiogenic tumor. Primarily the angiogenesis is mediated by vascular endothelial growth factor (VEGF) with blood vessels that distinctively differs from normal vessel but other proangiogenic factors play a role as well. Due to the ineffective therapy the prognosis of glioblastoma is poor and has driven the research to find new therapeutic agencies. An example is of this Bevacizumab (Avastin), a humanized monoclonal antibody against VEGF. However, despite advanced neuroimaging techniques it remains difficult to predict tumor response to anti-angiogenic therapy in individual patients. For example there is diminished contrast enhancement of the tumor and reduced surrounding edema most likely due to inhibition in vessel permeability early in the treatment with bevacizumab. This finding is named "pseudoresponse" since the decreased enhancement can be secondary to an antipermeability effect rather than the result of reduction in tumor size. The opposite is seen in the treatment with temozolamide and radiation where an increase in area of enhancement is seen that resolves over time - so called pseudoprogression. Both these conditions are well demonstrated on conventional MR imaging as well as on advanced MRI like diffusion and perfusion imaging. However they still may cause confusion and wrongly results in change of therapy as well as in the interpretation of results of Phase I and Phase II clinical trials. To partially address this issue the MacDonald criteria have recently been revised. The present lecture will focus present knowledge and research on the use of advanced imaging to support response or progression during ongoing therapy.

**O-5** **8:50 AM - 9:10 AM**

**Decision Making Following Anti-Angiogenic Therapy: The Neuro-Oncologist's Perspective**

Tracy T. Batchelor, MD, MPH

CERN Foundation  
Dayton, OH, USA

**O-6** **9:10 AM - 9:30 AM**

**Advanced Imaging and Non-FDG PET for Differentiating True From Pseudo-Progression**

Whitney B. Pope, MD, PhD

Radiology, UCLA  
Los Angeles, CA, USA

The role of advanced MRI and non-FDG PET in the evaluation of brain tumor patients, specifically the ability to differentiate true- from pseudoprogession will be presented.

**O-7** **9:30 AM - 9:50 AM**

**Review of RANO**

Patrick Y. Wen, MD

Dana-Farber/Brigham and Women's Cancer Center  
Boston, MA, USA

Dr. Patrick Wen graduated from St. Bartholomew's Hospital Medical College, University of London. He completed his internal medicine training at University of London affiliated hospitals. His neurology training was completed at the National Hospitals for Nervous Diseases at Queen Square, London, and in the Harvard-Longwood Neurology Training Program. Dr. Wen is currently a Professor of Neurology at Harvard Medical School, the Director of the Center for Neuro-Oncology at Dana-Farber/Brigham and Women's Cancer Center and Director of the Division of Neuro-Oncology in the Department of Neurology at Brigham and Women's Hospital. He was Vice President of the Society For Neuro-Oncology. He is Chair-Elect of the Neuro-Oncology Section of the American Academy of Neurology, Vice Chair of the Neuro-Oncology Committee in the Alliance for Clinical Trials in Oncology (ACTION) Cooperative Group, and chairs the New Agents Committee of the Adult Brain Tumor Consortium. His research is focused on novel treatments for brain tumors, including targeted molecular therapies and inhibitors of angiogenesis. In addition, he is interested in response assessment and optimal trial designs in neuro-oncology and is a leader of the Response Assessment in Neuro-oncology Working Group that recently proposed new response criteria for gliomas.

## Monday Morning

**8:30 AM - 10:00 AM**

### Trianon Ballroom

#### (4) ASPNR PROGRAMMING: FETAL AND NEONATAL IMAGING

**O-8** **8:30 AM - 8:55 AM**

**Advanced Fetal and Neonatal Imaging Techniques**

P. Ellen Grant, MD

Radiology, MGH  
Boston, MA, USA

**O-9** **8:55 AM - 9:20 AM**

**New Insights into Neurocognitive Deficits of Prematurity**

A. James Barkovich, MD

UCSF Medical Center  
San Francisco, CA, USA

Presentation Summary: Imaging Findings and Causes of Disability in Premature Infants

Currently, 12% of live births in the U.S. are premature; although most research has focused upon the subset with very low birthweight (slightly more than 10% of prematures), all prematurely born neonates are at increased risk for neurodevelopmental disorders. This presentation will focus on disorders of brain development in the prematurely born neonate and the state of maturation of the brain at various times of development. Late migrating neurons, connections with the cerebral subplate and the developing cerebral cortex, and cerebellar neuronal migration and connections all are ongoing in neonates who are born prematurely. A better understanding of the status of development helps to understand the significant incidence of neurodevelopmental delay and behavioral disorders in these children.

**O-10** **9:20 AM - 9:45 AM**

**Fetal and Neonatal Cerebellar Abnormalities**

Catherine Limperopoulos, PhD

George Washington Univ. Schl of Medicine & Health Sciences  
Washington, DC, USA



## Monday Morning

**8:30 AM - 10:00 AM**

**Murray Hill**

### (5) SYNAPTIC JUNCTION PROGRAMMING: MR SAFETY FOR PATIENTS WITH IMPLANTS

**0-11**

**8:30 AM - 8:55 AM**

Emanuel Kanal, MD

Univ of Pittsburgh Med Ctr  
Pittsburgh, PA, USA

#### Presentation Summary

The MR industry has come a long way since the initial introduction of MRI into the clinical arena, when many implants, and especially electromagnetically active implants, were considered absolute contraindications. This presentation will discuss the potential safety concerns of implants in the MR imaging environment. The static magnetic fields, the gradient magnetic fields, and the radiofrequency time varying magnetic fields associated with the MR imaging process each has the potential to interact with implants in various and unique mechanisms that introduce their own potential safety concerns. The rather unique role that the static magnetic field strength can play in determining the safety of MR scanning of certain implants or devices will also be reviewed. Specific devices that have been shown to be safe in MR environments will be highlighted, and specific solutions will be discussed that have enabled us to safely and diagnostically expose patients with numerous implanted devices to the potential diagnostic benefits of the MR imaging process. Among these will be the relatively recently FDA-approved first MR conditional labeling of a cardiac pacemaker system. We will also entertain a brief glimpse into the direction that our industry is taking towards developing even more ambitious MR conditionally labelled devices. Finally, we will introduce possible approaches that the MR industry is considering to accommodate the ever increasing number of patients in whom device have been implanted, including Fixed Parameter Mode scanning protocols, and explain how they work and the rationale behind the push for their adoption into our MR imaging industry.

**0-12**

**8:55 AM - 9:20 AM**

Alex Mamourian, MD

Radiology, University of Pennsylvania  
Philadelphia, PA, USA

#### Presentation Summary

In this presentation I will provide a reasonable approach to imaging patients with vagal nerve stimulators and programmable shunts using MR.

**0-13**

**9:20 AM - 9:45 AM**

Harold I. Litt, MD, PhD

Radiology, University of Pennsylvania  
Philadelphia, PA, USA

*Harold Litt MD-PhD is Associate Professor of Radiology and Medicine at the Perelman School of Medicine of the University of Pennsylvania and Chief of the Cardiovascular Imaging Section of the Department of Radiology. After obtaining AB and AM degrees in physics at Harvard University, and an MD and PhD in biophysics from SUNY at Buffalo, he undertook an internship at Mount Auburn Hospital-Harvard Medical School and residency in diagnostic radiology at the University of Pennsylvania School of Medicine. Following fellowship training in cardiothoracic radiology at the University of California at San Francisco, he returned to Penn. Dr. Litt's research concerns novel methods and applications of Computed Tomography and Magnetic Resonance Imaging in cardiovascular disease, including methods for visualization of large clinical imaging datasets, imaging of patients with implanted cardiac devices, and quantitative analysis of cardiac motion. He is principal investigator of a large, multicenter trial sponsored by the Commonwealth of Pennsylvania Tobacco Settlement Fund comparing CT with usual care for evaluation of patients presenting to emergency departments with chest pain.*

#### Presentation Summary

Recent experience is slowly overturning the long held belief that an implanted pacemaker or defibrillator is an absolute contraindication to MRI. Imaging of device patients may have an acceptable risk profile in certain circumstances. While the recent emergence of "MRI-compatible" devices addresses some safety issues, others remain and legacy devices will persist for many years. A program for imaging of device patients should include appropriate clinical and safety checks, and requires close collaboration between radiologists and electrophysiologists. Neuroradiologists have an important role to play in such a program, given the importance of brain, head and neck, and spine MRI to patient care.

There are many potential interactions between MRI, implanted devices, and patients' electrophysiology. Imaging of such patients requires choosing appropriate MRI hardware (field strength, gradients, coils) and software (pulse sequences), as well as device settings, to obtain diagnostic studies with minimum risk to a particular patient.

Implanted cardiac devices may also be affected by CT when automated tube current adjustment techniques are used, although these effects are limited to the short time period when the generator is exposed to the time-varying x-rays.

## Monday Morning

**8:30 AM - 10:00 AM**

**Beekman/Sutton North**

**(6) ADVANCED CT IMAGING**

**O-14**

**8:30 AM - 9:00 AM**

### **Dual Energy CT Fundamental Principles and Neuro**

Rajiv Gupta, MD, PhD

Neuroradiology, Mass Gen Hospital  
Boston, MA, USA

#### **Presentation Summary**

This presentation will provide a hands-on introduction to dual energy CT (DECT). Fundamental principles of this new modality and its technical implementations will be described. The main capabilities and limitations of DECT will be summarized and illustrated with the help of clinical examples.

**O-15**

**9:00 AM - 9:30 AM**

### **Interactive Reconstruction**

Stuart R. Pomerantz, MD

Neuroradiology, Massachusetts General Hospital  
Boston, MA, USA

**O-16**

**9:30 AM - 10:00 AM**

### **Wide Coverage CT**

Srini Mukundan, Jr, MD, PhD

Radiology, Brigham & Women's Hospital  
Boston, MA, USA

#### **Presentation Summary**

Over the past decade, the development of high-performance x-ray tubes, spiral scan acquisition and multi-row detectors has led to the use of computed tomography (CT) as a means for generating single-phase volumetric angiograms of the neurovascular system. More recently, additional advances including the development of extreme wide-area detectors, rapid translating table technology and dual-energy approaches have further enabled the transformation of neurological computed tomography angiography (CTA) into a four-dimensional technology capable of demonstrating the transit of x-ray contrast media through the cerebrovascular system as a function of time. The value of these techniques is enhanced by the fact that rapid acquisition approaches facilitates robust bone subtraction angiography. When combined with volumetric computer reconstructions, dynamic maximum intensity projection images are created that appear similar to traditional catheter-based neuroangiography. Moreover, 4D CTA studies are typically performed at lower kilovoltage than

traditional CTA which has lead to relatively modest radiation dose for these newer studies. Finally, if obtained at an appropriate sampling rate, the data may be used not only to generate angiographic images, but may be reprocessed with perfusion algorithms to generate whole brain perfusion maps -- all obtained with a single injection of contrast media and a single acquisition. The seminar will include discussions of wide area detectors, helical shuttle scanning, angiography, perfusion and dose.

## Monday Morning

**8:30 AM - 10:00 AM**

**Sutton Center/South**

**(7) CUTTING EDGE RESEARCH  
SUPPORT BY THE FOUNDATION OF  
THE ASNR**

**O-17**

**8:30 AM - 8:45 AM**

### **Foundation of the ASNR: Where Do Your Contributions Go?**

Howard A. Rowley, MD

Radiology Dept., Univ. Of Wisconsin  
Madison, WI, USA

#### **Presentation Summary**

The Foundation of the ASNR is dedicated to research and education in Neuroradiology. With your help, we fund multiple annual seed grants to young investigators who are developing tools for practice tomorrow. Our sponsorship touches every facet of Neuroradiology education, helps our fellows thrive, and keeps all of us refreshed in best practices. This is your specialty, and your chance to help give back. Please consider a donation to the Foundation in your charitable giving plans. *Thank you for investing in Neuroradiology!*

**O-18**

**8:45 AM - 9:05 AM**

### **2009 Scholar's Award: Optimizing Arterial Spin Label MRI for the Visualization of Collateral Flow in Moyamoya Disease**

Greg G. Zaharchuk, MD, PhD

Department of Radiology, Lucille Packard Children's Hospital at Stanford  
Stanford, CA, USA

#### **Presentation Summary**

This talk focuses on the research project that originated from a 2009 ASNR Foundation Scholar Award Grant, which focused on using arterial spin label (ASL) to assess collateral flow patterns in Moyamoya disease patients. Collateral pathways are known to support the cerebral circulation during acute and chronic stroke.



The gold-standard for assessing collaterals is digital subtraction angiography (DSA), but it is a non-tomographic technique that requires subjective grading. ASL is a noninvasive method of measuring cerebral blood flow (CBF) that applies a magnetic label to endogenous water protons of the blood, which then distribute into the brain in proportion to local CBF. Because the label decays with the blood T1, delayed flow is highlighted. Moyamoya disease patients have narrowing of the large cerebral arteries and often demonstrate exuberant collateral networks. We examined newly diagnosed Moyamoya patients with multi-time-delay ASL and velocity-selective ASL (VSASL), which is insensitive to arterial delay, and compared them to gold-standard DSA and stable xCT perfusion measurements. ASL was found to provide a good tomographic map of presence and intensity of collateral CBF. During the grant period, several new avenues were explored, including methods to extract quantitative CBF, to improve VSASL, and to assess cerebral oxygenation.

**O-19** **9:05 AM - 9:25 AM**

**2009 Cerebrovascular Disease Research Award: Comparison and Statistical Validation of Cerebral Flow Results Obtained Using Phase Contrast MRA and Computational Flow Dynamics in an In Vitro Cerebral Aneurysm Model**

Frank C. Tong, MD

Department of Radiology, Emory University School of Medicine  
Atlanta, GA, USA

**Presentation Summary**

This presentation will provide a project summary of the funded project - Comparison and Statistical Validation of Cerebral Flow Results Obtained Using Phase Contrast MRA and Computational Flow Dynamics in an In Vitro Cerebral Aneurysm Model. The experimental methods, challenges, and results will be presented as well as the future extensions of this project.

**O-019a** **9:25 AM - 9:45 AM**

**2008 Basic Science Research Award: Evolving Patterns of Functional Connectivity in the Developing Brain: An Arterial Spin Labeling Perfusion MRI and Computational Network Analytical Investigation**

Christopher T. Whitlow, MD, PhD

Radiology Dept, Wake Forest School of Medicine  
Winston-Salem, NC, USA

**Presentation Summary**

Neurodevelopmental outcomes related to preterm birth have remained poor despite a marked reduction in mortality associated with premature birth. While only 10-15% of preterm infants will develop cerebral palsy, more than 60% will develop non-motor cognitive impairments, frequently in the absence of MRI and ultrasound-detectable brain lesions. These impairments result in significant morbidity and high costs to society. Clinical

MRI has been largely unsuccessful in accurately identifying non-motor related neurodevelopmental brain abnormalities in preterm neonates, particularly at the individual patient level. As such, abnormalities are typically diagnosed clinically at later stages of development when targeted intervention may be less effective. Early diagnosis of impairments is essential for facilitating targeted treatment during critical periods of brain development to reduce the frequency and severity of disability. The purpose of this presentation is to discuss network connectivity determinants of normal brain development based upon work funded by the Foundation of the ASNR, and to introduce a new subsequently funded project to study neurodevelopmental outcomes of preterm birth that arose directly from Foundation support. The aims of this newly funded project are to 1) examine structural brain network connectivity determinants of poor developmental outcomes in preterm neonates, and 2) apply a machine learning framework for potential use as a diagnostic tool to predict future cognitive impairments on the basis of structural MRI data collected at term-equivalent age. This presentation highlights the importance of early research funding for individual career development, and how research support granted by the Foundation of the ASNR leads to subsequent funding success from other sources.

## Monday Morning

**10:30 AM - 12:00 PM**  
**Grand Ballroom Suite**

**(8a) Adult Brain - Cerebrovascular I**

**O-20** **10:30 AM - 10:38 AM**

**Can a Malignant CT Perfusion Profile Be Identified Using Noncontrast CT Hypodensity Alone? A Study in Acute Ischemic Stroke Patients Imaged within 4.5 Hours of Symptom Onset**

Zaharchuk, G. Inoue, M. Mlynash, M. Straka,  
M. Lansberg, M. Bammer, R. Albers, G. W.

Stanford University  
Stanford, CA

**PURPOSE**

The "malignant profile" is an MRI pattern based on diffusion and perfusion imaging that is associated with poor outcomes following reperfusion in the 3-6 hour time window. The aim of this study was to estimate the incidence and prognostic implications of the malignant profile, as identified by CT perfusion (CTP), in patients treated with tPA <4.5 hours from stroke onset. In particular, we assessed whether similar information could be obtained with noncontrast CT (nCT) alone, using a criteria of hypodensity >1/3<sup>rd</sup> of the MCA territory.

## MATERIALS & METHODS

This retrospective study included all patients treated with tPA at our institution from May 2009 to May 2011 who had CTP performed prior to tPA therapy and within 4.5 hours of symptom onset. Perfusion data were acquired on 16- and 64-row CT scanners; two separate scans were done yielding either 4 or 8 cm coverage depending on the scanner. The incidence of the malignant profile, based on the previously published definition of a Tmax >8 sec perfusion lesion >85 mL was assessed using an automated software program (RAPID). This program also estimates the infarct core based on cerebral blood flow and cerebral blood volume thresholds <30% of values in the contralateral hemisphere. Poor outcome was defined as a modified Rankin Score (mRS) of 5-6 at 30 days. A neuroradiologist reviewed the nCT images blinded to the CTP results to determine whether early ischemic changes were present, specifically the presence of nCT hypodensity >1/3<sup>rd</sup> of the MCA territory.

## RESULTS

One hundred twenty-one patients were treated during the prespecified time period and 50 of these patients had a diagnostic quality CTP study performed. Mean age was 75 ± 14 years, 54% were female, and median (IQR) NIHSS was 12 (5-18). Mean time to CT was 106 ± 52 min (range 42-246 min). Six patients (12%) met the prespecified CTP criteria for the malignant profile. The poor outcome rate in these patients was 100% (6/6 patients, all died in the hospital) vs 11% (5/44) in the nonmalignant patients (p<0.001). Noncontrast CT hypodensity >1/3<sup>rd</sup> the MCA territory was seen in 4/6 (67%) of CTP malignant patients and 2/44 (5%) of CTP nonmalignant patients. Based on this, the sensitivity, specificity, PPV, and NPV of nCT for predicting a malignant CTP profile was 0.67 (95% CI 0.24-0.94), 0.95 (0.83-0.99), 0.67 (0.24-0.94), and 0.95 (0.83-0.99), respectively.

## CONCLUSION

The CTP malignant profile is present in approximately 10-15% of tPA eligible patients imaged within 4.5 hours of symptoms onset. The clinical outcome of these patients is poor despite tPA therapy, consistent with data from patients treated with iv tPA in the 3-6 hour window. In this small cohort, lack of nCT hypodensity >1/3<sup>rd</sup> of the MCA territory was a specific predictor of a negative malignant CTP profile, but sensitivity appears somewhat lower. CT perfusion may therefore identify a subset of patients that do not have large nCT hypodensity in the tPA time window who will do poorly. More study in larger cohorts would help clarify this.

**KEY WORDS:** CT perfusion, stroke, mismatch

O-21

10:38 AM - 10:46 AM

## Automated Regional and Tissue-Specific Assessment of CT Perfusion Parameters in Acute Ischemic Stroke

Kemmling, A.<sup>1,2</sup>·Kamalian, S.<sup>1</sup>·Krumm, R.<sup>2</sup>·Payabvash, S.<sup>1</sup>·Souza, L.<sup>1</sup>·Lev, M. H.<sup>1</sup>

<sup>1</sup>Massachusetts General Hospital, Boston, MA,

<sup>2</sup>University of Munster, Munster, GERMANY

## PURPOSE

Dynamic CT-perfusion (CTP) frequently is used in acute stroke imaging; however, there is need for further standardization of this technique for reliable quantification of tissue at risk. Perfusion thresholds to identify salvageable tissue have been established, but there is evidence for significantly different regional ischemic vulnerability. The purpose of this study was to present a robust algorithm for fully automated assessment of regional tissue-specific CT perfusion (CTP) parameters in acute ischemic stroke.

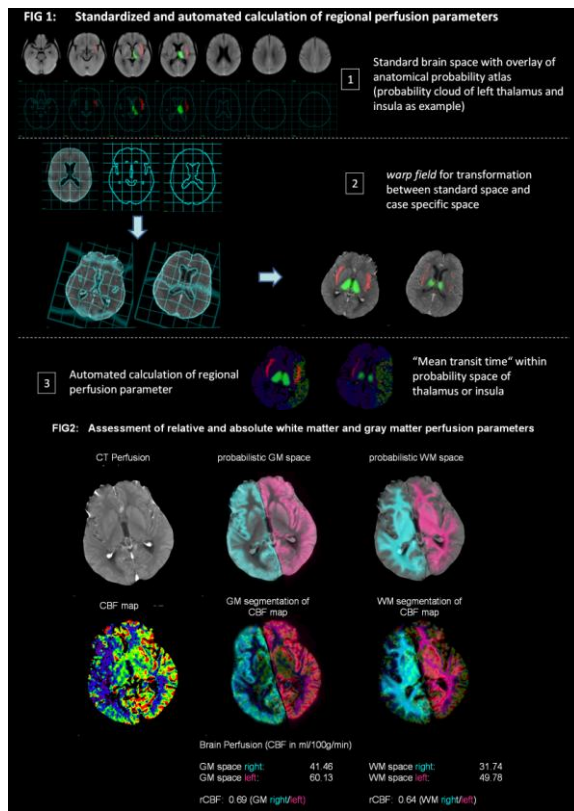
## MATERIALS & METHODS

Acute stroke imaging (native CT and dynamic CTP) was performed in 83 consecutive acute middle cerebral arterial strokes on a 128-slice CT scanner (Somatom Definition AS+, Siemens Medical Solutions). Regional CTP assessment was performed by an automated routine (Figure 1): (1) Robust nonlinear registration of CTP maps to MNI-152 space regardless of brain coverage was accomplished by registration of native CT to the anatomical CT perfusion image followed by inversion of the transformation matrix (CTPtoCT). The matrix CTPtoCT and nonlinear warpfield CTtoMNI were concatenated (CTPtoMNI). The warpfield CTPtoMNI was applied to perfusion maps. (2) Probabilistic atlases (Harvard-Oxford structural atlas) and highly refined probabilistic white and gray maps (in-house development) were used to calculate regional brain perfusion parameter. (3) Error correction excluded nonsignificant voxels within cerebrospinal fluid and vessels. (4) Automated relative and absolute CT perfusion values were calculated and compared to selected manually traced perfusion values for reference.

## RESULTS

Registration between perfusion maps and standard space was robust and reliable. Automated and manually obtained brain perfusion values were not significantly different; the average difference was less than 4.3% (SD 3.1%; p < 0.01). Figure 2 shows regional and tissue-specific assessment of perfusion parameters.





## CONCLUSION

The presented algorithm is robust and reliable and may be used to address the need for automated user independent assessment of regional perfusion parameters in acute stroke.

**KEY WORDS:** Stroke, CT perfusion, software

**O-22**

**10:46 AM - 10:54 AM**

## Pretreatment CT Angiography Source Image ASPECTS' Impact on Outcome in Endovascularly Treated Stroke Patients: Preliminary Results from the Penumbra START Trial

Frei, D. F.<sup>1</sup>•Yoo, A. J.<sup>2</sup>•Heck, D. V.<sup>3</sup>•Hellinger, F. R.<sup>4</sup>•McCollom, V. E.<sup>5</sup>•Fiorella, D. J.<sup>6</sup>•Turk, A. S.<sup>7</sup>•Malisch, T. W.<sup>8</sup>•Zaidat, O. O.<sup>9</sup>•Alexander, M. J.<sup>10</sup>•Devlin, T. G.<sup>11</sup>•Levy, E. I.<sup>12</sup>•Shah, Q. A.<sup>13</sup>•Hui, F. K.<sup>14</sup>•Goyal, M.<sup>15</sup>•Ghodke, B. V.<sup>16</sup>•Shaibani, A.<sup>17</sup>•Harrigan, M. R.<sup>18</sup>•Jovin, T. G.<sup>19</sup>•Madison, M. T.<sup>20</sup>•Chaudhry, Z. A.<sup>2</sup>•Gonzalez, R. G.<sup>2</sup>•Barraza, L.<sup>21</sup>•Sit, S. P.<sup>21</sup>•Bose, A.<sup>21</sup>•for the START Investigators

<sup>1</sup>Swedish Medical Center, Englewood, CO, <sup>2</sup>Massachusetts General Hospital, Boston, MA, <sup>3</sup>Forsyth Medical Center, Winston Salem, NC, <sup>4</sup>Florida Hospital, Orlando, FL, <sup>5</sup>Mercy Health Center, Oklahoma City, OK, <sup>6</sup>Stony Brook Medical Center, Stony Brook, NY, <sup>7</sup>Medical University of South Carolina, Charleston, SC, <sup>8</sup>Alexian Brothers Medical Center, Elk Grove Village, IL, <sup>9</sup>Medical College of Wisconsin, Milwaukee, WI, <sup>10</sup>Cedars-Sinai Medical Center, Los Angeles, CA, <sup>11</sup>Chattanooga Center for Neurologic Research, Chattanooga, TN, <sup>12</sup>Kaleida Health, Buffalo, NY, <sup>13</sup>Abington Memorial Hospital,

Abington, PA, <sup>14</sup>Cleveland Clinic, Cleveland, OH, <sup>15</sup>Alberta Health Services, Calgary, AB, CANADA, <sup>16</sup>Harborview Medical Center, Seattle, WA, <sup>17</sup>Northwest Community Hospital, Arlington Heights, IL, <sup>18</sup>University of Alabama at Birmingham, Birmingham, AL, <sup>19</sup>University of Pittsburgh Medical Center, Pittsburgh, PA, <sup>20</sup>St. Paul Radiology, St. Paul, MN, <sup>21</sup>Penumbra, Inc., Alameda, CA

## PURPOSE

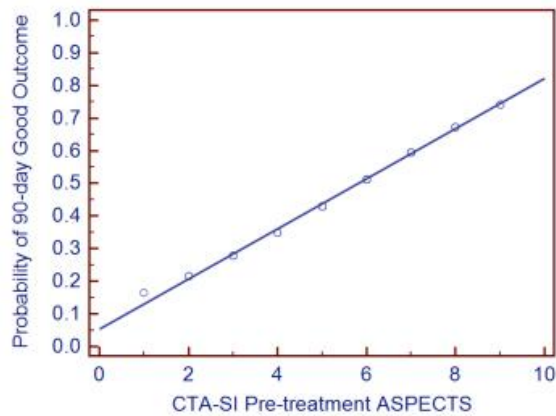
CT remains the most widely used modality for stroke evaluation, and ischemic change on noncontrast CT (NCCT) using ASPECTS has been demonstrated to predict clinical outcome to endovascular therapy (EVT). However, there is no standard imaging approach to select patients for EVT and data is lacking on the influence of pretreatment ASPECTS (pre-ASPECTS) from CTA source image (CTA SI) on outcomes following EVT.

## MATERIALS & METHODS

START was a prospective multicenter study to evaluate the impact of pretreatment core infarct size in patients undergoing EVT with the Penumbra System. The imaging approach included NCCT, CTA SI, CT perfusion or MRI diffusion imaging. This study focused on the CTA SI results. ASPECTS was graded in a blinded fashion and analyzed according to a priori classification (0-4, 5-7, 8-10) and the entire scale. Clinical outcomes were dichotomized as 90-day modified Rankin Scale scores (mRS) of 0-2 (good) vs 3-6. Univariate and multivariate analyses were performed to determine predictors of outcome.

## RESULTS

Of the 145 patients enrolled, 56 met study criteria for this preliminary analysis. Mean age was  $65.5 \pm 14.2$  years; median NIHSS was 19.5 (14-24). There were 30 (53.6%) females, and target vessel occlusions were in the ICA (n = 14), MCA M1 and M2 segments (n = 41). The median pre-ASPECTS on CTA SI was 6 (4.5-7). There were 14 (25%) patients with scores of 0-4, 34 (60.7%) with 5-7, 8 (14.3%) with 8-10. The rate of TIMI 2-3 revascularization was 87.3% (48/55). The median time from groin puncture to end of aspiration was 73.5 (40-108) minutes. Twenty-seven (48.2%) patients achieved a good 90-day outcome. Fifteen (26.8%) died. Only one (1.8%) patient had symptomatic hemorrhage. Higher pre-ASPECTS on CTA SI was associated with good outcomes (mRS 0-2) [median 6 (IQR 5-7) vs 5 (IQR 3-7),  $p < 0.05$ ]. The rate of good outcomes was 21.4% for ASPECTS 0-4, 55.9% for 5-7, and 62.5% for 8-10 ( $p = 0.08$ ). Adjusting for age and NIHSS, pre-ASPECTS was an independent predictor of good outcome (OR 1.5,  $p < 0.04$ ). In ROC analysis, ASPECTS  $> 4$  was the optimal threshold for identifying good outcomes (89% sensitivity, 38% specificity). Other univariate predictors of good outcome were lower age ( $p = 0.02$ ), lower NIHSS ( $p = 0.02$ ), more distal occlusion ( $p < 0.05$ ) and shorter time from groin puncture to stopping aspiration ( $p = 0.02$ ).



### CONCLUSION

These preliminary results show that higher pretreatment ASPECTS on CTA source images is associated with better outcomes following endovascular therapy. Comparative studies versus NCCT ASPECTS are necessary to determine their relative accuracy for outcome prediction.

**KEY WORDS:** Stroke, penumbra, ASPECTS

**O-23**

**10:54 AM - 11:02 AM**

### Poor Collateral Status on Timing-Invariant CT Angiography Is a Strong Predictor of Poor Clinical Outcome of Acute Large Vessel Occlusion Stroke Patients

Smit, E. J.<sup>1</sup>•Vonken, E. J.<sup>1</sup>•van Seeters, T.<sup>1</sup>•Dankbaar, J. W.<sup>1</sup>•Van Der Schaaf, I. C.<sup>1</sup>•Van Ginneken, B.<sup>2</sup>•Velthuis, B.<sup>1</sup>•Prokop, M.<sup>2</sup>

<sup>1</sup>UMC Utrecht, Utrecht, NETHERLANDS, <sup>2</sup>Radboud University Nijmegen Medical Centre, Nijmegen, NETHERLANDS

### PURPOSE

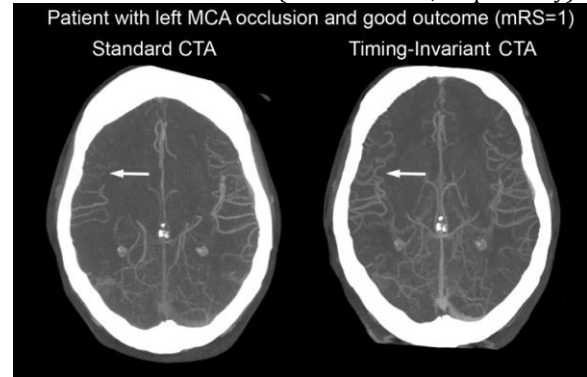
To assess whether timing-invariant CTA (TI CTA), which is insensitive to delayed contrast arrival, displays collateral arteries that are not visible on standard CTA, and compare their predictive values on clinical outcome.

### MATERIALS & METHODS

We selected 40 consecutive ischemic stroke patients with unilateral ICA and/or MCA occlusion from our clinical database. Standard CTA and CT perfusion (CTP) data were acquired at admission on a 128 detector row scanner. The CTP source images were used to reconstruct TI CTA. Clinical outcome data (modified Rankin Scale, mRS) after three months were available. Good clinical outcome was defined as mRS ≤2 and poor clinical outcome as mRS >2. Four experienced observers individually assessed collateral status on CTA and TI CTA in a blinded and randomized manner. Collateral status was rated good if ≥50% of collaterals were present and poor if <50% were present compared to the contralateral hemisphere. Scores were compared with a McNemar test (p<0.05).

### RESULTS

Collateral status was rated as being good on standard CTA in 49% of cases compared to 84% of cases on TI CTA (p<0.001). Of those patients rated with poor collateral status on standard CTA, 32% had good collateral status on TI CTA. Poor collateral status on TI CTA had a predictive value of 100% for poor outcome compared to only 69% for CTA. Good collateral status was a weak predictor of good clinical outcome for both standard CTA and TI CTA (64% and 56%, respectively).



### CONCLUSION

Poor collaterals status on timing-invariant CTA is a strong predictor of poor clinical outcome in acute large vessel occlusion stroke patients. Timing-invariant CTA shows collaterals that are not visible on standard CTA due to delayed contrast arrival.

**KEY WORDS:** CT perfusion, collaterals, stroke

**O-24**

**11:02 AM - 11:10 AM**

### Time-Resolved Intracranial CT Angiography Allows More Reliable Quantification of Intravascular Thrombus than Conventional CT Angiography

Frölich, A. M. J.<sup>1</sup>•Schrader, D.<sup>1</sup>•Schramm, R.<sup>1</sup>•Klotz, E.<sup>2</sup>•Knauth, M.<sup>1</sup>•Schramm, P.<sup>1</sup>

<sup>1</sup>University Medicine Göttingen, Göttingen, GERMANY, <sup>2</sup>Siemens AG, Healthcare Sector, Computed Tomography H IM CR R&D PA, Forchheim, GERMANY

### PURPOSE

In acute stroke patients with intracranial vessel occlusion, the location and extent of intravascular thrombus correlates with clinical and imaging outcomes and recently has been used to predict the success of intravenous thrombolysis. We hypothesized that four-dimensional, time-resolved CT angiography (4D CTA) reconstructed from whole-brain perfusion CT is more reliable than conventional arterial-phase CTA in assessing intracranial thrombus burden.

### MATERIALS & METHODS

Among 104 consecutive patients with angiographically proven anterior circulation arterial occlusion, whole-brain 4D CTA (45s total scan duration, 9.6 cm z-axis coverage) and bolus-triggered, arterial-phase CTA were available in 43 cases. For 4D CTA, temporal maximum intensity projections (tMIP) were calculated, combining all 30 individual spiral scans of the perfusion CT data



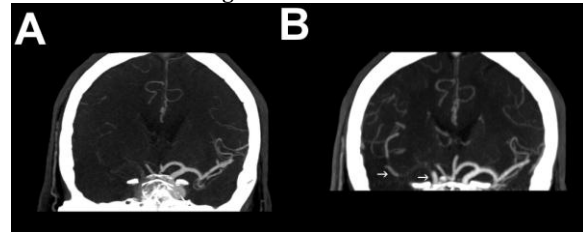
set into one CT volume. Intravascular thrombus extent was assessed with a previously described, semiquantitative clot burden score (CBS, 0-10; where 0 = complete infraclinoid ICA to distal MCA occlusion and 10 = patent vasculature). In patients with sufficient collateral flow, the length of the filling defect was measured on axial source images and coronal maximum intensity projections.

## RESULTS

Estimates of intravascular thrombus extent obtained from 4D CTA tMIP (median CBS: 8, interquartile range: 6-8) were significantly lower than those obtained from single-phase CTA (median CBS: 6, interquartile range: 4-7;  $p < 0.01$ ). Due to insufficient collateral flow, raters were unable to define the distal thrombus end in eight patients on CTA (18.6%) vs two patients on 4D CTA (4.7%). Mean length of the filling defect was significantly lower for 4D CTA (mean: 14.7 mm, SD: 8.8 mm) than for single-phase CTA (mean: 18.0 mm, SD: 8.0 mm;  $p = 0.01$ ).

## CONCLUSION

In acute stroke patients undergoing multimodal CT, analysis of 4D CTA (Fig. 1, B) offers a more reliable and narrow estimation of intravascular thrombus extent than conventional arterial-phase CTA alone (Fig. 1, A). As there is no current gold standard for assessing clot burden and thrombus length, further research is necessary to validate our findings and assess the use of 4D CTA in predicting outcomes and success of different recanalization strategies.



**KEY WORDS:** Stroke, CT perfusion, CT angiography

**0-25** **11:10 AM - 11:18 AM**

## Gray and White Matter CT Perfusion Thresholding for Outcome Prediction in 114 Patients with Acute Ischemic Stroke

Eilaghi, A.<sup>1,2</sup>Lee, T. Y.<sup>1</sup>Jakubovic, R.<sup>2</sup>Swartz, R. H.<sup>2</sup>Djalilvand, A.<sup>2</sup>Aviv, R. I.<sup>2</sup>

<sup>1</sup>Robarts Research Institute, UWO, London, ON, CANADA, <sup>2</sup>Sunnybrook Health Sciences Centre, Toronto, ON, CANADA

## PURPOSE

CT perfusion (CTP) is being evaluated increasingly to predict tissue fate in ischemic stroke although few large series report discrete thresholds for gray (GM) and white matter (WM). The purpose of this study is to define and evaluate the performance of baseline CTP-derived GM/WM thresholds for distinction of infarct versus noninfarct in a large cohort utilizing an automated GM/WM tissue probability map.

## MATERIALS & METHODS

Baseline noncontrast CT (NCCT) and CTP (CTP5, GE Healthcare, Waukesha, WI) imaging of 114 stroke patients within 4.5 hours of anterior circulation stroke onset were obtained. Recanalization was determined by CTA at 24 hours. Traced baseline CBV and 5-7 day FLAIR MRI ROIs defined the core and final infarct respectively. Baseline CTP TMAX ROI defined tissue at risk. Gray matter/WM tissue binary masks/ROIs were generated automatically by thresholding SPM8-derived probability maps and manually checked by an experienced neuroradiologist. Mirror ROIs were obtained from the contralateral GM and WM regions. Average CTP, FLAIR images, GM/WM tissue probability maps and all ROIs were coregistered with baseline NCCT using SPM8. Performance for tissue-specific thresholds to predict infarct was determined for GM and WM using a receiver operator characteristic curve (ROC) technique.

## RESULTS

The mean  $\pm$  SD age of 114 patients was  $69 \pm 14$  years; 56 male (49%). Intravenous rtPA was administered in 89 patients (78%) and recanalization occurred in 59 patients (49%). Infarct was right hemispheric in 55 patients (48%). Gray matter CBF and CBV were significantly different for all regions compared to WM ( $p < 0.001$ ). Expectedly, no significant WM/GM differences were found for MTT ( $p = 0.214-0.404$ ) or Tmax ( $p = 0.396-0.56$ ). Core, penumbra and benign oligemic regions were significantly different from each other for all perfusion parameters ( $p < 0.001$ ). Relative CBF thresholds best distinguished infarct from noninfarct for GM and WM demonstrating an area under the curve (AUC) of 0.85 and 0.83 respectively followed by absolute CBF, relative CBV and Tmax (Table 1).

Table 1: GM and WM thresholds for predicting total infarct versus noninfarct using 114 patients

CBF	GM	Abs.	13.51	0.83
		Rel.	0.5	0.85
	WM	Abs.	8.76	0.76
		Rel.	0.53	0.83
CBV	GM	Abs.	1.11	0.65
		Rel.	0.77	0.81
	WM	Abs.	0.71	0.65
		Rel.	0.84	0.80
MTT	GM	Abs.	7.00	0.61
		Rel.	1.56	0.61
	WM	Abs.	7.00	0.58
		Rel.	1.4	0.58
TMax	GM	Abs.	5.50	0.77
		Rel.	1.88	0.77
	WM	Abs.	5.50	0.71
		Rel.	1.64	0.71

## CONCLUSION

Significant different thresholds are demonstrated for infarct prediction for GM and WM emphasizing the need for independent consideration in predictive models. The

best discriminator between infarct and noninfarct is relative CBF.

**KEY WORDS:** CT perfusion, infarct prediction, gray and white matter

**O-26**

**11:18 AM - 11:26 AM**

### **Extended Brain Perfusion CT in the Detection of Crossed Cerebellar Diaschisis in Acute Ischemic Stroke**

Das, T.<sup>1</sup>•Thomas, O. M.<sup>1,2</sup>•Antoun, N. M.<sup>1</sup>•Scoffings, D. J.<sup>1</sup>

<sup>1</sup>Cambridge University Hospitals NHS Trust, Cambridge, UNITED KINGDOM, <sup>2</sup>University of Cambridge, Cambridge, UNITED KINGDOM

#### **PURPOSE**

Crossed cerebellar diaschisis (CCD) following supratentorial stroke is characterized by reduced blood perfusion in the contralateral cerebellar hemisphere, thought to be consequent to disruption of afferent inputs in cerebropontocerebellar pathways. Although reported in the context of PET, SPECT and MR brain perfusion studies, the detection rate during CT perfusion studies in the hyperacute or acute setting is not known.

#### **MATERIALS & METHODS**

Extended brain (100 mm coverage) perfusion CT studies of 67 out of 127 consecutive patients that presented with stroke-like symptoms during a 9-month period were analyzed retrospectively. Patients with non-MCA territory deficits or confirmed vertebrobasilar disease were excluded, as were studies that lacked coverage of the cerebellum or were otherwise of insufficient quality. Ten cases with no evidence of perfusion deficit and confirmation of an alternative diagnosis such as hemiplegic migraine were used as a control cohort. Cerebral blood flow (CBF), volume (CBV), mean transit time (MTT), time to peak (TTP) and time to drain (TTD) maps were calculated for each patient. In 57 cases with MCA territory ischemia or infarction, ROIs placed in the cerebellar hemispheres ipsilateral and contralateral to the affected MCA territory were used to measure CBF. A cerebellar asymmetry index (AI) was calculated for each case as  $[(\text{Ipsilateral CBF} - \text{Contralateral CBF}) / \text{Mean CBF}]$ . A threshold for hypoperfusion was defined as a CBF AI 2 standard deviations (2 SD) greater than the Mean CBF AI of the control cohort. Cases with an AI above this threshold were grouped as those demonstrating CCD. Asymmetry indexes for CBV, TTP, TTD and MTT were calculated in a similar manner. The Alberta Stroke Program Early CT Score (ASPECTS) was used to indicate the volume of affected tissue in the MCA territory on perfusion maps.

#### **RESULTS**

The mean CBF AI in the control cohort was -0.3% (SD 6.2%). Thus, a threshold of 12.1% (2 SD above the mean) was used to define cerebellar hypoperfusion. Thirty-seven per cent (21/57) of cases demonstrated cerebellar hypoperfusion in the hemisphere

contralateral to the affected MCA territory, consistent with CCD. Of these, 86% (18/21) also demonstrated an increase in TTP, TTD or MTT. Thirty-eight per cent (8/21) had reduced CBV but no evidence of cerebellar infarction of subsequent imaging. There was no significant difference in volume (as defined by ASPECTS) of ischemic tissue, infarcted tissue or ischemic penumbra between cases with or without CCD. Interestingly, two patients with lacunar infarcts confirmed by subsequent diffusion-weighted MRI demonstrated clear CCD.

#### **CONCLUSION**

Extended brain perfusion CT can demonstrate the presence of crossed cerebellar diaschisis in the hyperacute or acute setting. The presence of CCD is unrelated to supratentorial ischemic volume and can occur in the context of lacunar MCA territory infarction. In such cases, cerebellar hypoperfusion due to crossed cerebellar diaschisis may be indistinguishable from cerebellar ischemia.

**KEY WORDS:** Crossed cerebellar diaschisis, CT perfusion

**O-27**

**11:26 AM - 11:34 AM**

### **Perfusion Imaging Predicts Outcome in Transient Ischemic Attack and Minor Stroke: A Prospective Derivation-Validation Study**

Asdaghi, N.<sup>1</sup>•Coulter, J. I.<sup>2</sup>•Modi, J.<sup>2</sup>•Qazi, A.<sup>2</sup>•Goyal, M.<sup>2</sup>•Butcher, K. S.<sup>3</sup>•Demchuk, A. M.<sup>2</sup>•Hill, M. D.<sup>2</sup>•Coutts, S. B.<sup>2</sup>

<sup>1</sup>University of British Columbia, Vancouver, BC, CANADA, <sup>2</sup>Calgary Stroke Program, Calgary, AB, CANADA, <sup>3</sup>University of Alberta, Edmonton, AB, CANADA

#### **PURPOSE**

Patients presenting with transient or minor ischemic symptoms (TIA/MIS) are at risk for early deterioration. Identification of those at highest risk for progression may justify more aggressive acute reperfusion treatments. We tested the hypothesis that baseline perfusion (PWI) - diffusion (DWI) mismatch predicts clinical deterioration and infarct growth on follow-up imaging in this population.

#### **MATERIALS & METHODS**

Patients with TIA/MIS (NIH Stroke Scale  $\leq 3$ ) were enrolled prospectively and imaged within 24 hours of symptom onset as part of two sequential prospective imaging studies. All patients had clinical follow up. Baseline DWI and PWI (tmax+4s delay) and follow-up FLAIR infarct volumes [day 30 (derivation), day 90 (validation) cohort] were measured. Mismatch volumes were calculated as (Tmax+4s delay) - DWI lesion volume. Primary outcome was infarct growth on FLAIR imaging which was defined a priori as growth of at least 2.0 ml. Secondary outcome was clinical progression.

#### **RESULTS**

One hundred thirty-seven patients were included in the derivation and 281 patients in the validation cohorts.



The rates of DWI (54% vs 56%,  $p = 0.67$ ) and PWI lesions (42% vs 34.5%,  $p = 0.16$ ) at baseline were similar between the cohorts. The median time between symptom onset and baseline imaging was significantly shorter in the derivation (9.2 h, IQR=9.4) relative to the validation sets (15.1h, IQR=12.5  $p<0.001$ ). More patients had follow-up imaging in the derivation (87%) compared to the validation (76%) cohort ( $p = 0.021$ ). Primary and secondary outcome occurred in 18.5% and 9.5% in the derivation and 5.5% and 4.6% in the validation cohort. In the derivation cohort, baseline mismatch volumes adjusting for age, sex and time from symptom onset to MRI significantly predicted radiographic progression [OR = 1.06 (1.03-1.09),  $p<0.001$ ]. The optimal threshold for maximizing sensitivity (Sen) and specificity (Spec) in predicting infarct growth occurred at a mismatch volume of 10ml; which correctly predicted infarct expansion with 82% (Sen) and 91% (Spec) [Area under the curve (AUC) = 0.89 (0.80-0.98)]. In the validation cohort, this threshold was highly predictive of radiologic progression ( $p = 0.011$ , McNemars test). Linear regression showed that for every 10 ml of mismatch, there would be 2.5 ml infarct growth on day 30 FLAIR ( $R=0.80$ ,  $p<0.001$ ) (derivation set) and 1.1 ml of growth on day 90 FLAIR ( $R = 0.22$ ,  $p<0.001$ ) (validation set). Baseline mismatch showed a high discriminative value in predicting clinical deterioration in the derivation [AUC = 0.81 (0.67-0.96)] and moderate value in the validation cohort [AUC = 0.66 (0.46, 0.85)].

#### CONCLUSION

In a population of patients with minor stroke and TIA, early MR perfusion-diffusion mismatch predicts infarct growth and clinical progression. These findings suggest that there may be a group of patients with minor symptoms in whom reperfusion strategies may be beneficial.

**KEY WORDS:** TIA/minor stroke, perfusion imaging, MR imaging

**O-28**

**11:34 AM - 11:42 AM**

#### **Diffusion-Weighted Imaging Reversal after Thrombolysis in Acute Stroke Patients: A MR Correlate of Early Neurologic Improvement**

Labeyrie, M.<sup>1</sup>•Hess, A.<sup>2</sup>•Turc, G.<sup>3,1</sup>•Hervo, P.<sup>4</sup>•Roca, P.<sup>3,1</sup>•Mas, J.<sup>3,1</sup>•Baron, J.<sup>1</sup>•Meder, J.<sup>3,1</sup>•Touzé, E.<sup>3,1</sup>•Oppenheim, C.<sup>3,1</sup>

<sup>1</sup>INSERM 894, CH Sainte-Anne, Paris, FRANCE, <sup>2</sup>Hopital Bichat, Paris, FRANCE, <sup>3</sup>Université Sorbonne Paris-Cité, Paris, FRANCE, <sup>4</sup>General Electric Healthcare, Buc, FRANCE

#### **PURPOSE**

Diffusion-weighted imaging (DWI) commonly is considered a reliable marker of irreversible ischemia, although this view is challenged by reports on DWI lesion reversal. Recent pooled data from two prospective studies of patients imaged 3-6 hours after stroke onset suggest that the amount of DWI reversal is small and hence unlikely to be clinically relevant. Our

aim was to assess the prevalence, determinants and association with clinical outcome of reversible acute DWI lesions (RAD) in a large sample of patients treated by recanalization therapy within 4.5 hours after stroke onset.

#### **MATERIALS & METHODS**

Reversible acute DWI lesions were defined as baseline DWI lesions not incorporated into 24-hour DWI lesions. Reversible acute DWI lesions were determined both qualitatively by visual inspection and quantitatively by voxel-based comparison of coregistered initial and 24-hour follow-up DWI in 176 consecutive patients treated with recanalization therapy  $\leq 4.5$  hours after stroke onset. The association between the extent of RAD and each pre/posttreatment clinical and imaging variables was tested. The association with early neurologic improvement ( $\Delta$ NIHSS $\geq 8$  or NIHSS=0-2 at 24 hours) was assessed in multivariate analysis, and independent variables were tested further on excellent functional outcome, defined as modified Rankin Score  $\leq 1$  at hospital discharge.

#### **RESULTS**

Reversible acute DWI lesions were observed in 89 (50%) of patients. When present, the median (IQR) proportion of RAD voxels was 35% (18-65) of baseline DWI lesion, with a median (IQR) volume of 8mL (3-18). However, subtracting the volume of RAD from the initial DWI lesion altered the classification in PWI-DWI mismatch in only 5 of 100 patients with PWI, who shifted from "no mismatch" to "mismatch". The proportion of RAD voxels was significantly greater in patients treated within the first 3 hours than for others ( $p<0.05$ ), for patients with distal/no occlusion than for those with proximal occlusion ( $p<0.01$ ), and for patients with subsequent recanalization ( $p<0.01$ ). Early neurologic improvement was associated independently with age, recanalization, and most importantly with the presence of RAD [adjusted-OR = 5, CI95% (2.3-13),  $p<0.01$ ]. This association increased linearly with the extent of RAD. Reversible acute DWI lesions were also independently associated with an excellent outcome ( $p<0.01$ ).

#### **CONCLUSION**

Diffusion-weighted imaging reversal is common, albeit rarely complete, in stroke patients treated within the first 4.5 hours, and is strongly associated early neurologic improvement. These findings confirm that acute DWI lesions may contain symptomatic ischemic penumbra, (i.e., potentially salvageable tissue). However, with respect to clinical practice the impact of DWI lesion reversal on mismatch classification was minimal.

**KEY WORDS:** Stroke, diffusion-weighted imaging, prediction

O-29

11:42 AM - 11:50 AM

### Diffusion-Weighted Reversal Is Associated with Small Infarct Volume and Early Reperfusion in Patients with Transient Ischemic Attack and Minor Stroke

Asdaghi, N.<sup>1</sup>•Coulter, J. I.<sup>2</sup>•Modi, J.<sup>2</sup>•Qazi, A.<sup>2</sup>•Goyal, M.<sup>2</sup>•Butcher, K. S.<sup>3</sup>•Demchuk, A. M.<sup>2</sup>•Hill, M. D.<sup>2</sup>•Coutts, S. B.<sup>2</sup>

<sup>1</sup>University of British Columbia, Vancouver, BC, CANADA, <sup>2</sup>Calgary Stroke Program, Calgary, AB, CANADA, <sup>3</sup>University of Alberta, Edmonton, AB, CANADA

#### PURPOSE

One third of patients with TIA and minor ischemic stroke (MIS) have evidence of ischemic penumbra, defined as hypoperfused regions that have not been damaged irreversibly. Diffusion-weighted imaging (DWI) lesions are thought to represent irreversibly damaged tissue. Diffusion-weighted imaging reversal therefore has implications in accurate estimation of penumbra. We aimed to determine the rate of DWI reversal in this population.

#### MATERIALS & METHODS

Patients with TIA/MIS (NIH Stroke Scale  $\leq 3$ ) were enrolled prospectively and imaged within 24 hours of symptom onset as part of two prospective imaging cohorts. Patients were included if their baseline modified Rankin scale (mRS) score was  $\leq 1$ . All patients were followed clinically for 3 months and had a repeat MRI either at day 30 or 90. Baseline diffusion and perfusion lesions and follow-up FLAIR final infarct volumes were measured.

#### RESULTS

Four hundred eighteen patients were included; 55.5% had DWI lesions and 37% had PWI (Tmax + 2s delay) deficits at baseline. A total of 337 (81%) patients had follow-up imaging. Diffusion-weighted imaging reversal occurred in 22/192 (11.5%) of patients who had a diffusion lesion at baseline. The median time from symptom onset to follow-up imaging was not significantly different between those with or without DWI reversal (78.6 days, IQR = 33.3 vs 79.7 days, IQR = 59.4,  $p = 0.65$ ). The median DWI lesion volume was significantly smaller in those with reversal (0.27 ml, IQR = 0.75 ml) compared to those who did not reverse (1.45 ml, IQR = 3.8 ml,  $p < 0.001$ ). Patients with concurrent perfusion deficits (Tmax+2s) were significantly less likely to have DWI reversal (6%) compared to those without evidence of tissue hypoperfusion (20%;  $p = 0.003$ ). Diffusion-weighted imaging reversal occurred in 4% of patients with penumbral patterns [(Tmax + 2s)-DWI] and 18% of those without penumbra ( $p = 0.003$ ). Severity of hypoperfusion defined as greater prolongation of Tmax (+2, +4, +6, +8s) did not affect the likelihood of DWI reversal (linear trend  $p = 0.147$ ). No patient with DWI reversal had a mRS of  $\geq 2$  at 90 day, compared to 19% of those with evidence of infarction on follow-up imaging ( $p = 0.02$ ).

#### CONCLUSION

Diffusion-weighted imaging reversal is common in patients with TIA/MIS and is more likely to occur in those with smaller baseline lesions without concurrent tissue hypoperfusion. Diffusion-weighted imaging reversal therefore should not have a significant effect on the accuracy of penumbra definition. These data suggest early reperfusion is correlated with DWI reversal and better clinical outcome as measured by mRS.

**KEY WORDS:** DWI reversal, perfusion imaging, TIA/minor stroke

O-30

11:50 AM - 11:58 AM

### Diffusional Kurtosis Imaging Assessment of Motor Impairment in Stroke Patients

Helpern, J. A. • Hui, E. • Bonilha, L. • Tabesh, A. • Feng, W. • Adams, R. • Jensen, J.

Medical University of South Carolina  
Charleston, SC

#### PURPOSE

Diffusion tensor imaging (DTI) has been used to correlate the structural integrity of the corticospinal tracts with motor function impairment after stroke. Diffusion tensor imaging, however, is based on a Gaussian approximation of water diffusion distribution, which limits its ability to characterize complex cerebral tissue microstructure, such as that found in crossing white matter fiber bundles. Diffusional kurtosis imaging (DKI) is a new clinically feasible extension of DTI, which characterizes non-Gaussian diffusion by estimating the diffusional kurtosis. Here we investigate whether DKI can provide a better assessment of motor impairment than DTI in patients with acute ischemic stroke.

#### MATERIALS & METHODS

Acute ischemic stroke patients (N = 10, 11.25 - 53 hours postonset) were studied. Motor impairment was measured using the Fugl-Meyer Motor Scale (FMMS) with a lower FMMS indicating more severe motor impairment. MR imaging was performed with a 1.5 T Siemens Avanto scanner. Diffusional kurtosis imaging data were acquired with three b-values (0, 1000 and 2000 s/mm<sup>2</sup>) along 30 encoding directions using single-shot twice-refocused EPI (NEX = 1). Other parameters were: matrix = 74 x 74, 3 mm isotropic resolution, TR/TE = 5500/99 ms, BW/pixel = 1325 Hz. Fractional anisotropy (FA), mean (MD), axial (DA) and radial (DR) diffusivity along with mean (MK), axial (KA) and radial (KR) kurtosis were estimated using in-house software. Images were normalized to a T1-weighted template and segmented into gray and white matter masks. Corticospinal tracts, comprising the superior corona radiata, posterior limb of the internal capsule and cerebral peduncle, on the lesional hemisphere were segmented for each patient. All pixels within the tracts were averaged and the Pearson correlations with FMMS scores were calculated.



## RESULTS

None of the DTI metrics demonstrated a significant correlation with FMMS score. The DKI metric of axial kurtosis ( $K_A$ ), however, demonstrated a significant negative correlation ( $r = -0.89$  and  $p = 0.0005$ ) with FMMS score consistent with compromised tract integrity (Figure 1). Other diffusion metrics, including FA (Figure 1), did not demonstrate significant correlations. One explanation for these results is that diffusional non-Gaussianity measured with DKI allows for a more general and complete characterization of complex microarchitecture compared with DTI, which is limited by an assumption of Gaussian diffusion that fails to capture the full diffusional dynamics of complex media.

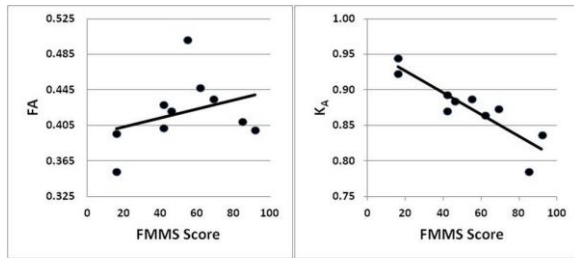


Figure 1: Correlation between the measurements of FA and Axial Kurtosis in the corticospinal tracts versus the FMMS. Lower score indicates more severe motor impairment.

## CONCLUSION

The current study demonstrates for the first time that the measurement of structural integrity of corticospinal tracts using diffusional kurtosis metrics significantly correlates with stroke patient's motor impairment in the acute phase.

**KEY WORDS:** Stroke, diffusion MR imaging, motor impairment

## Monday Morning

10:30 AM - 12:00 PM

Trianon Ballroom

(8b) Adult Brain: New  
Techniques/Post Processing - I

0-31

10:30 AM - 10:38 AM

**Selection of an Arterial Input Function Distal to Vasospasm Does Not Affect CT Perfusion Data in Aneurysmal Subarachnoid Hemorrhage**

Shin, B. Anumula, N. Ferrone, A. Masi, P. Campbell, R. Spandorfer, R. Rua, S. Sanelli, P. C.

Weill Cornell Medical College  
New York, NY

## PURPOSE

The postprocessing of CT perfusion (CTP) maps relies on the appropriate selection of an arterial input function (AIF). The purpose of this study is to determine

whether selecting an AIF distal to vasospasm affects the quantitative cerebral blood flow (CBF), cerebral blood volume (CBV), and mean transit time (MTT) values in aneurysmal subarachnoid hemorrhage.

## MATERIALS & METHODS

A retrospective analysis of 20 consecutive CTP exams was performed in 17 patients with aneurysmal subarachnoid hemorrhage. CT perfusion exams were included if at least one first order cerebral arterial segment (A1 or M1) had vasospasm in order to select the AIF distal to both vasospasm and nonvasospasm vessels within the same patient. Vasospasm was determined by the CT angiogram performed during the same acquisition time as CTP. Each CTP was postprocessed several times using standardized methods, only varying the selection of the AIF distal to both vasospasm and nonvasospasm arteries. Region-of-interest (ROI) analysis of the cortex was performed in a standardized fashion to acquire quantitative CTP values. Quantitative data for CBF, CBV and MTT were compared for AIF selection distal to vasospasm and nonvasospasm arteries. Paired-samples t-test was performed for statistical analysis; threshold for significance was defined as  $p < 0.05$ .

## RESULTS

All patients presented with acute aneurysmal subarachnoid hemorrhage on CT imaging. Median age was 53 years. The average thickness of subarachnoid hemorrhage was 7.55 mm, and 65% of imaging demonstrated intraventricular or parenchymal hemorrhage. The average Hunt-Hess score was  $2.24 \pm .83$  (STDev). The average number of days between clinical presentation and the concurrent CTA/CTP study was  $9.96 \pm 4.51$  (STDev). A total of 240 CTP maps were evaluated, including 80 CBF, 80 CBV and 80 MTT maps. The mean quantitative CBF, CBV, and MTT values and standard deviations are shown in Table 1. There was no statistically significant difference in the CTP values when an AIF is selected in a vessel distal to vasospasm compared to a nonvasospasm artery. Furthermore, subgroup analysis of the mean quantitative CTP values for each vascular territory (ACA, MCA, and PCA) also revealed no significant differences in the CBF, CBV and MTT values (Table 2).

Table 1. Quantitative CTP values for AIF selection

	Cerebral Blood Flow (mL/100gm/min)			Cerebral Volume (mL/100gm)			Blood			Mean Transit Time (seconds)	
	Mean	Std. Deviation	p-value	Mean	Std. Deviation	p-value	Mean	Std. Deviation	p-value		
Nonvasospasm AIF	53.06	15.01	0.639	2.59	0.69	0.112	4.84	0.91		0.556	
	Cerebral Blood Flow (mL/100gm/min)			Cerebral Volume (mL/100gm)			Blood			Mean Transit Time (seconds)	
	Mean	Std. Deviation	p-value	Mean	Std. Deviation	p-value	Mean	Std. Deviation	p-value		
R ACA (Nonvasospasm AIF)	40.01	11.88	0.80884	2.18	0.59	0.68816	5.10	1.59		0.62169	
R ACA (Vasospasm AIF)	39.63	9.69		2.17	0.59		5.00	1.92			
R MCA (Nonvasospasm AIF)	58.75	19.93	0.78991	2.78	0.67	0.50461	4.80	1.23		0.59343	
R MCA (Vasospasm AIF)	59.37	17.14		2.77	0.67		4.70	1.377			
R PCA (Nonvasospasm AIF)	52.16	25.93	0.96400	2.92	1.21	0.35138	5.48	1.17		0.56820	
R PCA (Vasospasm AIF)	52.27	23.68		2.90	1.16		5.36	1.16			
L ACA (Nonvasospasm AIF)	37.43	11.44	0.97697	2.03	0.61	0.74927	4.98	1.18		0.61295	
L ACA (Vasospasm AIF)	37.39	11.22		2.03	0.60		4.89	1.48			
L MCA (Nonvasospasm AIF)	57.03	17.53	0.89983	2.59	0.69	0.42841	4.51	0.98		0.58347	
L MCA (Vasospasm AIF)	57.29	14.71		2.58	0.68		4.42	1.08			
L PCA (Nonvasospasm AIF)	42.53	15.37	0.94294	2.34	0.74	0.45138	5.34	1.02		0.66126	
L PCA (Vasospasm AIF)	42.65	14.53		2.33	0.70		5.25	1.14			

## CONCLUSION

Placement of an AIF distal to vasospasm does not significantly affect the quantitative CTP data in aneurysmal subarachnoid hemorrhage. This information is helpful in evaluating perfusion abnormalities in patients with vasospasm involving multiple vessels.

**0-32** **10:38 AM - 10:46 AM**

# Evaluation of the Impact of Major Dose Reduction for Quantitative Brain Perfusion Studies Using a Low-Dose Simulation Algorithm and Iterative Reconstruction

Fardanesh, M.·Siegel, E.·Kouo, T.·Sterbis, K.

University of Maryland School of Medicine  
Baltimore, MD

## PURPOSE

Using a structured approach, we investigated the

minimum radiation dose required for quantitative brain perfusion, while maintaining diagnostic accuracy. We hypothesized that the regional nature of the flow analysis may be more tolerant than other types of imaging studies to radiation dose reduction.

## MATERIALS & METHODS

CT brain perfusion studies were acquired on 10 patients (8F, 2M; avg. age = 44.5 years, 18-70) using our routine institution protocol (80kVp, 125mAs) on a 256-slice CT scanner. The projection data were processed using a specially designed low-dose simulation algorithm, to generate datasets at 30%, 50%, and 70% dose reduction (relative original acquisition) levels with filtered back projection (FBP) reconstruction. Additionally, four cases with 70% simulated dose reduction were reconstructed using an iterative reconstruction technique (iDose<sup>4</sup>, Philips Healthcare). Quantitative perfusion parameters (MTT, CBF, CBV, and TTP) were measured for regions-of-interest in the ACA, MCA and PCA territories at the different dose levels (original and simulated). The qualitative evaluation of the low-dose simulated perfusion maps relative to the original routine dose was performed by two radiologists blinded to the dose-reduction level and reconstruction technique. A five-point scale was used to rate diagnostic confidence (0-25-50-75-100%). Data were analyzed using the Wilcoxon signed-rank test (reader scores) and Bland Altman analysis (quantitative measurements).

## RESULTS

Fifty percent dose reduction (relative to 80kVp, 125mAs) was achievable with no significant loss in quantitative perfusion parameters, when using FBP. The maps demonstrated different levels of dose reduction acceptability (Map, Max-Dose-Reduction, p-value; MTT, 50%, 0.181; CBF, 50%, 0.1; Summary Map, 70%, 0.371). A 70% dose reduction (relative to 80kVp, 125mAs) was achievable across all perfusion maps with the application of the iterative reconstruction technique. The diagnostic confidence scores were similar between the low-dose iDose<sup>4</sup> reconstructions (map, mean score: TTP, 3.8; CBF, 3.6; CBV, 3.8; MTT 3.5) and the routine-dose FBP reconstructions (mean score 4). These were both substantially higher than the low-dose FBP reconstructions (map, mean score: TTP, 1.5; CBF, 2.8; CBV, 2.4; MTT 2.1).

## CONCLUSION

Our study using low-dose simulations of clinical data suggests that the accuracy of CT brain perfusion assessment in evaluation of patients with acute stroke seems to be less dependent on radiation exposure than conventional anatomical brain imaging and that application of iterative reconstruction can allow further significant dose reductions of as much as 70% for CT brain perfusion studies without compromising diagnostic accuracy or confidence in evaluation of patients with suspected acute stroke. We are not aware of any prior studies that have determined the impact of iterative reconstruction in a quantitative fashion using automated image analysis and simulated exposure reduction.

**KEY WORDS:** Brain perfusion CT, low dose, iterative reconstruction

**O-33** **10:46 AM - 10:54 AM**

**Comparison of Arterial Spin Labeling and Dynamic Susceptibility Contrast-Enhanced MR Perfusion in Differentiating Tumor from Radiation Necrosis**

Colantoni, W.·Bert, R. J.·Borges, M. T.

University of Colorado Anschutz Medical Campus  
Aurora, CO

**PURPOSE**

MR contrast-enhanced susceptibility perfusion (CESP) has demonstrated its utility in differentiating central nervous system recurrent tumor from treatment-related changes. Arterial spin labeling (ASL) perfusion recently has been FDA approved for three MRI manufacturers. Preliminary studies and vendor-supplied literature suggest that ASL may be equal to CESP in posttreatment tumor evaluation. We have tested this hypothesis with a pseudo prospective reevaluation of tumors where ASL and/or CESP were obtained. Some cases now have a confirmed diagnosis.

**MATERIALS & METHODS**

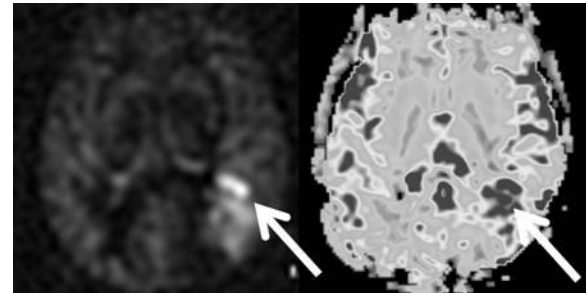
IRB exemption was obtained to collect and reevaluate tumor studies in our PACS database. Thirty-one patients, 36 total studies were selected from the PACS (McKesson) database where ASL (Philips, GE), and/or CESP (Philips, GE, Siemens) had been performed. Cases were stored in the teaching files section of the PACS (McKesson) and reevaluated by two of three trained neuroradiologists (each reading 2/3 of cases). Only primary tumors previously subjected to chemoradiation were evaluated. Most were glial tumors with two anaplastic meningiomas and one lymphoid tumor. Categorization used a 3 point scale: 1 = increased perfusion/persistent tumor, 2 = equivocal perfusion/indefinite, 3 = decreased perfusion/treatment necrosis. After independent scoring, data were transferred to a single spreadsheet. Two observers compared the prospective diagnosis to confirmed diagnoses by pathology or follow-up imaging demonstrating clear growth or necrotic encephalomalacia. Observer concordance, technique concordance and accuracy were scored.

**RESULTS**

Reader concordance, technique concordance and reader accuracy are shown in Table 1. The figure below demonstrates a typical case, where DSCP and ASL both predicted recurrent tumor later confirmed by biopsy and tumor growth. There were no completely discordant reads between readers or between CESP and ASL. Partial concordances, defined as one reader rating of intermediate and another rating clearly tumor or radiation necrosis, were few. Both ASL and CESP were generally accurate, in those cases with current available definitive diagnoses. The only clear error occurred in a case where only CESP was used and tumor recurrence was missed.

Table 1

Reader Concordance	Complete	Partial	Discordant
ASL	30/33	33/33	0/33
CESP	10/12	12/12	0/12
Concordance ASL vs. CSP	9/11	11/11	0/11
Accuracy	ASL	CSP	EQ
Reader 1	11/11	5/6	1 IND
Reader 2	12/12	3/4	2 IND
Reader 3	11/11	3/3	



**CONCLUSION**

Arterial spin labeling perfusion has promise as a reliable alternative to CESP in differentiating recurrent/persistent neoplasm from radiation necrosis and accurately supports low-grade tumor diagnosis. A controlled prospective study is warranted.

**KEY WORDS:** ASL, perfusion, necrosis

**O-34** **10:54 AM - 11:02 AM**

**Non-Gaussian Diffusion Imaging of Normal Pressure Hydrocephalus and the Effects of Microvascular Disease**

Eubig, J. A.·Johnson, G.·Babb, J. S.·Golomb, J. B.·George, A. E.

New York University Medical Center  
New York, NY

**PURPOSE**

Normal pressure hydrocephalus (NPH) is a debilitating but treatable disorder that is characterized by progressive gait apraxia, dementia and urinary incontinence. Diffusional kurtosis imaging (DKI), an extension of diffusion tensor imaging (DTI) which is based on the nongaussian distribution of proton diffusion, is believed to reflect neural tissue microstructural complexity. We recently have demonstrated in a pilot study that DKI is significantly decreased in periventricular parenchyma of patients with NPH (ASNR Award Paper 2011). However, the relative contribution of chronic microvascular disease (CMD), a commonly seen comorbidity in patients with NPH, to alterations in DKI and DTI has not been studied. We expanded our analysis to a larger group of patients to include DKI and standard DTI metrics including fractional anisotropy (FA). Correlations were



investigated between severity of hydrocephalus, severity of periventricular (CMD) and kurtosis, diffusion, and FA measures.

#### MATERIALS & METHODS

Retrospective study of NPH patients ( $n = 36$ ) compared to age-matched normal controls ( $n = 34$ ) with standard diffusion tensor imaging (DTI) and DKI. All patients were scanned at 1.5 T field strength (Siemens Avanto). Regions of interest included the bilateral frontal and parietal periventricular white matter, genu and splenium of the corpus callosum, and bilateral posterior limbs of the internal capsules. The severity of hydrocephalus and CMD were graded on a 4-point scale. T-test and Spearman correlation test were utilized for analysis.

#### RESULTS

Normal pressure hydrocephalus patients relative to normals demonstrated statistically significant decrease in  $kurtosis_{mean}$ ,  $kurtosis_{radial}$ ,  $kurtosis_{saxial}$ ,  $diffusion_{mean}$ ,  $diffusion_{radial}$ ,  $diffusion_{axial}$ , and FA in all regions of interest except the genu and splenium of the corpus callosum. Decreases in all kurtosis metrics ranged from 10-25% with the greatest changes seen in  $kurtosis_{radial}$  ( $p < 0.05$ ). There was no correlation between degree of ventriculomegaly and decrease in kurtosis. Decrease in kurtosis strongly correlated with severity of chronic CMD ( $p < 0.005$ ); however, statistically significant decrease in kurtosis ( $p < 0.05$ ) also was noted among NPH patients with no or minimal evidence of CMD with the magnitude of change ranging from 5-26%.

#### CONCLUSION

The severity of CMD significantly correlated with changes in kurtosis, diffusivity, and FA complicating the assessment of the relative contribution of hydrocephalus vs CMD to white matter kurtosis since many NPH patients have coexisting CMD. Our study however demonstrated significant differences in DKI and DTI among patients without evidence for CMD when compared to normal controls confirming that NPH plays an independent role in altering white matter integrity. Since kurtosis measurements are related to overall tissue complexity, the significantly decreased  $kurtosis_{mean}$ ,  $kurtosis_{radial}$ , and  $kurtosis_{saxial}$  of the periventricular and internal capsular white matter tracts suggests a loss of mechanical integrity of the corticospinal axons in NPH patients. Significant increases in  $diffusion_{mean}$ ,  $diffusion_{radial}$ ,  $diffusion_{axial}$  also suggest concomitant white matter edema. No significant correlation between degree of ventriculomegaly and kurtosis, diffusivity, or FA was demonstrated.

**KEY WORDS:** Normal pressure hydrocephalus, kurtosis, microvascular disease

O-35

11:02 AM - 11:10 AM

#### Feasibility of a New Metal Artifact Reduction Algorithm in the Noninvasive Follow Up with Flat-Panel Angiographic CT after Coiling, Clipping or Intracranial Stenting

Psychogios, M.·Knauth, M.

University Medicine Goettingen  
Goettingen, GERMANY

#### PURPOSE

Flat-panel angiographic CT after intravenous application of contrast media (ivACT) is used increasingly as a follow-up examination after coiling, clipping or intracranial stenting. Metal artifacts often deteriorate image quality around the implanted objects, especially around big coils, multiple clips or the markers of the Wingspan stent. Purpose of this study was to evaluate the feasibility of a new metal artifact reduction algorithm (MARA) in the aforementioned setting.

#### MATERIALS & METHODS

Fifteen patients were examined with ivACT 2 to 6 months after initial treatment. An intracranial aneurysm had been treated with multiple clips in eight cases, with coiling in two cases and two additional patients had been treated previously with both methods. Additionally, two patients were examined after stenting of a MCA stenosis with a Wingspan stent and one last patient after stent-assisted coiling. IvACT was performed on a flat-panel detector equipped angiography suite (Axiom Artis dBa, Siemens) after intravenous application of 80 ml contrast media. The uncorrected raw images then were transferred to a prototype reconstruction workstation where the MARA was applied. Two experienced neuroradiologists examined both corrected and uncorrected images on a commercially available workstation with a time break of 2 weeks, to reduce recall bias.

#### RESULTS

Image quality around the implants significantly improved after the application of the MARA. After clipping, examiners could correctly assess the number of the implanted clips and the patency of the parent vessel on the corrected images, while extensive artifacts limited the delineation of the clips and their surrounding structures on uncorrected images. Similarly, after coiling a small residual aneurysm could be depicted on the corrected ivACT images; the same case was tagged as "not diagnostic" on the uncorrected images due to metal artifacts. Streak artifacts around the markers of the Wingspan stent can be reduced with the MARA, but the exact depiction of a stenosis still is limited even on the corrected images. On the other hand, the use of the MARA did not lead to a image degradation in sections and slices beyond that of the implanted materials. For example the cerebral parenchyma on the opposite side of the implant could be delineated equally well on both corrected and uncorrected images. Small intracranial vessels, such as the superior cerebellar artery or the anterior choroidal

artery were depicted equally good both before and after correction. A restenosis within a small Wingspan stent was shown sufficiently before and after application of the MARA, demonstrating that the algorithm did not reduce contrast or spatial resolution of the ivACT.

#### CONCLUSION

Use of the MARA in our study significantly reduced artifacts around metallic implants on ivACT images and allowed for delineation of the surrounding structures (residual aneurysm, parent vessel, parenchyma). A degradation of image quality on other parts of the datasets could not be demonstrated after correction. An implementation of this algorithm in a commercially available angiography workstation could reverse or at least significantly reduce the known limitations of ivACT in the follow up of multiple clips, extensive coils, etc.

**KEY WORDS:** Metal artifact reduction, flat-panel angiographic CT, noninvasive follow-up methods

**O-36** **11:10 AM - 11:18 AM**

#### **New Structure-Preserving Denoising Technique Produces CT Head Images Comparable to Adaptive Statistical Iterative Reconstruction at Identical Reduced Radiation Dose**

Stein, E. G.<sup>1</sup>•Golan, S. S.<sup>2</sup>•Ng, S.<sup>3</sup>•Tanenbaum, L. N.<sup>2</sup>

<sup>1</sup>Maimonides Medical Center, Brooklyn, NY, <sup>2</sup>Mount Sinai Medical Center, New York, NY, <sup>3</sup>Mount Sinai Medical Center, Brooklyn, NY

#### PURPOSE

Low-radiation doses utilized for CT have high levels of noise when reconstructed with filtered back projection (FBP). Iterative reconstruction (ASIR) is a new technique that reduces image noise. Another method of noise reduction is structure-preserving denoising (SPD) which can be applied to any CT image of any generation or manufacturer. We evaluated quantitative and qualitative measures of dose-reduced CT of the head reconstructed with either FBP or ASIR, and FBP images processed with SPD (FBP-SPD).

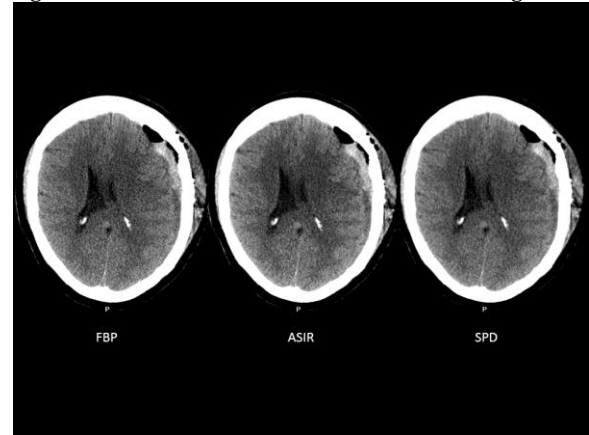
#### MATERIALS & METHODS

Nineteen head CT examinations performed using a reduced radiation dose were processed using both FBP and ASIR. A novel algorithm was applied to the FBP data set (FBP-SPD). Signal-to-noise (SNR) and contrast-to-noise ratios (CNR) for the datasets were calculated. Qualitative assessment of each study for overall quality and gray-white distinction was performed on a 4-point scale (1-best, 4-worst) by two radiologists blinded to the reconstruction method.

#### RESULTS

Compared to dose reduced FBP, SNR increased 31% and CNR increased 29% with the FBP-SPD images. The application ASIR increased SNR 15% and CNR 21%. The neuroradiologists scored gray-white distinction at  $2.5 \pm 0.6$  for FBP,  $1.8 \pm 0.4$  for FBP-SPD, and  $1.6 \pm 0.5$  for ASIR. Overall quality was scored at  $2.4 \pm 0.5$  for FBP,  $1.5$

$\pm 0.5$  for FBP-SPD and  $1.6 \pm 0.5$  for ASIR. Gray-white distinction and overall quality for the ASIR and FBP-SPD images were statistically significantly better than for the FBP images ( $p = 0.0001$ ) but there was no significant difference between ASIR and SPD images.



#### CONCLUSION

Structure-preserving denoising is manufacturer agnostic technique that produces images markedly better than those reconstructed with FBP and comparable in quality and gray-white distinction to those produced using ASIR.

**KEY WORDS:** Postprocessing, radiation dose, CT

**O-37** **11:18 AM - 11:26 AM**

#### **Cerebrovascular and Functional MR Imaging with the Blood Pool Agent Ferumoxytol: Initial Experience in Normal Subjects**

Zaharchuk, G. • Christen, T. • Qiu, D. • Ni, W. • Schmiedeskamp, H. • Bammer, R. • Moseley, M. E.

Stanford University  
Stanford, CA

#### PURPOSE

Long half-life or "blood pool" contrast agents potentially could improve imaging contrast in a wide variety of diseases. In particular, ferumoxytol (Feraheme, AMAG Pharmaceuticals Inc., Cambridge, MA) is an ultrasmall paramagnetic iron oxide particle compound recently approved for human use as a treatment for iron-deficiency anemia, but which has favorable contrast agent features, including long intravascular half-life (approximately 15 hours) and strong T2\* shortening effect. Herein, we report on our initial experience with ferumoxytol in humans for cerebrovascular and functional MRI (fMRI).

#### MATERIALS & METHODS

In this IRB-approved study, seven normal subjects received ferumoxytol at multiple doses up to a maximum of approximately 7 mg Fe/kg. High-resolution (0.7 mm<sup>3</sup> voxel size) T2 and T2\* mapping using multiecho SE and GE sequences was performed before and after contrast administration. These images were used to calculate molar relaxivity and to create high-resolution CBV maps. During contrast injection (4

ml injected at 1 ml/s), a lower resolution spin and gradient echo (SAGE)-EPI sequence (TR 1800, 5 echoes between 17 and 97 ms, 41 mm<sup>3</sup> voxel size) was used to track the bolus and create maps of CBV, CBF, and Tmax using automated software (RAPID). An fMRI brain activation paradigm (unilateral finger tapping 48 s on/48 s off, 6 epochs) was performed pre and postcontrast using a standard GE EPI pulse sequence (TR/TE 2000/35 ms). Additional imaging was performed in two subjects 6-24 hours following the initial dose.

## RESULTS

A marked reduction in T2\* was identified following ferumoxytol administration, which was about 1.5x greater in gray matter compared with white matter. Quantitative CBV maps in gray and white matter were  $5.4 \pm 0.5\%$  and  $3.1 \pm 0.3\%$ , consistent with prior literature values. Signal-to-noise ratio was adequate to create high-resolution CBV maps with voxel sizes of <1 mm<sup>3</sup>, in which fine vascular detail was visible. High signal on heavily T2\*-weighted images consistent with low CBV was seen easily in a subcentimeter periventricular white matter lesion ("UBO") in one volunteer 24 hours following contrast administration. Cerebral blood flow, CBV, and Tmax maps created using SAGE-EPI images during bolus passage demonstrated a pattern consistent with the higher resolution steady-state CBV maps. Functional MRI performed pre and postcontrast demonstrated expected signal behavior (i.e., positive signal change during tapping precontrast consistent with the BOLD effect and negative signal change postcontrast, consistent with the CBV response). The CBV hemodynamic response time for functional activation is approximately 20-30 sec, the first time this has been measured in humans. Lastly, we believe that the magnetic susceptibility difference between brain and air is favorably affected by ferumoxytol administration, resulting in decreased susceptibility artifact and signal dropout over the anterior temporal and inferior frontal lobes, characteristically difficult regions to assess with conventional fMRI.

## CONCLUSION

Ferumoxytol has many favorable properties for measuring cerebral hemodynamics and functional activation. High among them is the ability afforded by the long blood half-life to increase the spatial resolution of resultant maps by an order of magnitude, and subsequently to characterize smaller lesions and regions of activation more accurately than possible with prior techniques.

**KEY WORDS:** Ferumoxytol, functional MR imaging, perfusion

O-38

11:26 AM - 11:34 AM

## Reduced Patient Radiation from Adaptive Statistical Iterative Reconstruction Implementation for Neuroradiology T Protocols

Shepherd, T. M. • Prasad, V. R. • Hess, C. P. • Gould, R. • Dillon, W. P.

University of California San Francisco  
San Francisco, CA

## PURPOSE

Patient computed tomography (CT) radiation exposure can be reduced by lowering tube current or changing other acquisition parameters, but this can lead to unacceptable degradation of diagnostic image quality. Alternative CT data reconstruction methods, such as Adaptive Statistical Iterative Reconstruction (ASIR)(GE Healthcare) may be used to reduce image noise for low-dose CT acquisitions in real time. We assessed the radiation reductions associated with ASIR implementation across all neuroradiology CT protocols at our institution.

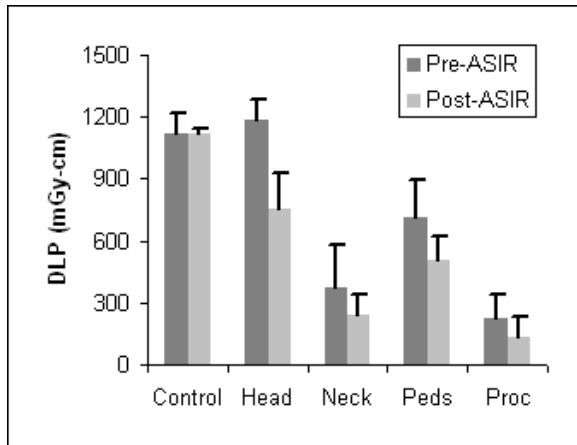
## MATERIALS & METHODS

In autumn 2010, our neuroradiology section adapted ASIR and increased noise index settings by consensus to reduce patient dose for all neuroradiology protocols on 4 CT scanners. Multiple CT parameters including ASIR and noise index, tube current, CT dose index and total exam dose-length product (DLP) were compared in consecutive cohorts of 25 patients for each protocol before and after these changes.

## RESULTS

CT protocol modifications for ASIR and noise index were reached iteratively by consensus within the section over a period of 3 months without difficulty. Figure 1 demonstrates DLP reductions of 29-42% were achieved for neuroradiology CT protocols after ASIR implementation, including noncontrast head ("Head"), contrast neck ("Neck"), pediatric head ("Peds") and CT-guided lumbar spine injections ("Proc") (mean  $\pm$  SD, all comparisons  $P < 0.01$ ). Noncontrast CT head studies ("Control") from a scanner without ASIR capability demonstrated no DLP change over the same period. DLP for stroke and subarachnoid hemorrhage CT angiograms (CTA) decreased 35% and 59% respectively ( $P < 0.01$ ) over the same time period. CT angiography protocol DLP reductions were multifactorial with contributions from ASIR, as well as reduced use of postcontrast and perfusion CT (e.g., down 55% and 60% respectively for subarachnoid hemorrhage CTAs).





#### CONCLUSION

Previous studies have demonstrated dose reductions with acceptable image quality for noncontrast CT head studies. Our results demonstrate that new advanced CT reconstruction algorithms, such as ASIR, can be used to reduce patient radiation by 30-40% in most neuroradiology CT protocols without reductions in diagnostic accuracy. Alternatively, ASIR can be used to improve image quality without dose penalty - for example, we now use thinner slices with ASIR in our low-dose noncontrast pediatric head without an increase in radiation dose ( $161 \pm 41$  mGy-cm). Newer model-based iterative reconstruction algorithms may lower CT radiation to patients even further.

**KEY WORDS:** Radiation, dose, ASIR

O-39

11:34 AM - 11:42 AM

#### High Quality Low Radiation Dose Unenhanced Head Computed Tomography Using a Fourth Generation Iterative Reconstruction Technique: Cadaver and Clinical Studies

Lahiji, K.·Daly, B.·Fardanesh, R. M.·Kouo, T. C.·Mehta, D.·Morales, R.·Steven, A.·Yang, Z.

University of Maryland  
Baltimore, MD

#### PURPOSE

The recent introduction of iterative reconstruction (IR) techniques for computed tomography (CT) allows for potential reduction of radiation dose without loss of diagnostic quality compared with conventional filtered back projection (FBP) techniques at standard dose. We investigated the use of a new fourth generation IR (IR4) technique for radiation dose reduction in cadaveric and clinical head CT studies.

#### MATERIALS & METHODS

Unenhanced head CT scans of two human cadavers were scanned at standard and reduced dose levels (19%-72% dose reduction) and image sets were reconstructed using both FBP and 4th-generation IR (IR4, iDose4, Philips Healthcare) to determine optimal techniques. Subsequently unenhanced head CT scans of 40 patients were performed at 33-43% reduced radiation level (120 kVp, 200 effective mAs) and image

sets were generated using the same IR4 and FBP reconstruction techniques. IR4 was tested at different strength applications determined by prior cadaveric scan findings: Level 2 (30%), Level 3 (40%), and Level 4 (50%), corresponding to appropriate compensation for increased image noise with incrementally greater dose reduction. All reconstructions were subjected to qualitative and quantitative analysis, using a recent standard dose (120kV, 300-350 effective mAs) head CT reconstructed with FBP in the same patient as a reference. Overall image quality, gray-white matter differentiation, posterior fossa and subarachnoid conspicuity, and artifacts were blindly scored by three neuroradiologists. Quantum noise was measured with standard regions of interest at the cerebral cortex, caudate head, and cerebellar hemisphere levels bilaterally.

#### RESULTS

Mean qualitative reader scores for gray-white matter differentiation, posterior fossa and subarachnoid conspicuity, and artifact presence showed no significant difference between low dose IR4 L2 and L3 datasets and standard-dose FBP datasets. No significant difference was seen for overall image quality in two of three readers. IR4 L2 and L3 scored significantly better than low dose FBP datasets for all criteria ( $P < 0.05$ , Wilcoxon rank test). Quantitative measurements of image noise showed no significant difference between the IR4 L2 & L3 datasets and the standard-dose FBP datasets. All IR4 levels had significantly lower noise than corresponding low dose FBP datasets ( $P < 0.05$  ANOVA). Compared to standard studies, mean CT dose index (CTDIvol) for low dose IR4 head studies dropped from standard dose level of 46.5 to 27.1 mGy, (brain dose from 40.8 to 25.5 mGy, lens dose from 46.5 to 29 mGy) and mean effective dose dropped from 1.86 to 1.18 mSv.

#### CONCLUSION

As predicted from cadaveric models, qualitative and quantitative data demonstrated that unenhanced head CT scans obtained at a 33-43% lower radiation dose with IR4 L2 and L3 reconstructions were of equal diagnostic quality to standard dose FBP reconstructed images for nearly all tested qualitative criteria and are suitable for routine clinical use. Low dose IR4 L2 and L3 reconstructions were equal to standard dose FBP for image noise. Mean absorbed and effective dose savings of 42% and 37% respectively were realized. This reduced radiation dose technique will be of greatest value in settings where patients may require multiple and frequent follow-up studies.

**KEY WORDS:** Computed tomography, head, iterative reconstruction

O-40

11:42 AM - 11:50 AM

# Graph Theoretical Analysis Applied to Structural MR Imaging Data Reveals Disease-Specific Gray Matter Changes in Patients with Diabetes Mellitus

Moody, E. A.<sup>1,2</sup>·Whitlow, C. T.<sup>1,3</sup>·Bowden, D. W.<sup>1</sup>·Maldjian, J. A.<sup>1</sup>

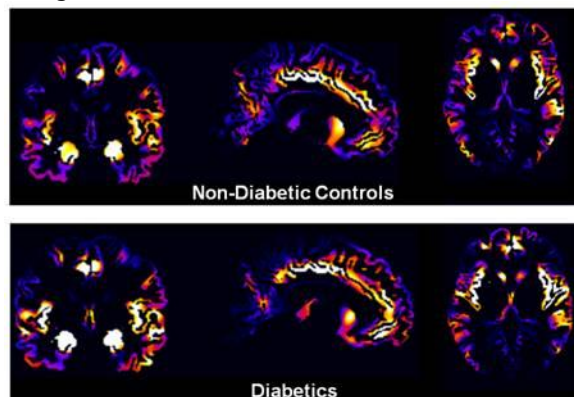
<sup>1</sup>Wake Forest School of Medicine, Winston-Salem, NC, <sup>2</sup>Virginia Tech - Wake Forest University Center for Injury Biomechanics, Winston-Salem, NC, <sup>3</sup>Translational Science Institute, Winston-Salem, NC

## PURPOSE

Diabetes mellitus (DM) is known to affect the brain, with development of progressive gray matter atrophy, white matter lesions, and cognitive impairments. Graph theoretic structural network methods have not been used yet to characterize DM-related changes in the brain that may reflect important disease-specific end-organ determinants of cognitive impairment. In this study, we applied graph theory network methods to structural MRI data hypothesizing that DM would be associated with a disease-specific pattern of gray matter volume change compared to nondiabetic controls.

## MATERIALS & METHODS

An institutional ethics committee approved this study. Two hundred diabetic and 92 nondiabetic control subjects were scanned in a 1.5 T GE scanner using an 8-channel head coil (GE Medical Systems, Milwaukee, WI, USA) for collection of structural anatomical MRI data. All data were motion-corrected, segmented and normalized to a standard template using the VBM8 toolbox within SPM8. Modulated gray matter maps from all subjects in each group were concatenated into a 4D image data file and used to construct a group-specific voxel-based 159,844x159,844 correlation matrix for graph theoretic analysis. Group-specific binarized adjacency matrices for diabetics and controls were constructed at a cost of 0.1 from which diabetic and nondiabetic degree maps were constructed (Figure 1). T-tests of degree between groups were performed for all regions.



## RESULTS

Figure 1 demonstrates group structural network degree maps for diabetics (bottom row) and nondiabetic

controls (top row). High (white) and low (purple) degree voxels correspond to relatively large or small number of associations with other voxels, respectively, based upon similarity in voxel gray-matter volume changes across subjects compared to all other brain voxels. These group-specific degree maps demonstrate striking right to left similarity, and that high and low degree voxels cluster in regions reflecting known anatomical structures. Regions containing highest degree voxels for DM-specific and nondiabetic degree maps include the amygdala, hippocampus, insular cortex, anterior cingulate cortex, and basal ganglia. T-tests corrected for multiple comparisons demonstrated significant differences in voxel degree for diabetics compared to controls, with increases in degree for putamen, temporal pole, and frontal superior regions, along with decreases in degree for occipital and inferior frontal regions ( $p < 3.1 \times 10^{-7}$ ).

## CONCLUSION

The application of graph theory network methods to structural MRI data revealed diabetes-specific patterns of volume change in gray matter areas that have been demonstrated to be important in cognitive function. These data demonstrate the utility of group-specific structural network maps to exploring brain diseases.

**KEY WORDS:** Diabetes mellitus, structural network, graph theory

O-41

11:50 AM - 11:58 AM

# Hyperpolarized <sup>13</sup>C Ascorbates as MR-Compatible Redox Sensors for Neuroimaging

Wilson, D. M.·Kurhanewicz, J.·Keshari, K.

University of California San Francisco  
San Francisco, CA

## PURPOSE

Reduction and oxidation (redox) chemistry plays a critical role in aging, neurodegenerative disease, and ischemia/reperfusion injury. Despite this strong relationship between redox and human disease, methods to interrogate a redox pair in vivo are limited. We have developed [<sup>1-13</sup>C] dehydroascorbate (DHA), the oxidized form of Vitamin C, as an endogenous redox sensor for in vivo imaging using hyperpolarized [HP] <sup>13</sup>C spectroscopy. In anesthetized rats, HP[<sup>1-13</sup>C] DHA was rapidly converted to [<sup>1-13</sup>C] Vitamin C within the brain, suggesting its utility in a variety of common cerebral disorders related to oxidative stress.

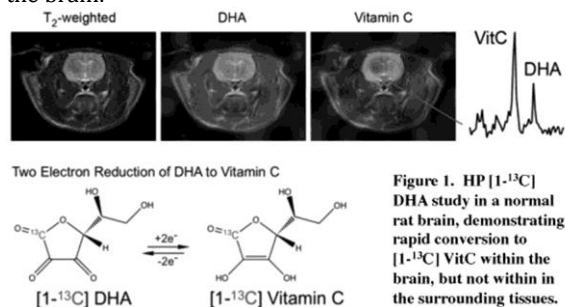
## MATERIALS & METHODS

**Synthesis of [<sup>1-13</sup>C] DHA:** [<sup>1-13</sup>C] DHA (Isotec, Miamisburg, OH) was synthesized using a published method, by air oxidation of [<sup>1-13</sup>C] ascorbic acid in the presence of catalytic amounts of copper (II) acetate. **Hyperpolarization and dissolution of [<sup>1-13</sup>C] DHA and [<sup>1-13</sup>C] Vitamin C:** [<sup>1-13</sup>C] DHA and [<sup>1-13</sup>C] VitC were hyperpolarized on a HyperSense DNP instrument (Oxford Instruments) as previously described. **3T Studies:** In vivo studies were performed using a 3 T MRI scanner (GE Healthcare, Waukesha, WI) equipped with

the MNS (multinuclear spectroscopy) hardware package.  $^{13}\text{C}$  MRSI studies were carried out as previously published.

## RESULTS

For HP  $[1-^{13}\text{C}]$  DHA studies, in voxels corresponding to brain, the average  $\text{VitC}/[\text{VitC} + \text{DHA}]$  was  $0.51 \pm 0.1$ , significantly higher than that seen in surrounding tissues. A corresponding image is seen in **Figure 1**, demonstrating localization of the  $[1-^{13}\text{C}]$  VitC metabolite within the brain. In contrast, following injection of HP  $[1-^{13}\text{C}]$  VitC, no observable metabolite was seen. In these studies, the magnitude of  $[1-^{13}\text{C}]$  VitC resonances was higher in surrounding tissues than in the brain.



## CONCLUSION

The steady-state concentration of Vitamin C in the brain is remarkably high, estimated to be 10 mM in neurons, while glia harbor high concentrations of GSH. On injection of HP  $[1-^{13}\text{C}]$  DHA into a normal rat, significant reduction to  $[1-^{13}\text{C}]$  Vitamin C was observed within the brain, with essentially no background conversion observed in surrounding tissues. Given the limited spatial resolution of this study, we were not able to determine whether this reduction took place primarily in gray matter (dominated by neurons) or white matter (predominantly glia). Rapid reduction of HP  $[1-^{13}\text{C}]$  DHA within the brain suggests a role for this probe in functional imaging (GLUT transporter density), determining local glutamate concentrations, as well as predicting vulnerability to reactive oxygen species (ROS).

**KEY WORDS:** Hyperpolarized, ascorbate, brain

# Monday Morning

**10:30 AM - 12:00 PM**

**Beekman/Sutton North**

**(8c) Pediatrics: New Techniques**

**0-42**

**10:30 AM - 10:38 AM**

## Model-Based Iterative Reconstruction for Pediatric Head CT Allows Greater Reductions in Radiation Dose than Adaptive Statistical Iterative Reconstruction

Mirza, N.·Delman, B.·Pawha, P.·Tanenbaum, L. N.

Mount Sinai School of Medicine  
New York, NY

## PURPOSE

The number of CT scans performed on children has increased substantially in the past 2 decades and approximately 11% of scans are performed on the pediatric population. The effective child's CT radiation dose is 2 (newborn) to 1.6 (5 years old) more than adults. Children undergoing CT examinations are more likely to have multiple scans. Growing tissues/organs are more sensitive to radiation effects and children have a longer latent time for potential radiation related cancers to develop. Adaptive statistical iterative reconstruction (ASIR) techniques provide standard image quality at substantially lower radiation dose than traditional filtered back projections (FBP) allow. Adaptive statistical iterative reconstruction leaves substantial information about the CT imaging chain untapped to permit rapid reconstruction times at the expense of quantum and system noise remaining in the image. Mode-based iterative reconstruction techniques (MBIR VEO) perform a more complex reconstruction, modeling system optics and statistics along with 3D three point beam analysis. While reconstruction times are longer, with fewer assumptions image noise is reduced drastically and dose reductions of up to 75% over FBP can be accomplished.

## MATERIALS & METHODS

Mode-based iterative reconstruction techniques images were obtained at a 30% lower dose (higher noise index) than currently in use for ASIR studies at our institution. Adaptive statistical iterative reconstruction and FBP images were reconstructed retrospectively for analysis from the dose reduced raw data. A quantitative (noise) and qualitative comparison (gray-white differentiation, overall quality) of the clinical MBIR VEO images was performed against the ASIR and FBP studies as well as against routine clinical expectations for pediatric head CT imaging. All examinations were performed on a clinical GE HD 750 scanner.

## RESULTS

Mode-based iterative reconstruction techniques produced images that were lower in noise than those



with ASIR and both were lower in noise than those with FBP. The MBIR VEO images were of standard quality, superior to those with ASIR and FBP and better than expected for dose conscious pediatric head CT in routine practice.

#### CONCLUSION

Mode-based iterative reconstruction techniques provide high image quality at radiation doses lower than can be provided with ASIR or FBP techniques and should become the standard for routine pediatric head imaging when widely available.

**KEY WORDS:** Radiation dose, model-based iterative reconstruction, CT

**O-43**

**10:38 AM - 10:46 AM**

#### "FAST" MR Imaging in the Evaluation of Pediatric Hydrocephalus

Eckel, L. J., Diehn, F., Hunt, C., Schwartz, K., Keating, G., Wetjen, N., Welker, K.

Mayo Clinic  
Rochester, MN

#### PURPOSE

Determine if MRI can be used successfully instead of CT for the routine evaluation of ventricular size in pediatric patients.

#### MATERIALS & METHODS

Over the course of more than 2 years, all pediatric patients needing an imaging evaluation of ventricular size were scheduled for MRI. In the past, these evaluations have been done by CT as it was quicker and provided the needed information. Utilizing a "fast" MRI sequence, such as FIESTA or T2 HASTE, two planes of imaging can be performed in less than 2 minutes. Utilizing MRI eliminates the radiation exposure from CT, an important consideration in this patient population group, which is young and often in need of multiple imaging evaluations.

#### RESULTS

During the time of our study, approximately 350 MRIs were performed in patients ranging in age from 0 to 14 years old. In every case, "fast" MRI was able to answer the clinical question. No CT exams were needed, eliminating radiation in these patients. In addition, no diagnostic MRI was needed, eliminating the need for pediatric sedation.

#### CONCLUSION

In the pediatric population, when evaluating ventricular size, "fast" MRI should be the first test of choice, as it is effective and reduces radiation exposure associated with CT.

**KEY WORDS:** Pediatric, hydrocephalus, MR imaging

**O-44**

**10:46 AM - 10:54 AM**

#### Clinical Applications for Fast Brain MR Imaging in Children

Aw, J., Schoeneman, S. E., Boylan, E. E., Burrowes, D.

Children's Memorial Hospital  
Chicago, IL

#### PURPOSE

Fast brain MRI imaging has been introduced recently for assessing brain ventricles in patients with ventriculo-peritoneal shunts (VPS). However, there is minimal literature on how this method could be beneficial for other indications. Compared to CT, this method reduces lifetime cumulative radiation dose and has multiplanar capabilities. It is much faster than full brain MRI, reducing exam costs and potentially reducing the need for sedation. However, fast brain MRI has lower resolution than a standard brain MRI and cannot detect hemorrhage. The goal of our study is to assess retrospectively additional clinical applications for fast brain MRI.

#### MATERIALS & METHODS

Patients who had undergone fast brain MRI were found in XenoBase, a database which references deidentified electronic medical records at our institution. XenoBase then was used to identify subgroups by diagnosis. One of the most common diagnoses was arachnoid cyst. After IRB approval, patients with fast brain MRI and arachnoid cyst were identified so that their fast brain MRI could be compared to any full brain MRI and to clinical outcomes. Fast brain MRI findings were excluded if there was not a full brain MRI within 1 year. Agreement with full brain MRI, and documented effect on clinical management were coded for statistical review.

#### RESULTS

Between 2008 and 2011, there were 14 arachnoid cyst patients with 16 fast brain MRI exams. In 12 members of this group, fast brain MRI was used alone or in comparison with a full brain MRI in the decision to follow or discharge the patient. Two exams failed to report a pituitary cyst and mass effect which were reported on prior exams. Six patients had no complications in the year following their fast brain MRI. The most common complication was headache (four cases).

#### CONCLUSION

Fast brain MRI reduces radiation exposure, time, cost, and the need for sedation in VPS patients. These benefits may be extended cautiously to other patient groups also requiring routine imaging, such as those with arachnoid cysts.

**KEY WORDS:** Brain ventricles, arachnoid cyst, fast brain MR imaging

O-45

10:54 AM - 11:02 AM

### Evaluating Pediatric Neuropathologies Using Multiple TE-Weighted Susceptibility Images Using Multi-Shot EPI Sequence

Soman, S.·Qiu, D.·Barnes, P. D.·Moseley, M.·Yeom, K.

Stanford University  
Stanford, CA

#### PURPOSE

Susceptibility-weighted imaging (SWI) has been proven clinically useful in a variety of clinical scenarios. However, for any susceptibility-weighted imaging, the length of the TE will determine the extent of susceptibility effects depicted. Sequences such as susceptibility-weighted imaging regularly employ a 3D gradient sequence at a single TE value to obtain isotropic susceptibility-weighted images. The multi-shot EPI sequence (3D MSME EPI) is an MRI pulse that allows for the acquisitions of images for multiple TE per each TR, and can effectively acquire images for multiple TEs in the same time as a single 3D GRE sequence. We sought to evaluate the utility of multiple TE images for evaluating pediatric pathologies compared to each other as well as against our standard 2D GRE sequence.

#### MATERIALS & METHODS

Fifty pediatric patients imaged as part of our clinical practice had multi-shot EPI sequences and 2D GRE sequences performed under an IRB approved protocol. TE = 15 (short), 25 (medium) and 60 (long) were used. Imaging of patients ranging from 1 to 21 years in age demonstrated various stages of tumors, hemorrhage, postoperative changes, or no abnormalities. A board-certified pediatric neuroradiologist and a second year neuroradiology fellow reviewed all images.

#### RESULTS

Numerous instances were found where long 3D TE images better depicted pathologies (such as blood products, postoperative changes, or siderosis, vessel prominence) than short or medium 3D TE images or 2D GRE images. In one case, a patient with elevated ferritin levels suspected of having hemophagocytic lymphohistiocytosis demonstrated siderosis on long TE images, while all other sequences appeared to be negative. Numerous cases also demonstrated that the extent of artifact (motion, braces, hardware) worsened with increasing TE.

#### CONCLUSION

Multi-shot EPI images can provide images that demonstrate susceptibility findings better seen on long TE 3D GRE images, can depict findings on short TE images that may be obscured by artifacts on longer TE images, and overall, often can show findings not visible on 2D GRE images, all in the same time as standard 3D GRE sequences (such as SWI). Additionally, this method produces multiple TE images that may be useful for advanced applications such as calculating T2\* values (which may be useful in characterizing neuropathologies), producing phase images or performing quantitative susceptibility mapping.

**KEY WORDS:** Susceptibility-weighted imaging, multiple TE imaging, pediatric neuroimaging

O-46

11:02 AM - 11:10 AM

### Identification and Quantification of Spatial Distortion and Other Imaging Artifacts in a 3.0 T Intraoperative MR Imaging Scanner

Choudhri, A. F.·Chin, E. M.·Whitehead, M. T.·Klimo, P.·Boop, F. A.

University of Tennessee Health Science Center  
Memphis, TN

#### PURPOSE

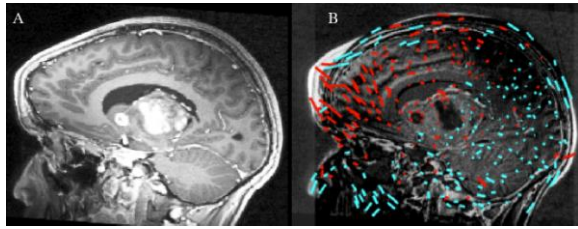
Intraoperative MRI (iMRI) is a new technology which allows acquisition of images during a surgical procedure, typically brain tumor resection, to assess for the presence of residual tumor. With 3.0 T iMRI equipment, susceptibility artifacts and field inhomogeneity due to surgical equipment and nonstandard patient positioning has reduced image quality and resolution. We performed a review of iMRI images to qualitatively and quantitatively characterize the presence and severity of spatial distortion.

#### MATERIALS & METHODS

We analyzed MRI scans from 50 consecutive pediatric patients undergoing surgery for primary brain tumors who were scanned with a 3.0 T iMRI (Siemens AG, Munich, Germany, and IMRIS, Winnipeg, CA) to quantify spatial distortion. DICOM datasets were evaluated in the MATLAB computing environment, and distortion was calculated by comparing to preoperative volumetric datasets performed for stereotactic navigation that were performed in a routine diagnostic MRI scanner. Images were analyzed both without and with vendor-provided distortion correction algorithms. Factors including head position, presence and location of external fixation frame, size of the resection cavity and quantity of postoperative/intraoperative pneumocephalus were evaluated.

#### RESULTS

Severity of spatial distortion most strongly correlated with distance from the isocenter of the magnetic field. In patients who were repositioned for further scanning without distortion, the repeat scans near the isocenter of the magnetic field had less distortion than was seen by application of vendor-provided distortion correction algorithms to the initial scans. Image A shows a sagittal intraoperative scan performed approximately 10 cm above isocenter of the magnetic field, with an elongated appearance of the anterior structures. A distortion map is shown demonstrating the magnitude and direction of distortion (Image B), as compared to preoperative structural imaging. In this patient, there was approximately 5 mm spatial shift of an 11 mm lesion that was being targeted for biopsy.



### CONCLUSION

We have performed a systematic study of sources of distortion in the high-field intraoperative MRI setting. Intraoperative MRI spatial distortion has the potential to negatively impact surgical outcomes if these images are used for surgical navigation, and neuroradiologists and neurosurgeons must be aware of the possibility and attempt to decrease distortion by positioning the patient as close to isocenter as possible and minimize pneumocephalus at the time of scanning. This information can help predict the presence of and severity of image distortion, which may be able to improve the effectiveness of iMRI guidance for brain tumor resection.

**KEY WORDS:** Intraoperative MR imaging, artifact, tumor

**O-47**

**11:10 AM - 11:18 AM**

### Arterial Spin Labeling Perfusion MR after Hypoxic-Ischemic Injury to the Brain in Children

Vossough, A.·Ziai, P.

Children's Hospital of Philadelphia  
Philadelphia, PA

### PURPOSE

To use arterial spin labeling (ASL) perfusion MRI for assessment of perfusion changes encountered after hypoxic-ischemic injury to the brain in children.

### MATERIALS & METHODS

We performed a retrospective study of ASL perfusion brain MRIs of children with acute hypoxic-ischemic injury to the brain who had undergone quantitative ASL imaging of the brain. All patients were studied with a pulsed ASL technique in addition to conventional and diffusion-weighted imaging. Many also had susceptibility-weighted imaging (SWI) MR venography performed as an indirect qualitative assessment of deoxyhemoglobin in the venous vasculature. Quantitative cerebral blood flow measurements of the cortical and deep gray matter were performed using regions of interest.

### RESULTS

Results of quantitative arterial spin labeling perfusion was available in 21 children with hypoxic-ischemic injury, as evidenced by diffusion and conventional MRI sequences. The patients demonstrated significantly increased gray matter cerebral blood flow measurements on arterial perfusion imaging after hypoxic-ischemic injury. In 18 patients the perfusion changes were more localized to the area of apparent ischemic injury, whereas in three, there was more

generalized hyperperfusion in the brain. Mean gray matter cerebral blood flow was measured at  $162 \pm 38$  mL/100g/minute in the areas of hyperperfusion. In patients that did have SWI MR venography, it generally demonstrated relative disappearance of the venous BOLD signal, presumably due to decreased deoxyhemoglobin in venous blood secondary to hyperperfusion.

### CONCLUSION

Marked local or global hyperperfusion can be seen in children with hypoxic-ischemic injury on arterial spin labeling perfusion MRI. Arterial spin labeling perfusion MRI can play an important role in detection of perfusion alterations in the brain in children with hypoxic-ischemic injury. It may have potential to serve as a marker in the assessment of secondary brain damage after hypoxic-ischemic injury and in the evaluation of neuroprotective treatment strategies for these patients.

**KEY WORDS:** Arterial spin labeling, hypoxic ischemic injury, children

**O-48**

**11:18 AM - 11:26 AM**

### Accuracy of Time-Resolved Dynamic Contrast-Enhanced MR Angiography in Classifying Soft Tissue Vascular Anomalies in the Head and Neck in Children

Tekes, A.·Esenkaya, A.·Weiss, C.·Ali, S.·Mitchell, S.·Huisman, T. A.

Johns Hopkins Hospital  
Baltimore, MD

### PURPOSE

Soft tissue vascular anomalies (VA) commonly present in the head and neck in children. Accurate classification is crucial since treatment and morbidity changes significantly between vascular tumors and vascular malformations. Further classification of vascular malformations is critical as the treatment method and agents are different for slow and fast flow vascular malformations. Conventional MRI with contrast is performed routinely for diagnosis and follow up of VA. Our objective is to evaluate accuracy of time-resolved dynamic contrast-enhanced MRA (TWIST) against conventional MRI with contrast in classification of soft tissue vascular anomalies in the head and neck in children.

### MATERIALS & METHODS

Children with suspected diagnosis of VA in the head and neck were referred for MRI from 2008 to 2011. Twenty-eight children from 0-17 years of age were enrolled. Time-resolved dynamic contrast-enhanced MRA and conventional MRI was performed (Triplanar T2-weighted imaging with fat saturation, precontrast axial T1-weighted imaging, and postcontrast triplanar fat-suppressed T1-weighted imaging). Time-resolved dynamic contrast-enhanced MRA was performed in coronal plane using blood-pool MR contrast agent (Ablavar-Lantheus) to enhance image quality and spatial resolution of MRA. Two pediatric



neuroradiologists evaluated all patients in two different sessions, 15 days apart: one session conventional MRI with contrast was evaluated, in the second session TWIST was evaluated. Clinical evaluation and/or percutaneous venogram/lymphogram data was the gold standard.

### RESULTS

Our patients had diagnosis of infantile hemangioma (n = 4), venous malformation (n = 12), and lymphatic malformation (n = 12). Time-resolved dynamic contrast-enhanced MRA alone could accurately classify 26/28, conventional MRI with contrast could accurately classify 22/28. Conventional MRI with contrast combined with TWIST could accurately classify all cases.

### CONCLUSION

Time-resolved dynamic contrast-enhanced MRA is superior to conventional MRI with contrast in classification of VA in the head and neck in children. Time-resolved dynamic contrast-enhanced MRA offers high temporal resolution in the order of seconds, and provides functional data about the dynamics of contrast enhancement comprising the arterial, venous and delayed venous phases, which reflects the nature of the vascular anomaly. MR imaging of soft tissue VA in the head and neck would be incomplete without TWIST. Use of Ablavar significantly reduces dose (1/3 of other gadolinium-based contrast agents), and does not require trigger imaging. Conventional MRI provides important information regarding the anatomical extent, size, and relation to critical anatomical structures, thus when combined with TWIST, MRI provides the best information without use of radiation in children.

**KEY WORDS:** Vascular anomalies, dynamic evaluation of vascular anomalies, TWIST, children

**O-49**

**11:26 AM - 11:34 AM**

### **MR Imaging Depicts Retinal Hemorrhages in Nonaccidental Trauma**

Zuccoli, G.·Panigrahy, A.·Halidpur, A.·Squires, J.·Wolford, J.·Berger, R.·Berger, R.

Children's Hospital of Pittsburgh  
Pittsburgh, PA

### **PURPOSE**

Abusive head trauma (AHT) is the leading cause of mortality from physical abuse in pediatric patients, and the leading cause of severe TBI in infants. Children who are victims of AHT often have nonspecific symptoms that overlap with relatively innocuous or self-limiting diagnoses, especially in cases without obvious superficial bruising. However, these patients usually demonstrate retinal hemorrhages (RH) which are highly specific for AHT. Dilated ophthalmologic exam by a trained clinician, the gold standard test for detection of RH, is not always available in the acute care setting. Purpose of this study is to evaluate for RH using MRI T2 Star weighted angiography (SWAN).

### **MATERIALS & METHODS**

Our study group included 14 pediatric patients with nonaccidental trauma who were selected retrospectively from the patients seen at our institution in 2011. In our study group, the average age was 10.6 months (range 2 to 24 months). The images were evaluated retrospectively by an experienced fellowship-trained neuroradiologist. Retinal hemorrhages were defined as foci of low signal intensity along the retina on SWAN. Lesions were classified into "point" like and "band" like based on their morphology. Two SWAN protocols were used: low resolution (3-5 mm thickness) and high resolution (1-2 mm thickness). Retinal hemorrhages were classified into bilateral, unilateral, intraretinal, preretinal, subretinal and intraretinal.

### **RESULTS**

*Clinical Findings* - All the patients had bilateral RH at eye exam. Extension of this hemorrhage into the preretinal (subhyaloid) space was identified in eight patients (57%), and subretinal hemorrhage was present in three patients (21.4%). In one of the patients, hemorrhage was found in all three compartments. *Imaging Findings* - MR SWAN images revealed abnormally hypointense periretinal signal consistent with blood products in the orbits of 11 out of the 14 patients confirmed to have retinal hemorrhages on dilated eye exam (78.5%). Two patients whose 5 mm SWAN images were initially negative showed findings positive for retinal hemorrhage using thinner slices of 1 mm. Of the patients whose SWAN images were assessed at thin 1 mm slices, only one patient conclusively demonstrated no discernable features of retinal hemorrhage. This patient showed only intraretinal hemorrhage at eye exam. Imaging features of RH could further be divided into "point-like" and "band-like" findings. In nine patients, the retinal hemorrhage was point-like (81.8%), while four patients demonstrated the band-like retinal hemorrhage (36.6%). Each of these patients had other signs of head trauma on multiple MR sequences such as subdural hemorrhages, edema and calvarial fracture.

### **CONCLUSION**

Dilated ophthalmologic exam by a trained clinician, the gold standard test for detection of RH, is not always available in the acute care setting. Our study suggests that high-resolution MRI SWAN imaging is useful in screening such patients for RH, especially in situations where nonaccidental trauma is suspected.

**KEY WORDS:** Nonaccidental trauma, retinal hemorrhages, eye

**O-50**

**11:34 AM - 11:42 AM**

### **Transfontanellar Contrast-Enhanced Ultrasound of Brain Injury in New Borns: Preliminary RESULTS**

Kastler, A.<sup>1</sup>·Manzoni, P.<sup>2</sup>·Chapuy, S.<sup>2</sup>·Aubry, S.<sup>2</sup>·Cattin, F.<sup>2</sup>·Biondi, A.<sup>2</sup>·Kastler, B.<sup>2</sup>

<sup>1</sup>University Hospital, Clermont Ferrand, FRANCE,

<sup>2</sup>University Hospital, Besancon, FRANCE

## PURPOSE

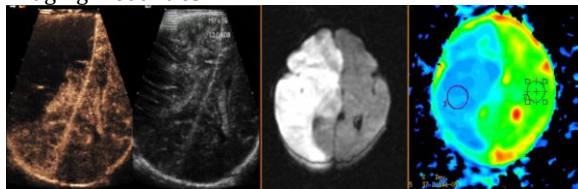
MR imaging is to date the best imaging modality in the early depiction of multiple types of neuropathologic lesions in newborns. Indeed, it offers excellent soft-tissue contrast and good spatial resolution and it is a noninvasive and nonionizing technique. Literature comparing the usefulness of US and MR examinations of the neonatal brain suggest that US is not as effective a modality as MR. However, in emergency settings, US remains better than MR regarding access and availability as it is a real-time bed side imaging modality. In order to improve US sensitivity and due to delayed MRI access, transfontanellar contrast-enhanced ultrasound (TCEUS) was performed as first line examination and compared to MRI in brain injury diagnosis in neonates.

## MATERIALS & METHODS

Five new borns were assessed during the neonatal period with TCEUS and brain MRI. Accuracy of the imaging findings were analyzed and compared. Three of these neonates presented with hypoxic-ischemic encephalopathy (HIE) symptoms, one suffered from severe epileptic seizures and another presented with postesophageal atresia repair neurologic impairment. All TCEU were realized under close neonatal intensive care supervision. Two separate injections of contrast material were systematically realized, subsequent arterial, venous and delayed phase US imaging were analyzed. The following MRI protocol was used: axial DWI, T1, T2, T2 and 3D TOF AngioMR.

## RESULTS

In all five patients, a good correlation between TCEU and MRI was found. In neonates with HIE (three cases), TCEUS and DWI sequences showed concordant impaired territories : hypovascularization on TCEUS versus hyperintensity on MRI (Figure 1). In the patient with postsurgical neurologic impairment, both MRI and TCEU showed intraventricular hemorrhage associated with subdural hematoma, but no ischemic lesions were seen. Finally, no abnormalities were detected in the patient with severe epileptic impairment on both imaging modalities.



## CONCLUSION

Transfontanellar contrast-enhanced ultrasound appears as a potential alternative and accessible imaging modality in the assessment of emergency neonatal brain injury. These promising preliminary results have to be confirmed by a larger prospective series of patients.

**KEY WORDS:** Transcranial ultrasound, contrast material

O-51

11:42 AM - 11:50 AM

## 3D Reconstruction of Fetal Brain MR Imaging

Kuklisova-Murgasova, M.<sup>1</sup>•Quaghebeur, G.<sup>2</sup>•Schnabel, J. A.<sup>2</sup>

<sup>1</sup>Institute of Biomedical Engineering, Oxford, UNITED KINGDOM, <sup>2</sup>University of Oxford, Oxford, UNITED KINGDOM

## PURPOSE

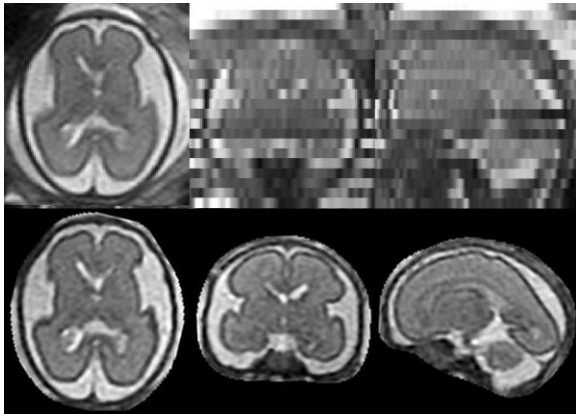
Fetal brain MRI has been used in clinical practice since fast single-shot techniques for acquisition of T2w 2D slices were developed to freeze fetal motion in time. Stacks of thick slices are acquired in three orthogonal directions. Slice thickness is usually 3 to 4 mm to obtain good contrast-to-noise ratio. Such images provide excellent delineation of fetal brain anatomy and are suitable for qualitative assessment of brain abnormalities. However, compromised fetal brain development (e.g., during IUGR) often is demonstrated by more subtle changes, which only can be assessed by quantitative analysis. Studies on preterm infants suggest that quantitative biomarkers, such as reduced cortical volume and sulcation index characterize IUGR. More advanced image analysis, currently used for research into brain development of preterm neonates, requires volumetric brain MR images. Due to their long acquisition times fetal motion presents a major challenge as 3D MR scanning sequences are not applicable in presence of unpredictable and fast fetal motion. We propose a method for the reconstruction of volumetric fetal MRI from 2D slices, comprising super-resolution reconstruction of the volume combined with intensity matching of acquired 2D slices and automatic exclusion of motion corrupted and misaligned slices.

## MATERIALS & METHODS

The motion between slices is corrected using automatic registration method. Initially all stacks are aligned using volumetric registration. Then a 3D volume is reconstructed using model of acquisition of a thick slice. The alignment then is iteratively refined by registering slices to the latest reconstructed volume. During reconstruction, inconsistencies in scaling of the slices and difference in the bias fields are estimated automatically and corrected. Slices corrupted by sudden fetal motion are detected automatically and excluded during reconstruction. The reconstruction method was applied to simulated data, as well as clinically acquired fetal MRI scans.

## RESULTS

We successfully reconstructed 10 clinically acquired fetal brain MR images with 3 and 4 mm thick slices. Our results show that the proposed method produces good quality reconstruction results for clinical data consisting of a small number of thick slices. The reconstructed volumes will be used to perform segmentation of brain structures to calculate volumes and assess cortical folding. Such measurement can enhance neurologic assessment of fetal brain development.



#### CONCLUSION

This method addresses the need for a comprehensive reconstruction model of 3D fetal MRI.

**KEY WORDS:** Fetal MR imaging, 3D reconstruction

**O-52**

**11:50 AM - 11:58 AM**

#### Non-Gaussian Diffusion-Weighted Imaging of the Developing Brain

Paydar, A.·Adisetiyo, V.·Fieremans, E.·Sheth, H.·Nwankwo, J.·Jensen, J.·Milla, S.

New York University School of Medicine  
New York, NY

#### PURPOSE

Significant brain development occurs in early childhood with growth and maturation of the brain seen at both macro- and microstructural levels. In vivo characterization and accurate diagnosis of microstructural abnormality currently remains challenging. Magnetic resonance imaging (MRI) has become the gold standard for high-resolution brain imaging during the course of development. Particularly, the advent of diffusion-weighted imaging (DWI) has improved detection of microstructural changes during brain maturation. However, standard DWI methods, such as the widely used diffusion tensor imaging (DTI) technique, are based on a Gaussian model of water diffusion that may limit sensitivity to microstructural tissue properties. Recently, diffusion-weighted techniques have been developed that utilize non-Gaussian modeling in order to better detect microstructural complexity in both white matter (WM) and gray matter (GM). One of these non-Gaussian diffusion techniques, diffusional kurtosis imaging (DKI), has demonstrated an increased sensitivity to changes in tissue microstructure as compared to Gaussian DTI in a rodent brain maturation study. Our purpose is to utilize DKI, a non-Gaussian diffusion model, to quantify microstructural changes that occur during brain maturation in both WM and GM and to compare this data with DTI metrics. We hypothesize that due to the improved ability to detect microstructural changes, non-Gaussian DWI will be able to detect alterations in myelination and brain development, as reflected by kurtosis metrics.

#### MATERIALS & METHODS

We have performed a retrospective review of 50 pediatric patients who underwent non-Gaussian DWI (DKI) from 2009-2011 on a 1.5 T MRI. These subjects ranged from 1 day to 754 days in age. Diffusional kurtosis imaging data was processed using the MatLab Diffusional Kurtosis Estimator software and the diffusion and kurtosis tensors were calculated to produce parametric maps for DTI diffusion metrics [mean diffusivity (MD) and fractional anisotropy (FA)], as well as a non-Gaussian metric called the mean kurtosis (MK). Subsequently, data were collected and analyzed from regions of interest (ROI) within multiple WM and GM structures, including the corpus callosum, basal ganglia, thalamus, and multiple subcortical WM areas. Diffusion metrics were analyzed with respect to age.

#### RESULTS

Gaussian-based DTI demonstrates expected increased anisotropy as measured by FA within the WM overtime, as myelination gradually takes place during early childhood [e.g., FA genu change from birth to 2 years of +82% ( $R^2 = 0.63$ ); FA splenium +70% ( $R^2 = 0.66$ )]. Diffusion tensor imaging data show changes within the GM [e.g., FA thalamus change of +63% ( $R^2 = 0.33$ ); FA putamen, change of -7% ( $R^2 = 0.024$ )]. Non-Gaussian DKI also demonstrates a consistent increase in kurtosis metrics within WM [e.g., MK genu, change of +116% ( $R^2 = 0.84$ ); MK splenium, change of +160% ( $R^2 = 0.82$ )] as well as in GM [e.g., MK thalamus, change of +138% ( $R^2 = 0.76$ ); MK putamen, change of +78% ( $R^2 = 0.66$ )] during brain maturation.

#### CONCLUSION

Diffusional kurtosis imaging metrics demonstrate significant change consistent with known patterns of brain maturation. This study suggests that DKI can detect progressive changes in microstructural complexity in both white matter and gray matter during human brain development.

**KEY WORDS:** Diffusional kurtosis imaging, DKI, brain development



## Monday Morning

**10:30 AM - 12:00 PM**  
**Sutton Center/South**

**(8d) Adult Brain: Trauma**

**O-53**

**10:30 AM - 10:38 AM**

### **Acute Diffusion Tensor Imaging Predicts Functional Outcomes at One Year Post Mild Traumatic Brain Injury**

Rosenbaum, S. B.<sup>1</sup>•Gardin, T. M.<sup>2</sup>•Kim, N.<sup>1</sup>•Zimmerman, M. E.<sup>1</sup>•Lipton, R. B.<sup>1</sup>•Lipton, M. L.<sup>1</sup>

<sup>1</sup>Albert Einstein College of Medicine, Bronx, NY,  
<sup>2</sup>Montefiore Medical Center, Bronx, NY

#### **PURPOSE**

Although most mTBI patients recover, approximately 30% have persistent symptoms (Alexander 1995). Our purpose was to determine if voxelwise assessment of whole-brain FA at the time of mTBI can predict the persistence of postconcussive symptoms (PCS) and health-related quality of life (HRQoL) at 1 year post injury.

#### **MATERIALS & METHODS**

This study was conducted with IRB approval and written, informed consent, and complied with HIPAA guidelines. Sixteen mTBI patients were recruited from a large emergency center. Diffusion tensor imaging (3.0 T, b = 1000, 32 directions) was performed within 2 weeks of injury, and tests of PCS [Post Concussion Symptoms Questionnaire (RPQ)] and HRQoL [Sickness Impact Profile (SIP)] were administered at 1 year post injury. Voxelwise assessment [p(individual voxel) <0.05, p(cluster size) <0.01] was performed in each patient to identify voxels with abnormally low FA in comparison to 40 healthy controls. Mean FA across the abnormal voxels and total number of abnormal voxels was calculated for each patient. Spearman's rank correlation analysis was used to test for significance of correlation between FA (total number of abnormal voxels and mean magnitude of abnormal voxels) and the RPQ and SIP outcome measures.

#### **RESULTS**

At 1 year post injury, mean FA across abnormal voxels was correlated significantly with measures of PCS and HRQoL. Mean low FA predicted worse HRQoL ( $r = -.595$ ,  $p < .012$ ), mediated by two measures of psychological functioning, namely psychological autonomy and communication ( $r = -.807$ ,  $p < .001$ ) and emotional stability ( $r = -.671$ ,  $p = .003$ ) as well as one measure of social functioning, namely social behavior ( $r = -.509$ ,  $p = .037$ ). Mean low FA also correlated with worse cognitive PCS on the RPQ ( $r = -.679$ ,  $p = .004$ ).

#### **CONCLUSION**

Abnormally low FA, previously shown to be a manifestation of traumatic axonal injury (e.g., Inglese et al., 2005; Li et al., 2011; MacDonald et al., 2007; Niogi et al., 2008; Rutgers et al., 2008) characteristic of mTBI, predicted more severe cognitive PCS (e.g., poor concentration, forgetfulness, taking longer to think) and worse HRQoL at >1 year post injury. Our findings suggest that severity of early trauma detected with DTI may be an effective predictor of long-term, real-world functional outcomes, particularly in psychological health and cognition, domains known to be important components of mTBI morbidity.

**KEY WORDS:** Mild traumatic brain injury, diffusion tensor imaging, post-concussive symptoms

**O-54**

**10:38 AM - 10:46 AM**

### **Personalized Medicine Approach to Determine Prognosis of Mild Traumatic Brain Injury: Combined Assessment of Diffusion Tensor Imaging and the Apolipoprotein E Genotype at Time of Injury Predicts Long-Term Cognitive Performance**

Gardin, T. M.<sup>1</sup>•Rosenbaum, S. B.<sup>2</sup>•Kim, N.<sup>2</sup>•Davies, P.<sup>2</sup>•Zimmerman, M.<sup>2</sup>•Lipton, R. B.<sup>2</sup>•Lipton, M. L.<sup>2</sup>

<sup>1</sup>Montefiore Medical Center, Bronx, NY, <sup>2</sup>Albert Einstein College of Medicine, Bronx, NY

#### **PURPOSE**

The apolipoprotein E4 allele (APOE4) confers worse prognosis for poor outcome and incident Alzheimer disease following TBI (Ariza et al., 2006; Isoniemi et al., 2006). Diffusion tensor imaging (DTI) demonstrates abnormalities in acute mTBI, but it remains uncertain how these abnormalities can determine long-term prognosis, a critical clinical need. The present study aimed to determine if APOE4 genotype, in conjunction with personalized assessment of acute DTI, could serve to predict sub-acute and chronic cognitive outcomes in patients following mTBI.

#### **MATERIALS & METHODS**

Sixteen mTBI patients, ages 24-62 years (mean: 36.5), were recruited from a large urban emergency center and gave informed consent in this HIPAA compliant study. Patients were genotyped and divided into two groups based on the presence (E4+) or absence (E4-) of the APOE E4 allele. Diffusion tensor imaging (3.0 T, b = 1000, 32 directions) was performed within 2 weeks following injury, and tests of memory and verbal fluency were administered 6 months and 1 year following injury. Voxel-wise analysis of fractional anisotropy (FA) images from DTI [p(voxel) <0.05, p(cluster size) <0.01] was performed in each patient to determine the number of brain voxels with abnormally low FA (termed 'low FA volume') as compared to 40 healthy controls, adjusted for age, gender and education (Kim et al., 2011). Five unpaired t-tests were performed to compare cognitive performance (memory and verbal fluency, important mTBI outcomes) and low FA volume between E4+ and E4- patients. Four hierarchical multiple regressions were performed to assess the

interaction effect of APOE4 and volume of abnormally low FA for prediction of memory and verbal fluency at 6 months and 1 year post injury.

## RESULTS

Six of 16 subjects carried at least one E4 allele. Initial t-tests revealed no significant difference between E4+ and E4- patients in low FA volume or cognitive performance. Hierarchical regressions, however, demonstrated significant interactions between E4 status and low FA volume for prediction of worse cognitive outcomes. E4+ interacted significantly with low FA volume to predict worse memory performance 6 months post injury ( $F = 5.516$ ,  $p < .04$ ), and worse verbal fluency 1 year following injury ( $F = 9.980$ ,  $p < .01$ ). Thus, volume of abnormally low FA at time of injury interacted with APOE genotype to predict cognitive performance at sub-acute (6 months) and chronic (1 year) time points.

## CONCLUSION

Although neither genotype nor DTI alone determined long-term prognosis, combined assessment of both factors at time of injury predicted cognitive performance at 6 months and 1 year. These preliminary results indicate that larger studies are warranted to confirm and refine the use of multimodal personalized assessments such as this for the assessment of mTBI outcome. Confirmation of effectiveness could guide management of mTBI patients and provide a much needed biomarker for the conduct of clinical treatment trials.

**KEY WORDS:** Mild traumatic brain injury, diffusion tensor imaging, apolipoprotein E

**O-55**

**10:46 AM - 10:54 AM**

### Could Heading Be Bad for Your Brain? Soccer Players Who Head Excessively Demonstrate Diffusion Tensor Imaging Abnormalities Similar to Traumatic Brain Injury, Which Are Associated with Cognitive Impairment

Kim, N.<sup>1</sup>•Zimmerman, M.<sup>1</sup>•Lipton, R. B.<sup>1</sup>•Stewart, W.<sup>2</sup>•Gulko, E.<sup>1</sup>•Branch, C. A.<sup>1</sup>•Lipton, M. L.<sup>1</sup>

<sup>1</sup>Albert Einstein College of Medicine of Yeshiva University, Bronx, NY, <sup>2</sup>Geisinger Health System, Danville, PA

## PURPOSE

Soccer heading may represent a form of repetitive mild trauma and be associated with long-term cognitive impairment. Because abnormally low white matter (WM) fractional anisotropy (FA) has been associated with cognitive impairment in patients with traumatic brain injury (TBI), we hypothesized that a threshold level ( $\beta$ ) exists for heading exposure above which evidence of white matter injury and cognitive impairment would be detectable.

## MATERIALS & METHODS

The study had IRB approval, included written informed consent, and complied with HIPAA. Thirty-two amateur

soccer players were recruited. Heading exposure was assessed with a standardized questionnaire and diffusion tensor imaging (DTI) (3.0 T; 32 directions;  $b = 1000$ ) was performed. Regions of interest (ROI) where FA was associated with heading exposure were determined using a voxelwise t-test comparing FA between subjects with the most heading exposure (upper quartile;  $> 1,320$  heads/year) and those with lesser exposure (lower 3 quartiles;  $< 1,320$  heads/year). Cognitive performance was assessed using a standardized battery (CogState; Collie et al., 2003; Maruff et al., 2009). Based on our threshold hypothesis we assumed that an S or inverse S shape related FA measures and cognitive performance against heading exposures. Such nonlinear shapes (S, inverse S) were modeled based on inverse logit (IL) functions with three parameters: (1) baseline ( $\alpha_1$ ) (2) association direction and scale factor ( $\alpha_2$ ) (3) departure position ( $\beta$ ) in heading exposure scales from baseline. These parameters were estimated utilizing a simulated annealing algorithm (Kirkpatrick et al., 1983) and gradient-based nonlinear regression algorithm (Bates and Watts, 1988) for each ROI and cognitive domain.

## RESULTS

Five ROIs were identified in temporooccipital WM and one in frontal WM where greater heading was associated with low FA. We found significant effects of  $\beta$  for all ROIs, and two cognitive domains (visual motor function, and verbal learning and memory). Estimates of  $\beta$  were ranged between 1080 and 1440 heads per year. Both cognitive domains showed significant correlations with FA measures (two ROIs in temporooccipital WM and one in frontal WM), mediated by heading exposures.

## CONCLUSION

Greater heading frequency is associated with low FA. Exceeding a threshold for heading frequency (1000-1500) may result in brain abnormalities similar to those seen in TBI, which confer cognitive impairment. If confirmed, these findings suggest that brain abnormalities related to heading are of clinical importance. Defining the appropriate exposure thresholds could facilitate public health interventions to limit heading exposure and its adverse consequences.

**KEY WORDS:** Soccer, DTI, cognition

**O-56**

**10:54 AM - 11:02 AM**

### Mild Traumatic Brain Injury Causes Reduction in Hippocampal Volumes over Time that Correlates with Patient-Reported Cognitive Impairment but Does Not Correlate with Verbal Memory Function

Venugopal, S.<sup>1</sup>•Sampat, M.<sup>1</sup>•LaHue, S.<sup>1</sup>•Cooper, S.<sup>1</sup>•Heffernan, A.<sup>1</sup>•Yue, J.<sup>1</sup>•Lee, H.<sup>1</sup>•Ghajar, J.<sup>2</sup>•Manley, G.<sup>1</sup>•Mukherjee, P.<sup>1</sup>

<sup>1</sup>University of California San Francisco, San Francisco, CA, <sup>2</sup>Brain Trauma Foundation, New York, NY

## PURPOSE

Mild traumatic brain injury (mTBI) is a growing epidemic often leading to significant long-term cognitive impairments, especially memory deficits. We explored volumetric changes in hippocampus and amygdala longitudinally after mTBI and correlated these results with verbal memory function as well as patient-reported cognitive impairments.

## MATERIALS & METHODS

Sixty-two adult patients, aged 17-57 years, with mTBI (GCS 13-15), loss of consciousness and posttraumatic amnesia, were enrolled prospectively and compared to 42 matched controls. The study protocol was approved by our institutional Committee on Human Research. Of the 62 patients, 33 had follow-up imaging at 1 year. Neuropsychological tests, including California Verbal Learning Test 2nd edition (CVLT-II), Center for Epidemiological Studies-Depression scale (CES-D), Cognitive Failure and PTSD questionnaires were administered to mTBI patients at both time points and to the controls once (except PTSD). Volumetric segmentation was performed with FreeSurfer (<http://surfer.nmr.mgh.harvard.edu>) on T1-FSPGR images acquired at 1-mm voxel resolution on a 3 T scanner. The segmentation was reviewed for accuracy by a board-certified neuroradiologist and data were analyzed after correction for intracranial volume (ICV). Pearson's correlation analysis was performed to evaluate association between hippocampal volumes and memory functions, both researcher-administered and patient reported.

## RESULTS

Statistically significant atrophy versus controls was found in both left and right hippocampi at 1 month and at 1 year post mTBI ( $p < 0.05$ ), with a trend towards decreasing volumes between 1 month and 1 year. At 1 year the left amygdala showed statistically significant atrophy ( $p < 0.05$ ), while the right amygdala showed a strong trend towards reduced volume ( $p = 0.06$ ), again trending towards lower amygdalar volumes bilaterally at 1 year compared to 1 month. All CVLT-II subtests, CES-D, and Cognitive Failure scores showed statistically significant decreases in performance at 1 month and at 1 year post mTBI versus controls ( $p < 0.05$ ). However both hippocampal volumes showed significant correlation ( $p < 0.05$ ) to self-filled questionnaires of depression (CES-D), PTSD, and cognitive failure at both 1 month and 1 year time-points with improvement over time. There was no significant correlation between patient reported cognitive failure and performance in CVLT.

## CONCLUSION

To our knowledge this is the first study to demonstrate structural changes in brain morphometry in mTBI. The lack of correlation between reduced hippocampal volumes and poor CVLT performance suggests other areas of brain might additionally contribute to the cognitive difficulties seen in mTBI patients. Correlation of the hippocampal volumes to cognitive impairment and depression in patients suggests that timely

management of such symptomatology could contribute to speedier recovery in mTBI victims.

**KEY WORDS:** Mild TBI, hippocampus, neurocognition

**O-57**

**11:02 AM - 11:10 AM**

## Resting-State Functional MR Imaging Reveals Altered Functional Connectivity in Cortical and Subcortical Networks One Month after Mild Traumatic Brain Injury

Li, Y.-LaHue, S.-Chen, R.-Cooper, S.-Yue, J.-Manley, G.-Mukherjee, P.

University of California San Francisco  
San Francisco, CA

## PURPOSE

It has been reported in several studies using resting-state fMRI (rs fMRI) that traumatic brain injury (TBI) affects functional connectivity. These prior studies have been limited by factors such as small sample size, a wide spectrum of injury severity, and evaluation of patients at variable time points late after injury. In this study, we analyzed rs fMRI in a cohort of 51 mild TBI (mTBI) patients at 1-month post injury and compared them with 45 healthy controls matched by age, gender, handedness and years of education.

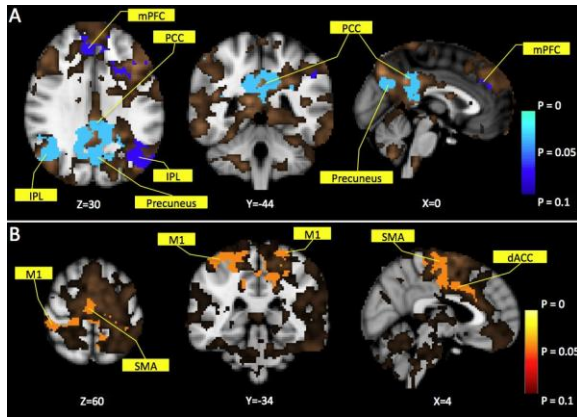
## MATERIALS & METHODS

Fifty-one mTBI patients (mean age  $30 \pm 8$  years, 34 male, 49 right-handed) and 45 healthy controls ( $29 \pm 9$  years, 28 male, 43 right-handed) underwent a 7-minute resting-state fMRI gradient-echo EPI sequence with 2s TR and 28ms TE, on a GE 3 T scanner. Preprocessing included motion correction, brain extraction, band-pass filtering, regression of irrelevant signals, registration onto the MNI152 template, and spatial smoothing using FSL tools. Functional connectivity maps were calculated from 15 seed regions summarized from currently published rs fMRI studies of TBI. Two-sample permutation testing was performed on all connectivity maps using the "randomize" function in FSL to determine statistically significant differences between patient and control groups after correction for multiple voxel-wise comparisons.

## RESULTS

Decreased functional connectivity of mTBI patients versus controls was found bilaterally in the default mode network and the hippocampal network, including the following regions: dorsal anterior cingulate cortex (dACC), posterior cingulate cortex (PCC), precuneus, medial prefrontal cortex (mPFC), inferior parietal lobule (IPL), hippocampus, and pons. The cortical regions of reduced connectivity are illustrated in Figure 1A. Increased functional connectivity of mTBI versus controls was found in a bilateral network encompassing supplementary motor area (SMA), primary motor cortex (M1), and dACC (Figure 1B).





## CONCLUSION

Resting-state fMRI of a relatively large cohort of mTBI patients reveals reduced functional connectivity of multiple networks, most prominently the default mode network and hippocampus; however, connectivity is increased in a motor-SMA network that includes the dACC. Further investigations are underway on correlation of these findings with neurocognitive performance. These initial results demonstrate that resting-state fMRI has promise as an imaging biomarker for clinical outcome after mTBI.

**KEY WORDS:** Traumatic brain injury, concussion, resting-state functional MR imaging

O-58

11:10 AM - 11:18 AM

## Characterization of Thalamocortical Association Using Resting-State Functional MR Imaging in Mild Traumatic Brain Injury

Zhou, Y.·Lui, Y. W.·Reaume, J.·Grossman, R. I.·Ge, Y.

New York University Langone Medical Center  
New York, NY

## PURPOSE

Previously using resting-state (rs) fMRI, we documented increased thalamocortical connectivity in patients with mild traumatic brain injury (mTBI). In order to further characterize thalamic injury in mTBI, in this study, we examined the amplitude of low-frequency fluctuations (ALFF) which is believed to reflect spontaneous brain activity intensity and temporal thalamocortical coherence between mTBI patients and controls.

## MATERIALS & METHODS

Thirty-three patients with clinically-defined mTBI were recruited in this study with a mean interval between MRI and trauma of 22 days (3~53 days). For comparison, 33 age-matched healthy controls also were recruited. All patients have various posttraumatic symptoms. MR imaging was performed at Siemens 3 T MR with a standard rs fMRI sequence (TR/TE = 2 sec/30 msec, flip angle = 75°, resolution = 1.72x1.72x6 mm<sup>3</sup>, 153 time points). In addition, conventional T2-weighted imaging and a 3D high-resolution T1-MPRAGE also were obtained. All rs fMRI datasets were realigned and coregistered to the 3D T1 image and then

normalized to the MNI template. The temporal coherence was computed based on the averaged time courses of the voxels between left and right thalamus (thalamo-thalamo) as well as between thalamus and each of 44 cortical Brodmann Areas (BAs) (thalamo-cortical). The fractional ALFF (fALFF) was computed using the REST software (www.restfmri.net).

## RESULTS

Consistent with previous data, we also found significantly increased thalamocortical functional connectivity in patients ( $P < 0.001$ ); as well as significantly increased temporal coherence between thalamus and cortex predominantly at low frequency band (0.025-0.05Hz) ( $P < 0.05$ ) with peak coherence value of 0.45 in controls and of 0.53 in patients (see Figures 1a and 1b). There was a positive correlation between low-frequency thalamocortical coherence and postconcussive syndrome score in MTBI patients (Spearman correlation  $r = 0.4$ ,  $P = 0.029$ ). We also found significantly reduced fALFF in the thalamus and its segments for sensory, temporal and frontal projections in patients ( $P < 0.05$ ), while in cortex there was no significant fALFF change between patients and controls.

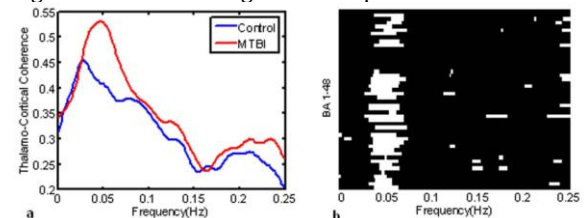


Figure 1. Significantly increased thalamo-cortical coherence ( $P < 0.05$ ) in MTBI patients compared to controls between average of all cortical Brodmann areas (BA 1-48) and thalamus (a) and between each of cortical Brodmann areas and thalamus (b, with white color indicates significant difference between two groups).

## CONCLUSION

We have shown reduced fALFF in the thalamus reflecting decreased spontaneous thalamic neuronal activity, believed to be secondary to thalamic injury after MTBI. This finding in conjunction with increased temporal thalamocortical coherence suggests that decreased regional activity in the thalamus may paradoxically be associated with an increase in thalamocortical synchrony. Alternatively there may be upregulation of cortical activity (rather than thalamic activity) which results in the observed increase in thalamocortical synchrony. This increased synchrony may influence the degree or severity of the posttraumatic symptoms in patients.

**Acknowledgement:** This work was supported by NIH grants numbers NS039135 and NS039135-08S1.

**KEY WORDS:** Traumatic brain injury, resting-state functional MR imaging, thalamo-cortical

O-59

11:18 AM - 11:26 AM

## Correlation of Imaging and ex vivo Features of Traumatic Brain Injury in a Trial of Pharmacologic Neurotrauma Prophylaxis

Larvie, M.·Whalen, M.

Massachusetts General Hospital  
Boston, MA

**PURPOSE**

Traumatic brain injury (TBI) is a major public health problem and is particularly significant in high-risk activities, such as certain contact sports and military action. The mechanisms of TBI vary depending upon the type and severity of trauma, and may include both primary injury that is a direct result of the impact as well as secondary injuries that may be related to intracranial hypertension, ischemia, cell death, and damage to the blood-brain barrier (BBB). In particular, loss of BBB integrity is associated with increased edema and subsequent brain injury, including seizure disorder. Consequently, we have investigated several pharmacologic agents in search of a method to decrease secondary injury, including several polymers that may function as putative membrane resealing agents that may help to restore BBB integrity.

**MATERIALS & METHODS**

We employed a model of TBI using a controlled cortical impact with adult mice. The sequelae of TBI were assessed with multiple animals and compared with controls. Multiple assays were performed, including MRI with T2 and DWI sequences using a small bore 9.4 T scanner, in vivo propidium iodide staining, ex vivo measurement of wet-dry brain weight, and BBB leakage assay using Evans blue extravasation. Motor and cognitive functions were tested using wire grip and Morris water maze tests, respectively. Controls included sham TBI and animals treated with control vehicle (PBS) in alternative to a pharmacologic agent.

**RESULTS**

One of the pharmacologic agents tested, a vinylpyrrolidone-vinyl acetate copolymer, was found to significantly reduce brain edema and subsequent lesion size. Lesion volume was assessed by MRI, using both T2 and ADC signal abnormality. Volumes derived from the T2 signal abnormality demonstrated a significant difference in lesion size, with the lesions in the treated animals approximately 38% ( $p < 0.05$ ) smaller than in the untreated animals. Ex vivo studies showed commensurate differences in brain edema, which was reduced approximately 45% ( $p < 0.005$ ) in treated animals. Blood-brain barrier leakage was decreased by 94% ( $p < 0.005$ ). Additionally, cognitive and motor functions were greater in treated animals compared to untreated.

**CONCLUSION**

We have identified an agent that results in improved outcomes in TBI when administered within 1 hour following injury, which represents a reasonable therapeutic window for application in a variety of clinical circumstances. This agent is a copolymer that acts to reseal cell membranes, which may be related to its pharmacologic mechanism of action. Brain lesion volumes as measured by MR imaging correlate with lesion size and characteristics as assessed by ex vivo analyses. These preclinical studies establish a paradigm for translation to human clinical trials, in which drug dose-response studies may be performed with noninvasive MR imaging.

**KEY WORDS:** Traumatic brain injury, animal model, prophylaxis

**O-60**

**11:26 AM - 11:34 AM**

### **Neuroimaging of Traumatic Brain Injury in the Military at the National Intrepid Center of Excellence**

Riedy, G.·Wolfowitz, R.·Harper, J.·Melford, C.·Oakes, T. R.  
National Intrepid Center of Excellence  
Bethesda, MD

**PURPOSE**

To describe the initial neuroradiology findings in a cohort of military members with traumatic brain injury (TBI) seen at the National Intrepid Center of Excellence (NICOE). The newly opened NICOE is dedicated to military personnel experiencing symptoms of TBI and psychological health conditions. The NICOE neuroimaging assessment involves an integrated 3.0 T MRI examination that incorporates high-resolution anatomical imaging, functional MRI, diffusion tensor imaging, perfusion, and MR spectroscopy. We present the initial findings from the structural imaging portion of the exam for 113 patients.

**MATERIALS & METHODS**

The study subjects were recruited from patients referred to the NICOE. Among the 113 subjects (94.7% male), the mean age was 33.0 years. The majority of subjects were deployed at least twice. Eighty-seven participants (77.0%) reported injuries with loss of consciousness, 103 participants (91.2%) reported blast exposure, and 94 participants (83.2%) reported multiple injuries or blast exposures. Of all subjects, 27.4% reported two or more blasts or injuries within 1 month. The median time since most recent injury was 773 days. Commonly reported symptoms included headaches, dizziness, irritability, and memory problems. Of the 113 subjects, 91.2% had mild TBI, 7.1% had moderate TBI, and 1.7% had severe TBI. MR imaging was performed using a 3.0 T GE 750 system with an integrated protocol that examined various aspects of TBI. The structural imaging portion included 1 mm isotropic voxels utilizing 3D volume sequences for T1, T2, and T2 FLAIR. Microhemorrhage was evaluated with routine GRE imaging and a customized susceptibility-weighted imaging sequence. In addition, pre and postcontrast T1 and T2 FLAIR images also were acquired.

**RESULTS**

One hundred thirteen patients were scanned over 8 months, using this TBI protocol. Of the patients referred to neuroimaging, 80.7% qualified for and received the integrated TBI protocol. Two subjects received truncated scans due to claustrophobia; three patients were excluded because of shrapnel in critical locations. Neuroradiologic assessment of the structural imaging demonstrated likely or possible TBI findings in 66.4% of the subjects ( $n = 75$ ). Of those with positive findings, 37.3% had received prior MRIs that were read as unremarkable. The most common finding was the

presence of T2 hyperintensities in the white matter (60.2%). Microhemorrhage was noted in 6.2% and encephalomalacia was noted in 8.0%. Postcontrast T2 enhancement was seen in 18.6%, with surface veins being the most likely source. Other findings include: Cavum septum pellucidum (21.2%), dilated perivascular spaces (27.4%), pituitary abnormalities (8.0%), and mastoid fluid (16.8%).

# CONCLUSION

Nearly all of the subjects referred for imaging at the NICOE had at least one blast exposure. Microhemorrhage was seen in a surprisingly small percentage of subjects. Of the patients with positive readings, 37.3% had prior MRIs without TBI findings. Structural imaging using 1 mm isotropic voxels may be more sensitive than routine imaging for the identification of intracranial abnormalities, which may be associated with brain injury. The presence of T2 hyperintensities within the white matter was the most common finding among the subjects. While these lesions are nonspecific, their presence in characteristic locations in this young age group could be representative of traumatic brain injury.

**KEY WORDS:** Traumatic brain injury

**O-61**

**11:34 AM - 11:42 AM**

## Traumatic Extravasation on Arterial Imaging Predicts Hematoma Expansion in Traumatic Head Injuries

Letourneau-Guillon, L.·Huynh, T.·Jakobovic, R.·Milwid, R.·Aviv, R. I.

Sunnybrook Health Sciences Centre  
Toronto, ON, CANADA

# PURPOSE

Several studies have suggested that intrahematoma contrast extravasation on computed tomography angiography (CTA) predicts hematoma expansion, poor outcome, and mortality in spontaneous intracerebral hemorrhages (ICH). The purpose of this study was to determine the predictive value of extravasation on CTA for hematoma expansion, need for surgical drainage and in-hospital mortality in traumatic head injuries.

# MATERIALS & METHODS

We retrospectively reviewed trauma patients presenting with at least one intracranial hematoma > 1 ml studied with CTA within 24 hours of admission. Intracerebral, subdural (SDH) and epidural (EDH) hematomas were included. Clinical, paraclinical and imaging data were reviewed. Two readers blinded to outcomes evaluated the CTA source images for the presence of extravasation within the hematomas. Volumetric assessment of the hematomas on both the initial and follow-up imaging was performed using a semiautomated software. Hematoma expansion was defined as growth of > 6ml or > 33%. Univariate analysis was performed with Fisher exact test and Wilcoxon rank sum test.

# RESULTS

Sixty patients admitted between July 2007 and August 2011 met the inclusion criteria. A total of 138 hemorrhagic lesions [83 (60%) intracerebral hematomas, 44 (32%) subdural hematomas, 11 (8%) epidural hematomas] were evaluated. Extravasation on CTA was present in 41 (30%) hematomas. The interobserver agreement for the presence of at least one focus of contrast extravasation was high ( $k = 0.89$ ; 95% CI 0.79 - 0.97). Ninety-eight (71%) lesions had imaging follow up. Lack of follow up was due to interval surgical drainage [ $n = 14$  (10%)] or mortality prior to follow up [ $n = 26$  (19%)]. Presence of contrast extravasation in intra and extra axial hemorrhage was associated with larger median final hematoma size (11.2 ml vs 2.2 ml,  $p < .001$ ), median absolute expansion (respectively 1.7 ml vs 0.2 ml,  $p < .01$ ), median percentage expansion (56.0% vs 12.3%,  $p = 0.02$ ), expansion of at least 6 ml (OR 7.7; 95% CI 2.3-25.9,  $p < .01$ ), expansion greater than 33% (OR 2.8; 95% CI 1.1-7.5,  $p = 0.04$ ), need for surgical drainage (OR 5.2; 95% CI 1.6-16.6,  $p < .01$ ) and trend towards higher in-hospital mortality (OR 1.8; 95% CI 0.8-3.7,  $p = 0.17$ ). Among the different subtypes of hematomas, contrast extravasation was associated with significantly larger median final hematoma volume for ICHs (6.7 vs 1.8 ml,  $p = 0.01$ ) and SDHs (31.1 vs 3.8 ml,  $p = 0.02$ ), median absolute expansion for ICHs (2.2 vs 0.2 ml,  $p < .001$ ), median percentage hematoma expansion for ICHs (328% vs 34%,  $p < .001$ ), expansion of at least 6 ml for ICHs (OR 8.3; 95% CI 1.6-41.3,  $p = 0.01$ ) and SDHs (OR 10.0; 95% CI 1.3-74.5,  $p = 0.03$ ), expansion greater than 33% for ICHs (OR 13.0; 95% CI 1.6-107.4,  $p = 0.005$ ), need for surgical drainage for ICHs (OR 10.9; 95% CI 1.1-112.0,  $p = 0.04$ ), and higher in-hospital mortality for SDHs (OR 5.5; 95% CI 1.4-22.2,  $p = 0.02$ ). Given the smaller sample size for epidural hematomas, no significant trend could be identified for this hematoma subtype.

# CONCLUSION

Contrast extravasation identified on admission CTA in the setting of traumatic head injuries provides prognostic information regarding hematoma expansion, need for surgical drainage and in-hospital mortality.

**KEY WORDS:** CT angiography, traumatic brain injury, hematoma

**O-62**

**11:42 AM - 11:50 AM**

## Practical Value of Canadian CT Head Rule in a Single Institution: A Ground Reality

Arab, A. F.<sup>1,2</sup>·Ahmed, M. E.<sup>1</sup>·Khankan, A. A.<sup>1</sup>·Hussein, M. A.<sup>3</sup>

<sup>1</sup>National Guard Hospital, Riyadh, SAUDI ARABIA, <sup>2</sup>King Saud Bin Abdulaziz University for Health Sciences, Riyadh, SAUDI ARABIA, <sup>3</sup>King Abdullah International Medical Research Center, Riyadh, SAUDI ARABIA

# PURPOSE

The controversy of performing a cranial computed tomography (CT) imaging for patients with minor head injury was supposed to be resolved by the foundation of



the Canadian CT Head Rule (CCHR) that was published 11 years ago. However, various reports in the current literature have challenged their practical value. The purpose of our study is to evaluate the compliance and effectiveness of using the CCHR in a busy emergency department in Saudi Arabia's main trauma center.

#### MATERIALS & METHODS

A cross-sectional retrospective study of 386 patients who presented to the emergency department from July 2010 to June 2011 with a mild head injury, was conducted following the institutional review board (IRB) approval. The patients were selected from the emergency department registry out of 1,200 patients with head trauma of the same period by systematic randomization. The CCHR was reapplied on the patients' charts. A survey was generated to evaluate emergency physicians' level of education and application of the CCHR and to evaluate their ability to determine the necessity of CT scans by giving scenarios of patients presenting to the emergency department with mild head injury. Two experienced neuroradiologists reviewed the CT scans of these patients to evaluate the significance of the injury according to the CCHR. The main outcome measure was the need for neurosurgical intervention and clinically important head injury on CT

#### RESULTS

The level of education regarding the CCHR was found to be optimal among emergency physicians using case-based scenario survey. However, 77.98% of the cranial CT scans conducted were unjustified suggesting noncompliance with CCHR by 36.54%. Patients who had abnormal cranial CT scans findings constituted 2.65% of the unjustified CT scans and 9.4% of the justified CT scans. Abnormalities that were found in the eight unjustified CT scans were not significant and no follow up scans were performed. Whereas abnormalities found on justified CT scans included a patient with subarachnoid hemorrhage and skull fracture that had a stable course on follow-up CT and a patient with extradural hemorrhage, subdural hemorrhage, and skull fracture which improved on follow-up CT.

#### CONCLUSION

The CCHR has a poor compliance potential in busy emergency departments of trauma centers and may not reduce the incidence of unjustified cranial CT scans. Even when the guidelines are applied, they may not prevent any unjustified CT scans.

**KEY WORDS:** CCHR, mild head injury, CT

O-63

11:50 AM - 11:58 AM

#### Combining Clinical Neuroimaging and Real-World Mechanical Impact Data to Investigate Motor Vehicle Crash-Related Subdural Hematoma

Urban, J.<sup>1,2</sup>·Whitlow, C. T.<sup>1,3</sup>·Maldjian, J. A.<sup>1</sup>·Powers, A. K.<sup>1</sup>·Stitzel, J. D.<sup>1,2</sup>

<sup>1</sup>Wake Forest University School of Medicine, Winston-Salem, NC, <sup>2</sup>Virginia Tech - Wake Forest University Center for Injury Biomechanics, Winston-Salem, NC, <sup>3</sup>Translational Science Institute, Winston-Salem, NC

#### PURPOSE

Approximately 1.7 million people sustain a traumatic brain injury (TBI) each year, with motor vehicle crash (MVC) representing the leading cause for hospitalization. Subdural hematoma (SDH) is a common and serious consequence of MVC-related TBI that is associated with high mortality and morbidity rates. Little is known, however, about the relationship between specific crash parameters and resulting intracranial trauma, particularly as a function of age. In this study, SDH volume and midline-shift were analyzed in order to better understand occupant injury, with the hypothesis that these traumatic neuroimaging findings would correlate with specific crash parameters and age.

#### MATERIALS & METHODS

Head computed tomography (CT) demonstrating SDH (n =57) were selected from the Crash Injury Research Engineering Network (CIREN) database. Semiautomated methods were used to quantify intracranial volume. Acute SDHs were segmented manually across serial axial CT images, providing total SDH injury volume that was expressed as a percentage of total intracranial volume for the purposes of normalization (Figure 1). Midline-shift was measured at the level of the Foramen of Monroe from the septum pellucidum to the midsagittal anterior-posterior line. The relationship between SDH volume, crash parameters and occupant age then were investigated using the Pearson product-moment correlation coefficient.



Figure 1. Example segmentation and three-dimensional reconstruction of a subdural hematoma from known crash characteristics and occupant parameters

## RESULTS

As expected, midline shift was positively correlated with percent subdural volume ( $r^2 = 0.3141$ ,  $p > 0.001$ ). Of all subdural hematoma patients who were drivers in near-side crashes, injury severity score was positively correlated with maximum crush of the vehicle ( $r^2 = 0.3771$ ,  $p = 0.0256$ ). For all patients with midline shift  $> 0$  who were drivers in frontal crashes, there was a trend for increasing midline-shift with age ( $r^2 = 0.6008$ ,  $p = 0.0702$ ). There was also a trend for positive correlation between percent subdural hematoma volume and  $\Delta V$  (change in velocity of the vehicle during the crash) for frontal crashes ( $r^2 = 0.1912$ ,  $p = 0.0792$ ).

## CONCLUSION

This study is the first volumetric analysis of real-world brain injuries using clinical CT and known mechanical impact data. Results demonstrate an increase in subdural volume by crash type that is correlated with age. That older patients have a greater volume of SDH suggests the possibility of traumatic rupture of bridging veins in the setting of age-related atrophy as a potential etiology for this finding. These data highlight the utility of combining clinical neuroimaging with demographics and mechanical crash data for investigating mechanisms of TBI. Such data may be used in the future to design safer cars and to inform diagnosis and treatment algorithms for MVC-related head trauma.

**KEY WORDS:** Subdural hematoma, motor vehicle crash, aging

O-063a

11:58 AM - 12:06 PM

### Differentiating Pseudo-Progression from True Tumor Progression in High-Grade Gliomas Using Morphologic Imaging Features and Radiation Dosimetric Analysis of Morphologic Features

Agarwal, A.<sup>1</sup>•Kumar, S.<sup>1</sup>•Narang, J.<sup>1</sup>•Schultz, L.<sup>1</sup>•Flanders, A.<sup>2</sup>•Mikkelsen, T.<sup>1</sup>•Jain, R.<sup>1</sup>

<sup>1</sup>Henry Ford Health System, Detroit, MI, <sup>2</sup>Thomas Jefferson University Hospital, Philadelphia, PA

## PURPOSE

Pseudo progression (PsP) is a term used to describe paradoxical increase of contrast enhancement within 12 weeks of chemoradiation therapy in gliomas attributable to treatment effects rather than true tumor progression (TTP). The purpose of this study was to evaluate the utility of morphologic imaging features and dosimetric analysis of MRI changes in differentiating PsP from TTP.

## MATERIALS & METHODS

Serial MRI examinations of 163 patients treated for a high-grade glioma at the Henry Ford Hospital between December 2008 and March 2011 were reviewed. Forty-six patients (30%; mean age 56.7 years, 30 females and 16 males) showed a recurrent or progressive-enhancing lesion (RPEL) within 12 weeks of radiotherapy. We used an in-house modified scoring system based on 17 different morphologic features (modified VASARI features) to assess the MRI studies. The size of the

enhancing component of the lesion was compared with the baseline study and the percentage increase in size was determined. The MRI changes were defined as recurrent volume ( $V_{rec}$ ) and registered with pretreatment CT dataset and the actual dose received by the  $V_{rec}$  during treatment was calculated using dose-volume histograms. The  $V_{rec}$  pattern was divided into: 1) "central," in which more than 95% of the  $V_{rec}$  was in the original high dose field (D95 or 95% isodose line); 2) "in-field," in which 80% to 95% of  $V_{rec}$  was inside the D95; 3) "marginal," in which 20 and 80% of  $V_{rec}$  was inside the D95; 4) "outside," in which less than 20% of  $V_{rec}$  was inside the D95. Comparisons among the two groups were done using Fisher's exact test for the categorical features and Kruskal-Wallis for the ordinal features.

## RESULTS

Out of the 17 different morphologic MRI features assessed to differentiate between PsP and TTP, the size of the T2-FLAIR signal abnormality was larger in the TTP group in comparison to PsP group ( $p = 0.002$ ). The percentage increase in size of the enhancing component from the base line study was also larger in the TTP group in comparison to the PsP group ( $p = 0.011$ ). The margins of the RPEL were poorly defined in PsP group (100%) in comparison to the TTP group (72%) ( $p = 0.088$ ). The enhancing lesion was seen to cross the midline in 28% of patients in the TTP group in comparison to none in the PsP group ( $p = 0.088$ ). The other morphologic MR features evaluated had no predictive value in differentiating between the PsP and TTP groups. Analysis of radiation dose distribution showed that MRI changes were centrally located in PsP and TTP groups with no significant difference.

## CONCLUSION

Morphologic imaging features have a very limited role in differentiating between PsP and TTP. Larger size of the recurrent enhancing lesion is a useful MRI feature favoring TTP rather than PsP. Lesions with poorly defined margins and crossing midline are more likely to represent TTP. There was no correlation between the pattern of MRI changes and radiation dose distribution between PsP and TTP. Hence, functional MR imaging may provide additional physiologic information needed in differentiating between PsP and TTP.

**KEY WORDS:** Glioma, pseudoprogession, tumor progression

## Monday Morning

10:30 AM - 12:00 PM

Murray Hill

(8e) Anatomy & Applications of  
Advanced Imaging

0-64

10:30 AM - 10:38 AM

### Asymmetry of the Hippocampus at 3 T: From the Dallas Heart Study

Lucarelli, R. T. King, K. S.

University of Texas Southwestern Medical School  
Dallas, TX

#### PURPOSE

A basic detection algorithm in neuroradiology is the use of asymmetry to identify abnormalities. This principle is essential to the lateralization of the seizure focus in intractable temporal lobe epilepsy. The imaging markers of mesial temporal sclerosis consist of hippocampal volume asymmetry, T2 prolongation, and loss of internal architecture. Asymmetry of hippocampal volumes also has been suggested to be more accurate than total volume in predicting cognitive impairment. Initial investigators asserted that even minor asymmetry in the hippocampus is highly specific for disease. It was soon recognized, however, that to understand the specificity and sensitivity of asymmetry for detection of disease it was necessary to establish the range of values in the general population. Previous meta-analysis of multiple smaller studies demonstrated right left asymmetry of the hippocampus in the general population, but was based primarily on studies using user-guided segmentation. Recently, it has been shown that there is a bias in these user-directed segmentations of right versus left structures. New programs, such as FSL and Freesurfer, have allowed automatic segmentation of the hippocampus and other deep brain nuclei. We report here an evaluation of a large community-based cohort, with right left hippocampal asymmetry data along with an evaluation of how this varies across the adult lifespan.

#### MATERIALS & METHODS

Whole-brain 3D-MPRAGE MR images were obtained at 3 T on 1545 Dallas Heart Study participants including 878 females and 667 males aged 19-85 years. Quantification of MR images was achieved with FMIRB software library (FSL) and hippocampal volume data were collected using FSLstats routine. Relative hippocampal difference was calculated using total hippocampal volume in each subject. Statistical significance was determined with two-tailed t-tests performed with SAS version 9.2.

#### RESULTS

Right relative hippocampal volume is greater than left hippocampal volume (mean 4.87%,  $p = 0.001$ ) in the Dallas Heart Study population. Men have slightly more asymmetry (5.38%,  $p = 0.001$ ) than females (4.53%,  $p = 0.001$ ). There is significant variability across the population in the degree of asymmetry, with most participants having less than 10% asymmetry, regardless of age. However there is an increase in the relative difference of right vs left hippocampal volumes associated with increasing age (Table 1).

Table 1 - Absolute Percent Difference Between Right and Left Hippocampi

Age	1st Quartile	Median	3rd Quartile	90%ile
20-29	1.81%	2.65%	5.46%	7.93%
30-39	1.48%	3.15%	5.36%	8.90%
40-49	1.70%	3.78%	6.56%	12.43%
50-59	1.57%	3.61%	6.75%	11.54%
60-69	1.56%	3.76%	6.80%	10.69%
70-79	3.06%	4.42%	7.24%	11.45%

#### CONCLUSION

Here we provide normal ranges of hippocampal asymmetry in a large community-based cohort with a wide range of ages and with diverse ethnic representation. We further demonstrate that these values vary with age and sex. These data will be useful in the neuroanatomical analysis of the hippocampus as it relates to a wide range of pathology.

**KEY WORDS:** Asymmetry, hippocampus, normal

0-65

10:38 AM - 10:46 AM

### Hippocampal Asymmetry in Patients with and without History of Seizure

Wycliffe, N. D. Volokhina, Y. Oyoyo, U. Kido, D.

Loma Linda University Medical Center  
Loma Linda, CA

#### PURPOSE

The diagnosis of subtle hippocampal sclerosis is difficult when there is normal asymmetry of the hippocampus. The purpose of this retrospective study was to see if the hippocampal asymmetry could be correlated to EEG abnormality in patients with history of seizure and to determine the incidence of asymmetry in patients with and without history of seizure.

#### MATERIALS & METHODS

This retrospective study is IRB and HIPPA compliant. High-resolution T2-weighted coronal images of the temporal lobes obtained for evaluation of seizure in 55 patients in 3 T Siemens Trio Tim MRI scanners were reviewed retrospectively. Presence or absences of EEG abnormality in the temporal lobes was noted in patients with seizure from chart review. MR imaging of a second group of 100 patients without history of seizure also was reviewed. For these patients 1 mm thick coronal images were reformatted in standard coronal viewing



plane for hippocampus from T2-weighted 3D acquired source images obtained at 3 T Siemens Trio Tim MRI scanners, using the Aquarius NET (AqNET) software. The hippocampi of the patients from both groups were examined for the size, shape and any abnormal T2 lengthening. For data acquisition, the hippocampus size were designated in a scale of 5, 1 being flat, 3 being oval and 5 being round, 2 being intermediate between 1 and 3 and 4 being intermediate between 3 and 5.

## RESULTS

Out of 55 cases of patients with history of seizure, five had abnormal EEG in the temporal lobes. Out of these five patients, three had symmetrical hippocampi and two had asymmetry of the hippocampus. One patient with symmetric hippocampus had T2 lengthening in both hippocampi consistent with hippocampal sclerosis. Of the remaining 50 patients in the seizure group with negative EEG, 22(44%) had symmetrical hippocampi and 28 (56%) had asymmetric hippocampi. The 100 nonseizure group of patients was divided equally with 50 patients (50%) showing symmetric hippocampi and 50 (50%) showing asymmetric hippocampi. The shape and area of the hippocampi were independent of the age and sex of patients in both groups. Majority of the symmetric hippocampi were of shape 2, intermediate between flat and oval, in both seizure (24%) and nonseizure (32%) groups. Symmetric oval shape was seen in 10% in the seizure patients and 12% in nonseizure patients. Among the patients with asymmetrical hippocampi, there was more frequent oval and round shape noted in the left side compared to the right side. The distribution patterns of asymmetry between the right and the left hippocampi did not correlate with history of seizure.

## CONCLUSION

Asymmetry of the hippocampus between the right and the left side is a common finding in both seizure and nonseizure patients and does not in itself represent hippocampal sclerosis.

**KEY WORDS:** Hippocampus, asymmetry, non-seizure

**O-66** **10:46 AM - 10:54 AM**

## Semi-Automated Landmark Identification Method Used to Quantify Age-Related Shape Change of Brain Structures

Urban, J. E.<sup>1</sup>·Maldjian, J. A.<sup>2</sup>·Whitlow, C. T.<sup>2,3</sup>·Stitzel, J. D.<sup>1</sup>

<sup>1</sup>Virginia Tech - Wake Forest University Center for Injury Biomechanics, Winston-Salem, NC, <sup>2</sup>Wake Forest University School of Medicine, Winston-Salem, NC, <sup>3</sup>Translational Science Institute, Winston-Salem, NC

## PURPOSE

Various structures within the brain are associated with aging. The ventricles are known to enlarge with age as the cerebrospinal fluid (CSF) increases. The hippocampus volume loss has been correlated closely with the development of Alzheimer disease. The objective of this study is to describe the size and shape changes of the adult ventricles and hippocampus using

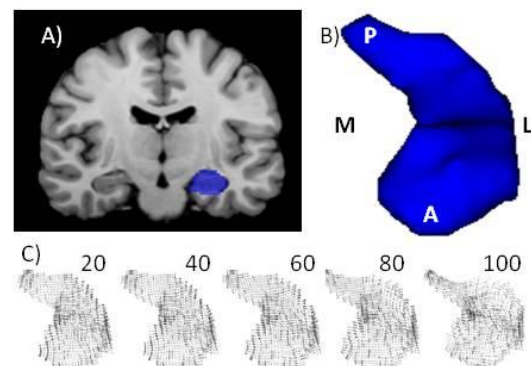
a semiautomated method for acquiring landmark data followed by a geometric morphometric analysis technique. The methodology developed is a multiple-step processing of magnetic resonance images (MRI) in a brain atlas.

## MATERIALS & METHODS

The MRI data were collected for patients ranging from ages 20 to 96 years old and grouped by decade to create group-specific templates. Each template was normalized to an atlas in Montreal Neurological Institute (MNI) space using a high-dimensional nonlinear transformation procedure. Preexisting label maps in MNI space and a manually segmented label map of the lateral ventricles were applied to segment structures of the brain and establish homologous landmarks surrounding the axial surface of the structures. The homologous landmarks were transformed back to patient space for output of each landmark as point cloud data. A Generalized Procrustes Analysis (GPA) was completed for the homologous landmarks to determine the size and shape differences of the ventricles and hippocampus. The coordinate locations were regressed onto age, which generated a model predicting the landmark location for each age. Permutation testing of  $1 \times 10^5$  random trials was used to assess the model significance.

## RESULTS

Complete landmark datasets were collected for all subjects. Significant differences in anterior/posterior (AP), medial/lateral (ML), and cranial/caudal (CC) directions were observed with age for the hippocampus ( $P < 0.0001$ ). A significant nonlinear decrease in the posterior CC measurement until age 80 was followed by an increase until age 100 ( $P < 0.0001$ ). Hippocampus landmarks remained relatively static until age 60 where a dynamic change was observed along the hippocampal tail. A significant nonlinear increase was observed in all directions along the lateral ventricle, exponentially increasing after age 40 ( $P < 0.0001$ ). All findings are in parallel with clinical findings associated with aging.



A. Two-dimensional segmentation of the hippocampus; B. Three-dimensional reconstruction of the hippocampus (front view); C. Quadratic model results for size and shape change of the hippocampus from age 20 to 100.

## CONCLUSION

This novel method of semiautomated landmark identification will allow for the creation of mapping functions to describe age-associated size and shape changes of the brain with regard to structure. This work may lead to a better understanding of how brain morphology is correlated to biomechanics and functional outcomes of traumatic brain injury.

**KEY WORDS:** Aging, image registration, morphometric analysis

O-67

10:54 AM - 11:02 AM

### Imaging Paleocortical Lamination Patterns of the Adult Human Olfactory Bulb and Tract: Comparison of Standard- and High-Resolution 3 T MR Imaging and MR Microscopy at 9.4 T

Burmeister, H. P.<sup>1</sup>Bitter, T.<sup>1</sup>Heiler, P. M.<sup>2</sup>Irintchev, A.<sup>1</sup>Froeber, R.<sup>1</sup>Dietzel, M.<sup>1</sup>Baltzer, P. A. T.<sup>1</sup>Reichenbach, J. R.<sup>1</sup>Schad, L. R.<sup>2</sup>Gudziol, H.<sup>1</sup>Guntinas-Lichius, O.<sup>1</sup>Kaiser, W. A.<sup>1</sup>

<sup>1</sup>University Hospital - Friedrich-Schiller-University Jena, Jena, GERMANY, <sup>2</sup>Heidelberg University, Mannheim, GERMANY

#### PURPOSE

Neurologic and smelling disorders (e.g., Alzheimer disease, sinonasal disease) negatively affect the microstructural integrity of the olfactory bulb's (OB) paleocortical layers. Recovery processes depend on active restoration of this microstructural integrity enabled by neurogenesis in the OB. The aim of this study was to evaluate lamination patterns of the OB and adjacent tract (OT) using high resolution MRI at 3 T as well as MR microscopy at 9.4 T in comparison with histologic sections.

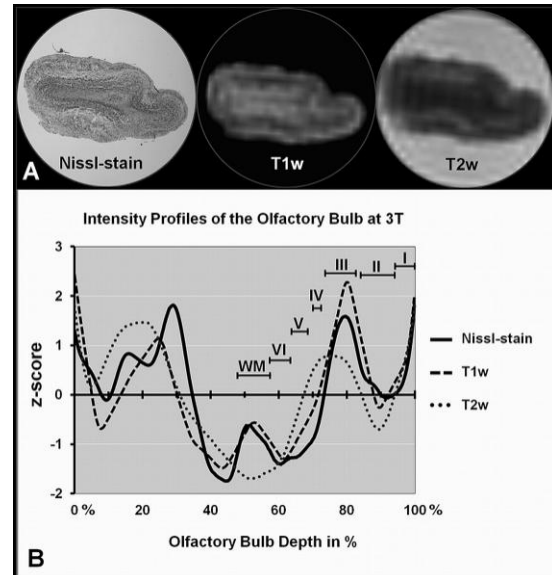
#### MATERIALS & METHODS

Twenty-four human OBs were imaged in vitro using standard (2 mm slice thickness) and high-resolution (0.2 mm slice thickness) T1-weighted and T2-weighted MR imaging at 3 T. Based on signal intensity differences, the number of OB layers and the OB lamination patterns were assessed by two observers in consensus. Results were compared using Wilcoxon test. Signal intensity profiles were compared to reference Nissl stained histologic sections and imaging results of MR microscopy. OT lamination patterns were assessed and different configurations of cross-sectional areas were compared to macroscopic results and OB/OT lamination patterns.

#### RESULTS

Standard resolution at 3 T identified three layers in 8.3%, two layers in 83.3%, and one layer in 8.3%. High-resolution at 3 T (4 layers in 91.7%, 3 layers in 8.3%) significantly performed better ( $P < 0.001$ ). Signal intensity profile analysis at 3 T (figure) and 9.4 T (yielding up to six different signal intensities) correlated with histologic sections and enabled quantitative evaluation of OB lamination patterns. 3 T MRI of the OT revealed two separate signal intensities in T2-weighted in 73%, a hyperintense core and a

hypointense sheath, and the number of OT signal intensities positively correlated ( $\rho = 0.541$ ,  $P = 0.006$ ) with the increasing complexity of the OT's cross-sectional area configurations. Additionally, cross-sectional area configurations correlated with macroscopic results ( $\rho = 0.558$ ,  $P = 0.002$ ) and OB lamination patterns ( $\rho = 0.446$ ,  $P = 0.022$ ).



#### CONCLUSION

Signal intensity profile analysis is suitable to differentiate OB and OT paleocortical layers. Therefore, signal intensity profile analysis may be used as a valuable tool to assess OB recovery processes in neurodegenerative/neuropsychiatric and smelling disorders or to estimate general regeneration abilities of the brain (as pars pro toto) at the level of group comparisons in future studies.

**KEY WORDS:** Olfactory bulb, MR microscopy, neurogenesis

O-68

11:02 AM - 11:10 AM

### Deformable Anatomical Templates Validation Using Functional MR Imaging of the Motor Hand Region

Hamilton, J. D.<sup>1</sup>Kumar, V. A.<sup>1</sup>Hayman, L.<sup>2</sup>Prabhu, S. S.<sup>1</sup>Hou, P.<sup>1</sup>Jackson, E. F.<sup>1</sup>Groneman, M.<sup>2</sup>Pagani, J.<sup>2</sup>Vabulas, M.<sup>2</sup>Kumar, A. J.<sup>1</sup>

<sup>1</sup>M.D. Anderson Cancer Center, Houston, TX, <sup>2</sup>Anatom-e Information Systems, Ltd., Houston, TX

#### PURPOSE

This study evaluated the concordance between the Deformable Anatomical Template (DAT)-identified origin of motor hand fibers and localization of the motor cortex of the hand (MCH) by functional magnetic resonance imaging (fMRI).

#### MATERIALS & METHODS

Preoperative fMRI during hand motor tasks was performed on 36 hemispheres in 26 patients with gliomas in or near eloquent areas, with a range of

histologies and patient ages. The DAT (Anatom-e Workstation, Houston, TX) is a 3D reference template of a normal volunteer's brain with 1,185 segmented labelled structures which undergo linear fitting to the global supratentorial cortical contours of the patients' MRI. The fMRI data were gathered using a one or two hand motor task with thresholding via an AFNI workstation (NIH Bethesda, MD) to the optimal balance of signal to noise. To facilitate visual analysis, the fMRI of the hand examinations were reformatted into a volume-rendered surface view superimposed on precontrast 3D T1 MR images containing the hand motor fibers of the DAT. Five reviewers assessed the data for concordance between DAT, fMRI and when necessary anatomical landmarks.

## RESULTS

Available fMRI data were diagnostically usable in 92% (33 of 36 analyzed hemispheres), with DAT anatomical accuracy in the remaining cases. The DAT prediction and fMRI findings were concordant in all nine normal hemispheres and in 20 of 24 (83%) glioma-bearing hemispheres. The inter-rater reliability was very good. The activity from fMRI tended to be located near the central sulcus while the DAT localized to the anatomical position of the MCH (i.e., the hand knob). The four discordant cases resulted from substantial mass effect by large frontal tumors. In these cases the DAT localized the fibers to the precentral sulcus with  $\frac{1}{2}$  to 1 gyrus of posterior shift (6-10 mm). Unlike tumor histology, gender or age, the location of the tumor was significant in predicting the mismatch between DAT and fMRI ( $P = 0.02$ ). A different pattern of mass effect was noted in the three patients who had previous operation, compared to the one surgically naïve patient.

## CONCLUSION

This study validated DAT's anatomical atlas and alignment process for the expected position of the MCH.

**KEY WORDS:** Brain atlas, functional MR imaging, glial tumor

**O-69** **11:10 AM - 11:18 AM**

## Parameters from Arterial Spin Labeling and DSC MR Imaging Identify Watershed Regions in the Human Brain

Thompson, G. Jackson, A.

University of Manchester  
Manchester, UNITED KINGDOM

## PURPOSE

Knowledge of arterial watershed regions in the brain is used to identify tissue which may be at risk during times of cerebral perfusion autoregulatory failure, or metabolic stress in the brain parenchyma. This applies to acute insults during systemic hypoperfusion and stroke, and longer-term insults through chronic metabolic or autoregulatory change implicated in diseases such as Alzheimer. While many hard copy atlases exist depicting watershed regions in the brain, and these areas are well known empirically among

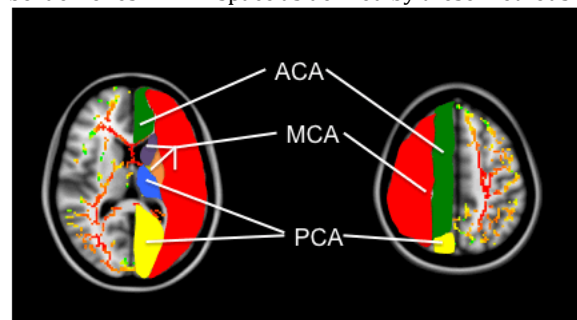
neuroradiologists, few if any atlases are available in commonly used template space for groupwise analysis of disease with respect to watershed zones. Vessel selective arterial spin labeling (ASL) can identify regional perfusion but it can be difficult to implement. We wished to identify methods to interrogate watershed regions from the timing parameters derived from perfusion-weighted imaging (PWI) that could be used individually, and in a template or atlas format in MNI space.

## MATERIALS & METHODS

Fourteen young, healthy volunteers [5 M:9 F, mean 29.2 (29-48) years] underwent ASL and DSC MRI imaging at 3 T on two separate occasions. Phase contrast angiography was used to ensure all participants had a nonvariant circle of Willis, and normal flow characteristics in the internal carotid and vertebrobasilar arteries. Arrival time (tA) was derived from multiinversion ASL, and mean transit time (MTT), arrival time (T0) and time to peak (TTP) were derived from DSC using gamma-variate fitting. These were constructed into templates in MNI space using FSL and skeletonized to identify border zones of delayed or prolonged timing parameters.

## RESULTS

The timing parameters from perfusion-weighted MR provide a probabilistic identification of major arterial territory watershed zones, in addition to perforating watershed zones in subcortical tissues. When constructed into a template in MNI space, there is good subjective correlation between the watershed zones identified here, and current hard copy atlases and MCA territory from a recent nuclear medicine study. The figure demonstrates the anterior, posterior, middle, thalamic and lenticulostriate territories and respective borderzones in MNI space as defined by these methods.



## CONCLUSION

We have demonstrated the use of PWI timing parameters for the identification of watershed regions in the brain, and used them to create a template in MNI space. While this currently is limited to those with normal cerebrovascular anatomy and flow, it may help in the analysis of imaging data in which subjective anatomical delineations of watershed regions currently are employed. An atlas also is definable.

**KEY WORDS:** ASL, DSC, watershed



O-70

11:18 AM - 11:26 AM

### Quantitative Magnetization Transfer and Diffusion Tensor Imaging Provide Complementary White Matter Information

Thompson, G.<sup>1</sup>·Zhao, S.<sup>1</sup>·Miller, P.<sup>2</sup>·Parker, G. J. M.<sup>1</sup>·Jackson, A.<sup>1</sup>

<sup>1</sup>University of Manchester, Manchester, UNITED KINGDOM, <sup>2</sup>University of Oxford, Oxford, UNITED KINGDOM

#### PURPOSE

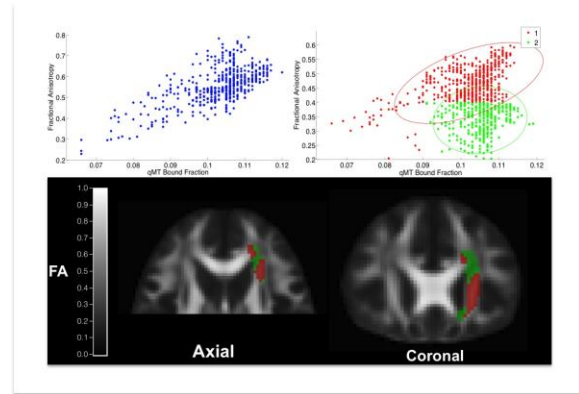
Diffusion tensor imaging (DTI) and magnetization transfer (MT) imaging have been used to study white matter (WM) in health and disease. Diffusion tensor imaging-derived fractional anisotropy (FA) correlates with fiber orientation, density, and caliber. Voxels with coherent fiber directions and greater density exhibit higher FA. The bound fraction (f) from quantitative MT imaging (qMT) relates to the macromolecular content of the voxel. In the brain, this has been shown to relate to myelination, although other macromolecules make this relationship more complex. The relationship between these parameters may provide further insights into WM in development and disease. We aimed to compare qMT f and FA values to assess the relationship between these two distinct WM parameters. A secondary objective was to determine whether whole brain qMT f could be derived without the need for B1 field correction, even at higher field strengths.

#### MATERIALS & METHODS

Whole brain qMT f and FA maps were generated for 26 healthy volunteers at 3 T. High-resolution (1x1x1mm) T1-weighted images were acquired and nonlinearly registered to MNI152 space. The resulting warps were applied to the f and FA maps to produce respective templates in MNI space. The JHU white matter atlas was used to extract the values of FA and f in six midline and 21 paired WM structures. Crossing fibers were identified using BedpostX.

#### RESULTS

In 35/48 of tracts examined, FA was correlated significantly directly to f (blue). In the corona radiata, however (6/48), voxels were found with high f but low FA (green). No significant relationships were observed for gray matter. The subcortical white matter exhibited low FA but intermediate f. Clustering of regions which did not exhibit direct FA/f correlation revealed a pattern consistent with crossing fibers. It was confirmed that for f, even at 3 T, there is no need for B1 correction.



#### CONCLUSION

Within major white matter tracts, qMT f is directly correlated with FA (blue, red), except in areas where lower FA is likely related to fiber crossing and directional heterogeneity within tracts (green). This pattern also is seen in the subcortical region, where U-fibers exhibit myelination and intermediate f, but intravoxel directional change and low FA. The combination of f and FA has potential to characterize WM structure, and may provide further complementary information to assess and quantify the structural changes occurring during development and disease. Finally, f can be measured at 3 T without the need for B1 homogeneity correction.

**KEY WORDS:** qMT, Diffusion tensor imaging, white matter

O-71

11:26 AM - 11:34 AM

### Structural Changes in the Central Nervous System of North Sea Divers

Moen, G.·Grüner, R.

Haukeland University Hospital  
N- 5021 Bergen, NORWAY

#### PURPOSE

Diving is associated with a risk of cerebral decompression illness, and the prevalence of neurologic symptoms is higher in divers compared with control groups. Microvascular dysfunction due to gas microembolism and exposure to hyperoxia are possible mechanisms which may result in the microstructural and microvascular deficits found in these divers. Early neuropathologic studies in few subjects have shown evidence of injury and focal degeneration in gray matter and white matter. The purpose of this study was thus to use conventional MRI to investigate if the following parameters would be more prevalent among symptomatic divers; volumetric changes of common brain structures, abundance of hyperintense lesions, abundance of focal hemorrhages.

#### MATERIALS & METHODS

Divers (N = 91, 51 ± 7 years) with an average experience of 15 years (range 3 - 38 years) of professional diving were compared to an age, height and body weight-matched control group (N = 45, 53 ± 7 years). On average, the divers performed work on

maximal diving depths of 176 meters (range 85 - 500 meters). Extensive conventional imaging of head, medulla and column, including diffusion and perfusion imaging, was performed on a 1.5 T MRI system. Structural images were assessed by two experienced neuroradiologists. Additionally, two MPRAGE (3D T1, TE/TI/TR = 4/20/9.7, 1 mm3) per participant were averaged and automatically segmented using the Freesurfer software. Significance was tested using two-tailed student t-tests ( $p < 0.05$ ).

## RESULTS

Significant volume reduction of the left hippocampus was seen in the divers compared to controls, while at the same time the volume of the left inferior lateral ventricle was larger. Also, the cortex and white matter of the left cerebellum were reduced. There was no difference in the number of hyperintense lesions in the right hemisphere, the left hemisphere, the brain stem, or in left of right cerebella hemisphere. Similarly, the number of focal hemorrhages did not differ in these regions between the two groups.

## CONCLUSION

Volumetric changes in the hippocampus and cerebellum are in agreement with the recently reduced ADC values reported in these areas in the same divers. The increase of ventricular size in the hippocampus region could be indicative of regional atrophy. In combination with negative findings of the prevalence of hyperintense lesion or focal hemorrhages, the results suggest the presence of subtle, microscale deficits. These findings may explain some of the long-term clinical symptoms reported among professional divers.

**KEY WORDS:** Anatomy, diving, MR imaging

**O-72** **11:34 AM - 11:42 AM**

## Added Information of FIESTA Sequence in Stenoocclusive Vertebrobasilar Dissection

Jun, S.-Chang, H.-Kim, M.

Keimyung University Hospital  
Daegu, KOREA, REPUBLIC OF

## PURPOSE

Time-of-flight (TOF) magnetic resonance angiography (MRA) provides useful information about pathologies in intracranial vessels. But, TOF MRA gives limited information in intracranial occlusion or severe stenosis due to decreased flow signal intensities. So we added and evaluated FIESTA sequence for detection of vertebrobasilar artery (VBA) dissection.

## MATERIALS & METHODS

We performed additional FIESTA sequence in 79 of patients diagnosed as VBA luminal abnormality (include stenosis, occlusion and dilatation) by means of TOF MRA. And we compared TOF MRA with FIESTA for detection of VBA dissection.

## RESULTS

In four aneurysmal type VBA dissections, both TOF MRA and FIESTA sequence could detect the lesions. In 23 steno-occlusion type VBA dissections, TOF MRA could not detect the lesions, whereas FIESTA sequence could depict the lesions. In remained 52 patients, 31 patients were diagnosed as hypoplasia and/or atherosclerosis, 19 patients were allocated as indeterminate group (1 patient was finally diagnosed as reversible vaso-constriction syndrome after the follow-up MRI).

## CONCLUSION

FIESTA sequence may give additional information in steno-occlusive VA dissection.

**KEY WORDS:** Dissection, angiography, MR imaging

**O-73** **11:42 AM - 11:50 AM**

## Evaluation and Classification of the Intracranial Dural Sinuses by Radiologic Imaging Methods

Gokce, E.-Pinarbasili, T.-Acu, B.-Firat, M. M.-Erkorkmaz, Ü.  
Gaziosmanpasa University  
Tokat, TURKEY

## PURPOSE

Dural venous sinuses (DVS) are often asymmetrical and have more variations than the arterial system. Cerebral vein configurations may show variations not only among individuals but also in the two hemispheres of the same person. The literature points out that the classification of the torcular herophili (TH) is carried mostly out by the anatomical studies. This study aims at evaluating the DVS, and classifying their types and variations by using imaging methods.

## MATERIALS & METHODS

In this study, the DVS of the 394 patients aged 7-85 were classified on the basis of TH. 209 of the patients were females and 185 were males. Between the years 2006 and 2011, they were examined by 2D TOF MRV, contrast-enhanced 3D SPGR MRI and cerebral DSA studies. Furthermore, occipital sinus (OS), transverse sinuses (TS), straight sinus, superior (SSS) and inferior (ISS) sagittal sinuses were evaluated one by one to determine eventual variations.

## RESULTS

The group in which SSS, straight and the two TS constituting TH were connected directly to each other was identified as the true confluence (Type I). The group with the connection of three out of four sinuses was defined as pseudo-confluence (Type II). The group with only two connected sinuses was considered as nonconfluence (Type III). The most common type was pseudo-confluence (Type II). Pseudo-confluence was divided into five sub-groups ranging from Type IIA to Type IIE. Occipital sinus was detected in 15% of the patients. As for the TS the codominant type with equal calibers was the most common. Straight sinus, superior was found duplicated in 90 (22.8%) cases and the straight sinus in 95 (24.1%) cases. The coexistence of the left TS agenesis and OS, the coexistence of pseudo-

confluence type torcular and OS, the coexistence of fenestrated straight sinus and OS, the fenestrated straight sinus existence in female gender were statistically significant.

#### CONCLUSION

Considering the possible complications, it is important to evaluate DVS and to determine their variations with appropriate imaging techniques for the assessment of radical neck dissections, cerebrovascular diseases, brain tumors, and making posterior cranial fossa or occipital surgical decisions. Flow gap is mistaken as the pseudo TS agenesis in 2D TOF MRV. Therefore, 2D TOF MRV examination is not sufficient by itself for the assessment of the DVS and it has to be correlated with other techniques. As the DVS demonstrate different filling in terms of the injected artery and the direction of the injection during the intraarterial DSA, the assessment should be performed with bilateral selective ICA and VA injections with all the projections. Dural venous sinuses were visualized satisfactorily by contrast-enhanced 3D SPGR MRI. Torcular herophili were classified more accurately with MIP images from different angles. Dural venous sinus are varied considerably, and the literature lacks of an exact classification of the variations detected in this study. Hence we reclassified the DVS on the basis of imaging findings and presented this work for clinical purposes.

**KEY WORDS:** Dural venous sinuses, radiologic imaging methods, torcular herophili

O-74

11:50 AM - 11:58 AM

#### Effect of Breathing Pattern on Hemodynamics during Spinal Angiography

Klostranec, J. M.<sup>1</sup>Gailloud, P.<sup>2</sup>

<sup>1</sup>University of Toronto, Toronto, ON, CANADA, <sup>2</sup>Johns Hopkins University, Baltimore, MD

#### PURPOSE

Spinal digital subtraction angiography (SpDSA) is the gold standard imaging technique for the investigation of spinal cord vascular disorders, and plays an important role in the planning of their endovascular or microsurgical management. Spinal DSA is performed most commonly under conscious sedation (CS), and endovascular treatment under general anesthesia (GA). In either case, changes in intrathoracic pressure (ITP) may occur with variations in breathing patterns, and have an impact on intrathoracic blood vessel patency and flow patterns. We report five observations in which a change in breathing pattern modified the content and significance of SpDSA images.

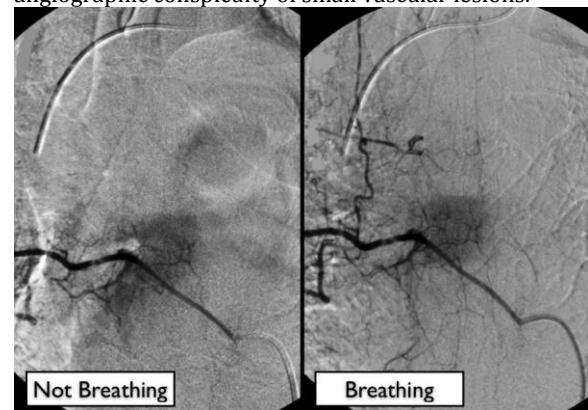
#### MATERIALS & METHODS

Case 1 - 60-year-old woman investigated for a suspicion of vascular malformation, negative angiogram. Case 2 - 54-year-old woman undergoing endovascular treatment of a spinal epidural arteriovenous fistula (SEAVF). Case 3 - 45-year-old woman undergoing endovascular treatment of a spinal arteriovenous fistula (SDAVF). Case 4 - 26-year-old man investigated for a

suspicion of vascular malformation, diagnosed with a SEAVF. Case 5 - 59-year-old woman undergoing endovascular treatment of a spinal epidural arteriovenous fistula (SEAVF). Breathing patterns were controlled either by ventilator settings in patients under GA (2, 3, 5), or by the patients themselves at the request of the angiographer when under CS (1, 4).

#### RESULTS

Case 1 illustrates the wide alterations in collateral branches documented with or without breath hold (Figure), showing that detection of potentially dangerous collateral pathways may depend on the breathing pattern. Cases 2 and 3 show two instances in which small anterior or posterior spinal arteries associated with vascular malformations were not detected during initial SpDSA performed under CS, but were visible at the time of treatment under GA with breath hold, leading in one case to a modification of the endovascular approach, in the other to a change from endovascular to surgical management. Cases 4 and 5 document the modification of the venous drainage of SEAVFs with change in breathing patterns; during breath hold, the drainage was towards intrathoracic paravertebral veins only, while during a Valsalva maneuver, it was mostly or only redirected towards the epidural plexus. Such changes may influence the angiographic conspicuity of small vascular lesions.



#### CONCLUSION

We present five cases in which ITP changes resulting from alterations in breathing pattern modified the content and significance of SpDSA images. Repeating injections under various breathing conditions may increase the collected angiographic information, in particular when characterizing spinal vascular malformations, or when facing suspicious angiographic findings.

**KEY WORDS:** Spinal angiography, intrathoracic pressure, hemodynamics



O-75

11:58 AM - 12:06 PM

**Common Peroneal Neuropathy: How Much 3 T MR Neurography Adds?**

Chalian, M. Thawait, G. K. Thawait, S. K. Del Grande, F. Chhabra, A.

The Johns Hopkins Hospital  
Baltimore, MD

**PURPOSE**

To examine diagnostic accuracy of semiquantitative and qualitative magnetic resonance neurography (MRN) criteria in common peroneal nerve (CPN) neuropathy.

**MATERIALS & METHODS**

Institutional review board approval was obtained with waiver of informed consent for this HIPPA compliant retrospective study. A review of 28 knees in 28 subjects (12 men, 16 women; age range 13 to 84 years, mean age  $42 \pm 20$  years) who had undergone MR neurography of the knee was performed. Thirteen patients who had a final diagnosis of CPN were classified as cases and 15 patients who lacked a final diagnosis of CPN neuropathy were classified as controls. Morphologic characteristics of the CPN including nerve T2 signal intensity, nerve size, nerve course, fascicles morphology, regional muscle edema and fatty infiltration, and an overall assessment of the CPN as being normal or abnormal were evaluated by two independent radiologists blinded to the clinical history. Overall sensitivity, specificity, and accuracy compared against our reference standards were expressed as percentages. Interobserver agreements were assessed using linear weighted kappa statistics.

**RESULTS**

Common peroneal nerve T2 signal abnormality had the highest sensitivity (77%) in identifying CPN neuropathy. Except for T2 signal abnormality, overall specificity for the nerve morphologic parameters and muscle denervation change assessed was fairly high, ranging from 73% to 100%. The consensus accuracy ranged from 68 to 79% for the morphologic characteristics assessed. The interobserver reproducibility was very good ( $k = 0.90$  to  $0.91$ ) for assessment of regional muscle denervation changes and moderate ( $k = 0.46$  to  $0.59$ ) for morphologic CPN characteristics.

**CONCLUSION**

MR neurography is a useful modality in supplementing the diagnosis of common peroneal neuropathy. Utilizing a predefined classification criteria helps standardize the morphologic criteria of CPN neuropathy diagnosis.

**KEY WORDS:** Common peroneal nerve, neuropathy, MR neurography

**Monday Afternoon****1:00 PM - 2:30 PM****Grand Ballroom Suite****(10) ASFNR PROGRAMMING: IMPLEMENTING FUNCTIONAL IMAGING IN THE CLINICAL SETTING (SAM # 1) (AR)**

\*Qualified by the American Board of Radiology (ABR) in meeting the criteria for Self-Assessment towards the purpose of fulfilling requirements in the ABR Maintenance of Certification program data 3/12.

O-76

1:00 PM - 1:25 PM

**fMRI**

Jeffrey R. Petrella, MD

Radiology, Duke University Medical Center  
Durham, NC, USA

**PRESENTATION SUMMARY**

Functional MRI (fMRI) has been on the medical imaging horizon for more than twenty years, and many commercial MRI scanners sold today are capable of implementing this fMRI; however, this technique is currently underutilized in clinical care. To date, the most important clinical application of fMRI is as an aid to identify functionally eloquent cortex for presurgical planning in patients with potentially resectable brain lesions, such as tumors and epileptogenic foci.

There are multiple barriers to adoption of fMRI in everyday clinical practice. Because fMRI requires a patient's active engagement in a task, it constitutes a fundamental departure from the traditional approach to clinical MRI scanning, in which technologists execute an appropriate series of pulse sequences and patients are instructed only to remain still. fMRI is most effective in a cooperative patient with adequate vision or hearing, capable of following directions, sometimes a significant challenge in critically ill, elderly or pediatric patients.

There is a significant learning curve involving both technical and interpretive aspects of fMRI. In addition to an MRI scanner with sufficient, field strength, gradient strength and speed, fMRI requires additional hardware and software for stimulus presentation and imaging analysis to make the scanner truly "fMRI-ready". Significant attention to quality control, particularly monitoring of patient motion and task engagement are needed to obtain adequate confidence in information for presurgical planning. The interpreting radiologist must gain considerable experience with a particular paradigm or set of paradigms. Apriori knowledge of putative eloquent activation sites can greatly aid in the interpretation of noisy scans, or those with weak activation. Knowledge

of gyral anatomy in three planes is important for accurately describing the location and extent of clinically relevant activation foci.

Incorporation of fMRI as a standard part of neuroradiology fellowship curriculum, as well as mini-fellowships consisting of case reviews and the opportunity to observe patient training and scanning, are methods to gain sufficient experience to begin implementation. A number of 3<sup>rd</sup> party vendors now offer “turn-key” solutions, involving hardware software as well as intensive one-on-one training to train technologists in performing fMRI exams. Several organizations, including the American Society of Functional Neuroradiology and the fMRI subcommittee of the Quantitative Imaging Biomarkers Alliance, are working with academia and industry to create standards for fMRI acquisition, analysis and interpretation. Such efforts should greatly facilitate widespread adoption of fMRI into clinical practice.

**O-77** **1:25 PM - 1:50 PM**

### ASL

Joseph A. Maldjian, MD

Wake Forest University School of Medicine  
Winston-Salem, NC, USA

#### PRESENTATION SUMMARY

ASL imaging has been in development for over a decade [1-3]. During this time, it has remained predominantly a research tool. With the recent availability of the technique from a variety of MRI vendors, ASL is now entering more broadly into the clinical realm. Unlike conventional bolus gadolinium techniques, ASL does not require intravenous contrast, is quantitative, and is readily repeatable. ASL applications are evolving as clinical experience is gained with this technique. At Wake Forest University School of Medicine, we have implemented an automated processing pipeline capable of handling a substantial clinical volume of perfusion acquisitions, allowing us to perform over 15,000 clinical ASL examinations in the past several years. These studies have revealed many pathologic and physiologic processes readily identified with quantitative perfusion imaging [4].

**Artifacts.** There are several frequently encountered artifacts in the clinical population with ASL. Susceptibility artifacts are present as is typical for any fast imaging based technique. ASL relies on a subtraction of imaging pairs to obtain the perfusion signal, also making it highly susceptible to slight motion artifacts, or transient gradient hardware instability. These artifacts can manifest in a variety of ways, most typically as rings of high signal, low signal, or signal in CSF spaces and can make the resulting images uninterpretable. Circulating gadolinium-based contrast agents significantly shorten T1 in all tissues in both the control and label conditions. The effect of this T1 shortening is to minimize the measurable differences between the spin tag and control conditions producing maps with almost no usable signal.

**Normal Perfusion Patterns.** ASL perfusion patterns demonstrate age-related changes in perfusion signal. Pediatric patients in the 5-15 year old range demonstrate high perfusion values. Adults demonstrate a gradual age-related decline in brain perfusion.

This talk will highlight the clinical experience with ASL including artifacts, normal perfusion patterns, and hyper and hypo-perfusion patterns in pathology.

**O-78**

**1:50 PM - 2:15 PM**

### Spectroscopy

Peter B. Barker, D.Phil, PhD

Radiology and Radiological Science  
Johns Hopkins University School of Medicine  
Baltimore, MD, USA

#### PRESENTATION SUMMARY

MR spectroscopy (MRS) offers a non-invasive way of measuring selected metabolites within the brain. Some of these compounds (NAA, glutamate) may represent neuronal integrity, while others (choline, *myo*-inositol) are thought to be more abundant in glial cells. Lactate may also be detected under certain pathological conditions, such as acute hypoxic or ischemic injury. The number of compounds that can be detected changes as a function of magnetic field strength and acquisition conditions used (in particular, the echo time (TE)).

MRS may be helpful in the diagnosis of a number of different neurological conditions. Most commonly it is used in the evaluation of brain tumors; pre-surgical MRS may help distinguish neoplastic from non-neoplastic or benign lesions, help establish tumor grade, and provide prognostic information. During and after treatment, MRS may be useful in evaluating therapeutic response and tumor regrowth. MRS may also be helpful in the diagnosis of hypoxic-ischemic injury, and characterizing various metabolic and demyelinating diseases.

This presentation will discuss optimal procedures for performing and interpreting MRS and MRSI, and will also describe normal regional and age-related variations. Characteristic examples of MRS in brain tumors, neurometabolic diseases and other neurological disorders will be presented.

## Monday Afternoon

**1:00 PM - 2:30 PM**

**Trianon Ballroom**

**(11) ASPNR PROGRAMMING:  
ADVANCED PEDIATRIC  
NEUROIMAGING TECHNIQUES**

**O-79**

**1:00 PM - 1:25 PM**

**Novel MR Techniques (DWI/DTI/fast SWI, etc)**

Roland Bammer, PhD  
Stanford University  
Stanford, CA, USA

**O-80**

**1:25 PM - 1:50 PM**

**Advanced MR Imaging in Patients with Focal Epilepsy: Focus Detection and Abnormal Connectivity**

Michael J. Paldino, MD  
Children's Hospital Boston  
Boston, MA, USA

### **PRESENTATION SUMMARY**

Most higher-order functions of the human brain emerge from parallel processing within sub-specialized, but distributed, functional systems. A complex neural network, formed by some  $10^{10}$  neurons, forms the structural substrate for efficient interaction between local and distributed areas of the cerebrum. To date, the impact of disordered developmental and electrical processes on this complex circuitry remains largely unknown.

Epilepsy is a common neurological condition defined by recurrent, unprovoked seizures that affects one percent of the population, including one in 200 children. Unlike in adults, developmental lesions predominate as the source of seizures in children; in particular, focal cortical dysplasia (FCD) is the most common anatomic substrate for intractable epilepsy in children. Although the workup has traditionally centered on detecting localized dysplastic abnormalities, there is evidence that malformations of cortical development (MCD) are associated with extensive alterations in tissue structure. Cortical structure outside of the region of MCD is normal, at least in the sense that it does not demonstrate the same histopathologic abnormalities that characterize dysplastic cortex. That patients with MCDs experience a wide range of functional deficits which often cannot be explained on the basis of the location of the structural abnormality therefore suggests abnormal cortico-cortical interaction. Regardless of whether such abnormal connectivity is established by genetic/developmental processes or by activity-dependent reorganization, such aberrancy has obvious potential implications for neuro-cognitive

development. Equally important, however, is the potential for developmental processes and seizure activity to establish and/or reinforce epileptogenic networks, which could predispose a patient to recurrent seizures after surgical management.

The goal of this lecture is to examine the potential of multi-modal magnetic resonance imaging: 1. to detect anatomic substrates of focal seizures and 2. to characterize network connectivity in pediatric patients with partial epilepsy.

**O-81**

**1:50 PM - 2:15 PM**

**Imaging Epileptic Discharges with Encephalographic MR**

Darren B. Orbach, MD, PhD  
Children's Hospital Boston / Harvard Medical School  
Boston, MA, USA

### **PRESENTATION SUMMARY**

Our group has developed a new approach to functional neuroimaging, which we call encephalographic MRI (eMRI). The technique combines simultaneous EEG and fast gradient-echo echo-planar imaging in patients with large amplitude, stereotyped electrical brain discharges. Our goal is to use MR to visualize fast phenomena which are more directly related to neuronal activity than are the metabolic/blood flow changes typically imaged with techniques such as BOLD and PET. We have demonstrated fast changes in both MR magnitude and phase images, concurrent with interictal epileptic spikes seen on simultaneously acquired EEG. Possible mechanisms underlying these fast changes, as well as potential applications, particularly in pediatric epilepsy, will be discussed.



## Monday Afternoon

**1:00 PM - 2:30 PM**

**Beekman/Sutton North**

**(12) SOCIOECONOMIC  
PROGRAMMING:  
HEALTHCARE/PAYMENT  
METHODOLOGY/HEALTH  
SERVICES**

**O-82**

**1:00 PM - 1:30 PM**

**Healthcare/Payment Methodology/Health Services**

Andrew W. Litt, MD

Dell Healthcare and Life Sciences  
Plano, TX, USA

### PRESENTATION SUMMARY

Healthcare payment is undergoing one of the most significant changes since the creation of Medicare and Medicaid in the 1960's. Both the public (government) and private (insurance) payors of health care are no longer willing to pay providers purely for the volume of care they deliver. Whether it's Accountable Care Organizations, episode of care payments, pay-for-performance models or other new forms of healthcare payment there is a clear shift of risk to the providers. These models will require physicians, hospitals and others to assume some or all of the financial risk as well as the outcome/quality risk. This talk will review the new payment models and discuss the key requirements towards managing those risk elements. In particular, it will focus on the use of information and information technology to manage patients as individuals and as populations. The role of data management and analytics will be explored as a key component of improving care while better managing cost. Finally, the use of new data storage and aggregation tools such as cloud computing will be presented as a means of developing a common, shared data platform that will allow for patients and their physicians to improve health.

**O-83**

**1:30 PM - 2:00 PM**

**Healthcare/Payment Methodology/Health Services**

Frank James Lexa, VII, MD

Wharton School, Univ. of Pennsylvania, Global  
Consulting Practicum  
Philadelphia, PA, USA

### PRESENTATION SUMMARY

The methods in the USA for paying for radiologist's services are likely to undergo a radical transformation during the next several years. This session will briefly review both historical and current mechanisms for valuation of radiologist's efforts and then move towards

projections of how radiologists could (or should) be paid for their work in the future in entities including: accountable care organizations, capitated and bundled payment schemes, medical homes, and beyond.

**O-84**

**2:00 PM - 2:30 PM**

**Healthcare/Payment Methodology/Health Services**

Marc D. Keshishian, MD

Blue Care Network  
Southfield, MI, USA

### PRESENTATION SUMMARY

Marc Keshishian is a graduate of Wayne State University School of Medicine and did his internal medicine residency at Detroit General/Receiving Hospital. He practiced medicine for 20 years. He has worked for Blue Cross Blue Shield of Michigan/Blue Care Network for the last ten years. He is the Senior Vice President and Chief Medical Officer of Blue Care Network where he is in charge of quality, utilization, credentialing, medical policy and pharmacy operations. Present information on the positive relationship between an insurance company, Blue Cross Blue Shield of Michigan, and the specialists in the state.

## Monday Afternoon

**1:00 PM - 2:30 PM**

**Sutton Center/South**

**(13) GENERAL PROGRAMMING:  
CNS INFECTIONS**

**O-85**

**1:00 PM - 1:20 PM**

**CNS Fungal Infections Masquerading as Bacterial and Mycobacterial Infections**

M. Judith Donovan Post, MD

Univ. of Miami, Miller School of Medicine  
Miami, FL, USA

### PRESENTATION SUMMARY

Fungal brain abscesses, such as those due to cryptococcal infection, aspergillosis (invasive and non-invasive allergic aspergillosis), mucormycosis, candidiasis, and dermatiaceous (darkly pigmented) fungal infection may be difficult to differentiate from bacterial and mycobacterial infections of the brain. This is due to the overlap in imaging findings on conventional MR. While certain imaging features such as signal heterogeneity on T2WI and diffusion imaging and multiplicity of lesions may be clues to the presence of fungal brain abscesses, as suggested by Mueller-Mang et al., they are not pathognomonic. More advanced imaging techniques such as proton MR spectroscopy and DTI with FA measurements may be needed to narrow the differential diagnosis. The different

biochemical environments of fungal brain abscesses as opposed to bacterial and mycobacterial abscesses may allow for a diagnostic differentiation. Knowledge of the immune status of the patient, the clinical presentation and laboratory data will also provide diagnostic insight.

**O-86**

**1:20 PM - 1:40 PM**

**CNS Lesions in AIDS: The HAART Era (to Include IRIS)**

Emerson L. Gasparetto, MD, PhD

Radiology, University Federal of Rio De Janeiro  
Rio De Janeiro, Brazil

**PRESENTATION SUMMARY**

This presentation aims to present the most common brain imaging findings in AIDS patients with CNS lesions in the HAART era. The importance of the HIV-related cognitive deficits and the most frequent imaging abnormalities is going to be emphasized. Also, all the imaging findings in patients with CNS-IRIS are going to be stressed. In addition, although uncommon nowadays, the imaging findings of toxoplasmosis, PML, cryptococcosis and tuberculosis are going to be reviewed. Finally, the future potential of advanced MRI techniques and post-processing techniques for the better understanding of the CNS damage in patients with HIV infection are going to be discussed.

**O-87**

**1:40 PM - 2:00 PM**

**Viruses: Difficulties in Diagnosing Viruses By Imaging**

Zoran Rumboldt, MD, PhD

Medical University of South Carolina  
Charleston, SC, USA

**PRESENTATION SUMMARY**

Neuroimaging constitutes an important component in the diagnostic process of viral CNS infections, along with the history, physical examination and cerebrospinal fluid analysis. Over 100 different invading viruses, the most common of which are herpes simplex, herpes zoster, arboviruses and enteroviruses, have been identified as causative agents of encephalitis. The etiology of encephalitis remains unknown in many cases of this complex syndrome, since probable etiologic agent is established in only 16-69% of cases. Viruses gain access through hematogenous dissemination or, less frequently, along the peripheral nerves, and many have a predilection for the gray matter, whether it is cortical, deep, or intramedullary. Some viruses, on the contrary, such as HIV and CJ virus, prefer the white matter. Acute viral encephalitis produces parenchymal infiltration with inflammatory cells, leading to neuronal injury and at times to extensive necrosis. The imaging findings reflect these pathologic changes, generally visualized as areas of low attenuation on CT, as well as of low T1 and high T2 signal intensity on MRI. Diffusion imaging is superior to conventional MR imaging for early detection of encephalitis, revealing bright DWI signal and reduced diffusion on ADC maps.

Radiological presentations of encephalitis are pleomorphic, but a fairly common finding is bilateral T2 hyperintensity in the thalami and/or basal ganglia, and viral infection should be taken into consideration whenever such bilateral deep gray matter lesions are found in an appropriate clinical setting. A number of viral infectious agents characteristically lead to specific localization and/or imaging appearance of CNS lesions. However, these viruses may also present with nonspecific findings, while other infections and non-infectious diseases may simulate their characteristic presentation. For instance, a transient lesion of high T2 signal and decreased diffusion in the corpus callosum splenium has been documented with influenza, adenovirus and rotavirus encephalitis, but also with E. coli infection, antiepileptic medication withdrawal, hypoglycemia, osmotic myelinolysis and other disease processes.

**O-88**

**2:00 PM - 2:20 PM**

**Spinal Infections: An Update**

E. Turgut Tali, MD

Radiology/Neuroradiology  
Gazi University School of Medicine  
Besevler Ankara, Turkey

**PRESENTATION SUMMARY**

Spinal infection is a significant cause of morbidity and mortality. This entity is notoriously difficult to differentiate clinically from degenerative processes, noninfective inflammatory disorders, and spinal neoplasm.

Recent epidemiologic studies point to an increasing prevalence of spinal epidural infection. MRI demonstrates soft tissue mass within the epidural space encroaching upon the theca or spinal nerves. MRI signal depends on the contents of the lesion. Frequently, long segment iso-hyperintense epidural mass lesion with hypointense thickened, displaced dura on T1- and T2WI is observed. Phlegmon has no liquid component or pus with almost uniform enhancement. Abscesses have a liquid component with rim enhancement.

Infective spondylitis accounts for approximately 2-7% of all cases of osteomyelitis. T1WI is useful to differentiate infected area. Low signal areas and interruption of the cortical continuity, destruction of the cortical margins are typical on T1WI whereas high signal of affected areas of the vertebral body and disc is typical on T2WI. Fat suppressed T2WI shows better conspicuity of the infected areas. Contrast enhancement is the earliest sign and pathognomonic in the acute inflammatory episode and even subtle infection then persists to a varying degree for several weeks or months. It is also helpful to differentiate the disc, the body and the phlegmon, which enhances homogeneously/inhomogeneously from abscess and necrosis, which appear as peripherally enhancing mass with hypointense liquefactive center. Fat suppressed T1WI can be helpful to obtain the better contrast between the tissues.

Pyogenic leptomeningitis is the most common bacterial infection of the spinal axis. On MRI, the precontrast

T1WI may be either normal or may reveal nonspecific abnormalities. T2WI are of limited use since the signal intensity of CSF may obscure the meningeal structures. Postcontrast T1WI may show inflamed dura or nerve sheath with possible involvement of the spinal cord. Three patterns of enhancement are defined: linear, nodular and diffuse; among which the linear enhancement is the most common pattern.

Infection of the spinal cord is relatively uncommon and may be caused by bacteria, virus, fungi and parasites. MRI findings of bacterial myelitis may differ in a wide spectrum from mild edema, swelling with mild or no contrast enhancement to prominent edema and abscess formation with diffuse, patchy or ring enhancement consistent with the stage of the infection. Viruses are the most common agents to infect the spinal cord. MR features of viral myelitis are nonspecific and indistinguishable from other forms of myelitis.

## Monday Afternoon

**1:00 PM - 2:30 PM**

**Murray Hill**

**(14) AN EXPERT: HOW I DO IT**

**O-89**

**1:00 PM - 1:30 PM**

### **Thyroid and Parathyroid Imaging**

Laurie A. Loevner, MD

Univ of Penn Medical Center  
Philadelphia, PA, USA

**O-90**

**1:30 PM - 2:00 PM**

### **Evaluation of Suspected Dural Sinus Thrombosis: Principles and Pitfalls**

James M. Provenzale, MD

Radiology, Duke University Medical Center and Emory  
University School of Medicine  
Durham, NC, USA

#### **PRESENTATION SUMMARY**

Dural sinus thrombosis (DST) is a potentially life-threatening entity that is often difficult to diagnose, for a variety of reasons. This presentation will systematically review the challenges inherent in imaging diagnosis of DST by using a classification system for categorizing errors; although this classification system can be applied to a wide variety of radiological diagnoses, in this presentation, solely DST will be considered.

Type 1 Error- Failure to detect finding ("miss")

One of the most common causes of failure to diagnose DST on MR images is failure to detect absence of a normal flow void within a dural sinus. Another common form of error is due to lack of conspicuity of the abnormality, i.e., low level of contrast between the

finding and adjacent normal tissue. For instance, the density of an abnormal structure seen on CT may not sufficiently differ from that of surrounding tissue.

Type 2 Error- Wrongly interpreting a finding as abnormal ("over-call")

On unenhanced CT, high density within a dural sinus due to causes other than thrombosis can produce a false-positive finding (or "over-call"). A primary example is increased density due to a high hematocrit, commonly seen in young children and in certain disease states (e.g., polycythemia vera).

Potential causes of error on MR imaging include asymmetry of size of the transverse sinuses, and misinterpretation of the bright signal from flow-related enhancement or in-plane flow as thrombus.

Type 3 Error- Recognizing abnormality but dismiss as normal or artifact ("under-call")

This type of error is due to failure to correctly interpret a finding as being abnormal. As an example, DST can appear dark on T2-weighted images and thus simulate a flow void. Therefore, particular attention must be given to the appearance of the dural sinus on other pulse sequences. Over-reliance on the presence of contrast-enhancement of a dural sinus as an indication of patency is another cause of a false-negative error. It is true that, in the vast majority of cases, contrast enhancement of a sinus is due to flow of contrast material within the sinus and an indication of patency. However, on occasion a thrombosed dural sinus can contrast-enhance.

Type 4 Error - Recognizing abnormality but assign incorrect etiology

In a type 4 error, the mistake is not in assuming that an abnormal finding is normal but in failing to correctly explain the abnormality, by assigning an incorrect cause to the abnormal finding. A primary example of this type of error is seen when venous infarction occurs secondary to DST. Failure to recognize the infarct as venous in origin (as opposed to the much more common arterial origin) is the origin of the problem. Such infarcts are often hemorrhagic and subcortical in location, an unusual appearance for arterial infarcts.

Type 5 Error - Failure to recognize limitations of imaging technique/recommend next imaging step

An example of failure to recognize limitations of a pulse sequence can be seen in the use of saturation pulses in MR venography. An arterial saturation pulse (which is placed caudad to the imaging slice in two-dimensional MR angiography) is frequently used to diminish the signal generated by flowing blood in arteries. However, this same saturation pulse can obliterate signal from flowing blood in the superior sagittal sinus, producing a false-positive study.

**0-91****2:00 PM - 2:30 PM****Imaging The Spinal Cord**

Gordon K. Sze, MD

Yale University  
New Haven, CT, USA**PRESENTATION SUMMARY**

On many levels, imaging of the spinal cord remains challenging, from clinical implementation to diagnosis to technical advances. First, clinically, MR scans of the spinal cord are often requested emergently. We have utilized a clinical algorithm to categorize requests into emergent (less than 2 hours), urgent (less than 6 hours), and routine (within 24 hours), thereby refining those clinical presentations which warrant mobilization of manpower and scanner time.

Second, diagnosis of certain spinal cord lesions remains perplexing. While most cases are routine, every center encounters cases in which the diagnosis is not readily apparent. For example, the abnormal spinal cord which exhibits hyperintensity on T2-weighted images with equivocal or patchy enhancement can be a diagnostic dilemma. This talk will discuss an organized pattern of analysis of these lesions, in the context of unusual etiologies.

Third, due to the small size of the spinal cord and its surrounding structures, technical advances remain difficult to implement in routine spinal cord imaging. This talk will conclude with a discussion of two technical aspects, demonstration of normal vascular anatomy and the characterization of vascular lesions of the spinal cord and their diagnosis with MR imaging, MR angiography and CT angiography, and the use of diffusion weighted imaging and diffusion tensor imaging in the analysis of spinal cord anatomy and potential spinal cord lesions.

**Monday Afternoon****3:00 PM - 4:30 PM****Grand Ballroom Suite****(15a) Adult Brain: Neoplasms I****0-97****3:00 PM - 3:08 PM****Probabilistic Radiographic Atlas of Glioblastoma Phenotypes**Ellingson, B. M.·Cloughesy, T. F.·Zaw, T.·Lai,  
A.·Nghiemphu, P. L.·Pope, W. B.David Geffen School of Medicine, University of California  
Los Angeles  
Los Angeles, CA**PURPOSE**

Tumor location is known to be a significant prognostic factor in glioblastoma, likely due to genetic profile of

tumor precursor cells and the state in the development cycle that these cells transform. The purpose of the current study was to construct and analyze probabilistic atlases examining preoperative tumor locations on MR imagines and corresponding biological and interventional phenotypes in order to provide insight in the niche locations of glioblastoma “cells of origin.”

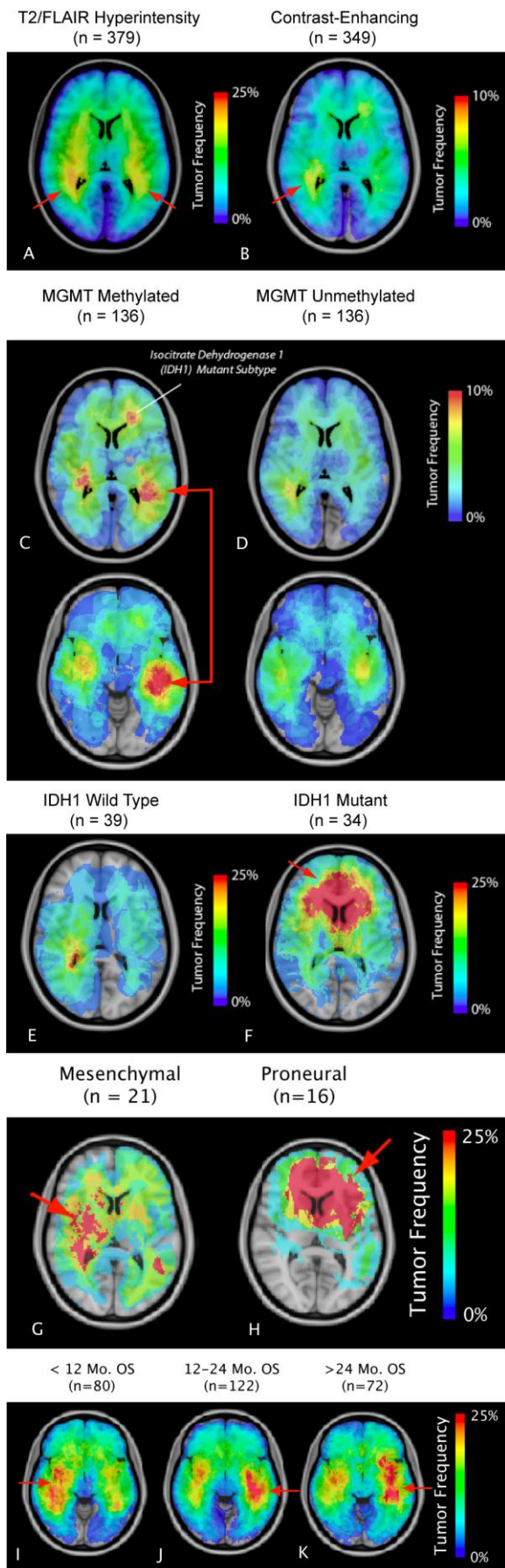
**MATERIALS & METHODS**

A total of 385 glioblastoma patients were enrolled in this HIPAA compliant retrospective study. Preoperative MR images in all patients were aligned to the MNI152 brain atlas. Contrast-enhancing regions on T1-weighted images (including regions of necrosis) and T2/FLAIR hyperintense regions were contoured on all images for all patients. Patients were stratified by age, MGMT promoter methylation status, IDH1 mutation status, and gene expression profile phenotypes. The frequency of tumor occurrence was calculated by counting the total number of times a contoured tumor occurred within an image voxel on the atlas divided by the total number of patients within that phenotype. A voxel-wise Fisher's exact test with a cluster-based correction using random permutations was used to find locations specific to different. A p-value of < 0.05 and a cluster size of more than 12 cc was required for statistical significance.

**RESULTS**

Probabilistic atlases demonstrate a high frequency of tumor occurrence in the periventricular white matter regions adjacent to the subventricular zone, which is known to harbor neural stem cells in the adult brain. Younger patients were more likely to have frontal lobe involvement at first presentation. MGMT promoter methylated tumors occur in a significantly higher frequency within the left temporal lobe. Patients with tumors in this region had a significantly longer survival independent of MGMT promoter methylation status. Patients with IDH1 mutated tumors were significantly more likely to have tumors in the frontal lobe. Similarly, the proneural genotype was localized more to the frontal lobe, whereas the mesenchymal subtype was more likely to be medial, in the right hemisphere, and posterior.





## CONCLUSION

Our data clearly demonstrates the inherent power of large-scale probabilistic radiographic atlases in identifying regions with the highest tumor incidence, which may be useful in identifying niche locations for glioma “cells of origin.”

**KEY WORDS:** Glioblastoma, atlas, genomic phenotype

0-98

3:08 PM - 3:16 PM

## Imaging Genomic Mapping in Glioblastoma Multiforme: A Novel Quantitative Merge between Imaging and Genomics. The Creation of a Signature for Tumor Necrosis Using Image Genomic Analysis in 12,764 genes and 555 microRNAs

Colen, R. R.<sup>1</sup> Mahajan, B.<sup>1</sup> Bruyere, J.<sup>1</sup> Jolesz, F. A.<sup>1</sup> Sathyan, P.<sup>2</sup> Zinn, P. O.<sup>2</sup>

<sup>1</sup>Brigham and Women's Hospital, Boston, MA, <sup>2</sup>M.D. Anderson Cancer Center, Houston, TX

## PURPOSE

To create a imaging genomic map, linking MR imaging traits with gene- and miRNA expression profiles, in patients with glioblastoma multiforme (GBM) to determine genomic correlates of necrosis to identify relevant MRI biomarkers and to find new genomic targets for GBM treatment. The introduction of gene microarrays, a method allowing for analysis of thousands of genes, has resulted in a greater insight into gliomagenesis, treatment response, and patient prognosis. However, specialized and invasive tissue sampling remains a limitation and bottleneck for its widespread use in the standard clinical realm. Here, we present the first study examining in a quantitative way imaging genomic in GBM to determine novel and targetable molecular necrosis correlates in GBM.

## MATERIALS & METHODS

We retrospectively identified 78 treatment naïve GBM patients from The Cancer Genome Atlas (TCGA) who had genetic expression profiles and pretreatment MR imaging. Image analysis was done on slicer 3.6 (slicer.org) and reviewed blindly in consensus by two neuroradiologists. The postcontrast T1-weighted images was used to quantitate necrosis volumes. Biostatistics analysis was performed for gene and miRNA sets whereas the median necrosis volume was taken as the cutoff to define high and low groups. These groups then were analyzed by Comparative Marker Selection (Broad Inst.). A total of 12,764 genes and 555 microRNAs were analyzed. Among the whole gene set the most upregulated mRNAs/miRNAs (N = 100), were analyzed with ingenuity pathway analysis (IPA).

## RESULTS

Ingenuity pathway analysis identified molecular networks, as well as canonical and functional pathways highly associated with cancer, cell death, cell cycle, and apoptosis in those patients with high necrosis.

## CONCLUSION

The necrosis radiophenotype identified genes and miRNAs and corresponding molecular networks that were highly associated with cell death and apoptosis. By these means we were able to identify possible key genes and miRNAs involved in cell cycle regulation and cell death. The uncovered genes and miRNAs represent new insight into necrosis as seen on MRI and an underlying possible molecular mechanisms of GBM aggressiveness and novel therapeutic approaches. Necrosis imaging biomarkers reflecting a specific molecular cancer composition will augment the predictive power for tumor aggressiveness and therapy response and identify novel targets GBM therapy.

**KEY WORDS:** Glioblastoma, imaging genomics, necrosis

**O-99**

**3:16 PM - 3:24 PM**

## MR Imaging to Predict Surgical and Radiation Dosimetry Borders: A Methodology Feasibility Study

Colen, R. R.<sup>1</sup>•Kovacs, A.<sup>1,2</sup>•Mahajan, B.<sup>1</sup>•Zinn, P. O.<sup>3</sup>•Schwarm, F. P.<sup>1</sup>•Jolesz, F.<sup>1</sup>

<sup>1</sup>Brigham and Women's Hospital, Boston, MA,

<sup>2</sup>University of Kaposvar, Kaposvar, HUNGARY, <sup>3</sup>M.D. Anderson Cancer Center, Houston, TX

## PURPOSE

To develop a robust methodology using MRI for predicting regions of relapse and thus help define the surgical resection and radiation dosimetry borders of the tumor beyond the area of enhancement and that which are used on conventional surgical and radiation treatment planning.

## MATERIALS & METHODS

We retrospectively identified 60 consecutive glioblastoma multiforme (GBM) patients (2005-2010) who had (presurgical, postsurgical, preradiation, and relapse) MRI studies and undergone radiation treatment (RT). The 3D Slicer software 3.6 (slicer.org) was used for all purposes of image analysis, manipulation and segmentation. All images were reviewed in consensus. Segmentation was carried out in a simple hierarchical model of anatomy, proceeding from peripheral to central. Three distinct structures were segmented (edema/invasion, enhancing tumor, and necrosis) on the presurgical scan. Five structures were segmented on the postoperative scans (edema/invasion, enhancing tumor, and necrosis and then also hemorrhage and surgical cavity). Subsequently, the models of edema, tumor and necrosis were generated and the quantitative volumes of the same were automatically calculated. MR perfusion (MRP) scans (N = 20) were registered to segmented images and quantitative perfusion parameters obtained.

## RESULTS

Accurate registration (within 2 mm) occurred among the images and the radiation planning CT images. In those scans in which complex rotation modifications and registrations were required, registration was

performed using more sophisticated techniques such as transformations on 3D slicer and registration was deemed adequate when error was 2 mm or less. Thirteen of 20 patients demonstrated increases in perfusion (reflective of tumor infiltration) beyond the border of enhancement and corresponding to regions of subsequent recurrence, suggesting that surgical resection and radiation planning to include those abnormal regions seen on advance imaging techniques (not on conventional MRI) might result in better tumor treatment and control of recurrence.

## CONCLUSION

We present a robust image analysis methodology/platform for accurate registration of conventional and advanced MRI sequences. MR perfusion abnormalities seen outside the area of enhancement predict regions of subsequent recurrence and relapse and thus registering and including these regions in the surgical resection and RT dosimetry planning system can be expected to decrease tumor recurrence and increase survival.

**KEY WORDS:** GBM, MR imaging, radiotherapy

**O-100**

**3:24 PM - 3:32 PM**

## Super Resolution Track Density Imaging of White Matter Signal Abnormality in Suspected Recurrent High Grade Glioma

Cohen, B. A. •Barajas, R. F. •Yu, J. J. •von Morze, C. •Hess, C. P. •Cha, S.

University of California San Francisco School of Medicine  
San Francisco, CA

## PURPOSE

White matter abnormality (WMA) in high grade glioma (HGG) patients following surgery and radiochemotherapy poses a diagnostic challenge due to heterogeneous underlying pathobiology of infiltrative tumor, treatment effects, and edema. Track density imaging (TDI) is a novel diffusion reconstruction method that achieves a unique image contrast at submillimeter resolution by using high angular resolution imaging (HARDI) and whole-brain fiber tractography. The purpose of our study was to assess WMA in recurrent HGG. We hypothesize that track density is decreased in both WMA and normal-appearing white matter (NAWM) in the diseased hemisphere compared to the contralateral side, and postulate that numerical values of track density are related inversely to the degree of tumor infiltration along white matter tracks.

## MATERIALS & METHODS

Nineteen patients with suspected recurrent HGG were enrolled. Of the 19, florid tumor recurrence was noted in 11 and >50% treatment effect in eight patients. Track density imaging maps were constructed from HARDI data at 250 micron isotropic spatial resolution. Nontargeted regions of interest (ROI) then were drawn manually on the WMA and NAWM. For each ROI, a

corresponding contralateral ROI was drawn. Across the entire cohort, track densities were compared to their contralateral values for both WMA and adjacent NAWM. Track densities, normalized to their homologous contralateral counterparts, then were compared between the recurrent tumor and treatment effect groups. For patients that subsequently recurred following resection ( $n = 12$ ), targeted ROIs were placed on sites of future recurrence. Finally, normalized track density was compared between the targeted sites and nontargeted WMA. A two-tailed Student's  $t$  test was used for statistical analysis.

## RESULTS

Normalized track densities for the surrounding WMA and adjacent NAWM were  $0.759 \pm 0.621$  and  $0.987 \pm 0.277$  (mean  $\pm$  SD), respectively, for recurrent tumor patients;  $0.901 \pm 0.668$  and  $0.923 \pm 0.139$  in those with predominantly treatment effect; and  $0.820 \pm 0.637$  and  $0.960 \pm 0.226$  across all subjects. For all 19, track density was decreased in the surrounding WMA ( $p = 0.0003$ ) but indistinguishable for NAWM ( $p = 0.602$ ) compared with the contralateral side. The track densities of WMA and adjacent NAWM were similar in the two groups ( $p > 0.514$ ). However, normalized track density in the targeted sites of future recurrence ( $0.444 \pm 0.196$ ) was significantly smaller than the nontargeted WMA ( $p = 0.003$ ).

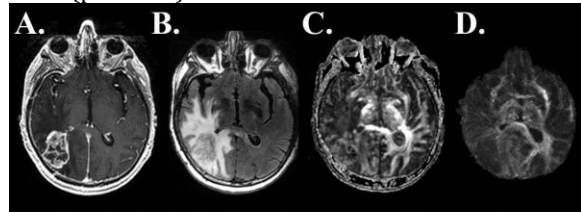


**Figure 1:** Track density imaging (TDI; 0.25 mm) provides superior spatial and contrast resolution when compared to fractional anisotropy (FA; 2.0 mm). A) T1 post contrast, B) FLAIR, C) FA map, and D) track density map in a patient with mixed radiation effect and tumor recurrence (50% viable tumor upon surgical biopsy) demonstrates improved visualization of contrast enhancing mass, peri-tumoral T2 hyperintense white matter, and normal appearing structures (anterior commissure) when compared to FA map. TDI was reconstructed from HARDI diffusion data (b-values = 0 and 2000 s/mm<sup>2</sup>, 55 directions, 2.2 mm isotropic resolution, TR/TE = 6500/90 ms, ASSET=2) imaged on a 3T clinical magnet in approximately 6 minutes. Fiber tracking was conducted using probabilistic streamlines and constrained spherical deconvolution, which resolves multiple fiber orientations. One million tracks were randomly seeded throughout the brain. The number of tracks passing through each element of a 250 µm isotropic grid was then counted, generating a TDI map.

## CONCLUSION

Track density imaging provides a novel tool for white matter evaluation in patients with recurrent HGG. The technique helps to distinguish between recurrent infiltrating tumor and treatment effects, and ultimately may be useful for predicting the site(s) of future recurrent disease.

**KEY WORDS:** Track density imaging, super resolution, high grade glioma

O-101

3:32 PM - 3:40 PM

## Suppression of Early Treatment-Related Effects on MR Imaging (Pseudoprogression) in Patients with Newly Diagnosed Glioblastoma Receiving a VEGF Signaling Inhibitor Combined with Temozolomide-Based Chemoradiation

Pinho, M. C.<sup>1,2</sup>Jennings, D. L.<sup>1</sup>Polaskova, P.<sup>1</sup>Batchelor, T.<sup>3</sup>Sorensen, A. G.<sup>4</sup>Gerstner, E. R.<sup>3</sup>

<sup>1</sup>Athinoula A. Martinos Center for Biomedical Imaging, Massachusetts General Hospital and Harvard Medical School, Boston, MA, <sup>2</sup>Hospital Israelita Albert Einstein, Sao Paulo, BRAZIL, <sup>3</sup>Pappas Center for Neuro-Oncology, Massachusetts General Hospital and Harvard Medical School, Boston, MA, <sup>4</sup>Siemens Healthcare USA, Malvern, PA

## PURPOSE

To evaluate the impact of anti-VEGF therapy on the incidence of early treatment-related effects, or pseudoprogression (PP), detected by MRI in patients with newly diagnosed glioblastoma treated with cediranib, a VEGF signaling tyrosine-kinase inhibitor.

## MATERIALS & METHODS

Patients with newly diagnosed glioblastoma enrolled in an IRB-approved clinical trial were evaluated longitudinally by serial MRIs. Treatment for all included standard temozolomide-based chemoradiation plus cediranib during initial chemoradiation and on maintenance. Serial 3 T MRI scans were performed prior to chemoradiation, weekly during the initial 6 weeks of treatment and every 4 weeks after chemoradiation. T1-weighted (pre/postcontrast) and FLAIR images were assessed for response using bidimensional and perimeter-based volumetric methods. Disease progression was defined according to updated RANO (Response Assessment in Neuro-oncology) criteria. Patients who presented with increasing/new contrast-enhanced lesions during the first 12 weeks after chemoradiation were considered to have apparent early progression (AEP) and kept on treatment. Lesions that subsequently stabilized or regressed on MRI follow up were classified as PP, while those that maintained growth despite treatment were classified as "true" early tumor progression (ETP).

## RESULTS

The initial group consisted of 40 patients (age = 22-74 years, mean age = 56 years; 27 males, 13 females). Mean volume of residual tumors at baseline was 29.39 cc ( $\pm$  23.40) on T1-weighted postcontrast and 68.18 cc ( $\pm$  62.98) on FLAIR. Currently, 21 patients are still alive and 19 have deceased, with a median follow up of 240 days for the whole group: 162 for the patients who died and 314 for the patients still living. Ten patients left the study due to treatment-related toxicity within 18 weeks of starting therapy and were excluded from the analysis. Considering the remaining 30 patients; 17 (54%) exhibited partial response and 11 (31%) were classified as stable disease. Only 2 (6%) patients presented with AEP, both of which were confirmed as ETP (one had biopsy confirmation and the other an early recurrence on the contralateral hemisphere). There were no cases of AEP that would fulfill the criteria for PP.

## CONCLUSION

In patients with newly diagnosed glioblastoma treated with temozolomide and radiation, the addition of a VEGF signaling inhibitor suppressed the development of early treatment-related effects (PP), which has been described in 26-58% of patients after standard chemoradiation alone at early postradiotherapy

imaging. This suppressive phenomenon likely is related to the powerful antipermeability effect of this class of agents, which modifies significantly the imaging appearance of these tumors. Although mechanistically expected, to our knowledge the preventive effect of anti-VEGF agents on the development of PP has not been described systematically, and has important implications for patient care. Suppressing the inflammatory process, edema and mass effect that accompanies chemoradiation may improve the tolerability of treatment and have a steroid-sparing effect. In patients with poor performance status or large, inoperable tumors, the addition of anti-VEGF agents is an interesting strategy to make chemoradiation feasible. Suppression of PP has the additional potential benefit of reducing the diagnostic dilemma surrounding increased contrast enhancement in early posttreatment evaluations and avoiding unnecessary invasive diagnostic interventions to evaluate these MRI changes.

**KEY WORDS:** Glioblastoma, pseudoprogression, VEGF

**O-102**

**3:40 PM - 3:48 PM**

**Quantitative Histogram Analysis of Diffusion and Diffusion Tensor Imaging of Glioblastomas for the Prediction of Clinical Outcome: A TCGA Glioma Phenotype Research Group Project**

Desai, H.<sup>1</sup>•Hwang, S. N.<sup>1</sup>•Holder, C. A.<sup>1</sup>•Flanders, A.<sup>2</sup>•Jilwan-Nicolas, M.<sup>3</sup>•Kirby, J.<sup>4</sup>•Saltz, J.<sup>5</sup>•Gutman, D. A.<sup>5</sup>•Raghavan, P.<sup>3</sup>•Buetow, K. H.<sup>6</sup>•TCGA Glioma Phenotype Research Group

<sup>1</sup>Emory University School of Medicine, Atlanta, GA, <sup>2</sup>Thomas Jefferson University Hospital, Philadelphia, PA, <sup>3</sup>University of Virginia, Charlottesville, VA, <sup>4</sup>SAIC-Frederick, Inc., Frederick, VA, <sup>5</sup>Emory University, Atlanta, GA, <sup>6</sup>National Cancer Institute, Bethesda, MD

**PURPOSE**

Investigate quantitative parameters derived by histogram analysis of diffusion and diffusion tensor imaging of glioblastomas as markers for clinical outcome.

**MATERIALS & METHODS**

As part of The Cancer Genome Atlas (TCGA) MRI characterization project of the National Cancer Institute, the multi-institutional TCGA Glioma Phenotype Research Group has been investigating MRI, including diffusion imaging and diffusion tensor imaging, as a means of predicting clinical outcomes for glioblastoma patients. For the current work, quantitative histogram analysis was performed on apparent diffusion coefficient (ADC) and fractional anisotropy (FA) maps for correlation with clinical outcomes. Small, noninclusive regions of interest (ROI) were selected manually within cerebrospinal fluid (CSF), normal-appearing corpus callosum (usually splenium but placed in the genu if tumor involved the splenium), and normal-appearing white matter (centrum semiovale) to obtain characteristic values for these sites. Voxel ADC and FA values were normalized by the characteristic

values measured in the ROIs. The volume of tumor was defined on the basis of the  $b = 0$  diffusion image by application of an Otsu thresholding method using the NIH ImageJ software. Mean, median, standard deviation, skew, and kurtosis of the normalized ADC and FA histograms were computed from voxels within tumor. Tumor volume also was computed. The diffusion histogram analysis has been performed on 39 of the TCGA glioblastomas at the current time. Eighteen of these data sets also included DTI. Clinical data including time to tumor progression and time to death are publicly available and were correlated with diffusion parameters. Linear correlation was performed between the diffusion and clinical parameters. As part of prior analysis, at least three neuroradiologists (from a panel of six) independently reviewed each MRI of 75 glioblastoma patients in the TCGA database. All images were evaluated according to 26 imaging features (VASARI feature set, <https://wiki.nci.nih.gov/display/CIP/VASARI>). Multireader assessment of each tumor was reduced to a single score for each feature. Correlations also were performed to assess agreement with the neuroradiologist interpretation.

**RESULTS**

Tumor volume obtained from the  $b = 0$  images strongly correlated with area measurements performed by neuroradiologists computed as the product of orthogonal tumor dimensions ( $p < 0.001$ ,  $r = 0.82$ ). No correlation was found between tumor volume and time to tumor progression or time to death. However, the mean tumor ADC normalized by CSF ADC is significantly correlated with time to tumor progression ( $p = 0.02$ ,  $r = 0.5$ ).

**CONCLUSION**

Higher ADC may reflect lower cellularity in tumors with delayed time to progression. Histogram analysis of diffusion and DTI potentially may assist in predicting clinical outcome.

**KEY WORDS:** Glioblastoma, diffusion, brain tumor

**O-103**

**3:48 PM - 3:56 PM**

**What "Dark Spots" on Principle of Echo-Shifting with a Train of Observation in Glioblastoma Reflects: Distribution of Dark Spots on Principle of Echo-Shifting with a Train of Observation in Glioblastoma and Its Relationship between Contrast Enhancement, Signals on Diffusion-Weighted Images and Pathologic Findings**

Ando, K.<sup>1</sup>•Ishikura, R.<sup>1</sup>•Mouri, M.<sup>1</sup>•Odawara, S.<sup>1</sup>•Katsuura, T.<sup>1</sup>•Yamasaki, M.<sup>1</sup>•Wakata, Y.<sup>1</sup>•Takada, Y.<sup>2,1</sup>•Yamano, T.<sup>1</sup>•Hirota, S.<sup>1</sup>•Mori, K.<sup>1</sup>•Arita, N.<sup>1</sup>

<sup>1</sup>Hyogo College of Medicine, Nishinomiya, JAPAN, <sup>2</sup>Meiwa Hospital, Nishinomiya, JAPAN

**PURPOSE**

PRESTO (principle of echo-shifting with a train of observation) is a novel imaging method that utilizes the magnetic susceptibility differences between tissues like susceptibility-weighted imaging (SWI). On PRESTO, we



can observe “dark spots” (DS) in glioblastomas (GB) like intratumoral susceptibility signal intensity (ITSS) on SWI. Intratumoral susceptibility signal intensity on GB already is reported, but its distribution in GB is not discussed fully in the literature. Because GB is a heterogeneous tumor with solid component of variable grade and cystic/necrotic component, it is important to know what DS on PRESTO in GB reflect. The aim of this study is to evaluate the distribution of DS on PRESTO in GB and clarify its relationship between contrast enhancement (CE), signals of diffusion-weighted image (DWI), and pathologic findings.

#### MATERIALS & METHODS

We retrospectively reviewed the cases with GB experienced in our institution from 2007-2010. Eighteen pathologically proven glioblastomas in 17 patients were involved in this study. T2-weighted image (T2WI), CE-T1-weighted image (CET1WI), DWI ( $b = 1000$ ) and PRESTO on 3 T MRI was obtained in all cases. Intratumoral component was classified as solid with CE, solid without CE, necrosis/cystic component, peritumoral edema, according to the findings of T2WI and CET1WI. Dark spots on PRESTO was graded from 0 to 2: (0) absent, (I) a few, (II) numerous to throughout the tumor. Dark spots in each component was compared to findings of CET1WI, DWI, and pathologic findings.

#### RESULTS

Solid component in GB was in 14/18 and DS was graded II in all 14, which also showed high signal intensity (HSI) on DWI (14/18). Five had non-CE solid component and DS was graded II in one and 0 in four. Among them, two of five showed HSI on DWI. Eight had necrotic or cystic component within solid component, and DS was graded in II in one, I in one and 0 in six. All showed low signal intensity (LSI) on DWI. Four were mainly cystic mass with thin cyst walls, which were with CE. Cyst walls were in grade II (two) and grade I (two) on PRESTO, and all showed HSI on DWI. Cystic component of cystic GB were grade II in two and grade 0 in two. All showed LSI on DWI. Peritumoral edema was in 11/18 and there were no DS in all cases, which showed LSI on DWI. Pathologic specimens obtained from solid component showed abundant tumor vessels in the solid part of the tumor in 14/17, with hemorrhage in four and without hemorrhage in ten. In cystic/necrotic components (12), only three of 12 showed intracystic hemorrhage.

#### CONCLUSION

Dark spots on PRESTO in GB mainly distribute in contrast-enhanced solid component with high signal on DWI, which suggested to be the highly malignant component of tumors. Compared to the pathologic findings, DS on PRESTO in solid component of GB may reflect abundant tumor vessels rather than intratumoral microhemorrhage.

**KEY WORDS:** Principle of echo-shifting with a train of observa, glioblastoma, pathology

O-104

3:56 PM - 4:04 PM

#### Arterial Spin Labeling Perfusion MR Imaging Differentiates Tumefactive Demyelinating Lesions from Glioblastoma Multiforme

Soun, J. E.<sup>1</sup> Pollock, J. M.<sup>2</sup> Maldjian, J. A.<sup>1</sup> Whitlow, C. T.<sup>1</sup>

<sup>1</sup>Wake Forest University School of Medicine, Winston-Salem, NC, <sup>2</sup>Oregon Health & Science University, Portland, OR

#### PURPOSE

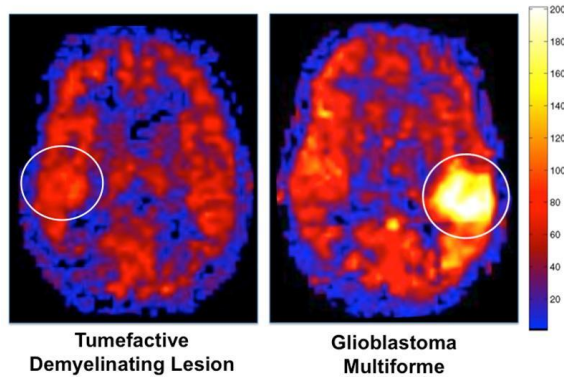
Tumefactive demyelinating lesions (TDL) and glioblastoma multiforme (GBM) can both present on MRI as rim-enhancing lesions, posing a diagnostic challenge. Glioblastoma multiformes are known to be exuberantly angiogenic, demonstrating greater intratumoral blood volume compared to TDL on gadolinium-based perfusion MRI. No studies to date, however, have extended these findings to pulsed arterial spin labeling (PASL) perfusion MRI. In the present study, we measured maximum intratumoral blood flow in GBM and TDL on PASL images, hypothesizing that GBM would demonstrate higher maximum intratumoral blood flow compared to TDL.

#### MATERIALS & METHODS

In this IRB-approved study, clinical MRI demonstrating TDL ( $n = 12$ ; eight subjects) or GBM ( $n = 18$ ; 14 subjects) that included PASL were identified retrospectively. Maximum intratumoral blood flow (mL/100 g/minute) was measured from a region of interest (ROI) manually drawn around each lesion on PASL images and confirmed on coregistered contrast-enhanced T1-weighted sequence using Aquarius iNtuition (TeraRecon, San Mateo, California). One-way between groups analysis of covariance (ANCOVA) was conducted, with tumor type (GBM, TDL) as the independent variable and maximum intratumoral blood flow as the dependent variable. Tumor volume and global whole-brain cerebral blood flow (CBF) were used as covariates. An additional ANCOVA was conducted with the same independent variable, but using the ratio of maximum intratumoral blood flow and global whole-brain CBF as the dependent variable to normalize ROI values by the magnitude of background whole-brain perfusion. Tumor volume was used as a covariate for this analysis.

#### RESULTS

ANCOVA controlling for differences in tumor volume and global brain CBF revealed a statistically significant difference in maximum intratumoral blood flow between tumor types, which was 68.2% higher in GBM (mean  $\pm$  SD;  $140.3 \pm 62.3$ ) compared to TDL (mean  $\pm$  SD;  $83.4 \pm 24.0$ ) [ $F(1,26) = 14.817$ ,  $p = .001$ ] (Figure 1). ANCOVA controlling for tumor volume and using tumor ROI values normalized by background whole-brain CBF demonstrated a similar statistically significant difference, with higher tumor blood flow ratio for GBM (mean  $\pm$  SD;  $3.3 \pm 1.6$ ) compared to TDL (mean  $\pm$  SD;  $1.5 \pm 0.4$ ) [ $F(1,27) = 11.733$ ,  $p = .002$ ].

**Figure 1****CONCLUSION**

Concordant with our hypothesis, maximum intratumoral blood flow measured with PASL was greater in GBM compared to TDL. This finding likely reflects histopathologic characteristics of GBMs, which are known to be exuberantly angiogenic. Measuring maximum intratumoral blood flow on PASL images at the clinical workstation using standard ROI tools represents a simple, noninvasive method for evaluating brain tumors, providing an additional approach for distinguishing GBM from TDL.

**KEY WORDS:** Arterial spin labeling, glioblastoma multiforme, tumefactive demyelination

**O-105****4:04 PM - 4:12 PM**

### Advanced 3.0 T MR Sequences in Assessing for Malignant Transformation of Low-Grade Gliomas

Craven, I. J.<sup>1</sup>•Romanowski, C. A.<sup>1</sup>•Jellinek, D. A.<sup>1</sup>•McKevitt, F.<sup>1</sup>•Larsen, J.<sup>1</sup>•Metherall, P.<sup>1</sup>•Currie, S.<sup>2</sup>•Griffiths, P. D.<sup>2</sup>•Wilkinson, I. D.<sup>2</sup>•Hoggard, N.<sup>2</sup>

<sup>1</sup>Royal Hallamshire Hospital, Sheffield, UNITED KINGDOM, <sup>2</sup>University of Sheffield, Sheffield, UNITED KINGDOM

**PURPOSE**

All patients with apparent low-grade gliomas (LGG) in our institution undergo a period of MR surveillance to try and identify the subpopulation who subsequently may undergo transformation into higher grade tumors and would thus benefit from adjuvant treatment. Imaging is performed at 3 monthly intervals until the tumor is characterized; if the tumor is felt to be benign the interval is increased to 6 months.

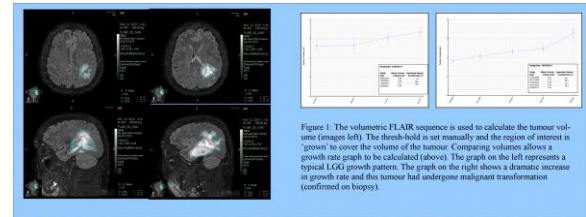
**MATERIALS & METHODS**

All patients undergoing surveillance are imaged using 3.0 T MR protocol including volumetric FLAIR, MR spectroscopy (MRS), MR perfusion and MR diffusion-weighted imaging. Semiautomated postprocessing software (MIM) utilizing thresholding and region growing techniques was used to calculate tumor volumes. In patients with sequential studies the growth rate of the tumor was calculated and spatial coregistration was used to assess apparent areas of tumor growth. We performed retrospective analysis of

all patients on our LGG surveillance program with respect to the following: • Tumor volumes. • MR spectroscopy. • MR perfusion. • MR diffusion. We compared a subgroup of patients who had histologic proof of transformation with the total population undergoing surveillance.

**RESULTS**

A total of 265 examinations on 121 patients were reviewed. Seventy-eight of 121 had more than one examination. Twenty of 78 patients underwent biopsy or resection based on clinical and/or radiologic suggestion of progression and 18/20 had confirmed grade 3 or 4 glioma. When compared to the nontransformers, the transforming group had a higher mean volume at presentation (53 ml vs 27 ml) and an increased equivalent annual growth rate (56.7% vs 27.6%). In those with suspected progression, MRS demonstrated a mean Cho/Cr peak ratio of 1.89 and mean rCBV ratio was 4.06. Of the 20 patients where transformation had been predicted radiologically, 13/20 either showed no abnormal contrast enhancement or no change in enhancement pattern from the previous study. Perfusion and diffusion data from the coregistered longitudinal studies also will be available.

**CONCLUSION**

Advanced MR techniques can be used to help predict tumors that transform and often before more conventional markers of progression (e.g., contrast enhancement). The semiautomated volumetric analysis can be used in a clinical setting and provides knowledge of the growth pattern which can help guide clinical management. Spatial coregistration of longitudinal studies allows subanalysis of the more active elements of the tumor and can help target biopsy.

**KEY WORDS:** Low-grade glioma, volumetric analysis, MR perfusion

**O-106****4:12 PM - 4:20 PM**

### Elevated Myoinositol in Diffuse Astrocytomas: A Marker of Anaplastic Phenotype, and Not Attributable to Microglial Infiltration

Updahyay, N. •Roncaroli, F. •Waldman, A. D.

Imperial College  
London, UNITED KINGDOM

**PURPOSE**

The relationship between MRS-visible metabolite levels in vivo and glioma grade has been investigated extensively, although the relevance of myoinositol (Myo) to grade and malignant transformation is less

well established. Moreover, the moieties and cell types that contribute to the detectable Myo pool have not been elucidated. Microglial infiltration has been associated with Myo elevation in inflammatory and neurodegenerative diseases, and has been implicated as having a role in neoangiogenesis and the malignant transformation of gliomas. The aim of this study was to examine the relationship between Myo, Cho and relative cerebral blood flow (rCBV), in grade II and III astrocytomas, and compare the imaging biomarkers with enzymatic markers of Myo synthesis and microglial cell type in tissue specimens from these gliomas.

#### MATERIALS & METHODS

Twenty-eight patients with histologically confirmed diffuse astrocytomas (14 diffuse low grade, WHO grade II; 14 anaplastic, WHO grade III) were included (13 stereotactic biopsies, 15 surgical specimens). All had multivoxel spectroscopic acquisition as part of a multimodal physiologic MRI protocol performed at either 1.5 T or 3 T (TE = 30ms, TR = 1500ms, 8x8 grid; Siemens Avanto/Verio, Erlangen, De). Metabolite ratios were estimated using proprietary software, following visual inspection of spectra for quality and satisfactory resonance peak fitting in the frequency domain. Relative cerebral blood volume (rCBV) was measured semiquantitatively using gradient echo dynamic susceptibility (DSC) MRI in 20 patients. Tissue immunostains with rabbit polyclonal antibodies directed against human inositol monophosphatase (IMPA1; Sigma - dilution 1:400; 25 cases) and Iba1 (Wako - dilution 1:750; 21 cases), were assessed semiquantitatively. The Kruskal-Wallis test was used to compare metabolite ratios and Wilcoxon rank-sum test was used to compare metabolite ratios and Iba-1 and IMPA1 levels between the groups. Spearman's rank correlation coefficient was used to compare Myo/Cr with Cho/Cr, and Myo/Cr with Iba1. Fisher's exact test was used to compare the proportion of voxels with the highest Myo/Cr co-localized with highest Cho/Cr and rCBV.

#### RESULTS

Myoinositol/Cr was significantly lower in grade II tumors compared with grade III tumors ( $p < 0.01$ ). The voxel with the highest Myo/Cr colocalized with the voxel with the highest Cho/Cr in 72% of cases, high Myo/Cr did not colocalize with regions of high CBV in the majority of gliomas. IMPA1 scores were significantly higher in grade III compared to grade II lesions ( $p < 0.01$ ). There was no correlation between semiquantitative microglial analysis using Iba1 antibody and Myo/Cr or tumor grade.

#### CONCLUSION

1. Positive correlation between Myo ratios and grade differs from other published data, but may reflect differences in MRS methodology and the previous comparisons including GBM (Grade IV) and oligodendrogliomas. 2. Higher Myo in grade III than grade II astrocytomas inferred from both MRS and immunohistochemistry suggests that this metabolite is not a marker of indolent tumor phenotype. 3. The lack

of correlation between Myo levels on MRS and microglial abundance does not support the hypothesis that microglia account for raised Myo levels in gliomas. 4. Poor spatial colocalization between high Myo/Cr and rCBV supports the view that they reflect different pathophysiologic processes associated with malignant transformation.

**KEY WORDS:** Glioma, spectroscopy, myoinositol

**O-107**

**4:20 PM - 4:28 PM**

#### Metabolic Characterization of Intracranial Lymphoma Using Hyperpolarized [1-<sup>13</sup>C] Pyruvate at Ultra-High Field (14 T)

Wilson, D. M. • Keshari, K. • Sukumar, S. • Rubenstein, J.

University of California San Francisco  
San Francisco, CA

#### PURPOSE

We tested the hypothesis that CSF metabolites reflect abnormal cerebral metabolism in CNS lymphoma patients and might lead to the identification of new diagnostic and prognostic biomarkers. Two novel approaches to model the metabolic microenvironment in CNS lymphoma were pursued: (1) Metabolic profiling of CSF and (2) Metabolic imaging using hyperpolarized (HP) <sup>13</sup>C probes in preclinical models.

#### MATERIALS & METHODS

**CSF metabolite analysis:** Gas chromatography- mass spectroscopy (GC-MS) was employed to profile a broad spectrum of metabolites (> 140) in CSF from CNS lymphoma. **Murine lymphoma xenografts:** Implantation of a Burkitt's cell line (Raji) into the brains RAG-deficient mice was performed, with tumor progression monitored by bioluminescence. **MR imaging methods:** In vivo MR studies were performed on a 14 T, 600WB micro-imaging spectrometer equipped with 100G/cm gradients (Varian Instruments). For <sup>13</sup>C pyruvate studies, an echo planar imaging-based pulse sequence has been constructed using frequency-specific pulses to generate a 3D image for each metabolite with an acquisition time of approximately 180 ms.

#### RESULTS

Metabolite concentrations in CSF from 15 subjects with active CNS lymphoma were compared to 15 controls without brain tumors. Seventeen metabolites were significantly higher in CSF (> two-fold) compared to controls ( $p < 0.05$ ). CSF concentrations of lactate were higher in patients with refractory lymphoma compared to chemotherapy-sensitive tumors. In vivo studies in Raj mice were performed at 14 T, with correlative histopathology. Typical results are shown in **Figure 1**, demonstrating significant differences between lymphoma and normal brain using both conventional <sup>1</sup>H imaging and HP <sup>13</sup>C pyruvate. HP [1-<sup>13</sup>C] pyruvate imaging demonstrated striking elevation in HP [1-<sup>13</sup>C] lactate in tumor.

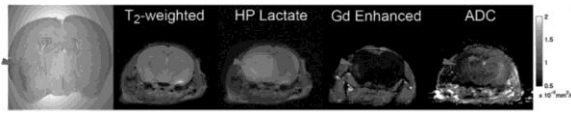


Figure 1. Typical MR data obtained for an implanted Burkitt's lymphoma (Raji) mouse at 14T. Corresponding to the region of infiltrating tumor identified on H&E staining, signal abnormality was seen on T<sub>2</sub> FSE, hyperpolarized <sup>13</sup>C lactate imaging, T<sub>1</sub> Gd post-gadolinium, and apparent diffusion coefficient (ADC) mapping.

## CONCLUSION

Elevated serum lactate dehydrogenase (LDH) is a hallmark of lymphoma, and is correlated with disease relapse/recurrence in several lymphoma subtypes. As for other cancers, enhanced expression of LDH (with a concomitant rise in lactate) reflects a primitive phenotype shifted away from oxidative phosphorylation and towards flux through glycolysis, consistent with the Warburg hypothesis. This phenotype not only reflects the elevated energy demands of tumor, but also relates to tumor progression, with acidification of the tumor microenvironment promoting local invasion. Our hypothesis that changes in CSF lactate seen in PCNSL patients relate directly to tumor adaptation and disease aggressiveness. GC-MS studies on the CSF of lymphoma patients demonstrated significant elevations in lactate. Studies in a murine model using HP <sup>13</sup>C spectroscopy suggest that metabolic imaging will provide new diagnostic and prognostic biomarkers for CNS lymphoma.

**KEY WORDS:** Hyperpolarized, lymphoma, pyruvate

## Monday Afternoon

**3:00 PM - 4:30 PM**  
**Trianon Ballroom**

**(15b) Adult Brain: New**  
**Techniques/Post Processing - II**

**O-108**

**3:00 PM - 3:08 PM**

**Noncontrast MR Angiography Using Pseudo-Continuous Arterial Spin Labeling and 3D Radial Sampling: Initial Clinical Experience**

Rusinak, D.·Wu, H.·Johnson, K.·Wu, Y.·Turski, P.

University of Wisconsin  
Madison, WI

## PURPOSE

To introduce a novel time resolved, noncontrast MRA technique that provides high-resolution whole brain MR angiograms with 200 ms temporal resolution.

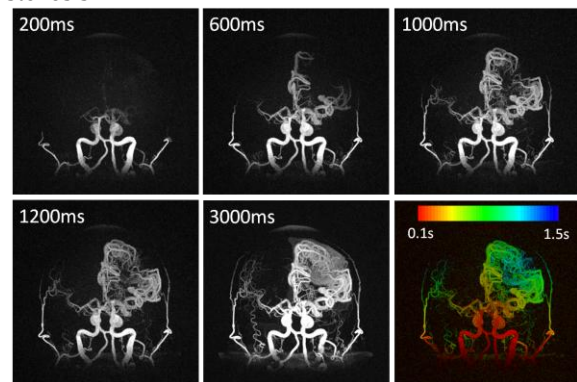
## MATERIALS & METHODS

PCASL-VIPR uses flow-driven adiabatic inversion to efficiently label spins passing through an axial slice just below the skull base. Varying the duration of the labeling pulse controls the length of the bolus allowing visualization of filling dynamics. PCASL-VIPR utilizes a

highly undersampled 3D radial SPGR readout to allow for high-resolution whole-brain PCASL angiograms in clinically feasible scan times. We have collected time-averaged acquisition with a single 3s tag and time-resolved images following labeling durations of 0, 200, 400, 600, 800, 1000, 1500 and 3000 msec (total scan time 6 min). To assess image quality two investigators were presented with source images and MIPs from 3D TOF and time-averaged PCASL-VIPR exams on a PACS workstation. Vessel conspicuity and saturation artifacts were evaluated on a four-point scale. Eight vessel segments were evaluated in 10 subjects and pathologic conditions (AVM, aneurysm, stenosis) were evaluated for each of the five patients. A Wilcoxon signed rank method was used to test for a significant ( $p < 0.05$ ). Time resolved images were evaluated for filling pattern visualization and time of arrival measurements.

## RESULTS

The figure shows 200, 600, 1000, 1200, and 3000 msec images from a patient with an AVM and the time of arrival map generated using the complete dataset. Our image quality evaluation in volunteer subjects demonstrated that the PCASL-VIPR provides diagnostic quality images equivalent to 3D TOF with less saturation artifacts (Wilcoxon signed rank method  $p < 0.5$ ). Our preliminary experience indicates that PCASL-VIPR is able to show differential filling rates in normal and pathologic vessels and is particularly useful for delineating the arterial supply to AVMs and detecting reduced flow in patients with arterial stenosis.



## CONCLUSION

PCASL-VIPR provides time-resolved images with temporal resolution of 200 msec. The images are free of limitations related to bolus dispersion or bolus timing. The initial clinical experience shows that the technique has fewer artifacts related to saturation effects compared to 3D TOF and provides quantitative measurement of arterial time of arrival.

**KEY WORDS:** MR angiography, noncontrast, ASL



O-109

3:08 PM - 3:16 PM

### **Combined Cerebral Perfusion Imaging, Contrast-Enhanced MR Angiography, and Phase-Contrast Flow Analysis of the Cerebrospinal Veins Using a Single Dose of Blood-Pool Contrast: Test-Retest Reproducibility**

Huston, J. M.·Vigen, K.·Field, A.

University of Wisconsin  
Madison, WI

#### **PURPOSE**

Altered cerebral white matter perfusion is a component of the current hypothesis linking chronic cerebrospinal venous insufficiency (CCSVI) to the pathogenesis of multiple sclerosis. Dynamic susceptibility contrast (DSC) MRI is the most common technique for imaging cerebral perfusion. Using conventional gadolinium contrast agents, multiple injections would be needed for first-pass perfusion imaging, contrast-enhanced magnetic resonance angiography (CE MRA) and phase-contrast analysis of venous flow. Use of a blood-pool gadolinium contrast agent, such as gadofosveset trisodium, allows perfusion imaging and CE MRA with a single injection. The purpose of this study is to evaluate the feasibility of a comprehensive CCSVI imaging protocol comprising perfusion, CE MRA, and venous flow quantitation from a single injection of blood-pool contrast, and to assess the test-retest reproducibility of cerebral perfusion parameters derived from this protocol.

#### **MATERIALS & METHODS**

A single dose of gadofosveset trisodium (Ablavar, Lantheus Medical Imaging, 0.03 mmol/kg at 3 mL/s) was used to obtain first-pass DSC perfusion, contrast-enhanced MRA, and time-resolved PC-VIPR MRV imaging in six healthy volunteers on a clinical 3 T system. Cerebral blood flow (CBF), cerebral blood volume (CBV), and mean transit time (MTT) maps were coregistered to axial T1-weighted MRI and symmetric regions of interest (ROI) were placed over bilateral centrum semiovale (fixed ellipse, area 265 mm<sup>2</sup>) to obtain mean white matter CBF, CBV, and MTT for each exam. Volunteers were repeatedly imaged on two separate days to assess reproducibility of hemodynamic parameters using Bland-Altman analysis.

#### **RESULTS**

T2\* signal change with single-dose Ablavar was seen less than typical for more conventional gadolinium contrast agents as previously reported in pigs but remained sufficient to generate comparable parametric maps. Cerebral blood flow measurements ranged between 9.14-21.71 mL/100g/min on day 1 and 9.31-22.48 mL/100g/min on day 2 (limits of agreement, 2.76 +/- 10.71) . Cerebral blood volume measurements ranged between 0.66-2.08 mL/100g on day 1 and 0.90-1.95 mL/100g on day 2 (limits of agreement, 0.29 +/- 1.15). Mean transit time measurements ranged between 5.44-7.80 s on day 1 and 5.12-8.61 s on day 2 (limits of agreement, 0.08 +/- 1.05).

#### **CONCLUSION**

Dynamic susceptibility contrast MRI with single-dose blood-pool contrast is feasible, reproducible, maintains a cost profile similar to more conventional gadolinium-based agents, and can be combined with CE MRA and quantitative flow MRV without the need for multiple injections.

**KEY WORDS:** Blood pool contrast agent, cerebral perfusion, PC-VIPR

O-110

3:16 PM - 3:24 PM

### **Visualization of Extracranial-Intracranial Bypass by Noncontrast Time-Resolved MR Angiography Using Arterial Spin Labeling**

Tsuchiya, K.·Gomyo, M.·Ohara, A.·Imai, M.·Tateishi, H.·Nitatori, T.

Kyorin University  
Tokyo, JAPAN

#### **PURPOSE**

Our purpose was to assess the visualization of the extracranial-intracranial (EC-IC) bypass by using noncontrast time-resolved MR angiography that has been developed based on the arterial spin labeling (ASL) technique.

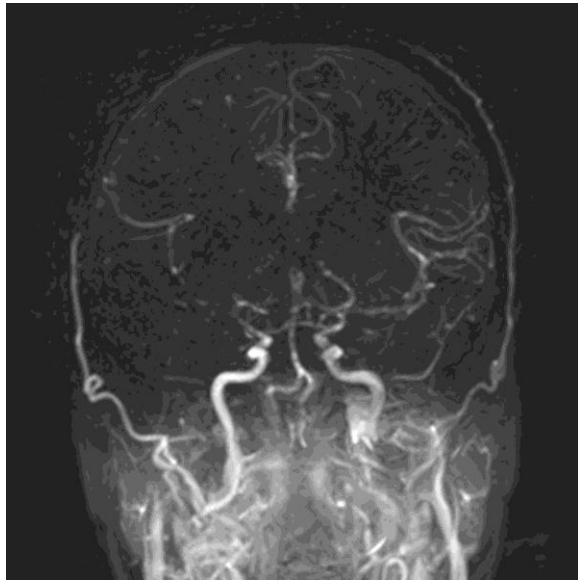
#### **MATERIALS & METHODS**

The patient group comprised a total of 26 patients (age range, 21-80 years; mean age, 59 years; 13 men and 13 women). Their disease included stenosis or occlusion of the internal carotid artery (14 patients) or the middle cerebral artery (MCA, five patients), moyamoya disease (five patients), and dissection in the vertebrobasilar system (two patients). Procedures of EC-IC bypass included a superficial temporal artery (STA) MCA bypass in 19 patients and a high-flow bypass by using a graft taken from the radial artery or other vessels in seven patients. Noncontrast time-resolved MR angiography was performed on a 1.5 T system using a 3D steady-state coherent gradient-echo sequence with parameters as follows: TR/TE/FA, 5.5 ms/2.5 ms/120 deg; FOV, 33x33 cm; imaging matrix, 256 x 256; slab thickness, 58 mm; and section thickness, 5 mm interpolated to 2.5 mm. In synchronization with the cardiac cycle by using the digital pulse wave, we performed 5-7 scans changing an inversion time by 200 ms in the coronal plane centered at the bypass site. Obtained images were compared visually with 3D time-of-flight (TOF) MR angiograms in all patients as well as digital subtraction angiograms in six patients regarding the visualization of the anastomosis and distal arterial branches. The assessment was done using a three-point grading system by consensus of two neuroradiologists.

#### **RESULTS**

Noncontrast time-resolved MR angiography better depicted anastomosis and distal arterial branches than 3D TOF MR angiography in 12 patients (46%), while the two techniques were equivalent in 14 patients (54%). Noncontrast time-resolved MR angiography

comparably demonstrated the bypass with digital subtraction angiography in the six patients.



#### CONCLUSION

Noncontrast time-resolved MR angiography is at least equivalent to 3D TOF MR angiography and conventional digital subtraction angiography to evaluate the postoperative status of EC-IC bypass.

**KEY WORDS:** Arterial spin labeling, MR angiography, bypass

**O-111**

**3:24 PM - 3:32 PM**

#### Cerebral Perfusion Postprocessing Using Vascular Territory-Based Region of Interest Analysis

Vakil, P.·Qian, R.·Habib, A.·Vranic, J.·Shaibani, A.·Ansari, S. A.·Carroll, T.·Hurley, M. C.

Northwestern University Feinberg School of Medicine  
Chicago, IL

#### PURPOSE

Sampling cerebral perfusion data involves the placement of discrete regions of interest (ROIs) on axial perfusion images. Regions of interest often are created by a radiologist in a simple clock face distribution which lacks vascular pathophysiologic coherence. This can result in a tailored but subjective assessment that cannot be compared easily serially or cross-sectionally. We illustrate an automated system of cerebral perfusion analysis using ROIs that conform to standard cerebrovascular anatomical landmarks.

#### MATERIALS & METHODS

Vascular territories were drawn by an experienced neuroradiologist on a normalized canonical T1 image using the MRIcron software. The following territories were considered: basilar; superior cerebellar, combined anterior inferior cerebellar/posterior inferior cerebellar; superior, inferior, and M1 perforator regions of the middle cerebral artery; posterior cerebral; and anterior cerebral arteries. These vascular territories

were registered automatically to each subject's cerebral MR perfusion (MRP) maps using the statistical parametric mapping software (SPM) package. MR perfusion parameters (cerebral blood flow and volume) were calculated in each vascular territory using MATLAB. The validity of this technique is demonstrated in 10 patients with neurovascular disease (six patients with acute ischemic stroke and four patients with chronic occlusive disease) who received DSC MRI perfusion and anatomical T1-weighted imaging as part of their neurovascular assessment. Automated vascular territory registration was assessed independently by two neuroradiologists to determine conformance to anatomical landmarks. A grade on a scale of 0-2 was assigned (0-poor, 2-excellent).

#### RESULTS

Vascular territory registration was performed with near perfect accuracy (average score of 1.9/2) for each territory. Figure 1a displays a canonical T1 image with overlaid vascular territories drawn as color coded ROIs. Figure 1b demonstrates the registered PCA territory of a single subject presenting with an acute embolic stroke in the right PCA. This can be visualized as reduced CBF in the right PCA vascular distribution in the MR CBF perfusion image (Figure 1c). This also is demonstrated in the vascular territory bar graph analysis which shows the qCBF values in gray matter of each vascular distribution (Figure 1d). In this figure, the blue line shows mean qCBF in healthy gray matter (55 ml/100g/min). The dotted blue lines demonstrate one standard deviation above and below the healthy mean.

#### CONCLUSION

We find that our automated ROI analysis may provide new insights into source of ischemia and an objective and reproducible means for evaluating vascular territory perfusion in patients with neurovascular disease.

**KEY WORDS:** Region of interest, vascular territory

**O-112**

**3:32 PM - 3:40 PM**

#### Evaluation of Cerebrospinal Venous Anatomy and Hemodynamics Using Isotropic-Voxel, Time-Resolved Phase Contrast Vastly Undersampled Radial Projection Imaging

Huston, J. M.·Schrauben, E.·Johnson, K.·Wieben, O.·Field, A.

University of Wisconsin  
Madison, WI

#### PURPOSE

Abnormal venous hemodynamics is a key concept in the current hypothesis of chronic cerebrospinal venous insufficiency (CCSVI) as a potentially causative factor in multiple sclerosis. Ultrasonography was the primary method used by Zamboni et al but several authors have since raised concerns regarding operator dependence and interobserver reproducibility of ultrasonography. PC VIPR is a novel magnetic resonance imaging (MRI) technique that may provide more objective,

reproducible imaging including both high-resolution 3D vascular anatomical images and hemodynamic measurements in 3D. The purpose of this study is to evaluate feasibility and reproducibility of PC VIPR imaging of the cerebrospinal venous system.

#### MATERIALS & METHODS

PC VIPR imaging of five healthy volunteers was performed on a clinical 3 T system. A single dose of gadofosveset trisodium (Ablavar, Lantheus Medical Imaging, 0.03-0.05 mmol/kg at 3 mL/s) performed "triple duty" as a contrast agent for first-pass perfusion, contrast-enhanced MRA, and PC VIPR. Cerebral, internal jugular (IJV) and azygous (AV) veins were imaged in three stages with neurovascular and cardiac phased-array coils. Maximum intensity projection imaging was performed with corresponding flow visualization in the form of vector fields. Peak and mean flow were measured from the dominant internal jugular vein at the levels of the jugular bulb and subclavian junction, and from the azygous vein. Volunteers were imaged repeatedly on two separate days for Bland-Altman analysis of test-retest reproducibility.

#### RESULTS

Cerebral veins, IJV, and AV were well depicted in 2D and 3D. At the level of jugular bulb, peak velocities within the dominant IJV ranged between 4.92-7.69 mL/s on day 1 and 3.40-9.30 mL/s on day 2 (limits of agreement, 0.78 +/- 4.68 mL/s). The mean velocities ranged between 3.25-4.95 mL/s on day 1 and 1.56-5.94 mL/s on day 2 (limits of agreement, 0.69 +/- 2.25 mL/s). At the level of the junction of the subclavian vein, peak velocities within the internal jugular vein ranged between 3.84-15.00 mL/s on day 1 and 2.32-19.96 mL/s on day 2 (limits of agreement, -2.80 +/- 12.68 mL/s). The mean velocities ranged between 1.11-7.95 mL/s on day 1 and 0.09-9.05 mL/s on day 2 (limits of agreement, -0.34 +/- 7.14 mL/s). At the level of the azygous veins, the peak velocities ranged between 5.45-9.11 mL/s on day 1 and 6.13-10.12 mL/s on day 2 (limits of agreement, -1.10 +/- 4.94 mL/s). The mean velocities ranged between 1.54-5.19 mL/s on day 1 and 1.02-4.63 mL/s on day 2 (limits of agreement, -0.36 +/- 1.79 mL/s).

#### CONCLUSION

PC VIPR is a feasible noninvasive technique that provides detailed evaluation of the cerebrospinal venous anatomy with flow quantitation in 3D and should provide more objective, reproducible imaging of CCSVI than operator-dependent ultrasonography. The addition of retrospective cardiac-respiratory double gating should further improve reliability of quantitative flow measurements.

**KEY WORDS:** Cerebrospinal venous anatomy, cerebrospinal venous hemodynamics, PC-VIPR

O-113

3:40 PM - 3:48 PM

#### Comparison between T1 TSE, T1 MPRAGE and Subtraction Postprocessing at 1.5 T and Comparison between T1 FLAIR, T1 MPRAGE and Subtraction Postprocessing at 3 T

Downs, R. K.·Bashir, M.·Heidenreich, J.

University of Louisville  
Louisville, KY

#### PURPOSE

Using contrast to background ratios to objectively compare the visibility of enhancing brain tumors (mostly metastases) of different sizes using 5 mm slice thickness T1 TSE and 1.5 mm slice thickness T1 MPRAGE for 1.5 T and compare 4 mm slice thickness T1 FLAIR with 1.5 mm slice thickness T1 MPRAGE at 3 T to determine which would be better for detection of small lesions. Each series also was subtracted digitally from its precontrast series and the contrast to background of lesions in the subtracted series was added to the comparison.

#### MATERIALS & METHODS

Approved IRB. Enrolled 13 patients with a total of 38 lesions at 1.5 T and 14 patients with a total of 55 lesions at 3 T. Used 1.5 T Siemens Espree and 3 T Siemens Verio. At 1.5 T precontrast and postcontrast T1 TSE (parameters TE 17, TR 400, FA 90, matrix 186 x 256, slice thickness 5 mm, gap 1.25 mm, FOV 200 x 220) and precontrast and postcontrast T1 MPRAGE (parameters TE 4.07, TR 894, FA 15, matrix 512 x 512, slice thickness 1.5 mm, gap 0 mm, FOV 350 x 350). At 3 T precontrast and postcontrast T1 FLAIR (parameters TE 12, TR 2610, TI 928, FA 120, matrix 202 x 320, slice thickness 4 mm, gap 1.2 mm, FOV 200 x 220) and precontrast and postcontrast T1 MPRAGE (parameters TE 2.89, TR 1190, FA 9, matrix 512 x 512, slice thickness 1.5 mm, gap 0 mm, FOV 350 x 350). Digital subtraction between each pre and postcontrast series type was performed. Contrast to background (C/B) signal intensity was measured using ROI over enhancement (centrally if solid, along the rim if ring enhancing) (Ce), ROI over contralateral normal brain of same type (Cb), and ROIs over nearest air (Ca) then calculating:  $C/B = (Ce - Ca) / (Cb - Ca)$ . For subtraction imaging Cb-Ca was occasionally zero or less, in these instances was defined as '1' to prevent inadvertent amplification. The data was graphed as C/B versus lesion size for each series and compared.

#### RESULTS

Subtraction provided the clear advantage in contrast to background with values ranging from 10x to 100x that of comparable sized nonsubtracted values. Thin section T1 MPRAGE provided increased contrast to background values compared to T1 TSE at 1.5 T but was inferior to T1 FLAIR at 3 T which increased with lesion size but for lesions less than 10 mm was not significant. One 2 mm lesion seen on 1.5 T MPRAGE was not seen on T1 TSE and in another patient one 3 mm lesion seen on 1.5 T T1 TSE was not seen on T1 MPRAGE.

## CONCLUSION

Subtraction provides a clear advantage in improved contrast to background for all lesion sizes compared to nonsubtracted T1 TSE, T1 FLAIR and MPRAGE at 1.5 T and 3 T. T1 MPRAGE provided mildly improved contrast to background compared to T1 TSE at 1.5 T but was mildly inferior to T1 FLAIR at 3 T, the difference progressed with lesion size. However, for small lesions (< 10 mm) which are what radiologists are most concerned about detecting there was no significant difference.

**KEY WORDS:** MR imaging, subtraction, postprocessing

**O-114**

**3:48 PM - 3:56 PM**

## Improved Subthalamic Nucleus Visualization Using Quantitative Susceptibility Mapping

Eskreis-Winkler, S.<sup>1</sup>Liu, T.<sup>2</sup>Kaplitt, M.<sup>1</sup>Tsiouris, A. J.<sup>1</sup>Wang, Y.<sup>1</sup>

<sup>1</sup>Weill Medical College of Cornell University, New York, NY, <sup>2</sup>MedImageMetric LLC, New York, NY

## PURPOSE

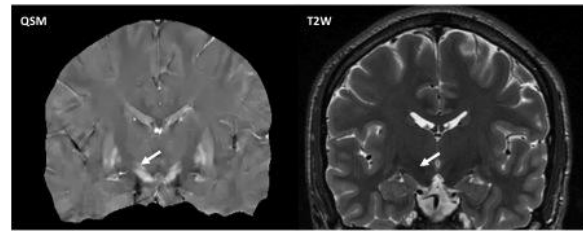
Neurosurgeons performing deep brain stimulation procedures on Parkinson's disease patients often must pinpoint the precise location of the subthalamic nucleus (STN). However, the STN can be difficult to visualize on conventional MR images, often T2-weighted (T2W) images. Since the STN is a site of iron deposition in the brain, it appears hyperintense on quantitative susceptibility mapping (QSM), a recently developed MRI technique that is sensitive to the presence of iron. The purpose of this study is to test the hypothesis that QSM is better than T2W for delineating the STN.

## MATERIALS & METHODS

Five healthy volunteers were imaged using a T2W fast spin-echo sequence and a multiecho gradient-echo sequence with identical resolution ( $0.75 \times 0.75 \times 2 \text{ mm}^3$ , 40 coronal slices) and similar scan time (under 5 min) on a 3 T MRI system. Quantitative susceptibility mapping was reconstructed from the gradient echo sequence. The contrast-to-noise ratios (CNRs) of the STNs in the T2W and QSM images for each subject were measured using a 1D signal intensity plot through the STN. The peak STN voxel value minus the minimum voxel value of the neighboring background was taken as the contrast. Noise was measured from a region of interest inside the lateral ventricle by calculating the standard deviation of the signal intensity. A paired t-test was performed on the STN CNRs to assess the difference between T2W and QSM.

## RESULTS

The CNRs of the STN were on average 3.89 on T2-weighted images and 51.18 on QSMs, a 13 fold improvement ( $p = 0.010$ ). An example case is illustrated in Fig.1 (arrow points to right STN).



## CONCLUSION

Quantitative susceptibility mapping provides better CNR for depicting the STN than conventional T2W imaging, and may be helpful to neurosurgeons planning deep brain stimulation procedures on Parkinson's disease patients.

**KEY WORDS:** QSM, STN, Subthalamic nucleus

**O-115**

**3:56 PM - 4:04 PM**

## Pitfalls of 3D FLAIR Brain Imaging: A Prospective Comparison with 2D FLAIR

Kakeda, S.<sup>1</sup>Korogi, Y.<sup>1</sup>Hiai, Y.<sup>2</sup>Ohnari, N.<sup>1</sup>Sato, T.<sup>1</sup>Hirai, T.<sup>3</sup>

<sup>1</sup>University of Occupational and Environmental Health School of Medicine, Kitakyushu-shi, JAPAN, <sup>2</sup>Kumamoto University, Kumamoto-shi, JAPAN, <sup>3</sup>Kumamoto University School of Medicine, Kumamoto-shi, JAPAN

## PURPOSE

Several authors have reported advantages of 3D fluid-attenuated inversion-recovery (FLAIR) over 2D FLAIR especially in the detection of MS lesions. To our knowledge, however, no previous studies have systematically compared 2D and 3D FLAIR. The purpose of our present study was to compare prospectively the image contrast of various brain lesions on 2D and 3D FLAIR images and to highlight the **pitfalls of 3D FLAIR**.

## MATERIALS & METHODS

In this prospective study, 130 patients suspected of having brain lesions on the basis of clinical history or neurologic findings underwent MR imaging with 2D and 3D FLAIR, and a total of 94 different lesions were evaluated. The conspicuity and detection of the various lesions were assessed qualitatively, and the contrast ratio between the gray or white matter and lesions was calculated as a quantitative assessment. We also performed a phantom study to investigate the effects of different flow velocities on 2D and 3D FLAIR.

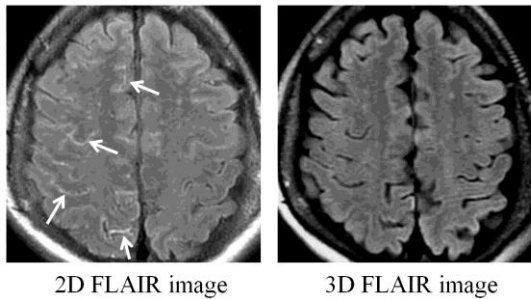
## RESULTS

With regard to the conspicuity and detection, 3D FLAIR was equal or superior to 2D FLAIR for multiple sclerosis, ischemic lesions or infarction, brain tumors, and chronic trauma. For these lesions, the mean contrast ratios were higher on 3D FLAIR than on 2D FLAIR images. In terms of the conspicuity of the extraaxial tumors (meningioma and schwannoma) and the subarachnoid hemorrhage, 3D FLAIR were also superior to 2D FLAIR due to the uniform suppression of the cerebral spinal fluid (CSF) signal eliminating CSF pulsation artifacts. However, 3D FLAIR was sometimes



inferior to 2D FLAIR in terms of lesion conspicuity in the patients with hippocampal sclerosis and leptomeningeal metastasis. Moreover, the ivy sign in patients with moyamoya disease frequently was obscured on 3D FLAIR compared with 2D FLAIR (**Fig., arrows**). The phantom study demonstrated that the signal intensity ratio on 3D FLAIR decreased more rapidly with increasing velocity than that on 2D FLAIR, which might result in a difference in the depiction of the ivy sign between both sequences.

Fig. Moyamoya disease in a 34-year-woman.



#### CONCLUSION

Although 3D FLAIR may replace 2D FLAIR images for most patients, the radiologists should keep in mind that 3D has some pitfalls.

**KEY WORDS:** 3D FLAIR, ivy sign, pitfall

**O-116**

**4:04 PM - 4:12 PM**

#### Cortical Volume Measurements in Freesurfer 4.5 and 5.0

Tanabe, J. L. • Krmpotich, T. • York, P. • Rojas, D. • Miller, D.

University of Colorado Denver  
Denver, CO

#### PURPOSE

Quantitative neuroimaging tools are useful for studying neurologic and psychiatric disorders but their application remains largely limited to research. Freesurfer (FS) is one tool that measures regional cortical volume and thickness based on 3 D surface modeling of cortical and sulcal topology. Editing and long computation times are major impediments to translating FS to the clinic. Updates to FS (v5.0) optimize algorithms and shorten computation time, but validations across versions have not been performed. The goal of this study was to evaluate the consistency of cortical volume measurements obtained from fully automated FS v5.0 to edited FS v4.5.

#### MATERIALS & METHODS

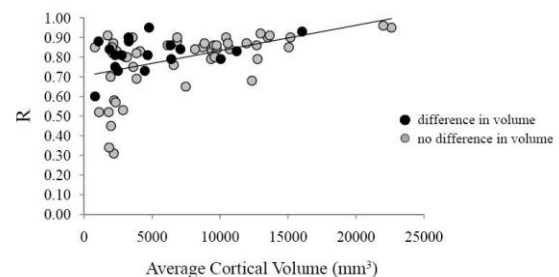
Fifty-four adults ( $35.6 \pm 8.1$  years) were scanned on a 3 T MR system using a quadrature head coil. T1-weighted SPGR-IR images were acquired (TR 45, TE 20, FA 45°, 256², .9 x .9 mm² in-plane, 1.7 mm thick). Images were processed with FS v4.5. A trained researcher corrected inaccuracies in white/gray matter boundary and pial surface. The same dataset then was analyzed with FS v5.0. Editing was not conducted on this dataset because

we wanted to assess the performance of fast and fully automated processing to a “gold standard” (i.e., edited and verified) dataset. Cortical volumes in 34 gyral-based regions (Desikan’s atlas) were obtained for each hemisphere. Statistical analyzes: Volumes were compared with 2-tailed, paired t-test,  $p < .001$ , corrected for 34 multiple comparisons. Volumes were correlated across versions.

#### RESULTS

Correlations are plotted as a function of volume, with each sphere representing a region. There was generally good correlation between versions of FS (r-value range: .31-.96, median: .84). The weakest correlations were in smaller regions. Differences in volume were found in 18/64 (28%) regions (black spheres) independent of region size or correlation strength. There was no consistent direction of volume differences.

Correlation between 4.5 vs 5.0 as a function of volume



#### CONCLUSION

Cortical volumes from fully automated FS v5.0 showed modest to strong correlations with FS v4.5. Weak correlations in smaller regions may be relate to statistical noise. Regardless of correlation, however, volumes differed significantly in a large number (28%) of regions in FS v5.0 compared to v4.5. Reasons for differences across versions are unknown and not likely due to editing as they were seen in regions that typically require no editing (cingulate, insula, and middle frontal gyrus). In conclusion, while computation is faster in FS v5.0 compared to v4.5, inconsistencies across versions and a continued need for editing are impediments to translating FS v5.0 into the clinical workflow.

**KEY WORDS:** Freesurfer, cortical volume, postprocessing

O-117

4:12 PM - 4:20 PM

### Evaluation of Metal Artifact Reduction Techniques Using 2D View Angle Tilting and Slice-Encoding for Metal Artifact and 3D Multi-Slab Acquisition with View Angle Tilting Gradient, Based on SPACE (MSVAT-SPACE) Techniques in Brain Imaging at 1.5 and 3 T

Trelles de Belaunde, M.<sup>1</sup>Goerner, F.<sup>1</sup>Ai, T.<sup>2</sup>Padua, A.<sup>3</sup>Nittka, M.<sup>4</sup>Runge, V.<sup>1</sup>

<sup>1</sup>University of Texas Medical Branch at Galveston, Galveston, TX, <sup>2</sup>Tongji Hospital, Huazhong University of Science and Technology, Wuhan, CHINA, <sup>3</sup>Siemens Healthcare, Houston, TX, <sup>4</sup>Siemens Healthcare, Erlangen, GERMANY

#### PURPOSE

To evaluate 2D standard FSE sequences (STANDARD), sequences with optimized BW for metallic artifact suppression (OPTIMIZED) and the work in progress sequences View Angle Tilting (VAT) and Slice-Encoding for Metal Artifact with View Angle Tilting (SEMAC-VAT) and the 3D sequence Multi-Slab Acquisition with VAT based on the SPACE Sequence (MSVAT-SPACE) in brain imaging for the reduction of metallic artifacts at 1.5 and 3 T.

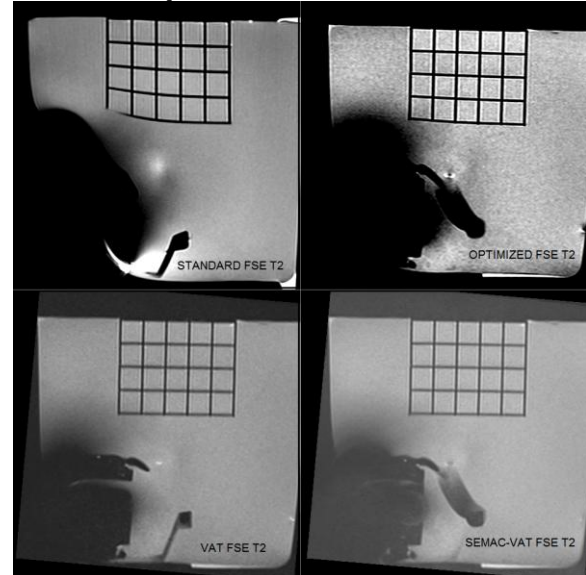
#### MATERIALS & METHODS

Agarose phantoms with two different aneurysm clips and an agarose phantom built to simulate a head with braces were imaged at 1.5 T (Espree, Siemens Healthcare) and 3 T (Verio, Siemens Healthcare) evaluating 2D FSE T1, T1 FLAIR (at 3 T), T2 and T2 FLAIR sequences using STANDARD, OPTIMIZED, VAT and SEMAC-VAT techniques and 3D MSVAT-SPACE, SPACE, MP-RAGE and FLASH sequences. A healthy volunteer with braces was imaged at 1.5 T. Artifact size was calculated for the aneurysm clips and SNR was obtained for all sequences. These values were reported as a percentage of the value on the STANDARD sequence to better quantitate the effect of BW optimization, VAT and SEMAC-VAT techniques. A blinded read was performed on images from the metal braces phantom and healthy volunteer to measure geometric distortion, blurring, size of artifact and overall image quality by an experienced neuroradiologist.

#### RESULTS

Overall aneurysm clip artifact size was reduced by 32.9%, 51.3% and 53.7% for OPTIMIZED, VAT and SEMAC-VAT. SNR was reduced by 34.4%, 49.7% and 44.4% respectively. At 1.5 T, VAT and SEMAC-VAT provide an additional 15.2% and 17.9% reduction in artifact size to bandwidth optimization. The results were more marked at 3 T with 21.6% and 23.8% additional reduction in artifact size. 3D imaging showed an overall artifact reduction of 38.5% for MS-VAT SPACE when compared to standard SPACE with MP-RAGE and FLASH showing even larger artifact sizes (approximately 376% and 665% larger than standard SPACE, respectively). The blinded read consistently ranked artifact size and geometric distortion from

largest to smallest STANDARD, OPTIMIZED and VAT = SEMAC-VAT. Blurring was greatest in the VAT and SEMAC-VAT sequences followed by the OPTIMIZED and STANDARD sequences.



#### CONCLUSION

MSVAT-SPACE, VAT and SEMAC-VAT sequences provide additional improvement for metallic artifacts on MRI by reducing artifact size and field distortion over that achievable with bandwidth optimization. The additional improvement was more evident at 3 T. Potential limitations include decreased SNR, blurring, incremental imaging time and increased SAR deposition especially at 3 T and with SEMAC technique.

**KEY WORDS:** Metal artifact, VAT, SEMAC

O-118

4:20 PM - 4:28 PM

### Effects of Increased Noise on Image Quality and Quantitative Interpretation in Low-Dose CT Perfusion

Shih, J.·Juluru, K.·Liu, Y.·Herrmann, C.·Hoelscher, A.·Raj, A.·Comunale, J.·Delaney, H.·Greenberg, E.·Sanelli, P.

Weill Cornell Medical College/New York Presbyterian Hospital  
New York, NY

#### PURPOSE

To determine the effects of increased noise on image quality and quantitative interpretation in low-dose CT perfusion (CTP).

#### MATERIALS & METHODS

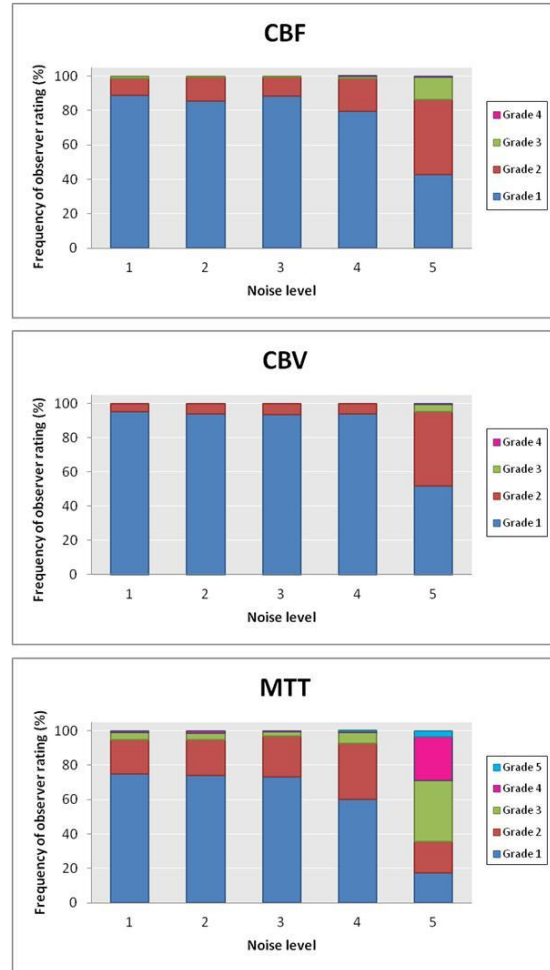
Retrospective analysis of 20 consecutive CTP in subarachnoid hemorrhage patients was performed. The acquired CTP was used as the reference dataset scanned with standard protocol (190mA, 80kVp, 5.0mm slices). Varying amounts of spectral noise were applied to the reference to generate noise-simulated datasets estimating different tube current levels (188, 177, 167, 127, 44mA). Standardized methods were used to postprocess datasets into cerebral blood flow (CBF),

cerebral blood volume (CBV), and mean transit time (MTT) maps. *Qualitative analysis:* Six blinded radiologists determined quality scores on a Likert scale (grade 1 as highest quality compared to reference image) using a software program that randomly displayed a noise-simulated CTP map with its reference for comparison. Spearman rank correlation coefficients determined the relationship between quality grade and noise level. Interobserver agreement was calculated by prevalence-adjusted bias-adjusted kappa values (PABAK). *Quantitative analysis:* Using standardized methods, 26 identical region-of-interest (ROI) placement sampling the cortex on each slice was performed. Mean and standard error of CBF, CBV and MTT were calculated. Paired two-tailed t-test determined statistical significance.

## RESULTS

A total of 1200 maps were generated; 400 CBF, 400 CBV and 400 MTT. There were 104 ROIs per subject per noise level for each map. *Qualitative analysis:* There were 7200 quality grades collected from six radiologists. The distribution of quality grades for each noise-simulated level for CBF, CBV and MTT is presented in Figure 1. The correlation coefficients for CBF ( $-0.34, p < 0.0001$ ), CBV ( $-0.35, p < 0.0001$ ) and MTT ( $-0.44, p < 0.0001$ ) were statistically significant. Interobserver agreement for noise levels 1-5 for CBF is 0.95, 0.98, 0.98, 0.95 and 0.52 respectively; CBV is 1, 1, 1, 1 and 0.83 respectively; and MTT is 0.83, 0.86, 0.88, 0.74 and 0.05, respectively. *Quantitative analysis:* Only noise level 5 showed statistically significant findings in the quantitative differences from the reference dataset for CBF ( $-1.8, p = 0.04$ ), CBV ( $0.07, p = 0.0006$ ) and MTT ( $0.45, p < 0.0001$ ). In a subgroup analysis of visual perfusion deficits, statistically significant differences also were seen only for noise level 5 for CBF ( $0.10, p < 0.0001$ ) and MTT ( $0.34, p = 0.0079$ ).

**Figure 1:** Distribution of quality scores for each noise-simulated level. (Noise level 5 has the greatest amount of spectral noise introduced, estimating 44mA.)



## CONCLUSION

Based on dose simulation techniques, CTP may be performed using 127mA to reduce radiation exposure while maintaining both image quality and quantitative interpretations. Statistically significant differences are only seen at the highest noise level (estimated 44mA) with worsening interobserver agreement potentially leading to interpretation variability. It may be possible to reduce radiation exposure further; however, continued investigation is warranted.

**KEY WORDS:** CT perfusion, radiation dose reduction

## Monday Afternoon

**3:00 PM - 4:30 PM**

**Beekman/Sutton North**

**(15c) Adult Brain:  
Degenerative/Demyelinating/Metabolic Diseases**

**O-119**

**3:00 PM - 3:08 PM**

### Scientific Paper (O)

Smith, E. A.

University of Michigan  
Ann Arbor, MI

**O-120**

**3:08 PM - 3:16 PM**

### White Matter Abnormalities in Late Life Depression: Relationship to Age and Treatment Response

Mettenburg, J. M.·Benzinger, T. L. S.·Shimony, J. S.·Snyder, A. Z.·Sheline, Y. I.

Washington University School of Medicine  
St. Louis, MO

#### PURPOSE

Traditional T2-weighted MR imaging results are nonspecific for the extent of underlying white matter structural abnormalities present in late life depression. Diffusion tensor imaging provides a unique opportunity to investigate the extent and nature of structural injury, but has been limited by examining only a subset of regions of interest and by confounds common to the study of an elderly population, including comorbid vascular pathology. Furthermore, comprehensive correlation of diffusion tensor imaging (DTI) measurements, including axial and radial diffusivity measurements, has not been demonstrated in the late life depression population.

#### MATERIALS & METHODS

Fifty-one depressed and 16 nondepressed, age- and cerebrovascular risk factor-matched elderly subjects underwent traditional anatomical T1- and T2-weight imaging, as well as DTI. The DTI data were skeletonized using tract-based spatial statistics (TBSS), and both regional and global analyses were performed. Relationships of the DTI findings with age and treatment response are explored and discussed.

#### RESULTS

Widespread structural abnormalities within white matter were detected, most prominent in uncinate and cingulate white matter, accounting for age, gender and education and matched for global T2 white matter hyperintensity volume. Regional differences generally were characterized by an increase in radial diffusivity. Age-related changes particularly in the cingulate bundle

were more advanced in individuals with late life depression relative to controls. Individuals in remission after 12 weeks demonstrate less extensive white matter abnormalities than individuals with persistent depressive symptoms, when compared to controls with TBSS.

#### CONCLUSION

White matter integrity is compromised in late life depression, largely manifested by increased radial diffusivity in specific regions, suggesting underlying myelin injury. A possible mechanism for underlying myelin injury is chronic white matter ischemia related to intrinsic cerebrovascular disease. In some regions such as the cingulate bundle, the white matter injury related to late-life depression appears to be independent of and compounded by age-related changes. White matter integrity may be necessary for successful treatment of late life depression, suggesting a need for intact functional networks.

**KEY WORDS:** Diffusion tensor imaging, late life depression, radial diffusivity

**O-121**

**3:16 PM - 3:24 PM**

### Interseptal Distance: A New Marker for Alzheimer Disease and Mild Cognitive Impairment

Gan, C. L.<sup>1</sup>·O'Sullivan, M.<sup>1,2</sup>·Halpin, S.<sup>1</sup>

<sup>1</sup>University Hospital of Wales, Cardiff, UNITED KINGDOM, <sup>2</sup>Cardiff University, Cardiff, UNITED KINGDOM

#### PURPOSE

Whilst the majority of the neuroimaging research in Alzheimer disease has been centered around mesial temporal lobe atrophy a few studies have shown subcallosal septal area atrophy in relation to Alzheimer disease. The subcallosal area and paraterminal gyrus, collectively known as the septal area, are part of the limbic system. The septal nuclei are subcortical gray matter nuclei deep to the septal area and are readily apparent on routine CT scans of the brain. Based on clinical observations, this paper tests a hypothesis that the distance between right and left septal nuclei is a surrogate measure for atrophy of these nuclei, and therefore potentially an easily quantifiable imaging marker for neurodegeneration.

#### MATERIALS & METHODS

(i) To observe the variation of the interseptal distance (ISD) within a population, ISD in 250 consecutive patients who had CT brain at University Hospital of Wales, Cardiff, U.K., excluding patients with intracranial mass lesions, large infarcts and history of neurosurgery, were measured independently by an experienced neuroradiologist and a second-year radiology trainee. Any history of Alzheimer disease, cognitive impairment or other chronic memory problems was noted. The measurements then were compared between the two assessors for reproducibility analysis. An optimum cut-off value was calculated between normal and abnormal values. (ii) To test our proposed ISD cut-off value in



Alzheimer disease patients, we measured the ISD from CT brain images in the first 20 patients from the memory clinic database who had established Alzheimer disease. (iii) To assess the value of applying the ISD cut-off value in mild cognitive impairment, ISD then was measured from MRI images of 66 datasets taken from a research study investigating structural correlates of ageing and mild cognitive impairment, including 21 patients with mild cognitive impairment and 45 age-matched healthy controls. The radiologists were blinded to clinical details.

## RESULTS

(i) Interseptal distance measurement was achieved in all 250 patients, taking only a few seconds each. Mean ISD for control patients was 2.3 mm; for those 28 patients with chronic memory problems was 5.9 mm ( $p = 0.001$ ), with an inter-rater coefficient of variation of 10.5% and an intraclass correlation coefficient of 0.96. The optimum cut-off between normal and abnormal ISD was assessed as 4 mm with sensitivity of 85.7% and specificity of 85.8%. (ii & iii) Mean ISDs for the different patient groups were: Alzheimer disease patients: 6.1 mm; mild cognitive impairment patients: 3.84 mm and healthy controls: 2.18 mm ( $p = 0.001$ ). All Alzheimer disease patients invariably had an ISD of more than 4 mm. Using a cut-off value of 4 mm, we correctly identified 10 mild cognitive impairment patients (47.6%) and 38 healthy controls (84.4%).

## CONCLUSION

To our knowledge, this is the first study that has demonstrated a highly accurate, simple, quick, reliable and reproducible quantitative measurement for septal area atrophy as a marker for neurodegenerative states. The results confirmed our hypothesis that Alzheimer disease and mild cognitive impairment patients have significantly wider ISD. Its use simplifies the imaging correlation of Alzheimer disease and mild cognitive impairment.

**KEY WORDS:** Interseptal distance, Alzheimer disease, mild cognitive impairment

O-122

3:24 PM - 3:32 PM

## Gray Matter Volume Loss in Patients with Alzheimer Disease: Is There a Gender Difference?

Weininger, M.<sup>1</sup>Vavro, H.<sup>1,2</sup>Patrick, K.<sup>1</sup>Parker, R. O.<sup>1</sup>Rumboldt, Z.<sup>1</sup>Spampinato, M. V.<sup>1</sup>

<sup>1</sup>Medical University of South Carolina, Charleston, SC,

<sup>2</sup>University Hospital Dubrava, Zagreb, CROATIA

## PURPOSE

Our purpose was to assess if there are gender specific differences in gray matter volume loss patterns in patients with newly diagnosed Alzheimer disease (AD) using voxel-based morphometry, a whole-brain analysis technique.

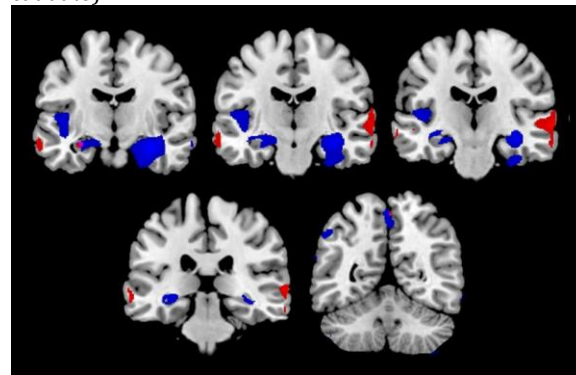
## MATERIALS & METHODS

Our study population included 83 patients (52 men, 31 women; mean age  $77 \pm 7$  years) from the Alzheimer's

Disease Neuroimaging Initiative (ADNI), who during study participation experienced progression from amnesic mild cognitive impairment (aMCI) to AD. Imaging and clinical evaluation of aMCI patients were obtained every 6 months as part of the ADNI protocol. Brain MRIs obtained 1 year before conversion from aMCI to AD, at the time of AD diagnosis, and after 12 months were available. Voxel-based morphometry with SPM5 was used to process MPRAGE images. The General Linear Model Repeated Measures was performed to evaluate for differences over time in disease severity, measured using the Clinical Dementia Rating (CDR) scale. Comparison between longitudinal imaging data was conducted using two-sample and paired t-tests. Results were considered significant when the  $p$ -value  $< 0.05$  after familywise error rate correction (FWER) for multiple comparisons.

## RESULTS

There was a significant progressive cognitive decline in both males and females ( $p < 0.001$ ) without significant interaction between CDR and gender. Baseline group comparison showed significantly greater atrophy in the posterior cingulate gyrus in females than males. Longitudinal analyzes revealed gender-specific differences in gray matter volume loss during the 12 months before AD diagnosis (women: bilateral uncus; men: right inferior frontal lobe; left inferior frontal lobe; right uncus;) and during the 12 months after AD diagnosis (women: left hippocampus; left superior and middle temporal gyrus; right superior and inferior temporal gyrus; right gyrus rectus; right superior parietal lobule; men: bilateral hippocampus and right parahippocampal gyrus; left insula; left superior frontal gyrus; left inferior parietal lobule; left precuneus, left caudate).



Coronal MRI images illustrating the areas of gray matter volume loss for women (red) and men (blue)

## CONCLUSION

Our data indicate that the extent and distribution of regional gray matter volume loss in patients with AD is strongly influenced by the gender, with men experiencing a faster rate of gray matter volume loss compared to women at the same disease stage. This finding has potentially important implications for therapeutic approaches in AD and should be taken into consideration in clinical trials.

**KEY WORDS:** Alzheimer disease, gray matter volume loss, voxel-based morphometry

O-123

3:32 PM - 3:40 PM

### 1H MR Spectroscopy Quantification and Partial Volume Effect Correction in Alzheimer Disease

Mato Abad, V.<sup>1,2</sup>•Hernández-Tamames, J.<sup>3,2</sup>•Álvarez-Linera, J. M.<sup>4,2</sup>•Pereira Loureiro, J.<sup>1</sup>•García-Álvarez, R.<sup>5</sup>•Ramos, A.<sup>6,2</sup>•Frank, A.<sup>7</sup>

<sup>1</sup>Centro IMEDIR. Universidad de A Coruña, A Coruña, SPAIN, <sup>2</sup>Laboratorio Neuroimagen Fundación CIEN-Fundación Reina Sofía, Madrid, SPAIN, <sup>3</sup>Universidad Rey Juan Carlos, Madrid, SPAIN, <sup>4</sup>Hospital Ruber Internacional, Madrid, SPAIN, <sup>5</sup>Research and Collaborations, General Electric Healthcare, Buc, FRANCE, <sup>6</sup>Hospital 12 de Octubre, Madrid, SPAIN, <sup>7</sup>Hospital Universitario La Paz, Madrid, SPAIN

#### PURPOSE

The aim of this study is to assess the convenience of applying methods of partial volume correction to reduce intersubject variability in <sup>1</sup>H magnetic resonance spectroscopy (<sup>1</sup>H MRS) studies. In particular, in studies of normal aging and neurodegenerative diseases, as Alzheimer disease.

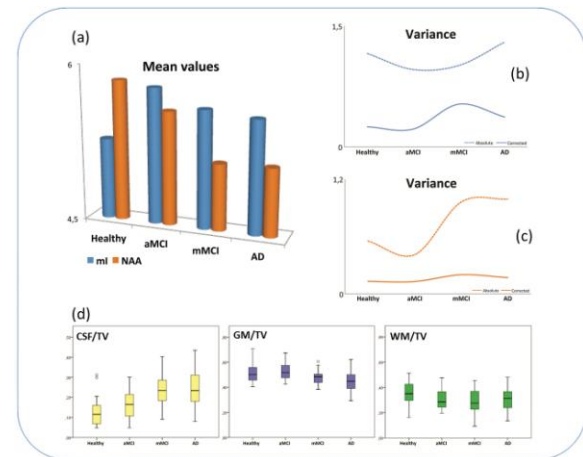
#### MATERIALS & METHODS

An automatic process has been developed with MATLAB software for: (1) Perform brain tissue segmentation from high-resolution 3D anatomical volume with SPM8 software; (2) Localize <sup>1</sup>H MRS voxel over the high-resolution 3D anatomical volume; (3) Calculate the partial volume of GM, WM and CBF within the voxel; (4) Quantify spectra using own in-house and LCModel software; (5) Finally, correct LCModel absolute quantifications by partial volume measurements. This process has been validated over 135 subjects belonging to DEMCAM project. These subjects (range 57-99 years) are classified into four groups as follows: 38 healthy participants, 20 amnesic mild cognitive impairment patients, 22 multidomain mild cognitive impairment patients (mMCI) and 55 Alzheimer disease patients (AD). <sup>1</sup>H MRS exam (single voxel PRESS: TR/TE=1500/35 ms) was performed from voxels placed in posterior cingulate and both hippocampus for each subject. Also, MRI 3D brain volume (SPGR TR/TE = 7/3 ms) was acquired for each subject. All MR data were acquired on a clinical 3.0T GE Signa HDx scanner.

#### RESULTS

Figure 1a shows mean values of ml and NAA metabolite concentrations along different groups. Figure 1b and Figure 1c show the variance values of ml and NAA respectively in each group for the absolute concentration and corrected by partial volume effect measures. It is very significant how increases the ml and decreases the NAA with the progression of the disease, varying the ratios behavior in each group, and the high reduction of the variability in each group after doing correction. Figure 1d shows how varying the voxel distribution of cerebrospinal fluid (CSF), gray

matter (GM) and white matter (WM) with respect to the total volume (TV) of the voxel for each group.



#### CONCLUSION

We found that quantification of metabolites after correction of the partial volume effect provides more accurate quantitative measurements, reduces the intersubject variability and improves the statistical results when performing group comparisons in studies of normal aging and neurodegenerative diseases. The automatic process developed facilitates the use of these techniques in statistical studies, improves the results of the <sup>1</sup>H MRS studies and reduces the sample size N, which suggests a potential for important research cost savings.

**KEY WORDS:** 1H MR spectroscopy, Alzheimer disease, quantification

O-124

3:40 PM - 3:48 PM

### Naming Impairment and Amnesic Mild Cognitive Impairment: A Cross-Sectional Voxel-Based Morphometry Study

Spampinato, M.<sup>1</sup>•Vavro, H.<sup>2</sup>•Patrick, K.<sup>1</sup>•Parker, R.<sup>1</sup>•Mintzer, J.<sup>1</sup>•Rumboldt, Z.<sup>1</sup>

<sup>1</sup>Medical University of South Carolina, Charleston, SC,

<sup>2</sup>University Hospital Dubrava, Zagreb, CROATIA

#### PURPOSE

Our goal was to evaluate gray matter volume loss patterns in patients with amnesic mild cognitive impairment (aMCI) with and without naming impairment using voxel-based morphometry (VBM).

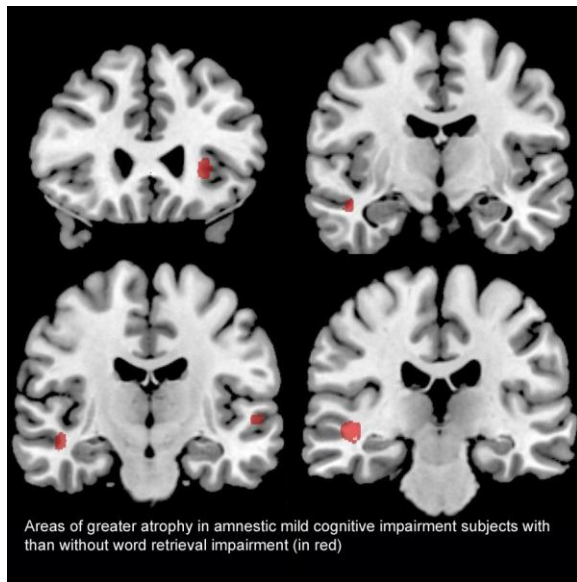
#### Materials & Methods

One hundred and one aMCI patients (73 males, median age 75 years) from the Alzheimer's Disease Neuroimaging Initiative (ADNI) with stable cognitive status over the course of at least 3 years were included in the study. The 30-item Boston Naming Test (BNT), a measure of word retrieval performance, was administered to all subjects at the time of recruitment in the study (median age 27 years, range 4-30 years). The sample was divided in two groups: 39 patients with BNT score below the median (low BNT), and 62 patients with BNT score equal or above the median (high BNT).

Clinical Dementia Rating (CDR) scale and CDR Sum of Boxes were obtained at baseline, and then after 12 and 24 months to assess disease severity. Pearson  $\chi^2$  test, one-way Anova, and General Linear Model Repeated Measures were used to compare demographic characteristics and disease severity between groups. Brain MRIs, obtained at the time of initial clinical evaluation and word retrieval performance assessment, were available for all subjects. Voxel-based morphometry with SPM5 was used to process MPRAGE images. Group comparison was conducted using a two-sample t-test. The results were considered significant if the p-value was less than 0.05 after familywise error rate correction (FWER) for multiple comparisons.

## RESULTS

There were no significant differences in gender distribution, years of education or disease severity at baseline, 12- and 24-month follow up between high BNT and low BNT aMCI subjects. There was a statistically significant difference in age between low and high BNT patients (low BNT median age [SD] = 76.8 [6.9]; high BNT median age [SD] = 73.6 [7.6],  $p = 0.038$ ); therefore age was included as a covariate in the VBM analysis. There was significantly lower GM volume in the low BNT than high BNT group in the right and left superior temporal gyri (respectively  $p < 0.001$  and  $p = 0.001$ ) and left insular cortex ( $p = 0.001$ ). There was no significant GM atrophy in the high BNT compared with the low BNT group.



## CONCLUSION

The spatial distribution and severity of GM atrophy differ in aMCI subjects with and without word retrieval impairment. MR imaging can improve our understanding of the complex relationship between GM volume loss, language impairment, and cognitive decline in patients with aMCI.

**KEY WORDS:** MR imaging, naming impairment, mild cognitive impairment

O-125

3:48 PM - 3:56 PM

## Phospho-Tau not APOE $\epsilon 4$ Modulates Amyloid- $\beta$ Associated Volume Loss in Cognitively Normal Older Individuals

Desikan, R. S.<sup>1</sup>McEvoy, L.<sup>1</sup>Thompson, W.<sup>1</sup>Holland, D.<sup>1</sup>Aisen, P.<sup>1</sup>Brewer, J.<sup>1</sup>Sperling, R.<sup>2</sup>Dale, A.<sup>1</sup>

<sup>1</sup>University of California San Diego, San Diego, CA,

<sup>2</sup>Harvard Medical School, Boston, MA

## PURPOSE

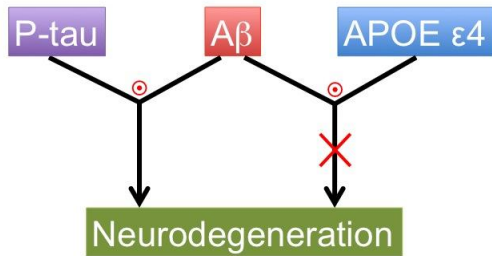
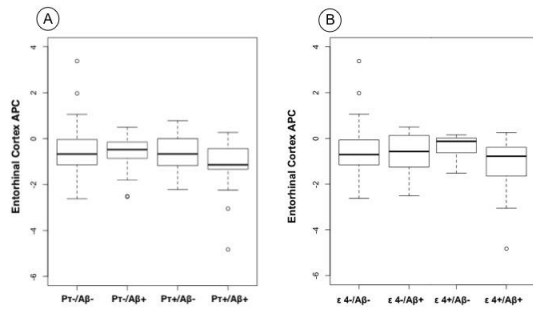
The relationship between neurodegeneration, the  $\epsilon 4$  allele of apolipoprotein E (APOE  $\epsilon 4$ ), and the two hallmark proteins of Alzheimer disease (AD), amyloid- $\beta$  ( $A\beta$ ) and tau, among cognitively normal older individuals is not well understood.

## MATERIALS & METHODS

We examined 107 clinically normal older participants (total of 417 longitudinal MRI scans). Using linear mixed effects models we investigated the interaction between CSF  $A\beta_{1-42}$  and both CSF p-tau<sub>181p</sub> (phospho-tau) and APOE  $\epsilon 4$  genotype on entorhinal cortex atrophy rate. We also examined the relationship between APOE  $\epsilon 4$  genotype, CSF  $A\beta_{1-42}$  and CSF p-tau<sub>181p</sub> on atrophy rate of other AD-vulnerable neuroanatomic regions.

## RESULTS

We found a significant interaction between CSF p-tau<sub>181p</sub> and CSF  $A\beta_{1-42}$  on entorhinal cortex atrophy rate. In the presence of CSF p-tau<sub>181p</sub>,  $A\beta$ -associated entorhinal cortex atrophy was increased; in the absence of CSF p-tau<sub>181p</sub>, the effect of CSF  $A\beta_{1-42}$  on longitudinal entorhinal volume loss was not significant. In comparison, we found no interaction between APOE  $\epsilon 4$  genotype and CSF  $A\beta_{1-42}$  on entorhinal atrophy rate. We found similar results in other AD-vulnerable regions.



#### CONCLUSION

In cognitively normal older individuals, phospho-tau modulates Aβ-associated degeneration. In contrast, the effect of APOE ε4 genotype on Aβ-associated volume loss is not significantly different from zero. Primary and secondary Ab prevention trials in cognitively normal older individuals should consider carefully this relationship between AD biomarkers.

**KEY WORDS:** Alzheimer disease, Tau, amyloid

**O-126**

**3:56 PM - 4:04 PM**

#### Microstructural Change of the Brain in Chronic Obstructive Pulmonary Disease: A Voxel-Based Investigation by MR Imaging

Ryu, C.<sup>1</sup>Jahng, G.<sup>1</sup>Rhee, H.<sup>1</sup>Choi, C.<sup>1</sup>Kim, S.<sup>1</sup>Kim, M.<sup>2</sup>

<sup>1</sup>Kyung Hee University Hospital, Seoul, KOREA, REPUBLIC OF, <sup>2</sup>Kyung Hee University, Seoul, KOREA, REPUBLIC OF

#### PURPOSE

A cognitive deficit is a common problem in patients with chronic obstructive pulmonary disease (COPD). The aim of this study was to evaluate prospectively if MRI can demonstrate the microstructural volume loss and the diffusion anisotropic change in subjects with COPD, compared with cognitively normal (CN) elderly subjects.

#### MATERIALS & METHODS

Institutional review board approval and informed consent were obtained. Six subjects with severe COPD (6 men, mean age, 69.8 years), 13 with moderate COPD (12 men, 1 women; mean age, 65.3 years), and 12 CN subjects (12 men, mean age, 63.9 years) underwent isotropic volumetric T1-weighted imaging and diffusion tensor imaging (DTI) with 32 directions and b-values of 0 and 800 sec/mm<sup>2</sup>. Voxel-based statistical analyzes among groups were performed on brain volumes, fractional anisotropy (FA) and trace. Cognitive function tests (CFT) were performed in all subjects, and the CFT scores were compared among three groups.

#### RESULTS

There wasn't any significant regional difference of gray matter in both severe and moderate COPD groups compared with the normal control group. Comparing between severe COPD and CN or between severe and moderate COPD, FA reduced extensively in both the cerebral cortex, frontoparietal periventricular white matter and the corticospinal tract. The trace value of the moderate COPD group was significantly higher in bilateral occipital cortices, left hippocampus and left superior frontal cortex than that of the CN group. The regions with increased trace in COPD groups were matched with the region with decreased FA in COPD compared with CN. The severe COPD group showed significantly lower scores in the language-related function, visuospatial function and frontal executive function than those of the CN and moderate COPD groups (Kruskal-Wallis test <0.05), and CFT scores did not show any significant differences between CN and moderate COPD.

#### CONCLUSION

This study demonstrated that COPD patients could affect the axonal integrity in multiple brain regions. The result of this study suggested the severity of COPD and the cognitive function might be correlated with the extent of microstructural change in brain. Voxel-based evaluation by MRI may be useful for preclinical detections of the cognitive dysfunction in patients with COPD.

**KEY WORDS:** Chronic obstructive pulmonary disease, diffusion tensor imaging, cognition disorders

**O-127**

**4:04 PM - 4:12 PM**

#### Serial 3-Year Proton MR Spectroscopic Imaging of Gray and White Matter in Relapsing Remitting Multiple Sclerosis

Kirov, I.<sup>1</sup>Tal, A.<sup>1</sup>Gorynski, E.<sup>1</sup>Babb, J.<sup>1</sup>Herbert, J.<sup>1</sup>Gonen, O.

New York University Medical Center  
New York, NY

#### PURPOSE

Since relapsing-remitting (RR) multiple sclerosis (MS) is, in addition to multifocal, a diffuse disease, our goal was to apply proton MR spectroscopic imaging (1H-MRSI) to characterize the diffuse component with



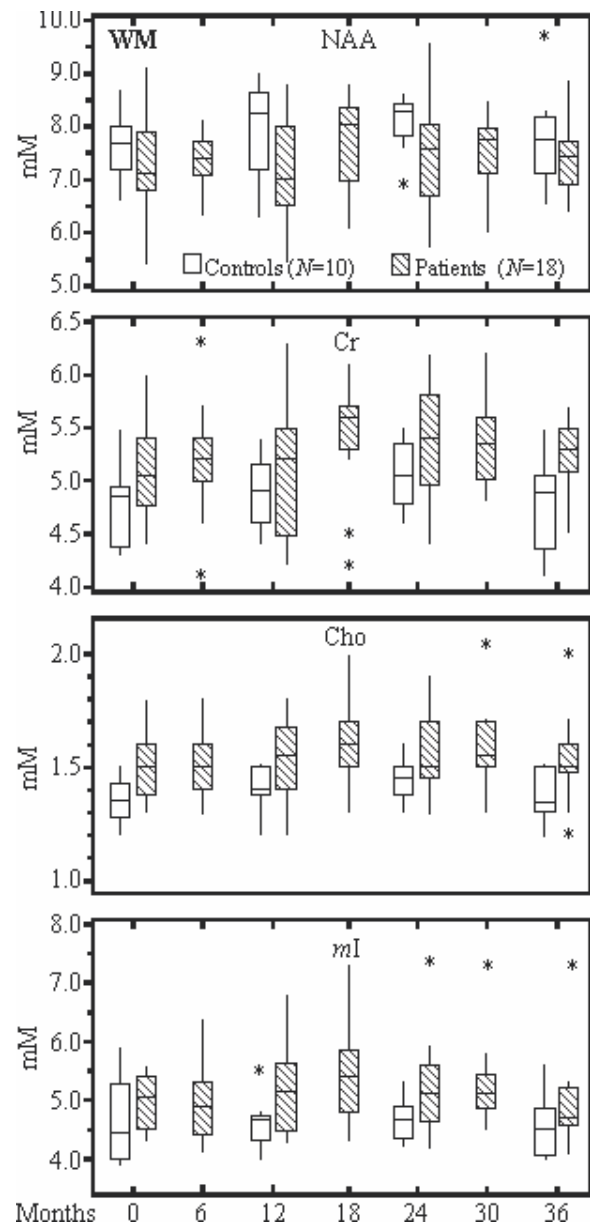
respect to gray and white matter (GM, WM) metabolism and follow its progression over 3 years.

#### MATERIALS & METHODS

Eighteen recently diagnosed, mildly disabled (baseline time from diagnosis: 32 months, mean Expanded Disability Status Scale score: 1.4) RR MS patients were scanned with MRI and 3D 1H-MRSI at 3 T semiannually for 3 years. Ten healthy gender- and age-matched controls were followed annually. Average absolute amounts of N-acetylaspartate (NAA), choline (Cho), creatine (Cr) and myo-inositol (mI) were obtained for all the GM and WM in the 360 cm<sup>3</sup> volume-of-interest (VOI). The VOI's cerebro-spinal-fluid (CSF), GM and WM fractions (CSFf, GMf, WMf) were obtained by segmentation of T1-weighted images and lesion volumes were calculated from T2-weighted MRI.

#### RESULTS

**Metabolism:** Only two patients were not on medications. At baseline, the average concentrations of WM Cr and Cho in patients,  $5.1 \pm 0.5$  and  $1.5 \pm 0.1$  mM were higher than controls',  $4.7 \pm 0.4$  and  $1.3 \pm 0.2$  mM. Lower WM NAA and higher WM mI were observed in almost all subsequent timepoints. The magnitude of the difference in any of these WM concentrations between baseline and 3 years was less than 3%. Boxplots of the distributions of metabolic concentrations of patients and controls at each time point (7 for patients, 5 for controls), is shown in Fig. 1. **Results, volumetry:** The patients' CSFf was normal at baseline, but higher than controls' thereafter. Finally, there was a significant increase in the rate of change of patients' average lesion volumes.



#### CONCLUSION

This study examined the presence and evolution of diffuse abnormalities in early RR MS. Metabolic changes in patients compared to controls were found only in WM (Fig. 1). In the context of increasing atrophy, these diffuse neuronal and glial abnormalities may include axonal dysfunction/loss, astrogliosis, inflammation and de-/re-myelination. These are present in the normal-appearing WM of patients between their 3rd and 6th year after diagnosis, but do not significantly change in magnitude over this time period. It is not known whether this represents the natural course of MS or the effect of immuno-modulatory medication.

**KEY WORDS:** Multiple sclerosis, proton MR spectroscopy, serial study

### Cumulative Double-Dose Gadobutrol at 3.0 T: Interim Analysis

Rovira, A.·Auger, C.·Hueriga, E.·Corral, J. F.·Mitjana, R.·Sastre-Garriga, J.·Montalban, X.

Hospital Vall d'Hebron  
Barcelona, SPAIN

#### PURPOSE

Several strategies have been proposed to increase the sensitivity of enhanced MRI for detecting disease activity in multiple sclerosis (MS), such as the use of contrast agents that achieve high T1 shortening, and a minimum 10-minute delay between gadolinium injection and scanning. There is now a large body of evidence indicating that a combination of these two strategies can lead to a significant increase in sensitivity compared to the standard technique. The aim of this study is to prospectively compare the gadolinium-enhancing lesion detection rate with a single and a cumulative dose of gadobutrol at 3.0 T with different delays after contrast injection in patients with a clinically isolated syndrome (CIS) and relapsing MS. The hypothesis is that the combined advantages of increasing delay and cumulative contrast dose will significantly increase the detection rate of active lesions.

#### MATERIALS & METHODS

Fifty-one patients with a CIS or relapsing MS [38 women (74%), mean age 34 years], who showed focal white matter lesions of the type seen in MS on previous brain MRI were included in this study. Sixteen patients were under treatment with immunomodulatory drugs (all but two with relapsing MS) at the time of the MRI examination. Patients underwent 3.0 T brain MRI consisting of transverse proton-density, T2-weighted and unenhanced T1-weighted sequences, and four sets of contrast-enhanced T1-weighted sequences performed 5 and 15 minutes after a single (0.1 mmol/kg) and a cumulative (0.1 + 0.1 mmol/kg) dose of gadobutrol. Each of the four sets of contrast-enhanced T1-weighted scans was evaluated for the presence and number of gadolinium-enhancing lesions in a random fashion and using objective image interpretation criteria by one of four experienced neuroradiologists blinded to the time point at which the enhanced sequences were obtained and using the unenhanced sequences as references. An independent reader not blinded to the timing of sequence acquisition identified the total number of enhancing lesions, and this number was used as the standard of reference. The data obtained were fitted to a negative binomial generalized linear model, with the two doses (single and cumulative) and the two time points at each dose as a repetitive measure.

#### RESULTS

Thirty patients (59%) had at least one gadolinium-enhancing lesion in the standard of reference. All active patients were identified in the 15 minutes-delay cumulative dose scan, whereas one was missed in the short-delay cumulative scan and two were missed in each of the single-dose scans. Relapsing MS patients had

a significantly higher number of active lesions compared to CIS patients only at the two single-dose time points. A significant increase in the mean number of active lesions was observed with increasing delay and dose: mean (median) number of lesions was 3.6 (1), 4.1 (1), 4.9 (2), and 5.4 (2) for each of the four time points

#### CONCLUSION

A cumulative gadobutrol dose associated with a longer delay time after contrast injection significantly increases detection of gadolinium-enhancing lesions in patients with CIS or relapsing MS. The cumulative dose increased identification of active patients by 3% to 7%.

**KEY WORDS:** Multiple sclerosis, gadolinium, contrast media

O-129

4:20 PM - 4:28 PM

### Differentiating Brain Lesions of Neuromyelitis Optica and Multiple Sclerosis Using Ultra-High-Field (7 T) MR Imaging

Ge, Y.·Kister, I.·Zhou, Y.·Herbert, J.·Jaggi, H.·Grossman, R. I.

New York University Langone Medical Center  
New York City, NY

#### PURPOSE

With increased clinical availability of MRI, brain lesions were found to be relatively common in patients with neuromyelitis optica (NMO); however, it is difficult to differentiate brain lesions of this entity from conventional multiple sclerosis (MS) based on the standard MR imaging. This study was to determine whether ultra-high-field (7 T) MR plays a role in demarcating the boundary of NMO and MS.

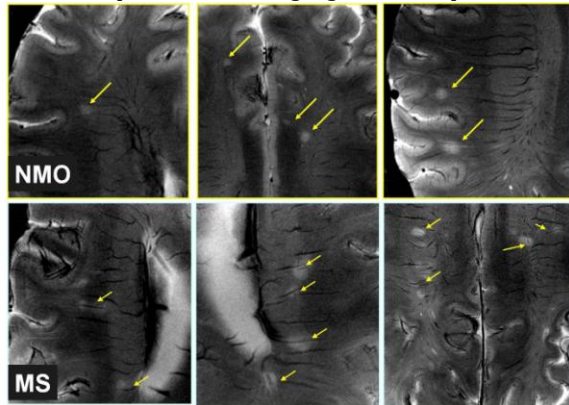
#### MATERIALS & METHODS

Six patients with NMO IgG-seropositive (all females, age of  $45.6 \pm 6.5$  years) and six patients with relapsing remitting (RR) MS patients (5 females, 1 male, age of  $47.5 \pm 12.5$  years) were recruited for this study. The imaging data were acquired at a 7 T whole-body human MR using a 24-element head array coil. NMO and MS patients were scanned using identical imaging protocol including a high-resolution 2D gradient echo sequence optimized to best visualize venous structures (TR/TE/flip angle = 500 ms/25 ms/35°, voxel size =  $0.23 \times 0.23 \times 2$  mm<sup>3</sup>), which is highly sensitive to venous vasculature and used to visually examine the presence of brain lesions and central venule within lesions. In addition, a multi-echo susceptibility weighted imaging (ME-SWI) was performed to generate T2\* mapping and MR venography with the following parameters: TR = 36 ms, TEs: six in-phase echoes from 6.15 to 31.62ms and echo spacing of 5.1ms; flip angle (FA) = 20°; and voxel size =  $0.5 \times 0.5 \times 1$  mm<sup>3</sup>.

#### RESULTS

In six NMO patients, we found a total of 24 supratentorial white matter lesions, all <15 mm<sup>2</sup>, of which only three had a visible central venule (16%). By

contrast, in six patients with MS, we found 156 small lesions ( $<15 \text{ mm}^2$ ), of which 132 (85%) contained a well-defined central venule (see Figure 1). In addition, the mean  $T2^*$  values of lentiform nucleus (putamen and globus pallidus) was  $15.2 \pm 2.1 \text{ ms}$  in NMO patients versus  $12.1 \pm 2.7 \text{ ms}$  in MS patients ( $P < 0.05$ ), suggesting less iron deposition in basal ganglia in NMO patients.



#### CONCLUSION

Ultra-high-field 7 T MR is useful in differentiating patients with NMO and MS. The perivenular abnormalities in MS has been well described in previous studies, and we found brain lesions in NMO are significantly less likely to contain a central venule compared to brain lesions of MS. There is also less degree of iron deposition in basal ganglia of NMO compared to MS. The different imaging features in the two disease entities may be reflective of their different underlying pathogenesis and pathophysiology.

**Acknowledgement:** This study was supported by Eurika grant from Guthy-Jackson Foundation.

**KEY WORDS:** Neuromyelitis, multiple sclerosis, 7 T MR imaging

**O-130**

**4:28 PM - 4:36 PM**

#### Morphologic Approach to White Matter Disease: SENRS Award Winner

Creasy, J. L.

Vanderbilt University  
Nashville, TN

Previously undiagnosed neurologic disorders primarily affecting white matter often are difficult to initially evaluate in clinical practice. A morphologic approach to white matter disease evaluation, using such features as global versus focal involvement, periventricular versus subcortical versus intervening white matter involvement and presence or absence of basal ganglia involvement to separate cases into several distinct groups will be described. Specific features of individual disease entities within each group will be highlighted. The purpose is to provide an approach for the initial diagnosis of the most prevalent and/or interesting white matter disease processes.

## Monday Afternoon

**3:00 PM - 4:30 PM**

**Sutton Center/South**

(15d) Pediatrics:  
Developmental/Congenital  
Malformations

**O-131**

**3:00 PM - 3:08 PM**

#### Prospective Assessment of Dynamic MR Scans and Phase-Contrast Cerebrospinal Fluid Flow MR Scans as Predictors of Surgical Outcome in Patients Undergoing Decompressive Surgery for Chiari I Malformations

Bapuraj, J. R.<sup>1</sup>Londy, F. J.<sup>1</sup>Quint, D. J.<sup>1</sup>Maher, C.<sup>1</sup>Martin, B. A.<sup>2</sup>Muraszko, K.<sup>1</sup>Maly Sundgren, P.<sup>1</sup>Chenevert, T.<sup>3</sup>

<sup>1</sup>University Hospital, University of Michigan, Ann Arbor, MI, <sup>2</sup>Swiss Federal Institute of Technology, Lausanne, SWITZERLAND, <sup>3</sup>University of Michigan, Ann Arbor, MI

#### PURPOSE

To evaluate the impact of neck position (flexion vs extension) on craniocervical (CVJ) and Sylvian aqueduct cerebrospinal fluid (CSF) flow rates in normal volunteers and Chiari I patients preoperatively and postoperatively.

#### MATERIALS & METHODS

Twenty-two normal volunteers were scanned on a 3 T scanner. Phase-contrast scans were performed perpendicular to the CVJ and the cerebral (Sylvian) aqueduct. Scan parameters were: TR/TE = min (typically 12.3ms/8.2 ms), 2 averages, 10° flip angle, 250 x 180 mm FOV, 252 x 179 matrix, 4 mm sections, and SENSE factor = 2, with flow compensation. Fifteen temporal phases during each cardiac cycle were acquired using a peripheral-pulse oxygenation signal for retrospective triggering. Sagittal and axial scans were performed with the neck in the flexed, extended and neutral positions for a total of six phase-contrast scans per patient. Velocity encoding was optimized for each subject (2 to 6 cm/sec). The data were analyzed with postprocessing software and the CSF flow velocities were calculated at the CVJ and within the cerebral aqueduct for all three neck position scans. Ten Chiari I patients also were scanned both preoperatively and 12 months postsurgery utilizing either a 1.5 or 3 T scanner. The same field strength scanner was used for all scans for each patient. Differing scan parameters (from above) when utilizing a 1.5 T scanner were: TR/TE = min (typically 19.0ms/7.9 ms), 1 average, 15° flip angle, 208 x 145 mm FOV, and 252 x 179 matrix. Anterior and posterior compartments of the CVJ CSF space were evaluated separately. All but one postoperative patient reported significant improvement of Chiari symptoms.

## RESULTS

With respect to CSF flow within the cerebral aqueduct, there was no statistical difference between the three neck positions in the normal volunteer group. Preoperative studies in the Chiari I group demonstrated a statistically significant difference ( $P = 0.03$  paired student t-test) in the maximum cephalic velocity of CSF flow between the neck neutral (4.3 cm/s) and flexed (3.7 cm/s) positions. This difference was not present in the postoperative Chiari group between the neck neutral (2.9 cm/s) and flexed (2.9 cm/s)  $P = 0.97$  positions. At the CVJ, the anterior compartment (anterior to the dentate ligament) maximum cephalic CSF velocity measurements did not demonstrate a significant statistical difference between the three neck positions for the normal volunteer group. However, the Chiari I patients showed a significant difference ( $P = 0.04$ ) between the neutral (3.0 cm/s) and flexed (4.0 cm/s) positions postoperatively though preoperatively there was no difference (4.1 vs 4.1 cm/s).

## CONCLUSION

Neck position affects CSF flow in symptomatic Chiari I patients. Flexion of the neck may cause cranial displacement of the tonsils, relieving the "ball-valve" effect of the low cerebellar tonsils which is present or accentuated with neutral/extended neck positioning. Cerebrospinal fluid flow in the cerebral aqueduct may be a sensitive indicator for predicting improvement in CSF flow postoperatively and may help to predict which patient may benefit from surgery.

**KEY WORDS:** Chiari I malformation, phase-contrast MR imaging, cerebrospinal fluid

**O-132**

**3:08 PM - 3:16 PM**

### Altered Sulcation in Fetuses with Chiari II Malformations

Glenn, O. A.<sup>1</sup>•Menon, P.<sup>1</sup>•Lee, H.<sup>1</sup>•Gupta, N.<sup>1</sup>•Farmer, D.<sup>2</sup>•Xu, D.<sup>1</sup>

<sup>1</sup>University of California San Francisco, San Francisco, CA, <sup>2</sup>University of California Davis, San Francisco, CA

## PURPOSE

To describe the appearance of primary sulcal formation in fetuses with Chiari II malformations.

## MATERIALS & METHODS

We reviewed brain MRI of fetuses aged 23-26 gestational weeks with Chiari II malformations during a 7-year period. We evaluated the sulcation pattern, subarachnoid space effacement (mild if CSF was seen anterior to the cerebellum and above the level of the lateral ventricles; moderate if there was no CSF anterior to the cerebellum and CSF was seen above the level of the lateral ventricles; severe if there was no CSF infratentorially and superior to the lateral ventricles), and lateral ventricular size. Postnatal MRIs were reviewed when available. This study was approved by our IRB.

## RESULTS

Forty-five fetal MRIs were reviewed. Mean GA at time of MRI was 24.3 weeks. Five fetuses had mild CSF effacement, 17 had moderate CSF effacement, 25 had severe CSF effacement. Eighteen fetuses had mild ventriculomegaly (<15 mm) and 20 had severe ventriculomegaly ( $\geq 15$ mm). Sylvian fissure was present in all cases and had an angled appearance. The parietooccipital sulcus was visible in 19 fetuses, and was angled horizontally. Calcarine sulcus was visible in two fetuses. Central sulcus was visible in eight cases. Eleven fetuses had anomalous sulcation pattern characterized by a visible superior temporal sulcus without visible central sulcus (mean GA 24.6 weeks; range 23.3 to 25.3 weeks). Seven fetuses had a visible superior frontal sulcus without visible central sulcus (mean GA 24.6 weeks; range 23.9 to 25.3 weeks). There was no correlation of anomalous sulcation pattern with ventriculomegaly or CSF effacement. In eight of the 13 fetuses with anomalous sulcation patterns, postnatal MRIs were performed and showed no evidence of polymicrogyria.

## CONCLUSION

In 29% of fetuses with Chiari II malformation, we observed an unusual pattern of sulcation characterized by early formation of normally late appearing sulci, and absence of normally early appearing sulci. In addition, the Sylvian fissure was abnormally angled. This altered formation of cerebral sulci has not been described previously in fetuses with Chiari II malformations and does not seem to represent polymicrogyria. Altered sulcation has been observed in neonatal sheep with untreated myelomeningoceles, but not in those with prenatal repair of myelomeningoceles suggesting that altered CSF dynamics may influence sulcal formation. In addition, children with Chiari II malformations are reported to have increased cortical complexity in temporal, parietal, and frontal regions. The identification of altered sulcation in some fetuses with Chiari II malformations hopefully will provide additional insight into the complexities underlying sulcal formation and conditions of abnormal sulcation. Importantly, these fetuses with unusual sulcation patterns detected by fetal MRI should not be mistakenly diagnosed with polymicrogyria.

**KEY WORDS:** Chiari II, fetal MR imaging, sulcation

**O-133**

**3:16 PM - 3:24 PM**

### Brain Apparent Diffusion Coefficient in Fetuses with Chiari Malformation Type II

Righini, A.<sup>1</sup>•Doneda, C.<sup>1</sup>•Parazzini, C.<sup>1</sup>•Re, T. J.<sup>2</sup>•Plebani, M.<sup>2</sup>•Milani, S.<sup>2</sup>•Triulzi, F.<sup>1</sup>

<sup>1</sup>ICP, Milan, ITALY, <sup>2</sup>University of Milan, Milan, ITALY

## PURPOSE

To determine apparent diffusion coefficient (ADC) values in select brain regions of fetuses affected by Chiari malformation type II (CM II) and to compare them with those of normal fetuses.



## MATERIALS & METHODS

Apparent diffusion coefficient values were measured in utero, by using an echo-planar three axes diffusion sequence (b-factor = 0 - 600 s/mm<sup>2</sup>), in frontal and occipital developing white matter (FWM and OWM), basal ganglia (BG) and cerebrospinal fluid (CSF) of 10 fetuses affected by CM II. Gestational age (GA) ranged from 19 to 35 weeks (mean 23.3). Results were compared with those determined in a population of 10 GA matched normal fetuses. The brain parenchyma compression index (CI), defined as the total area within the skull divided by the ventricular area (both areas measured on a single axial slice just above the thalami), also was calculated.

## RESULTS

In CM II fetuses, mean ADC value in FWM was 2.01 [sd] 0.28  $\mu\text{m}^2/\text{ms}$ , in OWM was 1.96 [sd] 0.33  $\mu\text{m}^2/\text{ms}$ , in BG was 1.36 [sd] 0.13  $\mu\text{m}^2/\text{ms}$ , and in CSF was 3.03 [sd] 0.25  $\mu\text{m}^2/\text{ms}$ . In controls, the mean ADC value in FWM was 1.75 [sd] 0.11  $\mu\text{m}^2/\text{ms}$ , in OWM was 1.71 [sd] 0.15  $\mu\text{m}^2/\text{ms}$ , in BG was 1.31 [sd] 0.17  $\mu\text{m}^2/\text{ms}$ , and in CSF was 3.01 [sd] 0.23  $\mu\text{m}^2/\text{ms}$ . A significant difference between mean ADC values of the two groups was found respectively in FWM ( $p = 0.02$ ) and OWM ( $p = 0.04$ ) (Figure 1). ADC values in FWM and OWM tended to correlate with CI without reaching a statistical significance.

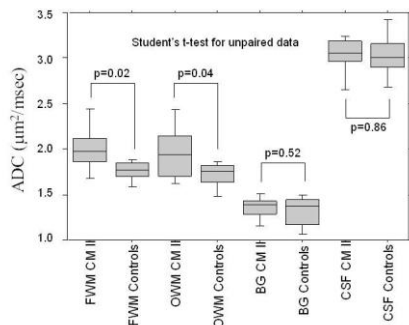


Figure 1. Graph showing ADC values in CM II and control groups.

## CONCLUSION

In CM II affected fetuses higher ADC values in the developing white matter could possibly be explained by interstitial water increase due to venous congestion, ventricular dilatation and cranial stenosis. Our data raise the question as to whether the ADC anomalies discovered in CM II affected fetuses may influence normal tissue development and merit further investigation.

**KEY WORDS:** Chiari malformation, ADC, fetal MR imaging

O-134

3:24 PM - 3:32 PM

## Diffusion-Weighted Imaging of the Cerebellum in the Fetus with Chiari 2 Malformation

Philpott, C.<sup>1</sup>Shannon, P.<sup>2</sup>Chitayat, D.<sup>2</sup>Ryan, G.<sup>2</sup>Blaser, S.<sup>1</sup>

<sup>1</sup>Hospital for Sick Children, Toronto, ON, CANADA, <sup>2</sup>Mt. Sinai Hospital, Toronto, ON, CANADA

## PURPOSE

Diffusion-weighted imaging, specifically apparent diffusion coefficient mapping (ADC maps) of the brain, is used to assess the integrity of neural tissue on a molecular level. In the developing brain, these values additionally reflect cellular maturation, tissue organization and reduction of water content. Apparent diffusin coefficient values in the pons and cerebellum have been shown to decrease from 23 gestational weeks (GW), thought to reflect brain maturation. Magnetic resonance imaging (MRI) of the fetus is employed in cases of suspected Chiari 2 malformations where further evaluation of the posterior fossa is required. Our aim was to evaluate whether there were any abnormalities of diffusion in the cerebellum associated with the abnormal cerebellar configuration in fetuses with Chiari 2 malformation.

## MATERIALS & METHODS

Fetuses with diagnoses of Chiari 2 malformations were identified using a text word search program (ISYSTM). All diffusion imaging had been performed on a 1.5 T Siemens AvantoTM system, with measurements from the calculated ADC map acquired from regions of interest placed in each cerebellar hemisphere and the pons. Values in groups of patients with Chiari 2 malformations were compared with those from fetuses with structurally normal brains, using statistical analysis accounting for the dependent variable of GW.

## RESULTS

There were seven fetuses with Chiari 2 malformation and 15 normal fetuses, ranging from 20 to 29 GW. The ADC values of the cerebellum with fetuses with Chiari 2 malformation were on average, 35% higher ( $1.82 \pm 0.1$  mm<sup>2</sup>/s), than ADC values in the normal fetuses ( $1.37 \pm 0.07$ ), statistically significant ( $p < 0.05$ ). There was no significant difference in the ADC values of the pons.

## CONCLUSION

There is a paucity of data published regarding diffusivity of the cerebellum in Chiari 2 malformations, particularly in the fetus. Decreased fractional anisotropy, (FA) in the middle cerebellar peduncle has been reported in one series of young adults with Chiari 2 malformation, with cause attributed to reduced fiber density, given presence of corpus callosal dysgenesis and decreased fractional anisotropy in this population. We propose that whilst abnormal white matter organization or early cerebellar degeneration could potentially contribute, the most plausible explanation pertains to abnormalities of CSF drainage in the posterior fossa, with increased extracellular water possibly accounting for this phenomenon.

**KEY WORDS:** Fetus, Chiari 2, diffusion

O-135

3:32 PM - 3:40 PM

### Atypical Hemispheric Asymmetry in Callosal Agenesis

Al-Mukhtar, A.

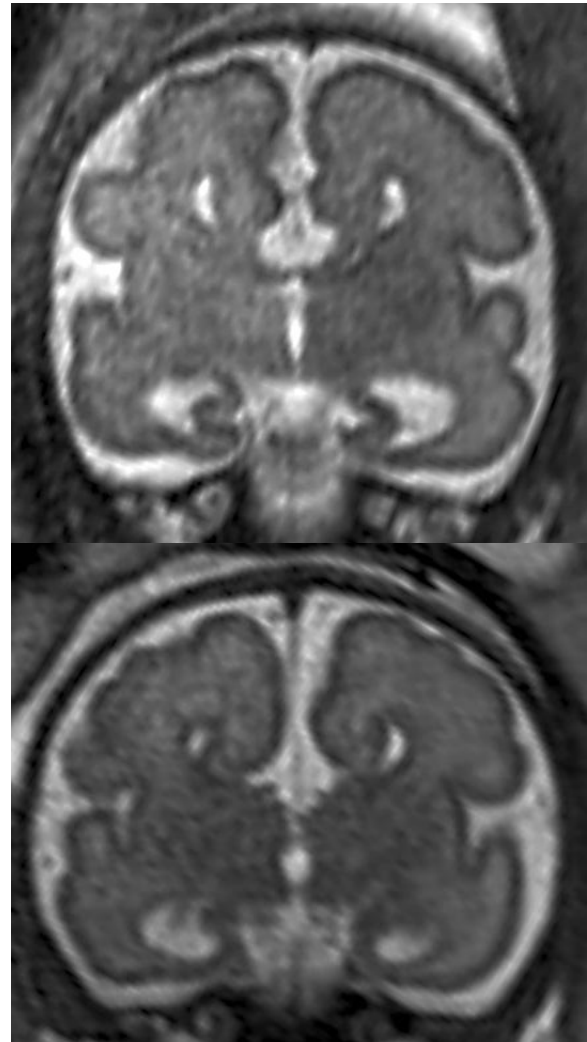
Medical University of Vienna  
Vienna, AUSTRIA

#### PURPOSE

To proof or rule out the hypothesis, that different types of commissural agenesis are associated with atypical developmental patterns of hemispheric asymmetry in the fetal brain.

#### MATERIALS & METHODS

In a retrospective analysis of 37 prenatal MR studies (1.5, orthogonal T2-weighted sequences in 3 section planes) in 37 fetuses (mean GW:27), with callosal a- (32/37) and hypogenesis (5/37), three raters blinded to the laterality of the systematically presented coronal T2-weighted fetal brain images, identified the right hemispheric (higher and deeper Sylvian fissure, earlier appearance of the superior temporal gyrus - STG, more flattened neocortical surface) or left hemispheric (shallower Sylvian fissure, more rounded lateral neocortex, later STG) surface pattern. The frequency of the different patterns [inverted or "atypically" asymmetric (Figure B), symmetric, "normal" leftward asymmetry (Figure A)] were compared to the data of a normal cohort.



#### RESULTS

The raters provided consistent results in 26/37 (70%) cases. The atypical asymmetry pattern was present in 19% (7/37) of cases with isolated callosal agenesis, whereas 3%(1/37) of cases with associated malformation showed this pattern (vs 3.5% in normal fetuses). The symmetric pattern was found in 8/37 (21%) and the typical pattern in 21/37 (57% vs 94.2% in normal fetuses).

#### CONCLUSION

Compared to normal fetuses, cases with callosal a- and hypogenesis are associated with an up to six times higher frequency of an atypical structural hemispheric lateralization pattern, as detected by fetal MRI. This emphasizes the widespread impact of laterality genes, which are frequently expressed abnormally in acallosal brains and potentially providing a new valuable functional prognostic marker in this condition.

**KEY WORDS:** Agenesis

O-136

3:40 PM - 3:48 PM

### Evaluation of the Normal Fetal Cerebellar Vermis on Fetal MR Imaging

Jasinski, T. H.<sup>1</sup>•Tanner, C. E.<sup>2</sup>•Wolfbreg, A.<sup>2</sup>•Madan, N.<sup>2</sup>

<sup>1</sup>Tufts University School of Medicine, Boston, MA, <sup>2</sup>Tufts Medical Center, Boston, MA

#### PURPOSE

Dandy-Walker malformation continuum (DWM) is a rare congenital malformation characterized by cerebellar vermian hypoplasia, cystic dilatation of the fourth ventricle, and enlargement of the posterior fossa. The spectrum of malformation, however, is variable. While the classic malformations are clearly identifiable on routine prenatal imaging, subtle variants with mild inferior vermian hypoplasia and widening of the foramen of Magendie (FM) are oftentimes difficult to distinguish from normal. Additionally, there is no normative data that exists for the size of the foramen of Magendie. Inability to make a definitive diagnosis increases patient's anxiety and hinders the patient's ability to make informed therapeutic decisions regarding the pregnancy. The purpose of this study was to establish retrospectively a range of normative values for the foramen of Magendie and the fetal cerebellar vermis.

#### MATERIALS & METHODS

All fetal MRI studies from 2004-2011 were reviewed retrospectively and all studies in pregnancies without neurologic abnormalities (determined by clinical and imaging follow up) were included in this study. In total, 88 patients were identified as part of this normal cohort. The cerebellar vermian area and the sagittal diameter of the foramen of Magendie were measured in all patients. Pearson product-moment correlation coefficients were determined with regard to each measurement and the fetal gestational age. The upper limits of normal for the FM then was determined, and applied retrospectively to the 110 patients not included in the normal cohort, including those subsequently diagnosed with DWM.

#### RESULTS

The cerebellar vermian area demonstrated linear growth during the pregnancy ( $r = 0.917$ ,  $p < 0.001$ ) in the normal cohort. However, the foramen of Magendie was found to be consistently less than 2.5 mm in all patients, with no significant interval change with regards to gestational age ( $r = 0.115$ ,  $p = 0.438$ ). This cutoff of 2.5 mm then was applied to those patients not included in the normal cohort. Twelve patients out of 110 were identified with an enlarged FM, 10 of whom were diagnosed with DWM by the radiologist. Two additional patients were identified, who on follow-up imaging and clinical examination, had evidence of a DWM variant.

#### CONCLUSION

Normative data support the use of 2.5 mm as the upper limits of normal for the size of the foramen of Magendie. This serves as a guide to the radiologist to help in borderline cases where DWM variants may be more

subtle, allowing improved confidence in diagnosis, and better patient counseling.

**KEY WORDS:** Dandy Walker malformation, fetal MR imaging, Foramen of Magendie

O-137

3:48 PM - 3:56 PM

### Periventricular Nodular Heterotopia: An Assessment of Additional Anomalies Associated with Location

Gonzalez, G.•Vedolin, L.•Barkovich, A.

University of California San Francisco  
San Francisco, CA

#### PURPOSE

To determine whether number, side or location of periventricular nodular heterotopia (PNH) are related to more complex malformations in the brain.

#### MATERIALS & METHODS

Patients or guardians gave their consent to be included in this group. Main and secondary diagnoses from 898 patients with brain malformations, from a personal collection of MRI cases gathered by one of the authors in the last 12 years, were reviewed to find those with PNH. The number (less than 5, 5 to 10 or more than 10), side (unilateral or bilateral) and location (*anterior*, if periventricular nodules were around frontal horns or bodies, or *posterior*, if they were around trigones, temporal or occipital horns) of the PNH were recorded, along with any anomalies of the cerebral cortex, white matter, major commissures, basal ganglia, posterior fossa elements, pituitary gland and olfactory structures. These observations were made independently by the three authors and a consensus was obtained in cases of disagreement.

#### RESULTS

One hundred cases were found to have PNH; 38% had less than five nodules, 20% between five and 10, and 42% more than 10. Bilateral PNH were found in 68%. Only 21% of patients had pure anterior PNH while 32% pure posterior PNH. Major differences were found in associated anomalies when PNH were divided by location (Table 1). Pituitary gland and basal ganglia anomalies were more common in anterior PNH. Malformations of cortical developmental, reduced white matter volume, delayed myelination, agenesis/hypogenesis of the corpus callosum, absence of hippocampal commissure, dysmorphic hippocampi, hypoplastic cerebellum and vermis, and abnormal brainstem were more frequent in posterior PNH.

Table 1	Periventricular Nodular Heterotopia			
	Anterior	n = 21%	Posterior	n = 32%
	n	%	n	%
Cortical anomalies	5	23.8	20	56.3
Abnormal hippocampi	4	19	8	25
Abnormal basal ganglia	3	14.3	1	3.1
White matter volume reduction	10	47.6	26	81.3
Delayed myelination	1	20	4	80
Corpus callosum agenesis	1	4.8	5	15.6
Corpus callosum hypogenesis	3	14.3	8	25
Absence of hippocampal commissure	2	9.5	6	18.8
Vermis hypoplasia	5	23.8	18	56.3
Cerebellar hypoplasia	2	9.5	9	28.1
Abnormal brainstem	4	19	15	46.9
Abnormal pituitary gland	3	14.3	2	6.3

#### CONCLUSION

Different malformation complexes are associated with PNH depending on their location. Posterior PNH are associated with more severe and more frequent malformations of the cerebral cortex, white matter, and posterior fossa elements.

**KEY WORDS:** Heterotopia, malformations of cortical developmental, MR imaging

**O-138**

**3:56 PM - 3:04 PM**

#### Temporal Lobe Features in Children with Hypochondroplasia/FGFR3 Gene Mutation

Philpott, C.·Widjaja, E.·Raybaud, C.·Branson, H.·Kannu, P.·Blaser, S.

Hospital for Sick Children  
Toronto, ON, CANADA

#### PURPOSE

Thanatophoric dysplasia and hypochondroplasia are both caused by fibroblast growth factor receptor 3 (FGFR3) gene mutations. Temporal lobe dysplasia has been well described on pathology and MRI in the fetus and infant with thanatophoric dysplasia, a lethal form of chondrodysplasia. These findings include hippocampal/parahippocampal dysplasia, polymicrogyria, sub-arachnoid neuroglial heterotopia of the temporal cortex and aberrant sulcation of the temporal lobe. Anecdotal cases of temporal lobe dysplasia in hypochondroplasia also have been described in the literature. We reviewed our cases of hypochondroplasia to ascertain the frequency of the findings.

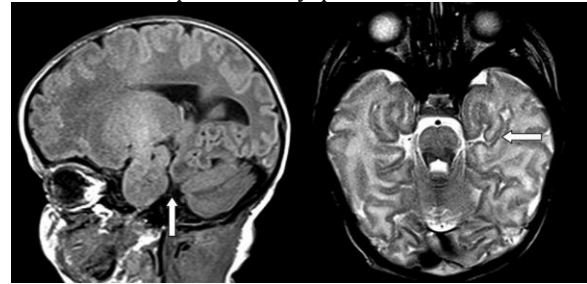
#### MATERIALS & METHODS

Brain imaging studies of eight children with hypochondroplasia were identified via a radiology text word search program (ISYSTM). The temporal lobes

were assessed on CT and MRI for size and configuration of the temporal horn and aberrant sulcation of the inferior surface of the temporal lobe.

#### RESULTS

Axial imaging (CT and MRI) demonstrated a triangular-shaped temporal horn in all. Inferior temporal lobe sulcation in the normal temporal lobe parallels the long axis of the temporal lobe. Axial CT and MRI in our cohort of hypochondroplasia patients revealed a deep transverse fissure of the inferior temporal lobe surface, in addition to medially arrayed inferior temporal lobe sulcation, with the medial aspect of the gyri "pointing" towards the circum-mesencephalic cistern. Coronal imaging revealed redundant folding of the inferior surface of the temporal lobe, while sagittal views sliced through the deep transverse fissure. Extent to the calcar avis was less common. Only a few of our patients suffered from seizures, apnea or symptoms directly referable to temporal lobe dysplasia.



#### CONCLUSION

We confirmed frequent inferomedial temporal lobe abnormalities, specifically hippocampal dysplasia and aberrant temporal lobe sulcation in our cohort of patients with hypochondroplasia. This may be associated with seizures or apnea or may be asymptomatic. Murine models with mutant FGF3 display increased neuroprogenitor proliferation, cortical thickness and surface area in the occipitotemporal cortex. This is thought to result in excessive convolution and likely explains the imaging findings in this patient cohort.

**KEY WORDS:** Medial temporal lobe, FGF3, hypochondroplasia

**O-139**

**3:04 PM - 3:12 PM**

#### Macrocephaly-Capillary Malformation Syndrome: Radiologic and Clinical Review

Sanchez-Montanez, A.<sup>1</sup>·Parra, P.<sup>2</sup>·Boronat, S.<sup>3</sup>·Delgado, I.<sup>3</sup>·Cano, P.<sup>3</sup>·Vazquez, E.<sup>3</sup>

<sup>1</sup>IDI Hospital Universitari Vall d'Hebron, Barcelona, SPAIN, <sup>2</sup>Complejo Hospitalario de Cáceres, Barcelona, SPAIN, <sup>3</sup>ICS Hospital Universitari Vall d'Hebron, Barcelona, SPAIN

#### PURPOSE

Macrocephaly-capillary malformation (M-CM) is a syndrome of unknown etiology whose main clinical symptoms are macrocephaly and capillary malformations, which frequently occur in the philtrum,



upper lip and nose, also found in limbs and trunk. Other features include neonatal hypotonia, developmental delay, hydrocephalus, overgrowth, polydactyly, body asymmetry and connective tissue disorders. The most valuable neuroimaging findings include white matter lesions, cerebral asymmetry, ventriculomegaly, cerebellar tonsillar herniation, cortical dysplasia and polymicrogyria. The pathogenesis of hydrocephalus and tonsillar herniation is attributed to a combination of several factors, being the initial event a cerebellar rapid growth difficult and distorting the dynamics of cerebrospinal fluid. To this date approximately 130 cases have been reported. The aim of this paper is to review the radiologic findings of five patients with M-CM recently studied in our institution, conducting a review of the literature.

#### MATERIALS & METHODS

We reviewed the medical records of five patients with M-CM from 2005 to the current date in our institution. We describe their clinical and radiologic findings, particularly MRI, compared with those described in the literature.

#### RESULTS

The most common radiologic findings in the five patients diagnosed with M-CM were tonsillar descent (5/5), ventriculomegaly (5/5), white matter lesions (4/5), dilated Virchow-Robin spaces (3/5), and abnormalities of venous sinuses and/or intracranial veins (3/5), findings consistent with those previously described. The most frequent clinical manifestations in our series were macrocephaly (5/5), developmental delay (4/5), overgrowth (5/5) and cutaneous manifestations such as midline facial nevus flammeus (5/5).

#### CONCLUSION

The recognition of typical imaging findings of this entity is very important, especially in order to achieve an early management of ventriculomegaly.

**KEY WORDS:** Macrocephaly, hydrocephalus, capillary malformation

**O-140**

**3:12 PM - 3:20 PM**

#### **Bilateral Cavitation of Ganglionic Eminence: A Fetal MR Imaging Sign of Halted Brain Development**

Righini, A.<sup>1</sup>Parazzini, C.<sup>1</sup>Doneda, C.<sup>1</sup>Re, T. J.<sup>2</sup>Triulzi, F.<sup>1</sup>

<sup>1</sup>ICP, Milan, ITALY, <sup>2</sup>University of Milan, Milan, ITALY

#### **PURPOSE**

The ganglionic eminence (GE) is pivotal for basal ganglia and cortical (i.e., interneurons) development, as extensively demonstrated in rat models. Data on human GE anomalies are very scarce. We report five lissencephalic fetuses, all showing similar bilateral GE region cavitations.

#### **MATERIALS & METHODS**

From 10 years prenatal MR imaging database, five cases (22, 29, 23, 22, 25 weeks gestation respectively, four

females, one male) with reported "cavitations or cysts in GE basal ganglia region" were collected. Two cases had familial recurrence.

#### **RESULTS**

At prenatal MR imaging, all cases displayed moderate microencephaly, corpus callosum agenesis (with rudimentary hippocampal commissure in four), defective opercularization, and bilateral symmetric cavitations in GE region (Figure 1). One case had bilateral frontal band heterotopias. Pathology (two cases), MR-autopsy (one case), and neonatal MR imaging (one case) confirmed lissencephaly and showed GE anomaly as to be of malformative rather than necrotic-clastic origin. One pregnancy was terminated without available pathology. Genotyping, aimed at determining the specific types of lissencephalies involved, is under investigation for cases with available material.

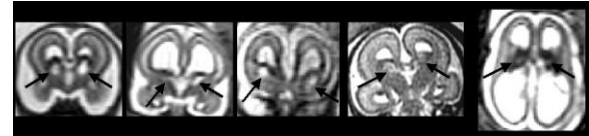


Figure 1. Four coronal and one axial T2-weighted sections showing each of the five reported cases with GE cavitations (black arrows).

#### **CONCLUSION**

The reported cases suggest how, in humans, defective GE region may play a key role in the development of complex brain malformations such as some lissencephalies.

**KEY WORDS:** Fetal MR imaging, ganglionic eminence, brain development

**O-142**

**3:20 PM - 3:28 PM**

#### **Delineation and Diagnostic Criteria of Oral-Facial-Digital Syndrome Type VI**

Poretti, A.<sup>1</sup>Vitiello, G.<sup>2</sup>Hennekam, R. C. M.<sup>3</sup>Huisman, T. A. G.<sup>1</sup>Valente, E.<sup>2</sup>Boltshauser, E.<sup>4</sup>

<sup>1</sup>The Johns Hopkins Medical School, Baltimore, MD, <sup>2</sup>IRCCS Casa Sollievo della Sofferenza Institute, San Giovanni Rotondo, ITALY, <sup>3</sup>Academic Medical Centre, Amsterdam, NETHERLANDS, <sup>4</sup>University Children's Hospital, Zurich, SWITZERLAND

#### **PURPOSE**

Oral-facial-digital syndrome type VI (OFD VI) represents a rare subtype of Joubert syndrome and related disorders (JSRD). Originally, polydactyly, enoral findings, intellectual disability, and vermian agenesis at post-mortem examination characterized the syndrome. Subsequently, MRI showed the molar tooth sign (MTS) in patients with OFD VI, prompting the inclusion of OFD VI in JSRD. We aimed to: 1) evaluate the spectrum of neuroimaging findings, 2) characterize the neurologic and dysmorphic features, the involvement of other organs, and the neurodevelopmental outcome, and 3) suggest diagnostic criteria for OFD VI.

## MATERIALS & METHODS

The inclusion criteria were 1) MTS and one enoral finding [tongue hamartoma(s), or multiple frenula, or cleft lip/palate] and polydactyly (pre-, meso-, or postaxial) or 2) MTS and more than one typical enoral finding. All images were evaluated retrospectively for qualitative assessment of infra-/supratentorial structural abnormalities. Information about neurologic and dysmorphic features, involvement of other organs, and neurodevelopmental/neurocognitive outcomes were collected by review of the clinical history and follow-up examination.

## RESULTS

Sixteen patients could be included in the study (11 males). At the last follow up at the median age of 10.5 years (2.5 months - 28.4 years), 14 patients were alive. The neuroimaging pattern included severe vermian hypoplasia (67%), hypoplastic (40%) and dysplastic (53%) cerebellar hemispheres, marked enlargement of the posterior fossa (67%), increased retrocerebellar collection of cerebrospinal fluid (47%), abnormal brainstem (73%), and supratentorial abnormalities such as ventriculomegaly (40%), callosal dysgenesis (27%), hypothalamic hamartomas (27%), and polymicrogyria (20%). We identified two new JSRD neuroimaging findings: ascending superior cerebellar peduncles (53%) and fused thalami (27%). The neurologic features included generalized muscular hypotonia (75%), truncal ataxia (present in all eight patients that could be evaluated), limb ataxia (present in four of five patients that could be evaluated), ocular motor apraxia (63%), strabismus (56%), nystagmus (19%), epileptic seizures (19%), and severe scoliosis (19%). All patients had motor developmental abnormalities. Developmental/cognitive outcome was abnormal in 93% of the patients (profound in 60%). The dysmorphic features included tongue hamartomas (81%), cleft lip/palate (31%), additional frenula (25%), upper lip notch (19%), postaxial (69%), preaxial (44%), and mesoaxial polydactyly (13%). Involvement of other organs was present in 11 patients and included particularly colobomas (31%).

## CONCLUSION

The OFD VI neuroimaging pattern was found to be more severe than in other JSRD subgroups. Tongue hamartomas, additional frenula, upper lip notch, and mesoaxial polydactyly are specific findings in OFD VI, while cleft lip/palate and other types of polydactyly are not specific. Involvement of other organs may include particularly colobomas. The majority of the patients have absent motor development and profound cognitive impairment. Compared with other JSRD subgroups, the neurologic findings and impairment of motor development and cognitive functions in OFD VI are significantly worse, suggesting a correlation with the more severe neuroimaging findings. Based on the literature and this study we suggest the following diagnostic criteria for OFD VI: MTS and 1) tongue hamartoma(s) and/or additional frenula and/or upper lip notch; and/or 2) mesoaxial polydactyly of one or more hands or feet; and/or 3) hypothalamic hamartoma.

**KEY WORDS:** Oral-Facial-Digital syndrome type VI, Joubert Syndrome and related disorders, cerebellar malformation

## Monday Afternoon

**3:00 PM - 4:30 PM**

**Murray Hill**

**(15e) Intracranial Manifestations of Rare Diseases/Miscellaneous**

**O-143**

**3:00 PM - 3:08 PM**

**Naming Impairment and Gray Matter Loss in Early Alzheimer Disease**

Vavro, H.<sup>1</sup>Parker, R.<sup>2</sup>Patrick, K.<sup>2</sup>Rumboldt, Z.<sup>2</sup>Mintzer, J.<sup>2</sup>Spampinato, M.<sup>2</sup>

<sup>1</sup>University Hospital Dubrava, Zagreb, CROATIA, <sup>2</sup>Medical University of South Carolina, Charleston, SC

## PURPOSE

Our goal was to evaluate gray matter (GM) volume loss patterns in patients with newly diagnosed Alzheimer disease (AD) with and without naming impairment using voxel-based morphometry (VBM).

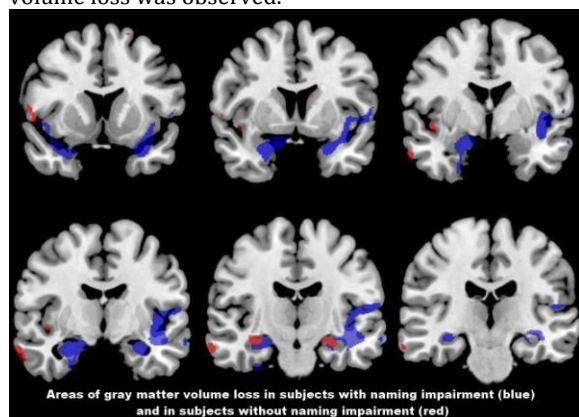
## Materials & Methods

We included in the study 76 subjects (32 women, 44 men; mean age 76 ±7 years) participating in the Alzheimer's Disease Neuroimaging Initiative (ADNI) with progression from amnesic mild cognitive impairment (aMCI) to AD during the course of the study. The 30-item Boston Naming Test (BNT), a measure of word retrieval performance, was administered to all subjects (median 25, range 7-30 years). Patients were divided in two groups, 41 subjects with BNT score equal or above the median (high BNT) and 35 subjects with BNT score below the median (low BNT). The Clinical Dementia Rating scale was used to assess disease severity. Pearson  $\chi^2$  test, one-way Anova, and General Linear Model Repeated Measures was used to compare demographic characteristics and disease severity between groups. Brain MRIs obtained at the time of the diagnosis of AD and 12 months later were available for each patient. VBM with SPM5 was used to process MPAGE images. Comparison between longitudinal imaging data was conducted using paired t-tests and results were considered significant when the p-value was less than 0.05 with familywise error rate correction (FWER) for multiple comparisons.

## RESULTS

There were no significant differences in demographic characteristics and disease severity between the two groups. Longitudinal analyzes of the imaging data revealed differences in the distribution and severity of GM volume loss between groups, with more widespread atrophy in the low BNT group. In low BNT subjects

there was greater involvement of the left cerebral hemisphere, including the temporal lobe, frontal lobe, insula, and parietal lobe; on the right in the frontal lobe and parietal lobe. In the high BNT group GM volume loss was bilateral with overall greater involvement of the right cerebral hemisphere, including bilateral temporal and frontal lobes, left caudate nucleus and right insula. In both groups bilateral hippocampal volume loss was observed.



#### CONCLUSION

The extent and distribution of GM volume loss in patients with early AD at the same disease stage significantly differs in the presence and absence of word retrieval impairment. These findings have potential implications for therapeutic approaches and prognostic considerations in AD.

**KEY WORDS:** Alzheimer disease, MR imaging, naming impairment

**O-144**

**3:08 PM - 3:16 PM**

#### Conventional Imaging Findings and Complications of Hereditary Hemorrhagic Telangiectasia in a Large Serial Cohort

McKenzie, G. A. • Hunt, C. H. • Thielen, K. R. • Kallmes, D. F. • Cloft, H. • Wood, C. P.

Mayo Clinic  
Rochester, MN

#### PURPOSE

Hereditary hemorrhagic telangiectasia (HHT) is an autosomal dominant disorder with widespread multiorgan angiodysplastic lesions. Central nervous system (CNS) complications can be from vascular abnormalities arising within the CNS or secondary to vascular abnormalities outside of the CNS. A large review was performed of a cohort of patients with HHT to better describe not only incidence and type of intrinsic CNS vascular abnormalities, but also the frequency and nature of the CNS complications. This included whether the complication was a result of an intrinsic CNS or extrinsic vascular abnormality.

#### MATERIALS & METHODS

From our institutional database of patients with the confirmed diagnosis of HHT, a retrospective review of all patients from 7/2003 to 3/2011 was performed. All

prior cross-sectional imaging studies (CT, MRI) were reviewed for common vascular abnormalities associated with HHT, including pulmonary and cerebral arteriovenous malformations (AVM), as well as for presence of right-to-left shunt on echocardiography and nuclear medicine perfusion studies. In addition, presumed complications of HHT also were documented from an imaging perspective, including stroke, cerebral abscess, and intracranial hemorrhage.

#### RESULTS

A total of 366 patients were identified with a diagnosis of HHT (229 male, 137 female) with an average age of 45.6 years at the date of their initial evaluation at our institution (SD +/- 18.0 years). The majority of these patients (228, 62.3%) had the classic history of significant bouts of epistaxis. A total of 155 patients (42.3%) had pulmonary AVMs with nuclear medicine pulmonary shunt indexes ranging from 1-66% (mean, 7.9%, SD 10.3%). Extracardiac shunting was also noted on 177 out of 366 patients (48.4%) with contrast echocardiography. Sixty-four patients (17.5%) had a CNS vascular anomaly with the most commonly identified abnormality being an arteriovenous malformation (11.7%). Major complications of HHT were not infrequent with 10.6% (21 stroke, 8 brain abscess, 10 intracranial hemorrhages).

#### CONCLUSION

Central nervous system vascular abnormalities are relatively common on cross-sectional imaging in this series of patients with HHT with the most common being an AVM. Hereditary hemorrhagic telangiectasia is not a benign disorder with frequent major complications related to intractable epistaxis, right-to-left extracardiac shunting, and intracranial hemorrhage. Careful follow up and long-term surveillance is needed in these patients to monitor for potential complications.

**KEY WORDS:** HHT, hereditary hemorrhagic telangiectasia, complication rate

**O-145**

**3:16 PM - 3:24 PM**

#### SMART Syndrome Is Not Always Benign: A Case Series

Black, D. F. • Lindell, E. P. • Morris, J. M. • Krecke, K. N. • Worrell, G. A. • Bartleson, J. D. • Lachance, D. H.

Mayo Clinic  
Rochester, MN

#### PURPOSE

The syndrome of stroke-like migraine attacks after radiation therapy (SMART) was described in 2003 but little is known about the cause, natural history, or long-term imaging findings. We report on ten SMART patients and review pertinent clinical, imaging, and pathologic findings in order to better understand this condition that was previously thought to be benign.

#### MATERIALS & METHODS

Following institutional review board approval, cerebral magnetic resonance imaging findings of 10 patients

seen by the authors and diagnosed with SMART syndrome at our institution between 3/1/2006 to 8/1/2010 were reviewed retrospectively. MR imaging results were correlated with clinical and pathologic data in a case series format.

## RESULTS

All ten subjects had remote cerebral irradiation for treatment of neoplasia and developed subsequent episodes of neurologic signs and symptoms. These attacks were accompanied by characteristic, unilateral, posterior gyral gadolinium enhancement often associated with gyral thickening and mild T2 hyperintensity best seen on FLAIR images. Five of the 10 patients had mildly restricted diffusion in these regions. Three subjects developed permanent cortical laminar necrosis following a SMART attack. Patient age at diagnosis ranged from 37-60 years (mean 49). The interval between radiation therapy and onset of SMART ranged from 6-32 years (mean 19). SMART attacks were associated with headaches in 70% and seizures in 60% of the cases. Unlike prior reports, half of the patients developed permanent neurologic deficits beyond their clinical baseline. Most commonly these included sensorimotor deficits, ataxia and cognitive impairment. None of the patients had tumor progression or recurrence as an explanation for their symptoms or findings. Patients who recovered returned to baseline within 2 months on average. Patients were treated symptomatically with a variety of medical therapies. Four of the five patients with permanent sequelae underwent brain biopsy which only demonstrated gliosis.

## CONCLUSION

Contrary to prior reports, SMART syndrome is not always benign. Some patients suffer persistent worsening from their baseline neurologic status. Typical imaging findings include thick, unilateral, gyral enhancement in the posterior cerebrum, which often correlates with the site of seizure activity, suggesting that seizures play a significant role in SMART syndrome. The anatomical localization of patients' deficits, seizures, and MRI findings were always within the previous radiation field. SMART is a delayed complication of cerebral irradiation but, in the four biopsied patients, results did not reveal a more specific pathophysiologic etiology. Various therapeutic options were employed but no definitely beneficial treatment is yet known.

**KEY WORDS:** Whole brain radiation, SMART syndrome, seizure

O-146

3:24 PM - 3:32 PM

## Frontal and Insular Cortical Thickness in Stimulant Dependent Individuals

Tanabe, J. L., York, P., Krmpotich, T., Miller, D., Dalwani, M., Sakai, J., Mikulich-Gilbert, S., Thompson, L., Rojas, D., Crowley, T.

University of Colorado  
Denver, CO

## PURPOSE

Structural changes in prefrontal cortex are reported frequently in drug-dependent subjects. Recent evidence suggests that insula, a component of the limbic system, is involved in addictive behavior. Few studies have focused on insula's role in substance abuse. We investigated whether there were differences in cortical thickness in substance-dependent individuals (SDI) compared to controls. *We hypothesized that compared to controls, SDI would have decreased prefrontal and insular cortical thickness.*

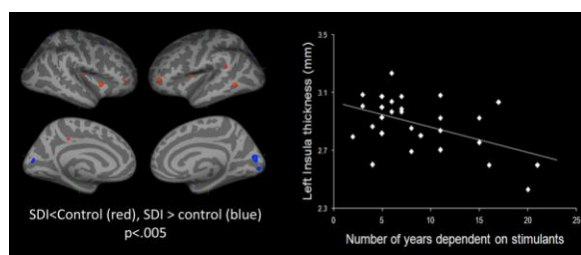
## MATERIALS & METHODS

Twenty-eight SDI (11M/17F,  $36 \pm 9$  years) were compared to 28 controls of similar gender and age (15M/13F,  $35 \pm 7$  years). Substance-dependent individuals were dependent on methamphetamine and/or cocaine (DSM-IV criteria). 3D T1-weighted MRI of the brain was acquired on a 3 T scanner. Cortical thickness was calculated with FreeSurfer(v4.5) (<http://www.surfer.nmr.mgh.harvard.edu>). Topological inaccuracies were corrected by an investigator blinded to group membership. Region of interest (ROI) and whole brain analyses were conducted. Three ROIs were selected a priori using an automated gyral-based parcellation method in FS: *orbitofrontal cortex, inferior frontal cortex, and insula*. Cortical thickness was compared across group using a 2-tailed ANCOVA, adjusted for age and total intracranial volume. Cortical thickness was correlated with duration of stimulant dependence. Whole brain: data were smoothed (10 mm FWHM) and tested for group differences, after adjusting for age and intracranial volume. To verify ROI results, statistical threshold was set at  $p < .005$ . To explore regions not hypothesized to differ a priori, a whole brain threshold was set at voxel-level  $p < .001$ , cluster level  $p < .05$ , after correcting for false positives using Monte Carlo Z-simulation (5000 iterations).

## RESULTS

ROI: There was thinning of the left insular cortex in SDI compared to controls ( $2.88 \pm 0.19$  vs  $2.97 \pm 0.18$  mm,  $p = 0.02$ ). No other regions differed in cortical thickness. Cortical thinning in the left insula was confirmed with whole brain analysis. Additional regions of cortical thinning were suggested in right insula, bilateral inferior frontal gyrus, and left temporal lobe (Figure 1, red). No regions exceed the whole brain threshold levels. The scatterplot shows the correlation between left insula thickness and duration of stimulant dependence ( $r = -.38$ ,  $p = .05$ ).





#### CONCLUSION

Thinning of the left insula in stimulant-dependent individuals is consistent with previous surface-based morphometric studies in patients dependent on cocaine, alcohol, and marijuana. Causality cannot be determined, but a negative correlation between duration of dependence and left insular thickness may suggest that chronic drug exposure could result in cortical thinning. These findings are consistent with a role for insula in the neurobiology of substance dependence.

**KEY WORDS:** Cortical thickness, insula, substance dependence

**O-147**

**3:32 PM - 3:40 PM**

#### Imaging of Dizziness in the ED: What Is the Diagnostic Yield and Are Clinical Factors Helpful in Predicting Imaging Outcome?

Buckle, C.<sup>1</sup>Lawhn- Heath, C.<sup>2</sup>Straus, C.

University of Chicago Hospitals  
Chicago, IL

#### PURPOSE

The purpose of this study was to determine the diagnostic yield of dizziness imaging in the ED and to identify clinical factors that might predict positive imaging findings in a large sample of patients presenting with acute dizziness to the emergency room.

#### MATERIALS & METHODS

Four hundred fifty-six consecutive head CTs performed on ER patients for the primary or secondary indication of vertigo and/or dizziness were reviewed retrospectively in this IRB-approved study. Clinical factors from the ED admission was obtained in 313, of these patients including age, gender, history (onset, duration, quality of dizziness), associated symptoms, past medical history, vascular risk factors and indication for the exam (r/o mass, bleed etc.). Head CT findings were classified into acute, subacute and chronic and were compared with follow-up imaging (repeat CT, MRI) where available. Multiple clinical factors coded in either an ordinal or binary fashion. Ordinal factors were entered into a logistical regression model. Pairwise comparisons of the final coding and the binary variables were performed using a 2x2 contingency table analysis of independence via Fisher's Exact Test and Pearson's Chi-Square Test. Subgroup analysis between the presence of neurologic disease and vascular risk factors with the presence of a positive acute imaging finding was performed using Pearson's Chi-Square test and

Fisher's Exact Test. All tests were performed at the  $\alpha = 0.05$  significance level.

#### RESULTS

The incidence of acute findings on CT was 1.9%. The incidence of any significant finding was 4.7%. Follow-up imaging, predominantly MRI was obtained 32% of the time, and changed the diagnosis 8% of the time. In particular, MRI detected several posterior fossa strokes not seen on CT. Of the clinical factors, only history of a mass (benign or malignant) and the type of dizziness (vertigo vs nonvertigo) were significant predictors for the presence of positive CT head findings. The presence of vascular risk factors, associated symptoms, and the known neurologic disease were not predictive of a acute cause for dizziness on either CT or MRI.

#### CONCLUSION

This study shows that the diagnostic yield of head CT for emergent findings in a large sample of patients presenting with acute dizziness is extremely low. However, MRI in appropriately selected patients changes the diagnosis a significant amount of the time. Furthermore, we show that the clinical evaluation of dizziness in the ER is challenging with few clinical factors (only a history of brain mass and the type of vertigo) predictive of imaging outcome. Surprisingly, vascular risk factors were not associated significantly with the presence of acute vertigo possibly because they are so common in the population at large. A small number of true positive findings and the retrospective design of our study limits generalizability of the data; however, the findings suggest that the evaluation of dizziness is a challenging problem faced by ER physicians and that more imaging with MRI (as opposed to CT) may be warranted, given the lack of reliable clinical factors to distinguish emergent from nonemergent causes of dizziness.

**KEY WORDS:** Dizziness, ER, vertigo

**O-148**

**3:40 PM - 3:48 PM**

#### Age-Related Degradation of Limbic System: A Quantitative Analysis with Diffusion Tensor Imaging

Gunbey, H. P.<sup>1</sup>Ercan, K.<sup>2</sup>Zan, E.<sup>3</sup>Findikoglu, A.  
S.<sup>4</sup>Karaoglanoglu, M.<sup>2</sup>Arslan, H.<sup>2</sup>

<sup>1</sup>Cankiri Government Hospital, Cankiri, TURKEY, <sup>2</sup>Ataturk Education and Research Hospital, Ankara, TURKEY, <sup>3</sup>Mardin Kadin Dogum ve Cocuk Hastaliklari Hastanesi, Mardin, TURKEY, <sup>4</sup>Erzincan Government Hospital, Erzincan, TURKEY

#### PURPOSE

The limbic system; a network of gray matter interconnected by white matter fibers is primarily responsible for emotions and memories. It is known to undergo degradation with aging as an important part of cerebral white matter. Although the gray matter components and the connecting fibers of this system have been studied separately, the integrity of the whole components including the hippocampus, amygdala,

parahippocampal gyrus, cingulum and fornix have not been yet analyzed with diffusion tensor imaging (DTI). We investigated the age-related changes of quantitative diffusivity parameters and fiber characteristics of limbic system in healthy volunteers.

#### MATERIALS & METHODS

Thirty-one healthy subjects aged 25-70 years were examined at 1.5 using standart DTI sequence. Quantitative fiber tracking was performed for 3D segmentation of the white matter tracts of fornix, cingulum and the parahippocampal gyrus to determine fractional anisotropy (FA) and mean diffusivity (ADC) measurements. The FA and ADC values of bilateral hippocampus, amygdala and parahippocampal gyrus also were obtained as the gray matter components.

#### RESULTS

Moderately significant negative correlations were found between the FA values of left hippocampus and right parahippocampal gyrus; and age ( $r = -0.486$ ,  $p = 0.006$ ). Also negative weak correlations were observed between the FA values of the left parahippocampal gyrus and fornix; and age ( $p < 0.05$ ). Interestingly right amygdala and left cingulum ADC values showed negative weak correlations ( $p < 0.05$ ) with age while the left hippocampal ADC values represented positive relation ( $r = 0.387$ ,  $p = 0.031$ ) as expected. In the cingulum, no correlation was observed between FA and age. The significant relative changes ( $p < 0.05$ ) per decade of age were found in the cingulum and parahippocampal gyrus FA measurements.

#### CONCLUSION

Quantitative fiber tracking enables identification of differences in diffusivity and fiber characteristics as a consequence of normal aging. As a novel finding we showed the effects of aging in the entire limbic microstructure that have not been described previously. Our approach shows that in course of time the hippocampus, parahippocampus and fornix are affected significantly while the cingulum is not.

**KEY WORDS:** Limbic system degradation, diffusion tensor imaging

O-149

3:48 PM - 3:56 PM

#### MR Imaging Findings in Adult Patients with Hemolytic Uremic Syndrome following an Infection with a Novel Mutation of E. Coli (Subtype O104:H4)

Löbel, U.<sup>1</sup>•Magnus, T.<sup>1</sup>•Meier-Cillien, M.<sup>2</sup>•Gerloff, C.<sup>1</sup>•Röther, J.<sup>2</sup>•Sedlacik, J.<sup>1</sup>•Eckert, B.<sup>2</sup>•Fiehler, J.<sup>1</sup>

<sup>1</sup>University Medical Center Hamburg-Eppendorf, Hamburg, GERMANY, <sup>2</sup>Allgemeines Krankenhaus Altona, Hamburg, GERMANY

#### PURPOSE

Infections with enterohemorrhagic E. coli (EHEC) typically occur in children causing renal dysfunction known as hemolytic uremic syndrome (HUS) and neurologic symptoms in a small percentage of patients. Therefore, very little information is available on the

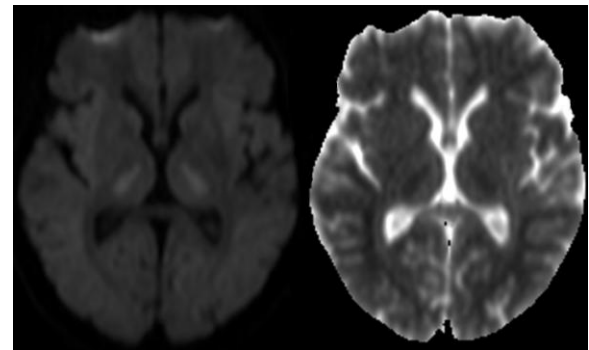
morphology of brain manifestations of EHEC and HUS in adults. During the recent epidemic with a novel mutation of Escherichia coli O104:H4 in Europe we performed MRI in adult cohort with HUS and neurologic symptoms.

#### Materials & Methods

MR imaging data of 58 (26 male, 32 female) adult patients (median:  $39 \pm 18$  years) with neurologic symptoms who were treated for proven EHEC infections at two hospitals were included in the evaluation. MR imaging was performed during May-July 2011 and included fluid-attenuated inversion recovery (FLAIR), diffusion-weighted imaging (DWI) and standard anatomical sequences. The decision to perform MRI was made on an individual basis with respect to the neurologic symptoms. In the acute stage, these included seizures, aphasia, hemiparesis and deterioration of consciousness.

#### RESULTS

Abnormal signal intensity based on FLAIR and/or DWI were found in the following anatomical structures (number of patients): bilateral thalamus (19), bilateral abducens nucleus (14), cortex (12), splenium of corpus callosum (11), centrum semiovale (9), basal ganglia (5), cerebellum (4), periaqueductal (4), hippocampus (3), tegmentum (2), insula (2), internal capsule (2) and dentate nucleus (1). In addition to hyperintense lesions of the centrum semiovale associated with restricted water diffusion in three patients and large bilateral infarcts observed in one patient, a peculiar pattern with symmetrical T2-hyperintensities and restricted water diffusion of the lateral thalamus and the region of the abducens nucleus was identified in nine patients (Figure). These findings suggest a systematic toxic effect on both structures which may be a characteristic for adult patients with neurologic symptoms after EHEC infection.



#### CONCLUSION

During the acute stage of adult patients with with neurologic symptoms after EHEC infection, a peculiar MRI pattern was identified which is characterized by symmetric T2-hyperintense lesions of the thalamus and pons. In addition, a pattern similar to MTX toxicity and large bilateral infarcts was observed. These patterns suggest a metabolic toxic effect of the disease or therapy on the brain.

**KEY WORDS:** MR imaging, escherichia coli, hemolytic uremic syndrome

O-150

3:56 PM - 4:04 PM

### Should We Be "Nervous" about Celiac Disease?

Currie, S.<sup>1</sup>·Hadjivassiliou, M.<sup>2</sup>·Clark, M. R. J.<sup>1</sup>·Craven, I. J.<sup>1</sup>·Sanders, D. S.<sup>2</sup>·Wilkinson, I. D.<sup>1</sup>·Griffiths, P. D.<sup>1</sup>·Hoggard, N.<sup>1</sup>

<sup>1</sup>Academic Unit of Radiology, Sheffield, UNITED KINGDOM, <sup>2</sup>Royal Hallamshire Hospital, Sheffield, UNITED KINGDOM

#### PURPOSE

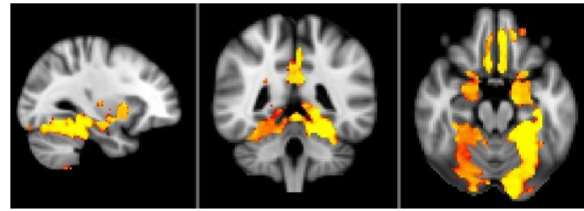
To establish the neurologic magnetic resonance (MR) imaging features of patients with celiac disease referred to the neurology clinic, Sheffield, UK.

#### MATERIALS & METHODS

Retrospective examination of MR images obtained from a consecutive cohort of patients (n = 36) with biopsy proven celiac disease referred for a neurologic opinion. Patients were divided into subgroups based on their primary neurologic complaint. All patients underwent 3 T MR imaging comprising axial T2-weighted, sagittal T1-weighted volume and single voxel point-resolved proton spectroscopy sequence (PRESS) of the cerebellar hemisphere and vermis (TE 144; TR 2000). Cerebellar volume, normalized to total intracranial volume and voxel-based morphometry (VBM) assessing differential gray matter volume loss was calculated using FSL (FMRIB Software Library). Cerebral white matter abnormalities (WMAs) were characterized using a previously published method, namely assessing size, number and distribution. MR spectroscopy, normalized cerebellar volume, cerebellar gray matter volume loss and WMAs were compared with age- and sex-matched controls.

#### RESULTS

Patient mean age =  $46.4 \pm 14.9$  years (range 19 to 73). Primary neurologic complaint comprised balance disturbance (n = 23; 63.9%), headache (6; 16.7%) and peripheral sensory loss (4; 11.1%). Compared with controls, cerebellar volume was reduced significantly in the patient group ( $6.83 \pm 0.76\%$  vs  $7.67 \pm 0.96\%$  of total intracranial volume,  $p = 0.002$ ). This significant difference was only apparent in the balance disturbance subgroup ( $6.76 \pm 0.83\%$  vs  $7.59 \pm 1.06\%$ ,  $p = 0.009$ ). VBM revealed statistically significant reduced gray matter primarily affecting the superior aspect of the cerebellum in celiac patients, compared to controls (uncorrected  $p < 0.01$ ). Compared with controls mean NAA/Cr ratio was lower in the patient group but this failed to reach statistical significance. Fourteen (39.9%) patients demonstrated cerebral white matter abnormalities (WMAs) unexpected for the patient's age with the highest incidence occurring in the headache subgroup (66.6% compared with 53% and 25% in the balance disturbance and peripheral sensory loss subgroups respectively). The headache subgroup averaged more than twice the number of WMAs per MR compared to the balance disturbance subgroup and six times more than peripheral sensory subgroup (mean = 19, 9 and 3 respectively).



#### CONCLUSION

Celiac patients referred to neurology demonstrate high rates of significant cerebellar abnormality on MR imaging. This suggests that gastroenterologists should have a low threshold for referral for celiac patients and has implications for health resources if screening for celiac disease commences.

**KEY WORDS:** Cerebellum, celiac, MR imaging

O-151

4:04 PM - 4:12 PM

### Imaging Features of Intracranial Textiloma: A Meta-Analysis and Three New Cases

Warren, A. L.<sup>1</sup>·Kleinschmidt-DeMasters, B. K.<sup>2</sup>·Salzman, K. L.<sup>1</sup>·Chin, B. M.<sup>1</sup>·Krisht, K.<sup>1</sup>·Couldwell, W. T.<sup>1</sup>·Osborn, A. G.<sup>1</sup>

<sup>1</sup>University of Utah School of Medicine, Salt Lake City, UT, <sup>2</sup>University of Colorado School of Medicine, Aurora, CO

#### PURPOSE

Textiloma, a foreign body reaction to retained surgical elements, can be mistaken for abscess or recurrent tumor on imaging. Although this phenomenon has been well described outside the central nervous system, only small series or case reports of intracranial textilomas exist. This paper reviews all published cases of intracranial textiloma with a meta-analysis of imaging features. We also present three new cases of intracranial textiloma.

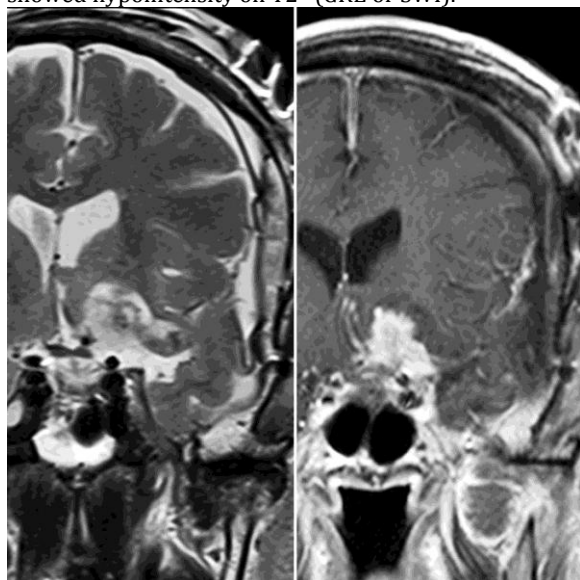
#### MATERIALS & METHODS

An exhaustive literature search identified 113 cases of iatrogenic intracranial foreign body reaction published since 1972. Cases included 46 foreign body reactions to hemostatic aids following tumor resection; 39 reactions to materials wrapped around intracranial aneurysms; 12 cases following microvascular decompression with Teflon, sponge, or other material; and 16 miscellaneous cases. Seventy-five cases had foreign body reaction confirmed on histopathology. Imaging illustrations for pathologically confirmed cases were reviewed to characterize CT and MR imaging features.

#### RESULTS

Of 75 pathology-proven cases, 62 cases had at least one CT or MRI illustration. Forty cases had CT imaging (16 NECTs, 35 CECTs, 11 both). Thirty-four of 35 CECTs showed textiloma enhancement, with 15/35 demonstrating ring, 11/35 homogeneously solid, and 8/35 heterogeneously solid patterns. Thirty-five cases had MR imaging and 12 had precontrast T1-weighted imaging, 30 T1C+, 10 T2-weighted imaging, and 5 FLAIR. Precontrast T1-weighted was predominantly

hypointense (9/12). Two of 12 were isointense and 1/12 was hyperintense. T2 features varied. Six of 10 were hyperintense while 4/10 were hypointense. MR enhancement patterns included heterogeneously solid (15/30), ring (12/30), and homogeneously solid (3/30) patterns. Of two cases with diffusion-weighted imaging (DWI), one case demonstrated restricted diffusion. All three of our cases had T1C+ scans. All enhanced strongly. Two of three had solid homogeneous enhancement while one demonstrated ring enhancement. All three cases were hypointense on T1-weighted imaging and partially or completely hypointense on T2-weighted imaging. Two had DWI scans; both showed mild restriction. Three of three showed hypointensity on T2\* (GRE or SWI).



#### CONCLUSION

Intracranial textiloma should be considered in the differential diagnosis of an enhancing mass lesion on CT or MRI at the site of previous neurosurgical resection. Intracranial textilomas virtually always enhance. When hypointense signal on T2-weighted MRI or blooming on T2\* is present, these features may help distinguish textiloma from abscess or recurrent tumor.

**KEY WORDS:** Foreign-body granuloma, neoplasm recurrence, diagnosis, hemostasis, surgical instrumentation

O-152

4:12 PM - 4:20 PM

#### Monitoring the Effects of Cumulative Radiation Exposure in Aneurysmal Subarachnoid Hemorrhage

Rosenbaum, D. G.<sup>1</sup>Minkowitz, S.<sup>2</sup>Loftus, M. L.<sup>1</sup>Shih, J.<sup>1</sup>Sanelli, P. C.<sup>1</sup>

<sup>1</sup>NewYork-Presbyterian Hospital, New York, NY, <sup>2</sup>Weill Cornell Medical College, New York, NY

#### PURPOSE

To monitor the cumulative radiation exposure due to CT imaging and the frequency of deterministic effects in aneurysmal subarachnoid hemorrhage (SAH).

#### MATERIALS & METHODS

We performed a retrospective study of consecutive aneurysmal SAH patients. Data collection included number and type of CT examinations of the head performed during hospitalization, including unenhanced CT, CT angiography (CTA), and CT perfusion (CTP). CT perfusion examinations were performed using 80 kVp and mA less than 200. The radiation exposure for each CT was recorded as dose-length product (DLP), an indicator of the energy imparted to organs and a surrogate for overall radiation burden. Chart reviews of both hospitalization and subsequent outpatient visits were undertaken for the following deterministic effects that may occur from ionizing radiation: delayed wound healing not attributable to other causes, skin erythema/burn, temporary or permanent epilation, and cataract formation. Length of outpatient follow up was documented as days from the last inpatient CT. Overall mean DLP and standard deviation (SD) were calculated for the study population and for each type of CT examination. Overall mean number of CT examinations was calculated for the study population and for each type of CT examination.

#### RESULTS

A total of 127 patients (mean age 52.7 years, SD12.5) admitted for aneurysmal SAH were included in this study. Mean cumulative DLP for the study population was 11,421 mGy-cm (SD5,024), with unenhanced CT, CTA, and CTP accounting for 33%, 28%, and 38% of the radiation burden, respectively. Patients underwent an average of 6.5 (SD3.6) CT examinations during hospitalization, consisting of 3.6 (SD3.6) unenhanced CT, 1.03 (SD0.82) CTA, and 1.83 (SD1.01) CTP. The mean length of outpatient follow up was 352 days (SD476). Adverse biologic events were found in 5.5% (7/127), with 3% (4/127) cataract formation and 2% (3/127) delayed wound healing. No cases of skin erythema/burn or epilation were noted. In two cases of cataract formation, the diagnosis was made within 4 months of the patient's last inpatient CT, possibly occurring too early to be attributed to radiation exposure. In the remaining two cases, cataract formation occurred within 3-5 years of the patient's last inpatient CT. In the cases of delayed wound healing, two cases involved persistent drainage not attributable to other causes (such as infection) and the third case involved frank dehiscence necessitating suture placement. Mean cumulative DLP for these seven patients who developed adverse biologic events was 13,446 mGy-cm (SD5,725) and mean number of CT examinations was 6.0 (SD2.7).

#### CONCLUSION

The frequency of adverse biologic events that have been described as deterministic effects occurring from radiation exposure was calculated as 5.5%, with cataract formation occurring in 3% and delayed wound healing in 2% of the study population. However, there is a reported 3-13% incidence of cataract formation in those over 40 years old and a 5-11% incidence of delayed wound healing for craniotomies in the general population. Although causation of these biologic events



cannot be determined, these findings may provide further support that there is a low incidence of deterministic effects from cumulative radiation exposure in aneurysmal SAH.

**O-153** **4:20 PM - 4:28 PM**

**Radiation Awareness in Patients Having a Head CT Scan: A Survey**

Adas, R. A. A.-Chakraborty, S.

The Ottawa Hospital/University  
Ottawa, ON, CANADA

**PURPOSE**

In light of ongoing media madness regarding increasing radiation exposure and possible ill-effects due to ever increasing number of CT scans, we conducted a survey to determine the level of 'radiation' awareness among patients being referred for a CT scan of the head.

**MATERIALS & METHODS**

The survey was conducted over a 6-month period following REB approval. Patients scheduled for a CT head scan received an information sheet that explained the purpose of the survey. The participants received a three-page questionnaire with 19 multiple choice questions about the indication, referring physicians and explanation about the benefit and risk of the scan that they were given. Questions also were directed to assess their awareness about radiation exposure, risk, organ dose. Finally they were asked about who they think should provide this information. After completing the survey the patients received a summarized information sheet explaining radiation exposure related to their scan and answers to some of the survey questions.

**RESULTS**

We received the feedback of 60 patients, age range (21-87 years) mean age of 62. One third of the patient was not aware about being exposed to radiation and it's relation to cancer. Twenty per cent of patients had no information why they were doing their scan. And more than 60% of patients had no information about their scan's dose, risks, and benefits. However most patients believe the radiologists would be the best person to explain this information to patients.

**CONCLUSION**

The increasing use of CT has led to several concerns regarding safety, dose, and radiation-induced cancers. Though this is a well discussed issue in imaging departments, the level of awareness in patients and referring physicians are unknown. The results of our survey showed that 60% of patients had no information about their scans prior to their booked appointments. We hope that by continuing this survey, we provide patients with brief proper information about radiation exposure and stimulate their curiosity. Also with this result we hope to improve dissemination of knowledge about radiation exposure to the general public, including prospective patients as well as the referring physicians.

**KEY WORDS:** Radiation awareness, CT head, survey

## Monday Afternoon

**4:45 PM - 6:15 PM**

**Grand Ballroom Suite**

**(16) ASPNR PROGRAMMING:  
PEDIATRIC HEAD AND NECK (SAM  
#2) (AR)**

\*Qualified by the American Board of Radiology (ABR) in meeting the criteria for Self-Assessment towards the purpose of fulfilling requirements in the ABR Maintenance of Certification program data 3/12.

**O-154**

**4:45 PM - 5:10 PM**

**Craniofacial Malformations: Radiological  
Perspective**

Susan I. Blaser, MD

Diagnostic Radiology. Hosp. for Sick Children  
Toronto, ON, Canada

**O-155**

**5:10 PM - 5:35 PM**

**Craniofacial Malformations: Clinical Perspective**

Gary F. Rogers, MD

Radiology, Children's National Medical Center  
Washington, DC, USA

*Gary F. Rogers, M.D., J.D., M.B.A., M.P.H., is the Chief of the Division of Plastic and Reconstructive Surgery at Children's National Medical Center in Washington, D.C., and an Associate Professor of Surgery and Pediatrics at George Washington School of Medicine. Dr. Rogers is a graduate of University of California, Los Angeles (B.S., 1987), Tulane University School of Medicine (M.D., 1991), Tulane University A.B. Freeman School of Business (M.B.A., 1991), Tulane University School of Public Health and Tropical Medicine (M.P.H., 1991), and the University of North Carolina, Chapel Hill School of Law (J.D., 1997). He completed residencies in orthopedic surgery (University of North Carolina, Chapel Hill 1996) and plastic surgery (University of Tennessee College of Medicine, Chattanooga, 1999), followed by fellowship training in pediatric plastic surgery (Children's Hospital Boston, 2001) and hand/microsurgery (Massachusetts General Hospital, 2002). He is certified by the American Board of Plastic Surgery, the American Board of Orthopedic Surgery, and holds a subspecialty certificate in surgery of the hand. He is an Associate Editor for the Journal of Craniofacial Surgery and has published over 80 peer-reviewed publications.*

**OBJECTIVES:**

1. Understand the pathogenesis of craniosynostosis
2. Recognize the associated clinical features of various forms of craniosynostosis.

3. Understand indications for treatment and surgical options.

#### PRESENTATION SUMMARY:

Craniosynostosis is the premature fusion of one or more cranial sutures. This pathologic process occurs in 1 in 2,000 to 2,500 live births and can occur in association with no less than 130 different syndromes. Any cranial suture can be affected, but fusion is most common in the sagittal suture (40-55%), followed by the coronal (20-25%), metopic (5-15%), and lambdoid (1%) sutures. Craniosynostosis results in characteristic changes to cranial shape that often suggest which suture(s) is involved (Virchow's Law). Some rare forms of craniosynostosis have unusual cranial shapes and require high resolution CT to make the diagnosis.

Intracranial hypertension has been documented in 10-15% of patients with single suture synostosis, and as many as 75% of patients with multiple sutures involved. Affected patients, especially those with an associated syndrome, may also have other physical findings such as midface hypoplasia, deafness, visual disturbances and blindness, speech impairments, learning and cognitive disabilities, nasopharyngeal airway obstruction, swallowing dysfunction, heart and lung abnormalities, and extremity anomalies.

The diagnosis, management, and treatment of craniosynostosis requires coordinated care. This is best accomplished by interdisciplinary team comprised of professionals from the following disciplines: anesthesiology, craniofacial surgery, genetics, hand surgery, intensive care, neurosurgery, nursing, ophthalmology, orthodontics, pediatrics, pediatric dentistry, prosthodontics, psychology, radiology, social work, and speech/language pathology. Treatment options include suturectomy, spring-mediated distraction, and open cranial remodeling procedures.

The pathogenesis of craniosynostosis is complex and, in most cases, is not fully understood. Contemporary research has demonstrated that the subjacent dura mater affects cranial suture patency by temporally and spatially supplying growth factors (e.g., FGF-2) and cellular elements (e.g., osteoblastic cells) to the overlying osteogenic fronts and suture mesenchyme. Mutations in TWIST, MSX, EFNB1, and FGFR1-3 genes have been associated with the development of some types of craniosynostosis, but most forms of have no identifiable genetic cause.

**O-156**

**5:35 PM - 6:10 PM**

#### Syndromic Hearing Loss

Caroline D. Robson, MB, ChB

Radiology, Children's Hospital  
Boston, MA, USA

## Monday Afternoon

**4:45 PM - 6:15 PM**

**Tranon Ballroom**

### (17) ASFNR PROGRAMMING: ADVANCED IMAGING IN PSYCHIATRIC DISEASE: OPPORTUNITIES AND TRENDS

**O-157**

**4:45 PM - 5:10 PM**

#### Advanced Imaging of Affective Disorders and Schizophrenia

Perry F. Renshaw, MD, PhD, MBA

The University of Utah  
Salt Lake City, UT, USA

*Dr. Renshaw received his M.D. and Ph.D. (biophysics) degrees from the University of Pennsylvania before completing his residency in adult psychiatry at the Massachusetts General Hospital. In 1992, he accepted a position at the the McLean Hospital Brain Imaging Center, where his NIH-funded work focused on the use of multinuclear MRS to study individuals with substance abuse and mood disorders. In 2008, Dr. Renshaw was recruited to the University of Utah as a USTAR Investigator and Professor of Psychiatry. He is an author of over 300 peer reviewed articles and has received numerous awards and honors for his research.*

#### PRESENTATION SUMMARY

Recently, three independent reports have suggested a strong association between regional suicide rates in the United States and altitude (Kim, 2001; Brenner, 2011; Betz, 2011). This association may be due to a poorly understood increase in rates of depression with elevation (DelMastro, 2011; Betz, 2011; Gamboa, 2011). We have evaluated whether there is a difference in brain chemistry with altitude by conducting proton (1H) magnetic resonance spectroscopy (MRS) studies of healthy volunteers in Salt Lake City (UT) and in Belmont (MA), which are 4,700 and 44 feet above sea level, respectively. 2D J-resolved 1H MRS was used to acquire MRS data from the anterior cingulate cortex (ACC) and the parietal-occipital cortex (POC) in ten age- and sex-matched healthy volunteers at each site. The UT cohort showed significantly decreased ACC glutamate ( $p = .01$ ), total creatine ( $p < .001$ ), and lactate ( $p = .05$ ). Significant differences were not observed for POC metabolites between the UT and MA cohorts. The present findings are of interest in light of commonly reported reductions in cortical glutamate/glutamine levels in major depression (Yuksel, 2010). Similarly, reductions in the proton MRS creatine resonance would be consistent with lower levels of phosphocreatine, which has been suggested as a marker for poor antidepressant treatment response (Iosifescu, 2008). This is the first report of changes in brain chemistry

with altitude and the findings suggest that novel therapeutic strategies may be necessary for treating depression at higher elevations.

**O-158** **5:10 PM - 5:35 PM**

### **Advanced Imaging for the Evaluation of Schizophrenia and Related Illnesses**

Martha Shenton, PhD

Psychiatry & Radiology, Brigham and Women's Hospital  
Boston, MA, USA

**O-159** **5:35 PM - 6:00 PM**

### **MR Techniques for Imaging in Psychiatric Disease: Current Status and Future Directions**

John D. Port, MD, PhD

Mayo Clinic  
Rochester, MN, USA

#### **PRESENTATION SUMMARY**

This presentation will review the major MR imaging techniques currently used to study psychiatric illness. MR volumetry, voxel-based morphometry, diffusion tensor imaging, functional MRI and MR spectroscopy will be discussed, including a summary of the technique, a brief review of the literature, and a discussion of the potential value and limitations of each technique. Finally, future MR tool development for psychiatric illness will be discussed in the context of what will be available in the next few years.

## **Monday Afternoon**

**4:45 PM - 6:15 PM**  
**Beekman/Sutton North**

### **(18) ADVANCED IMAGING SEMINAR: MOLECULAR NEURORADIOLOGY**

**O-160** **4:45 PM - 5:15 PM**

### **New Tracers for Tumor Imaging**

Hyunsuk Shim, PhD

Radiology, Emory University  
Atlanta, GA, USA

*POSITION TITLE: Tenured Associate Professor of Radiology*

#### **EDUCATION/TRAINING**

*Yonsei University at Seoul, Korea B.S. Physics*

*Univ of Illinois at Urbana-Champaign Ph.D. Biophysics*

*Johns Hopkins School of Medicine Post-doc Radiology*

*Johns Hopkins School of Medicine Post-doc Molecular Oncology*

**Research Interest:** *My laboratory has a diverse range of expertise in molecular imaging, cancer biology, and pharmacology. We have been studying the involvement of chemokine, stromal cell derived factor -1 (SDF-1) and its receptor CXCR4 in cancer invasion/metastasis. We are studying cancer invasion and metastasis, especially recruitment and homing of inflammatory and tumor cells at the distant organ sites. We have successfully led an interdisciplinary research team to discover a series of novel, potent anti-CXCR4 molecules, one of which is under clinical evaluation. We are also developing methods to detect metastatic tumor and tumor metabolism by using PET.*

#### **Honors**

*American Association for Cancer Research AFLAC Young Investigator Award 1997*

*Leukemia Society of America, Special Fellow Award 1998*

*Georgia Cancer Coalition, Distinguished Cancer Clinicians and Scientists 2002*

*The Phi Beta Kappa Society Excellent Teaching Recognition 2009*

*Radiology Department, Emory University, Outstanding Scientific Contribution Award 2011*

*Number of published articles: 47 peer reviewed articles, 50 International meeting abstracts.*

#### **PRESENTATION SUMMARY**

Molecular imaging is one of the fastest growing areas of medical imaging. Positron emission tomography (PET) and single photon emission tomography (SPECT) have been widely used in the clinical management of patients with cancer. Nuclear imaging provides biological information at the cellular, subcellular, and molecular level in living subjects with non-invasive procedures. In particular, PET imaging takes advantage of traditional diagnostic imaging techniques and introduces positron-emitting probes to determine the expression of indicative molecular targets at different stages of cancer.  $^{18}\text{F}$ -fluorodeoxyglucose ( $^{18}\text{F}$ -FDG), the only FDA approved oncological PET tracer, has been widely utilized in cancer diagnosis, staging, restaging, and even monitoring response to therapy; however,  $^{18}\text{F}$ -FDG is not a tumor-specific PET tracer. Over the last decade, many promising tumor-specific PET tracers have been developed and evaluated in preclinical and clinical studies. I will present an overview of the current non- $^{18}\text{F}$ -FDG PET tracers in oncology that have been developed based on tumor characteristics such as increased metabolism, hyperproliferation, angiogenesis, hypoxia, apoptosis, and tumor specific antigens and surface receptors. The corresponding SPECT tracers are discussed as well.

**O-161** **5:15 PM - 5:45 PM**

### **Imaging of Tumor Response - Pseudo or Real?**

Meng Law, MD

USC Medical Center  
Los Angeles, CA, USA

#### **EDUCATIONAL OBJECTIVES**

1. Understand the entities of pseudo-phenomena in the post therapeutic brain in the setting of novel therapies
2. Understand how to recognize pseudoprogression following treatment with temozolomide and radiation which is currently the standard of care for malignant glioma
3. Understand how to recognize pseudoresponse following treatment with novel anti-angiogenic therapies such as bevacizumab
4. Recognize some of the challenges and limitations with conventional MR imaging in the characterization of pseudophenomena
5. Appreciate how advanced MR techniques such as perfusion, permeability, diffusion and MR spectroscopy could be useful in characterization of pseudophenomena

**PRESENTATION SUMMARY** (Abstract from Reference 1 Wen P et al):

Currently, the most widely used criteria for assessing response to therapy in high-grade gliomas are based on two-dimensional tumor measurements on magnetic resonance imaging (MRI), in conjunction with clinical assessment and corticosteroid dose (the Macdonald Criteria). It is increasingly apparent that there are significant limitations to these criteria, which only address the contrast-enhancing component of the tumor. For example, chemoradiotherapy for newly diagnosed glioblastomas results in transient increase in tumor enhancement (pseudoprogression) in 20% to 30% of patients, which is difficult to differentiate from true tumor progression.

Antiangiogenic agents produce high radiographic response rates, as defined by a rapid decrease in contrast enhancement on CT/MRI that occurs within days of initiation of treatment and that is partly a result of reduced vascular permeability to contrast agents rather than a true antitumor effect. In addition, a subset of patients treated with antiangiogenic agents develop tumor recurrence characterized by an increase in the nonenhancing component depicted on T2-weighted/fluid-attenuated inversion recovery sequences. The recognition that contrast enhancement is nonspecific and may not always be a true surrogate of tumor response and the need to account for the nonenhancing component of the tumor mandate that new criteria be developed and validated to permit accurate assessment of the efficacy of novel therapies. Novel imaging techniques such as perfusion, permeability, diffusion and spectroscopic imaging technique are required to help characterize and understand these phenomena.

**O-162**

**5:15 PM - 5:45 PM**

### **PET/MR: Neuro Applications**

Zahi A. Fayad, PhD, FAHA, FACC

Mount Sinai School of Medicine  
New York, NY, USA

### **PRESENTATION SUMMARY**

Atherosclerosis-related diseases are projected to cost more than \$500 billion in the United States in 2010. The majority of life threatening consequences of

atherosclerosis, including myocardial infarction (MI) and stroke, result from acute thrombus formation on the surface of a plaque. The newly formed thrombus may completely occlude the lumen in situ, or embolize to occlude a distal narrower lumen, and in so doing cause infarction to the territory supplied by the artery. Most clinical investigations for atherosclerosis provide a readout on the degree of stenosis caused by the plaque. However, it is now well recognized that the plaque that is at risk of thrombus formation is not necessarily the plaque that impinges most on the lumen of the vessel. Numerous imaging techniques are currently being developed to provide information on both the composition and function of the plaques. Plaque rupture accounts for the majority of acute thrombus formation and is defined as a deep injury to the fibrous cap with consequent exposure of the underlying lipid-rich core to the arterial blood. The prerupture lesion that most closely resembles a ruptured plaque is the thin-cap fibroatheroma (TCFA), characterized by a large necrotic core underneath a thin, fibrous cap. TCFAs contain an abundance of macrophages and show signs of neovascularization with intraplaque hemorrhage. All of these features can now be probed by novel imaging techniques. Some of these techniques, such as ultrasound imaging of carotid intima-media thickness and intravascular ultrasound of the coronary arteries, are already in clinical use. Others, such as magnetic resonance imaging (MRI) and positron emission tomography (PET), have found application in research in the analysis of the compositional features of carotid artery plaque, and have potential clinical utility. In this article, we review the various imaging modalities used for the evaluation and quantification of atherosclerosis. We also review new methods based on nanomedicine for novel treatment of atherosclerosis.

## **Monday Afternoon**

**4:45 PM - 6:15 PM**

**Sutton Center/South**

### **(19) APPROPRIATE UTILIZATION OF CERVICAL SPINE IMAGING IN TRAUMA**

**O-163**

**4:45 PM - 5:05 PM**

### **Are We Currently Practicing Accounting to the ACR Appropriateness Criteria?**

Pina C. Sanelli, MD, MPH

Radiology, Weill Medical College of Cornell University  
New York, NY, USA



**O-164** **5:05 PM - 5:30 PM**

**What Are the Effects of Appropriate Utilization in Radiology Practice?**

Krystal Archer-Arroyo, MD

University of Maryland School of Medicine  
Baltimore, MD, USA

**O-165** **5:30 PM - 5:55 PM**

**What Are the Barriers to Implementing Appropriate Utilization Tools in Clinical Practice?**

Rahul Sharma, MD, MBA, FACEP

Weill Cornell Medical College  
New York, NY, USA

## Monday Afternoon

**4:45 PM - 6:15 PM**

**Murray Hill**

**(20) Pediatrics: Miscellaneous**

**O-548** **4:45 PM - 4:53 PM**

**Radiation Injury in Young Children Treated with Proton Beam Radiation Therapy for Brain Tumors: MR Imaging Features with Clinical Correlations**

Sabin, N. D. Merchant, T. M. Harreld, J. H. Patay,  
Z. Wright, K. D. Gray, J. Gajjar, A.

St. Jude Children's Research Hospital  
Memphis, TN

**PURPOSE**

Proton beam radiation therapy (PBRT) promises high dose conformity to the target volume while reducing radiation dose to normal tissues. Potential adverse effects, however, are poorly understood and sparsely documented in the literature, especially in the pediatric population. We report clinical and imaging findings of radiation-induced injury in eight children less than 3 years of age treated with PBRT for primary brain tumors.

**MATERIALS & METHODS**

Clinical and imaging data were collected for eight children (age 7 months to almost 3 years) with brain tumors who received 54 cobalt gray equivalent PBRT following chemotherapy and developed subsequent MRI evidence of radiation injury of brain parenchyma. Six patients had posterior fossa tumors; two had supratentorial neoplasms. Following PBRT, oral chemotherapy was continued for all but one patient. All patients had MRI of the brain just after completion of PBRT and at approximately 3-month intervals. Contours of areas of suspected radiation injury were drawn on coregistered MRI images and PBRT planning isodose

curves for each child and dose-volume histograms (DVH) were calculated for the abnormal areas.

**RESULTS**

On MRI obtained approximately 3 to 6 months after therapy, seven of eight patients had abnormal signal and enhancement consistent with necrosis in the posterior fossa, primarily in the brainstem. One had abnormal signal in the thalamus. Imaging findings resolved over 1 to 3 months in six of eight patients and were worse 2 months later in one patient. One patient expired before follow-up MRI. Two patients demonstrated potentially related clinical signs and symptoms; the remaining patients were asymptomatic. Coregistration of MRI images with isodose curves and associated DVH data reveal that most of the areas of abnormality are located along the deep margins of treatment regions receiving the highest radiation dose levels.

**CONCLUSION**

Radiation injury of brain may occur in young children treated with PBRT for primary central nervous system tumors and may be asymptomatic. In this series, injury was most commonly at the deep margins of the high-dose treatment region, possibly related to areas of highest energy deposition. These changes appeared unusually early after PBRT and improved relatively quickly in most patients. Possible etiologies for the unanticipated susceptibility of normal-appearing brain to PBRT in these very young children include age, focally intense deposition of energy related to the spread out Bragg peak and sensitization of brain tissue by chemotherapeutic agents. The brainstem may be particularly susceptible to the effects of PBRT.

**KEY WORDS:** Neoplasms, radiation injury, proton beam radiation therapy

**O-173** **4:53 PM - 5:01 PM**

**Comparison of Spin Echo and Gradient Echo T1-Weighted and Spin Echo T2-Weighted Images at 3 T for Term Neonatal Myelination Evaluation**

McKinney, A. Hanson, T. J. Sarikaya, B. Truwit, C. L.

University of Minnesota & Hennepin County Medical Centers  
Minneapolis, MN

**PURPOSE**

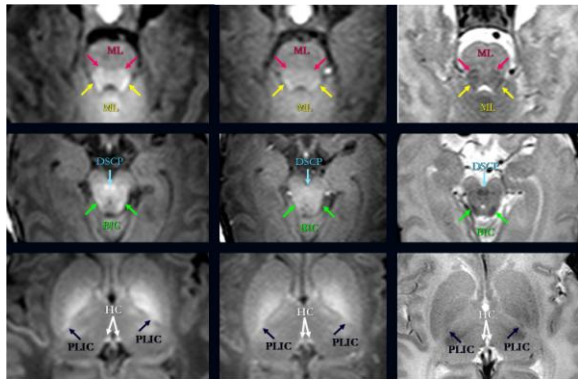
MR imaging often is utilized to assess myelination and to evaluate for hypoxic-ischemic insult (HII) in term infants. There is little data comparing myelination scoring between gradient echo T1-weighted imaging (GET1WI), spin echo T1-weighted imaging (SET1WI), and spin echo T2-weighted imaging (SET2WI) at 3 T. A prior study of term equivalent premature patients described that GET1WI leads SET1WI at 3 T, while SET2WI depicted the highest number of myelinated structures. Our purpose was to compare the extent of myelination on these sequences in developmentally normal term infants.

## MATERIALS & METHODS

IRB approval was obtained. Axial GET1WI, SET1WI, and SET2WI sequences are standard in our noncontrast 3 T MRI evaluation for HII. We retrospectively reviewed term neonates scanned at <3 weeks age for HII between 1/2005-1/2011 (n = 33), with the intent to include only developmentally normal children. We excluded 23 patients with: cerebral pathology on MRI (n = 9), residual neurologic deficit (n = 3), Apgar <3 at 10 minutes (n = 2), chromosomal anomaly (n = 2), no clinical follow up at >6 months age (n = 3), not all 3 sequences obtained (n = 3), or severe motion during MRI (n = 1). Thus, 10 infants who were developmentally normal at >6 months age were included. Two pediatric neuroradiologists independently reviewed the three sequences in 19 regions, based on previous studies.

## RESULTS

MR images were scored as +, -, or +/- for myelination, myelination being bright signal on GET1WI and SET1WI, and dark on SET2WI. Myelination was present in 60.5-75.3% of structures on GET1WI, 25.8-59.5% on SET1WI, and 58.9-65.3% on SET2WI. Interobserver kappa was "moderate" for GET1WI (k = 0.435, p<0.001), "fair" for SET1WI (k = 0.259, p<0.001), and "fair-moderate" for SET2WI (k = 0.387, p<0.001). Notably, there was 100% agreement between observers that myelination was present in all patients on GET1WI within the pyramidal decussation, medial lemniscus (ML), lateral lemniscus, brachium of inferior colliculus (BIC), superior cerebellar peduncle (SCP) and its decussation (DSCP), habenular commissure (HC), and posterior limb internal capsule (PLIC); on SET2WI there was 100% agreement that myelination was present in all patients in the ML, BIC, DSCP, and the inferior cerebellar peduncle.



## CONCLUSION

At 3 T, GRET1WI leads SET1WI in term myelination, as described previously in term equivalent premature infants. We again found that the highest interobserver agreement was on GRET1WI, but the current study noted that GRET1WI had a higher rate of myelinated structures than SET2WI, contrary to the prior study of term equivalent infants. Prospective studies are necessary to confirm our findings in developmentally normal, asymptomatic patients.

**KEY WORDS:** Neonatal, myelination, 3 T

O-174

5:01 PM - 5:09 PM

## Evaluation of Perinatal Arterial Ischemic Stroke by Arterial Spin Labeling Perfusion MR Imaging

De Vis, J. B.·Petersen, E. T.·de Vries, L. S.·Groenendaal, F.·Alderliesten, T.·Kersbergen, K.·Lemmers, P. M.·Hendrikse, J.·Benders, M.

University Medical Center Utrecht  
Utrecht, NETHERLANDS

## PURPOSE

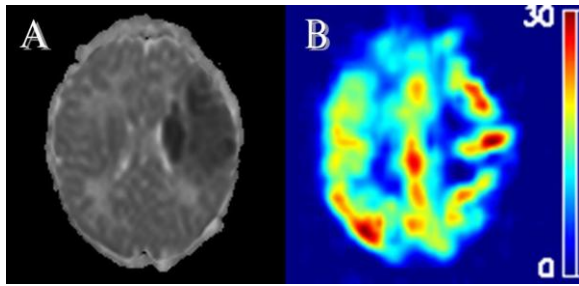
It was our aim to establish a noninvasive measurement of brain perfusion in neonates to evaluate the viability of brain tissue, especially in the penumbra, after perinatal arterial ischemic stroke (PAIS).

## MATERIALS & METHODS

For this we applied arterial spin labeling (ASL) perfusion imaging, which has been part of our neonatal imaging protocol in over 20 patients, for the first time in two PAIS patients.

## RESULTS

Two neonates suffered PAIS which was monitored by bilateral near infrared spectroscopy (NIRS). Conventional MR imaging with DWI and PC MRA was performed, next to pulsed ASL (3 T Philips); parameters: TR/TE/TI = 2500/20/1800 ms. A region of interest was drawn surrounding the stroke area, visualized on DWI, and surrounding the corresponding contralateral area. For accurate cerebral blood flow quantification the T<sub>1</sub> of blood was measured. A complete occlusion of the left middle cerebral artery as well as diffusion restriction in its supply area, illustrated on the ADC map (Fig. A: baby 1), was shown in both patients. Perfusion measured on the ASL images was lower in the stroke area compared with the corresponding contralateral area (baby1/baby2; 11.3/3.8 in the stroke area vs 13.5/8.5 ml/min in the corresponding contralateral area). In the first patient, higher perfusion signal was seen in the convexity of the left hemisphere probably due to luxury perfusion and collateral arteries (Fig. B). Furthermore, PC MRA in this patient measured higher flow in the left internal carotid artery (ICA) compared to the right ICA (41 vs 22 mL/min), probably due to ischemia-induced vasodilatation. In both patients NIRS showed a higher cerebral tissue oxygenation in both hemispheres immediately after the event followed by normalization on the right, but persistently higher values on the left. This might be due to initial bilateral hyperperfusion followed by decreased oxygen-use or ischemia-induced vasodilatation in the affected hemisphere.



#### CONCLUSION

Arterial spin labeling can reliably assess perfusion in perinatal arterial ischemic stroke. It may be used to assess tissue viability, to evaluate the effect of luxury perfusion and collateral arteries in the evolution of the penumbra and to monitor the effect of neuroprotective treatment after PAIS.

**KEY WORDS:** Arterial spin labeling, neonate, stroke

**O-175**

**5:09 PM - 5:17 PM**

#### Insensitivity of Diffusion Tensor Imaging to Neonatal White Matter Injury

Nagasunder, A. C.<sup>1</sup>Rollins, N. K.<sup>1</sup>Chalak, L.<sup>2</sup>Seo, Y.<sup>1</sup>Morriss, M. C.<sup>1</sup>Wang, Z.<sup>1</sup>

<sup>1</sup>Childrens Medical Center, Dallas, TX, <sup>2</sup>University Texas Southwestern Medical Center, Dallas, TX

#### PURPOSE

An abnormal conventional MR imaging (cMRI) in the perinatal period has high predictive value for neurodevelopmental impairment following neonatal hypoxic ischemic encephalopathy (HIE) although a normal MR does not insure a normal clinical outcome. Diffusion tensor imaging (DTI) may increase the prognostic value of MRI in this setting. The purpose of this study therefore was to compare diffusion tensor metrics of neonates at risk for ischemic brain injury to those neonatal "controls".

#### MATERIALS & METHODS

This study was IRB approved retrospectively. Subjects were selected from a database of neonates referred for MR imaging over the past 2 years for possible congenital brain malformation, apnea, or neonatal seizure in whom cMRI and neurologic examination were normal. Diffusion tensor imaging from this "control" group [n = 40; mean postconception age (PCA) 41.7 ± 5.1 weeks] was compared to 28 patients at risk for brain injury due to HIE (mean PCA, 38.4 ± 7.6 weeks; imaged 5-10 days of age); 20 were s/p therapeutic hypothermia, and eight patients s/p ECMO (mean PCA 40.3 ± 3.7 weeks; imaged 14-28 days of age) for neonatal respiratory failure not due to congenital diaphragmatic hernia or heart disease. MR imaging done at 3 T included T1, T2, and DWI; posterior limbs of internal capsules (PLIC), callosal genu (CG) and splenium (CS) were assessed as normal or abnormal on cMR. Diffusion tensor imaging parameters were SS-EPI, b = 700, 30 directions, TE = 84 ms, 2mm<sup>3</sup> voxel, 128<sup>2</sup> matrix size, SENSE = 2-2.5, 3 repetitions. After correction of eddy current distortion and motion

artifact, tensor data were postprocessed using FSL (FMRIB, Oxford, UK) and Tract-Based Spatial Statistics modified for use in neonates (Ball). Tensor metrics were analyzed using custom software written in IDL (IDL Research Systems Inc. Boulder, CO). The posterior limbs of internal capsules (PLIC), callosal genu (CG) and splenium (CS) were interrogated for fractional anisotropy (FA), and axial (AD) and radial diffusivity (RD). Ninety-five per cent confidence intervals for FA, AD, and RD were constructed from "control" data using linear regression analysis; FA, AD and RD for at-risk patients were considered abnormal if outside the confidence intervals. Findings on cMRI were compared to DTI.

#### RESULTS

Conventional MR imaging was abnormal in the PLIC, CS, and/or CC in five subjects s/p cooling HIE but in 0/8 ECMO patients. Of the HIE patients, FA values were outside the 95% confidence intervals in the PLIC in five subjects, in the CS in five, and the CG in four. With the use of FA+AD, there were six, six, and nine subjects outside the confidence intervals for the PLIC, CS, and CG, respectively. The use of FA+AD+RD increased number of the outliers to six, seven, and ten for the PLIC, CS, and CG, respectively. Diffuse atrophy and abnormal deep white matter was seen in seven of eight ECMO survivors; DTI in the PLIC, CS, and CC were consistently normal.

#### CONCLUSION

Diffusion tensor imaging is not sufficiently sensitive to detection of white matter injury in either patients at risk for or with HIE nor for survivors of neonatal ECMO in whom cMRI suggests white matter injury.

**KEY WORDS:** Neonatal HIE, diffusion tensor imaging

**O-176**

**5:17 PM - 5:25 PM**

#### Absolute Values and Interhemispheric Ratios of Cerebral Blood Flow Assessed by Arterial Spin Labeling and Transcranial Doppler Ultrasonography in Children with Sickle Cell Disease

Behpour, A. M.<sup>1,2</sup>Yu, J.<sup>2</sup>Leung, J.<sup>2</sup>Mikulis, D.<sup>1,3</sup>Kassner, A.<sup>1,2</sup>

<sup>1</sup>University of Toronto, Toronto, ON, CANADA, <sup>2</sup>Hospital for Sick Children, Toronto, ON, CANADA, <sup>3</sup>Toronto Western Hospital, Toronto, ON, CANADA

#### PURPOSE

Mechanisms responsible for cerebral ischemic events in sickle cell disease (SCD) are very complex and seem to be related to abnormal blood flow. Blood flow abnormalities can be due to narrowing or occlusion of cerebral vessels as well as hyperemia associated with chronic anemia. Advanced neuroimaging techniques such as arterial spin labeling (ASL) might be able to distinguish these mechanisms. The purpose of this study was to compare absolute values and interhemispheric ratios of blood flow obtained in the middle cerebral artery (MCA) territories with ASL

versus transcranial Doppler ultrasonography (TCD) in children with SCD.

#### MATERIALS & METHODS

Nine neurologically normal children with SCD (10 - 18 years old) along with five age-matched healthy controls underwent ASL and TCD. Arterial spin labeling data were acquired on a 3.0 T MRI system (Magnetom TrimTrio, Siemens Medical Solutions, Erlangen, Germany) using a PICORE Q2T sequence. Cerebral blood flow (CBF) was calculated in each subject for each MCA territory thresholded for gray matter using the ASL data processing toolbox (ASLtbx) provided by Wang et al. Blood flow velocities of the right and left MCAs were acquired with a TCD system (iU-22 xMatrix; Philips Electronics, Best, the Netherlands) equipped with an S5-1 transducer. The highest time average peak velocity (TAPV) between three consecutive measurements was obtained in each MCA. The mean CBF and TAPV were compared between patients and controls using a Mann-Whitney U-test. In addition, a left to right interhemispheric ratio was calculated for CBF and TAPV values. The correlation of ASL and TCD ratios was examined by a Spearman correlation coefficient ( $r_s$ ). Absolute values and ratios were defined as abnormal if they exceed two standard deviations of the mean of the control group.

#### RESULTS

The average CBF and TAPV were  $64.36 \pm 3.61$  ml/min/100 g ( $p = 0.003$ ) and  $97.06 \pm 5.1$  cm/s ( $p = 0.06$ ) in patients,  $40.47 \pm 1.15$  ml/min/100 g and  $77.98 \pm 3.25$  cm/s in controls, respectively. Individual CBF values in both MCA territories of all patients were higher than controls. However, abnormal TAPV values were identified only in five patients. The CBF and TAPV ratios varied between 0.83-1.2 and 0.73-1.01 in patients, 0.98-1.08 and 0.86-1.08 in controls, respectively. Cerebral blood flow ratios were significantly correlated with TAPV ratios in patients ( $r_s = 0.71$ ,  $p = 0.047$ ). Abnormal CBF ratios were observed in three patients, whereas only one of these three patients had an abnormal TAPV ratio.

#### CONCLUSION

Elevated CBF in SCD patients most likely is due to anemia with reduced oxygen delivery and a compensatory vasodilatory response in arterioles. Elevated TAPV also can be due to this effect but also could be due to MCA stenoses without anemia. Arterial spin labeling can be confounded by stenoses that result in increased transit times where flow underestimation is seen due to delay in the transit of magnetically labeled blood water protons. Application of either method should take into consideration these possible confounds through angiographic assessment of the large arterial supply vessels when applying absolute values or interhemispheric ratios for managing patients.

**KEY WORDS:** Neuroimaging, cerebral blood flow, sickle cell disease

O-177

5:25 PM - 5:33 PM

#### Intracranial Arterial Calcifications in a Pediatric Population: Prevalence and Possible Relationship to Childhood Disease

Harri, P. A.<sup>1</sup>Desai, N.<sup>1</sup>Chen, Z.<sup>2</sup>Mullins, M. E.<sup>1</sup>

<sup>1</sup>Emory University School of Medicine, Atlanta, GA,

<sup>2</sup>Rollins School of Public Health, Atlanta, GA

#### PURPOSE

The objective of this study was to retrospectively examine the prevalence of intracranial anterior and posterior circulation arterial calcification in a pediatric population as identified on routine, noncontrast head CT scans and to determine if correlations between specific underlying medical conditions and such calcifications exist.

#### MATERIALS & METHODS

This retrospective study was approved by our IRB. Consecutive noncontrast head CT scans on both male and female children ages 0-20 years between August 1, 2010 - October 31, 2010 at a large tertiary referral children's hospital were collected using the institutional picture archiving and communications system (PACS). Two fellowship-trained neuroradiologists independently interpreted these scans to determine the presence or absence of intracranial arterial calcification, and its location. The electronic medical records of all patients were reviewed for clinical history prompting the examination, demographics and medical history, especially disease processes that may predispose to premature arterial calcifications such as calcium metabolism disorders, diabetes mellitus, renal disease, and hyperlipidemia. Consensus conference was used to resolve disagreements. Chi-square and Fisher exact tests were used as appropriate to examine the potential significance of calcification incidence among aforementioned diseases. Statistical significance was defined as  $p$ -value  $< .05$ .

#### RESULTS

A total of 524 scans were included in the study. Arterial calcifications were observed in a total of 28/524 patients (5.3%) with calcifications isolated to the anterior circulation in 26/524 (5.0%), isolated to the posterior circulation in 1/524 (0.2%) and involving both systems in 1/524 (0.2%). There were no statistically significant differences in incidence of such calcifications between genders, but significantly more calcifications were found in children aged 6-12 years than any other age group. No significant associations were found with calcium metabolism disorder, diabetes mellitus, renal disease and hyperlipidemia and presence of calcification.

#### CONCLUSION

A previous study found intracranial carotid artery calcifications in 25% of pediatric patients undergoing a CT scan of the temporal bone. This study found intracranial arterial calcification to be a much rarer finding in the pediatric population. When present, such calcifications occur predominantly in the anterior



circulation and correlate poorly in our study sample with major diseases and risk factors that we expect to predispose adults to intracranial atherosclerotic disease. While the exact mechanism of such calcifications in children is unclear, further longitudinal studies are indicated to evaluate for long-term risk for atherosclerotic complication in these individuals or conversely to truly establish the benignity of this finding.

**KEY WORDS:** Intracranial arterial calcifications, prevalence

**O-178**

**5:33 PM - 5:41 PM**

### **Trend in the Use of Head and Cervical CT, and Brain and Spine MR Imaging for Children with Traumatic Brain Injuries in a Level I Trauma Center**

Roudsari, B.Jarvik, J. G.

University of Washington  
Seattle, WA

#### **PURPOSE**

To evaluate the recent trend in utilization of head and cervical CT and brain and spine MRI in pediatric trauma patients admitted from 2005-2009 to Harborview Medical Center, the only level I trauma center in the northwest of the United States.

#### **MATERIALS & METHODS**

We linked the HMC trauma registry to HMC billing department data and extracted the following variables: age, gender, race/ethnicity, insurance status, mechanism of injury, injury severity score, length of hospitalization, ICU admission status, final disposition, year of admission, and type and frequency of performed CTs. We classified age into 0-14 and 15-18 years. We plotted the rate of head CT and brain and cervical spine MRI against the year of admission. We used negative binomial regression to evaluate the 5-year trend in use of CT and MRI for these patients, after adjustment for age, gender, mechanism and severity of injury, and hospital disposition (dead vs alive). We present the results as incidence rate ratio (IRR) with the 95% confidence intervals.

#### **RESULTS**

There were 4,922 trauma patients 18 or younger admitted over the study period. For children 14 and younger, between 2005 and 2009, the use of head and cervical spine CT decreased 80% and 53%, respectively. The corresponding drop in the use of brain and spine MRI were 165% and 357%, respectively. For children 15-18 years, head CT dropped 15% between 2005 and 2006 and remained relatively unchanged between 2006 and 2009. The change in cervical spine CT, brain and spine MRI was comparable to children < = 14 years. Multivariable analyses demonstrated that after adjustment for previously mentioned covariates, among children ≤14 years, the use of head CT significantly dropped in 2009 compared to 2005 (IRR:0.71, 95% CI: 0.59-0.87). No significant change in the use of cervical spine CT, brain MRI or spine MRI was observed. Among

children 15-18 years, we did not observe any significant change in the use of head CT, brain MRI or spine MRI. However, cervical spine CT was less utilized in 2009 compared to 2005 (IRR: 0.69, 95% CI: 0.50-0.94).

Table 1: Unadjusted annual utilization rate (per 1000 patient) of head and cervical spine CT and brain and spine MRI, Harborview Medical Center, 2005-2009

Age	Year	Head CT	C-Spine CT	MRI brain	MRI spine
0-14	2005	859	348	45	32
	2006	699	329	27	26
	2007	608	326	18	38
	2008	610	282	25	31
	2009	478	227	17	7
15-18	2005	1193	456	46	64
	2006	1033	399	44	72
	2007	1008	472	53	46
	2008	993	345	36	53
	2009	1059	287	64	43

#### **CONCLUSION**

In contrast to published literature, we observed a declining trend in the use of CT for children ≤14 years in our trauma center without an increase in MRI use. However, the use of head CT for teenagers 15-18 has not changed during the most recent years. We observed a similar pattern for adults in our trauma center, indicating that teenagers are treated similarly to adults.

**KEY WORDS:** Trend analysis, CT and MR imaging, pediatric head and spine trauma

**O-179**

**5:41 PM - 5:49 PM**

### **Motion-Corrected Diffusion Tensor Imaging for Robust Pediatric Neuroimaging**

Holdsworth, S. J.<sup>1</sup>Yeom, K.<sup>2</sup>Skare, S.<sup>3</sup>Barnes, P.<sup>2</sup>Bammer, R.<sup>1,2</sup>

<sup>1</sup>Center for Quantitative Neuroimaging, Stanford, CA, <sup>2</sup>Pediatric Radiology Section, Stanford, CA, <sup>3</sup>Karolinska Institute, Stockholm, SWEDEN.

#### **PURPOSE**

A common problem with pediatric MR imaging is motion. Diffusion-weighted imaging (DWI) is highly sensitive to the effects of motion. The resulting artifacts can manifest in several ways, and include blurring (motion between volumes), slice "drop-outs" (motion during the diffusion encoding), and aliasing (motion during the parallel imaging/ghost calibration scan). In order to improve image quality in pediatric DWI and avoid repeat scans and prolonged scan time, we have implemented our GRAPPA-accelerated diffusion tensor (DT) EPI sequence on over 1,600 pediatric patients, and have developed tailored reconstruction software to correct for large motion and reduce the need for general anesthesia (GA).

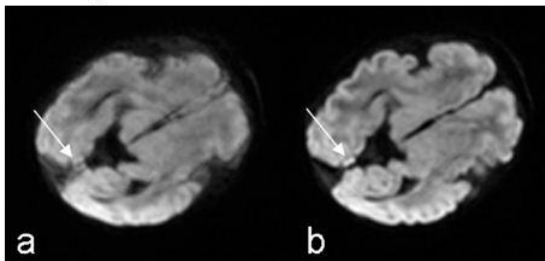
#### **MATERIALS & METHODS**

GRAPPA-accelerated EPI DTI data were collected on 100 patients at 1.5 T and 1,500 patients at 3 T between

the ages of 1 month and 18 years old. With these data, we investigated the use of a method to perform 3D rigid-body realignment with importance weighting and a new data rejection criterion for large motion.

## RESULTS

The figure shows a term infant *s.p.* cardiac arrest. Small blood products were inconspicuous on uncorrected DWI (a) but seen on motion-corrected DWI (b). Blood products along the right medial occipital region were equivocal without motion correction and similarly the signal within frontal interhemispheric region. The latter was a "pseudo lesion" caused by motion. Using the maximum motion detected from the 3D realignment procedure on the 1,600 DTI exams, 51% of patients did not move (either through cooperation or general anesthesia, denoted here by <1 mm of motion); 28% of patients moved between 1 - 3 mm; 13% between 3 - 5 mm; 6% between 5 - 10 mm; and 2% between 10-18 mm. Except for three patients, the motion correction steps employed were extremely robust in correcting for motion. In addition, the motion correction steps employed here do not blur or negatively affect the data on nonmoving patients.



## CONCLUSION

Our proposed integrated reconstruction scheme suggests that correcting for different types of motion at different stages of the DTI acquisition is critical to provide DTI scans of diagnostic quality. Apart from the very rare instance (0.2%) where the patient moved continuously and extensively throughout the scan, our motion correction procedures employed here are extremely robust at correcting for motion. Using this scheme, we show that highly diagnostic motion-corrected DTI data can be read routinely on our patient database within 10 minutes. Motion-corrected diffusion images improved diagnostic confidence, reduced equivocal lesions, and at times removed "pseudo lesions."

**KEY WORDS:** Pediatrics, diffusion tensor

O-180

5:49 PM - 5:57 PM

## Evaluation of Motion Correction Methods for Pediatric Spinal Cord Diffusion Tensor Imaging in Normals and Patients with Spinal Cord Injury

Middleton, D. M.<sup>1</sup>Mohamed, F. B.<sup>1</sup>Barakat, N.<sup>1</sup>Hunter, L. N.<sup>2</sup>Finsterbusch, J.<sup>3</sup>Faro, S. H.<sup>1</sup>Shah, P.<sup>1</sup>Samdani, A.<sup>2</sup>Mulcahey, M. J.<sup>2</sup>

<sup>1</sup>Temple University, Philadelphia, PA, <sup>2</sup>Shriners Hospital for Children, Philadelphia, PA, <sup>3</sup>University Medical Center Hamburg-Eppendorf, Hamburg, GERMANY

## PURPOSE

Motion correction is important in interpretation of medical images and plays a crucial role in diagnosis and treatment planning. While there has been intensive research into motion correction of brain images, little exists for spinal cord (SC) imaging. The goal of this study was to determine a reliable motion correction method for SC diffusion tensor imaging (DTI) and show effects of motion correction on DTI parameters in normal and injured SC in a pediatric population.

## MATERIALS & METHODS

Twenty subjects (age range 7-21 years), 10 controls without evidence of SC pathology and 10 patients with spinal cord injury (SCI), were recruited. Images were acquired using a newly developed inner-field-of-view sequence. Image registration was performed using the Automated-Image-Registration (AIR) package implemented in DTIstudio ([www.mristudio.org](http://www.mristudio.org)). Two transformation types, rigid and affine, using three cost functions, standard-deviation, least-square, and scaled-least-squares were evaluated. Transformation matrices generated for each registration were examined quantitatively using in-house developed Matlab code. The average and maximum displacements of vectors in a transformed image were calculated for R/L, A/P, and S/I directions. Using MedINRIA ([www.sop.inria.fr/asclepios/software/MedINRIA/](http://www.sop.inria.fr/asclepios/software/MedINRIA/)), fractional anisotropy (FA) and mean diffusivity (MD) were calculated pre and postcorrection. Regions-of-interest were drawn on midline sagittal FA color maps. After selection of a correction method, pre and postcorrection images were randomized and blindly evaluated by a neuroradiologist for cord edge conspicuity and cord homogeneity, scoring images from one to five in each category.

## RESULTS

Rigid methods produced more consistent and lower magnitude displacements compared to affine methods. Affine methods often resulted in large displacements and badly distorted images. Among rigid methods, rigid scaled-least-squares (RdSLS) showed greatest improvement (Figure 1). Statistically significant ( $p = 0.02$ ) decrease in FA values (14-21%) was found in postcorrection images for subjects with SCI, while control subjects showed minimal FA value reduction (<5%) and were not significant. This difference could be due to overestimation of FA values due to motion which was corrected successfully. Uncorrected images' median score was two in both edge conspicuity and cord homogeneity, and corrected images' median score was four in both categories. Using a Wilcoxon signed-rank test, differences were statistically significant for both edge conspicuity ( $p = 0.0015$ ) and cord homogeneity ( $p < 0.001$ ).

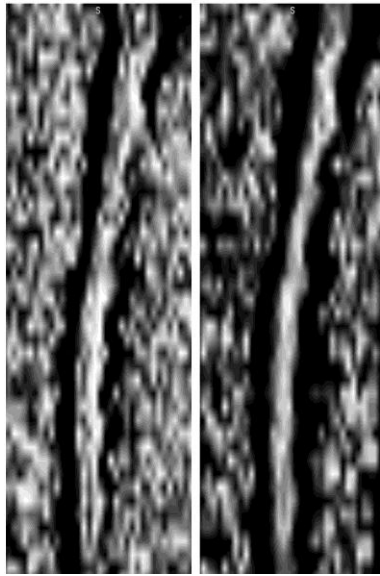


Figure 1 - Pre-correction (left) and post-correction (right) reconstructed sagittal FA maps for a control subject showing improved edge conspicuity and cord homogeneity.

#### CONCLUSION

Motion correction is an important consideration in pediatric SC DTI. In controls and subjects with SCI, analysis showed RdSLS to be an effective and reliable correction method. Development of SC specific correction methods would be an important step moving forward in SC DTI.

**KEY WORDS:** Pediatric, diffusion tensor imaging, spinal cord

O-181

5:57 PM - 6:05 PM

#### Diffusion Tensor Imaging of the Normal Pediatric Spinal Cord Using an Inner-Field-of-View EPI Sequence

Barakat, N.<sup>1</sup>•Mohamed, F.<sup>1</sup>•Hunter, L.<sup>2</sup>•Shah, P.<sup>1</sup>•Faro, S.<sup>1</sup>•Samdani, A.<sup>2</sup>•Finsterbusch, J.<sup>3</sup>•Betz, R.<sup>2</sup>•Gaughan, J.<sup>1</sup>•Mulcahey, M.<sup>2</sup>

<sup>1</sup>Temple University, Philadelphia, PA, <sup>2</sup>Shriners Hospital for Children, Philadelphia, PA, <sup>3</sup>University Medical Center Hamburg-Eppendorf, Hamburg, GERMANY

#### PURPOSE

The purpose of this study was to (a) evaluate the accuracy of cervical spinal cord DTI in children using a newly developed inner-field-of-view (iFoV) sequence with spatially selective 2D RF excitations and (b) examine reproducibility of the DTI measures.

#### MATERIALS & METHODS

Twenty-five subjects (mean age = 13.28 years) without evidence of spinal cord (SC) pathology were recruited. Subjects and their parents provided written informed assent and consent of the IRB-approved protocol. The iFoV sequence was implemented on a 3.0 T Siemens Verio MR scanner. High-resolution axial DTI images were acquired to cover the cervical SC (C1-C7). Diffusion tensor imaging parameters included: 20 directions,  $b = 1000 \text{ s/mm}^2$ , voxel size =  $1.2 \times 1.2 \times 3 \text{ mm}^3$ , axial slices = 35-45, TR = 6100-8000 ms, TE = 115ms, averages = 3 and TA = 7 min. Conventional T1- and T2-

weighted scans also were obtained. Anesthesia, cardiac and/or respiratory gating were not used. To test for reproducibility of the DTI measures, all subjects returned within 2 to 9 hours for a second scan. Motion correction of the DTI images was performed. Next, tensor estimation was done using MedINRIA. Diffusion tensor imaging indices were extracted from ROIs drawn at every axial slice location along the SC for both scans: fractional anisotropy (FA), axial diffusivity (AD), radial diffusivity (RD), mean diffusivity (MD), relative anisotropy (RA) and volume ratio (VR), planar index (Cp), linear index (Cl) and spherical index (Cs). The ROIs were carefully drawn so that there was a consistent sparing of the outer margin of the cervical cord that represented approximately one voxel width to minimize volume averaging with the CSF. Diffusion tensor imaging indices were reported at each disk level of the cervical SC as well as the middle portion of the cervical vertebral body. Statistical analysis was performed using intra-class-correlation (ICC) to test the reliability of the DTI datasets.

#### RESULTS

Imaging with the iFoV sequence resulted in reliable DTI data with reduced eddy current distortions and good delineation of gray white matter structures (Figure1). Subjects showed mean  $\pm$  standard deviation FA =  $0.50 \pm 0.11$ , AD =  $0.97 \pm 0.20 \times 10^{-3} \text{ mm}^2/\text{s}$ , RD =  $0.41 \pm 0.13 \times 10^{-3} \text{ mm}^2/\text{s}$ , MD =  $0.59 \pm 0.15 \times 10^{-3} \text{ mm}^2/\text{s}$ , RA =  $0.35 \pm 0.08$ , VR =  $0.03 \pm 0.00$ , Cp =  $0.13 \pm 0.07$ , Cl =  $0.29 \pm 0.09$  and Cs =  $0.58 \pm 0.11$ . Between C1 and C7 levels, there was a progressive decrease in FA (15%), AD (16%), MD (9%), RA (23%) and Cl (27%) and an increase in RD (1%), VR (11%), Cp (36%) and Cs (7%). Reliability test showed moderate to strong agreement between the two scans in all the subjects for all DTI parameters ( $0.72 < \text{ICC} < 0.97$ ).

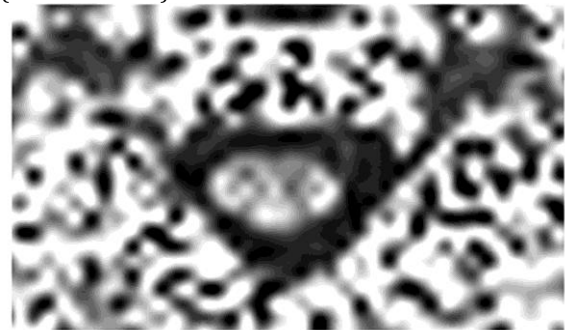


Figure 1: Axial FA image of a control subject's cervical SC (C5).

#### Conclusion

This study showed that accurate and reproducible DTI parameters can be estimated in pediatric cervical spinal cord using an iFoV EPI sequence.

**KEY WORDS:** Diffusion tensor imaging, spinal cord, pediatrics

O-182

6:05 PM - 6:13 PM

#### Complex Chiari (Chiari 1.5) Malformation

Moore, H.<sup>1</sup>•Chin, B. M.<sup>1</sup>•Moore, K. R.<sup>2</sup>

<sup>1</sup>University of Utah, Salt Lake City, UT, <sup>2</sup>Primary Children's Medical Center, Salt Lake City, UT

#### PURPOSE

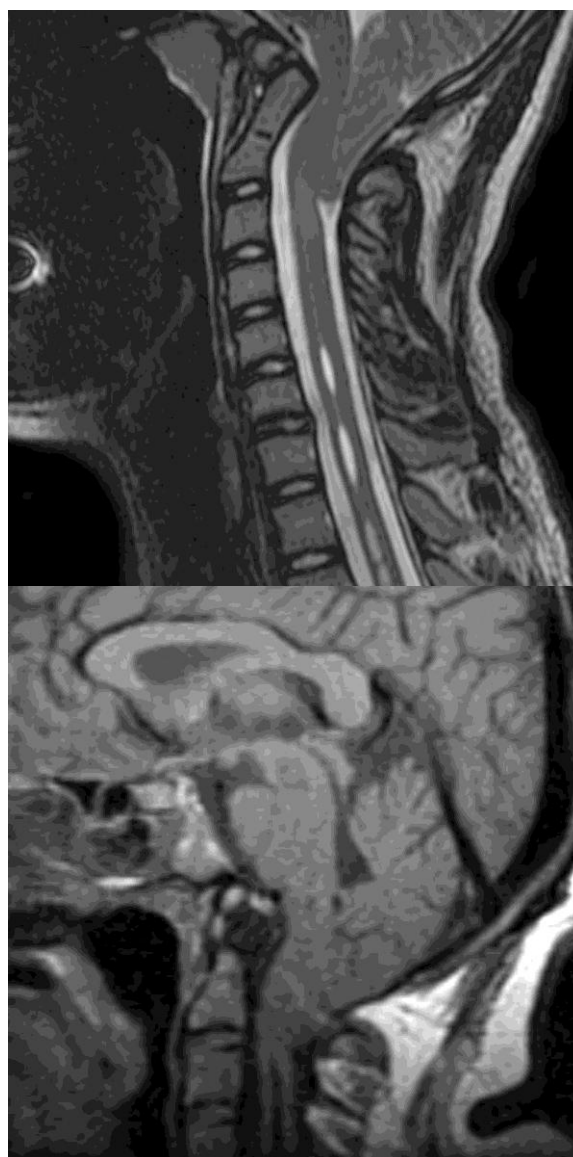
Complex Chiari Malformation, a newly defined term in the neurosurgical literature, includes Chiari 1.5 features as well as other anomalies of the craniovertebral junction. The purpose of this study was to characterize the relative frequency, clinical presentation, and radiologic spectrum of this entity at a large, pediatric tertiary care referral center.

#### MATERIALS & METHODS

A retrospective search of imaging databases using the keyword "Chiari 1" was performed for the time period 2006 to 2011. All studies with patients < 18 years of age were reviewed for features of Complex Chiari Malformation. Clinical data and imaging features were abstracted. Studies were excluded if pre or postoperative imaging or clinical notes were not available.

#### RESULTS

Twelve (13%) of the 92 patients characterized with Chiari 1 malformation had Complex Chiari Malformation features, including inferior herniation of the obex and cerebellar tonsils through the foramen magnum (Chiari 1.5 malformation), ventral brainstem compression due to odontoid retroflexion, medullary "kinking," basilar invagination, and/or other skull base abnormalities. The patients presented with signs and symptoms similar to those of Chiari 1 malformation patients (e.g., headache, weakness) as well as with similar incidences of scoliosis and syringohydromyelia. The Complex Chiari Malformation population more often required occipitocervical fusion and transoral odontoid resection for persistent symptoms and/or unresolved syringohydromyelia despite suboccipital craniectomy, C1 laminectomy, and duroplasty.



#### CONCLUSION

Knowledge of Complex Chiari Malformation and its distinctive clinical and radiologic features facilitates identification of patients most likely to present with severe symptoms and require extensive or repeated surgical procedures. Ongoing research suggests potential differences in imaging surveillance, operative strategies to treat brainstem compression and occipitocervical instability, and outcomes compared to those of routine Chiari 1 malformation.

**KEY WORDS:** Complex Chiari, Chiari 1.5



## Tuesday Morning

**7:30 AM - 8:30 AM**  
**Grand Ballroom Suite**

**(21) MAINTENANCE OF  
 CERTIFICATION (MOC) - REVIEW  
 SESSION (AR) HEAD AND NECK**

**O-183** **7:30 AM - 8:00 AM**

### Head & Neck

Gul Moonis, MD, BS

Radiology, Beth Israel Deaconess Medical Center  
 Boston, MA, USA

#### PRESENTATION SUMMARY

Discuss representative cases of Temporal bone/skull base.

2. Apply differential diagnoses in clinical practice.
3. Identify key imaging features of various lesions in the head and neck.
4. Identify and list the top radiographic differential considerations for each diagnosis.

**O-184** **8:00 AM - 8:30 AM**

### Head & Neck

Mary E. Cunnane, MD

Radiology, Massachusetts Eye and Ear Infirmary  
 Boston, MA, USA

## Tuesday Morning

**8:30 AM - 10:00 AM**  
**Grand Ballroom Suite**

**(22) GENERAL PROGRAMMING:  
 COLLABORATION WITH SOCIETY  
 FOR SILAN**

**O-185** **8:30 AM - 8:40 AM**

### Short Presentation about Dr. Juan Taveras

R Gilberto Gonzalez, MD, PhD

Neuroradiology, Massachusetts General Hospital  
 Boston, MA, USA

#### PRESENTATION SUMMARY

This will be an introduction into the life of Dr. Juan Taveras

**O-186**

**8:40 AM - 9:00 AM**

### Arteriovenous Malformations

Fernando Vinuela, MD

Interventional Neuroradiology, UCLA Medical Center  
 Los Angeles, CA, USA

#### PRESENTATION SUMMARY

Brain avms are the most frequent vascular malformation and those which cause most morbidity and mortality. The goals of endovascular management of cranial avms includes cure of the disease while maintaining normal structure and function, promoting quality of life and helping patients to cope with his/her condition. Multidisciplinary treatment is the best therapeutic approach in large and complex avms. It includes surgery, radiosurgery and embolization. The pre-diagnostic objectives involves avm localization, angioarchitecture and brain functional evaluation. The endovascular procedures must be tailored to achieve attainable and realistic objectives in order to decrease iatrogenia. The objectives of embolization includes: complete avm occlusion, embolization of risk targets and preparation for stereotactic radiosurgery or surgical removal. A temporal evolution of neuroendovascular techniques and examples of technical and clinical failures will be displayed in this presentation.

**O-187**

**9:00 AM - 9:20 AM**

### Neurocysticercosis and Other Tropical Infectious Diseases

Enrique Palacios, MD, FACP

Radiology, Tulane University  
 New Orleans, LA, USA

#### PRESENTATION SUMMARY

In the present era of worldwide rapid travel, immigration to and from developing countries and international commerce, the term "tropical diseases" could be considered outdated or even obsolete. In reviewing the current literature it is evident that parasitic and infectious diseases seen in the so-called endemic areas of the world are now encountered in non-endemic areas, including the United States. In addition, there has been a rise in immune suppression, particularly HIV-AIDS and that has caused an increase in opportunistic and tropical diseases, which often leads to poor treatment response.

Remarks will be concentrated on the most common manifestations of tropical diseases of the Central Nervous System that were found previously only in endemic areas and that are now seen worldwide, including the United States. Special attention with a brief epidemiological description will be paid to neurocysticercosis, protozoal, viral infections and other less common parasitic disorders that now appear sporadically or in the form of outbreaks in non-endemic areas. The recent outbreaks in New York, Louisiana and California of West Nile encephalitis, not previously seen in the United States, brings to light the association of some of these infections of the brain.

**REFERENCE:**

1. Centers for Disease Control and Prevention, Center for Global Health, Division of Parasitic Diseases and Malaria 1600 Clifton Road, N.E., Mailstop F-22 + Atlanta, Georgia 30333, USA, <http://www.cdc.gov/globalhealth/ntd/> +

2. Infectious Diseases in Immigrants from the perspective of a Tropical Medicine Referral unit. *Am J Trop Med Hyg* 69(1), 2003, 115-121.

3. Worldwide travel triggers spread of parasitic CNS infections. *Diagnostic Imaging Europe*. Vol. No February 1, 2009.

4. Neurocysticercosis: Radiologic-Pathologic Correlation *Neurocysticercosis RadioGraphics* 2010; 30:1705-1719. On-line 10.1148/rg.306105522.Content Code NR

5. Palmisano CT, Taylor V, Caillouet K, Byrd B, Wesson DM: Impact of West Nile virus outbreak upon St. Tammany Parish Mosquito Abatement District. *J Am Mosq Control Assoc*. 2005 Mar; 21(1):33-8.

**Questions**

1. Should the term tropical diseases be considered obsolete, since they now appear in non-endemic non tropical area?

2. Should neurocysticercosis considered to be endemic in some areas of the United States?

3. Is the increase in immunosuppression a risk for increase in the prevalence in the so called tropical diseases?

**O-188****9:20 AM - 9:40 AM****Multiple Sclerosis**

Alex Rovira, MD

Department of Radiology, Hospital Universitari Vall d'Herbron  
Barcelona, Spain

**PRESENTATION SUMMARY**

Conventional MR imaging techniques, such as T2-weighted and gadolinium-enhanced T1-weighted sequences are highly sensitive in detecting multiple sclerosis (MS) plaques and provide a quantitative assessment of inflammatory activity and lesion load. However, the changes identified by MR imaging in patients with MS are not completely disease-specific. Other disorders can cause white matter lesions with imaging characteristics similar to those seen in MS. Nevertheless, the MR imaging pattern of brain MS is usually relatively specific when age, clinical information, and the full range of MR imaging abnormalities are taken into consideration. MS lesions tend to affect specific regions of the brain hemispheres, including the periventricular white matter, the callosal-septal interface along the inferior surface of the corpus callosum, and the juxtacortical white matter ("U" fibers). Posterior fossa lesions preferentially involve the floor of the fourth ventricle, the middle cerebellar peduncles, and the brainstem. Most brainstem lesions are contiguous with the cisternal or ventricular cerebrospinal fluid spaces, and range from large confluent patches to solitary, well-delineated paramedian lesions or discrete "linings" of the cerebrospinal fluid border zones. These areas are a key

feature that helps to identify MS plaques and differentiate them from focal areas of ischemic demyelination and infarction, which preferentially involve the central pontine white matter. MS lesions of the spinal cord resemble those in the brain. On sagittal scans, the lesions characteristically have a cigar shape and rarely exceed two vertebral segments in length. On cross-section they typically occupy the lateral and posterior white-matter columns, extend to involve the central grey matter, and rarely occupy more than one half the cross-sectional area of the cord. The prevalence of cord abnormalities is as high as 92% in established MS. MRI identification of subclinical spinal cord lesions in patients with non-specific brain findings, particularly those >50 years old, can increase the diagnostic certainty because these lesions are relatively frequent in MS, but rare in other white matter diseases. Longitudinal and cross-sectional MR studies have shown that formation of new MS plaques is often associated with contrast enhancement. Incomplete ring enhancement on T1-weighted gadolinium-enhanced images, with the open border facing the gray matter of the cortex or basal ganglia is a common finding in active MS plaques and is a helpful feature for distinguishing between inflammatory-demyelinating lesions and other focal lesions such as tumors or abscesses.

**O-189****9:40 AM - 10:00 AM****Temporal Lobe Epilepsy, The Role of Neuroimaging**

Andres Arbelaez, MD

Neuroradiology, Corbic Cardio-neurovascular Institute - HPTU  
Medellin, Colombia

**PRESENTATION SUMMARY**

Focal epilepsy that is uncontrolled with antiepileptic drugs is potentially treatable with surgery. Such intervention is a consideration for 3% of patients with epilepsy. Temporal lobe epilepsy (TLE) encompasses a variety of disorders that have as a common feature seizures arising in a temporal lobe. Underlying pathologies include tumors, vascular malformations, cortical dysplasia, trauma, and hippocampal sclerosis. Each lesion has a unique pathophysiology and the type of seizure generated by them may vary according to its location.

In TLE patients resistant to current antiepileptic, surgery is the standard treatment. Best results are obtained when the abnormality that gives rise to seizures is entirely removed and the eloquent cortical regions and connecting white matter tracts are preserved. The principal role of MRI is to reveal lesions that might cause epilepsy. Identification of a resectable underlying structural lesion improves the chances of seizure freedom.

Structural imaging is essential in localization and lateralization of the seizure focus. MRI can reveal previously covert epileptic lesions, with quantitative and voxel-based analyses increasing its diagnostic yield. Despite improved techniques in neuroimaging that facilitate identification of surgical candidates, the success of epilepsy surgery has not changed

substantially. Recent observations from histopathology, neuroimaging, and neuroscience laboratory suggest that the syndrome is not always a uniform entity. Despite clinical similarities, not all patients become seizure free. If structural MRI does not indicate a structural cause of epilepsy or if data indicating a lesion are discordant with clinical and EEG data, functional imaging with FDG PET, and SPECT can identify the epileptic focus and guide intracranial electrode placement. New MRI techniques can help to delineate extent of mesial temporal lobe pathology and identify extra hippocampal neocortical changes, allowing individualized treatment planning. The purpose of this presentation is to show the selection process for surgery in some patients with TLE and the planning of the approach according to the multimodality findings. Presurgical Predictors of Seizure Control for mesial TLE:

**Positive:** Circumscribed hippocampal sclerosis or tumors, greater volume resected, atrophy ipsilateral to EEG abnormality, only hippocampal atrophy on MRI, concordant memory asymmetry on WADA(fMRI).

**Controversial:** Duration of epilepsy history. **Negative:** No histopathology in surgical specimen, lesion outside of resection, bilateral atrophy on MRI, history of secondary generalization, incomplete mesial resection, and wider FDG PET abnormality,

Reliable integration of structural and functional data into surgical image-guidance systems promises safer neurosurgery for epilepsy in the future.

## Tuesday Morning

**8:30 AM - 10:00 AM**

**Trianon Ballroom**

**(23) GENERAL PROGRAMMING:  
ALZHEIMER'S DEMENTIA**

**O-190**

**8:30 AM - 8:50 AM**

### **Preclinical Alzheimer's Dementia: A New Frontier in Treatment Trials**

Stephen Salloway, MD, MS

Neurology, Warren Alpert Medical School of Brown University  
Providence, RI, USA

#### **PRESENTATION SUMMARY**

There is an urgent need to develop treatments that delay the onset and slow the progression of Alzheimer's disease. Advances in imaging and fluid biomarkers have led to the development of new research criteria that view Alzheimer's disease (AD) as a multi-year illness with a long prodromal preclinical phase, a mildly symptomatic mild cognitive impairment (MCI) phase, and a more disabling dementia phase. There is general agreement among dementia experts that disease-

modifying and preventative treatments will have their greatest impact in reducing the severity of AD when initiated early in the course of the disease. This makes the preclinical phase an important target for secondary prevention trials. Recent data from the Alzheimer's Disease Neuroimaging Initiative (ADNI), the Dominantly Inherited Alzheimer's Network (DIAN), the Australian Imaging and Biomarker Lifestyle (AIBL) study and other biomarker studies have demonstrated changes in biomarkers more than 10 years before the onset of symptoms. The first changes are seen in amyloid markers with increases on amyloid PET and decreases in CSF amyloid beta 42. These are followed by increases in CSF tau, decreased metabolism on FDG PET, and hippocampal and cortical atrophy and ventricular enlargement on MRI. These changes occur earlier in a dose dependent manner in Apolipoprotein epsilon E4 carriers. Molecular imaging and MRI scanning, CSF testing of amyloid and tau, and genetic testing (Apolipoprotein E epsilon 4 allele and mutations in presenilin 1 and 2 and amyloid precursor protein genes) can be used to identify individuals at risk for AD, to monitor the progression of the disease, and to assess treatment outcomes. The new research diagnostic criteria for preclinical AD are being used as a basis for planning secondary prevention trials with amyloid-modifying agents which include imaging biomarkers and subtle changes on cognitive tests as primary outcome measures. This presentation will review the new research criteria and some of the challenges inherent in selecting biomarker outcomes for preclinical AD trials.

#### **REFERENCES:**

1. Rumboldt Z. Imaging of topographic viral CNS infections. *Neuroimaging Clin N Am* 2008; 18: 85-92.
2. Rumboldt Z, Thurnher MM, Gupta RK. Central nervous system infections. *Semin Roentgenol* 2007; 42: 62-91.
3. Fink KR, Thapa MM, Ishak GE, Pruthi S. Neuroimaging of pediatric central nervous system cytomegalovirus infection. *Radiographics* 2010; 30: 1779-96.
4. Handique SK, Das RR, Saharia B, Das P, Buragohain R, Saikia P. Coinfection of Japanese encephalitis with neurocysticercosis: an imaging study. *AJNR* 2008; 29: 170-5.
5. Shen WC, Chiu HH, Chow KC, et al. MR imaging findings of enteroviral encephalomyelitis: an outbreak in Taiwan. *AJNR* 1999; 20: 1889-95.
6. Thurnher MM, Post MJ, Jinkins JR. MRI of infections and neoplasms of the spine and spinal cord in 55 patients with AIDS. *Neuroradiology* 2000; 42: 551-63.
7. Provenzale JM, van Landingham KE, White LE. Clinical and imaging findings suggesting human herpesvirus 6 encephalitis. *Pediatr Neurol* 2010; 42: 32-9.
8. Lim CC, Lee KE, Lee WL, et al. Nipah virus encephalitis: serial MR study of an emerging disease. *Radiology* 2002; 222: 219-26.

**O-191****8:50 AM - 9:10 AM****Amyloid Imaging of Alzheimer's Dementia and Beyond**

Chester A. Mathis, PhD

University of Pittsburgh School of Medicine  
Pittsburgh, PA, USA

*Chester A. Mathis, Ph.D., is Professor of Radiology and Pharmaceutical Sciences at the University of Pittsburgh, Director of the University of Pittsburgh Positron Emission Tomography (PET) Facility, University of Pittsburgh Distinguished Professor, and inaugural holder of the UPMC PET Research Endowed Chair. Dr. Mathis has a long standing interest in applying synthetic radiochemistry techniques to develop PET radiopharmaceuticals to study brain function in vivo. Over the past 30 years, he has focused primarily on the development of radiotracers to image neuroreceptor systems using PET imaging methodology. Approximately 17 years ago, Dr. Mathis joined efforts with Dr. William E. Klunk of the Department of Psychiatry at the University of Pittsburgh to devise a PET radiotracer capable of imaging amyloid-beta plaques in living human brain. This work led to the development of Pittsburgh Compound-B (PiB) and other longer-lived analogues of PiB to non-invasively assess amyloid-beta plaque load in the brains of humans using PET imaging.*

**PRESENTATION SUMMARY**

Imaging agents capable of assessing amyloid-beta (A $\beta$ ) content in vivo in the brains of Alzheimer's disease (AD), mild cognitive impairment (MCI), and elderly normal control subjects will likely prove valuable as surrogate endpoints to assess the efficacy of anti-amyloid therapeutics (Rinne 2010), as diagnostic agents to assess beta-amyloidosis of the brain in AD, MCI, and elderly control subjects who would likely benefit from anti-amyloid therapies, and to test the amyloid cascade hypothesis of AD (Mathis 2007). While 11C-labeled Pittsburgh Compound B (PiB) is currently the most documented A $\beta$  imaging tracer in human studies throughout the world, the short half-life of 11C limits its clinical usefulness. At this time, three 18F-labeled A $\beta$  tracers are undergoing Phase III clinical trials as A $\beta$  PET imaging agents and show considerable promise. A brief overview of on-going studies using PiB and the 18F-labeled A $\beta$  tracers in human imaging studies will be presented along with a discussion of the future usefulness of these agents in clinical practice.

**O-192****9:10 AM - 9:30 AM****Quantitative Volumetric Imaging in AD Diagnosis and Treatment Trials**

Anders M. Dale, PhD

University of California at San Diego  
La Jolla, CA, USA**Presentation Summary**

Quantitative volumetric imaging shows great promise as biomarkers to evaluate treatment efficacy in clinical trials and for early diagnosis of Alzheimer's Disease.

Recent large scale, multi-site imaging studies, including the Alzheimer's Disease Neuroimaging Initiative (ADNI), have demonstrated the importance of using optimized cross-vendor image acquisition protocols and analysis procedures. In this presentation we will highlight some of the main lessons learnt from such studies. We will further discuss the value of integrating volumetric imaging biomarkers with molecular and genetic information, and outline how these can be translated into clinical practice.

**O-193****9:30 AM - 9:50 AM****Bridging the Gap: What Can Functional Neuroimaging Tell Us about the Pathophysiology in Alzheimer's Disease**

Jeffrey R. Petrella

Radiology, Duke University Medical Center  
Durham, NC, USA**PRESENTATION SUMMARY**

Aside from its use as a diagnostic tool in the central nervous system, one of the most exciting aspects of neuroimaging, particularly functional neuroimaging, is its ability to give us a window into the underlying pathology of diseases, such as Alzheimer's disease (AD). A little over 100 years ago, dementia was considered not a disease, but a normal part of the human aging process. Then, in 1906, a German psychiatrist named Alois Alzheimer made a seminal discovery in a patient who developed dementia in her 50's and died shortly thereafter. On autopsy, he described the plaques and tangles that we still consider to represent the underlying pathology of AD. Almost 70 years after Alzheimer's original discovery, a link was suggested between Alzheimer's discovery and the dementia of old age, suggesting the two conditions were pathologically identical [1]. Thereafter AD was no longer considered a rare condition of middle age, but the 4<sup>th</sup> or 5<sup>th</sup> most common cause of death in the U.S. A massive organized research effort on AD ensued, with subsequent studies suggesting how the pathology spread across the brain, and implicating the cholinergic system as a key part of the pathophysiology of AD, the first attempts at therapy aimed at enhancing this system as a means of improving cognitive performance [2].

Today, the predominant theory on the pathophysiology of AD is the amyloid hypothesis, which posits amyloid deposition as an early sentinel event, followed by a downstream cascade of inflammation, neuronal damage/death, atrophy and cognitive dysfunction. Biomarkers, including those from neuroimaging, can help us better understand this cascade [3]. Several emerging findings based on neuroimaging, as well as failure of several recent multi-center anti-amyloid therapeutic trials, have thrown the amyloid hypothesis into question [4]. Clinical trials in subjects with preclinical AD, a new and controversial diagnostic category of AD, will be critical in this regard. Functional neuroimaging may help bridge the gap in our understanding of the pathology of AD and its downstream cognitive effects. The mechanism of how amyloid plaques and neurofibrillary tangles spread



across the brain remains a mystery. Several recent studies using molecular imaging and functional MRI have given rise to theories on how this pathophysiology spreads and results in the phenotypic features of cognitive impairment and dementia [5-8]. As such, neuroimaging remains a powerful tool for understanding AD, and ultimately, in the search for a cure.

## Tuesday Morning

**8:30 AM - 10:00 AM**

**Beekman/Sutton North**

**(24) SYNAPTIC JUNCTION  
PROGRAMMING: DTI FOR  
DUMMIES**

**O-194**

**8:30 AM - 9:00 AM**

Andrew G. Bleicher, MD

Radiology, University of Pittsburgh Medical Center  
Pittsburgh, PA, USA

### PRESENTATION SUMMARY

Unlike standard DWI, DTI estimates the directionality of water diffusion, with FA and DTT providing indirect measures of white matter integrity. More advanced methods hope to address weaknesses of DTI, most notably the fiber crossing problem. More direct evaluation of fiber tract orientation and integrity could transform white matter imaging and assessment from the level of basic science to clinical diagnosis and treatment (including surgical localization and rehabilitation). While almost all publications have evaluated between group differences between patient groups and controls, more advanced processing methods hope to provide clinically actionable information for individual patients. White matter tracts, brain connectivity, and damage from pathologic entities may be represented in the near future with greater accuracy and higher fidelity than currently available with DTI. Clinical examples will accompany a brief overview of methods.

**O-195**

**9:00 AM - 9:30 AM**

Vikas Agarwal, MD

Department of Radiology, University of Pittsburgh  
Medical Center  
Pittsburgh, PA, USA

### PRESENTATION SUMMARY

Diffusion tensor imaging (DTI) is an emerging tool in clinical neuroradiology. Diffusion of water molecules in the brain is not necessarily the same in all directions. The idea that the direction of diffusion is more organized in a specific direction is known as anisotropy.

DTI is a more sophisticated form of diffusion based MRI which is obtained by applying diffusion gradients in at least 6 directions. It therefore allows for quantitative evaluation of the rate and direction of water motion within a voxel which in turn provides details on white matter tissue microstructure and organization which is beyond what is capable with conventional MRI sequences. With recent improvements in MR hardware, DTI has become a powerful non-invasive tool to evaluate the integrity and direction of fiber tracts in various pathological conditions. The most common clinical applications of DTI will be reviewed such as cerebral ischemia and wallerian degeneration, multiple sclerosis, traumatic brain injury and brain tumors.

**O-196**

**9:30 AM - 10:00 AM**

Michael L. Lipton, MD, PhD

Radiology, Albert Einstein College of Medicine  
Bronx, NY, USA

### PRESENTATION SUMMARY

This session is designed to be accessible to all neuroradiologists, but is especially appropriate for those without a high degree of familiarity with MR physics or DTI, including those who have not yet been exposed to DTI concepts at all. The explanations will not rely on mathematics. We will use a descriptive approach to review the basis of diffusion induced signal change and the nature of diffusion in tissue, with particular attention to the nature of diffusion anisotropy in white matter. The basic approach for directionally encoding diffusion images and extracting information about diffusion direction will be presented. The four principle diffusion metrics, fractional anisotropy (FA) and mean, axial and radial diffusivity will be explained and demonstrated. Microstructural and pathological correlates of various diffusion parameter scenarios will be covered, leaving the participant well-prepared for the second segment of this session, which covers clinical applications of DTI.

## Tuesday Morning

**8:30 AM - 10:00 AM**

**Sutton Center/South**

**(25) AN EXPERT: HOW I DO IT**

**O-197**

**8:30 AM - 9:00 AM**

**ASL in Neuropediatrics**

Francis Brunelle, MD

Hopital Necker-Enfants Malades  
Paris, France

### INTRODUCTION

In all fields of medicine understanding and analyze of the function of any organ relies on measurement of

organ perfusion. Up to now most techniques are using radionuclide imaging such as scintigraphy or PET. In children PET is relatively difficult to use as the availability of PET scanner and tracers is limited. More over all those techniques are qualitative and do not allow precise quantitative measurements. In the brain presence of the Blood Brain Barrier limits even more the use of tracers as most of the molecules do not cross this sealed barrier.

Several perfusion techniques were developed for study of the brain function: Xenon perfusion, contrast CT perfusion, O3 PET scan, and MRI perfusion with gadolinium.

Recently Arterial Spin labelling, ASL, became available and represents a real change in our practice for research and clinical use. Indeed ASL is non invasive and allows a quantitative measurement of brain perfusion. Up to now ASL is limited to the head and neck region for technical reasons.

Objectives:

To present new applications of ASL in the diagnosis and follow-up of head and neck and brain lesions in children.

Vascular malformations

ASL in measuring the blood flow in vascular lesion allows differentiation between high flow and low flow lesions, venous, lymphatic and hyper vascular ones.

Intracranial vascular malformations

After treatment, surgery, embolisation or radiotherapy it is necessary to follow up those lesions. MRI alone even thanks to MRI angiography may be controversial. ASL in demonstrating the flow in the residual malformation became a useful diagnostic tool in our department.

Moya Moya and vascular diseases

ASL is now the standard examination for the study and follow-up of brain perfusion after surgery in Moya Moya disease and vascular diseases.

ASL and epilepsy

The standard examination to study the brain perfusion in epilepsy in children is PET or SPECT. In our practice ASL has replaced it. It shows hyper perfusion during seizures and hypo perfusion during the inter-ictal period.

ASL and Autism

Our team and others has demonstrated reduced perfusion with PET in the temporal region in children with autism. ASL has replaced PET and shows the same findings.

Neurovascular coupling

In several diseases abnormal regulation of the brain perfusion occurs after brain injury. Migraine, near miss syndrome, stroke-like diseases. ASL allows to a better understanding the alterations of the neurovascular coupling.

In conclusion ASL offers a new tool in paediatric neuroradiology that will replace in many ways PET. Because of its non invasive nature, its possibility to quantify blood flow, it will also have a much larger use than PET.

**O-198**

**9:00 AM - 9:30 AM**

## **Challenges and Opportunities in Imaging the Complex Pediatric Patient**

Richard L. Robertson, MD

Radiology, Children's Hospital  
Boston, MA, USA

### **PRESENTATION SUMMARY**

Imaging of the complex pediatric patient can pose unique challenges that require attention to details specific to the child and to their disease state. Moyamoya is an example of a neurovascular condition that is illustrative of many issues faced in pediatric imaging.

Patient size, relative risks of exposure to ionizing radiation are all important considerations in pediatric imaging. Children with neurovascular diseases may have varying degrees of developmental delay, comorbidities or hemodynamic sensitivities that must be accounted for imaging procedures, especially those that require sedation or anesthesia.

Imaging techniques must be tailored to the pathophysiology of the child's disease to avoid misrepresentation of a neurovascular abnormality. For example, the use of an inappropriately long echo time in MR angiography in the evaluation of a child with sickle cell disease may result in signal loss in the branch vessels of the circle of Willis due to turbulence from a combination of anemia and sickled cells. This signal loss may simulate Moyamoya vasculopathy. Since children with sickle cell disease are at risk for the development of steno-occlusive vascular changes and stroke, the appearance of the signal loss on MRA may lead to the recommendation for catheter angiography. If the signal loss is not recognized as being artifactual, the child may be exposed to the risks of angiography unnecessarily.

Imaging of children with neurovascular disorders may stretch the limits of currently available techniques. An ideal MR exam in a child with Moyamoya would include an assessment of cerebral perfusion. Both contrast enhanced and arterial spin labeled MR techniques are limited in utility in children with Moyamoya due to the low velocity of blood flow and the variability in transit time for different regions of the brain due to the multi-vessel involvement in this condition.

Procedural safety in children with neurovascular conditions requires a coordinated team approach. An appropriate pre-procedural assessment should identify relevant factors that increase the risk of the procedure. Intra-procedural safety is achieved through the combined efforts of a multi-disciplinary team. Post-procedural care is particularly important in preventing complications in children with neurovascular disorders.

**O-199****9:30 AM - 10:00 AM****Pediatric Traumatic Brain Injury: What Advanced Neuroimaging Reveals**

Susan Palasis, MD

Radiology, Children's Healthcare Of Atlanta  
Atlanta, GA, USA**PRESENTATION SUMMARY**

Approximately half a million children sustain traumatic brain injury (TBI) in the USA each year. These are children of all different ages, sizes and at a particular state of development that effect how their brain responds to an injurious force. Anatomical and maturational characteristics of the pediatric brain make it more susceptible to traumatic injury than the adult's.

There are mechanisms of injury that are unique to the pediatric population such as non-accidental trauma (NAT). The forces generated during violent shaking of a young infant can yield patterns of closed head injury that can strongly suggest abuse. Another type of injury that is more often seen in the pediatric population is sports related "concussion". The Center of Disease Control (CDC) and World Health Organization (WHO) have now replaced this term with "mild traumatic brain injury" (mTBI). Young children have the highest rates of mTBI, with sports and bicycle accidents accounting for the majority of cases in the 5-14 age group. Approximately 30% of patients with mTBI and transient post-traumatic amnesia have persistent symptoms, and a significant number of those have decreased functional outcome. These findings suggest that there is an anatomic or physiologic disruption of the brain that occurs in mTBI. The lack of imaging tools with sufficient thresholds of detection can lead to underdiagnosis.

While CT remains the imaging modality of choice in the setting of acute TBI, MRI can reveal the presence or extent of brain injury that may not be readily apparent. Magnetic resonance spectroscopy (MRS), diffusion tensor imaging (DTI), and susceptibility weighted imaging (SWI) are some of the advanced MR techniques that can greatly enhance our ability to detect injury earlier and more accurately. This is helpful in subsequent clinical management and prognostication.

**Tuesday Morning****8:30 AM - 10:00 AM****Murray Hill****(26) YOUNG PROFESSIONAL PROGRAMMING: ENTERING AND THRIVING IN COMMUNITY PRACTICE****O-200****8:30 AM - 8:45 AM****Welcome to the Real World**

John E. Jordan, MD, M.P.P.

Advanced Imaging of South Bay, Inc.  
Torrance, CA, USA**PRESENTATION SUMMARY**

The challenges, opportunities, and key determinants of a successful transition into radiology private practice will be addressed. These factors will be presented against the backdrop of complex environmental influences encountered inside and outside of the practice setting. Successful practitioners require a broad understanding of the dual role radiologists must play as clinicians and practice managers. Key elements of those roles include understanding the business side of radiology, as well as patient-centered excellence in clinical care and service delivery. Successful transitions require that one embrace those roles, and navigate the practice environment(s) with an eye toward excellence in patient care. Engaging in quality improvement, practice efficiency/ flexibility, enhancement of productivity, and aggressive practice development are important approaches. Uncovering and promoting added- value to payers, administrators, colleagues, and patients through marketing, and service excellence will always prove a winning strategy, that most can achieve with the appropriate focus and determination. Flexible practices with strong leadership, and with mechanisms to unleash creative solutions to environmental challenges will thrive, and those individuals adapting with these traits will be best equipped to transition and thrive in private practice.

**O-201****8:45 AM - 9:00 AM****Understanding the Food Chain**

Robert M. Barr, MD

Mecklenburg Radiology Associates, P.A.  
Charlotte, NC, USA**PRESENTATION SUMMARY**

This session will be a brief review of the "alphabet soup" of coding, reimbursement, and coverage geared primarily for residents, fellows, and physicians entering private practice. What are the CPT and RUC, and why should Neuroradiologists care? What are RVUs and the

RAW? What is CMS's role, and what impact does it have on non-Medicare patients and payors? What about PPACA, PQRI, DRA, RAC, and LCDs? Quick definitions will be presented and key points will be highlighted, as well as simple steps that new physicians in practice can take to impact change, become involved, and potentially bring more revenue and better understanding of payment policy to their practices. Examples will be drawn from recent experience with general radiology and Neuroradiology procedures and imaging techniques.

#### **O-202 9:00 AM - 9:15 AM**

##### **The Corporate Environment**

Stephen T. Sweriduk, MD

Shields Healthcare Group  
Brockton, MA, USA

##### **PRESENTATION SUMMARY**

In the past, radiologists career choices were basically limited to two options, academic radiology and private practice. Today, radiologists also have the option to enter the corporate world. Corporate opportunities include working for private imaging companies, teleradiology companies, pharmaceutical and industry companies, as well as radiology benefits management companies. This talk will focus on the corporate environment, discussing various advantages and challenges associated with this career path.

#### **O-203 9:15 AM - 9:30 AM**

##### **The HMO Environment**

D. Christian Sonne, MD

Radiology, Kaiser Permanente Oakland Medical Center  
Oakland, CA, USA

##### **PRESENTATION SUMMARY**

This presentation is part of a panel discussion about working in a community radiology practice primarily directed toward recent and impending graduates. Presentation will describe working in an HMO environment as experienced at Kaiser Permanente. Will compare and contrast to 5 year experience in large private practice. Will discuss pros and cons of working in a large institution as a salaried employee including benefits, work effort, and job/life satisfaction. Will discuss efficiency (and inefficiency) issues, utilization, incentives, hospital/physician alignment, interactions with clinical colleagues and impact of ongoing health care reforms.

#### **O-204**

**9:30 AM - 9:45 AM**

##### **Making the Transition**

David J. Seidenwurm, MD, FACR

Radiological Associates  
Sacramento, CA, USA

##### **PRESENTATION SUMMARY**

The transition between academic practice and community practice requires shifting one's focus, but not too much. Instead of optimizing the design of a research project for grant funding, or to advance the progress of basic science, we optimize the design of systems for the delivery of care to our community. The existence of a great technique does not help patients if the service cannot be delivered reliably by your partners when you are on vacation or assigned to a different site. Because you have recently been in academic practice or fellowship, you are expert in the scientific and technical aspects of neuroradiology, and can expand and improve the practice you join by bringing new techniques and concepts to your community. In order to do this successfully, you must be able to communicate to your new partners and bring them up to speed. No service is truly useful until three radiologists can provide it. Additionally, you must also develop relationships with referring clinicians that support your new contributions, while enhancing the existing practice and the incumbent radiologists. A few specific suggestions. Take on any assignment offered you by your new partners. Start with the boring, the difficult or the frustrating. Do the hardest and most complex cases. Do that well and you will be indispensable. Be a teacher. Teach the clinical and radiological community to inform them of new developments. Make complex concepts simple. Anyone can make simple concepts complex. Keep your reports concise and comprehensible. Try not to suggest too many further studies. Above all, answer the clinical question. And above all that, answer the phone!

## **Tuesday Morning**

**10:30 AM - 12:00 PM**  
**Grand Ballroom Suite**

**(27a) Adult Brain: Neoplasms II**

#### **O-207**

**10:30 AM - 10:38 AM**

**Comparison of Dynamic Susceptibility Contrast MR Imaging Perfusion in Glioblastomas Treated with Bevacizumab vs Glioblastomas Treated without Bevacizumab: ENRS Award Winner**

Schweitzer, A. Graber, J. J. Young, R. J. Vaisfeld, J. Karimi, S. Holodny, A. I. Omuro, A. M.

Memorial Sloan-Kettering Cancer Center  
New York, NY



### PURPOSE

Bevacizumab is a monoclonal antibody targeting vascular endothelial growth factor A (VEGF-A) approved for treating recurrent malignant gliomas. Bevacizumab has direct effects on contrast enhancement and MRI determined vascular perfusion and permeability that does not necessarily indicate meaningful antitumoral activity. We hypothesize that MRI perfusion has limited utility in predicting progressive disease in patients with recurrent glioblastoma receiving bevacizumab. We compare perfusion changes in bevacizumab patients with perfusion changes in non-bevacizumab patients.

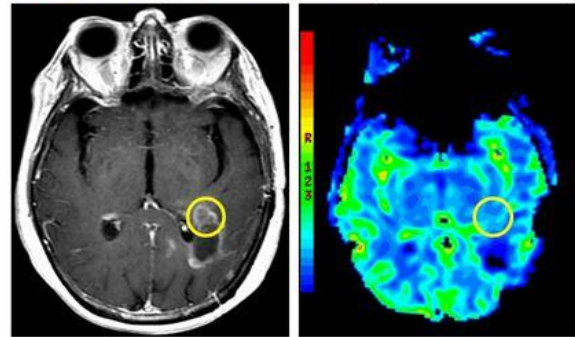
### MATERIALS & METHODS

We retrospectively reviewed 34 patients with glioblastoma who underwent dynamic susceptibility contrast (DSC) MRI perfusion prior to progression: 18 recurrent patients (median 54 years) treated with bevacizumab alone ( $n = 10$ ) or bevacizumab in combination with other agents ( $n = 8$ ); and 16 newly treated patients (median 61 years) who never received bevacizumab. Diagnosis of progressive disease was based on the Response Assessment in Neuro-Oncology (RANO) response criteria. Relative cerebral blood volume (rCBV), relative peak height (rPH) and percentage signal recovery (PSR) were measured by the tumoral regions-of-interest technique. Increases in rCBV  $\geq 1.75$ , a commonly applied threshold, were measured. Statistical analysis was performed using Wilcoxon rank-sum tests and logistic regression.

### RESULTS

No difference was found between the bevacizumab and the nonbevacizumab patients in median rCBV (1.76 vs 2.08,  $p = .62$ ), percent increase in rCBV (11.9 vs 17.7,  $p = .76$ ), rPH (1.65 vs 1.66,  $p = .93$ ), or PSR (.80 vs .89,  $p = .21$ ). Increases in rCBV  $\geq 1.75$  threshold occurred in 9/18 (50%) of bevacizumab patients and 10/16 (63%) of nonbevacizumab patients ( $p = .96$ ) with odds ratio = .6. When applying the rCBV threshold to bevacizumab patients, differences were found in rCBV (1.18 if  $< 1.75$  vs 2.96 if  $\geq 1.75$ ,  $p = .003$ ), percent increase in rCBV (-11.6 vs 107.5,  $p = .003$ ) and rPH (1.09 vs 1.99,  $p = .001$ ) but not PSR (.79 vs .88,  $p = .59$ ). Within nonbevacizumab patients, differences were found in rCBV (1.32 vs 2.08,  $p = .001$ ), percent increase in rCBV (-2.6 vs 71.9,  $p = .002$ ) and rPH (.95 vs 1.66,  $p = .002$ ) but not PSR (.80 vs .89,  $p = .21$ ).

Figure. Glioblastoma treated with bevacizumab shows new nodular enhancement (circle left) at the anterior margin of the resection cavity without increased rCBV (circle right, to 1.67 from 1.56).



### CONCLUSION

Some glioblastomas may not show increased perfusion prior to progression. Only one half of bevacizumab patients demonstrated increased perfusion prior to progression, as compared to nearly two thirds of nonbevacizumab patients. The differences between high perfusion and low perfusion groups may reflect the genetic and molecular heterogeneity of these tumors, as well as modulation of the perfusion response by bevacizumab. Additional research is necessary to develop new imaging tools and improved response criteria to guide the management of glioblastoma patients.

**KEY WORDS:** Glioblastomas

**O-208**

**10:38 AM - 10:46 AM**

### Simultaneous Perfusion and Permeability MR Imaging in Brain Tumor Patients

Bammer, R.<sup>1</sup>Andre, J.<sup>2</sup>Thomas, R.<sup>1</sup>Nagpal, S.<sup>1</sup>Recht, L.<sup>1</sup>Schmiedeskamp, H.<sup>1</sup>

<sup>1</sup>Stanford University, Stanford, CA, <sup>2</sup>Washington University, Seattle, WA

### PURPOSE

Cerebral blood volume (CBV) frequently is used to assess tumor vascularization. Conventional DSC-MRI suffers from T<sub>1</sub>-enhancement in the presence of contrast agent (CA) leakage and causes CBV to be in error. In addition, leakage into the extravascular-extracellular space (EES) affects both R<sub>2</sub>\*- and R<sub>2</sub> values and CBV measurements. To address these shortcomings, we present the application of a dynamic gradient- and spin-echo EPI (SAGE) sequence and combine it with a pharmacokinetic approach to improve quantitation and to derive the volume transfer parameter, K<sub>T</sub>, between intravascular plasma space (ISP) and EES for blood-brain barrier (BBB) integrity testing.

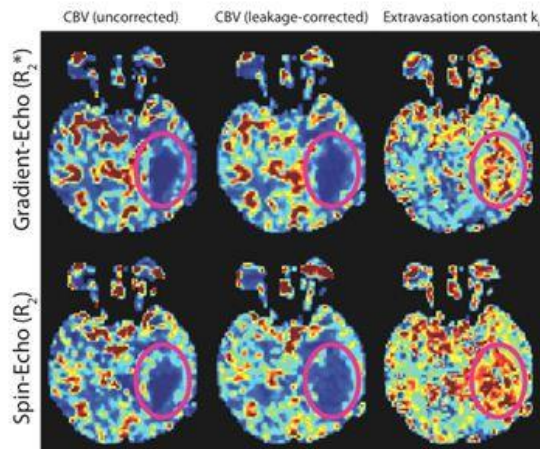
### MATERIALS & METHODS

Validation was performed on biopsy-confirmed GBM patients following chemoradiation therapy and administration of bevacizumab. The study was IRB

approved with informed consent obtained from each patient. **MR Scanning:** Dynamic SAGE-EPI scans acquired 4 GRE and 1 SE at every TR (1.8s) during the passage of a single-dose of gadolinium and allowed for computation of  $R_2(t)$  and  $R_2^*(t)$  maps without  $T_1$ -contamination. **Pharmacokinetic Modeling:** A two-compartment model was implemented into the RAPID software package. The model assumed different transversal relaxivities for IPS and EES, unidirectional flow from IPS to EES, and  $[Gd]_{EES} < [Gd]_{IPS}$  and allowed for the calculation of hemodynamic parameters and  $K_T$ .

## RESULTS

The figure shows different CBV values for conventional DSC and leakage-corrected CBV maps in areas of CA extravasation. The  $T_2^*$ -weighted DSC time signal continues to increase in areas of CA accumulation after the first pass. For the same area,  $R_2(t)$  overestimates the steady state IPS concentration due to added CA in the EES. A more accurate estimate of the time course is achieved when leakage correction is applied, reflected by an elevated  $K_T$ . The most pronounced differences in uncorrected vs leakage-corrected CBV can be seen at the rim of the tumor (also seen on post-Gad  $T_1$ ). Low tumor CBV was seen due to the antiangiogenic effect of bevacizumab. **Discussion:** We were able to correct hemodynamic parameter maps for confounding relaxation effects using SAGE DSC-PWI together with a parameter-free leakage correction. Similar to recent findings, regular DSC CBV processing underestimates CBV for leaky tissue. However,  $T_1$ -correction alone is insufficient and yields an overestimated CBV. Cerebral blood volumes of greater veracity can be obtained by considering the added distribution volume and corresponding  $T_2/T_2^*$  effects in the EES.



## CONCLUSION

Tumor CBV can be heavily biased by leakage and  $T_1$ -shortening. We recommend employing a multiecho readout (to eliminate  $T_1$  effects) and a permeability model to both improve accuracy and derive tissue permeability.

O-209

10:46 AM - 10:54 AM

## Diffusion Kurtosis Imaging in the Grading of Gliomas

Van Cauter, S.<sup>1</sup>·Veraart, J.<sup>2</sup>·Sijbers, J.<sup>2</sup>·Peeters, R. R.<sup>1</sup>·De Keyser, F.<sup>1</sup>·Van Gool, S.<sup>1</sup>·Himmelreich, U.<sup>3</sup>·Sunaert, S.<sup>1</sup>

<sup>1</sup>University Hospitals Leuven, Leuven, BELGIUM,

<sup>2</sup>University of Antwerp, Antwerp, BELGIUM, <sup>3</sup>Catholic

University Leuven, Leuven, BELGIUM.

## PURPOSE

Current routinely used magnetic resonance (MR) techniques are often insufficient in accurate grading of gliomas. In this study, we assessed the diagnostic accuracy of diffusion kurtosis imaging (DKI) parameters in grading gliomas. Diffusion kurtosis imaging is an extension of diffusion tensor imaging, in which the degree of non-Gaussian diffusion is quantified.

## MATERIALS & METHODS

Twenty-seven patients with cerebral gliomas prior to any treatment (8F/19M; age range: 20-76 years, median age: 54) underwent DKI imaging at a 3T MR scanner using a spin-echo diffusion-weighted imaging sequence with b-values of 0, 700, 1000 and 2800 s/mm<sup>2</sup>, applied in 10, 25, 40 and 75 uniformly distributed directions respectively. Diffusion parameters - mean diffusivity (MD), fractional anisotropy (FA), mean kurtosis (MK), radial and axial kurtosis (RK, AK) - were compared in the solid part of 17 high-grade gliomas (HGG) and 11 low-grade gliomas (LGG) (Mann-Whitney-U,  $p < 0.05$  significance, Bonferroni corrected). Mean diffusivity, FA, MK, RK and AK in solid tumor were furthermore normalized to the corresponding parameter value in contralateral normal appearing white matter (normWM) and the contralateral posterior limb of the internal capsule (PLIC) after age correction and compared among tumor grades.

## RESULTS

Mean kurtosis, RK and AK were significantly higher in HGG compared to LGG ( $p = 0.02$ ,  $p = 0.015$ ,  $p = 0.01$ ). Fractional anisotropy and MD did not differ significantly between glioma grades. All parameter values, except for AK, normalized to the contralateral white matter were significantly different between HGG and LGG (MK\_normWM,  $p = 0.02$ ; RK\_normWM,  $p = 0.03$ ; FA\_normWM,  $p = 0.025$ ; and MD\_normWM,  $p = 0.03$ ). When normalizing to PLIC, none of the considered parameters showed significant differences between HGG and LGG. Highest sensitivity and specificity to discriminate between HGG and LGG was found for MK and MK\_normWM in solid tumor (71%; 82% and 100%; 73% respectively). Optimal thresholds for MK and MK\_normWM to differentiate HGG from LGG were 0.52 and 0.51 respectively.

## CONCLUSION

We demonstrated significant differences in kurtosis parameters between HGG and LGG, thereby showing better separation compared to parameters from conventional diffusion imaging.

**KEY WORDS:** Diffusion kurtosis imaging, gliomas, grading

**O-210**

**10:54 AM - 11:02 AM**

### **Utility of Intraoperative MR Imaging in Improving Brain Tumor Resection: Single Center Initial Experience**

Ekram, T.·Jain, R.·Scarpance, L.·Rock, J.·Lee, I.·Omodon, M.·Rosenblum, M.·Kalkanis, S.

Henry Ford Health System  
Detroit, MI

#### **PURPOSE**

Safe, maximal resection of brain tumors is one of the most important predictors of patient survival. Intraoperative magnetic resonance imaging (iMRI) has improved the outcome in brain tumor patients by increasing the amount of safe tumor resection. The purpose of this project is to determine the impact of intraoperative MRI utilization on brain tumor resection volumes and operative time.

#### **MATERIALS & METHODS**

Patients who underwent craniotomy for brain tumors with the assistance of iMRI between 02/11-07/11 were evaluated retrospectively for tumor volumes at three time points: prior to resection, intraoperatively immediately following the first resection, and after the second or final resection, to assess the impact of intraoperative imaging. Tumor volumes for the enhancing part of the tumor were assessed using postcontrast T1-weighted imaging. Resection volumes were divided into four categories according to the neurosurgical literature and outcomes data: gross total resection (GTR) as 100% resection, major resection (MajR) as 90-99%, subtotal resection (STR) as 50-89%, and partial resection (PR) as below 50%.

#### **RESULTS**

Twenty-eight patients underwent tumor resection using iMRI during the above time period. Seventeen patients (gliomas n = 16, metastases n = 1) who underwent surgery for an intraaxial tumor were included for this analysis. The first surgical resection prior to intraoperative imaging resulted in average tumor volume reduction of 13.6 ml (range of 0 - 57.7 ml; CI 95% - 7.7 ml) and initial percentage reduction of 72% (0% - 100%; CI 95% - 16.8%) based on volumetric analysis of the enhancing component. In two cases, small enhancing nodules were missed on the first resection and iMRI identified those for subsequent resection. Fourteen patients (83%) underwent an additional surgical resection during the same procedure as intraoperative imaging identified residual enhancing tumor that was deemed safe for further resection. Second resection resulted in additional average tumor volume reduction of 2.6 ml (0 - 10.9 ml; CI 95% - 1.9 ml) and a percentage reduction of 25% (3% - 100%; CI 95% - 17%). After the first resection, two patients (11%) had GTR, four (24%) had MajR, eight (47%) had STR, and three (18%) had PR. With the iMRI-assisted second resection, overall resection grading for the 17 total

patients improved, and the percentage of patients with GTR increased from 24% to 47%, with only 6% of patients ultimately having a PR. Overall, combining the clinically relevant levels of resection (GTR and MajR), the percentage improved from 35% to 76% with the use of iMRI. Average intraoperative MRI scan time was 22 minutes. Postoperative clinical follow up demonstrated four (23%) patients with hemiplegia or aphasia with three demonstrating improvement or resolution at outpatient follow up. No significant postoperative complications were noted related to aggressive resection.

#### **CONCLUSION**

Intraoperative MRI improves safe resection of brain tumors in a majority of cases without significantly prolonging the operative time. A high percentage of patients benefited from intraoperative imaging. The real-time ability to identify residual enhancing tumor after initial resection improved the total tumor resection volume and percentage of patients with clinically significant tumor resection.

**O-211**

**11:02 AM - 11:10 AM**

### **Vasogenic Edema as a Marker of Treatment Response Demonstrated by MR Imaging in Newly Diagnosed Glioblastoma Receiving Anti-VEGF Therapy**

Fakhro, S. A.<sup>1</sup>·Pinho, M. C.<sup>2</sup>·Jennings, D. L.<sup>2</sup>·Polaskova, P.<sup>2</sup>·Emblem, K.<sup>2</sup>·Sorensen, A. G.<sup>3</sup>·Batchelor, T. T.<sup>4</sup>·Gerstner, E. R.<sup>4</sup>

<sup>1</sup>Athinoula A. Martinos Center for Biomedical Imaging, Massachusetts General Hospital and Harvard Medical School, Manama, BAHRAIN, <sup>2</sup>Athinoula A. Martinos Center for Biomedical Imaging, Massachusetts General Hospital and Harvard Medical School, Boston, MA, <sup>3</sup>Seimens Medical Solutions, Malvern, PA,

<sup>4</sup>Massachusetts General Hospital Cancer Center, Boston, MA

#### **PURPOSE**

To evaluate if the presence of vasogenic edema might be a predictive marker of treatment response in newly diagnosed glioblastomas receiving a vascular endothelial growth factor (VEGF) signaling tyrosine-kinase inhibitor (cediranib) as adjuvant therapy in addition to conventional temozolomide-based chemoradiation.

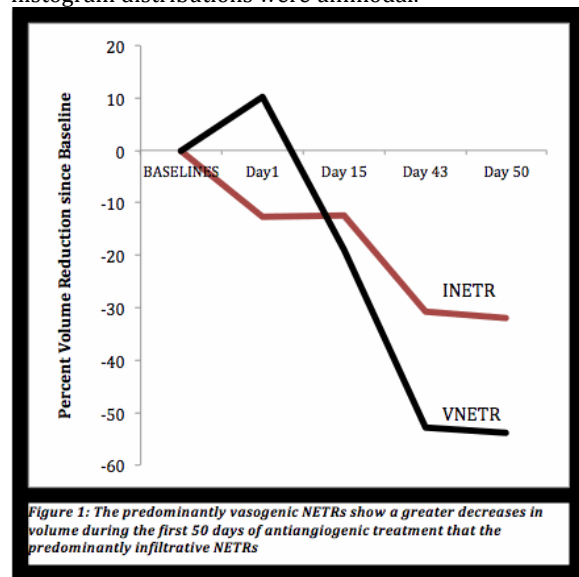
#### **MATERIALS & METHODS**

Thirty-seven patients with newly diagnosed glioblastomas were scanned at 3 T at two independent time points before adjuvant therapy (i.e., cediranib in combination with standard chemoradiation). Diffusion tensor imaging was performed at a TR = 7500 ms and TE = 84ms with b-values of 0 and 700s/mm<sup>2</sup> in 42 directions. Nonenhancing tumor regions (NETRs) were obtained by subtracting areas of contrast enhancement and necrosis from manually outlined regions of interest containing the entire MRI tumor abnormality. Based on published imaging criteria, a neuroradiologist with experience on brain tumor imaging (blinded to

posttreatment outcome and DTI data) classified the NETRs into *predominantly nonenhancing tumor*, *predominantly vasogenic edema* or *mixed/unspecific* cases. According to the radiologist's assessment, six tumor NETRs were classified as predominantly vasogenic edema and 15 as predominantly nonenhancing tumor. Sixteen patients had mixed components or were unclassifiable due to small volumes of residual tumor. The calculated NETR volumes from days 1, 8, 43, and 50 were compared for each group, and the greatest percent volume reduction in the NETR compared to baseline was considered the best response for each patient. Median values of FA and ADC histograms of the NETR were compared between the neuroradiologist-classified groups.

## RESULTS

The median volume percent change relative to baseline (best response) in the predominantly vasogenic NETR (VNETR) group was found to be significantly higher than that of the predominantly infiltrative NETR (INETR) group (-71.55% versus -32.52%;  $P < 0.01$ ). The FA values in the VNETR were found to be significantly lower than those of the INETR (median values 0.24 versus 0.28; Mann-Whitney test  $P < 0.05$ ). Half (3/6) of the VNETR ADC histograms had clearly defined bimodal distributions while all of the INETR (15/15) ADC histogram distributions were unimodal.



## CONCLUSION

It is a clinically relevant goal to validate imaging features that might be useful to select patients who would most benefit from expensive therapies that induce significant side effects. In this study, patients that were stratified qualitatively as VNETR demonstrated a significant response to cediranib. Furthermore, the quantitative analysis of NETR volumes in these two cohorts demonstrated differences in FA median values and ADC histogram distributions, which supports the concept that they do have different tissue microstructures.

**KEY WORDS:** MR imaging, glioblastoma, infiltration

O-212

11:10 AM - 11:18 AM

## Characterization of Brain Tumors Using BOLD Resting-State Functional Connectivity Maps: A Pilot Study

Chow, D. S. • Horenstein, C. I. • Grinband, J. • Jambawalikar, S. • Delapaz, R. L.

Columbia University Medical Center  
New York, NY

## PURPOSE

BOLD fMRI and functional connectivity are used increasingly for preoperative planning, prior to brain tumor resection. This functional information helps guide the extent of tumor resection and surgical trajectory. Brain tumors incite multiple pathophysiologic changes, including vascular compression or invasion, arteriovenous shunting, angiogenesis with proliferation of immature vessels lacking autoregulation and intratumoral hemorrhage, that alter intracerebral blood flow and may lead to decoupling of the neurovascular response. This study investigates whether BOLD functional connectivity mapping also can provide information about tumor type and pathologic classification.

## MATERIALS & METHODS

Retrospective review of 13 patients who had resting state BOLD fMRI at 3 T, prior to tumor resection (3 meningiomas, 2 metastatic adenocarcinomas, 1 anaplastic glioma, 7 glioblastomas). Motion and slice timing corrections were performed on the raw datasets. Two different functional connectivity (FC) maps were generated. Each voxel timeseries was correlated to its 26 nearest neighbors, to derive a measure of local (short range) connectivity. Each voxel timeseries was correlated to every other voxel in the brain, to derive a measure of global (long range) connectivity. Both FC maps were coregistered to structural images using FSL/FLIRT. Patterns of functional connectivity within the tumor and peritumoral white matter were characterized qualitatively.

## RESULTS

One meningioma demonstrated high connectivity on the local FC map, which spatially corresponded to low ADC values. Otherwise the meningiomas had low connectivity on the FC maps. All three meningiomas were well delineated on the FC maps, with accurate spatial extents, compared to T1 postcontrast images. Peritumoral brain parenchyma had normal connectivity values, relative to the contralateral side. One metastasis demonstrated local and global connectivity values similar to peritumoral white matter, masking the true extent of the lesion. The other metastasis demonstrated intermediate local FC values, between cortex and white matter, and global FC values, lower than cortex and white matter, allowing for good visualization of the lesion, with an accurate spatial extent. Peritumoral white matter demonstrated normal connectivity values. The anaplastic astrocytoma demonstrated high local connectivity with accurate delineation of the tumor on the FC map, and normal peritumoral connectivity. The



global FC map was degraded by artifact and was uninterpretable. One glioblastoma had local and global FC values similar to white matter, resulting in poor visualization and delineation of the tumor. One glioblastoma had high local and low global FC values, with good delineation of the tumor and accurate spatial extent. The other five glioblastomas had predominantly low connectivity on both the local and global FC maps, but two of these tumors showed patchy area of increased connectivity, which spatially corresponded to low ADC values. Two of the seven glioblastomas also had abnormal peritumoral functional connectivity values.

#### CONCLUSION

Due to alterations in BOLD signal, most tumors easily were visualized on functional connectivity maps. Two glioblastomas and one meningioma demonstrated focal regions of increased local (short range) connectivity, that spatially correlated with decreased ADC values. Two of the glioblastomas had abnormal functional connectivity in the peritumoral white matter, possibly reflecting their invasiveness. Further quantitative analysis is required to determine whether different class of tumors are associated with different signatures on BOLD imaging.

**KEY WORDS:** BOLD, functional connectivity, brain tumors

**O-213**

**11:18 AM - 11:26 AM**

#### Localization of Eloquent Cortex Using Resting-State Functional MR Imaging

Shimony, J. S. • Lee, M. • Hacker, C. • Zhang, D. • Mitra, A. • Snyder, A. • Leuthardt, E.

Washington University Medical School  
St. Louis, MO

#### PURPOSE

Currently, a challenge in the surgical treatment of brain tumors is to preserve eloquent areas of brain function while maximizing the extent of resection. The current gold standard for localization of eloquent cortex is direct electrocortical stimulation (DECS), during an awake craniotomy where the patient is able to participate in various cognitive tasks. The requirement for patient cooperation limits its use in a significant number of patients (e.g., children and medically tenuous patients) and thus prohibits an optimal resection for these individuals. Similarly task functional MR imaging (fMRI) requires patient cooperation. Resting-state functional connectivity MRI (fcMRI) has emerged as an alternative method for localization of brain networks that requires no active patient participation and can be done under sedation. The purpose of this study was to explore the use of fcMRI for localization of eloquent cortex in patients with brain tumors.

#### MATERIALS & METHODS

Fourteen subjects with a new diagnosis of brain tumor or metastasis were recruited prior to surgery. Twenty-one normal controls were scanned identically as part of

a different study. In addition to anatomical imaging, subjects also were scanned using BOLD sensitized resting state fMRI on a 3 T Siemens Allegra MR. For comparison, subjects also were scanned using a block design motor and language tasks, which were processed using standard techniques. Resting state analysis was performed using either a seed-based approach by placing seeds in the undistorted contralateral side of the brain. Alternatively, independent component analysis (ICA) was used to identify either the somatomotor or language networks.

#### RESULTS

The somatomotor cortex was identified consistently in all subjects using seed placement in the hand motor area in the undistorted side contralateral to the tumor using atlas coordinates. Identifying the language network required a more variable set of tools, depending on the tumor location. Placement of a seed region in Broca or Wernicke's regions was not always possible when tumors cause severe distortion of the left hemisphere. ICA analysis provided a robust alternative method of identifying the language network in distorted brain. Following identification of components of the language networks in ICA, these were checked by placement of seed regions and by comparison with the task-based fMRI scans.

#### CONCLUSION

Resting-state fcMRI can provide useful information on the location of eloquent cortex for presurgical planning and can be performed in many patients that can't benefit from traditional fMRI.

**KEY WORDS:** Functional MR imaging, brain neoplasm

**O-214**

**11:26 AM - 11:34 AM**

#### Characterization of Brain Tumors Using Quantitative Susceptibility Mapping: A Pilot Study

Horenstein, C. I. • Chow, D. S. • Jambawalikar, S.

Columbia University Medical Center  
New York, NY

#### PURPOSE

Quantitative susceptibility mapping (QSM) combines the magnitude and phase information from an susceptibility-weighted imaging (SWI) sequence to estimate tissue susceptibility, independent of acquisition parameters. The susceptibility of water is defined as zero. Positive QSM values reflect paramagnetic tissue and negative values reflect diamagnetic tissue. We characterized the distribution of tumoral and peritumoral susceptibility within different classes of tumor, and tested the following hypotheses: 1) intratumoral susceptibility increases with glioma grade, 2) glioblastomas have increased peritumoral susceptibility, compared to metastases, 3) intratumoral calcification on CT-scan spatially correlates with negative QSM values.

## MATERIALS & METHODS

We retrospectively analyzed 19 brain tumors (4 metastatic adenocarcinomas; 1 metastatic renal cell carcinoma (RCC); 5 meningiomas; 1 hemangioblastoma; 1 low-grade glioma (LGG); 3 intermediate-grade gliomas (IGG) and 4 glioblastomas (GBM)). Quantitative susceptibility maps were generated using MEDI, and coregistered to structural imaging. For intersubject comparisons, QSM values were transformed into z-scores, based on a control ROI in the contralateral white matter. Tumoral and peritumoral ROIs were hand drawn in AFNI on the structural datasets. ROI histogram analysis was performed in matlab.

## RESULTS

Displaying QSM maps in grayscale was better for visualizing normal anatomy. Displaying QSM maps as color overlays facilitated detection of intratumoral and peritumoral signal changes. Higher grade gliomas demonstrated a greater number of highly positive voxels, but also a greater number of highly negative voxels, resulting in small, variable shifts in the mean QSM values. Histogram analysis suggests that the standard deviation (std) of intratumoral QSM values [LGG:0.62; IGG:2.11; GBM:2.97] or range of intratumoral QSM values [LGG:(-2.2 to +3.1); IGG:(-21.4 to +21.3); GBM:(-21.5 to 40.9)] better correlate to tumor grade than mean intratumoral QSM value. Histogram kurtosis (LGG:3.02; IGG:6.93; GBM:13.58) and skewness (LGG: 0.03; IGG: 6.93; GBM: 13.58) both increased with tumor grade. The mean and std of peritumoral QSM was similar between GBMs(-0.01/+1.48) and metastases(-0.05/+1.31); however GBMs had a wider range of peritumoral QSM values [GBM:(-15 to +18.7); met:(-7.6 to +9.7)]. The results are confounded by the inclusion of an RCC metastasis, which has higher tumoral and peritumoral QSM values than the adenocarcinomas, due to blood products. If only adenocarcinomas are considered, group differences between GBMs and metastases are accentuated. GBMs demonstrated higher peritumoral kurtosis (GBM:17.94; mets:6.04) and skewness (GBM:1.04; met:0.40). Due to small sample sizes, the above results were not statistically significant. Visual inspection revealed that calcifications on CT scan were correlated spatially with negative QSM values. Several tumors displayed highly negative QSM values without corresponding calcification on CT, an unexpected finding.

## CONCLUSION

Quantitative susceptibility mapping is a novel MRI technique for characterization of brain tumors. Pilot data suggests that higher grade gliomas are associated with a wider range on intratumoral susceptibility than lower grade gliomas and that the GBMs are associated with a wider range of peritumoral susceptibility than metastases. Further evaluation is needed to determine whether these differences are significant between tumor classes. CT calcification had high spatial correlation with negative QSM voxels; however, several tumors displayed highly negative QSM values without corresponding calcification on CT, an unexpected finding. Further study is needed to define the sources of susceptibility as measured by QSM.

**KEY WORDS:** Quantitative susceptibility mapping, brain tumor, Susceptibility-weighted imaging

O-215

11:34 AM - 11:42 AM

## Noninvasive Differentiation of High-Grade and Low-Grade Glioma: A Pulsed Arterial Spin Labelling Study Using Relative Tumorous Blood Flow Values from Multiple Inversion Time Points

Furtner, J.·Schoepf, V.·Kasprian, G.·Weber, M.·Widhalm, G.·Wolfsberger, S.·Preusser, M.·Hainfellner, J.·Prayer, D.

Medical University Vienna  
Vienna, AUSTRIA

## PURPOSE

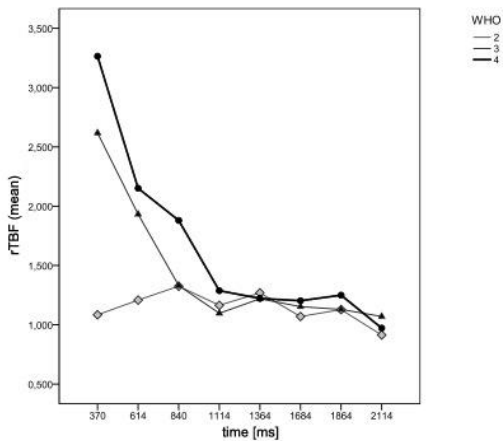
Pulsed arterial spin labelling (pASL) is a noninvasive MRI perfusion method using the water in the arterial blood as endogenous contrast agent. The purpose of this study was to determine the most suitable pulsed arterial spin labelling inversion time point (TI) for the differentiation between high-grade and low-grade glioma, using a multi-TI-pASL approach which tracks the labelled bolus dynamically over time.

## MATERIALS & METHODS

Thirty-three patients with gliomas, histologically classified as low-grade (n = 7) or high-grade gliomas (n = 26) according to the WHO brain tumor classification were included. A 3T MR scanner (Trio; Siemens Medical Solution, Erlangen, Germany) was used to perform pASL sequences at eight different inversion time points (370 ms, 614 ms, 864 ms, 1114 ms, 1364 ms, 1684 ms, 1864 ms, 2114 ms). The relative tumorous blood flow (rTBF) for all fixed inversion time points was calculated. A three-way mixed ANOVA was used to reveal potential differences in the rTBF between high-grade and low-grade gliomas.

## RESULTS

The difference of rTBF between high-grade and low-grade gliomas obtained statistically significant results at 370 ms (p = 0.003) and 640 ms (p = 0.012). No significant differences of signal intensity between high-grade and low-grade gliomas were obtained for all other inversion time points (p-values ranged from 0.129 to 0.955).



C

**CONCLUSION**

Our findings suggest that the most suitable inversion time point for differentiation of high-grade from low-grade glioma using pulsed arterial spin labelling is 370 ms. The application of the investigated pASL-inversion time point in this study will enable the noninvasive and fast characterization of such tumors in the future.

**KEY WORDS:** Arterial spin labelling, brain tumor, relative cerebral blood flow

**O-216****11:42 AM - 11:50 AM**

### Characterization of the Metabolic Changes at the Diffusion Tensor Defined Invasive Margins of Glioblastoma Using MR Spectroscopy

Young, A. M. H.·Thomas, O. M.·Mosen, L. A.·Frary, A. J.·Lupson, V. C.·Price, S. J.

Addenbrooke's Hospital  
Cambridge, UNITED KINGDOM

**PURPOSE**

Local white matter invasion is a key pathological hallmark of glioblastoma (GBM) and the major cause of treatment failure. Identification of the invasive tumor margin cannot be done on conventional MR imaging but is essential for appropriate treatment planning. Our work with diffusion tensor imaging (DTI) has shown it can accurately determine the invasive margin of gliomas. However, little is known about the metabolic activity of these regions. In this study, we have used magnetic resonance spectroscopy (MRS) to determine the metabolic profiles in the invasive region and compared this to normal-appearing white matter (both contralateral and adjacent, ipsilateral hemisphere white matter). In this way, we aim to characterize the changes in metabolic activity associated with tumor invasion.

**Materials & Methods**

The study group comprised 35 patients with newly diagnosed, subsequently histologically confirmed glioblastomas (24 males, 11 females; mean age 55, range 30 - 68 years). Imaging was performed at 3 T (Siemens TrioTim). Preoperatively, all patients underwent MR imaging which included DTI and multivoxel, short echo time (TE = 35ms) MRS sequences

as well as routine clinical imaging (T<sub>2</sub>, FLAIR and pre and postcontrast T<sub>1</sub> imaging) was used to plan the 2-dimensional MRS grid position. The isotropic (p) and anisotropic (q) components of the diffusion tensor were calculated as previously described. Comparing these parameter maps, peritumoral invasion was identified by those regions that demonstrated an increase in the isotropic component (p) but that had normal anisotropic diffusion (q). These regions then were used to select appropriate MRS voxels of interest for analysis and compared to normal-appearing adjacent and contralateral white matter. MR spectroscopy was analyzed using LCModel. The statistical significance of the measured metabolites was determined using an ANOVA (Tukey-Kramer multiple comparisons test; Sigma Plot 5, Systat). The significance level was taken as a p value of less than or equal to 0.05.

**RESULTS**

Seventeen metabolites presented sufficient data to perform the statistical analysis. Of these, seven metabolites demonstrated significant concentration differences in the invasive region compared to normal-appearing white matter. The invasive margin demonstrated a reduction in N-Acetylaspartate (NAA; p = 0.03) and Myo-inositol (Ins; p = 0.007), suggesting a reduction in neuron and astrocyte density respectively. Creatine (Cr) also was found to be significantly decreased in the invasive margin (p = 0.008). Interestingly, the phosphocreatine (PCr) appeared increased, but this did not reach statistical significance for the current sample size. Glutamate (Glu; p = 0.008) and the glutamate/glutamine cycle (Glx; p = 0.008) also demonstrated significant reduction in the invasive margin compared to adjacent white matter suggesting disruption of the glial-matrix integrity. Comparisons between normal-appearing and contralateral white matter demonstrated no difference.

**CONCLUSION**

We have observed, for the first time to our knowledge, a number of metabolic changes within the invasive tumor margin as defined by DTI imaging. These suggest underlying alterations in neuron and immune cell density as well as shifts in signalling metabolites fundamental to neuronal function.

**KEY WORDS:** Glioma, MR spectroscopy, invasive margin

**O-217****11:50 AM - 11:58 AM**

### MR Hypoxia Index: Detecting Hypoxic Regions within Gliomas

Toth, V.<sup>1</sup>·Preibisch, C.<sup>1</sup>·Hirsch, N.<sup>1</sup>·den Hollander, J.<sup>1</sup>·Foerschler, A.<sup>1</sup>·Ringel, F.<sup>1</sup>·Schlegel, J.<sup>1</sup>·Kooijman, H.<sup>2</sup>·Zimmer, C.<sup>1</sup>

<sup>1</sup>Klinikum rechts der Isar, Munich, GERMANY, <sup>2</sup>Philips, Best, NETHERLANDS

**PURPOSE**

An intratumoral hypoxic microenvironment promotes the development of stem cells, which in turn play an important role in tumor genesis, progression and

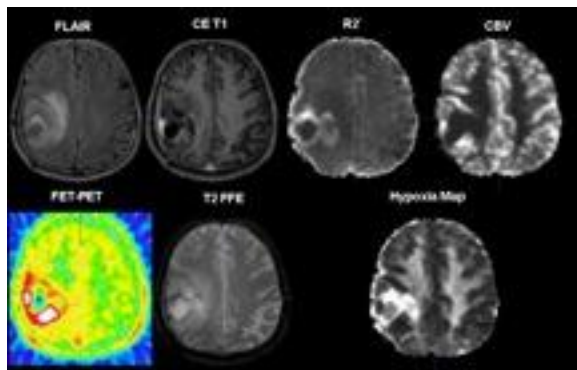
therapy resistance. In vivo identification of hypoxic regions in the brain is a target of new MRI techniques aiming at the noninvasive measurement of blood oxygenation. The detection of hypoxic niches in gliomas may predict the malignization of a low-grade tumor and hypoxic areas may serve as a hot spot for radiation therapy planning. In this work, a semiquantitative parameter, the Hypoxia Index is presented as a tool for a functional characterization of gliomas.

#### MATERIALS & METHODS

In a pilot study four healthy subjects (1 female, age  $32.5 \pm 15.2$  years) and 20 patients (9 females, age  $54 \pm 24.6$  years) with brain tumors were examined (histological grades: °II in 2 cases, °III in 4 cases and °IV in 14 cases). In addition to our conventional protocol measurements of transverse relaxation times  $T2^*$  and  $T2$  as well as of DSC-CBV were performed on a 3 T Philips Achieva.  $R2' = (1/T2^* - 1/T2)$  is sensitive for local susceptibility differences between blood and tissue and thus correlates with the blood oxygenation level. According to Yablonskiy and Haacke oxygen saturation  $Y = (1-q)$  and deoxygenation is related to  $q = R2'/(c \cdot CBV)$  where  $c = 4/3 \cdot \gamma \cdot \pi \cdot \Delta\chi \cdot B_0$ . The Hypoxia Index (HI) is calculated as a ratio of  $q/q_{max}$  with a threshold of  $q_{max} = \text{median}(q) + 3 \cdot \sigma(q)$  and hypoxia maps are created, which show increased hypoxia values as hyperintensities. Evaluation was performed with custom programs in MATLAB and SPM8. In two patients histological correlation was performed on intraoperatively sampled biopsy probes.

#### RESULTS

$R2'$  maps from healthy volunteers rendered homogenous maps with increased values in the basal ganglia due to iron deposition as well as in areas of macroscopic magnetic susceptibility gradients. Standard values for gray and white matter were collected. In nine patients we found hypoxic regions either in the contrast-enhancing solid tumor or in the non-enhancing infiltration zone. Hypoxia could be confirmed by HIF1 $\alpha$  immunohistochemistry in biopsy probes from hypoxic areas. In other cases the hyperintense signal corresponded to tumor necrosis or intratumoral bleeding. In one patient a postoperative ischemic lesion appeared hypoxic on the maps.



#### CONCLUSION

The Hypoxia Index is a new parameter able to detect hypoxic areas within brain tumors in the clinical setting. A systematic correlation of the hypoxia maps with

histology (HIF1 $\alpha$  staining) and PET (18F-FMISO) is being performed at our center.

**KEY WORDS:** Hypoxia, glioma, relaxometry

O-218

11:58 AM - 12:06 PM

#### Combined MR Imaging and Positron Emission Tomography Methionine Imaging for Assessing Pituitary Residual Secreting Adenomas in Surgically Treated Patients

Pezzulo, M.·Goldmann, S.·Massager, N.·Devuyst, F.·DeWitte, O.·Balériaux, D.

Universite Libre de Bruxelles  
Brussels, BELGIUM

#### PURPOSE

Postoperative evaluation of pituitary adenomas is challenging and often extremely difficult. The combined use of positron emission tomography (PET) methionine and MR imaging for identifying pituitary secreting residual adenomas in surgically treated patients as complementary imaging methods has become a routine and extremely useful procedure in our institution. The purpose of this presentation is to summarize the results of this experience.

#### MATERIALS & METHODS

Fifteen patients known for having pituitary adenomas surgically treated previously and with persisting endocrinopathy from hormonal hypersecretion, underwent MR imaging with high resolution T2 and T1 sequences, dynamic contrast-enhanced T1 acquisitions as well as a 3D T1 sequence for coregistration with a subsequent PET methionine scan.

#### RESULTS

In 12 patients there was a good anatomical correspondence of the dynamic-enhancing MR features and the functional methionine hypercaptation delineating the residual adenoma; in one patient there was no methionine selective captation in the supposed residual GH secreting adenoma explained by the medical hormonal treatment; in one patient the MR failed to identify the residual adenoma within a largely surgically rearranged parenchyma while the PET clearly identifies the lesion; in one patient MR imaging suggested the presence of a residual adenoma while there was no hypercaptation at PET imaging; therefore, follow up rather than surgical treatment was chosen.

#### CONCLUSION

We recommend the combined use of morphologic and functional imaging of the sellar region in patients surgically treated for pituitary adenomas with persisting endocrinopathy. This approach allows better and more reliable identification of a residual microadenoma in order to plan further surgical or medical treatment.

**KEY WORDS:** Pituitary adenoma, MR imaging, PET



## Tuesday Morning

10:30 AM - 12:00 PM

Trion Ballroom

### (27b) Functional Imaging I

O-219

10:30 AM - 10:38 AM

#### Relationship between Language Lateralization and the Corpus Callosum in Brain Tumor Patients Using Functional MR Imaging and Diffusion Tensor Imaging

Tantillo, G.·Holodny, A.·Lyo, J.·Brennan, N.·Peck, K. K.

Memorial Sloan-Kettering Cancer Center  
New York, NY

##### PURPOSE

Previous research demonstrates a correlation between language lateralization and corpus callosal (CC) morphology in healthy subjects. We assessed the relationship between the CC microstructure and degree of language lateralization in patients with left hemispheric tumors to examine how brain pathology influences language lateralization. Functional MRI was used to measure neural activation, and diffusion tensor imaging (DTI) fractional anisotropy (FA), a measure of diffusion directionality, was used to measure the microstructure of the CC.

##### MATERIALS & METHODS

Twenty right-handed and one left-handed patient with left hemispheric brain tumor were studied. The tumors were centered in or directly adjacent to the expected location of Broca's area. Functional MRI and DTI studies were performed on a 3 T GE scanner using EPI. Functional images were acquired with TR/TE = 4000/40 ms; 128×128 matrix; 4.5 mm thickness. Image analysis was performed with AFNI software. Functional activity from language tasks (phonemic and semantic fluency) was generated using cross-correlation analysis. Regions of interest (ROI's) were drawn using anatomical landmarks and the number of activated voxels were counted for Broca and Wernicke's areas. The lateralization index was calculated using the formula  $LI = (L-R)/(L+R)$ , and subjects were classified as right-dominant (RD), codominant (CD), or left-dominant (LD). For DTI analysis, color fractional anisotropy (FA) maps were generated. Regions of interest of the anterior, posterior, and body of the corpus callosum were drawn. The FA in the ROIs were calculated and then averaged per region of the CC for statistical analysis.

##### RESULTS

Average FA were compared across the three Broca group, with the CD group having higher FA than either the LD or RD group. There was a statistically significant difference between CD and RD patients ( $p = 0.013$ ). The difference between LD and CD Broca groups

approached significance ( $p = 0.091$ ), but did not reach it. The average FA also were compared across the three Wernicke groups, where there were no differences ( $p = 0.3$ ). Patients were further classified into a "lateralized" or "codominant" groups based on the LI. For Broca's area, codominant groups had significantly higher FA than lateralized groups ( $p = 0.02$ ).

##### CONCLUSION

As a group, patients who were LD or RD for language in Broca's area ROI's had lower FA in the anterior CC than those who were CD for language. When patients were sorted into lateralized vs codominant groups, codominant patients also had higher FA in the anterior CC than patients who displayed strong lateralization in either the left or right hemisphere. The greater FA in codominant patients may reflect a more directional microstructure for the CC in this region, suggesting a greater need for interhemispheric transfer of information. The presence of a brain tumor that encroaches upon functional cortical areas may trigger cortical reorganization as the brain adapts to tumor infiltration. This plasticity may be reflected in codominance as homologous language areas in the contralateral hemisphere may be recruited to assist in functional language tasks.

**KEY WORDS:** Functional MR imaging, diffusion tensor imaging

O-220

10:38 AM - 10:46 AM

#### Relationship between White Matter Tracts and Outcomes in Patients with Intracranial Tumors as Demonstrated on Diffusion Tensor Imaging

Giloon, B.<sup>1</sup>·Swan, B.<sup>1</sup>·Huss, D.<sup>1</sup>·Greenstein, M.<sup>2</sup>·Voss, J.<sup>2</sup>·Holdsworth, R.<sup>1</sup>·Moritz, C.<sup>1</sup>·Nair, V.<sup>1</sup>·Field, A.<sup>1</sup>·Kuo, J.<sup>1</sup>·Meyerand, E.<sup>1</sup>·Prabhakaran, V.<sup>1</sup>

<sup>1</sup>University of Wisconsin School of Medicine and Public Health, Madison, WI, <sup>2</sup>University of Wisconsin, Madison, WI

##### PURPOSE

Language deficits commonly are observed in patients afflicted with brain tumors after undergoing a surgical resection. Yet, the factors underlying the cause of this morbidity is not well understood. Similarly, even when controlling for tumor grade and stage, patient survival or mortality varies considerably. Our objective is to elucidate the relationship between tumor proximity to various white matter tracts in the brain and morbidity and mortality in these patients.

##### MATERIALS & METHODS

Adult patients with brain tumors ( $n = 32$ ) underwent preoperative diffusion tensor imaging (DTI) scans. These scans were analyzed and three major brain pathways identified. These are the right and left superior longitudinal fasciculi and the cingulum. Patient records were reviewed to determine postoperative language deficits as well as mortality information.

## RESULTS

Preliminary analyzes of the patients showed that there was a significant linear relationship between the distance of the tumor to the right ( $p = 0.013$ ) and left ( $p = 0.002$ ) superior longitudinal fasciculi and language deficits, with greater distances resulting in lesser impairment. There was also a significant increase in postoperative life span related to increasing tumor distance from the cingulum ( $p = 0.043$ ). analyzes of these patients are still underway and more patients are being added to the study as further DTIs are performed.

## CONCLUSION

There existed a linear relationship between the distance of the tumor to either the right ( $p = 0.013$ ) or left ( $p = 0.002$ ) superior longitudinal fasciculus and the presence of a postoperative language deficit. Patients who had tumors further away from their cingulum had longer postsurgical survival times ( $p = 0.043$ ).

**KEY WORDS:** Diffusion tensor imaging, brain tumor, functional MR imaging

O-221

10:46 AM - 10:54 AM

### Probabilistic Fiber Tracking of the Language and Motor White Matter Networks of the Supplementary Motor Area in Patients with Brain Tumor

Jenabi, M.·Peck, K. K.·Young, R. J.·Brennan, N.·Holodny, A. I.

Memorial Sloan-Kettering Cancer Center  
New York, NY

## PURPOSE

Accurate localization of the white matter pathways to and from the supplementary motor area (SMA) including SMA proper and pre-SMA is important for neurosurgical planning and to precisely determine if a lesion (tumor, infarct, etc.) correlates with a neurologic deficit. This study investigates the existence, location and relationship of pathways between the SMA and Broca's area using fMRI and probabilistic diffusion tensor tractography in patients with brain tumors.

## MATERIALS & METHODS

Twenty patients (10 males; mean age 43.8 years) with brain tumors (16 primary, 4 secondary) located in or adjacent to language pathways were studied. Functional MRI paradigms were performed on a 3 T scanner using gradient-echo echo-planar imaging (TR/TE = 4000/30 ms, 128 x 128 matrix, 90° flip angle, 4.5 mm slice thickness). We used block design motor (finger tapping) and language (phonemic fluency) paradigms. Diffusion tensor imaging was acquired using a single shot spin-echo echo-planar imaging with 25 noncollinear directions. Functional activity during the language task and the motor task was analyzed using analysis of functional neuroimaging (AFNI). Peak activated voxels were selected to define the SMA<sub>language</sub>, SMA<sub>motor</sub> and Broca's area seed regions for probabilistic fiber tracking performed with DTI&FiberTools (University Hospital, Freiburg, Germany) implemented in Matlab. Probabilistic tracts between SMA<sub>language</sub> and Broca's area

as well as SMA<sub>motor</sub> and Broca's area were generated. To evaluate the degree of the fiber connectivity, the number of voxels (volume), mean and standard deviation of each tract of individual patients were compared by using paired Student t-tests.

## RESULTS

Probabilistic tractography successfully showed the connectivity between SMA<sub>language</sub> and Broca's area and between SMA<sub>motor</sub> and Broca's area in both hemispheres via two, separate, unique paths for all subjects. The SMA<sub>language</sub> path was significantly more prominent than the SMA<sub>motor</sub> path in the degree of probabilistic connectivity ( $p < 0.0003$ ) and number of voxels ( $p < 0.0003$ ), independent of the location or laterality of tumors. No difference was found between the sides for the SMA<sub>language</sub> path (degree of connectivity:  $p < 0.58$  and number of voxels:  $p < 0.48$ ) or SMA<sub>motor</sub> path (degree of connectivity:  $p < 0.69$  and number of voxels:  $p < 0.56$ ).

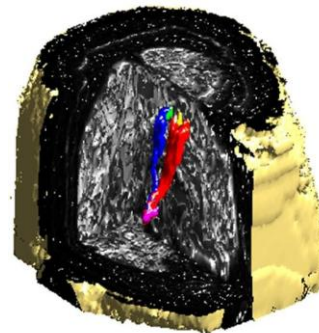


Figure. Oblique sagittal cut-away of 3D volume rendered probabilistic tractography shows the separate SMA<sub>language</sub> (red) and SMA<sub>motor</sub> (blue) pathways. The fMRI activated Broca's area (magenta), SMA<sub>language</sub> (yellow) and SMA<sub>motor</sub> (green) voxels used to seed the pathways are also labeled.

## CONCLUSION

Combination fMRI and probabilistic tractography identified two unique white matter pathways between Broca's area and SMA<sub>language</sub> and SMA<sub>motor</sub>. The connectivity between Broca's area and SMA<sub>language</sub> was stronger in all cases. Further work is necessary to determine the potential benefit of localization of these pathways for treatment decisions, such as in preoperative planning in patients with brain tumors.

**KEY WORDS:** Diffusion tensor imaging, probabilistic fiber tracking, supplementary motor area

O-222

10:54 AM - 11:02 AM

### Using a Functional Geometry Atlas to Map Brain Networks Affected by Tumor Growth

Langs, G.<sup>1</sup>·Sweet, A.<sup>2</sup>·Lashkari, D.<sup>2</sup>·Tie, Y.<sup>3</sup>·Rigolo, L.<sup>3</sup>·Golby, A. J.<sup>3</sup>·Golland, P.<sup>2</sup>

<sup>1</sup>Medical University of Vienna, Wien, AUSTRIA,

<sup>2</sup>Massachusetts Institute of Technology, Cambridge, MA,

<sup>3</sup>Harvard Medical School, Boston, MA

## PURPOSE

We propose a method that uses an atlas of functional connectivity patterns derived from healthy individuals to predict the location of corresponding networks in brains that exhibit pathology. The goal is to match

functional connectivity structures across subjects, even if substantial reorganization has occurred, and anatomical correspondences are not reliable.

#### MATERIALS & METHODS

We conducted experiments on language fMRI data of 13 subjects (6 control subjects, 7 tumor patients, for whom language areas were affected by the tumor). A functional geometry atlas was built from the control population. It captures the global connectivity structure that emerges during the cognitive task (anonym generation) while fMRI is acquired. For each subject we performed GLM analysis to detect activated areas. Subsequently a functional geometry map was built for the fMRI data of each tumor patient. Each map was matched to the atlas, and the activations in the control population were used to predict activation in the tumor patients. For comparison we conducted the same matching with an anatomical atlas (MNI). For this, we registered the anatomical T1 MRI data to a T1 MNI atlas template using FSL software. We compared the overlap between activated areas detected in the tumor patients, and the predicted activations. We used Dice score to quantify the overlap between predicted areas, and activated areas in the tumor patients.

#### RESULTS

The activation prediction based on the functional geometry atlas results in better overlap for all activated regions and activation p values smaller than 0.05. The average Dice score for functional matching is 0.1 to 0.2 higher than for anatomical mapping.

#### CONCLUSION

Mapping of functional networks across subjects based on the functional connectivity structure is feasible. The accuracy of matching functionally corresponding regions is higher compared to registration based on anatomy. This is particularly relevant in cases where substantial reorganization has occurred, such as in tumor patients. Future application of the method is the study of reorganization processes, and a support for the presurgical mapping of functional areas in tumor patients.

**KEY WORDS:** Functional geometry, functional networks

O-223

11:02 AM - 11:10 AM

#### Predicting Progression-Free Survival with Relative Cerebral Blood Volume in WHO Grade III Tumors

Mangla, R. Ekholm, S.

University of Rochester  
Rochester, NY

#### PURPOSE

We have studied the correlation between preoperative relative cerebral blood volume (rCBV) and prognosis of WHO grade III tumors. The hypothesis was that grade III tumors with high rCBV are more likely to behave as glioblastoma multiforme and would have a poor prognosis, whereas those with low rCBV are more likely to have favorable outcome, like low-grade glioma.

#### MATERIALS & METHODS

We have studied 34 patients (mean age = 39.6 years, 21 males and 13 females) who were diagnosed histopathologically as grade III anaplastic tumors and also had a preoperative MR perfusion scan. These include 20 cases of pure astrocytic tumor and 14 with oligodendroglial (OG) component. An increase in tumor size of 25 % on T1 contrast-enhanced images, or decline in the Karnofsky performance score were considered as progression.

#### RESULTS

For all grade III tumors (n = 34) mean rCBV was  $2.56 \pm 1.38$  with a progression-free survival (PFS) of  $492 \pm 397$  days. The mean rCBV of anaplastic astrocytomas (n = 20) was  $2.46 \pm 1.27$  with PFS  $453 \pm 361$  days. In contrast the mean rCBV of OG group (n = 14) was  $2.70 \pm 1.57$  with a PFS of  $946 \pm 556$  days. For grade III tumors as a group PFS was 1552.5 days ( $\pm 224.9$ ) when rCBV was 2.06 (p = .001). For the anaplastic astrocytomas PFS was  $851.6 \pm 171.1$  and  $301.3 \pm 74.4$  days, respectively (p < .00001 by log rank test). In the presence of an oligodendroglial component the PFS was  $1740.5 \pm 259.3$  and  $1422.6 \pm 306.4$  days comparing tumors with a high and low rCBV, respectively (p < .138 by Log Rank Mantel-Cox).

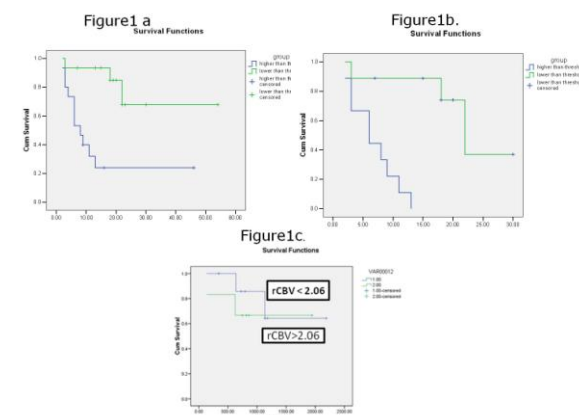


Figure 1a. Kaplan-Meier survival curves for all grade III tumors as a group, showed a difference in survival related to rCBV [ $\geq 2.06$  (blue) and  $< 2.06$  (green)].

Figure 1b. For astroglial tumors showed a difference in survival related to rCBV [ $\geq 2.06$  (blue) and  $< 2.06$  (green)].

Figure 1c. Survival curves tumors with oligodendroglial component no significant difference in survival [ $\geq 2.06$  (blue) and  $< 2.06$  (green)].

#### CONCLUSION

There was a strong correlation between rCBV and progression-free survival in pure astrocytic tumors. Within a single category of anaplastic astrocytomas those with higher rCBV had a worse prognosis than tumors with a low rCBV. Looking at grade III tumors overall, the rCBV had a significant but relatively weak correlation with regard to PFS. There was no significant correlation between rCBV and PFS in patients with grade III tumors containing an oligodendroglial component.

**KEY WORDS:** Glioma, cerebral blood volume, anaplastic astrocytoma

**O-224**

**11:10 AM - 11:18 AM**

# **Glioblastoma Multiforme Progression or Treatment-Related Pseudoprogression? A Direct Comparison of Common MR Imaging Diffusion and Perfusion Sequences at the Neuroradiology Clinical Workstation**

Whitlow, C. T.·Chan, M. D.·Wagner, J. S.·Sauer, R. N.·Lesser, G. J.·Bennett, M.·Tatter, S. B.·Ellis, T. L.·Paulsson, A. K.·Johnson, A. J.

Wake Forest University School of Medicine  
Winston-Salem, NC

## **PURPOSE**

In patients with glioblastoma multiforme (GBM) who are treated with concurrent radiation and temozolomide, differentiating between tumor progression and treatment-related pseudoprogression remains a challenge using MRI. The purpose of this pilot study was to conduct a direct comparison of dynamic-susceptibility contrast (DSC), pulsed arterial spin labeling (PASL) and diffusion-weighted imaging (DWI) for discriminating GBM progression from pseudoprogression, using a simple region of interest (ROI)-based analysis method amenable for use at the clinical workstation.

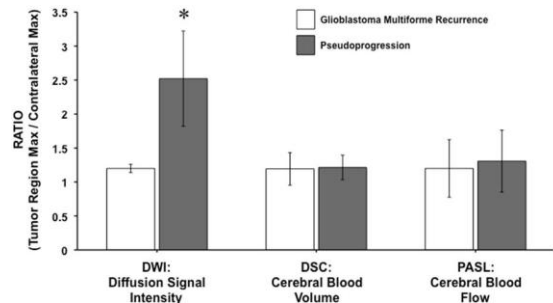
## **MATERIALS & METHODS**

In this HIPAA-compliant, IRB-approved case-control study, patients with clinically proven GBM progression (n = 15) or pseudoprogression (n = 14) and MRI examinations including diffusion-weighted imaging (DWI) (recurrence n = 14; pseudoprogression n = 13), DSC (progression n = 11; pseudoprogression n = 10), and/or PASL (recurrence n = 9; pseudoprogression n = 11) were identified retrospectively from a cancer center database. A circle ROI was placed manually to encompass the lesion on each sequence using Aquarius iNtuition (TeraRecon, San Mateo, CA), from which measures of maximum diffusion signal intensity (DSI), cerebral blood volume (CBV) and cerebral blood flow (CBF) were obtained, respectively. These data were normalized to maximum values obtained from a similar, contralateral, size-matched circle ROI, producing a dimensionless ratio of relative measures (rDSI, rCBV, rCBF). Serial t-tests were used to evaluate between-group demographic variables. Multivariate analysis of covariance (MANCOVA) controlling for between-group demographic differences then was conducted, with outcome (progression, pseudoprogression) as the independent variable and rDSI, rCBV and rCBF as dependent variables. Missing data for dependent variables were replaced with variable-associated means.

## **RESULTS**

Independent samples t-tests revealed no statistically significant difference between progression and pseudoprogression groups for age and total radiation dose. There was, however, a significant difference for

the time-interval from therapy completion to reference MRI, with a longer interval for the progression group [ $t(27) = 2.104$ ,  $p = .010$ ]. One-way between-groups MANCOVA controlling for the significant demographic variable revealed a significant between-group difference on the combined rDSI, rDSC, and rPASL dependent variable [ $F(3, 24) = 8.902$ ,  $p < .0005$ ; Wilks' Lambda = .473; partial eta squared = .527]. When results for the dependent variables were considered separately using a Bonferroni adjusted alpha level of .017, only the between-group difference for rDWI reached statistical significance [ $F(1, 26) = 16.469$ ,  $p < .0005$ ; partial eta squared = .559] (Figure).



## **CONCLUSION**

This combined analysis confirms findings of prior studies that have evaluated DWI, DSC and PASL on an individual basis, and further highlights the reproducible and robust ability of DWI to identify statistically significant differences between GBM progression and pseudoprogression, demonstrated in the present investigation using a simple method that can be performed at most neuroradiology clinical workstations.

**KEY WORDS:** Glioblastoma multiforme, pseudoprogression, pulsed arterial spin labeling

**O-225**

**11:18 AM - 11:26 AM**

# **Acute Alcohol Ingestion Significantly Affects Resting-State Networks and Induces Cerebellar Chemical Changes on Magnetic Resonance Spectroscopy**

Currie, S.<sup>1</sup>·Hadjivassiliou, M.<sup>2</sup>·Clark, M. R. J.<sup>1</sup>·Craven, I. J.<sup>1</sup>·Wilkinson, I. D.<sup>1</sup>·Griffiths, P. D.<sup>1</sup>·Hoggard, N.<sup>1</sup>

<sup>1</sup>Academic Unit of Radiology, Sheffield, UNITED KINGDOM, <sup>2</sup>Royal Hallamshire Hospital, Sheffield, UNITED KINGDOM

## **PURPOSE**

To establish possible changes in resting state network (RSN) connectivity and cerebellar spectroscopy following acute alcohol ingestion with a view to establishing a binge-drinking model.



## MATERIALS & METHODS

A 3 T single voxel MR spectroscopy (PRESS, TR = 2000 ms, TE = 144 ms) of the cerebellar hemisphere deep white matter and superior vermis and RS fMRI was performed on 10 healthy males (age  $26 \pm 4.8$  years; range 20-33) before and after ingestion of equivalent 31.56 g of ethanol (corresponding to 4 UK units: upper level of recommended daily limit, UK). All subjects were "social" drinkers with an average weekly alcohol consumption of  $179 \pm 83$  g (range 36-316).

MR imaging was performed prealcohol, immediately following alcohol and then at hourly intervals. End point was disappearance of alcohol peak at 1.3 parts per million on MR spectroscopy. Prior to each scan, all subjects had their percentage blood alcohol concentration (% BAC) measured using the breathalyzer AlcoSense™ Elite. To identify temporal differences in RSNs from pre to postalcohol states group comparison of RS fMRI data using multisubject independent component analysis (ICA) and dual regression (1) was performed with FSL (FMRIB Software Library). Temporal differences in area ratios of N-acetyl aspartate (NAA) and choline (Cho) referenced to creatine (Cr) were calculated using paired student t-test.

## RESULTS

MR spectroscopic alcohol peaks were detected in all subjects immediately following alcohol and disappeared at 4 hours postingestion, meaning that subjects were examined at 6 time points: pre, immediate, 1 hour, 2 hours, 3 hours and 4 hours postalcohol. Per cent of BAC peaked at 1 hour following alcohol ingestion then fell at subsequent intervals. Statistically significant temporal changes of RSNs are depicted in the Table and Figure. A significant increase in cerebellar NAA/Cr occurred from pre ( $0.96 \pm 0.04$ ) to 2 hours ( $0.99 \pm 0.03$ ) postalcohol consumption (CI 95%: 0.0457 to 0.0574;  $p = 0.026$ ). Conversely, Cho/Cr significantly fell from immediately ( $0.80 \pm 0.13$ ) to 4 hours ( $0.75 \pm 0.12$ ) after alcohol intake (CI 95%: 0.004 to 0.099;  $p = 0.037$ ).

Resting state networks that significantly intensify at time periods following alcohol ingestion.

	1hr post	2hr post	3hr post	4hr post
Pre-alcohol	Right Parietal-FrontalVisual	Right Parietal-FrontalLeft Parietal-FrontalVisualExtrastriatal Visual	Right Parietal-FrontalLeft Parietal-FrontalVisual	Left Parietal-Frontal

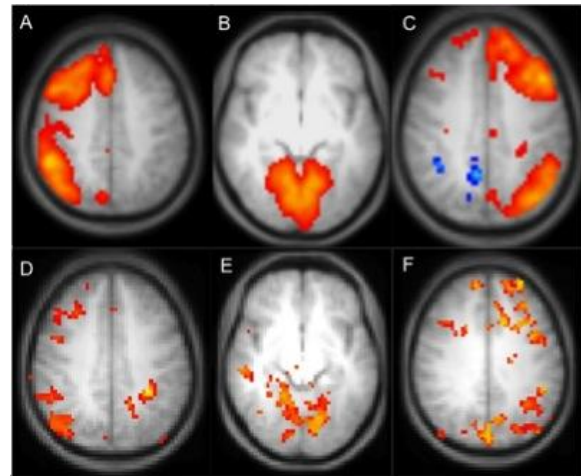


**Figure.** Alcohol significantly intensifies the functional connectivity of resting state networks (RSNs). Top row - identification of RSNs: A) Right parietal-frontal, B) Visual and C) Left parietal-frontal. Bottom row - corresponding statistically significant intensification of functional connectivity in the RSNs from pre-alcohol to 3h post-alcohol scan: D) Right parietal-frontal, E) Visual and, F) Left parietal-frontal.

## CONCLUSION

Single bolus alcohol ingestion significantly intensifies the functional connectivity of the visual and bilateral parietal-frontal networks and causes statistically significant alteration in cerebellar neurometabolites.

**KEY WORDS:** Alcohol, resting-state networks, functional imaging

O-226

11:26 AM - 11:34 AM

## Beyond the Tip of the Iceberg: Widespread pH Abnormalities Detected with $^{31}\text{P}$ -MR Spectroscopy in the Normal-Appearing Parenchyma of Patients with Cortical Malformations and Epilepsy

Andrade, C. S.<sup>1</sup>Otaduy, M. C. G.<sup>1</sup>Park, E. J.<sup>1</sup>Valente, K. D. R.<sup>1</sup>Tsunemi, M. H.<sup>2</sup>Leite, C. C.<sup>1</sup>

<sup>1</sup>Faculdade de Medicina da Universidade de Sao Paulo, Sao Paulo, BRAZIL, <sup>2</sup>Universidade Estadual Paulista Julio de Mesquita Filho, Botucatu, BRAZIL

## PURPOSE

The goal of this study was to evaluate the intracellular hydrogen-ion potential (pH) in the normal-appearing parenchyma (NAP) of patients with malformations of cortical development (MCD) and epilepsy.

## MATERIALS & METHODS

Three-dimensional phosphorus magnetic resonance spectroscopy ( $^{31}\text{P}$ -MRS) at 3.0 T was performed in 37 MCD patients and in 31 matched-control subjects. The patients were assigned into three main MCD subgroups: hemimegalencephaly/cortical dysplasia ( $n = 10$ ); heterotopia ( $n = 14$ ); schizencephaly/polymicrogyria ( $n = 13$ ). Voxels ( $12.5 \text{ cm}^3$ ) were selected in five homologous regions containing NAP: right putamen; left putamen; frontoparietal parasagittal cortex; right

centrum semiovale; and left centrum semiovale. Robust methods of quantification were applied, and the intracellular pH was calculated with the chemical shifts of inorganic phosphate (Pi) relative to phosphocreatine (PCr).

## RESULTS

In comparison to controls and assuming a p value < 0.05, MCD patients presented acidosis in the frontoparietal parasagittal cortex, right centrum semiovale, and left centrum semiovale (Table 1). Dunnet and Dunn tests demonstrated that the differences in pH values remained statistically significant in all MCD subgroups (Figure 1).

Table 1 - Comparisons of pH values between MCD patients and control subjects in five cerebral regions with normal appearing parenchyma

Region	Patients		Controls		p-value
	Mean	SD	Mean	SD	
Right putamen	6.914	0.033	7.007	0.046	p = 0.621
Left putamen	7.011	0.040	6.995	0.043	p = 0.170
Frontoparietal parasagittal cortex	6.985	0.022	7.087	0.048	p < 0.001*
Right centrum semiovale	7.004	0.029	7.096	0.042	p < 0.001
Left centrum semiovale	6.995	0.030	7.088	0.045	p < 0.001

Note: \*p-value obtained with Mann-Whitney test, other p-values obtained with Student's t test. p-values < 0.05 are printed in bold type. pH = hydrogen-ion potential, SD = standard deviation.

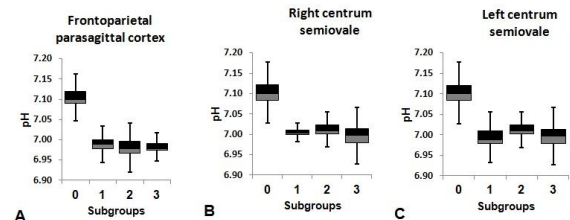


Figure 1: Box-plot graphics. Comparisons of mean hydrogen-ion potential (pH) values in the normal appearing parenchyma in the following regions: A) Frontoparietal parasagittal cortex, B) Right centrum semiovale, C) Left centrum semiovale. 0 = control-group; 1 = hemimegalencephaly or cortical dysplasia; 2 = heterotopia; 3 = schizencephaly or polymicrogyria. In all these regions, Dunnet and Dunn tests demonstrated statistically significant differences (p < 0.05) between the MCD subgroups compared to the control-group.

## CONCLUSION

There is a large body of evidence pointing to neurometabolic disturbances as key factors in epileptogenesis. Intracellular pH is an important parameter of brain bioenergetics and electrophysiologic status in neurons and glia. We recently have demonstrated pH disturbances in MCD lesions, but, to our knowledge, there are no <sup>31</sup>P-MRS studies in the evaluation of the NAP in MCD patients heretofore. The present study demonstrates widespread acidosis in the NAP, and reinforces the idea that MCD visible lesions are only the tip of the iceberg. This issue may be of particular importance in patients who are candidates for lesion resection. The NAP could be a secondary target for medical interventions, and understanding the biochemical abnormalities that occur beyond the visible lesions may facilitate this approach.

**KEY WORDS:** Phosphorus spectroscopy, epilepsy, malformations of cortical development

O-227

11:34 AM - 11:42 AM

### Arterial Spin Labeling Perfusion at 3 T in Mild Cognitive Impairment Enriched for Vascular Risk Factors

Aguilera, A. Singh, M. Law, M. Hajjar, I. Chui, H.

University of Southern California  
Los Angeles, CA

#### PURPOSE

To compare cerebral blood flow in subjects with mild cognitive impairment to elderly normal controls using arterial spin labeling MR perfusion at 3 T, in a sample enriched for vascular risk factors.

#### MATERIALS & METHODS

Sixteen subjects enrolled in the National Institute on Aging funded Aging Brain program project (10 females and 6 males, median age 76.6 years, range 69-91 years) underwent arterial spin MR perfusion at 3 T. Based on the subject's clinical dementia rating scale (CDR), Framingham cardiovascular risk profile (FCRP) and history of prior stroke or myocardial infarction, the subjects were stratified into three groups: 1. No cognitive impairment (n = 9), 2. Mild cognitive impairment with high vascular risk (n = 4) and 3. Mild cognitive impairment with low vascular risk (n = 3). We determined the cerebral perfusion in 38 regions of interest and compared the results between the three groups.

#### RESULTS

When comparing the normal aging subjects (group 1) and those with cognitive impairment (groups 2 and 3 combined) there was a significant reduction in CBF in the parietal peri-trigonal white matter ( $p < 0.05$ ). In comparisons between groups 1 and 3, a significant reduction in cerebral blood flow (CBF) was found in the posterior cingulate gyrus and parietal peri-trigonal white matter ( $p \leq 0.05$ ). No significant differences were found between groups 2 and 3, but the sample sizes were very small.

#### CONCLUSION

Arterial spin labeling MR perfusion can be a useful tool for characterizing regional decreases in cerebral blood flow in mild cognitive impairment. In a sample enriched for vascular risk factors, reductions were found in the parietal white matter. This region represents a vascular border zone and is known to be susceptible to the development of white matter hyperintensities.

**KEY WORDS:** Dementia, arterial spin labeling, perfusion

O-228

11:42 AM - 11:50 AM

### Using Arterial Spin Labeling-Derived Bolus Arrival Time to Demonstrate a Novel Compensatory Cerebrovascular Autoregulatory Mechanism during Two Normotensive Hypovolemic Stimuli

Cain, J. R.<sup>1</sup> Thompson, G.<sup>1</sup> Beards, S.<sup>2</sup> Parkes, L. M.<sup>1</sup> Jackson, A.<sup>1</sup>

<sup>1</sup>University of Manchester, Manchester, UNITED KINGDOM, <sup>2</sup>University Hospital of South Manchester, Manchester, UNITED KINGDOM

#### PURPOSE

Classical cerebrovascular autoregulation maintains cerebral blood flow (CBF) during fluctuations in cerebral perfusion pressure. Stimuli which decrease blood volume while blood pressure is maintained are normotensive hypovolemic challenges. This study was designed to investigate the cerebroautoregulatory changes seen during these stimuli and identify potential imaging biomarkers of cerebral autoregulation in normal subjects.

#### MATERIALS & METHODS

Twenty-two healthy volunteers (20-31 years old) underwent MRI (3.0 T Philips Achieva). Imaging included full brain arterial spin labeling (ASL) [measuring tissue perfusion and bolus arrival time (BAT)] and quantitative phase contrast angiography (PCA), measuring total blood inflow from internal carotid and basilar arteries at rest and during stimulation. Heart rate and blood pressure were measured during the experiments. In 11 subjects decreases in cardiac output were induced using a MRI compatible lower body negative pressure (LBNP) chamber (-20 mm Hg), the subjects' legs and lower torso were inside the chamber. In 11 subjects gases were delivered using a closed anesthetic gas circuit. Subjects were given the following gases for approximately 15 min: 100% O<sub>2</sub>, medical air and carbogen gas (95% O<sub>2</sub>, 5% CO<sub>2</sub>) delivered at a rate of 15L/min. Arterial spin labeling images were analyzed assuming a single blood compartment model. Control and labeled images were subtracted and a two-parameter fit for BAT and perfusion was performed on a voxel-by-voxel basis for gray matter. Phase contrast angiography data were analyzed using noncommercial software.

#### RESULTS

During LBNP heart rate increased ( $P=0.001$ ) but blood pressure was unaffected. During carbogen and O<sub>2</sub> there was no change in heart rate or blood pressure. Phase contrast angiography results showed a decrease in blood inflow to the brain during LBNP ( $p = 0.01$ ) compared to control but there was no difference in gray matter perfusion values between control and -20 mm Hg LBNP. However the BAT was significantly longer during LBNP than rest ( $p = 0.002$ ). Carbogen caused increases in blood inflow and O<sub>2</sub> decreases compared to air measured using PCA Bolus arrival time reductions occurred during O<sub>2</sub> inhalation ( $p < 0.001$ ), increases in

both perfusion and BAT during occurred carbogen administration ( $P < 0.001$ ) compared to air.

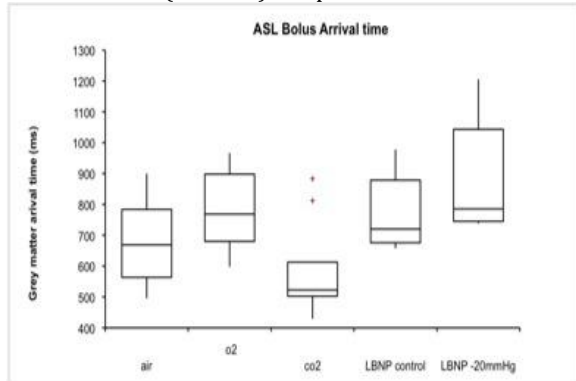


Figure: Box plot of bolus arrival time for each gas and before and during -20mmHg LBNP.

#### CONCLUSION

Stimuli that produce normotensive hypovolemic challenges (LBNP) or vasoconstrictory gases (O<sub>2</sub>) cause reductions in blood inflow, which is compensated in gray matter by an as yet unknown mechanism. This can be detected by the prolongation of BAT induced by these stimuli. There may be an underlying steal from white matter in order to maintain gray matter perfusion but resulting in a delay in blood arrival. Bolus arrival time provides a possible biomarker for autoregulatory studies.

**KEY WORDS:** Autoregulation, ASL, cerebral blood flow

O-229

11:50 AM - 11:58 AM

#### Extratemporal Abnormalities in Phosphorus MR Spectroscopy in Patients with Mesial Temporal Sclerosis

Park, E.·Lyra, K. P.·Andrade, C. S.·Castro, L. H. M.·Otaduy, M. C. G.·Leite, C. C.

São Paulo University  
Sao Paulo, BRAZIL

#### PURPOSE

<sup>31</sup>P MRS is a noninvasive method that allows measurement of several phosphorus metabolites related to energetic state and membrane composition. The aim of this study was to determine extratemporal metabolic changes by <sup>31</sup>P MRS in patients with mesial temporal sclerosis (MTS).

#### MATERIALS & METHODS

Three-dimensional <sup>31</sup>P MRS of 33 patients and 31 sex- and age-matched controls were performed on Intera Achieva 3.0 T system (Philips, Best, The Netherlands) using a double-tuned <sup>31</sup>P/<sup>1</sup>H head coil (AIRI, Cleveland, USA). All patients were diagnosed with unilateral MTS by conventional MRI and were seizure-free for at least 24 hours. Three-dimensional axial T1-weighted images also were acquired for the purpose of localization. Care was taken to position the three-dimensional MRS grid (six slices of 6 x 7) in the same way on all patients, with individual voxels of 30x30x20 mm. The voxels selected

for analysis were located in the anterior capsuloinular region (ACIR), posterior capsuloinular region (PCIR) and in the frontal region (FR). The location was considered ipsilateral or contralateral to the MTS. The <sup>31</sup>P MRS sequence was a pulse-acquire sequence with TE/TR = 0.31 ms/5093 ms, using an adiabatic pulse. Spectra processing and quantification was performed using the jMRUI software with the AMARES algorithm. Relative values of each metabolite divided by the sum of all metabolites (phosphodiesteres-PDE, phosphomonoesters-PME, inorganic phosphate - Pi, phosphocreatine-PCr, γ-, α-, β- adenosine triphosphate-ATP), as well as the PCr/ATP, PCr/Pi and ATP/Pi ratios and pH of patients and controls were obtained. T test was used to compare the differences between both groups and a p value less than 0.05 was considered statistically significant.

#### RESULTS

Compared to average values of controls, the following metabolites were significantly different, according to location: ipsilateral ACIR reduction of Pi (0.081 in patients, 0.089 in controls,  $p = 0.009$ ) and PCr/γ-ATP (1.966 in patients, 2.146 in controls,  $p = 0.027$ ), contralateral ACIR reduction of Pi (0.082 in patients, 0.089 in controls,  $p = 0.013$ ), increase of ATP (0.298 in patients, 0.286 in controls,  $p = 0.026$ ), ipsilateral PCIR reduction of Pi (0.077 in patients, 0.083 in controls,  $p = 0.009$ ) and PCr/γ-ATP (0.249 in patients, 0.286 in controls,  $p = 0.017$ ), increase of γ-ATP (0.098 in patients, 0.093 in controls,  $p = 0.024$ ), contralateral FR reduction of Pi (0.087 in patients, 0.093 in controls,  $p = 0.014$ ).

#### CONCLUSION

We found energetic dysfunction in the capsuloinular and frontal regions of patients with MTS, for both sides, ipsi and contralateral hemispheres. No changes in the metabolites related to membrane composition or pH were found. Previously, one study showed decreased PCr/γ-ATP ratio in the ipsilateral parietal lobe compared to controls. Our findings suggest that energetic dysfunction happens diffusely in the brain of patients with MTS, similar to what was shown in PET studies.

**KEY WORDS:** Neurometabolism, epilepsy, phosphorus spectroscopy



## Tuesday Morning

10:30 AM - 12:00 PM

Beekman/Sutton North

(27c) Adult Brain: Vascular,  
Intracranial

O-230

10:30 AM - 10:38 AM

### Ten-Year Experience of MDCT Angiography and the Detection of Brain Aneurysms: Is It Time to Go Straight to Aneurysm Repair or Conventional Angiogram?

Heit, J. J.·Sabbag, D.·Gonzalez, R. G.·Schaefer, P. W.·Hirsch, J. A.·Romero, J. M.

Massachusetts General Hospital  
Boston, MA

#### PURPOSE

Subarachnoid hemorrhage secondary to intracranial aneurysm (IA) rupture is a significant cause of morbidity and mortality. Two to three per cent of the population harbors an IA (ISUIA Trial, 1998; Rinkel et al., 1998), so the majority of IAs never rupture. Estimates of IA prevalence, distribution, and size are guided largely by studies that characterize IAs by conventional angiography and autopsy. CT angiography (CTA) is used increasingly for the evaluation of intracranial hemorrhage and other clinical concerns. There are few large studies describing IA characteristics in CTA patient populations, and existing studies have focused on patient populations undergoing CTA for specific indications, such as evaluation of carotid stenosis (Heman et al., 2009) or ischemic stroke (Oh et al., 2008). Here we describe the frequency, distribution, size, and incidence of IAs and IA rupture in a population undergoing CTA at a large referral center over a 10-year period.

#### MATERIALS & METHODS

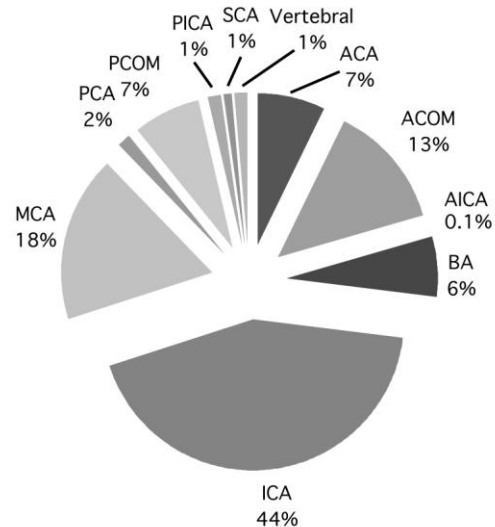
Our study was approved by the hospital's Institutional Review Board. We performed a review of all patients undergoing CTAs of the head from January 2000 to December 2010 at Massachusetts General Hospital with evidence of IA. Studies identifying an IA then were evaluated further for IA size, location, distribution, and the presence of associated intracranial hemorrhage. Patient records were reviewed for demographic information. Statistical analysis was performed using the SAS 9.1 software (SAS Institute Inc., Cary, NC).

#### RESULTS

Twenty-nine thousand three CTAs were identified, and IAs were identified in 2,933 patients (10%). Multiple IAs were identified in 544 patients (19%). IA distribution is summarized in the Figure. Intracranial aneurysm size was variable (1-35 mm). Large (>7 mm) IAs were most likely to occur at the anterior

communicating artery or at branches of the internal carotid artery (ICA). Larger (>7mm) IAs were associated more frequently with intracranial hemorrhage at presentation. Intracranial hemorrhage was present in 717 patients with an IA (24%). Aneurysm rupture was the cause of intracranial hemorrhage in 167 patients (6%). Incidental IAs were identified in 550 (19%) patients with intracranial hemorrhage. Seventy percent of IAs were identified in females and 30% were identified in males ( $p<0.001$ ).

### Aneurysm Distribution



#### CONCLUSION

These data represent the largest IA series published to date. The prevalence and frequency of incidental IAs was significantly higher than previously published reports. The distribution of IAs differed from prior studies (Schievink, 1997), with the ICA being the most common location (43%). Seventy-one percent of IAs were identified in females, higher percentage than published data.

**KEY WORDS:** Aneurysm, intracranial hemorrhage, epidemiology

O-231

10:38 AM - 10:46 AM

### Use of CT Perfusion for the Diagnosis of Vasospasm following Subarachnoid Hemorrhage: Which Combination of Perfusion Parameters Represents the Minimum Data Set?

Thomas, O. M.·Das, T.·Young, V. E.·Krishnan, A.·Sheikh-Bahaei, N.·Scoffings, D. J.·Bulters, D. O.·Gillard, J. H.

Addenbrooke's Hospital  
Cambridge, UNITED KINGDOM

#### PURPOSE

Although the use of CT perfusion (CTP) in the diagnosis of ischemic stroke has been the subject of extensive investigation, much less is known about the utility of

CTP following aneurysmal SAH-related delayed cerebral ischemia/vasospasm. We performed a receiver operating characteristic (ROC) analysis to find the most informative perfusion parameters, and to find the smallest possible combination of these parameters that was as informative as the data set as a whole.

#### Materials & Methods

We prospectively recruited 100 patients presenting with subarachnoid hemorrhage (SAH) over a 13-month period. Extended-coverage CTP (z-axis 100 mm) was performed on a Siemens Somatom Definition Flash on day 1, on day 3-10, and as clinically indicated. Of these patients, 21 were diagnosed with vasospasm jointly on clinical and radiologic grounds. A conventional deconvolution approach (syngo Volume Perfusion CT-Neuro) was used to derive the perfusion parameter maps [cerebral blood flow (CBF); cerebral blood volume (CBV); mean transit time (MTT); time to start (TTS); time to peak (TTP) and time to drain TTD]]. Volumetric regions of interest in areas of vasospasm and contralateral control regions were compared using an intra-subject ROC analysis, with area under curve (AUC) values calculated for each perfusion parameter. For each patient the maximum AUC value was calculated for every possible set of parameter maps, with set sizes ranging from 1 to 6 (all possible maps). The smallest set of maps with an AUC statistically indistinguishable from the maximum possible (i.e., an analysis of all six maps) was defined as the "minimum data set".

#### RESULTS

1) Individually, the TTD, TTP and TTS were the most informative parameters (median AUC: 0.852, 0.836 and 0.833 respectively; not significantly different, Wilcoxon ranksum). The MTT, CBF, and CBV were significantly less informative (AUC values 0.712, 0.741 and 0.573 respectively; all significantly lower than the TTD, TTP and TTS maps,  $P < 0.05$ , Wilcoxon ranksum). 2) The combination of the TTP and CBF parameter maps provided a minimum data set, (i.e., the AUC value (0.871) was statistically indistinguishable from an analysis of all six maps (0.890; Signtest,  $P = 1.000$ ). This is the only two-membered combination of parameter maps for which this was the case. Eight three-membered combinations of parameter maps were also statistically indistinguishable from an analysis of all six maps.

#### CONCLUSION

This combination of results indicates a high degree of mathematical redundancy between the maps. Strikingly, a pair of parameter maps carries almost as much information as the full complement of six.

**KEY WORDS:** Vasospasm, subarachnoid hemorrhage, CT perfusion

O-232

10:46 AM - 10:54 AM

### Hematoma Expansion and Intraventricular Perforation Is Predicted by CT Angiography Spot Sign and Postcontrast Leakage for Acute Intracerebral Hemorrhage

Tsukabe, A. Watanabe, Y. Tanaka, H. Nishizawa, M. Kunitomi, Y. Yoshiya, K. Tomiyama, N.

Osaka University Graduate School of Medicine  
Suita City, Osaka Prefecture, JAPAN

#### PURPOSE

Morbidity and mortality in spontaneous intracerebral hematoma (ICH) are correlated with hematoma expansion and intraventricular hemorrhage. The presence of computed tomography angiography (CTA) spot sign and postcontrast CT (PC CT) leakage (PCL) have been reported to be correlated with hematoma expansion. But previous studies have not taken into account the presence of intraventricular hemorrhage for hematoma progression. The purpose of this study is to elucidate whether CTA spot sign and PCL can predict hematoma progression more accurately if newly occurred intraventricular hemorrhage is defined as hematoma progression in addition to hematoma volume.

#### MATERIALS & METHODS

All patients with primary ICH who underwent CTA and PC CT within 6 hours of symptom onset, as well as follow-up noncontrast CT (NC CT) before discharge or death between January 2009 and August 2011 were recruited. All CT examinations were performed with 64 detector CT scanner. CT angiography studies were obtained using automatic triggering technique with 100 cc contrast media (300 mgI/ml), injection rate of 4 cc/sec. Postcontrast CT was obtained 120 seconds after contrast injection. One neuroradiologist reviewed admission and follow-up NC CT for measuring hematoma volume using ABC/2 method and determined the presence of intraventricular hemorrhage. He also reviewed CTA for spot sign and PC CT for PCL in another session. Predictive values of these two signs for hematoma progression were analyzed statistically respectively in two different definitions. Definition 1): Hematoma progression is defined as volume increase of hematoma size  $>20\%$  or  $>6$  mL. Definition 2): Hematoma progression is defined as hematoma volume increase as definition 1 or newly occurred intraventricular perforation regardless of volume change.

#### RESULTS

Twenty-six patients were recruited. The number of patients, whose hematoma size did not change, whose hematoma size increased, whose hematoma newly perforated into ventricle on follow-up NC CT was 19, 7, 6, respectively. Table shows sensitivity, specificity, positive predictive value (PPV), negative predictive value (NPV), accuracy for hematoma progression of CTA spot sign and PCL in two different definitions. In definition 2, both signs have better sensitivity, specificity, PPV and accuracy. Postcontrast leakage was

associated with higher likelihood for hematoma progression (in definition 1:  $p = 0.03$ , in definition 2:  $p < 0.01$ , Fisher's exact test).

		sensitivity	specificity	PPV	NPV	accuracy
CT A spot sign	definition 1	28.6%	73.7%	28.6%	73.7%	61.5%
	definition 2	41.7%	85.7%	71.4%	63.2%	65.4%
PCL	definition 1	100%	47.4%	41.2%	100%	61.5%
	definition 2	100%	64.3%	70.6%	100%	80.7%

#### CONCLUSION

CT angiography spot sign and PCL can predict hematoma progression more accurately if newly occurred intraventricular hemorrhage is defined as hematoma progression in addition to hematoma volume. Intraventricular hemorrhage is an important factor associated with hematoma progression.

**KEY WORDS:** Intracerebral hemorrhage, CT angiography spot sign, stroke

O-233

10:54 AM - 11:02 AM

#### Utility of CT Angiography in Primary Angiitis of the Central Nervous System

Johnson, J. M. • Franceschi, A. M. • Yoo, A. J. • Romero, J. M.

Massachusetts General Hospital  
Boston, MA

#### PURPOSE

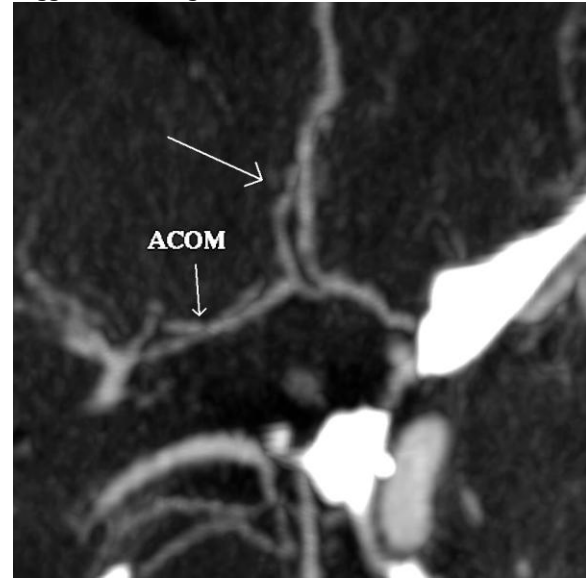
Primary angiitis (PA) of the central nervous system is a rare and poorly understood disease characterized by multifocal segmental inflammation of the small and medium vessels of the central nervous system (CNS), without signs of systemic or secondary vasculitis. Digital subtraction cerebral angiography (DSA) and brain biopsy typically are considered the "gold" standard diagnostic studies but are invasive procedures and in many reports have nonideal sensitivities of approximately 70%. Despite its noninvasive nature, ability for rapid acquisition and ready available, CT angiography (CTA) is traditionally not considered in the evaluation of suspected PACNS. We sought to evaluate the yield of CTA in a series of clinically definite cases of PACNS.

#### MATERIALS & METHODS

A retrospective database search was performed for cases between 2003 and 2011 with a clinical discharge diagnosis of CNS vasculitis and an evaluation with CT angiography of the head. Associated diagnostic imaging studies were also reviewed including MRI/MRA of the brain and DSA. Studies were reviewed for findings suggestive of vasculitis including multifocal narrowing in at least two vessels. Sensitivity analyses were performed for CTA and DSA using the final clinical diagnosis as the "gold" standard.

#### RESULTS

Twenty-one patients were identified with clinically definite PACNS and a CTA evaluation. Mean age was  $43.3 \pm 14.8$  years (age range: 15-70), and 57.1% of patients were female. Of our patients, 15/21 (71.4%) had CTA findings typical for CNS vasculitis including multifocal narrowing in multiple vascular distributions. This compares to 11/14 (78.6%) patients who had findings typical for CNS vasculitis on DSA. Fourteen patients had both CTA and DSA. Of these 9/14 (64.3%) were positive for vasculitis on both studies. All patients (9/9) with CTA findings of CNS vasculitis also had suggestive findings on DSA.



#### CONCLUSION

In this small group of clinically definite cases of PACNS, all patients with CTA findings suggestive of vasculitis were also positive for DSA findings suggestive of vasculitis. The diagnostic yield of CTA is similar to our experience and the published experience with DSA. Considering the high positive predictive value of CTA for a positive DSA, the risk associated with DSA may not be justified.

**KEY WORDS:** CT angiography, vasculitis, accuracy

O-234

11:02 AM - 11:10 AM

#### CT Perfusion Evaluation after Extracranial Bypass Surgery

Vos, P. C. • Smit, E. J. • Riordan, A. • Dankbaar, J. W.

University Medical Center Utrecht  
Utrecht, NETHERLANDS

#### PURPOSE

Extracranial bypass surgery is used to treat conditions like moyamoya disease, internal carotid artery occlusion or otherwise untreatable intracranial aneurysms. Postoperative evaluation of bypass patency on CT angiography (CTA) can be challenging due to small lumen size and artifacts from surgical clips. Small bypass lumen or bypass occlusion may result in hypoperfusion and thereby infarction. CT perfusion

(CTP) measurements therefore may have additional value over CTA. Altered hemodynamics and thereby contrast arrival time, in the area fed by the bypass can influence perfusion measurement. Perfusion algorithms that are delay sensitive may display incorrectly lower underestimated perfusion values, thereby causing unnecessary concern. The purpose of this study is to compare different perfusion algorithms in patients after extracranial bypass surgery and look at the differences in postoperative perfusion values between patients with and without infarction on follow-up imaging.

#### **MATERIALS & METHODS**

We retrospectively identified all patients that were treated between May 2007 and May 2011 at our institution with extracranial bypass surgery for moyamoya disease, internal carotid artery disease or otherwise untreatable intracranial aneurysms. Inclusion criteria were: age > 18, CTP and CTA imaging within 5 days after surgery, imaging follow up > 6 days after postoperative imaging. Data were collected on gender, age and surgery indication. The postoperative CTA was evaluated for bypass patency. CT perfusion images were analyzed with a tracer delay insensitive (bSVD) and a delay sensitive (sSVD) algorithm using the perfusion mismatch analyzer developed by ASIST, Japan. Quantitative perfusion values were measured in regions of interest in the middle cerebral artery flow territory cortex of both hemispheres, and compared between the two algorithms using a paired t-test. Presence of a new infarct in the treated hemisphere was evaluated on follow-up imaging. Differences in CTP values from the two different algorithms were compared between patients with and without infarction on follow up using an independent samples t-test.

#### **RESULTS**

Sixteen patients matched our inclusion criteria (median age 54 years (30-78); six men vs 10 women; three moyamoya disease, 10 aneurysm, three internal carotid artery disease. Two patients showed bypass occlusion. Six patients had new infarcts in the treated hemisphere on imaging follow up. In the treated hemisphere CBF was significantly lower when measured with sSVD compared to bSVD (median: 45.4 vs 61.3,  $p < 0.01$ ), MTT longer (8.2 vs 7.9  $p = 0.05$ ), and CBV lower (5.6 vs 6.7,  $p < 0.01$ ). In the untreated hemisphere similar differences were found for CBF and CBV, no significant difference was found for MTT. In patients that had an infarct on follow up compared to no infarct, MTT in the treated hemisphere was significantly longer when calculated with bSVD (8.49 vs 7.57,  $p = 0.039$ ). No significant difference in perfusion values could be found using sSVD.

#### **CONCLUSION**

In patients with extracranial bypass surgery a delay sensitive perfusion algorithm shows less favorable cerebral perfusion values than a delay insensitive algorithm. This confirms the fact that values calculated with sSVD underestimate CBF. With bSVD, and not with sSVD, a significant difference in MTT was found between patients that show infarction on follow up and patients without infarction.

**KEY WORDS:** Extracranial bypass, CT perfusion

**O-235**

**11:10 AM - 11:18 AM**

### **3C Score: Deriving Optimal CT-Based Imaging Characteristics for Predicting Clinical Outcome in Acute Ischemic Strokes with Proximal Occlusions**

Menon, B. K.<sup>1</sup>•Mayank, D.<sup>2</sup>•Smith, E. E.<sup>1</sup>•Modi, J.<sup>1</sup>•Sohn, S.<sup>3</sup>•Demchuk, A. M.<sup>1</sup>

<sup>1</sup>University of Calgary, Calgary, AB, CANADA, <sup>2</sup>Webber Academy, Calgary, AB, CANADA, <sup>3</sup>Keimyung University, Daegu, KOREA, REPUBLIC OF

#### **PURPOSE**

To derive a CT angiography-based imaging score based on extent of ischemic core, leptomeningeal collaterals and clot burden and determine its ability to discriminate clinical outcomes with or without therapy.

#### **MATERIALS & METHODS**

This was a study of patients with acute ischemic stroke and M1 MCA+/-intracranial ICA occlusions. Clot burden score is a 10-point score assessing extent of clot in the anterior circulation and the rLMC score is a 20-point collateral score based on scoring pial and lenticulostriate arteries in the anterior circulation. Good clinical outcome was defined as modified Rankin Score  $\leq 2$  at 90 days. Based on prior studies we have identified three characteristics based on CT imaging that are predictive of good outcome independent of age and initial NIHSS: CTASI, clot burden score and leptomeningeal collateral score. The 3C score (range 0-6) comprises three imaging measurements at baseline: 1.CTA-SI ASPECTS categorized as (0-4 = 0 points, 5-7 = 1, 8-10 = 2) 2.Collaterals (rLMC score 0-10 = 0, 11-16 = 1, 17-20 = 2) and 3. Clot burden (CBS 0-5 = 0, 6-7 = 1, 8-10 = 2). Primary measure of discrimination of clinical outcome was the c statistic.

#### **RESULTS**

The derivation cohort had 133 patients (mean age 66 years, median NIHSS 16). The c statistic for the 3C score was 0.75, indicating moderate to good discrimination of good outcomes. By comparison, the c statistic for NCCT ASPECTS was 0.62 and for CTA-SI ASPECTS was 0.66, and for a multivariable model containing age and NIHSS was 0.67. The relationship between 3C score and the probability of good outcome was similar across all treatment categories.

#### **CONCLUSION**

The 3C score combines information on extent of core, leptomeningeal collaterals and thrombus burden using CTA in patients with acute ischemic strokes caused by MCA occlusion. It is better at discriminating the chance of a good clinical outcome than NCCT, CTA-SI ASPECTS or the combination of age and NIHSS. We are now validating this score in a validation cohort of 225 patients from the prospectively collected Keimyung Stroke registry and will present the results at the meeting.

**KEY WORDS:** Ischemic stroke, CT, clinical outcome



O-236

11:18 AM - 11:26 AM

### Assessment of Cerebral Venous Thrombosis with Noncontrast Computed Tomography Using Corrected Hounsfield Unit Attenuation Values

Besachio, D. A.<sup>1</sup>Quigley, E. P.<sup>1</sup>Shah, L. M.<sup>1</sup>Salzman, K. L.

University of Utah  
Salt Lake City, UT

#### PURPOSE

Cerebral venous thrombosis is an uncommon, but potentially life-threatening condition with a variety of nonspecific clinical manifestations. Recent research has suggested that cerebral venous thrombosis may be predicted successfully through the use of Hounsfield unit (HU) attenuation values on noncontrast computed tomography (CT) scans while correcting for patient hematocrit values at the time of imaging through use of a hematocrit-Hounsfield ratio (H:H). The purpose of this study is to evaluate noncontrast CT examinations of the head in patients with known cerebral venous thrombosis as well as those without thrombosis and to determine if any reliable relationship exists between venous thrombosis, absolute noncontrast Hounsfield unit attenuation in the affected cerebral sinus or vein, and patient hematocrit.

#### MATERIALS & METHODS

Following institutional review board approval, a retrospective review of noncontrast head CTs performed on 18 patients with confirmed cerebral venous or dural sinus thrombosis and 18 patients without thrombosis were evaluated independently by three neuroradiologists. Maximum HU attenuation values in regions of known thrombosis were recorded with similarly placed measurements in normal control patients. Thirteen patients in each group had hematocrit levels drawn at the time of CT examination allowing for the calculation of an H:H.

#### RESULTS

The mean hematocrit between the two groups was not significantly different (39.0 and 39.4, respectively). The mean HU value for a thrombosed sinus was 69. The mean HU value for a nonthrombosed sinus was 51. There was some degree of overlap between the two groups. In cases of proven thrombosis, the mean HU values ranged from 57-83. Nonthrombosed mean HU values ranged from 32-63. Similarly, H:H demonstrated some overlap between cases of thrombosis and nonthrombosis. However, we found this overlap to be within a narrow range, with all thrombosis patients demonstrating an H:H of 1.4 or greater. Ninety-two per cent (12/13) of nonthrombosis cases were found to have an H:H of less than 1.5.

#### CONCLUSION

Our data suggests that high noncontrast HU values within a cerebral sinus or vein with elevated H:H may represent a simple, quantitative measure in determining the presence of cerebral venous thrombosis in noncontrast CT evaluation.

**KEY WORDS:** Venous, thrombosis, Hounsfield

O-237

11:26 AM - 11:34 AM

### T1 Gadolinium Enhancement of Intracranial Atherosclerotic Plaques Associated with Symptomatic Stenoses

Vakil, P.<sup>1</sup>Habib, A.<sup>2</sup>Vranic, J. E.<sup>2</sup>Korutz, A.<sup>2</sup>Hurley, M. C.<sup>2</sup>Shaibani, A.<sup>2</sup>Carroll, T. J.<sup>2</sup>Ansari, S. A.<sup>2</sup>

<sup>1</sup>Northwestern University, Chicago, IL, <sup>2</sup>Northwestern University Feinberg School of Medicine, Chicago, IL

#### PURPOSE

Inflammation in atherosclerotic plaques locally alters vascular endothelium permeability, allowing gadolinium (Gd) contrast uptake and visualization on T1-weighted MR imaging. Atherosclerotic plaque enhancement in the cervical carotid arteries has been correlated with a higher incidence of stroke. However, only a paucity of research has examined this relationship within the intracranial vasculature. We studied the relationship between intracranial plaque enhancement and acute symptomatic presentations of intracranial atherosclerotic disease.

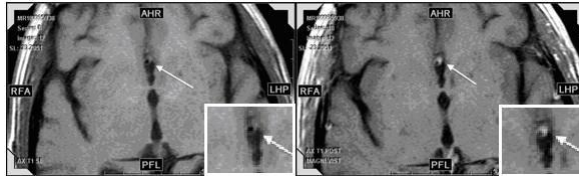
#### MATERIALS & METHODS

Using our institution's PACS and medical record databases, we retrospectively identified and analyzed 11 patients with high-grade atherosclerotic plaques (>70% stenosis) within the proximal intracranial vasculature (supraclinoid ICA, A1-A2 ACA, M1-M2 MCA, vertebral-basilar, P1-P2 PCA) that met inclusion criteria: 1) MRI/MRA 3D time-of-flight (TOF) imaging at time of diagnosis or symptomatic presentation and 2) visualization of intracranial plaques in vessels perpendicular to the imaging plane to minimize partial-volume averaging. Plaques were classified as asymptomatic or symptomatic if they induced acute physiologic symptoms (as determined by neurologic exam on presentation) and/or demonstrated DWI positive infarcts in the vascular distribution of the stenosed vessel. Two neuroradiologists conducted independent and blinded evaluation of each intracranial plaque using axial 3D TOF and T1 spin-echo imaging (pre and postcontrast injection) acquired as part of the initial neurovascular MR imaging evaluation. Scoring was performed on a five point scale (1-5) and results were subgrouped based on the probability of plaque enhancement (1-2 unlikely to be enhancing, 3 equivocal, 4-5 likely to be enhancing). Contralateral nonstenotic vessels served as internal controls.

#### RESULTS

In 11 patients, eight symptomatic and three asymptomatic intracranial plaques were subgrouped. In addition, seven intracranial plaques were scored as intermediate to highly enhancing (score of 4-5) and four plaques were scored as likely nonenhancing (score of 1-2). We found that six of seven (86%) enhancing plaques versus two of four (50%) nonenhancing plaques were symptomatic. We observed no associated vessel enhancement in the contralateral control symptomatic vessels. Figure 1a-b depicts pre and postcontrast T1 SE

images of a typical plaque that was scored as highly enhancing (score 5) and symptomatic involving the A2 ACA segment.



#### CONCLUSION

Our preliminary study demonstrates that T1 Gd-enhancing plaques may be an indicator of progressing or symptomatic intracranial atherosclerotic disease. We report an association between intracranial plaque enhancement and incidence of acute symptoms from severe intracranial stenoses. Our findings suggest that acute inflammation of intracranial stenoses may exacerbate luminal narrowing and/or plaque instability leading to symptomatic presentations.

**KEY WORDS:** Intracranial atherosclerosis, plaque imaging

O-238

11:34 AM - 11:42 AM

#### Association of MR Imaging Findings and Poor Visual Outcomes in Idiopathic Intracranial Hypertension

Saindane, A. M.<sup>1</sup>Riggeal, B. D.<sup>2</sup>Bruce, B. B.<sup>3</sup>Newman, N. J.<sup>1</sup>Biousse, V.

Emory University School of Medicine  
Atlanta, GA

#### PURPOSE

Idiopathic intracranial hypertension (IIH) is a condition characterized by elevated intracranial pressure (ICP) with normal cerebrospinal fluid (CSF) composition and no other identifiable cause. The clinical course of IIH is variable, resulting in irreversible vision loss in some patients, and a more benign course in others. Imaging is performed primarily to exclude an intracranial mass, hydrocephalus, or venous sinus thrombosis as a cause of elevated ICP. While imaging findings involving the orbits, sella turcica, and venous sinuses have been described in patients with IIH, their prognostic value for visual outcome has not been evaluated.

#### MATERIALS & METHODS

Fifty-seven patients with definite IIH were included in this IRB-approved study. All patients were evaluated by an experienced neuro-ophthalmologist and underwent funduscopy evaluation, visual field (VF) testing, lumbar puncture with opening pressure (OP) measurement, and MRI evaluation. Patients were divided into three groups: Group 1 - poor visual outcome with severe VF deficits (n = 9), Group 2 - good visual outcome with some VF deficits (n = 12), and Group 3 - good visual outcome with no VF deficits (n = 36). MR imaging studies were evaluated by an experienced neuroradiologist blinded to the patients' visual outcome. Orbital findings of optic nerve (ON) head protrusion, ON head enhancement, posterior scleral flattening, increased peri-ON CSF, and ON tortuosity

were evaluated, as were minimum optic canal diameter and presence or absence of optic canal CSF. Expansion of the sella turcica was graded, and the frequency of skull base cephaloceles was noted. MRVs were evaluated for transverse sinus (TS) stenosis and extent of calvarial venous channels. Gender, race, OP, BMI, and frequency of each MRI/MRV findings were evaluated as predictors of visual outcome. Patients also were divided into three groups based on OP (<30, 31-40, and >41) to determine differences in clinical and imaging findings associated with increasing OP.

#### RESULTS

No significant differences were found in mean BMI, patient age, race, or gender between the three visual outcome groups. The mean OP was significantly higher in group 1 than in group 3 (46 vs 35 cm water,  $p = 0.02$ ) but not between other groups. Despite worse visual outcomes and sometimes fulminant vision loss, there were no significant differences in the frequency of orbital findings suggestive of papilledema and elevated ICP between group 1 and the other groups. No significant differences in sellar enlargement, frequency of skull base cephaloceles, or presence of TS stenosis were present between the three groups. Optic canal diameter was significantly smaller (3.7 mm vs 4.1 mm,  $p = 0.04$ ) in patients with high OP (OP>41) than with low OP (OP<30). Otherwise, no significant differences in clinical or imaging findings were found related to OP.

#### CONCLUSION

While MRI findings may suggest the presence of elevated ICP and the diagnosis of IIH, they are not prognostic of visual outcome in IIH. Particularly, the absence of imaging findings does not exclude a diagnosis of IIH or portend a better visual prognosis. Increasing OP is associated with more severe vision loss.

**KEY WORDS:** Idiopathic intracranial hypertension, pseudotumor cerebri, MRV

O-239

11:42 AM - 11:50 AM

#### Vessel Wall MR Imaging to Differentiate between Reversible Cerebral Vasoconstriction Syndrome and Central Nervous System Vasculitis: Preliminary RESULTS

Mandell, D. M.<sup>1</sup>Matouk, C. C.<sup>2</sup>Swartz, R. H.<sup>3</sup>Silver, F. L.<sup>1</sup>Mikulis, D. J.<sup>1</sup>

<sup>1</sup>Toronto Western Hospital, Toronto, ON, CANADA,  
<sup>2</sup>Yale University, New Haven, CT, <sup>3</sup>Sunnybrook Health Sciences Centre, Toronto, ON, CANADA

#### PURPOSE

Proposed diagnostic criteria for reversible cerebral vasoconstriction syndromes (RCVS) are sudden-onset severe headache, multifocal segmental narrowing of cerebral arteries, lack of aneurysmal subarachnoid hemorrhage, near-normal cerebrospinal fluid, and spontaneous resolution of arterial narrowing within 3 months. Early discrimination between RCVS, and its principal differential, central nervous system (CNS) vasculitis, is important: RCVS is treated with

observation or possibly calcium channel blockers, whereas CNS vasculitis is treated with steroids and immunosuppression. However, the diagnosis of RCVS currently is confirmed only in retrospect, when arterial narrowing resolves. Large artery CNS vasculitis is associated with arterial wall thickening and enhancement. Reversible cerebral vasoconstriction syndrome is a disorder of arterial tone regulation, and the limited histopathologic data available suggests an absence of arterial wall inflammation; therefore, we hypothesized that patients with RCVS would lack arterial wall enhancement

#### MATERIALS & METHODS

From a database of 114 patients studied with high-resolution vessel wall MRI over a 4-year period, we identified all patients with multifocal segmental narrowing of large intracranial arteries and angiographic follow up, and performed a detailed chart review for each case. MR imaging was performed using a 3.0 T scanner with an 8-channel head coil. Vessel wall protocol included a time-of-flight MRA of the circle of Willis, T1-weighted black blood vessel wall sequence (single inversion recovery-prepared two-dimensional fast spin echo acquisition with field of view = 22x22 cm, acquired matrix = 512x512; slice thickness = 2 or 3 mm; total slab thickness 2 to 3 cm, TR/TI/TE = 2263/860/13 ms) before and after intravenous gadolinium. Images were obtained through the most severely narrowed arterial segments in each patient. Each vessel wall sequence was performed in both the short and long axis of the artery of interest. A neuroradiologist, blinded to vessel wall imaging and clinical data, graded the angiographic arterial narrowing as mild (<50%), moderate (50-79%), or severe (>80%) for each study. A different neuroradiologist, blinded to angiography and clinical data, categorized vessel wall thickness as "normal" (barely perceptible) versus "thickened," and comparing the pre and postgadolinium images, classified arterial wall enhancement in narrowed segments as "absent/minimal" versus "present" for each study.

#### RESULTS

Seven patients satisfied the inclusion criteria. Median age was 45 years (range 19 - 69) and six of seven patients were women. Presenting symptoms were acute headache (n = 2), neurologic deficit (n = 2), and headache with deficit (n = 3). Laboratory testing included a serum vasculitis workup in 7/7 patients and CSF analysis in 5/7 patients. Three patients lacked arterial wall enhancement, and these all had reversal of arterial narrowing within 3 months. Four patients demonstrated arterial wall enhancement, and these had persistent or progressive arterial narrowing at a median follow-up of 17 months (range 6-36), with final diagnoses of CNS vasculitis (3) and cocaine vasculopathy (1).

#### CONCLUSION

Preliminary results suggest that high-resolution contrast-enhanced vessel wall MRI may enable differentiation between reversible cerebral vasoconstriction and CNS vasculitis.

**KEY WORDS:** MR imaging, vessel wall, vasculitis

**O-240**

**11:50 AM - 11:58 AM**

#### **Intra-Voxel Incoherent Motion Revisited: Application to Quantitative Measurement of Brain Perfusion**

Federau, C.<sup>1</sup>•Maeder, P.<sup>1</sup>•O'Brien, K.<sup>2</sup>•Browaeys, P.<sup>1</sup>•Meuli, R.<sup>1</sup>•Hagmann, P.<sup>1</sup>

<sup>1</sup>CHUV, Lausanne, SWITZERLAND, <sup>2</sup>CIBM, Geneva, SWITZERLAND

#### **PURPOSE**

The MR-based methods in use in a clinical environment to measure brain perfusion are, in order of popularity, dynamic susceptibility contrast (DSC) MR, arterial spin labeling (ASL), and dynamic contrast-enhanced (DCE) MRI. The hypothesis, that perfusion could be measured with the Stejskal-Tanner diffusion sequence, was proposed 25 years ago by Le Bihan, under the name Intra-voxel Incoherent Motion (IVIM). Due to low signal-to-noise ratio, this idea could not be used clinically. The continued improvements over the last two decades of both the hardware and software technology, such as the use of stronger magnetic fields, multichannel receiver coils and better pulse sequences, enables the IVIM method for measuring perfusion to be reconsidered. Promising IVIM results were obtained recently in highly perfused organs such as the liver, kidney, and heart. The purpose of this study was to evaluate the feasibility of IVIM brain perfusion imaging in the clinical setting using current MRI technology.

#### **MATERIALS & METHODS**

Our experiments were performed on a 3 T scanner using a 32-multichannel receiver head coil. The Stejskal-Tanner diffusion pulse sequence was applied. Diffusion-weighted images of 16 different b-values were acquired in three orthogonal directions. The signal obtained was fitted to a double exponential following the IVIM theory, and the perfusion fraction *f* and the pseudo-diffusion coefficient *D\** were extracted. TR/TE = 4000 ms/99 ms, 4 averages, voxel size = 1.2 x 1.2 x 4 mm. We scanned 40 patients with various cerebral perfusion-related pathologic conditions.

#### **RESULTS**

Signal decay curves were bi-exponential in the brain parenchyma of all patients, and consistent parametric maps of brain perfusion fraction *f* and pseudo-diffusion coefficient *D\** were obtained. In patients with a primary brain tumor (Fig 1) or a metastasis, hyperperfusion was measured. In patients with sub-acute stroke, hypoperfusion or reactive hyperperfusion was measured.

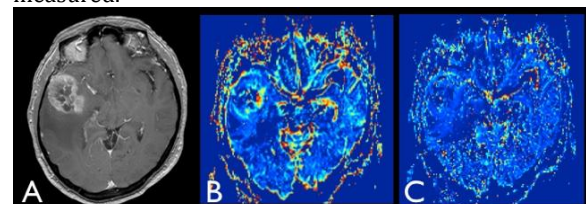


Fig 1: Glioblastoma multiforme of right temporal lobe

on T1 post-Gd image (A). Perfusion fraction  $f$  (B) and pseudo-diffusion coefficient  $D^*$  (C) obtained by IVIM method show hyper-perfusion compatible with neo-angiogenesis.

#### CONCLUSION

The IVIM method has the potential to become a key technique to measure brain perfusion in the clinical setting, since it is intrinsically quantitative, it is directly sensitive to blood flow within the capillary bed (independent of arterial transit and venous blood volume), it does not need iv-contrast injection, and it is based on a robust pulse sequence (Stejskal-Tanner).

**KEY WORDS:** Perfusion, IVIM, quantitative

## Tuesday Morning

**10:30 AM - 12:00 PM**

**Sutton Center/South**

(27d) Head & Neck: Anatomy, Face, Orbit and Congenital

**O-241**

**10:30 AM - 10:38 AM**

### Prevalence of Incidental "Pseudostenosis" of the Internal Jugular Vein Near the Craniocervical Junction

Diehn, F. E.·Schwartz, K. M.·Eckel, L. J.·Hunt, C. H.

Mayo Clinic  
Rochester, MN

#### PURPOSE

Narrowing of the internal jugular vein (IJV) near the craniocervical junction is not uncommonly reported on cross-sectional neuroimaging examinations. Some recent literature ascribes a relationship between IJV narrowing and disease, namely "chronic cerebrospinal venous insufficiency" as a pathophysiologic basis for multiple sclerosis. Our goal was to retrospectively investigate the prevalence of narrowing of the IJV near the craniocervical junction in a large group of consecutive patients imaged with CT angiography (CTA).

#### MATERIALS & METHODS

IRB approval was obtained for this HIPAA compliant research protocol. Consecutive patients who had undergone neck CTA at our institution were included. Exclusion criteria were: history of head and neck neoplasm, neck surgery and/or radiation therapy, IJV stenting or resection, IJV thrombosis, inadequate opacification of the IJV or lack of available 0.75 mm axial source images. The appearance of the bilateral IJVs near the craniocervical junction on the remaining CTAs was reviewed. At the narrowest point of the IJV near the craniocervical junction, each IJV was graded

subjectively according to degree of narrowing (occluded, nearly occluded, mild-moderate, none-minimal) and shape (absent, pinpoint, flattened, crescentic, ellipsoid), objectively measured (minimal diameter, diameter perpendicular to this, and area), and anatomically located (medial to, overlapping with, or lateral to the transverse foramen of C1).

#### RESULTS

From a group of 200 consecutive patients imaged with neck CTA, 18 were excluded for clinical criteria. Of the remaining 364 IJVs in 182 patients, 52 IJVs were excluded in 33 patients because of lack of adequate opacification (44 IJVs, 29 patients) or lack of available thin axial source images (8 IJVs, 4 patients). The final study group consisted of 312 IJVs (159 right and 163 left) in 149 patients. The mean age was 64 years, with a slight male predominance (54%). The most common subjective degree of IJV narrowing was mild to moderate [117 IJVs (38%)]. The most common subjective IJV shape was flattened [111 IJVs (36%)]. Subjective shape and degree of narrowing were highly correlated ( $p < 0.001$ ). Forty-six IJVs (15%) in 42 patients (28%) were categorized as occluded [2 (<1%)] or nearly occluded [44 (14%)], and 26 IJVs (8%) in 23 patients (15%) were rated to be absent [2 (<1%)] or have a pinpoint shape [24 (8%)]. None of these patients with the most narrowed/deformed IJVs had a diagnosis of multiple sclerosis. The mean measurements for all IJVs were: minimal diameter  $4 \pm 2$  mm, perpendicular diameter  $10 \pm 4$  mm, and area  $40 \pm 30$  mm. Both subjective shape and narrowing highly correlated with each of the three measurements ( $p < 0.0001$  for all comparisons). A lateral location with respect to the transverse foramen of C1 correlated with a smaller IJV area ( $p < 0.0001$ ).

#### CONCLUSION

The appearance of the IJV near the craniocervical junction is quite variable, with an occlusive or near occlusive appearance being relatively frequent (28% prevalence in our study population). Radiologists should be cautious to report this incidental finding, as these results suggest it is a frequent anatomical variant.

**KEY WORDS:** Internal jugular vein, pseudostenosis, anatomical variant

**O-242**

**10:38 AM - 10:46 AM**

### Unifocal versus Multifocal Mandibular Fractures: Demographics by Age and Injury Location

Abdel Mottalib, A.<sup>1</sup>·Sekiya, K.<sup>1,2</sup>·Nadgir, R. N.<sup>1</sup>·Kaneda, T.<sup>2</sup>·Sakai, O.<sup>1</sup>

<sup>1</sup>Boston University School of Medicine, Boston, MA,

<sup>2</sup>Nihon University School of Dentistry at Matsudo, Matsudo, JAPAN

#### PURPOSE

High incidence of unifocal mandibular fractures has been reported. The purpose of this study is to compare the age demographics of patients with unifocal and multifocal mandibular fractures in the largest imaging



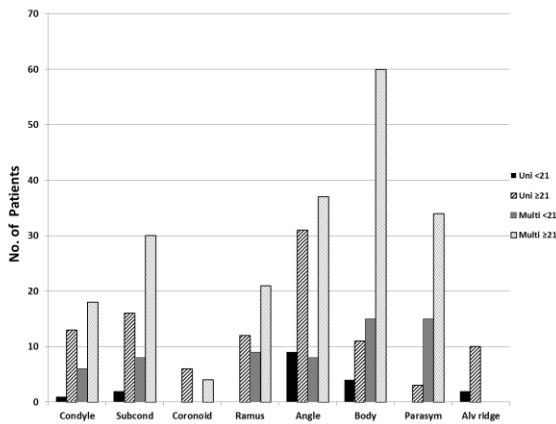
series to date, and to further characterize fracture subtype and location based on age.

#### MATERIALS & METHODS

Maxillofacial CT of patients with mandibular fractures over a 3-year period were reviewed retrospectively. All patients were scanned with 64 MDCT and axial 1.25 mm, sagittal and coronal 1.5 mm images were reviewed with optional 3D reconstructions. In addition to age and specific trauma history, fracture subtype (simple, comminuted, displaced) and site (parasymphysis, body, angle, ramus, coronoid, subcondyle, condyle) were recorded for each traumatized mandible.

#### RESULTS

We identified 243 patients (200 males, 43 females, age range 8 months to 95 years), with 385 fractures. Unifocal fractures were seen in 120 patients (49% of the total number of patients). Of these 243 patients, 41 pediatric/young adult patients (less than 21 years old) demonstrated 67 fractures and 202 adult patients (greater than 21 years old) demonstrated 318 fractures (see table). Among patients in both age groups, the mandibular angle was by far the most common site of fracture for unifocal injury. Among the younger age group, the body and parasymphysis were equivalently and most commonly affected regions of fracture in the setting multifocal injuries. Among the older age group, the body was by far the most commonly affected fracture site in the setting of multifocal injuries. Coronoid process fractures were less common but were only seen in the older age group, more frequently unifocally. Patients with mandibular body fractures tended to have additional injury affecting the contralateral mandibular angle or ramus.



#### CONCLUSION

Almost half of patients with mandibular fractures sustained unifocal injuries. Regardless of age, the mandibular angle was the most common site of unifocal injury. Among younger patients with multifocal injuries, the body and parasymphysis were affected most commonly, whereas among older patients, the body was the most common site of multifocal injury with additional fractures typically involving the contralateral angle or ramus.

**KEY WORDS:** Mandible, fracture

O-243

10:46 AM - 10:54 AM

#### Pathologic Expansion of the Jaw: A Useful Parameter in the Differentiation between Benign and Malignant Lesions

Gad, K.<sup>1</sup>Sciubba, J.<sup>2</sup>Antar, O.<sup>1</sup>Habba, M.<sup>1</sup>Hamed, M.<sup>1</sup>El-Nisr, M.<sup>1</sup>Yousem, D.<sup>2</sup>

<sup>1</sup>Suez Canal University, Ismailia, EGYPT, <sup>2</sup>Johns Hopkins University, Baltimore, MD

#### PURPOSE

To describe the pattern of pathologic bone expansion among benign and malignant jaw lesions.

#### MATERIALS & METHODS

Ninety-eight patients of different age groups (mean age: 39 + 18 years) with a clinically suspected jaw lesion were included in the study. Dental CT with panoramic and cross-sectional reconstruction was carried out on all patients.

#### RESULTS

Pathologic bone expansion occurred in 17% only of malignant lesions versus 44% of benign ones (P value= 0.02). A jaw lesion with bone expansion had an Odds ratio of only 0.19 to be malignant (P value = 0.39, CI = 95%). The direction of expansion (buccolingual versus mesiodistal) has shown an interesting relation to the type and location of jaw lesions.

#### CONCLUSION

Pathologic bone expansion was found to be an important imaging parameter that should be evaluated by dental CT when differentiating benign from malignant lesions of the jaw.

**KEY WORDS:** Jaw, bone expansion

O-244

10:54 AM - 11:02 AM

#### Effects of Aging on Facial Fat Using Quantitative MR Imaging and Spatial Resolution Enhancement Technique

Watanabe, M.·Jara, H.·Sekiya, K.·Liao, J. H.·Kussman, S.·Nadgir, R. N.·Sakai, O.

Boston Medical Center-Boston University School of Medicine  
Boston, MA

#### PURPOSE

To study the effect of aging on facial fat using quantitative MRI (qMRI) analysis of proton density (PD), T1 and T2 values.

#### MATERIALS & METHODS

Following IRB approval and after obtaining informed consent, 36 subjects (19 males, 17 females; age range 0.5-87 years, mean 32 years) underwent brain imaging which included the mixed-TSE pulse sequence using a 1.5 T magnet. Subjects consisted of three volunteers and 33 patients who were referred for various clinical reasons, including stroke, headache, seizure, epilepsy,

developmental delay, and dementia. None of the subjects carried a history that might result in facial tissue asymmetry (i.e., trauma, facial weakness, and perineural tumor spread). Proton density values of cerebrospinal fluid were normalized to 1.0 for each subject. Using spatial resolution enhancement technique, each voxel (size:  $0.94 \times 0.94 \times 3 \text{ mm}^3$ ) was subdivided into smaller voxels (size:  $0.31 \times 0.31 \times 3 \text{ mm}^3$ ). Then, T1, T2 and PD measurements were obtained within a rectangular voxel-based region-of-interest (ROI) in buccal fat, subcutaneous cheek fat, and four eyelid fat regions in medial and lateral portions of upper and lower eyelids bilaterally.

## RESULTS

The lateral lower eyelid region demonstrated characteristic age dependency; consistent decrease in T1 value with age was seen. The lateral upper eyelid and medial lower eyelid regions demonstrated slight T1 increase with age while medial upper eyelids showed relatively stable T1 measurements without age dependency. T2 values of the lateral lower eyelid showed greater increase with age compared to other regions of eyelid fat. Proton density values of all four eyelid regions demonstrated similar gradual increase with age. Subcutaneous cheek fat demonstrated slight increase in PD and T1 values and slight decrease in T2 values, while buccal fat demonstrated stable measurements in PD, T1 and T2 values without age dependency.

## CONCLUSION

Our results indicate differing aging patterns of regional facial fat, with most dramatic changes over time at the lateral lower eyelid. The noninvasive assessment of facial fat may be useful for quantitative monitoring of facial aging and evaluation of effectiveness of targeted antiaging strategies.

**KEY WORDS:** Facial fat, quantitative MR imaging, aging

**O-245**

**11:02 AM - 11:10 AM**

### Effects of Aging on Facial Muscles Using Quantitative MR Imaging

Watanabe, M.·Jara, H.·Sekiya, K.·Liao, J. H.·Kussman, S.·Nadgir, R. N.·Sakai, O.

Boston Medical Center-Boston University School of Medicine  
Boston, MA

## PURPOSE

To study the effect of aging on the facial muscles using quantitative MRI (qMRI) analysis of proton density (PD), T1 and T2 values.

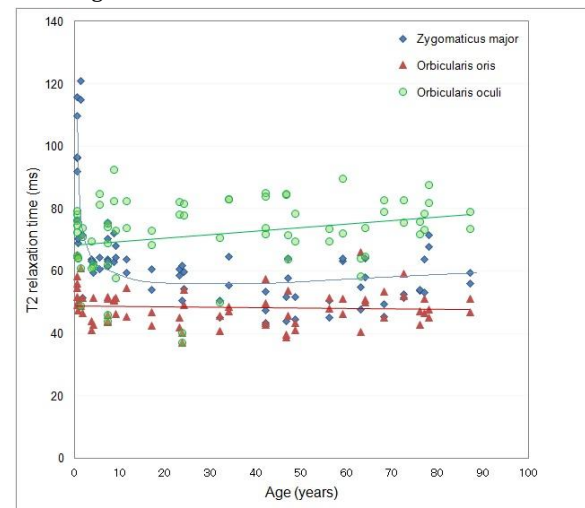
## MATERIALS & METHODS

Following IRB approval and after obtaining informed consent, 37 subjects (19 males, 18 females; age range 0.5-87 years, mean 32 years) underwent brain imaging which included the mixed-TSE pulse sequence using a 1.5 T magnet. Subjects consisted of three healthy volunteers and 34 patients who were referred for

various clinical reasons, including stroke, headache, seizure, epilepsy, developmental delay, and dementia. None of the subjects carried a history that might result in facial muscle abnormality (i.e., trauma, facial weakness, and perineural tumor spread). After PD values of cerebrospinal fluid were normalized to 1.0 for each subject, T1, T2 and PD measurements were obtained within a rectangular voxel-based region-of-interest (ROI) in five facial muscles, including masseter, buccinator, zygomaticus major, orbicularis oris and orbicularis oculi bilaterally.

## RESULTS

The zygomaticus major muscle exhibited characteristic age-related changes. A rapid decrease in T2 values was seen during infancy through early childhood; this decrease tapered in adolescence. A slight increase then was seen, beginning in middle age and continuing through the later years. Proton density and T1 values of the zygomaticus major muscle increased with age. Orbicularis oculi muscles showed a slight increase in PD, T1, and T2 values with increase in age. Masseter, buccinators and orbicularis oris muscles demonstrated relatively stable measurements in PD, T1, and T2 values for all ages.



## CONCLUSION

Our results indicate differing aging patterns of specific facial muscles, which could contribute to the morphologic changes in facial aging. The in vivo assessment of facial muscles would be useful for quantitative monitoring of facial aging, designing targeted antiaging strategies and evaluation of effectiveness of the antiaging strategies.

**KEY WORDS:** Facial muscle, quantitative MR imaging, aging

**O-246**

**11:10 AM - 11:18 AM**

### Parotid Gland Atrophy: A New Finding in Patients with Denervation of the Trigeminal Nerve

Raz, E.·Galheigo, D.·Som, P. M.·D' Ambrosio, F.·Fatterpekar, G.<sup>1</sup>

<sup>1</sup>New York University, New York, NY, <sup>2</sup>Mount Sinai Medical Center, New York, NY, <sup>3</sup>Sapienza University, Rome, ITALY

#### PURPOSE

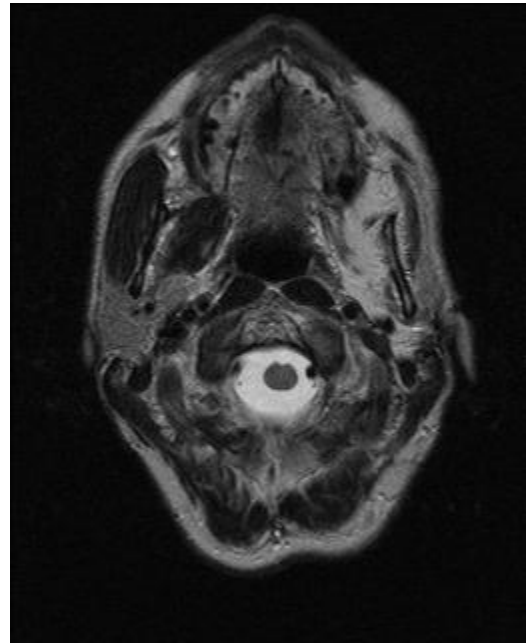
Trigeminal nerve (CN5) denervation is associated with atrophy of muscles innervated by the mandibular (V3) branch. Atrophy of the parotid gland accompanying such masticator muscle atrophy has not been described previously. The purpose of our study was to evaluate the association between parotid gland atrophy and CN5 denervation.

#### MATERIALS & METHODS

A multi-institutional retrospective study was carried out evaluating for cross-sectional (CT or MRI) imaging evidence of masticator muscle atrophy. Patients with myasthenia gravis, polymyositis, progressive systemic sclerosis, or rheumatoid arthritis which are systemic conditions known to cause masticator muscle atrophy were excluded from the study. In addition, patients with enhancement along the glossopharyngeal nerve and diffuse metastatic disease were excluded from the study. Based on these inclusion and exclusion criteria, 26 such cases of masticator space atrophy were identified. These cases then were evaluated for the degree of fatty replacement of the masticator group of muscles, and the presence of ipsilateral parotid gland atrophy. Fatty replacement of the masticator group of muscles was graded as 0 = partial, and 1 = complete. Ipsilateral parotid gland atrophy was graded as 0 = absent, and 1 = present. A two-tailed Fisher's exact test for categorical data was used to determine the correlation between the parotid gland atrophy in the side ipsilateral to the masticator space atrophy.

#### RESULTS

Partial fatty replacement of the masticator group of muscles was seen in five of the 26 patients (19%), and complete fatty replacement was seen in the remaining 21 patients (81%). Ipsilateral parotid gland atrophy was seen in nine of the 26 patients (35%). More specifically, such parotid gland atrophy was seen only in patients with complete fatty replacement of the masticator group of muscles (9/21 = 43%). Statistical analysis using Fisher's exact test demonstrated a p value < 0.0001, suggesting that this correlation between the parotid gland atrophy and CN5 denervation is significant. We presume that such atrophy of the parotid gland likely is influenced also by the chronicity of the event, and hence was not demonstrated in all our patients.



#### CONCLUSION

Ipsilateral parotid gland atrophy can sometimes be seen in the setting of trigeminal nerve denervation. Plausible hypothesis include: 1. Connections between the glossopharyngeal nerve and the auriculotemporal nerve, a branch of the mandibular division (V3) of the trigeminal nerve which provides parasympathetic innervation to the parotid gland. 2. Secondary disuse atrophy from atrophy of the masticator group of muscles.

**KEY WORDS:** Trigeminal nerve, parotid gland, denervation

O-247

11:18 AM - 11:26 AM

#### Optimization of Contrast-Enhanced Multidetector CT Protocol for Parotid Tumor: What Does Contribute the Better Lesion Conspicuity of Parotid Tumor in Neck CT Examination?

Lee, Y.<sup>1</sup>·Kim, T.<sup>1</sup>·Seo, H.<sup>1</sup>·Suh, S.<sup>2</sup>·Lee, N.<sup>3</sup>·Kim, J.<sup>3</sup>·Seol, H.<sup>2</sup>

<sup>1</sup>Ansan Hospital Korea University College of Medicine, Ansan, KOREA, REPUBLIC OF, <sup>2</sup>Guro Hospital Korea University College of Medicine, Seoul, KOREA, REPUBLIC OF, <sup>3</sup>Anam Hospital Korea University College of Medicine, Seoul, KOREA, REPUBLIC OF

#### PURPOSE

To determine the effect of various contrast media (CM)-enhanced MDCT scanning parameters for better lesion conspicuity of parotid tumor.

#### MATERIALS & METHODS

We enrolled pathologically proven 237 parotid tumors (mean size: 26 ± 10 mm) which consisted of 27 malignant tumors, 116 pleomorphic adenomas, 64 Warthin's tumors, 17 basal cell adenomas and 13 others. Their preoperative 64-channel CT images were obtained by monophasic or biphasic scanning including

following four acquisitions: without CM, and 40 s, 50 s and 70 s after intravenous injection. We recorded parotid-tumor difference (PTD) and contrast to noise ratio (CNR) by measuring Hounsfield values of parotid tumor, parenchyma and noise of ipsilateral masseter muscle. Their PTD and CNR were compared statistically to evaluate effects of scan delay, tumor size, iodine concentration of CM and pathologic types using multivariate analysis ( $p < .05$ ).

## RESULTS

Scan delay and pathologic types significantly affected PTD, CNR of parotid tumors, but tumor size and iodine concentration of CM did not. Compared with nonenhanced CT images, PTD and CNR of parotid tumors were best at CM-enhanced CT images with 50 s, which showed tendency to decline in more prolonged scan delay after 50 s. Significant differences of PTD, CNR depending on pathologic type were only found between pleomorphic adenoma and Warthin's tumor in CT examination with 50 s.

## CONCLUSION

For better lesion conspicuity of parotid tumor, MDCT scanning should begin 50 s after start of CM injection.

**KEY WORDS:** Parotid, CT, contrast media

**O-248**

**11:26 AM - 11:34 AM**

### **Parotid Gland Tumor Apparent Diffusion Coefficient Measurements: Effect of Region-of-Interest Methods on Apparent Diffusion Coefficient Values**

Saito, N.<sup>1</sup>·Nakahira, M.<sup>1</sup>·Nadgir, R.<sup>2</sup>·Sakai, O.<sup>2</sup>·Uchino, A.<sup>1</sup>·Kimura, F.<sup>1</sup>

<sup>1</sup>Saitama International Medical Center, Saitama Medical University, Saitama, JAPAN, <sup>2</sup>Boston Medical Center-Boston University School of Medicine, Boston, MA

## PURPOSE

Apparent diffusion coefficient (ADC) value has been reported to be a useful imaging biomarker to identify pathologic types and differentiate between benign and malignant tumors in salivary gland. However, ADC values are influenced by various methods for region of interest (ROI) placement. The purpose of this study is to assess the influence of ROI positioning on tumor ADC measurements in the patients with parotid gland tumors.

## MATERIALS & METHODS

Clinical charts and imaging data of 28 patients with 29 parotid gland tumors (17 males, 11 females: 11 pleomorphic adenomas, 13 Warthin's tumors, 5 malignant tumors) who underwent MR imaging prior to biopsy or surgical resection between April 2007 and March 2011 were evaluated retrospectively. MR imaging including diffusion-weighted imaging performed using a 1.5 T MR scanner. Tumor ADC values were measured according to three ROI placement methods: (1) whole-volume, (2) single-slice, and (3) small solid samples. Regions of interest were drawn manually along the entire tumor on each slice for

whole-volume method, and on a single slice containing the largest available tumor area for single-slice method. For small solid samples method, three small round ROIs were placed on the solid portion of the tumor. These three ROI methods were compared for differences in ADC measurements [mean ADC value (ADC mean), minimum ADC value (ADC min), relative ADC min (rADC min = ADC min/ADC mean), and standard deviation (SD)] and for differences among the tumor types.

## RESULTS

Significant differences were noted among three lesion types (pleomorphic adenoma, Warthin's tumor, and primary salivary gland malignancy) in terms of ADC mean and ADC min using each ROI placement method ( $p < 0.05$ , Kruskal-Wallis test). There were no significant rADC min differences among the lesion types using any of the ROI placement methods. Standard deviation for the whole-volume method showed significant differences among the lesions and the SDs for malignant tumors were the largest.

## CONCLUSION

Region-of-interest positioning may influence focal ADC measurements within a lesion, however ADC mean and ADC min values based on each ROI method did not differ significantly in terms of distinguishing parotid gland tumor types.

**KEY WORDS:** Parotid gland tumor, apparent diffusion coefficient, region of interest

**O-249**

**11:34 AM - 11:42 AM**

### **Open-Angle Glaucoma and Para-Optic Cyst: Initial Description in a Series of 12 Patients**

Bertrand, A.·Vignal, C.·Lafitte, F.·Koskas, P.·Bergès, O.·Héran, F.

Fondation Ophthalmologique A. de Rothschild  
Paris, FRANCE

## PURPOSE

To report for the first time, to our knowledge, the rare association of para-optic cyst and open-angle glaucoma; to discuss its pathophysiologic significance and prognostic value.

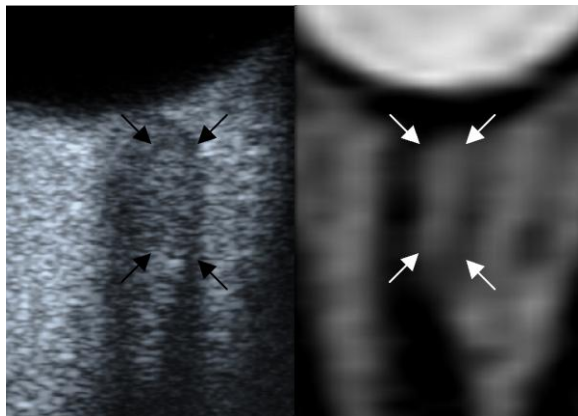
## MATERIALS & METHODS

During a period of 5 years, 12 patients addressed to our institution for a visual loss were diagnosed to have a para-optic cyst on MRI examination. We retrospectively collected the ophthalmologic reports of these patients (including fundus and visual field), and their MRI images (acquired on a 1.5 T MRI, always including a 2 mm thick coronal T2-TSE weighted sequence on the optic nerves). For seven patients, we completed the explorations by an Optical Coherence Tomography (OCT), a U.S. and Doppler examination of eyes and optic nerves with a bilateral measure of resistance index in the optic nerve arteries, and a high-resolution MRI of the optic nerves. High-resolution MRI was performed on a 1.5 T magnet using a surface coil, and included millimetric 3D T2 DRIVE and 2 mm thick coronal T1,

T2-TSE and FLAIR sequences. Volume of the cysts were measured manually on both 3D DRIVE and coronal T2-TSE sequences. Resistance index in the arteries of both eyes were compared using paired t-test or Wilcoxon signed rank test. Correlation between the size of the cysts on the one hand, and the indicators of glaucoma severity on the other hand (mean deviation and pattern standard deviation on visual field, thickness of the ganglionar fiber layer on OCT) were assessed using Pearson or Spearman correlation coefficient.

## RESULTS

All patients had an open-angle glaucoma. Cysts were always extra-optic and retrolaminar, mostly unilateral (11/12 patients), with a mean size of  $23 \text{ mm}^3 \pm 14$ . Cysts had a high signal on T2 and FLAIR sequences, and a variable signal in T1 and variable echogenicity, suggesting different proteinaceous contents. In 11/12 patients, the cyst had a mass effect on the adjacent optic nerve. There was no associated perturbation of the arterial vascularization of the optic nerve on the side of the cyst. Cyst volumes were correlated conversely with the severity of glaucoma on the same eye ( $p < 0.01$ , Pearson correlation coefficient ;  $p < 0.05$ , Spearman correlation coefficient).



## CONCLUSION

This is the first report, to our knowledge, of an association between open-angle glaucoma and para-optic cyst. If the exact nature of these cysts remains to be clarified, our initial data suggest that they are associated with a relatively preserved visual function. This could suggest that such cysts preserve the transcribleal pression in patients with open-angle glaucoma.

**KEY WORDS:** Glaucoma, cyst, optic nerve

O-250

11:42 AM - 11:50 AM

## MR Imaging Parameters and Clinical Scores in Thyroid-Associated Orbitopathy: Which One to Trust for Extraocular Muscle Evaluation?

Politi, L. S.<sup>1</sup>Godi, C.<sup>2</sup>Cammarata, G.<sup>1</sup>Ambrosi, A.<sup>2</sup>Falini, A.<sup>2,3</sup>Bianchi, S.<sup>1</sup>

<sup>1</sup>Ospedale San Raffaele, Milano, ITALY, <sup>2</sup>Vita-Salute San Raffaele University, Milano, ITALY, <sup>3</sup>San Raffaele Scientific Institute, Milan, ITALY

## Purposes

1) to find the magnetic resonance imaging (MRI) parameter best representing disease activity and extra-ocular muscle dysfunction in thyroid-associated orbitopathy (TAO); 2) to assess the role of diffusion-weighted imaging (DWI) of the orbits in TAO patients; 2) to compare clinical and MRI measures in patients affected by TAO at baseline and after treatment.

## MATERIALS & METHODS

Seventy-four patients affected by TAO underwent clinical and ophthalmologic evaluation and a MRI study including T2-SPIR, spin echo T1, postgadoliniumT1-SPIR (T1Gad) and DWI ( $b = 0-700$ ) sequences. According to the Clinical Activity Score (CAS), patients were divided into two groups, with inactive (CAS 0-2) or active (CAS 0-6) disease. A functional score (1 = normal; 4 = severe impairment) was assigned to every rectus muscle. Signal intensities and apparent diffusion coefficient (ADC), measured on all recti-muscles of both orbits, were normalized to the signal intensities of the right thalamus (SIRs) and then compared with those from 26 healthy subjects and with patients' clinical scores. Clinical, ophthalmologic examination and MRI follow up after intravenous steroid treatment were available in 35 patients. Mann-Whitney, Wilcoxon Signed Rank Test and Spearmann Correlation were applied for statistical analysis.

## RESULTS

Patients had T2-SPIR, T1Gad and ADC SIRs higher than healthy subjects ( $p < 0.001$ ). T2-SPIR and T1Gad SIRs showed significant increase ( $p < 0.001$ ) in the group of patients with active disease compared to the inactive one. Further, T2-SPIR, T1Gad and ADC SIRs were significantly higher in patients with inactive disease when compared to healthy controls. T2 and T1Gad SIRs, but not ADC, showed a significant correlation ( $p < 0.01$ ) with muscle dysfunction and CAS levels in the affected subjects. In addition, T2 and ADC SIRs of patients' muscles with no clinical evidence of dysfunction or active disease were significantly higher than those of healthy controls. All SIRs significantly reduced ( $p < 0.001$ ) in muscles that had clinical improvement after therapy; interestingly, even in the group of clinically stable-functioning muscles, a significant reduction ( $p < 0.01$ ) in MRI parameters was detected after therapy.

## CONCLUSION

MR imaging is able to depict disease involvement even in clinically spared extraocular muscle and could be more sensitive than ophthalmologic scores to modifications of muscle involvement. Thus MRI should be included in clinical trials for evaluation of therapeutic efficacy and in the clinical management of TAO patients.

**KEY WORDS:** Thyroid-associated orbitopathy, DWI, MR imaging



**O-251****11:50 AM - 11:58 AM****Procedure Times for MR Imaging-Guided Sclerotherapy of Low-Flow Vascular Malformations in Head and Neck at 1.5 T**

Sandhu, G. S.<sup>1</sup>•Derakhshan, J. J.<sup>1</sup>•Nour, S. G.<sup>2</sup>•Lewin, J. S.<sup>3</sup>•Griswold, M. A.<sup>1</sup>•Sunshine, J. L.<sup>1</sup>•Hsu, D. P.<sup>1</sup>

<sup>1</sup>University Hospitals of Cleveland, Cleveland, OH, <sup>2</sup>Emory University, Atlanta, GA, <sup>3</sup>Johns Hopkins University, Baltimore, MD

**PURPOSE**

MR imaging-guided sclerotherapy of low-flow vascular malformations was described initially at 0.2 T. Subsequently, the use of a 1.5 T system was reported, where the needle was placed into the lesion outside the magnet bore and the sclerosing agent then was injected under image guidance. Sclerotherapy now is performed at 1.5 T at our institution with the steps of needle placement as well as injection monitored by MRI. Here we study the times spent on various steps of sclerotherapy in all consecutive sessions conducted by a radiologist over a 2-year period.

**MATERIALS & METHODS**

A total of 29 sclerotherapy sessions were conducted on lesions located in the head/neck of 11 subjects (age 13 days to 67 years) between August 2009 and July 2011. During each session, diagnostic images were first obtained to plan the needle trajectory. Subsequently, the skin entry site for the needle was localized by moving a syringe filled with water along the skin surface while monitoring by continuous imaging using a tri-plane True fast imaging with steady-state precession (True-FISP; TR/TE/ $\alpha$  5.2 ms/2.6 ms/60°, voxel size 1.3×1.3×5 mm, averages 3) pulse sequence. Alignments of the three imaging planes of True-FISP were user-specified. Then an MRI-compatible needle was inserted into the lesion under image guidance using the same True-FISP. A sclerosing agent (ethanolamine/doxycycline) mixed with gadopentate dimeglumine (2 $\mu$ mol/1 cc) was administered while monitoring from images obtained using a tri-plane fast low-angle shot (FLASH; TR/TE/ $\alpha$  11.5 ms/5.3 ms/25°, voxel size 1.3×1.3×5 mm, averages 3) pulse sequence with similar alignments of the three planes to the True-FISP. Finally, diagnostic imaging was repeated to verify success of the injection. The first 26 sessions were conducted using our first-generation True-FISP and FLASH (time/frame 4 and 8 sec, respectively). The last three sessions were conducted using second-generation sequences with shorter frame times (250 ms-1 sec for True-FISP, 500 ms-2 sec for FLASH) constructed by removing averaging and varying spatial resolutions. Times spent on entry site localization, needle placement, sclerosing agent injection, total needle and total scanner times were noted for each session.

**RESULTS**

The mean value  $\pm$  standard deviation (min: sec) of times spent on entry site localization, needle placement and injection is 6:18  $\pm$  8:25, 5:02  $\pm$  7:38 and 3:21  $\pm$  2:45, respectively. Corresponding values of total needle and

scanner times are 10:36  $\pm$  9:59 and 97:10  $\pm$  23:48. Total needle time forms only 10.8% of total scanner time, the remaining fraction of which was spent on diagnostic imaging and operational planning. The mean value of total needle time in our study is  $\approx$ 33% of the interventional time previously described at 0.2 T. In our initial experience, the use of second-generation sequences has further reduced total needle time. Complications are limited to one subject who developed skin breakdown over the lesion, which healed without any further intervention.

**CONCLUSION**

Flexibility in choosing alignments of three planes of interventional imaging sequences helps reduce the risk of injury to structures located in vicinity to the needle and in reducing procedure times. Sclerotherapy of low-flow malformations in the head/neck region is successfully performed at 1.5 T using tri-plane imaging for guidance with a reduced needle time of  $\approx$ 10 min.

**KEY WORDS:** MR imaging-guided sclerotherapy, low-flow vascular malformations, interventional MR imaging

**Tuesday Morning****10:30 AM - 12:00 PM****Murray Hill****(27e) Pediatrics: Functional Imaging & Neonatal Imaging****O-252****10:30 AM - 10:38 AM****Pathologic Fetal Brain at "Rest"**

Schöpf, V. •Kasprian, G. •Brugger, P. C. •Prayer, D.

Medical University Vienna  
Vienna, AUSTRIA

**PURPOSE**

Functional magnetic resonance imaging (fMRI) has allowed insights into the spatiotemporal distribution of human brain networks. According to the neurophysiologic property of the fetal brain to generate spontaneous activity, it has been shown already that resting-state network (RSN) patterns constitute in utero (Schöpf et al., 2011). In this study we investigated how detectable morphologic abnormalities of the fetal brain influence the emergence and constitutions of RSNs in utero.

**MATERIALS & METHODS**

This study included eight singleton fetuses between gestational weeks (GW) 20 - 36 from fetuses with brain abnormalities. One hundred and six patients were measured, 71 data sets had to be excluded due to movement related issues, 16 fetuses did not show any

brain development abnormalities. Fetuses were diagnosed with an oligo hydramnion and complete kidney agenesis (fetus 1), a semilobar holoprocencephaly and hypertelorism (fetus 2), ventriculomegaly (fetus 3), Dandy Walker syndrome (fetus 4), an occipital tumor and clubfoot deformity (fetus 5), retrognathia, cardiomyopathy, bell-shaped thorax, and Noonan syndrome (fetus 6), and corpus callosum agenesis (fetus 7 and 8). MR imaging was performed on a 1.5 T unit (Philips Medical Systems, Best, The Netherlands) using a SENSE (sensitivity encoding) cardiac coil with five elements. Measurements were performed using single-shot gradient-recalled echo-planar imaging (EPI). Between 10 and 15 axial slices (5 mm thickness) were acquired with a matrix size of 144 x 144, FOV of 250 x 250 mm and TE/TR of 50/1000 ms and a flip angle of 90°. Measurements included 50 to 300 image volumes with slices obtained perpendicular to the brainstem. Image preprocessing was performed with FSL (FMRIB's Software Library, [www.fmrib.ox.ac.uk/fsl](http://www.fmrib.ox.ac.uk/fsl)) including motion correction as implemented in MCFLIRT (fMRI motion correction tool) version 5.5 and brain extraction as implemented in BET (brain extraction tool) version 2.1. The single-subject time series volumes then were analyzed using independent component analysis (ICA) as implemented in MELODIC (multivariate exploratory linear decomposition into independent components) version 3.10, a part of FSL, using FastICA (Beckmann et al., 2004).

## RESULTS

Resting-state network patterns were obtained in all fetuses with brain malformations investigated. The extent of the network patterns differed depending on the brain pathology. Activity clusters were constituted as consistent and coherent configuration located in nonpathologic subplate areas. Among these RSNs a frontal network composition was detected consistently across all gestational ages and investigated fetuses especially showed varying spatial and temporal extension.

## CONCLUSION

Information on connectivity and extend of functional resting-state networks in fetal pathologic brains can help to provide a predictive measure on the developmental outcome of the brain in the future.

**KEY WORDS:** Functional MR imaging, resting-state networks

**O-253**

**10:38 AM - 10:46 AM**

## Development of Functional Brain Network Interactions during Movie Watching

Gao, W.; Gilmore, J.; Lin, W.

University of North Carolina at Chapel Hill  
Chapel Hill, NC

## PURPOSE

It has been suggested that the frontoparietal control network (FPC) will selectively augment/decrease the

default network (DF) and dorsal attention network (DA), respectively, to cope with the cognitive demand elicited by movie watching in adults. In this study, we aimed to investigate the developmental processes of functional network interactions among the three networks during movie watching from children to adults.

## MATERIALS & METHODS

Twenty-one 4-year-old (10 male, 48~53 months), 25 6-year-old (11 male, 73~78 months) and 16 adult subjects (9 male, 25~33 years) were recruited to undergo fMRI scan during natural, continuous movie watching in a 3 T scanner. AT2\*-weighted EPI sequence was used with TR = 2 sec, TE = 32 ms; 33 slices; and voxel size = 4 x 4 x 4 mm<sup>3</sup>. One hundred fifty volume data were acquired. Anatomical images also were acquired with TR = 1820 ms; TE = 4.38 ms; inversion time = 1100 ms; 144 slices; and voxel size = 1 x 1 x 1 mm<sup>3</sup>. After preprocessing and warping all fMRI images into the MNI template space, the functional regions for each network were defined as spheres (8 mm radius) around previously published MIN coordinates (6, 9, and 6 regions for FPC, DA, DF, respectively). Functional interactions between pairs of regions were calculated as the Pearson correlation between the corresponding average time series.

Subsequently, both the within-network synchronization and the between-network interaction pattern were compared statistically across the three age groups to delineate their temporal evolution. Significance was defined as  $p < 0.05$  after FDR correction for multiple comparisons.

## RESULTS

For the individual networks, neither DA nor DF network shows significant age-dependent changes in mean connection strength and the connection density (number of significant connections over all possible ones) is above 50% for both networks in all three age groups. In contrast, the mean connection strength of the FPC shows significant, step-wise increases ( $p = 0.03$  from 4 to 6 year olds;  $p = 0.004$  from 6 year olds to adults) and the connection density similarly increases from 36.1% in 4 year olds to 86. One per cent in 6 year olds and adults. The between-network interaction patterns demonstrate more dynamic changes. Specifically, when comparing adults with the pediatric groups: (1) the positive interactions between FPC and DF significantly increase ( $p = 0.003/0.03$  for 4 year/6 year olds, respectively); (2) the negative correlations between DA-FPC significantly decrease (i.e., more negative,  $p = 2.8e-6/3.8e-5$  for 4 year/6 year olds, respectively); (3) the negative interactions between DA-DF also significantly decrease ( $p = 2.7e-5/7.5e-4$  for 4 year/6 year olds, respectively). Overall, the connection density between these three networks jumps from 13.2% in 4 year olds to 25.0% in 6 year olds and finally reaches 55.6% in adults.

## CONCLUSION

While the network architectures of DA and DF are already adult-like in 4 year olds, the executive control network-FPC demonstrates continuing age-dependent

integration process from 4 years olds to adults, which is consistent with the documented late emergence of related brain functions such as conflict resolution and self-control (6). More importantly, all between-network interactions show age-dependent improvements consistent with their matured architecture, suggesting that the maturation of FPC may play a critical role in the network-level interaction among the three networks.

**KEY WORDS:** Brain development, functional networks, resting state

O-254

10:46 AM - 10:54 AM

### Regional Involvement of Central Visual Pathways in Preterm Children with Periventricular Leukomalacia: Spatial Distribution Maps and "Along Tract" Probabilistic Tractography Analysis

Ceschin, R.<sup>1</sup>•Wisnowski, J.<sup>2,3</sup>•Bluml, S.<sup>2,3</sup>•Panigrahy, A.<sup>1,2</sup>

<sup>1</sup>Children's Hospital of Pittsburgh of University of Pittsburgh Medical College, Pittsburgh, PA, <sup>2</sup>Children's Hospital of Los Angeles, Los Angeles, CA, <sup>3</sup>University of Southern California, Los Angeles, CA

#### PURPOSE

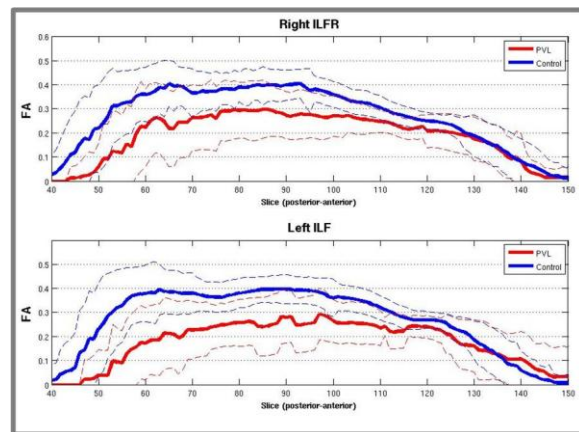
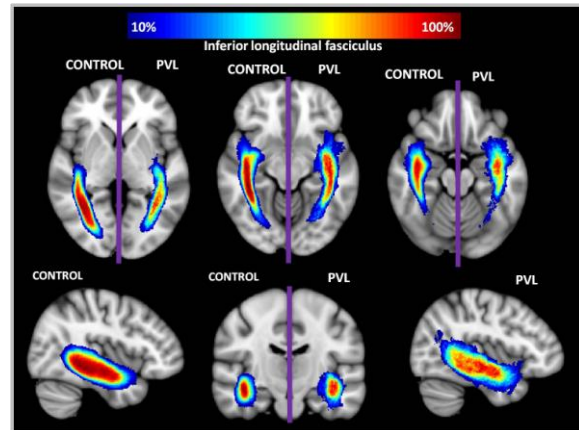
To test the hypothesis that there is preferential regional damage to central visual pathways in preterm children with periventricular leukomalacia (PVL). We use novel postprocessing methodology to improve spatial visualization of probabilistic tractography data and enhance the ability to see "along" tract distribution.

#### MATERIALS & METHODS

Diffusion tensor images were acquired on a 1.5 T GE scanner in 25 directions on 16 preterm children with PVL (mean age  $5.6 \pm 4$ ) and 75 controls (mean age  $5.7 \pm 3.4$ ). Probabilistic tractography and Tract-based spatial statistics (TBSS) were performed using Oxford's FMRIB to delineate central visual pathways [optic radiation, posterior thalamic radiation, inferior frontal orbital fasciculus (IFOF), inferior frontal fasciculus (ILF) and splenium]. Fractional anisotropy (FA) maps were coregistered into standard space using FSL's nonlinear registration method (FNIRT), and the resulting warps were applied to the previously delineated tracts. Spatial distribution maps were generated by overlaying each cohort's averaged bilateral tracts onto standard space and thresholding to only include voxels containing at least 10% of subject tracts. Mean FA was extracted at each slice along the principal longitudinal direction of the tract, for each subject in coregistered space.

#### RESULTS

Significant group differences were noted using both the TBSS and averaged probabilistic tractography metrics measurements in both dorsal and ventral stream central visual pathways ( $p < 0.001$ ), but no regional specificity could be determined. For cortical-cortical association pathways like the ILF (ventral visual pathway) both probability distribution maps and the "along" tract measurements revealed a preferential injury to the posterior regions of the tract compared to the anterior regions (Figures 1 and 2)



#### CONCLUSION

There is preferential posterior regional injury to central visual pathways in children with PVL which was best depicted by novel probabilistic tractography spatial distribution maps and "along" tract analysis compared to TBSS and averaged tractography based metric measurements.

**KEY WORDS:** Prematurity, tractography

O-255

10:54 AM - 11:02 AM

### Microstructural Abnormalities in Central Visual Pathways in Neonates with Congenital Heart Disease

Panigrahy, A.<sup>1,2</sup>•Paquette, L.<sup>2</sup>•Wisnowski, J.<sup>2,3</sup>•Del Castillo, S.<sup>2</sup>•Pruetz, J. D.<sup>2</sup>•Detterich, J. A.<sup>2</sup>•Ceschin, R.<sup>1</sup>•Nagasunder, A. C.<sup>2</sup>•Tavaré, J. C.<sup>2</sup>•Gilles, F. H.<sup>2</sup>•Seri, I.<sup>2</sup>•Williams, R. G.<sup>2</sup>•Bluml, S.<sup>2,3</sup>

<sup>1</sup>Children's Hospital of Pittsburgh of University of Pittsburgh Medical College, Pittsburgh, PA, <sup>2</sup>Children's Hospital of Los Angeles, Los Angeles, CA, <sup>3</sup>University of Southern California, Los Angeles, CA

#### PURPOSE

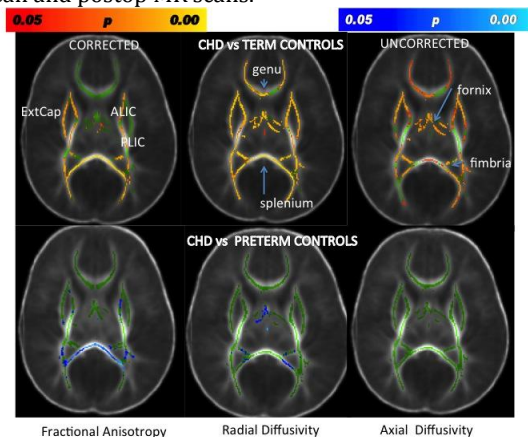
To test the hypothesis that there are selective microstructural abnormalities in central visual pathways in neonates with congenital heart disease (CHD) when compared to other critically-ill term and preterm neonates without CHD at term-equivalent age.

## MATERIALS & METHODS

A total of 96 term-equivalent neonates from a single institutional high-risk neonatal and cardiothoracic intensive care unit (ICU) population (42 CHD, 26 preterm controls and 28 term control infants) participated in this IRB-approved, HIPPA compliant study. Enrolled patients underwent clinically indicated MR studies with the addition of diffusion tensor imaging (DTI). Diffusion tensor imaging metrics were measured using two independent quantitative analyzes: (1) manually-traced standardized ROI placement and (2) automated voxel-based tract-based spatial statistics (TBSS). Statistical comparison was performed using ANOVA with Bonferroni correction. Correlation with peri-operative clinical variables also was performed.

## RESULTS

There was no difference in the postmenstrual age seen by MRI evaluation between the three neonatal groups at term-equivalent age. Widespread microstructural abnormalities were detected in multiple central visual-related tracts (inferior frontal orbital fasciculus, the optic radiation and the splenium) and multiple nonvisual related tracts (genu, posterior limb internal capsule) in the CHD group when compared to the control term group. In contrast, there were only little microstructural differences in the CHD cases compared to the preterm controls in the selected central visual pathways including the splenium. In the CHD patients, there was a high correlation ( $r$ ) between ADC/radial diffusivity of the thalamus and the preoperative pH level ( $r^2 = 0.6$ ) and the microstructure of the thalamus was also modified by age and timing of surgery ( $p < 0.05$ ). In addition, the thalamus was the only central visual pathway structure examined that demonstrated significant correlations between microstructural measurements and perioperative factors ( $p < 0.05$ ). There were no differences in the microstructure of the central visual pathways between the preoperative MR scan and postop MR scans.



## CONCLUSION

Neonates with CHD at term-equivalent age demonstrate diffuse microstructural abnormalities when compared to other high-risk term neonates without CHD. Marked similarity of microstructural changes with minimal differential involvement of central visual pathways between CHD neonates and preterm neonates without CHD suggest that there might be common mechanisms

of aberrant development which may underlie some of the similar long-term cognitive visual deficits that are seen in these patients.

**KEY WORDS:** Congenital heart disease

**O-256**

**11:02 AM - 11:10 AM**

## MR Imaging and Ultrasonography of the Brain in the Extreme Preterm Neonate

Barnes, P. D.<sup>1</sup>Bulas, D.<sup>2</sup>Slovis, T.<sup>3</sup>Wrage, L.<sup>4</sup>Cheng, H.<sup>4</sup>Hintz, S.<sup>1</sup>Higgins, R.<sup>5</sup>Finer, N.<sup>6</sup>Das, A.<sup>4</sup>

<sup>1</sup>Lucille Packard Children's Hospital at Stanford, Palo Alto, CA, <sup>2</sup>Children's National Medical Center, Washington, DC, <sup>3</sup>Children's Hospital of Michigan, Detroit, MI, <sup>4</sup>RTI International, Research Triangle Park, NC, <sup>5</sup>The Eunice Kennedy Shriver National Institute of Child Health and Human Development, Bethesda, MD, <sup>6</sup>University of San Diego, San Diego, CA

## PURPOSE

To compare near-term brain MRI with early and late brain ultrasound (US) in a large cohort of extreme preterm newborns.

## MATERIALS & METHODS

A prospective secondary study was done of near-term MRI (mean PMA 37.9 weeks) as compared with early (4-14 days postnatal age) and late (34-42 weeks PMA) US in 480 infants (mean 25.9 weeks EGA) as part of the multicenter, NICHD Neonatal Research Network NRN Surfactant Positive Airway Pressure and Oximetry Trial (SUPPORT). All had late US and MRI within 2 weeks of each other. Independent MRI and US central readers were masked to the clinical and other neuroimaging findings.

## RESULTS

Three hundred six (89.5%) of 342 infants with normal late US had normal near term MRI or only mild white matter abnormalities (WMA); the remaining 36 (10.5%) had moderate-severe WMA. All 18 infants with late US findings of moderate-severe ventriculomegaly (VMG) had MRI findings of moderate-severe WMA, moderate-severe VMG, or cystic lesions. Seventy-six per cent of 46 infants with grade 3 or 4 hemorrhage on early US had moderate-severe WMA on MRI. On MRI, cerebellar abnormalities were present in 79 (16.5%) and cerebral gray matter abnormalities were present in 6 (1%). Posterior fossa lesions were seen on US in 1.6%, but mastoid views were included in only about 50% of the centrally read US.

## CONCLUSION

In the largest extreme preterm cohort to date with near-term MRI and serial US, 19% had moderate to severe WMA on brain MRI, similar to previous reports. Cerebellar abnormalities were detected more frequently by MRI than by US. Neurodevelopmental outcomes at 18-22 months and school age will assess the relative and combined values of MRI and US as outcome predictors.

**KEY WORDS:** Neonatal, prematurity, MR imaging

**O-257**

**11:10 AM - 11:18 AM**

### **MR Imaging in Therapeutic Hypothermia for Term Hypoxic-Ischemic Encephalopathy**

Shankaran, S.<sup>1</sup>Barnes, P. D.<sup>2</sup>Hintz, S.<sup>2</sup>Laptook, A.<sup>3</sup>Higgins, R.<sup>4</sup>McDonald, S.<sup>5</sup>Zaterka-Baxter, K.<sup>5</sup>Das, A.<sup>5</sup>

<sup>1</sup>Wayne State University School of Medicine, Detroit, MI, <sup>2</sup>Lucille Packard Children's Hospital at Stanford, Palo Alto, CA, <sup>3</sup>Women's & Infants Hospital of Rhode Island Brown University, Providence, RI, <sup>4</sup>The Eunice Kennedy Shriver National Institute of Child Health and Human Development, Bethesda, MD, <sup>5</sup>RTI International, Research Triangle Park, NC

#### **PURPOSE**

To correlate brain MRI findings with neurodevelopmental outcomes in a retrospective study of term neonates enrolled in a NICHD Neonatal Research Network trial of whole body hypothermia.

#### **MATERIALS & METHODS**

Brain MRI findings were obtained by 44 weeks postmenstrual age in 136 infants with moderate-severe hypoxic-ischemic encephalopathy (HIE) who were randomized to cooling (33.5 degrees C for 72 hours). There were 73 in the hypothermia group and 63 in the control group. All MRIs were reviewed by a central reader masked to the clinical findings, groupings, and outcomes. The MRI findings were scored systemically according to pattern and extent of injury, including involvement of the cerebral hemispheres, basal ganglia, thalami, internal capsules, and other structures. Brain injury scores were correlated with death or disability at 18 months postnatal age.

#### **RESULTS**

No MRI abnormalities were observed in 38 of 73 infants (52%) in the cooled group and in 22 of 63 infants (35%) in the control group ( $P = 0.08$ ). Infants in the cooled group had fewer areas of injury (12%) as compared with the control group (22%,  $P = 0.02$ ). Fifty-one infants were dead or disabled by 18 months. The brain injury score correlated with outcome of death or disability ( $P = 0.001$ ) and disability among survivors ( $P = 0.0001$ ).

#### **CONCLUSION**

Fewer areas of brain injury on MRI were observed following whole-body cooling. The MRI brain injury score is a marker of death or disability at 18 months following hypothermia for term HIE.

**KEY WORDS:** Neonatal, hypoxia-ischemia, MR imaging

**O-258**

**11:18 AM - 11:26 AM**

### **Prognostic Utility of Combined Apparent Diffusion Coefficients and MR Spectroscopy in Infants with Hypoxic Ischemic Injury**

Johnson, J. M.<sup>1</sup>Ratai, E.<sup>1</sup>Chou, J.<sup>1</sup>Krishnamoorthy, K.<sup>1</sup>Caruso, P.<sup>1</sup>Grant, P. E.<sup>2,1</sup>

<sup>1</sup>Massachusetts General Hospital, Boston, MA,

<sup>2</sup>Childrens Hospital Boston, Boston, MA

#### **PURPOSE**

Hypoxic-ischemic injury (HII) is an important cause of perinatal mortality and morbidity. Because the prognosis is uncertain, reliable prognostic indicators are needed. MR spectroscopy (MRS) and diffusion-weighted imaging (DWI) have emerged as potential biomarkers for outcome. The purpose of this study was to evaluate combined use of ADC and MRS measurements retrospectively for prediction of outcome in neonates after HII.

#### **MATERIALS & METHODS**

A retrospective database search identified 17 neonates (mean gestational age 39.1 weeks) with HII. Patients were studied at 1.5 T within 5 days of life. Newborns with congenital malformations, inherited metabolic disorders, and evidence of intracranial infection were excluded. None underwent hypothermic treatment. Single voxel 1H-MRS (TR/TE = 1500/144 ms, NA = 128) was performed over a region of the right basal ganglia (BG). Absolute concentrations of choline (Cho), creatine (Cr), lactate (Lac) and N-acetylaspartate (NAA) were obtained. Apparent diffusion coefficient (ADC) regions of interest (ROI) were placed, matched to the SV MRS voxels. A receiver operating characteristic (ROC) analysis was conducted to determine the predictive value of the MRS and ADC measurements relative to survival. Patients were classified into favorable outcome (no, mild, and moderate developmental delay) and unfavorable outcome (severe developmental delay and death). Spearman Rank analysis was used to determine the relationship between ADC and spectroscopic markers.

#### **RESULTS**

Nine of 17 term neonates had unfavorable outcomes. Receiver operating characteristic analysis revealed an association between poor outcome and low ADC values in the basal ganglia. Low basal ganglia concentrations of Cho, Cr and NAA also were associated with poor outcome (Table 1). Spearman Rank analysis between ADC and spectroscopic markers revealed significant correlations between ADC and choline ( $p = 0.005$ ,  $R = 0.71$ ) as well as ADC and NAA ( $p = 0.003$ ,  $R = 0.73$ ) No correlation with lactate was found.

ROC analysis against favorable outcome	
Measurement	AUC
ADC	0.83
Cho	0.73
Cr	0.81
NAA	0.81
Lac	0.59

#### **CONCLUSION**

These results support prior studies that found that low ADC values and low concentrations of NAA and Cho in the BG correlate with poor outcome. Absolute concentrations yielded a better prognosis for the outcome compared to metabolic ratios. Lower Cr



concentrations in the basal ganglia were associated with poor outcome consistent with decreased energy stores. Higher choline levels were predictive of better outcome and correlated with ADC values, possibly indicating sparing of glial cells.

**KEY WORDS:** Hypoxic ischemic insult, apparent diffusion coefficient, MR spectroscopy

**O-259**

**11:26 AM - 11:34 AM**

### Use of Novel MR Imaging Tractography-Derived Metrics to Detect Axonal Pathway Damage in Neonatal Encephalopathy

Shen, P. Y.·Hess, C. P.·Von Morze, C.·Barkovich, A.

University of California San Francisco Medical Center  
San Francisco, CA

#### PURPOSE

Cerebral and brainstem white matter tracts commonly are affected by hypoxic-ischemic injury. However, the small size of many pathways limits their precise anatomical localization in neonates. The goal of this work is to determine whether two recently proposed fiber tractography metrics, track density imaging (TDI) and average path-length (APL), can identify tract-specific differences between infants with mild to severe neurologic outcome after neonatal encephalopathy.

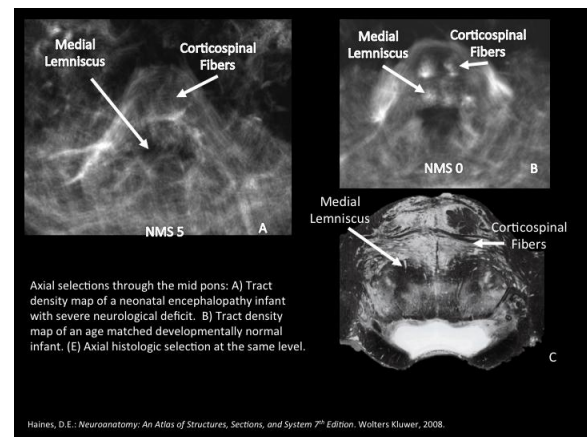
#### MATERIALS & METHODS

*Patient selection and outcome measures:* 23 preterm and term infants with neonatal encephalopathy were imaged at 3-4 days of life. Standardized neuromotor scores were obtained at 3 months of age. *Data acquisition:* Diffusion data were acquired on 1.5 T MRI scanner (General Electric Healthcare Waukesha, WI). Subjects were scanned utilizing a 30-direction DTI sequence with  $b = 700 \text{ s/mm}^2$  and voxel size of  $2.5 \times 2.5 \times 3 \text{ mm}^3$ . *Fiber-tracking:* Fiber tractography was performed utilizing constrained spherical deconvolution using MRtrix (Brain Research Institute, Melbourne, Australia) and in-house software developed by our group. *Tractography derived metrics:* Track density maps were constructed by counting the fraction of the total number of tracts passing through each voxel. Average path-length maps were constructed by adding the length of all streamlines passing through each voxel and dividing that by track density. *Image analysis:* Regions of interest were drawn manually over the white matter tracts of the corpus callosum, anterior and posterior limbs of internal capsule, ventrolateral and pulvinar thalamus and cerebral peduncles by a single neuroradiologist. Calculated track density and average path-length were normalized to average intracranial volume to account for differences in brain size.

#### RESULTS

Tractography-derived maps, including TDI and APL, reconstructed from the comparatively lower-resolution diffusion data yield a dramatic improvement in both spatial resolution and white matter contrast. Neonatal fractional anisotropy, TDI and APL of the corpus callosum (FA  $p = 0.002$ , TDI  $p = 0.006$ , APL  $p = 0.08$ ),

posterior internal capsule ( $p = 0.002$ ,  $0.09$ ,  $0.8$ ), ventrolateral thalamus ( $p = 0.03$ ,  $0.06$ ,  $0.07$ ), pulvinar ( $p = 0.15$ ,  $0.03$ ,  $0.03$ ) and cerebral peduncle ( $p = 0.008$ ,  $0.007$ ,  $0.15$ ) correlate inversely with severity of neurologic outcomes at 3 months of age.



#### CONCLUSION

High-resolution TDI and APL maps may help to prognosticate neurologic outcomes in encephalopathic neonates as has been shown with diffusivity and fractional anisotropy.

*Acknowledgement:* Project is supported by the GERRAF Academic Fellowship and by NIH R01EB009756, NIH R01NS046432 and NIH P50NS035902.

**KEY WORDS:** Hypoxic ischemic, track density imaging, average pathlength

**O-260**

**11:34 AM - 11:42 AM**

### Predicting Outcomes in Hypoxic-Ischemic Encephalopathy: Tract-Based Analysis of Corticospinal Tract and Corpus Callosum

de Macedo Rodrigues, K.<sup>1</sup>·Fons Estupina, M.<sup>1,2</sup>·McLean, A.<sup>3</sup>·Khawaja, O.<sup>1</sup>·Paldino, M.<sup>1</sup>·Grant, P.<sup>1</sup>

<sup>1</sup>Children's Hospital Boston, Boston, MA, <sup>2</sup>Sant Joan de Seu Hospital for Children, Barcelona, SPAIN, <sup>3</sup>Brigham and Women's Hospital, Boston, MA, <sup>4</sup>Children's Hospital Boston, Boston, MA

#### PURPOSE

Prior quantitative apparent diffusion coefficient (ADC) studies in hypoxic-ischemic encephalopathy (HIE) have been region of interest-based. We set out to determine if tract-based measures of CST and CC involvement showed selective CST involvement in HIE and if mean tract ADC decrease correlates with early motor outcomes.

#### MATERIALS & METHODS

Retrospectively included were neonates ( $\geq 36$  weeks of gestation) with clinical evidence of HIE and brain MR imaging (MRI) including 30 direction diffusion tensor imaging (DTI) at 3 T within 7 days of birth. Neonates with normal brain MRI in the first week without HIE were included as controls. Tracts were reconstructed using Diffusion Toolkit with 35-degree angular threshold. CST, CC, splenium of the corpus callosum

(SCC) and genu of the corpus callosum (GCC) were manually dissected in TrackVis. Motor outcome was assessed using the Gross Motor Function Classification System (GMFCS). The study was approved by the Committee on Clinical Investigation at Children's Hospital, Boston.

## RESULTS

Inclusion criteria were met by 37 HIE and nine controls. Mean age at MRI was  $2.9 \pm 1.5$  and  $4.2 \pm 0.9$  days respectively. Mean age at last follow up was  $12.7 \pm 7.6$  months. HIE versus Control: Mean ADC in CST and CC was lower in HIE neonates but was significant only in CST. Mean FA in CST and CC was significantly lower in HIE patients. HIE Good vs Bad Outcome: Outcome in HIE patients was poor in 10 and good in 27. The poor outcome group had significantly lower mean ADC in CST, GCC and SCC but not in the entire CC. HIE Hypothermia vs No Hypothermia: Hypothermia was performed in 22. All hypothermia had significantly higher ADC in SCC. Mean FA was also higher in cooled in all tracts except in GCC but differences were not significant. HIE without and with neonatal seizure (NS): HIE with NS had significantly lower mean ADC in SCC and GCC as well as CST. In addition, HIE with NS had elevated mean FA in these same tracts but this was only significant in the RCST. HIE Hypothermia, with and without NS: Within the cooled group, those with NS had lower mean ADC in all the tracts but this was significant only in SCC and GCC but not in the entire CC. HIE with NS had higher mean FA in all selected tracts but this was only significant in the SCC.

## CONCLUSION

Tract-based analysis demonstrated selective vulnerability of the CST in HIE compared to controls, with lower mean ADC correlating significantly with early neurologic outcome (neuromotor scores). Mean tract FA was also lower in HIE with poor motor outcome. Treatment with hypothermia was associated with a significant increase in mean ADC in SCC and significantly higher mean tract FA suggesting less metabolic compromise and preservation of white matter microstructure. Neonatal seizure were associated with lower ADC but higher FA in the SCC similar to other reports of transient seizure injury.

**KEY WORDS:** Hypoxic-ischemic encephalopathy, diffusion tensor imaging, tractography

O-261

11:42 AM - 11:50 AM

## Visualization of the Anisotropic Organization of the Transient Fetal Ganglionic Eminence Proliferative Zone Using In Utero Tractography

Mitter, C. S. • Kasprian, G. • Brugger, P. C. • Hainfellner, J. A. • Prayer, D.

Medical University of Vienna  
Vienna, AUSTRIA

## PURPOSE

The fetal brain exhibits several transient structures and layers that are not found in the infant or adult brain and

that play important roles in cerebral development. Located adjacent to the lateral ventricle, an enlarged portion of the ventricular/subventricular zone forms the ganglionic eminence that contains the proliferative zone for developing GABAergic neurons that form the interneurons of the cerebral cortex as well as the principal neurons of the basal ganglia. In order to identify the normal 3D imaging patterns of this structure, we used in utero diffusion tensor imaging (DTI)-based tractography to three-dimensionally display the normal organization of the ganglionic eminence proliferative zone based on its cell density related high anisotropy in living unsedated fetuses.

## MATERIALS & METHODS

Preselected nonmotion degraded DTI examinations of 13 living unsedated fetuses [21 - 27 gestational weeks (GW)] without gross cerebral malformations were included. Orthogonal axial diffusion tensor sequences (16 directions, reconstructed voxel size  $0.94 \text{ mm} \times 0.94 \text{ mm} \times 3 \text{ mm}$ , b-values of  $0 \text{ s/mm}^2$  and  $700 \text{ s/mm}^2$ ) were performed using a 1.5 T superconducting MR unit. Color coded FA maps were coregistered geometrically with multiplanar T2-weighted MR sequences. The ganglionic eminence was defined anatomically using a multiple ROI approach and visualized using a FACT algorithm (Philips Extended MR Workspace 2.6.3.2).

## RESULTS

Tractography of the ganglionic eminence was successful in 10/13 subjects in both hemispheres and in 3/13 subjects in only the right hemisphere. According to its anisotropic diffusion properties multiple "pseudofiber" tracts were identified within the ganglionic eminence. Coregistered T2-weighted sequences confirmed the location to be within the strongly hypointense cell rich proliferative layers of the ganglionic eminence. "Pseudofiber" tracts showed a C-shaped course with an anterior-posterior orientation along the body of the lateral ventricle and a superior-inferior orientation in front of the trigone.



Figure: Twenty-three GW-old fetus: Tractography of ganglionic eminence results in C-shaped "pseudofibers" along lateral ventricle, thus confirming strongly

anisotropic diffusion properties of ganglionic eminence proliferative zone.

#### CONCLUSION

This in utero and in vivo study demonstrates the potential of DTI-based tractography to visualize the three-dimensional structure of the ganglionic eminence based on its anisotropic microstructure in unsedated fetuses as early as 21 GW. Anisotropic organization of the ganglionic eminence may be related to tangential migration of developing neurons in this region. Due to its important role in the formation of GABAergic neurons, pathologies of the ganglionic eminence have the potential to cause a range of neurodevelopmental disorders, including epilepsy.

**KEY WORDS:** Fetal MR imaging, tractography, ganglionic eminence

**O-262**

**11:50 AM - 11:58 AM**

#### Assessment of Diffusion Images Acquired Using the American College of Radiology Phantom: A Comparison of Three Vendors

Rollins, N. K.<sup>1</sup>•Panigrahy, A.<sup>2</sup>•Babcock, E.<sup>3</sup>•Holshouser, B.<sup>4</sup>•Huang, H.<sup>3</sup>•Wang, Z.<sup>1</sup>

<sup>1</sup>Childrens Medical Center, Dallas, TX, <sup>2</sup>Childrens Hospital of Pittsburgh, Pittsburgh, PA, <sup>3</sup>University Texas Southwestern Medical Center, Dallas, TX, <sup>4</sup>Loma Linda Childrens Hospital, Loma Linda, CA

#### PURPOSE

Technical differences in MR scanners may result in measurable differences in scalar metrics that could be attributed erroneously to biological differences in patients; an important issue in conducting a multisite study using diffusion imaging. The American College of Radiology (ACR) phantom is widely available. We used the ACR phantom to compare quality measures for diffusion tensor images (DTI) acquired on different MR vendors using standardized protocols.

#### MATERIALS & METHODS

Diffusion tensor imaging was acquired using the ACR phantom on 3 T scanners: Siemens [TrioTim Syngo B17 (n = 2)], GE [HDXT 15.0 and HD16.0 (n = 2)], and Philips Achieva R3.2-3.6 (n = 4)]. Participating sites followed mutually agreed upon vendor-specific DTI protocols used for neonates in clinical practice: SS-EPI; b = 700; ~2 mm 3 voxel; 30-32 directions; TE ~84 msec; 1 acquisition; parallel imaging; multichannel (8-32) head coil. Tensor data were analyzed using internally developed software in IDL. B0 and eddy current distortion were assessed by analyzing grid line distortion on ACR slice 5; deviations from linearity were measured in the phase encoding direction. ACR slice 7 was used to assess SNR of the center and periphery of the b=0 image, and fractional anisotropy (FA) of the phantom, which should approach 0. Deviations from specified sequence parameters were recorded.

#### RESULTS

Both Siemens scanners had some image degradation due to vibration. Nonlinear gridline distortion was highest on the GE followed by Philips but was corrected with the subsequent use of second order shimming. Eddy current distortion was consistently smaller than acquisition voxel size after image registration. TE was the most variable parameter (74- 92 msec); acquisition bandwidth range was 1563-2928 Hz/pixel. The 2 mm slice thickness was problematic on clinical GE scanners resulting in nonisotropic voxels. Across vendors, SNR was consistently higher in the image periphery than center by a factor of 1.3-2.0. Signal to noise normalized by the voxel size was greatest at image center for GE and 14% lower on average on Siemens and Philips scanners. Fractional anisotropy deviated from 0 .07-2.4%. The highest FA values were seen on Philips scanners.

#### CONCLUSION

In the absence of an affordable widely available anisotropic phantom, the ACR phantom can be used to objectively assess image quality across vendors and sites; knowledge of which aids both the vendors and sites.

**KEY WORDS:** Diffusion imaging, quality assurance, multisite comparison

## Tuesday Afternoon

**1:00 PM - 2:30 PM**

**Grand Ballroom Suite**

**(29) ASPNR PROGRAMMING: 2012  
ASP NR INTERESTING CASE  
SESSION (AR)**

**O-263**

**1:00 PM - 1:30 PM**

A. James Barkovich, MD

UCSF Medical Center  
San Francisco, CA, USA

#### PRESENTATION SUMMARY

I will look at and discuss cases that are presented to me.

**O-264**

**1:30 PM - 2:00 PM**

Andrea Rossi, MD

Head, Neuroradiology, G. Gaslini Children's Hospital  
Genoa, Italy

#### PRESENTATION SUMMARY

A variety of interesting and informative spine cases will be shown and discussed with illustrations of the differential diagnosis and final diagnosis.

**O-265**

**2:00 PM - 2:30 PM**

Caroline D. Robson, MB, ChB

Radiology, Children's Hospital  
Boston, MA, USA

Presentation Summary  
Head and neck

## Tuesday Afternoon

**1:00 PM - 2:30 PM**  
**Beekman/Sutton North**

**(30) ASFNR PROGRAMMING:  
EMERGING TECHNIQUES IN  
FUNCTIONAL NEURORADIOLOGY**

**O-266** **1:00 PM - 1:25 PM**

### **Florbetapir-PET Imaging for Beta Amyloid Evaluation**

Dean F. Wong, MD, PhD

Johns Hopkins Medical Institutions  
Baltimore, MD, USA

#### **PRESENTATION SUMMARY**

Until the last decade, the measurement of brain  $\beta$ -amyloid, an Alzheimer's disease marker, could only be performed post mortem. In 2003, the first PET imaging in a living human brain with  $^{11}\text{C}$ -PIB was performed. Since then, there has been an explosion of such studies globally, expanding our understanding of amyloid deposition in normal aging mild cognitive impairment (MCI) and dementia, such as Alzheimer's disease (AD).  $^{11}\text{C}$ -PIB PET has been a major research tool both cross-sectionally and longitudinally. Baseline  $^{11}\text{C}$ -PIB has also been shown to predict longitudinal cognitive decline as well as correlate with clinical diagnoses and current cognitive status. Further, various methods of quantification of  $^{11}\text{C}$ -PIB have been attempted to help predict which patients with MCI are more likely to go on to develop AD.

In 2010,  $^{18}\text{F}$  - AV45 (florbetapir F 18) was first demonstrated to show dramatic differences between patients with AD and matched healthy controls (HC). A major advantage of  $^{18}\text{F}$  is its 110-minute half life, versus the 20-minutes of  $^{11}\text{C}$ , which expands the availability of the PET imaging of brain amyloid geographically to centers that do not have onsite cyclotrons. In addition to florbetapir, a number of other  $^{18}\text{F}$  tracers, including AV-1 and [ $^{18}\text{F}$ ] flutemetamol, are being developed, at least two of which are being considered for future NDAs by the FDA for use as clinical radiopharmaceuticals in general nuclear medicine.

Recently, the Alzheimer's Disease Neuroimaging Initiative - 2 (ADNI-2) adopted the use of florbetapir, based on similar studies done with MRI and FDG in ADNI-1, as one of the principal outcome measures for studying the natural course of Alzheimer's Disease. Such data will not only provide significant information

on the characteristics and course of the disorder, but a guide by which drugs for the treatment of dementia might slow or change the progression of amyloid deposition.

This presentation will emphasize the development of florbetapir studies and their quantification. The second portion will include how florbetapir has been expanded to numerous sites in North America and Europe and Asia and will give a general summary of the research to date. We will also document attempts at the validation of florbetapir for use in pathology; in January 2011, for example, amyloid deposition detected with PET in patients shortly before death was confirmed at autopsy. Finally, we will discuss potential future clinical and research usage of such tracers for other related disorders.

**O-267**

**1:25 PM - 1:50 PM**

### **Brain MR Imaging with Use of Iron Oxide Nanoparticle, Ferumoxytol, in Preclinical and Clinical Studies**

Edward A. Neuwelt, MD

Oregon Health & Science University  
Portland, OR, USA

#### **PRESENTATION SUMMARY**

Brain MR Imaging with Use of Iron Oxide Nanoparticle, Ferumoxytol, in Preclinical and Clinical Studies

The objectives of our ferumoxytol studies are to improve magnetic resonance imaging (MRI) approaches for characterizing tumor inflammation and vascular properties in animal brain tumor models and patients with central nervous system (CNS) lesions. Increased permeability of the blood-brain barrier (BBB) as well as inflammation both at the BBB and in brain tissue, are fundamental components of brain tumors and CNS injury from chemotherapy or radiation therapy. Conventional gadolinium-based contrast agents (GBCA) are low molecular weight extracellular chelates that rapidly and transiently detect nonspecific BBB permeability changes due to tumor or inflammation. Ferumoxytol iron oxide nanoparticle MR contrast agent, by contrast, is initially localized in the blood pool, and slowly leaks across the BBB to become intracellularly trapped in resident phagocytic cells. These nanoparticles will therefore function first as a blood pool agent for the accurate measurement of tumor relative cerebral blood volume (rCBV) with dynamic MRI at early time points (30 min), and then as cellular contrast agents for assessment of tumor inflammation (1-2 days). In animal models of primary and metastatic brain tumors, ferumoxytol dynamic MRI showed that the anti-angiogenic agent bevacizumab decreases tumor blood volume, equivalent to high dose steroid, while targeting vascular  $\alpha\text{V}$ -integrins increased tumor blood volume. In clinical studies, we have optimized dynamic and anatomical MRI of brain tumors with ferumoxytol at different magnetic field strengths. Ferumoxytol appears to be a superior contrast agent, compared to GBCA, for assessing therapy-induced changes in tumor vasculature and can be used to clearly differentiate true tumor progression from pseudoprogression after

chemoradiotherapy, and true tumor response from pseudoresponse after anti-angiogenic therapy. We are evaluating ferumoxytol for imaging inflammation, assessing nanoparticle uptake into tumor-associated macrophages. Our overall hypothesis is that MRI with ferumoxytol will be complimentary to GBCA, to improve diagnosis and provide better and earlier demonstration of tumor response to treatments. Ultimately, our goal is to validate dynamic MRI of vascular properties with ferumoxytol followed by anatomical imaging of inflammation, so that this becomes the new standard of care for both diagnosis and treatment response assessment in primary and metastatic brain tumors.

**O-268** **1:50 PM - 2:10 PM**

### **VASO MR Imaging for Blood Volume Imaging**

Hanzhang Lu, PhD

UT Southwestern Medical Center  
Dallas, TX, USA

#### **PRESENTATION SUMMARY**

Imaging of cerebral blood volume (CBV) can also be achieved by taking advantage of differences in intrinsic MR properties between blood and surrounding tissues. In this lecture, I will describe a technique called Vascular-Space-Occupancy (VASO) MRI (Lu et al., 2003), which utilizes T1 difference between tissue and blood to separate signals from these two compartments. This technique can operate in two different modes, one without exogenous contrast agent and the other with the injection of Gd-DTPA contrast agent. Both modes are introduced in this lecture. The first mode is completely based on intrinsic properties of the brain, thus has two advantages. First, relative changes in CBV can be measured without the need for exogenous contrast agent. Second, one can perform the measurement at a relatively high temporal resolution (e.g. 6 seconds) compared to the previous methods which requires considerable waiting for the contrast agent to be washed out. The first mode can only give relative changes in CBV but not absolute CBV values at baseline. To obtain absolute CBV values at baseline, the second mode can be used which employs pre- and post-contrast scans, between which a dose of Gd-DTPA is injected (Lu et al., 2005; Lu et al., 2008). Compared to the other contrast-agent based methods, the VASO approach provides higher sensitivity, does not require the knowledge of arterial input function, and is relatively less sensitive to variations in contrast agent concentrations.

#### **Key Points**

VASO imaging is based on intrinsic T1 differences between blood and tissue

The technique uses non-selective inversion recovery sequence and the inversion time is set to null the blood signal

This method can be used to non-invasively detect CBV changes due to brain activation or physiologic challenge  
Absolute values of CBV can be measured by performing image subtraction between post- and pre-contrast scans when Gd-DTPA is used

The post/pre signal difference has a straightforward relationship with CBV as the pre-contrast blood magnetization is 0 and the post-contrast blood signal is at equilibrium magnetization

CBV quantification in VASO is therefore simpler compared to DSC and DCE methods, and does not require the knowledge of arterial input function

**O-269** **2:10 PM - 2:30 PM**

### **Resting State fMRI for Mapping Brain Networks**

Haris Sair, MD

Radiology/Neuroradiology, Johns Hopkins Medicine  
Baltimore, MD, USA

#### **PRESENTATION SUMMARY**

Resting state functional Magnetic Resonance Imaging (rs-fMRI) has been used for examination of the brain as an interconnected network of varied brain regions, each subserving a particular role in the context of integrated functioning. These networks represent anatomically distinct however temporally correlated regions of the brain, and disruptions both within and between these networks have been demonstrated in various clinical disorders. Rs-fMRI acquisition, processing, and analysis methods will be briefly introduced for mapping brain networks. The application of graph theory to brain mapping and functional connectivity will be reviewed. Common intrinsic brain networks that have been identified using rs-fMRI will be reviewed.

## **Tuesday Afternoon**

**1:00 PM - 2:30 PM**  
**Sutton Center/South**

**(31) ASHNR PROGRAMMING:**  
**SKULL BASE**

**O-270** **1:00 PM - 1:25 PM**

### **Skull Base Anatomy/Developmental Lesions**

C. Douglas Phillips, MD, FACR

Weill Med. College Of Cornell/NY Presby'n  
New York, NY, USA

#### **PRESENTATION SUMMARY**

The central skull base is a complex osteo-cartilaginous structure that interfaces with the sinonasal cavity, the orbits, the soft tissue of the supra hyoid neck, and the upper cervical spinal canal. Knowledge of the embryology and early development contribute to understanding the potential maldevelopmental conditions there, such as encephaloceles, and also the myriad malformations of the craniocervical junction. This introductory talk of the skull base will cover the normal and abnormal development of the skull base, and cover some more common malformations of the



skull base. Complex anterior skull base lesions which may involve the sinonasal cavity will be discussed in more detail. Central skull base maldevelopmental lesions, including encephaloceles, will be discussed. Craniocervical junction pathology will be discussed briefly.

**O-271****1:25 PM - 1:50 PM****Intrinsic Skull Base Pathology**

Richard H. Wiggins, III, MD, CIIP

Radiology, University Of Utah Health Sciences Center  
Salt Lake City, UT, USA**PRESENTATION SUMMARY**

Intrinsic Skull Base Pathology. The rare intrinsic lesions of the skull base are those arising from the bones of the skull base themselves. There are more common extrinsic lesions of the skull base, which invade the skull base from the surrounding structures. Both CT and MRI are complimentary for evaluation of lesions of the skull base. CT is best for osseous matrix evaluation, while MRI demonstrates improved soft tissue evaluation. Both intrinsic and extrinsic lesions of the skull base can have similar appearances, and their imaging appearances will be compared and described, including fibrous dysplasia, metastasis, meningioma, multiple myeloma, non-Hodgkin lymphoma, pituitary macroadenoma, arachnoid granulation, Langerhans histiocytosis, chordoma, Paget disease, and chondrosarcoma.

**O-272****1:50 PM - 2:10 PM****Nasopharyngeal Neoplasms**

Christine M. Glastonbury, MBBS

Radiology/Neuroradiology, University Of California, San Francisco  
San Francisco, CA, USA**PRESENTATION SUMMARY**

Imaging already plays a central role in the evaluation of nasopharyngeal disease as this region may be difficult to examine clinically. While nasopharyngeal carcinoma (NPC) is the most common primary malignancy of the nasopharynx it is an uncommon malignancy in much of the western world. The 2010 revised AJCC brought important changes to the TNM staging of NPC and additionally there have been important changes in the World Health Organization (WHO) terminology used for the histologic classification of nasopharyngeal carcinoma. This lecture will update you on these modifications and new terminologies while emphasizing the important nasopharyngeal anatomy landmarks, the imaging appearances and pitfalls of nasopharyngeal carcinoma and other common and rare nasopharyngeal neoplasms.

**Tuesday Afternoon****1:00 PM - 2:30 PM****Tranon Ballroom****(32) GENERAL PROGRAMMING:  
INTRACRANIAL VESSEL WALL  
IMAGING****O-273a****1:00 PM - 1:20 PM****The Epidemiology and Clinical Implications of  
Intracranial Atherosclerotic Disease**

Rick Swartz, HBS, MD, PhD, FRCPC

Sunny Brook Health Sciences Centre  
Toronto, ON, Canada**PRESENTATION SUMMARY**

Stroke is the leading cause of adult neurological disability in North America and the second leading cause of death worldwide. Intracranial atherosclerosis is the most common cause of stroke worldwide, accounting for nearly 50% of all strokes in Asia and over 10% in North America. This presentation will review the incidence and prevalence of intracranial atherosclerosis and its importance as a cause of stroke both nationally and globally. The clinical impact of intracranial atherosclerosis will be reviewed, highlighting recent changes in clinical management of symptomatic intracranial stenosis. The need for accurate diagnosis and improved prognostication will be discussed in the context of evolving treatment options for intracranial atherosclerosis.

**O-273****1:20 PM - 1:40 PM****From Extracranial to Intracranial Disease: A New  
Frontier in Vascular Imaging**

Bruce A. Wasserman, MD

Radiology, Johns Hopkins University  
Baltimore, MD, USA**O-274****1:40 PM - 2:00 PM****Vessel Wall MRI Imaging of Intracranial  
Vasculopathies**

David J. Mikulis, MD

Toronto Western Hospital  
Toronto, ON, Canada**PRESENTATION SUMMARY**

Ischemic stroke occurs as an ictal event where there is a sudden severe reduction in blood flow leading to permanent tissue injury. The temporal evolution of this injury can be categorized into acute, subacute, and chronic phases. The acute phase occurs within hours of symptom onset. The subacute phase occurs in the ensuing days, weeks, and months in which the injury

and response to injury is completed. The chronic phase is the stable state of the tissue after these events have occurred. We have found evidence of an additional unrecognized phase that is associated with chronic blood flow insufficiency not associated with sudden onset of symptoms. This injury is occurring inter-ictally, and is a type of injury that has not been extensively studied and is not in the mindset of most clinicians and Neurologists. Evidence for this consists of thinning of the cerebral cortex and increased water diffusion in the adjacent white matter in patients who have severe vascular stenoses but with normal brain MRI studies. These patients have a very specific defect in flow physiology: they cannot increase blood flow in response to the increased metabolic demands of the tissue. Normally, blood flow increases 50-100% above resting values when a neural network becomes active. This increase fails to occur in these patients. Flow has therefore become "uncoupled." Persistent ischemia does not occur because flow is adequate to match resting metabolic demand. The ischemia is episodic only occurring during neuronal activation. Chronic exposure of neural networks to inadequate flow during increased functional activity may lead to slow but progressive tissue injury. As expected the effect appears to be independent of the cause of the vascular narrowing as it has been observed in patients both atherosclerosis and moyamoya disease. The abnormal flow physiology occurs in the setting of severely stenotic or occluded cervical or circle of Willis vessels. From an autoregulation perspective, the impact of these narrowed vessels on vascular reserve can be severe with lack of vasodilatation during a flow stimulus. Under these conditions, the autoregulatory mechanism is incapable of lowering flow resistance any further (maximal arterial vasodilatation has been reached) and the increase in flow associated with increased neural activity does not occur. The purpose of this presentation therefore, is to show evidence of this phenomenon and the effect it has on patients in the absence of stroke-like events.

**0-275** **2:00 PM - 2:20 PM**

#### **Intracranial Vascular Imaging at 7T**

Jeroen Hendrikse, MD

UMC Utrecht  
Utrecht, Netherlands

#### **PRESENTATION SUMMARY**

7 Tesla MRI gains sensitivity especially at high resolution with 2.3 fold increase in signal compared to 3 Tesla MRI and 4.6 fold signal increase compared to 1.5 Tesla MRI. With this signal to noise increase 7 Tesla MRI will make ultra high resolution 3D imaging possible with ~5 times shorter scan times for the same amount of signal compared to 3 Tesla. Three-dimensional (3D) MR imaging methods with a high isotropic resolution make it now possible to image the intracranial arteries beyond the intracranial segment of the carotid artery, basilar artery or M1 segment. Still, 7 Tesla MRI has also significant challenges that need to be dealt with such as an increase in susceptibility effects (these effects can

also be exploited for the detection of blood breakdown products). Optimal intracranial vessel wall MRI sequences at 7 Tesla should combine an optimal blood and liquor suppression to show the vessel wall. A promising 7 Tesla MRI sequence is the 3D turbo spin-echo (TSE) sequence with a 0.8x0.8x0.8mm isotropic resolution. In addition to detection of focal thickening and plaque of intracranial vessel walls 7 Tesla MRI has shown enhancement after contrast administration of small branches and signal loss due to thrombus. With the 3D TSE method 20% of the detected lesions showed enhancement.

## **Tuesday Afternoon**

**1:00 PM - 2:30 PM**

### **Murray Hill**

#### **(33) YOUNG PROFESSIONAL PROGRAMMING: ACADEMIC SESSION**

**0-276**

**1:00 PM - 1:15 PM**

#### **Getting Your First Job**

Carolyn C. Meltzer, MD, FACR

Radiology, Emory University School Of Medicine  
Atlanta, GA, USA

**0-277**

**1:15 PM - 1:30 PM**

#### **Building a Research Program**

Soonmee Cha, MD

Radiology, University of California, San Francisco  
Medical Center  
San Francisco, CA, USA

#### **PRESENTATION SUMMARY**

This presentation will focus on illustrating the basic steps to building a successful research program for junior faculty in academic neuroradiology. It will present unique challenges and pitfalls associated with developing a research program in neuroimaging. Scientific strategies, support system and key elements needed for developing the research team will be discussed. The importance of focusing on a specific disease topic or hypothesis-driven mechanistic approach rather than on a latest imaging technique or observational approach will be emphasized as the essential first step toward building a rewarding successful career in academic neuroradiology.

**O-278****1:30 PM - 1:45 PM****The Different Components of Academic Radiology**

Suresh K. Mukherji, MD, FACR

Radiology, University of Michigan Health System  
Ann Arbor, MI, USA

This session will review the different components of academic career. In addition to research, important components include teaching, administration and excellent clinical work.

**O-279****1:45 PM - 2:00 PM****Getting Promoted: The Different Promotion Tracks**

David M. Yousem, MD, MBA

Radiology Dept., Johns Hopkins Medical Institution  
Baltimore, MD, USA**PRESENTATION SUMMARY**

This lecture will discuss the major promotion tracks for academic advancement focusing on Clinician, Educator, Research Scientist, Program Builder tracks. Emphasis on publication records vs. grants vs. presentations vs. society work vs. leadership efforts and how they help will be highlighted. Tips for advancement that are immediately applicable will be provided.

**Tuesday Afternoon****3:00 PM - 4:30 PM****Grand Ballroom Suite****(34a) Adult Brain Neoplasms III****O-285****3:00 PM - 3:08 PM****Survival Prediction in Glioblastoma: Role of Tumor Blood Volume versus Molecular Subclassification Using Genomic Mapping -- A TCGA Glioma Phenotype Research Group Project**Jain, R.<sup>1</sup>Poisson, L.<sup>1</sup>Narang, J.<sup>1</sup>Gutman, D.<sup>2</sup>Flanders, A.<sup>3</sup>Daniel, B.<sup>2</sup>Jaffe, C.<sup>4</sup>Mikkelsen, T.<sup>1</sup>TCGA Glioma Phenotype Research Group

<sup>1</sup>Henry Ford Health System, Detroit, MI, <sup>2</sup>Emory University, Atlanta, GA, <sup>3</sup>Thomas Jefferson University Hospital, Philadelphia, PA, <sup>4</sup>Boston University, Boston, MA

**PURPOSE**

Molecular subclassification of glioblastoma (GBM) has led to a better understanding of tumor cell origin and biology; however, it has not shown any significant difference in survival in this subgroup of very aggressive neoplasms. The purpose of this study was to evaluate the role of tumor blood volume estimated using DSC T2\* MR perfusion in survival prediction compared to the molecular subclasses of GBM.

**MATERIALS & METHODS**

Fifty-seven patients with treatment naïve GBM underwent DSC T2\* MR perfusion studies at two different institutes. Of these, 50 patients had gene expression data available from TCGA. Relative cerebral blood volume (rCBV) maps were generated using NordicICE (Nordic Neuro Lab) software using leakage correction. rCBV<sub>max</sub>, rCBV<sub>mean</sub> of the contrast enhancing part of the lesion (CEL) as well as rCBV<sub>NEL</sub> of the nonenhancing part of the lesion (NEL) were measured. All the patients were subclassified into classical, mesenchymal, neural and proneural based on Verhaak classification and also into mesenchymal, proneural and proliferative based on Phillips classification system. We correlated the perfusion parameters with the molecular subclasses as well as with patient survival. Cox regression was used to model the association of overall survival with perfusion parameters accounting for potential confounders. Additionally we included each of the Verhaak and Phillips classification groups as predictors. P-values were derived from Wald chi-square tests of the hazard ratio.

**RESULTS**

No statistically significant differences were noted for rCBV<sub>max</sub>, rCBV<sub>mean</sub> of CEL as well as rCBV<sub>NEL</sub> between the four classes using Verhaak or three classes using Phillips classification system. However, increasing rCBV measures appear to relate to poor survival in GBM. rCBV<sub>max</sub> (p = 0.0131) seems to be the most significant regardless of the potential confounders (MR scanner type, patient age) or molecular classification. rCBV<sub>NEL</sub> showed marginally significant increasing risk of death (p = 0.0555). Interestingly, the Verhaak classifier appears to have a confounding effect on the hazard ratio for rCBV<sub>mean</sub> (p = 0.0299) and potentially to a lesser degree for rCBV<sub>NEL</sub> (p = 0.0974); though not with rCBV<sub>max</sub>. It is additionally interesting that the Phillips subclasses neither associate with patient survival nor affect the association of rCBV measures with survival.

**CONCLUSION**

In the future, molecular subclassification of gliomas potentially could lead to individualized therapy regimens targeting specific biologic pathways. However in the present study, the hemodynamic imaging biomarkers (i.e., rCBV measures) did not show any difference between different subclasses of glioblastomas using Verhaak or Phillips classification system based on genomic/molecular mapping. rCBV measures predicted patient overall survival better than the molecular subclasses, suggesting an important role non-invasive imaging biomarkers could play in patients prognosis and survival.

**KEY WORDS:** Genomic mapping, tumor blood volume, glioblastoma

O-286

3:08 PM - 3:16 PM

# **Dynamic Susceptibility Contrast MR Imaging in Glioblastomas: Correlation of Whole-Tumor Histogram Analysis of the Normalized Cerebral Blood Volume and Vascular Permeability with Histopathologic and Molecular Markers of Tumor Aggressiveness**

Gasparotti, R.<sup>1</sup>•Liserre, R.<sup>2</sup>•Ferrara, M.<sup>3</sup>•Grisanti, S.<sup>2</sup>•Buglione di Monale, M.<sup>1</sup>•Poliani, P. L.<sup>1</sup>

<sup>1</sup>University of Brescia, Brescia, ITALY, <sup>2</sup>Spedali Civili di Brescia, Brescia, ITALY, <sup>3</sup>Ospedale A. Manzoni, Lecco, ITALY

## **PURPOSE**

To date, molecular subtypes of glioblastoma only can be identified by genetic analysis of surgical specimens. Aim of the study is to determine whether whole-tumor histogram analysis of the normalized cerebral blood volume (CBV) and vascular permeability can identify subtypes of glioblastomas (GBMs) with different histopathologic and molecular patterns of aggressiveness.

## **MATERIALS & METHODS**

Dynamic susceptibility contrast (DSC) MR imaging (Avanto 1.5 T, Siemens, Erlangen, Germany) was obtained in a consecutive series of 30 patients (10 females, 20 males; mean age 59 years; age range, 32-78 years) with histologically confirmed GBMs, with a whole-brain T2\*gradient-echo echo planar sequence during iv injection of a bolus of gadolinium-DTPA. Perfusion data were processed off-line with a dedicated software (NordicIce, NordicNeuroLab, Bergen, Norway) to create color-coded maps of rCBV and volume transfer coefficient (Ktrans). Regions of interest (ROIs) were manually drawn encompassing the whole contrast-enhancing lesion and nonenhancing peritumoral area in normalized rCBV and Ktrans maps overlaid on axial postcontrast T1-weighted images. Data analysis was performed with the histogram analysis of normalized CBVs and Ktrans from the entire tumor volume. Brain MR examination also included DWI sequences with ADC map calculation. The following histopathologic markers were included into the statistical analysis: GBM cell proliferation (MIB), migration/invasion (Gemistocytes), angiogenesis (expression of the enhancer of Zeste 2, EZH2), epidermal growth factor receptor (EGFR), p53 mutation.

## **RESULTS**

For whole-tumor histogram analysis mean rCBV ( $p < .001$   $r = .605$ ), and rCBV maximum value ( $p < .05$ ,  $r = .460$ ) were found to be significantly associated with EGFR over expression. Mean and maximum rCBV values tended to be higher in patients showing increased over expression of EGFR, with significant differences between subgroups as shown by post-hoc analysis ( $p < .05$ ). According to ROC curve analysis mean whole-tumor CBV values helped to distinguish GBMs with EGFR over expression with 74% sensitivity and 70% specificity at a cutoff value of 1.79. Whole-tumor ADC mode ( $p < .05$   $r = -.440$ ) and median ( $p < .05$   $r = -.430$ )

also were found to be inversely correlated with EGFR over expression. No significant associations were found between Ktrans and histopathologic markers.

## **CONCLUSION**

According to our data analysis GBMs over expressing EGFR are characterized by increased mean whole-tumor CBV, which could represent a new potential preoperative predictor of tumor aggressiveness. The correlation between rCBV values and EGFR over expression supports the role of EGFR in tumor angiogenesis and invasion. EGFR over expression is in fact related to increased angiogenesis, likely due to increased secretion of vascular endothelial growth factor and tumor invasion, likely due to increased secretion of matrix metalloproteinases, both promoting resistance to radiation therapy and rapid postoperative regrowth. Imaging methods that assess molecular differences among GBMs may represent a useful resource to improve outcome by potentially allowing individualized patient management.

**KEY WORDS:** Brain tumors, DSC MR perfusion, histology

O-287

3:16 PM - 3:24 PM

# **Analysis and Prognostic Informations of Apparent Diffusion Coefficient Values and MGMT Promoter Methylation in Patients Affected by Glioblastoma Multiforme**

Romano, A. • Calabria, L. F. • Tavanti, F. • Minniti, G. • Finocchi, V. • Fantozzi, L. M. • Bozzao, A.

S. Andrea Hospital University  
Rome, ITALY

## **PURPOSE**

The status of MGMT promoter methylation in glioblastomas (GBM) currently is obtained after surgery since considered a prognostic marker of the disease and more frequently related to pseudo-progression. The purpose of this study was to evaluate whether apparent diffusion coefficient (ADC) values can predict the status of MGMT of GBM and correlate with overall survival (OS) and progression free survival (PFS).

## **MATERIALS & METHODS**

This retrospective study included 47 patients with pathologic proven glioblastoma. All of them underwent MR DWI study before surgery and the status of MGMT promoter methylation was searched. Minimum ADC values were evaluated drawing multiple regions of interest within the enhancement component of the tumor thus transferred on ADC maps. Overall survival and PSF parameters were calculated and Student T-test, Kaplan-Meier curves, linear and cox regression were performed.

## **RESULTS**

Twenty-five patients showed positive methylation of the MGMT promoter. Patients showing MGMT promoter methylation had higher minimum ADC values ( $p < .05$ ) and they survived more over a long time than those without MGMT promoter methylation (OS,  $p < 0.05$ ;

PFS,  $p < 0.05$ ). Chosen the median values of 80 as ADC cut-off, 25 patients showing minimum ADC values higher than 80 survived more over a long time than 22 patients with minimum ADC lower than 80 (OS,  $p = 0.02$ ; PFS,  $p < 0.05$ ). A linear correlation between minimum ADC values vs the OS and PFS was observed ( $R = 0.458$  and  $R = 0.520$  respectively). A cox regression showed that ADC and positive methylation of the MGMT promoter were independent factors.

#### CONCLUSION

Minimum ADC values in GBM could be used as a preoperative parameter to estimate the survival of patients independently by the status of MGMT promoter methylation. This observation may have clinical impact in those patients in which surgery or biopsy could not be performed.

**KEY WORDS:** MGMT promoter methylation, apparent diffusion coefficient, glioblastoma multiforme

**O-288**

**3:24 PM - 3:32 PM**

#### Quantitative Analysis of Diffusion Restriction in the Subependymal Spread of Primary Brain Neoplasms

Khaleel, Z. L.·Rassner, U.·Shah, L. M.·Quigley, E. P.

University of Utah Medical Center  
Salt Lake City, UT

#### PURPOSE

This paper analyzes the diffusion parameters for subependymal or intraventricular dissemination of high-grade primary brain neoplasm.

#### MATERIALS & METHODS

Retrospective review of 196 patients with high-grade brain neoplasms (specifically; glioblastoma, anaplastic astrocytoma, anaplastic oligodendroglioma) was performed. Axial T2, FLAIR, diffusion-weighted imaging, and axial and coronal gadolinium-enhanced imaging of all the prior studies was reviewed to determine which patients demonstrated diffusion restriction preceding contrast enhancement of intraventricular or subependymal tumor spread. In such subjects, the apparent diffusion coefficient (ADC) values were measured at the sites of intraventricular diffusion restriction. Control ADC values for unaffected parenchyma also were measured.

#### RESULTS

Of 196 patients with high-grade primary brain neoplasm, 41 cases demonstrated intraventricular or subependymal tumor spread with associated diffusion restriction that preceded the development of contrast enhancement. The mean ADC values for subependymal spread of tumor measured  $0.46 \times 10^{-3} \text{ cm}^2/\text{s}$  with a standard deviation of  $.146 \times 10^{-3} \text{ cm}^2/\text{s}$ . The mean ADC values for unaffected brain was  $.751 \times 10^{-3} \text{ cm}^2/\text{s}$  with standard deviation of  $.101 \times 10^{-3} \text{ cm}^2/\text{s}$ .

#### CONCLUSION

Intraventricular or subependymal dissemination of neoplasm often is considered a near terminal event.

Intraventricular or subependymal disease can be treated with intraventricular chemotherapeutics. Highly cellular tumors have been shown to restrict diffusion. In this series, we demonstrate that significant decrease in ADC values at the ventricular margin or the subependyma allows the early detection of subependymal spread. These changes in ADC parameters may precede subependymal tumor enhancement. Such an early detection may allow earlier treatment with intraventricular chemotherapeutics.

**KEY WORDS:** Neoplasm, diffusion tensor imaging, subependymal

**O-289**

**3:32 PM - 3:40 PM**

#### Associations between Genomic Features and Quantitative Histogram Analysis of Diffusion and Diffusion Tensor Imaging of Glioblastomas: A TCGA Glioma Phenotype Research Group Project

Hwang, S. N.<sup>1</sup>·Holder, C. A.<sup>1</sup>·Desai, H.<sup>1</sup>·Clifford, R.<sup>2</sup>·Huang, E.<sup>2</sup>·Hammoud, D.<sup>3</sup>·Wintermark, M.<sup>4</sup>·Colen, R. R.<sup>5</sup>·Jain, R.<sup>6</sup>·Freymann, J.<sup>7</sup>·Flanders, A.<sup>8</sup>·TCGA Glioma Phenotype Research Group

<sup>1</sup>Emory University School of Medicine, Atlanta, GA, <sup>2</sup>National Cancer Institute, Bethesda, MD, <sup>3</sup>National Institute of Health, Bethesda, MD, <sup>4</sup>University of Virginia, Charlottesville, VA, <sup>5</sup>Brigham and Womens Hospital, Boston, MA, <sup>6</sup>Henry Ford Health System, Detroit, MI, <sup>7</sup>SAIC-Frederick, Inc., Frederick, VA, <sup>8</sup>Thomas Jefferson University Hospital, Philadelphia, PA

#### PURPOSE

Investigate associations between genomic features and quantitative parameters derived by histogram analysis of diffusion and diffusion tensor imaging of glioblastomas.

#### MATERIALS & METHODS

As part of The Cancer Genome Atlas (TCGA) MRI characterization project of the National Cancer Institute, the multiinstitutional TCGA Glioma Phenotype Research Group has been investigating MRI, including diffusion imaging and diffusion tensor imaging, as a means of predicting the genomic features of glioblastomas. For the current work, quantitative histogram analysis was performed on apparent diffusion coefficient (ADC) and fractional anisotropy (FA) maps for correlation with genomic features. Small, noninclusive regions of interest (ROI) were selected manually within cerebrospinal fluid (CSF), normal-appearing corpus callosum (usually splenium but placed in the genu if tumor involved the splenium), and normal-appearing white matter (centrum semiovale) to obtain characteristic values for these sites. Voxel ADC and FA values were normalized by the characteristic values measured in the ROIs. The volume of tumor was defined on the basis of the  $b = 0$  diffusion image by application of an Otsu thresholding method using the NIH ImageJ software. Mean, median, standard deviation, skew, and kurtosis of the normalized ADC and FA histograms were computed from voxels within tumor. Tumor volume also was computed. The diffusion histogram analysis



has been performed on 39 of the TCGA glioblastomas at the time current time. Eighteen of these data sets also included DTI. Genomic features of the tumors were obtained from TCGA's publicly available information (TCGA, Nature 455:1061, 2008), including mutation status (presence versus absence of a gene mutation) for the TP53, PTEN, EGFR, NF1, and IDH1 genes. On the basis of copy number data, subgroups were identified, including tumors with high-level EGFR gene amplification, high-level PDGFRA amplification, homozygous deletions of CDKN2A, and deletions of NF1. Student's t-test was applied for statistical analysis.

## RESULTS

Tumors with a TP53 mutation were found to have lower ADC normalized by CSF ( $p = 0.037$ , mean 34 versus 40). Tumors with high EGFR amplification demonstrated histograms with a narrowed distribution of FA normalized by the corpus callosum as demonstrated by decreased standard deviation ( $p = 0.027$ ). Tumors with PDGRFA amplification demonstrated significant broadening of the ADC histogram normalized by CSF as demonstrated by increased standard deviation ( $p = 0.03$ ). Tumors with PDGRFA amplification also demonstrated decreased FA normalized by white matter ( $p = 0.037$ , mean 36 versus 48;  $p = 0.03$ , median 32 versus 44). Tumors with CDKN2A homozygous deletion demonstrated a small but statistically significant increase in ADC normalized by the corpus callosum compared to tumors without the deletion ( $p = 0.05$ , median 38.5 versus 37.0).

## CONCLUSION

Quantitative histogram analysis of ADC and FA maps may provide a noninvasive means of predicting genomic features of tumors. This information may be helpful in predicting outcomes and tailoring treatment.

**KEY WORDS:** Glioblastoma, diffusion, brain tumor

**O-290**

**3:40 PM - 3:48 PM**

### Persistent Restricted Diffusion Abnormalities in Bevacizumab-Treated Glioma Patients: Relationship to Outcomes

Mong, S. Ellingson, B. M. Nghiemphu, P. L. Kim, H. J. Mirsadraei, L. Lai, A. Yong, W. H. Zaw, T. M. Cloughesy, T. F. Pope, W.

David Geffen School of Medicine at the University of California Los Angeles  
Los Angeles, CA

## PURPOSE

A fraction of patients with malignant glioma develop lesions with restricted diffusion during treatment with bevacizumab that persist for long periods of time. Etiologies proposed have included aggressive tumor versus atypical necrotic tumor. Our aim was to retrospectively characterize the evolution of these lesions and their relationship to patient outcome.

## MATERIALS & METHODS

Twenty patients with malignant glioma treated with bevacizumab developed persistent diffusion abnormalities near the original tumor site for at least 2 months. Change in mean ADC value and volume of the diffusion-restricted abnormality was computed for each time-point during follow up. Controls were matched by sex, age, bevacizumab treatment, grade and tumor diagnosis. An unpaired Student's t-test was used to compare the mean ADC values across tumor grade. The relationships between the change in mean ADC over time and the change in volume of diffusion-restricted abnormality over time to survival outcomes, including time to progression (TTP), progression-free survival from the time of bevacizumab treatment (TTS) and overall survival from initial diagnosis (OS), were analyzed using Kaplan Meier analysis with log-rank test and Cox hazard models. Survival analysis was performed additionally to compare the outcomes from restricted diffusion cases with matched controls.

## RESULTS

Of these patients with restricted diffusion lesions, 14 (70%) had glioblastoma, and the rest were grade III gliomas. Of the patients with restricted diffusion lesions occurring after initiation of bevacizumab (75%), lesions occurred at a mean of 189 days after the start of treatment and persisted for a mean of 375 days from lesion onset. The average of mean ADC values for these lesions was not significantly different across tumor grades (unpaired t-test,  $p = 0.97$ ). Positive change in mean ADC over time trended towards longer TTP when compared with stable or decreasing temporal changes in mean ADC (Log-rank;  $p = 0.09$ ). Similarly, patients with increasing volume of restricted diffusion over time tended to trend with shorter TTS compared to patients demonstrating stable or decreasing volume, though this was not statistically significant (Log-rank,  $p = 0.08$ ). Interestingly, patients with diffusion-restricted lesions had significantly greater TTP (Log-rank,  $p = 0.005$ ), TTS (Log-rank,  $p = 0.01$ ) and OS (Log-rank,  $p < 0.001$ ) compared to matched controls. For patients with advanced physiologic imaging, regions of diffusion signal abnormality were hypoperfused and showed decreased activity on PET scans. Necrosis of the diffusion abnormality was confirmed by surgical resection in one patient.

## CONCLUSION

Patients with malignant glioma treated with bevacizumab and who develop persistent restricted diffusion lesions had better survival outcomes than matched controls. The diffusion signal abnormality remained stable over time, and changes in the degree of signal abnormality and volume of diffusion restriction did not predict difference in outcomes in these patients. These lesions spatially colocalized with areas of hypoperfusion and decreased radiotracer uptake on advanced imaging studies, and with atypical necrosis on selected histologic specimens. Taken together, the biopsy results, survival outcomes and advanced imaging correlations provide evidence that the development of persisting diffusion-restricted lesions is related to

treatment effect, rather than development of aggressive, hypercellular tumor in a majority of cases.

**KEY WORDS:** Glioblastoma, bevacizumab, restricted diffusion

**O-291**

**3:48 PM - 3:56 PM**

### Probabilistic Functional Diffusion Maps in Glioblastoma

Ellingson, B. M.·Cloughesy, T. F.·Lai, A.·Nghiemphu, P. L.·Pope, W. B.

David Geffen School of Medicine, University of California Los Angeles  
Los Angeles, CA

#### PURPOSE

Functional diffusion mapping (fDM) uses the voxel-wise changes in apparent diffusion coefficient (ADC) measured in the same patient over time as a biomarker for cancer response to treatment. This technique has shown to be sensitive to multiple treatment paradigms; however, fDM quantification remains highly dependent on the quality of image coregistration between sequential ADC maps. The current study develops a probabilistic approach to fDM quantification, where finite translational and rotation perturbations are performed after initial registration of ADC maps.

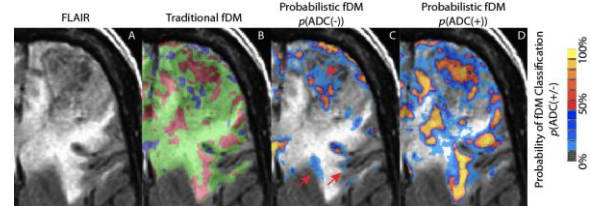
#### MATERIALS & METHODS

A total of 143 histologically confirmed newly diagnosed glioblastoma patients with high quality diffusion MR images before and after initiation of radiochemotherapy (external beam radiotherapy combined with temozolomide) were included in the current study. Baseline scans were obtained 1 week prior to treatment and posttreatment scans were obtained 4-6 weeks after concurrent radiotherapy and chemotherapy. Apparent diffusion coefficient maps were coregistered. Then, a total of 1000 finite perturbations in translation ( $\pm 5$  mm) and rotation ( $\pm 15$  deg) were applied, followed by repeated fDM quantification. The total probability of decreased ADC [ $p(\text{ADC}(-))$ ] and increased ADC [ $p(\text{ADC}(+))$ ] were quantified within pretreatment FLAIR hyperintense regions and used as biomarkers for treatment response.

#### RESULTS

Probabilistic fDMs illustrating the probability of obtaining fDM-classification per voxel during random, finite perturbations, showed regions of increasing and decreasing ADC with the tumor of newly diagnosed glioblastoma patients. Patients with probabilistic fDM-classified volume fraction of decreasing ADC in more than 20% of pretreatment FLAIR abnormal regions [ $\% \text{ADC}(-) > 20\%$ ] had a significantly shorter PFS compared with patients having a lower volume fraction (Log-rank,  $P < 0.0001$ ; HR = 3.3). Median PFS for patients with probabilistic fDM-classified  $\% \text{ADC}(-) > 20\%$  was 239 days compared with 602 days for patients having  $\% \text{ADC}(-) < 20\%$ . Log-rank analysis was suggested patients with probabilistic fDM-classified volume fraction of increasing ADC in more than 20% of

pretreatment FLAIR abnormal regions [ $\% \text{ADC}(+) > 20\%$ ] had a significantly longer PFS compared with patients having a lower volume fraction (Log-rank,  $P < 0.0001$ ; HR = 0.39).



#### CONCLUSION

Probabilistic fDMs provide a robust alternative to the use of traditional fDMs with respect to visualization and quantification. Probabilistic fDMs allow for a relatively registration-independent estimate of fDM parameters, resulting in increased clinical sensitivity.

**KEY WORDS:** Functional diffusion maps, glioblastoma, biomarker

**O-292**

**3:56 PM - 4:04 PM**

### Super-Resolution Track Density Imaging: Initial Clinical Experience and Biological Correlation within Glioblastoma Multiforme

Barajas, R. F.·Hess, C.·Yu, J.·Phillips, J.·Von Morze, C.·Cha, S.

University of California San Francisco  
San Francisco, CA

#### PURPOSE

Track-density imaging (TDI) allows for visualization of fine anatomical detail at submillimeter spatial resolution. The purpose of our study was to determine whether MR track density imaging (TDI) is influenced by and directly correlates with aggressive cellular expression patterns of treatment-naïve glioblastoma multiforme (GBM).

#### MATERIALS & METHODS

Eighteen patients with treatment-naïve GBM were recruited prospectively prior to surgical resection. Preoperative MRI on a 3 T MR scanner was performed with standard anatomical sequences in addition to high angular resolution diffusion imaging (HARDI; TR/TE = 9s/94 ms,  $b = 2000$  s/mm<sup>2</sup>, 55 directions, slice thickness 2.2 mm) reconstructed at 250 micron resolution using probabilistic streamline tractography with constrained spherical deconvolution (model order = 8, 0.1 mm step size, 1 million seed points) allowing for the production of track density (TD) and fractional anisotropy (FA) maps. Forty-three tissue samples were collected utilizing stereotactic neurosurgical techniques. Histologic tissue analysis characterized aggressive features of GBM (tumor presence or absence, hypoxia, peri-axonal infiltration, and cellular proliferation) using a four tier scale. Track density and FA maps were coaligned with anatomical images allowing for measurements from each biopsy site and contralateral brain producing relative values (rTD and rFA). Logistic regression assessed for differential rTD

and rFA expression between biopsy sites based on low and high aggressiveness patterns. Linear regression tested for significance between imaging variables and histologic parameters.

## RESULTS

Mean rTD was not found to be significantly different between contrast-enhancing and nonenhancing regions. Mean rTD was more likely to be elevated within biopsy regions expressing aggressive cellular features ( $P < 0.05$ ). A strong positive correlation between relative track density and regional expression of tumor, vascular hyperplasia (Factor VIII), hypoxia (CA-9), per-axonal infiltration (SMI-31), and cellular mitosis (Ki-67) was observed irrespective of the presence or absence of contrast enhancement ( $P < 0.05$ ). No significant differential expression or correlation was observed between rFA and histologic measures.

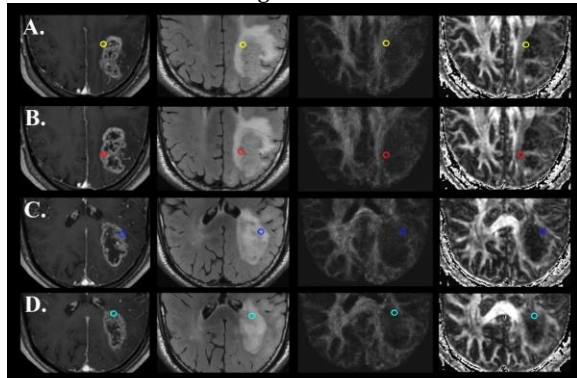


Figure 1: Post contrast T1 weighted (first column), FLAIR (second column), track density (TD; third column), and fractional anisotropy (FA; fourth column) images from a patient with newly diagnosed GBM demonstrates improved spatial and contrast resolution of white matter track integrity depicted by track density imaging when compared to FA. A-D) TD values obtained from image guided biopsy sites (colored circles) demonstrate differential expression of TD between regions of aggressive tumor growth (elevated cellular proliferation and axonal architecture destruction; rows A and B) compared to regions of low aggressive characteristics (rows C and D). Unlike track density values, FA measures did not correlate with histologic characteristics or demonstrate differential regional expression.

## CONCLUSION

Track density imaging provides submillimeter spatial resolution of white matter integrity and can quantify cellular features of GBM aggressiveness suggesting TDI provides unique spatial resolution of white matter tracts that is not achieved by conventional FA maps. Correlation of rTD with cellular features of GBM aggression suggests TDI may be clinically useful in noninvasively identifying regions of glioma malignancy prior to surgical intervention.

**KEY WORDS:** Track density imaging, glioblastoma, pathologic correlation

O-293

4:04 PM - 4:12 PM

## "Diffusion-Contrast and Perfusion-Contrast Mismatching": Useful Findings in Differentiating Glioblastomas from Other Solitary Nonhemorrhagic Intraaxial Tumors

Baek, H. Kim, H. Kim, S. Lee, H.

University of Ulsan College of Medicine, Asan Medical Center

Seoul, KOREA, REPUBLIC OF

## PURPOSE

To investigate the diagnostic utility of "diffusion-contrast (DC) and perfusion-contrast (PC) mismatching" in differentiating glioblastomas from other solitary nonhemorrhagic intraaxial tumors.

## MATERIALS & METHODS

After approval from the institutional ethics committee was obtained, the MR imaging studies of 112 consecutive patients with a solitary nonhemorrhagic enhancing tumor (glioblastoma = 59, metastasis = 39, lymphoma = 24), and without previous surgery or treatment, were reviewed. To determine the degree of DC or PC mismatching, we evaluated whether the area of contrast-enhancement (CE) corresponded with the area of decreased apparent diffusion coefficient (ADC) or increased normalized cerebral blood volume (nCBV). According to the degree of DC and PC mismatching, we were classified into four categories: matching (category 1), positive mismatching (the area of CE is larger than that of decreased ADC or increased nCBV (category 2), negative mismatching (the area of CE is smaller than that of decreased ADC or increased nCBV (category 3), and discrepancy between the area of CE and that of decreased ADC or increased nCBV (category 4). Quantitative perfusion parameters obtained from the histogram of nCBV and T2\* relaxivity curve were compared with categories of DC and PC mismatching. Statistical analysis consisted of a Chi-square test, receiver operating characteristic (ROC) curve, and one-way ANOVA.

## RESULTS

There was a significant difference among the glioblastoma, metastasis, and lymphoma in the DC mismatching with excellent interobserver agreement ( $\kappa = 0.87$ ). Glioblastoma and metastasis had a significantly highest prevalence of negative mismatching (category 3) (37 of 59, 62.7%;  $P < .0001$ ) and matching (category 1) (23 of 39, 59.0%;  $P < .0001$ ), respectively. In PC mismatching, category 3 (negative mismatching) and category 1 (matching) were detected most frequently in glioblastoma (30 of 59, 50.8%) and metastasis (21 of 39, 53.8%), respectively. Among the DC mismatching categories, percent recovery of T2\* relaxivity was significantly lowest in category 2 (mean = 52.3,  $P = 0.001$ ). The sensitivity, specificity and positive predictive value of DC mismatching for differentiating glioblastoma from other tumors were 62.7%, 87.3% and 82.2%, respectively.

Categories of DC- and PC- contrast Mismatching according to the Pathology			
Diffusion-contrast Mismatching	Glioblastoma	Metastasis	Lymphoma
1. Matching	20/59 (33.9%)	23/39 (59.0%)	12/24 (50.0%)
2. Positive Mismatching	2/59 (3.3%)	8/39 (20.5%)	12/24 (50.0%)
3. Negative Mismatching	37/9 (62.7%)	2/39 (5.1%)	0/24 (0%)
4. Discrepancy	0/59 (0%)	6/39 (15.4%)	0/24 (0%)
Perfusion-contrast Mismatching	Glioblastoma	Metastasis	Lymphoma
1. Matching	21/59 (35.6%)	21/39 (53.8%)	4/24 (16.7%)
2. Positive Mismatching	8/59 (13.6%)	15/39 (38.5%)	20/24 (83.3%)
3. Negative Mismatching	30/59 (50.8%)	3/39 (7.7%)	0/24 (0%)
4. Discrepancy	0/59 (0%)	0/39 (0%)	0/24 (0%)

#### CONCLUSION

Diffusion-contrast mismatching may be useful in differentiating glioblastomas from other nonhemorrhagic intraaxial tumors including metastasis or lymphoma when a negative mismatching is present.

**KEY WORDS:** Nonhemorrhagic brain tumor, diffusion-weighted image, perfusion MR image

**O-294 4:12 PM - 4:20 PM**

#### Glioblastoma Multiforme: Relationship to Subventricular Zone and Recurrence

Kimura, M. C. G. Lee, R. Y. Miller, C. R. Castillo, M.

University of North Carolina  
Chapel Hill, NC

#### PURPOSE

To determine if the initial location of glioblastoma (GB) and its relationship to the subventricular zone (SVZ) determines the pattern of recurrence.

#### MATERIALS & METHODS

We analyzed the initial (prior to any treatment) and last follow-up MR studies in 48 patients with GB. On postcontrast images all nontreated GB were divided into three groups according to the relationship of their enhancing margins to the SVZ as follows: in continuity with the SVZ (group I), distant (subcortical, SC) (group II) and abutting both the SVZ and SC region (group III). Recurrences or continuous growth seen as enhancing areas on follow-up studies were characterized as "local" when they occurred within surgical bed, as "spread" when they occurred within 1 centimeter of the surgical bed, and as "distant" when they did not have any contact with surgical bed. Statistical analysis: The averages and p-values were calculated using Microsoft

Excel 2007. A Fisher Exact Test was performed on the contingency table.

#### RESULTS

There were 48 patients with GB, 16 female and 32 male. The mean ages at presentation were for 36.8 +/- 20.4 group I, 61.1 +/- 14.4 for group II, and 54.9 +/- 14.2 for group III. Forty-eight per cent of GBs were in contact with the SC and SVZ (Group III). Group II was the second most common (42%) and Group I the least frequent (10%). Overall, "Spread" and "local" patterns of recurrence/growth occurred essentially equally (45 and 43% each, respectively) and "distant" in 12%. In Group I, 80% showed a "spread" pattern, 20% a "local" pattern, and none a "distant" pattern. In Group II, 48% showed a "spread" pattern, 33% a "local" pattern, and 19% a "distant" one. In Group III, 56% showed a "local" pattern, 35% a "spread" pattern, and 9% a "distant" one. The type and location of recurrences and/or progressive growth had no specific relationship to the location of the initial tumors, with p = 0.275.

Fisher Exact Test of GBs Recurrence					
	Group I (SVZ)	Group II (SC)	Group III (both)	Totals	%
Spread	4	10	9	23	0.45098
Local	1	7	14	22	0.431373
Distant	0	4	2	6	0.117647
Totals	5	21	25	51	
Spread %	80	47.62	36		
Local %	20	33.33	56		
Distant %	0	19.05	8		

#### CONCLUSION

The location of our GBs in relationship to the SVZ did not predict the pattern of tumor recurrence and/or extension. Our observation disagrees with the literature that suggests that types of recurrences can be predicted according to initial location of GBs. Most GBs recurred/grew in their surgical bed or slightly beyond it; distant recurrences and growth were the least common pattern.

**KEY WORDS:** Glioblastoma recurrence, stem cell, subventricular

**O-295 4:20 PM - 4:28 PM**

#### Contrast-Enhanced 3D T1 FLAIR with Vascular Suppression to Improve Conspicuity of Enhancing Lesions

Butman, J. A.

The Clinical Center of the National Institutes of Health  
Bethesda, MD

#### PURPOSE

Contrast-enhanced 3D T1-FFE sequences demonstrate high signal in tissues due to blood-brain barrier breakdown and also in vessels due to intravascular contrast. The latter reduces conspicuity of small lesions

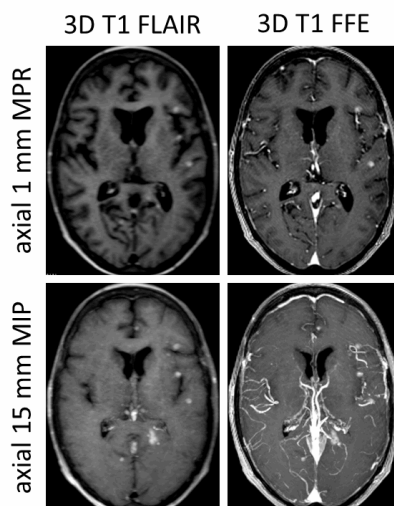
and renders tumor segmentation difficult. The observation that vascular signal is nearly completely suppressed on 3D T2 FLAIR suggests that the dephasing of moving spins during the FLAIR echo train could be applied to eliminate vascular signal from T1-weighted sequences. Thus, we test the feasibility of suppressing vascular signal from high resolution 3D isotropic T1-weighted contrast-enhanced images to improve conspicuity of enhancing lesions by using 3D T1 FLAIR technique.

#### MATERIALS & METHODS

3D T1-FLAIR was implemented on a 1.5 T Philips Achieva system. Contrast parameters: TR 1600 ms, TI 750 ms, TE 32 ms, ETL 20, FA 90, variable FA, BW 872Hz/px, 1 average. Geometric parameters: sagittal acquisition, 256 × 249, FOV 250 cm, sense × 3 in slice × 2 in phase. Imaging time: 4 m 13 s. Contrast-enhanced 3D T1-FLAIR was performed on five patients with brain tumors and compared with contrast-enhanced 3D T1-FFE sequences. Contrast parameters were TR 6.8 ms, TE 3.1 ms, BW 271 Hz/px. Geometric parameters were sagittal acquisition 256 × 253, FOV 240 cm, no sense acceleration. Imaging time: 5 m 26 s.

#### RESULTS

Complete suppression of vascular signal from the arterial circulation was achieved in each case on the 3D T1-FLAIR. Near complete suppression of venous signal was achieved from the venous sinuses as well as the deep cortical venous system. Typically only a few superficial cortical veins draining into the sagittal sinus exhibited enhanced signal. Most of the normal enhancing tissues (i.e., pituitary, choroid plexus, sinus mucosa) were well seen on 3D T1-FLAIR. The exception was the dura of the falx and tentorium which was not visualized at all. All enhancing tumors that were identified on the 3D T1-FFE also were identified readily on the 3D T1 FLAIR. For detection of small lesions using maximum intensity projection, the advantage of vascular suppression is readily apparent (Figure).



#### CONCLUSION

Suppression of vascular signal on contrast-enhanced T1-weighted imaging is achievable by using a 3D T1-FLAIR readout. Thus, high-resolution isotropic imaging of contrast-enhancing brain lesions not confounded by vascular enhancement is now achievable. Further sequence optimization to achieve greater image contrast, signal to noise, and to reduce image blurring is likely achievable and the goal of future work.

**KEY WORDS:** FLAIR, metastases, vasculature

## Tuesday Afternoon

**3:00 PM - 4:30 PM**  
**Trianon Ballroom**

**(34b) Pediatrics: Other**

**O-296**

**3:00 PM - 3:08 PM**

### Brain Structural Development during the First 18 Months of Life: A Longitudinal MR Imaging Study

Lin, W.·Zhu, H.·Shen, D.·Shi, F.·Linglong, K.·Wang, L.·Gao, W.·Smith, J. K.

University of North Carolina at Chapel Hill  
Chapel Hill, NC

#### PURPOSE

To characterize normal overall and regional brain growth trajectories during the first 18 months of life with a longitudinal MR imaging study.

#### MATERIALS & METHODS

Thirteen normal and healthy pediatric subjects were recruited and imaged every 3 months starting from 26.3 ± 7.8 days till 368.8 ± 12 days, and again at 557.5 ± 24 days of age [total 6 time points (tps)] using 3T MRI. T1 (MP-RAGE) and T2-weighted images were obtained. Images from each subject at different tps were coregistered using an intensity-based 4D HAMMER and subsequently warped onto the MNI brain atlas. Tissue segmentation was performed to separate gray (GM) and white (WM) matter. Brain parcellation based on the MNI coordinates was accomplished and through which volumetric measurements of the primary motor, sensory, visual (Calcarine fissure), auditory (Heschl's gyrus), and language (Broca's and Wernicke's areas) cortices were assessed.

#### RESULTS

The ICV increases 78.6% ± 15% in year one although the most dramatic growth occurs during the first 3 months (34.1% ± 6%). White matter grows about 16% every 3 months between month 0-6, followed by a much slower pace (8%) between 6-12 months. However, the growth of WM reverses and exhibits a rapid growth (28%) between 12-18 months. A remarkable growth of GM is observed between 0-6 months (33.7% 0-3



months and 37.7% 3-6 months), followed by a slight reduction to 27.2% 6-9, 22.7% 9-12, and 22.8% 12-18 months. Together, our findings suggest that the first 6 months of life are of critical importance with remarkable increase of GM and WM volumes whereas the second half of the first year is dominated by GM increase. In contrast, a marked increase in WM outpacing the GM is observed between 12-18 months, suggesting a potential shift of developmental focus to establish connections among different brain regions. The five functional areas exhibit distinctly different growth trajectories. In particular, the growth trajectories of GM within these five functional areas shed new light on the developmental processes. The visual, motor and sensory areas have a similar trajectory with the exception that the growth rate of the visual cortex decreases after month 12, suggesting active pruning in the visual cortex after year 1. In contrast, the trajectories of the auditory and language areas exhibit a faster pace than other functional areas after month 3 with the language area showing the fastest growth. More importantly, the increased growth rate of the auditory area appears short-lived where its trajectory returns to a similar level as that of motor/sensory after year 1 while the language area continues its rapid growth. Although the reduced growth rate in the auditory cortex is not as apparent as that in the visual cortex, it may suggest that pruning process also takes place after year 1 in the auditory cortex.

#### CONCLUSION

Our study represents the first longitudinal study with an extremely short time interval between scans and in very young pediatric subjects. Results not only provide unprecedented insights into normal brain development but offer invaluable normative data for the study of neurodevelopmental disorder.

**KEY WORDS:** Early brain development, MR imaging

**O-297**

**3:08 PM - 3:16 PM**

#### Use of In Utero MR Imaging in Prenatal Investigation of Enlarged Dural Venous Sinuses with Thrombus

Fanou, E. M.<sup>1</sup>Reeves, M. J.<sup>2</sup>Howe, D.<sup>3</sup>Joy, H.<sup>4</sup>Morris, S.<sup>5</sup>Russell, S.<sup>6</sup>Griffiths, P.<sup>2</sup>

<sup>1</sup>University Hospital of North Staffordshire, Stoke-on-Trent, UNITED KINGDOM, <sup>2</sup>Academic Unit of Radiology, Sheffield, UNITED KINGDOM, <sup>3</sup>Princess Anne Hospital, Southampton, UNITED KINGDOM, <sup>4</sup>University Hospital of Southampton, Southampton, UNITED KINGDOM, <sup>5</sup>University Hospital of Wales, Cardiff, UNITED KINGDOM, <sup>6</sup>St Mary's Hospital, Manchester, UNITED KINGDOM

#### PURPOSE

To describe and evaluate the diagnostic value of in utero MR (iuMR) imaging, in the prenatal diagnosis of dural venous sinus thrombosis (DVST) and its clinical significance.

#### MATERIALS & METHODS

We report a series of ten fetuses with DVST, imaged at four centers (Southampton, Manchester, Cardiff and Sheffield). The women were referred for iuMR imaging due to space-occupying lesions identified on antenatal ultrasound (all cases in the second trimester).

#### RESULTS

In eight cases the dilated dural sinus with thrombus was in the vicinity of the Torcular Herophili (straight sinus, posterior portion of the superior sagittal sinus or transverse sinus). In one case it was confined to the straight sinus and in one case thrombus was seen at the lateral aspect of the cranium. Follow-up imaging (either iuMR or ultrasound) was performed in seven cases and showed complete resolution in two cases, regression in two cases, stable appearances in two and progression in one case. Mild ventriculomegaly was present in two cases. Termination of the pregnancy was performed in four cases. Clinical follow up is ongoing with the other six cases.

#### CONCLUSION

To our knowledge this is one of the largest series of cases of prenatal DVST reported in the literature. In a previous report Merzoug et al (2008), described 13 cases, all involving the vicinity of the torcula. Early clinical follow up suggests a good prognosis in the cases available for study so far.

**KEY WORDS:** In utero MR imaging, dural venous sinus thrombosis, Torcular Herophili

**O-298**

**3:16 PM - 3:24 PM**

#### Childhood Posterior Reversible Encephalopathy Syndrome: Increased Leptomeningeal FLAIR Signal

Agarwal, A. Altinok, D.

Children's Hospital of Michigan  
Detroit, MI

#### Purpose

Posterior reversible encephalopathy (PRES) is a clinico-radiologic syndrome characterized clinically by headache, seizures and altered sensorium and radiologic changes which are reversible. The purpose of this study was to describe the spectrum of MR imaging findings in childhood PRES and to have an insight into the pathophysiology.

#### MATERIALS & METHODS

MR imaging of 20 clinically diagnosed cases of PRES between July 2009 and June 2011 were reviewed. Out of the 20 patients, 12 (60%) were girls and 8 (40%) were boys with mean age of 9 years (range, 5-13 years). The final diagnosis of PRES was made based on the clinical presentation and the MR imaging features at the time of presentation which were reversible on the follow-up imaging. The medical records of the patients were reviewed to find the underlying medical disease.

#### RESULTS

The most common MR imaging finding was high T2-FLAIR signal in the cortex and subcortical white matter

of both cerebral hemispheres, particularly in the parieto-occipital lobes (n = 16). The second most common MR imaging finding was increased leptomeningeal signal on FLAIR sequence (n = 7). Four out of these seven patients had no other parenchymal findings. There was leptomeningeal enhancement in five out of the seven patients with increased leptomeningeal FLAIR signal. There were atypical imaging findings like involvement of the cerebellum (n = 5), brain stem (n = 3), basal ganglia (n = 4), corpus callosum (n = 1) and deep white matter (n = 1). Some of the other imaging findings were diffusion restriction (n = 3), parenchymal hemorrhage (n = 2) and focal parenchymal enhancement (n = 3). Eight out of the 20 patients included in the study were on immunosuppressant therapy for organ transplant. Four patients had severe hypertension at the time of presentation. Some of the other underlying medical conditions were neurofibromatosis (n = 1), autoimmune disorders (n = 1), acute on chronic renal failure (n = 1) and Henoch Schonlein purpura (n = 1).

#### CONCLUSION

Childhood PRES commonly is seen in the setting of immunosuppressant therapy for organ transplant and severe hypertension. Childhood PRES also may develop in patients with systemic conditions such as neurofibromatosis, acute or chronic renal failure, autoimmune disease and after cancer chemotherapy. The most characteristic imaging pattern is cortical and subcortical vasogenic edema, particularly in the parieto-occipital lobes. This pattern is also the most common pattern described in adults. Fairly high incidence of abnormal increased leptomeningeal FLAIR signal and leptomeningeal enhancement in our study makes us propose sepsis/systemic inflammation with meningeal involvement plays an important role in the pathophysiology of PRES.

**KEY WORDS:** Childhood, PRES, encephalopathy

**O-299**

**3:24 PM - 3:32 PM**

#### **HIMAL Is a Malformation that Predisposes to Prolonged Febrile Seizures: Baseline MR Imaging Data from the FEBSTAT Study**

Chan, S.<sup>1</sup>Bello, J. A.<sup>2</sup>Shinnar, S.<sup>2</sup>Hesdorffer, D. C.<sup>1</sup>Lewis, D. V.<sup>3</sup>MacFall, J.<sup>3</sup>Shinnar, R. C.<sup>2</sup>Gomes, W. A.<sup>2</sup>Nordli, D.<sup>4</sup>Pellock, J.<sup>5</sup>Frank, L. M.<sup>6</sup>Moshe, S. L.<sup>2</sup>Sun, S.<sup>5</sup>and the FEBSTAT Study Team

<sup>1</sup>Columbia University, New York, NY, <sup>2</sup>Montefiore Medical Center & Albert Einstein College of Medicine, Bronx, NY, <sup>3</sup>Duke University, Durham, NC, <sup>4</sup>Children's Memorial Hospital, Northwestern University Feinberg School of Medicine, Chicago, IL, <sup>5</sup>Virginia Commonwealth University, Richmond, VA, <sup>6</sup>Eastern Virginia Medical School, Norfolk, VA

#### **PURPOSE**

HIMAL is a form of hippocampal malrotation with a normal corpus callosum, which is characterized by incomplete inversion of the hippocampus with a rounded shape and blurred internal architecture.

HIMAL is seen much more often on magnetic resonance (MR) imaging examinations of people with epilepsy, than in people without epilepsy. It has been unclear whether HIMAL represents a pathologic finding or an anatomical variant.

#### **MATERIALS & METHODS**

FEBSTAT is a prospective multicenter study of febrile status epilepticus (FSE) (lasting 30 minutes or longer) designed to determine whether or not a prolonged febrile seizure causes acute hippocampal damage and, if so, whether or not the damage leads to mesial temporal sclerosis. As part of this research study, eligible subjects have a baseline MR imaging study within 72 hours of the episode of status epilepticus, and a follow-up MR imaging study at 1 year. All MR imaging exams undergo both quantitative analysis of hippocampal volume and T2 signal by two research scientists, and visual analysis by two experienced neuroradiologists, all of whom were blinded to the clinical details. The control group consisted of a cohort of children with a first simple febrile seizure who had previously undergone MR imaging using a similar study protocol.

#### **RESULTS**

Among the 190 children with FSE, HIMAL occurred in 15 children (7.9%), of which 13 (86.7%) were on the left side and 2 were bilateral (13.3%). Increased T2 signal in the right hippocampus occurred in one child who had bilateral HIMAL; no other increased T2 signal was seen in HIMAL. HIMAL was not associated with age at FSE, or with peak temperature, but it was associated with gender. Fourteen of the 15 HIMALs occurred in males and one in females (exact p = 0.000525). Among 96 controls with a first simple febrile seizure (FS), 2 (2.1%) had HIMAL: one on the left and one bilateral. Using logistic regression, the odds ratio for having HIMAL in cases with FSE compared with simple FS was 4.01 (95% CI = 0.90-17.9).

#### **CONCLUSION**

These data indicate that HIMAL is a developmental malformation that predominantly affects the left hippocampus, and is found much more frequently among male children. The higher frequency of HIMAL in children with prolonged FS suggests that it is a pathologic finding. Long-term clinical follow up and subsequent MR imaging will be needed to ascertain whether or not there is a higher rate of subsequent temporal lobe epilepsy and mesial temporal sclerosis in these children.

*Acknowledgement:* Supported by Grants NS 43209 "Consequences of Prolonged Febrile Seizures in Childhood" from NINDS, and HD 36867 from NICHD.

**KEY WORDS:** HIMAL, hippocampal malrotation, febrile seizures

**O-300**

**3:32 PM - 3:40 PM**

#### **Spectrum of MR Imaging Abnormalities in Children with Epilepsy and SCN1A Gene Mutation**

Patay, Z.<sup>1</sup>Van Poppel, K.<sup>2</sup>Roberts, D.<sup>3</sup>Clarke, D.<sup>2</sup>McGregor, A.<sup>2</sup>Perkins, F. F.<sup>2</sup>Wheless, J.<sup>2</sup>

<sup>1</sup>St. Jude Children's Research Hospital, Memphis, TN,  
<sup>2</sup>LeBonheur Neuroscience Institute, Memphis, TN,  
<sup>3</sup>Medical University of South Carolina, Charleston, SC

#### PURPOSE

SCN1A gene mutations have been found in multiple epilepsy syndromes, ranging from benign entities to severe epileptic encephalopathies. At our institution, we diagnosed several children with SCN1A mutations and observed abnormalities involving mesial temporal (MT) structures on MRI. We therefore set out to retrospectively evaluate MRI findings in all of our patients with SCN1A mutations focusing on the incidence and spectrum of MT abnormalities.

#### MATERIALS & METHODS

We carried out a retrospective review of 20 patients (M/F: 15/5, age range: 10 months-14 years) with epilepsy and confirmed SCN1A gene abnormalities diagnosed between 2005 and 2010. All but four had onset of epilepsy within the first year of life (range: 3 months-4 years). MR imaging was performed on 1.5 or 3 T units. Imaging protocols were inconsistent but always included coronal thin-section T2-weighted imaging of the temporal lobes. Two neuroradiologists reviewed MRIs independently. Brain abnormalities were categorized as temporal or extratemporal. Temporal lobe abnormalities were divided into five groups: 1) Definite MT sclerosis (MTS) (hippocampal volume loss, T2/FLAIR hypersignal and internal architecture alteration), 2) Possible MTS (two of the above), 3) Other MT abnormalities (only one of the above or other abnormality, such as malrotation or dysmorphia), 4) Nonparenchymal temporal lobe changes (NPTLC) and 5) Normal.

#### RESULTS

Abnormalities were found in 19 patients. Definite MTS was found in six patients (30%), two of which were bilateral, possible MTS in four patients (20%), two of which were bilateral, and other MT abnormalities in three patients (15%). In the NPTLC group one patient had a right hippocampal fissure cyst and one patient had hippocampal inclusion cysts. Extratemporal abnormalities were found in six patients: diffuse brain atrophy (two patients), enlarged perivascular spaces within centrum semiovale (one patient), nonspecific globus pallidus lesion (one patient), nonspecific centrum semiovale T2 hyperintensities (one patient) and persistent cavum Vergae (one patient). Of the six patients with definite MTS, 4 had classic severe myoclonic epilepsy of infancy (SMEI) with prolonged febrile seizures (FS) and one had a history of simple FS. Of the 4 patients with possible MTS, 1 had SMEI and 2 had simple FS. Among the 3 with other MT abnormalities, one had SMEI and one patient had multiple episodes of status epilepticus. In the seven patients with normal MRIs, two had SMEI, one had prolonged and one had a simple FS.

#### CONCLUSION

The incidence of MTS in pediatric epilepsy is unknown, but believed to be relatively uncommon. In our series of children with SCN1A gene mutation, 50% had findings

of definite or possible MTS, many without history of prolonged FS. While the MRI appearance of MTS was not different from that observed in older patients, the most striking finding of our study was indeed the remarkably high percentage of MT abnormalities (in particular MTS) for the patients' age. It is unclear whether these MRI findings are related to the genetic abnormality itself or are a consequence of the intractable seizures. We believe that testing for SCN1A mutation should be considered in young children with epilepsy and MRI evidence of MT abnormalities.

**KEY WORDS:** Epilepsy, mesial temporal sclerosis, SCN1A mutation

**O-301**

**3:40 PM - 3:48 PM**

#### Resting-State Functional Connectivity MR Imaging Identifies Epileptic Foci Localized with Magnetoencephalography

Stufflebeam, S. M.<sup>1</sup>Liu, H.<sup>1</sup>Sepulcre, J.<sup>1</sup>Madsen, J. R.<sup>2</sup>Tanaka, N.<sup>1</sup>Grant, P. E.<sup>2,1</sup>

<sup>1</sup>Massachusetts General Hospital-Martinos Center, Charlestown, MA, <sup>2</sup>Children's Hospital Boston, Boston, MA

#### PURPOSE

The best hope of cure in a medically refractory patient with epilepsy is the surgical removal of the epileptogenic cortex with preservation of the eloquent cortex. Despite use of invasive methods to find an epileptic focus, about one third of patients have recurrent seizures or suffer from significant motor or cognitive deficits. We previously have identified areas of abnormal connectivity using rsfMRI and showed good correlation with invasive localizations in a pilot study. Here we identify areas of abnormal connectivity using rsfMRI and compare localization to magnetoencephalography (MEG) in a larger number of patients.

#### MATERIALS & METHODS

We retrospectively studied 14 patients with epilepsy who were candidates for surgical resection. Structural MRI: T1 MPRAGE acquired on a 3T Tim-Trio scanner with a commercial 32-channel head coil (Siemens, Erlangen, Germany). Functional MRI: Standard MGH BOLD fMRI sequences were used for the resting-state and task fMRI scans. Subjects were asked to keep eyes open and fixate on a cross-hair during a BOLD EPI resting-state fMRI (3 mm isotropic voxels). MEG: Whole-head MEG was obtained using a Elekta-Neuromag device. Equivalent current dipole (ECD) source analysis was performed on the inter-ictal discharges using a single layer boundary element model. The ECDs were fused to the MPRAGE anatomical volume from each patient's MRI. Epileptic discharges were localized by experienced magnetoencephalographers, and the lobar localizations of interictal discharges were determined. rsfMRI analysis: We chose a neighborhood strategy to define local and remote limits. Specifically, the low-pass filtered fMRI signal time course of each voxel from the subject's brain was correlated (Pearson correlation) to

every other voxel time course, at the local (all voxels in a 3 mm radius beyond the original voxel) and remote level (voxels outside a 25 mm radius sphere). The degree of coupling was calculated by summing the number of voxels above a correlation threshold of 0.25 both locally and remotely. In order to determine statistically significant differences between the patients and controls, we calculated the Z value at each voxel in the individual patients using our ad hoc normative control sample of subjects. The lobar localization of the abnormal local and remote rsfMRI coupling was compared to that of the localization of the MEG observed interictal discharges.

## RESULTS

Three subjects had excessive head motion and were excluded. Two subjects had no statistically abnormal coupling, although MEG identified foci in the frontal lobes. In the remaining nine subjects, the rsfMRI was overlapped by the MEG results in eight cases.

## CONCLUSION

Using a single 10-minute rs-fMRI acquisition, it might be possible to determine the epileptic foci. This will be further assessed with surgical outcomes.

**KEY WORDS:** Presurgical mapping, seizure localization, magnetoencephalography

**O-302**

**3:48 PM - 3:56 PM**

## Brain MR Imaging Abnormalities in Infantile GM2 Gangliosidosis

Caruso, P. A.<sup>1</sup>Loes, D. J.<sup>2</sup>Pan, J. J.<sup>1</sup>Eichler, F. S.<sup>1</sup>

<sup>1</sup>Massachusetts General Hospital, Boston, MA,

<sup>2</sup>Suburban Radiologic Consultants, Ltd., Minneapolis, MN

## PURPOSE

GM2 gangliosidosis are autosomal recessive disorders caused by deficiency of  $\beta$ -hexosaminidase. The deficiency results in excess accumulation of glycolipids in the lysosomes of neuronal cells and leads to neurodegeneration. The infantile variant is rapidly progressive and leads to death before 4 years of age. Changes in the brain can be detected by neuroimaging techniques. We set out to examine brain MRIs in the largest cohort of infantile GM2 patients to date.

## MATERIALS & METHODS

Brain MRIs of infantile GM2 gangliosidosis patients were collected by the National Tay Sachs and Allied Diseases Association (NTSAD) and examined by two independent neuroradiologists. Changes were evaluated in both white matter and gray matter regions on conventional imaging (T1, T2, and FLAIR).

## RESULTS

A total of 10 brain MRIs of patients with infantile GM2 gangliosidosis was examined. The average age at time of MRI is 11.8 months (range 9-18 months). All (10/10) patients displayed hypomyelination on the MRI with relative preservation of myelin in the splenium and

genu of the corpus callosum. Most patients had hyperintensities in the caudate (8/10) and putamen (9/10) on T2-weighted images, with a few displaying swelling of these structures as well (3/10). A minority of patients displayed subtle cerebellar white matter abnormalities as well (3/10). No atrophy and no ventricular enlargement was present.

## CONCLUSION

We find hypomyelination and gray and white matter changes in specific structures on the brain MRIs of GM2 patients. We propose a scoring system based on these abnormalities to evaluate the progression of GM2 gangliosidosis. Prospective validation of this scoring system is needed in a separate cohort. We hope that the scoring system will be of utility in future clinical trials of this devastating disorder.

**KEY WORDS:** GM2 gangliosidosis, Infantile

**O-303**

**3:56 PM - 4:04 PM**

## Neuroradiologic Correlates of Clinical Disability and Progression in the X-Linked Leukodystrophy Pelizaeus-Merzbacher Disease

Laukka, J. J.<sup>1,2</sup>Kamholz, J.<sup>2</sup>

<sup>1</sup>Michigan State University, Detroit, MI, <sup>2</sup>Detroit Medical Center, Detroit, MI

## PURPOSE

To determine whether quantitative measures of MRI data from patients with Pelizaeus-Merzbacher disease (PMD), an X-linked dysmyelinating disorder, caused by mutations affecting the proteolipid protein, correlates with clinical severity or progression. Consistent with this notion, brain MRI studies in patients with PMD have demonstrated patterns consistent with hypomyelination (Figure 1), although patients with *PLP1* null mutations also have evidence of axonal degeneration. Development of reliable noninvasive quantitative biomarkers of disease activity would be useful not only for following the natural history of the disease, but also potential for evaluating future therapies.

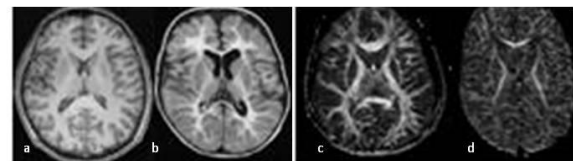


**Figure 1:** MR images showing the difference in white matter contrast between seen in 3D T1W image (a) and FA map (c) of healthy control subject compared 3D T1W (b) and FA map (d) of a typical PMD patient.

## MATERIALS & METHODS

In our current work we have analyzed the clinical phenotypes and MRI scans of 52 male patients with PMD and 9 female carriers for whom the *PLP1* genotype had been determined. In addition, we developed a 32-point functional disability scoring system for PMD, and validated it for inter-rater reliability. We quantified total brain volume, white matter volume, inter-caudate ratio, and corpus callosum area for our cohort of patients using conventional T1- and T2-weighted MRI

sequences, and correlated these data to the patient's functional disability score.

## RESULTS

The results of this study demonstrate that decreased white matter volume is a common finding for all the PMD patients in this cohort, regardless of genotype. In addition, clinical severity is correlated with white matter volume, inter-caudate ratio and corpus callosum volume. Although there are multiple genetic and molecular mechanisms causing PMD in this cohort, these data imply that white matter atrophy is the major pathologic determinant of the clinical disability in most patients.

## CONCLUSION

MR imaging analysis of patients with PMD will not only further our understanding of this inherited leukodystrophy, but also will provide important insights into molecular pathogenesis of other more common, acquired white matter diseases, such as multiple sclerosis (MS). For example, the role of demyelination in causing the clinical signs and symptoms in MS is complex, and long-term disability in this disease may be caused by axonal degeneration, not by demyelination and/or abnormalities of nerve conduction. Our studies of patients with PMD will help further elucidate the role of axonal degeneration in disease progression in a disease where the specific cause is known. These studies may also help to identify new cellular and molecular targets that will be relevant for the treatment of patients with both PMD and MS.

**KEY WORDS:** Pelizaeus-Merzbacher disease, proteolipid protein, leukodystrophy

**O-304**

**4:04 PM - 4:12 PM**

### Successful Treatment and Brain Creatine Restoration in Knockout Mice with Creatine Transporter Deficiency

Cecil, K. M.<sup>1</sup> Lindquist, D. M.<sup>1</sup> Pyne-Geithman, G. J.<sup>2</sup> Clark, J. F.<sup>2</sup>

<sup>1</sup>Cincinnati Children's Hospital Medical Center, Cincinnati, OH, <sup>2</sup>University of Cincinnati, Cincinnati, OH

#### PURPOSE

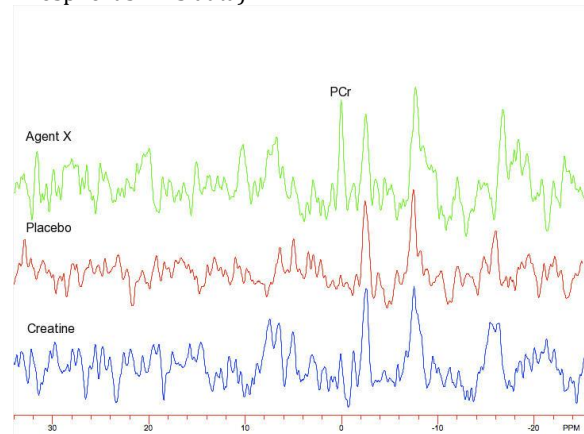
Creatine transporter deficiency (CTD) is an untreatable X-linked mental retardation syndrome with severe cognitive and speech impairment. Patients are identified by an absence of creatine in the brain on proton MR spectroscopy (MRS) and distinguished from two creatine synthesis deficiency syndromes with genetic testing. For CTD, defects of the transporter (gene-SLC6A8 on Xq28) prevent creatine from crossing the blood-brain barrier and entering brain cells. A brain specific CTD knockout mouse was developed replicating key features of the human disease and establishing an animal model for treatment of CTD. We report the successful treatment of the CTD knockout mouse and present confirmation by MRS.

## MATERIALS & METHODS

Brain specific knockout and litter-mate control mice were assigned randomly and treated with on one of three supplements: AgentX (confidential), creatine or maltodextrine as placebo. Proton and phosphorus MRS data were collected on a 7 T MR system. Mice (N = 16) were studied with MRS after 9 weeks of supplementation. Single voxel proton data were acquired on a 144 uL voxel covering the cerebrum using a double spin-echo sequence. Phosphorus MRS data were acquired with an ISIS sequence from the same voxel. Metabolite quantification was performed with jMRUI and compared between groups and over time with statistical tests for significance (t-tests, ANOVA).

## RESULTS

Creatine and phosphocreatine levels in the brain were significantly higher after 9 weeks supplementation of AgentX in knockout mice, compared to creatine and placebo supplemented knockout mice (Figure 1-Phosphorus MRS data).



## CONCLUSION

Successful treatment was achieved in a brain specific knockout mouse model for the second largest known cause of X-linked mental retardation in humans, CTD.

**KEY WORDS:** Creatine deficiency, phosphorus, spectroscopy

**O-305**

**4:12 PM - 4:20 PM**

### Diffusion Tensor Imaging Findings in Autosomal Recessive Spastic Ataxia of Charlevoix-Saguenay

Oguz, K. K.<sup>1,2</sup> Gocmen, R.<sup>2</sup> Turk, S.<sup>3</sup> Sanverdi, E.<sup>2</sup> Doerschner, K.<sup>3</sup>

<sup>1</sup>Bilkent University, National Magnetic Resonance Research Centre, Ankara, TURKEY, <sup>2</sup>Hacettepe University, Ankara, TURKEY, <sup>3</sup>Bilkent University, Ankara, TURKEY

#### PURPOSE

Autosomal recessive spastic ataxia of Charlevoix-Saguenay (ARSACS) is a rare neurodegenerative disorder characterized by early-onset cerebellar ataxia, spasticity, nystagmus, peripheral neuropathy, pyramidal tract signs, extremity deformities, and hypermyelination of the retinal nerve fibers. Magnetic



resonance imaging (MRI) findings in ARSACS include early, progressive atrophy of the predominantly superior vermis, cerebellar hemispheres, and linear hypointensity in the pons on T2-weighted images. Bilateral paramedian linear T2 hypointensities in the pons might reflect abnormality of the corticospinal tract. A recent article suggested hypertrophy of the crossing pontine tract (CPT) as the principle abnormality compressing corticospinal tract (CST)s at basis of the pons. We aimed to determine diffusion tensor imaging (DTI) abnormalities mainly in the brainstem to further enhance our understanding of etiology in ARSACS.

#### **MATERIALS & METHODS**

Four patients (M/F: 3/1, mean age:18.75 years (range:3-51years) and 4 age- and sex matched healthy subjects were examined on 1.5 T MR scanner (Magnetom TIM, Siemens, Germany). A routine MR imaging and T2\* GRE axial (TR/TE; 850/26 ms, FA:20 °) were obtained. Diffusion tensor imaging applied a single-shot echo-planar imaging sequence with a b factor of 1000s/mm<sup>2</sup>, 64 independent directions, TR/TE =5814 /98 ms, FOV=230x230 mm, matrix = 128x128, voxel-size = 1.5X1.8X1.8 mm<sup>3</sup>, 25 sections with 3 mm thickness without intersection gap. Fiber tractography of CSTs were generated using available software (syngoDTI, Siemens). Vermian and cerebellar atrophy, presence of linear hypointensities on T2-weighted and T2\*GRE images were recorded from MRI. Diffusion-sensitized image sets were analyzed using FSL (www.fmrib.ox.ac.uk/fsl). All scans were corrected for head motion and eddy currents using the affine registration (FDT, FMRIB's Diffusion Tool). b0 volumes of each subject were extracted and averaged. The main diffusion tensor was fitted in each voxel with FSL DTIFit and the FA and MD maps were calculated. Then ROIs were drawn on color-coded FA maps at CPTs, and along CSTs from brainstem up to precentral gyri using JHU white matter atlas. Extracted ROIs were verified using an FA template in the MNI space .To test for differences in diffusion indices between groups the Mann-Whitney U test was used and p values below 0.05 were accepted for significance.

#### **RESULTS**

All four patients had vermian and cerebellar atrophy, linear parallel T2 hypointensities with no apparent susceptibility signal on T2\*GRE images. In the brainstem CSTs showed significantly lower FA (right: 0.33 vs 0.56, left:0.35 vs 0.51; p:0.02) and higher MD (right: 0.72x10<sup>-3</sup> vs 0.64x10<sup>-3</sup>, left: 0.76x10<sup>-3</sup> vs 0.66x10<sup>-3</sup> mm<sup>2</sup>/s; p:0.04) in the patients without significant change in upper segments of the CSTs (p>0.05). Although CPTs had higher FA than healthy subjects (mean: 0.67 vs 0.53), this difference didn't reach statistical significance (p>0.05).

#### **CONCLUSION**

In a limited number of ARSACS patients, diffusion abnormalities mainly localized in the brainstem where fiber tractography of CSTs showed weakening and decrease in thickness. Increased FA values of CPTs may arise from increases in myelination as observed in

retinal nerve fibers and increased ADC with decreased FA in CST in the brainstem from distorted myelination and various microstructural changes.

**KEY WORDS:** Autosomal recessive spastic ataxia of Charlevoix-S, diffusion tensor imaging

**O-306**

**4:20 PM - 4:28 PM**

#### **Arterial Spine Labeling Perfusion MR Imaging in Children with Hemiplegic Migraine**

Ziai, P.·Vossough, A.·Zimmerman, R. A.

Children's Hospital of Philadelphia  
Philadelphia, PA

#### **PURPOSE**

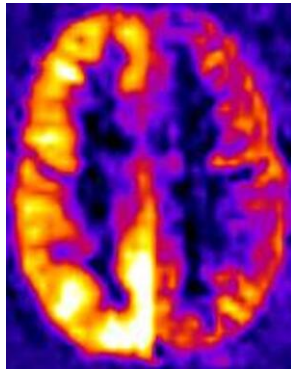
Hemiplegic migraine is a serious and potentially debilitating form of migraine. The purpose of this study was to assess arterial spin labeling (ASL) perfusion in the imaging of hemiplegic migraine in children.

#### **MATERIALS & METHODS**

We performed a retrospective study of ASL perfusion brain MRIs of children with a final clinical diagnosis of hemiplegic migraine that had quantitative ASL imaging and had negative diffusion imaging. All patients underwent pulsed arterial spin labeling (PASL). Quantitative assessment of cerebral blood flow (CBF) of the cortical regions of the hemispheres was performed. Two regions of interest were assessed and averaged on each hemisphere and compared to similar location and size regions in the contralateral hemisphere. Mean blood flow and ratio between the two hemispheres was calculated. An asymmetry index between the two hemispheres also was calculated and assessed in the context of clinical lateralization.

#### **RESULTS**

Results of quantitative arterial spin labeling perfusion was available in seven children with hemiplegic migraine. Arterial spin labeling perfusion MRI revealed hyperperfusion of the cerebral hemisphere contralateral to the side of the patients' symptoms and hemiparesis in all these cases. The cerebral blood flow measurement in the involved hemisphere was 169.4+/-29.0 mL/100g/min and in the normal hemisphere was 75+/-17.3 mL/100g/min. The ratio of CBF of the involved to the normal side was 2.29+/-0.42. The calculated asymmetry index between the two hemispheres was 39.6+/-6.6 (range 30.8 to 49.3). In the subset that had follow-up imaging, the hyperperfusion resolved spontaneously and without any permanent damage or sign of ischemia visible on follow-up MRI.

**CONCLUSION**

Arterial spin labeling perfusion MRI can play an important role in detection of perfusion alterations in the brain in children with complicated or hemiplegic migraine. It should be considered as a useful tool in imaging assessment of children presenting with hemispheric stroke-like symptoms that do not demonstrate diffusion abnormalities. Arterial spin labeling has potential to become a useful imaging modality in this group of patients to evaluate the sequential changes of cerebral perfusion in order to better understand the pathogenesis of the disease.

**KEY WORDS:** Perfusion, migraine, children

**O-307**

**4:28 PM - 4:36 PM**

### Elucidating Subresolution Microstructure with Oscillating Diffusion Gradient MR Imaging

Van, A. T.<sup>1</sup>Holdsworth, S. J.<sup>1</sup>Bammer, R.

Stanford University  
Stanford, CA

**PURPOSE**

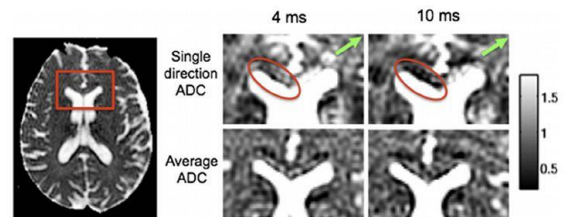
Tissue membranes and different cell organelles restrict diffusion in tissue. The restrictions microstructure imposes on diffusive motion lead to apparent diffusion coefficients (ADCs) that depend on the "shutter speed" of the diffusion probing tool and allows one to infer further detail beyond conventional ADC measurements/spatial resolution. As the motion probing interval increases, ADC measurements reveal increased diffusion restrictions due to an increased likelihood for spins to be affected by cellular obstacles within their diffusion trajectory. Here, we report on the first results of oscillating diffusion gradient MRI (OGMRI) in humans.

**MATERIALS & METHODS**

The study was IRB-approved and informed consent was obtained from each subject ( $n = 3$ ). Apodized cosine-modulated gradients were designed to replace the traditional trapezoid diffusion-encoding gradients in 2D SE DWI-EPI. A tetrahedral diffusion-encoding scheme was used. The diffusion-encoding parameters were: TE = 116 ms,  $G_{\max} = 50$  mT/m, diffusion times of 4 ms, 6 ms, 8 ms, and 10 ms, corresponding to the cosine gradient frequencies of 62.5 Hz, 41.7 Hz, 31.3 Hz, and 25 Hz.

**RESULTS**

The figure shows a trace ADC map. To illustrate the observed diffusion time dependence of the ADC, zoomed ADC maps are shown for the shortest (4 ms) and longest (10 ms) diffusion time. When ADC maps were computed from a single diffusion direction (top row), the long diffusion time result shows significantly lower ADC values at locations where fibers are running predominantly perpendicular to the diffusion-encoding direction (in-plane diffusion encoding direction is shown by the green arrow on the top right corner of each sub figure). At shorter diffusion time (4 ms), the measured ADC in these fibers increases as fewer restrictions occur. However, the ADC is still lower than ADC values measured at the contra-lateral side, where fibers run predominantly parallel to the gradient. This suggests that the effects of diffusion restriction imposed by boundaries just starts to increase ADC at diffusion time of 4 ms. When multiple diffusion directions are averaged (bottom), the time-dependency effect is mostly drowned by the ADC along fibers.

**CONCLUSION**

The use of cosine-modulated diffusion gradient at reasonably low diffusion times has been shown for the first time in in vivo human studies without the use of high-performance gradients. The added microstructural information that can be inferred from the time-dependency of ADC may have utility in early detection of disease to the brain, such as AD, CJD, or in MS.

**KEY WORDS:** Oscillating diffusion, MR imaging

## Tuesday Afternoon

**3:00 PM - 4:30 PM**

**Beekman/Sutton North**

**(34c) Interventional:  
Arteriovenous Malformations,  
Fistulae & Other Vascular Lesions**

**O-308**

**3:00 PM - 3:08 PM**

**Utility of Targeted Digital Subtraction Angiography and Flat Panel Detector CT for Evaluation of Complex Cerebral Developmental Venous Anomalies**

Chen, J. X.<sup>1</sup>Kathuria, S.<sup>2</sup>Gandhi, D.<sup>3</sup>

<sup>1</sup>Johns Hopkins School of Medicine, Baltimore, MD, <sup>2</sup>Johns Hopkins Hospital, Baltimore, MD, <sup>3</sup>University of Maryland Medical Center, Baltimore, MD

#### PURPOSE

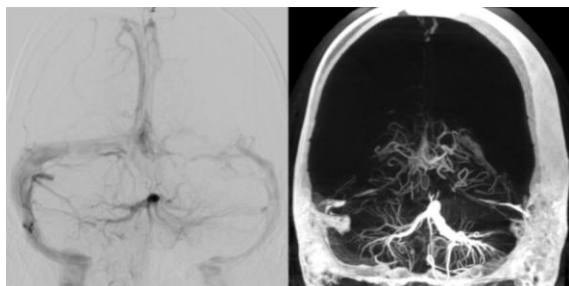
Developmental venous anomalies (DVAs) are the most common asymptomatic cerebral vascular malformation. The vast majority of these lesions are detected incidentally and associated with a benign clinical course. However, there is increasing recognition of the small subset of DVAs that present with sequelae of venous hypertension, cerebral hemorrhage, thrombosis or in association with related parenchymal abnormalities. Digital subtraction angiography (DSA) is infrequently performed for the evaluation of DVAs, but can have an important role in the investigation of complex or symptomatic lesions, particularly when combined with flat panel detector CT (FPCT). This study demonstrates the utility of FPCT as an adjunct to DSA in delineating DVA drainage territory size, outflow tract abnormalities, and venous hypertension associated with symptomatic lesions.

#### MATERIALS & METHODS

Ten cases of symptomatic DVAs were evaluated by DSA and FPCT between February 2010 and October 2011. Clinical symptoms, noninvasive imaging findings, DSA, and FPCT results were recorded retrospectively in an IRB-approved database. Qualitative analysis of DVA characteristics on noninvasive imaging (CT/MRI), DSA and FPCT was performed by two neurointerventionalists, with differences resolved by consensus.

#### RESULTS

Digital subtraction angiography and FPCT were technically successful in all cases without any complications. The extent of DVA drainage territory visualized on FPCT was 30% or greater than DSA in eight cases (80%) including one case in which a small DVA was only appreciated on FPCT. Outflow stenosis was better seen or appreciated only on FPCT in three cases (30%), of which two cases had a calcific ring at the dural interface and was visualized only on FPCT. The presence of venous hypertension was appreciated better on FPCT than DSA alone in seven cases (70%). In one patient, there was demonstration of previously unsuspected DVA at the center of a capillary telangiectasia. Dynamic DSA images were superior to FPCT in visualizing 1 case of an arterialized DVA. In 9 cases, conservative management was undertaken.



#### CONCLUSION

In symptomatic or complex DVAs, FPCT is a valuable adjunct to DSA for detailed resolution of lesion angioarchitecture. In comparison to noninvasive modalities, angiographic evaluation with DSA and FPCT can better characterize the size of the drainage territory, presence of venous hypertension, and degree of outflow tract stenosis. Flat panel detector CT also may shed some light on the etiopathogenesis of cryptic malformations like capillary telangiectasia. This additional information has the potential to increase our understanding of the symptomatology of these lesions and may perhaps influence management strategies in the future.

**KEY WORDS:** Developmental venous anomaly, flat panel detector CT, digital subtraction angiography

O-309

3:08 PM - 3:16 PM

#### Elaboration of a Semi-Automated Algorithm for Brain Arteriovenous Malformations Segmentation: Initial Results

Clarençon, F.<sup>1,2</sup>•Maizeroi-Eugène, F.<sup>3</sup>•Gory, B.<sup>4,2</sup>•Sourour, N.<sup>1</sup>•Bresson, D.<sup>5,2</sup>•Mounayer, C.<sup>4,2</sup>

<sup>1</sup>Pitié-Salpêtrière Hospital, Paris, FRANCE, <sup>2</sup>EA 3842; Constellation de Recherche Médicale Appliquée, Limoges, FRANCE, <sup>3</sup>Segmentix, Limoges, FRANCE, <sup>4</sup>University Hospital of Limoges, Limoges, FRANCE, <sup>5</sup>Lariboisière Hospital, Paris, FRANCE

#### PURPOSE

Brain arteriovenous venous malformations (bAVMs) are serious vascular malformations. Distinction between the different components in the angio-architecture of the bAVM is of tremendous importance for the understanding of these complex lesions and in order to tailor the treatment. The purpose of our study was to elaborate a semiautomated segmentation algorithm in order to distinguish, on 3D rotational acquisition (3D RA) volume, the different components of the bAVM (arterial feeders, nidus and draining veins).

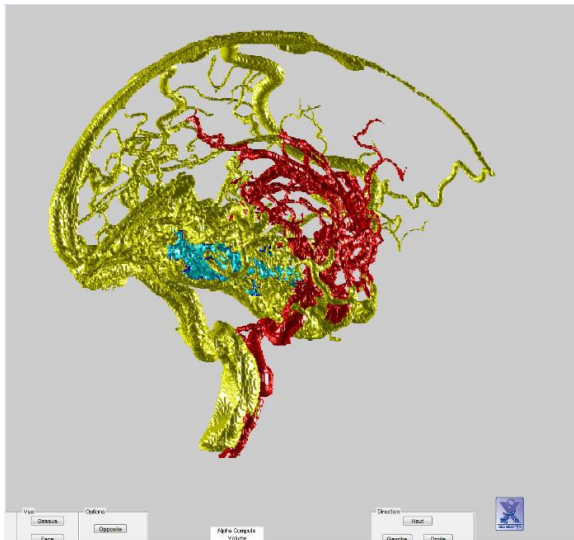
#### MATERIALS & METHODS

The semiautomated algorithm was elaborated on Matlab software (version R2009b). The data from 3D RA of seven patients (3 males, 4 females; 6 supratentorial bAVMs; 1 infratentorial bAVM) were used to elaborate the algorithm. The nidus was individualized on axial slice from the 3D RA. Then, the upper and lower edges of the nidus were specified. Given the fact that the nidus has a poor homogeneity [disorganized structure leading to a low compacity (rate between surface and volume)], nidus segmentation was performed on the low compacity structures adjacent to the selected point. Feeding arteries and draining veins were selected on axial slice from the 3D RA. These taggings were applied only when the nature of the vessel was certain. Finally, segmentation of the vessels was performed using density, shape characteristics and with a propagation algorithm. Mean duration for the segmentation was assessed. The quality of the segmentation was evaluated by comparison with the six

frames rate images from AP, lateral and oblique views acquired from the DSA.

## RESULTS

Segmentation was satisfying in all the cases. No major error was observed; only mild errors were depicted that were related to crossing between veins and arteries. These errors could be corrected easily by additional tagging of the vessels. Mean duration for the bAVM segmentation, including the vessels tagging, was about 15 min.



## CONCLUSION

This segmentation algorithm is a promising tool for the recognition, on the 3D RA reconstructions, of the different components of the bAVMs; it may help in a better understanding of the angio-architecture of these complex vascular lesions.

**KEY WORDS:** Brain AVM, algorithm, segmentation

**O-310**

**3:16 PM - 3:24 PM**

### Overlying Live Fluoroscopy with 3D MR Imaging for Brain Arteriovenous Malformations Angiographic Assessment and Endovascular Embolization

Blanc, R. P. B.<sup>1</sup>Chauvet, D.<sup>1</sup>Savatovsky, J.<sup>1</sup>Babic, D.<sup>2</sup>Pistocchi, S.<sup>1</sup>Bartolini, B.<sup>1</sup>Piotin, M.<sup>1</sup>

<sup>1</sup>Rothschild Foundation, Paris, FRANCE, <sup>2</sup>Philips Healthcare, Best, NETHERLANDS

## PURPOSE

We describe our preliminary experience combining superselective angiography, real-time fluoroscopy and 3DRoadmap navigation with preacquired magnetic resonance imaging (MRI) isotropic datasets for brain AVM embolization.

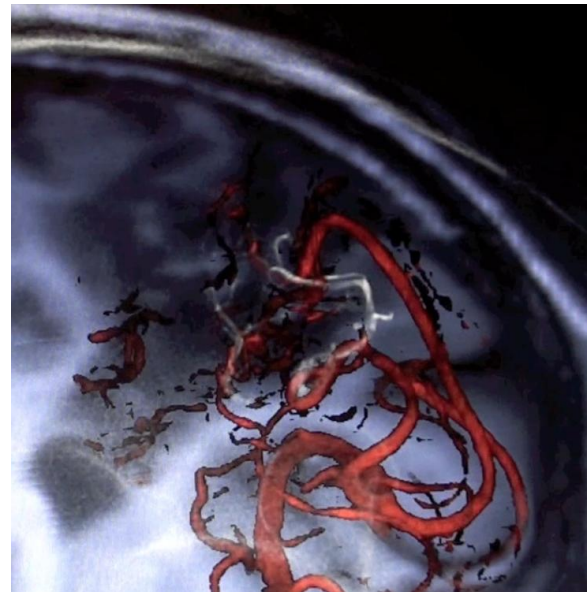
## MATERIALS & METHODS

Roadmaps are generated through fusion of preacquired magnetic resonance imaging (MRI) isotropic datasets and a 3D rotation angiography (3D RA) generated by the 3D workstation (Xtravision, Philips Healthcare, The Netherlands B.V.). Datasets were coregistered according

to a semiautomatized mutual information coregistration technique. Accuracy of coregistration of arterial feeders for brain AVM was assessed by recording the maximal discrepancy between feeders imaged by 3D RA and feeders visible on 3D MR after multiplanar reformation. Then endovascular navigation toward the nidus was realized under live fluoroscopy and 3DRoadmap. Images could be adjusted to different angles by altering the C-arm position to provide multiple working projections for the purpose of navigation and superselective catheterization of AVM arterial feeders.

## RESULTS

The technique provides important informations on anatomical landmarks. The fluoroscopic navigation, overlaid on the corresponding soft tissue of the underlying anatomy, is accurate and efficient tool for catheter guidance in intracranial vessels and for control of the progression of embolic agents in the targeted vascular lesions while performing embolization of arteriovenous malformations.



## CONCLUSION

Coregistration of 3D RA with 3D MR T1 appears reliable with millimetric accuracy and can be implemented in the critical brain AVM embolization settings. The superimposition of live fluoroscopy combined with 3D Roadmapping could improve the understanding of the microcatheter navigation towards the complex AVM vessel network and helped for control of the progression of embolic agents in the nidal vessels.

**KEY WORDS:** Brain arteriovenous malformation, embolization, 3D angiography

**O-311**

**3:24 PM - 3:32 PM**

### Outcomes of Modern Endovascular Treatment of Vein of Galen Malformations

Berenstein, A.<sup>1</sup>Niimi, Y.<sup>2</sup>Molofsky, W.<sup>2</sup>Fifi, J.<sup>2</sup>Ortiz, R.<sup>2</sup>

<sup>1</sup>St. Luke Roosevelt Hospital, New York, NY, <sup>2</sup>Roosevelt Hospital, New York, NY

#### PURPOSE

Vein of Galen aneurysmal malformations (VGAM) if untreated carry almost 100% morbidity and mortality. We are reporting the outcome of modern endovascular therapy in a consecutive series of 56 patients with vein of Galen aneurysmal malformations requiring treatment.

#### MATERIALS & METHODS

A consecutive series of 56 children presenting to our hospital with VGAM, from June 2004 to December 2010. All were treated by transarterial liquid embolization with cyanoacrylate tissue adhesive (NBCA) as the primary agent; targeting the fistula sites via percutaneous femoral artery access. Coils were used only to rearrange the anatomy or protect normal arteries. The goal of embolization in these patients was to reduce arteriovenous shunting so that heart failure becomes medically manageable, in the newborn period, and then staged embolizations to obtain closure of the malformation. A Total of 225 procedures were done.

#### RESULTS

Fifty-six cases (16 cure, 13 near total occlusion, 3 death) underwent treatment by us in 2004 or after. Among them, one cure, one near total occlusion and five partial occlusions had treatment at an outside institution. Out of the 56 patients total obliteration was achieved in 16 (28.5%). Near total obliteration >90% in 13 (23.2%), in seven (12.5%) significant malformation remained open, but targeted embolization was done, and 20 (35.7%) are still undergoing treatment. Twelve complications occurred in 225 procedures. Seven were technical with no clinical manifestation. In the other five (8.9%) children there were three dead, two from hemorrhages (3.7%) and one of CHF, and there were two infarction (3.7%), with residual clinical consequences.

#### CONCLUSION

Present management of VGAM with modern endovascular techniques and in conjunction with specialized neuroanesthetic, pediatric intensivist and neurointensive care results in significantly improved outcomes with cure and normal neurologic development. Multiple stages are often necessary. These patients require long-term care by an interdisciplinary team; and should be treated in specialized centers catering to this group of diseases.

**KEY WORDS:** Vein of Galen malformations, embolization, treatment

**O-312**

**3:32 PM - 3:40 PM**

#### **Mandible Arteriovenous Malformations Management**

Yakes, W. F.

Vascular Malformation Center  
Englewood, CO

#### PURPOSE

To determine optimal management strategies for the treatment of mandibular AVM.

#### MATERIALS & METHODS

Ten patients (9 females, 1 male), age 9 -14 years; mean age 15, underwent endovascular therapy to treat their mandibular AVMs. Five patients had distinct intraosseous AVM and one patient had periosteal mandibular AVM. Three patients had prior PVA and gel foam embolization, one patient had a lip graft, one had prior mandible surgery, all that had failed.

#### RESULTS

All ten patients have demonstrated MR and angiographic cure of their AVM. The follow up is 11 months - 35 months, with a mean follow up of 18 months. No complications were noted.

#### CONCLUSION

Endovascular approaches to manage mandibular AVM are curative. The intraosseous variety is largely a fistula between artery and vein within the bone. All respond well to endovascular ethanol therapy alone. Surgery was not required in any patient.

**KEY WORDS:** Arteriovenous malformation, mandible, ethanol

**O-313**

**3:40 PM - 3:48 PM**

#### **Spinal Arteriovenous Malformations in Patients with Spinal Dysraphism**

Stockley, H. M.·Williams, T.·Herwadkar, A.

Greater Manchester Neurosciences Centre, Salford  
Royal Hospital  
Manchester, UNITED KINGDOM

#### PURPOSE

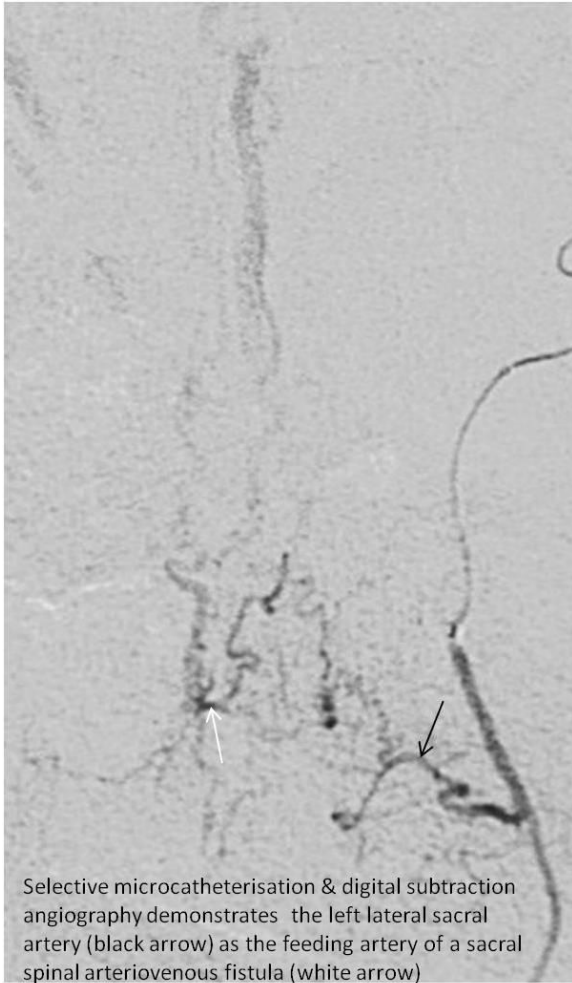
Spinal vascular malformations are rare entities. Furthermore there is minimal published evidence of spinal vascular malformations in patients who have an underlying spinal dysraphism, with most of these being single case reports. Using a combination of magnetic resonance imaging, computed tomography and digital subtraction angiography, we present a series of four patients with varying features of spinal dysraphism who were identified as also having a spinal arteriovenous malformation. We describe imaging features which may assist in determining the level of fistulous communication in this small subgroup of patients.

#### MATERIALS & METHODS

A review of the Interventional Neuroradiology database for the last ten years at Greater Manchester Neurosciences Centre identified 76 patients who underwent spinal angiography. This resulted in 87 digital subtraction angiograms, of which 52 examinations were for investigation of a potential spinal vascular malformation. Review of the imaging findings, clinical notes and operative notes identified a subgroup of four patients who had an arteriovenous



malformation and demonstrated varying features of spinal dysraphism.



Selective microcatheterisation & digital subtraction angiography demonstrates the left lateral sacral artery (black arrow) as the feeding artery of a sacral spinal arteriovenous fistula (white arrow)

## RESULTS

Imaging characteristics	% of patients
High signal on sagittal T2 MR imaging of the spinal cord	100%
Perimedullary flow voids	100%
Low lying termination of spinal cord	100%
Intraspinal tumour	50% (2/2 Lipoma)
Open neural tube defect (Occult)	75% (3/3 Bony)
Level of arteriovenous fistula	100% sacral
Feeding artery	Medial sacral artery (25%), lateral sacral artery (50%) and anterior spinal artery arising from L3 (25%)

## CONCLUSION

1. High T2 signal within the spinal cord in patients with an underlying spinal dysraphism may represent an arteriovenous fistula. 2. If an intraspinal tumor is present then the adjacent vessels should be assessed carefully for a fistulous connection. 3. Pelvic splanchnic arteries should be fully interrogated if routine angiography fails to determine a point of fistulous communication.

**KEY WORDS:** Arteriovenous malformation, spinal dysraphism

**O-314**

**3:48 PM - 3:56 PM**

## MR Imaging/MR Angiography and CT Imaging of Indirect and Direct Cavernous Carotid Fistula

Mossa-Basha, M. Gailloud, P. Pearl, M. Lin, D. D.

Johns Hopkins University  
Baltimore, MD

## PURPOSE

Cavernous carotid fistulae (CCF) represent abnormal connections between the cavernous sinus and the cavernous carotid artery (direct), or dural branches of the internal carotid artery or external carotid artery (indirect). Affected patients typically present with chemosis, proptosis, conjunctival injection, retro-orbital pain and decreased visual acuity. Although definitive diagnosis is made by catheter angiography (DSA), MRI with MRA or CTA is indispensable as the initial, noninvasive evaluation and to rule out other pathologic processes with a similar clinical presentation. In this study, we intend to analyze the CTA and MRI/MRA features of angiographically confirmed CCFs, evaluate the accuracy of these characteristics, and determine what factors may contribute to differentiation of direct from indirect CCF.

## MATERIALS & METHODS

Cases of angiographically confirmed CCF that also had pretreatment cross-sectional imaging were collected by searching our radiology database from 1/1/01 to 9/30/11. The preembolization MRI/MRA and CTA imaging studies were analyzed retrospectively. Ipsilateral and contralateral superior ophthalmic vein (SOV) and cavernous sinus (CS) diameter were measured. The affected cavernous sinuses were evaluated for intracavernous flow voids on both T2 and T1 postcontrast sequences. Flow-related signal of the affected cavernous sinus also was evaluated specifically on 3D TOF MRA source images. The lesion characteristics were compared between direct and indirect cavernous carotid fistulae by unpaired T-test with correction for multiple comparisons.

## RESULTS

There were a total of 16 cases, including 11 indirect (one patient had bilateral lesions) and five direct CCF. In 13 cases where MRI/MRA was available, 12 cases (93%) showed intracavernous flow-related signal on TOF MRA, with the one exception representing a case of indirect CCF with superimposed cavernous sinus thrombosis that was revealed on DSA. Intracavernous sinus flow voids on T2 and T1 postcontrast sequences were identified in seven of 10 indirect CCF and in three of three direct CCF, with two of three direct CCF cases demonstrating prominent intracavernous flow voids bilaterally. CT angiography and postcontrast MRI provided different measurements in 16 cases between the two types of CCFs in SOV and CS. The mean diameter of the ipsilateral SOV in direct CCF measured  $6.0 \pm 2.4$  mm, significantly larger compared to  $2.4 \pm 1.1$  mm of indirect CCF ( $p < .01$ ), and the mean diameter of the contralateral SOV of direct CCF measuring  $2.0 \pm .76$  mm was also larger than the indirect CCF of  $1.5 \pm .67$  mm. Additionally, affected CS averaging  $13 \pm 5$  mm in diameter in direct CCF is larger compared to  $9.3 \pm 2.7$  mm in indirect CCF, and the CS measuring  $9.7 \pm 1.1$  mm in direct CCF is slightly larger compared to  $8.2 \pm 0.6$  mm in indirect CCF.

## CONCLUSION

MR imaging/MR angiography and CTA provide an important evaluation of patients presenting with suspected CCF, and intracavernous flow-related signal on TOF MRA is the most reliable feature depicting 13/14 (93%) of cases in this study. The mean diameter measurements of SOV and CS obtained from CTA and MRI allow differentiation between direct and indirect CCF. Specifically, the ipsilateral SOV and CS are enlarged less commonly with indirect CCF as compared to the direct type.

**KEY WORDS:** Cavernous carotid fistula, dural arteriovenous fistula, vascular malformation

O-315

3:56 PM - 4:04 PM

### Long-Term Follow Up of Intracranial Dural Arteriovenous Fistulas with Cortical Venous Drainage Treated with Onyx Embolization of a Single Pedicle

Tejada, J. G.<sup>1</sup>•Escobar, W.<sup>2</sup>•Pedroza, A.<sup>2</sup>•Useche, N.<sup>3</sup>

<sup>1</sup>Indiana University, Indianapolis, IN, <sup>2</sup>Universidad del Valle, Cali, COLOMBIA, <sup>3</sup>Fundacion Santa Fe de Bogota Hospital, Bogota, COLOMBIA

#### PURPOSE

The therapeutic strategy for intracranial dural arteriovenous fistulas (DAVFs) is not yet well established. We now report on the treatment of intracranial DAVFs using Onyx-18, a nonadhesive liquid embolic agent.

#### MATERIALS & METHODS

We retrospectively identified all patients with intracranial DAVFs who were treated with Onyx as the single treatment technique at our institutions between April 2006 and October 2011. We documented age, gender, presenting symptoms, DAVF site, number of feeders per DAVF, whether cortical venous reflux was present, posttreatment angiography results, follow-up angiography results and clinic follow up when available.

#### RESULTS

Fourteen male patients were identified, who underwent 14 procedures for DAVF repair using Onyx-18. The mean age was  $56 \pm 12$  years. Thirteen patients presented with symptoms related to the fistula. There was an average of five feeders per DAVF (range 1-9). Cortical venous reflux was present in all patients. All patients underwent transarterial superselective catheterization of the pedicle arising from the branch of the middle meningeal artery, and Onyx-18 was injected under continuous road map guidance. Complete resolution of the DAVF on immediate posttreatment angiography was achieved in 13 patients. One patient had residual flow after the embolization and was taken to surgery the next day and complete cure of the fistula was achieved. In 13 patients complete cure of the fistula was achieved by Onyx injection on a single feeder arising from the middle meningeal artery. All patients all had cortical venous drainage (Borden type III). There were no reported complications related to the procedure. Follow-up angiography was available for 13 patients (mean, 6.4 months); one patient was lost to follow up. None of the patients who returned for follow up had any signs of angiographic recurrence. Resolution of the symptoms was noted in all angiographically cured patients at the time of the clinical follow up.

#### CONCLUSION

In our experience, the endovascular treatment of intracranial DAVFs with Onyx-18 is feasible, safe, durable and highly effective. No recurrence of the DAVF was demonstrated on follow-up catheter angiography. If a feeder from the middle meningeal artery is identified, it is highly probable to achieve a cure with the Onyx

injection of this single pedicle with treatment in one session.

**KEY WORDS:** Onyx, dural fistula, follow up

O-316

4:04 PM - 4:12 PM

### Pediatric Intracranial Dural Arteriovenous Fistulas: Clinical Features, Angioarchitecture, and Treatment Outcomes

Maluste, N.<sup>1</sup>•Fullerton, H. J.<sup>2</sup>•English, J. D.<sup>2</sup>•Halbach, V. V.<sup>2</sup>•Dowd, C. F.<sup>3</sup>•Higashida, R. T.<sup>2</sup>•Young, W. L.<sup>2</sup>•Gupta, N.<sup>2</sup>•Hetts, S. W.<sup>2</sup>

<sup>1</sup>Case Western Reserve University Medical School, Cleveland, OH, <sup>2</sup>University of California San Francisco, San Francisco, CA, <sup>3</sup>University of California San Francisco Medical Center, San Francisco, CA

#### PURPOSE

Intracranial dural arteriovenous fistula (DAVF) is rare in children. We sought to better characterize its presentation, angioarchitectural features, and outcomes of its treatment.

#### MATERIALS & METHODS

Under an IRB-approved protocol, 21 patients with intracranial DAVF were identified retrospectively from a neurointerventional radiology database out of a total of 388 patients aged 18 years or less. Medical records and imaging studies were reviewed. Demographics, clinical presentation, lesion angioarchitecture, treatment approaches, angiographic outcomes, and clinical outcomes were categorized and assessed.

#### RESULTS

Eleven boys and ten girls presented between 1 day and 18 years of age, with boys presenting at a median of 1.3 years and girls presenting at a median of 9.6 years. The most common presenting symptoms were focal neurologic deficits (35%), respiratory distress (22%), seizures (13%), CHF (13%), and recent trauma (13%). Twenty-two percent of patients had additional vascular lesions at the time of diagnosis, including capillary hemangioma, cystic hygroma, venous sinus thrombosis, and neck arteriovenous fistulas. At initial angiography, 15 patients harbored single intracranial DAVFs and six patients had between two and six DAVFs. The number of feeding arteries and arteriovenous connections ranged from one to greater than 10. The most common fistula locations were the torcula (8 fistulas), transverse sinus (7), superior sagittal sinus (6), and cavernous sinus (6). Whereas torcular fistulas were more common in young children, traumatic cavernous sinus fistulas were more common in teenagers. A median of 1.5 and an average of four diagnostic and therapeutic procedures were performed per patient, with a range of one to 20. Of these interventions, 53 were embolizations (66%), 12 were diagnostic angiograms (15%), five were surgical resections (6%), three were stereotactic radiosurgeries (4%), and two were balloon angioplasties of stenotic draining dural venous sinuses (2.5%). Among those receiving endovascular therapy, 10 patients were treated with coils, 10 with particulate

embolics, seven with liquid adhesives, three with absolute ethanol, three with detachable balloons, and one with silk sutures. Six patients (26%) had DAVF obliteration by the end of treatment. One patient had spontaneous DAVF resolution without treatment. At last follow up, four patients had a normal neurologic exam, four patients had focal neurologic deficits, two patients had seizure disorders, and one patient had developmental delay. Five patients died during follow up.

#### CONCLUSION

Dural arteriovenous fistula constituted 6% of pediatric intracranial arteriovenous shunting lesions at our institution. Boys presented at younger ages than girls. Complex congenital fistulas were predominantly present in young children presenting with CHF symptoms and traumatic fistulas were more common in teenagers. In comparison to vein of Galen malformations, nontraumatic DAVF had lower rates of angiographic obliteration and poorer clinical outcomes.

**KEY WORDS:** Dural arteriovenous fistula, pediatric cerebrovascular disease, endovascular therapy

**O-317**

**4:12 PM - 4:20 PM**

#### Endovascular Treatment in "Benign" Intracranial Hypertension: Clinical Result and Mid-Term Follow Up

Aguilar Perez, M.<sup>1</sup>Fischer, S.<sup>1</sup>Horvath-Rizea, D.<sup>1</sup>Unsöld, R.<sup>2</sup>Bäzner, H.<sup>1</sup>Henkes, H.<sup>1</sup>

<sup>1</sup>Klinikum Stuttgart, D-70174 Stuttgart, GERMANY, <sup>2</sup>Augenheilkunde Düsseldorf, 40212 Düsseldorf, GERMANY

#### PURPOSE

Idiopathic intracranial hypertension (IIH) is a disorder of increased intracranial pressure in the absence of any known causative factor, previously referred to as pseudotumor cerebri or benign intracranial hypertension. The term "benign" was dropped after several reports of severe visual loss and significant risk of blindness. Although the severity of the symptoms can affect the activities of daily living, the most important factor to plan the treatment is the amount and progression of the visual loss. Recently stenting of stenotic dural sinuses has gained popularity as treatment of IIH since these stenoses may contribute to an obstruction of the venous return and hence CSF outflow. We prospectively evaluated the safety and efficacy of endovascular treatment in these patients.

#### MATERIALS & METHODS

A total of 25 patients underwent endovascular treatment of idiopathic intracranial hypertension. Most of them were women (76%) and clinically obese (88%), as defined by overweight > 20% or a BMI (body mass index) > 25 kg/m<sup>2</sup>. The mean age was 38-76 years (range 5-64). All the patients referred headache as clinical manifestation and the majority of them also any type of visual problems with all the patients presenting papilledema in the ophthalmologic evaluation. Elevated

intracranial pressure was documented in all the patients with an opening pressure >20 cm H<sub>2</sub>O in the lateral decubitus position. Magnetic resonance imaging was performed in order to exclude another cause of intracranial hypertension. In 23 of the 25 patients (92%) hyperintensity of the optic nerve sheath was observed and in 18 (72%) an empty sella syndrome was present, one of them with associated rhinoliquorhea. All the patients presented any grade of venous stenosis, three of them (12%), unilateral and 22 (88%), bilateral. Patients were treated with angioplasty and stenting of the venous stenosis if symptoms persisted under medical treatment (acetazolamide), repeated lumbar punctures, cerebrospinal fluid (CSF) diversion procedures (such as lumbo- or ventriculoperitoneal shunts) or a combination of them. Stent was placed in all 25 patients, in eight (32%) unilaterally and in 17 (68%) bilaterally.

#### RESULTS

Resolution of the venous stenosis was possible in all the patients. There were no periprocedural or long-term complications in relation with the endovascular treatment. Improvement of papilledema was observed in all the patients and 22 of 25 (88%) reported improvement of the headache after the treatment. In the midterm follow-up (median 19-42 months, cumulative 369 months) only five patients (20%) presented restenosis, which were retreated.

#### CONCLUSION

Endovascular treatment with sinus stenting is an easy, safe and effective treatment in patients with idiopathic intracranial hypertension. The far majority of patients have a persistent clinical benefit.

**KEY WORDS:** Idiopathic intracranial hypertension, pseudotumor cerebri, angioplastia and stenting

**O-318**

**4:20 PM - 4:28 PM**

#### MR Angiographic Staging Systems of the Anterior and Posterior Circulations in Moyamoya Disease: Interobserver and Intraobserver Reproducibility and Intermodality Agreement with Conventional Angiography

Mugikura, S.·Murata, T.·Takahashi, S.·Fujimura, M.

Tohoku University School of Medicine  
Sendai, JAPAN

#### PURPOSE

Moyamoya disease shows stenoocclusive changes at or around the terminal part of the internal carotid artery (ICA) bifurcation bilaterally and often involves also the posterior cerebral artery (PCA). Conventional angiography and their staging systems of the severity of ICA and PCA lesions have been used for the diagnosis and grading of the lesions, but the use of conventional angiography is being replaced by time of flight MR angiography (MRA) only in the diagnosis due to its noninvasiveness. However, staging systems in MRA of ICA and PCA lesions necessary to the grading of the lesions have not been introduced to our knowledge. Our

purpose is to apply the two ICA and PCA staging systems originally introduced in conventional angiography to MRA, and to assess the interobserver and intraobserver reproducibility in MRA and the intermodality agreement between MRA and conventional angiography.

#### MATERIALS & METHODS

In 104 hemispheres of 52 consecutive Japanese patients diagnosed with moyamoya disease (ranging from 4 to 60 years of age, mean age 30 years), the two 4-grade ICA and PCA staging systems documented in previous studies were applied on both conventional angiography and MRA. In brief, for both ICA and PCA staging, as occlusive changes in the main trunk of ICA or PCA progress, moyamoya vessels from ICA or PCA develop. When the occlusive changes of the ICA or PCA become extremely severe, these vessels subsequently decrease, respectively. To assess the interobserver reproducibility of the ICA and PCA stages in MRA, we compared the stages determined independently by the two observers and to assess the intraobserver reproducibility of the two stages in MRA, we compared the stages determined at the first and the second evaluation after an interval of 2 weeks by one of the two observers. To assess the intermodality agreement of the ICA and PCA stages between MRA and conventional angiography, we compared the stages in MRA determined by each of the two observers and the stages in conventional angiography determined by consensus of the two observers. MR angiography was performed by using a 1.5 T (Signa Horizon LX CVi; GE Healthcare, Milwaukee, WI) scanner.

#### RESULTS

In ICA and PCA staging systems, MRA showed excellent interobserver reproducibility (weighted kappa: 0.9 in ICA stages and 0.85 in PCA stages), excellent intraobserver reproducibility (0.9 in ICA stages and 0.8 in PCA stages) and excellent intermodality agreement with conventional angiography (weighted kappa in observer 1: 0.9 in ICA stages and 0.8 in PCA stages, in observer 2: 0.8 in ICA stages and 0.8 in PCA stages).

#### CONCLUSION

In ICA and PCA staging systems of moyamoya disease used in this study, MRA showed excellent inter and intraobserver reproducibility and intermodality agreement with conventional angiography. Internal carotid artery and PCA staging systems used in this study are useful in evaluations of lesion severity in MRA.

**KEY WORDS:** Moyamoya, MR angiography, posterior circulation

## Tuesday Afternoon

**3:00 PM - 4:30 PM**

**Sutton Center/South**

**(34d) Head & Neck: Pharynx, Larynx, Soft Tissue Neck, Sinonasal and Temporal Bone**

**O-319**

**3:00 PM - 3:08 PM**

**MR Imaging Demonstration of Endolymphatic Hydrops Associated with Endolymphatic Sac Tumors**

Butman, J. A.<sup>1</sup>Kim, H. J.<sup>2</sup>Lonser, R. R.<sup>3</sup>

<sup>1</sup>The Clinical Center of the National Institutes of Health, Bethesda, MD, <sup>2</sup>NIDCD/The National Institutes of Health, Bethesda, MD, <sup>3</sup>NINDS/The National Institutes of Health, Bethesda, MD

#### PURPOSE

To characterize alterations in the internal architecture of the labyrinth resulting from endolymphatic sac tumors (ELSTS) in a consecutive series of patients with von-Hippel Lindau (VHL) disease.

#### MATERIALS & METHODS

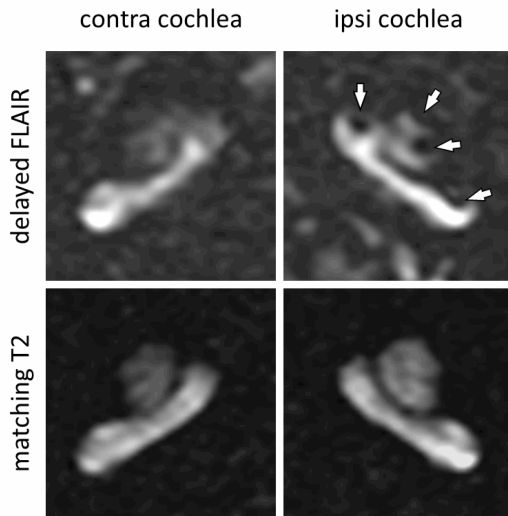
Eight VHL patients with nine small unoperated ELSTS were enrolled in a VHL natural history study (ClinicalTrials.gov identifier: NCT00005902). Prior to surgery, delayed FLAIR imaging was performed to evaluate the architecture of the membranous labyrinth. Delayed FLAIR images were obtained from 6 to 18 hours following injection of 0.1 mM/kg gadoteridol (used clinically to evaluate the brain and spine). Images were obtained on a 3.0 T Philips Achieva using a 6 channel 8 coil whole-head phased array. Contrast parameters were TR 11000, TE 120, ETL 27, TI 2550. Geometric parameters were: FOV 150 mm, thickness 1.7 mm, gap 0, matrix 320 x 243. Imaging time was ~3:25 per signal average, and four averages were performed. Care was taken to ensure that axial slices paralleled that of the horizontal semicircular canal. T2-weighted images were obtained with an identical geometry for anatomical reference.

#### RESULTS

In three ears, increased FLAIR signal throughout the labyrinth (involving both the endolymph and perilymph) representing residua of prior intralabyrinthine hemorrhage obscured the internal architecture of the labyrinth so that endolymphatic hydrops could not be assessed. In three ears, dilation of the membranous labyrinth confirmed the presence of endolymphatic hydrops. Figure shows dilation of the scala media as filling defects surrounded by enhancing perilymph in the cochlea ipsilateral to the ELST, as compared with the normal appearance of the



contralateral cochlea. In two ears, the membranous labyrinth appeared normal.



#### CONCLUSION

Previously, we have shown that even very small ELSTs can result in audiovestibular function which may present acutely resulting from acute intralabyrinthine hemorrhage or may present gradually, in a manner suggestive of Meniere's disease. Subsequently, methods to interrogate the internal architecture of the inner ear with delayed FLAIR imaging allowed us to directly demonstrate endolymphatic hydrops in patients who previously had undergone ELST resection. This report extends the prior observation of endolymphatic hydrops to a series of patients with ELSTS confirming that development of endolymphatic hydrops is a mechanism of audiovestibular dysfunction in this cohort.

**KEY WORDS:** Hearing, FLAIR, VHL

**O-320**

**3:08 PM - 3:16 PM**

#### Improved in vivo Visualization and Evaluation of Endolymphatic Hydrops Using High-Field MR Imaging in Meniere's Disease and Correlation with Audiovestibular Function

Flatz, W. H. Gurkov, R. Ertl-Wagner, B. B. Reiser, M. F.

University of Munich - Grosshadern Campus  
Munich, GERMANY

#### PURPOSE

The objective of our study was to detect and evaluate endolymphatic hydrops in Meniere's disease in vivo using MRI.

#### MATERIALS & METHODS

Forty-six previously untreated patients suffering from clinical symptoms of Meniere's disease according to AAO-HNS criteria were examined in a prospective study. Diluted gadolinium was administered intratympanically 24 hours prior to the MR scan. MR imaging was performed using a 3 T scanner using a dedicated 8 channel surface coil and a head-coil

acquiring a 3D FLAIR sequence, a 3D IR TSE sequence and a high resolution True-FISP Dual Excitation sequence (CISS). Correlation with clinical symptoms and audiovestibular function testing was performed using audiometric hearing tests, caloric stimulation, electrocochleography (ECoChG) and vestibular evoked myogenic potentials (VEMP).

#### RESULTS

Inner ear fluid spaces could be well delineated in high resolution using all three employed MR-sequences. 3D FLAIR clearly depicted gadolinium distribution in the perilymphatic space and thus allowed delineation between peri- and endolymphatic regions. Using 3D IR-TSE imaging allowed for differentiation between fluid-filled spaces of the inner ear and bony structures, as well as between peri- and endolymphatic spaces. Patients suffering from severe clinical signs and functional impairment of Meniere's disease showed smaller perilymphatic spaces and larger endolymphatic spaces compared to patients with not so severe symptoms. Additionally, in patients showing severe clinical and functional impairment evaluated by ECoChG and VEMP, lack of vestibular gadolinium distribution was found. We found significant correlation between the degree of hydrops on the one hand and the averaged hearing level at 0.25-1 and 0.5-3 kHz and the vestibular evoked myogenic potential interaural amplitude ratio on the other hand. A trend toward a correlation was noticed between the hydrops and the caloric response; no correlation was noticed between the hydrops and the SP/AP ratio. The degree of endolymphatic hydrops correlates with a progressive loss of auditory and sacculus function in patients with Meniere's disease. No adverse events were found using intratympanic administration of diluted gadolinium.

#### CONCLUSION

Endolymphatic hydrops can be detected and evaluated using 3D FLAIR and 3D IR-TSE after intratympanic administration of gadolinium. Using 3D IR-TSE imaging allows differentiation between fluid-filled spaces and bone. MR-morphologic changes found in patients suffering from Meniere's disease correlate with the severity of clinical symptoms.

**KEY WORDS:** Meniere, MR imaging, hydrops

**O-321**

**3:16 PM - 3:24 PM**

#### Characteristic Imaging Findings in Temporal Bone Facial Meningoceles

Hamilton, B. E.<sup>1</sup>Baugnon, K.<sup>2</sup>Hudgins, P.<sup>2</sup>Harnsberger, H. R.<sup>3</sup>

<sup>1</sup>Oregon Health and Sciences University, Portland, OR,  
<sup>2</sup>Emory University School of Medicine, Atlanta, GA,  
<sup>3</sup>University of Utah, Salt Lake City, UT

#### PURPOSE

Facial nerve (fallopian canal) meningoceles are rare temporal bone lesions that may be incidental findings. Since they may allow communication with the intracranial subarachnoid fluid space, they may

predispose to cerebrospinal fluid (CSF) leak or meningitis, prompting some authors to advocate surgical repair. They mimic other pathology such as facial schwannoma on CT that could lead to therapeutic misadventure. We reviewed a series of meningoceles in order to review the pertinent imaging and correlated with clinical history and presenting findings.

#### MATERIALS & METHODS

A single experienced head and neck radiologist retrospectively reviewed a series of facial meningoceles that were identified by review of teaching files from three institutions. Available clinical history and presenting symptoms were reviewed in all patients. Imaging findings were correlated to clinical findings based on review of electronic medical records.

#### RESULTS

Nine patients aged 4 to 69 years had 11 meningoceles on high-resolution temporal bone CT and internal auditory canal MRI studies (two with bilateral lesions). Five patients had findings of meningitis and/or CSF leak. Three presented with sensorineural hearing loss. None had documented facial nerve weakness. One patient presented with moderate conductive hearing loss. Facial meningoceles demonstrated benign-appearing expansile enlargement of the geniculate fossa without permeative lucencies or overt destructive changes on temporal bone CT (Figure 1). More extensive facial nerve involvement was variable. MR imaging showed fluid signal intensity within an enlarged geniculate fossa without nodular soft tissue component or enhancement (Figure 2).

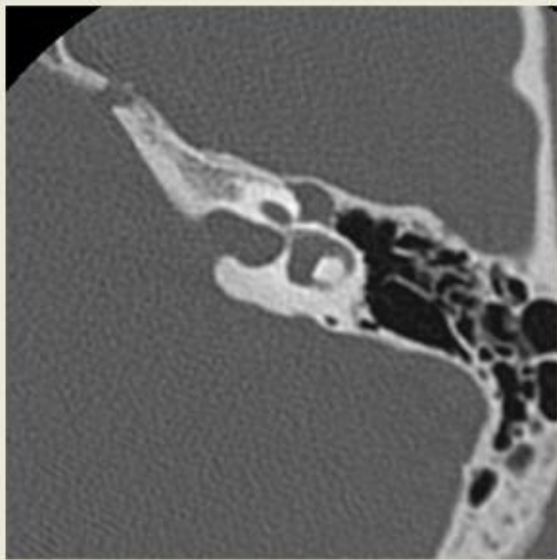


Figure 1.

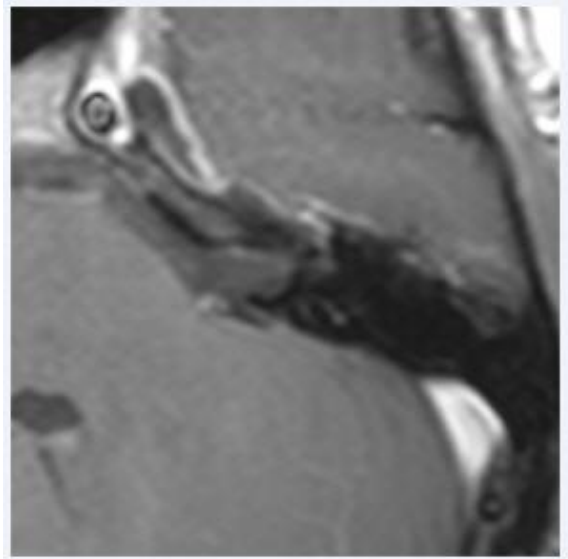


Figure 2.

#### CONCLUSION

Facial meningoceles are rare lesions that are associated with meningitis and CSF leak, however other cases occur incidentally. Temporal bone CT appearance mimics facial schwannoma, therefore MRI is an important confirmatory test to distinguish between meningocele and schwannoma as diagnostic considerations. Surgical therapy is indicated for facial meningoceles when presenting with signs and symptoms of CSF leak and/or meningitis.

**KEY WORDS:** Meningocele, facial nerve, fallopian canal

O-322

3:24 PM - 3:32 PM

#### Diagnostic Value of Screening Acoustic MR Imaging in Patients with Hearing Loss: Overutilization?

Osborn, D.<sup>1</sup>Jain, R.<sup>1</sup>Standring, R.<sup>1</sup>Shah, P.<sup>2</sup>Succar, E.<sup>2</sup>Seidman, M.<sup>1</sup>

<sup>1</sup>Henry Ford Health System, Detroit, MI, <sup>2</sup>Wayne State University School of Medicine, Detroit, MI

#### PURPOSE

Hearing loss and the possibility of a retrocochlear pathology often presents a diagnostic quandary for physicians. While "asymmetric sensorineural hearing loss" could be an indicator of retrocochlear pathology, screening MRI scans are often negative. With increasing healthcare costs, excessive imaging has come under scrutiny. The purpose of this study was to assess the diagnostic yield of screening MRI in patients with hearing loss. We also evaluated additional clinical criteria to see if their presence could improve the diagnostic yield of screening MRI.

#### MATERIALS & METHODS

Six hundred fifteen patients (52% male, mean age 59.8 years) who underwent an acoustic protocol MRI for "hearing loss" between 10/2005 and 5/2011 at our institution were identified through a search of the radiology information system. We also looked for

documentation of additional clinical criteria used to perform the MRI study, including “asymmetric hearing loss”, “acute” onset of symptoms, “unilateral tinnitus”, “bilateral tinnitus”, and “dizziness”. To better define “asymmetric hearing loss”, audiograms were categorized as having asymmetries of 10 dB difference at three frequencies, 15 dB difference at two frequencies, and 15 dB difference at 3000 Hz. Patients with a 15% decrease in word recognition between ears also were recorded. MR imaging findings were categorized as “normal” (no abnormalities), “incidental” (findings do not explain symptoms), or “abnormal” (findings explain symptoms).

## RESULTS

Of the 615 MRIs reviewed, 562 (91.4%) cases were normal or had only incidental findings. Only 56 (8.6%) patients had abnormal findings consistent with the clinical presentation. Regarding the clinical criteria, 21.3% had associated “unilateral tinnitus”, of which 17% ( $p < 0.001$ ) had a MRI classified as “abnormal”.

Clinical Criteria	All Patients (N=615)	Abnormal MRI N(%)	p-value
Unilateral Tinnitus	131 (21%)	22 (17%)	<0.001
Acute Onset	103 (17%)	15 (15%)	0.018
Asymmetric hearing loss	520 (85%)	49 (9%)	0.096
Bilateral Tinnitus	105 (17%)	2 (2%)	0.007
Dizziness	185 (30%)	19 (10%)	0.338

Of the 410 audiograms analyzed, 12.4% of those with an asymmetry of 15 dB difference at 3000 Hz had a MRI categorized as “abnormal”.

Type of Asymmetry	All Patients (N=410)	Abnormal MRI	% Abnormal
15 dB difference at 3000 Hz	251	31	12
15 dB difference at 2 frequencies	354	33	9
10 dB difference at 3 frequencies	364	35	10
15% decrease in word recognition	146	12	8

## CONCLUSION

In summary, screening acoustic MRI has a low diagnostic yield (8.6%) in patients presenting with hearing loss. However, screening patients with additional “unilateral tinnitus” (17% vs 8.6%), “acute” onset of symptoms (15% vs 8.6%), and asymmetric hearing loss characterized by 15 dB difference at 3000 Hz (12.4% vs 8.6%) can lead to improvement in the diagnostic yield of MRI suggesting that patients with the presence of these clinical criteria in addition to hearing loss could benefit from screening MRI. Applying stricter clinical criteria to screen these patients can improve the diagnostic yield of screening MRI and ultimately lead to meaningful benefits for patients and improve the delivery of healthcare.

**KEY WORDS:** Hearing loss, asymmetric sensorineural hearing loss, overutilization

O-323

3:32 PM - 3:40 PM

## Signal Intensity Changes of the Cochlea in Patients with Cerebellopontine Angle Meningioma on Isotropic 3D Fluid-Attenuated Inversion Recovery MR Imaging at 3 T: Comparison with Vestibular Schwannoma

Kim, H.<sup>1</sup>Choi, J.<sup>1</sup>Lee, H.<sup>2</sup>Kim, H.<sup>1</sup>Cha, J.<sup>1</sup>Kim, S.<sup>1</sup>

<sup>1</sup>Samsung Medical Center, Seoul, KOREA, REPUBLIC OF,  
<sup>2</sup>Sanggye Paik Hospital, Inje University School of Medicine, Seoul, KOREA, REPUBLIC OF

## PURPOSE

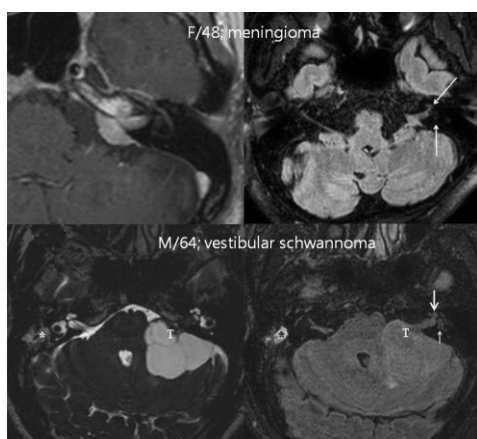
The signal intensity (SI) of the labyrinth in patients with vestibular schwannoma (VS) is known to be increased on FLAIR MR imaging due to increased protein concentration within the perilymph. It has been proposed that mechanical obstruction of the internal auditory canal (IAC) can cause increased perilymph protein concentration by either breakdown of the blood-perilymph barrier due to increased filtration from plasma or blockage of neuroaxonal transport of proteins by compression of the cochlear nerve. To validate this theory, we compared SI changes of the cochlea in patients with cerebellopontine angle (CPA) meningioma with those in patients with VS on isotropic 3D FLAIR imaging.

## MATERIALS & METHODS

This study included 18 patients with unilateral CPA meningioma extending to the IAC and 77 patients with unilateral VS. In each group, we qualitatively and quantitatively compared the SIs of the cochlea on the affected side with those on the unaffected side on 3D FLAIR imaging. The SI ratios (SIRs) of the cochlea on the affected side in patients with meningioma were compared with those in patients with VS.

## RESULTS

Qualitatively, compared with the brain stem, the SI of the cochlea on the affected side was increased markedly in 6% (1/18) and 82% (63/77), mildly increased in 33% (6/18) and 14% (11/77) and not increased in 61% (11/18) and 4% (3/77), in patients with meningioma and VS, respectively. Quantitative study revealed significantly greater SIRs of the cochlea on the affected side in both patients with meningioma ( $0.57 \pm 0.22$ ;  $p = 0.007$ ) and VS ( $1.03 \pm 0.40$ ;  $p < 0.0001$ ), compared with those on the unaffected side (meningioma,  $0.45 \pm 0.12$ ; VS,  $0.60 \pm 0.33$ ). The SIRs of the cochlea on the affected side in patients with meningioma were statistically significantly lower than those in patients with VS ( $p < 0.0001$ ).



#### CONCLUSION

The SIs of the cochlea in patients with CPA/IAC meningioma are significantly lower than those in patients with VS on 3D FLAIR imaging. There may exist more complex mechanism(s) other than mechanical obstruction of the IAC to explain the cause of increased protein concentration in the perilymph in patients with VS.

**KEY WORDS:** Three-dimensional FLAIR MR imaging, inner ear, temporal bone, cerebellopontine angle meningioma

O-324

3:40 PM - 3:48 PM

#### Inner Ear Anomalies Seen on CT Images in Patients with Down Syndrome

Intrapiromkul, J.·Aygun, N.·Yousem, D. M.

The Johns Hopkins University  
Baltimore, MD

#### PURPOSE

A higher than normal prevalence of hearing loss (42-82%) has been observed in Down syndrome (DS). Inner ear anomalies are thought to be much less frequent and tend to be overlooked, yet they play a part in the etiology of mixed or sensorineural hearing loss in 17-46% of DS cases. Although dysplasia of inner ear structures in DS has been reported in several histopathologic studies, the imaging findings have been chronicled in only one radiologic study. The purpose of this study is to evaluate the prevalence of inner ear anomalies detected on computerized tomography (CT) images in DS patients.

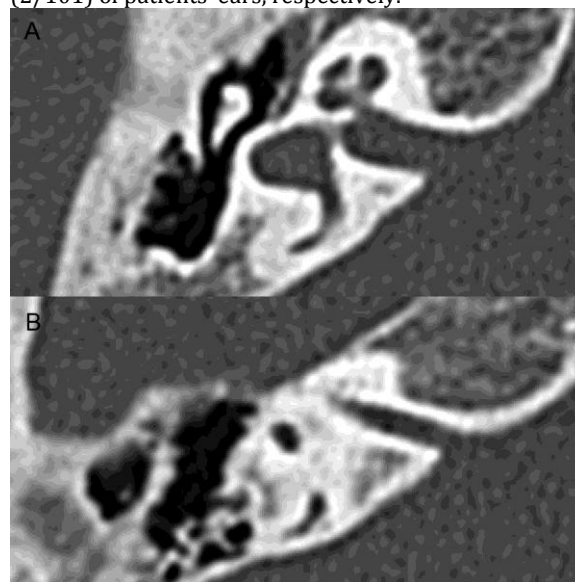
#### MATERIALS & METHODS

The radiologic database was reviewed retrospectively for DS patients with CT scans that included the temporal bones. The study was approved by the institutional review board. The CT images were evaluated by two experienced neuroradiologists separately and in consensus. The CT images of the temporal bones were qualitatively assessed for malformed bony island of lateral semicircular canal (LSCC), internal auditory canal (IAC) stenosis (< 3.3 mm at midpoint), cochlear aperture stenosis (< 1.4 mm in width), semicircular canal (SCC) dehiscence, and enlarged vestibular aqueducts (>1.5 mm in width). The

size of the bony island of the LSCC was measured with < 3 mm in maximal diameter considered abnormal.

#### RESULTS

Ninety-two DS patients with CT images including the temporal bones were identified. Forty-one cases with suboptimal scans due to low resolution or motion artifact were excluded. Fifty-one patients (102 ears), aged  $23.5 \pm 18.7$  years (mean  $\pm$  SD) were included in this study. Inner ear anomalies were observed in 74.5% (38/51) of DS patients. Of all patients' ears, malformed (small or absent) bony island of LSCC (Figure 1A) was seen in 24.8% (25/101) by qualitative assessment and 53.5% (54/101) by quantitative assessment (<3 mm in diameter). Internal auditory canal stenosis (Figure 1B), cochlear aperture stenosis, SCC dehiscence, and enlarged vestibular aqueducts were detected in 20.6% (21/102), 18.4% (18/98), 8.8% (9/102) and 2% (2/101) of patients' ears, respectively.



#### CONCLUSION

Inner ear anomalies are common (74.5%, 38/51) in DS patients. Malformed small (< 3 mm) bony island of LSCC is the most common (53.3%, 54/101) inner ear anomaly, followed by IAC stenosis and cochlear aperture stenosis. The correlation between radiographic findings of inner ear dysplasia and vestibulocochlear symptoms remains to be determined.

**KEY WORDS:** Down syndrome, inner ear, trisomy 21

O-325

3:48 PM - 3:56 PM

#### Diagnostic Accuracy of Nonecho Planar Diffusion-Weighted Imaging in the Detection of Residual and/or Recurrent Cholesteatoma of the Temporal Bone

Dremmen, M. H. G.·Hofman, P. A. M.·Hof, J. R.·Stokroos, R. J.·Postma, A. A.

Maastricht University Medical Centre  
Maastricht, NETHERLANDS

**PURPOSE**

Nonecho planar imaging (non-EPI) diffusion-weighted (DW) magnetic resonance imaging (MRI) is a promising alternative to second-look surgery for the detection of residual and/or recurrent cholesteatoma. We evaluated the diagnostic accuracy, expressed as positive predictive value, of MRI for the detection of residual and/or recurrent cholesteatoma in our hospital.

**MATERIALS & METHODS**

Fifty-six MR imaging studies were performed from 2005 to 2010 in patients previously operated for cholesteatoma. Pre and postgadolinium T1-weighted, T2-weighted and non-EPI DWI sequences were performed and correlated with clinical and intraoperative findings. Twenty-seven cases underwent second-look surgery; seven cases are under close clinical follow up. Twenty-two cases without evidence of cholesteatoma are under regular follow up (range 14-44 months).

**RESULTS**

Non-EPI DWI sequences showed increased DW signal intensity in 36 cases. Of those, 27 had second-look surgery, confirming cholesteatoma in 25 cases; in one case an empyema was diagnosed and in one other case no cholesteatoma was found at surgery. In two nonoperated cases, increased DW signal intensity was accompanied by hyperintense signal on T1-weighted images, consistent with transplanted fat in the postoperative cavity.

The positive predictive value for detection of cholesteatoma was 93% (25/27).

**CONCLUSION**

Residual and/or recurrent cholesteatomas after primary cholesteatoma surgery can be detected accurately by increased DW signal intensity on non-EPI DW MR imaging. However, DWI without conventional sequences increases the risk of misdiagnosis in our patient setting, because transplanted fat within the postoperative cavity may show increased DW signal intensity.

**KEY WORDS:** Diagnostic accuracy, nonecho planar diffusion-weighted imaging, residual recurrent cholesteatoma

**O-326****3:56 PM - 4:04 PM**

### **Radiographic Findings of Sinonasal Respiratory Epithelial Adenomatous Hamartoma: A Closer Look at the Olfactory Clefts**

Hawley, K.·Ahmed, M.·Sindwani, R.

Cleveland Clinic Foundation  
Cleveland, OH

**PURPOSE**

Respiratory epithelial adenomatoid hamartoma (REAH) is a benign glandular proliferation with ciliated epithelium located in the sinonasal cavities. It was originally described in 1995 and since, has only been published as small case series. Respiratory epithelial

adenomatoid hamartoma can present as an isolated polypoid lesion commonly originating from the olfactory cleft (OC), or found in association with an inflammatory process, most commonly sinonasal polyposis (SNP). Little is currently known about the implications and radiographic findings of these two distinct clinical presentations. Because the isolated disease is noted often in the OC, it has been suggested that this region may appear widened on CT imaging. We aim to better understand the radiologic features in the different forms of REAH, and closely examine changes in the OC that may occur with this entity.

**MATERIALS & METHODS**

This is a case control study comparing patients with histologic evidence of REAH to a control group with SNP without evidence of REAH, both groups have opacified OC on CT. To account for the different presentations of REAH, comparisons were made between: patients with isolated REAH (group A), those with REAH and concurrent SNP (group B), and those with SNP and no pathologic diagnosis of REAH (group C). Clinical and radiographic findings were compared between the groups. Specifically, Harvard sinus CT scores and the width of the OC in each group were analyzed. When measuring the width of the OC, the width between middle turbinates (x), between each lamina papyracea (y) and the ratio of the two (x/y) was recorded. Patients without opacification of the OC were excluded.

**RESULTS**

There were 29 patients with REAH: seven in group A, mean age 69 years and 22 in group B, mean age 58 years. Group C consisted of 26 patients, mean age 48 years. Harvard CT scores were found to be statistically different ( $p < 0.01$ ) between groups A and B and between groups A and C. CT scores of groups B and C were similar. Olfactory cleft width measurement x was significantly larger in groups A and B when compared to C, and the ratio x/y was significantly smaller in groups A and B compared to C ( $p < 0.01$ ). Measurements x, y, or ratio x/y were not different between groups A and B, and the measurement y was not found to be different between any groups. When diffuse SNP is present and the olfactory clefts are involved, if measurement x is 10 mm or greater, then the sensitivity and specificity for the presence of REAH is 73% and 81% respectively; the PPV and NPV are 76 and 78% respectively.

**CONCLUSION**

Both distinct clinical presentations of REAH (isolated and concurrent with SNP) correlate with a widening of the OC on CT when compared to patients with SNP only. There is no difference in dimensions in patients with isolated when compared to patients with concurrent REAH. Although directed biopsies from the OC are not performed routinely in the operating room when a patient has diffuse SNP, our findings suggest that this may be the true anatomical origin of REAH.

**KEY WORDS:** Paranasal sinus disease, hamartoma, radiographic findings



O-327

4:04 PM - 4:12 PM

### Repeatability of Pretreatment FDG-PET Compared to Early Treatment-Induced Changes for Head and Neck Cancer

Hoang, J. K. • Peterson, B. L. • Broadwater, G. • Das, S. • Yoo, D. • Brizel, D. D.

Duke University Medical Center  
Durham, NC

#### PURPOSE

Several studies have evaluated reproducibility of FDG-PET with double baseline scans and show metabolic activity can vary by 10% and 16%. To date no prior studies have compared directly this variability with early treatment response metabolic changes. This study aims to compare the pretreatment intrinsic variability of SUV with early treatment-induced change in head and neck cancer (HNC) patients undergoing serial FDG-PET scans.

#### MATERIALS & METHODS

Seventeen subjects with AJCC stages III-IV HNC receiving curative intent chemoradiation (CRT) were imaged with two baseline PET-CT scans (PET1 and 2) and a third scan (PET3) after 1-2 weeks of CRT. A radiologist manually delineated volumes for the primary tumor and the most metabolically active nodal metastasis to determine SUVmax, SUVmean, and SUVpeak. Relative differences in these SUV parameters were calculated for the two baseline PET scans [ $d1 = \text{Abs}(\text{PET1}-\text{PET2})/\text{AvPET1and2}$ ;  $\text{AvPET1and2} = (\text{PET1} + \text{PET2})/2$ ] and the intratreatment PET scan [ $d2 = \text{AvPET1and2}-\text{PET3}/\text{avPET1and2}$ ]. The differences in d1 and d2 means were evaluated with the t-test. SUV repeatability was quantified with intraclass correlation coefficient (ICC). A p-value of <0.05 was statistically significant.

#### RESULTS

Sixteen patients had double baseline scans (median interval 10 days, interquartile range 7-13.5) and 15 patients had intratreatment scans (median interval 13.5 days, interquartile range 12-17). The median radiation dose at the time of the intratreatment scan was 12 Gy (interquartile range 10-14). thirteen patients had no residual disease after CRT. Three patients had pathologically confirmed residual disease. Table 1 shows the mean SUV differences and ICC. Mean d1 SUV (baseline differences) was lower for nodal disease than primary tumor. All mean d2 SUV (intratreatment changes) were higher than d1 SUV for primary and nodes, but the differences in means were not statistically significant. When patients were divided by treatment response, patients with residual disease had smaller intratreatment decreases in SUV for nodal disease compared to patients with no residual disease. All baseline primary tumor and nodal SUV values had excellent ICC > 0.85 suggesting excellent reproducibility of quantitative measurements, but only nodal SUVmax and nodal SUVmean had nonoverlapping 95% confidence intervals with PET2 and PET3 ICC 95% confidence intervals.

Table 1. Mean SUV difference and intraclass correlation (ICC).

	Baseline difference (d1) (%)	Intratreatment change (d2) (%)	No residual disease intratreatment change (%)	Residual disease intratreatment change (%)	d1 d2 t-test p-value	ICC of PET 1 & 2	ICC of PET 2 & 3
Primary tumor							
SUVmax	11.2 (7.8)	14.9 (22.3)	12.03 (22.5)	25.4 (22.5)	0.49	0.94 (0.76-0.97)	0.67 (0.27-0.87)
SUVmean	9.7 (9.9)	9.9 (22.6)	8.6 (21.4)	14.9 (31.5)	0.95	0.91 (0.76-0.97)	0.67 (0.27-0.87)
SUVpeak	12.2 (8.6)	13.5 (22.4)	11.4 (22.8)	21.5 (23.1)	0.66	0.92 (0.80-0.97)	0.72 (0.36-0.89)
Nodal disease							
SUVmax	8.0 (5.2)	11.0 (23.7)	11.3 (22.3)	9.2 (43.1)	0.24	0.95 (0.81-0.98)	0.57 (0.11-0.83)
SUVmean	9.6 (7.7)	11.3 (23.9)	14.0 (20.0)	-4.6 (49.3)	0.31	0.93 (0.81-0.97)	0.46 (0.03-0.78)
SUVpeak	13.9 (11.2)	15.0 (25.3)	16.7 (21.8)	4.6 (53.2)	0.23	0.86 (0.65-0.95)	0.51 (0.03-0.80)

Note: Values in parentheses for baseline and intratreatment differences are the standard deviation. Values in parentheses for ICC are 95% confidence intervals.

#### CONCLUSION

There is excellent repeatability between baseline SUV for HNC relative to intratreatment changes, particularly for nodal disease. The implications are that evaluation of early treatment response should be measured quantitatively in nodal disease rather than the primary tumor and assessment of positive response should account for the intrinsic baseline variability.

**KEY WORDS:** Head and neck cancer, FDG-PET, early treatment response

O-328

4:12 PM - 4:20 PM

### CT Imaging Correlates to Genomic Expression of Squamous Cell Carcinoma of the Oral Cavity

Pickering, C. R. • Shah, K. • Ahmed, S. • Frederick, M. J. • Ginsberg, L. E. • Kumar, A. J. • Myers, J. N. • Hamilton, J. D.

M.D. Anderson Cancer Center  
Houston, TX

## PURPOSE

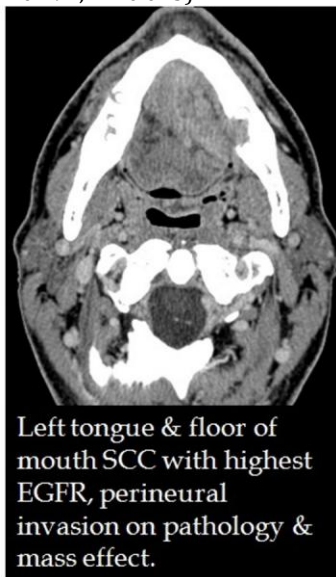
Genomic expression has become important for the prognosis and treatment of some malignancies; including those affecting breast and brain. However, clinically useful biomarkers for squamous cell carcinoma of the oral cavity (SCC OC) are limited. Imaging biomarkers that correlate with genomic alterations or gene expression of SCC OC have not been studied, despite successful correlations in other tumor types.

## MATERIALS & METHODS

After IRB approval, surplus frozen tissue from 43 patients with SCC OC was analyzed for gene expression. A team of neuroradiologists, blinded to the genomic analysis, reviewed the available imaging in 27 patients for an extensive list of possible imaging biomarkers, which then were correlated to genomic expression in tumor suppressor protein TP53, epidermal growth factor receptor (EGFR), cyclin D1 (CCND1) and angiogenesis-related genes.

## RESULTS

The enhancement [in Hounsfield units (HU)] of the primary tumor correlated with vascular endothelial growth factor (VEGF) receptor-1 (FLT-1) gene expression [Pearson Coefficient (PC) = 0.451;  $P = 0.018$ ]. Epidermal growth factor receptor expression correlated with mass effect (measured by midline displacement and airway compromise; PC = 0.432;  $P = 0.024$ ), estimated percentage of necrosis in metastatic lymph nodes (PC = 0.694,  $P = 0.026$ ) and increased risk of perineural invasion by pathology. The largest tumors (by cross-sectional area on axial images) related to VEGF ligand A (PC = 0.486,  $P = 0.010$ ) and VEGF Receptor 2 (KDR; PC = -0.421,  $P = 0.029$ ), as well as the amount of mass effect and an increased risk of perineural invasion by pathology. The cross-sectional area of the largest metastatic lymph node correlated to CCND1 (PC = 0.491,  $P = 0.015$ ).



## CONCLUSION

To the authors' knowledge, this preliminary data is the first report of the CT imaging correlates with genomic

expression in untreated SCC OC. The analysis of additional genomic and imaging biomarkers is still in process. The relationship between VEGF expression and enhancement, as well as EGFR and nodal necrosis, confirmed an apriori hypothesis generated from data in brain tumors. Many of the correlations identified so far are the targets of chemotherapeutic agents and this information could be helpful in tailoring individual treatment of patients with SCC of the head and neck. Further confirmation and evaluation of these imaging correlates is needed to ascertain their clinical utility, such as predicting prognosis or treatment outcomes. It is unknown if these imaging features could apply to other SCC locations.

**KEY WORDS:** Gene expression, oral cavity squamous cell carcinoma, computed tomography

**O-329**

**4:20 PM - 4:28 PM**

## Radiofrequency Ablation of Benign Nonfunctioning Thyroid Nodules: 3-Year Follow-Up Results in 111 Patients

Lim, H.<sup>1</sup>·Lee, J.<sup>1</sup>·Ha, E.<sup>1</sup>·Sung, J.<sup>2</sup>·Kim, J.<sup>3</sup>·Baek, J.<sup>1,2</sup>

<sup>1</sup>Asan Medical Center, Seoul, KOREA, REPUBLIC OF, <sup>2</sup>Daerim St. Mary's Hospital, Seoul, KOREA, REPUBLIC OF, <sup>3</sup>Chung-Ang University College of Medicine, Seoul, KOREA, REPUBLIC OF

## PURPOSE

The purpose of this study is to evaluate the clinical outcomes and safety of radiofrequency (RF) ablation for patients with benign nonfunctioning thyroid nodules followed up longer than 3 years.

## MATERIALS & METHODS

From June 2002 to December 2007, 538 thyroid nodules of 505 patients were treated using ultrasound (US)-guided radiofrequency (RF) ablation. Among them, 126 nodules of 111 patients were enrolled as they fulfilled the following criteria: reporting cosmetic and/or symptomatic problems; largest diameter of the nodule exceeding 2 cm; cytologic confirmation of benignancy at two separate US-guided fine-needle aspiration biopsy; thyroid function was within normal limit; followed up more than 3 years; and refusal of or ineligibility for surgery. We used moving shot technique with Cool-Tip RF system and an internally cooled electrode. Thyroid nodule volume, cosmetic and symptomatic scores were evaluated before treatment and during follow-up periods. We evaluated factor related to the efficacy. Complications during the procedure and follow-up periods also were evaluated.

## RESULTS

The mean follow-up duration after RF ablation was  $49.4 \pm 13.6$  months (mean  $\pm$  SD). The mean number of treatment session was  $2.2 \pm 1.4$ . Thyroid nodule volume decreased significantly from  $9.8 \pm 8.5$  mL to  $0.9 \pm 3.3$  mL ( $P < .001$ ) at final evaluation with volume reduction ratio of  $93.4 \pm 11.7$  %. The mean symptom ( $P < .001$ ) and cosmetic score ( $P < .001$ ) improved significantly. Factors related to the efficacy were initial solidity and initial volume. Regrowth was observed in seven nodules

due to marginal regrowth. Overall complication rate was 3.6% (4/111). All patients with complications recovered without sequelae.

#### CONCLUSION

Our study demonstrated that RF ablation is effective in achieving shrinkage of benign thyroid nodules as well as in controlling nodule-related problems at 3 years. There were no life-threatening complications or sequelae. Therefore, RF ablation can be used as a nonsurgical treatment modality for benign nonfunctioning thyroid nodules.

**KEY WORDS:** Radiofrequency ablation, thyroid nodule, ultrasound

## Afternoon

**3:00 PM - 4:30 PM**

**Murray Hill**

**(35) GRANT WRITING SEMINAR**

**O-330**

**3:00 PM - 3:20 PM**

#### Early Career Awards

Timothy P.L. Roberts, PhD

Radiology, Children's Hospital of Philadelphia  
Philadelphia, PA, USA

#### Presentation Summary

This presentation will discuss the options for junior neuroradiology fellows and faculty to obtain extramural funding. While considerable emphasis will be placed on NIH K-awards, alternative strategies (e.g. Foundations) will be introduced. Key elements in successful grant applications will be emphasized and key red flags to be avoided will be identified.

**O-331**

**3:20 PM - 3:40 PM**

#### How to Prepare Your First Grant Submission

Elizabeth A. Krupinski, PhD

Radiology and Psychology, University of Arizona  
Tucson, AZ, USA

*Dr. Krupinski is a Professor at the University of Arizona in the Department of Radiology. She received her BA from Cornell, MA from Montclair State and PhD from Temple, all in Experimental Psychology. Her interests are in medical image perception, observer performance, decision making, and human factors. She is Associate Director of Evaluation for the Arizona Telemedicine Program. She has published extensively in these areas, and has presented at conferences nationally and internationally. She is Past Chair of SPIE Medical Imaging Conference, Past President of the American Telemedicine Association, President of the Medical Image Perception Society, and Chair of the Society for Imaging Informatics*

*in Medicine. She has served as a reviewer on NIH, FDA, DoD and other funding agencies for over 20 years.*

#### Presentation Summary

This workshop will provide information and practical advice on writing a grant proposal with particular emphasis on submitting to the National Institutes of Health (NIH). The benefits of considering other funding agencies as well as other mechanisms than the classic R01 will be addressed. The workshop is designed primarily for junior faculty in academic centers who wish to pursue a career in radiologic research. The workshop will begin with an overview of the NIH, the institutes, and the various funding mechanism available to investigators. The application process will then be covered, providing tips on what to include in what sections, what aspects to emphasize when writing your grant, and tips on deciding what to include and what not to include in the proposal. What happens to the proposal once submitted will be covered as well. Although a significant amount of information is available on how the review process works, many investigators (new and experienced) have questions that are best answered in person by those who have first-hand experience. Therefore, attendees will also be provided with a clearer understanding of the review process in order to be better prepared to write grants that are more likely to be well received. Review criteria will be covered as will what happens behind closed doors during a typical review session.

**O-332**

**3:40 PM - 4:00 PM**

#### How to Avoid Common Pitfalls in Grant Submission

Peter B. Barker, D.Phil PhD

Radiology, Johns Hopkins University  
Baltimore, MD, USA

## Tuesday Afternoon

**4:45 PM - 6:15 PM**

**Beekman/Sutton North**

**(36) ASHNR PROGRAMMING:  
SINUS / ORBIT**

**O-333**

**4:45 PM - 5:10 PM**

#### Orbit Tumors and Vascular Lesions

Deborah R. Shatzkes, MD

Radiology, Lenox Hill Hospital  
New York, NY, USA

#### Presentation Summary

Most pathology in the orbit can be categorized into one of a limited number of patterns of orbital disease, with lesions of widely varying biologic behavior and clinical

relevance presenting virtually identical imaging appearances. As such, the generation of a limited and clinically useful differential diagnosis requires a modicum of clinical information. Combining the patient's age with two clinical features, namely the presence or absence of pain and the rapidity of onset of symptoms, will help direct differential considerations into appropriate categories. For example, when there is rapid onset of a painful orbital process, primary considerations are infectious and inflammatory, so that an infiltrative orbital process is more likely to represent cellulitis or pseudotumor than sarcoidosis or metastatic disease. Other diseases that can present a virtually identical imaging appearance of diffusely infiltrative process include such widely varying clinical entities as Wegener granulomatosis, retrobulbar hemorrhage and cavernous sinus thrombosis. Clearly, a differential that includes all these entities is not a useful one to the referring clinician.

Conversely, there are several disease processes that affect the orbit that can present with widely varying imaging patterns. For example, lymphoma most often presents in the orbital anterior compartment, but can appear as a retrobulbar infiltrate, a discrete retrobulbar mass, a lesion of the extraocular muscles, bilateral lacrimal masses, and a bony orbital lesion. As such, in the absence of appropriate clinical information, lymphoma must be included in virtually every differential diagnosis in the orbit. Other diseases that may have myriad manifestations in the orbit include pseudotumor, sarcoidosis and metastatic disease. While some entities have distinguishing imaging features, such as enophthalmos in the setting of the scirrhous variant of breast carcinoma, in most cases these entities are radiographically indistinguishable.

**O-334****5:10 PM - 5:35 PM**

### **Sinonasal Anatomy**

Michelle A. Michel, MD

Radiology, Medical College of Wisconsin/Froedtert Hospital  
Milwaukee, WI, USA

#### **Presentation Summary**

The frontal sinuses are separated by an intersinus septum and each drains via its ostium into the frontal recess. The nasolacrimal duct drains into the inferior meatus. The middle meatus receives drainage from the frontal sinus, the anterior ethmoid air cells, and the maxillary sinuses. The posterior ethmoid cells and sphenoid sinuses drain into the superior meatus via the sphenoethmoidal recess. The roof of the ethmoid labyrinth is derived from the orbital plate of the frontal bone or fovea ethmoidalis. Medial to the fovea ethmoidalis is the cribriform plate derived from the ethmoid bone. The structures comprising the ostiomeatal complex include the uncinate process, ethmoid infundibulum, hiatus semilunaris, middle meatus, ethmoid bulla, and middle turbinate. The infundibulum connects the maxillary ostium to the middle meatus at the hiatus semilunaris. The middle turbinate is attached superiorly to the cribriform plate

by the vertical lamella and posteriorly to the lamina papyracea by the basal lamella. The sphenoid sinuses are bordered by the sella turcica, anterior cranial fossa and optic nerves, cavernous sinuses, foramen rotundum, vidian canals, internal carotid arteries, and the clivus.

Anatomic variations are common. They may make a patient more susceptible to recurrent disease or prone to injury during surgery. Deviation of the nasal septum is a common anatomic variant and may be diffuse and broad-based, focal, or S-shaped. Septal spurs are frequently seen in association with deviation of the septum and may be bony or cartilaginous. Agger nasi cells are the most anterior of the ethmoid air cells. Infraorbital ethmoid cells (Haller cells) extend along the medial aspect of the orbital floor. Sphenoethmoidal cells (Onodi cells) are posterolateral extensions of posterior ethmoid air cells. An asymmetric, "low-lying" ethmoid roof is a potential risk factor for intracranial injury during endoscopic ethmoidectomy. Dehiscence of the lamina papyracea may predispose a patient to orbital injury during endoscopic surgery. Pneumatization of the middle turbinate (concha bullosa) and may be unilateral or bilateral and may narrow the middle meatus. Paradoxical curvature of the middle turbinate is present when the curvature of the concha is concave towards the nasal septum. The uncinate process may be pneumatized, deviated, or atelectatic. Pneumatization of the sphenoid sinus is highly variable. Septations within the sphenoid sinus may terminate on the bony covering over the internal carotid artery. The bony covering over the artery may be thin or absent placing the vessel at risk during endoscopic sphenoid surgery.

**O-335****5:35 PM - 6:00 PM**

### **Sinonasal and Orbital Infections**

Daniel W. Williams, III, MD

Radiology, Wake Forest School of Medicine  
Winston-Salem, NC, USA

#### **LEARNING OBJECTIVES**

1. Review pertinent sinonasal and orbital anatomy
2. Discuss imaging techniques
3. Describe the imaging appearance of sinonasal and orbital infections
4. Recognize local and distant complications of sinusitis

#### **OUTLINE**

1. Introduction
  - a. Anatomy
  - b. Imaging issues
2. Clinical/imaging features of acute and chronic sinusitis
3. Complications of sinusitis
  - a. Local
  - b. Regional
  - c. Distant (intracranial)
4. Potential imaging pitfalls
5. Orbital infections
  - a. Cellulitis (pre-septal vs. post-septal)
  - b. Abscess (subperiosteal, orbital)
  - c. Ophthalmic vein and cavernous sinus thrombosis

d. Orbital apex syndrome

## Tuesday Afternoon

**4:45 PM - 6:15 PM**

**Trionon Ballroom**

**(37) GENERAL PROGRAMMING:  
ANEURYSMS**

**O-336**

**4:45 PM - 5:05 PM**

### **Aneurysm Biology and Implications for Treatment**

Ajay K. Wakhloo, MD, PhD

Neuroimaging, University of Massachusetts Medical  
School  
Worcester, MA, USA

#### **Presentation Summary**

Intracranial aneurysms represent a challenging pathological entity found in 2-6% of the world population. They may present infrequently with devastating and often fatal intracranial hemorrhage. Multiple mechanisms have been proposed in their formation and rupture. More recently evidence is accumulating that this disease may be multifactorial and genetic predisposition, specific hydrodynamic conditions at the aneurysm formation site, inflammatory changes of the aneurysm wall with degeneration and subsequent rupture, all may play a role. Treatment options specifically targeted at the aneurysm/parent artery complex will be presented.

**O-337**

**5:05 PM - 5:25 PM**

### **Flow Diversion**

David J. Fiorella, MD, PhD

Neurosurgery Surgery, Stony Brook University Medical  
Center  
Stony Brook, NY, USA

#### **Presentation Summary**

Flow diversion represents a conceptually new approach to the endovascular treatment of brain aneurysms. These new devices have provided us with the ability to achieve a durable and complete reconstruction of even the most complex cerebral aneurysms, many of which were not previously amenable to surgical or endovascular repair. As this technology is increasingly applied, we are continuously learning more about its capabilities and limitations. We will review the theoretical basis for the mechanism of action of flow diverters, the existing clinical data and the existing indications and contraindications for treatment.

**O-338**

**5:25 PM - 5:45 PM**

### **Biologically Active Coils**

Cameron G. McDougall, MD, FRCS

Barrow Neurosurgical Assoc.  
Phoenix, AZ, USA

**O-339**

**5:45 PM - 6:05 PM**

### **Aneurysm Clinical Trials and Tribulations**

Andrew J. Molyneux, FRCR

Oxford Neuroradiology and Neurovascular Research  
Unit, Oxford University  
Oxford, United Kingdom

#### **Presentation Summary**

The objective of this presentation is to review the latest evidence from randomized clinical trials of endovascular coil treatment of cerebral aneurysms, in respect of the both clinical outcomes and the risk of delayed re-bleeding and where possible comparing these with the results of neurosurgical clipping.

The talk will highlight the difficulties and challenges of conducting rigorous clinical trials, in respect of both ruptured and unruptured aneurysms. It will review some of the reasons behind the failure of the Trial of Endovascular Aneurysms Management (TEAM), a randomized trial of unruptured cerebral aneurysm treatment, which was stopped prematurely.

It will examine the shortcomings and the strengths of randomized clinical trials and the criticisms which arise and assist the audience in understanding the validity or otherwise of such criticisms.

Based on the most recent published data for patients with ruptured cerebral aneurysms suitable for coiling there is overwhelming evidence of improved clinical outcomes in coiled patients at follow up compared with neurosurgical clipping.

There remains considerable uncertainty concerning the best management for small incidental unruptured cerebral aneurysms.

## Tuesday Afternoon

**4:45 PM - 6:15 PM**

**Grand Ballroom Suite**

**(38) WHAT IS QUALITY? ...  
PERSPECTIVES FROM PATIENT,  
THE PAYERS AND (LEAST  
IMPORTANTLY) US? (SAM #3)**

\*Qualified by the American Board of Radiology (ABR) in meeting the criteria for Self-Assessment towards the purpose of fulfilling requirements in the ABR Maintenance of Certification program data 3/12.



**O-340****4:45 PM - 4:57 PM****Academic Neuroradiology**

Suresh K. Mukherji, MD, FACR

Radiology, University of Michigan Health System  
Ann Arbor, MI, USA**Presentation Summary**

The intent of this presentation is to present the academic radiology perspective of quality. Academic neuroradiologists feel that patients should choose their center because all neuroradiologists in their group are fellowship-trained with many of top tier academic centers requiring faculty to complete a two-year neuroradiology fellowship. All faculty are required to be eligible of Senior membership in the American Society of Neuroradiology. All neuroradiologists are required to have or be eligible to take their Certificate of Added Qualification in Neuroradiology.

Academic medical centers (AMC) tend to have larger Neuroradiology sections that permit to faculty to further specialize in different areas such as Head & Neck, Pediatric neuroimaging, stroke, and biologic imaging. This permits even greater quality of interpretation for the more complex imaging studies. AMC tend to be early adopters of acquiring new technologies. Companies tend to form relationships that permit early deployment of new CT, MR and angio to major AMC. This permits integration of these new technologies that allow us to perform research that may benefit patient care.

minute time to final read on emergent stroke CT's) can be important for hospital based clinicians. The second similarity is our customers. The primary customer for neuroradiology services is the referring clinician. The secondary customer is the patient (the consumer of services). Another secondary customers is the payors. We'll hear from them directly. High level, timely services enable referring clinicians to diagnose and treat conditions quickly and can generate patient satisfaction. An important component of referring clinician and hospital satisfaction is turn around time. A fast turn around time is important for all practices and hospitals in the competitive imaging market. It speeds diagnosis, treatment, and billing. The direct access to neuroradiologists both during normal business hours and after hours is also an important factor for clinicians. A difference between private practice and academic practice is our hospital partners. Academic practices typically work with one hospital system. Private practices may work with multiple hospital systems, sometimes ones that directly compete with each other. Navigating the sea of administrators can be challenging in this environment, but it is important to work closely with our hospital partners to fulfill their expectations and drive their business. Radiology departments are typically some of the most important profit centers that institutions have. Keeping radiology departments profitable is an important measure of quality for our hospital partners.

**O-341****4:57 PM - 5:09 PM****Private Practice Neuroradiology**

Sean Meagher, MD

Radiology, Central Illinois Radiological Assoc. Ltd  
Peoria, IL, USA

Quality in private practice Neuroradiology is service driven. Service has multiple facets, but can generally be divided into service to referring clinicians, patients, and hospital/business partners. Service in private practice has many similarities to academic Neuroradiology and a couple of fundamental differences. The first similarity is the provision of high level, accurate diagnosis in a timely manner. The focus on excellent technology coupled with it's effective implementation is a universal goal in Neuroradiology. Both groups strive to use imaging technology such as MR and CT to accurately diagnose conditions for referring clinicians and patients. The effective and efficient application of these technologies can differentiate hospitals and practices. The appropriate choice of imaging modality coupled with tailored protocoling can speed diagnosis, increase scanner throughput, and increase profitability for hospitals and businesses that own the imaging equipment. Effective throughput can be measured with data such as 3rd available appointment for patient and the time to completed exam once ordered. Keeping backlogs down is important for patient and referring clinician satisfaction. Additionally, implementation of tailored imaging measures (for example, less than 20

**O-342****5:09 PM - 5:21 PM****Government**

David J. Seidenwurm, MD, FACR

Radiological Associates  
Sacramento, CA, USA**Presentation Summary**

The government's definition of quality is multifaceted, and sometimes obscure for numerous reasons. Publically funded healthcare payment programs like Medicare are evolving to incorporate value along with volume in the compensation mechanisms for physicians and hospitals suggesting that value is part of the definition of quality. Industrial models of quality are embedded in these programs in the form of zero payment for never events, and the use of geographic variation and ethnic disparities in care delivery as evidence of gaps in care for performance measure development, for example. Proposed volume based criteria for certain procedures exemplify the quality construct of exemplary luminary physicians demonstrating excellence at major regional centers. The use of multispecialty practice guidelines as the foundation for performance measures employed in value based purchasing programs suggest that public payers understand quality, at least in part, as conformity with evidence based medicine, and value quantitative definitions of quality even if they fall short of outcome data. Programs that reward the processes leading to board certification and recertification suggest that peer defined competence is part of the public's definition of quality, as well. Severe penalties for failure to provide service to patients presenting at hospital facilities suggest that access for hard to serve populations is also a strong component of quality in government healthcare programs.

**O-343****5:21 PM - 5:33 PM****Clinical**

Michael G. Stewart, MD, MPH

Otolaryngology, Weill Medical College of Cornell  
New York, NY, USA**Presentation Summary**

There are some basics to providing quality radiology care such as customer service, maintenance of privacy, radiation safety, billing practices, and communication with patients and providers. I will review those briefly, but focus on the communication between the radiologist and the clinician, and address both aspects of that communication.

As ordering clinicians, we have a responsibility to communicate our questions and appropriate clinical background to the radiologist, and to order appropriate studies.

From the radiologist, we expect some basics, such as no clinically significant misses, clear descriptions, and focusing on what is clinically important. Defining high quality would include the following: having reviewed the request and any specific questions, focusing on important findings, a reasonable differential diagnosis,

suggested additional imaging only if truly helpful, and person-to-person communication of important findings or questions. While rapid report generation might be important - and perceived as a proxy for quality - for some providers and patients, I value accuracy and reliability over speed, so a longer turnaround for a consistent product is high-quality to me. Of course, all else being equal, then more rapid reporting is generally better. Each of these points will be discussed in some detail.

There are also some subtleties and annoyances, which may be perceived as "poor quality" by clinicians, although this topic is open for discussion, as there may be aspects of the reporting process which are opaque to the clinician. Some potential issues include: routinely recommending additional imaging or testing, excessive reporting of incidental findings, overly cautious (cover yourself) interpretations or making recommendations for potential diagnosis with "alarmist" language, or recommendations which are outside of standard clinical guidelines (for example, thyroid FNA of tiny masses). These points will also be discussed in some detail, with some examples.

**REFERENCES:**

1. Strife JL, Kun LE, Becker GJ, et al. American Board of Radiology Perspective on Maintenance of Certification: Part IV - Practice Quality Improvement for Diagnostic Radiology. *RadioGraphics* 2007;27:769-774.
2. Hoe J. Quality service in radiology. *Biomed Imaging Interv J* 2007;3(3):e24.

**O-344****5:33 PM - 5:45 PM****Patient**

Crystal A. Jones

Radiology, University of Michigan Health System  
Ann Arbor, MI, USA

*Mrs. Jones has worked as an administrative assistant for 17 years. She has experience in the public and private sectors, most recently the healthcare field, which has given her the pleasure of working with individuals from all walks of life. Over the years, Crystal has taken numerous courses educating and guiding herself to meet the requirements of today's dynamic and demanding responsibilities of a professional administrative assistant. Her experience in the public and private sectors, when combined with her compassion for the wellbeing of individuals, has given her a unique point of view enabling her to excel in the healthcare environment. Crystal's primary focuses outside of work are her three young daughters and tackling the challenge of raising them in today's world. Currently, she is an active leader for her two youngest daughters' Girl Scout troop and enjoys participating in "Girls on the Run" with her oldest daughter. Her other interests include working out, spending time with her family and baking!*

**Presentation Summary**

The intent of this presentation is to present the patients perspective of quality. The criteria patients use to form perspectives in great service, quality and satisfaction, while on the road of their experience, tends to shy away

from the technical framework that some radiologist use to define these terms. Most patients are not technical experts, and will then rely on their experience and third-party information to form their perspective on great service and quality.

Quality will vary depending on the patient. What one patient might feel is important to form their point of view, quite possibly might not even be on the radar of another. Perspective is most often obtained from a point of view. Appearance and experience play a major part in forming one's point of view.

Great service and quality are on opposite sides of the road between patient and radiologist, yet sometimes pass each other. What each side uses to assess radiology services, differ greatly. The key is to understand how to identify the patients' needs and then fulfill those needs. Some believe that the practice of radiology would be considerably different if it were more patient-centered. Beginning with the clerical staff, to the technologist and then the radiologist, thinking about patients would make a huge difference in many ways. If medical staff thought that they were the patient, it might force some to go that extra mile.

## Tuesday Afternoon

**4:45 PM - 6:15 PM**  
**Murray Hill**

**(39) SYNAPTIC JUNCTION  
PROGRAMMING: POINT/COUNTER  
POINT: COMMUNICATING  
RESULTS DIRECTLY TO PATIENTS**

**O-345** **4:45 PM - 5:30 PM**

**Synaptic Junction Programming: Point/Counter  
Point: Communicating Results Directly to Patients**

Annette J. Johnson, MD, MS

Radiology, Wake Forest University School of Medicine  
Winston Salem, NC, USA

Please see Dr. Branstetter's presentation summary for this Synaptic Junction programming.

**O-346** **5:30 PM - 6:15 PM**

**Synaptic Junction Programming: Point/Counter  
Point: Communicating Results Directly to Patients**

Barton F. Branstetter, IV, MD

Univ. of Pittsburgh Med. Ctr.  
Wexford, PA, USA

Presentation Summary

Synaptic Junction's Point-Counterpoint series highlights an area of controversy in Radiology. The debate format allows the two sides of the argument to be presented and

rebutted. This year's topic is "Direct-to-Patient Communication". The presenters will discuss the relative merits and risks of alerting patients directly about their radiologic test results, instead of communicating only with the referring physician. Different options for patient communication will be explored.

## Tuesday Afternoon

**4:45 PM - 6:15 PM**  
**Sutton Center/South**

**(40) ADVANCED IMAGING  
SEMINAR: NEUROTRANSMITTERS  
AND IMAGING**

**O-347**

**4:45 PM - 5:15 PM**

**MEG and Neurotransmitters**

William C. Gaetz, PhD

Dept. of Diagnostic Imaging, The Hospital for Sick  
Children  
Toronto, ON, Canada

Presentation Summary

Non invasive measures of human brain function include electroencephalography (EEG) and magnetoencephalography (MEG). These EEG and MEG measures are thought to depend critically on specific neurotransmitters such as the inhibitory neurotransmitter GABA and the excitatory neurotransmitter Glutamate. In this presentation we will begin with an introduction to the neural cell assemblies thought to give rise to the signals measured with EEG and MEG. The functional dependence of these cortical oscillations on local neurotransmitters GABA and Glutamate will be briefly reviewed. The presentation will then focus on recent findings related to beta (15-30Hz) and Gamma (60-90Hz) MEG rhythms and MRS measures of GABA and Glutamate concentration. Finally, the clinical relevance of these measures, specifically in the context of diseased states such as Schizophrenia, Epilepsy, and Autism will be addressed. These cortical oscillations might provide a window into the efficacy of the neurotransmitter systems in patients and thus provide a potential biomarker for treatment efficacy.

**O-348****5:15 PM - 5:45 PM****Psychiatric Disease and Neurotransmitters**

Laura M. Rowland, PhD

University of Maryland School of Medicine  
Baltimore, MD, USA

*Laura Rowland, Ph.D. is an assistant professor at the Maryland Psychiatric Research Center (MPRC), Department of Psychiatry, University of Maryland School of Medicine. Her research interests include in vivo neurochemical measurements of glutamatergic and GABAergic function, multimodal assessments of learning, translational behavioral neuroscience, and pharmacological challenge studies as they relate to schizophrenia and related disorders. Research funding sources include NIH and NARSAD (now Brain and Behavior Research Foundation). She was the recipient of NARSAD and ICOSR (International Congress on Schizophrenia Research) young investigator awards, as well as several internal research awards. She previously served as an officer on for the ISMRM psychiatry spectroscopy and imaging workgroup. Actively involved in post-doctoral training, she is the co-director for an NIH funded T32 research fellowship program and the coordinator for the young investigator program for the ICOSR.*

**Presentation Summary**

Effective brain and behavior function depends on a carefully orchestrated balance of inhibition and excitation in the central nervous system. That dynamic is dependent on the actions of glutamate, the principal excitatory neurotransmitter, and gamma-aminobutyric acid (GABA), the principal inhibitory transmitter. A disturbance in the actions of these neurotransmitters is implicated in the pathophysiology of severe psychiatric disorders such as schizophrenia. This presentation will focus on the application of a noninvasive imaging technique, proton magnetic resonance spectroscopy (<sup>1</sup>H-MRS), to study these neurotransmitters in schizophrenia and related psychotic disorders. This presentation will also cover <sup>1</sup>H-MRS applications for measuring two modulators of glutamatergic and GABAergic neurotransmission, glutathione (GSH) and N-acetylaspartylglutamate (NAAG). The impact of drug treatment, disease course spanning from "high-risk" to chronic phases, and psychiatric state will be discussed. The functional significance of these metabolites, especially as they relate to cognition, will be highlighted. The objective of this presentation is to highlight recent research devoted to understanding the glutamatergic and GABAergic systems in psychotic disorders.

**O-349****5:45 PM - 6:15 PM****Alcohol, Smoking, Drugs and Neurotransmitters**

Graeme F. Mason, PhD

Psychiatry, Yale University, School of Medicine,  
Diagnostic Radiology & Psychiatry  
New Haven, CT, USA

*Dr. Mason received a B.S. in Nuclear Engineering with a minor in Spanish from the Pennsylvania State University in 1986. He spent a summer training at Hershey Medical Center with Richard Briggs, Ph.D., and moved to Yale University in the fall of 1986, where he pursued a Ph.D. in Molecular Biophysics & Biochemistry with Professor Robert Shulman. His doctoral work led to the development of mathematical modeling approaches to assess metabolic parameters using isotopic measurements performed with magnetic resonance spectroscopy. A postdoctoral period of training at Yale and the University of Alabama at Birmingham expanded his skills to projects with humans at high magnetic field strengths, and he returned to Yale in 1997, where is now an Associate Professor in the Departments of Diagnostic Radiology and Psychiatry. Dr. Mason's primary interests today are the evaluation of metabolic pathways with <sup>13</sup>C MRS and the application of MRS to evaluate neurotransmitter and energy metabolism in the brain, particularly as applied to study the effects of alcohol and nicotine.*

**Presentation Summary**

Ethanol and nicotine have unique roles as the most prevalent drugs of abuse and dependence in the world. Ethanol has a unique double role as a source of energy and a neuromodulator, and its oxidation for energy also results in neuromodulation. Nicotine affects a variety of neurotransmitter systems, and they interact with ethanol's effects. A non-invasive method to evaluate effects of ethanol and nicotine on the neurotransmitters glutamate and glutamine without the use of radioactivity is Magnetic Resonance Spectroscopy (MRS). This presentation will begin with an explanation of the basic theory behind MRS and how the technology can be used to measure neurotransmitters in the human brain. The methods include <sup>1</sup>H MRS to measure the concentrations of neurochemicals and <sup>13</sup>C MRS to measure kinetics of neurotransmitter turnover. Next will be shown applications of <sup>1</sup>H and <sup>13</sup>C MRS to study effects of ethanol and nicotine. Included among these are observations of studies of acute administration of ethanol and nicotine on the brain and how they may illuminate what is observed with chronic consumption. Of particular interest are observations of effects of alcohol withdrawal in smokers relative to non-smokers. In summary, the objective of this presentation is the dissemination of non-invasive methods that can be used to evaluate the effects of alcohol and nicotine on amino acid neurotransmitters and what light that information may shed on addiction and vulnerability to dependence.

## Wednesday Morning

**7:30 AM - 8:30 AM**  
**Grand Ballroom Suite**

**(41) MAINTENANCE OF  
 CERTIFICATION (MOC) - REVIEW  
 SESSION (AR) CEREBROVASCULAR**

**O-350** **7:30 AM - 8:00 AM**

**Maintenance of Certification (MOC) - Review Session  
 (AR) Cerebrovascular**

Maresh V. Jayaraman, MD

Diagnostic Imaging, Warren Alpert School of Medicine  
 at Brown University  
 Providence, RI, USA

Presentation Summary

Through a case presentation format, we will review key topics in vascular neuroradiology. The diagnosis, pathophysiology and treatment of vascular pathology of the brain, spine, and head and neck will be covered in an interactive program employing the audience response system. This problem-based strategy will include a discussion of advanced imaging techniques and state-of-the-art, evidence-based treatment.

**O-351** **8:00 AM - 8:30 AM**

**Maintenance of Certification (MOC) - Review Session  
 (AR) Cerebrovascular**

Clifford J. Eskey, MD, PhD

Radiology, Dartmouth-Hitchcock Medical Center  
 Lebanon, NH, USA

Presentation Summary

Through a case presentation format, we will review key topics in vascular neuroradiology. The diagnosis, pathophysiology and treatment of vascular pathology of the brain, spine, and head and neck will be covered in an interactive program employing the audience response system. This problem-based strategy will include a discussion of advanced imaging techniques and state-of-the-art, evidence-based treatment.

## Wednesday Morning

**8:30 AM - 10:00 AM**  
**Grand Ballroom Suite**

**(42) GENERAL SESSION:  
 LUMINARY SESSION: PAST,  
 PRESENT AND FUTURE**

**O-352** **8:30 AM - 8:40 AM**

**Founding the American Society of Neuroradiology**

Michael S. Huckman, MD

Rush University Medical Center  
 Chicago, IL, USA

Presentation Summary

The American Society of Neuroradiology was founded in 1962 at a meeting called by Juan Taveras at Keen's Chophouse in New York City. This talk will outline the prehistory of the Society, why it was founded, who were the 14 founding members, and early history of the Society.

**O-353** **8:40 AM - 8:55 AM**

**General Session : Luminary Session: Past, Present  
 and Future**

Anne G. Osborn, MD

Radiology, University of Utah Medical Center  
 Salt Lake City, UT, USA

Presentation Summary

The past presages the present and influences the future. This presentation will highlight important milestones in the evolution of the diagnostic tools we have used, currently use, and will probably employ in our future clinical practices. It will emphasize the importance of knowing neuroanatomy and understanding neuropathology and neurogenetics for the accurate interpretation of neuroimaging studies. How did we, as neuroradiologists, come to "peek" inside the brain as we do and learn what we now may almost take for granted?

**O-354** **8:55 AM - 9:10 AM**

**We've Come A Long Way. Key Technologic Advances  
 in the Last 50 Years, Creating Images Then and Now**

R. Nick Bryan, MD, PhD

Radiology, University of Pennsylvania Health System  
 Philadelphia, PA, USA

Presentation Summary

There have been two evolutionary stages of neuroradiology: The Dark Age, during which the brain was invisible and the Light Age, when the living brain could be imaged non-invasively. The transition was abrupt, beginning in 1974 with the advent of x-ray CT



and reaching early maturity in the early 1980's with MRI. The Light Age is still evolving and can be subdivided into two sequential eras: the Structural and the Functional. The former involves seeing what the brain looks like; the latter involves seeing what the brain is doing. The Functional Era began in the 1990's with the development of fMRI. An undertone to structural and functional imaging has been molecular imaging, which may well form the basis of the next neuroradiological era. Amazingly, and fortunately, the increased ability to image finer structure and more physiological parameters of the brain has come with less invasion, discomfort and risk to the patient. The ASNR has provided critical leadership and a robust scientific forum for these remarkable advances in neuroimaging, which will fondly be remembered in this presentation.

**O-355** **9:10 AM - 9:25 AM**

**Neurointerventional Radiology: 50 Years Ago and 50 Years from Now**

Alex Berenstein, MD  
Roosevelt Hospital  
New York, NY, USA

**O-356** **9:25 AM - 9:40 AM**

**Where Neuroradiology Stands Today**

Patricia A. Hudgins, MD  
Radiology, Emory University School of Medicine  
Atlanta, GA, USA

**Presentation Summary**  
It is appropriate for us to reflect on the current state of Neuroradiology as we celebrate our 50th anniversary. Our neuroradiology clinical work, training organizations, and research are thriving. The ASNR is one of the most respected medical societies, with a stable or growing membership of almost 5,000, a robust annual meeting, and a journal of quality manuscripts and a high impact factor. Did the Founding Fathers envision the extraordinary growth of Interventional Neuroradiology, and subspecialization in head and neck, pediatric, functional and spine neuroradiology? Could they imagine that 50 years after that meeting in Keens Steakhouse their specialty would become so complex that a Radiology resident would need one or two years additional training after residency to just begin to understand the disease processes that affect the central nervous system?

Requests for neuroimaging continue to grow, although changes in healthcare reimbursement and concerns about radiation dose to the public may impact our field in the near future. Just 5 years ago, the term "maintenance of certification" and the core competencies were novel ideas; now they are part of our daily lexicon. I will summarize "Neuroradiology: Where We Are Today," but know that things are changing so quickly, that by the time you all return home, this presentation will be ancient history!

**O-357**

**9:40 AM - 10:00 AM**

**Neuroimaging Studies of the Future**

Bruce R. Rosen, MD, PhD  
Radiology Department, Massachusetts General Hospital  
Charlestown, MA, USA

**Wednesday Morning**

**10:30 AM - 11:00 AM**  
**Grand Ballroom Suite**

**(43) KEYNOTE SPEAKER:**  
**ROBERT I. GROSSMAN, MD**

**O-358**

**10:30 AM - 11:00 AM**

**Healthcare and Neuroradiology - Nexus of Practice, Politics, and the Practical**

Robert I. Grossman, MD  
Dept of Radiology, NYU Medical Center  
New York, NY, USA

**Presentation Summary**

Over the past 40 years the imaging revolution has transformed healthcare in the United States. It has enabled shorter lengths of stay, minimally invasive procedures, markedly improved diagnostic acumen, and encouraged a generation of the brightest medical students to choose diagnostic radiology (and Neuroradiology) as their profession. Coincident with the ascendancy of imaging has been the escalation of healthcare expenditures. The unsustainable nature of this growth has catalyzed significant political debate as well as passage of the Affordable Care Act (2010). Today, neuroradiology (and radiology) is in a most precarious position. While it has greatly enhanced the diagnosis and treatment of neurological disorders the associated expenses have made it a target for payers, physicians, policy makers, and pundits. Accountable Care Organizations, bundled payment initiatives, and other attempts to limit costs directly impact the future growth and welfare of imaging. There are several essential components for Neuroradiology to survive and thrive in the hostile climate of diminishing revenues and dwindling resources. Non-radiologists, insurance companies, and regulators must recognize unequivocal evidence indicating radiology's value and role in cost-effective care. Radiology (and Neuroradiology) should advocate for a seat at the policy table whether it be at the federal, state, or hospital level. It should seek to train researchers (basic and translational) and pursue activities that create innovations and insights into neurological diseases. All of these elements necessitate a focus on leadership and leadership training. To sustain the pre-eminence of neuroradiology in the 21<sup>st</sup>

Century requires continuous discovery, objective value, and inspired leaders.

## Wednesday Morning

**11:00 AM - 11:15 AM**  
**Grand Ballroom Suite**

**(44) ASNR PRESIDENTIAL ADDRESS**

**O-359**

**11:00 AM - 11:15 AM**

**ASNR PRESIDENTIAL ADDRESS**

David B. Hackney, MD, FACR, ASNR 2012 President  
 Radiology, Beth Israel Deaconess Medical Center  
 Boston, MA, USA

## Wednesday Afternoon

**1:00 PM - 2:30 PM**  
**Grand Ballroom Suite**

**(48) ASHNR PROGRAMMING:  
 HEAD AND NECK CANCER (SAM #  
 4) (AR)**

\*Qualified by the American Board of Radiology (ABR) in meeting the criteria for Self-Assessment towards the purpose of fulfilling requirements in the ABR Maintenance of Certification program data 3/12.

**O-360**

**1:00 PM - 1:25 PM**

**PET: Current Thoughts**

Suresh K. Mukherji, MD, FACR  
 Radiology, University of Michigan Health System  
 Ann Arbor, MI, USA

Presentation Summary  
 The intent of this presentation is to discuss the current and future role of PET-CT in head and neck imaging. We will also discuss current recommendations regarding when to perform PET-CT in Head & neck Cancer.

**O-361**

**1:25 PM - 1:50 PM**

**HPV-Related Head & Neck Malignancy**

Lawrence E. Ginsberg, MD  
 Radiology, M.D. Anderson Cancer Center  
 Houston, TX, USA

Presentation Summary

Over the last 10-15 years there has been a fundamental shift in the prototypical head and neck mucosal cancer patient. Previously, such patients were generally older, median age 60 years, and the cancers were typically smoking and drinking-related. Most such lesions were not associated with Human Papilloma Virus (HPV). Smoking rates have subsequently declined, and more recently there has been a significant increase in lesions that are positive for HPV; the vast majority of these lesions arise in the oropharynx, specifically the tonsil and base of tongue.

Oral oncogenic HPV, particularly type-16 infection has a proven association with the development of oropharyngeal malignancy. This same virus is the cause of nearly all cervical cancers, as well as most malignancies of the penis, vulva and anus. Oncogenic HPV is sexually transmitted, and oropharyngeal HPV-related cancers typically occur in middle aged, white, affluent men, those with a high lifetime number of vaginal and oral sex partners. Though controversial, there is some evidence to suggest that poor oral hygiene and drinking/smoking increases the risk of such malignancies.

Research is ongoing, to be reported in this presentation, to determine if the imaging appearance at the mucosal primary site has any distinguishing features between HPV +ive and HPV -ive tumors. With respect to the lymph nodes, there is evidence that cystic lymph nodes are uniquely associated with HPV +ive metastases. Further research is looking to confirm these initial reports.

Radiologic misdiagnosis of cystic nodal metastases as second branchial cleft cysts is a major problem. Such cases present to MD Anderson Cancer Center on a regular basis. In some cases, the oropharyngeal malignancy is evident on the very study in which nodal metastasis is not considered in the differential diagnosis. Additionally, because aspiration of such nodes may yield only cyst fluid and no obvious tumor, or be unapparent to an inexperienced pathologist, the mistaken diagnosis of branchial cleft cyst may continue until the offending malignancy presents at a more advanced stage, diminishing prognosis.

Fortunately, the vast majority of HPV-related oropharyngeal cancers are very responsive to standard treatments with radiation and often chemotherapy. Ongoing studies seek to identify those cases in which less aggressive and presumably less debilitating therapeutic regimens may be appropriate for patients with HPV-associated oropharyngeal cancer.

Experts in the field fear a burgeoning epidemic of oropharyngeal malignancies is underway. Vaccination of young girls has been recommended for some time, and because not all girls are vaccinated, the risk for sexually transmitted HPV infection to males has been

recognized, and the CDC has recently recommended routine vaccination for boys aged 11-12. While controversial to those who would argue such vaccinations promote promiscuity, they are crucial in stemming the epidemic of oropharyngeal cancer cases tied directly to sexually transmitted HPV infection.

**O-362****1:50 PM - 2:15 PM****Laryngeal/Hypopharyngeal Cancer**

Ilona M. Schmalfuss, MD

Radiology, NF/SG Veterans Administration and University of Florida  
Gainesville, FL, USA

**Presentation Summary**

Squamous cell carcinoma is the most common type of cancer involving the larynx and hypopharynx. Chronic tobacco and alcohol abuse represent the main risk factors with HPV playing only a minor role.

**Larynx** is divided into supraglottis, glottis and subglottis. These communicate along their mucosal surfaces and their deeply located paraglottic and preepiglottic fat planes. Infiltration of the fat planes is often missed on clinical examination as it occurs in submucosal fashion.

*Glottic cancers* (65%) usually originate from the anterior true vocal cords and tend to involve into the anterior commissure and spread into the contralateral cord, paraglottic fat planes as well as supraglottic and subglottic larynx.

*Supraglottic tumors* (30%) arising from the epiglottis like to infiltrate the preepiglottic space and subsequently grow inferiorly to gain access to the glottis. Lesions originating from other supraglottic sites tend to infiltrate the paraglottic fat planes and to spread to the glottis larynx.

*Subglottic malignancies* (5%) like to invade the cricoid ring, trachea, thyroid gland and upper esophagus.

**Hypopharynx** is divided into pyriform sinuses, post-cricoid region and posterior hypopharyngeal wall. Since the hypopharynx is collapsed during scanning, the assessment of the hypopharynx relies upon detection of intramural fat planes.

*Postcricoid region cancers* like to invade the posterior larynx causing vocal cord paralysis and to grow inferiorly to involve the trachea and esophagus.

*Pyriform sinus malignancies* arising from the lateral wall like to involve the posterior thyroid cartilage and the lateral neck compartment while tumors arising from the medial wall show early laryngeal invasion and vocal cord fixation.

*Posterior hypopharyngeal wall cancers* like to grow in craniocaudal direction potentially spanning from the nasopharynx to the esophagus.

**Special considerations:**

Laryngeal cartilage involvement is associated with lower response and higher recurrence rates with organ preservation therapies. It can manifest as cartilage sclerosis, cortical erosions and bone marrow replacement. Cartilage sclerosis is the most sensitive criterion but has a positive predictive value of only

50%. MR is most sensitive; however, it suffers from low specificity.

Nodal involvement: The different tumor sites have different lymphatic drainages: supraglottic cancers: group II and III, glottic tumors: nodal metastasis rare; subglottic lesions: group VI and mediastinal lymph nodes; postcricoid tumors: group III, IV and VI; pyriform sinus tumors: group II, III, and V; posterior hypopharyngeal wall cancers: retropharyngeal lymph nodes.

**Wednesday Afternoon****1:00 PM - 2:30 PM****Trion Ballroom****(49) SNIS PROGRAMMING: VENOUS DISEASE****O-363****1:00 PM - 1:15 PM****Diagnosis**

Aseem Sharma, MD

Mallinckrodt Institute of Radiology, Washington  
University School of Medicine  
St. Louis, MO, USA

**Presentation Summary**

This presentation will introduce the audience to the role of various neuroimaging techniques in the diagnosis of pathologic diseases affecting the intracranial venous system.

**O-364****1:15 PM - 1:30 PM****Treatment**

Donald F. Frei, Jr, MD

Radiology Imaging Associates  
Englewood, CO, USA

**Presentation Summary**

Discuss the literature and the range of thrombolytic and mechanical treatment options for the treatment of cerebral venous sinus thrombosis.

**O-365****1:30 PM - 1:45 PM****CCSVI**

Howard L. Dorne, MD

Vascular and Interventional Specialists of Orange  
County  
Orange, CA, USA

**Presentation Summary**

Chronic cerebrospinal venous insufficiency (CCSVI), a radically different and controversial concept regarding the pathogenesis of multiple sclerosis, suggests that

macro-occlusive abnormalities of the extracranial venous drainage pathways of the brain and spinal cord can cause or contribute to multiple sclerosis (MS). As a consequence of this theory, it has been suggested that angioplasty and possibly stenting of the internal jugular and/or azygos veins can improve the signs and symptoms of MS. These interventions have been performed sporadically across the globe in an open-label fashion. This lecture will examine the origin of the CCSVI theory and discuss the data supporting and refuting its existence.

**O-366****1:45 PM - 2:00 PM****Idiopathic Intracranial Hypertension**

David A. Kumpe, MD, FACR

Radiology, University of Colorado Hospital  
Aurora, CO, USA**Presentation Summary**

The clinical presentation of Idiopathic Intracranial Hypertension (IIH), also called pseudotumor cerebri, is headache, visual obscurations, possibly pulsatile tinnitus and diplopia. In more severe cases there is papilledema which can diminish visual acuity and visual fields, and can eventually cause optic nerve atrophy with irreversible visual damage, and even cause blindness. A subgroup of IIH patients has venous outflow obstruction in the transverse and sigmoid sinuses. Stent placement can alleviate such outflow obstruction.

We have performed stent placement in 22 IIH patients to date, and in 1 patient with subacute dural sinus thrombosis. Patient selection criteria include the presence of papilledema, and elevated opening pressures on lumbar puncture ( $>25$  cm H<sub>2</sub>O). Patients are evaluated with cerebral arteriography and dural sinus manometry. Stenting is performed when there is a pressure gradient between the torcular and the internal jugular vein of  $\geq 10$  mm Hg (normal gradient is  $\leq 4$  mm Hg). There was 100% technical success with uniform decrease in the pressure gradient.

In appropriate cases, papilledema is relieved. On the other hand, in our experience, headaches usually change in character but are not eliminated in female patients. Stents have uniformly remained patent in angiographic followup as long as 99 months. In approximately 24% of patients there is hemodynamic failure due to collapse of the dural sinuses above the stent. The cause for this phenomenon remains unclear. There is a need for improving patient selection criteria.

Nonetheless, these results are superior to the conventional surgical treatments for advanced IIH with papilledema, which include lumboperitoneal or ventriculoperitoneal shunting, and optic nerve sheath fenestration.

**Wednesday Afternoon****1:00 PM - 2:30 PM****Beekman/Sutton North****(50) ASSR PROGRAMMING:  
ADVANCED IMAGING OF THE  
SPINE AND DISK****O-367****1:00 PM - 1:15 PM****Biology of Disk Degeneration**

Jeffrey C. Lotz, PhD

University of California, San Francisco  
San Francisco, CA, USA**Presentation Summary**

The intervertebral disc is a fibrocartilaginous joint that supports spinal forces while facilitating compound movements. To meet these demands, it has a complex structural organization that imparts unique physical properties. The nucleus is composed of mainly high molecular weight glycosaminoglycans (GAG) with a fixed negative charge that induces osmotic swelling. Nuclear swelling and intervertebral movement is constrained by the annular ligament that is composed type I collagen organized in a lamellar arrangement. These biomechanical properties cause the disc to be large, avascular, and aneural. Unfortunately, these features also cause the disc to have a limited capacity for self-repair.

Disc cell survival is dependent upon diffusion from capillaries in the adjacent vertebra and surrounding vascularized tissues. This disc transport limitation causes nucleus oxygen levels to be low, between 0.5% and 5%. Because of this, nucleus cells produce energy through anaerobic glycolysis, which generates lactic acid as a byproduct. Accumulation of lactic acid decreases disc pH to near 6.3.

Age-related remodeling leads to physiologic degeneration of matrix. The disc's limited diffusional capacity worsens over time as vertebral blood vessel density decreases. Increasing hypoxic conditions inhibit matrix synthesis: glycosaminoglycan (GAG) production at 1% oxygen is one-fifth that at 5%. Additionally, matrix reorganization is stimulated by load-mediated cell behaviors. Cells respond pressure, which can be anabolic within certain ranges, and catabolic in others. Excessive stimulation leads to formation of arachidonate-derived prostaglandins, up-regulation of proinflammatory cytokines, and secretion of matrix metalloproteinases that degrade matrix. Poor transport between the disc and capillaries leads to accumulation of cleaved matrix fragments that bind to cell surface receptors and further stimulate catabolic responses. Over time, stress-induced changes in cell phenotype lead to increased secretion of type I collagen and senescence.

Pathologic, painful degeneration can occur when matrix damage accumulates. Increased production of growth factors such as bFGF, IGF-1, and PDGF within annular fissures can encourage granulation tissue formation. IL-1 stimulation of disc cells produces secretion of neurotrophic factors that, along with decreases in GAG, encourage neo-innervation and neo-vascularization at the vertebral endplate and annulus. Inflammatory and neurotrophic factors may diffuse into the adjacent vertebra to recruitment of polymorphonuclear cells, leading to bone marrow edema (BME). Endplate nociceptors in fibrovascular bone marrow can be further sensitized by inflammatory nucleus properties, principally TNF-alpha. Consequently, data from multiple studies suggest that BME adjacent to the endplate is among the most specific of all MRI observations for predicting concordant discography-induced pain.

**O-368** **1:15 PM - 1:30 PM**

**High Field Strength MR Imaging of Spine and Spinal Cord Anatomy**

Thomas P. Naidich, MD

Radiology, Mount Sinai Medical Center  
New York, NY, USA

**O-369** **1:30 PM - 1:45 PM**

**Advanced Imaging of Disk Degeneration**

David B. Hackney, MD, FACR

Radiology, Beth Israel Deaconess Medical Center  
Boston, MA, USA

**O-370** **1:45 PM - 2:00 PM**

**Diffusion Tensor of the Spine and Cord**

Meng Law, MD

USC Medical Center  
Los Angeles, CA, USA

**EDUCATIONAL OBJECTIVES**

1. Understand the challenges with imaging the spine and spinal cord such as the small FOV, susceptibility, field inhomogeneity
2. Understand some of the sequence limitations with clinical DWI, DTI and Fiber Tractography
3. Demonstrate some new techniques such as "reduced FOV" or "zoomed EPI" techniques which can substantially improve image quality for spine DWI and DTI
4. Demonstrate the clinical impact of these sequences
5. Demonstrate DWI and DTI of the spine, spinal cord and surrounding structures.

**PRESENTATION SUMMARY**

Currently, DWI and DTI are almost performed routinely in the brain as part of most clinical protocols. It has demonstrated important clinical utility which would be good to be translated to the spine and spinal cord. There are a number of applications of DWI and DTI in

the evaluation of the diseases of the spinal cord listed below, keeping in mind that this is a short subset of a long list of potential applications:

- Normal Anatomy (Ultra-High Field Imaging In Vivo and Ex-Vivo Imaging)
- Multiple sclerosis and other demyelinating diseases
- Spinal cord tumors and arterio-venous malformations
- Degenerative myelopathy - cord compression and canal stenosis
- HIV-associated spinal cord abnormalities
- Transverse myelitis
- Spinal cord injury
- Spinal cord ischemia

Due to the small FOV, susceptibility and field inhomogeneity of the spine and spinal cord, imaging the spine is a considerable challenge, particularly with standard EPI and gradient echo techniques. There are some new sequences and techniques, namely "reduced FOV" or "zoomed EPI" techniques which can substantially improve image quality for spine DWI and DTI. We will review some of these techniques and demonstrate the clinical impact of these in improving our diagnostic sensitivity and specificity.

## Wednesday Afternoon

**1:00 PM - 2:30 PM**

**Murray Hill**

**(51) SYNAPTIC JUNCTION  
PROGRAMMING: DOSE  
EXTRACTION**

**O-371** **1:00 PM - 2:30 PM**

**Synaptic Junction Programming: Dose Extraction**

Tessa Cook, MD

Radiology, Hospital of the University of Pennsylvania  
Philadelphia, PA, USA



## Wednesday Afternoon

**1:00 PM - 2:30 PM**

**Sutton Center/South**

**(52) AN EXPERT: HOW I DO IT**

**O-372**

**1:00 PM - 1:30 PM**

### **Multimodal Brain Tumor Imaging: Pearls and Pitfalls**

Andrei I. Holodny, MD

Radiology, Memorial Sloan-Kettering Cancer Center  
New York, NY, USA

#### **Presentation Summary**

This presentation will discuss the role Multimodal Brain Tumor Imaging, including advanced techniques in the current evaluation of brain tumors. I will discuss how current therapeutic options affect the MR appearance of tumors.

**O-373**

**1:30 PM - 2:00 PM**

### **CT and MR Perfusion Imaging in Cerebrovascular Disease**

Pamela W. Schaefer, MD

Radiology, Massachusetts General Hospital  
Boston, MA, USA

#### **Presentation Summary**

This talk will predominantly address the use of MR and CT perfusion imaging for the evaluation of acute stroke patients. Specifically, it will address the utility of cerebral blood volume, cerebral blood flow and tissue transit time measures for identifying infarct core and ischemic penumbra. The use of perfusion maps to predict hemorrhagic transformation will also be presented. MR and CT perfusion will be compared and contrasted. The advantages and disadvantages of both techniques will be presented. How technical factors such as selection of arterial input function and delay correction affect image interpretation will be covered. The lack of standardization of post processing software perfusion packages and how this affects our ability to identify infarct core and penumbra will also be discussed. How chronic carotid occlusions and stenoses and underlying chronic cerebrovascular disease affect acute stroke image interpretation will be covered. Semiquantitative and quantitative methods of measuring infarct core and penumbra volumes will be presented. The use of these volumes in combination with clinical stroke scales to determine treatment will also be included.

**O-374**

**2:00 PM - 2:30 PM**

### **CFS Flow Imaging**

Rafeeqe A. Bhadelia, MD

Radiology, Beth Israel Deaconess Medical Center  
Boston, MA, USA

#### **LEARNING OBJECTIVES:**

1. Review clinical applications of CSF flow imaging.
2. Discuss the techniques of CSF flow imaging.
3. Illustrate clinical examples and discuss role of CSF flow imaging.

#### **Presentation Summary**

MR imaging is able to detect cardiac cycle related pulsatile CSF motion as 'flow artifacts' or 'flow voids' on routine pulse sequences (T2/FLAIR) or on specialized motion sensitive sequences like SSFP. The cardiac cycle induced pulsatile CSF flow can also be qualitatively or quantitatively assessed using the cine phase-contrast (cine-PC) sequence. Although research is being conducted at many centers around the world on the subject of CSF flow imaging with cine-PC, there is little consensus on utilization and interpretation of it in clinical practice. This presentation will focus on CSF flow imaging with cine-PC MRI in routine clinical practice while providing examples of other techniques. Various technical aspects of cine-PC imaging of CSF flow will be discussed to familiarize the audience about how to successfully employ it in clinical settings. Clinical examples of obstructive hydrocephalus, normal pressure hydrocephalus, endoscopic 3rd ventriculostomy, Chiari I malformation, and intracranial and spinal cysts will be shown to discuss the role of CSF flow imaging. Finally, brief discussion of the future of CSF flow imaging will be presented.

## Wednesday Afternoon

**3:00 PM - 4:30 PM**

**Grand Ballroom Suite**

**(53a) Adult Brain: Vascular, Extracranial & Intracranial**

**O-389**

**3:00 PM - 3:08 PM**

### **Model-Based Iterative Reconstruction Allows Further Dose Reductions for CT Neuroangiography with Higher Spatial Resolution and Reduced Noise over ASIR and FBP**

Mirza, N. Pawha, P. Tanenbaum, L.

Mount Sinai School of Medicine  
New York, NY

#### **PURPOSE**

The relatively high radiation dose associated with CT neuroangiography recently has drawn a great deal of

attention. Adaptive statistical iterative reconstruction (ASIR) is a commercially available reconstruction technique that, compared to filtered back projection (FBP) methods typically used in CT, provides a reduction in image noise and improvement in low contrast detectability (LCD). MBIR-VEO is a new reconstruction technique that, compared to ASIR methods, provides an improvement in spatial resolution and further reduction in image noise allowing for even lower dose imaging with the same, or better, diagnostic value.

#### MATERIALS & METHODS

Adaptive statistical iterative reconstruction (ASIR) techniques provide standard image quality at substantially lower radiation dose than traditional filtered back projections (FBP) allow. Adaptive statistical iterative reconstruction leaves substantial information about the CT imaging chain untapped to permit rapid reconstruction times at the expense of quantum and system noise remaining in the image. Model-based iterative reconstruction techniques (MBIR-VEO) perform a more complex reconstruction, modeling system optics and statistics along with 3D three-point beam analysis. While reconstruction times are longer, with fewer assumptions image noise is reduced drastically and dose reductions of up to 75% over FBP can be accomplished. MBIR-VEO images were obtained at a 40% lower dose (higher noise index) than currently in use for ASIR studies at our institution. Adaptive statistical iterative reconstruction and FBP images were retrospectively reconstructed for analysis from the dose reduced raw data. A quantitative (noise) and qualitative comparison (spatial resolution, overall quality) of the clinical MBIR-VEO images was performed against the ASIR and FBP studies as well as against routine clinical expectations of CT angiography of the head and neck. All examinations were performed on a clinical GE HD 750 scanner.

#### RESULTS

Clinical neuro CTA images reconstructed with MBIR-VEO demonstrated better than expected edge definition, vessel conspicuity and overall quality on 2D maximum intensity projections as compared with images reconstructed with ASIR or FBP. The dose-reduced source MBIR-VEO images showed significantly less noise than ASIR and FBP.

#### CONCLUSION

Model-based iterative reconstruction image quality was equivalent or superior to ASIR and FBP utilizing a clinical reduced dose protocol (40% dose reduction compared to ASIR). Model-based iterative reconstruction images were visually sharper and contained less noise than those with ASIR or FBP.

**KEY WORDS:** Iterative reconstruction, model-based, CT angiography, radiation dose

O-390

3:08 PM - 3:16 PM

#### High-Pitch Dual-Source CT Angiography of Supra-Aortic Arteries

Brodoefel, H.<sup>1</sup>·Korn, A.<sup>2</sup>·Danz, S.<sup>2</sup>·Ernemann, U.<sup>2</sup>·Moonis, G.<sup>1</sup>

<sup>1</sup>Beth Israel Deaconess Medical Center, Boston, MA,

<sup>2</sup>University of Tuebingen, Tuebingen, GERMANY

#### PURPOSE

Noninvasive imaging is accepted increasingly for evaluation of extracranial atherosclerotic disease in stroke patients. High-pitch dual-source CT angiography (CTA) is a recent innovation that allows reduction of overlapping projections and shortens scan time to less than 1 sec. The aim of our study was to assess this technique in terms of image quality and radiation dose in supra-aortic CTA.

#### MATERIALS & METHODS

CT angiography of supra-aortic arteries was performed with using a standard contrast injection and two different CT acquisition protocols: conventional single-source 64-slice spiral (pitch 0.61) and ECG-synchronized high-pitch dual-source 128-slice CT (pitch 3.2). For each protocol, 25 sex-, age- and BMI-matched patients were identified. Quantitative and qualitative image quality of intra and extracranial vessel segments was assessed by blinded, independent readers and radiation dose compared between the different algorithms.

#### RESULTS

Conventional and high-pitch CTA achieved comparable signal-to-noise ratios in both arterial ( $54.2 \pm 15.4$  vs  $60.6 \pm 16.4$ ;  $p = 0.16$ ) and venous segments ( $24.0 \pm 11.5$  vs  $19.7 \pm 9.5$ ;  $p = 0.15$ ). High-pitch scanning was, however, associated with sharper delineation of vessel contours and image quality was graded significantly better in the brachiocephalic trunk ( $p < 0.0001$ ), the subclavian arteries ( $p < 0.0001$ ), proximal common carotid arteries ( $p < 0.03$ ) and vertebral V1 segments ( $p < 0.0001$ ). With use of the high-pitch approach, the dose-length-product was reduced by nearly 50% ( $275 \pm 38$  vs  $142 \pm 21$  mGy\*cm).



Blurring of vessel walls due to motion with conventional 64-slice CT (A) are Eliminated by high-pitch imaging (B)

#### CONCLUSION

High-pitch CTA of supra-aortic arteries improves image quality in proximal segments while significantly lowering radiation dose. The technique thus qualifies as a promising alternative to conventional spiral CTA and may be particularly useful for identification of ostial stenosis.

**KEY WORDS:** High-pitch CT angiography, supra-aortic arteries, image quality

**O-391**

**3:16 PM - 3:24 PM**

**Correlation of Internal Carotid Artery Minimal Lumen Diameter with NASCET-Based Percent Stenosis on Mean Diffusivity CT Angiography: What Should We Do When the "Normal" Distal Reference Lumen Is Not So Normal?**

Sabbag, D. J.<sup>1</sup>Waldron, N.<sup>1</sup>Tardie, N.<sup>1</sup>Jatt, M.<sup>1</sup>Gonzales, R.<sup>1</sup>Riascos, R.<sup>2</sup>Romero, J.<sup>1</sup>

<sup>1</sup>Massachusetts General Hospital, Boston, MA,  
<sup>2</sup>University of Texas Medical Branch at Galveston, Galveston, TX.

**PURPOSE**

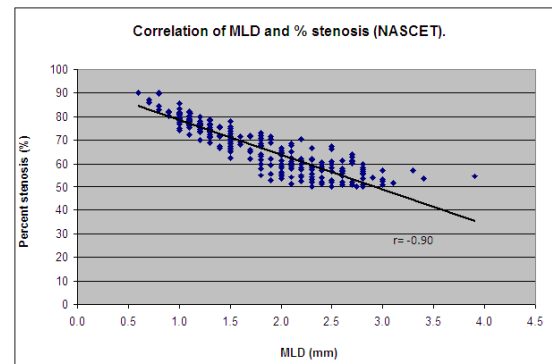
The NASCET criteria have been the gold standard for angiographic evaluation of carotid artery stenosis secondary to atheromatous disease. In current practice, the application of the NASCET criteria requires determining a "normal distal" segment, which in a large proportion of patients is not obtainable due to extensive atheromatous disease or to distal vessel diameter changes when severe stenosis is present. The purpose of this study is to correlate minimal lumen diameter (MLD) and percent stenosis of the internal carotid artery.

**MATERIALS & METHODS**

A review of the Neurovascular Laboratory-MDCT angiography database was used to identify patients with 50% stenosis or more based on NASCET criteria. The MLD and NASCET-based percent stenosis were measured prospectively on all cases. Correlation of the MLD and percent stenosis was performed using Pearson correlation coefficient.

**RESULTS**

Two hundred seventy-one patients were identified with a mean age of 72 years, male/female ratio of 1.5:1, with 376 carotid arteries with >50% were identified. The mean MLD was of 1.65 mm and the mean stenosis was of 69.5%. The Pearson coefficient correlation of MLD and percent stenosis was  $r = 0.90$  (two-sided P value of <0.001). See graph #1.



**CONCLUSION**

Minimal lumen diameter is a reliable measurement to determine degree of stenosis particularly in arteries where a normal distal lumen is not obtainable. Based on these results MLD of less than 1.25 mm is strongly related to a 70-99% stenosis, MLD of more than 1.9 mm to 3 mm are related to a stenosis of 50-69% and lesions between 1.25 mm and 1.9 mm overlap and are likely moderate to severe lesions.

**KEY WORDS:** Carotid stenosis, NASCET, minimal lumen diameter

**O-392**

**3:24 PM - 3:32 PM**

**Cerebral Ischemia after Thoracic Endovascular Aortic Repair: A Diffusion-Weighted MR Imaging Study**

Schlamann, M. U.·Eggebrecht, H.·Tsagakis, K.·Goericke, S.·Kahlert, P.

Universitiy Hospital Essen  
Essen, GERMANY

**PURPOSE**

The risk of intracranial stroke after thoracic endovascular aortic repair (TEVAR) due to dislodgment and subsequent embolization of debris during intravascular manipulation of guidewires and catheters ranges between 2% and 6%. The rate of clinically silent cerebral ischemia is yet unknown, but may be even higher.

**MATERIALS & METHODS**

Twenty patients who underwent TEVAR were included into this prospective study. Periprocedural apparent and silent cerebral ischemia was assessed by neurologic testing and serial cerebral diffusion-weighted (DW) magnetic resonance imaging (MRI) at baseline and within 1-10 days after the procedure.

**RESULTS**

Thoracic endovascular aortic repair was successful in all patients without immediate clinically apparent neurologic deficits. Postinterventional DW MRI detected a total of 33 new focal brain lesions in 13 of the 20 patients (65%). Lesions were usually multiple (1-6 lesions per patient) and equally dispersed in both hemispheres. There were no additional apparent neurologic events during the in-hospital period.

## CONCLUSION

Thoracic endovascular aortic repair resulted in substantial ischemic brain embolizations in the majority of patients as detected by serial DW MRI. Although even multiple lesions per patients were found, these lesions were not associated with apparent neurologic events. Further developments should be directed towards reducing the risk of periprocedural cerebral embolization.

**KEY WORDS:** TEVAR, ischemia, diffusion-weighted imaging

**O-393**

**3:32 PM - 3:40 PM**

## Comparison of Common Carotid Compliance Measured with Cardiac-Gated 3D Time of Flight MR Imaging and Ultrasound

Mihlon, F.·Hildreth, K.·Moreau, K.·Bert, R.

University of Colorado  
Aurora, CO

## PURPOSE

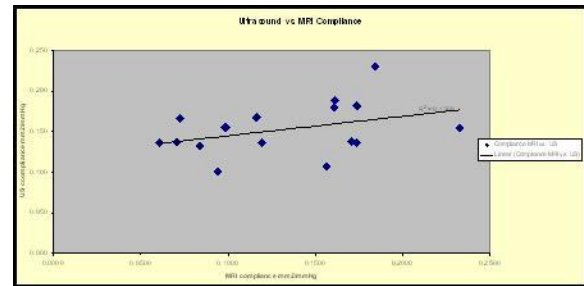
We previously have tested an MRI method of directly measuring arterial compliance and capacitance using cardiac-gated 3D time of flight (CG3DToF) MRI in a phantom model. Such a technique could allow direct intracranial measurement of arterial compliance. We now are comparing compliance measurements with this technique against common carotid ultrasound measurements in humans.

## MATERIALS & METHODS

This study was granted IRB expedited approval. Thus far, eight young normal volunteers, without cardiovascular disease (age range 24-32 years), have been tested. Standard ultrasound compliance measurements were recorded for each common carotid artery, 1 cm below the bifurcation, immediately before MRI measurements. Three to five blood pressure cuff measurements were measured in each arm before each ultrasound measurement, before and after each MRI study. A 2 cm segment of the CCA was imaged on a 1.5 T (Achieva, Philips Medical System) using CG3DToF, with varying delays of 95 - 120 msec and gate widths from 185 - 485 msec; gate interval set to longest. Phase contrast (PC) flow measurements (2D quantitative, cardiac triggered, 20 time points) also were obtained for correlation with gate placement. Postprocessing of ultrasound and MRI was performed off line. Five 1 mm slices were trimmed from the top and bottom of the MRI series to avoid edge of field and inflow effects. The resulting MRI vascular volumes were measured with the same manufacturer's volume rendering software and is presented as a scatter plot (Microsoft Excel).

## RESULTS

Chart 1 presents a scatter plot of compliance measured with ultrasound (US) vs MRI. When variability of BP measurements was eliminated, variance improved to about 0.4. This variance will be updated at the meeting with additional patient data and corrections for variations in delay time and gate widths.



## CONCLUSION

We expected our MRI technique methods to underestimate the carotid compliance, as the finite gate width required for this MRI technique would produce a lower systolic volume than ultrasound, which measures lumen diameter near maximum peaks and troughs. In many cases the agreement between US and MRI was excellent, but results were sensitive to the delay time and gate width. Optimal performance was obtained when delay was set to full width, half maximum of the flow upslope curve from PC data and the gate width less than 240 msec. Data will be updated at the meeting. Cardiac-gated 3D time of flight shows great promise as a volumetric means of directly measuring arterial compliance and can be used intracranially.

**KEY WORDS:** Arterial, compliance, MR imaging

**O-394**

**3:40 PM - 3:48 PM**

## Doppler Ultrasonography and Time-Resolved Contrast-Enhanced MR Angiography versus Rotational Digital Subtraction Angiography in Internal Carotid Artery Stenosis

Gokce, E.·Altankus, A.·Acu, B.·Firat, M. M.·Çelikyay, F.·Ekorkmaz, Ü.

Gaziosmanpasa University  
Tokat, TURKEY

## PURPOSE

In this study, rotational (3 dimensional) digital subtraction angiography (DSA) being taken as a reference, the sensitivity, specificity, positive and negative predictive values, and diagnostic accuracy of Doppler ultrasonography and time-resolved imaging of contrast kinetics (TRICKS) MR angiography were used in the detection of internal carotid artery (ICA) stenosis in patients with cerebrovascular disease symptoms.

## MATERIALS & METHODS

From January 2011 to September 2011, 22 (17 male, 5 female; age range 53-82 years) consecutive patients were included in this study. MR angiography was performed 1.5 T MR. Digital subtraction angiography were obtained lateral, anteroposterior planes and rotational. The stenotic segments were evaluated with eight different parameters (for DSA subjective, conventional lateral, 3D MIP sagittal, axial plane area and for TRICKS MR angiography subjective, MIP sagittal, VR sagittal, axial area) of DSA and TRICKS MR angiography techniques. Results of TRICKS MR angiography, and DSA were read independently by two

observers. Velocity, area and diameter measurements were performed with Doppler ultrasonography which was performed by another radiologist for determining stenosis ratio. Stenosis ratio was determined by the North American Symptomatic Endarterectomy Trial (NASCET) method. Area and diameter information from the nonstenotic ICA were obtained by Doppler US to adapt NASCET. Area measurement by 3D DSA was accepted as gold standard method. The parameter variabilities of three imaging tests were calculated by using k statistics with the categorized stenosis.

## RESULTS

All segments throughout in 44 ICAs compared at 39 point of stenosis in Doppler US, TRICKS MR angiography and DSA. Coherence between observers was very good and excellent according to kappa statistics for both methods (TRICKS MR angiography and DSA) and analyzed parameters. For all parameters, sensitivity, specificity, PPV, NPV, and diagnostic accuracy of three imaging methods are given in the table.

	Doppler Velocity	Doppler Diameter	Doppler Area	Subjective DSA	Subjective TRICKS	MIP Sagittal DSA	VR Sagittal TRICKS	Lateral DSA	MIP Sagittal TRICKS	Area TRICKS
Sensitivity	100%	72%	90,9%	90,9%	90,9%	45,4%	63,6%	72,7%	72,7%	81,8%
Specificity	96,4%	92%	85,7%	96,4%	92,9%	100%	96,4%	100%	96,4%	92,8%
P.P.V	91,7%	80%	71,4%	90,9%	83,3%	100%	87,5%	100%	88,8%	81,8%
N.P.V	100%	89,6%	96%	96,4%	96,3%	82%	87,1%	90,3%	90%	92,8%
Diagnostic Accuracy	97,4%	87,2%	87,2%	94,9%	92,3%	84,6%	87,2%	92,3%	89,7%	89,7%

## CONCLUSION

Area measurement of axial plane on rotational DSA can be more accurately measured especially in patients whose stenotic segments could not measure optimal because of superposition on lateral plane. Stenosis rates of lateral plane measurements of five patients' stenosis which described ulceration on DSA moved to superior class on area measurements. On TRICKS MR angiography only one stenosis rate moved to superior class (51% to 77%). We evaluated that area measurements on DSA and TRICKS MR angiography increase diagnostic accuracy especially on irregular plaques. Doppler ultrasonography is a cheap, fast and easily accessible method and can be used safely in detecting carotid stenosis. TRICKS MR angiography is superior to Doppler US and DSA on analysis of all CCA segments' different projections after one contrast injection. Furthermore, TRICKS MR angiography is a noninvasive, nonionization, higher diagnostic accuracy of all parameters and safe so is an alternative to DSA for diagnosing ICA stenosis.

**KEY WORDS:** Carotid stenosis, rotational DS angiography, TRICKS MR angiography

O-395

3:48 PM - 3:56 PM

## Effect of Region-of-Interest Placement in Bolus Tracking Cerebral CT Angiography

Huang, R.-Chai, B.-Lee, T.

Brigham and Women's Hospital  
Boston, MA

## PURPOSE

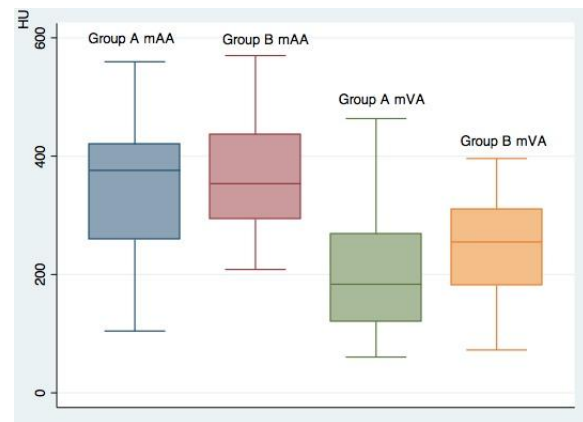
Premature or delayed triggering of semiautomatic bolus tracking during computed tomography angiography (CTA) can occur due to streak artifact from venous contrast near the ascending aortic arch. We study the effect on the quality of head CT angiogram after changing the region of interest of bolus tracking to the descending aorta.

## MATERIALS & METHODS

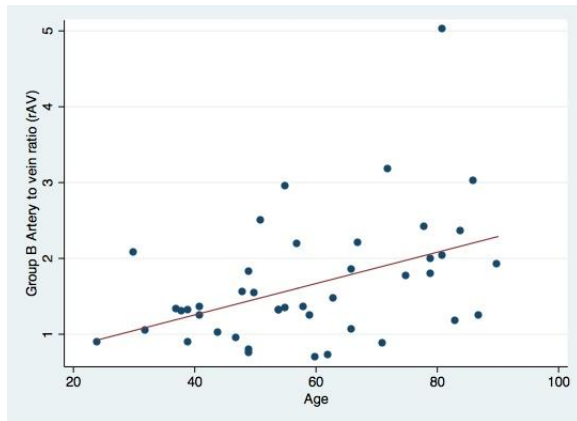
Head CTA examinations from 81 patients performed in the same scanner with the same contrast dose were reviewed retrospectively. Region of interest for semiautomatic bolus tracking was placed in the ascending aorta in 37 patients (group A) and in the descending aorta in 43 patients (group B). The mean arterial attenuation (mAA) in the proximal middle cerebral arteries and the mean venous attenuation (mVA) in the superior sagittal and straight sinuses were measured. The attenuation ratios of artery to vein (Rav) were calculated and compared between the two groups. The calculated ratios also were correlated with patients' age within each group.

## RESULTS

Group A had lower mVA (201 HU vs 250 HU,  $p = 0.0017$ ) and higher Rav (2.1 vs 1.6,  $p = 0.032$ ) compared to group B. However, five out of 37 patients (14%) in group A had mAA less than 200 HU, while none of the 44 patients in group B had arterial attenuation below 200 HU. Within group B, there is moderate correlation between the Rav and patient age ( $R = 0.42$ ,  $p = 0.004$ ). Greater variance of Rav was observed in group A (1.21) compared to group B (0.68) ( $p = 0.036$ ).







#### CONCLUSION

Placement of region of interest in the descending aorta can minimize the chance of suboptimal arterial contrast in head CTA at the cost of introducing greater venous contamination, particularly at younger age group.

**KEY WORDS:** CT angiography, region of interest, bolus tracking

O-396

3:56 PM - 4:04 PM

#### Addition of a Low-Dose Contrast-Enhanced MR Angiography at 3.0 T in the Assessment of Acute Stroke: A More Efficient and Accurate Stroke Protocol

Nael, K.-Linetsky, M.-Pirastehfar, M.-Villablanca, P. J.-Salamon, N.

David Geffen School of Medicine, University of California Los Angeles  
Los Angeles, CA

#### PURPOSE

A comprehensive MR stroke protocol should determine the ischemic core, penumbra and the status of neck and brain arteries, all essential for treatment decision-making in the acute setting. Further improvement in acquisition time (AT) and image quality may have important therapeutic and prognostic implications for patients with acute stroke. **Our purpose is to evaluate the feasibility of a 3.0 T MR stroke protocol that combines a low-dose contrast-enhanced MRA (CE MRA) and perfusion, without the need for additional contrast, and to compare the results with more routine stroke protocol using time-of-flight MRA (TOF MRA).**

#### MATERIALS & METHODS

Twenty patients (11M, age range: 42-95 years) presenting with acute stroke underwent our routine MR stroke protocol: DWI/ADC, FLAIR, GRE, T2, TOF MRA of the neck (voxel:  $1.2 \times 1.0 \times 2.0 \text{ mm}^3$ , AT: 3 min 40 sec), and brain ( $0.7 \times 0.7 \times 0.7 \text{ mm}^3$ , AT: 6 min 20 sec), and EPI perfusion. Additionally, we incorporated a low-dose 3D CE MRA (voxel size:  $0.8 \times 0.8 \times 0.9 \text{ mm}^3$ , covering from arch to vertex, AT: 20 sec), integrated with 2-dimensional parallel acquisition (GRAPPA  $\times 6$ ) just before the perfusion imaging. A total of 20 ml of gadolinium, used routinely for MR perfusion, was

diluted with saline and utilized with a modified 2-phase contrast injection scheme to accomplish both CE MRA and perfusion, without the need for additional contrast. The degree of arterial stenosis on CE MRA and TOF MRA were assessed independently by two neuroradiologists using a 4-grade scoring scale (1: 0-49%, 2: 50-70%, 3: 71-99%, 4: occlusion) and the results were compared with a consensus reading of the corresponding segments on digital subtraction angiography (DSA) available in eight patients. The intermodality and interobserver agreement for determination of categorized stenosis was calculated by kappa test. The sensitivity and specificity were calculated for each technique in comparison to DSA.

#### RESULTS

A total of 600 arterial segments were evaluated without statistically significant difference for grading of arterial stenosis between the readers or modalities ( $p > 0.2$ ). Seventy-four arterial stenoses were detected with CE MRA and 81 with TOF MRA. There was good interobserver agreement for CE MRA ( $k = 0.76$ ) and TOF MRA ( $k = 0.8$ ). The intermodality agreement was lower ( $k = 0.43$ , 95% CI: 0.35, 0.51), mainly due to overestimation of arterial stenosis by TOF MRA. Twenty arterial segments with mild disease and 15 segments with high-grade stenosis read as occluded on TOF MRA. The sensitivity and specificity for diagnosis of overall arterial stenosis were 83% and 96% for CE MRA and 85% and 74% for TOF MRA, using DSA as the standard of reference. The average examination time with CE MRA only (12 min) was significantly less ( $p < 0.05$ ) in comparison to routine protocol using TOF MRA (22 min).

#### CONCLUSION

The described MR stroke protocol is feasible and results in significant reduction in scan time and improved diagnostic accuracy for evaluation of arterial stenosis, when compared to routine stroke protocol using TOF MRA. The inherent higher SNR at 3.0 T and a modified contrast injection scheme, this low-dose CE MRA can be implemented into routine stroke protocol without contrast penalty.

**KEY WORDS:** Contrast-enhanced MR angiography, 3 T, stroke protocol

O-397

4:04 PM - 4:12 PM

#### Prediction of Leptomeningeal Collateral Formation in Acute Ischemic Stroke Using an Assessment for Vascular Reactivity

Christoforidis, G.<sup>1</sup>•Zhu, F.<sup>1</sup>•Khan, S.<sup>1</sup>•Garg, N.<sup>2</sup>•Theyel, B.<sup>1</sup>•Benayoun, M.<sup>1</sup>

<sup>1</sup>University of Chicago, Chicago, IL, <sup>2</sup>University of Illinois at Chicago, Chicago, IL

#### PURPOSE

Leptomeningeal collateral perfusion to an ischemic territory during acute ischemic stroke depends on the density of native pial vessels present but is variable from patient to patient. As a result infarct volumes vary

significantly depending on the extent of leptomeningeal collateral formation. Noninvasive predictors for the extent of leptomeningeal collateral formation during acute ischemic stroke have not been developed. Methods predictive of leptomeningeal collateral formation could help assess a patient's ability to withstand a large vessel occlusion. In theory vascular reactivity in the normal state may be a predictor for leptomeningeal collateral formation. This work examines whether CO<sub>2</sub> and acetazolamide challenges can be used to predict infarct volumes during acute ischemic stroke.

#### **MATERIALS & METHODS**

Dynamic susceptibility contrast magnetic resonance imaging (MRI) (3 T Achieva, Philips) was performed in five mongrel dogs (20-30 kg) while breathing medical air (baseline), 5% carbon dioxide (CO<sub>2</sub> challenge) and 20 minutes following infusion of 1 g acetazolamide (combined CO<sub>2</sub> and acetazolamide challenge) with attention to end tidal CO<sub>2</sub>. Cerebral blood volume (CBV), cerebral blood flow (CBF) and mean transit time (MTT) values through symmetric left and right hemisphere regions of interest derived from separate gray matter and white matter structures at baseline and during each challenge were calculated. The following day, a previously described angiographically based methodology allowed for permanent middle cerebral artery occlusion in the same animals. Leptomeningeal collateral formation was assessed using arterial arrival times (AAT) from regions of interest within normal and collateralized branches of the distal M3 segment using a custom-made program. MR imaging was performed following the occlusions. Infarct volumes were calculated using a threshold technique by two blinded observers using 1 hour postocclusion mean diffusivity (MD) maps. Bivariate linear fit analyses were used to assess any correlation between challenged versus baseline ratio of cerebral blood volume and cerebral blood flow infarct volume determinations.

#### **RESULTS**

Cerebral blood flow values derived from cortical gray matter during simultaneous CO<sub>2</sub> challenge demonstrate a statistically significant correlation ( $p = 0.0415$ ,  $r^2_{adj} = 0.729$ ) to infarct volumes and leptomeningeal collateral formation ( $p = 0.462$ ,  $r^2_{adj} = 0.710$ ). Cerebral blood volume values from white matter during acetazolamide and CO<sub>2</sub> challenge demonstrate a statistically significant correlation to infarct volumes ( $p = 0.0109$ ,  $r^2_{adj} = 0.886$ ) and leptomeningeal collateral formation ( $p = 0.0161$ ,  $r^2_{adj} = 0.952$ ). Changes in CBV values from cortical gray matter, CBF from white matter and MTT values were not found to have a statistically significant correlation with infarct volumes or AAT assessment of leptomeningeal collateral formation.

#### **CONCLUSION**

Preliminary data presented here suggest that cerebral blood volume and cerebral blood flow changes associated following CO<sub>2</sub> and acetazolamide challenge may have predictive value for leptomeningeal collateral formation and infarct volumes during acute ischemic

stroke. Additional investigation is necessary to derive a more definitive conclusion.

**KEY WORDS:** Ischemic stroke, leptomeningeal collaterals, cerebrovascular reactivity

**O-398**

**4:12 PM - 4:20 PM**

#### **Optimizing Temporal Resolution to Minimize CT Dose in CT Brain Perfusion**

Riordan, A. J., Velthuis, B., Bennink, E., de Jong, H. W. A.

Utrecht Medical College  
Utrecht, NETHERLANDS

#### **PURPOSE**

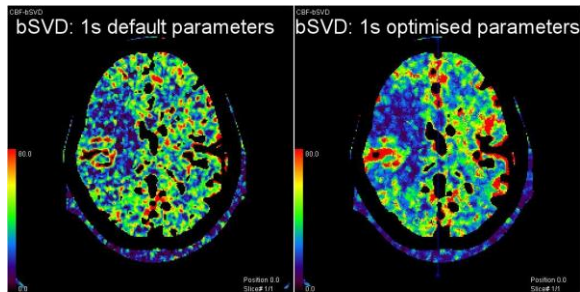
Advised CT perfusion (CTP) protocols vary from 0.5 to 4 seconds between frames, resulting in CT doses between 66 and 452 CTDI-vol (mGy) per series. This dose range implies there is room for optimization. Clinical studies are less suitable for protocol optimization due to ethical objections. Therefore we developed and applied an anthropomorphic head phantom to emulate a wide range of CT protocols to optimize temporal sampling, using known "true" cerebral blood flow (CBF) values to quantify bias.

#### **MATERIALS & METHODS**

An anthropomorphic head phantom with realistic resolution and noise features was constructed by combining high-resolution cerebral MRI data and CTP acquisitions of a skull phantom. CT perfusion data were generated with combinations of frame interval of 1, 2 or 4 seconds and 150 mAs or 75 mAs. These data were processed using two major CTP software packages [i.e., block Circulant Singular Value Decomposition (bSVD) (Asist group, Japan)] and Fit Based Deconvolution (FBD) (Philips Brain Perfusion package, 4.0) methods. Using the ground truth of the phantom, the protocols are assessed for quantitative accuracy (CBF bias and contrast) and image noise. To substantiate the phantom as a reliable tool, results of the simulated data were compared to clinical data (with informed consent) at 75 mAs with 1, 2 and 4 seconds frame intervals and 150 mAs with 2 and 4 second frame interval.

#### **RESULTS**

Clinical data showed similar dependence on protocol and algorithm as the phantom in terms of CBF bias and noise which proved its applicability. For the FBD software, higher scan dose resulted in less image noise and accuracy. However, at equal dose (75 mAs with 1 second sample rate, versus 150 mAs with 2 second sample rate) it was found that 2's frame intervals were preferable. For the bSVD perfusion software the 2's protocol was most useful in terms of image quality and quantitative accuracy regardless of CT dose. However, if adjustment of specific algorithm parameters settings was allowed, 1's frame intervals was preferred (see perfusion maps from the phantom in attached figure).



#### CONCLUSION

For the FBD, 2 seconds is preferred over 1 or 4 seconds in terms of dose efficiency. For the SVD-based methods 1 second is potentially better in terms of quantitative accuracy, but requires alteration of algorithm parameter settings. Finding an optimal protocol depends heavily on algorithm choice and settings, and can be accomplished using a realistic anthropomorphic phantom.

**KEY WORDS:** CT brain perfusion, stroke, scan protocol

**O-399**

**4:20 PM - 4:28 PM**

### 3 T MR Imaging Evaluation of the Relationship of White Matter Hyperintensities and Cognitive Scores

Cairns, B.<sup>1</sup>Bowes, J.<sup>1</sup>Stroman, P.<sup>1</sup>Alvarado, B.<sup>1</sup>Islam, O.<sup>1</sup>Garcia, A.

Queen's University  
Kingston, ON, CANADA

#### PURPOSE

White matter hyperintensities (WMH) are common among older people and are believed to result from vascular abnormalities compounding the cognitive decline in aging and dementia. Yet, the clinical significance attributed to the WMH remains unclear and controversial. We have analyzed the presence and stage of WMH and their relationships with scores of a battery of cognitive tests in cognitively normal older adults, patients diagnosed with mild cognitive impairment (MCI) and Alzheimer disease (AD).

#### MATERIALS & METHODS

Forty-nine persons (mean age  $73 \pm 7$  years) were included in the study: Twenty were cognitively normal control subjects (age  $71.24 \pm 5.68$  years), eight patients had MCI (age  $72.00 \pm 7.75$  years) and 21 patients had mild AD (age  $73.20 \pm 8.94$  years). The battery of psychometric tests including the Montreal Cognitive Assessment (MoCA), the California Verbal Learning Test Version II (CVLT-II), the Mattis Dementia Rating Scale (DRS), the Stroop Test (Stroop) and the Trail Making Test: Part B (TMT-B) was administered within 2 weeks of the magnetic resonance imaging (MRI) study. The CVLT was not administered to patients with AD as they could not complete it. Fifty axial slices of 3 mm thickness (voxel size  $1 \times 1 \times 3$  mm<sup>3</sup>) T2-weighted FLAIR scans were acquired in a 3 T magnetron and evaluated by a board-certified neuroradiologist blinded to cognitive scores. White matter hyperintensities were graded following a modified Fazekas scale as follows:

grade 0 (no WMH); grade I, mild (single lesions  $<10$  mm, and/or grouped lesions  $<20$  mm of any diameter); grade II, moderate (single lesions 10-20 mm, and/or grouped lesions  $>20$  mm linked by no more than "connecting bridges"); grade III, severe (single lesions  $>20$  mm, and/or confluent hyperintense areas  $>20$  mm diameter). Data were analyzed by ANOVA.

#### RESULTS

Three persons had no WMH (grade 0) and all had AD. All normal controls had WMH. Three persons had severe WMH: 1 was a normal control and 2 had AD. Thirty persons had grade 1 (mild) and 13 had grade 2 (moderate) WMH. Because of the low frequency of grades 0 and 3, comparisons were made after combining WMH grades 0 and 1 as group A (none and mild WMH) and grades 2 and 3 as group B (moderate and severe WMH). Eighty percent of controls, 62% MCI and 57% AD patients were in group A. Group A were significantly younger than group B ( $p < .05$ ). Group B had significantly lower MoCA scores than group A (mean of 2.3 points lower), DRS, Stroop and the Short Delay Cued Recall (SDCR) sub-score of the CVLT (all  $p < .05$ ), while there was no difference in the Trails-B or among any other sub-scores of the CVLT.

#### CONCLUSION

Most subjects (43/49) had either grade I or II WMH, regardless of cognitive category. Although patients had more WMH than controls, the distribution of WMH argues against a clinically significant association between WMH seen in 3 T MR and cognitive tests scores. Combining grade 0 with 1, and grade 2 with 3, forming a two-tiered system (normal-mild vs moderate-severe) could be of potential clinical relevance. Larger studies are warranted.

**KEY WORDS:** White matter, dementia, cognitive score

## Wednesday Afternoon

**3:00 PM - 4:30 PM**

**Tranon Ballroom**

**(53b) Spine: Other**

**O-400**

**3:00 PM - 3:08 PM**

### Postoperative Intraspinal Subdural Hygromas in a Pediatric and Young Adult Patient Population: Incidence, Predisposing Factors, Imaging and Clinical Features

Patay, Z.<sup>1</sup>Mohammed, N.<sup>1</sup>Goldsberry, G.<sup>2</sup>Li, Y.<sup>1</sup>Harreld, J. H.<sup>1</sup>Gajjar, A.<sup>1</sup>Boop, F.<sup>1</sup>Sanford, R.<sup>1</sup>Sablauer, A.<sup>1</sup>

<sup>1</sup>St. Jude Children's Research Hospital, Memphis, TN,  
<sup>2</sup>Medical University of South Carolina, Charleston, SC

#### PURPOSE

The natural history and course of intracranial (posttraumatic, postsurgical) subdural hygromas is well documented. Literature data suggest that intraspinal-enhancing subdural fluid collections are not uncommon after surgery for posterior fossa tumors (PFT) in children. In this study we sought to describe: a.) the imaging features of postoperative intraspinal subdural hygromas (PISH) at diagnosis and follow up and determine their b.) incidence rate, c.) predisposing factors and d.) possible neurologic correlates.

#### MATERIALS & METHODS

In this retrospective study we reviewed the medical files of 263 patients (age-range: 2 months -21 years), who received surgery for PFTs (medulloblastoma = 145, ependymoma = 80, atypical teratoid rhabdoid tumor = 23, astrocytoma = 14, spongioblastoma = 1). Once patients with PISH were identified (n = 22), an age-matched internal control group was established (n = 44), which was used for comparative risk factor analysis. Preoperative brain MRI studies were evaluated for location and size of PFT, presence and magnitude of tonsillar herniation, presence and magnitude (using the index of Evans) of supratentorial hydrocephalus, as well as presence and grade of empty sella. For each case, the first postoperative brain MRI study was evaluated for the presence of intracranial subdural hygromas. First and second postoperative spine MRI studies were evaluated for the presence of PISH and in positive cases, the extent, magnitude and signal properties of PISH were assessed on precontrast T1- and T2-weighted (when available) and postcontrast T1-weighted (in all patients) images. Fisher's exact, Wilcoxon rank and two-sample t-tests were used for statistical analysis.

#### RESULTS

The overall incidence rate of PISH was 8.37% (exact 95% CI: 0.0532, 0.1239) in our series. Characteristically, PISH showed intermediate signal on precontrast T1-weighted and signal enhancement on postcontrast T1-weighted imaging. In 15 patients PISH involved the entire spine. All PISHs resolved on the second postoperative study and none were associated with neurologic signs or symptoms. Location, size, histological type of the PFT and hydrocephalus did not show correlation with the development of PISH. Significant correlation was found between PISH and the presence of tonsillar herniation ( $p = 0.0041$ ). Association was found between PISH and postoperative intracranial subdural hygromas ( $p = 0.0050$ ) as well as PISH and empty sella ( $p = 0.0892$ ).

#### CONCLUSION

The incidence of PISH in our series is lower but comparable to that described by other investigators in a smaller patient cohort (15.5%). Our data suggest that the development of PISH is linked to abrupt pressure and hydrodynamic changes due to posterior fossa decompression and reestablishment of communication between the intracranial and intraspinal CSF compartments following surgery. Tonsillar herniation prior to surgery, causing sequestration of the intracranial and intraspinal CSF spaces, perhaps with excessive pressure values within the intrathecal space,

seems to be the sole significant predisposing factor for the "ex vacuo" development of PISH. Hence PISH is a surrogate imaging indicator of benign transient postoperative cerebral spinal fluid (CSF) hypotension following preoperative intraspinal hypertension. Postoperative intraspinal subdural hygromas are clinically benign, yet may pose differential diagnostic challenges, hamper the accuracy of CSF cytology and impair the diagnostic imaging evaluation of possible metastatic leptomeningeal dissemination. The typically rapid and spontaneous resolution of PISH, however, allows for early reassessment.

**KEY WORDS:** Spine, subdural hygroma, MR imaging

**O-401**

**3:08 PM - 3:16 PM**

#### MR Imaging Findings and Clinical Characteristics of Intramedullary Spinal Cord Metastases: A Large Case Series

Rykken, J. B.·Diehn, F. E.·Hunt, C. H.·Eckel, L. J.·Schwartz, K. M.·Kaufmann, T. J.·Wood, C. P.

Mayo Clinic  
Rochester, MN

#### PURPOSE

Intramedullary metastases to the spinal cord are rare. Our goal was to review retrospectively the MRI appearance and clinical characteristics of a large series of intramedullary spinal cord metastases from a single institution.

#### MATERIALS & METHODS

Our radiology and clinical databases were used to identify patients with potential intramedullary spinal cord metastases from 1999 to 2011. Exclusion criteria were: lack of confirmed diagnosis (e.g., patients where the clinical differential diagnosis was radiation myelitis/necrosis) and lack of available initial pretreatment MRI. The initial MRI examination of each remaining patient was reviewed in consensus by two radiologists. Specific features that were evaluated included: number of intramedullary metastases, location, position within the cord, morphology, size, cord expansion, T1 and T2 signal characteristics, gadolinium enhancement characteristics, cystic change/necrosis, other visible central nervous system (CNS) metastases, and visible primary tumor and/or non-CNS metastases. The clinical records were reviewed for patient age at MRI, presenting symptoms, and if applicable, date of death.

#### RESULTS

Among 54 total patients, nine were excluded (4 for lack of firm diagnosis, 5 for lack of available initial pretreatment MRI). The remaining 45 patients (mean age 58.3 +/- 13.5 years) had 65 spinal cord metastases. Thirty-six of 45 (80.0%) patients presented with a solitary cord metastasis. Lung carcinoma was the most common primary tumor [21 of 45 (47%) patients]. Twenty-six of 45 (58%) patients presented with weakness as the dominant symptom. Of those patients who expired, mean survival from the date of MRI was

26.9 +/- 39.4 weeks. Thirty-seven of 65 (57%) metastases were located in the thoracic spine. Thirty-three of 65 (51%) of lesions were located eccentrically, compared to 30 of 65 (46%) located centrally within the cord. Two of 65 (4%) were exophytic. Fifty-nine of 65 (91%) were well circumscribed. Cord expansion was associated with 40 of 65 (62%) lesions. Metastases tended to be T1 isointense [43 of 61 (70%)] and T2 hyperintense [51 of 65 (78%)]. For those cases which received gadolinium, almost all enhanced [58 of 59 (98%)]. The enhancement pattern was variably homogeneous [29 of 58 (50%)] and heterogeneous [28 of 58 (48%)]. There was only one ring-enhancing, centrally necrotic/cystic lesion [1 of 58 (2%)]. The mean longitudinal extent of the enhancing lesions was 1.3 +/- 1.1 (range, 1-8) vertebral segments. The mean longitudinal extent of associated T2 signal hyperintensity was 4.4 +/- 4.1 vertebral segments (range, 1-15). In 26 of 45 patients (58%), either the primary tumor and/or non-CNS metastases were also visible on the reviewed MRI. Other CNS metastases, such as cerebellar, leptomeningeal or vertebral metastases, were visualized in 27 of 45 (60%) patients.

#### CONCLUSION

On MRI, spinal cord metastases tend to be solitary, well circumscribed, expansile, and T1 iso and T2 hyperintense. Almost all enhance, with adjacent T2 signal abnormality much larger than the enhancing component. Associated additional CNS metastases and/or the primary tumor/non-CNS metastases are commonly present on the initial MRI. Patients have a poor prognosis, with a mean survival of 6 months from the MRI date.

**KEY WORDS:** Spinal cord, intramedullary metastasis, MR imaging

**O-402**

**3:16 PM - 3:24 PM**

#### **Cord Compression: How Often Is It Really Acute?**

Potigailo, V. Katzman, G.

University of Chicago  
Chicago, IL

#### **PURPOSE**

The objective of this study is to examine the efficacy of utilization of spine magnetic resonance imaging (MRI) as ordered by the Emergency Department (ED) at a tertiary care academic medical center for diagnosis of a suspected acute cord compression. Our clinical observations suggest that this advanced imaging modality may be over-utilized.

#### **MATERIALS & METHODS**

The HIPAA-compliant study was approved by the institutional review board with informed consent waived. Electronic medical records for ED patients who presented with an indication of "acute cord compression" were retrieved from the medical center database. Only records for patients that received STAT MRIs ordered between May 1, 2010 and May 31, 2011

were included in this study. The final result set contained electronic records for 70 patients.

#### **RESULTS**

Seventy patients' emergency MRIs were investigated for signs of acute cord compression. Of the 70 patients studied, one case (1.4%) was positive for acute cord compression with the remaining 69 cases (98.6%) demonstrating degenerative changes, internal derangement of the cord or chronic cord compression. The following studies were ordered: 24 total spine (cervical, thoracic and lumbar), four cervical spine, one cervical and thoracic, one cervical and lumbar, five thoracic, 13 thoracic and lumbar, and 22 lumbar MRIs. Twenty-five studies (36%) were requested and performed during normal business hours (8 am-5 pm), 31 (44%) were performed between 5 pm and 12 am and the final 14 (20%) between 12am and 8am. Overall, 45 studies (64%) were ordered after hours. The frequency with which STAT spine MRI were ordered differed slightly between ER physicians, ranging between 1 and 7 studies for the reviewed period (1 year). Neurology and/or neurosurgery services were consulted in 30 of the 70 cases, other services were consulted in eight cases, and consultation was not documented by the ordering ED physician for the remaining 32 cases.

#### **CONCLUSION**

This study exemplifies a universal trend in overutilization of advanced imaging modalities, specifically MRI, by the emergency department in a tertiary care academic medical center. It also demonstrates poor correlation between the indication for the examination and the final radiologic diagnosis. The use of emergency resources, including staff, technologists and hospital facilities, were skewed disproportionately after business hours, which has been shown previously to increase the cost of healthcare to the patients and, ultimately, society.

**KEY WORDS:** Cord, compression, spine

**O-403**

**3:24 PM - 3:32 PM**

#### **Effect of Partial Obstruction of the Subarachnoid Space on Cerebrospinal Fluid Velocity and Pressure Studied with Computational Fluid Dynamics**

Støverud, K. H.<sup>1</sup> Mardal, K. A.<sup>1</sup> Haughton, V.<sup>2</sup> Langtangen, H. P.<sup>1</sup>

<sup>1</sup>Simula Research Laboratory, Lysaker, NORWAY,

<sup>2</sup>University of Wisconsin School of Medicine and Public Health, Madison, WI

#### **PURPOSE**

Altered cerebrospinal fluid (CSF) pressures distal to partial obstruction of CSF flow has a role in production of syringomyelia, according to contemporary theories. The purpose of this study was to measure the effect of partial obstruction on CSF pressure and velocities.

#### **MATERIALS & METHODS**

A simple, idealized model of an unobstructed subarachnoid space (SAS) based on normal anatomical



dimensions was made by placing a cylinder inside another larger cylinder, 10 cm in length. For obstruction, focal expansion of the inner cylinder was added to the model. We converted the geometric model in NETGEN to a tetrahedral computational mesh consisting of interconnected nodes. Fluid flow through the model was simulated with FEniCS 0.9.8. At the inflow and outflow boundaries we defined a plug-shaped velocity profile, varying sinusoidally or constant in time. For the sinusoid, a period  $T = 0.85$  was selected based on a heart rate of 70 beats per minute. Peak velocities and maximum pressure difference throughout the model were sampled from calculations in all geometries and plotted versus degree of obstruction and a curve fitting was performed. The pressure difference between top and bottom in all geometries was plotted as a function of time. The pressure at every point along the z-axis was tabulated at  $t = T/4$ ,  $t = T/3$ ,  $t = T/2$  and for the constant inflow rate.

### RESULTS

The models had 0%, 35%, 60%, 75% or 85% reduction of the cross-sectional area of the SAS. Velocity and pressure varied with location and phase of the cardiac cycle. At the time of peak inflow the velocity profile in the unobstructed model was uniform throughout the length of the model. With obstruction of the SAS, velocity was greater at the level of the obstruction. Velocity increased exponentially as the cross-sectional area decreases. Bidirectional flow was evident throughout the SAS at the time of zero inflow in the 0% and 35% obstruction models. With 75% or 85% obstruction, bidirectional flow was not present at the obstructed region, although present proximal and distal to the obstruction. Pressure changed linearly in the unobstructed model. Pressure decreased minimally at the level of the obstruction for 35% obstruction and more considerably as the cross-sectional area decreases. In the unobstructed geometry and with a 35% obstruction the pressure gradient reached maximum when the flow turned. With a 60% obstruction or greater the phase between peak velocity and peak pressure gradient changed until at 85% obstruction the velocity and pressure gradient peak at the same point in time. Distal to the obstruction, peak velocity was constant in the z-direction and pressure changed linearly with distance in the z-direction.

### CONCLUSION

Fluid pressure in the SAS increased ( $\sim 1.2$  mmHg) with obstructions up to 85% of the SAS, associated with considerable increases in peak velocities. Pressure decreased abruptly at the level of obstruction, as theorized by Greitz, when the SAS was narrowed by 60% or more. Pressure did not increase distal to the obstruction. Partial obstructions of the SAS caused a change in the phase of the pressure gradient.

**KEY WORDS:** Cerebrospinal fluid flow, syringomyelia, Chiari 1

O-404

3:32 PM - 3:40 PM

### Dorsal Thoracic Arachnoid Web and the "Scalpel Sign": A Distinct Clinico-Radiologic Entity

Reardon, M. A. • Carpenter-Bailey, K. • Matsumoto, J. • Mukherjee, S. • Raghavan, P.

University of Virginia  
Charlottesville, VA

### PURPOSE

We report a series of 11 patients with a characteristic MRI/myelographic appearance of the upper thoracic spinal cord, which we term the "scalpel sign", produced by an arachnoid web(s). We propose that the existence of arachnoid webs in the dorsal subarachnoid space in these patients can result in a progressive myelopathy that is potentially curable by surgical lysis of the web. We aim to discuss the pathophysiology of how an arachnoid web eventually may lead to syringohydromyelia.

### MATERIALS & METHODS

We performed retrospective review of imaging studies of 11 patients (7 females and 4 males, age range: 31 to 67 years) with imaging demonstrating focal dorsal deformity of the upper thoracic spinal cord. Patient presenting symptoms included back pain and lower extremity weakness/numbness. MR imaging and CT myelography were performed on five patients. Five patients underwent only MRI examination of the thoracic spine, and one patient underwent CT myelogram alone.

### RESULTS

All 11 patients demonstrated a characteristic "scalpel"-shaped deformity of the upper thoracic cord. Eight of 10 patients undergoing MRI examination demonstrated T2 cord signal changes cephalad to the level of focal ventral deviation. Five of the eight patients with cord signal changes also demonstrated syringohydromyelia cephalad to the level of ventral deviation. The arachnoid web itself was not evident on MRI or CT myelography. Five patients with T2 cord signal abnormality underwent surgery which demonstrated dorsal arachnoid web(s) in four patients. A myelotomy was performed in one patient as the cord signal abnormality was mistakenly diagnosed as a tumor and a web was not sought retrospectively.



#### CONCLUSION

Arachnoid webs play a role in the etiology of syringohydromyelia. The scalpel sign is a reliable indicator of a dorsal thoracic arachnoid web. Recognition of this entity enables planned surgical lysis of the offending web which may be curative.

**KEY WORDS:** Arachnoid web, syringohydromyelia

**O-405**

**3:40 PM - 3:48 PM**

#### Proximal Kink of the Upper Left Thoracic Intersegmental Arteries: Anatomical Variant or Pathologic Process Potentially Resulting in Spinal Cord Ischemia?

Gailloud, P.<sup>1</sup>•Ponti, A.<sup>2</sup>•Chen, J.<sup>1</sup>•Pardo, C.<sup>1</sup>•Fasel, J. H. D.<sup>2</sup>

<sup>1</sup>The Johns Hopkins Medical Institutions, Baltimore, MD,

<sup>2</sup>University of Geneva Medical School, Geneva, SWITZERLAND

#### PURPOSE

This study was prompted by recurrent observations made during spinal digital subtraction angiography (SpDSA) of kinks of various severities involving the proximal segment of left upper thoracic intersegmental arteries (ISA) (Figure 1A, white arrow).

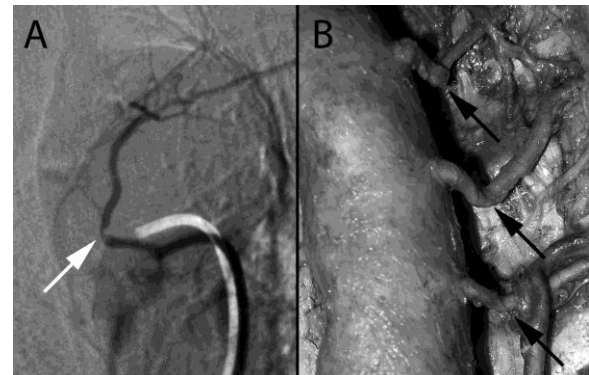
#### MATERIALS & METHODS

Radiologic data: Thoracic ISA were investigated in 56 consecutive diagnostic spinal angiograms performed during an 11-month period. Patients were divided in two groups for subsequent analysis according to the presence or absence of the studied anomaly. Thoracic contributions to the anterior spinal artery (ASA) also were recorded. Anatomical data: The topographic relationships of the upper thoracic ISA with surrounding structures were investigated in three cadavers.

#### RESULTS

Radiologic data: Forty-nine angiograms with complete bilateral documentation of the thoracic ISA were included. One or more kinks were found in 13 patients (26.5%). All involved arteries were on the left side, with the following distribution: T2 = 9%, T3 = 14%, T4 = 18%, T5 = 32%, T6 = 9%, T7 = 14%, T8 = 4%. One or

more ASA contributors were documented at corresponding levels (left T2 to T8) in 22 of 36 patients without kinks (61.1%), and six of 13 patients with kinks (46.2%). While not statistically significant, this trend might indicate a tendency for patients with kinks to have a lower number of functional ASA contributors at the upper thoracic level. No significant difference in gender or age was found between the two groups. In one patient, a 32-year-old woman investigated for acute left leg paralysis and incontinence suggestive of a spinal stroke, a prominent ASA contributor originating from a severely kinked left T4 ISA was opacified through collaterals only. Anatomical data: Upper ISA kinks were documented on the left side of all specimens. The kinked segments, located along the dorsal aspect of the aortic wall, were visible only after gentle dextroversion of the aorta (Figure 1B, black arrows, after dissection of the endothoracic fascia); the kinks appeared related to the recurrent course of the upper thoracic ISA, due in large part to the leftward position of the aorta at this level, accentuated by the passage of these arteries behind longitudinal strands of reinforced connective tissue within the endothoracic fascia.



#### CONCLUSION

Proximal kinks of upper left thoracic ISA frequently noted on SpDSA appear to be linked to the recurrent course of these arteries and their passage behind connective reinforcements within the endothoracic fascia. The frequent presence of ASA contributors at corresponding levels suggests a possible etiology for thoracic ischemic myelopathy.

**KEY WORDS:** Spinal angiography, spinal vascular disorders, spinal stroke

**O-406**

**3:48 PM - 3:56 PM**

#### Molecular Imaging Detects Impairment in the Retrograde Axonal Transport Mechanism after Radiation Injury

Bredow, S.•LeRoux, L.•Grosshans, D.•Schellingerhout, D.

M.D. Anderson Cancer Center  
Houston, TX

#### PURPOSE

The goal of this study was to determine whether molecular imaging is a suitable technique to detect changes in the spinal cord in response to radiation injury.

## MATERIALS & METHODS

The lower thoracic spinal cord of adult female BALB/c mice was irradiated with single doses of 2, 10, and 80 Gy. An optical imaging method utilizing the fluorescently labeled nontoxic C-fragment of tetanus toxin (TTc) was used to evaluate changes in the retrograde axonal transport mechanism, while Luxol fast blue staining served to assess demyelination in radiated cords.

## RESULTS

Transport of TTc in the thoracic spinal cord was impaired in a dose-dependent manner as early as 2 days after radiation. Transport was decreased significantly by 16 d in animals exposed to either 10 or 80, while animals exposed to 2 Gy remained unaffected. Further, animals exposed to the highest dose also experienced significant weight loss by 9 d and developed posterior paralysis by 45 d. Demyelination in radiated cords could be observed after 30 d in mice exposed to 80 Gy.

## CONCLUSION

Radiation of the spinal cord induces dose-dependent changes in the axonal transport mechanism which can be monitored by molecular imaging. This approach suggests a novel diagnostic modality to assess nerve injury and monitor therapeutic interventions.

**KEY WORDS:** Molecular imaging, radiation toxicity, neurography

O-407

3:56 PM - 4:04 PM

## Diffusion-Weighted MR Imaging "Claw Sign" Is Useful in Differentiation of Infectious from Degenerative Modic I Signal Changes of the Spine

Poplawski, M. M.·Pawha, P. S.·Delman, B. N.·Naidich, T. P.·Tanenbaum, L. N.

Mount Sinai School of Medicine  
New York, NY

## PURPOSE

Modic signal changes, a common observation in MR imaging, are signal intensity findings in vertebral body marrow adjacent to endplates of degenerative disks. Type I Modic change is more likely to be clinically symptomatic and is characterized by decreased signal on T1-weighted imaging and increased signal on T2-weighted imaging, that can be difficult to differentiate from and often suggestive of vertebral osteomyelitis and diskitis. Of late, diffusion-weighted MR imaging (DWI) has been shown to be a useful tool in imaging of osseous and epidural spinal lesions, including spinal infection. In this retrospective observational study of patients who were referred for spinal MRI, we characterize and correlate the MRI appearance of spinal levels in patients with Modic I signal changes, and in patients with confirmed spinal infection, with particular attention to the presence or absence of the DWI "claw sign".

## MATERIALS & METHODS

Seventy-four patients with Modic I type endplate abnormalities were selected and classified into three groups: clinically confirmed diskitis/osteomyelitis (n = 21), degenerative Modic I change (n = 33), and suggestive of infection but clinically disproved (n = 20). Each abnormal spinal level was blindly and independently evaluated by two neuroradiologists in terms of MR endplate and disk signal changes, enhancement, and appearance on DWI (b value of 500 s/mm<sup>2</sup>). The presence of diffusion "claw sign" was scored on a scale of 1 = definite, 2 = probable, 3 = questionable, 4 = absent (diffuse DWI signal).

## RESULTS

Type I changes in the absence of infection invariably correlated with a characteristic DWI "claw sign" of high diffusion signal at the boundary of the active marrow process and the normal marrow, while patients with type I Modic signal and confirmed spondylodiskitis exhibited significant absence of the "claw sign" (average "claw" scores by neuroradiologist #1 of  $1.21 \pm 0.07$  vs  $3.67 \pm 0.17$ ,  $p < 0.01$ ; neuroradiologist #2:  $1.58 \pm 0.14$  vs  $3.52 \pm 0.16$ ,  $p < 0.01$ ). Similarly, the group in which infection was suggested initially, but subsequently discounted, had an average score in independent reads of  $1.45 \pm 0.13$  and  $1.70 \pm 0.18$ . Suggestion of infection seemed to be related to the presence of high T2 signal in the disk space, which in this study had a high sensitivity, but low specificity for infection. On the other hand, absence of the "claw sign" (combined score 3 and 4) had a high sensitivity (86-90%), specificity (85-98%) and predictive values for infection.

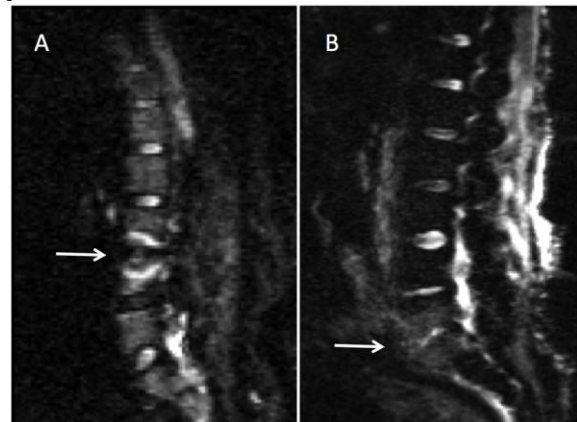


Fig. Diffusion-weighted imaging (DWI) of the spine showing characteristic "claw sign" of restricted diffusion in a 52yo patient with Modic I degenerative change (A), and absence of the "claw sign" with diffuse DWI signal in a 55yo patient with osteomyelitis. Both studies showed similar type I pattern with low T1WI and high T2WI.

## CONCLUSION

Diffusion-weighted imaging offers powerful characterization information in patients with Type I Modic MR signal changes and assists in the differentiation of degenerative disease from spondylodiskitis of the spine.

**KEY WORDS:** diffusion-weighted imaging, spine, infection

**O-408****4:04 PM - 4:12 PM**

### **HIV Positive Adults Presenting with Acute Myelopathy or Cauda Equina Syndrome: A 4-Year Retrospective Review of MR Imaging Findings with Clinical, Biochemical and Pathologic Correlation**

Candy, S. E. • Macingwane, N. • Chang, G.

Groote Schuur Hospital  
Cape Town, SOUTH AFRICA

#### **PURPOSE**

Cape Town is the center of an HIV tuberculosis co-epidemic. Spinal involvement with paraplegia and loss of sphincter function is a dreaded complication. This presentation reviews the MRI and clinicopathologic findings of HIV positive adults with acute myelopathy or cauda equina symptoms at our hospital over a 4-year period, 2008 - 2011.

#### **MATERIALS & METHODS**

Two hundred sixteen cases were identified from hospital records. The MR imaging, CD4 count, cerebrospinal fluid (CSF) analysis and pathology reports were correlated.

#### **RESULTS**

The majority were HAART naive. Mean age at presentation was 37.1 years and 58% were female reflecting population prevalence. Median CD4 count at presentation was 185 cells/ul. 30% (n = 65) had MR features of TB osteitis and in this group TB was confirmed either on biopsy or CSF analysis in 88% of those tested (n = 51). The median CD4 count was higher in patients with osteitis than in the remainder: 225 (range 117-397) vs 147 (range 56-274) p = 0.0017. The involved spinal level followed the expected distribution described in immune competent patients (62% thoracolumbar, 18% lumbosacral, 20% cervicothoracic). Of the 151 osteitis negative cases (70%), 42% had MR features of infective/inflammatory arachnoiditis (thickened, enhancing nerve roots, leptomeningeal or loculated enhancement of the CSF, abnormal CSF signal), mostly in association with long segment cord signal abnormality on T2-weighted imaging. In this group for whom either CSF or biopsy results were available, 47% had proven TB. CMV (n = 2), Herpes Zoster (n = 2) and Cryptococcal antibodies (n = 2) were present in the CSF of a further six cases. Eight patients, two of whom met the criteria for TB IRIS (immune reconstitution inflammatory syndrome) had enhancing intramedullary lesions. Another 11 had HIV associated tumors (9 lymphoma, 1 angioleiomyoma and 1 myopericytoma). Only 12 patients had causes incidental to their immune status (7 acute disk herniations, 3 plasmacytoma/myeloma, 3 vertebral metastases and 2 cystic cord lesions). Even where there was no discernible MR abnormality 30% of those tested had CSF proof of TB.

#### **CONCLUSION**

This study represents the largest reported series of clinical cord/cauda equina compression in HIV positive adults imaged with MRI. In our setting tuberculosis is

the most common etiologic agent with infectious arachnoiditis (often without clinical evidence of meningitis) being more common than osteitis and associated with a lower CD4 count. Lymphoma was found to be relatively uncommon. Unusual HIV-associated tumors were rare. Although nonspecific inflammatory myelitis is represented almost certainly in our group, the threat of exacerbation of an underlying infection cautions against the empiric use of steroids.

**KEY WORDS:** HIV spine, myelopathy, tuberculosis

**O-409****4:12 PM - 4:20 PM**

### **Diagnosis of Early Sacroiliitis in Seronegative Spondylarthropathies by Diffusion-Weighted Imaging and Correlation of Clinical and Laboratory Findings with Apparent Diffusion Coefficient Values**

Gezmis, E. • Donmez, F. Y. • Kural, F. • Agildere, M.

Baskent University  
Ankara, TURKEY

#### **PURPOSE**

Seronegative spondylarthropathies (SpA) are a group of diseases affecting the axial skeleton predominantly. Sacroiliitis is one of the diagnostic criteria of seronegative SpA. Differentiating inflammatory low back pain from mechanical pain clinically is challenging in most of the cases; even ESSG (European SpA Study Group), modified New York and ASAS (Assessment of Spondylarthropathy International Society) criteria may not be sufficient for early diagnosis of the disease; therefore imaging gains importance. Diffusion-weighted imaging (DWI) promises to show the microscopical movement of the molecules, which may help the routine sequences to evaluate the medullary signal changes. The purpose of our study is to show the signal characteristics of the sacral and iliac surfaces by DWI which may contribute in early diagnosis of the disease and investigate the correlation between the apparent diffusion coefficient (ADC) values and clinical and laboratory parameters (enthesitis, arthritis, sedimentation and CRP).

#### **MATERIALS & METHODS**

Sixty-two patients (35 female, 27 male; aged 16-62 years) with inflammatory low back pain, with a history or suspect of seronegative SpA admitted to our department between May 2010 and August 2011 are enrolled into the study.

Forty age- and sex-matched subjects whose pain was not of inflammatory type, with no laboratory or clinical findings compatible with seronegative spondylarthropathy constituted the control group. MR studies were done on a 1.5 T unit, with a body coil. After routine T1-weighted, T2-weighted and STIR sequences, DWI was obtained at b values of 50, 400 and 800, in the coronal oblique plane. Apparent diffusion coefficient values at three points (upper, middle, lower) on both surfaces of the both sacroiliac joints (total of 12 points) were measured in all 102 subjects. Also ADC values of the areas, showing pathologic signal intensity were measured and compared with the ADC values of the

control group. The CRP and sedimentation results of the patients at the time of MRI study and the presence or absence of arthritis and enthesitis also were correlated with the ADC values.

#### RESULTS

Only in 11 patients, there was a visible signal change consistent with edema on DWI. Apparent diffusion coefficient values at the upper, middle and lower points of both surfaces of the both sacroiliac joints were found  $0.23 \times 10^{-3} \text{ mm}^2/\text{sn}$  in the control group. In the patient group, mean ADC value of  $0.48 \times 10^{-3} \text{ mm}^2/\text{sn}$  was obtained, which was statistically significant, compatible with the increased diffusion due to medullary edema in the early sacroiliitis. Therefore, although there were no signal changes, ADC measurements showed sacroiliitis in 51 patients. The ADC values obtained from the edema areas were found more significantly higher than the ADC values of the control group. There was a slight correlation between CRP and ADC values; presumed to be showing the relation between the activity of the disease and the active inflammation on DWI. There was no correlation between arthritis and enthesitis and the ADC values. There was neither no correlation between the sedimentation rates and the ADC values.

#### CONCLUSION

Diffusion-weighted imaging, by measuring ADC values, adds significant information in the early diagnosis of sacroiliitis and may help to evaluate the efficiency of the treatment.

**KEY WORDS:** Sacroiliitis, diffusion-weighted imaging, spondylarthropathy

**O-410**

**4:20 PM - 4:28 PM**

#### Image-Guided Percutaneous Disk Sampling: Impact of Antecedent Antibiotics on Yield

Agarwal, V.·Delfyett, W. T.·Tsay, J.

University of Pittsburgh Medical Center  
Pittsburgh, PA

#### PURPOSE

Diskitis/osteomyelitis accounts for 2-4% of all bone infections. An aging population, higher numbers of immunocompromised patients, and increasing use of intravascular devices may all contribute to possibly rising incidence. Given the often insidious onset of pain, when suspected, prompt initiation of therapy is encouraged. A variety of blood tests and cultures are performed routinely, but lack negative predictive value. Considering the overlap in the imaging appearance of infectious and noninfectious conditions, both of which can cause back pain, percutaneous disk space sampling frequently is requested. The purpose of this study is to evaluate the effect of antecedent antimicrobial therapy on diagnostic yield from percutaneous disk space sampling.

#### MATERIALS & METHODS

An IRB-approved, HIPAA compliant, retrospective review of the electronic health records of all patients

who have undergone image-guided percutaneous sampling procedures for suspected diskitis/osteomyelitis in the last 5 years at our institution was performed. A total of 134 patients were identified. Demographics, medical history and culture results were recorded as well as duration of presenting symptoms and whether antecedent antibiotic therapy had been administered.

#### RESULTS

Of the 134 patients identified who underwent percutaneous disk space sampling, 74 had received antecedent antibiotic treatment compared with 50. The positive culture rate from patients previously on antibiotics was 20% ( $n = 15$ ) compared with 30% ( $n = 15$ ) for patients who had not received prior antibiotic treatment. The overall positive culture rate for our study population was 22% ( $n = 30$ ).

#### CONCLUSION

Antecedent antibiotic therapy did not result in diminished diagnostic yield from percutaneous sampling of suspected diskitis/osteomyelitis. Given similar diagnostic yields, percutaneous sampling may be warranted despite presence of antecedent therapy, allowing for optimal tailoring of the therapeutic regimen. A hallmark of antibiotic management is to withhold therapy until cultures have been obtained. Our results suggest that delaying initiation of therapy may not be warranted; nonetheless, individual clinical scenarios and careful consideration of antimicrobial resistance remain important parts of the decision-making process.

**KEY WORDS:** Diskitis, osteomyelitis, biopsy

**O-411**

**4:28 PM - 4:36 PM**

#### Role of MR Imaging of the Sciatic Nerves in Diagnosis of Peripheral Noncompressive Sciatic Neuropathy

Naeini, R. M.·Brian, S.·Dillon, W. P.·Chin, C. T.

University of California at San Francisco  
San Francisco, CA

#### PURPOSE

The most common etiology of sciatica is compression and entrapment of the nerve by herniated disk or foraminal stenosis. High-resolution MRI of the peripheral nerves allows us to detect peripheral neuropathy in a variety of other etiologies including infectious, inflammatory, and toxic causes. These conditions have not been described extensively in the radiographic literature. The purpose is to describe abnormal findings on MRI of the sciatic nerves in patients with noncompressive sciatic neuropathy.

#### MATERIALS & METHODS

Retrospective review of patients (2003-2010) diagnosed with sciatic neuropathy without evidence of sciatic nerve compression on conventional spine imaging who were referred for MRI of the sciatic nerves by neurologists and surgeons. We assessed patient

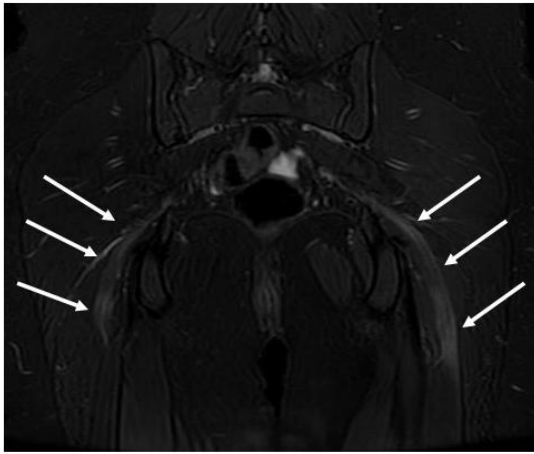


demographics, signal changes on MRI, distribution of nerve involvement and correlated with clinical and EMG findings. MRI: Coronal and axial inversion recovery sequences of the sciatic nerves; axial and coronal T1 fatsaturated postgadolinium in selected patients. (1.5 T magnet TR 2530 TE 20 TI 160 3/3.5 mm FOV 34 NEX 3).

## RESULTS

Eight patients, 4M, 4F; 19-81 years old (mean 42.1) had MRI of sciatic nerves. All eight patients had increased T2 signal within the sciatic nerves. Additional roots involved included the L5 nerve root (all patients) followed by less commonly S1, L4, L3 and S2. Etiologies included infection (Herpes, HIV, MRSA bactremia); inflammatory (systemic lupus erythematosus); toxins (heroin- and alcohol-induced neuropathy); and trauma/surgery. The five patients who underwent electrodiagnostic testing had corresponding abnormal EMGs. The one patient who underwent nerve biopsy demonstrated intraneural vasculitis.

Patient/Age/Sex	Clinical Diagnosis	Involved Nerve Roots, Short segment (<5cm) or Long segment(>5cm)	EMG/Biopsy	Enhancement if gadolinium was given
1 19/F	SLE peripheral neuropathy	Bilateral Sciatic (Long segment) Bilateral Femoral nerves (Long segment)	Severe axonal and motor polyneuropathy	N/A
2 28/F	Heroin Induced neuropathy	Bilateral Sciatic nerves (Long segment)	Acute demyelination polyneuropathy	N/A
3 33/M	Alcohol induced chemical neuritis	Left L5-S2 nerves (Long segment)	Acute denervation by dorsal ganglia involvement	Lack of enhancement of Left L5 through S2 nerves
4 81/ F	Post surgical neuropathy	Right L4-S1 and Left L3-L4 nerves (Short segment)	Chronic active right L5 and left L3-L4 radiculopathy	N/A
5 60/ M	Inflammatory neuropathy, likely flu vaccine related	Right L4 and L5 nerves (Short segment)	Chronic denervation and reinnervation in vastus medialis muscle supplied by the right L4 nerve root	Enhancement of extraforaminal segments of right L4 and L5 nerve roots
6 49/ M	Varicella Zoster neuropathy	Right L5 nerve (Long segment)	No EMG	N/A
7 20/ F	Necrotizing pancreatitis and MRSA bacteremia	Bilateral sciatic nerves (Long segment)	No Sural nerve biopsy consistent with leukocytoclastic vasculitis	No Enhancement
8 47/ M	HIV related neuropathy	Bilateral sciatic nerves and L5 and S1 nerve roots (Long segment)	No EMG	N/A



Coronal STIR demonstrates abnormal patchy segmental T2 signal abnormality in bilateral sciatic nerves (arrows) in a patient with Heroin induced neuropathy.

#### CONCLUSION

Patients with clinical symptoms of sciatica and no nerve compression on conventional imaging can present a diagnostic dilemma. Inflammatory, infectious and toxic injury to peripheral nerves can result in symptoms of sciatica and abnormal T2 hyperintensity on MRI. These radiographic findings have not been described previously. MR imaging of the sciatic nerves can play an important role not only to confirm clinically suspected neuropathy, but also to demonstrate the extent of abnormality.

**KEY WORDS:** Sciatic nerve, peripheral neuropathy, MR imaging

## Wednesday Afternoon

**3:00 PM - 4:30 PM**

**Beekman/Sutton North**

**(53c) Interventional: Aneurysms I**

**0-412**

**3:00 PM - 3:08 PM**

**Cerecyte Coil Trial: Angiographic and Clinical Outcomes of Endovascular Coiling in Patients with Ruptured and Unruptured Intracranial Aneurysms Treated with Cerecyte Coils Compared with Bare Platinum Coils - Final Results of a Prospective Randomized Trial**

Molyneux, A. J.<sup>1</sup>•Fox, A.<sup>2</sup>•Sneade, M.<sup>1</sup>•Clarke, A.<sup>1</sup>•Mehta, Z.<sup>1</sup>•Coley, S.<sup>3</sup>

<sup>1</sup>Oxford University, Oxford, UNITED KINGDOM,

<sup>2</sup>Sunybrook Health Sciences, Toronto, ON, CANADA,

<sup>3</sup>Royal Hallamshire Hospital, Sheffield, UNITED KINGDOM

#### PURPOSE

To report the angiographic and clinical outcomes of the Cerecyte Coil trial.

#### MATERIALS & METHODS

Four hundred ninety-seven patients were randomized and eligible for analysis, in 23 centers worldwide. Two hundred sixty-three patients were treated for a previously unruptured aneurysm (UIA) and 234 with a recently ruptured aneurysm (RA) who were in Grade 1 or 2 after SAH. The primary objective of the trial was to determine whether Cerecyte polymer-loaded coils improved the proportion of patients with angiographic occlusion of the aneurysm. The secondary objectives were to compare the clinical outcomes and retreatment rates in the two groups. Analysis was by intention to treat.

#### RESULTS

Four hundred eighty-one patients underwent coil treatment of their aneurysm: 227 patients with recently ruptured aneurysms RA and 254 with UIA. Four hundred thirty-three follow-up angiograms were assessed by the Core lab, there was no significant difference between the groups, 127 of 215 (59%) and 118 of 218 (54%) in the Cerecyte and bare platinum groups respectively ( $p = 0.17$ ), fulfilled the definition of success. Late retreatment was performed in 25 of 452 (5.5%) patients with follow-up angiography between 4 and 34 months, 17 (7.7%), 8 (3.5%) in the Cerecyte and bare platinum groups respectively ( $p = 0.064$ , nonsignificant). The clinical outcomes did not differ between the groups. At 6 months patients with RA 213/221 (96%) had a modified Rankin  $\leq 2$ , and 237/242 (98%) with UIA. There was one late rebleed in the RA group at 4 months.

#### CONCLUSION

There was no significant difference in the angiographic outcomes between the coil types. The clinical outcomes are better than any previously reported randomized trials.

**KEY WORDS:** Aneurysm, coiling, randomized trial

**0-413**

**3:08 PM - 3:16 PM**

**Buenos Aires Experience with the Pipeline Embolization Device for the Treatment of Complex Intracranial Aneurysms: Safety, Efficacy and Long-Term Follow Up**

Lylyk, P.•Ferrario, A.•Ceratto, R.•Scrivano, E.•Lundquist, J.•Nella Castro, R.•Bleise, C.•Chudyk, J.

ENERI

Buenos Aires, ARGENTINA

#### PURPOSE

Hemodynamic flow is considered to be one of the major factors in the progression and rupture of intracranial aneurysms. Flow diverter devices reduce blood flow in the aneurysm sac, allow gradual stagnation, thrombosis and neointimal remodeling while maintain outflow in the side branches and perforators. Also, enable us to

treat complex intracranial aneurysms. The purpose is to present our experience and long term follow up in endovascular reconstruction of complex intracranial aneurysms using a flow diverter device Pipeline (PED).

#### **MATERIALS & METHODS**

Since March 2006 to January 2011, 272 patients with 330 intracranial aneurysms were treated with 506 devices. Subjects were included if they had wide-neck intracranial aneurysm (neck of  $>4$  mm or dome/neck ratio of  $\geq 1.5$ ) or previous failure endovascular treatment attempts of intracranial aneurysm.

#### **RESULTS**

All patients received dual platelet antiaggregation before and for a 6-months period. Angiographic follow up was performed at 3, 6, 12 months and 2, 3 and 4 years. Seventy-eight percent of the patients were female; mean age was 55 years; 78% were symptomatic due to: mass effect, 32%; subarachnoid hemorrhage, 27%; headache, 14%; others, 27%. A total of 437 PED were implanted and procedural success was 98%; 19% had previous treatment (clipping, coiling and/or stenting); anterior circulation aneurysms, 85%. Technical complications were presented in 7%: stent partially opened, 10 patients; undelivered stent, 6 patients; micro-wire complications, 4 patients; others, 11 patients. Peri-procedure (30 days) related adverse events were 4.4%: 2.6% had transient or definitive neurologic defects; death rate, 1.8%. One-year aneurysm angiographic occlusion rates were 90.5% (124 of 137 patients); 2-year, 94.3% (66 of 70 patients); 3-4-year, 100% (19 patients).

#### **CONCLUSION**

Endovascular treatment of complex intracranial aneurysms with PED is a safe and effective procedure, with an acceptable morbi-mortality rate. Serial angiographic follow up showed gradually occlusion, with total occlusion at 3-4 years. To our knowledge, this is the largest angiographic follow up of this type of devices. The PED represents a promising new endovascular technology for the treatment of cerebral aneurysms.

**KEY WORDS:** Intracranial aneurysm, flow diverter, pipeline embolization device

**O-414**

**3:16 PM - 3:24 PM**

#### **SILK Arterial Reconstruction in 87 Intracranial Aneurysms on 76 Patients**

Korkmazer, B.<sup>1</sup>Kizilkilic, O.<sup>1</sup>Velioglu, M.<sup>2</sup>Kocak, B.<sup>1</sup>Tureci, E.<sup>1</sup>Islak, C.<sup>1</sup>Kocer, N.<sup>1</sup>

<sup>1</sup>Cerrahpasa Medical School, Istanbul, TURKEY, <sup>2</sup>GATA Haydarpasa Training Hospital, Istanbul, TURKEY

#### **PURPOSE**

Endovascular treatment is currently the method of choice for intracranial aneurysms. One of the major concerns is recurrence after treatment; especially for the large, wide-necked saccular aneurysms and fusiform aneurysms. The advent of flow diverter

technology has provided new instruments for the treatment of these complex aneurysms. Flow diverter stents aim to reconstruct the vessel wall and to create hemodynamic changes that induce progressive aneurysm thrombosis. There are currently two commercially available flow diverters, the Pipeline Embolization Device (EV3, Irvine California) and SILK Flow Diverter stent (Balt, Montmorency, France). The aim of this study is to report our experience in 76 consecutive patients with 87 intracranial aneurysms treated with SILK stents.

#### **MATERIALS & METHODS**

Seventy-six patients (age range, 24-74 years; average age, 47.9 years; 58 female), whose aneurysms were not eligible for conventional endovascular techniques or surgery, were treated with SILK stent in the last 3.5 years. Fifty-two (59.7%) of the aneurysms were carotid-ophtalmic aneurysms and 18 (20.6%) were cavernous ICA aneurysms. There were totally 11 supraclinoid aneurysms, one cervical ICA aneurysm and one middle cerebral artery aneurysm. There were only four posterior circulation aneurysms in our series (4.6%). Mean aneurysm size was 15.1 mm (range, 1.3 mm - 50 mm). Except three patients who presented with subarachnoid hemorrhage, all patients were pretreated with dual antiplatelet medications for at least 5 days before surgery and continued taking both agents for at least 3 months after treatment. Occlusion rates in angiographic follow-up were analyzed by using the grading schema which was described by Kamran et al.

#### **RESULTS**

The SILK stents were placed in a proper position across the whole length of the aneurysm neck in all patients. Overall mortality rate was 6.6%. There were three (3.9%) transient morbidity and two (2.6%) permanent morbidities due to embolic events. Immediate angiographic results at the end of the endovascular treatment included 13 complete occlusions (Grade IV), 11 Grade III occlusions, 17 Grade II occlusions, 32 Grade I occlusions and 14 with no changes in the sac filling (Grade 0). Control angiographic studies were performed in 60 patients with 69 aneurysms (84.5%). Overall control angiographic occlusion rates were; 81.1% (56/69) Kamran Grade IV, 15.9% (11/69) Grade III and 2.9% (2/69) Grade II.

#### **CONCLUSION**

As a flow diverter, despite deployment difficulties and early/delayed complications, SILK stent can be used in challenging aneurysms which have previously higher regrowth rates with conventional endovascular treatment.

**KEY WORDS:** SILK stent, flow diverter stents, aneurysm

**O-415****3:24 PM - 3:32 PM****Initial Experience with "Woven Endobridge" at ENERI for the Treatment of Terminal Aneurysms**

Lylyk, P.·Ceratto, R.·Ferrario, A.·Lundquist, J.·Scrivano, E.·Nella, R.·Chudyk, J.·Bleise, C.

ENERI

Buenos Aires, ARGENTINA

**PURPOSE**

Endovascular reconstruction with endoprosthesis such as flow diverters produces a very low rate of aneurysm recanalization with a high recovery outcome compared with endosaccular coiling, although the use of antiplatelet agents in the acute stage of hemorrhage and lateral aneurysms carries the risk of side branch occlusion and represents a limitation to this method. The WEB device "Woven Endobridge" (Sequent Medical, Aliso Viejo, California) is intended as a new alternative in the treatment of terminal and bifurcation aneurysms. Our purpose is to present our initial experience with the WEB device.

**MATERIALS & METHODS**

Between May 2009 and May 2010, seven patients with lateral, terminal, cerebral aneurysms, either ruptured or unruptured, were treated. Clinical and angiographic controls were performed during 39 months at an average 19-month schedule.

**RESULTS**

Seven patients with eight aneurysms were treated (4 women, 38-75 years, median age 50). Seven aneurysms were incidental, all were small in size, and five located at the internal carotid artery. Five aneurysms were treated successfully with the WEB device, observing complete occlusion at 3-month follow up in three cases. Two patients died due to unrelated events with the endovascular procedure.

**CONCLUSION**

The WEB device is an alternative for the treatment of lateral and bifurcation aneurysms, especially in the acute stage of SAH, although more studies, more cases and longer follow-up periods are needed in order to test safety and assess recanalization.

**KEY WORDS:** Aneurysms, web endoprosthesis, sequent device

**O-416****3:32 PM - 3:40 PM****Development of Quantifiable Indices of Time-Contrast Curves to Assess the Hemodynamic Effect of Flow Diverting Devices: A Feasibility Study in the Rabbit Elastase Aneurysm Model**

Struffert, T.<sup>1</sup>·Ott, S.<sup>1</sup>·Kowarschik, M.<sup>2</sup>·Bender, F.<sup>2</sup>·Adamek, E.<sup>1</sup>·Doerfler, A.<sup>1</sup>

<sup>1</sup>University Erlangen-Nuremberg, Erlangen, GERMANY, <sup>2</sup>Siemens AG, Healthcare Sector, Forchheim, GERMANY.

**PURPOSE**

Flow diverters (FD) are used increasingly to treat aneurysms. An objective method to measure the hemodynamic effect of a FD is desirable.

**MATERIALS & METHODS**

In 10 rabbits aneurysms (elastase model) were induced and treated with a FD (n = 5, Pipeline) or a conventional stent (n = 3, Neuroform). Two animals served as controls. Before and after implantation, angiography series were obtained with 30 frames per second. Applying a new software for the analysis of DSA series (prototype development of syngo iFlow, Siemens AG, Healthcare Sector, Forchheim) time-contrast curves of the contrast in/outflow of the aneurysm were created. Time to peak (TTP, maximum contrast within the aneurysm), the full width at half maximum (FWHM) and the average slope of the curve (contrast density alteration/time) to represent the in and outflow (IF, OF) was calculated.

**RESULTS**

The mean values before treatment were TTP = 0.6 sec, HTCD = 0.9 sec, IF = 216.1 and OF = 81.5. After FD treatment, the TTP of 1.4 sec and FWHM of 14.6 sec were extended. The IF was 60.7 and the OF was 6.2 and therefore delayed. The values after stent treatment (TTP = 0.6 sec, FWHM = 0.8 sec, IF = 198, AOF = 81.3) did not differ from the values of all animals before therapy. After 6 months, all aneurysms of the FD group were occluded. The aneurysms of the stent and control group were still perfused.

**CONCLUSION**

Using prototype software for analysis of DSA series it was feasible to create time-contrast curves. Parameters to measure the hemodynamic efficacy of endovascular implants could be calculated. The presented parameters could possibly serve as predictive markers.

**KEY WORDS:** Flow diverter, hemodynamic effect, quantifiable indices

**O-417****3:40 PM - 3:48 PM****Does Balloon Assistance in Intraprocedural Aneurysmal Rupture During Coil Embolization of Brain Aneurysms Influence Outcome?**

Gobin, Y. P.·Santillan, A.·Greenberg, E.·Leng, L. Z.·Stieg, P. E.·Patsalides, A.

New York Presbyterian Hospital-Weill Medical College of Cornell University  
New York, NY

**PURPOSE**

Intraprocedural aneurysmal rupture (IAR) is a feared complication of coil embolization of intracranial aneurysms and is associated with high rates of morbidity and mortality. We report the incidence, endovascular management, and clinical outcome of patients with IAR, with emphasis on the role of the balloon assisted coiling.

**MATERIALS & METHODS**

We conducted a retrospective analysis of all intracranial aneurysms treated by coil embolization between September 2001 and June 2011. All patients with IAR were studied. Comparison of immediate clinical outcomes was performed using univariate analysis (Fisher's test).

#### RESULTS

Of 652 intracranial aneurysms treated with coil embolization, an IAR occurred in 22 (3.4%). Rupture occurred during placement of coils in 18 cases, microcatheters in 2 cases, guidewire in 1 case, and during induction of anesthesia in 1 case. Before treatment, 15 out of 22 (68%) patients were in good clinical condition (WFNS Grade 1). After IAR, the WFNS grade was either unchanged or improved for 12 out of 13 (92.3%) patients where balloon assistance was used and 4 out of 9 (44.4%) patients where it was not. Unchanged or improved clinical grades on the WFNS scale were significantly associated with the use of the balloon assisted technique in the setting of an IAR ( $p=0.023$ ). Death occurred in 2 (9.1%) patients.

#### CONCLUSION

When an aneurysm ruptures during coil embolization, balloon-assistance is helpful to obtain rapid hemostasis, which results in better outcome.

**KEY WORDS:** Balloon assistance, intraprocedural aneurysmal rupture, coil embolization

**O-418**

**3:48 PM - 3:56 PM**

Periprocedural Complications of Balloon-Assisted Coiling for Intracranial Aneurysms

Patsalides, A. Santillan, A. Mazura, J. Leng, L. Z. Riina, H. A. Gobin, Y. P.

New York Presbyterian Hospital-Weill Medical College of Cornell University  
New York, NY

#### PURPOSE

The balloon-assisted coiling (BAC) technique represents an effective tool for the treatment of intracranial aneurysms with unfavorable anatomy. Some studies however, showed increased incidence of adverse events with BAC compared to embolization with coils alone and the safety of this technique has generated a matter of debate. In this study, we provide our institutional experience regarding the safety of the BAC technique and we compare our results with the patients treated with coils alone.

#### MATERIALS & METHODS

We retrospectively reviewed 428 consecutive patients with 491 intracranial aneurysms (274 acutely ruptured and 217 unruptured) treated via the endovascular approach with BAC or coils alone. Patients who were treated with stent-assisted coiling were excluded from the analysis, even if the BAC technique was used initially. All procedure-related adverse events were reported, regardless of clinical outcome. Adverse events were separated into three categories: thromboembolic events, intraprocedural aneurysm rupture, and device-

related problems. A thromboembolic event was defined as parent vessel occlusion secondary to thrombus formation, a new filling defect in the parent vessel near the aneurysm neck, or a new filling defect in more distal branches in the vascular territory of the treated aneurysm. Intraprocedural aneurysm rupture was defined as violation of the aneurysmal sac by coil loops or the microcatheter, with or without associated contrast extravasation. Device-related problems included significant problems inability to navigate the microcatheter into the aneurysm neck, and coil migration after detachment. Clinical outcomes of any adverse event were classified as none, transient neurologic deficit, permanent neurologic deficit, and death. Procedure-related morbidity was defined as the presence of new permanent neurologic deficit, or the need to perform a repeat procedure (endovascular or surgical) attributed to any procedure-related complication. The incidence of adverse events, morbidity and mortality were compared between the BAC and coil alone groups.

#### RESULTS

Two hundred twenty-four patients with 236 aneurysms were treated with the remodeling technique and 204 patients with 255 aneurysms were treated with coils alone. Aneurysms among patients treated with coils alone were more likely to be acutely ruptured. The total rate of periprocedural adverse events was 9.6% (47/491 embolizations). Thromboembolic events, intraprocedural aneurysmal rupture, and device-related complications occurred in 2.4%, 3.9% and 3.3% procedures, respectively. The risk of thromboembolic events and device-related problems was similar between the BAC and coil alone groups. A trend towards a higher risk of intraprocedural aneurysm rupture was observed in the balloon-remodeling group but the difference was not statistically significant. The total cumulative morbidity and mortality for both groups was 2.6% (11/428 patients) and there was no statistically significant difference in the morbidity, mortality and cumulative morbidity and mortality rates between the two groups.

#### CONCLUSION

In our series of patients with acutely ruptured and unruptured aneurysms, the BAC technique allowed us to treat aneurysms with unfavorable anatomical characteristics without increasing the incidence of periprocedural complications.

**KEY WORDS:** Balloon assistance, periprocedural complication, coil embolization

**O-419**

**3:56 PM - 4:04 PM**

**Intraaneurysmal Flow Disruption: A New Approach for the Endovascular Treatment of Intracranial Aneurysms - Basic Concepts and Preliminary Clinical Experience**

Pierot, L.<sup>1</sup> Kadziolka, K.<sup>1</sup> Jiang, J.<sup>2</sup> Strother, C. M.<sup>2</sup>

<sup>1</sup>Hopital Maison-Blanche, Reims, FRANCE, <sup>2</sup>Methodist Hospital, Houston, TX



**PURPOSE**

Over several years, standard coiling is the first line approach for the treatment of intracranial aneurysms. However, this technique has some limitations, including treatment of wide-neck and large and giant aneurysms and recanalizations. Therefore, new techniques and devices are needed. The objective of intrasaccular flow disruption is the modification of aneurysmal flow by placing a device not in the parent vessel but in the aneurysm sac. Computational fluid dynamics, preclinical testing, and preliminary clinical experience are discussed.

**MATERIALS & METHODS**

Computational fluid dynamics (FLUENT) and preclinical testing (canine cross-over carotid bifurcation model) were used to develop an intrasaccular flow disrupter design, designated as WEB, for both unruptured and ruptured aneurysms. WEB is a self-expanding, oblate, braided nitinol mesh. The WEB implant is deployed -- or retrieved prior to detachment -- similar to endovascular coil systems through microcatheters with an internal diameter > 0.027". The detachment system is electrothermal and instantaneous. Clinically, four patients (4 females, age: 50-74 years) harboring unruptured aneurysms (basilar artery: 1, internal carotid artery: 1, anterior communicating artery: 1, and middle cerebral artery: 1) were treated between June and October 2011 using an intraaneurysmal flow-disrupter (WEB, Sequent, Aliso Viejo, CA). All procedures were performed under heparin discontinued 24 hours after the procedure. Premedication with clopidogrel was given to one patient as a stenting was not excluded. The remaining patients did not receive antiplatelet premedication. Per our standard coiling protocol, aspirin was given for 1 month after the procedure.

**RESULTS**

Based on computational fluid dynamic modeling and preclinical data, the selected intraaneurysmal design, WEB, demonstrated profound intraaneurysmal stasis within 30 min of device deployment. Clinically, the device was successfully deployed in all cases. No clinical complications were encountered. In one case, the device was not selected appropriately and was too small. Additional coiling was performed. In all cases, disruption of the intraaneurysmal flow was rapidly obtained. Midterm follow-up results are presented.

**CONCLUSION**

Intrasaccular flow disruption using WEB is a new way to treat some types of aneurysm, particularly wide-neck bifurcation aneurysms. This preliminary clinical experience shows the safety and efficacy of the device when used in appropriately selected cases.

**KEY WORDS:** Aneurysm, embolization

**O-420****4:04 PM - 4:12 PM****Delayed Ipsilateral Brain Parenchymal Hemorrhage after Aneurysm Treatment with Pipeline Stent**

Cruz, J.<sup>1</sup>·Chow, M.<sup>2</sup>·O'Kelly, C.<sup>2</sup>·Marotta, B.<sup>3</sup>·Spears, J.<sup>4</sup>·Montanera, W.<sup>4</sup>·Fiorella, D.<sup>5</sup>·Marotta, T. R.<sup>4</sup>

<sup>1</sup>University of Toronto, Toronto, ON, CANADA, <sup>2</sup>University of Alberta, Edmonton, AB, CANADA, <sup>3</sup>University of Sidney, Sidney, AUSTRALIA, <sup>4</sup>Saint Michael's Hospital, University of Toronto, Toronto, ON, CANADA, <sup>5</sup>Stony Brook University Medical Center, State University of New York, Stony Brook, NY

**PURPOSE**

The pipeline embolization device (PED) is a flow-diverting stent designed for the treatment of cerebral aneurysms. New unexpected complications recently have been published. We report four cases of delayed ipsilateral parenchymal hemorrhage (IPH) following technically successful treatment of anterior circulation aneurysms with PED.

**MATERIALS & METHODS**

Clinical and imaging data from all patients undergoing aneurysm treatment with the PED at two institutions were analyzed to assess the incidence of delayed parenchymal hemorrhage.

**RESULTS**

A total of 66 patients (47 anterior circulation) with cerebral aneurysms underwent treatment with PED between January 2008 and November of 2010. Four patients experienced delayed, peri-procedural, IPH. All hemorrhages occurred after treatment of anterior circulation aneurysms (8.5%). Aneurysm size was 5 - 21 mm. All IPHs were ipsilateral to the treated aneurysm (average 5.3 cm) and remote from the treated aneurysms. All procedures were technically successful and uncomplicated. All patients remained well during the immediate postoperative period. The hemorrhages became clinically evident 1-6 days after the procedure (average 2.3 days). Three patients presented with hemiplegia or hemiparesis, one patient presented with loss of consciousness. One patient fully recovered, one patient died, and two had persisting neurologic deficits.

**CONCLUSION**

Delayed, ipsilateral parenchymal hemorrhage may occur after the treatment of anterior circulation aneurysms with flow diverters. This complication appears independent of aneurysm size, and does not seem related to intraprocedural complications or solely attributable to dual antiplatelet therapy.

**KEY WORDS:** Pipeline embolization device, aneurysm, parenchymal hemorrhage

O-421

4:12 PM - 4:20 PM

### Diagnostic Yield of Catheter Angiography in Patients with Subarachnoid Hemorrhage and Negative Initial Noninvasive Neurovascular Examinations

Delgado Almandoz, J. E.·Crandall, B. M.·Fease, J. L.·Scholz, J. M.·Anderson, R. E.·Kadkhodayan, Y.·Tubman, D. E.

Abbott Northwestern Hospital  
Minneapolis, MN

#### PURPOSE

To determine the yield of catheter angiography for the detection of causative vascular lesions in patients with subarachnoid hemorrhage (SAH) who have a negative initial noninvasive neurovascular examination.

#### MATERIALS & METHODS

Between January 1st, 2006 and October 21st, 2011, we instituted a prospective protocol by which patients who presented to our institution with SAH and had a negative initial noninvasive neurovascular examination [CT or MR angiogram (CTA, MRA)] were examined with catheter angiography to detect causative vascular lesions. Two experienced neuroradiologists evaluated the NCCTs to determine the pattern of SAH (diffuse, perimesencephalic or peripheral) and the catheter angiograms to assess for the presence of a causative vascular lesion. All differences in reader interpretation were resolved by consensus.

#### RESULTS

Fifty-two patients were included in our study, with a mean age of 59 years (median 60 years, range 25-88 years). Twenty-seven patients were male (51.9%) and 25 female (48.1%). Thirty-one patients had diffuse SAH (59.6%), 12 peripheral SAH (23.1%) and nine perimesencephalic SAH (17.3%). The initial noninvasive neurovascular examination was a CTA in 44 patients (84.6%) and an MRA in eight patients (15.4%). A second catheter angiogram was performed in 31 patients (59.6%). Mean time interval between the initial noninvasive neurovascular examination and the first catheter angiogram was 0.8 days (median 1 day, range 0-7 days) and the second catheter angiogram was 11.9 days (median 8.0 days, range 2-69 days). Catheter angiography demonstrated a causative vascular lesion in five patients (9.6%), three of which had diffuse SAH (yield of 9.7%) and two had peripheral SAH (yield of 16.7%). Of note, one of the causative vascular lesions was identified in a second catheter angiogram performed 8 days after the CTA in a patient with diffuse SAH. The vascular lesions identified were two dural arteriovenous fistulas, one pial cerebellopontine angle arteriovenous malformation with a 2 mm feeding artery aneurysm located in the internal auditory canal (Figure), a 3 mm anterior communicating artery aneurysm, and one case of drug-induced vasculopathy in a patient with peripheral SAH. Two of the vascular lesions underwent endovascular embolization, one radiosurgery and one endovascular embolization followed by radiosurgery. In retrospect, the vascular

lesion could be seen in the initial noninvasive examination in two patients.



#### CONCLUSION

Catheter angiography is a valuable tool in the evaluation of patients with diffuse and peripheral SAH who have a negative initial noninvasive neurovascular examination, demonstrating a causative vascular lesion in 9.7% and 16.7% of patients, respectively.

**KEY WORDS:** Subarachnoid hemorrhage, angiogram, aneurysm

O-422

4:20 PM - 4:28 PM

### Size and Location of Ruptured Intracranial Aneurysms in a Consecutive Series of 612 Patients with Acute Subarachnoid Hemorrhage Treated at a Tertiary Referral Medical Center during a 16-Year Period

Delgado Almandoz, J. E.·Fease, J. L.·Crandall, B. M.·Kadkhodayan, Y.·Scholz, J. M.·Anderson, R. E.·Tubman, D. E.

Abbott Northwestern Hospital  
Minneapolis, MN

#### PURPOSE

To assess the size and location of ruptured intracranial aneurysms in patients with acute subarachnoid hemorrhage (SAH) treated with endovascular coil embolization over a 16-year period at a tertiary referral medical center.

#### MATERIALS & METHODS

We retrospectively reviewed the size and location of ruptured intracranial aneurysms in all patients that presented to our institution with acute SAH and underwent endovascular coil embolization from June 1st, 1995 until October 15th, 2011. The aneurysm location and maximum sac diameter were recorded

utilizing catheter angiography. In patients with multiple aneurysms, we recorded data for the aneurysm thought most likely to be responsible for the SAH based upon SAH distribution as well as maximum aneurysm size and morphology.

## RESULTS

During the study's time period, a total of 1,619 intracranial aneurysms underwent endovascular coil embolization at our institution. Of these, 612 (37.8%) ruptured aneurysms were treated emergently in 583 patients with SAH (389 females and 194 males, mean age 54.9 years, range 7-97 years). In 21 patients (3.6%), two or more intracranial aneurysms were treated emergently due to the inability to definitely identify the causative aneurysm. The most common ruptured aneurysm locations were anterior communicating (36.6%), posterior communicating (19.6%), middle cerebral (13.7%), internal carotid (11.4%) and basilar (7.8%) arteries. Mean ruptured aneurysm maximum sac diameter was 6.5 mm (range 1.6-42 mm, median 5.6 mm). Nearly half (48.9%) of the ruptured intracranial aneurysms treated at our institution had a maximum sac diameter  $\leq 5$  mm, including 72.7% of the anterior cerebral artery, 61.9% of the posterior inferior cerebellar artery and 58.5% of the anterior communicating artery aneurysms (Table). In our series, 375 (61.3%) of the ruptured intracranial aneurysms had a maximum diameter  $< 7$  mm and only 102 (16.7%) ruptured intracranial aneurysms were  $\geq 10$  mm in maximum diameter.

Ruptured Aneurysm Location Distribution by Maximum Aneurysm Diameter

Aneurysm Location:	$\leq 5$ mm	6-9 mm	$\geq 10$ mm	Total:
All:	299 (48.9%)	211 (34.4%)	102 (16.7%)	612
Anterior circulation:	207 (51.8%)	122 (30.5%)	71 (17.7%)	400
ACOM	131 (58.5%)	68 (30.4%)	25 (11.2%)	224
MCA	37 (44.0%)	25 (29.8%)	22 (26.2%)	84
ICA	23 (32.9%)	26 (37.1%)	21 (30.0%)	70
ACA	16 (72.7%)	3 (13.6%)	3 (13.6%)	22
Posterior circulation (including PCOM):	92 (43.4%)	89 (42%)	31 (14.6%)	212
PCOM	53 (44.2%)	56 (46.7%)	11 (9.2%)	120
Basilar	16 (33.3%)	17 (35.4%)	15 (31.3%)	48
PICA	13 (61.9%)	5 (23.8%)	3 (14.3%)	21
Vertebral	4 (40.0%)	5 (50.0%)	1 (10.0%)	10

PCA	3 (50.0%)	2 (33.3%)	1 (16.7%)	6
SCA	3 (60.0%)	2 (40.0%)	0 (0.0%)	5
AICA	0 (0.0%)	2 (100.0%)	0 (0.0%)	2

ACA: anterior cerebral artery; ACOM: anterior communicating artery; AICA: anterior inferior cerebellar artery; ICA: internal carotid artery; MCA: middle cerebral artery; PCA: posterior cerebral artery; PCOM: posterior communicating artery; PICA: posterior inferior cerebellar artery; SCA: superior cerebellar artery.

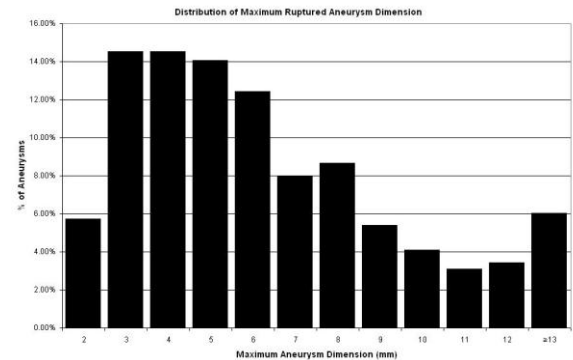


Figure. Maximum aneurysm dimension was measured in millimeters and rounded to the nearest whole number.

## CONCLUSION

The majority (61%) of ruptured intracranial aneurysms treated with endovascular coil embolization for acute SAH at our institution were  $< 7$  mm in maximum diameter and nearly half (48.9%) were  $\leq 5$  mm in maximum diameter. These findings suggest that the data from the ISUIA trial which reported that the risk of SAH from intracranial aneurysms  $< 7$  mm in size is very low should be interpreted with caution.

**KEY WORDS:** Subarachnoid hemorrhage, aneurysm

## Wednesday Afternoon

**3:00 PM - 4:30 PM**  
**Sutton Center/South**

(53d) Head & Neck: Other, New  
 Techniques & Temporal Bone

**O-423**

**3:00 PM - 3:08 PM**

**Vascular Washout Signature of Hypercellular/Adenomatous Parathyroid Lesions on 4D CT**

Ginat, D. T. Kelly, H. R. Hamberg, L. M. Hunter, G. J.

Massachusetts General Hospital  
 Boston, MA

## PURPOSE

The purpose of this study is to establish the vascular washout signature of abnormal parathyroid tissue in comparison with thyroid and lymph nodes on 4D CT

and to determine whether or not this technique can be used to differentiate abnormal parathyroid glands from other structures in the head and neck that potentially could be mistaken for diseased parathyroid tissue.

#### MATERIALS & METHODS

Informed consent was waived by the institutional review body for this retrospective, chart review study. Patients who had undergone 3-phase 4D CT for preoperative localization of parathyroid tissue with a biochemically proven diagnosis of sporadic primary hyperparathyroidism and who underwent pathology proven parathyroid tumor removal between March 1 and June 30, 2011 were evaluated. Patients with concomitant thyroid or lymph node disease, prior total thyroidectomy, or multiple endocrine neoplasia were excluded from the study. The 4D CT studies were all acquired using a GE 16-Slice Lightspeed scanner. Three phases were collected; precontrast baseline (PCB), an early vascular (EV) phase 30 seconds after commencement of injection of 100 ml of iopamidol 370 at 4 ml/sec into an antecubital vein, and a late vascular (LV) phase 30 seconds after the end of the EV phase. Regions of interest (ROI) were drawn over parathyroid lesions, normal-appearing thyroid, and lymph nodes on the PCB, EV and LV phases of the study. Visual anatomical coregistration was performed between each phase to ensure the same tissue was being evaluated at each time point. A percent washout (PW) was computed using the ROIs for each tissue for each phase, by applying the following equation:  $PW = 100 \times [(EV\ PCB) - (LV\ PCB)] / (EV\ PCB)$ . The null hypothesis tested was that "there is no difference in vascular washout signature between parathyroid lesions, normal thyroid tissue, and lymph nodes." A two-tailed Student's t-test with unequal variances was used. A value of  $P < 0.05$  was considered statistically significant.

#### RESULTS

There were 32 patients that met inclusion criteria. Hyperplastic/adenomatous parathyroid lesions demonstrated rapid washout of contrast with an average percent washout of 65.6% (95% CI: 5.4%), compared with thyroid tissue, which had an average percent washout of 44.2% (95% CI: 9.9%). Lymph nodes exhibited a distinctive pattern of continuous increase in enhancement over the three phases, with an average percent washout of -11.5% (95% CI: 17.7%). The null hypothesis was rejected with a significant difference in the percent washout between hyperplastic/adenomatous parathyroid lesions and thyroid tissue ( $P < 0.001$ ) and between parathyroid lesions and lymph nodes ( $P < 0.0001$ ).

#### CONCLUSION

The vascular dynamic signatures of abnormal parathyroid tissue, normal thyroid tissue, and lymph node tissue are statistically different from each other. This parameter is very useful in differentiating abnormal parathyroid lesions from other nodular head and neck structures that could mimic parathyroid adenoma/hyperplasia. Application of this test potentially could improve preoperative localization of target parathyroid lesions on 4D CT.

**KEY WORDS:** 4D CT, parathyroid, washout

**O-424**

**3:08 PM - 3:16 PM**

#### 4D CT for Primary Hyperparathyroidism: How Many Phases Do You Need?

Gafton, A. R. · Sze, G. · Jaba, I. M. · Carling, T. · Staib, L. · Mahajan, A.

Yale University School of Medicine  
New Haven, CT

#### PURPOSE

To assess the enhancement characteristics of parathyroid lesions on multiphase (4D CT) neck scans.

#### MATERIALS & METHODS

The study was based on a retrospective review of 13 pathologically confirmed parathyroid hormone (PTH)-secreting lesions detected on 4D CT exams in 13 patients between August 2010 and July 2011. Neck CT exams (from mandibular angle to aortic arch) were performed on a 64-MDCT scanner with a protocol consisting of noncontrast (phase 0) and three postcontrast phases (phase 1 at 30 seconds, phase 2 at 90 seconds and phase 3 at 210 seconds after contrast injection). Attenuation values (HU) were measured on axial CT images in all phases for parathyroid lesions, common carotid artery (CCA), and soft tissue (ST) structures including thyroid gland, lymph node, and submandibular gland. Three predictive indices were calculated: "relative enhancement washout percentage" by formula  $[(HU\ tissue\ phase\ 1 - HU\ tissue\ phase\ 2) / HU\ tissue\ phase\ 1] \times 100$ ; "tissue-CCA enhancement ratio" in all phases by formula  $(HU\ tissue / HU\ CCA)$ ; "relative arterial enhancement" by formula:  $[(HU\ tissue\ phase\ 1 - HU\ tissue\ phase\ 0) / HU\ tissue\ phase\ 0] \times 100$ . These calculated variables for parathyroid lesions were compared to those of other ST structures with Student t-test.

#### RESULTS

All parathyroid lesions were enlarged pathologically and cellular, benign-appearing parathyroid glands. The lesion locations were: right upper ectopic retroesophageal (2), right upper eutopic (1), right lower eutopic (5), left lower intrathyroid (1), left upper ectopic paraesophageal (1), left upper eutopic (1) and left lower eutopic (2). The mean relative enhancement washout percentage of parathyroid lesions (6.9%, sd 52.5) was significantly higher than that of lymph nodes (-68.7%, sd 39.1) ( $p < 0.009$ ) and submandibular gland (-102%, sd 54.5) ( $p < 0.0002$ ), but not significantly different from the thyroid (-14.5, sd 17.8) ( $p = 0.1$ ). The parathyroid lesion-CCA ratio in the arterial phase (0.5) was significantly higher compared to lymph nodes and submandibular glands ( $p < 0.0001$ ) and significantly lower compared to the thyroid gland ( $p < 0.009$ ). In the venous phases (phases 2 and 3), parathyroid lesion-CCA ratios (0.68 and 0.71) were only significantly lower than the thyroid ( $p < 0.0001$ ). There was no significant difference between parathyroid lesion-CCA ratios in the last two phases of scanning to suggest an added utility of phase 4. The mean relative arterial enhancement of

parathyroid lesions (161.4%, sd 130.8) was significantly higher than thyroid (47.1%, sd 24.2) ( $p < 0.01$ ) and lymph nodes (46.5%, sd 36.5) ( $p < 0.007$ ), but not statistically different than the mean relative arterial enhancement of submandibular glands (116.9%, sd 124.1), suggesting that the noncontrast and arterial phases alone are not sufficient for diagnosis.

#### CONCLUSION

Parathyroid lesions have higher arterial phase tissue-CCA ratio compared to lymph nodes and submandibular glands and lower tissue-CCA ratio compared to thyroid gland. Parathyroid lesions have higher mean relative arterial enhancement compared to thyroid and lymph nodes, but not statistically different from submandibular glands. While the noncontrast phase may be helpful in differentiating hyperdense thyroid tissue from parathyroid lesions, the delayed venous phase (phase 4) was not useful in diagnosing parathyroid lesions and can be eliminated from the 4D CT protocol.

**KEY WORDS:** Hyperparathyroidism, 4D CT, enhancement

**O-425**

**3:16 PM - 3:24 PM**

#### Fine Needle Aspiration for Thyroid Nodule with Macrocalcification

Lee, J.-Lee, S.

Chungbuk National University  
Cheongju, KOREA, REPUBLIC OF

#### PURPOSE

The purpose of this study is to evaluate the diagnostic yield and the accuracy of ultrasound (US)-guided fine needle aspiration (FNA) of thyroid nodules with macrocalcification and investigate the association between macrocalcification subtypes and the risk of malignancy.

#### MATERIALS & METHODS

We retrospectively reviewed sonographic findings of thyroid nodules with macrocalcification in 151 patients who underwent US-guided FNA in our hospital from January 2009 to December 2010. Thyroid nodules with macrocalcification were classified into four groups; smooth total (eggshell) calcification, smooth partial calcification, irregular calcification, and nodular calcification as tumor in tumor shape. Nodule size, calcification size, preoperative FNA cytologic diagnosis, and surgically confirmed pathologic diagnosis were included in our analysis. Diagnostic yield of FNA for thyroid nodule with macrocalcification was determined by cytologic report. Sensitivity, specificity and diagnostic accuracy based on preoperative FNA cytologic diagnosis were calculated compared with surgically confirmed pathologic diagnosis.

#### RESULTS

There were 167 nodules with macrocalcification in 151 patients; 95 were benign, 60 were malignant and 12 were nondiagnostic. Diagnostic yield of FNA for thyroid

nodule with macrocalcification was 92.81%. Of 167 FNA materials, 106 nodules not surgically confirmed were excluded. Most of the nodules in patients who did not undergo surgery after FNA were diagnosed benign. Sixty-one nodules with macrocalcification that underwent US-guided FNA and surgery were included. Among four groups, sensitivity, specificity, positive predictive value, and false negative value were 93.75%, 76.92%, 95.74%, and 4.25%. Our diagnostic accuracy was 90.16% (Kappa value = .815). There was no statistically significant difference in association between macrocalcification subtypes and the risk of malignancy ( $P = .114$ ).

#### CONCLUSION

Diagnostic yield of FNA for thyroid nodule with macrocalcification is significantly high and diagnostic accuracy is reliable. Fine needle aspiration can be a good screening method for cytologic evaluation of thyroid nodule with macrocalcification.

**KEY WORDS:** Thyroid nodule, macrocalcification, fine needle aspiration

**O-426**

**3:24 PM - 3:32 PM**

#### Analysis of Primary and Recurrent Adenoid Cystic Carcinoma after Radiation Therapy Using MR Imaging and Diffusion-Weighted Imaging

Kontzialis, M.-Teknos, T.-Wakely, P.-Kirsch, C.

Ohio State University  
Columbus, OH

#### PURPOSE

Adenoid cystic carcinoma (ACC) is an uncommon malignancy of the minor salivary glands with a propensity for perineural spread. The tumor also may recur with skip lesions beyond surgical and radiation therapy treatment margins. The purpose of this paper was to analyze diffusion-weighted imaging characteristics of primary ACC and ACC tumor recurring after treatment with radiation therapy.

#### MATERIALS & METHODS

After IRB approval (IRB # 2011C0031) a total of 18 patients, with histologically proven primary or recurrent ACC that had been imaged with magnetic resonance diffusion-weighting imaging (DWI), were reviewed retrospectively. There was a total of 12 female and six male patients with an age range at time of diagnosis of 32-77 years, and a mean age of 53.3. Thirteen patients ( $n = 13$ ) had DWI magnetic resonance imaging (MRI) of primary ACC. Six patients had tumor recurrence postradiation therapy. In the subgroup ( $n = 6$ ) with recurrent tumor postradiation, a total of nine recurrent lesions were evaluated. Apparent diffusion coefficient (ADC) values were calculated for primary lesions and for recurrent lesions after radiation therapy, with avoidance of measurements in necrotic or cystic regions, and with placement of the region of interest (ROI) for the ADC measurement over the most enhancing portion of the tumor. The ADC values of the



primary and recurrent tumors after radiation therapy were compared with unpaired student t-test.

## RESULTS

A statistical significant difference in the ADC value between primary and recurring ACCs after radiation was observed ( $p < 0.0001$ ). The mean ADC value of the primary lesions was approximately  $0.87 \pm 0.07 \times 10^{-3} \text{ mm}^2/\text{s}$  and the range of the values was  $(0.73-1.1) \times 10^{-3} \text{ mm}^2/\text{s}$ . The mean ADC value for tumor recurrence post radiation therapy was  $1.18 \pm 0.08 \times 10^{-3} \text{ mm}^2/\text{s}$  and the range of the values was  $(0.98-1.3) \times 10^{-3} \text{ mm}^2/\text{s}$ .

## CONCLUSION

In this preliminary study, although limited by a small sample size, the mean ADC value of histopathologically proven primary ACC was  $0.87 \pm 0.07 \times 10^{-3} \text{ mm}^2/\text{s}$ , and the mean ADC value of recurrent tumor after radiation was  $1.18 \pm 0.08 \times 10^{-3} \text{ mm}^2/\text{s}$  demonstrating a statistically significant difference. These values may reflect findings in previous DWI tumor research correlating lower tumor ADC values to increased cellularity. The preliminary data are suggestive of statistically significant increased ADC values in recurrent ACC after radiation therapy, that may reflect alterations in tumor membrane permeability and extracellular matrix. The utilization of DWI MRI for assessment of primary and recurrent ACC may improve the radiographic evaluation and treatment planning of this unique salivary gland neoplasm.

**KEY WORDS:** Adenoid cystic carcinoma, recurrence, diffusion-weighted imaging

O-427

3:32 PM - 3:40 PM

## Quantitative Assessment of Extracranial Venous Drainage and Cerebral Perfusion in Multiple Sclerosis Patients and Normal Controls Using Arterial Spin Labeling and 4D Flow

McTaggart, R. A. • Elkins, C. J. • Hsiao, A. • Cutalo, M. J. • Rosenberg, J. • Dake, M. D. • Fischbein, N. J. • Zaharchuk, G.

Stanford University  
Stanford, CA

## PURPOSE

Chronic cerebrospinal venous insufficiency (CCSVI) hypothesizes an association between venous stenoses/impaired extracranial venous drainage and multiple sclerosis (MS). We recently found MS patients have greater IJ flattening and a trend toward more non-IJ collaterals than healthy controls. We now seek to determine any corresponding quantitative differences in extracranial venous drainage and cerebral perfusion.

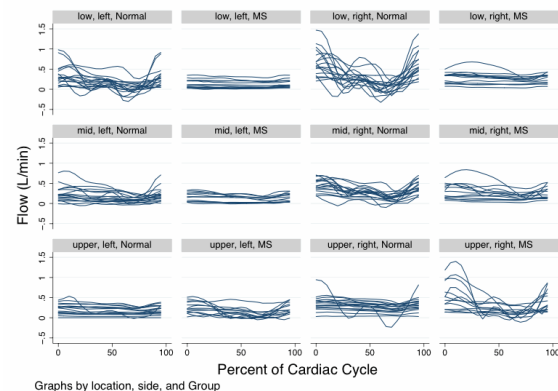
## MATERIALS & METHODS

Gender and age-matched healthy control ( $n = 17$ ) and MS patients ( $n = 13$ ) underwent arterial spin labeling (ASL), and time-resolved, 3D velocity encoded MR imaging (4D Flow) at 3T. Arterial spin labeling and 4D Flow data were analyzed using in-house software

programs. Subjects were considered to have codominant internal jugular venous drainage if the difference between sides was less than 200 ml/minute. Otherwise, a dominant side was assigned. Venous pulsatility index (VPI) was calculated  $(F_{\text{max}} - F_{\text{min}}/F_{\text{max}}) \times 100$  at the upper, mid, and low neck segments. Comparison of jugular venous flow and total cerebral blood flow between groups was done using a Mann-Whitney test stratified by location (upper, mid, lower).

## RESULTS

There were 11 (65%) and 10 (77%) women in the healthy control and MS cohorts, respectively. The mean ages of the two cohorts were 44.5 and 46.8, respectively. The mean EDSS of our MS cohort was 3.25 (1-6.5). All patients had relapsing-remitting MS. Dominant IJ drainage was seen in nine (53%) of normal patients and eight (62%) of MS patients. When dominance was present it was right sided in 88%. There are significant differences in flow between normal and MS patients at the upper ( $P = 0.0017$ ), mid ( $P = < 0.001$ ) and low ( $P = 0.0017$ ) neck segments. There were significant differences in pulsatility between normal and MS cohorts in the upper, mid, and low neck segments ( $P < 0.00001$ ) (Figure 1). There was no difference in total CBF (ml/min) in normal patients 688.4 vs MS patients 710.1 ( $P = 0.46$ ).



## CONCLUSION

Despite similar intracranial inflow (total CBF) as measured by ASL in healthy control and MS patients, there are significant and profound differences in jugular venous outflow between healthy control and MS patients. We cannot determine, using the methods described herein, that extracranial venous drainage in MS patients is physiologically impaired, but the observed differences in jugular venous drainage between healthy controls and MS patients deserve further study.

**KEY WORDS:** Multiple sclerosis, chronic cerebrospinal venous insufficiency, internal jugular vein

O-428

3:40 PM - 3:48 PM

## Mastoid Sign of Dural Sinus Thrombosis: The Signal, Not the Source

Shah, L. • Khaleel, Z. • Wiggins, R. • Harnsberger, R.

University of Utah  
Salt Lake City, UT

#### PURPOSE

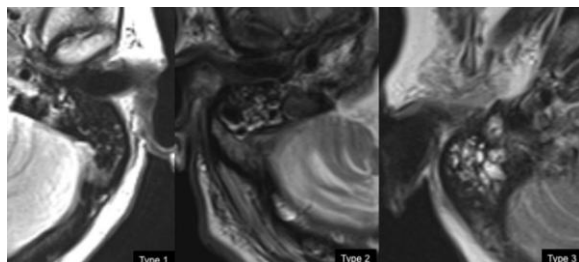
The mastoid emissary veins are part of an extensive venous drainage system connecting the sigmoid and transverse sinuses with the posterior auricular and/or suboccipital venous plexus. Obstruction of this elaborate network can lead to mucosal hyperemia and transudation of fluid into the mastoid air cells, which can have a continuum of manifestations. The variable mastoid imaging appearance in patients may be due to the variable venous anatomy and the extent and chronicity of dural sinus venous thrombosis (DSVT). We propose that mastoid imaging findings identified in the setting of posterior fossa DSVT are a phenomenon of craniocervical venous congestion.

#### MATERIALS & METHODS

After IRB approval and RIS search from 2001 to 2011, CT and MRI studies for acute DSVT were evaluated by two neuroradiologists. Mastoid involvement was graded: 0 = no mastoid involvement; 1 = linear T2 hyperintensity along mastoid air cells representing mucosal congestion, not visible on CT; 2 = crescentic T2 hyperintensity along mastoid air cells representing mucosal thickening, not visible on CT; 3 = T2 hyperintensity and soft tissue attenuation on CT opacifying mastoid air cells representing effusion.

#### RESULTS

Of 291 cases produced from the RIS search of acute DSVT, 26 cases were positive (specifically, transverse sinus, sigmoid sinus, internal jugular vein and vein of Labbe). The spectrum of mastoid involvement ranged from no findings to complete opacification. Of the 26 cases positive for DSVT, 22 had mastoid findings. Eight subjects had type 1 mastoid involvement, 11 had type 2 mucosal thickening and three subjects had type 3. Of the 22 cases with mastoid air cell involvement, 20 had thrombosis of the ipsilateral transverse sinus, one had ipsilateral IJV thrombosis, and one case showed thrombosis of the ipsilateral vein of Labbe. Bilateral DSVT was seen in one patient. Parenchymal or subarachnoid hemorrhage was noted in five cases. Increased parenchymal T2 hyperintensity likely representing edema was observed in seven cases, three of which showed hemorrhage. None of the patients with DSVT and mastoid involvement had clinical findings of infectious mastoiditis. There was a significant association between dural venous thrombosis and mastoid findings ( $X^2$  ( $N = 26$ ),  $p < 0.0001$ ).



#### CONCLUSION

The intracranial dural venous sinuses drain into a complex craniocervical venous anatomical landscape, which can lead to a spectrum of mastoid air cell findings from mucosal congestion to effusion. In the setting of DSVT, it is important to recognize this as a secondary finding rather than a primary infectious process.

**KEY WORDS:** Dural sinus thrombosis, mastoid effusion

**O-429**

**3:48 PM - 3:56 PM**

#### Mandible at Prenatal MR Imaging

Nemec, U.<sup>1</sup>Nemec, S. F.<sup>1</sup>Weber, M.<sup>1</sup>Brugger, P. C.<sup>1</sup>Bettelheim, D.<sup>1</sup>Rimoin, D. L.<sup>2</sup>Graham, J. M.<sup>2</sup>Prayer, D.<sup>1</sup>

<sup>1</sup>Medical University of Vienna, Vienna, AUSTRIA,

<sup>2</sup>Cedars Sinai Medical Center, Los Angeles, CA

#### PURPOSE

This study sought to evaluate normal mandibular growth on prenatal magnetic resonance (MR) imaging by constructing a fetal growth chart.

#### MATERIALS & METHODS

Retrospectively, 561 prenatal MR scans of 483 fetuses [19+0 to 36+6 gestational weeks (GW)], with normal anatomy or anomalies that did not involve the fetal face, were included in the study. On axial T2-weighted MR imaging, the mandibular width was measured 10 mm posterior to the anterior mandibular margin. In addition, on a mid-sagittal plane, the inferior facial angle was defined by the crossing of a line orthogonal to the vertical forehead and another line joining the mentum and the anterior margin of the upper lip. Statistical description, Pearson correlation, and linear regression analysis were used to evaluate mandibular width and inferior facial angle in relation to gestation. By t-testing, mandibular width on MR imaging was compared with published ultrasound data.

#### RESULTS

Minimum and maximum values, mean values, and percentiles were defined. Mandibular growth as a function of gestational age was expressed by the formula: mandibular width =  $1.622 + .928 * (* = GW)$ . The correlation coefficient ( $r = .890$ ) was statistically significant ( $p < .001$ ). There was a significant difference between mandibular width obtained by MR imaging and ultrasound ( $p < .001$ ). The inferior facial angle did not correlate with gestation.

#### CONCLUSION

Our MR imaging study charted normal mandibular growth in utero, which, in addition to ultrasound, may be helpful to objectively determine a normal mandible as well as micrognathia and retrognathia by MR imaging. Differences in visualization on ultrasound and MR imaging emphasize the value of our preliminary MR growth chart.

**KEY WORDS:** Normal mandible, prenatal MR imaging, fetal growth chart

O-430

3:56 PM - 4:04 PM

### Mild Congenital Aural Dysplasia: Identifying the Subtle Findings

Janse van Rensburg, P.·Yorgason, J. G.·Harnsberger, H. R.·Wiggins, R. H.

University of Utah  
Salt Lake City, UT

#### PURPOSE

The mild spectrum of congenital external and middle ear dysplasia often is misdiagnosed clinically and radiologically because of near normal external ear anatomy and mild external auditory canal stenosis and/or subtle middle ear findings. The goal of this study is to characterize the high-resolution CT (HR CT) findings of mild congenital aural dysplasia so that radiologists will recognize these findings as part of a spectrum of congenital aural dysplasia and avoid diagnostic pitfalls.

#### MATERIALS & METHODS

Following IRB approval, a retrospective case review was performed at a tertiary referral center. Patients with congenital aural dysplasia with no previous ear surgery were identified from a clinical and radiographic database dating from 1998 to 2009. High-resolution CT scans were reviewed, and the imaging characteristics were documented by a senior CAQ neuroradiologist.

#### RESULTS

One hundred six cases of congenital aural dysplasia (118 ears) were identified on review of the clinical and radiologic database. The HR CT scans of 49 patients with 56 affected temporal bones were available for review. Thirty-one temporal bones (55%) had overt external auditory canal atresia. Twenty-five temporal bones (45%) had mild aural dysplasia without overt external auditory canal atresia. In cases with mild dysplasia, we identified HR CT findings including the degree of EAC narrowing, the appearance of the ossicles, oval and round windows, and the course of the facial nerve.

#### CONCLUSION

The commonly used term "congenital aural atresia" often misleads clinicians and radiologists by implying that atresia of the external auditory canal is present in all cases. Thus mild congenital aural lesions may be misinterpreted or missed altogether by the radiologist. The spectrum of congenital aural disease is described better as "congenital aural dysplasia" to remind the radiologist of the mild spectrum of HR CT findings, which can be observed in these more subtle cases. The most common HR CT findings in this patient group include focal or diffuse external auditory canal narrowing, ossicular malposition and fusion anomalies and mastoid segment facial nerve anterior displacement.

**KEY WORDS:** Congenital aural atresia, temporal bone, CT

O-431

4:04 PM - 4:12 PM

### CT Findings in Conductive Hearing Loss and Correlation with Surgical Findings and Audiometry

Ozgen, B.·Aslan Dundar, T.·Genc, A.·Sennaroglu, L.

Hacettepe University  
Ankara, TURKEY

#### PURPOSE

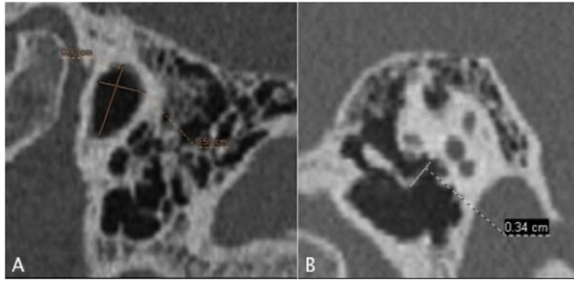
The computed tomography (CT) is an excellent technique for the evaluation of the middle ear (with detailed demonstration of the ossicular anatomy). CT also was shown to depict otosclerotic foci early in the course of the disease. This technique has thus an increasing role in the evaluation of the conductive hearing loss (CHL) as a noninvasive alternative to exploratory tympanotomy. The aim of this study was to evaluate the reliability of CT findings in predicting the etiology of CHL, to correlate the degree of radiologic abnormalities with the audiological findings and to investigate the value of tomographic measurements as a preoperative guide before tympanotomy.

#### MATERIALS & METHODS

Forty-three patients (45 ears) were evaluated prospectively with preoperative audiometric evaluation and temporal bone CT, followed by exploratory tympanotomy. External auditory canal diameter (EACD) was measured by CT on the sagittal and coronal reformats and compared with speculum diameter used in surgery (Figure A). Similarly, incus long process - stapes footplate distance were measured with CT on the Poschl reformatted images (Figure B) and compared with the Teflon piston size used during surgery. In cases with otosclerosis, the otosclerotic focus was measured on CT, classified according to Symons and Fanning and was compared with the audiological data.

#### RESULTS

At surgery, otosclerosis was found in 39 ears. In the remaining 6 ears the underlying pathologies were ossicular anomalies with absence of stapes suprastructure, deficiency of the long process of incus, fracture of stapedial crura and fusion of the malleolus. Superior semicircular dehiscence was not detected. 42 of 45 ears were correctly diagnosed with the CT scan (with a sensitivity of %93.3). The detection of otosclerosis with CT had a sensitivity of %94.4 (2 cases was missed) and a specificity of 100%. There was no significant correlation between tomographic EACD measurement and speculum diameter. The CT could not correctly assess the incus-footplate distance ( $p>0.05$ ). The diameter of the otosclerotic foci and its classification revealed no significant correlation with the audiological data ( $p>0.05$ ).



#### CONCLUSION

CT of the temporal bone is an important preoperative tool for the evaluation of patients with CHL. Although we found it to be useful for assessing the underlying pathology, the CT measurements could not predict the size of the speculum to be used nor the length of the Teflon piston to be implanted. The size of the otosclerotic foci was not correlated with the hearing level of the patient.

**KEY WORDS:** Computed tomography, conductive hearing loss

**O-432**

**4:12 PM - 4:20 PM**

#### Evaluation of Endosteal Ossification of the Otic Capsule with CT in Children

Ozgen, B. Sanverdi, E. Dolgun, A. Cila, A.

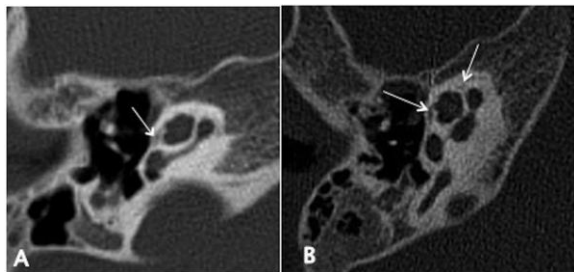
Hacettepe University  
Ankara, TURKEY

#### PURPOSE

Endosteal ossification (EO) of the otic capsule (OC) is a continuous process in the postnatal term. Incomplete ossification is seen as a pericochlear hypodensity on CT. We evaluated the evolution of EO with age using temporal bone CT. The effect of accompanying SNHL with or without radiologically detectable inner ear abnormalities (IEA) also was assessed.

#### MATERIALS & METHODS

Consecutive temporal bone CT studies of 493 children (986 ears) (mean age: 5.2 years, F/M: 245/248) present in our institution's PACS archive were reviewed. Incomplete EO (iEO) areas were defined and then classified as mild, moderate (Figure A) and severe (Figure B) according to the extent. Results were analyzed with one-way variance analysis and chi-square tests.



#### RESULTS

The EO was complete in 387 temporal bones. In the remaining iEO group the most frequent finding was mild focal hypodensity at the fissula ante fenestram

(FA) (n = 453, 45.9%). No significant difference was found in respect to the presence iEO among the genders (p = 0.8). Younger age was associated with an increased level of iEO (P <0.001). Eight hundred twelve of temporal bones did not reveal any radiologic inner ear abnormality and those had no significant difference from the IEA group in respect to the presence of iEO (p = 0.2). The development EO also showed no correlation with the presence of SNHL (p = 0.08).

#### CONCLUSION

Presence of focal hypodensity in the region of the FA by CT is independent from underlying SNHL or radiologically detectable IEAs. Incomplete EO could be accepted as a normal finding in younger children as a part of bone maturation and can be seen up to 17 years of age.

**KEY WORDS:** Endosteal ossification, temporal bone, CT

**O-433**

**4:20 PM - 4:28 PM**

#### Imaging Temporal Bone Trauma

Bulakbaşı, N.<sup>1</sup> Ilıca, A.<sup>2</sup> Alıcıoğlu, B.<sup>1</sup> Tosun, Ö.<sup>1</sup> Akpınar, H.<sup>1</sup>

<sup>1</sup>Near East University, Nicosia/TRNC, TURKEY,

<sup>2</sup>Gülhane Military Medical Academy, Ankara, TURKEY

#### PURPOSE

To evaluate traumatized temporal bone, anatomical structures mimicking fracture lines and posttraumatic complications.

#### APPROACH/METHODS

All patients were scanned by 64 channel multislice CT imager. High resolution images with 0.625 mm slice thickness were obtained by multiplanar reconstruction. Temporal bone MR imaging were used when it was necessary. The full range of CT and MR imaging abnormalities were reviewed to increase the specificity of radiologic imaging in the evaluation of temporal bone trauma.

#### FINDINGS/DISCUSSION

Temporal bone is affected in up to 40% of high energy closed head traumas and in up to 25% of skull base fractures. Because of its complex anatomical structure, evaluation of temporal bone is very difficult. Many of normal anatomical structures such as sphenosquamosal and occipitomastoid sutures, squamotympanic, tympanomastoid, petrosquamous, petrotympanic, and petromastoid fissures, singular and petromastoid canals, cochlear and vestibular aqueducts, glossopharyngeal sulcus, and mastoid and inferior tympanic canaliculi can mimic the fracture lines. In the evaluation of traumatized temporal bone, individual assessment of critical anatomical structures whose affection causing serious complications are more important than the classification of temporal bone fractures (either transverse, oblique, longitudinal and complex, or otic capsule involving and sparing). These critical structures include facial canal and nerve (for peripheral facial paralysis), carotid canal (for internal

carotid artery thrombosis or dissection), jugular foramen (for jugular vein thrombosis), bony labyrinth (for vertigo or sensory-neural hearing loss), ossicles (for conductive hearing loss), tegmen tympani (for otorrhea or otomeningitis), mastoid air cells (for meningitis or sigmoid sinus thrombosis). On the other hand some fracture lines can remain silent at first and become prominent in time. This is mainly a result of improper imaging techniques used for routine evaluation of trauma patients. Patients with head trauma routinely evaluated by cranial, maxillofacial and servikal CT examinations but none of them had adequate spatial resolution for temporal bone evaluation. For this reason, secondary findings such as opacification in mastoid air cells, external auditory canal or middle ear cavity, air/fluid levels in sphenoid sinus, adjacent pneumocephalus, extra-axial fluid collection, air in glenoid or infratemporal fossae. CT is not always adequate to evaluate the full extent of temporal bone trauma and its complications, but especially in traumas affecting the membranous labyrinth and brain stem, MRI should be the choice of imaging modality. Intralabyrinthine hemorrhages caused by physical trauma or barotraumas can only be seen in MR images. Furthermore posttraumatic meningitis, venous thrombosis, meningoceles, otorrhea can be evaluated more accurately by MRI.

#### SUMMARY/CONCLUSION

Although the temporal bone traumas are not so frequent in head trauma patients, the clinical consequences can include very serious morbidities such as permanent hearing loss, facial paralysis, vertigo, otomeningitis, and vascular complication. The early diagnosis and proper treatment can significantly reduce the morbidity and prevent complications. Special care must be taken to temporal imaging especially in posttraumatic patients having a clinical or radiologic suspicion of temporal bone fracture.

**KEY WORDS:** Temporal bone, trauma, computed tomography

## Wednesday Afternoon

**3:00 PM - 4:30 PM**

**Murray Hill**

**(53e) Socioeconomics**

**O-434**

**3:00 PM - 3:08 PM**

**Post-Publication Errors in AJNR Compared with Other Imaging Journals**

Northam, M. C.<sup>1</sup>Halm, K.<sup>2</sup>Castillo, M.<sup>1</sup>

<sup>1</sup>University of North Carolina at Chapel Hill, Chapel Hill, NC, <sup>2</sup>American Journal of Neuroradiology, Oak Brook, IL

#### PURPOSE

The quantity and types of post-publication errors in AJNR are not known. We analyzed and compared numbers and types of errata in AJNR with four other high impact factor (IF) imaging journals.

#### MATERIALS & METHODS

Using the Web of Knowledge ISI database we selected the five imaging-related journals with the highest IF. In each journal's website we searched for the terms "erratum" and "errata" anywhere in titles, abstracts, and author lists for a 5-year period (2006-2011). These were counted and categorized as minor: typographical and image-related or major: factual, statistics, and foundational errors. The number and types of errors found in AJNR then were compared with the other four journals.

#### RESULTS

Journals assessed were: JNM (IF = 7.022), Radiology (6.066), AJNR (3.464), AJR (2.797), and RadioGraphics (2.760). There were a total of 158 errata and each was placed in one of the following categories: typographical (94), factual (6), image-related (48), statistical calculation (7), or serious foundational errors (3) and then grouped into minor and major. Errata also were labeled as authors' (107) or journal responsibilities (51). Total errata per journal were as follows: AJNR (25), RadioGraphics (22), Radiology (42), AJR (20), and JNM (49). In AJNR 5 errata were the journal's and 20 authors' responsibilities; other journals were as follows: RadioGraphics: 10 and 12, Radiology: 10 and 32, AJR: 16 and 4, and JNM: 10 and 39, respectively. Major errors were distributed as follows: AJNR (3), RadioGraphics (1), Radiology (2), AJR (2), and JNM (8) and minor as: AJNR (22), RadioGraphics (21), Radiology (40), AJR (18), and JNM (41). The numbers and types of errata did not correlate with the numbers of articles published by each journal during the period studied. Total errata as percentage of total articles published in the 5-year period were: AJNR (1.3%), RadioGraphics (2.8%), Radiology (2.0%), AJR (0.6%), and JNM (3.6%).

#### CONCLUSION

The numbers and types of post-publication errors identified as errata in AJNR compares favorably with those of four other imaging journals with high IF. Most errors in AJNR were minor and reflected authors' responsibilities.

**KEY WORDS:** Post-publication errors, AJNR

**O-435**

**3:08 PM - 3:16 PM**

**Personal Patient Consultations with the Radiologist: A Novel Tool in Garnering Loyalty and Referrals in Outpatient Radiology**

Keiper, M. D.<sup>1</sup>Mead, L.<sup>2</sup>Murphy, R.<sup>2</sup>Horsley, W.<sup>2</sup>

<sup>1</sup>University of Nebraska Medical Center, Omaha, NE,

<sup>2</sup>Scottsdale Medical Imaging, Scottsdale, AZ



## PURPOSE

Traditional outpatient radiology center marketing has been directed primarily towards referring clinicians as the key referral source of patient populations. Although direct patient marketing has increased in utilization, it typically remains a secondary tool in the development of niche radiology and interventional procedures in most radiology markets. The purpose of this study is to determine the efficacy of direct patient consultations with radiologists in providing value added to referring clinicians and increased direct patient loyalty and referrals in outpatient radiology.

## Material & Methods

CT, MRI and PET/CT patients referred to an outpatient radiology center over a 1-year period were given the option of setting an appointment with a specialty radiologist (musculoskeletal, neuroradiology or oncologic) to personally review the imaging study and ask pertinent questions relative to imaging findings within 1 week after completion of the initial study. At the time of enrollment, patients were required to complete a general survey regarding quality of service, staff and overall experience at the imaging center. The same survey subsequently was completed immediately after the personal consultation with the radiologist. A portion of the survey was designed in an attempt to determine if the program would be a useful tool in garnering loyalty within the patient population and increase direct patient and physician referrals. Four specific statements were offered and graded by the patient in order to determine the likelihood of success of this program: 1. "I will personally utilize the imaging center again for radiology tests." 2. "I will recommend the imaging center to family and friends for radiology tests." 3. "I will insist that my doctor refers me and my family to the imaging center for radiology tests." 4. "I would travel significant distances (>25 miles) to have radiology tests performed at the imaging center." The patient was asked to rate the statements based on a 1-5 scale with one representing complete disagreement with the statement and five representing complete agreement with the statement. Scores were tabulated, analyzed and compared. Statistical evaluation of the scores before and after consultation was performed utilizing the Wilcoxon match-pair signed-rank test. A total of 430 patients enrolled in the study. Twenty-four patients did not report for the consultations and were excluded from the study.

## RESULTS

The results of the survey before and after the personal radiology consultations are tabulated below.

Survey Question	Mean Initial Visit	Mean Final Visit	Mean Difference	Significance
1	4.07	4.9	0.83	p<0.0001
2	4.01	4.91	0.9	p<0.0001
3	3.31	4.74	1.43	p<0.0001
4	3.16	4.6	1.44	p<0.0001

## CONCLUSION

Direct patient consultations with radiologists provided statistically significant greater patient satisfaction in outpatient imaging visits. Survey data indicate that this

effect may ultimately serve to garner increased patient loyalty and direct patient and physician referrals in outpatient radiology.

**KEY WORDS:** Marketing, business development, referral sources

**O-436**

**3:16 PM - 3:24 PM**

## Variation in Radiology Resident Experience: Will Training Minimums Be Met?

Delfyett, W. T. • Savino, M. R. • Tsay, J.

University of Pittsburgh Medical Center  
Pittsburgh, PA

## PURPOSE

The ACGME has mandated participation in a resident caseload system, which, for diagnostic radiology, includes documentation of representative exam types with a future goal of setting minimum benchmarks for each resident. Presently, the ACGME provides annual program national percentile ranks in various exam types. While useful for external stratification, program-level data may not reflect the range of cases that residents dictate, which is more pertinent when considering minimum benchmarks. Hence, with individual-level information, programs may need to readdress their curricula to meet benchmarks if discrepancies exist. In advance of defined minima set by the ACGME, we sought to evaluate the numerical variation of cases dictated by residents in the University of Pittsburgh Medical Center Diagnostic Radiology Residency Program.

## MATERIALS & METHODS

With IRB approval, using the UPMC Radiology information system (GE Healthcare, Centricity RIS-IC), HIPAA-compliant reports were generated which summed individual resident dictations from 2008-2011. As a sample of case exposure, a subset of neuroradiology exams were queried, regardless of contrast administration, including CT Head, MRI Brain, CTA head, MRA brain, and a grouped ENT CT category consisting of orbital, maxillofacial, and soft tissue neck imaging. Basic statistical analysis was performed for each resident training year within the three academic years available.

## RESULTS

For illustrative purposes, only CT head data from the graduating class of 2011 are presented. This resident subgroup dictated a mean of 243 cases with a median of 215, a range of 414, and a coefficient of variation (CV) of 42.6% in their second training year; a mean of 188 exams with a median of 153, a range of 341, and a CV of 54.6% in their third training year; and a mean of 137 cases with a median of 123, a range of 443, and a CV of 78.6% in their fourth training year. In each academic year investigated, certain residents from each training year dictated a number of CT head cases which was less than the value of one standard deviation below the mean calculated from those of their training level peers, indicating performance in the lowest 15.6<sup>th</sup> percentile.

In the 2008-09 academic year, this group included two first-year residents, one second-year resident, three third-year residents, and two fourth-year residents. In the 2009-10 academic year, three first-year residents, two second-year residents, two third-year residents, and two fourth-year residents fell into this lowest percentile group. In the 2010-11 academic year, the lowest-ranking fraction included three first-year residents, two second-year residents, one third-year resident, and one fourth-year resident.

#### CONCLUSION

Dramatic variability occurs in the volumes of neuroradiology exam types dictated by UPMC Radiology residents as evidenced by large coefficients of variation. In addition, several residents each year fell in the lowest 15.6<sup>th</sup> percentile compared to the mean, highlighting the desire for minimum benchmarks. The data observed for the neuroradiology exams presented likely applies to other radiology divisions. As such, individual training programs may need to evaluate their resident volume ranges in advance of ACGME-set minima to ensure minimum competency upon completion of training.

**KEY WORDS:** ACGME, resident training, competency

**O-437**

**3:24 PM - 3:32 PM**

#### **Lack of Correlation between Increasing Neuroradiology Exam Volumes On-Call and Major Discrepancies in Primary Reads Performed by Residents**

Verdoorn, J. T.<sup>1</sup>•Hunt, C. H.<sup>1</sup>•Luetmer, M. T.<sup>2</sup>•Wood, C. P.<sup>1</sup>•Kalmes, D. F.<sup>1</sup>

<sup>1</sup>Mayo Clinic, Rochester, MN, <sup>2</sup>College of St Benedict, St Joseph, MN

#### PURPOSE

A common perception is that increased on-call workload by residents can lead to increased error rate when interpreting complex studies. We correlated whether increased volume of cases has led to an increased major discrepancy rate at our institution.

#### MATERIALS & METHODS

After obtaining IRB approval, a retrospective review was made of all neuroradiology CT exams with a primary read by a resident between the hours of 2300 to 0800 from 1/2006 through 12/2010. All studies performed during these hours were read by the resident on-call with a staff neuroradiologist over-reading the studies in the morning at 0800. As the volume of on-call studies is typically larger during the weekend, studies read on Friday, Saturday, or Sunday night were examined separately. Discrepancies were classified by the staff radiologist as either minor or major. "Major" discrepancy was defined as any discrepancy that the staff radiologist felt was significant enough to affect patient care, thereby necessitating not only correcting the report in the electronic medical record, but also contacting the ordering physician by phone. The total number of revisions was recorded by quarter for each year. In addition, the total number of

neuroradiology studies read overnight on-call was recorded. These only included CT examinations of the head (included CT angiography), neck, and spine. Paired t-test was performed to determine statistical significance for the trends with a p-value of <0.05 being considered significant.

#### RESULTS

The mean number of neuroradiology cases per night read during the weekdays increased from 3.0 in 2006 to 5.2 in 2010 ( $p<0.001$ ), with a maximum of number of cases per weeknight increasing from 8.2 to 11.0 ( $p<0.001$ ). During the weekend, even higher volumes typically are encountered and the mean number of neuroradiology cases per night read during the weekend increased from 5.4 in 2006 to 7.6 in 2010 ( $p<0.001$ ), with a maximum number of cases per weekend night increasing from 10.4 to 15.0 ( $p<0.001$ ). Despite this increase in case workload, the neuroradiology major discrepancy rate decreased slightly from 2.7% in 2006 to 2.3% in 2010 ( $p = 0.34$ ).

#### CONCLUSION

Despite an increase in neuroradiology exam volumes read by on-call residents during the night, there continues to be a very low major discrepancy rate. While continued surveillance of on-call volumes is crucial to maintaining an appropriate educational environment for residents, concern of increased major errors should not be used as the sole argument for limiting resident autonomy during their training.

**KEY WORDS:** Quality, on-call volume, error rate

**O-438**

**3:32 PM - 3:40 PM**

#### **Critical Findings Lists in Neuroradiology: Survey of Neuroradiology Training Programs**

Babiarz, L. S.•Trotter, S.•Viertel, V. G.•Nagy, P.•Lewin, J. S.•Yousem, D. M.

Johns Hopkins Hospital  
Baltimore, MD

#### PURPOSE

Recently the Joint Commission has identified the need for a list of critical findings and timely and effective communication of such findings for diagnostic radiology tests as one of the National Patient Safety Goals. We surveyed directors of neuroradiology fellowship training programs in order to assess and compare critical findings lists across programs.

#### MATERIALS & METHODS

A three-question survey was sent out via email to all the neuroradiology fellowship training directors listed by the ASNR: (1) "Do you have a critical findings list for neuroradiology?", (2) "How is that list distributed to residents and fellows?", and (3) "Was this list vetted by neurology, neurosurgery, and otolaryngology (ENT)?" Programs with a critical findings list were asked for a copy of the list. Each program director received the original request email as well as a reminder email. Additional communication took place for programs with

lists. Summary and comparative statistics were made for all the responses and submitted lists.

## RESULTS

Forty of 89 programs responded to the survey. Seventeen programs had critical findings lists and 23 did not. Thirteen programs sent a copy of their list. Programs distribute their lists during orientation/initial training (eight programs) and via websites (eight) and emails (five), post lists in work areas (six), include lists in their policy booklets (three), present during conferences (one), and allow access to the lists via an electronic system (one). One of 17 lists was vetted with neurology, neurosurgery, or ENT, and two of 17 were drafted by a hospital-wide committee with representatives from all departments. Nine of 17 lists were comprised by radiology departments. The origin of the remaining five lists was not clear. A total of 37 critical finding entities were seen in 13 submitted lists. List length ranged from four to 23 items (average = 10.5). The top five entities include: hemorrhage (12 of 13 lists), acute stroke (10 of 13), herniation (10 of 13), cord compression (10 of 13), and spinal fracture/instability (nine of 13). Two lists included the "anything clinically important" critical finding category. Programs with no critical findings lists call referring physicians based on "common sense", "clinical judgment", or "word of mouth". Some programs communicate all positive findings for urgent/"stat" studies. Programs with and without lists document their communication with clinicians.

## CONCLUSION

Of the surveyed neuroradiology programs that responded, less than half (43%) have critical findings lists which they disseminate during orientation, via websites and emails, and which they post at work stations. The vast majority of neuroradiology critical findings lists are created by radiology departments without input from neurology, neurosurgery, or ENT. There is a great variability in the length and content of the lists with the most common entities being hemorrhage, stroke, herniation, cord compression, and spinal fracture/instability.

**KEY WORDS:** Critical findings, neuroradiology training

**O-439**

**3:40 PM - 3:48 PM**

### Screening Cervical Spine CT in the Emergency Department: A Collaborative Quality Improvement Initiative

Griffith, B. Vallee, P. Slezak, M. Narayan, A. Krupp, S. Nagarwala, J. Loeckner, C. P. Jain, R. Kelly, M.

Henry Ford Hospital  
Detroit, MI

## PURPOSE

To analyze the use of screening cervical spine CT performed following blunt trauma by establishing the number of potentially avoidable studies when strict clinical criteria (NEXUS criteria - National Emergency X-Ray Utilization Study) are applied and to determine the

indications for ordering studies in the absence of these strict criteria.

## MATERIALS & METHODS

All patients presenting to the Henry Ford Hospital Emergency Department between March and September 2011 for whom a screening cervical spine CT was ordered in the setting of blunt trauma were eligible for enrollment in the study. For each study ordered, the requesting clinician was instructed to complete a survey regarding mechanism of injury, indication for ordering the study, and clinical suspicion of injury. The cervical spine CT examinations of these patients then were evaluated by a board certified radiologist blinded to the survey data to determine the presence or absence of cervical spine injury. Exclusion criteria included: age < 18 years, penetrating injury, known C-spine fracture or dislocation/subluxation, transfer patient, or remote injury (>48 hours).

## RESULTS

Four hundred forty-nine patients have been enrolled in the study to date, of which 30 were excluded. Of the 419 included patients, four (1%) were positive and 410 (97.9%) were negative for acute cervical spine injury. Five studies (1.2%) were indeterminate for acute injury, but failed to demonstrate an acute abnormality upon subsequent imaging and further review of clinical records. Of the 415 studies without acute cervical spine injury, 63 (15.2%) had none of the five NEXUS criteria. Of patients without any of the five NEXUS criteria, the most common reason for ordering a screening cervical spine CT was dangerous mechanism of injury (52%; 30% dangerous mechanism by Canadian Cervical Spine Rule criteria, 22% non-CCR dangerous mechanism) followed by subjective complaint of neck pain (38%). The rate of studies performed without any NEXUS criteria during the study period was 15%. This was a drop from 24% found at the same institution in a prior retrospective study.

## CONCLUSION

Despite its acceptance as a screening tool for cervical spine imaging in blunt trauma patients, many patients continue to be imaged without meeting the NEXUS criteria. Strict adherence to these criteria has the potential to significantly decrease the number of screening cervical spine CT studies ordered for patients following blunt trauma, which would help limit patient radiation exposure and improve the cost-effectiveness of these studies. Radiologists, radiology departments, and emergency physicians all must play an active role in ensuring appropriate utilization of medical imaging. As demonstrated with this study, even small changes in policy or practice, such as the initiation of a simple survey, has the potential to alter ordering practices of clinicians and ultimately lead to meaningful benefits for patients and improve the delivery of healthcare. This study's collaboration between the departments of radiology and emergency medicine indicates a broad desire to improve healthcare delivery and utilization. This study, hopefully, can serve as a model for future quality improvement initiatives in our department.

**KEY WORDS:** NEXUS, cervical spine

**O-440**

**3:48 PM - 3:56 PM**

**Reducing Radiation Dose in Fluoroscopy-Guided Lumbar Punctures and Myelograms by Decreasing the Fluoroscopic Frame Rate**

Sabat, S. • Kalapos, P. • Brown, K. • Bigger, J.

Penn State Milton S. Hershey Medical Center  
Hershey, PA

**PURPOSE**

Fluoroscopy-guided lumbar puncture/myelogram is a common procedure in a radiology department and is done most commonly in our institute (and at least many others) under a continuous fluoroscopy mode. There is almost no published literature on the use of continuous versus pulsed fluoroscopy in lumbar puncture/myelograms and the resultant dose savings. We hypothesized that in a procedure where there is not much temporal change in image data, a pulsed fluoroscopic technique in the lowest possible frame (pulse) rate should be sufficient and should achieve substantial reduction in radiation doses. We did this study as a QA process in our Radiology Department.

**MATERIALS & METHODS**

Appropriate IRB approval was obtained. The study was prospective in nature. Fluoroscopic-guided lumbar puncture/myelograms were done on 35 patients. Patients were divided into a control group of 17 patients and an actual study group of 18 patients. In the first 17 patients fluoroscopy was done using a "continuous mode" setting (control group). In the next 18 patients, fluoroscopy was done in a pulsed mode (study group) with the lowest possible setting of three pulses/sec; a low dose setting also was kept as some systems are known to automatically adjust the dose to a higher level. Skin entry dose was measured in all patients using a OSL dosimeter (OSL nanodots). Only the fluoroscopic doses were used. Dosimeters were removed when spot films/overhead exposures were to be taken. Dosimeters were analyzed for skin entry dose; DAP (dose area product) also was calculated. Mathematical mean dose and DAP numbers of the study and control groups were compared. The groups were almost similar in average weight, the BMI in the control group being 30 while the BMI of the control group was 30.8. Other possible confounding variables also were tried to be as closely matched as possible.

**RESULTS**

Technical success was 100%. In none of the 18 cases with the lower frame rate, image quality was considered suboptimal. The average skin entry dose in the control group (group with routine continuous fluoroscopic setting) was 2245 mRads while the entry dose in the study group (group with reduced frame rate of 3 pulses/sec) was 398 mRads (5.6 times lower). The mean DAP in the control group was 65 Gy.cm<sup>2</sup>, while that in the study group was 11 Gy.cm<sup>2</sup> ( 5.9 times lower). The average fluoroscopic time, often a surrogate of total procedure time, in the control group was 39

seconds while that in the control group was 33 seconds (15% lower).

**CONCLUSION**

Pulse fluoroscopy done with a pulse rate of 3/s is adequate for most lumbar punctures/myelograms and can reduce the fluoroscopic skin doses by more than five times as compared to continuous fluoroscopy. The overall fluoroscopic time also does not increase but rather shows a small decrease.

**KEY WORDS:** Fluoroscopy, lumbar puncture, myelogram

**O-441**

**3:56 PM - 4:04 PM**

**Sequential vs Helical CT Technique for Adult Brain Imaging: A Clinical and Phantom Image Quality Study Utilizing 128 Row Detector CT**

Ozsvath, J. A. • Vega, E. • Davis, A.

New York University Langone Medical Center  
New York, NY

**PURPOSE**

At many institutions the commonly accepted standard protocol for routine imaging of the adult brain remains thick section multisequential acquisition, an anomaly in a specialty where thin section (<1 mm) helical acquisition has become a standard of care. The aim of this study was to compare CT phantom test results with regards to low contrast and line pair resolution of conventional multisequential versus helical acquisition and to retrospectively compare the image quality of brain scans acquired with multisequential technique versus helical technique utilizing the latest generation 128 row detector CT (128 RDCT) scanners. The primary statistical endpoint was to determine if the new practice (helical) is equivalent or superior to the standard practice (sequential).

**MATERIALS & METHODS**

Initial nonclinical investigation was performed by scanning an ACR low resolution phantom on a 128 RDCT with (A) thin and thick acquisition multisequential technique and (B) helical 40 row detector CT acquisition. A line pair and low resolution phantom was scanned on a 128 RDCT with (A) thin multisequential, (B) helical 40 and (C) helical 128 acquisition. All other scanning parameters for the protocols within compared groups were held constant including field of view, gantry rotation time, kVp CTDI, reconstruction algorithm and final slice thickness. Clinical investigation involved retrospective review of two separate comparative groups undergoing head CTs performed on two identical 128 RDCT scanners from 03/01/2011 through 09/01/2011 each utilizing either multisequential or thin slice helical acquisition, in which all other acquisition parameters as described above were identical. Scans whose qualities were degraded from external factors including patient motion or metallic streak artifact were eliminated. Qualifying scans were reviewed by three experienced evaluators (neuroradiologists) and two inexperienced evaluators (senior level radiology residents) to mitigate the effects

of experience. Cases were presented in random, blinded fashion with readers evaluating five specific criteria of both image quality and artifact at specific anatomical locations. Criteria were graded on a five-point scale which ranged from nonvisualization (nondiagnostic quality) to superior visualization (superior diagnostic quality).

## RESULTS

Phantom tests demonstrated no significant difference regarding low contrast resolution between either the thin or thick acquisition multisequential and the 40 detector helical technique. One hundred twenty-eight detector imaging demonstrated increased noise although greatest signal to noise ratio. One hundred of twenty-eight and 40 detector helical techniques were superior to multisequential technique for line-pair resolution. Preliminary results regarding randomized, blinded evaluation of 128 RDCT multisequential versus helical technique indicate no difference in overall image quality score between the two groups. A trend was detected towards reduced artifact although worse low contrast resolution for helical technique; a larger sample set analysis for increased statistical power and a criteria subset analysis is pending.

## CONCLUSION

Preliminary study results support replacing standard multisequential protocol with helical technique for adult brain imaging given there is at least no overall difference in image quality. The benefits that volume acquisition helical imaging provide including improved multiplanar reformat imaging, advanced postprocessing capability and faster scan time may be realized for routine brain imaging.

**KEY WORDS:** Helical, sequential

**O-442**

**4:04 PM - 4:12 PM**

### **Economic Model for Gadobutrol-Enhanced MR Imaging in the Detection of Brain Metastases**

Law, M.<sup>1</sup>•Benedict, A.<sup>2</sup>•Anzalone, N.<sup>3</sup>•Combs, S. E.<sup>4</sup>•Enterline, D.<sup>5</sup>•Essig, M.<sup>6</sup>•Nguyen, T.<sup>7</sup>•Rovira, A.<sup>8</sup>•Provenzale, J.<sup>9</sup>

<sup>1</sup>University of Southern California, Los Angeles, CA, <sup>2</sup>United Biosource Corporation, London, UNITED KINGDOM, <sup>3</sup>Ospedale San Raffaele, Milan, ITALY, <sup>4</sup>Universitätsklinikum Heidelberg, Heidelberg, GERMANY, <sup>5</sup>Duke Medical Center, Durham, NC, <sup>6</sup>Universitätsklinikum Erlangen, Erlangen, GERMANY, <sup>7</sup>Ottawa Hospital, Ottawa, ON, CANADA, <sup>8</sup>Vall d'Hebron University Hospital, Barcelona, SPAIN, <sup>9</sup>Duke University, Durham, NC

## PURPOSE

Brain metastases (BMets) are the most common form of brain cancer, originating most commonly from lung, breast, melanoma and kidney. Treatment of BMets is associated with a substantial healthcare burden. The purpose of our study was to evaluate the short-term cost impact of increased diagnostic accuracy on selection of primary treatment for patients with BMets,

additional therapies indicated at 3 months, and costs of treatment in the first 3 months from diagnosis. As the vasculature of brain metastases have no or no intact blood-brain barrier (BBB), contrast-enhanced magnetic resonance (MR) imaging with gadolinium-based contrast agents is the most sensitive imaging modality for the detection and characterization of cerebral metastases. The basis of the study was that at gadolinium dosage 0.1mmol/kg, gadobutrol demonstrated advantages over gadopentetate dimeglumine for visualization of BMets, improving conspicuity of detected lesions.

## MATERIALS & METHODS

A decision analytical model was developed to reflect the decision process for selecting primary interventions for patients with BMets and outcomes at 3 months. Structured interviews with a panel of eight neuroradiologists, radiooncologist and radiosurgeons established the factors that contribute to the decision about the primary therapy including conventional surgery, stereotactic radiosurgery (SRS) and whole brain radiation therapy (WBRT), on their own or in combination. Tumor prognosis (based on histology and performance status), number of lesions, lesion size and lesion location were identified as playing role in initial treatment decisions. To reflect variations across practices, thresholds for small/medium/large number of lesions; small/large tumor diameter and % distribution of patients across treatment options are made modifiable in the model. Three-month survival data were obtained from literature, by primary tumor. Data on 27 patients in Anzalone et al. (2009) has been incorporated into the model, including age, histology as baseline characteristics, number of lesions identified and lesion conspicuity. Using re-sampling of these patients, various decision algorithms have been applied to a cohort of 1000 patients to establish the final primary treatment selection and cost of treatment. Therapy costs were based on published US treatment costs. Detailed sensitivity analyzes were conducted.

## RESULTS

Under the base case scenario with large number of lesions defined as >4 and large lesion size >35 mm in a cohort of 1000 patients, use of gadobutrol was associated with a resulting therapy of 296 conventional surgeries, 495 SRS and 205 WBRT. Use of gadopentetate was associated with 329 conventional surgeries, 462 SRS and 209 WBRT. This resulted in \$596,079 cost savings for the use of gadobutrol vs gadopentetate. Results were sensitive to cutoff for large number of lesions.

## CONCLUSION

We built a model to compare impact of improved diagnostic imaging in any given setting by using a macrocyclic contrast agent with higher relaxivity. Current results show that there may be cost savings possible due to increased diagnostic accuracy. These are limited due to small sample size, lack of tumor size data and performance scores in the Anzalone study. However, with more detailed patient level data from



future studies with contrast agents, the model will enable more robust comparisons.

**KEY WORDS:** Gadobutrol, brain metastases, cost

**O-443**

**4:12 PM - 4:20 PM**

### **Impact of Neuroradiologist's Second Opinion Reporting on the Staging of Head and Neck Cancer**

Lysack, J. T.<sup>1</sup>Hoy, M.<sup>1</sup>Hudon, M. E.<sup>1</sup>Nakoneshny, S. C.<sup>2</sup>Dort, J. C.

University of Calgary  
Calgary, AB, CANADA

#### **PURPOSE**

The primary role of imaging in head and neck cancer is to stage the disease. Accurate staging is important for determining prognosis and guiding treatment. Patients referred to our regional cancer center frequently present with imaging studies that were performed and interpreted elsewhere. These undergo a formal reinterpretation by a neuroradiologist with expertise in head and neck imaging. In our experience, it is not uncommon for significant differences in interpretation to arise. A retrospective study was performed to determine the discrepancy rate between the original and second opinion reports with specific regard to local (T) and regional lymph node (N) staging for known or suspected cases of head and neck cancer.

#### **MATERIALS & METHODS**

All cases (N = 97) of biopsy proven or clinically suspected head and neck cancer for which a second opinion report by a neuroradiologist with expertise in head and neck imaging (JL) had been issued during the 2010 calendar year were identified. For each case, the original and second opinion radiology reports were collected, randomized, and distributed to an experienced head and neck surgeon (JD). The surgeon reviewed each report separately and recorded the TN staging as was stated explicitly or determined from the information provided in each report. The discrepancy rate was calculated for differences in staging between the original and second-opinion reports.

#### **RESULTS**

The staging changed between the original and second-opinion reports in 80% (78/97) of cases. The T staging changed in 70% (68/97), the N staging changed in 55% (53/97), and both the T and N staging changed in 44% (43/97) of cases. Further work is underway to define and determine the frequency of "clinically important" differences, including those that would result in a change from surgery to radiotherapy and/or chemotherapy as the primary treatment modality, and vice versa.

#### **CONCLUSION**

We found an 80% discrepancy rate for radiologic staging of head and neck cancer following neuroradiologist second-opinion reporting. A similarly high rate of clinical impact was found in a recent study by Brook et al; in 84% of cases, new information

resulted from radiologist consultation at multidisciplinary oncology rounds. In an earlier study focusing on head and neck cancer, Loevner et al found changes in interpretation following neuroradiologist review in 41% of cases. Regarding neuroradiology second opinions, in general, Briggs et al found a 13% major discrepancy rate for cases specifically requested by clinicians while, in the context of an institutional policy requiring second-opinion consultations on all outside neuroradiology studies, Zan et al found clinically important differences in 8% of cases. It thus appears that discrepancy rates are higher when clinical cases are more frequently complex, as would be expected. It seems that oncology cases, in general, and head and neck oncology cases, in particular, present a challenge to general radiologists. In an effort to guide continuing medical education and quality improvement initiatives, further work is underway to determine the specific imaging findings that most frequently are misinterpreted in head and neck oncology cases.

**KEY WORDS:** Second opinion, head and neck cancer, value added

**O-444**

**4:20 PM - 4:28 PM**

### **Use of Semi-Automated Time-Driven Activity-Based Cost Analysis to Track the Technical Cost of Performing Imaging Studies**

Andoh, H. M.<sup>1</sup>Balkman, J.<sup>2</sup>Cheung, Y. Y.<sup>2</sup>Belden, C. J.<sup>2</sup>

<sup>1</sup>Dartmouth Medical College, Hanover, NH, <sup>2</sup>Dartmouth-Hitchcock Medical Center, Lebanon, NH

#### **PURPOSE**

Tools that enable accurate, reproducible analysis of the direct and indirect costs of performing imaging studies are becoming ever increasingly important. Time-driven activity-based costing (TDABC) analysis has emerged as a technique that is well suited for this purpose. We developed a semiautomated method and spreadsheet model to track the technical cost of imaging studies using TDABC to calculate the technical cost of two common procedures in neuroradiology, MR Brain w/o contrast and MR Lumbar spine w/o contrast, in order to validate the methodology.

#### **MATERIALS & METHODS**

A time motion study of conventional MR Brain w/o contrast and MR Lumbar Spine w/o contrast examinations was performed using stopwatches to time activities to the nearest minute. Timed activities included a) scanner idle time, b) patients changing into gowns, c) patients being brought into the MR room and placed onto the scanner and d) patient dismissal from the MR room, room cleaning and other related activities performed before the next patient. Scan time, defined as the period from start of the first obtained sequence to end of last obtained sequence, was obtained directly from DICOM files through automated export and processing of MR data. Equipment and building costs were calculated using the 3T MR acquisition cost, yearly service and maintenance costs, yearly software and hardware upgrade costs and construction room costs

which included magnetic and RF shielding costs. The combined equipment and building costs were amortized annually over the useful life of the MR machine and these future costs were discounted at 3% per year. Equipment and building use cost per hour then were calculated using the average number of hours each day the MR machine is available for scanning while factoring in an optimal 80% utilization rate. Personnel costs were calculated using annual compensation including fringe benefits divided by the average clinical hours per week.

#### RESULTS

The mean scan time for MR Brain w/o contrast examinations was 24 minutes. The mean scan time for MR Lumbar spine w/o contrast examinations was 23 minutes. After adding statistically allocated fixed costs, digital imaging costs and overhead to the equipment, building and personnel costs, the mean technical cost of a MR Brain w/o contrast examination was \$320 and the mean technical cost of a MR Lumbar spine w/o contrast examination was \$317.

#### CONCLUSION

Time-driven activity-based costing (TDABC) represents a relatively simple, low resource and minimally time-consuming method to develop relevant and accurate cost information on which to base pricing and strategic decisions. Unlike other cost accounting methods in health care which calculate costs based on relative value units or reimbursement for the entire examination, TDABC allows for analysis of the cost of each activity or process within the examination. This approach allows managers to more accurately evaluate the effectiveness of specific initiatives aimed at decreasing costs associated with each activity.

**KEY WORDS:** Cost, economics, MR imaging

## Wednesday Afternoon

**4:45 PM - 6:15 PM**

**Trion Ballroom**

**(54) ASSR PROGRAMMING:  
EPIDEMIOLOGY BASICS FOR SPINE  
IMAGING AND INTERVENTIONS**

**O-445**

**4:45 PM - 5:05 PM**

**Epidemiology of Low Back Pain and Sciatica:  
Historically Fundamental Studies**

Walter S. Bartynski, MD

Radiology, Presbyterian University Hospital  
Pittsburgh, PA, USA

**O-446**

**5:05 PM - 5:25 PM**

**The SPORT Trial: Review of Results for HNP, Stenosis and Spondylolisthesis**

Alan S. Hilibrand, MD

Jefferson Medical College  
Philadelphia, PA, USA

*Dr. Hilibrand is Professor of Orthopaedic Surgery as well as Director of Medical Education for the Department of Orthopaedic Surgery at the Rothman Institute and Jefferson Medical College in Philadelphia. He specializes in the treatment of adult spinal disorders. Dr. Hilibrand has authored or co-authored 130 articles in peer-reviewed journals, including The New England Journal of Medicine and The Journal of the American Medical Association. He currently serves as a deputy editor for The Journal of the American Academy of Orthopaedic Surgeons and The Journal of Bone and Joint Surgery (Am). He was recognized with the Jefferson Medical College AOA Clinical Faculty Teaching Award in 2001 and the Dean's Citation for Significant Contributions to the Advancement of Education in 2004. In the Spring of 2007, he represented the American Orthopaedic Association as an ABC Travelling Fellow. Dr. Hilibrand also recently served as vice-chair to the AAOS Communications Cabinet. Dr. Hilibrand earned his undergraduate degree from the Massachusetts Institute of Technology and his medical degree from the Yale University School of Medicine in New Haven, CT. He completed his Orthopaedic training at the University of Michigan Hospitals in Ann Arbor and a fellowship in spine and spinal cord injury at Case Western Reserve University in Cleveland.*

#### PRESENTATION SUMMARY

The Spine Patient Outcomes Research Trial (SPORT) was the largest federally (NIH) - funded trial in clinical medicine to date. Over two thousand patients at 13 sites around the USA with lumbar disc herniation, lumbar spinal stenosis, and lumbar stenosis with degenerative spondylolisthesis were enrolled and followed for at least five years. SPORT was designed as a randomized clinical trial comparing nonoperative and operative management of patients with these conditions who had failed initial nonoperative treatment, although a parallel observational cohort of patients who chose their treatment was also followed. Despite significant crossover in both randomized and observational cohorts, there was a significantly greater improvement in physical function and significantly less disability and bodily pain among patients who underwent surgical treatment when compared with those who underwent continued nonoperative treatment. Further subgroup analyses of the outcome data from SPORT have been used to better define which patients with these conditions stand to benefit most from operative intervention or nonoperative treatment

**O-447****5:25 PM - 5:45 PM****Objective Outcome Criteria for Assessment Spine Interventional Treatment: Basic Paradigms and Implementation in a Spine Intervention Practice**

Jeffrey G. Jarvik, MD, MPH

Radiology, University of Washington  
Seattle, WA, USA**O-448****5:45 PM - 6:05 PM****The Statistics of Controlled Trials**

Howard E. Rockette, PhD

University of Pittsburgh  
Pittsburgh, PA, USA**PRESENTATION SUMMARY**

When ethical concerns do not preclude its use, the randomized double-blinded clinical trial remains the gold standard of medical research. In this presentation we discuss the advantages of the randomized clinical trial in terms of the important statistical concepts of bias and precision. We consider aspects of the design of a clinical trial as well as standard practices used in the analysis. Design issues covered include eligibility criteria, stratification variables, the role of randomization, specification of the primary hypothesis, the need for interim analysis, and sample size estimation. The discussion on analysis includes the principle of intent to treat, use of confidence intervals, and subgroup analysis. Although randomized clinical trials are the method of choice, they have their problems and limitations and these will be discussed. The presentation is targeted to clinicians who have no formal course work or background in statistics. Examples of randomized trials from the medical literature are provided to illustrate concepts. After attending the presentation, the attendee should (1) understand the advantages and disadvantages of the randomized clinical trial, (2) know the statistical aspects that must be addressed in designing a randomized clinical trial, (3) understand some of the issues that affect the statistical analysis of the trial, and (4) be better able to interpret the results of clinical trials in the medical literature.

**Wednesday Afternoon****4:45 PM - 6:15 PM****Murray Hill****(55) SOCIOECONOMICS  
PROGRAMMING: THE NUTS &  
BOLTS OF HEALTH CARE  
PAYMENT AND REFORM: WHAT  
YOU NEED TO KNOW!****O-449****4:45 PM - 4:58 PM****Current Procedure Terminology (CPT)**

Jacqueline A. Bello, MD

Montefiore Med. Ctr.  
Bronx, NY, USA**PRESENTATION SUMMARY**

CPT®, a registered trademark of the American Medical Association is an acronym for "Current Procedural Terminology". It is a collection of descriptive terms and identifying codes for medical, surgical and diagnostic services and procedures. CPT allows for effective, reliable communication among physicians, other healthcare providers, patients, and third parties. In addition to its use by public and private health insurance programs, CPT is also used for administrative management, and is applicable to medical education & research. The universal nomenclature provides a basis for local, regional, and national utilization comparisons. There are three categories of CPT Codes. Only Category I codes undergo valuation by the RUC for assignment of RVUs. A given service or procedure must meet certain criteria to be designated as a Category I code. These are:

- the service/procedure is FDA approved
- the service/procedure is distinct, and is performed by many physicians/ practitioners across the US
- the service/procedure is **NOT**:
  - A fragment of an existing service/procedure
  - Reportable by one or more existing codes
  - Reporting extraordinary circumstances for an existing code
- the clinical efficacy of the service/procedure is well established and documented in the US peer reviewed literature.

Category II codes are optional codes for performance measurement. These codes facilitate data collection regarding the quality of care, or may relate to compliance with state or federal law.

Category III codes refer to emerging technology. They facilitate data collection and assess new services and procedures for the FDA approval process, and/or to substantiate widespread usage. Category III codes do not indicate that a service is experimental or of limited utility. Payment for these codes is based on the policies of payers and local Medicare Carriers.

The CPT structure and process includes three annual meetings convened by the CPT Editorial Panel. The majority of the 17 member panel consists of physician specialty society representatives. Additional seats are held by non-physician healthcare providers, experts in performance measurement, and representatives from hospitals and payers. The CPT Advisory Committee proposes new codes, or code revisions to the panel for their consideration and action. Standing and ad hoc Workgroups are used to facilitate the process to achieve consensus among various stakeholders in a given code. The Panel will approve, reject or table a code proposal for more information. Once approved, Category I codes are sent to the RUC for valuation.

---

**O-450 4:58 PM - 5:10 PM**


---

**AMA/Specialty Relative Value Scale Updated Committee (RUC)**

William D. Donovan, MD, MPH, FACR

Diagnostic Imaging, William W. Backus Hospital  
Norwich, CT, USA

**PRESENTATION SUMMARY**

The RVS Update Committee establishes RVU values for new/revised medical and surgical procedures. A brief overview of Medicare payment policy with focus on Neuroradiology will be given, along with current radiology-related trends and activities at the RUC.

---

**O-451**


---

**5:10 PM - 5:22 PM**
**Relativity Assessment Workgroup (RAW)**

Geraldine McGinty, MB, MBA

NRAD Medical Associates PC  
Garden City, NY, USA

*Dr Geraldine McGinty is a radiologist in private practice on Long Island. She serves as the ACR's advisor to the Relative Value Update Committee and is the incoming Chair of the ACR's Commission on Economics. She completed her residency at the University of Pittsburgh followed by a fellowship in Womens' Imaging at the Massachusetts General Hospital. She has an MBA from Columbia University.*

Presentation Summary

The Relativity Assessment workgroup and its effect on imaging reimbursement.

---

**O-452**


---

**5:22 PM - 5:34 PM**
**Patient Protection and Affordable Care Act (AC)**

Carolyn C. Meltzer, MD, FACR

Radiology Dept., Emory University School Of Medicine  
Atlanta, GA, USA

**PRESENTATION SUMMARY**

On March 23, 2010, sweeping healthcare legislation, in the form of the *Patient Protection and Affordable Care Act* (PPACA), was signed into law by President Barack Obama. There are many highly interdependent challenges in the current US health care system, including rising costs, variable access and quality, fragmented delivery, geographic workforce misalignments, and barriers to translation of innovation. PPACA focuses most heavily on cost containment and, to a lesser extent, on matters of access and delivery integration. In this presentation we will focus on the portions of PPACA that most directly impact radiologists and their implications for the way we practice today and in the future.

---

**O-453**


---

**5:34 PM - 5:46 PM**
**Accountable Care Organizations**

Suresh K. Mukherji, MD, FACR

Radiology, University of Michigan Health System  
Ann Arbor, MI, USA

**PRESENTATION SUMMARY**

The intent of this presentation is to provide an update of Accountable Care Organizations and opportunities for Radiologists to be participatory in these organizations.

## Wednesday Afternoon

**4:45 PM - 6:15 PM**

**Grand Ballroom Suite**

**(56) SNIS PROGRAMMING: DURAL  
ARTERIOVENOUS FISTULAE**

**O-454**

**4:45 PM - 5:15 PM**

### Diagnosis

Katie D. Vo, MD

Radiology, Mallinckrodt Inst. of Radiology, Washington University  
St. Louis, MO, USA

### PRESENTATION SUMMARY

Intracranial dural arteriovenous fistulae (DAVF) are uncommon vascular lesions and account for 10% of all intracranial arteriovenous malformations. They consist of a group of vascular malformation characterized by either a single or network of abnormal vascular connection between dural arteries and veins. The majority of DAVFs are locating at the skull base and involve the transverse, sigmoid, torcular, or cavernous sinuses. Since venous sinus thrombosis or stenosis is commonly seen at the time of DAVF diagnosis, it has been postulated that the DAVF formation represents an attempt at revascularization and recanalization of the sinus. Clinical manifestations of DAVF are related to location and venous drainage pattern. Clinical diagnosis, classification and imaging findings of DAVF are discussed.

**O-455**

**5:15 PM - 5:45 PM**

### Classification and Natural History

Gregory J. Zipfel, MD

School of Medicine, Washington University in St. Louis  
St. Louis, MO, USA

*Gregory J. Zipfel, MD, FACS, FAHA is Associate Professor of Neurological Surgery and Neurology at Washington University in St. Louis School of Medicine. He is also Co-Director of the Stroke and Cerebrovascular Center and Program Director of the Neurological Surgery Residency Training Program at Washington University. Dr. Zipfel is an expert in the surgical treatment of cerebrovascular disease and skull base tumors. He also directs the Cerebrovascular Research Program in the Department of Neurosurgery at Washington University. This program - which includes both an NIH-funded basic science laboratory and an array of clinical research studies - has three primary areas of interest: 1) Examining the pathophysiologic effects of amyloid- $\beta$  peptide (A $\beta$ ) on cerebral arteriole function and the manner in which these effects contribute to ischemic stroke, intracerebral hemorrhage, and Alzheimer's Disease; 2) Exploring the molecular basis and developing novel therapeutics for*

*vasospasm-induced delayed cerebral ischemia following aneurysmal subarachnoid hemorrhage; and 3) Determining and classifying the pathophysiology and natural history of dural arteriovenous fistulae.*

### Presentation Summary

I will review the definition, epidemiology, classification, and natural history of cranial dural arteriovenous fistulas, with a special emphasis on recent natural history studies and their impact on patient management.

**O-456**

**5:45 PM - 6:15 PM**

### Treatment

DeWitte T. Cross, III, MD

Department of Radiology, Washington University School of Medicine  
St Louis, MO, USA

### PRESENTATION SUMMARY

Dural arteriovenous fistulae may be managed, depending on type and presentation, by observation, endovascular treatment, surgery, radiosurgery, or combined treatment strategies. Endovascular treatment may be performed via trans-arterial, trans-venous, or direct-puncture routes. Embolic agents used for endovascular treatment include Onyx® (ethylene vinyl alcohol copolymer), fibered or detachable platinum microcoils, n-butyl cyanoacrylate (NBCA) glue, polyvinyl alcohol (PVA) particles, and dehydrated alcohol. Treatment is sometimes staged and is often performed under general anesthesia. Goals of treatment are to limit or prevent intracranial bleeding and neurological deficits or to reduce associated symptoms such as intolerable pulsatile tinnitus, chemosis, diplopia, or proptosis. Surgical treatment may be performed to disconnect an arteriovenous fistula from its draining vein(s) or a venous sinus. Complications of treatment include intracranial bleeding and stroke. Recurrences are seen in a minority of successfully treated patients, so follow-up imaging studies are often recommended in addition to clinical follow-up care. These points will be discussed and illustrated.

## Wednesday Afternoon

**4:45 PM - 6:15 PM**

**Beekman/Sutton North**

**(57) ASHNR PROGRAMMING:  
TEMPORAL BONE**



**O-457****4:45 PM - 5:15 PM****The Internal Auditory Canal: Anatomy and Pathology**

John I. Lane, MD

Radiology, Mayo Clinic  
Rochester, MN, USA**PRESENTATION SUMMARY**

This presentation will focus on the anatomy and pathology of the internal auditory canal. Imaging techniques to include high resolution multidetector CT and MR will be discussed. The imaging characteristics of major pathologic entities involving the IAC encountered in the work-up of 7th and 8th cranial nerve deficits will be covered. The discussion will also familiarize the audience with the different surgical approaches to the resection of IAC masses and its expected post-operative imaging appearance.

**O-458****5:15 PM - 5:45 PM****Temporal Bone Neoplasia**

H. Ric Harnsberger, MD

University Of Utah  
Salt Lake City, UT, USA**PRESENTATION SUMMARY**

In this presentation an anatomy-based differential diagnosis list of tumors that are found in the external auditory canal (EAC), middle ear, inner ear, and facial nerve will be reviewed. In each location the specific imaging findings of the tumors found there will be presented. Each tumor discussion will contain information regarding clinical presentation, CT and MR findings, and differential diagnosis. Where possible, characteristic imaging findings unique to a specific tumor will be highlighted.

By area benign and malignant tumors reviewed include:

External auditory canal

Benign: Exostoses, osteoma

Malignant: EAC squamous cell carcinoma

Middle ear

Benign: Glomus tympanicum & jugulare paraganglioma, facial nerve schwannoma, adenoma and meningioma, Langerhans cell histiocytosis

Malignant: Rhabdomyosarcoma

Inner ear

Benign: Intralabyrinthine schwannoma, endolymphatic sac tumor, meningioma

Facial nerve

Benign: Facial nerve schwannoma, facial nerve hemangioma (venous malformation)

Malignant: Perineural parotid malignancy

**O-459****5:45 PM - 6:15 PM****Acute and Chronic Inflammatory Disease of the Temporal Bone**

Joel D. Swartz, MD

Germantown Imaging  
Gladwyne, PA, USA**PRESENTATION SUMMARY**

Temporal bone inflammatory disease is usually organized into three anatomic regions: (1) the external ear, (2) the middle ear, mastoid, and petrous apex and (3) the inner ear. Acute external otitis is the most common external ear infection. Chronic external otitis often occurs secondary to subepithelial infiltration of inflammatory cells and may result in a fibrous plug, most common at the medial margin of the bony EAC in direct apposition to the tympanic annulus (medial canal fibrosis). Necrotizing external otitis (NEO) or malignant external otitis typically presents with otorrhea and severe otalgia in diabetics. *Pseudomonas aeruginosa* is the most common pathogen. As with the middle ear variety, external auditory canal cholesteatoma (EACC) is caused by the disruption of normal lateral migration of keratin debris from the tympanic membrane. Keratosis Obturans (KO) occurs in a younger age group than EACC. These patients often present with severe pain and conductive hearing loss; otorrhea is rare. Unlike EACC, KO is commonly associated with sinusitis and bronchitis. Despite the obvious interrelationship, acute otomastoiditis (AOM) and chronic otomastoiditis (COM) are two different disease processes. AOM is usually caused by bacterial infection, and chronic otomastoiditis by eustachian tube dysfunction. Similarly, each disease has its own specific set of complications. With respect to AOM, complications include coalescence, subperiosteal abscess, labyrinthitis, petrous apicitis, as well as intracranial involvement such as meningitis, abscess formation, and dural sinus occlusive disease. COM may result in middle ear effusion, tympanic membrane retractions, acquired cholesteatoma, granulation tissue, cholesterol granuloma, ossicular fixation, and ossicular erosion. Facial nerve dysfunction may occur as a result of acute or chronic disease. Labyrinthitis is an inflammatory disease of the perilymphatic spaces of the inner ear which result in secondary changes within the endolymphatic spaces (membranous labyrinth). The sole imaging finding in individuals with acute/subacute labyrinthitis is enhancement of the normally nonenhancing fluid-filled spaces of the labyrinth as seen on contrast-enhanced T1-weighted images. If acute labyrinthitis does not resolve, a progression to chronic disease initially results in fibrous changes followed by ossification in a process transpiring over as little as a few weeks to several years.

## Wednesday Afternoon

**4:45 PM - 6:15 PM**

**Sutton Center/South**

**(58) ADVANCED IMAGING  
SEMINAR: FASTER AND FASTER**

**O-460**

**4:45 PM - 5:15 PM**

### **Fast MRI**

Daniel K. Sodickson, MD, PhD

Radiology, NYU Langone Medical Center  
New York, NY, USA

*Dr. Sodickson is Vice-Chair for Research and Director of the Bernard and Irene Schwartz Center for Biomedical Imaging in the Department of Radiology at NYU Langone Medical Center. He received a B.S. in Physics and a B.A. in Humanities from Yale College. He earned his Ph.D. in Medical Physics from MIT and his M.D. from Harvard Medical School, both as a part of the Harvard-MIT Division of Health Sciences and Technology (HST). In 1996-7, he introduced the SiMultaneous Acquisition of Spatial Harmonics (SMASH) technique, and he has been involved ever since in the ongoing development of parallel MRI. Dr. Sodickson is a Fellow of the International Society for Magnetic Resonance in Medicine (ISMRM), and, in 2006, he received the ISMRM's highest honor, the Gold Medal, for pioneering scientific contributions to magnetic resonance in medicine and biology. His current research centers on new approaches to the formation and use of medical images, through basic development and clinical application of rapid MRI, exploration of the fundamental capabilities of high-field MRI, investigation of new scanner architectures, and noninvasive detection of tissue electromagnetic properties.*

### **PRESENTATION SUMMARY**

This presentation will review recent advances in rapid magnetic resonance imaging, in historical context and with an eye towards how these advances promise to change the way day-to-day imaging is performed and interpreted. Particular emphasis will be placed on the burgeoning new field of compressed sensing for rapid medical imaging. In essence, compressed sensing represents a form of "pre-compression," which allows dramatic reductions in the number of data points required to generate a complete image. Rather than devoting precious scan time to the acquisition of a traditionally defined complete dataset in order to create images whose inconsequential features would only be discarded by a faithful image compression algorithm, compressed sensing techniques take advantage of the knowledge that nearly all images in medicine (and, for that matter, in nature) may be faithfully represented by a number of parameters smaller than the number of voxels. This knowledge, combined with appropriate irregular sampling and nonlinear reconstruction

strategies, enables reconstruction of images from highly undersampled, and hence highly accelerated, datasets. Unlike other constrained or model-based image reconstruction approaches, compressed sensing techniques do not ever presuppose which are the most important image features, and they can therefore be remarkably successful in preserving true image content in a largely unbiased fashion. In the presentation, basic principles of compressed sensing will be reviewed, productive combinations with parallel imaging in suitable detector arrays will be discussed, and various practical methods and applications (in neuroimaging and elsewhere) will be surveyed. The presentation will conclude with an exploration of how, in addition to providing access to new spatial and temporal scales, modern rapid imaging techniques such as compressed sensing may change the way clinicians and researchers look at images, and may even require re-evaluation of what we mean by an "image."

**O-461**

**5:15 PM - 5:45 PM**

### **Fast CT**

Howard A. Rowley, MD

Radiology Dept., Univ. Of Wisconsin  
Madison, WI, USA

### **PRESENTATION SUMMARY**

CT protocols can be made both better and faster. Strategies for improvement include larger array scanners, streamlined workflow which prospectively identifies some patients for comprehensive CT-CTA-CT perfusion exams, and combined CT perfusion - time resolved CT angio techniques using a single injection. A key goal in acute stroke imaging triage is to capture comprehensive multimodal CT studies quickly and efficiently during the first "Golden Hour" after presentation. Done properly, comprehensive CT protocols need not slow down time to decision for TPA, can provide added diagnostic value, and are cost-effective. Radiation dose limitation and reduction can easily be achieved through a variety of approaches, while still maintaining high quality.

**O-462**

**5:45 PM - 6:15 PM**

### **Fast Spectroscopy**

Peter B. Barker, D.Phil. PhD

Radiology, Johns Hopkins University  
Baltimore, MD, USA

## Thursday Morning

**7:30 AM - 8:30 AM**  
**Grand Ballroom Suite**

**(59) MAINTENANCE OF  
 CERTIFICATION (MOC) - REVIEW  
 SESSION (AR) SPINE**

**O-463** **7:30 AM - 8:30 AM**

**Maintenance of Certification (MOC) - Review Session  
 (AR) Spine**

Jeffrey S. Ross, MD

Neuroradiology, Barrow Neurological Institute, St.  
 Joseph's Hosp.  
 Phoenix, AZ, USA

### PRESENTATION SUMMARY

MOC type spine pathology is presented with appropriate differential diagnostic possibilities

**O-464** **7:30 AM - 8:30 AM**

**Maintenance of Certification (MOC) - Review Session  
 (AR) Spine**

Michael T. Modic, MD

Cleveland Clinic Foundation  
 Cleveland, OH, USA

## Thursday Morning

**8:30 AM - 10:00 AM**  
**Grand Ballroom Suite**

**(60) ASSR PROGRAMMING: THE  
 SACROILIAC JOINT AND PELVIS:  
 IMAGING AND INTERVENTIONS  
 (SAM #5) \*(AR)**

\*Qualified by the American Board of Radiology (ABR) in meeting the criteria for Self-Assessment towards the purpose of fulfilling requirements in the ABR Maintenance of Certification program data 3/12.

**O-465**

**8:30 AM - 8:50 AM**

**Anatomy and Imaging of the SIJ and Pelvis for the  
 Spine Interventionalist**

Alyssa T. Watanabe, MD

Voxel Imaging, Inc., USC School Of Medicine  
 Manhattan Beach, CA, USA

### OBJECTIVES:

1. Discuss the anatomy of the sacro-iliac joint and sacrum
2. Understand methods for imaging sacral anatomy and pathology and relevance for spinal interventions

### PRESENTATION SUMMARY

The sacrum is a large triangular and complex bone at the caudal end of the spinal axis. There are five sacral segments. The intervertebral disc spaces of the sacrum are typically fused by the third decade. The sacral hiatus represents an aperture in the posterior wall of the caudal sacrum marked by the unfused sacral cornua of S5. This aperture is utilized for caudal epidural injections. The thecal sac typically ends at S2 but may end as low as S4. The sacral hiatus may be absent in a small percentage of patients. The sacrum tends to have a more acute curve in females than males.

The sacral ala are found lateral to S1 and are a common site of insufficiency fracture. Sacroplasty has been employed for treatment of these fractures, and the challenge is in treating the large surface area of these wing-shaped bones. The anatomy, fracture patterns, and various fluoroscopic projections and techniques for visualizing and approaching sacral fractures will be discussed.

There are four paired sacral foramina, located inferior to the promontory and medial to the lateral masses of the sacrum. The anterior foramina are larger than the posterior foramina.

The sacro-iliac joints are comprised of the ligamentous (2/3) and synovial (1/3) components. Sacro-iliac joint injections are directed to the synovial part of the joint which is in the caudal part of the joint. The posterior joint is medial to the anterior joint. Treatment of the S-I joint with radiofrequency requires knowledge of the complex and rich neural innervation of this area.

The L4 and L5 nerves comprise the lumbosacral trunk. The sciatic nerve is comprised of the lumbosacral trunk plus S1-S3 nerve contributions. Oblique axial imaging is the key sequence for evaluating for piriformis syndrome. An entrapped nerve may demonstrate increased T12 signal, enlargement, abnormal enhancement which is typically focal. Examples of the L5 nerve root sign will also be presented. Imaging techniques for depicting and diagnosing nerve entrapment syndromes will be covered.

O-466

8:50 AM - 9:10 AM

### Innervation of the Sacroiliac Joint: Implications for Diagnostic Testing and Selection for RF Ablation

Paul Dreyfuss, MD

Washington Interventional Spine Associates  
Kirkland, WA, USA

#### PRESENTATION SUMMARY

The sacroiliac joint has the necessary anatomical substrate to be painful. In patients with persistent pain after lumbosacral arthrodesis there is a 32% prevalence of sacroiliac joint pain whereas in those with chronic low back pain the prevalence is 10-15%.

The specificity of intra-articular blocks is limited. Local anesthetics injected into the joint can escape, through defects in the ventral or dorsal capsule, and can anesthetize nearby structures. Additionally, intra-articular blocks might anesthetize the synovial portion of the joint, but they do not necessarily anesthetize the interosseous or dorsal sacroiliac ligaments which could be an additional or alternative source of pain.

An alternative to intra-articular injections are nerve blocks, in which the nerves that supply the joint are anesthetized. Some investigators maintain that the joint is innervated both posteriorly and anteriorly. Others maintain that the innervation is exclusively posterior stemming from the lateral branches of the sacral dorsal rami. Thus, the innervation of the sacroiliac joint has not been properly resolved to determine if blockade of the accessible sacral lateral branches would adequately anesthetize the joint.

One method of testing the validity of diagnostic nerve blocks in this context is to perform the blocks on normal volunteers to see if they are protected from experimentally-induced pain from the target structure. When this was done for conventional (single site, single depth) sacral lateral branch blocks (LBBs), they were found to be ineffective in protecting volunteers from pain evoked from either the sacroiliac joint or its posterior ligaments. The deficiency of the single site, single depth technique arose because sacral lateral branches vary in depth and location. In order to accommodate these variations, a multi-site, multi-depth technique was developed. A subsequent randomized placebo controlled study demonstrated that active multi-site, multi-depth LBBs blocks protected 70% of normal volunteers from pain evoked from the interosseous and dorsal sacroiliac ligaments. This proportion was significantly different from that observed in the volunteers who received placebo injections confirming the affect was not attributable to placebo.

There were only a small proportion of subjects in this study who were protected from intraarticular pain when LBBs were shown to be physiologically effective. The inability of LBBs to reliably anesthetize the intraarticular portion of the sacroiliac joint indicates the joint must have an innervation that is not exclusively through the sacral lateral branches. An additional ventral innervation is likely.

LBBs can be used as a test specifically for pain stemming from the posterior sacroiliac ligaments, but

they do not replace intra-articular blocks. Intraarticular blocks test for intraarticular joint pain, and LBBs primarily test for ligament pain. Thus, these tests are complementary.

Sacral lateral branch radiofrequency (RF) neurotomy has been used to treat sacroiliac joint pain. Although intraarticular blocks have been used to select patients for RF neurotomy in light of current data, intra-articular blocks should no longer be the primary prognostic test for subsequent sacroiliac joint neurotomy. More compelling would be relief of pain following controlled blocks of the sacral lateral branches. In principle, this diagnostic test should yield more robust outcomes from lateral branch RF neurotomy than have been reported to date. This is analogous to the validated use of medial branch blocks and not intrarticular joint blocks for selection of patients for medial branch RF neurotomy in the cervical and lumbar spine.

O-467

9:10 AM - 9:30 AM

### Diagnostic and Therapeutic Injections of the Sacroiliac Joint and Pelvis

Jeffrey A. Stone, MD

Radiology, Mayo Clinic Florida  
Jacksonville, FL, USA

#### PRESENTATION SUMMARY

There are a host of conditions that present with pain in the low back, gluteal and pelvic region that are not attributable to degenerative lumbar spine disease. Familiarity and recognition of these entities is important for accurate diagnosis and treatment. Sacroiliac joint (SIJ) pain is a very common cause of low lumbar and gluteal pain and causes significant morbidity and loss of function. It is often the result of osteoarthritis of the synovial portion of the joint and may also be related to instability of the joint particularly after trauma. The complex innervation of the SIJ makes treatment difficult. Various injection techniques have been utilized to treat SIJ pain refractory to medications and physical therapy including intra-articular and periarticular injections of anesthetic and steroid as well as hypertonic dextrose (prolotherapy) in an effort to strengthen the ligaments that support the SIJ. Surgical options remain limited in the treatment of this difficult disease.

Pain in the sacrococcygeal region often occurs after trauma or childbirth and is referred to as coccygodynia. It is most problematic with the seated position and is often difficult to control with conservative therapies. There are also several pelvic region conditions that can mimic spinal origin radicular syndromes. Piriformis syndrome is a distinct entity due to dysfunction or inflammation of the piriformis muscle and results in localized pain and sciatica due to its intimate anatomic relationship with the sciatic nerve. Peri-anal or groin pain can be seen as a result of injury or compression of the pudendal nerve as it enters the pelvis. Lateral thigh pain suggesting lower lumbosacral radiculopathy may be the result of trochanteric bursitis. It is easily differentiated however; on physical exam by local tenderness

These entities can often be differentiated based on clinical presentation, physical exam, imaging and electrodiagnostic studies. The radiologist may play a role in the treatment of these conditions when they are refractory to non-interventional therapies and image guided injection can assist in their treatment. This lecture covers the typical presentation, diagnosis and interventional treatment options for these disorders as well as existing evidence for their efficacy.

**O-468****9:30 AM - 9:50 AM**

### **RF Ablation of the SIJ: Review of Technique Options and Treatment Success**

Wade H. M. Wong, DO

Radiology Dept, UCSD Medical Center  
San Diego, CA, USA

#### **PRESENTATION SUMMARY**

This presentation will discuss the role of Radiofrequency denervation of the SIJ particularly when traditional intraarticular steroid injection therapy for chronic painful sacroiliitis is effective but disappointingly short lasting. The complex innervation of the SIJ will be reviewed. Considering that the L5 dorsal ramus, and the lateral branches of S1, S2, and S3 are most conventionally targeted, a variety of methods for performing Radiofrequency Ablation will be described including the common monopolar and bipolar techniques in addition to the newer needle arrayed Simplicity and the Sinergy cooled RF techniques. Results from the literature will be reviewed as to both short and long term efficacy. In addition practical technical pitfalls and pearls from personal experience will be included.

This presentation is appropriate for Neuroradiologists and other physicians who perform image guided interventions for back pain.

## **Thursday Morning**

**8:30 AM - 10:00 AM****Trianon Ballroom**

**(61) COLLABORATION WITH  
EUROPEAN SOCIETY OF  
NEURORADIOLOGY (ESNR): WHITE  
MATTER DISEASES**

**O-469****8:30 AM - 8:50 AM**

### **State of the Art MR Imaging of Multiple Sclerosis and Other Demyelinating Disease**

Frederik Barkhof, MD

Image Analysis Centre (IAC) & Department of  
Radiology, VU University Medical Center  
Amsterdam, Netherlands

*Frederik Barkhof received his MD from VU University, Amsterdam, The Netherlands in 1988 and defended his PhD in 1992, for which he received the Philips Prize for Radiology in 1992 and the Lucien Appel Prize for Neuroradiology in 1994. He currently serves as a full Professor in Neuroradiology at VU University Medical Centre. He is a senior staff member of the MS Center Amsterdam, and senior consultant of the Alzheimer Center, Amsterdam. He is the Scientific Director of the Image Analysis Centre (IAC), involved in analysis of multicentre drug trials. Prof. Barkhof is the chairman of the Dutch Society of Neuroradiology and the MAGNIMS study group. He serves on the Editorial boards of Brain, Eur Radiology, Neuroradiology, and Journal of Neurology. Prof. Barkhof's research interests focus on multiple sclerosis (spinal cord MRI, grey matter, atrophy, histopathology correlations), on ageing (white matter lesions and microbleeds), and on dementia (hippocampal atrophy in Alzheimer and functional MR). He authored more than 570 papers referenced in PubMed, has an H-factor of 75 and is author of the books "Neuroimaging in Dementia" and "Clinical applications of functional brain MRI".*

#### **PRESENTATION SUMMARY**

For diagnostic purposes, MRI is often used to demonstrate dissemination of lesions in the CNS in patients with multiple sclerosis (MS), with special relevance for juxtacortical, periventricular and infratentorial brain lesions. In the McDonald diagnostic criteria for MS, MRI can also provide evidence for dissemination in time, allowing an even earlier diagnosis and treatment initiation in MS, certainly now the 2010 revision considers the simultaneous occurrence of enhancing and non-enhancing lesions seen on a single scan as evidence for dissemination in time. The occurrence of spinal cord lesions is quite specific for MS, especially in elderly subjects and may help to avoid false-positive diagnosis. New developments like DIR hold great promise, but await validation in a multicenter setting.

Serial MRI shows a vast amount of disease activity that goes undetected clinically. To a large extent, the significance of such subclinical activity remains undetermined. The number of active (gadolinium-enhancing) lesions is closely linked to (concurrent) relapse-activity, but its predictive value wears off over time, and the predictive value for evolution of disability is limited (as is the case for relapses). Measures of cerebral atrophy from (serial MRI) may prove more effective in this regard. While MRI plays a major role in evaluating the effect of new therapies in randomized clinical trials, its importance in monitoring individual patients remains uncertain. If any, the usefulness of MRI may be to rule out subclinical relapses in patients, when



there is doubt about the institution or modification of anti-inflammatory treatment. MRI is used to monitor side-effects, such as PML

**O-470**

**8:50 AM - 9:10 AM**

**Pediatric Multiple Sclerosis, ADEM and Other Demyelinating Diseases: Where Do We Stand?**

Andrea Rossi, MD

Head, Neuroradiology, G. Gaslini Children's Hospital  
Genoa, Italy

**PRESENTATION SUMMARY**

This presentation will focus on the peculiarities of multiple sclerosis presenting in children as well as on other pediatric demyelinating diseases, including acute disseminated encephalomyelitis and its variants, and neuromyelitis optica. Other immune mediated encephalopathies will also be covered.

**O-471**

**9:10 AM - 9:30 AM**

**Demyelinating Diseases of the Spinal Cord**

Majda M. Thurnher, MD

Department of Radiology, Medical University Vienna  
Vienna, Austria

**PRESENTATION SUMMARY**

The most common demyelinating diseases affecting the spinal cord are multiple sclerosis (MS), acute disseminated encephalomyelitis (ADEM), neuromyelitis optica (NMO) and transverse myelitis (TM). Recent studies have clearly shown complexity and heterogeneity of demyelinating diseases indicating the need of redefinition of current concepts and classification. Multiple Sclerosis (MS) is by far the most common demyelinating disorder.

MS lesions have been found in the spinal cord up to 99% of autopsy cases. Additionally, diffuse changes and spinal cord atrophy may be present. Spinal cord atrophy correlates with clinical disability, it is more prominent in the upper part of the cord, and the duration of the disease is the most important determinant of cord atrophy. Post-mortem studies have shown that cord damage is not limited to lesions visible on T2-WI

Neuromyelitis optica (NMO) has been known as Devic's disease causes extensive demyelination of optic nerve and of the affected segments of the spinal cord. Discovery of highly specific NMO-antibody (anti-aquaporin-4-antibody) with high sensitivity and specificity for NMO has significantly improved the early diagnosis of NMO. A new concept of "NMO spectrum disorders" was recently introduced.

Acute disseminated encephalomyelitis is an immune-mediated inflammatory CNS disorder, frequently affecting the spinal cord. Recent studies have shown that the anti-myelin oligodendrocyte glycoprotein (MOG) humoral immune response is exclusively found in pediatric patients with demyelinating CNS disorders. In children suspected to be affected by ADEM, the measurement of highly

reactive anti-MOG IgG may help to differentiate from acute encephalitis.

There is also growing evidence that the length of the lesion in acute transverse myelitis (ATM) is likely important from pathogenic and prognostic standpoint. Patients with acute partial TM (APTM) have lesion extending less than 2 segments on MRI, and those with acute complete (ACTM) have abnormalities extending for multiple segments. Patients in the first group are at higher risk for developing MS in comparison to those in the second group where the risk is very low.

In this lecture imaging findings as well as new pathogenetic concepts of demyelinating diseases affecting the spinal cord will be discussed.

**O-472**

**9:30 AM - 9:50 AM**

**White Matter Damage in Neurodegenerative Diseases Assessed Using Advanced MRI Techniques**

Federica Agosta, MD

San Raffaele Scientific Institute, Vita-Salute San Raffaele University  
Milan, Italy

*Federica Agosta was born in Milano on 01/04/1978, took her Graduation in Medicine in 2003 and her Post-Degree Graduation in Neurology in 2008. Federica Agosta has a broad background in clinical neurology and neuroimaging, with specific training and expertise in neurodegenerative diseases. As research fellow at the Scientific Institute San Raffaele, Milan, Italy she collaborated in several research projects on the use of conventional and quantitative MRI in the study of normal aging, ALS, PD, and MS. As a postdoctoral fellow at the Memory and Aging Center, UCSF, she expanded her knowledge on AD, frontotemporal dementia, and primary progressive aphasia. Federica Agosta is currently a clinical researcher at the Institute of Experimental Neurology, University Vita-Salute San Raffaele, Milan, Italy, where she conducts research projects in patients with dementia and other neurodegenerative conditions. She is member of the ENS, in which she participates actively to the Neuroimaging Subcommittee, and Neuroimaging Symposium in ALS. Dr. Agosta is author or co-author of more than 100 scientific papers published on peer-reviewed journals (H index: 20).*

**PRESENTATION SUMMARY**

Neurodegenerative diseases are progressive, hereditary or sporadic diseases. Progressive neurodegeneration of the nervous system may cause loss of movement ability, like in motor neuron diseases and movement disorders, or cognitive deficits, like in dementia. Methods for early detection of specific disease processes need to be identified and reliable techniques for monitoring disease progression will likely be critical in demonstrating the effects of disease-modifying therapies when available. Structural MRI showed that each syndrome is associated with a specific pattern of brain atrophy. White matter (WM) alterations are also a major pathological characteristic of neurodegenerative diseases. By measuring directional changes in water diffusivity, diffusion tensor (DT) MRI allows to investigate brain WM microstructure. DT MRI studies

provided insights into the similarities and differences of the spatial patterns of WM damage in different neurodegenerative conditions. Moreover, studies combining the assessment of grey matter and WM damage in these patients suggested that WM alterations may be due either to axonal degeneration associated with injury/death of neuronal cell bodies or to pathological protein deposition in the WM of the affected brain regions. In conclusion, advanced MRI techniques investigating WM damage are useful to enrich our understanding of pathophysiology of neurodegenerative processes. As the biology of these diseases is elucidated, hope is beginning to emerge for specific treatments targeted at modification of pathological processes, which most likely will require objective and accurate markers to monitor their efficacy, such as those offered by neuroimaging.

## Thursday Morning

**8:30 AM - 10:00 AM**  
**Beekman/Sutton North**

**(62) SOCIOECONOMIC  
 PROGRAMMING: CURRENT ISSUES  
 IN STROKE IMAGING AND  
 TREATMENT: WHAT IS THE  
 EVIDENCE?**

**0-473** **8:30 AM - 8:50 AM**

### **How Much Evidence is Truly Available?**

Pina C. Sanelli, MD, MPH

Radiology, Weill Cornell Medical College  
 New York, NY, USA

#### **PRESENTATION SUMMARY**

A review of the principles and goals in evidence based medicine will be presented. The evidence pyramid will be reviewed to demonstrate the different levels of evidence available for application in addressing current day medical questions. Specifically, the available evidence to support acute stroke imaging algorithms and treatment protocols will be discussed.

**0-474** **8:50 AM - 9:15 AM**

### **Neuroimaging In Acute Ischemic Stroke**

Katie D. Vo, MD

Radiology, Mallinckrodt Inst. of Radiology, Washington  
 University  
 St. Louis, MO, USA

#### **PRESENTATION SUMMARY**

Stroke is the fourth leading cause of mortality after heart disease, cancer and chronic lower respiratory disease, accounting for 134,000 deaths per year in the United States. The socio-economic impact from the disease is equally high. It is the leading cause of severe long-term disability and the leading diagnosis from hospital to long-term care. The estimated direct and indirect costs of stroke totaled 74 billion dollars in 2010 with 60% of the cost related directly to medical expenditures. Acute inpatient hospital cost accounts for 70% of the first-year post-stroke costs with diagnostic tests during the initial hospitalization contribute nearly 20% to total hospital costs. The cost relating to neuroimaging will likely increase with time as it is not only being used to diagnosis but also to select patient with focal ischemia for thrombolytic and interventional thrombectomy. The focus of this talk is on the neuroimaging of acute ischemia within the first few hours of stroke onset when issues relating to therapeutic decision-making are of paramount importance. The goals of neuroimaging in patients presenting with acute neurological deficits and suspected ischemic stroke, and the levels of evidence for its use in this population will be discussed.

**0-475** **9:15 AM - 9:45 AM**

### **Endovascular Treatment of the Stroke Patient**

Danial K. Hallam, MD, MSc

Radiology, University of Washington  
 Seattle, WA, USA

#### **PRESENTATION SUMMARY**

The lecture examines evidence regarding endovascular treatment of acute ischemic stroke. Extensive data support the value of specialized stroke centers in improving outcome. As IV treatment directly impacts the decision as to when and how to treat by endovascular means, data summarizing IV treatment will be discussed. Currently, IV thrombolysis is the standard of care for treatment of acute anterior ischemic infarct within 3 hours of symptom onset and may reasonably be used up to 4.5 hours. Data supporting IV treatment is level 1, as is data to support IA thrombolysis. Intra-arterial thrombolysis may be used at a qualified stroke center to treat patients with major stroke due to MCA occlusion < 6h who cannot receive IV alteplase. In consideration of the need to proceed with IA treatment, especially by mechanical means, evidence suggests lower canalization rates of large more proximal clots with IV treatment. Noting the correlation of revascularization with outcome, these data support proceeding to endovascular approach in a patient already undergoing IV treatment with known large proximal clot. The FDA has approved two devices for mechanical intracranial clot retrieval, Merci Retriever and Penumbra System. Although considered appropriate for emergency stroke treatment, the effect on outcomes of these two systems has not been established. Recent interest focuses on the use of self-expanding removal stents for revascularization in acute stroke. A multi-center trial comparing this technique to

the Merci clot retrieval device is nearing completion. Other stents along with angioplasty have been employed but there is insufficient data to support their utility.

## Thursday Morning

**8:30 AM - 10:00 AM**  
**Sutton Center/South**

(63) Interventional and Spine:  
 Miscellaneous

**O-483** **8:30 AM - 8:38 AM**

### **Patients Presenting with Cranial Nerve(s) Paresis/Palsy Due to an Intracranial Aneurysm: Clinical Results after Treatment Using Flow Diversion Stenting**

Biondi, A.<sup>1</sup>•Jirari, M.<sup>1</sup>•Clarençon, F.<sup>2</sup>•Vuillier, F.<sup>1</sup>•Cattin, F.<sup>1</sup>

<sup>1</sup>Besancon University Hospital, Besancon, FRANCE,

<sup>2</sup>Pitié-Salpêtrière Hospital, Paris, FRANCE

#### **PURPOSE**

To evaluate clinical results after endovascular treatment using flow diversion stenting (FDS) in patients with cranial nerve(s) paresis/palsy due to an intracranial aneurysm.

#### **MATERIALS & METHODS**

Fourteen patients with 16 unruptured aneurysms responsible for cranial nerve(s) paresis/palsy. All aneurysms were located in the internal carotid artery and were large/giant. Clinical evaluation before treatment, after treatment, at 1 month and one year follow up was performed independently. Results were compared to a group of 10 patients with cranial nerve(s) paresis/palsy due to an intracranial aneurysm treated by coils and a group of 10 patients treated by parent artery occlusion.

#### **RESULTS**

After treatment, transient worsening of cranial nerve(s) deficits was observed in two patients. In two patients no improvement was observed despite of treatment. At 1 month transient worsening of cranial nerve(s) deficits was observed in five cases. Symptoms resolved after steroid therapy in four cases and persisted in one. One-year follow-up results are under analysis. Preliminary data seem to suggest that symptoms due to cranial nerve involvement regress or disappear more rapidly in the group of patients treated by PAO while at 1-year follow up there are not significant differences.

#### **CONCLUSION**

The advent of FDS represents an important step in the therapy of large/giant aneurysms in patients presenting

with cranial nerve(s) paresis/palsy. The obvious advantage of the FDS therapy is the preservation of the parent artery. At long-term follow up clinical results are similar to those obtained with other endovascular technique.

**KEY WORDS:** Flow diverting stent, aneurysm, stenting

**O-484**

**8:38 AM - 8:46 AM**

### **Surpass Flow-Disruption Device for Endovascular Treatment of Distal Aneurysms beyond the Carotid and Basilar Arteries: Clinical and Angiographic Results**

de Vries, J.<sup>1</sup>•Wakhloo, A.<sup>2</sup>•Lylyk, P.<sup>3</sup>•Boogaarts, J.<sup>1</sup>

<sup>1</sup>Radboud University Medical Center Nijmegen, Nijmegen, NETHERLANDS, <sup>2</sup>University of Massachusetts, Worcester, MA, <sup>3</sup>ENERI, Clínica Médica Belgrano, Buenos aires, ARGENTINA

#### **PURPOSE**

A new generation of flow disruption (FD) device (Surpass FD, Tel Aviv, Israel) was used for distal aneurysms beyond the carotid and basilar arteries.

#### **MATERIALS & METHODS**

A total of 15 aneurysms in 13 patients were treated. Four aneurysms originated in the M2 segment, two in the MCA bifurcation, one in the M1 segment, one in the M3 segment, two in the ACoA, one in the A1 segment, one in the A2 segment, and three in the P2/P3 segment. Nine aneurysms were of fusiform/dissecting type and six were saccular. To achieve the calculated flow disruption between the parent artery and aneurysm and required for an occlusion, single devices, tailored to local boundary conditions, were placed endovascularly in parent arteries and covering the aneurysm. Implanted devices measured 2.9 mm in diameter with a length of 15-20 mm. Immediate control angiography demonstrated various degrees of flow reduction within aneurysm up to a complete flow stagnation.

#### **RESULTS**

There was no postprocedural neurologic morbidity and mortality. Procedure-related thromboembolic complications were seen in two patients and resolved after administering of Abciximab in both. None of the patients ruptured their aneurysm during follow up. Results of 6 months follow-up angiography will be presented.

#### **CONCLUSION**

Preliminary data demonstrate the safety and feasibility of a new generation of FD device in the treatment of distal aneurysms beyond the carotid and basilar arteries.

**KEY WORDS:** Flow diverter, aneurysm, intracranial

**O-485****8:46 AM - 8:54 AM****Pipeline Flow Diverter Stents for Endovascular Treatment of Intracranial Aneurysm in Hong Kong Chinese Populations**

Lo, S. S. M.·Cheung, Y. L.·Tang, K. W.·Chan, C. M.·Cheng, K. M.

Queen Elizabeth Hospital  
Kowloon, HONG KONG**PURPOSE**

Pipeline embolization device (PED) was approved by FDA to treat wide-necked cerebral aneurysms. The safety of the procedure and aneurysm outcome are still equivocal, especially for small ( $\leq 3$  mm) aneurysms. Our aim of this study was to evaluate the safety, efficacy and complication rate of the PED in the treatment of nonrupture and rupture wide neck intracranial aneurysms in local Chinese population.

**MATERIALS & METHODS**

Pipeline embolization device were performed in patients with ruptured or unruptured aneurysms that were wide neck ( $>4$  mm or dome-neck ratio  $<1.5$ ), or had failed previous treatment. We prospectively evaluate all patient performed PED since 2008. All patients were pretreated with dual antiplatelet medication and continued taking both drugs for at least 6 months after operation. A control digital subtraction angiogram (DSA) was performed at 6 months after the operation. Angiographic and clinical results were recorded after treatment and at 6 months following operation.

**RESULTS**

Thirty-eight patients with 42 intracranial aneurysms (31 female; 20-80 years of age; average age, 55; 20 ruptured and 22 unruptured aneurysms) were treated with PED since 2008. A total of 48 PEDs were used. Aneurysm size ranged from 2 mm-27 mm, with 17 (40%) aneurysm  $\leq 3$  mm in size. All aneurysms were wide neck except two, with a mean dome-neck ratio of 1.25. Pipeline embolization device placement was technically successful in all patients. Thirty aneurysms were treated by implantation of PEDs alone and 12 by a combination of PED and coils. Single PED was placed in 31 aneurysms, with two overlapping PEDs in seven aneurysms, and three overlapping PEDs in one aneurysm. Immediate angiographic occlusion was achieved in two and significant flow reduction in another 26 aneurysms. Six-month follow-up angiography were performed in 27 patients (31 aneurysms; 16 unrupture and 15 rupture), which demonstrated complete occlusion in 28 (90%) and partial filling in three (10%) out of 31 aneurysms. Eight patients were pending follow up and three patients did not have follow-up angiography. No aneurysm demonstrated a deterioration of angiographic occlusion during the follow-up DSA. There were a total of five (13%) major complications (permanent stroke or death) encountered after the procedure. Four occurred in ruptured group and one in unruptured group. Three patients (8%) experienced major periprocedural stroke

or intracranial hemorrhage; and two procedure-related deaths within the study period, one is related to delay rupture of an aneurysm with PED alone treatment, another is related to massive cerebral infarction. The clinical outcome for PED treated unrupture group was excellent, all patients have full GCS score and Modified Rankin Scale (mRS) of 0 at hospital discharged and clinical follow up. Whereas the clinical outcome of ruptured group was fair, with mRS of 0-2 in 67% patients.

**CONCLUSION**

In our prospective analysis of PED placement, PED device is an effective treatment for rupture and nonrupture wide-neck intracranial aneurysms, with a very high (90%) complete angiographic occlusion. Pipeline embolization device is also a safe treatment, especially for unrupture aneurysm, with a complication rate  $< 5\%$ . Our data also demonstrate the effectiveness of PED in treatment of wide-neck small ( $\leq 3$  mm) aneurysms.

**KEY WORDS:** Aneurysm, stent, pipeline**O-486****8:54 AM - 9:02 AM****Acute Ischemic Stroke Treatment: The Capillary Index Score and Breaking the Fifty Percent Barrier**

Al-Ali, F.

Borgess Medical Center  
Kalamazoo, MI**PURPOSE**

Despite increased recanalization rates in acute ischemic stroke treatment, the clinical improvement rates have not risen above 50%. Can acute ischemic stroke treatment break this 50% barrier?

**MATERIALS & METHODS**

This is a nonrandomized, single-center registry on consecutive subjects admitted for intraarterial acute ischemic stroke treatment. The Capillary Index Score (CIS), an indicator of remaining viable tissue in the ischemic area, was calculated from preintervention catheter cerebral angiogram. TIMI flow of 2 or 3 was considered successful recanalization. mRS 0-2 at 3 months was considered good outcome.

**RESULTS**

Forty-six of 58 patients who were admitted for intraarterial acute ischemic stroke treatment had occlusion in the internal carotid or middle cerebral artery (M1). Seventy-two percent of patients had successful recanalization and 27% had good outcome. Capillary Index Score was available for 26 patients; 42% were favorable (CIS 2 or 3) and 58% were poor (CIS 0 or 1). Good outcome was found only in the favorable CIS group ( $P = 0.0148$ ). Successful recanalization ( $P = 0.0029$ ) and time from ictus to revascularization ( $P = 0.0039$ ) predicted good outcome. In patients with favorable CIS and TIMI 3, 83% had good outcome.

**CONCLUSION**

If the strong prognostic value of the CIS demonstrated in this study is proven by a large prospective trial, selecting for those patients with favorable CIS should allow us to break the 50% barrier.

**KEY WORDS:** Stroke, blood flow, collateral circulation

**O-487****9:02 AM - 9:10 AM**

### **CT-Guided Cryoablation for Palliation of Secondary Trigeminal Neuralgia from Head and Neck Malignancy**

Dar, S.<sup>1</sup>·Love, Z.<sup>2</sup>·Prologo, J.<sup>2</sup>·Hsu, D.<sup>2</sup>

<sup>1</sup>Case Western Reserve University, Cleveland, OH,

<sup>2</sup>University Hospitals, Case Medical Center, Cleveland, OH

**PURPOSE**

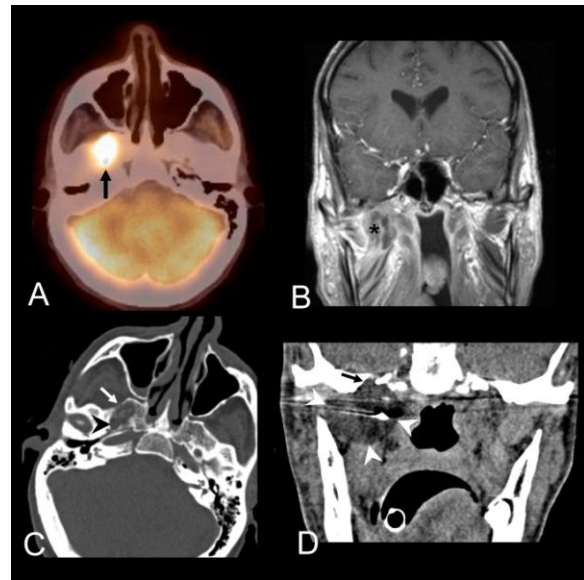
To perform and report experience with percutaneous cryoablation, a novel palliative treatment of trigeminal neuralgia (TN) secondary to recurrent invasive head and neck carcinoma. Head and neck cancer accounts for approximately 2.4% of new cancer cases in the United States every year. Conventional treatment for these patients has been chemotherapy, radiotherapy, or combination chemo/radiation therapy (CRT). Facial pain is a common presentation secondary to tumoral invasion, rendering an individual unable to perform basic activities such as eating and talking. Cryotherapy may provide immediate pain relief, much like the way in which it now is utilized increasingly in pain palliation in patients with metastases to the musculoskeletal system.

**MATERIALS & METHODS**

We retrospectively analyzed palliative cryoablation procedures performed on recurrent head and neck malignancy between September 2010 and June 2011. The procedure was performed under general anesthesia or conscious sedation. For each patient 1-2 cryoprobes were placed in the tumor and 2 or 4 freeze-thaw cycles were performed. Patients were evaluated for facial pain relief immediately following treatment with a telephone follow up.

**RESULTS**

A total of three patients underwent treatment for three masses using CT-guided percutaneous cryoablation. On imaging, technical success was achieved in all cases with hypodense ice formation seen encompassing symptomatic lesions on CT. No procedural complications were encountered with postprocedure pain relief and reduction in required pain medication noted in all patients. Of note, one patient in our study had 1 month of pain relief before return of symptoms.

**CONCLUSION**

Percutaneous cryoablation is a novel, efficient, minimally invasive method for the palliative treatment of invasive head and neck carcinoma in patients suffering from TN as a result of direct tumoral invasion of the extracranial divisions of the trigeminal nerve. Our results suggest it currently may not be a curative technique as one patient's symptoms returned, but it would provide useful as an adjunctive therapy of current palliative therapies for TN secondary to invasive head and neck carcinoma with minimal procedural morbidity and immediate pain relief.

**KEY WORDS:** Trigeminal neuralgia, cryoablation, head and neck

**O-488****9:10 AM - 9:18 AM**

### **Use of the Axera Device in Neurovascular Procedures as a Novel Way of Obtaining Vascular Access**

Fortes, M.·Jindal, G.·Patel, R.·Gandhi, D.

University of Maryland  
Baltimore, MD

**PURPOSE**

After the development of the Seldinger's technique in 1953, the use of this ingenious method for safe vascular access increased enormously and became standard practice in the interventional fields. Multiple devices have been created to close or suture the femoral artery access site in an attempt to reduce manual compression time and complications. However, the known disadvantages of closure devices include increased risk of infection, limb ischemia, limitations in the capacity to reaccess the site in the short term and the unknown long effects of having these implants. The Axera™ (Arstasis, Redwood City, CA) access device modifies the Seldinger's technique to create a 10 degrees puncture angle in an attempt to reduce manual compression time necessary to obtain hemostasis as well as ambulation time, without the use of implants. This study aims to



evaluate the efficacy of Axera™ in reducing time to hemostasis, bed elevation and ambulation in patients undergoing neurovascular procedures, in comparison to historic published data.

#### **MATERIALS & METHODS**

This study is a single center, prospective trial. Fifty patients were enrolled in this ongoing study over a 2-month period. Vascular access was performed in an Artis Zee biplane angiographic suite (Siemens, Erlangen, Germany) using the Axera™ device. Five or 6 french vascular sheaths were introduced to the right or left common femoral arteries. At the end of the procedure, sheaths were removed and hemostasis obtained with manual compression. Type of procedure, procedural duration, use of heparin, antiplatelets or anticoagulant medications, time to hemostasis, bed elevation and ambulation times were recorded.

#### **RESULTS**

Fifty-two neurovascular procedures were performed in 38 females (76%) and 12 males (24%) with ages between 15 and 86 years old (average 54.8 years). Five french sheaths were used for all 38 diagnostic angiograms. All but one of the 16 interventional procedures were performed through a 6 french sheath. Sixteen patients were on antiplatelets therapy. Heparin was used in 34 procedures, with an average of 3647 units. Two patients received intraarterial TPA (6-9 mg). Average time to hemostasis in this series was 5 minutes (range 2-9). In the subgroup of 16 patients that received no heparin and were on low dose (81 mg aspirin) or no antiplatelets therapy, median time to hemostasis was only 3 minutes. Patients that were able to have their beds elevated to 45 degrees and walk, did so in 1 hour and 2 hours, respectively. No significant hematomas or other device-related complications were observed in our series.

#### **CONCLUSION**

Axera™ device provides neurointerventionalists with a new perspective regarding the use of closure devices. There is significant safety advantage, reduction in manual compression and ambulation times in comparison to historic standards for patients receiving manual compression as well as some closure devices.

**KEY WORDS:** Vascular access, closure device, cerebral angiography

**O-489**

**9:18 AM - 9:26 AM**

#### **Findings of Patients Referred for Flexion MR Imaging for Hirayama Disease in North America: A Multisite Study**

Lehman, V. T.<sup>1</sup>•Luetmer, P. H.<sup>1</sup>•Sorenson, E. J.<sup>1</sup>•Fletcher, G. P.<sup>2</sup>•Gupta, V.<sup>3</sup>•Hu, L. S.<sup>2</sup>•Kotsenas, A. L.<sup>1</sup>

<sup>1</sup>Mayo Graduate School of Medical Education, Rochester, MN, <sup>2</sup>Mayo Graduate School of Medical Education, Scottsdale, AZ, <sup>3</sup>Mayo Graduate School of Medical Education, Jacksonville, FL

#### **PURPOSE**

Hirayama disease (HD) is a rare condition characterized by asymmetric muscle weakness and atrophy typically in the C8-T1 distribution. MR findings include loss of attachment (LOA) of dura to the lamina, asymmetric lower cervical spinal cord atrophy, spinal cord T2 signal, loss of cervical lordosis in the neutral position, and forward displacement of the dura with flexion MR. This condition is reported primarily in Southeast Asia with few reports from North America.

#### **MATERIALS & METHODS**

We identified all patients referred for flexion MR for consideration of HD between 1995 and 2011 at three large group practices located in the Midwestern, Southeastern and Southwestern USA. Chart and EMG review by a board-certified neurologist established the clinical diagnosis using accepted criteria. First the neutral and then neutral and flexion MR were evaluated by consensus of three blinded readers. Each MR was evaluated for findings of HD listed above and scored for likelihood of HD.

#### **RESULTS**

Thirty-eight patients were referred for flexion MR, 21 who met clinical criteria for HD and 17 who did not. With HD, the average age was 24 years (range 17-61), all were male, all resided in North America, and 20 were Caucasian. Without HD, the average age was 41 years (range 15-68), 11 were male and 14 were Caucasian. Loss of attachment was present in 14/21 patients (66%) with HD and equivocally present in 1/17 (6%) without HD. Anterior dural shift averaged 2.7 mm (range 0-7) in patients with HD and 0.1 mm (range 0-1) in patients without HD. Five patients with HD had no anterior dural shift, three of whom were over the age of 30. The sensitivity and specificity, respectively, for HD was 70% and 100% for neutral images and 71% and 100% with addition of flexion images. There were six false negative assignments both without and with flexion, four of which had no LOA and four of which had no dural shift.

#### **CONCLUSION**

Hirayama disease occurs in the North American Caucasian population. We report high MR specificity and moderate sensitivity, even without flexion. Findings of HD are often present on neutral studies, which can prompt flexion MR. Loss of attachment, reported to be the most accurate neutral sign of HD, was present in only 70% of our patients. Contrary to a report identifying anterior dural shift in a large percentage of normal individuals, this was absent in nearly everyone without HD, although our group was comparatively older. Hirayama disease was clinically diagnosed in a relatively high number of patients without overt findings on MR. This may be due to diminished MR findings with age or due to the presence of a spectrum of MR findings with HD.

**KEY WORDS:** Hirayama, flexion MR imaging, flexion myelopathy

O-490

9:26 AM - 9:34 AM

### Selective Intraarterial Chemotherapy in the Treatment Strategy for Spinal Metastatic Disease: Phase I Study

Patsalides, A.<sup>1</sup>•Lis, E.<sup>2</sup>•Bilsky, M.<sup>2</sup>•Yamada, J.<sup>2</sup>•Gobin, P.<sup>1</sup>

<sup>1</sup>Weill Cornell Medical College, New York, NY,

<sup>2</sup>Memorial Sloan-Kettering Cancer Center, New York, NY

#### PURPOSE

The treatment objective of spinal metastatic disease (SMD) is to achieve local tumor control and prevent progression of the tumor in the spinal canal and subsequent cord compression with neurologic compromise. Radiation therapy and surgery are the standard treatments and are usually effective. Recurrence however is not infrequent, especially with radioresistant metastases such as colon, lung, renal carcinomas and melanoma. In these cases reirradiation is limited by spinal cord toxicity and resurgery is often futile; thus, the therapeutic options are limited. This IRB-approved phase I clinical trial tested the hypothesis that selective spinal intraarterial chemotherapy can be applied safely in patients with SMD that failed the standard treatments. This experimental treatment consists of infusion of a chemotherapy agent selectively into the arteries supplying the SMD with the intention to prevent tumor progression and spinal cord compression.

#### MATERIALS & METHODS

Inclusion criteria were the presence of recurrent epidural SMD in patients who were not candidates for the standard treatments of radiation therapy or surgery. Exclusion criteria were high-grade cord compression, rapidly worsening neurologic symptoms, and life expectancy less than 3 months. The procedure consisted of selective catheterization of the arteries supplying the epidural disease and infusion of an alkylating agent, provided there was not concomitant supply to the spinal cord. The chemotherapy dose was adjusted to white cell and platelet count and was divided among the arteries supplying the tumor. Detachable coils were used to occlude the ventral branch of the lumbar or intercostal artery and divert the drug into the tumor. Postprocedure follow up consisted of weekly complete blood counts (CBC) and the procedure could be repeated up to three times in 3-6 week intervals, based on the results of CBC and the patients overall condition. Spinal MRI was repeated 1 month after the last procedure.

#### RESULTS

Six patients were enrolled in the study and underwent a total of 13 procedures. Three patients had metastatic colorectal carcinoma, two had metastatic sarcoma and one had metastatic melanoma. The targeted lesions were located in the thoracic (n = 5) and lumbar spine (n = 1). Three patients had a total of three procedures, one had two procedures and two patients had only one procedure. The follow-up duration ranged from 3 to 9 months (median: 5 months). There was no periprocedural complication. One patient who was

pretreated heavily with chemotherapy, radiation and bone marrow transplant developed grade 4 myelotoxicity and neutropenic fever, requiring hospital admission. The postprocedure MRI results showed local control at the treated level in four of six patients, tumor regression in one patient and tumor progression in one patient. All patients had evidence of progression of either systemic metastatic disease or spinal metastatic disease at a different level from the one we treated.

#### CONCLUSION

Selective spinal intraarterial chemotherapy is feasible, safe and has encouraging results in terms of local tumor control. Systemic toxicity remains a concern. These results need to be validated in larger clinical trials.

**KEY WORDS:** Intraarterial chemotherapy

O-491

9:34 AM - 9:42 AM

### Effect of the CT Table Restraint Strap on Shoulder Position in Cervical Spine CT: Implications for Dose and Image Quality

Wylie, J. D. •Kranz, P. G.

Duke University Medical Center  
Durham, NC

#### PURPOSE

CT is being used increasingly as the primary imaging modality to evaluate the cervical spine in the setting of trauma, resulting in increased patient dose compared to conventional radiography. We have observed that the use of the CT table restraint strap can impair the ability of many patients to appropriately lower their shoulders. The purpose of this study was to evaluate the effect of the CT table restraint strap on shoulder position, image quality, and patient dose in patients undergoing cervical spine CT.

#### MATERIALS & METHODS

In this prospective investigation, patients undergoing cervical spine CT for suspected cervical spine trauma were randomized to having their arms placed within or outside the CT table restraint strap. Both groups were instructed to lower their shoulders as much as possible immediately prior to scanning. Patients were scanned using identical protocols on a single scanner using automated tube current modulation. Z-axis coverage was identical for each patient. Shoulder level, image noise, subjective image quality (determined by the lowest level the spinal cord was clearly visible), and dose were examined. Neck diameter was measured from the scout image to assess body habitus.

#### RESULTS

Fifty patients were enrolled, with 25 patients randomized into each group. Body habitus was similar between the two arms (neck diameter 12.9 cm vs 12.6 cm, p = 0.39). Patients whose arms were placed outside the restraint strap were able to lower their shoulders an average of 1.2 vertebral levels more than those with their arms in the strap (p = 0.002). In the group whose arms were placed outside the strap, there was a 19%

reduction in dose (average DLP 554.9 vs 682.5,  $p = 0.02$ ), and increased ability to visualize the cord by 0.9 vertebral levels ( $p = 0.02$ ). There was no difference between the two groups in image noise measured at the C4 level ( $p = 0.34$ ), but a reduction in image noise at the T1 level in the group with arms placed outside the strap ( $p = 0.05$ ).

#### CONCLUSION

The use of the CT table restraint strap to immobilize the arms and torso can impair the ability of patients undergoing cervical spine CT to lower their shoulders. This results in increased dose, increased image noise, and decreased subjective image quality for patients whose arms are placed within the restraint strap compared with patients whose arms are not restrained. In selected patients, allowing patients to place their arms outside the strap provides a no-cost method for reducing dose and improving image quality.

**KEY WORDS:** Dose reduction, spine, CT

**O-492**

**9:42 AM - 9:50 AM**

#### **Cervical Fractures Pattern and CT Angiography Indication for Vertebral Artery Dissection Suspicion**

Cuvinciuc, V.·Mehdizade, A.·Haller, S.·Barnaure, I.·Tessitore, E.·Vargas, M.·Lovblad, K.

University Hospitals of Geneva  
Geneva, SWITZERLAND

#### PURPOSE

To identify patterns of cervical fractures and luxation most likely associated to vertebral artery dissection, as identified with CT angiography.

#### MATERIALS & METHODS

Retrospective analysis for 5 years of patients with cervical fractures. Sixty-one patients with cervical fractures and head and neck CT angiography were identified. Patterns of cervical fractures and luxation, such as involvement of the transverse foramen, vertebral body, articular facets, laminae, and spinous processes were noted. In 12 patients, the diagnosis was uncertain and it was confirmed with MR imaging.

#### RESULTS

Twenty-six patients (42.62%) with vertebral arterial dissection were identified. No significant statistical correlation ( $p < 0.05$ ) was found between the involvement of the various cervical segments and the vertebral artery dissection. The involvement of the transverse foramen and articular facets had the highest sensitivity in predicting the vertebral artery dissection (both 73.08%), but with low specificity (31.43%, respectively 28.57%). Fractures of both the transverse foramen and the articular facets have a lower sensitivity (57.69%), but with a higher specificity (51.43%). No case of vertebral dissection associated to isolated transverse foramen or articular facet fracture was found. Vertebral body fractures had sensitivity of 46.15%, and specificity of 54.29%. In one case of isolated vertebral body fracture (out of four), we have

found a vertebral artery dissection. The highest specificity was noted for fractures of laminae and spinous processes, of 77.14%, respectively 85.71%, but with low sensitivity (38.46%, respectively 23.08%). No cases of isolated fractures of the laminae or spinous processes, associated to the vertebral artery dissection, were identified.

#### CONCLUSION

CT angiography should be performed in all cases of multiple fractures of transverse foramen, articular facets and/or vertebral body, due to the relatively high risk of vertebral artery dissection. No case of vertebral artery dissection was found in our series associated to isolated fractures of the transverse foramen or articular facets.

**KEY WORDS:** Cervical fracture, vertebral artery dissection, CT angiography

**O-492a**

**9:50 AM - 9:58 AM**

#### **Improved Outcomes with Percutaneous Image-Guided Lumbar Synovial Cyst Treatment: Novel Approaches and Techniques - ASSR Mentor Award**

Tekchandani, L.

Winthrop University Hospital  
Mineola, NY

## **Thursday Morning**

**10:30 AM - 12:00 PM**  
**Grand Ballroom Suite**

(65a) Adult Brain:  
Degenerative/Demyelinating/  
Metabolic Diseases II

**O-500**

**10:30 AM - 10:38 AM**

#### **Amyloid- $\beta$ Associated Volume Loss Occurs Only in the Presence of Phospho-Tau**

Desikan, R. S.<sup>1</sup>·McEvoy, L. K.<sup>1</sup>·Thompson, W. K.<sup>1</sup>·Roddey, C.<sup>1</sup>·Holland, D.<sup>1</sup>·Blennow, K.<sup>2</sup>·Aisen, P. S.<sup>1</sup>·Brewer, J. B.<sup>1</sup>·Hyman, B. T.<sup>3</sup>·Dale, A. M.<sup>1</sup>

<sup>1</sup>University of California San Diego, San Diego, CA, <sup>2</sup>Sahlgrenska Academy at Goteburg University, Goteburg, SWEDEN, <sup>3</sup>Massachusetts General Hospital, Boston, MA

#### PURPOSE

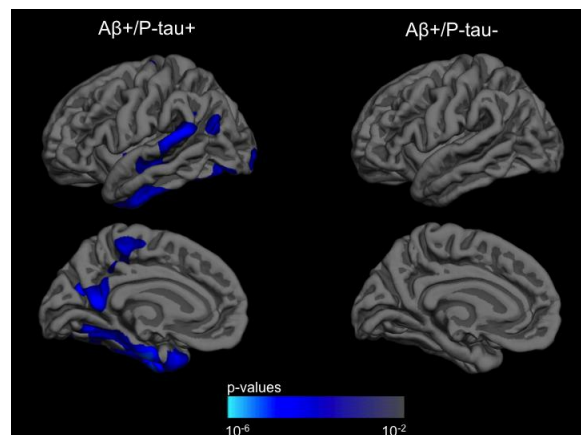
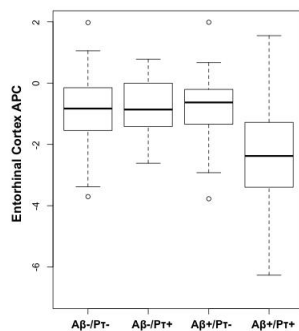
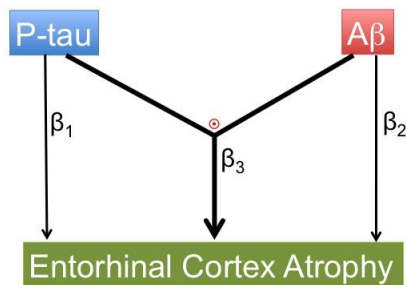
The relationship between neurodegeneration and the two hallmark proteins of Alzheimer disease (AD), amyloid- $\beta$  (A $\beta$ ) and tau, is still unclear.

## MATERIALS & METHODS

Here, we examined 286 nondemented participants (107 cognitively normal older adults and 179 memory impaired individuals) who underwent longitudinal MR imaging and lumbar puncture. Using mixed effects models, we investigated the relationship between longitudinal entorhinal cortex atrophy, CSF p-tau181p and CSF A $\beta$ 1-42.

## RESULTS

We found a significant relationship between elevated entorhinal cortex atrophy and decreased CSF A $\beta$ 1-42 only with elevated CSF p-tau181p. We observed a similar relationship in other AD-vulnerable regions and with clinical decline over time, as assessed using CDR-Sum of Boxes and the cognitive component of the Alzheimer's Disease Assessment Scale.



## CONCLUSION

Our findings indicate that in humans at risk for dementia A $\beta$ -associated volume loss occurs only in the presence of phospho-tau.

**KEY WORDS:** Phospho-tau, amyloid, neurodegeneration

**O-501**

**10:38 AM - 10:46 AM**

## MR Imaging Grading Scale for Amyloid-Related Imaging Abnormalities

Daams, M.<sup>1</sup>Barkhof, F.<sup>1</sup>Wattjes, M. P.<sup>1</sup>Brashear, H. R.<sup>2</sup>Arrighi, H. M.<sup>2</sup>Morris, K.<sup>2</sup>Scheltens, P.<sup>1</sup>

<sup>1</sup>VU University Medical Center, Amsterdam, NETHERLANDS, <sup>2</sup>Janssen Alzheimer Immunotherapy, South San Francisco, CA

## PURPOSE

Amyloid-related imaging abnormalities (ARIA) have been reported in clinical trials of amyloid-lowering therapies for Alzheimer disease. Amyloid-related imaging abnormalities-E is the subgroup of ARIA characterized by parenchymal and sulcal hyperintensities on FLAIR images that are believed to represent cerebral edema and sulcal effusions. Amyloid-related imaging abnormalities-E is heterogeneous and no clear correlation has been established with clinical symptoms or outcomes, thus a radiologic grading scale that accurately measures these findings is proposed and tested for inter-rater reliability.

## MATERIALS & METHODS

Based on case reviews of ARIA-E, a scale was developed that measured its two components, sulcal and parenchymal hyperintensities and in addition, gyral swelling. All three characteristics were graded in 12 regions using a six-step scale according to spatial extent per lobe. Two neuroradiologists applied the scale in a blinded fashion to serial MRIs of 20 subjects from a Phase 2 clinical trial of anti-beta amyloid immunotherapy (bapineuzumab). Ten cases were identified previously with varying degrees of ARIA-E and 10 were non-ARIA-E cases. Agreement was calculated between the two raters using the intraclass correlation coefficient (ICC).

## RESULTS

The ARIA-E grading process was reported as acceptably easy to implement and resulted in a high level of inter-rater reliability with 100% agreement on the interpretation of non-ARIA-E cases. High inter-rater agreement was observed for parenchymal hyperintensities (ICC = 0.831), sulcal hyperintensities (ICC = 0.892), and the two findings together (ICC = 0.887). Scoring of gyral swelling had the greatest variability between the two raters (ICC = 0.542) but appeared to add value with regard to radiologic severity by increasing the range of total scores.

## CONCLUSION

A simple visual grading scale for reporting ARIA-E findings is proposed. The scale demonstrated good inter-rater reliability and ease of use when tested in a

blinded fashion. Following wider testing and training among neuroradiologists, this scale may make possible more precise description and categorization of the various manifestations of ARIA-E on MRI.

**KEY WORDS:** Alzheimer disease, amyloid, grading scale

**O-502**

**10:46 AM - 10:54 AM**

### Rates of Decline in Alzheimer Disease Decrease with Age

Holland, D.·McEvoy, L. K.·Desikan, R. S.·Dale, A. M.

University of California San Diego  
La Jolla, CA

#### PURPOSE

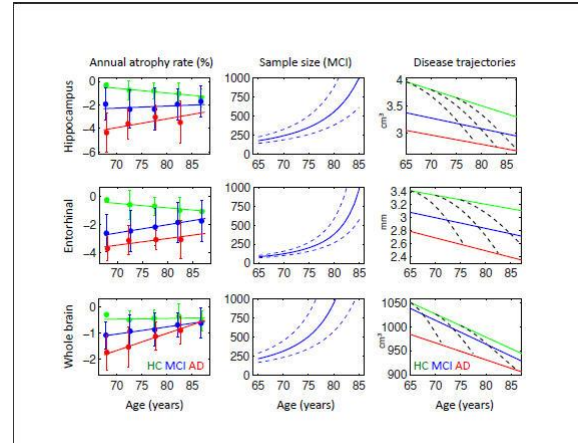
Age is the strongest risk factor for late-onset Alzheimer disease (AD), but the effect of age on clinical and atrophic rates of decline in AD has been largely unexplored. Since the elderly population is growing, and proportionally growing faster with increasing age, our purpose was to better understand whether and how age interacts with the disease process to affect rate of decline; to model disease trajectories; and to assess implications for clinical trial sample sizes.

#### MATERIALS & METHODS

We examined longitudinal rates of change as a function of baseline age for measures of clinical decline and structural MRI-based regional brain atrophy, in cohorts of AD, mild cognitive impairment (MCI), and cognitively healthy (HC) older individuals (total  $n = 722$ ) from the Alzheimer's Disease Neuroimaging Initiative. The effect of age was modeled using mixed effects linear regression. We used the age-specific annual rates of change, relative to HCs, in power calculations to estimate sample sizes needed to adequately power a clinical trial when individuals of a given age comprise the study sample. From baseline measures and rates of atrophy as a function of age, disease trajectories were modeled assuming the annual atrophy rate increases linearly with time.

#### RESULTS

There was pronounced deceleration with age in the rates of clinical and atrophic decline for AD and MCI individuals, while HCs showed evidence of an increase in rates of decline with age. This resulted in convergence in rates of change for HCs and patients near 90 years of age. Baseline cerebrospinal fluid densities of AD-relevant proteins,  $A_{1-42}$ , tau, and phospho-tau<sub>181p</sub> (ptau), showed a similar pattern of convergence across cohorts, particularly for ptau. In contrast, baseline clinical measures did not change with age, indicating uniformity of clinical severity at baseline. Sample sizes based on rates of change in clinical or morphometric measures, relative to HCs, showed dramatic increases with age of study sample. Calculated disease trajectories show the rapid decline from HC to MCI to AD in ~10 years.



#### CONCLUSION

These results imply that the phenotypic expression of AD is relatively mild in individuals older than approximately 85 years. This may affect the ability to distinguish AD from normal aging in the very old. Our results also demonstrate that inclusion of older individuals in clinical trials can reduce substantially the power to detect beneficial effects of a disease-modifying treatment. Finally, plausible disease trajectories can be modeled based on longitudinal morphometric data.

**KEY WORDS:** Alzheimer disease, aging, biomarkers

**O-503**

**10:54 AM - 11:02 AM**

### Comparison of Brain Atrophy in Progressive Supranuclear Palsy Subtypes

Saini, J.·Pal, P. K.·Bagepally, B. S.·Yadav, R.

Nimhans  
Bangalore, INDIA

#### PURPOSE

Purpose of the present study is to identify differences in the cortical thickness and volumes of subcortical structures in progressive supranuclear palsy (PSP)-Parkinsonism (PSP-P) and PSP- Richardson's syndrome (PSP-RS) subtypes of PSP using fully automated methodology.

#### MATERIALS & METHODS

Twenty-eight patients of PSP were evaluated. They included 17 patients of PSP-RS (8 men, age  $59.18 \pm 9.27$  years) and 11 patients of PSP-P (12 men, age  $62.74 \pm 6.60$  years). All patients fulfilled the standard criteria for the diagnosis of PSP and were recruited from the movement disorder unit of the National Institute of Mental Health and Neurosciences (NIMHANS). All patients were evaluated clinically by Hoehn-Yahr (HY) staging and PSP rating scale. The 1 mm<sup>3</sup> structural 3D T1-weighted images were acquired on 3 T MRI scanner. Volumetry of subcortical structures was performed using FSL-FIRST software and cortical thickness estimation and analysis was done using Freesurfer software. The volumes of hippocampus, amygdala, caudate, putamen and thalamus were extracted. Two groups were compared statistically for age, sex, intracranial volume (ICV), gray matter volume (GMV),



white matter volume (WMV) and clinical scores. Volumes of the subcortical structures also were compared. Statistical comparisons were performed using R software. Whole brain cortical thickness was compared between the subgroups using age, sex and ICV as nuisance regressors (at  $p < 0.001$ , uncorrected).

## RESULTS

The patients with PSP-RS showed significantly lower PSP rating scale. Rest of the demographic and clinical parameters did not show any statistical difference ( $P > 0.05$ ). Intracranial volume, GMV and WMV comparison showed significantly decreased WMV in the PSP-RS subgroup ( $383.35 \pm 62.54$  ml) as compared to PSP-P subgroup ( $424.60 \pm 29.81$  ml,  $p = 0.03$ ). None of the deep subcortical structures showed statistically significant volume difference between the two subgroups. On cortical thickness analysis small areas of reduced cortical thickness was observed in PSP-RS as compared to PSP-P in the left postcentral gyrus, right supramarginal gyrus and insula.

## CONCLUSION

The subcortical structures atrophy is not differing between the two PSP subgroups. Cortical thickness analysis shows areas of cortical thinning in the sensory and insular region supporting the clinical observations of sensory, cognitive abnormalities in the PSP-RS group. Lowered global WMV in PSP-RS subjects along with the higher clinical severity might indicate that PSP-RS is the severe subtype of PSP with possibly impaired cortical connectivity. Further studies should direct towards better understanding of white matter impairment as well as its functional implications in various subtypes of PSP.

**KEY WORDS:** PSP-RS, PSP-P, MR imaging

**O-504**

**11:02 AM - 11:10 AM**

### Ventricular and Cerebral Gray Matter Volumes Predict Cognitive Improvement in Normal Pressure Hydrocephalus following Shunt Treatment

Serulle, Y.·Milch, H.·Kirov, I.·Golomb, J. B.·Rusinek, H.·Gonen, O.·George, A. E.

New York University School of Medicine  
New York, NY

## PURPOSE

In an accompanying abstract (Serulle et al. 12-O-669-ASNR) we have demonstrated that brain volume segmentation obtained using automated methods can be used to differentiate normal pressure hydrocephalus (NPH) from normal age-related brain volume loss and Alzheimer disease (AD). The purpose of this study is to investigate neuroimaging factors, including total gray matter (GM), white matter (WM), cerebrospinal fluid (CSF) and ventricular volumes that are associated with cognitive outcome of shunt placement surgery.

## MATERIALS & METHODS

Cognitive data were available for ten out of 16 NPH patients selected for surgery based on their clinical

improvement following a high volume large bore spinal tap procedure. Each patient underwent a comprehensive cognitive assessment before and after surgery. Preoperative MPRAGE sequences were analyzed. Brain segmentation into total GM, WM and CSF was performed using the Statistical Parametric Mapping 8 (SPM8) software in MATLAB1. Ventricular volume was obtained using Firevoxel2 software. T tests were used to determine statistical significance.

## RESULTS

Fifteen of 16 shunted NPH patients showed gait response ranging from mild improvement to total resolution of gait impairment (94%) and nine out of 13 (69%) showed improvement in urinary incontinence. Five out of ten patients (50%) had cognitive improvement (responders) while five did not have discernible cognitive improvement (nonresponders) following shunt surgery. There was no significant difference in age between responders (77) and nonresponders (78). Responders had higher ventricular volumes (43% higher) prior to surgery compared to nonresponders (responders  $187 \pm 15$  ml, nonresponders  $132 \pm 11$  ml,  $P < 0.01$ ). Total GM volume was higher in responders ( $652 \pm 71$  ml) compared to nonresponders ( $460 \pm 51$ ) ( $P < 0.05$ ). There was no significant difference on WM volume (responders  $390 \pm 79$ , nonresponders  $385 \pm 20$ , or total CSF volume (responders  $658 \pm 88$  ml, nonresponders  $658 \pm 96$  ml) between responders and nonresponders.

## CONCLUSION

Normal pressure hydrocephalus patients with higher GM volume and larger ventricles on preoperative brain MRIs are more likely to have improvement of their cognitive function following ventricular shunt surgery. The lower GM volume in nonresponders may represent AD comorbidity in the NPH population. These data suggest that automated computerized brain segmentation is a useful tool to help predict potential cognitive outcome in NPH patients undergoing ventricular shunt surgery.

**KEY WORDS:** Hydrocephalus, NPH, segmentation

**O-505**

**11:10 AM - 11:18 AM**

### Clinical and Imaging Features of Hypertrophic Olivary Degeneration in a Large Retrospective Cohort

Carr, C. M.·Hunt, C.·Kotsenas, A.·Wood, C.·Krecke, K.·Timothy, K.

Mayo Clinic  
Rochester, MN

## PURPOSE

Hypertrophic olivary degeneration (HOD) is an uncommon type of transneuronal degeneration. Hypertrophic olivary degeneration typically is caused by lesions occurring in the dento-rubro-olivary pathway (triangle of Guillain-Mollaret). The purpose of this retrospective review was to evaluate the imaging findings of HOD in the largest case series to date,

identify common etiologies of HOD, evaluate findings in atypical and idiopathic cases and correlate with clinical symptomatology.

#### **MATERIALS & METHODS**

This retrospective study was reviewed and approved by the Mayo Clinic Institutional Review Board. Querying our institutional radiology database for all patients with reported hypertrophic olivary degeneration, a retrospective review was performed on all patients from 7/1/2002 to 7/1/2011. The reports and imaging were reviewed for the presence of HOD and any associated lesions in the dento-rubro-olivary pathway. The patient's electronic medical record was reviewed for any history of palatal myoclonus, associated symptoms and for the indication for the MRI examination that was performed. Patients were considered to have findings of HOD if there was focal increased T2 signal with lack of enhancement in either or both inferior olivary nuclei (ION). Other criteria used to support the diagnosis of HOD included associated hypertrophy of the ION, a lesion in the triangle of Guillain-Mollaret, and presence of palatal myoclonus. Patients were excluded if there was any associated enhancement in the area of increased T2 signal of the ION or lesional extension into the ION.

#### **RESULTS**

The initial search resulted in 123 patients. After review of the reports and imaging, a total of 108 patients had findings consistent with HOD as confirmed by at least one neuroradiologist. Thirty-two percent (35/108) had palatal myoclonus. Fifty-five percent (59/108) had an associated lesion in the dento-rubro-olivary pathway. The most common lesional etiologies for HOD were postsurgical resection of a tumor (15/59), infarct (15/59) or a vascular malformation (15/59). Of the cases that did not have a definite lesion in the dento-rubro-olivary pathway (49/108), the largest single diagnosis in this group of patients was progressive ataxia and palatal myoclonus (PAPT) (9/49). Seventy-six percent (82/108) had findings of HOD bilaterally although findings were not always symmetric.

#### **CONCLUSION**

Hypertrophic olivary degeneration may present with either unilateral or bilateral olivary involvement, with a bilateral asymmetric presentation being most typical. A wide variety of lesions can cause HOD with postsurgical change, infarction, and vascular malformations being the most common etiologies. The majority of patients in this series did not have the classic symptom of palatal myoclonus. Although the majority of patients with palatal myoclonus have been reported to have findings of HOD, the converse does not appear to be true. Hypertrophic olivary degeneration frequently can be seen as an incidental finding without any visualized abnormality in the brain and without symptoms.

**KEY WORDS:** HOD, hypertrophic olivary degeneration, palatal myoclonus

O-506

11:18 AM - 11:26 AM

#### **Reduced White Matter Volume Associated with Childhood Lead Exposure**

Beckwith, T.<sup>1</sup>•Dietrich, K. N.<sup>2</sup>•Cecil, K. M.<sup>1</sup>

<sup>1</sup>Cincinnati Children's Hospital Medical Center, Cincinnati, OH, <sup>2</sup>University of Cincinnati, Cincinnati, OH

#### **PURPOSE**

The overall goal of our research is to better understand the effects of childhood environmental lead exposure on brain development. We previously reported adult gray matter volume loss was inversely associated with increased mean childhood blood lead levels (MeanPb). This association was primarily observed in the prefrontal cortex and anterior cingulate and found almost exclusively in males. Our original analysis did not appreciate white matter changes. In this new analysis, we performed voxel-based morphometry (VBM) of high-resolution T1-weighted imaging acquired in an lead exposed cohort and improved our covariate modeling strategy to identify volumetric differences in adult parenchymal white matter associated with early childhood blood lead levels. We also examined the influence of the participant's sex.

#### **MATERIALS & METHODS**

A total of 157 adult participants (mean age  $20.8 \pm 0.9$  years) from the Cincinnati Lead Study (CLS) (M = 83, F = 74), a birth cohort established between 1979 and 1984 that recruited pregnant women from areas with high levels of childhood lead poisoning, consented and completed this study. Blood lead levels were assessed for participants starting at birth, and measurements were taken every 3 months through age 5 years, then every 6 months through age 6.5 years. High-resolution, three dimensional, whole brain T1-weighted imaging was acquired on a 1.5 T scanner. Data was processed and analyzed in Matlab version 7.9 using SPM8 and VBM8 software. Voxel-based morphology was performed on white matter tissue with volume and probability density maps produced for each participant and compared using a multiple linear regression model that included MeanPb, as well as significant confounding variables which were established using forward and backward elimination strategies in SPSS 12.0.

#### **RESULTS**

Several regions demonstrated an inverse association between childhood MeanPb and white matter volume. Most pronounced are areas of association located in the cingulum, orbital frontal and prefrontal white matter with additional foci in cortical white matter near the superior frontal gyrus and precentral gyrus. When separated by sex, females displayed no significant volume loss. In contrast males presented with an inverse association between increased MeanPb and white matter volume loss predominately in the prefrontal region and adjacent to the precentral motor cortex. Covariate inclusion was necessary for identifying white matter associations.

**CONCLUSION**

These findings show volume loss associated with increased MeanPb in white matter regions adjacent to previously reported regions of gray matter volume loss within the same cohort. Tissue loss within the prefrontal region and cingulum may account for cognitive and behavioral impairments seen within the CLS. Tissue loss in motor regions also may explain abnormalities in motor control observed in the CLS. The sex differences observed are consistent with previous studies, including those assessing juvenile delinquency and adult, criminality suggesting that males are more susceptible to developmental effects of childhood lead exposure.

**KEY WORDS:** Volume, lead, environment

**O-507****11:26 AM - 11:34 AM**

### **Sex Differences in Diffusion Tensor Imaging Metrics in Adults with Childhood Lead Exposure**

Cecil, K. M.<sup>1</sup>•Beckwith, T.<sup>1</sup>•Dietrich, K. N.<sup>2</sup>

<sup>1</sup>Cincinnati Children's Hospital Medical Center, Cincinnati, OH, <sup>2</sup>University of Cincinnati, Cincinnati, OH

**PURPOSE**

The overall objective of our research is to better understand the effects of childhood environmental lead exposure on brain development. Our previous work found that aberrations in diffusion tensor imaging (DTI) metrics were associated with mean childhood blood lead levels (MeanPb). This association was observed mainly in the corona radiata, internal capsule, and splenium of the corpus callosum. This pattern of altered DTI metrics is thought to be indicative of axonal damage and altered patterns of myelination. However, we did not evaluate the important effects of sex on these metrics. In this study, a voxel-based analysis of four DTI metrics was performed with imaging in a previously lead-exposed cohort to identify abnormal diffusion patterns associated with sex and MeanPb levels.

**MATERIALS & METHODS**

Ninety-one adult participants (mean age  $22.9 \pm 1.54$  years) from the Cincinnati Lead Study (CLS), a birth cohort established between 1979 and 1984 that recruited pregnant women from areas with high levels of childhood lead poisoning, consented and completed this study. Participants were separated into subcohorts based on sex (F = 52, M = 39). Blood lead levels were assessed for participants starting at birth, and measurements were taken every 3 months through age 5 years, then every 6 months through age 6.5 years. Imaging was performed on a 3 T scanner. A whole-brain, three dimensional, MPRAGE, high-resolution anatomical T1-weighted scan and 46 section diffusion-weighted spin-echo echo-planar scan in the axial plane were acquired. Diffusion-weighted data were reconstructed in DTIStudio, and individual maps for fractional anisotropy (FA), mean diffusivity (MD), axial diffusivity (AD), and radial diffusivity (RD) were created for each participant. Anatomical images were processed using SPM5 software. Voxel-based statistical analyses

were performed using CCHIPS-Cincinnati Children's Image Processing Software. A multiple linear regression was performed for each sex subcohort comparing MeanPb with the values of each DTI metric. Confounding variables for each cohort were established using backward and forward regression models in SPSS version 12.0 and included in the analyses.

**RESULTS**

Diffuse patterns of decreased FA, and increased MD and RD values were observed in the female subcohort in areas including the internal capsule and centrum semiovale. Increased AD values also were observed in the centrum semiovale. In the male subcohort, sporadic increases and decreases in FA and AD were seen in the centrum semiovale, with reduced MD in the inferior longitudinal fasciculus and increased RD in the internal capsule.

**CONCLUSION**

Analysis demonstrated an association between MeanPb and the four DTI metrics related to sex. Females presented with more robust and diverse abnormalities in DTI measurements than males, especially in the internal capsule and white matter of the centrum semiovale. Though previous studies have shown that males seem to be more susceptible to the effects of childhood lead exposure on brain volume and measures of criminality, both sexes demonstrate similar deficits in neurobehavioral testing and these results may help explain the deficits observed in females.

**KEY WORDS:** Diffusion tensor imaging, lead, sex

**O-508****11:34 AM - 11:42 AM**

### **Brain Hemodynamic Changes Associated with Chronic Cerebrospinal Venous Insufficiency Are Not Specific for Multiple Sclerosis and Do Not Contribute to Its Severity**

Marziali, S. • Garaci, F. • Meschini, A. • Fornari, M. • Melis, M. • Fabiano, S. • Stefanini, M. • Centonze, D. • Simonetti, G. • Floris, R.

University of Rome Tor Vergata  
Rome, ITALY

**PURPOSE**

Aim of our study was to investigate the relationship between chronic cerebrospinal venous insufficiency (CCSVI) and cerebral hemodynamic parameters, to disclose their possible involvement in pathophysiology of multiple sclerosis (MS).

**MATERIALS & METHODS**

Values of cerebral blood volume (CBV), cerebral blood flow (CBF), and mean transit time (MTT) were assessed by dynamic susceptibility contrast-enhanced (DSC) magnetic resonance imaging (MRI) in normal-appearing white matter (NAWM) of 39 patients with MS, 25 positive to CCSVI (CCSVI+) and 14 negative to CCSVI (CCSVI-), and of 26 healthy controls (14 CCSVI+ and 12 CCSVI-).

## RESULTS

Multiple sclerosis patients, both CCSVI+ and CCSVI-, showed a reduced CBF and an increased MTT, without any significant variation of CBV. Otherwise, all CCSVI+ subjects showed cerebral hemodynamic anomalies, such as a decreased CBF and CBV, without any delaying of MTT when compared to CCSVI subjects. No correlation was found between values of CBV and CBF from all NAWM and disability scales; a positive correlation was found in the periventricular NAWM for MTT value.

## CONCLUSION

Our data supported a role of CCSVI in cerebral hemodynamic changes, such as decreasing of CBV and CBF, regardless of the presence of MS. Our results showed that CCSVI has no impact on neurologic functions and disability progression in patients with MS. Hence the question of whether CCSVI still can be considered as a pathologic condition.

**KEY WORDS:** Dynamic susceptibility contrast-enhanced MRI, multiple sclerosis, CCSVI

**O-509**

**11:42 AM - 11:50 AM**

### Prevalence of Longitudinal Extensive Spinal Cord Lesions and Opticospinal Multiple Sclerosis in Hispanic Americans Compared to Nonhispanic Whites with Multiple Sclerosis

Lerner, A.·Amezcu, L.·Weber, C.·Shiroishi, M. S.·Kim, P. E.·Go, J. L.·Law, M.

University of Southern California  
Los Angeles, CA

## PURPOSE

High prevalence of optic and spinal cord symptoms at presentation in MS patients has been reported recently in Latin America and in a cohort in USA (Southern California) in Hispanic white (HW) patients suggesting a higher prevalence of opticospinal multiple sclerosis (OSMS) in Hispanic population. However, little is known about longitudinal extensive cord lesions (LESCLs) common to OSMS in U.S. populations. These cord lesions are defined as longitudinal and spanning >3 segments. The primary objective of this study is to determine the prevalence of LESCLs within a cohort of HW multiple sclerosis (MS) and non-Hispanic white (NHW) patients. The secondary objective is to correlate presence of LESCL lesions with clinical presentation of opticospinal multiple sclerosis (OSMS) in these populations.

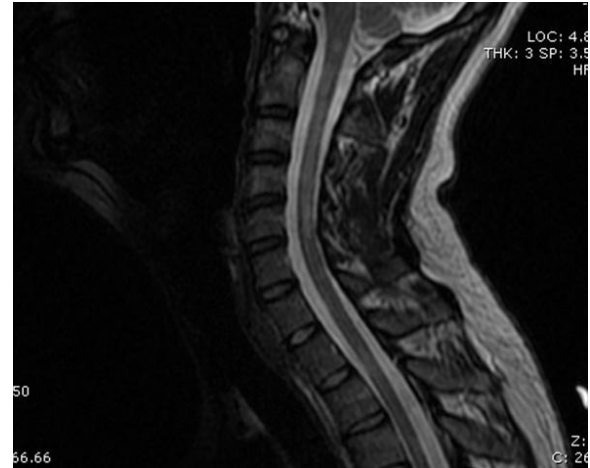
## MATERIALS & METHODS

Medical records and MRI studies were investigated retrospectively for 148 patients with clinical definitive MS meeting the spatial distribution diagnostic criteria of Barkhof et al (1997) on brain MRI, consisting of 84 HW patients and 64 NHW patients. Patients not meeting Barkhoff or meeting definite Wingerchuk criteria for neuromyelitis optica (NMO) were excluded from the study. All first available spinal cord MRI studies were reviewed for presence of LESCLs. Longitudinal extensive cord lesions were defined as spinal cord

lesions extending over three or more vertebral levels on sagittal spinal MR. Presence of LESCLs lesions were correlated with clinical history of opticospinal multiple sclerosis (OSMS).

## RESULTS

Cervical spinal cord lesions and LESCLs were more prevalent in HW cohort when compared to NW cohort. In HW patients 14% of spinal cord lesions represented LESCLs. These lesions were seen most frequently in the cervical spinal cord. Higher prevalence of clinical OSMS was observed in HW cohort compared to NW and correlated with presence of LESCLs.



## CONCLUSION

Hispanic white patients with MS compared to NHW patients with MS demonstrate higher prevalence of LESCLs and opticospinal MS, which may suggest differences in pattern of CNS damage in this population and corresponding clinical presentation. Similar differences in spinal cord involvement in MS have been reported more commonly in non-European populations, particularly in Asian populations suggesting that ethnic background is an important marker of CNS involvement in MS.

**KEY WORDS:** Multiple sclerosis, longitudinal extensive spinal cord lesion, opticospinal multiple sclerosis

**O-510**

**11:50 AM - 11:58 AM**

### Do Nonenhancing Hypointense Lesions (Black Holes) Add Information to MR Imaging Criteria for Dissemination in Space in Clinically Isolated Syndromes?

Mitjana, R.<sup>1</sup>·Tintoré, M.<sup>1</sup>·Auger, C.<sup>1</sup>·Filippi, M.<sup>2</sup>·Rocca, M.<sup>2</sup>·Barkhof, F.<sup>3</sup>·Polman, C.<sup>3</sup>·Fazekas, F.<sup>4</sup>·Montalban, X.<sup>1</sup>·Rovira, À.<sup>1</sup>

<sup>1</sup>Hospital Vall d'Hebron, Barcelona, SPAIN, <sup>2</sup>San Raffaele, Milan, ITALY, <sup>3</sup>VU University Medical Centre, Amsterdam, NETHERLANDS, <sup>4</sup>Medical University of Graz, Graz, AUSTRIA

## PURPOSE

To analyze the prevalence of nonenhancing black holes in a large population of clinically isolated syndrome (CIS) patients, on MRI scan obtained within the first 6

months following symptoms onset, and its value for predicting early conversion to clinically definite MS (CDMS).

#### MATERIALS & METHODS

Observational prospective multicentric study based on pre-existing MRI data obtained on CIS patients coming from different MAGNIMS centers. Inclusion criteria were: (1) a CIS suggestive of CNS demyelination involving the optic nerve, brainstem, spinal cord, or other topography, not attributable to other disease; (2) age between 16 and 50 years; (3) onset of symptoms within 3 months of clinical examinations; (4) performance of a brain MR examination within the first 6 months after CIS onset. In a subgroup of patients a follow-up MRI scan was performed 12 months after symptoms onset. All MR scans were performed on a 1.5 T and included the following sequences: 1) transverse T2-weighted dual-echo; and 2) contrast-enhanced transverse T1-weighted. All sequences 3-5 mm slice thickness covering the whole brain. MR imaging scans were assessed by a neuroradiologist blinded to clinical data, who determined the number and location of high signal lesions on T2-weighted images and of nonenhancing hypointense lesions on T1-weighted images. Patients were classified based on the number of Barkhof-Tintoré (BT) criteria fulfilled, and on the presence or absence of nonenhancing black holes on baseline scan. Clinically definite MS was diagnosed when a second attack with a new neurologic abnormality was confirmed by examination.

#### RESULTS

We included 520 patients (69% females) with CIS followed for a mean of 45.7 months. Mean age at symptoms onset was 31 years; range 16-50 years. One hundred seventy-three patients (33.3%) presented with optic neuritis, 153 (29.4%) with brainstem symptoms, 138 (26.5%) with spinal cord syndrome and the remaining 56 patients (10.8%) had a different presentation (hemispheric, polyregional or undetermined). Two hundred nineteen patients (42.1%) converted to CDMS (mean time 17.6 months). Four hundred fifty-six patients (87.7%) showed focal brain lesions of the type seen in MS. Criteria for dissemination in space (3-4 BT criteria) were fulfilled in 286 of these patients (55%). One hundred eighty-nine of these patients showed at least one nonenhancing black hole (36%) (mean number 3.19; range:1-23). These proportions varied depending on the number of BT criteria fulfilled: 13% in patients with 0-2 BT criteria and 45% with 3-4 BT criteria. Patients with nonenhancing black holes had a higher risk of conversion to CDMS [55.2% vs 44.8%; hazard ratio (HR)] 1.3; 95% confidence interval (CI) 1.0-1.8;  $p = 0.031$ . However no significant increase of conversion to CDMS adjusted by number of BT criteria was associated with presence of nonenhancing black holes (HR 0.8; CI 0.6-1.0;  $p = 0.094$ ).

#### CONCLUSION

Presence of hypointense nonenhancing lesions on T1-weighted images, which are frequent in CIS patients,

does not increase the risk of early conversion to CDMS independently of number of BT criteria fulfilled.

**KEY WORDS:** Black holes, multiple sclerosis, CIS

## Thursday Morning

**10:30 AM - 12:00 PM**

**Trianon Ballroom**

**(65b) Interventional: Aneurysms II**

**O-511**

**10:30 AM - 10:38 AM**

**Diagnostic Quality and Accuracy of Low Dose 3D Digital Subtraction Angiography Protocols in the Evaluation of Intracranial Aneurysms**

Pearl, M. S.<sup>1</sup>•Katz, Z.<sup>1</sup>•Messina, S. A.<sup>1</sup>•Blasco, J.<sup>2</sup>•Tamargo, R. J.<sup>1</sup>•Huang, J.<sup>1</sup>•Leigh, R.<sup>1</sup>•Zeiler, S. R.<sup>1</sup>•Radvany, M. G.<sup>1</sup>•Ehtiati, T.<sup>3</sup>•Gailloud, P.<sup>1</sup>

<sup>1</sup>The Johns Hopkins Hospital, Baltimore, MD, <sup>2</sup>Hospital Clinic, Barcelona, SPAIN, <sup>3</sup>Siemens Corporate Research Division, Baltimore, MD

#### PURPOSE

3D digital subtraction angiography (DSA) is the gold standard imaging technique for the diagnosis and characterization of intracranial aneurysms. This study analyzes the subjective assessment of image quality and the measured differences in aneurysm size in low dose versus standard 3D DSA protocols.

#### MATERIALS & METHODS

Based on preliminary studies in a swine model, three low dose 3D DSA protocols (0.10  $\mu\text{Gy/f}$ , 0.17  $\mu\text{Gy/f}$ , 0.24  $\mu\text{Gy/f}$ ) were compared against the standard 5s 0.36 $\mu\text{Gy/frame}$  setting. Twelve patients with intracranial aneurysms were enrolled (4 in each low dose protocol). The standard and one low dose 3D DSA protocol were performed in each patient. Multiplanar (2D) and 3D reconstructions were created to optimize aneurysm assessment for treatment planning. Three interventional neuroradiologists measured two predefined components of aneurysm size in each protocol. The difference between corresponding measurements obtained from the low dose and standard protocols was calculated. 0.5 mm was defined as the threshold for a clinically acceptable difference. Three interventional neuroradiologists, two neurosurgeons, and two neurologists rated the quality of the 3D reconstructions as good (3), acceptable (2), or poor (1).

#### RESULTS

Dose (mGy): Delivered system doses ranged from 26.6 to 101.2. Delivered dose average and ranges per protocol: 0.36  $\mu\text{Gy/f}$  (87.7; 73.0 - 101.2); 0.24  $\mu\text{Gy/f}$  (58.7; 50.0 - 69.4); 0.17  $\mu\text{Gy/f}$  (45.6; 36.6 - 53.8); 0.10  $\mu\text{Gy/f}$  (28.4; 26.6 - 31.8). The 0.24  $\mu\text{Gy/f}$  protocols



delivered 28% to 32% less dose compared with the standard 0.36  $\mu\text{Gy}/\text{f}$ . Measurement accuracy: 144 measurements of aneurysm size were made. Ranges of measured differences (standard vs low dose) (mm) per protocol: 0.24  $\mu\text{Gy}/\text{f}$  (0.33 - 0.39); 0.17  $\mu\text{Gy}/\text{f}$  (0.47 - 0.60); 0.10  $\mu\text{Gy}/\text{f}$  (0.71 - 0.74). Measured differences in the 0.24  $\mu\text{Gy}/\text{f}$  group were clinically acceptable. The greatest measured differences were in the 0.10  $\mu\text{Gy}/\text{f}$  group. 3D Morphologic assessment: Seven reviewers provided a total of 168 evaluations of 3D image quality. Average rating per protocol: 0.36  $\mu\text{Gy}/\text{f}$  (2.76); 0.24  $\mu\text{Gy}/\text{f}$  (2.71); 0.17  $\mu\text{Gy}/\text{f}$  (2.64); 0.10  $\mu\text{Gy}/\text{f}$  (1.89). Eleven "poor" ratings were noted, of which eight were from the 0.10  $\mu\text{Gy}/\text{f}$  group.

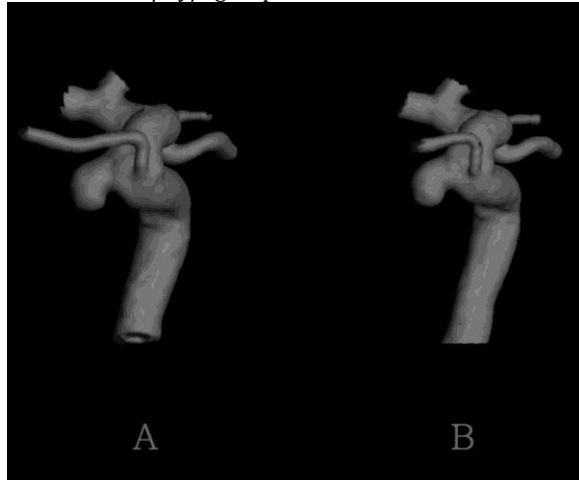


Figure 1. 3D reconstructions from patient with right clinoid segment aneurysm. (A). Low dose (5s 0.24  $\mu\text{Gy}/\text{f}$ ) and (B) standard (5s 0.36  $\mu\text{Gy}/\text{f}$ ) 3D DSA protocols. 0.24 $\mu\text{Gy}/\text{f}$  protocols were most difficult to distinguish from standard.

#### CONCLUSION

Low dose 5s 0.24  $\mu\text{Gy}/\text{f}$  3D DSA protocols generate accurate, diagnostic quality images that deliver doses of up to 32% less than the standard 5s 0.36  $\mu\text{Gy}/\text{f}$  setting.

**KEY WORDS:** Low dose, 3D DSA, aneurysm

**O-512**

**10:38 AM - 10:46 AM**

#### Practical Techniques for Dose Reduction during Cerebral Digital Subtraction Angiography

Pearl, M. S. Gailloud, P.

The Johns Hopkins Hospital  
Baltimore, MD

#### PURPOSE

Digital subtraction angiography (DSA) is the gold standard imaging method for the evaluation of cerebrovascular disorders. This study compares doses delivered during cerebral DSA in a phantom model using various dose reduction techniques.

#### MATERIALS & METHODS

Three components of a diagnostic angiogram were analyzed: femoral artery access, roadmap guidance, and DSA. Variables included fluoroscopic pulses per second

(p/s), DSA frames per second (f/s), and collimation. Pediatric and adult settings were applied to each protocol. Delivered skin doses (mGy) were measured. *Femoral artery access:* 12 protocols were developed. All had five seconds of fluoroscopy and five additional seconds of either fluoroscopy or DSA. *Roadmap guidance:* five protocols were analyzed with fluoroscopic pulse rates of 15, 10, 7.5, 4, and 3 p/s. *DSA:* four biplane imaging protocols were tested including neck and cranial AP and lateral views for carotid and vertebral angiography, with DSA frame rates of 2 and 3 f/s.

#### RESULTS

*Femoral artery access:* Ranges of delivered doses (mGy): four protocols without a DSA component: Adult (0 to 0.1); Pediatric (0 to 0.1); eight protocols utilizing DSA: Adult (0.8 to 1.9); Pediatric (0.3 to 0.7). Protocols using fluoroscopy alone delivered 86% to 95% less dose than those utilizing DSA. *Roadmap guidance:* Delivered doses (mGy) per protocol: 15 p/s, 10 p/s, 7.5 p/s, 4 p/s, and 3 p/s. Adult: (0.9, 0.6, 0.5, 0.2, 0.2); Pediatric: (0.8, 0.5, 0.4, 0.2, 0.2). Roadmaps performed at 3 or 4 p/s delivered 50% to 78% less dose than higher pulse rate protocols. *Cerebral DSA:* Average and ranges of delivered doses (mGy): Adult (1021.3; 541.4 to 1562.8); Pediatric (308.2; 182.5 to 454.1). Pediatric protocols delivered an average of 70% less dose than adult protocols. Collimation reduced the delivered dose by 49% to 54% (adult) and 37% to 41% (pediatric) for identical DSA frame rates.

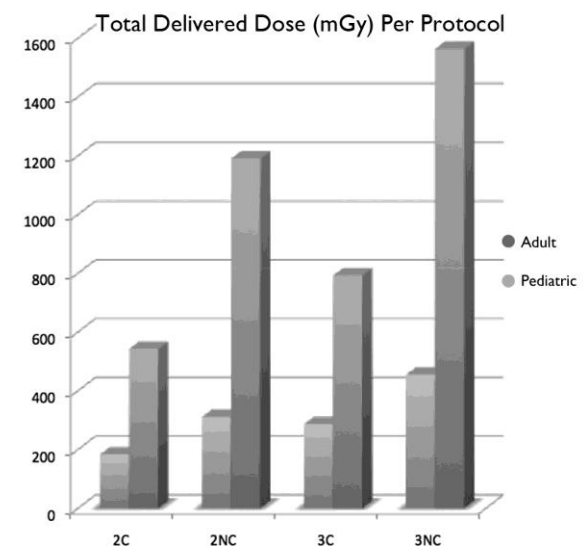


Figure 1. Total adult and pediatric delivered doses per protocol. Pediatric doses were an average of 70% less than adult doses. Doses from 2NC group were 109% to 150% higher than those from 3C group despite being performed at lower DSA rate. DSA rates: 2 = f/s; 3 = f/s. C = collimate. NC = no collimation.

#### CONCLUSION

Tailoring cerebral DSA protocols and adhering to basic principles of fluoroscopy significantly reduce cumulative delivered doses. In this phantom model, pediatric protocols offered on average a 70% dose reduction when compared to adult protocols.

Collimation alone reduced the delivered dose by 37% to 54%.

**KEY WORDS:** Dose reduction techniques, 3D DSA, aneurysm

**O-513**

**10:46 AM - 10:54 AM**

### **Coil Embolization Using Enterprise Stent for Intracranial Saccular Aneurysm: a Single Center Experience of 289 Consecutive Aneurysms**

Cho, Y.-Yu, M.-Lee, S.-Kang, H.-Han, M.

Seoul National University Hospital  
Seoul, KOREA, REPUBLIC OF

#### **PURPOSE**

Development of the intracranial self-expandable stents has made it possible to treat cerebral aneurysms with difficult configurations by coil embolization. We present the clinical and radiologic outcomes of coil embolization using the Enterprise stent for intracranial saccular aneurysms.

#### **MATERIALS & METHODS**

Clinical and morphologic outcomes of 261 consecutive patients with a total of 289 aneurysms were assessed retrospectively, which were treated by Enterprise stent-protected coil embolization during the period from June 2008 to August 2011. There were 20 acutely ruptured aneurysms (6.9%) and 51 recanalized aneurysms (17.6%).

#### **RESULTS**

Stents were implanted prior to insertion of the first coil in 162 aneurysms (56.1%), in the course of coiling in 68 (23.5%), and after completion of coil insertion in 59 (20.4%). Satisfactory aneurysmal occlusion could be achieved in 205 aneurysms (70.9%; total occlusion in 20 and near-total in 185). Procedure-related complications occurred in 36 patients (13.8%) and permanent neurologic sequelae remained in four (1.5%). Follow-up imaging (mean interval,  $12.0 \pm 5.8$  months) of 229 aneurysms demonstrated stable occlusion in 183 (80.0%) and major recanalization in 29 (12.7%). Follow-up angiography of 102 aneurysms demonstrated in-stent stenosis in 14 (13.7%). Eleven patients (4.2%) suffered delayed cerebral infarction.

#### **CONCLUSION**

Stent-protection technique using the Enterprise stent is effective for coil embolization of wide-necked aneurysms thanks to easy navigation and precise placement. Possibility of procedure-related complications, in-stent stenosis, and delayed cerebral infarction needs to be cautioned.

**KEY WORDS:** Aneurysm, coil embolization, Enterprise stent

**O-514**

**10:54 AM - 11:02 AM**

### **Endovascular Treatment Results and Follow Up in Patients with Aneurysms $\leq 3$ mm: A Single Center Experience**

Bink, A.<sup>1</sup>Engeler, S.<sup>2</sup>Güresir, E.<sup>2</sup>du Mesnil de  
Rochemont, R.<sup>2</sup>Berkefeld, J.<sup>2</sup>

<sup>1</sup>Johann Wolfgang Goethe-University, Frankfurt/Main, Germany, Münster, GERMANY, <sup>2</sup>Johann Wolfgang Goethe-University, Frankfurt/Main, Germany, Frankfurt, GERMANY

#### **PURPOSE**

Retrospective analysis of patients treated for ruptured or unruptured very small aneurysms by means of coiling to evaluate feasibility, complication rates and outcome.

#### **MATERIALS & METHODS**

The university patients' database was searched for patients admitted between 1999 and 2011 with endovascular treatment of aneurysms  $\leq 3$  mm. Configuration and site of the aneurysms, number of coils needed to treat, occlusion rate and clinical outcome were assessed.

#### **RESULTS**

Forty-four consecutive patients with 45 aneurysms  $\leq 3$  mm were included in this retrospective analysis. Thirty-nine of 45 (87%) very small aneurysms caused subarachnoid haemorrhage, 13% of the aneurysms were incidental findings. Thirty-four aneurysms belonged to the anterior and 11 to the posterior circulation. Coiling was performed successfully in 38 aneurysms. Seven aneurysms were treated by clipping after endovascular treatment had not been successful. In six of these cases coils could not be placed adequately in the aneurysms and in one patient intraprocedural partial thrombosis of the aneurysm with the risk of a thromboembolic event led to early termination of the intervention. Mean coil number used was 1.4 (range: 1-3). Complete occlusion was achieved in 31 of 38 aneurysms, a residual neck was observed in seven aneurysms. As complications two intraprocedural ruptures occurred during 45 treatment procedures. No procedure-related death was observed. At admission Hunt&Hess scores of 0-2 were seen in 25 patients and H&H scores of 3-5 were found 19 patients. After a mean follow up of 10 months modified Rankin Scale scores of 0-2 were found in 26 patients. Fourteen patients had mRS of 3-5. Four patients had expired.

#### **CONCLUSION**

A procedure-related rupture rate of 4.4 % in ruptured versus 0% in unruptured aneurysms was found. The intraprocedural ruptures had no influence on mortality. Although one aneurysm showed partial thrombosis during the intervention no thromboembolic event was present. Endovascular coil embolization of very small aneurysms is feasible but long-term efficacy still has to be determined.

**KEY WORDS:** Aneurysm, endovascular, outcome

**O-515****11:02 AM - 11:10 AM**

### **Flow Diverter Stents for Unruptured and Recurrent Aneurysms: Considerations after Our First 70 Patients with Long Follow Up**

Isalberti, M.·Paolucci, A.·Civelli, V.·Filizzolo, M.·Triulzi, F. M.

Fondazione IRCCS Ca' Granda - Ospedale Maggiore Policlinico  
Milan, ITALY

#### **PURPOSE**

After our first cases, performed in November 2008 for large and giant or wide-neck aneurysms, we started to use flow diverter stents even for small aneurysms, thinking to tackle aneurysms in a different way that could be treated with coils. We evaluated our first elective 70 patients.

#### **MATERIALS & METHODS**

Since November 12, 2008 we treated more than 70 patients (mostly females), with age ranging from 29 and 75 years old in our center. We also treated a few cases of ruptured aneurysms. All the patients were given double antiplatelets therapy 4/5 days before the endovascular procedure, except for two patients who had loading dose before delivering the stent. We performed angiographic control before discharge, after 3 and 12 months.

#### **RESULTS**

During treatment we had one fatal hemorrhagic complication after thromboembolic phenomena. Late hemorrhage happened in two patients one of which was fatal. We had four technical complications without clinical impact on the patients. We observed three asymptomatic and complete stent occlusion: in one patient the aneurysm remained patent and we occluded the artery with detachable balloons. In a couple of cases the stent was not deployed properly. Two patients had transient ischemic attacks after double therapy suspension. The majority of the patients healed completely, reduction of the size of the aneurysm was diagnosed in the other patients.

#### **CONCLUSION**

We believe that flow diverter stents, for unruptured aneurysms, is a very useful tool, even for small aneurysms. The double antiplatelets therapy is still a disadvantage.

**KEY WORDS:** Flow diverter, stents, aneurysms

**O-516****11:10 AM - 11:18 AM**

### **Sixteen-Year Experience of Endovascular Treatment of Intracranial Aneurysms at a Single Center**

Gorelik, N.<sup>1</sup>·La Piana, R.<sup>2</sup>·del Pilar Cortes, M.<sup>2</sup>·Tampieri, D.<sup>2</sup>

<sup>1</sup>McGill University, Montreal, QC, CANADA, <sup>2</sup>Montreal Neurological Institute and Hospital, Montreal, QC, CANADA

#### **PURPOSE**

The past two decades have witnessed an ever increasing use of endovascular treatment (EVT) for intracranial aneurysms. This approach entails a lesser degree of invasiveness, possible use in sicker patients, easier access to the vertebrobasilar system, lower infection risks, and shorter recovery period. However, it carries the risk of regrowth and reopening of the aneurysm with consequential risks of morbidity and mortality associated with retreatment or rupture. To this day, data on the long-term outcome of EVT remains limited. The aim of our study is to provide a retrospective review of all the endovascular procedures for intracranial aneurysms performed at our Institution between June 1995 and July 2011 and present the demographics of the treated population, the aneurysmal characteristics, the initial and final angiographic results, as well as the rates of recanalization, retreatment, and post-EVT rupture.

#### **MATERIALS & METHODS**

We reviewed the charts of all the patients treated endovascularly for intracranial aneurysms at the Montreal Neurological Institute from June 1st, 1995 to July 31st, 2011. For each patient, the following information was collected: age, gender, aneurysmal location, shape, size, and status (ruptured vs intact), Hunt-Hess grade of subarachnoid hemorrhage, symptoms at presentation for unruptured lesions, presence and type of previous treatment of the aneurysm, date of EVT, type and quantity of devices employed, initial and final angiographic outcomes, angiographic outcome prior to retreatment, date of last angiographic and neuroradiologic follow ups, occurrence of retreatment with reason for retreatment and type of procedure, as well as occurrence of post-EVT rupture with clinical outcome.

#### **RESULTS**

A total of 460 aneurysms in 434 patients were treated at our Institution in the past 16 years. Three hundred eighteen aneurysms were ruptured and 142 were intact. Initial angiography showed 70% complete occlusions, 11% residual necks, and 19% residual aneurysms. Angiographic follow up was available for 76% of the treated aneurysms and neuroradiologic follow up (CTA, MRI, MRA) was available in 91% of the cases. The final angiographic results revealed 65% complete occlusions, 18% residual necks, and 17% residual aneurysms. Sixty-one percent of aneurysms remained morphologically unchanged, 18% thrombosed further, and 21% recanalized. Forty-nine aneurysms were retreated. Ruptures occurred in nine cases from 1 day to 7 years post-EVT with a 44% mortality.

#### **CONCLUSION**

In accordance with the literature, our study demonstrates that complications of EVT remain infrequent, but have potentially serious consequences. With over 60% of aneurysms in our sample totally occluded at long-term follow up, our work demonstrates a high success rate over years, which is consistent with the range of total occlusion at follow up

seen in previously published articles. Knowledge of the long-term outcomes of EVT is critical in establishing follow-up guidelines.

**KEY WORDS:** Intracranial aneurysms, endovascular embolization, long-term follow up

**O-517**

**11:18 AM - 11:26 AM**

### **"Y" and "X" Stent-Assisted Coiling of Complex Intracranial Bifurcation Aneurysms**

Bartolini, B. M.·Blanc, R.·Pistocchi, S.·Piotin, M.

Fondation A. de Rothschild  
Paris, FRANCE

#### **PURPOSE**

Stent-assisted endovascular treatment of intracranial aneurysms currently is performed in many endovascular centers. Unfortunately, some parent vessel bifurcation aneurysms are not treatable with single stent-assisted coiling. Recently, small series presented a novel treatment using double stents in "Y" and "X" configuration. We present our experience with "Y" and "X" stent-assisted coiling of complex bifurcation intracranial aneurysms, with emphasis on clinical and angiographic outcomes.

#### **MATERIALS & METHODS**

Clinical and angiographic outcomes of 74 patients harboring 82 intracranial aneurysms, treated with "Y" and "X" stent-assisted coiling in 77 procedures from June 2006 to November 2011, were analyzed retrospectively.

#### **RESULTS**

We treated 74 patients (27 men and 47 women, ages ranging from 28 to 86 years, average: 53 years), harboring 82 aneurysms (sac sizes from 2.1 mm to 22.0 mm, mean: 7.6 mm; neck sizes from 1.8 mm to 10.7 mm, mean: 5.3 mm), 59.7% (49/82) localized at the middle cerebral artery bifurcation, 23.2% (19/82) on the anterior communicating artery and 17.1% (14/82) at the apex of the basilar artery, in 77 procedures. Clinical presentations were: incidental discovery 73.2% (60/82), recanalizations of previously coiled aneurysms 20.7% (17/82), subarachnoid hemorrhages 6.1% (5/82). All but two procedures (in cases of acutely ruptured aneurysm) were carried out under full heparinization and dual antiplatelet medication (clopidogrel and aspirin). In two case of acutely ruptured aneurysm abciximab was administrated intraarterially and intravenously during the procedure, aspirin and clopidogrel being started after the treatment. We performed 77 procedures, 87.0% (67/77) with "Y" stenting, 5.2% (4/77) with "X" stenting, while 7.8% (6/77) attempted "Y" or "X" stenting failed. Out of 71 successful procedures, we delivered the stents before coiling in 91.5% (65/71), after in 7.1% (5/71), without coils in 1.4% (1/71). Complications associated with transient or reversible neurologic deficit (<7 days) were encountered in 7.8% (6/77) of the procedures, while complications associated with permanent neurologic deficits or death

were noted in 10.4% (8/77). The 14 procedure-related complications were the following: two stent occlusions, five thromboembolisms, four intraprocedural ruptures, two delayed intraparenchymal hematoma and one stroke secondary to iron-deficit anemia. The immediate angiographic control showed a complete occlusion in 48.8% (40/82) of the aneurysms, a partial (neck or sac remnant) occlusion in 51.2% (42/82). To date, 56.1% (46/82) of the aneurysms had been followed up (average: 11 months) with angiography, disclosing a recanalization in 13.0% (6/46), and an improvement in 39.1% (18/46). No aneurysm (re)bled during the follow-up period. At discharge and follow up, the modified Rankin Scale score was 0 in 86.5% (64/74) of the patients, 1 in 1.3% (1/74), 2 in 1.3% (1/74), 3 in 2.7% (2/74), 4 in 6.7% (5/74), 6 in 1.3% (1/74).

#### **CONCLUSION**

"Y" and "X" stent-assisted coiling of complex bifurcation intracranial aneurysms is a feasible and effective technique. Our major concern is the high rate of complications with permanent neurologic deficits. Improvement of stent design and technology may reduce permanent morbidity in the future.

**KEY WORDS:** Stent, aneurysm, bifurcation

**O-518**

**11:26 AM - 11:34 AM**

### **Pipeline Embolization Device for Neurovascular Reconstruction: Initial and Follow-up Experience in the Treatment of 167 Intracranial Aneurysms and Dissections**

Henkes, H.·Fischer, S.·Vajda, Z.·Aguilar Perez, M.·Schmid, E.·Hopf, N.·Bäzner, H.

Klinikum Stuttgart  
D-70174 Stuttgart, GERMANY

#### **PURPOSE**

The purpose of this study was to evaluate the safety and efficacy of a flow diverter "Pipeline Embolization Device" (PED) for the treatment of intracranial aneurysms and dissections.

#### **MATERIALS & METHODS**

One hundred forty-eight consecutive patients underwent an endovascular treatment of 167 intracranial aneurysms or dissections using the PED between September 2009 and September 2011. Target vessels included the anterior circulation in 129 (77%) and the posterior circulation in 38 (23%). Lesions were aneurysms (n = 150) and vessel dissections (n = 17).

#### **RESULTS**

No technical failure of the procedure was encountered. Immediate exclusion of the target lesion was not observed. Angiographic follow-up examinations were carried out in 131 (78%) cases, and revealed complete cure of the target lesion(s) in 66 (50%), morphologic improvement in 40 lesions (31%), and no improvement in 25 lesions (19%). Six major complications were encountered: one fatal aneurysm rupture, one acute and

one delayed PED thrombosis and three hemorrhages in the dependent brain parenchyma.

#### CONCLUSION

Our experience reveals that the Pipeline Embolization Device (PED) is a well controllable treatment option for wide-necked saccular aneurysms, fusiform aneurysms, remnants of aneurysms, aneurysms with a high likelihood of failure with conventional endovascular techniques, and dissected vessels in selected cases. While vessel reconstruction, performed after dissection, is achieved within days, vessel remodeling may take several months. Dual platelet inhibition is obligatory. Parenchymal bleeding into brain areas dependent on the target vessel is rare.

**KEY WORDS:** Aneurysm, dissection, pipeline embolization device (PED)

**O-519**

**11:34 AM - 11:42 AM**

#### Biomechanical Wall Properties of Human Intracranial Aneurysms Resected following Surgical Clipping: IRRAs Project

Costalat, V.

CHU Gui de Chauliac  
Montpellier, FRANCE

#### PURPOSE

Individual rupture risk assessment of intracranial aneurysms is a major issue in the clinical management of asymptomatic aneurysms. Aneurysm rupture occurs when wall tension exceeds the strength limit of the wall tissue. At present, aneurysmal wall mechanics are poorly understood and thus, risk assessment involving mechanical properties is nonexistent. Aneurysm computational hemodynamics studies make the assumption of rigid walls, an arguable simplification. We therefore aim to assess mechanical properties of ruptured and unruptured intracranial aneurysms in order to provide the foundation for future patient-specific aneurysmal risk assessment. This work also challenges some of the currently held hypotheses in computational flow hemodynamics research.

#### MATERIALS & METHODS

A specific conservation protocol was applied to aneurysmal tissues following clipping and resection in order to preserve their mechanical properties. Sixteen intracranial aneurysms (11 female, 5 male) underwent mechanical uniaxial stress tests under physiologic conditions, temperature, and saline isotonic solution. These represented 11 unruptured and five ruptured aneurysms. Stress/strain curves then were obtained for each sample, and a fitting algorithm was applied following a 3-parameter [C(10), C(01), C(11)] Mooney-Rivlin hyperelastic model. Each aneurysm was classified according to its biomechanical properties and (un)rupture status.

#### RESULTS

Tissue testing demonstrated three main tissue classes: soft, rigid, and intermediate. All unruptured aneurysms

presented a more rigid tissue than ruptured or prruptured aneurysms within each gender subgroup. Wall thickness was not correlated to aneurysmal status (ruptured/unruptured). An intermediate subgroup of unruptured aneurysms with softer tissue characteristic was identified and correlated with multiple documented risk factors of rupture.

#### CONCLUSION

There is a significant modification in biomechanical properties between ruptured aneurysm, presenting a soft tissue and unruptured aneurysms, presenting a rigid material. This finding strongly supports the idea that a biomechanical risk factor based assessment should be utilized to improve the therapeutic decision making.

**KEY WORDS:** Biomechanical, rupture risk, aneurysm

**O-520**

**11:42 AM - 11:50 AM**

#### 4D Flow MR Imaging Quantifies Hemodynamics in Large and Giant Intracranial Aneurysms

Ansari, S. A.·Schnell, S.·Vakil, P.·Hurley, M. C.·Bendok, B. R.·Batjer, H.·Carroll, T. J.·Carr, J.·Markl, M.

Northwestern University Feinberg School of Medicine  
Chicago, IL

#### PURPOSE

Unruptured intracranial aneurysms (IA) are potentially life threatening conditions, often developing at vascular bifurcation points. Intracranial aneurysms size and patient risk factors have been linked to aneurysm rupture, but specific data regarding interval growth or destabilization is lacking. We studied the feasibility of 4D flow MRI to analyze 3D flow patterns (vorticity) and aneurysm wall shear stress (WSS) in large or giant IAs.

#### MATERIALS & METHODS

Seven patients (4 F:3 M, age  $53.6 \pm 15.4$  years) with large or giant IAs (mean largest dimension =  $2.6 \pm 0.9$ , range = 1.4-4.2 mm) were studied. Intracranial aneurysms were located near the ICA bifurcation (n = 5) with saccular/spherical morphology or the basilar artery (n = 2) with fusiform morphology. 4D flow MRI (3 T TRIO and 1.5 T Avanto, Siemens, Germany, spatial-res = 0.99-1.8 mm x 0.78-1.46 mm x 1.2-1.4 mm, TE/TR = 2.9-3.3 ms/5.5-6 ms, temporal-res = 44-48 ms, 3-directional velocity encoding with  $v_{enc} = 70-80$  cm/s) data were analyzed using Matlab-based tools and 3D blood flow visualization software. Intra-aneurysmal flow was visualized using time-resolved pathlines and vector graphs mapped onto a 2D plane aneurysm center. The WSS pattern along the aneurysm wall was calculated by cubic spline interpolation of the velocity gradient along the aneurysm contour as described previously. The vorticity defined as  $Vort = \text{abs}(\zeta_x, \zeta_y, \zeta_z)$  (with  $\zeta_x = \delta w / \delta y - \delta v / \delta z$ ,  $\zeta_y = \delta u / \delta z - \delta w / \delta x$ ,  $\zeta_z = \delta v / \delta x - \delta u / \delta y$  and  $u, v, w$  being the velocity vector components) was calculated for 48x48 points within the plane transecting the aneurysm. Vorticity was denoised with a 3x3 2D median filter for all cardiac phases, outliers were rejected.



## RESULTS

3D spatial and 3-directional velocity encoding allowed for the 3D visualization of complex intracranial flow patterns. Intracranial aneurysms could be well segmented using the velocity data combined with magnitude data. Flow patterns in the aneurysms could be classified in two morphologic groups. Narrow high-flow channels in combination with large central low flow regions were identified in saccular/spherical IAs (ICA or MCA, group 1, n = 5). Slow flow with less defined flow channels were noted in fusiform IAs (VA or BA, group 2, n = 2). The distribution of WSS was significantly more heterogeneous and increased for group 1 compared to group 2 ( $WSS = 0.63N/m^2 \pm 0.33N/m^2$  versus  $0.038N/m^2 \pm 0.016$ ). Vorticity in the plane through the center of the aneurysm was significantly higher for group 1 versus group 2 ( $0.073 \pm 0.028$  versus  $0.018 \pm 0.005$ , paired t-test,  $p < 0.01$ ).

## CONCLUSION

Our feasibility study shows the potential of 4D flow MRI to identify differences in flow characteristics such as vorticity and WSS patterns in two IA morphology groups. Future longitudinal studies based on the measurement, analysis and visualization of intracranial aneurysm hemodynamics using 4D flow MRI have the potential to correlate disease progression with authentic regional hemodynamics and may improve risk stratification and treatment planning.

**KEY WORDS:** 4D Flow MR imaging, intracranial aneurysms

**O-521**

**11:50 AM - 11:58 AM**

### Reossification of the Eroded Sinus(es) Wall after Endovascular Treatment of Giant/Large Intracranial Aneurysms

Biondi, A.<sup>1</sup>•Jirari, M.<sup>1</sup>•Clarençon, F.<sup>2</sup>•Billon-Grand, C.<sup>1</sup>•Cattin, F.<sup>1</sup>

<sup>1</sup>Besancon University Hospital, Besancon, FRANCE,  
<sup>2</sup>Pitié-Salpêtrière Hospital, Paris, FRANCE

## PURPOSE

Cataclysmic epistaxis is a rare but frightening complication of intracranial giant/large aneurysms (G/LAs). This life-threatening complication occurs secondary to erosion of the adjacent sinuses wall and rupture of the aneurysm sac in the sinus. The purpose of our study was to evaluate the reossification of the sinus(es) wall on CT follow up after endovascular treatment of the G/LA intracranial aneurysms.

## MATERIALS & METHODS

Thirty out of 62 patients (mean age of 53 years) treated for an intracranial G/L aneurysm of the carotid siphon, presented an erosion of the sinus(es) wall related to the contiguous aneurysm. The bone erosion was evaluated on pretreatment CT scan. Fifteen of the 30 patients were treated by occlusion of the parent artery, four by coils (with stent-assisted coil placement in two) and 11 patients with a flow diverter (FD) stent (silk stent in five and pipeline stent in six). All the patients had

imaging follow up(s) ranging from 3 to 18 months. The reossification of the sinus wall was assessed on CT follow up in 21 patients. Three patients are still under evaluation. Three patients underwent only MR studies and three patients were lost at follow up.

## RESULTS

On CT follow up, a reossification of the sinus bone adjacent to the aneurysm sac was observed in 19 out of 21 patients independently of the endovascular technique used. All 19 patients presented complete or nearly complete occlusion and a dramatic shrinkage of the aneurysm. In two patients (aneurysm treated by coils), persistent bone erosion was associated with residual/recurrent aneurysm.

## CONCLUSION

In our experience, after endovascular occlusion of an intracranial G/L aneurysm, CT imaging follow up shows reossification of the previously eroded sinus wall in all patients in whom aneurysm occlusion and shrinkage is obtained.

**KEY WORDS:** Aneurysm, flow diverter stents, parent artery occlusion

**O-522**

**11:58 AM - 12:06 PM**

### Ophthalmic Artery Sacrifice: Diagnostic Utility of Balloon Test Occlusion Study with Photopic Electroretinography

Ansari, S. A.<sup>1</sup>•Towle, V. L.<sup>2</sup>•Roth, S.<sup>2</sup>•Gemmete, J. J.<sup>3</sup>•Christoforidis, G.<sup>2</sup>

<sup>1</sup>Northwestern University Feinberg School of Medicine, Chicago, IL, <sup>2</sup>University of Chicago, Chicago, IL,  
<sup>3</sup>University of Michigan, Chicago, IL

## PURPOSE

Vessel deconstruction of the ophthalmic artery (OA) occasionally is required in the treatment of periorbital internal carotid artery (ICA) intracranial aneurysms, or more rare lesions such as dural AVF/AVMs, or symptomatic intraorbital OA aneurysms. Multiple external carotid artery (ECA) to OA collaterals can prevent ocular ischemia in >90% of cases. However, despite visualization of ECA collateral supply to the distal ophthalmic-retinal artery and/or preservation of a choroidal blush on angiographic assessment, vision loss may still occur due to inadequate retinal perfusion and delayed thromboembolic complications.

## MATERIALS & METHODS

We studied four separate endovascular interventions that required proximal OA deconstruction: Patient 1 with a fusiform OA aneurysm treated with coil embolization; Patient 2-4 with a periorbital ICA aneurysms incorporating the OA treated with ethylene vinyl alcohol (Onyx) liquid or coil embolization. In all patients, baseline visual field testing was documented prior to the procedure. Common carotid angiograms were performed prior to, during ICA balloon test occlusion (BTO) across the OA origin, and after OA

sacrifice. Photopic electroretinography (PERG) was recorded in both eyes using surface/needle infraorbital electrodes by measuring a-wave (cone system) and b-wave (Mueller cell) responses before and intermittently at 5, 15, and 25 minutes after ICA BTO. Additionally, diffuse flash visual evoked potentials were recorded from scalp electrodes over the occipital cortex.

#### RESULTS

Angiographic ECA OA collaterals with an intact choroidal blush were present in all patients during ICA BTO, though the choroidal blush fluctuated in visibility and correlated with PERG b-values. In patients 1 and 4, ~50% reduced b-values from baseline were noted at 15-25 minutes during the BTO. In contrast, preserved or transiently <30% reduced b-values were observed in patients 2 and 3 during the BTO and following OA sacrifice. Visual evoked potentials remained intact throughout the procedure. Following coil/liquid embolization, OA sacrifice was confirmed on angiography in patients 1-3. All patients were visually and neurologically intact postprocedure. However, patient 1 returned 4 days later with spontaneous vision loss and branch central retinal artery occlusion. In patient 4, the periorbital aneurysm was partially coiled to salvage the OA due to PERG results and experience with patient 1.

#### CONCLUSION

We report a novel intraoperative application of PERG to assess retinal perfusion in preparation for OA sacrifice. During a BTO study across the OA origin, concomitant PERG may assist in predicting retinal ischemia or delayed thromboembolic complications quantitatively (>50% reduced baseline b-values) rather than the qualitative assessment of ECA OA collaterals or choroidal blush with angiography. The BTO PERG technique is a unique diagnostic assessment of collateral retinal perfusion with implications for altering treatment planning or postprocedure management such as fluid augmentation, hypertensive therapy, and utilization of dual antiplatelet medications.

**KEY WORDS:** Ophthalmic artery, photopic electroretinography, balloon test occlusion

## Thursday Morning

10:30 AM - 12:00 PM

Beekman/Sutton North

(65c) Spine Intervention

O-523

10:30 AM - 10:38 AM

### Vertebral Artery Position in the Setting of Cervical Degenerative Disease: What Is a "Safe Position" for Selective Cervical Nerve Root Block?

Fitzgerald, R. T.·Bartynski, W. S.

University of Pittsburgh  
Pittsburgh, PA

#### PURPOSE

CT-guided or fluoroscopic selective cervical nerve root block (SCNRB) commonly is utilized as a diagnostic/therapeutic tool in patients with cervical radiculopathy. Potential complications include spinal cord injury (potentially related to particulate injection into a radiculomedullary artery) and stroke (potentially related to interaction with the vertebral artery). When performing SCNRB with CT fluoroscopy, we commonly observe that the vertebral artery lies in close proximity to the entry point of the target neural foramen and/or the target nerve root, often secondary to uncovertebral and facet arthropathy. The purpose of this study is to assess the position of the vertebral artery relative to the typical SCNRB injection point.

#### MATERIALS & METHODS

CT fluoroscopically guided SCNRBs were performed at 70 levels in 68 patients with cervical radiculopathy and/or neck pain over a 1-year period (age range 19-83 years, mean 50.6 years; C4: 6, C5: 21, C6: 21, C7: 22). Vertebral artery position was categorized as: anterior (normal), partially covering the lateral aperture of the neural foramen, and completely/nearly completely covering the lateral aperture of the neural foramen. Degenerative neural foraminal narrowing at each treated level was characterized as: normal, moderate narrowing, severe narrowing. Vertebral artery position relative to degree of foraminal narrowing was compared.

#### RESULTS

Results are summarized in Table 1. Complete neural foramen covering was identified in 15 of 23 (65%) severely narrowed foramina (Figure) and 11 of 37 (30%) moderately narrowed foramina. Partial neural foraminal covering was most commonly present in moderately narrowed foramina (17 of 37). Normal vertebral artery anatomical position was typically seen with normal or moderately narrow foramina.

Vertebral Artery Position Relative to Neural Foraminal Narrowing			
		Vertebral Artery Position	
Neural Foramen Size	Anterior (normal)	Partial Coverage	Complete or Near-Complete Coverage
Normal	7	2	1
Moderate Narrowing	9	17	11
Severe Narrowing	4	4	15



#### CONCLUSION

The vertebral artery commonly lies at the aperture of the neural foramen in patients undergoing SCNRB related to displacement from uncinate/facet hypertrophy. Awareness of this typical aberrant vertebral artery position can aid the operator in selection of needle trajectory and tip target point prior to injection.

**KEY WORDS:** Selective cervical nerve root block, vertebral artery, neural foramen

**O-524**

**10:38 AM - 10:46 AM**

#### Spinal Cord Hypothermia without Systemic Hypothermia

Purdy, P. D.<sup>1</sup>•Novakovic, R. L.<sup>1</sup>•Giles, B. P.<sup>2</sup>•Miller, S. L.<sup>1</sup>•Riegel, M. S.<sup>1</sup>

<sup>1</sup>University of Texas Southwestern Medical Center, Dallas, TX, <sup>2</sup>Veterans Administration Medical Center, Dallas, TX

#### PURPOSE

Hypothermia has been shown to be beneficial in the setting of acute spinal cord injury (SCI). However, widespread use has been hindered by the need for

systemic hypothermia as the vehicle for achieving spinal cord hypothermia. This study demonstrates that localized spinal cord hypothermia can be achieved via a percutaneous approach while maintaining systemic normothermia.

#### MATERIALS & METHODS

Five Yucatan swine underwent catheterization of the subarachnoid space and infusion of room temperature, chilled, and iced Plasma-Lyte A (Baxter Healthcare Corporation) solutions into the cervical spinal canal, with drainage from the lumbar canal. Thermocouples were placed within the spinal cord and in the subarachnoid space and recorded during infusions and recovery from hypothermia (Fig. 1).

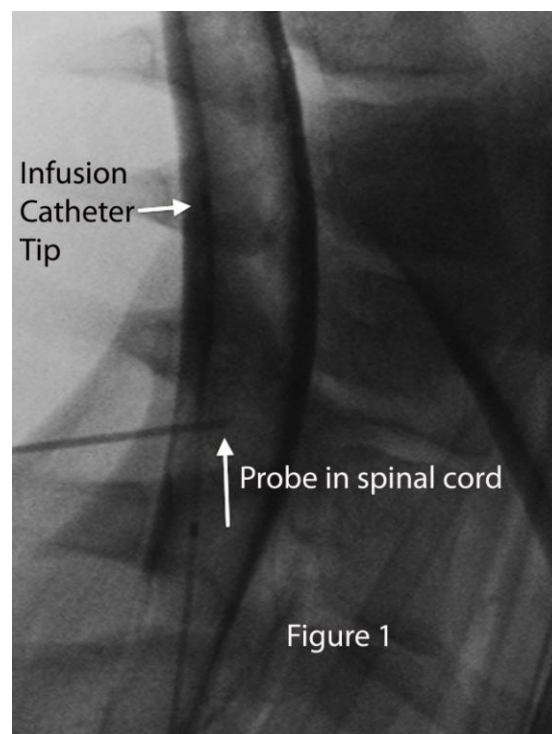
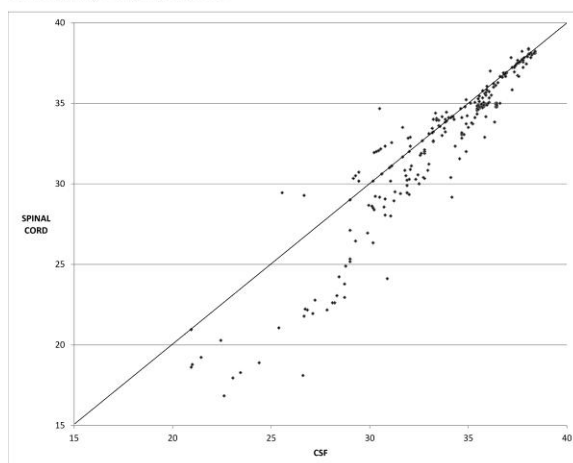


Figure 2

Spinal Cord (y-axis) vs. CSF (x-axis) Temperature



#### RESULTS

Hypothermia as low as 16.8°C was achieved in the spinal cord with retention of systemic normothermia, with strong ( $r = .95$ ) correlation between the spinal

cord temperature and the cerebrospinal fluid (CSF) temperature (Fig. 2). Degrees of cooling varied with flow rates and with infusate temperature.

#### CONCLUSION

While the data are preliminary in a small group of animals, the ability to rapidly create a wide range of controlled spinal cord hypothermia while preserving normal body temperature warrants wider exploration. The study also indicates that further investigation of the hypothesis that CSF temperature monitoring may be an acceptable surrogate for direct spinal cord temperature monitoring should be pursued. The value of profound vs mild cooling may be investigated with this model.

**KEY WORDS:** Spinal cord injury, hypothermia, cerebrospinal fluid

**O-525**

**10:46 AM - 10:54 AM**

#### **Improved Outcomes with Percutaneous Image-Guided Lumbar Synovial Cyst Treatment: Novel Approaches and Techniques**

Tekchandani, L. Ortiz, O.

Winthrop University Hospital  
Mineola, NY

#### PURPOSE

To show improved outcomes following lumbar synovial cyst rupture in previously symptomatic patients using aggressive tandem and/or coaxial percutaneous image-guided techniques.

#### MATERIALS & METHODS

Thirteen consecutive patients underwent CT-guided percutaneous treatment for their symptomatic lumbar synovial cysts. All patients presented with unilateral lower extremity radiculopathy with or without lower back pain. These patients chose to undergo attempted percutaneous management of their symptomatic lumbar synovial cysts. All procedures were performed under strict aseptic technique using intravenous anesthesia and CT fluoroscopic guidance. A facet arthrogram was attempted using a low osmolar nonionic contrast agent in all patients. Cyst rupture, using a tandem and/or coaxial technique, was performed in all patients using an 18 ga guide needle and a 22 ga insert needle. In those instances where the facet arthrogram demonstrated the presence of a communicating cyst, the tandem approach consisted of simultaneous cyst opacification via repeat arthrography and subsequent cyst puncture, attempted aspiration and rupture with a second needle (18 and or 22 ga). Isolated, noncommunicating cysts were accessed via an interlaminar or transforaminal approach using coaxial technique with an 18 ga spinal (guide) needle and a 22 ga (insert) Chiba needle. Following attempted cyst aspiration, cyst rupture is performed using a 1 to 3 mL mixture of methylprednisolone (2 mL, 80 mg) and bupivacaine (3 mL, 0.5%). All patients have been followed for a minimum of 3 weeks after their procedure.

#### RESULTS

Ten patients were male and three were female, with an average age of 65.0 years. All patients presented with severe (9-10/10) unilateral lower extremity radiculopathy, with or without low back pain. These patients had their cysts accessed either through the facet joint (indirect) or through an interlaminar or transforaminal approach (direct). The cysts did not communicate with the parent facet joint in four patients. Five patients underwent coaxial technique cyst rupture and eight patients underwent tandem technique cyst rupture. Cyst aspiration was performed successfully in three patients, yielding straw-colored, viscous fluid. Cyst rupture was documented in all cases by the eradication of the cyst as seen with postprocedure imaging and the presence of small amounts of contrast agent within the epidural space. The mean surveillance period in these patients was 38.08 months, with a range of 95 months and a median of 22 months. Three patients were retreated for recurrent, though smaller cysts, which occurred within 3 months of initial treatment. These patients have not had a recurrence at a minimum of 1 year follow up. Also, to date, none of the remaining patients have had a recurrence. No treatment-related complications were observed.

#### CONCLUSION

Aggressive tandem and/or coaxial percutaneous image-guided techniques for rupture and treatment of lumbar synovial cysts reduces recurrence rates and therefore helps avoid more invasive, open surgical procedures in this group of patients.

**KEY WORDS:** Lumbar synovial cyst, percutaneous treatment

**O-526**

**10:54 AM - 11:02 AM**

#### **Does T2 Signal Intensity of Synovial Cysts Predict Outcomes following Percutaneous Rupture?**

Cambron, S. C. Pastel, D. McIntyre, J. J. Guerin, S.

Dartmouth Hitchcock Medical Center  
Lebanon, NH

#### PURPOSE

Synovial cysts of the lumbar spine facet joints are an uncommon cause of radiculopathy. Incidence of synovial cysts is estimated at 0.6% of symptomatic patients, and 1.6% of pathologic specimens on retrospective review. Degeneration of facet joints is the most common etiologies of cyst formation. The most common symptoms are painful radiculopathy (85%), neurogenic single-root or multiroot claudication (44%), sensory loss (43%), and motor weakness (27%). Treatment options range from no treatment to surgical removal. Percutaneous treatments include CT-guided rupture, and steroid injection. The cysts have a variable T2 appearance on MRI. In our clinical experience, the T2 hypointense cysts are more difficult to rupture and tend to have a less favorable outcome. We will present a case series of treated patients, and compare outcomes based on the T2 signal characteristics of the cysts.

## MATERIALS & METHODS

Diagnosis was made by MRI. Symptoms included radiculopathy corresponding to the location of the cyst. Prone positioning and moderate sedation was used. Intermittent CT fluoroscopic guidance was used to gain direct access to the facet joint. Continuity of facet joint to cyst was confirmed with dilute contrast. Cysts then were ruptured with a forceful injection of contrast. Cyst rupture was confirmed by the presence of contrast material in the epidural space, and by the loss of resistance to injection. After rupture, 80 mg of DepoMedrol was injected. Assessment of clinical outcome was by review of electronic medical records.

## RESULTS

Eighty procedures were attempted in 59 patients. There were 46 females and 13 males, ages 40-87 years (average 64). Twelve patients had repeated procedures at a single facet, one patient had six procedures over 2 years. Injected facets included; 38 L4-5 (64%), 13 L5-S1 (22%), 6 L3-4 (10%), and 2 L2-3 (3%). Cyst rupture was technically successful in 72 out of 80 attempts (90%). Cysts were characterized on MRI and divided into three groups, T2 hyperintense, mixed T2 signal intensity, and T2 hypointense. Forty (50%) procedures resulted in complete resolution of radicular symptoms. After resolution, pain recurred in 13 of 40 cases. Recurrence of pain ranged from 2 weeks to 3 years. Twenty procedures resulted in partial relief of radicular symptoms. Eleven procedures (14%) resulted in no change in clinical symptoms, including four cases with technically successful cyst rupture. The rupture rate and clinical outcome for each group of cysts based on T2 signal intensity will be compared with examples of each. Pathology of surgical cases will be reviewed and correlated to MR imaging features.

## CONCLUSION

Percutaneous rupture of lumbar spine facet synovial cysts is a safe procedure for management of synovial cysts. In our experience, T2 hyperintense cysts are easier to rupture, perhaps due to the cysts containing a higher proportion of fluid and being less gelatinous or calcified than cysts of mixed signal intensity and T2 hypointensity. We plan to report the rupture rate and clinical outcomes of synovial cysts based on T2 signal intensity. These results will allow improved patient selection for this minimally invasive procedure.

**KEY WORDS:** Synovial cyst, percutaneous, spine

O-527

11:02 AM - 11:10 AM

## Multicenter Study to Assess the Efficacy and Safety of Sacroplasty in Patients with Osteoporotic Sacral Insufficiency Fractures

Ortiz, A.<sup>1</sup>Kortman, K.<sup>2</sup>Miller, T.<sup>3</sup>Brook, A.<sup>3</sup>Tutton, S.<sup>4</sup>Mathis, J.<sup>5</sup>Georgy, B.<sup>6</sup>

<sup>1</sup>Winthrop-University Hospital, Mineola, NY, <sup>2</sup>Sharp Memorial Hospital, San Diego, CA, <sup>3</sup>Montefiore Medical Center, Bronx, NY, <sup>4</sup>Medical College of Wisconsin, Milwaukee, WI, <sup>5</sup>Center for Advanced Diagnostic

Imaging, Roanoke, VA, <sup>6</sup>North County Radiology, San Diego, CA

## PURPOSE

To assess the outcomes and safety after CT-guided percutaneous sacroplasty in patients with sacral insufficiency fractures.

## MATERIALS & METHODS

A retrospective multicenter analysis of consecutive patients undergoing image-guided sacroplasty for painful sacral insufficiency fractures. All procedures were performed with CT, CT and fluoroscopy or CT fluoroscopy. The inclusion criteria consisted of severe sacral pain not responding to conservative medical management with imaging (MRI, CT and/or skeletal scintigraphy) evidence of unilateral or bilateral sacral insufficiency fractures. The presence of other pelvic or spinal fractures also was recorded. The number of bone needles (13 or 11 g) and the volume of injected acrylic bone cement also were documented. Outcome measures included hospitalization status (inpatient or outpatient), pretreatment and posttreatment visual analog scale (VAS) scores, analgesic use and complications. Patients were followed at approximately 1 month and up to 1 year and beyond their sacroplasty procedure.

## RESULTS

One hundred seventy-eight patients were included in this study. One hundred fifty-one patients were female and 27 were male with an average patient age of 77.4 years. One hundred forty-six patients had bilateral sacral insufficiency fractures and 32 had unilateral fractures. Forty-six patients had additional fractures of the axial skeleton consisting of 32 pelvic fractures, 19 vertebral compression fractures and one coccyx fracture. One hundred one patients were evaluated and treated as inpatients and 72 patients were managed as outpatients. The average pretreatment VAS score of 9.1 (1.1 standard deviation) was improved significantly after sacroplasty to 1.6 (1.7 standard deviation). Furthermore 67 of the 178 patients (37%) reported complete pain relief. Significant reductions in analgesic use were observed. Sacroplasty facilitated inpatient discharge in those patients who already were hospitalized. There were no procedure-related deaths, infections, pulmonary emboli, significant cement extravasations or hemorrhages. One patient experienced transient radiculitis, which was treated with steroids. This yields a minor complication rate of 0.56%.

## CONCLUSION

CT-guided percutaneous sacroplasty is a safe and effective procedure in the treatment of painful sacral insufficiency fractures. CT-guided sacroplasty is associated with prompt and durable pain relief and should be considered as an effective treatment option in this patient population.

**KEY WORDS:** Sacroplasty, sacral fracture, osteoporosis

**O-528****11:10 AM - 11:18 AM****Multicenter Study to Assess the Efficacy and Safety of Sacroplasty in Patients with Pathologic Sacral Lesions**

Ortiz, A.<sup>1</sup>•Kortman, K.<sup>2</sup>•Miller, T.<sup>3</sup>•Brook, A.<sup>3</sup>•Tutton, S.<sup>4</sup>•Mathis, J.<sup>5</sup>•Georgy, B.<sup>6</sup>

<sup>1</sup>Winthrop University Hospital, Mineola, NY, <sup>2</sup>Sharp Memorial Hospital, San Diego, CA, <sup>3</sup>Montefiore Medical Center, Bronx, NY, <sup>4</sup>Medical College of Wisconsin, Milwaukee, WI, <sup>5</sup>Center for Advanced Diagnostic Imaging, Roanoke, VA, <sup>6</sup>North County Radiology, San Diego, CA

**PURPOSE**

To assess the outcomes and safety after CT-guided percutaneous sacroplasty in patients with symptomatic sacral lesions.

**MATERIALS & METHODS**

A retrospective multicenter analysis of consecutive patients undergoing image-guided sacroplasty for painful sacral lesions. All procedures were performed with CT, CT and fluoroscopy or CT fluoroscopy. The inclusion criteria consisted of severe sacral pain imaging (MRI, CT and/or skeletal scintigraphy) a sacral lesion. A biopsy was performed in all cases. The number of bone needles (13 or 11 g) and the volume of injected acrylic bone cement also were documented. Outcome measures included hospitalization status (inpatient or outpatient), pretreatment and posttreatment visual analog scale (VAS) scores, analgesic use and complications. Patients were followed at approximately 1 month.

**RESULTS**

Nineteen patients were included in this study, 15 of whom were female and 4 were male. The average patient age was 64.5 years. Malignant lesions were diagnosed in 17 of the patients; eight patients had multiple myeloma, six had metastatic disease, two had leukemia and one had lymphoma. Two patients had benign lesions, one patient with a hemangioma and the other with a cyst. Bilateral sacral lesions were identified in eight patients and unilateral lesions were seen in 11 patients. Eight patients were evaluated and treated as inpatients and 11 patients were managed as outpatients. The average pretreatment VAS score of 8.9 (0.97 standard deviation) was improved significantly after sacroplasty to 2.4 (2.38 standard deviation). Only five of the 19 patients (25%) reported complete pain relief. Significant reductions in analgesic use were observed in this latter group of patients. There were no procedure-related deaths, infections, pulmonary emboli, significant cement extravasations or hemorrhages.

**CONCLUSION**

CT-guided percutaneous sacroplasty is a safe and effective procedure in the treatment of painful sacral benign and neoplastic sacral lesions.

**KEY WORDS:** Sacroplasty, neoplasm, sacrum

**O-529****11:26 AM - 11:34 AM****Cryoablation/Vertebroplasty versus Radiofrequency Vertebroplasty in Neoplastic Vertebral Localization**

Masala, S. • Massari, F. • Fiori, R. • Simonetti, G.

University of Rome  
Rome, ITALY

**PURPOSE**

The aim of our study was to emphasize the state of the art in vertebral neoplastic percutaneous palliative treatment by comparing the Visuale Analogue Scale (VAS) scores in cryoablation plus vertebroplasty versus radiofrequency plus vertebroplasty, and their feasibility, reliability and efficacy in short-term series.

**MATERIALS & METHODS**

Combined procedure of radiofrequency (RF) thermal ablation plus vertebroplasty or cryoablation plus vertebroplasty were performed in osteolytic neoplastic localizations in 45 consecutive patients suffering for pain refractory to conservative therapies. We evaluated pain with a "Visual Analogue Scale" (VAS), performed in the preoperative period and at 4 hours, 24 hours, 1 week, 1 month, 3 months and 6 months from the procedure.

**RESULTS**

There were no statistical significant differences in the VAS score between patients treated with cryoablation and vertebroplasty and those treated with RF ablation and vertebroplasty at 1 week ( $p = 0.34$ ), 1 month ( $p = 1$ ), 3 months ( $p = 0.68$ ) and 6 months ( $p = 0.65$ ). Patients treated with cryoablation and vertebroplasty have less pain at 4 hours ( $p < 0.001$ ) and at 24 hours ( $p < 0.001$ ) than patients treated with RF ablation and vertebroplasty.

**CONCLUSION**

Both RF ablation and cryoablation are optimal techniques in the treatment of painful vertebral neoplastic lesions. Cryoablation achieves reduced treatment-related pain in the early follow-up time and a better volume control by real-time depiction of ablation margins.

**KEY WORDS:** Neurointerventional radiology, spine, cryoablation

**O-530****11:34 AM - 11:42 AM****Comparison between Radiofrequency Targeted Vertebral Augmentation Kyphoplasty, Balloon Kyphoplasty and Vertebroplasty Using High Viscosity Cement in Treatment of Vertebral Compression Fractures**

Georgy, B.

North County Radiology  
San Diego, CA

**PURPOSE**



Both vertebroplasty and balloon kyphoplasty have been described for treatment of vertebral compression fractures. Targeting and control of cement has long been a topic of debate and goal of minimally invasive (MI) treatment of vertebral compression fractures. Balloon kyphoplasty was developed to create a cavity within which cement can be contained. Vertebroplasty is known for its high leakage rate compared with balloon kyphoplasty. In vitro studies showed that high-viscosity cements were shown to significantly decrease the incidence of leakage in cancellous bone-like substrates compared with low-viscosity cements. In this study, we compare the incidence and pattern of cement leakage in cases treated with high-viscosity cement vertebroplasty (VP) (DePuy Spine, Raynham, MA), standard balloon kyphoplasty (BKP) (Medtronic, Sunnyvale, CA) and radiofrequency targeted vertebral augmentation (RF TVA) (StabiliT System, Dfine, San Jose, CA).

#### MATERIALS & METHODS

Retrospective analysis of postoperative radiographs of patients treated with the three MI cement augmentation techniques were analyzed for the incidence and location of cement leakage. One hundred twelve consecutive patients with 159 treated levels were included in this review. There were 66 VP levels and 46 levels in BKP and 47 levels in RF TVA groups treated ranging from T3 to L5.

#### RESULTS

In the VP group, a total of 33 leakages were reported (17 diskal, 11 venous, 4 paravertebral and 1 epidural). In the KP group a total of 31 leakages were reported (15 diskal, 11 venous, 3 paravertebral and 2 epidural). In the RF KP group a total of 16 leakages were reported (8 diskal, 5 venous, 3 paravertebral and nonepidural). No significant leakage that required any surgical intervention was noted.

#### CONCLUSION

These findings show that targeted cement augmentation using RF TVA technique may provide approximately 50% reduction in leakage rate when compared to conventional VP with high viscosity cement and standard BKP. These results may be related to targeted cement delivery as a result of the unique combination of controlled delivery of radiofrequency activated (very high viscosity) cement at a low rate of injection after creation of multiple site-specific channels using the navigational osteotome. The system also allows a unipedicular access and remote controlled cement delivery to decrease procedural invasiveness and physician radiation exposure.

**KEY WORDS:** Vertebroplasty, kyphoplasty, radiofrequency

O-531

11:42 AM - 11:50 AM

#### Patients with Osteoporotic Compression Fractures: Comparison of Balloon Kyphoplasty or Radiofrequency Kyphoplasty

Pflugmacher, R.·Bornemann, R.·Deml, M.·Kabir, K.·Wirtz, D. C.

Universitätsklinikum Bonn  
Bonn, GERMANY

#### PURPOSE

Since the 1990s, balloon kyphoplasty has been proven as an effective method of treating patients with painful vertebral compression fractures (VCF). However, due to the low viscosity of the PMMA cement uncontrollable cement leakage with corresponding risks is often the focus of discussions on this procedure. The radio-frequency kyphoplasty is an innovative procedure available since 2009, for which an ultra-high viscosity cement is used. It also offers the advantage of over 30 minute's constant processing time. For the statistical comparison of the two methods of augmentation clinical and radiologic data of two larger patient groups were evaluated.

#### MATERIALS & METHODS

As part of the surgical treatment of patients with conservative therapy-resistant osteoporotic vertebral fractures a prospective study of radiofrequency kyphoplasty (RFK) was performed between 2009 and September 2010. From the clinical aspect, measurement parameters for efficacy and safety were the course of pain intensity using a visual analog scale (VAS: 0 to 100 mm) and the Oswestry Disability Score (0-100%). For the radiologic outcome the increase in the middle and anterior parts of the treated vertebra and the reduction of kyphosis after surgery and after 6 months were evaluated. Furthermore, the extent of cement extrusion and the duration of operation time were compared. There were two groups of patients chosen with the same indication, and with the same average VAS prior to treatment. For the balloon kyphoplasty (BKP) the Kyphon ® technology was used. For the BKP group the same parameters as in the first group were evaluated (matched pairs). To compare the data statistically parametric and nonparametric tests were applied.

#### RESULTS

For the radiofrequency kyphoplasty group (RFK) 114 patients were recruited, and for the balloon kyphoplasty group (BKP) 114 appropriate patients were selected. In 48% of the RFK patients and in 44% of the BKP patients more than one vertebral body was treated (thoracic or lumbar). Prior to treatment 84 mm on the VAS were calculated in both groups. The decrease in VAS values was (RFK vs BKP) immediately after surgery, 58.8 mm vs 54.7 mm ( $p = 0.02$ ), and 73.0 vs 58.9 mm after 6 months ( $p < 0.001$ ). In both groups improvements in the Oswestry scores were registered after 6 months without a statistically significant difference. In both groups, the middle part of the vertebral bodies was increased by an average of 3.1 mm. Radiofrequency yielded a decrease in the average

kyphosis angle of 4.4, the BKP resulted in about 3.8 degrees. Concerning cement leakage a key difference in favor of the radiofrequency kyphoplasty was detected (6.1% vs 27.8%;  $p < 0.0001$ ). For RFK a significant shorter duration of operation time was calculated (28.2 vs 49.6 min;  $p < 0.001$ ).

#### CONCLUSION

The RFK has proven to be a clinically very effective procedure that does somewhat better than BKP in long-lasting pain relief. No differences could be detected regarding improvement of functioning and the mean restoration of mid- and anterior vertebral height. As the safety aspect is concerned the RFK offers the advantage of a statistically significant lower proportion of cement extrusion.

**KEY WORDS:** Vertebral compression fractures, kyphoplasty, osteoporosis

**O-532** **11:50 AM - 11:58 AM**

#### Reducing Patient Dose for CT-Guided Lumbar Injections: A Body Habitus Tailored Technique Targeting the Planning CT

Schauburger, J.·Kranz, P. G.·Hoang, J. K.

Duke University Medical Center  
Durham, NC

#### PURPOSE

A recent study from our group showed that the major contributor to radiation dose for CT-guided spine interventions was the planning CT which could be up to six times the CT fluoroscopy dose. The purpose of this study was to review a newly implemented radiation dose reduction technique for CT-guided spine injections which tailors the planning CT tube current (mA) to body habitus.

#### MATERIALS & METHODS

We retrospectively reviewed 80 CT-guided lumbar spine injections. Forty procedures were performed with Protocol 1 using automatic tube current modulation for the planning CT (min 100, max 440, NI 10). Forty procedures were performed with Protocol 2 which tailored the planning CT mA to body size: 50 mA and 100 mA fixed tube current was used for patients with lateral scanogram anteroposterior (AP) diameter  $\leq 30$  cm and  $> 30$  cm, respectively. The 30 cm cut-off is based on a prior study. In both protocols, the z-axis length of the planning CT was at the discretion of the interventionalist; however, Protocol 2 called for minimized scanning. Data collected included patient AP diameter on the scout image, planning CT mA, number of injections per procedure, z-axis coverage, and the radiation dose parameters for the planning CT and total procedure, measured by CTDI and DLP.

#### RESULTS

The mean mA in Protocol 1 was 435 mA (sd 0.7). For Protocol 2, 26/40 patients were scanned with 50 mA and 14/40 were scanned with 100 mA. Using Protocol 2, only one patient (2.5%) required rescanning due to

inadequate visualization of anatomy. Protocol 2 resulted in a 9-fold decrease in CTDI and 11-fold decrease in DLP for the planning CT (Table 1). For the total procedure, the CTDI and DLP for Protocol 2 was 2 and 4.5 times lower than Protocol 1, respectively. For Protocol 1 the planning CT represented 72% of the total DLP; whereas, with Protocol 2, the planning CT represented 30% of the total DLP.

Table 1.

	Protocol 1	Protocol 2	p-value
Patient age (years)	60.9 (15.2)	61.6 (15.2)	0.85
Number of injections/procedure	1.68 (0.57)	1.70 (0.52)	0.84
Patient AP diameter (cm)	28.3 (4.2)	27.3 (5.2)	0.28
Z-axis, planning CT (cm)	9.6 (4.2)	6.5 (1.8)	$< 0.0001$
Planning CT CTDI	38.5 (24.4)	4.2 (2.5)	$< 0.0001$
Planning CT DLP	313.1 (116.3)	27.9 (21.7)	$< 0.0001$
Total Procedure CTDI	275.6 (168.7)	136.5 (92.6)	$< 0.0001$
Total Procedure DLP	432.1 (153.6)	94.2 (52.0)	$< 0.0001$

Note - Numbers in parentheses are standard deviation.

#### CONCLUSION

Total radiation dose for CT-guided lumbar injections can be markedly reduced by almost five-fold when using low tube current for the planning CT tailored to patient's body habitus. This technique can be applied to CT spine injections and also potentially some lumbar spine biopsies. Institutions should actively review their protocols for opportunities for radiation dose reduction.

**KEY WORDS:** Pain management, dose reduction, spine injections

**O-533** **11:58 AM - 12:06 PM**

#### Detection and Treatment of Cerebrospinal Fluid Leaks in Idiopathic Intracranial Hypotension

Albes, G.·Weng, H.·Horvath-Rizea, D.·Hopf, N.·Bäzner, H.·Henkes, H.

Klinikum Stuttgart  
D-70174 Stuttgart, GERMANY

#### PURPOSE

To evaluate the diagnostic imaging findings and the treatment results of patients with idiopathic intracranial hypotension (IIH) due to cerebrospinal fluid (CSF) leaks.

#### MATERIALS & METHODS

Between 2/2009 and 10/2011 20 patients (13 male, median age 49 years) 14 presenting with orthostatic headache, 16 with spontaneous subdural effusions or SAH due to IIH were enrolled. All patients underwent a whole spine CT and MR myelography starting 45 minutes after the intrathecal injection of 9 cc of Iomeprol (Imeron 300 M) and 1 cc of gadobutrolum 604,72 mg (Gadovist). Adjacent to the level of the

detected CSF leak(s) 20 cc autologous fresh venous blood mixed with 0.5 cc Gadovist were injected epidurally (blood patch). The location and distribution of the blood patch was visualized with MRI the following day. Two weeks after the blood patch the treatment result was evaluated clinically and eventually by CT/MRI myelography.

#### RESULTS

The CSF leaks were detected at the cervical ( $n = 7$ ), thoracic ( $n = 19$ ) or lumbar ( $n = 14$ ) spine. In 16 patients more than one spine segment was affected. Blood patches were applied in one ( $n = 7$ ) or several ( $n = 13$ ) levels. Clinical and/or radiologic improvement was achieved after one ( $n = 11$ ), two ( $n = 5$ ), three ( $n = 3$ ) or five ( $n = 1$ ) blood patch sessions. The only complication was an episode of transient global amnesia in one patient.

#### CONCLUSION

The incidence of IIH seems higher than reported. CT and MR myelography allows the detection of spinal CSF leaks. Targeted epidural blood patch is a safe and effective treatment. Several sessions are mostly necessary.

**KEY WORDS:** Idiopathic intracranial hypotension, spinal CSF leak, epidural blood patch

## Thursday Morning

**10:30 AM - 12:00 PM**  
**Sutton Center/South**

**(65d) Epilepsy & Other**

**O-534**

**10:30 AM - 10:38 AM**

### Graph-Theoretical Analysis of Functional MR Imaging BOLD Activation Maps for Language Localization in Patients with Complex Partial Seizures Reveals Small-World Structure of Brain Connectivity Network: Initial Experience

Karmonik, C.<sup>1</sup>Fung, S. H.<sup>2</sup>Verma, A.<sup>1</sup>Dulay, M.<sup>1</sup>Grossman, R. G.<sup>1</sup>

<sup>1</sup>The Methodist Hospital Neurological Institute, Houston, TX, <sup>2</sup>The Methodist Hospital, Houston, TX

#### PURPOSE

To investigate the structure of brain connectivity network while performing a block-design language task in patients with complex partial seizures (CPS) towards the goal of separating language activation into distinct functional subunits and improving laterality index (LI) computation for determining language dominance.

#### MATERIALS & METHODS

As part of surgical workup in six CPS patients (age: 21-35 years, mean: 31, 3 male, 2 left-handed) functional

magnetic resonance imaging (fMRI) BOLD activation maps were created using a block-design language task [language comprehension with hand motor feedback ( $n = 3$ ), word generation ( $n = 3$ ), alternating off-on periods of 30 seconds length, total of 9 periods, TR = 3000 ms]. Weighted networks were created with nodes representing voxels where activation was larger than 60% of maximum activation. Connection weights were derived from correlation coefficients between voxel time-intensity curves (neglecting weights smaller than 0.85). Networks were imported into Cytoscape (version 2.8.1, NCIBI, NIH). Edge-weighted force-directed layouts were used to create network graphs. The MCODE clustering algorithm (Bader Lab, University of Toronto, Canada) was employed to identify clusters corresponding to functional subunits within each network. Voxels belonging to different clusters were overlaid onto structural brain images of each patient employing a pseudo-color scheme.

#### RESULTS

Graphs of brain connectivity networks showed a small-world structure with large number of short-scale connections between nodes belonging to each cluster and small number of large-scale connections between clusters (Figure 1). Clusters corresponded in general to anatomical localized regions commonly associated with distinct function (visual, language, and motor).

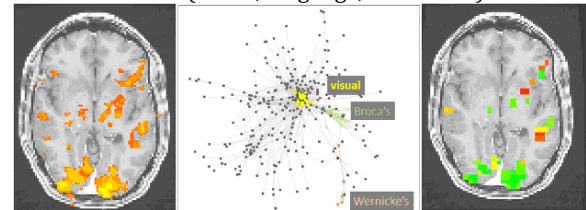


Figure 1: Left: fMRI BOLD activation map for 'block-design' language task (orange: voxels of positive activation). Center: Graph of corresponding brain connectivity network. Right: Functional subunits (clusters distinguished by different colors) identified with MCODE mapped back onto structural brain images.

#### CONCLUSION

Graph-theoretical cluster analysis employing the MCODE algorithm aids in the separation of functional subunits in the brain when performing a language task. Identifying subunits only involved in language processing might improve LI calculation aimed at localizing language function and determining language dominance for presurgical planning in patients with complex partial seizures.

**KEY WORDS:** Complex partial seizures, functional MR imaging, brain connectivity

**O-535**

**10:38 AM - 10:46 AM**

### Usefulness of Brain Perfusion Maps Obtained with Arterial Spin Labeling in Refractory Epilepsy

Bargallo, N.·Setoain, X.·Rubi, S.·Carreno, M.·Donaire, A.·Guitard, J.·Oleaga, L.

Hospital Clinico Y Provincial de Barcelona  
Barcelona, SPAIN

## PURPOSE

The aim of this study is to determine the usefulness of arterial spin labeling (ASL) in clinical diagnosis of refractory epilepsy.

## MATERIALS & METHODS

This is an exploratory study. We have performed perfusion maps using arterial spin labeling in all patients monitored in the epilepsy unit during the last year in our hospital. Forty-five patients were included, 26 females and 18 males (mean age 35 years; age range 4-66). All the patients underwent video EEG monitoring, 3 T scan MRI exam with dedicated epilepsy protocol consisting of 3D FLAIR, coronal DIR, coronal T2-weighted imaging, 3D T1 MPRAGE and axial T2-weighted imaging and pulsed ASL. Relative cerebral blood flow (CBF) maps were generated using manufacturer's software (3D NEURO; Siemens) and coregistered with 3D FLAIR Image. Positron emission tomography (PET) or SISCOM data were obtained in all patients (28 and 32 respectively). Kappa and Kendall's coefficients of concordance were obtained between structural MRI, ASL, PET and SPECT images.

## RESULTS

Thirty-six patients (80%) show structural lesion on MR examination and nine (20%) subjects show negative MRI. Findings observed were: 13 mesial sclerosis, five of them with temporal pole signal abnormalities, six tumors, six cortical dysplasia, four enlarged amygdale (possible hamartoma or dysplasia), three heterotopias, two Rasmussen or chronic encephalitis, one polymicrogyria, and one posttraumatic malacic changes. Quality of ASL acquisition was good in 34 patients, in seven patients all brains were not studied completely (mainly temporal poles) and in four patients the data were too much degraded by movement artifacts that was dismissed. Relative CBF maps showed abnormalities in 24 patients (58.5%) and were negative in 17 patients (41.5%). Decrease on rCBF maps was detected in 18/24 patients (40.9%) and increase rCBF in 6/24 (13.3 %). PET scan was positive in 20/28 patients (71.4%) and negative in 8/28 patients (28.6%). SISCOM exams show abnormalities in 28/32 cases (87.5%) and were negative in 4/32 cases (12.5%). Statistically significant concordance was observed between structural MRI and ASL perfusion maps (0.53 Tau-b de Kendall and 0.92 Kappa) and between PET and ASL perfusion maps (0.31) (Tau-b de Kendall and 0.49 Kappa). However no significant concordance was observed between ASL perfusion maps and SISCOM (0.15 Tau-b de Kendall and -0.13 Kappa).

## CONCLUSION

Arterial spin labeling perfusion map is a new tool that can detect abnormalities in patients with refractory epilepsy. Further studies are needed to determine its diagnostic value, mainly in MRI negative patients. Given the correlation between ASL and PET perfusion with ASL could become part of the standard workup in patients with epilepsy.

**KEY WORDS:** Epilepsy, arterial spin labeling

## O-536

10:46 AM - 10:54 AM

## Atlas-Based Diffusion Tensor Imaging and Volumetric Analysis Classify Temporal Lobe Epilepsy with and without Hippocampal Sclerosis

Gan, S.<sup>1,2</sup>•Qian, G.<sup>1</sup>•Seneviratne, U.<sup>3</sup>•Cook, M.<sup>2</sup>

<sup>1</sup>The University of Melbourne, Melbourne, AUSTRALIA,

<sup>2</sup>St Vincent's Hospital, Melbourne, AUSTRALIA, <sup>3</sup>Monash Medical Centre, Melbourne, AUSTRALIA

## PURPOSE

White matter tracts diffusion tensor imaging (DTI) changes were reported in temporal lobe epilepsy (TLE). Fornix and cingulum DTI changes were shown in patients with hippocampal sclerosis (TLE HS) and those with a normal structural MRI (TLE NH). This study aims to determine if atlas-based analysis (ABA) of deep white matter (DWM) DTI and volumetric parameters can discriminate these TLE subtypes, and determine the best MRI parameter and DWM discriminants. Relationships between the best DWM discriminants for TLE HS patients and the sclerotic hippocampal MRI parameters is investigated.

## MATERIALS & METHODS

Twenty TLE patients (8 TLE HS and 12 TLE NH) and 15 controls were recruited. Atlas-based analysis was performed by registering JHU-DTI-MNI-single subject atlas DWM region of interest (ROIs) to subject's native DTI space. Hippocampal volumetric ROIs were delineated manually on T1 images. Ipsilateral, contralateral and (ipsilateral-contralateral)/(ipsilateral+contralateral) asymmetry index (INDEX) of 5 MRI parameters Volume (VOL), fractional anisotropy (FA), mean diffusivity (MD), parallel ( $\lambda||$ ) and perpendicular diffusivity ( $\lambda\perp$ ) were calculated from the hippocampal ROIs and 12 DWM ROIs [Fornix Cres/Stria Terminalis (FS), column and body of fornix (FX), cingulum temporal lobe portion (CGH), cingulum cingulate gyrus portion (CGC), uncinate fasciculus (UNC) sagittal stratum (SS), superior longitudinal fasciculus (SLF), SFO (superior fronto-occipital fasciculus), inferior fronto-occipital fasciculus (IFO), genu (GCC), body (BCC) and splenium (SCC) of corpus callosum]. MANOVAs followed by ANOVAs and discriminant function analysis were computed for the 5 MRI parameters of DWM. Correlations of DWM with hippocampal parameters were analyzed.

## RESULTS

At  $p < 0.05$  significance level, compared to controls, both TLE subgroups have 1) decreased FA and increased ADC in the ipsilateral and contralateral\_FX and SCC, and 2) decreased FS\_VOL-INDEX and SLF\_λ||-INDEX. Discriminant analysis shows FS\_VOL-INDEX best discriminate controls from the TLE patients. Compared to controls and TLE NH subgroups, TLE HS group has 1) decreased FS and CGH\_VOL-INDEX, decreased FS\_λ||-INDEX and SCC\_λ||-INDEX, and increased FS\_ADC-INDEX, FS\_λ⊥ INDEX, SCC\_ADC-INDEX and SCC\_λ⊥ INDEX, 2) increased Ipsilateral\_FX\_VOL with decreased contralateral\_FX\_VOL, 3) decreased contralateral\_SLF\_FA with increased SLF\_FA-INDEX,

increased SLF\_ADC-INDEX, and increased contralateral\_SLF\_λ with decreased SLF\_λ INDEX. Among them, FS\_ADC-INDEX, SCC\_ADC-INDEX and SLF\_FA-INDEX best discriminate HS from controls and TLE-NH patients. Compared to controls and TLE-HS subgroups, TLE-NH have 1) decreased Ipsilateral and contralateral\_GCC\_VOL and SCC\_VOL, 2) decreased CGH\_λ|-INDEX, 3) decreased SS\_ADC-INDEX and SS\_Radial-INDEX, and increased SFO\_FA-INDEX. CGH\_λ|-INDEX, SS\_ADC-INDEX and SS\_λ-INDEX best discriminate TLE-NH patients. Discriminant analysis categorized 100% of cases correctly using the volume and DTI parameter-INDEXes of the best DWM discriminants for the three groups demonstrated above (FS, FX, CGH, SS, SLF, SCC). λ|-INDEX is the best discriminator MRI parameter, correctly categorizing 85.7% of cases using all 12 DWM\_λ|-INDEXes. Among the best DWM discriminants for TLE HS patients, SLF\_VOL-INDEX, ipsilateral\_FS\_FA, ipsilateral\_FS\_ADC, SCC\_ADC-INDEX and SCC\_λ|-INDEX correlates positively with the respective hippocampal MRI parameter.

#### CONCLUSION

Atlas-based analysis of volumetric and DTI parameters can discriminate between TLE with normal structural MRI and TLE HS and controls. λ|-INDEX demonstrated as the best discriminant MRI parameter, while FS, CGH, SCC, SLF and SS volumetric and DTI changes may serve as DWM discriminant markers for these TLE subtypes. FS, SCC, and SLF associate with worse sclerotic hippocampi volumetric and DTI parameters, and may be used as disease markers with hippocampal MRI parameters in TLE HS group.

**KEY WORDS:** Temporal lobe epilepsy, diffusion tensor imaging, hippocampal sclerosis

0-537

10:54 AM - 11:02 AM

#### Resting-State BOLD Functional MR Imaging Shows Visual Default Mode Network Abnormalities in Migraine with Perpetual and Transient Aura

Waldman, A. D. Honeyfield, L. Sharp, D. J. Leech, R. West, D. Beckmann, C. Weatherall, M. Peatfield, R.

Imperial College  
London, UNITED KINGDOM

#### PURPOSE

Migraine with perpetual or persistent aura is a rare, debilitating disorder where sensory abnormalities, usually visual, persist for weeks to months. It is believed that symptoms arise due to a disturbance in brain energy metabolism and altered perfusion, although there is little imaging data to substantiate this. Previous studies have reported marked hypo- and hyperperfusion in typical transient migrainous aura, although a small series of four patients with persistent aura showed no changes in water diffusion or brain perfusion. BOLD fMRI suggests correlation between the BOLD signal and spreading cortical depression in the visual cortex. The aim of this study was to investigate perfusion, diffusion-weighted imaging (DWI), and

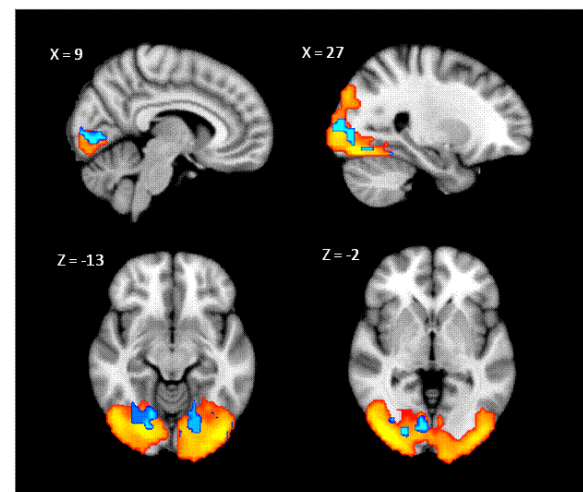
resting state (default mode) BOLD fMRI abnormalities in patients with migrainous perpetual aura and migraine with nonpersistent aura.

#### MATERIALS & METHODS

Pulsed ASL perfusion, DWI and resting-state (RS) BOLD fMRI data were acquired from five patients with migraine with persistent visual aura, seven patients with typical transient migrainous aura and 10 age-matched healthy volunteers, using a Siemens 3 T Verio MRI system (Siemens, Erlangen, De). Apparent diffusion coefficient (ADC) and relative CBF (rCBF) were calculated from manually selected regions of interest (ROIs) in bilateral frontal, parietal, temporal and visual cortices. Relative CBF measurements from visual cortex were normalized to the mean frontal and parietal values. RS fMRI data were analyzed using MELODIC (FSL; fMRIB, Oxon, UK) and established default state models, following brain segmentation.

#### RESULTS

Visual inspection identified no focal abnormality of water diffusion or perfusion in any of the subjects. No significant individual subject or group differences were detected in ADC or corrected rCBF. Decreased functional connectivity in primary and associated visual default mode networks were detectable in persistent aura migraine subjects ( $p = 0.038$ ) and intermittent aura subjects ( $p = 0.001$ ) compared with controls. Migraineurs with nonpersistent aura showed borderline greater decrease in connectivity compared with those with persistent visual aura ( $p = 0.063$ ).



#### CONCLUSION

1. Our novel preliminary RS fMRI data reveal decreased functional connectivity in visual networks in migraineurs with visual aura. 2. Patients with perpetual visual aura show less decrease in connectivity than those with intermittent visual auras, which may reflect compensatory vasoregulatory mechanisms related to spreading cortical depression in the former group. 3. RS fMRI provides a potential objective imaging biomarker for use in trials of novel targeted therapies for migraine. 4. Brain perfusion and DWI is normal in patients with perpetual visual aura.

**KEY WORDS:** Migraine, functional MR imaging

O-538

11:02 AM - 11:10 AM

### Comparison of Imaging Connectivity with Electrophysiologic Connectivity in Epilepsy Patients with Intracranial Electrodes

Jones, S. E.<sup>1</sup>Gonzalez-Martinez, J.<sup>1</sup>Nair, D.<sup>1</sup>Najm, I.<sup>1</sup>Phillips, M.<sup>1</sup>Sakaie, K.<sup>1</sup>Zhang, M.<sup>2</sup>

<sup>1</sup>Cleveland Clinic Foundation, Cleveland, OH, <sup>2</sup>Cornell University, Ithaca, NY

#### PURPOSE

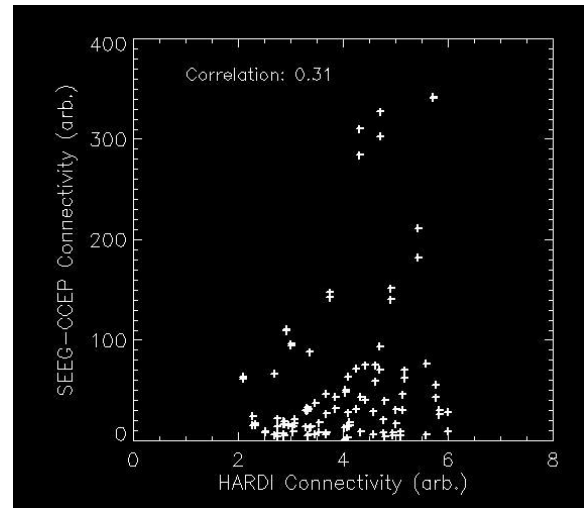
To compare the patterns of imaging connectivity to electrophysiologic connectivity in epilepsy patients with multiple intracranial electrodes. Imaging connectivity includes structural imaging from high angular resolution diffusion imaging (HARDI) and functional imaging from resting-state MRI. Electrophysiologic (EP) connectivity includes cortico-cortico evoked potentials (CCEP) stimulated using numerous intracranial electrodes.

#### MATERIALS & METHODS

Six epilepsy patients with medically refractory epilepsy underwent standard invasive evaluation using multiple stereotactic EEG (SEEG) intracranial electrodes. Prior to implantation, patients underwent 3 T MRI including anatomical imaging, HARDI imaging and resting-state MRI. The locations of electrode contacts were coregistered using postimplantation CT. Stereotactic EEG electrode contacts were stimulated using a CCEP protocol while the patient was monitored during long-term intensive care setting for up to 10 days. Ultra-fast probabilistic tracking was performed using partial differential equation (PDE) methods between the stimulating electrode and all recording electrodes. Imaging connectivity was derived from the difference of track density maps using anisotropic HARDI data from the isotropic control state. Similarly, rsMRI correlations were performed between all electrode pairs. Imaging connectivity was compared with electrophysiologic connectivity for all electrodes within a patient's brain parenchyma.

#### Results

The attached figure is one example of many comparisons possible with this data set, showing a single patient with 14 bilateral multicontact-SEEG electrodes in the occipital lobes, containing 153 contacts. Here, the stimulating electrode was located near the primary visual cortex, and each point represents both the EP and HARDI connectivity (arbitrary scale). The ensemble of points shows a modest correlation coefficient of 0.31. Such plots can be made for all simulated electrodes, over all patients. Overall, correlation coefficients are modest. Many instances of strong HARDI connectivity show minimal EP response; and many instances of strong EP connectivity show minimal HARDI response. Contributing factors include the possibility of inhibitory effects confounding EP connectivity, the contribution of other cortical regions not directly involved with the stimulating-receiving pair, and the relatively coarse resolution of HARDI voxels compared with the size of a gyrus.



#### CONCLUSION

Imaging connectivity (based on HARDI data) correlates modestly with imaging connectivity (based on electrophysiologic recordings), based on data derived from human intracranial electrodes.

**KEY WORDS:** HARDI, connectivity, intracranial electrodes

O-539

11:10 AM - 11:18 AM

### Selection of Functional Imaging to Identify the Epileptogenic Zone in Focal Intractable Epilepsy: Magnetoencephalography, Positron Emission Tomography, or Single-Photon Emission Tomography?

Widjaja, E.

Hospital for Sick Children  
Toronto, ON, CANADA

#### PURPOSE

Surgical resection of the epileptogenic zone could potentially render patients with focal intractable epilepsy seizure free. Those with focal seizure and normal MRI or a questionable lesion on MRI would undergo further diagnostic investigation to identify the epileptogenic zone. If further investigation identified the epileptogenic zone, then these patients would be considered potential candidates for epilepsy surgery. Currently there is no consensus as to which diagnostic test is optimal, magnetoencephalography (MEG), FDG-PET and combined ictal-interictal SPECT. The objective of the study was to determine the optimal diagnostic strategy that will identify the epileptogenic zone in children with suspected focal intractable epilepsy, so that appropriate treatment could be provided to reduce seizures and optimize their quality adjusted life years (or utilities).

#### MATERIALS & METHODS

Markov-based decision model was used to simulate the course of events of pediatric patients with suspected focal intractable epilepsy being workedup for epilepsy surgery. We took the perspective of the epileptologists. The best case scenario was a 10-year child with



clinically suspected focal intractable epilepsy based on clinical semiology or electroencephalography (EEG) and had undergone MRI. The three diagnostic strategies were (i) MEG, (ii) FDG-PET, and (iii) ictal-interictal SPECT. If the diagnostic test was positive, the patient would proceed with surgical resection of the epileptogenic zone. If the test was negative, the patient would continue with medical treatment. Following surgery or medical treatment, the patient could enter one of the four health states: no seizures, >50% improvement in seizures, <50% improvement in seizures or death. If the patient survived, the patient can continue in that particular health state or die from epilepsy-associated death or death from other causes based on the background mortality rate for their age. Probabilistic sensitivity analyses were conducted on the sensitivity and specificity of the tests and utilities.

## RESULTS

For the base case analysis, the model predicted FDG-PET yielded the highest utility. Magnetoencephalography yielded the second highest utility, and ictal-interictal SPECT yielded the lowest utility. Probabilistic sensitivity analysis showed that for the range of sensitivities and specificities of the three different test strategies tested, FDG-PET remained the preferred test and yielded the highest utility. The incremental utility of FDG-PET was greater compared to MEG, but this increment was small. Probabilistic sensitivity analysis for the range of utilities tested showed that FDG-PET remained the preferred test.

## CONCLUSION

In this preliminary study, we have found that in children with suspected focal intractable epilepsy, the model predicted FDG-PET yielded the highest utility compared to MEG and ictal-interictal SPECT. Further work is needed to evaluate if combinations of the different diagnostic strategies could further improve identification of the epileptogenic zone and also to incorporate cost into the analysis.

**KEY WORDS:** Magnetoencephalography, PET, SPECT

**O-540**

**11:18 AM - 11:26 AM**

### Neuroimaging Findings in Patients with Newly Diagnosed Epilepsy

Hourani, R.<sup>1</sup>•Bou Ayache, J.<sup>1</sup>•Nasreddine, W.<sup>2</sup>•Hmaimess, G.<sup>3,4</sup>•Sabbagh, S.<sup>5</sup>•Beydoun, A.<sup>1</sup>

<sup>1</sup>American University of Beirut Medical Center, Beirut, LEBANON, <sup>2</sup>Rafic Hariri University Hospital, Beirut, LEBANON, <sup>3</sup>Saint George Hospital University Medical Center, Beirut, LEBANON, <sup>4</sup>University of Balamand, Beirut, LEBANON, <sup>5</sup>Hotel Dieu de France, Beirut, LEBANON

## PURPOSE

The yield of MRI in patients with newly diagnosed epilepsy has not been adequately assessed yet. In this study, we evaluated the frequency of epileptogenic lesions in patients with newly diagnosed epilepsy.

## MATERIALS & METHODS

In this study, neurologists from across Lebanon referred their patients (at least 6 months of age) with one or more suspected unprovoked seizures to the American University of Beirut medical center where they underwent a full evaluation. This included a detailed description of the spells, full physical and neurologic examinations, sleep deprived 3 hours video-EEG study, an epilepsy protocol MRI, bone densitometry, and quality of life questionnaire. All patients diagnosed with epilepsy underwent a 1.5 T epilepsy protocol MRI including 1 mm 3D SPGR images, axial and coronal thin cuts FLAIR, axial diffusion and T2\* sequences. All MRIs were reviewed by a neuroradiologist with expertise in epilepsy who was blinded to the clinical history and diagnosis. The MRIs were classified as normal, abnormal and epileptogenic, or abnormal and nonepileptogenic based on previously published criteria.

## RESULTS

Of the 334 patients diagnosed with epilepsy, 219 patients already had an MRI performed. In the whole group, 89/219 (41%) had an epileptogenic lesion detected on their MRI. When stratified by syndrome type, the frequencies of epileptogenic lesions were 3%, 59%, and 51% in patients diagnosed with idiopathic generalized, symptomatic generalized and localization-related epilepsy, respectively. When further stratified by age groups, the frequencies of epileptogenic lesions in adults were 0% and 70% in patients diagnosed with idiopathic generalized and localization-related epilepsy, respectively. In patients less than 18 years of age, the frequencies of epileptogenic lesions were 5% and 39%, in those diagnosed with idiopathic generalized and localization related epilepsy, respectively. The difference in the frequency of epileptogenic lesions in localization-related epilepsy between adults and children was statistically significant (36/53 in adults vs 29/75 in children,  $p < 0.01$ ). A variety of epileptogenic lesions was detected and will be discussed.

## CONCLUSION

A high percentage of patients with newly diagnosed epilepsy who underwent a dedicated epilepsy MRI protocol were found to have an epileptogenic lesion. This underscores the importance of obtaining a high quality MRI interpreted by an expert especially in patients with newly diagnosed localization related epilepsy.

**KEY WORDS:** Epilepsy, neuroimaging

**O-541**

**11:26 AM - 11:34 AM**

### Optimal Diffusion-Weighted Imaging Protocol to Evaluate Transient Global Amnesia at Critical Phase and Follow Up at 3 T MR Imaging

Billon-Grand, C.•Cattin, F.•Medeiros de Bustos, E.•Muzard, E.•Moulin, T.•Biondi, A.

Besançon University Hospital  
Besançon, FRANCE

**PURPOSE**

To evaluate patients with transient global amnesia (TGA) during critical phase and to find an optimal diffusion-weighted imaging (DWI) protocol for lesion detection.

**MATERIALS & METHODS**

Five patients (5 females) aged from 50 to 76 years with TGA as defined by Hodges and Warlow were enrolled consecutively over a 4-month period. 3 T MRI was performed from 6 to 15 hours after the onset of symptoms and 48 hours later. In all patients the MRI protocol was DWI with b value/section thickness 1000/5 mm; 2000/5 mm and diffusion tensor imaging (DTI).

**RESULTS**

At initial MRI three patients had single or double punctuate hyperintense lesion on DWI with b 1000/5 mm thickness. Among these patients two had an added lesion diagnosed with b 2000. One patient had one lesion diagnosed only on DWI with b 2000/5 mm with normal b 1000. One patient was normal. Sequences with b 2000/5 mm showed the better lesions in all four patients at critical phase. Diffusion tensor imaging was not providing further informations. In 48-hour follow-up MRI, further lesions were detected with b 1000/5 mm and b 2000/5 mm. One patient was already normal.

**CONCLUSION**

On the basis of these preliminary results, highest lesion detection is possible with DWI using b value/section thickness 2000/5 mm at 3 T MRI. Follow-up DWI performed 48 hours later might be recommended because it allows visualization of a greater number of lesions at 3 T MRI.

**KEY WORDS:** Diffusion, transient global amnesia, 3 T MR imaging

**O-542****11:34 AM - 11:42 AM**

### **Functional Significance of the Arcuate Fasciculi in Pediatric Epilepsy Patients with Malformations of Cortical Development**

Paldino, M. J.-Hedges, K.-Rodrigues, K. M.-Grant, P. E.

Children's Hospital Boston  
Boston, MA

**PURPOSE**

Patients with malformations of cortical development (MCD) experience a wide range of functional deficits which often cannot be explained on the basis of the location of the structural abnormality. The goal of this study was to characterize the arcuate fasciculus (AF) and its relationship to language development in pediatric epilepsy patients with MCD.

**MATERIALS & METHODS**

Patients from an existing imaging database were included with inclusion criteria: 1. MCD. 2. Thirty-direction diffusion tensor imaging (DTI) performed at 3 T. 3. Language characterized by a pediatric-neurologist.

Twenty-two subjects presenting with headache without neurologic deficit, language impairment, or MRI abnormality served as a comparative cohort; these subjects underwent identical imaging sequences. Diffusion tensor imaging data were used for deterministic tract reconstruction. The AF was categorized as present on the left-only, right-only, or bilaterally. Mean ADC and FA were calculated within all tracts. Patients were divided into three language development groups: 1. Intact: age-appropriate. 2. Mild-to-moderate impairment: some language development but delayed compared to peers. 3. Profound impairment: absent verbal language. Proportions were compared using the Fisher exact test; continuous variables with the Wilcoxon rank sum test.

**RESULTS**

Thirty-seven MCD patients met criteria: 16 with polymicrogyria, 15 with focal cortical dysplasia, one lissencephaly, four schizencephaly, and one gray-matter heterotopia. Twenty-one MCD patients had intact language, 11 mild-to-moderate, and five profound impairment. All normative subjects had intact language and an identifiable left AF; 17/22 had an identifiable right AF. Tract parameters (ADC and FA) in normatives did not differ from MCD patients. One hundred percent (11/11) of MCD patients without a left AF had language impairment (six mild-to-moderate, five profound). Twenty-three percent (6/26) of patients with a left AF were impaired (five mild-to-moderate). This difference was significant ( $p < 0.0001$ ). There was no significant difference between frequency of language impairment in patients with (10/26) versus without (7/11) a right AF ( $p = 0.15$ ). One hundred percent (21/21) of MCD patients with intact language had an identifiable left AF. The frequency of absent left AF in patients with intact language was significantly less than that in patients with some degree of impairment ( $p < 0.0001$ ). Of the 11 MCD patients with absent left AF, four had no identifiable right AF. One hundred percent of patients with bilateral absence were profoundly impaired. Of seven with no left AF but an identifiable right AF, six were mild-moderately impaired while only one was profoundly impaired. The frequency of profound language impairment among those with an absent left AF was higher in those patients whose right AF was also absent ( $p < 0.01$ ).

**CONCLUSION**

These preliminary results demonstrate that clinically relevant alterations in structural connectivity can be detected in individual patients using this straightforward tract-based paradigm. Furthermore, the left AF may be necessary, though not sufficient, for normal language development. The right AF is neither necessary nor sufficient, but may play an important role in language development in the absence of the left AF.

**KEY WORDS:** Arcuate fasciculus, language

O-543

11:42 AM - 11:50 AM

### Evaluation of Cranial CT Utilization in Minor Head Trauma in Children

Kessler, M. M.<sup>1</sup>•Linscott, L.<sup>1</sup>•Kitchin, D.<sup>1</sup>•Quayle, K.<sup>2</sup>•Hildebolt, C.<sup>3</sup>•McKinstry, R. C.<sup>1</sup>•Don, S.<sup>1</sup>

<sup>1</sup>Mallinckrodt Institute of Radiology, Saint Louis, MO,

<sup>2</sup>Saint Louis Children's Hospital, Saint Louis, MO,

<sup>3</sup>Washington University, Saint Louis, MO

#### PURPOSE

An informal polling of pediatric radiologists in 2001 suggested that up to 30% of pediatric computed tomography (CT) scans were not indicated. Given the concern for unnecessary radiation exposure to children, this warranted objective study. For acute, minor head trauma, two published guidelines (in 2002 and 2009) with decision tree analysis help guide emergency physicians with regard to the need for head CT. Quantitative evaluation was performed to determine whether or not CT scans of the head performed for acute, minor head trauma consistently follow published guidelines. The objective was to test the hypothesis that at a free-standing children's hospital, 70% of head CT scans obtained for acute, minor head trauma followed published guidelines. Further, to identify any significant imaging findings when the study was not indicated based on these guidelines.

#### MATERIALS & METHODS

Clinical and imaging data were reviewed retrospectively for 184 consecutive patients who had acute, minor head trauma and presented to the emergency unit from 15 February 2009 to 16 January 2010. The null hypothesis was that 30% of head CT studies ordered after minor trauma did not follow established guidelines. The binomial test was used to test this percentage against the actual percentage of head CT studies that did not meet established guidelines. Statistical testing was performed and 95% confidence intervals (CIs) were calculated for children < 2 years old and for children 2 to 20 years old.

#### RESULTS

For children < 2 years old, 2 of 78 [2.6% (CI: 0.5% - 8.3%)] and for children 2 to 20 years old 12 of 104 [11.5% (CI: 6.4% - 18.7%)] did not meet guidelines. These percentages were significantly less than the hypothesized value of 30% ( $P < 0.001$ ). No significant imaging finding was seen in the 14 cases for which the guidelines were not followed.

#### CONCLUSION

Currently head CT scans obtained for acute, minor head trauma in children follow established guidelines significantly more often than pediatric radiologists assumed in 2001.

**KEY WORDS:** Minor head trauma, children, radiation safety

O-544

11:50 AM - 11:58 AM

### MR Imaging Features of Novel Influenza A (H1N1) Infection with Neurologic Complications: Case Series in a Pediatric Population with Clinical and Pathologic Correlation

Zeng, H.<sup>1</sup>•Quinet, S.<sup>2</sup>•Huan, X.<sup>1</sup>•He, Y.<sup>1</sup>•Gan, Y.<sup>1</sup>•Huang, W.<sup>1</sup>•Wang, Y.<sup>2</sup>•Haughton, V.<sup>2</sup>

<sup>1</sup>Shenzhen Children's Hospital, Shenzhen City, CHINA,

<sup>2</sup>University of Wisconsin, Madison, WI

#### PURPOSE

To describe and correlate clinical features and neurologic complications of 15 pediatric patients with confirmed novel influenza A (H1N1) infection hospitalized in Shenzhen Children's Hospital in China between September 2009 and April 2011 with associated magnetic resonance imaging (MRI) features.

#### MATERIALS & METHODS

Clinical information and imaging of 15 pediatric patients with neurologic complications after infection with influenza A (H1N1) were analyzed retrospectively. All patients underwent unenhanced and enhanced MRI of the brain. Additionally, MRI was performed on two patients immediately after brain death, prior to autopsy.

#### RESULTS

Six children died, five due to complications of acute necrotizing encephalopathy (ANE) and one due to intracranial fungal infection. The remaining nine were ultimately discharged, two of whom were diagnosed with meningitis, and the other seven diagnosed with influenza-associated encephalopathy with normal brain MRI. On histology, diffuse cerebral and cerebellar edema, vascular injury and parenchymal necrosis were the main pathologic features seen with ANE. Additionally, gross evidence of hemorrhage and necrosis were apparent in the thalami and brain stem. MR imaging features of ANE include multiple symmetric brain lesions in the thalami, frequently involving the internal capsule, lenticular nucleus, pontine tegmentum and white matter of cerebrum and cerebellum with prolonged T1 and T2 signal. The thalami demonstrated central low and peripheral high signal on diffusion-weighted imaging. MR imaging of the patient with intracranial fungal infection demonstrated significant meningeal enhancement and fungal granuloma, with associated prolonged T1 and T2 signal and ring enhancement. Two MRI scans performed after brain death showed diffuse gray and white matter involvement, with blurring of the gray-white junction, cerebellar tonsillar herniation, and swollen, edematous brain stem, with MRI signal abnormalities suggestive of hemorrhage, edema and/or necrosis.

#### CONCLUSION

Observed neurologic complications after influenza A (H1N1) infection included influenza-associated encephalopathy (ANE), uncomplicated meningitis and opportunistic fungal infection. Although prognosis of ANE is poor, its MRI findings are relatively specific.

**KEY WORDS:** Influenza (H1N1), acute necrotizing encephalopathy, MR imaging

## Thursday Morning

**10:30 AM - 12:00 PM**

**Murray Hill**

**(65e) Neoplasms - Spine and Brain**

**O-545**

**10:30 AM - 10:38 AM**

### **Spinal Blood Flow Maps: A Minimally Invasive Alternative to Spinal Angiography in the Evaluation of Extramedullary Spinal Tumors**

Mazura, J. C.<sup>1</sup>Patsalides, A.<sup>1</sup>Pauliah, M.<sup>2</sup>Peck, K. K.<sup>2</sup>Santillan, A.<sup>1</sup>Bilsky, M. H.<sup>2</sup>Karimi, S.<sup>2</sup>

<sup>1</sup>Weill Cornell Medical College, New York, NY,

<sup>2</sup>Memorial Sloan-Kettering Cancer Center, New York, NY

#### **PURPOSE**

While primary spinal tumors are rare, metastatic disease to the spine is relatively common, affecting 5-10% of patients with cancer. Symptomatic lesions resistant to chemotherapy and radiation often require surgical intervention to preserve neurologic function and maintain spinal structural integrity. Corpectomy provides superior long-term decompression compared to posterior laminectomy. Corpectomy, however, is an involved surgery with higher rates of perioperative hemorrhage especially when treating hypervascular tumors that are not embolized preoperatively. Currently, there is no minimally invasive way to determine extramedullary spinal tumors vascularity and the potential need for preoperative embolization. The purpose of this study is to compare MR perfusion to the gold standard, DSA, in evaluating the vascularity of extramedullary spinal tumors.

#### **MATERIALS & METHODS**

A retrospective chart review revealed 11 patients (with tumors involving 12 spinal levels) who had spinal MR perfusion studies at Memorial Sloan-Kettering Cancer Center (MSKCC) and subsequently underwent spinal angiography at New York Presbyterian Hospital. MR perfusion was performed on a 1.5 T GE scanner using 8-channel-CTL surface spinal coil. The postprocessed perfusion maps were generated using an algorithm developed at MSKCC where a small ROI was placed on the tumor and on an adjacent normal vertebral body to determine blood flow (BF) to these respective regions. A BF ratio comparing the blood flow to the tumor (TBF) and the blood flow to an adjacent normal vertebral body (VBF) was then calculated (BF ratio = TBF/VBF). Three neurointerventionalists performed all angiography using a transfemoral approach. Spinal tumor vascularity was graded on a scale from 0 to 4 as follows: 0 = decreased enhancement compared to a normal nondiseased vertebral body (NVB); 1 = same degree of

enhancement compared to a NVB; 2 = mild tumor blush; 3 = moderate tumor blush; 4 = marked tumor blush with early arteriovenous shunting. All studies were reviewed by a blinded neurointerventionalist with 5 years of experience and compared to the clinical read. In situations of discordance, a second blinded researcher reviewed the study to establish consensus.

#### **RESULTS**

See Table 1.

Patient #	MRP BF ratio	DSA score	Tumor location	Tumor type
1a	5.14	4	T12	Renal cell carcinoma
2	3.10	3	L4	Hepatocellular carcinoma
3	2.39	4	L1/2	Renal cell carcinoma
4	2.32	4	T12	Renal cell carcinoma
5	2.17	4	T10	Renal cell carcinoma
6	1.99	3	T12	Adenocarcinoma of the colon
7	1.90	3	T1	Renal cell carcinoma
8	1.84	3	T12	Thyroid carcinoma
9	1.66	1	L3	Renal cell carcinoma
10	1.14	1	L2	Schwannoma
11	0.55	1	T12	Renal cell carcinoma
1b	0.43	0	T2	Renal cell carcinoma

Statistical analysis using Spearman's rank correlation coefficient (Spearman's rho), a nonparametric measure of statistical dependence between two variables, showed a strong correlation between CBF ratio and DSA score with a Spearman's rho = 0.87 (p value = 0.00012).

#### **CONCLUSION**

These data show a statistically significant correlation (rho = 0.87) between CBF ratio and DSA and suggest that MR perfusion can serve as a surrogate to DSA for determining tumor vascularity in patients with extramedullary spinal tumors. Using MR perfusion to evaluate vascularity could minimize unnecessary invasive spinal angiography and its potential associated complications. A larger study is required to bolster these results and to establish BF ratio ranges for corresponding DSA grade.

**KEY WORDS:** DSA, MR perfusion, tumor

**O-546**

**10:38 AM - 10:46 AM**

### **Dynamic Contrast-Enhanced MR Imaging of Osseous Spine Metastasis before and One Hour after High Dose Image-Guided Radiation Therapy**

Lis, E. Zahaczewsky, M. L. Karimi, S. Billsky, M. Yamada, J. Peck, K. Zelefsky, M.

Memorial Sloan-Kettering Cancer Center  
New York, NY

**PURPOSE**

Single fraction high dose image-guided radiation therapy (HD-IGRT) does not follow the conventional stochastic effects of fractionated radiotherapy. This project was to evaluate the near immediate effects on the dynamic contrast-enhanced MRI (DCE MRI) perfusion parameters, plasma blood volume ( $V_p$ ) and permeability ( $K_{trans}$ ) of spine metastasis that have undergone single fraction high dose image-guided radiation therapy (HD-IGRT).

**MATERIALS & METHODS**

Five patients (mean age = 62 years) with documented spine metastasis, four prostate and one thyroid underwent standard MRI (1.5 T GE scanner using an 8-channel cervical-thoracic-lumbar (CTL) surface spinal coil). For pre- and post-MRI scans, T1-weighted DCE MRI was performed utilizing 3D fast SPGR sequence with the following parameters: number of phases = 80, TR/TE = 3.6/1.1 msec, slice thickness = 10 mm, flip angle = 30°, FOV = 34 cm, matrix size = 256 × 128 in the sagittal plane. Gd-DTPA at a dose of 0.1 mmol/kg of body weight was administered at a rate of 2.5 ml/s by power injector. Data pre and postprocessing was performed using dynamic image processing software (NordicICE). Preprocessing steps included background noise removal, spatial and temporal filtering, and automatic detection of the arterial input function (AIF) from the aorta. The metastasis subsequently underwent HD-IGRT, 24Gy. Within 1 hour of completion of the radiation therapy repeat DCE MRI was performed. To assess the perfusion parameters as predictors of treatment response,  $V_p$  and  $K_{trans}$  of the metastasis were calculated pre- and post-RT. These parameters were normalized as a ratio to adjacent nonirradiated marrow and compared pre- and post-RT.

**RESULTS**

The 1-hour post-HD-IGRT showed a significant drop in the ( $V_p$ ) of all five metastasis ( $p = 0.03$ ), indicating lower vascular plasma volume in the tumors after treatment. Permeability,  $K_{trans}$  remained stable for one case and slightly decreased for four cases ( $p = 0.03$ ).

**CONCLUSION**

Dynamic contrast-enhanced MR perfusion of the spinal marrow is sensitive in detecting hemodynamic changes following HD-IGRT with our data suggesting that the immediate effect of HD-IGRT on spine metastasis is on the vascularity of the lesion, probably occlusion of the microvasculature as demonstrated by a precipitous drop in the ( $V_p$ ).

**KEY WORDS:** Radiation therapy, dynamic contrast-enhanced MR imaging, spine metastases

O-547

10:46 AM - 10:54 AM

### Distinguishing Malignant from Benign Peripheral Nerve Sheath Tumors with Diffusion-Weighted Imaging

Lagemann, G. M.·Chou, D.·Weinstein, P. R.·Chin, C. T.  
University of California San Francisco  
San Francisco, CA

**PURPOSE**

Differentiating malignant from benign peripheral nerve sheath tumors is an important diagnostic dilemma. Imaging features such as degree of enhancement, signal heterogeneity and rate of growth by serial MR imaging often overlap between benign and aggressive tumors. High metabolic activity is demonstrated routinely in benign NSTs on PET imaging and biopsies are prone to sampling error. A definitive radiographic marker would be invaluable in the diagnosis and subsequent treatment for these patients given the range from surveillance imaging, radiation to surgical resection. Literature review shows a case report of diffusion-weighted imaging (DWI) of a malignant peripheral nerve sheath tumor. We sought to determine whether DWI could be used to differentiate reliably between benign and malignant nerve sheath tumors.

**MATERIALS & METHODS**

MR imaging with DWI was performed in patients with spinal nerve sheath tumors referred by neurosurgeons and oncologists between 2003 and 2011 (Philips 1.5 Gyroscan Intera, the Netherlands). Diffusion-weighted scanning was performed in three directions (singleshot echoplanar: TR 2 x pulse-pulse interval; TE 15 ms; FOV 22; 256x144; 5.0/0.5 mm; B-value 400 s/mm<sup>2</sup>). Apparent diffusion coefficient (ADC) maps were obtained, and regions of interest were drawn and analyzed for mean ADC values using software available on the scanner. Mean ADC values were compared. Correlation with pathology reports and clinical follow up was performed additionally. Statistical analysis was performed with the Student T test.

**RESULTS**

Sixteen patients with spinal nerve sheath tumors underwent MRI with DWI (7-77 years, mean 50 years; 10 male; 6 female). Nine of 16 patients underwent diagnostic biopsy or resection. Mean follow up was 1.8 years (0-5.6 years). Five tumors were cervical and 11 lumbosacral in location. Eleven tumors involved nerve roots, one involved brachial plexus cords, and four involved peripheral nerves. There were 10 benign tumors (3 neurofibromas, 7 schwannomas; 7 pathologically confirmed, 3 confirmed with stable radiographic follow-up). Two were malignant tumors (confirmed pathologically). Mean diameter for benign tumors was 20 mm (11-35 mm) and for malignant tumors 69 mm (10-127 mm). All tumors demonstrated enhancement. Five of the 10 benign tumors and one of the two malignant tumors demonstrated homogeneous enhancement. Six of the 10 benign tumors and one of two malignant tumors demonstrated homogenous T2 signal. Mean ADC value for benign tumors was  $1.60 \pm$

$0.26 \times 10^{-3} \text{ mm}^2/\text{s}$  and for malignant tumors was  $0.89 \pm 0.33 \times 10^{-3} \text{ mm}^2/\text{s}$ . P value was less than 0.01.

#### CONCLUSION

Malignant nerve sheath tumors demonstrate relative reduced diffusion compared to benign nerve sheath tumors. Classical imaging characteristics such as tumor size, pattern of enhancement, and T2 signal intensity, however, have considerable overlap between benign and malignant groups. Diffusion-weighted imaging may be a promising tool for prospectively differentiating benign from malignant nerve sheath tumors. Relatively reduced diffusion in malignant nerve sheath tumors may be due to increased tumor cellularity, as has been demonstrated in other malignant neoplasms.

**KEY WORDS:** Nerve sheath tumor, NST, diffusion

**O-549**

**11:02 AM - 11:10 AM**

#### **"Occult" Signal Enhancement in Pediatric Diffuse Intrinsic Pontine Glioma Is the MR Imaging Marker of Angiogenesis**

Conway, A. E.·Reddick, G. W.·Li, Y.·Glass, J. O.·Sablaue, A.·Baker, J. N.·Kun, L.·Broniscer, A.·Patay, Z.

St. Jude Children's Research Hospital  
Memphis, TN

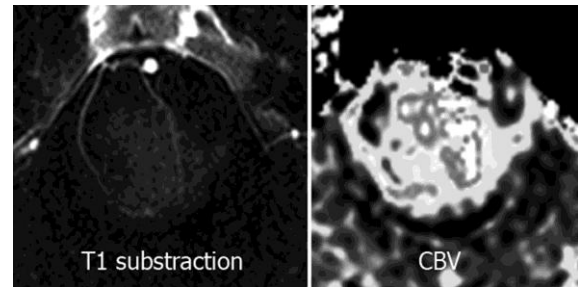
#### PURPOSE

In diffuse intrinsic pontine gliomas (DIPG) subtraction of precontrast T1-weighted images (T1WIs) from postcontrast T1WIs occasionally reveals subtle, "occult" enhancement (oE). We hypothesized that oE represents "intravascular" enhancement related to angiogenesis, rather than the more common "extravascular" enhancement, secondary to blood-brain barrier disruption, and if so, should be characterized by increased relative blood volume compartment compared to nonenhancing (NE) tumor. To test our hypothesis, we used dynamic susceptibility-contrast perfusion MRI to compare cerebral blood volume (CBV) values in oE and NE tumor, as well as in normal-appearing deep cerebellar white matter (DCWM). Since increased CBV in cerebral gliomas has been shown to be associated with poor prognosis, we also wanted to compare robust clinical outcome metrics, specifically progression-free survival (PFS) and overall survival (OS), of patients with tumors exhibiting oE to those not showing signal enhancements.

#### MATERIALS & METHODS

We retrospectively reviewed pretreatment MRI studies of 70 patients (M/F: 34/36; median age: 6.4 years; age-range: 2.3-17.3 years) diagnosed with DIPG for the presence of oE on T1-subtraction images (T1SIs). "Occult" enhancement was defined as signal enhancement not appreciated on post-contrast T1WIs, but visible with a web-like, "cloudy" appearance on postcontrast T1SIs (Fig.1). We identified 11 patients (16.6%) with oE. No enhancement was found in six patients (9.1%). Using an ROI-based approach we compared CBV values in areas of oE with CBV in 1) NE areas of the same tumor, 2) normal-appearing DCWM in

patients with oE and 3) anatomically corresponding tumor areas in patients with NE tumors. PFS and OS were determined by Kaplan-Meier analysis and log-rank testing.



#### RESULTS

The average CBV in areas of oE was significantly higher than in NE areas of the same tumor (7.91 vs 3.66,  $p = 0.0156$ ), within DCWM in the same patient (7.91 vs 3.80,  $p = 0.0156$ ), and in anatomically corresponding tumor areas in patients with no enhancement at all (7.91 vs 1.95,  $p = 0.0027$ ). There was no statistically significant difference in clinical outcome metrics between the oE and the NE groups (OS,  $p = 0.5203$ ; PFS,  $p = 0.7994$ ) but a trend towards faster clinical deterioration in the oE group was suggested by the Kaplan-Meier curves.

#### CONCLUSION

Our data suggest that in DIPG, oE may indeed be a surrogate MRI marker for angiogenesis, underscoring the utility of T1SIs in the diagnostic MRI evaluation of DIPG and other cerebral neoplasms. This previously unappreciated semiologic element may have an impact on overall tumor evaluation including "grading" and response to therapy, biopsy guidance and outcome prediction.

**KEY WORDS:** Diffuse intrinsic pontine glioma, MR imaging, angiogenesis

**O-550**

**11:10 AM - 11:18 AM**

#### **Evaluating Changes during Treatment of Pediatric Diffuse Intrinsic Pontine Glioma Using Diffusion Tensor Imaging**

Steffen-Smith, E. A.·Sarlls, J.·Bent, R. S.·Walker, L.·Pierpaoli, C.·Warren, K. E.

National Institutes of Health  
Bethesda, MD

#### PURPOSE

Diagnosis and management of children with diffuse intrinsic pontine glioma (DIPG) is reliant upon MRI, as biopsy tissue rarely is obtained. Diffusion tensor imaging (DTI) provides noninvasive analysis of the tissue microstructure and has been shown to be useful in evaluating response to therapy in some cancers. Studies of DTI in DIPG have reported increased diffusivity compared to normal tissue and other brain tumors. The global diffusion metrics used in most studies provide a limited view of the tumor structure, whereas histogram analyzes may provide more specific



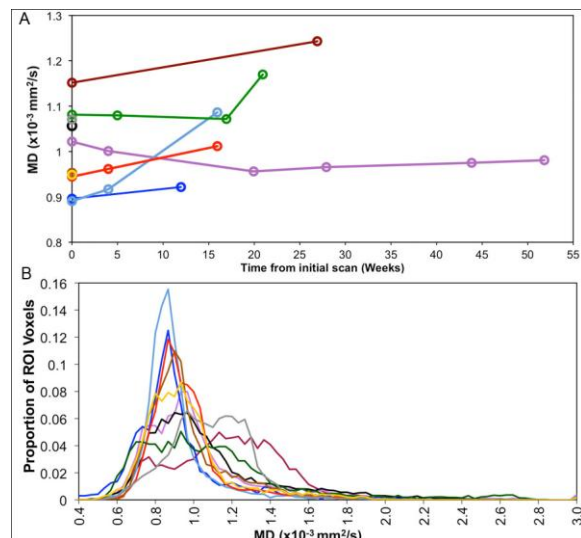
information of diffusion properties throughout the lesion. This study evaluated pediatric DIPGs over the course of treatment using global metrics and histogram analysis of DTI parameters.

#### MATERIALS & METHODS

Diffusion tensor imaging was acquired at 2.5 mm isotropic voxels with 60 diffusion directions and b-value =  $1100 \text{ s/mm}^2$  in 10 pediatric patients (range = 4 - 8 years, median = 5 years) enrolled in a clinical study of Pegylated Interferon Alfa-2b (PEG-Intron®) for treatment of DIPG following radiation therapy. Scans were performed prior to disease progression at multiple time points over the course of treatment, with a median of 18 weeks from the initial scan to progression (range = 5 - 59.9 wks). Mean diffusivity (MD) was evaluated in a region of interest (ROI) that encompassed the entire tumor, as identified by signal abnormality on T2 fluid attenuated inversion recovery (FLAIR) images. Tumor histograms were calculated from MD values. Histogram characteristics including the mean, median, and kurtosis were evaluated with time to progression.

#### RESULTS

As seen in Figure 1A, mean MD values at initial scan (range =  $0.89 - 1.15 \times 10^{-3} \text{ mm}^2/\text{s}$ ) were higher than normal tissue (normal brain tissue =  $0.7 \times 10^{-3} \text{ mm}^2/\text{s}$ ) and were found to significantly increase during treatment ( $p < 0.05$ ). However, mean MD was not predictive of time to progression. The range of initial mean MD was quite broad, thus the histogram of ROI values was analyzed in an attempt to find common features. Shape of the MD histograms was heterogeneous (median kurtosis = 8, range 2.2 - 34.7) with no clear pattern of MD distribution (Figure 1B).



#### CONCLUSION

While global measures of MD showed increased tumor diffusivity in all patients, the range of values was large. Mean diffusivity histograms revealed diverse diffusion characteristics in DIPG. These findings illustrate the vastly heterogeneous structure of these tumors, which can confound evaluation of treatment response.

**KEY WORDS:** Diffusion tensor imaging, brain tumor, children

O-551

11:18 AM - 11:26 AM

#### Arterial Spin Labeling: A Noninvasive Means for Grading Pediatric Tumors?

Mitchell, L. A.<sup>1</sup>Zaharchuk, G.<sup>1</sup>Edwards, M. S. B.<sup>2</sup>Campen, C. J.<sup>2</sup>Barnes, P. D.<sup>2</sup>Fisher, P. G.<sup>2</sup>Yeom, K. W.<sup>2</sup>

<sup>1</sup>Stanford University Medical Center, Stanford, CA,

<sup>2</sup>Lucile Packard Children's Hospital, Stanford, CA

#### PURPOSE

To investigate correlation between arterial spin label (ASL) cerebral blood flow (CBF) and pediatric brain tumors WHO grade classification.

#### MATERIALS & METHODS

Twenty-four children (age 0.15-17 years, mean 8.3 years) with ASL CBF MRI obtained prior to treatment with surgical pathology were evaluated retrospectively after local IRB approval. Arterial spin labeling was performed using a pseudocontinuous labeling period of 1500 ms, followed by a 1500 ms postlabel delay on 3 T MRI. Whole-brain images were acquired with a 3D background suppressed fast spin-echo (FSE) stack-of-spirals method, with a TR of ~5s. Proton density images were obtained for CBF quantitation, which was performed using the microsphere methodology described by Buxton (2005). Quantitative tumor ASL CBF was obtained by placing a region of interest (ROI) over the solid portions of the tumor. The CBF was normalized to contralateral gray and white matter and expressed as a percentile of the normal CBF  $\pm$  standard deviation. The resultant data were compared using a one way analysis of variance with a post-hoc Dunn's test.

#### RESULTS

Of the 24 tumors, nine were high-grade (WHO grade III/IV), including glioblastoma (2), primitive neuroectodermal tumors (1), medulloblastoma (3), diffuse intrinsic pontine glioma (1), melanoma (1), ependymoma grade III (1); and 15 were low-grade (WHO grade I/II), including ganglioglioma (2), grade I pilocytic astrocytoma (5), grade II astrocytoma (1), craniopharyngioma (2), ependymoma (1), choroid plexus papilloma (3), DNET (1). High-grade tumor mean ASL CBF ( $146.9 \pm 49.7\%$ ) was significantly different than low-grade tumors ( $89.7 \pm 16.3\%$ ) or contralateral brain parenchyma,  $P < 0.05$ . Low-grade tumors and contralateral brain parenchyma were not different,  $P < 0.05$ .

#### CONCLUSION

Mean ASL CBF values were significantly higher in high-grade than in low-grade pediatric brain tumors or normal parenchyma. Arterial spin label CBF, a noninvasive means of assessing CBF, may assist in grading pediatric brain tumors.

**KEY WORDS:** Neoplasm, pediatric, ASL

**O-552****11:26 AM - 11:34 AM**

### **Characterization of Brain Tumor Pseudoprogession with C11 Methionine and FDG Brain Positron Emission Tomography in Pediatric Patients**

Naidu, P. K. • Miller, J. H. • Egelhoff, J. C. • Curran, J. G.

Phoenix Children's Hospital  
Phoenix, AZ

#### **PURPOSE**

Central nervous system (CNS) tumors are the second most common childhood cancer after hematologic malignancies. Many treatments for these tumors worsen lesional enhancement and edema. Such treatment-related changes (TRCs), can be confused for worsening malignancy, hence the synonym "pseudoprogession". While the term pseudoprogession is applied most often to adult high-grade glioma patients treated with temozolamide and concurrent radiotherapy, analogous findings are seen in a range of pediatric CNS malignancies. Pseudoprogession in the pediatric population has not yet been well characterized. Similar to adults, conventional MRI cannot distinguish between pseudoprogession and early progression in pediatric patients. Complementary brain PET studies utilizing C11 Methionine (an amino acid radiotracer), and FDG (a glucose analog) may help clarify the true nature of TRCs with characteristic tracer distribution patterns. We present six cases of pediatric brain tumors in which C11 Methionine and FDG assisted in the diagnosis of pseudoprogession, thus demonstrating their utility in evaluating TRCs in both glial and nonglial-based pediatric brain malignancies.

#### **MATERIALS & METHODS**

We retrospectively reviewed the imaging of nine pediatric patients with a primary brain malignancy that underwent posttreatment C11 methionine and FDG brain PET to evaluate for worsening or suspicious findings on posttherapeutic conventional MRI. Both the posttherapeutic MRI as well as the brain PETs were analyzed and compared to pretherapeutic studies. For each patient, information about tumor histopathology, location, grade, treatment regimen, and chronology thereof were obtained from chart review and correlated to the imaging findings.

#### **RESULTS**

Average patient age at initial presentation was 8.8 years old. Malignancies were all high grade, and ranged from anaplastic astrocytoma, anaplastic ependymoma, medulloblastoma, to PNET. New areas of pathologic enhancement were present on postcontrast T1-weighted MRI in eight of nine patients, with progression of perilesional T2 FLAIR hyperintensity in five of nine patients. Six out of nine C11 PET examinations demonstrated corresponding lesion positivity, and three of nine were C11 negative. Three of nine lesions showed significant metabolism FDG PET. Patterns of brain PET radiotracer distribution were analyzed.

Subsequent MRI was available in eight of nine patients, and showed resolution of suspicious findings in four.

#### **CONCLUSION**

A pattern of C11 Methionine positivity or lack of activity with FDG hypometabolism in areas of new lesional or perilesional MRI abnormality was indicative of pseudoprogession rather than early progression of primary brain malignancy in six of nine patients. While pseudoprogession in the adult population near exclusively refers to posttherapy high-grade glioma patients, pseudoprogession in the pediatric population is poorly characterized to date, and can be seen in both glial and nonglial origin tumors, mostly high-grade, but also occasionally in low-grade lesions. While conventional CE MRI remains inconclusive with regard to differentiating early progression from pseudoprogession in all patients, C11 Methionine in combination with FDG brain PET can aid in clarifying the diagnosis in pediatric patients, thereby helping oncologists determine if an immediate alteration in treatment regimen is necessary.

**KEY WORDS:** Pseudoprogession, malignancy, PET

**O-553****11:34 AM - 11:42 AM**

### **Decreasing Apparent Diffusion Coefficient Values in Successfully Treated Optic Pathway Gliomas**

Grimm, J. P.<sup>1</sup> • Greenblatt, K.<sup>1</sup> • Finlay, J. L.<sup>1</sup> • Bluml, S.<sup>1,2</sup> • Nelson, M. D.<sup>1</sup>

<sup>1</sup>Childrens Hospital Los Angeles, Los Angeles, CA, <sup>2</sup>Rudi Schulte Research Institute, Santa Barbara, CA

#### **PURPOSE**

This study evaluates apparent diffusion coefficient (ADC) values of optic pathway gliomas (OPG) during treatment and proposes that decreasing ADC values are seen in successfully treated OPGs. OPGs are well defined tumors and typically are not resected making them ideal candidates for following changes in ADC values during treatment. Low ADC values typically are associated with high tumor cellularity and grade. Accordingly, previous studies have indicated that increasing ADC values are a favorable treatment response in adult gliomas. In contradistinction, in pediatric pontine gliomas decreasing ADC values may be a favorable prognostic indicator. This study aims to improve our understanding of changes in ADC values during the treatment of brain tumors.

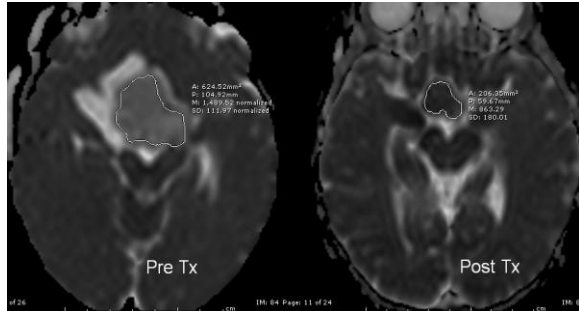
#### **MATERIALS & METHODS**

Eight patients with OPG demonstrating a favorable response to chemotherapy were identified from neurooncology patients imaged at our institution over the last 6 months. Favorable response was defined as a large decrease in tumor volume with stable or improving clinical status. Regions of interests (ROI) were drawn over the tumor both at the beginning and end of therapy to measure ADC values. Areas containing cysts/necrosis, hemorrhage and blood vessels were excluded from the ROIs. Additional ROIs were drawn over portions of the tumor with the lowest ADC values.

Regions of interest of normal frontal white matter were drawn for comparison. Values were compared using paired Student t-tests.

### RESULTS

There was a significant decrease in ADC values of OPGs during a favorable chemotherapeutic response. The average ADC value of the tumors decreased from 1.49 ( $\times 10^{-3}$  mm<sup>2</sup>/s) to 1.12 ( $p = 0.0001$ ) and the average lowest ADC value of the tumors decreased from 1.33 to 0.97 ( $p = 0.003$ ). All ADC values for the tumors were significantly higher ( $p < 0.05$ ) than that of normal white matter except for ROIs placed over the lowest ADC value of the tumor after treatment.



### CONCLUSION

Apparent diffusion coefficient values were found to decrease significantly with successful treatment of OPG. This is similar to findings in pontine gliomas, and may represent a decrease in extracellular fluid and edema within these tumors. This finding highlights the importance of cautiously evaluating ADC values, and correlating them to the tumor type. Decreasing ADC values do not always mean increasing tumor cellularity/progression and can be a favorable sign. This is most likely true in tumors with high baseline ADC values, and it is notable that the lowest ADC values within these OPGs after treatment approached that of normal white matter.

**KEY WORDS:** ADC, glioma, astrocytoma

**O-554**

**11:42 AM - 11:50 AM**

### Impact of Sedation on FLAIR Imaging of the Pediatric Brain

Harreld, J. H. • Sabin, N. D. • Kaddoum, R. N. • Parish, M. E. • Gajjar, A. • Patay, Z.

St. Jude Children's Research Hospital  
Memphis, TN

### PURPOSE

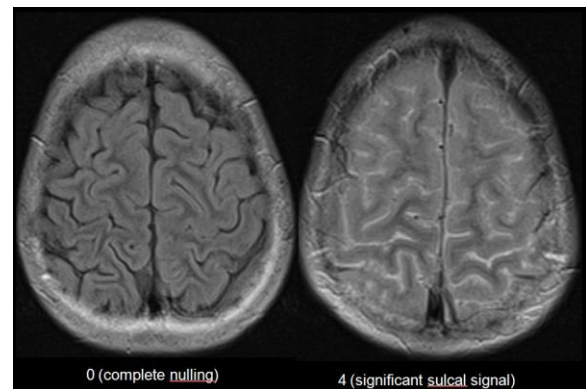
Accurate detection of leptomeningeal metastatic disease is critical for risk stratification of patients with central nervous system (CNS) malignancies. Optimization of MR imaging for metastasis detection therefore is crucial. Postcontrast fluid-attenuated inversion recovery (FLAIR) MR imaging is sensitive for detection of leptomeningeal metastasis, but is subject to artifactual sulcal signal intensity (SSI) variations. We studied the relationship of this signal intensity to sedation factors.

### MATERIALS & METHODS

Sulcal signal intensity on pre and postcontrast FLAIR images acquired in nonsedated (NS,  $n = 6$ , mean age 12.3 years), IV propofol sedated (IV,  $n = 8$ , mean age 5.2 years) and combination inhalational sevoflurane and IV propofol sedated (INH,  $n = 6$ , mean age 5 years) pediatric brain tumor patients with no history of leptomeningeal disease was rated from 0 (complete nulling) to four (significant hyperintensity) by two independent neuroradiologists (Figure 1). Sedated patients received supplemental oxygen; nonsedated patients breathed room air. Mean pre- and post-SSI and change in SSI from pre to postcontrast imaging were compared between sedation groups (Student's t-test) and correlated (Pearson correlation coefficient) with inspired oxygen percentage (FiO<sub>2</sub>), mean arterial pressure (MAP), time after contrast administration (t post), and hematocrit (Hct).

### RESULTS

Intravenous (IV) and INH sedated patients were statistically equivalent in age but significantly younger than NS ( $p < 0.01$ ). Mean IV FiO<sub>2</sub> of 51% was significantly greater than INH FiO<sub>2</sub> of 35% and NS FiO<sub>2</sub> of 21% (room air;  $p < 0.01$ ). Sulcal signal intensity increased from pre to postcontrast in 17/20 patients (INH 25%, IV 88%, NS 117% increase). Overall, pre, post or change in SSI was not correlated with FiO<sub>2</sub> ( $r = 0.168, 0.228, 0.1644$ ), but INH FiO<sub>2</sub> correlated strongly with precontrast ( $r = 0.90$ ), postcontrast ( $r = 0.76$ ) SSI, and moderately negatively with pre to post -contrast SSI change ( $r = -0.7$ ). Pre and postcontrast SSI was significantly greater in INH compared to IV and NS, and in IV compared to NS. Correlation of SSI with MAP was moderately negative precontrast ( $r = -0.27$ ), and postcontrast ( $r = -0.32$ ). Mean arterial pressure was strongly negatively correlated with FiO<sub>2</sub> ( $r = -0.858$ ). Hematocrit and t post were not correlated with SSI or other factors.



### CONCLUSION

Though FiO<sub>2</sub> was greater in IV (propofol) sedates, sedation with inhalational sevoflurane resulted in increased SSI and sensitivity to FiO<sub>2</sub>-induced signal changes relative to propofol-only sedation and no sedation, in contrast to prior studies implicating high FiO<sub>2</sub> in increased SSI regardless of anesthetic. Further study will enhance understanding of the interplay between sedation and FiO<sub>2</sub> and facilitate FLAIR imaging optimization.

**KEY WORDS:** Sedation, FLAIR, oxygen

**O-555**

**11:50 AM - 11:58 AM**

### Effects of Sedation on Cerebral White Matter Perfusion in the Pediatric Brain

Harreld, J. H. Kaddoum, R. N. Helton, K. J. Glass, J. O. Patay, Z. Sansgiri, R. Parish, M. E. Gajjar, A. Reddick, W. E.

St. Jude Children's Research Hospital  
Memphis, TN

#### PURPOSE

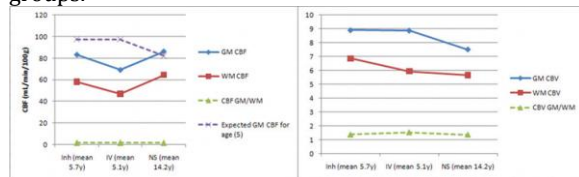
Significant alterations in cortical cerebral blood flow (CBF) and cerebral blood volume (CBV) in children sedated for dynamic susceptibility contrast (DSC) perfusion MRI with IV propofol and combined IV propofol/inhalational sevoflurane anesthesia have been described (Harreld et al, RSNA 2011), in keeping with known effects of these agents on vessels and cerebral metabolic rate (CMR) and potentially impacting interpretation of MR perfusion data. Given that cortical CMR is three-fold greater than white matter (WM) CMR and that CMR and CBF are tightly coupled in the usual state, effects of sedation on gray matter (GM) and WM perfusion may differ. We retrospectively reviewed DSC MR perfusion imaging and sedation data in a pediatric neuro-oncology population to investigate the effects of anesthesia on WM CBF and CBV.

#### MATERIALS & METHODS

Dynamic susceptibility contrast MR perfusion images acquired supratentorially (Magnevist IV contrast, 0.8-1 cc/sec) in 49 pediatric patients without visible supratentorial brain abnormalities (age 1.4 - 18 years, mean 8.6) sedated with IV propofol (IV, n = 20), combination sevoflurane and propofol (INH/IV, n = 10) or nonsedated (NS, n = 19) underwent segmentation of GM and WM. Middle cerebral artery territory (MCA) GM, WM and GM/WM CBV and CBF then were calculated and statistically compared Student's t-test between groups.

#### RESULTS

Statistically significant decreases in MCA WM (and GM) CBF with IV propofol ( $p = 0.04$ ,  $p = 0.01$ ) were attenuated by the addition of sevoflurane. In both sedation groups, WM CBV was not altered significantly, while GM CBV was significantly increased ( $p = 0.02$ ,  $0.02$ ). Though IV GM/WM CBV trended slightly higher (IV = 1.55, NS and INH/IV = 1.38), there was no significant difference in GM/WM CBF or CBV between groups.



#### CONCLUSION

Anesthesia-induced alterations in WM CBF appear to mirror those in GM. Sedative-induced increases in WM

CBV were not statistically significant, in contrast to significant elevation of GM CBV with IV and INH/IV sedation. Though this may support the validity of WM comparison across sedation groups, lack of statistical power, possibly due to small sample size, may obscure true differences and larger, prospective studies are necessary for confirmation.

**KEY WORDS:** Sedation, perfusion, brain

## Thursday Afternoon

**1:00 PM - 2:30 PM**

**Grand Ballroom Suite**

**(66a) Adult Brain:  
Cerebrovascular II**

**O-556**

**1:00 PM - 1:08 PM**

### Refining the Pretreatment Noncontrast CT ASPECTS Threshold for IAT Selection: Pooled Analysis of the Penumbra Pivotal Study and the PICS Registry

Chaudhry, Z. A.<sup>1</sup>Yoo, A. J.<sup>1</sup>Gonzalez, R.<sup>1</sup>Goyal, M.<sup>2</sup>Demchuk, A.<sup>2</sup>Mualem, E.<sup>3</sup>Bose, A.<sup>3</sup>Sit, S.<sup>3</sup>

<sup>1</sup>Massachusetts General Hospital, Boston, MA,  
<sup>2</sup>University of Calgary, Calgary, AB, CANADA,  
<sup>3</sup>Penumbra, Inc., Alameda, CA

#### PURPOSE

Previous studies have demonstrated that the Alberta Stroke Program Early CT Score (ASPECTS) on pretreatment noncontrast CT (NCCT) can be used to identify patients who will benefit from intraarterial therapy (IAT). Specifically, an ASPECTS threshold of seven has been identified as clinically important. We sought to test this threshold and further characterize the clinical impact of pretreatment ASPECTS (pre-ASPECTS) in a large IAT cohort.

#### MATERIALS & METHODS

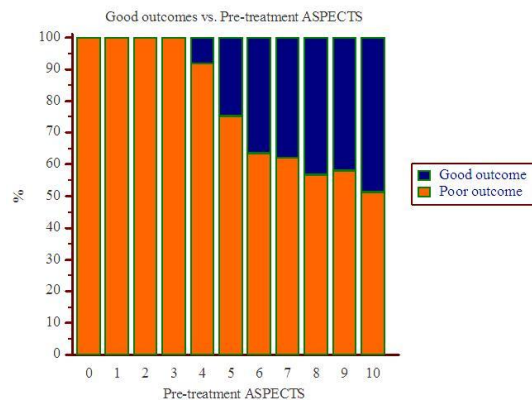
We identified anterior circulation acute ischemic stroke patients treated with the Penumbra Stroke System in the Pivotal Study and the Penumbra Imaging Collaborative Study (PICS). Inclusion criteria for this analysis were evaluable pretreatment NCCT and available 90-day modified Rankin Scale (mRS) score. Expert readers graded ischemic change on NCCT using ASPECTS and blinded to all clinical information except stroke side.

#### RESULTS

Of 221 patients who fulfilled study criteria, the mean age was  $66.0 \pm 15.1$  years, and median NIHSS score was 16 (IQR 12-21). The cohort was 50.9% (112/220) female. There were 111 (50.2%) right-sided strokes. The target vessel occlusion involved the ICA in 21.9%



(48/219), MCA in 77.6% (170/219) and ACA in 0.5% (1/219). The median ASPECTS was 7 (IQR 6-9). TIMI 2-3 reperfusion was achieved in 83% (181/218). Good outcome (mRS 0-2) was achieved in 77 (34.8%) patients at 90 days. Adjusting for age, NIHSS and reperfusion, pretreatment ASPECTS was an independent predictor of good outcome (O.R. 1.47; 95% C.I.:1.23 to 1.76). Pre-ASPECTS >7 predicted good outcome with a relative risk of 1.80 (95% C.I.:1.23 to 2.64). The proportion of good outcomes was exceedingly low among pre-ASPECTS 0-4 2.8% (1/36); Figure. When trichotomizing pre-ASPECTS at 0-4 (n = 36), 5-7 (n = 76) and 8-10 (n = 109), the median 90-day mRS scores were 6 (IQR 4-6), 3.5 (IQR 2-6) and 3 (IQR 1-4), respectively ( $p < 0.0001$ ). In pairwise comparison, the only significant differences were between pre-ASPECTS 0-4 and the other groups. While there was no effect of reperfusion on outcome among pre-ASPECTS 0-4, TIMI 2-3 reperfusion ( $p = 0.04$ ) and earlier timing of reperfusion (none vs <300 minutes vs  $\geq 300$  minutes;  $p = 0.03$ ) were associated with better outcomes among pre-ASPECTS 5-10.



## CONCLUSION

Pretreatment NCCT ASPECTS is a critical determinant of outcome following IAT. Pre-ASPECTS 0-4 identifies a population of patients who are highly likely to have dismal outcomes and do not benefit from endovascular reperfusion.

**KEY WORDS:** Ischemic stroke, IA therapy, noncontrast CT ASPECTS

O-557

1:08 PM - 1:16 PM

## Penumbra Imaging Collaborative Study: Results of Patient Functional Outcome from Image-Guided Patient Selection

Zaidat, O.<sup>1</sup>•Meagher, S.<sup>2</sup>•Brant-Zawadzki, M.<sup>3</sup>•Farkas, J.<sup>4</sup>•Malek, R.<sup>5</sup>•Crandall, B.<sup>6</sup>•Frei, D.<sup>7</sup>•Hui, F.<sup>8</sup>•Alexander, M.<sup>9</sup>•Chong, B.<sup>10</sup>•Janjua, N.<sup>11</sup>•Shaff, D.<sup>12</sup>•Yavagal, D.<sup>13</sup>•Heck, D.<sup>14</sup>•Malisch, T.<sup>15</sup>•Turk III, A.<sup>16</sup>•Hayakawa, M.<sup>17</sup>•Miskolczi, L.<sup>18</sup>•Tarr, R.<sup>19</sup>•Ortiz, R.<sup>20</sup>•Zauner, A.<sup>21</sup>•Klucznik, R.<sup>22</sup>•Zylak, C.<sup>23</sup>•Yoo, A.<sup>24</sup>•Mualem, E.<sup>25</sup>•Bose, A.<sup>25</sup>•Sit, S.<sup>25</sup>•For the PICS Investigators

<sup>1</sup>Medical College of Wisconsin, Milwaukee, WI, <sup>2</sup>OSF Saint Francis Medical Center, Peoria, IL, <sup>3</sup>Hoag Hospital, Newport Beach, CA, <sup>4</sup>Maimonides Medical Center, Brooklyn, NY, <sup>5</sup>Good Samaritan Hospital, San Jose, CA, <sup>6</sup>Abbott Northwestern Hospital, Minneapolis, MN, <sup>7</sup>Swedish Medical Center, Englewood, CO, <sup>8</sup>Cleveland Clinic, Cleveland, OH, <sup>9</sup>Cedars-Sinai Medical Center, Los Angeles, CA, <sup>10</sup>Mayo Clinic, Phoenix, AZ, <sup>11</sup>Long Island College Hospital, Brooklyn, NY, <sup>12</sup>Lehigh Valley Health Network, Allentown, PA, <sup>13</sup>Jackson Memorial Hospital, Miami, FL, <sup>14</sup>Forsyth Medical Center, Winston-Salem, NC, <sup>15</sup>Alexian Brothers Medical Center, Elk Grove Village, IL, <sup>16</sup>Medical University of South Carolina, Charleston, SC, <sup>17</sup>University of Iowa Health Care, Iowa City, IA, <sup>18</sup>Holy Cross Hospital, Fort Lauderdale, FL, <sup>19</sup>University Hospital of Cleveland, Cleveland, OH, <sup>20</sup>St. Luke's-Roosevelt Hospital Center, New York, NY, <sup>21</sup>Santa Barbara Cottage Hospital, Santa Barbara, CA, <sup>22</sup>The Methodist Hospital, Houston, TX, <sup>23</sup>Providence Sacred Heart Medical Center, Spokane, WA, <sup>24</sup>Massachusetts General Hospital, Boston, MA, <sup>25</sup>Penumbra, Inc, Alameda, CA

## PURPOSE

Several imaging techniques currently are used to triage patients for acute ischemic stroke intervention. However, definitive evidence is lacking on which imaging modality is best for identifying patients most likely to benefit from mechanical thrombectomy (MT). The PICS registry sought to determine the imaging modalities being used to guide patient triage for MT and assess their impact on patient functional outcome after treatment.

## MATERIALS & METHODS

Patients treated by the Penumbra System per institutional standard of care were enrolled across 35 centers in the United States. Baseline imaging modality was captured to identify usage rates of three principal imaging techniques: noncontrast CT (NCCT), CT perfusion (CT-P), and MRI diffusion-weighted imaging (DWI). The modified Rankin Scale (mRS) was used to assess 90-day patient functional outcome.

## RESULTS

Among 305 patients enrolled in the PICS registry, 267 had the requisite imaging modalities and were used for this analysis. Their mean age was  $66.6 \pm 15.9$  years; 49.4% (132/267) were females, and the median NIHSS score at presentation was 17.0 (IQR 12-21). The median time from stroke onset to presentation was 2.3 (IQR 1-

4) hours, onset to arterial puncture was 4.8 (IQR 3.6-6.2) hours, and puncture to end of thromboaspiration was 73.0 (IQR 49-110) min. Posttreatment, 83.5% of patients were recanalized successfully to TIMI 2/3 (from TIMI 0/1) with 43.5% achieving functional independence at 90 days (mRS of 0-2). All cause mortality was 19.9% (53/267) with symptomatic intracranial hemorrhage reported in 4.5% (12/267) of the patients. The principal imaging modalities used for patient triage were NCCT in 61.8% (165/267), CT-P in 27.3% (73/267) and DWI in 10.9% (29/267) of the study population. There was no significant difference between groups for patient age, baseline NIHSS, and time from puncture to end of thromboaspiration. The time from stroke symptom onset to groin puncture was significantly different in the DWI cohort ( $p < 0.0001$ ) with a median of 6.5 hours as compared to 4.4 hours for NCCT, and 4.8 hours for CTP. This may be related to the longer duration required for this imaging modality. Of the patients selected for NCCT, 42.5% (57/134) were functionally independent at 90 days, whereas for CT-P and DWI, the rates were 45.9% (28/61) and 42.9% (12/28), respectively, indicating there is no difference among the three groups.

#### CONCLUSION

These data suggest that in the United States, there is a wide variability in the types of imaging modality used to guide patient selection for acute stroke intervention by mechanical thrombectomy. In addition, the imaging approach appears to have little impact on patient functional outcome after treatment.

**KEY WORDS:** Stroke, Penumbra, thrombectomy

**O-558**

**1:16 PM - 1:24 PM**

#### **CT/CT Angiography and MR Imaging Findings Predict Recurrent Stroke after Transient Ischemic Attack and Minor Stroke: Results of the Prospective CATCH Study**

Goyal, M. Hill, M. D. Modi, J. Patel, S. K. Demchuk, A. M. Coutts, S. B.

University of Calgary  
Calgary, AB, CANADA

#### **PURPOSE**

Transient ischemic attack (TIA) and minor stroke portend a substantial risk of recurrent stroke. Identification of a DWI lesion on brain MRI can identify patients at the highest risk for a recurrent stroke. However most patients already get a CT head completed and large artery disease, which is easily identifiable by CTA, is the stroke mechanism with the highest risk of early stroke recurrence. We therefore hypothesized that with the fast assessment of the intracranial and extracranial vasculature, CTA could predict recurrent stroke in TIA and minor stroke patients. We secondarily sought to compare prediction of recurrent stroke with CT/CTA with acute DWI

#### **MATERIALS & METHODS**

Five hundred ten consecutive TIA and minor stroke patients (NIHSS < 4) underwent CT/CTA within 24 hours of symptom onset and subsequent MRI. A stroke neurologist assessed all patients within 24 hours of symptom onset. We assessed the risk of recurrent stroke within 90 days using standard clinical variables and predefined abnormalities on the CT/CTA (acute ischemia on CT and/or intracranial or extracranial occlusion or stenosis  $\geq 50\%$ ) and MRI (DWI positive). A secondary analysis to compare the accuracy of prediction of recurrent stroke with CT/CTA and DWI MRI then was completed using receiver operator characteristics curves.

#### **RESULTS**

Over a period of 29 months, 510 patients were enrolled of whom 491 (96.3%) were admitted to hospital. Median patient age was 69 years (range 27-99). The CT/CTA positive metric was present in 171 patients (34%). Four hundred twenty (82%) patients had an MRI for their acute event (before any recurrent event) and 243 of these were DWI positive (58%; 95% CI 53-63). MR imaging results were imputed for 90 patients. After imputation of missing MRI results, the rate of DWI positivity was unchanged ( $n = 295$ , 58%; 53-62). Median time from onset to CTA was 5.5 hours (IQR: 6.4 hours), to MRI was 17.5 hours (IQR: 12 hours). Follow up was available on 98% of patients. There were 36 recurrent strokes (7.1% 95% CI: 5.0-9.6). Median time to event was 1 day (IQR 7.5). Symptoms ongoing at first assessment, HR 2.2 (95% CI: 1.02-4.9), CT/CTA abnormalities, HR 4.0 (95% CI: 2.0-8.5) and DWI positivity, 2.2 (1.05-4.7) predicted recurrent stroke. In the multivariable analysis only CT/CTA abnormalities predicted recurrent stroke. In a secondary analysis CT/CTA and MRI were not significantly different in their discriminative value in predicting recurrent stroke (0.67, (95% CI: 0.59-0.76) versus 0.59, (95% CI: 0.52-0.67),  $p = 0.09$ ).

#### **CONCLUSION**

Early assessment of the intracranial and extracranial vasculature using CT/CTA predicts recurrent stroke and clinical outcome in patients with TIA and minor stroke. In many institutions CTA is more readily available than MRI and physicians should access whichever technique is available quicker at their institution. Using CT/CTA to assess TIA and minor stroke patients is a practical solution to assessment of these patients and has the potential to benefit many people worldwide. Adoption of CT/CTA into clinical practice for the assessment of TIA and minor stroke patients identifies a high-risk group suitable for aggressive acute stroke prevention treatment.

**KEY WORDS:** Minor stroke, TIA, CTA



O-559

1:24 PM - 1:32 PM

### Visual Estimation of MR Imaging Core/Penumbra Mismatch versus Quantitative Measurement

Dahlgren, R. M. Saraf-Lavi, E. Ghitis, J. Sidani, C. Nagornaya, N. Yavagal, D.

University of Miami  
Miami, FL

#### PURPOSE

Imaging patients in the acute stroke setting impacts the decision on whether to take the patient to the angio suite for intraarterial thrombolysis. Diffusion-weighted imaging (DWI) is used to estimate infarct core, and MR perfusion-weighted time to peak maps (TTP) imaging to estimate salvageable ischemic penumbra. Inclusion criteria for enrollment of acute stroke patients into clinical trials aimed at extending the time window for IV thrombolysis beyond 3 hours are DWI/TTP lesion volume mismatch greater than 20%. We sought to determine how well visual estimation of infarct and mismatch size compares with quantitative measurement.

#### MATERIALS & METHODS

Acute diffusion-weighted image (DWI) and perfusion time to peak maps (TTP) in 85 strokes and established infarct volumes in 32 acute strokes were measured by computerized planimetry. Mismatch was defined as  $TTP/DWI \geq 1.2$ . Two experienced, neuro-fellowship trained interpreters, blinded to planimetric values, then were asked to subjectively estimate the percent penumbra at increments of 0-20%, 20-40%, 40-60%, 60-80%, 80-100%, defining percent penumbra as:  $((\text{volume of TTP abnormality} - \text{volume of diffusion restriction}) / \text{volume of TTP abnormality}) \times 100$ . MR imaging was performed on two 1.5 T imaging systems (Siemens Avanto - Erlangen, Germany, and Phillips Infineon - Eindhoven, Netherlands) with a 25 mT/m maximum gradient strength and head coil. FLAIR protocol imaging was an axial sequence (TR: 8,000 ms; TE: 125 ms; TI: 2,500 ms; 22 slices (variable); slice thickness: 5 mm; interslice gap: 2 mm; matrix size: 162 ! 256). The PWI sequence was a single shot EPI used to acquire whole brain images with temporal resolution of approximately 2 seconds. The PWI maps generated rCBV, rCBF, TTP and MTT images.

#### RESULTS

The mean quantitative DWI/TTP mismatch was 68% (range 4% to 100%). The first interpreting neuroradiologist correctly qualitatively estimated the mismatch in 27 of the 32 cases (84%). The second interpreting neuroradiologist correctly qualitatively estimated the mismatch in 25 of the 32 cases (78%). Interrater agreement was calculated using kappa statistics and found to be very high. Taken together, an average of 19% of the cases were incorrectly categorized. However, all the incorrect qualitatively mismatch interpretations underestimated the penumbra into the 0-20% category, which in clinical scenarios would have excluded patients from potential intervention.

#### CONCLUSION

Visual estimation of admission DWI/MTT images in acute stroke patients, compared to quantitative measurement, leads to underestimation of mismatch size in some cases. This underestimation would have effectively excluded patients from intervention, whom by computerized planimetry calculations would have been eligible for treatment. Automated quantitative segmentation tools may therefore be desirable to optimize patient selection for entry into stroke clinical trials.

**KEY WORDS:** Penumbra, stroke

O-560

1:32 PM - 1:40 PM

### Quantitative Cerebral Blood Flow Thresholds May Predict the Absolute Penumbra and Final Infarct Volume Using Bookend Dynamic Susceptibility Contrast MR Perfusion-Weighted Imaging Technique with Concentric Region of Interest Analysis

Vranic, J. E. Vakil, P. Habib, A. Korutz, A. Hurley, M. C. Shaibani, A. Carroll, T. J. Ansari, S. A.

Northwestern University Feinberg School of Medicine  
Chicago, IL

#### PURPOSE

One of the purposes of neuroimaging in the setting of hyperacute stroke is to determine tissue that is at risk for infarction, yet potentially reversible (ischemic penumbra) with implications for intravenous or intraarterial thrombolytic therapy. Traditional MR diffusion/perfusion-weighted imaging (DWI/PWI) can depict infarcted tissue and relative regional hemodynamic compromise, but does not provide a quantitative metric of cerebral blood flow (CBF) to delineate the absolute penumbra. Recent studies have suggested that quantitative CBF (qCBF) values may precisely localize ischemic tissue that would benefit from reperfusion therapy and be salvaged from infarction. In this study, we explored whether qCBF as measured by the Bookend dynamic susceptibility contrast (DSC-MR PWI) technique can accurately predict the absolute ischemic penumbra or final infarct volume in the hyperacute stroke setting.

#### MATERIALS & METHODS

Using our institution's PACS and medical record databases, we retrospectively identified and analyzed seven patients (3M:4F, mean age  $64 \pm 11$  years) that suffered a large vessel (ICA/A1-A2 ACA/M1-M2 MCA) thromboembolic occlusion in the anterior intracranial circulation (mean NIHSS  $16 \pm 9.8$ ), received the MR DWI/PWI using the Bookend DSC-MRI protocol within 8 hours of symptom onset, and follow-up CT imaging at 48-72 hours after presentation confirmed an expanding infarct volume. A trained neuroradiologist mapped regions of interest (ROIs) surrounding the initial infarct volume on DWI, final infarct volume on follow-up CT, and qCBF abnormality on PWI color maps. Both CT and MR DWI/PWI images were coregistered using MATLAB software and qCBF values were calculated in four

separate concentric ROIs encompassing the initial infarct core, final infarct volume, qCBF abnormality, and normal tissue peripherally. Concentric ROI values were extracted volumetrically cross-sectionally, analyzed among individual patients and averaged for standard deviation analysis.

## RESULTS

The average qCBF value of the initial infarct volume was  $6.6 \pm 2.7$  ml/100g/min. The ischemic absolute penumbra, determined by tissue peripheral to the initial DWI core, but internal to the final CT infarct volume, had an average qCBF of  $14.5 \pm 0.4$  ml/100g/min. The false penumbra was tissue identified as abnormal on qCBF color map analysis, but peripheral to the final CT infarct volume, had an average qCBF of  $16.9 \pm 0.6$  ml/100g/min. Finally, normal tissue peripheral to the qCBF abnormality had an average value of  $41.5 \pm 4.3$  ml/100g/min.

## CONCLUSION

Our preliminary study indicates that an appropriate qCBF threshold measurement as determined by the Bookend DSC-MR PWI technique, may serve as a quantitative predictor of the absolute penumbra and final infarct volume. With clinical validation of this technique to accurately assess tissue at risk in the hyperacute stroke setting, thrombolytic therapy may be planned with improved judgment or caution.

**KEY WORDS:** Stroke volume, quantitative MR perfusion, penumbra

**O-561**

**1:40 PM - 1:48 PM**

### **Preliminary Results from the Penumbra START Trial Confirm the Clinical Importance of Pretreatment Infarct Volume in Acute Stroke Intervention by the Penumbra System**

Frei, D. F.<sup>1</sup>•Yoo, A. J.<sup>2</sup>•Heck, D. V.<sup>3</sup>•Hellinger, F. R.<sup>4</sup>•McCollom, V. E.<sup>5</sup>•Fiorella, D. J.<sup>6</sup>•Turk, A. S.<sup>7</sup>•Malisch, T. W.<sup>8</sup>•Zaidat, O. O.<sup>9</sup>•Alexander, M. J.<sup>10</sup>•Devlin, T. G.<sup>11</sup>•Levy, E. I.<sup>12</sup>•Shah, Q. A.<sup>13</sup>•Hui, F. K.<sup>14</sup>•Goyal, M.<sup>15</sup>•Ghodke, B. V.<sup>16</sup>•Shaibani, A.<sup>17</sup>•Harrigan, M. R.<sup>18</sup>•Jovin, T. G.<sup>19</sup>•Madison, M. T.<sup>20</sup>•Chaudhry, Z. A.<sup>2</sup>•Gonzalez, R. G.<sup>2</sup>•Barraza, L.<sup>21</sup>•Sit, S. P.<sup>21</sup>•Bose, A.<sup>21</sup>•for the START Investigators

<sup>1</sup>Swedish Medical Center, Englewood, CO, <sup>2</sup>Massachusetts General Hospital, Boston, MA, <sup>3</sup>Forsyth Medical Center, Winston Salem, NC, <sup>4</sup>Florida Hospital, Orlando, FL, <sup>5</sup>Mercy Health Center, Oklahoma City, OK, <sup>6</sup>Stony Brook Medical Center, Stony Brook, NY, <sup>7</sup>Medical University of South Carolina, Charleston, SC, <sup>8</sup>Alexian Brothers Medical Center, Elk Grove Village, IL, <sup>9</sup>Medical College of Wisconsin, Milwaukee, WI, <sup>10</sup>Cedars-Sinai Medical Center, Los Angeles, CA, <sup>11</sup>Chattanooga Center for Neurologic Research, Chattanooga, TN, <sup>12</sup>Kaleida Health, Buffalo, NY, <sup>13</sup>Abington Memorial Hospital, Abington, PA, <sup>14</sup>Cleveland Clinic, Cleveland, OH, <sup>15</sup>Alberta Health Services, Calgary, AB, CANADA, <sup>16</sup>Harborview Medical Center, Seattle, WA, <sup>17</sup>Northwest Community Hospital, Arlington Heights, IL, <sup>18</sup>University of Alabama at Birmingham, Birmingham, AL,

<sup>19</sup>University of Pittsburgh Medical Center, Pittsburgh, PA, <sup>20</sup>St. Paul Radiology, St. Paul, MN, <sup>21</sup>Penumbra, Inc., Alameda, CA

## PURPOSE

Recent evidence suggests that the pretreatment core infarct volume is an independent predictor of clinical outcome following endovascular stroke therapy in acute ischemic stroke. We report the preliminary results of a prospective study aimed to confirm this hypothesis in stroke patients treated with the Penumbra Stroke System.

## MATERIALS & METHODS

The START trial was a prospective multicenter study to evaluate the clinical impact of pretreatment core infarct size in patients undergoing endovascular stroke therapy using the Penumbra Stroke System. The imaging approach was left to each center's discretion, and included CTA source images, CT perfusion (CTP) or MRI diffusion imaging (DWI). Infarct volumes were prospectively determined on these modalities prior to endovascular stroke therapy using the Penumbra System. Infarct volumes were analyzed as both continuous and trichotomized (<50 mL, 50-100 mL, >100 mL) variables. Clinical outcomes were dichotomized as 90-day modified Rankin Scale scores of 0-2 (good outcome) vs 3-6 (poor outcome). Univariate analysis was performed to determine predictors of outcome.

## RESULTS

Of the 145 patients enrolled, 49 met study criteria for this preliminary analysis. The mean age was  $67.1 \pm 12.7$  years; median NIHSS was 19 (15-24). There were 30 (61.2%) females, and target vessel occlusions were in the internal carotid artery (ICA) (n = 6), MCA M1 and M2 segments (n = 43). The median pretreatment infarct volume was 15.8 (3.5-44.8). There were 41 (83.7%) patients with volumes <50 mL, 4 (8.2%) with 50-100 mL, 4 (8.2%) with >100 mL. The imaging modality was CTA-SI in 13 (26.5%), CTP in 27 (55.1%), DWI in 9 (18.3%). The median time from groin puncture to discontinuation of aspiration was 63.5 (39-97) minutes. Nineteen (38.8%) patients achieved a good 90-day outcome. Thirteen (26.5%) died. No patients suffered a symptomatic hemorrhage. Smaller pretreatment infarct volume was associated significantly with good outcomes (p = 0.02). The median pretreatment core infarct volume was 12 (0-19) for the good outcome group (Rankin Scale scores 0-2) as compared to 21 (10-48) for the Rankin Scale scores 3-6 group. The rate of good outcomes (Rankin Scale scores 0-2) was 43.9% for <50 mL, 0% for 50-100 mL, and 25% for >100 mL (p = 0.19). Infarct volume <50 mL was 95% sensitive for a good outcome in this cohort. The only other univariate predictor of outcome was age (p = 0.02).

## CONCLUSION

Preliminary START results confirm that smaller pretreatment infarct volume is associated with better outcomes following endovascular therapy. Ongoing imaging review and analysis are being conducted to

better characterize specific infarct volume thresholds for outcome prediction.

**KEY WORDS:** Stroke, penumbra, core infarct volume

**O-562**

**1:48 PM - 1:56 PM**

### Arterial Occlusion on CT Angiography Is Not a Specific Predictor of Mismatch between Diffusion-Weighted Imaging and Perfusion-Weighted Imaging Lesions in Acute Ischemic Stroke

Bezerra, R.·Copen, W. A.·McIntosh, E.·Diwan, I.·Garg, P.·Mocking, S.·Kimberly, W. T.·Arsava, E. M.·Ji, R.·Ay, H.·Singhal, A. B.·Schaefer, P. W.·Wu, O.

Massachusetts General Hospital  
Boston, MA

#### PURPOSE

Fewer than 5% of acute stroke patients receive thrombolytic therapy. Perfusion-weighted MRI (PWI) has been postulated to be an essential tool for extending therapy to a greater number of patients by identifying those with still salvageable tissue. Some argue that PWI is unnecessary in this role, because the presence or absence of arterial stenosis or occlusion on vascular imaging predicts the occurrence of diffusion-weighted MRI (DWI) and PWI mismatch. To assess the added value of PWI, we investigated the relationship between arterial occlusion or stenosis on CT angiography (CTA) and DWI and PWI mismatch.

#### MATERIALS & METHODS

We retrospectively analyzed intracranial CTAs from 95 ischemic stroke patients who underwent DWI and PWI within 12 hours of the time when they were last seen well, who received neither intravenous nor intraarterial recanalization therapy nor experimental therapy, had DWI lesions  $> 1 \text{ cm}^3$  and, had follow-up imaging  $\geq 4$  days from stroke onset. Based on CTA, patients were divided into two groups: those with total occlusion or visually estimated stenosis  $\geq 50\%$ , in the stroke territory, and those with no such CTA finding. Perfusion-weighted imaging data were processed using deconvolution with automatically selected arterial input functions using oscillation index regularized singular value decomposition. Two perfusion maps were evaluated: mean transit time (MTT) and time to the maximum value of the residue function (Tmax). Lesion volumes on DWI, Tmax ( $\geq 6$  seconds) and MTT (subjectively visible lesion) were measured. Follow-up lesions, either FLAIR MRI or noncontrast CT, were manually outlined. Holes in the outlines on the MTT, DWI, and follow-up lesions were filled using an automated algorithm. All images were coregistered to the acute PWI maps. Mismatch was defined as (PWI-DWI)/DWI  $> 20\%$  and PWI-DWI  $\geq 10 \text{ cm}^3$ .

#### RESULTS

Seventy-four patients presented with occlusion or stenosis, four of these involving stenosis and the remainder occlusions. Twenty-one patients had no arterial occlusion/stenosis. The sensitivity of occlusion/stenosis in predicting DWI-PWI mismatch

was 89% (95% confidence interval: 78-95%) when MTT was used, and 89% (77-95%) when Tmax was used. The specificity of occlusion/stenosis in predicting mismatch was 42% (26-61%) for MTT and 41% (25-59%) for Tmax. Other results are summarized in the Table, expressed as mean  $\pm$  SD or mean (interquartile range).

Demographic and imaging findings in patients with and without occlusion/stenosis on CTA. *P<0.05			
	Arterial Occlusion/Stenosis (N=74)	No Arterial Occlusion/Stenosis (N=21)	P-value
Age (years)	63.6 $\pm$ 17.3	63.0 $\pm$ 17.5	0.83
Sex (%male)	61%	76%	0.30
Admission NIHSS*	6 [3-13]	2 [2-7]	0.04
Time-to-MRI (h)	6.0 $\pm$ 2.6	5.3 $\pm$ 3.1	0.26
Time-to-FU (days)*	22.6 $\pm$ 23.7	40.2 $\pm$ 31.6	0.02
Follow-up Type (%MR)	72%	81%	0.58
DWI lesion (cm <sup>3</sup> )*	12.6 [4.1-45.0]	4.2 [1.1-20.8]	0.01
FU lesion (cm <sup>3</sup> )*	18.5 [7.3-77.3]	7.1 [1.5-21.5]	0.003
MTT lesion (cm <sup>3</sup> )*	72.8 [23.5-151.5]	16.6 [0.81-33.7]	<0.0001
Tmax lesion (cm <sup>3</sup> )*	51.5 [12.5-117.4]	6.1 [0-20.3]	<0.0001
MTT mismatch (Prevalence)*	74% (55/74)	33% (7/21)	0.001
Tmax mismatch (Prevalence)*	73% (54/74)	33% (7/21)	0.002

#### CONCLUSION

Although patients with arterial occlusion or stenosis on CTA were significantly more likely to have DWI and PWI mismatch, mismatch was seen in one third of patients without occlusion or stenosis. Additionally, more than one quarter of patients with arterial occlusion or stenosis did not have mismatch. In more than 30% of patients, PWI provided information that was not available on CTA and could have influenced the decision to offer thrombolytic therapy.

**KEY WORDS:** Perfusion-weighted imaging, diffusion-weighted imaging, CT angiography

### Diffusion Tensor Imaging Metrics as a Surrogate Marker of Lesion Age in Acute Ischemic Stroke: A Preliminary Study

Puig Alcantara, J.<sup>1</sup>•Daunis-i-Estadella, J.<sup>2</sup>•Blasco, G.<sup>3</sup>•Soria, G.<sup>4</sup>•Prats, A.<sup>5</sup>•Boada, I.<sup>2</sup>•Castellanos, M.<sup>3</sup>•Serena, J.<sup>3</sup>•Pedraza, S.<sup>3</sup>

<sup>1</sup>Department of Radiology (IDI), Girona, SPAIN, <sup>2</sup>Universitat de Girona, Girona, SPAIN, <sup>3</sup>Hospital Universitari Dr Josep Trueta, Girona, SPAIN, <sup>4</sup>Institut d'Investigacions Biomèdiques August Pi i Sunyer, Barcelona, SPAIN, <sup>5</sup>Universitat de Barcelona, Barcelona, SPAIN, <sup>6</sup>Universitat de Girona, Girona, SPAIN, <sup>7</sup>Hospital Universitari Dr Josep Trueta, Girona, SPAIN

#### PURPOSE

Intravenous tissue plasminogen activator (IV t-PA) is only approved within 4.5 hours of acute ischemic stroke (AIS) onset. However, AIS occurs during sleep in approximately 25% of patients and these are automatically excluded from treatment. An MRI surrogate marker of lesion age might help identify patients with unknown AIS onset. Negative FLAIR findings identify patients within 4.5 hours of onset moderately accurately. Diffusion anisotropy detects microstructural changes from ischemic injury, but its value remains unclear. We compared FLAIR and diffusion tensor imaging (DTI) metrics for detecting cerebral infarctions up to 4.5 hours of onset.

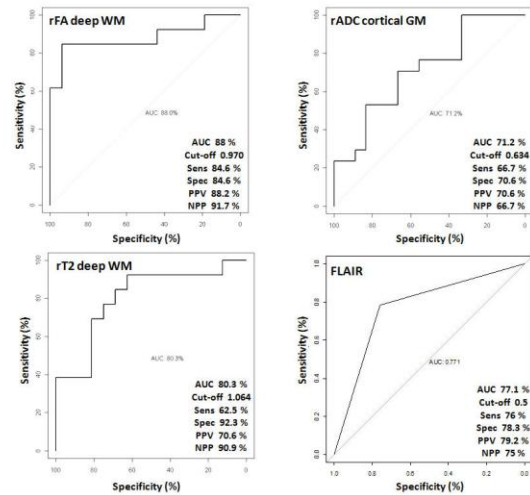
#### MATERIALS & METHODS

We enrolled patients with middle cerebral artery (MCA) AIS onset clearly within 12 hours. All patients underwent multimodal MRI including DTI on a 1.5 T scanner. We analyzed deep and cortical gray matter (GM) and deep and subcortical white matter (WM) affected by stroke. In these regions, we measured fractional anisotropy (FA), eigenvalues ( $\lambda_1$ ,  $\lambda_2$ ,  $\lambda_3$ ), mean diffusivity (MD), apparent diffusion coefficient (ADC), and T2-weighted signal intensity on coregistered maps using regions of interest encompassing the hyperintensity depicted on diffusion-weighted MRI. We also determined the values for the normal homologous contralateral regions in the same slice and calculated the ratios (r) with the affected side. FLAIR-positive was defined as a new hyperintense signal in totally infarcted tissue.

#### RESULTS

From 60 consecutive patients, we analyzed the 48 (17 women, mean age  $68 \pm 14$  years) with known onset. In 25 (52.1%), onset was  $\leq 4.5$  hours (mean  $182.3 \text{ min} \pm 65.6$ ). Variables with significant differences between infarcts  $\leq 4.5$  were (Table) rFA deep WM ( $p = 0.001$ ), rMD cortical GM ( $p = 0.036$ ), rADC cortical GM ( $p = 0.009$ ), rT2 deep WM ( $p = 0.006$ ), and FLAIR ( $p < 0.001$ ). Logistic binary regression models and receiver operating characteristic demonstrated that rFA deep WM was the most reliable to discriminate infarcts  $< 4.5$  h (Goodman-Kruskal = 0.76; Kendall = 0.39). The sensitivity, specificity, and positive and negative predictive values

for infarct 0.970 were 93.8%, 84.6%, 88.2%, and 91.7%, respectively.



Diffusion Anisotropy Metrics and Signal Intensity on FLAIR According Stroke Time Evolution

	< 4.5 hours	> 4.5 hours	p-value
FLAIR (normal/hyperintensity)	19/6	5/18	0.000
rFA cortical GM (SD)	1.209 (0.295) n=18	1.064 (0.278) n=17	0.146
rFA subcortical WM (SD)	1.189 (0.392) n=13	1.416 (0.522) n=10	0.247
rFA deep GM (SD)	1.175 (0.184) n=13	1.030 (0.296) n=9	0.170
rFA deep WM (SD)	1.178 (0.287) n=16	0.826 (0.209) n=13	0.001
r MD deep WM (SD)	0.703 (0.235) n=17	0.622 (0.248) n=17	0.339
r MD cortical GM	0.682 (0.122) n=13	0.528 (0.212) n=11	0.036
r MD subcortical WM (SD)	0.632 (0.148) n=13	0.607 (0.180) n=8	0.733
r MD deep GM (SD)	0.695 (0.166) n=16	0.728 (0.255) n=13	0.679
r ADC deep WM (SD)	0.707 (0.178) n=18	0.574 (0.132) n=17	0.018
r ADC cortical GM (SD)	0.670 (0.139) n=13	0.506 (0.132) n=10	0.009
r ADC subcortical WM (SD)	0.670 (0.214) n=13	0.581 (0.119) n=9	0.273
r ADC deep GM (SD)	0.680 (0.185) n=16	0.756 (0.206) n=12	0.311
r T2 deep WM (SD)	1.113 (0.255) n=18	1.166 (0.242) n=17	0.537
r T2 cortical GM (SD)	1.172 (0.297) n=13	1.158 (0.139) n=10	0.889
r T2 subcortical WM (SD)	1.076 (0.218) n=13	1.295 (0.397) n=8	0.117
r T2 deep GM (SD)	1.036 (0.143) n=16	1.221 (0.192) n=13	0.006

#### CONCLUSION

Diffusion tensor imaging metrics, especially rFA deep WM, may be a surrogate marker of stroke age.

**KEY WORDS:** Stroke, MR imaging, diffusion tensor imaging

**O-564**

**2:04 PM - 2:12 PM**

# **Reduced CO<sub>2</sub> BOLD MR Cerebrovascular Reactivity Is Associated with Ischemic Events in Patients with Carotid Artery Occlusion**

Mandell, D. M.<sup>1</sup>•Battisti-Charbonney, A.<sup>1</sup>•Pucci, O.<sup>1</sup>•Han, J. S.<sup>1</sup>•Spano, V. R.<sup>1</sup>•Sam, K.<sup>1</sup>•Poublanc, J.<sup>1</sup>•Crawley, A. P.<sup>1</sup>•Fisher, J. A.<sup>2</sup>•Mikulis, D. J.<sup>1</sup>

<sup>1</sup>Toronto Western Hospital, Toronto, ON, CANADA,

<sup>2</sup>Toronto General Hospital, Toronto, ON, CANADA

## **PURPOSE**

In patients with carotid artery occlusion, cerebral hemodynamic impairment yields increased risk of subsequent ischemic stroke. Cerebral hemodynamic status may be evaluated by measuring cerebrovascular reactivity (CVR), the change in cerebral blood flow induced by a vasodilatory stimulus. Recent studies validate the use of blood oxygen level-dependent (BOLD) MR imaging during a precisely controlled oscillation of end-tidal partial pressure of carbon dioxide (PETCO<sub>2</sub>) to measure CVR. The CO<sub>2</sub> BOLD CVR technique is quick, nonionizing, and it can be performed at the same session as routine MRI. The aim of this study was to determine whether there is a difference in CO<sub>2</sub> BOLD CVR between carotid artery occlusion patients with versus without prior ischemic events.

## **MATERIALS & METHODS**

We performed a cross-sectional analysis of 30 consecutive patients with carotid artery occlusion who underwent CO<sub>2</sub> BOLD MR mapping of CVR at the Toronto Western Hospital between January 2006 and June 2011. Following a detailed chart review, subjects were categorized as "occlusion associated with prior ischemic event" if there was a prior transient ischemic attack or ischemic stroke attributable to the ipsilateral middle cerebral artery territory, and otherwise, categorized as "occlusion without prior ischemic event." MR imaging was performed on a 3.0 T whole body scanner. Following a T1-weighted three-dimensional sequence for anatomical coregistration, CVR data was acquired with a T2\*-weighted single-shot gradient echo echo-planar sequence during precisely controlled oscillation of PETCO<sub>2</sub> between 40 and 50 mm Hg. Cerebrovascular reactivity was calculated as %ΔBOLD MR signal intensity per mm Hg ΔPETCO<sub>2</sub> on a voxel-wise basis. We segmented the ipsilateral middle cerebral artery territory cortex using an automated algorithm, and calculated mean CVR for this segment. Subjects with infarction involving greater than one third of the segment were excluded, and we manually segmented any smaller infarcts and removed these regions from the mean CVR calculations. Using normative data, and defining reduced CVR as two standard deviations below the mean for healthy subjects, our thresholds for reduced and paradoxical CVR were CVR < 0.16% ΔMR signal intensity per mm Hg ΔPETCO<sub>2</sub>, and < 0%, respectively. We applied Fisher's exact test to determine whether the proportion of

subjects with reduced CVR differed between those with versus without prior ischemic events. We similarly tested whether the proportion of subjects with paradoxical CVR differed between the two groups.

## **RESULTS**

There were 30 patients with 33 carotid artery occlusions, of which 25 occlusions were associated with ipsilateral ischemic events and eight were not. Twenty of the 25 occlusions with ischemic events were associated with reduced CVR (80%) whereas only three of the eight occlusions without ischemic events had reduced CVR (38%, two-tailed P = 0.036). Six of the 25 occlusions with ischemic events were associated with paradoxical CVR (24%), whereas none of the occlusions without ischemic events had paradoxical CVR (two-tailed P = 0.296).

## **CONCLUSION**

Reduced CO<sub>2</sub> BOLD CVR is associated with prior ipsilateral ischemic events in patients with carotid artery occlusion. This raises the possibility of using CO<sub>2</sub> BOLD CVR for prognostication in patients with carotid occlusion, but prospective validation is needed.

**KEY WORDS:** Cerebrovascular reactivity, carotid artery occlusion

**O-565**

**2:12 PM - 2:20 PM**

# **How Do Clinical Predictors Affect the Utility of CT Perfusion in Delayed Cerebral Ischemia?**

Killeen, R. P.<sup>1,2</sup>•Gupta, A.<sup>1</sup>•Delaney, H.<sup>1</sup>•Johnson, C.<sup>1</sup>•Comunale, J.<sup>1</sup>•Tsiouris, A. J.<sup>1</sup>•Sanelli, P. C.<sup>1</sup>

<sup>1</sup>NewYork-Presbyterian Hospital, New York, NY,

<sup>2</sup>Hermitage Medical Clinic, Dublin, IRELAND

## **PURPOSE**

To evaluate the effect of clinical predictors on the utility of CT perfusion (CTP) for determining delayed cerebral ischemia (DCI) in aneurysmal subarachnoid hemorrhage (ASAH).

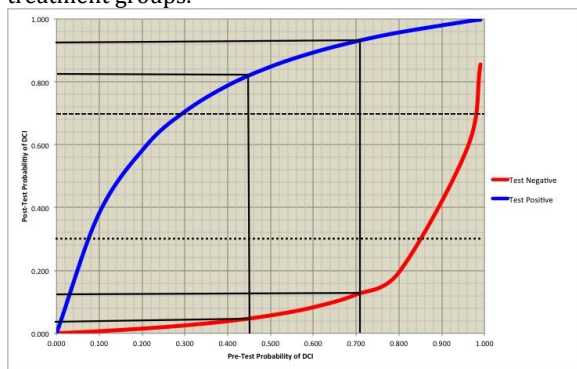
## **MATERIALS & METHODS**

Retrospective study of consecutive ASAH patients with CTP performed between days 6-8 following aneurysm rupture in asymptomatic patients or on the same day symptoms occurred in patients with clinical deterioration. Qualitative analysis of CTP was performed by three blinded neuroradiologists to identify perfusion deficits. Reference standard for determining DCI consisted of both imaging and clinical criteria. Test characteristics of CTP were calculated and graphs of conditional probabilities (GCP) constructed using Bayesian analysis. Literature review was performed to identify common clinical predictors and their probabilities of DCI. These probabilities were applied to the GCP as the pretest probabilities to represent different clinical and imaging scenarios.

## **RESULTS**

Ninety-seven patients were included; 41%(40/97) had DCI. Qualitative CTP deficits were seen in 95% (38/40)

patients with DCI and 18% (10/57) without DCI. Sensitivity, specificity, positive and negative predictive values for CTP were 0.95 (95% CI 0.88-1.0), 0.83 (95% CI 0.73-0.92), 0.79 (95% CI 0.68-0.91) and 0.96 (95% CI 0.90-1.0), respectively. The likelihood ratios of positive and negative CTP were 5.4 (95% CI 3.1-9.6) and 0.6 (95% CI 0.02-0.24), respectively. Bayes' theorem calculated the posttest probability of DCI for any given pretest probability using the GCP for CTP (Figure 1). The following clinical predictors were evaluated to represent different patient scenarios: (1) Hunt and Hess: grades 1-2 have 35% probability of DCI and grades 3-5 have 61% probability, (2) Fisher: grade 2 has 33% probability, grade 3 has 54%, and grade 4 has 70%, (3) Glasgow coma scale (GCS): score <9 has 71% probability and >9 has 45%. Figure 1 illustrates an example when the pretest probabilities are in close range using GCS less than or greater than 9. The posttest probability (y-axis) of DCI when CTP is negative (red line) is <15% and posttest probability is 80% when CTP is positive (blue line) in both groups. If treatment threshold (dashed lines) is set arbitrarily at >70% probability of DCI and no treatment at <30% probability, CTP will significantly change the posttest probability and categorize patients into treatment or no treatment groups.



## CONCLUSION

CT perfusion has high sensitivity for determining DCI and significantly contributes to its posttest probability in a wide range of patient scenarios. Thus, CTP may add important information along with common clinical predictors in treatment decisions of ASAH patients.

**KEY WORDS:** CT perfusion, Bayesian analysis, delayed cerebral ischemia

**O-566**

**2:20 PM - 2:28 PM**

## Assessment of the Integrity of Hemodynamic Reserve, as Measured by Dynamic Susceptibility Contrast MR Perfusion before and after Vasodilation Is Compromised by Collateral Circulation

Thulborn, K. R. Atkinson, I. C. Alexander, A. Singal, M. Amin-Hanjani, S.

University of Illinois at Chicago  
Chicago, IL

## PURPOSE

To test if worsening perfusion asymmetry, identified by DSC MR perfusion after vasodilation, classically interpreted as compromised HR, is consistent with loss of regional activation from blood oxygenation level dependent (BOLD) fMRI that also implies loss of HR.

## MATERIALS & METHODS

Patients with technically adequate imaging evaluation of cerebrovascular disease were classified as single vessel (SV, N = 10), two-vessel (TV, N = 9), multivessel (MV, N = 14), and moyamoya disease (MM, N = 18). Loss of HR was assessed by: (1) worsening asymmetry in regional tissue transit times (TTT) measured by DSC MR perfusion from before to after vasodilation with acetazolamide, and (2) loss of regional activation during blood oxygenation level dependent (BOLD) functional MRI. The concentration-normalized time courses of the perfusion studies were analyzed by voxel-wise by multivariate nonlinear, least squares fitting of a gamma variate function to obtain TTT (full width at half maximum height). For each patient, the differences in TTT values between the vascular territory distal to the diseased vessel and contralateral normal tissue before and after vasodilation were compared (paired student t-test,  $p < 0.05$ ) in each of six vascular territories (left and right anterior, middle and posterior cerebral arteries). The fMRI test used a two-condition (30s), block-design, 4-cycle fMRI paradigm comparing an audiovisual bilateral hand grasping with flashing checkerboard stimulus condition to fixation. The BOLD activation was obtained by t-test and classified as positive or negative for activation in each vascular territory. The percentages of congruent and incongruent results across both methods were tabulated for the vascular territories distal to and remote from the diseased vessel.

## RESULTS

The percent congruency of the perfusion to fMRI results across disease category are tabulated for vascular territories distal to and remote from disease in Table 1. There is a large portion (30-51%) of incongruent results in the potentially compromised vascular territory but not in other regions. The proportion of incongruent results appears to be related to leptomeningeal collateral circulation that is greatest in single vessel disease and moyamoya disease and least in two and multivessel disease.

Congruency (%) between loss of HR by MR perfusion and loss of BOLD fMRI

Cerebrovascular Disease Patient Group	Territory relative to diseased vessel	Number of Cases	Congruency (%)	Incongruency (%)
SV	distal	10	50	50
TV	distal	9	70	30
MV	distal	14	58	42
MM	distal	20	49	51
SV	remote	10	98	2
TV	remote	9	94	6
MV	remote	14	97	3



**CONCLUSION**

The classic interpretation of worsening perfusion asymmetry on vasodilation as indicating compromised HR distal to a diseased vessel is not consistent with the intact regional BOLD activation in a large proportion of cases. This contradiction, more common when significant collateral circulation is present, is explained by violation of the assumption of a single arterial input function in the perfusion analysis.

**KEY WORDS:** Brain perfusion, arterial input function, collateral circulation

**O-567****2:28 PM - 2:36 PM****Affect of Diabetes on Brain Structure: ACCORD-MIND MR Imaging Baseline Data**

Bryan, N.<sup>1</sup>Bilello, M.<sup>1</sup>Davatzikos, C.<sup>1</sup>Lazar, R. M.<sup>2</sup>Murray, A.<sup>3</sup>Horowitz, K.<sup>4</sup>Lovato, J.<sup>5</sup>Miller, M. E.<sup>5</sup>Williamson, J.<sup>5</sup>Launer, L. J.<sup>6</sup>

<sup>1</sup>University of Pennsylvania, Philadelphia, PA, <sup>2</sup>Columbia University, New York, NY, <sup>3</sup>Hennepin County Medical Center, Minneapolis, MN, <sup>4</sup>Case Western Reserve University, Cleveland, OH, <sup>5</sup>Wake Forest University, Winston Salem, NC, <sup>6</sup>National Institute on Aging, Bethesda, MD

**PURPOSE**

Type II diabetes is associated with stroke and cognitive decline, including dementia. MR imaging offers the opportunity to evaluate brain both normal brain and pathologic lesion volumes. ACCORD was a clinical trial of standard vs intense management of glycemia, hypertension and blood lipid profile. The MIND sub-study evaluated the effects of these treatments on the structure and function of the brain, using brain MRI to evaluate brain structure. In this report, baseline data from ACCORD/MIND MRI relate duration and severity of diabetes to brain structure, testing whether more severe metrics of diabetes are correlated inversely with brain volume and positively correlated with lesion load.

**MATERIALS & METHODS**

Baseline diabetes for ACCORD/MIND participants was evaluated by fasting plasma glucose (FPG), hemoglobin A1C (HgbA1C) and duration of diabetes. MR imaging was performed with Flair, PD, T2- and T1-weighted sequences. An automated, multisignal computer algorithm classified all brain tissue as gray or white matter, normal or abnormal. Separate linear regression models were used to investigate the relationship of the three diabetes measures to the MRI outcomes.

**RESULTS**

Six hundred fourteen participants were included. The mean volumes of total gray (463.8cm<sup>3</sup>) and total white matter (463.6cm<sup>3</sup>) were similar. There was very little abnormal gray matter (0.15 cc; <0.02% of total gray matter), with an order of magnitude more abnormal white matter (2.02 cc; 0.4% of total white matter). The volume of abnormal basal ganglia tissue was 0.33 cc. Of the total abnormal tissue, approximately 81% was in the white matter, 14% in the basal ganglia, and 5% in

the gray matter. An inverse relationship between diabetes duration and FPG was found with total and normal gray matter volumes. A 10-year difference in diabetes duration was predictive of a 4.28 m<sup>3</sup> difference in total gray matter volume. Fasting plasma glucose inversely correlated with ischemic lesion volume. Hemoglobin A1C was not associated with any MRI measure.

**CONCLUSION**

In the diabetic population of the ACCORD-MIND sub-study, duration of diabetes and, to a lesser extent, FPG were associated most strongly with brain, specifically gray matter, atrophy. Our findings raise the possibility that both neurodegenerative disease such as AD and vascular pathology play roles in the cognitive changes observed in diabetes.

**Acknowledgements:** This study was supported by the National Heart, Lung and Blood Institute and the National Institute on Aging at NIH.

**KEY WORDS:** Diabetes, ischemia, MR imaging

**Thursday Afternoon****1:00 PM - 2:30 PM****Trianon Ballroom**

**(66b) Interventional:  
Thrombolysis/Stroke**

**O-568****1:00 PM - 1:08 PM****Single Center Experience with Trevo Stent Retriever Device in Acute Ischemic Stroke: Safety and Efficacy in 60 Consecutive Patients**

San Roman, L.<sup>1</sup>Blasco, J.<sup>1</sup>Macho, J.<sup>1</sup>Lopez Rueda, A.<sup>1</sup>Obach, V.<sup>1</sup>Tomasello, A.<sup>2</sup>Campodonico, D.<sup>1</sup>Perandreu, J.<sup>3</sup>Branera, J.<sup>3</sup>Chamorro, A.<sup>1</sup>

<sup>1</sup>Hospital Clinic of Barcelona, Barcelona, SPAIN, <sup>2</sup>Hospital Sant Pau, Barcelona, SPAIN, <sup>3</sup>Hospital Parc Tauli, Sabadell, SPAIN

**PURPOSE**

We sought to explore the safety and efficacy of the new TREVO stent-like retriever in 60 consecutive patients with acute stroke.

**MATERIALS & METHODS**

Prospective, single-center study of patients (n =60, mean age 71.3 years, 45% males) with stroke lasting < 8 hours in the anterior circulation, or < 12 hours in the vertebrobasilar circulation were treated if CT perfusion /CT angiography confirmed an artery occlusion, ruled out a malignant profile, or showed target mismatch if symptoms > 4.5 hours. Successful recanalization (TICI 2b-3), good outcome (modified Rankin Scale score 0 to 2) and mortality at day 90, device-related

complications, and serious bleeding (NIHSS score increase > 4 points), were prospectively assessed.

#### RESULTS

The median (IQR) NIHSS score on admission was 18 (12-22), the median (IQR) time from stroke onset to arterial puncture was 210 (173-296) minutes. Thirty-three (55%) patients also had received intravenous rtPA. Overall, 49 patients were only treated with the TREVO device, while 11 had additional devices because TREVO was unable to reopen the occluded vessel. Successful recanalization TICI 3 or 2b was achieved in 87% of the patients with 45% of good clinical outcome (mRs 0-2) at 90 days, 28% mortality rate, and 12% of symptomatic intracranial bleeding in the first 36 hours.

#### CONCLUSION

The TREVO device was reasonably safe and effective in terms of revascularization and good clinical outcomes in patients with severe stroke. These results support the formal investigation of the TREVO device in randomized clinical trials.

**KEY WORDS:** Acute ischemic stroke, endovascular treatment

**O-569**

**1:08 PM - 1:16 PM**

#### **Recanalization Rate and Periprocedural Complications of Mechanical Thrombectomy with Retrieable Stents in Acute Stroke: A Retrospective Analysis of 119 Cases**

Yilmaz, U.·Papanagiotou, P.·Roth, C.·Viera, J.·Körner, H.·Alexandrou, M.·Ziegler, K.·Reith, W.

Saarland University Hospital  
Homburg, GERMANY

#### PURPOSE

Currently endovascular treatment of acute intracerebral artery occlusions by mechanical thrombectomy got impetus by a new technique using fully retrievable self-expanding stents. First results reported in the last year showed promising angiographic outcome with recanalization rates between 89-94%. The prospective ReFlow-Study with favorable clinical outcome as primary measure is pending. The purpose of this study was to analyze data on angiographic outcome and complications of mechanical thrombectomy with retrievable stents in a large collective.

#### MATERIALS & METHODS

Data of 119 consecutive patients with acute intracerebral artery occlusions who underwent endovascular treatment with retrievable stents were analyzed regarding angiographic outcome, periprocedural complications and the influence of additional proximal extracranial artery occlusions and of the presence of collaterals.

#### RESULTS

Recanalization with postinterventional TICI  $\geq 2$  was achieved in 91.5%. Occlusions were located in the M1 segment of the MCA in 43.7%, in the M2 segment in

5.9%, in the carotid T in 30.3% and in the basilar artery in 11.8%. The mean time to recanalization was 58 minutes with a standard deviation of 36 minutes. The mean number of maneuvers needed was 1.8. Periprocedural complications included perforations (0.8%), dissections (1.7%) and transient vasospasms (24.4%). Neither additional proximal artery occlusions nor the presence or absence of collaterals had significant influence on angiographic outcome.

#### CONCLUSION

Mechanical thrombectomy with retrievable stents in acute stroke is a promising new technique with a high recanalization and low periprocedural complication rate.

**KEY WORDS:** Stroke, mechanical thrombectomy, retrievable stents

**O-570**

**1:16 PM - 1:24 PM**

#### **Histopathologic Clot Composition in Ischemic Stroke and Its Influence on Mechanical Recanalization and Patient Outcome**

Boeckh-Behrens, T.·Förschler, A.·Prothmann, S.·Kreiser, K.·Zimmer, C.·Bauer, J.·Poppert, H.

Klinikum Rechts der Isar, Technische Universität  
München  
Munich, GERMANY

#### PURPOSE

The recent progress in interventional techniques in acute ischemic stroke therapy - mainly based on the development of stent retriever systems- not only leads to a significant improvement of recanalization rates in cerebral main stem occlusions but also increasingly opens up the opportunity to retrieve thrombi for histopathologic examination. Aim of this study was to evaluate possible correlations and connections between histopathologic clot characteristics and clinical data concerning the mechanical extraction procedure as well as clinical course and outcome of patients with acute ischemic stroke.

#### MATERIALS & METHODS

All patients treated by mechanical recanalisation between 10/2010 and 07/2011 with main stem occlusion in the anterior circulation were included in the analysis if evaluable thrombi could be obtained. This was the case in 34 out of 54 patients with an altogether recanalization rate of 89% TICI2b/3. A semiautomated histopathologic analysis of the retrieved thrombi was performed and the percentage fractions of fibrin, erythrocytes and leukocytes per cut were evaluated, respectively. These data were correlated to clinical and interventional data with regard to etiology, NIHSS score before treatment, at discharge and their difference, recanalization time (start to end angiography), number of recanalization maneuvers and achieved TICI score.

#### RESULTS

The analyzed very inhomogeneous thrombi were in 53% fibrin-dominant (more than 60% fibrin), in 12%

erythrocyte-dominant (more than 60% erythrocytes) and in 35% mixed. There was a moderate but significant positive correlation between the leukocyte count of the thrombi and the NIHSS value at discharge ( $p = 0.05$ ) as well as the recanalization time ( $p = 0.037$ ). Additionally, the leukocyte count was significantly higher in the group of patients with an achieved TICI score of only 2b in contrast to the group with a TICI score of 3.

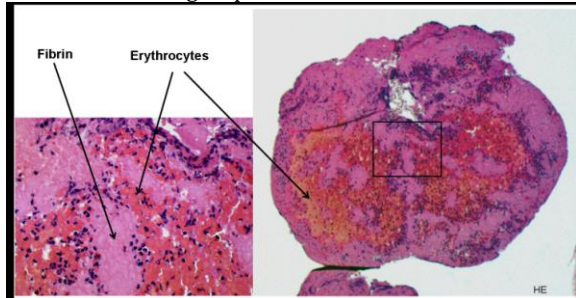


Figure 1. Example of well organized thrombus with central accumulations of erythrocytes enclosed by fibrin components and islets of leukocytes

#### CONCLUSION

The histopathologic structure of clots in ischemic stroke seems to have an impact on patient outcome and on the recanalization procedure. The present study shows a relation between higher leukocyte fractions in the clot and worse outcome data of patients, longer recanalization time as well as a decrease in achieved recanalization success. Our findings are consistent with prior studies that showed a substantial impact of white blood cells in thrombus formation and stroke development and may contribute to a better understanding of the underlying pathophysiologic processes.

**KEY WORDS:** Thrombus, stroke, histology

**O-571**

**1:24 PM - 1:32 PM**

#### Distal Embolization Predicts Infarct Growth and Futile Recanalization after Endovascular Stroke Therapy

Almekhlafi, M. A. Modi, J. Goel, A. Menon, B. Demchuk, A. Goyal, M.

University of Calgary  
Calgary, AB, CANADA

#### PURPOSE

With the growing use of intraarterial devices in acute stroke therapy, distal embolization (DE) is increasingly encountered. Reports described the incidence of these emboli but none so far linked them to the futile recanalization phenomenon. We report DE impact on clinical and radiographic outcomes in relation to futile recanalization.

#### MATERIALS & METHODS

This is a retrospective longitudinal cohort including all anterior circulation stroke patients treated using intraarterial therapy in our center between 2005 and 2011. Patients enrolled in randomized trials were excluded. Baseline and follow-up CT scans were scored

by a stroke neurologist and a neuroradiologist blinded to the clinical and angiographic data. Angiograms were reviewed by an experienced interventional neuroradiologist blinded to the clinical and radiographic outcome. Distal embolization is defined as any luminal filling defect in the arterial tree distal to the thrombus or any new luminal filling defect in a different arterial territory evaluated at final cerebral angiogram. Infarct growth was defined as a drop of two points in ASPECTS on noncontrast CT follow-up scan compared to baseline.

#### RESULTS

Eighty-two patients [mean age 68 (13.8) years, median NIHSS 17(IQR 7), median ASPECTS 8(2)] were studied. Intravenous tPA was used in 63%. The median onset-to-puncture time was 209 (119) minutes. The occlusion site was the L/T-type carotid occlusion in 22%, proximal MCA in 53.7%, and M2-MCA in 24.3%. The Merci device was used in 28%, Penumbra system in 31.7%, angioplasty balloon in 18.3%, and retrievable stents in 11%. Intraarterial tPA also was used in 59% of cases. Successful recanalization (TICI 2b/3) was achieved in 43%. Distal emboli occurred in 45.1% of cases, 10% of which were in the ACA territory. Despite successful recanalization, infarct growth occurred in 28.6% of patients. Distal embolization occurred in 80% (8/10) of those with infarct growth and recanalized vs 60% (15/25) in those who had no infarct growth and recanalized. Good clinical outcome (mRS 0-2) at discharge was noted in 58.3% of patients with successful recanalization and no DE, 30.4% in those with successful recanalization and DE, and 17% in those who did not recanalize (TICI 0-2a) ( $p = 0.015$ ).

#### CONCLUSION

Distal embolization is common in the setting of endovascular stroke therapy and is associated with infarct growth and worse outcomes despite successful recanalization. Distal embolization may be one factor contributing to the futile recanalization phenomenon. This retrospective, single center experience needs to be validated in endovascular clinical trials.

**KEY WORDS:** Stroke, recanalization, emboli

**O-572**

**1:32 PM - 1:40 PM**

#### Frequency and Relevance of Peripheral Embolism Caused by Loss of Thrombus Material during Mechanical Thrombectomy for Treatment of Acute Stroke

Kurre, W.<sup>1</sup> Vajda, Z.<sup>1</sup> Aguilar Perez, M.<sup>1</sup> Fischer, S.<sup>1</sup> Schmid, E.<sup>2</sup> Bätzner, H.<sup>2</sup> Henkes, H.<sup>1</sup>

<sup>1</sup>Katharinenhospital, Stuttgart, GERMANY, <sup>2</sup>Klinikum Stuttgart, Stuttgart, GERMANY

#### PURPOSE

Loss of thrombus material causing new peripheral embolic vessel occlusions is one of the potential hazards in mechanical recanalization procedures. Our purpose was to evaluate the frequency of these incidents and the

relevance measured by new infarcts in primarily not affected vessel territories.

#### MATERIALS & METHODS

We retrospectively analyzed all cases of mechanical thrombectomy performed in our department for treatment of acute ischemic stroke. To find a valuable measure for the frequency of thrombus loss during retraction of the device we selected cases with isolated M1 occlusion, present A1 segment on the affected side and absent signs of anterior cerebral artery (ACA) emboli on the initial angiographic run. Images of the primary and last run of the intervention were carefully assessed for signs of any distal vessel occlusion in the middle cerebral artery (MCA) territory and new occlusions in ACA vessels. Since the clinical relevance of these new occlusions is hard to assess due to predominance of clinical symptoms caused by the MCA infarct we used demarcation of new ischemic areas in the ACA territory on follow-up imaging as a surrogate parameter.

#### RESULTS

We analyzed 90 consecutive mechanical thrombectomy procedures for isolated M1 occlusion. Eleven patients with an absent or significantly hypoplastic ipsilateral A1 segment were excluded from the analysis. In the remaining 79 cases successful recanalization (TICI 3 and 2b) of the M1 segment was achieved in 92.4% (n = 73). In the final angiographic run distal MCA branch occlusions persisted in 54 patients (68.4%). Within the MCA territory we were unable to undoubtedly distinguish between procedure-induced and preexistent emboli. New vessel occlusions in the ACA territory were observed in 11 cases (13.9%). One patient received an additional thrombectomy in the ACA to restore flow. Follow-up imaging was done by CT in 48 patients, the remaining 25 MRI was performed. New infarcts in the territory of the ACA were detectable in four patients (5%).

#### CONCLUSION

Peripheral embolism due to loss of thrombus material during mechanical thrombectomy occurs in 13.9% of cases leading to new infarcts in 5%. Although it is unlikely that the overall clinical benefit of patients receiving mechanical recanalization is significantly hampered by this side effect, efforts should be taken to improve devices and techniques to reduce the frequency of thrombus loss.

**KEY WORDS:** Thrombectomy, stroke, embolism

O-573

1:40 PM - 1:48 PM

#### Acute Histologic Changes Observed in Swine Arteries Treated with a Mechanical Thrombectomy Device

Yuki, I.<sup>1</sup>Kan, I.<sup>1</sup>Golshan, A.<sup>1</sup>Vinters MD, H. V.<sup>1</sup>Kim, R. H.<sup>1</sup>Yin, N.<sup>1</sup>Duckwiler, G.<sup>1</sup>Vinuela, F. A.<sup>1</sup>Murayama, Y.<sup>2</sup>Vinuela, F.<sup>1</sup>

<sup>1</sup>University of California Los Angeles, Los Angeles, CA,

<sup>2</sup>Jikei Medical School of Medicine, Tokyo, JAPAN

#### PURPOSE

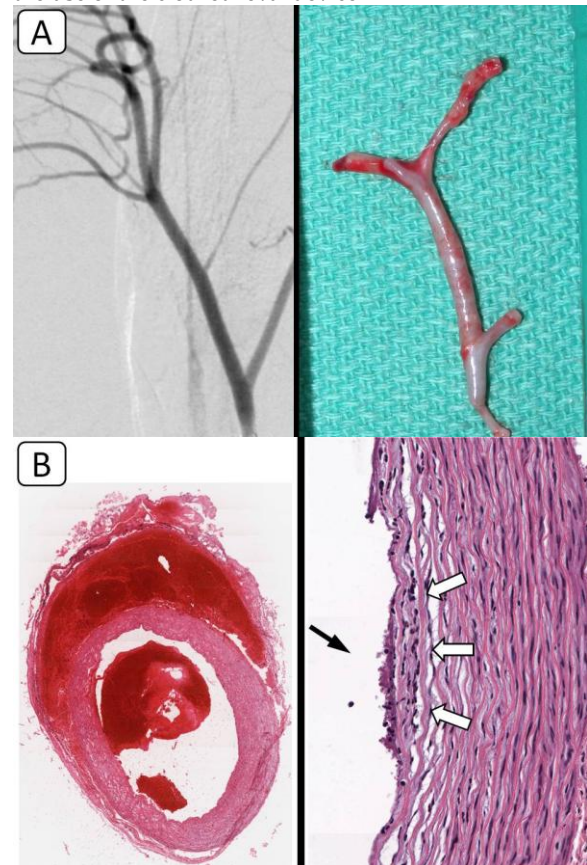
To evaluate acute arterial histologic changes induced by mechanical thrombectomy using a dedicated swine stroke model.

#### MATERIALS & METHODS

A total of eight superficial cervical arteries (SCAs) in four swine were occluded with experimental thrombus and treated using the Merci Clot Retrieval System®. Each treated artery was harvested immediately after the procedure and histologic analysis of each arterial sample was performed. Four untreated SCAs were used as controls.

#### RESULTS

A total of 24 attempts at clot retrieval were made. The average number of retrieval attempts per artery was three. Circumferential intimal denudation and separation of smooth muscle layers in the tunica media were seen in all samples. The intimal denudation was seen regardless of the number of retrieval attempts. A minor sub-intimal dissection was seen in one artery. Arterial perforation with sub-adventitial hematoma was seen in two arteries and these findings were associated with microwire/microcatheter navigation rather than the use of the clot retrieval device.



#### CONCLUSION

Mild histologic changes including intimal denudation and separation of smooth muscle layers in tunica media were seen in every artery treated by mechanical thrombectomy. Two cases of subadventitial hematoma both were associated with microwire/catheter

navigation rather than the use of the clot retrieval device.

**O-574**

**1:48 PM - 1:56 PM**

**Prediction of Periprocedural Ischemic Complication in Carotid Artery Stenting with Filter Embolic Protection Device by Using MR Plaque Imaging: Comparison between Open Cell and Closed Cell Stent**

Takayama, K.<sup>1</sup>•Myouchin, K.<sup>1</sup>•Wada, T.<sup>2</sup>•Sakamoto, M.<sup>2</sup>•Taoka, T.<sup>2</sup>•Nakagawa, H.<sup>2</sup>•Kichikawa, K.<sup>2</sup>•Kurokawa, S.<sup>1</sup>

<sup>1</sup>Ishinkai Yao General Hospital, Yao, Osaka, JAPAN,

<sup>2</sup>Nara Medical University, Kashihara, Nara, JAPAN

**PURPOSE**

Our purpose is to investigate the feasibility of magnetic resonance (MR) plaque imaging to predict the high risk lesion for ischemic complication during carotid artery stenting (CAS) using filter embolic protection device (EPD) and evaluate the difference between open cell stent (Precise) and close cell stent (Carotid Wallstent).

**MATERIALS & METHODS**

One hundred thirty-six carotid artery stenotic lesions in 129 patients before CAS (116 male and 13 female; mean age, 72.4 years) were evaluated by MR plaque imaging with black blood T1-weighted images. The population consisted of 45.6 % symptomatic stenosis more than 50% at the common or internal carotid artery, and 54.4% asymptomatic stenosis more than 80% stenosis. All CAS procedures were performed by standard procedure using two types filter EPD and stent [Angioguard XP/Precise (A/P): 75, Filter wire EZ/Carotid Wallstent (F/W): 61]. Main plaque components were classified into unstable plaque (intraplaque hemorrhage and lipid-rich/necrotic core) and stable (fibrous tissue and dense calcification) from the signal pattern. Development of new ischemic lesions on diffusion-weighted imaging (DWI) was assessed within 48 hours after CAS. We made statistical assessment on the plaque classification and the number of new ischemic lesions.

**RESULTS**

Technical success with the CAS procedures was achieved in 136 (100%) of 136 procedures. Ipsilateral new ischemic lesions were observed in 23 (32.4%) in A/P group (unstable plaques 36%) and in 11 (18.1%) in F/W group (unstable plaques 47.5%). Ipsilateral multiple ischemic lesions (>10) were observed in five (6.7%) in A/P group and in two (3.3%) in F/W group. In seven patients with multiple ischemic lesions, four showed minor strokes, two showed TIA, and one was asymptomatic. New ischemic lesions except multiple ischemic lesions were all asymptomatic. There was no significant difference between unstable and stable plaque about the presence of new ischemic lesion in both groups. However in A/P group, multiple ischemic lesions occurred significantly ( $P < 0.01$ ) more frequently in patients with unstable plaque, but in F/W group did not occur significantly.

**CONCLUSION**

Presence of unstable carotid plaques showed a higher risk of ischemic complication of CAS using open cell stent, but there were no significant complications in using close cell stent.

**KEY WORDS:** Carotid artery stenting, filter protection device, MR plaque imaging

**O-575**

**1:56 PM - 2:04 PM**

**Evaluation of an Intravenous-Endovascular Strategy in Patients with Acute Proximal Middle Cerebral Artery Occlusion**

Vendrell, J.•Mernes, R.•Nagot, N.•Milhaud, D.•Lobotesis, K.•Costalat, V.•Machi, P.•Maldonado, I. L.•Riquelme, C.•Arquiza, C.•Bonafe, A.

Gui de Chauliac Hospital

Montpellier, FRANCE

**PURPOSE**

Intravenous thrombolysis (IVT) administered in acute ischemic stroke provides low recanalization rates in proximal intracranial occlusions, with consequently poor clinical outcome. The purpose of this study was to assess the safety and efficacy of an intravenous-endovascular strategy (IES) using mechanical thrombectomy in cases of IVT failure for patients presenting with acute middle cerebral artery (MCA) occlusion.

**MATERIALS & METHODS**

From January 2007 to September 2010, all patients presenting with an acute MCA occlusion within 4.5 hours and an NIHSS score between 8 to 25 were eligible. All of them were methodically selected by using magnetic resonance imaging. Intravenous thrombolysis contraindication, diffusion-weighted imaging (DWI) - ASPECT score <5, and associated occlusion in another intracranial arterial territory were the main exclusion criteria. From September 2009 to September 2010, following a review of our stroke management, mechanical thrombectomy using the Solitaire FR® device was performed systematically if there was an NIHSS improvement  $\leq 4$  points 1 hour after IVT (IES group). Results in terms of clinical outcome were compared to those from an historic standard IVT series from January 2007 to August 2009 (IVT group) by using NIHSS at 24 hours and mRS score at 3 months. A mRS score ranging from 0 to 2 was considered as a favorable clinical result.

**RESULTS**

Alteplase was administered in 123 patients with proximal intracranial occlusion. Among them, 56 had a confirmed MCA occlusion, 32 were included in the IVT group and 24 in the IES group. At baseline, patient characteristics were similar between the two groups although NIHSS score was slightly worse in the IES group (15.2 vs 13.3,  $p = 0.25$ ). At 24 hours, the mean NIHSS improvement was 8.0 points in the IES group and 2.8 points in the IVT group ( $p = 0.001$ ). At 3 months, 17/22 (77%) patients from the IES group and 15/30

(50%) from the IVT group had a mRS  $\leq 2$ . After adjustment for initial NIHSS, DWI - ASPECT score and diabetes, IES was strongly associated with favorable clinical outcome (mRS  $\leq 2$ ) at 3 months (77% vs 50%, adjOR = 11.9, 95%CI:1.6-89.1,  $p < 0.02$ ). No symptomatic intracranial hemorrhage was observed during the two periods.

#### CONCLUSION

IES using systematic mechanical thrombectomy after IVT failure seems to safely improve the clinical outcome at 3 months and could represent an interesting alternative in the management of patients with acute ischemic stroke due to MCA occlusion.

**KEY WORDS:** Acute stroke, MCA occlusion, thrombectomy

**O-576**

**2:04 PM - 2:12 PM**

#### Comparison of Stroke Intervention Modalities: Mechanical Thrombectomy Devices

Soltanolkotabi, M.<sup>1</sup>Habib, A.<sup>1</sup>Sozzer, A. R.<sup>2</sup>Shaibani, A.<sup>1</sup>Hurley, M. C.<sup>1</sup>Miller, J. W.<sup>1</sup>Bendok, B. R.<sup>1</sup>Ansari, S. A.<sup>1</sup>

<sup>1</sup>Northwestern University Feinberg School of Medicine, Chicago, IL, <sup>2</sup>Midwestern University, Downers Grove, IL

#### PURPOSE

Stroke is the third leading cause of death in the United States. Intraarterial thrombolysis or mechanical thrombectomy has shown promising results in the treatment of hyperacute stroke, but there is no current class 1 evidence. Both the MERCI and Penumbra thrombectomy devices have demonstrated near equivalence in single arm trials with respect to the NINDS IV tPA trial, with the benefit of an extended time window for intervention. However, these devices have yet to be juxtaposed to address superiority or sequence of device utilization in a critical time period for intervention. We compared the safety and efficacy of the MERCI and Penumbra devices in the management of hyperacute ischemic stroke patients.

#### MATERIALS & METHODS

We retrospectively reviewed a consecutive series of hyperacute ischemic stroke interventions that underwent mechanical thrombectomy with the MERCI and/or Penumbra devices between January 2008 and March 2011. Patient demographics, technical outcomes, complications (ICH-ECASS classification), and clinical outcomes (30 day-NIHSS and 90 day-mRS scores) were recorded. Recanalization success was defined with respect to TIC1 reperfusion scale scores  $\geq 2a$ . Statistical analysis was performed to study categorical and numerical data using the  $\chi^2$  and one-way ANOVA tests.

#### RESULTS

Seventy endovascular stroke interventions were treated with MERCI (n = 27), Penumbra (n = 30), or combination of MERCI/Penumbra (n = 13) thrombectomy devices. Subgroups matched in terms of age, gender, and baseline NIHSS. Thromboembolic

occlusions were predominantly anterior circulation strokes (95%) with baseline TIC1 scores of 0/1. Both MERCI and Penumbra devices were not found to be statistically different in terms of successful recanalization, complications, patient outcome, or mortality. We noted a nonstatistical trend toward more successful recanalization rates with the MERCI device. However, the increased utilization of IA tPA with the MERCI device could have contributed to higher recanalization success. There were no device-related procedural complications. Symptomatic ICH at 24-48 hours postprocedure was noted in five (7.1%) of the 70 cases. The overall mortality rate was six of 70 (8.6%). Device crossover was attempted in difficult cases, where one device fails to recanalize the vessel, and may have contributed to the lower recanalization rates in the MERCI/Penumbra subgroup. All five operators were inclined to use the Penumbra device in the last 28/32 single device cases due to subjectively lower recanalization times, superior handling or ease of use; however, no objective data for recanalization times was available for comparison due to retrospective limitations.

Characteristic	MERCI (n=27)	Penumbra (n=30)	MERCI/Penumbra (n=13)	P Value
Mean Age (yrs.)	73.2	73.6	72.7	0.9
Mean NIHSS Baseline	17.5	18.0	20.9	0.4
Mean NIHSS Discharge	9.4	8.6	12.8	0.2
Mean NIHSS 30days	6.9	5.1	9.3	0.3
Mean IA tPA Dose (mg/procedure)	9.6	4.6	5.4	<0.05
Recanalization	22.2%(n=6)	33.3%(n=10)	46.2%(n=6)	0.4
TIC1 2a	33.3%(n=9)	23.3%(n=7)	7.7%(n=1)	0.3
TIC1 2b			15.4%(n=2)	0.5
TIC1 3	37.0%(n=10)	33.3%(n=10)	69.2%	0.07
TIC1 $\geq 2a$	92.6%	90.0%		
Device Related Complications	0	0	0	N/A
Symptomatic ICH Rate	7.4% (n=2)	3.3% (n=1)	15.4% (n=2)	0.3
mRS $\leq 2$ 90 days	66.7% (n=18)	64.3% (n=18)	40.0% (n=4)	0.5
Mortality Rate	3.7% (n=1)	10% (n=3)	15% (n=2)	0.6

#### CONCLUSION

In our single center experience of mechanical thrombectomy devices, we noted no statistical difference in the safety or technical/clinical efficacy of the MERCI or Penumbra systems. Subjective superiority or operator preference may lead to a specific sequence of device utilization, but both devices can be complementary and device crossover may be required to achieve recanalization success in recalcitrant cases.



**KEY WORDS:** Acute ischemic stroke, mechanical thrombectomy

**O-577**

**2:12 PM - 2:20 PM**

### Degree of Clot-Related Susceptibility Artifact is an Independent Risk Factor for Parenchymal Hematoma following Mechanical Thrombectomy

Franceschi, A. M.·Chaudhry, Z. A.·Kamalian, S.·Yoo, A. J.·Hirsch, J. A.·Schwamm, L. H.·Lev, M. H.

Massachusetts General Hospital  
Boston, MA

#### PURPOSE

We observed that in several cases of embolectomy-treated acute stroke patients complicated by parenchymal hematoma (PH), there was marked susceptibility change ("blooming artifact") on admission gradient-echo MRI sequences surrounding the occlusive thrombus. We sought to determine if this imaging feature was associated with hemorrhagic risk.

#### MATERIALS & METHODS

We identified 89 consecutive embolectomy-treated patients who had admission susceptibility-weighted MRI sequences (50 MPGR, 26 perfusion-GRE and 13 low-B) and follow-up imaging. Parenchymal hematoma was defined as PH1 or PH2 per ECASS criteria. A "susceptibility ratio score" (SRS) was determined by dividing the maximum width of the blooming artifact of the involved vessel ( $n = 67$  proximal-MCA, 13 ICA/MCA, and 10-terminal ICA) by that of the corresponding segment of the contralateral uninvolved vessel. Patients were stratified according to SRS  $<2$  (Group 1), 2-4 (Group 2), or  $>4$  (Group 3). Univariate and multivariate analyses were performed to test the association between SRS scores and PH on posttreatment follow-up imaging.

#### RESULTS

Mean age was  $67.6 \pm 17.4$  years, and median NIHSS score was 16 (IQR 14-20). The mean SRS was  $2.8 \pm 1.2$ . Using ECASS criteria, no hemorrhages were seen in 46 (50.5%); HI1 in 26 (28.6%); HI2 in 10 (11.0%); PH1 in 3 (3.4%); and PH2 in 4 (4.5%). The PH rate was 0% (0/22) for Group 1, 5.8% (3/50) for Group 2, and 24% (4/17) for Group 3 ( $p = 0.02$ , two-tailed Fishers Exact Test). Adjusting for age, NIHSS score, TICI reperfusion, and IV tPA pretreatment, ordinal SRS was an independent predictor of parenchymal hematoma (O.R. 8.50, 95% C.I.: 1.5-47.7;  $p = 0.01$ ). There was an interaction between ordinal SRS and IV tPA such that IV tPA prior to embolectomy resulted in a higher rate of PH in the SRS  $>4$  group (30% vs 2.6%).

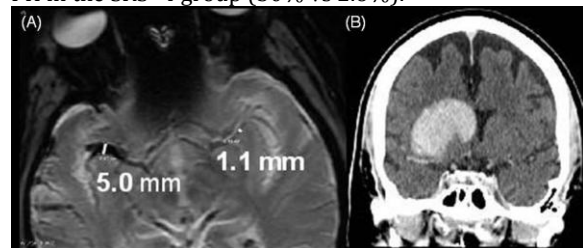


Figure 1A. Sample measurement for calculation of SRS from MPGR image (SRS = 4.5; high risk, Group 3).

Figure 1B. CT scan post mechanical thrombectomy demonstrates acute development of PH bleed.

#### CONCLUSION

An easy to calculate "susceptibility ratio score" appears to be associated with development of parenchymal hematoma in acute stroke patients treated with mechanical thrombectomy, with low risk (SRS  $<2$ , 0% hematoma incidence) and high risk (SRS  $>4$ , 24% hematoma incidence) groups. For the high risk group, PH was more likely in those with IV tPA pretreatment. We speculate that this imaging sign may be a biomarker for occlusive thrombus burden and/or the degree of baseline vessel wall injury surrounding the occlusive clot. Replication of this novel observation in independent cohorts is needed.

**KEY WORDS:** MR imaging susceptibility artifact, mechanical thrombectomy, parenchymal hematoma

**O-578**

**2:20 PM - 2:28 PM**

### Degree of Clot Enhancement on Admission CT Predicts Revascularization Efficacy in Acute Ischemic Stroke: An Investigation of 90 Patients

Mohtakhar, P.·English, J. D.·Dowd, C. F.·Higashida, R.·Halbach, V. V.·Hets, S. W.

University of California San Francisco  
San Francisco, CA

#### PURPOSE

Thrombi in the setting of acute ischemic stroke have been classified in pathology studies as "red clots" (erythrocyte rich) versus "white clots" (platelet/fibrin rich). Current strategies in lysing these clots include pharmacologic agents and mechanical devices. Despite these treatment options, thrombolysis fails in a significant portion of patients and may lead to hemorrhagic complications. Insight into clot composition may allow improved triage of patients to the appropriate treatment. The purpose of the study was to investigate whether the lysability of thrombi in acute ischemic stroke can be predicted by measuring the Hounsfield (HU) on the admission nonenhanced CT (NECT), postcontrast-enhanced CT (CECT) and CTA.

#### MATERIALS & METHODS

We studied 90 patients with acute anterior and posterior circulation large vessel ischemic strokes treated at our institution with IV tPA, IA tPA, and/or mechanical thrombectomy devices (Merci). The HU of the clot was measured on NECT, CECT and CTA. The HU of the homologous contralateral cerebral artery also was measured for standardization purposes. The obtained HU was corrected for hematocrit by using an accepted correction formula  $HU_{clot}/HU_{contralateral}$ . The volume of the clot was calculated using the formula for a cylinder with an elliptical base ( $\pi \times R \times r \times h$ ). Recanalization was assessed by TICI grade (0-3).

## RESULTS

There is a strong correlation between the HU of the thrombus on preintervention NECT and postintervention TICI grade among all patients regardless of pharmacologic or mechanical treatment (Table 1). Patients with TICI $\geq$ 2 demonstrated higher HU on NECT compared to patients with TICI $<$ 2 among all treatment modalities. On CECT and CTA, patients with higher TICI scores tended to have a higher HU; however, this did not reach statistical significance. There was no correlation between clot volume and lysisability.

Table 1.

	IV TPA patients (N=45)	p-value	IA TPA patients (N=43)	p-value	MERC1+TPA patients (N=77)	p-value
Correlation HU & TICI on NECT	0.69	<0.0001	0.72	<0.0001	0.73	<0.0001
Mean corrected HU on NECT for TICI $\geq$ 2	1.58	0.01	1.66	0.006	1.7	<0.0001
Mean corrected HU on NECT for TICI <2	1.39		1.40		1.3	
Correlation HU & TICI on CECT	0.02	0.44	0.09	0.28	0.09	0.21
Mean HU on CECT for TICI $\geq$ 2	55 $\pm$ 24.8	0.37	55 $\pm$ 24.5	0.12	51 $\pm$ 22.3	0.12
Mean HU on CECT for TICI <2	52 $\pm$ 14.2		45 $\pm$ 19.1		45 $\pm$ 13	
Correlation HU & TICI on CTA	0.13	0.19	0.18	0.12	0.008	0.47
Mean HU on CTA for TICI $\geq$ 2	80 $\pm$ 29.7	0.54	77 $\pm$ 28.0	0.12	76 $\pm$ 29.9	0.37
Mean HU on CTA for TICI <2	75 $\pm$ 26.4		65 $\pm$ 28.5		78 $\pm$ 26.9	
Thrombus volume mm <sup>3</sup> for TICI $\geq$ 2	139 $\pm$ 124	0.28	129 $\pm$ 115	0.44	124 $\pm$ 127	0.27
Thrombus volume mm <sup>3</sup> for TICI <2	106 $\pm$ 92		121 $\pm$ 90		153 $\pm$ 228	

HU=Hounsfield Unit  
TICI=Thrombolysis in Cerebral Infarction  
NECT=Non-enhanced CT  
CECT=Post-contrast enhanced CT  
CTA=CT angiogram

## CONCLUSION

Thrombi with lower HU on NECT appear to be more resistant to pharmacologic and mechanical thrombectomy and likely represent "white clots." Conversely, thrombi with higher HU are less resistant to lysis and thrombectomy and likely represent "red clots." Measuring the HU of the thrombus on the admission NECT provides the stroke team with a rapid method to analyze the clot composition, a potentially useful discriminator in selecting the most appropriate reperfusion strategy for an individual patient.

**KEY WORDS:** Stroke, thrombolysis, clot composition

O-579

2:28 PM - 2:36 PM

## Relationship between Thrombus Density and Different Stroke Subtypes

Nielsen, J., van der Schaaf, I., Biessels, G., van Seeters, T., Horsch, A., Luitse, M., van der Graaf, Y., Kappelle, J., Mali, W., Velthuis, B.

University Medical Center Utrecht  
Utrecht, NETHERLANDS

## PURPOSE

To determine the relationship between thrombus density and different stroke subtypes in patients with acute ischemic stroke.

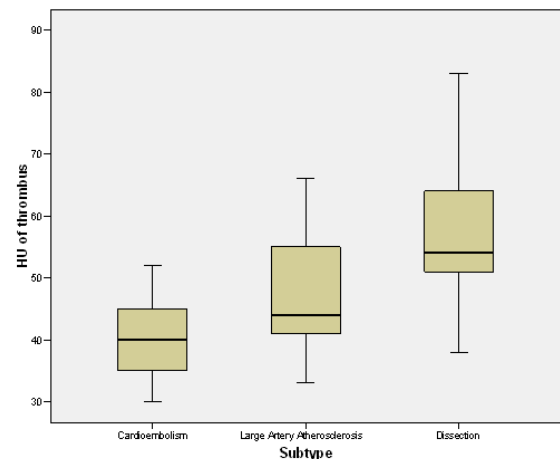
## MATERIALS & METHODS

We prospectively included 91 patients with acute ischemic anterior circulation stroke who had a visible occlusion on CT angiography that was presumed to be

caused by cardioembolism (n = 35), large artery atherosclerosis (n = 39) or dissection (n = 17). All patients underwent native CT, CT perfusion and CT angiography on admission within 9 hours after stroke onset. Presence or absence of a dense vessel sign in the middle cerebral artery or internal carotid artery was assessed on native CT and thrombus density was measured in Hounsfield Units on native CT. Subsequently, occurrence of dense vessel signs and thrombus density were related with stroke subtypes.

## RESULTS

The presence of dense vessel signs differed significantly among subtypes. Dense vessel sign was found in 46%, 59% and 94% of patients with cardioembolism, large artery atherosclerosis, and dissection respectively (X<sup>2</sup>-test; p = 0.002). The mean Hounsfield Units of the presumed thrombus location in all vessels was 39.9 (95%CI 37.9-42.0) in cardioembolism, 47.1 (95%CI 43.0-51.2) in large artery atherosclerosis and 57.0 (95%CI 51.9-62.1) in dissection (ANCOVA-test, p<0.0001). We found the same significant ranking order in the density of thrombi with dense vessel signs [mean Hounsfield Units: cardioembolism 43.3 (95%CI 40.0-46.5); large artery atherosclerosis 49.3 (95%CI 46.0-52.6); dissection 58.2 (95%CI 53.3-63.1), ANCOVA-test; p = 0.003].



## CONCLUSION

Thrombus density is related to stroke subtype and probably reflects different thrombus composition.

**KEY WORDS:** Stroke, CT perfusion, density

## Thursday Afternoon

**1:00 PM - 2:30 PM**

**Beekman/Sutton North**

**(66c) Interventional: New Devices  
& Techniques**

**O-580**

**1:00 PM - 1:08 PM**

### **Efficacy of a New Generation of Flow Disruption Device for Endovascular Treatment of Intracranial Aneurysms: Angiographic Results**

de Vries, J.<sup>1</sup>Wakhloo, A.<sup>2</sup>Lylyk, P.<sup>3</sup>Hartmann, M.<sup>4</sup>von Kummer, R.<sup>5</sup>Schumacher, M.<sup>6</sup>

<sup>1</sup>Radboud University Medical Center Nijmegen, Nijmegen, NETHERLANDS, <sup>2</sup>University of Massachusetts, Worcester, MA, <sup>3</sup>ENERI, Clínica Médica Belgrano, Buenos Aires, ARGENTINA, <sup>4</sup>University of Heidelberg, Heidelberg, GERMANY, <sup>5</sup>University of Technology, Dresden, GERMANY, <sup>6</sup>University of Freiburg, Freiburg im Breisgau, GERMANY

#### **PURPOSE**

Based on previous in vitro and in vivo experimental studies a new generation of flow disruption (FD) device (Surpass FD, Tel Aviv, Israel) was developed and evaluated for the treatment of intracranial aneurysms.

#### **MATERIALS & METHODS**

A total of 93 aneurysms in 77 patients were treated. To achieve the calculated flow disruption between the parent artery and aneurysm and required for an occlusion, single devices, tailored to local boundary conditions, were placed endovascularly in parent arteries and covering the aneurysm. Implanted devices measured 2.9-5.3 mm in diameter with a length of 10-80 mm. Immediate control angiography demonstrated various degrees of flow reduction within aneurysm up to a complete flow stagnation.

#### **RESULTS**

Up to 12-month follow-up angiography available in 55 patients showed a complete occlusion in 44 aneurysms, a 70-90% occlusion in seven, and a less than 50% occlusion in four. In this latter group the FD was placed over a previously implanted Wingspan stent in one patient. In two complex giant fusiform basilar aneurysms remodeling of the diseased segment was seen. All perforating arteries covered by the implant remained patent during the follow-up period.

#### **CONCLUSION**

Preliminary data demonstrate in treatment of complex aneurysms the efficacy of a new generation of FD device.

**KEY WORDS:** Flow diverter, aneurysm, intracranial

**O-581**

**1:08 PM - 1:16 PM**

### **Pipeline Retrospective European Multicenter Study**

Machi, P.<sup>1</sup>Piotin, M.<sup>2</sup>Moreno, A.<sup>3</sup>Boulanger, T.<sup>4</sup>Gascou, G.<sup>1</sup>Bonafé, A.<sup>1</sup>

<sup>1</sup>Chu Montpellier, Montpellier, FRANCE, <sup>2</sup>Fondation Rothschild, Paris, FRANCE, <sup>3</sup>Universidad de Murcia, Murcia, SPAIN, <sup>4</sup>Hopital S. Jean, Bruxelles, BELGIUM.

#### **PURPOSE**

In the endovascular treatment of cerebral aneurysms, the reconstruction of the parent artery with flow diverting devices is a recent technical advance. In the present study (PREMS study), we report and discuss a retrospective multicenter series of brain aneurysms treated with the Pipeline Embolization Device.

#### **MATERIALS & METHODS**

We retrospectively retrieved from four European centers clinical and radiologic data of all patients treated with the PED device for ruptured or unruptured cerebral aneurysms. Immediate and midterm morphologic results, as well as the incidence of neurologic adverse events was recorded and analyzed.

#### **RESULTS**

Between September 2008 and April 2011, 83 patients (24 men) harboring 86 aneurysms were included (average age 56 years). Seventy-eight of them were located in the anterior circulation. There were ten ruptured aneurysms. In 28 cases (32.5%) PEDs were used after a previous treatment fail. Five cases (5.8%) of postoperative major stroke were observed. A follow-up angiography, available for 68 patients, showed complete occlusion in 63 (92.6%). An in-stent stenosis of less than 50% of the artery diameter was identified in two cases (2.3%). The rate of permanent morbidity was 2.4% (two patients) and the mortality was 3.4% (three patients). The period of follow up ranged from 3 to 29 months (mean 10.3 months).

#### **CONCLUSION**

The management of cerebral aneurysms is feasible using PED. This device allows obtaining a very high rate of complete aneurysm occlusion. The morbidity and mortality rates seem to be similar to those previously reported with conventional endovascular techniques.

**KEY WORDS:** Flow diverters

**O-582**

**1:16 PM - 1:24 PM**

### **Noninvasive Assessment of Vasospasm following Aneurysmal Subarachnoid Hemorrhage Using C-Arm CT Perfusion Blood Volume Measurements in the Neurointerventional Suite**

Kamran, M.<sup>1</sup>Downer, J.<sup>1</sup>Deuerling-Zheng, Y.<sup>2</sup>Byrne, J. V.<sup>1</sup>

<sup>1</sup>University of Oxford, Oxford, UNITED KINGDOM, <sup>2</sup>Siemens AG Healthcare Sector, Forchheim, GERMANY

## PURPOSE

Digital subtraction angiography (DSA) is the current gold standard for detecting cerebral vasospasm - a major cause of morbidity following aneurysmal subarachnoid hemorrhage (SAH). Digital subtraction angiography, however, can reliably identify only the major vessel spasm and is unable to estimate its hemodynamic significance. To overcome these issues and to enable comprehensive noninvasive assessment of vasospasm inside the interventional suite, a novel protocol involving measurement of perfused blood volume (PBV) using C-arm angiographic systems was implemented.

## MATERIALS & METHODS

Twenty-five patients from the neurointensive treatment unit with suspected vasospasm following aneurysmal SAH were scanned using a biplane angiography system (Axiom Artis dBA; Siemens Healthcare, Germany). The imaging protocol included two 8-seconds rotational acquisitions, each comprising approximately 400 projection images at 0.50 steps. Perfused blood volume maps were constructed using dedicated prototype software (Siemens AG, Healthcare). Contemporaneous MR scan including a perfusion-weighted sequence (MR PWI) was obtained for comparison. For robust quantitative analysis, an automated approach using FSL (FMRIB Software Library) package with standardized cortical and subcortical regions of interest (ROIs) was used. Statistical agreement between the two modalities was explored using Bland-Altman test. Correct identification or exclusion of hemodynamically significant vasospasm was used as diagnostic endpoint to evaluate the utility of C-arm CT PBV in the management of vasospasm.

## RESULTS

Twenty-five patients (9 male, 16 female; mean age 53.1 years) underwent MR-PWI and C-arm CT scans performed within 12 hours of each other. Fisher CT grades were: 4 in 15, 3 in 7, and 2 in 3 patients; and WFNS scores were: 5 in 5, 4 in 11, 3 in 6, and 2 in 3 patients. Angiographic vasospasm was present in 19 patients, of whom 16 had hemodynamic abnormalities detectable on MR PWI images (criterion-standard). C-arm CT MIP reconstructions showed spastic vessels in 17 patients (sensitivity 89.5%). Hemodynamic abnormalities were correctly identified in all 16 patients with C-arm CT PBV maps. The two techniques correlated well in estimating the volume of tissue with perfusion abnormality  $p < 0.5$  ( $r = 0.91$ ). Bland Altman analysis of agreement for C-arm rPBV and MR-PWI rCBV showed: (a) 95% limits of agreement for cortical ROIs -1.2 to 1.1 and for subcortical ROIs -1.05 to 0.81 (b) bias in measurements for cortical ROIs -0.1 and for subcortical ROIs -0.12. Comparison of C-arm PBV with MR-PWI rCBF showed: (a) 95% limits of agreement for cortical ROIs -1.1 to 1.3 and for subcortical ROIs -0.73 to 0.49 (b) bias in measurements for cortical ROIs -0.1 and for subcortical ROIs -0.12. Limits of agreement for both comparisons included clinically significant rCBV and rCBF discrepancies.

## CONCLUSION

Our results demonstrate: (a) feasibility of C-arm CT PBV measurements for neuro-ITU patients with vasospasm following aneurysmal SAH and (b) C-arm PBV parameter carries weightings for both cerebral blood volume and cerebral blood flow. A comprehensive, single scan, noninvasive assessment of the vasospasm and its hemodynamic significance in an optimized interventional environment, improves the workflow by avoiding patient transfer between the diagnostic and the interventional set-ups. Implications exist for the use of technique in the management of acute ischemic stroke.

**KEY WORDS:** SAH, vasospasm, C-arm PBV

**O-583**

**1:24 PM - 1:32 PM**

## Treatment of Intracranial Atherosclerotic Stenoses with a Balloon-Expandable Paclitaxel Eluting Coronary Stent (Coroflex Please): Preliminary Results

Vajda, Z.<sup>1</sup>-Fischer, S.<sup>1</sup>-Schmid, E.<sup>2</sup>-Albes, G.<sup>1</sup>-Bäzner, H.<sup>2</sup>-Henkes, H.<sup>1</sup>

<sup>1</sup>Klinik für Neuroradiologie, Klinikum Stuttgart, D-70174 Stuttgart, GERMANY, <sup>2</sup>Klinik für Neurologie, Klinikum Stuttgart, D-70174 Stuttgart, GERMANY

## PURPOSE

Procedural safety and high rates of in-stent recurrent stenotic lesions (ISR) remain a concern in the endovascular treatment of intracranial atherosclerotic disease (ICAD). Here we present technical feasibility, safety and efficiency of the paclitaxel eluting balloon-expandable coronary stent Coroflex Please in the endovascular treatment of ICAD.

## MATERIALS & METHODS

Ninety-five patients (79 male; median age: 68 years) with 106 intracranial atherosclerotic stenotic lesions underwent endovascular treatment using Coroflex Please stents (B.Braun, Germany). Location and degree of target stenoses before and after treatment and at follow up and adverse clinical sequelae of treatment were registered. Postprocedural medication included 100 mg ASA and 75 mg clopidogrel for 1 year. Angiographic follow up was scheduled for 6, 12, 26 and 52 weeks after the treatment.

## RESULTS

Lesion locations were: ICA petrous ( $n = 44$ , 42%), ICA cavernous ( $n = 43$ , 41%), ICA supraclinoid ( $n = 4$ , 4%), intradural VA ( $n = 11$ , 10%) and BA ( $n = 4$ , 4%). Seven lesions could not be treated due to difficult anatomy and stent stiffness (7% technical failure rate). The combined postinterventional neurologic morbidity and mortality rate (stroke, ICH, SAH and CCF) was  $n = 4$  (3.7%) within and  $n = 1$  (0.9%) at and beyond 30 days, respectively. Angiographic and clinical follow-up examinations were obtained in 77 (78%) of the lesions (mean 12.5 months, maximum 46 months). Asymptomatic recurrent stenosis was seen in three out

of 77 (3.8%) lesions. There was one case of late stent thrombosis (0.9%).

#### CONCLUSION

Treatment of ICAD using drug-eluting coronary stents is safe and effective. Technical failure due to stent stiffness remains a problem. Application of the more flexible, newest generation thin-strut stents may overcome this problem.

**KEY WORDS:** Atherosclerotic stenosis, stent, angioplasty

**O-584**

**1:32 PM - 1:40 PM**

#### **Mechanical Thrombectomy with the Trevo Stent Device in Proximal Intracranial Arterial Occlusions of the Posterior Circulation**

Berkhemer, O. A.<sup>1</sup>·van den Berg, R.<sup>1</sup>·van der Kallen, B. F. W.<sup>2</sup>·Lycklama, G. J.<sup>2</sup>·van Zwam, W.<sup>3</sup>·Nederkoorn, P. J.<sup>1</sup>·Sprengers, M. E.<sup>1</sup>·Bot, J.<sup>1</sup>·Boiten, J.<sup>2</sup>·van Doorn, M. M.<sup>1</sup>·van Oostenbrugge, R. J.<sup>3</sup>·van der Lugt, A.<sup>4</sup>·Dippel, D.<sup>4</sup>·Roos, I.<sup>1</sup>·Majoie, C. B.<sup>1</sup>

<sup>1</sup>Academic Medical Center, Amsterdam, NETHERLANDS, <sup>2</sup>Medisch Centrum Haaglanden, The Hague, NETHERLANDS, <sup>3</sup>Maastricht University Medical Center, Maastricht, NETHERLANDS, <sup>4</sup>Erasmus Medical Center, Rotterdam, NETHERLANDS

#### PURPOSE

To evaluate the safety and effectiveness of a self-expanding and fully retrievable stent (Trevo; Concentric Medical Inc., Mountain View, CA, USA) in revascularization of patients with acute ischemic stroke.

#### MATERIALS & METHODS

Retrospective analysis of 16 consecutive patients (mean age 56 years; M:F = 13:3) with an acute ischemic stroke caused by a basilar artery occlusion treated with a fully retrievable stent within the first 13 hours from symptom onset [median National Institutes of Health Stroke Scale, 24 (range 8-32)]. Thrombectomy was used as rescue therapy in patients who failed (n = 6) or were ineligible (n = 10) for IV rtPA. Complications related to the procedure and outcome at 3-6 months were assessed.

#### RESULTS

Stent placement was feasible in all procedures and successful recanalization defined as TICI grade 2b or 3 was achieved in 12 of 16 treated vessels (75%). The mean number of passes for maximal recanalization was 2 (range 1-4). The median time from groin puncture to recanalization was 105 (26 - 180) minutes. No significant procedural event occurred. Twenty-five percent of all patients had a good outcome (mRS 0 to 2), none of the patients had a moderate outcome (mRS 3), and 75% a poor outcome (mRS 4 to 6).

#### CONCLUSION

These results suggest that the Trevo device can safely and effectively remove clots from basilar artery occlusions in acute ischemic stroke. The high

percentage of poor outcome was probably related to high NIHSS at presentation.

**KEY WORDS:** Thrombectomy, Trevo, acute ischemic stroke

**O-585**

**1:40 PM - 1:48 PM**

#### **Imaging Findings in MR-Guided Focused Ultrasound Treatment for Patients with Essential Tremor**

Wintermark, M.<sup>1</sup>·Druzgal, J.<sup>1</sup>·Huss, D. S.<sup>1</sup>·Khaled, M. A.<sup>1</sup>·Monteith, S.<sup>1</sup>·Loomba, J. J.<sup>1</sup>·Huerta, T.<sup>1</sup>·Kassell, N.<sup>1</sup>·Elias, W.

University of Virginia  
Charlottesville, VA

#### PURPOSE

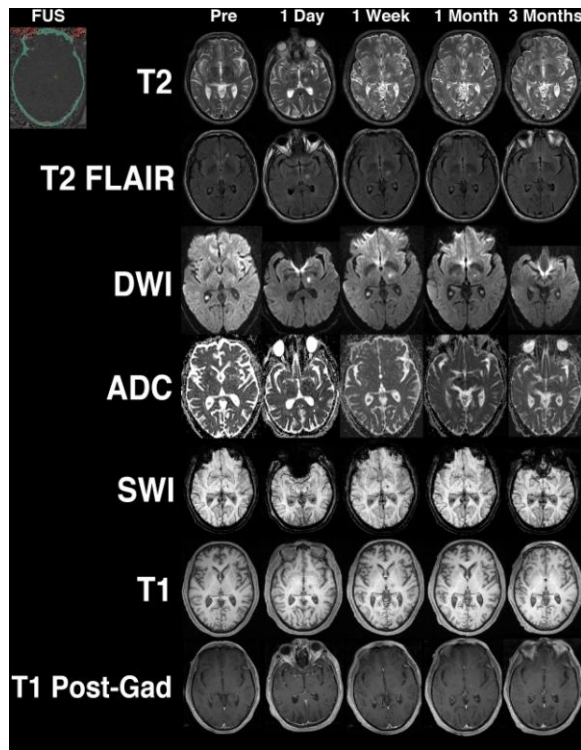
To describe findings on MR imaging postlesioning of the Vim nucleus of the thalamus by MR-guided focused ultrasound as treatment for essential tremor.

#### MATERIALS & METHODS

Ten patients with medication-refractory essential tremor were consented prospectively, enrolled in a single-site, FDA-approved pilot clinical trial and treated with MR-guided focused ultrasound targeting the VIM nucleus of the thalamus contralateral to the hand dominance side. The MR-guided focused ultrasound thalamotomies were performed in a clinical 3 T MR system (HD750; GE, Milwaukee, WI) using a clinical system for focused ultrasound surgery (ExAblate 4000; InSightec, Haifa, Israel) featuring a hemispheric 1,024-element phased array transducer operating at 650kHz. MR imaging studies were obtained on a 3 T scanner prior to the procedure, and 24 hours, 1 week, 1 month and 3 months following the procedure. The MRI protocol was the same at all five time points, and included the following sequences: sagittal MPRAGE; axial T1 SE; axial T2 TSE; axial FLAIR; axial SWI; axial and coronal DWI; axial T1 SE postcontrast. Imaging findings on the respective sequences were recorded, and evaluated as potential predictor of the change in CRST from prior to treatment to 3 months posttreatment.

#### RESULTS

Among the ten patients were nine males and one female, age: 66 ± 8 years. T2-weighted images showed three zones in the location of the target: a central relatively dark zone I, a bright T2 zone II delineated by a dark rim, and a surrounding zone III of edema. Zone III was maximum at 24 hours posttreatment and decreased afterwards. Diffusion-weighted imaging showed reduced ADC values at 24 hours and 1 week posttreatment, and normalization of the ADC values at 1 and 3 months. Enhancement at the target was typically observed at 1 month. A cavity was observed at 1 week and 1 month, and collapsed by 3 months. No macrohemorrhage was observed but microbleeds were visible at the target on SWI



#### CONCLUSION

MR-guided focused ultrasound is a new treatment modality for essential tremor and potentially for numerous other brain lesions. Typical imaging features are observed at specific time points after the treatment.

**KEY WORDS:** MR-guided focused ultrasound, essential tremor, MRI-guided treatment

0-586

1:48 PM - 1:56 PM

#### Quantitation of Neointimal Hyperplasia Using High-Resolution Contrast-Enhanced Cone-Beam CT for Follow-up Imaging of Intracranial Stenting

Mehra, M.·van der Bom, I. M. J.·Wakhloo, A. K.·Gounis, M. J.

University of Massachusetts  
Worcester, MA

#### PURPOSE

The gold-standard follow-up imaging modality of intracranial atherosclerotic disease (ICAD) treated with neurovascular stents is digital subtracted angiography. However, accurate assessment of the degree of restenosis requires an appropriate projection of the stented vessel in order to disclose the true lumen. Since the vessel path is tortuous and the neointimal hyperplasia (NH) is generally eccentric, restenosis may be under or overestimated using 2 dimensional (2D) techniques. Previous research has shown that by using a nonbinned reconstruction algorithm, contrast-enhanced cone-beam computed tomography (CE CBCT) data acquired with a small field of view enables visualization of stent and host vessel with great detail. Here we propose using 3D CE CBCT to quantitatively

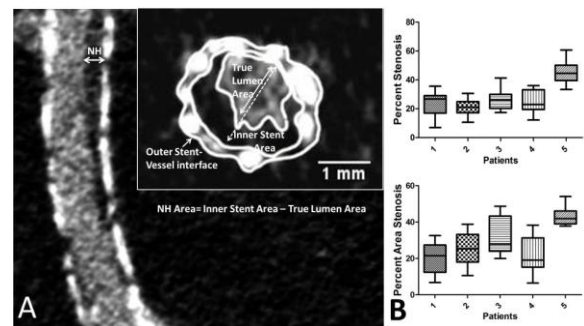
determine the restenosis in patients with neurovascular stents.

#### MATERIALS & METHODS

Contrast-enhanced CBCT data of five patients (mean age 65.6 years, 4 female) treated with intracranial stenting for ICAD acquired during follow-up angiography (mean follow up 5.6 months) were retrospectively analyzed for presence of NH. Cone-beam computed tomography data were acquired using a bi-plane angiographic C-arm system (FD20, Philips Healthcare, Best, The Netherlands) with a detector size of 22 cm and 20% iodinated contrast (iopamidol 51%, Isovue-250; Bracco Diagnostics, Princeton, NJ) injection of 3 ml/s for 23 seconds into the common carotid artery with a 2 second imaging delay. Data were reconstructed (512<sup>3</sup> matrix) using a nonbinned algorithm and were truncated as to only include the stented portion of the parent vessel. Morphometry was performed by calculating the outer stent vessel interface, inner stent and true lumen cross-sectional area respectively. Percent area stenosis (NH area/inner stent area \* 100) and the percent vessel stenosis  $\{[1 - (\text{True lumen diameter}/\text{Inner stent diameter})] * 100\}$  were the parameters analyzed. Vessel cross-sections were sampled every 0.5 mm along the length of the stent (Figure 1A, inset) using Image J software (NIH, Bethesda, MD).

#### RESULTS

The NH was visualized as the absence of contrast opacification within the inner stent cross-sectional area (Figure 1A). The percent area stenosis (mean  $\pm$  standard deviation;  $26.81 \pm 11.50\%$ ) and percent vessel diameter stenosis ( $26.64 \pm 10.74\%$ ) calculated for the five patients is illustrated (Figure 1B, box-whiskers plot).



#### CONCLUSION

Contrast-enhanced CBCT offers a promising technique for the visualization and standardized quantitative assessment of NH across the vessel cross-section. Our current ongoing research is to validate this technique by histomorphometry in preclinical models of NH

**KEY WORDS:** Intracranial atherosclerotic disease, cone-beam CT, intracranial stenting



O-587

1:56 PM - 2:04 PM

#### 4D Omni-Plane Fluoroscopy: Alleviating the Problem of Forbidden View Angles

Oberstar, E.<sup>1</sup>•Davis, B.<sup>1</sup>•Royalty, K.<sup>1</sup>•Kowarschik, M.<sup>2</sup>•Strother, C. M.<sup>1</sup>•Mistretta, C.<sup>1</sup>

<sup>1</sup>University of Wisconsin Madison, Madison, WI,

<sup>2</sup>Siemens Healthcare, Forchheim, GERMANY

##### PURPOSE

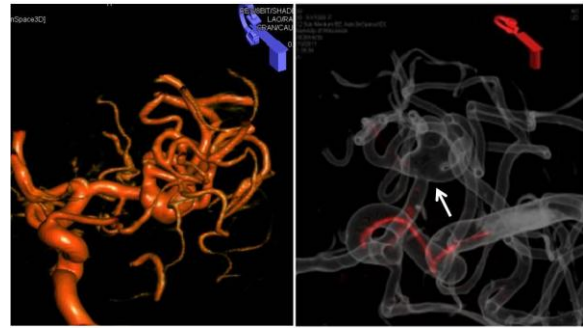
To develop a 4D interventional fluoroscopy mode that permits viewing of device placement from any desired view without gantry rotation.

##### MATERIALS & METHODS

A novel algorithm uses bi-plane fluoroscopy to generate virtual 4D fluoroscopic images of interventional device manipulations and then embeds these into a conventional 3D DSA acquired using a rotational C-arm acquisition. For each time frame, the two fluoroscopic views are backprojected into the 3D volume. The intersection in the 3D volume then defines the current position of the interventional device in 3D space. Once the two fluoroscopic images are embedded in the 3D volume the image can be rotated in arbitrary directions giving the operator the ability to view the devices in any desired projection without the need for a change in gantry position. The feasibility of this method has been shown using postprocessing of animal and human examinations using MATLAB. The technique currently is being implemented in GPU hardware to facilitate eventual real time fluoroscopic operation.

##### RESULTS

Below, the figure on the left shows the original 3D volume in the best working projection that was obtainable using conventional roadmap techniques. The user can rotate the reconstructed 3D volume to define an optimal working projection and, then embed the two fluoroscopic views. Then, the reconstructed 4D volume can be viewed showing virtual device manipulation in an optimal working projection. On the right is the virtual fluoroscopic view showing clearly, on this transparent surface rendering, the aneurysm ostium and adjacent branches (arrow). Note that this view, as indicated by the red icon, is not accessible for traditional fluoroscopy due to mechanical C-arm joint kinematics. This technique has been developed in conjunction with our recent work on 4D DSA that provides a new dimension to traditional DSA by generating time series of 3D volumes rather than 2D images.



##### CONCLUSION

4D fluoroscopy should provide a new degree of flexibility in interventional procedures and, by eliminating the need to use suboptimal working projections also increase the safety and efficacy of many procedures. In combination with 4D DSA there are also significant opportunities for x-ray and contrast dose reduction.

**KEY WORDS:** Roadmap, angiography, image-guided interventions

O-588

2:04 PM - 2:12 PM

#### Use of Onyx and Coils for Occluding Direct Type of Carotid Cavernous Fistulas via the Arterial Route

Prasad, C. R, A. H. •Sabbharwal, P. S. •Saini, J.

National Institute of Mental Health and Neuro Sciences  
Bangalore, INDIA

##### PURPOSE

The authors conducted this study to determine if the liquid embolic agent, ethylene vinyl alcohol copolymer, Onyx, could be used in combination with detachable coils to achieve successful occlusion of direct type (Barrow type A) of carotid-cavernous fistulas through the arterial route.

##### MATERIALS & METHODS

We prospectively collected clinical data in all patients who underwent embolization of carotid-cavernous fistulas at our institution over a period of 1 year. Only patients with direct type of carotid-cavernous fistula (Barrow type A) were included in the study. The clinical parameters, extent of fistula, presence of cortical venous reflux, duration of fistula, viscosity of Onyx used, volume of Onyx used, number and type of coils used, extent of embolization and complications were recorded.

##### RESULTS

A total of 11 patients (7 men and 4 women aged between 17 to 48 years) with Barrow type A fistula underwent embolization with coils and Onyx. All patients had trauma as the etiology in our series and all had proptosis and ophthalmoplegia of varying degrees. Embolization was done through the arterial route in all cases. Complete obliteration of the fistula was achieved in all cases. In all patients only a single session of embolization was done. No neurologic complications occurred in any of the patients. All patients reported some relief of symptoms at varying intervals.

## CONCLUSION

The adjuvant use of the liquid embolic agent, Onyx, with detachable coils in direct type of carotid-cavernous fistulas through the arterial route is a safe and very effective method for embolization with complete occlusion of the fistula in a single session. To our best knowledge this is the first demonstration of use of Onyx with detachable coils in the treatment of direct type of carotid-cavernous fistulas through the arterial route.

**KEY WORDS:** Carotid cavernous fistula, Onyx, coils

**O-589**

**2:12 PM - 2:20 PM**

## Progress in 4D Digital Subtraction Angiography Implementation: Technical Aspects

Davis, B.<sup>1</sup>•Kowarschik, M.<sup>2</sup>•Royalty, K.<sup>3,1</sup>•Oberstar, E.<sup>1</sup>•Szczykutowicz, T.<sup>1</sup>•Mistretta, C.<sup>1</sup>•Strother, C.<sup>1</sup>

<sup>1</sup>University of Wisconsin Madison, Madison, WI, <sup>2</sup>Siemens HealthCare, Forchheim, GERMANY, <sup>3</sup>Siemens Medical Solutions, Madison, WI

## PURPOSE

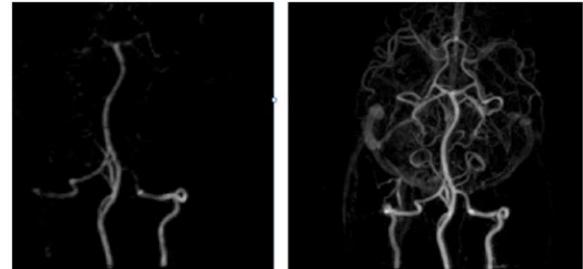
To report recent progress in the implementation of a 4D DSA method, implemented on rotational C-arm apparatus, that adds an additional dimension to the time series of 2D images provided by conventional DSA.

## MATERIALS & METHODS

4D DSA is a constrained reconstruction in which time-resolved 3D volumes are constructed following a single contrast injection. Since our previous reports, additional algorithmic modifications have been employed to reduce the effects of vessel overlap artifacts. Temporal information contained in the rotational projections is deposited in the reconstructed 3D volumes. Preinjection and postinjection projections are subjected to sub-pixel registration to correct for potential motion. The projections are convolved to enhance their SNR, and are backprojected into the rotational DSA constraining volume. The backprojected, temporally varying projection data essentially provide a weighting image that selects those components of the constraining image that are present in each time frame. In order to minimize overlap artifacts, backprojection is carried out at two or more angles. When multiple angles are used, the minimum voxel values obtained following the backprojections are assumed to result from nonoverlapping observations. Given the sparsity of angiographic data sets, this strategy works well. In principle all projections within the angular range that defines the temporal aperture can be used. Sinogram analysis and normalization of projections by the nonzero vascular voxel count also may be used to reduce overlap artifacts. For nonoverlapping vessels the temporal resolution corresponds to the acquisition rate of the projection images. When the minimum is acquired at a larger angle, then the frame duration is increased and the temporal resolution for that voxel is decreased. Worst case 4D DSA frame rates on the order of 4-5 per second should be possible.

## RESULTS

The Figure shows early and late MIPs through reconstructed 4D DSA time-frame volumes obtained after a vertebral artery injection. Successful examinations also have been obtained with intravenous injections. This reconstruction provides time-dependent frames with higher SNR than the acquired projections as well as the ability to fully rotate each time frame in arbitrary directions.



## CONCLUSION

4D DSA provides fully rotatable time of arrival analysis and is part of a diagnostic and interventional portfolio of algorithms that also enable 4D fluoroscopy, thus eliminating forbidden views in interventional procedures.

**KEY WORDS:** DSA, vascular disease, 3D DSA

**O-590**

**2:20 PM - 2:28 PM**

## Sphenopalatine Ganglion Alcohol Neurolysis under CT Guidance in the Management of Craniofacial Pain in 53 Procedures

Kastler, A.<sup>1</sup>•Aubry, S.<sup>2</sup>•Cadel, G.<sup>2</sup>•Kastler, B.<sup>2</sup>

<sup>1</sup>University Hospital, Clermont ferrand, FRANCE,

<sup>2</sup>University Hospital, Besancon, FRANCE

## PURPOSE

The sphenopalatine ganglion is involved in various facial pain syndromes such as cluster headaches, trigeminal neuralgia, local neoplastic compression mechanisms, atypical facial pain syndromes or myofascial pain of head and neck. The management of these facial pain syndromes can be challenging as the accurate diagnosis, especially in atypical facial pain syndromes, can be difficult to obtain due to repeated failure of conventional therapies. These last few years, a number of interventional minimally invasive techniques have been used to manage sphenopalatine-involved facial pain. We therefore propose an alternate to existing treatment of facial pain with alcohol neurolysis of the sphenopalatine (SPN) ganglion under CT guidance.

## MATERIALS & METHODS

Thirty-eight patients were included in this retrospective monocentric study between December 1995 and December 2010. A total of 53 sphenopalatine neurolysis (SPN) were performed at our Institution using absolute alcohol. The SPN was considered to be effective when pain relief was equal to or greater than 50% lasting for at least 1 week. The mean pain relief period following

the procedure for each patient was noted. In case of recurring pain, both duration and intensity of pain were noted. All procedures were realized ambulatory under local anesthesia. CT guidance was the rule.

## RESULTS

Mean duration of facial pain before procedure was 6.1 years. Thirty-six out of the 53 SPN (67.9%) procedures performed were successful. The overall mean duration of pain relief was 8.7 months after SPN procedure. In 27% of the successful cases no recurrence of pain occurred. In 26/36 successful SPN, recurring pain occurred with a mean duration of 5.4 months after initial procedure. Success rate of SPN depending of pain type are as follows: atypical facial pain: 85.7%; cluster headache: 83.3%, trigeminal neuralgia: 50%, compression by neoplasm: 100%, radiotherapy sequelae: 0%. Statistical analysis showed significant results ( $p < 0.05$ ) in favor of atypical pain and cluster headache. Complications encountered were as follows: short term: four local hematomas seen on control slices (7.5%), four transient hemipalate anesthesia (7.5%) and three pain increase after procedure (5.7%); long term: two cases of persisting hemipalate paresthesia (3.8%), two cases of persisting hemipalate anesthesia (3.8%). No epistaxis or lachrymal dryness were noted.

## CONCLUSION

CT-guided alcohol neurolysis of the sphenopalatine ganglion is a safe and effective treatment of refractory chronic craniofacial pain syndromes especially in cases of cluster headaches and atypical facial.

**KEY WORDS:** Sphenopalatine, neurolysis, pain

# Thursday Afternoon

**1:00 PM - 2:30 PM**  
**Sutton Center/South**

**(66d) Spine: New Techniques & Degenerative**

**0-591**

**1:00 PM - 1:08 PM**

**Back Pain Outcomes Using Longitudinal Data (BOLD) Project**

Jarvik, J. G.<sup>1</sup>Avins, A. L.<sup>2</sup>Bauer, Z.<sup>1</sup>Bresnahan, B. W.<sup>1</sup>Comstock, B. A.<sup>1</sup>Deyo, R. A.<sup>3</sup>Friedly, J.<sup>1</sup>Heagerty, P. J.<sup>1</sup>James, K. T.<sup>1</sup>Kessler, L. G.<sup>1</sup>Nedeljkovic, S. S.<sup>4</sup>Nerenz, D. R.<sup>5</sup>Sullivan, S. D.<sup>1</sup>Turner, J. A.<sup>1</sup>

<sup>1</sup>University of Washington, Seattle, WA, <sup>2</sup>Northern California Kaiser-Permanente and UCSF, Oakland, CA, <sup>3</sup>Oregon Health and Sciences University, Portland, OR, <sup>4</sup>Brigham and Women's Hospital, Boston, MA, <sup>5</sup>Henry Ford Health System, Detroit, MI

## PURPOSE

The back pain outcomes using longitudinal data (BOLD) project is an Agency for Healthcare Research and Quality (AHRQ)-funded, multicenter study focused on building the infrastructure to perform comparative effectiveness research in low back pain. The overall goal of this project is to establish a sustainable, rich registry to evaluate prospectively the effectiveness, safety, and cost-effectiveness of interventions for patients age 65 and older with low back pain. In addition to establishing the registry, we will conduct a prospective, observational cohort study comparing patients who do versus do not receive early imaging (within 6 weeks of presentation) in terms of disability, pain and health-related quality of life at 3, 6 and 12 months. Also part of the BOLD grant is a randomized, double-blind controlled trial comparing injections of epidural steroid with local anesthetic to local anesthetic injections alone for pain patients with spinal stenosis.

## MATERIALS & METHODS

We are enrolling registry participants from three geographically diverse health care organizations that are members of the HMO Research Network: Kaiser-Permanente Northern California, Henry Ford Health System in Detroit, and the Harvard Pilgrim/Harvard Vanguard System in Boston. Our goal is to enroll 5,000 patients aged 65 and older when they present to a primary health care provider for a new episode of care for back pain. We obtain patient-reported outcome measures at baseline and 3, 6 and 12 months. These include the Roland-Morris Disability Questionnaire (RMDQ), numerical rating scales (NRS) of average back pain and average leg pain in the last 7 days, the Brief Pain Inventory, the EuroQoL 5D, and a question about falls in the past 3 weeks. In addition, we will have access to extensive information available as part of the electronic medical record in the information systems at these HMO Research Network sites.

## RESULTS

As of 10/25/11, we have enrolled 1,136 patients into the BOLD registry. The most common primary ICD-9 diagnosis was lumbago ( $n = 518$ ), followed by back pain with radiation ( $n = 157$ ) and backache ( $n = 103$ ). Thirty percent (337) had pain for less than 1 month. The mean age is 74.4 (SD = 7.0) years; 66% (749) are female; 18% (199) are African-American; 54% (612) are married; 35% (388) have at least a college degree; 12% (138) are working full- or part-time; and 53% (598) have never smoked. Baseline values for the patient-reported outcome measures are summarized in the Table.

Baseline Values of Outcome Measures for BOLD Registry Participants	
Measure	Value (SD)
Roland-Morris Disability Questionnaire (RMDQ)	10.9 (6.3)
Back pain numerical rating scale (0-10NRS)*	3.6 (3.4)
Leg pain 0-10 NRS*	4.4 (3.0)
Brief Pain Inventory (BPI)- General activity	2.7 (2.8)
BPI- Mood	4.7 (3.2)
BPI- Walking	4.4 (3.1)
BPI- Work	1.9 (2.5)
BPI- Relations with others	3.5 (3.2)
BPI- Sleep	3.6 (3.0)
BPI- Enjoyment	1.7 (2.4)
PHQ-4**	0.73 (0.18)
EuroQoL 5D	8% (n=92)
Fell in last 3 weeks	10.9 (6.3)
*average pain in last 7 days**Patient Health Questionnaire for Depression and Anxiety (2 items each)	

## CONCLUSION

We have demonstrated the feasibility of assembling a large registry of seniors with back pain with expected enrollment of 5,000 patients by mid-2012. The first project for which we will use the registry is to investigate the effects of early imaging for seniors with back pain.

**O-592**

**1:08 PM - 1:16 PM**

## Model-Based Iterative Reconstruction (MBIR-VEO) Allows Further Dose Reductions for CT of the Spine with Higher Spatial Resolution and Reduced Noise over ASIR and FBP

Tanenbaum, L. N. • Pawha, P. • Delman, B.

Mount Sinai School of Medicine  
New York, NY

## PURPOSE

The relatively high radiation dose associated with CT of the spine is a concern. Adaptive statistical iterative reconstruction (ASIR) is a commercially available reconstruction technique that, compared to filtered back projection (FBP) methods typically used in CT, provides a reduction in image noise and improved low contrast detectability (LCD). MBIR-VEO is a new reconstruction technique that, compared to ASIR methods, provides an improvement in spatial resolution and further reduction in image noise allowing for even lower dose imaging with the same, or better, diagnostic value.

## MATERIALS & METHODS

Adaptive statistical iterative reconstruction techniques provide standard image quality at substantially lower radiation dose than traditional filtered back projections allow. Adaptive statistical iterative reconstruction leaves substantial information about the CT imaging chain untapped to permit rapid reconstruction times at the expense of quantum and system noise remaining in the image. Model-based iterative reconstruction techniques (MBIR-VEO) perform a more complex reconstruction, modeling system optics and statistics along with 3D three-point beam analysis. While reconstruction times are longer, with fewer assumptions image noise is reduced drastically and dose reductions of up to 75% over FBP can be accomplished. MBIR-VEO images were obtained at a 40% lower dose (higher noise index) than currently in use for ASIR studies at our institution. The dose employed for ASIR studies previously was reduced 40% from that traditionally used for FBP. Adaptive statistical iterative reconstruction and FBP images were reconstructed retrospectively for analysis from the dose-reduced raw data. A quantitative (noise) and qualitative comparison (spatial resolution, overall quality) of the clinical MBIR-VEO images was performed against the ASIR and FBP studies as well as against routine clinical expectations for CT of the spine. All examinations were performed on a clinical GE HD 750 scanner.

## RESULTS

Clinical spine CT images reconstructed with MBIR-VEO demonstrated better than expected edge definition, low contrast detectability and overall quality as compared with images reconstructed with ASIR or FBP. The dose-reduced source MBIR-VEO images showed significantly less noise than ASIR and FBP.

## CONCLUSION

Model-based iterative reconstruction image quality was equivalent or superior to ASIR and FBP utilizing a clinical reduced dose protocol (40% dose reduction compared to ASIR). Model-based iterative reconstruction images were visually sharper and contained less noise than those with ASIR or FBP.

**KEY WORDS:** Iterative reconstruction, model based, radiation dose, CT

**O-593**

**1:16 PM - 1:24 PM**

## Applicability of Diffusion Tensor Imaging in the Assessment of Degeneration of the Lumbar Intervertebral Disks

Puig Alcantara, J.<sup>1</sup> • Blasco, G.<sup>1</sup> • Daunis-i-Estadella, J.<sup>2</sup> • Molina, X.<sup>1</sup> • Guergue, C.<sup>1</sup> • Motos, N.<sup>1</sup> • Pedraza, S.<sup>1</sup>

<sup>1</sup>Hospital Universitari Dr Josep Trueta, Girona, SPAIN,

<sup>2</sup>Universitat de Girona, Girona, SPAIN

## PURPOSE

Degeneration of the lumbar intervertebral disks (LIVD) is highly prevalent in adults and contributes to pain syndromes. Qualitative differentiation between the

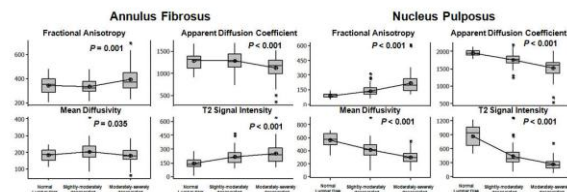
nucleus pulposus and annulus fibrosus on T2-weighted imaging, based on water content, has been used to assess LIVD degeneration. We investigated whether quantitative assessment using diffusion tensor imaging (DTI) metrics of LIVD correlates with visual grading of degeneration on T2-weighted imaging.

#### MATERIALS & METHODS

One hundred seventy-eight consecutive patients (82 women; age,  $46 \pm 15$  years) with low back pain underwent 1.5 T MRI including sagittal and axial T1- and T2-weighted FSE and DTI sequences acquired in 12 directions. All imaging analyzes focused on the L4-L5 LIVD. Quantitative evaluations of the annulus fibrosus and nucleus pulposus were based on fractional anisotropy (FA) values, mean diffusivity (MD), apparent diffusion coefficient (ADC), and T2 signal intensity (SI) on coregistered maps using multiple regions of interest. The qualitative assessment categorized disks as normal (hyperintense), slightly-moderately degenerated (intermediate signal), and moderately-severely degenerated (hypointense) on T2-weighted images. Bulging and herniated disks also were recorded.

#### RESULTS

Sixty-two (34.8%) disks had normal T2-SI; 44 (27.7%) were bulging and 41 (23%) were herniated. Lower FA values on the annulus fibrosus correlated strongly with degenerative LIVD (Student's  $t$ -test = 3.14;  $p = 0.011$ ). Mean FA values tended to decrease significantly with degeneration (normal > bulging > herniated disks) ( $p = 0.004$ ). Increased mean FA (Fisher test = 6.34;  $p = 0.002$ ), decreased mean ADC (Fisher test = 8.55;  $p = 0.001$ ), decreased median MD (Kruskal-Wallis test = 6.76;  $p = 0.021$ ), and decreased median T2-SI (Kruskal-Wallis test = 24.21;  $p < 0.001$ ) on the nucleus pulposus correlated significantly with degenerative LIVD.



#### CONCLUSION

Diffusion tensor imaging-metrics evaluation seems able to characterize LIVD degeneration. Quantitative imaging techniques like DTI-metrics may help clinicians and researchers understand the development and clinical course of degenerative disk disease.

**KEY WORDS:** Degenerative, diffusion tensor imaging, MR imaging

O-594

1:24 PM - 1:32 PM

#### Physiology-Based Quantitative Assessment of Cerebrospinal Fluid Flow with Valsalva Maneuver in Normal Subjects

Bhadelia, R. A.<sup>1</sup>Madan, N.<sup>2</sup>Zhao, Y.<sup>3</sup>Butler, J.<sup>4</sup>Heilman, C.<sup>2</sup>Patz, S.<sup>1</sup>

<sup>1</sup>Beth Israel Deaconess Medical Center, Chestnut Hill, MA, <sup>2</sup>Tufts Medical Center, Boston, MA, <sup>3</sup>Phillips Medical Systems, Boston, MA, <sup>4</sup>Brigham and Women's Hospital, Boston, MA

#### PURPOSE

Our overall goal is to develop a MRI method to assess cerebrospinal fluid (CSF) flow obstruction in patients with Chiari I malformation (CMI). The purpose of this preliminary study was to quantitatively measure CSF flow pulsations in response to a physiologic challenge, the Valsalva maneuver in normal subjects.

#### MATERIALS & METHODS

Using parallel imaging, the acquisition time of routine cine phase-contrast (cine PC) was decreased from several minutes to <15s. The measured flow waveform was validated by comparing with the input waveform on a programmable MRI compatible pump. In eight normal subjects, CSF flow pulsations were assessed at the foramen magnum at rest and during and immediately after a controlled Valsalva maneuver. Cerebrospinal fluid oscillatory flow volume (CSF OFV = sum of absolute volumes of CSF systolic and diastolic flows) and flow waveform amplitudes (CSF Amp) were determined.

#### RESULTS

The measured flow was in very good agreement with the programmed pump flow using fast cine-PC (within 5%). During Valsalva, CSF OFV decreased from  $1.13 \pm 0.22$  ml to  $0.77 \pm 0.11$  ml ( $p < 0.002$ ) and CSF AMP decreased from  $4.51 \pm 2.69$  ml/s to  $3.69 \pm 2.14$  ml/s ( $p = 0.03$ ). Immediately after Valsalva, CSF OFV increased to  $1.32 \pm 0.18$  ml ( $p = 0.001$ ) and CSF Amp increased to  $5.13 \pm 2.68$  ml/s ( $p = 0.004$ ) compared to Valsalva period.

#### CONCLUSION

Using ultrafast MRI, it is feasible to quantitatively assess dynamic changes in CSF flow in response to physiologic challenges. The observed changes in CSF flow pulsations are similar to those reported by Williams using CSF pressure measurements. This method potentially can be used to assess CSF flow obstruction in patients with CMI at the foramen magnum.

**KEY WORDS:** CSF flow, MR imaging, physiology

**O-595****1:32 PM - 1:40 PM****Diagnostic Impact of Gadolinium in the Postoperative Lumbar Spine**

Mahady, K. F. Menon, N. Rankine, J. Warren, D.

Leeds Teaching Hospitals NHS Trust, UK  
Leeds, UNITED KINGDOM**PURPOSE**

Differentiating postoperative fibrosis and recurrent disk herniation after discectomy is important to clinical management, with revision surgery being of proven benefit in recurrent disk herniation and potentially detrimental in fibrosis.

The role of gadolinium-enhanced MRI in distinguishing recurrent disk herniation from fibrosis in the postoperative lumbar spine has become controversial. Advances in MRI technology have led to images of greater resolution allowing the diagnosis of recurrent disk protrusion based on anatomical and morphologic characteristics present on unenhanced sequences. The aim of this study is to investigate the diagnostic impact and continuing role of gadolinium in light of these technologic advances.

**MATERIALS & METHODS**

Patients with clinical features of a recurrent disk protrusion following discectomy were identified. All patients were imaged at 1.5 T and had received gadolinium routinely as part of our institution's imaging protocol (axial and sagittal T1, T2, and T1 with gadolinium). Patients who were within 6 weeks of the discectomy procedure were excluded. The images without gadolinium were reviewed retrospectively by an experienced consultant radiologist. The presence of a disk protrusion or fibrosis and the degree of confidence for each was assessed at the operated level. Cases where it was considered gadolinium may be of diagnostic benefit were identified. On a separate occasion the images with the gadolinium sequences were analyzed using the same criteria.

**RESULTS**

Fifty-one patients were examined. Gadolinium made no change to the diagnosis in 35/51 (69%). Of these cases 30 had a definite disk protrusion and five were normal. In six of 51 (12%) gadolinium improved the diagnostic confidence, but did not change the diagnosis: a mixed picture of disk herniation and fibrosis was demonstrated on the unenhanced sequences. In 10/51 (20%) gadolinium-enhanced sequences changed the diagnosis. Of these seven patients had a diagnosis of disk protrusion on the unenhanced sequences changed to fibrosis. In one patient a diagnosis of fibrosis was changed to disk herniation. In two patients the size of the disk was downgraded and the unexpected presence of fibrosis demonstrated. In six of 51 (12%) the diagnosis was unclear on unenhanced sequences and these were identified as cases where gadolinium may be of diagnostic benefit. The postgadolinium imaging improved the diagnostic confidence in four of six of these cases but did not change the diagnosis. In two of

six the diagnosis was changed from a disk protrusion to fibrosis.

**CONCLUSION**

Gadolinium is useful in distinguishing recurrent or residual disk herniation from postoperative fibrosis. Although gadolinium did not affect the diagnosis in 69% of patients, 20% (10/51) patients would have been given an incorrect diagnosis if gadolinium had not been administered routinely. If gadolinium had only been given to the 12% of cases where it was thought likely to be beneficial following assessment of the unenhanced scans, eight of 51 (16%) would have received the wrong diagnosis. Fibrosis extending into the disk/annulus can mimic recurrent disk protrusion and in the absence of gadolinium-enhanced MRI, revision surgery may have been considered inappropriately.

**KEY WORDS:** Postoperative, lumbar spine, MR imaging**O-596****1:40 PM - 1:48 PM****In vivo Quantification of T1 Rho within Lumbar Spine Disk Spaces at 3.0 T with Parallel Transmission: Preliminary Findings**Filippi, C. G.<sup>1</sup> Nickerson, J. P.<sup>1</sup> Watts, R.<sup>1</sup> Gonyea, J. V.<sup>1</sup> Hipko, S. G.<sup>1</sup> Andrews, T.<sup>2</sup><sup>1</sup>University of Vermont College of Medicine, Burlington, VT, <sup>2</sup>Philips Health Care, Cleveland, OH**PURPOSE**

MR imaging with T1rho contrast is an emerging imaging modality that has been shown to correlate with glycosaminoglycan content within the disk space in vitro. Studies at 1.5 T have shown a correlation between T1rho values and disk degeneration. The purpose of this study was to quantify T1rho values in a small cohort of asymptomatic young individuals compared to an asymptomatic group of older patients and to qualitatively compare T1rho images to standard sagittal T2 images in the lumbar spine at 3.0 T.

**MATERIALS & METHODS**

Seven healthy volunteers (4 male, 3 female; age range: 27-34 years, mean age: 28.5 years) and five older, healthy volunteers (5 male, no female, age range 41-54 years, mean age: 47.5 years) were scanned using a Philips 3 T Parallel Transmission MR system (Philips Healthcare, Best, Netherlands). A sagittal T2W turbo spin echo (TSE) scan was performed with the following parameters: TE/TR = 2800/110ms, flip = 90 deg, FOV = 240x240 mm, thickness = 3 mm, 18 slices, matrix = 480 x 480. For the T1rho acquisition, a sagittal 3D gradient echo sequence was repeated with five spin lock times (TSL): TR/TE = 3.35/1.76 ms, flip = 10 deg, 240 x 240 mm, thickness = 3mm, 18 slices, matrix = 160 x 160, TSL (spin lock times) = 1/25/50/75/100 ms, spin lock frequency = 350 Hz. For quantitative analysis, on sagittal images, an ROI was placed centrally within L3/L4, L4/L5, and L5/S1 disk spaces on TSL = 100 msec images. Average and standard deviations for the T1rho values were determined and student t-test was performed for statistical analysis. Images were



qualitatively assessed by two neuroradiologists, and interobserver variability determined with Kappa statistic.

## RESULTS

At L3/L4: T1rho values for younger volunteers 145.4 +/- 37.8 (range 107.6-183.2). At L4/L5: T1rho values for younger volunteers 136.3 +/- 30.8 (range 105.5-167.1). At L5/S1: T1rho values for younger volunteers 144.7 +/- 28.1 (range 116.6-172.8). At L3/L4: T1rho values for older volunteers 70.1 +/- 20.1 (range 50.0-90.2). At L4/L5: T1rho values for older volunteers 99.1 +/- 24.8 (range 74.3-123.9). At L5/S1: T1rho values for older volunteers 65.4 +/- 28.1 (range 54.1-77.7). T1rho values were lower at all disk space levels in older volunteers which was statistically significant at L3/L4 ( $P < .025$ ) and L5/S1 ( $P < .01$ ) but not at L4/L5. Qualitatively, disk desiccation or loss of signal was seen equally well with both T1rho and T2 images. Kappa statistic was greater than 0.75 for excellent interobserver agreement.

## CONCLUSION

T1rho quantitative values can be obtained using parallel transmission MR at 3.0 T, and values were significantly lower at L3/L4 and L5/S1 disk spaces in older, healthy volunteers whose disk spaces demonstrated greater desiccation on both standard T2W TSE and T1rho imaging. This lends support to the potential development of T1rho contrast as a quantitative, in vivo, bioimaging marker of disk degeneration.

**KEY WORDS:** T1 Rho imaging, lumbar spine MR, disk degeneration

O-597

1:48 PM - 1:56 PM

## Measurement of Blood Perfusion in Spinal Metastases with Dynamic Contrast-Enhanced MR Imaging: Evaluation of Tumor Response to Radiation Therapy

Chu, S. Karimi, S. Peck, K. K. Yamada, Y. Lis, E. Lyo, J. Bilsky, M. Holodny, A. I.

Memorial Sloan-Kettering Cancer Center  
New York, NY

## PURPOSE

We use dynamic contrast-enhanced MRI (DCE MRI) before and after radiation therapy (RT) to investigate the correlation between perfusion parameters and changes on conventional MRI.

## MATERIALS & METHODS

Fifteen patients with 19 known spinal metastases underwent DCE MRI before and after RT. Treated lesions were classified as treatment successes ( $n = 17$ ) and failures ( $n = 2$ ). Perfusion parameters including plasma volume ( $V_p$ ), permeability ( $K_{trans}$ ), area under the curve (AUC), and peak enhancement (PE) were measured. Percent change in parameter values was calculated for each tumor. Outflow hemodynamics were assessed qualitatively based on the morphologies of the

signal intensity (SI) time curves in 13 pre and 13 posttreatment scans.

## RESULTS

Plasma volume was the strongest predictor of treatment response. All successfully treated lesions showed a decrease in  $V_p$ , and the two cases of tumor progression both showed drastic increases in  $V_p$ . The false-positive rate of  $\Delta V_p$  as a predictor was  $9.38 \times 10^{-9}$  and the false-negative rate was 0.055. Changes in AUC and PE demonstrated similar relationships to the observed treatment response, but had higher false-positive and false-negative rates. No significant trends were found in  $K_{trans}$ . Signal intensity curves from successfully treated lesions had characteristic "untreated" and "treated" patterns in 11 pre and 8 posttreatment scans, respectively.

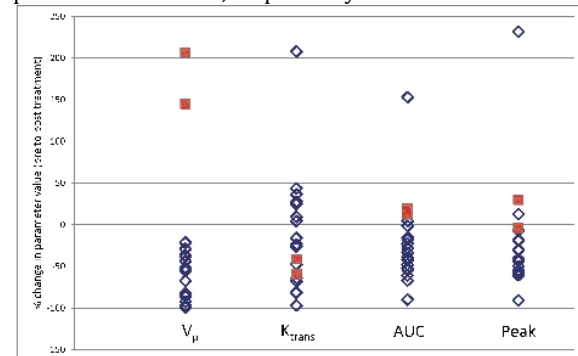


Figure 1

Scatter plot showing percent change of each parameter. 1 outlier from each of  $\Delta K_{trans}$ ,  $\Delta AUC$ , and  $\Delta PE$  (seen in the scatter plot as the datapoints with % change > 150%) was removed prior to statistical analysis.  $\Delta V_p$ ,  $\Delta AUC$ , and  $\Delta PE$  showed significant differences in means between treatment successes and failures ( $p = 1.49 \times 10^{-9}$  for  $\Delta V_p$ ,  $p = 0.006$  for  $\Delta AUC$  and  $p = 0.007$  for  $\Delta PE$ ).  $\Delta K_{trans}$  showed no significant difference in means between treatment successes and failures.

◆ = successful treatment  
■ = treatment failure

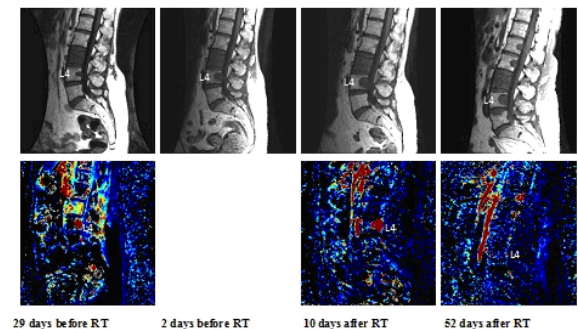


Figure 2

Case of leiomyosarcoma metastasis to the spine. The tumor in L4 is observed to progress between the 1<sup>st</sup> and 2<sup>nd</sup> pre-treatment scans on T1-weighted imaging (upper row). No changes in tumor size are apparent on the T1 images on either the 1<sup>st</sup> or 2<sup>nd</sup> post-treatment scans.  $V_p$  on the other hand (lower row), decreased from 7.30 on the scan 29 days before RT to 3.27 on the scan 10 days after RT (55.12% decrease). On the scan 52 days after RT, a visible reduction on the  $V_p$  heatmap can be seen in the region of L4.  $V_p$  on this day was 0.45 (93.83% decrease from the original pre-treatment scan). Perfusion data was not acquired with the pre-treatment scan 2 days before RT.

## CONCLUSION

Changes in perfusion, particularly  $V_p$ , reflects tumor responses to RT in bone metastases. Perfusion parameters measured early after treatment appear to predict positive outcomes earlier than tumor contraction on structural imaging. The ability of DCE MRI to detect early treatment response has potential to improve patient care and outcome.

**KEY WORDS:** Dynamic contrast-enhanced MR imaging, spine metastases, radiation therapy

**O-598**

**1:56 PM - 2:04 PM**

**Improved MR Conspicuity of Fat Composition in Vertebral Lesions by Using Iterative Decomposition of Water and Fat with Echo Asymmetric and Least-Squares Estimation Compared to T1-Weighted Spin Echo at 1.5 and 3 T**

Vachha, B. A.·Sarkar, S.·Greenman, R.·Hackney, D.

Beth Israel Deaconess Medical Center  
Boston, MA

**PURPOSE**

Iterative decomposition of water and fat with echo asymmetric and least-squares estimation (IDEAL) has been shown to effectively suppress fat and this has been used to replace short tau inversion recovery (STIR) imaging for detecting vertebral body lesions. However, the role of IDEAL imaging in characterizing fat composition has been overlooked. We evaluated IDEAL fat images for depiction of vertebral body lesions, as compared to conventional T1-weighted spin-echo (SE) images.

**MATERIALS & METHODS**

Twenty patients referred for spine MRI for a variety of indications underwent 2D FSE imaging with asymmetrically timed 3-point echo detection optimized at 1.5 T and 3 T. In addition to conventional T1-weighted spin-echo images, IDEAL images were acquired with an intermediate T2-weighting at 1.5 T: TR/TE = 3500/70 ms and a high T2-weighting at 3 T: TR/TE = 3500/100 ms. Thirty-two lesions distributed within the cervical, thoracic and lumbar vertebrae were identified. Contrast characteristics of the lesions were obtained by computing signal ratios for each of the lesions compared to background fat in adjacent vertebrae (Lesion: Background signal ratio) within the fat-selective IDEAL and the T1-weighted SE image slices. A comparison was made of signal intensity in the depot fat posterior to the spine to the cerebrospinal fluid within thecal sac (Fat: Water ratio) to assess overall contrast between fat and water.

**RESULTS**

Ten of 32 lesions demonstrated lesion: background signal ratios < 1, suggesting less fat content within the lesion compared to the background fat in the adjacent vertebra, or "fat-depleted" lesions. The remaining 22 lesions were noted to have signal ratios > 1, suggesting higher fat content within the lesion compared to background, or "fat-accumulating" lesions. Mean signal ratios for fat-depleted lesions were 0.64 (SD 0.15) on T1-weighted images, and 0.31 (SD 0.32) on IDEAL fat images. The difference was significant by two-tailed t-test;  $p < 0.05$ . For fat-accumulating lesions, the results were 1.46 (0.21) for T1-weighted and 1.93 (0.58) for IDEAL;  $p < 0.05$ . Fat-selective IDEAL images showed significantly higher fat-water contrast of 70.23 (SD 32.11) than conventional T1 images 14.34 (SD 5.35);  $p < 0.001$ .

**CONCLUSION**

At both field strengths, the IDEAL fat images demonstrated significantly higher contrast between vertebral lesions and adjacent vertebral bodies than conventional T1-weighted SE images. This implies that IDEAL fat images may be more sensitive in detecting vertebral body lesions. We are currently expanding the application of IDEAL fat images for characterizing a larger set of vertebral abnormalities, but clinical observation has confirmed the objective impression of greater conspicuity compared to conventional T1-weighted technique. We note that the parameters of the IDEAL acquisition used for this study are T2-weighted and the contrast we observe is based on the fat/water chemical shift, rather than T1 differences. Thus, although the quantitative contrast ratios may change with different parameters, our results suggest that the advantage of IDEAL fat images over conventional T1 may be robust to the timing parameters.

**KEY WORDS:** Spine lesions, MR imaging, IDEAL

**O-599**

**2:04 PM - 2:12 PM**

**Intramedullary Contrast Enhancement in Cervical Compressive Myelopathy**

Galheigo, D.<sup>1</sup>·Raz, E.<sup>1</sup>·Cruz, L. H.<sup>2</sup>·George, A.<sup>1</sup>·Goodgold, A.<sup>1</sup>·Fatterpekar, G. M.<sup>1</sup>

<sup>1</sup>New York University School of Medicine, New York, NY,  
<sup>2</sup>CDPI - Clínica de Diagnóstico por Imagem, Rio de Janeiro, BRAZIL

**PURPOSE**

Intramedullary spinal cord enhancement typically is associated with tumors, infections, inflammatory disease conditions, and vascular malformations. It has only been described uncommonly in patients with compressive myelopathy. The purpose of our study is to illustrate the characteristic imaging appearance of intramedullary enhancement in patients with such compressive myelopathy.

**MATERIALS & METHODS**

We retrospectively reviewed MR imaging findings in six cases of cervical compressive myelopathy. Specifically, we evaluated the intramedullary enhancement with respect to the involved "compressive" disk level, the number of vertebral segments involved, its relationship to the T2-signal abnormality, and its enhancement pattern.

**RESULTS**

The intramedullary cord enhancement was seen at or below the level of the involved disk, and was less than one vertebral segment in length. It was less than the T2-signal abnormality, especially in its caudal extent. Typically a striated (corduroy) pattern of enhancement was seen on the sagittal postcontrast images. Diffuse shaggy enhancement was seen on the axial images sparing only a thin rim of the peripheral aspect of the cord. There was no cystic lesion, hemorrhage or enhancing nodule seen in any of these patients.



### CONCLUSION

The presence of enhancement in the spinal cord reflects breakdown of the blood-spinal cord barrier. It can be seen uncommonly in patients with compressive myelopathy related to degenerative disk disease, and is thought to be related to venous congestion. It is therefore critical to recognize the characteristic imaging appearance of such compressive myelopathy so as to distinguish it from other causes of intramedullary enhancement, helping in appropriate patient management.

**KEY WORDS:** Compressive myelopathy, intramedullary enhancement, MR imaging

**O-600**

**2:12 PM - 2:20 PM**

### Diffusion Tensor MR Imaging of the Cervical Spinal Cord in Patients with Multisegmental Cervical Spinal Canal Stenosis: Preliminary Results

Lutz, J.·Lummel, N.·Brückmann, H.·Wesemann, T.·Linn, J.

University Hospital of Munich (LMU) Grosshadern  
Munich, GERMANY

### PURPOSE

Aim of the study was to preoperatively evaluate microstructural tissue changes of the cervical spine in patients with symptomatic multisegmental stenosis due to cervical spondylosis using diffusion tensor imaging (DTI) in comparison to conventional MRI to assess the leading stenosis.

### MATERIALS & METHODS

Ten patients with symptomatic cervical spondylosis (mean age 55.4 years) at different levels were examined prior to surgical decompression using a 3.0 T MR scanner (Signa HDx, GE, USA). We used an axial single shot DTI EPI sequence along 15 different diffusion directions with a b-value of 700 s/mm<sup>2</sup> and a slice thickness of 2 mm, ranging from C1-C7. For anatomical correlation, a 2 mm sagittal and axial T2-weighted sequence was acquired for coregistration with the functional DTI maps. Additionally, all patients underwent myelography. The fractional anisotropy (FA) and the apparent diffusion coefficient (ADC) were

studied. The DTI indices were correlated with surgical and clinical findings.

### RESULTS

The patients had lower FA at the symptomatic height, compared to control levels: C2-C3 and C6-C7. The ADC was elevated at the narrowed height but did not reach statistical significance. Fractional anisotropy values were directly correlated with increased signal intensity on T2-weighted sequences, however did not correlate either with FA or ADC.

### CONCLUSION

These findings suggest that DTI could allow the identification and quantification of anisotropic changes between normal cervical spine tissue and compressed areas. Additionally, the DTI indices could help to determine the leading stenosis equally as conventional MRI. Diffusion tensor imaging of the cervical spine is achievable for the delineation of the spondylosis, and can detect the leading area in patients with multisegmental cervical stenosis.

**KEY WORDS:** DTI, spinal canal stenosis, MR diffusion

**O-601**

**2:20 PM - 2:28 PM**

### Oxaliplatin-Induced Neuropathy Can Be Demonstrated by Molecular Neurography: Proof-of-Principle in an Animal Model

Schellingerhout, D.·Bredow, S.·LeRoux, L.

M.D. Anderson Cancer Center  
Houston, TX

### PURPOSE

The purpose of our study was to utilize a new imaging technology, neurography, based on the retrograde transport of a molecular imaging agent, to determine if oxaliplatin neurotoxicity affects retrograde axonal transport.

### MATERIALS & METHODS

Female adult BALB/c mice (n = 8) were treated with oxaliplatin to a cumulative dose of 30 mg/kg by giving 10 divided intraperitoneal doses using 5 days of treatment, 5 days rest, 5 days treatment administration paradigm. Animals were imaged at baseline and weekly for 149 days after commencement of therapy. Control animals (n = 8 from 8 to 28 days, n = 4 from 35 to 65 days) were mock treated with saline and were imaged similarly out to 65 days. All animals received fluorescently labeled TTc-Alexa790 (15 ug in 20 uL) via intramuscular injection into the calf muscles at every imaging session. Fluorescent imaging (Xenogen IVIS 200) was used to image the distribution of TTc over 60 minutes, with ROI measurements taken from the thoracic spine to quantitate fluorescent uptake. Region of interest measurements had background activity subtracted, and were normalized to the signal intensity at time = 0.

## RESULTS

With sham treatment, TTF transport through the sciatic nerve and spinal cord causes the fluorescent signal intensity over the thoracic ROI to gradually increase (Figure, legend indicates number of days after start of study). At 60 minutes the grouped mean normalized fluorescence was 562% ( $\pm$  210% SD). With oxaliplatin treatment, transport is abruptly and severely impaired with baseline values of 836%  $\pm$  375% falling to 396%  $\pm$  140%, 247%  $\pm$  63%, 213%  $\pm$  58%, 162%  $\pm$  46%, 147%  $\pm$  63% with each successive week and stabilizing around 175% ( $\pm$  45%) for grouped means from 6 weeks out to the end of the study. The difference between normalized fluorescence grouped mean values from 6 weeks after oxaliplatin treatment to the end of study, and control animals is highly statistically significant (T-test  $p < 0.0001$ ).

## CONCLUSION

Oxaliplatin causes a rapid and apparently irreversible (to our current follow-up of 149 days) decrease of retrograde axonal transport in the sciatic nerves and spinal cord, as demonstrated with a neurographic molecular imaging agent.

**KEY WORDS:** Molecular imaging, neuropathy, chemotoxicity

**O-602**

**2:28 PM - 2:36 PM**

### Neurography: Imaging Neural Transport with a Molecular Probe

Schellingerhout, D. LeRoux, L. G. Bredow, S.

M.D. Anderson Cancer Center  
Houston, TX

## PURPOSE

To develop an agent for imaging retrograde axonal transport in nerve tissues based on the optical labeling of a nontoxic fragment of tetanus toxin.

## MATERIALS & METHODS

A His-tagged recombinant tetanus toxin fragment (TTF) was produced in *E. coli*, purified, and labeled with a variety of Alexa fluorophors for optical imaging studies. Gel electrophoresis (SDS-PAGE) and quantitative immunodetection studies were performed. Cell uptake studies were performed to assess in vitro efficacy. Labeled TTF was injected into the soleus muscle of C57bl and Balb/C mice, and Wistar rats, and imaging performed with the IVIS 200 (Xenogen). In situ validation was performed with laser scanning confocal microscope FV 1000 (Olympus) utilizing intact glycerol mounted samples, and cryosections.

## RESULTS

Gel electrophoresis and quantitative immunodetection indicated that the integrity and immune reactivity of the protein was preserved after labeling. Cell uptake assays indicated robust uptake in differentiated PC12 cells. In vivo optical imaging demonstrated the uptake of TTF-Alexa in the sciatic nerve and spinal cord. Progressive uptake and transport of the agent could be seen along

the course of the sciatic nerve and spinal cord. Confocal microscopy studies on intact excised nerve segments and cryosections confirmed the compound uptake in nerve fascicles of the sciatic nerve. Axonal nerve uptake and superficial lymphatic uptake were clearly distinguishable, and transport was shown to be nerve-specific. Immunohistochemistry on cord sections demonstrated the presence of the agent in spinal cord neurons.

## CONCLUSION

Fluorescently labeled TTF is taken up into motor nerve endings after intramuscular injection, and is retrogradely transported in nerve axons. This process can be demonstrated with noninvasive in vivo imaging, and allows nerve anatomy and function to be studied.

**KEY WORDS:** Molecular imaging, neurography, nerve imaging

## Thursday Afternoon

**1:00 PM - 2:30 PM**

**Murray Hill**

### (66e) Adult Brain: Functional Imaging II

**O-603**

**1:00 PM - 1:08 PM**

### Diffusion Tensor Imaging in Parkinson Disease

Gencturk, M. Anik, Y. Bozkurt, P. Demirci, A.

Kocaeli University School of Medicine  
Kocaeli, TURKEY

## PURPOSE

The aim of this study is to evaluate the role of diffusion tensor imaging (DTI) parameters in Parkinson disease.

## MATERIALS & METHODS

Twenty-four patients with Parkinson disease in several stages of the disease according to Hoehn and Yahr scale as the study group and 30 healthy volunteers as the control group were included in the study. Parkinson disease severity was measured with the Unified Parkinson Disease Rating Scale (UPDRS). All patients were examined via 3 T MR scanner. Fractional anisotropy (FA) and mean diffusivity (MD) measurements via DTI were obtained from substantia nigra, red nucleus and dentate nucleus. Findings were compared among both groups.

## RESULTS

Fractional anisotropy values of substantia nigra, red nucleus and dentate nucleus were significantly decreased ( $p = 0.02$ ,  $p = 0.030$  and  $p = 0.042$  respectively) and inversely MD values were significantly increased ( $p = 0.04$ ,  $p = 0.046$  and  $p =$

0.047) in Parkinson disease group compared with that of the control group. There were also correlations among FA and ADC values with UPDRS scores.

#### CONCLUSION

These findings provide evidence that DTI measurements of substantia nigra, red nucleus and dentate nucleus seem useful in Parkinson disease.

**KEY WORDS:** DTI, Parkinson

**O-604**

**1:08 PM - 1:16 PM**

#### Diffusion Tensor Tractography-Guided Deep Brain Stimulator Placement for Parkinson's Disease

Said, N.·Raghavan, P.·Elias, W. J.·Cupino, A.·Tustison, N. J.·Patrie, J.·Wintermark, M.

University of Virginia  
Charlottesville, VA.

#### PURPOSE

Deep brain stimulators (DBS) are used to treat Parkinson's disease. One of the accepted locations for placement of DBS leads is within the globus pallidus internus (GPi). Currently, positioning is assessed by placing a lead into the region of the GPi and performing intraoperative testing by turning on the DBS, increasing the stimulator voltage, and monitoring for a motor response. A motor response indicates proximity to the corticospinal tract (CST) thereby approximating position within the GPi. A voltage setting between two and four volts is ideal, indicating that the lead is in ideal proximity to the CST, therefore likely in an optimal location within the GPi. If a motor response occurs at a setting of less than two volts then the DBS lead is likely too close to the CST and it may need to be repositioned. Likewise if no motor response is elicited until the voltage is increased to greater than four volts, the lead may be too far from the CST and it may need to be repositioned. The purpose of this study is to retrospectively determine whether a correlation exists between intraoperative voltage test results for DBS lead placement and distance from the CST using diffusion tensor imaging (DTI) with tractography.

#### MATERIALS & METHODS

The study was approved by the institutional review board. We retrospectively reviewed pre and postoperative MRI studies and intraoperative test results in eight patients - 12 leads as four patients had bilateral DBS placement. Preoperative T1 images including DTI information were coregistered with the postoperative T1 MRI for each patient. Tractography of the CST was performed, and the shortest distance from each contact of each DBS lead to the CST was automatically calculated using software-based analysis. The distance measurements calculated for each contact were evaluated for linear regression with respect to the intraoperative voltage measurements which elicited a motor response at each contact.

#### RESULTS

Voltage measured at the different DBS contacts was  $4.54 \text{ V} \pm 2.54$ . Distance between the DBS contacts and the CST was  $3.84 \text{ mm} \pm 1.75$ . Linear regression analysis yielded a significant coefficient of 0.132 ( $p = 0.025$ ) with a correlation coefficient of 0.349.

#### CONCLUSION

A positive correlation between intraoperative test voltage and measured distance to the CST for DBS leads indicates that DTI of CST is reliable. In the future, one could envisage using DTI as a preoperative guidance tool to plan DBS lead approach and final position thereby limiting the need for repositioning.

**KEY WORDS:** Diffusion, tensor, tractography

**O-605**

**1:16 PM - 1:24 PM**

#### White Matter Abnormality in Parkinson Disease: Evaluation with Diffusion Tensor Imaging Using Tract-Based Spatial Statistics Study

Kim, S.·Kim, H.·Kim, N.·Choi, C.·Kim, H.·Lee, C.

University of Ulsan Asan Medical Center  
Seoul, KOREA, REPUBLIC OF

#### PURPOSE

Idiopathic Parkinson disease (PD) is a neurodegenerative disease primarily involving basal ganglia and midbrain. White matter abnormality in PD patients is not well known yet and conventional MR imaging is not sufficient to evaluate white matter changes in PD. Our purpose is to evaluate white matter abnormality on diffusion tensor MR imaging in patients with PD using tract-based spatial statistics (TBSS).

#### MATERIALS & METHODS

Diffusion tensor imaging (DTI) was obtained with a 3.0 T MR system in 74 patients [mean age  $62.9 \pm 9.2$  (SD)] with PD, and 74 age- and sex-matched normal control (NC) subjects [mean age  $62.4 \pm 9.5$  (SD)]. Patients were selected on the basis of clinical criteria. Patients with history of chronic hypertension, diabetes, stroke or head injury, or prominent high signal in the white matter on T2-weighted images were excluded from the study. Fractional anisotropy (FA) and mean diffusivity (MD) maps were generated using FDT in the FMRIB's Software Library (FSL) package and processed to perform tract-based comparisons of FA and MD between the two groups using TBSS in FSL. To address multiple comparison issue, this result is corrected for family-wise error using threshold-free cluster enhancement (TFCE) method across the white matter skeleton.

#### Results

There was a significant difference in MD between PD and NC groups. In PD group, there were wide-spread changes in MD in both cerebral hemispheres mainly involving frontal and parietal lobes, with sparse alterations in occipital lobes. There were changes in MD in corpus callosum, bilateral internal capsules, corona radiata, thalamic radiation, superior longitudinal fasciculus, cingulum and cerebral tectum of the brain in

PD patients compared to NC group. Involvement was more prominent in the left hemisphere than the right. There was no significant difference in FA map between PD and NC groups.

#### CONCLUSION

Diffusion tensor imaging with TBSS revealed wide spread abnormality of white matter in patients with PD compared to NC

**KEY WORDS:** Parkinson disease, diffusion tensor imaging, tract-based spatial statistics

**O-606**

**1:24 PM - 1:32 PM**

#### Systematic Analysis of Association White Matter Tracts of Language

Honce, J.-Ree, A.

University of Colorado Anschutz Medical Campus  
Aurora, CO

#### PURPOSE

The pathways that underlie language function are supported by a number of white matter tracts that are likely to go well beyond the traditionally held white matter connection between Broca's and Wernicke's areas, the arcuate fasciculus as a single undifferentiated pathway. As an anatomical investigation, this study uses diffusion tensor imaging (DTI) to systematically bring to light the greater diversity of potential white matter tracts, many of them novel, which might underlie language processing. Furthermore, the types of artifacts encountered in the parcellation of tracts are explored and classified. This latter purpose is not ancillary but integral to the careful anatomical interpretation of these parcellations and prerequisite along with the tracts themselves to approach a more comprehensive network model of language.

#### MATERIALS & METHODS

Seven healthy adult right-handed males gave written informed consent. Data was acquired on a GE 3.0 T MRI system (General Electric, Milwaukee, WI), using a DTI sequence, providing isotropic resolution (2.0 x 2.0 x 2.0 mm) and coverage of the whole head. The DTI was performed using 60 directions, b value of 1000, a 256 x 256 matrix and number of b0 volumes equal to one. The data were postprocessed with Diffusion ToolKit, using angle threshold of 35 degrees, and a Runge Kutta algorithm. The region of interest (ROI) analysis was carried out on TrackVis. Regions of interest were constructed to correspond with the white matter underlying gyri of the left cerebral hemisphere. The connectivities between the ROIs were documented as relates to anatomical course, regions of termination, and number of streamlines.

#### RESULTS

In this study we establish diverse connections between the ventrolateral frontal lobe and the temporal lobe gyri, incorporating tracts such as the extreme capsule, subcomponents of the superior longitudinal fasciculus (SLF), a cortical region called Geschwind's territory and

incorporate the tracts that underlie Glasser's superior temporal gyrus - middle temporal gyrus (STG-MTG) segmentation of the arcuate fasciculus as well as the tracts that underlie Catani's 3 part segmentation of the arcuate fasciculus. Five different types of artifacts were encountered that relate to tracts extending beyond cortical confines, conflation of adjacent tracts, premature terminations of tracts, artificial inflation of tract number between adjacent gyri, and artificial low tract numbers related to exclusion of tract extension artifacts.

#### CONCLUSION

We show that the connectivity in the left hemisphere as it subserves possible language networks is far more an elaborate system than currently proposed anatomical models. This elaboration of perisylvian pathways may help guide future gross anatomical validation studies and attempts at network models for language as well as other interrelated brain functions.

**KEY WORDS:** Language, diffusion tensor imaging, white matter tracts

**O-607**

**1:32 PM - 1:40 PM**

#### Investigation of Effective Connectivity between BA 22, 44 and 45 during Sentence Completion and Word Generation BOLD Functional MR Imaging

Nandiraju, D.<sup>1</sup>Mohamed, F. B.<sup>1</sup>Stefanatos, G.<sup>2</sup>Saad, M.<sup>3</sup>Conklin, C.<sup>1</sup>DiMarco, A.<sup>2</sup>Faro, S. H.<sup>1</sup>

<sup>1</sup>Temple University Hospital, Philadelphia, PA, <sup>2</sup>Temple University, Philadelphia, PA, <sup>3</sup>University of Alexandria, Alexandria, EGYPT

#### PURPOSE

To compare effective connectivity between BA-22, 44 and 45 during two clinically used fMRI tasks: Sentence completion (SC) and verb generation (VG).

#### MATERIALS & METHODS

Eight right-handed normal volunteers were scanned on a 3 T scanner using a 12-channel head coil. The visual stimulus was delivered through MRI compatible goggles. A block-design with 14 alternating blocks (7 Activity and 7 Control), TR 3 sec, eight TRs per block was used to collect BOLD images. The two commonly used clinical fMRI tasks, SC task with scrambled letters as a control and a VG task with a blank screen as a control was used. The data were analyzed using Statistical Parametric Map (SPM8) software. In every individual subject three regions of interest (ROI) pertaining to primary language (BA-22, 44 and 45) were identified and defined using Pick-atlas software. The effective connectivity between these three ROIs was calculated using dynamic causal modeling implemented in SPM8 (DCM-10). Based on the cognitive understanding of the two tasks eight different models were specified. All the models included left BA-22, 44 and 45 but varied in initial input and connections that were modulated during each task. Using Bayesian model selection (BMS), random effects analysis (REA) was performed and an optimal model was identified.



Next, parameter estimates from all subjects for the optimal model were entered into one sample t-test to test statistically whether the mechanisms represented by optimal model were expressed consistently across the subjects.

## RESULTS

Statistical parametric map analysis showed highest number of activated voxels in BA-22 and BA-45 during SC task and in BA-45 and BA-44 in VG task. In SC task, BMS showed that Model-1 was superior to other models (Figure-1a) and task-related modulatory influences showed a modest increase of 6% in connection strength from BA-22 to BA-45. During the VG task Model-3 was found to be superior compared to other alternative models (Figure-1b) and task-related modulatory influences resulted in increase of connection strength from BA-45 to BA-44 by 33%.

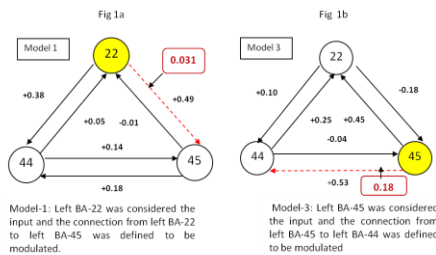


Figure 1 shows the strengths of the intrinsic connections and the modulatory input of optimal model averaged across all subjects for sentence completion (1a) and verb generation (1b) tasks. The numbers along side of the connections indicate the average of intrinsic connection strength. The numbers in rectangular box indicate the parameter for modulation. Input for a specific model is grayed out and the connection that is being modulated is marked with dotted lines.

## CONCLUSION

1. Dynamic casual modeling and BMS revealed the optimal network connectivity models for the SC and VG tasks. a. For SC task the optimal model showed that BA-22 plays an important role and BA-45 receives input from BA-22 during this task. b. For VG task the optimal model showed that BA-45 plays an important role and BA-44 receives input from BA-45 during this task. 2. Effective connectivity analysis also confirmed the importance of BA-45 in both these tasks.

**KEY WORDS:** Language fMRI, effective connectivity

**O-608**

**1:40 PM - 1:48 PM**

## Monitoring of Glucose Metabolism with Standard $^1\text{H}$ MR Spectroscopy on Clinical MR Scanners

Grimm, J. P.<sup>1</sup>•Ashoori, I.<sup>2</sup>•Choi, S.<sup>3</sup>•Panigrahy, A.<sup>1,4</sup>•Greenblatt, K.<sup>1</sup>•Nelson, M. D.<sup>1</sup>•Bluml, S.<sup>1,2</sup>

<sup>1</sup>Childrens Hospital Los Angeles, Los Angeles, CA, <sup>2</sup>Rudi Schulte Research Institute, Santa Barbara, CA, <sup>3</sup>Brain and Creativity Institute, University of Southern California, Los Angeles, CA, <sup>4</sup>University of Pittsburgh, School of Medicine, Pittsburgh, PA

## PURPOSE

Recent progress in MR technology has resulted in improved reproducibility of MR spectra. The goal of this study was to demonstrate that the uptake and breakdown of glucose (Glc) in the human brain could be monitored with standard  $^1\text{H}$  MRS on clinical MR scanners.

## MATERIALS & METHODS

After a baseline MRS study, regular glucose (three control subjects, four studies, 1.1 - 1.8 gr/kg body weight) or U- $^{13}\text{C}$  enriched glucose (one control subject, two studies, 0.9 gr/kg) was administered orally. MR spectra were acquired up to  $\approx 100$  min after glucose administration. Subjects fasted 4-12 hours for the regular glucose studies and 12 hours overnight for  $^{13}\text{C}$  glucose studies. In addition, one adult brain tumor patient (12 hours overnight fasting) and four pediatric patients with brain tumors were studied after oral administration of U- $^{13}\text{C}$  enriched glucose (4 hours of fasting). All studies were carried out on a clinical MR system (Philips, Achieva 3.0 T, Best, The Netherlands) using an 8-channel head coil. Single-voxel PRESS spectra (TR = 2s, TE = 35 ms, 128 averages,  $10\text{-}15\text{ cm}^3$  of parietal/occipital gray matter (GM) and parietal white matter (WM) were acquired in controls. In patients with tumors, voxels were placed in tumor tissue. Fully automated LCModel software (S. Provencher Inc.) was used for processing and quantitation.

## RESULTS

Oral  $^{12}\text{C}$  Glc administration resulted in increased tissue Glc concentrations. When  $^{13}\text{C}$  enriched Glc was used,  $^{13}\text{C}$  label replaced  $^{12}\text{C}$  and resulted in an apparent reduction of the  $^1\text{H}$  MRS detectable breakdown products of glucose such as glutamate (Glu) (Fig. 1A). In a tumor, an apparent reduction of lactate was detected consistent with an increase of glycolysis relative to aerobic oxidation in the TCA-cycle (Warburg effect, Fig. 1B).

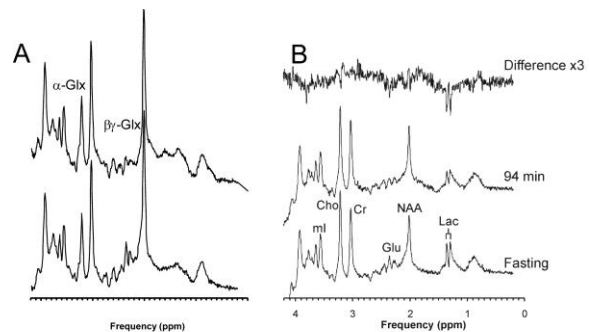


Fig. A: PRESS spectrum of GM before (bottom) and  $\approx 90$  min after oral administration of  $^{13}\text{C}$  Glc. The signal in the  $\beta\text{-Glx}$  (glutamate and glutamine) is reduced reflecting the accumulation of  $^{13}\text{C}$  label in the molecules. B: In a comparable experiment in an adult brain tumor, a significant reduction of lactate was observed.

## CONCLUSION

The improved stability of MR systems allows the monitoring of glucose metabolism in the brain with no need for additional hardware using FDA-approved MRS methods. The simplicity of this approach comes at the cost of an inferior specificity when compared with more advanced approaches such as direct  $^{13}\text{C}$  detection, polarization transfer, and methods that employ more complex editing for indirect detection. Still, this method may be useful to answer important biological questions in clinical settings where the logistical challenges of more advanced methods cannot be overcome.

**KEY WORDS:** Spectroscopy, glucose, metabolism

O-609

1:48 PM - 1:56 PM

### Cortical Adaptation to Visual Blurring: A 3 T Functional MR Imaging Comparison between Corrected Myopia and Emmetropia

Nguyen, T. H.<sup>1</sup>•Stievenart, J.<sup>1</sup>•Yoshida, M.<sup>2</sup>•Baranton, K.<sup>3</sup>•Abanou, A.<sup>1</sup>

<sup>1</sup>C.H.N.O. des XV-XX, Paris, FRANCE, <sup>2</sup>Jikei University School of Medicine, Tokyo, JAPAN, <sup>3</sup>Essilor, Paris, FRANCE

#### PURPOSE

To compare through functional MR imaging (fMRI) the visual cortex response to blurred and unblurred visual stimuli, in myopic and normal subjects.

#### MATERIALS & METHODS

We explored 40 subjects aged from 18 to 35 years corresponding to two groups of 20 emmetropic subjects and 20 corrected myopic patients. 3T fMRI examinations alternated sequences of blurred or unblurred images, including natural scenes and optotypes. The subject's time reaction to the changing of image resolution was recorded. Functional data underwent individual and group statistical analyzes, using Statistical Parametric Mapping (SPM8©), then superimposed on anatomical MNI templates.

#### RESULTS

Emmetropic and corrected myopic subjects presented a comparable extension, but a different amplitude in cortical response. While the primary visual cortex is mainly activated in emmetropic subjects, with a temporary recruitment of associative areas, strong activations were observed mainly in the visual secondary visual networks in myopic patients, outlining the dorsal and ventral pathways, as well as parietal, frontal and prefrontal areas. The myopic patients showed a shorter time reaction to the image blurring or unblurring phenomenon. Enhanced activations in secondary and associative visual networks in myopic patients suggest a cortical plasticity in the perception and the reconstruction of a blurred image, as myopia is a long-term habituation to altered spatial resolution. The shorter reaction to resolution alteration in myopic patients may correspond to a larger tolerance in the perception of a blurred image.

#### CONCLUSION

At an equivalent visual acuity, the myopic patients present a higher connection of visual primary, secondary and associative networks when compared to emmetropic subjects, in order to enhance the cortical perception and reconstruction of a visual stimulus.

**KEY WORDS:** Functional MR imaging, cortical plasticity, vision

O-610

1:56 PM - 2:04 PM

### Diffusion Tensor Imaging Findings during Spontaneous Migraine Attacks

Kara, B.<sup>1</sup>•Atamer, A.<sup>2</sup>•Selcuk, H.<sup>1</sup>•Onat, L.<sup>2</sup>•Ulusoy, L.<sup>2</sup>•Mutlu, A.<sup>2</sup>

<sup>1</sup>Bakirkoy Dr. Sadi Konuk Teaching Hospital, Istanbul, TURKEY, <sup>2</sup>Florence Nightengale Hospital, Istanbul, TURKEY

#### PURPOSE

The studies using positron emission tomography (PET) showed that the brainstem may have an important role in migraine. Recently, diffusion tensor imaging (DTI) studies demonstrated that structural alterations in migraineurs may extend beyond the normal-appearing brain tissues in conventional sequences. In light of the previous studies, the aim of our study was to find out if DTI may detect any abnormality in brainstem and white matter structures during the spontaneous migraine attacks.

#### MATERIALS & METHODS

The patients were recruited from the migraine population attending the neurology department. Only patients who met all of the following criteria were enrolled in the study: a) the criteria of the International Classification of Headache Disorders for the diagnosis of migraine, b) age between 18-55, c) absence of any systemic or metabolic disorders including hypertension, hypercholesterolemia, diabetes mellitus, and cardiovascular diseases. Patients with any signal abnormality in brain parenchyma in conventional T2- and FLAIR-weighted sequences were excluded. The DTI images obtained in a 3 T system (GE Healthcare, Milwaukee, WI, USA) were processed using commercially available software (Functool DTI processing, GE Healthcare, Milwaukee, WI, USA) to produce ADC and FA maps. We measured the fractional anisotropy (FA) and apparent diffusion coefficient (ADC) values of red nuclei, periaqueductal gray matter (PGM), thalami, posterior limb of internal capsule (PLIC) and subcortical white matter (SWM). Fifteen healthy volunteers with normal neurologic exam and no personal or family history of migraine served as control group.

#### RESULTS

A total of 14 patients (12 females, 2 males) enrolled in the study. Patients' age varied between 21 and 54 years (mean 36.4 years). All patients presented without aura. The mean duration of disease was 10.8 years (ranged 1 to 26 years). The mean frequency of attacks was 5.2 times per month. The pain was generalized in four patients, on the right side in five patients and on the left side in five patients. The mean time from attack onset to the MRI was 1 hour. In control group (8 females, 7 males), mean age was 27.3 years. By using Student's t-test; the FA and ADC values in PGM, PLICs, thalami and SWMs showed no statistical differences between healthy and migraine group. In patient group, the ADC values of right and left red nuclei were statistically higher than healthy subjects ( $p = 0.024$  and  $p = 0.005$ ;

respectively). The FA measurements of red nuclei showed no differences between patient and healthy cohorts. Pearson correlation analysis depicted that there was no correlation between DTI metrics and clinical characteristics of the patients.

#### CONCLUSION

The present study showed increased ADC values in red nuclei during spontaneous migraine attacks. Our results support the findings of previous PET studies which concluded that the brainstem may play a central role in the pathogenesis of migraine episode. However, the underlying mechanism for our findings is unclear and we do not know whether these changes are responsible for triggering an attack or are they the consequence of the attack itself.

**KEY WORDS:** DTI, migraine

**O-611**

**2:04 PM - 2:12 PM**

#### Concurrent Transcranial Magnetic Stimulation and Functional MR Imaging during Speech Arrest for Exploring Language Networks

Roberts, D. R.·Fox, J.·Krishna, V.·Brodle, J.·Barr, D.

Medical University of South Carolina  
Charleston, SC

#### PURPOSE

Mapping of language functions relies on neuropsychological testing, invasive procedures such as intraoperative mapping and Wada, or on neuroimaging methods including PET or functional MRI (fMRI). Although functional neuroimaging has greatly expanded our understanding of language networks, there are issues related to the use of these procedures. For example, even though a cortical area is shown to be "active" during an fMRI language task, there is no indication as to whether or not the area is crucial for language function. We propose solving this problem by performing transcranial magnetic stimulation (TMS) during fMRI to delineate essential cortical areas that actively participate in language production. Transcranial magnetic stimulation is a noninvasive, nonpainful technique that employs active cortical stimulation allowing an investigator to safely and repeatedly create temporary "virtual" cortical lesions in normal subjects.

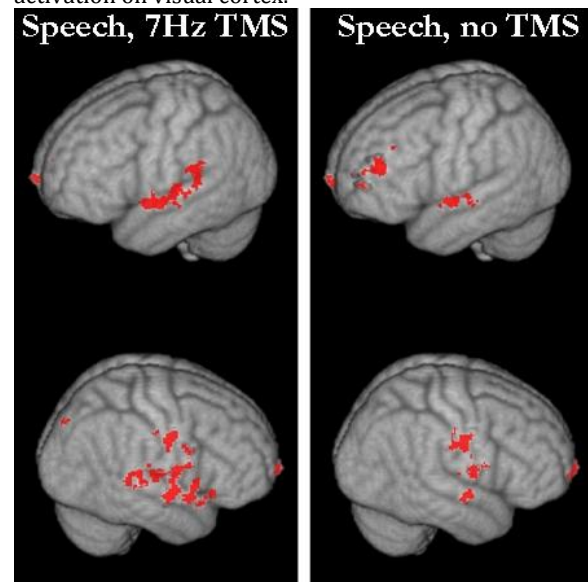
#### MATERIALS & METHODS

Following IRB approval, four subjects underwent concurrent TMS/fMRI. First the subject's resting motor threshold (rMT) was determined. Transcranial magnetic stimulation then was applied at 7 Hz, 100% rMT. The TMS coil was positioned systematically along the left scalp to identify the site of TMS-induced speech arrest. This site was marked on the scalp. Video recordings were acquired for off-line review to ensure speech arrest was produced. The subject then was taken to the MRI scanner. The TMS coil was placed at the previously identified site of speech arrest inside the MRI head coil. Each participant underwent structural scanning and concurrent TMS/fMRI. A sparse fMRI

sequence was acquired during a language task (rote counting) both with and without 7Hz TMS applied in a randomized fashion. Epochs of TMS applied at 2Hz (not sufficient to induce speech arrest) also were included as a control condition.

#### RESULTS

Group analysis during speech without TMS identified expected language areas. Group analysis of speech arrest with 7 Hz TMS compared with the speech-no TMS condition showed increased bilateral temporal activation, inhibition of left frontal activation, increased right frontal activation and new visual cortex activation. We hypothesize the increased bitemporal activation may be related to coil noise. We hypothesize that the visual cortex activation seen only during 7 Hz TMS may indicate a release of normal speech-induced visual inhibition suggesting a causal influence of left frontal activation on visual cortex.



#### CONCLUSION

Our data support a previously proposed fronto-parietal "attention network" that may modulate visual processing via back-projection. Concurrent TMS/fMRI is a technique useful for exploring the causal interactions between remote but functionally interconnected brain regions.

**KEY WORDS:** Functional MR imaging, TMS, language

**O-612**

**2:12 PM - 2:20 PM**

#### BOLD Functional MR Imaging of Theory of Mind in Autism

Wigginton, T.<sup>1</sup>·Froehlich, A. L.<sup>2</sup>·DuBray, M. B.<sup>2</sup>·Anderson, J. S.<sup>2</sup>·Lainhart, J. E.<sup>2</sup>·Druzgal, J.<sup>1</sup>

<sup>1</sup>University of Virginia, Charlottesville, VA, <sup>2</sup>University of Utah, Salt Lake City, UT

#### PURPOSE

Autism is a neurodevelopmental disorder characterized by core deficiencies in social interaction and communication. Despite affecting approximately 0.5%

of the population, the cause of autism remains unknown. One of the prevailing neuropsychological theories of autism suggests a central deficiency in the "theory of mind" mechanism. Theory of mind (TOM) refers to the ability of one person to predict another person's behavior or beliefs by attributing them to independent mental states. Blood oxygen level dependent (BOLD) functional magnetic resonance imaging (fMRI) data from our laboratory indicates that a simple manipulation of a two-player game like scissors, paper, rock (SPR) can be used as a reliable assay for brain activation of TOM regions in normal subjects. The manipulation consists of telling subjects they are competing against two different opponents - either a live person, or a computer employing a rule-based strategy - when in reality they are always competing against randomly generated responses. This simple belief regarding the nature of your opponent robustly recruits the TOM network in normal people. The present study uses the SPR task to test the hypothesis that autistic patients demonstrate deficient BOLD fMRI activity related to TOM tasks.

#### **MATERIALS & METHODS**

Subjects were selected from the Utah Autism Research Project. We scanned 25 young adults with high-functioning autism and 24 age-matched typically developing controls. The experimental design consisted of each subject undergoing multiple trials of the SPR paradigm while BOLD fMRI data were collected. Subjects were practiced on the SPR paradigm prior to MRI scanning. At the beginning of each trial, subjects learned who their opponent would be (computer algorithm or live person) from a written instruction. Pictures of a scissors, paper, and rock appeared in the subject's visual field, and subjects were given time to determine which object they wished to choose for that trial. After subjects made their choice via a button press, a visual cue indicated which object their opponent chose for the round. Based on the rules of the game, subjects immediately knew whether they won, lost, or tied. In reality, subjects always played against a randomly generated sequence of responses, and the only difference between trial types was the subject's belief about the nature of their opponent (computer algorithm or live person). Standard statistical analysis of fMRI data with the fMRI Software Library (FSL) was used to test differences between the autism and control patients with regard to the TOM contrast (Live vs Computer).

#### **RESULTS**

Preliminary whole brain analysis shows that activity related to the TOM contrast (belief of playing a live opponent vs belief of playing a computer algorithm) is greater in several regions of the control brains when compared to the autistic population. Most of these differences co-localize to regions previously associated with the theory of mind mechanism.

#### **CONCLUSION**

Based on the preliminary data, autistic patients demonstrate decreased task-related activation in networks previously associated with the theory of mind

mechanism. These findings provide biological support the neuropsychology theory that autistic patients have a central deficiency in the TOM mechanism.

**KEY WORDS:** BOLD fMRI, autism, theory of mind

**O-613**

**2:20 PM - 2:28 PM**

#### **Preoperative Cortical Localization by Magnetic Source Imaging for Endovascular Treatment of Arteriovenous Malformations in Eloquent Brain Tissue**

Cho, A.-Lee, R.-Pakbaz, R.

University of California San Diego  
San Diego, CA

#### **PURPOSE**

Preoperative localization of functionally eloquent brain tissue helps physicians plan and tailor the extent of endovascular embolization and surgical resection of AVMs. Combined magnetoencephalography and MR data can be used to localize functional somatosensory, auditory, and motor cortical organization.

#### **MATERIALS & METHODS**

Retrospective review of all AVMs treated at our institution (endovascular, surgical and radiosurgery) over the past 2 years. We identified eight cases of AVMs involving eloquent cortical brain tissue with associated magnetic source imaging for localization of cortical organization. Case records were reviewed for patient outcome, and impact of functional cortical localization on treatment and management.

#### **RESULTS**

Combined magnetoencephalography and MR data had a high degree of reliability in localizing motor cortex in areas adjacent to and incorporated by AVMs. Functional cortical localization affected AVM treatment plans, focusing on preservation of eloquent cortex function.

#### **CONCLUSION**

Functional mapping of the cortex is indispensable for optimal treatment of AVMs involving eloquent brain tissue. These cases demonstrate the utility of preoperative functional brain mapping using magnetoencephalography.

**KEY WORDS:** AVM, MEG, endovascular

## Thursday Afternoon

**3:00 PM - 4:30 PM**

**Grand Ballroom Suite**

### (67) SNIS PROGRAMMING: CAROTID DISEASE (SAM #6) (AR)

\*Qualified by the American Board of Radiology (ABR) in meeting the criteria for Self-Assessment towards the purpose of fulfilling requirements in the ABR Maintenance of Certification program data 3/12.

**0-614**

**3:00 PM - 3:20 PM**

#### Diagnosis

Colin P. Derdeyn, MD

Radiology, Mallinckrodt Institute of Radiology,  
Washington University School of Medicine  
St. Louis, MO, USA

#### PRESENTATION SUMMARY

Atherosclerotic stenosis of the cervical carotid arteries is a common cause of ischemic stroke. Both embolic and hemodynamic factors play a role in this (1). Surgical revascularization (carotid endarterectomy, CEA) is a proven method for reducing stroke risk in some patient populations (2, 3). Carotid angioplasty and stenting is also an emerging option for treatment in some patients (4).

The two most important factors in determining whether patients with known or suspected carotid disease will benefit from intervention are whether they are symptomatic and the degree of stenosis. While area and length of plaque are important physiologically, the empiric evidence from the clinical trials that demonstrated benefit from intervention requires linear diameter stenosis. Catheter angiography (digital subtraction angiography, DSA) provides the most accurate method for measurement, but also carries the most risk and expense. This talk will review the relative advantages and disadvantages of DSA, and the non-invasive imaging modalities: Doppler ultrasound, Magnetic Resonance (MR) and Computed Tomography. Given the marginal benefit of revascularization in asymptomatic patients, a great deal of current research is focused on tools for the identification of high-risk subgroups. Factors that may portend high risk include embolic (transcranial Doppler (5), plaque imaging by MR(6)) and hemodynamic factors (7). We will conclude with an overview of ongoing research in this area.

**0-615**

**3:20 PM - 3:40 PM**

#### Treatment

Donald V. Heck, MD

Forsyth Radiology Associates  
Winston-Salem, NC, USA

#### PRESENTATION SUMMARY

Carotid stenting *may* be preferable to carotid endarterectomy because it is less invasive. Randomized trials of carotid stenting compared with carotid endarterectomy have consistently shown carotid stenting is efficacious in preventing stroke for the first few years after the initial perioperative period. Hence the utility of carotid stenting hinges on low risk in the perioperative period (first 30 days), which is the subject of intense scrutiny, and long term durability, which is under study.

Factors affecting the safety of carotid stenting, in addition to operator training and experience and overall patient condition, include anatomic factors such as aortic arch characteristics, arterial tortuosity, and lesion calcification. The latter anatomic factors can be evaluated on pre-operative non-invasive imaging. The most important goal during a carotid stent procedure is the prevention of cerebral embolization. This requires pharmacologic preparation of the patient pre-operatively, and management of anti-coagulation during the procedure. As with any neurointervention, attention to good catheterization technique and catheter flushing is crucial. In addition, "cerebral protection" either with a filter placed distal to the stenosis or flow reversal with an occlusion balloon placed proximal to the lesion is usually employed. There are multiple FDA-approved devices for this purpose.

**0-616**

**3:40 PM - 4:00 PM**

#### CEA Versus CAS Trials

Christopher J. Moran, MD

Washington Univ. School Of Medicine  
St. Louis, MO, USA

#### PRESENTATION SUMMARY

Ischemic stroke has been shown to be associated with carotid artery atherosclerotic disease. Surgical therapy with carotid endarterectomy (CEA) has been proven to be more effective than medical therapy in symptomatic patients with greater than 70% stenosis and in asymptomatic patients with stenosis greater than 60%. These trials help to establish criteria for the evaluation of patients (angiography and ultrasound) and for the operators (complications less than 6% for symptomatic and 3% for asymptomatic patients).

Interventionalists had experience with atherosclerotic disease in areas other than the carotid artery and began to apply the techniques of angioplasty and stenting to this vessel. As experience was gained, the balloons and stents were improved, and eventually cerebral protection devices were introduced to improve procedural results. The proof of efficacy remained comparison of CEA to the new techniques of CAS.

European investigators conducted three trials: EVA-3S, SPACE, and ICSS. These trials found that CEA was safer than CAS in the overall analyses. Operator training and experience as well as patient selection have been used to explain the results of these trials.

In North America, a large National Institute of Health (NIH)-supported trial comparing CEA and CAS was conducted from 2000 to 2008. Symptomatic patients had an angiographic stenosis greater than 50% and asymptomatic patients greater than 60%. The surgeons' complication rate was less than 5% for symptomatic patients and less than 3% for asymptomatic patients. The interventionalists' endovascular experience and CAS results were evaluated prior to hands-on training and lead-in phase training.

A total of 2502 patients were enrolled by the 108 centers. The primary endpoint of stroke, myocardial infarction, or death during the periprocedural period or any ipsilateral stroke within four years of randomization was achieved by 6.8% of the CEA patients and 7.2% of the CAS patients. Strokes were more frequent after CAS (4.1% versus 2.3% for CEA,  $p=.01$ ). Myocardial infarction was more common after CEA (2.3% versus 1.1% for CAS,  $p=.03$ ). At long-term follow-up, there was no major difference in major ipsilateral strokes (CEA 0.8% versus CAS 1.4%,  $p=.28$ ).

These results and further subgroup analysis have shown similar findings and have led to discussion on the severity of procedure-associated strokes and myocardial infarctions on patients' quality of life. The outcome and the low morbidity and mortality with both techniques are an indication of improvement in surgical and interventional care of patients with carotid disease.

*neuroimaging variables in cognitive and neurobehavioral disorders. He is board certified in clinical neuropsychology by the American Academy of Clinical Neuropsychology/American Board of Professional Psychology, has authored or co-authored 9 textbooks and over 250 peer-reviewed articles in neuropsychology, neuroimaging, and neuroscience. He is currently the Associate Editor of Brain Imaging & Behavior and has served in a number of elected positions in professional neuropsychological societies.*

#### **PRESENTATION SUMMARY**

**MILD TBI:** What is it, what can be done and what can imaging bring to the table? A brief overview of mild traumatic brain injury (mTBI) will be presented that includes how it is defined, underlying neuropathology along with the limits of conventional neuroimaging in assessing the effects of mTBI. The perspective that mTBI occurs as a disruption in brain connectivity will be emphasized with particular vulnerability to long white matter tracts and inter-hemispheric connectivity across the corpus callosum, as well as a frontotemporolimbic focus of injury. From this perspective, neuroimaging methods like diffusion tensor imaging (DTI), functional MRI (fMRI) including resting state functional MRI (rsfMRI) and magnetic resonance spectroscopy (MRS) are best suited to detect the more subtle pathology associated with mTBI. Furthermore, these advanced neuroimaging methods provide the opportunity to identify and track potential recovery and/or the development of chronic changes as well as provide neuroimaging metrics for the study of neurobehavioral and neurocognitive outcome. From these methods a much improved understanding of mTBI is emerging.

## **Thursday Afternoon**

**3:00 PM - 4:30 PM**

**Tranon Ballroom**

**(68) GENERAL PROGRAMMING:  
MILD TRAUMATIC BRAIN INJURY**

**0-617**

**3:00 PM - 3:20 PM**

**MILD TBI: What is it? What Can Be Done? What Can Imaging Bring to the Table?**

Erin D. Bigler, PhD

Psychology, Brigham Young University  
Provo, UT, USA

*Erin D. Bigler is Professor of Psychology and Neuroscience at Brigham Young University, where he was the Department Chair from 1996-2002 and an Adjunct Professor of Psychiatry at the University of Utah and a member of the Utah Brain Institute. From 1977 to 1990 he was a Professor of Psychology and Psychiatry at the University of Texas. Upon returning to BYU he established the Brain Imaging and Behavior Laboratory, researching*

**0-618**

**3:20 PM - 3:40 PM**

**Animal Models Reveal the Pathologic Basis for Clinical Imaging Findings**

Craig A. Branch, PhD

Albert Einstein College of Medicine  
Bronx, NY, USA

#### **PRESENTATION SUMMARY**

MRI Diffusion Tensor Imaging (DTI) findings in mild traumatic brain injury (mTBI) suggest white matter pathology of unknown origin. DTI in animal models of nTBI can be used to investigate these findings, and may be correlated with pathology. Here, we examine the relevant literature on the use of DTI in animal models of mild and more severe traumatic brain injury. We present our own experience in an animal model of mild TBI and discuss the best acquisition methods for high field - small animal DTI.



**O-619****3:40 PM - 4:00 PM****White Matter Injury in mTBI: Why it Matters Most and How Imaging Can Improve Detection**

Pratik Mukherjee, MD, PhD

Univ. California, San Francisco  
San Francisco, CA, USA**O-620****4:00 PM - 4:20 PM****Translating Advanced Imaging Approaches to Patient Care: Promise and Pitfalls**

Michael L. Lipton, MD, PhD

Radiology, Albert Einstein College of Medicine  
Bronx, NY, USA**PRESENTATION SUMMARY**

This session will review the use of neuroimaging for the clinical assessment of patients with mild traumatic brain injury (mTBI). The focus will be on the use of diffusion imaging methods, particularly diffusion tensor imaging (DTI), to detect evidence of traumatic axonal injury after mTBI. The limitations of visual assessment of DTI-based maps and tractograms and the need for quantitative analyses for detection of abnormalities will be discussed. Methodological considerations for the implementation of quantitative analyses will be presented with particular attention to the need for rigorous validation of analytic methods and ongoing quality control. Specific pitfalls in the performance and interpretation of DTI in the clinical setting will be discussed.

**Thursday Afternoon****3:00 PM - 4:30 PM****Beekman/Sutton North****(69) ASSR PROGRAMMING: SPINE  
POTPOURRI****O-621****3:00 PM - 3:30 PM****Making Imaging Interpretation Clinically Relevant to the Spine Surgeon**

Robert M. Quencer, MD

Radiology, Univ. of Miami Miller School of Medicine  
Miami, FL, USA**PRESENTATION SUMMARY**

The objectives of this presentation will be twofold:

1. to describe spine imaging features which a) often **are not** mentioned in radiology reports or b) **are not** observed but in both instances the findings nonetheless are important to the surgeon in operative planning

2. to describe how the surgeon uses findings which **are** contained in radiology reports in the operative management of patients.

With the examples shown, the intent is to encourage radiology interpretations to be more strategic in nature, in which the radiologist has a deeper understanding of the surgical implications of the findings and conveys that information in a meaningful report.

**O-622****3:30 PM - 4:00 PM****Spinal Alignment: Why Pelvic Incidence, Cob Angles and Kyphosis are Important in Spinal Balance, Scoliosis and Spondylolisthesis**

Johan W. Van Goethem, MD, PhD

Radiology, University Hospital of Antwerp  
Antwerp (Edegem), Belgium**PRESENTATION SUMMARY**

Spinal alignment can be abnormal in the frontal plane and/or the sagittal plane. In the frontal plane the normal load-bearing spine is straight. Scoliosis is defined as a deviation from the midline in a frontal plane. A small deviation ( $<10^\circ$ ) is sometimes called spinal asymmetry, while 'true' scoliosis has a deviation of  $\geq 10^\circ$ . This deviation is accompanied by a rotation that is maximally at the apex of the curve. Imaging in scoliosis is very important. Most cases of scoliosis are idiopathic and imaging is used routinely in monitoring the changes of the deformity that take place during growth. Imaging is also crucial in determining the underlying etiology in non-idiopathic cases of scoliosis. Finally, imaging is used in pre- and postoperative monitoring.

Normal alignment of the spine in a sagittal plane is determined by a set of spinal curves in the sagittal plane. In the normally aligned human these include a cervical lordosis that averages - depending on the endpoints - 20 to 50 degrees (C2-C7) or 30 to 70 degrees (C1-T1), a thoracic kyphosis averaging 30 to 35 degrees (T5-T12) and a lumbar lordosis averaging 50 to 60 degrees (T12-S1). These curves give strength and stability, and balance with minimal effort by allowing to position the center of gravity of the trunk. This is accomplished by keeping a vertical through the center of mass that usually runs in front of the shoulder joint, just behind the femoral heads and 3-4 cm in front of the ankle joint. The sagittal curves also provide functionality, including horizontal gaze, flexibility, shock absorption and spring function. These curves adapt during standing, sitting or running in order to maintain this functionality as best as possible. Lumbar lordosis is mainly determined by sacral slope and to a lesser extent by pelvic incidence. Thoracic kyphosis is determined by lumbar lordosis, all while maintaining balance with the least possible effort. Cervical lordosis adjusts for maintaining horizontal gaze and head functionality in general.

Abnormal frontal alignment, i.e. scoliosis, also affects sagittal alignment. In scoliosis there is higher pelvic incidence, higher pelvic tilt, lower sacral slope, lower lumbar lordosis and lower thoracic kyphosis. In spondylolysis there is a higher rate of anterolisthesis in

cases of lower pelvic incidence, lower pelvic tilt, higher sacral slope and higher lumbar lordosis.

**O-623**

**4:00 PM - 4:30 PM**

### **Hot Topics in Vertebral Augmentation**

Allan L Brook, MD

Montefiore Medical Center  
Bronx, NY, USA

## **Thursday Afternoon**

**3:00 PM - 4:30 PM**

**Sutton Center/South**

**(70) 70 - INTERVENTIONAL AND  
SPINE: MISCELLANEOUS**

**O-634**

**3:00 PM - 3:08 PM**

### **Admission CT Perfusion Is Not Predictive of Final Infarct Size According to ASPECTS after Recanalization with Intraarterial Thrombolysis for Anterior Circulation Ischemic Stroke**

Khaw, A. V. · Angermaier, A. · Kirsch, M. · Hosten, N. · Kessler, C. · Langner, S.

Ernst Moritz Arndt University  
Greifswald, GERMANY

#### **PURPOSE**

As compared with volumetric approaches, the semiquantitative ASPECTS system (Alberta Stroke Program Early CT Score) offers the advantage of easy and rapid assessment of the extent of perfusion disturbance in acute ischemic stroke. The aim of this study was to evaluate the relationship between admission ASPECT scores for the CT perfusion (CTP) parameters cerebral blood flow, cerebral blood volume, time-to-peak (CBF, CBV, TTP, resp.), and final infarct size after intraarterial thrombolysis (iaT) for acute ischemic stroke.

#### **MATERIALS & METHODS**

In this prospective, IRB-approved study, 26 ischemic stroke patients (17 women, 9 men, mean age  $\pm$  SD: 67.5  $\pm$  12.1 years, range 43-83) with M1, proximal M2, or distal internal carotid artery occlusion were consecutively enrolled to undergo a prespecified imaging protocol with noncontrast CT (ncCT), CTP and CT angiography (CTA), followed by iaT within 6 hours after symptom onset (mean  $\pm$  SD: 4  $\pm$  1.2h). Three raters who were experienced in acute stroke imaging and blinded for ncCT, CTA, all clinical and demographic data created color-coded CTP maps and scored for CBF, CBV, and TTP according to the ASPECTS algorithm on a consensus base. These scores were compared with the

final ischemic lesion size in the day 5 follow-up ncCT using ASPECTS.

#### **RESULTS**

Recanalization (TIMI 2 & 3) was successful in 19 patients (73%), two patients (8%) each had asymptomatic and symptomatic parenchymal hemorrhage. The median improvement of NIH Stroke Scale score was 7.5 (range -12 to 19), 15 patients (58%) had favorable functional outcome (modified Rankin Scale score  $\leq$  2) at 90 days after stroke. Intraarterial thrombolysis occurred within 3 hours of onset in eight patients, between 3 and 6 hours in the remaining 18 (69%). Four CTP studies were technically insufficient. The median ASPECTS CBF was 3 points (range: 1-8), ASPECTS CBV 5 (1-8), and ASPECTS TTP 1.5 (0-5). Final infarct size was scored with a median of 6.5 (1-10) points. All ASPECTS PCT parameters were significantly lower than ASPECTS CT values ( $p < 0.004$ ). This applied to the subgroup with successful recanalization ( $p = 0.08$ ). None of the ASPECTS PCT parameters showed a significant correlation with ASPECTS CT values ( $p > 0.36$ ).

#### **CONCLUSION**

The initial ASPECTS lesion was assessed significantly larger in all three CTP parameters CBF, CBV, TTP as compared with the ischemic lesion on day 5 ncCT, and was not predictive of final infarct size by ASPECTS when recanalization was achieved successfully with intraarterial thrombolysis. This observation supports increasing findings suggesting the initial perfusion lesion, especially CBV which has been reported as the best parameter indicating final infarct size, may be partially reversible in the event of recanalization. Our findings also reinforce the paradigm of rapid and effective recanalization (i.e., by implementing endovascular techniques) to salvage critically ischemic brain tissue in acute stroke.

**KEY WORDS:** Ischemic stroke, intraarterial thrombolysis, CT perfusion

**O-635**

**3:08 PM - 3:16 PM**

### **Reliability of Clinical Tools for Assessment of Noncontrast CT, CT Angiography Source Images and CT Perfusion in Patients with Acute Ischemic Stroke**

van Seeters, T.<sup>1</sup> · Biessels, G. J.<sup>1</sup> · van der Schaaf, I. C.<sup>1</sup> · Niesten, J. M.<sup>1</sup> · Dankbaar, J. W.<sup>1</sup> · Horsch, A. D.<sup>1,2</sup> · Kappelle, L. J.<sup>1</sup> · van der Graaf, Y.<sup>1</sup> · Velthuis, B. K.<sup>1</sup>

<sup>1</sup>University Medical Center Utrecht, Utrecht, NETHERLANDS, <sup>2</sup>Rijnstate Hospital, Arnhem, NETHERLANDS

#### **PURPOSE**

Several scoring tools exist to assess the extent of ischemia in acute stroke patients. Reliability of these tools is important for implementation in routine clinical practice. The aim of this study is to determine the inter and intraobserver variability of the one third middle cerebral artery (MCA) rule and the Alberta Stroke

Program Early CT Score (ASPECTS) in a multimodal CT workup of patients suspected of ischemic stroke.

#### MATERIALS & METHODS

We prospectively included 116 consecutive patients with a suspected ischemic stroke. All patients are participants of the Dutch acute Stroke Trial (DUST). Noncontrast CT (NC CT), CT angiography (CTA), and CT perfusion (CTP) were acquired at admission in all patients. Inclusion criteria were acute neurologic deficit of less than 9 hours duration, and a NIH Stroke Scale  $\geq 2$ . Exclusion criteria were poor image quality ( $n = 2$ ), and absence of one or both image slices required for ASPECTS ( $n = 9$ ). Two neuroradiologists and four experienced radiology trainees independently evaluated the NC CT, CTA source images (CTA SI), and CTP for  $>1/3$  MCA involvement and ASPECTS. On CTP, cerebral blood volume (CBV), mean transit time (MTT), and predicted penumbra and infarct core maps were evaluated. To determine intraobserver agreement, all observers evaluated ten consecutive scans twice. Kappa statistics were used to calculate overall agreement.

#### RESULTS

For NC CT, inter and intraobserver agreement for the  $1/3$  MCA rule were moderate ( $\kappa = 0.428$ ) and fair ( $\kappa = 0.268$ ); and were fair ( $\kappa = 0.219$ ) and moderate ( $\kappa = 0.509$ ) for ASPECTS. For CTA SI, inter and intraobserver agreement were only poor ( $\kappa = 0.168$ ) and moderate ( $\kappa = 0.576$ ) for the  $1/3$  MCA rule, but were moderate ( $\kappa = 0.583$ ) and good ( $\kappa = 0.686$ ) for ASPECTS. For CTP however, inter and intraobserver agreement for the  $1/3$  MCA rule were excellent (range:  $\kappa = 0.820$ , CBV maps; to  $\kappa = 0.955$ , penumbra maps) and good to excellent (range:  $\kappa = 0.732$ , infarct core maps; to  $\kappa = 0.915$ , both MTT and penumbra maps); and were excellent (range:  $\kappa = 0.852$ , infarct core maps; to  $\kappa = 0.980$ , penumbra maps) and moderate to excellent (range:  $\kappa = 0.457$ , CBV maps; to  $\kappa = 0.965$ , MTT maps) for ASPECTS.

#### CONCLUSION

The reliability of the  $1/3$  MCA rule and ASPECTS is similar, but is much better for CT perfusion than for NCCT and CTA SI.

**KEY WORDS:** Ischemic stroke, reliability, CT

**O-636**

**3:16 PM - 3:24 PM**

#### Effects of Positive and Negative Shifts in Bolus Arrival Time on Deconvolution Methods for CT Brain Perfusion

Bennink, E.·Riordan, A. J.·de Jong, H. W.

Utrecht University Medical Center  
Utrecht, NETHERLANDS

#### PURPOSE

CT brain perfusion analysis requires measurement of an arterial input function (AIF). Ideally, the bolus arrival time of the selected AIF coincides with the bolus arrival time in the tissue. However, in many cases the selection of the AIF can result in positive time shifts (delays, e.g., AIF in carotid artery) or negative shifts (e.g., AIF in a

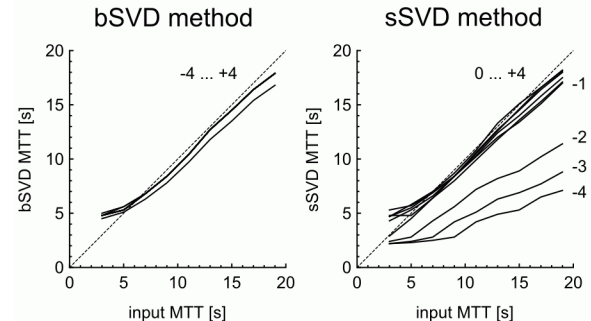
collateral artery behind an occlusion) with respect to the tissue. Since these time shifts can cause bias in the resulting tissue mean transit times (MTT), we studied the response of commonly used deconvolution methods on positive and negative time shifts.

#### MATERIALS & METHODS

The sSVD and bSVD methods, as described, and the arrival time sensitive (ATS) and arrival time insensitive (ATIS) methods found in the Philips brain perfusion package version 4.5 were included. Since calculation of a bias requires knowledge of the real value a digital phantom was created based on detailed modeling of the contrast agent dynamics. This phantom contains a matrix of tissue regions in which the time shift was varied from +4 (carotic) to -4 (collateral) seconds, while tissue MTT varied from 3 (healthy) to 19 (diseased) seconds. In order to solely compare the responses of the deconvolution methods, other filters were disabled.

#### RESULTS

Biases for a range of time shifts and tissue MTTs were calculated. The figure summarizes the response of the bSVD and sSVD methods to time shifts. Without time shift all methods gave MTTs that were within 11% of the real value. As for positive time shifts the sSVD, bSVD and ATIS methods showed no dependence, while the MTT as measured by ATS appeared to be linear dependent on the shift. For negative time shifts (collateral AIF) the sSVD, ATIS and ATS methods significantly underestimated the MTT, as can be seen in the figure, while the bSVD again showed no bias.



#### CONCLUSION

Only bSVD is insensitive to all time shifts, while the ATIS and sSVD methods show similar behavior and can handle positive time shifts only. Since positive time shifts are most likely to occur, it is advisable to use a deconvolution method that is at least insensitive to positive shifts. Philips software users are therefore advised to use the "arrival time insensitive" method for quantification and to prevent measuring the AIF distal to an occlusion or in a collateral artery.

**KEY WORDS:** CT, perfusion, delay

O-637

3:24 PM - 3:32 PM

### Infarct Risk Factors Related to Ethnicity: The SABRE Cohort Study

Shibata, D. K.<sup>1</sup>•Tillin, T.<sup>2</sup>•Beauchamp, N.<sup>1</sup>•Heasman, J.<sup>3</sup>•Gedroyc, W.<sup>3</sup>•Stewart, R.<sup>4</sup>•Hughes, A.<sup>5</sup>•Chaturvedi, N.<sup>2</sup>

<sup>1</sup>University of Washington, Seattle, WA, <sup>2</sup>Imperial College, London, UNITED KINGDOM, <sup>3</sup>St. Marys NHS Trust, London, UNITED KINGDOM, <sup>4</sup>King's College, London, UNITED KINGDOM, <sup>5</sup>Imperial College at St. Mary's, London, UNITED KINGDOM

#### PURPOSE

Stroke mortality has been related to ethnicity and is increased in people of African descent compared with Caucasians, but factors responsible are unclear. The purpose of this study is to compare infarcts on MRI by ethnicity and the role of risk factors.

#### MATERIALS & METHODS

SABRE (Southall and Brent Revisited) is a community-based multiethnic cohort of men and women aged 40-69 years at baseline (1988-1990), and 58-86 years at follow up (2008-2011). At follow up, a questionnaire was completed and investigations performed including resting and ambulatory blood pressure (BP), anthropometry, glucose and lipids. Brain MRI scans were performed on 590 Caucasians and 207 people of African descent. The majority of the scans were performed at 3 T and included axial T1, T2, FLAIR and coronal 3D SPGR images. The scans were scored for infarcts independently by two readers according to the Cardiovascular Health Study protocol. Any discrepant scores were adjudicated.

#### RESULTS

Mortality was greater in Caucasians (605, 25%) than those of African descent (121, 15%) ( $p < 0.0001$ ), although stroke was more likely the underlying cause in the latter group (23, 19% vs (43, 7%,  $p < 0.0001$ ). Baseline systolic/diastolic BP was similarly higher in those of African descent than Caucasians in attendees (8/5 mmHg), nonresponders (7/6 mmHg), and those who died (8/5 mmHg). At follow up, stroke risk factors were worse in those of African descent, apart from smoking (table). Prevalence of infarcts was similar by ethnicity, not differing when those <65 years were analyzed separately, or when those with stroke/TIA history were excluded. Associations between infarcts and risk factors did not differ by ethnicity. But prescribed treatment in those with elevated clinic BP ( $\geq 140$  mmHg systolic, or  $\geq 90$  mmHg diastolic) was 83% in those of African descent, 63% in Caucasians ( $p < 0.0001$ ). Further, in those with an infarct, 95% of those of African descent, and 69% ( $p < 0.0001$ ) of Caucasians were on treatment.

Risk Factors of Infarct on MRI			
Risk Factor	Caucasian	African Descent	P value
Age (years)	69.7 +/- 6.2	70.5 +/- 5.9	0.2
Male	78%	51%	<.0001
BP systolic	138 ± 16.9	142 ± 17.4	0.02
BP diastolic	77 ± 9.7	78 ± 9.0	0.2
Anti-Htn Meds	51%	76%	<.0001
H/O stroke/TIA	5%	7%	0.2
Known Diabetes	12%	33%	<.0001
Ever Smoker	62%	35%	<.0001
microalbuminuria	18%	20%	0.5
Infarcts on MRI	22%	21%	0.8
Model	Odds ratio (Cauc vs African)		P value
Age, sex	0.94 (0.77, 1.16)		0.6
Age, sex, risk factors	0.83 (0.66, 1.04)		0.1
Age, sex, risk factors, smoking	0.90 (0.72, 1.13)		0.4

#### CONCLUSION

Equivalence of infarct rates in these two ethnic groups was unanticipated, given the greater stroke mortality in those of African descent. Mitigating against selective mortality as the explanation of our findings is the similar ethnic differential in baseline BP in survivors and nonsurvivors, the lower overall mortality in those of African descent, and overall small numbers of stroke deaths. A more likely explanation is that in the population studied, there may be better targeted more aggressive treatment in those of African descent, reducing their potential burden of infarcts.

**KEY WORDS:** Infarct, MR imaging, ethnicity

O-638

3:32 PM - 3:40 PM

### Hospital-Acquired Pneumonia is Linked to Right Peri-Insular and Infratentorial Stroke

Kemmling, A.<sup>1</sup>•Lev, M. H.<sup>1</sup>•Payabvash, S.<sup>1</sup>•Kamalian, S.<sup>1</sup>•Betensky, R.<sup>2</sup>•Pervez, M. A.<sup>1</sup>•Masrur, S.<sup>1</sup>•Schwamm, L. H.<sup>1</sup>

<sup>1</sup>Massachusetts General Hospital, Boston, MA, <sup>2</sup>Dana-Farber/Harvard Cancer Center, Boston, MA

#### PURPOSE

Hospital-acquired pneumonia (HAP) is a major complication of stroke. We sought to determine if infarction in specific brain regions was associated with HAP, using a rigorous case-control study design and an independently validated regional/voxel-based statistical methodology.

#### MATERIALS & METHODS

Two hundred fifteen acute stroke patients with HAP were randomly selected from our stroke database (2003-2009) and matched to 215 nonpneumonia acute stroke controls. Admission CT and MR DWI images and binary masks of infarction were registered to MNI-152 space. Regional atlas-based and voxel-based log-odds

were calculated to assess the relationship between infarct location and the likelihood of developing HAP. Penalized conditional logistic regression was used to identify imaging regions and clinical variables independently associated with pneumonia; log-odds ratios (OR), p-values, and q-values (false discovery rates) were calculated.

## RESULTS

The 215 HAP and 215 control patients were well matched with regard to gender (100%); age ( $R^2 = 0.97$ ); admission infarct volumes ( $13.9 \pm 1.7$  ml vs  $13.4 \pm 2.0$  ml;  $p = 0.73$ ), admission NIHSS ( $R^2 = 0.99$ ), and eight other clinical variables. In HAP patients, mean hemispheric percent infarction was 57% higher in the right and 25% lower in the left hemisphere compared to controls. Infarction in the cerebellum ( $n = 33$ ) and brainstem ( $n = 13$ ) was also more common with HAP. Of the 10 regions most frequently infarcted with HAP, only right insular cortex volume was significantly different versus controls (20 versus 12 ml,  $p = 0.02$ ). In univariate analyzes, the highest log-ORs for pneumonia were observed in the cerebellum, brain stem and right hemisphere (Table 1). The best performing multivariate model selected seven brain regions of infarction and two binary infarct volume-based variables independently associated with HAP. The voxel-based odds ratio for HAP was substantially higher infratentorially (OR up to 8), than in either the right (OR up to 3) or left (OR~1) hemispheres (Figure 1).

Table 1. Univariate log OR for anatomic brain regions potentially associated with HAP (as defined by  $p < 0.05$ ). Associated false discovery rate (q-value) is listed.

Brain region	log-OR	p-value	q-value
R Sagittal stratum	0.8544	0.0014	0.0415
R Fornix / Stria	1.0704	0.0014	0.0415
R temporooccipital Inferior Temporal Gyrus	1.0460	0.0012	0.0415
R Lateral Occipital Cortex	0.8557	0.0031	0.0708
R Posterior thalamic radiation	0.7691	0.0056	0.0865
R Middle Frontal Gyrus	0.6554	0.0057	0.0865
R Uncinate fasciculus	0.7178	0.0085	0.1099
R Posterior corona radiata	0.6286	0.0129	0.1168
L Superior Frontal Gyrus	-0.6286	0.0129	0.1168
L Juxtapositional Lobule Cortex	-0.7885	0.0113	0.1168
R Cerebral peduncle	0.8755	0.0200	0.1372
R retrolenticular Internal capsule	0.5653	0.0240	0.1372
R Inferior Frontal Gyrus	0.5831	0.0221	0.1372
R Superior Parietal Lobule	0.6391	0.0242	0.1372
R Frontal Operculum Cortex	0.5543	0.0217	0.1372
R Parietal Operculum Cortex	0.5831	0.0221	0.1372
R Heschl's	0.5596	0.0287	0.1533
R Insular Cortex	0.4855	0.0307	0.1546
R Inferior Frontal Gyrus	0.5534	0.0345	0.1644
R posterior Inferior Temporal Gyrus	0.6592	0.0382	0.1648
R Lingual Gyrus	0.6592	0.0382	0.1648
R Anterior corona radiata	0.5031	0.0429	0.1689
R Middle Temporal Gyrus	0.5819	0.0422	0.1689
R posterior limb Internal capsule	0.4884	0.0458	0.1697

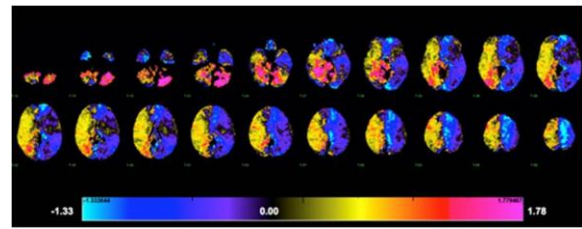


Figure 1. Brain voxels with significant odds of developing hospital acquired pneumonia in stroke patients, expressed as log-odds ratio ( $p < 0.05$ ).

## CONCLUSION

Hospital-acquired pneumonia is associated with right peri-insular and infratentorial stroke. This novel structure-function correlation might be mediated through autonomic (vagal) modulation of swallowing and/or immune mechanisms. Indeed, two recent studies in Science (Oct 2011) have linked stroke to infection - potentially reflecting sympathetically mediated immune compromise.

**KEY WORDS:** Hospital-acquired pneumonia, stroke, peri-insular and infratentorial stroke

O-639

3:40 PM - 3:48 PM

## Role of Perifocal Apparent Diffusion Coefficient in Differentiating High- and Low-Grade Gliomas

Manzoor, M. U·Rumboldt, Z·Tabesh, A·Topiwala, P·Morgan, P·Giglio, P·Spampinato, M. V.

Medical University of South Carolina  
Charleston, SC

## PURPOSE

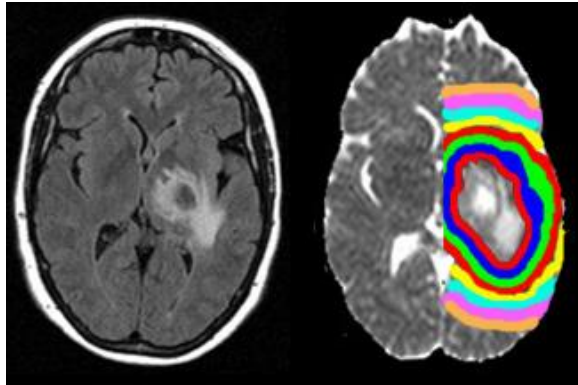
Our aim was to assess water diffusivity within the brain parenchyma surrounding gliomas. We hypothesized that perifocal apparent diffusion coefficient (ADC) values will differ between high- and low-grade gliomas.

## MATERIALS & METHODS

Twenty-one treatment-naïve patients with pathology-proven gliomas (WHO grade II = 5; grade III-IV = 16) were evaluated retrospectively. MR imaging data obtained before treatment initiation were collected. A tumor volume-of-interest (tumor VOI), including the lesion and any surrounding T2 prolongation, was outlined on FLAIR. Eight incrementally dilated VOIs around the tumor VOI were obtained in 3D ranges away from the tumor VOI for a distance of 4 cm, with 5 mm incremental steps (0-5, 5-10, 10-15, 15-20, 20-25, 25-30, 30-35 and 35-40mm). A VOI was drawn within the contralateral normal-appearing white matter (NAWM) in the centrum semiovale. After exclusion of the contralateral hemisphere and cerebrospinal fluid, the mean and lowest 25th percentile (Q1) ADC values within the dilated perifocal VOIs were obtained using in-house Matlab software and normalized to the contralateral NAWM ADC. Mann-Whitney test and receiver operating characteristics (ROC) curves were used for statistical analyzes. Results were considered significant when  $p < 0.05$ .

## RESULTS

Normalized mean and Q1 ADC values of the dilated perifocal VOIs were different between the high- and low-grade groups, with lower ADC values in high-grade gliomas group. Specifically, mean ADC values were significantly different in the 3D range of 10 to 25 mm away from the tumor VOI (from the center to the periphery: mean ADC at 10-15mm  $p = 0.026$ ; at 15-20 mm  $p = 0.026$ ; at 20-25 mm  $p = 0.013$ ). Q1 ADC values were significantly different in the 3D range of 10 to 30 mm away from the tumor VOI (from the center to the periphery: Q1 ADC at 10-15 mm  $p = 0.013$ ; at 15-20 mm  $p = 0.008$ ; at 20-25 mm  $p = 0.010$ ; at 25-30 mm  $p = 0.017$ ). ROC analyzes revealed greatest area under the curve (AUC) for the perifocal normalized Q1 ADC 20-25 mm away from the tumor VOI (AUC = 0.9, confidence interval = 0.724-1). Normalized average Q1 ADC values (SD) 20-25 mm away from the tumor VOI were respectively 1.05 (0.03) for low-grade and 0.98 (0.05) for high-grade tumors.



## CONCLUSION

Perifocal ADC measurement in gliomas may reflect the magnitude of tumor infiltration beyond the abnormality on conventional MRI. Perifocal ADC measurements could be helpful in determining tumor aggressiveness and thereby potentially guiding patient management.

**KEY WORDS:** Glioma, apparent diffusion coefficient, tumor

O-640

3:48 PM - 3:56 PM

### Correlation between MR Imaging-Positron Emission Tomography Data and Survival Data in Newly Diagnosed Glioblastoma Multiforme Patients Receiving Cediranib

Stemkens, B.<sup>1,2</sup>•Chonde, D. B.<sup>2</sup>•Jennings, D. L.<sup>2</sup>•Pinho, M.<sup>2</sup>•Gerstner, E. R.<sup>3</sup>•Batchelor, T. T.<sup>3</sup>•Catana, C.<sup>2</sup>

<sup>1</sup>University of Technology Eindhoven, Eindhoven, NETHERLANDS, <sup>2</sup>Athinoula A. Martinos Center for Biomedical Imaging, Massachusetts General Hospital and Harvard Medical School, Boston, MA,

<sup>3</sup>Massachusetts General Hospital Cancer Center, Harvard Medical School, Boston, MA

## PURPOSE

To determine the correlation between MR imaging positron emission tomography (MR PET) data, and the progression free survival and overall survival in patients with newly diagnosed glioblastoma receiving the vascular endothelial growth factor receptor inhibitor Cediranib.

## MATERIALS & METHODS

Nine patients (age range = 22 to 74 years; mean = 52 years) with newly diagnosed glioblastoma were scanned on the Brain PET, a prototype MRI-compatible PET scanner designed to fit inside the 3 T human MAGNETOM Trio MRI scanner (Siemens Healthcare Inc.). Immediately after the intravenous injection of ~5 mCi 18-FDG, a ninety-minute dynamic PET scan was performed and data were stored in list-mode format. MR data were collected simultaneously using our standard brain tumor imaging protocol. Attenuation maps were generated from the CT volumes coregistered to the high-resolution MPRAGE. Volumes were reconstructed for the 40- to 60-minute time frame with the ordinary Poisson ordered-subset expectation maximization 3D algorithm from prompt and expected random coincidence, normalization, attenuation, and scatter coincidence sinograms using one subset and 64 iterations. The nonenhancing region was defined as the ROI drawn on FLAIR images minus the ROI drawn on T1 axial post images. This is the region where the most information about the tumor metabolism is found. The standardized uptake values (SUV) in the nonenhancing region were normalized to the contralateral hemisphere. These normalized values were used to determine the total glycolysis, computed as. The relationship between changes in total glycolysis at day 1 and day 50 after the start of treatment compared to the baseline value at day -5  $\pm 1$  and 1-year progression-free and overall survival was investigated. The time of death was categorized into within 1 year after start of treatment, between 1-2 years, or after 2 years/still alive. Statistical analysis was performed with Pearson correlation.

## RESULTS

A positive correlation was observed between the total glycolysis change at day 1 of treatment and the date of progression ( ) with a specificity of 67% and sensitivity of 83%. Furthermore there was a correlation found between the change at day 1 and the time of death ( ) with a specificity of 75% and sensitivity of 80%. There was no correlation between the change in total glycolysis at day 50 and the date of progression ( ) or time of death ( ).

## CONCLUSION

The change in total glycolysis within the nonenhancing tumor region, one day after administration of cediranib is a good predictor for disease progression and survival. It is known that cediranib has a rapid onset (within 1 day), and PET data in combination with MRI data seem to be a good predictor for progression and survival in this group of patients and may be a useful early biomarker of response.

**Acknowledgements:** This work was partly supported by NIH grants (R01 CA129371-03, R01 CA137254-01A1)



and ARRA (U01CA062490) awards and the Harvard Catalyst grant.

**KEY WORDS:** PET, glioblastoma, VEGF

**O-642**

**4:04 PM - 4:12 PM**

### **Radiologic Extent of Traumatic Subarachnoid Hemorrhage Is Predictive of Cognitive Outcome in Traumatic Brain Injury**

Wong, G. K. C.

The Chinese University of Hong Kong  
Hong Kong, HONG KONG.

#### **PURPOSE**

We explored the radiologic predictors of long-term cognitive profiles of traumatic brain injury patients with computed tomography evidence of traumatic subarachnoid hemorrhage (tSAH).

#### **MATERIALS & METHODS**

Patients with tSAH were contacted to obtain their consent to participate in the study. Forty-seven (42%) of 111 eligible patients completed all the cognitive assessments. Extent (number of anatomical sites), anatomical sites, and thickness of tSAH.

#### **RESULTS**

Time from ictus to assessment ranged from 3 to 5 years. No difference in patient characteristics was observed between those who participated and those who did not. Number of cognitive domain deficits was predicted by the extent of tSAH (B coefficient, 0.68; 95% CI, 0.24-1.11;  $p = 0.003$ ; semipartial correlation coefficient, 0.433), in addition to age and GCS on admission, with a total  $R^2$  value of 50%. Anatomical sites per sec and thickness of tSAH did not predict cognitive outcome.

#### **CONCLUSION**

In addition to follow-up neurologic outcome (GOSE), the extent of tSAH is an independent risk factor for the number of cognitive domain deficits that occur.

**KEY WORDS:** Traumatic brain injury, subarachnoid hemorrhage

**O-643**

**4:12 PM - 4:20 PM**

### **Progressive Multifocal Leukoencephalopathy: Revisiting "Atypical" Imaging Features**

Busselberg, P. D.·Delfyett, W. T.·Tsay, J.

University of Pittsburgh Medical Center  
Pittsburgh, PA

#### **PURPOSE**

The lack of contrast enhancement and mass effect are generally described among the "classic" magnetic resonance (MR) imaging features of progressive multifocal leukoencephalopathy (PML). When present, they are regarded as "atypical" features, with reported incidences in the literature rarely exceeding 10%. In an individual MR examination, this perception could lead

radiologists to discount PML as a diagnostic consideration when the diagnosis might be otherwise suspected. The purpose of this study is to reassess the frequency of contrast enhancement and mass effect associated with PML in our institution's experience.

#### **MATERIALS & METHODS**

Following IRB approval and in HIPAA compliant fashion, a retrospective review of the institution's electronic medical record was performed to identify cases of pathologically confirmed PML with brain MR imaging from 2001 to 2011. MR imaging studies were reviewed by three radiologists and brain lesions were characterized by consensus with respect to the distribution, presence of enhancement, and mass effect. Enhancement was characterized by distribution (central versus peripheral) and intensity (none, faint, moderate, or avid). The degree of mass effect was graded as volume loss, none, mild, moderate, or marked. Incidences of enhancement and mass effect of any degree were compared with previously reported values.

#### **RESULTS**

Seventeen pathologically confirmed cases of PML with brain MR imaging were identified (13 male, 4 female). Patient risk factors included HIV infection (7), lymphoma (5), multiple myeloma (2), natalizumab therapy for multiple sclerosis (2), and combined variable immune deficiency (1). A total of 33 brain MR studies was performed. One patient never received contrast. No enhancement was observed on any study in 8/16 patients, and 8/16 (50%) demonstrated enhancement on at least one study. No mass effect was observed on any MR in 2/17 patients, and 12/17 (71%) showed some degree of mass effect on at least one study. Volume loss was observed in 3/17 patients.

#### **CONCLUSION**

Enhancement and mass effect associated with PML lesions were found more commonly than reported in the literature. The reasons for these discrepancies are likely multifactorial, and possibly related to underlying medical conditions, variations in treatment, and the degree of specific contrast agent T1 shortening. Future studies may elucidate these relationships. Given our results, reconsideration of whether historically "atypical" features deserve this designation may be warranted.

**KEY WORDS:** Progressive multifocal leukoencephalopathy, MR imaging, atypical

**O-644**

**4:20 PM - 4:28 PM**

### **Adult Cystic Fibrosis Sinonasal CT Findings - WNRS: Gabriel Wilson Award**

Stilwill, S. E.·Orlandi, R.·Wiggins, R. H.

University of Utah  
Salt Lake City, UT

**PURPOSE**

The purpose of this study is to evaluate the CT imaging features of the paranasal sinuses in adult patients with cystic fibrosis.

**MATERIALS & METHODS**

Sinus CT imaging studies of adult cystic fibrosis (CF) patients were reviewed retrospectively at an academic medical center over a 10-year period. The paranasal sinuses were evaluated for development, extent of inflammatory change, presence and location of bone sclerosis, possible mucocoele formation and possible prior surgery. A random subset of 100 cases from noncystic fibrosis (non-CF) patients were evaluated to assess the prevalence of sphenoid sinus hypoplasia.

**RESULTS**

Seventy-eight adult CF patients were identified and included in this study (average age 28.8 years). Sphenoid sinus aplasia or hypoplasia in this cohort is prevalent (71.1%). Prevalence of sphenoid sinus hypoplasia in noncystic fibrosis patients is virtually nonexistent (1%). Frontal sinus hypoplasia was slightly less common (62.3%). Maxillary sinus hypoplasia was least common (22.4%). Sclerosis was seen frequently (91%), and 17% of patients had presence of mucocoele formation. Paranasal sinus inflammation was widespread in our CF cohort.

**CONCLUSION**

Sinonasal underdevelopment and inflammatory change in adult cystic fibrosis patients are akin to findings previously described in pediatric patients. A higher rate of prior ethmoid surgery, significant mucocoele formation, and osseous sclerosis was demonstrated in our adult exclusive retrospective study. High prevalence of bone sclerosis in the maxillary and sphenoid sinuses suggests evolution of osteoneogenesis secondary to longstanding chronic sinonasal inflammation. Additionally, the presence of sphenoid sinus hypoplasia on sinonasal CT imaging should direct one's attention to the possible diagnosis of cystic fibrosis given the close statistical association in comparison to non-CF patients.

**KEY WORDS:** Cystic fibrosis, sinonasal

## Thursday Afternoon

**4:30 PM - 4:45 PM**

**Grand Ballroom Suite**

**(72) CLOSING REMARKS**

**0-651**

**4:30 PM - 4:45 PM**

### Closing Remarks

Pamela W. Schaefer, MD, ASNR 2012-2013 President

Radiology, Massachusetts General Hospital  
Boston, MA, USA

### PRESENTATION SUMMARY

I will summarize the highlights of the meeting and thank the audience for participating.

**Monday, April 23 -  
Wednesday, April 25**

**6:30 AM - 9:00 PM**

**Thursday, April 26**

**6:30 AM - 3:00 PM**

**Americas Hall II**

**Excerpta Extraordinaire 1 - 46**

**(EE1) - Adult Brain**

**Note: A missing printed number indicates an abstract has been withdrawn.**

### EE-1

**Susac's Syndrome: Neuroradiology Makes all the Difference**

Keiper, M. D.<sup>1</sup>•Jones, W.<sup>2</sup>•Horsley, W.<sup>2</sup>•White, M.<sup>1</sup>•Omojola, M.<sup>1</sup>•Poage, D.<sup>1</sup>•Helvey, J.<sup>1</sup>

<sup>1</sup>University of Nebraska Medical Center, Omaha, NE,

<sup>2</sup>Scottsdale Medical Imaging, Scottsdale, AZ

### PURPOSE

Susac's syndrome has protean manifestations and is difficult to diagnose based on clinical findings alone unless the classic triad of retinal branch occlusion, hearing loss and encephalopathy is present and recognized by an astute clinician. The purpose of this abstract is to illustrate the pivotal role of the neuroradiologist in assimilating clinical information and imaging findings to successfully diagnose Susac's

syndrome and lead the referring clinician and patient to the appropriate treatment.

#### CASE REPORT

A 34-year-old male with clinical history of hypertension, migraine headaches and diabetes presented to the Emergency Department (ED) of a community hospital every 2 weeks over a 4-month period with complaints of headache, intermittent blurred vision and difficulty with concentration. Laboratory and CT imaging of the brain at the time of several ED visits were unremarkable with the exception of mild nonspecific white matter attenuation changes attributed to small vessel ischemia in the brain on CT. The patient was evaluated repeatedly and treated for his chronic medical conditions with recommendations for psychiatric evaluation for increasingly bizarre behavior as witnessed by family. A subsequent ED visit for more severe headache, blurred vision, and anisocoria prompted an emergent MRI of the brain. After preliminary evaluation of the MRI and assimilation of previously recorded clinical data, the neuroradiologist contacted the ED physician and requested evaluation of the patient's hearing. Further evaluation at the bedside by the ED physician elicited a several month history of hearing loss not previously disclosed by the patient. A diagnosis of Susac's syndrome subsequently was offered by the neuroradiologist and ultimately confirmed through audiology, retinal evaluation and additional clinical parameters. The patient was treated with intravenous immunoglobulin and steroids which produced near resolution of hearing deficits, headaches, blurred vision and behavioral anomalies.

#### IMAGING FINDINGS

MR imaging of the brain demonstrated multiple hemispheric and callosal white matter lesions with associated variable enhancement. Callosal lesions were both central and marginal. No regions of restricted diffusion were noted. Diffuse leptomeningeal hyperemia and swelling also was noted in the cerebral hemispheres. All findings dramatically improved after initiation of therapy as demonstrated on follow-up MR imaging.

#### SUMMARY

The neuroradiologist can play a pivotal role in the assimilation of clinical information and imaging findings in the ultimate diagnosis of Susac's syndrome particularly in the setting of protean clinical manifestations.

**KEY WORDS:** Susac's syndrome

#### EE-2

##### Nibbled Cerebral Cortex: A New Sign Characteristic of Sneddon's Syndrome

Politi, L. S.<sup>1</sup>Vivoda, M.<sup>1</sup>Godi, C.<sup>1,2</sup>Rodegher, M.<sup>1</sup>Colombo, B.<sup>1</sup>Martinelli, V.<sup>1</sup>Falini, A.<sup>1,2</sup>

<sup>1</sup>San Raffaele Scientific Institute, Milano, ITALY, <sup>2</sup>Vita-Salute San Raffaele University, Milano, ITALY

#### PURPOSE

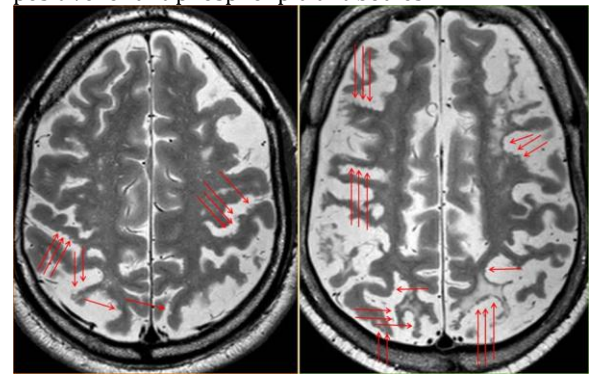
Sneddon's syndrome is a rare disorder characterized by the association of livedo racemosa and neurologic symptoms. It usually occurs in young adults and has been associated with antiphospholipid syndromes. There is no biologic or histological marker, so the diagnosis is based on clinical and nonspecific neuroradiologic findings. We identified characteristic magnetic resonance imaging (MRI) features and propose them as a typical aspects of Sneddon's syndrome.

#### CASE REPORT

Three patients (1 woman and 2 men), who presented with livedo racemosa and progressive cognitive decline were diagnosed with Sneddon's syndrome. Imaging findings, performed on a 1.5 and 3 T MR scanners, were related to clinical and laboratory findings.

#### IMAGING FINDINGS

In all three patients, besides nonspecific small hyperintense lesions of the white matter on T2-weighted images, we observed punctiform cortical lesions, giving the appearance of a nibbled cerebral cortex. Lesions appeared hyperintense on T2-weighted and hypointense on T1-weighted images, with parieto-occipital predominance. Parieto-occipital atrophy was particularly evident with enlargement of the posterior portions of the lateral ventricles. The patients disability related with the duration of the disease and the site and extent of the cortical involvement. Two patients tested positive for antiphospholipid antibodies.



#### SUMMARY

Sneddon's syndrome should be considered in cases with nibbled cerebral cortex appearance together with parieto-occipital atrophy.

**KEY WORDS:** Sneddon, MR imaging, cortical alteration

#### EE-3

##### Subacute Methotrexate Neurotoxicity: Stroke-Like Clinical Presentation with Restricted Diffusion in the Bilateral Centrum Semiovale White Matter

Millar, W. S.·Foreman, B.·Mandel, A.

Columbia University Medical Center  
New York, NY

### PURPOSE

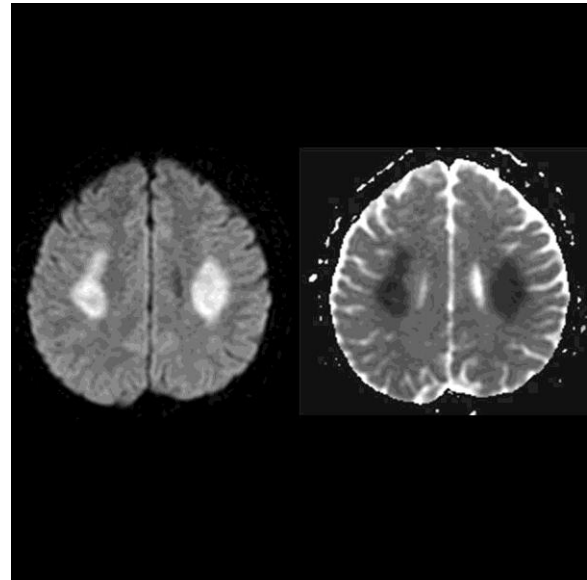
To illustrate the unusual stroke-like sequelae of subacute methotrexate neurotoxicity to the bilateral centrum semiovale white matter using MRI and MRS.

### CASE REPORT

A 20-year-old man, undergoing chemotherapy for pre-B cell acute lymphoblastic leukemia (ALL), received intrathecal methotrexate, cytarabine, and hydrocortisone, followed by systemic methotrexate without immediate complications. Soon after, the patient presented to clinic with a headache and mild nausea. He was afebrile and his clinical exam was reportedly normal. When standing to leave the clinic, he suddenly felt dizzy and nauseous. When the clinic staff addressed him, he was able to nod, but was completely unable to speak. He was placed on a stretcher, a rapid response team was called, and he was transported to the emergency department (ED). In the ED, his initial vital signs, and peripheral glucose, were normal. Additional laboratory studies including serum electrolytes, kidney function, blood count, and coagulation studies were negative. His noncontrast head CT was normal. Intravenous tissue plasminogen activator (tPA) criteria were reviewed, and IV tPA was administered at 2 hours and 15 minutes from onset of symptoms. A lumbar puncture subsequently was performed (opening pressure, slightly elevated; normal glucose, protein, and cells). Left focal slowing was noted on EEG without epileptiform discharges or seizures.

### IMAGING FINDINGS

MR imaging of the brain demonstrated bilaterally symmetric regions of significantly restricted diffusion limited to the centrum semiovale white matter (Figure: DWI (left); ADC map (right)). MR spectroscopy (MRS) of the left frontal white matter lesion (not illustrated) showed no lactate doublet. CT angiography demonstrated no vascular abnormalities, and CT perfusion was symmetric. The patient improved significantly over the next 3 days, and was neurologically normal by day 7. Six weeks later, MRI brain follow-up demonstrated resolution of the restricted diffusion with persistent leukoencephalopathy in the bilateral centrum semiovale white matter on T2 FLAIR images.



### SUMMARY

Subacute methotrexate neurotoxicity can present as acute stroke, both clinically and radiographically. Rapid resolution of clinical and DWI findings, as well as normal CT angiography, normal CT perfusion, and absence of lactate on MR spectroscopy, suggests a transient metabolic encephalopathy, as has been suggested in prior case reports, rather than a vasculopathic ischemic etiology. Awareness of this unusual pattern of acute DWI sequelae localized to the deep cerebral white matter can lead to faster diagnosis, accurate prognosis and improved clinical care of patients with subacute methotrexate neurotoxicity.

**KEY WORDS:** Methotrexate, DWI, neurotoxicity

### EE-4

#### Cortical Hemosiderosis in Familial Acaeruloplasminemia

Postma, A. A. • Hoeberigs, M. C.

Maastricht University Medical Centre  
Maastricht, NETHERLANDS

### PURPOSE

To demonstrate the MR findings in aceruloplasminemia in a symptomatic 51-year-old patient and her asymptomatic brother.

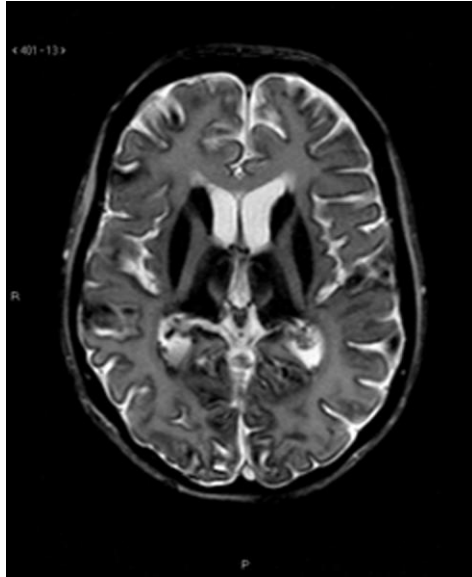
### CASE REPORT

A 51-year-old female presented with cognitive decline since a few years. Her medical history revealed type I diabetes and severe depressions, for which she received psychiatric therapy. Previous imaging was read as normal. Repeated MR of the brain was requested.

### IMAGING FINDINGS

Coronal inversion recovery and transverse T2-weighted images showed marked atrophy, with widening of sulci and ventricular system. The atrophy was progressive from 2005 until 2009. No hyperintense focal signal abnormalities were noted on T2- and FLAIR images. Gradient-echo T2-weighted images demonstrated

marked hypointensity in basal ganglia, thalami, brainstem nuclei and dentate nuclei of the cerebellum. There was a distinct hypointense lining of the bilateral cerebellar and cerebral cortices.



#### SUMMARY

The imaging findings of the brain with involvement of basal ganglia and cortices were suggestive of an iron metabolism disorder, more specifically aceruloplasminemia because of involvement of both basal ganglia and cortices. Serum analysis demonstrated an increased ferritin and an absence of ceruloplasmin. The diagnosis of aceruloplasminemia was made. T1- and T2-weighted images of the liver show marked signal loss in the liver parenchyma, consistent with liver iron loading. Aceruloplasminemia is an autosomal recessive disorder affecting iron metabolism. Therefore screening was offered to first degree relatives. Laboratory analysis of the asymptomatic brother revealed he also was affected. MR imaging of the brain demonstrated hypointense basal ganglia, thalami and dentate nucleus, and partially hypointense lining of part of the cortex. No atrophy was present; therapy was started.

**KEY WORDS:** Hemosiderosis, aceruloplasminemia, cortical involvement

#### EE-5

##### Transient Restricted Diffusion in the Splenium of Corpus Callosum in Migraine with Aura

Agarwal, A.·Maller, V.·Vijay, K.·Kaneekar, S.

Penn State Milton S. Hershey Medical Center  
Hershey, PA

#### PURPOSE

Reversible lesion in the central area of the splenium of the corpus callosum is a unique phenomenon occurring in widespread conditions, particularly in patients with encephalitis or encephalopathy and in patients receiving antiepileptic drugs. We describe a patient suffering from migraine with aura associated with a

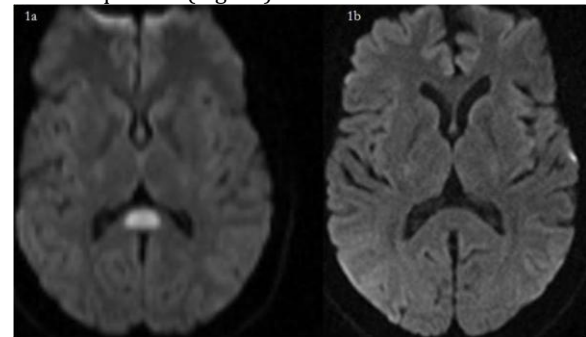
transient abnormality in the midline of the splenium of the corpus callosum, showed by magnetic resonance imaging.

#### CASE REPORT

A 51-year-old man with clinical diagnosis of migraine for last 18 years and multiple prior episodes was admitted again due to very severe throbbing headache, vomiting, and severe general condition. Patient had transient right-sided homonymous hemianopia, however the ophthalmic examination was unremarkable on admission.

#### IMAGING FINDINGS

Magnetic resonance imaging (MRI) revealed a solitary discrete ovoid area of signal abnormality with restricted diffusion in the central part of the splenium of corpus callosum (Fig 1a), with no abnormal enhancement. The imaging findings were nonspecific for any particular pathology and the probability of ischemic stroke was low. Patient had complete resolution of symptoms on the second day of admission and was discharged after being scheduled for follow-up MR in 2 weeks. Follow-up MR showed complete resolution of signal abnormalities on all sequences (Fig 1 b).



#### SUMMARY

There have been reports of various etiologies associated with a temporary focal lesion in the splenium of the corpus callosum manifested as obviously restricted diffusion. We describe a rare case where migraine was considered to be the cause of the reversible focal injury of the splenium.

**KEY WORDS:** Splenium, transient

#### EE-6

##### Adult-Onset Ornithine Transcarbamylase Deficiency: Case Report and Imaging Findings

Suzuki, K.<sup>1</sup>·Hori, M.<sup>2</sup>·Okada, Y.<sup>1</sup>·Tsunoo, M.<sup>1</sup>·Suzuki, H.<sup>1</sup>·Kobayashi, M.<sup>1</sup>·Kodera, J.<sup>1</sup>·Mizumura, S.<sup>1</sup>·Shiraga, N.<sup>1</sup>

<sup>1</sup>Toho University, Tokyo, JAPAN, <sup>2</sup>Juntendo University, Tokyo, JAPAN

#### PURPOSE

Ornithine transcarbamylase deficiency (OTCD) is an X-linked inherited disease and the most common inborn error in urea cycle disorder. There are few data reported on MRI imaging findings of patients with adult-onset OTCD. We report a case of 29-year-old

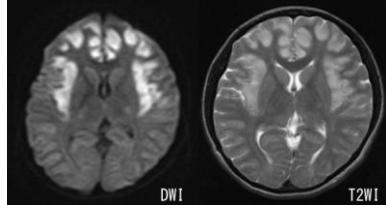
woman of OTCD related hyperammonaemia encephalopathy.

#### CASE REPORT

A 29-year-old woman at 8 weeks of gestation presented with disorientation, repeating speech and bradykinesia without motor dysfunction. During the past 3 weeks, unsuccessful communication can be observed by her husband. Few days before admission, she had nausea and vomiting. There is neither medical history nor family history of disease. No remarkable findings in physical examination. In laboratory investigations, serum ammonia showed abnormal higher value (583 µg/dL). Organic acid analysis in urine revealed a urea cycle disorder. Since the rise of citrulline was not accepted, the patient was diagnosed as OTCD. Symptom and imaging findings have been improved after symptomatic therapy.

#### IMAGING FINDINGS

Hyperintense area spreads out in the wide area of the cerebral cortex, especially in the insular cortex and cingulate gyrus, on diffusion-weighted image (DWI). No signal change in occipital lobes and cerebellum. Also by T2-weighted Image (T2WI), the hyperintense area was observed in the cerebral cortex. Distribution of signal change was the same as that of T2WI.



#### SUMMARY

We report a case of adult-onset OTCD. Characteristic distribution of abnormal intensities have been demonstrated by MR imaging. Hyperintense area accepted the cerebral cortex, especially in the insular cortex and cingulate gyrus, in T2WI and DWI seemed to be characteristic of this disease. Adult-onset OTCD is rare disease but should be added to the differential diagnosis of cortical lesions. Early diagnosis and treatment of OTCD are important to prevent chronic impairment because early changes of this disease can be reversible.

**KEY WORDS:** Ornithine transcarbamylase deficiency

#### EE-7

#### Idiopathic Bilateral Stenosis of the Foramina of Monro: What the Neuroradiologist Needs to Know

Raz, E.·Fatterpekar, G.·Loh, J.·Harter, D.·Davis, A.

New York University  
New York, NY

#### PURPOSE

Idiopathic bilateral stenosis of the foramina of Monro is an uncommon disease condition presenting with biventricular hydrocephalus. The purpose of our study

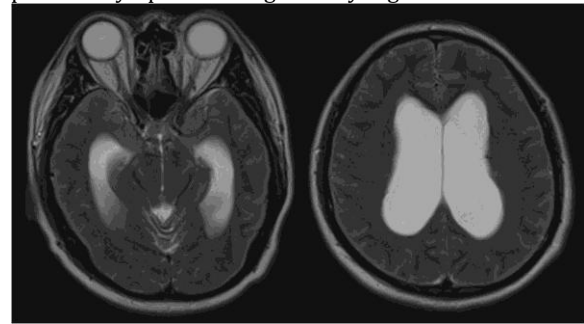
was to demonstrate the typical imaging findings of such a stenosis at the foramina of Monro.

#### CASE REPORT

A 42-year-old man presented with chronic headache and change in mental status.

#### IMAGING FINDINGS

Cross-sectional imaging studies including CT and MRI demonstrated symmetric, moderate to severe enlargement of the lateral ventricles. The third ventricle was slit-like. Downward displacement of the third ventricle and midbrain also was seen. No mass lesion was seen in the region of the foramina of Monro. No abnormal enhancement was seen. A diagnosis of idiopathic bilateral stenosis of foramina of Monro was considered. The patient underwent endoscopic foraminoplasty and septoplasty. Follow-up studies demonstrated reduction in the size of the lateral ventricles and resolution of the downward displacement of the third ventricle and midbrain. The patient's symptoms also gradually regressed.



#### CONCLUSION

Only nine cases of idiopathic stenosis at the foramina of Monro in adults have been reported in the radiology literature. Biventricular hydrocephalus in the absence of abnormal enhancement or any focal mass at the foramina of Monro should raise a red flag for the uncommon but treatable entity of idiopathic stenosis at the foramina of Monro.

**KEY WORDS:** Hydrocephalus, web, Monro foramen

#### EE-8

#### Maple Syrup Urine Disease: MR Imaging Features of Acute Exacerbation in an Adult Patient

Rawal, S.·Faghfoury, H.·Krings, T.

Toronto Western Hospital, University of Toronto  
Toronto, ON, CANADA

#### PURPOSE

Maple syrup urine disease (MSUD) is an inherited disorder of branched-chain amino acid (BCAA) metabolism that manifests in early infancy; the disorder only rarely presents in adulthood. We present a case of an adult with MSUD exacerbation to demonstrate the discrepancy between imaging findings in adults versus children with this disorder, which has not been reported previously.

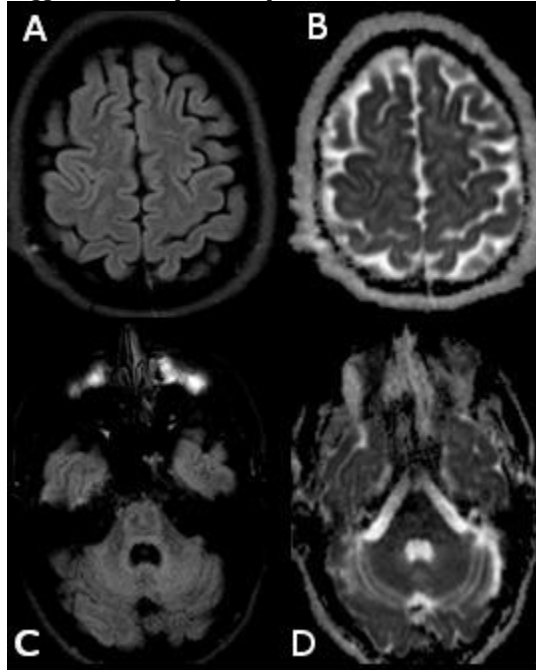


### CASE REPORT

A 36-year-old male patient presented to our emergency department with a 5-day history of decreased oral intake, altered mental status, memory disturbance, impaired balance, nausea and urinary retention. He had a past medical history of classical MSUD diagnosed in infancy, with multiple childhood hospitalizations for disease control. Neurologically, he was at baseline, with stable signs of cerebellar dysfunction. Laboratory studies revealed significantly elevated BCAA levels.

### IMAGING FINDINGS

Cortical thickening with increased FLAIR signal (A) and restricted diffusion on ADC map (B) was identified involving the cerebral cortex, most striking at the superior frontal cortical regions, suggestive of acute cytotoxic edema. Increased FLAIR signal was identified involving the pons and brachium pontis (C) in the absence of restricted diffusion on ADC map (D) suggestive of sequelae of prior exacerbations of MSUD.



### SUMMARY

Prior literature has concentrated on the MRI findings of neonates and children affected by MSUD. In acute neonatal exacerbations, the classic form demonstrates T2 hyperintensity with diffusion restriction predominantly involving the cerebellar white matter, the dorsal brainstem, the posterior limb of the internal capsule, the globus pallidus, and thalamus - areas which are thought to correspond to early myelinated regions within the infant brain. It has been demonstrated in very few cases in the literature that older patients may have additional involvement of the cerebral cortex, rather than the typical childhood pattern of MSUD edema. The MRI findings in our patient support a hypothesis of shifting neurotoxic effects, such that, for reasons that remain to be determined, the pathologic mechanisms that preferentially affect myelinated regions in younger patients, may, with age, progressively involve the cortical gray matter. Despite

the paucity of reported literature as to the adult findings in acute MSUD exacerbation, there is adequate evidence to suggest a discrepancy between the MRI manifestations of exacerbation in adults versus younger patients. An awareness of the expected MRI findings in adults is essential to avoid misdiagnoses in these patients.

**KEY WORDS:** Maple syrup urine disease, MR imaging

### EE-9

#### Concurrent Marginal B-Cell Lymphoma and Oligoastrocytoma, WHO Grade II: MR Spectroscopy and Perfusion Is the Key

Chang, J. P. · Wang, A. · Olson, R.  
William Beaumont Hospital  
Royal Oak, MI

### PURPOSE

To demonstrate the integral role advanced MR imaging techniques, particularly MR spectroscopy and perfusion, played in the diagnosis of a difficult rare case of concurrent oligoastrocytoma and B-cell lymphoma.

### CASE REPORT

A 38-year-old Caucasian male patient with no significant past medical history with an enlarging lump in the left neck for the past 10 months. CT scan demonstrated diffuse lymphadenopathy throughout the body suggestive of lymphoma, confirmed with biopsy as marginal B-cell lymphoma. The patient developed dizziness and blurry vision and was diagnosed with hyperviscosity syndrome and started on plasmapheresis. Ophthalmologic exam showed papilledema and brain MRI was obtained.

### IMAGING FINDINGS

The patient underwent a brain MRI with functional sequences which included speech and motor activation maps, MR spectroscopy and perfusion. Diffusion tensor imaging also was performed for fiber tractography. The MRI demonstrated a 5.5 cm complex cystic mass centered in the left posterior frontal lobe with both solid and cystic components. The mass was both subcortical and cortical with mild inhomogeneous enhancement. There was moderate mass effect and left to right midline shift of 4-5 mm. MR spectroscopy showed no NAA, Choline or creatinine peak in the cystic component of the lesion and significant decrease of the NAA, a creatinine peak and elevation of the Choline peak with the presence of lactate and lipid in the solid portion. There was significant increase of regional cerebral blood volume and flow of the solid component of the left frontal lobe lesion as compared to the contralateral normal brain. Conversely, there was decrease in both regional cerebral blood volume and flow of the cystic component. Fiber tractography showed significant displacement of the fibers surrounding this mass. Functional imaging showed Broca's speech cortex was at the anterior margin and the compensation speech cortex at the posterior margin of the left frontal lobe neoplasm. Wernicke's speech cortex was at the left superior temporal gyri,

approximately 2.8 cm posterior to the posterior margin of the neoplasm. The motor cortex of the right upper extremity was approximately 2.1 cm posterior to the posterior margin of the neoplasm.

#### SUMMARY

This case report highlights the integral role advanced MR imaging plays in diagnosing difficult cases. With the MR spectroscopy and perfusion showing two different distinct patterns, we were able to correctly diagnose separate processes concurrently within one intracranial lesion, confirmed with pathology as oligoastrocytoma, WHO grade II and marginal B-cell lymphoma. In terms of treatment, our patient's lesion was predominantly related to the oligoastrocytoma and as such was treated with successful surgical resection with the aid of DTI and functional imaging, followed by radiation therapy. The patient also is undergoing treatment with chemotherapy for his lymphoma. The value of addition of chemotherapeutic agents to treatment of oligodrogliomas has yet to be studied, but in our patient with a lymphomatous component, parallel treatment is under way hopefully with good results to follow.

**KEY WORDS:** Spectroscopy, perfusion, lymphoma

#### EE-10

##### **Susceptibility-Weighted Imaging Suggests Hyperperfusion as a Compensatory Mechanism in Adult Patients with Hemolytic Uremic Syndrome following an Infection with E. Coli Subtype O104:H4**

Löbel, U.·Sedlacik, J.·Magnus, T.·Gerloff, C.·Fiehler, J.  
University Medical Center Hamburg-Eppendorf  
Hamburg, GERMANY

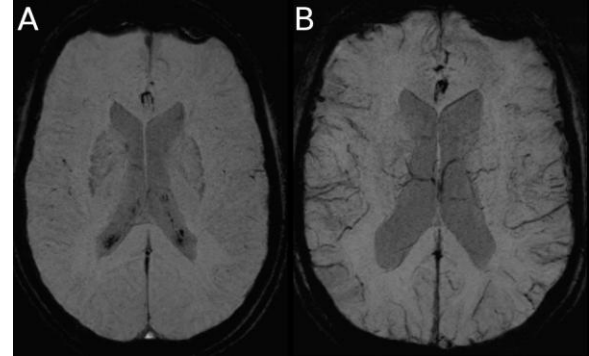
#### PURPOSE

During the recent epidemic with a novel mutation of *Escherichia coli* O104:H4 in Europe (May-July), magnetic resonance imaging (MRI) was performed in adult patients with hemolytic uremic syndrome (HUS) and neurologic symptoms. The MRI protocol included standard conventional sequences and susceptibility-weighted imaging (SWI) which was added for the detection of hemorrhages and hemorrhagic infarcts suspected based on the pathophysiology causing HUS. Interestingly, hemorrhagic lesions were not identified, but the venous contrast on SWI was pathologic in several patients. Our purpose was to describe the relationship of SWI and conventional MRI findings.

#### CASE REPORT

MR imaging was performed in 47 patients (17 male, 30 female) on a 1.5 T scanner using the following parameters for SWI: TE/TR/FA=30 ms/46 ms/15°, matrix =256x256x64, FOV=249x249x128 mm<sup>3</sup>. The data of four patients were excluded from the analysis due to motion artifacts. The signal intensity of the SWI was scored based on the minimum intensity projection image as follows: 1=signal of venous vessels vanished (Figure A), 2=intermediate contrast of deep veins, no contrast of cortical veins, 3=good contrast of deep veins, intermediate contrast of cortical veins and 4=normal SWI contrast (Figure B). In addition, the end tidal CO<sub>2</sub>

(etCO<sub>2</sub>) was recorded if patients were scanned during general anesthesia because etCO<sub>2</sub> influences the cerebral blood flow and consequently the venous blood oxygen level dependent (BOLD) signal. The etCO<sub>2</sub> should be kept <30-35 mmHg to ensure that the signal loss is not due to the general anesthesia. Therefore, the SWI data of three patients were excluded. The etCO<sub>2</sub> for the remaining 40 patients ranged 18-32 mmHg.



#### IMAGING FINDINGS

Conventional MRI was pathologic in 15/40 patients with lesions of bilateral thalamus, bilateral abducens nucleus, cortex, splenium of corpus callosum, centrum semiovale, basal ganglia and cerebellum by T2-weighted and diffusion-weighted imaging suggesting a metabolic toxic effect on the brain. No micro or macrohemorrhages were observed (0/40). Signal intensity on SWI was abnormal in 22/40 patients with the following scores: 1=11 patients, 2=7 patients, 3=4 patients, 4=18 patients. Both conventional MRI and SWI were abnormal in 11 patients, while four patients showed a pathologic conventional MRI and normal SWI. Interestingly, 11 patients showed abnormal MRI findings only by SWI, but not by conventional MRI. No pathology by MRI was identified in 14 patients.

#### SUMMARY

While hemorrhages were not identified, the detected loss of the venous BOLD signal on SWI suggests hyperperfusion as a compensatory mechanism in HUS patients with neurologic symptoms.

**KEY WORDS:** Susceptibility-weighted imaging, *Escherichia coli*, hemolytic uremic syndrome

#### EE-11

##### **Case of Rheumatoid Meningoencephalitis Presenting as Innumerable Subarachnoid Microabscesses**

Lipshutz, G.·Wu, L.·Dodge, J.·Pollock, J. M.  
Oregon Health and Science University  
Portland, OR

#### PURPOSE

A 45-year-old female with a history of rheumatoid arthritis presents with 1 month of progressively worsening neurologic symptoms including severe lower extremity weakness and numbness, headaches, confusion, and falls.

### CASE REPORT

She had been taking methotrexate and prednisone since 2005 and Remicaide was added in April of 2009. She reports a long history of neurologic and ophthalmologic symptoms including waxing and waning arm and leg weakness as well as uveitis. However, when she initially presented to the emergency department, she explained that her weakness, numbness and confusion were much worse. An MRI was performed which showed meningeal enhancement involving the frontal lobes diffusely with T2 hyperintensity/edema extending into the subcortical white matter bilaterally. Cerebrospinal fluid (CSF) studies and blood cultures were negative and she was given a diagnosis of aseptic meningitis secondary to Remicaide. Remicaide then was stopped and the patient was discharged. One month later the patient presented to the hospital again with persistence of leg weakness and numbness, headaches, and forgetfulness. Exhaustive CSF and serum studies for infectious agents as well as autoimmune and inflammatory conditions were performed. Except for a positive RF factor and oligoclonal bodies found in CSF, all tests were negative. Cerebrospinal fluid analysis showed a mildly elevated WBC and a very mildly elevated protein. Her PPD and CSF gram stain and culture were negative. A brain biopsy then was performed which revealed rheumatoid meningoencephalitis. Steroids were restarted and her symptoms improved drastically and she was discharged from the hospital.

### IMAGING FINDINGS

T1 postcontrast images show multiple 4-5 mm nodular ring enhancing lesions diffusely extending into the subarachnoid spaces. The lesions show diffusion restriction centrally. T2 images show paramedian bi-hemispheric areas of T2 hyperintensity within the white matter. The imaging resembles multiple micro-abscesses centered in the subarachnoid spaces around the falx and frontal convexities.



### SUMMARY

Rheumatoid meningoencephalitis is a rare condition associated with rheumatoid arthritis that is often fatal with a mortality of up to 30%. The diagnosis can be

difficult to make, particularly given many rheumatoid patients are on immunosuppressive therapies. Rheumatoid meningoencephalitis should be considered in a rheumatoid patient with severe neurologic dysfunction and no identifiable pathogen to account for the infectious imaging findings.

**KEY WORDS:** Rheumatoid, meningitis, encephalitis

### EE-12

#### Unusual Radiologic Manifestation of Central Nervous System Schistosomiasis Presenting as Fleeting Lesions within the Brain

Jocson, V. D.

London Health Sciences Centre  
London, ON, CANADA

### PURPOSE

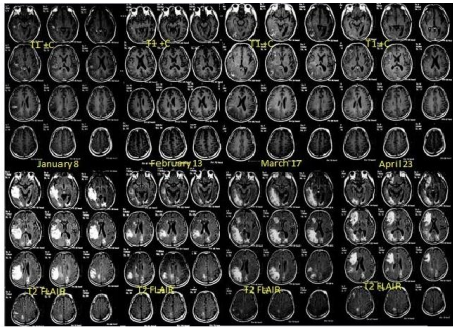
To describe additional features of central nervous system (CNS) schistosomiasis presenting as fleeting lesions during disease evolution within the brain making diagnosis more difficult.

### CASE REPORT

Patient is 39-year-old male, right-handed from southern province in the Philippines who was admitted in the local hospital due to clinical presentation of seizure. History started 8 months prior to admission when he experienced numbness of left lower extremity from knee down, with stiffening of the left side of the body accompanied by headache. There also was documented postictal loss of consciousness. On admission to a local hospital, he was worked up with series of cranial MR imaging prior to eventual surgical biopsy.

### IMAGING FINDINGS

Initial MR examination of the brain on admission shows an apparent irregular and infiltrative lesion within the right temporo-parietal region with mass effect. Enhancement pattern is somewhat nodular with some central linear enhancement like those being described by Liu, et.al. Smaller focus with irregular enhancement also is seen in the right frontal lobe. There are T2 FLAIR edema changes centered to the right temporo-parietal lesion. Investigation led to presumptive diagnosis of an infiltrative high-grade glioma. Subsequent MRI after 1 month redemonstrates the lesion in a more posterior parietal location with corresponding edema shift posteriorly, slightly regressed from before. The previously seen right frontal enhancing focus is no longer seen. After 2 months, the lesions are conspicuously more posterior parietal with evolved and thicker nodular enhancement as well as worsening yet again of the white matter edema. The right frontal lobe lesions reappeared. On the third month before contemplated surgical biopsy, the follow-up cranial MRI showed near total resolution of the previous findings within the right posterior parietal region. The lesions dramatically became prominent within the right frontal lobe with shifting edema changes noted frontally. The biopsy findings in the right frontal lobe revealed chronic granulomatous inflammation with schistosoma eggs.



#### SUMMARY

This case report highlights yet another unusual radiologic presentation of CNS schistosomiasis that makes diagnosis still confusing even in the setting of high disease prevalence. Despite well documented enhancement patterns for this disease entity, this additional feature of apparent fleeting distribution within the brain during disease evolution in the absence of ongoing empirical treatment remains to be elucidated.

**KEY WORDS:** Schistosomiasis, central nervous system, fleeting

#### EE-13

### Imaging Findings of an Unusual *Alternaria* Fungal Brain Infection in an Immunocompetent Patient

Leake, D. R.  
Austin Radiological Association  
Austin, TX

#### PURPOSE

To describe unusual imaging findings of *Alternaria* fungal brain infection in an immunocompetent patient.

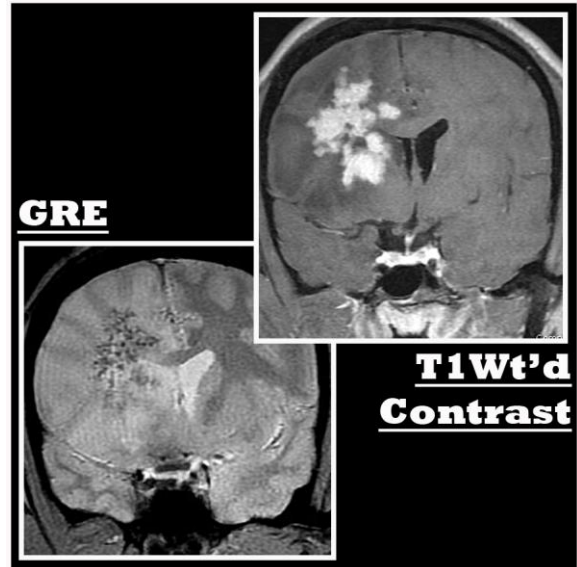
#### CASE REPORT

A 32-year-old male in good health presented to our emergency room with new onset seizure. No significant past history. Normal Labs. CT head exam and MRI head exam revealed a right frontal mass. The imaging findings suggested a high-grade malignancy with nodular enhancement and hemorrhage within its center. At surgery, biopsy revealed necrotizing granulomatous inflammation with yeast and hyphae (path slides available). Subsequent microbiology cultures documented unusual *Alternaria* fungal infection. Subsequent workup by infectious disease consult: no evidence of immunodeficiency; no known predisposing factor to developing this infection (e.g., HIV negative, no underlying malignancies, no travel history, no wound history). Patient was medicated with oral antifungal medication, voriconazole, and is doing well with monthly MRI brain follow-up exams.

#### IMAGING FINDINGS

(CT and MRI obtained on the same day). **CT head:** Inhomogenous mass (hypodense and isodense) right frontal and basal ganglia region. Surrounding vasogenic edema. No hemorrhage, cavitation, or calcification. **MRI head:** T1-weighted inhomogenous mass (hypointense

and isointense). D-weighted: No restriction. Some areas of hypointensity. T2-weighted: inhomogenous mass (hyperintense and isointense) with surrounding vasogenic edema and mass effect. GRE: Nodular areas of hypointensity within the center of the mass (blooming of Ca<sup>+</sup> and/or blood products?) No Ca<sup>+</sup>/hemorrhage seen on CT head. T1-weighted postcontrast: Numerous nodular (cauliflower-like) areas of enhancement within the mass. No cavitation or ring enhancement.



#### SUMMARY

This case report demonstrates how an unsuspected *Alternaria* brain fungal infection caused an unusual imaging pattern on CT/MRI mimicking a malignant brain tumor. The combined MRI findings of cauliflower-like enhancement and hypointensity on GRE may alert the neuroradiologist to include fungal brain infection in the differential diagnosis in future cases.

**KEY WORDS:** Brain/microbiology, alternaria, fungal infections

#### EE-14

### Unique Case of Immune Reconstitution Inflammatory Syndrome

Shah, S.-Kwon, M.-Kanagal Shamanna, R.-Young, K. H.  
M.D. Anderson Cancer Center  
Houston, TX

#### PURPOSE

Immune reconstitution inflammatory syndrome (IRIS) is a rare idiopathic inflammatory syndrome that can be seen following the commencement of antiretroviral therapy in AIDS patients with underlying opportunistic infections. Approximately 15-20% of patients with progressive multifocal leukoencephalopathy (PML) develop IRIS following the onset of therapy. Patients with PML IRIS usually present with worsening neurologic symptoms, and MRI imaging reveals enlarging T2 hyperintense white matter lesions that may demonstrate postcontrast enhancement. The purpose of this excerpt is to describe a unique case of

biopsy-proven PML IRIS presenting with marked mass effect and confluent enhancement, a variant to our knowledge that has not been described previously.

#### CASE REPORT

A 44-year-old male with history of Hodgkin's lymphoma was admitted with increasingly severe headache and dizziness. Initial MR imaging revealed nonenhancing, T2 hyperintense white matter lesions suggestive of PML prompting testing which revealed positive HIV serology. A few weeks after the initiation of highly active antiretroviral therapy (HAART), there was marked progression of symptoms and signs with new onset right lower extremity weakness, dysarthria, and a right-sided visual field defect. Repeat MR imaging revealed new and progressive enhancing, T2 hyperintense white matter lesions resulting in midline shift. Immune reconstitution inflammatory syndrome and lymphoma were offered as presumptive top differential diagnoses based on imaging and clinical history. The patient underwent a brain biopsy that revealed active and chronic inflammatory cells without evidence of lymphoma. Immunohistochemistry revealed cells infected with JC virus. The clinical and laboratory data also supported a diagnosis of PML IRIS, as the symptoms and signs progressed after the initiation of effective antiretroviral therapy (CD4 count increased from 74 to 194) and improved with continued therapy.

#### IMAGING FINDINGS

Initial MR imaging prior to treatment with HAART demonstrated nonenhancing, T2 hyperintense lesions in the subcortical U fibers (Figure 1), suggestive of PML. A few weeks following initiation of HAART, MR imaging revealed marked progression of T2 hyperintense white matter lesions resulting in 1.1 cm rightward midline shift. These lesions demonstrated new confluent enhancement (Figure 2) without restricted diffusion.

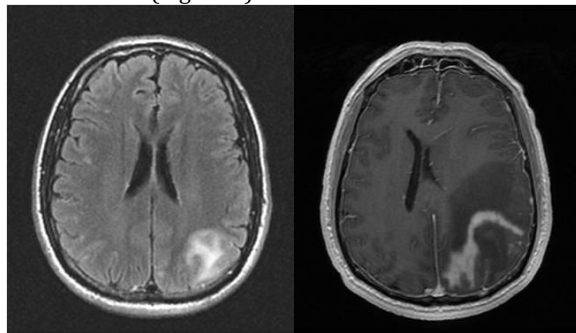


Figure 1: FLAIR

Figure 2: T1+C

#### SUMMARY

Progressive multifocal leukoencephalopathy associated IRIS usually presents with T2 hyperintense white matter lesions with mild or no enhancement. Our case reveals a unique presentation of PML-associated IRIS that presented with confluent enhancement and midline shift. The diagnosis should be included in the differential based on these imaging findings.

**KEY WORDS:** IRIS, PML, HIV

#### EE-15

#### MR Imaging Findings of Rheumatoid Meningitis: A Case Report

Hasiloglu, Z. I.-Asik, M.-Erer, B.-Dikici, A. S.-Altintas, A.-Albayram, S.

Istanbul University  
Istanbul, TURKEY

#### PURPOSE

To present the clinical and cranial magnetic resonance (MR) imaging findings of a 62-year-old rheumatoid arthritis (RA) patient who has been followed up for 4 years and diagnosed as rheumatoid meningitis (RM) by demonstrating findings of meningitis on cranial MR scan and excluding other etiologic factors.

#### CASE REPORT

A 62-year-old woman with a 4-year history of RA who was admitted to our hospital after experiencing headache over 1 month and newly developed paresis and paresthesia on her left arm. Physical examination showed arthritis with synovial hypertrophy on her hand, foot and wrist joints, compatible with RA. There was no abnormal findings in neurologic examination and mental status. Laboratory data showed increased rheumatoid factor as high as 351 IU/mL and anticyclic citrullinated peptide (120 IU/mL). Serum examination for other autoantibodies were normal. Cerebrospinal fluid (CSF) analysis revealed mildly increased white cell count (40 cells/mm<sup>3</sup>) and protein levels (40 mg/dL) without any atypical cells.

#### IMAGING FINDINGS

Cranial MR imaging revealed hyperintensity in the right frontoparietal subarachnoid space on fast fluid-attenuated inversion recovery (FLAIR) images and meningeal thickening and pathologic contrast enhancement on T1-weighted images. Diffusion-weighted images showed restriction of diffusion at the same localizations. Reasons that may lead to leptomeningeal and pachymeningeal enhancement by imaging characteristics are sought. These are; infectious, tumoral, inflammatory and other causes. But with the patient's clinical history, physical examination, blood count, biochemistry results, CSF analysis findings, lung x-ray, thoracic and abdominal CT, other diseases except RM were excluded. Definite diagnosis of RM is done by pathologic examination but, we couldn't perform biopsy because of disapproval of the patient. According to the imaging and laboratory findings and 4 years of RA history, we assumed the diagnosis was RM. Then we started methylprednisolone 1000mg/day for 5 days, continued with oral prednisolone 60 mg/day and added 20 mg/week MTX and 10 mg/week folic acid treatment. We gradually decreased the oral prednisolone dose until reaching to maintenance dose of 4 mg/day. Both the clinical response and normalized CSF examination findings supported the RM diagnosis.

#### SUMMARY

Rheumatoid arthritis is a treatable disease with high mortality rate. For treatment, accurate diagnosis has a

crucial role. Cranial MR imaging and biopsy findings have primary importance on RM diagnosis. In RA patients, meningeal thickening and contrast enhancement on cranial MR should bring RM to mind. To make accurate diagnosis, as we elucidated, other conditions that may cause meningeal enhancement should be excluded.

**KEY WORDS:** Rheumatoid arthritis, rheumatoid meningitis, MR imaging

#### EE-16

##### **Acute Cerebellitis Associated with H1N1 Influenza Vaccination**

Ferreira, R. M.<sup>1</sup>Cini, F.<sup>2</sup>Albino, P.<sup>2</sup>

<sup>1</sup>Clinica Imagem, Florianopolis, BRAZIL, <sup>2</sup>Hospital Governador Celso Ramos, Florianopolis, BRAZIL

#### **PURPOSE**

Neuroinflammatory disorders have been associated to autoimmune diseases and following viral infections. Opsoclonus myoclonus syndrome is a rare disorder that has been described in the setting of central nervous system malignancies and following viral infection. Clinical features of involuntary saccades, myoclonus, and ataxia are pathognomic for this condition, which may be reversible with steroid or iv immunoglobulin therapy. We herein describe a patient with acute cerebellitis and opsoclonus myoclonus syndrome following H1N1 vaccination.

#### **CASE REPORT**

A 62-year-old female, with diabetes mellitus II, started with dizziness and nausea two days after H1N1 influenza vaccination. On the fifth day, the patient could not stay in orthostatic position, with a paresis in all the limbs. Two days after, she presented with cephalic tremor and horizontal opsoclonus with ocular flutter, beyond a marked dysmetria in the upper limbs. Intravenous methylprednisolone was administered for 3 days. After that, she started with urinary retention. Endovenous immunoglobulin was administered for 5 days with little response. The patient got worse and couldn't eat anymore. Finally, she evolved to a coma state, responding only for pain stimulus.

#### **IMAGING FINDINGS**

Brain MRI performed at day 30 after vaccination demonstrated diffuse cerebellar swelling with cortical hypersignal on T2WI and Flair imaging. Second MRI at day 60 showed regression of cerebellar swelling with persistent hypersignal intensity on T2WI involving cerebellar white matter.

#### **SUMMARY**

This is the first report of acute cerebellitis and opsoclonus myoclonus syndrome following H1N1 vaccination. Cerebellar swelling was presumed an autoimmune response triggered by H1N1 vaccination. There is no previous report of any sort of brain MRI abnormalities associated with such vaccination.

**KEY WORDS:** Inflammatory, H1N1

#### EE-17

##### **Neurosarcoidosis Mimicking Cerebral Contusions in the Setting of Trauma**

Farid, N.

University of California San Diego  
San Diego, CA

#### **PURPOSE**

To report an interesting case of neurosarcoidosis mimicking cerebral contusions in a patient status post motor vehicle accident.

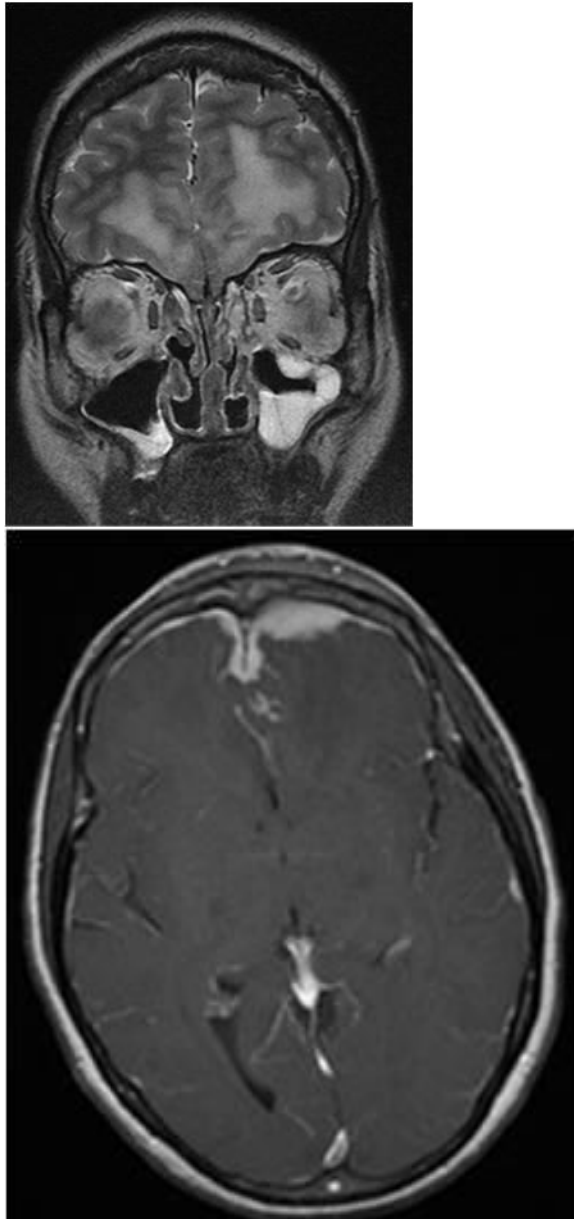
#### **CASE REPORT**

A 54-year-old female presented to the emergency department following a motor vehicle accident. Initially noncontrast CT of the head was performed with findings highly concerning for bifrontal cerebral contusions. The patient subsequently was transferred to a tertiary care center for further neurologic workup, and MRI of the brain was obtained. Based on the MRI findings, the patient underwent a sinonasal biopsy demonstrating nonnecrotizing granulomata which, together with the imaging findings, was consistent with a diagnosis of neurosarcoidosis.

#### **IMAGING FINDINGS**

Initial noncontrast head CT demonstrated large patchy areas of hypodensity in the bifrontal lobe white matter. Subsequent MRI of the brain with gadolinium demonstrated marked nodular dural thickening and enhancement overlying the bifrontal convexities and along the anterior falx with associated T2/FLAIR hyperintensity in the bifrontal lobe white matter. In addition, MRI demonstrated a homogeneously enhancing dural mass in the left cavernous sinus, an enhancing nodule in the left lateral pterygoid muscle, and extensive paranasal sinus inflammatory disease.





#### SUMMARY

It is well known that MRI is highly valuable in the setting of head trauma in order to detect findings which may not be evident on CT such as diffuse axonal injury. However, this case highlights the additional utility of MRI in excluding other entities which may mimic traumatic head injury such as inflammatory disorders, as in the present case, and nontraumatic causes of intraparenchymal hemorrhage such as neoplasms and vascular malformations. Furthermore, this case highlights the fact that extensive imaging findings of neurosarcoidosis may not be associated with symptoms and that involvement of the paranasal sinuses is a fortuitous finding as it offers the clinician a relatively safe target for biopsy.

**KEY WORDS:** Neurosarcoid

#### EE-18

#### Orbital Myositis Associated with Crohn's Disease

Rahman, F. N.·Castillo, M.

University of North Carolina Chapel Hill  
Chapel Hill, NC

#### PURPOSE

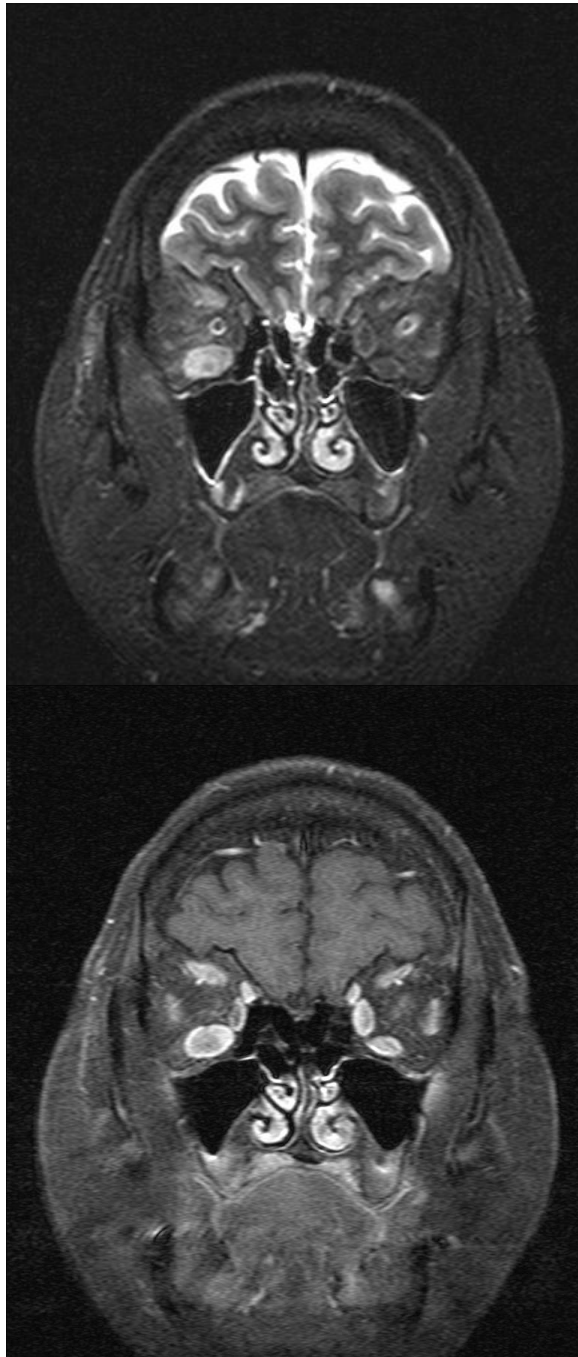
Ocular myositis is an entity within the spectrum of idiopathic orbital inflammatory syndrome, formerly known as orbital pseudotumor. Orbital myositis represents inflammation of one or more unilateral or bilateral extraocular muscles. Although orbital myositis can be idiopathic, it often is associated with infectious processes such as Lyme disease, cysticercosis, poststreptococcal, and herpes zoster as well as systemic inflammatory conditions such as sarcoidosis, systemic lupus erythematosus, Crohn's disease, giant cell arteritis, and scleroderma.

#### CASE REPORT

A 44-year-old female with Crohn's disease presents to the hospital from her physician's office for "eye infection and swelling". On examination, she has decreased vision in her right eye. Over the last few days, her vision has deteriorated from mild diplopia to seeing only dark and light with her right eye. In addition, she has been suffering from severe right periorbital pain and photophobia exacerbated by eye movements. The patient has had similar symptoms in the past intermittently associated with both eyes. Her ocular symptoms usually have occurred in association with flare-ups of her intestinal Crohn's symptoms. The patient was given solumedrol iv and discharged on oral steroids. Her symptoms improved. On a future admission, the symptoms and imaging findings occurred contralaterally with resolution of the right-sided findings.

#### IMAGING FINDINGS

T2 and postcontrast T1 coronal MRI of the orbits reveals enlargement, edema, and enhancement of primarily the right inferior rectus muscle, although other extraocular muscles are involved to a lesser degree. Thyroid associated ophthalmopathy appears similar, although it is usually symmetric.



## EE-19

### Simultaneous Development of a Brain Abscess and Endogenous Endophthalmitis Due to *Klebsiella Pneumoniae*

Kim, Y.·Chang, H.·Kim, M.

Keimyung University Hospital  
Daegu, KOREA, REPUBLIC OF

#### PURPOSE

To present simultaneous development of a brain abscess and endogenous endophthalmitis.

#### CASE REPORT

A 55-year-old man with poorly controlled diabetes mellitus was admitted to a local community hospital due to headache and fever. Cerebrospinal fluid (CSF) study revealed bacterial meningitis. The patient's symptoms improved after antibiotic treatment. However, on the third hospital day, he developed blurred vision in right eye and was transferred to our hospital.

#### IMAGING FINDINGS

Diffusion-weighted imaging (DWI) showed bright signal intensities in right orbit and brain. On gadolinium-enhanced T1-weighted image (Gd-enhanced T1WI, not shown), there were ring enhancing lesions in brain, but right orbital lesion was not visible. On FLAIR, there were high signal intensities in corresponding area.

#### SUMMARY

Ocular myositis is a rare inflammatory condition of the extraocular muscles that can be associated with Crohn's disease along with many other systemic inflammatory as well as infectious conditions. The disease process can be severely debilitating due to pain and vision loss. With steroid administration, the imaging findings and symptoms usually resolve.

**KEY WORDS:** Orbital myositis, Crohn's, inflammatory



#### SUMMARY

The purulent fluid of the intraocular abscess has restricted free motion of water producing hyperintensity on DWI and hypointensity on apparent diffusion coefficient (ADC) map. FLAIR is designed for suppression of free water, such as cerebrospinal fluid (CSF). Intraocular purulent fluid appears as high signal intensity foci relative to the vitreous on FLAIR due to a difference in relaxation between proteinaceous inflammatory fluid and the relatively free water in the vitreous. So, high signal intensity in globe on DWI, corresponding low signal intensity on ADC map and hyperintensity on FLAIR are useful for the diagnosis of endogenous endophthalmitis. However, Gd-enhanced T1WI is useless in the diagnosis of endophthalmitis, because the vitreous humor is avascular and an intravitreal abscess may not produce an enhancing wall before the occurrence of inflammatory neovascularization. Similarly, high signal intensity of brain abscess on DWI is due to viscosity and dense cellular packing of purulent material. On FLAIR or Gd-enhanced T1WI, there is nonspecific finding such as high signal intensity or ring enhancing lesion.

**KEY WORDS:** Infectious disease, neuroradiology, MR imaging

#### EE-20

#### Aggressive Papillary Glioneuronal Tumor with First Reported Incidence of Extracranial Metastasis

Pamorthy, S.·Gandhe, A.·Slone, W. H.·Newton, H. B.·Ray-Chaudhury, A.·Bourekas, E. C.

Ohio State University Medical Center  
Columbus, OH

#### PURPOSE

Papillary glioneuronal tumors (PGNT) were first identified as a distinct group of brain neoplasms by Komori et al (1998). They are a relatively new entity within the "neuronal and mixed neuronal-glia" tumor subset in the revised WHO brain tumor classification (2007). To date 37 cases of PGNT have been reported, most commonly in the second and third decade. While PGNT is usually a low-grade malignancy, we present a rare case of a supratentorial tumor with an aggressive postsurgical local recurrence and first ever reported extracranial metastasis to the pleural space. To our knowledge this is the first reported incidence of extracranial metastasis from a PGNT. The current literature, highlights of the clinical and radiologic course over a span of 5 years and histopathologic characterization will be discussed.

#### CASE REPORT

A 19-year-old caucasian female presented 5 years ago with progressive headaches and intermittent right-sided visual field deficits for 2 months. MRI examination of the brain revealed a large left parieto-occipital tumor, initially considered a high-grade glioma. However, histopathologic exam of the resected tumor indicated a rare papillary glioneuronal tumor with an unusually high Ki-67 index of 26% (usually 1-3% in PGNT). The clinical management necessitated an aggressive clinical approach with chemoradiation, on the lines of high-grade glioma management. A total of nine revision surgeries, whole brain irradiation and 13 cycles of systemic chemotherapy failed to contain PGNT recurrence and eventual extracranial dissemination. When she presented with shortness of breath and chest pain earlier this year, chest imaging uncovered a large right pleural effusion and pleural nodularity. Histopathology confirmed pleural metastasis from the primary brain tumor, 5 years after initial diagnosis.

#### IMAGING FINDINGS

The initial MRI exam revealed an irregular, rim-enhancing left parieto-occipital mass. The tumor was thought to be completely resected. At 18 months, follow-up MRI revealed a recurrent ring-enhancing lesion. Recurrent tumor and radiation necrosis were in the differential. However, hypermetabolic activity of the enhancing component on PET CT brain imaging confirmed by histopathology reiterated tumor recurrence. More recently, chest radiography, CT chest and PET CT exams were obtained due to new onset chest pain and shortness of breath. A large right pleural effusion and hypermetabolic pleural nodularity were confirmed histopathologically as pleural metastasis from the primary brain tumor.

**SUMMARY**

Recurrence and distant metastasis of a typically low-grade malignant lesion warrants close interval monitoring, confirmation of the identity of the tumor at recurrence, and also potential transformation into high-grade gliomas. Reporting rare cases like PGNT is very useful in recognizing unknown clinical and imaging patterns of the disease process. It also aids appropriate characterization and identification of specific subsets within the neuronal-glial group of tumors. Comparison and extrapolation of information from multiple cases would help track temporal prognosis, formulate time sensitive and clinically relevant imaging protocols that eventually result in successful treatment strategies.

**KEY WORDS:** Papillary glioneuronal tumor, extracranial metastasis, MR imaging

**EE-21**

### **Adult Cerebellar Medulloblastoma: Striated Enhancement in the Large Cell Subtype**

Zhang, J.<sup>1</sup>•Millar, W. S.<sup>2</sup>•Lignelli, A.<sup>2</sup>

<sup>1</sup>New York-Presbyterian Hospital, New York, NY,

<sup>2</sup>Columbia University Medical Center, New York, NY

**PURPOSE**

To describe the unusual MR imaging features of an atypical case of cerebellar medulloblastoma presenting in an older adult.

**CASE REPORT**

A 48-year-old woman presented with headache, nausea and positional suboccipital pain. MRI brain demonstrated a midline posterior fossa mass. The patient underwent a subtotal tumor resection, followed by radiation therapy and chemotherapy. The frozen section favored lymphoma over medulloblastoma. Permanent sections, however, confirmed the diagnosis as medulloblastoma, large cell type, the least common (about 4%) of four medulloblastoma subtypes, based on WHO classification.

**IMAGING FINDINGS**

MRI images revealed an enhancing midline mass centered on the cerebellar vermis and involving both medial cerebellar hemispheres without subarachnoid seeding. Contrast-enhanced sagittal T1-weighted MR image showed an unusual pattern of striated enhancement (Fig 1a). Adult medulloblastomas usually demonstrate less enhancement compared with that seen in pediatric medulloblastomas, and are more lateral in location. The finding of a striated enhancement is generally atypical for medulloblastoma. Atypical medulloblastoma has been noted to mimic the morphologic appearance of Lhermitte-Duclos disease, however, the dramatic enhancement pattern seen in the current case is not reportedly present. In the current case, MR spectroscopy (TE = 144 ms) demonstrated a markedly increased choline peak with decreased NAA, consistent with high grade of tumor (Fig 1b) and the histopathologic finding of large cell medulloblastoma. In the 5 years of MRI follow up, however, there has been

no evidence of abnormal signal or enhancement to suggest the presence of residual, recurrent or metastatic tumor.

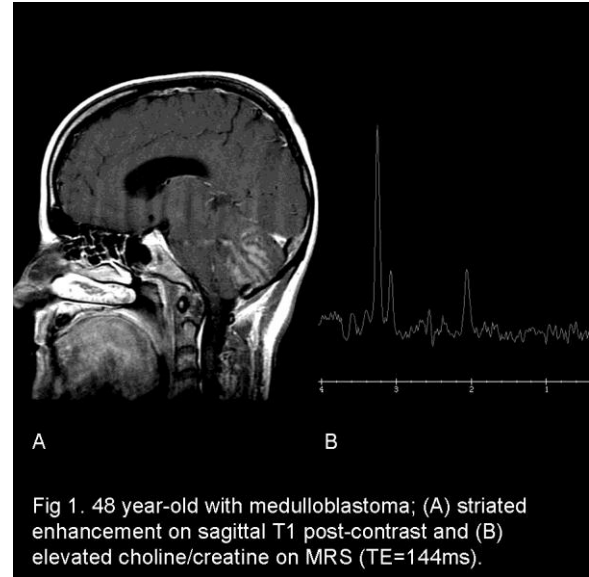


Fig 1. 48 year-old with medulloblastoma; (A) striated enhancement on sagittal T1 post-contrast and (B) elevated choline/creatine on MRS (TE=144ms).

**SUMMARY**

Adult cerebellar medulloblastomas are much less common than their pediatric counterparts, accounting for 0.4%-1% of adult tumors. Almost two thirds of adult cases occur in younger adults (20-40 years), with rare cases reported in adults older than 50 years. The midline vermian presentation with marked striated enhancement in this 48-year-old patient was notably atypical, perhaps reflecting the more aggressive large cell subtype; this subtype usually has a poor prognosis. Awareness of these unusual imaging findings and presentation may assist in the correct diagnosis of medulloblastoma in older adults.

**KEY WORDS:** Medulloblastoma, brain neoplasm, MR imaging

**EE-22**

### **Cerebellar Liponeurocytoma: A Case Report of this Extremely Rare Tumor**

Castanho, P.•Novais, G.•Fragata, I.

Centro Hospitalar Lisboa Central  
Lisbon, PORTUGAL

**PURPOSE**

Cerebellar liponeurocytoma is an extremely rare tumor of the adults, with only a few cases reported worldwide so far.

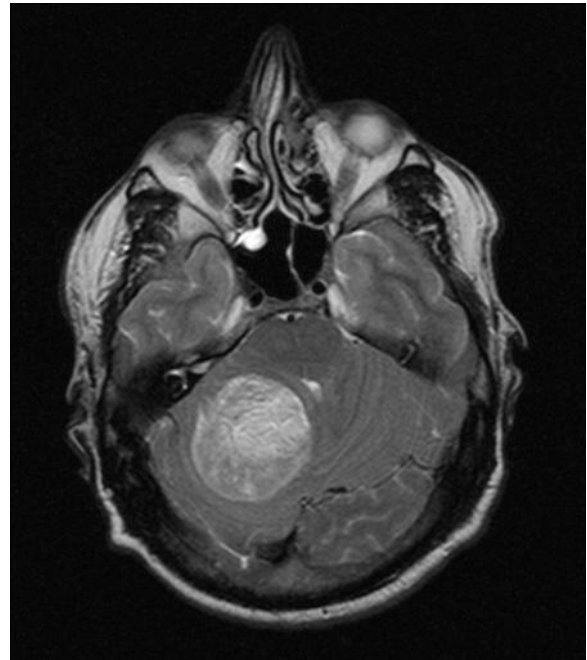
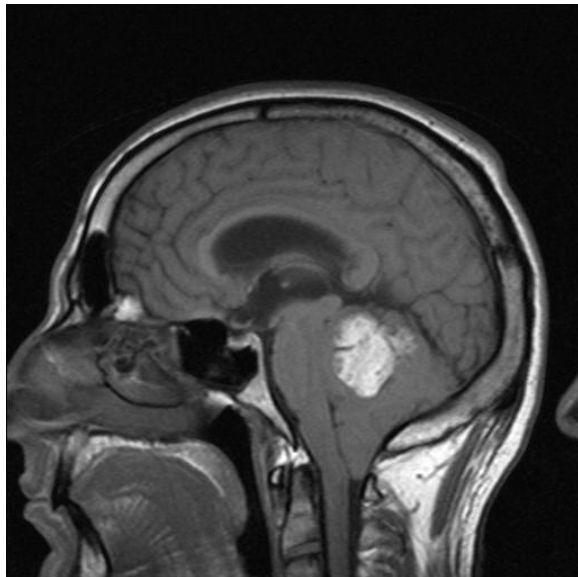
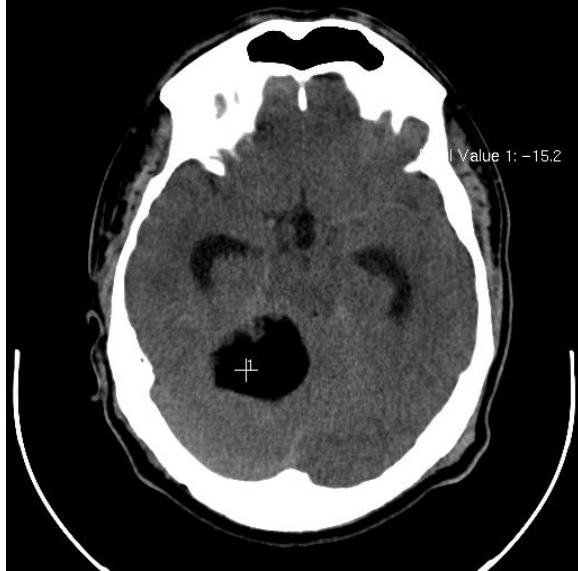
**CASE REPORT**

The authors report the case of a 43-year-old male who presented with long-standing ataxia.

**IMAGING FINDINGS**

MR imaging (MRI) showed a superior vermian and right hemispheric cerebellar solid mass, with high intensity signal on T1- and T2-weighted images, with scant nodular enhancement. Subtotal surgical removal was

performed, with complete recovery of the symptoms. There was no growth of the residual tumor at 6 months.



#### SUMMARY

Cerebellar liponeurocytoma is an extremely rare tumor, that nevertheless should be sought whenever in face of a solid mass of the cerebellum in an adult, particularly with a lipidic component. It usually bears a favorable prognosis.

**KEY WORDS:** Liponeurocytoma, cerebellum

#### EE-23

#### Sella Paraganglioma Arises in the Clivus: Case Report and Literature Review

Hill, J. A. • Aulino, J. • Nickols, H. H. • Russell, P. T. • Ramachandra, T.

Vanderbilt University Medical Center  
Nashville, TN

#### PURPOSE

We present a case of paraganglioma involving the sella and clivus, and suggest that sellar paragangliomas arise in the clivus.

#### CASE REPORT

An 86-year-old female presented with generalized weakness. Cross-sectional imaging revealed a mass centered within the clivus. Following transnasal endoscopic excisional biopsy, the diagnosis of paraganglioma was confirmed by pathologic evaluation, following morphologic and immunohistochemical analysis. MR studies 8 years prior to presentation suggest a clivus origin of this paraganglioma. Review of the 22 reported sellar paraganglioma cases since 1978 suggests that sellar paragangliomas invariably involve the clivus.

#### IMAGING FINDINGS

CT demonstrates a mildly lobular 45 mm mass centered within and eroding the clivus, with involvement of the

sella, clivus, and sphenoid sinuses, without internal calcifications. The lesion demonstrates moderate, relatively homogeneous enhancement with encasement of the internal carotid arteries. No other internal vascular flow voids were present, and the tumor did not display a "salt and pepper" appearance on any sequences.

#### SUMMARY

Paraganglioma arising in the sellar region is a rare diagnosis. MR studies of our patient, obtained 8 years prior to presentation, suggest that sellar paragangliomas arise in the clivus and extend into the sella, a theory supported by literature review.

**KEY WORDS:** Paraganglioma, sella, clivus

#### EE-24

##### Olfactory Nerve Ganglioglioma

Guha-Thakurta, N.·Debnam, J. M.·Langford, L. A.

M.D. Anderson Cancer Center  
Houston, TX

#### PURPOSE

To describe the first case of an olfactory nerve ganglioglioma.

#### CASE REPORT

An 18-year-old male with persistent headaches.

#### IMAGING FINDINGS

MR imaging revealed a 6 cm x 2.5 cm extra-axial mass along the floor of the left anterior cranial fossa demonstrating T2 hyperintensity and homogeneous enhancement with a cystic component posteriorly. Its anterior-posterior extent was from the cribriform plate and the fovea ethmoidalis to the optic chiasm. CT angiogram identified circumferential encasement of the A1 segment of the left anterior cerebral artery and downward bowing of the floor of the anterior cranial fossa. There was lack of FDG avidity on PET imaging. The patient underwent an orbitofrontal craniotomy through a subfrontal approach for resection of the mass. Intraoperatively the neoplasm followed the olfactory nerve from the cribriform plate to the olfactory trigone posteriorly. Histologic examination revealed a neuroectodermal neoplasm with a large percentage of astrocytic cells positive for S-100 and a subset positive for GFAP. Also noted was positive immunoreactivity for synaptophysin of the ganglion-like cells and a final diagnosis of ganglioglioma of the olfactory nerve.

#### SUMMARY

Gangliogliomas are mixed glioneuronal tumors and commonly involve the temporal lobe. We describe the first case of a ganglioglioma of the olfactory nerve with radiologic-pathologic correlation, discuss the differential diagnosis on imaging, its management and outcome.

**KEY WORDS:** Ganglioglioma, olfactory nerve

#### EE-25

##### Central Giant Cell Reparative Granuloma Presenting as a Parasellar Mass

Muzzafar, S.·Luttrull, M. D.·Bourekas, E. C.·Slone, H.

Ohio State University Medical Center  
Columbus, OH

#### PURPOSE

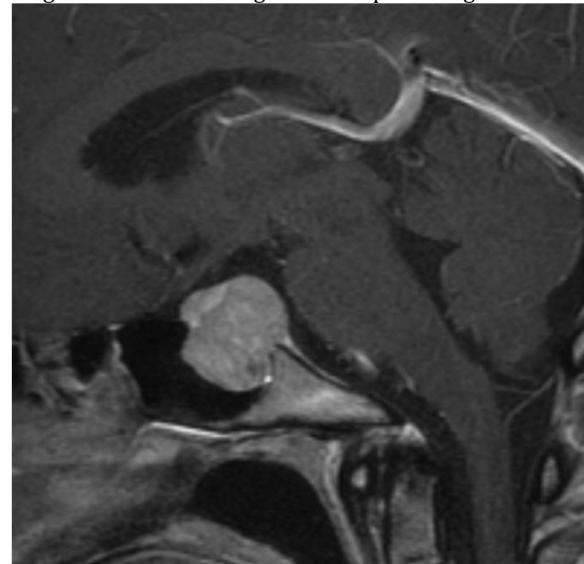
We report a rare case of a parasellar mass which was pathologically proven to represent a central giant cell reparative granuloma. Central giant cell granulomas rarely have been reported in the sphenoid bone. However, to our knowledge, this is the first case of a central giant cell reparative granuloma presenting as a parasellar mass with pituitary dysfunction.

#### CASE REPORT

A 19-year-old male presented with a 3-month onset of weight loss, headache, blurry vision and drooping left eyelid. He had evidence of pituitary dysfunction with low levels of growth hormone and testosterone. Physical examination was significant for a dilated left pupil and ptosis suggestive of left 3<sup>rd</sup> cranial nerve palsy.

#### IMAGING FINDINGS

MRI showed an expansile, enhancing mass centered in the posterosuperior sphenoid bone and dorsum sellae with cavernous sinus and sphenoid sinus extension. MRI showed the pituitary gland to be compressed and displaced anteriorly by the mass. CT images showed calcific densities within the mass. Histopathology revealed spindle cell proliferation, scattered osteoclastic giant cells, prominent multifocal reactive new bone formation and no osteoblastic atypia or pleomorphism. Ki-67 stain showed a proliferation index of about 10 - 12% and the reticulin stain showed focal investment of reticulin around cells. The histologic differential was a giant cell reparative granuloma versus a brown tumor of hyperparathyroidism. The serum biochemistry did not support the latter. The final diagnosis was a central giant cell reparative granuloma.





**SUMMARY**

Central giant cell reparative granulomas are benign fibroosseous lesions. In the head and neck, they are found most commonly in the mandible and maxilla and less frequently within the ethmoid, sphenoid, temporal bones and the cranial vault. The name has been coined by Jaffe who believed that it was not a neoplasm in the real sense but represented a local reparative granulomatous reaction following trauma or inflammation. Hyperparathyroidism should be ruled out as brown tumors appear identical on histopathology. To our knowledge, 4 cases involving the sphenoid bone have been reported in the English literature. We believe this is the first report of a central giant cell reparative granuloma presenting as a parasellar mass and leading to pituitary dysfunction.

**KEY WORDS:** Central giant cell reparative granuloma, parasellar, pituitary

**EE-26**

### **Giant Neurofibroma of the Occipital Scalp Associated with Lambda Defect for 50 Years**

Nakamura, H.·Uchiada, M.·Yoshida, Y.·Tanaka, Y.·Nakajima, Y.

St.Marianna University of Medicine  
Kawasaki, JAPAN

**PURPOSE**

We are to demonstrate the huge neurofibroma with lambda defect for almost 50 years. In the review of literature, there were reports which were published 30 or 40 years ago. We have not read the imaging findings such as computed tomography (CT) and magnetic resonance imaging (MRI). We would like to demonstrate the huge neurofibroma including the CT and MRI imaging.

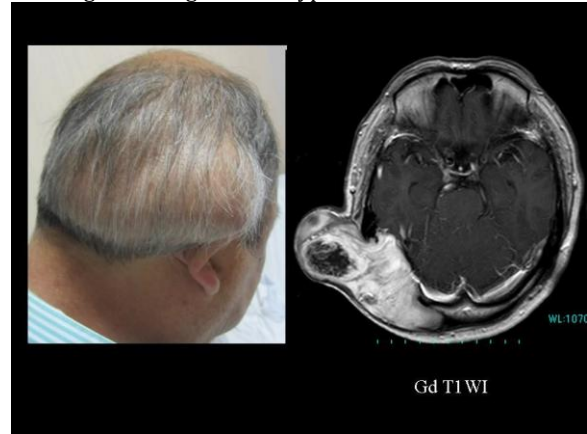
**CASE REPORT**

The patient was a 61-year-old male. He first noticed the occipital scalp mass at the age of 9 years. Since then, it has been increasing gradually for almost 50 years. Because he noticed that it had seemed to be rapidly increasing for the last 2 or 3 years, he came to our hospital. Skull plain radiograph shows the huge mass around the lambda defect. CT and MRI show a hypervascular huge tumor with punctuate calcification around the lambda defect. He had no clinical profile of neurofibromatosis such as café au lait spot, Lisch nodules and so on. Our preoperative diagnosis was hemangioma, hemangiopericytoma. Operation was performed and the pathologic diagnosis was neurofibroma. Our inspection is that although he has no proof of neurofibromatosis, he has neurofibroma in the region of lambda defect with neurofibromatosis.

**IMAGING FINDINGS**

The CT shows a huge soft tissue mass with punctuate calcification in the lambda defect. Around the defect, it has osteoblastic change probably due to the tumor. Contrast CT shows hypervascular. MRI shows the mass has low signal intensity on T1-weighted image and T2-

weighted images and it has prominent flow-voids. Gd T1-weighted image shows hypervascular.

**SUMMARY**

We have experienced a huge neurofibroma in the region of lambda defect. We would like you to be reminded of such a case including CT and MRI findings.

**KEY WORDS:** Neurofibroma, neurofibromatosis, scalp mass

**EE-27**

### **Primary Central Nervous System Extranodal NK/T-Cell Lymphoma, Nasal Type: A Case Report**

Prajapati, H. J.·Vincentelli, C.·Hwang, S. N.·Voloschin, A.·Dehkharghani, S.

Emory University Hospital  
Atlanta, GA

**PURPOSE**

Primary central nervous system (CNS) extranodal NK/T-cell lymphoma, nasal type (NKTCL), is an extraordinarily rare neoplasm, with only five reported cases to date. All existing reports have been in male patients, suggesting a possibly exclusive gender predilection. Here we present a case of primary CNS NKTCL in a 60-year-old immunocompetent woman, representing the index case of this neoplasm in any female or in a patient of African American descent. Given the extreme rarity of this condition, and dearth of radiologic literature, we felt an expanded discussion of the radiopathologic features and presentation of this unique case would be timely.

**CASE REPORT**

A 60-year-old African American woman presented to an outside hospital with acute onset of right-sided weakness and clinical suspicion of acute stroke. Initial CT scan demonstrated a mass in the left frontal lobe. The patient subsequently was transferred to our institution for higher level care. During admission the patient's clinical status declined, with worsening right-sided paralysis and expressive aphasia. Three sequential MRI brain exams with contrast were performed in the following 20 days, all including dynamic susceptibility contrast T2\* MR perfusion (MRP). Stereotactic biopsy of the lesion was deemed

prudent for definitive diagnosis. Subsequent laboratory tests, whole body CT PET, MRI of the whole spine, and biopsy of a suspicious skin lesion also were performed during the course of her workup.

#### IMAGING FINDINGS

Initial MRI revealed a single 2.6 x 2.6 x 2.2 cm left frontal lobe mass with heterogeneous intensity on T1-weighted and intermediate signal on T2-weighted images. Marked perilesional edema and midline shift were noted. The mass demonstrated hyperperfusion on MRP, and features of hypercellularity with a putatively elevated nuclear-cytoplasmic ratio and hindered diffusion (mean ADC = 836 cm<sup>2</sup>/sec). MRI 8 days later revealed enlargement of the lesion to 3 x 3 x 2.5 cm, worsening edema and progression in midline shift. Microscopic examination revealed a malignant lymphoid population infiltrating the brain tissue with an angiocentric pattern and extensive necrosis. Malignant cells were immunoreactive for leukocyte common antigen (LCA, CD45), T-lymphocyte marker CD3, and cytotoxic molecule TIA1, and negative for B-cell markers CD20/PAX5. NK-cell marker CD56 was notably negative. In situ hybridization for EBV encoded RNA was positive. The patient was HIV negative. Complete blood count was normal. Bone marrow biopsy was negative for lymphoma. Of note, no sinonasal/nasopharyngeal primary lesions were noted by history, direct ENT examination, MRI, or PET CT scan. High-dose methotrexate was initiated, but subsequent MRI showed disease progression, and as such was discontinued. The patient was scheduled for impending radiation treatment and continues to be followed at our institution.

#### SUMMARY

Primary central nervous system (CNS) extranodal NKTCL is a highly aggressive but exquisitely uncommon neoplasm. This case represents the first ever reported in a woman, or patient of African American descent. This case expands the narrow clinicopathologic spectrum of NKTCL, however the uniformly aggressive behavior of this disorder is highlighted in the rapid progression of our case, and underscores the need for ongoing investigation towards nosologic clarity and expanded treatment strategies.

**KEY WORDS:** Extranodal NK/T-cell lymphoma, primary CNS lymphoma

#### EE-28

##### Intracranial Solitary Fibrous Tumor

Oswood, M. C.

Consulting Radiologists, Ltd  
Minneapolis, MN

#### PURPOSE

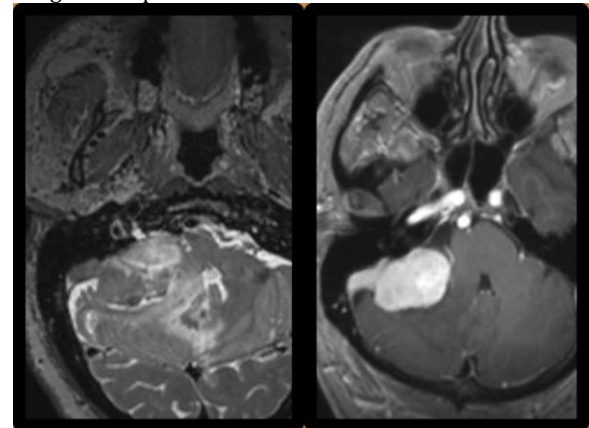
Describe imaging features of intracranial solitary fibrous tumor (SFT), a rare neoplasm which mimics meningioma.

#### CASE REPORT

The patient is a 69-year-old man who presented with neck pain, dizziness and ataxia. He had no cranial neuropathy. Magnetic resonance imaging (MRI) showed a posterior fossa tumor. The patient underwent craniotomy and subtotal tumor resection. A preliminary diagnosis of meningioma was based on imaging findings and frozen section pathology. Permanent pathologic sections with immunohistochemical stains identified the mass as SFT. The patient underwent stereotactic radiosurgery for residual tumor. He is symptom free with no evidence of recurrence at 6-month follow up.

#### IMAGING FINDINGS

An extra-axial enhancing mass is present in the posterior fossa. The mass has a broad dural attachment. There is mass effect on the brainstem and cerebellum, with edema in the cerebellum. The mass has a patchy pattern of increased and decreased signal on the T2-weighted sequence.



#### SUMMARY

Solitary fibrous tumor is a rare neoplasm of mesenchymal origin (Carneiro 1996). Approximately 200 intracranial cases have been reported in the literature (Bisceglia et al. 2011). When the tumor occurs intracranially, its clinical and imaging features are similar to the more common meningioma. Solitary fibrous tumor characteristically has patchy increased and decreased T2 signal which may differentiate SFT from meningioma on MRI (Kim 2004, Clarencon 2011).

**KEY WORDS:** Solitary, fibrous

#### EE-29

##### Case of Lhermitte-Duclos Disease in Undiagnosed Cowden's Syndrome

Cain, J. R.<sup>1</sup>Braham Chaouch, R.<sup>2</sup>Kamaly, I.<sup>3</sup>Mills, S.<sup>3</sup>Evans, G.<sup>4</sup>Soh, C.

<sup>31</sup>University of Manchester, Manchester, UNITED KINGDOM, <sup>2</sup>University Hospital of South Manchester, Manchester, UNITED KINGDOM, <sup>3</sup>Salford Royal Hospital, Manchester, UNITED KINGDOM, <sup>4</sup>Central Manchester University Hospitals, Manchester, UNITED KINGDOM

#### PURPOSE

To describe a classical appearance of a case of Lhermitte-Duclos disease and highlight the importance

of screening patients with this condition for Cowden's syndrome.

#### CASE REPORT

A 36-year-old previously healthy woman presented to neurology with a history of tension headache. She underwent brain and cervical spine MR imaging.

#### IMAGING FINDINGS

The MRI showed a right cerebellar mass, which was T1-hypointense, T2-hyperintense and nonenhancing. The mass contained multiple striations of increased signal intensity. The mass was causing a mild degree of tonsillar herniation and tri-ventricular hydrocephalus. The lesion was consistent with dysplastic cerebellar gangliocytoma (Lhermitte-Duclos disease) and had the classical appearance of multiple striations known as "corduroy" or "tiger-stripe" sign. The patient also was noted to be macrocephalic and was known to have multiple skin lesions. The radiologist alerted the clinicians about Lhermitte-Duclos disease and its association with Cowden's disease. The patient was referred to the genetics service for a review and Cowden's syndrome was diagnosed.

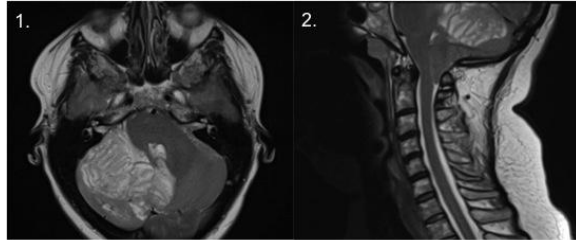


Image 1: T2 axial imaging showing right sided dysplastic cerebellar gangliocytoma with classical tiger-stripe appearance.

Image 2: Sagittal T2 cervical spine image showing dysplastic cerebellar gangliocytoma and mild degree of tonsillar herniation.

#### SUMMARY

Less than 300 cases of Lhermitte-Duclos disease have been described in the literature. In more than 50% of cases there also has been an underlying diagnosis of Cowden's syndrome. The syndrome also known as multiple hamartoma syndrome, it is autosomal dominant and associated with PTEN mutation on chromosome 10. It has a number of associated extracranial neoplasms including breast, thyroid adenomas, GI polyps, and genitourinary malignancy's. Cowden's also is associated with macrocephaly and mucocutaneous lesions including trichilemmomas and facial acral keratoses. Patients with a diagnosis of Cowden's syndrome undergo regular surveillance screening of thyroid, breast, gastrointestinal and genitourinary systems to identify occult malignancies. Lhermitte-Duclos disease is a very rare slow growing neoplasm with a characteristic appearance but all patients with this condition should be screened for Cowden's syndrome due to the high risk of other malignancies.

**KEY WORDS:** Cerebellum, tumor, Cowden syndrome

#### EE-30

#### Use of Coronal Diffusion-Weighted Imaging for the Evaluation of Optic Nerve Ischemia: A CASE REPORT

Vittori, J., Guida, P., Gorelick, J., Tishkoff, N. .

Hospital of Saint Raphael  
New Haven, CT

#### PURPOSE

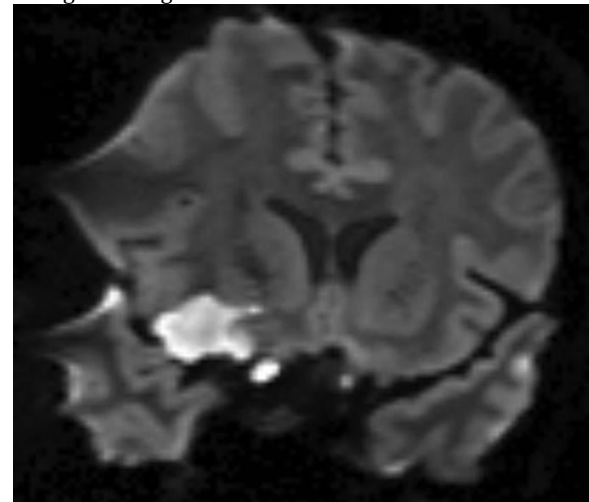
To demonstrate the clinical utility of diffusion-weighted imaging in the coronal plane for the purposes of confirming the diagnosis of ischemic optic neuropathy. Clinical presentation, imaging findings and differential diagnoses will be discussed.

#### CASE REPORT

A 28-year-old male presented with left-sided visual symptoms. Physical exam revealed temporal hemianopsia. A suprasellar mass with findings consistent with a tuberculum sella meningioma was found on initial MR imaging. The patient underwent surgical resection via a right frontotemporal craniotomy. On postoperative day 1, the patient developed progressive loss of vision in the right eye. Ophthalmologic exam was suggestive of posterior ischemic optic neuropathy.

#### IMAGING FINDINGS

MR imaging of the optic nerves was performed postoperative day 2 on a Siemens Magnetom 3 T magnet. Coronal T2-weighted images demonstrated questionable subtle increased T2 signal in the right prechiasmatic optic nerve. Routine axial diffusion-weighted images were limited at the skull base secondary to susceptibility artifact and postoperative changes. For clarification, coronal diffusion-weighted images were obtained which clearly demonstrated restricted diffusion in the right prechiasmatic optic nerve. Subtle restricted diffusion also was noted in the left prechiasmatic optic nerve without corresponding T2 signal changes.



#### SUMMARY

We present an interesting case of postoperative right optic nerve ischemia for which the diagnosis was unequivocally confirmed using thin slice DWI in the

coronal plane. Subclinical subtle ischemic changes in the left optic nerve also were detected with this technique. A search of the literature revealed no prior reports using this technical approach for the evaluation of optic nerve ischemia. Although restricted diffusion has been reported in cases of acute optic nerve inflammation, optic nerve sheath meningiomas and lymphatic lesions, diffusion-weighted imaging, in association with conventional sequences, may be of benefit in differentiating ischemia from other optic nerve pathologies in the appropriate clinical setting. As signal changes on T-2 weighted imaging initially may be extremely subtle or absent, coronal DWI should improve the detection of optic nerve ischemia, particularly within the optic canal and suprasellar cistern, by minimizing susceptibility effects in the region of interest, and should be considered when acute optic nerve pathology is suspected.

**KEY WORDS:** Optic nerve ischemia, diffusion, coronal

## EE-31

### **Caution in the Callosum - Signal Change in the Body of the Corpus Callosum Status Postshunting: Case Presentation and Review of the Literature**

Parker, S. Kirsch, C.

The Ohio State University  
Columbus, OH

#### **PURPOSE**

This case illustrates the presence of a benign signal change in the corpus callosum that can occur postshunting.

#### **CASE REPORT**

A 72-year-old female presented with balance complaints, urinary incontinence, and decreased memory. Magnetic resonance image (MRI) at an outside institution demonstrated dilated lateral and third ventricles. She was given a diagnosis of normal pressure hydrocephalus (NPH) and underwent a trial of lumbar drain with placement of a ventriculoperitoneal (VP) shunt which resulted in resolution of symptoms. After a 2-month period of improvement, the patient had vague visual symptoms and a follow-up MRI at an outside institution noted increased T2 signal, without enhancement in the body of the corpus callosum, and suggested possible neoplasm. However, a PET at this outside institution demonstrated no FDG localization. The patient presented to our institution for possible biopsy and a preoperative Stealth MRI at our institution demonstrated increased T2 and FLAIR signal within the body of the corpus callosum, with no enhancement and preservation of the transverse white matter tracts. A corresponding CT also showed decreased attenuation in the body of the corpus callosum. Although these findings were called immediately at time of review to neurosurgery as likely postshunting benign-appearing signal change with no biopsy required, the neurosurgical service still performed the biopsy based on concerns from the outside report. The biopsy specimen and histopathology revealed benign white

matter with reactive gliosis and no definite tumor. Following the biopsy procedure, the shunt was clamped resulting in recurrence of hydrocephalus (with the lateral ventricles having a bifrontal diameter of 4.4 cm and third ventricular measurement of 1.6 cm) and resolution of the signal change in the body of the corpus callosum. Two days after the shunt was reopened, the hydrocephalus improved (with bifrontal ventricular size decreased to 2.9 cm, and third ventricular measurement to 4 mm) and a recurrence of low signal change in the body of the corpus callosum was demonstrated.

#### **IMAGING FINDINGS**

The timing and presentation of this lesion in the corpus callosum is characteristic of the benign signal change that can occur postshunting for NPH. On MRI the linear high signal preserves the transverse white matter tracts that would be expected to be disrupted by tumoral pathology. In this patient, there is also recurrence and resolution of the low attenuation correlating to the degree of hydrocephalus. Gliomas of the corpus callosum are rare tumors, especially in the elderly. The MR images prior to biopsy also demonstrated no enhancement postgadolinium, and no restricted diffusion on ADC. These findings are all suggestive of a benign appearance postshunting rather than tumor pathology, and although biopsy confirmed the diagnosis of reactive gliosis and no tumor, it is hoped that awareness of these findings will prevent unnecessary invasive surgical biopsy in the future.

#### **SUMMARY**

These findings further emphasize the importance of identifying this as a benign change to avoid unnecessary invasive biopsies.

**KEY WORDS:** Corpus callosum, signal change, shunting

## EE-32

### **Pseudo-Arteriovenous Shunting with MR Perfusion Due to Venous Reflux from Transient Functional Central Venous Stenosis Due to Valsalva**

Chen, J. Y.-U, H. S.-Oygar, A. E.-Imbesi, S. G.-Ciacci, J. D.-Lee, R. R.

San Diego VA Medical Center/University of California  
San Diego Health System  
San Diego, CA

#### **PURPOSE**

To describe a previously unreported MR perfusion artifact resulting in a striking pattern of abnormality on postprocessed perfusion maps, simulating arteriovenous shunting.

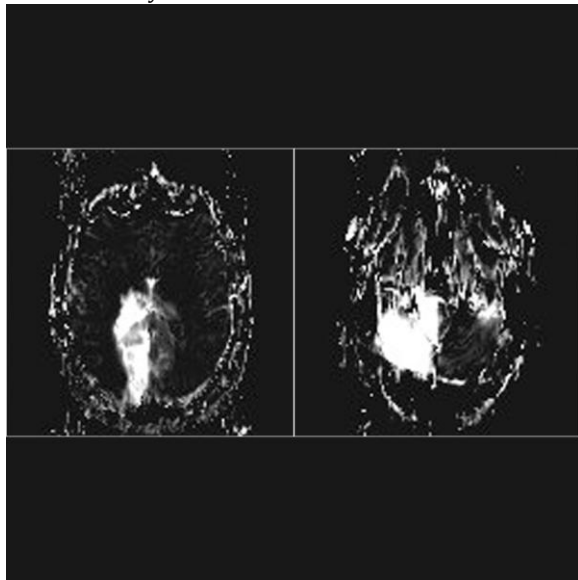
#### **CASE REPORT**

A 46-year-old male presented with a cystic lesion centered in the cerebellar vermis, which had developed new curvilinear areas of enhancement. MR spectroscopy and perfusion were performed to further evaluate the lesion. MR perfusion was acquired using GRE EPI technique during a 3 mL/sec injection into the

right antecubital vein. Perfusion data were postprocessed using the basilar artery for the arterial input function due to the location of the lesion in the posterior fossa. The MR perfusion maps demonstrated apparent marked asymmetric perfusion abnormality in the posterior fossa, and medial occipital/inferior parietal lobes, disproportionate to the size of the vermian lesion and generally corresponding to the posterior circulation territories across all perfusion maps (rCBV, rCBF, MTT, and TTP). To evaluate the perfusion abnormality further, perfusion source images were reviewed, which demonstrated temporally earlier contrast arrival in the areas of perfusion abnormality than in the cerebral arterial system, suggesting retrograde venous perfusion through the jugular vein. Contrast-enhanced CT of the chest to evaluate for areas of central venous stenosis and to exclude venous compression from an intrathoracic mass was unremarkable. When interviewed, the patient recalled being surprised at the start of the bolus contrast injection, resulting in a brief, sharp inhalation and breath-hold - functionally a Valsalva maneuver, transiently increasing intrathoracic pressure. MR angiography of the circle of Willis, MRV of the brain and repeat MR perfusion were performed with the patient at quiet respiration using the same route of injection, contrast dose and imaging parameters as the initial study. The findings of the MRA/V were unremarkable. The new perfusion maps and source data were normal and symmetric.

#### IMAGING FINDINGS

Selected rCBF maps demonstrate abnormal asymmetric blood flow in the right cerebellum and posterior cerebral artery territories.



#### SUMMARY

In our patient, the best explanation for this pattern of perfusion abnormality, which mimics arteriovenous shunting, is retrograde venous perfusion due to impaired central venous flow related to transiently increased intrathoracic pressure during unintended Valsalva. This explanation reinforces the importance of reviewing perfusion source images and also reinforces

preexisting recommendations for performing dynamic contrast-enhanced studies, such as CT or MR angiography or perfusion with techniques to minimize venous reflux.

**KEY WORDS:** Perfusion, artifact, Valsalva

#### EE-33

#### Acquired Ependymal Cyst with Appearance Similar to a Craniopharyngioma Implant

Sabin, N. D. • Ellison, D. W. • Klimo, P. • Harreld, J. H. • Patay, Z. • Kun, L. E.

St. Jude Children's Research Hospital  
Memphis, TN

#### PURPOSE

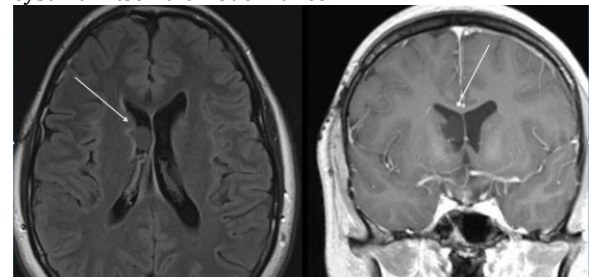
To present the clinical history and MR imaging features of an acquired ependymal cyst that resembled a metastatic cystic craniopharyngioma implant.

#### CASE REPORT

A 20-year-old woman with a history of a suprasellar craniopharyngioma that had been partially resected and treated with radiation developed a cyst, detected on surveillance magnetic resonance imaging (MRI) studies, that extended from a defect associated with a prior right frontal drainage catheter tract into her right lateral ventricle. The cyst enlarged over an approximately 4-year period until it measured approximately 1.4 cm x 1.4 cm x 1.1 cm. The patient demonstrated no signs or symptoms potentially related to the enlarging structure. Due to the increase in the size of the cystic lesion and the fact that it might represent a metastatic craniopharyngioma implant along the catheter tract, the cyst was removed surgically. The histologic diagnosis of the cystic structure was an ependymal cyst.

#### IMAGING FINDINGS

MR imaging demonstrated a cystic lesion that extended into the right lateral ventricle from a defect in the lateral wall of the anterior aspect of the body of that ventricle (arrows). The defect was associated with a prior right frontal drainage catheter tract. The signal intensity of the cyst was slightly greater than CSF on unenhanced T1-weighted images and isointense to CSF on T2-weighted images. The lesion was moderately hyperintense on postcontrast FLAIR images. Water diffusion in the lesion was slightly lower than that of CSF, suggesting macromolecular contents. Enhancing vessels were present along portions of the cyst, but the cyst wall itself did not enhance.





**SUMMARY**

Ependymal cysts are ependymal lined cystic structures that contain fluid that usually follows cerebrospinal fluid (CSF) signal intensity on MRI. They are characterized as developmental cysts and are usually incidental asymptomatic findings on imaging although there are reports of symptomatic ependymal cysts. To our knowledge, there are no reports of acquired ependymal cysts. Metastatic implants of craniopharyngioma along the routes of previous surgical approaches are reported although they are rare. In this case, the apparent proteinaceous contents of a cystic lesion along the course of a prior drainage catheter tract in a craniopharyngioma patient caused concern for a metastatic craniopharyngioma implant. The unexpected tissue diagnosis of an ependymal cyst suggests that such cysts may be acquired subsequent to procedures that extend into a ventricle and, in the proper context, may appear similar to a craniopharyngioma cyst.

**KEY WORDS:** Ependymal cyst, postoperative findings

**EE-34****Rare Presentation of a Vidian Nerve Schwannoma**

Willy, R. Paz, D.  
Naval Medical Center San Diego  
San Diego, CA

**PURPOSE**

1. Describe a rare presentation of vidian nerve schwannoma. 2. Review the clinical and diagnostic imaging manifestations of cranial schwannomas. 3. Define the anatomy of the vidian nerve and the clinical findings of vidian nerve dysfunction. 4. Describe the surgical approaches for biopsy and treatment of a vidian nerve schwannoma.

**CASE REPORT**

1. Epidemiology and clinical implications of cranial schwannomas. 2. Appropriate imaging modalities and techniques to investigate suspected schwannomas. 3. Expected surgical management for diagnosis and treatment.

**IMAGING FINDINGS**

Vidian nerve schwannomas are exceedingly rare with only three cases reported in the current medical literature. In this case, the patient was being evaluated initially for asymmetric right-sided sensorineural hearing loss with an MRI of the internal auditory canals that incidentally revealed an expansile mass within the greater wing of the right sphenoid bone. MR imaging and CT angiography, in addition to transthyroid biopsy, was consistent with schwannoma in the expected location of the vidian nerve. Further clinical workup was consistent with reduced lacrimation on the right also consistent with a vidian nerve lesion. Complete surgical resection was not possible secondary to suspected carotid involvement by this presumed vidian nerve schwannoma.

**SUMMARY**

1. Vidian nerve schwannomas are very rare tumors. 2. Proper imaging findings can suggest the diagnosis and guide surgical approach for diagnosis and management.

**KEY WORDS:** Schwannoma, vidian

**EE-35****Advanced Imaging of Cerebral Fat Embolism**

Eckel, L. J. Gilbertson, J. Campeau, N.  
Mayo Clinic  
Rochester, MN

**PURPOSE**

Provide an update to the imaging appearance of cerebral fat embolism.

**CASE REPORT**

A young male was involved in a motor vehicle crash, fracturing his femur. He was treated initially with closed reduction, and external fixator application on the day of admission. Surgery was performed on hospital days 1 and 3 for treatment of open inferior right patellar fracture with tendon avulsion. Following surgery, on day 3 of hospitalization, he developed hypoxic respiratory failure and acute respiratory distress syndrome (ARDS). He remained comatose and was found to have diffuse skin petechiae. Additional clinical findings included high fever, tachycardia, hypertension, tachypnea, diaphoresis, and decerebrate posturing.

**IMAGING FINDINGS**

Head CT examinations obtained at the time of admission were negative. A head CT obtained on the third hospital day was interpreted as negative, but in retrospect showed subtle hypointense foci within bilateral centrum semiovale white matter. Brain MRI was obtained and showed the typical pattern associated with fat embolism, notably the "starfield" pattern on diffusion-weighted imaging. In addition, the fat droplets could be seen on susceptibility-weighted imaging and on MR perfusion imaging, subtle changes of decreased blood volume, corresponding to the foci of restricted diffusion, also were evident. This case also illustrates the appearance of fat emboli on CT, conventional pre and postgadolinium MR imaging, and on advanced MRI pulse sequences including susceptibility-weighted imaging, diffusion imaging, and dynamic susceptibility contrast perfusion imaging.

**SUMMARY**

Using the full complement of CT and MR imaging tools available, cerebral fat embolism can be diagnosed definitively.

**KEY WORDS:** Embolism, fat, trauma



## EE-36

**Internal Carotid Artery Pseudo-Aneurysm with Associated Lower Cranial Nerve Palsies following Orthognatic Surgery: Endovascular Reconstruction**

Hacein-Bey, L.<sup>1</sup>Blazun, J. M.<sup>2</sup>Jackson, R. F.<sup>3</sup>

<sup>1</sup>Radiological Associates of Sacramento, Sacramento, CA,

<sup>2</sup>Sutter ENT Medical Group, Sacramento, CA, <sup>3</sup>Sutter Oral Surgery, Sacramento, CA

**PURPOSE**

Reported complications following orthognatic surgical procedures such as Le Fort osteotomies are rare. The most common neurologic complications are neurosensory deficits in the region innervated by the inferior alveolar nerve (after mandibular manipulation) and the greater palatine and infraorbital nerves (after maxillary osteotomy), while reported vascular complications include epistaxis from pseudo-aneurysms of distal branches of the maxillary artery (i.e., descending palatine and sphenopalatine arteries), blindness and arteriovenous fistulas of the carotid arteries (external and internal). The mechanisms of injury include direct trauma, such as tearing with surgical instruments, stretching during manipulation of the osteotomized bone segments, or downfracture of the maxilla extending to the foramen lacerum.

**CASE REPORT**

An 18-year-old male with facial bone dysplasia, apertognathia, maxillary hypoplasia and mandibular hyperplasia was treated with maxillary Le Fort I osteotomy with internal fixation and elastic intermaxillary fixation. Following surgery, the patient gradually developed palsies of the vagus and accessory nerves manifesting as dysphagia, cough, vocal cord paralysis and trapezius muscle atrophy. Cross-sectional imaging revealed a small, laterally pointing pseudoaneurysm of the high cervical internal carotid artery (ICA) at the skull base, exerting pulsatile mass effect on adjacent lower cranial nerves. The patient was treated with carotid artery stent reconstruction and pseudoaneurysm coil obliteration, and kept on dual antiplatelet therapy for 2 months, and clinical recovery followed.

**IMAGING FINDINGS**

A small, broad-based, irregular, laterally pointing pseudoaneurysm of the high cervical ICA at the exit of the carotid canal without surrounding hematoma was clearly demonstrated on CTA, which visualization was rendered difficult on MRA due to considerable metallic artifact from surgical hardware.

**SUMMARY**

Angiography exquisitely demonstrated the lesion, which was repaired fully with the combination of ICA stenting and pseudoaneurysm coil obliteration, allowing total carotid reconstruction.

**KEY WORDS:** Le Fort osteotomy, carotid, pseudoaneurysm

## EE-37

**Cerebral Myxomatous Aneurysms in the Setting of Atrial Myxoma**

Desai, M. P.·Shah, P. D.·Sauvageau, E.·Bourekas, E. C.·Slone, H.

The Ohio State University Medical Center  
Columbus, OH

**PURPOSE**

Cardiac myxomas are the most common primary tumors of the heart; however, it is rare to find cerebral aneurysm formation secondary to a cardiac myxoma. Up to 10% of patients with an atrial myxoma present with no clinical symptoms; however, when symptoms do present, they manifest as obstruction of the mitral valve or systemic embolisms (peripheral or cerebral). Neurologic events secondary to the myxoma have been reported in 26-45% of cases, predominantly consisting of embolic cerebral infarct, with aneurysm formation a much rarer complication. We present a case of cerebral myxomatous aneurysms discovered in a patient that initially presented with infarcts caused by an atrial myxoma.

**CASE REPORT**

A 33-year-old man, with a history of seizures, meningioma, hypertension, iv drug use, migraines and recurrent syncope, presented to the Emergency Department with left hemiplegia, slurred speech and another syncopal episode. Neurologic imaging found multiple cerebral infarcts along with numerous peripheral aneurysms. Of these aneurysms, the larger two were located in the pericallosal region of the anterior cerebral artery circulation. Cardiac imaging demonstrated a left atrial mass attached to the interatrial septum which was confirmed to be a myxoma. This was determined to be the source of thromboemboli resulting in the patient's recurrent cerebral infarctions, as well as the source of the cerebral aneurysms which formed from weakening of the arterial wall by tumor microemboli. The myxoma was removed surgically and the patient had an uneventful postoperative course without further neurologic complication.

**IMAGING FINDINGS**

Brain MR imaging at the time of presentation revealed scattered areas of signal abnormality in the distribution of the anterior circulation compatible with chronic infarcts. Areas of restricted diffusion were seen in the posterior circulation compatible with acute infarcts. Postcontrast imaging revealed multiple aneurysms, the largest of which were seen in the anterior cerebral artery distribution. These were confirmed with CTA and conventional angiography. Cardiac MRI revealed a mass in the left atrium attached to the interatrial septum.

**SUMMARY**

Cerebral myxomatous aneurysm formation is a rare complication of cardiac atrial myxoma and results from weakening of the arterial wall from tumor microemboli. Seeding of these microemboli can result in delayed

aneurysm formation, even after the mass has been resected. While cerebral infarcts are the most common neurologic complication, intracranial hemorrhage from aneurysms can be a delayed presentation in a patient with known cardiac myxoma and this potential complication should be considered when working up the patient. Cerebral CT angiography or MR angiography should be considered in the evaluation of any patient with an atrial myxoma.

**KEY WORDS:** Myxomatous aneurysms, cardiac atrial myxoma

#### EE-38

### **Bilateral Hypertrophic Olivary Degeneration Secondary to a Distal Dissecting Posterior Inferior Cerebellar Artery Aneurysm**

Burns, P. A.·Flynn, P. A.·Rennie, I. M.·McKinstry, C. S.·O'Leary, S. M.·Smyth, G. P.

Royal Victoria Hospital  
Belfast, UNITED KINGDOM

#### **PURPOSE**

To discuss a hitherto unreported cause of bilateral hypertrophic olivary degeneration (HOD).

#### **CASE REPORT**

A previously well, 61-year-old male was admitted with sudden onset headache and reduced GCS of 14. Initial unenhanced CT demonstrated subarachnoid and right cerebellar parenchymal hemorrhage. A shallow right subdural hemorrhage also was evident. CT angiography was negative. Catheter angiography confirmed the presence of a dissecting aneurysm of the right posterior inferior cerebellar artery (PICA). Parent vessel coil occlusion was performed just proximal to the point of dissection. Inpatient post-embolisation MRI demonstrated a small distal PICA territory infarction. Follow-up MRI at 9 months noted bilateral enlargement of and T2 hyperintensity within the inferior olivary nuclei which was not present on inpatient MRI. Clinical examination of the patient confirmed palatal myoclonus.

#### **IMAGING FINDINGS**

Microcatheter exploration of the right PICA confirmed dissection distal to the telovelotonsillary loop. Dissection at this site explains the concurrent findings of subarachnoid and subdural hemorrhage. Follow-up MRI at 9 months shows hemosiderin staining secondary to right cerebellar hemorrhage. In addition, enlargement of and T2 hyperintensity within the inferior olivary nuclei is consistent with bilateral HOD.



#### **SUMMARY**

Hypertrophic olivary degeneration is secondary to disruption of the dentatorubro-olivary pathway (Guillain-Mollaret Triangle), which is composed of the ipsilateral inferior olivary nucleus in the medulla, the contralateral dentate nucleus in the cerebellum and the red nucleus. The findings of T2 hyperintensity and enlargement within the inferior olivary nuclei typically occur 6 months after the primary insult. A primary lesion affecting the central tegmental tract and superior cerebellar peduncle is associated classically with bilateral HOD, although this does not explain the findings in this case. The intraparenchymal hemorrhage was medial within the right cerebellar hemisphere, centered on the dentate nucleus. Bilateral innervation of each inferior olivary nucleus from the right dentate nucleus may account for these findings.

**KEY WORDS:** Dissection, degeneration

#### EE-39

### **Trigeminal Hemangioma: Imaging Characteristics**

Derman, A. Y.·Ozsvath, J.·Jafar, J. J.·Zagzag, D.·Fatterpekar, G.

New York University Langone Medical Center  
New York, NY

## PURPOSE

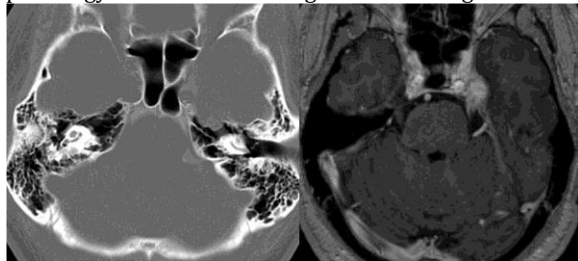
Hemangiomas involving the trigeminal ganglion are rare. The purpose of our study was to describe the CT and MR imaging findings of a trigeminal hemangioma.

## CASE REPORT

A 53-year-old previously healthy male presented with several months history of left-sided occipital headaches, facial numbness, and facial pain exacerbated by eating or grimacing.

## IMAGING FINDINGS

Noncontrast CT head demonstrated an ill-defined slightly hyperdense, extraaxial mass, centered in left Meckel's cave scalloping and remodeling the left petrous apex. MRI brain demonstrated a multilobulated heterogeneous mass predominantly isointense on T1-weighted imaging (WI), and hyperintense on T2WI extending from the Meckel's cave up to, but not beyond the foramina rotundum and ovale. A focal area of hyperintense signal was seen within this lesion on T1WI. The mass demonstrated moderate-intense enhancement. Abnormal linear enhancement contiguous with the mass was noted along the walls of the cisternal portion of trigeminal nerve and the proximal mandibular and maxillary divisions. There was no enhancing dural tail. Cerebral angiogram demonstrated a slightly hypervascular left Meckel's cave mass with persistent venous contrast pooling, with vascular supply from internal and external carotid arteries. Stereotactic computer-assisted microsurgical resection of the mass was performed, and surgical pathology demonstrated a trigeminal hemangioma.



## SUMMARY

The current presentation describes a rare case of a hemangioma of the trigeminal ganglion. Only a handful of cases of Meckel's cave hemangiomas have been described in the literature. The unique imaging finding in the current case is the abnormal linear enhancement along the walls of the cisternal portion of trigeminal nerve proximal to the mass, as well as along the walls of maxillary and mandibular portions of the trigeminal nerve more distally, likely reflecting the lesion's association with the perineural vascular plexus. To our knowledge, this finding has never been documented before, and can help distinguish a hemangioma from other etiologies.

**KEY WORDS:** Hemangioma, trigeminal, Meckle's cave

## EE-40

### Hyperintense Ipsilateral Cortical Sulci on FLAIR Imaging in Carotid Stenosis: Ivy Sign Equivalent from Enlarged Leptomeningeal Collaterals

Hacein-Bey, L.<sup>1</sup>•Mukundan, G.<sup>1</sup>•Shahi, K.<sup>2</sup>•Chan, H.<sup>3</sup>•Tajlil, A. T.<sup>4</sup>

<sup>1</sup>Radiological Associates of Sacramento, Sacramento, CA,

<sup>2</sup>Neurosurgical Associates, Sacramento, CA, <sup>3</sup>Mercy Medical Group, Internal Medicine, Sacramento, CA,

<sup>4</sup>Vascular Surgery, Sacramento, CA

## PURPOSE

Fluid-attenuated inversion recovery (FLAIR) is used routinely in magnetic resonance imaging (MRI) of the brain because of its high lesion-to-tissue contrast from T2 prolongation with nulling of normal cerebrospinal fluid (CSF) background. It is recognized widely to be particularly sensitive for disease states that affect the CSF in the subarachnoid space, which then appears hyperintense on those images, including subarachnoid hemorrhage, meningitis, meningeal carcinomatosis, leptomeningeal metastasis, subdural hematoma, adjacent neoplasms, dural venous thrombosis, and status epilepticus. It also has been described as a diagnostic pitfall in patients undergoing MR imaging on propofol or supplemental oxygen, and in case of prior administration of iodinated contrast material.

## CASE REPORT

A 69-year-old woman presented with intermittent right hemispheric transient ischemic attacks (TIAs). MRI of the brain did not show restricted diffusion consistent with strokes, but showed diffuse serpentine hyperintensities within the left hemispheric convexity on FLAIR images, interpreted as possible subarachnoid hemorrhage (SAH) or meningitis. The patient denied headaches, and declined a spinal tap. Computed tomographic angiography (CTA) showed a severe left carotid stenosis, the most likely source of the patient's TIAs, and a small aneurysm of the contralateral middle cerebral artery. As there was concern for possible aneurysmal SAH, a cerebral angiogram was obtained, which confirmed a small, incidental right anterior temporal artery origin aneurysm, and showed relatively poor collateral circulation to the left hemisphere, with dilated, late-filling convexity collaterals. Following multidisciplinary assessment, it was elected to treat the patient with carotid endarterectomy, as there was a remaining doubt as to the FLAIR MRI findings representing prior, clinically silent SAH which could interfere with the administration of dual antiplatelet therapy.

## IMAGING FINDINGS

Follow-up MRI showed complete resolution of left convexity sulcal serpentine hyperintensities. The finding of hyperintensities on FLAIR imaging within the convexity sulci remains incompletely understood, and commonly is linked to CSF abnormalities. In the moyamoya patient population, enlarged leptomeningeal collaterals presenting as serpiginous hyperintense structures, correlating with ipsilateral decrease in

cerebrovascular reserve have long been recognized as the “ivy sign”.

#### SUMMARY

In the context of severe arterial disease causing cerebral hypoperfusion, maximally dilated leptomeningeal collateral vessels should be considered a likely cause for serpiginous hyperintense structures within convexity sulci on FLAIR imaging.

**KEY WORDS:** FLAIR imaging, Ivy sign, leptomeningeal collaterals

#### EE-41

##### Arterialized Venous Angioma

Stefani, M. A.·Franciscatto, A. C.

Hospital de Clínicas de Porto Alegre  
Porto Alegre, BRAZIL

#### PURPOSE

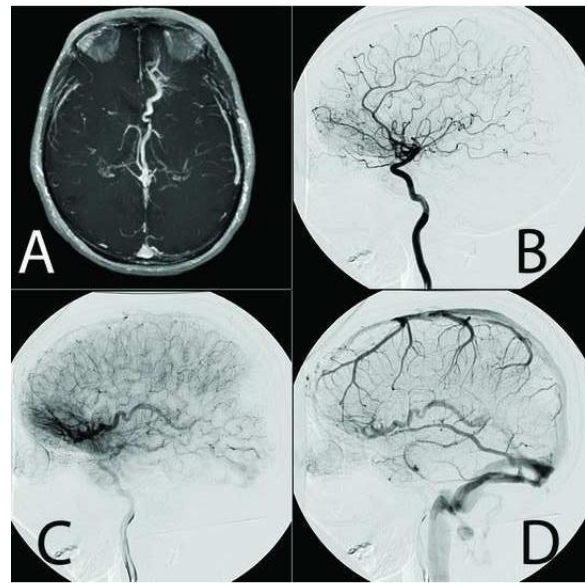
Developmental venous anomalies (DVA) are common findings described on MR exams performed for neurologic investigations. It is thought to represent a primary dysplasia of capillaries and small transcerebral veins or a compensatory mechanism caused by an intrauterine accident resulting in thrombosis of normal venous pathways. When digital subtraction angiography (DSA) is performed, it is found on the venous phase. Based on few studies of natural history they usually are quoted as innocent incidental, as they rarely bleed or present with symptoms. The current practice for DVA is conservative management without specific treatment targeting the vascular lesion. There is a different subgroup arterialized DVA with hemorrhagic presentation in 36% of the cases.

#### CASE REPORT

Between 2007 and 2010 three patients (1 man and 2 women) presented on this series were seen in clinic for recent onset of seizures in one case, other had an incidental finding during investigation of a headache and the other one with an episode of intracerebral hemorrhage attributed to the vascular abnormality. Ages of presentation were between the third and fifth decades of life.

#### IMAGING FINDINGS

On MR examinations there were classical features of venous angioma (caput medusa and dilated veins). However, the precocious appearance of the abnormal vein on the arterial phase of a DSA is a disturbing feature and immediately raises the concern of a potential risk of hemorrhage or other neurologic complication. No therapy was used in the two cases without bleeding and stereotactic radiosurgery was performed for the hemorrhagic one. After an average of 3 years of follow up there were no new hemorrhagic episodes. Seizures and headaches were managed easily with pharmacologic therapy.



#### SUMMARY

Recognizing arterialized DVA as a different disease may increase the number of diagnosed lesions and help to define more precisely its prevalence in the clinical practice. In any instance, however, there is a controversy if these lesions should be treated or left untouched. Considering the limited knowledge present in the literature about natural history and therapeutic results of these conditions, the outcomes are unpredictable. Although it seems logical, angiographic factors associated with a hemorrhagic presentation do not necessarily predict a higher subsequent risk of bleeding, as it was observed on arteriovenous malformations. The impact of these factors on the natural history requires prospective follow-up studies.

**KEY WORDS:** Developmental venous anomalies, angiography, hemorrhage

#### EE-42

##### Imaging Findings in Cerebroretinal Microangiopathy with Calcifications and Cysts

Safder, S.·Castillo, M.

University of North Carolina Chapel Hill  
Chapel Hill, NC

#### PURPOSE

To describe imaging findings and clinical constellation for cerebroretinal microangiopathy with calcifications and cysts (CRMCC).

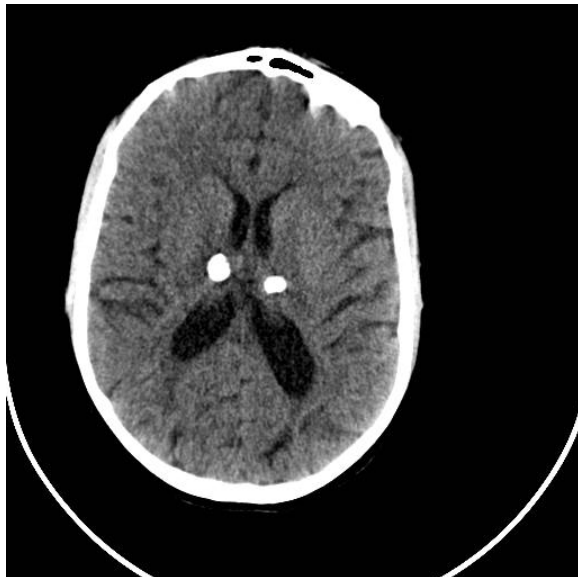
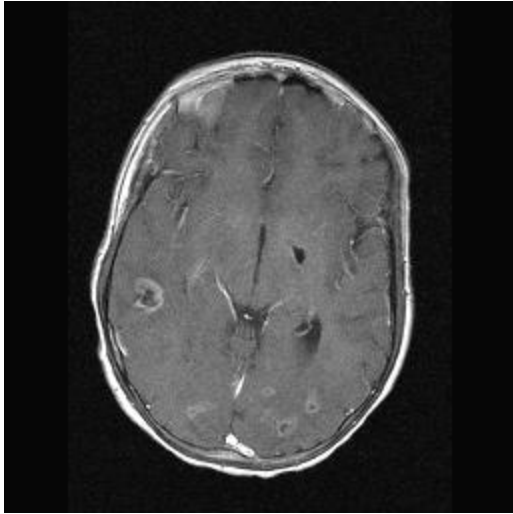
#### CASE REPORT

A 14-year-old male with right-sided weakness, right eye deviation and seizure. Pontine cyst seen on imaging with subsequent craniectomy for removal. Subsequently patient was found to have subretinal hemorrhages and exudative retinopathy. A few months later patient had GI bleeding with biopsy demonstrating telangiectatic capillaries; thickened vessels with hyalinization. Colonic biopsy showed patchy mucosal

hemorrhage. Patient's CT scan showed several intracerebral calcifications and cysts. Constellation of patient's symptoms and imaging findings are consistent with cerebroretinal microangiopathy with calcifications and cysts. We have additional images from a second patient as well.

#### IMAGING FINDINGS

Bilateral bulky calcifications, usually centered at the thalamus, basal ganglia, and subcortical white matter. Additionally, leukodystrophy with or without enhancement may be seen.



#### SUMMARY

Cerebroretinal microangiopathy with calcifications and cysts is a rare disorder with several key distinctive clinical and imaging findings. Being familiar with the imaging findings may expedite the diagnosis in order to implement preventative measures for other aspects of the disease such as gastrointestinal bleeding.

**KEY WORDS:** Cerebroretinal, Microangiopathy

#### EE-43

#### Reversal of Dementia Caused by Dural Arteriovenous Fistula following Endovascular Therapy

Zarghouni, M.·Henderson, J. B.·Hise, J. H.·Opatowsky, M. J.·Layton, K. F.

Baylor University Medical Center  
Dallas, TX

#### PURPOSE

We report two cases in which patients' dementia secondary to dural arteriovenous fistulas (dAVF) was cured following endovascular treatment.

#### CASE REPORT

Case 1: A 53-year-old female presented with a 4-month history of dysarthria, ataxia, and severe memory loss. Initial imaging revealed a calcified superior sagittal sinus wall in addition to dilated deep collateral veins. A cerebral angiogram demonstrated a left middle cranial fossa high-flow dAVF (Figure 1). Transvenous endovascular coil embolization at the fistula site resulted in occlusion of the dAVF (Figure 2). Clinical follow up at 6 months revealed marked improvement in her memory dysfunction and dysarthria. Case 2: A 74-year-old male presented with a 6-month history of visual disturbances, memory loss, and intellectual decline. Outside imaging revealed a right-sided "arteriovenous malformation." Pretreatment angiographic images revealed a high-flow superior sagittal sinus dAVF fed by bilateral middle meningeal

and superficial temporal arteries. Following two staged transarterial endovascular embolization procedures, posttreatment angiography revealed successful occlusion of the dAVF. Clinical follow up at 1 year revealed marked improvement with return of cognitive function to baseline.

#### IMAGING FINDINGS

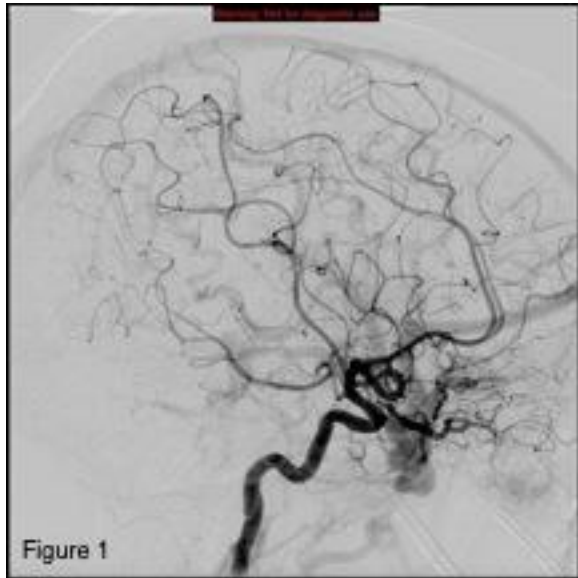


Figure 1. Pretreatment angiogram shows enlarged ophthalmic artery with multiple branches supplying high-flow arteriovenous fistula involving middle cranial fossa

Figure 2. Posttreatment angiogram shows cure of fistula and complete resolution of early venous drainage

#### SUMMARY

We describe two patients who presented with dementia as the primary neurologic manifestation of their dural arteriovenous fistula. Although dementia is not the most common presentation for a dAVF, these cases

show that obliterating the fistula can eliminate this dreadful manifestation. This awareness may facilitate the diagnosis of dementia in cases caused by a dAVF and allow for a minimally invasive treatment that restores cognitive function back to baseline.

**KEY WORDS:** Arteriovenous fistula, neuro-interventional, dementia

#### EE-44

#### Complex Dural Fistulae after Cerebral Venous Thrombosis: A Witnessed Evolution within a 7-Month Follow Up

Caçador, N.·Patricio, M.·Pamplona, J.·Braz, A.·Rios, A.·Fragata, I.·Capela, C.·Reis, J.

Centro Hospitalar Lisboa Central  
Lisbon, PORTUGAL

#### PURPOSE

The purpose of this work is to present a well documented case of cerebral venous thrombosis, with complex secondary dural fistulization. The sequential exams performed to the patient during a 7-month follow up, using MRI and angiography, allow us to understand the evolution of this rare pattern of vascular complication, after an initial uncomplicated venous cerebral thrombosis.

#### CASE REPORT

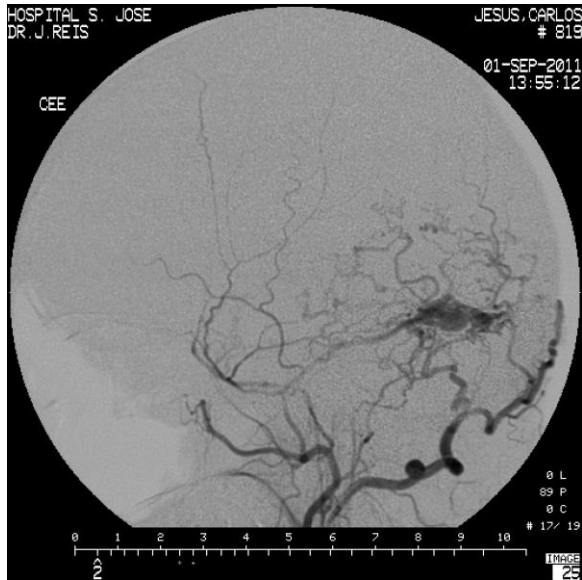
Male patient, 42 years old, admitted because of worsening headache and partial visual loss. Observation revealed bilateral papillary edema and reduction of visual acuity. Noncontrast head CT at admission suggested venous thrombosis, later confirmed by MRI and MRV. Anticoagulation therapy (heparin) and acetazolamide were started. After 15 days, there was a partial repermeabilization of the transverse sinus. During the following months, the patient developed permanent intracranial hypertension and severe visual loss with optic nerve atrophy. A lumbar-peritoneal shunting was performed. At this time, no new imaging findings were found. Six months after the initial ictus, new symptoms arose, with psychomotor and speech lentification. The MRI reveals at this time signs of congestive venous encephalopathy with parenchymal involvement. The angiographic study clearly demonstrated multiple and complex dural fistulae between external carotid and meningeal branches of the vertebral artery, to the superior sagittal sinus. Endovascular treatment is scheduled.

#### IMAGING FINDINGS

Head CT at admission showed spontaneous hyperdensity of the superior sagittal sinus and left transverse sinus. MR imaging at admission showed no parenchymal involvement, and confirmed venous thrombosis of superior sagittal sinus and left transverse sinus. After 6 months, brain MRI showed vasogenic edema of the right middle cerebellar peduncle and hemisphere, with hyperintensity in T2 and FLAIR, without restriction on diffusion-weighted imaging sequences. Multiple flow voids in the posterior fossa



were noted. Digital subtraction angiography demonstrated multiple complex dural fistulae between external carotid and meningeal branches of the vertebral artery, to superior sagittal sinus and left transverse sinus.



#### SUMMARY

This case clearly demonstrates the evolution of a simple venous thrombosis, to a complex and multiple dural fistulization process between external carotid and meningeal branches of the vertebral artery, to the superior sagittal sinus, a rare vascular complication.

**KEY WORDS:** Dural fistula, venous thrombosis

#### EE-45

#### Unusual Case of Arteriovenous Malformation Masquerading as a Neoplasm

Dumeer, S.<sup>1</sup>•Lignelli, A.<sup>2</sup>•Millar, W. S.<sup>2</sup>

<sup>1</sup>New York Presbyterian Hospital, New York, NY,

<sup>2</sup>Columbia University Medical Center, New York, NY

#### PURPOSE

To describe an unusual case of cerebral arteriovenous malformation masquerading as a neoplasm.

#### CASE REPORT

A 46-year-old, right-handed male presented to an outside hospital with new onset seizures. He had a past history of memory deficits and multiple episodes of right leg numbness. Computed tomography (CT) and magnetic resonance imaging (MRI) obtained at an outside hospital demonstrated findings consistent with a right medial temporal lobe neoplasm. He was referred to our hospital for biopsy and tumor resection. Patient was referred to radiology department for a preoperative MRI.

#### IMAGING FINDINGS

CT head obtained at outside hospital was read as mild hypodensity in right posterior medial temporal lobe. Outside hospital MRI report described a hyperintense

FLAIR lesion without significant enhancement in the posterior medial temporal lobe suspicious for neoplasm. Brain MRI (Figure 1A) obtained at our institution demonstrated swelling and hyperintense FLAIR signal in right medial temporal lobe including the hippocampus. No significant enhancement was seen. There was associated mass effect with entrapment and enlargement of right temporal horn. Along the posterior margin of this abnormal FLAIR signal, a curvilinear region of low T2 signal was noted, suspicious for prominent flow-voids. The possibility of vascular malformation was raised. MR spectroscopy did not reveal elevated choline or lactic acid to suggest a neoplasm. Clinicians were encouraged to postpone the biopsy and order a magnetic resonance angiography (MRA) study as these findings were suspicious for arteriovenous malformation with venous congestion. MR angiography showed a small arteriovenous malformation in the posterior right thalamus, bordering the right lateral ventricle. The nidus measured approximately 1 cm, possibly fed by the right posterior cerebral artery and drained into anterior superior straight sinus. Conventional cerebral angiography (Figure 1B) revealed an arteriovenous malformation in the right posterior choroidal artery distribution with a 1 cm nidus being drained by two large tortuous veins into the deep venous system.

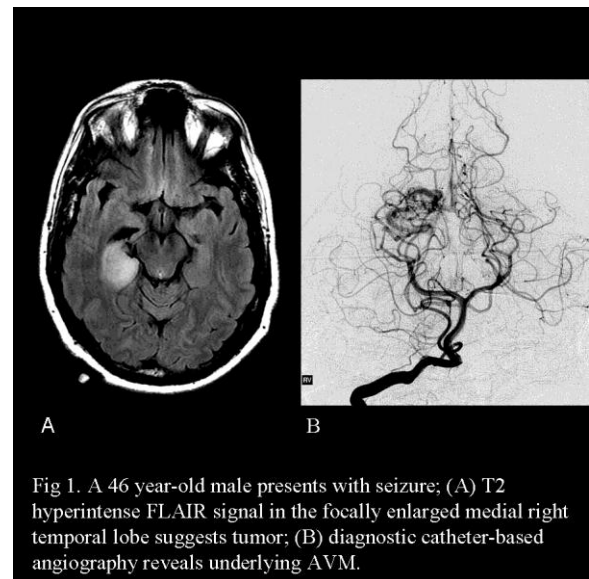


Fig 1. A 46 year-old male presents with seizure; (A) T2 hyperintense FLAIR signal in the focally enlarged medial right temporal lobe suggests tumor; (B) diagnostic catheter-based angiography reveals underlying AVM.

#### SUMMARY

Brain arteriovenous malformations are abnormal vascular connections within the brain that are presumably congenital in nature. They frequently masquerade as hemorrhagic and nonhemorrhagic tumors. They may lead to nonhemorrhagic neurologic deficits due to venous congestion, gliosis, hydrocephalus, or arterial steal. A high index of suspicion is required to recognize an AVM with venous congestion and prevent inadvertent biopsies.

**KEY WORDS:** Arteriovenous malformation, MR angiography

## EE-46

### Fenestration of the Petrous Internal Carotid Artery with Short Segment Duplication Mimicking an Arterial Dissection

Hacein-Bey, L.<sup>1</sup>•Raghavan, N.<sup>1</sup>•Mukundan, G.<sup>1</sup>•Sekhon, A. K.<sup>2</sup>•Dodrill, L. K.<sup>3</sup>•Park, T. C.<sup>2</sup>

<sup>1</sup>Radiological Associates of Sacramento, Sacramento, CA, <sup>2</sup>Sutter Medical Group, Sacramento, CA, <sup>3</sup>Sutter General Hospital, Sacramento, CA

#### PURPOSE

The diagnosis of craniocervical artery dissection is commonly difficult, and patients often are seen multiple times, or present with neurologic signs before the diagnosis is made. Thus, a high level of suspicion must be present. Conversely, since anticoagulation therapy has its own morbidity, firmly establishing the diagnosis is important, requiring cerebral angiography in difficult cases.

#### CASE REPORT

A 59-year-old right-handed female with a history of coronary artery disease, hypertension and hypercholesterolemia presented to her primary physician with the complaint of a vague low-intensity headache, which had been present for a few months, was confined mostly to the posterior occipital area and may have been concomitant to a recent cardiac catheterization which revealed a 70% stenosis of the left anterior descending coronary artery. MR imaging and MRA of the brain and cervical arteries. The findings on MRA of a vascular irregularity of the petrous portion of the internal carotid artery with a central filling defect, suspicious for a carotid dissection, and of absence of ischemic lesions on MRI, were immediately reported. The patient was instructed to go to an emergency room. Angiography showed a fenestration of the petrous segment of the left ICA, causing a short segment duplication. The patient's neurologic examination was totally unremarkable, in particular for cervicgia or a Horner's syndrome. She was discharged to home on amitriptyline, which relieved her headache.

#### IMAGING FINDINGS

Angiography established the diagnosis of a fenestration of the petrous portion of the ICA with a short duplicated arterial segment at that level on the basis of a complete septum within the carotid canal, the smooth appearance of both arterial channels, one of which was slightly tortuous, and the lack of blood products within the periarterial spaces. Fenestrations and duplications of the ICA are extremely rare, with only five cases of cervical or petrous ICA fenestration reported to date to our knowledge, one displaying a multichannel pattern within the exact same arterial segment as in our patient.

#### SUMMARY

The embryologic development of the ICA results from several complex evolving changes and regressions of the dorsal and ventral aorta and its arches. Fenestrations, on the other hand, are not thought to be related to developmental anomalies of aortic arches, but

rather to the persistence of the cranial portion of the carotid duct (ductus caroticus), a segment of the embryonic dorsal aorta which connects the third and fourth aortic arches, and which normally is destined to complete regression during early development.

**KEY WORDS:** Carotid artery, fenestration, duplication

**Monday, April 23 –  
Wednesday, April 25**

**6:30 AM – 9:00 PM**

**Thursday, April 26**

**6:30 AM – 3:00 PM**

**Excerpta Extraordinaire 47 – 50**

(EE2) EE 2 - ANATOMY

**Note: A missing printed number indicates an abstract has been withdrawn.**

## EE-47

### Idiopathic Herniation of Gyrus Rectus Resulting in Visual Loss

Shankar, J. J. S. • Clark, D. • Mishra, A.

QE II Hospital  
Halifax, NS, CANADA

#### PURPOSE

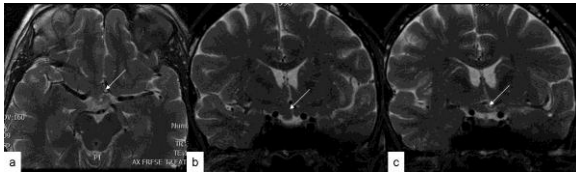
Herniation of gyrus rectus is a known phenomenon. Usually it is secondary to mass effect. Very rarely the herniation of gyrus rectus results in neurologic deficits. Idiopathic herniation of gyrus rectus is known but has never been reported to be associated with neurologic symptoms. We report a case of idiopathic gyrus rectus herniation resulting in bilateral visual field defect.

#### CASE REPORT

A 61-year-old male presented with progressive visual loss with pale optic disk. Visual field examination located the lesion to be around posterior optic nerve or optic chiasm. CT head was normal. MRI head did not reveal any mass lesion responsible for the patients' symptoms.

#### IMAGING FINDINGS

Coronal T2-weighted images showed herniation of the posterior part of the right gyrus rectus causing compression and displacement of the optic chiasm. On ophthalmologic examination, there was bitemporal field defect which could be explained by the compressive lesion at the level of optic chiasm. The patient currently is being evaluated for the surgical decompression of the optic chiasm.



#### SUMMARY

Idiopathic herniation of gyrus rectus is a rare entity and can be associated with neurologic deficits.

**KEY WORDS:** Gyrus rectus herniation, progressive visual loss

#### EE-48

##### Pars Nervosa Mimicking Jugular Venous Thrombus

Hernandez, R. J. • Minja, F. J.

Yale University  
New Haven, CT

#### PURPOSE

Briefly revisit the normal anatomy of the jugular foramen to help avoid misidentification of the pars nervosa as a pathologic filling defect such as jugular venous thrombus.

#### CASE REPORT

A 24-year-old gentleman presented to the emergency department with low-grade fever and left neck pain 10 days status post left tympanomastoidectomy for cholesteatoma removal. Clinical concern was for dural or jugular venous thrombus. Contrast-enhanced MRI of the brain was performed initially for further evaluation. Thin tubular filling defects were noted along the anteromedial aspect of the jugular foramen. Preliminary interpretation raised the possibility of jugular venous thrombus with final interpretation identifying these defects as the pars nervosa. Contrast CT of the neck subsequently was performed again demonstrating cranial nerves IX-XI traversing the jugular foramen while revealing prominent bilateral cervical lymphadenopathy. The latter was suggested as a potential etiology for the young man's neck pain.

#### IMAGING FINDINGS

Contrast-enhanced MRI at the skull base revealed expected postoperative changes related to left tympanomastoidectomy. Thin serpiginous filling defects were noted along the anteromedial aspect of the left jugular foramen in the expected location of the pars nervosa. Findings were similar in the right jugular foramen. Upon close examination, both cisternal and extracranial components were identified. Contrast CT redemonstrated these findings at the skull base in addition to prominent bilateral cervical lymphadenopathy measuring up to 2.4 cm at level II on the left.



#### SUMMARY

The complex anatomy of the jugular foramen is well studied both with extensive cadaveric dissection and more recent in vivo descriptions as seen with various imaging modalities. The jugular foramen may be subdivided into three compartments. Moving from anteromedial to posterolateral, there is the inferior petrosal compartment, the intrajugular compartment or pars nervosa which includes cranial nerves IX-XI, and the sigmoid compartment. When interpreting potential filling defects of the jugular foramen, the pars nervosa should be considered as a potential false positive. One should reference its expected location anterior and medial to the jugular spine, compare with the contralateral side, and look closely for cisternal and extraforaminal extension. While much emphasis is placed on this anatomy to help develop a differential diagnosis and to characterize clinical manifestations of lesions involving the foramen, familiarity with expected anatomy and available imaging techniques can help avert misinterpretation of normal anatomical detail.

**KEY WORDS:** Pars nervosa, jugular foramen, anatomy

#### EE-49

##### Arterial Steal from the Anterior Spinal Artery: A Cause of Ischemic Myelopathy

Patel, N. V. • Katz, Z. M. • Gailloud, P. E.

Johns Hopkins Medicine  
Baltimore, MD

#### PURPOSE

Vascular steal from the anterior spinal artery (ASA) has been described as a potential cause of ischemic myelopathy. Of the few cases reported in the literature, most have been in the setting of aortic coarctation and are associated with marked dilatation of the ASA, confounding the distinction between compressive and ischemic effects. Our purpose is to describe two unique cases of ASA steal resulting from conditions besides

aortic coarctation and to review the pathophysiology and clinical features of these cases.

#### **CASE REPORT**

Case 1: A 57-year-old male presented after acute worsening of bilateral lower extremity weakness that had been progressing more gradually over several months. The exacerbation left him unable to walk. Electromyography and nerve conduction studies of the lower extremities were normal, CT myelography showed no findings of cord compression, and a lumbar puncture was also normal. Spinal angiography revealed findings of anterior artery steal resulting from collateralization to an isolated left subclavian artery. The collateral pathway was embolized from a left transradial approach and the patient's lower extremity strength improved. Case 2: A 30-year-old female with Takayasu arteritis presented with transient, paroxysmal heaviness and numbness on the left side of her body, including her back and lower face. Brain MRI showed no abnormality to explain these symptoms and MRI of the spine showed no evidence of cord compression. Spinal angiography showed extensive arterioocclusive disease of the carotid and vertebral arteries with collaterals to the brain that included a pathway through the ASA.

#### **IMAGING FINDINGS**

Case 1: Spinal angiography revealed congenital isolation of an aberrant left subclavian artery. The distal segment of the left subclavian was reconstituted through multiple collaterals including a prominent supply through the artery of the cervical enlargement, shunting through the anterior spinal artery to the left costocervical trunk. After embolization, shunting through this spinal pathway was obliterated. Case 2: Spinal angiography showed occlusion of both common carotid arteries, the right vertebral artery, and the more distal right subclavian artery. The left vertebral artery was patent and there were extensive collaterals to the occluded carotid and vertebral arteries, including a prominent pathway across the ASA from left T2.

#### **SUMMARY**

Anterior spinal artery steal is a rarely described cause of gradually progressive and acute-onset myelopathy. The condition typically occurs in the setting of arterial occlusion, whether congenital or acquired. In some cases, endovascular treatment may be feasible and can result in clinical neurologic improvement. This diagnosis is an important consideration in the evaluation of patients with progressive myelopathy.

**KEY WORDS:** Anterior spinal artery, vascular steal, myelopathy

#### **EE-50**

#### **High-Resolution MR Neurography Findings in Diabetic Neuropathy**

Thakkar, R. S.·Chalian, M.·Del Grande, F.·Thawait, G.·Thawait, S.·Chhabra, A.

Johns Hopkins University  
Baltimore, MD

#### **PURPOSE**

Diabetic neuropathy (DN) is the most common cause of neuropathy and is associated with a wide range of clinical manifestations. The most common form of diabetic neuropathy is the distal symmetrical form of the disorder. Focal diabetic neuropathy although less common, clinically manifests with a confusing picture or as an entrapment neuropathy. The goal of this abstract is to depict the spectrum of imaging abnormalities in diabetic subjects on MR neurography as well as discuss relevant differential diagnosis.

#### **CASE REPORT**

A case series of subjects with various manifestations of DN and related differential diagnoses (entrapment neuropathy, multifocal motor neuropathy, chronic inflammatory demyelinating neuropathy, hereditary motor-sensory polyneuropathy). The spectrum of imaging abnormalities of DN on high-resolution 3 T MR neurography will be depicted.

#### **IMAGING FINDINGS**

Imaging abnormalities in diabetic subjects vary from abnormal T2 hyperintensity and fascicular enlargement in acute-subacute stages to atrophic-appearing fascicles with intraepineural fat deposition in chronic stage of neuropathy. Nerve enlargement may be seen in all stages of neuropathy. Associated regional muscle denervation changes (edema-like T2 signal abnormality in acute-subacute stages and fatty replacement with or without atrophy in subacute-chronic stages of the disease) are helpful findings to confirm the diagnosis of neuropathy. Other key roles of imaging to exclude mass lesions or entrapment neuropathy and differentiate from above-mentioned polyneuropathy conditions will be highlighted.

#### **SUMMARY**

A spectrum of imaging abnormalities of diabetic neuropathy is depicted on high-resolution 3 T MR neurography, which also aids in its differential diagnosis.

**KEY WORDS:** Diabetic neuropathy, MR neurography, fascicles

**Monday, April 23 –  
Wednesday, April 25**

**6:30 AM – 9:00 PM**

**Thursday, April 26**

**6:30 AM – 3:00 PM**

**Americas Hall II**

**Excerpta Extraordinaire 51 – 62**

**(EE3) E3 – Head and Neck**

**Note: A missing printed number indicates an abstract has been withdrawn.**

#### **EE-51**

##### **Dumbbell-Shaped Cranio-Orbital Solitary Fibrous Tumor: A Novel Route of Intracranial Spread**

Chakraborty, A. K.·Helvey, J. T.·White, M.·Poage, D.·Omojola, M.·Keiper, M.

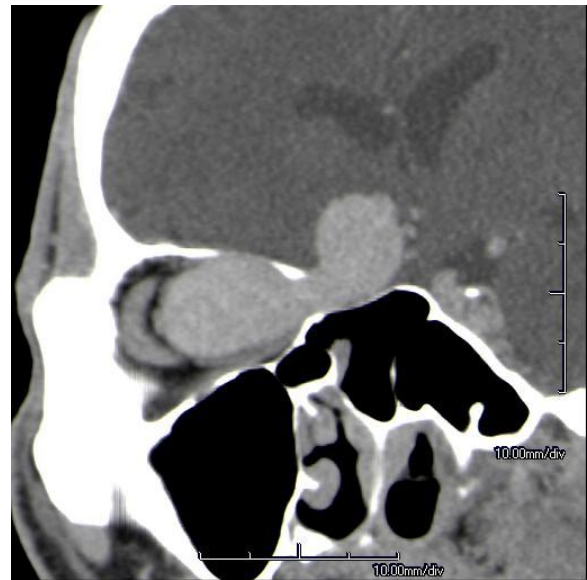
University of Nebraska Medical Center  
Omaha, NE

#### **PURPOSE**

Solitary fibrous tumor (SFT) is a rare spindle cell tumor of mesenchymal origin originally described as a tumor of the pleura. Extrathoracic presentations of SFTs also have been reported, including involvement of the central nervous system (CNS) and orbit where it classically follows a benign course. Cranio-orbital SFT has been reported three times previously in the English literature to our knowledge. The route of intracranial spread was noted via the superior orbital fissure in these cases. We discuss a case of cranio-orbital SFT with a dumbbell configuration extending through the optic canal, believed to be a unique route of intracranial spread.

#### **CASE REPORT**

A 46-year-old gentleman presented to the Emergency Department after a 2-day history of worsening headache, right periorbital pain and proptosis with a remote history of right-eye blindness for which he did not seek medical care. Contrast-enhanced head CT revealed a 4.7 cm discrete, intensely enhancing bilobed mass extending from the right orbit through the optic canal to the suprasellar cistern and planum sphenoidale (Figure 1). Meningioma, schwannoma, hemangioma and aneurysm were diagnostic considerations.



Imaging: Reformatted oblique coronal contrast-enhanced CT of the head

#### **IMAGING FINDINGS**

MR imaging and MRA of the head confirmed a homogeneously enhancing, dumbbell mass extending through the optic canal. An unusual meningioma was considered the most likely preoperative diagnosis. A right frontal craniotomy and mass resection were performed. Final pathologic diagnosis with positive immunostaining for CD34, CD99 and Bcl-2 was consistent with solitary fibrous tumor. Features to suggest malignant solitary fibrous tumor such as >4 mitosis/10 HPF, necrosis or cellular atypia were absent.

#### **SUMMARY**

Cranio-orbital solitary fibrous tumor is exceedingly rare, with merely three cases reported in neurosurgery and ophthalmology literature. The route of intracranial spread in these cases was the superior orbital fissure in two and not specifically discussed in the third. To our knowledge, our case of cranio-orbital SFT gaining access to the cranial vault via the optic canal is a unique route of intracranial spread. In addition to our case, the three published cases of cranio-orbital SFT had a preoperative presumptive diagnosis of meningioma. We will discuss the differential diagnosis of cranio-orbital mass lesions, particularly involving the optic canal and superior orbital fissure. We also will discuss past misdiagnosis of orbital solitary fibrous tumor with hemangiopericytoma due to their similar imaging and pathologic characteristics.

**KEY WORDS:** Solitary fibrous tumor, cranio-orbital, optic canal

#### **EE-52**

##### **MR Imaging of Intraneural Perineurioma of the Brachial Plexus**

Schallert, E. K.·Saraf Lavi, E.·Levi, A. D.·Brown, A. D.·Norenberg, M. D.

University of Miami/Jackson Memorial Hospital  
Miami, FL

#### PURPOSE

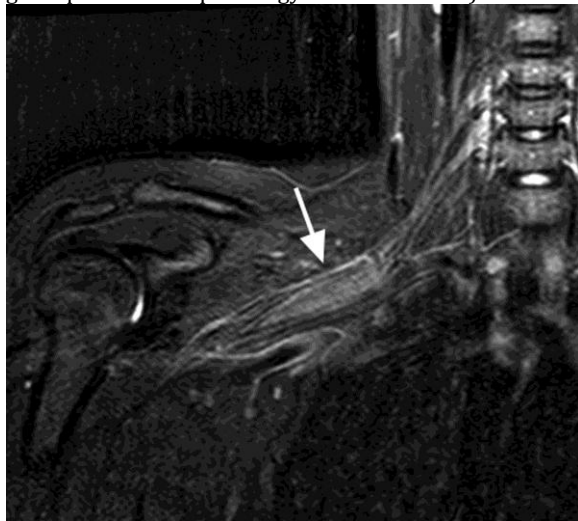
To present the case of a 18-year-old woman with progressive right hand weakness, numbness and severe atrophic changes of the hand secondary to an intraneural perineurioma involving the right brachial plexus, in whom the initial diagnosis was suggested by MRI.

#### CASE REPORT

A 18-year-old female was referred for evaluation of progressive right hand weakness and numbness over the past year. Her illness began with a slight inability to bend her distal second digit. Eight months prior to presentation she began to experience intermittent ventral hand numbness lasting for periods of 30-40 min with handwriting changes and pain with writing. Six months prior to presentation, the numbness in the hand became permanent and for the next 6 months, she noted that the muscles in her hand were severely atrophied. On examination, there was weakness and severe atrophic changes in all of the intrinsic muscles of the hand. There was absent sensation in the 4th and 5th digits as well as the medial aspect of the forearm. Clinical and electrophysiologic evaluation localized the lesion to the lower trunk of the brachial plexus. The patient was referred to a neurologist for evaluation of possible thoracic outlet syndrome versus a structural abnormality of the brachial plexus and MRI was performed.

#### IMAGING FINDINGS

MR imaging of the right brachial plexus was performed with a 1.5 T MR scanner and demonstrated a 4 cm long segment of fusiform enlargement, hyperintense T2 signal and diffuse enhancement of the lower trunk of the right brachial plexus extending to the divisions. (In addition to the MRI images, we have intraoperative gross pictures and pathology slide correlates.)



#### SUMMARY

Intraneural perineurioma is an uncommon benign tumor of the perineurium of peripheral nerve sheaths occurring primarily in adolescents or young adults. MR

imaging is a valuable tool in suggesting this diagnosis and in surgical planning. The diagnosis should be entertained in cases of a diffuse lesion affecting the brachial plexus when coupled with the clinical history or progressive motor/sensory disturbance in a young person.

**KEY WORDS:** Perineurioma, brachial plexus, MR imaging

#### EE-53

#### Hyperplasia of Reimplanted Intramuscular Parathyroid Tissue Identified by Dynamic CT

Pawha, P. S. Som, P. M.  
Mount Sinai School of Medicine  
New York, NY

#### PURPOSE

Dynamic CT has been shown to be useful in localization of both normotopic and ectopic parathyroid adenomas. Recurrent hyperparathyroidism after surgery can present additional challenges in localization. Parathyroid tissue may be reimplanted in muscle tissue during parathyroidectomy to preserve function. If further revision surgery is needed, both normotopic and reimplantation sites may need to be explored. We report a case of preoperative dynamic CT localization of hyperplastic reimplanted intramuscular parathyroid tissue in a patient with recurrent hyperparathyroidism.

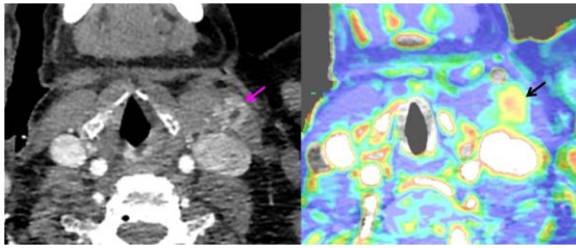
#### CASE REPORT

A 61-year-old female with a history of tertiary hyperparathyroidism secondary to chronic renal disease, underwent four gland parathyroid resections in 1999. As part of the surgery, she had neck reimplantation, which involved mincing a portion of one gland and implanting this within a pocket created in the left sternocleidomastoid muscle. In 2009 she underwent revision surgery for recurrent hyperparathyroidism, with forearm reimplantation. Following surgery, she had persistent hyperparathyroidism, for which she underwent evaluation with dynamic CT in 8/2010.

#### IMAGING FINDINGS

Dynamic CT of the neck was performed on a GE VCT 64-slice scanner, with reduced dose protocol. CT revealed a focal region of patchy but avid early enhancement (30 seconds post injection) within the left sternocleidomastoid muscle, adjacent to a surgical clip which had been placed during reimplantation. The margins of the enhancement were ill-defined, and muscle attenuation was interspersed with the avidly enhancing tissue. At surgery, this was found to be hyperfunctioning parathyroid tissue embedded within the muscle. Intraoperative parathyroid hormone levels dropped dramatically after resection.





#### SUMMARY

Reimplanted parathyroid tissue occasionally may become hyperplastic, causing persistent/recurrent hyperparathyroidism and presenting a challenge for planning further revision surgery. This case suggests that hyperplastic reimplanted intramuscular tissue may be localized with dynamic CT. The hyperplastic minced tissue in this case had similar enhancement characteristics to encapsulated parathyroid adenomas, but demonstrated a more ill-defined morphology, interspersed with muscle.

**KEY WORDS:** Parathyroid, dynamic CT

#### EE-54

#### Inflammatory Pseudotumor of the Nasopharynx and Skull Base: Mimicking an Aggressive Neoplasm/Infection

Chwang, W. B.<sup>1</sup>•Jain, R.<sup>2</sup>•Narayan, A.<sup>1</sup>•McHugh, J.<sup>2</sup>•Ghanem, T.<sup>1</sup>•Seidman, M.<sup>1</sup>•Jain, R.<sup>1</sup>

<sup>1</sup>Henry Ford Hospital, Detroit, MI, <sup>2</sup>University of Michigan, Ann Arbor, MI

#### PURPOSE

Inflammatory pseudotumor of the nasopharynx and skull base is a rare disease of idiopathic etiology, which can mimic an aggressive neoplasm or infection both clinically and radiographically. In this presentation, we illustrate the radiographic appearance of inflammatory pseudotumor in an elderly diabetic patient, highlighting features which may be helpful in distinguishing pseudotumor from the other entities. A brief discussion of the differential diagnosis of an aggressive-appearing infiltrative mass of the nasopharynx and skull base follows.

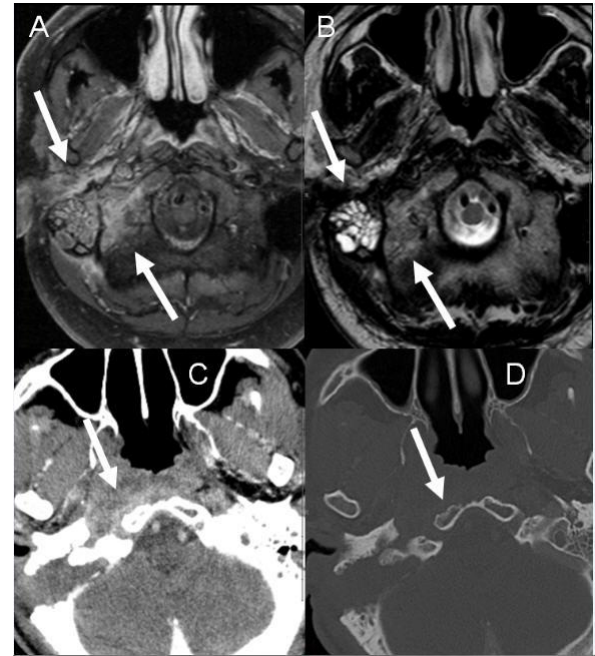
#### CASE REPORT

A 47-year-old man presented with right-sided facial paralysis, muffled hearing sensation, and pain in the right face and neck regions. The patient was a known insulin-dependent diabetic since 1 year of age, and recent glucose levels had been uncontrolled. On physical examination, the patient's right face was immobile from paralysis of the right seventh cranial nerve. There was a large, fleshy mass in the lateral aspect of the external auditory canal just medial to the entrance of the meatus. Three separate biopsies were performed via percutaneous, open surgical, and transnasal approaches. The biopsies demonstrated fibrous tissue and mild chronic inflammation, and were negative for tumor. Cultures were also negative. After treatment with antibiotics and hyperbaric oxygen therapy, the patient's condition was not improved

significantly. The patient had multiple consultations with otolaryngology, infectious disease, and endocrinology specialists. He was placed on more aggressive control of his diabetes, and after a course of several months, repeat imaging showed improvement of the patient's mass without any antineoplastic treatment.

#### IMAGING FINDINGS

CT scan revealed an ill-defined soft tissue mass around the right mastoid tip, with infiltration of the right carotid space and erosion of the right skull base. MR imaging demonstrated that the mass had intracranial extension, and there was fluid opacification of the right middle ear mastoid air cells due to eustachian tube obstruction.



#### SUMMARY

We illustrate the radiographic findings of inflammatory pseudotumor of the nasopharynx and skull base, and emphasize the importance of including inflammatory pseudotumor in the differential diagnosis of infiltrative nasopharyngeal and skull base masses.

**KEY WORDS:** Inflammatory pseudotumor, nasopharynx, skull base

#### EE-55

#### Laryngeal Candidiasis

Arabi, M.•Shah, G.•Owens, S.•Srinivasan, A.

University of Michigan  
Ann Arbor, MI

#### PURPOSE

To illustrate the imaging findings in a rare case of laryngeal candidiasis with discussion of its differential diagnosis.

### CASE REPORT

A 86-year-old man with history of atrial fibrillation, bladder cancer, prostate cancer and chronic lymphocytic leukemia presented with shortness of breath, fever, dysphagia and dysphonia. He was evaluated with a contrast-enhanced CT that revealed asymmetric soft tissue thickening at the left base of tongue, presumed to be lingual tonsillar hypertrophy. After a 6-week treatment with broad-spectrum antibiotics (fluconazole and Nystatin for pancytopenia, candida esophagitis, and recurrent neutropenic fever due to *Pseudomonas bacteremia*) he reported continuing hoarseness, worsening pain, worsening dysphagia, solids worse than liquids and right ear pain. At this time, a repeat contrast-enhanced CT was ordered.

### IMAGING FINDINGS

The repeat contrast-enhanced CT neck demonstrated asymmetric hypoattenuating soft tissue thickening of the right aryepiglottic fold with minimal enhancement, supraglottic laryngeal narrowing and near complete effacement of the right pyriform sinus. Patchy enhancement also was seen along the right true vocal cord. These findings were new since the previous CT performed 6 weeks earlier. Due to rapid progression of these abnormalities within a short duration, possibility of infection was considered and chances of this being neoplastic considered less likely. The patient underwent endoscopic biopsy with pathologic and microbiologic analysis that revealed laryngeal candidiasis.

### SUMMARY

Primary laryngeal candidiasis is a rare infection that occurs in immunocompromised patients and often is associated with involvement of other sites along the aerodigestive tract. Patients typically present with nonspecific symptoms such as hoarseness, dyspnea, dysphagia and sore throat. Endoscopically, the lesions appear as white plaques, pseudomembranes or vegetative masses. Histopathologically, hyperplastic and inflammatory epithelial changes are seen and the diagnosis is confirmed by the presence of candida hyphae on periodic acid-Schiff (PAS) or Gömöri methenamine silver staining. While the appearance of asymmetric hypoattenuating laryngeal soft tissue swelling with variable enhancement should raise the suspicion of neoplasm in most occasions, imaging findings need to be interpreted in the light of clinical information. The key feature that suggested a non-neoplastic diagnosis was the rapid interval progression of findings on successive scans. A high degree of clinical suspicion for infection in this immunocompromised patient combined with the unusual chronological progression of imaging findings helped guide the surgeon towards endoscopic biopsy that clinched the diagnosis. In summary, laryngeal candidiasis, while rare, can mimic neoplasm on a neck CT. Obtaining relevant clinical information and comparison with any recent CT scans are very helpful in guiding the radiologist to this possibility.

**KEY WORDS:** Laryngeal candidiasis

### EE-56

#### Report of an Iatrogenic Origin of Collet-Sicard Syndrome

Novais, G.·Castanho, P.·Oliveira, A.·Fragata, I.

Centro Hospitalar Lisboa Central  
Lisbon, PORTUGAL

### PURPOSE

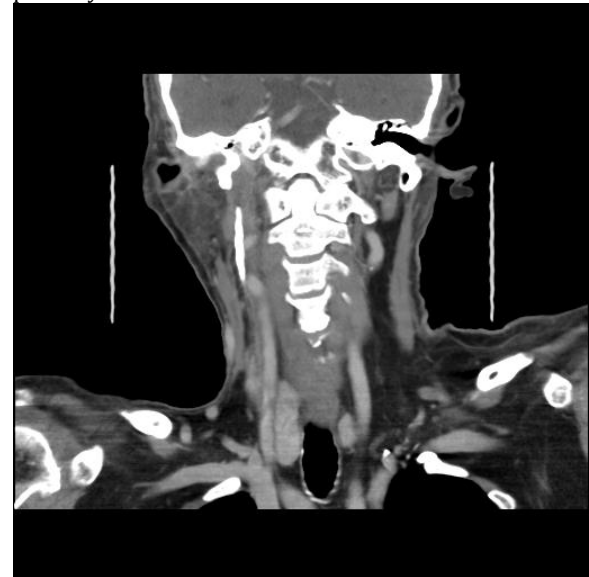
Collet-Sicard syndrome is a rare neurologic entity, corresponding to unilateral lesions of cranial nerves IX, X, XI, and XII.

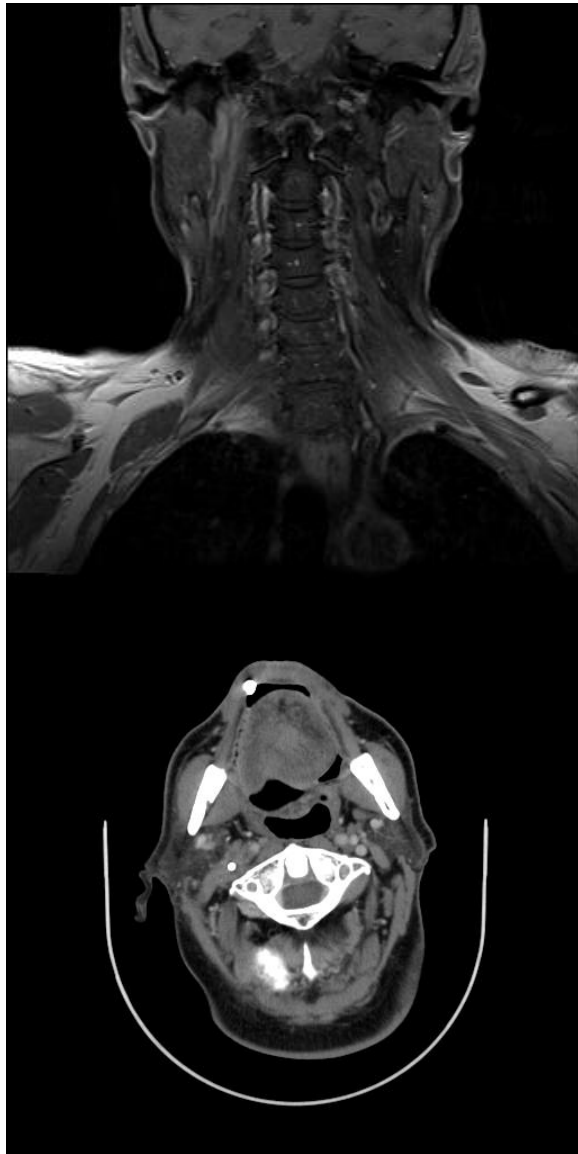
### CASE REPORT

The authors report the case of a 73-year-old male under chemotherapy for colon cancer. He had a misplaced subcutaneous intravenous reservoir, directed upwards to the jugular bulb, and developed a Collet-Sicard syndrome 1 month after a chemotherapy session, administered through the same misplaced intravenous catheter.

### IMAGING FINDINGS

Imaging showed an inflammatory mass around the jugular vein, with jugular venous thrombosis. After removal of the misplaced vascular device and a short period of steroid therapy, the patient recovered partially from his deficits.





#### SUMMARY

Collet-Sicard syndrome, although rare, provides important semiological information, as it points to pathology of a very precise location. To our knowledge, this is the only iatrogenic case reported in medical literature so far. This case highlights the importance of the clinical features as a guide to the imaging exams.

**KEY WORDS:** Collet-Sicard, iatrogenic

#### EE-57

### Papillary Carcinoma of Thyroid with Metastasis to Ectopic Sublingual Thyroid

Agarwal, A.·Maller, V.·Kaneekar, S.·Thamburaj, K.

Penn State Milton S. Hershey Medical Center  
Hershey, PA

#### PURPOSE

Papillary carcinoma of thyroid is the most common type of thyroid neoplasm which usually is confined to the

thyroid and tends to metastasize to regional lymph nodes. It commonly metastasizes to regional lymph nodes, but at the time of diagnosis, 10-15% of patients have distant metastases to the bones and lungs. We report a case of papillary carcinoma of thyroid metastasizing to ectopic sublingual thyroid, which has not been reported previously.

#### CASE REPORT

A 60-year-old female presented with a progressively enlarging painless swelling in the anterior part of the neck since 1 year. Ultrasound and CT of the neck documented a large mass in left thyroid gland with complex cystic and solid components without any associated cervical lymphadenopathy (Figure 1a). Thyroid function test was within normal range and FNAC of the thyroid swelling revealed papillary carcinoma. Incidental sublingual thyroid also was seen on CT (Figure 1a). Left hemithyroidectomy was performed. Four months postoperatively, patient presented with enlarging nodule in the submental/sublingual region.

#### IMAGING FINDINGS

Contrast-enhanced CT performed subsequently revealed postsurgical changes of left hemithyroidectomy in the neck. There was no evidence of recurrent disease in the surgical bed. Study, however, revealed significant interval enlargement of the ectopic sublingual thyroid gland with new hypodense nodules (Figure 1b). Given the patient's hypothyroid status, this was interpreted as compensatory enlargement. However, given the imaging appearance of new hypodense nodules within the ectopic gland and superficial location, biopsy was performed. Histopathology revealed papillary thyroid carcinoma, similar to the primary thyroid mass.



#### SUMMARY

We describe a rare case of thyroid papillary carcinoma metastasizing to ectopic sublingual thyroid.

**KEY WORDS:** Ectopic, thyroid, papillary

#### EE-58

### Perineural Invasion of Sinonasal Lymphoma: A Rare Cause of Trigeminal Neuropathy

Agarwal, A.·Vijay, K.·Nguyen, D.·Maller, V.

Penn State Milton S. Hershey Medical Center  
Hershey, PA

**PURPOSE**

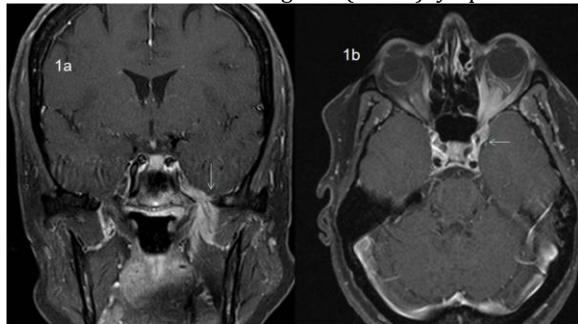
Trigeminal neuropathy secondary to perineural invasion of sinonasal lymphoma is extremely rare. Likewise, sinonasal lymphoma is demonstrated infrequently, initially with cranial neuropathy. Especially, low-grade lymphomas commonly do not involve the central or peripheral nervous system. The present case served to broaden the differential diagnosis of secondary trigeminal neuropathy and to alert clinicians to cautiously assess perineural spread of occult neoplasm in sinonasal tract and larynx or pharynx.

**CASE REPORT**

A 55-year-old female patient presented with numbness, altered sensation, and intermittent pain over left face for a couple of months. Detailed neurologic exams showed reduced perception to light touch and pinprick, numbness sensation, and a dull ache in the distribution of left mandibular division of the trigeminal nerve.

**IMAGING FINDINGS**

Brain MRI revealed marrow signal alteration of the hard palate, with infiltrative soft tissue extending along the V2 and V3 branches of trigeminal nerve. The enhancement and thickening of nerve extended transneurally to cavernous sinus, through the foramen rotundum and ovale (Figures 1 a, b). The initial diagnostic impression was secondary trigeminal neuropathy associated with hard palate neoplasm, likely adenocarcinoma/acinic cell carcinoma from the minor salivary gland. The histopathologic exams however documented low-grade (MALT) lymphoma.

**SUMMARY**

Perineural spread of head and neck cancer uncommonly is encountered as the cause of cranial neuropathy. Adenoid cystic carcinoma and squamous cell carcinoma in naso and oropharynx, salivary glands, and paranasal cavities accounted for most of cases of perineural tumor spread. There are very few reports of secondary trigeminal neuropathy associated with perineural invasion of sinonasal lymphoma, with fewer from low-grade lymphomas. Occult neoplasm in pharynx or larynx may extend to invade trigeminal nerve and therefore thorough examination of these sites for unexplained, evolving trigeminal neuropathy is mandatory.

**KEY WORDS:** Perineural, sinonasal

**EE-59****Petrous Apex Teratoma**

Harreld, J. H.<sup>1</sup>•Klimo, P.<sup>1</sup>•Jenkins, J. J.<sup>1</sup>•Lasater, O. E.<sup>2</sup>•Armstrong, G. T.<sup>1</sup>

<sup>1</sup>St. Jude Children's Research Hospital, Memphis, TN,

<sup>2</sup>LeBonheur Children's Hospital, Memphis, TN

**PURPOSE**

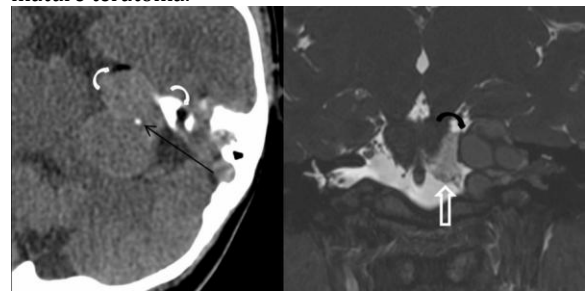
To review conventional and advanced imaging findings in a rare case of petrous apex teratoma.

**CASE REPORT**

An 11-year-old girl with a history of deafness in the left ear since birth presented with progressive left facial droop and ptosis of 3 months' duration and recent onset of daily headache. Physical examination revealed a left facial palsy, mild bilateral abducens palsy, and erythema of the left eye conjunctiva.

**IMAGING FINDINGS**

CT imaging demonstrated a predominantly multicystic, rim-enhancing lesion in the left cerebellopontine angle with extension into, and expansion of, all labyrinthine structures via the internal auditory canal and fairly significant mass effect on the left pons, middle cerebellar peduncle and cerebellum. There was minimal extension of soft tissue to the middle ear epitympanum. A punctate intralesional calcification was present (arrow), as well as at least three small foci of fat density at the periphery of the cysts (curved white arrows). MR imaging demonstrated an additional diffusion-restricted component consistent with epidermoid cyst in the left prepontine cistern (open arrow), with compression of the left 5<sup>th</sup> nerve (curved black arrow) between this and the multicystic component. The lesion was hypoperfused by dynamic susceptibility contrast perfusion imaging. Single-voxel MR spectroscopy demonstrated a lone large NAA peak, with no significant choline or creatine peaks. Pathologic diagnosis was mature teratoma.

**SUMMARY**

Mature teratoma of the petrous apex, rarely described in the literature, is in the differential diagnosis of cystic temporal bone lesions. Conventional and advanced imaging findings are described.

**KEY WORDS:** Temporal bone, teratoma, petrous



**EE-60****Giant-Cell Tumor of the Temporal Bone: Case Report of a Rare Cause of Trigeminal Neuralgia**

Castanho, P. R.·Novais, G.·Fragata, I.

Centro Hospitalar Lisboa Central  
Lisbon, PORTUGAL

**PURPOSE**

Giant-cell tumors are rare lesions that may seldom involve the skull base.

**CASE REPORT**

The authors report the case of a 56-year-old female who presented with left trigeminal neuralgia that was proven to be caused by a temporal mass compressing the trigeminal nerve.

**IMAGING FINDINGS**

Imaging studies showed a skull base temporal mass with destruction of the temporal bone and extension to the infratemporal fossa. The pathology confirmed the diagnosis of giant-cell tumor. Total surgical removal was performed, with complete recovery of the neuralgia and no tumor relapse so far. The patient also has findings suggestive of right orbital fibrous dysplasia.

**SUMMARY**

Temporal giant-cell tumor is a rare cause of trigeminal neuralgia that may have a benign course if aggressive surgical treatment is undertaken.

**KEY WORDS:** Giant-cell tumor, trigeminal neuralgia, temporal bone

**EE-61****Arachnoid Granulations of the Temporal Bone: Treatable Causes of Spontaneous Cerebrospinal Fluid Leaks**

Trimble, C. R.<sup>1</sup>·Harnsberger, H. R.<sup>2</sup>·Hildenbrand, P. G.<sup>3</sup>·Eisenman, D.<sup>1</sup>·Morales, R. E.<sup>1</sup>

<sup>1</sup>University of Maryland Medical Center, Baltimore, MD,

<sup>2</sup>University of Utah School of Medicine, Salt Lake City, UT, <sup>3</sup>Lahey Clinic, Burlington, MA

#### PURPOSE

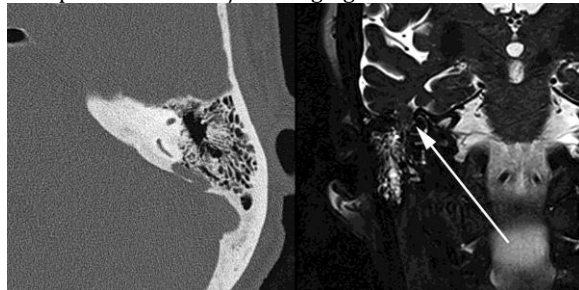
Arachnoid granulations (AGs) are meningotheelial protrusions which resorb cerebrospinal fluid (CSF) from the contiguous subarachnoid space into the venous circulation. Most AGs communicate with the dural venous sinuses. Less commonly, AGs are identified along the petrous and mastoid portions of the temporal bone. These may not communicate directly with the dural venous sinuses. Though traditionally viewed as incidental findings, AGs are recognized increasingly as a potential cause of CSF leak, associated meningitis, and spontaneous cephaloceles. Their identification plays an integral role in the surgical management of symptomatic patients.

#### CASE REPORT

Multimodality imaging from nine patients demonstrating 12 AGs was collected from several institutions. Inclusion criteria included AGs located adjacent to the petrous or mastoid portions of the temporal bone and the exclusion of other significant pathology. Intra-AG signal was compared to fluid in the adjacent CSF spaces. Atraumatic, spontaneous CSF leaks were present in six patients and meningitis in one patient. Intraoperative findings confirmed CSF leaks from AGs in three of six patients. Intra-AG cephaloceles were confirmed at surgery in two patients.

#### IMAGING FINDINGS

CT imaging of these patients demonstrated arachnoid granulations eroding into the posterior petrous temporal bone or laterally into the mastoid air cells. Mastoid fluid was present in six of six patients with CSF leak and the patient with meningitis. Additional macroscopic dural venous sinus arachnoid granulations were demonstrated in some of the cases. Intra-AG MR signal paralleled CSF. Additional soft tissue intensity signal was demonstrated on the two patients with confirmed intra-AG cephaloceles. There was no enhancement of intra-AG contents in the seven cases with postcontrast MR/CT imaging.



#### SUMMARY

It is important to recognize temporal bone arachnoid granulations as potential cases of CSF leak and resulting meningitis for preoperative surgical localization. Representative imaging findings often include erosion along the posterior portion of the petrous temporal bone or directly into the mastoid air cells, lack of solid enhancement (differentiating the lesions from

endolymphatic sac tumors or other destructive neoplasms) and possible opacification of adjacent mastoid air cells. The AGs that erode into the temporal bone are at risk for causing CSF leak if they extend towards a pneumatized region or directly into adjacent mastoid air cells. Intra-AG MR signal is usually isointense to CSF, but AGs containing cephaloceles may contain additional foci of soft tissue signal.

**KEY WORDS:** Arachnoid granulation, CSF leak

#### EE-62

#### Duplicated Internal Auditory Canal: A Rare Anomaly of the Inner Ear

Dombrowski, A.·Abdullah, A.·Bapuraj, R.·Shah, G.·Mukherji, S. K.

University of Michigan Health System  
Ann Arbor, MI

#### PURPOSE

Duplicated internal auditory canal (IAC) is a rare anomaly of the temporal bone, which usually is associated with ipsilateral sensorineural hearing loss. Only a few cases have been described previously in literature. We describe a rare case of duplicated right internal auditory canal in a 6-month-old patient with a history of Down syndrome.

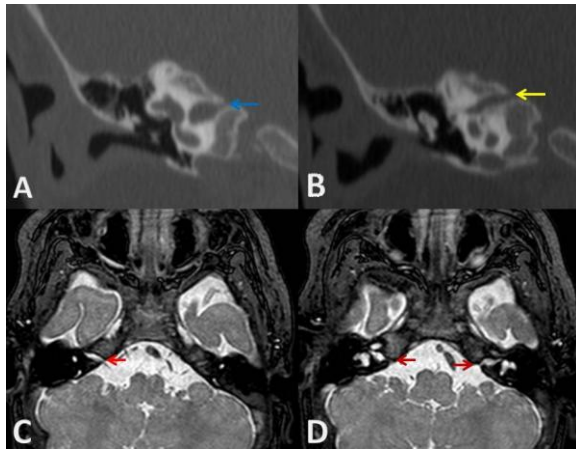
#### CASE REPORT

A 6-month-old male with Trisomy 21 presented with profound bilateral sensorineural hearing loss. The patient failed the newborn hearing screening and had no waveforms at 90 decibels on Auditory Brainstem Response testing. Past medical history was unremarkable for recurrent ear infections. On focused physical examination, the auricles were normal appearing. External auditory canals were patent bilaterally revealing clear and translucent tympanic membranes. Patient did not reveal evidence for facial palsy. There were no oral cavity lesions or masses. On palpation, child's neck revealed no evidence for cervical or supraclavicular lymphadenopathy.

#### IMAGING FINDINGS

Subsequently, a high-resolution computed tomography (HRCT) of the temporal bone was performed. Duplicated appearance of the right internal auditory canal with separation of facial and vestibulocochlear segments was noted. The facial nerve canal demonstrated normal caliber, located anterior and superior to vestibulocochlear canal, while there was significant narrowing of the cochlear canal near the fundus. Significant stenosis of the vestibulocochlear segment of the duplicated IAC was identified at the porus acousticus. Dehiscent right posterior semicircular canal also was seen. An enlarged right vestibule was also noted. A single IAC was identified on the contralateral side that demonstrated significant stenosis at the porus acousticus. High-resolution magnetic resonance imaging (HR MRI) of IAC was recommended which revealed absent right cochlear nerve. The left cochlear nerve was identified, however.





#### SUMMARY

Duplication of the IAC is an extremely rare anomaly involving a redundant osseous canal extending from the cerebellopontine angle through the otic capsule bone toward the labyrinth or cochlea. A duplicated IAC may or may not be associated with congenital sensorineural hearing loss secondary to aplasia or hypoplasia of the vestibulocochlear nerve. In patients with an abnormal IAC, the diameter of the canal does not predict reliably the presence or absence of the eighth cranial nerve, thus limiting the accuracy of HRCT in this situation. The ability to perform reconstructions with a steady-state sequence in a sagittal oblique plane of the IAC is crucial in examining the IAC contents and therefore, identifying cochlear nerve hypoplasia or aplasia.

**KEY WORDS:** Internal auditory canal, facial nerve, atresia

**Monday, April 23 –  
Wednesday, April 25**

**6:30 AM – 9:00 PM**

**Thursday, April 26**

**6:30 AM - 3:00 PM**

**Americas Hall II**

**Excerpta Extraordinaire 63 – 71**

(EE4) E4. – Interventional

**Note: A missing printed number indicates an abstract has been withdrawn.**

#### EE-63

#### Endovascular Treatment of Flow-Induced Anterior Spinal Artery Aneurysm Secondary to Aortic Coarctation

Soltanolkotabi, M.<sup>1</sup>•Marden, F. A.<sup>2</sup>•Hurley, M. C.<sup>1</sup>•Shaibani, A.<sup>1</sup>•Bendok, B. R.<sup>1</sup>•Batjer, H. H.<sup>1</sup>•Ansari, S. A.<sup>1</sup>

<sup>1</sup>Northwestern University Feinberg School of Medicine, Chicago, IL, <sup>2</sup>Alexian Brothers Neurosciences Institute, Elk Grove Village, IL

#### PURPOSE

Neurologic complications associated with coarctation of the aorta are generally intracranial. Less familiar, but equally disastrous are the spinal cord complications of this congenital heart lesion. We report on the endovascular treatment of a unique case of a ruptured anterior spinal artery aneurysm caused by a severe, unrepaired, and previously undiagnosed aortic coarctation.

#### CASE REPORT

A 56-year-old female with a past medical history of chronic hypertension and coronary artery disease, presented with severe, acute neck pain. Physical examination revealed hypertension, fever, a wide pulse pressure, and aortic regurgitation. Neurologic examination was within normal limits at the time of presentation.

#### IMAGING FINDINGS

A CT scan revealed an acute subarachnoid hemorrhage (SAH) with a small amount of blood in the fourth ventricle and a larger amount at the cisterna magna with extension to the C1 level. CT angiography (CTA) of the head/neck and spinal MR imaging/MR angiography (MRI/MRA) demonstrated an aneurysm ventral to the spinal cord at C6-7, associated with a markedly dilated anterior spinal artery (ASA). The ASA aneurysm was believed to be the source of the SAH. Additionally, a severe aortic coarctation was identified in the thorax.

Multiple dilated intercostal spinal collateral arteries communicating with the ASA were noted bypassing the aortic coarctation. The patient rapidly lost consciousness during the CTA (GCS = 6) and as a result she was intubated. Transfemoral spinal angiography was attempted, but failed due to an inability to access the ascending aorta across the coarctation. The patient was transferred to our tertiary center for further evaluation and treatment. We attempted a spinal angiogram via right transbrachial approach elucidating the 7 mm ASA aneurysm with a wide neck (4 mm) at the C6-7 level, supplied from a hypertrophied branch of the right thyrocervical trunk. The dome of the aneurysm had an irregular morphology and a daughter sac suggestive of recent rupture. However, endovascular therapy was delayed due to the significant contrast exposure and development of contrast-induced nephrotoxicity. Despite our recommendations, aortic coarctation repair was deferred by the cardiothoracic service due to multiple comorbidities. Ten days later, the patient underwent successful endovascular coil embolization of the wide necked ASA aneurysm. Although there was partial encroachment of the parent artery, patent antegrade flow remained secondary to flow demand from this significant collateral route.

#### SUMMARY

In the rare cases of spinal artery aneurysms, caused by the high-flow collaterals bypassing an aortic coarctation, correction of the aortic coarctation usually will lead to regression of these aneurysms. However, in our case, the ASA aneurysm had ruptured resulting in cord compression and progressive myelopathy with risk for rerupture and devastating complications. A multidisciplinary approach is required to address the multifaceted treatment plan in these complex presentations including aortic coarctation repair, securing the spinal artery aneurysm via endovascular/microsurgical approach, and balancing the hemodynamics of renal perfusion versus aneurysm stabilization.

**KEY WORDS:** Anterior spinal artery aneurysm, aortic coarctation, endovascular treatment

#### EE-64

#### Ruptured Intrameatal Anterior Inferior Cerebellar Artery Aneurysm: Endovascular Management Is a Viable Treatment Option

Lee, S.<sup>1</sup>•Christoforidis, G.<sup>1</sup>•Hreib, K.<sup>2</sup>•David, C.<sup>2</sup>

<sup>1</sup>The University of Chicago, Chicago, IL, <sup>2</sup>Lahey Clinic Medical Center, Burlington, MA

#### PURPOSE

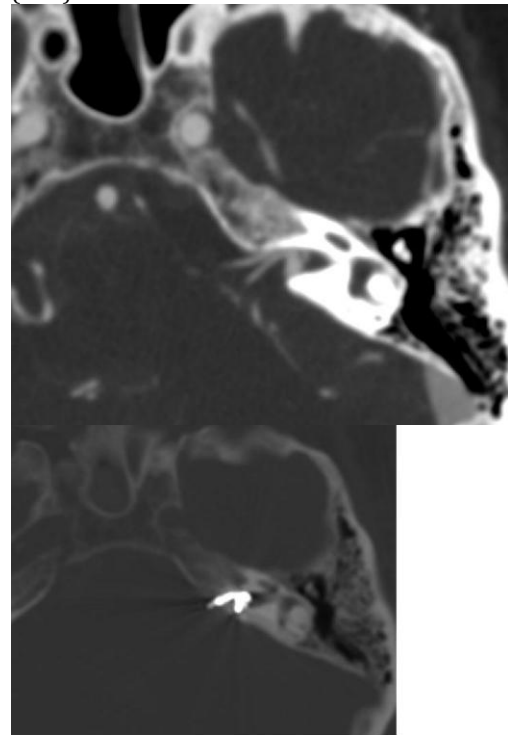
Ruptured intrameatal AICA aneurysm is extremely rare. As far as authors know, there are only 13 cases reported in the literature which all were treated with either surgical clipping or trapping. There is no case report which was treated with endovascular coiling. We present this case to demonstrate technical feasibility of endovascular treatment of the lesion and its clinical outcome.

#### CASE REPORT

An 87-year-old female presented with acute subarachnoid hemorrhage (SAH) due to ruptured left intrameatal AICA aneurysm. Her Hunt and Hess Scale on admission was grade 2, Glasgow Coma Scale was 13 and her CT scan showed Fischer grade 4 SAH. Considering her age and progressive deterioration of mental status, endovascular coiling of the aneurysm and sacrifice of AICA at or beyond the lateral pontine segment was recommended and was performed successfully. Follow-up physical examination on 1 month showed mild gait difficulty but no other neurologic deficit. In particular, there was no hearing loss, no facial asymmetry, no motor or sensory deficits. Her modified Rankin Scale (mRS) on 30-day follow up was 2.

#### IMAGING FINDINGS

Initial brain CT scan showed acute SAH mainly posterior fossa with intraventricular hemorrhage. CT angiography and DSA showed 3.5 mm x 4 mm fusiform AICA aneurysm within the left internal auditory canal. Endovascular coil embolization of the aneurysm as well as parent artery sacrifice beyond the lateral pontine segment of AICA was performed. There was no AICA territorial ischemia on 1-month follow-up MR imaging (MRI) examination.



#### SUMMARY

Endovascular coil embolization of a ruptured intrameatal AICA aneurysm with the parent artery sacrifice is technically feasible and resulted in favorable clinical outcome in our case.

**KEY WORDS:** AICA aneurysm, coil embolization

## EE-65

### Cerebral Hyperperfusion Syndrome following Balloon-Assisted Coil Embolization of an Unruptured M1 Bifurcation Aneurysm

Tubman, D. E. • Crandall, B. M. • Scholz, J. M. • Fease, J. L. • Delgado Almandoz, J. E. • Anderson, R. E.

Abbott Northwestern Hospital  
Minneapolis, MN

#### PURPOSE

Cerebral hyperperfusion syndrome is known to occur following recanalization of acute embolic stroke, carotid endarterectomy, stent-assisted angioplasty and arteriovenous malformation resection. It is a rare complication reported following surgical clipping of cerebral aneurysm. The authors present a case of cerebral hyperperfusion syndrome occurring following elective endovascular treatment of an unruptured right M1 aneurysm using balloon remodeling technique for coil embolization in a 70-year-old female.

#### CASE REPORT

Angiography demonstrated a very wide necked right middle cerebral artery aneurysm measuring 8.5 x 12.2 x 8.6 mm with incorporation of the inferior M2 branch into its base. Balloon assistance was utilized to aid in coil placement. Initial postprocedure examination demonstrated signs and symptoms of ischemia in the right middle cerebral artery territory. Blood pressure was maintained normotensive and symptoms completely resolved within 72 hours.

#### IMAGING FINDINGS

Postoperative imaging revealed increased perfusion and edema in the territory of the right middle cerebral artery with increased contrast in this distribution. Repeat imaging 24 hour's postprocedure demonstrated interval return to normal.

#### SUMMARY

Hyperperfusion syndrome is a rare complication following aneurysm surgery and to our knowledge has not been reported following use of balloon remodeling technique for endovascular embolization.

**KEY WORDS:** Balloon-assistance, hyperperfusion, aneurysm embolization

## EE-66

### Macro Embolus from Carotid Plaque Rupture during Carotid Stent-Assisted Angioplasty

Lee, S.<sup>1</sup> • Kim, M.<sup>2</sup> • Farb, R.<sup>3</sup> • Agid, R.<sup>3</sup> • Croul, S.<sup>3</sup> • Christoforidis, G.<sup>1</sup>

<sup>1</sup>The University of Chicago, Chicago, IL, <sup>2</sup>Pohang St. Mary Hospital, PoHand, KOREA, REPUBLIC OF, <sup>3</sup>Toronto Western Hospital, Toronto, ON, CANADA

#### PURPOSE

Reported captured emboli by embolic protection devices (EPD) during the carotid stent-assisted

angioplasty (CSA) ranged around  $300 \pm 500 \mu\text{m}$  by  $100 \pm 200 \mu\text{m}$ . We report a flow arresting macro-embolus from carotid plaque rupture (3.5 mm x 12 mm) during CSA which we captured and retrieved successfully.

#### CASE REPORT

A 63-year-old male who presented with right upper extremity weakness, mild expressive dysphasia and cognitive dysfunction showed left internal carotid artery stenosis (70% with NASCET method). The CSA was performed with EPD. Immediately after the stent deployment, poststenting angiography of the left ICA showed large filling defect in the EPD with significantly decreased ante-grade blood flow. Assuming filling defects can be related to acute platelet aggregation, 2B3A inhibitor was infused but did not resolve the filling defect. Thus we attempted retrieval of the embolus with EPD and the procedure was successful. The postretrieval angiography did not show any evidence of filling defects and the patient was discharged home post CSA 2<sup>nd</sup> day without additional neurologic deficit. Neurologic improvement was observed on post CSA 30<sup>th</sup> day clinical follow-up examination.

#### IMAGING FINDINGS

Pre CAS angiography showed 70% of luminal stenosis on the left extracranial internal carotid artery (ICA). A 4 by 15 mm sized balloon angioplasty of the lesion was performed followed with 7 mm by 40 mm sized carotid stent deployment. Immediate poststent deployment angiography showed 4 by 10 mm sized sausage-shaped filling defect caught by the EPD with near total antegrade flow arrest. We successfully retrieved the embolus together with the EPD. The dimension of the retrieved embolus was about 12 x 3.5 mm. Histopathologic examination of the embolus showed relative acellular matrix with frequent cholesterol clefts, focal calcifications and focal fibrous strands which are consistent with typical organized atherosclerotic plaque.



#### SUMMARY

Macro embolus from carotid plaque rupture during the CSA procedure may occur and potentially complicate the CSA procedure. In our particular case, the usage of EPD provided an opportunity of capturing and retrieval of the embolus successfully. This case report may

provide an explanation for acute carotid artery occlusion after CSA.

**KEY WORDS:** Carotid stent-assisted angioplasty, plaque rupture, atheromatous plaque

#### EE-67

### **New Indication for Flow Diversion Using "Pipeline" Intracranial Endovascular Device: Cavernous Carotid Artery Injury during Transsphenoidal Pituitary Surgery**

Ugurel, M. S.<sup>1</sup>•Karaman, B.<sup>1</sup>•Aslan, A.<sup>1</sup>•Cekirge, S.<sup>2</sup>

<sup>1</sup>Gülhane Military Medical Academy, Ankara, TURKEY,

<sup>2</sup>Hacettepe University, Ankara, TURKEY

#### **PURPOSE**

To present an unusual and off-label use of flow-diverting intracranial embolization device "Pipeline" in reconstructing an iatrogenically injured internal carotid artery (ICA).

#### **CASE REPORT**

Right ICA was injured during transsphenoidal pituitary surgery and patient was transported to DSA unit immediately. Mild contrast extravasation was evident during first angiogram, which vanished in the second run and a dissecting pseudoaneurysm remained (**Figure 1**). Next day following Clopidogrel loading, three overlapping "Pipeline" flow-diverting intracranial embolization devices were deployed at the site of pseudoaneurysm.

#### **IMAGING FINDINGS**

Follow-up angiogram a month later revealed perfect remodelling of the cavernous ICA, free from the dissecting aneurysm with patent ophthalmic, posterior communicating and anterior choroidal arteries (**Figure 2**).



#### **SUMMARY**

Previous reports usually mention about life-saving ICA sacrifice procedure following injury during hypophyseal surgery. This technique may represent a new approach in such cases, providing a more acceptable outcome for both the patient and neurosurgeon.

**KEY WORDS:** Cavernous carotid artery, iatrogenic injury, endovascular treatment

#### EE-68

### **Embolization of a Massive Right Frontal Lobe Non-Galenic Pial Arteriovenous Fistula Using Novel Penumbra 400™ Detachable Coils in a Neonate**

von Ritschl, R.•Murph, D.•Nakamura, L.•Casey, K. L.•Chaljub, G.•Swischuk, L.

University of Texas Medical Branch  
Galveston, TX

#### **PURPOSE**

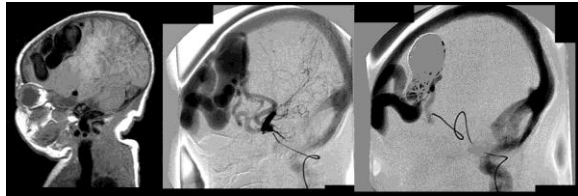
The novel Penumbra 400™ coiling system, utilizing coils with longer length and greater diameter than other currently available platinum coils led to successful embolization with greater packing density, reduced procedural time, and lower radiation dose in a neonate with a massive right frontal lobe non-Galenic pial arteriovenous fistula.

#### **CASE REPORT**

A 5-day-old girl presented with high output heart failure at birth and a palpable bruit with thrill noted over the anterior fontanel. Subsequent neuroimaging revealed a massive cortical, non-Galenic arteriovenous fistula along the right frontal convexity. Fifteen Penumbra 400™ detachable coils, ranging in size from 8 mm - 24 mm x 20 cm - 60 cm (607 cm total length), 0.020 in diameter, were placed into the arteriovenous fistula via transumbilical arterial route. Near complete embolization of the proximal arteriovenous fistula was obtained with persistent inferior fistula remaining. The patient's cardiovascular status is improving. A planned transvenous approach will be performed depending on the patient's clinical response.

#### **IMAGING FINDINGS**

**Head US:** Multiple middle cerebral artery and anterior cerebral artery feeders with multiple dilated varices are seen in the midline and to the right consistent with arteriovenous fistula, not draining to the vein of Galen. **MRI brain, MRV, MRA:** A large cortical arteriovenous fistula is noted within the right frontal lobe. Prominent venous varices are seen measuring up to 3.5 cm in oblique dimension. **Percutaneous transumbilical artery digital subtraction angiography of cerebral arteriovenous fistula embolization, procedure:** 3F microcatheter was advanced through the aortic arch. The left vertebral was selected, the microcatheter was advanced through the vertebral-basilar system terminating into right middle cerebral artery via posterior communicating artery collateral from the vertebral-basilar into the right middle cerebral artery. A large feeding vessel was accessed that was located at the superior aspect of the arteriovenous fistula. Fifteen Penumbra 400™ detachable coils, ranging in size from 8 mm - 24 mm x 20 cm - 60 cm (607 cm total length), were placed into the arteriovenous fistula via transumbilical arterial route. Significant decreased flow was observed.



#### SUMMARY

We believe the Penumbra 400™ coiling system will achieve greater packing density, shorten procedural time, and will lead to lower radiation dose in these exceptional cases, though further investigation is needed.

**KEY WORDS:** Embolization, cerebral arteriovenous fistula, penumbra longer coils

#### EE-69

#### Rotational Vertebral Artery Syndrome (Bow Hunter's Syndrome): Angiographic and CT Angiography Imaging Techniques and Findings

Koonce, J. D.<sup>1</sup>Heck, D.<sup>2</sup>Neal, M.<sup>1</sup>Wilson, J.<sup>1</sup>Morris, P.<sup>1</sup>

<sup>1</sup>Wake Forest, Winston-Salem, NC, <sup>2</sup>Forsyth Medical Center, Winston-Salem, NC

#### PURPOSE

Rotational vertebral artery syndrome (RVAS) or Bow Hunter's syndrome is a rare and potentially under-diagnosed condition in which vertebral artery flow is compromised by positional rotation of the neck in the setting of absent alternative pathways of flow. This will cause neurologic symptoms and may even lead to stroke. The vertebral artery looks normal in all or almost all cases in the neutral position, and therefore a high index of suspicion is needed to diagnose this condition. However, this is not sufficient. It is also necessary to engage the cooperation of the patient to rotate his/her head to a point of becoming symptomatic

to document the angiographic compromise of the artery. Our purpose is to explain the optimal angiographic technique to image RVAS as well as briefly discuss CT findings that may be suggestive of RVAS.

#### CASE REPORT

Three patients with positional dizziness and other TIA-like symptoms underwent imaging evaluation at our institution. Angiography in the neutral position was obtained as a baseline, and incremental angiographic images were obtained through a range of positions of the neck until the patient became symptomatic. Hesitant or reluctant patients were exhorted to provoke their symptoms, even at considerable discomfort to themselves, with the explanation that their surgical cure depended on these images. CT angiography also was obtained for surgical planning.

#### IMAGING FINDINGS

Despite the occurrence of neurologic symptoms catheter angiographic images were obtained without permanent adverse consequence. Neutral position images were normal in all patients. Incremental angiography subsequently demonstrated severe stenosis or occlusion of the vertebral artery in all three patients; two related to spondylosis and one due to C1-C2 hypermobility. The CTA images in patients with RVAS secondary to spondylosis demonstrated focal large osteophytes abutting the vertebral artery outside of the transverse foramen, and turning the head accentuated the vertebral artery narrowing. All three patients had clinical resolution of the vertebrobasilar insufficiency symptoms after surgical intervention.



Figure 1a. A large osteophyte abuts the right vertebral artery at C4 - C5

Figure 1b. Appropriate angiographic protocol allows one to obtain quality images of the right vertebral artery occlusion at C4 - C5 despite concurrent neurologic symptoms

#### SUMMARY

Rotational vertebral artery syndrome is rare; however, potentially under-diagnosed as supported by our cohort of three patients in less than 1 year. Even with a good patient history, a half-hearted angiographic protocol is not sufficient to diagnose this condition. Consistent encouragement of the patient to comply with the instructions given during catheter angiography is paramount to obtain quality images of RVAS. The aforementioned imaging findings combined with a proper clinical exam allow confident diagnosis of RVAS, a surgically treatable cause of vertebrobasilar insufficiency.

**KEY WORDS:** Positional vertebral artery occlusion, Bow-Hunter's syndrome, vertebral artery

**EE-70****Endovascular Recanalization of Supraclinoid Internal Carotid Artery Occlusion in the Subacute Setting**

Vranic, J. E.·Hurley, M. C.·Shaibani, A.·Bendok, B. R.·Batjer, H.·Ansari, S. A.

Northwestern University Feinberg School of Medicine  
Chicago, IL

**PURPOSE**

Managing subacute or chronic cervical/intracranial thromboembolic occlusions can be challenging. Medical management is recommended with respect to the recent COSS trial findings. When medical treatment fails and ischemic symptoms persist, surgical bypass procedures may be considered to preserve neuronal survival and function. We report on the rare endovascular recanalization of a supraclinoid left internal carotid artery (LICA) occlusion via mechanical thrombectomy in the subacute setting, discussing both its feasibility and potential risks.

**CASE REPORT**

A 20-year-old male presented with transient aphasia and right-sided hemiplegia.

**IMAGING FINDINGS**

CT/MR imaging identified a left temporal lobe infarct and angiographic studies (DSA) confirmed supraclinoid LICA occlusion, but with robust collateral flow across the anterior communicating artery (Acomm) supplying the left anterior cerebral (ACA) and middle cerebral arteries (MCA). The patient was discharged on antiplatelet and statin therapy. The patient returned 1 week later, again with transient right-sided weakness/numbness and facial droop. Repeat MRI revealed new acute infarcts in the left corona radiata and left insular cortex. Repeat DSA showed thrombus progression into the carotid terminus restricting flow across the Acomm into the left MCA distribution, with collateral flow now limited to pial collaterals. Two weeks later, the patient was transferred to our institution for a surgical bypass procedure on heparin anticoagulation and hemodynamic augmentation to stabilize the patient's ongoing TIAs. Gross cerebral blood flow (CBF) abnormality and progression of "silent" left MCA infarcts were noted on repeat MR perfusion/diffusion-weighted scanning. In preparation for a superficial temporal artery-to-MCA bypass, a normotensive challenge was attempted, but the patient collapsed into a densely hemiparetic/aphasic state not responsive to hemodynamic augmentation. Emergent endovascular intervention was initiated, but since an underlying obliterative vasculopathy (moyamoya) could not be excluded by imaging, angioplasty and stenting strategies were deferred. Instead, endovascular recanalization was achieved successfully by probing the thromboembolic occlusion with a microcatheter/microwire complex and subsequently with Penumbra vacuum aspiration thrombectomy device and low-dose 10 mg intraarterial tPA, resulting in TICI 2b antegrade reperfusion of the left ACA/MCA

Postprocedure, the patient was hemodynamically relaxed to normotension without any neurologic deficits and continued on heparin anticoagulation followed by antiplatelet therapy. Follow-up CT and MRI/MR perfusion studies demonstrated significantly improved CBF in both left ACA/MCA distributions, but asymptomatic complications of distal iatrogenic emboli and mild petechial and perisylvian subarachnoid hemorrhagic conversion were noted and managed by intermittently terminating anticoagulation/antiplatelet therapy.

**SUMMARY**

Endovascular recanalization of subacute, intracranial thromboembolic occlusions is feasible and may represent an alternative strategy when patients' neurologic and hematologic status cannot tolerate a surgical bypass procedure. Since significant risk for complications exist including distal iatrogenic emboli, reocclusion, reperfusion hemorrhage, and hemorrhagic conversion of subacute infarcts, it should be reserved until multidisciplinary consultation documents failure of optimum medical management, recurring TIAs/strokes, severe regional hypoperfusion or ischemia dependent on hemodynamic augmentation. In addition, vigilant attention to postprocedure management is crucial in limiting complications by titrating hemodynamic control, anticoagulation and especially antiplatelet medications if stenting is performed.

**KEY WORDS:** Recanalization, intervention, stroke

**EE-71****Sagittal Sinus Clot Retrieval Using a Solitaire AB Neurovascular Stent**

Blair, P. S.·Rennie, I.·Flynn, P.·O'Leary, S.

Royal Victoria Hospital  
Belfast, UNITED KINGDOM

**PURPOSE**

We present a case of cerebral venous sinus thrombosis treated with endovascular clot retrieval using a Solitaire AB stent. To our knowledge, this is the first documented use of this technique.

**CASE REPORT**

A 61-year-old man presented with a 1-day history of sudden onset frontal headache and associated vomiting. He was admitted to hospital for investigation. Lumbar puncture was negative. CT brain revealed extensive cerebral venous sinus thrombosis within the superior sagittal sinus, right transverse and sigmoid sinuses and within the right jugular vein. The patient was anticoagulated with low molecular weight heparin. Following a deterioration with collapse, generalized seizure and a drop in consciousness, the patient was transferred to the Regional Neuroscience Centre. CT venogram showed propagation of the venous sinus thrombosis. The patient's Glasgow Coma Score fluctuated with continued seizure activity and left hemiparesis. On the fifth day, after discussion with the



interventional neuroradiologists, catheter venography was performed with a view to retrieve clot. A DAC microcatheter was navigated through the extensive clot in the venous sinuses and tissue plasminogen activator was injected directly. A Solitaire AB stent was deployed to retrieve clot. The patient was extubated the following day with no neurologic deficit and was well enough to be discharged within the following week.

#### IMAGING FINDINGS

CT scanning of the head demonstrated the “dense delta” sign within the venous sinuses along with asymmetric increased density within the right transverse, sigmoid sinus and right jugular vein. CT venography confirmed the diagnosis with an “empty delta” sign. Catheter venography allowed navigation of a Solitaire AB stent to retrieve clot. Postprocedural venography showed adequate recanalization of the venous sinuses. A follow-up MRI brain showed good flow within the superior sagittal sinus with no evidence of venous infarction.

#### SUMMARY

Cerebral venous sinus thrombosis is a common condition with high morbidity and mortality. The mainstay of treatment is anticoagulation following prompt diagnosis. We present a case where clinical deterioration followed despite adequate anticoagulation. Failed medical therapy led the interventional neuroradiologists to attempt intrasinus thrombolysis followed by clot retrieval using a Solitaire AB stent. The patient made an excellent recovery and postprocedural imaging showed adequate recanalization of the cerebral venous sinus system. To our knowledge, this is the first use of a Solitaire AB stent for clot retrieval in venous sinus thrombosis. We advocate its use in those cases where medical therapy alone fails to prevent clot extension and clinical recovery.

**KEY WORDS:** Sagittal sinus thrombosis, clot retrieval

**Monday, April 23 –  
Wednesday, April 25  
6:30 AM – 9:00 PM  
Thursday, April 26  
6:30 AM – 3:00 PM  
Americas Hall II**

**Excerpta Extraordinaire 72 – 96**

(EE5) E5. – Pediatrics

**Note: A missing printed number indicates an abstract has been withdrawn.**

#### EE-72

#### **Concurrent Cranial and Spinal Subdural Hematomas in a Teenage Football Player: An Extremely Rare Entity**

Singh, M.<sup>1</sup>•Zada, G.<sup>2</sup>•Jones, J. G. A.<sup>2</sup>•Lerner, A.<sup>2</sup>•Boyko, O. B.<sup>2</sup>•Law, M.<sup>2</sup>•Rahmanuddin, S.<sup>2</sup>•Rajamohan, A.<sup>2</sup>•Shiroishi, M. S.<sup>2</sup>

<sup>1</sup>New York Medical College, Valhalla, NY, <sup>2</sup>Keck School of Medicine, University of Southern California, Los Angeles, CA

#### **PURPOSE**

To describe a unique presentation of concurrent spinal and cranial subdural hematomas, an extremely rare entity.

#### **CASE REPORT**

A 16-year-old male high school football player presented with episodes of headache and complete body stiffness, especially in the arms, lower back, and thighs immediately following a football game. This was accompanied by severe nausea and vomiting for several days. Viral meningitis was suspected by the primary clinician, and treatment with corticosteroids was initiated. Over the next several weeks, there was gradual symptom improvement and the patient returned to his baseline clinical status. This patient experienced a severe recurrence of the previous myriad of symptoms following a subsequent football game, without an obvious isolated traumatic episode. In addition, he experienced a new left-sided headache, fatigue and difficulty ambulating. He was admitted and an extensive workup was performed.

#### **IMAGING FINDINGS**

MR imaging of the brain showed a thin 2-3 mm subdural hematoma over the entire left cerebral hemisphere with extension into the interhemispheric fissure, as well as the posterior fossa. Additionally, lumbar spine imaging demonstrated an approximately 3 mm subdural hematoma dorsal to the thecal sac

extending from approximately the L1 to L4 levels. Cervical and thoracic MRI were negative for hematoma or evidence of vascular anomalies. Extensive workup, including laboratory evaluation and MR angiography of the brain, failed to reveal a bleeding diathesis or vascular malformation. The patient was treated conservatively with pain management and returned to baseline without any further sequelae.

#### SUMMARY

Coinciding spinal and cranial subdural hematomas are extremely rare, as less than 20 cases have been reported in the literature. Even more uncommon are posttraumatic concomitant hematomas, most of which are secondary to trauma to multiple sites. Multiple traumatic injuries, specifically to the head and lumbar region in our case, likely play an important role in the underlying etiology. However, specific mechanisms for the development of nontraumatic, concomitant spinal and cranial subdural hematomas have been hypothesized. There have been reported cases of spinal hematoma secondary to redistribution from cranial hematomas. Wong et al postulated that an amplification of shearing forces from increased intracranial pressure may cause tearing of the inner dura within the spine leading to hematoma formation in this area. Treatment of simultaneous cranial and spinal subdural hematomas, in which no predisposing factor has been identified, has not been established due to a limited amount of cases. Our patient received conservative management, consistent with previously treated patients within the same demographic.

**KEY WORDS:** Subdural hematoma, trauma

#### EE-73

##### **Susceptibility-Weighted Imaging in Migraines: Appearance of the Cerebral Veins**

Mirsky, D. M.·Vossough, A.·Zimmerman, R. A.

The Children's Hospital of Philadelphia  
Philadelphia, PA

#### PURPOSE

Migraine is the most common acute and recurrent headache syndrome in children. Characterized by periodic episodes of paroxysmal headache and accompanied by nausea, vomiting, abdominal pain, it typically is relieved with sleep. The pathophysiology of migraine is complex and not completely understood. Classically it was thought to be vascular in etiology with hypoperfusion due to vasoconstriction resulting in the preceding aura, and hyperfusion due to vasodilatation leading to the headache. Recent data suggest that primary neuronal dysfunction within the brainstem affects the trigeminal somatosensory and modulatory pain systems including the spinal trigeminal nucleus and thalamus. This neuronal dysfunction results in excessive excitation followed by spreading depression leading to the described phases of vasoconstriction and vasodilatation. Over the past two decades, neuroimaging has played a role in characterizing this phenomenon, particularly with the aid of perfusion-

weighted imaging. Hypoperfusion and hyperfusion have been described in association with migraine headaches both in the absence and presence of abnormal arterial imaging. Utilizing susceptibility-weighted imaging in conjunction with arterial spin labeled perfusion imaging, we describe an unusual appearance to the cerebral veins in pediatric migraine patients presenting with cerebral hypoperfusion. There is an increase in conspicuity of the cerebral veins ipsilateral to the hypoperfused hemisphere.

#### CASE REPORT

Several pediatric patients presenting with migraine were evaluated by MR susceptibility and perfusion imaging. A retrospective review of the imaging findings and perfusion correlates was performed in these cases.

#### IMAGING FINDINGS

We observed an unusual appearance to the cerebral veins on susceptibility-weighted imaging in pediatric patients with migraines which was associated with perfusion abnormalities. Asymmetric increased conspicuity of the ipsilateral cerebral veins was observed in patients who demonstrated decreased perfusion to a given cerebral hemisphere.

#### SUMMARY

Migraine is a common cause of acute and recurrent headache in children. While the underlying etiology remains unclear, neuroimaging plays a role in characterizing the perfusion changes associated with migraine headaches. This finding of increased conspicuity of the cerebral veins in pediatric migraine patients in association with ipsilateral cerebral hypoperfusion is illustrated. This characteristic of the cerebral veins is related to increased circulating deoxyhemoglobin resulting in increased magnetic susceptibility effect. Vasoconstriction of the arterial system can lead to decreased cerebral perfusion downstream resulting in delayed transit time of blood, increased oxygen extraction and increased deoxyhemoglobin content.

**KEY WORDS:** Migraine, susceptibility-weighted imaging, venous system

#### EE-74

##### **Fludarabine-Induced Severe Necrotizing Leukoencephalopathy in Pediatric Hematopoietic Stem Cell Transplantation**

Helton, K. J.·Patay, Z.·Triplett, B. M.

St. Jude Children's Research Hospital  
Memphis, TN

#### PURPOSE

Initially nearly discarded due to severe neurotoxicity, fludarabine at lower doses has been a major component in successful reduced intensity conditioning (RIC) hematopoietic stem cell transplants (HSCT) for thousands of patients each year. Of 157 patients who received fludarabine containing RIC HSCT in our

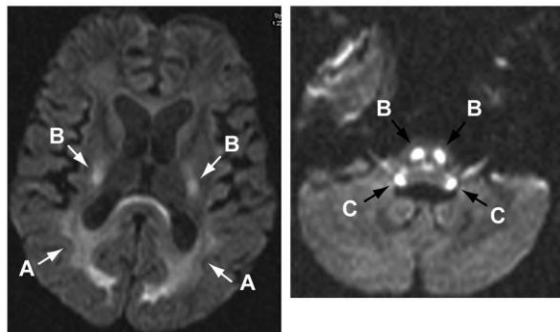
institution, two patients developed fludarabine-induced severe necrotizing leukoencephalopathy.

#### CASE REPORT

Case 1. A 14-year-old boy underwent HSCT for acute lymphocytic leukemia. Two weeks following transplant, he developed paresthesia, foot drop, patellar hyperreflexia, and ankle clonus, which progressed to difficulty walking and upper body hypersensitivity, with ascending paresthesia. Loss of motor reflexes and emotional lability followed. Lumbar puncture showed elevated myelin basic protein (16 ug/L). He next developed cortical blindness, progressive autonomic instability, and eventually required mechanical ventilation. By day +100, he was in a persistent vegetative state, and succumbed to sepsis 9 months posttransplant. Case 2. A 16-year-old girl underwent HSCT for secondary myelodysplastic syndrome. Two weeks following transplant she developed progressive bilateral burning foot pain and poor ambulation. Upper chest hyperesthesias and cortical blindness soon followed. She became confused and required aggressive control of severe total body neuropathic pain. Lumbar puncture showed elevated myelin basic protein (6.6 ug/L). Her deterioration continued to the point of no purposeful movement or vocalization. Intermittent apneic spells led to tracheostomy placement; she was discharged on hospice care, and died 6 months posttransplant with urosepsis.

#### IMAGING FINDINGS

Case 1. Follow-up MRI (Figure) showed progressive restricted water diffusion within retrogeniculate optic radiations (A) motor (B) and brainstem sensory tracts (C), interpreted as vacuolating myelinopathy in the context of acute myelinotoxicity. The final MRI (not shown) demonstrated diffuse atrophy, extensive leukoencephalopathy, and new areas of restricted diffusion of the optic nerves, chiasm, mamillary bodies and hypothalamus. Case 2. Similarly, the initial MRI showed a diffuse acute demyelinating process of the retrogeniculate optic radiations, motor and sensory tracts which became progressive, leading to rarefaction of tissue matrix in involved areas with time.



#### SUMMARY

Although pediatric HSCT frequently is associated with neurologic toxicities, our review is the first to describe the complete clinical and concomitant distinguishing imaging features fludarabine-induced severe necrotizing leukoencephalopathy. Both patients developed distinctive restricted diffusion lesion

patterns that coincided with development of lower extremity sensory neuropathy, retrogeniculate blindness, rapidly progressive total body sensory and motor neuropathies, and eventual global neurologic devastation. Fludarabine-induced severe necrotizing leukoencephalopathy has unique clinical and radiologic features that should aid early diagnosis and prognostication for afflicted patients.

**KEY WORDS:** Fludarabine-induced, severe necrotizing leukoencephalopathy, clinical/diffusion patterns

#### EE-75

##### Pediatric Wernicke Encephalopathy

Harreld, J. H. • Perko, R. • Helton, K. J. • Wright, K. D.

St. Jude Children's Research Hospital  
Memphis, TN

#### PURPOSE

To illustrate the imaging findings in two cases of pediatric Wernicke encephalopathy at our hospital during a recent TPN vitamin shortage and to emphasize the importance of recognizing this potentially fatal but treatable condition in the pediatric population.

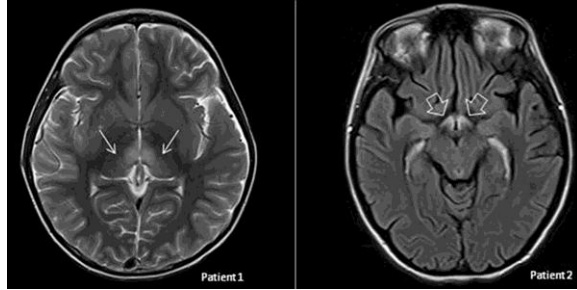
#### CASE REPORT

A five-year-old girl with metastatic medulloblastoma on TPN for 8 weeks due to poor appetite and weight loss following postoperative craniospinal irradiation ate multiple carbohydrate snacks in a single sitting. The following morning she woke with vertical nystagmus. Over the next 2 days, she developed progressive, predominantly postprandial somnolence, ataxia and word finding difficulty. Wernicke encephalopathy (thiamine deficiency) was suspected based on MR imaging and clinical presentation. Additional history revealed that an oral multivitamin prescribed due to TPN vitamin shortage had not been taken as directed. Symptoms improved within 6 hours of 25 mg iv thiamine; the patient's symptoms continued to improve on twice daily dosing with near complete resolution by day 4. Several days later a second patient, with a history of acute myelogenous leukemia postallogeic bone marrow transplant and on TPN for protracted nausea, vomiting and diarrhea, presented with acute mental status changes and blurry vision following a recent improvement in appetite. IV thiamine was administered for suspected Wernicke encephalopathy after emergent MRI. Rapid resolution of clinical and imaging findings ensued.

#### IMAGING FINDINGS

Patient 1: MRI demonstrated edema in the bilateral medial thalami (arrows), tectal plate and periaqueductal gray matter with small foci of cytotoxic edema in the thalami and tectum; MRA and MRV were normal. Follow-up MRI 2 weeks later demonstrated only minimal residual signal abnormality in the thalami, corresponding to pretreatment cytotoxic edema. Patient 2: MR imaging demonstrated only subtle bilateral hypothalamic T2 hyperintensity (open arrows) and

enhancing prominence of the tuber cinereum, which were resolved at MR imaging 6 days later.



#### SUMMARY

Wernicke encephalopathy, more commonly seen in adult alcoholics, should be suspected in malnourished or chronically ill pediatric patients with acute mental status changes, vision changes, vertical nystagmus and/or ataxia. Prompt recognition and treatment with thiamine is essential to averting a potentially fatal outcome.

**KEY WORDS:** Wernicke, encephalopathy, pediatric

#### EE-76

##### Brain MR Imaging Findings in Patients with Menkes Disease Including MR Spectroscopy

Ferreira, R. M. F.<sup>1</sup>•Laner, C.<sup>1</sup>•Kini, J.<sup>2</sup>•Grant, G. P.<sup>3</sup>

<sup>1</sup>Clinica Imagem, Florianopolis, BRAZIL, <sup>2</sup>Massachusetts General Hospital, Boston, MA, <sup>3</sup>Boston Children's Hospital, Boston, MA

#### PURPOSE

Report two cases of Menkes disease with their neuroimaging features, one of them with spectroscopy study and MRI follow up demonstrating sequentially the appearance of imaging findings. Findings on DWI also are commented.

#### CASE REPORT

Two patients with Menkes disease were studied with brain MRI. In one of the cases, the patient was followed with multiples MRI examinations, in which spectroscopy and DWI were performed.

#### IMAGING FINDINGS

Our two infants presented with neurologic degeneration, with prior history of seizures, hypotonia and failure to thrive. MR imaging of both patients demonstrated brain atrophy, swollen temporal lobes, dysmyelination, and elongation and tortuosity of intracranial vessels. At the final stage, severe volume loss associated with bilateral subdural collections were observed, mimicking child abuse. In one of the patients, the MRI follow up showed sequentially the appearance of such neuroimaging findings. This is the first report of MR spectroscopy study in a patient with Menkes disease showing high lactate levels.

#### SUMMARY

Although the association of brain volume loss, swollen temporal lobes and tortuous intracranial vessels are the

most described imaging findings, the classic findings can be absent or may appear sequentially in the early onset of the disorder. MR spectroscopy may show lactate peak.

**KEY WORDS:** Metabolic, MR spectroscopy

#### EE-77

##### Cranial MR Imaging Findings of Central Nervous System Toxicity of Isoniazid

Hasiloglu, Z. I. •Albayram, S. •Asik, M. •Kilic, O. •Unver, O. •Erdemli, H. •Kocer, N.

Istanbul University  
Istanbul, TURKEY

#### PURPOSE

To present cranial magnetic resonance (MR) imaging findings of central nervous system toxicity in a patient who received isoniazid (INH) usage as tuberculosis prophylaxis.

#### CASE REPORT

A 12-year-old girl referred to hospital with the complaints of weight loss and growth retardation. INH (10 mg/kg/day) prophylaxis was started because of hilar enlargement, parenchymal infiltration and two positive PPD tests with an interval of 2 months. After 4 months of treatment, patient referred to hospital with tremors and dizziness. In the neurologic examination, intentional tremor, ataxia, dysdiadochokinesia and dysmetria were detected. Romberg test was found positive. There was no abnormal findings in routine blood count, biochemical, metabolic and hormonal tests.

#### IMAGING FINDINGS

In the regions that lie symmetrically and bilaterally from thalamus to mesencephalon and bilateral dentate nuclei of cerebellum, no contrast fixations were seen; hyperintensity was detected on T2-weighted and fast fluid attenuated inversion recovery (FLAIR) images. Diffusion-weighted images showed restriction of diffusion at the same localizations. MR spectroscopy examination did not differ compared with the normal parenchyma. Laboratory data showed increased blood INH level as high as 16 microgram/mL (normal<3). According to the imaging and laboratory findings, we assumed the diagnosis was INH toxicity. Then we decided to discontinue INH treatment and pyridoxine replacement therapy. After 1 month, the clinical and cranial MR imaging findings regressed completely.

#### SUMMARY

Isoniazid causes toxicity by inhibiting pyridoxine (vitamin B6) metabolism and decreasing  $\gamma$ -aminobutyric acid (GABA) level. Decreasing of GABA, which is an inhibitor neurotransmitter, causes convulsions and tremors. Isoniazid half-life may show variability in children. Because of that, during INH therapy, serum levels of INH should be monitored, pyridoxine replacement should be done as prophylaxis, and patient should be monitored in terms of possible complications.

**KEY WORDS:** Isoniazid, toxicity, central nervous system

## EE-78

### **Case of Acyl-CoA Oxidase 1 Deficiency: Longitudinal MR Imaging Evaluation Including MR Spectroscopy and Diffusion Tensor Imaging**

Bernardi, B.·Longo, D.·Verdolotti, T.·Macchiaiolo, M.·Napolitano, A.·Cannatà, V.·Bartuli, A.

Bambino Gesù Pediatric Hospital  
Rome, ITALY

#### **PURPOSE**

To show neuroradiologic evolution of a case of Acyl-CoA oxidase 1 deficiency (SCOX) from the onset of symptoms to a late stage of the disease by a retrospective longitudinal MR study. We present and discuss serial conventional MRI findings and serial functional studies including DTI and MR spectroscopy in a child with SCOX.

#### **CASE REPORT**

SCOX is a peroxisomal disease that belongs to the group of fatty acids beta-oxidation disorders and is characterized by elevated levels of very long chain fatty acids (VLCFAs) in blood and tissues. Typical symptoms are neonatal seizures, hypotonia and neurologic regression, usually starting at 24 months. We present the case of a male child of unrelated parents, with unremarkable pregnancy and uneventful birth. The patient showed only marked neonatal hypotonia, but all early developmental milestones were reached normally. At the age of 12 months he showed severe developmental delay, followed by neurologic regression. Once a metabolic disease was suspected, several exams were performed to reach the diagnosis, including VLCFAs serum dosage, immunoblot analysis and genetic mutational analysis.

#### **IMAGING FINDINGS**

The first MRI, performed at the age of 1 year, revealed bilateral polymicrogyria involving perisylvian and frontal cortex, without significant white matter (WM) abnormalities. Subsequent MR studies, starting from the first, performed at the age of 5 years, showed wide and progressive WM abnormalities with a typical dynamic pattern of distribution (centrifugal, caudo-cranial, and posterior-anterior) sparing the subcortical U fibers. The MRI performed at the age of 5 years was characterized by the appearance of ponto-medullary and cerebellar WM abnormalities and vermis atrophy. In a later phase of the disease, a MR study, performed at 6 years, showed the appearance of a marked atrophy of brainstem, frontal and temporal lobes, due to extensive involvement of supratentorial WM. At this age the optic pathways and the corpus callosum clearly were involved. The periventricular WM showed a pattern of signal changes characterized by an inner zone hypointense on T1WI and hyperintense on T2WI with increased ADC and reduced FA, consistent with WM vacuolation. The outer zone showed hyperintensity on T2WI and normal signal on T1WI, with almost preserved myelination. Between these two zones, we

noted the presence of an intermediate, thin and linear area of high signal on T1WI and low ADC values, with mild enhancement after contrast administration, likely representing a line of active demyelination. This finding has been described in another peroxisomal disease: Child Cerebral X-linked Adrenoleukodystrophy. Single voxel H<sup>+</sup> MRS acquired on 3T MR unit (Skyra, Siemens) with PRESS technique and short echo time (TE = 30 ms) was localized in abnormal paratrigonal WM and occipital cortex. Postprocessing was performed on "Tarquin" software. Results showed reduced NAA peak and increased Cho peak in abnormal WM compared to cortex; we also noted two peaks, Lip09 and Lip13, probably representing lipids or macromolecules.

#### **SUMMARY**

We present a retrospective longitudinal MRI study of a rare case of SCOX with some uncommon neuroradiologic features. To our knowledge, it's the only report in literature including H<sup>+</sup> MRS and DTI.

**KEY WORDS:** Acyl-CoA oxidase deficiency (SCOX), peroxisomal disorder, MR imaging

## EE-79

### **Ectopic Cervical Thymus as a Cause of Horner's Syndrome**

Morozova, L. V.·Rarey, K.·Stout, A.·Pollock, J. M.

Oregon Health and Science University  
Portland, OR

#### **PURPOSE**

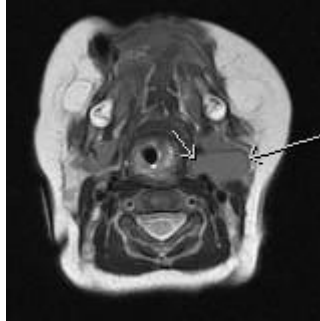
To describe the history, clinical presentation, and imaging findings of a young infant with Horner's syndrome secondary to ectopic cervical thymic tissue.

#### **CASE REPORT**

LM is a 3-week-old girl who presented with unequal pupil size. Her parents noticed anisocoria at 6 days of age, reporting the right pupil being larger than the left. At initial presentation, the parents reported no ptosis or other neurologic symptoms. LM was the product of a full-term, uncomplicated pregnancy and otherwise healthy. There was no history of birth trauma. Due to patient's young age, additional testing was deferred and close clinical follow up was planned. At 2 months the parents reported development of left upper lid ptosis and the patient underwent apraclonidine test. Apraclonidine test was positive, suggesting Horner's syndrome. MR imaging of the chest, abdomen, and pelvis was performed to evaluate for neuroblastoma, but did not reveal an abnormality. Normal thymic tissue was seen in the chest. The patient underwent neck MRI which demonstrated a soft tissue mass just anterior to the left carotid space adjacent to the submandibular gland. Spot urine check for the presence of excessive catecholamine was performed and was normal. The patient underwent operation to remove mass pressing on the left sympathetic chain. Review of the surgical specimen by pathology demonstrated ectopic thymus.

#### **IMAGING FINDINGS**

There is a 12 x 20 x 19 mm soft tissue mass within the left submandibular space of the neck at the level of the angle of the mandible. The mass is situated just anterior to the left common and internal carotid arteries and slightly compresses the carotid space.



#### SUMMARY

Ectopic cervical thymus is a very rare condition. This is the first reported case of an isolated supra-hyoid ectopic cervical thymus causing Horner's syndrome. In evaluating an infant/child with Horner's syndrome, ectopic cervical thymus should be considered if a mass is identified.

**KEY WORDS:** Cervical thymus, Horner's syndrome

#### EE-80

##### Conventional MR Imaging and Diffusion Tensor Imaging Findings in a Patient with Mutation in TUBA1A

Bernardi, B. • Colafati, G. S. • Figà Talamanca, L. • Randisi, F. • Zanni, G. • Cannatà, V. • Genovese, E. • Bertini, E. S.

Bambino Gesù Pediatric Hospital  
Rome, ITALY

#### PURPOSE

Mutations in alphetubulin1a (TUBA1A), located on chromosome 12, have been associated with a wide spectrum of disorders of cortical development, ranging from focal perisylvian pachygyria to agyria, but with a specific combination of features not observed in other mutations, such as dysgenesis of the corpus callosum, dysgenesis of the anterior limb of the internal capsule and mild to severe cerebellar and brainstem hypoplasia. Main objectives of this case report are to contribute in defining the phenotypic spectrum associated with mutations in TUBA1A by means of conventional MRI adding the exploration of DTI features (FA maps and fiber tractography).

#### CASE REPORT

This female patient was born at term after an uncomplicated pregnancy and delivery. At the age of 4 months, she developed febrile seizures. Electroencephalography did not show epileptiform abnormalities but inter-hemispheric asynchrony and a pattern of multifocal slow waves were evident. The diagnosis of TUBA1A mutation was based on polymerase chain reaction (PCR) and DNA sequencing of the four coding exons of the TUBA1A gene. Brain MR

imaging was performed on a 1.5 T scanner at age 4 and 11 months.

#### IMAGING FINDINGS

The first MR imaging scan, at 4 months, showed cortical malformation consisting in abnormal gyral pattern characterized by bilateral polymicrogyria with antero-posterior gradient. The white matter was hypoplastic bilaterally with thinning of corpus callosum; the trigones and occipital horns of the left lateral ventricle appeared severely dilated and both frontal horns had a "hooked" aspect resulting from the hypoplastic corpus callosum. The left basal ganglia were abnormally shaped resulting from poorly myelination and hypoplasia of the anterior limb of the internal capsule that lead to a lack of clear separation of the striatum into caudate nucleus and putamen and the rather full appearance of these structures. The brainstem was thin with severe hypoplasia involving mainly the right part of the pons, the inferior portion of the right cerebral peduncle and the right superior cerebellar peduncle. Diffuse cerebellar dysplasia involving mainly the vermis and less the left hemisphere was also evident. MR imaging performed at 11 months included DTI. Conventional MRI confirmed the previously described features. Fractional anisotropy maps and fiber tractography were obtained. The FA maps showed decreased anisotropy in the anterior limb of the left internal capsule. Fiber tractography revealed a significant decrease in volume of the left cortical-spinal tract and of the fibers of the corpus callosum.

#### SUMMARY

Our data confirm, as previously reported, the existence of specific brain abnormalities associated with gyral malformation in patients with TUBA1A mutations and highlight the presence of abnormal DTI features that may suggest the differentiation of TUBA1A-related disorders of cortical development from those related to other gene abnormalities.

**KEY WORDS:** Alphetubulin 1A, cortical development, diffusion tensor imaging

#### EE-81

##### Hypothalamic Adhesion: An Incidental Finding?

Branson, H. M. • Blaser, S. I. • Laughlin, S. • Raybaud, C.

The Hospital for Sick Children  
Toronto, ON, CANADA

#### PURPOSE

The aim of this study is to describe a midline congenital normal variant of the hypothalamus demonstrated on MRI.

#### CASE REPORT

To date we have found several cases of an accessory gray matter bundle that appears to cross the midline to connect the hypothalamus anterior to the mamillary bodies and within the third ventricle.

#### IMAGING FINDINGS



This bundle appears of gray matter signal and also appears connected to the optic chiasm by a thin linear gray matter strand. Initial reports included a differential diagnosis of hypothalamic hamartoma, although this is thought incorrect as the gray matter tissue runs through the third ventricle and is not located in the classic location of a hypothalamic hamartoma. This hypothalamic adhesion has been reported in some patients with Chiari II malformation.

#### SUMMARY

An entity demonstrated on MRI of an accessory gray matter adhesion/bundle within the third ventricle and bridging the hypothalamus is a presumed congenital anomaly. Associations with other congenital anomalies is being sought. This has been reported previously in some patients with Chiari II malformations.

**KEY WORDS:** Hypothalamus, adhesion, anatomy

#### EE-82

##### **Case of Atretic Occipital Cephalocele with Dandy-Walker Variant and Subependymal Heterotopia: Mean Diffusivity CT vs MR Imaging**

Ando, K.·Ishikura, R.·Mouri, M.·Odawara, S.·Igarashi, Y.·Yamasaki, M.·Katsuura, T.·Wakata, Y.·Hirota, S.·Fujita, S.·Arita, N.

Hyogo College of Medicine  
Nishinomiya, JAPAN

#### PURPOSE

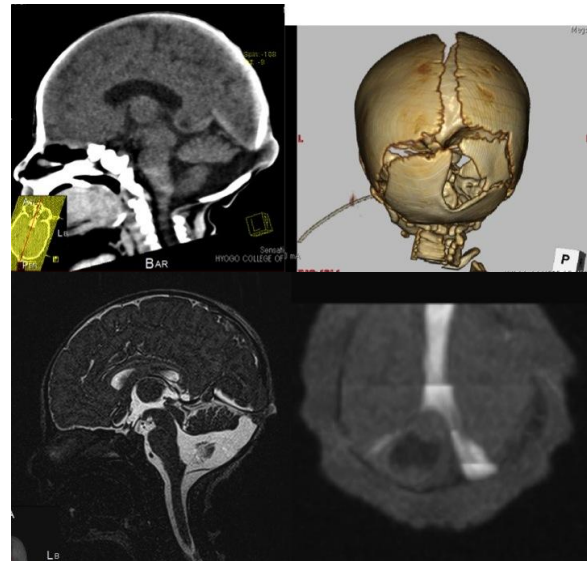
Atretic occipital cephalocele is a uncommon congenital anomaly, which usually presents as nodular, small masses just above the external occipital protuberance. Patients with atretic occipital cephaloceles appear to have a low incidence of associated anomalies and a good prognosis for normal development. We herein present a case of atretic occipital cephalocele with Dandy-Walker variant and subependymal heterotopia. Usefulness of noncontrast mean diffusivity (MD) CT and MRI are discussed.

#### CASE REPORT

A male newborn baby of 2 days after birth presented with cranial mass with bone defect and abdominal distention. Abdominal distention turned out to be due to Hirschsprung disease.

#### IMAGING FINDINGS

Noncontrast MD CT and noncontrast MRI were performed. Noncontrast MD CT including MPR and 3D images was useful to visualize the bone defect, cephalocele itself, and intracranial anomalies of Dandy-Walker variant and subependymal heterotopia. Noncontrast MRI with CISS and MRV could not visualize bone defect itself, but was equally useful to MD CT to visualize cephalocele, fibrous connection tissue and intracranial anomalies, and could visualize the venous anomaly and relationship between cephalocele and surrounding venous sinus, which were important for the following surgical intervention.



#### SUMMARY

Mean diffusivity CT with MPR and 3D images and MRI are equally useful for diagnosing atretic occipital cephalocele to visualize cephalocele and intracranial anomalies. Mean diffusivity CT is superior to MRI in visualizing bone abnormality. On the other hand, CISS and MRV on MRI was superior to MD CT to visualize fibrous connective tissue and venous anomaly, respectively.

**KEY WORDS:** Atretic occipital cephalocele, MD CT, MR imaging

#### EE-83

##### **Fatal Case of H1N1 Acute Necrotizing Encephalopathy in a 2-Year-Old Boy**

Burns, P. A.·Rennie, I. M.·McKinstry, C. S.·Flynn, P. A.·Smyth, G. P.·O'Leary, S. M.

Royal Victoria Hospital  
Belfast, UNITED KINGDOM

#### PURPOSE

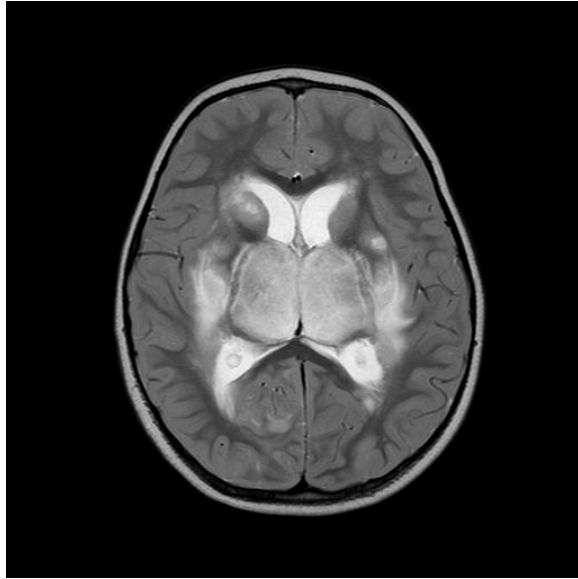
To discuss the imaging findings in a case of acute necrotizing encephalopathy secondary to novel influenza H1N1 infection.

#### CASE REPORT

A previously well, 2-year-old caucasian boy was admitted to hospital with increasing shortness of breath. There had been a short preceding history of a viral illness. Routine immunization was up to date. Initial examination revealed bilateral crepitations on auscultation and low oxygen saturation. Chest radiograph was reported as normal. The following morning he became increasingly unresponsive with a GCS of 4 and was transferred to the regional pediatric intensive care unit. He continued to rapidly deteriorate and subsequently developed multiorgan failure. H1N1 influenza infection was confirmed in respiratory secretions. He passed away 5 days later.

### IMAGING FINDINGS

MR imaging revealed extensive abnormality with marked swelling and T2 hyperintensity within the thalami, midbrain and pons. Similar signal change was observed within the caudate nuclei, putamina, external capsules, periventricular white matter and cerebellar white matter. These areas all demonstrated diffusion restriction, which appeared concentric within the thalami and pons. Multifocal frontal lobe cortical infarction also was present. There was no evidence of contrast enhancement. Mass effect was noted with hydrocephalus, effacement of basal cerebrospinal fluid (CSF) spaces and approximately 8 mm of tonsillar herniation. MR angiography and venography were normal.



### SUMMARY

Influenza A-associated acute necrotizing encephalopathy has been well described previously in East Asian patients, particularly in Japan. Other associated infections include human herpesvirus-6, measles, parainfluenza and mycoplasma. However, to the best of our knowledge this is the youngest reported case fatality secondary to novel H1N1 influenza. Although the pathogenesis remains unknown, it is speculated to be an immune-related phenomenon. The imaging findings of multifocal lesions within the thalami, cerebral and cerebellar white matter and brainstem have been described previously. Diffuse meningeal enhancement also has been reported, although not observed in this case. The additional finding of multifocal cortical infarction is however unusual.

**KEY WORDS:** H1N1, encephalopathy

### EE-84

#### 5-Year-Old Male with Systemic Lupus Erythematosus Presenting with Bilateral Moyamoya and Chronic Stroke

Javadi, P.·Ansari Gilani, K.·Dreyer, S.·Blackham, K. A.

University Hospital Case Medical Center  
Cleveland, OH

### PURPOSE

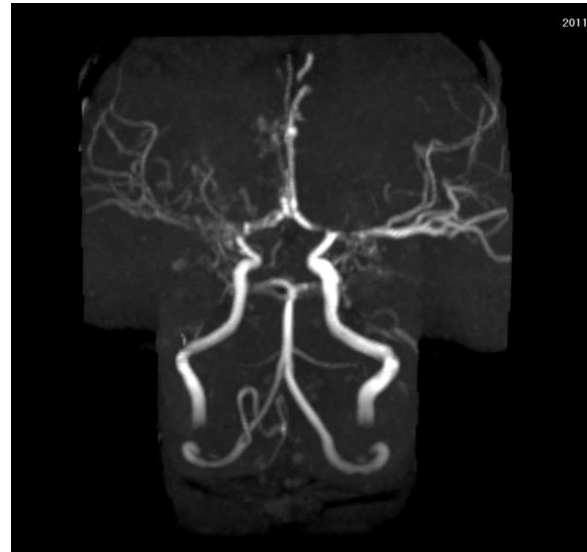
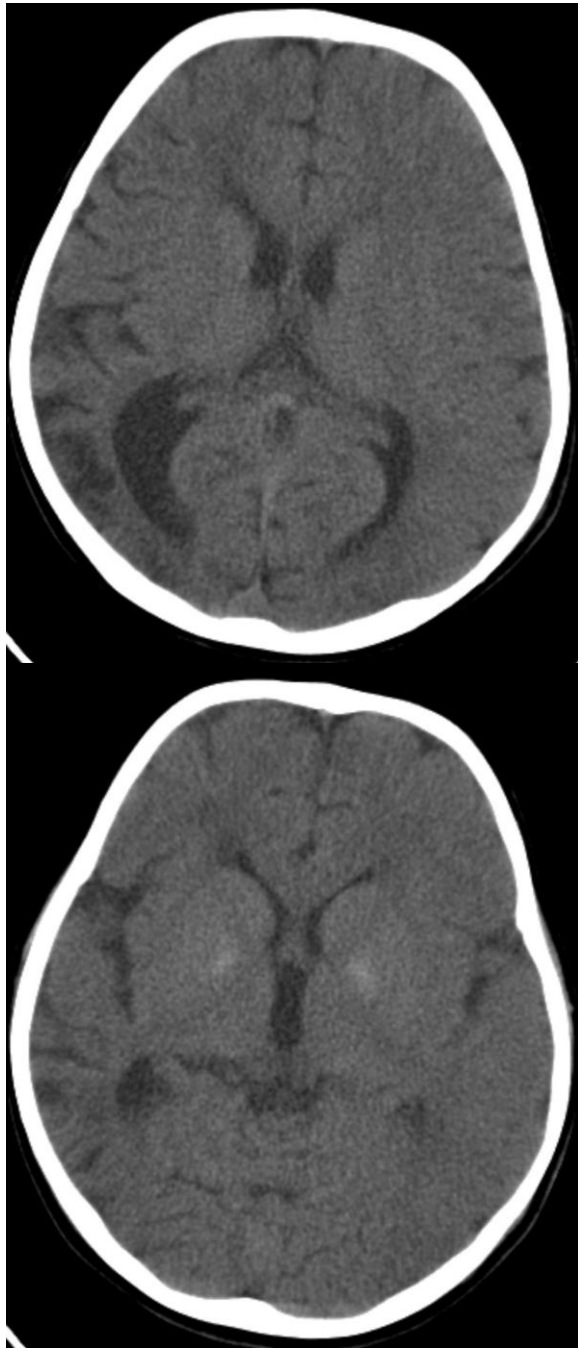
The purpose of this report is to discuss clinical manifestations and imaging findings of a pediatric patient presenting with a rare manifestation of neuropsychiatric systemic lupus erythematosus (SLE).

### CASE REPORT

A 5-year-old male from a rural community was referred to the pediatric rheumatology clinic following few months of nodular rash in feet and fingers and pain in the extremities. Patient's mother had concern about the child's recurrent headaches and persistent fatigue. The child was lost to follow up until he had an accident of falling from a pony 4 months later. CT of the head demonstrated extensive right hemispheric encephalomalacia and bilateral basal ganglia calcifications. Patient subsequently was admitted to a children's hospital and diagnosis of SLE was made based on combined clinical and serological findings.

### IMAGING FINDINGS

A. CT of head demonstrates right parieto-occipital encephalomalacia. B. CT image demonstrates bilateral basal ganglia calcification. C. MR angiography demonstrates bilateral constricted ICA termini with extensive distal collateral flow.



#### SUMMARY

Neuropsychiatric manifestations of pediatric lupus include headache, seizure, cognitive dysfunction, and stroke with suspected underlying immune-complex mediated vasculopathy. This case highlights that when stroke and moyamoya pattern is seen in the pediatric population a prothrombotic state such as SLE should be considered.

**KEY WORDS:** Systemic lupus erythematosus, moyamoya, stroke

#### EE-85

#### Brain and Spine MR Imaging Findings in a Rare Case of Polymerase Chain Reaction Proven Ureaplasma Meningitis

Dumeer, S.<sup>1</sup>•Millar, W. S.<sup>2</sup>•Lignelli, A.<sup>2</sup>

<sup>1</sup>New York-Presbyterian Hospital, New York, NY,

<sup>2</sup>Columbia University Medical Center, New York, NY

#### PURPOSE

To describe the MRI brain and spine findings in a neonate with polymerase chain reaction (PCR) proven ureaplasma meningitis. Neonatal meningitis secondary to ureaplasma is very rare and is difficult to diagnose and treat. A high index of suspicion is required to diagnose ureaplasma meningitis in setting of meningitis not responding to standard antibiotic therapy.

#### CASE REPORT

A 12-day-old, full term neonate, presented with fever of unknown origin, irritability, poor feeding and upper respiratory infection for 4 days. Cerebrospinal fluid (CSF) analysis was consistent with nonspecific bacterial meningitis. Blood, urine, CSF cultures obtained before starting antibiotics were all negative. Despite antiviral and antibacterial therapy, the patient continued to be symptomatic. Additional tests to rule out herpes simplex virus (HSV), respiratory syncytial virus (RSV), influenza, enterovirus, human herpes virus 6 (HHV6), cytomegalovirus (CMV), fungal, and tuberculosis infections were all negative. The patient was not

immunocompromised. After 10 weeks, the patient became completely asymptomatic, and was without neurologic sequelae. A PCR test subsequently performed on a CSF sample obtained at admission revealed a 16S ribosome sequence unique to ureaplasma. The diagnosis of ureaplasma meningitis was made retrospectively.

#### IMAGING FINDINGS

Cranial MRI performed on day of admission showed subtle but extensive leptomeningeal enhancement on post-contrast T1-weighted images. Dilatation of bilateral lateral, third and fourth ventricles indicated hydrocephalus. The abnormal leptomeningeal enhancement was more conspicuous on postcontrast FLAIR images obtained the next day. Enhancement was seen predominantly in basal cisterns, Sylvian fissures and along circle of Willis. Follow-up MRI brain at 4 days (Figure 1A) showed progression of the leptomeningeal enhancement and an increase in hydrocephalus despite antibiotic therapy. Subtle ependymal enhancement along lateral ventricles now was noted. MR imaging of the total spine (Figure 1B) also showed diffuse leptomeningeal enhancement along entire length of spinal cord, especially dorsally. Follow-up MR imaging 10 weeks later showed complete resolution of the abnormal findings.

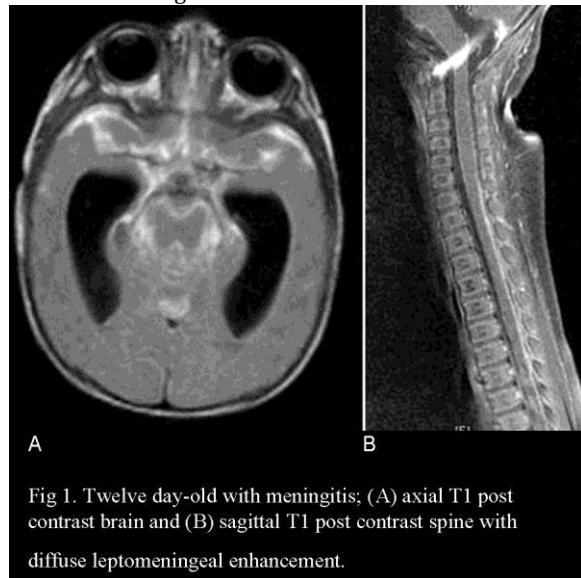


Fig 1. Twelve day-old with meningitis; (A) axial T1 post contrast brain and (B) sagittal T1 post contrast spine with diffuse leptomeningeal enhancement.

#### SUMMARY

Only a few cases with ureaplasma meningitis and the associated radiologic findings have been reported in the literature. MRI findings, in this case, consisted of diffuse leptomeningeal enhancement of the brain and spinal cord as well as mild ependymitis and hydrocephalus. Postcontrast FLAIR images assisted in demonstrating the intracranial leptomeningeal enhancement. In a neonate, ureaplasma infection should be considered in the setting of bacterial meningitis that does not respond to standard antibiotic therapy.

**KEY WORDS:** Ureaplasma, meningitis, MR imaging

#### EE-86

#### Interesting Case of Amoebic Encephalitis

Koerber, A. J.·Challa, H.·Goldstein, S.

University of Kentucky Hospital  
Lexington, KY

#### PURPOSE

The patient is a previously healthy 2-year-old white male. He presented with acute onset fevers, ataxia, and abnormal eye movements. He had an EEG on the date of admission, which demonstrated severe diffuse encephalopathy, possibly worse in the left hemisphere. There was no epileptiform activity during the exam. A lumbar puncture also was performed on the date of admission, which demonstrated a WBC of 178 cells/uL, neutrophil count of seven cells/uL, lymphocyte count of 166 cells/uL, and monocyte count of five cells/uL. The cerebrospinal fluid (CSF) glucose was 27 mg/dL, protein was 251 mg/dL, and lactic acid was 3.9 mmol/L. The cytology of the CSF demonstrated lymphocytosis with admixed plasma cells and rare atypical cells, which possibly could be reactive lymphocytes. Results were nonspecific and were consistent with an infectious process.

#### CASE REPORT

CT of the head without contrast done on the date of admission demonstrated multiple low density lesions located throughout both sides of the brain, including the left basal ganglia and the high right parietal lobe. MRI of the brain with and without contrast was performed on the second day of admission, which demonstrated nodular leptomeningeal enhancement throughout the basal cisterns and coating the ependymal lining of the ventricular system. There also were scattered areas of parenchymal enhancement throughout both hemispheres (including the bilateral basal ganglia), but most prominent in the right parietal convexity. This area also was associated with abnormal leptomeningeal enhancement. Differential considerations included infection, Langerhans cell histiocytosis, central nervous system (CNS) lymphoma, or a germ cell tumor. He was started on multiple antimicrobial regimens, but his symptoms continued to worsen, and he became obtunded and started having seizures.

#### IMAGING FINDINGS

Repeat EEGs were performed, but these were similar to the first (severe encephalopathy without seizure activity). A repeat head CT without contrast performed 4 days after admission redemonstrated the multiple low density lesions, but there was now mild ventriculomegaly. MR angiography and MRV of the brain performed on day 5 of the hospitalization demonstrated no acute abnormalities. The patient underwent a bone marrow biopsy on day 6 of the hospitalization, which was unremarkable. Also on day 6 of the hospitalization, he underwent a craniotomy and brain lesion resection from the right frontal lobe. The brain biopsy demonstrated amoebiasis. The tissue was sent to the CDC for PCR testing, which confirmed the presence of *Balamuthia mandrillaris*. The patient was

started on diflucan, flucytosine, and sulfadiazine. Despite these medications, the patient's ventriculomegaly worsened and he required a ventriculoperitoneal shunt. He also required a Nissen fundoplication with gastrostomy tube placement and tracheostomy. His ventriculomegaly stabilized, and his symptoms slightly improved, but he had severe residual neurologic deficits and seizures.

#### SUMMARY

He was transferred to a rehabilitation facility after a hospital stay of 2.5 months. He is currently in stable condition living at home with his mother. He continues to have severe neurologic deficits, but his seizures are improved. He still has a tracheostomy, gastrostomy tube, and VP shunt.

**KEY WORDS:** Amoebic, encephalitis, balamuthia

#### EE-87

##### **Isolated Intraparenchymal Cerebellar Rosai-Dorfman Disease in a Child**

Wang, B. • Ketonen, L. M.

M.D. Anderson Cancer Center  
Houston, TX

#### PURPOSE

To illustrate the imaging findings of a case of isolated intraparenchymal cerebellar Rosai-Dorfman disease (RDD) in a child, which to our knowledge is the first reported case of such lesion in a child.

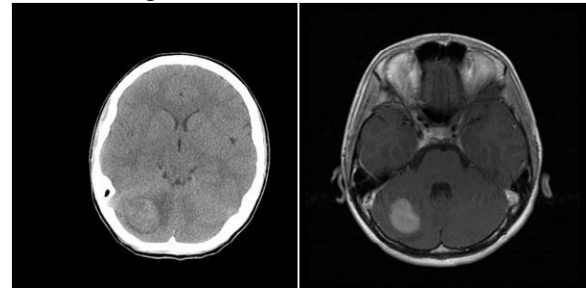
#### CASE REPORT

The patient is a 14-year-old boy without significant past medical history. On 01/04/2011, he developed a sudden headache in the back of his head and was taken to the emergency room. He was sent home after blood and urine tests were normal. Two days later he had severe headaches again. He had a CT scan, followed by an MRI that demonstrated a right cerebellar mass. The patient underwent gross total resection of the lesion on 02/10/2010. Frozen pathology was consistent with histiocytic process with granulomata. Gross pathology shows ovoid resection of cerebellum. Within the specimen is a firm yellow-tan well circumscribed tumor. Histologic sections show the classic appearance of RDD with lobular aggregates of histiocytes surrounded by thin connective tissue septae containing mature lymphocytes. Within the cytoplasm of histiocytes, scattered lymphocytes are noted (emperipolesis). The adjacent cerebellum shows Rosenthal fiber formation and reactive gliosis. Immunohistochemistry shows strong diffuse reactivity in the histiocytes for CD68 and focal strong reactivity for S-100 protein.

#### IMAGING FINDINGS

CT shows a hyperdense lesion in the right cerebellar hemisphere, with surrounding edema. MR imaging demonstrates a solitary 3 x 2.6 cm homogeneously enhancing lesion in the right cerebellar hemisphere. On the T2 FLAIR images, the lesion has slightly low central signal, with surrounding edema. On the gradient image,

a tiny focus of susceptibility signal void is present which could represent tiny focus of hemorrhage. On the T1 image, the lesion is isointense to the brain tissue. On the diffusion image, there is no restricted diffusion.



#### SUMMARY

Rosai-Dorfman disease, sinus histiocytosis with massive lymphadenopathy, rarely involves the intracranial structure without other sites of involvement. When it does, it commonly is dural-based, involving the frontal and parietal regions and the skull base. Isolated intraparenchymal Rosai-Dorfman disease is extremely rare. We found only two reported cases in the literature of isolated intraparenchymal RDD involving the cerebellum, both cases are in adults, even though the disease predominantly affects children and young adults. To our knowledge, this case is the first reported case of such lesion in a child. Despite its rarity, one should be aware of this entity and take it into consideration when treating solitary cerebellar lesions even in children.

**KEY WORDS:** Rosai-Dorfman disease, pediatric, cerebellum

#### EE-88

##### **Infantile Melanoma: A Case of Transplacental Melanoma Transmission to the Neuraxis and Tongue**

Naidu, P. K. • Miller, J. H. • Egelhoff, J. C. • Curran, J. G.

Phoenix Childrens Hospital  
Phoenix, AZ

#### PURPOSE

To describe a case of transplacental transmission of metastatic melanoma characterized on MRI, the third reported to involve the neuraxis, and the first to involve the oral cavity.

#### CASE REPORT

A 3-month-old female presented with multiple cutaneous lesions on her head that had developed over the previous 1.5 months. She was born at full term, healthy, delivered by cesarean section. Five years prior, her mother had been diagnosed with cutaneous melanoma of the face, treated by wide excision. One month postpartum the patient's mother had a seizure. Her brain MRI showed multiple intracranial lesions. Her body imaging demonstrated diffusely metastatic melanoma. The infant's cutaneous lesions progressed and a biopsy confirmed transplacental transmission of

metastatic melanoma. An MRI of the head and neck was performed.

#### IMAGING FINDINGS

Contrast-enhanced MRI of the brain and neck revealed multiple intracranial and neck lesions compatible with melanoma metastases. The intracranial lesions were largely right-sided, including a 5-6 mm T1 hyperintense, T2 hypointense intraaxial mass in the right frontal corona radiata and another in the right occipital lobe. An 8 mm extraaxial lesion superficial to the right frontal lobe contained a hemorrhagic fluid-fluid level. A 6 mm diameter pineal gland showed thick circumferential enhancement greater than anticipated for the patient's age. From a developmental standpoint, the brain was structurally normal outside of these lesions. Within the neck, a 6 mm oval-shaped T1 hyperintense mass was present in the left tongue. Additional enlarged left posterior triangle lymph nodes were also T1 hyperintense. The cutaneous lesions noted on the patient's forehead during physical examination were not obvious on MRI despite the inclusion of fat saturated sequences.

#### SUMMARY

Approximately 1 of every 1000 pregnant patients is diagnosed with a malignancy, with melanoma representing approximately 8% of such cancers. Despite its rarity, maternal melanoma is the malignancy most often transmitted transplacentally to the fetus. Only eight cases of transplacental transmission of melanoma have been reported in the literature to date. We present the 9th case, the 3rd with metastatic lesions to the neuraxis, and the 1st with involvement of the oral cavity. Prior reports have described intracranial lesions within the posterior fossa and mastoid regions, the former with poor outcome and the latter with lesion regression. While the prognosis for both the mother and fetus in this situation is poor, new advances in oncologic treatment may yield a therapeutic impact, possibly increasing the incidence of this rare but fascinating entity in the near future.

**KEY WORDS:** Melanoma, transplacental

#### EE-89

##### **Focal Spinal Cord Atrophy: Is There a Germinoma Nearby?**

Maller, V. G.·Choudhary, A. K.·Agarwal, A.·Nguyen, D. T.

Penn State Milton S. Hershey Medical Center  
Hershey, PA

#### PURPOSE

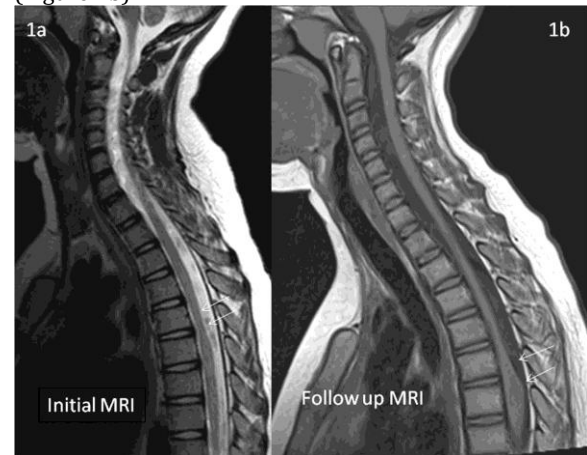
We describe a case of thoracic intramedullary germinoma presenting in a 11-year-old female in whom the diagnosis was made 2 years after onset of progressive myelopathy. Initial MR imaging studies revealed focal atrophy of the thoracic spinal cord with no definite mass.

#### CASE REPORT

A 11-year-old female presented with history of progressive bilateral lower extremity weakness and scoliosis. She was evaluated by pediatric neurologist and clinical diagnosis of muscular dystrophy was considered. Serial MRI performed at regular intervals for 2 years after onset of her symptoms revealed no significant finding, except for focal atrophy of the spinal cord at T5-6 level. Subsequent follow-up MRI revealed an expansile enhancing mass in the thoracic spinal cord at T6 level, by which time the patient was wheel chair bound and incontinent. The tumor was resected surgically and the pathology report was consistent with intramedullary germinoma.

#### IMAGING FINDINGS

Initial MRI of the spine at the onset of symptoms showed focal spinal cord atrophy at T5-6 level (Figure 1a). Subsequent follow-up MRI revealed an expansile mass in the thoracic spinal cord at T6 level after 2 years (Figure 1b).



#### SUMMARY

We report a unique case of primary intramedullary germinoma with prolonged period of clinical signs and symptoms which preceded radiologic visualization of the lesion in the spinal cord. Presence of focal cord atrophy in a patient with progressive neurologic deterioration should raise the suspicion of an underlying germinoma. This could be similar to hemiatrophy preceding or accompanying the imaging depiction of a basal ganglia mass lesion thought to be caused by a paraneoplastic process.

**KEY WORDS:** Germinoma, intramedullary, atrophy

#### EE-90

##### **Primary Intracranial Rhabdomyosarcoma of the Pineal Region**

Naidu, P. K.·Miller, J. H.·Curran, J. G.·Egelhoff, J. C.

Phoenix Childrens Hospital  
Phoenix, AZ

#### PURPOSE

To describe a case of primary intracranial rhabdomyosarcoma located within the pineal region, the first reported in this location.



### CASE REPORT

A 13-year-old female with no significant past medical history presented with 3 weeks of worsening headache and intermittent vomiting. No other symptoms were present. Neurologic examination was remarkable for papilledema. Upgaze was intact, with neurologic examination otherwise unremarkable. Imaging was performed.

### IMAGING FINDINGS

Noncontrast CT of the brain revealed a 2.5 cm hyperdense mass in the third ventricle with resultant lateral and anterior third ventricular outflow obstruction. MR imaging showed a T1 hypointense, T2 hyperintense 2.8 cm lobular contrast-enhancing pineal region mass extending into the midbrain and posterior aspect of the third ventricle. No intracranial or spinal metastases were identified. A surgical biopsy was performed. The initial result was reported as a "malignant small cell tumor" without further description. The final pathologic diagnosis was rhabdomyosarcoma. The densely packed tumor cells expressed both desmin and myogenin by immunohistochemical staining. Neural immunohistochemical markers such as GFAP and neurofilament were negative. The proliferative index (MIB-1) was high. An alveolar subtype initially was suspected, confirmed by the presence of a PAX3/FOXO1 fusion transcript upon RT-DNA analysis.

### SUMMARY

4.5 of every 1 million children younger than 14 years old are diagnosed with rhabdomyosarcoma each year, with head and neck the most common location. Although rhabdomyosarcoma is the most common sarcoma of childhood, it is rarely encountered intracranially. Less than 40 primary intracranial rhabdomyosarcomas had been reported in the literature as of 2007. We present rhabdomyosarcoma of the pineal region, a location which, to our knowledge, has not been reported in the literature as of yet. Intracranial rhabdomyosarcomas pose a treatment challenge by virtue of their rarity. No standard of treatment has been defined. While the tumor often is debulked surgically followed by radiation, the optimal radiation dose is unknown. Similarly, the most favorable chemotherapeutic drugs are not clear, with regimens proven effective in the treatment of extracranial rhabdomyosarcomas often used. Prognosis for both pediatric and adult patients with primary intracranial rhabdomyosarcomas is poor, with only 11% of those reported surviving for greater than 2 years after initial diagnosis.

**KEY WORDS:** Rhabdomyosarcoma, intracranial

### EE-91

#### MR Imaging Features of Infantile Embryonal Tumor with Abundant Neuropil and Ependymoblastic Rosettes in the Pons

Patay, Z.·Reddick, G. W.·Harreld, J. H.·Sabin, N.·Helton, K.·Sablaue, A.·Glass, J. O.·Klimo, P.·Broniscer, A.·Ellison, D.

St. Jude Children's Research Hospital  
Memphis, TN

### PURPOSE

Embryonal tumor with abundant neuropil and ependymoblastic rosettes (ETANER) is a rare but distinctive embryonal tumor of the central nervous system, typically encountered in young children with a clear female preponderance and a dismal prognosis. Most are supratentorial in location, but involvement of brainstem and cerebellum also occurs. Only five pontine tumors have been reported to date and advanced MRI data are even sparser, limited to MR spectroscopy (MRS) in a supratentorial ETANER. We report conventional and advanced magnetic resonance imaging (MRI) features in pontine ETANER.

### CASE REPORT

An 11-month-old female patient presented with head tilt, ataxia and eye deviation. MR imaging revealed a brainstem tumor. Because of the unusual appearance of the lesion on follow-up conventional and advanced MRI performed at our institution 2 weeks later, stereotactic biopsy was performed. Histopathologic evaluation confirmed the diagnosis of ETANER.

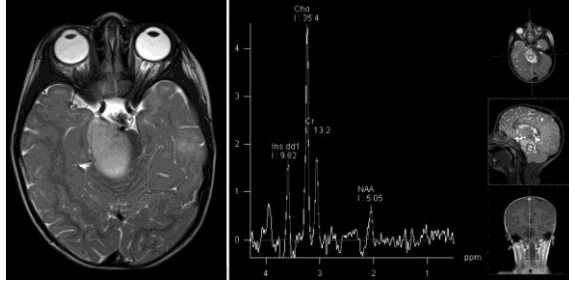
### IMAGING FINDINGS

Conventional MRI showed a well defined intraaxial brainstem lesion involving 80% of the pons, eccentric to the right, with an upper ventral exophytic component growing supratentorially into the right mesial temporal fossa. The lesion demonstrated minimal dorsal necrosis and virtually no enhancement. Apparent diffusion coefficient (ADC) values were elevated compared to uninvolved brainstem and cerebellum (0.66 mm<sup>2</sup>/sec vs 0.53 mm<sup>2</sup>/sec and 0.54 mm<sup>2</sup>/sec respectively), consistent with relative hypocellularity. The tumor was hypoperfused (rCBV of tumor vs uninvolved pons = 0.58; tumor vs cerebellum = 0.43), indicating a lack of significant angiogenesis. Choline:N-acetylaspartate ratios varied between 1.6 and 7.02 within the tumor field and myo-inositol was elevated, consistent with malignant neoplasm.

### SUMMARY

In the pontine location, ETANER may represent a differential diagnostic dilemma with diffuse intrinsic pontine glioma (DIPG) and pilocytic astrocytoma (PA), typically necessitating biopsy prior to management decisions. Recognition of the potentially distinctive features of this rare entity, therefore, is important. Pontine ETANER, in the literature and in this case, typically is well defined, homogeneously T2 hyperintense, usually solid (but occasionally with areas of necrosis) and shows little or no enhancement. In an appropriate clinical setting, conventional MRI findings may be suggestive, facilitating differentiation of ETANER from DIPGs and PAs. The discrepancy between the low-grade appearance on conventional MRI and diffusion/perfusion imaging and the high-grade malignancy features on MRS may enhance the specificity of the diagnostic imaging workup (Figure 1). Prospective advanced MRI data, however, are needed to

further evaluate the utility of the advanced techniques in the imaging diagnosis of ETANER in the brainstem.



**KEY WORDS:** Embryonal tumor, MR imaging

## EE-92

### Multimodal MR Imaging Findings of a Congenital Glioblastoma Multiforme

Donmez, F. Y. • Kural, F. • Aslan, H. • Coban, G. • Ozen, O. • Agildere, M.

Baskent University  
Ankara, TURKEY

#### PURPOSE

To demonstrate the imaging findings of a congenital glioblastoma multiforme.

#### CASE REPORT

An 8-month-old female patient from North Iraq presenting with an enlarging head was admitted to our hospital. The parents stated, they were told that the head circumference was larger than normal limits at birth. No investigation was made further at that time. On her routine follow up on the second month, a CT was performed because of the enlarged head, which revealed a supratentorial mass. The parents did not seek any treatment at that time. Six months later, the baby was seen at our hospital, with the complaint of increasing enlargement of the head circumference. On physical examination, the patient was fine, with normal reflexes and normal responses to the stimuli, except for the macrocephaly.

#### IMAGING FINDINGS

MR imaging showed a huge mass in the right frontoparietal lobes, with multiple small and large cystic areas and solid components which were isointense to gray matter on both T1W and T2W images. The mass had a partially extraparenchymal appearance, especially on coronal slices. On diffusion-weighted images, the solid portions showed restriction, probably due to high cellularity. A multivoxel MR spectroscopy performed at TE: 30, 135 and 270 ms depicted very high Choline/Creatine ratios and a significant decrease in NAA. Based on the cystic and partially extraparenchymal appearance, desmoplastic infantile ganglioglioma was the primary diagnosis, with astrocytoma and PNET also in the differential. The patient was operated the next day by subtotal resection of the tumor. Pathologic examination revealed a glioblastoma multiforme. The patient did fine after the operation and high-dose chemotherapy was planned.

#### SUMMARY

Congenital glioblastoma multiforme is a rare tumor, with less than 50 cases reported in English literature. Published reports are based mostly on clinical, genetical and pathologic behavior, reports of radiologic appearance are relatively uncommon. The imaging in those reports most commonly involved antenatal diagnoses by ultrasound, we did not recognize any report of MRI with diffusion and spectroscopy so far. Diagnosis by imaging among the most common congenital tumors is difficult. However, there are some clues which can direct the radiologist to the diagnosis. In this case, the partially extraparenchymal and cystic appearance of the tumor misled us to the possible diagnosis of desmoplastic infantile ganglioglioma, which has a better prognosis, and does not need aggressive chemotherapy as glioblastoma does. However, pathology showed highly mitotic glial proliferation with necrosis. In conclusion, differential diagnosis of a supratentorial heterogeneous hemispheric mass in an infant may include any of the glial and embryonic tumors. We need more clues radiologically, to help us predict the histologic type.

**KEY WORDS:** Congenital, glioblastoma multiforme, MR imaging

## EE-93

### Juvenile Pilocytic Astrocytoma in Association with Arteriovenous Malformation

Soltanolkotabi, M.<sup>1</sup>•DiPatri, A. J.<sup>2</sup>•Hurley, M. C.<sup>1</sup>•Ansari, S. A.<sup>1</sup>•Rajaram, V.<sup>2</sup>•Tomita, T.<sup>2</sup>•Shaibani, A.<sup>1,2</sup>

<sup>1</sup>Northwestern University Feinberg School of Medicine, Chicago, IL, <sup>2</sup>Children's Memorial Hospital, Chicago, IL

#### PURPOSE

Juvenile pilocytic astrocytomas (JPA) are highly vascular, relatively common primary brain tumors in the pediatric population; however, their association with a true arteriovenous malformation (AVM) is extremely rare. We report an 8-year-old girl with right supratentorial JPA with an angiographically documented AVM entangled in the tumor mass who presented with intracranial hemorrhage due to a ruptured anterior choroidal artery pseudoaneurysm encased in the lesion. The AVM nidus and the hemorrhage site were embolized with Onyx.

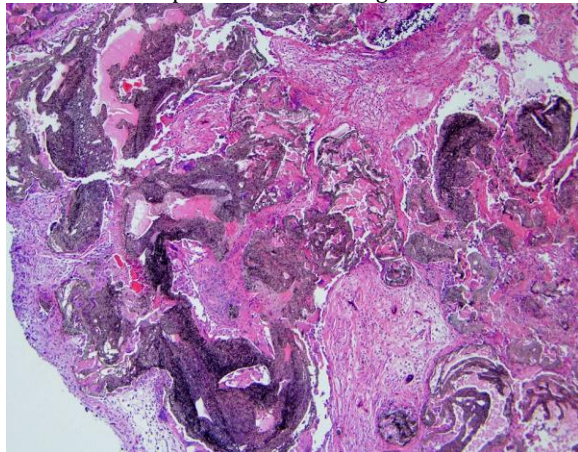
#### CASE REPORT

An 8-year-old female with a past medical history of intermittent headaches for approximately 2 months, presented with loss of consciousness (GCS=7). Prior to presentation, she had experienced sudden onset of severe right temporal headache, ataxia, and slurred speech followed by emesis and unresponsiveness. Physical examination revealed hypertension and bradycardia with a nonreactive, dilated right pupil and left spastic hemiplegia.

#### IMAGING FINDINGS

Brain CT scan demonstrated a large (4.5-5 cm), hyperdense, acute intraparenchymal hemorrhage in the

right basal ganglia and thalamus with midline shift and secondary obstructive hydrocephalus. Conventional angiography demonstrated an AVM nidus supplied by the right anterior choroidal artery without evidence of a tumor blush. Two intranidal aneurysms and a prenidial pseudoaneurysm of the anterior choroidal artery were identified. The prenidial pseudoaneurysm was centered within the hematoma and therefore considered the most likely site of rupture. The patient underwent Onyx embolization of the anterior choroidal artery and the AVM nidus. A small trickle of Onyx extending from the base of the pseudoaneurysm into the extravascular space identified as the rupture site. Control angiogram following embolization confirmed obliteration of the pseudoaneurysm and AVM nidus. Follow-up MR brain imaging revealed a right-sided, heterogeneous mass involving the thalamus and basal ganglia. The mass had increased in size and appeared to be contrast enhancing at the tumor hemorrhagic site. At this time, the coexistence of a neoplasm with the AVM was suspected. The patient underwent surgical resection of a 3-3.5 cm heterogeneous mass entangled with the AVM. Histopathologic examination revealed a pilocytic astrocytoma-WHO grade I, intermingled with large embolized vessels consistent with an AVM. Clinically, the patient continued to suffer from left hemiplegia and left homonymous hemianopsia; however, she recovered ambulation and partial muscle strength.



#### SUMMARY

Although the presence of a true AVM entangled with a JPA in the present case may be a coincidence; a growing number of such reports would point to the existence of a distinct entity and/or a relationship between the two lesions.

**KEY WORDS:** Juvenile pilocytic astrocytoma, arteriovenous malformation, pediatrics

#### EE-94

##### **Pediatric Anteroinferior Atlantoaxial Rotatory Dislocation with Resultant Basilar Invagination**

Birchansky, S. B.<sup>1</sup>Jea, A.<sup>1</sup>Rauch, R.<sup>2</sup>

<sup>1</sup>Texas Children's Hospital, Houston, TX, <sup>2</sup>Texas Children's Hospital, Pearland, TX

#### PURPOSE

A severe form of atlantoaxial rotatory fixation manifest as anteroinferior rotatory dislocation and secondary basilar invagination is described in pediatric patients with pertinent imaging findings.

#### CASE REPORT

Cervical spine CT and MR images in two school-age children with anteroinferior atlantoaxial rotatory dislocation were reviewed retrospectively, one child presenting acutely after trauma and the other with complaints of chronic neck pain and limited motion; neither had any known predisposing condition associated with cranial settling. Both children required subsequent craniocervical fusion.

#### IMAGING FINDINGS

Images in the child with acute injury demonstrated severe C1 leftward rotatory subluxation including frank anteroinferior rotatory dislocation of the right C1 anterolateral arch with respect to C2, inferior slippage of the anterior tubercle with respect to the dens, only slight widening of the anterior atlantodental interval, atlantooccipital rotatory subluxation and relative "cranial settling" with slightly high riding dens. The second patient had evidence of a chronic atlantoaxial rotatory dislocation with the left C1 lateral mass dislocated anteroinferior to C2, secondary bony remodeling along the craniocervical junction, severe anterior atlantodental widening, rotatory atlantooccipital subluxation with secondary chronic arthrosis, and "cranial settling" with dens invaginating into the foramen magnum impinging on the cervicomedullary cord.

#### SUMMARY

Although classic descriptions of atlantoaxial rotatory fixation emphasize the rotatory component on dynamic imaging and importance of assessing the degree of anterior atlantodental subluxation, this study illustrates CT and MRI findings in a severe form of rotatory fixation, manifest as frank anteroinferior dislocation of the C1 ring with respect to C2, thus locking the joint in an inferior slipped position accompanied by basilar invagination as the buttressing effects of the craniocervical junction articulations are lost.

**KEY WORDS:** Rotatory dislocation, atlantoaxial, basilar invagination

#### EE-95

##### **Intramedullary Cervical Cord Cavernous Angioma: A Case Report**

Gabriel, G. E.·Tumkur, S. M.·Challa, H

University of Kentucky  
Lexington, KY

#### PURPOSE

To present a case report of an intramedullary cervical cavernous angioma in a 14-year-old girl.

#### CASE REPORT

A 14-year-old female presented with progressive numbness in the right hand over the past several months. Motor power was 5/5. She also was complaining of tenderness over the cervical spine. MR imaging of the cervical spine was performed demonstrating a 2.1 x 1.4 cm intramedullary lesion centered at the C3 level which nearly replaces the spinal cord at this level. The lesion demonstrated heterogeneous signal on T1- and T2-weighted images with a rim of hemosiderin characteristic of a cavernous angioma. There was no associated edema or contrast enhancement. Given the progressive nature of symptoms, neurosurgery was consulted and the patient underwent resection. A diagnosis of a vascular malformation with local hemosiderosis was rendered by the pathologist. Follow-up imaging 2 weeks later revealed postoperative changes with total resection of the intramedullary lesion. Clinically, the patient's right hand dexterity had diminished from her preoperative state. Follow-up postoperative imaging 4 years later revealed myelomalacic changes within the cervical spinal cord. Clinically, there was still residual diminished dexterity in the right hand with no other significant clinical change.

#### IMAGING FINDINGS

ICVAs are rare lesions within the spinal cord specifically in the pediatric population. MR imaging is the modality of choice. Familial distribution and multiplicity also has been noted with cavernous angiomas and thus the entire central nervous system (CNS) must be screened. In our case, no other lesions were demonstrated and there was no positive family history. In adult ICVAs, there is a slight female predominance, however pediatric ICVAs tend to occur slightly more frequently in males. In children, the distribution of the cavernous angiomas in the spinal cord tends to be equal in distribution between cervical and thoracic cord as compared to adults who predominantly present with lesion in the thoracic cord. Clinical presentation of ICVAs in the pediatric population varies from motor or sensory deficits, myelopathy or even may be asymptomatic. Most of the presenting symptomatology may be attributable to hemorrhages within ICVAs and may have slow and stepwise deterioration with periods of recovery or have a gradual functional decline. Neurologic deterioration due to hemorrhage is most common presentation in the pediatric population and is considered rare in adults. In our case, the patient presented with sensory dysfunction with no definite evidence of acute hemorrhage seen on the MRI. The risk of hemorrhage within the spinal cord from ICVAs has been reported to be 1.4-1.6% per year. Management of ICVAs must encompass a multitude of factors such as size of lesion, location, patient symptomatology, and lesion progression. More favorable outcomes have been seen after surgical resection of ICVAs in the pediatric population as compared to adults. The entire lesion must be resected to prevent future hemorrhages.

#### SUMMARY

ICVAs are rare lesions in the pediatric population and are seen easily on MRI. In most cases, complete

resection of the lesion is recommended in order to decrease risk of hemorrhage and resulting morbidity.

**KEY WORDS:** Angioma, cavernous, pediatric

#### EE-96

#### Segmental Spinal Dysgenesis

Naidu, P. K. • Miller, J. H. • Curran, J. G. • Egelhoff, J. C

Phoenix Childrens Hospital  
Phoenix, AZ

#### PURPOSE

To describe a case of segmental spinal dysgenesis (SSD) that presented to our institution, review its embryology, characteristic imaging findings on MRI, and clinical implications.

#### CASE REPORT

A 7-year-old male with lower extremity paralysis, history of club foot, and prior spinal fusion for congenital scoliosis presented with fever, vomiting and drainage from his surgical site. An MRI of the spine was performed for further evaluation.

#### IMAGING FINDINGS

The MRI demonstrated pronounced spinal deformity, with kyphotic angulation of the lower thoracic spine superimposed upon a levoconvex curvature. The vertebral bodies at the level of kyphosis were hypoplastic. The spinal cord parenchyma abruptly thinned within the mid-thoracic spine, with minimal strands descending inferiorly. At the level of the sacrum, there was revisualization of normal-appearing spinal cord parenchyma, which extended inferiorly to end in a dorsal lipoma. Posterior fusion hardware extended from C7 inferiorly throughout the entirety of the spine. A horseshoe kidney was present. Additionally, there was a malformed, small sacrum compatible with sacral dysgenesis.

#### SUMMARY

Segmental spinal dysgenesis is one of the rarer developmental spine abnormalities, consisting of absence or dysgenesis of a portion of the vertebral column, underlying spinal cord, and nerve roots together with a focal severe kyphosis/kyphoscoliosis. The incidence of this abnormality is not widely published, presumably on the basis of its rarity. While usually found in the thoracolumbar spine, a rare instance has been reported at the cervicothoracic junction. While the embryologic basis of SSD is not entirely clear, it is thought to be due to an insult during gastrulation, with abnormal apoptosis and chorda-mesodermal derangement in the developing notochord. Clinically, the diagnosis may be discovered on prenatal ultrasound. Neurologic deficits are variable, and depend upon the amount of functional spinal cord parenchyma left. Most patients have some degree of impaired lower extremity function, often paraplegia (as in this case) or paraparesis. Focal spinal stenosis can be seen at the level of kyphosis, potentially worsening baseline neurologic deficits. Renal anomalies such as cross-fused

ectopia or horseshoe kidney also are associated, with neurogenic bladder, incontinence, and frequent UTIs also present in these patients. Management of patients with SSD is controversial and should be tailored to the individual case. While some surgeons advocate surgical fusion for stabilization upon diagnosis, others defer such intervention with interval bracing to promote bony maturity. The paucity of vertebral elements makes fusion in these patients more complex as well. Spinal stenosis may necessitate surgical decompression in select cases.

**Monday, April 23 –  
Wednesday, April 25  
6:30 AM – 9:00 PM  
Thursday, April 26  
6:30 AM – 3:00 PM**

**Americas Hall II  
Excerpta Extraordinaire 97**

**(EE6) E6 – Socioeconomics**

**Note: A missing printed number indicates an abstract has been withdrawn.**

**EE-97**

#### **Time and Cost Analysis of IV Access for Contrast-Enhanced MR Imaging**

Fischer, I. Tomsick, T.

University of Cincinnati  
Cincinnati, OH

#### **PURPOSE**

To analyze the potential time and cost savings of starting ivs outside the MRI scanner itself prior to contrast-enhanced MR neuro studies, as opposed to starting ivs during the exam, between pre and postcontrast series, inside the magnet room.

#### **CASE REPORT**

We measured the interval between the time stamps on the last precontrast and first postcontrast sequences for inpatient (n = 117) and outpatient (n = 182) neuro MRIs performed at our facility in a given month. This was subtracted from the scan time for the last precontrast sequence of each exam, giving an estimated iv access time for each study. The average estimated iv access time for outpatients and inpatients were compared to give a theoretical amount of time that could be saved by having all outpatients arrive at the MRI suite with iv access. A brief trial of starting ivs on all outpatient studies with contrast before they came into the scanner then was initiated, and the actual inpatient and outpatient iv access times were calculated.

#### **IMAGING FINDINGS**

A total of 384 MRIs were reviewed. The average theoretical time saved by changing our current iv access procedure was 6.76 minutes (+/- 7.4 min, p = 5E<sup>-10</sup>). Given our average weekday outpatient MRI (with contrast) study volume, this yields 54 minutes per day in theoretical average savings, which is greater than the scheduling time slot of an additional Brain MRI per day (40 minutes): an opportunity cost of \$990,000 in billing annually. However, the average actual time saved by obtaining iv access prior to scan initiation was 5.32 minutes per exam (p = 6E<sup>-6</sup>), or 42.6 minutes per day. Sensitivity analysis of the time and cost savings in a variety of clinical practice patterns will be discussed. Discussion: It should be noted that, although the theoretical and actual time saved after changing iv access practice on outpatient exams was sufficient to accommodate an additional outpatient Brain MRI each day, time savings was spread over 4 outpatient scanners; therefore, a theoretical average maximum of 27.0 and actual average maximum of 22.2 minutes was saved on any one magnet daily: insufficient time to facilitate a complete additional brain exam scheduling time slot, given our current local practice of randomly assigning patients to magnets. Other practical factors that may impact the decision to adopt this policy, including institutional resistance to change, will be discussed.

#### **SUMMARY**

Current economic stressors increase the value of identifying and addressing needless waste and opportunity costs, no matter how small. As evidenced by our analysis of outpatient MRI iv access start times, even small time savings can compound to a significant dollar amount, given sufficient scan volume.

**KEY WORDS:** IV access, outpatient MRI with contrast, efficiency

**Monday, April 23 –  
Wednesday, April 25**

**6:30 AM – 9:00 PM**

**Thursday, April 26**

**6:30 AM – 3:00 PM**

**Americas Hall II**

**Excerpta Extraordinaire 98 – 106**

**(EE7) E7. – Interventional**

**Note: A missing printed number indicates an abstract has been withdrawn.**

#### **EE-98**

##### **Toxoplasma Myelitis Simulating Cord Neoplasm on MR Imaging: A Rare and Underdiagnosed Infection**

Post, M. Sidani, C. Bhatia, R.

University of Miami School of Medicine  
Miami, FL

#### **PURPOSE**

To characterize the MR findings in a patient with a thoracic spinal cord mass unexpectedly found at surgery to be due to the rarely encountered toxoplasma myelitis so that this diagnosis might be entertained in future cases, thereby obviating the need for surgical exploration.

#### **CASE REPORT**

An otherwise healthy 54-year-old Haitian female with no known underlying conditions developed progressive bilateral leg weakness and excruciating back pain without fever, prompting a visit to two different outside hospitals without any definitive diagnosis being established. At the second hospital, an MR revealed a mid thoracic spinal cord mass which led to a wide differential, including posttraumatic or ischemic myelopathy, transverse myelitis or a posttraumatic or postinfectious syrinx. The patient was transferred to our institution for biopsy. Preoperatively the neurosurgical diagnosis was spinal cord tumor in this patient who had developed a waxing and waning mental status, making a detailed history not possible. However, a T5-T8 laminectomy revealed an inflamed spinal cord with gliotic and necrotic tissue. Histopathologic examination revealed acute and chronic coagulative necrosis with extracellular tachyzoites and pseudocysts. H and E and immunoperoxidase stains demonstrated *Toxoplasma gondii*, prompting medical therapy. Nine days after surgery because of an increasing encephalopathy, a brain MR revealed multiple ring-enhancing lesions with edema and mass effect and a variable diffusion pattern (with the majority of lesions showing increased central diffusibility with fewer

lesions demonstrating minimal patchy and peripheral restricted diffusion), felt to be compatible with toxoplasma encephalitis, with some improvement in these lesions on medical therapy. Thallium scan was negative for tumor, including lymphoma. Only postoperatively the patient then was discovered to be HIV positive with a CD4 count of 22.

#### **IMAGING FINDINGS**

MR imaging showed a single slightly heterogeneously enhancing T5 to T8 intramedullary mass expanding the spinal cord with marked surrounding edema extending into the cervical cord as well as into the conus. On T1-weighted imaging the lesion was iso to mildly hypointense; on T2-weighted imaging the mass had a high signal center surrounded by an iso to slightly hypointense rim, compatible with the coagulative necrosis that characterizes infection with *Toxoplasma gondii*.

#### **SUMMARY**

In a patient with a discrete enhancing spinal cord mass on MR, even in the absence of typical infectious symptomatology and any previously established immunosuppression, spinal cord infections always should be considered in the differential since they are potentially medically treatable. Since toxoplasma infection is characterized by a coagulative necrosis rather than a liquefactive necrosis, *Toxoplasma gondii* should be included in the differential diagnosis of a spinal cord mass when an imaging pattern consistent with coagulative necrosis is seen. Diffusion imaging of the spine as well as susceptibility-weighted imaging could be added to the conventional spinal MR as further diagnostic aides. Finally, a corollary MR of the brain is vital to suggesting the correct diagnosis while serial scans of the brain and spine can illustrate the effectiveness of medical therapy without the need for operative intervention.

**KEY WORDS:** *Toxoplasma myelitis*, spinal cord infection, immunocompromised

#### **EE-99**

##### **CT and MR Features in a Case of Crowned Dens Syndrome with Atypical Unilateral and Positional Headache**

Stecco, A. Viana, M. Perchinunno, M. Carriero, A.

AOU Maggiore della Carità  
Novara, ITALY

#### **PURPOSE**

Crowned Dens syndrome (CDS) is a clinical-radiologic entity characterized by calcification of the periodontoid articular structures and by acute attacks of neck pain with fever, rigidity, and general sign of inflammation. The crystal deposit frequently can be due to pseudogout, but also to rheumatoid arthritis and osteoarthritis.

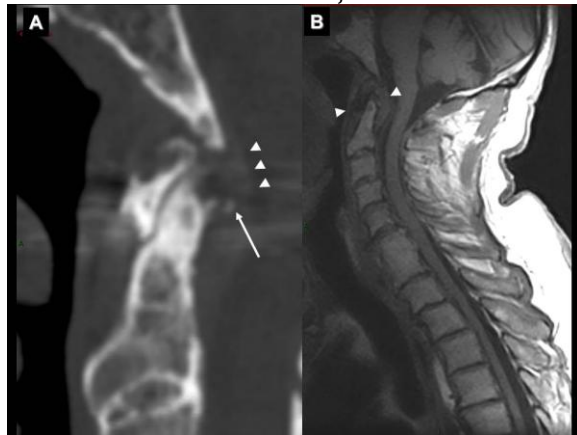
#### **CASE REPORT**



This is a case report with a 12-month follow up of a patient with an atypical presentation of CDS. An 81-year-old man, who had never suffered from headache before July 2010, developed progressively a strictly left-side headache that after a couple of weeks became daily. The pain was localized on the whole left scalp but it was more intense on the frontal area, the intensity was moderate to high and the quality of the pain was throbbing. There were no associated symptoms. The headache intensity was constant during the day but the pain was aggravated by gaining the orthostatic position, neck hyperextension or Valsalva. We saw him 15 days after the headache onset.

#### IMAGING FINDINGS

The neurologic examination was normal except for a reduced range of motion in the neck. A brain MRI with Gd and cervical MRI were ordered and the patient was prescribed with Indometacin. He partially responded to Indometacin orally 25 mg t.i.d. and after a week he was given a dosage of 50 mg t.i.d. with a complete regression of the pain. The brain MRI was normal while an MRI of the cervical spine showed (Figure 1B) a nonhomogeneous 12 mm mass behind and around the odontoid process of C2, narrowing the subarachnoid space in C1, stretching the posterior longitudinal ligament and touching the left vertebral artery. A CT scan (Figure 1A) focused on C1-C2 showed calcification in the soft tissue around odontoid process and an inflammation thickening of C2 left root. Rheumatologist concluded there was spinal osteoarthritis with involvement of the atlanto-axial joint.



#### SUMMARY

This is a case with typical radiologic findings for CDS. Indeed the clinical picture was not at all typical for CDS for the unilaterality, the localization and the quality of the head pain, the aggravation by position and Valsalva, and the lack of either fever or inflammatory signs. This clinical picture was never described in a patient with CDS. This case widens the spectrum of the clinical presentation of CDS, a condition that we should keep in mind in front of that neuroradiologic appearance.

**KEY WORDS:** Crowned Dens, crystal deposit, headache

#### EE-100

##### Iatrogenic Pneumocephalus after Epidural Anesthesia in the Obstetric Patient

Gidwani, G.·Werhun, E.·Sukerkar, A.·Nadimpalli, S.

Advocate Illinois Masonic Hospital  
Chicago, IL

#### PURPOSE

Pneumocephalus is a rare complication of epidural anesthesia which occurs when air is introduced inadvertently into the cranial vault, or more specifically, the subarachnoid space.

#### CASE REPORT

We present a case of an obstetric patient who suddenly became unresponsive shortly after epidural anesthesia.

#### IMAGING FINDINGS

After conversion to general anesthesia for emergent cesarean section, the patient was found to have evidence of pneumocephalus on postoperative computed tomography (CT). Few articles exist in the English literature on this topic, so it is important that clinicians be aware of this iatrogenic complication.

#### SUMMARY

Knowledge of complications and a thorough explanation of the risks, benefits, and alternatives to the patient is paramount.

**KEY WORDS:** Pneumocephalus, iatrogenic

#### EE-101

##### Spinal Schwannoma Presenting with Acute Hemorrhage in the Spinal Canal

Donmez, F. Y.·Kural, F.·Akpınar, B.·Ozen, O.·Agildere, M.

Baskent University  
Ankara, TURKEY

#### PURPOSE

To demonstrate the imaging findings of a spinal schwannoma presenting with acute hemorrhage in the spinal canal.

#### CASE REPORT

A 82-year-old woman presented with the complaint of monoplegia. She could walk well until the last 10 days. Her walking deficit started since, and at the time of her admission, she could not move her right lower extremity. She was otherwise healthy except for the history of a coronary stent operation 2 years ago. On her neurologic examination, she was fully cooperative and oriented. Her neurologic examination was normal except for the right monoplegia and hypoesthesia in the right L2-3-4-5 and S1 dermatoma.

#### IMAGING FINDINGS

A thoracolumbar MRI with contrast was performed promptly. There was a hemorrhagic mass in the conus medullaris which was hypointense on T1-weighted and

heterogeneous on T2-weighted images. Only a small component of 14 mm showed contrast enhancement. A subdural hematoma at late subacute stage, which was hyperintense on both T1-weighted and T2-weighted images, extending from T1 to S1, in both anterior and posterior of the canal was evident. The differential diagnosis of an hemorrhagic intradural intramedullary mass included a hemorrhagic ependymoma, hemangioblastoma or a cavernoma. On the next day, she was operated. A huge hematoma and an intradural extramedullary mass were resected. Pathologic examination showed a mass composed of spindle cells, hemorrhagic and degenerative areas and vascular proliferation which also had S100 and GFAP expression, compatible with a schwannoma.

#### SUMMARY

A spinal subdural hemorrhage due to a schwannoma is very rare. Spinal cord tumors most commonly present with a chronic, progressive course, an acute presentation may be because of a tumor bleeding. At that time emergent surgery is needed. This case emphasizes the fact that some benign tumors also may present acutely and dramatically. Radiologically, it was challenging for this tumor to decide whether it is intra or extramedullary. The hemorrhagic lesion in the conus medullaris included the diagnosis of an hemorrhagic ependymoma, the most common tumor which has a tendency to bleed, a hemangioblastoma or a vascular malformation such as a cavernoma. A spinal schwannoma was not in the differential. However, this case of schwannoma showed an infrequent cause of spinal hemorrhage, which should also be kept in mind in a patient presenting with rapid onset and sudden worsening of neurologic deficits.

**KEY WORDS:** Spinal schwannoma, hemorrhage

#### EE-102

##### **Persistent Neck Pain after Anterior Cervical Discectomy and Fusion Surgery: Look for Facet Subluxation**

Maller, V. G. • Agarwal, A. • Nguyen, D. T.

Penn State Milton S. Hershey Medical Center  
Hershey, PA

#### PURPOSE

To describe a case of persistent neck pain after anterior cervical discectomy and fusion (ACDF) surgery resulting from bilateral facet joint subluxation, probably due to excessive traction.

#### CASE REPORT

A 35-year-old gentleman who underwent anterior cervical discectomy and fusion surgery for disk protrusion at C5-6 and C6-7 levels, presented with persistent neck and bilateral shoulder pain. There was no history of radiation of pain, weakness, or tingling sensation in the arms.

#### IMAGING FINDINGS

X-ray and MRI of the cervical spine revealed subluxation of the C6-7 facet joint bilaterally (Figure 1a, b). There was no residual or recurrent disk or significant scar tissue on MRI.



#### SUMMARY

Excessive distraction during ACDF may lead to facet joint subluxation, which may be a cause for persistent postoperative neck pain. It is important for the radiologist to be aware of this condition.

**KEY WORDS:** ACDF, facet, subluxation

#### EE-103

##### **Extradural Spinal Gout Causing Cord Compression**

Arani, K. N. • Wang, A. • Olson, R. • Silbergleit, R.

William Beaumont Hospital  
Royal Oak, MI

#### PURPOSE

Although gout is a common metabolic disorder, involvement of the axial skeleton and, specifically, urate deposition in the spine is rare. This excerpt describes a rare case of gout presenting as an extradural cervical spine mass resulting in cord compression.

#### CASE REPORT

We present a case of a 66-year-old Caucasian male who had a 3-4 week history of weakness in his lower extremities with difficulty walking and recurrent falls. Symptoms started gradually with progressive worsening. Patient had a history of gout diagnosed 40 years ago involving his right toe. He had no recent episode of gout involving any of his other joints. Due to only remote history of gout, patient was not taking medications for gout prior to admission. Uric acid level was only 5.3 at the time of presentation. Upon presentation, he had weak bilateral lower extremities. He was barely able to lift his right leg off the bed and his left leg was also weak. Patient underwent a cervical laminectomy at C7 with removal of the mass. Pathology demonstrated fragments of soft tissue with extensive deposits of uric acid and surrounding inflammatory reaction consistent with gout. He was transferred to inpatient rehabilitation and his strength was greatly improved, 4/5 out of all extremities.

### IMAGING FINDINGS

The cervical spine MR imaging demonstrated an extradural hypointense mass at the C7-T1 level on the right side (Figure 1) leading to moderate displacement and compression of the spinal cord. CT demonstrated endplate destruction with soft tissue mass that contained calcifications (Figure 2).



### SUMMARY

Most cases of spinal gout note extradural location of tophus, although even rarer cases of intradural deposition have been seen in literature. As in all cases of gout, cervical spine involvement of gout has a male predominance. Axial skeletal deposits usually represent a complication of long-standing and poorly controlled hyperuricemia. Unlike other cases, our patient had no hyperuricemia. Another rare feature in this case is that there was tophaceous gout of the spine with no peripheral tophi (except for remote history described 40 years earlier). In conclusion, we present an unusual case of a patient with cord compression secondary to an extradural cervical spine gout. Although spine involvement of gout is rare, it is prudent to include in the differential diagnosis of a patient known to have history of gout.

**KEY WORDS:** Gout, spinal cord compression, extradural mass

### EE-104

#### Hirayama Disease: The Importance of Flexion MR Imaging

Garlick, C. Kim, J. Goyal, K. Liem, J.

Oakwood Hospital and Medical Center  
Dearborn, MI

### PURPOSE

To provide a brief review of the imaging findings of this rare disease and reiterate the importance of obtaining flexion MR imaging when it is suspected.

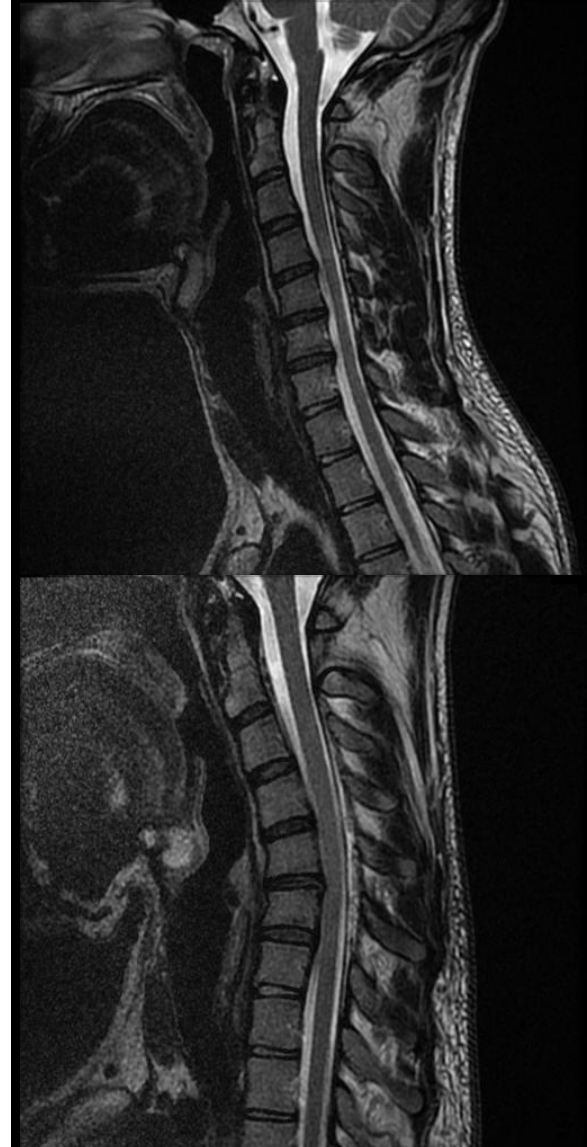
### CASE REPORT

We report a 21-year-old Caucasian male who presented with progressive weakness in his left forearm and hand, beginning at the age of 18, with eventual involvement of the right forearm as well, however less severe. On physical examination he demonstrated atrophy of the

forearms, hands and triceps bilaterally, left more involved than right, and absent reflexes. Electromyography (EMG) was performed and was suggestive of a motor nerve etiology.

### IMAGING FINDINGS

Initial routine MRI of the cervical spine showed asymmetric cord atrophy at C5 and C6 levels without abnormal signal intensity within the cord. Because of concern for Hirayama disease, a flexion MRI was performed which demonstrated obliteration of the subarachnoid space, anterior displacement of the posterior dura as well as multiple flow voids in the widened epidural space, consistent with engorgement of the posterior venous plexus.



### SUMMARY

Hirayama disease is a rare myelopathy of the lower cervical spine. Juvenile onset, usually unilateral upper extremity muscular atrophy and a nonprogressive course in the later stage are cardinal clinical features. Asymmetric cord atrophy with or without abnormal signal intensity on nonflexion routine MR in young

males with distal upper extremity weakness should raise suspicion of Hirayama disease. Flexion MR should be performed for confirmation of the diagnosis. Classic findings include anterior displacement of the cervical cord and posterior dural wall, obliteration of the subarachnoid space with enhancing posterior venous plexus engorgement in the expanded epidural space as well as asymmetric lower cervical cord atrophy. Early recognition is necessary as avoidance of neck flexion as well as treatment options including cervical collar placement and/or therapy, can halt or significantly reduce the progression in select patients.

**KEY WORDS:** Hirayama, myelopathy of the cervical spine

#### EE-105

##### **Intradural Capillary Hemangioma of the Cauda Equina**

Malhotra, A.·Kalra, V.·Laurans, M. S. H.·Hutner, A.

Yale University School of Medicine  
New Haven, CT

##### **PURPOSE**

We report an unusual imaging appearance of a intradural lobular capillary hemangioma, in close relation to the conus and cauda equine nerve roots. Capillary hemangiomas in this location are exceedingly rare and all the cases described in the literature have been reported to have intense enhancement on postcontrast MRI. Our case showed only mild enhancement in the lobulated lesion, not previously described.

##### **CASE REPORT**

A 46-year-old female presented with history of radicular pain in the left lower extremity and on subsequent testing was found to have signs of gastrocnemius wasting.

##### **IMAGING FINDINGS**

MR imaging lumbar spine demonstrated a well circumscribed, lobulated, intradural mass just below the conus measuring approximately 1 cm. There was no expansion of the bony canal or extension into the neural foramina. The lesion was isointense to the adjacent neural structures on T1 WI and iso to mildly hyperintense on T2 WI. Postcontrast images showed mild, somewhat heterogeneous enhancement in the lesion. No further cranio-spinal lesions were found on MRI. At surgery, the lesion appeared raspberry-like collection of blood vessels, intimately involved with the cauda equine nerve roots. Surgical resection was performed and pathology was consistent with a lobular capillary hemangioma.

##### **SUMMARY**

Capillary hemangioma is a benign vascular lesion, usually found in the skin or soft tissues of children. There are rare case reports of these vascular lesions arising from the cauda equine nerve roots, the dura or the pial surface of the cord. Unlike cavernomas which

are more frequent, this entity has a lobular architecture with septae and consists of small capillaries lined by endothelial cells. Intense, homogeneous enhancement is described in all the previous case reports of this rare entity. We report an unusual imaging appearance of this very rare entity.

**KEY WORDS:** Conus, hemangioma, capillary

#### EE-106

##### **Case of Segmental Neurofibromatosis Type I (Radiologic/Dermatologic Correlation) Presenting with Acute Cord Compression**

Cain, J. R.<sup>1</sup>·Laws, P. M.<sup>2</sup>·Ealing, J. J.<sup>1</sup>·Huson, S. M.<sup>3</sup>·Ghosh, K.<sup>2</sup>·Soh, C.<sup>2</sup>

<sup>1</sup>University of Manchester, Manchester, UNITED KINGDOM, <sup>2</sup>Salford Royal Hospital, Manchester, UNITED KINGDOM, <sup>3</sup>Central Manchester University Hospitals, Manchester, UNITED KINGDOM

##### **PURPOSE**

To describe a case of segmental neurofibromatosis type I (NF1) presenting with acute cord compression and the potential diagnostic importance of correlating neurologic, dermatologic and radiologic findings.

##### **CASE REPORT**

A 41-year-old previously healthy woman presented with a history of progressive weakness in upper and lower limbs for 6 months. This had progressed rapidly over a week and the patient was now wheelchair bound. She was transferred to the regional neuroradiology centre and underwent MRI imaging of her cervical spine.

##### **IMAGING FINDINGS**

MR imaging revealed that there was a large intraspinal tumor spanning seven vertebral heights from foramen magnum to C7. The mass was filling the entire cervical canal causing severe cord compression. The tumor extended out through the left C4 and C5 exit foramen into a larger extraspinal tumor on the left side of the neck, in keeping with a large plexiform neurofibroma. There was a chain of similar tumors on the left side of the neck, along the line of the vagus nerve, extending into the mediastinum. There were no lesions on the right side. All tumors had same signal characteristics. Due to the localized clustering of lesions the neuroradiologist raised the potential diagnosis of segmental neurofibromatosis type I, and recommended examination of the patient's skin for café au lait lesions. On examination the patient had a well defined patch of café au lait macules over the left side of neck and upper torso and no other skin lesions.

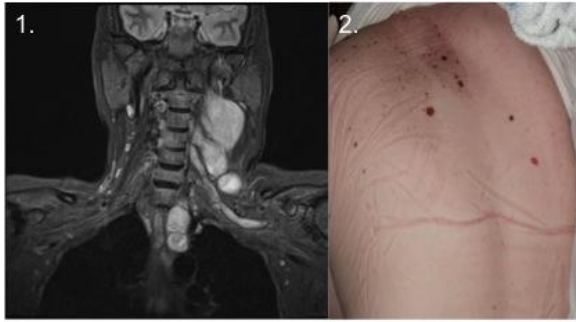


Image 1: Coronal T1 inversion recovery MR images showing chain of neurofibroma on left side of neck and upper torso.  
Image 2: Photograph of patient's back showing isolated patch of café au lait macules in corresponding region.

#### SUMMARY

Assessment by the Manchester Neurofibromatosis Clinic team (SH and JE) confirmed a clinical diagnosis of segmental NF1. As expected NF1 genetic analysis on lymphocyte DNA was normal and has not been undertaken on any other tissues. The condition has different inheritance characteristics and prognostic features to generalized NF1. However, in cases like this with a significant internal burden the neurofibromas are at risk of malignant change. The cutaneous features of segmental neurofibromatosis characteristically are localized in a blaschkoid distribution, thought to represent pathways of epidermal cell migration during fetal development. The case highlights the importance of requesting clinical correlation of findings to ensure diagnosis is not overlooked.

**KEY WORDS:** Neurofibromatosis, NF1, cord compression

**Monday, April 23 –  
Wednesday, April 25  
6:30 AM – 9:00 PM  
Thursday, April 26  
6:30 AM – 3:00 PM**

**Americas Hall II  
Scientific Posters Printed 1 – 74**

**(P1) Adult Brain**

**Note: A missing printed poster number indicates an abstract has been withdrawn.**

#### P-1

##### **Frequency of Eye Deviation in Patients Undergoing Head CT for All Reasons versus Head CT for Acute Ischemic Stroke**

Schwartz, K. M. • Ahmed, A. T. • Fugate, J. E. • Hunt, C. H. • Diehn, F. E. • Eckel, L. J. • Kallmes, D. F.

Mayo Clinic Rochester  
Rochester, MN

#### **PURPOSE**

Conjugate eye deviation (CED) is a well known phenomenon occurring in stroke patients, with eye deviation to the side of the infarct in the acute phase of stroke. Evaluation of gaze deviation on computed tomography (CT) has been helpful in predicting acute ischemic stroke. However, the frequency of eye deviation in the general population of patients undergoing head CT is unknown. Therefore, the specificity of conjugate eye deviation for acute ischemic stroke is unclear. The aim of our study was to determine the frequency and degree of eye deviation in patients undergoing head CT in the emergency department (ED) or hospital setting for all reasons compared to patients undergoing head CT for signs and symptoms of acute ischemic stroke.

#### **MATERIALS & METHODS**

IRB approval was obtained for this HIPAA compliant research protocol. Three groups of patients were included. Group 1 (n = 120) included consecutive inpatient and ED patients who had undergone head CT at our institution for indications other than acute stroke. Group 2 (n = 48) included a cohort of patients who received intravenous tissue plasminogen activator (tPA) for clinical signs of acute ischemic stroke. Group 3 (n = 67) included patients referred for intraarterial stroke therapy. Exclusion criteria included prior cataract surgery or extensive motion precluding evaluation of the ocular lenses. The presence or absence of subjective eye deviation as well as the angle of the

eyes were recorded. This angle was measured using a line drawn through midline structures compared to a line drawn through the long axis of the ocular lens. Additional patient information was collected from the medical record including gender, age, pertinent clinical history, additional imaging evaluation, and pertinent imaging findings.

## RESULTS

In Group 1, 17 (14%) of 120 patients had conjugate eye deviation (CED) with a mean deviation of 19 degrees, 42 (35%) had lone eye deviation (LED), and 8 (7%) had skew deviation (SD). In Group 2, 14 (29%) of 48 patients had CED, with a mean deviation of 25 degrees, 7 (15%) had LED, and 2 (4%) had SD. In Group 3, 32 (48%) of 67 patients had CED with a mean deviation of 26 degrees, 4 (6%) had LED, and 1 (1%) had SD. There was a statistically significant difference between the three groups for CED ( $p < 0.0001$ ) and LED ( $p < 0.0001$ ) but no significant difference between the groups for skew deviation ( $p = 0.21$ ).

## CONCLUSION

Conjugate eye deviation is common in patients presenting with acute stroke. Such deviation also may be seen in patients presenting without acute stroke, but with degrees of deviation less than stroke patients. Lone eye deviation frequently occurs in the ER/inpatient setting but only rarely in patients with severe stroke.

**KEY WORDS:** Eye deviation, acute stroke

## P-2

### Prevalence and Predictors of the Tissue at Risk of Infarction in Acute Stroke Patients Treated Beyond 8 Hours after Symptom Onset

Leiva Salinas, C.<sup>1</sup>·Jovin, T.<sup>2</sup>·Aghaebrahim, A.<sup>2</sup>·Patrie, J. T.<sup>3</sup>·Zhu, G.<sup>3</sup>·Wintermark, M.<sup>3</sup>

<sup>1</sup>Hospital Universitario la Fe, Valencia, SPAIN,

<sup>2</sup>University of Pittsburgh, Pittsburgh, PA, <sup>3</sup>University of Virginia, Charlottesville, VA

## PURPOSE

To assess the prevalence and extent of tissue at risk of infarction in a population of acute stroke patients treated with endovascular recanalization therapies beyond 8 hours from symptom onset. To investigate the baseline imaging and clinical features that predict the fate of this tissue at risk.

## MATERIALS & METHODS

We retrospectively reviewed a series of patients with acute ischemic stroke treated with endovascular recanalization therapies beyond 8 hours from symptom onset. The tissue at risk was calculated as the difference between the infarct volumes on baseline and follow-up images ( $\Delta$  volume of infarct). Imaging variables included baseline infarct volume on admission CT and/or MRI, carotid stenosis  $\geq 70\%$  on baseline CT angiography (CTA), predicted infarct core and penumbra volumes on admission PCT, arterial recanalization on therapeutic digital subtraction

angiography (DSA) and final infarct volume on follow-up CT and/or MRI. Clinical and demographic data included age, time to baseline, time to treatment, diabetes, hypertension, hypercholesterolemia and NIHSS and blood glucose at baseline. First, we analyzed the frequency and distribution of the  $\Delta$  volume of infarct. Then, we used a multivariate regression analysis to show which baseline demographic, clinical and imaging variables predict the  $\Delta$  volume of infarct.

## RESULTS

We identified 74 patients (mean age 64, mean baseline NIHSS 14, male gender 55%, mean time to baseline 12.3 h, mean time to treatment 15.2 h). There was a mean  $\Delta$  volume of infarct from baseline to follow-up of 78.6 cc [ $p < 0.001$ , 95% CI: (56.8, 100.5 cc)]. The multivariate regression analysis showed that the  $\Delta$  volume of infarct was greater when the baseline volume of infarct tissue was small ( $p < 0.001$ ), and smaller in case of recanalization ( $p = 0.001$ ). For those patients without recanalization, there was a trend for larger perfusion CT penumbral volume to be associated with larger  $\Delta$  volume of infarct from baseline to follow-up ( $p = 0.090$ ).

## CONCLUSION

There is potentially salvageable tissue at risk in acute stroke patients treated even beyond 8 hours of symptom onset.

**KEY WORDS:** Stroke, tissue at risk of infarction, endovascular recanalization therapies

## P-3

### Radiologic Predictors of Progression to Hemispherectomy in Patients with Large Territory Middle Cerebral Artery Stroke

Edasery, D.·Mian, A.·Camargo Faye, E.·Cervantes, A.·Koyfman, F.·Holsapple, J.·Sakai, O.·Nguyen, T.

Boston University Medical Center  
Boston, MA

## PURPOSE

Hemispherectomy is a life-saving procedure following proximal middle cerebral artery (MCA) stroke associated with malignant edema. Early hemispherectomy is thought to result in better outcomes than later hemispherectomy, particularly in young patients. Predicting whether a patient will need hemispherectomy can be helpful to triage patients accordingly. We evaluated basal ganglia predictors indicating the need for early surgical intervention in patients with large territory MCA stroke.

## MATERIALS & METHODS

This was a retrospective study evaluating patients admitted with ischemic stroke to a university hospital center. In general, patients with malignant cerebral edema refractory to medical therapy, or with herniating signs (depressed level of consciousness, anisocoria, contralateral leg weakness) were triaged to hemispherectomy. Patients aged 10 to 80, with large territory MCA infarct, ASPECTS score less than seven,



were included. Patients triaged to comfort measures early in their admission were excluded. A neuroradiologist, blinded to whether the patients were to undergo hemispherectomy, reviewed admission CT or MRI scans of each patient meeting inclusion criteria for presence of caudate or lentiform nucleus infarction.

## RESULTS

There were 31 patients with large territory MCA infarcts admitted from January 2005 to December 2010, of which 10 (32%) underwent hemispherectomy. Mean age of this cohort was 55 (range 11 to 74) and 44% were female. The mean ASPECTS score on admission CT or MRI studies (up to 48 hours) was three. Presence of infarction of the caudate nucleus or basal ganglia (both caudate and lentiform nucleus) predicted progression to hemispherectomy (9/10 vs 6/21,  $p = 0.002$  and 5/10 vs 2/21,  $p = 0.02$  respectively, Fisher's exact). Infarction of the lentiform nucleus alone did not predict progression to hemispherectomy.

## CONCLUSION

In patients with large territory middle cerebral artery stroke, infarction of the caudate nucleus or basal ganglia (caudate and lentiform nucleus) predicted patients progressing to hemispherectomy.

**KEY WORDS:** Stroke, hemispherectomy, basal ganglia

## P-4

### Altered Resting-State Connectivity in Stroke Patients

Tsai, Y.<sup>1,2</sup>·Biswal, B. B.<sup>3</sup>·Lin, C.<sup>2</sup>·Weng, H.<sup>1</sup>·Gohel, S.<sup>3</sup>

<sup>1</sup>Chang Gung Memorial Hospital at Chiayi, Chiayi, TAIWAN, <sup>2</sup>National Yang Ming University, Taipei, TAIWAN, <sup>3</sup>New Jersey Medical School/University of Medicine & Dentistry of New Jersey, Newark, NJ

## PURPOSE

Changes that occur in the brain after a stroke have been described at the cellular/molecular and behavioral levels. While the results of "activation" studies using functional magnetic resonance imaging (fMRI) have generated working hypotheses regarding how plasticity is expressed in a damaged brain after stroke, discrete regions of interest and localized "activation" results have not been interpreted in the context of an integrated neural network. Abnormal resting-state connectivity has been demonstrated recently in stroke patients. However, it remains unclear how functional connectivity in this case changes over time. The primary goal of this study is to investigate the longitudinal changes in resting-state functional connectivity in stroke patients.

## MATERIALS & METHODS

Twenty-two first-ever ischemic stroke patients with motor deficits were enrolled for clinical evaluation and **MRI scans** at the (1) first week and (2) 6 months after stroke. Twenty age- and gender-matched healthy subjects also were enrolled. The fMRI data were collected using a **1.5 T human MRI scanner (Gyrosan**

**Intera; Philips Medical Systems, Best, The Netherlands)**, with a gradient-echo echo-planar sequence (EPI) sequence sensitive to BOLD contrast. Each scan consisted of 80 image volumes and lasted for 5 minutes and 28 seconds. The functional connectivity was determined by independent component analysis (ICA) using the MELODIC program available through FSL software ([www.fmrib.ox.ac.uk/fsl](http://www.fmrib.ox.ac.uk/fsl)).

## RESULTS

**We found** significant differences in functional connectivity between stroke patients and matched controls. Furthermore, a significant increase in the spatial extent of the motor, medial frontal, and default mode networks after 6 months compared to 1 week was observed (Fig). Significant correlation between the z-score of functional connectivity and clinical measurements such as muscle power, the National Institutes of Health Stroke Scale, and the Modified Rankin Scale were obtained during the first-week and six-month measurements for each individual subject.

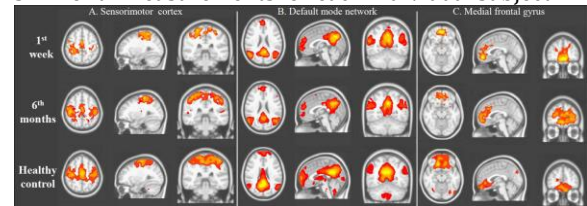


Fig 1. Group ICA map representing (A) sensorimotor cortex, (B) default mode network, and (C) medial frontal gyrus in first week and 6 months after stroke as well as in healthy controls.

## CONCLUSION

This preliminary study suggests the use of resting-state analysis as a method to study and assess brain function in stroke patients, due to its ability to complement existing approaches. This study also suggests that impaired resting-state functional connectivity changes with stroke progression can be used as a measurement to assess functionality and predictors of rehabilitation.

**KEY WORDS:** Stroke, functional imaging, resting-state

## P-5

### Ischemic Cerebrovascular Disease of Posterior Circulation and Calcified Intracranial Vertebrobasilar Artery: A Case-Control Study

Chawalparit, O.·Chareewit, S.

Siriraj Hospital  
Bangkok, THAILAND

## PURPOSE

To evaluate the association of intracranial vertebrobasilar artery calcification and ischemic cerebrovascular disease of the posterior circulation.

## MATERIALS & METHODS

A cross-sectional, retrospective, case-control study was performed on 198 patients with cranial CT. Presence of the posterior fossa infarction was disclosed in 104 patients of the case group and absence of the posterior

fossa infarction in 94 patients was age and sex matched and defined as a control group. Circumferential and thickness of calcification were graded for the intracranial vertebral and basilar arteries. Association between vascular wall calcification and posterior fossa infarction was analyzed.

## RESULTS

No statistically significant relationship between the present of vertebrobasilar (VB) calcification and posterior fossa infarction was found ( $p = 0.08$ , OR = 1.75, 95% CI = 0.94 - 3.26). In subgroup analysis, by reclassifying occipital lobe and thalamus as areas supplied by VB system, there was a statistically significant relationship between the VB calcification and infarction ( $p = 0.02$ , OR = 2.08, 95% CI = 1.10 - 3.94). No relationship between degree of calcification and the area of infarction was observed.

## CONCLUSION

This study implied a trend of association between the VB artery calcification and ischemic posterior circulation. Complete evaluating of the true territory of posterior circulation is needed to confirm the finding.

**KEY WORDS:** Posterior fossa, infarction, vertebrobasilar calcification

## P-6

### Using Clinician Treatment Thresholds in Comparing Effectiveness of Digital Subtraction Angiography and CT Perfusion for Delayed Cerebral Ischemia

Gupta, A. Killeen, R. P. Delaney, H. Johnson, C. E. Comunale, J. P. Tsiouris, A. J. Dunning, A. Sanelli, P. C.

Weill Cornell Medical Center/New York Presbyterian Hospital  
New York, NY

## PURPOSE

To compare CT perfusion (CTP) and digital subtraction angiography (DSA) for determining delayed cerebral ischemia (DCI) in aneurysmal subarachnoid hemorrhage (A-SAH) based on clinicians' treatment thresholds.

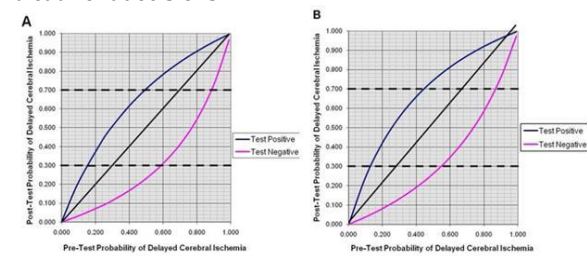
## MATERIALS & METHODS

Retrospective study of consecutive A-SAH patients with both CTP and DSA obtained at days 6-8 following aneurysm rupture. Qualitative and quantitative analyses of CTP deficits were performed by three blinded neuroradiologists. Digital subtraction angiography was classified as presence or absence of vasospasm. The reference standard for DCI was based on clinical deterioration and/or infarction on follow-up CT/MR imaging not attributed to other causes. The test characteristics of CTP and DSA were calculated and graphs of conditional probabilities (GCP) were constructed using Bayesian analysis. To determine clinicians' treatment thresholds for DCI using hypervolemic-hemodilution-hyperdynamic (HHH) and intraarterial (IA) vasodilators/angioplasty therapies,

independent surveys of five neuro-ICU physicians was performed.

## RESULTS

Fifty-seven patients were included in the study; 79% (45/57) had DCI. Seventy percent (40/57) had CTP deficits; of which were 80% (36/45) DCI and 33% (4/12) no DCI patients. Sixty-three percent (36/57) had DSA demonstrating vasospasm; of which were 73% (33/45) DCI and 25% (3/12) no DCI patients. Quantitative analysis of CTP revealed a significant difference in CBF for DCI (29.4 mL/100gm/min) and no DCI (40.5 mL/100gm/min,  $p=0.0213$ ) groups. The sensitivity, specificity, positive and negative predictive values for CTP were 0.80, 0.67, 0.90, and 0.47; for DSA were 0.73, 0.75, 0.92, and 0.43, respectively. Consensus treatment threshold for HHH and IA-therapy were 30% and 70%, respectively (interpreted as a posttest probability of >30% or >70% initiates treatment with HHH or IA-therapy, respectively). Graphs of conditional probabilities for CTP (Figure 1A) and DSA (Figure 1B) for determining DCI revealed no clinically significant difference. However, treatment thresholds (dashed lines) guide the optimal imaging strategy for A-SAH at different pretest probabilities. A pretest probability of 16% is needed with a positive CTP to initiate treatment with HHH compared to 12% for DSA. In addition, a pretest probability of 50% is needed with a positive CTP to initiate IA-therapy compared to 44% for DSA. Furthermore, when pretest probabilities are higher than 85% or lower than 10%, a positive or negative result with either CTP or DSA will not alter posttest probabilities significantly enough to influence treatment decisions.



## CONCLUSION

Though CTP and DSA have similar test characteristics for determining DCI in A-SAH, clinicians' treatment threshold is a valuable component in assessing the optimal imaging strategy for patients with different pretest probabilities. Further work is needed to study the rationale for determining these treatment thresholds.

**KEY WORDS:** CT perfusion, digital subtraction angiography, aneurysmal subarachnoid hemorrhage

## P-7

### Positive Effects of False-Negative Diffusion-Weighted MR Imaging in Acute Cerebellar Stroke

Ding, X. Chen, L. Tong, D. Wang, J.

The First Hospital of Jilin University  
Changchun, CHINA

**PURPOSE**

To improve the awareness of physicians about false-negative diffusion-weighted (DW) magnetic resonance imaging (MRI) findings in patients with acute cerebellar infarction and the importance of periodically observing nystagmus after symptom onset.

**MATERIALS & METHODS**

We retrospectively reviewed the medical records of 12 patients who all had complained of severe isolated dizziness or vertigo between May 2009 and December 2010. All patients had visited the emergency department within 2-6 hours of its onset. Findings of initial MRI were negative. All patients had gone to the neurology department for peripheral vestibular disorders. Spontaneous and positional nystagmus 6-24 hours after symptom onset was observed periodically.

**RESULTS**

In six of the patients, severe vertigo, nausea, and vomiting persisted after the nystagmus had been resolved. In five of the patients, the direction and/or type of nystagmus changed periodically. Repeat MR examinations were performed 24 hours after symptom onset because of the atypical pattern of nystagmus for benign peripheral vestibular disorders, at which point cerebellar infarction was detected.

**CONCLUSION**

Physicians who examine patients with acute severe isolated vertigo or dizziness should consider the possibility of false-negative DW MRI findings in case of hyperacute ischemic stroke. It is vital to observe the nystagmus periodically after onset. The MR examination should be repeated more than 24 hours after symptom onset in patients with an atypical pattern of nystagmus for benign peripheral vestibular disorders.

**KEY WORDS:** Acute cerebellar stroke, MR imaging

## P-8

### Comparison of Four-Dimensional CT Angiography with MR Angiography in Acute Ischemic Stroke Patients with Probable Internal Carotid Artery Occlusion

Miyazaki, Y.<sup>1</sup>Mori, T.<sup>1</sup>Tajiri, H.<sup>1</sup>Iwata, T.<sup>1</sup>Nakazaki, M.

Shonan Kamakura General Hospital  
Kamakura, Kanagawa, JAPAN

#### PURPOSE

Emergency MR angiography (MRA) can provide useful information to find the internal carotid artery (ICA) occlusion in an acute stroke setting. However, the usefulness of four-dimensional CT angiography (4D CTA) using 320 rows area detector CT remains uncertain for emergency diagnosis of cerebral vasculature in acute ischemic stroke. The aim of our retrospective study was to investigate whether or not there were some differences between 4D CTA and MRA findings in acute ischemic stroke patients with probable internal carotid artery occlusion.

#### MATERIALS & METHODS

Included for analysis were acute ischemic stroke patients 1) who were admitted to our institution within 48 hours of symptom onset from September 2010 to September 2011, 2) who underwent whole brain 4D CTA within 24 hours following emergency MRA on admission and 3) in whom the affected ICA absolutely was not visualized on MRA. We compared 4D CTA findings with MRA findings.

#### RESULTS

During study period, 446 acute ischemic stroke patients were admitted within 48 hours from symptom onset and emergency MRA showed no visualization of the affected ICA in 39 of them. Among the 39 patients, 23 patients underwent 4D CTA following MRA. The 4D CTA demonstrated delayed antegrade flow of the affected ICA in nine of the 23 patients and the affected ICA supplied by collateral flow in one of them (43.5%, 10/23). In the rest (56.5%, 13/23), 4D CTA could not visualize the affected ICA at all.

#### CONCLUSION

In an acute stroke setting, 4D CTA can provide more accurate information of the affected ICA which absolutely is not visualized in MRA.

**KEY WORDS:** 4D CT angiography, acute ischemic stroke, internal carotid artery occlusion

## P-9

### Modified "ABC/2" Method for Diffusion-Weighted Imaging Stroke Measurement Has Good Inter-Rater Reliability

Diaz, K.<sup>1</sup>Smolak, A.<sup>2</sup>Bulic, S.<sup>3</sup>Linden, C.<sup>1</sup>Janjua, N.<sup>3</sup>

<sup>1</sup>State University of New York Downstate Medical Center at Long Island College Hospital, Brooklyn, NY, <sup>2</sup>Columbia University School of Social Work, New York, NY, <sup>3</sup>State University of New York Downstate Medical Center, Brooklyn, NY

#### PURPOSE

Diffusion-weighted magnetic resonance imaging (DWI MRI) has great sensitivity for ischemia, and may be a reliable tool for triaging stroke patients for therapy, compared with CT, particularly in instances of unknown time windows, where risk of revascularization therapies may be potentially higher. Studies evaluating bedside techniques of DWI volume measurement, similar to previously described techniques for measuring intracerebral hemorrhage (ICH) on computed tomography (CT) have been compared with automated planimetry. The inter-rater reliability (IRR) of similar bedside techniques for ICH measurement on CT is well established, but the IRR for DWI stroke measurement has not been studied. We sought to evaluate the IRR of physicians involved in screening stroke patients' radiology studies.

#### MATERIALS & METHODS

This study is a subgroup of a larger study of the benefits and safety of endovascular revascularization in patients with acute ischemic stroke beyond 8 hours who fulfill criteria of a clinical-diffusion mismatch. Three raters (attending neuroradiologist, a 3rd-year radiology resident and a 3rd-year neurology resident) were provided with written instructions on using the modified ABC/2 method as follows: dimension A defined as largest linear diameter within abnormal area on a single slice; B, largest linear diameter perpendicular to A; C, number of slices minus 1 multiplied by depth in centimeters. Measurements were examined for inter-rater reliability through the interclass correlation (ICC) statistic, to give a composite score of intraobserver and interobserver variability. Multiple imputation with 10 iterations was performed to correct for two deleted outlier scores on the DWI stroke rating. The ICC was tested for being significantly different from zero and this gave the reported p-value, which evaluates if an ICC is significant.

#### RESULTS

The greatest inter-rater variability was seen in the diffusion-weighted images and with small lesions. The modified ABC/2 method was more precise in the ICH group. The ICC results were as follows: CT stroke = 0.979, 95% CI: 0.894 to 0.998, p = 0.000; CT ICH = 0.998, 95% CI: 0.988 to 1.000, p = .000; DWI stroke = 1, 95% CI: 0.998 to 1.000, p = 0.000.

**CONCLUSION**

The modified ABC/2 method can be performed rapidly and has good IRR for DWI stroke and excellent IRR for both stroke and ICH on CT. This may be considered as an alternative to computer automated planimetry for evaluation of MRI and other radiologic studies for rapid triage of stroke patients for potential therapy.

**KEY WORDS:** ABC/2 method, stroke

**P-10****T2\*-Weighted Gradient-Echo MR Imaging for Diagnosis of Cerebral Venous Thrombosis**

Ihn, Y.-Jung, W.

St. Vincent's Hospital  
Suwon, KOREA, REPUBLIC OF

**PURPOSE**

Cerebral venous thrombosis (CVT) can have severe clinical outcome, some even leading to death. Intravascular clot disintegration as well as flow changes due to thrombosis can lead to signal changes in T2- and T1-weighted sequences. In our study, nine patients with CVT (including sinus thrombosis) were analyzed retrospectively in spin-echo sequence before and after administration of contrast medium, T2\*-weighted conventional GRE, MR venography or conventional angiography.

**MATERIALS & METHODS**

Eleven patients with venous sinus thrombosis were examined (six women, five men, ages 1 - 68 years). The clinical symptoms were nonspecific (acute paresis, seizure, hemiplegia). Ten of these patients were in acute stage (< 7 days), one was in the subacute stage (> 7 days). We retrospectively reviewed the MR image findings and MR venography or transfemoral catheter angiography (TFCA) finding. Transverse T2-weighted fast spin-echo, FLAIR, T1-weighted spin-echo, T2\*-weighted conventional GRE sequence, enhanced T1-weighted and MR venography were analyzed.

**RESULTS**

The venous thromboses were best detectable in the T2\*-weighted GRE sequence in nine patients. In the remaining two patients, it was detectable only with difficulty. The T2\*-weighted GRE sequence was superior to the T2-weighted fast spin echo, FLAIR, T1-weighted spin echo sequence in all patients. MR venography image findings were correlated with TFCA venographic findings in all case.

**CONCLUSION**

The T2\*-weighted GRE sequence was possibly the best method of detection of acute CVT. Therefore, it seems to be of benefit to integrate a T2\*-weighted conventional GRE sequence into the MR protocol for the diagnosis of cerebral venous thrombosis.

**KEY WORDS:** MR imaging, gradient-echo, cerebral venous thrombosis

**P-11****Variable MR Sequences for Iron Detection of Motor Cortex in Amyotrophic Lateral Sclerosis**

Adachi, Y.-Sato, N.

National Center Hospital of Neurology and Psychiatry  
Tokyo, JAPAN

**PURPOSE**

Several reports about radiologic finding of amyotrophic lateral sclerosis (ALS) patients have been published. The presence of low signal intensity in the motor cortex and high signal intensity in the pyramidal tract on T2-weighted images and atrophy of motor cortex are described using conventional MR imaging techniques. Previous studies suggested that abnormal iron deposition caused low signal intensity in the motor cortex of ALS patients. Susceptibility-weighted imaging (SWI) now is the most advanced and sensitive MR imaging sequence for susceptibility differences including iron deposition. The purpose of this study was to evaluate the sensitivity of SWI compared with conventional spin-echo T2-weighted and GRE imaging sequences in detection of low signal intensity of motor cortex in ALS patients compared with age-matched normal volunteers.

**MATERIALS & METHODS**

This study included 23 patients (13 male and 10 female) clinically diagnosed by neurologist as ALS and we retrospectively reviewed their brain MR images. Patients ranged in age from 43 to 77 year old. Twenty-eight age-matched normal volunteers (13 males and 15 females, ranging in age from 33 to 82 years old) also were examined by MRI as controls. The standard protocol included axial conventional spin-echo T2-weighted imaging, T2-weighted GRE imaging and SWI. The SWI sequences were reconstructed with minimum intensity projection (MIP) technique. We used two transverse images on each sequence for evaluation of signal intensity of motor cortex; superior image was at the level of central semiovale and inferior image was at the level of the top slice of lateral ventricle. Signal intensity of motor cortex was compared with that of superior frontal cortex and graded with a three-point scoring system; isointense (score 0), mildly hypointense (score 1) or markedly hypointense (score 2). In statistical analysis, we used total score of superior and inferior images.

**RESULTS**

On SWI, two patients had score 4, five patients had score 3, eight patients had score 2, six patients had score 1 and one patient had score 0. Both patients who assessed total score 4 had laterality. These lateralities corresponded with clinical symptom. On conventional spin-echo T2-weighted images, five patients had score 1 and remaining 15 patients had score 0. All patients were scored 0 on GRE. In group of normal volunteers, three out of 28 normal volunteers were assessed total score 2, 11 volunteers were score 1 and 14 volunteers were score 0 on SWI. Statistical analysis showed that total scores of precentral cortical signal intensity on



SWI in ALS patients were significantly higher than normal volunteers ( $p < 0.0001$ ).

## CONCLUSION

This study demonstrated that SWI was the most sensitive sequence to detect the low signal intensity of precentral cortex in ALS patients compared with conventional and gradient T2-weighted sequences. This finding could be useful and easily obtainable imaging findings for early diagnosis of ALS.

**KEY WORDS:** Amyotrophic lateral sclerosis, susceptibility-weighted imaging, motor cortex

## P-12

### Alteration of Brain Default Mode Network in Liver Cirrhosis with and without Spontaneous Portosystemic Shunt: A Resting-State Functional MR Imaging Study

Lin, T.<sup>1</sup>·Hsu, T.<sup>2,3</sup>·Lin, W.<sup>1,2</sup>

<sup>1</sup>Kaohsiung Chang Gung Memorial Hospital and Chang Gung University, Kaohsiung, TAIWAN, <sup>2</sup>National Yang-Ming University, Taipei, TAIWAN, <sup>3</sup>Taipei Veterans General Hospital, Taipei, TAIWAN

## PURPOSE

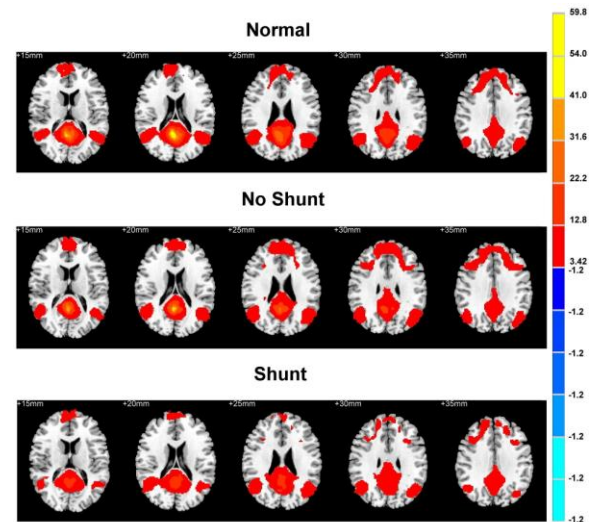
Spontaneous portosystemic shunt (PSS) is a well known complication of liver cirrhosis and portal hypertension. However, its impact to brain default mode network (DMN) still is not well delineated. The purpose of this study is to evaluate the intrinsic connectivity of DMN with resting-state functional MRI (fMRI) in cirrhotic patients with and without spontaneous PSS.

## MATERIALS & METHODS

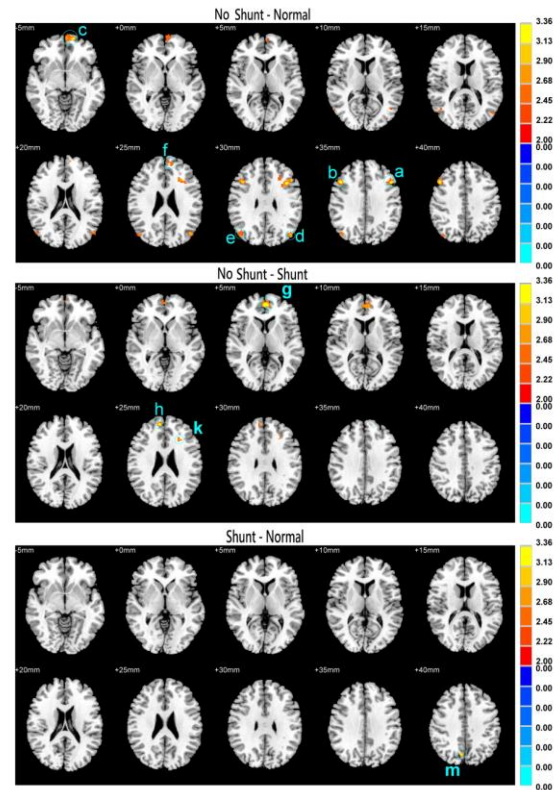
The resting-state fMRI data were collected from 48 cirrhotic patients without overt hepatic encephalopathy (spontaneous PSS = 22, without PSS = 26), and 40 age/gender-comparable healthy controls. We investigated differences in cortico-cortical connectivity of DMN between three subgroups. Strength of functional connectivity correlation coefficient (fc-CC) was determined by resting-state fMRI. Partial correlations among intercortical fc-CC, severity of PSS, main portal flow and laboratory tests were analyzed.

## RESULTS

Cirrhotic patient without PSS showed increase strength of executive control network after comparing with PSS group and health controls. In cirrhotic patients, the decrease fc-CC of medial prefrontal cortex was associated with increased severity of PSS, decreased albumin, increase INR value and decrease main portal flow.



Functional connectivity relative to the PCC seed (4, -54, 20) region. Statistical threshold was set at FDR correction  $P < 0.001$



a: L Middle Frontal Gyrus; b: R Middle Frontal Gyrus; c: L Medial Frontal Gyrus; d: L Middle Temporal Gyrus; e: R Middle Temporal Gyrus; f: L Superior Frontal Gyrus; g: L Medial Frontal Gyrus; h: R Medial Frontal Gyrus; k: L Middle Frontal Gyrus; m: R Precuneus

## CONCLUSION

Cirrhotic patients without spontaneous PSS may elicit a compensational executive control system enhancement, and further downhill corresponding to PSS severity and poor clinical profiles. Through appropriate targets, the resting-state fMRI technology may provide relevant supplemental information for monitoring early hepatic encephalopathy and serve as a new biomarker for clinical diagnosis.



**KEY WORDS:** Portosystemic shunt, default mode network, resting-state functional MR imaging

#### P-14

##### Diffusional Kurtosis Imaging of Normal-Appearing White Matter in Multiple Sclerosis

Yoshida, M.<sup>1</sup>•Hori, M.<sup>1</sup>•Fukunaga, I.<sup>2</sup>•Yokoyama, K.<sup>1</sup>•Suzuki, M.<sup>3</sup>•Kamagata, K.<sup>1</sup>•Aoki, S.<sup>1</sup>•Masutani, Y.<sup>4</sup>

<sup>1</sup>Juntendo University School of Medicine, Tokyo, JAPAN, <sup>2</sup>Graduate School of Health Promotion Science, Tokyo Metropolitan University, Tokyo, JAPAN, <sup>3</sup>Juntendo Urayasu Hospital, Juntendo University School of Medicine, Chiba, JAPAN, <sup>4</sup>Graduate School of Medicine, The University of Tokyo, Tokyo, JAPAN

##### PURPOSE

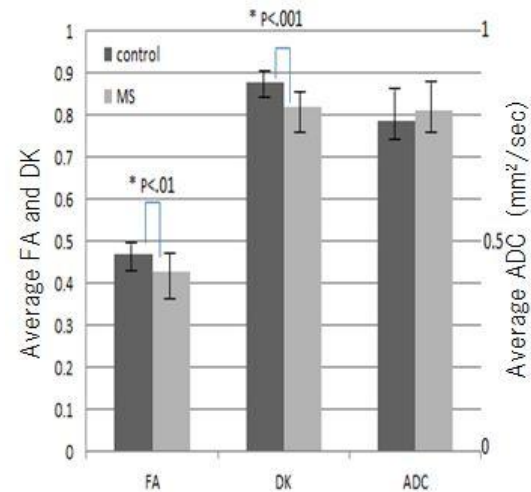
The purpose of this study is to evaluate diffusional changes of the normal-appearing white matter (NAWM) regions remote from multiple sclerosis (MS) plaques using a new method, diffusional kurtosis imaging (DKI), for investigating the non-Gaussian behavior of water diffusion.

##### MATERIALS & METHODS

Twelve patients with known MS and six age-matched healthy volunteers participated in this study. Diffusional kurtosis imaging was performed on a 3 T MR scanner. Diffusion metric maps were calculated by using the free software dTV IIFZR (Image Computing and Analysis Laboratory, Department of Radiology, The University of Tokyo). Fractional anisotropy (FA) and apparent diffusion coefficient (ADC) maps of conventional model and DK maps were computed. Regions of interest (ROIs) were placed on 24 cerebral regions such as frontal, parietal, temporal lobe white matter between MS patients and controls.

##### RESULTS

The mean FA of all ROIs was  $0.468 \pm 0.015$  in the control group,  $0.428 \pm 0.031$  in the MS group. The mean ADC was  $0.785 \times 10^{-3} \text{ mm}^2/\text{sec} \pm 0.035$  in the control group,  $0.811 \pm 0.044$  in the MS group. The mean DK of all ROIs was  $0.879 \pm 0.021$  in the control group,  $0.820 \pm 0.030$  in the MS group. Significant differences in mean FA ( $P < .01$ ) and particularly DK ( $P < .001$ ) were observed between normal WM and NAWM. In analysis of individual ROIs, significant differences in DK were observed in three ROIs (right superior longitudinal fasciculus, right temporal lobe WM, splenium of corpus callosum) between normal WM and NAWM. Only one ROI showed significant difference in ADC and FA.



##### CONCLUSION

Diffusional kurtosis imaging may have the potential to be a sensitive biomarker to detect tissue damage in patients with MS in comparison with conventional diffusional evaluations such as diffusion tensor imaging.

**KEY WORDS:** Diffusional kurtosis imaging, non-Gaussian, multiple sclerosis, normal-appearing white matter

#### P-15

##### MR Imaging of Thai Patients with Negative Anti-AQP4 Antibody

Ngamsombat, C.•Wongsripuemtet, J.•Chawalparit, O.•Pienpuck, W.•Jitpratoom, P.•Siritho, S.•Prayoonwiwat, N.

Siriraj Hospital Mahidol University  
Bangkok, THAILAND

##### PURPOSE

Neuromyelitis optica (NMO)-IgG is a specific autoantibody marker for neuromyelitis optica (NMO). It binds selectively to aquaporin 4 (AQP4). Opticospinal multiple sclerosis (OSMS) in Asians has similar features to the relapsing-remitting form of neuromyelitis optica (NMO) seen in Westerners and OSMS is suggested to be NMO based on the frequent detection of specific NMO-IgG. However, it remains unknown in Thai patients whether anti-AQP4 antibody positive and negative OSMS patients possess an identical disease. The objective is to study the characteristics of MRI findings in brain and spinal cord in Thai patients with negative serum aquaporin-4 antibody.

##### MATERIALS & METHODS

Eighty-seven Thai patients attending Siriraj MS clinics with negative anti-AQP4 antibody were study retrospectively. After excluding three patients with inconclusive diagnosis, five patients with other diagnosis, 15 patients with CIS and 24 patient with no available MRI study on PACS, 40 cases with available MRI were included. The available brain and spinal MRIs

in the hospital archive system were reviewed by three neuroradiologists and finalized by consensus. Clinical data and MRI findings were analyzed.

## RESULTS

There were 37 brain MRIs and 32 spinal MRIs (29 with brain MRIs) for the analysis. The mean age of the patients was 38.95 years old (range 8-67 years) with 31 females and nine males. Clinical diagnosis was made in four cases of NMO, 12 high risk NMOS, 21 RRMS, one PPMS, one PRMS and one OSMS. For brain MRIs, 17 patients (42.5%) were fulfilled (3/4) Barkhof's criteria, and 11 patients (27.5%) had negative findings. Only eight patients (20%) had enhancement lesions. The cloud-like enhancement pattern were five cases (62.5%), nodular enhancement pattern were found in three cases (37.5%). The involvement of brain in common location of AQP-4 were found: subependymal lateral ventricle 12 patients (30%), extensive hemispheric lesion 10 patients (25%), subependymal third/fourth ventricle three patients (7.5%), medullar extending to cervical cord three patients (7.5%) and corticospinal tract lesion one patient (2.5%). There were 21 patients (52.5%) with nonspecific pattern. Most of the lesions (58.33%) had vasogenic edema. For spinal cord MRI - negative finding was found in 17 cases (53.12%) and positive in 15 cases (37.5%). Among the positive cases, most lesions (12 patients, 80%) are at thoracic level. There were nine cases (60%) with enhancing lesions, eight cases (53.33%) with cord swelling, eight cases (53.33%) with long extensive lesions (three or more vertebral body), 10 cases (66.6%) with peripheral location on axial plane, two cases (13.33%) with central cord location, and two cases (13.33%) with mixed pattern.

## CONCLUSION

The MRI findings of Thai patients with negative anti-AQP4 antibody had high incidence of brain lesion along subependymal lateral ventricle and extensive hemispheric lesion and most are vasogenic edema. Most common thoracic location is noted. Long extensive cord lesions as in anti-AQP4 positive patient also are observed.

**KEY WORDS:** Neuromyelitis optica, AQP4 negative

## P-16

### Feasibility of Advanced MR Imaging and Imaging Phenotype of Ictal-Interictal EEG Patterns in Critically Ill Patients with Nonstructural, Severe Brain Injury

Parikh, G.·Wen, Y.·He, X.·Xu, D.·Peterson, B. S.·Delapaz, R. L.·Claassen, J.

Columbia University Medical Center  
New York, NY

## PURPOSE

MR imaging is challenging in critically ill patients who often are intubated and hemodynamically unstable. Prior studies described qualitative ADC signal changes in the thalamus, hippocampus, and cortical regions in

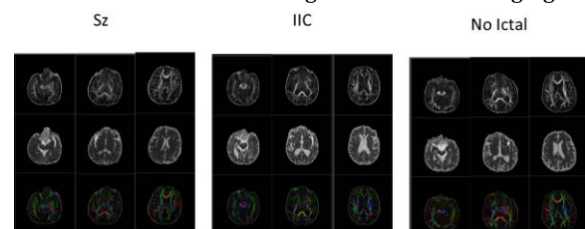
patients with seizures and status epilepticus. The purpose of this study was to show the feasibility of MRI during the acute phase of severe brain injury and to define the imaging signature of ictal interictal EEG patterns which may warrant aggressive antiepileptic therapy.

## MATERIALS & METHODS

This is an IRB-approved observational study of all patients admitted to the Neuro ICU with acute brain injury that undergo 3 T MR imaging as part of their routine clinical care. Images were acquired on a GE Signa 3 T whole body scanner (Milwaukee, WI), equipped with an 8-channel head receiver coil. Patients were included if they had acute nonstructural brain injury (e.g., status epilepticus, CNS infection), continuous EEG available within 24 hours postictus, and ADC and DTI sequences available. Diffusion tensor imaging slices were acquired in an axial orientation parallel to the AC-PC line using echo-planar DTI imaging sequence, with TR = 6000 ms, TE = minimum, FOV = 24 cm, acquisition matrix = 128 x 128, and slice thickness = 5.0 mm. We acquired 1 baseline image with b = 0 s/mm<sup>2</sup> and 1 diffusion-weighted image at b = 1000 s/mm<sup>2</sup> with diffusion gradients applied in 25 directions sampling 3D space uniformly. Diffusion-weighted imaging data first were inspected visually to guarantee no obvious motion. The DWI data then were corrected for eddy-current induced distortion using FSL software functions, and optimized and converted to diffusion tensors using software developed here at CUMC.

## RESULTS

We safely obtained high quality MR imaging in 18 critically ill patients with nonstructural brain injury (31 MRIs). FA, ADC, and directional FA color maps were created for 14 MRI scans (11 patients; see attached figure). Three patients had seizures, two ictal interictal, and nine nonictal EEG findings at the time of imaging.



## CONCLUSION

These data show the feasibility of acquiring advanced structural MRI sequences in critically ill patients with acute brain injury. Whole-brain and region-of-interest quantitative analyses including ADC and FA values are being performed with between-group and inpatient comparisons.

**KEY WORDS:** Interictal, diffusion tensor imaging, seizure

## P-17

### Application of Cine MR Imaging in Low Cerebrospinal Fluid Syndrome

Yang, I.<sup>1</sup>•Chen, H.<sup>1,2</sup>•Chen, M.<sup>1</sup>•Lui, C.<sup>1</sup>•Lin, W.<sup>1,2</sup>

<sup>1</sup>Kaohsiung Chang Gung Memorial Hospital and Chang Gung University College of Medicine, Kaohsiung, Taiwan, Kaohsiung, TAIWAN, <sup>2</sup>National Yang-Ming University, Taipei, TAIWAN

#### PURPOSE

Low cerebrospinal fluid (CSF) syndrome is characterized by orthostatic headache. Abnormal MR imaging results have been considered to be the *sine qua non* of low CSF syndrome, but a sizeable minority of patients have normal results on conventional MR imaging. The purpose of this study was to evaluate CSF flow on cine MRI in low CSF syndrome patients before and after treatment.

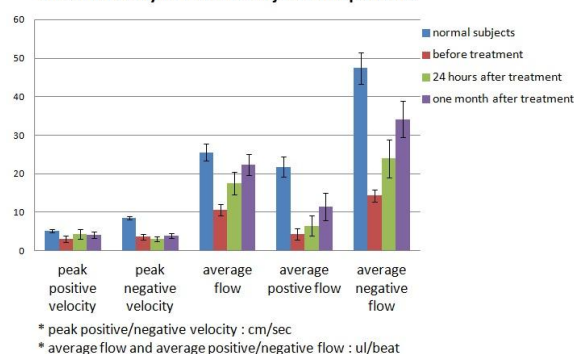
#### MATERIALS & METHODS

From 2007 to 2011, there were 20 patients with low CSF syndrome (10 males and 10 females; mean age 40.9 years old; from 30 to 62) and 31 age- and gender-matched healthy volunteers were enrolled (15 males and 16 females; mean age 46.32 years old). Cine MRI was used to measure the flow of CSF in the aqueduct, including average flow, peak positive/negative velocity, and average positive/negative flow in all subjects. Repeated cine MRI study was assessed in patients immediate and 1 month later after treatment. Statistical analysis was performed to find out the difference between patients and health controls, and in patients before and after treatment.

#### RESULTS

After conservative treatment, 18 of 20 patients (90%) received epidural blood patch (EBP). Among them, 15 patients received one, two patients had two and one patient received three EBPs. All subjects experienced resolution of symptoms after treatment. Before treatment, patient had significant lower average CSF flow than healthy controls (10.67 vs 25.57 ul/beat,  $F = 20.852$ ,  $p = 0.000$ ). By using ANOVA analysis with Benferroni correction, the average CSF flow of patients significantly elevated after EPB 24 hours later (17.58 ul/beat), and gradually increased in 1 month follow-up study (22.43 ul/beat) ( $F = 5.929$ ,  $p = 0.005$ ).

Cine MRI study in normal subjects and patients



#### CONCLUSION

Cine MRI was useful for noninvasively assessing the state of CSF dynamics and for confirming the effectiveness of treatment in patient with low CSF pressure syndrome.

**KEY WORDS:** Cine MR imaging, low CSF syndrome, average flow in aqueduct

## P-18

### Classification and Quantification of Diffusion Tensor Imaging in Normal-Aged Adults

Chen, C. C. C.<sup>1</sup>•Chai, J.<sup>1</sup>•Fu, J.<sup>2</sup>•Chiang, C.<sup>1</sup>•Wu, Y.<sup>1</sup>

<sup>1</sup>Taichung Veterans General Hospital, Taichung, TAIWAN, <sup>2</sup>National Yunlin University of Science and Technology, Yunlin, TAIWAN

#### PURPOSE

Diffusion tensor imaging (DTI) is a promising tool for providing in vivo characterization of white matter information, which has been used to analyze the data of age-related neurodegenerative diseases such as Alzheimer disease. In this study, DTIs in normal-aged adults were quantified and analyzed to provide the baseline information for further study.

#### Materials & Methods

A total of 35 subjects meeting the following criteria were enrolled: 1) a mini-mental status examination (MMSE) of no less than 28; 2) a clinical dementia rating (CDR) scale equals to 0; and 3) age above 55 years old. The MR imaging was performed on Siemens Symphony 1.5 T MR scanner. Except the conventional T1W, T2W and FLAIR MRI, DTIs were acquired by using a single-shot EPI sequence (TR/TE/acquisitions, 9600 ms/98 ms/4) with gradients applied in 12 directions and 2 b-values (0, 1000 s/mm<sup>2</sup>). The white matter was segmented using statistical parametric mapping (SPM) software from sagittal 3D MPRAGE T1-weighted images. The T1 images were registered with the DTI using mutual information combining with the quasi-Newton method. Two measurements, the fractional anisotropy (FA) and the mean diffusivity (MD), were calculated from the white matter in the DTI. The output analysis was arranged in three diagrams, showing the relationships between: 1) age and FA; 2) age and MD; and 3) FA and MD

#### RESULTS

The diagram for age vs FA showed that as age increases, FA decreases. The slope of the age-FA-linear regression coefficient was -0.0011 ( $R^2 = 0.4218$ ). The diagram for age vs MD showed that as age increases, so does the MD. The slope of the age-MD linear regression coefficient was 0.0024 ( $R^2 = 0.4921$ ). The diagram for MD vs FA showed that as MD increases, FA decreases as a whole. The slope of the MD-FA linear regression coefficient was -0.3889 ( $R^2 = 0.6311$ ). The data were divided into two groups, group 1 for the age ranged from 56 to 70 years old and group 2 for the age ranged from 71 to 90 years old. The results in the MD vs FA diagram revealed that the two groups of data were divided into clusters. The slope of the linear regression coefficient in group 1 was -0.7202 ( $R^2 = 0.3441$ ). The slope of the linear

regression coefficient in group 2 was  $-0.2224$  ( $R^2 = 0.8451$ ). A  $t$ -test of the difference between the regression coefficients showed that the slope in group 1 was significantly different from the slope in group 2.

#### CONCLUSION

The experimental results showed that with age, the FA decreased and the MD increased. Those results corresponded to the natural degeneration of nerve fibers in normal-aged people. After grouping the data by the age, the MD vs FA diagram revealed the clustering phenomenon. In the group above 71 years old, the effect of white matter degeneration on FA and MD was significantly different from the group younger than 70 years old.

**KEY WORDS:** Fractional anisotropy, mean diffusivity, diffusion tensor imaging

#### P-19

##### **Multimodal Biological Parametric Mapping Reveals the Effect of Gray-Matter Atrophy on Positron Emission Tomography Measures of Hypometabolism Associated with Alzheimer Disease**

Westcott, G.·Maldjian, J. A.·Whitlow, C. T.

Wake Forest University School of Medicine  
Winston-Salem, NC

#### PURPOSE

Structural magnetic resonance imaging (MRI) and fluorodeoxyglucose positron emission tomography (FDG-PET) have been used to identify regions of gray-matter atrophy and hypometabolism in patients with Alzheimer disease (AD). The degree to which gray-matter atrophy contributes to these metabolic decreases identified with FDG-PET have not been explored. We hypothesize that the regional cerebral metabolic changes in AD are greater than those accounted for by underlying decreases in gray-matter volume.

#### MATERIALS & METHODS

T1-weighted structural MRI and FDG-PET images were obtained from the Alzheimer's Disease Neuroimaging Initiative for 102 cognitively normal (CN) and 92 AD patients. The Statistical Parametric MappingVBM8 toolbox was used for segmentation and normalization of MRI images to the ICBM MNI template. The resulting Jacobian images were masked for gray matter to prevent contamination of the analysis with expansion in the volume of surrounding cerebrospinal fluid. Positron emission tomography images were coregistered to the MRI using SPM and the warps generated from MRI normalization were applied to PET data. An SPM voxel-based analysis was performed to compare AD to CN PET data without correcting for gray matter. Finally, a biological parametric mapping analysis was used to compare normalized PET data while using corresponding normalized gray matter maps as a voxel-wise regressor.

#### RESULTS

An unregressed voxel-based analysis of ADNI subjects reproduced the temporoparietal and cingulate FDG-hypometabolism in AD, as reported in the literature. When BPM regression was applied to correct PET data for the degree of gray matter atrophy, the difference in activity between CN controls and AD patients within the parietal lobe was absent, while the difference in the cingulate gyrus remained. Furthermore, correcting for gray matter atrophy greatly reduced the metabolic decreases in the hippocampus, but did not abolish it completely.

#### CONCLUSION

Controlling for gray-matter volume reveals that differences in regional cerebral metabolic activity described in parietal areas in AD patients is due to atrophy. Although some of the hippocampal FDG-hypometabolism appeared to be due to gray-matter atrophy, our results also suggest a degree of intrinsic metabolic dysfunction that cannot be explained by changes in gray-matter volume.

**KEY WORDS:** Alzheimer disease, positron emission tomography

#### P-20

##### **Preoperative Localization of the Sensorimotor Area in Brain Tumor Patients Using Resting-State Functional MR Imaging**

Ramalho, J.·Ferreira, H.·Reis, J.

Centro Hospitalar de Lisboa Central  
Lisbon, PORTUGAL

#### PURPOSE

Blood oxygenation level-dependent (BOLD) functional magnetic resonance imaging (fMRI) is a noninvasive method for mapping eloquent brain cortices. A novel technique in functional neuroimaging termed "resting-state fMRI", in contrast to task-based fMRI, measures BOLD signal without the patient being subjected to any task. Resting-state fMRI has been shown to be a robust noninvasive method for localization of functional connectivity in sensorimotor areas as well as other resting-state networks in healthy subjects. The purpose of this study is to determine if this technique also can be used to localize the sensorimotor areas in patients with brain tumors.

#### MATERIALS & METHODS

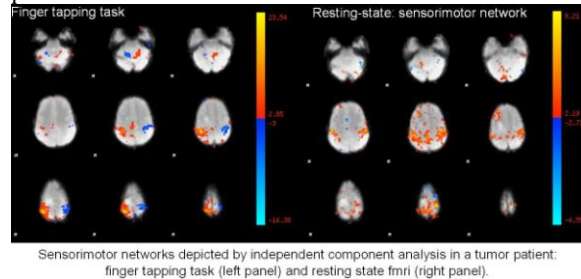
Resting-state fMRI was acquired in 10 healthy young adults and 10 brain tumor patients. A data-driven multivariate technique for analyzing resting-state fMRI data, named independent component analysis (ICA) was used (MELODIC/FSL). Conventional fMRI motor mapping (finger tapping protocol) also was performed in both groups.

#### RESULTS

Consistent delineation of sensorimotor cortex was obtained using the resting-state BOLD data in patients with brain tumors in the same way as in healthy



controls. Resting-state functional mapping in all cases performed as well or better than task-based fMRI.



## CONCLUSION

It is possible to localize the sensorimotor area from resting-state BOLD data in patients with brain tumors. Resting-state fMRI offers several practical advantages over task-based fMRI and it can be used in presurgical planning of brain tumor resections, particularly in patients who have difficulties in performing motor paradigms.

**KEY WORDS:** Resting-state functional MR imaging, brain tumor, independent component analysis

## P-21

### Truncation of FACT-Based Tractography of the Arcuate Fasciculus in Patients with Brain Tumors Due to Crossing Motor Fibers

Li, Z.·Patel, G.·Peck, K. K.·Brennan, N.·Holodny, A. I.·Young, R. J.

Memorial Sloan-Kettering Cancer Center  
New York, NY

## PURPOSE

To compare the efficacy of deterministic and probabilistic tractography in the reconstruction of the arcuate fasciculus in regions of fiber crossings in patients with brain tumors.

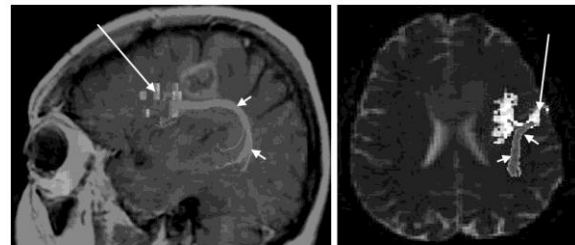
## MATERIALS & METHODS

We retrospectively identified 30 patients with left brain tumors <2cm from the arcuate fasciculus. Patients were right-handed and left language dominant. Functional MRI was performed using gradient-echo echo-planar imaging (TR/TE=4000/30ms, 128x128 matrix, 90° flip angle). Block-design phonemic fluency, semantic fluency and verb generation paradigms were analyzed in Analysis of Functional Neuroimaging. Diffusion tensor imaging (DTI) was acquired using single shot spin-echo echo-planar imaging with 25 noncollinear directions. Arcuate fasciculus was reconstructed using a deterministic fiber assignment by continuous tracking (FACT) algorithm and a probabilistic index of connectivity (PICO) algorithm in DTI&FiberTools (University Hospital, Friburg, Germany) software implemented in Matlab (Mathworks, Natick, MA). Tracking was controlled using two regions-of-interest corresponding to fMRI activated Broca's and Wernicke's areas, fractional anisotropy (FA)>0.15 and turning angle <45 degrees. Tracts were examined for extension between Broca's and Wernicke's areas, configuration

near tumors and/or edema, and compared with normal contralateral tracts. Fibers were scored for their anterior termination to Broca's area: 0-none; 1-few; 2-some; or 3-all. Corticospinal and corticobulbar motor fibers also were reconstructed by probabilistic tractography to compare their relationships with arcuate fasciculus fibers.

## RESULTS

In 26/30(86.7%) cases, both probabilistic and FACT reconstructed the posterior and middle parts of the left arcuate fasciculus. Fiber assignment by continuous tracking failed to reconstruct the anterior-most fibers of the arcuate fasciculus in 22/26(84.6%) cases, whereas probabilistic reconstructed the entire arcuate fasciculus. Mean scores for the anterior termination were 0.30 for FACT and 1.97 for probabilistic, with truncation occurring at the level of the crossing corticospinal and corticobulbar fibers. In 4/30 cases, neither probabilistic nor FACT produced any tract through regions of extensive tumor and/or edema. In the normal right hemisphere, FACT failed to reconstruct the anterior-most fibers of the arcuate fasciculus in 18/30 (60%) cases, whereas probabilistic reconstructed the entire arcuate fasciculus in all cases. Mean scores for the anterior termination were 0.67 for FACT and 2.23 for probabilistic.



Patient with left frontal lobe glioblastoma. FACT tractography of the arcuate fasciculus (short arrows) overlaid on a sagittal contrast T1-weighted image (left) and an axialB0 diffusion tensor image (right) shows truncation of the arcuate fibers (short arrows) prior to rostral termination at Broca's area by descending corticospinal and corticobulbar fibers (long arrows) shown by probabilistic tractography.

## CONCLUSION

The anterior arcuate fasciculus usually is truncated by FACT due to crossing corticobulbar and corticospinal fibers. Probabilistic outperformed FACT in achieving more complete cortical-cortical connectivity between Broca's and Wernicke's areas, although both techniques failed in a few cases with extensive tumor and/or edema. Additional work is needed to validate the location and functionality of the reconstructed tracts.

**KEY WORDS:** Diffusion tensor imaging, probabilistic, tractography

## P-22

### Detailed Analysis and Comparison of MR Spectroscopy Acquired at the Parietal Lobe of Normal Brain Using 1.5 T and 4.0 T MR Imaging Equipments

Khan, M. N. -<sup>1</sup>K. Karakach, T. K.<sup>2</sup>Mohsin, H.<sup>1</sup>Kashgari, A.<sup>1</sup>

<sup>1</sup>IWK Health Centre, Halifax, NS, CANADA, <sup>2</sup>Dalhousie University, Halifax, NS, CANADA

#### PURPOSE

To acquire short TE, single voxel, point-resolved spatially localized spectroscopy in a healthy adult subject using 1.5 T and 4.0 T field strengths outputs. Pictorially and graphically display all detectable metabolites individually with absolute quantification and in a common spectrum. Assess the difference in spectra acquired at both field strengths.

#### MATERIALS & METHODS

Using PROBE P - PRESS sequence which is point-resolved spectroscopy (PRESS) uses a 90°-180°-180° pulse train and detects the spin echo following the second 180° pulse, a short TE (35 ms) single voxel at parietal white matter is performed. GE 1.5 T HDX signa HD MR at IWK health centre and Varian INOVA 4T MR at NRC-IBD (Atlantic), NRL at the QEII Health Sciences Centre are used to acquire spectra. True axial T2 used for planning with 4 mm thickness and 0 interspaces. TE used is 35 and Voxel size used is 2x2x2 cm with ROI at periventricular parietal white matter. Spectra acquired are analyzed using LC Model and graphs plotted for individual metabolite. Spectra are compared for any difference.

#### RESULTS

Full spectrum of metabolites from both field strengths plotted in comprehensive manner and better quality and more informative spectrum showing more sensitive metabolic profile is achieved from 4 T MRI.

#### CONCLUSION

A comprehensive pictorial display and review of all possible adult brain metabolites detectable on 1.5 T and 4 T field strength MRI.

**KEY WORDS:** Technique, single voxel spectroscopy, short TE

## P-23

### Functional MR Imaging of Brazilian Sign Language in Congenitally Deaf Showing Cortical Reorganization of Primary Auditory Cortex

Rosset, S.<sup>1</sup>Valadao, M. N.<sup>1</sup>Isaac, M. L.<sup>1</sup>Lima, P. F.<sup>1</sup>De Araujo, D. B.<sup>2</sup>Santos, A. C.<sup>1</sup>

<sup>1</sup>University of São Paulo, Ribeirão Preto, BRAZIL,

<sup>2</sup>Federal University of Rio Grande do Norte, Natal, BRAZIL

#### PURPOSE

Sign language signs are natural languages that share the properties of spoken languages, with several studies demonstrating cortical activation in classical language areas in the left hemisphere with more bilateral representation. Measuring brain activation using functional MRI in congenitally deaf subjects make it possible to observe the process of cortical reorganization of primary auditory cortex. This study aimed at determining the activation of cortical areas engaged in receptive and expressive language tasks in three groups of subjects a) congenitally deaf who communicate only with LIBRAS (Brazilian Language of signs), hereafter named MD (monolingual deaf); b) monolingual hearing subjects who communicate via Portuguese speech alone (MH), and c) congenitally deaf subjects who communicate either with LIBRAS and oral speech (BD: bilingual deaf).

#### MATERIALS & METHODS

Twenty-five congenitally deaf subjects (12 MD and 13 BD), and 13 hearing controls (MH) were studied using fMRI with a 1.5 equipment (Magnetom Vision Plus, Siemens, Erlangen, Germany).

#### RESULTS

Deaf signers showed activation in the right inferior frontal cortex, in the temporal and inferior parietal cortex bilaterally compared with hearing participants for a task involving perception of sign language. Hearing subjects showed activation in the left inferior frontal, superior temporal and fusiform gyrus. For MD subjects, sign production tasks produced activation in the following regions: 1) unilateral (left) activation of precentral gyrus, supramarginal gyrus, inferior parietal lobule; 2) bilateral activation of middle and superior temporal gyrus, inferior frontal gyrus, cingulate gyrus. For MH subjects, sign production tasks produced no significant activation. In the second place, we found that deaf signers and speakers in task of speech production generated activations in left middle and superior temporal cortex and cingulate gyrus when contrasted with the task of sign production. Instead, the task of sign production showed activations in the left inferior parietal, postcentral, superior occipital and supramarginal cortex, right middle and inferior temporal gyrus, fusiform gyrus, lingual gyrus and bilateral middle frontal gyrus.

#### CONCLUSION

Our findings were concordant with the literature, confirming the existence of a common cortical substrate for both sign language and for speech, with the involvement of superior temporal cortex. The right hemisphere is more activated with sign language and the area of the primary auditory cortex is activated in deaf subjects for language tasks.

**KEY WORDS:** Brazilian sign language (Libras), deafness, functional MR imaging



## P-24

## New Semantic Language Paradigms for Clinical Functional MR Imaging

Zacá, D.·Jarso, S.·Pillai, J. J.

Johns Hopkins University  
Baltimore, MD

### PURPOSE

Language mapping by fMRI has been clinically validated both for language localization and lateralization. However in light of the newly developed dual stream model of language processing, new fMRI paradigms for presurgical mapping should be designed to elicit activation beyond the classical expressive and receptive areas. In this study we compared localization and lateralization between three new semantic language paradigms and two clinically used language paradigms.

### MATERIALS & METHODS

Seven adult right-handed, native English-speaking, healthy volunteers participated in this study performed on a 3 T MR Siemens Trio scanner. 3D T1 MPRAGE images were acquired to provide high-resolution reference frame (voxel size 1 mm<sup>3</sup>) for anatomical coregistration. BOLD images were acquired by a single-shot T2\*-weighted gradient-echo EPI sequence (TR=2,000 ms; TE=30 ms; 90° flip angle; voxel size 3 mm<sup>3</sup>). Subjects performed two clinical language paradigms, Silent Word Generation (SWG) and Sentence Completion (SC) and three newly designed semantic paradigms, visual antonym (VA) and auditory antonym (AA) discrimination and noun to verb association (NVA). All paradigms were block design with six alternating active and control blocks lasting 20 seconds. Images were processed using AFNI software and transformed to Talairach coordinates. A non Parametric Friedmann test was used to determine a significant paradigm effect in percentage signal change (PSC) at a group level. Then Mann tests were performed between pairs of paradigms in five regions of interest for language activation: inferior frontal gyrus (IFG), superior frontal gyrus (SFG), middle frontal gyrus (MFG), middle temporal gyrus (MTG) and superior temporal gyrus (STG). A laterality index (LI) was calculated using a statistical threshold independent model for each paradigm in all five regions of interest (ROIs). A one sample Wilcoxon test was performed and an asymmetric activation pattern was defined for an absolute LI value greater than 0.1.

### RESULTS

Significant differences were detected in the MTG. Visual antonym and NVA demonstrated stronger activation than the clinical paradigms SWG and SC (Figure 1). In this ROI, VA was the only paradigm with LI statistically significantly higher than 0.1 ( $z = 1.94$ ,  $p < 0.02$ ).

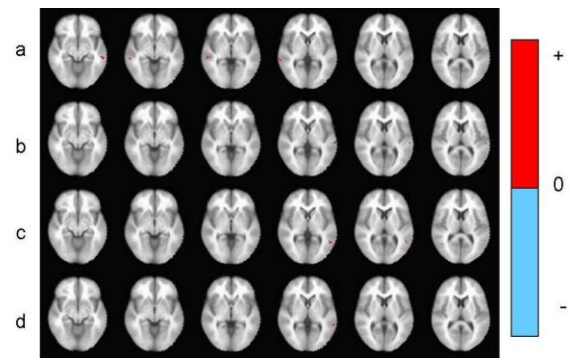


Figure 1: Paired Mann tests results in MTG: a) NVA minus SC; b) VA minus SC; c) NVA minus SWG; d) VA vs SWG. Maps were thresholded at significance level of  $p < 0.05$ , with 5 voxels cluster size

### CONCLUSION

Visual antonym and NVA should be added to the current battery of clinical language paradigms to provide a more complete representation of the language network.

**KEY WORDS:** Semantic paradigm, language localization and lateralization, dual stream model

## P-25

## Tractography of the Facial Nerve in Tumors of the Cereb

Gonçalves Pereira, P.<sup>1</sup>·Neto d'Almeida, G.<sup>1,2</sup>·Escada, P.<sup>2</sup>·Mataças, R.<sup>1,3</sup>·Taoka, T.<sup>4</sup>

<sup>1</sup>HPP - Hospital dos Lusíadas, Lisboa, PORTUGAL, <sup>2</sup>Hospital Egas Moniz, Lisboa, PORTUGAL, <sup>3</sup>Hospital dos Capuchos, Lisboa, PORTUGAL, <sup>4</sup>Nara University Hospital, Nara, JAPAN

### PURPOSE

To determine the course of the facial nerve by diffusion tensor (DT) tractography in the vicinity of cerebellopontine angle (CPA) schwannomas and arachnoid cysts, and to evaluate the agreement with surgical findings.

### MATERIALS & METHODS

We have evaluated eight patients with CPA masses at 1.5 T, six cases with vestibular schwannoma who had undergone surgery and two patients with arachnoid cysts. Diffusion tensor images were obtained with a single-shot echo-planar sequence (TR 4900 msec, TE 85 msec, b 1000 sec/mm<sup>2</sup>, six-axis encoding, FOV 230 mm, matrix 128 x 128, spacing 3 mm, 4 averages, 35 slices). Two independent observers (PMGP and TT) traced the facial nerve tract accordingly to the method of Taoka T. et al. The preoperative position of the presumed facial nerve was correlated with the surgical findings and the postoperative outcome in the patients with schwannomas. The feasibility of this technique was assessed in all eight cases.

### RESULTS

The facial nerve was illustrated by DT tractography in every patient. Fiber bundles were more difficult to trace in patients with arachnoid cysts. One observer missed

the correct position in one case, a grade 4 (Koos scale) vestibular schwannoma, possibly due to the large size of the mass. However, the course of the constructed tracts agreed with surgical findings in all six operated cases. The surgical outcome was favorable, leaving these patients without permanent facial paralysis. The facial nerve was shifted anteriorly with regard to the mass in all eight patients.

#### CONCLUSION

Diffusion tensor tractography of the facial nerves is feasible, reproducible and delivers useful preoperative information. Care should be taken when evaluating CPA grade 4 masses. Also, the fluid content of large arachnoid cysts may lower the anisotropy of small fiber bundles and limit a precise tracing.

**KEY WORDS:** Tractography, facial nerve, schwannoma

#### P-26

##### Relationship Between pH-Weighted Endogenous Amide Proton Chemical Exchange Saturation Transfer MR Imaging and Tissue Lactic Acidosis in Acute Ischemic Stroke

Ding, X.-Tong, D.-Wang, J.-Chen, L.

The First Hospital of Jilin University  
Changchun, CHINA

#### PURPOSE

The ischemic tissue becomes acidic after initiation of anaerobic respiration. It may result in impaired tissue metabolism and, eventually, in severe tissue damage. Their spatiotemporal resolution often is not sufficient for routine examination of fast-evolving and heterogeneous acute stroke lesions, although the changes in the major cerebral metabolites can be studied using magnetic resonance spectroscopy (MRS)-based techniques. To assess tissue acidosis by probing the pH-dependent chemical exchange of amide protons from endogenous proteins and peptides using pH-weighted MR imaging (MRI).

#### MATERIALS & METHODS

We characterized acute ischemic tissue damage using localized proton MRS and multiparametric imaging techniques that included perfusion, diffusion, pH, and relaxation MRI.

#### RESULTS

Our study showed that pH-weighted MRI can detect ischemic lesions and strong relationship with tissue lactate content measured by MRS, indicating lactic acidosis. Our study also confirmed the correlation between apparent diffusion coefficient (ADC) and lactate. However, no significant relationship was found for perfusion, T1, and T2.

#### CONCLUSION

By sensitizing to local tissue pH, optimized endogenous pH-weighted MRI remains a promising tool for providing a substitute imaging marker of lactic acidosis

and altered tissue metabolism, and augments conventional techniques for stroke diagnosis.

**KEY WORDS:** Acute ischemic stroke, endogenous amide proton, lactic acidosis

#### P-27

##### Chronic Neuropsychological Sequelae in HIV-Negative Tuberculous Meningitis and Cryptococcal Meningitis: Voxel-Based Diffusion Tensor Imaging Study

Chen, P.-Lu, C.-Chen, H.-Chen, M.-Hsu, N.-Chou, K.-Lin, C.-Lin, W.

<sup>1</sup>Kaohsiung Chang Gung Memorial Hospital and Chang Gung University College of Medicine, Kaohsiung, TAIWAN, <sup>2</sup>National Yang-Ming University, Taipei, TAIWAN

#### PURPOSE

Tuberculous (TBM) and cryptococcal meningitis (CM) are two of the most common types of chronic meningitis. The study was performed to assess whether the occurrence of chronic neuropsychological sequelae is associated with microstructure white matter (WM) damage in HIV-negative chronic meningitis.

#### MATERIALS & METHODS

Nineteen HIV-negative TBM patients, 13 HIV-negative CM patients and 32 sex- and age-matched healthy volunteers were evaluated and compared. The clinical relevance of WM integrity was studied using voxel-based diffusion tensor imaging (DTI) MRI. All subjects underwent complete medical and neurologic examinations, and neuropsychological testing. Differences in DTI indices were correlated with present neuropsychological rating scores, and cerebrospinal fluid (CSF) analysis during their initial hospitalization.

#### RESULTS

Chronic meningitis patients had higher cognitive deficits than healthy subjects, especially in TBM. There were changes in WM integrity in several WM regions in the hippocampus, inferior longitudinal fasciculus, cingulum, superior corona radiata, forceps major, superior longitudinal fasciculus and globus pallidus (Figure 1). Declined WM integrity in the globus pallidus and the hippocampus was associated with worse CSF analysis profiles, including higher protein and lower glucose concentration (Figure 2). Poorer DTI parameters were further linearly related to worse cognitive performance during follow up.

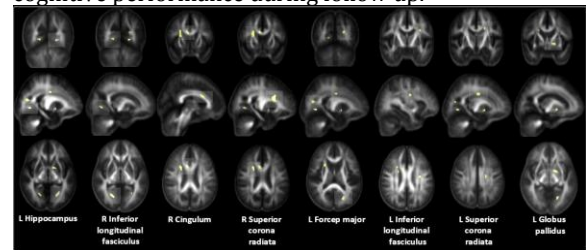


Figure 1. Comparison of fractional anisotropy (FA) between chronic meningitis patients and healthy volunteers

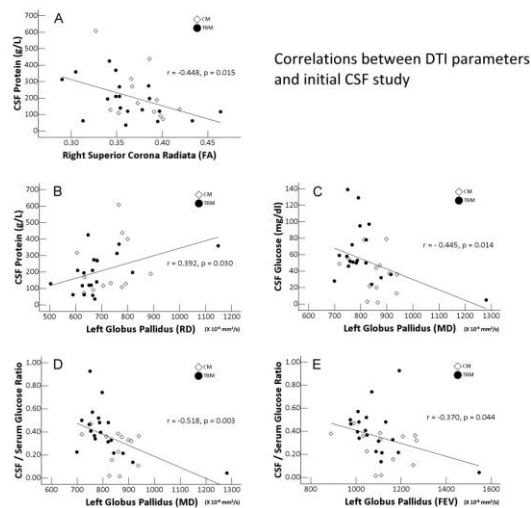


Figure 2. Correlation between DTI parameters and initial CSF study

#### CONCLUSION

HIV-negative TBM and CM survivors have significant WM damages. The correlations between decreased DTI indices and initial disease severity suggest that WM alterations may be involved in the psychopathology and pathophysiology of co-morbidities in chronic meningitis.

**KEY WORDS:** Diffusion tensor image, HIV-negative cryptococcal meningitis, HIV-negative tuberculous meningitis

#### P-28

##### Differentiation of Tumefactive Demyelinating Lesions from High-Grade Gliomas with Use of Diffusion Tensor Imaging

Toh, C.<sup>1</sup>Wei, K.<sup>1</sup>Wong, H.<sup>1</sup>Ng, S.<sup>1</sup>Lin, C.<sup>2</sup>Castillo, M.<sup>3</sup>

<sup>1</sup>Chang Gung Memorial Hospital, Linkou, TAIWAN,

<sup>2</sup>National Yang-Ming University, Taipei, TAIWAN,

<sup>3</sup>University of North Carolina, Chapel Hill, NC

#### PURPOSE

Tumefactive demyelinating lesions (TDLs) may be indistinguishable from high-grade gliomas on conventional MR imaging. The role of diffusion tensor imaging (DTI) in differentiating TDLs from high-grade gliomas is not clear and quantitative comparison between the two has not been reported. Here we aimed to differentiate TDLs from high-grade gliomas using DTI.

#### MATERIALS & METHODS

Diffusion tensor imaging was performed in eight TDLs and 13 high-grade gliomas. The presence of three findings [i.e., intralesional hyperintensities on fractional anisotropy (FA) map], restricted diffusion in lesion periphery and perilesional hyperintense FA rim were

assessed by visual inspection. The FA and MD values were measured in the central nonenhancing portion, peripheral enhancing portion and perilesional edema for each lesion and compared between two groups respectively.

#### RESULTS

Tumefactive demyelinating lesions had significantly higher incidence of intralesional hyperintensities on FA maps ( $P = 0.049$ ) but lower incidence of perilesional hyperintense FA rim ( $P < 0.001$ ), as compared with those of high-grade gliomas on visual inspection. Tumefactive demyelinating lesions had significantly higher FA ( $P = 0.004$ ) and lower MD ( $P = 0.001$ ) values in the peripheral enhancing portions of the lesions as compared with those of high-grade gliomas. In perilesional edema, FA values were significantly higher in high-grade gliomas ( $P = 0.001$ ).

#### CONCLUSION

Diffusion tensor imaging is helpful in differentiating TDLs from high-grade gliomas by using visual inspection and quantitative analysis.

**KEY WORDS:** Diffusion tensor imaging, tumefactive demyelinating lesion, high-grade glioma

#### P-29

##### BOLD Functional MR Imaging Mapping of First and Second Language Areas in Bilingual Patients with Brain Tumors

White, E.<sup>1</sup>Rigolo, L.<sup>1</sup>Tie, Y.<sup>1</sup>Golby, A.<sup>1</sup>Mukundan, S.

Brigham and Women's Hospital  
Boston, MA

#### PURPOSE

Functional magnetic resonance imaging (fMRI) is a powerful, noninvasive tool to map brain areas associated with task performance. Functional MRI commonly is used to identify critical cortical areas including language areas during presurgical mapping, and can contribute to physician confidence in resection of tumors near eloquent cortical regions. Differences in size and precise location of cortical activation attributable to first and second languages have been described in healthy subjects. For these reasons we hypothesized that different regions of activation also will be demonstrated for first and second languages in patients with brain tumors, hence, it would be important to map each language independently in bilingual patients for presurgical planning.

#### MATERIALS & METHODS

Four bilingual patients (age range 30-70 years) with left-sided brain lesions participated in this study, which was conducted under the auspices of the IRB. All subjects spoke English, Russian, Portuguese, and Italian were first languages in three of the four patients. English was the first language for the fourth patient fluent in sign language. Antonym generation and noun categorization tasks were performed by each subject in their first (L1) and second (L2) languages. Images were

acquired on a 3 T General Electric Signa scanner. Blood oxygenation level dependent (BOLD) fMRI data were analyzed using Statistical Parametric Mapping software (SPM5) and Matlab (MathWorks). The WFU Pickatlas was used to define language regions of interest (ROIs). The left-sided Brodmann areas 44 and 45 were used to create a Broca's ROI; left-sided supramarginal, angular, and posterior half of superior temporal gyri were used to create a Wernicke's ROI. Then the ROIs in the Montreal Neurological Institute (MNI) space were reverse-normalized to each patients' own brain space, taking into account the distorted brain anatomy caused by brain tumors.

## RESULTS

Nonidentical regions of activation attributable to first and second languages were demonstrated in all patients. The overall area of activation attributable to L2 was larger than the area attributable to L1 for all patients. Spatial overlap was seen for L1 and L2 activations located within the Broca's ROI. Conversely, distinct spatial mapping of L1 and L2 was observed within the Wernicke's ROI in three of four patients.

## CONCLUSION

Independent mapping of each language in bilingual patients is critical to identify eloquent regions and to avoid postoperative deficits. This is of particular importance in Wernicke's area due to spatial separation of L1 and L2 activations within this ROI. In addition data suggests that the areas of activation of L2 would be underestimated by mapping L1 alone.

**KEY WORDS:** Functional MR imaging, brain tumors

## P-30

### Mirror Neuron Abnormalities in Patients with First-Episode Schizophrenia

Saito, Y.<sup>1,2</sup>•Kubicki, M.<sup>2</sup>•Otsuka, T.<sup>2</sup>•Rathi, Y.<sup>2</sup>•Pasternak, O.<sup>2</sup>•Eckbo, R.<sup>2</sup>•Kikinis, Z.<sup>2</sup>•Clemm, C.<sup>2</sup>•Roppongi, T.<sup>2</sup>•Koerte, I.<sup>2</sup>•Kinoshita, T.<sup>1</sup>•Shenton, M.<sup>2</sup>

<sup>1</sup>Kansai Medical University, Osaka, JAPAN, <sup>2</sup>Harvard Medical School, Boston, MA

## PURPOSE

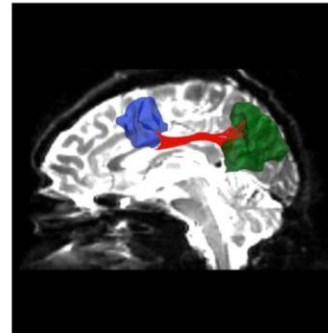
How can we access and understand the mind of others? Mirror neurons fire when an animal performs a goal-directed action and when it sees others performing the same action. Mirror neurons, insula, and some limbic structures provide the ability to empathize with others through the representation and "inner imitation" of the actions (facial expressions, body postures) of others. Dysfunction of mirror neurons may be one of the core deficits of socially isolating disorders such as autism and schizophrenia. The purpose of the current study is to identify and to evaluate mirror neuron integrity in patients with schizophrenia compared with healthy controls.

## MATERIALS & METHODS

Diffusion tensor imaging (DTI) scans were analyzed from 21 patients and 27 controls. Mean fractional

anisotropy (FA), trace (T), radial diffusivity, and axial diffusivity were measured from the mirror neuron tracts (Figure 1). The assessment of negative symptoms (SANS) and the assessment of positive symptoms (SAPS) were used to evaluate clinical symptoms.

Figure 1.



The mirror neurons (red) were extracted from the premotor area (blue) and the inferior parietal lobe (green).

## RESULTS

The primary findings of this study were that there was the group difference for the T of the mirror neurons between the schizophrenia patients and the controls ( $F(1, 46) = 4.207, p = .046, r^2 = .084$ ). There was no group difference for the FA but the scores of the severity of patients' symptoms which are related with the functions of mirror neurons, SANS - unchanging facial expressions ( $\rho = -0.50, p = .033, \rho = .558, p = .016$ ), global rating of affective flattening or blunting ( $\rho = -0.672, p = .002, \rho = .574, p = .013$ ), and ability to feel intimacy and closeness ( $\rho = -0.616, p = .007, \rho = .636, p = .005$ ) were correlated negatively with the FA and radial diffusivity of the tracts.

## CONCLUSION

Diffusion tensor imaging measures may not be apparent in first-episode schizophrenia but may be observed as the disease progresses. Our patients were first-episode subjects so maybe that was why we didn't have the group differences of the FA but the T. However, to our knowledge, no previous study has evaluated prospectively the clinical correlation between the severity of the first-episode schizophrenia patients' symptoms and the FA of the mirror neuron tracts. We revealed that the severity of patients' symptoms, SANS - unchanging facial expressions, global rating of affective flattening or blunting, and ability to feel intimacy and closeness were correlated negatively with the mirror neuron FA.

**KEY WORDS:** Diffusion tensor imaging, mirror neuron, schizophrenia



## P-31

### Mapping Microstructural Correlations of White Matter in the Human Brain Using Seed-Voxel Correlation Analysis of Diffusion Tensor Imaging

Shetty, C.<sup>1</sup>Li, Y.<sup>1</sup>Owen, J.<sup>1</sup>Malter Cohen, M.<sup>2</sup>Casey, B.<sup>2</sup>Mukherjee, P.<sup>1</sup>

<sup>1</sup>University of California San Francisco, San Francisco, CA, <sup>2</sup>Weill Cornell Medical College, New York, NY

#### PURPOSE

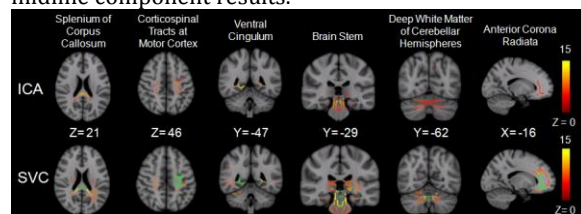
Microstructural correlations reflect phylogenetic and functional similarities between different white matter pathways. Independent component analysis (ICA) has been used on group diffusion tensor imaging (DTI) data to characterize spatial covariation of white matter microstructure across subjects. In addition to ICA, seed-voxel correlation (SVC) analysis often is used to detect functional connectivity in resting-state fMRI. These two methods are compared in a recent paper finding complementary, but not entirely overlapping, information. We demonstrate the first use of SVC on group DTI data to map white matter microstructural correlations and compare these novel results to those of ICA

#### MATERIALS & METHODS

Two hundred normal adult volunteers (mean  $26.4 \pm 6.5$  years, 108 men) underwent 3 T DTI with 55 directions at  $b = 1000$ . The fractional anisotropy (FA) values were computed using TBSS and we performed ICA as described. Due to our larger cohort, we estimated 50 independent components instead of 25. Seed regions for SVC were obtained from the largest cluster in each thresholded IC spatial map. The FA values in the seed region were averaged and the correlation was computed between the seed and every voxel on the FA skeleton. The Z scores for the IC maps were thresholded at 2.5 and the Z scores for the SVC maps were thresholded according to  $p < 0.05$ , with false discovery rate correction.

#### RESULTS

As in the recent ICA of DTI study, voxels with the strongest FA correlations in most IC spatial maps corresponded to anatomically distinct white matter tracts, tracts segments, and/or homologous pairs of tracts. In addition to the five main groups previously found, we identified another dominant feature that could be classified as prefrontal tracts, such as the anterior corona radiata. The figure shows a representative example from each group; the seed is shown in green for SVC maps. We found 36 similar SVC and ICA pairs; SVC confirmed unilateral, bilateral and midline component results.



#### CONCLUSION

In this study, we extended the findings by performing a higher dimensional ICA decomposition of normal white matter, demonstrating additional spatial correlations, such as in prefrontal fiber tracts. We also demonstrated that SVC can be used to map white matter microstructural correlations and produces results similar to ICA when the seed is derived from ICA. Advantages of SVC over ICA include the ability to perform hypothesis-driven mapping of microstructural correlations of specific white matter regions and the ability to specify a principled statistical significance threshold.

**KEY WORDS:** Diffusion tensor imaging, microstructural correlations, seed-voxel correlation

## P-32

### Progressive Multifocal Leukoencephalopathy MR Imaging Patterns in Multiple Sclerosis Patients Treated with Natalizumab: An Update of Natalizumab Progressive Multifocal Leukoencephalopathy MR Imaging Guidelines

Richert, N.<sup>1</sup>Yousry, T. A.<sup>2,3</sup>Pelletier, D.<sup>4</sup>Cadavid, D.<sup>1</sup>Gass, A.<sup>5</sup>Radue, E.<sup>6</sup>Filippi, M.<sup>7</sup>

<sup>1</sup>Biogen Idec, Cambridge, MA, <sup>2</sup>UCLH National Hospital for Neurology and Neurosurgery, London, England, UNITED KINGDOM, <sup>3</sup>UCL Institute of Neurology, London, England, UNITED KINGDOM, <sup>4</sup>Yale University School of Medicine, New Haven, CT, <sup>5</sup>University Hospital Mannheim, Mannheim, GERMANY, <sup>6</sup>University Hospital Basel, Basel, SWITZERLAND, <sup>7</sup>Scientific Institute and Vita-Salute University San Raffaele, Milan, ITALY

#### PURPOSE

To update existing guidelines for early diagnosis of progressive multifocal leukoencephalopathy (PML) with magnetic resonance imaging (MRI) based on common characteristics of PML and PML-related immune reconstitution inflammatory syndrome (IRIS) in natalizumab-treated multiple sclerosis (MS) patients. Natalizumab is an effective treatment in MS patients that is associated with a small but devastating risk of PML. Guidelines were published in 2006 to improve early diagnosis of PML using MRI. However, because of the small number of MS patients initially diagnosed with PML, the imaging criteria could be derived only from PML lesions in HIV patients. There is therefore an urgent need to assess the MR characteristics of PML in MS patients and to update the existing guidelines accordingly.

#### MATERIALS & METHODS

In the postmarketing phase, the first 40 cases of PML in natalizumab-treated MS patients were identified, of whom 22 (7 with IRIS) fulfilled the inclusion criteria for this study. The MR images were analyzed according to predefined criteria by five independent readers.

#### RESULTS

The typical, most frequent pattern in early PML patients is that of large (83%), confluent (94%), subcortical

(100%) lesions, a low signal on T1-weighted images (94%) and a high signal on T2-weighted (100%) and diffusion-weighted (DW) images (100%). The border is sharp towards the gray matter, and ill-defined towards the white matter (100%). Additionally, punctate T2 hyperintensities in the vicinity of PML lesions were observed in 72% of patients, and contrast enhancement was observed in 59-76% of the patients. Finally, T1 hyperintense signals were found during and after the IRIS phase but not in the PML phase.

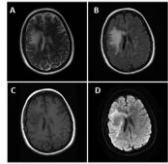


Figure 1. PML presentation. A, T2-weighted; B, FLAIR; C, T1-weighted precontrast; D, DW images

### CONCLUSION

For the purpose of screening and the essential early diagnosis of PML in MS patients treated with natalizumab, attention to characteristic MRI patterns, especially the subcortical location with destruction of U-fibers and the high-signal intensity on DWI, is critical. Finally, the T1 hyperintense signal could help differentiate PML from PML IRIS.

**KEY WORDS:** Progressive multifocal leukoencephalopathy (PML), natalizumab, PML diagnosis guidelines

### P-33

#### Long-Term Neuropsychological Sequelae in HIV-Negative Tuberculous Meningitis: A Cine MR Imaging Study

Hsu, N.<sup>1</sup>•Lu, C.<sup>1</sup>•Chen, M.<sup>1</sup>•Chen, H.<sup>1,2</sup>•Chang, C.<sup>1</sup>•Lin, W.<sup>1,2</sup>

<sup>1</sup>Kaohsiung Chang Gung Memorial Hospital, Chang Gung University College of Medicine, Kaohsiung, TAIWAN, <sup>2</sup>National Yang-Ming University, Taipei, TAIWAN

### PURPOSE

Tuberculous meningitis (TBM) is the most severe form of tuberculous infection, still complicated with neurologic deficits even with aggressive treatment. Cognitive dysfunction and hydrocephalus are the well known late sequelae of chronic TBM, but the relationship between them is not well studied yet. In this study we evaluate the relationship between cognitive dysfunction and hydrocephalus by cine MRI in TBM.

### MATERIALS & METHODS

There were 19 patients with TBM (15 males and 4 females; mean age 51.84 years old; from 21 to 78) and 37 age- and sex-matched healthy volunteers were enrolled. All subjects underwent complete neurologic examination, neuropsychological test and MRI study during follow up. The cine phase-contrast MRI technique was applied to all subjects to assess the dynamic CSF flow in the aqueduct by the following five parameters: peak positive velocity (PPV), peak negative

velocity (PNV), average positive flow (APF), average negative flow (ANF), and mean average flow (AF). Correlations among the cine MRI parameters, initial clinical presentation and presented neuropsychological rating score were assessed.

### RESULTS

The neuropsychological scores are worse in TBM patients than in normal controls. In cine MRI, the AF ( $p = 0.011$ ), APF ( $p = 0.002$ ), and ANF ( $p = 0.016$ ) in TBM group was significantly higher than normal controls, suggesting hydrocephalus (Figure 1). The higher CSF flow parameters were associated with declined neuropsychological rating score. The worse initial clinical presentations also were associated with poorer long-term cognitive function performance. There was no significant correlation between initial clinical profiles and CSF flow parameters.

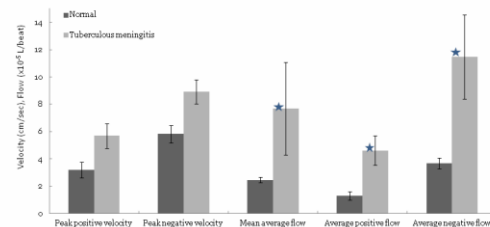


Figure 1 Comparison of Cine MRI parameters in TBM patients and normal control group. Significant difference between TBM and normal control in mean average flow ( $p=0.011$ ), average positive flow ( $p=0.002$ ) and average negative flow ( $p=0.016$ ).

### CONCLUSION

Neuropsychological dysfunction is a multifactor-related late complication in TBM. In addition to initial disease severity, chronic hydrocephalus might played an important role in long-term cognitive function performance. Using cine MRI for acquisition of CSF flow could help us to explore the relationship with the disease which may cause hydrocephalus and the neuropsychological sequelae.

**KEY WORDS:** Cine MR imaging, tuberculous meningitis, neuropsychological sequelae

### P-34

#### Neurolisteriosis: Not only Rhombencephalitis

Agostinis, C.•Rizzi, M.•Gritti, P.•Rottoli, M.•Manara, O.•Bonaldi, G.

Ospedali Riuniti  
Bergamo, ITALY

### PURPOSE

*Listeria monocytogenes* (LM), an anaerobic gram-positive intracellular bacillus, is a known cause of rhomboencephalitis due to anatomical predilection for this region. The presence of multiple cranial neuropathies and brainstem lesions on MR scan in a patient with central nervous system (CNS) infection can address the diagnosis of neurolisteriosis. We present



the imaging findings of our series of 24 patients with LM meningoencephalitis.

#### MATERIALS & METHODS

We reviewed the CT and MRI features of patients diagnosed of CNS infection by LM at our Hospital between January 2000 and October 2011. Inclusion criteria were: adults, with blood or cerebrospinal fluid (CSF) positive cultures for LM and symptoms of CNS infection.

#### RESULTS

Twenty-four patients were recruited, 15 men and 9 women, mean age 57 years (range 26-79). Ten patients (45.5%) were not immunocompromised. A CT scan of the brain was performed in all patients at onset, being altered in 25% of them. MR imaging the brain was obtained in 14 patients (56%) and showed abnormal findings in all but one of cases. Rhombencephalitis was present in all 13 MR-positive cases. Supratentorial lesions were found in eight patients. Meningeal enhancement was present in seven cases.

#### CONCLUSION

Because of the importance of early treatment in the prognosis of this potentially fatal condition, LM meningoencephalitis must be suspected promptly in patients with symptoms of CNS infection associated with lower cranial nerve deficits and infratentorial involvement on MR examination. In our experience, however, concomitant supratentorial lesions can be in some cases confounding, making the diagnosis more difficult. The conditions we considered most frequently in the differential diagnosis were acute disseminated encephalomyelitis, Behcet disease, sarcoidosis, multiple sclerosis and Whipple disease.

**KEY WORDS:** *Listeria monocytogenes*, MR imaging, meningoencephalitis

#### P-35

##### **Differentiation of Pyogenic Brain Abscesses from Necrotic Glioblastomas with Use of Susceptibility-Weighted Imaging**

Toh, C.<sup>1</sup>Wei, K.<sup>1</sup>Wong, H.<sup>1</sup>Lin, C.<sup>2</sup>

<sup>1</sup>Chang Gung Memorial Hospital, Linkou, TAIWAN,

<sup>2</sup>National Yang-Ming University, Taipei, TAIWAN

#### PURPOSE

The presence of hypointense rim at the lesion margins on T2-weighted imaging (T2WI) is a common imaging feature of brain abscesses and necrotic glioblastomas. The prevalence and morphology of the hypointense rims have never been studied using susceptibility-weighted imaging (SWI) with greater sensitivity to magnetic susceptibility. We aimed to differentiate abscesses from glioblastomas by assessing the morphology of their lesion margin using SWI

#### MATERIALS & METHODS

T2-weighted imaging and SWI were performed in eight abscesses and 20 rim-enhancing glioblastomas. On

T2WI and SWI, the prevalence and the border types (complete vs incomplete) of hypointense rim were assessed by visual inspection. On SWI, the contour (smooth vs irregular) and the location of hypointense rims relative to the contrast-enhancing rim, as well as the prevalence of dual rim sign, defined as two concentric rims at lesion margin, with the outer one being hypointense and the inner one hyperintense were analyzed further.

#### RESULTS

The prevalence and the border types of hypointense rim on T2WI were not different between abscesses and glioblastomas. On SWI, there were significantly greater proportion of hypointense rims that were complete ( $P < 0.001$ ), smooth ( $P < 0.001$ ) and having same location as the contrast-enhancing rim ( $P < 0.001$ ). A dual rim sign was present in nine abscesses but absent in all of the glioblastomas ( $p < 0.001$ ).

#### CONCLUSION

Susceptibility-weighted imaging can differentiate pyogenic abscesses from necrotic glioblastomas. Dual rim sign is the most specific imaging features distinguishing the two.

**KEY WORDS:** Susceptibility-weighted imaging, brain abscess, glioblastoma

#### P-36

##### **Immuno-Serologically Negative Pachymeningitis Associated with Immunoglobulin G4 (IgG4)-Related Disease**

KAN, I.<sup>1,2</sup>Matsumoto, M.<sup>1</sup>Yasue, M.<sup>1</sup>Sakamoto, A.<sup>1</sup>Abe, T.<sup>2</sup>

<sup>1</sup>Omori Red Cross Hospital, Tokyo, JAPAN, <sup>2</sup>Jikei University School of Medicine, Tokyo, JAPAN

#### PURPOSE

Immunoglobulin (Ig) G4-related disease is a recently defined disease entity that is characterized by elevated serum IgG4 levels and extensive IgG4-positive plasma cell infiltration of various organs. The purpose is to report a rare case of pachymeningitis with extensive IgG4-positive plasma cell infiltration; despite the serum IgG and IgG4 level have not increased.

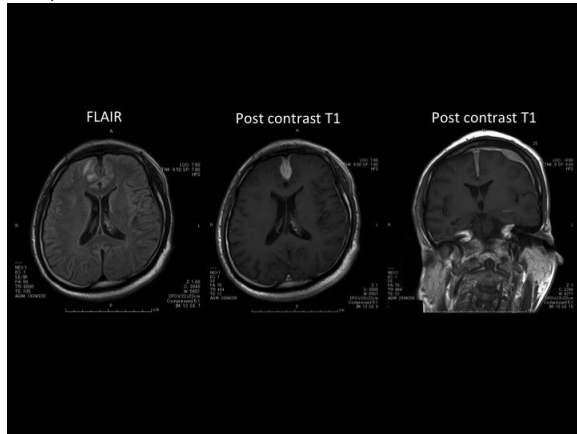
#### MATERIALS & METHODS

A 42-year-old male with a history of diabetes presented with a month-long headache. MR imaging showed thickening of dura matter and extraaxially nodular mass. Immunoserological examination, including serum IgG and IgG4, were all within normal range. Thus, biopsy of the extraaxial nodule, which supposed to hypertrophic change of dura matter, was performed for diagnosis. In pathologic finding, hematoxylin-eosin (H-E) stain showed that extensive infiltration of inflammatory cells (e.g., lymphocyte, plasma cells) was observed. Immunohistochemical staining showed prominent IgG-positive plasma cell infiltration as well as IgG4-positive cell. The ratio of IgG4-/IgG-positive plasma cells is more than 70%. According to those

finding, steroid therapy was started with 30 mg of oral prednisolone, and follow-up MRI showed that hypertrophic change of dural matter was improved.

## RESULTS

MR imaging showed that near-circumferential thickening of the dura mater and a 2 cm extraaxial nodular mass at the left convexity area, which were isointense on T1 images, hypointense on T2 images and demonstrated enhancement following administration of gadolinium. There was associated edema at bi-frontal lobe, which is close to falx cerebri.



## CONCLUSION

Recently, there has been an increasing number of reports describing the relationship of hypertrophic pachymeningitis and IgG4-related disease. As mentioned before, characteristics of IgG4-related disease are elevated serum IgG4 levels and extensive IgG4-positive plasma cell infiltration of various organs. However, it is rare that prominent IgG-positive plasma cell infiltration is observed under the situation that the serum IgG and IgG4 level have not increased. Examination and biopsy, considering IgG4-related disease, should be planned even if the serum IgG and IgG4 levels have not increased.

**KEY WORDS:** IgG4 related disease, pachymeningitis

## P-37

### Progressive Multifocal Leukoencephalopathy with Discrete Involvement of Pyramidal Tract

Umino, M.·Maeda, M.·Matsushima, N.·Tomimoto, H.

Mie University School of Medicine  
Tsu, JAPAN

## PURPOSE

Progressive multifocal leukoencephalopathy (PML) is a demyelinating disease caused by reactivation of JC virus in immunosuppressed patients. The diagnosis usually is inferred from imaging and confirmed by cerebrospinal fluid (CSF) polymerase chain reaction (PCR) for JC virus DNA. To date, PML with discrete involvement of the pyramidal tract has been described in only two patients. This report describes a case with PML showing discrete involvement of a pyramidal tract on T2-weighted and FLAIR images, which was difficult to distinguish from

tumors such as lymphomatosis cerebri and gliomatosis cerebri.

## MATERIALS & METHODS

A 61-year-old woman with systemic lupus erythematosus, hepatocellular carcinoma, and diabetic mellitus developed a progressive right hemiparesis for several months. MR imaging sequences included T1-weighted imaging, FLAIR imaging, T2-weighted imaging, diffusion-weighted imaging (DWI), contrast-enhanced T1-weighted imaging, and MR spectroscopy (MRS). The patient underwent brain biopsy followed by CSF PCR analysis of JC virus DNA.

## RESULTS

Brain MR imaging showed high-intensity lesions predominantly involving the left temporal lobe white matter. Lesions extended along the left pyramidal tract into brain stem (Figures 1A, 1B). No contrast enhancement of lesions was observed. Diffusion-weighted imaging showed a high signal partially in the lesions. MR spectroscopy revealed a decreased NAA and increased choline. Based on clinical information and MR imaging findings, the tentative diagnoses included PML and brain tumor such as gliomatosis cerebri and lymphomatosis cerebri. Brain biopsy revealed no tumor cells but instead showed demyelinated brain tissue with large nucleated cells. Cerebrospinal PCR revealed JC virus infection leading to the diagnosis of PML.

Fig. 1A

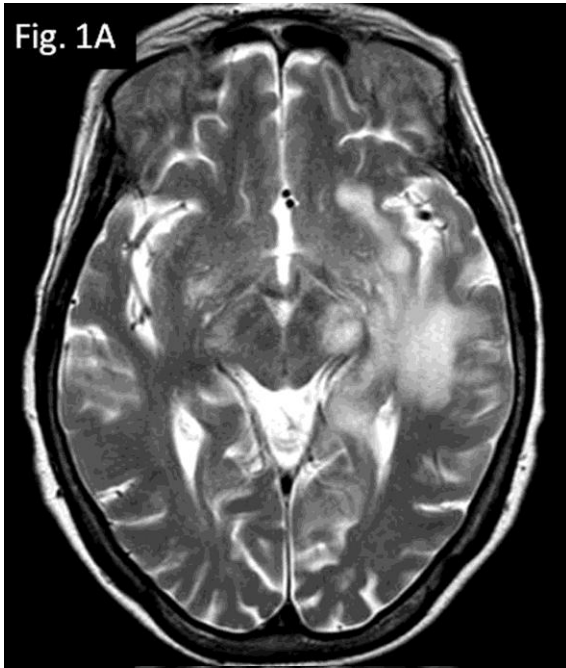
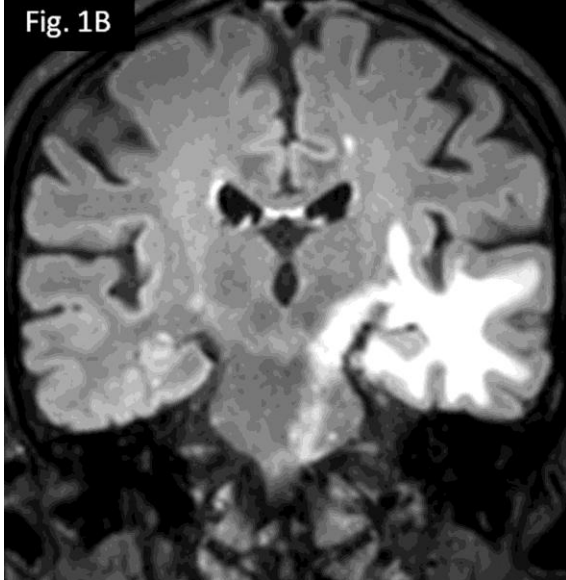


Fig. 1B



### CONCLUSION

The present case underscores the difficulty of making a differential diagnosis between PML and a brain tumor. It is noteworthy that discrete involvement of pyramidal tract is apparent in PML.

**KEY WORDS:** PML, MR imaging, pyramidal tract

### P-38

#### Structure Deficits and Chronic Cognitive Impairments in Tuberculous Meningitis

Chen, H.<sup>1,2</sup>•Lu, C.<sup>1</sup>•Chen, P.<sup>1</sup>•Chang, C.<sup>1</sup>•Hsu, N.<sup>1</sup>•Chou, K.<sup>2</sup>•Lin, C.<sup>2,2</sup>•Lin, W.<sup>1,2</sup>

<sup>1</sup>Kaohsiung Chang Gung Memorial Hospital, and Chang Gung University College of Medicine, Kaohsiung, TAIWAN, <sup>2</sup>National Yang-Ming University, Taipei, TAIWAN

### PURPOSE

Chronic neuropsychological sequelae may occur in patients with tuberculous meningitis (TBM). Impact of structural abnormalities in TBM patients on clinical performance is unknown. We applied “diffeomorphic anatomical registration using exponentiated lie algebra” (DARTEL) voxel-based morphometry (VBM) to determine whether gray matter deficits on TBM are associated with acute presentations and chronic cognitive impairments.

### MATERIALS & METHODS

Magnetic resonance imaging (MRI) and neuropsychological tests were conducted on 17 patients with TBM, and 17 age-, sex-, and education-matched healthy subjects. Various demographic, clinical, and laboratory findings at presentation were evaluated. Differences in gray matter volume (GMV) between patient and normal subjects were investigated using DARTEL-VBM to determine which structural abnormalities existed. The severity of disease was scored by clinical profiles and imaging findings. Correlations among structural deficits, disease severity, and diminished cognitive functioning were assessed.

### RESULTS

The patient groups performed worse neuropsychological subtests than healthy controllers. Compared to healthy subjects, TBM patients showed smaller GMV in right thalamus, right caudate head, right superior and middle temporal gyrus, right precuneus, and left putamen ( $P < 0.001$ , uncorrected). The smaller GMV in right thalamus, right superior temporal gyrus, right precuneus, left putamen, and right caudate ( $P < 0.05$ ) were associated further with declined cognitive function. The worse disease severity, based on clinical profile and conventional MRI findings at the time of admission, is correlated with smaller GMV in right caudate head ( $P < 0.05$ ).

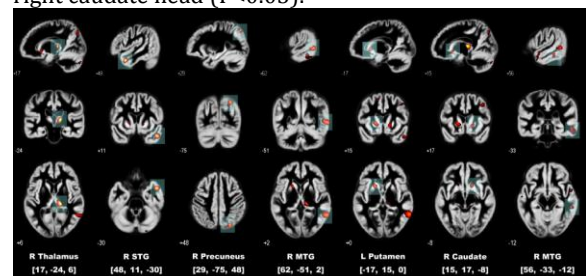
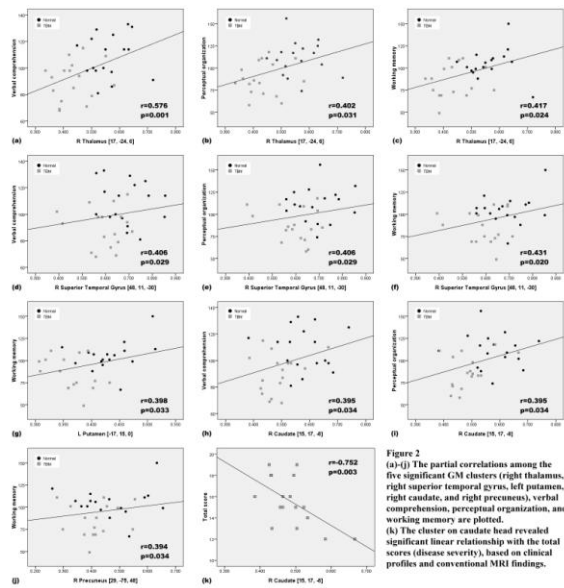


Figure 1. Smaller gray matter volumes (GMV) in TBM patients versus normal subjects, with highlighted significant areas in right thalamus, right superior and middle temporal gyrus, right precuneus, and right caudate ( $p < 0.001$ , uncorrected). R = right, STG = superior temporal gyrus, MTG = middle temporal gyrus.



## CONCLUSION

Initial disease severity of TBM is associated with vulnerably structure damages and subsequent neuropsychological consequences. Early diagnosis and early treatment are essential for long-term cognition function preservation.

**KEY WORDS:** Tuberculous meningitis

## P-39

### Man vs Machine - Validation of the Qualitative Imaging Feature Set VASARI Using Volumetric Analysis by 3 D Slicer of the TCGA GBM Dataset: A TCGA Glioma Phenotype Research Group Project

Gutman, D. A.<sup>1</sup>Huang, E.<sup>2</sup>Flanders, A.<sup>3</sup>Mikkelsen, T.<sup>4</sup>Scarpace, L.<sup>4</sup>Holder, C.<sup>1</sup>Hwang, S.<sup>1</sup>Aurora, T.<sup>1</sup>Jolesz, F. A.<sup>5</sup>Saltz, J.<sup>1</sup>Colen, R.<sup>5</sup>TCGA Glioma Phenotype Research Group, ..<sup>2</sup>

<sup>1</sup>Emory University, Atlanta, GA, <sup>2</sup>National Cancer Institute, Bethesda, MD, <sup>3</sup>Thomas Jefferson, Philadelphia, PA, <sup>4</sup>Henry Ford Hospital, Detroit, MI, <sup>5</sup>Brigham and Womens Hospital, Boston, MA

## PURPOSE

Glioblastoma (GBM) was the first tumor to undergo comprehensive genetic analysis as part of the NCIs The Cancer Genome Atlas (TCGA). Clinical images were collected in The Cancer Imaging Archive (TCIA) to augment this genomic repository. While volumetric analysis is likely more precise, the current tooling available to support such analysis (e.g., 3D SLICER, MIPAV, etc.) require a significant amount of domain expertise. Thus, volumetric analysis remains difficult in clinical practice, and qualitative assessments of imaging features are still critical, particularly if they have clinical relevance. The purpose of this study was to assess the correlation between semiquantitative image (human-generated) features generated by the current gold standard (i.e., neuroradiologists) against quantitative imaging volumetric measurements (machine-aided).

## MATERIALS & METHODS

Each image was assessed by at least three independent neuroradiologists who recorded a set of 30 imaging features describing the size, location, and morphology of the tumor. To perform a systematic evaluation of these images, a set of qualitative imaging features (the VASARI feature set) was developed which included a visual assessment of key features of the MRI data. For practical reasons, a number of these imaging features were scored visually including the contribution of individual tumor compartments (e.g., the necrotic component, the contrast enhancing portion, edematous component, and noncontrast enhancing tumor) to the overall tumor volume. For each tumor, radiologists reviewed a series of images which included a T1 axial image both before and after gadolinium contrast administration, and a T2 axial FLAIR image. These features involved the trained neuroradiologists estimating the total volume of abnormal tissue noted on the image stack. Estimating from within the mass of abnormal tissue four compartments were defined as the percentage of tumor that showed contrast enhancement, the proportion of tumor showing no-contrast enhancement, the proportion of the volume that appeared to be necrotic tissue, and the proportion of the estimated volume that appeared to be edematous tissue. In parallel, we performed volumetric analysis using the 3 D slicer platform to quantitatively measure actual volumes of each individual region. The flair-volume, contrast-enhancing region, and necrotic core were independently segmented and verified by a trained neuroradiologist (RRC).

## RESULTS

Univariate linear regressions of the volumetric contrast-enhancing portion, edema, and necrosis measurements upon the neuroradiologist-generated contrast enhancing, edema, and necrosis estimates respectively, were performed. These analyzes indicated very strong correlations between the volumetric and human measurements (p-value < 0.0001 in each case).

## CONCLUSION

This study, which included consensus reads by three neuroradiologists in 75 patients, indicated a high-degree of concordance between these two methodologies. Given that quantitative volumetry is not performed in every day cancer clinical practice, this work suggests that clinical visual semiquantitative estimations of tumor volume are both reproducible and valid.

**KEY WORDS:** Glioblastoma, TCGA, volumetrics

## P-40

### Is Quantitative Information from Advanced MR Imaging and from Fluorodeoxyglucose- and Methionine-Positron Emission Tomography Analogous in Malignant Gliomas?

Kitajima, M.<sup>1</sup>Hirai, T.<sup>1</sup>Nakamura, H.<sup>1</sup>Uetani, H.<sup>1</sup>Iwashita, K.<sup>1</sup>Makino, K.<sup>1</sup>Nakashima, R.<sup>2</sup>Shigematsu, Y.<sup>1</sup>Nishimura, S.<sup>1</sup>Shiraishi, S.<sup>1</sup>Kuratsu, J.<sup>1</sup>Yamashita, Y.<sup>1</sup>

<sup>1</sup>Kumamoto University, Kumamoto, JAPAN, <sup>2</sup>Japanese Red Cross Kumamoto Health Care Center, Kumamoto, JAPAN

## PURPOSE

Multimodality advanced imaging, specifically magnetic resonance (MR) dynamic susceptibility contrast (DSC) perfusion-, diffusion-weighted imaging (DWI) and positron emission tomography (PET) imaging using <sup>18</sup>F-fluorodeoxyglucose (FDG) and <sup>11</sup>C-methionine (MET) can provide useful information about the proliferative potential and clinical prognosis in patients with malignant gliomas. However, the reciprocal correlation between those MR imaging and PET imaging findings has not been evaluated fully. Our aim was to assess the correlation of the quantitative parameters derived from MR DSC perfusion-weighted imaging and DWI with PET imaging using FDG and MET in patients with malignant gliomas.

## MATERIALS & METHODS

As part of a clinical audit, we reviewed 3 T MRI data from DSC perfusion imaging and DWI and FDG and MET PET imaging data in 25 patients with histologically proven malignant gliomas (12 glioblastomas, 5 anaplastic astrocytomas, 7 anaplastic oligodendrogliomas, 1 anaplastic oligoastrocytoma). The indices characterizing solid lesions were the ratio of the lesional maximum relative cerebral blood volume (rCBV) to the contralateral normal-appearing white matter (max rCBV ratio), the ratio of the minimum lesional apparent diffusion coefficient (ADC) to the contralateral white matter (min ADC ratio), and the ratio of the lesional maximum standardized uptake (SUVmax) to the uptake in the contralateral normal-appearing gray matter (L/Nmax) on FDG and MET PET scans. Spearman's rank order correlation test was used to analyze the relationship between the data derived from MR (max rCBV and min ADC ratios) and L/Nmax PET using FDG and MET.

## RESULTS

There was a strong significant positive correlation between the min ADC ratio and L/Nmax on FDG PET ( $r = -0.718$ ,  $p = 0.0004$ ). The other pairs with a significant correlation were the max rCBV ratio and L/Nmax on MET PET ( $r = 0.681$ ,  $p = 0.001$ ), and the max rCBV ratio and L/Nmax on FDG PET ( $r = 0.583$ ,  $p = 0.004$ ).

Spearman's rank order correlation between each MR parameter and L/Nmax on PET

		PET	
		L/N max FDG PET	L/N max MET PET
MR	min ADC ratio	$r = -0.718$ , $p = 0.0004$	$r = 0.583$ , $p = 0.004$
	max rCBV ratio	$r = -0.393$ , $p = 0.059$	$r = 0.681$ , $p = 0.001$

## CONCLUSION

Quantitative parameters derived from advanced MRI and PET scans of malignant glioma correlated with each other. As potential imaging biomarkers for the metabolism of malignant gliomas, quantitative

information from DWI and DSC may be analogous to FDG and MET PET information.

**KEY WORDS:** Glioma, MR imaging, positron emission tomography

## P-41

### Differentiating Malignant Central Nervous System Lymphoma from Glioblastoma: Assessment Using Arterial Spin Labeling, Diffusion-Weighted Imaging and <sup>18</sup>F-fluorodeoxyglucose Positron Emission Tomography

Yamashita, K. Yoshiura, T. Hiwatashi, A. Togao, O. Kikuchi, K. Abe, K. Maruoka, Y. Mizoguchi, M. Yoshimoto, K. Honda, H.

Kyushu University  
Fukuoka, JAPAN

## PURPOSE

Differentiation between malignant central nervous system (CNS) lymphoma and glioblastoma is sometimes difficult on conventional MR images, while their discrimination is essential for the therapeutic decision. Previous reports have revealed the usefulness of apparent diffusion coefficient (ADC) value derived from diffusion-weighted imaging, dynamic susceptibility contrast perfusion MR imaging and <sup>18</sup>F-fluorodeoxyglucose positron emission tomography (FDG PET). Arterial spin labeling (ASL) is a noninvasive and quantifiable method for blood flow measurement and has been reported to be useful in differentiating high- and low-grade gliomas. Our purpose was to evaluate the diagnostic performance of ASL, ADC and FDG PET in differentiating malignant CNS lymphomas from glioblastomas.

## MATERIALS & METHODS

A total of 59 patients including 22 with malignant CNS lymphoma (mean age,  $65.4 \pm 10.4$  years) and 37 with a pathologically proven glioblastoma (mean age,  $58.5 \pm 16.7$  years) were enrolled in this study. Arterial spin labeling was performed using a pulsed ASL method at a 3 T unit. An absolute tumor blood flow (aTBF) was measured as a mean blood flow value within a region-of-interest drawn in the tumor. In addition, a relative tumor blood flow (rTBF) was obtained by normalizing the aTBF by a blood flow measured in the normal-appearing cortical gray matter in the contralateral hemisphere. The aTBF and rTBF values, minimum ADC (ADCmin), and maximum standard uptake value (SUVmax) by using FDG PET were compared between glioblastomas and malignant lymphomas using Mann-Whitney U test. In addition, the area under the ROC curves (AUC) value for the discrimination between glioblastoma and malignant lymphoma was calculated with the aTBF, rTBF, ADCmin and SUVmax, respectively.

## RESULTS

The aTBF, rTBF and ADCmin values were significantly higher in glioblastomas (mean aTBF  $\pm$  SD =  $91.6 \pm 56.0$  mL/100 g/min, mean rTBF  $\pm$  SD =  $2.61 \pm 1.61$ , mean ADCmin  $\pm$  SD =  $0.78 \pm 0.19 \times 10^{-3}$  mm<sup>2</sup>/s) in comparison

with malignant lymphomas (mean aTBF  $\pm$  SD =  $40.9 \pm 16.4$  mL/100 g/min, mean rTBF  $\pm$  SD =  $1.27 \pm 0.37$ , mean ADCmin  $\pm$  SD =  $0.60 \pm 0.13 \times 10^{-3}$  mm<sup>2</sup>/s) ( $p < 0.005$ , respectively). In addition, SUVmax value was significantly lower in glioblastomas (mean SUVmax  $\pm$  SD =  $13.1 \pm 6.34$ ) in comparison with malignant lymphomas (mean SUVmax  $\pm$  SD =  $21.3 \pm 8.11$ ) ( $p < 0.005$ ). The AUC values for the aTBF, rTBF, ADCmin and SUVmax were 0.855, 0.793, 0.779 and 0.802, respectively.

#### CONCLUSION

Our results demonstrated that aTBF and rTBF obtained with ASL technique as well as ADCmin and SUVmax provide useful information to differentiate between malignant CNS lymphoma and glioblastoma. The aTBF showed the highest AUC value among the 4 measurements.

**KEY WORDS:** CNS lymphoma, glioblastoma, arterial spin labeling

#### P-42

##### **Imaging of Metastatic Brain Tumors after Gamma Knife Radiosurgery on Principle of Echo-Shifting with a Train of Observation: Preliminary Report**

Wakata, Y. Ando, K. Odawara, S. Mori, M. Igarashi, Y. Katsuura, T. Ishikura, R. Hirota, S.

Hyogo College of Medicine  
Nishinomiya city, Hyogo, JAPAN

#### PURPOSE

The signal voids "dark spots" are observed in metastatic brain tumors on PRESTO (principle of echo-shifting with a train of observation) of MRI, suggesting intratumoral microhemorrhage and they increase after gamma knife radiosurgery (GKR). The aim of this study is to clarify the relationship between the tumor prognosis and "dark spots" on PRESTO in metastatic brain tumors after gamma knife radiosurgery.

#### MATERIALS & METHODS

Fourteen metastatic brain tumors in seven patients 7-80 years (mean: 61.3 years, 4 male and 3 female) were involved in this study. The primary cancers were lung cancer (4 cases), renal cell carcinoma (1 case), colon cancer (1 case). The principle of echo-shifting with a train of observation and contrast-enhanced T1-weighted (CET1WI) images were acquired in all cases using 3 T Achieva (Phillips, Best, Nederland) on pre GKR, 1 month after GKR, and on follow up (5-28 months, mean: 11.7 months). We evaluated the tumor size on CET1WI and compared it to "dark spots" in tumor on PRESTO.

#### RESULTS

On images of pre GKR, tumor size was 2.9 to 24.9 mm (mean 10.3 mm) on CE-T1WI, and "dark spots" on PRESTO was observed in 6/12 tumors. On images of 1 month after GKR, the tumors decrease in size, 2.1 to 23.3 mm (mean 8.6 mm). "Dark spots" on PRESTO increased and observed in 11/14 tumors (78.6%). On

the follow-up images, when the tumor size decreased or had no changes (10/14, 71.4%) compared to 1 month after GKR, "dark spots" increased (7/10, 70%) or had no change (3/10, 30%). But when the tumor size increased (4/14, 28.6%), "dark spots" decreased (4/4, 100%).

#### CONCLUSION

"Dark spots" on PRESTO increases in metastatic brain tumors after GKR, suggesting the effect of GKR. Decrease of "dark spots" in metastatic brain tumor on follow-up images may indicate tumor regrowth.

**KEY WORDS:** PRESTO, metastatic brain tumor, gamma knife

#### P-43

##### **Lymphomas, Glioblastomas and Metastatic Tumors: Differences in the Apparent Diffusion Coefficient Evaluated with High b-Value Diffusion-Weighted MR Imaging at 3 T**

Yamasaki, F. Kajiwar, Y. Watanabe, Y. Takayasu, T. Nosaka, R. Sugiyama, K. Kurisu, K.

Hiroshima University Hospital  
Hiroshima, JAPAN

#### PURPOSE

The usefulness of the apparent diffusion coefficient (ADC) obtained from diffusion-weighted images (DWI) for a differential diagnosis among glioblastoma, metastatic tumors, and primary central nervous system lymphoma is controversial. We assessed whether high b-value DWI at b 4,000 s/mm<sup>2</sup> could discriminate among them. We also compared the power of high- (b-4,000) and standard b-value (b-1,000) imaging on a 3 T magnetic resonance (MR) instrument.

#### MATERIALS & METHODS

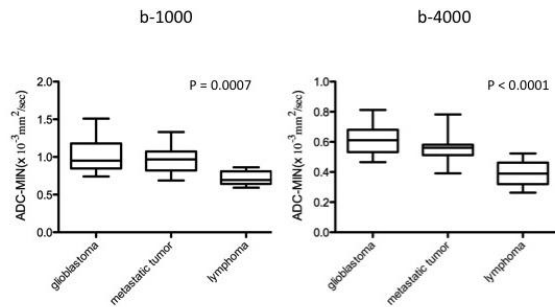
This study was approved by our institutional review board. We acquired DWI at 3 T with b = 1,000 and b = 4,000 s/mm<sup>2</sup> in 10 patients with lymphoma, 10 patients with metastatic tumors, and 14 patients with glioblastoma. The ADC was measured by placing multiple regions of interest (ROI) on ADC maps of the site of enhanced lesions on contrast-enhanced T1-weighted MR images. We avoided hemorrhagic and cystic lesions by using T1-, T2-, FLAIR-, and T2\* MR images. The ADC value of each tumor was determined preoperatively from several ROI and expressed as the minimum, mean, and maximum ADC value (ADC MIN, ADC MEAN, ADC MAX). We evaluated the relationship between ADCs and histologic information including tumor cellularity.

#### RESULTS

The ADC MIN of glioblastomas ranged from 0.741 to  $1.510 \times 10^{-3}$  mm<sup>2</sup>/sec at b-1,000 and from 0.465 to  $0.812 \times 10^{-3}$  mm<sup>2</sup>/sec at b-4,000. In metastatic tumors these values ranged from 0.687 to  $1.330 \times 10^{-3}$  mm<sup>2</sup>/sec at b-1,000 and from 0.391 to  $0.782 \times 10^{-3}$  mm<sup>2</sup>/sec at b-4,000 and in lymphomas they ranged from 0.592 to  $0.863 \times 10^{-3}$  mm<sup>2</sup>/sec at b-1,000 and from 0.263 to  $0.523 \times 10^{-3}$  mm<sup>2</sup>/sec at b-4,000. All ADC



values were associated statistically with tumor cellularity. Apparent diffusion coefficient MIN at b-4,000 was associated with tumor cellularity more significantly than ADC-MIN at b-1,000. All ADC values were lower for lymphomas than glioblastomas and metastatic tumors and the statistical difference was larger at b-4,000 than b-1,000. However, there was no statistical difference in the ADC of glioblastomas and metastatic tumors at either b-1,000 or b-4,000.



#### CONCLUSION

Calculating the ADC value is useful for distinguishing lymphoma from glioblastoma and metastatic tumors. The lowest degree of overlapping and a better inverse correspondence with tumor cellularity were obtained with ADC MIN at b-4,000 s/mm<sup>2</sup> at 3 T MRI.

**KEY WORDS:** Diffusion-weighted imaging, high b value, apparent diffusion coefficient

#### P-44

### 3 D Volume Intensity Histogram Analysis Predicts Tumor Outcome in Patients Treated by Surgery and Radiation Therapy for Metastatic Brain Lesions

Izadi, K.·Rahmanuddin, S.·Christian, S.·Cen, Y.·Ferre, J.·Martinez, M.·Aguilera, A. L.·Shiroishi, M. S.·Kim, M. J.·Kim, P. E.·Law, M.

Keck School of Medicine, University of Southern California  
Los Angeles, CA

#### PURPOSE

Metastatic lesions of the brain can be treated by both surgical resection and concurrent radiation therapy. The difficulty arises in separating posttreatment recurrence of tumor versus radiation necrosis along the surgical cavity when enhancement is visualized on follow-up MR. Using 3 D volume intensity histogram curves, we compared the enhancement patterns in patients with tumor recurrence versus radiation necrosis.

#### MATERIALS & METHODS

Using retrospective analysis of imaging reports, we obtained a list of 14 patients who had enhancing, metastatic lesions in the brain from a nonbrain primary tumor. Primary malignancies included breast, renal cell, lung and testicular carcinomas. These patients were treated by both complete surgical resection followed by radiation (gamma or cyber knife). They all had at least

one follow-up MRI of the brain at least 3 months following treatment that revealed suspicious enhancement along the surgical margins. Of the 14 patients, seven had tumor recurrence (3 pathologically proven) and seven had radiation necrosis based on no change or improvement in imaging findings on continued MRI surveillance. 3 D volume intensity histogram curves were used to analyze the enhancement patterns in these 14 patients along the surgical cavities. Baseline and follow-up MR images and tumor treatment outcome were reviewed from a 3 to 36 months interval. T1 pre and postcontrast images were postprocessed and ROI were drawn including all postgadolinium-enhanced part by using the Fuji 3D advanced imaging software. Average, maximum and minimum volume intensity values were compared after surgery and radiation treatment follow up.

#### RESULTS

Based on our volume intensity histogram curves, there was a statistically significant difference ( $p < .01$ ) in the mean value in the patients with tumor recurrence (976  $\pm$  435 AU) versus the patients with radiation necrosis (246  $\pm$  394 AU). There was also a statistically significant difference ( $p = .03$ ) in the maximum value in the tumor recurrence group (1824  $\pm$  1111 AU) versus the patients with radiation necrosis (605  $\pm$  620 AU). Lastly, there was also a statistically significant difference ( $p = .01$ ) in the minimum values between the tumor recurrence group (362  $\pm$  277 AU) and the radiation necrosis group (-48  $\pm$  186 AU).

#### CONCLUSION

Values extracted from 3 D volume intensity histogram analysis could help to differentiate tumor recurrence versus radiation necrosis in treated brain metastases.

**KEY WORDS:** Histogram, volume, intensity

#### P-45

### Added Value of Proton MR Spectroscopy in the Differentiation of Primary Central Nervous System Lymphoma from Other Solid Enhancing Lesions

Yoon, W.·Kim, S.·Jeong, M.·Kang, H.

Chonnam National University Hospital  
Gwangju, KOREA, REPUBLIC OF

#### PURPOSE

The purpose of this study was to evaluate the added value of proton MR spectroscopy (MRS) in the differentiation of primary central nervous system lymphoma (PCNSL) from other solid-enhancing lesions, compared with conventional MR imaging only.

#### MATERIALS & METHODS

Conventional MR imaging and proton MRS obtained from 14 patients with PCNSL (7 men and 7 women; mean age, 63 years) and 48 patients with other solid-enhancing lesions (28 high-grade gliomas, 10 metastases, and 10 tumefactive demyelinating lesions) were evaluated retrospectively. Ratios of Lac+Lip/Cr were calculated and thresholds between PCNSL and

other enhancing lesions were selected with receiver operating characteristic (ROC) curves. The diagnostic accuracy of conventional MR imaging plus proton MRS for differentiating PCNSLs from other solid-enhancing lesions was compared with that of conventional MR imaging alone.

#### RESULTS

The median Lac+Lip/Cr ratios of PCNSL were significantly higher than that of other solid-enhancing lesions (6.65 versus 2.85;  $P < 0.0001$ ). From ROC curve analysis, the cut-off value at 4.48 Lac+Lip/Cr provided 92.9% sensitivity and 70.8% specificity for the diagnosis of PCNSL. The diagnostic accuracy of conventional MR imaging plus proton MRS was also significantly higher than that of conventional MR imaging alone (87.1% vs 75.8%,  $P = 0.008$ ).

#### CONCLUSION

The characteristic increase of Lac+Lip/Cr ratio on proton MRS provides valuable information to differentiate PCNSL from other solid-enhancing brain lesions.

**KEY WORDS:** Lymphoma, MR spectroscopy, brain tumor

#### P-46

##### **Clinical Value of Concurrent Use of MR Spectroscopy and Perfusion MR Imaging for Differentiating Demyelinating Lesions from Neoplasm**

Goss, J. • Mendelsohn, D. B. • Patel, R. • Yetkin, Z. F.

University of Texas Southwestern Medical Center  
Dallas, TX

#### PURPOSE

Demyelinating diseases of the brain may present as a brain mass that is indistinguishable from brain neoplasms on clinical exam and conventional MR imaging. Furthermore, proton MR spectroscopy (MRS) findings of some demyelinating lesions may be similar to gliomas. In these challenging cases, perfusion MR imaging (MRP) may provide additional information that may improve noninvasive diagnosis of these lesions. The aim of the present study was to evaluate the clinical value of concurrent use of MRS and MRP in distinguishing demyelinating lesions from neoplasms.

#### MATERIALS & METHODS

Charts of patients who underwent MRS and MRP for evaluation of brain lesion were reviewed. Data included relevant history, MRS and MRP findings, and histopathologic exam results.

#### RESULTS

Fifty-two patients, aged from 17 to 76 years, underwent MRS and MRP to evaluate brain lesions. All patients had biopsy of the brain lesion to establish a final diagnosis. Seventeen patients had demyelinating disease and 35 patients had glial tumors. MR spectroscopy findings showed increased choline/creatine for both demyelinating and neoplastic lesions. Twenty-nine patients with glial tumors showed increased regional

cerebral blood volume (rCBV). Three patients with glial tumors showed increased choline/creatine and normal rCBV. Normal choline/creatine and increased rCBV was observed in three patients with glioma. Eleven cases of demyelination showed minimal to significantly decreased rCBV. Six cases of demyelination showed perfusion findings similar to that of contralateral normal brain.

#### CONCLUSION

Concurrent use of MRS and MRP provides advantage over conventional MR imaging in distinguishing demyelinating lesions from neoplasm.

**KEY WORDS:** MR spectroscopy, MR perfusion, adult brain

#### P-47

##### **Positron Emission Tomography Findings of Pituitary Adenomas: Different Uptake of Atypical Adenomas**

Tomura, N. • Ikeda, H. • Saginoya, T.

Southern TOHOKU Research Institute for Neuroscience  
Koriyama, JAPAN

#### PURPOSE

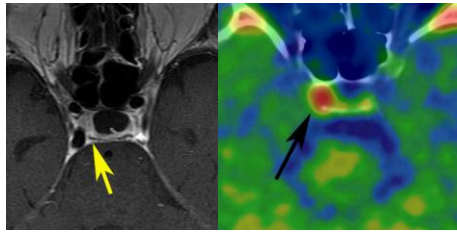
Findings of positron emission tomography (PET) using  $^{18}\text{F}$ -fluorodeoxyglucose (FDG) and  $^{11}\text{C}$ -methionine (MET) in cases of pituitary adenomas are presented.

#### MATERIALS & METHODS

Positron emission tomography CT using FDG and MET was performed in 69 patients with pituitary adenomas. They include nine patients with atypical pituitary adenoma (MIB-1 index; 3%). After the CT scan, PET imaging using MET (MET PET) was performed 20 min after injection of MET. Positron emission tomography using FDG (FDG PET) was injected 60 min. after MET PET. Fluorodeoxyglucose PET was performed 90 min after the injection of FDG. Coregistered images were displayed on a workstation. Fusion images with MRI also were made. The maximum of standardized uptake value (SUVmax) of both FDG and MET of the adenomas was measured and compared with that of normal pituitary gland in patients with suspected tumors of the brain ( $n = 42$ ). The SUVmax of both FDG and MET in atypical pituitary adenomas was compared with that of other adenomas.

#### RESULTS

The SUVmax of MET and that of FDG in patients with pituitary adenomas was  $3.8 \pm 2.4$  and  $6.5 \pm 7.8$ , respectively. It was significantly ( $p < 0.001$ ) higher than that (the SUVmax of FDG and MET was  $2.1 \pm 0.9$  and  $3.3 \pm 0.7$ , respectively) in normal pituitary gland. There was a significant difference ( $p < 0.001$ ) of SUVmax of MET and FDG between atypical adenomas (SUVmax of MET =  $5.9 \pm 2.4$ , SUVmax of FDG =  $13.5 \pm 12.1$ ) and other adenomas (SUVmax of MET =  $3.5 \pm 2.2$ , SUVmax of FDG =  $5.5 \pm 6.5$ ).



#### CONCLUSION

Both FDG PET and MET PET provide more information in the diagnosis of pituitary adenomas, and they also are feasible to differentiate atypical adenomas from other adenomas.

**KEY WORDS:** Pituitary adenoma, PET

#### P-48

##### Rating Scale of Combined Conventional and Advanced MR Imaging in Differentiating Tumor Progression from Posttreatment Change (Preliminary Study)

Wongsripumtet, J.·Tritrakarn, S.·Boosaruxapong, K.·Sangruchi, T.·Witthiwei, T.·Veerasarn, V.·Chawalparit, O.

Siriraj Hospital, Mahidol University  
Bangkok, THAILAND

#### PURPOSE

The radiographic differentiation of brain tumor recurrence from posttreatment change is difficult and remains a challenge for radiologists and neurologists. The conventional MR imaging (MRI) and different advanced MRI techniques offer the potential information that may help to distinguish between these two conditions. Aim of our study was to combine findings in both conventional MRI and advanced MRI and using multiparametric scoring system to determine recurrent disease in patients with treated gliomas.

#### MATERIALS & METHODS

Posttreatment 3 T conventional and advanced MR imaging (perfusion MRI, DWI and MR spectroscopy) were obtained in 10 patients (5 male and 5 female) who were diagnosed with glioma and previously treated with surgery or combined surgery with chemoradiation. The findings on conventional MRI were evaluated in terms of degree of perilesional edema (mild< 50%, moderate 50-75 % and severe >75% ), pattern of enhancement (thin linear, thick linear or nodular enhancement), hemorrhage and new enhancing lesion. Apparent diffusion coefficient (ADC) ratio, regional cerebral blood flow and blood volume (rCBF and rCBV), MR spectroscopy, Choline/Creatine, Choline/N-acetyl-aspartate ratio (Cho/Cr and Cho/NAA ratio) within the lesions compared with contralateral normal white matter were evaluated and calculated for the optimum cut-off point based upon thresholds derived from our own data. All data were correlated to final diagnoses established by histopathologic and MR imaging follow up. Each finding was scored as positive (one point, except for severe edema, rating was 2 points) and

negative (zero point). The combined multiparametric scores (0 to 8) were analyzed and found the optimal cut-off point to improve diagnostic accuracy for diagnosis of recurrent glioma.

#### RESULTS

Moderated to severe perilesional edema, hemorrhage and new enhancing lesion are associated highly with recurrent glioma on conventional MRI ( $p = 0.046, 0.038$  and  $0.038$ , respectively). Thick linear and nodular enhancements occurred in 4/5 (80%) recurrent glioma and 1/5 (20%) posttreatment cases ( $p = 0.15$ ). We found the optimum threshold for rCBV = 1 (sensitivity = 75%, specificity = 100%), rCBF = 0.8 (sensitivity = 75%, specificity = 66.7%), ADC ratio = 2 (sensitivity = 50%, specificity = 50%) but could not get the appropriate cut-off point for Cho/Cr and Cho/NAA in our study. Combined multiparametric score of conventional MRI and advanced MRI of 2/8, the sensitivity and specificity for detection of recurrent tumor was 83.3% and 100%, respectively. If we used the data from previous published study, the Cho/Cr or Cho/NAA ratio with diagnostic value greater than 2 on MRS will give high accuracy for diagnosis of recurrent tumor (sensitivity and specificity > 85%) as optimum value in our study, the multiparametric scores threshold of 3/9 yielding high diagnostic accuracy (sensitivity = 83.3%, specificity = 100%) for prediction of tumor recurrence or posttreatment change.

#### CONCLUSION

Combination findings from conventional and advanced MRI has potential to improve overall diagnostic accuracy in differentiating tumor progression from the posttreatment change.

**KEY WORDS:** Glioma, posttreatment change, conventional and advanced MR imaging

#### P-49

##### Regional Definition of High-Grade Glioma by Using 3D Imaging Volume Intensity Histogram Analysis

Martinez, M.

University of Southern California  
Los Angeles, CA

#### PURPOSE

Currently, GBM is characterized and followed by using size measurements of the enhancing lesion both pre and posttreatment. At this point, the outer FLAIR positive portion associated with lesions is not being characterized. We propose the use of 3D volumetric histogram analysis as a parameter to define the three different regions of GBM, inner necrotic portion, active enhancing portion, and peripheral most aspect of the lesion which may be described as possible tumor vs edema.

#### MATERIALS & METHODS

Imaging reports were reviewed retrospectively and nine patients were selected who demonstrated the classic appearing GBM lesion. Patients who had no

baseline imaging or who had anything other than the classic appearing GBM were excluded. T1 postcontrast and FLAIR images were reviewed on baseline MRIs and regions of interest (ROI) were placed over all three regions using the Fuji 3D advanced imaging software. 3D volume intensity histogram curves then were obtained and used to define the regions of the GBM, the central defined as "necrotic" regions, enhancing tumor defined as "perinecrotic" region and the peripheral flair positive edematous defined as "progression" region. Average, maximum and minimum volume intensity values in all three regions were compared. Paired T-tests were used to explore the difference in average, maximal and minimal volume intensity (VI) histogram values between the normal, necrotic, perinecrotic and progression regions. Bonferroni adjustment for multiple testing also performed.

## RESULTS

Results showed that the average VI is significantly higher in perinecrotic region compare to necrotic and progression region. There is also a significant difference in VI between the necrotic region and the "progression" region (perinecrotic-  $2552.5 \pm 1213.5$ , necrotic-  $977.5 \pm 527.8$  and "progression"- $1217.5 \pm 495.5$ ). These differences are seen even after Bonferroni adjustment for multiple testing ( $\alpha$  reduced to 0.008).

## CONCLUSION

3D volume intensity histogram is an important tool to define the region of GBM lesion on both pre and posttreatment imaging. This may be a better parameter than direct size measurements to evaluate response to treatment.

**KEY WORDS:** GBM, 3D- volume intensity analysis

## P-50

### Central Nervous System and Head/Neck Histiocytoses: Spectrum of Imaging Findings in 26 Patients

Shah, S. Sedrak, P. Guha-Thakurta, N. Ketonen, L. Williams, M. D. Debnam, J. M.

M.D. Anderson Cancer Center  
Houston, TX

## PURPOSE

The histiocytoses are a rare collection of diseases characterized by the proliferation of histiocytes, a component of the mononuclear phagocyte system, that can cause tumor formation and destructive changes. The purpose of this study is to review the imaging appearances of the histiocytoses in the central nervous system (CNS) and the head/neck region.

## MATERIALS & METHODS

CT, MR and PET/CT studies of the brain, maxillofacial region/neck, and spine were reviewed in 26 patients with pathologically proven histiocytosis. The studies were evaluated for the presence of disease in the following locations: intraaxial and extraaxial intracranial compartments, calvarium, skull base, sella,

orbit, paranasal sinuses, spine, and the head and neck region.

## RESULTS

Specific diseases included Rosai-Dorfman disease (n = 12), Erdheim-Chester disease (n = 7), Langerhans cell histiocytosis (n = 5), juvenile xanthogranuloma (n = 1), and malignant histiocytosis (n = 1). The most common locations of the histiocytoses were the intraaxial intracranial compartment, calvarium/skull base, and the orbits. Imaging characteristics included FLAIR hyperintense foci with enhancing components in the brainstem, cerebellum and periventricular white matter. Histiocytoses of the calvarium, skull base, and orbits demonstrated enhancing lesions as did disease involving the extraaxial intracranial compartment, sella, paranasal sinuses, spine, and tongue base.

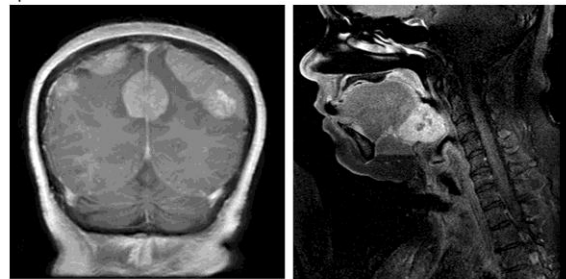


Figure 1: Coronal post contrast image demonstrates large bilateral extra-axial masses (Erdheim-Chester)

Figure 2: Sagittal post contrast image demonstrates enhancing tongue base mass (malignant histiocytosis)

## CONCLUSION

The histiocytoses have variable imaging appearances in the CNS and the head/neck region. Neuroradiologists should be aware of the spectrum of findings and thus avoid mistaking them for other disease processes.

**KEY WORDS:** Histiocytosis, Langerhans cell histiocytosis, Rosai-Dorfman

## P-51

### Differentiating Glioblastoma from Metastasis with Pretreatment Dynamic Contrast-Enhanced MR Imaging Perfusion

Vaisfeld, J. A.<sup>1,2</sup> Shah, A. D.<sup>1</sup> Patel, G. V.<sup>1</sup> Peck, K. K.<sup>1</sup> Karimi, S.<sup>1</sup> Holodny, A. I.<sup>1</sup> Young, R. J.<sup>1</sup>

<sup>1</sup>Memorial Sloan-Kettering Cancer Center, New York, NY, <sup>2</sup>Charite Universitaetsmedizin Berlin, Berlin, GERMANY

## PURPOSE

Glioblastoma multiforme and brain metastasis are the two most common forms of malignant brain tumors. Conventional MRI has limited capacity to differentiate between these entities, both of which usually present as enhancing mass lesions. The purpose of this study is to determine whether T1-weighted dynamic contrast-enhanced (DCE) MRI perfusion is useful in discriminating glioblastoma from metastasis.

## Materials & Methods

T1-weighted DCE MRI perfusion was performed in 30 patients with untreated solitary contrast-enhancing brain tumors (15 glioblastomas and 15 metastases)

before surgical resection. Dynamic contrast-enhanced MRI perfusion was acquired using an axial 3D spoiled gradient-recalled acquisition in the steady-state sequence with following parameters: TR/TE = 3.2/1.1 ms, 128 x 128 matrix, 3 mm slice thickness, 25 flip angle. The data were processed on an off-line workstation using Nordiclce (NordicNeuroLab, Milwaukee, Wis). Absolute metrics and ratios normalized to the contralateral white matter were measured using region-of-interest analysis in the enhancing tumor and nonenhancing peritumoral abnormality for following perfusion parameters: 1) volume transfer coefficient for leakage of contrast from plasma volume to extravascular extracellular space (K12 or Ktrans); 2) reflux of contrast back to plasma space (k21); 3) plasma volume (Vp); 4) extracellular volume (Ve); 5) area under the DCE curve (AUC); and 6) wash-in rate. Statistical analysis was performed using Wilcoxon rank-sum tests with  $p = .05$ .

## RESULTS

The peritumoral wash-in ratio was significantly different between glioblastoma (median = .726) and metastasis (median = .573) with  $p < .05$ . The remaining peritumoral measurements and normalized ratios, and all the tumoral measurements and normalized ratios were not significant with  $p > .19$  and  $p > .15$ , respectively.

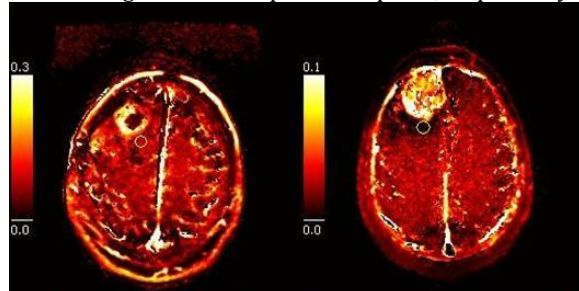


Figure: Wash-in map for patient with glioblastoma (left) and metastasis (right). ROI is placed in the peritumoral edema. The peritumoral wash-in ratio is significantly higher in glioblastoma as compared to metastasis.

## CONCLUSION

These results suggest that the peritumoral wash-in ratio can differentiate between glioblastoma and metastasis. None of the perfusion parameters of the enhancing part of the tumor reached statistical significance. The wash-in ratio is a measure of the slope of the kinetic curve and may reflect increased vascularity in the peritumoral abnormality of glioblastoma, which is expected to harbor vasogenic edema and infiltrating tumor cells with relatively intact vascularity. In contrast, the peritumoral abnormality of metastasis only contains bland vasogenic edema that may decrease vascularity due to compression of the microcirculation from excessive fluid in the extravascular space. Further work is necessary to better define the optimal imaging strategy to noninvasively distinguish between glioblastoma and metastasis, and in particular the role of DCE MRI perfusion for diagnosis and prognostication.

**KEY WORDS:** Perfusion brain, glioblastoma, metastasis

## P-52

### Diffusion Tensor Imaging in Erdheim-Chester Disease

Guha-Thakurta, N. Wang, J. Ketonen, L. Ketonen, L. Debnam, J. M.

M.D. Anderson Cancer Center  
Houston, TX

## PURPOSE

To evaluate the changes in white matter fiber tract patterns using diffusion tensor imaging (DTI) in Erdheim-Chester disease (ECD).

## MATERIALS & METHODS

Retrospective review of MR brain imaging in biopsy proven ECD cases presenting to our institution from 2005-2011 was performed. Fractional anisotropy (FA) and apparent diffusion coefficient (ADC) were measured in white matter (WM) tracts including the transverse pontine fibers. Serial FA and ADC measurements were obtained over time, before and after initiation of treatment. Additionally, fiber tracking of the WM tracts in relation to the lesion was performed using DTI tractography tool.

## RESULTS

Intracranial ECD lesions can be infiltrative or focal. White matter tracts demonstrate alteration in the region of the lesions. Following successful treatment, restoration of the normal fiber tract morphology was observed. Fractional anisotropy values were reduced at presentation, but recovered following response to treatment. These changes were concordant with the tractography analysis of white matter tracts. Apparent diffusion coefficient values also decreased after institution of therapy.

## CONCLUSION

The normal WM fiber tract patterns are altered in intracranial ECD at presentation, and restored following appropriate therapy. Early response in FA and ADC may serve as an imaging biomarker to assess treatment response.

**KEY WORDS:** Erdheim-Chester disease, brain, diffusion tensor imaging

## P-53

### Diffusion-Weighted Imaging of Intracranial Myeloid Sarcomas

Guha-Thakurta, N. Langford, L. A. Debnam, J. M.

M.D. Anderson Cancer Center  
Houston, TX

## PURPOSE

Intracranial myeloid sarcoma is a rare tumor comprised of extramedullary accumulation of immature myeloid cells. Herein we describe the common and atypical imaging features of these tumors and their characteristics on diffusion-weighted imaging (DWI).



## MATERIALS & METHODS

Retrospective review of MR imaging, including DWI, of the brain was performed of cases diagnosed with intracranial myeloid sarcomas at our institution from 2005-2011.

## RESULTS

Intracranial myeloid sarcomas typically present as extraaxial masses. Parenchymal lesions are less common, demonstrate homogeneous enhancement on postcontrast images and exhibit restricted diffusion. Ring-enhancing appearance has not been reported before and can occur either in the presence or absence of systemic infection. Such lesions do not demonstrate restricted diffusion and thus can be differentiated from pyogenic abscesses.

## CONCLUSION

The diagnosis of intracranial myeloid sarcoma can be a challenge and a high index of suspicion is warranted in cases with atypical imaging features. Diffusion-weighted MRI characteristics vary based on the morphology of the lesion and can be helpful in ascertaining the appropriate diagnoses in clinically complex patients.

**KEY WORDS:** Myeloid sarcoma, granulocytic sarcoma, intracranial

## P-54

### Relative Insensitivity of T1 Gradient Echo MR Imaging at 3 T to Low Concentrations of Contrast: In Vitro Validation

Cloran, F. J. • Mamourian, A. C.

University of Pennsylvania Medical Center  
Philadelphia, PA

## PURPOSE

The inherent low soft tissue T1 contrast on MR at 3T imaging led to replacement of spin echo T1 imaging with gradient echo (GRE) techniques at most sites. This occurred without critical evaluation of their relative merits. While 3T MR was promoted as increasing conspicuity of contrast agents, theoretical and experimental studies suggest there may be decreased contrast sensitivity on 3D GRE sequences relative to spin echo sequences at low gadolinium concentrations. Anecdotally, we noticed contrast enhancement of brain lesions appeared less conspicuous when imaged at 3T than 1.5T at our institution. To determine the magnitude of this effect, we compared signal to background in a phantom using magnetization-prepared rapid gradient-echo imaging (MP-RAGE) at 3T and conventional T1 spin-echo imaging at 1.5T over a wide range of gadolinium concentrations using our clinical scanners.

## MATERIALS & METHODS

Starting with a solution of gadobenate dimeglumine (MultiHance, 0.25mmol MultiHance/L distilled water), we filled a series of nine plastic tubes with sequential dilutions from 0.25 mmol/L to 0.00125 mmol/L; a

phantom control of distilled water also was used. Based on pilot testing, we found these phantoms approximated the range of visible contrast seen on typical MR examinations. These tubes were imaged in a control water bath using our standard GRE technique (MP-RAGE TR 1760, TI 950.0, TE 3.1) for the 3T unit and a fat-suppressed spin-echo T1-weighted sequence (TR 476.0, TE 9.5) at 1.5T. Relative contrast was calculated by subtracting the local average signal intensity of the adjacent water bath from the signal intensity of each tube determined with our PACS tools (Figure 1).

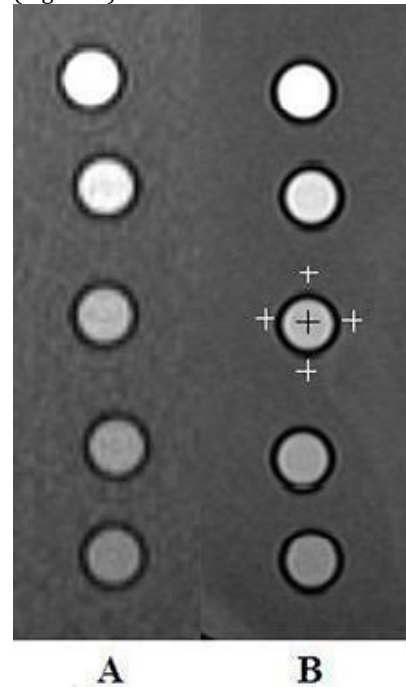


Figure 1. Representative phantoms in decreasing order of osmolality from 0.25mmol/L to 0.0625mmol/L imaged at 3T utilizing our MP-RAGE sequence (Column A) and at 1.5 T utilizing our fat-suppressed spin echo T1-weighted sequence (Column B). "+" connotes where signal intensities were sampled for assessment of the phantom and water bath signal intensities.

## RESULTS

At 3T and 1.5T, there was a linear relationship between concentration of gadolinium and relative signal intensity on both sequences and scanners. At the highest concentration, 0.25mmol/L, relative contrast was higher (104%) on the GRE technique at 3T than T1 spin echo at 1.5T. However, at subsequent dilutions, relative contrast was much lower at 3T compared with 1.5T, i.e., 73% at 0.025mmol/L and 66% at 0.00125mmol/L.

## CONCLUSION

Our phantom data support theoretical and clinical observations that conspicuity of low concentrations of gadolinium enhancement is superior at 1.5T using conventional spin echo T1 technique compared with 3D GRE technique at 3T. This has significant implications



for the primary detection at 3 T of lesions that cause interruption of the blood-brain barrier as well as follow-up imaging of lesions at 3T when previous imaging was performed at 1.5T.

**KEY WORDS:** Gradient recall echo, MP-RAGE, contrast

**P-55**

### Multiparametric Classification of BOLD Hyperoxia and Dynamic Susceptibility Contrast Maps: Study of the Healthy Brain

Aizenstein, O.<sup>1</sup>·Artzi, M.<sup>1,2</sup>·Abramovitch, R.<sup>3</sup>·Hendler, T.<sup>1,2</sup>·Ben Bashat, D.<sup>1</sup>

<sup>1</sup>Tel Aviv Sourasky Medical Center, Tel-Aviv, ISRAEL, <sup>2</sup>Tel Aviv University, Tel-Aviv, ISRAEL, <sup>3</sup>Hadassah Hebrew University Medical Center, Jerusalem, ISRAEL

#### PURPOSE

Blood-oxygenation level-dependent(BOLD) contrast and dynamic susceptibility contrast(DSC) imaging are used commonly to evaluate brain hemodynamics. Aim of this study was to use unsupervised multimodal classification on combined data of BOLD hyperoxia challenge and DSC imaging, in order to characterize brain tissue vascularity and regional differences between brain lobes and hemispheres in healthy subjects.

#### MATERIALS & METHODS

**Subjects and scan parameters:** Eight healthy subjects were included(28±4 years). MR imaging scans were performed on a 3.0T GE scanner. Hyperoxia challenge induced using inhalation of carbogen(95%O<sub>2</sub>+5%CO<sub>2</sub>), with room-air at baseline. Dynamic susceptibility contrast images were acquired during injection of a double dose Gd-DOTA. **Data analysis** was performed using SPM5 and FSL software. Hyperoxia challenge: preprocessing included timing and motion corrections. A statistical mask( $p \leq 0.05$ ) was calculated using first-level GLM analysis. Percent signal change( $\Delta S$ ) maps were calculated for voxels which passed the statistical threshold. Dynamic susceptibility contrast data: cerebral blood volume and flow(CBV/CBF), mean-transit-time(MTT), time-to-peak(TTP) and signal-recovery(SR) maps were calculated using PENGUIN and FSL software. A KMeans, unsupervised multimodal clustering, was applied on all parameters for each subject. Volumes of interest(VOI) were defined on right and left hemispheres, and four brain lobes.

#### RESULTS

**Brain clusters:**Tissue clustering results are presented in Figure 1. The three clusters were classified as major blood-vessels and dura(BvasD-red), gray-matter(GM-green) and white-matter(WM-blue), approved by a senior neuroradiologist. Means and standard deviations of the hemodynamic indices obtained in three clusters are given in Table 1. Gray matter/WM ratio was higher for the  $\Delta S$  relative to the DSC data sets. **Brain lobe differences:**Significantly longer TTP values were found in the occipital relative to all other lobes. Significant differences between brain lobes were detected for rCBV

and rCBF with: Temporal>Occipital>Frontal/Parietal. **Brain hemisphere asymmetry:**A trend of higher vascularity was detected in the GM of the right versus left hemispheres, in the rCBV and  $\Delta S$ .

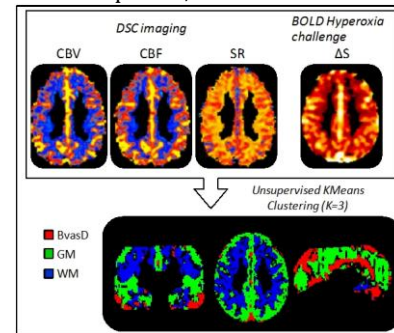


Table 1: hemodynamic values.

Hemodynamic index	BvasD	GM	WM
DSC_rCBV <sub>relative units</sub>	1.84±0.10	1.14±0.06	0.53±0.02
DSC_rCBF <sub>relative units</sub>	1.44±0.11	1.22±0.06	0.58±0.02
DSC_MTT <sub>sec</sub>	8.09±1.56	5.5±1.02	5.60±1.22
DSC_TTP <sub>sec</sub>	10.5±1.37	9.54±0.95	10.16±1.05
DSC_SR <sub>%</sub>	72±3	87±2	94±1
BOLD_ΔS <sub>%</sub>	7.51±1.45	2.98±0.49	1.14±0.26

#### CONCLUSION

In this study we integrated several hemodynamic parameters obtained from two independent methods in order to study the vascular properties of the healthy brain. This provides comprehensive information which may be used by future studies to improve characterization of the hemodynamic features as baseline for the healthy and pathologic brain.

**KEY WORDS:** Multiparametric classification, dynamic susceptibility contrast, hyperoxia

**P-56**

### Structural Deficits in the Emotion Circuit and Cerebellum Are Associated with Depression, Anxiety and Cognitive Dysfunction in Methadone Maintenance Patients: A Voxel-Based Morphometric Study

Lin, W.<sup>1,2</sup>·Chou, K.<sup>2</sup>·Chen, H.<sup>1</sup>·Chen, C.<sup>1</sup>·Lin, C.<sup>2</sup>

<sup>1</sup>Chang Gung University, Kaohsiung Chang Gung Memorial Hospital, Kaohsiung, TAIWAN, <sup>2</sup>National Yang-Ming University, Taipei, TAIWAN

#### PURPOSE

Heroin users on methadone maintenance treatment (MMT) have elevated rates of comorbid depression and are associated with higher relapse rates for substance abuse. Structural abnormalities in MMT patients have been reported but their impact on clinical performance is unknown.

#### MATERIALS & METHODS

We investigated differences in gray matter volume (GMV) between 27 MMT patients and 23 healthy

controls by voxel-based morphometry and correlated the differences with Beck Depression Inventory, Beck Anxiety Inventory scores, and diminished cognitive functioning.

## RESULTS

Methadone maintenance treatment patients exhibited higher emotional deficits than healthy subjects. There was significantly smaller GMV in multiple cortices, especially in the left inferior frontal gyrus and left cerebellar vermis in the MMT group. The smaller GMV in the prefrontal cortices, left subcallosal cingulate gyrus, left postcentral gyrus, left insula, and right cerebellar declive correlated with worse depression scores. The smaller GMV in the prefrontal cortices, left subcallosal cingulate gyrus, and left postcentral gyrus also correlated with worse anxiety scores, while the smaller GMV in the cerebellum and bilateral insula was associated with worse executive performance.

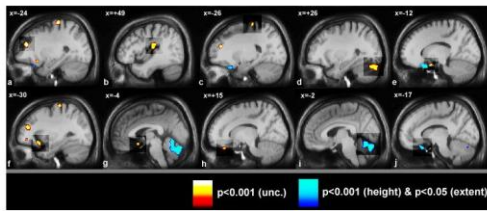


Figure 1. Hot colormap: uncorrected  $p < 0.001$ , Cold colormap: uncorrected  $p < 0.001$  with cluster extent correction family-wise error (FWE) corrected  $p < 0.05$ , clusters overlap with partial uncorrected  $p < 0.001$  clusters. a: Left medial frontal gyrus, BA9; b: Right insula, BA13; c: Left postcentral gyrus, BA3; d: Right cerebellar declive; e: Left subcallosal cingulate gyrus, BA34; f: Left insula, BA13; g: Left anterior cingulate gyrus, BA25; h: Right inferior frontal gyrus, BA11; i: Left cerebellar vermis; j: Left inferior frontal gyrus, BA47

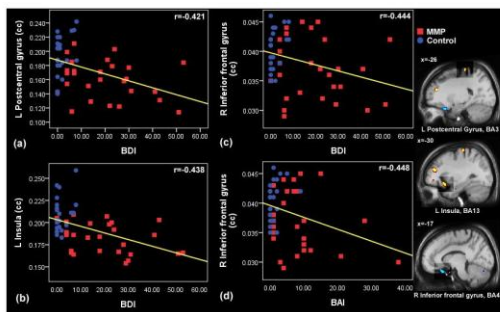


Figure 2. Correlations between depression and anxiety symptom ratings and gray matter volume. BDI, Beck Depression Inventory; BAI, Beck Anxiety Inventory. a, regional volume of the left post-central gyrus significantly negatively correlated with BDI; b, regional volume of the left insula significantly negatively correlated with BDI; c, regional volume of the right inferior frontal gyrus significantly negatively correlated with BDI; d, regional volume of the right inferior frontal gyrus significantly negatively correlated with BAI

## CONCLUSION

These results reveal that MMT patients have GMV changes of certain brain regions hypothesized to influence cognition and emotion and might thus be involved in the psychopathology of those comorbidities in MMT.

**KEY WORDS:** Cingulate gyrus, heroin, voxel-based morphometry

## P-57

### Improving Accuracy and Reproducibility of Quantification of Brain Volume by Multispectral MR Imaging

Chen, C. C. C.<sup>1</sup>•Chen, H.<sup>2</sup>•Chai, J.<sup>1</sup>•Chen, S.<sup>3</sup>•Lee, S.<sup>1</sup>•Chang, C.<sup>3</sup>

<sup>1</sup>Taichung Veterans General Hospital, Taichung, TAIWAN, <sup>2</sup>Hungkuang University, Taichung, TAIWAN, <sup>3</sup>University of Maryland, Baltimore, MD

## PURPOSE

Quantification of brain volume is one of the medical diagnosis basis rules on brain disease. Recently, a new application of independent component analysis (ICA) implemented with support vector machine (SVM) has been investigated to perform in multispectral MR image analysis for classifying tissues and quantifying brain volume. However, it generally performs slice by slice in which case training samples are slice-dependent. Each slice requires its own specific training samples and training samples obtained from one slice are not applied to another slice. This study develops a volume-based technique, called volume sphering analysis (VSA) which can process all MR image slices as an image cube using only one set of training samples obtained from a single image slice to perform image classification on all image slices. To evaluate the accuracy, reproducibility, and speed of the proposed VSA method for quantifying gray and white matters with respect to ICA implemented with SVM.

## MATERIALS & METHODS

Synthetic data from the BrainWeb Simulated Brain Database and real normal brain MR data of ten healthy volunteers (mean age  $41.4 \pm 9.6$  years old) were used to evaluate the accuracy and reproducibility of gray matter (GM), white matter (WM) volume measurements by using the proposed method to analyze three sets of T1-weighted, T2-weighted and proton density images.

## RESULTS

The mean processing times of seven synthetic data sets (different noise levels) were  $462.6 \pm 60.2$  seconds for ICA implemented with SVM and  $42.9 \pm 0.2$  seconds for VSA classification. Intra and interoperator coefficients of variation (CVs) in WM/GM volume measurements were 3.2%/5.6% and 3.8%/7.2% for ICA implemented with SVM and 1.5%/2.0% and 1.9%/2.3% for VAS methods.

## CONCLUSION

Our experimental results revealed significantly high accuracy and reproducibility of the VSA method in classification of synthetic and clinical brain data. The preliminary results also save significant effort in multislice MR image classification.

**KEY WORDS:** Brain volume, quantification, volume sphering analysis



moderate or severe, by comparing the amount of fluid on either side of the nerve with the diameter of the nerve itself.

### RESULTS

The results showed that flattening of the posterior sclera and intraocular protrusion of the optic nerve were significantly more likely to be found in patients with papilledema than in controls across all readers ( $p$  values  $<0.001$ ). A moderate or severe amount of subarachnoid fluid was more likely to be seen in patients with papilledema, but this was only statistically significant for one expert reader. The sensitivity of flattening of the posterior sclera for the detection of papilledema ranged from 64-92%, and its specificity from 68-88%. The sensitivity of intraocular protrusion of the optic nerve for the detection of papilledema ranged from 48-60%, and its specificity ranged from 88-100%. A moderate or severe amount of fluid surrounding the optic nerve had a sensitivity ranging from 36-56% and was between 68% and 100% specific for the detection of papilledema. When two of three or all three signs were positive, the specificity for detecting papilledema increased to 92-100% among the expert readers.

### CONCLUSION

Our results confirm that posterior sclera flattening and intraocular protrusion of the optic nerve are statistically more likely in patients with elevated intracranial pressure. In addition, compared with the largest prior study to demonstrate statistical significance of any of these signs, our results show an approximately equal ability to detect posterior sclera flattening and perioptic subarachnoid space distention, but a nearly two-fold increase in the ability to detect intraocular protrusion of the optic nerve by employing high resolution T2 imaging. Previous mixed results regarding the statistical significance of the presence of these MRI signs among patients with increased intracranial pressure may have been secondary to volume averaging from the relatively thick sections employed in conventional T2-weighted imaging. High resolution T2-weighted imaging can help eliminate this problem and appears to be a useful adjunct MRI series in any patient with a question of increased intracranial pressure.

**KEY WORDS:** Papilledema, 3D T2

### P-60

#### Effects of Alcohol on Neurocognitive Functions and the Brain

Koçuk, N.<sup>1</sup>·Ada, E.<sup>2</sup>·Akgün, B.<sup>2</sup>·Akdede, B. B.<sup>2</sup>·Akvardar, Y.<sup>3</sup>

<sup>1</sup>Bingöl State Hospital, Bingöl, TURKEY, <sup>2</sup>Dokuz Eylül University, İzmir, TURKEY, <sup>3</sup>Marmara University, İzmir, TURKEY

### PURPOSE

The aim of this study is to investigate changes of neuropsychological functioning and hippocampal,

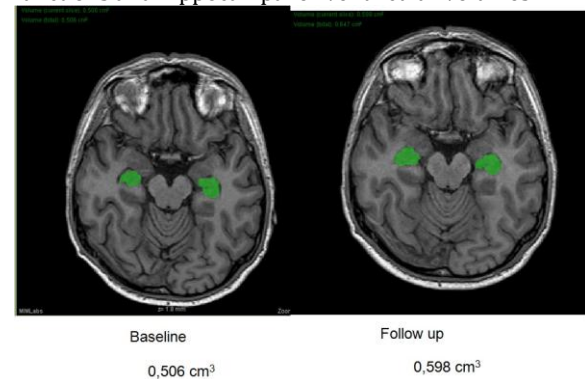
ventricular volume and their relationships during early abstinence of alcohol in comparison to healthy controls.

### MATERIALS & METHODS

Eighteen male right-handed alcohol-dependent patients were tested in the first week of detoxification and after 8 weeks of abstinence. Hippocampal and ventricular volumes were assessed using magnetic resonance imaging (MRI). Eighteen age/education-wise matched and right-handed male healthy controls were conducted neuropsychological tests and MRI once. Executive functions, verbal/nonverbal memory, verbal fluency, working memory, attention, upper limb motor function and visuo-spatial abilities were assessed.

### RESULTS

At baseline alcohol-dependent patients had smaller hippocampal volumes, larger ventricular volumes and impairments in executive functions, immediate and delayed verbal/nonverbal memory, verbal fluency, visuo-spatial functions, upper limb motor function and attention than controls. At follow up there was a significant increase in hippocampal volumes, decrease in ventricular size in alcohol-dependent patients. Except the executive functions, semantic part of verbal fluency and upper limb motor functions there was a significant improvement in all other neuropsychological functions. No relationships were found between neurocognitive functions and hippocampal or ventricular volumes.



### CONCLUSION

Our results indicate a substantial improvement in brain structure and neurocognition in alcohol-dependent patients during early weeks of abstinence. Some of the brain functions and regions remain impaired despite abstinence. Understanding the mechanisms underlying partial recovery may help to create a model of brain regeneration in order to develop new and more effective treatment strategies for alcohol dependence.

**KEY WORDS:** Alcohol, neuropsychological testing, MR brain imaging

### P-61

#### Planning of Safe Endoscopic Third Ventriculostomy: A Morphometric MR Imaging and MR Angiography Study of Tuber Cinereum Proximity to Critical Major Arteries

Horsburgh, A.·Kirolos, R. W.·Massoud, T. F.



Addenbrooke's Hospital, University of Cambridge  
Cambridge, UNITED KINGDOM

#### PURPOSE

Acute arterial hemorrhage in the interpeduncular fossa is a dreaded complication of endoscopic third ventriculostomy (ETV). When the posterior tuber cinereum (TC) is fenestrated, the basilar artery tip (BT) or its branches may be encountered and damaged below the floor of the third ventricle. The formation of traumatic basilar tip aneurysm also may complicate ETV. Major arterial injuries can be avoided by careful preoperative planning and meticulous technique. It also is uncertain whether partial obstruction of an ETV stoma by the P1 segments of the posterior cerebral arteries might contribute to postoperative failure of an ETV. We studied normal MRI and MR angiographic morphometry and configuration of the BT and the P1 segments relative to the floor of the third ventricle.

#### MATERIALS & METHODS

We retrospectively analyzed the images of 82 patients with normal findings, nondilated ventricles (mean Evans index of 0.26), and lying in a neutral head position (mean cervico-medullary angle of 141°). We cross-referenced MRAs with sagittal and axial MRIs to measure distances of BT and P1 segments to the middle of the TC, halfway between the mammillary bodies and the infundibular recess. We also classified the location of the BT in the interpeduncular and suprasellar cisterns. We correlated the combined sagittal areas of these two cisterns and the prepontine cistern, and the patients' ages, with the TC-to-artery distances using regression analysis.

#### RESULTS

The patients were 76% female and 24% male, with a mean age 53 years (range 14-86 years). The BT, right P1 and left P1 segments were a mean 4.9 mm (range 0-11 mm), 5.5 mm (range 0-11 mm), and 5.7 mm (range 0-12 mm) respectively from the TC. On axial images 10 (12%) BTs were in the interpeduncular cistern, and 72 (88%) were in the suprasellar cistern. On sagittal images 74% of BTs were in front of the mammillary bodies and 26% were behind them. These distances and locations did not correlate with age or sagittal area of the three basal cisterns combined (mean 359 mm<sup>2</sup>).

#### CONCLUSION

The most important vascular complication to avoid during ETV is injury to the basilar artery and its nearby branches. In the presence of normal-sized ventricles, the BT and P1 segments are anatomically close to the TC and potentially at risk during ETV in adults of all ages. This is pertinent to the small subset of patients requiring an ETV when the ventricles are nondilated. Moreover, it is known that the floor of the third ventricle balloons downwards in the presence of hydrocephalus, approximating even further the TC to the basilar tip and pons. Careful scrutiny of preoperative MR images and the morphometric data presented can help reduce vascular complications during and after ETV.

**KEY WORDS:** Neuroendoscopy, anatomy, tuber cinereum

#### P-62

#### Should Postcontrast T2 FLAIR Replace Precontrast T2 FLAIR? A Large Series Comparison

Rydberg, C. H.·Watson, R. E.·Port, J. D.·Koeller, K. K.

Mayo Clinic  
Rochester, MN

#### PURPOSE

With continuing pressure to better image our patients in less time, it is important that we select our pulse sequences wisely. Postcontrast T2 FLAIR has been shown superior to noncontrast T2 FLAIR and postcontrast T1-weighted images in evaluation of meningeal disease and certain neoplasms. Our purpose is to compare precontrast and postcontrast T2 FLAIR sequences in a large series of patients to determine if precontrast T2 FLAIR should be replaced by postcontrast T2 FLAIR in routine scanning.

#### MATERIALS & METHODS

Over a 5-week period, a postcontrast T2 FLAIR sequence was added to the routine contrast-enhanced MRI exams of 217 consecutive patients including both hospitalized patients and out-patients. Scans were performed on GE and Siemens 1.5 T and 3.0 T magnets. All cases were reviewed by three experienced neuroradiologists. The indication for scanning was available. Routine sequences including FSET2, precontrast T2 FLAIR, and postcontrast T1 sequences. Evaluation criteria included: Does the postcontrast T2 FLAIR provide additional information? If yes, to what extent was the information helpful? Are there additional artifacts associated with the postcontrast T2 FLAIR images and if present do they interfere with interpretation? Given a choice would you prefer a precontrast T2 FLAIR, a postcontrast T2 FLAIR, or both?

#### RESULTS

The postcontrast T2 FLAIR was judged to offer additional information in 37% of cases compared to precontrast T2 FLAIR. This additional information was deemed vital in 4%, helpful in 32% and not helpful in 1% of overall cases. The postcontrast T2 FLAIR was particularly helpful in meningeal and perivascular processes and with tumors including metastases, lymphoma, meningiomas, and gliomas. No additional artifacts were noted on the postcontrast T2 FLAIR images. Reviewer preference was for precontrast T2 FLAIR sequence in 38% of cases, postcontrast T2 FLAIR in 36% of cases, and in 26% of the time reviewers would prefer to have both for interpretation.

#### CONCLUSION

Postcontrast T2 FLAIR has been shown to demonstrate particular pathologies better than precontrast T2 FLAIR and enhanced T1 images. If both pre and postcontrast T2 FLAIR images are available for side-by-side comparison the enhancing lesions are easy to visualize. With ever-increasing time pressure, performing both

sequences on all patients is not a likely option. Without a precontrast T2 FLAIR sequence, the radiologist must mentally integrate the T1-shortening of an enhancing lesion with the possible background T2 prolongation of a T2 FLAIR image. The ease of this integration improves with experience. Reviewer's comfort level interpreting postcontrast T2 FLAIR without the benefit of precontrast T2 FLAIR increased with the number of cases reviewed. Our evaluation demonstrated that postcontrast T2 FLAIR provided additional information compared to precontrast T2 FLAIR in 37% of cases. In 4% of cases this information was judged to be vital. There are no additional artifacts associated with postcontrast T2 FLAIR. If time permits only one T2 FLAIR sequence, our data supports that it should be performed after contrast administration.

**KEY WORDS:** FLAIR, postcontrast

## P-63

### **Rathke Cleft Cysts: MR Criteria for Presumptive Diagnosis**

Gaddikeri, S. Vattoth, S. Riley, K. O. Combs, J. T. Smith, C. B. DeHoff, G. W. Roberson, G.

University of Alabama at Birmingham  
Birmingham, AL

#### **PURPOSE**

The objective of this study is to define MR criteria to distinguish Rathke's cleft cyst (RCC) from other cystic lesions of the sella.

#### **MATERIALS & METHODS**

Records of 252 patients with MR scans suggesting RCC were reviewed retrospectively for indication for initial MR study, location of cyst, signal intensity on T1 and T2, dimensions of the cyst, encroachment on the optic chiasm, pattern of enhancement and stability of the cyst for more than 1 year on follow-up MR studies. Of those who had surgical resection/decompression, the indication for surgery and the histopathology of the cyst were reviewed. One hundred sixty patients were excluded from the study based on the following exclusion criteria: 1). Hormonally active (hyper functioning) pituitary lesion, 2). Cysts with enhancing mural nodule, 3). Histologically proven non RCC cystic lesions and 4). Cysts with less than 1 year follow up (n = 114).

#### **RESULTS**

In our study of 252 patients, the age group ranged from 20 to 86 years at the time of initial MR study. After exclusion criteria were applied, 103 remaining patients were analyzed. Usually the suggestion of RCC was an incidental finding (n = 85). Headache was presenting symptom in 13, including one patient with a visual field defect. Visual field deficit were present in five patients. The cyst in 57 patients had T1 hyperintensity, in 28 had T1 hypointensity and isointense T1 in 18. T2 signal intensity was hyperintense in 59 and iso- to hypointensity in 54. Postcontrast images demonstrated no enhancement in 83 and thin marginal enhancement

in 20. One hundred two patients demonstrated stable appearance of the cyst after at least 1 year follow-up MR study. Of the five patients histologically verified as RCC, the surgical indication was visual field deficit in two patients, progressive headache in two, and increasing size with headache in one.

#### **CONCLUSION**

Rathke's cleft cysts typically have cystic appearance with T1 hyperintensity, sometimes with T1 iso or hypointensity, variable T2 signal, and no or thin marginal enhancement plus stability over extended time with no growth.

**KEY WORDS:** Rathke cleft cyst, T1, T2 signal intensity, follow up

## P-64

### **Review of the Pathologies Associated with High T1-Weighted Signal in the Basal Ganglia on MR Imaging**

Zaitout, Z.<sup>1</sup>Connolly, D.<sup>1</sup>Batty, R.<sup>1</sup>Karunasaagarar, K.<sup>2</sup>Romanowski, C.<sup>1</sup>

<sup>1</sup>Royal Hallamshire Hospital, Sheffield, UNITED KINGDOM, <sup>2</sup>Worcestershire Acute Trust, Worcester, UNITED KINGDOM

With several functions and a fundamental influence over cognition and motor functions, the basal ganglia is the cohesive center of the brain. As a consequence, there are several conditions which affect the basal ganglia and have various clinical and radiologic manifestations. Nevertheless, on magnetic resonance imaging (MRI) there is a limited differential diagnosis for those conditions presenting with T1-weighted spin echo hyperintensity within the central nervous system in general and the basal ganglia in particular. The three main causes of high T1-weighted signal that we have addressed are: blood products, calcification and metal deposition. The aim of our poster is to explore these basal ganglia pathologies and provide image illustrations.

**KEY WORDS:** MR imaging, basal ganglia, T1-weighted signal

## P-65

### **Soccer Heading Impact on the Brain and Cognition**

Kim, N.<sup>1</sup>Zimmerman, M.<sup>1</sup>Lipton, R. B.<sup>1</sup>Stewart, W.<sup>2</sup>Gulko, E.<sup>1</sup>Branch, C. A.<sup>1</sup>Lipton, M. L.<sup>1</sup>

<sup>1</sup>Albert Einstein College of Medicine of Yeshiva University, Bronx, NY, <sup>2</sup>Geisinger Health System, Danville, PA

#### **PURPOSE**

Soccer heading may represent a form of repetitive mild trauma and be associated with long-term cognitive impairment. Because abnormally low white matter (WM) fractional anisotropy (FA) has been associated with cognitive impairment in patients with TBI, we hypothesized that a threshold level ( $\beta$ ) exists for heading exposure above which evidence of white



matter injury and cognitive impairment would be detectable.

#### **MATERIALS & METHODS**

The study had IRB approval, included written informal consent, and complied with HIPAA. Thirty-two amateur soccer players were recruited. Heading exposure was assessed with a standardized questionnaire and DTI (3.0 T; 32 directions;  $b = 1000$ ) was performed. Regions of interest (ROI) where FA was associated with heading exposure were determined using a voxelwise t-test comparing FA between subjects with the most heading exposure (upper quartile;  $\geq 1,320$  heads/year) and those with lesser exposure (lower 3 quartiles;  $< 1,320$  heads/year). Cognitive performance was assessed using a standardized battery (CogState; Collie et al., 2003; Maruff et al., 2009). Based on our threshold hypothesis we assumed that an S or inverse S shape related FA measures and cognitive performance against heading exposures. Such nonlinear shapes (S, inverse S) were modeled based on Inverse Logit (IL) functions with three parameters: (1) baseline ( $\alpha_1$ ) (2) association direction and scale factor ( $\alpha_2$ ) (3) departure position ( $\beta$ ) in heading exposure scales from baseline. These parameters were estimated utilizing a simulated annealing algorithm (Kirkpatrick et al., 1983) and gradient-based nonlinear regression algorithm (Bates and Watts, 1988) for each ROI and cognitive domain.

#### **RESULTS**

Five ROIs were identified in temporooccipital WM and one in frontal WM where greater heading was associated with low FA. We found significant effects of  $\beta$  for all ROIs, and two cognitive domains (visual motor function, and verbal learning & memory). Estimates of  $\beta$  were ranged between 1080 and 1440 heads per year. Both cognitive domains showed significant correlations with FA measures (two ROIs in temporooccipital WM and one in frontal WM), mediated by heading exposures.

#### **CONCLUSION**

Greater heading frequency is associated with low FA. Exceeding a threshold for heading frequency (1000-1500) may result in brain abnormalities similar to those seen in TBI, which confer cognitive impairment. If confirmed, these findings suggest that brain abnormalities related to heading are of clinical importance. Defining the appropriate exposure thresholds could facilitate public health interventions to limit heading exposure and its adverse consequences.

**KEY WORDS:** Soccer, DTI, cognition

#### **P-66**

##### **Functional MR Imaging Evaluation of Driving in Patients with Traumatic Brain Injury**

Andrews, S.·Mendelsohn, D. B.·Yetkin, Z. F.

University of Texas Southwestern Medical Center  
Dallas, TX

#### **PURPOSE**

Patients with traumatic brain injury (TBI) might suffer from varying degrees of cognitive impairment despite a similar level of injury. Cognitive impairment in TBI may place patients at higher risk for accidents. Driving is a complex task that requires coordination of motor and cognitive skills. Evaluation of the brain activation elicited by a task designed to simulate decisions frequently made during driving may provide prognostic information for TBI patients with high-risk of accident. The aim of the present study was to determine the feasibility and resultant brain activation of a driving task in patients with TBI.

#### **MATERIALS & METHODS**

Patients with TBI and control subjects were recruited to perform a novel driving task during functional magnetic resonance imaging (fMRI) using a 1.5 T scanner. The driving task was presented visually and simulated the required perception and decision-making during driving. The accuracy and timing of the responses were documented.

#### **RESULTS**

Thirteen patients with TBI (10 male, 3 female, age range: 19-37 years) and five healthy controls (2 males, 3 females, age range: 17-42 years) were enrolled in this study. All TBI patients and healthy controls performed the task without motion artifacts. Traumatic brain injury patients and healthy controls showed activation in similar brain regions: bilateral parietal and bilateral posterior temporal lobes including visuospatial association areas, motor cortices, bilateral middle frontal gyri, anterior cingulates, and the visual cortices. Traumatic brain injury showed increased activation in the similar regions compared to controls. Traumatic brain injury patients also showed additional regions of activation in the bilateral basal ganglia, thalami, posterior cingulates and hippocampi. Extent of brain activation in TBI patients showed interindividual differences.

#### **CONCLUSION**

Traumatic brain injury patients and healthy controls were able to perform the driving task. The visually presented driving task elicited brain activation including motor, visual cortices and visuospatial association areas in all subjects. Further studies are needed to investigate the utility of fMRI of driving tasks in identifying the individuals with decreased driving skills.

**KEY WORDS:** Functional MR imaging, traumatic brain injury, driving

#### **P-67**

##### **Clinical Usefulness of 3D Basiparallel Anatomical Scanning for Evaluating Aneurysms of the Vertebral Artery**

Morikawa, M.·Ideguchi, R.·Enokizono, M.·Uetani, M.·Horie, N.·Hayashi, K.·Nagata, I.

Nagasaki University  
Nagasaki, JAPAN

#### PURPOSE

Basiparallel anatomical scanning (BPAS) was designed to visualize the surface appearance of the vertebrobasilar artery within the cistern. In this study, we aimed to evaluate the efficacy of 3-dimensional BPAS (3D BPAS) and to present a retrospective analysis of our experience with the diagnosis.

#### MATERIALS & METHODS

Between 2007 and 2010, we experienced 12 patients of vertebral artery (VA) aneurysm, including seven dissections (5 in VA and 2 in posterior inferior cerebellar artery), four fusiform aneurysms, and one saccular aneurysm at our institution. We obtained images of 3D BPAS and 3D TOF MRA in all patients, and digital subtraction angiography in 11 of the 12 patients. The mean age of the 12 patients (7 males and 5 females) was 56 years old (range 18-80). Five of the 12 patients presented with ischemia, three with headache, two with cranial nerve dysfunction and one with SAH. Coil embolization was performed in five patients. In 3D BPAS, we evaluated the external diameter of the affected artery. We compared the findings in 3D BPAS with MRA to evaluate the discrepancy.

#### RESULTS

All patients presented with dilatation of the external diameter on 3D BPAS. In two dissections of posterior inferior cerebellar artery, 3D BPAS contributed to accurate diagnosis. By comparing the findings in 3D BPAS with MRA, we found a discrepancy in seven of 12 patients (58%) due to intramural hematoma of dissection or due to occlusion of aneurysm. In 10 of 12 patients received follow-up MRI, temporal shrinkage of the arterial shape was confirmed in four dissections and one treated fusiform aneurysm.

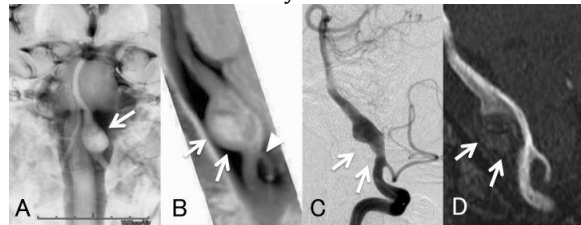


Figure. Partially thrombosed left VA aneurysm. 3D BPAS raysum image (A) and MPR image (B) show fusiform dilatation of left VA aneurysm (arrows) and demonstrate the relationship of the left posterior inferior cerebellar artery and the aneurysm (arrowhead). Left vertebral angiogram (C) and MRA MIP image (D) fail to demonstrate entire aneurysm lumen due to intraaneurysmal thrombus (arrows).

#### CONCLUSION

3D BPAS is a noninvasive and useful method as follow up for the VA aneurysms, and can provide additional information for treatment planning.

**KEY WORDS:** Basiparallel anatomical scanning, vertebral artery, aneurysm

P-68

**Is Higher Choroid Plexus "Load" an Etiologic Factor in Idiopathic Intracranial Hypertension? Testing a**

#### Hypothesis in a Correlative Clinical Imaging Morphometric Study

Horsburgh, A. Massoud, T. F.

Addenbrooke's Hospital, University of Cambridge  
Cambridge, UNITED KINGDOM

#### PURPOSE

Idiopathic intracranial hypertension (IIH) is a condition of raised cerebrospinal fluid (CSF) pressure in the presence of normal ventricular size. The exact etiology of IIH remains controversial, and although many causes have been considered, IIH is thought to result from disordered CSF dynamics, either through increased CSF formation (CSF form) or through reduced CSF drainage secondary to increased resistance, e.g., associated with raised venous sinus pressure. Previous ventricular infusion and velocity sensitive MRI studies have demonstrated elevated CSF form in a few IIH patients. Although there is no consensus regarding the precise pathogenesis of raised ICP in IIH, increased CSF form may be important, at least as a cofactor. We therefore hypothesized that if increased CSF form played a role in IIH that it may result in, or from, macroscopic increase in size of the CP. This higher CP "load" may represent an etiologic factor in IIH, one potentially amenable to novel treatments if present.

#### MATERIALS & METHODS

We retrospectively studied 50 patients who all had met the modified Dandy criteria for the diagnosis of IIH: CSF pressure >25 cmH<sub>2</sub>O, appropriate clinical symptoms, and no other significant findings on neuroimaging. Axial head CT venograms within 6 weeks of a documented lumbar puncture were examined by two radiologists. A representation of the size or "load" of CP was considered as the axial area of CP at three separate levels and locations (the body of the lateral ventricle, the glomus at the trigone, and at the 4th ventricle) measured using electronic calipers. Results were compared with 50 matched controls in whom the three axial CP areas were measured on normal postcontrast head CT images. The Evans Index (EI) of ventricular size was measured to exclude ventriculomegaly. We used a Student t-test for independent samples to statistically compare IIH and control groups, with significance set at P<0.05. The effect of the variable of ICP also was tested on the dependent variable (area of CP) using regression analysis.

#### RESULTS

Patients with IIH were a mean age 35 years (98% female, 2% male). Matched controls were a mean age 38 years (97% females, 3% male). None of the CT studies demonstrated ventriculomegaly (EI<0.3). There was no significant difference in the total measured axial areas of the CP between IIH patients (183 mm<sup>2</sup>) and controls (178 mm<sup>2</sup>). In particular, the mean diameter of the CP glomus was 6.5 mm and 6 mm in the two groups respectively. There was no correlation between the 'load' of CP and the degree of ICP (R<sup>2</sup><0.02).

#### CONCLUSION

There is no appreciable macroscopic increase in size of the CP in patients with IIH. If increased CSF form is an etiologic factor in the pathogenesis of IIH, this is not reflected in a corresponding raised "load" of CP.

**KEY WORDS:** Intracranial hypertension, choroid plexus, ventricles

**P-69**

### Comparing Prevalence of MR Imaging Biomarkers of Microvascular Angiopathy between Subtypes of Open Angle Glaucoma and Controls

Cain, J. R.<sup>1</sup>Hansen, T.<sup>1</sup>Mercieca, K.<sup>2</sup>Steeple, L.<sup>2</sup>Spencer, F.<sup>2</sup>Jackson, A.<sup>1</sup>

<sup>1</sup>University of Manchester, Manchester, UNITED KINGDOM, <sup>2</sup>Central Manchester University Hospitals, Manchester, UNITED KINGDOM

#### PURPOSE

Cerebrovascular disease has been linked to abnormal cerebrospinal fluid pulsation. This is thought to cause damage to the brain parenchyma, known as pulse wave encephalopathy. Studies have linked open angle glaucoma to cerebrovascular conditions. Open angle glaucoma is linked to raised intraocular pressure, but glaucoma can occur without raised intraocular pressure. This subtype is known as normal tension glaucoma and indicates an alternative etiology. This study investigates biomarkers of abnormal cerebrospinal fluid pulsation and cerebrovascular disease in subtypes of open angle glaucoma.

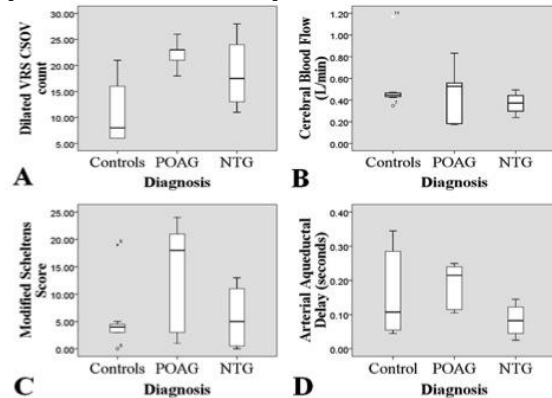
#### MATERIALS & METHODS

Sixteen subjects were recruited for the study. Five primary open angle glaucoma (POAG) patients, four normal tension glaucoma (NTG) patients, and seven normal controls were recruited. All subjects underwent a magnetic resonance imaging scan (Achieva 1.5 T) sequences included; 3D T1 inversion recovery, FLAIR, phase contrast imaging flow studies of the carotid and basilar arteries (VENC 120cm/s), jugular veins (VENC 40cm/s), cerebral aqueduct (VENC 8cm/s), and foramen magnum (8 cm/s), Axial SPIR FLAIR of orbits, Coronal T2 SPIR orbits. Phase contrast angiography was used to assess cerebrospinal fluid (CSF) pulsation including arterial aqueductal delay. Cerebrospinal fluid pulsation, MRI images were used to biomarkers of microvascular angiopathy including dilated Virchow Robin spaces (VRS), Scheltens white matter scores, optic nerve and brain atrophy were compared between groups. Subjects also underwent visual acuity measurement, intraocular pressure measurement, central corneal thickness measurement, visual fields testing, optic disk examination, and optic disk stereo photography.

#### RESULTS

Biomarkers of microvascular angiopathy (dilated Virchow Robin spaces) were significantly higher in POAG compared to controls ( $p = 0.008$ ), and were also higher than in NTG. Arterial aqueductal delay was significantly shorter ( $p = 0.05$ ) in NTG than POAG. There

were no significant differences in ratios of brain matter CSF and modified Scheltens scores with controls. There were no significant differences in mean optic nerve and optic nerve subarachnoid space measurements.



**Box and whisker diagrams showing dilated Virchow Robin spaces in the centrum semiovale (VRS CSOV, A), cerebral blood flow (B), Modified Scheltens score (C), and arterial aqueductal delay (D). POAG – primary open angle glaucoma, NTG – normal tension glaucoma.**

#### CONCLUSION

Primary open angle glaucoma patients have more microvascular disease than controls or NTG patients, indicating this may play a role in its etiology. The results indicate a greater association for POAG with microvascular angiopathy than NTG. Narrowing of small vessels of the eye has been noted previously in POAG. Short arterial aqueductal delay in NTG compared to POAG indicates CSF pulsation could be part of its etiology. This study provides some evidence of differing pathologic processes occurring between different subtypes of glaucoma.

**KEY WORDS:** Glaucoma, MR imaging, microvascular disease

**P-70**

### Measurement of Thrombus Volume in Acute Ischemic Stroke Using Thin-Slice Noncontrast CT: Comparison of Conventional Axial CT and Helical CT

Ahn, S.Kim, E.

Yonsei University Health System  
Seoul, KOREA, REPUBLIC OF

#### PURPOSE

The accurate assessment of thrombus burden using noncontrast CT (NCT) is important for determining treatment strategy and predicting prognosis in acute ischemic stroke. Thin-slice helical NCT can be used to this end. However, it brings additional radiation exposure, impeding its use by researchers. Conventional axial (sequential) images obtained by multidetector row CT scanners can be reconstructed into thin-slice images. Therefore, we hypothesized that these images could be used to measure thrombus volume and possibly replace helical NCT. The purpose of this study was to evaluate the usefulness of conventional axial NCT for

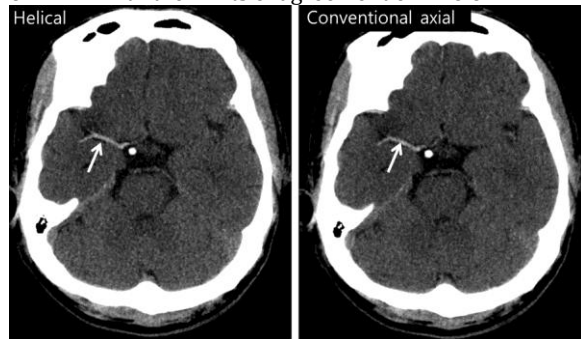
measurement of thrombus volume compared with helical NCT.

#### MATERIALS & METHODS

We enrolled 58 consecutive patients who underwent both 5 mm conventional axial NCT and 1.25 mm helical NCT, and had occlusion on CTA in the anterior circulation within 6 hours of symptom onset. Each of conventional axial NCT images subsequently was reconstructed into four 1.25 mm images. Eight patients were excluded because of severe motion. Thrombus volumes were measured semiautomatically with both axial and helical NCT images. The intraclass correlation coefficient (ICC) and Bland-Altman plot were used to assess measurement agreement.

#### RESULTS

Thrombi were detected in all patients on both NCT images, and occlusion sites were as follows: middle cerebral artery (MCA) alone in 35 patients, MCA and internal cerebral artery (ICA) in 14 patients and ICA alone in one patient. The mean thrombus volumes were 124.25 mm<sup>3</sup> and 117.84 mm<sup>3</sup> on conventional axial NCT and helical NCT, respectively, without statistical significance ( $P > 0.05$ ). The agreement between conventional axial NCT and helical NCT measurements of thrombus volume was almost perfect with the ICC being 0.981. The mean thrombus volume difference was 6.4 mm<sup>3</sup> with the limits of agreement of  $\pm 46.6$  mm<sup>3</sup>.



#### CONCLUSION

Thin-slice NCT reconstructed from 5 mm conventional axial images can provide sufficiently accurate measurement of thrombus volume without additional helical NCT in acute ischemic stroke.

**KEY WORDS:** Acute ischemic stroke, thrombus volume, noncontrast CT

#### P-71

##### Surveillance Imaging after Intracranial Stent Implantation: Noninvasive Imaging Compared with Digital Subtraction Angiography

Golshani, B.·Lazzaro, M. A.·Darkhabani, Z.·Raslau, F.·Baruah, D.·Fitzsimmons, B.·Zaidat, O. O.

Medical College of Wisconsin and Froedtert Hospital Milwaukee, WI

#### PURPOSE

An approximately 30% rate of in-stent restenosis (ISR) has been reported in intracranial atherosclerotic disease (ICAD). Digital subtraction angiography (DSA) is the gold standard imaging for detection of ISR; however, there is limited literature on optimal noninvasive surveillance imaging. We compared the ability of CTA and MRA to DSA in recognizing ISR.

#### MATERIALS & METHODS

A single-center database of patients treated with stent implantation for ICAD was accessed. All patients who underwent follow-up imaging with DSA paired with either MRA or CTA within 30 days were included in the analysis. Two angiography readers and two noninvasive imaging readers measured restenosis with a submillimeter digital caliper. In-stent restenosis was categorized as: none/minimal, mild ( $< 50\%$ ), moderate ( $\geq 50\text{--}70\%$ ), and severe ( $\geq 70\%$ ). Analysis was performed with weighted kappa statistics.

#### RESULTS

We identified 18 cases of individual stents that underwent surveillance imaging with paired DSA and CTA and six stents that underwent imaging with paired DSA and MRA. Of those undergoing DSA and CTA ( $n = 18$ ), lesion locations included ICA ( $n = 6$ ), MCA ( $n = 6$ ), PCA ( $n = 3$ ), ACA ( $n = 1$ ), intracranial vertebral artery ( $n = 1$ ), basilar artery ( $n = 1$ ). Stents included Wingspan ( $n = 17$ ) and Neuroform ( $n = 1$ ). Interreader agreement produced  $\kappa = 0.64$  (95% CI: 0.36-0.91) for DSA and  $\kappa = 0.70$  (95% CI: 0.48-0.91) for CTA. CT angiography and DSA agreement was  $\kappa = 0.37$  (95% CI: 0.24-0.50). Of those undergoing DSA and MRA ( $n = 6$ ), lesion locations included ICA ( $n = 2$ ), MCA ( $n = 2$ ), PCA ( $n = 1$ ), ACA ( $n = 1$ ). Interreader agreement produced  $\kappa = 0.74$  (95% CI: 0.33-1.0) for DSA and  $\kappa = 1.0$  (95% CI: 1-1) for MRA. MR angiography and DSA agreement was  $\kappa = 0.30$  (95% CI: 0.17-0.43).

#### CONCLUSION

Good reader agreement exists within DSA, CTA, and MRA. However, when comparing noninvasive imaging (CTA and MRA) to DSA, only fair agreement exists. This data suggests that CTA and MRA are not comparable to DSA for evaluation of in-stent restenosis.

**KEY WORDS:** In-stent, restenosis, imaging

#### P-72

##### Visual Grading Scales of Intracranial Internal Carotid Artery Calcifications on CT: A Comparison Study with Quantitative Measurements

Ahn, S.·Kim, E.·Shin, N.

Yonsei University Health System  
Seoul, KOREA, REPUBLIC OF

#### PURPOSE

Intracranial carotid artery calcifications (ICACs) are detected frequently on noncontrast brain CT in elderly people. However, their clinical significance has shown some discrepancy between previous reports; some investigators demonstrated that ICAC did not show a

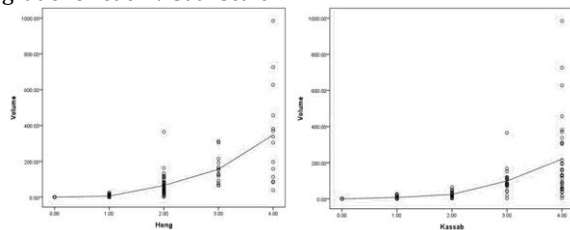
significant correlation with cerebral ischemia, while others reported that ICAC correlated well with ischemic stroke and white matter hyperintensity. These studies used different visual grading scales, which might have led to inconsistent results in the degree of calcification and consequently in the clinical significance. Therefore, to accurately investigate the clinical significance of ICAC, evaluation of various visual grading scales with respect to quantitative measurements is needed. In the present study, we aimed to evaluate the performance of each visual grading scale by comparing with ICAC volume.

#### MATERIALS & METHODS

In this retrospective study, 49 consecutive patients older than 50 years (mean 65.3 years old) who had undergone noncontrast CT were included regardless of their underlying medical history. In a retrospective manner, five visual grading scales were evaluated: the scales of Babiarz et al., Erbay et al., Kassab et al., Chung et al., and Hong et al. ICAC volumes also were measured semiautomatically by applying a threshold of 130 HU. The relationship between the visual grading scales and volumetric measurements was assessed by the Spearman's rho. A linear regression model was applied to test the hypothesis of a linear relationship between the visual grades and the volumetric measurements. Differences in ICAC volume between visual grades in each scale were evaluated using ANOVA with Bonferroni correction.

#### RESULTS

Overall, a high correlation between visual grades and volumetric measurements of ICAC was present with Spearman  $\rho$  ranging from 0.836 to 0.874. However, scatter increased with higher visual grades as ICACs with higher grades contained a wide range of volumes. The relationship between visual grades and volume was evaluated by using a linear model and their  $R^2$  ranged from 0.28 to 0.43; 0.35 for Babiarz's, 0.35 for Erbay's, 0.28 for Kassab's, 0.30 for Chung's, and 0.43 for Hong's. The mean volumes were not significantly different between visual grades except the cases with the highest grade for each visual scale.



#### CONCLUSION

Although visual grading grades show a good correlation with volumes of ICAC, visual grades poorly reflect the actual volume; consequently, they may be less sensitive in differentiating clinical groups. Among the visual grading scales, the Hong's scale reflects ICAC volume better than the other scales.

**KEY WORDS:** Intracranial carotid artery calcification, visual grading scales, volume

#### P-73

#### MR Imaging and CT Imaging of Indirect and Direct Cavernous Carotid Fistula

Mossa-Basha, M. Gailloud, P. Pearl, M. Lin, D. D.

Johns Hopkins University  
Baltimore, MD

#### PURPOSE

Cavernous carotid fistulae (CCF) represent abnormal connections between the cavernous sinus and the cavernous carotid artery (direct), or dural branches of the internal carotid artery or external carotid artery (indirect). Affected patients typically present with chemosis, proptosis, conjunctival injection, retro-orbital pain and decreased visual acuity. Although definitive diagnosis is made by catheter angiography (DSA), MRI with MRA or CTA is indispensable as the initial, noninvasive evaluation and to rule out other pathologic processes with a similar clinical presentation. In this study, we intend to analyze the CTA and MRI/MRA features of angiographically confirmed CCFs, evaluate the accuracy of these characteristics, and determine what factors may contribute to differentiation of direct from indirect CCF.

#### MATERIALS & METHODS

Cases of angiographically confirmed CCF that also had pretreatment cross-sectional imaging were collected by searching our radiology database from 1/1/01 to 9/30/11. The preembolization MRI/MRA and CTA imaging studies were analyzed retrospectively. Ipsilateral and contralateral superior ophthalmic vein (SOV) and cavernous sinus (CS) diameter were measured. The affected cavernous sinuses were evaluated for intracavernous flow voids on both T2 and T1 postcontrast sequences. Flow-related signal of the affected cavernous sinus also was specifically evaluated on 3D TOF MRA source images. The lesion characteristics were compared between direct and indirect cavernous carotid fistulae by unpaired T-test with correction for multiple comparisons.

#### RESULTS

There were a total of 16 cases, including 11 indirect (one patient had bilateral lesions) and five direct CCF. In 13 cases where MRI/MRA was available, 12 cases (93%) showed intracavernous flow-related signal on TOF MRA, with the one exception representing a case of indirect CCF with superimposed cavernous sinus thrombosis that was revealed on DSA. Intracavernous sinus flow voids on T2 and T1 postcontrast sequences were identified in 7/10 indirect CCF and in 3/3 direct CCF, with 2/3 direct CCF cases demonstrating prominent intracavernous flow voids bilaterally. CT angiography and postcontrast MRI provided different measurements in 16 cases between the 2 types of CCFs in SOV and CS. The mean diameter of the ipsilateral SOV in direct CCF measured  $6.0 \pm 2.4$  mm, significantly larger compared to  $2.4 \pm 1.1$  mm of indirect CCF ( $p < .01$ ), and the mean diameter of the contralateral SOV of direct CCF measuring  $2.0 \pm .76$  mm was also larger than the indirect CCF of  $1.5 \pm .67$  mm. Additionally, affected

CS averaging  $13 \pm 5$  mm in diameter in direct CCF is larger compared to  $9.3 \pm 2.7$  mm in indirect CCF, and the contralateral CS measuring  $9.7 \pm 1.1$  mm in direct CCF is slightly larger compared to  $8.2 \pm 0.6$  mm in indirect CCF.

#### CONCLUSION

MR imaging/MRA and CTA provide an important evaluation of patients presenting with suspected CCF, and intracavernous flow-related signal on TOF MRA is the most reliable feature depicting 13/14 (93%) of cases in this study. The mean diameter measurements of SOV and CS obtained from CTA and MRI allow differentiation between direct and indirect CCF. Specifically, the ipsilateral SOV and CS are less commonly enlarged with indirect CCF as compared to the direct type.

**KEY WORDS:** Cavernous carotid fistula, vascular malformation

#### P-74

#### Enhancing Acute Ischemic Stroke Interpretation through Online ASPECTS Training ([www.aspectsinstroke.com](http://www.aspectsinstroke.com))

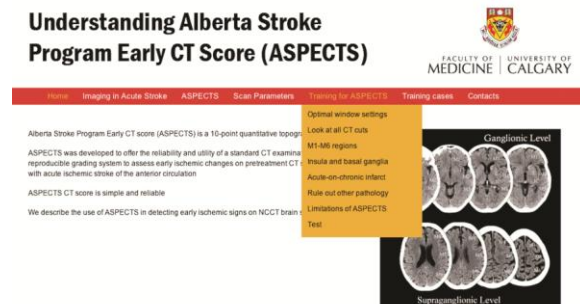
Modi, J.-Bai, D. H.-Almekhlafi, M.-Menon, B. K.-Goyal, M.

University of Calgary  
Calgary, AB, CANADA

#### PURPOSE

The Alberta Stroke Program Early CT Score (ASPECTS) is a simple, validated and reliable semiquantitative scale used for the detection and risk stratification of acute brain ischemia. To help clinicians optimize the use of ASPECTS in acute ischemic stroke diagnoses, we have developed an online teaching website ([aspectsinstroke.com](http://aspectsinstroke.com)), that offers an interactive training experience (Figure 1).

#### Understanding Alberta Stroke Program Early CT Score (ASPECTS)



#### MATERIALS & METHODS

The website design was structured on four principles: engaging presentation, quality content, user-friendliness, and openness to improvement. The website training section consists of interactive examples with brief clinical history, early and follow-up NCCT scans with expert interpretations. A feedback system through email is included within the website to further facilitate learning. To study how much the website was being used and how it was being used, a third-party website statistics collection service called Google Analytics was employed.

#### RESULTS

From its launch in September 2010, the website has attracted 4,288 visits from 2,945 unique users worldwide viewing 20,381 pages (Figure 2). Over the first 12 months after launch, there was a trend towards increasing usage. The number of visits in the first 3 months was 392, the second 3 months was 746, and the most recent 3 months was 1,548.



#### CONCLUSION

An interactive web approach is an efficient and effective alternative method for teaching the interpretation of early ischemic changes using ASPECTS on noncontrast CT. This teaching website could potentially play a role in the standardization of acute ischemic stroke (AIS) diagnoses, be a tool for image selection in multicenter clinical trials, and hopefully play a part in the establishment of AIS treatment guidelines in the future.

**KEY WORDS:** ASPECTS, stroke, online training

**Monday, April 23 –  
Wednesday, April 25**

**6:30 AM – 9:00 PM**

**Thursday, April 26**  
**6:30 AM - 3:00 PM**

**Americas Hall II**  
**Scientific (Printed) Posters 75 – 77**

**(P2) Anatomy**

**Note: A missing printed poster number indicates an abstract has been withdrawn.**



## P-75

### Displacement of Basal Brain Structures upon Flexion and Extension: Kinematic MR Imaging Morphometry and Relevance to Neuroendoscopic Procedures

Horsburgh, A. • Kirolos, R. W. • Massoud, T. F.

Addenbrooke's Hospital  
Cambridge, UNITED KINGDOM

#### PURPOSE

Therapeutic neuroendoscopy is an increasingly common option in minimally invasive neurosurgical practice. An appreciation of normal intracranial anatomy allows optimal planning of endoscope trajectories, necessary for safe and effective neuroendoscopic procedures. To date little information exists on the displacement of the caudal brain relative to the skull upon head movement. Potential displacement of basal brain structures upon head placement in different operative positions could have profound implications for the planning and performance of neuroendoscopic procedures. We used kinematic MRI studies to examine the morphometric displacement and changing anatomical relationships between the clivus and basal brain structures, intracranial vessels, and subarachnoid spaces.

#### MATERIALS & METHODS

We retrospectively evaluated the studies of 15 patients undergoing sagittal T2 kinematic MRI of the head and neck in modest flexion and extension. Using electronic calipers we first established the horizontal axial reference plane as a line drawn along the inferior borders of the anterior and posterior arches of the atlas. The angle between this line and a line between the opisthion and the hard palate defined the degree of flexion and extension. We then measured the following parameters in maximum flexion and extension: 1) The cervico-medullary angle (CMA); 2) Displacement of the ventral surface of the brainstem by measuring the change in depth of the prepontine and premedullary cisterns; 3) Total sagittal area of the basal, prepontine and premedullary cisterns; 4) The basilar tip to tuber cinereum (TC) distance; and 5) The angle of approach to the aqueduct of Sylvius through foramen magnum.

#### RESULTS

A mean extension angle of  $-15.8^\circ$  ( $-6^\circ$  to  $-22^\circ$ ) was achieved in all 15 patients. A mean flexion angle of  $+9.9^\circ$  ( $+9.2^\circ$  to  $+11.2^\circ$ ) was achieved in six patients. The mean CMA was  $157.2^\circ$  ( $150^\circ$ - $174^\circ$ ) in extension, and  $146^\circ$  ( $132^\circ$ - $149^\circ$ ) in flexion. We found mild displacement of brainstems toward the clivus even on modest degrees of flexion. The mean reduction in prepontine and premedullary cistern depth was 0.8 mm and 0.4 mm, respectively. The combined area of basal cisterns was minimally reduced from 402 mm<sup>2</sup> in flexion to 399 mm<sup>2</sup> in extension. The basilar tip did not move significantly from its position in extension to flexion, 5.2 mm to 5.3 mm from the TC, respectively. We found that  $22^\circ$  of head flexion were required to optimize a direct approach to the cerebral aqueduct from foramen

magnum during a potential suboccipital endoscopic approach to aqueductoplasty.

#### CONCLUSION

Preliminary studies using kinematic MRI show a small displacement of the brainstem relative to the clivus even within minor physiologic changes to head position. However, these changes are small and there is no significant movement of the basilar tip in modest flexion and extension. These results should be useful for presurgical planning of optimal patient positioning during neuroendoscopic procedures such as third ventriculostomy, trans-fourth ventricular aqueductoplasty, and the expanded endonasal transphenoidal approach to the retroclival space.

**KEY WORDS:** Morphometry, neuroendoscopy, kinematic MR imaging

## P-76

### Gender Influences Vascular Diameter during MR Angiographic Evaluation of the Circle of Willis

Stefani, M. A.<sup>1</sup> • Schneider, F. L.<sup>1</sup> • Marrone, A. C. H.<sup>1</sup> • Aesse, F.<sup>2</sup> • Pinheiro, C. P.<sup>2</sup> • Mazzola, A.<sup>2</sup>

<sup>1</sup>Hospital de Clínicas de Porto Alegre, Porto Alegre, BRAZIL, <sup>2</sup>Hospital Moinhos de Vento, Porto Alegre, BRAZIL

#### PURPOSE

The present study evaluates the calibers and anatomical configurations based on the magnetic resonance examinations, examining vascular territories and sex-linked variations.

#### MATERIALS & METHODS

A randomized sample of 30 angiographic examinations with magnetic resonance (MRA) in adult patients of both sexes was obtained and components of the circle of Willis were identified. Branch diameters were measured on a transversal cut 5 mm from the vessel origin in a typical angiographic frontal incidence and for comparative statistical analysis, examinations were divided in groups considering the patients' sex and age. The examination of the vascular distributions and calibers were blinded and performed by two examiners.

#### RESULTS

The classical circle of Willis configuration was verified in only 15 examinations (50%). Greater calibers were observed in the arteries of the posterior circulation and multiple linear regression analysis established that the caliber of the posterior circulation was influenced by an independent variable related to the gender. Additional variations included unilateral and bilateral fetal and hypoplastic posterior communicating arteries. In the anterior cerebral artery (ACA), the presence of an accessory developed ACA, an ACA giving branches to the distal portion of the two hemispheres and a third median ACA the variants observed.

**CONCLUSION**

Gender influences the variations on internal diameters of posterior circulation vessels, with larger measurements in men.

**KEY WORDS:** Arteries, anatomical variation, MR angiography

**P-77**

**Prevalence of the Caroticoclinoid Foramen as Determined by CT**

Rubinstein, D.-Otero, A. V.-Ree, A. A.  
University of Colorado School of Medicine  
Aurora, CO

**PURPOSE**

To determine the frequency of ossification of the ligament between the anterior and middle clinoid processes (arrow in the figure). Ossification of this structure forms the caroticoclinoid foramen (asterisk in the figure) and its presence will affect the approach to and difficulty of surgery in the cavernous sinus region.

**MATERIALS & METHODS**

The CT scans of the paranasal sinuses or the face of 100 hundred consecutive patients were reviewed to determine the incidence of completely ossified bars connecting the anterior, middle and posterior clinoid processes of the sphenoid bone. All scans consisted of 1 mm helically acquired sections and were evaluated using multiplanar reformatted images on a workstation.

**RESULTS**

A complete ossified bar between the anterior and middle clinoid processes was identified on the right in 16 subjects and on the left in nine. Seven subjects had bilateral caroticoclinoid foramina. Of the 16 on the right, seven also had a complete ossified bar connecting the anterior and posterior clinoid processes. Two of the seven on the left had an anterior-posterior clinoid bar. In addition, there were separate anterior-posterior clinoid bars in three subjects on the right and one on the left. The subject with the left-sided anterior-posterior clinoid bar also had anterior-middle clinoid bar on the right.

**CONCLUSION**

Ossification of the anterior-middle clinoid ligament to form a caroticoclinoid foramen occurred in 18% of the subjects. It can be identified on thinly collimated CT scans that include the cavernous sinuses. Additional or separate ossification of the anterior-posterior clinoid ligament also can be identified.

**KEY WORDS:** Skull base, CT, anatomy

**Monday, April 23 –  
Wednesday, April 25**

**6:30 AM – 9:00 PM**

**Thursday, April 26**

**6:30 AM - 3:00 PM**

**Americas Hall II**

**Scientific Posters (Printed) 78 –  
86**

**(P3) Head and Neck**

**Note: A missing printed poster number  
indicates an abstract has been withdrawn.**

**P-78**

**Imaging of Vidian Canal**

Sathyakumar, V. D.<sup>1</sup> Ginsberg, L. E.<sup>2</sup>

<sup>1</sup>Baylor College of Medicine, Houston, TX, <sup>2</sup>The University of Texas M.D. Anderson Cancer Center, Houston, TX

**PURPOSE**

The purpose of this exhibit is to describe the anatomy of the vidian canal and its contents, and discuss various pathologies that can affect this deep-seated, skull-based foramen.

**MATERIALS & METHODS**

1. Describe the anatomy and contents of vidian canal. 2. Discuss the pathologies that can affect vidian canal.

**RESULTS**

The vidian canal, also known as the pterygoid canal, is housed deep in the sphenoid bone and visualized on most of the CT or MRI studies of the skull base. It transmits the nerve of pterygoid canal, also known as the vidian nerve, along with its corresponding artery (artery of the pterygoid canal). The greater superficial petrosal nerve, (a branch of the facial nerve) and deep petrosal nerve (a branch from carotid sympathetic plexus) join to form the vidian nerve. Among the other neural functions to be described attributable to the vidian nerve is lacrimation. The vidian canal may be

involved primarily by diseases that arise from the contents of the canal, or secondarily, by virtue of its location in the skull base. The pathologies reviewed include tumor arising from vidian nerve (including benign and malignant), metastatic processes, and diseases that arise from surrounding structures such as nasopharynx and skull base, and perineural spread to involve the canal secondarily.

#### CONCLUSION

The vidian canal is a small and frequently overlooked foramen in the skull base. Since lesions affecting this canal are relatively uncommon, and potentially asymptomatic, the radiologist should be careful to evaluate this potential blind spot. This is especially true in cases of perineural spread of tumor, in which case failure to recognize tumor may lead to subsequent involvement of the intratemporal facial nerve, with potentially grave consequences.

**KEY WORDS:** Skull base, vidian canal, anatomy

#### P-79

##### Dynamic Contrast-Enhanced MR Imaging of Orbital and Anterior Visual Pathway Lesions

Chi, T. L. · Al-Ibraheemi, A. K. · Hou, P. · Schiffman, J. S.

University of Texas M.D. Anderson Cancer Center  
Houston, TX

#### PURPOSE

The purpose of this study was to evaluate the utility of T1-weighted dynamic contrast-enhanced MR imaging (DCE MRI) as an adjunct to conventional MRI of the orbit. Findings on conventional MRI of orbital tumors are often nonspecific. High-resolution imaging at 3T has improved our ability to differentiate between intrinsic and extrinsic optic nerve pathology and therefore improved our confidence with our differential diagnosis. However, significant overlap exists with routine imaging alone and for certain lesions that are risky to biopsy, additional imaging parameters are needed for further lesion characterization. For example, optic nerve gliomas accompanied by arachnoid proliferation have imaging findings similar to those of optic nerve sheath meningiomas, and differentiation between leukemic infiltration of the nerve and sequelae of treatment, i.e., radiation-induced optic neuropathy, is difficult if not impossible. We hypothesized that DCE MRI is useful in the overall assessment of orbital and anterior visual pathway pathology.

#### MATERIALS & METHODS

We retrospectively reviewed T1-weighted DCE MRI findings of 12 patients with radiation-induced optic neuropathy (1 patient), optic nerve sheath meningioma (4), optic nerve gliomas (3), intraorbital metastasis (2), and neurofibromatosis (1) (1- chiasmal glioma; 1- intraconal mass). Dynamic contrast-enhanced MRI protocol at 3T consisted of 3D axial fast spoiled gradient echo T1-weighted scan. Images were acquired with a 22 cm field of view, 2 mm slice thickness, and 0 mm gap with 256x128 matrix. The total acquisition time varied

from 7 to 11 minutes. Intravenous contrast at 0.1 mmol/kg was injected with a power injector at 4 cc/sec followed by a 20 cc saline bolus. Average dynamic contrast resolution was around 10 sec with average acquisition pixel size of 0.86 x 1.72x2 mm<sup>3</sup>. Data were analyzed off-line on a GE AW workstation (General Electric Medical Systems, Milwaukee, WI). Regions of interest were selected, and perfusion parameters analyzed included positive enhancement integral (PEI) at 90 sec and maximum slope of signal intensity (SI<sub>max-slope</sub>).

#### RESULTS

The SI-time curves of orbital lesions demonstrated different perfusion characteristics. The perfusion curves for all optic nerve sheath meningiomas were similar. Positive enhancement integrals ranged from 202.73 - 275.9. The SI<sub>max-slope</sub> was elevated (321.69 - 465.15), and SI reached a plateau, and then slowly declined. For the single untreated optic nerve glioma, PEI was 307.69, SI<sub>max-slope</sub> was 419.75, and the SI-time curve was similar to those for meningiomas, but peaked slightly later and demonstrated a slow washout. The SI-time curves for intraorbital metastases demonstrated a much gradual increase in SI over time. The enhancement curve of the orbital mass in the patient with neurofibromatosis 1 paralleled that of a typical subcutaneous neurofibroma found on the same scan, allowing us to assume that these two lesions had the same histology. The patient with radiation-induced optic neuropathy had the lowest PEI (25.75) and SI<sub>max-slope</sub> (112.9) with no washout.

#### CONCLUSION

Our preliminary DCE MRI data show discernible differences in the enhancing characteristics of orbital tumors and anterior visual pathway lesions. A larger study will be needed to show that DCE MRI has added value in differentiation of these processes.

**KEY WORDS:** DCE MR imaging, orbit, perfusion

#### P-80

##### Ocular Adnexal IgG4-Related Disease: CT and MR Imaging Findings

Park, S.<sup>1,2</sup> · Jung, H.<sup>1</sup> · Kim, J.<sup>3</sup> · Seo, H.<sup>3</sup> · Son, C.<sup>3</sup> · Choi, S.<sup>3</sup> · Han, M.<sup>2</sup> · Chang, K.<sup>2</sup> · Chun, J.<sup>3</sup>

<sup>1</sup>Boramae Medical Center, Seoul, KOREA, REPUBLIC OF, <sup>2</sup>Seoul National University College of Medicine, Seoul, KOREA, REPUBLIC OF, <sup>3</sup>Seoul National University Hospital, Seoul, KOREA, REPUBLIC OF

#### PURPOSE

IgG4-related sclerosing disease is a systemic inflammatory disease that recently has been regarded as a new clinicopathologic entity that has characterized with lymphoplasmacytic infiltration, fibrosis, obliterative phlebitis of medium and small veins, and variable degree of eosinophilia. It is a multiorgan involving autoimmune disease that is responsive to steroids. The most common site is the pancreas but orbit involvement also has been reported. The purpose

of this study is to evaluate the CT and MR imaging findings of IgG4-related sclerosing disease involving orbit.

#### **MATERIALS & METHODS**

CT (n = 10) and MR (n = 3) images obtained in 11 patients (7 men and 4 women: mean age, 53 years: age range, 35-67 years) with histologically proved IgG4-related sclerosing disease in orbit, were reviewed retrospectively. We analyzed imaging findings with particular attention to the multiplicity and bilaterality, location, size, margin, CT attenuation, enhancement degree on CT and MR, bone involvement, and MR signal intensity. Among the multiple follow-up images, initial CT and MR images only were included for the evaluation. When new lesions developed, the image also was included in the evaluation.

#### **RESULTS**

A total of 18 lesions were found in 11 patients. Seven patients had bilateral lesions and four patients had unilateral lesions. The lacrimal gland was the most frequent location involved in all 11 patients. Bilateral lacrimal gland involvement was in five, bilateral lesion with one lacrimal gland and another orbital lesion was in two (1 intraconal, 1 medial canthal lesion), unilateral lacrimal gland lesion was in four. Mean size of the lesion was 23 mm. Most (17/18) of the lesions had well demarcated margin with ovoid shape. On precontrast CT (10 lesions in 7 patients), six had iso-attenuation and four had high attenuation compared with muscle. On postcontrast-enhanced CT (13 lesions in 8 patients), most (10/13) lesions had moderate enhancement (similar degree with mucosal enhancement). On three MR images (5 lesions in 3 patients), all of the five lesions showed iso-signal intensity on T1-weighted images, and three low signal intensity lesions and two iso-signal intensity lesions on T2-weighted images in comparison with cerebral gray matter. After contrast media injection, two had moderate enhancement (similar degree with mucosa) and three had mild enhancement (similar degree with muscle). Bone destruction was not noted.

#### **CONCLUSION**

Lacrimal gland involving well demarcated ovoid mass with moderate enhancement is the most common CT and MR imaging findings of IgG4-related sclerosing disease in orbit. The low or iso-signal intensity on T2-weighted MR imaging probably reflect the various amounts of fibrosis contained in the individual lesion.

**KEY WORDS:** IgG4, orbit, CT MR imaging

#### **P-81**

#### **Patterns of Local, Malignant Disease Spread in the Floor of Mouth and Oral Tongue**

Ahmad, I. Mosier, K. M.

Indiana University - Purdue University Indianapolis  
Indianapolis, IN

#### **PURPOSE**

1. To review the CT/MR, floor of mouth and oral tongue anatomy. 2. Learn the patterns of local malignant disease spread in the floor of the mouth and oral tongue. The floor of mouth (FOM), is structurally formed by the mylohyoid muscle and consists of the oral mucosa and the subjacent sublingual space (SLS). The oral tongue is the anterior 2/3rd of the tongue, anterior to the circumvallate papilla. These oral cavity subsites commonly harbor malignant disease processes. Knowledge of radiologic anatomy, routes of spread and pathophysiology facilitate the radiologist in accurately determining disease extent and assisting the clinician in adequate treatment planning.

#### **Material & Methods**

We performed a retrospective review of our imaging data base for FOM lesions. Since 2001 to June 2011, a total of 765 cases of malignant lesions were available, and we selected lesions based on their potential for spread to adjacent or distant sites. In addition we reviewed the specific appearance of these lesions on CT and MR. We then evaluated patterns of local disease spread based on mucosal, submucosal, perimuscular, perineural, direct or perivascular routes.

#### **RESULTS**

Common malignant entities of the floor of mouth with potential for spread to adjacent or distant sites are squamous cell carcinoma, sublingual or minor salivary gland tumors and lymphoma. The FOM and oral tongue malignancies may spread to the other oral cavity subsites such as mandible, submandibular space, parapharyngeal space, preepiglottic space and the hyoid bone by mucosal, submucosal, perimuscular, perineural or perivascular or direct spread to the adjacent mandible. Extension of malignant disease to adjacent sites in the oral cavity, oropharynx or surrounding spaces will upstage the disease. In our review the predominant modality used to characterize the lesion was contrast-enhanced CT for most benign and malignant lesions, followed by contrast-enhanced MR.

#### **CONCLUSION**

The extent of malignant disease in the FOM and the application of this information ensure accurate staging and determine the proper treatment planning. The specific imaging appearance of these lesions, the infiltration of different structures and the mechanism of spread helps to predict the disease extent. A combination of CT and MRI is complimentary and problem solving in certain complex cases. Adequate anatomical knowledge of possible local spread mechanism helps to understand disease extent and thus ensure appropriate management.

**KEY WORDS:** FOM

## P-82

**Patients with Congenital Hyposmia Exhibit a Spectrum of Anatomical Brain Abnormalities**

Sethi, I. Sharma, S. Agarwal, R. Henkin, R. Levy, L. M.

George Washington University Medical Center  
Washington, DC

**PURPOSE**

Patients with congenital hyposmia have been considered to have absent olfactory bulbs as the cause of their smell loss. To evaluate this concept, anatomical changes in the brains of patients with congenital hyposmia were studied critically by use of magnetic resonance imaging (MRI).

**MATERIALS & METHODS**

Thirty-four patients with congenital hyposmia were studied [age  $29 \pm 18$  years (mean  $\pm$  SD), 13 men, 21 women]. All patients had Type I hyposmia (ability to detect but inability to recognize any odor). All patients also had Type 2 congenital hyposmia (spontaneous smell loss without hypogonadism). Patients were evaluated with a standard MRI protocol including high-resolution T2-weighted coronal images. Structural abnormalities were evaluated in regions of the olfactory bulbs, olfactory grooves, olfactory sulci, orbitofrontal cortex, temporal lobes and hippocampi. Diffusion tensor imaging (DTI) tractography with high-resolution 3D anatomical reconstructions also were obtained.

**RESULTS**

In all 34 patients, olfactory bulb size varied widely, with most bulb volumes less than that of normal controls. There was a significant degree of bilaterality in abnormalities involving decreases in olfactory bulb sizes, olfactory groove depth, olfactory sulcal depth and in hippocampal deformations ( $r > 0.7$ ,  $p < 0.01$ ). Ipsilaterally, decreased bulb size was significantly correlated with decreased ipsilateral olfactory groove depth ( $r > 0.7$ ). Normal olfactory sulci were present despite the presence of smaller than normal olfactory bulbs in seven patients (21%). Abnormal hippocampal malrotations were observed bilaterally in 10 patients (30%) and unilaterally in 24 patients (70%). In five patients (15%) olfactory sulci were absent with fusion of the gyrus rectus with the medial orbital gyrus, and fusion of associated fiber tracts; these latter observations were best observed by DTI and 3D reconstructions. In some cases, fused gyri extended inferiorly, either unilaterally or bilaterally.

**CONCLUSION**

Anatomical structural abnormalities are present in the brain of most patients with congenital hyposmia. Anatomical abnormalities can vary greatly and include changes in olfactory bulbs, grooves, sulci and hippocampi. While the mechanisms of smell loss in patients with congenital hyposmia may vary, anatomical changes involve a spectrum of abnormalities of varying degrees and severity in several brain regions.

**KEY WORDS:** Hyposmia, congenital, olfactory bulbs

## P-83

**Supernumerary Olfactory Bulbs Are Present in MR Imaging Studies of Brain Anatomy**

Sharma, S. Agarwal, R. Sethi, I. Kelahan, L. Henkin, R. Levy, L. M.

George Washington University Medical Center  
Washington, DC

**PURPOSE**

To study olfactory bulb characteristics in normal subjects and in patients with smell loss.

**MATERIALS & METHODS**

Magnetic resonance imaging (MRI) studies of anatomical structures in the region of the olfactory bulbs were acquired from a series of 220 subjects referred to our Medical Center for evaluation of several clinical complaints (e.g., headache, possible seizure, TIA, etc.). All patients had a standard MRI brain protocol including high-resolution T2-weighted coronal images. All images were evaluated carefully for olfactory bulb morphology and structural abnormalities in the orbitofrontal cortex, rectus gyrus region, olfactory grooves, hippocampi and temporal lobes.

**RESULTS**

Supernumerary olfactory bulbs were discovered in 16 patients (7.3%) [N = 16, age  $43 \pm 16$  years (mean  $\pm$  SD), range 6-68 years], which included six males and 10 females. Bilateral duplication of bulbs was present in 15 patients (94%) with unilateral duplication in one patient (6%). Patients exhibited normal olfactory sulci but widened and flattened olfactory grooves [15 of 16 patients (94%)]. Olfactory bulb size was within normal limits in 10 patients (62%) with mild to moderate asymmetry of bulb size in six of 16 patients (38%). Olfactory groove depth was decreased with respect to normal in five patients (31%). Hippocampal malrotations were increased compared to normal in five patients (31%). In the one patient with unilateral bulb duplication, a contralateral left fronto-temporal arachnoid cyst was present. Smell function was known to be impaired in only one of these patients (6%) who had congenital hyposmia.

**CONCLUSION**

On the basis of these observations, olfactory bulb duplication may be more common than currently is recognized. This is the first report of supernumerary olfactory bulbs. This may have occurred since olfactory bulb anatomy has been difficult to image with prior techniques and olfactory bulb anatomy has not been the focus of neuroradiologic attention in the past. Functional studies of olfaction among these patients have not been evaluated systematically, with only one patient among the 16 with a known significant loss of smell. The other patients among the 16 studied had no stated clinical changes related to olfactory function.

**KEY WORDS:** Olfactory bulbs, supernumerary, duplication

#### P-84

##### Otalgia: Rational Imaging Approach

Bidari, S. S. Shushrutha Hedna, V. De Jesus, R. Waters, M. F. Mancuso, A. A.

University of Florida  
Gainesville, FL

##### PURPOSE

Progressive referred otalgia (PRO) is a very important symptom in upper aero-digestive tract disease and needs cross-sectional imaging evaluation as the etiology behind it may not be entirely benign. The pathology most often is in temporal bone, TMJ, parotid gland, nasopharynx, oropharynx, tonsils, tongue-base and pyriform sinus. In this review we highlight the importance of understanding detailed innervation of the temporal bone, its role in protocol design and various clinical scenarios causing PRO.

##### MATERIALS & METHODS

This is a review of the data from our institutional protocol for the last 10 years and literature search.

##### RESULTS

Progressive referred otalgia may come from middle ear disease caused by eustachian tube dysfunction such as that caused by nasopharyngeal carcinoma. It may be via the glossopharyngeal nerve from the tongue base, tonsil or via the vagus nerve from the pyriform sinus. The cause, if found, may be a carcinoma at one of these sites. The pain refers back to the temporal bone due to innervation by Jacobson's nerve (IXth nerve branch) or by Arnold's nerve (Xth nerve branch). The principal end innervation of the glossopharyngeal nerve is sensory to the oropharynx. The most common structural cause of a glossopharyngeal nerve pain pattern is squamous cell carcinoma or lymphoma of the palatine tonsil, glossotonsillar fossa or tongue base seen in patients with throat pain or referred otalgia. These are sometimes entirely submucosal cancers that can only be found with CT or MRI and confirmed with the endoscopist's biopsy site guided by the imaging study areas of suspicion; so called imaging directed biopsy. CT is better than MRI as there are more artifacts on MRI due to swallowing. Imaging protocol is designed to evaluate the temporal bones and the neck, at least extending up to the pyriform sinuses.

##### CONCLUSION

Progressive referred otalgia must be viewed with a very high index of suspicion even in light of negative upper aero-digestive tract endoscopy especially in the smoking/drinking population. Once TMJ syndromes and similar sources of pain that may have a periauricular location been excluded clinically, it is important that these patients also have a complete clinical evaluation of the nasopharynx, oropharynx and hypopharynx as well as otoscopy by an experienced otolaryngologist. Depending on this initial triage they may be referred for

imaging. Understanding the innervation, anatomy and pathophysiology is crucial in designing the appropriate protocols that would help clinch the correct diagnosis.

**KEY WORDS:** Otalgia, referred neuralgia, submucosal cancer

#### P-85

##### Syphilis of the Inner Ear Mimicking Schwannoma

Agostinis, C. Marini, B. Galtelli, C. Gallizioli, G. Bonaldi, G.

Ospedali Riuniti  
Bergamo, ITALY

##### PURPOSE

To present a rare case of luetic infection with bilateral involvement of the inner ear causing sensorineural hearing loss, vertigo and left facial palsy in a 28-year-old man with HIV infection.

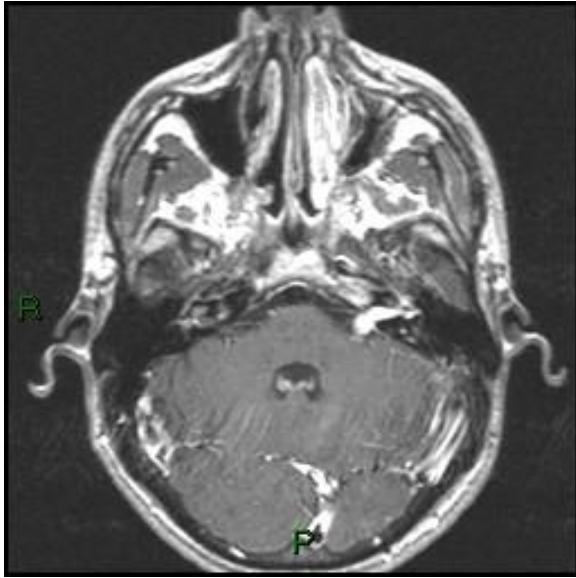
##### MATERIALS & METHODS

This young patient from Brazil was admitted to our hospital with a 2-month history of progressive hearing loss in the left ear and a more recent development of left facial paralysis and right hypoacusis.

##### RESULTS

On admission, a first contrast-enhanced MR scan showed a lesion occupying the left internal auditory canal and a limited portion of the adjacent cerebello-pontine angle cistern. A clear enhancement also was noted at the level of the labyrinth and most part of the intratemporal facial nerve, bilaterally. The normal hyperintensity on MR cisternogram was reduced in the left inner ear. A CT scan of the temporal bone was unremarkable except for a slight apparent enlargement of the labyrinthine segment of the left facial nerve canal. Serology tests for most common infections also were performed on admission and showed HIV and VDRL (Venereal Disease Research Laboratories) positivity. Cerebrospinal fluid (CSF) VDRL also was positive. High-dose penicillin G therapy was started. After about 4 weeks a follow-up MRI showed a significant reduction of the solid lesion and a less marked enhancement of the membranous labyrinth. Facial palsy as well as hypoacusis improved.





#### CONCLUSION

The peculiar, interesting aspect of our case is the tumor-like appearance of the left auditory canal lesion. The association with diffuse inner ear involvement as well as the presence of facial nerve palsy suggested a diagnosis different from acoustic schwannoma, i.e., an inflammatory-infectious condition, which was defined by serology and, ultimately, confirmed by response to treatment.

**KEY WORDS:** Infectious disease, temporal bone, acoustic schwannoma

#### P -86

#### Measurements of T2 Relaxation Times of the Articular Disk of Temporomandibular Joint on Temporomandibular Joint Dysfunction Patients and Asymptomatic Volunteers

Kakimoto, N., Tsujimoto, T., Kataoka, M., Tomita, S., Shimamoto, H., Murakami, S., Furukawa, S.

Osaka University Graduate School of Dentistry  
Suita, Osaka, JAPAN

#### PURPOSE

Measuring T2 relaxation times by MR imaging has been reported to detect degenerated cartilage on knee cartilage and lumbar intervertebral disk. The aim of this study was to measure T2 relaxation time of the articular disk of temporomandibular joint (TMJ) on temporomandibular joint dysfunction (TMD) patients and asymptomatic volunteers.

#### MATERIALS & METHODS

One hundred four patients with TMD and 17 asymptomatic volunteers were examined by 1.5 T MR scanner (Signa HDxt 1.5 T, GE Healthcare, WI, USA). The imaging protocol consisted of oblique sagittal multiecho spin-echo T2-weighted sequence performed with the following parameters; TR/TE, 1000/8.9, 17.8, 26.7, 35.6, 44.5, 53.4, 62.4, 71.3 msec, FOV, 120 x 120 mm,

matrix size, 256 x 160, slice thickness, 4 mm, gap, 1 mm, and total acquisition time, 5 minutes 22 seconds. T2 relaxation times of the articular disk of TMJ were calculated on Advantage Workstation (GE Healthcare, WI, USA). Temporomandibular joint patients were divided by disk position (normal superior, partial anterior disk displacement with reduction, partial anterior disk displacement without reduction, anterior disk displacement with reduction, and anterior disk displacement without reduction), disk formation (biconcave, biplanar, hemiconvex, thickening of the posterior band, biconvex, and folded), joint effusion (none or minimal, moderate, marked, and extensive), bone change (none and osteoarthritis), and bone edema (none and edema).

#### RESULTS

The T2 relaxation time of the articular disk of anterior disk displacement without reduction group was significantly longer than that of asymptomatic volunteer group and normal superior position in patients group ( $P < 0.01$ ). The T2 relaxation time of the articular disk of folded type group was significantly longer than that of asymptomatic volunteer group ( $P < 0.01$ ). The T2 relaxation time of the articular disk of extensive joint fluid group was significantly longer than that of asymptomatic volunteer, none or minimal joint fluid in patients, and moderate joint fluid groups ( $P < 0.01$ ). The T2 relaxation time of the articular disk of osteoarthritis group was significantly longer than that of asymptomatic volunteer and no osteoarthritis finding in patients groups ( $P < 0.01$ ). The T2 relaxation time of the articular disk of bone edema group was significantly longer than that of asymptomatic volunteer and no bone edema finding in patients groups ( $P < 0.01$ ).

#### CONCLUSION

T2 relaxation times of the articular disk of TMD patients were longer than that of asymptomatic volunteers. The severe MR findings were correlated with the longer T2 relaxation time of the articular disk of TMJ.

**KEY WORDS:** TMJ, T2 mapping, articular disk

**Monday, April 23 –  
Wednesday, April 25  
6:30 AM - 9:00 PM  
Thursday, April 26  
6:30 AM - 3:30 PM**

**Americas Hall II  
Posters (Printed) 87 – 99**

**(P4) Interventional**

**Note: A missing printed poster number  
indicates an abstract has been withdrawn.**

#### **P-87**

**Pseudoaneurysm of the Inferolateral Trunk after Right Hemifacial Arteriovenous Malformation Resection Presenting with Periorbital Excruciating Pain and Lateral Gaze Palsy: Discussion of the Symptoms Considering the Anatomical and Radiologic Findings as well as Treatment Options and Outcome**

Erdem, E.·Akdol, M. S.·Amole, A.

University of Arkansas for Medical Sciences  
Little Rock, AR

#### **PURPOSE**

We are reporting an interesting case of a right facial arteriovenous malformation (AVM) presenting with right periorbital pain and double vision following surgical treatment of the AVM.

#### **MATERIALS & METHODS**

The patient is a 12-year-old male with long-standing history of AVM resection and facial reconstruction surgeries. He had recent treatment of recurrent AVM with endovascular Onyx embolizations of the external carotid artery branches followed by surgical resection 3 months after the last embolization. He presented with right-sided periorbital excruciating pain, double vision and lack of the lateral movement of the right orbital globe consistent with abducens nerve (CN VI) palsy. No obvious oculomotor and trochlear nerve symptoms were observed. The symptoms appeared 4 months after the AVM surgery that involved wide resection of the AVM nidus within the right pterygoid space and the cranial base. Noninvasive diagnostic studies, especially contrast-enhanced MR angiogram of the cranial base, demonstrated suspicious findings for a small aneurysm in the cavernous sinus. Catheter angiogram confirmed this finding however; disclosed a 12x 6 mm pseudoaneurysm arising from the right inferolateral trunk (ILT) branch itself, 1 cm beyond the origin of the right internal carotid artery.

#### **RESULTS**

Definitive treatment was performed by embolizing the pseudoaneurysm using detachable coils. The periorbital pain subsided immediately after the occlusion of the aneurysm. The abducens nerve palsy continued with decreasing intensity and the patient was symptom-free at 2 months follow up.

#### **CONCLUSION**

In this presentation, radiologic findings were discussed in detail with emphasis on the regional anatomy as well as treatment options and outcome. The anterolateral triangle of the cavernous sinus and the superior ophthalmic fissure are anatomically complex. This area is particularly important in microsurgical removal of cavernous sinus tumors and therefore thoroughly investigated in the literature. Deep and medial location, concentration of ocular sensory and motor nerves, small arterial branches within and in close proximity to venous component of the cavernous sinus makes the surgical approach difficult. The inadvertent ILT injury during the surgery presented itself as a pseudoaneurysm, rather than carotico-cavernous fistula. This aneurysm then became symptomatic by entrapment of the trigeminal nerve V1 division and CNVI palsy at the anterolateral triangle close to the superior orbital fissure. Consistent with the current observations in the literature, endovascular coil embolization of this aneurysm was highly effective in controlling the patient's complaints and full recovery of the neurologic symptoms and immediate control of the pain.

**KEY WORDS:** Pseudoaneurysm, coil embolization, cranial nerve palsy

#### **P-88**

**MR Angiography at 3.0 T with Volume Rendering-Coil Imaging for Coiled Intracranial Unruptured Aneurysm**

Kiura, Y.·Matsushige, T.·Sakamoto, S.·Okazaki, T.·Shinagawa, K.·Kurusu, K.

Hiroshima University  
Hiroshima, JAPAN

#### **PURPOSE**

To evaluate the stability of coiled aneurysm, the ideal examination should demonstrate all related components: aneurysms, coils, and parent arteries in one image. The purpose of this study was to validate volume-rendering coil (VR coil) technique at 3 T MR angiography (MRA) in comparison with digital subtraction angiography (DSA).

#### **MATERIALS & METHODS**

Twenty-one aneurysms from 20 patients underwent 3 T MRA in the initial assessment for endovascular treatment of cerebral aneurysm. 3 T MRA was performed within 2 days after endovascular surgery for unruptured aneurysms. Two neuroradiologists with over 10 years of experience, blinded to pertinent

clinical information, independently assessed VR coil image and DSA to evaluate aneurysm occlusion.

## RESULTS

The mean interval between MRA and angiography was  $1.3 \pm 0.7$  days. The size of aneurysm included was 5.6 mm in average. The interobserver reading agreement was very good ( $k = 0.793$ ) in VR coil and perfect ( $k = 1.000$ ) in DSA. Referenced on DSA as a standard, the overall sensitivity and specificity of VR coil were 87.5% and 93.8%, respectively. Regarding the demonstration of coils in aneurysm, parent and branch arteries, Volume-rendering coil was considered comparable to DSA. Aneurysm neighboring the skull base or originating from small parent artery, however, still was visualized poorly on VR coil image.

## CONCLUSION

Volume-rendering coil imaging has a good agreement with DSA in the initial evaluation of coil embolization for intracranial aneurysms. 3 T MRA VR coil technique enabling the evaluation of neck morphology and coil compaction appeared effective for screening of the neck remnant and was helpful to decide further treatment strategy.

**KEY WORDS:** Coil embolization, aneurysm, 3 T MR imaging

## P-89

### Peri-Stent Aneurysm Formation after Stent Implant for Stenotic Intracranial Vertebral Artery Dissection: Report of Two Cases Successfully Treated with Coil Embolization

Ishimaru, H.·Nakashima, K.·Takahata, H.·Matsuoka, Y.  
National Hospital Organization Nagasaki Medical Center  
Omura, JAPAN

## PURPOSE

Although stenting for stenotic vertebral artery dissection (VAD) improves compromised blood flow, delayed peri-stent aneurysm formation is not well known. We report two cases with delayed peri-stent aneurysm formation successfully treated with coil embolization.

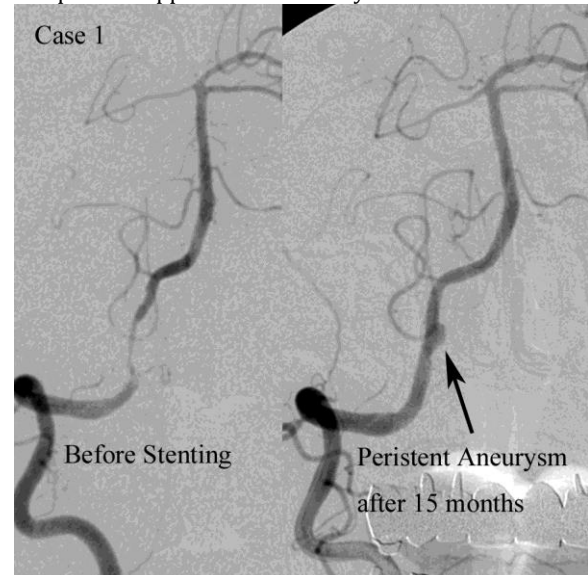
## MATERIALS & METHODS

Since 2004, three patients with stenotic intracranial VAD underwent endovascular angioplasty at our institution. All three patients had acute infarction in posterior circulation territory and clinical evidence of hemodynamic insufficiency. Neuroimaging studies revealed intracranial vertebral artery stenosis caused by dissection, contralateral vertebral artery occlusion, and hypoplasia of posterior communicating arteries in all patients. In two of three patients, balloon angioplasty at first session was successful. One of these two patients had clinical evidence of hemodynamic insufficiency 2 months after the first session, and a balloon-expanded coronary stent was implanted. Angiography immediately after stenting showed no definite aneurysm beside the stent (Case 1). In the remaining patient, balloon angioplasty at first session failed due to

recoil, a balloon-expanded coronary stent was implanted at the first session. Angiography immediately after stenting showed minimal slit-like projection at proximal edge of the stent (Case 2). These two cases were included in this study.

## RESULTS

In case 1, CT angiography obtained 5 months later revealed peri-stent aneurysm. In case 2, catheter angiography performed 3 months later showed that the projection at proximal edge enlarged and formed an aneurysm beside the stent. Because follow-up neuroimaging showed growth of the aneurysm, endovascular aneurysmal embolization was planned in both cases. We advanced a microcatheter into the aneurysm through the strut of the stent and delivered detachable coils into the aneurysm lumen successfully in both cases. The postprocedural course was uneventful and follow-up examination revealed complete disappearance of aneurysm in both cases.



## CONCLUSION

Peri-stent aneurysm formation probably represents enlargement of underlying false lumen that was not visible on angiography during the procedure. Stenting for stenotic intracranial VAD may result in delayed peri-stent aneurysm formation, which would be managed with coil embolization through the strut.

**KEY WORDS:** Vertebral artery dissection, stent, aneurysm formation

## P-90

### Rapidly Evolving Large Extracranial Vertebral Artery Pseudoaneurysm in Behcet's Disease

Rao, S.·Morón, F.·Bhanusali, N.·Benndorf, G.

Baylor College of Medicine  
Houston, TX

## PURPOSE

Behcet's disease is a multisystem chronic autoimmune disease of unknown etiology with a wide spectrum of

symptoms and organ system involvement. Behcet's vasculitis usually affects veins of all sizes with superficial thrombophlebitis and thrombosis of major vessels. Arterial manifestation, particularly of the extracranial vertebral arteries is rare. We report an unusual case of a patient with Behcet's disease, who presented with bilateral spontaneous vertebral artery pseudoaneurysms.

#### MATERIALS & METHODS

A 26-year-old African American female with known Behcet's disease initially presented with radiating left neck and arm pain. A 6 mm left spontaneous vertebral artery (VA) pseudoaneurysm of the V2 segment was found on computed tomography angiography (CTA) and managed conservatively with steroids and medical anticoagulation. She returned 4 months later due to new onset right neck and arm pain with accompanying weakness. A second, new, 1.2x1.6x0.8 cm right VA (V1 segment) pseudoaneurysm was identified on CTA and confirmed by angiography. Over 4 days, the patient developed escalating right upper extremity sensory and motor deficits with rapid enlargement of the right VA pseudoaneurysm. Given the large size of the pseudoaneurysm along with the presumed underlying fragility of the vessel wall, parent vessel occlusion was considered the best treatment option rather than stenting. Repeat angiography at the beginning of the endovascular treatment revealed subtotal occlusion of the right proximal VA by the enlarging pseudoaneurysm. A microcatheter was navigated into the distal most portion of the patent proximal right vertebral artery segment just proximal to the pseudoaneurysm at C6 and multiple detachable coils (Codman Neurovascular; Raynham, Massachusetts) were deployed.

#### RESULTS

Endovascular occlusion of the remaining right vertebral artery inflow was performed successfully. Posttreatment, retrograde reconstitution of the distal and intracranial right vertebral artery was visualized via cervical collaterals and retrograde filling from the left vertebral artery. Patient was treated with high dose prednisone and counseled on compliance. Follow-up postprocedure angiogram at 4 months showed complete coil occlusion of the right VA and decreased size of the left VA. Clinically, the patient recovered well with improvement of pain to baseline and normal sensory-motor neurologic exam.



#### CONCLUSION

This case is notable for its presentation in an African American patient, the unusual location and bilaterality of the vertebral artery pseudoaneurysms. In our case, Behcet's disease presented spontaneously with a rapidly evolving large pseudoaneurysm of the cervical arterial circulation, which warranted endovascular management in combination with optimized medical management of the underlying disease.

#### P-91

##### Staged Coil Occlusion for Giant Spinal Perimedullary Arteriovenous Fistula

Burns, P. A.<sup>1</sup>Rennie, I. M.<sup>1</sup>Flynn, P. A.<sup>1</sup>Nahser, H. C.<sup>2</sup>O'Leary, S. M.<sup>1</sup>Smyth, G. P.<sup>1</sup>McKinstry, C. S.<sup>1</sup>

<sup>1</sup>Royal Victoria Hospital, Belfast, UNITED KINGDOM, <sup>2</sup>Walton Hospital, Liverpool, UNITED KINGDOM

#### PURPOSE

To discuss the use of endovascular coil occlusion for giant type III spinal perimedullary arteriovenous fistula (GAVF).

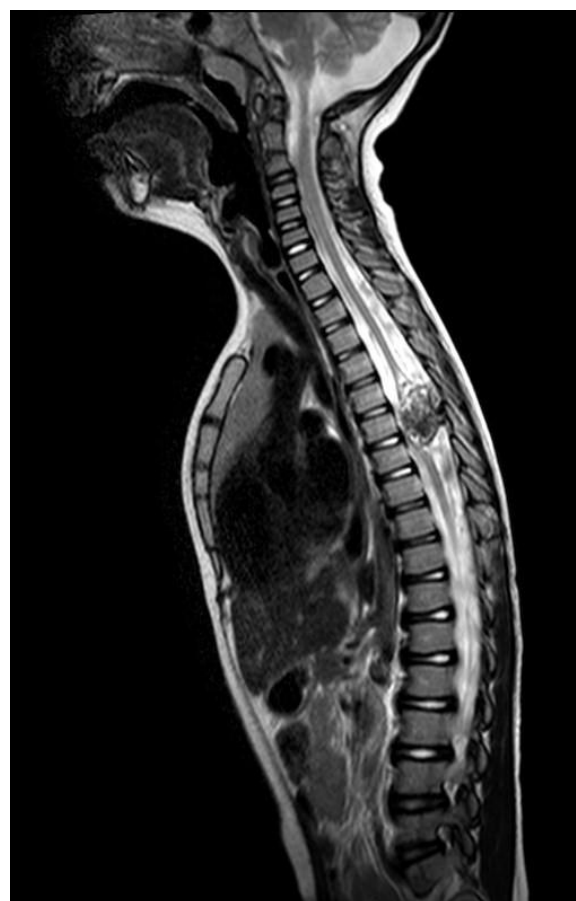
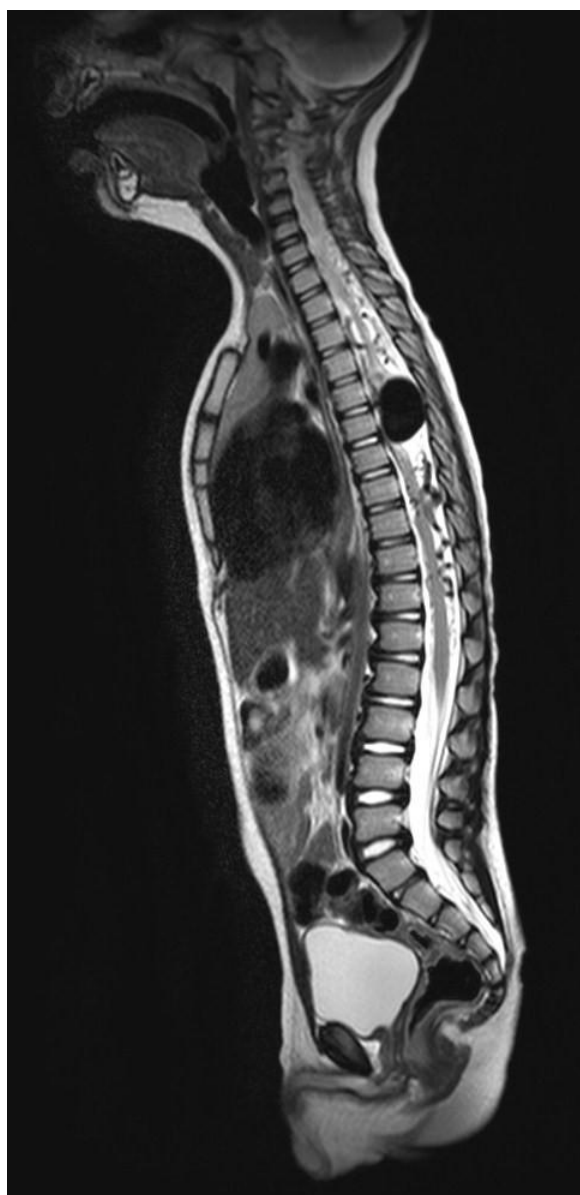
#### MATERIALS & METHODS

Retrospective case review of three pediatric patients exclusively treated via coil occlusion. GAVF are high flow shunts with associated venous aneurysms or pouches which generally present in childhood.

#### RESULTS

Case 1 was a 7-year-old female who presented with back pain and leg weakness. Initial MRI demonstrated a fistula in the thoracolumbar region with a large venous pouch. Coil occlusion of the venous pouch was performed on two separate occasions, 5 months apart. Follow-up MRI confirmed occlusion of the fistula. Her symptoms improved, although she required a tendon-lengthening procedure. Case 2 was a 5-year-old male who presented with increasing spastic diplegia. Initial MRI demonstrated a mid-thoracic perimedullary fistula with an associated venous pouch. Coil occlusion was performed on two separate occasions, 2 months apart. Follow-up MRI confirmed occlusion of the fistula (refer to attached images). His symptoms ultimately stabilized and no longer deteriorated. Case 3 was a 6-year-old male who presented with sudden onset headache. This

was found to be due to subarachnoid hemorrhage secondary to a cervical perimedullary fistula, which was associated with two large venous pouches supplied via the right thyrocervical artery and vertebral artery. There was a known history of hereditary hemorrhagic telangiectasia. Coil occlusion was performed via the thyrocervical artery. Supply via the vertebral artery was part-occluded with onyx as tortuous anatomy precluded coil deployment. Further treatment was intended again via the vertebral artery, however interval follow-up MRI demonstrated complete occlusion of the fistula. He made a full recovery.



#### CONCLUSION

Occlusion of giant type III spinal perimedullary fistulas via staged coil occlusion is a safe and effective treatment option.

**KEY WORDS:** Perimedullary fistula, embolization

#### P-92

#### Analysis of Genetic Polymorphisms in Patients with Brain Arteriovenous Malformations

Franciscatto, A. C.·Matte, U. S.·Sperb, F.·Motta, S.·Stefani, M. A.

Hospital de Clínicas de Porto Alegre  
Porto Alegre, BRAZIL

#### PURPOSE

Brain arteriovenous malformations (AVM) are a cause of intracranial hemorrhage. Prevention of AVM bleeding or rebleeding is the aim of treatment. Improving genetics knowledge of AVMs could help to develop new forms of treatments or future prevention therapies. The aim of this study is to evaluate the association of some genetical polymorphisms with brain AVM.

#### MATERIALS & METHODS

We studied polymorphisms in Endoglin (207G>A), Activine-like kinasis (IVS3-35A>G), Interleucin 1 beta (511C>T), Interleucin 1 beta (IL1B -31T>C), Interleucin



6 (174G>C), TNF- $\alpha$  (238G>A) and ApoE. PCR analysis of 44 AVM patients and 96 controls were done.

## RESULTS

We found no significant differences between AVM patients and controls (Table 1).

Comparison between AVM patients and controls regarding studied genetic polymorphisms

Genetic Polymorphisms		AVM	Controls	P value
ApoE	E2/E3	9.09	14.58	.566
	E2/E3/E4	2.27	2.08	
	E3	63.63	62.5	
	E3/E4	22.72	20.83	
TNF $\alpha$	AG	13.63	10.41	.416
	GG	86.36	89.58	
IL1B (-511C>T)	AA	9.09	17.70	.416
	AG	56.82	48.95	
	GG	34.09	33.33	
IL1B (-31T>C)	AA	34.09	23.95	.402
	AG	47.73	51.04	
	GG	18.18	25	
ALK-1	AA	38.64	31.25	.676
	AG	50	57.29	
	GG	11.36	11.45	
ENG	CC	79.54	75	.476
	CT	20.45	21.87	
IL6	CC	9.09	10.41	.969
	CG	38.63	38.54	

## CONCLUSION

Other studies with more patients will be necessary to evaluate these results.

**KEY WORDS:** Arteriovenous malformation, genetic polymorphism

## P-93

### Revascularization of Acute Arterial Occlusions of the Anterior Cerebral Circulation Using the Penumbra System with Pulse Flow Restoration and Aspiration Components: A Single Center Assessment

Schramm, P.<sup>1</sup>•Schramm, R.<sup>1</sup>•Aceves, M.<sup>2</sup>•Mohr, A.<sup>1</sup>•Knauth, M.<sup>1</sup>

<sup>1</sup>University Goettingen Medical Center, Goettingen, GERMANY, <sup>2</sup>Penumbra Inc., Alameda, CA

## PURPOSE

The Penumbra System® is a continuous aspiration-based mechanical thrombectomy device for acute stroke intervention. This single center assessment describes our experience using a new investigational Pulse™ Flow Restoration component with the existing Penumbra System®, and the clinical outcome of treated patients

presenting with acute ischemic stroke due to occlusion of a large vessel of the anterior cerebral circulation.

## MATERIALS & METHODS

Eleven patients with acute ischemic stroke (median NIHSS 17, range 13 -22) due to occlusion of either internal carotid artery, middle cerebral artery or anterior cerebral artery (TICI 0) were treated with the Penumbra System with Pulse Flow Restoration and aspiration components within 8 hours after symptom onset. The investigational Pulse component of this System operates by temporary deployment of a self-expanding Nitinol Flow Restoration Device intended to restore vessel lumen and capture thrombus. Thrombectomy with both components of the System was performed as the initial mechanical treatment in all 11 cases. TICI flow in the target vessel segment was assessed before and after the recanalization procedure. Patients' clinical outcomes were evaluated using the NIHSS and mRS scores at discharge and at day 30 postprocedure respectively.

## RESULTS

In nine patients, TICI 2a or higher was achieved after using both components of the System as primary mechanical intervention (81.8%). Immediate flow restoration while deploying the Pulse component was accomplished in all of those nine cases. The mean time from first angio run to first perfusion was 34.9 min (range 22-54 min). However, in two cases implantation of a permanent intracranial stent had to be performed to achieve permanent perfusion. The mean number of Pulse deployments to effect maximal recanalization was  $2.0 \pm 1.1$ , and the mean time from first to last deployment of all Penumbra devices was  $38.9 \text{ min} \pm 28.3$ . Mean NIHSS at discharge improved from a baseline value of  $17 \pm 3.5$  to  $10.5 \pm 7.1$ . Good outcome at 30 day postprocedure (mRS 0-2) was observed in 54.5% of patients. Two patients experienced hemorrhage (HI-1), none of which were considered serious, and the serious device-related adverse event rate was 9%.

## CONCLUSION

Stent-assisted thrombectomy using the Penumbra System with Pulse Flow Restoration and aspiration components is a fast and effective way to treat acute occlusions of the anterior cerebral circulation. In this series of 11 patients, the combined components of the System led to a high recanalization rate (81.8 %) and favorable clinical outcome in a majority (55.5%) of patients, with an acceptable serious device-related complication rate.

**KEY WORDS:** Penumbra system, thrombectomy, flow restoration

**P-94****Hemodynamic Effects and Safety of Intraarterial Milrinone in Vasospasm Patients**

Rayes, M. Narayanan, S.

Wayne State University/Detroit Medical Center  
Detroit, MI

**PURPOSE**

To evaluate the hemodynamic effects, safety profile, and efficacy of intraarterial Milrinone in patients with cerebral vasospasm. Cerebral vasospasm is a common complication of aneurysmal SAH and relates to higher morbidity and mortality. When aggressive medical therapy (hypervolemia, hypertension, and hemodilution) fails, endovascular therapies, including mechanical and/or chemical options are utilized. Milrinone, a selective phosphodiesterase type III isoenzyme inhibitor with positive inotropic and vasodilator effects (arterial and venous) and minimal chronotropic effect, has been used occasionally to improve cerebral perfusion.

**MATERIALS & METHODS**

We reviewed our prospectively maintained database of patients who received intraarterial (IA) Milrinone at one academic medical center. Inclusion criteria for this study were cerebral vasospasm demonstrated by angiography and treated with IA Milrinone. Safety profile was based on immediate hemodynamic effects of Milrinone, including tachycardia and hypotension, the presence of cardiac arrhythmia during the procedure and immediate postprocedure period, and neurologic sequelae.

**RESULTS**

Thirteen cerebral angiograms with IA Milrinone infusion were performed in 12 women over 15 months (March 2010 - July 2011). Average age was 48 years (range 31-63 years). Vasospasm was due to aneurysmal subarachnoid hemorrhage in nine cases, posterior reversible encephalopathy syndrome (PRES) in two cases, and reversible cerebral vasoconstriction syndrome (RCVS) in one case. Three patients were treated with Verapamil and one patient with Milrinone initially with angiographic and clinical improvement, but vasospasm recurred within 2-4 days. Two patients underwent combined balloon angioplasty with IA Milrinone, and three patients received combined IA Verapamil and IA Milrinone. Six patients received only IA Milrinone; the remainder were started on an intravenous (IV) Milrinone infusion (0.375-0.5 mcg/kg/min) for 2-5 days afterwards. Injections were performed in the cervical internal carotid artery, V2 segment of the vertebral artery, or A1, M1, or P1 segments over 5-15 minutes/vessel. The average dose/extracranial vessel was 7.8 mg (range 2-20 mg), and the average dose/intracranial vessel was 2.7 mg (range 2-4 mg). Average total IA dose was 16.2 mg (range 10-26 mg). Eight patients experienced mild, asymptomatic tachycardia during the infusion; in only one case did this result in limitation of the Milrinone dose. Two patients had mild decrease in systolic blood

pressure post-IA Milrinone. No cardiac arrhythmias occurred during/postprocedure. All Milrinone infusions resulted in moderate improvement to complete resolution of the vasospasm.

**CONCLUSION**

Intraarterial Milrinone is a promising, relatively understudied, treatment for cerebral vasospasm. Intraarterial Milrinone may be associated with transient, dose-related, tachycardia and less commonly, hypotension. Cardiac arrhythmia and neurologic sequelae were absent in this case series. Further studies are required to determine the optimal dose/duration of IA/IV Milrinone.

**KEY WORDS:** Milrinone, vasospasm, hemodynamic

**P-95****Results of Mechanical Thrombolysis for Acute Ischemic Stroke: Comparison with Intraarterial Urokinase Infusion**

Choi, S. Jeon, S. Lee, Y.

Wonkwang University Hospital  
Iksan, KOREA, REPUBLIC OF

**PURPOSE**

To evaluate the efficacy and safety of mechanical thrombolysis in acute ischemic stroke compared with results of intraarterial (IA) pharmacologic thrombolysis.

**MATERIALS & METHODS**

We retrospectively reviewed patients who were performed IA thrombolytic treatment because of acute thromboembolic occlusion of major vessels. Total patients were 101 and divided into three groups: group I [pure urokinase (UK) infusion,  $n = 31$ ], group II [mechanical thrombolysis (clot disruption) by using microwire and microcatheter,  $n = 40$ ], group III [mechanical thrombolysis by using angioplasty balloon, retrievable self-expandable stent, or aspiration thrombectomy catheter,  $n = 30$ ]. We assessed treatment results which were compared by recanalization rate, clinical outcome, mortality, and symptomatic hemorrhage rate.

**RESULTS**

The recanalization rate was 51.6% in group I, 75% in group II, and 78.6% in group III. Mechanical thrombolysis groups had higher recanalization rate and group III had the best result of recanalization rate ( $p < .05$ ). We assessed clinical outcome by using modified Rankin Scale (mRS) after 3 months and favorable outcome was the best in group III, followed by group II, and group I ( $p < .05$ ). The symptomatic hemorrhage rate and mortality was 12.9%, 19.4%, in group I, 15%, 17.5% in group II, and 3.3%, 6.7% in group III, respectively. The symptomatic hemorrhage rate and mortality was the lowest in group III. This difference was not significant statistically ( $p > .05$ ). However, it could be explained: group III has tendency that symptomatic hemorrhage and mortality are low.

**CONCLUSION**

Mechanical thrombolysis has higher rate of recanalization and good clinical outcome than UK thrombolysis. From among two different mechanical thrombolytic therapies, by using mechanical devices have less rate of hemorrhage and mortality than by using microwire and microcatheter. Therefore, mechanical thrombolysis by using devices might be safer and more effective than other existing thrombolytic treatments.

**KEY WORDS:** Acute stroke, thrombolysis, angiography

**P-96****Stenting for Postirradiation Vasculopathy**

Liu, H.-Lee, C.-Wang, Y.-Chen, Y.

National Taiwan University Hospital  
Taipei, TAIWAN

**PURPOSE**

To report our experience of stenting for the patients who had radiotherapy treatment for head and neck cancer.

**MATERIALS & METHODS**

In the last 6 years, we had 10 patients with severe stenosis or occlusion of cervical carotid artery after local irradiation. They were all male, age ranging between 45 and 63 years old. They had history of local irradiation therapy for the head and neck cancer (nasopharyngeal cancer in 6, buccal cancer in 2, tongue cancer in 1, and oropharyngeal cancer in 1) 6 to 19 years ago. Among them, unilateral severe stenosis was found in seven, bilateral disease in two, and bilateral occlusion in one. Regarding the location, supra-bulb lesion was shown in three vessels, common carotid disease in two, and at the bulb in eight. Balloon expandable coronary stent was used in two (1 for petrous segment, 1 for VA orifice in patient with bilateral carotid occlusion), the rest were treated with self-expandable stents.

**RESULTS**

All the procedures were performed successfully. Intractable fluctuation of blood pressure was found in four patients after the stent deployment. Two had to stay in intensive care unit for 7 days, two for 4 days in order to maintain a normal blood pressure. Fluctuation of blood pressure still occurred in two patients after discharge, and one suffered from fainting attacks occasionally due to severe hypotension. Significant in-stent stenosis was noted in two stents and they were found at regular 3-month follow-up.

**CONCLUSION**

The procedure for stenting to patients with stenosis due to irradiation vasculopathy may be similar to atherosclerotic lesions, but the postprocedure care is different, especially the fluctuation of blood pressure and the in-stent stenosis is probably more frequent.

**KEY WORDS:** Head and neck cancer, irradiation, stenosis

**P-97****Usefulness of Perfusion-Weighted Imaging-Based Time Intensity Curve to Predict Neurologic Deterioration after Onset in Acute Ischemic Stroke Patients with Severe Stenosis or Occlusion of the Internal Carotid or Middle Carotid Artery**

Nakazaki, M.-Mori, T.-Tajiri, H.-Iwata, T.-Miayazaki, Y.

Shonan Kamakura  
Kamakura, JAPAN

**PURPOSE**

Some acute ischemic stroke patients present mild neurologic symptoms at admission and deteriorate day by day. The purpose of our study was to investigate whether or not perfusion-weighted imaging(PWI)-based time intensity curve(TIC) easily can predict their neurologic deterioration after admission.

**MATERIALS & METHODS**

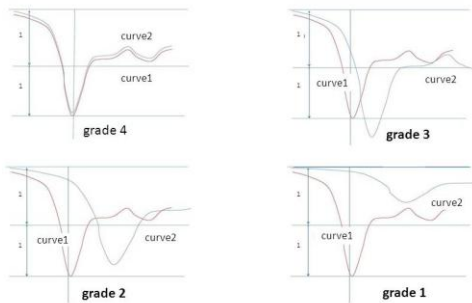
Included for retrospective analysis were acute stroke patients 1) who were admitted to our institution from October 2008 to September 2011 within 48 hours from onset, 2) with mild neurologic symptoms of NIHSS score of 10 or less, 3) who underwent emergency MRI study on admission, demonstrating severe stenosis(70% or more) or occlusion of the ICA or MCA and an ischemic stroke in the ipsilateral MCA territory, 4) who were treated without reperfusion therapy, and 5) who had no stenosis or occlusion lesion in the contralateral ICA or MCA by DSA. We evaluated PWI findings by time intensity curve grade(1 to 4). Time intensity curves were generated on region of interests set at symmetrical positions of the bilateral MCA territories, were classified into four grades according to the time to peak(TP) and the reduction value of the peak signal (PS) (Figure). We investigated patient's baseline features, DWI-ASPECTS, TIC grades, NIHSS on admission(adm\_NIHSS), NIHSS on the 7th day(7d\_NIHSS) and difference between 7d\_NIHSS and adm\_NIHSS (7d-adm\_NIHSS). We defined neurologic deterioration on the 7th day as 7d-adm\_NIHSS of more than 0.

**RESULTS**

Seventy-one patients were analyzed. Their median age was 73 years, women were 36 patients, median NIHSS at admission was four. There were 50 patients in large-vessels stenosis or occlusion, 13 in cardioembolism, six in TIA, and two in other. Median DWI ASPECT score was 9, and 18% patients had grade 1 of TIC, 53% had type 2, and 28.2% had type 3. Thirty-five patients were treated by dual-antiplatelet therapy, 21 patients mono-antiplatelet therapy, and 13 patients anticoagulation therapy. Two patients discontinued antiplatelet or anticoagulant therapy due to hemorrhagic infarction. Median NIHSS score on the 7th day was one. In 60 patients(84%), 7d-adm\_NIHSS was 0 or less. However, in 11 patients (16%), 7d-adm\_NIHSS was more than 0. Among the 11 patients, nine patients (82%) had grade 1

of TIC at admission. Logistic regression analysis also demonstrated grade 1 of TIC was an independent significant predictor of neurologic deterioration (OR,62.5; 95%CI,10.0-333,  $P<0.001$ ).

#### Time-Intensity Curves grade



#### CONCLUSION

In acute ischemic stroke patients with severe stenosis or occlusion of the IC or MCA, PWI-based TIC was useful in predicting neurologic deterioration after admission.

**KEY WORDS:** MR imaging/perfusion, acute ischemic stroke, emergency MR imaging

#### P-98

##### Combination of the ReStore™ Thrombectomy Device and the ReFlex™ Intracranial Access and Aspiration Catheter for the Treatment of Acute Ischemic Stroke: Initial Clinical Results

Schramm, P. • Schramm, R. • Knauth, M. University  
Goettingen, GERMANY

#### PURPOSE

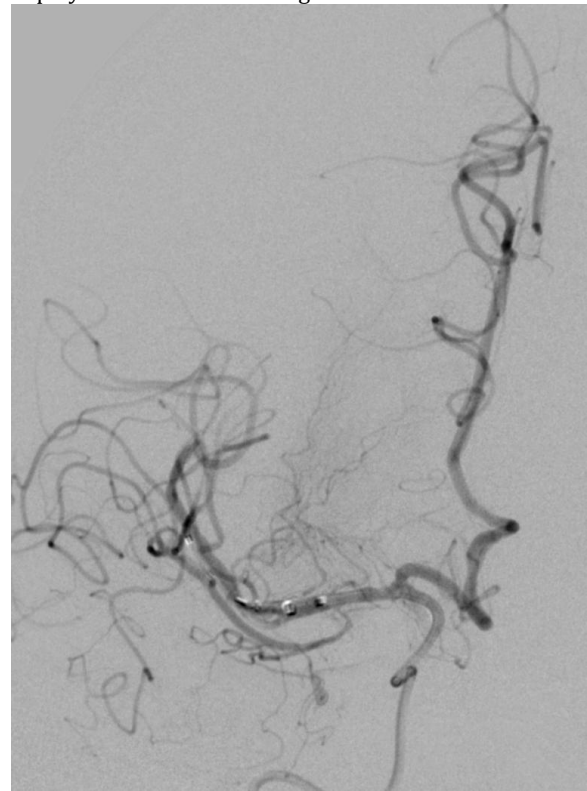
Recently, a variety of intracranial access catheter systems have been developed for treatment of acute cerebral vessel occlusion. Larger access catheters enable both clot aspiration and introduction of flow restoration devices like the new ReStore™ thrombectomy microcatheter. This device consists of a flexible, tapered microcatheter with a braided mesh retrieval element attached to its distal segment. The retrieval element is deployed through the advancement of a guidewire or the ReAct™ stylet through the lumen to radially expand the retrieval element.

#### MATERIALS & METHODS

We present the first clinical data of a new large lumen hyperflexible intracranial aspiration catheter (ReFlex™ 5F, 058" ID x 125 cm, Reverse Medical, Irvine, CA) combined with the ReStore™ thrombectomy device for the endovascular treatment of acute ischemic stroke. In detail, four patients (63 - 88 years, 2 M/2 F) with acute occlusion of the ICA or MCA (symptom onset < 6 hours) were treated with the combination of ReStore™ thrombectomy device and the ReFlex™ intracranial access and aspiration catheter. We evaluated the performance of the combination of both devices regarding flow restoration and recanalization.

#### RESULTS

Occlusion sites included right M1, right carotid T and left M2. Pretreatment TIC grade was 0 in all patients according to digital subtraction angiogram. Using the combination of ReStore™ thrombectomy device and ReFlex™ catheter, average time to first flow restoration was 28 minutes ( $\pm 21$  min). In all patients, persistent recanalization was achieved (TICI 3 in three patients, TICI 2b in one patient). In three cases, ReFlex™ aspiration catheter was navigated into the M1 using two microwires for stability. In no case, vessel dissection or impairment of intracranial perfusion appeared. Flow restoration worked in all cases and resulted in significant improvement of TIC score. In all cases, additional rt-PA (10 mg) was administered directly into the thrombus through the ReStore™ device. To achieve complete recanalization the ReStore™ devices were deployed 2.6 times on average.



#### CONCLUSION

The combination of ReStore™ thrombectomy device and the ReFlex™ aspiration catheter is a promising new treatment option for both flow restoration and aspiration in patients suffering from acute intracranial arterial occlusion. ReFlex™ catheter enables quick distal access into the M1.

**KEY WORDS:** Acute ischemic stroke, ReStore™ thrombectomy device, intracranial access and aspiration catheter

#### P-99

##### Prereperfusion Diffusion-Weighted Imaging/Perfusion-Weighted Image-Combined Predictor of Favorable 3-Month Clinical Outcome in Acute Ischemic Stroke Patients Who Underwent

## Endovascular Reperfusion Therapy for Internal Carotid or Middle Carotid Artery Occlusion

Nakazaki, M.·Mori, T.·Tajiri, H.·Iwata, T.·Miayazaki, Y.

Shonan Kamakura  
Kamakura, JAPAN

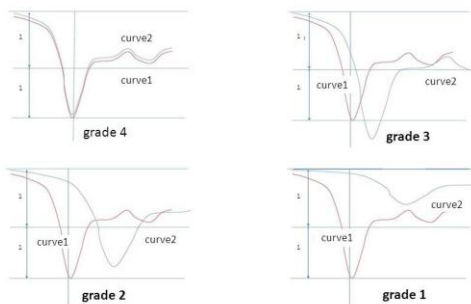
### PURPOSE

Emergency diffusion-weighted imaging (DWI) and/or perfusion-weighted imaging (PWI) are performed in an acute stroke setting, but it is difficult to predict favorable clinical outcome before endovascular treatment (ET). The purpose of our study was to investigate whether or not a DWI/PWI-combined factor can predict favorable 3-month clinical outcome or in-hospital survival before emergency ET in acute ischemic stroke patients with occlusion of the internal carotid artery (ICA) or the middle cerebral artery (MCA).

### MATERIALS & METHODS

Included for retrospective analysis were acute stroke patients 1) who were admitted to our institution from January 2004 to June 2011, 2) who had serious neurologic symptoms of NIHSS score of 8 or more, 3) who underwent emergency MRI study, displaying occlusion of the ICA or MCA, and 4) who underwent emergency endovascular reperfusion therapy within 8 hours from stroke onset. We evaluated DWI findings by DWI ASPECTS and PWI findings by time-intensity-curve (TIC) grade (1 to 4). Time intensity curves were generated on regions of interest set at symmetrical positions of the bilateral MCA territories, and were classified into four grades according to the time to peak (TP) and the reduction value of the peak signal (PS) (Figure). We defined DWI/PWI-combined factor (DPCF) as DWI ASPECTS of 6 or more and TIC of 2 or more, defined successful recanalization as TIC 2B or 3, and defined favorable 3-month clinical outcome as modified Rankin scale (3M-mRS) of 0-2.

### Time-Intensity Curves grade



### RESULTS

Eighty-two patients were analyzed. Their median age was 77 years, women were 36 patients, mean admission NIHSS was  $17.5 \pm 5.2$ , median DWI ASPECT score was 7. Seventy patients had cardiogenic stroke, successful recanalization was achieved in 46 patients (57.0%). Twenty-six patients (32%) had 3M-mRS of 0-2 and 68 patients (83%) survived for 3 months. There were 21

patients with DPCF. The median 3M-mRS in the patients with DPCF was 3 statistically significantly ( $P < 0.001$ ) better than 5 in the patients without DPCF. Logistic regression analysis also demonstrated that DPCF was the independent prereperfusion predictor of favorable 3-month clinical outcome (OR, 11.5; 95%CI, 1.38-100,  $P = 0.024$ ) and survival (OR, 6.76; 95%CI, 1.71-26.7,  $P = 0.006$ ).

### CONCLUSION

In ischemic stroke patients who underwent endovascular reperfusion therapy for the ICA or MCA occlusion within 8 hours from onset, DPCF was the independent prereperfusion predictor of favorable 3-month clinical outcome and survival.

**KEY WORDS:** MR imaging/perfusion, reperfusion therapy, MR imaging/diffusion

**Monday, April 23 –  
Wednesday, April 25  
6:30 AM – 9:00 PM  
Thursday, April 26  
6:30 AM – 3:00 PM**

**Americas Hall II  
Posters (Printed ) 100 – 112**

(P5) P5 - Pediatrics

**Note: A missing printed poster number indicates an abstract has been withdrawn.**

### P-100

#### Twelve Years of Experience with Pediatric Ischemic Stroke: Imaging, Etiology and the Role of Angiography

Mortimer, A. M.·Bradley, M.·Likeman, M.·Stoodley, N. G.·Sun, K.·Sharples, P.·Renowden, S. A.

Frenchay Hospital  
Bristol, UNITED KINGDOM

### PURPOSE

Pediatric ischemic stroke is relatively rare. The etiology of ischemic stroke in the pediatric population is, however, diverse and neuroimaging has a significant role to play in identification of the underlying diagnosis in order to optimize care. This study aimed to review 12-years experience of imaging in pediatric stroke in order to identify the range of imaging diagnoses and allow illustration of this as part of a visual display. This study concentrates on vascular etiologies and aims to investigate the potential benefit of catheter digital subtraction angiography (DSA) over magnetic resonance angiography (MRA) in the diagnosis of the underlying cause for stroke.

## MATERIALS & METHODS

A retrospective database and case note review of 12 years (1999-2011) of practice in a regional neuroscience center was performed to identify all cases of childhood ischemic stroke. Neonatal and traumatic etiologies were excluded.

## RESULTS

Forty-one cases of childhood ischemic stroke were identified, median age 4.9 years, range 2-16 years. All cases had evidence of ischemia demonstrated using either computed tomography or magnetic resonance imaging. The underlying etiologies were prior cardiac surgery in six (14.6%), meningitis in three (7.3%), Varicella infection in six (14.6%), unknown in eight (19.5%) and vascular etiologies in 18 (43.9%) patients. Vascular causes comprised arterial dissection in seven, fibromucular dysplasia in three, thromboembolism in two, moyamoya in three and vasculitis in three patients. The majority of patients underwent both CT and MR imaging with 30 (73%) undergoing MR angiography. Sixteen (39%) of these patients underwent catheter angiography. Importantly, MRA failed to identify the location of vascular abnormality in three cases. This included two cases of underlying vasculitis, seen as subtle vessel irregularity and beading on DSA, and one case of dissection that failed to be identified by MRA. Although MRA was useful in correctly identifying the location of the abnormality in the majority of patients, DSA was successful in characterizing the lesion further, notably in seven cases including two patients with a new diagnosis of fibromuscular dysplasia, two patients with underlying vasculopathies and three patients with arterial dissection. All patients with normal conventional angiograms also had normal magnetic resonance angiograms. The imaging findings in these cases are illustrated on a visual display to provide the radiologist with a comprehensive guide to imaging in this clinical setting.

## CONCLUSION

The etiology of pediatric stroke is varied and imaging can certainly aid the diagnosis. Characteristic findings may be seen on MR imaging but conventional angiography improved diagnostic confidence in a number of patients in our series and we believe that it has a significant role to play in the investigation of this population.

**KEY WORDS:** Pediatric stroke, catheter angiography, moyamoya

## P-101

### Pallister-Hall Syndrome

Zhu, F. Yang, E. Katzman, G.

University of Chicago  
Chicago, IL

## PURPOSE

Pallister-Hall syndrome was first reported by Hall et al. in 1980 based on a group of six patients who shared similar congenital abnormalities. Common manifesta-

tions include hypothalamic hamartoma, limb abnormalities such as polydactyly and dysplastic nails, craniofacial deformity, imperforate anus, and various visceral abnormalities. Genetic studies of familial cases revealed an autosomal dominant inheritance pattern with variable expressivity. The disease is not invariably lethal and the main cause of death is likely a combination of structural malformation and hypothalamic-pituitary-adrenal insufficiency.

## MATERIALS & METHODS

We analyzed the radiologic manifestations of 21 cases of patients diagnosed with Pallister-Hall syndrome from three medical institutions. Extremity radiographic studies were available for 18 patients and 73 limbs were imaged. Brain MRI was available for all 21 patients and 10/21 had follow-up MRI evaluations to assess for growth of the hamartoma.

## RESULTS

Poly(syn)dactyly was present in nearly 50% of the imaged limbs (36/73) and was preaxial, postaxial, or central, dependent on extra digit location. Hypothalamic hamartomas were found in all patients with volumes ranging from 0.2 to 41.5 cm<sup>3</sup>. They appeared noninvasive and remained proportionate to the brain growth on follow-up imaging.

## CONCLUSION

Pallister-Hall syndrome is a rare congenital disorder. Recognition of the constellation of radiologic features will assist clinical diagnosis and help distinguish it from other syndromes.

**KEY WORDS:** Pallister-Hall syndrome, congenital malformation

## P-102

### Diastematomyelia: Prenatal Diagnosis with Fetal MR Imaging

Sintini, M. Brisigotti, M. Barbisan, F.

Infermi Hospital Rimini  
Rimini, ITALY

## PURPOSE

Diastematomyelia is a sagittal clefting of the spinal cord into two "hemicords" each lined by its own pia mater. Such clefting may extend through the full thickness of the cord or may involve only its ventral/dorsal half (partial clefting). Partial clefting frequently is observed as a transitional state at the cranial and caudal extreme of a full-thickness cleft.

## MATERIALS & METHODS

We describe the case of a 18-week-old female fetus with a sonographic diagnosis of Chiari 2 malformation and spinal dysraphism at the thoracic-lumbar junction with meningocele. MR imaging was performed with a 1.5 T (Philips Achieva) machine employing standard 16-channel "torso" surface coil and three planes single-shot T2W TSE, 3D gradient-echo T1-weighted, DWI (b-factor 800). The Chiari 2 malformation was confirmed together



with the spinal dysraphism starting at the caudal end of the thoracic spine where a bony spur and a double canal were clearly showed. Pregnancy was terminated and an post-mortem MRI performed (3 planes T1W SE and T2W TSE 1-2 mm thickness) looking for the spinal cord clefting at the bony spur site without disclosing it. The diastematomyelia was found by the pathologist at the fetal dissection and each "hemicord" had an overall length of about 6 mm without spinal roots. Therefore the meningocele was empty.

## RESULTS

Histologic hallmarks were a double ependymal canal lined with cylindrical epithelium and immature nervous tissue around each one.

## CONCLUSION

In conclusion fetal MRI proved to be able to disclose diastematomyelia when the bony spur and the double canal are present at 18 weeks. To our knowledge this is the earliest MRI diagnosis of this malformation.

**KEY WORDS:** Fetal MR imaging

## P-103

### Spectrum of Fetal MR Imaging Findings in Developmental Central Nervous System Anomalies

Amundson, P., Gonzalez, A., Carbone, J., Shimony, J.

Mallinckrodt Institute of Radiology  
St Louis, MO

## PURPOSE

To demonstrate the most common spectrum of findings in central nervous system (CNS) anomalies as seen in fetal MR imaging.

## MATERIALS & METHODS

A retrospective review of patients presenting for fetal MRI was performed at our tertiary care Children's Hospital over a 9-year period. All exams were referred for an anomaly diagnosed at our prenatal ultrasound unit. A total of 351 fetal MRI exams were reviewed at an average gestational age of 27.1 weeks (range 16.3 - 38.3). Average maternal age was 28.3 years (range 14 - 45). This exhibit displays statistics of the different findings and discusses the salient MR features used to detect and diagnose these CNS anomalies.

## RESULTS

Three hundred fifty-one prenatal MRI exams were performed following abnormal ultrasounds. Of these, 293 were of singleton fetuses, 26 twins, and 2 triplets. The most common findings in the supratentorial brain included: Ventriculomegaly (n = 58), Primary Hydrocephalus (n = 16), Dysgenesis of the CC (n = 15), Agenesis of the CC (n = 10), Aqueductal Stenosis (n = 9), Subdural Hematoma (n = 8), and Parenchymal injury (PVL, infarct, gliosis) (n = 7). The most common findings in the posterior fossa included: Mega Cisterna Magna (n = 22), Meningocele (n = 15), Dandy-Walker variant (n = 11), Encephalocele (n = 10), Chiari II (n = 9), and Dandy Walker malformation (n = 8). The most common facial

findings included: Micrognathia (n = 3), Anophthalmia/Microphthalmia (n = 2), and Cleft lip/palate (n = 2). The most common neck and spine findings included: Cystic Hygroma (n = 4), neck masses (n = 3), and Sacrococcygeal Teratoma (n = 2). In 67% of the cases, the MRI either changed the US diagnosis or made additional findings to it. In 43% of the cases, MRI findings changed management, primarily in how patients are counseled.

## CONCLUSION

Fetal MRI is an important adjunct to fetal ultrasound and provides valuable additional information to the Maternal Fetal Medicine service that affects counseling of patients in many cases. It is important that the interpreting radiologist be familiar with the most common findings on fetal MRI.

**KEY WORDS:** Fetal, MR imaging, CNS

## P-104

### Semiautomated Volumetric Measurements of Optic Pathway Gliomas in NF1: The Effect of Coregistration on Accuracy and Variability

Ben-Sira, L.<sup>1</sup>, Shofty, B.<sup>2</sup>, Precel, R.<sup>1</sup>, Weizman, L.<sup>3</sup>, Joskowicz, L.<sup>3</sup>, Yonash, T.<sup>1</sup>, Constantini, S.<sup>1</sup>, Shiran, S.<sup>1</sup>, Ben Bashat, D.<sup>1</sup>

<sup>1</sup>Sourasky Medical Center, Tel Aviv, ISRAEL, <sup>2</sup>Tel Aviv University, Tel Aviv, ISRAEL, <sup>3</sup>The Hebrew University, Jerusalem, ISRAEL

## PURPOSE

The volumetric assessment of optic pathway gliomas (OPGs) is important in identifying fast-growing tumors prior to clinical deterioration thus enabling therapy and prevent vision loss. Precise estimation and follow-up of the lesions is imperative, hence the need to develop an appropriate quantification method. An ideal method for quantifying these irregular lesions should be fast, objective, specific, sensitive and accurate. Our study assesses the benefit of a novel method of volumetric measurement of OPGs, specifically in NF-1 patients, over linear measurements.

## MATERIALS & METHODS

We compared two semiautomatic volumetric measurement methods; one using T1+Gad in the axial plane, the other included coregistered-normalized combined T1+Gad and T2 (CRCM) in the axial plane. Coregistration was performed using the SPM package. Semiautomated measurements were all performed using ANALYZE 9.0 software. Ten NF patients with diagnosed OPG were included in the study, each with 2-7 consecutive exams, with a total of 37 exams. Measurements were performed twice in each method by radiology resident, and once in the CRCM method by a senior pediatric radiologist (this last measurement was considered "gold standard").

## RESULTS

One-way repeated measurements ANOVA showed no significant difference between OPG volumes in

recurrent measurements. The intraobserver average disagreement was 13.63% for the single AxT1+Gad method and 11.36% for the CRCM method. The interobserver average disagreement was 14.17% for the CRCM method.

#### CONCLUSION

Both methods are repeatable and reproducible. The CRCM method has a lower average disagreement compared to the single axial T1+Gad method when compared to the gold standard. We suggest a novel volume assessment method that may provide efficient, time sparing and reliable follow up for OPGs in NF patients.

**KEY WORDS:** Optic pathway glioma, volumetric measurements, neurofibromatosis

#### P-105

##### Resting-State Intrinsic Connectivity and Intelligence Indexes in Children

Rosset, S.<sup>1</sup>•Rondinoni, C.<sup>1</sup>•Souza-Oliveira, C.<sup>2</sup>•Salmon, C. E. G.<sup>1</sup>•Santos, A. C.<sup>1</sup>•University of São Paulo

<sup>1</sup>University of São Paulo, Ribeirão Preto, BRAZIL,  
<sup>2</sup>Federal Fluminense University, Campos de Goytacazes, BRAZIL

#### PURPOSE

Delineation of a normality scenario is a prerogative for the study of brain disease. Recently, the approach to the resting brain and its intrinsic functional connectivity has become the method of choice of many researchers given its simplicity and adaptability to a variety of cohorts. The present study aimed to identify the main resting-state networks in the normal infant brain and to verify the relationships between the maturation of the intrinsic networks and the intelligence quotients defined by the Brazilian version of Wechsler Intelligence Scale for Children-III. Results may be useful in early identification of deviations of normality.

#### MATERIALS & METHODS

Sixteen volunteers were recruited for the study (8 females, group mean age 11 ± 2.1 years old). The subjects had no neurologic or psychiatric disorder as confirmed by a clinical examination. The research protocol was approved by the local Ethical Committee and the parents signed an informed consent. The images were acquired in a Achieva 3 T MRI scanner (Philips, Best, The Netherlands) using a standard resting state functional design (TR/TE = 2000/30 ms, 200 volumes). The images were acquired under soft-tone mode, which attenuated the acoustic noise by reducing the slew rate of the gradient. Tridimensional T1-weighted images were acquired for spatial registration of functional volumes. Functional data were submitted to default preprocessing in BrainVoyager QX (Brain Innovations, The Netherlands). Procedures for group random effects Independent Component Analysis and Granger Causality Mapping are described elsewhere. The default-mode network (DMN) identified among the RFX group maps defined a frontal region-of-

interest (Brodmann Area 10), which was used as a seed for Granger Causality calculation across the whole brain. An analysis of covariance (ANCOVA) was accomplished considering two age groups (younger and older, with younger ≤ 10 years old) and the IQ scores given by WISC-III (Full, Verbal and Execution). The value of Granger causality (effective connectivity) inside the Salience network was tested for covariance depending on age group and IQ score.

#### RESULTS

Two main results can be drawn from our study. First, the Default-mode networks of our voluntary children seem to be coupled with somatosensory areas. This conclusion is based on the fact that the positive signal of the group independent component defining the DMN has its negative counterpart in the central areas of the brain, more specifically, Brodmann areas 6, 4, 3, 1, 2 and 40. Second, the ANCOVA showed significance of covariance between IQ score, Granger causality values inside Salience Network and age group. Covariance was significant for Full IQ and Verbal IQ scores ( $p < 0.05$ ).

#### CONCLUSION

The normal development of the brain may result in strengthening of effective connectivity between frontal areas and areas related to salience of outside world stimuli. Caution should be taken in the diagnosis of ADHD, once the standard functioning in the infant brain is naturally coupled to the sensory and motor areas, indicating that the modulation of general activity must be approached by taking into account subtle balances between the normal behavior and disease.

**KEY WORDS:** Functional MR imaging, resting-state, IQ

#### P-106

##### Improving the Success Rate of Functional MR Imaging in Assessment of Language Lateralization in Children with Intractable Epilepsy

Patel, R.•Mendelsohn, D.•Yetkin, Z. F.

University of Texas Southwestern Medical Center  
Dallas, TX

#### PURPOSE

Assessment of language lateralization using Wada and surgical cortical mapping is difficult and has a low success rate in young children. Functional MRI has been increasingly used for preoperative assessment of language localization and lateralization in children with intractable epilepsy; however, success rates of fMRI language tasks are also low compared to those of adults. The aim of the present study was to evaluate the success rate of category fluency task in the assessment of language lateralization in children with intractable epilepsy.

#### MATERIALS & METHODS

Charts and images of children with intractable epilepsy who underwent fMRI for preoperative assessment of language lateralization were reviewed. All patients were asked to perform an age-appropriate category

fluency task. Data included relevant history, fMRI maps of language task, and language outcomes after surgery.

### RESULTS

Forty-six children with intractable epilepsy (21 male, 25 female, age range: 2 to 18 years) underwent fMRI for preoperative assessment of language lateralization. Due to motion artifacts, nine patients had to perform the task twice and one patient performed the task three times. Functional maps of the brain consistently showed activation in bilateral superior temporal and transverse temporal gyri, right and/or left posterior temporal lobe, bilateral inferior and middle frontal gyri, supplementary motor area, bilateral motor cortices and the cerebellar hemispheres. Functional brain maps showed the dominant hemisphere for language in all patients.

### CONCLUSION

Category fluency tasks were performed by children within a wide age range. Consistent activation of language regions was obtained in younger children as well as adolescents. Preoperative fMRI assessment of language localization and lateralization was completed successfully using category fluency tasks in this group of children with intractable epilepsy.

**KEY WORDS:** Functional MR imaging, epilepsy, children

### P-107

#### MR Spectroscopy of Developing Brain in First Year of Life

Yahyavi-Firouz-Abadi, N.-Shimony, J. S.

Mallinckrodt Institute of Radiology  
St Louis, MO

### PURPOSE

Magnetic resonance imaging is being used increasingly to evaluate neonatal brain. Proton magnetic resonance spectroscopy (MRS) can be performed routinely on most clinical magnetic resonance scanners and has been applied in a wide range of pediatric applications. Neonatal magnetic resonance spectra are different from those of adult brain. Brain maturation is characterized by increase in N-acetyl aspartate (NAA) and creatine and concomitant decrease in choline, myoinositol and lipids. In the newborns, NAA/choline ratio is much smaller than adults. Few studies have looked at perinatal changes of brain metabolites during the first month of life. No large study has been performed looking at changes in preterm versus term infants during the first year of life.

### MATERIALS & METHODS

We performed a retrospective review of MRS exams done during 2010 in a large metropolitan pediatric hospital in children less than 1 year of age. Single voxel proton spectroscopic data were acquired in the left basal ganglia with an intermediate TE (144 msec) and metabolite ratios were calculated. Preliminary data consisted of 88 exams from 50 term (gestational age of

37 weeks and more) and 38 preterm (gestational age less than 37 weeks) children.

### RESULTS

Data analysis demonstrated significant positive linear correlation ( $R^2 = 0.69$ ,  $P < 0.001$ ) between adjusted gestational age (postconception age) and NAA/Choline ratio. This positive correlation was present in both preterm ( $R^2 = 0.67$ ,  $P < 0.001$ ) and term ( $R^2 = 0.69$ ,  $P < 0.001$ ) subgroups. There was no significant difference in this ratio between preterm and term children. NAA/Choline ratio reached 1.0 at 66 weeks postconception in term and 68 weeks postconception in preterm children. There was no statistically significant difference between the two groups.

### CONCLUSION

This study investigated changes in metabolite concentrations and their ratios during development in a large number of term and preterm infants during the first year of life. NAA/Choline ratio increased linearly in both groups without significant difference, and reached a ratio of 1.0 at 66-68 weeks postconception in both groups.

**KEY WORDS:** Choline, N-acetyl aspartate, ratio

### P-108

#### Probabilistic MR Diffusion Tensor Imaging at 3.0 T in Perilesional White Matter in Pediatric Periventricular Nodular Gray Matter Heterotopia

Maxwell, A. W. P.<sup>1</sup>Watts, R. P.<sup>2</sup>Filippi, C. G.<sup>2</sup>

<sup>1</sup>University of Vermont College of Medicine, Burlington, VT, <sup>2</sup>Fletcher Allen Health Care, Burlington, VT

### PURPOSE

Periventricular nodular gray matter heterotopia (PVNH) is thought to result from aberrant neuronal migration in utero and is strongly associated with a postnatal clinical presentation of seizure. Even with aggressive pharmacologic and surgical interventions, a subset of PVNH patients remain refractory to treatment, a finding suggestive of more diffuse pathology potentially involving those white matter tracts surrounding the heterotopic nodules. The purpose of this study was evaluate for the presence of such abnormalities within white matter surrounding these areas of PVNH and to quantify their distribution within the brain.

### MATERIALS & METHODS

Seven pediatric patients (5 females, 2 males, average age 8.7 years, range 0-21 years) with clear radiographic evidence of PVNH and a clinical history of seizures were selected retrospectively for analysis, all of whom were imaged at 3.0 T with magnetic resonance diffusion tensor imaging (DTI). Using probabilistic DTI, values for fractional anisotropy (FA), mean diffusivity (MD), radial diffusivity (RD), and the principal Eigen value ( $\lambda_1$ ) were calculated within perinodular white matter at distances of five, 10, 15, and 20 millimeters from well defined regions-of-interest (ROI). These values then were

compared to those calculated within age- and location-matched ROIs in healthy control patients (6 females, 1 male, average age 9.5 years, range 0-17 years) to assess for the presence and magnitude of differences.

## RESULTS

As demonstrated in Table I, perinodular white matter in all seven PVNH patients showed significantly decreased FA ( $p < 0.05$ ) and significantly elevated MD and RD (MD:  $p < 0.05$ ; RD:  $p < 0.05$ ) at all evaluated distances (up to 20 mm circumferentially) as compared to healthy control patients. No significant differences were detected in  $\lambda_1$  at any distance between PVNH and control patients.

Diffusion Parameter	Distance	Heterotopia	Control	p-value
Fractional Anisotropy (FA)	5 mm	0.375 +/- 0.066	0.497 +/- 0.091	$p = 0.012^a$
	10 mm	0.349 +/- 0.087	0.459 +/- 0.061	$p = 0.048^a$
	15 mm	0.319 +/- 0.087	0.398 +/- 0.058	$p = 0.025^a$
	20 mm	0.315 +/- 0.094	0.379 +/- 0.061	$p = 0.013^a$
Mean Diffusivity (MD) (mm <sup>2</sup> /sec.)	5 mm	$0.944 \times 10^{-3} \pm 2.10 \times 10^{-4}$	$0.835 \times 10^{-3} \pm 6.27 \times 10^{-5}$	$p = 0.023^a$
	10 mm	$0.876 \times 10^{-3} \pm 1.62 \times 10^{-4}$	$0.792 \times 10^{-3} \pm 4.51 \times 10^{-5}$	$p = 0.015^a$
	15 mm	$0.901 \times 10^{-3} \pm 1.91 \times 10^{-4}$	$0.783 \times 10^{-3} \pm 4.94 \times 10^{-5}$	$p = 0.012^a$
	20 mm	$0.909 \times 10^{-3} \pm 1.94 \times 10^{-4}$	$0.781 \times 10^{-3} \pm 4.67 \times 10^{-5}$	$p = 0.010^a$
Radial Diffusivity (RD) (mm <sup>2</sup> /sec.)	5 mm	$0.756 \times 10^{-3} \pm 2.03 \times 10^{-4}$	$0.585 \times 10^{-3} \pm 8.15 \times 10^{-5}$	$p = 0.006^a$
	10 mm	$0.708 \times 10^{-3} \pm 1.77 \times 10^{-4}$	$0.582 \times 10^{-3} \pm 5.62 \times 10^{-5}$	$p = 0.030^a$
	15 mm	$0.751 \times 10^{-3} \pm 2.14 \times 10^{-4}$	$0.605 \times 10^{-3} \pm 5.35 \times 10^{-5}$	$p = 0.016^a$
	20 mm	$0.757 \times 10^{-3} \pm 1.99 \times 10^{-4}$	$0.615 \times 10^{-3} \pm 5.49 \times 10^{-5}$	$p = 0.005^a$
Principal Eigen value ( $\lambda_1$ ) (mm <sup>2</sup> /sec.)	5 mm	$1.32 \times 10^{-3} \pm 2.31 \times 10^{-4}$	$1.33 \times 10^{-3} \pm 1.67 \times 10^{-4}$	$p = 0.298$
	10 mm	$1.21 \times 10^{-3} \pm 1.71 \times 10^{-4}$	$1.21 \times 10^{-3} \pm 1.06 \times 10^{-4}$	$p = 0.324$
	15 mm	$1.20 \times 10^{-3} \pm 1.48 \times 10^{-4}$	$1.20 \times 10^{-3} \pm 8.53 \times 10^{-5}$	$p = 0.153$
	20 mm	$1.21 \times 10^{-3} \pm 2.19 \times 10^{-4}$	$1.21 \times 10^{-3} \pm 6.12 \times 10^{-5}$	$p = 0.118$

a = statistically-significant result

## CONCLUSION

Periventricular nodular gray matter heterotopia is associated with statistically significant abnormalities in DTI metrics (elevated mean and radial diffusivity and decreased FA) within the surrounding perilesional white matter circumferentially and for distances no less than 20 millimeters from visible nodular lesions. These findings may indicate diffuse microstructural abnormality within this white matter such as aberrant myelination, ectopic gray matter microfoci, or other pathologic changes in axonal integrity or neuronal migration. Further research will be helpful in determining the extent to which such perinodular white

matter changes affect clinical outcomes in patients who are refractory to standard medical and surgical treatments.

**KEY WORDS:** Diffusion tensor imaging, heterotopia, 3.0 T

## P-109

### Longitudinal Comparison of Metabolite Ratios in Neonates with Hypoxic Ischemic Encephalopathy

Lee, P. N.<sup>1</sup>Ferriero, D. M.<sup>1</sup>Barkovich, J. A.<sup>1</sup>Xu, D.<sup>1,2</sup>

<sup>1</sup>University of California San Francisco, San Francisco, CA, <sup>2</sup>University of California Berkeley, Berkeley, CA

## PURPOSE

Proton MR spectroscopy (1H-MRS) is a valuable method for studying the neurodevelopment in infants with hypoxic ischemic encephalopathy (HIE). Studies have illustrated prognostic value in determining ratios between Lactate (Lac), N-acetyl aspartate (NAA), and Choline (CHO) from newborn infants. We studied neonates with signs of HIE by looking at the metabolite ratio differences between normal and abnormal outcome groups at approximately 4 days after birth and follow up at 6 months of age. A longitudinal comparison also was performed to determine changes in metabolite ratio across outcome groups.

## MATERIALS & METHODS

A comprehensive MRI exam with lactated edited 3D MRS was performed at approximately 4 days and at 6 months of life for 25 newborns with HIE using methods previously described. All subjects were examined by a pediatric neurologist at 6 months of age and were evaluated neurologically using a Neuromotor Scoring system validated at our institution. Nine patients had abnormal neurologic outcome (NMS $\geq$ 2), and 16 patients had normal outcome (NMS $\leq$ 1). The MRS data were sent to an off-line Sun Workstation (Sun Microsystems, Mountain View, Ca) for postprocessing quantification and analysis. A basal ganglia (BG) region of interest (ROI) was drawn bilaterally on T2 images, in which spectroscopic data were collected. Left and right ROIs were found to be statistically similar and were combined for analysis. Mann-Whitney U tests were performed for statistical comparison.

## RESULTS

Infants in the abnormal cohort had statistically higher LAC/CHO and CHO/NAA ratios at the 6-month time point in comparison with the normal outcome cohort. Both normal and abnormal outcome groups showed a decrease in CHO/NAA and LAC/NAA ratios over time, suggesting increases in NAA as the brain matures despite the hypoxic insult. Percent change in LAC/NAA was higher, while percent change in CHO/NAA was lower for the abnormal outcome group (Table 1).

Table 1

Mean $\pm$ SD	At Term		6 Months	
	Normal	Abnormal	Normal	Abnormal
		P-Value		P-Value

	e					
CHO/N	1.797±0.08	2.101±0.10	0.06	0.992±0.087	1.346±0.113	0.042
AA			45			0*
LAC/N	0.109±0.028	0.203±0.035	0.15	0.051±0.004	0.072±0.005	0.004
AA			22			6*
LAC/C	0.075±0.013	0.099±0.015	0.17	0.053±0.005	0.057±0.006	0.712
HO			56			9
	Normal			Abnormal		
	% Change	Term	vs.	Term	vs.	
		6mo	P-	6mo	P-	
		Value		Value		
CHO/N	44.7	0.0001*	35.9	0.0080*		
AA						
LAC/N	53.2	0.0167*	64.5	0.0036*		
AA						
LAC/C	29.3	0.5815	42.4	0.2730		
HO						

\*Statistically significant at the 5% level

\*\*% Change=(Mean Scan1-Mean Scan2)/Mean Scan1

## CONCLUSION

The study has confirmed previous findings that HIE patients with worse outcome have substantial lactate levels and higher CHO/NAA ratios resulting from cellular breakdown and damage. This pattern persists after 6 months, which may indicate that the effects are long lasting and the patients are still recovering from injury. Due to the small number of patients included in this study, this pattern must be confirmed in a larger cohort which could point to needs for further treatment during management of these patients.

**KEY WORDS:** Spectroscopy, ischemia

## P-110

### Mild White Matter Changes Detected in Preterms by Ultrasound and MR Imaging as Predictors of Neurobehavioral Outcome

Ben-Sira, L.<sup>1</sup> Weinstein, M.<sup>1</sup> Gros-Tsur, V.<sup>2</sup> Marom, R.<sup>1</sup> Berger, I.<sup>1</sup> Shiran, S.<sup>1</sup> Leitner, Y.<sup>1</sup> Uliel, S.<sup>1</sup> Geva, R.<sup>3</sup> Ben-Bashat, D.<sup>1</sup>

<sup>1</sup>Tel-Aviv Sourasky Medical Center, Tel Aviv, ISRAEL, <sup>2</sup>Shaare-Zedek Medical Center, Jerusalem, ISRAEL, <sup>3</sup>Bar-Ilan University, Ramat-Gan, ISRAEL

## PURPOSE

Prematurity is a risk factor for mild to severe neurodevelopmental impairments, which occur in more than 50% of preterm infants. In preterms, increased echogenicity often is detected using cranial ultrasound (cUS) and recently diffuse excessive high signal intensity (DEHSI) was documented with MRI. Little is known about the correlation between the spatial distribution and severity of these findings and their clinical relevance. In this study we initially evaluated the total white matter (WM) changes using both conventional MRI and cUS, and then focused specifically on WM changes in the frontal (FR), posterior parietal (PPR) and occipital (POR) areas. Left FR is engaged in language while PPR and POR are engaged in selective attention and visual attention. We hypothesized that

WM integrity in these regions would correlate with neonatal attention regulation in infancy and with language and performance skills at 1 year.

## MATERIALS & METHODS

Thirty-three premature infants born at <34 weeks' gestational age with mild to moderate echogenicity identified on routine cUS underwent MRI at 36-40 weeks, on a 3 T MRI system. Diffuse and focal echogenic regions were defined on the first cUS (cUS1) and on a second cUS examination performed close to the MRI (cUS2). Regions with DEHSI were defined on T1- and T2-weighted MRI images. These parameters were evaluated separately for frontal, periventricular, parietal and occipital areas. Identical rating criteria were applied to both modalities and a total score of WM changes across areas was calculated. Behavioral outcome was assessed at term (44 weeks) using the Rapid Neonatal Neurobehavioral Assessment Procedure (NB), to assess the integrity and organization of the sensory-motor system in the neonatal period; and at 1 year using the Griffiths Mental Development Scales (GMDS).

## RESULTS

A significant correlation was detected between WM changes as measured on cUS2 and on MRI ( $r=0.405$ ,  $p=0.019$ ). The WM changes score was higher on cUS1 than on cUS2, which implies that some of the echogenicity is transient as expected. Only the total WM changes score calculated on MRI, significantly correlated with neurobehavioral outcome, specifically with hearing and language scales ( $r=-0.7$ ,  $p=0.01$ ). When looking specifically at WM changes in the FR, PPR and POR, WM changes detected in the right PPR in cUS2 correlated with NB score at term ( $r=0.45$ ,  $p=0.047$ ) and MRI WM score detected in the POR correlated with NB score at 44 weeks ( $r=0.48$ ,  $p=0.027$ ). The NB attention item at 44 weeks correlated with the performance and hand-eye coordination scales of the GMDS, respectively ( $r=0.761$   $p=0.007$ ;  $r=0.723$   $p=0.012$ ). Finally, MRI WM score detected in the left and right FR correlated with the language scale ( $r=-6.4$ ,  $p=0.02$ ) and left and right PPR correlated with the performance scale at 1 year of age ( $r=0.569$   $p=0.034$ ).

## CONCLUSION

Our preliminary data emphasize the notion that MRI at term is more sensitive than cUS for evaluating WM integrity. Even mild WM abnormalities at that age in specific regions may be related to visual attention regulation at infancy and to hand-eye coordination, language and performance skills at 1 year.

**KEY WORDS:** Preterm, white matter, development

**P-111****Role of Multimodality Imaging in the Diagnosis, Staging and Treatment Monitoring of Nasopharyngeal Carcinomas in the Pediatric Population**

Ponisio, M. R. • Fischer, K. C. • Khanna, G. • Rajderkar, D.

Mallinckrodt Institute of Radiology  
Saint Louis, MO

**PURPOSE**

Nasopharyngeal carcinoma (NPC) in the pediatric population is rare with imaging studies playing a key role in diagnosis, staging and treatment planning. We review clinical and imaging features in patients with a diagnosis of NPC, and discuss the salient multimodality radiologic features in the diagnosis and treatment.

**MATERIALS & METHODS**

The clinical and imaging history of 10 pediatric patients (age range 10-19 years) with biopsy proven NPC was reviewed retrospectively. All patients underwent computed tomography (CT) or magnetic resonance (MR) imaging at clinical presentation. Fluorine-18 fluorodeoxyglucose positron emission tomography/computed tomography (<sup>18</sup>F-FDG PET/CT) imaging was performed on eight patients and nine patients underwent follow-up imaging.

**RESULTS**

Ten pediatric patients (9 male and 1 female; mean age 14.8 years) with biopsy-confirmed diagnosis of nasopharyngeal carcinoma (NPC) were reviewed. The most common initial presentation was neck masses. The other symptoms include nasal obstruction, tinnitus, and nasal/ear discharge. Surgical pathology confirmed that 9 of the 10 patients were positive for the Epstein-Barr virus (EBV). Histopathology of these carcinomas included undifferentiated carcinoma (n = 4), nonkeratinizing undifferentiated carcinoma (n = 5) and poorly differentiated carcinoma (n = 1). Key imaging features at presentation revealed invasion of the skull base (n = 7), extension into the adjacent anatomical spaces (n = 5), bilateral neck lymphadenopathy (n = 9), and unilateral opacification in the mastoid air cell and asymmetric mass in the posterior nasopharynx (n = 8). Imaging with <sup>18</sup>F-FDG PET/CT, available in eight patients, provided a total of 27 scans for review. <sup>18</sup>F-FDG PET/CT played an important role in the initial staging, in the localization of the primary tumor especially in patients with bulky lymphadenopathy, in monitoring treatment response, and to evaluate progression of the local/distant metastatic disease.

**CONCLUSION**

Nasopharyngeal carcinoma accounts for less than 1% of all childhood cancers and is unlikely to be considered in the differential diagnosis unless the radiologist is aware of NPC's salient characteristic multimodality imaging appearances. <sup>18</sup>F-FDG PET/CT imaging directly impacted treatment planning by providing accurate tumor mapping and monitoring of the treatment response.

**KEY WORDS:** Nasopharyngeal carcinoma (NPC), multimodality imaging, pediatric

**P-112****Primary Glioblastoma Multiforme of the Spine in a Teenager: Case Description and Literature Review**

Valente, M.

Centro Infantil Dr. Domingos Boldrini  
Campinas - São Paulo, BRAZIL

**PURPOSE**

The authors describe an unusual case of a primary spinal cord glioblastoma multiforme in an male teenager (16 year old) presented with sudden right leg paresthesia after exercise.

**MATERIALS & METHODS**

Clinical evaluation and MRI were performed and a tumefactive lesion of the thoracic spine was detected.

**RESULTS**

Biopsy was done and the histopathologic study showed a primary glioblastoma of the spinal cord. The lesion was partially removed and radiation therapy was done.

**CONCLUSION**

The review of the literature corroborates that the primary intramedullary glioblastoma multiforme is seen only rarely in children/young adults. The clinical presentation and the level of the spinal cord involvement also is unusual.

**KEY WORDS:** Glioblastoma multiforme of the spine, spinal cord tumors, pediatric spinal tumors



**Monday, April 23 –  
Wednesday, April 25**

**6:30 AM – 9:00 PM**

**Thursday, April 26**

**6:30 AM – 3:00 PM**

**Americas Hall II  
Posters (Printed) 113**

(P6) P6 - Socioeconomics

**Note: A missing printed poster number indicates an abstract has been withdrawn.**

#### **P-113**

#### **Efficacy of Checklist-Style Structured Reporting in Reducing Missed Findings in Resident Preliminary Reports**

Lin, E.<sup>1</sup>•Powell, D. K.<sup>2</sup>•Kagetsu, N.<sup>1</sup>

<sup>1</sup>St. Luke's-Roosevelt Hospital Center, New York, NY,

<sup>2</sup>Beth Israel Medical Center, New York, NY

#### **PURPOSE**

Many benefits have been attributed to the use of structured radiology reporting, including improved quality and consistency of reports, decreased report turn-around time, and increased clarity of reports (Schwartz et al, 2011). The effective use of checklists in medicine to promote patient safety raises the question of their role in structured radiology reporting (Pronovost et al, 2006). A checklist-style structured radiology report for cervical spine CTs was introduced at a community and tertiary care hospital with a level-one trauma center, and the rates of reported and missed findings were examined in preliminary reports by on-call residents before and after their introduction.

#### **MATERIALS & METHODS**

A retrospective cohort study was performed, examining 2,913 cervical spine CT preliminary reports generated by on-call residents between July 2009 and October 2011. One thousand eight-one reports generated between December 2010 and October 2011 using the checklist-style reporting template were compared with 1,832 reports generated between July 2009 and March 2011 using other templates. Reported findings later confirmed by an attending neuroradiologist and missed findings later detected by an attending neuroradiologist were counted. Only findings considered relevant to emergency department management were considered, which included all acute fractures, all causes of severe spinal canal stenosis, prevertebral soft tissue swelling or masses, intracranial hemorrhage, abnormal spinal cord densities, abnormal extradural densities, and

emergent lung findings (consolidation, pneumothorax, or pleural effusions).

#### **RESULTS**

In 1,832 reports generated without use of the checklist-style template, 117 (82.4%) out of 142 emergent findings were identified by on-call residents. In 1,081 reports generated with the checklist-style template, 96 (88.1%) out of 109 emergent findings were identified by on-call residents, representing a 32.4% relative reduction in missed findings when using the checklist-style reporting template. Larger differences were noted in the detection of emergent nonfracture findings, with 43 (71.7%) out of 60 findings identified on reports without checklist-style templates and 49 (90.7%) out of 54 findings identified on reports with checklist-style templates, representing a 67.1% relative reduction in missed nonfracture findings.

#### **CONCLUSION**

The use of checklists in standardized reporting templates for cervical spine CTs reduced the number of missed emergent findings by on-call residents. A particularly large reduction was noted in the number of emergent nonfracture findings missed, an expected result given that residents' search patterns naturally include fracture detection. The implementation of checklists in structured radiology reporting can increase the accuracy of reports and improve patient safety.

**KEY WORDS:** Structured, reporting, checklist

**Monday, April 23 –  
Wednesday, April 25**

**6:30 AM – 9:00 PM**

**Thursday, April 26**

**6:30 AM – 3:00 PM**

**Americas Hall II  
Scientific Posters (Printed) 114 –  
124**

(P7) P7 – SPINE

**Note: A missing printed poster number indicates an abstract has been withdrawn.**

**P-114****Diffuse Hypertrophy of Cranial and Peripheral Nerves, Spinal Roots and Cervical and Lumbosacral Plexi in Chronic Demyelinating Polyradiculoneuropathy**Peltz, M.<sup>1</sup>•Manconi, F.<sup>2</sup><sup>1</sup>Aob G. Brotzu Cagliari, Cagliari, ITALY, <sup>2</sup>AO SS. Trinità Cagliari, Cagliari, ITALY**PURPOSE**

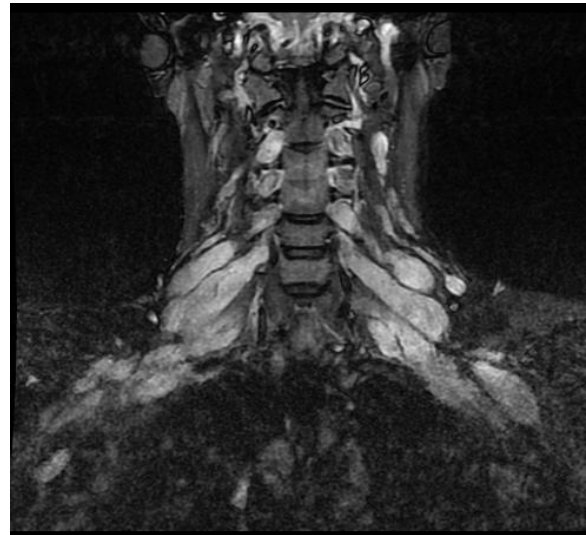
Case report of chronic inflammatory polyradiculoneuropathy (CIPD) with diffuse very marked enlargement of cranial nerves, spinal roots, cervical and lumbosacral plexi and peripheral nerves visible on MRI.

**MATERIALS & METHODS**

Neuroimaging data were collected by the senior author using a 1.5 T unit (GE Signa Healthcare, Milwaukee, Wisconsin) using multiplanar FSE T2, T1 and FIESTA 3D at the brain and spine levels with gadolinium and STIR sequences for the body study. Electrodiagnostic studies, CSF profile and physical examination were conducted by a senior neurologist.

**RESULTS**

A 52-year-old woman, 26 years prior our examination developed a relatively symmetric motor weakness, paresthesias, sensory loss, muscle limbs atrophy, more severe distally. Hereditary motor sensory neuropathy (HMSN) was suspected. Electrodiagnostic findings were consistent with severe diffuse sensorimotor demyelinating polyneuropathy and CSF profile showed elevated total protein. Hypertrophic nerves were detected on physical exam. Patient was placed on high doses of Deflazacort (60 mg/d) with improvement of symptoms and maintained lower doses with good function. Later she developed a peripheral facial neuropathy, bilateral proptosis, steppage gait and Romberg sign. Several nerves limbs were enlarged to palpation. Electrodiagnostic examination showed signs of peripheral demyelination and axonal loss. Cerebrospinal fluid (CSF) protein was elevated. Using multiplanar capabilities, T2 sequences and gadolinium, MRI clearly depicted hypertrophy and contrast enhancement of cranial nerves, except for I, II and XI pairs as well of cauda equina roots, emerging spinal nerves, brachial and lumbar plexi and intercostal nerves with sparing of splanchnic branches. Differential diagnosis versus other more frequent hypertrophic neuropathies such as HMSN, neurofibromatosis, is easily done by MRI.

**CONCLUSION**

Our patient met the diagnostic criteria for CIDP. Cranial and spinal nerves thickening has been reported on MRI studies in CIDP. This is the first reported case with diffuse dramatic hypertrophy of cranial nerves, spinal roots, brachial and lumbosacral plexi and intercostal nerves visible on MRI. Chronic inflammatory polyradiculoneuropathy should be considered in case of hypertrophic neuropathy.

**KEY WORDS:** Nerves, spinal, cranial**P-115****Patterns of Epidural Contrast Spread and the Impact of Plica Mediana Dorsalis**Mohamed, M. A.<sup>1</sup>•Nada, E.<sup>2</sup><sup>1</sup>Johns Hopkins University, Baltimore, MD, <sup>2</sup>Cleveland Clinic, Cleveland, OH**PURPOSE**

The epidural space is an important anatomical space that anesthesiologists in particular use extensively. The plica mediana dorsalis (PMD) is a band that divides the epidural space dorsally in the midline (Figure 1); its anatomy and clinical implications on the spread of epidural injections are not well studied.



Figure 1. Lumbar epidurogram showing appearance of PMD as vertical midline translucency

#### MATERIALS & METHODS

Thirty patients who were suffering from chronic back pain underwent lumbar epidural steroid (Depo-Medrol) and bupivacaine injection under fluoroscopy. Strict midline introduction of the epidural needle tip with its bevel directed upward was assured using fluoroscopy of five milliliter of iohexol 200 mg/ml was injected in the epidural space. Prospective readings of the epidurograms by three neuroradiologists were done separately to check for the distribution, the appearance of the spread of the contrast and the radiologic evidence of the presence of PMD

#### RESULTS

The PMD was observed in 80% of the patients studied. Denser contrast spread on one side was found in 79% of patients who had the PMD and 33% who did not ( $P = 0.03$ ). Asymmetrical spread of the contrast vertically and horizontally was observed in 67% and 50% of patients with and without PMD, respectively, and was not associated significantly with the presence of PMD ( $P = 0.45$ ) (Figure 2).



Figure 2: Lumbar epidurogram showing strictly unilateral spread of contrast

#### CONCLUSION

The PMD is present in the majority of patients. Plica mediana dorsalis favors denser contrast spread on one side and hence preferential spread of medication on that side, but it does not reflect the symmetry of contrast spread longitudinally and horizontally on either side of it. These features carry important clinical implications for understanding unilateral epidural analgesia, inadequate block, difficulties passing, threading and troubleshooting epidural catheters.

#### P-116

### Evaluation of the Quantitative and Qualitative Effects of Adaptive Statistical Iterative Reconstruction on CT-Guided Lumbar Spine Nerve Blocks

Kim, E. Y. · Hess, C. P. · Dillon, W. P.

University of California San Francisco  
San Francisco, CA

#### PURPOSE

Adaptive statistical iterative reconstruction (ASIR), a recently introduced CT reconstruction technique, can be used to lower radiation dose when used in the abdomen, chest, coronary angiography, and head. However, the role of ASIR during spine intervention procedures has not been reported, to our knowledge. The aim of this study was to assess whether the use of ASIR during CT-guided lumbar spine nerve blocks improves the depiction of structures critical to accurate needle placement.

#### MATERIALS & METHODS

This IRB-approved retrospective study included 23 consecutive patients who underwent CT-guided lumbar spine nerve blocks between July 2011 and October 2011. Images were obtained on a 64-detector CT scanner (LightSpeed VCT, GE Healthcare) using a fixed tube voltage and current (140 kV, 10 mA) for all patients undergoing lumbar spinal nerve root block procedures. Images were reconstructed using both ASIR 0% (referred to as the filtered-back projection, or FBP, group) and ASIR 100% (referred to as the ASIR group) and uploaded to the clinical PACS for quantitative and qualitative analysis. For quantitative analysis, the mean and standard deviation of attenuation values were measured for four regions of interest: psoas muscle, fat, CSF fluid, and bone. Image noise and contrast-to-noise ratio (CNR) were calculated. Qualitative analysis was conducted by two subspecialty-certified neuroradiologists, blinded to reconstruction algorithm and all clinical data. Visualization of nerve target and epidural fat were graded on a 3-point scale (0, not visualized; 1, barely perceptible; 2, confidently visualized). Overall confidence in needle advancement also was graded on a 3-point scale (0, requires rescan; 1, partially advance needle; 2, advance needle to target). Finally, overall preferred image reconstruction (FBP vs ASIR 100%) was assessed. Wilcoxon signed rank tests were used to compare scores for each reconstruction technique, and a chi-squared test was used to assess whether there was a difference in preferred reconstruction technique. The degree of interobserver agreement was determined using kappa statistics.

#### RESULTS

There were 12 men and 11 women included in this study (mean age 64.4 years, range 47 to 88 years). The mean weight for all patients was 154.8 pounds (range 105 to 208 pounds). When comparing image noise measured in the FBP and ASIR groups, there was significantly less noise in the ASIR groups for all tissues measured (psoas muscle,  $P = 0.006$ ; fat,  $P < 0.001$ ; CSF

fluid,  $P < 0.04$ ; bone,  $P < 0.003$ ). In addition, CNR was significantly higher in the ASIR group when comparing psoas muscle versus fat ( $P < 0.001$ ), CSF fluid versus fat ( $P < 0.006$ ), and psoas muscle versus bone ( $P < 0.05$ ). There were significantly higher scores for the ASIR group when compared to the FBP group for subjective visualization of nerve and fat ( $P < 0.001$  for each) and for overall confidence in needle advancement ( $P < 0.001$ ). Kappa scores for ASIR were higher than for FBP for visualization of nerve root and for confidence in needle advancement, but were higher for FBP for epidural fat.

#### CONCLUSION

Adaptive statistical iterative reconstruction appears to improve the depiction of structures critical to accurate needle placement for CT-guided lumbar spine nerve blocks.

**KEY WORDS:** Adaptive statistical iterative reconstruction, CT, lumbar spine nerve blocks

#### P-117

##### Effect of Music on Anxiety in Patients Undergoing Spinal Interventional Procedures

Iqbal, A.<sup>1</sup>Gregson, B.<sup>2</sup>Sowiak, S.<sup>1</sup>Birchall, D.<sup>1</sup>

<sup>1</sup>Royal Victoria Infirmary, Newcastle, UNITED KINGDOM, <sup>2</sup>Newcastle University, Newcastle, UNITED KINGDOM

#### PURPOSE

The use of intraoperative music is widely suggested to reduce patient anxiety, but there are very few studies validating this concept and none relating to interventional radiology procedures. We aimed to investigate the anxiolytic potential of music therapy in patients undergoing spinal nerve and facet joint blocks.

#### MATERIALS & METHODS

Anticipation of an invasive procedure in hospital is likely to provoke feelings of anxiety and stress in patients. Seventy patients (M:F 34:36 years) undergoing spinal nerve or facet joint blocks were randomized into a control or music group. Music was played in the background during the procedure although the patients were not made aware of this. Pre and postprocedural anxiety levels were measured using an internationally recognized and established scoring scale (State-Trait Anxiety Inventory) which has been used extensively in research and clinical practice.

#### RESULTS

The mean age for the control group was 49.3 and the music group 51.5. There was no difference in the preanxiety scores between the control ( $42.8 \pm 14.8$ ) and music ( $37.5 \pm 13.0$ ) groups ( $p = 0.11$ ). There was a significant reduction between the pre and postprocedural anxiety scores for the control group ( $42.8 \pm 14.8$  to  $35.7 \pm 13.8$ ,  $p = 0.004$ ) and music group ( $37.5 \pm 13.0$  to  $30.6 \pm 10.7$ ,  $p = 0.001$ ). In the control group there was a significant change for males ( $p = 0.02$ ) and age  $>45$  ( $p = 0.03$ ) but not for females ( $p = 0.09$ ) and age  $<45$  ( $p = 0.07$ ). In the music group there

was a significant change specifically for females ( $p = 0.004$ ) and age  $<45$  ( $p = 0.006$ ).

#### CONCLUSION

Listening to background music during spinal nerve and facet joint blocks is a simple and effective strategy, which helps to significantly reduce anxiety, particularly in females and those  $<45$  years in age.

**KEY WORDS:** Intervention

#### P-118

##### Cavity Creation, Vertebroplasty, and Image-Guided Radiation Therapy-Intensity-Modulated Radiation Therapy: A Combined Treatment Strategy for Vertebral Metastases

Nguyen, T. H.·Kuo, J. V.·Hoang, B. H.·Keyak, J. H.

University of California Irvine Medical Center  
Orange, CA

#### PURPOSE

We present a safe and effective treatment strategy for vertebral metastases, particularly those affected by pain symptoms, pathologic compression fracture, and/or canal or cord impingement.

#### MATERIALS & METHODS

Eleven patients with a total of 22 vertebral metastatic levels were evaluated from 2008 - present at our institution. Cavity creation within the involved vertebral body (by nonballoon techniques to avoid hematologic dissemination), followed by cement injection (vertebroplasty) and fiducial marker placement, was performed at each level via trans or extrapedicular, and uni or bilateral approach. The involved vertebra then was treated within 2 weeks of the above spinal intervention by targeted radiation therapy [i.e., image-guided radiation therapy (IGRT) or intensity modulated radiation therapy (IMRT)]. The technique, safety, efficacy, and outcome of this treatment strategy were analyzed and assessed.

#### RESULTS

All patients achieved durable pain relief and spinal stability with cessation of any further compression. Three patients with epidural tumor, one with cord impingement, resolved completely after treatment. There was no major complication. There was no tumor recurrence at any of the treated levels during extended follow up.

#### CONCLUSION

This treatment strategy combines the strengths of interventional radiology/neuroradiology in providing immediate pain relief, bone strengthening and structural stability, and the strengths of radiation oncology in delivering accurate and maximum targeted radiation to the tumor while minimizing the dose to critical structures such as spinal cord. This combined treatment is a safe and effective treatment option, which can provide excellent long-term palliation for metastatic disease in the spine.

**KEY WORDS:** Spine, metastases, vertebroplasty

#### P-119

### Sacral and Coccygeal Remodeling with CT-Guided Vertebroplasty

Manfrè, L.

Miniinvasive Spine Interventional Dept.  
Catania, ITALY

#### PURPOSE

Painful sacral insufficiency or tumoral fractures are clearly detected on MRI and bone scanning. Moreover, coccygeal subluxation after trauma can be responsible for unsustainable pain when the patient is seated. The purpose of our investigation was to obtain sacral and coccygeal vertebroplasty using CT-guided percutaneous fractionated injection of polymethylmethacrylate.

#### MATERIALS & METHODS

Among 1244 patients undergone vertebroplasty procedure, 21 cases with osteoporotic or neoplastic sacral involvement were selected. All the patients referred had severe local pain and motion disability. Pain intensity was scored on a VAS scale ranging from 0 (no pain) to 10 (unsustainable pain). Motion disability was graded using a 5-points scale. In patients with osteoporotic fractures, bilateral paraspinal approach through the sacral body-to-wing lines was used. In sacral malignancy, trans-alar route and/or trans-foraminal route were adopted. Multiple 2-3 cc PMMA microinjections were performed under CT-guide, to remodel the original sacral shape. In the three patients with coccygeal luxation, the coccyx was fused to S5 using a single shot of PMMA and transsacral-coccygeal route.

#### RESULTS

All the patients were painless or referred significant pain reduction after 4 weeks. Complete sacral remodel was achieved in all the patients, without foraminal or extrasacral leakage nor complications. In patients with coccygeal subluxation, the pain was resolved immediately after the treatment, the patients being painless in seated position.



#### CONCLUSION

CT-guided fractionated PMMA injections allows efficient sacral and coccyx remodeling preventing PMMA foraminal leakage, resolving the pain of patients.

**KEY WORDS:** Coccygeplasty, sacroplasty, sacrococcygeal pain

#### P-120

### C-Arm Cone Beam Computed Tomography for Guidance of Epidural Steroid Injections

Rao, S. Saadeh, T. Benndorf, G.

Baylor College of Medicine  
Houston, TX

#### PURPOSE

C-arm cone beam computed tomography (CBCT) is a three-dimensional imaging technology that provides nearly real-time guidance for interventional spine procedures. It offers a high degree of spatial resolution and allows for fast image reconstruction in axial planes. Our study describes the use of CBCT technology for monitoring and guidance of spinal epidural steroid interventions.

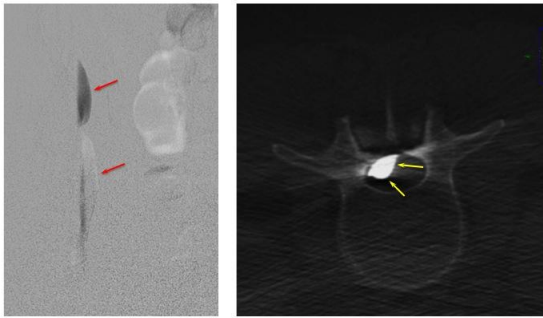
#### MATERIALS & METHODS

We retrospectively reviewed 48 patients (out of 393 total procedures) who underwent image-guided lumbar interlaminar epidural steroid injections (ESI) at Ben Taub General Hospital from February 2009 through October 2011. All patients had chronic lower back pain and lumbar radiculopathy refractory to medical therapy. A 20-gauge Tuohy needle was inserted into the soft tissues of the back and advanced in the midline into the lumbar epidural space. Tip position was verified with biplanar digital subtraction fluoroscopy and

injection of 3-5 mL of Iohexol contrast (Omnipaque 180; GE Healthcare). Prior to injecting the medication, additional imaging via cone beam CT (XPerCT, Allura, Phillips Medical Systems) was performed to verify needle position and evaluate contrast distribution in the spinal canal using the following parameters: 10 sec rotation, "Abdominal Fast HD", 512 x 512 pixel matrix.

## RESULTS

The majority of ESI procedures were completed without imaging evidence of complication (45/48), the epidural space well visualized in axial planes. In two patients, 2D biplane images were suspicious for contrast injection in the subdural space, while another patient had contrast in both the epidural and subdural spaces. In all three cases, C-arm CBCT readily confirmed these findings, while the patient was still on the table. The procedures were discontinued and rescheduled. Of the successfully completed procedures, the majority had visualization of contrast into the anterior epidural space.



## CONCLUSION

C-arm CBCT for epidural steroid injections is feasible and represents a useful adjunct to traditional fluoroscopy or radiographic imaging. It may help to decrease the risk of complications compared to "loss of resistance techniques" performed solely under fluoroscopic guidance. In our study, CBCT image resolution was of sufficiently high quality for precise anatomical visualization of the epidural, subdural, and subarachnoid space. Cone beam CT may be useful in patients with complex anatomy in which visualization of needle path is difficult in spinal interventions.

**KEY WORDS:** C-arm cone beam computed tomography, epidural steroid injections, real-time imaging

## P-121

### Painful Nonfractured Vertebral Body Edema: New Application for Vertebroplasty?

Manfrè, L.

Miniinvasive Spine Interventional Dept.  
Catania, ITALY

## PURPOSE

Vertebroplasty has been recognized as a powerful technique for vertebral fractures treatment, reducing

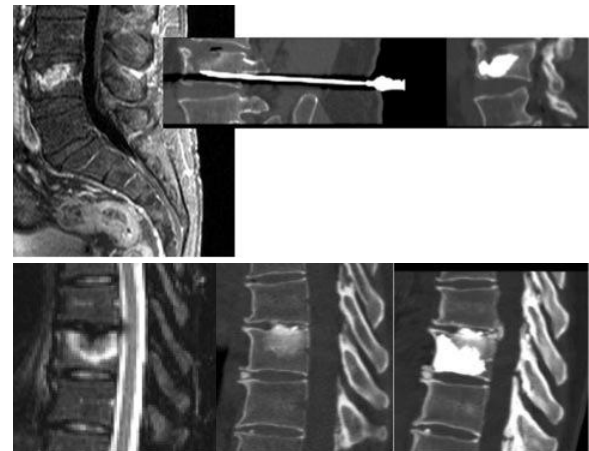
the pain related with minimal risk. Sometimes, painful vertebral edema can occur in nonfractured vertebra, related to abnormal compression on the vertebral body. We evaluate the possibility to treat painful patients affected by vertebral edema using CT-guided PMMA injection in nonfractured edematous vertebral body.

## MATERIALS & METHODS

Among 1244 patients undergoing vertebroplasty procedures, eight cases were affected by focal vertebral pain related to compressive Schmorl nodes (6 patients) or thoracic totally calcified disk degeneration (2 patients). In all the patients the pain was referred during the normal day activities and even during the night, at bedrest. MR imaging revealed abnormal signal intensity compatible with edema inside the vertebra inferior to the Schmorl node or calcified disk, while CT scans excluded fracture and only mild sclerotic changes were appreciated. Vertebroplasty was performed with whole-body augmentation of the pathologic vertebra body.

## RESULTS

The patients became painless in 24 hours and no complication was detected at 1 week-3 months follow-up controls.



## CONCLUSION

In conclusion, vertebroplasty using PMMA seems to be a powerful technique in the treatment of nonfractured vertebrae affected by painful edema.

**KEY WORDS:** Vertebral edema, aseptic spondylitis, vertebroplasty

## P-122

### Subclavian Artery and Brachial Plexus Compression by Cervical Ribs: Incidence and Clinical Correlates

Patel, N. V.·Alluwaimi, F.·Viertel, V.·Intrapiromkul, J.·Walden, M.·Yousem, D. M.

Johns Hopkins Medicine  
Baltimore, MD

## PURPOSE

Cervical ribs are an important cause of thoracic outlet syndrome, which can develop as a result of brachial



plexus or vascular compression within the costoscalene triangle. Earlier population studies on cervical ribs have relied on conventional radiography, but the detection of ribs and evaluation of resulting neurovascular compression may be improved with computed tomography. Our purpose was to use CT to determine the incidence of neurovascular compression in patients with cervical ribs and to examine the correlation between the imaging findings and clinical symptoms.

#### **MATERIALS & METHODS**

Patients with cervical ribs were identified from a retrospective review of 3300 consecutive cervical spine CT scans interpreted at a university hospital. Cases were identified initially by fellows before confirmation by an attending neuroradiologist. Each case then was assessed for imaging findings suggesting neurovascular compression, defined as contact between a cervical rib and the brachial plexus or subclavian artery. The patients' medical records were reviewed for the presence of clinical signs and symptoms referable to compression of these neurovascular structures.

#### **RESULTS**

Amongst 62 patients initially identified as having cervical ribs, 80 cervical ribs were confirmed in 59 patients. The fellow and attending agreed on the presence or absence of cervical ribs in 91% of the 124 left and right sides evaluated (Cohen's  $\kappa = 0.8$ ). Of the confirmed cases, four patients were excluded from analysis due to confounding neurologic problems (cervical cord compression, absent cortical activity). There were CT findings of neurovascular compression associated with 53.3% (40/75) of cervical ribs, more commonly of the brachial plexus (36.0%, 27/75) than the subclavian artery (21.3%, 16/75) in the arms down CT position. Both the brachial plexus and subclavian artery were compressed in three cases (4.0%). Amongst the cases of neurovascular compression, two (5.0%) were associated with ipsilateral thoracic outlet syndrome and one (2.5%) was associated with weak ipsilateral grip strength. No symptoms of neurovascular compromise were present on the contralateral side in these three patients.

#### **CONCLUSION**

Our study shows that imaging findings of neurovascular compression are present in the majority of patients with cervical ribs, even in the arms down position. Amongst these patients, we found that up to 7.5% have clinical symptoms of neurovascular compromise. This retrospective analysis did not employ provocative maneuvers, which could identify additional patients with clinical symptoms and may have lead to false negative results. Nonetheless, our findings underscore the importance of routinely identifying and reporting the presence of cervical ribs.

**KEY WORDS:** Cervical ribs, thoracic outlet syndrome, brachial plexopathy

#### **P-123**

##### **Cervical Ribs: Anterior Terminations**

Alluwaimi, F.·Patel, N. V.·Viertel, V.·Intrapiromkul, J.·Walden, M.·Yousem, D. M.

Johns Hopkins University  
Baltimore, MD

#### **PURPOSE**

To study the anterior terminations of normal variant cervical ribs.

#### **MATERIALS & METHODS**

The cervical CT scans of 5,000 consecutive patients were reviewed retrospectively to determine if a cervical rib was present. After exclusion criteria, 3404 cases were reviewed by trained observers for laterality, the anterior termination of the cervical rib end, and compression of the brachial plexus or subclavian artery. After expert review, 67 patients with 93 cervical ribs, 41 patients with a unilateral rib and 26 with bilateral ribs, were enrolled.

#### **RESULTS**

Of the 93 cervical rib cases, 46 (49.5%) were found to end blindly with attachment to the C7 transverse process, 20 (21.5%) to the C7 transverse process only, 9 (9.7%) only blindly, 8 (8.6%) to the sternum and the C7 transverse processes, and 5 (5.4%) to the C7 transverse process and T1 rib. There was 1 (1%) case with attachment to T1 rib, 1 (1.1%) ending blindly and attaching to T1 rib and 3 (3.3%) undetermined. Most cases had no compression of the subclavian artery or the brachial plexus (49.5%). The brachial plexus was compressed more often than the subclavian artery (30% vs 16%) and 4.3% of cervical ribs compressed both.

#### **CONCLUSION**

Most cervical ribs end with an attachment to the C7 transverse process (88%) and/or blindly (61%). Cervical ribs usually do not compress the subclavian artery or the brachial plexus in the arms down CT position.

**KEY WORDS:** Cervical ribs, Cervical ribs termination and attachment, thoracic outlet syndrome

#### **P-124**

##### **Comparison of FIESTA, 3D MERGE, 3D COSMIC and T2 Fast Spin-Echo High-Resolution Acquisitions for Evaluation of Craniocervical and Atlantoaxial Ligament Morphology**

Lake, J. R.·Thomas, J.·Baird, S. H.·Cornwell, B.·Alleman, A.  
University of Oklahoma  
Oklahoma City, OK

#### **PURPOSE**

Traumatic cervical spine injuries, particularly those with potential atlantoaxial and craniocervical ligament involvement require emergent imaging evaluation to

facilitate appropriate surgical or nonsurgical management. Optimizing MR pulse sequences for visualization of these structures is necessary to achieve efficient and accurate diagnosis of these potentially devastating injuries. We hypothesize that volumetric sequences such as FIESTA may provide equivalent resolution of the craniocervical and atlantoaxial ligaments compared with T2 triplane fast spin-echo sequences, which require longer scan times. In this investigation, we compared four separate cervical spine MRI sequences, and evaluated them based on each sequence's ability to resolve ligament morphology in a prospective group of normal patients. Results of this study will be used to implement changes to our current cervical spine trauma protocols.

#### **MATERIALS & METHODS**

A total of 40 patients with nontraumatic neck pain, and no prior history of cervical injuries were recruited for this study. The patients were imaged on 1.5 T MR scanners (GE, Milwaukee, Wisconsin). In addition to routine MRI sequences (Sagittal T1, T2, STIR, Axial T2, T2\*), 3D FIESTA (15cm FOV, 1 mm sl. thickness, TR 6.4, TE 2.7, flip angle 55 degrees, 256 x 192 matrix, 3 NEX, 4 min 6 sec scan time) 3D MERGE (15 cm FOV, 1.5 mm sl. thickness, TR 46.8, TE 17.7, 256 x 192 matrix, 8 min 34 sec scan time), 3D COSMIC (18 cm FOV, 3 mm sl. thickness, TR 5.7, TE 2.7, 224 x 288 matrix, 2 min 10 sec scan time) and Tri-plane T2 fast spin-echo sequences were obtained (18 cm FOV, 3 mm sl. thickness, TR 3000/TE 125, 256 x 224 matrix, echo train 19, 5 NEX, sequence times varying between 3 min 7 sec and 3 min 36 sec). 3D volumetric sequences were obtained in the axial plane and reconstructed prior to interpretation using AW suite software (GE Healthcare, Barrington, IL). Each of the studies were evaluated by three neuroradiologists who directly compared the conspicuity of the apical dental, anterior atlantoccipital membrane, tectorial membrane, transverse and cruciate ligaments between the four pulse sequences and graded their relative appearance on a four-point scale (0 = least conspicuous, poorly resolved, 4 = easily resolved and delineated from the surrounding tissues, clearly demonstrated). Interobserver variability amongst the investigators was calculated using the Kappa statistic.

#### **RESULTS**

Due to inherent contrast in signal intensities between the craniocervical ligaments and surrounding structures, the craniocervical ligament complex was best demonstrated on high-resolution triplane T2-weighted sequences. Subjective evaluation (interobserver variability) of the volumetric pulse sequences graded on a four-point scale were: FIESTA 3.5(0.82), MERGE 3.3(0.67) COSMIC 3.1(0.61).

#### **CONCLUSION**

While T2 triplane sequences provided the best visualization of the craniocervical ligament complex and atlantoaxial ligaments, the axial 3D FIESTA sequence and reconstructions provided acceptable image quality and structure resolution at a fraction of the scan time of the triplane T2 sequences. We believe FIESTA

sequences can be a viable and efficient option in MR imaging of the craniocervical and atlantoaxial ligaments in the trauma patient.

**KEY WORDS:** MR imaging, craniocervical, ligaments

**Monday, April 23 –  
Wednesday, April 25  
6:30 AM – 9:00 PM  
Thursday, April 26  
6:30 AM - 3:00 PM  
Americas Hall II  
Electronic Posters (ePosters)  
1 – 124**

**eP1 – ADULT BRAIN**

**Note: A missing printed number indicates an abstract has been withdrawn.**

#### **eP-1**

**Significance of Slow Flow on FLAIR and Hypointense Thrombi on GRE before Endovascular Treatment in Acute Ischemic Stroke in Comparison with Diffusion and Perfusion MR and Angiographic Findings**

Moritani, T.·Elison, A.·Hayakawa, M.·Starkey, L. J.·Sato, Y.

University of Iowa Hospitals and Clinics  
Iowa City, IA

#### **PURPOSE**

Hyperintense vessels on FLAIR is an indicator of slow flow of the blood proximal and distal to thrombi, stenoses or occlusions. GRE can directly visualize thrombi that contain certain blood products as hypointense in the vessel with blooming artifacts. The location, size and age of thrombi are useful information for endovascular treatment. However, exact mechanism and clinical significance of these findings on FLAIR and GRE have not been defined clearly. Diffusion-perfusion mismatch has been used for determining the applicability of endovascular treatment. We assessed the significance of the FLAIR and GRE findings in comparison with diffusion and perfusion MR and angiographic findings.

#### **MATERIALS & METHODS**

We reviewed 38 consecutive patients (40-90 years old, M:F=15:23) with acute ischemic stroke that have both MRIs (3-9 hours from onset) and angiograms (6-13 hours from onset). IVtPA were performed in 13 patients before MRIs. Endovascular treatments (chemical and mechanical thrombolysis and stent) were performed in

33 patients. The distribution of slow flow on FLAIR and hypointense thrombi on GRE were correlated with diffusion and perfusion MR and angiographic findings. Conventional MRIs including FLAIR and GRE, diffusion-weighted images (spin-echo type echo-planar with parallel imaging and the ADC maps with  $b = 0$  and 1000 sec/mm<sup>2</sup>) and perfusion-weighted images (color maps of rCBV, rCBF, and MTT) were obtained with 1.5 T or 3 T scanners.

## RESULTS

Hyperintense MCAs on FLAIR were identified in 97% (36/38) with variable distributions from M1 through M4 branches. Corresponding variable perfusion MR abnormalities with the same distribution as slow flows on FLAIR were observed in all patients, which included 34 elongated MTT and two shortened MTT; 30 increased CBV, four decreased CBV, and two normal CBV; and 26 decreased CBF, five increased CBF and five normal CBF. Two patients with no FLAIR slow flow had mild perfusion MR abnormalities; one patient had increased MTT, mildly increased CBV and normal CBF with a MCA stenosis on angiogram, and another had increased MTT, normal CBV and mildly decreased CBF with an ICA stenosis. Angiograms show corresponding abnormalities including thrombi, stenoses, occlusions, and associated slow flows and collaterals in all patients. Hyperintense ICAs on FLAIR also were seen in 12 patients in which slow flows with ICA stenoses or occlusions were proven on angiogram. Hypointense MCA thrombi on GRE were identified in 66% (25/38) with variable distributions in M1 through M4 with variable sizes measuring 2-25 mm. On angiogram, thrombi with or without stenoses were visualized in 35 patients, therefore, in which isointense thrombi on GRE were expected to be present in nine patients.

## CONCLUSION

Hyperintense vessels (slow flow) on FLAIR are seen frequently on MRI in applicants for endovascular treatment. The distribution of FLAIR slow flows corresponds to perfusion MR abnormalities. FLAIR (slow flow)-diffusion mismatch is thought to be another useful index for determining the applicability of endovascular treatment, especially if perfusion MRI cannot be performed. Identifying the location, size and age of thrombi (hypointense or isointense on GRE) are thought to be useful information for endovascular treatment.

**KEY WORDS:** FLAIR, GRE, stroke

## eP-2

### Mechanism of Acute Ischemic Stroke in Patients with Severe Intracranial Atherosclerotic Disease

Dubow, J.·Salamon, E.·Greenberg, E.·Patsalides, A.

Weill Cornell Medical College  
New York, NY

## PURPOSE

Intracranial atherosclerotic disease (ICAD) is a common cause of ischemic stroke worldwide. Although the

pathogenesis of cerebral infarction in ICAD has been reported from autopsy series, the mechanism of stroke remains elusive. This study utilized baseline perfusion and MRI or CT imaging to help identify the mechanism of acute stroke in severe ICAD.

## MATERIALS & METHODS

We retrospectively reviewed baseline CT or MR perfusion studies and DWI MRI or CT scans in patients with severe (>70%) symptomatic ICAD. Only patients with established acute ischemic stroke were included; transient ischemic attacks were excluded. The location of stenosis was the supraclinoid internal carotid artery in three patients, the middle cerebral artery in 14 patients, the anterior cerebral artery in one patient and the vertebral artery in two patients. The perfusion scans were performed without hemodynamic challenge and were classified as abnormal if there was a perfusion deficit outside of known core infarct. Perfusion images were further classified according to the three stages of hemodynamic changes seen in occlusive disease. A normal perfusion study was classified as stage 0. Stage 1 was defined as elevated mean transit time (MTT), elevated cerebral blood volume (CBV) and normal cerebral blood flow (CBF). Stage 1 represented autoregulatory vasodilation. Stage 2 was defined as decreased CBF, with concurrent prolonged MTT and normal to increased CBV. Stage 3 occurred when autoregulatory vasodilation was not adequate to maintain normal cerebral blood flow, so CBF began to fall. The infarct pattern was categorized as borderzone (watershed), cortical or penetrating artery, based on CT or MRI. A blinded neuroradiologist reviewed all imaging studies.

## RESULTS

Twenty consecutive patients were included in this analysis, 18 with anterior and two with posterior circulation ICAD. All patients with anterior circulation lesions had borderzone infarcts, whereas the two patients with posterior circulation lesions did not have borderzone infarcts. Of the 18 patients with anterior circulation ICAD, seven had borderzone infarcts only, five had borderzone and cortical and penetrating artery infarcts, five had borderzone and cortical infarcts, and one had borderzone and penetrating artery infarcts. Sixteen of the 18 patients with any form of borderzone infarction had concordant perfusion deficits (stage 2 in 13 patients, stage 1 in 3 patients), while the two patients with nonborderzone infarctions had no perfusion deficits.

## CONCLUSION

We found that most patients with severe ICAD and acute stroke had either borderzone or a combination of borderzone and cortical or perforating artery infarcts. In patients with severe ICAD, the mechanism of stroke is multifactorial, but hemodynamic insufficiency plays the primary role in anterior circulation infarcts. The fact that 10 out of 20 patients had a combination of borderzone and cortical infarcts with perfusion deficits supports the theory that the combination of embolism and hypoperfusion can lead to impaired clearance of emboli and produce infarcts. Only patients with

vertebrobasilar stenosis did not have borderzone infarcts. The mechanism of stroke may differ between anterior versus posterior ICAD.

**KEY WORDS:** Intracranial atherosclerotic disease, intracranial atherosclerosis

### eP-3

#### 4D Phase-Contrast MR Angiography of the Carotid Artery: Initial Experiences from Flow Phantoms to Patients

Kusumawidjaja, D.<sup>1</sup>•Lopez-Gonzalez, R.<sup>1</sup>•Foster, J.<sup>2</sup>•Watson, A.<sup>2</sup>•Lanaghan, K.<sup>2</sup>•Forbes, K.<sup>2</sup>

<sup>1</sup>The University of Glasgow, Glasgow, UNITED KINGDOM, <sup>2</sup>NHS Greater Glasgow and Clyde, Glasgow, UNITED KINGDOM

#### PURPOSE

Four-dimensional phase contrast MR angiography (4D MRA) is a new development in vascular imaging, offering significant improvements for the noninvasive characterization of blood flow. It offers simultaneous acquisition of 3D morphology and time-resolved blood flow velocities in three directions. Data can be used to derive secondary flow parameters such as wall shear stress. AIMS: To explore the utility of 4D MRA to characterize flow and wall biomechanics in the carotid artery with 3.0 T MRI, in phantom studies, normal volunteers and patients with carotid stenosis. These parameters are important in development of atherosclerosis.

#### MATERIALS & METHODS

Validation of flow velocities with conventional 2D PC MRA using MRI flow phantoms. Further experiments were conducted with anthropomorphic carotid phantoms and healthy volunteers. Finally, patients with at least 50% internal carotid stenosis were scanned. Extrapolated shear stress measurements were analyzed using an in-house built mathematical package and qualitatively compared between patients and healthy volunteers.

#### RESULTS

Bland-Altman plots revealed comparable flow velocities between 2D and 4D MRA. Utilization of 4D flow analysis software allowed visualization of 3D vessel geometry and flow patterns within phantoms and normal carotid bifurcation. Visualization of color-coded flow and 3D pathlines allowed for the temporal assessment of complex flow. Data was used to calculate shear stress forces on the vessel wall.

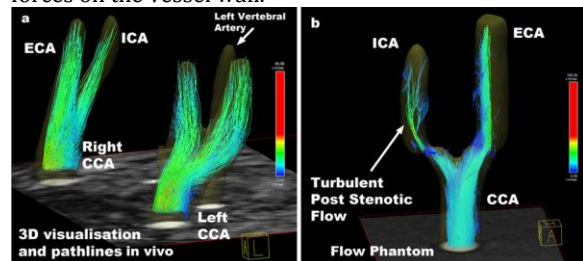


Figure 1. (a) 4D flow visualization of both carotid bifurcations in healthy volunteer. 3D flow visualization of both carotid bifurcations using time-resolved pathlines showing normal (laminar) and straight flow. (b) 4D flow visualization of both carotid bifurcations in anthropomorphic MRI flow phantom with 70% stenosis

#### CONCLUSION

4D MRA is a feasible and potentially useful method of quantifying complex flow in vascular territories. It also allows for biomechanical analysis such as shear stress derivation, which may prove to be a useful surrogate marker for future neurovascular events. Future directions will include formal assessment of carotid atherosclerosis and other vessels.

**KEY WORDS:** MR imaging, carotid, stroke

### eP-4

#### CT Workup of Acute Stroke Patients: Does Perfusion CT Add Value Compared to Noncontrast CT, CT Angiogram and Clinical Evaluation?

Zhu, G.<sup>1,2</sup>•Jovin, T.<sup>3</sup>•Aghaebrahim, A.<sup>3</sup>•Salinas, C. L.<sup>1,4</sup>•Wintermark, M.<sup>1</sup>

<sup>1</sup>University of Virginia, Charlottesville, VA, <sup>2</sup>Military General Hospital of Beijing PLA, Beijing, CHINA, <sup>3</sup>University of Pittsburgh, Pittsburgh, PA, <sup>4</sup>Hospital Universitario y Politécnico la Fe, Valencia, SPAIN

#### PURPOSE

To determine whether penumbral imaging adds value to noncontrast head CT, CT angiogram (CTA) and clinical assessment in patients with acute ischemic stroke.

#### MATERIALS & METHODS

We retrospectively review the clinical and imaging data collected in 60 patients with acute ischemic stroke. ASPECTS score was calculated from noncontrast head CT. CT angiography was reviewed for site of arterial occlusion and degree of collateral flow. Perfusion CT was used to calculate the volumes of infarct core and ischemic penumbra on admission. Recanalization and final infarct size were assessed on the follow-up imaging. Clinical data included age, time from onset to CT, NIHSS at baseline, treatment type and modified Rankin score (mRS) 90 days. In a first analysis, we used volume of penumbra as an outcome, and assessed whether it could be predicted from clinical variables, NCT ASPECTS or CTA occlusion of collaterals. In a second set of analyzes, we used final infarct and mRS as outcomes, and we assessed which imaging and clinical variables predicted them best. Both analyzes used multivariate regression analyzes.

#### RESULTS

The average time from onset to CT is 8.5 hours (min = 1 hour, max = 19.5 hours). Ninety-five percent of all patients received endovascular treatment, 19% also received intravenous thrombolysis with rtPA. The average time from onset to treatment is 10.3 hours (min = 1.5 hours, max = 48 hours). Penumbral volume

could be predicted by NIHSS and occlusion ( $P = 0.08$ ), but correlation was poor ( $R^2 = 0.136$ ). Penumbra could not be predicted by ASPECTS and site of arterial occlusion. The only variables significantly associated with final infarct size were NIHSS ( $P = 0.023$ ), penumbra ( $P = 0.018$ ) and recanalization ( $P = 0.014$ ). The  $R^2$  is 0.54 for the corresponding multivariate model. Though there was no significant association, only recanalization and mRS showed a trend in terms of association with mRS at 90 days ( $P = 0.084$ ,  $R^2 = 0.4$ ).

#### CONCLUSION

Penumbra is an important determinant of final infarct size and clinical outcome, and penumbra imaging adds relevant clinical information compared to a stroke CT workup including only noncontrast CT and CTA.

**KEY WORDS:** Perfusion CT, penumbra, acute ischemic stroke

#### eP-5

##### Evaluation of Cerebral Vascular Reactivity with Acetazolamide Challenge Dynamic Susceptibility Contrast MR Imaging: Preliminary Experience

Oda, S.·Kikuchi, K.·Hiratsuka, Y.·Watanabe, H.·Mochizuki, T.

Ehime University School of Medicine  
Ehime, JAPAN

#### PURPOSE

Cerebral vascular reactivity(CVR) estimation is crucial information for presurgical planning of revascularization. Acetazolamide(ACZ) challenge SPECT is performed to estimate CVR. Recently, dynamic susceptibility contrast MRI(DSC MRI) is used for evaluation of cerebral perfusion. In this study, we attempt to estimate CVR with ACZ challenge DSC MRI.

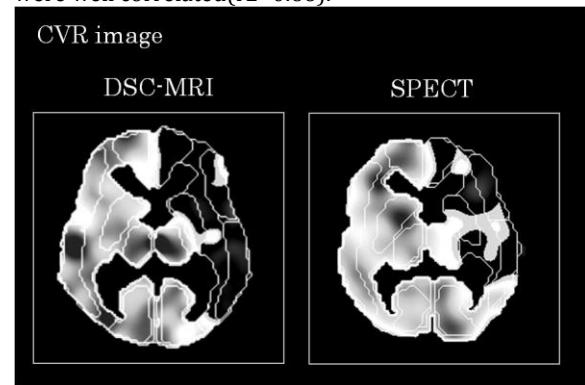
#### MATERIALS & METHODS

Eight patients with cerebral artery occlusive disease were included in this study. Rest and ACZ challenge brain-perfusion I-123 IMP SPECT data were acquired with a triple- or two-head gamma-camera equipped with fanbeam collimators. Acetazolamide challenge was induced by injection of 1g of ACZ 15 minutes before the administration of the second I-123 IMP injection. The quantitative SPECT reconstruction was accomplished by using dual-table autoradiographic method and a dual administration of 123I-IMP. Dynamic susceptibility contrast MRI was performed with a 3.0 T MRI unit. Dynamic susceptibility contrast MRI data were obtained with single-shot 2D GEEPI( $TR/TE/FA=1200/20/70$ ). Sixty dynamic images were obtained at 1.2 seconds time resolution per image during an intravenous bolus injection of Gd contrast agent. A 7.5 mL dose of contrast agent was injected by an MR-compatible power injector at a rate of 3 mL/s then a 20 mL saline flush was administered. After rest DSC MRI, 1 g of ACZ was administered intravenously. Fifteen minutes later, ACZ challenge DSC MRI was performed in the same manner as the rest study. These DSC MRI data were processed by perfusion mismatch analyze (software from ASIST-

Japan). To calibrate arterial input function in the two studies, values of venous input function were set to equal in both studies. Cerebral blood flow(CBF) images were generated with a block-circulant singular value decomposition algorithm which fully compensate for the bolus time delay. Cerebral vascular reactivity images were generated after realignment and spatial normalization to the standard brain atlas using the SPM2 function of NUEROFLEXER(software from Nihon Medi-Physics Co.,Ltd.). Regions of interest(ROIs) in the cerebral cortical area were drawn automatically by NUEROFLEXER. Cerebral vascular reactivity was defined by the increased rate of CBF after ACZ as follows:  $CVR=[(ACZ-CBF)-(rest-CBF)]/(rest-CBF) \times 100$ .

#### RESULTS

All SPECT and DSC MRI studies were performed successfully and adverse effects were not evident. Cerebral blood flow and CVR values/images were adequately obtained with above procedures. Correlations of CBF values at rest and challenged were moderate ( $r^2 = 0.42$ ), however CVR values of each study were well correlated( $r^2=0.66$ ).



#### CONCLUSION

Cerebral vascular reactivity obtained by ACZ challenge DSC MRI is a comparable parameter to ACZ challenge SPECT examination.

**KEY WORDS:** Cerebral perfusion reserve, MR imaging

#### eP-6

##### Value of Noncontrast Time-Resolved MR Angiography Using Arterial Spin Labeling in the Diagnosis of Moyamoya Disease

Tsuchiya, K.·Tateishi, H.·Gomyo, M.·Ohara, A.·Imai, M.·Nitatori, T.

Kyorin University  
Tokyo, JAPAN

#### PURPOSE

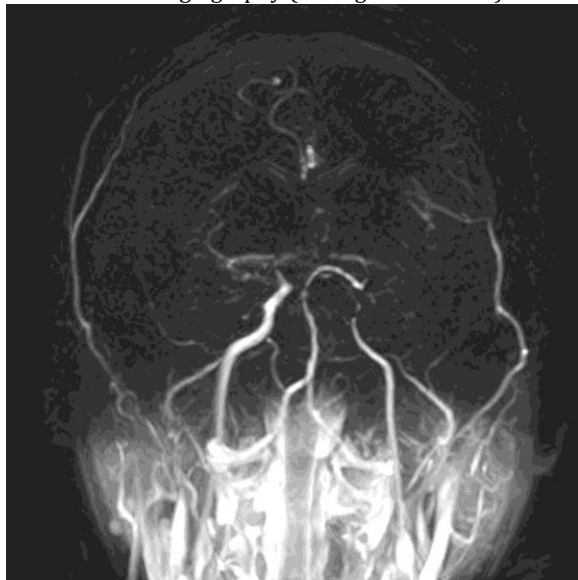
The purpose of our study was to assess the value of noncontrast time-resolved MR angiography (NTMRA) that has been developed based on the arterial spin labeling (ASL) technique in the diagnosis of moyamoya disease.

#### MATERIALS & METHODS

Our patient group comprised a total of 12 patients (age range, 21-75 years; mean age, 52.6 years; 5 men and 7 women). Among them, seven patients were after bypass surgery, while the remaining five had had no surgery. Noncontrast time-resolved MR angiography was performed on a 1.5 T system using a 3D steady state coherent gradient-echo sequence with parameters as follows: TR/TE/FA, 5.5 ms/2.5 ms/120 deg; FOV, 33x33 cm; imaging matrix, 256 x 256; slab thickness, 58 mm; and section thickness, 5 mm interpolated to 2.5 mm. In synchronization with the cardiac cycle by using the digital pulse wave, we performed 5-7 scans changing an inversion time by 200 ms in the coronal plane. Obtained images were compared visually with 3D time-of-flight (TOF) MR angiograms regarding the visualization of the stenosis/occlusion of the internal carotid artery and moyamoya vessels in the nonsurgery group. Meanwhile, in postsurgery group, we assessed the visualization of the anastomosis and distal arterial branches. The assessment was performed using a four-point grading system (0 = poor to 3 = best) by consensus of two neuroradiologists.

## RESULTS

No significant difference was present between NTMRA (average score = 2.4) and 3D TOF MR angiography (average score = 2.2) in the nonsurgery group. Classification according to Suzuki's staging (I-VI) was possible in all patients. In the postsurgery group, NTMRA (average score = 2.7) was significantly superior to 3D TOF MR angiography (average score = 2.1).



## CONCLUSION

Noncontrast time-resolved MR angiography is at least equivalent to 3D TOF MR angiography in the preoperative diagnosis of moyamoya disease. Noncontrast time-resolved MR angiography is of more value in the assessment of post bypass status than 3D TOF MR angiography. Noncontrast time-resolved MR angiography is a technique that can noninvasively enable the morphologic and functional diagnosis of moyamoya disease.

**KEY WORDS:** Arterial spin labeling, MR angiography, moyamoya disease

## eP-7

### MR Imaging in Thai Patients with Seropositive Anti-AQP4 Antibody

Chawalparit, O.·Pienpuck, W.·Jitpratoom, P.·Siritho, S.·Prayoonwiwat, N.

Siriraj Hospital  
Bangkok, THAILAND

## PURPOSE

To study the characteristics of magnetic resonance imaging (MRI) findings in Thai patients with seropositive aquaporin-4 (AQP-4) antibody.

## MATERIALS & METHODS

Fifty-three Thai patients attending Siriraj Hospital MS Clinic with positive anti-AQP4 antibody (Sendai's technique) were studied retrospectively. The available brain and spinal MRI in the hospital archive system were reviewed by two neuroradiologists and finalized by consensus. Clinical data and MRI findings were analyzed.

## RESULTS

Thirty-three patients with available MRI were included. There were 32 brain MRI and 27 spinal MRI (26 with brain MRI) for the analysis. The mean age was 42.7 years old (range 17-81); 31/33 were female. Clinical diagnosis were as follows: neuromyelitis optica:- NMO (9 cases), high risk NMO (8 cases), multiple sclerosis:- MS (8 cases; 5 relapsing remitting MS, 1 primary progressive MS, 1 progressive relapsing MS and 1 opticospinal MS) and Sjogren syndrome (2 cases). At the time of data analysis, diagnosis was inconclusive in five cases. Interval from an attack to the imaging study varied from 1 day to 5 years. Follow-up MRI was done in 13 cases, mostly more than 3 months interval. For brain MRI, 50% fulfilled Barkhof's criteria, 25% showed corpus callosum involvement, 12.5% had brain atrophy and 15.6% had negative findings. Nodular pattern of T2 lesions was found in most cases and 13 cases (40.6%) had only nodular lesions. The remaining 43.7% had either confluent, patchy, or mixed pattern of T2 lesions. Brain lesions typical for NMO were found: subependymal third/fourth ventricle (37.5%), subependymal lateral ventricle (28.1%), and medullary lesion extending to cervical cord (18.8%). Extensive hemispheric lesion and corticospinal tract lesion were found in 12.5% and 15.6%, respectively. There was 43.8% with nonspecific pattern. Most lesions had cloud-like enhancement and vasogenic edema. For spinal cord MRI, gadolinium enhancement was performed in all but one case. Negative finding was found in four cases (14.8%) and positive in 23 cases (85.2%). Among the positive cases, 47.8% had one T2 lesion and 52.2% had more than one lesion, mostly at thoracic cord. There were 15 cases (57.7%) with enhancing lesions, five cases (18.5%) with cord swelling, 18 cases (66.7%) with long extensive lesion (more than 3 vertebral body). Thirteen cases (48.1%) with central cord location on



axial plane, five cases (21.3%) with peripheral location, and five cases (21.3%) with mixed pattern. When comparing patients who fulfilled and not fulfilled Barkhof's brain criteria and their spinal lesions, no significant difference was found. Typical NMO brain lesions were associated significantly with clinical diagnosis ( $p < 0.05$ ) but not with length of spinal cord lesion.

#### CONCLUSION

The MRI findings in Thai patients with seropositive for anti-AQP4 antibody had high incidence of typical brain NMO lesion as well as long extensive cord lesion as described in other Asian countries.

**KEY WORDS:** Neuromyelitis optica, MR imaging, AQP-4

#### eP-8

##### Primary Motor Cortex Iron Content in Sporadic Amyotrophic Lateral Sclerosis: A Potential Biomarker of Disease Status

Zhang, J.·Luo, C.·Cai, P.·Chen, K.·Wang, J.

Southwest Hospital, Third Military Medical University  
Chongqing, CHINA

#### PURPOSE

To characterize iron deposition in the brains of patients with sporadic amyotrophic lateral sclerosis (ALS) and to correlate them to the clinical status of ALS.

#### MATERIALS & METHODS

Seventeen patients with ALS and 17 control subjects underwent MRI. The phase shift values of the bilateral caudate nucleus, globus pallidus, putamen, primary motor cortex (PMC) and frontal white matter were calculated. Clinical features were rated with the ALS Functional Rating Scale (ALSFRS).

#### RESULTS

A difference in the measured phase shift values between patients and controls was observed in the PMC ( $P = 0.000$ ). Correlation between the phase shift values from the PMC and the ALSFRS score ( $r = 0.581$ ,  $P = 0.015$ ) has been founded, but not between the phase shift values from the PMC and duration ( $r = -0.319$ ,  $P = 0.211$ ). Receiver operating characteristic analysis on the phase shift values of the PMC in patients with ALS showed that the area under the curve was 0.789.

#### CONCLUSION

Abnormal iron metabolism exists in ALS patients. Iron deposition in the PMC can be considered as a biomarker for diagnosing ALS and serve as a clinical index to assess the severity of ALS.

**KEY WORDS:** Iron deposition, amyotrophic lateral sclerosis, susceptibility-weighted imaging

#### eP-9

##### Correlations between Cerebellar Volume Changes and Clinical Dysfunction in Patients with Spinocerebellar Ataxia Type 6

Sato, K.<sup>1</sup>·Ishigame, K.<sup>1</sup>·Ying, S.<sup>1</sup>·Oishi, K.<sup>1</sup>·Miller, M. I.<sup>1</sup>·Mori, S.<sup>1,2</sup>

<sup>1</sup>The Johns Hopkins University School of Medicine, Baltimore, MD, <sup>2</sup>Kennedy Krieger Institute, Baltimore, MD

#### PURPOSE

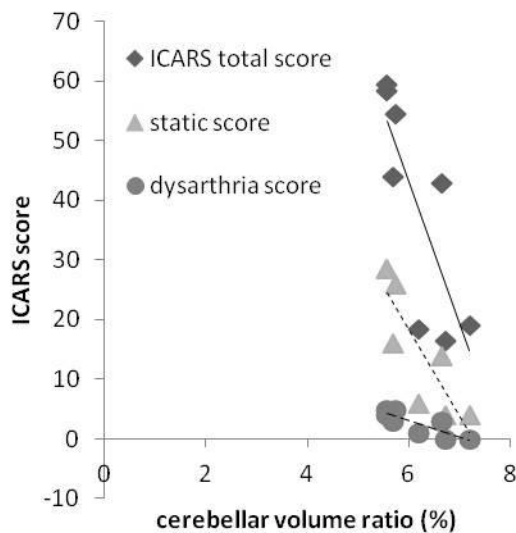
Spinocerebellar ataxia type 6 (SCA6) is a rare autosomal dominant disease that is associated with neurodegeneration of the cerebellum. The aim of this study was to investigate whether fractional volumetric changes of cerebellum and its subdivisions, using an automated cerebellar parcellation algorithm, correlate with clinical dysfunction measured with the International Cooperative Ataxia Rating Scales (ICARS) in patients with SCA6.

#### MATERIALS & METHODS

Eight patients (4 women/4 men, mean age:  $58.3 \pm 7.67$  years) with genetically confirmed SCA6 and seven age-matched healthy volunteers (4 women/3 men, mean age:  $57.0 \pm 5.03$  years) were studied using Philips Intera 3T MR. ICARS was used to measure clinical symptoms, including incoordination, visual disturbances, and dysarthria. Conventional T2-weighted imaging was acquired to rule out other cerebellar pathology. A 3D T1-MPRAGE imaging (TR/TE=10.33ms/6ms, flip angle=8°, voxel size=0.8x0.8x1.1 mm) was used for atlas-based analysis using automated parcellation of cerebellum based on the Large Deformation Diffeomorphic Metric Mapping (LDDMM) algorithm. Then we performed fractional volumetric analysis (ratio of whole cerebellum or its subdivisions divided by total intracranial volume). Spearman's rank correlation coefficient was used as a nonparametric test to analyze the relationships between volumetric measures and ICARS and its subscales including static (posture and gait) score and dysarthria score.

#### RESULTS

There was significant smaller fractional cerebellar volume in patients (mean±SD:  $6.16\% \pm 0.62$ ) as compared to controls (mean±SD:  $9.36\% \pm 0.57$ ) ( $p < 0.0001$ ). We also found significant reduction of fractional volume of all cerebellar subdivisions except the anterior vermis with pronounced reduction found in the anterior and posterior lobe in patients ( $P < 0.0001$ ). The reduction of fractional volume of cerebellum strongly correlated with ICARS (Spearman's rho= -0.857,  $p = 0.006$ ), static score (Spearman's rho= -0.93,  $p = 0.0005$ ), and dysarthria score (Spearman's rho= -0.80,  $p = 0.01$ ) in patients (Figure 1). Despite diffuse atrophic changes, only the fractional volume of posterior lobe and cerebellar white matter showed significant correlation with ICARS and static score ( $p < 0.05$ ). There was no significant correlation between either fractional volume of anterior lobe or the vermis and ICARS scales in these patients.



### CONCLUSION

Our findings suggest there is significant neuronal degeneration of cerebellum involving all subdivisions except the anterior vermis in patients with SCA-6. Our results of strong correlation between cerebellar atrophic measures and total and sub-ICARS scales indicate that the fractional volumetric analysis may have potential as a biomarker of clinical dysfunction and atrophic changes of entire cerebellum, the posterior lobe, and cerebellar white matter has better predictive value of disease severity than other subdivisions.

**KEY WORDS:** Spinocerebellar ataxia type 6, MR imaging, large deformation diffeomorphic metric mapping

### eP-10

#### In vivo Detection of Cortical Microinfarcts on 3 T MR Imaging

Maeda, M.·Ii, Y.·Umino, M.·Tomimoto, H.

Mie University School of Medicine  
Tsu, JAPAN

### PURPOSE

Cortical microinfarcts (CMIs) are reportedly an important risk factor for dementia. These lesions, detected frequently as small (< 3-5 mm) foci restricted to the cerebral cortex in autopsy specimens, are distributed predominantly in the area of predilection for cerebral amyloid angiopathy (CAA) with or without Alzheimer disease (AD) pathology. Information related to CMIs has remained limited to that of autopsy brains because CMIs remain invisible on conventional MRI. We therefore aimed to visualize CMIs using double inversion recovery (DIR) and 3D fluid attenuated inversion recovery (3D FLAIR) on 3 T MRI.

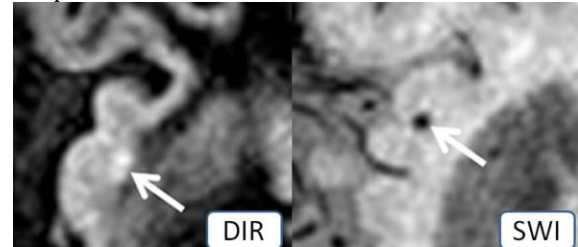
### MATERIALS & METHODS

We prospectively performed analyses of MR images from 70 cognitively compromised subjects with AD ( $n = 47$ ), mild cognitive impairment ( $n = 14$ ), AD with

vascular dementia (VaD) ( $n = 3$ ), VaD ( $n = 2$ ), CAA-associated intracerebral hemorrhage (ICH) ( $n = 2$ ), and one each of normal pressure hydrocephalus and dementia with Lewy bodies (DLB). The MR scan protocol included 2D, 3D DIR, and 3D FLAIR images for CMIs and susceptibility-weighted images (SWI) to detect cerebral microbleeds (CMBs). Intracortical lesions (CMIs) were determined as positive if they were detected exclusively as high signal foci both on DIR and 3D FLAIR images.

### RESULTS

Nine of 70 patients (5 of AD and one each of AD with VaD, ICH, VaD, and DLB) had small intracortical high signal lesions indicating CMIs on both DIR and 3D FLAIR images (Figure). These lesions were located proximal to CMBs (Figure). In a patient with AD, CMIs apparently increased in number during 1 year follow up. All nine subjects with CMIs invariably had multiple lobar CMBs on SWI, predominantly in the parieto-occipital lobe.



### CONCLUSION

Combined use of DIR and 3D FLAIR on 3 T MRI may present a means to visualize CMIs in vivo, which are putative biomarkers for CAA in combination with lobar CMB.

**KEY WORDS:** Alzheimer disease, cerebral amyloid angiopathy, MR imaging

### eP-11

#### Presence of Pineal Cysts in Patients with Multiple Sclerosis versus the General Population in Western New York

Ahmed, T. F.·Scott, B.·Ifthikharuddin, S.

Rochester General Hospital  
Rochester, NY

### PURPOSE

To assess the incidence of pineal cysts in a population of patients from Western New York with an established diagnosis of multiple sclerosis (MS) and to compare those findings with an age- and sex-matched control group from the same region.

### MATERIALS & METHODS

A retrospective review of prior brain magnetic resonance imaging scans (MRIs) in patients with clinically established MS over the course of a 5-year period in a community hospital and a outpatient imaging clinic in Western New York is being performed. A similar review of age- and sex-matched individuals

without a history of MS from the same institutions also will be performed. The studies are being reviewed independently by two fellowship-trained neuroradiologists and a senior radiology resident using standard pulse sequences and scan acquisitions from 1.5 T GE magnets. The presence of cystic changes (pineal cysts measuring <2 mm in short axis diameter), pineal cysts (cysts measuring > 2 mm in short axis diameter), or the absence of cystic findings are being noted. Data concerning cyst size, sex, patient age, and lesion burden also will be compiled. Standard statistical analyzes will be performed on the findings to demonstrate statistical significance.

## RESULTS

The total cohort will include approximately 300 patients and the control cases will contain a similar matched number. Preliminary results demonstrate the presence of cysts or cystic changes in 55.88% [cystic changes in 10 of 34 patients (29.41%) and cysts in nine of 34 patients (26.47%)] of the patients with a clinically established diagnosis of multiple sclerosis. Of the sampled population 70.58% were female and 29.41% were male.

## CONCLUSION

There is a higher incidence of pineal cysts and cystic changes in a population of patients with a clinical diagnosis of multiple sclerosis from the western New York region. The pathophysiologic significance of these findings is unclear and warrants further investigation.

**KEY WORDS:** Pineal cyst, multiple sclerosis

## eP-12

### Tract-Based Spatial Statistics of Diffusion Tensor Imaging in Hereditary Spastic Paraplegia with Thin Corpus Callosum

Oguz, K. K.<sup>1,2</sup>•Sanverdi, E. S.<sup>2</sup>•Turk, S.<sup>1</sup>•Doerschner, K.<sup>1</sup>

<sup>1</sup>Bilkent University, Ankara, TURKEY, <sup>2</sup>Hacettepe University, Ankara, TURKEY

## PURPOSE

Hereditary spastic paraplegia (HSP) is a clinical group of neurodegenerative disorders characterized by slowly progressive spastic gait, ataxia and cognitive impairment. Hereditary spastic paraplegia with thin corpus callosum (HSP TCC) is the most common form of complicated HSPs and has autosomal recessive inheritance. Until now there existed only a very limited number of case reports describing changes in white matter diffusivity associated with this condition. Our aim was to systematically investigate and quantify diffusivity changes in HSP patients. We used tract-based spatial statistics (TBSS) to identify possible candidate white matter tracts that exhibit marked changes in diffusion properties.

## MATERIAL & METHODS

Three HSP TCC cases (M/F:2/1; mean age: 22.3) and three age- and sex-matched healthy subjects were examined using a 1.5 T MR scanner (Magnetom TIM,

Siemens, Germany). The study was approved by the IRB of Hacettepe University, Ankara, Turkey. The MR imaging protocol consisted of a sagittal FLAIR (TR/TE/TI; 8900/100/2100 ms) and DTI sequence (single-shot echo-planar imaging sequence, b factor: 1000s/mm<sup>2</sup>, 64 independent directions, TR/TE = 5814/98 ms, FOV = 230 x 230 mm, matrix = 128 x 128, voxel-size = 1.5 x 1.8 x 1.8 mm<sup>3</sup>, 25 sections with 3 mm thickness without intersection gap). Following evaluation of the abnormalities on MRI by a neuroradiologist, voxelwise statistical analysis of fractional anisotropy (FA) and mean diffusivity (MD) maps was carried out using TBSS implemented within the FSL software package (<http://www.fmrib.ox.ac.uk/fsl/>). The preprocessing of the diffusion-weighted data included head motion and eddy current correction, diffusion tensor fitting (FSL DTIFit) and calculation of the FA and MD maps. Fractional anisotropy maps were registered and aligned to the average space, and the mean FA skeleton computed. Voxelwise statistics on the skeletonized FA, and corresponding MD, data was computed at a threshold level of p=0.05. White matter structures with significant group differences in FA and MD were extracted as ROIs, registered to and overlaid onto an anatomical template ([www.fmrib.ox.ac.uk/fsl/data/FMRIB58](http://www.fmrib.ox.ac.uk/fsl/data/FMRIB58)), and labelled using the MRI Atlas of Human White Matter (Oishi et al., 2011).

## RESULTS

All three patients had classically described periventricular mild T2 signal increase predominantly in the frontal lobes and atrophy of corpus callosum markedly in the genu and anterior corpus. Corticospinal tract, entire internal capsule, anterior thalamic radiation, superior longitudinal fasciculus, uncinate fasciculus, inferior fronto-occipital fasciculus showed significantly greater MD and lower FA compared to healthy subjects.

## CONCLUSION

Our findings show a more widespread white matter involvement microstructurally in HSP TCC as assessed by TBSS DTI than appeared on conventional MRI which shows more prominent anterior callosum and frontal lobe involvement.

**KEY WORDS:** Spastic paraplegia, hereditary, diffusion MR imaging

## eP-13

### Value of Routine Head MR Imaging following Resective Epilepsy Surgery

Rosebrock, R. E.•Krecke, K. N.•Britton, J. W.•Truitt, K. A.

Mayo Clinic  
Rochester, MN

## PURPOSE

The practice at Mayo Clinic for several years had been to perform a head MRI 3 months following resective epilepsy surgery in addition to an EEG and other selected tests. The estimated charges, based on the National Market Reference Point (NMRP) 85%-ile, for

head MRI without contrast is \$3543 and exam without and with contrast is \$5175. We sought to evaluate the value of a routine postsurgical MRI in management of our epilepsy patients.

#### **MATERIALS & METHODS**

Following IRB approval, epilepsy surgery cases were obtained from a log of all electrocorticography (ECOG) studies performed at Mayo Clinic, Rochester. One hundred seventy-three patients underwent ECOG from 2006-2008. Of these, 76 were excluded (31 = MRI not performed, 22 = ECOG done as part of surgical mapping for brain tumor surgery, 23 = surgical resection not done), leaving 97 patients for inclusion. Preoperative MRI findings were categorized as lesional or nonlesional. Postoperative MRI findings were categorized as expected, unexpected clinically significant, or unexpected clinically insignificant. Surgeries were categorized as temporal, extratemporal, or both; and lesionectomy, corticectomy, or both. The electronic medical record (EMR) was reviewed to determine surgical outcome (seizure free, auras only, significant seizure reduction, or no reduction) and to identify postoperative neurologic complaints and imaging findings.

#### **RESULTS**

Ninety-seven patients underwent 98 surgeries. Fifty-two (53%) were male. Median age at time of surgery was 33.7 years (range 10-76 years). Median time between surgery and routine postsurgical follow-up MRI of the head was 105 days (range 38-364 days). Sixty-six (67%) surgeries were lesional (35 = mesial temporal sclerosis) and 32 (31%) nonlesional. Thirty-eight (39%) surgeries were corticectomies, 4 (4%) were lesionectomies and 56 (57%) were combined lesionectomy and corticectomy. Postoperatively, 74 (76%) of the patients were seizure free, 2 (2%) reported continued auras, 12 (12%) had a significant seizure reduction and 10 (10%) had no reduction. Three (3%) patients complained of headaches and 1 (1%) complained of tingling in the fingers. In 96 (98%) of the surgeries, the postoperative MRI showed expected findings. In 2 (2%) surgeries, the postoperative MRI showed an unexpected clinically insignificant finding. One had a convexity extradural hematoma and one had a small region of infarction deep to the cortical resection. None of the patients had an unexpected clinically significant finding on the postoperative MRI.

#### **CONCLUSION**

The total charges for follow-up MR imaging performed during this study of nearly 100 patients were in excess of \$400,000, based on NMRP estimate. In our comparative effectiveness analysis of cost-benefit, we did not demonstrate value for head MRI as part of the routine postsurgical follow-up process, in terms of clinically significant findings or altered management, and have since discontinued this practice at our institution.

**KEY WORDS:** Epilepsy, postsurgical MR imaging, comparative effectiveness

#### **eP-14**

#### **Pulsed Arterial Spin Labeling Perfusion MR Imaging in Mesial Temporal Lobe Epilepsy: Initial Report**

Eryurt, B.Öner, A. Ucar, M. Bilir, E. Kurt, G. Capraz, & Tali, T.

Gazi University School of Medicine  
Ankara, TURKEY

#### **PURPOSE**

Quantification of the mesial temporal lobe perfusion asymmetry is a complementary method in presurgical management of patients with mesial temporal lobe epilepsy. The purpose of this study was to evaluate and compare pASL and dynamic susceptibility contrast (DSC)-based perfusion MR imaging, in detecting perfusion abnormalities of patients with mesial temporal lobe epilepsy.

#### **MATERIALS & METHODS**

This study was approved by the local ethical committee, and written informed consent was obtained in each patient. Fifteen patients (8 males, 7 female, ages 22-49 years) with medically refractory temporal lobe epilepsy and documented evidence of lateralization in noninvasive EEG and/or PET was enrolled in this study. Following conventional brain MRI, pASL with quantitative imaging and DSC perfusion MRI was performed in all subjects with a 3 T scanner. Regional cerebral blood flow (CBF) values in both right and left mesial temporal lobe were evaluated, by means of qualitative and quantitative analysis of perfusion image by two neuroradiologists blinded to the lateralization data in one sitting. Pulsed arterial spin labeling- and DSC-based perfusion MR imaging were compared with each other in detection of mesial temporal lobe perfusion abnormalities and the lateralization data.

#### **RESULTS**

Pulsed arterial spin labeling showed hypoperfusion in 13 of 15 cases, and correlated well with PET/EEG lateralization in all except one. Dynamic susceptibility contrast perfusion depicted hypoperfusion in all cases, but failed to correlate with PET/EEG in the same one case.

#### **CONCLUSION**

The results of this initial report shows that pASL provides accurate lateralizing information, which is comparable to that of DSC perfusion. Therefore pASL MRI can be used as an imaging adjunct in the evaluation of mesial temporal lobe epilepsy, and may be considered as an alternative to DSC perfusion imaging.

**KEY WORDS:** pASL, epilepsy

## eP-15

### Contribution of Insular Cortex in Determining Epileptic Focus in Temporal Lobe Epileptic Cases and Research on Its Importance on Hippocampus Lateralization Using Evidence by Spectroscopic Detection MR and Positron Emission Tomography/CT

Cavusoglu, I. G.<sup>1</sup>Inecikli, M. F.<sup>2</sup>Hakyemez, B.<sup>3</sup>

<sup>1</sup>Ahi Evren Chest Heart and Vessel Surgery Education and Research Hospital, Trabzon, TURKEY, <sup>2</sup>Kastamonu State Hospital, Kastamonu, TURKEY, <sup>3</sup>Uludag University School of Medicine, Bursa, TURKEY

#### PURPOSE

There is a complex electrophysiologic and anatomical relationship between insular cortex and temporolimbic structures. In patients with temporal lobe epilepsy (TLE) sensitive centers such as insular cortex often are affected. There are many studies in the literature about hippocampal and parahippocampal structures. Research on insular cortex is limited. The aim of our study is to show whether insular cortex is affected in TLE patients by means of MR spectroscopy (MRS) and positron emission tomography/computer tomography (PET/CT) and to define the contribution of hippocampus in lateralization of epileptic focus.

#### MATERIALS & METHODS

In our study, 19 patients and 15 healthy control cases were analyzed. Brain PET/CT analysis was done on 19 TLE patients and point-resolved spectroscopic (PRESS) sequence and single voxel spectroscopy (MRS) of both hippocampus and insular cortex was done in all cases. Amplitude values from MR spectrum belonging to NAA, Cho, Cr metabolites were assessed quantitatively. NAA/Cho+Cr, NAA/Cho, NAA/Cr and Cho/Cr values were obtained.

#### RESULTS

According to clinical and electroencephalography (EEG) findings, the most sensitive lateralization on both hippocampi was established through MRS parameters with NAA/Cho+Cr in 17 cases out of 19 (89%). Hypometabolism on the epileptic side was found in 12 cases in PET/CT (64%) in accordance with clinical and EEG findings. All MRS parameters were abnormal in all these cases. Statistically significant decrease in NAA and NAA/Cho+Cr, NAA/Cho, NAA/Cr proportions was found in insular cortex localization on the same side as epileptic focus in 12 out of 19 cases compared to the control group ( $p < 0.001$ ). In seven out of 12 PET/CT (58%) cases where abnormality in terms of epileptic focus was found, hypometabolism in the insular cortex on same side also was found.

#### CONCLUSION

Metabolic and functional abnormalities occurring in insular cortex of TLE cases can be determined with MRS and PET/CT. These metabolic abnormalities could be related with epilepsies originating from insular cortex or insular spread of seizures. In these cases radiologically determined metabolic abnormalities

which are supported with clinical and EEG findings can make important contributions to predict expected surgical success ratios and help planning surgical treatment.

**KEY WORDS:** Insular cortex, MR spectroscopy, positron emission tomography

## eP-16

### Magnetization Transfer Ratio Can Lateralize Hippocampal Sclerosis

Santos, A. C.<sup>1</sup>Diniz, P. P. R. B.<sup>2</sup>Salmon, C. E. G.<sup>1</sup>Rosset, S.<sup>1</sup>Velasco, T.<sup>1</sup>Leite, J. P.<sup>1</sup>Sakamoto, A. C.<sup>1</sup>

<sup>1</sup>University of Sao Paulo, Ribeirao Preto - SP, BRAZIL, <sup>2</sup>Federal University of Pernambuco, Recife - PE, BRAZIL

#### PURPOSE

Mesial temporal sclerosis (MTS) is characterized by cell loss and gliosis mainly in the hippocampus which is detected by volumetric loss and prolonged T2. Magnetization transfer ratio (MTr) allows access to water bound to macromolecular proteins and has potential to provide new insight to the synapse reorganization and sprouting. However, only two preliminary studies used MTr to hippocampal sclerosis (HS) with contradictory results, both with a few patients. The goal of this study is to investigate the possible contribution of MTr to identify HS for future pathophysiologic references.

#### MATERIALS & METHODS

We studied 32 patients with epilepsy and MTS in a 3 T MRI scanner. All patient had unilateral HS proved by temporal lobectomy and histological diagnosis, 18 on the right hippocampus. All images were automatically segmented with FreeSurfer package. The MTr maps were calculated as well as quantitative T2 for comparison. The segmentation labels were used to extracted values for MTr, volume and quantitative T2. The data were analyzed using a discriminant analysis with cross-validation and the normalized difference between hippocampus also was calculated.

#### RESULTS

Using the normalized difference between hippocampi we saw that volumetric data lateralized correctly 30 of 32 cases, the MTR lateralized 29 cases and T2 time lateralized 28 cases. Using the values of MTR, volume and T2 times for each hippocampus we did a discriminant analysis that showed: when we use, individually, the volumetric data the hit rate was 94%, MTR data was 84%, T2 relaxometry was 84%. Higher lateralization ratios were acquired combining volume MTR relaxometry (97%).

#### CONCLUSION

Magnetization transfer ratio can detect HS and may be used to provide complementary information of hippocampal pathology. For lateralization of epileptogenic focus and preoperative examination, the combination of techniques represents better accuracy.

**KEY WORDS:** Mesial temporal sclerosis, magnetization transfer ratio, temporal lobe epilepsy

#### eP-17

### High-Resolution in vivo Mapping the Human Brain White Matter Pathways: A Diffusion Tensor Tractography Study on 3.0 T

Kamali, A.<sup>1</sup>Brody, J.<sup>1</sup>Hasan, K. M.<sup>2</sup>

<sup>1</sup>University of Medicine & Dentistry of New Jersey/Cooper University Hospital, Camden, NJ,

<sup>2</sup>University of Texas, Houston, TX

#### PURPOSE

To prospectively investigate the utility of high spatial resolution diffusion tensor imaging (DTI) in mapping the projection, association, commissural, and brainstem fiber pathways in the healthy adult human brain.

#### MATERIALS & METHODS

This work was approved by the local institutional review board (IRB) and was health insurance portability and accountability act (HIPAA) compliant. *Subjects:* Five healthy men (age range 24-37 years) were studied and written informed consent was obtained from all subjects. *Conventional and DT-MRI Acquisition:* Data were acquired using a Philips 3.0 T Intera system using a SENSE receive head coil. Diffusion-weighted image (DWI) data were acquired axially using a single-shot multi-slice 2D spin-echo diffusion with the balanced *Icosa21* tensor encoding scheme. The b-factor = 500 sec mm<sup>-2</sup>, TR/TE = 14460/60 msec, FOV = 256 mm x 256 mm and slice thickness/gap/# slices = 1 mm/0 mm/120. The EPI phase encoding used a SENSE k-space undersampling factor of two, with an effective k-space matrix of 112 x 112 and an image matrix after zero-filling of 256 x 256. The acquisition spatial resolution for DTI data was ~ 2.2 9 mm x 2.29 mm x 1 mm, and the nominal resolution after image construction was 1 mm x 1 mm x 1 mm. *Fiber Tracking:* We used the FACT algorithm (DTIStudio) to reconstruct the projection, association, commissural, and brainstem pathways with a fractional anisotropy (FA) threshold of 0.22 and angle threshold of 60 degrees.

#### RESULTS

We demonstrate the feasibility of fiber tracking of projection, association, commissural and brainstem pathways using high SNR, angular and spatial resolution DTI on 3 T which provides data with high fidelity to map the white matter network of the human brain in both health and disease.

#### CONCLUSION

We demonstrate for the first time the feasibility and utility of high spatial resolution DTI to map brain white matter pathways relative to cortical and deep gray matter on healthy controls in an affordable amount of time. Our study is a good incentive to combine the anatomical (this study) with physiologic (fMRI, PET) studies.

**KEY WORDS:** High resolution, diffusion tensor imaging, brain white matter

#### eP-18

### Tracing Prefrontal Connectivity of the Caudate Head Using High-Resolution Diffusion Tensor Tractography

Kamali, A.<sup>1</sup>Hasan, K. M.<sup>2</sup>

<sup>1</sup>University of Medicine & Dentistry of New Jersey/Cooper University Hospital, Camden, NJ,

<sup>2</sup>University of Texas Medical School Houston, Houston, TX

#### PURPOSE

Lack of adequate imaging sensitivity and spatial resolution, so far, impeded depiction of prefronto-caudate pathway in lower resolution studies. This work aimed to explore the acuity and feasibility of visualization of white matter sub-structure within the human caudate nuclei in vivo such as frontostriatal pathway using a high-resolution diffusion tensor imaging technique and deterministic tractography approach. The caudate and putamen (Striatum) are the principal input of the basal ganglia circuit in the human brain. The caudate nucleus curves around the ventricular system and receives most of the projections from association areas of the cortex. The projections are particularly heavy from prefrontal cortex and frontal pole which project to the head of the caudate. The noninvasive mapping of the frontal lobe connections to the thalamus and basal ganglia would help advance our knowledge of brain-behavior relations as a result of natural aging, or pathologies such as Huntington's disease, bipolar disorders, Tourette's syndrome, and attention-deficit/hyperactivity disorder. Diffusion tensor tractography of white matter connections between the cortex and deep gray matter structures is challenged by the signal-to-noise ratio (SNR) due to overestimation of anisotropy at low SNR and partial volume averaging upon using large voxel volumes.

#### MATERIALS & METHODS

*Subjects:* Five healthy men (age range 24-37 years) were studied and written informed consent was obtained. *Conventional and DT-MRI Acquisition:* Data were acquired using a Philips 3.0 T Intera system using a SENSE receive head coil. Diffusion-weighted image (DWI) data were acquired axially using a single-shot multi-slice 2-D spin-echo diffusion with the balanced *Icosa21* tensor encoding scheme. The b-factor = 500 sec mm<sup>-2</sup>, TR/TE = 14460/60 msec, FOV = 256 mm x 256 mm and slice thickness/gap/# slices = 1 mm / 0 mm / 120. The EPI phase encoding used a SENSE k-space undersampling factor of two, with an effective k-space matrix of 112 x 112 and an image matrix after zero-filling of 256 x 256. *Fiber Tracking:* We used the FACT algorithm (DTIStudio) to reconstruct *prefronto-caudate and the anterior thalamic radiation connections* with a fractional anisotropy (FA) threshold of 0.22 and angle threshold of 60 degrees. Statistical comparisons were made using analysis of variance (Student t-test) and the Mann-Whitney tests.



## RESULTS

Using higher resolution combined with higher magnetic field strength improved the detectable anisotropy in gray matter (caudate) along with reducing partial volume effects. This allowed us to reveal more anatomical details and to map the prefronto-caudate pathway. In our experience, anterior thalamic radiation is traceable using slice thickness  $\sim 3$  mm, while the prefronto-caudate pathway was not traceable using the FACT approach at  $\sim 3$  mm which is attributable to mixing of fibers in different orientations within the voxel leading to lack of needed anisotropy in gray matter in larger voxel volume which was solved by using thinner slices and smaller voxel volume.

## CONCLUSION

In this report we demonstrated that using higher resolution along with thinner slices reduce the partial volume effect and enabled the tracing of the prefronto-caudate pathway within the gray matter (caudate nuclei) in vivo.

**KEY WORDS:** Diffusion tensor imaging, caudate, prefrontal cortex

## eP-19

### Difference in Vulnerability to Radiation-Induced Changes among Major Cerebral White Matter Bundles: Longitudinal Diffusion Tensor Imaging Observation

Tha, K. K.<sup>1</sup>•Terae, S.<sup>1</sup>•Onodera, S.<sup>1</sup>•Aoyama, H.<sup>2</sup>•Popy, K. A.<sup>1</sup>•Shirato, H.<sup>1</sup>

<sup>1</sup>Hokkaido University Graduate School of Medicine, Sapporo, JAPAN, <sup>2</sup>Niigata University Graduate School of Medical and Dental Sciences, Niigata, JAPAN

## PURPOSE

Cerebral white matter is known to be vulnerable to radiation-induced changes. However, it is not well documented if the radiation-induced changes occur equally among various cerebral white matter structures. This study was aimed to evaluate if vulnerability to radiation-induced changes differed among major cerebral white matter bundles, by using diffusion tensor imaging (DTI).

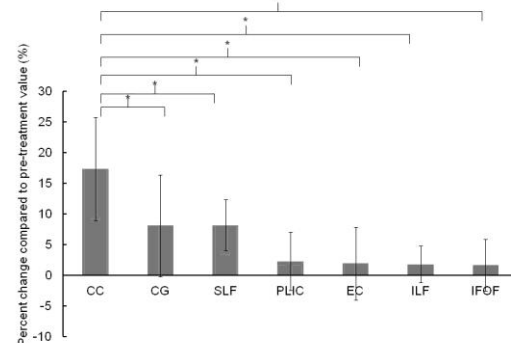
## MATERIALS & METHODS

Seventeen patients (mean age = 63.1 years, range = 53-75 years), who were scheduled to undergo whole brain radiation therapy (WBRT; 35Gy in 14 fractions) to treat cerebral metastases, were enrolled in this prospective study. Diffusion tensor imaging, along with routine MRI sequences, was performed before WBRT, immediately after WBRT, 1.5, 4, 8, and 12 months after WBRT. Temporal changes in the absolute values of major DTI indexes -- fractional anisotropy (FA), mean diffusivity (MD), longitudinal ( $\lambda_{//}$ ) and perpendicular ( $\lambda_{\perp}$ ) diffusivities, were compared among seven normal-appearing major white matter bundles [i.e., corpus callosum (CC), posterior limb of internal capsule (PLIC), cingulate (CG), superior (SLF) and inferior longitudinal fasciculi (ILF), inferior fronto-occipital fasciculus

(IFOF), and external capsule (EC)]. For comparison, temporal changes in the absolute values of major DTI indexes also were evaluated in six normal subjects. One way analysis of variance (ANOVA) and post-hoc Tukey's tests were used for statistical analysis, and  $P < 0.05$  was considered significant.

## RESULTS

Compared to pretreatment values, trend toward decrease in FA and increase in MD,  $\lambda_{//}$  and  $\lambda_{\perp}$  after WBRT was observed in major cerebral white matter bundles of the patients -- reaching statistical significance at 1.5 and 8 months for FA of PLIC, 1.5, 4, 8, and 12 months for FA of SLF, 4, 8, and 12 months for MD of CC, 8 and 12 months for MD of CG, 12 months for MD of SLF, 12 months for  $\lambda_{//}$  of CG, 4 and 8 months for  $\lambda_{\perp}$  of CC, 8 months for  $\lambda_{\perp}$  of CG, and 8 and 12 months for  $\lambda_{\perp}$  of SLF. Percent changes in the absolute values of major DTI indexes varied significantly among the bundles: CC, CG, and SLF exhibited larger percent changes than PLIC, ILF, IFOF, and EC (Figure).



Percent changes in MD values of major cerebral white matter bundles at 8 months after WBRT, relative to pre-treatment values. Mean values and standard deviation are shown. \* indicates statistical significance.

## CONCLUSION

The results suggest vulnerability to radiation-induced changes differs among major cerebral white matter bundles. This knowledge may be helpful for future planning or modification of radiation field, to preserve neural function and maintain quality of life.

**KEY WORDS:** Whole brain radiation therapy, diffusion tensor imaging, cerebral white matter

## eP-20

### Brain Tumors Visualization on Contrast-Enhanced MR Imaging Based on Gadoteridol Extravasation and Ferumoxytol Uptake by Tumor-Associated Macrophages

Gahramanov, S.<sup>1</sup>•Isidro, R. A.<sup>2</sup>•Woltjer, R.<sup>1</sup>•Hamilton, B. E.<sup>1</sup>•Muldoon, L. L.<sup>1</sup>•Neuwelt, E. A.<sup>1</sup>

<sup>1</sup>Oregon Health and Science University, Portland, OR, <sup>2</sup>Ponce School of Medicine, Ponce, PR.

## PURPOSE

Current contrast-enhanced MR imaging of brain tumors is based on extravasation of gadolinium-based contrast agent across permeable tumor vasculature. The

magnitude of contrast enhancement depends on the level of blood-brain barrier disruption. The presence of tumor-associated macrophages in brain tumors and their ability to uptake iron oxide nanoparticles may provide an attractive alternative contrast agent for tumor visualization. The magnitude of contrast enhancement would depend on the extent of immune-competent cells present in the tumors. We evaluated and compared contrast-enhanced MR images of brain tumors using two contrast agents acting through two different tumor properties and correlated with histologic appearance.

#### **MATERIALS & METHODS**

Fourteen patients with newly diagnosed brain lesions underwent an imaging study under three institutional reviewed board-approved research protocols on a 3 T MRI system. T1- and T2-weighted images were acquired before and 10-20 minutes after 0.1 mmol/kg gadoteridol intravenous administration. Ferumoxytol was given intravenously the next day at a dose of either 4 mg/kg or 510 mg regardless of body weight according to the protocols with post-ferumoxytol T1- and T2-weighted images acquisition 24 hours later. Immediately after the imaging study, all patients had a tissue biopsy. Postcontrast enhancement characteristics (location, size, intensity, pattern) on T1 (hyperintensity) and T2 (hypointensity) were evaluated after each contrast agent in all patients and correlated with histologic diagnosis. Immunohistochemical staining is being pursued in conjunction with Perl's iron stain to determine the different immune-competent cells in the pathology tissue and iron localization.

#### **RESULTS**

Eight patients had high grade primary brain tumors (6 GBMs, 1 anaplastic astrocytoma, 1 anaplastic oligodendroglioma), two patients B-cell CNS lymphoma, two patients metastatic tumors (1 melanoma, 1 lung adenocarcinoma), one patient demyelinating disease, and one patient subacute infarct. No differences were observed in T1 enhancement characteristics of both contrast agents in all patients with brain tumors except one lymphoma case where the ferumoxytol enhancement size was larger than after gadoteridol. T2 hypointensity was apparent in 11 out of 12 patients with brain tumors after ferumoxytol and none after gadoteridol. Immunohistochemical staining is in process to assess colocalization of CD68, CD163 macrophage/monocyte cells with iron particles.

#### **CONCLUSION**

Despite different mechanisms of action, gadoteridol and ferumoxytol showed similar T1 enhancement characteristics of malignant brain tumors. This finding suggests a close relationship between blood-brain barrier disruption and presence of macrophages/monocytes. It would be of particular interest to noninvasively visualize the presence of tumor-associated macrophages in different brain tumors and determine their prognostic value and treatment response prediction.

**KEY WORDS:** Brain tumors, ferumoxytol, tumor-associated macrophages

#### **eP-21**

#### **Consecutive Acquisition of Time-Resolved Contrast-Enhanced MR Angiography and Perfusion MR Imaging of Suspected Brain Metastasis through the Addition of a Supplementary Dose of a Gd-Based Contrast Agent**

Tsuchiya, K.<sup>1</sup>•Aoki, S.<sup>2</sup>•Shimoji, K.<sup>2</sup>•Mori, H.<sup>3</sup>•Kunimatsu, A.<sup>3</sup>

<sup>1</sup>Kyorin University, Tokyo, JAPAN, <sup>2</sup>Juntendo University, Tokyo, JAPAN, <sup>3</sup>University of Tokyo, Tokyo, JAPAN

#### **PURPOSE**

To assess the feasibility and value of time-resolved contrast-enhanced MR angiography (TCMRA) and additionally performing perfusion MR imaging (PWI) of suspected brain metastasis by employing a supplementary injection of a Gd-based contrast agent.

#### **MATERIALS & METHODS**

Our study group comprised 69 cases of suspected brain metastasis. Their final diagnosis included brain metastasis in 31, high-grade glioma (HGG) in 13, low-grade glioma (LGG) in three, lymphoma in seven, meningioma in six, and others in nine. Using an identical 1.5 T scanner and parameters at three institutions, we first obtained precontrast T1/T2-weighted images (T1/T2WIs), FLAIR images, and diffusion-weighted images. Then, we obtained TCMRA images and first postcontrast T1WIs. When their findings were negative or equivocal, we obtained PWI and second postcontrast T1WIs. We employed a Gd-based contrast agent, which can be supplementarily given with the FDA approval in such cases, at a dose of 0.2 mL/kg followed by a 20 mL saline flush at a rate of 3 mL/sec for both TCMRA and PWI. We evaluated perfusion maps (rCBF, rCBV, and MTT) as well as TCMRA images with respect to contrast of a lesion with normal brain using a three-point grading scale (1 = poor/2 = fair/3 = good). Furthermore, we assessed whether these techniques added information to conventional MR imaging in the differential diagnosis with reference to the final diagnosis. We also evaluated whether the second injection improved the number and visibility in cases of multiple lesions.

#### **RESULTS**

In all patients, we obtained PWI maps and TCMRA images that allowed assessment of tumor hemodynamics with average assessment scores of 2.0 and 2.3, respectively. In 14 cases (20%), PWI and/or TCMRA provided additional information to conventional MR findings. In 10 of the 31 cases of brain metastasis (32%), the number of detected lesions increased after the second injection, while the lesion visibility was improved in 59 of the 69 cases (86%).

#### **CONCLUSION**

Consecutive acquisition of TCMRA and PWI by employing a supplementary injection of a Gd-based

contrast agent can facilitate the preoperative differential diagnosis in case of suspected brain metastasis. It is also valuable as it improves the number and visibility of lesions.

**KEY WORDS:** MR angiography, perfusion, contrast agent

## eP-22

### MR Imaging Brain Dynamic Contrast-Enhanced Characteristics in a Pilot Study Using Intracerebral Microdialysis to Determine the Neuropharmacokinetics of Bafetinib in Patients with Recurrent High-Grade Glioma

Chen, B. T.<sup>1</sup>•Ortiz, A. O.<sup>2</sup>•Muradyan, N.<sup>3</sup>•Badie, B.<sup>1</sup>•Portnow, J.<sup>1</sup>

<sup>1</sup>City of Hope Medical Center, Duarte, CA, <sup>2</sup>Winthrop-University Hospital, Mineola, NY, <sup>3</sup>iCAD, Inc., Nashua, NH

#### PURPOSE

Bafetinib (INNO-406, NS-187, CML-187) is an oral potent BCR-ABL/LYN dual tyrosine kinase inhibitor and is expected to be effective in treating gliomas. MRI dynamic contrast-enhanced (DCE) data have been used to estimate the blood-brain barrier (BBB) permeability, an imaging biomarker for monitoring treatment response. The purpose of this study was to analyze the DCE MRI brain characteristics of study patients with recurrent high-grade gliomas being treated with bafetinib, to correlate this with the results of intracerebral microdialysis and to determine the neuropharmacokinetics of bafetinib.

#### MATERIALS & METHODS

Seven patients were enrolled in this pilot study. All patients had pathology proven high-grade gliomas confirmed by either surgical debulking or stereotactic brain biopsy, during which an intracerebral microdialysis catheter for neuropharmacokinetic analysis was placed in the viable tumor or peritumoral tissue for measuring intracerebral levels of bafetinib. Posttreatment MRI exams were obtained after oral bafetinib therapy varying from 2 to 8 weeks. Serial MRI brain studies with DCE sequences were obtained including preoperative, postoperative day #1 and posttreatment examinations. The DCE MRI portion of data was processed using iCAD software. Whole tumor ROIs were drawn manually. The maps of permeability surface area product per unit volume of tissue  $K^{trans}$  (1/min), initial area under gadolinium curve iAUGC (60sec) (mMsec), extracellular extravascular volume fraction  $V_e$  were generated from DCE analysis.

#### RESULTS

Four of seven patients had complete serial MRI examinations. The mean  $K^{trans}$  values pre-op and posttreatment were 0.092 and 0.074 min<sup>-1</sup> for Pt1, 0.112 and 0.136 min<sup>-1</sup> for Pt4, 0.083 and 0.061 min<sup>-1</sup> for Pt5, 0.072 and 0.119 min<sup>-1</sup> for Pt6. The enhancing volume of tumors increased considerably from pre-op to posttreatment for three patients [27.66 to 38.18 cc for Pt 1 (38%), 58.86 to 94.15 cc for Pt 4 (60%), 3.9 to

25.33 cc for Pt 5 (550%)] indicating progression of disease. It slightly decreased for Pt 6 8.65 to 7.31 cc (-15.5%), however there was significant increase of  $K^{trans}$  (65%) indicating progression of the disease. The mean  $V_e$  values did not show considerable changes, except in Pt 4 (+79%) who also had 21.4% increase of  $K^{trans}$  and 60% increase of the enhancing volume of the tumor. All four patients showed progression of disease on both MRI imaging and clinical evaluation. The dialysate of the neuropharmacokinetic analysis showed no evidence of bafetinib in the cerebrospinal fluid sample.

#### CONCLUSION

Orally administered bafetinib does not appear to be clinically effective in treating high-grade gliomas. The low BBB permeability observed by DCE MRI analysis and confirmed by neuropharmacokinetic analysis further supports the notion that this drug is not present in sufficient concentration within the brain tissue to be effective.

**KEY WORDS:** MR imaging brain DCE, Bafetinib, high-grade glioma

## eP-23

### Primary Melanocytic Lesions of the Central Nervous System and Metastatic Melanoma: Pictorial Review

Leon, J. L. •Garcia-Ferrer, L. •Aliaga, R. •Campos, S.

Hospital Clinico Universitario de Valencia  
Valencia, SPAIN

#### PURPOSE

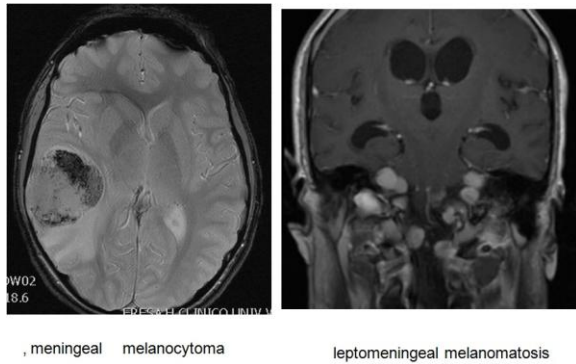
We present the variety of pigmented lesions of the central nervous system (CNS) with patients diagnosed in our diagnostic imaging unit.

#### MATERIALS & METHODS

Primary melanocytic lesions of the CNS and metastatic melanoma are pigmented lesions of the CNS. Their imaging appearances are influenced by the degree of melanin content as well as the presence or absence of hemorrhage. Melanocytic lesions of the CNS arise from melanocytes located within the leptomeninges, and this group includes diffuse melanocytosis and meningeal melanomatosis (seen in neurocutaneous melanosis), melanocytoma, and malignant melanoma. Primary melanin-containing lesions of the CNS must be differentiated from metastatic melanoma because these lesions require different patient workup and therapy.

#### RESULTS

During the last 2 years, ten patients with CNS pigmented lesions (all of them have pathologic correlation) have been diagnosed. In this pictorial review we present neurocutaneous melanosis, meningeal melanocytoma, primary leptomeningeal melanomatosis and CNS melanoma (primary and metastasis).



### CONCLUSION

Pigmented lesions of the CNS are rare entities that may simulate other CNS neoplasm at both imaging and histologic evaluation. It is important to know the appearance of the pigmented lesions with melanin content in order to differentiate benign from malignant lesions. Metastatic melanoma should be ruled out when these lesions are encountered, since the prognosis and therapeutic options for pigmented lesions differ substantially from what is expected for melanoma.

**KEY WORDS:** Pigmented lesions, CNS, melanocytic lesions

### eP-24

#### Supratentorial Ependymomas: Review of Imaging Findings in 24 Patients

Anantaram, G.·Sainil, J.·Paramveer, S.

National Institute of Mental Health and Neurosciences  
Bangalore, INDIA

### PURPOSE

To compare the age distribution and characteristic CT and MR imaging findings of supratentorial ependymomas.

### MATERIALS & METHODS

During a recent 11-year period, CT and MR images of 24 patients with histologically proven supratentorial ependymomas were obtained and retrospectively reviewed in terms of incidence, peak age, location, size, signal intensity, the presence or absence of cyst, enhancement pattern, and other associated findings.

### RESULTS

Among the 24 patients, most supratentorial ependymomas (in 12 of 24 patients) developed in children less than 10 years. Approximately half of these developed between 6 to 8 years. Intraventricular location was seen in 12% (3/24) of cases. Four imaging appearances were noted. Heterogenous solid-cystic mass was seen in 54% (13/24), cystic mass with mural nodule in 29% (7/24), solid mass with multiple peripheral cysts was seen in 4% (1/24) solid mass was seen in 8% (2/24) of tumors. Few imaging appearances (solid mass with multiple peripheral cysts, solid mass), enhancement pattern (mild and homogenous enhancement) and type of calcification (chunky

calcification) was noted in children and young adults (3-16 years) only. The signal intensity of ependymomas was nonspecific, regardless of their location. Intraventricular tumors had heterogenous solid-cystic mass appearance only. Mild peritumoral edema 29% (7/24) was seen in tumors with appearance of cyst with mural nodule. Gross peritumoral edema was seen in tumors with appearance of heterogenous solid cystic mass.

### CONCLUSION

Even though the CT and MR imaging findings of supratentorial ependymomas vary and are nonspecific, awareness of imaging findings and of tumor distribution according to age [large supratentorial intraparenchymal (tumor, focally abutting the adjacent ventricle)], is helpful and increases the likelihood of correct preoperative clinical diagnosis.

**KEY WORDS:** Supratentorial ependymomas

### eP-25

#### Peritumoral T2 Mapping of Glioblastoma Multiformes and Metastatic Brain Tumors

Nakai, K.·Nawashiro, H.·Kosuda, S.·Kaji, T.

National Defense Medical College  
Tokorozawa, Saitama, JAPAN

### PURPOSE

Vasogenic edema on glioblastoma multiforme (GBM) or a metastatic brain tumor (METS) might have different values of T2 relaxation time because the vasogenic edema involves an increased water component. In this study, we assessed the diagnostic utility of T2 mapping techniques in distinguishing GBM from METS.

### MATERIALS & METHODS

We studied 13 patients with glioblastoma (GBM group, n = 7) or metastatic brain tumor (METS group, n = 6) without previous surgery or treatment. All MR imaging was carried out using a 3.0 T whole-body unit, and axial T2 maps were generated with 5 TEs (TE = 20, 40, 60, 80, and 100 ms). Data were analyzed by using image processing and analysis software.

### RESULTS

There was a significant difference at 230 ms of T2 relaxation time between the GBM and METS groups (p = 0.004). Indexes derived from combinations of frequency counts of 102, 160 and 230 ms for T2 relaxation time were evaluated for the possibility to distinguish GBM from METS using ROC analysis. A ratio by frequency count of 160 ms to 230 ms and inverse of normalized counts at 230 ms yielded a higher ROC-AUC (0.905).

### CONCLUSION

The distribution of T2 relaxation time in the peritumoral area shows different patterns in glioblastoma and a metastatic brain tumor. The ratio of 160 ms to 230 ms at T2 relaxation time appears to be a good predictor for differential diagnosis between these lesions.

**KEY WORDS:** T2 mapping, glioblastoma multiforme, metastatic brain tumor

#### eP-26

### Differentiation of Radiation Necrosis from Recurrent Brain Tumors: Role of Perfusion CT

Yildirim, O.·Cebeci, H.·Hakyemez, B.·Inecikli, F.·Parlak, M.

Uludag University School of Medicine  
Bursa, TURKEY

#### PURPOSE

Differentiation of recurrent brain tumor from radiation necrosis after radiation therapy on patients who had undergone brain tumor surgery is important for planning the treatment. It is very difficult with conventional CT and MRI in some cases. Accurate diagnosis of these two lesions is critical for determining treatment protocol. Our purpose in this study is the discrimination of radiation necrosis from recurrent tumor with perfusion CT.

#### MATERIALS & METHODS

Our study included 13 female and 11 male patients, who had undergone surgery for brain tumors and radiation therapy after surgery and then later in the control MR imaging had new or progressively enhancing lesions. Fourteen of the cases were glioblastoma multiforme (GBM) (58%), five were oligodendroglioma (21%) and five were metastasis (21%). Normalized cerebral blood volume (nCBV), normalized cerebral blood flow (nCBF), normalized mean transit time (nMTT) and normalized permeability (nPM) measurements of lesions are evaluated with perfusion CT. Eight (33%) of cases had histopathologic diagnosis with surgical resection or stereotactic biopsy, remaining 16 (67%) patients were evaluated clinically and radiologically at the 18-month follow-up period. Mann-Whitney U test was performed to compare the perfusion CT parameters between the 2 groups. In addition, ROCs were performed to determine the best cut-points for the perfusion CT parameters in differentiating radiation necrosis and recurrent tumor.

#### RESULTS

Thirteen cases were radiation necrosis and 11 were recurrent tumor depending on perfusion CT parameters. There was statistically significant difference on nCBV, nCBF and nMTT parameters between radiation necrosis and recurrent tumor groups ( $p < 0.001$ ), and no significant difference on PM parameter ( $p = 0.093$ ). Mean nCBF and nCBV values were higher and nMTT values were lower in recurrent tumor group compared with radiation necrosis group.

#### CONCLUSION

As a result, CT perfusion may help differentiate radiation necrosis from recurrent tumor on the basis of various perfusion parameters. Recurrent tumor group has higher nCBV and nCBF values and lower nMTT values than radiation necrosis group. Normalized permeability values were not significantly different.

**KEY WORDS:** Cerebral radiation necrosis, recurrent tumor, perfusion computerized tomography

#### eP-27

### Cortical Tumors with Hyperintense Rim on FLAIR Imaging: Radiologic and Pathologic Features

Gocmen, R.<sup>1</sup>·Oguz, K. K.<sup>1,2</sup>·Soylemezoglu, F.<sup>1</sup>·Arslankoz, S.<sup>1</sup>

<sup>1</sup>Hacettepe University, Ankara, TURKEY, <sup>2</sup>Bilkent University, Ankara, TURKEY

#### PURPOSE

Since original description by Parmer et al. in 2007, hyperintense ring sign on fluid-attenuated inversion recovery (FLAIR) image has been considered as a sign with 90% specificity for dysembryoplastic neuroepithelial tumor (DNET). However, the nature of this sign still remains uncertain. The present study aims to revisit this sign documenting histopathologic spectrum of lesions with FLAIR hyperintense rim on MR imaging.

#### MATERIALS & METHODS

This institutional review board-approved retrospective study included nine patients (M/F:5/4; 5-27 years, mean age 18.9) who had cortical tumors with hyperintense rim on FLAIR imaging and histopathologic examination between January 2009 to October 2011. All patients had cranial MRI in a 1.5 T MR scanner (Magnetom TIM, Siemens, Erlangen, Germany) using contrast material. Two neuroradiologists evaluated studies with respect to the location of the tumor, size, signal features on FLAIR, T1- and T2-weighted imaging (WI), mass effect, enhancement characteristics, thickness and completeness of the hyperintense rim. All tumor specimens were fixed in formalin and embedded in paraffin. In addition to hematoxylin and eosin staining, immunohistochemistry for isocitrate dehydrogenase 1 (IDH1), p53, glial fibrillary acidic protein (GFAP), Ki-67, synaptophysin and other antibodies was performed. Briefly, after deparaffinization and boiling for antigen retrieval (citrate buffer, pH 9) when necessary, five micrometer sections were stained with listed antibodies and the avidin-biotin complex method.

#### RESULTS

All nine were intracortical as confirmed histopathologically. All tumors were supratentorial with a predilection of the frontal lobes [frontal (n = 4), parietal (n = 2), frontoparietal (n = 2), and temporal lobes (n = 1)]. All tumors were hypointense on T1- and hyperintense on T2-WI compared to gray and white matter and had well demarcated borders. None of them showed peritumoral edema or mass effect. Only three cases showed minimal contrast enhancement. Two tumors were cystic, the rest were solid. Hyperintense rim around the tumors was complete in the three cases while incomplete in six cases. Thickness of the hyperintense rim ranged from 1 to 3.5 mm (mean: 2.2 mm). All patients underwent gross total surgical resection. All cases were postsurgically diagnosed on

the basis of histopathologic findings according to the 2007 WHO classification of tumors of the central nervous system: grade II oligoastrocytoma (n = 3), grade III oligoastrocytoma (n = 1), DNET (n = 2), grade II infiltrative astrocytoma (n = 1), angiocentric glioma (n = 1), pleomorphic xanthoastrocytoma (PXA) (n = 1).

#### CONCLUSION

Our study showed hyperintense FLAIR rim sign in various cortical-based tumors such as grade II and III oligoastrocytoma, grade II astrocytoma, angiocentric glioma, PXA in addition to DNET. Although radiologically well demarcated, tumors with this finding could show infiltrative transition zones and presence of this finding does not state low grade of the tumor histopathologically.

**KEY WORDS:** Fluid-attenuated inversion recovery, dysembryoplastic neuroepithelial tumor, oligoastrocytoma

#### eP-28

##### Comparison between the Two Separate Injections Method and the Single Injection Method for Double Dose Contrast Study in Lesion Delineation of Metastatic Brain Tumors

Ochi, T.<sup>1</sup>•Taoka, T.<sup>2</sup>•Akashi, T.<sup>2</sup>•Miyasaka, T.<sup>3</sup>•Sakamoto, M.<sup>2</sup>•Hidaka, S.<sup>1</sup>•Sakaguchi, H.<sup>1</sup>•Kichikawa, K.<sup>2</sup>

<sup>1</sup>Nara Prefectural Mimuro Hospital, Ikoma, JAPAN, <sup>2</sup>Nara Medical University, Kashihara, JAPAN, <sup>3</sup>Nara Prefectural Nara Hospital, Nara, JAPAN

#### PURPOSE

MR imaging with higher dose contrast media for metastatic brain tumor is established method for detecting smaller nodes. Besides the detection, as widespread of stereotactic radiation in the clinical practice, the delineation of the tumor margin has become important for making radiation plan. We conducted the current study to evaluate the order of the injection and imaging in performing double dose contrast-enhanced MRI for brain metastasis. We compared two separate injections method and single injection method for the margin delineation of the tumor as well as the number, intensity of the tumors.

#### MATERIALS & METHODS

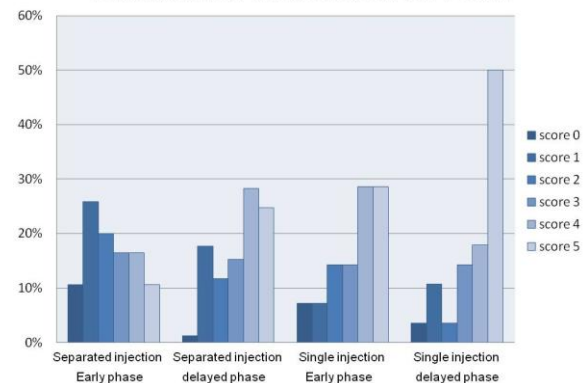
Twenty-seven patients with brain metastasis divided into two groups. Group A: Two separate injections (0.2 + 0.2 ml/kg); 16 patients. Group B: Single injection (0.4 ml/kg); 11 patients. The group A underwent spin-echo (SE) T1-weighted sequence and MPRAGE (magnetization prepared rapid acquisition with gradient echo) sequence after each injection, and the group B underwent the same MR studies at the same timing as group A. Numbers of the lesions were compared between early and delayed studies by the two methods. Signal intensity of lesions was measured to give signal noise ratio (SNR). Margin delineation of lesions was evaluated by classifying as follows: Score 0, no enhancement; Score 1, ill-defined; Score 2, between

3 and 1; Score 3, half circumference; Score 4, between 5 and 3; Score 5, whole circumference.

#### RESULTS

The number of the detected lesions was largest on delayed studies of MPRAGE in both groups. Signal to noise ratio of lesions is statistically lower on early studies of group A than other studies. About margin delineation, on both SE and MPRAGE studies, the score for the single dose study of the group A showed statistically significant lesser score compared to other groups. There was no statistically significant difference between delayed studies of group A and early studies of group B. Delayed studies of group A showed statistically superior scores to delayed studies of group B.

Distribution of score on SE T1WI



#### CONCLUSION

Lesions showed equal delineation on early studies of group B, acquired immediately after single injection of double dose, and delayed studies of group A, acquired immediately after second injection of standard dose. Thus, reducing examination time by single injection did not affect margin delineation of lesions. Delayed studies of group B showed better delineation than delayed studies of group A. Therefore single injection may shorten examination time or improve delineation of lesions for the study of brain metastasis.

**KEY WORDS:** Brain metastasis, contrast media, double dose

#### eP-29

##### Usefulness of Continuous Arterial Spin Labeling Image for MR Monitoring of Radiotherapy of Nonglial Brain Tumors

Yamamoto, T. • Takeuchi, H. • Kimura, H.

University of Fukui  
Fukui, JAPAN

#### PURPOSE

To illustrate the usefulness of continuous arterial spin labeling (CASL) for MR monitoring of radiotherapy for nonglial brain tumor.

#### MATERIALS & METHODS

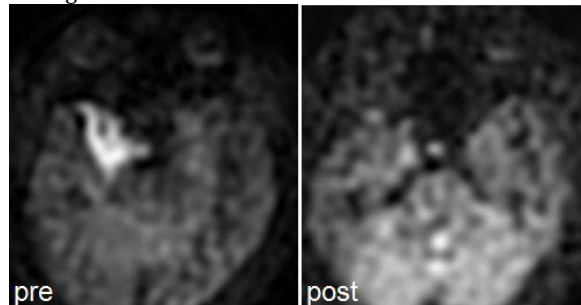
Between January 2009 and July 2010, seven patients with nonglial brain neoplasms underwent radiotherapy



only and were scanned using a 3 T MR unit to follow the course before and after radiotherapy. These tumors included three meningiomas, three vestibular schwannomas and one craniopharyngioma confirmed by pathologic examination. MR examinations employing routine protocols and CASL imaging were performed at 3-month to 1-year intervals after radiotherapy. Routine protocols included axial T1-weighted gradient-echo sequences (TR/TE/TI, 11.3/5.3/300). Continuous arterial spin labeling was prepared using a three-dimensional (3D) spiral FSE sequence with background suppression for perfusion imaging covering the entire brain. A pseudo-continuous scheme was employed with a 1.5-second duration for ASL. Other acquisition parameters were as follows: 8 arms with 32 points in each spiral arm, phase encoding in the z direction=34, section thickness=5 mm, TR=6 seconds, post label wait=1.5 seconds, image reconstruction matrix=128 × 128, and NEX=3. Gross tumor size was delineated on postcontrast T1-weighted MR images of each patient and the differences were noted. We used our own analysis software (IDL7.0, ITT Visual Information Solutions, Boulder, CO, USA) to fuse postcontrast T1-weighted images and CASL images and recognized portions of tumors precisely and located the region of interest in the tumor and a normal cortex on the CASL image. We also measured average blood flow and reviewed the images comparatively.

## RESULTS

Decreased tumor blood with time was observed in six of seven cases. Even if a size change was not present, we were able to observe decreasing blood flow on the CASL image. Tumor blood flow increased in one schwannoma case treated once 3 months later, and tumor blood flow decreased slightly thereafter. On post -contrast T1-weighted imaging, it was difficult to delineate tumor size change and contrast effects on the tumor soon after treatment because of a persistent enhancement effect. As for cases showing increased tumor blood flow, tumor size was transiently increased on postcontrast T1-weighted imaging. Cerebrocortical blood flow at the periphery of the middle cerebral artery area, which we measured as contrast, was approximately constant during each course.



## CONCLUSION

Continuous arterial spin labeling allows visual determination, which is superior to conventional postcontrast MRI for therapeutic monitoring. Continuous arterial spin labeling is a potentially noninvasive tool for judging the efficacy of radiotherapy for brain neoplasms.

**KEY WORDS:** Continuous arterial spin labeling, nonglial brain tumors, radiotherapy

## eP-30

### Analyses of Perfusion CT Parameters in the Evaluation of Brain Gliomas and Metastases

Kajiwara, Y.·Yamasaki, F.·Watanabe, Y.·Takayasu, T.·Nosaka, R.·Sugiyama, K.·Kurusu, K.

Hiroshima University  
Hiroshima, JAPAN

## PURPOSE

Perfusion computed tomography (CT) can provide additional information about tumor vascularity and angiogenesis for characterizing brain tumors. The aim of our study is to evaluate the usefulness of various perfusion CT (PCT) parameters in diagnosing the glioblastoma multiforme (GBM) and metastatic brain tumors (MBT).

## MATERIALS & METHODS

Perfusion CT was performed in 59 patients (39 GBM, 20 MBT). Normalized ratios of the PCT parameters [normalized cerebral blood flow (nCBF), normalized cerebral blood volume (nCBV), normalized mean transit time (nMTT)] were used for final analysis. All parameters were obtained from tumor-enhanced region (nCBFt, nCBVt, and nMTTt) and peritumoral region (nCBFp, nCBVp, and nMTTp).

## RESULTS

Mean nCBFt and nCBVt in GBM were  $4.98 \pm 2.17$  and  $3.94 \pm 1.2$  and significantly higher than MBT ( $2.77 \pm 2.15$ ,  $P < 0.005$  and  $2.99 \pm 1.85$ ,  $P < 0.005$ ). Mean nCBFp and nCBVp were statistically significantly difference between GBM and MBT (nCBFp; GBM  $0.79 \pm 0.25$  vs MBT  $0.56 \pm 0.22$ ,  $P < 0.001$ , nCBVp; GBM  $0.81 \pm 0.2$  vs MBT and  $0.73 \pm 0.28$ ,  $P < 0.005$ ). Mean nMTTt and nMTTp were most significantly higher in MBT ( $1.33 \pm 0.51$  and  $1.69 \pm 0.65$ ) than GBM ( $0.84 \pm 0.26$  and  $1.18 \pm 0.23$ ) ( $P < 0.005$ ).

## CONCLUSION

Perfusion CT provides useful information for preoperative diagnosis and valuable complementary information about tumor hemodynamics. Using statistical analyzes both the tumor region data and peritumoral region resulted significant for diagnosis in malignant brain tumors.

**KEY WORDS:** Perfusion CT, glioblastoma, metastatic brain tumor

## eP-31

### Role of MR Spectroscopy in Intracranial Malignant Tumors: Correlation with Histopathologic Findings

Kayahan Ulu, E. M.<sup>1</sup>·Hunca Memis, C.<sup>2</sup>

<sup>1</sup>Medical Park Samsun Hospital, Samsun, TURKEY,

<sup>2</sup>Baskent University, Ankara, TURKEY

## PURPOSE

The aim of this study was to evaluate the role of magnetic resonance spectroscopy (MRS) values in the differential diagnosis and grading of intracranial malignant tumors and to describe the relationship between the MRI and histopathologic findings.

## MATERIALS & METHODS

We retrospectively evaluated the conventional brain magnetic resonance imaging (MRI) and MRS of 67 patients diagnosed with intracranial malignant tumor. We divided the patients into four groups according to the histologic characteristics [grade II glial tumor (group 1), grade III glial tumor (group 2), grade IV glial tumor (group 3) and metastasis (group 4)]. In MRS, we evaluated Cho, NAA, Cr, Cho/NAA, NAA/Cr ve Cho/Cr values in the lesions and contralateral normal white matter. We reported the conventional MRI findings of tumors (the contrast enhancement, hemorrhage, cyst-necrosis, and distant tumor foci). In pathologic examination, Ki-67 labeling index (LI) was calculated in patients with glial tumors.

## RESULTS

Twenty-four (35.8%) high-grade glial tumors, 22 (32.8%) low-grade glial tumors and 21 (31.3%) metastasis were detected. There were statistically significant differences between groups in terms of the conventional MRI findings of tumors (the contrast enhancement, hemorrhage, cyst-necrosis, and distant tumor foci) ( $p < 0.0001$ ). The contrast enhancement, hemorrhage, cyst-necrosis and distant tumor foci was less prominent in the grade II glial tumors. All of the patients with grade III and grade IV glial tumors had peritumoral edema. The hemorrhage was most common in grade IV glial tumors (57.9%). The distant tumor foci was detected most commonly in patients with grade IV glial tumors and metastases, but not observed in patients with grade II glial tumors. The mean Cho, NAA, Cr, Cho/NAA, NAA/Cr values were higher in the patients with grade II glial tumors than other groups (high-grade glial tumors and metastases) and the difference was statistically significant ( $p < 0.0001$ ). Mean of Ki-67 LI were not significantly different between groups ( $p > 0.05$ ).

## CONCLUSION

The combination of MRS parameters and conventional MRI findings provide useful information for differentiating low-grade glial tumors from high-grade glial tumors and for preoperatively predicting the degree of malignancy in gliomas.

**KEY WORDS:** MR imaging, brain neoplasm, magnetic

## eP-32

### Physiologic Effect of Caffeine on Susceptibility-Weighted Imaging

Gonçalves Pereira, P.<sup>1,2</sup>·Caseiro, A.<sup>2</sup>·Sousa, P.<sup>1,2</sup>·Mananças, R.<sup>1,3</sup>

<sup>1</sup>HPP - Hospital dos Lusíadas, Lisboa, PORTUGAL,

<sup>2</sup>Instituto Politécnico de Lisboa, Escola Superior de Tecnologia da Saúde de Lisboa, Lisboa, PORTUGAL,

<sup>3</sup>Hospital dos Capuchos, Lisboa, PORTUGAL

## PURPOSE

Susceptibility-weighted imaging (SWI) is a relatively new contrast in MR imaging. Previous studies have found an effect of caffeine in the contrast generated by SWI images. The present study investigates the effect of caffeine on contrast-to-noise ratio (CNR) in SWI

## MATERIALS & METHODS

Twenty-four healthy volunteers (12 female, 26 - 54 ± 3 - 12 years) were enrolled in the study after being interviewed to exclude those with neurologic diseases. All participants gave their written informed consent. All the volunteers were caffeine-free for 24 hours prior to the test. After ingestion, there was no report of any undesirable side effect. Susceptibility-weighted images were acquired pre and postingestion of 100 ml of coffee (≈200 mg of caffeine). The volunteers were divided into four groups of six subjects and evaluated sequentially (15, 25, 30, 45 min after caffeine). High-resolution T2\*-weighted 3D gradient-echo (SWI) sequence was acquired on the axial plane on a 1.5 T (Siemens Avanto) whole body scanner using the manufacturer's standard head coil and the parameters: TR=49; TE=40; flip-angle=15; FOV=87 x 230; matrix=221 x 320. The caffeine effect on SWI was quantified by calculating the contrast-to-noise ratio [CNR = (Sa - Sb)/Sref], in magnitude and MIP images, pre and postingestion of caffeine, whereas Sa corresponds to signal intensity measured by a ROI placed at the internal cerebral vein, Sb at the white matter of the corona radiata and Sref at the lateral ventricle (CSF). Image processing was performed using OsiriX. Statistics were performed with GraphPad Prism.

## RESULTS

The SWI images postcaffeine showed an enhanced contrast in brain venous vasculature in all participants. Precaffeine CNR differed significantly from CNR measured postcaffeine in images of magnitude ( $p < 0.0001$ ) and MIP ( $p < 0.0001$ ). There was no difference between groups evaluated at different time-points postcaffeine.

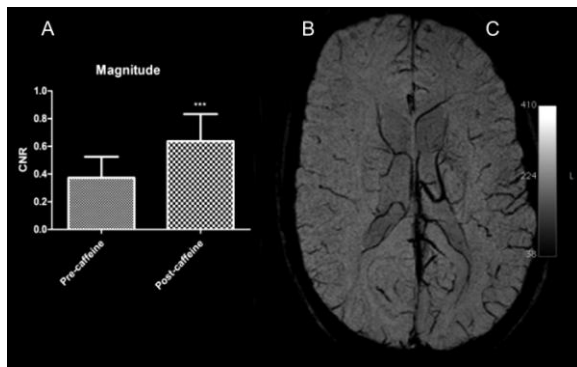


Figure: A - Mean and standard deviation of CNR pre and post-ingestion of  $\approx 100$  ml of coffee, (\*\*\*,0.0001), obtained in internal cerebral vein for entire sample ( $n = 24$ ) in magnitude images. B - Right hemisphere precaffeine (MIP image). C - Left hemisphere 15 min postcaffeine (MIP) with same window settings.

### CONCLUSION

There was a significant reduction of signal within the veins in all the patients solely due to the effect of caffeine intake. Contrast differences pre and postcaffeine were not significant in white matter and in CSF. We speculate that caffeine can be used as a cost-effective, safe and easy way to administrate contrast agent on SWI images.

**KEY WORDS:** Susceptibility-weighted imaging, brain venous system, caffeine

### eP-33

#### Volumetric Brain Mapping of T1/T2 Ratios with Multispectral qMR Imaging: Preliminary Age-Related Effects over the Human Lifespan

Abdel Mottalib, A. Sekiya, K. Watanabe, M. Nadgir, R. N. Saito, N. Sakai, O. Jara, H.

Boston University School of Medicine  
Boston, MA

### PURPOSE

To study the age-related changes of T1/T2 ratios of the normal brain across the human lifespan using quantitative MR imaging (qMRI).

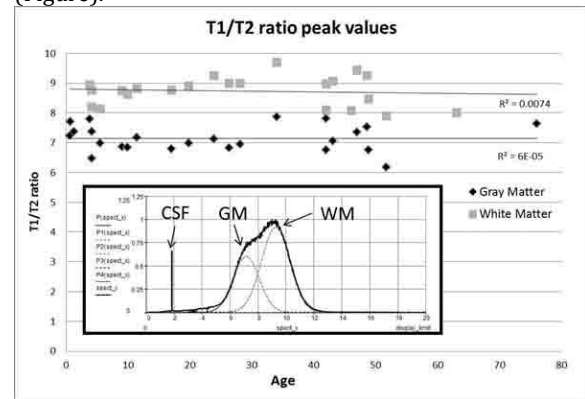
### MATERIALS & METHODS

Following IRB approval and following informed consent, 30 subjects (15 males, 15 females, age range of 0.6-76 years) were enrolled for this study. Study population consisted of nine volunteers and 21 patients who were referred for brain MRI for various clinical indications. In addition to routine clinical brain imaging, all subjects were imaged with the mixed-TSE pulse sequence with a 1.5 T MR scanner (Intera or Achieva, Philips Medical Systems, Cleveland, OH). Interpretation of clinical brain imaging component by subspecialty trained neuroradiologists indicated normal appearance without focal lesion on all patient subjects. The intracranial structures including gray matter (GM), white matter (WM), meninges, and cerebrospinal fluid (CSF) were segmented using a dual-clustering

segmentation algorithm. T1/T2 ratio histograms were generated with a pixel counting algorithm and further modelled with Gaussian functions. Peak values were derived from the histograms and plotted as a function of age.

### RESULTS

The T1/T2 ratio histograms of the intracranial structure were primarily bimodal, consisting of distinct GM and WM peaks. These peaks were tissue specific and remained relatively constant throughout all ages (Figure).



### CONCLUSION

The peak values of T1/T2 ratio histograms appear comparatively stable throughout the human lifespan, although it has been reported that there are marked age-related changes in both T1 and T2 values of human brain. The constancy of the T1/T2 ratio could be a useful indicator of brain normalcy.

**KEY WORDS:** qMR imaging, T1/T2 ratio, brain aging

### eP-34

#### Evaluation of the Pituitary Gland: Postcontrast T1-Weighted Imaging vs Volumetric Interpolated Breath-Hold Examination Imaging

Davis, M. A. Castillo, M.

University of North Carolina Chapel Hill  
Chapel Hill, NC

### PURPOSE

Volumetric interpolated breath-hold examination (VIBE) is a fast, efficient, and high-resolution modality commonly used for abdominal imaging. Our goal was to compare coronal spin-echo (SE) T1-weighted and VIBE sequences in pituitary gland imaging. We hypothesized that VIBE images are of higher quality and are clinically useful when compared to the SE sequence.

### MATERIALS & METHODS

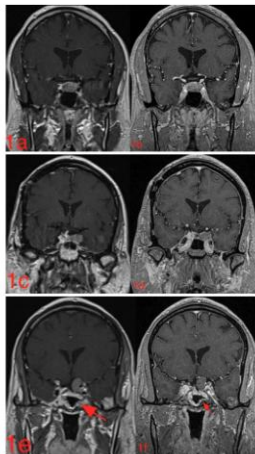
In 32 patients postcontrast SE T1-weighted and VIBE sequences were evaluated qualitatively. After dynamic imaging (part of our standard protocol), 50% of patients underwent VIBE before SE and 50% SE before VIBE. Features of the two sequences that were compared included: intensity of pituitary gland contrast enhancement, lesion depiction, and ability to view the

internal anatomy of the cavernous sinuses and separate them from the gland. These were rated as VIBE being better, equal, or worse in comparison to the SE images. Statistical analysis using chi-square statistics was performed.

## RESULTS

The degree of contrast enhancement on 18 VIBE studies was considered better than SE, six were considered equal, and eight were worse. With respect to lesion depiction, 18 VIBE studies were considered better than SE, six were equal, and eight were worse. Finally, with respect to cavernous sinus anatomy, 18 VIBE studies were considered better than SE, six were equal, and eight were worse. These results were all statistically significant ( $p = .02$ ). When looking at micro/macro adenomas and postsurgical patients specifically, VIBE imaging was judged as superior, however these data were not statistically significant.

Figure 1: Multiple SE T1 weighted (a,c,e) and corresponding VIBE (b,d,f) images of the pituitary gland. A and B demonstrate diffuse enlargement of the pituitary gland. Note that anatomy is better depicted on VIBE than on the conventional post contrast T1 image. C and D (different patient) show a mass in the left aspect of the gland causing rightward deviation of the pituitary stalk. The mass is better seen on the VIBE image and its borders are better defined. E and F demonstrate a mass with suprasellar extension (different patient). Visualization of the mass and delineation of the cavernous sinuses is improved with VIBE imaging. Post surgical changes seen in the sphenoid sinus (arrows) are more clearly differentiated from the surrounding structures with VIBE imaging.



## CONCLUSION

We conclude that VIBE is superior to SE for evaluation of the pituitary gland especially in respect to greater contrast enhancement and depiction of anatomy. A trend towards VIBE being superior in the evaluation of adenomas was seen, although not statistically significant which may reflect sample size. Volumetric interpolated breath-hold examination may be added to or supplant the traditional postcontrast T1-weighted SE sequence resulting in better image quality.

**KEY WORDS:** Volumetric interpolated breath-hold examination, spin echo T1-weighted imaging, pituitary

## eP-35

### Efficacy of Parabolic Flip Angle Used in Noncontrast-Enhanced 4D MR Angiography for the Evaluation of Arteriovenous Malformation in Central Nervous System

Sakamoto, M.<sup>1</sup>•Taoka, T.<sup>1</sup>•Wada, T.<sup>1</sup>•Akashi, T.<sup>1</sup>•Miyasaka, T.<sup>2</sup>•Ochi, T.<sup>3</sup>•Kichikawa, K.<sup>1</sup>•Uchikoshi, M.<sup>4</sup>•Schmidt, P.<sup>5</sup>

<sup>1</sup>Nara Medical University, Kashihara, JAPAN, <sup>2</sup>Nara Prefectural Nara Hospital, Nara, JAPAN, <sup>3</sup>Nara Prefectural Mimuro Hospital, Oji, JAPAN, <sup>4</sup>Siemens Japan K.K., Tokyo, JAPAN, <sup>5</sup>Siemens AG Healthcare Sector, Erlangen, GERMANY

## PURPOSE

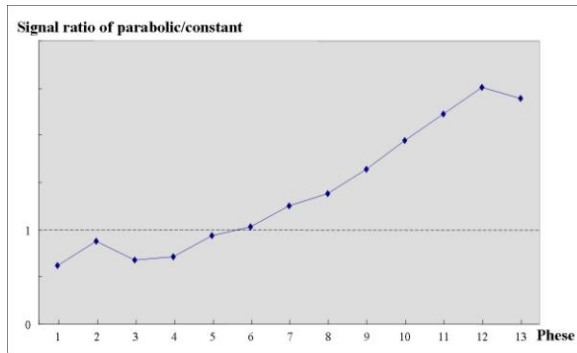
The imaging diagnosis of arteriovenous malformation (AVM) requires a high temporal resolution for the delineation of arteriovenous shunting and a high spatial resolution for the delineation of nidus and draining veins. Flow-sensitive alternating inversion recovery noncontrast-enhanced (CE) 4D MR angiography (MRA) accomplishes the high temporal and spatial resolution as an alternative to conventional angiography. Moreover the parabolic flip angle (FA) is reported as an improvement and enables a longer persistence of the blood signal compared to constant FA approach. We evaluated clinical cases with AVM in central nervous system (CNS) in order to assess the efficacy of parabolic FA by comparing with constant FA.

## MATERIALS & METHODS

Nine cases (4 males and 5 females, average age 62.6 years) with AVM in CNS were evaluated by nonCE 4D MRA using parabolic and constant FA. Noncontrast-enhanced 4D MRA was acquired with 3.0 T MR scanner (MAGNETOM Verio, Siemens, Germany) and following protocol; FoV: 220x189, Matrix: 224x179, slice thickness: 1, FA: parabolic=variable from 6 to 36, consistent=25, acquisition window: 1RR (50 msec/phase), voxel size=0.98x1.06x1.00. Two experienced neuroradiologists evaluated the images for the visualization of nidus and draining vein with four grading score (1: poor, 2: fair, 3: good and 4: excellent). The kappa value was evaluated for the interobserver agreement and the scores of parabolic and constant FA groups were analyzed statistically. In order to assess the difference of signal persistence, signal ratio of parabolic to constant in each phase was calculated from the signal measured by ROI set on each AVM structure visualized in both scans.

## RESULTS

The kappa value among two investigators was 0.78. The score of parabolic FA group was  $3.07 \pm 0.73$  and that of constant FA group was  $2.36 \pm 1.01$  and there was significant difference ( $P < 0.01$ ) by Wilcoxon signed-rank test. The average signal ratio was below 1.0 from the first to fourth phases and continued to increase over 1.0 after the sixth phase (Figure).



### CONCLUSION

The signal persistence was proved to be better in parabolic than constant FA group, therefore the AVM structures with delayed delineation such as draining vein and low flow shunt were considered to be visualized better in non-CE 4D MRA using parabolic FA. This prediction also was supported by our result that the parabolic FA group counted significantly higher score than constant FA group. We conclude that non-CE 4D MRA with parabolic FA provides more valuable information in the diagnosis of AVM.

**KEY WORDS:** non CE 4D MR angiography, AVM, parabolic

### eP-36

#### Combined Whole-Brain Time-Resolved CT Angiography and Perfusion CT in Evaluation of Moyamoya Disease

Yazbek, S.·Tanenbaum, L. N.

The Mount Sinai School of Medicine  
New York, NY

### PURPOSE

Moyamoya disease is a progressive occlusive disease of the supraclinoid internal carotid arteries with secondary collateralization. While conventional catheter angiography (CCA) is the gold standard for diagnosis, single-phase (SP) CTA and time-of-flight (TOF) MRA commonly are employed as primary diagnostic modalities, primarily due to their noninvasive nature. Both techniques suffer from artifact challenges and neither offers the spatial resolution to adequately delineate the smallest collateral vessels. Even more critically lacking in SP CTA and TOF MRA is the physiologic information provided in time-resolved imaging of the dynamics of flow about an occlusion and the functional contribution of collateral vessels pre and postintervention. Time-resolved (TR) MRA techniques exist, but require greater compromises as spatial resolution and anatomical coverage are traded off to obtain adequate temporal resolution. Information about tissue perfusion, important for understanding the significance of stenotic disease requires a unique contrast injection with traditional CT and MR techniques. Conventional catheter angiography does not provide direct information about brain perfusion. Combined TR CTA and perfusion techniques (TR CTA PCT) offer whole-brain dynamic vascular assessment

similar to that provided by CCA along with perfusion imaging in a single contrast injection and scan. We evaluated the role of whole-brain time-resolved CT angiography and simultaneous perfusion CT (PCT) in depicting primary and collateral vascular anatomy and dynamics as well as brain perfusion in the management of patients with moyamoya disease.

### MATERIALS & METHODS

We report the cases of five patients presenting with moyamoya disease and evaluated with combined 4D CTA PCT as well as cerebral angiography. All examinations were performed on conventional clinical CT scanners (64 channel-40 mm detector height) with dynamic shuttle capabilities. Nine time-resolved CT angiography and perfusion CTs were reviewed retrospectively and compared with CCA findings. We discuss the protocol for TR CTA PCT including iodinated contrast and radiation implications as well as delineate the advantages of TR CTA PCT and its impact on surgical decision making and follow up.

### RESULTS

When compared with CCA in moyamoya disease, 4D CTA accurately delineated the collateral vasculature, the patency of the graft and the antegrade versus retrograde filling of the stenotic artery and graft. Two TOF MRA and one static CTA of the head also were compared with the result of TR CTA in the same patients. These studies were limited in the delineation of the collateral vasculature because of artifacts and limited spatial resolution with the MRA and lack of dynamic information. 4D CTA PCT also helped evaluate the state of perfusion of the brain supplied by the diseased vasculature. A decrease in CBF and increase in parameters such as CBV, Tmax, TTP and MTT suggested the need for surgical intervention and vascular bypass and restoration of normal perfusion parameters.

### CONCLUSION

4D CTA PCT is a widely available valuable new adjunct in the noninvasive diagnostic workup of moyamoya disease, in the treatment planning and in the postoperative follow up.

**KEY WORDS:** Moyamoya, time-resolved CT angiography, perfusion

### eP-37

#### Practical Approach to Analyzing Pontine Lesions

Altmeyer, W.·Tranvinh, E.·Rodriguez, P.·Tantiwongkosi, B.

University of Texas Health Science Center at San Antonio  
San Antonio, TX

### PURPOSE

Provide a practical approach to analysis of pontine lesions utilizing a pictorial review of common pontine pathology.

## MATERIALS & METHODS

The pons is a central relay station of the midbrain with white matter tracts coursing to the cerebrum, spinal cord, thalamus and cerebellum. The pons also contains multiple nuclei; including nuclei of cranial nerves V, VI, VII and VIII. The pons is home to certain unique disease processes that should be considered whenever a pontine lesion is encountered. The diseases that have a predilection for the pons can be considered in multiple broad categories. Vascular lesions include capillary telangiectasias, cavernomas, developmental venous anomalies, and infarctions. Tumors that have a predilection for the pons include diffuse pontine glioma, ependymoma, and periventricular lymphoma. Certain neurodegenerative diseases may affect the pons; including multiple system atrophy and olivopontocerebellar atrophy. With the abundance of white matter tracts coursing through the pons, demyelinating diseases are common. Central pontine myelinolysis, multiple sclerosis, and acute disseminated encephalomyelitis often affect the white matter of the pons. Generation of an appropriate differential diagnosis for a pontine lesion can be achieved after analyzing a few important variables. Like most pathology, patient age is of paramount importance. Diffuse pontine gliomas occur almost exclusively in children while multiple system atrophy presents around the sixth decade of life. One particularly important characteristic to examine is the presence or lack of pontine enlargement. Gliomas and infection tend to expand the pons while neurodegenerative diseases lead to regional atrophy. Pontine infarctions typically will respect the midline while demyelinating diseases often follow the transverse pontine white matter fibers. Enhancement pattern is an important factor when evaluating a pontine mass lesion. Diffuse pontine gliomas typically demonstrate minimal if any enhancement. Lymphomas classically show uniform central enhancement. Active demyelination often exhibits thin peripheral enhancement.

## RESULTS

Providing particular attention to certain characteristics of pontine lesions will help the radiologist craft an appropriate differential diagnosis.

## CONCLUSION

Certain lesion characteristics, including patient age, enhancement pattern, pontine expansion and location with respect to the midline are particularly helpful when evaluating a pontine lesion.

**KEY WORDS:** Pons, pontine

eP-38

## T2-Weighted versus Intrathecal Contrast-Enhanced MR Cisternography in the Evaluation of Cerebrospinal Fluid Leakage

Ecın, G.·Oner, A.·Tokgoz, N.·Ucar, M.·Aykol, S.·Tali, T.

Gazi University School of Medicine  
Ankara, TURKEY

## PURPOSE

Radiologic identification of the location of the cerebrospinal fluid (CSF) leakage is important for proper surgical planning. A variety of imaging techniques including MRI with heavily T2-weighted images have been employed for this purpose. However intrathecal contrast-enhanced MR cisternography is reported to be a more effective imaging tool in this setting. The purpose of this study is to evaluate and compare conventional T2-weighted MR cisternography (T2MRC) with intrathecal contrast-enhanced MRI technique (CEMRC) in identifying the presence and site of CSF rhinorrhea.

## MATERIALS & METHODS

Sixty MRI examinations performed in patients with suspected CSF rhinorrhea between 2002 and 2011 were reviewed. Imaging included heavily T2-weighted images in the coronal plane and intrathecally enhanced fat suppressed T1-weighted images in three orthogonal planes. Both sets of images were reviewed by two blinded radiologists in one sitting for the presence and location of a CSF leakage. In patients with detected leakage, imaging data results were compared with surgical findings.

## RESULTS

With surgery-proven CSF leakage in 20 instances as reference, CEMRC detected 18 (90%), whereas T2MRC reported only 13 (65%) correctly. Detected leakage was in three different locations: the ethmoidal region in 11 examinations (55%), the wall of the sphenoid sinus in six examinations (30%) and wall of the frontal sinus in three examinations (15%). In two instances where both imaging sets failed to depict any leakage, surgery revealed a defect at the sphenoid sinus wall and the ethmoidal region. Apart from these instances, eight patients with T2MRC and seven patients with CEMRC were depicted falsely as having leakage, with no supporting surgical findings. Overall, the sensitivity, specificity, positive predictive value and negative predictive values in detecting CSF fistulae were 0.92, 0.80, 0.76 and 0.93 for CEMRC, and 0.56, 0.77, 0.64 and 0.71 for T2WMRC, respectively.

## CONCLUSION

In our experience intrathecal contrast-enhanced MR cisternography is a more sensitive and specific imaging technique in identifying the presence and site of CSF rhinorrhea than conventional T2-weighted MR cisternography. Intrathecal contrast-enhanced MR cisternography represents an effective and a minimally invasive method for evaluating suspected CSF fistulae.

**KEY WORDS:** CSF leakage, intrathecal, MR imaging



## eP-39

### Ecchordosis Physaliphora: A Broad Spectrum of Imaging Findings on Fast Imaging Employing Steady-State Acquisition

Chihara, C.·Korogi, Y.·Kakeda, S.·Nishimura, J.·Ohnari, N.  
University of Occupational and Environmental Health,  
Japan  
Kitakyushu-shi, JAPAN

#### PURPOSE

Ecchordosis physaliphora (EP) is a benign lesion which arises from ectopic notochordal remnants and is found incidentally on the clivus in 0.4-2.0% of autopsies. Only a few studies provided the radiologic features of retroclival EP using conventional MRI. Fast imaging employing steady-state acquisition (FIESTA), which has a high spatial resolution and signal to noise ratio (SNR), may depict the microanatomy of EP. We investigated the FIESTA findings of EP in large series.

#### MATERIALS & METHODS

From radiology database for a 6-year period, we selected 974 patients who underwent a brain FIESTA. This patient cohort was used to further select consecutive 78 (8.0%) MRI based on the following criteria; FIESTA shows the excrescence on the dorsal surface of the clivus and/or the abnormal signal intensity within clivus. On the basis of characteristics of EP observed in prior reports, the lesions were defined as "definite EP" when they appeared as the hyperintense excrescence (HE) on the dorsal surface of the clivus on FIESTA, and the remaining cases without HE were defined as "undetermined EP".

#### RESULTS

There were 17 definite EP (17/974, 1.7%) and 61 undetermined EP (61/974, 6.3%); according to the configuration of the clivus excrescence (Figure), 17 definite EP were further classified into three groups as Group A (n=3), Group B (n=8), and Group C (n=6), and 61 undetermined EP also were classified further into three groups as Group D (n=36), Group E (n=19), and Group F (n=6). Of 17 definite EP and 61 undetermined EP, 14 (82.4%) and 50 (82.0%) were located at the same slice level as the Dorello canal, and 17 (100%) and 57 (93.4%) were located in midline of the craniospinal axis, respectively. Therefore, FIESTA findings of undetermined EP were nearly equal to those of definite EP except for the lack of the HE.

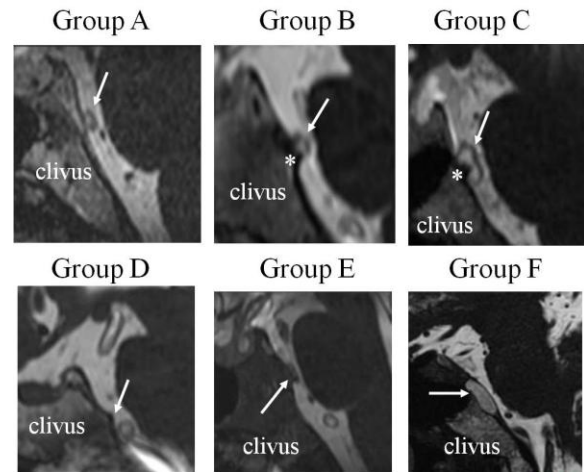


Figure: FIESTA sagittal images of six types of EP. Definite EP; Group A: HE alone (arrow), Group B: HE plus hypointense bulge of clivus (asterisk), and Group C: HE plus hypointense protrusion of clivus (asterisk). Undetermined EP; Group D: hypointense bulge of clivus alone (arrow), Group E: hypointense protrusion of clivus (arrow) alone, and Group F: intraclival lesion (arrow) alone

#### CONCLUSION

Excrescence on the dorsal midline surface of the clivus at the level of Dorello canal, either with HE or without HE, was observed frequently on FIESTA. Our results suggest that the MR imaging appearances of EP are diverse.

**KEY WORDS:** Ecchordosis physaliphora, FIESTA

## eP-40

### Meningoceles and Meningoencephaloceles of the Skull Base - Imaging Pre and Postsurgery: Pictorial Essay and Literary Review

Pollice, S.·Maggialetti, A.·Scarabino, T.

ASL BT  
Andria, ITALY

#### PURPOSE

Assessment and follow up of meningoceles and meningoencephaloceles of the cranial base.

#### MATERIALS & METHODS

Evaluation with CT and MR of meningoceles meningoencephaloceles of skull base. Differential diagnosis, pitfalls, pre and postoperative imaging and pictorial essay.

#### RESULTS

The etiology of meningoceles and meningoencephaloceles include congenital skull base defect and traumatic events. The knowledge of ontogeny of skull bone is the key to differentiate acquired and congenital forms.

**CONCLUSION**

MR imaging and CT are optimal tools to diagnose this pathology and to evaluate postsurgery effects.

**KEY WORDS:** Meningocele, CT, MR imaging

**eP-41**

### **Role of 3D Fast Imaging Employing Steady-State Acquisition in Modern Neuroimaging**

Raslan, O.·Spilberg, G. Z.·Dundamadappa, S.·Takhtani, D.

University of Massachusetts Medical Center  
Worcester, MA

**PURPOSE**

Fast imaging employing steady-state acquisition (FIESTA) sequence has become a mainstay in the evaluation of the cerebellopontine angles and the inner ear. Other uses of FIESTA include demonstration of cranial nerve pathology, assessment of the ventricular system before and after surgery, evaluation of complex cystic lesions, characterization of spine lesions and to study abnormalities in fetal neuroimaging. Our aim is to illustrate the applications of FIESTA in neuroimaging.

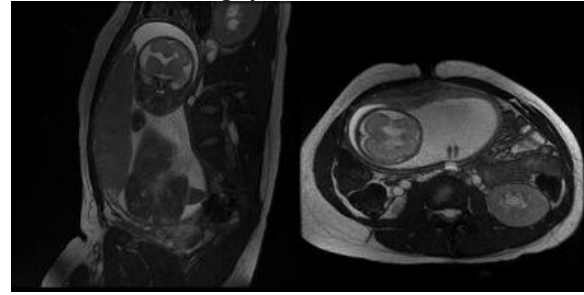
**MATERIALS & METHODS**

Fast imaging employing steady-state acquisition was acquired in a 1.5 T GE machine, with the following parameters; FOV of 18 cm, matrix of 320 x 256, TR~4.5 msec, TE~1.5 msec, FA 65 degrees, NEX 4 and slice thickness of 0.8. Multiplanar reformats were obtained when required, from this volumetric data. Twenty-six patients from our hospital neuroimaging database were selected for this review. The pathologies studied included: tumors, spine lesions, hydrocephalus, fetal malformations and intracranial cysts.

**RESULTS**

FIESTA is a gradient-echo technique (GE), using balanced steady-state free precession. The sequence exhibits high signal to noise ratio and a T2/T1 weighting. There is high contrast between CSF/fluid and other structures. The sequence uses short TR and TE, minimizing artifacts and making this a faster sequence. FIESTA is capable of depicting the cisternal segments of all 12 cranial nerves. FIESTA demonstrates exquisite ventricular anatomy, not only diagnosing hydrocephalus, but also points to the level and cause of obstruction. It can be helpful in demonstrating aqueductal, cisternal, and ventricular obstruction. It can be used as an adjunct to CSF flow studies in the evaluation of CSF dynamics in cases of third ventricle, pineal region and tectal tumors. FIESTA can be used in delineation of purely cystic intraspinal lesions, such as arachnoid cysts which are difficult to detect using routine T2. Fast imaging employing steady-state acquisition can be used to differentiate true spinal arteriovenous malformations, from flow-related artifacts. Using FIESTA nerve root avulsion and pseudomeningocele formation are well demonstrated. The internal architecture and septations of a spinal cord syrinx are better demonstrated using FIESTA. MR imaging gives important additional information in

fetuses shown to have brain or spinal abnormalities. FIESTA is a valid tool in diagnosis of encephalo/myeloceles, structural malformations, and severe ventriculomegaly.

**CONCLUSION**

FIESTA imaging is a valuable tool in assessment of IAC, temporal bone, cranial nerve and complex cystic lesions. FIESTA has an important role in assessment of the ventricular system, spinal lesions and fetal malformation.

**KEY WORDS:** FIESTA, MR imaging

**eP-42**

### **Update of Gadolinium Contrast Agent Stability and Relaxivity: Impact on Clinical Practice**

Enterline, D. S.

Duke University Medical Center  
Durham, NC

**PURPOSE**

Understanding gadolinium-based contrast agent (GBCA) stability and relaxivity is important for improving patient safety and optimizing image quality and interpretation. This exhibit reviews the critical literature and highlights key factors and common misconceptions associated with the concept of relaxivity. Contrast agent stability also is addressed. These properties directly impact contrast agent use in clinical practice and are important for all radiologists to appreciate.

**MATERIALS & METHODS**

R1 relaxivity is a measure of the signal-producing capacity of a given gadolinium and is defined as the inverse of longitudinal recovery time (T1); the shorter the T1 relaxation time, the higher the r1. Gadolinium agents have characteristic relaxivity that depends on measurement conditions (biologic environment, temperature, field strength). Higher relaxivity agents provide more enhancement than standard extracellular GBCA and there are marked differences between agents. Gadolinium is a toxic heavy metal, and avoiding dissociation of the gadolinium-chelate complex is critical for patient safety. Stability is measured in various ways and under various conditions. We reviewed thermodynamic, kinetic, and conditional stability data for the available gadolinium agents, as well as the result of challenge studies in which gadolinium agents are incubated with competitor ions under physiologic conditions.

## RESULTS

The relaxivity of a gadolinium agent is related to the way it interacts with serum proteins once injected. The agents with "standard" relaxivity exhibit minimal to no protein interaction upon injection. Higher relaxivity agents exhibit various degrees of protein interaction, from weak, transient interaction (gadobenate dimeglumine) to strong and lasting protein binding (gadofosveset). A number of studies have demonstrated the benefit of higher relaxivity gadolinium agents for various neuroimaging applications. Some higher relaxivity agents (gadobenate dimeglumine and gadoxetic acid) are also lipophilic molecules which are taken up by normal hepatocytes in the liver, making them useful for delayed imaging of the biliary system. The macrocyclic agents (gadoteridol and gadobutol) are the most stable agents by a number of measures, followed by certain of the linear ionic agents (gadobenate dimeglumine and gadopentetate dimeglumine, gadofosveset) and lastly by the nonionic linear agents (gadodiamide, gadoversetamide). The stability of gadolinium agents is inversely related to their association with the development of nephrogenic systemic fibrosis (NSF) in patients with poor kidney function.

## CONCLUSION

The relaxivity and chemical stability of gadolinium-based MR contrast agents differ among the various agents and these differences have relevant clinical implications for the practicing neuroradiologist.

**KEY WORDS:** Gadolinium, contrast, relaxivity

## eP-43

### Value of Consecutive Performance of CT Perfusion and CT Angiographic Surface Anatomical Scanning in the Diagnosis of Skull Metastasis

Ohara, A.·Tsuchiya, K.·Tateishi, H.·Gomyo, M.·Nitatori, T.  
Kyorin University  
Tokyo, JAPAN

## PURPOSE

To assess the value of consecutive acquisition of CT perfusion (CTP) and CT angiographic surface anatomical scanning (CTA SAS), which generates surface images of the brain and skull from a CTA data set, in the diagnosis of metastatic skull tumors.

## MATERIALS & METHODS

Our study group comprised three cases of skull metastasis (two men and one woman; age range, 62-80 years; primary site, esophagus, thyroid, and liver) examined on a 64-row CT. First, we performed precontrast scan of the whole brain followed by CTP using 25 mL of contrast agent (350 mgI/mL) and a saline flush (40 mL). Then, CT angiography (CTA) was obtained using 75 mL of contrast agent followed by a saline flush (40 mL). In postprocessing, we first generated CTP maps of cerebral blood volume/flow (CBV/CBF) and a mean transit time. Then, we obtained CTA images followed by creating surface images with

and without removing the skull and scalp. We assessed CTP maps regarding tumor vascularity. CT angiographic images were evaluated whether they depicted tumor-related findings or other vascular lesions. CT angiographic surface anatomical scanning images were assessed regarding visualization of the tumor and adjacent brain.

## RESULTS

In all cases, we could obtain CTP maps that revealed elevated CBV and CBF to a variable degree. CT angiography images visualized feeding arteries from the middle meningeal artery in all cases and a tumor stain in two cases. In each case, CTA SAS images including the skull well depicted bone destruction and a soft-tissue mass, while CTA SAS images after removing the skull and scalp demonstrated the adjacent sinus and cortical veins.

## CONCLUSION

Although in a limited series, CTP and CTA SAS, which can be performed consecutively, are found to effectively show the hemodynamic and anatomical findings of skull metastasis.

**KEY WORDS:** Skull metastasis, CTP, CTA-SAS

## eP-44

### Pseudoarachnoiditis Appearance in Spontaneous Intracranial Hypotension

Alkan, O.·Yildirim, T.·Akin, S.·Demir, S.·Altinkaya, N.  
Baskent University  
Adana, TURKEY

## PURPOSE

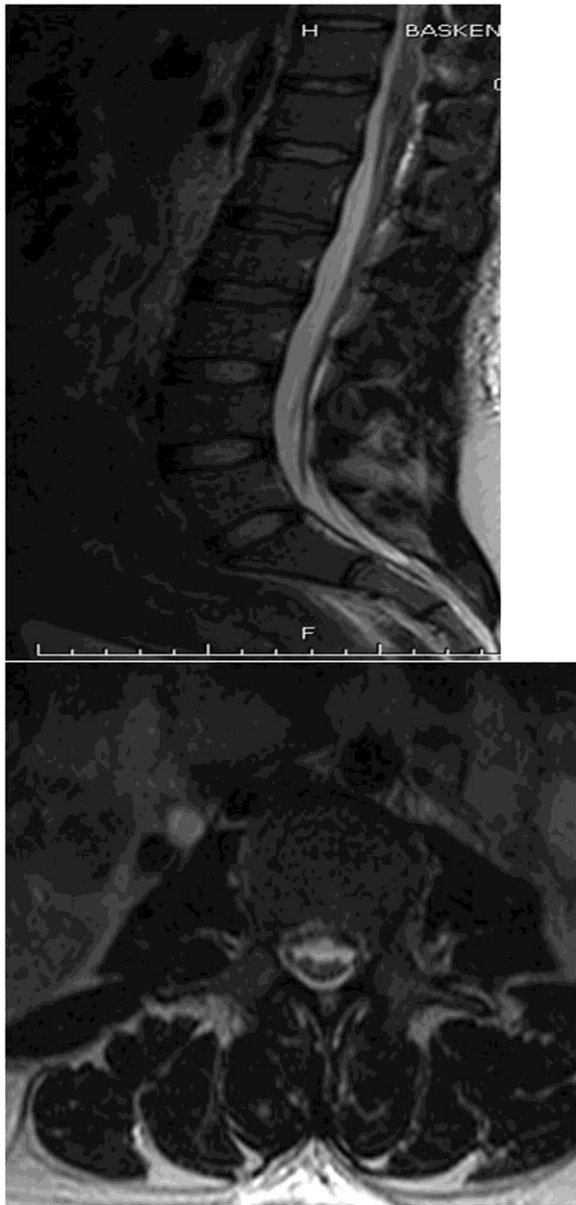
To present spinal MR imaging findings in three cases with spontaneous intracranial hypotension (SIH).

## MATERIALS & METHODS

The patients presented with a sudden-onset headache associated with blurred vision. Their neurologic and physical examinations revealed no abnormalities. We performed spine and brain MR images.

## RESULTS

Brain MR of the first case showed minimally subdural effusion. Brain MR of the second case was normal. Brain MR of the third case showed subdural effusion and pachymeningeal enhancement. Lumbar spinal MR showed clustering of the cauda equina fibers mimicking arachnoiditis in the all cases (Figure 1a, b). Since the patients did not respond to analgesics, the epidural leaks were treated with an epidural blood patch. The patients' symptoms improved to almost complete resolution within 24 hours, and the arachnoiditis-like spinal MRI findings completely resolved.



#### CONCLUSION

The most common clinical manifestation of SIH is an orthostatic headache. Typical findings on brain MR of SIH were well documented, although brain MR is sometimes normal. Spinal MR imaging in SIH usually reveals a collapsed dural sac, extradural fluid collections, spinal meningeal enhancement, and dilatation of the epidural venous plexus, meningeal diverticula, and the presence of retrospinal fluid collections at C1-C2. The collapsed dural sac has a characteristic hexagon-like contour, which has been described as a “festooned appearance”. The pseudoarachnoiditis appearance probably resulted from a secondary loss of CSF volume. A possible explanation for this finding is that decreased intrathecal CSF leads to collapse of the dural sac in the spinal subarachnoid space, resulting in clustering of the nerve roots. In conclusion, when SIH is suspected based on clinical symptoms but is not supported by brain MRI

results, spinal MR can be helpful in establishing the diagnosis.

**KEY WORDS:** Pseudoarachnoiditis appearance, spontaneous intracranial hypotension

#### eP-45

##### First and Foremost: Findings at the Level of the Cranio-Cervical Junction on a Head CT

Khashper, A.<sup>1</sup>Anghel, T.<sup>2</sup>Radu, A.<sup>1</sup>Del Carpio-O'Donovan, R.<sup>1</sup>

<sup>1</sup>McGill University Health Centre, Montreal, QC, CANADA, <sup>2</sup>McGill University, Montreal, QC, CANADA

#### PURPOSE

This exhibit will illustrate the importance of the first image of a computed tomography (CT) brain scan where significant imaging findings can be detected. The aim of the exhibit is to: 1. Highlight the importance of a careful inspection of the first image on a brain CT. 2. Provide a systematic approach of the first image evaluation. 3. Present a concise checklist based on the anatomical zones.

#### MATERIALS & METHODS

Imaging findings and their clinical relevance will be illustrated using an interactive, visually oriented, case-based approach. Various pathologies will be classified based on anatomical zones, including medulla-cervical junction and intrathecal space, bony cranio-cervical junction, vascular structures and soft tissue.

#### RESULTS

The most inferior cut of a brain CT can reveal a clinically significant abnormality, even if it is partially visualized. Such findings require further clinical and imaging workup leading to a correct diagnosis. Selected cases will be presented according to anatomical zones and teaching points will be outlined.

#### CONCLUSION

The first image of the brain CT scan contains no less information than the rest of the study and should not be neglected. It might not only suggest the diagnosis, but also provide useful information guiding further investigation, treatment and management.

**KEY WORDS:** Cranio-cervical junction, computed tomography, foramen of magnum

#### eP-46

##### Common Diagnostic Challenges in Neuroimaging: A Survey of Trainee Radiologists

Adams, A.<sup>1</sup>Mankad, K.<sup>2</sup>

<sup>1</sup>Barts and the London NHS Trust, London, UNITED KINGDOM, <sup>2</sup>Great Ormond Street Hospital, London, UNITED KINGDOM

## PURPOSE

The aim of the study was to elucidate the most common diagnostic neuroimaging problems encountered by trainee radiologists. This included diagnostic imaging problems encountered during normal working hours as well as common neuroimaging dilemmas encountered during on-call/"out of hours" work.

## MATERIALS & METHODS

A survey was conducted across all radiology trainees and neuroradiology fellows within the London Deanery. Each trainee was asked to list the most common and/or difficult neuroimaging problems they had encountered. In addition, the trainees were asked how they managed the situation in terms of communication with other colleagues and what was subsequently performed in terms of further imaging/advice provided.

## RESULTS

A number of diagnostic neuroimaging dilemmas were recorded (e.g., How to image the patient with acute visual disturbance? When to report a dense transverse sinus as a sinus thrombosis?). The 10 most common neuroimaging problems encountered by trainees were investigated further with regards to the current national (National Institute for Clinical Excellence) and international guidelines. The recommended imaging protocols for each diagnostic challenge are provided.

## CONCLUSION

Trainee radiologists and neuroradiology fellows in training often encounter various diagnostic challenges in neuroimaging that require the application of further imaging techniques in terms of cross-sectional imaging. The aim of this study was to highlight some of these common diagnostic dilemmas and provide current protocols and advice based on current guidelines and current literature.

**KEY WORDS:** Neuroimaging, diagnostic, challenges

eP-47

## Severe Traumatic Head Injury: Prognostic Value of Brainstem Injuries Detected by MR Imaging

Ramos, A.<sup>1,2</sup>•Hilario, A.<sup>1</sup>•Salvador, E.<sup>1</sup>•Cicuendez, M.<sup>1</sup>•Millan-Juncos, J.<sup>1,2</sup>•Lagares, A.<sup>1</sup>

<sup>1</sup>Hospital Universitario 12 de Octubre, Madrid, SPAIN,

<sup>2</sup>Universidad Complutense de Madrid, Madrid, SPAIN

## PURPOSE

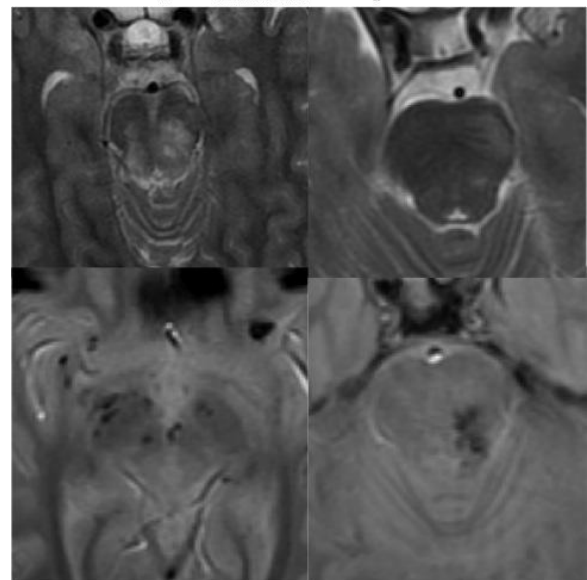
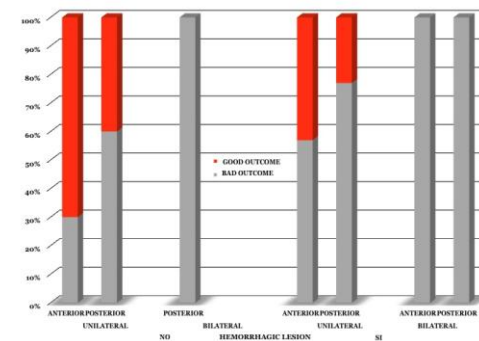
Despite advances in radiology and clinical prognostic models, prognostic assessment in head trauma remains unclear. Using conventional MR sequences for the detection of associated lesions to diffuse axonal injury has demonstrated great utility as a prognostic factor. Brainstem injuries traditionally have been associated with worse prognosis. However, some patients with traumatic brainstem lesions have a benign course. The aim of this study is to correlate brainstem injuries detected by conventional MR with final outcome in patients with severe traumatic brain injury (TBI).

## MATERIALS & METHODS

We retrospectively reviewed data obtained from patients with severe TBI and brainstem lesions admitted to our hospital between 2002 and 2011. MR imaging was obtained in the subacute phase of head injury (during the first 30 days after trauma). The MR imaging protocol included: T2-weighted FSE, FLAIR and gradient-echo T2\*-weighted images in the axial plane. Lesion location and characteristics were determined on MR. The relationship between neuroimaging and outcome was estimated at least 6 months after injury using the dichotomized Glasgow Outcome Scale-Extended (GOSE): good outcome and bad outcome.

## RESULTS

The study population consisted of 51 patients with brainstem lesions after severe TBI. Lesions tend to occur more frequently in the mesencephalon (84%), followed by medulla oblongata (6%), pons (4%) and multiple locations (6%). Most lesions were hemorrhagic (64%) and unilateral (74%). According to final prognosis, 16 patients with brainstem lesions showed good outcome. Bilateral lesions led to a poor outcome independent of location. Factors associated with the worse prognosis were hemorrhage [ $p < 0.01$ , O.R. 4.94 (IC 95% 1.3-18.7)], and posterior location in mesencephalic lesions [ $p < 0.05$ , O.R. 2.7 (IC95% 1.2-9.6)].



## CONCLUSION

Brainstem lesions detected at MR invariably are not associated with a bad outcome. Location, extension and lesion characteristics must be considered in the assessment of final outcome. A worse prognosis is associated with bilateral lesions.

**KEY WORDS:** Head trauma, brainstem, MR imaging

#### eP-48

##### **Diffuse Vascular Injury: Convergent-Type Hemorrhage in the Supratentorial White Matter on Susceptibility-Weighted Imaging in Cases of Severe Traumatic Brain Damage**

Iwamura, A.·Taoka, T.·Fukusumi, A.·Sakamoto, M.·Miyasaka, T.·Ochi, T.·Akashi, T.·Okuchi, K.·Kichikawa, K.

Nara Medical University  
840 Shijo-cho, Kashihara, Nara, JAPAN

#### **PURPOSE**

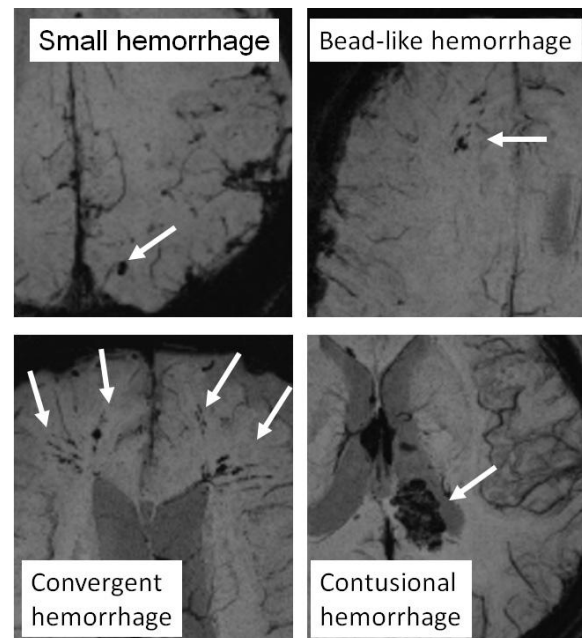
Although diffuse axonal injuries (DAI) are accompanied by microbleeding in many instances, DAI lesions without microbleeding as well as isolated microbleeding are reported. Bleeding within the brain parenchyma, including microbleeding in the white matter, is one of major features of traumatic brain damage. The purpose of this study is to delineate the character and importance of supratentorial deep white matter hemorrhages detected by susceptibility-weighted imaging (SWI) in cases of traumatic brain damage.

#### **MATERIALS & METHODS**

Twenty-five consecutive cases with severe traumatic head injury were included in the current study. MR imaging examinations were made within 1 month after injury. Images were created using a clinical scanner and the protocol for severe brain injury including T1WI, T2WI, FLAIR, diffusion-weighted image (DWI) with apparent diffusion coefficient (ADC) image and SWI. Diagnosis for DAI was made on T1WI, T2WI, FLAIR and DWI. On SWI, we evaluated the degree and distribution of the supratentorial hemorrhages. We classified the degree of bleeding on SWI into four grades: "small hemorrhage," "bead-like hemorrhage," "convergent-type hemorrhage," and "contusional hemorrhage." We correlated the degree and distribution of the hemorrhage to clinical outcomes. We also evaluated the ADC image of lobes with "convergent-type hemorrhage."

#### **RESULTS**

Existence of "contusional hemorrhage" correlated with a poor outcome, that is, worse than "severely disabled" on the Glasgow outcome scale. There was a statistically significant ( $p < 0.01$ ) correlation between the number of lobes affected by "convergent hemorrhage" and the clinical outcome. There were 45 lobes with "convergent hemorrhage" and 27 of them showed increased diffusivity on ADC images.



#### **CONCLUSION**

Supratentorial contusional hemorrhages and supratentorial convergent-type multiple hemorrhages were associated with poor prognosis after traumatic brain injury. These scattered supratentorial white matter microbleedings in traumatic brain injury frequently were visualized on SWI. Based on their linear arrangement, convergent distribution, and frequent elevation of diffusivity, these microbleedings may be due to injury at the proximal medullary veins and subsequent venous congestion. This finding may be important in predicting the duration of consciousness disturbances and impaired clinical outcome.

**KEY WORDS:** Susceptibility-weighted image, diffuse axonal injury, diffuse vascular injury

#### eP-49

##### **Initial and Follow-Up Imaging Findings of Spontaneous Symptomatic Intracranial Vertebrobasilar Dissection**

Ahn, S.<sup>1</sup>·Kim, B.<sup>1</sup>·Suh, S.<sup>2</sup>·Kim, D.<sup>1</sup>·Kim, D.<sup>1</sup>

<sup>1</sup>Yonsei University Health System, Seoul, KOREA, REPUBLIC OF, <sup>2</sup>Yonsei University College of Medicine, Gangnam Severance Hospital, Seoul, KOREA, REPUBLIC OF

#### **PURPOSE**

This study aims to evaluate initial radiographic findings of symptomatic intracranial vertebrobasilar dissection (si-VBD) as well as the follow-up imaging of conservatively managed si-VBD.

#### **MATERIALS & METHODS**

We retrospectively evaluated the initial radiographic findings of 210 patients with 230 si-VBDs (48 ruptured and 192 unruptured), who underwent catheter angiography as well as MR and/or CT angiography, so



that angiographic shapes (e.g., dilatation without stenosis, pearl-and-string, or steno-occlusive without dilatation) and pathognomonic findings (e.g., intramural hematoma, intimal flap) could be reviewed. Furthermore, the natural radiographic evolution of conservatively managed unruptured si-VBDs was evaluated.

## RESULTS

Primary shape differed significantly between ruptured and unruptured si-VBD. Ruptured si-VBD presented with two main morphologies in most cases: dilatation without stenosis or pearl-and-string appearance, with the primary shape of unruptured si-VBDs being evenly distributed. Intramural hematomas were found most frequently in stenosis without dilatation (42/60) followed by pearl-and-string group (27/90). Intimal flap was found most frequently in pearl-and-string lesions (21/90) followed by stenosis without dilatation (8/60). Follow-up results significantly differed by initial si-VBD shape: 73.5% of the dilatation without stenosis group showed no change, while improvement was observed in 90.7% of the stenosis without dilatation group ( $p < 0.05$ ). Symptomatic intracranial VBDs with intramural hematoma showed improvement in 63% and progression in 20.4%, with only 16.7% exhibiting no change ( $p < 0.05$ ). Follow-up results did not differ significantly according to intimal flap presence.



## CONCLUSION

Primary angiographic shapes of si-VBDs differ between ruptured and unruptured lesions. Stenosis without dilatation-type most frequently exhibited radiographic improvement, followed by pearl-and-string and dilatation without stenosis-type on follow-up imaging.

**KEY WORDS:** Stroke in young adults, vertebrobasilar artery dissection

## eP-50

### Atherosclerotic Plaque Enhancement of Middle Cerebral Artery in High-Resolution Contrast-Enhanced MR Intracranial Vessel Wall Imaging: Striatocapsular and Lenticulostriate Infarctions

Choi, B. Kim, J. Jung, C. Kim, E.

Seoul National University Bundang Hospital  
Seongnam-si, KOREA, REPUBLIC OF

## PURPOSE

Striatocapsular infarction is related most often to middle cerebral artery atherosclerosis, whereas lenticulostriate infarction usually is attributed to small vessel lipohyalinosis. We investigate the relationship

between middle cerebral arterial wall enhancement in high-resolution contrast-enhanced MR (CE MR) vessel wall imaging and infarct type categorized as striatocapsular or lenticulostriate infarctions.

## MATERIALS & METHODS

Consecutive patients with basal ganglia and corona radiata infarction underwent MR angiography and CE MR vessel wall imaging to assess the degree of stenosis and the presence and eccentricity of plaque enhancement. MR angiography was scored as "mild," "moderate" or "severe" and contrast enhancement of middle cerebral arterial wall in CE MR vessel wall imaging was scored as "no enhancement," "equivocal enhancement" or "enhancement". Infarcts were divided into striatocapsular infarction and lenticulostriate infarction groups.

## RESULTS

Thirty-seven patients with basal ganglia and corona radiata infarction were included, 11 with striatocapsular infarction and 26 with lenticulostriate lesion. Among patients with striatocapsular infarction, 10 (91%) patients had plaque enhancement and among patients with lenticulostriate infarct 14 (54%) patients had plaque enhancement on CE MR vessel wall imaging ( $p = 0.03$ ). There were no statistical differences in the stenotic degree and the eccentricity of plaque enhancement between the two groups.

## CONCLUSION

Our study showed that striatocapsular infarction could be due to atherosclerosis in the middle cerebral artery, but lenticulostriate infarction possibly has mixed causes of large or small arterial disease. High-resolution CE MR vessel wall imaging could help precise stroke subtyping.

**KEY WORDS:** Atherosclerosis, plaque, infarction

## eP-51

### Features of Intracranial Arterial Dissection on Postcontrast 3D Time-of-Flight MR Angiography: Additional Value of Rescanning after Contrast Injection

Ishimaru, H. Nakashima, K. Takahata, H. Matsuoka, Y.

National Hospital Organization Nagasaki Medical Center  
Omura, JAPAN

## PURPOSE

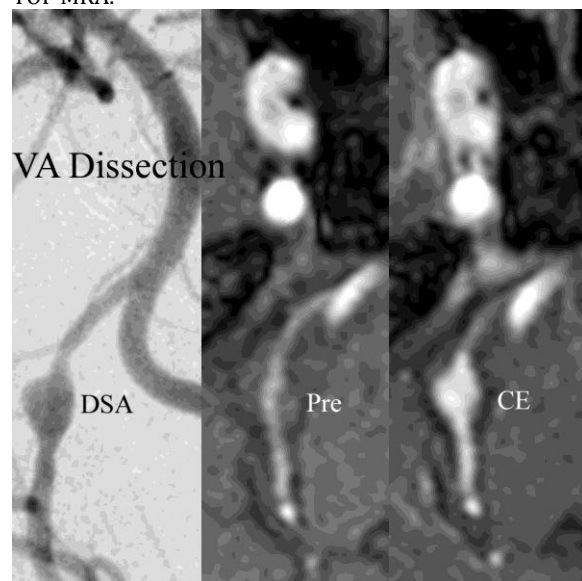
On conventional angiography, false lumen in dissected artery often retains contrast media during late arterial and venous phase because of slow flow. On 3D time-of-flight MR angiography (3D TOF MRA) the slow flow causes luminal low signal, which complicates the diagnosis of the disease on 3D TOF MRA. Postcontrast 3D TOF MRA is more sensitive to slow blood flow than routine 3D TOF MRA; therefore, we aimed to clarify the efficacy of postcontrast 3D TOF MRA in the diagnosis of intracranial arterial dissection (IAD).

## MATERIALS & METHODS

We performed pre and postcontrast 3D TOF MRA simultaneously in 29 cases of IAD confirmed by double lumen on catheter angiography ( $n = 21$ ) or T1 hyperintense intramural hematoma (IMH) ( $n = 8$ ). Vertebral ( $n = 13$ ), basilar ( $n = 4$ ), anterior cerebral ( $n = 5$ ), middle cerebral ( $n = 5$ ), posterior cerebral ( $n = 1$ ), and posteroinferior cerebellar ( $n = 1$ ) arteries were involved. 3D TOF MRA was performed with a 1.5 T MR system. Multiplanar reformatted images (MPR) parallel and orthogonal to the affected vessel were reconstructed retrospectively from the source images of pre and postcontrast 3D TOF MRA, and the luminal enhancement was assessed.

## RESULTS

In 15 (71%) of 21 patients confirmed by double lumen on catheter angiography, postcontrast 3D TOF MRA depicted a false lumen as a thin enhanced channel parallel to the true lumen showing high signal on precontrast 3D TOF MRA. In six of these 15 patients, false lumen did not show high signal on precontrast 3D TOF MRA. In the remaining nine patients, the enhancement of false lumen was observed beyond the range of double lumen on precontrast 3D TOF MRA. In five of these nine patients, the enhancement of false lumen was observed beyond the range of double lumen on catheter angiography. In one patient with double lumen on catheter angiography, both lumens showing low signal on precontrast 3D TOF MRA were enhanced; however, both lumens were indistinguishable. In five patients with double lumen on catheter angiography and all eight patients confirmed by IMH, there was no significant difference between pre and postcontrast 3D TOF MRA.



## CONCLUSION

Postcontrast 3D TOF MRA had advantage in depiction of slow-flowing (false) lumen that was low signal on precontrast 3D TO FMRA. In suspicious case, postcontrast 3D TO FMRA should be added to routine MR examination.

**KEY WORDS:** Dissection, MR angiography, Gd-enhanced

## eP-52

### Quantitative Analysis of Flow-Related Signal of Intracranial Arteries on 3D Time-of-Flight MRA in Patients with Sickle Cell Disease

Brahler, T.·Arya, R.·Shah, B.·Nadgir, R.·Saito, N.·Jara, H.·Sakai, O.

Boston Medical Center  
Boston, MA

## PURPOSE

High incidence of intracranial arterial stenosis/occlusion is well known in patients with sickle cell disease (SCD); however, quantitative analysis of magnetic resonance angiography (MRA) signal intensity has not been described previously. The purpose of this study is to quantify the signal intensities of intracranial arteries in patients with SCD on 3D time-of-flight (TOF) MRA.

## MATERIALS & METHODS

Retrospective review was performed after institutional review board approval. Intracranial 3D TOF MRA source images from patients with SCD ( $n = 24$ , average age of 19.7 years) examined at our institution from 2004 to 2008 using 1.5T MR units were analyzed. Images from age-matched patients without SCD ( $n = 24$ , average age of 21.4 years) and normal MRA findings from the same time period also were reviewed. Regions of interest measurements were placed at the bilateral anterior cerebral arteries (A1 segments), bilateral middle cerebral arteries (M1 segments), and the distal basilar artery to measure maximum and average signal intensities. Inter-exam signal variability was standardized with air and right masseter muscle signal intensities.

## RESULTS

Statistical analysis was completed using the Student's *t*-test. Significantly higher maximal signal intensities were noted in patients with SCD for all investigated vessels ( $p < 0.001$ ) and significant increase in average signal intensities for the A1 and M1 segments ( $p < 0.001$ ). Increase in average intensity for the basilar artery was nearly significant ( $p = 0.057$ ).

## CONCLUSION

On 3D TOF MRA, intracranial arterial signal intensity, which corresponds to increased flow velocity, is significantly greater in patients with SCD compared with age-matched controls. This suggests unique vascular dynamics, which may have prognostic implications.

**KEY WORDS:** Sickle cell, flow, MR angiography

## eP-53

**Acute Sick Cell Crisis Associated with Near Total Occlusion of Intracranial Arteries**

Low, S. B. L. Chawda, S. Derakhshani, S.  
Queens University Hospital  
Romford, Essex, UNITED KINGDOM

**PURPOSE**

To illustrate a severe cerebral vaso-occlusive complication of sickle cell anemia.

**MATERIALS & METHODS**

A 34-year-old female with sickle cell disease and sickle cell nephropathy presents with new-onset seizures, blurred vision and hypertension. A plain CT scan of the head showed multiple hypodense ischemic lesions within bilateral cerebral hemisphere, mainly over the right basal ganglia, left corona radiata and left parietal lobe. Also distal basilar artery was hyperdense and enlarged. As a result, a MRI of the brain including MR angiogram was done. MR angiogram showed total occlusion of both internal carotid arteries at their origins with filling of the supraclinoid parts of both internal carotid arteries and their main branches from the posterior circulation, through posterior communicating arteries. There was also stenosis at the distal basilar artery and an enlargement at the point of its bifurcation.

**RESULTS**

Blood pressure was maintained between 140-160 mmHg systolic with Amlodipine and Labetolol. The patient was anticoagulated with iv heparin and later, Warfarin, maintaining an INR of 2-3. Seizures were terminated initially with benzodiazepine and phenytoin. Patient developed further seizures, which required HDU care. Seizures were managed effectively with the introduction of Levetiracetam. Patient was reviewed by the ophthalmologists who ruled out any adverse causes for her blurred vision. No treatment was given. Her nephropathy was managed conservatively. MR imaging of the brain repeated a week later showed significant regression of the previously identified ischemic lesions with absence of flow voids in the internal carotid arteries.

**CONCLUSION**

Sickle cell disease causes occlusion of large arteries, as in this case both internal carotid and basilar arteries. However, this can be reversed effectively with anticoagulation if identified early, to prevent the development of permanent infarctive stroke. There should be a low threshold for CT head scans in patients presenting with sickling crisis.

**KEY WORDS:** Sickle cell disease, sickle cell crisis, vascular thrombosis

## eP-54

**Angiographically Derived Arterial Arrival Time as a Measure of Leptomeningeal Collateral Formation in Experimental Acute Stroke**

Christoforidis, G.<sup>1</sup> Benayoun, M.<sup>1</sup> Theyel, B.<sup>1</sup> Khan, S.<sup>1</sup> Garg, N.<sup>1</sup> Rink, C.<sup>2</sup> Kontzialis, M.<sup>2</sup> Sen, C.<sup>2</sup>

<sup>1</sup>University of Chicago, Chicago, IL, <sup>2</sup>The Ohio State University, Columbus, OH

**PURPOSE**

An angiographically derived, temporally based quantitative method assessing leptomeningeal collateral perfusion in a large animal minimally invasive middle cerebral artery occlusion (MCAO) model was developed. It was compared to other methods assessing collateral perfusion and determined whether it is predictive of infarct volume.

**MATERIALS & METHODS**

A previously described angiographically-based methodology allowed transient (n=8) and permanent (n=5) middle cerebral artery (MCA) and carotid terminus occlusion in mongrel dogs (20-30 kg). Arterial arrival times (AAT) were measured from regions of interest (ROIs) within normal and collateralized distal M3 segment MCA branches identified on angiographic images (Figure) using a custom made MATLAB based program which measured contrast density over time within the ROIs. Additionally, relative cerebral blood volumes (rCBV) were measured as contrast density within centimeter square symmetric ROIs within the middle cerebral artery territories using a MATLAB-based custom made program which measured contrast density over time within the regions of interest. Leptomeningeal collateral formation was assessed on a previously published leptomeningeal collateral extent 10 point scoring system. Using bivariate linear fit analysis the derived AAT values were compared to rCBV, collateral scores and infarct volumes derived from MRI (3 T Achieva, Philips) mean diffusivity maps. Arterial arrival times reproducibility was assessed between two observers.

**RESULTS**

Arterial arrival times was reproducibly assessed and predictive of infarct volume measured on mean diffusivity maps acquired on animals undergoing 1 hour postreperfusion following 1 hour transient occlusion ( $p < 0.0001$ ;  $r^2_{adj} = 0.890$ ,  $n=8$ ) and 1 hour post permanent MCAO ( $p = 0.0125$ ,  $r^2_{adj} = 0.875$ ,  $n=5$ ). Arterial arrival time correlated with rCBV ( $p < 0.0011$ ,  $r^2_{adj} = 0.828$ ,  $n=8$ ), and collateral scoring system ( $p < 0.0001$ ,  $r^2_{adj} = 0.916$ ,  $n=8$ ).

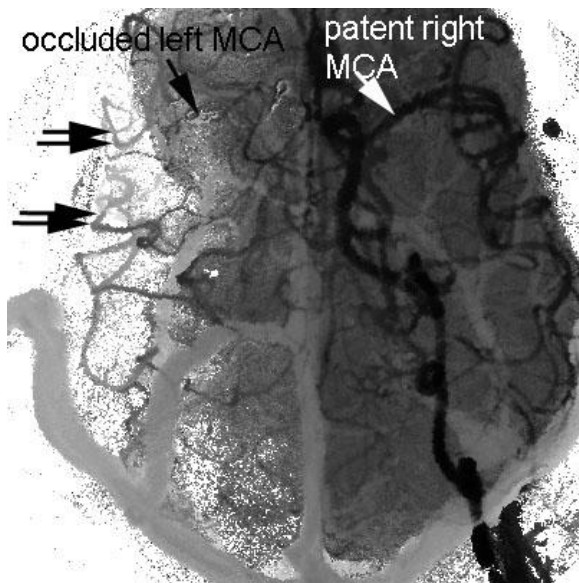


Figure. Compiled angiographic images over time demonstrate leptomeningeal collateral formation with reverse reconstitution of occluded MCA territory. Vascular arrival times were measured at M3 segments (double arrows) within occluded MCA territory. Time is coded based on gray scale

#### CONCLUSION

Quantitative leptomeningeal collateral assessment using the methods described indicate that AAT assessment is a predictor for infarct volume following transient and permanent MCA occlusion in experimental stroke. It is noteworthy that angiographically based parameters for leptomeningeal collateral formation differ from CT and MRI-based methods due to differences in the time frame and the relative density of the vasculature on the derived color or gray scale maps. Further analysis is needed to assess discrepancies between angiographically based and MRI or CT-based assessment of cerebral perfusion during acute cerebral ischemia.

**KEY WORDS:** Leptomeningeal collaterals, cerebral angiography, acute stroke

eP-55

#### Stroke Patients with Brain Parenchyma Contrast Staining on CT after Digital Subtraction Angiography: What Is the Prognosis for Hemorrhage or Infarction?

Amans, M. R. • Hetts, S. W.

University of California San Francisco  
San Francisco, CA

#### PURPOSE

In the setting of acute ischemic stroke, brain parenchyma contrast staining following digital subtraction angiography (DSA) has been described as a rare phenomenon. This is thought to be secondary to transient breakdown of the blood-brain barrier. Contrast staining presents an imaging interpretive challenge, as it often is confused with, and sometimes

difficult to differentiate from, parenchymal hemorrhage, although staining is not associated with mass effect. Given the increasing frequency of endovascular thrombolysis and thrombectomy, we sought to identify prognostic significance to parenchymal staining on postprocedure CT.

#### MATERIALS & METHODS

Under an IRB-approved protocol, we retrospectively analyzed our institution's neurointerventional radiology database to identify acute ischemic stroke patients who underwent DSA with or without intraarterial therapy, had a subsequent noncontrast head CT within 48 hours and had a follow-up brain imaging study after the initial postprocedure CT. For those patients meeting inclusion criteria, imaging studies were reviewed to determine the absence, presence, and extent of brain parenchymal contrast staining on initial postprocedure CT. Absence, presence, and extent of intracranial hemorrhage and cerebral infarction also were determined. Odds ratios and Fisher's exact tests were performed using STATA SE version 11 (College Station, TX).

#### RESULTS

Of 23 patients meeting inclusion criteria, 14 (61%) demonstrated brain parenchymal contrast staining on postprocedure CT. Of these two (14%) went on to intraparenchymal hemorrhagic transformation, one in the deep gray matter matching area of contrast stain, and one in the temporal cortex matching area of contrast staining. No patients without staining had hemorrhagic transformation. All 13 patients with basal ganglia staining developed infarction in the contrast stained areas. Patients with anterior circulation ischemia were more likely to exhibit parenchymal staining than those with posterior circulation ischemia (71% versus 17%, OR 12, 95% CI 0.9 to 600,  $p = 0.05$ ).

#### CONCLUSION

Contrast staining has been described as a rare postangiographic phenomenon secondary to transient breakdown of the blood-brain barrier in part due to the stroke, as well as secondary to the inherent toxic effects of contrast. Changes in patient management, particularly the ease and availability of CT, have led to increasing numbers of CT examinations in patients within the first 48 hours after DSA. Contrast staining may be much more prevalent than initially anticipated, and the observed increased prevalence, with relative paucity of hemorrhagic transformation, brings into question the accepted etiology. Perhaps staining is not secondary to blood-brain barrier breakdown, but rather represents contrast stasis in capillaries in areas of core infarction. As such, brain parenchymal contrast staining may provide further insight into the concept of no-reflow at the microvascular level, particularly in deep gray matter, during acute ischemic stroke.

**KEY WORDS:** Stroke, thrombolysis, contrast staining

## eP-56

### Effectiveness of Intravenous Thrombolysis in Acute Ischemic Stroke Can Be Quantified by Clot Length Reduction Using Thin-Slice Nonenhanced Computed Tomography Scans

Riedel, C. H.·Jansen, O.

University of Kiel  
Kiel, GERMANY

#### PURPOSE

To evaluate the amount of thrombotic clot that can be dissolved by intravenous thrombolysis (IVT) in cases of acute middle cerebral artery (MCA) stroke.

#### MATERIALS & METHODS

Patients suffering from acute ischemic MCA stroke treated with IVT within 3 hours after symptoms onset were included in this retrospective case series that was conducted between April 2007 and June 2010. In all patients, thin-slice nonenhanced CT (NECT, 2.5 mm slice width) had to demonstrate a hyperdense middle cerebral artery sign (HMCAS) before and within 24 hours after IVT. The HMCAS was segmented semiautomatically and reduced to a middle axis in order to measure clot length before and after IVT. Descriptive statistics of clot length reduction were calculated.

#### RESULTS

Seventy-three patients (54% male) with a mean age of 69 years (SD:  $\pm 13.2$ ) matched the inclusion criteria. The mean reduction of thrombus length was found to be 3.1 mm (SD:  $\pm 1.4$  mm). We found only one clot with a length reduction (lr) of more than 7 mm (lr: 12 mm) in which an initial CTA study showed only partial thrombotic occlusion. Five clots (7%) had grown significantly after IVT.

#### CONCLUSION

In most stroke cases in which IVT failed to completely dissolve a thrombus in the MCA, clot length reduction was found to be within a small range of values around a well defined mean. This length can be used to define a threshold beyond which IVT is most likely to fail.

**KEY WORDS:** Computed tomography, thrombus, intravenous thrombolysis

## eP-57

### Comparison of CT Perfusion Deconvolution Algorithms in Estimation of Penumbra in Acute Ischemic Stroke

Dehkharghani, S.·Noorian, A. R.·Hwang, S. N.

Emory University School of Medicine  
Atlanta, GA

#### PURPOSE

Investigate the impact of placing the user-defined arterial input function (AIF), ipsilateral or contralateral to the side of vascular occlusion, on the standard perfusion metrics computed with various deconvolution

algorithms. Background: CT perfusion (CTP) is used widely in the evaluation of acute ischemic stroke. Phantom and clinical studies have highlighted the potentially significant differences in perfusion metrics computed with different deconvolution algorithms, particularly underscoring concerns of overestimating hypoperfusion in regions with benign arrival-time delay. Various singular value decomposition (SVD) techniques frequently are employed for deconvolution of the tissue residue function, and determination of perfusion parameters such as mean transit time (MTT) and time-to-maximum of the residue function (Tmax), commonly used for characterizing tissue at risk and penumbra. Bolus delay and dispersion effects are known to confound perfusion measurements, depending on the deconvolution technique, AIF placement, and other user-defined parameters.

#### MATERIALS & METHODS

After institutional review board approval, consecutive series of patients with ipsilateral occlusion of the internal carotid artery (ICA) or middle cerebral artery (MCA) with acute stroke were characterized retrospectively with CT angiography of the head and neck and CTP. CT perfusion was acquired in cine mode with two separate injections of 40-45 cc nonionic iodinated intravenous contrast. Two separate slabs, each with eight contiguous 5 mm sections covering 4 cm of brain were acquired with one-second temporal resolution carried over 45-seconds dynamic bolus passage. CT perfusion was analyzed with free software (Perfusion Mismatch Analyzer: <http://asist.umin.jp/index-e.htm>). Subjects were characterized for the site and extent of acute thrombus, by duration of stroke-like symptoms, lateralization of clinical findings, and NIH stroke scale. Six separate perfusion data sets were obtained for each patient: standard (sSVD); delay-insensitive, block-circulant SVD (bSVD); and delay-corrected (dSVD) deconvolution maps, each acquired separately with the AIF placed either ipsilateral or contralateral to the occluded vessel. Manual ROIs were placed over the perfusion abnormality defined by Tmax as well as MTT, with mirror image ROIs in the contralateral normal brain. Lesion volumes and mean pixel values were computed and followed by computation of CBF within these ROIs. Repeated measure analysis of variance was performed to identify significant differences among different analyzes.

#### RESULTS

CT perfusion was performed on four MCA stroke patients (mean age 66.2, 40% male, mean NIHSS 20.75) and two ICA stroke patients (mean age 51.3, 50% male, mean NIHSS 23.5). Arterial input function placement ipsilateral to the side of occlusion resulted in an apparent underestimation of hypoperfusion, as defined by decreased CBF, which was statistically significant for sSVD ( $p=0.02$ ) and dSVD ( $p=0.02$ ). A suggestion of a mild underestimation using bSVD was not significant ( $p=0.09$ ). No significant differences were identified with the other perfusion metrics.

## CONCLUSION

The difference in CT perfusion metrics using different deconvolution techniques observed in previous phantom/clinical studies is less apparent in our stroke patients. This may relate to dispersion effects, not accounted for in phantom simulations. Further evaluation of AIF dependency in stroke patients accounting for bolus dispersion thus may be necessary. However, the results do suggest bSVD may be less sensitive to bolus arrival delay.

**KEY WORDS:** Stroke, perfusion, deconvolution

eP-58

## Probabilistic Integration of Thrombus Location in CT Perfusion Imaging for Improved Prediction of Tissue Outcome

Kemmling, A.<sup>1,2</sup>•Kamalian, S.<sup>1</sup>•Krumm, R.<sup>2</sup>•Souza, L.<sup>1</sup>•Seyedmehdi, P.<sup>1</sup>•Lev, M. H.<sup>1</sup>

<sup>1</sup>Massachusetts General Hospital, Boston, MA,

<sup>2</sup>University of Munster, Munster, GERMANY

## PURPOSE

CT perfusion (CTP) is used frequently in acute stroke imaging; however, there is need for further standardization for reliable quantification of tissue at risk. Using a global threshold to predict infarct is not precise. Vascular status, in particular proximal branch occlusion, is an important predictor for outcome. The purpose was to present a holistic stroke imaging approach by combining CTP maps with a priori infarct probability defined by site of vessel occlusion to improve prediction of infarct.

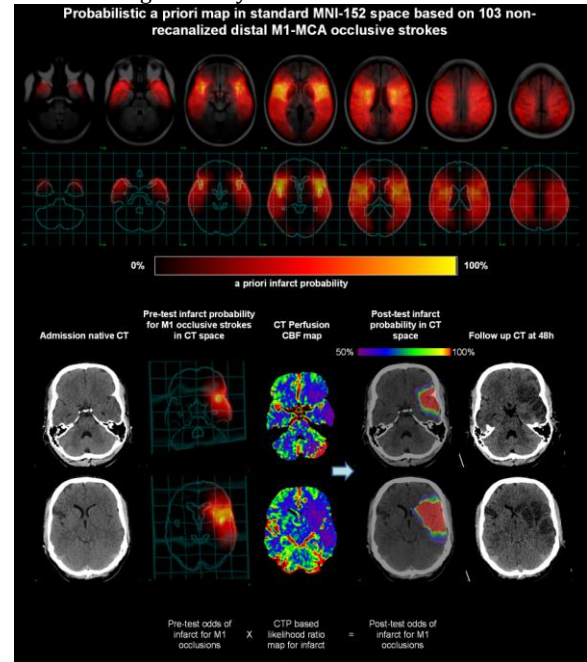
## MATERIALS & METHODS

A novel method is presented to derive CTP-based images displaying voxel-wise probability of infarction: 1) In 83 MCA occlusive stroke, voxel-wise sensitivity and specificity for infarction for incremental perfusion thresholds was measured with respect to tissue-outcome lesion maps at 48 hours. CT perfusion parameters (gray value at any voxel) in CTP images were converted to likelihood ratios defined by sensitivity/(1-specificity). Thus, the discriminative power for every perfusion value with respect to tissue outcome was encoded directly within the perfusion image. 2) A probabilistic a priori map in standard space based on 103 nonrecanalized distal M1-MCA occlusive strokes at 48 hour after onset was generated (Figure). Lesion masks were registered to standard MNI-152 space. 3) The pretest probability map for M1-occlusive strokes was transformed to CTP space and multiplied by the CTP-based likelihood ratio to obtain a post-test map displaying voxel-wise probability of infarction.

## RESULTS

In 10 sample cases, infarct probability in admission imaging was displayed and compared to follow-up imaging at 48 hours. Areas of >95% infarct probability correlated very well with actual tissue outcome. In contrast to original CTP maps, the resulting probability

map exclusively displays voxels at risk of infarction. Noise was significantly reduced.



## CONCLUSION

Infarct prediction can be improved combining CT perfusion maps with a priori infarct probability defined by site of vessel occlusion. Further studies are warranted.

**KEY WORDS:** Stroke, CT perfusion, software

eP-59

## Admission "NIHSS Score/NCCT Aspects" Ratio Correlates with Length of Stay and Discharge Disposition in Acute Stroke

Arneja, A. K.<sup>1</sup>•Byrns, K.<sup>2</sup>•Kamalian, S.<sup>3</sup>•Gilani, S.<sup>2</sup>•Lev, M. H.<sup>3</sup>•Lev, S.<sup>2</sup>

<sup>1</sup>New York Medical College, Valhalla, NY, <sup>2</sup>Nassau University Medical Center, East Meadow, NY, <sup>3</sup>Massachusetts General Hospital, Boston, MA

## PURPOSE

In cases of middle cerebral artery (MCA) infarction, the extent of territorial involvement is a critical factor in management. To provide greater accuracy in evaluating the volume of critically ischemic brain, the Alberta Stroke Program Early CT Score (ASPECTS) was developed. Admission NIH stroke scale (NIHSS) score and admission ASPECTS are both established predictors of patient outcome in acute stroke. The ratio between admission NIHSS score and NCCT ASPECTS provides a measure of baseline acute stroke severity, with NIHSS providing a sensitive measure of "clinical penumbra" and NCCT ASPECTS providing a specific measure of "infarct core". Our goal was to test the hypothesis that a stroke scale score measuring symptom severity by combining these two outcome predictors would provide a more powerful predictor of length of stay (LOS) and discharge disposition in acute stroke patients.

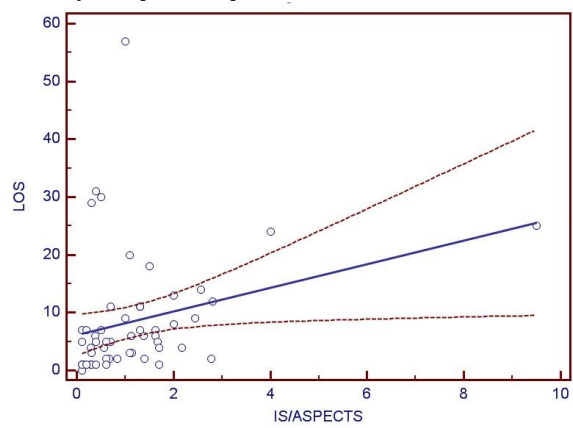


## MATERIALS & METHODS

We identified 55 consecutive acute stroke patients presenting to our emergency department with symptoms suggesting cerebral ischemia, between May 2010 and April 2011, for whom admission nonenhanced CT scans, NIHSS scores, final diagnoses, length of stay and discharge disposition data were available. Clinicians performing NIHSS scores were certified through the American Stroke Association's NIHSS training program. Two radiologists evaluated the CT studies after completing the online ASPECTS training module created by the University of Calgary, blinded to other patient data. We defined the Stroke Scale Ratio Score (SSRS) as the ratio between the admission NIHSS score and admission ASPECTS. We used a four point scale to assess discharge disposition (home, rehabilitation facility, nursing home, death). Statistical tests included regression analysis, ANOVA, Fisher's test, and ROC for binary outcome.

## RESULTS

There was a strong correlation between LOS and discharge disposition, including all outliers ( $p < .04$ ); validating that these two variables are related measures of patient outcome. Although the correlation between SSRS and LOS was significant ( $R^2 = 0.08$ ,  $p = 0.036$ , Figure 1), when the four outliers with confounding medical issues were removed, a much stronger correlation was demonstrated ( $R^2 = 0.45$ ,  $p < 0.001$ ). In a multivariate model comparing NIHSS, ASPECTS and SSRS, SSRS was the only independent predictor of outcome.



## CONCLUSION

A stroke scale score combining the ratio between admission NIHSS data and ASPECTS can help predict LOS and discharge disposition in acute stroke patients with statistical significance and may provide a clinically simple, potent and more accurate tool to predict stroke outcome. These results need to be validated with a larger, prospective well selected cohort.

**KEY WORDS:** Ischemic stroke, ASPECTS, NCCT

## eP-60

### Effect of Chronic Hemodynamic Impairment on Cortical Thickness in Moyamoya Patients

Sagar, J. R.<sup>1</sup>•Lee, J.<sup>1</sup>•Snyder, A.<sup>1</sup>•Shimony, J.<sup>1</sup>•Zazulia, A.<sup>1</sup>•Aiyagari, V.<sup>2</sup>•Davis, P.<sup>3</sup>•Ivan, C.<sup>4</sup>•Prabhakaran, S.<sup>5</sup>•Zipfel, G.<sup>1</sup>•Derdeyn, C.<sup>1</sup>

<sup>1</sup>Washington University School of Medicine, St. Louis, MO, <sup>2</sup>University of Illinois Chicago School of Medicine, Chicago, IL, <sup>3</sup>University of Iowa School of Medicine, Iowa City, IA, <sup>4</sup>University of Indiana School of Medicine, Indianapolis, IN, <sup>5</sup>Rush University School of Medicine, Chicago, IL

## PURPOSE

Chronic hemodynamic impairment may lead to reduced cortical thickness, perhaps related to metabolic downregulation in cortical neurons. The purpose of this study was to determine whether hemodynamic impairment could be correlated to decreased cortical thickness in patients with idiopathic moyamoya phenomenon.

## MATERIALS & METHODS

The study was a retrospective analysis of a prospective, blindly-adjudicated, multicenter patient cohort from five Midwestern sites. Inclusion criteria required unilateral or bilateral moyamoya phenomenon by catheter angiography and presumed idiopathic basal arterial occlusive disease. Baseline measurements of oxygen extraction fraction (OEF) were made using positron emission tomography (PET). Hemodynamic impairment was determined by comparing the ratio of the left or right middle cerebral to cerebellar count-based OEF to normal control subjects. Those with values beyond the 95% confidence limit were considered increased. MR imaging was obtained concurrently with PET to provide anatomical data for cortical thickness measurements. MR imaging also was used to identify areas of previous ischemia or infarction. Measurements of OEF in the MCA territory of each hemisphere then were compared to measurements of cortical thickness calculated using FreeSurfer imaging software.

## RESULTS

Complete MR datasets were available in 40 subjects. Mean age was 44 years. Eleven were male. Thirty-one had bilateral disease. Three had increased OEF in both hemispheres and four had unilateral increased OEF. Nine patients had repeat MRI and PET exams 1-2 years after enrollment. Three of these patients underwent revascularization surgery during follow up. Two of the three patients initially had elevated OEF that became normal by the time of post-op imaging. The third patient had normal OEF values throughout the follow-up period. Another patient initially had elevated OEF in one hemisphere that spontaneously decreased to normal by the time of their follow-up imaging. The cortical thickness of hemispheres with normal OEF was 2.52 mm (95%CI 2.52 +/- 0.4 mm). In contrast, the cortical thickness of hemispheres with elevated OEF was 2.40

mm (95%CI 2.40 +/- 0.23 mm). This difference approached statistical significance,  $p = 0.068$ .

#### CONCLUSION

Chronic hemodynamic impairment may be associated with reduced cortical thickness. This may reflect reversible downregulation or irreversible subclinical ischemic injury.

**KEY WORDS:** Hemodynamics, moyamoya, cortical thickness

#### eP-61

##### Significance of CT Perfusion Deficits on Admission in Aneurysmal Subarachnoid Hemorrhage

Anumula, N. S. Hoang, A. Johnson, C. Comunale, J. Tsiouris, A. Mangat, H. Rosengart, A. Kapinos, G. Parikh, G. Sanelli, P.

Weill Cornell Medical College  
New York, NY

#### PURPOSE

CT perfusion (CTP) has been used in patients with aneurysmal subarachnoid hemorrhage for detection of delayed cerebral ischemia (DCI). Efforts to improve outcomes in these patients have been focused on earlier detection of DCI to initiate prompt treatment. Our hypothesis is that CTP deficits on admission may assist in identifying patients at high risk for DCI. The purpose of this initial study is to understand the significance of CTP deficits on admission in relationship to development of clinical and imaging findings of DCI.

#### MATERIALS & METHODS

A retrospective study of consecutive aneurysmal subarachnoid hemorrhage patients from December 2007 to August 2011 was performed. Inclusion criteria were CTP performed during the baseline period (day 0-3 following aneurysm rupture) with a qualitative perfusion deficit. All CTP exams were reviewed by two blinded neuroradiologists independently for a perfusion deficit. A third neuroradiologist performed a tie-breaker review in cases of disagreement. Thorough chart review was performed by three neuro-intensivists blinded to all imaging data for consensus agreement regarding the development of new clinical findings attributed to DCI. Chart review also was performed for transcranial Doppler ultrasonography (TCD) results. Digital subtraction angiography (DSA) exams were reviewed by two neuroradiologists independently for vasospasm. A third neuroradiologist performed a tie-breaker review. Correlation of the location of CTP deficits with clinical and imaging data was determined by consensus agreement with two neuroradiologists and three neuro-intensivists blinded to the treatment management of these patients.

#### RESULTS

Fifty-one patients (median age 50 years, 67% (34/51) female) with CTP deficits on admission were included in the analysis. Mean day CTP performed was 1.2 days following aneurysm rupture. CT perfusion deficits were

located in the following vascular territories: 19.8% right anterior cerebral artery (ACA), 34.3% right middle cerebral artery (MCA), 5.2% right posterior cerebral artery (PCA), 17.7% left ACA, 15.6% left MCA, 2% left PCA and 5.2% diffuse deficits.

Fifty-nine percent (30/51) of patients demonstrated new clinical findings (mean 7.0 days) and 27% (14/51) had infarction on follow-up CT/MR imaging (mean 8.9 days) attributed to DCI. Of the 51 patients, 36 underwent DSA (mean 7.6 days). Ninety-four percent (34/36) had vasospasm; of these 76% (26/34) received medical treatment with hypervolemic-hemodilution-hyperdynamic therapy, 82% (28/34) underwent inter-arterial therapy with verapamil and 15% (5/34) underwent balloon angioplasty. Thirty-nine patients had TCD performed (mean 6.7 days) and 74% (29/39) of them had elevated velocities indicative of vasospasm. Correlation of the CTP deficit vascular territory revealed 83% (30/36) agreement with the location of vessels demonstrating vasospasm on DSA, 69% (27/39) agreement with location of vessels that had elevated velocities on TCD, 57% (29/51) agreement with symptoms attributed to DCI, and 22% (11/51) agreement with location of infarction detected on follow-up CT/MR imaging.

#### CONCLUSION

CT perfusion deficits on admission had the highest agreement with development of arterial narrowing on DSA and TCD. This preliminary data support the need for further investigation of identifying CTP deficits on admission to assist in early classification of high risk patients for developing clinical and imaging findings of DCI.

#### eP-62

##### CT-Negative, Susceptibility-Weighted Imaging-Positive Studies for Acute Hemorrhage in Acute Stroke: A Survey of Clinical Management Decisions by Stroke Neurologists

Eshetu, T. Leigh, R. Yousem, D. M.

Johns Hopkins Hospital  
Baltimore, MD

#### PURPOSE

In the acute ischemic stroke setting, thrombolytic therapy has been the standard of care for over a decade. It is also known that hemorrhage on CT of the brain is an absolute contraindication for thrombolysis. The purpose of this study is to gain insight into the management decisions by stroke neurologists in the setting of acute stroke, where CT is negative but MRI/susceptibility-weighted imaging (SWI) is positive for hemorrhage.

#### MATERIALS & METHODS

A 22-point multiple choice format questionnaire was sent via email to members of the stroke service in the department of neurology at our institution. The questionnaire was based on a scenario where a patient with acute stroke was admitted and underwent both CT and MRI evaluations within 1 hour of each other. There

were subsequent questions regarding factors that may influence management decisions by the clinicians. The factors considered included: the pattern and distribution of the SWI abnormality, distribution of the infarct, patient age, NIHSS scale, and preexisting white matter disease. There were separate sections for intravenous and intraarterial thrombolysis. Additional assessment of the clinicians' attitude towards MRI as the first line modality for evaluation of acute stroke was made. The survey will be extended to involve neurologists in multiple stroke centers throughout the nation.

#### RESULTS

The majority of the respondents (86%) stated that they will administer thrombolytic agents as long as the CT was negative for hemorrhage, regardless of the MRI/SWI findings. One respondent stated that they will thrombolize only if the SWI pattern was restricted to petechial-pattern of bleed. Eighty-six percent responded that the size of SWI abnormality would influence their decision for cortical/subcortical microbleeds (CAA pattern). Other factors that influenced the management of the patients included the arterial distribution of the infarct (57%), NIH stroke scale, NIHSS (70%), and age (14%). None of the respondents stated that their decision would be influenced by preexisting extensive white matter disease or hypertensive pattern of chronic bleed. Seventy-one percent felt that MRI should be the preferred modality in the initial evaluation of patients with ischemic stroke, as long as it did not delay thrombolytic administration. Fourteen percent responded that MRI should be the primary modality even if it slightly delayed thrombolysis.

#### CONCLUSION

The majority of the stroke neurologists at our institution believe that thrombolysis should be administered in the setting of acute stroke as long as CT is negative for hemorrhage, even if SWI is positive for hemorrhage. However, the majority also prefer MRI as the primary modality of choice in the evaluation of patients in the acute stroke setting. The survey will be extended to include stroke neurologists in multiple major institutions.

**KEY WORDS:** Acute stroke, susceptibility-weighted imaging

#### eP-63

##### Contrast Enhancement following Endovascular Intervention for Acute Stroke

Burns, J.·Gamss, C.·Shifteh, K.·Farinhas, J. M.·Brook, A. L.·Bello, J. A.·Miller, T. S.

Montefiore Medical Center  
Bronx, NY

#### PURPOSE

Endovascular management of acute stroke is performed increasingly, with potential for both revascularization of at-risk brain tissue as well as reperfusion injury as the therapeutic window is extended. Both basal ganglia and

parenchymal enhancement have been described following endovascular treatment of aneurysms. The purpose of this study is to determine the incidence of intracranial enhancement following intraarterial treatment of acute stroke.

#### MATERIALS & METHODS

Imaging of 35 consecutive patients undergoing intraarterial mechanical or chemical thrombolysis was analyzed retrospectively. Posttreatment CT scans were reviewed for the presence of either basal ganglia or other parenchymal enhancement following intraarterial treatment. Follow-up imaging was evaluated for resolution of contrast density, as well as the presence of intracranial hemorrhage. Variables such as the intervals between procedure and follow-up imaging were assessed with respect to the presence of hemorrhage on follow-up exams.

#### RESULTS

Twenty-one female (age 39-95 years, median 70) and 14 male (age 31-84 years, median 66) patients underwent endovascular intervention for acute stroke. The time elapsed between intervention and first follow-up imaging ranged from 1-16 hours (median 2 hours, mean 3.25 hours). Density of the basal ganglia, cortex or subarachnoid space was demonstrated in 21/35 (60%) of patients following intraarterial stroke therapy. Basal ganglia density was present in nine patients; parenchymal density in two patients; subarachnoid density in four patients; a mixed pattern of density was seen in six patients. Findings resolved on follow-up imaging in 15/21 (71%). On follow-up exams, 6/21 patients demonstrated persistent hyperdensity on CT, including five patients with parenchymal hemorrhage and a single patient with subarachnoid hemorrhage.

#### CONCLUSION

Parenchymal density on CT following intraarterial treatment of acute stroke is common, seen in nearly two thirds of patients in this study. In most cases, short-term resolution of this finding suggests contrast enhancement as its etiology. In cases where this finding did not resolve in the short term, follow-up imaging demonstrated frank hemorrhage. The overall incidence of hyperdensity following treatment was greater than in prior series evaluating patients undergoing endovascular coil embolization of intracranial aneurysms, likely due to ischemic vulnerability of the blood-brain barrier in the acute stroke setting.

#### eP-64

##### Quantification of Wallerian Degeneration on Diffusion Tensor Imaging as an Independent Biomarker of Long-Term Motor Outcome after Stroke

Puig Alcantara, J.·Blasco, G.·Daunis-i-Estadella, J.·Figueras, J.·Castellanos, M.·Serena, J.·Pedraza, S.·

<sup>1</sup>Hospital Universitari Dr Josep Trueta, Girona, SPAIN, <sup>2</sup>Hospital Universitari Dr Josep Trueta, Girona, SPAIN, <sup>3</sup>Universitat de Girona, Girona, SPAIN, <sup>4</sup>Hospital Universitari Dr Josep Trueta, Girona, SPAIN, <sup>5</sup>Hospital Universitari Dr Josep Trueta, Girona, SPAIN

## PURPOSE

Motor impairment is common after stroke and contributes significantly to patients' ability to live independently. Over 50% of AIS patients have residual motor deficits. Reduced diffusion anisotropy values have been interpreted as Wallerian degeneration (WD), i.e., the anterograde degeneration of axons after proximal axonal or cell body injury. The extent of WD in the corticospinal tract (CST) has been suggested as one of the major determinants of motor deficit. We aimed (1) to develop a model to predict which variables in the first month after stroke are most accurate in predicting long-term (2 years) motor outcome, (2) to assess whether anisotropy using diffusion tensor imaging (DTI) in the CST correlates with long-term motor outcome after middle cerebral artery acute ischemic stroke (AIS), and (3) to calculate the best fractional anisotropy (FA) cutoff to discriminate long-term motor deficit.

## MATERIALS & METHODS

Consecutive patients with anterior circulation AIS underwent multimodal MRI including DTI <12 hours, 3 days, and 30 days after symptom onset. Clinical and demographic data were recorded. Imaging analysis included assessment of infarct volume, level of vascular occlusion, location of CST damage on diffusion tensor tractography [motor and premotor cortex, centrum semiovale, corona radiata, and posterior limb of the internal capsule (PLIC), FA ratio (rFA) between affected and unaffected sides of the CST at the level of the pons, recanalization after iv rt-PA (TIMI score 0-3), and hemorrhagic transformation. Motor outcomes obtained at 2-year follow up were classified as good [Motoricity Index Score (MI) 100], intermediate (MI 99-55), or poor (MI 49-0).

## RESULTS

We evaluated 70 patients (28 women; age  $72 \pm 15$  years). Median NIHSS score was 12 (IQR 6-18). At admission, 55 (78.6%) had some motor deficit and CST damage was seen in 76.7%. Infarct volume at day 30 was 10.1 (4.1-40.3). Motor outcome was classified as intermediate in 18 (25.75%) patients and poor in 13 (18.6%). Lower rFA values correlated with motor deficit at day 30 ( $p < 0.001$ ;  $r = -0.801$ ) (Table). Independent predictors of long-term motor outcome were rFA at day 30, infarct volume at day 3, motor deficit at day 3, motor deficit at day 30, and PLIC damage on admission. rFA at day 30 was the best predictor of long-term motor outcome (OR, 35.45; 95%CI, 32.23-39.87;  $p < 0.001$ ). The best rFA cutoffs for discriminating good vs intermediate and intermediate vs poor outcome at 2 years were 0.978 and 0.685, respectively (AUC = 0.99,  $p < 0.001$ ).

Imaging, Clinical Data and Follow up According Long-Term Motor Outcome at 2 years

	Overall (N=70)	MI 100 (N=39, 55.7%)	MI 50 - 99 (N=18, 25.7%)	MI 0 - 49 (N=13, 18.6%)	p-value
Age, median (IQR)	72 (61-78.3)	71 (61-79)	67 (51.8-76.5)	75 (70.5-80)	0.481
Female, n (%)	28 (40.0%)	13 (33.3%)	8 (44.4%)	7 (53.8%)	0.385
Vascular recanalization after IV rt-PA, n (%)	14 (38.9%)	5 (26.3%)	3 (30%)	6 (85.7%)	0.018
Symptomatic hemorrhagic transformation, n (%)	5 (8.9%)	1 (3.4%)	3 (18.8%)	1 (9.1%)	0.386
rFA at admission	1.01 (1.05-1.01)	1 (1.05-1)	0.98 (1.08-0.98)	1.02 (1.05-1.02)	0.282
rFA at day 3	1.01 (1.05-1.01)	1.01 (1.05-1.01)	1.01 (1.05-1.01)	1 (1.04-1)	0.429
rFA at day 30	0.98 (1.02-0.98)	1.02 (1.07-1.02)	0.91 (0.94-0.91)	0.59 (0.63-0.59)	<.001
Motor cortex damage at admission, n (%)	18 (25.7%)	8 (20.5%)	3 (16.7%)	7 (53.8%)	0.035
Premotor cortex damage at admission, n (%)	15 (21.4%)	7 (17.9%)	4 (22.2%)	4 (30.8%)	0.619
Centrum semiovale damage at admission, n (%)	12 (17.1%)	4 (10.3%)	2 (11.1%)	6 (46.2%)	0.009
Corona radiata damage at admission, n (%)	35 (50.0%)	14 (35.9%)	2 (66.7%)	9 (69.2%)	0.030
PLIC damage at admission, n (%)	14 (20.0%)	0 (0.0%)	6 (33.3%)	8 (61.5%)	<.001
Infarct volume at admission, mL, median (IQR)	19.1 (9.2-53.5)	10.4 (7.1-22.6)	26.1 (14-61.3)	83.7 (41.5-148.8)	<.001
Infarct volume at day 30, mL, median (IQR)	10.1 (4.1-40.3)	7.5 (3.2-11.3)	15.1 (7.5-49)	69.4 (31.8-120.2)	<.001
Total NIHSS scores at admission, median (IQR)	12 (6-18)	9 (5-12)	15.5 (10.3-20)	19 (16-20)	<.001
Total NIHSS scores at day 30, median (IQR)	2 (0-9)	1 (0-2)	5 (2-10)	16 (10-19)	<.001
Motor NIHSS scores at admission, median (IQR)	4.5 (1-8)	2 (0-5)	7 (1.8-8)	8 (7-8)	<.001
Motor NIHSS scores at day 30, median (IQR)	0 (0-4)	0 (0-0)	3 (0-4.3)	7 (5.5-8)	<.001
Rankin Index Score at day 30, median (IQR)	2 (1-4)	2 (1-2)	3 (2.8-4)	4 (4-4)	<.001

## CONCLUSION

Wallerian degeneration in the CST revealed by DTI at day 30 is an independent predictor of long-term motor outcome after stroke. Diffusion tensor imaging metrics would provide more accurate prediction of motor function, enabling clinicians and patients to set realistic goals and allocate resources efficiently.

**KEY WORDS:** Stroke, diffusion tensor imaging, outcome

## eP-65

### Temporal Evolution of High-Density Lesions on Noncontrast CT after Intraarterial Thrombolysis in Patients with Acute Ischemic Stroke

Sabel, B.·Phan, C.·Parikh, A.·Chaudhry, Z.·Romero, J.·Yoo, A.·Gupta, R.

Massachusetts General Hospital, Harvard Medical School  
Boston, MA

#### PURPOSE

This study investigates the temporal decay of hyperattenuation due to contrast staining versus that from hemorrhage after reperfusion therapy. The earliest follow-up time to differentiate these two etiologies on a noncontrast CT is derived.

#### MATERIALS & METHODS

This retrospective study was approved by the Institutional Review Board and was compliant with HIPAA regulations. Sixty-one patients, all of who had at least one intraparenchymal hyperattenuating focus on CT scans of the brain, were divided into two subsets. Patients were included in this study if they had between two and five follow-up CT scans. The first subset of 21 men and 19 women had hemorrhage, as confirmed by a subsequent MRI. The second subset (9 female and 12 male patients) consisted of patients given reperfusion therapy postacute stroke. They were confirmed to have no hemorrhagic component in the hyperattenuating lesion, as evidenced by lack of susceptibility on posttreatment MRI. A standard PACS workstation (AGFA Impax ES) was used to measure and follow the time course of the maximum density within each hyperdense lesion. The difference between the maximum density in the lesion and that in the corresponding anatomical structure in the contralateral hemisphere, was recorded as the maximum relative density. The time course of maximum relative density due to hemorrhage and that due to contrast staining was compared by plotting their two washout curves as a function of time. The half-washout time (HWT: the time it takes the relative density to decrease by 50%) for hemorrhage and contrast staining was computed. The accuracy of HWT in differentiating hemorrhage from contrast staining was quantified as a receiver-operator characteristic (ROC) curve.

#### RESULTS

Intraparenchymal hemorrhage and contrast staining follow an exponential decay pattern. The mean HWT for hemorrhage was 102.7 hours while that for pure contrast staining was 12.1 hours. Receiver operating characteristic (ROC) analysis of HWT showed excellent discrimination between hemorrhage and contrast staining. For example, a HWT threshold of <20 hours is 98% sensitive and 78% specific for excluding hemorrhage in a hyperdense lesion. These results also can be used to estimate the minimum time required for follow-up CT scan: a scan performed 9 hours after the initial scan will show an expected decay of at least 25 percent if the lesion is purely iodinated contrast

staining. This much washout is above the standard deviation for the observed fluctuations in hemorrhage washout time (mean half-washout time of ~103 hours). A less than 25% drop in the maximum relative density at 9 hours is suspicious for hemorrhagic conversion of infarct postintraarterial therapy.

#### CONCLUSION

Intraparenchymal hemorrhage and contrast staining have markedly different half-washout times of 102.7 hours and 12 hours respectively. In cases where it is essential to exclude hemorrhage as early as possible (for example to start anticoagulation), a drop of 25% or more in the maximum relative enhancement at 9 hours essentially excludes hemorrhagic conversion.

**KEY WORDS:** Stroke, hemorrhage, intraarterial thrombolysis

## eP-66

### Characterization of Normal Pressure Hydrocephalus Using Brain Imaging Segmentation Metrics

Serulle, Y.·Milch, H.·Kirov, I.·Rusinek, H.·Golomb, J. B.·Gonen, O.·George, A. E.

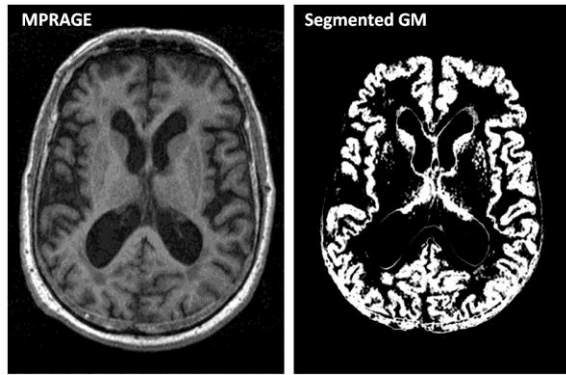
New York University School of Medicine  
New York, NY

#### PURPOSE

Normal pressure hydrocephalus (NPH) is a treatable debilitating neurologic disorder characterized by severe motor deficits, urinary incontinence and cognitive impairment. Objective imaging metrics to characterize NPH are not well defined, and differentiating NPH from other neurodegenerative diseases such as Alzheimer disease (AD) is often a challenge. To characterize NPH using commonly available and automatically determined structural imaging metrics, we have compared brain tissue distribution in a group of NPH patients relative to normal and AD control groups.

#### MATERIALS & METHODS

Sixteen NPH patients, 16 AD patients, and 20 age-matched normal controls were enrolled and received detailed clinical evaluation and cognitive testing as per NYU Aging and Dementia Center protocols. Normal pressure hydrocephalus diagnosis was established based on positive response to shunt. Preshunt MR images of the NPH patients were used in the study. High resolution 3D T1-weighted (MPRAGE: 1 mm slices/TR 2300/TE 3.97/Matrix 256 x 256) were processed to derive total GM, WM and CSF volumes (Statistical Parametric Mapping 8 software) and ventricular volumes (Firevoxel) (Figure 1). T tests were used to compare imaging metrics across groups.



## RESULTS

Total CSF volume did not differ between controls, NPH and AD. However, ventricular volume in NPH patients ( $166 \pm 11$  ml) was over two and a half times higher than controls' ( $64 \pm 4$  ml,  $P < 0.001$ ), and nearly two times higher than AD patients' ( $91 \pm 6$  ml,  $P < 0.001$ ). While there was no difference in GM volume between NPH patients and controls, GM volume was decreased by 30% in AD patients ( $406 \pm 11$  ml) relative to NPH patients ( $577 \pm 35$  ml,  $P < 0.001$ ) and by 33% relative to controls ( $610 \pm 15$  ml,  $P < 0.001$ ). Controls had higher WM volume ( $467 \pm 17$  ml) than both NPH ( $405 \pm 28$  ml,  $P < 0.05$ ), and AD ( $358 \pm 17$  ml,  $P < 0.001$ ). There was no difference in WM volume between AD and NPH.

## CONCLUSION

Normal pressure hydrocephalus is characterized by ventricular volume nearly twice that of AD patients and over 2.5 times normal controls with global CSF measures being similar across the three groups suggesting that generalized atrophy assessments are not helpful for differential diagnosis. Decreased GM (30% to 33%) characterized the AD group. These findings suggest that brain segmentation metrics especially GM and ventricular volumetry have an important role in the clinical diagnosis of NPH from controls and AD.

**KEY WORDS:** NPH, segmentation, hydrocephalus

## eP-67

### Amyloid- $\beta$ Modulates: The Effect of TOMM40 on Alzheimer-Associated Neurodegeneration

Desikan, R. S.<sup>1</sup>Hess, C. P.<sup>2</sup>McEvoy, L. K.<sup>1</sup>Holland, D.<sup>1</sup>Thompson, W. K.<sup>1</sup>Roddey, C.<sup>1</sup>Brewer, J. B.<sup>1</sup>Aisen, P. S.<sup>1</sup>Sperling, R. A.<sup>3</sup>Hyman, B. T.<sup>3</sup>Dale, A. M.<sup>1</sup>

<sup>1</sup>University of California San Diego, San Diego, CA, <sup>2</sup>University of California San Francisco, San Francisco, CA, <sup>3</sup>Harvard Medical School, Boston, MA

## PURPOSE

Recent genome wide association studies have identified TOMM40 as a novel susceptibility locus for Alzheimer disease (AD). However, the mechanism by which

TOMM40 exerts its effect on the neurodegenerative process underlying AD is unclear.

## MATERIALS & METHODS

We examined longitudinal MRI scans (total of 1,042 scans), and baseline CSF measurements in 355 older individuals (107 cognitively normal older individuals (HC), 176 individuals with mild cognitive impairment, and 72 patients with AD). Using linear mixed effects models, we investigated the interaction between TOMM40 (rs2075650) and CSF A $\beta$ 1-42 on entorhinal cortex atrophy rate, while covarying for the effects of age, sex, disease severity (CDR-Sum of Boxes), and APOE  $\epsilon$ 4 genotype. In a similar fashion, we also examined the relationship between TOMM40, and CSF A $\beta$ 1-42 on atrophy rate of other AD-vulnerable regions.

## RESULTS

Across all individuals, we found a significant interaction between TOMM40 and CSF A $\beta$ 1-42 on entorhinal cortex atrophy rate. In the presence of CSF A $\beta$ 1-42, TOMM40 significantly associated with entorhinal cortex volume loss; in the absence of CSF A $\beta$ 1-42, the effect of TOMM40 on entorhinal cortex atrophy rate was not significantly different from zero. We found similar results in other AD-vulnerable regions. Finally, examining only the HC individuals, we found a similar interaction between TOMM40 and CSF A $\beta$ 1-42 on volume loss, even after covarying for the effects of APOE  $\epsilon$ 4 genotype.

## CONCLUSION

We present novel evidence suggesting that TOMM40 likely exerts its effect on AD-associated neurodegeneration via an A $\beta$ -related mechanism. Our findings also demonstrate that this relationship between TOMM40, A $\beta$ , and volume loss is present in cognitively normal older individuals indicating that A $\beta$  modulates the effect of TOMM40 on the neurodegenerative process underlying the preclinical phase of AD.

**KEY WORDS:** Alzheimer disease, neuroimaging, amyloid

## eP-68

### Brain MR Imaging Findings in the Antiphospholipid Antibody Syndrome of Systemic Lupus Erythematosus

Kaichi, Y.<sup>1</sup>Kakeda, S.<sup>1</sup>Moriya, J.<sup>1</sup>Ohnari, N.<sup>1</sup>Saito, K.<sup>1</sup>Tanaka, Y.<sup>1</sup>Tatsugami, F.<sup>2</sup>Date, S.<sup>2</sup>Awai, K.<sup>2</sup>Korogi, Y.<sup>1</sup>

<sup>1</sup>University of Occupational and Environmental Health School of Medicine, Kitakyushu, JAPAN, <sup>2</sup>Graduate School of Biomedical Sciences, Hiroshima University, Hiroshima, JAPAN

## PURPOSE

The antiphospholipid syndrome (APS) may affect the incidence and pathogenesis of cerebrovascular diseases in the patients with systemic lupus erythematosus (SLE). A few authors have reported the brain MR findings of SLE with APS in small series. Our purpose is



to reveal the characteristic MR findings in the patient group with APS by comparing the group without APS in large series of SLE.

#### MATERIALS & METHODS

This retrospective study was approved by the institutional review board and informed consent was not required. A computerized search of the patient database at our university hospital for a period from May 2004 through June 2011 revealed the data for patients whose diagnosis was SLE. This patient cohort was used to further select 261 patients who underwent a brain MR examination after a diagnosis of SLE. Five of those patients were excluded on the basis of the following exclusion criteria; MR images showed an inadequate image quality ( $n = 2$ ); the patient had the brain tumor ( $n = 1$ ), osmotic myelinolysis ( $n = 1$ ), or multiple sclerosis ( $n = 1$ ). Finally, 256 SLE patients (45 with APS, 211 without APS = non-APS) fulfilled the criteria and two neuroradiologists assessed the abnormalities on their initial MRI. The abnormalities were categorized as large territorial infarctions, lacunar infarctions, localized cortical infarctions, watershed infarctions, microembolisms, basal ganglial lesions, callosal lesions, white matter lesions on T2-weighted and/or FLAIR images (Fazekas rating scale), and macro or microhemorrhages. The occlusions of each artery on MR angiography also were evaluated as present or absent.

#### RESULTS

No significant difference was found between the APS group and the non-APS group in the baseline characteristics, including age, sex, disease duration, and cerebrovascular risk factors (diabetes, hypertension, smokers, hyperlipidemia, obesity). Abnormal MR findings were more common in the APS group (73%: 33/45) than in the non-APS group (53%: 112/211). The localized cortical infarction in the middle cerebral artery area (20% vs 2.4%) and bilateral watershed infarction (13% vs 1.4%, Figure) were significantly more common in the APS group than in the non-APS group at any age groups ( $P < .001$ ).

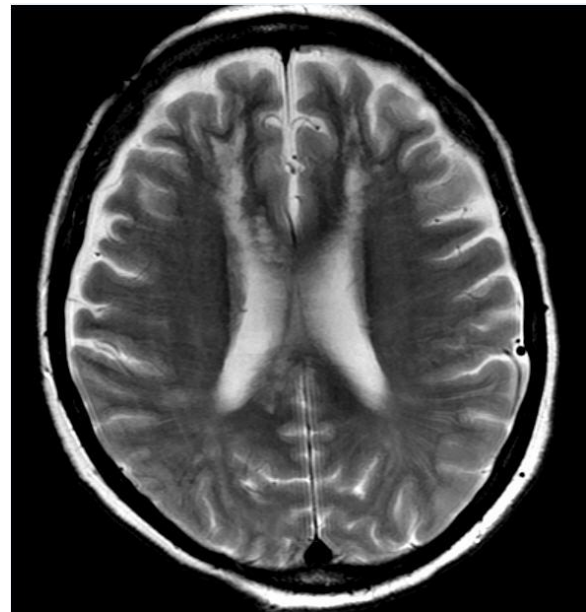


Figure. SLE patient with APS. T2-weighted image shows bilateral watershed infarction (arrows)

#### CONCLUSION

The SLE patients with APS showed abnormal MR findings more commonly. Localized cortical infarction and bilateral watershed infarction may be characteristic MR findings for APS.

**KEY WORDS:** Brain MR imaging, antiphospholipid antibody syndrome, systemic lupus erythematosus

#### eP-69

##### Comparison of Number of Enhancing Lesions on T1 Turbo-Spin Echo and T1 Fluid-Attenuating Inversion Recovery Images at 1.5 T and 3 T in Multiple Sclerosis

Hoffman, B.<sup>1</sup>McKinney, A. M.<sup>1,2</sup>Truwit, C. L.<sup>2</sup>

<sup>1</sup>University of Minnesota, Minneapolis, MN, <sup>2</sup>Hennepin County Medical Center, Minneapolis, MN

#### PURPOSE

T1-weighted inversion recovery (T1IR) imaging demonstrates higher brain tissue contrast than T1-weighted spin-echo imaging (T1SE), while T1SE demonstrates a higher contrast ratio of enhancing tumor to both white and gray matter, suggesting greater sensitivity in detecting enhancing lesions. To our knowledge, only one study has compared the number of contrast-enhancing lesions in multiple sclerosis on fluid-attenuated T1IR to T1SE. The objective of this report was to determine which sequence depicts a greater number of enhancing demyelinating lesions, and to determine if this occurs at both 1.5 T and 3 T.

#### MATERIALS & METHODS

Institutional review board approval was obtained. Since January 2010, our "demyelinating disease" brain protocol at both 1.5T and 3T has included both postcontrast fluid-attenuating T1IR and T1 turbo-spin echo, the acquisition time for each being about 5

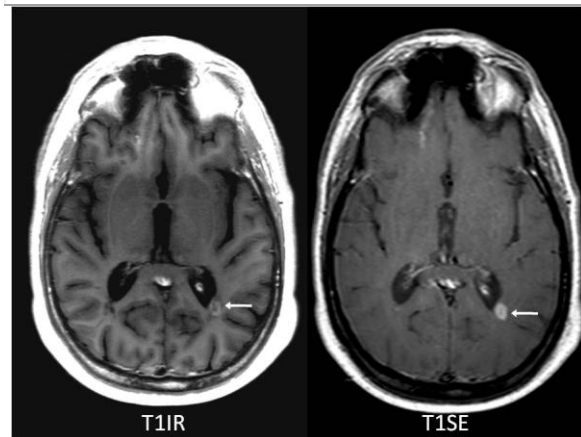
minutes. A PACS search for "Multiple Sclerosis" yielded 48 MRI examinations in 37 patients who had clinically definite MS during that time period. Two staff neuroradiologists reviewed the MRIs independently both from each other and from the other sequence, using T2-weighted and FLAIR images in conjunction. Kappa values were calculated for interobserver agreement between sequences, as well as intraobserver-intersequence agreement between T1IR and T1SE both at 1.5T and 3T.

## RESULTS

Of 48 MRIs reviewed; 23 were at 1.5 T and 25 at 3 T, with 72 total enhancing lesions noted by Reader 1 (R1), and 59 by Reader 2 (R2). On T1SE, R1 found 42 enhancing lesions (33 at 1.5T and 9 at 3T), while R2 found 33 lesions (24 at 1.5T and 9 at 3T). On T1IR, R1 found 30 lesions (25 at 1.5T and 5 at 3T) while R2 found 26 lesions (21 at 1.5T and 5 at 3T). There was quite strong agreement between observers for both T1IR and T1SE, but T1IR was consistently higher. Intraobserver-intersequence agreement was higher at 1.5 T than 3 T (**Table**).

Inter- and Intraobserver Agreement Kappa and p-values (Note: R1=Reader 1, R2=Reader 2)

Agreement Measured	Kappa	p-valued
R1 vs. R2: T1SE at 1.5T (n=23)	0.725	<0.001
R1 vs. R2: T1IR at 1.5T (n=23)	0.864	<0.001
R1 vs. R2: T1SE at 3T (n=25)	0.701	<0.001
R1 vs. R2: T1IR at 3T (n=25)	0.874	<0.001
R1 vs. R2: T1SE Overall (n=48)	0.727	<0.001
R1 vs. R2: T1IR Overall (n=48)	0.873	<0.001
R1: T1IR vs. T1SE at 1.5T (n=23)	0.750	<0.001
R1: T1IR vs. T1SE at 3T (n=25)	0.552	<0.001
R1: T1IR vs. T1SE Overall (n=48)	0.720	<0.001
R2: T1IR vs. T1SE at 1.5T (n=23)	0.935	<0.001
R2: T1IR vs. T1SE at 3T (n=25)	0.648	<0.001
R2: T1IR vs. T1SE Overall (n=48)	0.862	<0.001



## CONCLUSION

In agreement with previously reported data, our study demonstrates that T1SE has a higher sensitivity in detection of enhancing MS lesions as compared to T1IR.

However, T1IR has a higher interobserver agreement at both 1.5 T and 3 T.

**KEY WORDS:** Multiple sclerosis

## eP-70

### Diagnostic Value of Cortical-Juxtacortical in Clinically Isolated Syndromes

Auger, C.·Pla, J.·Pareto, D.·Mitjana, R.·Tintoré, M.·Corral, J. F.·Montalban, X.·Rovira, A.

Hospital Vall d'Hebron  
Barcelona, SPAIN

## PURPOSE

To evaluate the presence and the spatial distribution of cortical-juxtacortical lesions in patients diagnosed of a first clinical isolated syndrome (CIS) by using MRI-based lesion probability maps, and to determine its impact to diagnose lesion dissemination in space (DIS) according to the 2010 McDonald Criteria for multiple sclerosis (MS).

## MATERIALS & METHODS

Forty-nine patients (29 females) aged between 20 and 50 years old (mean 34 years) who presented with a CIS (19 optic neuritis, 14 spinal cord syndromes, 13 brainstem syndromes and three cerebral hemispheric syndromes) underwent brain and spinal cord MRI scanning within the first 5 months after symptoms onset. Brain MRI was obtained with a 3.0 T magnet using a 32 channel head coil. The following sequences were obtained: 1) Transverse proton-density and T2-weighted fast spin-echo; 2) 2D Transverse T2-fast FLAIR; 3) Un-enhanced and contrast-enhanced transverse T1-weighted gradient-echo, and 4) 3D transverse double inversion-recovery (DIR). All sequences 3 mm slice thickness. Cortical-juxtacortical lesions of each patient, defined as focal T2 hyperintensities within or in contact to the cortical ribbon, were identified, manually outlined and segmented into a binarized CL mask. A cortical-juxtacortical MRI-based lesion probability map was obtained.

## RESULTS

Cortical-juxtacortical lesions were identified in 22 patients (44.9%). Frontal lobe was the most affected area with an incidence of 52% of the lesions. Temporal and parietal lobes also had a significant incidence (22% and 20%). No lesions were detected on the occipital lobe (1%). According to the MS 2010 McDonald diagnostic criteria, identification of cortico-juxtacortical lesion contributed to demonstrate lesions disseminated in space (DIS) in six of the 22 patients (27%).

## CONCLUSION

Cortical-juxtacortical lesions are a common MRI finding in patients with a CIS, predominantly involving the frontal and temporal lobes. Its demonstration has a high relevance for the diagnosis of dissemination in space according to the MS 2010 McDonald diagnostic criteria.

**KEY WORDS:** Multiple sclerosis, diagnosis, MR imaging

## eP-71

### Atrophy in Subcortical Structures Related to the Papez Circuit in Alzheimer Disease

Garcia-Polo, P.<sup>1</sup>•Pajares, G.<sup>2</sup>•Hernández-Tamames, J.<sup>3</sup>•Alfayate, E.<sup>1</sup>•Frank, A.<sup>4</sup>•Álvarez-Linera, J.<sup>5</sup>

<sup>1</sup>Fundación Cien - Centro Alzheimer Fundación Reina Sofía, Madrid, SPAIN, <sup>2</sup>Centre for Biomedical Technology - UPM, Madrid, SPAIN, <sup>3</sup>Universidad Rey Juan Carlos, Móstoles, SPAIN, <sup>4</sup>Hospital Universitario La Paz, Madrid, SPAIN, <sup>5</sup>Hospital Ruber Internacional, Madrid, SPAIN

#### PURPOSE

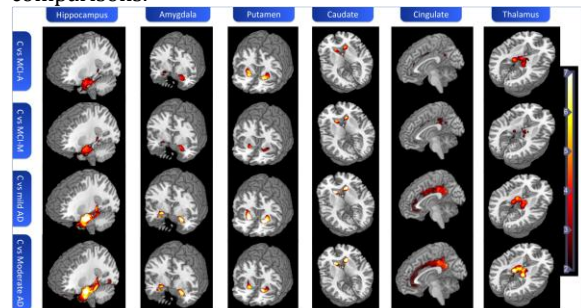
Alzheimer disease (AD) is the most common cause of dementia. Neuronal and synaptic losses occur initially and predominantly in the medial temporal lobe structures including hippocampus, amygdala and thalamus, structures that belong to the Papez circuit. The integrity of the connections amongst them is essential for episodic memory, which is specifically impaired in AD. For this reason we have investigated the degeneration pattern of subcortical structures and its relation to early stages of AD, i.e., mild cognitive impairment (MCI), both in the amnesic and multidomain types using structural magnetic resonance imaging (using a 3T GE scanner) and VBM-DARTEL.

#### MATERIALS & METHODS

A structural MRI 3D T1 volume was acquired from 163 subjects (44 control, 30 MCI-Amnesic, 29 MCI-Multidomain, 47 AD-mild, 13 AD-Moderate). A segmentation of the images into gray matter (GM), white matter (WM) and cerebrospinal fluid (CSF) was performed using SPM8. Normalization, modulation and smoothing (kernel of FWHM = 4 mm) of the GM, WM and CSF masks was performed using DARTEL. Finally, several statistical maps using a multiple regression analysis within the general linear model were obtained.

#### RESULTS

The comparisons between groups (control vs MCI-A, control vs MCI-M, control vs AD-m and control vs AD-M) showed a clear gradation [ $t = (2.7)$ ,  $p_{\max} < 0.001$ ] of volume loss regarding hippocampus, putamen, amygdala, cingulate, fusiform gyrus and thalamus, with a linear trend in volume loss in the progression control < MCI-A < MCI-M < AD in nearly all of the comparisons.



#### CONCLUSION

The posterior cingulate is affected more severely in MCI-M than in MCI-A (this result also arises in a PET-ASL study done by the group), and the volume loss in this region is higher for AD-m and even more for AD-M. The linear trend in volume loss has its exception in thalamus and putamen, probably due to the heterogeneity of the MCI-M group. Despite this fact, the group's division MCI-A > MCI-M > AD-m > AD-M seems to be a reliable approximation in the evolution of the Alzheimer disease. We conclude that the integrity of structures within the Papez Circuit is crucial in the role of episodic memory and is highly correlated with memory impairment and the evolution of Alzheimer disease.

## eP-72

### Prospective Comparison of 3D Double Inversion Recovery versus 3D FLAIR for the Detection of Brainstem Plaques in 100 Multiple Sclerosis Patients

Shapiro, M. D.<sup>1</sup>•Lees, J. S.<sup>2</sup>

<sup>1</sup>Neuroskeletal Imaging of Winter Park, Winter Park, FL,

<sup>2</sup>Neuro Imaging of Winter Park, Winter Park, FL

#### PURPOSE

To determine whether 3D FLAIR or 3D DIR is better for detecting MS plaques in the brainstem and cerebellar peduncles at 3 T.

#### MATERIALS & METHODS

One hundred patients with the known diagnoses of multiple sclerosis were imaged prospectively on a 3 T MRI (SiemensVerio) system using a 32 channel head coil with both 3D FLAIR and 3D DIR pulse sequences obtained in the sagittal plane with 1.3 mm slice thickness. The DIR sequence was performed prior to injection of gadolinium. The FLAIR sequence was performed postcontrast. Any lesions identified on the FLAIR sequence that enhanced on the conventional T1 conventional spin echo sequence (CSE) were eliminated from the study. In addition, all routine sequences were obtained except for the T1 coronal postcontrast sequence. All scans were reviewed by a CAQ neuroradiologist. The parameters for the two sequences were as follows: 3D FLAIR 3D DIR, TR 6,000 7500, TE 404 324, TI 2,100 3,000 (fat saturation) and 450, BW 781 814, TF (ETL) 141 222, FOV 240 240, NEX 1 1, TA 6:20 7:15.

#### RESULTS

Ninety-six MS plaques were identified on the 3D DIR sequence in the brainstem or cerebellar peduncles. Eighty-eight plaques were detected on the 3D FLAIR sequence. No plaque was identified on FLAIR that wasn't identified on DIR.

#### CONCLUSION

3D DIR is superior to 3D FLAIR in the detection of MS plaques involving the brainstem and/or cerebellar peduncles at 3 T using a 32 channel head coil.

**KEY WORDS:** 3 T, 3D double inversion recovery-FLAIR, brainstem multiple sclerosis

#### eP-73

### **Nosocomial Herpes Encephalitis: Rare but Treatable with Early MR Diagnosis**

Doshi, P. M. • Post, J. D. • Saigal, G. • Nagornaya, N. • Podda, A. • Quencer, R.

Jackson Memorial Hospital/University of Miami  
Miami, FL

#### **PURPOSE**

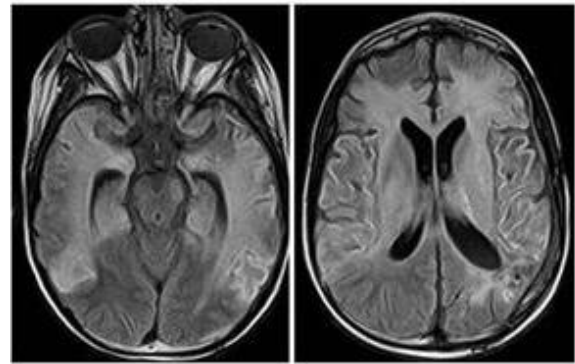
To describe three cases of nosocomial herpes simplex encephalitis (NHSE) and determine imaging clues that might lead to an early diagnosis of this disease.

#### **MATERIALS & METHODS**

We retrospectively reviewed the clinical and imaging findings in three patients with NHSE proven by CSF PCR. CT and plain and contrast MR scans were obtained in all with serial scans covering a 5 to 7 weeks time period. Noncontrast CT represented the initial study in two.

#### **RESULTS**

Prior to development of NHSE, initial presentations of the three patients, were in the settings of recurrent tumor, postsurgery with hydrocephalus, and traumatic nonhemorrhagic contusion. Following clinical/surgical management, a change/deterioration of their clinical status prompted further investigation and neuroimaging. New areas of abnormal imaging findings were seen between days 4 to 10 of the hospital stay. One patient (with hydrocephalus) showed new hypodensity in left temporal lobe on CT. Another (with nonhemorrhagic contusion) showed mild extension of the primary hypodensity with new hypodensities in the contralateral frontotemporal lobes on follow-up CT, not initially suspected to be due to NHSE. Third patient (with recurrent tumor) showed new subtle abnormal high FLAIR signal with restricted diffusion in both frontotemporal and insular regions with gyriform enhancement pattern on left side extending beyond the surgical bed in the parietal lobe, interpreted as hypoxic ischemic injury. These imaging findings went unrecognized as a sign of NHSE due to (1) myriad of other findings from these patients' underlying conditions and posttreatment changes; (2) lack of clinical suspicion for NHSE. Follow-up MR in all three patients, showed more extensive FLAIR signal (Figure) and restricted diffusion in both cerebral hemispheres (one patient in frontotemporal lobes and other two involving all lobes to varying degree), hippocampal formations and cingulate gyri with high T1 signal in a gyriform pattern, findings suggestive but not pathognomonic for HSE. Although acyclovir was given, imaging done between 4-6 weeks, following initial hospitalization, showed worsening and extension of signal abnormalities with cortical necrosis and clinical deterioration.



#### **CONCLUSION**

While rare, HSE can develop in the hospital and should be considered when new and rapidly evolving parenchymal abnormalities (especially temporal lobe) incongruous with the patient's admitting diagnosis are seen on imaging. Early neuroradiologic suspicion for NHSE can be achieved using MR, alerting the clinician to this diagnosis, which can be further confirmed by CSF analysis, resulting in institution of appropriate medical therapy and improved patient outcome.

**KEY WORDS:** Herpes encephalitis, nosocomial

#### eP-75

### **Time-Dependent Cell Invasion, Motility, and Proliferation Level Estimate Map Characteristics of Malignant Gliomas Treated with Paclitaxel Poliglumex**

Ellingson, B. M.<sup>1</sup> • Boxerman, J. L.<sup>2</sup> • Jeyapalan, S.<sup>2</sup> • Elinazano, H. D.<sup>2</sup> • Goldman, M.<sup>2</sup> • Dipetrillo, T.<sup>2</sup> • Safran, H.<sup>2</sup> • Pope, W. B.<sup>1</sup>

<sup>1</sup>David Geffen School of Medicine, University of California Los Angeles, Los Angeles, CA, <sup>2</sup>Brown University and Rhode Island Hospital, Providence, RI

#### **PURPOSE**

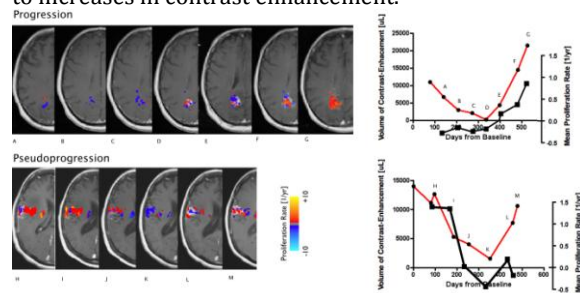
Paclitaxel poliglumex (PPX; Cell Therapeutics, Inc., Seattle, WA) is a microtubule stabilizer and mitotic inhibitor with a radiosensitization index of 4-8, and has been proposed as a radiosensitizing agent for patients with high-grade gliomas undergoing radiation therapy with the purpose of increasing acute cytotoxicity and effectiveness of radiotherapy. Initial observations of PPX-treated gliomas demonstrated substantial transient increases in the degree and number of contrast-enhancing lesions, many of which were later found to be quiescent tumor or due to treatment-related changes in the tumor mimicking progressive disease (i.e., pseudoprogression). The purpose of the current study was to determine whether time-dependent cell invasion, motility, and proliferation level estimate (CIRCLE) maps derived from serial diffusion MRI data could distinguish pseudoprogression from recurrent tumor in a phase II study of PPX added to standard IMRT and TMZ therapy for newly diagnosed high-grade (WHO III-IV) gliomas.

#### **MATERIALS & METHODS**

A total of 15 histologically confirmed newly diagnosed high-grade glioma patients with diffusion MR images before and after completion of PPX and who demonstrated progressive post-PPX enhancement by RANO criteria were included in the current study. Time-dependent CIMPLE maps were generated from three sequential ADC maps evaluated over time using a moving three scan window according to previously established algorithms. The largest extent of each spatially distinct contrast-enhancing lesion was contoured for CIMPLE map evaluation, and each enhancing lesion was evaluated separately to determine tumor recurrence.

## RESULTS

In enhancing lesions either histologically confirmed to be recurrent tumor or suspected to be such based on clinical or temporal imaging features, time-dependent proliferation rates appeared to be increasing and positive within the majority of the enhancing lesion. Alternatively, in lesions either histologically confirmed to be pseudoprogression or with a waxing and waning appearance, the mean proliferation rate was low or steadily decreasing over time. In a few cases, an increase in mean proliferation rate was observed prior to increases in contrast enhancement.



## CONCLUSION

Time-dependent CIMPLe map estimates of proliferation rate is a unique and potentially promising biomarker for studying PPX treatment response in individual high-grade glioma patients.

**KEY WORDS:** Glioblastoma, CIMPLe maps, diffusion MR imaging

## eP-76

### Radiation-Induced Tumors of the Brain, Neck, and Spine

Chundru, R.·Glastonbury, C.

University of California San Francisco  
San Francisco, CA

## PURPOSE

Approximately 60% of all patients with cancer will receive radiation treatment at some point in the course of their treatment. There are many acute and late expected effects and complications of radiation therapy which involve any of the tissues in the radiated field. Radiation-induced second primary tumors are a rare complication but can be difficult to detect due to posttreatment changes in the neck inhibiting clinical

examination. These iatrogenic tumors are defined by specific oncology criteria: they must occur within a prior radiation field, they must have histology different from the initial tumor and there must be a sufficient latency period between the two tumors. The purpose of our study was to evaluate the clinical and imaging characteristics of radiation-induced neoplasms including the most common histologic types, locations, and time of onset relative to treatment (latency).

## MATERIALS & METHODS

Following IRB approval a search of imaging records was performed to identify brain, head and neck scans using search keywords, "radiation-induced", "sarcoma", "secondary tumor" and "secondary malignancy" from 1993 to 2011. This resulted in 1,066 patients with 2,489 imaging examinations. The radiology reports and clinical records were reviewed to determine the presence of 72 distinct pathologically confirmed radiation-induced tumors in 66 patients which were included in the study. Subsequently, the clinical records were reviewed to determine the primary tumor, age at radiation, type and dose of radiation therapy, latency period, and location and histology of secondary tumor. The inclusion criteria for radiation-induced tumor had been designated previously by the oncologic team.

## RESULTS

The MRI and CT reports of 1,066 patients were reviewed and a total of 72 pathologically distinct radiation induced tumors in 66 patients were evaluated. The largest pathologic group was sarcomas (n=25), of which the most common tumor type was osteosarcoma (n=2). Most patient groups had been treated with radiation for retinoblastoma (n=7) followed by nasopharyngeal carcinoma (n=6). The second most common pathologic group was meningioma (n=22), of which seven patients had multiple meningiomas, and at least six meningiomas showed histologic atypia. There were eight radiation-induced glial neoplasms, and six cases followed had been radiated during childhood. Glioblastoma (n=4) was the most common histologic subtype and the temporal lobe was the most common location (n=4). Six salivary gland neoplasms were found and all occurred in the parotid. The specific tumor histology was varied, with mucoepidermoid (n=2) the most common, but five different types evident including, cystadenocarcinoma (n=1), adenocarcinoma (n=1), rhabdomyosarcoma (n=1), and spindle cell carcinoma (n=1). Eleven other tumor types in patients also were found: Mucosal squamous cell carcinoma (n=2), skin external auditory canal squamous cell (n=1), basal cell carcinoma (n=3), adenocarcinoma (n=2), schwannoma (n=1), papillary thyroid cancer (n=1) and esthesioneuroblastoma (n=1).

## CONCLUSION

It is important for the radiologist and oncologist to have a good understanding of radiation-induced neoplasms and their clinical and imaging characteristics, in order to make the earliest diagnosis, allowing the best chance of treatment success.

**KEY WORDS:** Radiation-induced neoplasm, radiation-induced sarcoma, radiation-induced meningioma



## eP-77

### Higher Gadolinium Concentration or Higher Relaxivity for Improved Morphologic Assessment of Brain Tumors? Results of a Multicenter Intraindividual Crossover Comparison of Gadobutrol and Gadobenate Dimeglumine (The MERIT Study)

Goyal, M.<sup>1</sup>·Seidl, Z.<sup>2</sup>·Vymazal, J.<sup>3</sup>·Mechl, M.<sup>4</sup>·Herman, M.<sup>5</sup>·Colosimo, C.<sup>6</sup>·Pasowicz, M.<sup>7</sup>·Yeung, R.<sup>8</sup>·Paraniak-Gieszczyk, B.<sup>9</sup>·Yemen, B.<sup>10</sup>·Anzalone, N.<sup>11</sup>·Citterio, A.<sup>12</sup>·Schneider, G.<sup>13</sup>·Bastianello, S.<sup>14</sup>·Ruscalleda, J.<sup>15</sup>

<sup>1</sup>University of Calgary, Calgary, AB, CANADA, <sup>2</sup>Lekarska Fakulta - Neurologicka Klinika, Prague, CZECH REPUBLIC, <sup>3</sup>Na Homolce Hospital, Prague, CZECH REPUBLIC, <sup>4</sup>University Hospital, Brno, CZECH REPUBLIC, <sup>5</sup>University Hospital, Olomouc, CZECH REPUBLIC, <sup>6</sup>Policlinico "Agostino Gemelli", Rome, ITALY, <sup>7</sup>John Paul II Hospital, Krakow, POLAND, <sup>8</sup>Sunnybrook Health Sciences Centre, Toronto, ON, CANADA, <sup>9</sup>NZOZ Slaskie Centrum Diagnostyki Obrazowej, Katowice, POLAND, <sup>10</sup>Hamilton Health Sciences Corporation, Hamilton, ON, CANADA, <sup>11</sup>Ospedale San Raffaele, Milan, ITALY, <sup>12</sup>Ospedale Niguarda Ca' Granda, Milan, ITALY, <sup>13</sup>University Hospital, Homburg/Saar, GERMANY, <sup>14</sup>Fondazione Istituto Neurologico Casimiro Mondino, Pavia, ITALY, <sup>15</sup>Hospital de la Santa Cruz y San Pablo, Barcelona, SPAIN

#### PURPOSE

The higher r1 relaxivity of gadobenate dimeglumine has proven advantageous compared to other gadolinium-based contrast agents for contrast-enhanced brain MRI. Gadobutrol is more highly concentrated (1.0 M) compared to other agents. This study was performed to intraindividually compare 0.1 mmol/kg doses of these agents for qualitative and quantitative assessment of brain tumors.

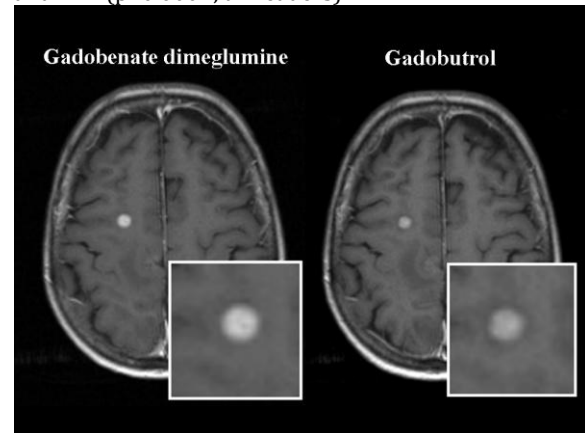
#### MATERIALS & METHODS

Adult patients with suspected or known brain tumors underwent two identical MRI exams at 1.5 T, one with gadobenate dimeglumine and the other with gadobutrol both at a dose of 0.1 mmol/kg bodyweight. The agents were injected in randomized order separated by 3-14 days. Imaging sequences and acquisition timing were identical for the two exams. Three blinded readers evaluated images qualitatively for diagnostic information (lesion extent, delineation, morphology, enhancement, global preference) and quantitatively for % lesion enhancement, contrast-to-noise ratio (CNR) and lesion-to-background ratio (LBR). Interreader agreement was assessed for all qualitative assessments.

#### RESULTS

One hundred fourteen of 123 enrolled patients successfully underwent both examinations. Final diagnoses were intra-axial tumors, metastases, extra-axial tumors, "other" tumors and "nontumor" (49, 46, 8, 7 and 4 subjects, respectively). Readers 1, 2 and 3 demonstrated preference for gadobenate dimeglumine

in 46 (40.7%), 54 (47.4%) and 49 (43.0%) patients, respectively, compared with six, seven and seven patients for gadobutrol ( $p < 0.0001$ ; all readers). Highly significant ( $p < 0.0001$ ; all readers) preference for gadobenate dimeglumine was similarly demonstrated for all other qualitative endpoints. Interreader agreement was good for all evaluations. The mean percent enhancement of lesions was highly significantly greater with gadobenate dimeglumine (reader 1:  $119.9 \pm 68.7$  vs  $97.3 \pm 58.2$ ; reader 2:  $121.6 \pm 65.9$  vs  $99.8 \pm 56.9$ ; reader 3:  $111.9 \pm 62.3$  vs  $89.7 \pm 55.9$ ;  $p < 0.0001$ ; all readers). Likewise, highly significant increases with gadobenate dimeglumine compared to gadobutrol was noted by all three readers for both CNR ( $p = 0.0186$ ,  $p < 0.0001$ ,  $p = 0.0007$ ; readers 1, 2 and 3, respectively) and LBR ( $p < 0.0001$ ; all readers).



#### CONCLUSION

High relaxivity rather than high gadolinium concentration results in significantly greater morphologic information and lesion enhancement when gadobenate dimeglumine and gadobutrol are compared at equivalent 0.1 mmol/kg doses. The results confirm expectations based on considerations of molecular structure and physicochemical properties.

**KEY WORDS:** Tumors, contrast agents, Comparative studies

## eP-78

### Advanced MR Imaging in Glioblastoma Multiforme: A Potential Approach to Determine Tumor Aggressiveness in Elderly Patients

Jabehdar Maralani, P.·Mohan, S.·Wang, S.·Voluck, M.·Melhem, E. R.

Hospital of the University of Pennsylvania  
Philadelphia, PA

#### PURPOSE

Glioblastoma multiforme (GBM) is the most common primary malignant brain neoplasm with an overall low survival rate. Age has consistently been shown as a negative prognostic factor. In particular, patients over the age of 70 have the lowest survival rate. There is recent evidence that advanced MRI correlates with cellular and molecular indices of GBM aggressiveness. In this study, we investigate advanced MRI-derived

parameters in patients 70 and over 70 (70+) and below 70 (70-) years of age with GBM. We hypothesize that aggressive GBMs in the elderly patients are associated with specific MRI indices of tumor behavior.

## MATERIALS & METHODS

After approval by institutional review board, MRIs of 20 consecutive patients referred to our institution with pathology-proven GBM aged 70 and over were compared to MRIs of 20 patients aged less than 70. Contrast-enhanced T1 images, diffusion tensor imaging (DTI) and relative cerebral blood volume (rCBV) maps were coregistered to achieve maximum mutual pixel information across images. Diffusion tensor imaging metrics including apparent diffusion coefficient (ADC), fractional anisotropy (FA), linear anisotropy coefficient (CL), planar anisotropy coefficient (CP) and CS spherical anisotropy coefficient (CS) and rCBV were measured both in the solid enhancing part of the neoplasm and in the brain parenchyma immediately adjacent to the neoplasm. The data are presented as mean  $\pm$  SD. Two-tailed unpaired t-test is used for comparison.

## RESULTS

The age of the patients in 70+ and 70- groups were  $77.2 \pm 5.6$  and  $52.8 \pm 12.9$  years, with a male to female ratio of 12/8 and 14/6, respectively. Advanced MRI data is summarized in Table 1. Mean rCBV values in solid tumor components and immediate peritumoral areas were 41% and 23 % higher in 70+ compared to 70-group ( $4.68 \pm 1.87$  vs  $3.32 \pm 1.32$ ,  $p = 0.01$  and  $2.93 \pm 0.95$  vs  $2.38 \pm 0.73$ ,  $p = 0.04$ ; respectively). Among DTI metrics, CP values were slightly, but statistically significant, lower in both tumor and peritumoral areas in 70+ compared to 70- group ( $p = 0.01$  and  $p = 0.03$ , respectively). There was also a trend towards lower ADC and FA values in the solid component of the tumor in 70+ patients which did not reach statistical significance ( $p = 0.08$  and  $p = 0.09$ , respectively).

Table 1. Advanced MRI data.

	70+ group	70- group	p value
rCBV tumor	$4.68 \pm 1.87$	$3.32 \pm 1.32$	0.01
rCBV peritumoral area	$2.93 \pm 0.95$	$2.38 \pm 0.73$	0.04
ADC tumor	$0.0011 \pm 0.0001$	$0.0012 \pm 0.0002$	0.08
FA tumor	$0.161 \pm 0.038$	$0.188 \pm 0.061$	0.09
CL tumor	$0.058 \pm 0.019$	$0.065 \pm 0.030$	0.37
CP tumor	$0.096 \pm 0.020$	$0.119 \pm 0.036$	0.01
CS tumor	$0.845 \pm 0.034$	$0.813 \pm 0.058$	0.04
ADC peritumoral area	$0.0012 \pm 0.0001$	$0.0011 \pm 0.0001$	0.98
FA peritumoral area	$0.208 \pm 0.058$	$0.230 \pm 0.069$	0.23
CL peritumoral area	$0.078 \pm 0.030$	$0.083 \pm 0.032$	0.67
CP peritumoral area	$0.120 \pm 0.034$	$0.145 \pm 0.037$	0.03
CS peritumoral area	$0.800 \pm 0.054$	$0.767 \pm 0.065$	0.08

## CONCLUSION

Both the solid components and the immediate peritumoral areas of the GBM in the 70+ patients

demonstrated significant increased perfusion, evident as higher rCBV values, compared to 70- patients. The result of the current study suggests advanced MR imaging may reflect the biologic behavior of the tumor and improve prediction of patient prognosis and therapeutic response.

**KEY WORDS:** Glioblastoma multiforme, advanced MR imaging, age

## eP-79

### Introduction into Imaging Genomic Mapping in Brain Tumors

Colen, R. R.<sup>1</sup>•Mahajan, B.<sup>1</sup>•Jolesz, F. O.<sup>1</sup>•Zinn, P. O.<sup>2</sup>

<sup>1</sup>Brigham and Women's Hospital, Boston, MA, <sup>2</sup>M.D. Anderson Cancer Center, Houston, TX

## PURPOSE

To introduce, define and detail the concept of imaging genomics and how to perform imaging genomic mapping in brain tumors, specifically glioblastoma, using large scale genomic and imaging analysis. Large scale gene- and microRNA-based cancer characterization is commonly not performed due to high cost, time and manpower required for large dataset analysis and interpretation. In order to leverage genomic data for therapy so that personalized medicine transpire, a cost-effective biomarker that accurately reflects underlying molecular cancer compositions is urgently needed. Imaging, specifically MRI is a promising biomarker to reflect underlying tumor pathology and biologic function. It follows that if imaging phenotypes of tumors obtained from routine clinical MRI studies can be associated with specific gene and microRNA expression signatures, imaging phenotypes can serve as noninvasive surrogates for tumor gene expression information and routinely provide information at a large-scale genomic level regarding the diagnosis, prognosis, and optimal treatment indicated. Thus, a new field termed imaging genomics has emerged and links specific MRI radiophenotypes with gene expression profiles.

## MATERIALS & METHODS

We identified 78 treatment-naïve GBM patients from The Cancer Genome Atlas (TCGA) who had both gene and microRNA expression profiles and pretreatment MR neuroimaging. In each patient, a total of 13,628 genes (22,267 hybridization probes) and 555 microRNAs (1,510 hybridization probes) were analyzed for significance and differential fold regulation using Comparative Marker Selection (Broad Institute, MIT, <http://www.broadinstitute.org/cancer/software/genepattern/>), Ingenuity Pathway Analysis (<http://www.ingenuity.com>), and then associated with the imaging characteristics. Image data used in this research were obtained from The Cancer Imaging Archive (<http://cancerimagingarchive.net/>) sponsored by the Cancer Imaging Program, DCTD/NCI/NIH. Using the 3D slicer software 3.6 (<http://www.slicer.org>), FLAIR was used for segmentation of the edema, and postcontrast T1-weighted imaging (T1WI) for

segmentation of enhancement (defined as tumor) and necrosis (Figure). Two neuroradiologists reviewed the images in consensus. Affymetrix level 1 mRNA and Agilent level 2 microRNA data were used for genetic analysis (<http://cancergenome.nih.gov/>). The Kaplan Meier method was used to calculate overall- and progression-free survival. Mean gene expression across GBM subgroups was calculated using ANOVA and Tukey-Kramer tests. For gene and microRNA correlations we used R square statistics.

## RESULTS

Top upregulated and downregulated genes and microRNAs not previously described in the literature were identified which had underlying concordant biologic processes of edema/invasion, necrosis, and enhancing tumor MRI phenotypes. Kaplan Meier analysis demonstrated that these resulted in significantly decreased survival ( $P=0.0008$ ) and shorter time to disease progression ( $P=0.0009$ ). In some cases, the gene expression was a stronger prognostic variable than either molecular subtype (as defined by Veerak and colleagues) in the Cox proportional hazards ratio ( $P=0.03$ ). This subsequently was confirmed in in vitro and in vivo studies.

## CONCLUSION

Imaging genomics links imaging phenotypes to underlying genotypes in GBM patients. It allows for bidirectional imaging phenotype-genotype correlations and discoveries. Imaging genomic mapping can be used to discover biologically meaningful genes that can be used for development of therapeutic targets, identify candidates which have the target gene, and help predict response and nonresponse to specific target therapies based on genomic targets and tumor genetic composition.

**KEY WORDS:** Glioblastoma, genomics, radiogenomics

## eP-80

### Correlation of Probabilistic Tractography of the Corticospinal Tract with Neurologic Weakness in Brain Tumor Patients

Qian, J.·Patel, G.·Vaisfeld, J.·Jenabi, M.·Peck, K. K.·Holodny, A. I.·Young, R. J.

Memorial Sloan-Kettering Cancer Center  
New York, NY

## PURPOSE

Diffusion tensor imaging (DTI) can be reconstructed via probabilistic tractography algorithms to provide in vivo information about white matter microstructure. The purpose of this study is to evaluate the correlation of probabilistic tractography to clinical motor deficits in patients with brain tumors near the corticospinal tract.

## MATERIALS & METHODS

We retrospectively queried the institutional PACS to find patients who had DTI from 2010 to 2011. From an initial cohort of 98 patients, we excluded patients without tumor ( $n=16$ ), whose tumor and/or edema did

not directly involve the corticospinal tract ( $n=47$ ), or had incomplete clinical follow up ( $n=3$ ). The interim study cohort consisted of 21 patients with a median age of 57 years (range, 4-66). All patients had unilateral primary ( $n=17$ ) or metastatic ( $n=4$ ) tumors. Diffusion tensor imaging was acquired using a single shot spin-echo echo-planar-imaging sequence with 15-25 noncollinear directions with GE 3 T scanner. Probabilistic tractography of the corticospinal tract was performed using DTI and FiberTools (University Hospital, Freiburg, Germany) implemented in Matlab (Mathworks, Natick, MA). The morphology of each hemispheric corticospinal tract was graded visually as normal, displaced, reduced, or displaced and reduced. Connected voxel volumes were measured by calculating the nonzero voxels in each hemisphere, and voxel ratios were obtained by dividing the voxel volume of the tumor side tract with that of the normal contralateral tract. The voxel ratio analysis was correlated with clinical deficits ascertained through chart review.

## RESULTS

Of the 11 patients with hand and/or foot motor weakness, nine (81.8%) patients showed reduced corticospinal tract volumes. Grading the tract morphology as displaced, reduced, or displaced and reduced correctly correlated with the side of weakness in 33%, 75% and 80% of patients, respectively. Voxel ratio analysis showed that the voxel ratio ranges of 60-70%, 70-80%, 80-90% and 90-100% (when comparing tumor vs normal tracts) were correlated with motor weakness in 100%, 75%, 44% and 29% of patients. Of the remaining 10 patients without motor weakness, a normal corticospinal tract correctly indicated no motor symptoms in 83%.

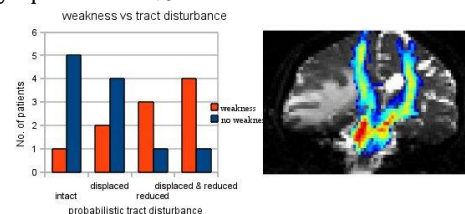


**Figure.** Table (left) shows the number of patients with motor weakness and corresponding tract disturbances. Probabilistic tractography of the corticospinal tract overlaid on a coronal B0 DTI image (right) shows a right hemispheric tumor and edema causing medial displacement of the right corticospinal tract.

## CONCLUSION

Probabilistic tractography appears to correlate well with motor weakness in patients with tumors near the corticospinal tract. More work is necessary to precisely localize and correlate the tractography abnormalities with clinical signs and symptoms, to validate the tractography results with intraoperative stimulation, and to determine the potential role in treatment planning.

**KEY WORDS:** DTI probabilistic tractography, corticospinal tract, brain tumor

## eP-81

### Evaluation of P-Glycoprotein Inhibition in Glioma and Implications for Treatment: A Combined Positron Emission Tomography and MR Imaging Study

Thompson, G.<sup>1</sup>Feldmann, M.<sup>2</sup>Pathmanaban, O.<sup>3</sup>Wang, S.<sup>1</sup>McMahon, A.<sup>1</sup>Koepp, M.<sup>2</sup>Asselin, M.<sup>1</sup>Jackson, A.<sup>1</sup>

<sup>1</sup>University of Manchester, Manchester, UNITED KINGDOM, <sup>2</sup>University College London, London, UNITED KINGDOM, <sup>3</sup>Salford Royal Foundation Trust, Salford, UNITED KINGDOM

#### PURPOSE

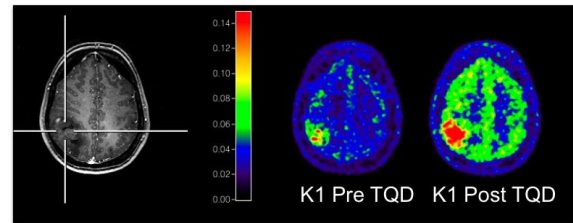
High-grade gliomas (HGG) are characterized by treatment resistance. P-glycoprotein (P-gp) is the product of multidrug resistance 1 gene (MDR1) and is present on luminal neuroendothelium, acting as an efflux pump and integral part of the blood-brain barrier. P-gp is also present on glioma cells and is overexpressed in tumor stem cells. Treatment of HGG is guided currently by contrast-enhanced MRI. At diagnosis, microinvasive tumor deposits exist beyond the enhancing regions and, in addition to residual macroscopic disease, these are thought to be largely responsible for treatment resistance. By increasing chemotherapy uptake into solid tumor, tumor periphery and infiltrated but normal-appearing brain tissue, P-gp blockade may increase chemotherapeutic efficacy. It may also target chemotherapy drugs to tumor and tumor stem cells. Tariquidar (TQD) is a potent third generation noncompetitive inhibitor of P-gp, which had been shown to reduce intrinsic and acquired resistance in a variety of solid tumors, and increase target delivery to privileged sites.

#### MATERIALS & METHODS

Four patients with suspected HGG underwent dynamic PET imaging with [<sup>15</sup>O]H<sub>2</sub>O followed by the P-gp substrate (R)-[<sup>11</sup>C]Verapamil before and after administration of 2 mg/kg of the P-gp inhibitor tariquidar. Parametric maps of perfusion, transport rate constant (K<sub>1</sub>) of (R)-[<sup>11</sup>C]Verapamil from plasma to brain (influx), and extraction fraction (EF) were derived for each patient. Tumors were segmented manually using a combination of contrast-enhanced and FLAIR MR imaging, and remaining normal-appearing tissue segmented automatically using FAST. Targeted biopsies were taken in each region of interest to confirm grade and for correlations with immunohistochemical data.

#### RESULTS

TQD increased the K<sub>1</sub>, and EF of the labelled P-gp substrate in: NAWM (n=3, p<0.0001), gray matter (n=3, p<0.0001), peri-enhancing FLAIR abnormality (n=2, p<0.0001), enhancing high-grade glioma (n=3, p<0.0001), and low-grade glioma (n=2, p<0.0001). There was no significant increase in perfusion attributable to the TQD. The figure shows an example of the change in K<sub>1</sub> following TQD in a transforming LGG.



#### CONCLUSION

These preliminary data suggest that tariquidar inhibits P-gp in vivo and differentially increases the uptake of P-gp substrates into WM, GM, peritumoral FLAIR abnormality and low- and high-grade regions of glioma. This is a promising indicator of potential utility as an adjuvant chemotherapy in primary or secondary HGG, and also may promote synergy with concomitant radiotherapy. Further work is ongoing, including correlation of imaging and biopsy findings, and investigation of the underlying mechanisms and effect on temozolomide using an animal model of glioma.

**KEY WORDS:** Glioma, P-gp, tariquidar

## eP-82

### Functional Perfusion Maps Derived from Serial Dynamic Susceptibility Contrast-MR Imaging Estimates of Relative Cerebral Blood Volume Can Differentiate Pseudoprogression and Quiescent Tumor from Progressive Disease in Malignant Glioma Patients Treated with Paclitaxel Poliglumex

Ellingson, B. M.<sup>1</sup>Boxerman, J. L.<sup>2</sup>Jeyapalan, S.<sup>2</sup>Elinzano, H. D.<sup>2</sup>Goldman, M.<sup>2</sup>Dipetrillo, T.<sup>2</sup>Safran, H.<sup>2</sup>Pope, W. B.<sup>1</sup>

<sup>1</sup>David Geffen School of Medicine at the University of California Los Angeles, Los Angeles, CA, <sup>2</sup>Brown University and Rhode Island Hospital, Providence, RI

#### PURPOSE

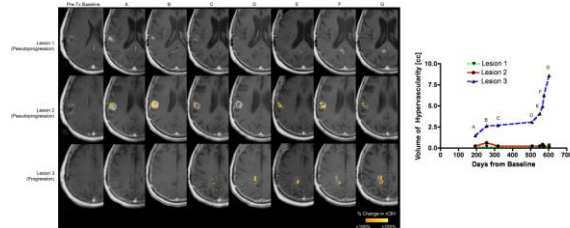
Paclitaxel poliglumex (PPX; Cell Therapeutics, Inc., Seattle, WA) is a microtubule stabilizer and mitotic inhibitor recently proposed as a novel radiosensitizing agent for patients with high-grade gliomas undergoing radiation therapy. The purpose of PPX treatment is increase acute cytotoxicity and effectiveness of radiotherapy; however, initial observations of PPX-treated gliomas illustrated substantial transient increases in the degree and number of contrast-enhancing lesions. Many of these lesions were later found to be quiescent tumor or due to treatment-related changes in the tumor mimicking progressive disease (i.e., pseudoprogression). Since growing tumor is thought to exhibit increased vascular proliferation resulting in higher relative cerebral blood volume (rCBV) compared with pseudoprogression, we hypothesized a voxel-wise temporal analysis rCBV, termed functional perfusion mapping (fPMs), may be useful for separating pseudoprogressive lesions from true progression.

## MATERIALS & METHODS

Ten histologically confirmed high-grade glioma patients with perfusion MR images before and at least four time points during initiation of PPX and who demonstrated progressive post-PPX enhancement by RANO criteria were included in the current study. A total of 16 lesions were identified from these 10 patients during their treatment. Of these 16 lesions, seven were identified as progressive tumor and nine lesions were determined to be pseudoprogression, based on histologic validation from biopsy samples or radiographic characteristics over time. Relative CBV maps calculated from dynamic susceptibility contrast (DSC) MRI scans acquired posttreatment were coregistered with pretreatment rCBV maps, and all images were aligned to standard MNI atlas space. Voxel-wise subtraction was performed between baseline and follow-up rCBV maps. Voxels with an increase in rCBV greater than 100% with respect to baseline (pretreatment) CBV maps were labeled and the volume of tissue with an increase in rCBV greater than 100% (hypervascular volume) was quantified for each follow-up time point.

## RESULTS

In tumors with quiescent tumor or pseudoprogression, fPM temporal trends showed a stable or decreasing volume of hypervascularity with increasing volume of contrast enhancement. In lesions with a stable volume of contrast enhancement over time, the volume of hypervascularity also remained stable from baseline. Increasing temporal trends in the volume of hypervascularity were suggestive of recurrent tumor. FPMs had a 57% sensitivity, 89% specificity, 80% positive predictive value, and 73% negative predictive value for delineating pseudoprogression from recurrent tumor.



## CONCLUSION

Temporal changes in the volume of hypervascularity estimated from fPMs have a high specificity for delineating pseudoprogression from recurrent tumor in malignant glioma patients treated with PPX.

**KEY WORDS:** Perfusion MR imaging, PPX, glioblastoma

## eP-83

### Reincreased Perfusion of Recurrent Glioblastomas under Bevacizumab Treatment

Liu, X.<sup>1</sup>Tian, W.<sup>1</sup>Hussain, A.<sup>1</sup>Ekholm, S.

University of Rochester School of Medicine & Dentistry  
Rochester, NY

## PURPOSE

Bevacizumab is the humanized monoclonal antibody that blocks vascular endothelial growth factor (VEGF) and inhibits angiogenesis. Previous studies reported decreased relative cerebral blood volume (rCBV) of glioblastomas treated by Bevacizumab. The purpose of this study was to evaluate whether there was increased perfusion in recurrent glioblastomas under Bevacizumab treatment.

## MATERIALS & METHODS

Fourteen cases with recurrent glioblastomas under Bevacizumab treatment were reviewed. Serial dynamic susceptibility-weighted contrast-enhanced MR perfusion imaging (DSC PWI) examinations were performed after Bevacizumab treatment. The maximal rCBV ratios in the examinations when the glioblastomas showed minimal enhancement after Bevacizumab treatment were enrolled as reference, the continuing increase of enhancing lesions (>25%) over a minimum 4 months was defined as recurrence/progression. The differences of maximal rCBV ratio between reference and recurrent glioblastomas were evaluated with paired t test.

## RESULTS

The mean maximal rCBV ratio of reference glioblastomas after Bevacizumab treatment was  $1.65 \pm 0.52$ ; the mean maximal rCBV ratio of recurrent glioblastomas was significantly higher,  $6.11 \pm 4.58$ . The *p* value of paired t test was 0.013 (t value of 3.166),

## CONCLUSION

Our preliminary results show that recurrent glioblastomas under Bevacizumab treatment with reincreased perfusion, suggests new angiogenesis and represent early feature of tumor recurrence.

**KEY WORDS:** Perfusion-weighted imaging, glioblastoma, Bevacizumab

## eP-84

### Quantitative Magnetization Transfer in Brain Tumors

Thompson, G.<sup>1</sup>Zhao, S.<sup>1</sup>Soh, C.<sup>2</sup>Mills, S. J.<sup>2</sup>Parker, G. J. M.<sup>1</sup>Jackson, A.<sup>1</sup>

<sup>1</sup>University of Manchester, Manchester, UNITED KINGDOM, <sup>2</sup>Salford Royal Foundation Trust, Salford, UNITED KINGDOM

## PURPOSE

The bound pool fraction (f) from quantitative magnetization transfer imaging has been shown to relate to myelin content in animal models. Since gliomas preferentially arise in and affect white matter tracts, f was hypothesized to aid detection of disease and white matter involvement in primary brain tumors through invasive disruption of white matter integrity. Furthermore, the effect of differing microstructural features across histologic glioma subtypes may be reflected in different ranges of f, which is known to be affected by other macromolecular constituents,



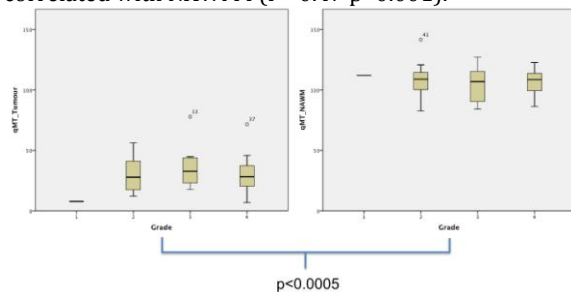
particularly in solid tumors which do not contain myelinated tissue.

#### MATERIALS & METHODS

Forty-seven patients with histologically proven glioma underwent routine preoperative tumor imaging at 3 T in addition to qMT imaging according to the method of Cercignani et al. The following WHO grades of lesions were identified I=1, II=16, III=8, IV=22. Age was 24-73 years (mean 51). Within oligo grade II, six were 1p/19q deleted and three not. Regions of interest were placed on regions of solid tumor (ST) and normal-appearing white matter (NAWM) and in the high-grade gliomas (HGG) within peritumoral FLAIR abnormality (PA), which is known to represent a combination of edema and microinvasive disease.

#### RESULTS

There was no significant difference between the mean  $f$  values for ST across grades, nor between deleted and nondeleted grade II. There were significant differences between ST, PA and NAWM ( $p < 0.0005$ ). The figure shows the comparison of qMT  $f$  ( $\times 10$ ) in ST and NAWM in different grades. Age was significantly negatively correlated with NAWM  $f$  ( $r = -0.47$   $p = 0.001$ ).



#### CONCLUSION

This is the largest group of glioma patients to be assessed with qMT to date. Bound pool fraction from qMT is sensitive for tumor presence in white matter but not specific for grade. Within oligoendroglial tumors, it is not able to distinguish 1p/19q deletion. In invasive HGG, there is a significant difference between solid tumor, peripheral FLAIR abnormality and NAWM. It is related inversely to age in NAWM in keeping with pathophysiologic models of aging, and reflecting the sensitivity of the technique for detecting WM change. Fraction provides a quantitative measure which distinguishes solid tumor from peripheral edema or FLAIR hyperintensity and NAWM, and may prove useful for treatment planning and disease follow up in glioma. This includes automatic segmentation of LGG from brain, and detection of early peripheral WM change.

**KEY WORDS:** qMT, glioma

#### eP-85

#### Prediction of Recurrence and Progression-Free Survival in Patients with Glioblastoma Multiforme: The Role of MR Perfusion Monitoring during Radiation-Temozolomide Therapy

Bisdas, S.<sup>1</sup>•Surlan-Popovic, K.<sup>2</sup>

<sup>1</sup>Eberhard Karls University, Tuebingen, GERMANY,

<sup>2</sup>University Hospital of Ljubljana, Ljubljana, SLOVENIA

#### PURPOSE

To evaluate the early perfusion parameter changes in patients with glioblastoma multiforme during the concomitant radiation and temozolomide therapy (RT TMZ) and examine the predictive value of such changes for progression-free survival (PFS) and overall survival (OS).

#### MATERIALS & METHODS

Institutional review board approval was obtained, and HIPAA guidelines were followed. Sixteen consecutive patients with primary glioblastoma multiforme underwent prospectively dynamic contrast-enhanced T1-weighted MR imaging in a 3T scanner before therapy initiation, after completion of 30Gy, and after completion of 60Gy RT, while they were concomitantly treated with TMZ. The pharmacokinetic modelling was based on a two-compartment model that allowed for the calculation of Ktrans (transfer constant between intra and extravascular, extracellular space), Ve (extravascular, extracellular space), and iAUC (initial area under the signal intensity-time curve). Regions of interest (ROIs) were drawn around the entire contrast-enhanced tumor region. Linear regression analysis was performed to correlate changes in tumor size (based on Macdonald criteria), Karnofsky performance score and perfusion parameters with PFS and OS. ROC curves were used to examine the sensitivity and specificity of the MR-perfusion values for outcome prediction, whereas log-rank testing was used to assess the survival rates.

#### RESULTS

The median clinical follow-up of the patients was 2 years. Initial reduction ( $\geq 42\%$ , sensitivity: 95%, specificity: 88%,  $P = 0.002$ ) in Ktrans and iAUC values after 30Gy of RT TMZ therapy, followed by further reduction at the end of the RT TMZ therapy was a significant predictor of longer PFS. Patients with reduction of the baseline Ktrans and iAUC values more than 64% and 40%, respectively at the end of therapy experienced no recurrence after 2 years. The patients with longer PFS had an initial decrease of Ve values after 30Gy RT TMZ, followed by an increase at the end of therapy ( $P = 0.001$ ). Patients with increase of the Ve values after 30Gy experienced recurrence during the first year ( $P = 0.001$ ). The ROC curves for recurrence and 1-year survival showed a greater area under the curve with perfusion parameter changes than with tumor size ( $0.002 \leq P \leq 0.01$ ). A combination of Ktrans and Ve changes showed the best sensitivity (98%) for predicting recurrence and shorter PFS. The perfusion changes during the therapy showed a tendency to correlate with the OS ( $P = 0.07$ ). When combined with the Karnofsky performance score and the tumor size (based on Macdonald criteria), the iAUC change at the end of RT TMZ therapy was predictive for shorter OS ( $P = 0.02$ ).

#### CONCLUSION



These preliminary findings suggest the potential value of early monitoring of MR-perfusion biomarkers (Ktrans, Ve, and iAUC) during the course of RT TMZ therapy as a measure of treatment response and recurrence prediction in patients with glioblastoma multiforme.

**KEY WORDS:** Glioblastoma, MR perfusion, radiation therapy

#### eP-86

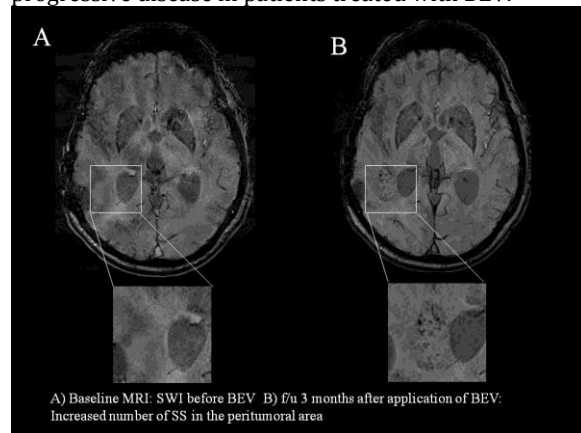
### Susceptibility-Weighted Imaging Predicts Progressive Disease in Patients with Recurrent Glioblastoma Treated with Bevacizumab

Radbruch, A.·Kramp, L.·Wiestler, B.·Bäumer, P.·Heiland, S.·Wick, W.·Bendszus, M.

University of Heidelberg  
Heidelberg, GERMANY

#### PURPOSE

Antiangiogenic treatment with the vascular endothelial growth factor-directed antibody Bevacizumab(BEV) is used increasingly in the therapy of recurrent glioblastoma. Assessing response to BEV treatment is nonetheless challenging as permeability of the blood-brain barrier(and hence contrast agent uptake) is reduced through BEV. It is reported, however, that BEV may induce T2 progress by co-opting existing blood vessels, resulting in increased invasiveness of the tumor. This event precedes recurrent contrast enhancement. Susceptibility-weighted imaging(SWI) is a new imaging technique that has been shown to be a useful tool in the differential diagnosis of enhancing brain lesions due to the assessment of dotlike hypointensities, so termed susceptibility signals(Figure 1). Here, we analyzed if the increase of SS in the peritumoral area of glioblastoma may predict progressive disease in patients treated with BEV.



#### MATERIALS & METHODS

Thirty patients with histologically proven recurrent glioblastoma were examined at 3 T using with SWI(TR:26, TE:19,2, flipangle:15°). All patients received a baseline MRI prior to the first application of BEV followed by three monthly f/u MRIs. All patients presented T1 progress in one of the subsequent f/u. Two neuroradiologists assessed independently if and in

which f/u the number of SS in the peritumoral area increased.

#### RESULTS

Twenty-seven of 30 patients showed an increasing number of SS within the peritumoral area. Sixteen patients presented an increasing number of SS when T1 progress was diagnosed. In 11 patients an increasing number of SS was diagnosed in the precedent f/u before T1 progress was diagnosed. Of those 11 patients five presented T2 progress in the f/u when the number of SS increased. Three patients did not show any increase in the number of SS at all.

#### CONCLUSION

Our study shows that an increasing number of SS predicts the upcoming T1 progress in patients that are treated with BEV. However the source of the SS is not fully understood yet. One hypothesis is that migrating tumor cells in the invasion front cause microbleeds. In case of standard radiochemotherapy these microbleeds may be accompanied by a vascular reach and leaky tumor boarder, causing contrast-enhancing T1 progress. This T1-progress may not be present in case of BEV therapy due to its antiangiogenic effect. Ultimately the fact that T2-progress was regularly accompanied by SS increase may be caused by the same phenomenon: BEV may suppress blood-brain barrier disruption but may not avoid infiltrative tumor progress causing T2-progress as well as SS in the peritumoral area.

**KEY WORDS:** Glioblastoma, Bevacizumab, susceptibility-weighted imaging

#### eP-87

### Atypical MR Imaging Findings of Intracranial Epidermoid Cyst

Lee, H.·Al-Khalili, R.

New Jersey Medical School  
Newark, NJ

#### PURPOSE

Intracranial epidermoid cysts are estimated to constitute 0.2 to 1.8% of all intracranial tumors. It is most commonly paramedian in location. On CT scans, most epidermoid cysts are well defined hypoattenuated masses that resemble CSF and do not enhance with contrast. Calcification is present in 10-25% of cases. Most epidermoid cysts are isointense or slightly hyperintense to CSF on both T1- and T2-weighted MR images. They do not suppress completely on FLAIR images and typically restrict water (high signal intensity) on diffusion-weighted images (DWI). We present two rare cases of a suprasellar epidermoid cyst with high T1-weighted signal intensity and no water restriction on DWI. To our knowledge, these atypical presentations have not been reported in the literature.

#### MATERIALS & METHODS

The first case is a 68-year-old woman who presented with symptoms of pituitary dysfunction with cold

intolerance. The second case is a 38-year-old woman who initially presented with symptoms of stroke-like symptoms. MR imaging of both patients demonstrated a suprasellar mass causing mass effect on the optic nerves and optic chiasm. The mass showed high T1-weighted and low T2-weighted signal intensity and no water restriction on DWI. There was no postcontrast enhancement. The differential diagnosis of this suprasellar mass included craniopharyngioma and Rathke's cleft cyst. Pituitary adenoma and epidermoid cyst were less likely.

## RESULTS

Both patients underwent transphenoidal resection of the mass. Upon removal of the cyst, contents appeared to be more reminiscent of keratin which suggested epidermoid cyst. Squamous epithelial lining was discovered on pathologic evaluation containing macrophages, foam cells, cholesterol clefts and foreign body giant cell reaction. The basaloid appearance of the adamantinomatous variant of craniopharyngioma was not seen, nor was the papillary features that would indicate the presence of a papillary variant of craniopharyngioma. The final pathologic diagnosis was epidermoid cyst. Discussion: Epidermoid cysts arise from ectodermal inclusion during neural tube closure in the 3rd-5th week of embryogenesis. Epithelial cell rests may be transplanted to regions such as the cerebellopontine angle by the laterally migrating otic capsule or developing neurovasculature. It is atypical for the epidermoid cyst to grow along the midline. The cyst interior is filled with "unpleasant" soft, waxy, or flaky keratohyalin material that results from the progressive desquamation of the cyst wall. Cystic contents usually include debris, keratin, water, and cholesterol laid down in a lamellar fashion. The major differential consideration for the epidermoid cyst is an arachnoid cyst. On CT, epidermoid cyst resembles arachnoid cyst which has CSF density. On MRI, the epidermoid cyst presents as high signal intensity on both Flair sequence and DWI in contrast to the arachnoid cyst that shows low signal intensity.

## CONCLUSION

An epidermoid cyst in the suprasellar region with high T1 signal intensity and no water restriction is a very rare case. The high T1-weighted signal intensity is secondary to the contents of cholesterol clefts. The location and signal characters on MRI findings as seen in our cases are atypical for epidermoid cyst.

**KEY WORDS:** Epidermoid cyst, suprasellar mass

## eP-88

### Interobserver and Intraobserver Agreement of Relative Cerebral Blood Volume Values in Glial Tumor Using Different Proprietary Software Analysis Tool

Fallatah, S. M.<sup>1</sup>Krishnan, A.<sup>1</sup>Brisson, M.<sup>1</sup>Adams, M.<sup>1</sup>Golay, X.<sup>2</sup>Jäger, H.<sup>1</sup>

<sup>1</sup>National Hospital for Neurology and Neurosurgery, London, UNITED KINGDOM, <sup>2</sup>UCL Institute of Neurology, London, UNITED KINGDOM

## PURPOSE

The aim of this study was to assess interobserver and intraobserver reliability and reproducibility of relative cerebral blood volume (rCBV) measurements in patients with glial brain tumors. For proper implementation of rCBV measurements in the clinical management of brain tumors the technique should fulfil the following criteria: firstly, it should reliably identify the areas of high rCBV value; secondly it should be reproducible, independent of manufacturer; thirdly the degree of inter and intraobserver errors should be known to enable critical interpretation; finally it should be time efficient.

## MATERIALS & METHODS

Dynamic susceptibility contrast (DSC) MR perfusion images of 14 histologically confirmed glial brain tumors (six glioblastoma multiforme, three astrocytoma grade II, two astrocytoma grade III and three oligodendroglioma grade II) were analyzed by two independent operators blinded to the histopathologic diagnosis. Measurements of rCBV were performed using a previously described validated method choosing the means of the higher rCBV value of several intratumoral regions of interest (ROIs) and ROIs in the contralateral white matter for normalization. The observers used three different commercial perfusion analysis software packages (including two from MRI equipment manufacturers). Patients were classified into two groups: group A, rCBV <1.7 and group B, rCBV ≥1.7. Calculations of the intraclass correlation coefficient, Pearson's correlation coefficients and Bland Altman analysis were used to determine the levels of agreement. The data obtained were compared also to rCBV values mentioned in the clinical reports.

## RESULTS

The interobserver agreement appears substantial with intraclass correlation coefficient (ICC) of 0.74. The intraobserver agreement was good (ICC was 0.59). Both observers showed almost perfect agreement in grouping patients as A and B. The variations between observers are correlated with increasing rCBV values.

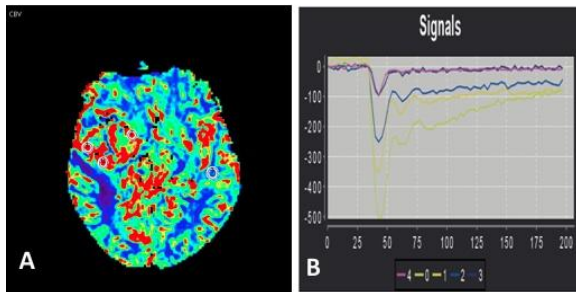


Figure: A, rCBV map shows several intratumoral ROIs placed over areas of high rCBV and one ROI in contralateral white matter. Signal-intensity curve, B represents different ROIs.

#### CONCLUSION

There were some differences in the rCBV values obtained from the three perfusion analysis softwares with an increasing divergence for high rCBV values. Distinction between tumors with low (1.7) rCBVs showed very good agreement however between all observers and types of analysis software.

**KEY WORDS:** Relative cerebral blood volume, interobserver agreement, glioma

#### eP-89

##### **Differentiation between Noncontrast-Enhancing Tumor Areas and Perifocal Edema in Glioblastoma Using Diffusion Tensor Imaging**

Janssen, H.·Schneider, D.·Lutz, J.·Kreth, F.·Schnell, O.·Linn, J.

University Hospital Munich  
Munich, GERMANY

#### PURPOSE

Differentiating the noncontrast-enhancing parts of high-grade glioma from perifocal edema can be challenging in conventional MR sequences. This impedes delineation of the exact tumor borders. The aim of this study was to investigate whether diffusion tensor imaging could be a supporting parameter.

#### MATERIALS & METHODS

Forty untreated patients with histologically proven glioblastoma were examined prospectively at a 3 T clinical MRI scanner (Signa HDx, GE Healthcare). The sequence protocol included T2-weighted and FLAIR images, a 3D-fast-spoiled-gradient-echo (FSPGR) sequence before and after contrast media application and an EPI diffusion tensor sequence with 10 directions of gradient sampling ( $b = 1000$ ). Fractional anisotropy (FA) was measured in five regions of interest (ROIs), within the contrast-enhancing part of the tumor (ROI 1), directly adjacent to the enhancement within the nonenhancing tumor region, in the T2 hyperintense white matter (assumed perifocal edema, ROI 3), within the normal-appearing ipsilateral white matter (ROI 4), and in the contralateral white matter (ROI 5).

#### RESULTS

There were significant differences between the FA values of enhancing and nonenhancing tumor regions (mean value ROI 1 =  $0.198 \pm 0.05$ ; mean value ROI 2 =  $0.238 \pm 0.066$ ;  $p < 0.01$ ), between nonenhancing tumor regions and perifocal edema (mean value ROI 3 =  $0.205 \pm 0.078$ ;  $p < 0.05$ ), and between perifocal edema and normal-appearing white matter (ROI 4 =  $0.386 \pm 0.078$ ;  $p < 0.01$ ). There were no significant differences of FA values between ROI 4 and ROI 5 ( $p < 0.31$ ).

#### CONCLUSION

Our results show that FA measurements are helpful to differentiate noncontrast-enhancing tumor regions from perifocal edema in high-grade gliomas. Therefore the identification of tumor borders may be more precise using this technique compared to conventional MRI.

**KEY WORDS:** Glioblastoma, fractional anisotropy

#### eP-90

##### **Differentiation between Primary Central Nervous System Lymphoma and Glioblastoma: Which Indices from Perfusion MR or Positron Emission Tomography Images Yield Optimal Diagnostic Values?**

Kitajima, M.<sup>1</sup>·Hirai, T.<sup>1</sup>·Nakamura, H.<sup>1</sup>·Makino, K.<sup>1</sup>·Uetani, H.<sup>1</sup>·Iwashita, K.<sup>1</sup>·Shigematsu, Y.<sup>1</sup>·Nishimura, S.<sup>1</sup>·Nakashima, R.<sup>2</sup>·Shiraishi, S.<sup>1</sup>·Kuratsu, J.<sup>1</sup>·Yamashita, Y.<sup>1</sup>

<sup>1</sup>Kumamoto University, Kumamoto, JAPAN, <sup>2</sup>Japanese Red Cross Kumamoto Health Care Center, Kumamoto, JAPAN

#### PURPOSE

The incidence of primary central nervous system lymphoma (PCNSL) has increased in the last decades. Typical features of PCNSL on advanced magnetic resonance (MR) or positron emission tomography (PET) images have been reported; however, it is sometimes difficult to distinguish between PCNSL and glioblastoma multiforme (GBM). Furthermore, it has not been evaluated which are the most useful findings for differentiation between PCNSL and GBM on perfusion MR and PET imaging studies. Our aim of this study was to evaluate which quantitative indices derived from perfusion MR or PET imaging yield the best diagnostic value for differentiating between PCNSL and GBM.

#### MATERIALS & METHODS

As part of a clinical audit, we retrospectively evaluated 3 T MRI data from conventional MRI, dynamic susceptibility contrast perfusion MR, and <sup>18</sup>F-fluorodeoxyglucose (FDG) and <sup>11</sup>C-methionine (MET) PET imaging studies performed on 23 immunocompetent patients with surgically proven PCNSL ( $n = 11$ ) or GBM ( $n = 12$ ). Indices characterizing solid areas of the largest lesions were determined; they included the ratio of the lesional maximum relative cerebral blood volume (rCBV) to the contralateral normal-appearing white matter (max rCBV ratio) and the ratio of the maximum standardized uptake values

(SUVmax) of the lesion to the uptake in the contralateral normal-appearing gray matter (L/Nmax) on FDG and MET PET images. These indices were compared in the two groups using an independent t-test. Receiver operating characteristic (ROC) curves and the area under the curve (AUC) were calculated to evaluate diagnostic performance; we also performed pairwise comparison of the ROC curves.

## RESULTS

The max rCBV ratio was higher in GBM than PCNSL ( $5.63 \pm 3.42$  vs  $1.34 \pm 1.09$ ;  $p < 0.0007$ ). The L/Nmax on FDG PET was lower in GBM than PCNSL ( $1.11 \pm 0.48$  vs  $2.08 \pm 0.70$ ;  $p < 0.0008$ ). There was no significant intergroup difference in MET PET. In ROC analysis, the best diagnostic performance was obtained for the max rCBV ratio (sensitivity 90.9%; specificity 91.7%; AUC 0.947; cut-off 2.07) followed by the L/Nmax on FDG PET (sensitivity 81.8%; specificity 83.3%; AUC 0.879; cut-off 1.67). Pairwise comparison of the two ROC curves revealed no significant differences.

## CONCLUSION

The max rCBV ratio tends to yield the best diagnostic performance for differentiating between PCNSL and GBM, although there were no significant differences among the three indices derived from perfusion MRI and PET.

**KEY WORDS:** MR imaging, positron emission tomography, primary central nervous system lymphoma

## eP-91

### FLAIR Volume Distinguishes True Progression from Pseudoprogression Regardless of Radiation Treatment Effects in Glioblastoma

Jones, J. G. A.·Shiroishi, M.·Mandelin, P.·Singh, M.·Law, M.  
University of Southern California  
Los Angeles, CA

## PURPOSE

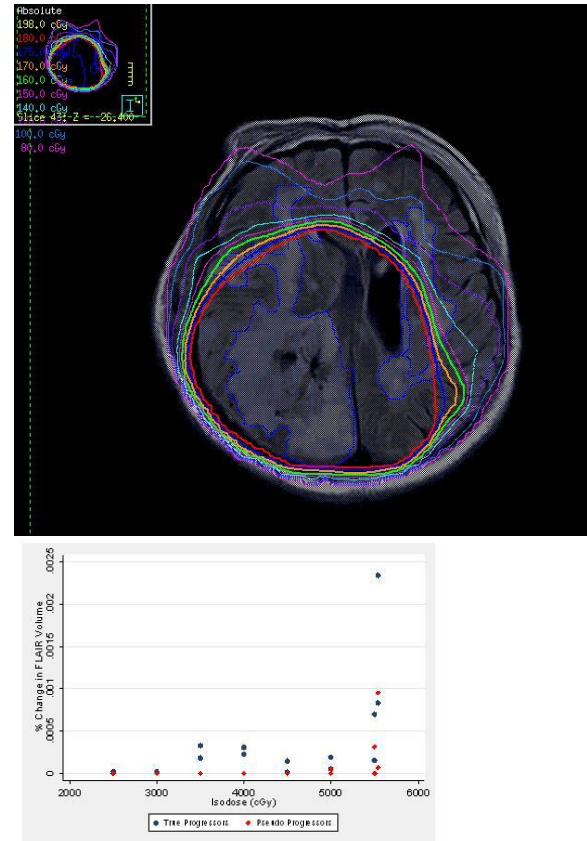
To determine whether T2 FLAIR signal on conventional MRI can differentiate true tumor progression (TP) from pseudoprogression (PsP) in glioblastoma patients treated with radiation and temozolomide.

## MATERIALS & METHODS

Ten patients who developed worsening contrast enhancement within 6 months of completing chemoradiation were followed with serial MRI exams. Based on subsequent radiographic progression, or lack thereof, subjects were divided into TP (N = 7) and PsP (N = 3) cohorts. Radiation dose plans were overlaid onto T2 FLAIR MR images from the initial scan of concern and from radiographic follow up. The volume of T2 hyperintensity was outlined manually and then computed on a workstation. The percent change in FLAIR volume between initial and follow-up scans also was calculated.

## RESULTS

The percent increase in FLAIR volume was significantly greater in TP than PsP, regardless of radiation dose ( $p = 0.005$ ). Most FLAIR change occurred adjacent to the initial tumor site, consistent with known patterns of recurrence.



## CONCLUSION

Radiation-induced T2 signal does not prevent accurate determination of tumor progression using volumetric assessment of FLAIR changes in glioblastoma patients.

**KEY WORDS:** Pseudoprogression, T2 signal intensity, radiation effects

## eP-92

### Is Contrast-Enhanced 3D FLAIR Imaging Useful for Differentiating Rathke's Cleft Cyst from Cystic Craniopharyngioma?

Hirai, T.·Yano, S.·Kitajima, M.·Shigematsu, Y.·Uetani, H.·Yamashita, Y.

Graduate School of Medical Sciences Kumamoto University  
Kumamoto, JAPAN

## PURPOSE

It can be difficult to discriminate between Rathke's cleft cyst (RCC) and cystic craniopharyngioma by conventional MRI alone. The purpose of this study was to assess whether enhancement of the wall of RCC and of cystic craniopharyngioma is different at contrast-

enhanced 3D T2 fluid-attenuated inversion-recovery (3D T2-FLAIR) imaging at 3 T.

#### MATERIALS & METHODS

We prospectively evaluated pre and postcontrast T1-weighted and 3D T2-FLAIR images of 17 surgically confirmed patients (10 RCC and 7 cystic craniopharyngioma patients). All patients underwent the MR studies on a 3 T unit prior to surgery. In the two patient groups, two neuroradiologists independently recorded contrast enhancement of the cystic wall as involving most of the wall (grade 3), a portion of the wall (grade 2), and no enhancement (grade 1). Final judgments of the two observers were performed by consensus. Differences in the mean grade between the two groups were analyzed with the Mann-Whitney test. Interobserver agreement was determined by calculating the  $\kappa$  coefficient.

#### RESULTS

On postcontrast T1-weighted images all RCCs and craniopharyngiomas were classified as grade 2 or 3 (interobserver agreement,  $\kappa = 0.824$ ); the difference between the two patient groups was not significant. On postcontrast 3D T2-FLAIR images, nine RCCs were grade 1, the other was grade 2; five craniopharyngiomas were grade 3, two were grade 2 ( $\kappa = 0.867$ ). The difference between the two groups was significant ( $p = 0.0011$ ).

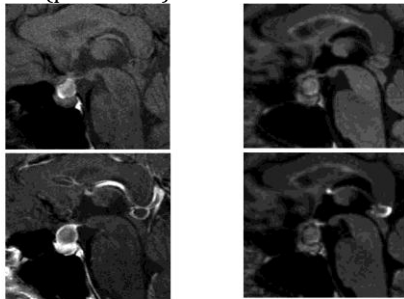


Figure 1. A 40-year-old woman with Rathke's cleft cyst. Postcontrast T1WI (lower left) shows contrast enhancement of the entire wall (grade 3) compared with precontrast T1WI (upper left). Postcontrast 3D FLAIR (lower right) reveals no definite enhancement of the cystic wall (grade 1) compared with precontrast 3D FLAIR (upper right).

#### CONCLUSION

On contrast-enhanced 3D T2-FLAIR images, enhancement of the wall of RCCs and cystic craniopharyngiomas was significantly different. Contrast-enhanced 3D T2-FLAIR images are useful for differentiating the two types of cystic lesion.

**KEY WORDS:** 3D FLAIR, contrast-enhanced MR imaging

#### eP-93

#### Changing Patterns of Tumor Progression Remote to the Primary Site in Bevacizumab-Treated Glioma Patients

del Prado, G.·Neuwelt, E.·Gahramanov, S.·Hamilton, B. E  
Oregon Health and Sciences University  
Portland, OR

#### PURPOSE

There is a recently reported pattern of distant tumor progression in patients treated with bevacizumab therapy for high-grade primary brain gliomas. This can be seen as a new area of nonenhancing T2 signal abnormality remote to the surgical resection cavity. This is particularly problematic since the primary tumor site may show concurrent local radiographic improvement. We review our imaging current experience in bevacizumab-treated patients in order to characterize the typical and atypical patterns of glioma relapse.

#### MATERIALS & METHODS

We performed a retrospective review of pre and post-bevacizumab MRI studies in 40 patients who received bevacizumab therapy for high-grade glioma in a single neuro-oncology clinical at a tertiary care teaching hospital. All studies were reviewed by an experienced neuroradiologist and radiology resident. Images were evaluated to assess for new T2 and FLAIR signal abnormality, enhancement, and mass effect. Sequential MRI studies before and following bevacizumab therapy were used to characterize patterns of disease over time. The last scan obtained was used to confirm the final pattern. Patterns of disease were considered local when abnormalities were confined to the immediate primary tumor and/or perioperative site without noncontiguous distant abnormalities. Multifocal disease was defined as multiple discrete signal abnormalities or enhancement without contiguous T2 signal abnormality between lesions. Diffuse disease was defined as predominantly ill-defined disease affecting both hemispheres, with more than three lobes involved. Distant disease was considered new discrete signal abnormality and/or enhancement without contiguous signal abnormality with respect to the primary or perioperative site. Electronic medical records were reviewed to determine the pertinent operative and treatment history including the timing and dose of bevacizumab.

#### RESULTS

A total of 35/40 (87.5%) patients who received bevacizumab for treatment of high-grade primary CNS neoplasm had all pertinent imaging for inclusion. Eighteen patients had local patterns of involvement prior to bevacizumab therapy. Of these, nine showed local progression, three became diffuse patterns, two stable, two partial response (one still alive), and one each became distant and multifocal in pattern on follow up. There were 10 multifocal tumors at prebevacizumab baseline, with 8/10 showing progression on surveillance. One showed no change and one showed partial response (still alive). Seven patients had diffuse patterns of involvement, with four showing progression, one worsening carcinomatosis, one stable, and one partial response (still alive) on follow up. Overall, a change in the tumor pattern compared to prebevacizumab scans was seen in 5/35 (14.3%); three local disease patients transitioned to diffuse, one to multifocal, and one to distant patterns of tumor involvement.

#### CONCLUSION

We observed a change in the pattern of disease in 5/35 (14.3%) patients after bevacizumab therapy. Such progression can be less obvious given distant areas of increasing T2 signal abnormality and/or mass effect despite diminished enhancement after bevacizumab treatment. Radiologists must be alert to evolving patterns of distant disease progression in primary brain gliomas despite radiographic improvement at the primary tumor site in the perioperative site in patients treated with bevacizumab.

**KEY WORDS:** Bevacizumab, primary CNS neoplasms

#### eP-94

### **Radiogenogram: MR Imaging as a Screening Tool for Uncovering Novel Genomic Drug Targets**

Colen, R. R.<sup>1</sup>Sathyan, P.<sup>2</sup>Jolesz, F. A.<sup>1</sup>Zinn, P. O.<sup>2</sup>

<sup>1</sup>Brigham and Women's Hospital, Boston, MA, <sup>2</sup>M.D. Anderson Cancer Center, Houston, TX

#### **PURPOSE**

To validate MRI as a screen tool to screen for glioblastoma genomic targets in order for subsequent pharmaceutical development of therapeutic gene targets. Recent genomic data are overwhelmingly vast; and, for the most part, clinical applicability of such large discoveries remains indeterminate. Selecting a clinical meaningful target to pursue after sifting through myriads of genomic data will not necessarily result in a clinically applicable target for drug development; and, importantly, this trial-and-error method is not cost-effective. Thus, these discoveries have resulted in only limited advancements in GBM treatment.

#### **MATERIALS & METHODS**

We identified 78 treatment-naïve GBM patients from The Cancer Genome Atlas (TCGA) who had both gene and microRNA expression profiles and pretreatment MR neuroimaging. In each patient, a total of 13,628 genes (22,267 hybridization probes) and 555 microRNAs (1,510 hybridization probes) were analyzed for significance and differential fold regulation using Comparative Marker Selection (Broad Institute, MIT, <http://www.broadinstitute.org/cancer/software/genepattern/>), analyzed with Ingenuity Pathway Analysis (<http://www.ingenuity.com>), and then associated with the imaging characteristics. Image data used in this research were obtained from The Cancer Imaging Archive (<http://cancerimagingarchive.net/>) sponsored by the Cancer Imaging Program, DCTD/NCI/NIH. Using 3D slicer software 3.6 (<http://www.slicer.org>), FLAIR was used for segmentation of the edema, and postcontrast T1-weighted imaging (T1WI) for segmentation of enhancement (defined as tumor) and necrosis. Two neuroradiologists reviewed the images in consensus. Affymetrix level 1 mRNA and Agilent level 2 microRNA data were downloaded from the public TCGA dataportal (<http://cancergenome.nih.gov/>). The Robust Multi-Array algorithm was used for normalization. The Kaplan Meier method was used to calculate overall- and progression-free survival. Mean gene expression across GBM subgroups was calculated using ANOVA and

Tukey-Kramer tests. For gene and microRNA correlations we used R square statistics. All calculations were performed in Microsoft Excel 2010 and JMP 9.01 (SAS Institute, CA). In vitro and in vivo studies in mice were performed to confirm these genomic targets.

#### **RESULTS**

Our MRI screen identified top upregulated and down regulated genes and microRNAs which were novel and not previously described in the literature. These were concordant with the underlying biologic processes of edema/invasion, necrosis, and enhancing tumor MRI phenotypes. Kaplan Meier analysis demonstrated that these resulted in significantly decreased survival ( $P = 0.0008$ ) and shorter time to disease progression ( $P = 0.0009$ ). In some cases, the gene expression was a stronger prognostic variable than either molecular subtype (as defined by Veerakak and colleagues) in the Cox proportional hazards ratio ( $P = 0.03$ ). In vitro and in vivo animal models as well as loss and gain of function models subsequently confirmed the genomic target's function which was concordant with the underlying biologic processes measured by MRI.

#### **CONCLUSION**

MR imaging is an effective screening tool to uncover clinically meaningful genomic targets that can be used in drug development of therapeutic targets for GBM treatment. Furthermore, these might serve as better prognostic predictors than those currently used.

**KEY WORDS:** Glioblastoma, genomics, radiogenomics

#### eP-95

### **Frequency of Pseudoprogression in Patients with Glioblastoma According to RANO Criteria**

Radbruch, A.·Fladt, J.·Wiestler, B.·Lutz, K.·Bäumer, P.·Heiland, S.·Wick, W.·Bendszus, M.

University of Heidelberg  
Heidelberg, GERMANY

#### **PURPOSE**

It is reported that 20-30% of patients with high-grade glioma undergoing their first or second radiation MRI show increased contrast enhancement that eventually subsides without any change in treatment. Because of this phenomenon, that is termed pseudoprogression, the recently introduced Response Assessment in Neuro-Oncology Criteria (RANO criteria) suggest that within 12 weeks of completion of radiotherapy, progression can be determined only if the majority of the new enhancement is outside the radiation field. To validate this concept we assessed the frequency of pseudoprogression in a large cohort of patients with glioblastoma at different time-points.

#### **MATERIAL & METHODS**

Patients with glioblastoma ( $n = 233$ ) were examined between 1.1.2008-12.31.2010. All patients received a baseline MRI after resection or biopsy of the glioblastoma, and further follow-up examinations every 3 months. All patients underwent standard



radiotherapy with combined temozolomide subsequent to the operation. All patients who received external MRI or who received study-medication were excluded. Two experienced neuroradiologists (M.B. and A.R.) assessed if an enhancement increase of at least 25% appeared within the radiation field at the follow-up examinations that qualifies for progressive disease (PD) at 3, 6, 9 and 12 months. In patients with MRI that demonstrated this progressive enhancement and hence progressive disease or pseudoprogression assessment of the evolution, over the next 6 months was done. Variables were increased or stable enhancement, enhancement that decreased less than 50%, more than 50% or that disappeared completely.

## RESULTS

One hundred fifty-eight patients had to be excluded due to study participation (30), external MRI (70), no progression within one year (27) or insufficient MRI examination (21). Eighty-five patients presented PD within the radiation field within 1 year after radiochemotherapy. Only 7.7% of the patients presented increase of the enhancement 3 months after completion of radiochemotherapy that subsequently subsided. This percentage did not differ significantly after 6 and 9 months. Detailed results are presented in the Table.

	Increase	Stable	Decrease < 50 %	Decrease > 50 %	Decrease 100 %	Total
3 Months	23 (88,5%)	1 (3,85%)	2 (7,7%)	0 (0%)	0 (0%)	26
6 Months	33 (82,5%)	3 (7,5%)	1 (2,5%)	2 (5%)	1 (2,5%)	40
9 Months	13 (86,6%)	1 (6,6%)	0 (0%)	0 (0%)	1 (6,6%)	15
12 Months	4 (100%)	0 (0%)	0 (0%)	0 (0%)	0 (0%)	4
Total	73 (85,9%)	5 (5,9%)	3 (3,5%)	2 (2,4%)	2 (2,4%)	85

## CONCLUSION

Our data challenge the introduced concept of pseudoprogression according to RANO Criteria. We could not confirm the supposed value of 20-30% of pseudoprogression nor the arbitrary cut-off at 3 months for enhancing lesion that disappear without change of management. Therefore the supposed limitation of 3 months is questionable. Furthermore a low frequency of pseudoprogression may result in a delay for the necessary change in therapy for the majority of patients who present real progression. To avoid these consequences frequency of pseudoprogression and other MR imaging modalities such as perfusion-, diffusion- or susceptibility-weighted imaging should be investigated for better sensitivity than T1/T2/FLAIR

and a collaborative effort should be made on this topic in a multicenter study.

**KEY WORDS:** Glioblastoma, pseudoprogression, RANO criteria

## eP-96

### Preoperative Metabolic Mapping of Gliomas with Hybrid MR Imaging-Positron Emission Tomography Imaging: Feasibility of the Method and Spatial Distribution of the Metabolic Changes

Bisdas, S.·Nägele, T.·Ritz, R.·Braun, C.·Ernemann, U.

Eberhard Karls University  
Tuebingen, GERMANY

## PURPOSE

In clinical practice, the most powerful adjunct to histopathology for the grading of gliomas and detection of anaplastic foci seems to be the metabolic imaging using positron emission tomography (PET) tracers as well as MR spectroscopy (MRS). Purpose of this study is to examine the feasibility of both techniques in a newly launched hybrid MR PET unit for tumor grading as well as to examine the spatial distributions of metabolic changes in diffuse gliomas.

## MATERIALS & METHODS

Twenty-four consecutive patients with gliomas underwent simultaneous methionine (MET) MR PET imaging for detection of the most malignant tumor part prior to surgical sampling and histologic diagnosis. Prior to image coregistration and fusion of MR PET and MRS data, tumor to normal brain (T/N) uptake ratios and the corresponding metabolites peaks (Cho: choline; Cr: creatine; NAA: N-acetyl-aspartate) in MRS were calculated. The cases were divided into three types, based on the relation between the MET uptake area and the increased metabolite ratios: type I, the increased MET uptake area had at least 50% overlap or was completely within the area of increased Cho/NAA ratio; type II, the increased MET uptake site had less than 50% overlap of increased Cho/NAA ratio site; type III, the increased MET uptake region had no spatial relationship with the "hot" lesions in the MRS maps. If increased accumulation of MET was absent or not clear, the cases were classified as type III.

## RESULTS

Sixteen low-grade gliomas and eight anaplastic gliomas were included and histologically verified. No lesions of type I were identified. Three lesions were classified as type II and 21 lesions were classified as type III. In four of the type III lesions the increased MET uptake region had no spatial relationship with the "hot" lesions in the MRS maps, while in 17 patients there was no increased MET accumulation and tumor was sampled from the area with the highest Cho/NAA ratio. The Cho/NAA and Cr/NAA maps showed a close spatial relationship in the majority of the patients. The median MET uptake in the pooled surgically sampled tumor sites was 1.5 (range: 1-3), whereas the median Cho/NAA and Cho/Cr ratios were 2.0 (0.9-5.8) and 1.4 (0.5-8.3), respectively. The

Spearman's  $\rho$  correlations of the metabolic markers in the low-grade gliomas showed significant correlations between MET uptake and Cr/NAA ratio ( $\rho = 0.59$ ,  $p = 0.015$ ) as well as between Cho/NAA and Cr/NAA ratios ( $\rho = 0.79$ ,  $p = 0.0002$ ).

#### CONCLUSION

Metabolic mapping prior to histologic sampling is feasible using simultaneous MR PET imaging. High methionine uptake, which is indicative of tumor cell infiltration, doesn't always spatially correlate with neuronal cell loss and cell membrane proliferation (Cho/NAA). It seems that creatine (Cr) as marker of tissue energy metabolism is associated with increased methionine uptake. Thus, the spatial distribution differences in gliomas should be taken into account and guide the surgical sampling.

**KEY WORDS:** Gliomas, MR spectroscopy, PET

#### eP-97

##### "Marginal Line Profile" on $\Delta R2^*$ Map: A Specific Sign for Differentiating Glioblastoma from Solitary Brain Metastasis

Suh, C. H.-Kim, H. S.

Asan Medical Center  
Seoul, KOREA, REPUBLIC OF

#### PURPOSE

To determine whether "Marginal Line Profile" (MLP) of dynamic susceptibility contrast (DSC) perfusion MR imaging could differentiate glioblastoma from metastasis and to assess correlations between the MLP and quantitative perfusion parameters.

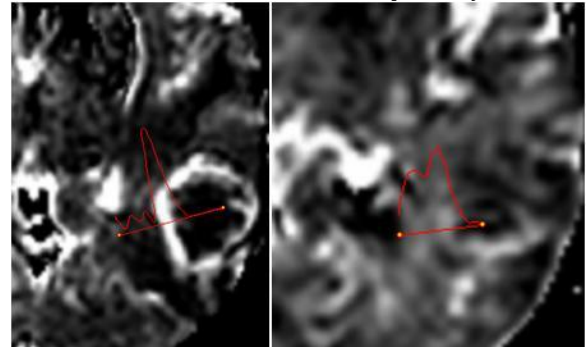
#### MATERIALS & METHODS

After approval from the institutional ethics committee was obtained, the DSC perfusion MR imaging studies of 104 consecutive patients with histopathologic diagnosis of glioblastoma ( $n = 57$ ) or metastasis ( $n = 47$ ) without previous surgery or treatment, were reviewed. Two neuroradiologists, who were blinded to clinical data, independently calculated MLP for  $\Delta R2^*$  and normalized cerebral blood volume (nCBV) around the border between contrast-enhancing lesion and perienhancing lesion. The MLP type was classified into acute MLP and oblique MLP. Quantitative histogram perfusion parameters obtained from whole-tumor voxels in perienhancing lesions were compared with the MLP type. Statistical analysis consisted of a chi-square test, receiver operating characteristic (ROC) curve and independent T-test.

#### RESULTS

There was significant difference between glioblastoma and metastasis with respect to the MLP with excellent interobserver agreement ( $\kappa = 0.89$ ). Metastasis had a significantly higher prevalence of acute MLP than glioblastoma [45 of 47 (96%) patients vs 20 of 57 (35%) patients;  $P < .0001$ ]. Among the quantitative histogram parameters, range and maximum of nCBV in perienhancing lesion were associated significantly with

the MLP type. Sensitivity, specificity, positive predictive value and negative predictive value of the MLP for differentiating glioblastoma from metastasis were 64.9%, 95.7%, 94.9%, and 69.2%, respectively.



Tumor pathology and quantitative perfusion parameters for the different 'Marginal Line Profile' type

#### CONCLUSION

The findings of our study show that acute MLP of DSC perfusion MR imaging is a specific imaging sign for differentiating between glioblastoma and metastasis.

**KEY WORDS:** Marginal line profile, glioblastoma, solitary brain metastasis

#### eP-98

##### Diagnostic Value of Susceptibility-Weighted Imaging in Differentiating Schwannoma from Meningioma

Choi, H.-Jung, S.-Ahn, K.-Kim, B

Seoul St. Mary's Hospital  
Seoul, KOREA, REPUBLIC OF

#### PURPOSE

Meningioma and schwannoma are the most common and second most common extraaxial tumors in adult patients. Generally, there is more frequent microhemorrhage in schwannomas and there is more frequent calcification in meningioma. Susceptibility-weighted image (SWI) is sensitive in detecting microhemorrhage, which shows blooming of dark signal intensity on SWI. The purpose of this study was to evaluate diagnostic value of SWI in differentiating schwannoma from meningioma.

#### MATERIALS & METHODS

Between June 2009 and April 2011, 118 meningiomas and 53 schwannomas were pathologically proven. Among those susceptibility-weighted image were preoperatively taken in 27 meningiomas and 11 schwannomas. We retrospectively analyzed imaging feature of those tumors: size; signal intensity on T2-weighted image of entire tumor (normalized to caudate); calcification on precontrast CT; dark spots on SWI (less than 50% or more than 50%); and enhancement portion (less than 50% or more than 50%). Univariate and multivariate analysis were performed to find associated variables to differentiate schwannoma from meningioma.

#### RESULTS

Univariate analysis showed high T2-signal intensity, dark spots on SWI, and enhancing portion of less than 50% were associated with schwannoma. Multivariate analysis showed dark spots (more than 50%) on SWI was the most predictive variable among them ( $p < 0.05$ ).

#### CONCLUSION

Dark spots (more than 50%) on SWI can be a predictive sign of schwannoma in differentiation from meningioma.

**KEY WORDS:** SWI, schwannoma, meningioma

#### eP-99

#### Atypical Imaging Features of Primary Central Nervous System Lymphomas in Immunocompetent Patients: Their Relationships to Epstein-Barr Virus - Initial Experience

Chung, W.-Kim, H.

University of Ulsan College of Medicine, Asan Medical Center  
Seoul, KOREA, REPUBLIC OF

#### PURPOSE

To evaluate atypical MR imaging features of Epstein-Barr virus (EBV)-positive primary central nervous system lymphomas (PCNSL) in immunocompetent patients and to compare these imaging findings with those of EBV-negative PCNSL.

#### MATERIALS & METHODS

This retrospective study was approved by the institutional review board with waiver of informed consent. Advanced and conventional MR images were obtained from 20 consecutive patients (15 men, 5 women; mean age, 63 years; age range, 34-83 years) with pathologically proven EBV-positive ( $n = 8$ ) or -negative ( $n = 12$ ) PCNSLs. Between group differences in the occurrence of tumor necrosis or hemorrhage, the apparent diffusion coefficients (ADC) of the area of necrosis and solid tumor, the maximum and range of relative cerebral blood volume (rCBV<sub>max</sub> and rCBV<sub>r</sub>, respectively) and the choline to N-acetyl aspartate ratio (Cho/NAA ratio) in the area of solid tumor were analyzed statistically.

#### RESULTS

Tumor necrosis and hemorrhage mimicking glioblastoma were observed in six (75%) and three (38%) of eight patients with EBV-positive PCNSLs, respectively, and in none of 12 patients with EBV-negative PCNSLs ( $P < 0.0001$ ). Of the six patients with necrotic EBV-positive PCNSLs, three showed decreased ADC in the area of necrosis (normalized ADC,  $4.16 \pm 7.69$ ). ADCs in the area of solid tumor did not differ significantly. Patients with EBV-positive PCNSLs tended to have a lower rCBV<sub>max</sub> ( $2.56 \pm 0.89$  vs  $2.79 \pm 0.92$ ,  $P > 0.05$ ) and rCBV<sub>r</sub> ( $1.76 \pm 0.87$  vs  $1.83 \pm 0.73$ ,  $P > 0.05$ ) than those with EBV-positive PCNSLs, and their Cho/NAA ratios did not differ significantly ( $5.55 \pm 7.74$  vs  $9.10 \pm 6.41$ ,  $P = 0.125$ ). The sensitivity, specificity, and accuracy in differentiating between EBV-positive

and -negative PCNSLs were 87.5 %, 91.7 %, and 90.0 %, respectively, for conventional and advanced MR imagings.

Table. Conventional and advanced MR imaging findings in patients with EBV-positive and -negative PCNSL at time of diagnosis.

Conventional Imaging Findings			EBV+ PCNSL, n=8 (%)	EBV- PCNSL, n=12 (%)
Number of lesions (n=patients)	Single		5 (63)	6 (50)
	Multiple		3 (37)	6 (50)
	Total number of lesions		15	24
Location (n=lesions)	Periventricular		3 (20)	2 (8)
	Lobar		7 (47)	12 (50)
	BG/thalamus/stem/Cbll		2 (13) / 0 / 1 (7) / 2 (13)	4 (17) / 5 (21) / 1 (4) / 0
Hemorrhage (n=patients)			3 (38)	0
Extensive necrosis (n=patients)			4 (50)	0
Contrast enhancement pattern (n=patients)	Homogeneous		3 (38)	12 (100)
	Inhomogeneous		5 (63)	0
	Rim-enhancing		4 (50)	0
Advanced imaging findings			EBV+ PCNSL (n=7)	EBV- PCNSL (n=10)
Diffusion weighted imaging	ADC <sub>core</sub> (10 <sup>-3</sup> mm <sup>2</sup> /sec)	$3.22 \pm 2.13$	$4.37 \pm 1.53$	
	ADC <sub>core</sub> /ADC <sub>wm</sub>	$4.16 \pm 7.69$	$5.19 \pm 6.23$	
Perfusion MRI			rCBV <sub>max</sub> (mean / range)	$2.79 \pm 0.92$ / $2.56 \pm 0.89$ /
MR Spectroscopy	rCBV <sub>r</sub> (mean / range)	$1.83 \pm 0.73$ /	$1.76 \pm 0.87$ /	
	Cho/NAA ratio(mean/range)	$5.55 \pm 7.74$ / $1.24 - 22.79$	$9.10 \pm 6.41$ / $1.3 - 22.36$	

#### CONCLUSION

Initial experience with a small number of patients suggests that EBV-positive PCNSLs in immunocompetent patients tend to present with atypical advanced and conventional MR imaging features resembling those of patients with glioblastomas.

**KEY WORDS:** Epstein-Barr virus-positive primary CNS lymphoma, Immunocompetent patients, atypical MR findings

## eP-100

### Diffusion-Weight Imaging, MR Perfusion-Weighted Imaging and Diffusion Tensor Imaging in Microcystic Meningiomas

Liu, X.-Tian, W.-Ekholm, S.

University of Rochester School of Medicine & Dentistry  
Rochester, NY

#### PURPOSE

Microcystic meningioma is a rare variant of meningioma, and characterized with masses of meningeal syncytium in the process of vacuolization with numerous lacunae or elongated slits and a very rich network of vessels. The reports of radiologic findings in the microcystic meningiomas are variable. We report four cases of the microcystic meningiomas, including the findings of diffusion-weight imaging, MR perfusion-weighted imaging and diffusion tensor imaging.

#### MATERIALS & METHODS

There are four cases with histology-confirmed microcystic meningiomas, the diffusion-weight imaging was performed in all of these cases, MR perfusion-weighted imaging and diffusion tensor imaging were performed in three of them. Retrospectively, 41 patients with other variants of meningiomas, including meningothelial, transitional, psammomatous, fibroblastic atypical and anaplastic meningiomas, and 18 cases of intracranial dural-based metastases were enrolled for comparison.

#### RESULTS

The four microcystic meningiomas cases included three males and one female, mean age is  $46 \pm 10$  years. The minimal apparent diffusion coefficient (ADC), maximal fractional anisotropy (FA), maximal rCBV ratio in each case and the mean values were listed in the Table. The mean values of minimal ADC, maximal FA and maximal rCBV ratio in other meningiomas are  $0.722 \pm 0.123$ ,  $0.375 \pm 0.085$ , and  $11.39 \pm 6.56$  respectively, and there was no significant difference in minimal ADC and maximal rCBV ratio between microcystic meningiomas and other meningiomas ( $p > 0.05$ ), the mean value of maximal FA in microcystic meningiomas is significantly lower. The mean values of minimal ADC, maximal FA and maximal rCBV ratio in dural based metastases are  $0.78 \pm 0.23$ ,  $0.161 \pm 0.036$ , and  $5.01 \pm 3.27$  respectively. There was no significant difference in minimal ADC and maximal FA between microcystic meningiomas and dural-based metastases ( $p > 0.05$ ), the mean value of maximal rCBV ratio in microcystic meningiomas is significantly higher.

Table: MR perfusion-weighted imaging and diffusion imaging measurement in microcystic meningiomas

Index	Case 1	Case 2	Case 3	Case 4	Mean $\pm$ SD
Maximal FA	0.2538	0.072	0.1423	-	$0.156 \pm 0.09$
Minimal ADC	1.2057	1.0013	0.652	0.881	$0.935 \pm 0.23$
Maximal rCBV ratio	22.09	2.172	9.902	-	$11.388 \pm 10.04$

#### CONCLUSION

The findings of MR perfusion-weighted imaging and diffusion imaging in microcystic meningiomas are variable. Combination analysis of multiple imaging parameter is useful for imaging diagnosis.

**KEY WORDS:** Microcystic meningioma, diffusion tensor imaging, perfusion-weighted imaging

## eP-101

### Imaging Appearance of Spontaneous Retroclival Hematoma in Pituitary Apoplexy

Azzam, R. I.-Maya, M. M.-Famini, P.-Moser, F.  
G.-Pressman, B. D.

Cedars Sinai Medical Center  
Los Angeles, CA

#### PURPOSE

To determine the incidence and appearance of retroclival epidural hematoma in the setting of spontaneous pituitary apoplexy.

#### MATERIALS & METHODS

Single institution review of over 10,000 brain imaging studies utilizing computerized tomography (CT) or magnetic resonance imaging (MRI) yielded 2598 patients with sellar and parasellar masses over a 10-year period. A detailed review of medical records and imaging identified 16 patients who presented with pituitary apoplexy due to a mass.

#### RESULTS

Sixteen patients with pituitary apoplexy were identified. In nine patients, retroclival epidural hemorrhages were detected. We describe the imaging appearance based on size, location, irregular contour, mild enhancement, evolution of T1 and T2 signal and resolution on follow-up imaging as characteristics of spontaneous (nontraumatic), retroclival hemorrhage secondary to pituitary apoplexy. Surgical decompression of the sellar/suprasellar component was undertaken in most patients due to neurologic deficits. Majority of patients had follow-up serial imaging for evaluation of retroclival hemorrhage with resolution seen in most.



#### CONCLUSION

Pituitary apoplexy is a rare but sometimes life threatening disorder most commonly characterized by a combination of sudden headache, visual disturbance, and hypothalamic/hormonal dysfunction. Hemorrhagic infarction of an underlying pituitary tumor most commonly contributes to sudden onset of symptoms with unique MR imaging and histopathologic findings. Spontaneous retroclival hemorrhage is a rarely reported complication of pituitary apoplexy. Interestingly, it was a common finding in our series. The evaluation for blood product signal on T1 (Figure) and T2-weighted sequences can be confusing in the early stages of hemorrhage. We describe nine separate patients with unique imaging appearances that highlight the importance of identifying retroclival hemorrhage and differentiating blood products from other retroclival masses.

**KEY WORDS:** Pituitary, apoplexy, hematoma

#### eP-102

##### Neuroanatomical Correlates of Neuropsychological and Psychopathologic Domains in First Episode Schizophrenia: A Multimodal Analysis

Rossi Espagnet, M.<sup>1</sup>•Romano, A.<sup>1</sup>•Rigucci, S.<sup>1</sup>•Carducci, F.<sup>2</sup>•Bonamini, M.<sup>1</sup>•Comparelli, A.<sup>1</sup>•Girardi, P.<sup>1</sup>•Fantozzi, L.<sup>1</sup>•Bozzao, A.<sup>1</sup>

<sup>1</sup>Sant'Andrea Hospital, Rome, ITALY, <sup>2</sup>University La Sapienza, Rome, ITALY

#### PURPOSE

A few studies explored the relationships between gray matter (GM) volume and neuropsychopathologic features in first episode schizophrenia (FES). The aims

of our study were to explore gray and white matter (WM) abnormalities comparing FES patients to healthy controls (HCs) and to evaluate possible relationships between gray matter volume and neuropsychopathologic features in FES.

#### MATERIALS & METHODS

Both FES and HCs underwent MRI (1.5 T) acquisitions. Gray matter volumes were evaluated using voxel-based morphometry and DARTEL algorithm whereas WM analysis was performed by the Tract-Based Spatial Statistics method after calculation of fractional anisotropy (FA) maps. For multiple regression analysis, symptoms and neuropsychological performances were scored by PANSS scale and by a neuropsychological comprehensive assessment (MATRICS), respectively.

#### RESULTS

Patients showed significantly decreased volume of left Brodmann area (BA) 37 and decreased FA of all major WM tracts ( $p < 0.005$ ). Left cerebellar volume was related inversely to disorganized/cognitive PANSS factor. Trail-Making A, Wisconsin Test and Facial-Affect Recognition scores significantly correlated with right BA32, BA28 and BA36 volumes, respectively ( $p < 0.005$ ).

#### CONCLUSION

We confirm the presence of morphologic alterations of both gray and white matter in FES with an involvement of the fronto-limbic structures, consistently with a synthesis between a neurodevelopmental perspective and a neo-Bleulerian model.

**KEY WORDS:** First episode schizophrenia, voxel-based morphometry, diffusion tensor imaging

#### eP-103

##### Tract-Specific Analysis of 30-Direction Diffusion Tensor Imaging Data Localizes Diffusion Abnormalities in Amyotrophic Lateral Sclerosis

Brun, C. C. • Newman, S. A. • Wang, S. • Yushkevich, P. A. • Melhem, E. R. • Elman, L. B. • McCluskey, L. F. • Gee, J. C. • Woo, J. H.

University of Pennsylvania  
Philadelphia, PA

#### PURPOSE

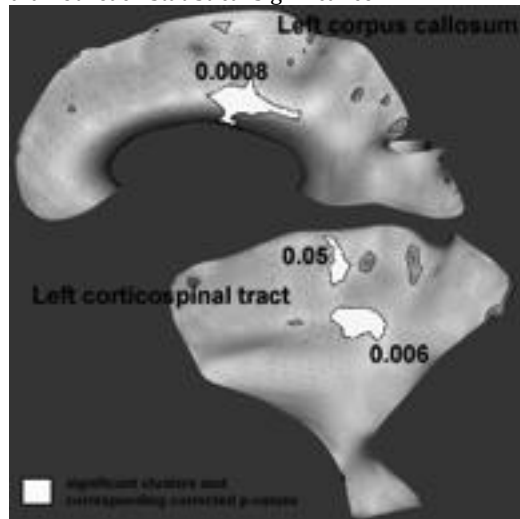
To localize significant decreases in fractional anisotropy (FA) in the white matter (WM) of patients with amyotrophic lateral sclerosis (ALS). ALS is a degenerative disease of motor neurons. Using diffusion tensor imaging (DTI), previous studies found significant reductions in FA in the corticospinal tract (CST) and corpus callosum (CC) of patients with ALS compared to controls, a finding thought to reflect axonal degeneration. Tract-specific analysis (TSA), a novel method for assessing local differences in WM integrity, has been applied previously to 12-direction DTIs in ALS. Here, we apply TSA to 30-direction DTI data.

#### MATERIALS & METHODS

We recruited 33 patients with ALS and 13 healthy controls (age: 54.6±10/55±5.4 years old, respectively). Diffusion-weighted images were acquired in 30 directions ( $b=1000\text{s/mm}^2$ ) on a 3.0 T Siemens Trio scanner using an 12-channel coil and single-shot spin-echo diffusion-weighted echo-planar sequence, with four unweighted images ( $b=0$ ), GRAPPA of three. Other parameters: NEX=3, TR=6700ms, TE=85ms, FOV=245x245mm, matrix=112x112, slice=2.2mm, gap=0mm, voxel dimension 2.19x2.19x2.2mm<sup>3</sup>, scan time=13min. After correcting for motion and eddy-current artifacts, DTIs were reconstructed using standard linear fitting methods, and then normalized to a DTI template built using healthy controls (age 60-80 years) from the public IXI database. The CST and CC tracts were segmented and extracted from whole brain tractography of the template, converted to 3D binary structures, then modeled as medial meshes with corresponding boundaries. These predefined volumetric tracts were used to sample subjects' DTI data and project average FA onto the tract's medial surface. Comparisons between groups were performed using a cluster-based analysis. We report the locations of significantly reduced FA in ALS patients compared to controls (10000 permutation test,  $p<0.05$ , corrected for multiple comparisons).

## RESULTS

Fractional anisotropy was reduced in the left and right posterior body of the CC ( $p=0.008$  and  $0.011$ , respectively) and adjacent regions of the left CST ( $p=0.006$ ). Interestingly, FA reductions in the right CST did not reach statistical significance.



## CONCLUSION

Significant clusters of decreased FA were localized in the expected region of the primary motor pathway (CST) and in the expected region of motor strip commissural fibers (CC). Our results, while being statistically more powerful, confirm findings obtained with 12 directions DTIs. One difference lies in the absence of significance in the right CST, perhaps caused by a stronger right hemispheric dominance within our group of patients. This study highlights the effectiveness of TSA at detecting local diffusion alterations in large white matter tracts.

**KEY WORDS:** ALS, white matter, specific tracts

## eP-104

### First Results of Quantitative Cerebrovascular Reserve with MR Imaging

Qian, R.<sup>1</sup>•Vakil, P.<sup>1</sup>•Hurley, M. C.<sup>2</sup>•Ansari, S. A.<sup>2</sup>•Sammet, C.<sup>2</sup>•Mouannes-Srour, J.<sup>2</sup>•Batjer, H.<sup>2</sup>•Bendok, B. R.<sup>2</sup>•Carroll, T. J.<sup>1</sup>

<sup>1</sup>Northwestern University, Evanston, IL, <sup>2</sup>Northwestern University, Chicago, IL

## PURPOSE

Cerebrovascular reserve (CVR) measures the autoregulatory dilatation of intracranial vessels in the setting of ischemic pathologies. Hemodynamic failure is characterized by altered CBV, CBF, CVR and oxygen extraction fraction predisposing a patient to infarcts. We have developed a novel approach to quantify and score CVR (qCVR).

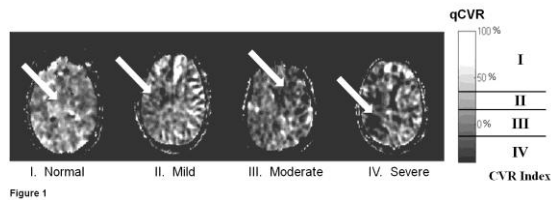
## MATERIALS & METHODS

All subjects were scanned on a 1.5T MRI scanner in this IRB approved study. Patients referred for Diamox challenge (1000 mg) were reviewed retrospectively using the previously published quantitative perfusion pulse sequence. Cerebral perfusion was measured prior to and 10 minutes after administration of Diamox. Asymptomatic healthy volunteers were scanned without Diamox as experimental controls. The intravascular compartmentalization of Gd-DTPA produces a predictable bias in that depends on water exchange rate ( $\tau_{ex} = 0.9\text{ s}^{-1}$ ) and precontrast T1 value of blood. We derived a response curve that is relevant to the second contrast agent infusion and validated the accuracy in controls. QCVR ( $\text{QCVR} = \frac{\text{qCBF}_{\text{baseline}} - \text{qCBF}_{\text{Diamox}}}{\text{qCBF}_{\text{baseline}}} \times 100\%$ ) was calculated in normal and hemodynamically compromised vascular territories. Statistical Analysis: The quality of the compartmentalization model was determined by a McNair F-test. We compared 1<sup>st</sup> and 2<sup>nd</sup> injection volunteer perfusion to verify the scan-to-scan variability of the techniques in the absence of Diamox challenge based on Wilcoxon signed rank test. In patients, we compared the degree of CVR in normal regions with expectations based on historical reference data. In all tests significance was defined at the 5% level.

## RESULTS

We found the second injection WCF modeling equation:  $\text{WCF} = 0.003(\text{dR1}_1)^2 + 0.8(\text{dR1}) + 0.1$  at 1.5T ( $F(3,14) = 14.0$ ,  $P < 0.001$ ). Mean qCVR in controls was  $3.9 \pm 8.1\%$ , in agreement with the test-retest reliability of the technique ( $0 \pm 14\%$ ). In patients normo-perfused territories exhibited the expected 30% flow augmentation for the dose of Diamox applied. We derived a quantitative scale for the flow augmentation based on the severity of CVR reduction on a four-point scale (Figure): I = Normal ( $\text{qCVR} > 30\%/1000\text{ mg Diamox}$ ), II = mild impairment ( $10\% < \text{qCVR} < 30\%$ ), III = moderate impairment ( $-10\% < \text{qCVR} < 10\%$ ), IV = severe impairment (vascular steal) ( $\text{qCVR} < -10\%$ ).





### CONCLUSION

We found that quantification of CVR is possible with MRI with a Diamox challenge. Our proposed index correlates with the presence of hemodynamic compromise resulting from neurovascular disease. Assigning a quantitative CVR score has the potential to track longitudinal changes in hemodynamic status in response to therapy.

**KEY WORDS:** Quantitative cerebrovascular reserve

### eP-105

#### Bolus-Tracked CT Perfusion: Technical Note

Tyndall, A. J.·Karwacki, G.·Tumminelli, T.·Kummer, S.·Ahlhelm, F. J.·Stippich, C.·Ulmer, S.

University Hospital Basel  
Basel, SWITZERLAND

### PURPOSE

CT perfusion has become a mainstay in stroke imaging. Patients undergoing CT perfusion often suffer from other medical conditions such as left cardiac failure. In these patients it is difficult to predict the ideal bolus timing, thus interpretation of the results might be hampered.

### MATERIALS & METHODS

Inspired by the concept of bolus tracking for pulmonary embolism we performed a bolus tracking prior to CT perfusion in 30 patients. The trigger slice was positioned in the proximal supraaortic ascending aorta. A bolus of 30 cc Ultravist 370 (Schering, Berlin, Germany) was injected and images were acquired every 2 seconds on a clinical 128 row multidetector CT scanner (Siemens Definition AS, Forchheim, Germany). The time until enhancement was measured based on visual control. For CT perfusion (80 kV, 200 mAs, collimation of 32x1.2 mm) we injected 40 cc Ultravist intravenously and started the measurement delayed by the individual ejection time. The image stack included the skull base to depict the arterial input function acquiring images every 2 seconds (45 seconds total) allowing a coverage of 7 cm.

### RESULTS

In all patients an arterial input function as well as a venous output function could be analyzed in the defined time gap of 45 seconds. Perfusion maps (time to peak, mean transit time, cerebral blood volume and flow) could be created to reliably predict the likelihood of a stroke to enrol these patients in either intravenous or intraarterial thrombolysis or recanalization therapy.

### CONCLUSION

Heart failure (HF) has been recognized as a risk factor for stroke, as well as an independent risk factor for severe strokes. Patients with cerebral ischemia often suffer from other medical conditions such as left cardiac failure. Our proposed simple press button method avoids dropouts from cerebral CT perfusion studies in patients with reduced cardiac output at time cost of additional 2 minutes and may influence clinical management.

**KEY WORDS:** CT, perfusion, bolus

### eP-106

#### Noninvasive Cerebrovascular Reactivity Assessment Using Apparent Spin Labeling and Blood Oxygenation Level Dependent

Portelo, A.<sup>1</sup>·Vilela, P.<sup>2</sup>·Sousa, I.<sup>1</sup>·Figueiredo, P.<sup>1</sup>

<sup>1</sup>Instituto Superior Técnico, Lisbon, PORTUGAL,

<sup>2</sup>Hospital da Luz, Lisbon, PORTUGAL

### PURPOSE

We aimed to develop a reproducible protocol for noninvasive assessment of cerebrovascular reactivity (CVR) combining a breath hold (BH) challenge with cerebral blood flow (CBF) measurements using apparent spin labeling (ASL), in comparison with a matching BOLD protocol.

### MATERIALS & METHODS

A group of 10 healthy subjects was studied over two sessions on a 3 T MRI. Blood oxygenation level dependent (BOLD) images were obtained using GE-EPI sequence and ASL images were obtained using Q2TIPS-PICORE sequence from nine contiguous slices. The BH protocol consisted of three (BOLD)/eight (ASL) cycles of 20s BH alternated with normal breathing. The data were analyzed using FSL, including standard preprocessing steps and general linear model statistical analysis. Both BOLD and CBF maps of CVR were obtained for each subject and session, showing significant responses to BH, especially in gray matter. Cerebrovascular reactivity measurements were obtained as percent signal changes averaged across the activation maps associated with the BOLD and CBF responses. Intra and intersubject variability was measured in terms of the respective coefficients of variation (CV).

### RESULTS

The mean percent signal change averaged across the CVR maps was  $1.0 \pm 0.2\%$  and  $1.6 \pm 0.2\%$  for BOLD sessions 1 and 2,  $0.6 \pm 0.1\%$  and  $0.7 \pm 0.1\%$  for BOLD ASL sessions 1 and 2, and  $74 \pm 7\%$  and  $73 \pm 9\%$  for CBF sessions 1 and 2. The intra and intersubject variability were:  $CV_{intra} = 12\%$  and  $CV_{inter} = 36\%$  for BOLD,  $CV_{intra} = 17\%$  and  $CV_{inter} = 25\%$  for BOLD ASL, and  $CV_{intra} = 31\%$  and  $CV_{inter} = 36\%$  for CBF.

**CONCLUSION**

Noninvasive CVR assessed by fMRI by measuring the BOLD and CBF responses to breath hold challenges is a reproducible method.

**KEY WORDS:** Cerebrovascular reactivity, ASL, MR imaging

**eP-107****Eyeshields in Cranial CT Exams: Reduction of X-ray Dosage in Clinical Routine**

Harder, D.·Ulmer, S.·Tumminelli, T.·Lieb, J. M.·Ahlhelm, F. J.·Stippich, C.·Roser, H. W.  
University Hospital Basel  
Basel, SWITZERLAND

**PURPOSE**

In cranial CT the lenses are at risk of radiation exposure without any additional diagnostic benefit. Various manufacturers offer protection devices (eyeshields) to cover the eyes during scanning. We determined the radiation dose in patients' lenses in three clinical protocols with two different devices.

**MATERIALS & METHODS**

Thermoluminescent dosimeters (lithium borate,  $\text{Li}_2\text{B}_4\text{O}_7$ ) were attached to the lenses of the head of an anthropomorphic Rando Alderson phantom. Simulating the clinical set-up on a 64-multirow detector CT (Siemens Somatom Sensation, Forchheim, Germany) we performed three exams (serial cranial CT, 120 kV, 380 mA, collimation 24 x 1.2 mm; spiral cranial CT 1, 120 kV, 380 mA, collimation 24 x 1.2 mm and spiral cranial CT 2, 120 kV, 130 mA, collimation 64 x 0.6 mm) using either one, CT-Eye Protex (Admedics Advanced Medical Solutions AG, Zuchwil, Switzerland), and CT-eyeshield (Promedics, Biel, Switzerland), in four separate runs each.

**RESULTS**

Mean dosage was 57.7 mSv, 35.3 mSv and 46.2 mSv for the serial exam, 63.5 mSv, 39.5 mSv, and 47.8 mSv for spiral exam 1 and 7.8 mSv, 5.6 mSv, and 6.3 mSv for spiral exam 2, respectively. Dose reduction ranged between 28.2 and 38.8% for CT-Eye Protex, and between 19.1 and 24.7% for CT-eyeshield.

**CONCLUSION**

Dosage reduction varied considerably between manufacturers. For daily routine, however, a significant reduction can be achieved in each patient using either device and should be performed especially in patients undergoing repetitive CT scans.

**KEY WORDS:** Radiation, eyeshield, CT

**eP-108****Utility of CT Perfusion Compared with SPECT Scans in Acute Stroke Patients with Carotid Artery or Middle Cerebral Artery Disease**

Tajiri, H.·Mori, T.·Iwata, T.·Miyazaki, Y.·Nakazaki, M.  
Shonan Kamakura General Hospital Stroke Center  
Kamakura, JAPAN

**PURPOSE**

The purpose of our retrospective study was to investigate the utility of CT perfusion using whole-brain 320 rows area detector for assessing cerebral blood flow (CBF) in acute ischemic stroke patients with the carotid artery (CA) or middle cerebral artery (MCA) disease compared with  $^{99\text{m}}\text{Tc}$ -ECD single photon emission computed tomography (SPECT).

**MATERIALS & METHODS**

Included for retrospective analysis were patients, (1) who were admitted from January 2011 to October 2011 due to acute ischemic stroke, (2) who had the carotid artery or middle cerebral artery disease, and (3) who underwent both CT perfusion (CTP) using 320 row area detector CT and  $^{99\text{m}}\text{Tc}$ -ECD SPECT within 3 days of admission. Excluded were patients (1) who underwent emergency reperfusion therapy between CTP and SPECT, (2) had bilateral stenosis/occlusion of the CA or MCA, or (3) who had large old cerebral infarction. Cerebral blood flow (CBF) of CTP and SPECT was measured on the MCA territory in the affected side (Aff CBF) and in the contralateral side (Con CBF). Asymmetry index was defined as Aff CBF divided by Con CBF. We evaluated Aff CBF, Con CBF, and AI of CTP compared with those of SPECT. In addition, we evaluated crossed cerebellar diaschisis (CCD) visually in CTP and SPECT images.

**RESULTS**

Thirty-six patients were matched to our criteria. Twenty-two patients had the CA lesions and 14 had the MCA lesions. Age was  $71.3 \pm 11.4$  years (mean  $\pm$  SD), Man (%) was 75%, Right-sided lesion (%) was 39%. The rank correlation coefficient was 0.591 ( $p = 0.000$ ) in Aff CBF, 0.526 ( $p = 0.001$ ) in Con CBF, and 0.713 ( $p = 0.000$ ) in AI. CT perfusion showed CCD in nine cases and SPECT in eight of the nine patients ( $R^2 = 0.77$ ,  $p = 0.000$ ).

**CONCLUSION**

CT perfusion using 320 rows area detector CT, particularly AI, had diagnostic performance equivalent to  $^{99\text{m}}\text{Tc}$ -ECD SPECT to assess CBF in acute stroke patients with the CA or MCA disease. CT perfusion was able to find CCD.

**KEY WORDS:** 320 detector row CT, CT perfusion, SPECT

## eP-110

### Downsloping of the Third Ventricle: A Reliable Indicator of Intracranial Hypotension?

Tan, J. C.·Dillon, W. P.

University of California San Francisco  
San Francisco, CA

#### PURPOSE

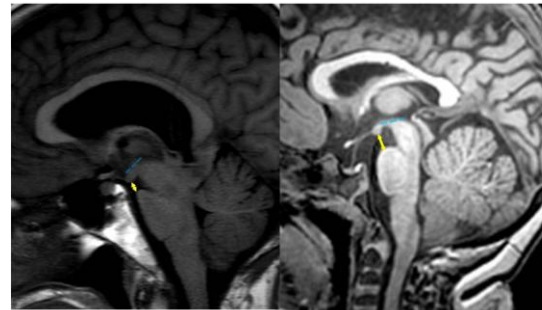
Chiari I malformation and intracranial hypotension can be difficult to differentiate. Both clinical entities may present with chronic daily headache. Both may demonstrate low-lying cerebellar tonsils on imaging. Reliable imaging features to differentiate the two entities are critical, as the therapy for Chiari I malformation - usually posterior fossa decompression and duraplasty - differs drastically from the therapy for intracranial hypotension - epidural blood patch. We have noticed that, in patients with intracranial hypotension, qualitative assessment of the floor of the third ventricle demonstrates a draping of the anterior aspect of the ventricular floor over the dorsum sella (Figure 1, blue line). This can be more quantitatively assessed by measuring the distance between the mammillary bodies and the pons (Figure 1, yellow arrow). We propose downsloping of the third ventricle as a helpful imaging feature of intracranial hypotension.

#### MATERIALS & METHODS

In a retrospective review, our hospital's radiology reporting system database was searched for the keywords of intracranial hypotension and Chiari I malformation. Out of the generated brain MRI studies, we selected patients with histories suggesting intracranial hypotension or Chiari I malformation. Criteria for intracranial hypotension included postural headache and one or more of the following: cerebrospinal fluid leak, dural tear, lumbar puncture demonstrating low pressure, and symptoms responding to epidural blood patch. Criteria for Chiari I malformation included low-lying cerebellar tonsils and normal pressure on lumbar puncture or symptomatic response to surgical decompression. Two neuroradiologists reviewed brain MRI studies for the criteria of downsloping of the third ventricle, decreased pontomammillary body distance (defined as less than or equal to 5 mm), diffuse dural enhancement, enlargement of dural venous sinuses, subdural fluid collections, and low-lying cerebellar tonsils (defined as greater than or equal to 5.5 mm below the foramen magnum).

#### RESULTS

Forty patients were found that met criteria for intracranial hypotension. Forty patients were found that met criteria for Chiari I malformation. All of the patients with intracranial hypotension had a downsloping third ventricle and a decreased pontomammillary body distance. None of the patients with Chiari I malformation had a downsloping third ventricle or a decreased pontomammillary body distance.



A. Intracranial hypotension

B. Chiari I malformation

#### CONCLUSION

The imaging feature of a downsloping third ventricle is a useful addition to the armamentarium of known imaging characteristics of intracranial hypotension. A downsloping third ventricle was sometimes seen without inferior displacement of the cerebellar tonsils, suggesting that it is an early finding.

**KEY WORDS:** Spontaneous intracranial hypotension, Chiari malformation, third ventricle

## eP-111

### Isolated Involvement of Occipital Cortex in Patients with Hypoxic Ischemic Encephalopathy

Parmar, H. A.·Trobe, J.

University of Michigan  
Ann Arbor, MI

#### PURPOSE

Hypoxic-ischemic encephalopathy (HIE) results from a global insult, either due to ischemia from hypoperfusion or hypoxia in the setting of sufficient perfusion. Although there are multiple causes of HIE, the most common are cardiac arrest and respiratory failure. The clinical deficits and imaging abnormalities typically reflect damage to the neocortex, deep cerebral gray nuclei, hippocampus, cerebellum, and parieto-occipital watershed regions. The primary visual cortex is not widely recognized as an isolated target in HIE.

#### MATERIALS & METHODS

We undertook a retrospective evaluation of our departmental electronic medical records over last 6 years. We identified patients presenting with cortical blindness following cardiac arrest, systemic hypotension or global hypoperfusion. CT and MRI studies were evaluated in all these patients. We selected only patients with isolated or predominant involvement of occipital lobes on imaging and all who had clinical evidence of visual abnormalities.

#### RESULTS

Seven patients met our inclusion criteria of visual field abnormalities on clinical inspection and isolated (or predominant) involvement of the occipital lobes on neuroimaging. There were six male and one female

patients (age range of 15 years to 56 years). Five patients had documented cardiac arrest (2 due to motor vehicular accident, 1 from electrocution and 2 with myocardial infarction) and two patients had systemic hypotension sustained during cardiac surgery. Two patients presented with acute vision abnormalities (within 7 days) and abnormal signal in the occipital lobes on the diffusion-weighted imaging. In the subacute period (1-3 weeks) (2 patients), abnormal signal were demonstrable on the T2 and FLAIR sequences, subtle obscuration of gray-white matter differentiation and enhancement after contrast administration is. In the chronic period (after 3 weeks) (3 patients), conventional MRI showed signs of laminar necrosis and volume loss. One patient had changes of volume loss on CT scan as he could not get MRI due to cardiac pacemaker.

### CONCLUSION

Our study is notable for demonstrating hypoxic-ischemic damage to the primary visual cortex without other enduring neurologic deficits. Recognition of this phenomenon was delayed in five patients because the visual field lacked the typical hemianopic features associated with visual cortical damage, and the MRI signs were so subtle - on the early and the late studies - as to be initially overlooked. Although not traditionally acknowledged as a vulnerable region in HIE, the primary visual cortex has features that could make it susceptible to damage in this condition. It lies at a remote region of arterial blood supply, the terminus of the posterior cerebral artery. Under hypotensive conditions, perfusion may not be adequate. Other possible explanation is that the granular cells in the occipital striate cortex are more developed and may be more sensitive to an hypoxic state than other neuronal cells. It is noteworthy that the same striate cortex is preferentially involved in cases with methyl mercury poisoning. It has not been clarified why the striate cortex is vulnerable in cases with methyl mercury poisoning, but there might be some factors which overlap with those in cases with cortical blindness due to an hypoxic state.

**KEY WORDS:** Hypoxic- ischemic encephalopathy, occipital lobe, cortical blindness

### eP-113

#### Diffuse Axonal Abnormalities after Mild Traumatic Brain Injury: A Multivoxel Proton MR Spectroscopy at 3 T

Kirov, I. Tal, A. Babb, J. Grossman, R. Gonen, O.

New York University Medical Center  
New York, NY

### PURPOSE

While most mild traumatic brain injury (mTBI) patients have unremarkable clinical MRI, many have neurologic complaints. Since quantitative MR is sensitive to microscopic pathology, our goal was to test whether metabolic abnormalities are quantifiable with multivoxel proton MR spectroscopic imaging ( $^1\text{H}$ -MRSI)

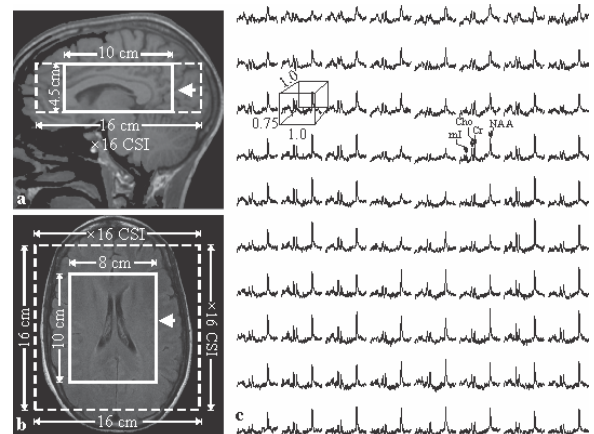
via surrogates: N-acetylaspartate (NAA) for neuronal integrity, creatine (Cr) for cellular energy/density, choline (Cho) for membrane turnover and myo-inositol (ml) for astroglial proliferation.

### MATERIALS & METHODS

All experiments were done at 3 T. Clinical T1- and T2-weighted MRI was used to center the 3D  $^1\text{H}$ -MRSI (480 voxels over  $360\text{ cm}^3$ , ~30% of the brain) on the diencephalon and corpus callosum as shown in Figure 1a-b. Spectra from the axial slice in Fig.1b are shown in Fig.1c. Twenty-six mTBI patients (mean Glasgow Coma Scale score 14.7), 18-56 years old, 3-55 days postinjury and 13 matched controls were scanned. Metabolite levels, along with gray-, white-matter and cerebrospinal fluid (GM/WM/CSF) fractions were obtained in each voxel. Global GM and WM absolute metabolic concentrations were estimated using linear regression and patients were compared with controls using two-way analysis of variance.

### RESULTS

Of the four mTBI patients who had positive MRI findings, only two had any MRI findings that may have been related to their mTBI. Sixteen patients reported at least one neurologic symptom that they attributed to their mTBI. Five of those patients were on physician-prescribed medications. Patients' average concentrations of NAA, Cr, Cho and ml in GM and of Cr, Cho and ml in WM were not different from controls'. However, NAA significantly lower in patients' than in controls' WM ( $7.2 \pm 0.8$  versus  $7.7 \pm 0.6$  mM,  $p=0.0125$ ). Patients who reported at least one symptom had lower WM NAA than those who did not have complaints ( $7.0 \pm 0.6$  versus  $7.6 \pm 1.1$  mM). Finally, the Cho and Cr levels in WM of all patients correlated with time from mTBI.



### CONCLUSION

Since the metabolic concentrations were deduced by linear regression using the entire dataset of 480 voxels, they represent the global concentrations of GM and WM inside the  $360\text{ cm}^3$  region-of-interest. Importantly, any abnormalities detected this way must be diffuse since focal changes would be averaged out. Given that NAA is a surrogate marker for neuronal damage, the findings of decreased WM NAA support the hypothesis that the initial mTBI sequelae are axonal and diffuse. Absence of GM damage and WM glial abnormalities that may

accompany axonal degeneration suggest that dysfunction rather than degeneration dominate at least shortly after mTBI.

**KEY WORDS:** Mild traumatic brain injury, proton MR spectroscopy, diffuse axonal injury

#### eP-114

### Cerebrospinal Venous Stenosis: A Common Radiologic Finding

Alahmadi, K. O. A. • Fox, A. J. • Symons, S. P. • Howard, P. • Yeung, R. • Aviv, R. I.

Sunnybrook Hospital  
Toronto, ON, CANADA

#### PURPOSE

One hundred thirty patients undergoing CT for various nonmultiple sclerosis reasons had images retrospectively entered into a database of vein diameters. The purpose was to show prevalence and characteristics of venous narrowings in a variety of locations, for non-MS patients. CT shows not only venous luminal size, but also adjacent extravenous tissues. Contrarily, the published works by Zamboni and colleagues used Duplex ultrasound to assess.

#### MATERIALS & METHODS

Veins were analyzed consistently by measuring the widest and narrowest diameters of main neck and cerebral veins, and calculating percentages for each narrowing. Adjacent tissues also were assessed for potential extrinsic venous compression. Variables of gender, CT indication, and level of narrowing for each were recorded. Percent venous narrowing was calculated by dividing narrowest measurements by the widest, subtracted from 1, multiplied by 100, as for carotid stenosis, and described with mean, standard deviation (SD), median, minimum and maximum.

#### RESULTS

A total of 130 patients were studied with 27 (20.8%) for trauma, 55 (42.3%) for malignancy, 38 (29.2%) for infection and 1 (0.8%) for bleeding. Forty-seven patients (36%) were female and 83 (64%) male. Mean age at CT was 60 years (SD = 17.24) with a range from 19 to 100 years old (median age 61). While some patients had two studies for the same reason, one had two different indications (stroke and trauma). A substantial number of veins showed measurable narrowing more than 50% stenosis. Locations of stenosis we most commonly at C1-2, with others scattered through the neck veins. Most narrowings were associated with identified extrinsic compressive tissues, including 12 by blood vessels, 10 by muscles, 17 partial and 14 severe by lateral mass of C1 (with digastric muscle), 18 by lymph node, abscess, or mass. Discussion: This study investigated vein diameters from enhanced CT assessing morphology of extracranial veins and surrounding tissues, and found common venous narrowings explained by compression from adjacent structures. Zamboni et al based the diagnosis on venous hemodynamic, not morphologic features with Doppler,

reporting multiple significant stenoses of internal jugular, azygous, and lumbar veins caused by intrinsic anomalies like annulus, septum, and valve malformations, hypoplasia, twisting, membranous obstruction or segmental agenesis. They may not have fully studied surrounding tissues to exclude extrinsic vascular stenoses, as we have found to be common. They arbitrarily considered significant stenosis as any venous lumen reduction greater than 50% on selective images.

#### CONCLUSION

Contrast CT (including CTA) is noninvasive, less operator-dependent, less time consuming than Doppler. CT can evaluate anatomical and morphologic features of extracranial veins and surrounding anatomical structures, also causing venous stenosis. CT lacks dynamic real time. It can show collapse of veins under multiple circumstances such as Valsalva, another intrinsic reason for vascular collapse. It may be that Zamboni's diagnosis of venous stenosis did not fully study for extrinsic tissues.

**KEY WORDS:** Cerebrospinal veins, multiple sclerosis, enhanced CT neck

#### eP-115

### Image-Based Automated Prediction of Disability in Acute Stroke Patients by Leveraging Lesion Topography and Statistical Models

Bammer, R. • Straka, M. • Albers, G.

Stanford University  
Staford, CA

#### PURPOSE

Diffusion-weighted imaging (DWI) and perfusion-weighted imaging (PWI) are used to identify infarct core and at-risk tissue in acute stroke. A substantial mismatch between core and at-risk tissue predicts a favorable outcome if tissue is reperfused successfully, whereas either a large DWI or PWI lesion represent a malignant profile and indicate that patients will most likely sustain harmful reperfusion injuries (see DEFUSE study). Thus far, imaging-based prediction of clinical outcome has been primarily on overall lesion size or volumetric mismatch. However, volumetric mismatch neglects the impact of lesion topography on clinical disability. Here, we introduce a per-pixel importance-weighting,  $w(r)$ , to the mismatch analysis, in which voxels contribute more or less to the scoring metric, based on local stroke incidence.

\$\$\$MISSING OR BAD TABLE SPECIFICATION {0472D329-0D47-402B-80A7-5D7DDAB510BF}\$\$\$

#### MATERIALS & METHODS

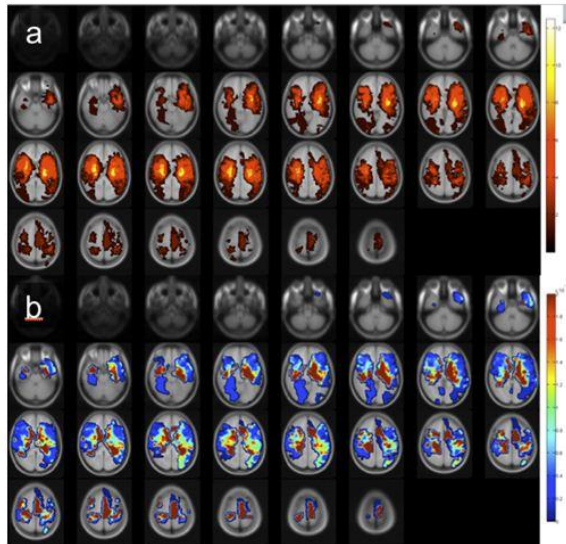
To derive  $w(r)$  we built a statistical model that combined existing manually segmented day-5 FLAIR imaging data and nonlinearly coregistered (to MINC atlas) with day-5 NIHSS scores from the acute stroke data repository ( $n=44$ ) of the DEFUSE trial. Specifically, we averaged over all existing  $j = 1 \dots n$  patients so that local weighting coefficients were:  $w(r_j) = M$



$\frac{1}{N} \sum (L_j(r_i) \cdot \text{NIHSS}_j / \text{LV}_j)$ , where  $\text{NIHSS}_j$  and  $\text{LV}_j$  are the disability score and lesion volume for the  $j$ -th patient, respectively.

## RESULTS

The figure (a) shows the stroke incidence on a per-voxel basis derived from 44 acute stroke patients in atlas space. Since DEFUSE enrolled mostly MCA strokes, the counts in the ACA territory and the posterior circulation were relatively sparse. Both hemispheres had very similar stroke incidence rates for the MCA territory. In (b), the corresponding relative contributions of individual voxels to the final NIHSS are shown. Note the considerable hemispheric asymmetry of the spatial weight distributions. The latter is due mostly to the composition of the NIHSS, which accounts more points to the dominant hemisphere. Thus, lesions in the dominant hemisphere contribute more to disability. Using leave-one-out analysis, the relationship between the predicted NIHSS and true NIHSS demonstrated high correlation ( $r > 0.9$ ).



## CONCLUSION

Previous work on stroke atlases has been limited to ASPECT-derived or expert-based scores from predetermined regions. Our approach is related to a population-averaged variant of the data-driven method suggested by Menezes et al (Stroke-38:194-197) applied to a selected acute stroke population. This pilot study demonstrates very encouraging results that suggest the feasibility of automated prediction of disability. Most striking was the regionally localized contributions to NIHSS. Currently, our atlas is limited to MCA territories but will be expanded to ACA and the posterior circulation in the near future.

**KEY WORDS:** Stroke

## eP-116

### GRAPPA-Accelerated Dual-Echo Diffusion-Weighted Echo Planar Imaging with Intensity Correction

Holdsworth, S. J.<sup>1,3</sup>Skare, S.<sup>2</sup>Straka, M.<sup>1,3</sup>Inoue, M.<sup>3</sup>Bammer, R.<sup>1</sup>

<sup>1</sup>Stanford University, Stanford, CA, <sup>2</sup>Karolinska Institute, Stockholm, SWEDEN, <sup>3</sup>Stanford University Medical Center, Stanford, CA

## PURPOSE

Parallel imaging affords reduced geometric distortion and blurring in diffusion-weighted single-shot (ss)-EPI (DWI) as well as shorter echo time. The latter reduces "T<sub>2</sub>-shine-through", but in turn may result in reduced lesion conspicuity on DWI. To retain DWI's sensitivity to lesions and improve quality, we present a novel GRAPPA-accelerated dual-echo EPI DWI sequence and validated it on stroke patients. In addition, we introduce a new technique to remove equivocal coil-induced intensity modulations.

## MATERIALS & METHODS

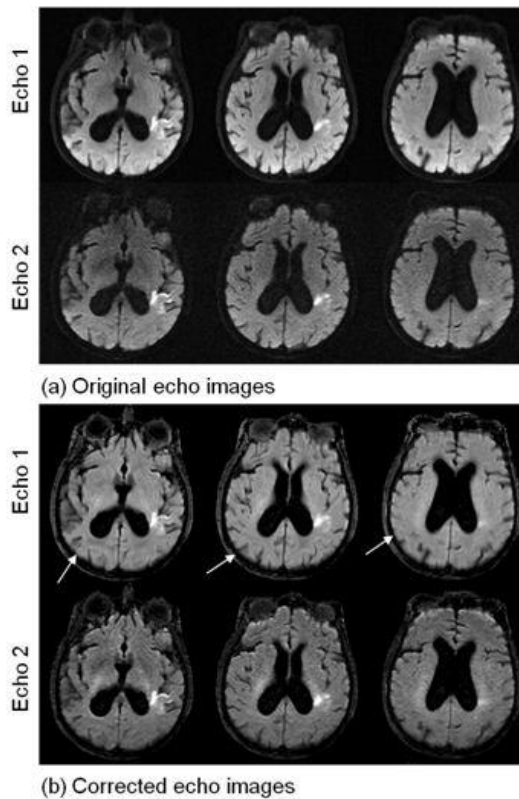
The study was IRB approved and after obtaining consent, 15 stroke patients were imaged using a 1.5T GE system and an 8-channel head coil: tetrahedral encoding ( $b=1000\text{s/mm}^2$ ), matrix =  $192^2$ ,  $R = 3$ , NEX = 2, TR/TE<sub>1</sub>/TE<sub>2</sub> = 3s/51ms/115ms, 24cm FOV, and slthck/gap=5mm/1.5mm. Both echoes were corrected for signal intensity variations across the images using a new data-driven, calibration free method.

## RESULTS

The figure shows one example of the new GRAPPA-accelerated dual-echo EPI scan acquired on a 91-year-old stroke patient with a left MCA occlusion. The increased lesion conspicuity of echo 2 is apparent. Fig. 1b shows coil sensitivity-corrected maps, which remove the hyperintensity of the signal - particularly in the posterior regions where cortical regions are closer to individual coil elements. In all 15 cases, the second echo was more conspicuous, particularly in smaller embolic lesions and lacunes, or cortical lesions, whilst the first echo offered pristine ADC maps with high SNR.

**Discussion:** The use of a long-TE echo goes against the common teaching that TE should be kept short to avoid "T<sub>2</sub>-shine-through". While this might be true for separating acute from subacute lesions, general lesion conspicuity suffered from short echo times despite the greater SNR. Note that the combined effect of diffusion-restriction, diffusion-based attenuation of normal tissue, and slightly prolonged lesion T<sub>2</sub> gives additional lesion contrast that is not achievable on T<sub>2</sub>-wFSE or FLAIR. Moreover, the added information from quantitative ADC and T<sub>2</sub> furthered our ability to differentiate between acute and subacute lesions. Lastly, the removal of coil-induced intensity bias improved diagnostic confidence in cortical areas close to coil elements. One could argue that a calibration scan could be acquired for coil-sensitivity correction, however this adds scan time.





#### CONCLUSION

Diffusion-weighted imaging with short-TE, due to parallel MRI, can miss stroke lesions. Dual-echo DWI should be used to boost lesion conspicuity (late echoes) and afford high SNR ADC maps (early echoes). Coil bias fields can be removed from the echoes without extra calibration scans.

**KEY WORDS:** Diffusion weighted

#### eP-117

#### Usefulness of Magnitude Image for Susceptibility-Weighted Imaging to Evaluate the Treatment of Dural Arteriovenous Fistula

Miyasaka, T.<sup>1</sup>•Taoka, T.<sup>2</sup>•Ochi, T.<sup>2</sup>•Akashi, T.<sup>2</sup>•Myochin, K.<sup>2</sup>•Wada, T.<sup>2</sup>•Takayama, K.<sup>2</sup>•Nakagawa, H.<sup>1</sup>•Kichikawa, K.<sup>2</sup>

<sup>1</sup>Nara Prefectural Nara Hospital, Nara, JAPAN, <sup>2</sup>Nara Medical University, Kashihara, JAPAN

#### PURPOSE

To evaluate the role of signal intensity of magnitude images for SWI (SWImag) in diagnosis and followup in patients with draining veins of dAVF.

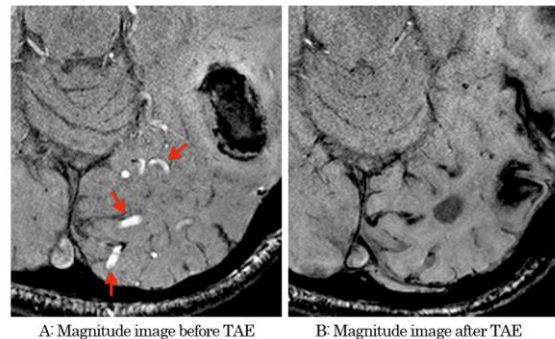
#### MATERIALS & METHODS

Seven patients (3 male, 4 female, aged 54-76 years: mean 66.1 years) with angiographically proven dAVF (5 patients of TS-SS dural AVF, 1 patient of tentorial AVF, 1 patient of cavernous dural AVF) were included. Two patients had hemorrhage, three patients had dizziness, a patient had tinnitus and a patient had exophthalmos.

Susceptibility-weighted imaging using 3D-FLASH was undergone in 3 T MR suite. The scanning parameters were: TE value = 20 ms, TR = 27 ms, FA value = 15 and slice thickness = 1.3 mm. The draining veins of seven patients were identified on cerebral angiography and the signal intensity of the SWImag before the treatment was assessed. Then, on SWImag, the change of the signal intensity of the draining veins before and after the treatment was assessed in reference to follow-up angiography.

#### RESULTS

Fifteen draining veins were identified on angiography. On SWImag before the treatment, nine veins (60%) were visualized as high intensity (arrows), three veins (20%) as moderate intensity, three veins (20%) as unidentified. Three patients were treated by TAE, four patients were treated by TVE and the arteriovenous shunt completely disappeared in five patients, decreased residual shunt was still found in two patients. In nine high-intensity veins before the treatment, all of eight draining veins, which completely disappeared on angiography after the treatment, were lower signal intensity. One draining vein, which had decreased residual shunt after the treatment, showed lower intensity. In three moderate-intensity veins, which completely disappeared on angiography after the treatment, one draining vein showed lower signal intensity, one draining vein showed the same intensity, and one draining vein was not depicted by coil artifacts.



#### CONCLUSION

SWImag depicted the majority of the draining veins of dAVF as bright intensity. We speculate that higher concentration of oxy-Hb within draining veins is one of the causes of high-signal intensity. Draining veins, which disappeared on angiography after the treatment, showed lower signal intensity than before treatment due to decreased velocity and lower concentration of oxy-Hb.

**KEY WORDS:** SWI, dAVF, red vein

## eP-118

### Hemodynamic Effects of Carotid Artery Stenting on Cerebral Vascular and Cerebrospinal Fluid Flow: Quantitative Analysis of 2D Phase-Contrast Cine MR Imaging

Youn, S.<sup>1</sup>•Lee, J.<sup>2</sup>•Kim, H.<sup>1</sup>•Lee, H.<sup>2</sup>

<sup>1</sup>Daegu Catholic University Medical Center, Daegu, KOREA, REPUBLIC OF, <sup>2</sup>Kyungpook National University Hospital, Daegu, KOREA, REPUBLIC OF

#### PURPOSE

Carotid artery stenting (CAS) has been expected to prevent acute stroke and to reverse chronic cerebral ischemia in patients with severe carotid artery stenosis. However, little has been revealed on hemodynamic effect of CAS on cerebral vein, cerebrospinal fluid (CSF) as well as artery. We prospectively evaluated the hemodynamic changes after CAS by using 2 D phase-contrast magnetic resonance imaging (2D PC MRI).

#### MATERIALS & METHODS

A total of 15 severe carotid artery stenosis (14 patients; 11 men; mean age, 72.1 years old) were treated with CAS, and 2D PC MRI of five scan plane was performed before and within 48 hours after CAS. From region of interest of vessels and CSF, the time-to-flow volume curve was produced by using software (CImage, GE, Wisconsin). The cerebral blood flow volumes (CBFVs), peak systolic velocities (PSVs) were compared between pre-CAS and post-CAS by paired T-test.

#### RESULTS

At both neck and brain levels, the total CBFV of arteries, the CBFV and PSV of stented-side carotid artery, the percentage of CBFV of stented-side carotid artery among total CBFV increased after CAS, respectively ( $p < 0.05$ ). The total CBFV of both side internal jugular vein (IJV), sum of superior sagittal sinus (SSS) and straight sinus (SS), and CBFV of right IJV, SSS, and SS increased respectively without change of PSV after CAS ( $p < 0.05$ ). At both neck and brain levels, the CBFV and PSV of CSF did not change after CAS.

#### CONCLUSION

2D PC MRI is a useful technique to evaluate the effect of CAS on the artery, vein, and CSF. Carotid artery stenting improves total CBFV of both artery and vein by increasing CBFV and PSV of stented-side carotid artery, with no change on the CSF.

**KEY WORDS:** Carotid artery stenting, phase contrast MR imaging, hemodynamic effect

## eP-119

### Risk Factors for Rebleeding of Aneurysmal Subarachnoid Hemorrhage Based on the Analysis of On-Admission Information

Wu, C. •Liu, Y. •Zhao, Z. •He, M. •You, C.

West China Hospital, Sichuan University  
Chengdu, CHINA

#### PURPOSE

Rebleeding was still a commonly devastating complication of aneurysmal subarachnoid hemorrhage (aSAH), especially when early surgical intervention was not applicable due to many reasons. Our aim was to provide a quick evaluation of rebleeding risk based on the on-admission information and to guide the management of patients.

#### MATERIALS & METHODS

A retrospective review of 630 consecutive cases of SAH in our institution from January 2005 to December 2008 has been preceded and 458 cases were included for analysis. Sixty-three cases of in-hospital rebleeding were identified by clinical symptoms or computed tomography (CT) scan. Chi-square or Mann-Whitney test were used to screen for the possible risk factors from clinical variables and hematologic parameters. The predictive values of the associated risk factors were assessed by logistic multivariate regression.

#### RESULTS

The identified risk factors were time interval between the first attack and admission less than 2 days, male, poor Hunt-Hess grade (III~V), high systolic pressure ( $>140$  mmHg), intracerebral or intraventricular hematoma, high level of serum glucose ( $>6.32$  mmol/L) and white blood cell counting (WBC counting  $>12 \times 10^9/L$ ). Logistic regression analysis showed that intracerebral or intraventricular hematoma ( $p = 0.010, OR = 1.478$ ), blood glucose above 6.32 mmol/L ( $p = 0.011, OR = 2.126$ ) were independent risk factors.

#### CONCLUSION

We found that a particularly high risk of rebleeding was observed among patients who had intracerebral or intraventricular hematoma on the initial CT scan or had a relatively high serum glucose level on admission. The finding of high level of serum glucose and WBC as risk factors for rebleeding might indicate that patients stress response status could relate to rebleed. Based on the on-admission information, an earlier and more aggressive intervention may be applied to patients at high risk.

**KEY WORDS:** Aneurysmal subarachnoid hemorrhage, rebleeding, risk factor

## eP-120

### Thalamic Pseudomass Secondary to Venous Hypertension

Sabby, T. L. •Hunt, C. H. •Black, D. F. •Morris, J. M. •Miller, G. M. •Campeau, N. G.

Mayo Clinic  
Rochester, MN

#### PURPOSE

Hypertension involving the deep cerebral venous system, with or without deep internal cerebral vein thrombosis, has a protean appearance and can lead to changes ranging from reversible unilateral or bilateral thalamic edema to thalamic infarction. The imaging

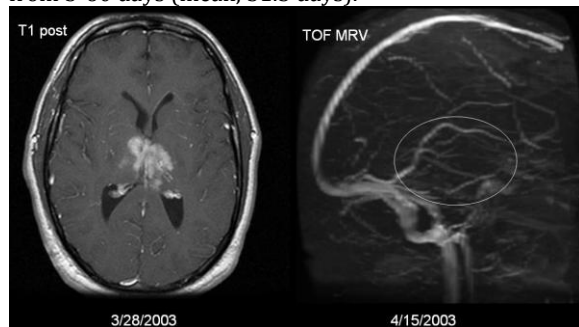
appearance may mimic that of glioma and lymphoma, leading to delayed or misdiagnosis of a potentially treatable entity. We present a subset of patients with the common imaging feature of enhancing thalamic pseudomass due to venous hypertension in order to better characterize and aid in the detection of this disorder.

#### MATERIALS & METHODS

At our institution, we have encountered four patients since 2002 who have presented with thalamic pseudomass due to venous infarction. A retrospective chart review was performed with attention to clinical presentation, MRI appearance, initial differential diagnosis, any interventions performed, and ultimate cause of the venous infarction.

#### RESULTS

The four patients ranged in age from 18 to 71 years (two males and two females). All of these patients presented with a stuttering neurologic course that was not typical for arterial infarction. The time course from initial presentation to initial imaging varied from 0 to 4 days. MR imaging demonstrated that all patients had mass-like enlargement of the bilateral thalami with minimal diffusion restriction. Upon gadolinium administration, intense, patchy enhancement was noted throughout the bilateral thalami in all of our patients. Venous pathology was not suspected initially or recognized in three of four patients, with early differential considerations including lymphoma and high-grade glioma. One patient underwent stereotactic brain biopsy which yielded a nondiagnostic result. A second brain biopsy was being considered when repeat MRI yielded the diagnosis of evolving thalamic infarction. Two patients underwent lumbar puncture for cytology to exclude lymphoma. All of our patients had venous hypertension as a common mechanism for venous infarction, with three having venous sinus thrombosis and one with a dural arteriovenous fistula. The time from initial symptom to final diagnosis ranged from 3-60 days (mean, 31.5 days).



#### CONCLUSION

Venous hypertension can be a common cause of bithalamic infarction. Delayed presentation and imaging can lead to imaging of the infarct during the subacute phase, mimicking the appearance of an underlying mass from either a high-grade glioma or lymphoma. Recognition of the imaging characteristics we describe is essential for making a timely and correct diagnosis and avoiding delayed treatment and invasive interventions.

**KEY WORDS:** Venous infarction, thalamic infarction, pseudomass

#### eP-121

#### Mean Transit Time Thresholds for Penumbra Characterization: Difficulties in Definition and in Application beyond the Individual

Ahmed, A.<sup>1</sup>An, H.<sup>2</sup>Ford, A. L.<sup>3</sup>Kumar, G.<sup>3</sup>Vo, K. D.<sup>1</sup>Lin, W.<sup>2</sup>Lee, J.<sup>3</sup>

<sup>1</sup>Mallinckrodt Institute of Radiology, St Louis, MO,

<sup>2</sup>University of North Carolina at Chapel Hill School of

Medicine, Chapel Hill, NC, <sup>3</sup>Washington University in St Louis School of Medicine, St Louis, MO

#### PURPOSE

The MR diffusion-perfusion mismatch (DPM) is a commonly used model to delineate the ischemic penumbra, which has been hypothesized to represent reversibly injured, but potentially salvageable tissue in patients presenting with acute stroke. However, it remains challenging to define the optimal perfusion-based threshold for identifying this tissue at risk for infarction, both in individual patients and in a population. In this study, we calculated the ischemic thresholds for gray matter in a cohort of acute stroke patients using cerebral blood flow (CBF) and mean transit time (MTT), and assessed the ability of these parameters' thresholds to predict penumbral tissue infarction. In addition, we evaluated the variability of the penumbral thresholds across patients and tried to determine if a population-based, mean ischemic threshold value could feasibly be applied to all individuals.

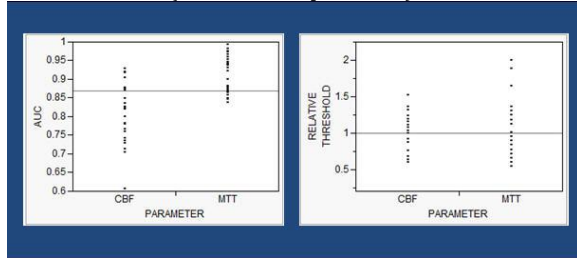
#### MATERIALS & METHODS

Twenty-seven patients were studied prospectively using dynamic susceptibility contrast (DSC) perfusion-weighted imaging (PWI) and diffusion-weighted imaging (DWI) within 3 hours of stroke symptom onset. FLAIR images obtained at 1 month were used to define final infarct region. Rigid image registration was performed to align patient images, and segmentation performed to isolate gray matter. Cerebral blood flow and MTT were computed, with MTT prolongation (MTT of affected tissue - mean MTT of the contralateral hemisphere) used to define the severity of the perfusion deficit. Histograms were constructed to demonstrate the relative frequency of MTT prolongation and CBF values for tissue destined to die or survive. ROC analysis was performed to measure the predictive value of CBF and MTT relative to the final infarct. Areas under the ROC curve (AUCs) for both parameters were generated and compared. Population means and variances for the CBF and MTT prolongation thresholds were calculated and compared.

#### RESULTS

The mean AUCs for MTT and CBF were 0.92 ( $\pm 0.08$ ) and 0.82 ( $\pm 0.16$ ), respectively, demonstrating that MTT is superior to CBF at predicting final tissue infarction in individual patients ( $p < 0.001$ ). The mean population threshold values for MTT prolongation and CBF were

5.47 seconds ( $\pm 4.4$ ) and 0.45 mL 100 g<sup>-1</sup> min<sup>-1</sup> ( $\pm 0.21$ ), respectively. Mean transit time thresholds, however, demonstrated a significantly higher variance than the CBF thresholds (F ratio = 4.6,  $p = 0.036$ ).



## CONCLUSION

While MTT prolongation performs better than CBF at predicting tissue infarction on an individual level, the high degree of MTT threshold variance may limit the utility of a population average in individual patients.

**KEY WORDS:** Ischemic penumbra, perfusion MR, mean transit time

## eP-122

### Analysis of Vein and Venous Sinus on Susceptibility-Weighted Imaging in Consideration of Vessel Size, Flow Velocity, and Oxygen Saturation

Choi, H.<sup>1</sup>Jung, S.<sup>2</sup>Ahn, K.<sup>3</sup>Kim, B.

Seoul St. Mary's Hospital  
Seoul, KOREA, REPUBLIC OF

## PURPOSE

Susceptibility-weighted image (SWI) is sensitive in small venous structure on behalf of phase difference with brain parenchyma, flow velocity, and paramagnetic effect of deoxy-hemoglobin. However, venous sinus which is larger than cortical vein shows brighter on magnitude image and SWI. It is known that vessel signal intensity is affected by flow direction, flow velocity, and oxygen saturation. The purpose of this study was to evaluate patterns of signal intensity in venous system on SWI in consideration of vessel size, flow velocity, and oxygen saturation.

## MATERIALS & METHODS

We hypothesized those veins with larger diameter, higher velocity, and higher oxygen saturation show higher signal intensity on magnitude image and SWI. Shunted flow of AVM might be larger diameter, higher velocity, and higher oxygen saturation than normal cortical vein. We included cortical vein, superior sagittal sinus (SSS), and venous side of arteriovenous malformation (AVM) as target veins of analysis: those veins are different in diameter, flow velocity, and oxygen saturation. We measured signal intensities of those venous structures both on magnitude image and SWI. Measured signal intensities were normalized with signal intensity of centrum semiovale. There were eight patients with AVM who underwent both DSA and SWI between June 2009 and April 2011. Normal age-matched controls were found on PACS in the same period: same parameters for SWI were used.

## RESULTS

Superior sagittal sinus and draining venous side of AVM showed higher signal intensity than cortical vein on magnitude image and SWI. Superior sagittal sinus in patients with AVM showed higher signal intensity than cortical vein both on magnitude image and SWI. Signal intensities of cortical vein were not different between normal subject and patients with AVM. Magnitude image and SWI showed significant signal difference in SSS of normal subject. However, magnitude image and SWI showed no significant signal difference in venous side of AVM.

## CONCLUSION

Veins and venous sinuses on magnitude image and SWI were affected by vessel diameter, flow velocity, and oxygen saturation. Further quantitative analysis should be followed for functional imaging of venous system.

**KEY WORDS:** SWI, vein, AVM

## eP-123

### Susceptibility-Weighted Imaging: Technical Aspect as Shortening Acquisition Time

Shih, Y. Y.<sup>1</sup>Tsai, P. H.<sup>2</sup>Tsai, F. Y.<sup>3,2</sup>Chan, W. P.<sup>2</sup>Chung, H. W.<sup>4</sup>

<sup>1</sup>Siemens Limited Healthcare Sector, Taipei, TAIWAN, <sup>2</sup>Taipei Medical University, Taipei, TAIWAN, <sup>3</sup>University of California, Irvine, Orange, CA, <sup>4</sup>National Taiwan University, Taipei, TAIWAN

## PURPOSE

We have used susceptibility-weighted imaging (SWI) to evaluate acute stroke patients to identify thrombosis and possible penumbra. The acquisition has been too long for examining acute stroke patients due to motion from agitation and mental changes. We developed new technique to shorten the acquisition to have diagnostic quality SWI with those acute stroke patients.

## MATERIALS & METHODS

Susceptibility-weighted imaging sequence parameters were performed in 1.5 T Siemens Avanto magnet (Siemens Medical Solution, Erlangen, Germany) as recommended by manufacturer: TE (Echo time) 40 ms; TR (reception time) 49 ms; Flip angle 15 degrees; Slice thickness 2 mm; Bandwidth 80 Hz/pixel and Voxel size 1.1x0.9x2.0 mm; Slices per slab 60; Slice resolution 80%; Matrix 224x256; iPAT = 2 and scanning time 3.46 min. We have tried five different parameters on matrix size, voxel size, slice resolution as well as partial Fourier to compare with better diagnostic quality of SWI with volunteers, focusing on altering the parameters related to phase encoding directions.

## RESULTS

We were able to shorten the scanning time from 3.46 min to 2.14 min with maintaining diagnostic quality of SWI images.

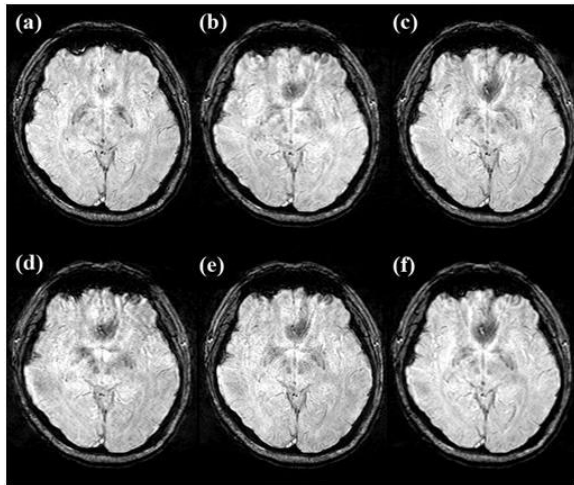
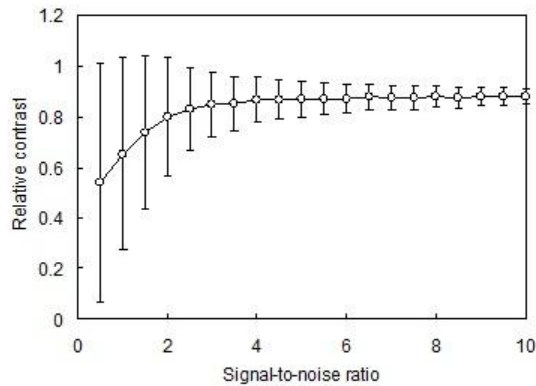


Fig. 1. Simulation results of SNR vs contrast between veins and normal white matter

Fig. 2. Images from 28<sup>th</sup> slice with different parameters: default settings (a) and other five trials (b-f)

#### CONCLUSION

We have successfully achieved shortening acquisition time of SWI from 3.46 min to 2.14 min by altering the several parameters but maintaining diagnostic quality. We also have applied this modified SWI to clinical acute stroke patients.

**KEY WORDS:** Stroke, SWI, MR imaging

#### eP-124

##### Cerebral Aneurysms in Patients with Coarctation of the Aorta: Prevalence and Need for Screening

Mortimer, A. M.<sup>1</sup>•Curtis, S. L.<sup>2</sup>•Wilde, P.<sup>2</sup>•Aw, J.<sup>2</sup>•Chakrabarti, S.<sup>2</sup>•Hamilton, M.<sup>2</sup>•Martin, R.<sup>2</sup>•Turner, M.<sup>2</sup>•Stuart, G. A.<sup>2</sup>•Bradley, M.<sup>1</sup>

<sup>1</sup>Frenchay Hospital, Bristol, UNITED KINGDOM, <sup>2</sup>Bristol Heart Institute, Bristol, UNITED KINGDOM

#### PURPOSE

Angiographic and autopsy studies suggest that cerebral aneurysms are found in 0.4-6.0% of adults, whereas those studies based on magnetic resonance angiography (MRA) suggest a prevalence of 0.1-1.8% (a prevalence is <0.5% has been demonstrated in young adults). Older studies suggested that 10-50% of coarctation of the

aorta patients have cerebral aneurysms; however, screening recommendations are variable, with some organizations failing to mention screening in this circumstance, and others making only vague suggestions. The prevalence of cerebral aneurysms and the role of aneurysm screening in coarctation treated in the modern era are unknown. We aimed to: 1. quantify the prevalence of cerebral aneurysms in our cohort of patients with aortic coarctation; 2. investigate the relationship between clinical factors, such as aortopathy and hypertension, and cerebral aneurysms in coarctation of the aorta; 3. determine the need for screening patients with aortic coarctation for cerebral aneurysms.

#### MATERIALS & METHODS

Consecutive patients > 16 years with coarctation undergoing brain magnetic resonance angiography (MRA) between May 1999 and October 2007 were included. MR angiography was performed using a Siemens Symphony 1.5 T scanner using a 3D time of flight protocol, and at the same time magnetic resonance imaging (MRI) was performed of the heart and aorta. Cerebral MRA scans were double-reported by a neuroradiologist. Statistics are described as mean  $\pm$  s.d. and median  $\pm$  range. Continuous variables were compared using Student t-tests and Mann-Whitney U tests (categorical variables using Fisher's Exact test).

#### RESULTS

One hundred seventeen were retrieved for double-reporting. Median age of the patients was  $29 \pm 11$  years (range 16-59 years). IAs were found in 12 patients (10.3%). Mean diameter of the aneurysms was 3.9 mm (range 2.0-8.0 mm). Patients with aneurysms were older than those without (aneurysm group-median 37 years, range 16-50 years; no aneurysm group-median 23 years, range 16-59 years;  $Z = -2.01$ ;  $p = 0.04$ ). However, these patients were younger than those identified with aneurysms in population studies. Hypertension was more common in the aneurysm group (aneurysm group-83% vs no aneurysm group-43%;  $p = 0.01$ ). There was no association between ascending aortopathy, bicuspid aortic valve and cerebral aneurysms.

#### CONCLUSION

Coarctation patients have a higher prevalence of cerebral aneurysms, occurring at an earlier age than in population studies. This study suggests that routine screening for cerebral aneurysms in coarctation may be necessary and may prevent avoidable cerebral hemorrhage. Hypertension is likely to be an important pathophysiologic factor.

**KEY WORDS:** Coarctation, cerebral aneurysm, screening

#### eP-125

##### Immediate Flow Restoration and Clot Extraction for Acute Ischemic Stroke by Using Retrievable Self-Expandable Stent: Initial Experiences of 30 Patients in a Single Institution

Youn, S.<sup>1</sup>•Kim, H.<sup>1</sup>•Lee, H.<sup>2</sup>



<sup>1</sup>Daegu Catholic University Medical Center, Daegu, KOREA, REPUBLIC OF, <sup>2</sup>Kyungpook National University Hospital, Daegu, KOREA, REPUBLIC OF

#### PURPOSE

The purpose of this study was to present our experience of immediate flow restoration (IFR) and clot extraction (CE) by using self-expandable retrievable intracranial stents for the revascularization of acute ischemic stroke.

#### MATERIALS & METHODS

A total of 30 patients with an acute ischemic stroke attributable to a large artery occlusion (mean National Institutes of Health Stroke Scale (NIHSS), 15.8; after intravenous tissue plasminogen activator,  $n = 16$ ; mean symptom-needle time, 210 minutes) were treated prospectively with the Enterprise ( $n = 7$ ) or Solitaire stent ( $n = 23$ ). The occlusion site was middle cerebral artery in 18 (3 with coexisting fetal-type-posterior cerebral artery occlusion), internal carotid artery in nine (8 with involvement of terminal carotid artery and 2 with tandem occlusion of middle cerebral artery), and top of basilar artery in three patients. Immediate flow restoration and CE were performed by unfolding and withdrawing stent. Urokinase ( $n = 5$ ) or antiplatelet agent ( $n = 20$ ) was infused to sustain IFR.

#### RESULTS

Thrombolysis in cerebral ischemia grade (TICI)  $\geq 2$  (2b) was achieved in 90.9% (66.6%). Thrombolysis in cerebral ischemia  $\geq 2$  was achieved in 81.6% of IMF (58/66) and 51.5% of CE (34/66), respectively (mean number of passes per patient, 2.2; mean times of procedure, 118 minutes; mean tirofiban, 412.5 microgram). Five patients (16.7%) had procedural events: two leak by microwire, a side-branch compromise due to clot mobilization, two inadvertent detach. Four patients (13.3%) died from severe brain swelling and hemorrhagic transformation. Sixteen patients (53.3%) demonstrated the improvements of NIHSS within 1 week, and 13 patients (43.3%) had a modified 3 months Rankin Score  $\leq 2$ .

#### CONCLUSION

Despite procedural events, IFR and CE by using the self-expanding retrievable stent can achieve a high rate of recanalization and favorable clinical outcomes in acute ischemic stroke.

**KEY WORDS:** Immediate flow restoration, clot extraction, acute ischemic stroke

#### eP-126

##### Ruptured Cerebral Aneurysms, Large Prevalence of Small Size

Miller, T. S.<sup>1,2</sup>•Baxi, N.<sup>1,2</sup>•Altschul, D.<sup>1,2,2</sup>•Farinhas, J.<sup>1,2</sup>•Pasquale, D.<sup>1,2</sup>•Brook, A.<sup>1,2</sup>•Flamm, E.<sup>1,2</sup>

<sup>1</sup>Montefiore Medical Center, Bronx, NY, <sup>2</sup>Albert Einstein College of Medicine, Bronx, NY

#### PURPOSE

To determine the absolute size of ruptured aneurysms in a population diagnosed with cerebral catheter

angiography. Most practitioners agree that if a patient harbors an unruptured aneurysm, has a personal or strong family history of subarachnoid hemorrhage, and has several years of life expectancy, that patient's aneurysm poses a significant risk, and treatment will improve overall outcome. The situation is not as clear for those patients without a personal or family history of ruptured aneurysm. In patients with aneurysms over 1 cm in size, or with aneurysms located in the posterior circulation, or those with an observed increase in size, or those that are symptomatic, a risk benefit analysis usually favors treatment. Debate rages on the optimal management of small-unruptured cerebral aneurysms.

#### MATERIALS & METHODS

We retrospectively reviewed the medical records of all patients presenting to our institution with aneurysmal subarachnoid hemorrhage.

#### RESULTS

Table.

4 year Data Results								
	<7mm	7-10mm	11-15mm	16-20mm	21-25mm	>25mm	Total	Avg.
ACoM/A	37	14	0	1	0	0	52	5.4
PCoM/A	19	13	0	0	0	0	32	6.2
MCA	20	12	3	0	0	0	35	6.6
ICA	24	6	5	3	0	0	38	7.2
AntChor	5	1	0	0	0	0	6	4.5
ACA	3	0	0	0	0	0	3	4.3
Basilar	5	1	1	1	0	0	8	7.5
PICA	2	1	0	0	0	0	3	5.0
Peric	2	2	0	0	0	0	4	5.5
Total	117(64.6%)	50(27.6%)	9(4.9%)	5(2.7%)	0	0	181	6.3

Four years ruptured aneurysm data at a single institution.

#### CONCLUSION

The 64.6% of aneurysmal SAH from the cohort have aneurysms <7 mm in diameter. Average size of aneurysms rupturing from ACA, ACOM, Pericallosal is smaller than other sites. There is a definite population of small aneurysms that are at high risk of rupture. The cost of aneurysmal SAH to our population is great. Further investigation is warranted to better define this population in order to treat and prevent subarachnoid hemorrhage.

**KEY WORDS:** Aneurysm, subarachnoid hemorrhage

#### eP-127

##### Diffusion-Weighted Imaging of Intravascular Clots in Cerebral Venous Thrombosis

Agarwal, A. •Kanekar, S. •Thamburaj, K. •Maller, V.

Penn State Milton S. Hershey Medical Center  
Hershey, PA

#### PURPOSE

The appearance of intravascular clots, in patients with cerebral venous thrombosis (CVT), has been well



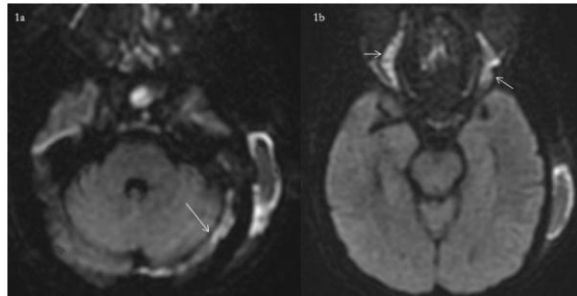
described on conventional MRI. On diffusion-weighted imaging (DWI), some authors previously reported an increased signal corresponding to the presence of intravascular clots in cases of CVT (venous sinuses and cortical veins), in the presence or absence of parenchymal lesions. Both the frequency and diagnostic value of diffusion signal changes in CVT are unknown. For this purpose, in this series of patients with CVT, we investigated the frequency of diffusion signal changes in sinuses or veins, at the time of diagnosis.

#### MATERIALS & METHODS

From January 2007 and July 2011, we selected 54 consecutive patients (30 men, 24 women; age range, 4 to 59 years; mean age, 35 years) with CVT. The diagnosis of CVT was made on the basis of the following criteria: (1) absence of flow or partial flow void in thrombosed sinuses or veins, (2) typical signal abnormalities corresponding to the intraluminal clot on T1 (pre and postcontrast) and/or T2-weighted MRI (including FLAIR and T2 gradient images), (3) complete or partial filling defect on MR venogram. Furthermore, the diffusion images were reviewed for the presence or absence of increased signal in veins or sinuses by visual inspection. Apparent diffusion coefficient (ADC) measurements were made in patients with occluded superior sagittal sinus, because the close vicinity of cerebrospinal fluid (CSF) in other locations could alter the exact evaluation of water diffusion.

#### RESULTS

Diffusion-weighted images revealed bright signal of the intravascular clots in 22 patients (41%). This included 7 patients with DW bright clots in the venous sinus and the cortical veins, 11 patients with increased signal in the venous sinuses only, three patients with isolated cortical vein thrombosis. One of the patients had concurrent left transverse sinus and cavernous sinus thrombosis [Figure 1a,b], along with thrombosis of the superior ophthalmic veins, all of which were bright on the diffusion images. ADC measurement in six patients with superior sagittal sinus thrombosis showed decreased absolute values ( $0.42\text{--}0.61 \times 10^{-3} \text{ mm}^2/\text{s}$ ). Associated parenchymal changes were seen only in 10 of the 22 patients with bright diffusion intravascular clot.



#### CONCLUSION

Diffusion-weighted MRI can directly demonstrate the presence of an intravenous clot in patients with cerebral venous thrombosis; both in the venous sinuses and cortical veins, and can increase the diagnostic accuracy of MRI.

**KEY WORDS:** Clot, venous, diffusion

#### eP-128

#### Acute Ischemic Stroke in Nonhuman Primate Models: Prospective Sequential MR Imaging Observations in First 24 Hours after Middle Carotid Artery Branch Occlusion and Reperfusion

Cha, S.<sup>1</sup>•Lee, S.<sup>2</sup>•Lee, S.<sup>1</sup>

<sup>1</sup>Chung Buk National University Hospital, Cheongju, KOREA, REPUBLIC OF, <sup>2</sup>National Primate Research Center, Cheongwon, KOREA, REPUBLIC OF

#### PURPOSE

To observe sequential MRI findings in the hyperacute stage of reperfused acute ischemic stroke using temporary endovascular occlusion of the middle cerebral artery branches in nonhuman primate models.

#### MATERIALS & METHODS

Four Rhesus monkeys weighing 4.5–6.5 Kg were imaged with 3 T MRI to acquire preinfarction brain controls under general anesthesia. With neurointerventional techniques, superior division branch of right MCA in each animal was occluded temporarily. Immediately after arterial occlusion, each animal was evaluated repeatedly with 3 T MRI for 6 hours. When MR diffusion change appeared in the ischemic territory, arterial branch was recanalized and patency was confirmed by TOF MRA. After endovascular procedure and MRIs during hyperacute phase of ischemic brain infarction, each animal was recovered from the anesthesia and nursed to survive. At 24 hours, MRI was repeated under general anesthesia to detect any progression of the induced.

#### RESULTS

All 4 animals developed acute ischemic brain infarction in the corresponding territories of occluded M2 division branches of the middle cerebral arteries. Prospective sequential MRIs demonstrated changes of the hyperacute brain infarction during the first 24 hours.

#### CONCLUSION

We were successful to occlude MCA branches temporarily, to induce acute ischemic stroke in small nonhuman primates using endovascular technique, and to repeat MRI follow-ups during the first 24 hours after the onset of ischemic brain infarction. We were able to maintain the nonhuman primate models beyond the hyperacute phase to the acute stage. This preliminary experience would lead to more reliable and more reproducible model of preclinical in vivo ischemic stroke.

**KEY WORDS:** Ischemic stroke, MR imaging, primate model

## eP-129

**4D Flow MR Imaging in the Evaluation of Intracranial Arteriovenous Malformations**

Ansari, S. A.·Carroll, T. J.·Vakil, P.·Rahme, R. J.·Hurley, M. C.·Bendok, B. R.·Batjer, H.·Markl, M.

Northwestern University Feinberg School of Medicine  
Chicago, IL

**PURPOSE**

Arteriovenous malformations (AVM) are an important cause of hemorrhagic stroke. Risk stratification is based on the Spetzler-Martin grade (SMG), size, location, and venous drainage patterns. However, these parameters represent empirical measures without assessment of AVM flow properties. To gain further insights into AVM hemodynamics, we investigated the feasibility of 4D flow MRI for analysis of AVM flow patterns within and surrounding the lesion and the potential to monitor postembolization changes in AVM vascularization and hemodynamics.

**MATERIALS & METHODS**

Twelve patients with AVMs (age=38±13 years, 6 female) were examined using 1.5 T and 3 T MR systems (Avanto & Trio, Siemens, Germany). The study cohort included three ruptured and eight unruptured AVMs with SMG=1 (n=2), SMG=2 (n=5), SMG=3 (n=4), and SMG=4 (n=1). X-ray angiography demonstrated deep AVM location in four patients and deep venous drainage in eight patients. Additional follow-up 4D flow MRI after interventional treatment by staged embolization was performed in three patients. ECG synchronized 4D flow MRI was performed covering the AVM in an axial oblique 3D slab (venc=100cm/s, flip angle=15°, temporal resolution=45ms, spatial resolution=(1.2-1.6)3mm<sup>3</sup>). Data were corrected for eddy currents, Maxwell terms, and velocity aliasing. A 3D PC-MR angiogram was calculated from the 4D flow data. AVM hemodynamics were visualized using time-resolved 3D pathlines originating from 15000-25000 emitter points equally distributed within the 3D PC MRA vessel lumen (EnSight, CEI, USA). Time-integrated pathlines were calculated to depict the complete path of blood flow over one cardiac cycle and were color coded according to blood flow velocity.

**RESULTS**

AVM hemodynamics were evaluated successfully in 11 of 12 patients; one patient could not be analyzed due to head motion artifacts. Using time-integrated pathlines, blood flow distribution, vascularization, and velocity distributions were assessed within the AVM nidus and surrounding vessels. Large, deep and superficial draining veins were clearly identified in all cases. Blood flow velocities were highly variable between patients indicating intersubject heterogeneity in the AVM compartment. Venous blood flow velocities in the sagittal and transverse sinuses in the patient population were substantially higher (>30cm/s) than that of healthy normals (15-25cm/s). In patients with postembolization follow-up imaging (n=3), 4D flow analysis depicted significant changes in AVM

vascularization, velocity distribution and draining patterns. Pre-embolization, highly complex vascularization of the AVM with low and high flow regions were observed. Venous drainage was channeled mostly through one large posterior vessel with peak velocities above 50cm/s. Post-embolization, 3D pathline analysis demonstrated significant compaction of the AVM as well as blood flow velocity reduction.

**CONCLUSION**

The high variability in AVM blood flow velocities and venous drainage patterns indicate the need for individual evaluation of flow characteristics. 3D blood flow visualization reveals intricate vascularization of AVMs of different size, location, and severity as specified by the SMG. Our ability to identify changes in AVM hemodynamics following embolization further indicate the sensitivity of 4D flow MRI for comprehensive hemodynamic monitoring during therapy. Further serial studies are required to evaluate its potential for improving the planning of intervention and postinterventional monitoring.

**KEY WORDS:** AVM, 4D, hemodynamics

## eP-130

**Novel Insights into the Differential Diagnosis of Acute Multiple Sclerosis Plaques from an International Cohort of 3643 Patients**

Mueller-Lenke, N.<sup>1</sup>·Kappos, L.<sup>2</sup>·Pehrs-Jurvillier, A. C.<sup>1</sup>·Naegelin, Y.<sup>2</sup>·Bendfeldt, K.<sup>1</sup>·Sprenger, T.<sup>1,2</sup>·Stippich, C.<sup>2</sup>·Radue, E. W.<sup>1</sup>

<sup>1</sup>Medical Image Analysis Center Basel, Basel, SWITZERLAND, <sup>2</sup>University Hospital Basel, Basel, SWITZERLAND

**PURPOSE**

With the increasing importance of contrast-enhancing plaques for diagnosing multiple sclerosis (MS) in the recently revised Mc-Donald criteria it is crucial to avoid a misinterpretation of other contrast-enhancing abnormalities as MS lesions. Little is known about the prevalence and best possible differential diagnosis of developmental venous anomaly (DVA) as one of these pitfalls. The purpose of this prospective study was to analyze the prevalence and appearance of DVA on magnetic resonance imaging (MRI) in a large cohort of MS patients.

**MATERIALS & METHODS**

We prospectively evaluated the MRI scans of 3643 MS patients from four international multicenter trials. All patients had brain MRIs performed according to a predefined MRI protocol including proton density/ T2-weighted, pre and postgadolinium enhanced T1weighted scans. All scans were done with 3 mm slice thickness, no gap, axial plane, in subcallosal line, on 1.5 or 3.0 T scanners. Contrast-enhancing T1-weighted scans were screened by a single experienced neuroradiologist for possible DVAs that had to be confirmed on follow-up scans. Possible DVAs were defined by pattern of location, anatomical area, size,

shape, presence or absence of flow void or chemical shift artifacts and were counted as definite DVAs if confirmed on a follow-up scan at least 6 months apart.

## RESULTS

Overall, 490 (13.1%) of the 3643 MS patients had a total of 664 confirmed DVAs. There was an equal distribution between the left and the right hemisphere. Seventy-eight percent of DVAs were supratentorial, 22% were infratentorial, and 47% were small. Two other types of VM were identified (34 teleangiectasias, 5 cavernomas). Other imaging patterns were observed including examples of DVAs mimicking acute MS plaques. Due to different size, shape and location the typical appearance of a DVA with multiple enlarged vessels converging on a dilated parenchymal vessel was often incompletely visible.

## CONCLUSION

Our study shows that intracerebral DVAs are a very common incidental finding with at least every tenth MS patient having such a vascular lesion. It is mandatory to recognize and to know the different MRI appearances of DVAs to avoid misjudging it as acute contrast-enhancing MS lesions. Small solitary contrast-enhancing MS plaques seen on a single MRI scan without follow up should be checked for a clear T2 correlate, no flow void and no tubular structure before considering it for the diagnosis of MS.

**KEY WORDS:** Multiple sclerosis plaques, developmental venous anomaly, differential diagnosis

## eP-131

### Evaluation of Corpus Callosum Involvement in MS Patients via Diffusion Tensor Imaging, Arterial Spin Labeling, Magnetization Transfer Ratios, Volumetric Analysis and Correlation with Expanded Disability Status Score

Duzgol, C.·Anik, Y.·Bickin, H.·Efendi, H.·Demirci, A.

Kocaeli University School of Medicine  
Kocaeli, TURKEY

## PURPOSE

The aim of this study is to evaluate callosal involvement in MS patients via DTI, MTR, ASL, volumetric analysis and correlate these findings with EDSS.

## MATERIALS & METHODS

Thirty MS patients and 30 healthy volunteers were examined with 3 T MRI. Fractional anisotropy (FA) ve mean diffusivity (MD) measurements of DTI, MTR, ASL and volumetric analysis of corpus callosum were performed. All findings of MS patients were compared with the control group and also correlated with EDSS.

## RESULTS

Callosal volume was significantly decreased in MS patients. Magnetization transfer ratios and FA measurements of callosum also were decreased significantly. Mean diffusivity was slightly increased. Arterial spin labeling also was altered. Correlation of

MTR, FA, MD, ASL and volumetric analysis revealed significant correlation with EDSS.

## CONCLUSION

Magnetization transfer ratios of callosum were found to be the most significant parameter in MS patients. Abnormalities in corpus callosum can be assessed with MTR, ASL, DTI, volume analysis and associated with EDSS in MS.

**KEY WORDS:** MS, ASL, EDSS

## eP-132

### Individual Detection of Parkinson Disease Patients Using Support Vector Machine Analysis of Susceptibility-Weighted Imaging: Initial Results

Haller, S.<sup>1</sup>·Badoud, S.<sup>1</sup>·Nguyen, D.<sup>2</sup>·Garibotto, V.<sup>1</sup>·Barnaure-Nachbar, I.<sup>1</sup>·Lovblad, K.<sup>1</sup>·Burkhard, P.<sup>1</sup>

<sup>1</sup>University Hospital Geneva, Geneva, SWITZERLAND,

<sup>2</sup>CDRC, Carouge, SWITZERLAND

## PURPOSE

Brain iron accumulation was assessed in patients with suspected Parkinson disease (PD) using susceptibility-weighted imaging (SWI). In a two-stage analysis, we performed a group level analysis to detect regions of brain iron deposition in PD, and a pattern recognition analysis to detect PD subjects at the individual level.

## MATERIALS & METHODS

The study was approved by the local ethical committee. We included 36 consecutive patients with parkinsonism suggestive of PD who had (i) SWI at 3 T, (ii) brain 123I-ioflupane SPECT (DaTScan) and (iii) extensive neurologic testing including follow up (16 PD, 67.4 ± 6.2 years, 11 females; 20 OTHER 65.2 ± 12.5 years, 6 females). Group-level analysis included region of interest (ROI) and voxel-wise statistics, individual-level analysis included support vector machine (SVM) classification.

## RESULTS

At the group level, the visual ROI analysis yielded no differences between groups. In contrast, the voxel-wise analysis demonstrated decreased iron deposition in bilateral, right-dominant thalamus in PD patients versus OTHER. The inverse comparison yielded no supra-threshold clusters. At the individual level, SVM correctly classified PD patients with accuracies up to 86%.

## CONCLUSION

Support vector machine-based pattern recognition of SWI data provides accurate discrimination of PD patients in suspected PD disease at an individual level, despite the absence of visually detectable alterations.

**KEY WORDS:** Parkinson disease, SWI, SVM

## eP-133

### Evaluation of Optic Nerve in Multiple Sclerosis Patients with Magnetization Transfer Ratios,

## Diffusion Tensor Imaging and Blood Oxygenation Level Dependent

Gencturk, M.·Anik, Y.·Cakir, O.·Efendi, H.·Bickin, H.·Demirci, A.

Kocaeli University School of Medicine  
Kocaeli, TURKEY

### PURPOSE

The aim of this study is to evaluate magnetization transfer ratio (MTR), diffusion tensor imaging (DTI) of the optic nerve and optic radiation, functional MRI following visual stimulation in multiple sclerosis (MS) patients with and without optic neuritis history and correlate these findings with normal healthy volunteers.

### MATERIALS & METHODS

Forty MS patients; 20 that had optic neuritis attack previously and 20 that had no optic neuritis attack before and 20 healthy volunteered patients without eye pathology as the control group were included. All patients were examined with 3T MR equipment. Magnetization transfer ratio, DTI and functional MRI following visual stimulation were acquired. Magnetization transfer ratio and fractional anisotropy (FA) and mean diffusivity (MD) measurements from DTI of the optic nerve, chiasma and optic radiation were obtained. Volumetric analysis of blood oxygenation level dependent (BOLD) following visual stimulation was performed. All those findings among three groups were compared.

### RESULTS

In MS patients with optic neuritis attack previously, FA and MTR values of the optic nerves and BOLD visual volumetric analysis were decreased significantly, and MD values were increased compared with that of the control group ( $p < 0.001$ ) and of the MS patients with no optic neuritis attack ( $p < 0.01$ ). Significant correlation was found among FA MTR and BOLD activation area reduction and MD elevation ( $p < 0.01$ ).

### CONCLUSION

Magnetization transfer ratio and DTI and visual BOLD analysis are found to be sensitive to optic nerve damage in patients with MS.

**KEY WORDS:** DTI, MS, optic nerve

## eP-134

### Functional MR Imaging of Theory of Mind: Game Paradigms

Druzgal, J.·Krishnamurthy, B.

University of Virginia  
Charlottesville, VA

### PURPOSE

Theory of mind refers to the ability of people to form mental representations about the goals and beliefs of other people in the social environment. This ability is central to normal human social interaction, and is thought to be selectively impaired in the autism

spectrum of disease. Previous functional imaging studies of theory of mind have relied, to differing degrees, on three classes of paradigms: 1) attributing mental states to a fictional character, 2) interpretation of goal-directed actions performed by a human actor, and 3) simple games played with an unseen opponent or computer. The game paradigm has received the least attention, despite the significant advantage of controlling for both stimulus effects and motor responses that may be beneficial in evaluating pathologic conditions like autism.

### MATERIALS & METHODS

The present experiment uses BOLD fMRI of two different paradigms to test hypotheses-related belief about the nature of the second participant in a game situation. The first paradigm uses the game "Scissors, Paper, Rock" to create a situation where individuals believe they are in direct two-way competition with an unseen opponent outside the MRI scanner - either a live person, a computer using rule-based algorithms to compete, or a randomly generated response. The second paradigm - the "Beauty Contest" - was designed to mirror the visual and motor requirements of the "Scissors, Paper, Rock" task. In the Beauty Contest, participants chose from a panel of faces, which face they believed an unseen person outside the scanner would find the most attractive. Participants were again told that they were either interacting with a live person, a computerized "face assessment" algorithm, or a random response. For both paradigms, the reality was that subjects were always playing against a randomly generated response. Thus, the only thing that varied from trial-to-trial in either game was the subject's belief about the nature of the opponent. Fifteen young healthy subjects performed these two tasks while BOLD fMRI data were collected on a Siemens 3 T Trio scanner. Standardized postprocessing of the data was performed using the fMRI Software Library (FSL), including spatial realignment, slice timing correction, coregistration of anatomical and functional data, normalization to a standard brain template, and statistical analysis with a general linear model.

### RESULTS

In both tasks, the primary comparison of believing the unseen agent outside the scanner is a live person versus belief of a computer algorithm activates an extensive network of regions previously associated with the theory of mind mechanism. These regions include: medial prefrontal cortex, anterior cingulate gyrus, posterior cingulate gyrus, precuneus, superior temporal sulcus, and temporal parietal junction. All regions are significantly active at Z-values corrected for a mapwise cluster threshold level of  $p < 0.05$ . Despite the different cognitive demands of the two games, this contrast of Live vs Computer activates identical regions in both tasks.

### CONCLUSION

Game paradigms may provide an effective way to interrogate the entire theory of mind network in a way that controls for confounds relative to conditions such as autism.

**KEY WORDS:** BOLD fMRI, theory of mind

### eP-135

#### **Impact of CT Perfusion on Acute Stroke Management Decision in All-Comers within Three Hours of Symptoms Onset**

Yen, P.·Gubitz, G.·Bhan, V.·Shankar, J.

Dalhousie University  
Halifax, NS, CANADA

#### **PURPOSE**

The advent of perfusion CT imaging for patients presenting with acute ischemic stroke symptoms has widened the window of intravenous or intraarterial thrombolytic intervention and identified cases where thrombolytic therapy will have no benefit. This additional diagnostic tool can be performed with rapidity and is cost-effective. The effect of thrombolytic treatment in patients treated within 3 hours of stroke symptom onset has been variable in different trials and studies. This can be attributed to the presence of a penumbra and also the individual variability of penumbra viability and neuronal population vulnerability. Though there are numerous accounts of the value of CT perfusion, it is unknown how it alters the actual patient management. We aim to evaluate the use of CT perfusion in the acute stroke patients presenting within 3 hours of symptom onset at our institution and whether the CTP findings alters patient management.

#### **MATERIALS & METHODS**

We prospectively performed nonenhanced CT (NECT), CT angiography (CTA), and perfusion CT (CTP) in acute stroke patients presenting within 3 hours of symptom onset. CT angiography and CTP were performed using the standard protocol at our institution. Color maps of the hemodynamic parameters including cerebral blood flow, volume, and time to peak were obtained. An ASPECT score was determined for the NECT and CTP images. We collected clinical information and outcome data for all patients from a centralized clinical database. One stroke neurologist and a general neurologist involved in stroke patient care were asked to make retrospective management decisions for all patients. First, a management plan was arrived based solely on the clinical information and NECT ASPECT score. Next, a second management decision was determined with consideration of CTA and CTP findings. These were compared with the actual therapy received.

#### **RESULTS**

Fifteen patients including seven females and eight males with a mean age of 63 years underwent complete neurovascular imaging study at our institution for acute stroke. Two of the 15 patients did not receive intravenous thrombolysis based on the lack of objective CTA and CTP evidence of stroke. The same patients did not have any residual clinical deficits or infarct on follow-up CT. Two different patients had matched defects on CTP (i.e., no penumbra) and on follow-up scans had infarcts that corresponded to the CTP defect.

Nevertheless, upon retrospective analysis, the stroke neurologists did not alter their management plan despite CTP findings because its accuracy and effectiveness have not been rigorously tested by randomized control trials and therefore deemed unreliable.

#### **CONCLUSION**

The treating neurologists are reluctant to change management decisions based on CTP results in the absence of any randomized control trial for acute ischemic stroke treatment. Currently, CTP is not part of the Canadian Best Practice recommendations for stroke care. The acceptance of CTP and implementation of its findings in the acute ischemic stroke management is improving but in the absence of randomized controlled trial, the treating physicians are still hesitant in utilizing this technique.

**KEY WORDS:** CT Perfusion, stroke

### eP-136

#### **Imaging Findings on Brain CT and MR Imaging of Patients with Neurosyphilis**

Goldsher, D.<sup>1,2</sup>·Shreiber, R.<sup>1</sup>·Khamaysi, Z.<sup>1</sup>·Bergman, R.<sup>1,2</sup>

<sup>1</sup>Rambam Health Care Campus, Haifa, ISRAEL,

<sup>2</sup>Technion - Israel Institute of Technology, Haifa, ISRAEL

#### **PURPOSE**

To present the imaging findings on cerebral CT and MRI of patients with asymptomatic neurosyphilis.

#### **MATERIALS & METHODS**

Six consecutive patients with proven neurosyphilis, based on abnormal CSF findings, underwent cerebral CT and MRI between 2003 and 2010. Their mean age was 39 years. All of them were males. Detailed histories were taken from all patients. They all underwent complete physical and neurologic examinations and were asked and examined for vascular risk factors including diabetes mellitus, hyperlipidemia and hypertension as well as medication histories, toxic exposure and tobacco use. Baseline routine blood counts and chemistries also were performed. In addition, all six patients were examined for cardiac involvement including electrocardiography (ECG) and cardiac ultrasound. The cerebrospinal fluid (CSF) analysis included protein concentrations, glucose levels and cell counts. Venereal Disease Research Laboratory Test (VDRL) test, rapid plasma regain (RPR) test and treponema pallidum hemagglutination (TPHA) test. The latter were performed in both the serum and the CSF samples. HIV serology was performed in all of the patients.

#### **RESULTS**

Despite the lack of subjective complaints, the neurologic and ophthalmologic examinations revealed abnormalities in five of the six patients, most commonly cranial nerve involvement (3 pts) and hemiparesis (2 pts). CT studies revealed abnormalities in four of the six patients, and MRI in all six. The CT and MRI findings

were congruent in three pts showing brain infarcts in two and mild generalized atrophy in one. In more than half of the patients, mainly those with cranial nerve involvement, the neuroimaging studies were not congruent with the neurologic and ophthalmologic findings.

#### CONCLUSION

1. The most common neuroimaging finding in patients with neurosyphilis is stroke. This might be due to meningovascular endarteritis. 2. Neuroimaging findings often are not congruent with the neurologic findings. 3. Neurosyphilis should always be considered in young patients with brain infarcts without known risk factors.

**KEY WORDS:** Stroke

#### eP-137

##### **Permeability and Perfusion MR Imaging to Distinguish Residual/Recurrent Metastatic Brain Tumor from Radiation Necrosis in Patients Treated with Radiation Therapy**

Shiroishi, M. S.<sup>1</sup>•Cen, Y.<sup>1</sup>•Muradyan, N.<sup>2</sup>•Rahmanuddin, S.<sup>1</sup>•Ozhand, A.<sup>1</sup>•Wagle, N.<sup>1</sup>•Chen, B. T.<sup>3</sup>•Pagnini, P.<sup>1</sup>•Chen, T. C.<sup>1</sup>•Go, J. L.<sup>1</sup>•Boyko, O. B.<sup>1</sup>•Lerner, A.<sup>1</sup>•Lebel, R. M.<sup>4</sup>•Commins, D. L.<sup>1</sup>•Kim, P. E.<sup>1</sup>•Zada, G.<sup>1</sup>•Liu, C. Y.<sup>1</sup>•Christian, S.<sup>1</sup>•Law, M.<sup>1</sup>

<sup>1</sup>Keck School of Medicine, University of Southern California, Los Angeles, CA, <sup>2</sup>iCAD, Inc, Nashua, NH, <sup>3</sup>City of Hope, Duarte, CA, <sup>4</sup>University of Southern California, Los Angeles, CA

#### PURPOSE

To distinguish between recurrent/residual metastatic brain tumor from radiation necrosis using permeability and perfusion MRI in patients treated with radiation therapy.

#### MATERIALS & METHODS

This is a retrospective study in which 15 patients with systemic malignancy were treated with radiation therapy for metastatic brain tumors and underwent T1-weighted dynamic contrast-enhanced (DCE) permeability and T2\*-weighted dynamic susceptibility contrast (DSC) perfusion MR imaging. Primary malignancies included breast, renal cell, lung, and testicular carcinoma. Five patients were found to have increase in the size of enhancing lesions on follow-up imaging and underwent repeat surgery. Ten patients demonstrated stable/improvement in the size of enhancing lesions on follow up. This was presumed to represent radiation necrosis. The time period of follow-up imaging after radiation treatment ranged from 3 months to 32 months. Dynamic contrast-enhanced/DSC datasets were postprocessed retrospectively using iCAD and GE ADW software. In six patients, quantitative pharmacokinetic analysis of DCE data was not possible due to protocol differences and therefore qualitative permeability assessment was performed using color overlay maps. In four patients, rCBV max could not be determined due to susceptibility artifact.

#### RESULTS

All five patients with increasing size of enhancing lesions on follow-up imaging were confirmed pathologically to represent residual/recurrent metastatic tumor. rCBV max was elevated significantly in patients with residual/recurrent tumor compared to those with presumed radiation necrosis ( $p < 0.05$ ). There was trend towards higher volume transfer constant  $K^{trans}$  in those with recurrent/residual tumor. For those patients in whom pharmacokinetic analysis was not possible, qualitative permeability assessment using color overlay maps demonstrated elevated permeability in tumors and low permeability in presumed radiation necrosis. The mean size of the extravascular-extracellular space ( $v_e$  mean) was significantly lower in those with presumed radiation necrosis ( $p < 0.05$ ).

#### CONCLUSION

Permeability and perfusion MR imaging has the potential to serve as imaging biomarkers to monitor therapeutic efficacy of radiation therapy for metastatic brain tumors.

**KEY WORDS:** Perfusion MR imaging, permeability MR imaging, metastatic brain tumor

#### eP-138

##### **Comparison between Gadopentetate Dimeglumine and Gadobutrol for MR Perfusion at 3 T**

Safriel, Y.<sup>1,2</sup>•Dale, B.<sup>3</sup>

<sup>1</sup>University of South Florida, Clearwater, FL, <sup>2</sup>Radiology Associates of Clearwater, Clearwater, FL, <sup>3</sup>Siemens Medical Systems, Erlangen, GERMANY

#### PURPOSE

To use the Global Bolus Plot (GBP) graph to investigate differences of high- versus low-relaxivity contrast agent on dynamic susceptibility contrast (DSC) perfusion at 3 T. Automatically generated GBP graphs measure whole brain signal changes over time during the dynamic injection of contrast.

#### MATERIALS & METHODS

This study was performed as part of our health systems Value Added Committee mandate to evaluate a new contrast agent (Gadobutrol) as compared to the existing agent (Gadopentetate) prior to adding a new agent to the formulary. Eleven patients with gliomas or metastatic brain tumors underwent a DSC perfusion exam in addition to a routine brain exam. Patients were imaged before and after brain surgery with the different contrast agents. Imaging was performed using standard, FDA-approved sequences on a Siemens Tim Trio 3 T (Siemens AG, Erlangen, Germany). Parameters for the GRE-based sequence were TR = 1450, TE = 45, 13 slices, slice thickness = 5 mm, gap = 1 mm (20%), average = 1, FOV = 230 at 100% phase and no phase over sampling, EPI factor = 128, measurements = 50, matrix = 128 x 128. FDA-approved 8-channel head coil shipped with the MRI system was used in all studies. 0.1 ml/kg of Gadobutrol or 0.2ml/kg of Gadopentetate (both Bayer



AG, Berlin, Germany) was injected at 4-5 cc/sec via power injector. Image parameters and injection rates were similar for all studies. Postprocessing was performed on the scanner console using Syngo version B17.0 (Siemens AG, Erlangen, Germany). The whole brain automatically generated GBP graphs were used to determine maximal signal change from baseline (Cmax) and tightness of curve (Ct).

## RESULTS

Eleven patients underwent 23 examinations. Nine examinations were performed with Gadopentetate and 14 with Gadobutrol. ANOVA (JMP 9.0.0, SAS Institute, Cary, NC) testing was used for the main effects of Gadobutrol vs Gadopentetate and pre op vs post op. There was no significant effect for either Cmax ( $p = .3277$ ) or Ct ( $p = .9130$ ) with an adjusted  $R^2$  of 0.0198 and -0.1058 respectively. A stepwise ANOVA using the minimum Bayes Information Criterion shows that none of the models met the Bayes information criterion.

## CONCLUSION

As opposed to previously published results showing differences between high and low relaxivity agents in region of interest measurements taken at tumors, the automatically generated whole brain GBP graphs do not show a difference in the Cmax or Ct in the perfusion characteristics of Gadobutrol versus Gadopentetate.

**KEY WORDS:** Perfusion, gadavist, magnevist

## eP-139

### Glioblastoma Multiforme: Perfusion and Its Relation to the Subventricular Zone

Kimura, M. C. G. • Lee, R. • Miller, C. R. • Castillo, M.

University of North Carolina Chapel Hill  
Chapel Hill, NC

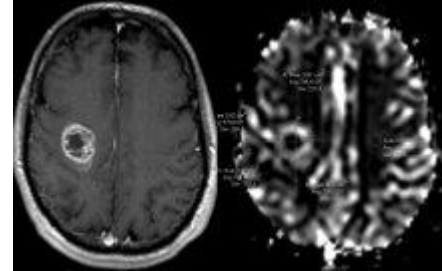
## PURPOSE

Some glioblastomas (GB) are thought to arise from the subventricular zone (SVZ) while others arise from the subcortical (SC) regions. Since these regions are highly neurogenic and hyperperfused we sought to assess if relative cerebral blood volume (rCBV) maps are able to show increased perfusion on the borders of GB corresponding to the SVZ and SC regions.

## MATERIALS & METHODS

We analyzed preoperative MR imaging including contrast-enhanced perfusion studies in 38 patients with GB. Imaging studies were reviewed and GB were divided into three groups according to their relationship to SVZ as touching the SVZ (group 1), SC and not touching the SVZ (group 2), and touching the SVZ + SC (group 3). Perfusion analysis was done using the rCBV maps and tumors were divided in four parts by orthogonal lines creating quadrants, medial-anterior (MA), medial-posterior (MP), lateral-anterior (LA) and lateral-posterior (LP). Regions of interest (ROIs) were drawn manually for any fourth-part of tumor (Figure 1) and numbers were acquired, registered separately, and normalized. An ROI on the corresponding contralateral

white matter (WM) was used to normalize GB borders intensity values and accomplished by dividing ROIs numbers of all quadrants (MA, MP, LA and LP) for the ROI number of contralateral WM. Statistical analysis: Mean and standard deviation values of rCBV for the subtype regions were calculated. Statistical comparisons were made between the regions using a Tukey's multiple comparisons test.



## RESULTS

Fifty-four percent of GB were categorized as group 3, 34% as group 2, and 12% as group 1. Nine percent of GB were multicentric or multifocal at diagnosis. Perfusion demonstrated random values for ROI analysis of rCBV maps. There was no statistically significant evidence of higher rCBV on GB borders, either at the SVZ or SC zones.

## CONCLUSION

Our study could not confirm previous reported findings indicating that both the SVZ and SC zone have increased perfusion in GB due to neuro- and gliomagenesis. Thus perfusion cannot be used to assess the origin of GB nor can it identify zones related to activity neural stem cell activity in them. Figure 1- GB T1 contrast-enhanced axial image and corresponding rCBV map with orthogonal lines dividing the tumor in four parts and ROIs drawn circumscribing increased perfusion in lesion borders. Region of interest in the contralateral white matter is delineated and its intensity value was used to normalize.

**KEY WORDS:** Glioblastoma, neural stem cells, perfusion

## eP-140

### Dynamic Contrast-Enhanced and Dynamic Susceptibility Contrast MR Imaging Metrics Correlate in Follow Up of Patients with High-Grade Gliomas

Ferré, J.<sup>1</sup> • Shiroishi, M. S.<sup>1</sup> • Jones, J. G.<sup>1</sup> • Lebel, R. M.<sup>1</sup> • Cen, Y.<sup>1</sup> • Muradyan, N.<sup>2</sup> • Rahmanuddin, S.<sup>1</sup> • Law, M.<sup>1</sup>

<sup>1</sup>University of Southern California, Los Angeles, CA,  
<sup>2</sup>iCAD, Inc, Nashua, NH

## PURPOSE

To determine if metrics obtained with dynamic contrast-enhanced (DCE) MR imaging correlate with cerebral blood volume (CBV) obtained with dynamic susceptibility contrast (DSC) MR imaging in follow up of patients with high-grade glioma. Dynamic contrast-enhanced MRI has the potential to give both permeability and perfusion metrics with less sensitivity to susceptibility artifacts, even more important in

postoperative status. In addition, the problem of leakage correction is avoided.

#### MATERIALS & METHODS

Thirteen high-grade glioma patients with MR imaging findings of postradiation therapy enhancing lesions were evaluated. Eight patients had pseudoprogression (PsP) and five had true early progression (TEP). Dynamic contrast-enhanced and DSC MRI sequences were acquired during the same exam at 3 T. Dynamic contrast-enhanced MR images were postprocessed on an iCAD workstation, a semiautomated image analysis suite. Dynamic susceptibility contrast MR images were postprocessed using Penguin, a freeware perfusion tool operating through Matlab. Total enhancing tumor volume was drawn manually to create a 3D region of interest (Figure). Cerebral blood volume was extracted from DSC MRI. Metrics extracted from DCE MRI were: vascular permeability ( $K^{trans}$ ), fractional plasma volume ( $V_p$ ), fractional volume of extravascular-extracellular space (EVF), rate constant  $K_{ep}$ , initial area under gadolinium curve (iAUGC) and tissue relaxation rate  $T_{10}$ . Pearson correlation coefficient ( $r$ ) was calculated between CBV and each DCE metric.

#### RESULTS

Mean values  $\pm$  SD of metrics were: CBV:  $1.8 \pm 1$  ml/100g,  $K^{trans}$ :  $0.19 \pm 0.07$  min<sup>-1</sup>,  $V_p$ :  $0.06 \pm 0.03$ , EVF:  $0.40 \pm 0.09$ ,  $K_{ep}$ :  $0.50 \pm 0.11$  min<sup>-1</sup>, iAUGC:  $2.86 \pm 1.18$  mMsec, and  $T_{10}$ :  $1.47 \pm 0.29$  sec. Cerebral blood volume was significantly correlated with  $V_p$  ( $r = 0.624$ ,  $p = 0.023$ ),  $K_{ep}$  ( $r = 0.681$ ,  $p = 0.010$ ), and iAUGC ( $r = 0.680$ ,  $p = 0.011$ ). No significant correlation was found with  $K^{trans}$ , EVF and  $T_{10}$ .

#### CONCLUSION

Preliminary results showed correlation between DCE MRI metrics and CBV measured with DSC MRI in follow up of patients with high-grade glioma. These results could be explained because CBV and  $V_p$  measure theoretically the same compartment in tumor, CBV and  $K_{ep}$  increase both with the grading of tumor and iAUGC of DCE MRI shows the initial amount of contrast/blood in the tissue thus the correlation with CBV would be expected. Further studies are needed to validate these findings.

**KEY WORDS:** Perfusion, permeability, glioma

#### eP-141

##### Imaging Genomic Mapping of Edema/Cellular Invasion MR Imaging-Phenotypes in Glioblastoma Multiforme

Zinn, P. O.<sup>1</sup>Mahajan, B.<sup>2</sup>Sathyan, P.<sup>1</sup>Singh, S.<sup>1</sup>Majumder, S.<sup>1</sup>Flanders, A.<sup>3</sup>Huang, E.<sup>4</sup>Jain, R.<sup>5</sup>Gutman, D.<sup>6</sup>Hwang, S.<sup>6</sup>Kirby, J.<sup>7</sup>Freyman, J.<sup>7</sup>TCGA Glioma Phenotype Research Group·Jolesz, F. A.<sup>2</sup>Colen, R. R.<sup>2</sup>Holder, C.<sup>2</sup>Wintermark, M.<sup>2</sup>

<sup>1</sup>M.D. Anderson Cancer Center, Houston, TX, <sup>2</sup>Brigham and Women's Hospital, Boston, MA, <sup>3</sup>Thomas Jefferson University Hospital, Philadelphia, PA, <sup>4</sup>National Cancer Institute, Bethesda, MD, <sup>5</sup>Henry Ford, Detroit, MI,

<sup>6</sup>Emory University, Atlanta, GA, <sup>7</sup>SAIC-Frederick, Bethesda, MD

#### PURPOSE

Despite recent discoveries of new molecular targets and pathways, the search for an effective therapy for glioblastoma multiforme (GBM) continues. A newly emerged field, imaging genomic, links gene expression profiles with MRI phenotypes. MR imaging FLAIR is a noninvasive diagnostic modality and previously was found to correlate with cellular invasion in GBM. Thus, our imaging genomic screen has the potential to reveal novel molecular determinants of invasion. Here, we present the first comprehensive imaging genomic analysis using quantitative MRI volumetrics and large-scale gene- and microRNA expression profiling in GBM.

#### MATERIALS & METHODS

Based on molecular data from The Cancer Genome Atlas (TCGA) and imaging data from The Cancer Imaging Archive (TCIA), discovery and validation sets with gene, microRNA, and quantitative MR imaging data were created. Top concordant genes and microRNAs correlated with high FLAIR volumes from both sets were further characterized by Kaplan Meier survival statistics, microRNA-gene correlation analyzes, and GBM molecular subtype-specific distribution.

#### RESULTS

The top upregulated gene in both the discovery (4 fold) and validation (11 fold) sets was PERIOSTIN (POSTN). The top downregulated microRNA in both sets was miR-219, which is predicted to bind to POSTN. Kaplan Meier analysis demonstrated that above median expression of POSTN resulted in significantly decreased survival and shorter time to disease progression ( $P < 0.001$ ). High POSTN and low miR-219 expression were significantly associated with the mesenchymal GBM subtype ( $P < 0.0001$ ).

#### CONCLUSION

Here, we propose a novel diagnostic method to screen for molecular cancer subtypes and genomic correlates of cellular invasion. Our findings also have potential therapeutic significance since successful molecular inhibition of invasion will improve therapy and patient survival in GBM.

**KEY WORDS:** Brain tumor, genomics, radiogenomics

#### eP-142

##### Postoperative Surgical Cavity Size Change, over First 30 Days after Gross Total Resection of Brain Metastasis, Is Predicted by Surrounding Vasogenic Edema

Ahmed, S.<sup>1</sup>Hamilton, J.<sup>1</sup>Vu, T.<sup>1</sup>Rao, G.<sup>1</sup>Cahill, D. P.<sup>2</sup>Reasonda, L. G.<sup>1</sup>McAleer, M. F.<sup>1</sup>Mahajan, A.<sup>1</sup>

<sup>1</sup>M.D. Anderson Cancer Center, Houston, TX, <sup>2</sup>Mass General Hospital, Boston, MA

#### PURPOSE

Following gross total resection of brain metastasis, patients at our institution are offered stereotactic radiosurgery (SRS) to the operative bed versus observation as an alternative to whole brain radiation on an ongoing protocol. Stereotactic radiosurgery is administered within 30 days of the gross total surgical resection provided the maximum diameter of the resection cavity is less than 40 mm. The purpose of our study was to determine the relationship, if any, between the extent of vasogenic edema surrounding the resection cavity on the immediate postoperative MRI, and the degree of change in size of the resection cavity on a treatment planning/follow-up study performed within 30 days.

#### MATERIALS & METHODS

Of 71 patients with resection of brain metastasis who were considered for the trial, 44 patients met inclusion criteria. Thirty-seven of 44 patients had a follow-up imaging study within 30 days of the postoperative MRI. Two of the patients had two lesions resected, for a total of 39 resection cavities reviewed. Cavity size was measured by two neuroradiologists on the immediate postoperative MRI, and on a follow-up/treatment planning study performed within 30 days. The maximum axial dimension of hyper-intensity on T2-weighted imaging (vasogenic edema) surrounding the resection cavity on the postoperative MRI also was recorded.

#### RESULTS

Of the 39 resection cavities evaluated, only one of 10 patients (10%) with vasogenic edema from 0-10 mm had a decrease of >10% in the cavity size, while three of five (60%) of patients with 10-20 mm edema and 19 of 24 (80%) of >20 mm had such decreases. The correlation for edema and cavity size was statistically significant (Pearson coefficient of -0.35,  $P = 0.02$ ). An arbitrary cut-off value of 15 mm yielded a sensitivity of 91% and specificity of 63% ( $P < 0.001$ ).

#### CONCLUSION

There are changes observed in the size of the surgical cavity following resection of brain metastasis within the first 30 days. Following gross total resection of brain metastasis, a resection cavity with moderate/extensive surrounding vasogenic edema on the immediate postoperative MRI is significantly more likely to decrease in size by 10% in the first 30 days, when compared to a resection cavity with little or no surrounding vasogenic edema. Patients with resection cavity size of greater than 4 cm and with moderate/extensive surrounding edema thought ineligible for SRS, on our current ongoing study, may in fact demonstrate decreased resection cavity size within 30 days. This would make them a candidate for SRS. So far, there have been four such instances within our study population. Additionally, 7/7 patient less than 40 years of age demonstrated 10% decrease in cavity size, while 15/33 patients greater than 40 years demonstrated such change ( $P = 0.03$ ), which could be attributable to age-related differences in brain volumes.

**KEY WORDS:** Brain metastasis, radiosurgery, edema

#### eP-143

#### Clinical Applicability in Determination of Significant Carotid Stenosis Using Mean Transit Time and Cerebral Blood Flow Calculated by Circulant and Standard Decomposition Methods in the Postprocessing of MR Perfusion

Teng, M. M. H.<sup>1,2</sup>•Kao, Y.<sup>1</sup>•Chiu, F.<sup>1</sup>•Chen, W.<sup>1</sup>•Chang, F.<sup>1,2</sup>•Guo, W.<sup>1,2</sup>•Chang, C.<sup>1,2</sup>

<sup>1</sup>National Yang Ming University, Taipei, TAIWAN, <sup>2</sup>Taipei Veterans General Hospital, Taipei, TAIWAN

#### PURPOSE

We evaluated the lesion-to-normal ratios of cerebral blood flow (CBF) and mean transit time (MTT) on MR perfusion processed with two different deconvolution methods - standard singular value decomposition (sSVD) and circulant singular value decomposition (cSVD).

#### MATERIALS & METHODS

We postprocessed MR perfusion data and evaluated the lesion-side-to-normal-side ratio (LNR) of CBF and MTT before and after CSF and vessel pixel elimination (CVPE). Totally 31 patients with significant unilateral carotid stenosis (90% or more) diagnosed on digital subtraction angiography, CT angiography, or MR angiography were included. The CBV was calculated as the ratio of areas under the concentration-time curves between a tissue voxel and the arterial input function. The area was calculated as a summation of the concentration-time curve. We calculated CBF twice, including sCBF and cCBF. The sCBF was calculated using sSVD. The cCBF was calculated by cSVD. We calculated MTT using central volume theory, including sMTTc and cMTTc. sMTTc was calculated by CBV divided by sCBF. cMTTc was calculated by CBV divided by cCBF. The CSF pixels were removed using the mask generated by the first several images of brain perfusion and Otsu's thresholding technique. The threshold used for vessel pixels removal was mean CBV + 2 standard deviations. We selected two levels of the brain for measurement of perfusion: one high ventricular level (the level at the body of lateral ventricle), and one supraventricular level (the first level above lateral ventricle). The supraventricular level was not included in MR perfusion study thus was not available for measurement in five patients. Totally 57 levels were evaluated, including 31 high ventricular levels and 26 supraventricular levels. For each level, we drew two ROI equal to the size of each hemisphere and calculated the lesion-side-to-normal-side ratio of MTT and CBF.

#### RESULTS

All measured LNR of sMTTc were larger than one as expected before and after CVPE, same as TTP ratios. The ratios of cMTTc was inverted in five (19%), and one (4%) before and after CVPE respectively in supraventricular level, and in six (19%) and five (16%) cases before and after CVPE respectively in high ventricular level. The sCBF LNRs were smaller than one as expected in majority of cases: 23 (88%), 24 (92%) cases before and after CVPE in supraventricular level,

and 27 (87%), 29 (94%) cases before and after CVPE in high ventricular level. However, the cCBF LNRs were smaller than one as expected only in 12 (46%), nine (35%) cases before and after CVPE in supraventricular level, and 17 (55%), 17(55%) cases in high ventricular level.

#### CONCLUSION

Same as TTP, the sMTTc obtained by sSVD and central volume theory can be used to indicate the side with arterial stenosis in patients with significant unilateral carotid stenosis. cMTTc is less reliable in determination of the lesion side. sCBF obtained by sSVD can indicate the lesion side by reduced sCBF. cCBF is not reliable in determination of the lesion side.

**KEY WORDS:** MR perfusion, carotid stenosis, postprocessing

#### eP-144

##### Portable Head CT in the Critically Ill Patient: Utility and Accuracy

Byington, K. E.·Grilli, C. J.·Reznikov, B.·Liu, X.

Christiana Care Health System  
Wilmington, DE

#### PURPOSE

There are well documented, inherent risks in the intrahospital transportation of the critically ill patient. Potential risks include the compromise of support equipment as well as the intrinsic danger of being temporarily removed from the resources of the critical care unit. To reduce or eliminate such concerns, portable CT has been implemented at our institution since 2009 for imaging surveillance of these patients. The downside of such a scheme lies within the reduced imaging quality of the portable CT scan. The purpose of this study is to assess the utility and diagnostic accuracy of the portable head CT. To our knowledge, this is the first preliminary study to compare the rate of discrepancy of the portable head CT with respect to conventional stationary CT or MRI, the correlation of such discrepancy with quality of the exam, and the validity of the use of portable CT in the critically ill patient.

#### MATERIALS & METHODS

A retrospective review of 302 portable CTs of the head was performed. Of those examinations, in 193 instances there was a subsequent conventional stationary CT or MRI within 1 month of the original portable study. Fifty-two of these 193 examinations were excluded secondary to interval surgery between the portable and conventional examinations, leaving 141 studies for comparison. Comparison was made by a review of the official reports of the portable and conventional imaging and any discordance in the findings was divided into either a major or minor discrepancy group. Major discrepancies, as determined by board certified neuroradiologists, were defined as those that directly affected patient care or clinical outcome. The quality of each portable study also was assessed and classified

into three categories: 1 near diagnostic, 2 suboptimal, or 3 nondiagnostic. Cross-reference then was made to assess for any correlation between the quality of the examination and rate of discrepancy.

#### RESULTS

Ninety-one and one half percent (129 of 141) of portable CTs showed no discrepancy compared to the subsequent stationary study; 7.8% (11 of 141) showed a minor discrepancy; and 0.7% (1 of 141) showed a major discrepancy. Quality ratings were as follows: 65 studies were rated as near diagnostic, 69 suboptimal, and seven nondiagnostic. The quality of the portable CT study had no significant effect on the rate of discrepancy.

#### CONCLUSION

Our preliminary review indicates that there is high agreement between portable and conventional CT. Only a small percentage of the cases showed a minor discrepancy which we believe primarily related to the techniques of portable CT. There was a single instance of a major discrepancy which, in retrospect, likely is related to human error rather than the limitations of portable CT as determined by two board certified neuroradiologists. We feel that portable CT is a very useful technique in eliminating the safety concerns of transporting critically ill patients and is of acceptable diagnostic value in this specific patient population.

**KEY WORDS:** Portable CT, head CT

#### eP-145

##### Imaging Intracranial Calcification: A Comparison between CT and Quantitative Susceptibility Mapping

Chen, W.<sup>1</sup>·Liu, T.<sup>2</sup>·Zhu, W.<sup>1</sup>·Wang, Y.<sup>3</sup>

<sup>1</sup>Tongji Hospital, Tongji Medical College, Huazhong University of Science & Technology, Wuhan, CHINA, <sup>2</sup>MedImageMetric LLC, New York, NY, <sup>3</sup>Weill Medical College of Cornell University, New York, NY

#### PURPOSE

Although the appearance of calcification on a gradient echo MR image is not specific and may be confounded by other findings such as hemorrhage, additional CT confirmation often is needed for making proper diagnosis, prognosis, and therapy. Recently, a novel MRI technique, quantitative susceptibility mapping (QSM) has shown the capability to differentiate paramagnetic material including hemorrhage from such diamagnetic material including calcification. The purpose of this study is to evaluate the utility of QSM for detecting intracranial calcifications.

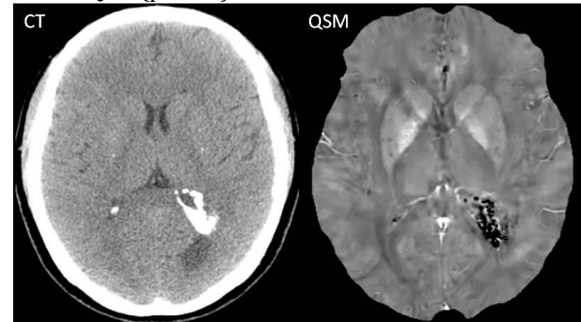
#### MATERIALS & METHODS

Two experienced neuroradiologists retrospectively reviewed on workstations CT and QSM images of 38 consecutive patients (ages 6-75 years; 24M/14F) with intracranial calcifications. All patients had undergone a CT follow-up study within 7 days after the MRI scan. Abnormal signal variations were identified on CT and

QSM as lesions. These lesions were split into putative calcifications and putative hemorrhages based on their signal intensities on QSM and CT, respectively. These findings were compared with a reference standard that was a combination of pathologic proof, conclusive imaging findings, and consensus between the two readers. Sensitivities and specificities, receiver operating characteristic curves (ROC), and the areas under the curves (AUC) were calculated for CT and QSM. Differences between CT and QSM were evaluated using the McNemar test and the method described by DeLong et al.

## RESULTS

A total of 220 lesions were detected on CT and QSM images, 168 (76.4%) of which were calcifications and 52 (23.6%) were hemorrhages. On QSM, calcifications appeared either totally hypo-intense (98.7%) or mostly hypo-intense with some heterogeneity (Figure). The sensitivities, specificities, and AUCs of two methods are summarized in the Table. No significant differences were found in sensitivity, specificities and AUC between CT and QSM ( $p > 0.05$ ).



Diagnostic performance of QSM and CT in detecting intracranial calcifications

	QSM	CT
Sensitivity (95%CI)	0.917(0.864-0.954)	0.952(0.908-0.979)
Specificity (95%CI)	0.981(0.897-1)	1(0.932-1)
AUC (95%CI)	0.949(0.916-0.982)	0.976(0.957-0.995)

## CONCLUSION

No significant difference was found in calcification detection between QSM and CT. Quantitative susceptibility mapping is an accurate MRI technique for calcification identification without ionizing radiation.

**KEY WORDS:** Quantitative susceptibility mapping, calcification

## eP-146

### Early Detection of Brain Tumor Progression Using a Novel Imaging-Based Biomarker

Ross, B. D.<sup>1</sup>Lemasson, B.<sup>1</sup>Chenevert, T. L.<sup>1</sup>Mikkelsen, T.<sup>2</sup>Boes, J.<sup>1</sup>Johnson, T. D.<sup>1</sup>Galban, S.<sup>1</sup>Rehemtulla, A.<sup>1</sup>Galban, C. J.<sup>1</sup>

<sup>1</sup>University of Michigan, Ann Arbor, MI, <sup>2</sup>Henry Ford Hospital, West Bloomfield, MI

## PURPOSE

The purpose of this study was to develop and evaluate a new voxel-based method, referred to as parametric response mapping (PRM), for early detection of brain tumor progression using standard MR images (FLAIR and T1-weighted postcontrast). Parametric response mapping results were evaluated to standard MRI-based criteria of progression assessment in patients with Grade III/IV gliomas.

## MATERIALS & METHODS

Fourteen patients with grades III/IV glioma underwent MRI before and during treatment (every 2 months). MR imaging scans, acquired on a 1.5 T or a 3 T clinical scanner, consisted of FLAIR and postcontrast T1-weighted (T1w Gd) images. All images were spatially registered to T1w Gd pretreatment scans and tumors were contoured manually on the T1w Gd images. Subsequent to PRM analysis, FLAIR images were normalized to the signal from the white matter tracks (rFLAIR). Parametric response mapping, applied to the whole brain volume on rFLAIR, was performed by first generating voxel-based difference maps at each longitudinal follow-up scan using the baseline as the subtrahend.

## RESULTS

Baseline was defined as either the pretreatment or subsequent rFLAIR image. Individual voxels were classified based on the extent of change observed in the rFLAIR difference maps. Three classifications were used: voxels with a significant increase in rFLAIR values ( $PRM_{rFLAIR+}$ : red), significant decrease ( $PRM_{rFLAIR-}$ : blue) or statistically unchanged ( $PRM_{rFLAIR0}$ : green). Disease recurrence was defined by PRM as the sum of red voxels that exceed 20% of the tumor volume as delineated on T1w Gd. Figure 1 illustrates a temporal MRI series from a representative chemo-RT treated GBM patient at baseline and follow-up scan dates. Disease progression was determined on week 35 by the MacDonald criteria. The area of increased rFLAIR detected at week 18 (shown as PRM red voxels) overlapped with the region designated recurrent tumor by T1w Gd on week 35.  $PRM_{rFLAIR}$  detected tumor recurrence on average  $18 \pm 3$  weeks (SEM) earlier than the MacDonald criteria. We also observed that  $PRM_{rFLAIR+}$  (red voxels) found outside the tumor T1w Gd regions revealed the location in which the tumor would progress on subsequent scans based on current standard progression criteria (Figure 1. Right image).

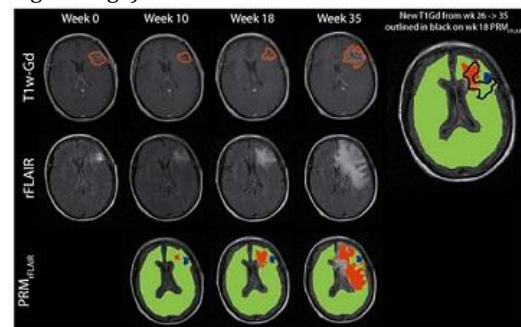


Figure 1: Serial MRI of a treated GBM showing T1w-Gd, rFLAIR and  $PRM_{rFLAIR+}$  in 1<sup>st</sup>, 2<sup>nd</sup> & 3<sup>rd</sup> rows respectively. The regions of increased rFLAIR are in red. Red regions corresponds to eventual progressive tumor called on week 35 as shown on the right by overlay of the new tumor (new T1w-Gd volume between week 18 & week 35) onto  $PRM_{rFLAIR+}$  at week 18.

## CONCLUSION

These results show that the PRM approach provides early detection and spatial depiction of brain tumor progression prior to detection by currently available conventional MRI-based criteria. Further validation of PRM for detection of tumor recurrence will require a larger cohort of patients and evaluation in a multisite clinical trial.

**KEY WORDS:** Glioma, imaging biomarker, progression

## eP-147

### Quantitative Susceptibility Mapping Image Quality Evaluation in Clinical Setting

Wang, S.<sup>1</sup>•Chen, W.<sup>2</sup>•Tsiouris, A.<sup>3</sup>•Liu, T.<sup>4</sup>•Wang, Y.<sup>5</sup>

<sup>1</sup>University of Electronic Science and Technology of China, Cheng Du, CHINA, <sup>2</sup>Tongji Hospital, Tongji Medical College, Huazhong University of Science & Technology, Wuhan, CHINA, <sup>3</sup>Weill Cornell Medical College, New York, NY, <sup>4</sup>MedImageMetric LLC, New York, NY, <sup>5</sup>Cornell University, Ithaca, NY

## PURPOSE

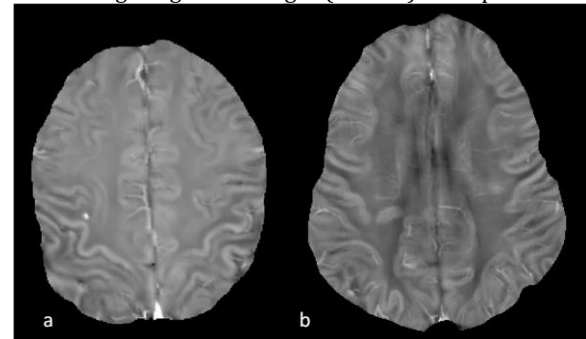
Quantitative susceptibility mapping (QSM) is a newly established MRI technique that quantifies tissue magnetic susceptibility property. In this study, we assess the feasibility of applying QSM in clinical practice by examining image quality.

## MATERIALS & METHODS

A radiologist reviewed QSMs of 114 consecutive patients (50 F/64 M, 17-87 years) imaged from 9/12/2011-10/10/2011 at our hospital. Overall image quality and four regions of the brain (substantia nigra/red nucleus, basal ganglia, Galen's vein, and gray matter/white matter border) were scored using the following scale: 1 = severe artifacts/blurring; 2 = moderate artifacts/blurring; 3 = no artifacts/blurring. Indications of pathology were noted. A chi-squared test was performed to compare image scores among eight age intervals, between the four brain regions, and between normal and pathologic subjects.

## RESULTS

Fifty patients showed no QSM indication of pathology. In the remaining 64 patients, 279 hyperintense lesions were identified, including 136 diffuse white matter lesions of slightly higher susceptibility than surrounding white matter (Fig.1b) (suspected as demyelinating lesions) in 24 MS patients, 45 isolated points of very high susceptibility value (suspected as microbleeds) in 15 patients (Fig.1a), 25 hemorrhages in 15 patients, three venous malformations in three patients, and 70 other lesions in seven patients. There was no statistically significant difference in image quality with respect to the presence of pathology ( $p = 0.14$ ), age of subject ( $p = 0.17$ ) or brain regions ( $p = 0.90$ ). Overall image quality was  $2.86 \pm 0.43$  for all subjects and  $2.89 \pm 0.36$  for pathologic subjects. Motion corrupted images (score 1) in two patients and hemorrhage degraded images (score 2) in six patients.





Scores of groups		Score 1	Score 2	Score 3
Age	10-19	0	1	4
	20-29	1	1	10
	30-39	0	0	23
	40-49	0	0	21
	50-59	1	1	21
	60-69	0	2	7
	70-79	0	1	7
	80-89	2	2	9
Area	substantia nigra/red nucleus	4	7	103
	galen's vein	4	5	105
	basal ganglia	4	10	100
	gray matter/white matter	4	6	104
Diseases	no QSM indication	0	3	47
	microbleeds	0	1	14
	Demyelination	0	0	24
	Venous Malformation	0	0	3
	Other	2	3	17

#### CONCLUSION

Quantitative susceptibility mapping is an imaging technique capable of high image quality in a wide range of subject ages and pathologies. Quantitative susceptibility mapping is potentially useful for evaluating hemorrhages, microbleeds, venous malformations, and the demyelinating lesions of multiple sclerosis.

**KEY WORDS:** Quantitative, susceptibility

#### eP-148

#### Quantitative Cerebral Blood Flow Measurements in Symptomatic versus Asymptomatic Intracranial Atherosclerotic Disease Using Bookend Dynamic Susceptibility Contrast MR Perfusion-Weighted Imaging Technique with Vascular Territory Region of Interest Analysis

Korutz, A. Vakil, P. Qian, R. Habib, A. Vranic, J. E. Hurley, M. C. Shaibani, A. Carroll, T. J. Ansari, S. A.

Northwestern University Feinberg School of Medicine  
Chicago, IL

#### PURPOSE

The third-leading cause of death in the United States is stroke with approximately 800,000 victims per year. Intracranial atherosclerotic disease (ICAD) is responsible for 7-10% of all strokes, but the risk of recurrent stroke in this population approaches nearly 12-22% at 1 year despite optimum medical management with antiplatelet/antithrombotic medications. Although the role of surgical or endovascular intervention in severe ICAD has been definitively relegated to patients failing medical

management, we have yet to develop a risk stratification scheme to identify this susceptible population prior to refractory TIAs/strokes. We studied the differences in quantitative cerebral blood flow (qCBF) value measurements as measured by the Bookend dynamic susceptibility contrast (DSC MR PWI) technique using vascular territory ROI analysis in symptomatic and asymptomatic patients with ICAD.

#### MATERIALS & METHODS

Using our institution's PACS and medical record databases we retrospectively identified 10 patients (6M:4F; 61+/-14 years) with moderate to severe intracranial stenoses (>50%) as identified with MRA within or immediately distal to the circle of Willis (A1/A2 ACA, M1/M2 MCA, and P1/P2 PCA) that had a correlative DSC-MR PWI scan at time of diagnosis or presentation. Vascular territories were divided into symptomatic and asymptomatic subgroups that contained acute infarcts on diffusion-weighted MRI versus those that were infarct free respectively. Automated vascular territory ROI analysis was performed to include both gray and white matter within each respective arterial distribution on each subject's MR PWI maps. Individual qCBF values were generated for each vascular distribution from the DSC MR PWI scan. Vascular territory ROI analysis for the MCA distribution was further subdivided into the inferior division (iMCA), superior division (sMCA), and M1 perforators (pMCA). Quantitative CBF values for individual territories downstream of intracranial stenoses were compared using the two-tailed Student's t-test.

#### RESULTS

Seven vascular territories (1 ACA, 2 sMCA, 2 iMCA and 2 pMCA) were placed in the symptomatic subgroup, presenting with acute infarcts, and nine vascular territories (2 sMCA, 2 iMCA, 2 pMCA and 3 PCA) were placed in the asymptomatic subgroup, infarct free. The mean qCBF for all vascular territories (gray and white matter) containing acute infarcts was 27.7 +/- 5.8 mL/min/100g and for all vascular territories which were infarct free was 39.9 +/- 9.4 mL/min/100g. The difference between qCBF values in vascular territories with and without infarcts was statistically significant ( $p < 0.01$ ).

#### CONCLUSION

Quantitative CBF measurements using the Bookend DSC MR PWI sequence and vascular territory ROI analysis may assist in stratifying patient risk in the setting of moderate to severe ICAD as a marker for stage 2 hemodynamic compromise. Statistical differences in qCBF values between symptomatic and asymptomatic patients suggest earlier detection of unstable or refractory intracranial stenoses may be possible, allowing for more aggressive medical management or intervention.

**KEY WORDS:** Atherosclerosis, perfusion, intracranial

## eP-149

**Another Reversal Sign: The Use of Dynamic CT Angiography in Suspected Cases of Brain Death**

Chakraborty, S.·Adas, R. A. A.

The Ottawa Hospital/University  
Ottawa, ON, CANADA

**PURPOSE**

Neurologic determination of death or brain death is primarily a clinical diagnosis. The diagnosis of brain death must respect all guarantees required by law and be determined as early as possible to avoid unnecessary treatment and to allow organ harvesting for transplantation. Ancillary testing is used in situations where clinical assessment is impossible or confounded by other factors. This study is to determine the utility of the new dynamic CT angiogram (dCTA) technique ancillary to the diagnosis of brain death.

**MATERIALS & METHODS**

Dynamic CTA is a noninvasive technique to acquire a time series of bone subtracted or nonsubtracted CTA images of the whole brain. This provides temporal flow information on entire cranial circulation. We retrospectively analyzed the charts of eight adult suspected brain death patients who had undergone a dynamic CT angiography. Control group included acute stroke patients who on follow-up scan showed no strokes. All studies were analyzed using Vitrea FX workstation. The earliest contrast enhancement times of both internal (ICA), external carotid arteries (ECA) and their branches were recorded for both patient groups.

**RESULTS**

While having the same benefit of easy availability and noninvasiveness of the standard CTA, dCTA could show us brain blood flow during the whole scanning period of 80 seconds, making it possible to analyze the pattern of flow qualitatively. So, trickle flow and presence of small amount of contrast in the basal arteries does not confuse us to confidently diagnose lack of global intracranial flow. It also images the entire cranial vasculature simultaneously and allows comparison to the extra cranial arterial flow that can be used as internal control. So, significant delay in intracerebral flow can be seen in comparison to extracranial circulation. In normal individuals, we have noted appearance of contrast in the internal carotid artery is slightly earlier or at the same time as the external carotid branches at the skull base. There is a reversal of this pattern in brain dead patients. In all brain death patients, compared to the control, ICA only enhanced after ECA branches were opacified. This could be surrogate marker of lack of intracranial flow in brain death.

**CONCLUSION**

Dynamic CTA can be used to reliably demonstrate the lack of cerebral blood flow in patients with suspected brain death with extracranial circulation as an internal reference. The "reversal sign" sign has been described

in brain death patients as the reversal of gray-white matter density in noncontrast CT. The "dCTA reversal sign" results from the delayed enhancement of the ICA, relative to a normal ECA

**KEY WORDS:** Brain death, dynamic CT angiography, DCTA

## eP-150

**Combining Graph Theoretical Analysis and Conventional Anatomical MR Imaging: A New Voxel-Wise Approach for Constructing Disease-Specific Structural Brain Networks Applied to Alzheimer Disease**

Whitlow, C. T.·Maldjian, J. A.

Wake Forest University School of Medicine  
Winston-Salem, NC

**PURPOSE**

Graph theoretical analysis applied to MRI has begun to shed light upon neurodegenerative diseases at the level of whole-brain distributed network connectivity. In the present study, we applied graph theory methods to voxel-wise data from a T1-weighted MRI sequence, hypothesizing that the construction of group-specific structural brain networks from conventional anatomical imaging would yield important disease-associated patterns of change in cerebral gray matter.

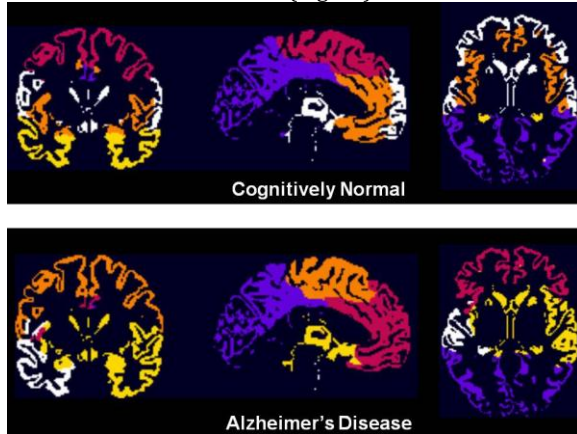
**MATERIALS & METHODS**

T1-weighted structural MRI data from 102 cognitively normal (CN) and 92 Alzheimer disease (AD) patients were obtained from the Alzheimer's Disease Neuroimaging Initiative. All data were motion-corrected, segmented and normalized to a standard template using VBM8 toolbox within SPM8. Modulated gray matter maps from all subjects in each group were concatenated into a 4D image data file to construct group-specific voxel-based 159,844 x 159,844 correlation matrices. Binarized adjacency matrices then were generated at a cost of 0.1, from which AD- and CN-specific degree and modularity maps were constructed. Serial t-tests were used to evaluate between-group differences in degree, including a priori hypothesized differences for specific structures known to be abnormal in AD (e.g., hippocampus and components of the default mode network).

**RESULTS**

High and low degree voxels are those with a relatively large or small number of connections with other brain voxels, respectively, based upon similarity in voxel gray-matter volume changes across subjects compared to all other brain voxels. T tests corrected for multiple comparisons demonstrated between-group AD-associated decreases in degree for hippocampus and increases for default mode structures (medial prefrontal cortex, posterior cingulate cortex, precuneus, and inferior parietal lobe) ( $p < .0008$ ). Figure 1 presents modularity maps that demonstrate the distribution of individual voxels into a striking mosaic of regional clusters that reflect the known distributed anatomical

organization of the brain. Alzheimer disease modularity maps demonstrate a pattern of lateralization and loss of anatomical complexity. This is characterized by the collapse of two intra-hippocampal and -frontal lobe modules in CN into single respective modules for AD, as well as hippocampal lateralized into separate right and left modules that contain additional ipsilateral temporal lobe and insular structures (Figure).



#### CONCLUSION

This novel voxel-wise approach for constructing disease-specific brain networks using an anatomical T1-weighted sequence yielded important information about AD, replicating known abnormalities involving the hippocampus and default mode network, but also revealing a global whole-brain pattern of lateralization and loss of anatomical complexity, and may lead to the development of new disease-specific imaging biomarkers in the future.

**KEY WORDS:** Graph theoretical analysis, Alzheimer disease

#### eP-151

##### Recommendations for Selecting the Vascular Input Functions to Optimize the Validity in CT Perfusion Imaging in 256- (or More) Slice Scanners

Niessen, J.·van der Schaaf, I.·Riordan, A.·de Jong, H.·Mali, W.·Velthuis, B.

University Medical Center Utrecht  
Utrecht, NETHERLANDS

#### PURPOSE

To improve accuracy and reproducibility of quantitative perfusion by the assessment of the optimal artery for the arterial input function (AIF) and re-evaluating the necessity of the venous output function (VOF).

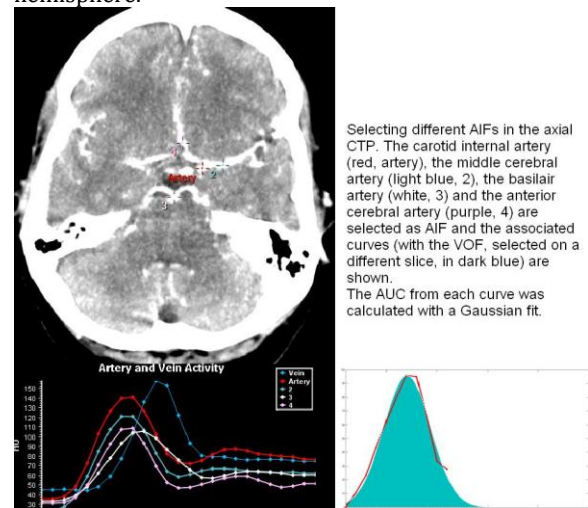
#### MATERIALS & METHODS

Forty-four patients with acute middle cerebral artery (MCA) ischemic stroke underwent noncontrast CT, CT perfusion (CTP) and CT angiography using a 256-slice CT scanner. In the CTP measurements, anterior cerebral artery (ACA), contralateral MCA, contralateral internal carotid artery (ICA) and the basilar artery (Abas) were selected as the AIF and the area under the AIF curve ( $AUC_{AIF}$ ) was calculated. To investigate the AIF

accuracy, we compared the quantitative perfusion measurements in both symptomatic and asymptomatic hemisphere for each AIF location (repeated Measures' test). To investigate the operator steps and reproducibility we examined if the VOF could be deleted and compared the resulting quantitative measurements with the VOF in a large vein (paired t-test).

#### RESULTS

The ICA had the largest  $AUC_{AIF}$  followed by Abas, MCA and ACA. The differences in AUC were statistically significant between all arteries ( $p < 0.0001$ ). Selecting the ICA and Abas as AIF resulted in the lowest (i.e., most accurate) quantitative mean CBV and CBF and accordingly the highest quantitative MTT (all  $p < 0.0001$ ). Not correcting the AIF by the VOF showed significantly higher mean CBV (i.e., overestimation) on both the hemisphere ipsi- and contralateral to the thrombus ( $p = 0.003$  and  $p = 0.001$  respectively), and a significantly higher CBF ( $p = 0.016$ ) on the ipsilateral hemisphere.



#### CONCLUSION

To improve validity of quantitative perfusion values we recommend to select the ICA as the AIF and a large vein as the VOF.

**KEY WORDS:** Stroke, CT perfusion, AIF

#### eP-152

##### Time-Resolved CT Angiogram Protocol for Confirmation of Brain Death

Shankar, J. J. S.·Maloney, W.·Vandorpe, R.

QE II Hospital  
Halifax, NS, CANADA

#### PURPOSE

Computed tomography angiography (CTA) has been accepted as one of the ancillary test for confirmation of brain death. The protocol for CTA for the confirmation of brain death can vary considerably between different centers. The most common protocol used is two acquisitions of CTA after a single bolus of contrast injection. However the time interval between the two

acquisitions varies in different centers and can be operator-dependent. Delay of the second acquisition may lead to diffusion of contrast into the distal cortical branches causing false negative results on the CTA. The purpose of our study is to devise a standardized protocol for CTA for confirmation of brain death which will not be operator-dependent.

#### **MATERIALS & METHODS**

All patients referred to our department for CTA for confirmation of brain death prospectively underwent CT perfusion protocol on the 64-slice dual energy CT scanner (Siemens Sensation definition). A total of 40 ml of contrast media was injected at a rate of 4 ml/sec. A total of 22 volumes of the approximately whole brain were acquired with the total time of acquisition of 42 seconds after the injection of contrast media. The axial source images were reconstructed into 5 mm thick slice and sent to PACS. The images were analyzed for the presence of contrast media in the superficial temporal artery branches to the scalp to confirm the successful intravascular injection. The presence of contrast in the different segment of intracranial arteries was analyzed. All images were evaluated on a 4- and 7-point scale described in the literature based on the presence of contrast in the intracranial ICA, M4 segment of MCA, A2 segment of ACA, internal cerebral vein and great cerebral vein of Galen. Sensitivity and specificity of the 4- point and 7-point scale were calculated.

#### **RESULTS**

In the last 6 months a total of eight patients, all of whom were declared clinically brain dead, were referred to us for the ancillary test of CTA for confirmation of brain death. One of the patients also underwent nuclear medicine flow study for brain death confirmation 15 minutes before undergoing our CTA protocol. Six out of the seven patients were declared brain dead on our CTA protocol. One of the patients had no perfusion in the brain stem but had preserved perfusion to the rest of the brain and we could not declare him brain dead. This patient subsequently died 12 hours after the CTA. The sensitivity and specificity of the 4- and 7-point scale in our study were 100%.

#### **CONCLUSION**

We found 100% sensitivity and specificity with our new time-resolved CTA protocol with a shorter time of acquisition, lower radiation and contrast dose with less operator dependence.

**KEY WORDS:** Brain death, time-resolved CT angiogram, CT perfusion

#### **eP-153**

##### **Comparison of Full Dose Optimark and Half Dose Multihance Postcontrast T1 Sequences of the Brain**

Kessler, M. M.<sup>1</sup>·Benzinger, T.<sup>1</sup>·Soriano, C. J.<sup>2</sup>·Wippold, F. J.<sup>1</sup>

<sup>1</sup>Mallinckrodt Institute of Radiology, Saint Louis, MO,

<sup>2</sup>Resomasa, Lima, PERU

#### **PURPOSE**

This review evaluates the enhancement characteristics of human brain tumors imaged with standard dose (0.1 mmol/kg) gadoversetamide and half dose (0.05 mmol/kg) gadobenate dimeglumine.

#### **MATERIALS & METHODS**

Patients with a suspected or known brain tumor are imaged routinely at our institution with a contrast-enhanced MRI, using standard dose (0.1 mmol/kg) gadoversetamide. These patients subsequently undergo a stereotactic brain MRI performed with half dose (0.05 mmol/kg) gadobenate dimeglumine for anticipated stereotactic radiosurgery or surgery. A postcontrast 3D T1-weighted gradient echo sequence is included in both protocols. The full-dose gadoversetamide and half-dose gadobenate dimeglumine postcontrast T1 weighted sequences of 20 patients with various brain tumors were reviewed retrospectively by three radiologists. The radiologists were blinded to the contrast agent and dose. This study received approval from the institutional review board.

#### **RESULTS**

No enhancing were missed on half dose gadobenate dimeglumine, examinations (100% concordance).

#### **CONCLUSION**

In our clinical practice, brain MRI exams performed with application of half dose (0.05 mmol/kg) gadobenate dimeglumine have equivalent diagnostic utility to those with standard dose (0.1 mmol/kg) gadoversetamide on postcontrast T1-weighted imaging. Clinical relevance/application: The results of this study could decrease the cost-per-study of brain MRI exams in regards to the volume of injected iv contrast and potentially lower the incidence of contrast-related complications.

**KEY WORDS:** Gadobenate dimeglumine, brain, half dose

#### **eP-154**

##### **Every Bright Blob on a MR Angiogram is not an Aneurysm! Unusual Features of Intracranial Lipomas in Adults: An Observational Study**

Siripurapu, R.·Herwadkar, A.

Salford Royal NHS Foundation Trust  
Manchester, UNITED KINGDOM

#### **PURPOSE**

To review the imaging features and distribution of intracranial lipomas in adults. To review the

embryology and pathogenesis of intracranial lipomas with emphasis on the embryology of meninx primitiva. To make aware the potential pitfall of labeling some of these as aneurysms.

#### MATERIALS & METHODS

Imaging database at Salford Royal Foundation Trust from January 2007 to September 2011 identified 38 adult patients (16 years to 90 years) with intracranial lipomas. CT and/or MR imaging in all 38 patients was reviewed retrospectively by two neuroradiologists for location, imaging characteristics, relation to adjacent vessels and brain. The presence of other congenital anomalies also was reviewed. Eleven excluded cases were parafalcine fat (8), ecchordosis (1) and dermoid (1).

#### RESULTS

The distribution of various lipomas is depicted in Table 1. Of the 27 cases, six were related closely to the vessels mimicking aneurysms on the T2 sequence or on time of flight MR angiogram. Of these, two were close to the middle cerebral artery (Figure 1) and four to the basilar artery. Contrary to the published literature, our study identified only four cases of pericallosal lipomas and very few cases of associated congenital malformations, presumably as the study involved only adult patients. As previously illustrated, our study also supports that the relative frequency of location of these corresponds to the temporal sequence of dissolution of meninx primitiva.

Table 1: Distribution of intracranial lipomas

Suprasellar cistern	8	29.7%
Quadrigeminal cistern	5	18.5%
Pericallosal and velum interpositum extending to callosum	4	14.8%
Interpeduncular cistern	3	11.1%
Cerebellar	2	7.4%
Sylvian	2	7.4%
Others	3	11.1%
Total	27	100%



#### CONCLUSION

Intracranial lipomas are rare, tend to occur in specific characteristic locations within the brain and can be seen in the absence of other malformations in adults. When they occur in isolation and in unusual location, close to a vessel, it is important to be aware of the potential pitfall of labeling them as aneurysms.

**KEY WORDS:** Lipoma, intracranial

#### eP-155

#### Complications of Deep Brain Stimulator Implantation

Chin, B. M.<sup>1</sup>Salzman, K. L.<sup>1</sup>House, P.<sup>1</sup>Glastonbury, C.<sup>2</sup>

<sup>1</sup>University of Utah, Salt Lake City, UT, <sup>2</sup>University of California San Francisco, San Francisco, CA

#### PURPOSE

Deep brain stimulator (DBS) implantation is a stereotactic neurosurgical technique increasingly used to treat movement disorders, including Parkinson's disease, dystonia, and essential tremor. Knowledge of the potential complications is important. The purpose of this study was to characterize the incidence, presentation, and radiologic appearances of DBS complications.

#### MATERIALS & METHODS

A retrospective search of imaging databases using keywords "deep brain stimulator" and "DBS" was performed from 2001 to 2011. Clinical data and imaging features were reviewed. Studies were excluded if

preoperative or postoperative imaging or clinical follow up were not available.

## RESULTS

One hundred seventy-two patients with DBS procedures were identified, with a total of 324 lead placement procedures. Twenty patients (12%) required repeat surgery for lead adjustment or replacement, based on failure to achieve expected clinical results after multiple programming attempts. Thirty-one complications (10% of total procedures) occurred, including infection (7 patients), subdural hematoma or hygromas (7 patients), symptomatic lead tract edema (5 patients), and stroke (3 patients). Asymptomatic patients with small amounts of intra-axial or extra-axial hemorrhage were followed with imaging. Patients with infection, stroke, or inflammatory edema along the leads presented with altered mental status, weakness, seizures, or other forms of neurologic impairment. Occasionally, diagnosis was delayed when signs or symptoms were attributed to medications or the patient's primary disease process. Due to concerns of MRI compatibility with the DBS leads, CT is the primary postprocedure imaging modality utilized at our institution. However, MRI is possible with appropriate safeguards. Knowledge of the artifacts is essential to avoid over- or under-diagnosis of complications.

## CONCLUSION

Knowledge of DBS complications and their clinical and radiologic presentations is imperative for optimal patient outcomes.

**KEY WORDS:** Deep brain stimulator, DBS, complications

## eP-156

### Automated Vessel Extraction for Assessment of Leptomeningeal Collateral Status

Lee, Y. Z.<sup>1</sup>•Aylward, S.<sup>2</sup>•Huang, D. Y.<sup>1</sup>•Faber, J. E.<sup>1</sup>•Matheus, G.<sup>3</sup>•Smith, J. K.<sup>1</sup>

<sup>1</sup>University of North Carolina at Chapel Hill, Chapel Hill, NC, <sup>2</sup>Kitware, Carrboro, NC, <sup>3</sup>Medical University of South Carolina, Charleston, SC

## PURPOSE

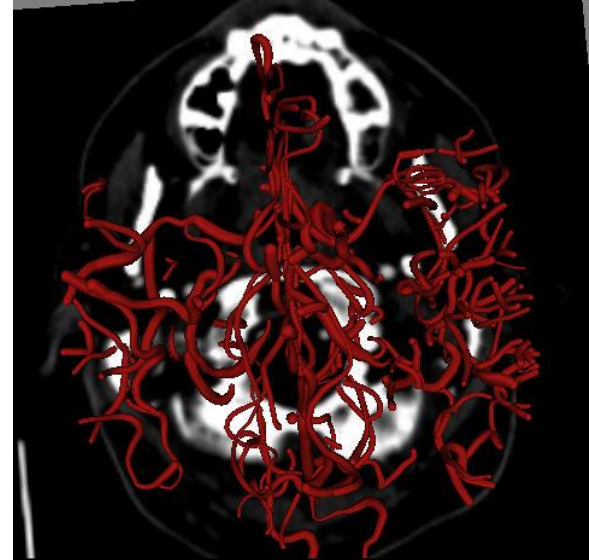
The decision to initiate therapy in acute ischemic stroke remains a balance between potentially worsening disability versus promoting significant salvage of brain tissue. Although it is well known that collateral status is an important determinant of penumbral volume, final infarct size and clinical outcome, rapid and systematic non- or minimally invasive assessment of status remains challenging. While the gold standard for evaluating leptomeningeal collaterals remains digital subtraction angiography (DSA), more recent work has focused on manual evaluation based on computed tomographic angiography (CTA) and MRI-based approaches. The goal of this study was to explore automated vessel extraction techniques for the evaluation of leptomeningeal collaterals on CTA.

## MATERIALS & METHODS

Five patients with acute stroke and an M1/A1 occlusion were identified retrospectively. Technically adequate data sets were identified that did not have evidence of significant venous contamination or patient motion. CTA data were anonymized and transferred offline for analysis. Custom software was written using the ITK/VTK framework and TubeTK libraries for the identification and extraction of vessels within the CTA. Arterial vessels were extracted in a semiautomatic fashion. No specific effort was made to exclude venous vessels. The extracted vessels then were rendered in 3D for evaluation by a neuroradiologist. The presence of vessels identified as leptomeningeal collaterals was graded based on comparison to the contralateral side. Leptomeningeal collaterals also were evaluated independently after blinding to the 3D data, based on maximum intensity projections (MIPs) of the data set in the axial plane.

## RESULTS

Good agreement was obtained between leptomeningeal collateral grade based on the semiautomated vessel extraction relative to the MIP data sets. Vessel geometries could be identified readily on the 3D images.



## CONCLUSION

The rapid evaluation of leptomeningeal collaterals can provide important diagnostic information for acute stroke patients. Our preliminary work demonstrates that this evaluation may be performed in a semiautomated manner, which is an important component in a systematic, quantitative evaluation of collateral flow. Furthermore, this will provide the framework for more advanced analysis and research in the future. Work is ongoing to further improve collateral detection, extraction and flow for correlation with clinical outcomes.

**KEY WORDS:** Computer analysis, stroke, CTA

## eP-157

### Cost-Effectiveness of CT Angiography, MR Angiography and Intraarterial Digital Subtraction



## Angiography in Patients with Ruptured Intracranial Aneurysms: A Decision Model

Sailer, A. M. H.<sup>1</sup>•Grutters, J. P. C.<sup>2</sup>•van Zwam, W. H.<sup>1</sup>

<sup>1</sup>Maastricht University Medical Center, Maastricht, NETHERLANDS, <sup>2</sup>CAPHRI School for Public Health and Primary Care, Maastricht, NETHERLANDS

### PURPOSE

In patients with nontraumatic subarachnoid hemorrhage, intraarterial digital subtraction angiography (IA DSA) is the gold standard for the detection of ruptured intracranial aneurysms and determination of their feasibility of endovascular coiling. Contrast-enhanced magnetic resonance angiography (MRA) and computed tomography angiography (CTA) are two noninvasive alternatives to current standard. With imaging deeming no feasibility of endovascular treatment, surgical clipping is an alternative treatment option with slightly higher costs and minor outcome over a 1 year period. The goal of this study was to compare the cost-effectiveness of MRA, CTA and IA DSA in patients with nontraumatic subarachnoid hemorrhage based on a 1-year period.

### MATERIALS & METHODS

A decision model was used to calculate costs and benefits [in quality-adjusted life-years (QALYs)] that accrued to hypothetical cohorts of patients with presentation of subarachnoid hemorrhage in the emergency department. Sensitivity and specificity of MRA, CTA and IA DSA in both detecting aneurysms and determining feasibility of coiling were based on a prospective study in 75 patients. Costs of the diagnostic test, therapy (either coiling or clipping), as well as patients' quality of life for the first year period and associated costs were taken into account. In a scenario analysis a strategy was examined where in each patient for whom coiling was not deemed feasible IA DSA was performed.

### RESULTS

Intraarterial DSA was the most effective diagnostic option, yielding 0.6224 QALYs (SD 0.0191) over 1 year, followed by CTA (0.6173 QALYs; SD 0.0193) and MRA (0.6129 QALYs; SD 0.01914). The total one year costs were lowest for IA-DSA (\$48,099; SD \$3,343), followed by CTA (\$49,525; SD \$3,385) and MRA (\$51,474; SD \$3,394). As IA DSA was both more effective and less costly over 1 year, it dominated CTA and MRA. CT angiography was more effective and less costly, and thus dominated, MRA. The strategy that included IA DSA for each patient for whom coiling was not deemed feasible, led to equal effectiveness for IA DSA, MRA and CTA. In this strategy CTA was less costly, and therefore cost-effective compared to MRA and IA DSA.

### CONCLUSION

Comparing the noninvasive imaging modalities, CTA was superior to MRA in terms of cost-effectiveness. However, IA DSA dominated both MRA and CTA due to higher quality of life and less overall one-year costs. A strategy where CTA was followed by IA DSA if coiling

was not deemed feasible, was found to be the most cost-effective option.

**KEY WORDS:** Aneurysm, Cost-effectiveness, IA-DSA, MRA, CTA

### eP-158

## Can Patient Selection for Intraarterial Stroke Therapy Be Optimized without "Advanced Imaging"?

Jayaraman, M. V. •Boxerman, J. L. •Silver, B. •Rogg, J. M.

Warren Alpert School of Medicine at Brown University Providence, RI

### PURPOSE

Imaging-based triage has the theoretical advantage of better selecting stroke patients for acute revascularization therapy than time alone. However, advanced imaging techniques such as diffusion-weighted MRI may not be consistently attainable at all hospitals. The purpose of this study was to determine whether the combination of clinical examination, arterial occlusion on CT angiography (CTA) and noncontrast CT (NCCT) ASPECTS can identify patients presenting with acute anterior circulation stroke who may be most likely to benefit from recanalization.

### MATERIALS & METHODS

Retrospective review of hospital records was performed to identify all patients presenting within 8 hours of symptom onset with suspected anterior circulation stroke with an NIH stroke scale (NIHSS)  $\geq 8$  between January 1, 2009 and December 30, 2010. As part of our clinical protocol, all of these patients underwent NCCT and CTA. Imaging was reviewed to score ASPECTS on NCCT and the presence of proximal arterial occlusion [defined as the internal carotid artery (ICA), M1 or first 1cm of an M2 branch of the middle cerebral artery (MCA)]. For patients who underwent intraarterial therapy (IAT), angiograms were reviewed and final recanalization status was classified as none for Thrombolysis in Cerebral Ischemia (TICI) 0-1, partial for TICI 2a and complete for TICI 2b/3. Discharge disposition was recorded for all patients and categorized as Home (with or without services), Rehabilitation (short or long-term) or Death (including discharge to Hospice). Based on imaging findings, patients were placed into three groups (all with NIHSS  $> 8$ ): Group 1, No proximal arterial occlusion, NCCT ASPECTS  $\geq 8$ ; Group 2, Proximal occlusion, NCCT ASPECTS  $\geq 8$ ; Group 3: Proximal occlusion, NCCT ASPECTS  $< 8$ .

### RESULTS

Fifty-two patients met inclusion criteria, with 10 in Group 1, 30 in Group 2 and 12 in Group 3. Intraarterial therapy was performed in 25/30 Group 2 patients and 2/12 Group 3 patients. Of Group 2 patients who underwent IAT, final TICI score was TICI 2b/3 in 11/25 (44%), TICI 2a in 7/25 (28%) and TICI 0-1 in 7/25 (28%). Discharge status was home in 60% of Group 1 patients, 23% of Group 2 patients and 0% of Group 3

patients. Among Group 2 patients, 55% with TIC1 2b/3a were discharged home compared with 5% with TIC1 0-1 or 2a. Of the 2 Group three patients who underwent IAT, one achieved TIC1 2b recanalization, but that patient died. In hospital mortality was 0% for Group 1, 27% for all Group 2 (0% for TIC1 2b/3 and 42% for TIC1 0-1 or 2a) and 58% for Group 3. The odds ratio for discharge home with successful recanalization in Group 2 patients was 21.6 (95% Confidence Interval 2.1-223.6).

#### CONCLUSION

In this retrospective analysis, patients with an NIHSS  $\geq 8$ , proximal arterial occlusion on CTA and NCCT ASPECTS  $\geq 8$  appear to benefit from recanalization. Further validation of these clinical and imaging selection criteria in a prospective trial is warranted, especially for patients who may otherwise be ineligible based on time criteria alone.

**KEY WORDS:** Stroke, thrombectomy, thrombolysis

#### eP-159

##### **Detection of Cerebral Vasospasm Using Dynamic CT: Analysis of Volume Perfusion CT Maps and 4D CT Angiography**

Schramm, P.<sup>1</sup>Dolatowski, K.<sup>1</sup>Schramm, R.<sup>1</sup>Froelich, A.<sup>1</sup>Klotz, E.<sup>2</sup>Knauth, M.<sup>1</sup>

<sup>1</sup>University Goettingen Medical Center, Goettingen, GERMANY, <sup>2</sup>Siemens Healthcare, Forchheim, GERMANY

#### PURPOSE

Cerebral vasospasm with a raised risk for secondary ischemia is a frequent complication after subarachnoid hemorrhage (SAH). We tested, whether "whole brain" volume perfusion CT (VPCT) delivers relevant information about the localization and characteristics of arterial vasospasm and the volume at risk of secondary infarction.

#### MATERIALS & METHODS

Eleven consecutive patients with suspicion of cerebral vasospasm due to SAH underwent VPCT of the brain. CT angiographic maximum-intensity projections were generated from thin slice recons of the VPCT dataset at peak arterial time. Images were assessed for presence of arterial vasospasm and compared with conventional CTA or DSA. The distribution of ischemic lesions was analyzed on 3D perfusion parameter maps of cerebral blood flow (CBF), cerebral blood volume (CBV), mean transit time (MTT) and time to drain (TTD).

#### RESULTS

In all 11 patients, focal areas of cerebral hypoperfusion were detected on color-coded VPCT parameter maps. The highest sensitivity was found for MTT and TTD. Focal reductions of CBV strongly correlated with infarction on follow-up CT. Eight patients (73%) had vasospastic lesions of intracranial arteries on MIP reconstructions of the 4D CTA. All of these stenotic lesions were also visible on conventional CTA or DSA,

resulting in 100% sensitivity of the 4D CTA reconstructions.

#### CONCLUSION

Volume perfusion CT is a noninvasive method that allows detecting cerebral vasospasm in patients suffering from SAH. It has the potential to demonstrate focal perfusion deficits as well as vasospastic arterial segments and might therefore improve diagnosis and treatment decisions in those patients.

**KEY WORDS:** Cerebral vasospasm, 4D CT angiography, volume perfusion CT

#### eP-160

##### **Can CT Perfusion Assist in Guiding Treatment Management for Vasospasm in Aneurysmal Subarachnoid Hemorrhage?**

Anumula, N. S.Gold, R.Johnson, C.Comunale, J.Tsiouris, A.Sanelli, P. C.

Weill Cornell Medical College  
New York, NY

#### PURPOSE

CT perfusion (CTP) provides hemodynamic information that may assist clinicians in assessing the need for immediate treatment of vasospasm with medical and/or interventional therapies. The purpose is to evaluate qualitative and quantitative CTP for different treatment options of vasospasm in aneurysmal subarachnoid hemorrhage (A-SAH).

#### MATERIALS & METHODS

Retrospective study of consecutive A-SAH patients enrolled in a prospective IRB-approved clinical trial was performed. CT perfusion was performed 6-8 days following A-SAH. Qualitative analysis of perfusion deficits were performed by two blinded neuroradiologists. Quantitative CTP was performed using standardized protocol with region-of-interest placement sampling cortical cerebral blood flow (CBF), cerebral blood volume (CBV), and mean transit time (MTT). Diagnosis of vasospasm was assessed by clinical and imaging criteria. Three treatment outcome groups were studied: (1) medical treatment with only hypertension-hemodilution-hypervolemia(HHH), (2) interventional therapies with intraarterial(IA) vasodilators and/or angioplasty, (3) no treatment. Clinical decisions for treatment management were based on clinical exam, transcranial Doppler ultrasound and cerebral angiography. Mean quantitative CTP values were compared for treatment groups using two tailed t-test and pairwise comparisons. Receiver operating characteristic(ROC) curves determined accuracy from the area-under-the-curve(AUC) with its standard error(SE). Optimal threshold values were calculated using the northwest corner method.

#### RESULTS

Ninety-six patients (median age 49 years) were classified into three treatment groups: 21%(19/96) HHH, 34%(33/96) IA-therapy and 46%(44/96) no

treatment. Vasospasm was diagnosed in 42%(40/96); of which 18%(7/40) had HHH, 80%(32/40) IA-therapy, and 2%(1/40) no treatment. No vasospasm was classified in 58%(56/96); of which 21%(12/56) had HHH, 2%(1/56) IA-therapy, and 77%(43/56) no treatment. Qualitative CTP deficits were seen in 50%(48/96); occurring in 95%(38/40) with vasospasm and 18%(10/56) with no vasospasm. These deficits were seen in 63%(12/19) HHH, 94%(31/33) IA-therapy, and 11%(5/44) no treatment. Presence of CTP deficit had 83% sensitivity, 89% specificity, 90% positive predictive and 81% negative predictive values for treatment. Mean quantitative CTP values for each treatment group are shown in Table 1. Statistically significant differences in CBF and MTT occurred amongst all three treatment groups. Pairwise comparisons also showed a significant difference for CBF ( $p<0.0001$ ), CBV ( $p<0.05$ ) and MTT ( $p<0.0001$ ) between the IA-therapy and no treatment groups. Only CBF ( $p<0.05$ ) had a significant difference between the HHH and IA-therapy groups. Further analysis with ROC demonstrated that CBF had the highest AUC of 0.82 (SE 0.04) for comparing treatment groups. Threshold analysis revealed CBF of 30mL/100gm/min (71% sensitivity, 89% specificity) for determining patients requiring treatment versus no treatment and CBF of 26mL/100gm/min (79% sensitivity, 74% specificity) for determining HHH versus IA-therapy.

Table 1: Mean quantitative CTP values and standard deviation (SD) for each treatment group

Mean (SD)	No treatment	HHH	IA-therapy	p-value
CBF (mL/100gm/min)	40.6 (11.1)	33.2 (15.4)	24.4 (11.9)	<0.0001
CBV (mL/100gm)	2.01 (0.51)	1.99 (0.68)	1.71 (0.66)	0.0825
MTT (seconds)	4.7 (1.7)	6.6 (4.3)	7.4 (2.7)	0.0001

## CONCLUSION

Given the risks and benefits of treatment for vasospasm, CTP may have potential in guiding treatment management decisions. Presence of CTP deficits has a high likelihood of requiring treatment for vasospasm. However, quantitative analysis of these perfusion deficits requires further investigation.

## eP-161

### Which Intracranial Arterial Segments Are Frequently Affected by Artifact on Susceptibility-Weighted Imaging?

Choi, H.·Jung, S.·Ahn, K.·Kim, B.  
Seoul St. Mary's Hospital  
Seoul, KOREA, REPUBLIC OF

## PURPOSE

Susceptibility-weighted image (SWI) was initially developed to visualize small vessels, especially veins. However, artery is visualized as high signal intensity in the lumen on SWI. Arterial luminal high-signal often is affected by dark signal artifact from local magnetic field

inhomogeneity or flow direction. Susceptibility-weighted imaging can demonstrate intraarterial thrombus as dark signal intensity in acute stroke patients. Therefore, differentiating true intraarterial thrombus from artifact is important. The purpose of this study is to investigate which intracranial arterial segment is affected frequently by artifact and which arterial segment is visualized consistently on SWI

## MATERIALS & METHODS

Thirty patients with normal MRA were recruited from June 2010 to May 2011. They underwent intracranial TOF MRA, cervical contrast-enhanced MRA, and SWI using 3.0 T MR system (Magnetom Verio, Siemens Medical Solution, Erlangen, Germany). Susceptibility-weighted imaging was reconstructed from magnitude image and phase map. Their age was ranged from 16 to 84 years old: five patients below 30 years old; five patients between 30 and 39 years old; five patients between 40 and 49 years old; five patients between 50 and 59 years old; five patients between 60 and 69 years old; and five patients over 70 years old. Two radiology trainees were introduced about arterial signal on SWI and then they evaluated magnitude image and SWI in terms of which intracranial arterial segment is affected by dark signal intensity. They were blinded from normal MRA results.

## RESULTS

Arterial segments frequently affected by artifact were distal ICA (100%), A1 (93.3%), A2 (86.7%), basilar artery (51.7%), and M1 (38.3%). Arterial segments which were visualized consistently were only M2 (100%) on magnitude image. Susceptibility-weighted imaging was more affected by artifact than magnitude image in M1 and P1 ( $p<0.05$ ).

## CONCLUSION

When evaluating intraarterial thrombus using SWI, careful interpretation is required in distal ICA, A2, A1, basilar artery, and M1. Magnitude image is preferred in M1 and P1 segments when evaluating intraarterial thrombus.

**KEY WORDS:** Artery, artifact, SWI

## eP-162

### Quantitative MR Imaging Measurements of Transverse Sinus Areas in Idiopathic Intracranial Hypertension

Roux, P.<sup>1</sup>·Savatovsky, J.<sup>1</sup>·Senage, T.<sup>2</sup>·Bertrand, A.<sup>3</sup>·Vignal, C.<sup>1</sup>·Heran, F.<sup>1</sup>

<sup>1</sup>Fondation Ophthalmologique A. de Rothschild, Paris, FRANCE, <sup>2</sup>CHU Nantes, Nantes, FRANCE, <sup>3</sup>CHU Pitié Salpêtrière, Paris, FRANCE

## PURPOSE

Idiopathic intracranial hypertension (IIH) is an increasing cause of headache in young patients; its early diagnosis is crucial as a delay in treatment exposes to a risk of nonreversible blindness. The diagnosis of IIH currently relies on the modified Dandy diagnostic

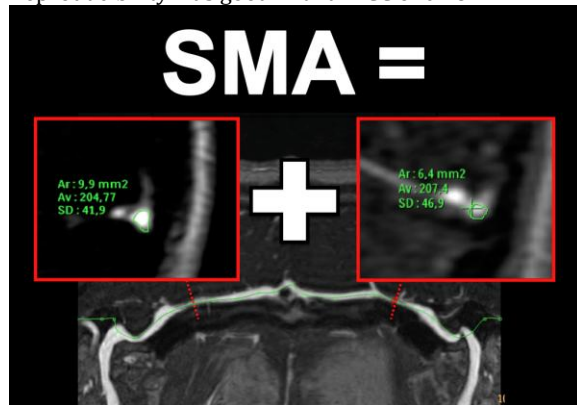
criteria. Bilateral transverse sinus stenosis has been found in previous studies to be predictive of IIH, and venous outflow tract abnormalities are thought to be involved directly in the pathophysiology of IIH. So far, the assessment of transverse sinus stenosis has been subjective only. The aim of our study was to quantitatively assess transverse sinus stenosis on contrast-enhanced MR venography and to propose a threshold value which could be used for diagnostic purpose.

#### MATERIALS & METHODS

We retrospectively analyzed 70 MR examinations of 41 patients (mean age  $34 \pm 12$ ) who had a final diagnosis of IIH according to the Dandy criteria, including an elevated CSF lumbar pressure. We compared them to a control group of 29 patients (mean age  $32 \pm 11$ ) who underwent imaging for headaches, and for whom the investigations excluded the diagnosis of idiopathic or secondary intracranial hypertension. All patients underwent an MRI including contrast-enhanced MRV. Images were analyzed independently by two neuroradiologists using vessel extraction technique on curved planar reconstructions. Each reader visually determined, for each transverse sinus, the narrowest segment and manually measured its area on a sectional image orthogonal to the sinus axis. The two values were summed for each patient (sum of minimal cross-sectional area or SMA) in order to reflect the global venous outflow. Interobserver reliabilities were calculated with intraclass correlation coefficient (ICC). Sum of minimal cross-sectional area was compared between patients and controls using Mann-Whitney U-test. Different threshold values were tested to find the best accuracy and measure the area under the receiver operator characteristic curve (AUC).

#### RESULTS

Sum of minimal cross-sectional area was significantly lower in patients (Mean  $17.9 \text{ mm}^2 \pm 8.8$ ) than controls (Mean  $80.8 \pm 52.7$ );  $p < 0.0001$ . For a threshold value of  $32 \text{ mm}^2$ , the sensitivity and a specificity were respectively of 90.2% and 89.7%. The AUC was 0.973. Reproducibility was good with an ICC of 0.78.



#### CONCLUSION

Our results demonstrate that in patients with a suspicion of IIH, quantitative assessment of the sum of cross-sectional areas of transverse sinuses is reproducible, sensitive and specific. Nevertheless it

should still be associated to other MR signs to further improve accuracy. This value might furthermore be used as a noninvasive marker for follow up during and after IIH treatments.

**KEY WORDS:** Idiopathic intracranial hypertension, MR venography, venous stenosis

#### eP-163

##### Intracranial Atherosclerotic Plaque Enhancement in Patients with Ischemic Stroke

Skarpathiotakis, M.<sup>1</sup>•Mandell, D. M.<sup>2</sup>•Swartz, R. H.<sup>3</sup>•Tomlinson, G.<sup>4</sup>•Mikulis, D.<sup>2</sup>

<sup>1</sup>University of Toronto, Toronto, ON, CANADA, <sup>2</sup>The Toronto Western Hospital, Toronto, ON, CANADA, <sup>3</sup>Sunnybrook Health Sciences Centre, Toronto, ON, CANADA, <sup>4</sup>University Health Network, Toronto, ON, CANADA

#### PURPOSE

Inflammation of an atherosclerotic plaque is a well known risk factor in the development of ischemic stroke and myocardial infarction. MR imaging is capable of characterizing inflammation by assessing plaque enhancement in both extracranial carotid arteries and coronary arteries. Our goal was to determine whether enhancing intracranial atherosclerotic plaque was present in the vessel supplying the territory of infarction using high-resolution MRI wall imaging at 3 T.

#### MATERIALS & METHODS

A retrospective review was performed in 29 patients with a history of ischemic stroke and intracranial vascular stenoses who were scanned on a 3 T MRI system using a high-resolution intracranial blood vessel wall imaging protocol. The stroke territory, time of ictus relative to the time of imaging, site of atherosclerotic plaque and degree of plaque enhancement were documented.

#### RESULTS

Sixteen patients had 3 T MRI vessel wall imaging performed during the acute phase of their ischemic stroke, defined as  $< 4$  weeks. In all of these patients, atherosclerotic plaque in the vessel supplying the stroke territory demonstrated strong enhancement. There was a clear trend of decreasing enhancement as the time of imaging relative to the ischemic event increased. One of the five patients imaged in the subacute phase, defined as 4-12 weeks, had strong enhancement, three had mild enhancement and one had no enhancement of the atherosclerotic plaque in the vessel supplying the stroke territory. One out of eight patients imaged in the chronic phase of their ischemic stroke, defined as  $> 12$  weeks, had strong enhancement, three had mild enhancement and four had no enhancement of the atherosclerotic plaque in the vessel supplying the stroke territory.

#### CONCLUSION

Strong pathologic enhancement of intracranial atherosclerotic plaque was seen in all patients in the acute phase of ischemic stroke in the vessel supplying the stroke territory. The strength and presence of enhancement of the atherosclerotic plaque decrease with increasing time after the ischemic event. These findings suggest that the presence of enhancing intracranial atherosclerotic plaque may be a risk factor for acute ischemic stroke.

**KEY WORDS:** Intracranial vessel wall imaging, atherosclerotic plaque enhancement, ischemic stroke

#### eP-164

##### Real-Time Motion Correction

Bammer, R.·Ooi, M.·Koppeinigg, D.·Fischbein, N.·Aksoy, M.

Stanford University  
Stanford, CA

##### PURPOSE

Correction of head motion artifacts is an ongoing challenge in MRI. Sadly, motion is often the worst in patients that are acutely ill and in which time cannot be afforded to repeat failed exams. Different retrospective and prospective approaches have been suggested, thus far. However, these approaches rely frequently on the need to acquire extra MR navigator data or are restricted to a subset of MR pulse sequences. Here, a radically different approach is presented in which camera tracking is used and which is applicable to any MR pulse sequence.

##### MATERIALS & METHODS

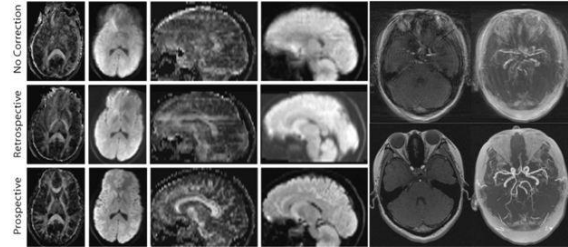
An MR-compatible in-bore video tracking system with submillimeter accuracy to track motion was mounted on the head coil of a 1.5 T GE scanner. This NIH-funded study was IRB approved and informed consent was obtained from each subject (n=10) participating in the study. The tracking device yields pose information every 1/25sec and was used to adapt the scan plane to patient motion. To demonstrate clinical utility, 3D TOF (5 slab MOTSA) sequences and diffusion tensor EPI scans were performed under normal conditions and under motion.

##### RESULTS

The four left columns in this figure show an example of a diffusion tensor exam in a heavily moving patient. Conventional DTI reconstruction was technically inadequate(top). Due to spin-history effects and incomplete volume coverage as a result of motion, retrospective motion correction(middle) failed, too. Real-time motion correction(bottom) yielded pristine isoDWI and fractional anisotropy maps. Similarly, 3D TOF MRI was applied to a second subject who was moving excessively in the MR scanner. Both MRA raw images and MIPs were deemed technically inadequate. A repeat scan with real-time motion correction ON yielded images almost entirely free of motion artifacts.

**Discussion:** Patient motion can impair the quality of MRI exams leading to reduced diagnostic confidence,

false interpretations, and incomplete or costly repeat studies. Here, real-time adaptive motion correction was demonstrated successfully for DTI and 3D TOF studies. Some minor residual artifacts remained due to a slight response delay of the current system to react to pose updates, changes of susceptibility distortions due to motion relative to the main magnetic field, and altered coil sensitivity exposure during motion.



##### CONCLUSION

Clinical MRI studies can strongly benefit from real-time motion correction, especially when a motion tracking system is used that does not interfere with MR contrast and scanner performance, and which is universally applicable. Such motion correction scheme is recommended in pediatric or agitated patients.

**KEY WORDS:** Motion

#### eP-164a

##### Quantitative MR Imaging Evaluation of Cranial Nerve Pathology in Familial Dysautonomia

Hwang, J.<sup>1</sup>·Lui, Y.<sup>1</sup>·Milch, H.<sup>2</sup>·Milla, S.<sup>1</sup>

<sup>1</sup>New York University School of Medicine, New York, NY,  
<sup>2</sup>Boston University Medical School, Boston, MA

##### PURPOSE

Familial dysautonomia (FD), also known as Riley-Day syndrome, is an autosomal recessive nervous system disorder seen primarily in Ashkenazi Jews. The IKBKAP gene on chromosome 9q has been implicated in FD. It encodes the IkappaB kinase complex-associated protein (IKAP/hELP1) which is expressed in the central and peripheral nervous systems. Nearly all FD patients have a frame-shift mutation which results in a truncated protein. Familial dysautonomia patients have widespread, variable symptoms affecting the central and peripheral nervous systems. Due to religious restrictions, limited information thus far has been obtained from postmortem examination. Neuroimaging offers an important means of assessing structural changes in vivo. There is new data suggesting a primarily afferent nerve abnormality in these patients, including cranial nerve dysfunction (Kaufmann et al). As the trigeminal nerve is the largest of the cranial nerves and predominantly afferent in function, it is an ideal nerve to study using high-resolution MR imaging. The purpose of this study is to compare the caliber of the trigeminal nerves in FD patients to a control group.

##### MATERIALS & METHODS

We performed a retrospective study of patients with an established diagnosis of FD being followed at a major

FD treatment facility. Patients with prior brain MRI performed between 11/03 and 4/11 were included. To obtain cross-sectional area measurements of the trigeminal nerves, we utilized 3D T1-weighted high-resolution data obtained in the axial plane. Data were imported to a 3D workstation (Aquarius iNtuition, TeraRecon, Inc). Axial images centered at the level of the cisternal portion of each trigeminal nerve were used to prescribe double-oblique sections oriented perpendicular to the long axis of the nerve. The section representing the thickest diameter or clearest cross-sectional view of the nerve was chosen. A region of interest (ROI) was drawn around the nerve using a "polygon" measuring tool to account for irregular nerve shapes and the area within the ROI was generated by the program.

#### RESULTS

Twelve FD patients had brain MRI studies during the study period. One patient was excluded because a 3D sequence was not performed, and therefore we could not perform volumetric analysis. Thus, a total of 11 patients, or 22 trigeminal nerves, were evaluated. The patients ranged from 8-61 years of age at the time of their MRI exams. We found a statistically significant smaller trigeminal nerve cross-sectional area in the FD patients compared to a control group. The mean cross-sectional area of the trigeminal nerve in FD patients was 0.034 cm<sup>2</sup>, significantly smaller compared to the control group which had a mean area of 0.134 cm<sup>2</sup> (2-tailed Student t-test using significance level  $p < 0.05$ ).

#### CONCLUSION

Our study showed a smaller caliber of the trigeminal nerves in FD patients compared to a control group suggesting trigeminal nerve atrophy or congenitally small size. Future work already is underway to correlate these findings with clinical symptoms of trigeminal nerve dysfunction. Our findings support the notion that there is an afferent nerve abnormality in FD patients.

**KEY WORDS:** Dysautonomia, cranial nerves

**Monday, April 23 -  
Wednesday, April 25  
6:30 AM - 9:00 PM  
Thursday, April 26  
6:30 AM - 3:00 PM  
Americas Hall II  
Electronic Posters (ePosters)  
165 - 166**

**eP2 - ANATOMY**

**Note: A missing printed number indicates an abstract has been withdrawn.**

#### eP-165

#### **Evaluation for Detectability of the Artery of Percheron on 3 T 3D Time-of-Flight MR Angiography**

Hiratsuka, Y.<sup>1</sup>•Kikuchi, K.<sup>1</sup>•Oda, S.<sup>1</sup>•Miki, H.<sup>2</sup>•Mochizuki, T.<sup>1</sup>

<sup>1</sup>Ehime University School of Medicine, Toon, JAPAN,

<sup>2</sup>Ehime Prefectural Central Hospital, Matsuyama, JAPAN

#### **PURPOSE**

The paramedian territory of thalamus is supplied by the paramedian (or thalamoperforating) arteries, which arise from the P1 segment of the PCA. The arteries have great variability with respect to number, size, and territorial contribution to the thalamus. Percheron have been classified into three types as the arterial configurations. Type II (asymmetrical type), designated as the artery of Percheron, is an uncommon anatomical variant, in which a single dominant paramedian artery supplies the bilateral medial thalami with variable contribution to the rostral midbrain. 3 T MRA has higher spatial resolution and higher SNR than 1.5 T MRA, and are expected to depict the small arteries without using contrast media. The purpose of this study is to evaluate the detectability and the anatomical variation of the paramedian artery using 3D TOF MRA on 3 T MRI.

#### **MATERIALS & METHODS**

3 T 3D MRA of 134 patients were analyzed retrospectively. The patients with moyamoya disease or abnormalities on posterior circulation such as vascular stenosis, occlusion or aneurysms were excluded from this study. The patients of more than 60 years old also were excluded to reduce the influence from arteriosclerotic change. Imaging parameters for 3D TOF MRA were as follows: 285 x 512 matrix (512 reconstructed), with parallel imaging (SENSE factor 2.0), TR/TE: 23/3.45 ms, a ramped radio-frequency pulse with a central flip angle of 18°, one slab of 90



sections, bandwidth: 31.2 kHz, FOV: 160 x 160 mm, NEX: 1, and 1.1 mm thick (ZIP2 0.5 mm). Two radiologists evaluated the detectability of the paramedian artery and classified the arteries into three types according to pattern of the origin with MPR and partial MIP on a workstation.

#### RESULTS

The paramedian artery of 122 patients could be identified. Twenty-five cases (20.5%) were classified as the artery of Percheron (type II), and 97 cases (79.5%) were classified as type I (symmetrical type) or type III (arcade type). The artery of Percheron was depicted clearly on 3 T MRA compared to the other types of paramedian artery, and it was difficult to distinguish between the arteries of type I and type III.



#### CONCLUSION

The paramedian artery was well depicted on 3 T 3D TOF MRA, and we could evaluate accurately the variation and distribution of this artery. That will be useful for diagnosis of midbrain and thalamic ischemia, such as bilateral thalamic ischemic lesions.

**KEY WORDS:** Artery of Percheron, time-of-flight MRA, 3 T MR imaging

#### eP-166

#### When the Optic Nerve Is too Large or too Small: Standard Measurements for the Optic Nerve and Optic Nerve Complex

Lo, E.<sup>1</sup>•Bobra, S. J.<sup>2</sup>•Valvassori, G.<sup>1</sup>•Michals, E.<sup>1</sup>

<sup>1</sup>University of Illinois, Chicago, IL, <sup>2</sup>Gottlieb Memorial Hospital, Melrose Park, IL

#### PURPOSE

In our practice, radiologists interpret optic nerve diameter based on a qualitative determination of whether the nerve diameter appears too large or too small for that patient. We aim to establish standard measurements for both the optic nerve and optic nerve complex for radiologists to quantitatively interpret

abnormal optic nerve anatomy. After establishing a normative diameter for the optic nerve, we were able to compare these measurements with 10 patients with optic nerve atrophy or hypoplasia.

#### MATERIALS & METHODS

The first part of this presentation demonstrates the measurement of the diameter of the optic nerves of 94 patients with no optic nerve pathology. Since by CT and T1 MR sequences, the nerve cannot be distinguished from the surrounding meningeal sheath, all measurements were obtained from coronal T2 MR fat-suppressed images obtained with the axis of the nerve perpendicular to the plane of section. The retrobulbar and orbital segments of the bilateral optic nerves were measured. The age of the patients ranged from 2 months to 81 years. The second part of this presentation accumulates similar measurements in 10 patients with abnormal visual acuity given an ophthalmologic diagnosis of optic nerve atrophy or hypoplasia.

#### RESULTS

In 94 patients, the mean diameter of the retrobulbar portion of the optic nerve complex was 5.3 mm on the right and 5.3 mm on the left. The mean optic nerve diameter in its retrobulbar portion was 2.9 mm on the right and 2.8 mm on the left. In patients with optic nerve atrophy/hypoplasia, the mean diameter of the retrobulbar portion of the optic nerve complex was 3.5 mm and the mean diameter of the abnormal optic nerve was 1.6 mm. Measurements for the orbital portion of the optic nerves also are included. These measurements were further stratified by age. Examples of abnormally enlarged optic nerves in patients with optic neuritis and optic glioma are demonstrated for comparison.

#### CONCLUSION

Coronal T2 MR fat-suppressed images are ideal for distinguishing the optic nerve from the optic nerve sheath and measuring the nerve diameter. Quantitative measurements of the optic nerve can aid radiologists in the diagnosis of optic nerve atrophy and other optic nerve pathology. We establish a mean diameter of 2.9 mm for the retrobulbar portion of the optic nerve and 2.3 mm for the orbital portion of the optic nerve. The mean diameter of atrophic or hypoplastic optic nerves in the retrobulbar and orbital portions was 1.6 mm and 0.9 mm, respectively.

**Monday, April 23 –  
Wednesday, April 25  
6:30 AM - 9:00 PM  
Thursday, April 26  
6:30 AM - 3:00 PM  
Americas Hall II  
Electronic Posters (ePosters)  
167 – 192**

**eP3 – HEAD AND NECK**

**Note: A missing printed number indicates an abstract has been withdrawn.**

#### **eP-167**

##### **Irradiation-Induced Damage to Submandibular Salivary Glands: The Role of CT Perfusion**

Surlan Popovic, K.<sup>1</sup>•Strojan, P.<sup>1</sup>•Popovic, P.<sup>1</sup>•Bisdas, S.<sup>2</sup>

<sup>1</sup>University Medical Center Ljubljana, Ljubljana, SLOVENIA, <sup>2</sup>Eberhard Karls University Hospital, Tübingen, GERMANY

#### **PURPOSE**

Perfusion computed tomography is a noninvasive functional imaging method that can detect changes of tissue perfusion parameters. The hallmarks of radiation-induced damage to salivary glands are functional changes in salivary output and xerostomia. One of the main causes of xerostomia is the damage of blood vessels in irradiated glands. The aim of our study was to detect whether the changes of submandibular gland volume values during and after radiochemotherapy (RT-ChT), as measured with CT volumetry, correspond to the radiation dose received by the submandibular glands; and to detect whether the changes of perfusion parameters in submandibular glands during and after RT-ChT correspond to the changes of submandibular gland volume values.

#### **MATERIALS & METHODS**

The study enrolled 12 patients with local and/or regional inoperable squamous cell carcinoma of the oral cavity and/or oropharynx, treated with concomitant RT-ChT with cisplatin. Patients underwent CT volumetry and perfusion CT scans before the therapy (t0), after the completion of 40 Gy (t1) and 70 Gy of RT-ChT (at the end of therapy, t2) and 3 months after the therapy (t3). Submandibular gland volume, blood volume (BV), permeability surface area product (PS) and blood flow (BF) of submandibular glands were quantified. Data were analyzed statistically with Kolmogorov-Smirnov test, paired t-test and Pearson's correlation analysis (Rp).

#### **RESULTS**

Submandibular gland volume at t1, t2 and t3 was significantly lower compared to the baseline value ( $p = 0.000$ ). Blood volume values showed a reduction in the first period (t0-t1:  $p = 0.000$ ), followed by an increase (t1-t2:  $p = 0.000$ ) and once again a reduction in the last period (t2-t3:  $p = 0.000$ ). Permeability surface values showed an initial increase (t0-t1:  $p = 0.000$ ), followed by a PS value reduction (t1-t2:  $p = 0.004$ ; t2-t3:  $p = 0.000$ ). Blood flow values initially showed a trend of increase (t0-t1:  $p = 0.000$  and t1-t2:  $p = 0.014$ ), followed by a reduction in BF values (t2-t3:  $p = 0.000$ ). A significant linear correlation was found between changes of submandibular gland volume values and changes of perfusion parameter BV (t0-t3:  $p = 0.012$ ,  $R_p = -0.697$ ).

#### **CONCLUSION**

Perfusion CT is clinically feasible for monitoring the effects of concomitant RT-ChT in submandibular glands. Changes of submandibular gland volume values, as measured with CT volumetry, correlate with radiation dose received by the gland and with changes of BV. The results suggest that perfusion parameter BV can be used to predict the development of xerostomia.

**KEY WORDS:** Salivary gland, CT perfusion

#### **eP-168**

##### **Apparent Diffusion Coefficient Analysis of Parotid Gland of Sjögren's Syndrome Response to Cevimeline Treatment**

Wu, M.<sup>1,2</sup>•Shen, C.<sup>1</sup>•Tyan, Y.<sup>1</sup>•Wei, C.<sup>1,2</sup>

<sup>1</sup>Chung Shan Medical University Hospital, Taichung, TAIWAN, <sup>2</sup>Chung Shan Medical University, Taichung, TAIWAN

#### **PURPOSE**

Sjögren's syndrome is considered a systemic autoimmune disease with the exocrine glands as main target organs. Cevimeline is indicated for the treatment of symptoms of dry mouth in patients with Sjögren's syndrome. Apparent diffusion coefficient (ADC) can provide biologic tissues with the local microstructural characteristics of water diffusion. The purpose of this study is to use ADC to analyze the response of the parotid gland of Sjögren's syndrome to cevimeline treatment.

#### **MATERIALS & METHODS**

A total 36 subjects with Sjögren's syndrome presenting with xerostomia were enrolled. Initial MR imaging was performed before treatment, and performed at the second MR study after 4 weeks of proper cevimeline treatment.

#### **RESULTS**

Regarding response to salivary stimulation, there was a significant increase of the mean ADC values on precevimeline treatment. Also significant increase of the mean ADC values on postcevimeline treatment. After 4 weeks of cevimeline treatment, the salivary secretion

response revealed a significant increase from 5.3% to 11.3%.

#### CONCLUSION

Apparent diffusion coefficient values can be a monitor of salivary secretion. Diffusion-weighted imaging is able to evaluate response sensitivity of the salivary flow of the Sjogren's syndrome in postcevimeline treatment.

**KEY WORDS:** Sjögren's syndrome, apparent diffusion coefficient, cevimeline

#### eP-169

##### Internal Derangements of the Temporomandibular Joint: Is there Still a Place for Ultrasound?

Dupuy-Bonafé, I.<sup>1</sup>Picot, M.<sup>1</sup>Maldonado, I. L.<sup>1</sup>Bonafé, A.

Montpellier University Hospital  
Montpellier, FRANCE

#### PURPOSE

The aim of this study was to assess the diagnostic value of articular sounds, standardized clinical examination and standardized articular ultrasound in the detection of internal derangements of the temporomandibular joint.

#### MATERIALS & METHODS

Forty patients and 20 asymptomatic volunteers underwent a standardized interview, physical examination, and static and dynamic articular ultrasound. Sensitivity, specificity, and predictive values were calculated using magnetic resonance as the reference test.

#### RESULTS

One hundred twenty joints were examined. Based on our findings, the presence of articular sounds and physical signs are often insufficient to detect disk displacement. Imaging by static and dynamic high-resolution ultrasound demonstrates considerably lower sensitivity when compared with magnetic resonance. Some of the technical difficulties resulted from a limited access due to the presence of surrounding bone structures.

#### CONCLUSION

The present study does not support the recommendation of ultrasound as a conclusive diagnostic tool for internal derangements of the temporomandibular joint.

**KEY WORDS:** Temporomandibular joint, ultrasonography, disk displacement

#### eP-170

##### Reliability of Short TI Inversion Recovery MR Imaging Sequence in Measuring Tongue Tumor Thickness: Correlation with Histologic Tumor Thickness

Manzoor, M. U.<sup>1</sup>Bashir, U.<sup>2</sup>Majeed, Y.<sup>2</sup>Spampinato, M. V.<sup>1</sup>Uddin, N.<sup>2</sup>Faruqui, Z.<sup>2</sup>

<sup>1</sup>Medical University of South Carolina, Charleston, SC,

<sup>2</sup>Shaukat Khanum Memorial Cancer Hospital & Research Centre, Lahore, PAKISTAN

#### PURPOSE

To compare tongue tumor thickness measured at 1.5 T MRI, using T2-weighted and short TI inversion recovery (STIR) sequences with tumor thickness determined by histology following glossectomy.

#### MATERIALS & METHODS

We retrospectively reviewed hospital records for patients who had undergone resection of tongue cancer in our tertiary care referral center between July 2008 and December 2010. We included all subjects who underwent partial glossectomy, and for whom preoperative MR imaging was available. Patients who had received neoadjuvant chemotherapy or inoperable tumors (T3 and T4 disease) were excluded. Also the patients in whom gap between MR imaging and surgery exceeded 6 weeks were excluded. MR imaging was performed with a 1.5 T scanner (GE Healthcare, Wisconsin, USA). Sequences obtained were: T2 coronal (3000/98/1), STIR axial (5000/60/1). Slice thickness was of 4 mm for T2-weighted and of 8 mm for STIR sequences. Radiologic as well as histopathologic data analysis was conducted in a standardized fashion: a horizontal line was drawn joining the tumor-mucosa junction at both ends of the tumor (referred to as "reference line"), from which a perpendicular line was drawn at the point of maximum tumor thickness. This was considered to represent tumor depth. For exophytic masses, an additional line was drawn in the opposite direction from the reference line and both measurements were added (i.e., tumor depth + exophytic component) to give the total tumor thickness. Statistical analysis of the data was performed using SPSS 17 software. Pearson's correlation analysis was done separately between T2 and STIR MRI measured tumor thickness and histologic thickness. For all analyzes, a two-tailed p-value of <0.05 was considered the reference standard for statistical significance.

#### RESULTS

We initially evaluated 33 patients, four were excluded because of unavailability of histology slides. An additional patient was excluded because the tumor was not visible on any MR imaging sequence. In 18 subjects the neoplasm could be identified only on STIR imaging; in 10 subjects the tumor was identified on both T2 and STIR. The mean age of our patients was 50 years (19-79), with male-to-female ratio of 18:10. All patients had either T1 or T2 stage disease. Histologic tumor thickness ranged from 4 mm to 16 mm (mean 8.54 mm). On imaging, the minimum detected tumor

thickness on STIR axial was 4 mm, and the minimum detected tumor thickness for T2 coronal was 5 mm. Both techniques failed to demonstrate tumor of 2 mm thickness ( $n=1$ ). Pearson correlation analysis demonstrated a positive correlation between histologic tumor thickness and MR-measured tumor thickness yielding R value of 0.71 and 0.87 for STIR axial and T2 coronal imaging respectively. Results were statistically significant in both cases.

#### CONCLUSION

Tongue tumor thickness measured on MRI (T2 and STIR-weighted sequences) has a good positive correlation with histologic tumor thickness and can be used reliably for this purpose. Additionally, though more precise in measurement, conventional T2-weighted sequences are not sensitive for the detection of small tongue cancers, and preference should be given to STIR sequences in measurement of local disease in such cases.

**KEY WORDS:** Tongue, tumor, MR imaging

#### eP-171

##### Actinomycosis in the Mandible: CT and MR Findings

Sasaki, Y.<sup>1</sup>•Kaneda, T.<sup>1</sup>•Mori, S.<sup>1</sup>•Uyeda, J. W.<sup>2</sup>•Sakai, O.<sup>2</sup>

<sup>1</sup>Nihon University School of Dentistry at Matsudo, Matsudo, Chiba, JAPAN, <sup>2</sup>Boston Medical Center, Boston University School of Medicine, Boston, MA

#### PURPOSE

Differentiating actinomycosis in the mandibular region from other inflammatory/infectious conditions or malignant tumors is clinically challenging yet essential for accurate diagnosis. The purpose of this study was to evaluate the characteristic MR and CT findings of actinomycosis in the mandible.

#### MATERIALS & METHODS

We reviewed the CT and MR findings in five patients with pathologically proved mandibular actinomycosis. CT ( $n = 5$ ) and MR images ( $n = 5$ ) were evaluated for the location, margin, density or signal intensity, osteolytic or sclerotic changes, periosteal reaction, presence of sequestra, presence of gas, inflammation of the masseter muscles and pterugoid, presence of cellulitis including the skin, presence of fistula, and lymphadenopathy in the neck.

#### RESULTS

CT showed an ill-defined mass-like lesion ( $n = 5$ ) with osteolytic ( $n = 5$ ), periosteal reaction ( $n = 4$ ), gas ( $n = 3$ ), sequestra ( $n = 4$ ), and presence of lymphadenopathy ( $n = 5$ ). All locations included the mandible ( $n = 5$ ). MR imaging revealed low signal ( $n=5$ ) on T1-weighted and high signal ( $n = 5$ ) on T2-weighted images in the mandible, cellulitis including the skin ( $n = 5$ ), inflammation of masseter muscles ( $n = 4$ ), inflammation of pterugoid ( $n = 4$ ), and presence of lymphadenopathy in the neck ( $n = 5$ ). CT and MR imaging demonstrated infiltration or invasion into the adjacent soft tissues of the face ( $n = 5$ ).

#### CONCLUSION

Our findings suggest that CT and MRI are beneficial diagnostic tools used to assess for actinomycosis in the mandible.

**KEY WORDS:** Actinomycosis, mandible, CT and MR findings

#### eP-172

##### Efficacy Oral Propranolol for the Treatment of Head and Neck Infantile Hemangioma

Al Azri, F.•Ganesh, A.•Harikrishna, B.•Al-Zuahibi, S.•Al-Jabri, S.•Al-Waily, A.•Al-Riyami, A.•Abdullah, A.•Al-Senaidi, K.

Sultan Qaboos University Hospital  
Muscat, OMAN

#### PURPOSE

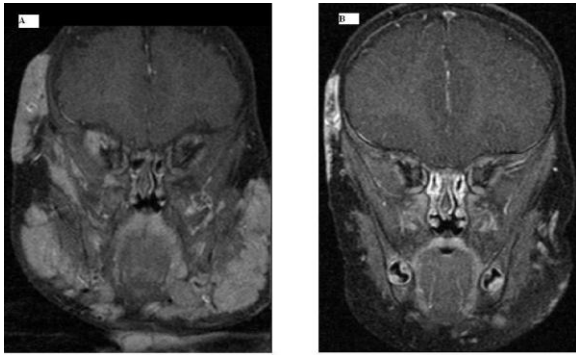
Infantile hemangiomas (IH) are common benign orbital tumors in children. They have a predictable natural history with a proliferative phase in the first few months of life followed by a spontaneous involution phase. Intervention is indicated when lesions interfere with a vital function. Recently, oral propranolol has been found effective and safe in the treatment of IH. Our purpose is to investigate the efficacy and safety of oral propranolol in the management of head and neck IH.

#### MATERIALS & METHODS

Six patients between three and 19 months of age with IH were treated with oral propranolol (2mg/kg/day). All patients underwent detailed specific (regional), systemic, and radiologic evaluations before treatment and at periodic intervals after starting treatment with particular attention to side effects from therapy. Four patients had IH head and neck with peri-orbital involvement and two neck IH without peri-orbital involvement. Two patients had undergone treatment with oral corticosteroids and one patient was treated with percutaneous sclerotherapy with sodium diatrizoate tetrahydrate earlier with unsatisfactory response.

#### RESULTS

All four patients with peri-orbital involvement had severe ptosis with potential for deprivation amblyopia. Three patients had orbital involvement. Two patient had deep cervical IH. Oral propranolol was commenced in all patients after admission, with monitoring by the pediatric cardiologist. Subsequent treatment was carried out with periodic out-patient monitoring. All patients showed excellent response to the treatment with regression of IH. No side effects from therapy were encountered.



#### CONCLUSION

Oral propranolol is effective and safe therapy when used in selected patients with life or organ specific function threatening IH. It should be considered in patients not responding to the conventional methods of therapy, such as intralesional sclerosing agents or systemic steroids. In patients with significant orbital involvement and lesions causing vision-threatening complications, propranolol may be used as a primary treatment modality.

**KEY WORDS:** Orbital hemangioma, infants, propranolol

#### eP-173

##### **Differences between Proximal versus Distal Intraorbital Optic Nerve Diffusion Tensor MR Imaging Properties in Glaucoma Patients**

Garaci, F.·Marziali, S.·Melis, M.·Bolacchi, F.·Martucci, A.·Nucci, C.·Simonetti, G.·Floris, R.

University of Rome Tor Vergata  
Rome, ITALY

#### PURPOSE

To analyze in vivo the diffusion tensor magnetic resonance imaging (DT MRI) properties of the intraorbital optic nerve at two different levels: Proximal to the optic nerve head (ONH) and distal to the ONH at the level of the orbital apex in glaucoma patients.

#### MATERIALS & METHODS

Twenty-four patients with primary open-angle glaucoma were examined. The categorization into early and severe glaucoma was performed by Hodapp's classification. Fifteen healthy individuals served as control subjects. DT MR imaging was performed with a 3 T MR unit. Region of interest analysis was performed on each intraorbital optic nerve.

#### RESULTS

At early glaucoma clinical stages alterations of the mean diffusivity (MD) and fractional anisotropy (FA) values accompanied by an increase of the principal diffusivities were observed in the proximal segment, whereas the distal part showed a slight but not statistically significant increase in the MD and a statistically significant decrease in the FA accompanied by a decrease of the largest principal diffusivity, lambda 1, and an increase of the intermediate and smallest principal diffusivities, lambda 2 and lambda 3. At severe

disease stages an increase in overall diffusivities together with a decrease in FA was observed both in the proximal and in the distal segments.

#### CONCLUSION

Our results indicate that according to DT MRI intraorbital optic nerve degeneration is a complex biological process that affects differently the proximal and the distal segments of the intraorbital optic nerve at early disease stages.

**KEY WORDS:** DTI, optic nerve, glaucoma

#### eP-174

##### **Chronic Optic Neuropathy: Correlation of MR Imaging Characteristics with Etiology**

Rives, A. F.·Nadgir, R.·Subramanian, M.·Jara, H.·Cheng, J. F.·Sakai, O.

Boston Medical Center  
Boston, MA

#### PURPOSE

To correlate the MR imaging characteristics of chronic optic neuropathy with the clinically determined etiology.

#### MATERIALS & METHODS

Following IRB approval, we searched our imaging database for dedicated orbital MRI studies performed at our institution between 11/2007 and 1/2009. Images were reviewed by a neuroradiologist, and optic nerve size, signal, and enhancement characteristics were documented for all cases of radiographically suspected chronic optic neuropathy. A chart review then was performed on this subset of patients to determine the suspected etiology for the optic neuropathy. MRI findings were correlated with the clinical impressions.

#### RESULTS

Review of our imaging database yielded 105 orbital MRI examinations. Twelve patients (5 males, 7 females; mean age 44 years) demonstrated radiologic evidence of unilateral or bilateral chronic optic neuropathy. All 12 patients had a small caliber, nonenhancing optic nerve on MRI. Ten patients demonstrated increased T2 signal in the affected optic nerve(s), and two patients demonstrated normal T2 signal in the affected optic nerve(s). Etiologies of chronic neuropathy associated with a high signal optic nerve included inflammation (n = 4), ischemia (n = 2), radionecrosis (n = 1), optic nerve sheath neoplasm (n = 1), iatrogenic injury (n = 1) and drug toxicity (n = 1). Etiologies associated with a normal signal optic nerve included nutritional deficiency (n = 1) and congenital hypoplasia (n = 1).

#### CONCLUSION

Our preliminary data suggest that increased T2 signal in the setting of chronic optic neuropathy can be seen with processes resulting in demyelination, gliosis or direct nerve injury, whereas preservation of nerve signal is more likely to be associated with systemic/congenital conditions.

**KEY WORDS:** Optic neuropathy, optic nerve

#### eP-175

### Combined B-Mode Ultrasound and Real-Time Qualitative Elastography for the Preoperative Diagnosis of Cervical Metastatic Lymph Nodes in Papillary Thyroid Carcinoma: Comparison with Computed Tomography

Lee, Y.-Yoo, W.

Catholic University of Korea  
Bucheon, KOREA, REPUBLIC OF

#### PURPOSE

To compare the diagnostic accuracy of combined B-mode ultrasound and real-time qualitative elastography (US/UE) with that of contrast-enhanced computed tomography (CE CT) in the preoperative evaluation of cervical metastatic lymph nodes in patients with papillary thyroid carcinoma.

#### MATERIALS & METHODS

From July 2009 to October 2009, 46 consecutive patients with papillary thyroid carcinoma, confirmed by aspiration cytology assessment, underwent US/UE and CE CT. The color-coded elastographic representation of the relative stiffness of cervical lymph nodes was qualitatively scored by two independent observers to determine the proportion of stiff areas from ES1-4 (ES1, soft to ES4, stiff). The sensitivity, specificity, and diagnostic accuracy of US/UE and CE CT were compared for the final status of 552 cervical node levels. The final status of cervical nodes was determined from surgical pathology and follow-up data.

#### RESULTS

At all lymph node levels, the sensitivity, specificity, and diagnostic accuracy of US/UE were 64.3%, 87.1%, and 77.4%, respectively, while those of CE CT were 54.2%, 85%, and 71.4%, respectively. A moderate interobserver agreement was observed in scoring real-time qualitative elastography, as indicated by weighted kappa statistics ( $k = 0.59$ ).

#### CONCLUSION

The US/UE combination is superior to CE CT for an accurate preoperative evaluation of cervical metastatic nodes in patients with papillary thyroid carcinoma.

**KEY WORDS:** Lymph node, ultrasound, elastography

#### eP-177

### Airway Collapsibility on Sleep Cine MR Imaging Is Related to Small Vessel Disease on Brain MR Imaging in Obstructive Sleep Apnea

Seo, H.<sup>1</sup>Kim, J.<sup>2</sup>Kim, H.<sup>1</sup>Park, S.<sup>3</sup>

<sup>1</sup>Seoul National University Hospital Healthcare System Gangnam Center, Seoul, KOREA, REPUBLIC OF, <sup>2</sup>Seoul National University Hospital, Seoul, KOREA, REPUBLIC OF, <sup>3</sup>Borame Medical Center, Seoul, KOREA, REPUBLIC OF

#### PURPOSE

Obstructive sleep apnea (OSA) is associated with ischemic stroke and hypertension. However, a relationship between OSA and small vessel disease (SVD) is still uncertain. Sleep magnetic resonance imaging (MRI) is the advanced imaging tool to evaluate upper airway obstruction during sleep. This study is to examine the relationship between OSA and SVD in patients who had sleep MRI scan.

#### MATERIALS & METHODS

From April 2009 to October 2011, 69 consecutive subjects were evaluated with sleep MRI and brain MRI. A balanced fast field-echo sequence and turbo field-echo mode were used to create the cine MR images for sleep MRI using 1.5 T MRI machine. Normal respiration before sedation was recorded for 140 seconds. Thereafter, sleep was induced with intravenously administered midazolam. The upper airway was classified into two (retropalatal and retroglossal) levels. The axial and sagittal cine images were provided. We retrospectively measured anterior-to-posterior (AP) and transverse diameter at two levels on presedation and postsedation images. The airway collapsibility was calculated as same method with previous study. For this calculation, we used the largest airway diameter on presedation image and the shortest airway diameter on postsedation image. To differentiate the true obstruction from a swallow, we measured the diameter of airway when obstruction lasted more than 3 seconds. Degree and location of SVD, lacunar infarction, microhemorrhage and large vessel disease (LVD) were evaluated on brain MRI, retrospectively. We also obtained medical history, medication, familial medical history, laboratory finding, endoscopic result and the result of OSA evaluation from electronic medical record.

#### RESULTS

Airway collapse was observed at the retropalatal level (65 patients, 47.9%) and at the retroglossal level (69 patients, 60.0%) ( $p > 0.05$ ). There are 21 patients with grade 1 SVD, three patients with grade 2 SVD and three patients with LVD. The progression of SVD or LVD is in five or one patients among 32 patients who had brain MRI follow up. Airway collapse was more severe in SVD or LVD patient group than in patients who had no brain lesion ( $p < 0.05$ ). However, only grade of SVD was associated significantly with airway collapse (postsedation retroglossal AP diameter, retroglossal AP collapsibility and presedation retropalatal AP diameter) after the other confounding factors (age, systolic blood pressure, previous medical history of hypertension, cerebrovascular disease, coronary artery disease or atrial fibrillation, low-density lipoprotein, cholesterol, hemoglobin A1c, aspirin) were eliminated by statistical analysis ( $p < 0.05$ ).

#### CONCLUSION

Airway collapse in patient with OSA is related to SVD and may be an indicator of ischemic change in intracranial small vessels.

**KEY WORDS:** Obstructive sleep apnea, sleep MR imaging, small vessel disease



## eP-178

# Obstructive Sleep Apnea and Cardiovascular Disease: Evaluation with Sleep Cine MR Imaging, Coronary CT Angiography and Carotid Doppler Ultrasonography

Seo, H.<sup>1</sup>Kim, H.<sup>1</sup>Kim, J.<sup>2</sup>Park, S.<sup>3</sup>

<sup>1</sup>Seoul National University Hospital Healthcare System Gangnam Center, Seoul, KOREA, REPUBLIC OF, <sup>2</sup>Seoul National University Hospital, Seoul, KOREA, REPUBLIC OF, <sup>3</sup>Boramae Medical Center, Seoul, KOREA, REPUBLIC OF

## PURPOSE

Obstructive sleep apnea (OSA) is a sleep-disordered breathing condition, which is being implicated increasingly in a multitude of cardiovascular diseases (CVD). Nowadays, sleep magnetic resonance imaging (MRI) is introduced to evaluate the dynamic motion and obstruction of upper airway during sleep. The purpose of this study is to verify the association between OSA and atherosclerotic change of coronary artery, aorta and carotid arteries via sleep MRI, coronary computed tomography angiography (CTA) and carotid doppler ultrasonography (US).

## MATERIALS & METHODS

From April 2009 to October 2011, 67 consecutive subjects were evaluated with sleep MRI and carotid doppler US. Among them coronal CTA was performed in 47 patients. A balanced fast field-echo sequence and turbo field-echo mode were used to create the cine MR images for sleep MRI using 1.5 T MRI machine. Normal respiration before sedation was recorded for 140 seconds. Thereafter, sleep was induced with intravenously administered midazolam. The upper airway was classified into two (retropalatal and retroglossal) levels. The axial and sagittal cine images were provided. We retrospectively measured anterior-to-posterior (AP) and transverse diameter at two levels on presedation and postsedation images. The airway collapsibility was calculated as same method with previous study. For this calculation, we use the largest airway diameter on presedation image and the shortest airway diameter on postsedation image. To differentiate the true obstruction from a swallow, we measured the diameter of airway when obstruction lasting greater than 3 seconds. We assessed the coronary artery stenosis > 50%, vulnerable plaque, number of involved major vessels, aortic atherosclerosis and patent foramen ovale (PFO) on coronary CTA images. We also evaluated the intima-media thickness and plaque (calcified, mixed and noncalcified) of carotid artery on carotid Doppler images.

## RESULTS

Airway collapse was significantly observed in patient with PFO, coronary artery stenosis > 50%, aortic atherosclerosis and mixed plaque on carotid Doppler US ( $p < 0.05$ ). There is no relation between numbers of involved major coronary or vulnerable plaque. However, mixed plaque at carotid artery, stenosis > 50% and aortic atherosclerosis were significantly

associated with airway collapse (postsedation retroglossal or retropalatal transverse diameter, retroglossal transverse collapsibility, postsedation retropalatal AP or transverse diameter, retropalatal AP or transverse collapsibility and retropalatal circumferential collapsibility) after the other confounding factors were eliminated by statistical analysis ( $p < 0.05$ ).

## CONCLUSION

Airway collapse in patient with OSA is related to coronary artery stenosis and atherosclerotic change of large arteries (greater than carotid artery).

**KEY WORDS:** Obstructive sleep apnea, sleep MR imaging, coronary CTA

## eP-179

# Prevalence of Vocal Cord Paralysis in Patients with Enlarged Lymph Nodes along the Expected Course of Recurrent Laryngeal Nerve

Agarwal, R. Akin, E. A. Taheri, M. R.

The George Washington University Hospital  
Washington, DC

## PURPOSE

We tested the null hypothesis that enlarged lymph nodes along the expected course of the recurrent laryngeal nerve would result in vocal cord paralysis.

## MATERIALS & METHODS

Positron emission tomography/CT examination of 416 consecutive patients who were referred with a variety of diagnoses were reviewed. This database was chosen for the large fraction of studies being performed for tumor staging. Patients with enlarged lymph nodes along the course of the recurrent laryngeal nerves were identified and selected for the study. CT scans of the neck were reviewed for evidence of vocal cord paralysis, including asymmetric widening of the pyriform sinus as well as medialization of the arytenoid cartilage and vocal cord. We subsequently reviewed the patients' medical records for evidence of changes in voice quality or impairment in vocal cord movement.

## RESULTS

Enlarged lymph nodes along the course of the recurrent laryngeal nerve were identified in forty-five patients. Over 85% of these patients were diagnosed with malignancy. Breast, lung and colon constituted 66% of the diagnoses with lymphoma accounting for slightly less than 10%. Forty-nine percent of the nodes had detectable metabolic activity. Twenty-seven percent of the patients had evidence of subcapsular invasion on CT scan, as identified by an ill-defined or irregular margin of the lymph node. The short axis dimension of the lymph nodes measured greater than 2 cm in about 15% of the patients. The shortest transverse diameter of the remaining nodes measured greater than 1 cm. None of these patients had definitive CT evidence of vocal cord paralysis (i.e., medialized arytenoid cartilage and vocal cord and asymmetrically enlarged pyriform sinus).

Review of the medical records revealed no clinical evidence of vocal cord paralysis in these patients.

#### CONCLUSION

The prevalence of vocal cord paralysis in patients with enlarged lymph nodes along the course of recurrent laryngeal nerve is low.

**KEY WORDS:** Recurrent laryngeal nerve, lymphadenopathy, vocal cord paralysis

#### eP-180

##### **Retrospective Study of High-Resolution MR Imaging Internal Auditory Canal-Cranial Nerve VIII in Patients with Central Vertigo to Assess Morphology of Superior Semicircular Canal**

Abdullah, A.·Rivas-Rodriguez, F.·Mukherji, S. K.

University of Michigan Health System  
Ann Arbor, MI

#### PURPOSE

To evaluate the presence of imaging findings suggestive of semicircular canal dehiscence (SCCD) on high-resolution heavily T2-weighted MRI (HR T2W MR) sequence in patients presenting with central vertigo and/or conductive hearing loss, in whom pre and postcontrast high-resolution MRI internal auditory canal (IAC) did not reveal abnormalities in CN VIII, pons, medulla, internal auditory canal or CPA cisterns. Additionally, we assessed the diagnostic performance of IAC MRI by comparing imaging findings suggestive of SCCD on HR T2W MR with and without multiplanar reformats with HRCT temporal bone as reference standard.

#### MATERIALS & METHODS

IAC MRI scans of 138 patients with clinical presentation of central vertigo and/or conductive hearing loss were evaluated for MRI imaging findings suggestive of SCCD on high-resolution heavy weighted T2 MRI sequence. None of these patients demonstrated MR imaging abnormalities involving CN VIII, pons, medulla, internal auditory canal or CPA cisterns. Continuation of fluid signal from superior semicircular canal into the adjacent middle cranial fossa subarachnoid space along with lack of intervening septum between these structures was considered suggestive of SCCD. High-resolution CT of temporal bone with multiplanar reformats were available for imaging correlation in 45 patients. High-resolution CT was considered positive for SCCD when osseous septum covering the superior or posterior semicircular canal was absent. Subsequently, sensitivity, specificity, positive and negative predictive values for HR T2W MR with and without multiplanar reformats in Poschl and Stenver planes suggestive of SCCD were calculated with HRCT temporal bone considered as reference gold standard for the diagnosis of SCCD.

#### RESULTS

High-resolution heavily T2-weighted sequence of IAC identified imaging findings suggestive of SCCD in 36

ears (14%). Imaging evaluation of morphology of SCC on high resolution heavily weighted T2 MRI sequence were correlated with HRCT of the temporal bone with multiplanar reconstructions in 45 patients (90 ears). Twenty ears out of 90 ears approximately 22% that were scanned with both HR MR and HRCT were positive for SCCD on HR MR and correlated to HRCT findings. High-resolution T2W MR imaging findings showed a sensitivity of 68%, specificity of 83%, PPV of 68% and NPV of 91% for diagnosing SCCD without reconstruction in Poschl and Stenver planes. With MPR in Poschl and Stenver planes, HR T2W MR imaging findings showed a sensitivity of 90%, specificity of 98%, PPV of 95%, and NPV of 97%.

#### CONCLUSION

High-resolution T2W MR sequence demonstrates findings suggestive of SCCD in a significant percentage (14%) of patients consulted for central vertigo and or conductive hearing loss in which alternative differential diagnoses were excluded on HR IAC MRI. We postulate that high resolution heavily T2-weighted MRI sequence of IAC on patients with central vertigo or conductive hearing loss should be screened carefully for imaging findings suggestive of SCCD. If suggestive MR imaging findings are present, a HRCT temporal bone should be performed to confirm or exclude this diagnosis. Additionally, HR T2W MR images with multiplanar reconstruction in Stenver and Poschl planes provide higher sensitivity and specificity for detection of superior semicircular canal dehiscence.

**KEY WORDS:** Superior semicircular canal, dehiscence, MR imaging

#### eP-181

##### **<sup>18</sup>F-Fluoride Positron Emission Tomography/CT Scan for Quantification of Bone Metabolism in the Inner Ear in Patients with Otosclerosis: A Pilot Study**

Waterval, J. J.·Brans, B.·Vallinga, M.·Stokroos, R. J.

Maastricht University Medical Centre  
Maastricht, NETHERLANDS

#### PURPOSE

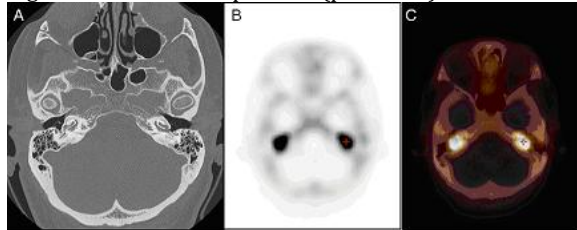
In case of clinical suspicion of fenestral and/or cochlear otosclerosis, audiometry and high-resolution computed tomography (HRCT) are the gold standard to evaluate the *presence* of disease (Figure A). The *activity* of disease has only been described histopathologically as active or quiescent. High-resolution CT is a static diagnostic tool whereas quantification of the bone metabolism could be useful to indirectly predict the course of otosclerosis, the course of future hearing loss or vestibular function. The degree of abnormal bone metabolism might influence the decision of performing surgery. <sup>18</sup>F-fluoride positron emission tomography (PET) has the potential to give reliable dynamic information in vivo. The aim of this pilot study is to assess <sup>18</sup>F-fluoride activity in patients diagnosed with otosclerosis and to evaluate the use of a complementary PET scan.

## MATERIALS & METHODS

Patients with otosclerosis underwent a PET scan and a HRCT scan. A control group was composed retrospectively, consisting of patients who had undergone a PET/CT scan of the same region for a different purpose. In all PET scans regions of interest were drawn on standardized places in the temporal bone to measure bone metabolism using standardized uptake values (SUV). Maximal SUV values in the otic capsules were measured.

## RESULTS

Group 1: otosclerosis, n=11 patients with n=16 positive for otosclerosis. Group 2: control patients n=6 PET scans, temporal bones n=10. Otosclerosis on CT scan was graded according to the Symons/Fanning classification: four temporal bones were classified as grade 1, three were classified grade 2B, three grade 2C and six grade 3 otosclerosis. Positron emission tomography scan: visual assessment of temporal bones showed visible increased activity in the otic capsules on PET in 11 of 16 cases (Figure B and C), none were positive in the control group. Significant higher SUV<sub>mean</sub> values were found in the otosclerosis group in the fenestral area (p=0.0003) and saccule area (p=0.047). The maximal SUV<sub>max</sub> in the entire otic capsule was higher in otosclerosis patients (p=0.0001).



## CONCLUSION

<sup>18</sup>F-fluoride PET is the first imaging technique that has the potential to be a reproducible method to quantify bone metabolism in bone disorders such as otosclerosis. A larger study has to prove whether hearing deterioration really can be predicted with this imaging technique. This could influence the decision and planning to perform stapes surgery in patients with fenestral otosclerosis or cochlear implantation in patients with cochlear otosclerosis and severe sensorineural hearing loss.

**KEY WORDS:** Otosclerosis, dynamic imaging

## eP-182

### Necessity of T2-Weighted Imaging through the Entire Brain for the MR Imaging of the Ear

Ozgen, B. Sanverdi, E. K. Oguz, K. Dolgun, A. Cila, A.

Hacettepe University  
Ankara, TURKEY

## PURPOSE

Magnetic resonance (MR) imaging is the study of choice for the evaluation of the inner ear structures in patients presenting with vestibulocochlear symptoms. The selected scanning protocol may vary, however it usually

includes axial T2-weighted imaging (T2WI) through the entire brain in addition to the dedicated temporal bone sequences. The purpose of this study was thus to evaluate the necessity of the T2WI through the brain for the evaluation of vestibulocochlear dysfunction.

## MATERIALS & METHODS

MR imaging of 440 adult patients (M/F: 224/216; mean age: 49 years  $\pm$  14.2) scanned for audiovestibular symptoms such as sensory neural hearing loss, tinnitus, vertigo were reviewed retrospectively. The abnormal findings on T2WI were recorded and classified. Small vessel disease (SVD) was classified according to the localization of lesions; in the territory of deep perforants (SVDdp) and in the subcortical white matter (SVDswm). Receiver operating characteristic (ROC) curve analysis was calculated to show the relation between the age and the inner ear and/or brain parenchyma lesions.

## RESULTS

T2-weighted imaging revealed abnormalities in 143 patients (32.5%). In this group 109 patients (76.2%) showed chronic ischemic changes with SVD in 78.8% cases (33.9% SVDdp and 44.9% SVDswm). Twenty-two patients had major arterial infarcts with four cases of temporal lobe infarct. One young patient had basal ganglia lesions raising concern for vasculitis. The statistical analysis revealed a positive correlation between the age and evidence of accompanying T2 abnormalities (Student's sample test,  $P < 0.001$ ), revealing increased incidence of brain lesion with advancing age. By ROC curve analysis, a cut-off point of 58.5 years was found for this increasing T2 lesion load with age (sensitivity: 52% and specificity: 84%). There was no significant association between the gender and the presence of abnormal T2 findings (chi-square test,  $P = 0.9$ ). In our case series, T2WI from the whole brain was crucial for the diagnosis in three patients [two with multiple sclerosis (MS) and one with probable vasculitis].

## CONCLUSION

Given increasing needs for high throughput in MR units, our study suggest that T2WI of the brain may not be mandatory, for the evaluation of the SNHL, tinnitus, vertigo and Meniere's disease as it does not provide additional information related to the audiovestibular system that could change patients' management. It might be of value in younger population with additional neurologic findings or atypical presentation.

**KEY WORDS:** Temporal bone, MR imaging

## eP-183

### MR Imaging of Acoustic Neuromas to Assess Poststereotactic Radiosurgery/Radiotherapy Response

Peri, N. Mahadevan, A. Bhadelia, R.

Beth Israel Deaconess Medical Center  
Boston, MA

## PURPOSE

To review the MR studies on patients with acoustic neuromas, treated with stereotactic radiosurgery/radiotherapy (SRS/SRT) to assess the response.

## MATERIALS & METHODS

Eighteen patients were treated with SRS/SRT from 2006-2010. MR studies performed prior to the procedure and at the latest follow up available were reviewed. Signal intensity on the different sequences and tumor measurements (linear in three dimensions and volumes) were obtained. Correlation with clinical symptoms at treatment and follow up was performed.

## RESULTS

Posttreatment changes included appearance of new cystic foci in the tumor, heterogeneous appearance on FLAIR and postcontrast sequences and slightly decreased intensity of the hyperintense signal on FLAIR sequence. These were predominantly seen at follow-up studies within 1 year. There was no significant change in the diffusion signal posttherapy in most cases; only 2/18 patients had further decrease in the DWI signal to a very minor degree. Four of 18 (22%) patients had mild increase in the size of the tumor, three of these were within 1.5 years of treatment, and felt to represent cystic/necrotic changes in the tumor. Fourteen of 18 (78%) patients had mild decrease in size at follow up ranging from 1-2.5 years.

## CONCLUSION

Stereotactic radiosurgery/radiotherapy is a noninvasive treatment of acoustic neuromas with good response. Assessment of follow-up MR studies helps us to understand the natural course of these tumors and assess tumor response after radiation treatment.

**KEY WORDS:** Acoustic neuroma, imaging, postradiosurgery

## eP-184

### What Are the Most Specific CT Markers for Residual Nodal Disease after Nonsurgical Treatment for Oropharyngeal Cancer?

Hamilton, J. D.<sup>1</sup> Sandulache, V. C.<sup>1</sup> Daram, S. P.<sup>1</sup> Ow, T. J.<sup>1</sup> Skinner, H. D.<sup>1</sup> Ginsberg, L. E.<sup>1</sup> Myers, J. N.<sup>1</sup> Ahmed, S.<sup>2</sup>

<sup>1</sup>M.D. Anderson Cancer Center, Houston, TX, <sup>2</sup>MD Anderson Cancer Center, Houston, TX

## PURPOSE

Although CT criteria are sensitive for detection of residual nodal disease in previously treated head and neck tumors, their low specificity can lead to nodal dissections based on image findings of uncertain significance. This study seeks the most specific and best positive predictive valued (PPV) imaging features by CT for residual nodal tumor.

## MATERIALS & METHODS

The outcomes of patients with oropharyngeal squamous cell carcinoma with nodal disease treated with definitive radiation therapy, with or without chemotherapy, were evaluated by subsequent nodal dissection between 1995 and 2009. Among the 201 patients, 139 had pre and post therapy contrast-enhanced CTs and 16 had only posttherapy exams. All imaging was reviewed by a radiologist initially blinded to the pathology who recorded the imaging parameters.

## RESULTS

Residual disease was found in 30 patients, within 85 of 2,428 dissected lymph nodes (15% of patients; 3.5% of lymph nodes). The best performing measures for specificity and PPV were new low density necrotic or cystic areas (99% and 83%, respectively) or a lack of significant size change (<20% in cross-sectional area; 96% and 57%). The latter further improved if only larger pathologic-appearing lymph nodes were used to decrease measurement error. Extracapsular nodal spread (ECS) had modest performance (86% and 88%). Absolute nodal size as isolated criteria was not a good predictor. However, a combination of > 1.5cm maximal axial dimension and any focal finding (low density, calcification or enhancement) had 100% sensitivity for detection and a lack of these findings a 100% negative predictive value (NPV). The next best performer for NPV at 90% was a combination of significant size decrease and no new necrosis. **Discussion:** Negative predictive value was relatively high for all criteria due to the low prevalence of residual nodal disease in this population. A limitation of this retrospective study is the long time period with heterogeneity in treatment and indications for nodal dissection. Extracapsular nodal spread was assessed on pretreatment imaging because loss of fat planes and tissue stranding is common posttreatment. Extracapsular nodal spread was less specific than initially reported in our pilot data. The CT criteria by Ojiri et al including a combination of >1.5cm maximal axial dimension, focal finding or extracapsular spread were sensitive but nonspecific as previously reported, with poor performance by modified RECIST criteria. Improved CT spatial resolution may increase sensitivity and detection but lower the specificity of focal nodal findings. New necrosis or the lack of a significant size change are specific markers for residual disease whose novel combination also yields an acceptable NPV, present in 124 patients compared to four by previous CT criteria. The improved specificity and applicability may be important clinically as alternative treatment pathways other than nodal dissection, such as systemic therapy, are utilized.

## CONCLUSION

New focal lucency or lack of significant decrease in size of affected nodes are the most specific CT imaging markers for residual nodal disease after treatment. The combination of these findings rivals NPV performance of prior reported CT criteria but emphasizes the need for comparison with pretreatment imaging exams.

**KEY WORDS:** Residual nodal disease, squamous cell carcinoma of oropharynx, specific findings

#### eP-185

##### Utility of Laryngeal CT in the Preoperative Evaluation of Revision Laryngoplasty

Ludwig, B. J.·Raduazo, P. A.·Witsell, D. L.·Eastwood, J. D.·Hoang, J. K.

Duke University Medical Center  
Durham, NC

##### PURPOSE

For patients with persistent dysphonia after medialization laryngoplasty, functional evaluation with videostroboscopy is the gold standard. Some otolaryngologists also utilize CT prior to revision surgery to evaluate for malposition of previous injectables/implants and to estimate implant size. The objective of this study was to determine the utility of CT in assessing dysphonia in the postlaryngoplasty larynx relative to videostroboscopy.

##### MATERIALS & METHODS

We performed a retrospective review of CT neck and videostroboscopic findings in patients with a history of dysphonia after medialization laryngoplasty. A total of 16 CT examinations were identified from a patient data portal search of diagnosis and procedure codes. The materials used for laryngoplasty included VoCoM implants, Gore-Tex, silicone, fat and gelfoam. In one patient (2 exams) videostroboscopies were unsuccessful due to supraglottic hyperactivity. Fourteen remaining cases had CTs with axial and coronal images. Four of 14 CTs included phonation images with adducted true vocal cords (TVC). CT images were evaluated retrospectively by two radiologists blinded to the videostroboscopy results. The following CT findings were evaluated: 1) TVC position in axial and craniocaudal plane with and without phonation, 2) presence of anterior or posterior glottic gaps on axial phonation CT images, and 3) position of injectables/implants. These findings were correlated with videostroboscopy reports and discussion with the treating surgeon.

##### RESULTS

Nine of 14 patients had videostroboscopy TVC asymmetry in the axial plane at rest with six patients having a persistent asymmetry with phonation. Four of 14 patients had videostroboscopy TVC asymmetry in the craniocaudal plane. Table 1 summarizes the sensitivity, specificity and accuracy of CT compared to videostroboscopy. CT images without phonation had a sensitivity of 75-78% for abnormalities in TVC medialization or craniocaudal position. The sensitivity of CT for TVC craniocaudal position increased with use of phonation images. Phonation CT successfully identified one case of a posterior glottic gap, but failed to identify one case of anterior glottic gap detected on videostroboscopy. In addition to the prescribed findings, readers found three cases in which injectables were reabsorbed or injected in extraglottic sites, but not

appreciated on videostroboscopy. There were also two cases of silicone granulomas in which CT provided further information about the extent of disease.

Table 1. Diagnostic ability of neck CT compared with videostroboscopy

CT Findings*	N	Sensitivity	Specificity	Accuracy
1. Axial position without phonation	14	78%	80%	79%
2. Craniocaudal position without phonation	14	75%	50%	57%
3. Axial position with phonation	4	0	100%	50%
4. Craniocaudal position with phonation	4	100%	67%	75%
5. Anterior glottic gap	4	0	100%	75%
6. Posterior glottic gap	4	100%	67%	75%

\*Note that Findings 1 and 2 were determined on standard neck CT with reformatted coronal images and Findings 3-6 required CT with phonation (TVC in adducted position).

##### CONCLUSION

CT cannot replace videostroboscopy for dynamic assessment of the larynx, but for patients who have an unsuccessful videostroboscopy study, CT has moderate correlation with direct visualization. CT is superior to videostroboscopy in detecting implant malposition and deep extent of granulomatous complications.

**KEY WORDS:** Laryngeal computed tomography (CT), laryngoplasty, vocal cord paralysis

#### eP-186

##### Cerebrospinal Fluid Leak: Comparison of Computed Tomography Cisternography and Nuclear Medicine Cisternography

Ikram, N.<sup>1</sup>·Hogg, J.<sup>2</sup>·Roberts, T.<sup>2</sup>·Marano, G.<sup>2</sup>·Hobbs, G.<sup>1</sup>

<sup>1</sup>West Virginia University, Morgantown, WV, <sup>2</sup>West Virginia University Hospitals, Morgantown, WV

##### PURPOSE

Cerebrospinal fluid (CSF) leak occurs from defects in dura mater and skull base. Detection and repair of CSF leak are important to avoid intracranial hypovolemia and recurrent meningitis. Positive contrast CT cisternography MR cisternography, and nuclear medicine (NM) cisternography have been used to diagnose CSF leaks. Our purpose was to review our experience with CT and nuclear cisternography approaches in this diagnosis.

##### MATERIALS & METHODS

Our IRB-approved study found 162 patients with simultaneous NM cisternogram and positive contrast CT cisternogram between January 2001 and December 2010. The cases were reviewed and data were collected on age, gender, clinical presentation, etiology, reported results of the CT and NM cisternograms, and surgical findings. In addition, the CT studies were reviewed retrospectively for osseous defects and were tabulated separately. Forty-one cases were excluded because their evaluation was performed for hydrocephalus. Ninety-

one more were excluded because there was no surgical confirmation of presence or absence of CSF leak. Our study group included only the 30 patients who had surgical confirmation.

## RESULTS

Symptoms were limited to rhinorrhea in 14/30 (46.7%). Another 14/30 (46.7%) had multiple symptoms. One patient suffered meningitis (3.3%). The remaining patient (3.3%) had no symptoms. Etiologic factors related to the CSF leaks included prior surgery in 11/30 (36.7%), spontaneous leak in 10/30 (33.3%), and prior trauma in 4/30 (13.3%). Multiple etiologies were identified in 4/30 (13.3%) of patients. Sensitivities of the modalities reviewed are as listed: CT cisternography alone 80% (24/30). Nuclear medicine alone (regardless of the method) 70% (21/30). CT cisternography + nuclear cisternography combined 93.3% (28/30). Intranasal pledget counts alone 93.8% (15/16). CT without consideration of intrathecal contrast 80% (24/30). 2011 retrospective review of CT alone (admitting bias from known CSF leak) 90% (27/30). In all cases when variations on nuclear techniques were used, simple intranasal pledget counts had the highest sensitivity. There was 100% agreement in the nuclear studies in all 5 cases when pledgets counts and SPECT (Single Photon Emission Computed Tomography) were both used. There was agreement in 8/9 (88.9%) cases when pledgets and SPECT CT was used. In the other case, pledgets were positive, but SPECT CT was not.

## CONCLUSION

We found pledgets for nuclear cisternography to have the same sensitivity separately in detecting a CSF leak as CT cisternography and NM cisternography have combined. The data suggest that the radiation dose and cost associated with adding more imaging modalities may not be offset by an increase in diagnostic performance. Moreover, careful inspection and reporting of the presence of an osseous defect in the skull base can significantly contribute to preoperative planning.

**KEY WORDS:** CSF leak, CT cisternography, NM cisternography

## eP-187

### Early Diagnostic Findings of Invasive Fungal Rhinosinusitis Prior to Osseous Destruction

LaPlante, J.<sup>1</sup>•McNally, S.<sup>1</sup>•Nguyen, R.<sup>2</sup>•Davidson, H.<sup>1</sup>•Orlandi, R.<sup>1</sup>•Harnsberger, H.<sup>1</sup>•Wiggins, R.<sup>1</sup>•Quigley, E.<sup>1</sup>

<sup>1</sup>University of Utah, Salt Lake City, UT, <sup>2</sup>Columbia Basin Imaging, Richland, WA

## PURPOSE

Acute invasive fungal rhinosinusitis (AIFRS) is a rapidly progressive often fatal disease without pathognomonic early imaging characteristics. We present two key imaging features of AIFRS: absent mucosal enhancement and mucosal intrinsic T1 shortening.

These signs may serve as an early indicator of devascularized mucosa, microhemorrhage or angioinvasive fungal infection. Detectability prior to the late signs of osseous destruction or extra sinus extension is critical in decreasing morbidity and mortality associated with invasive fungal disease.

## MATERIALS & METHODS

Retrospectively reviewed the CT and MR imaging studies of nine immunocompromised patients who were subsequently diagnosed with invasive fungal rhinosinusitis in order to identify early imaging characteristics. We assessed the pattern of sinonasal mucosal enhancement, MR imaging characteristics in addition to the classic imaging signs of AIFRS such as sinus opacification, osseous destruction and evidence for disease extension beyond the sinuses.

## RESULTS

Nine immunocompromised patients with AIFRS were identified. All nine cases demonstrated lack of mucosal enhancement in the affected areas. Three of nine patients demonstrated evidence of osseous destruction on CT imaging at the time of presentation. Eight of nine cases demonstrated intrinsic T1 shortening of the mucosa corresponding to regions of decreased mucosal enhancement. These signs guided early biopsy, debridement, and/or at least partial resection or exenteration. Pathologic analysis in biopsy, resection, and exenteration specimens demonstrated invasive fungal infection and tissue necrosis. Fungal hyphae consistent with *Aspergillus* and *Mucormycosis* were present.

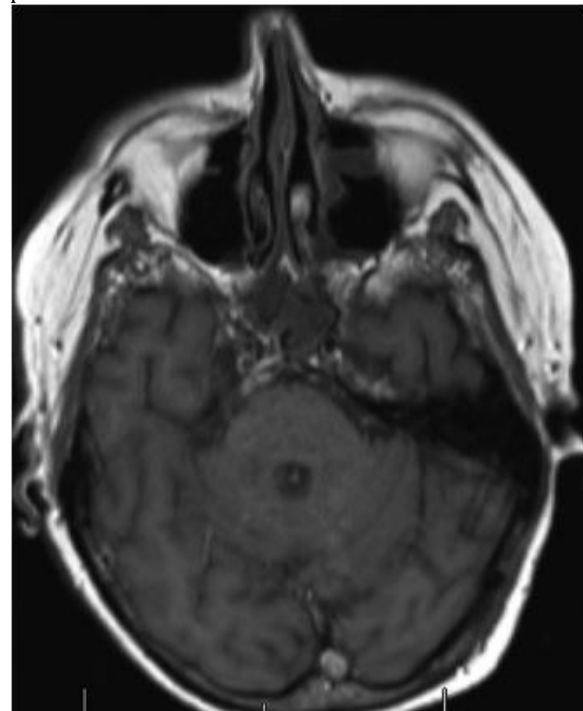


Fig 1. T1 shortening is demonstrated within left turbinate correlating with lack of postcontrast enhancement and angio-invasive mucormycosis on pathology



## CONCLUSION

Given the critical mortality associated with invasive fungal sinusitis in the immunocompromised patient, early recognition of key imaging features provides opportunity for early treatment and surgical intervention. Loss of normal mucosal enhancement and mucosal intrinsic T1 shortening correlates with devascularized mucosa, tissue necrosis or fungal angioinvasion. These imaging characteristics present prior to the late comorbid signs of osseous destruction and extrasinus extension. Earlier disease recognition is critical in this rapidly progressive and often fatal disease and may serve as a diagnostic method to decrease morbidity and mortality.

**KEY WORDS:** Sinonasal, fungal, rhinosinusitis

## eP-188

### MR Imaging Score System on Spatium Perilymphaticum Gadolinium Opacification and Its Application for Diagnosis of Meniere's Disease

Zheming, F.·Ying, L.·Xi, C.·Dairong, C.

The First Affiliated Hospital of Fujian Medical University Fuzhou, CHINA

## PURPOSE

Proposed a conception of spatium perilymphaticum gadolinium opacification and MRI scoring methods and explore the value of their diagnosis of Meniere's disease.

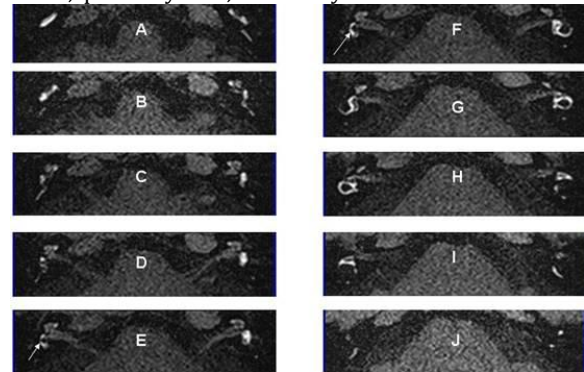
## MATERIALS & METHODS

Fifty-one asymptomatic ears and 65 ear lesions with Meniere's disease were enrolled in this study. We analyzed MR imaging of spatium perilymphaticum after intratympanic gadolinium injection with the following scoring method: (1) Semicircular canal not developed equal score 0; some developed equal score 1; fully developed equal score 2. (2) There are high-signal and low-signal areas in the vestibule, low-signal areas above the lateral semicircular canal plane equal score 6; low signal areas down to lateral semicircular canal plane equal score 3; no higher signal in the vestibule area equal score 0. (3) Basal turn of cochlea: fully developed equal score 3; partly developed equal score 2; scala vestibule of basal turned smaller than scala tympani equal score 1 regardless of full or developed in basal turn; none developed equal score 0. Medial turn of cochlea: fully developed equal score 2; partly developed equal score 1; none developed equal score 0. Apical turn of cochlea: developed equal score 1; none developed equal score 0. One radiologist, double blinded, scored all cases. SPSS17.0 software (SPSS Inc., Chicago, IL, USA) was used to conduct multiple independent samples of nonparametric tests, multivariate logistic regression, and receiver operating characteristic (ROC) curve analysis. Evaluate the sensitivity and specificity for diagnosis of Meniere's disease with the scoring system.

## RESULTS

(1) Meniere's disease summation score 0-12, median nine (quarter spacing 4.5); no symptoms group

summation score 15-18, median 17 (quarter spacing 3), two group differences had statistical significance (Wilcoxon rank and inspection  $P=0.00$ ); (2) based on summation score for the diagnosis of Meniere's disease, tangent point was 14.5, Youden index 0.969, specificity 1.00, sensitivity 0.969; (3) let cochlear, vestibular, semicircular canal scoring for association variable, logistic regression model:  $\text{Logit}P=61.216-7.381 \times \text{vestibular} -3.056 \times \text{canal}$ , based on the p value of ROC curves, diagnostic cut-off point 0.651 (vestibular  $\leq 3$  or semicircular canals  $\leq 4$  points), Youden index 0.969, specificity 1.00, sensitivity 0.969.



## CONCLUSION

Perilymphatic space of gadolinium contrast MRI score in distinguishing Meniere's disease has practical value (specific 1, sensitivity 0.969), any case meeting one of the following points could be diagnostic: (1) perilymphatic space of gadolinium contrast MRI total less than 14.5, (2) vestibular low signal areas down more than lateral semicircular canal plane, namely vestibular score value  $\leq 3$ , (3) semicircular canal scoring value  $\leq 4$ .

**KEY WORDS:** Patium perilymphaticum, gadolinium, inner ear

## eP-189

### Prevalence of Anterior Internal Auditory Canal "Diverticulum" on CT in Patients with Otosclerosis

Hoeberigs, M. C.·Waterval, J. J.·Stokroos, R. J.·Stadler, A. A. R.

Maastricht University Hospital  
Maastricht, NETHERLANDS

## PURPOSE

In patients with otosclerosis an otosclerotic hypodense cavitating plaque at the medial margin of the otic capsule, seen as an indentation or "diverticulum" of the anterior margin of the internal auditory canal (IAC), might be present. We aimed to determine the prevalence of this easily identifiable anterior IAC indentation on CT in patients with otosclerosis.

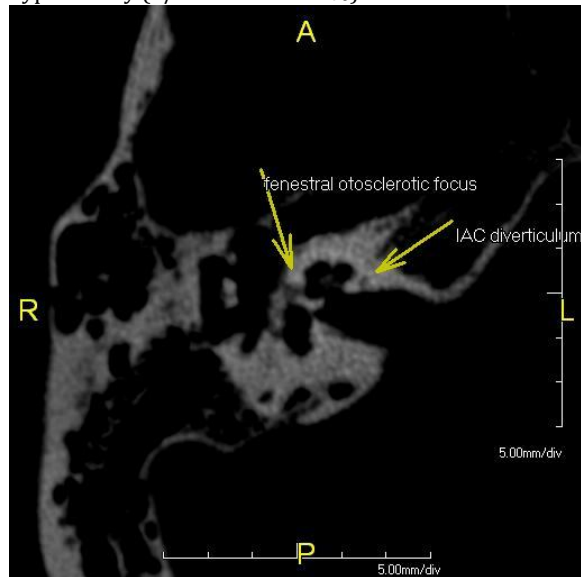
## MATERIALS & METHODS

Two hundred twenty-two consecutive high-resolution CT scans (0.4-0.6 mm) of the mastoid bone in patients with conductive or mixed hearing loss from January 2008 to December 2010 were retrospectively reviewed

by two neuroradiologists and 1 ENT surgeon. A total of 444 ears was scored for presence and severity of otosclerosis (graded according to the Symons/Fanning classification: 1 fenestral; 2 patchy pericochlear; 3 extensive pericochlear) and for the presence of anterior IAC diverticulum/plaque (defined as an obvious notch in the anterior IAC margin, isodense to the IAC itself; a faint curvature of the wall was scored negative).

## RESULTS

Anterior IAC diverticulum was observed in 9/92 ears (10%) with only fenestral otosclerosis; in 9/35 (25%) of grade 2 patchy cochlear otosclerosis and in 14/20 (70%) with grade 3 otosclerosis. Only one patient without CT signs of otosclerosis, but with clinical stapedial fixation, demonstrated bilateral IAC hypodensity (2/297 ears or 0.6%).



## CONCLUSION

Evaluation of the anterior IAC might aid in the detection of not only cochlear, but also in the more subtle fenestral.

**KEY WORDS:** Otosclerosis, anatomy

## eP-190

### Incidence of Superior Semicircular Canal Dehiscence in Patients with Hearing Loss Using Submillimetric Temporal Bone CT

Lee, Y.<sup>1</sup>•Rodriguez, F.<sup>2</sup>•Mukherji, S.<sup>2</sup>

<sup>1</sup>Ansan Hospital Korea University College of Medicine, Ansan, KOREA, REPUBLIC OF, <sup>2</sup>University of Michigan Medical School, Ann Arbor, MI

## PURPOSE

Superior semicircular canal dehiscence (SSCD) is known to be a cause of pressure-induced vertigo (Tulio's phenomena). Recently, it has become more accepted that SSCD is also being a cause of unexplained hearing loss (HL). However, multiplanar reconstructions (MPR) that specifically evaluate the superior semicircular canals are not performed routinely as part of a temporal

bone CT at most institutions. The intent of this study was to evaluate the incidence of SSCD in patients with conductive hearing loss (CHL), mixed hearing loss (MHL) by high-resolution TBCT.

## MATERIALS & METHODS

We retrospectively enrolled a total of 404 patients with hearing loss who underwent TBCT (0.6 mm) examination at our institution over the past 5 years. After excluding the 232 patients with sensorineural hearing loss, based on their audiometric tests, we recorded the TBCT and clinical findings of both ears in patients with CHL (n = 127) and MHL (n = 45). Presence of SSCD was decided by reviewing coronal and additional reformatted images in the planes of Stenver and Pöschl, which allowed detailed evaluation of the SCC. We performed multinomial logistic regression statistical analysis to find the relationship between SSCD and hearing status (p value: 0.05).

## RESULTS

The overall incidences of SSCD in ears as follows; CHL: 6.6% (11/166), MHL: 7.2% (5/69), normal hearing function: 3.0% (3/100) (p>0.05). After excluding ears with confounding clinical abnormalities that could cause HL (e.g., tympanic membrane, TBCT abnormalities, otosclerosis, etc.), the presence of SSCD is associated significantly with MHL [4/27, odd ratio: 5.35 (95% CI: 1.11-25.81), p<0.01] compared to normal hearing function, while five cases of SSCD were detected in 61 ears with CHL (odd ratio: 3.31), thus we did not find a statistical difference between CHL and normal hearing function.

## CONCLUSION

Our results suggest that the integrity of the SSC should be evaluated specifically with MPR in all patients with HL.

**KEY WORDS:** Temporal bone, CT, hearing loss

## eP-191

### MR Imaging Evaluation of Endoscopic Cranial Base Reconstruction with Pedicled Nasoseptal Flap following Endoscopic Endonasal Skull Base Surgery

Learned, K. O. • Lee, J. Y. K. • Adappa, N. D. • Palmer, J. N. • Newman, J. • Loevner, L. A.

University of Pennsylvania  
Philadelphia, PA

## PURPOSE

Endoscopic cranial base reconstruction is the essential component of expanded endonasal approaches for resections of the skull base lesions. Pedicled nasoseptal flaps (NSFs), mucoperiosteum-mucoperichondrium flaps from one or both sides of nasal septum with vascular pedicles from sphenopalatine arteries, are used increasingly because they are readily available and allow the successful closures of the surgical defects at the skull base with faster healing. This project illustrates the normal appearance of the NSFs and their

relationship with multilayer reconstructions during the critical immediate postoperative period.

#### **MATERIALS & METHODS**

We retrospectively reviewed patients who underwent endoscopic endonasal surgical resections for a spectrum of complex skull base pathologies from 2008 to 2011, identifying those who had cranial base reconstructions with NSFs. The immediate postoperative-enhanced MR imaging of NSFs were evaluated for vascular pedicles, enhancement, relationship with free grafts and coverage of skull base defects. Imaging findings were correlated with surgical techniques and clinically evident cerebrospinal fluid (CSF) leak.

#### **RESULTS**

Twenty-three patients had their cranial defect reconstructions utilizing NSFs and enhanced MR imaging performed within 48 hours after surgeries. Nasoseptal flaps were harvested from one or both sides of nasal septum in 18 and five patients respectively (18 unilateral and 10 bilateral NSFs). Nineteen patients had multilayer reconstructions with free grafts (Duragen, fat and fascia lata). Of total 28 harvested NSFs, 21 flaps (14 unilateral and 7 bilateral) were confidently identified by their enhancement and vascular pedicles arising from sphenopalatine foramen. Neither flap enhancement nor vascular pedicle was identified in five flaps (4 unilateral and 1 bilateral). In two cases of bilateral flap harvesting, the enhancing smaller flaps were not distinguished confidently from nasal mucosa without clear visibility of vascular pedicles. Eighteen of 21 confidently identified NSFs approximated cranial defects on the nasal sides; 16 multilayer reconstructions demonstrated close abutment of the NSFs to the free graft layers in their entirety. Three confidently identified NSFs were displaced and lost their abutment with the free grafts and denuded mucosa, and CSF leaks occurred in two cases. In two cases, the clinically evident CSF leak occurred at the edge of the viable NSFs and well constructed skull base defects.

#### **CONCLUSION**

Nasoseptal flaps can be identified confidently by their enhanced sphenopalatine vascular pedicles. The enhancing NSFs approximate denuded edges of the skull base defects on the nasal side and closely abut the free grafts. Any discontinuity and displacement of the NSFs and reconstructive layers should be viewed with caution and may indicate the site of CSF leak.

#### **eP-192**

#### **Cystic Lesions of the Nasopharynx: Prevalence and Clinical Relevance**

Sekiya, K.<sup>1,2</sup>•Watanabe, M.<sup>1</sup>•Nadgir, R. N.<sup>1</sup>•Flower, E. N.<sup>1</sup>•Kaneda, T.<sup>2</sup>•Sakai, O.<sup>1</sup>

<sup>1</sup>Boston University School of Medicine, Boston, MA,  
<sup>2</sup>Nihon University School of Dentistry at Matsudo,  
Matsudo, JAPAN

#### **PURPOSE**

The purpose of this study is to investigate the prevalence, imaging features, and clinical relevance of Tornwaldt and nasopharyngeal mucous retention cysts in the largest patient series to date.

#### **MATERIALS & METHODS**

Head MRI of 3,000 patients (1,254 males, 1,746 females; age 0-97 years, mean age 49 years) were reviewed retrospectively to identify cystic lesions in the nasopharynx. All studies were performed at 1.5 T MR units for various clinical indications. The routine sequences included 5 mm sagittal SE T1-weighted and axial GRASE, FLAIR, FFE T2-weighted images. Location, size, and signal characteristic of cystic lesions were recorded along with patient age. Midline cystic lesions contacting the posterior wall of the nasopharynx were defined as Tornwaldt cysts. Cystic lesions located lateral to the peak of the longus colli muscles or without midline posterior pharyngeal attachment were defined as mucous retention cysts. Clinical records of patients with cystic lesions were reviewed for possible associated symptoms.

#### **RESULTS**

Among 3,000 patients, 164 (5.3%) (71 males, 89 females; age range 13-86 years, mean age 49 years) demonstrated imaging findings consistent with Tornwaldt cyst, with the greatest prevalence in patients in their 50s. Three hundred two patients (10.1%) (139 males, 163 females; age range 2-95 years, mean age 47 years) demonstrated imaging findings consistent with mucous retention cysts with or without Tornwaldt cysts. Tornwaldt cysts were seen in eight adolescent patients, but not seen in patients less than 12 years old. Mucous retention cysts were seen in all age groups, also with peak prevalence in patients in their 50s. Mean Tornwaldt cyst size was  $6 \pm 3$  mm in long axis (range, 2-15 mm) and the mean mucous retention cyst size was  $5 \pm 3$  mm in long axis (range, 1-16 mm). Regarding Tornwaldt cysts, T1 signal was high in 22%, intermediate in 56%, and low in 22%; T2 signal was high in 60%, intermediate in 31%, and low in 9%. Regarding retention cysts, T1 signal was high in 10%, intermediate in 65%, and low in 25% while the majority demonstrated high signal intensity on T2-weighted images. Only one patient with Tornwaldt cyst presented with halitosis, pain, and foul smelling discharge; surgical resection improved the symptoms.

#### **CONCLUSION**

Nasopharyngeal cystic lesions are not uncommon, with 5.3% prevalence of Tornwaldt cyst and 10.1% prevalence of mucous retention cyst, and highest prevalence in patients in their 50s for both lesion types. These lesions are unlikely to be of clinical significance. Awareness of the commonality of these lesions can allow for a relatively specific diagnosis and limit further unnecessary workup.

**KEY WORDS:** Nasopharynx, Tornwaldt cyst, MR imaging

**Monday, April 23 –  
Wednesday, April 25**

**6:30 AM - 9:00 PM**

**Thursday, April 26**

**6:30 AM - 3:00 PM**

**Americas Hall II**

**Electronic Posters (ePosters)  
193 – 271**

**eP4 – INTERVENTIONAL**

**Note: A missing printed number indicates an abstract has been withdrawn.**

#### **eP-193**

##### **Coil Protection Technique Using Small Helical Coil in Wide-Neck Aneurysms**

Cho, Y.<sup>1</sup>•Kang, H.<sup>1</sup>•Han, M.<sup>1</sup>•Lim, J.<sup>2</sup>

<sup>1</sup>Seoul National University Hospital, Seoul, KOREA, REPUBLIC OF, <sup>2</sup>Sun Hospital, Daejeon, KOREA, REPUBLIC OF

#### **PURPOSE**

Several remodeling or protection techniques are used increasingly to treat wide-neck intracranial aneurysms. These techniques have limitations to treat some aneurysms if the aneurysm configuration, diameter of vessel, or course of vessel is not conducive to their use. We describe a novel coil protection technique for treatment of aneurysm with wide neck.

#### **MATERIALS & METHODS**

This technique consisted of a series of aneurysmal selection of a microcatheter, selection of entrance of branch artery with another microcatheter, deploying a part of small helical coil into branch artery, and framing coil insertion within aneurysmal sac under the protection of the helical coil. After completion of the first coil insertion, helical coil should be retrieved to confirm the stability of the framing coil. The helical coil can be used as filling coil.

#### **RESULTS**

This technique was applied to treat aneurysm located in the middle cerebral artery bifurcation in four patients, and A1, M1, anterior communicating artery and basilar tip aneurysm in one, respectively. We successfully filled wide-neck aneurysms with coils using coil protection technique. Seven intracranial saccular aneurysms were treated successfully with this technique. None of them experienced complications related to applying this technique.

#### **CONCLUSION**

We suggest that the coil protection technique is a good alternative to traditional remodeling or protection technique. This technique is particularly suitable for the treatment of broad-neck aneurysms originating from small branch with acute angle.

**KEY WORDS:** Aneurysm, embolization, coil

#### **eP-194**

##### **Immediate Angiographic Outcome after Endovascular Therapy for Anterior Communicating Artery Aneurysms: Correlation with Vascular Morphologic Features**

Uemura, A. • Kamo, M.

St. Luke's International Hospital  
Tokyo, JAPAN

#### **PURPOSE**

The purpose of this study is to analyze the impacts of morphologic features on angiography after endovascular embolization for anterior communicating artery (AcoA) aneurysms.

#### **MATERIALS & METHODS**

We conducted a retrospective study of 32 AcoA aneurysms in 31 patients treated with endovascular coil embolization between February 2003 and July 2011. There were 18 males and 13 females. Age ranged from 32 to 90 years (mean 60.6). Evaluated morphologic subjects included direction of the dome, dome size, dome/neck ratio, presence of irregularity and angle between A1 segment of the anterior cerebral artery and C1 segment of the internal carotid artery. Immediate angiographic results (complete occlusion or incomplete) and presence of procedural complications (aneurysmal rupture and thromboembolic events) were correlated with the morphologic subjects. Fisher exact test was used for the statistical analysis.

#### **RESULTS**

A single factor significantly associated with incomplete occlusion was superior dome direction ( $p = 0.037$ ). There was no correlation between morphologic features and procedural complications.

#### **CONCLUSION**

Incomplete occlusion after coil embolization for AcoA aneurysms is more common in cases of superior dome direction.

**KEY WORDS:** Anterior communicating aneurysm, embolization, angiography

## eP-195

### Subarachnoid Hyperdensity on Flat Panel Detector-Based Cone-Beam CT Immediately after Uneventful Coil Embolization of Unruptured Intracranial Aneurysms

Shinohara, Y.<sup>1</sup>•Sakamoto, M.<sup>1</sup>•Takeuchi, H.<sup>2</sup>•Uno, T.<sup>1</sup>•Watanabe, T.<sup>1</sup>•Kaminou, T.<sup>1</sup>•Ogawa, T.<sup>1</sup>

<sup>1</sup>Tottori University, Yonago, JAPAN, <sup>2</sup>Nojima Hospital, Kurayoshi, JAPAN

#### PURPOSE

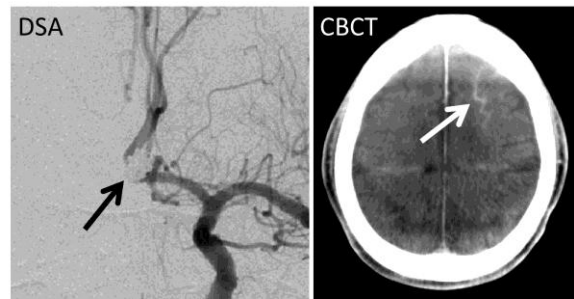
Flat panel detector-based cone-beam CT (CB CT) can provide CT-like images of the brain. Using this equipment, brain CT images can be obtained without transferring patients from the angiography suite to a conventional CT facility. According to the previous articles, conventional brain CT after uneventful endovascular treatment of cerebral aneurysms sometimes shows subarachnoid hyperdensity mimicking subarachnoid hemorrhage. Purpose of this study was to investigate the potential to detect subarachnoid hyperdensity on CB CT immediately after coil embolization of unruptured intracranial aneurysms.

#### MATERIALS & METHODS

Thirty patients underwent CB CT immediately after uncomplicated coil embolization were included. No acute infarction or hemorrhage was found on conventional CT or MR imaging before endovascular treatment of each patient. Cone-beam CT imaging was performed by a biplane flat panel detector angiographic system (Allura Xper FD20/10, Phillips or AXIOM Artis dBA, Siemens) immediately after embolization. Several parameters such as total volume of contrast medium injected, size and location of the aneurysms, embolization with whether balloon inflation and stent assistance or not were investigated related to the presence of subarachnoid hyperdensity on CB CT. Statistical analyzes were performed by using chi-square test and Pearson correlation test, as necessary ( $P < 0.05$ ).

#### RESULTS

Six of 30 patients (20%) showed focal subarachnoid hyperdensity within the relevant parent artery territory harboring treated aneurysm. The locations of the subarachnoid hyperdensity were as follows: superior frontal sulcus in four, superior and middle frontal sulci in one, and middle frontal sulcus in one. Postprocedural CT or MR imaging within 1 week demonstrated no evidence of hemorrhage in these six patients. A statistically significant difference was observed between the presence of subarachnoid hyperdensity and total volume of the contrast medium injected and the size of aneurysms ( $P < 0.001$ ,  $P < 0.05$ , respectively), which showed significant correlation among each other ( $R = 0.558$ ,  $P < 0.01$ ). On the other hand, the location of aneurysms, balloon inflation, and stent assistance did not show statistically significant differences in relation to the presence of subarachnoid hyperdensity ( $P = 0.420$ ,  $0.719$ ,  $0.126$ , respectively).



#### CONCLUSION

Cone-beam CT immediately after coil embolization can detect subarachnoid hyperdensity almost equal to the conventional CT as previously reported, presumably due to the temporal disruption of blood-cerebrospinal fluid interface, in relation to the total volume of contrast medium injected. It is important to recognize this finding because it mimics subarachnoid hemorrhage, which may hamper the immediate postprocedural medical management including anticoagulant/antiaggregant treatment.

**KEY WORDS:** Flat panel detector-based cone-beam CT, subarachnoid hyperdensity, unruptured intracranial aneurysm

## eP-196

### ARUBA: A Randomized Trial of Unruptured Brain Arteriovenous Malformations

Mohr, J. P.<sup>1</sup>•Stapf, C.<sup>2</sup>•Moskowitz, A. J.<sup>3</sup>•Parides, M. J.<sup>3</sup>•Moquete, E.<sup>3</sup>•Moy, C. S.<sup>4</sup>•Young, W. L.<sup>5</sup>•Houdart, E.<sup>2</sup>•Vicaud, E.<sup>2</sup>•Pile-Spellman, J.<sup>6</sup>

<sup>1</sup>Columbia University, New York, NY, <sup>2</sup>Hopital Lariboisiere, Paris, FRANCE, <sup>3</sup>Mt Sinai Medical Center, New York, NY, <sup>4</sup>NINDS/NIH, Bethesda, MD, <sup>5</sup>University of California San Francisco, San Francisco, CA, <sup>6</sup>Winthrop University Hospital, Mineola, NY

**Rationale:** Current invasive treatment for brain arteriovenous malformations (AVMs) is varied and includes endovascular procedures, neurosurgery, and radiotherapy. However, no controlled treatment data for any comparison of treatments, immediate or deferred, on the benefit of preventive therapy for unruptured brain AVMs have yet been performed. **Design:** ARUBA is an international, multicenter, randomized, controlled, open, prospective clinical trial. **NINDS**

(<http://clinicaltrials.gov/ct/show/NCT00389181>).

**Sample Size:** 400 patients (1:1 random assignment). **Population studied:** Patients aged  $\geq 18$  years, diagnosed with an unruptured brain AVM considered by the local investigators to be suitable for attempted eradication. **Outcome measures:** The primary outcome is the composite event of death from any cause or stroke (hemorrhage or infarction confirmed by imaging). Clinical outcome status will be measured by the Rankin Scale, NIHSS, SF-36, and EuroQol. **Interventions:** Patients are randomly assigned to best possible invasive therapy (medical management plus endovascular, surgical, and/or radiation therapy)

versus medical management alone. Patients will be followed for 5-10 years from randomization. Primary aim: To determine whether a strategy of medical management alone is superior, or not inferior, for preventing the composite outcome of death from any cause or stroke (symptomatic hemorrhage or infarction) in the treatment of unruptured BAVMs. Secondary aim: To determine whether treatment of unruptured BAVMs by medical management alone decreases the risk of death or clinical impairment (Rankin Score  $\geq 2$ ) at 5 years post-randomization compared to invasive therapy. Trial status: More than 170 patients have been enrolled worldwide. Interested multidisciplinary treatment teams are welcome to join. Sponsor: NIH/NINDS (NCT00389181). Contact: jpm10@columbia.edu (www.arubastudy.org)

**KEY WORDS:** Arteriovenous malformations, intervention, natural history

#### eP-197

##### **Stent-Assisted Coil Embolization of Wide-Necked Intracranial Aneurysms: Long-Term Follow-up Experience at a Single Institute**

Santillan, A.-Greenberg, E.-Patsalides, A.-Salvaggio, K.-Riina, H. A.-Stieg, P. E.-Gobin, Y. P.

New York Presbyterian Hospital-Weill Medical College of Cornell University  
New York, NY

##### **PURPOSE**

Stent-assisted coil embolization facilitates the endovascular treatment of wide-necked intracranial aneurysms. We retrospectively examine the long-term results of stent usage in conjunction with coil embolization in wide-necked intracranial aneurysms.

##### **MATERIALS & METHODS**

Between November 2002 and December 2010, 86 patients harboring 88 wide-necked intracranial aneurysms were treated using the Neuroform, Enterprise, and Ultralink coronary stents. Patient and aneurysm characteristics and occurrence of complications were analyzed. Follow-up imaging included digital subtraction angiography (DSA) or magnetic resonance angiography (MRA).

##### **RESULTS**

The stenting procedure failed in two patients due to technical difficulties such as poor navigability through tortuous vessels and inability to reach the target artery. Therefore, 84 patients harboring 86 intracranial aneurysms were included for analysis. Immediately after treatment, complete aneurysm occlusion was observed in 42.4% (n = 38), neck remnant in 38.4% (n = 33), and residual aneurysm in 17.4% (n = 15) of the cases. Angiographic and clinical follow up were available in 74 and 78 patients, respectively. The mean angiographic follow up was 30.1 months (range, 0-98 months). At last follow up, complete aneurysm occlusion was seen in 76.7% (n = 66), neck remnant in 8.1% (n = 7), residual aneurysm in 1.2% (n = 1), and

lost on follow up in 14% (n = 12) of the cases. Eleven aneurysms (12.8%) were retreated with no complications. Seventy-five patients (89.3%) had favorable clinical outcome with a modified Rankin Scale (mRS)  $\leq 1$ , three patients (3.6%) had an mRS of two and five patients (5.9%) did not have a clinical follow up. The mean clinical follow-up time was 39.9 months (range, 0-98 months). One patient (1.2%) died from a procedure-related hemorrhage.

##### **CONCLUSION**

Stent-assisted coil embolization of wide-necked intracranial aneurysms can be performed with few complications and provides a high rate of aneurysm occlusion at long-term follow up.

**KEY WORDS:** Stent, coil embolization, aneurysm

#### eP-198

##### **Transvenous Coil Embolization by Using Pnumbra Coil 400 Embolization System in a Combined Arterial and Venous Endovascular Occlusion of a Dural Arteriovenous Fistula: A Case Report**

Derakhshani, S.<sup>1,2</sup> Low, S. B. L.<sup>1</sup> Butler, P.<sup>2</sup>

<sup>1</sup>Queens University Hospital, Romford, Essex, UNITED KINGDOM, <sup>2</sup>The Royal London Hospital, London, UNITED KINGDOM

##### **PURPOSE**

We describe combined transarterial and transvenous embolization of a dural arteriovenous fistulae (dAVF) using new coil embolization system on the venous side treatment.

##### **MATERIALS & METHODS**

An adult male suffering from neurologic impairment due to a dAVF was treated first by dual arterial and venous embolization. He was listed for gamma knife surgery postoperatively. Coils were used for the purpose of embolization on arterial and venous side. We used Pnumbra 400 coil embolization system on the venous side.

##### **Result**

Complete elimination of flow was achieved after endovenous embolization after transarterial treatment. No preoperative or postoperative complications were observed.

##### **CONCLUSION**

It is necessary to eliminate a dural fistula completely. We presented complete occlusion by dual endovascular approach using both transarterial and transvenous embolization. High volume occupancy of new Pnumbra 400 coils can be used to achieve embolization of large structures such as major cerebral veins effectively.

**KEY WORDS:** Endovenous coil embolization, arterial occlusion, dural arteriovenous malformation



## eP-199

**Intraarterial Techniques for Blood-Brain Barrier Disruption and Gene Therapy in Mice**

Foley, C. P.·Rubin, D. G.·Santillan, A.·Sondhi, D.·Crystal, R. G.·Gobin, Y.·Ballon, D. J.

Weill Cornell Medical College  
New York, NY

**PURPOSE**

One treatment that has shown promise for treating neurologic disease (lysosomal storage disorders, Parkinson's, cancer, etc.) is gene therapy. However, since this therapy cannot pass from the bloodstream to the brain because of the blood-brain barrier (BBB), it generally has been administered to the central nervous system by directly infusing a solution containing the therapy into brain tissue, which requires multiple needle insertions to cover large volumes of tissue. Intraarterial (IA) delivery coupled with BBB disruption potentially could treat larger volumes of neural tissue to achieve high drug tissue concentrations with reduced systemic exposure. The goal of this work was to evaluate the utility of IA delivery in administering adeno-associated viral vectors in mice.

**MATERIALS & METHODS**

We surgically positioned custom built polyimide microcatheters (169  $\mu$ m outer diameter) in the internal carotid artery (ICA) of mice. Mice were moved to the bore of a small-animal MRI system (Biospec 70/30 USR, Bruker-Biospin) and injected IA with 750  $\mu$ l of Gd-DTPA (1:19 dilution of Magnevist®, Bayer Healthcare Pharmaceuticals, in saline) at a flow rate of 800  $\mu$ l/min while monitoring the distributed volume and rate of tissue uptake/washout of the injected agent in real time using a FLASH gradient-echo pulse sequence with TR = 25 ms, TE = 3.8 ms, FOV = 25 mm  $\times$  25 mm, and a matrix = 192  $\times$  256. This was performed both with and without prior IA injection of a hyperosmolar mannitol solution (25 wt/v%) to locally disrupt the BBB. This procedure permitted quantification of the extent of BBB disruption in different brain territories. These data were used to optimize delivery parameters for use in IA gene therapy experiments. Mice received IA injection of AAVrh.10CLN2 particles after IA mannitol-mediated BBB disruption and were analyzed for gene expression after 5 weeks.

**RESULTS**

We found that the volume and flow rate of injected mannitol affected the degree of BBB disruption (observed as an increase above baseline in normalized time courses of signal intensity in a region of interest). For a given mannitol flow rate, the degree of BBB disruption increased with increasing injection volume. More importantly, different territories of the brain exhibited different levels of BBB disruption related to the order in which the feeding arteries branch from the ICA. Mice that received IA injection of AAVrh.10CLN2 particles after IA mannitol mediated BBB disruption showed extensive gene expression after 5 weeks.

**CONCLUSION**

The techniques demonstrated in this work enabled us to reproducibly disrupt the BBB in different territories of the mouse brain to varying degrees by changing the volume and flow rate of the mannitol injection. This should serve as a platform for future work on IA delivery in preclinical mouse models of human disease. Further, we have demonstrated that this technique is a viable way to obtain wide scale gene-expression in neural tissue following a single administration of a viral vector solution.

## eP-200

**Superselective Ophthalmic Artery Chemotherapy for Intraocular Retinoblastoma**

Bracco, S.·Romano, D.·Cioni, S.·Galluzzi, P.·Hadjistilianou, T.·Cerese, A.·Venturi, C.

Universitaria Senese  
Siena, ITALY

**PURPOSE**

To report our experience in superselective ophthalmic artery infusion of melphalan (SOAIM) for intraocular retinoblastoma.

**MATERIALS & METHODS**

From June 2008 to October 2010, 38 patients (18 females, 20 males; age range at first treatment, 7 months to 22 years) with 41 eyes with retinoblastoma were scheduled for SOAIM, for 17 newly diagnosed retinoblastomas tumor, node and metastasis (TNM) [TNM 1A (n = 1), 1B (n = 1), 2A (n = 7), 2B (n = 4) and 3A (n = 4)], and 24 retinoblastomas with partial remission or relapse [TNM 1B (n = 13), 2A (n = 1) and 2B (n = 10)]. Eight patients (ten eyes) have been treated by SOAIM alone. Follow up was 6-27 months in 28 patients (30 eyes).

**RESULTS**

Ophthalmic artery cannulation failed in two patients. Thirty-six patients underwent 140 treatments by internal (n = 112) or external (n = 28) carotid arteries. No major procedural complications occurred. Two patients have been lost to follow up. Remaining 34 patients (37 eyes) had no metastatic disease. Four patients suffered permanent ocular complications: chorioretinal dystrophy (n = 2), ptosis (n = 1) and strabismus and exotropia (n = 1). Eight (22%) eyes in eight (24%) patients underwent enucleation: seven out of 16 (43%) newly diagnosed retinoblastomas and one out of 22 (4.5%) retinoblastomas undergoing partial remission or relapse. For all treated eyes, Kaplan-Meier eye enucleation-free rates (K-M) were 85.4% (95% CI, 73.3-97.5%), 74.4% (95% CI, 57-91.8%) and still stable at 6, 12 months and 2 years, respectively. For eyes with partial remission or relapse, and eyes at presentation, K-M at 2 years were 95.5% (95% CI, 86.9-100%) and 45.6% (95% CI, 16.6-74.6%), respectively.

**CONCLUSION**

Superselective ophthalmic artery infusion of melphalan was safe and powerful, especially following other

therapies. Superselective ophthalmic artery infusion of melphalan should be added to focal therapies spectrum. In selected cases, melphalan should be combined with other chemotherapeutic agents.

**KEY WORDS:** Retinoblastoma, superselective intraarterial, chemotherapy

#### eP-201

### Carotid Artery Stenting Using Filter Embolic Protection Device for High-Grade Stenosis: Examination about the Frequency of Ischemic Complications

Wada, T.<sup>1</sup>•Takayama, K.<sup>2</sup>•Myouchin, K.<sup>2</sup>•Sakamoto, M.<sup>1</sup>•Taoka, T.<sup>1</sup>•Nakagawa, H.<sup>3</sup>•Kichikawa, K.<sup>1</sup>

<sup>1</sup>Nara Medical University, Kashihara, JAPAN, <sup>2</sup>Ishinkai Yao General Hospital, Yao, Osaka, JAPAN, <sup>3</sup>Nara Prefectural Nara Hospital, Nara, Nara, JAPAN

#### PURPOSE

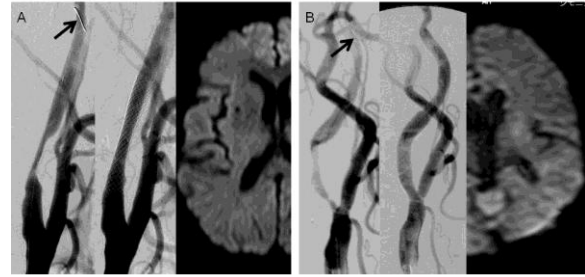
On carotid artery stenting (CAS) procedure, passage of filter embolic protection device (EPD) at the site of severe stenosis may have potential risk for ischemic complication due to generating emboli. Some operators use proximal protection in order to prevent the complication; however, there is no published evidence to support this potential risk. In order to estimate the potential risk for generating emboli at the passage of EPD at the site of severe stenosis, we evaluated the frequency of the ischemic complications in CAS procedure using filter EPD in the cases with severe carotid stenosis and compared it with the mild stenosis cases.

#### MATERIALS & METHODS

Our subjects were 232 carotid artery stenotic lesions on 223 cases (201 males, 51-86 years of age with average age 72.7 years, NASCET 50-99% stenosis with an average of 81.4%). We performed CAS by standard procedure using filter EPD and acquired diffusion-weighted imaging (DWI) within 48 hours after procedure. Applied EPD were Angioguard in 146 cases and Filterwire EZ in 86 cases, and applied stents were Precise in 159 cases and Carotid Wallstent in 73 cases. The population was classified into severe stenosis group (more than 90% stenosis: 60 cases) and mild stenosis group (stenosis from 50% to 90%: 172 cases). We evaluated the frequency of appearance of postoperative ischemic lesions on DWI and the frequency of symptomatic ischemic strokes by CAS procedure.

#### RESULTS

Ischemic lesions on DWI were observed in 15 cases of severe stenosis group (25%) and 48 cases of mild stenotic group (28%). Minor symptomatic ischemic strokes occurred in two cases of severe stenosis group (3.3%) and six cases of mild stenosis group (3.5%). As for a postoperative ischemic change on DWI and symptomatic stroke, there were no statistically significant differences between both groups.



A case of mild stenosis group (A); 68 years old male with asymptomatic right ICA 81% stenosis, and a case of severe stenosis group (B); 70 years old male with symptomatic left ICA 90% stenosis.

In both cases, filter EPD (→) could be passed through the stenosis alone. After CAS, both cases had no ischemic stroke and no appearance of acute ischemic lesion on DWI.

#### CONCLUSION

The ischemic complications of CAS using EPD in the cases with severe stenosis did not showed higher frequency compared with mild stenotic group. Thus, EPD passage at the site of severe stenosis itself does not seem to raise the frequency of ischemic complications. It seems that factors other than passage of EPD are responsible for ischemic complication in CAS procedure.

**KEY WORDS:** Carotid artery stenting, filter embolic protection device, high-grade stenosis

#### eP-202

### Intraarterial Verapamil Challenge: A New Diagnostic Tool for Reversible Cerebral Vasoconstriction Syndrome

Shivashankar, R.<sup>1</sup>•Rahme, R.<sup>1</sup>•Jimenez, L.<sup>1</sup>•Khan, U.<sup>1</sup>•Ringer, A. J.<sup>1,2</sup>•Kleindorfer, D.<sup>1</sup>•Abruzzo, T. A.<sup>1,2</sup>

<sup>1</sup>University of Cincinnati, Cincinnati, OH, <sup>2</sup>Mayfield Clinic, Cincinnati, OH

#### PURPOSE

In patients with consistent clinical features, the initial diagnosis of reversible cerebral vasoconstriction syndrome (RCVS) typically relies on characteristic angiographic findings, commonly described as "sausages on a string" appearance. However, diagnostic confirmation remains retrospective and is obtained only when spontaneous resolution of clinical and angiographic findings is demonstrated 1-3 months later. Thus, differentiating RCVS from other, less benign cerebrovascular disorders, particularly primary angiitis of the central nervous system (PACNS), is often challenging early in the course of the disease. We sought to analyze the angiographic response to intraarterial (IA) verapamil as a potential diagnostic tool in patients with suspected RCVS.

#### MATERIALS & METHODS

All patients who underwent IA verapamil infusion for medically refractory RCVS at our institution between January 2007 and June 2011 were identified by searching a prospectively maintained institutional neuroangiography database. Medical records and angiographic images were reviewed retrospectively.

Clinical and imaging data were extracted and the dose of IA verapamil and corresponding angiographic response were specifically recorded.

### RESULTS

During the study period, four patients with severe RCVS (3 women and 1 man, age range 19-58 years) were treated by IA infusion of verapamil at the time of the initial diagnostic cerebral angiogram. Clinical presentation included thunderclap headaches in three patients, cerebral ischemia or infarction in two, and subarachnoid hemorrhage in one. The dose of verapamil ranged from 10 to 20 mg per vessel. Complete resolution of angiographic abnormalities and restoration of a normal arterial luminal diameter was observed within 15 minutes of verapamil infusion in all patients. There was no procedure-related mortality or permanent morbidity. One patient had a verapamil-induced self-limited generalized tonic-clonic seizure with no significant clinical consequences.

### CONCLUSION

Intraarterial verapamil challenge may help confirm the diagnosis of RCVS during the initial angiographic study and differentiate it from other cerebral angiopathies with a less benign course, particularly PACNS. The therapeutic value of this intervention is less certain and remains to be demonstrated.

**KEY WORDS:** Reversible cerebral vasoconstriction syndrome, intraarterial, verapamil

### eP-203

#### **In vivo Evaluation of Carotid Artery Stents Using Multidetector Row CT Angiography: Comparison of Three Different Kernels**

Lee, Y.-Yoo, W.

Catholic University of Korea  
Bucheon, KOREA, REPUBLIC OF

### PURPOSE

To assess the lumen visibility of carotid artery stents using multidetector row computed tomography (MDCT) angiography in vivo, compare a medium-smooth kernel (B30s), a medium-sharp kernel (B50s), and a sharp kernel (B60s), and correlate these results to digital subtraction angiography (DSA) as a reference standard.

### MATERIALS & METHODS

Thirty-two stents from 31 patients (28 men, 3 women) who underwent CT angiography with 16- and 64-slice MDCT were analyzed retrospectively. In CT angiograms using B30s, B50s, and B60s, the lumen diameters of the stented vessels were measured independently three times by two observers, and the artificial luminal narrowing (ALN) was calculated. Digital subtraction angiography served as the reference standard for the measurement of the lumen diameter on CT angiography.

### RESULTS

For the interobserver reliability, the intraclass correlation coefficients for the lumen diameters on the CT angiograms with B30s, B50s and B60s were 0.99, 0.99, and 0.99. The lumen diameters were  $3.57 \pm 0.99$  mm on B30s images,  $3.88 \pm 0.97$  mm on B50s images and  $3.98 \pm 0.99$  mm on B60s images. The mean ALN was  $24.7 \pm 8.9\%$  on B30s images,  $17.8 \pm 9.5\%$  on B50s images, and  $15.6 \pm 9.6\%$  on B60s images. The CT angiography using B60s had the highest coincidence of in-stent lumen diameters with DSA and the smallest ALN. There were statistically significant differences in the lumen diameter and ALN among the CT angiograms using B30s, B50s, and B60s ( $p < 0.001$ ).

### CONCLUSION

The CT angiography with a sharp kernel is considered to be a useful diagnostic modality to assess the stented vessels after carotid angioplasty and stenting.

**KEY WORDS:** Carotid artery, stents, CT angiography

### eP-204

#### **Effect of ASPECT Score on Functional Outcome in Endovascular Recanalization of Acute Symptomatic Carotid Artery Occlusions**

Ranawat, N. S.<sup>1,2</sup>•Chaudhary, S.<sup>2</sup>•Qureshi, A. I.<sup>2</sup>

<sup>1</sup>Central Florida Health Alliance, Leesburg, FL,

<sup>2</sup>University of Minnesota Medical Center, Minneapolis, MN

### PURPOSE

Treatment of occluded carotid arteries in patients with acute symptoms has not been defined clearly. With bypass surgery not being a viable option as shown in the EC/IC bypass and COSS trials, alternative treatments need to be evaluated. Objective: To review functional outcomes in patients undergoing endovascular recanalization (EVR) of occluded carotid arteries with ipsilateral acute stroke or TIA symptoms.

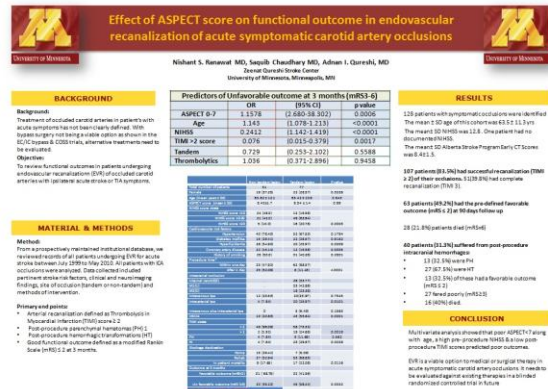
### MATERIALS & METHODS

From a prospectively maintained institutional database, we reviewed records of all patients undergoing EVR for acute stroke between July 1999 to May 2010. All patients with ICA occlusions were analyzed. Data collected included pertinent stroke risk factors, clinical and neuroimaging findings, site of occlusion (tandem or nontandem) and methods of intervention. Primary end points: •Arterial recanalization defined as thrombolysis in myocardial infarction (TIMI) score  $\geq 2$ . •Postprocedure parenchymal hematomas (PH) 1, •Postprocedure hemorrhagic transformations (HT). •Good functional outcome defined as a modified Rankin Scale (mRS)  $\leq 2$  at 3 months.

### RESULTS

One hundred twenty-eight patients with symptomatic occlusions were identified. The mean  $\pm$  SD age of this cohort was  $63.5 \pm 11.3$  years. The mean  $\pm$  SD NIHSS was 12.8. One patient had no documented NIHSS. The mean  $\pm$  SD Alberta Stroke Program Early CT Scores was

8.4 ± 1.5. One hundred seven patients (83.5%) had successful recanalization (TIMI ≥ 2) of their occlusions. Fifty-one (39.8%) had complete recanalization (TIMI 3). Sixty-three patients (49.2%) had the predefined favorable outcome (mRS ≤ 2) at 90 days follow up. Twenty-eight (21.8%) patients died (mRS = 6). Forty patients (31.3%) suffered from postprocedure intracranial hemorrhages: 13 (32.5%) were PH, 27 (67.5%) were HT, 13 (32.5%) of these had a favorable outcome (mRS ≤ 2). Twenty-seven fared poorly (mRS ≥ 3). Sixteen (40%) died.



## CONCLUSION

Multivariate analysis showed that poor ASPECT < 7 along with age, a high preprocedure NIHSS and a low postprocedure TIMI scores predicted poor outcomes. Endovascular recanalization is a viable option to medical or surgical therapy in acute symptomatic carotid artery occlusions. It needs to be evaluated against existing therapies in a blinded randomized controlled trial in the future.

**KEY WORDS:** ASPECT, carotid occlusion, endovascular revascularization

## eP-205

### Forced-Suction Thrombectomy after Carotid Stenting in Patients with Massive Thrombus and Acute Extracranial Internal Carotid Artery Occlusion

Kwak, H.-Chung, G.

Chonbuk National University Hospital and Medical School  
Jeonju, KOREA, REPUBLIC OF

## PURPOSE

We evaluated the safety and efficacy of emergent carotid stenting and modified PS technique for cases of acute extracranial internal carotid artery (ICA) occlusion and massive thrombus with acute ischemic stroke symptoms.

## MATERIALS & METHODS

From December 2009 and June 2011, we retrospectively reviewed the clinical outcomes of five patients with tandem occlusion of the ICA and middle cerebral artery (MCA) and who underwent recanalization by modified PS technique after carotid

artery stenting. Direct wedging between the tip of the reperfusion catheter and the distal part of the clot followed by forceful suction by using 10mL syringe is a unique feature of this technique.

## RESULTS

The median NIHSS score on admission was 13 and ranged from 9 to 18. Median time from symptom onset to arrival at hospital was 216 minutes. The mean time lag between arrival at hospital and IAT ranged from 69 minutes. Recanalization by stenting of carotid artery occlusion was performed successfully in all patients. Mean number of modified PS technique about distal migrated thrombus was three. Recanalization of MCA (TICI grade III) was observed in all the patients. Symptomatic hemorrhage transformation did not occurred during the hospital day. At discharge, the median NIHSS score was 2.2 (range; 1 - 6). At the 3-month follow up, the functional outcome was excellent in three of the five patients, good in one patient and poor in one patient.

## CONCLUSION

The modified PS technique after carotid artery stenting is safe and effective treatment for treatment in patients with massive thrombus into the distal portion of ICA obstruction and tandem occlusion of the ICA and MCA occlusion.

**KEY WORDS:** Stroke, thrombectomy

## eP-206

### Influence of Stent Design on Outcome of Carotid Artery Stenting

Kim, D.<sup>1</sup> Park, K.<sup>1,2</sup> Kim, B.<sup>1</sup> Kim, Y.<sup>1</sup> Nam, H.<sup>1</sup> Heo, J.<sup>1</sup> Kim, D.<sup>1</sup>

<sup>1</sup>Yonsei University College of Medicine, Seoul, KOREA, REPUBLIC OF, <sup>2</sup>National Health Insurance Corp. Ilsan Hospital, Goyang-si, Gyeonggi-do, KOREA, REPUBLIC OF

## PURPOSE

Carotid stenosis is a common cause of ischemic stroke. Carotid artery stenting (CAS) can be an alternative treatment of carotid endarterectomy (CEA). The purpose of the present study was to assess the outcome of CAS by stent design.

## MATERIALS & METHODS

One hundred sixty-four patients with moderate or severe carotid stenosis (132 males and 32 females; mean age 69.3 years) were treated by CAS between 2007 and 2010. All patients were divided into two groups (82 in closed cell stent and 82 in open cell stent) and the clinical, procedural, and imaging outcomes were assessed and compared. They also were divided into two groups by initial symptom presence (122 in symptomatic group and 42 in asymptomatic group) to evaluate the influence of stent design between each group.

## RESULTS

"New embolism" including "captured emboli" by protection device and "new embolic lesions" on postprocedural DWI was significantly more frequent in open cell stent group comparing with closed cell stent group ( $n = 45$  in closed cell versus  $n = 60$  in open cell,  $P = .015$ ). Thirty-day clinical outcome was not different between two groups. In symptomatic group, stent design was a strong risk factor of "new embolism" [ $P = .021$ , odds ratio (OR) 2.817], while diabetes was a risk factor of "new embolism" in asymptomatic group ( $P = .033$ , OR 10.626).

## CONCLUSION

The stent design may have an influence on outcome of CAS. The selection of appropriate stent design is necessary for improvement of treatment outcome.

## eP-207

### Value of Volume of Interest C-Arm CT Imaging in the Endovascular Treatment of Intracranial Aneurysms: A Feasibility Study

Chintalapani, G.<sup>1</sup>•Chinnadurai, P.<sup>1</sup>•Maier, A.<sup>2</sup>•Shaltoni, H.<sup>3</sup>•Morsi, H.<sup>3,4</sup>•Mawad, M.<sup>3,4</sup>

<sup>1</sup>Siemens Medical Solutions USA Inc., Hoffman Estates, IL, <sup>2</sup>Siemens AG, Forchheim, GERMANY, <sup>3</sup>St. Luke's Episcopal Hospital, Houston, TX, <sup>4</sup>Baylor College of Medicine, Houston, TX

## PURPOSE

During endovascular treatment of intracranial aneurysms, it is very crucial to understand the relationship of deployed devices such as stents, flow diverters, and coils to the parent artery and adjacent normal branches. Although existing C-arm CT imaging techniques provide such information, the repeated intraprocedural use of C-arm CT is limited due to increased radiation dose delivered to the patient. We propose to evaluate the feasibility of a new VOI imaging technique that creates high quality 3D images of the selected region of interest for intermediate updates and image guidance during the procedure without significant increase in radiation.

## MATERIALS & METHODS

Volume of interest images were obtained in 10 patients undergoing endovascular treatment of intracranial aneurysms. The VOI images were acquired by iso-centering the C-arm around the implanted device using a standard 20s DR DynaCT (Axiom Artis Zee, Siemens AG, Forchheim, Germany) acquisition with the x-ray source collimated on the VOI. The size of the VOI is approximately 12% of the full volume. The VOI images are reconstructed using reconstruction software provided by the angiographic systems as well as using an offline prototype reconstruction algorithm.

## RESULTS

Images from full volume and VOI acquisitions are reconstructed with similar reconstruction parameters with a resolution of 0.2 mm/pixel and compared to each other. Qualitative analysis shows that VOI images are

comparable to secondary reconstructions from a full volume acquisition (Figure 1). The cumulative dose is significantly reduced with VOI scan resulting in a reduction of 91.8% in dose area product when compared to full volume scan.

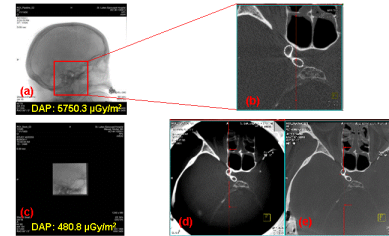


Fig 1(a): (a) Full volume scan, (b) secondary reconstruction from a full volume scan, (c) VOI scan, (d) standard reconstruction of VOI scan, (e) offline prototype reconstruction of VOI scan

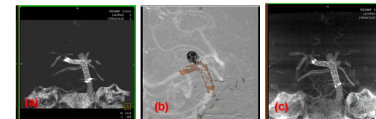


Fig 1(b): (a) Standard reconstruction of VOI scan after stent deployment and before coiling, (b) Stent segmented from (a) and overlaid on to fluoroscopy image for image guidance during coiling, (c) Offline prototype reconstruction of the same VOI scan with truncation artifact correction.

## CONCLUSION

Volume of interest imaging allows additional and repeated C-arm CT acquisitions on the same patient during the endovascular treatment without significant increase in radiation exposure. Volume of interest imaging after a stent/flow diverter deployment or during the coiling of the aneurysm provides immediate feedback on the device placement and the vessel apposition of the implanted devices. Moreover, the implanted devices from VOI images can be segmented and overlaid on fluoroscopic images for image guidance during the procedure. The acquisition of VOI images can be difficult due to the dependency on iso-centering the C-arm around the aneurysm or the deployed devices. Further improvements are needed to adaptively collimate the C-arm around the region of interest. Nevertheless, VOI imaging technique can be a valuable tool to provide image guidance during the treatment, to assess treatment efficacy and to potentially improve the clinical outcomes, all without increasing the radiation dose.

**KEY WORDS:** Volume of interest imaging, VOI, devices

## eP-208

### Angiographic Analysis of Flow Diversion for Intracranial Aneurysms

Jou, L.•Shaltoni, H.•Morsi, H.•Mawad, M.

Baylor College of Medicine  
Houston, TX

## PURPOSE

Hemodynamic factors are important to the development and rupture of intracranial aneurysms. Reconstruction of parent vessel with flow diverters is an attractive alternative for treatment of complex aneurysms, but monitoring intraaneurysmal hemodynamics during the endovascular procedure is critical to the success of a treatment. Flow stasis within an aneurysm after flow diversion can be misleading in some cases and does not reflect the true

intraaneurysmal hemodynamics as flow stasis is observed more often for the posteriorly oriented aneurysms than for the anteriorly oriented aneurysms due to contrast settling driven by the gravity. A new technique based on high frame rate digital subtraction angiography (HFR DSA) is developed for the evaluation of flow diversion.

#### MATERIALS & METHODS

Fourteen patients (average age of 60 years old) with at least one saccular aneurysm at the internal carotid artery were treated with flow diversion and imaged using our protocol both before and after deployment of the Pipeline Embolization Device (PED). The average aneurysm size was 10 mm. Additional five aneurysms (averaged 15 mm) were treated by a Neuroform stent and embolic coils using the same protocol for the purpose of comparison. High frame rate angiographic images were analyzed based on our technique to determine the efficiency of flow diversion. Computational fluid dynamics (CFD) of patient-specific aneurysm models also was employed for determination of intraaneurysmal flow. The intraaneurysmal flow rates from HFR DSA and CFD were compared against each other; the flow diversion efficiency after flow diversion also was evaluated.

#### RESULTS

There is a linear relationship between the flow diversion coefficients obtained from the DSA and CFD. Nearly 49% of blood flow remains within the aneurysm after deployment of three PEDs, followed by 56% after one PED and 92% for a Neuroform stent alone. On the contrary, the average flow reduction for coiled aneurysms is 96%. A high frame rate DSA (30 f/s) provides a better estimate on the intraaneurysmal flow than the DSA at lower frame rates (<15 f/s). In addition, the locations of flow impingement in CFD are in good agreement with the HFR DSA.

#### CONCLUSION

Our CFD calculation validates the flow diversion estimated by our DSA technique. Because of this linear relationship, it does not require a lengthy CFD simulation to derive the intraaneurysmal flow rate that often demands a long computation time. Therefore, one can rely on the HFR DSA for real-time assessment of intraaneurysmal hemodynamics and for an analysis of therapeutic effect of flow diversion.

**KEY WORDS:** Aneurysms, flow diverter, stents

#### eP-209

#### Metal Artifact Reduction of Coil Mass Artifacts in High-Resolution Flat-Detector Cone-Beam Computed Tomography of Cerebral Stent-Assisted Coiling

van der Bom, I. M. J.<sup>1</sup>Ruijters, D.<sup>2</sup>Spilberg, G.<sup>1</sup>Hou, S. Y.<sup>1</sup>van de Haar, P.<sup>2</sup>Carelsen, B.<sup>2</sup>Gounis, M. J.<sup>1</sup>Wakhloo, A. K.<sup>1</sup>

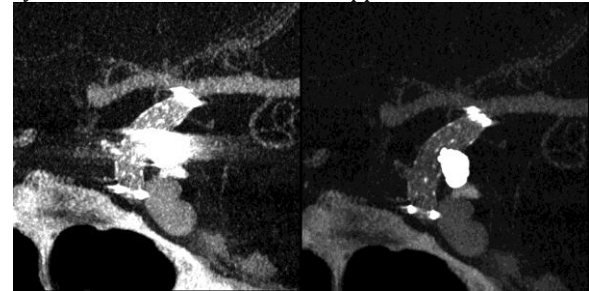
<sup>1</sup>University of Massachusetts, Worcester, MA, <sup>2</sup>Philips Healthcare, Best, NETHERLANDS

#### PURPOSE

C-arm systems equipped with flat-detector technology do not only provide 2D fluoroscopy, but also enable in situ 3D cone-beam computed tomography (CB CT) that can be utilized for peri-interventional evaluation. Recently, it was shown that both neurovascular stents and host arteries could be visualized in great detail. However, visibility of these structures are impeded by artifacts generated by adjacent coil masses. Here, we report the use of a metal artifact reduction (MAR) algorithm for high-resolution contrast-enhanced CB CT (VasoCT) with the objective to improve visualization in cases of stent-assisted aneurysm embolization.

#### MATERIALS & METHODS

VasoCT data were acquired in 25 patients that underwent stent-assisted coiling. Nonbinned reconstructions were generated (FOV: 34<sup>3</sup>cm, 256<sup>3</sup> matrix) with and without MAR (Figure). For all 25 cases, both reconstructions were reviewed by three neuroradiologists on a dedicated workstation. Visibility of the stent, vessel, and the relationship between stent, vessel and coil mass were scored using a 3-point scale. The observers were asked whether the metal artifact was obscuring the vessel beyond the actual coil mass, and which of both reconstructions offered overall better visibility. The results were analyzed using raw agreement statistics and robustness of the rating system was tested with Fleiss' kappa-method.



Representative VasoCT data without (left) and with MAR (right)

#### RESULTS

In more than half of all cases, observers agreed that visibility of stent, vessel, and the relationship was insufficient for evaluation (score of 1) ( $\kappa=0.66$  to 0.72) and in 56% that the artifact was obscuring adjacent anatomy ( $\kappa = 0.5$ ) without MAR. With MAR, observers agreed that the visibility of the stent, vessel, and the relationship was improved by at least one point on the scoring system in ~50% of all cases ( $\kappa=0.6$ ) and that the artifact was not obscuring the vessel in 64% of the cases. The visibility was sufficient for evaluation (score  $\geq 2$ ) with MAR in 68% of cases. Overall, the observers concluded that the visibility of the reconstruction with MAR was better than without in 92% of the cases ( $\kappa = 0.9$ ).

#### CONCLUSION

Although MAR is not capable of fully removing metal artifacts, our study shows that the image quality of VasoCT improves visualization of the parent vessel, stent and coil mass as well as adjacent anatomy previously obscured by the streak artifacts. The impact



of the artifacts on the visibility varied between cases, and yet the overall visibility of the contrast-enhanced CB CT improved in the majority of the cases.

**KEY WORDS:** Stent-assisted coiling, flat-detector cone-beam CT, metal artifact reduction

#### eP-210

### Endovascular Treatment of Unruptured Intracranial Aneurysms: A Systematic Review of the Literature on Safety and Efficacy with Emphasis on Subgroup Analyses

Naggara, O.<sup>1</sup>•Leclerc, A.<sup>1</sup>•Oppenheim, C.<sup>1</sup>•Meder, J.<sup>1</sup>•Raymond, J.<sup>2</sup>

<sup>1</sup>Université Descartes, Sorbonne Paris Cité, Paris, FRANCE, <sup>2</sup>Notre Dame Hospital, University of Montreal, Montreal, QC, CANADA

#### PURPOSE

To report subgroup analyses of an updated systematic review on endovascular treatment (EVT) of unruptured intracranial aneurysms (UAs); to compare types of embolic agents, adjunct techniques such as balloon or stent-assisted coiling, and new devices such as flow diverters, and to identify potential risk factors for poor outcomes.

#### MATERIALS & METHODS

The manuscript was prepared in accordance with the MOOSE and PRISMA guidelines. The literature was searched using PubMed, EMBASE, and Cochrane database. Eligibility criteria were (1) explicit procedural complications rates; (2) at least 10 patients; (3) saccular, nondissecting UAs; (4) original study published in English or French between January 2003 and July 2011; and (5) a methodological quality score > 6, according to modified STROBE criteria. Endpoints included procedural mortality and unfavorable outcomes, defined as any death or modified Rankin Scale of 3-6 at one month.

#### RESULTS

Ninety-seven studies, including 26 new studies, were included in the updated analysis. Unfavorable outcomes occurred in 4.7% of patients [99% confidence interval (CI), 3.8-5.7, 242/6941]. Patients treated after 2004 had better outcomes than patients treated during the 2001-2003 period ( $p = 0.01$ ) or in 2000 and before ( $p < 0.0001$ ). A significantly higher risk was associated with the use of a liquid embolic agent ( $p = 0.002$ ). Unfavorable outcomes occurred in 11.5% (99% CI: 4.9-24.6%) of patients treated with flow diversion.

#### CONCLUSION

Procedure-related poor outcomes occurred in 4.7% of patients, but risks seem to decrease in recent years. Liquid embolic agents and flow diversion were associated with higher risks.

**KEY WORDS:** Unruptured intracranial aneurysm, endovascular treatment, meta analysis

#### eP-211

### Discriminant Model of the Rupture Status of Aneurysm: Analysis by the Data Mining Method

Ryu, C.•Koh, J.•Kim, E.•Choi, W.

Kyung Hee University Hospital  
Seoul, KOREA, REPUBLIC OF

#### PURPOSE

Many clinical and geometric variables of cerebral aneurysms have been studied widely to determine rupture risk. However, there have been only a few studies about the comprehensive analysis of the variables related to the rupture status of intracranial aneurysms. The aim of this study is to choose the valuable variables within numerous clinical and geometric variables to discriminate between ruptured and unruptured aneurysms. To process the large volume of data, we used the data-mining method.

#### MATERIALS & METHODS

Five hundred fifty-three aneurysms in consecutive 448 patients (mean age,  $57.44 \pm 11.21$  years; males, 157; females, 291) who performed 3D rotational angiography were included in this study. There were 327 unruptured and 226 ruptured aneurysms. Eight clinical variables (age, sex, hypertension, DM, smoking, drinking, body mass index, multiplicity of the aneurysm) and 17 geometric variables [location 1, 2, 3, shape, number of the daughter sac, the axis, maximum diameter, parent artery diameter, volume, CI, Cp, Cs, volume neck ratio, the aspect ratio (AR); bottleneck ratio (BR); height to width ratio (HWR); and the size ratio] were evaluated from chart review and analysis of 3D angiography. The logistic regression and the decision tree model consisting of data mining algorithms were used as decision method to obtain an effective discriminant model of the rupture risk of aneurysm. Eighty percent of data were used to train the decision tree model and 20% of data were used as the subset for a valid model. Three different algorithms (entropy, chi-square, and Gini) were used for decision tree models.

#### RESULTS

As the result of the stepwise logistic regression, independent variables were correlated to aneurysm rupture were location 2, 3, shape, number of daughter sac, diameter, bottleneck factor, size ratio, BMI, HTN, DM, and age. In the entropy, chi-square, and Gini algorithms of decision tree models, the numbers of leaves that misclassification rate of the test model was matched with valid model were 5, 36, and 35, respectively. In chi-square decision tree, independent variables correlated to aneurysm rupture were HWR, BNF, Cp1 and number of aneurysms. The analysis by decision tree suggests an accuracy of 68% for the ruptured aneurysms.

#### CONCLUSION

This study showed multiple independent variables were correlated with aneurysm rupture status. The comparison between classic analysis and data mining

analysis showed us that data mining analysis was easier to understand. Data mining methods could help clinicians to predict the aneurysm rupture and then adapt their practices accordingly.

**KEY WORDS:** Data mining, aneurysms, intracranial, statistical model

## eP-212

### Embolization of Ruptured Intracranial Aneurysms in Elderly Patients

Iosif, C.·Clarençon, F.·Sourour, N.·Colonne, C.·DiMaria, F.·Szatmary, Z.·Le Jean, L.·Chiras, J.

Pitie-Salpetriere  
Paris, FRANCE

#### PURPOSE

We report our experience in endovascular coiling of ruptured cerebral aneurysms in patients aged 70 years and over, with emphasis on feasibility, technical challenge and clinical outcome.

#### MATERIALS & METHODS

We retrospectively analyzed our database of 991 consecutive patients who were admitted at our institution for aneurysmal subarachnoid hemorrhage during an 8-year period (from 2002 to 2010). Fifty of 991 patients aged 70 and over (mean age = 76, range 71-84), with 55 aneurysms, were treated by endovascular means [regular coiling: n = 49 (89%), balloon-assisted technique: n = 4 (7%) and stent-and-coils technique: n = 2 (3.5%)]. Mean World Federation of Neurosurgery Score (WFNS) at admission was 2.36 (+/- 1.30, median: 2) and mean Fisher Grade on initial CT was 3.62 (+/- 0.69, median: 4). We statistically analyzed our data with emphasis on technical difficulties, complications and clinical outcome (death and GOS at 6-month follow up), by univariate and multivariate statistical analyzes (Medcalc electronic statistical software).

#### RESULTS

Favorable outcome (GOS: 4-5) at 6 months was ascertained for 62% of patients. Mortality at 6 months was 20% (GOS: 1). No rebleeding occurred during postembolization follow up. Failure of catheterization was observed in 1.8% of aneurysms. Dissection of parent vessel occurred in 1.8% of aneurysms embolized and rupture of the aneurysm during embolization occurred in 3.6% of aneurysms. Clinical situation postembolization was unchanged in 82% of patients and deteriorated in 8%, while delay in awakening and absence of awakening was present in 4% and 6%, respectively. Thromboembolic complication during the embolization was observed in 12% (of which 6% were symptomatic) of patients and postembolization ischemic stroke was present in 16% of the patients. Multivariate analysis showed that advancing age was not correlated with higher probability of poor clinical outcome. On the contrary, higher initial WFN Score was positively correlated with poor clinical outcome.

#### CONCLUSION

Endovascular treatment of ruptured intracranial aneurysms in patients aged 70 years and over appears to be feasible. Nevertheless, poor WFNS at admission is associated with poor clinical outcome.

**KEY WORDS:** Aneurysm, embolization, elderly

## eP-213

### Antiaggregation with Clopidogrel: Correlation between the Level of Platelet Inhibition and the Incidence of Adverse Events in Interventional Neuroradiology

Maldonado, I. L.·Seris, C.·Costalat, V.·Machi, P.·Bonafé, A.

Montpellier University Hospital  
Montpellier, FRANCE

#### PURPOSE

In patients undergoing procedures intended for the implantation of intracranial stents or coils, platelet antiaggregation is a necessity. Insufficient antiaggregation may be associated to a higher risk of thromboembolic complications. Since recently, it is possible to quantify the individual response to clopidogrel thanks to point of care assays that may be used in the operating room. In the present study, we assess the incidence of perioperative thromboembolic and hemorrhagic complications in function of the level of platelet inhibition using the VerifyNow assay in a single center series of neuroendovascular procedures.

#### MATERIALS & METHODS

The medical files of all patients between February 2008 and June 2010 undergoing nonurgent endovascular treatments intended for intracranial or supra-aortic stenting were retrieved for an institutional database. Perioperative thromboembolic and hemorrhagic adverse events were recorded from the time of the anesthetic induction to postoperative day 2.

#### RESULTS

A total of 286 patients underwent endovascular procedures that were performed for treating cerebral aneurysms, intracranial stenosis or arteriovenous fistulas in the period of study. Fifteen were excluded because of incomplete data. Two analysis of incidence of adverse events were performed, by grouping the procedures in two categories according to the level of platelet inhibition:  $\leq 40\%$  versus  $> 40\%$  and  $\leq 20$  versus  $> 20\%$ . In both situations, a higher incidence of thromboembolic complications was observed in patients presenting with levels of platelet inhibition above the selected cut-off (9.5% versus 1.9% for the 40% cutoff and 10.8% versus 3.3% for the 20% cutoff,  $p = 0.01$ ). We did not observed any correlation between the level of antiaggregation and the incidence of hemorrhagic complications. However, the two cases of severe intracranial hemorrhage were observed in the  $PI > 20\%$  group.

## CONCLUSION

The present study confirms the importance of obtaining a minimal level of platelet inhibition in the prevention of thromboembolic complication in therapeutic neuroendovascular procedures, which confirms the utility of point of care assays. A minimal level of 20% may be suggested.

**KEY WORDS:** Platelets, stents, thromboembolism

## eP-214

### How Might CFD Predictions Help? A Case Study of Pipeline Embolization Device in a Large Intracranial Aneurysm?

Jiang, J.<sup>1</sup>•Strother, C.<sup>1</sup>•Neimann, D.<sup>1</sup>•Royalty, K.<sup>2</sup>•Aagaard-Kienitz, B.<sup>1</sup>

<sup>1</sup>University of Wisconsin, Madison, WI, <sup>2</sup>Siemens Medical Solutions (USA) Inc., Mountain View, CA

## PURPOSE

Treating cerebral aneurysms with endovascular flow-diverting stents is becoming a popular option, particularly, for wide-neck or segmental cerebral aneurysms. To demonstrate potential clinical utility of image-based CFD simulations, we performed a comprehensive data analysis for a clinical case where a patient was treated successfully using a Pipeline Embolization Device (PED) but unfortunately suffered a nonaneurysmal parenchymal hemorrhage originating from lenticulostriate arteries (LSA; autopsy confirmed) on postoperative day three. Assuming a variety of possible physiologic conditions, as guided by imaging and autopsy findings, our main goals of this case study are 1) to predict flow reduction entering the aneurysm posttreatment and 2) to investigate potential acute pressure changes in and around the treated aneurysm.

## MATERIALS & METHODS

3D pretreatment angiographic data were first obtained with a bi-plane C-arm system (Axiom Artis, Siemens, Germany). However, the segmented vasculature was modified using in-house software as follows. First, since LSAs were too small in size (typically 0.4-0.8 mm) to be clearly depicted by the 3D angiographic data, a computational geometry method was used to stitch two small (0.6 mm diameter) LSAs onto the vasculature. Second, under the guidance of posttreatment CTA findings, we also modified the vessel geometry to incorporate a partial opening of a preexisting severe (approximately 80%) stenosis proximal to the ICA aneurysm after stenting. We then utilized in-house software based on Tetgen, an open source package, to perform CFD mesh generation. To simulate the flow-diverting stent, a virtual PED was first embedded as a thin porous (65% porosity) membrane. Mathematical treatments then were applied onto the membrane interface to mimic the flow alternation effect. All models are solved by a commercial CFD solver (Ansys FLUENT, USA) by using a physiologic flow waveform (280 mL/min under 80 beat per minute) derived from MR measurements in normal ICAs. Flow diversion rates among vessel outlets (MCA, ACA and PCA) distal to the

ICA aneurysm were varied by assuming both intact and compromised auto-regulations.

## RESULTS

CFD simulation predicted that the PED can dramatically divert the flow away from the ICA aneurysm, thereby significantly reducing hemodynamic stresses (approximately 80% and 60% reduction of flow and kinetic energy, respectively), consistent with angiographic imaging findings. Our simulation results also indicated that there is little change in the intraaneurysmal pressure after the partial opening of the proximal stenosis. However, the peak systolic pressure could increase as high as 8 mm Hg at the LSAs if the flow auto-regulation mechanism was intact, largely due to the drastically altered hemodynamic environment.

## CONCLUSION

We recognize that CFD-calculated flow is not fully validated and thus not ready for comprehensive posttreatment evaluations of flow-diverting stent treatments in vivo. However, it does, in our opinion, provide insight to altered hemodynamics (due to the PED) that is not readily available in the neurointerventional suite. In this case study, by mathematically modeling physiologic possibilities, we found that the altered hemodynamic environment could have led to an acute pressure increase in small vessels distal to the treated large ICA aneurysm that resulted in a fatal hemorrhage.

**KEY WORDS:** Flow diverting stent, computational fluid dynamics

## eP-215

### Time-Resolved MR Angiography for Monitoring of Coiled Intracranial Aneurysms

Saindane, A. M. • Dehkharghani, S. • Tong, F. • Dion, J.

Emory University School of Medicine  
Atlanta, GA

## PURPOSE

Cerebral aneurysm evolution following coil-embolization is unpredictable, and extended imaging surveillance has been advocated. Noninvasive monitoring with 3D time-of-flight (3D TOF MRA) and contrast-enhanced MRA (CE MRA) techniques has been proposed. We hypothesize that multiphasic time-resolved MRA (TR CE MRA) may prove superior to alternative techniques, given its immunity to suboptimal timing inherent to bolus-chase methods, and exquisite temporal profile of residual aneurysmal flow.

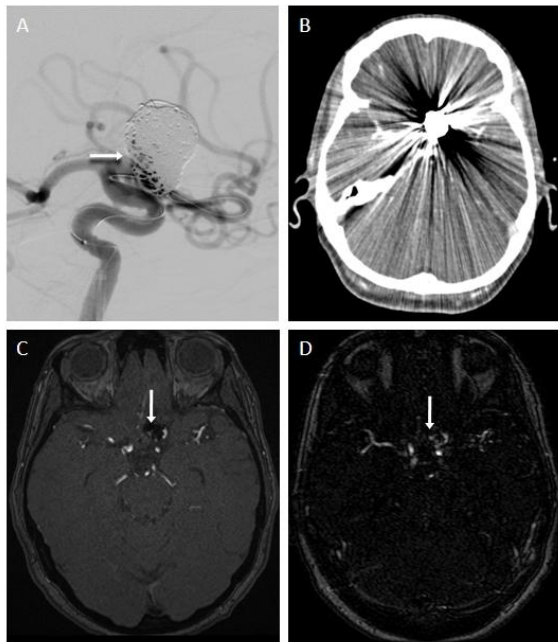
## MATERIALS & METHODS

Over a 1-year period, 28 coil-embolized intracranial aneurysms in 25 consecutive patients (3 subjects with paired aneurysms) were evaluated. Subjects underwent MRA on a 1.5 T GE unit using 1) 3D TOF MRA (TR=26, TE=3.1, flip angle=20, 1.4-mm slice thickness) and 2) TR CE MRA using TRICKS (TR=2.54, TE=1.97, flip angle=35,

2.0-mm slice thickness) prior to and during administration of a standard weight-based dose (0.1 mmol/kg) of intravenous gadobenatimeglumine. Ten total acquisitions with submillimeter in-plane resolution and 4-second temporal resolution were obtained. Eleven patients underwent catheter angiography within 60 days of the MRA examination for evaluation of coiled aneurysms. 3D TOF MRA, TR CE MRA, and catheter angiograms were evaluated for presence and size of residual aneurysm neck and interstitial filling.

## RESULTS

All MRAs were diagnostic for evaluation of the coiled aneurysms. The distribution of coiled aneurysms were: 8 ophthalmic, 6 posterior communicating, 5 anterior communicating, 5 superior hypophyseal, 2 middle cerebral, 1 internal carotid terminus, and 1 basilar tip. 3D TOF MRA demonstrated a residual neck or interstitial filling in 11/28 aneurysms. Time-resolved CE MRA demonstrated a residual neck or interstitial filling in 14/28 aneurysms. Of note, TR CE MRA demonstrated the residual neck to be larger in 4/11 coiled aneurysms than did 3D TOF MRA. Concordance of TR CE MRA with catheter angiographic findings was confirmed in all 11 patients undergoing conventional angiography within 1 month of the MRA examination. In one case where the TR CE MRA demonstrated a small residual neck and the 3D TOF MRA did not, the catheter angiogram showed a residual neck. The figure below shows: A) coiled giant left ophthalmic segment aneurysm with a small area of residual filling. B) CTA examination was nondiagnostic due to extensive streak artifact. C) 3D TOF MRA shows a small area of flow-related enhancement within the aneurysm sac. D) TR CE MRA shows a larger area of contrast-filling of the aneurysm sac.



## CONCLUSION

Time-resolved CE MRA is a reliable, noninvasive method for monitoring coil embolized intracranial

aneurysms. Multiphasic imaging in a clinically relevant timeframe provides superior detection of the presence and temporal nature of residual aneurysmal filling, and immunity to limitations inherent to conventional MRA techniques.

**KEY WORDS:** Aneurysm, coil embolization, time resolved MRA

## eP-216

### Diagnostic Yield of Repeat CT Angiography in Patients with Subarachnoid Hemorrhage and Negative Initial CT and Catheter Angiograms

Delgado Almandoz, J. E.·Crandall, B. M.·Fease, J. L.·Scholz, J. M.·Anderson, R. E.·Kadkhodayan, Y.·Tubman, D. E.

Abbott Northwestern Hospital  
Minneapolis, MN

## PURPOSE

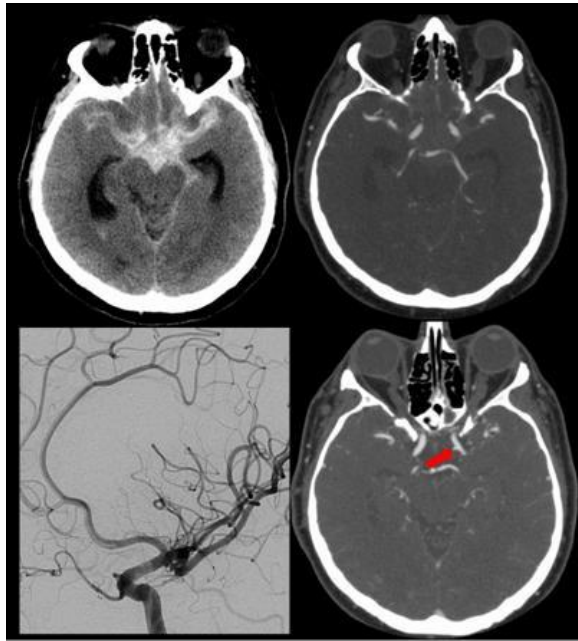
To determine the yield of repeat CT angiography for the detection of causative vascular lesions in patients with subarachnoid hemorrhage (SAH) who have negative initial CT and catheter angiograms.

## MATERIALS & METHODS

We conducted a retrospective review of patients who presented to our institution between January 1st, 2008 and October 21, 2011 with SAH and negative initial CT and catheter angiograms who were examined with repeat CT angiography in order to determine the yield of this imaging modality for the detection of causative vascular lesions. Two experienced neuroradiologists evaluated the NCCTs to determine the pattern of SAH (diffuse, perimesencephalic or peripheral) and the CT angiograms (CTA) to assess for the presence of a causative vascular lesion. All differences in reader interpretation were resolved by consensus.

## RESULTS

Twenty-three patients were included in our study, with a mean age of 55 years (median 56 years, range 28-78 years). Sixteen patients were male (67.6%) and seven female (30.4%). Eighteen patients had diffuse SAH (78.3%), four perimesencephalic SAH (17.4%) and one peripheral SAH (4.3%). Mean time interval between the initial neurovascular examination and the repeat CTA was 25.7 days (median 20 days, range 2-150 days). The repeat CTA demonstrated a causative vascular lesion in two patients (8.7%), all of which had diffuse SAH (yield of 11.1%). The vascular lesions identified were one small pontine arteriovenous malformation and a 2 mm supraclinoid internal carotid artery aneurysm (Figure). The pontine arteriovenous malformation underwent radiosurgery and the internal carotid artery aneurysm underwent surgical clipping. In retrospect, none of these vascular lesions were evident in the initial CT or catheter angiograms.



### CONCLUSION

Repeat CT angiography is a valuable tool in the evaluation of patients with diffuse SAH who have negative initial CT and catheter angiograms, demonstrating a causative vascular lesion in 11.1% of patients.

**KEY WORDS:** Subarachnoid hemorrhage, CT angiography, aneurysm

### eP-217

#### Effect of Intracranial Stent Implantation on the Geometry of the Cerebrovasculature

Gounis, M. J.<sup>1</sup>King, R. M.<sup>1</sup>Chueh, J.<sup>1</sup>Carniato, S. L.<sup>2</sup>Silva, C. F.<sup>1</sup>Spilberg, G.<sup>1</sup>Wakhloo, A. K.<sup>1</sup>

<sup>1</sup>University of Massachusetts, Worcester, MA, <sup>2</sup>Stryker Neurovascular, Fremont, CA

### PURPOSE

Simulations that investigate the impact of stents or flow diverters on patient-specific brain aneurysms often assume rigid walls with anatomy ascertained prior to implantation of the device. Prior research performed on 2D angiograms demonstrated an increase of the angle between the A1 and A2 segment after stent-assisted coil embolization of anterior communicating artery (Acom) aneurysms. However, due to the tortuosity of the cerebrovasculature, 3D assessment of the radius of curvature (RC) can more accurately characterize the impact of stenting on the host vessel. We hypothesize that stent implantation into the cerebrovasculature, which lacks perivascular support as compared to systemic arteries, imposes changes to the RC of the native parent vessel.

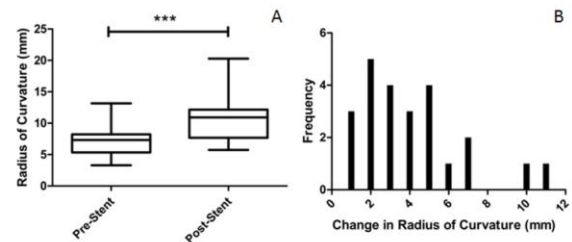
### MATERIALS & METHODS

We reviewed our database of 238 aneurysms that were embolized by stent-assisted coiling. Aneurysms were selected based on the following criteria: 1. Availability

of pretreatment and immediate posttreatment contrast-enhanced cone-beam CT (CB CT), 2. Use of a FDA-cleared self-expanding stent to support coil embolization, 3. Location of the stent within the anterior, intracranial circulation, and 4. Streak artifacts caused by the platinum coils within the aneurysm did not interfere with postimaging processing to segment the stented vessel. The images were reconstructed and vessel centerline in the segment of the implanted stent was extracted. From the centerline, the RC was calculated. Importantly, all calculations were performed on 3D datasets.

### RESULTS

Twenty-four patients were included in this study based on the aforesaid criteria. Locations of the aneurysms were: five Acom, 16 intracranial internal carotid artery, and three internal carotid artery terminus. The average pre and postimplant centerline lengths were  $28.5 \pm 6.0$  mm and  $28.4 \pm 5.6$  mm, respectively. The mean difference in lengths of  $0.02 \pm 2.3$  mm ( $p > 0.05$ , paired t-test) suggested reliable selection of the vascular segment. Mean RC was  $7.1 \pm 2.1$  mm pre-stent implantation and  $10.7 \pm 3.5$  mm postimplantation. The average RC was increased by more than 50% from the preimplantation values (Figure,  $p < 0.001$ ). There was no difference in the change of the RC as a function of stent location.



### CONCLUSION

The implantation of neurovascular stents has been shown to have a large impact on the RC of the host vessel. Pursuant to these results, models to study the effect of stents or flow diverters on intraaneurysmal hemodynamics should consider changes imposed upon the parent vessel geometry.

**KEY WORDS:** Radius of curvature, stent, cone-beam computed tomography

### eP-218

#### Place of the Adjunctive Techniques (Remodelling and Stenting) in the Management of Intracranial Aneurysms: Evaluation in a Single-Center Series

Pierot, L.·Rajpal, G.·Kadziolka, K.·Barbe, C.

Hopital Maison-Blanche  
Reims, FRANCE

### PURPOSE

Coiling is now the first line treatment of intracranial aneurysms. Techniques using adjunctive devices are used increasingly to enlarge indications of the endovascular treatment, singularly for wide-neck and

large and giant aneurysms. The place of remodelling technique and stenting are analyzed in a single center in a 3-years period (2008-2010).

#### **MATERIALS & METHODS**

During the study period, 253 patients (age: 16-87 years, mean:  $51.0 \pm 13.4$  years) were proposed for the endovascular treatment of 288 aneurysms.

#### **RESULTS**

Treatment failed in 3/288 aneurysms (1.0%). The remodelling technique was used in 23.9% in 2008, in 40.0% in 2009, and in 43.9% in 2010. Stenting was used in 4.6% in 2008, in 14.8% in 2009, and in 20.7% in 2010. The remodelling technique was used in 36.3% of ruptured aneurysms and 36.0% of unruptured aneurysms, in 38.7% of ACA/Acom aneurysms, 28.4% of ICA aneurysms, 39.0% of MCA aneurysms, and 43.8% of VB aneurysms, in 35.3% of aneurysms less or equal to 10 mm and 42.4% of aneurysms greater than 10 mm, in 35.5% of aneurysms with a neck  $\leq 4$  mm and 38.6% of aneurysms  $> 4$  mm. The rate of specific adverse events (thromboembolism and intraoperative rupture) was similar in 2008 (4.6%), 2009 (6.1%), and 2010 (7.3%).

#### **CONCLUSION**

In our series, the remodelling technique as well as the stenting are used increasingly in the endovascular treatment of intracranial aneurysms. The frequency of use of remodelling technique is not modified by aneurysm status (ruptured/unruptured) and aneurysm characteristics (aneurysm location and size, neck size).

**KEY WORDS:** Aneurysm, coiling, adjunctive techniques

#### **eP-219**

#### **Cerebral Microembolism during Endovascular Treatment of Unruptured Aneurysms: Successful Reduction by Modification of Coiling Technique and Maintenance of Intraprocedural Blood Pressure**

Lee, D. Park, E. Kwak, J. Suk, E. Ahn, J. Kwon, D. Kwun, B.

Asan Medical Center  
Seoul, KOREA, REPUBLIC OF

#### **PURPOSE**

Diffusion-weighted MR images (DWI) obtained after endovascular treatment of cerebral aneurysms frequently show multiple high signal intensity (HSI) dots, which are believed to be asymptomatic in most of the cases. However, we cannot conclude the clinical consequences of those lesions in terms of long-term effect. Recently we suffered from unusually prevalent DWI abnormalities, which could be reduced successfully by modification of our coiling technique to minimize air embolism and active maintenance of intraprocedural blood pressure on top of strict antiplatelet function monitoring.

#### **MATERIALS & METHODS**

From December 2010 to March 2011, a total of 79 patients with unruptured cerebral aneurysms were treated with various endovascular methods. In the earlier period, 44 patients were treated with our conventional embolization technique (group A). Following 35 patients were treated with our newly modified coiling technique while intraprocedural mean blood pressure (BP) was maintained over 80 mmHg (group B). Diffusion-weighted imaging was obtained on the following day. We compared occurrence of any DWI HSI lesions, occurrence of HSI lesions more than five, occurrence of HSI lesions in other arterial territories between the two groups (chi-square test).

#### **RESULTS**

Diffusion-weighted imaging HSI lesions, 90.9% were in group A and 34.3% in group B. More than five DWI HSI lesions were noted in 84.1% in group A and 22.9% in group B. Diffusion-weighted imaging HSI lesions were observed in other arterial territories in 40.9% in group A and 14.3% in group B. Those differences were statistically significant ( $p < 0.0001$ ).

#### **CONCLUSION**

We could reduce successfully cerebral microembolism by modification of our embolization technique and active maintenance of blood pressure during endovascular treatment of unruptured cerebral aneurysms.

**KEY WORDS:** Cerebral aneurysm, microembolism, coiling

#### **eP-220**

#### **LUNA™ Aneurysm Embolization System for Treatment of Intracranial Aneurysms**

Piotin, M.<sup>1</sup> Sourour, N.<sup>2</sup> Mounayer, C.<sup>3</sup> Blanc, R.

<sup>1</sup>Fondation Ophthalmologique A. de Rothschild, Paris, FRANCE, <sup>2</sup>Hôpital de la Pitié-Salpêtrière, Paris, FRANCE, <sup>3</sup>CHU Dupuytren Limoges, Paris, FRANCE

#### **PURPOSE**

The LUNA™ aneurysm embolization system (AES) is a self-expanding ovoid device that serves as a scaffold for endothelialization across the aneurysm neck. The objective of this clinical study was to evaluate the ability of the AES to occlude intracranial aneurysms while maintaining patency of the parent artery.

#### **MATERIALS & METHODS**

Six patients with intracranial aneurysms underwent treatment with AES. Immediate postimplantation occlusion grade [complete obliteration of the aneurysm including the neck], near-complete (persistence of any portion of the original defect of the arterial wall), or incomplete (any opacification of the sac) compared to baseline, and parent vessel compromise were evaluated. Patients underwent neurologic and neurocognitive testing with the Modified Rankin Scale and the National Institute of Health Stroke Scale (NIHSS) at baseline and time of discharge. Follow up



included clinical assessment at 1 month and 3 months, clinical and angiographic follow up at 6 and 12 months.

## RESULTS

Six patients (5 women, 1 man) with six unruptured saccular aneurysms (2 MCA, 1 para-ophthalmic, 1 ICA bifurcation, 1 carotido-cave, 1 ICA-Pcom; sizes from 5.0 to 6.4 mm) were enrolled to date in the study. One AES was deployed per aneurysm. In two cases, the AES embolization was carried out with balloon microcatheter assistance. In three cases, the immediate postdeployment angiogram showed a near complete aneurysm occlusion, the three other cases showed persisting sac opacification around the AES. There were no parent vessel compromises of parent vessels. Two adverse events occurred during two procedures (1 distal clot embolization, 1 aneurysm perforation) without any clinical consequence. In the first four treated patients, clinical follow up at 1 and 3 months were uneventful. In the remaining two patients, the 1-month clinical follow up was uneventful. The 6-month clinical angiographic follow up is still pending for the six patients.

## CONCLUSION

Preliminary results demonstrate good safety profile. Angiographic follow up is pending.

**KEY WORDS:** Aneurysms, endovascular treatment, embolic device

## eP-221

### Initial Clinical Experience in Buenos Aires with SURPASS Flow Diverter

Lylyk, P. • Lundquist, J. • Chudyk, J. • Bleise, C. • Scrivano, E. • Ferrario, A. • Ceratto, R. • Nella, R.

ENERI  
Buenos Aires, ARGENTINA

## PURPOSE

To present our initial clinical experience with the Surpass flow diverter, as well as preliminary follow-up results in a series of 44 patients. The Surpass (SP) device is indicated for the treatment of saccular aneurysms, wide-neck or fusiform, originated at a main vessel with a diameter of  $\geq 2$  mm and  $\leq 6$  mm.

## MATERIALS & METHODS

We selected patients with complex aneurysms that were considered to have a high probability of failure or recurrence with conventional endovascular treatment. All patients were treated previously with two antiplatelet agents, at least 72 hours before surgery and for at least 6 months after treatment. Angiographic and clinical follow up were performed at 6 months.

## RESULTS

We enrolled 44 patients with 49 intracranial aneurysms, 34 women, 40 saccular aneurysms, seven fusiform and two blister like. A total of 54 SP were used. In 80% of the cases only one SP was used. Complete occlusion was achieved in 20 of the 25 cases controlled

with angiography at 3-month follow up, and there was no side branch occlusion reported. Two patients had thromboembolic complications, asymptomatic in one and left hemiparesis in the second. This patient died 2 months later. Four device-related complications were observed without clinical consequences.

## CONCLUSION

The SURPASS flow diverter device allows endovascular arterial reconstruction for the treatment of complex aneurysms with a high rate of aneurysm occlusion.

**KEY WORDS:** Aneurysms, flow diverter, Surpass device

## eP-222

### Endovascular Catheter for Magnetic Navigation under MR Imaging Guidance: Evaluation of Heating in vivo at 1.5 T

Hetts, S. W. • Martin, A. J. • Saeed, M. • Evans, L. • Bernhardt, A. • Malba, V. • Settecasse, F. • Do, L. • Wilson, M. W.

University of California San Francisco  
San Francisco, CA

## PURPOSE

Endovascular navigation under MRI guidance can be facilitated by a catheter with electrical current carrying microcoils on the tip. Not only do the microcoils create a visible artifact to allow catheter tracking, but also they create a small magnetic moment that attempts to align with the strong B0 magnetic field of the MR scanner, thus permitting remote controlled catheter tip deflection. We determined the upper boundary of electrical currents safely usable at 1.5 T in a coil-tipped microcatheter in vivo.

## MATERIALS & METHODS

A 2.7F Tracker-18 microcatheter served as the substrate. A solenoid of 75 turns was created from 0.0015 inch copper wire on the outer surface of a 1.3 mm diameter alumina tube, with wire wound into thermal epoxy for adherence. Final layers of epoxy and heat shrink were applied over the solenoid. Two lead wires were attached to microcoil leads proximal to the catheter tip. The leads were pulled through the catheter lumen and a modified Thuoy-Borst Y-adaptor at the microcatheter hub, allowing saline to be infused through the side port. A solenoidal coil-tipped catheter with luminal saline drip was navigated under x-ray guidance to the common carotid artery (CCA) of a pig via transfemoral percutaneous access. The pig was moved to a 1.5 T clinical MR scanner and imaging was performed with a steady state-free precession (SSFP) sequence (TR = 5.5 ms, TE = 1.6 ms, flip angle = 30°, 128 x 128 matrix, 5-6 mm slice thickness, SAR = 3.7 W/kg). Continuous direct current (0 mA to 600 mA) then was applied to the catheter microcoils for zero to 5 minutes at various points in the CCA. The catheter then was navigated to the contralateral CCA, the CCA was ligated or balloon-occluded proximal to the catheter tip (in order to achieve zero flow conditions in the artery) and the experiments were repeated. Postmortem histologic analyzes of the CCAs were performed to assess potential

thermal or mechanical damage. We conducted in vivo experiments on six swine carotid arteries.

## RESULTS

No damage to the catheterized porcine common carotid arteries was detected by gross examination or histologic analysis at 0 to 300 mA of current application for up to 5 minutes. Under conditions of zero arterial flow, platelet and fibrin coagulum was detected adherent to the endothelium of the ligated artery or detached in the arterial lumen in three of six samples. Under conditions of normal arterial flow, however, no histologic damage or coagulum was identified. At 600 mA tip current, carotid wall damage and luminal thrombus was evident, thus establishing that this catheter system can deliver detrimental levels of energy to the arterial wall at levels of current higher than those that are likely necessary for tip navigation.

## CONCLUSION

Preliminary in vivo testing of our magnetic catheter system demonstrated no thermal injury to vessel walls at normal and zero arterial flow at 300 mA, but damage was evident at 600 mA. These experiments will serve as the basis for further testing under different scenarios of catheter navigation.

**KEY WORDS:** Catheter, remote control, ASNR Foundation

## eP-223

### Surpass Flow-Disruption Device for Endovascular Treatment of Aneurysms of the Posterior Circulation: Clinical and Angiographic Results

de Vries, J.<sup>1</sup>•Wakhloo, A.<sup>2</sup>•Lylyk, P.<sup>3</sup>•Boogaarts, J.<sup>1</sup>

<sup>1</sup>Radboud University Medical Center Nijmegen, Nijmegen, NETHERLANDS, <sup>2</sup>University of Massachusetts, Worcester, MA, <sup>3</sup>ENERI, Clínica Médica Belgrano, Buenos Aires, ARGENTINA

## PURPOSE

A new generation of flow disruption (FD) device (Surpass FD, Tel Aviv, Israel) was used for aneurysms at the posterior circulation.

## MATERIALS & METHODS

A total of 10 aneurysms in 10 patients were treated. Three aneurysms originated in the vertebral artery, one in the posterior inferior cerebellar artery, three in the basilar artery, and three in the P2/P3 segment. Nine aneurysms were of fusiform/dissecting type and one was saccular. To achieve the calculated flow disruption between the parent artery and aneurysm and required for an occlusion, single devices, tailored to local boundary conditions, were placed endovascularly in parent arteries and covering the aneurysm. Implanted devices measured 2.9-5.3 mm in diameter with a length of 15-50 mm. Immediate control angiography demonstrated various degree of flow reduction within aneurysm up to a complete flow stagnation.

## RESULTS

One patient with a large fusiform midbasilar artery aneurysm developed a major stroke 2 days after intervention and died due to a pseudomonas pneumonia. One vertebral aneurysm ruptured 2 weeks after procedure without neurologic sequelae. Digital subtraction angiography disclosed complete occlusion of this aneurysm. Five patients had follow-up angiography. In all a complete or near-complete occlusion of the aneurysm could be documented.

## CONCLUSION

Preliminary data demonstrate in treatment of aneurysms of the posterior circulation, the feasibility of a new generation of FD device.

**KEY WORDS:** Flow diverter, aneurysm, intracranial

## eP-224

### Predictors of New Lesions on Diffusion-Weighted Imaging Postcarotid Stenting: A Prospective Study Using Procedural Transcranial Doppler Monitoring

Almekhlafi, M. A. • Bal, S. • Stephenson, C. • Stewart, E. • Menon, B. • Demchuk, A. • Goyal, M.

University of Calgary  
Calgary, AB, CANADA

## PURPOSE

Carotid angioplasty and stenting (CAS) carries a 4.1% risk of periprocedural stroke. 1. Protective devices during CAS are inadequate to mitigate this risk as the International Carotid Stenting Study showed evidence of at least one new diffusion-weighted imaging (DWI) lesion on post-CAS MR in 50% of 124 patients. 2. We aimed to identify the procedure step(s) associated with embolization.

## MATERIALS & METHODS

This is a prospective study correlating the size and number of micro embolic signals (MES) on transcranial Doppler during each step of CAS, with the development of new diffusion lesions on postprocedure MR brain. Carotid angioplasty and stenting was divided into 11 steps: crossing the arch, cannulating the common carotid artery, crossing the lesion with the protection device, deploying the protection device, crossing the lesion with the pre-stenting balloon, inflating/deflating the pre-stenting balloon, crossing lesion with the stent, deploying the stent, crossing the lesion with the post-stenting balloon, inflating/deflating the post-stenting balloon, retrieving the protection device and guide catheter. The number and size of embolic signals were evaluated by an investigator blinded to the patients' clinical information. The size of the embolic signals was estimated based on the relative energy index MES (REIM) as described before. 3. The REIM was divided into micro-emboli (REIM ≤ 1), macro-emboli (1.1-2 REIM) and malignant (REIM > 2).

## RESULTS

Thirteen male patients were recruited with a median age of 67 years (range 53 to 83 years). Four (31%) patients were asymptomatic. The median onset to CAS

in the symptomatic group was 14 days (interquartile range "IQR" 6). Protection devices were used in all patients. The median (IQR) number of embolic signals was highest during stent deployment: 58 (13), protection device deployment: 33 (17), and preexisting balloon inflation and deflation: 20 (18). Crossing the aorta: four (7) and crossing the lesion: nine (17) revealed lower MES counts. A majority of embolic signals were micro-embolic signals; however a significant number of "malignant" embolic signals were seen (REIM>2 ~1 mm diameter). Postprocedure MR was done within 2 days in all patients. Nine patients (69%) had at least one new DWI lesion on the postprocedure MRI. The median number of new DWI lesions was six (range 1 to 37). A new DWI lesion was symptomatic in only one patient (11.1%) causing worsening of baseline weakness. Patients without new DWI lesions were 5 years younger on average (median age of 63 years vs 68 years). Large embolic signals tended to be associated with the development of new DWI lesions post CAS. Poststenting angioplasty was the only step that tended to have higher counts of embolic signals in those with vs without new DWI lesions.

#### CONCLUSION

Device deployment (protection device, balloons, and stent) had the highest number of embolic signals compared to other CAS steps. The majority of patients had new DWI lesions post CAS but these were symptomatic in only one. Studies are needed to investigate the incidence of new DWI lesions with new protection methods and in patients with vs without poststenting angioplasty.

**KEY WORDS:** Carotid stenting, MR imaging, transcranial doppler

#### eP-225

#### 4D Digital Subtraction Angiography: A New Angiographic Tool for Evaluation of Cerebrovascular Abnormalities

Aagaard-Kienitz, B.·Niemann, D.·Kowarschik, M.·Davis, B.·Royalty, K.·Oberstar, E.·Szczykutowicz, T.·Mistretta, C.·Strother, C.

University of Wisconsin Madison  
Madison, WI

#### PURPOSE

To evaluate the potential value of time-resolved 3D DSA (4D DSA) in the diagnostic assessment of complex cerebrovascular abnormalities.

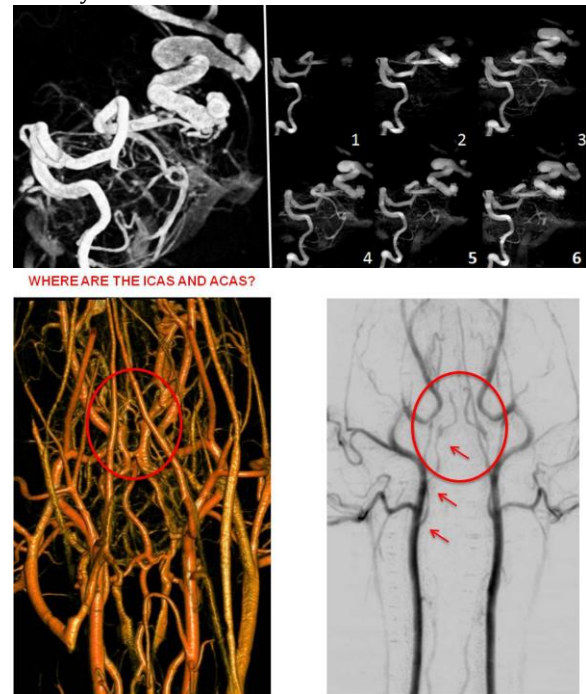
#### MATERIALS & METHODS

4D DSA is a constrained reconstruction in which time-resolved 3D volumes are constructed following an IV or IA injection. Using a previously described algorithm we have reconstructed a series of 3D DSA volumes from normal and abnormal studies to provide 4D DSA time frames. The resulting 4D DSA time frames enjoy the same spatial resolution as does the conventional 3D volume. 4D DSA reconstructions are compared for the ease of displaying and understanding complex vascular

relationships to standard 2D DSA acquisitions and standard 3D DSA reconstructions.

#### RESULTS

By providing the ability to look at a conventional 3D volume as a time-resolved sequence in any desired viewing angle, 4D DSA improves the ability to visualize complex vascular relationships. The time-resolved feature of 4D DSA largely eliminates the problem of arterial and venous overlap in acquisitions done with an intravenous selection of contrast. On the left in Figure 1 below is a standard 3D DSA of an AVM with a venous outflow obstruction. Individual time frames from the 4D DSA reconstruction of this volume are shown on the right. The venous obstruction is seen easily on the 4D time frames; over 10 2D DSA acquisitions were required to demonstrate this. Figure 2 shows an IV 3D DSA acquisition in which the ICAs and ACAs are obscured by veins. A single time frame from the 4D DSA clearly demonstrates these structures. Finally, by decreasing the need for multiple 2D DSA acquisitions, the technique offers the possibility of significant savings in x-ray and contrast dose.



#### CONCLUSION

4D DSA adds value to the ability to visualize complex vascular abnormalities. Because of the ability to view the time-resolved 4D volume from any desired angle, it should allow examinations to be performed with less x-ray and contrast dose.

**KEY WORDS:** Angiography, new technique, DSA

## eP-226

### Preoperative Embolization of Thoracic, Lumbar, and Sacral Spinal Tumors: Technique and Outcomes from a Single Center

Nair, S.<sup>1</sup>Gobin, Y. P.<sup>1</sup>Leng, L. Z.<sup>1</sup>Hartl, R.<sup>1</sup>Bilsky, M. H.<sup>2</sup>Patsalides, A.<sup>1</sup>

<sup>1</sup>New York Presbyterian Hospital/Weill Cornell Medical Center, New York, NY, <sup>2</sup>Memorial Sloan-Kettering Cancer Center, New York, NY

#### PURPOSE

To describe our experience with preoperative angiography and embolization of primary and metastatic thoracic, lumbar, and sacral spinal tumors causing spinal instability and/or high-grade spinal cord compression. The indication for angiography was tumor pathology consistent with a hypervascular tumor. The goal of embolization was to reduce tumor hypervascularity to reduce intraoperative blood loss and surgical morbidity.

#### MATERIALS & METHODS

Retrospective review was conducted for 228 spinal angiograms performed in 198 patients between December 2001 and December 2010. Vascularity was graded as normal (0, similar to the normal vertebral body blush), mild hypervascularity (1, slightly more prominent than normal vertebral body blush), moderate hypervascularity (2, significant tumor blush without arteriovenous shunting), and severe hypervascularity (3, severe tumor blush with arteriovenous shunting). The criteria for embolization included tumor hypervascularity, absence of a radiculomedullary artery arising from the tumor feeder, and ability to achieve stable catheter position thereby avoiding reflux into the aorta and resulting embolic complications. Thoracic procedures typically were performed under general anesthesia to improve image acquisition. Lumbar and sacral procedures typically were performed with sedation alone. Embolization materials included polyvinyl alcohol (PVA) particles, detachable platinum coils, and liquid embolics. The embolization endpoint was absence of residual tumor hypervascularity.

#### RESULTS

Spinal angiography revealed hypervascularity in 201/228 cases in 174/198 patients. The most common pathology was metastatic renal cell carcinoma (44.2%), followed by metastatic thyroid carcinoma (9.2%) and leiomyosarcoma (6.6%) with mean vascularity of 2.0, 2.0, and 1.0 respectively. Embolization of tumor-feeding branches was undertaken in 188/201 hypervascular tumors. Contraindications to embolization of a tumor-feeding branch included the presence of a radiculomedullary artery (48.1%), minimal hypervascularity from the feeder (42.3%), and technical inability (9.6%). Thirteen patients with hypervascular tumors did not undergo embolization of any tumor-feeding branches owing to the presence of a radiculomedullary artery and/or minimal hypervascularity. Fifteen patients underwent repeat

embolization of the same lesion because of tumor recurrence and repeat surgery. Twelve patients underwent embolization of new, different lesions. Mean vascularity of embolized tumors was 2.0 with a mean number of embolized tumor-feeding branches of 2.4 (range 1-8). All embolizations were performed with PVA particles. In 51.6% of embolizations, detachable coils also were utilized, most commonly to occlude the ventral branch of the lumbar or intercostal artery to divert the particles into the tumor. Liquid embolic material was used in 2.7% of embolizations. Eighty-six percent of hypervascular tumors were embolized completely, 12.7% were embolized nearly completely, and 1.3% were embolized only partially. Complete embolization with PVA particles only versus PVA particles and coils was 80% vs 92.0%. One patient suffered a cardiac event secondary to anesthesia and another had a large groin hematoma; neither resulted in long-term morbidity. There were no other complications including new postoperative neurologic deficit following either angiography or embolization.

#### CONCLUSION

This is the largest reported series of preoperative spinal tumor embolizations. We conclude that preoperative angiography of thoracic, lumbar, and sacral spinal tumors and embolization of hypervascular tumors is safe when performed at a high volume center with a rigorous protocol and criteria for embolization.

**KEY WORDS:** Embolization, tumor, spine

## eP-227

### Frameless Multimodal Image-Guidance of Localized Convection-Enhanced Delivery of Therapeutics in the Brain

van der Bom, I. M. J. Moser, R. P. Gao, G. Sena-Esteves, M. Aronin, N. Gounis, M. J.

University of Massachusetts  
Worcester, MA

#### PURPOSE

Convection-enhanced delivery (CED) is an effective method to administer macromolecular compounds that are unable to cross the blood-brain barrier, into the brain. Because the resulting administration is highly localized, accurate cannula placement by minimally invasive surgery is an important requisite. Here, we report on the use of an angiographic C-arm system which enables truly frameless multimodal image guidance during CED surgery.

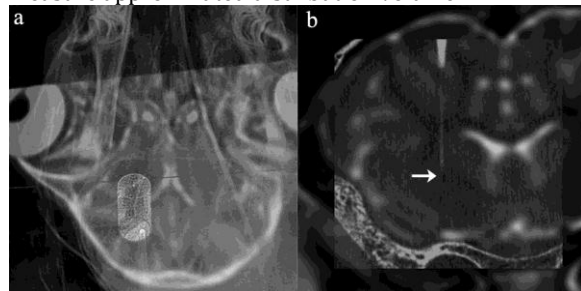
#### MATERIALS & METHODS

Adeno-associated viral vector (AAV)-10 designed to deliver small interfering RNA (siRNA), was administered into the striatum of five purposely bred sheep by CED in order to assess safety and distribution. Prior to surgery, magnetic resonance imaging (MRI) data were acquired for surgery planning. Animals were transferred to the angiography suite and prepared for surgery. In each animal, a single burr hole was created in the skull and a noninvasive frame, designed to hold

and manipulate the microcannula, was attached. In situ cone-beam computed tomography (CB CT) data were obtained using a flat-detector C-arm system and was registered with MRI data. Cannula trajectory was planned on fused CB CT MRI data and progression depth to striatum was measured. Due to calibration of the C-arm system, a patient-image (CB CT and MRI data) relationship was achieved automatically. To align guide sheath with planned trajectory, x-ray images acquired under oblique views were superimposed onto CB CT and MRI data enabling frameless 3D navigation. After alignment of sheath with planned path, cannula was progressed into brain by measured depth, since cannula tip, with an outer diameter of 300  $\mu\text{m}$ , was not visible with x-ray imaging. High-resolution CB CT was acquired and registered with MRI to confirm cannula tip end position. Compound mixed with 2.0 mM gadolinium (Gd) was infused with 3.0  $\mu\text{l}/\text{minute}$  for a total of 100.0  $\mu\text{l}$ . Upon completion, animals were transferred to MR scanner to assess approximated compound distribution by measuring volume of spread of Gd.

### RESULTS

Cannula was introduced successfully under multimodal image guidance (Fig 1a). Cannula tip was visualized using high-resolution CBCT and registration with MRI enabled validation of position relative to striatum (Fig 1b). Gd-enhanced MR imaging post CED confirmed localized administration of compound and was used to measure approximated distribution volume in ml.



### CONCLUSION

We have demonstrated use of a calibrated angiographic C-arm system as a truly frameless multimodal navigation tool during a minimally invasive procedure. The nonalloy, 300  $\mu\text{m}$  diameter canula tip was well visualized using CB CT, enabling confirmation of tip end position relative to anatomy.

**KEY WORDS:** Image-guided procedures, frameless neuronavigation, minimally invasive surgery

eP-228

### Digital Subtraction Angiography Color Maps: Initial Clinical Experience

Spilberg, G.-van der Bom, I. M. J.-Kuhn, A. L.-Gounis, M. J.-Wakhloo, A. K.

University of Massachusetts  
Worcester, MA

### PURPOSE

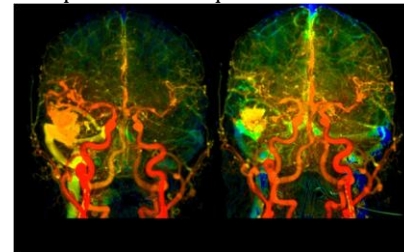
Previously, it was shown that temporally compressed, color-coded maps (CCM) derived from digital subtraction angiography (DSA) improve visualization of findings as compared to standard DSA. The time sequence of images replaced by one single composite image is capable of summarizing dynamic information. Interpretation of DSA requires not only comprehensive knowledge of cerebrovascular anatomy, but also an understanding of hemodynamics and experience. Color-coded maps offers a simplification to translate technical information to broader groups of people.

### MATERIALS & METHODS

Twenty patients with vascular pathologies were studied: fourteen stroke/intracranial atherosclerosis, three vasospasm, one aneurysm, one balloon test occlusion and one AVM. Depending on the vascular pathology and its arterial supply, injection of contrast was performed either through a 6F pigtail catheter positioned in the ascending aorta or selectively in the internal carotid or vertebral artery. Digital subtraction angiography acquisitions were obtained using a flat panel angiographic system (FD20/20, Philips Healthcare, Netherlands). The same coupled, automatic injection was repeated before and at the end of the procedure, when treatment was performed. The DSA acquisitions were postprocessed to generate the parametric maps that translate the kinetics of contrast transport at the pixel-level into colors representing temporal parameters such as time to peak or arrival time. Additionally, difference maps were constructed following treatments to evaluate subtle changes.

### RESULTS

Color-coded maps were generated using the same parameters as a regular acquisition, so there is no increase in radiation to the patient. The postprocessing is quick, immediately available, and is easy to understand. The use of CCM enhanced the analysis of different components of the vasculature in one single image. In patients with intracranial stenosis, it was possible to understand temporal asymmetry in perfusion easily. In patients with AVMs, CCM depicted the magnitude of steal. In patients with vasospasm, it was possible to compare pre and posttreatment CCM to evaluate improvement. Although the images simplify the dynamic information, no new data are generated. Color-coded maps is an enhanced feature of the information available in the conventional DSA. Because it is not a quantitative perfusion map, subjective interpretation is required.



Arrival time color maps before and after 1 session of AVM Onyx embolization. Note decrease of steal in contralateral hemisphere following partial embolization

**CONCLUSION**

The necessity of physiologic information in the angiography suite is the ultimate goal. Color-coded maps is an initial step in this direction; and also an attempt at simplifying complex hemodynamic data.

**KEY WORDS:** Interventional neuroradiology, digital subtraction angiography, image processing

**eP-229**

### **Multimodality Image Fusion: A Novel Technique for Management of the Endovascular and Surgical Management of Brain Arteriovenous Malformations**

Kocak, B.·Kizilkilic, O.·Korkmazer, B.·Tureci, E.·Islak, C.·Kocer, N.

Cerrahpasa Medical School  
Istanbul, TURKEY

**PURPOSE**

We describe a three-dimensional digital subtraction angiography (3D DSA) and multiplanar reconstructed magnetic resonance imaging (MPR MRI) fusion technique to facilitate the endovascular and surgical management of the brain arteriovenous malformations especially in challenging cases.

**MATERIALS & METHODS**

The DSA MRI fusion technique was performed in eight patients with brain AVMs. A biplane neuroangiography suit (Allura Xper FD20; Philips Healthcare) was used to perform endovascular procedures including acquisition of the 3D DSA images and endovascular embolization. 3D DSA and MPR MRI images were fused on a 3D workstation (Xtra Vision, Philips Healthcare) used for 3D DSA reconstruction by using of a prototype DSA MRI fusion software (Philips Healthcare, Best, the Netherlands) based on an algorithm for semiautomated registration. The technique was used for two main purposes: to provide neuronavigation before the endovascular or surgical treatments, real-time neuronavigation during the endovascular procedure.

**RESULTS**

The image fusion was performed approximately within 3 minutes per patient in all of the patients. The image fusion provided determination of the exact location of malformation before the embolization in four patients; endovascular navigation, surgical navigation and combined navigation, respectively in five, one and one patients. The fused images were used for neuronavigation in real-time for six patients during endovascular treatment. The technical success was achieved in all patients. There was no mortality and morbidity in all of treatment procedures which were navigated by the image fusion.

**CONCLUSION**

Using the image fusion of 3D DSA and multiplanar reconstructed MRI in brain AVMs integrates the advanced visualization of the complex vasculature and the detailed visualization of the adjacent brain parenchyma; and provides considerable data and

neuronavigation for the neurointerventionalists and neurosurgeons for the management of the brain arteriovenous malformations in real-time or before the treatment.

**KEY WORDS:** Image fusion, brain arteriovenous malformations

**eP-230**

### **Monitoring of Balloon Test Occlusion of the Internal Carotid Artery by Parametric Color Coding of Digital Subtraction Angiography and Perfusion Imaging within the Angio Suite: A Feasibility Study**

Struffert, T.·Deuerling-Zheng, Y.·Engelhorn, T.·Kloska, S.·Gölit, P.·Bozzato, A.·Doerfler, A

University Erlangen-Nuremberg  
Erlangen, GERMANY

**PURPOSE**

Temporary balloon test occlusion (BTO) of the internal carotid artery (ICA) is performed to evaluate patients who are scheduled to undergo endovascular or surgical procedures in which permanent occlusion of the ICA might be necessary. We tested the hypothesis that parametric color coding (PCC) with the possibility to measure time to peak (TTP) (iFlow, Siemens AG Healthcare Sector, Forchheim, Germany) and perfusion imaging (CBV mapping) within the angio suite (Neuro PBV IR, Siemens AG Healthcare Sector, Forchheim, Germany) would simplify the identification of good candidates.

**MATERIALS & METHODS**

Ten patients were scheduled for BTO PCC series and perfusion imaging before and after temporary ICA occlusion was performed. Angiographic series were evaluated for venous delay (comparison of contralateral cortical veins) by "eyeballing" and by measurement of TTP by PCC. Comparison of CBV values in six defined regions on both hemispheres was performed.

**RESULTS**

Values of venous delay by eyeballing and PCC showed a high correlation ( $r = 0.9$ ,  $p = 0.01$ ). Analysis of CBV mapping showed that before occlusion the difference between absolute CBV values of the six defined regions was  $\pm 10\%$ . In nine patients the CBV maps were symmetrical during BTO. We recognized one patient with an asymmetrical CBV map during BTO with an increase of CBV of  $+15\%$  on the side of occlusion in two of the six regions. This patient showed the greatest difference in time of 2.5 seconds. Before occlusion the CBV values were slightly less dispersed than after and during BTO. The program used did not prolong the occlusion time of 20 minutes.

**CONCLUSION**

Perfusion imaging within the angio suite and PCC during BTO is feasible. The use of PCC enables a more objective and simple way to measure the venous delay. Perfusion imaging (CBV mapping) may add value though patients with an increased CBV seem to



represent those at the limits of the reserve capacity. These patients then could be unsuitable for permanent ICA occlusion.

**KEY WORDS:** Balloon test occlusion, parametric color coding, perfusion imaging

#### eP-231

### Safety and Efficacy of Titrated High-Dose Intraarterial Nicardipine for the Treatment of Cerebral Vasospasm

Bahl, M.<sup>1</sup>Eskey, C. J.

Dartmouth-Hitchcock Medical Center  
Lebanon, NH

#### PURPOSE

The use of high-dose intraarterial nicardipine, a calcium channel blocker, for cerebral vasospasm has become increasingly popular, but reported data on its safety and efficacy are limited. We report our experience with intraarterial nicardipine for medically refractory subarachnoid hemorrhage-associated vasospasm.

#### MATERIALS & METHODS

A retrospective review of a consecutive series of patients with angiographic vasospasm over a 5-year period was performed. Clinical evaluation, transcranial Doppler (TCD) imaging, and CT angiography were used to determine presence and degree of vasospasm. After angiographic confirmation of vasospasm, nicardipine was infused into the affected arteries at a high dose rate (0.5 mg/min) with angiography performed after each 5 mg aliquot to assess response. Posttreatment clinical evaluation and imaging studies were reviewed.

#### RESULTS

Thirty-three consecutive patients underwent a total of 60 sessions of intraarterial nicardipine treatment. Between 5.5 mg and 40.0 mg of nicardipine with an average of 17.3 mg was used per treatment session. All treated vessels demonstrated angiographic dilatation. Mean velocities with TCD imaging were reduced significantly from pretreatment values immediately after infusion ( $p < 0.001$ ) with sustained effect several days after infusion ( $p < 0.001$ ) (Figure 1). Only one patient was unable to tolerate intraarterial nicardipine due to systemic hypotension. Given lack of sustained responses to intraarterial nicardipine, two patients ultimately underwent transluminal balloon angioplasty. Five patients died from complications of initial hemorrhage. No major neurologic or other major procedure-related complications occurred. Posthospital discharge clinical data and imaging studies were available for 25 patients, all of whom demonstrated neurologic improvement with residual minor or no deficits.

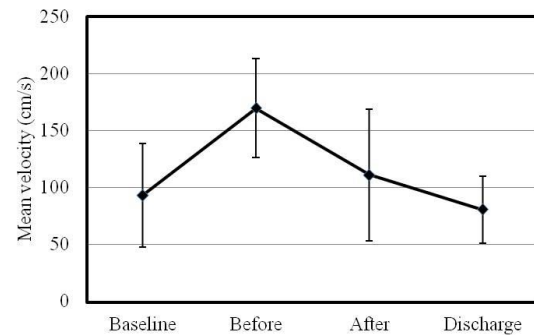


**Figure 1.** Comparison of mean velocities at baseline, on the day of treatment (before), within two days after treatment (after), and by day of hospital discharge.

#### CONCLUSION

High-dose intraarterial nicardipine, titrated to effect, results in rapid and sustained improvement in cerebral vasospasm and is associated with favorable long-term neurologic status.

**KEY WORDS:** Vasospasm, nicardipine

#### eP-232

### Sclerotherapeutic Management of Recurrent and de novo Salivary Gland Cysts with Doxycycline and Bleomycine: An Alternative to Conventional Methods

Berenstein, A.<sup>1</sup>Urkin, M.<sup>2</sup>Niimi, Y.<sup>2</sup>Weiss, I.<sup>2</sup>

<sup>1</sup>St. Luke Roosevelt Hospital, New York, NY, <sup>2</sup>Roosevelt Hospital, New York, NY

#### PURPOSE

Salivary gland cysts (SGC) present as cystic lesions in the submental and neck area and can be categorized as oral or plunging. Successful treatment by marsupialization or surgical resection have been difficult as complete obliteration of the lesion is rarely possible without risking damaging vital structures, and recurrence is frequent. Advances in sclerotherapy have created a viable treatment option which has been safe, may be complete and renders no surgical scar. We here present a series of six patients treated successfully with sclerotherapy using Doxycycline alone or in conjunction with Bleomycine.

#### MATERIALS & METHODS

We conducted a retrospective chart review of patients with complicated plunging SGC who were treated at our institution from 2008-2010. The first five were recurrent lesions from one or more surgeries. We included six patients and relevant parameters.

#### RESULTS

Five out of six patients presented with recurrence of plunging SGC which had been treated previously with surgery up to six times at other institutions. Two were located primarily in the submental space, one of them involving also the deep portion of the parotid space. The rest were located in the neck. Half of the patients were

treated with combination therapy with Doxycycline and Bleomycin. The mean number of treatment was 2.5. In all patients no residual lesion was seen in up to 14 months average f/u, no adverse effects were noted.

#### CONCLUSION

To our knowledge this is the first report of direct puncture image-guided sclerotherapy with Doxycycline alone or coupled with Bleomycine; our results suggest it as a safe and efficient treatment for de novo or recurrent SGC and should be considered before an extensive surgical approach.

**KEY WORDS:** Salivary gland cysts, sclerotherapy, bleomycine

#### eP-233

##### Intraarterial MR Perfusion Imaging of Meningiomas: Comparison to Digital Subtraction Angiography

Hetts, S. W. • Martin, A. J. • English, J. D. • Dowd, C. F. • Halbach, V. V. • Higashida, R. T. • McDermott, M. • Cha, S. • Saloner, D.

University of California San Francisco  
San Francisco, CA

#### PURPOSE

Meningiomas often benefit from preoperative embolization to reduce operative blood loss and associated morbidity. Intraarterial (IA) administration of contrast into the external carotid artery (ECA) and internal carotid artery (ICA) branches supplying the tumor during the embolization procedure maps out the blood vessels supplying the tumor as well as evaluating which portions of the tumor are devascularized successfully. Whereas IA digital subtraction x-ray angiography (DSA) is the gold standard for embolization guidance, IA perfusion MRI may offer increased sensitivity to residual vascularized tumor.

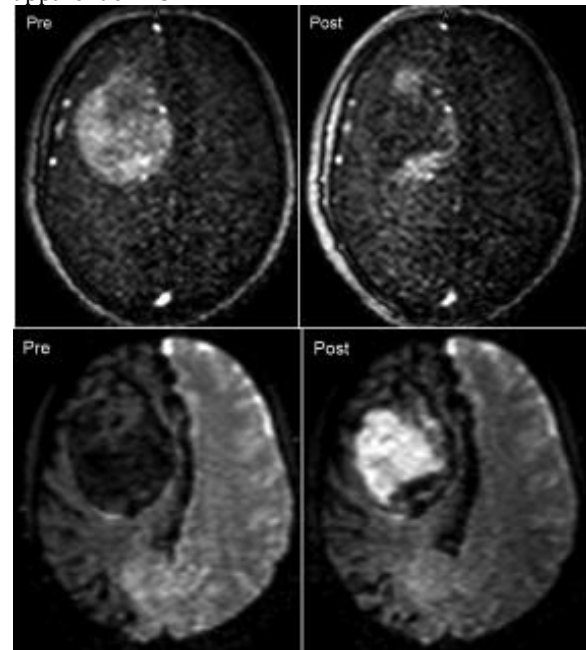
#### MATERIALS & METHODS

Studies were performed in a combined XMR suite wherein an x-ray angiography unit (Integris V5000, Philips) is coupled in-line to a 1.5 T MR scanner (Intera, Philips), allowing easy patient movement between the two imaging modalities during endovascular procedures. We evaluated 14 patients with IA T2\* dynamic susceptibility contrast (DSC) perfusion MR during preoperative embolization. Eight of these patients also were evaluated with intraprocedural IA T1-weighted perfusion MR. Intraarterial perfusion was performed with dilute gadolinium injected initially into the ECA and subsequently into the CCA. The selected carotid artery was confirmed to provide vascular supply to the tumor by prior DSA. The portions of the tumor demonstrated to be associated with ECA or ICA supply, based on IA MR perfusion measures, were compared to DSA.

#### RESULTS

Both T2\* and T1 IA perfusion MR techniques were more sensitive than DSA at detecting vascularized tumor

prior to or following embolization. The T1 technique (Figure, top row, pre and postembolization) was subject to less susceptibility artifact, and thus performed better than the T2\* technique (Figure, bottom row, pre and postembolization) at the skull base. Both IA MR perfusion techniques demonstrated tighter arterial input functions than the IV MRI perfusion technique due to contrast administration directly into cervicocerebral arteries. Similarly, time enhancement curves for the IA MR perfusion methods demonstrated reduced mean transit time (MTT) and lack of a recirculation peak as compared to the IV MR perfusion method. Intraarterial MR perfusion methods were good at differentiating ECA from ICA supply to individual tumors. However, vascular variants such as anterior falx artery or meningohipophyseal artery tumor supply (ICA branches outside the blood-brain barrier) presented interpretive challenges for MRI but were readily apparent on DSA.



#### CONCLUSION

Intraarterial MR perfusion techniques appear to be a useful adjunct to DSA in determining tumor vascularity and the source of that blood supply during preoperative embolization procedures.

**KEY WORDS:** Intraarterial perfusion imaging, meningioma, interventional MR imaging

#### eP-234

##### Percutaneous Biopsy of Cavernous Sinus Tumor through the Foramen Ovale: Technique and Results

Escobar, W.<sup>1</sup> • Gomez, F.<sup>1,2</sup>

<sup>1</sup>Universidad del Valle Centro Medico Imbanaco, Cali, COLOMBIA, <sup>2</sup>DIME, Cali, COLOMBIA

#### PURPOSE

Various tumors can affect the skull base and cavernous sinus. Their histologic diagnosis and treatment is quite

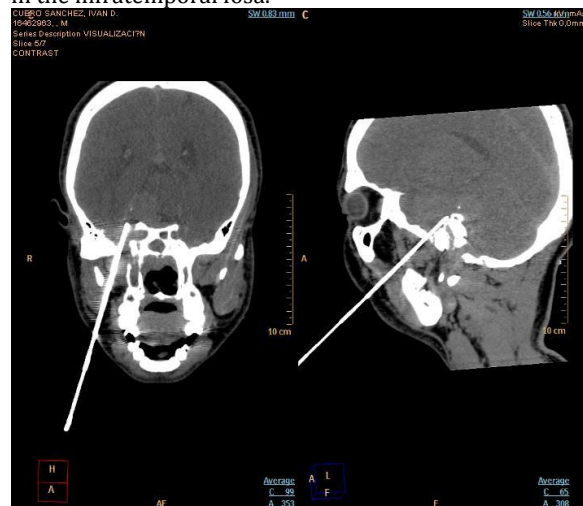
complex, requiring in many opportunities major surgical interventions to expose the tumor to obtain a biopsy and subsequently resect the lesion to attempt its complete eradication. Some cases require additional treatment - or can only be treated - with radiation therapy and/or chemotherapy. Knowing the histologic diagnosis before the therapeutic surgical intervention allows for better therapeutic planning. We present a series of cases demonstrating that with the appropriate technique it is possible to perform percutaneous skull base biopsies to obtain a histologic diagnosis. We are presenting a series of cases, which demonstrate that with the appropriate technique it is possible to perform percutaneous biopsies of cavernous sinus via foramen ovale, in order to obtain a histologic diagnosis.

#### MATERIALS & METHODS

Between the years 1998 and 2011, 57 percutaneous image-guided biopsies were performed at our center in different regions of the skull base, including the anterior cranial fossa, middle fossa, parasellar region, clivus and infratemporal fossa. To reach the lesions we used different approach routes, including: trans-foramen ovale, trans-orbital, trans-nasal, supra and infrazygomatic. Thirteen procedures were performed of cavernous sinus. Ten patients under fluoroscopic guidance alone in the angiography suite using tandem technique. Two biopsies were obtained under CT guidance and one case required both CT and fluoroscopic guidance. A 22G needle was inserted first to identify the safest pathway and choose the biopsy site; subsequently a 14, 16 or 18G biopsy needle with automatic firing was placed to obtain the core biopsy.

#### RESULTS

Tissue samples were obtained in 13 lesions and a diagnosis was possible in 12 cases. Histologic diagnosis included: chordoma, chondrosarcoma, rhabdomyosarcoma, carcinoma, metastasis, pituitary adenoma, lymphoma, meningioma and schwannoma. No mortality and low morbidity, two small hematomas in the infratemporal fossa.



#### CONCLUSION

Percutaneous biopsy of cavernous sinus is possible. It is a safe procedure, and allows histologic diagnosis to plan

for appropriate surgical, radiation or chemotherapy treatment and it is a new development in neuroradiology.

**KEY WORDS:** Percutaneous biopsy, cavernous sinus, tumors

#### eP-235

#### Vascular Complications of Penetrating Head Injuries to the Intracranial Arteries: Diagnostic and Endovascular Treatment

Escobar, W.·Pedroza, A.

Universidad del Valle-Centro Medico Imbanaco  
Cali, COLOMBIA

#### PURPOSE

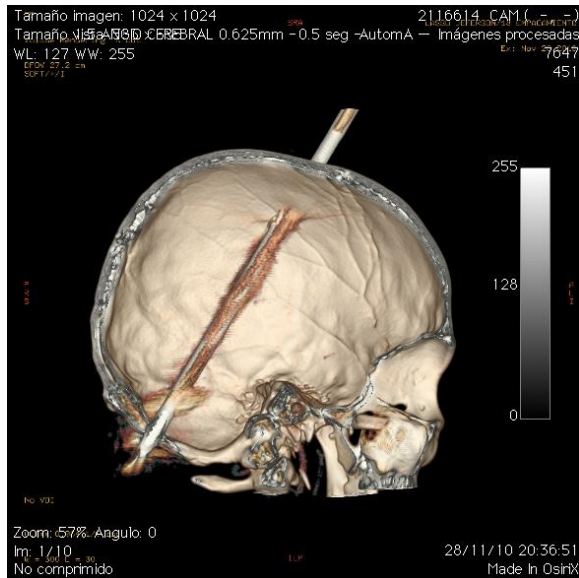
Penetrating head injuries can result from numerous intentional or unintentional events, including missile wounds, stab wounds, motor vehicle or occupational accidents. Traumatic injuries to the intracranial arteries can be divided into three main categories: dissections, aneurysms and fistulas. These may have an individual or a combined presentation. Diagnosis: Angiography is the gold standard. Multidetector tomography can make a diagnosis and localize the exact areas compromised, but in some occasions it is difficult to diagnose because of the artifacts generated by metal objects. Endovascular therapeutic techniques are frequently the treatment of choice for these lesions, since direct surgical treatment can be limited by inaccessibility, urgency, and the presence of co-morbid conditions. Objective: Demonstrate that endovascular treatment for vascular lesions caused by penetrating trauma is feasible, safe, durable and highly effective.

#### MATERIALS & METHODS

Between the years 2005 and 2011 we treated 11 consecutive patients with vascular lesions secondary to penetrating wounds at our Hospital: seven gunshot wounds and four stab wounds, seven pseudoaneurysms and two arteriovenous fistulas. We realized multidetector tomography to six of the patients diagnosing lesions in three of them and on the fourth one the splinters of the bullet blocked visualization of the pseudoaneurysms. Cerebral angiography of the six vessels with digital subtraction and endovascular treatment of the lesions was realized on all patients. Follow-up cerebral angiography could be done on seven of the patients.

#### RESULTS

Two traumatic aneurysms and two arteriovenous fistulas were excluded immediately from circulation after stent graft placement without contrast material filling into the aneurysm cavity. Four were excluded with coils and one with bare stent plus coils. We did not have complications. The mean mid-term follow up was 32 months. All patients showed exclusion of the pseudoaneurysms and of the fistulas from the circulation on the angiographic follow ups.



### CONCLUSION

Our experience demonstrates that endovascular treatment of intracranial traumatic aneurysms is feasible, safe, durable and highly effective. On follow-up angiography there were no reports of pseudoaneurysms or fistulae recurrence.

**KEY WORDS:** Vascular, complications, penetrating injury

### eP-236

#### Improved Device Visualization Using Flat Detector Angiographic Systems

Aagaard-Kienitz, B.<sup>1</sup>Niemann, D.<sup>1</sup>Royalty, K.<sup>2</sup>Consigny, D.<sup>1</sup>Pulfer, K.<sup>1</sup>Strother, C. M.<sup>1</sup>

<sup>1</sup>University of Wisconsin Madison, Madison, WI,

<sup>2</sup>Siemens Medical Solutions, Madison, WI

### PURPOSE

To assess the ability of currently available C-arm CT (ACT) angiographic systems to image implantable devices in vivo and in vitro.

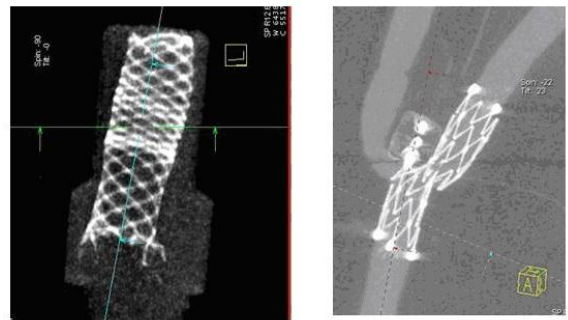
### MATERIALS & METHODS

All imaging was done using an Artis-Zeego angiographic system (Siemens HealthCare, Germany). The flat detector is 40 X 30 cm<sup>2</sup> with 2480 X 1920 pixels with a pixel size of 154 X 154 μm<sup>2</sup>. Standard C-arm CT acquisitions use a 2 x 2 detector pixel binning strategy to reduce noise and improve contrast resolution. For this study, the angiographic system was configured to acquire images at the native detector resolution (unbinned) at a 22 x 22 cm<sup>2</sup> field of view centered on the detector. This resulted in projection images of 1024 x 1024 pixels at the native pixel resolution of 154 x 154 μm<sup>2</sup>. A focal spot size of 0.3 mm was used for all scans. Three-dimensional volumes then were reconstructed at an isotropic voxel size of 0.80 μm<sup>3</sup> using the commercial product reconstruction algorithms (syngo X-Workplace, Siemens Healthcare, Germany). A variety of implantable devices used for endovascular therapy as well as

anatomical structures were imaged both in vitro and in vivo.

### RESULTS

The high spatial resolution ACT reconstructions demonstrated superior image quality for high contrast objects such as stents, implants, contrast enhanced vessels, and bone, compared to conventional ACT acquisitions. The high resolution ACT images demonstrated reduced contrast resolution, as well as increased truncation artifacts for objects that are at the edge of the acquisition field of view. The figure below on the left shows a Pipeline stent deployed in a phantom. Changes in the pore distribution and configuration can be seen clearly. On the right a Wingspan stent and Sequent WEB are seen in a canine bifurcation aneurysm model. Deformity of the Wingspan stent is evident. The horizontal layer of the WEB is visible. Little metal artifact is caused by the high density elements of the devices.



### CONCLUSION

High-resolution ACT can provide isotropic 3D resolution of less than 100 μm, that allows for improved in vivo imaging of devices, contrast-filled vascular structures and bone. This capability should improve the ability to assess the relationship of devices, e.g., stents to vascular structures.

**KEY WORDS:** Device visualization, flat detector, device evaluation

### eP-237

#### Targeting of Fluoroscopically Occult Lesions in the Angiography Suite Using 3D MR Imaging Overlay Guidance

Tao, Y.<sup>1</sup>Ehtiaty, T.<sup>2</sup>Edelstein, W.<sup>1</sup>Klostranec, J.<sup>3</sup>Pearl, M.<sup>1</sup>Wang, G.<sup>1</sup>El-Sharkawy, A.<sup>1</sup>Gailloud, P.<sup>1</sup>Radvan, M. G.<sup>1</sup>

<sup>1</sup>The Johns Hopkins School of Medicine, Baltimore, MD,

<sup>2</sup>Siemens Corporate Research, Princeton, NJ, <sup>3</sup>University of Toronto School of Medicine, Toronto, ON, CANADA

### PURPOSE

Magnetic resonance imaging (MRI) is an excellent modality for identifying pathology, but performing interventional procedures in the MRI environment remains difficult. Many procedures are performed under CT guidance for this reason. Procedures performed under fluoroscopic guidance have the

potential to have an even lower radiation dose than those performed under CT guidance. This study evaluates if fluoroscopically occult lesions identified by MRI can be biopsied using fluoroscopic guidance by coregistering MRI with cone-beam CT (CBCT) data sets obtained in the angiography suite.

#### **MATERIALS & METHODS**

After creation of a multimodality phantom in which fluoroscopically occult lesions measuring 5 mm and 10 mm were created, we performed MRI on the phantom to generate a three dimensional (3D) data set. Using CBCT, a second 3D data set was generated in the angiography suite and coregistered with the MRI data set (MRI overlay). The 3D/3D registration of the MRI to CBCT coupled with the 3D/2D calibration-based registration between the CBCT images and the fluoroscopic projection images allow the lesions segmented on the MRI datasets to be overlaid onto the live fluoroscopy. Using path planning software for needle navigation procedures (iGuide, Siemens Medical) we targeted the lesions segmented on the fused MR images and performed biopsy of the lesions.

#### **RESULTS**

Using the MRI overlay technique, 5 mm and 10 mm fluoroscopically occult lesions were biopsied successfully using real-time fluoroscopy guidance.

#### **CONCLUSION**

Fluoroscopically occult lesions identified with MRI can be biopsied successfully under fluoroscopic guidance using image coregistration techniques.

**KEY WORDS:** Image overlay, biopsy

#### **eP-238**

##### **Flat Panel Detector Computed Tomography of the Spinal Venous System: An Enhanced Venous Phase for Spinal Digital Subtraction Angiography**

Chen, J. X.<sup>1</sup>•Ethiati, T.<sup>2</sup>•Gaillood, P.<sup>3</sup>

<sup>1</sup>Johns Hopkins School of Medicine, Baltimore, MD, <sup>2</sup>Siemens, Baltimore, MD, <sup>3</sup>Johns Hopkins Medical Institutions, Baltimore, MD

#### **PURPOSE**

Digital subtraction angiography (DSA) remains the gold standard modality for spinal vascular imaging, but investigation of the spinal venous system continues to be challenging due to small vessel size and effect of motion artifact. The advent of flat panel detector computed tomography (FPCT) has provided a means to overcome these obstacles. Its superior spatial resolution and multiplanar reconstruction capability allow for delineation of small and complex venous structures, which can be essential for diagnostic and therapeutic decision-making. The purpose of this study was to evaluate the utility and safety of FPCT as an adjunct to spinal DSA for evaluation of spinal vascular disorders.

#### **MATERIALS & METHODS**

In this prospective series, we assessed 63 consecutive spinal FPCTs performed over a 25-month period at our institution. Flat panel detector CT mean entrance skin radiation dose was compared to doses for SpDSA runs aimed at documenting the venous phase (n = 7) and cerebral FPCTs (n = 20). Patient demographics, technical procedural information, incidence of procedural complications, and angiographic diagnoses were recorded in an IRB-approved database. Diagnostic contribution of FPCT to 2D DSA was qualitatively stratified into the following groups: A) no additional information added; B) complemented or enhanced DSA findings; C) essential to therapeutic planning; D) diagnosis principally based on FPCT findings.

#### **RESULTS**

There were no intraprocedural or postprocedural complications in the studied cohort. Flat panel detector CT was technically successful in 61 of 63 cases (96.8%). The mean entrance skin dose for spinal FPCT was 419 mGy (SD: 58.5) as compared to 170.4 mGy (SD: 48.7) for SpDSA venous phase runs and 309 mGy (SD: 53) for cerebral FPCTs. Angiographic diagnoses included vascular malformation (44%), stroke (10%), spinal venous anomalies (10%), other (8%), and unremarkable (27%). Spinal FPCT was the principal contributor to the diagnosis in 16 cases (25%), was valuable for endovascular or surgical planning in 13 cases (21%), complemented SpDSA findings in 12 cases (19%), and did not add additional diagnostic information in 20 cases (31%). Among the 20 cases for which no additional diagnostic contribution was assessed, X cases demonstrated the spinal venous system, which was not or poorly visualized on SpDSA.

#### **CONCLUSION**

Spinal FPCT demonstrated an excellent safety profile and only a moderate increase in radiation dose as compared to SpDSA venous phase runs or cerebral FPCT. The modality enhanced SpDSA findings in a majority of cases, allowing precise visualization of spinal venous anatomy, which was particularly valuable for therapeutic planning and elucidation of diagnostically challenging venous abnormalities. These findings highlight the benefits of FPCT for overcoming traditional challenges to spinal venous imaging and suggest its potential role as an adjunct to SpDSA.

**KEY WORDS:** Flat panel detector CT, digital subtraction angiography, spinal venous anatomy

#### **eP-239**

##### **C-Arm CT Dynamic Cerebral Perfusion Measurement for Ischemic Stroke: An Experimental Study in Canines**

Royalty, K.<sup>1,2</sup>•Strother, C.<sup>2</sup>•Pulfer, K.<sup>2</sup>•Deuerling-Zheng, Y.<sup>3</sup>•Manhart, M.<sup>4,3</sup>•Fieselmann, A.<sup>3</sup>

<sup>1</sup>Siemens Medical Solutions, USA, Hoffman Estates, IL, <sup>2</sup>University of Wisconsin, Madison, WI, <sup>3</sup>Siemens Healthcare, Forchheim, GERMANY, <sup>4</sup>University of Erlangen, Erlangen, GERMANY



## PURPOSE

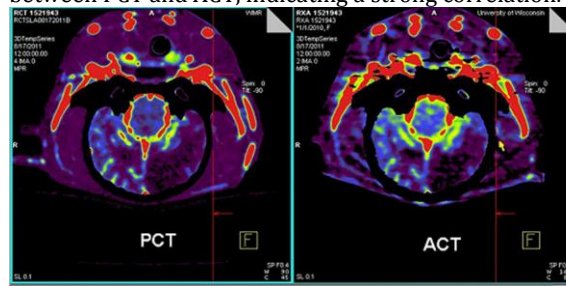
To compare relative cerebral blood flow (rCBF) measurements acquired with standard perfusion CT (PCT) with ones obtained with angiographic C-arm CT (ACT) using a canine ischemic stroke model.

## MATERIALS & METHODS

Under an institutionally approved protocol, ischemic strokes were induced in seven healthy canines. Four hours after stroke creation, PCT was acquired and immediately followed by CBF measurements with ACT (Artis Multi-axis system, Siemens Healthcare) using a novel high-speed acquisition protocol that consisted of seven consecutive bidirectional rotations (total scan time of 30 s). Each sweep acquired 133 projections over a period of 2.8 seconds, which then were reconstructed with prototype processing software that used a 4D interpolation-based analytical image reconstruction algorithm to generate volumes with 1 s temporal resolution. The PCT and ACT data then were processed to provide rCBF maps using a standard deconvolution-based algorithm. The canine's basilar artery was used to define the arterial input function in the coregistered PCT and ACT slices. A region of interest (ROI) was placed manually on co-registered PCT and ACT CBF maps to match as closely as possible the center of any abnormality on the CBF images for a single 5 mm slice. A symmetrical ROI was proscribed in the opposite hemisphere. A ratio of the stroke to normal hemisphere CBF values was calculated for each pair of ROIs.

## RESULTS

A hemispheric stroke was created and confirmed in six of the seven animals. There was good qualitative agreement between the dynamic perfusion maps calculated with PCT and those calculated with ACT. The figure below shows a side-by-side comparison of a coregistered PCT and ACT CBF map. In the six canines with confirmed ischemic lesions, both PCT and ACT relative CBF measurements showed a greater than 50% reduction in rCBF for the ischemic territory relative to the corresponding normal contralateral hemisphere. A linear regression analysis shows an r-squared value of 0.93 when comparing the relative CBF measurements between PCT and ACT, indicating a strong correlation.



## CONCLUSION

Using ACT, measurement of rCBF seems to be feasible in the interventional suite. Further work is required to establish the limits of this technique, validate the absolute measurements for CBF, and calculate the cerebral blood volume (CBV), mean transit time (MTT), and time to peak (TTP) perfusion parameters.

**KEY WORDS:** CBF, C-arm, stroke

## eP-240

### Preoperative Embolization of Cervical and Cervico-Thoracic Spinal Tumors: Technique and Outcomes from a Single Center

Leng, L. Z.<sup>1</sup>•Nair, S.<sup>1</sup>•Patsalides, A.<sup>1</sup>•Laufer, I.<sup>2</sup>•Bilsky, M. H.<sup>2</sup>•Gobin, Y. P.<sup>1</sup>

<sup>1</sup>Weill Cornell Medical College - New York Presbyterian Hospital, New York, NY, <sup>2</sup>Memorial Sloan-Kettering Cancer Center, New York, NY

## PURPOSE

To describe our experience with preoperative angiography and embolization of cervical spinal tumors. Preoperative angiography of 40 cervical and cervico-thoracic primary and metastatic spinal tumors was performed in 36 patients. The indications for surgery were spinal instability and/or high-grade spinal cord compression. The indication for preoperative angiography was tumor pathology consistent with a hypervascular tumor. The goal of embolization was to reduce tumor opacification in an effort to reduce intraoperative blood loss and surgical morbidity.

## MATERIALS & METHODS

Retrospective review of angiograms and peri-procedural charts was conducted for 40 procedures performed between April 2002-December 2010. Embolization was undertaken in 21 cases. No patients underwent multiple embolizations of the same lesion. Vascularity was graded as none (0, same as normal adjacent vertebral body); mild (1, slightly more prominent than normal vertebral body blush); moderate (2, significant tumor blush without arteriovenous shunting); and severe (3, severe tumor blush with arteriovenous shunting). The criteria for embolization included the presence of significant tumor vascularity, ability to achieve stable microcatheter position without reflux into carotid or vertebral arteries and the resulting embolic stroke risk, and absence of a spinal cord artery arising from the tumor feeder. The criteria for vertebral artery occlusion was significant tumor vascularity, risk of reflux into vertebral artery despite selective catheterization of tumor feeder, tumor involvement of the vertebral artery resulting in high likelihood of vessel sacrifice during surgery, and robust collateral flow during balloon test occlusion. Embolization procedures were all performed under general anesthesia. Embolization materials utilized include polyvinyl alcohol (PVA) particles (95.2%), detachable platinum coils (33.3%), detachable balloons (14.3%), and the liquid embolic agent, Onyx (9.5%).

## RESULTS

Hypervascular tumors were identified in 85% of cases. The most common pathology was renal cell carcinoma (35% of all procedures) and the second most common was thyroid carcinoma (15%). Mean vascularity score of renal cell carcinoma and thyroid carcinoma tumors was 2.23 and 1.83, respectively. The most commonly visualized tumor feeders were vertebral artery



branches (67.7%), ascending cervical artery (35.3%), deep cervical artery (35.3%), thyrocervical trunk branches other than ascending cervical (20.6%), and occipital artery (14.7%). Complete or near-complete embolization of targeted tumor feeders was achieved in 85.7% of cases. Vertebral artery occlusion was performed in 23.8% of embolization cases. A spinal cord artery feeder was identified in 32.5% of cases. Embolization of one or more feeders was not undertaken because of minimal tumor opacification (15 cases), inability to achieve stable catheter position without risk of cerebral embolization (10 cases), and presence of spinal cord artery (2 cases). One patient experienced an allergic anaphylactic response during angiography that was managed successfully and did not result in any long-term morbidity. There were no other complications or new postprocedure neurologic deficits.

#### CONCLUSION

Preoperative angiography and embolization cervical and cervico-thoracic spinal tumors is safe when performed at a high-volume center that adheres to a rigorous protocol and criteria for embolization.

**KEY WORDS:** Preoperative embolization, tumor, cervical spine

#### eP-241

##### **Symptomatic Atherosclerotic Middle Cerebral Artery Stenosis Treatment with Self-Expandable Intracranial Stents: Single Center Experience**

Gandini, R.·Pampana, E.·Massari, F.·Reale, C. A.·Del Giudice, C.·Simonetti, G.

University of Rome  
Rome, ITALY

#### PURPOSE

Endovascular treatment of intracranial stenosis with self-expandable stents (SES) is a new challenge for prevention and treatment of acute stroke. We report our single center experience in middle cerebral artery stenosis treatment focusing on the adequate preprocedural and post procedural management.

#### MATERIALS & METHODS

In this prospective, multicenter, single-arm study, medically refractory patients with symptoms evaluated with Rankin score attributable to angiographically demonstrated intracranial stenosis >50% were enrolled. Intracranial lesions were predilated with an undersized balloon catheter to 80% of the native vessel diameter, followed by deployment of the self-expanding Wingspan stent to facilitate further remodeling of the atherosclerotic plaque and to maintain vessel patency. All patients underwent postprocedural neurologic examinations and angio-MR were performed 3 and 6 months after the procedure.

#### RESULTS

Twenty-six patients were enrolled in our study. Seventeen patients had an acute ischemic stroke (AIS),

the remaining had transient ischemic attacks (TIA). There was successful deployment of the Wingspan stents in all patients. The M1 (n = 19) and M2 (n = 7) middle cerebral artery segments were treated. Successful recanalization occurred in 100% of patients with reduction of the stenosis from  $84 \pm 4\%$  down to  $18 \pm 2\%$ . No immediate postprocedural complications occurred. Twenty-four hours postprocedural MR diffusion analysis showed absence of acute ischemic lesions. No restenosis were showed at 6 months angio-MR follow up.

#### CONCLUSION

Our experience with SES in treatment of middle cerebral stenosis demonstrated the technical feasibility and high rate of recanalization with acute stenting. Good planning associated with adequate devices in dedicated centers permitted us to obtain excellent results.

**KEY WORDS:** MCA stenosis, intracranial stenting

#### eP-242

##### **One Hundred Fifty-Two Patient Comparison of Interventional Acute and 90-Day Outcomes in Acute Ischemic Stroke - Stentriever™ Technology, Merci® and Intraarterial rt-PA: A Retrospective Single Center Experience**

Fragata, I. R.·Reis, J. L.·Ribeiro, C.·Baptista, T.

Centro Hospitalar Lisboa Central  
Lisbon, PORTUGAL

#### PURPOSE

Interventional options provide more direct interaction with larger thrombus burden, and may result in recanalization and good clinical outcomes for selected patients with acute ischemic stroke. PROACT II study demonstrated a benefit in recanalization and modified Rankin score in a select group of patients with M1 and M2 occlusions. The MERCI and Multi MERCI Studies demonstrated that revascularization was a predictor for better patient outcomes and studied the first mechanical thrombectomy device in AIS: the Merci retriever. Newer devices such as Trevo® and Solitaire® are stent-like devices utilized for mechanical thrombectomy. Each of these modalities has been studied in trials and registries. This is a "real world" analysis of how these technologies are employed in clinical practice and the benefit of interventional techniques for cerebrovascular occlusions.

#### MATERIALS & METHODS

Retrospective analysis of 152 consecutive interventional cases where IA lytic, Merci retrieval system, Penumbra, Solitaire and the Trevo system were employed, between January 2010 and September 2011. General inclusion criteria were NIHSS >10 or CTA showing large vessel occlusion; age > 18; time from symptoms < 8 hours. Patients with signs of hemorrhage on CT at admission, signs of acute lesion >1/3 of MCA territory; glucose <50 or >400, platelets <100 000, uncontrolled BP (SBP>185 and/or DBP>110) were

excluded. If there was no contraindication, iv tPA 0.6 mg/kg was administered before procedure; if possible, intervention was performed under sedation only.

## RESULTS

Median age was  $63.8 \pm 14.6$ , and median NIHSS was 18 (Q1 - Q3) (15 - 22). Time from symptom onset was  $201 \pm 172$  (mean  $\pm$  SD) minutes. Occlusions locations were: proximal ICA = 19(12%); ICA-T = 39 (26%); MCA = 71 (48%); ACA = 3 (2%); Vertebrobasilar = 18 (12%). High revascularization results were achieved with 45.4% achieving TIC1 2 and 40.1% achieving TIC1 3 for a total of 85.6% of patients with a TIC1 score of  $>2$ . Clinical results were positive showing a shift from the median baseline NIHSS = 18 to median NIHSS at discharge = 10. Analysis is on-going for mRS but 108 patients have been followed to the 90 day endpoint. At discharge mRS 0-2 = 29.9% of patients, and for those currently followed at 90 days, mRS 0-2 = 40.8%. A comparison of mechanical thrombectomy modalities of Merci® and Trevo® also were compared and results are as follows (Table).

	Merci (n = 42)	Trevo (n = 50)
Number of Passes (median)	3	2
Recanalization with 1 pass	14%	28%
TICI $\geq 2$	78.5%	96%
TICI 3	33%	48%
Duration of procedure (minutes)	$102.9 \pm 48.2$	$77.6 \pm 42.4$

## CONCLUSION

High revascularization rates can be achieved with interventional techniques, especially with mechanical thrombectomy. This also translated into good clinical outcomes for many patients. In our experience, the use of the newest stentriever technology has brought a significant improvement in revascularization rates, clinical outcomes and also shorter procedural times.

**KEY WORDS:** Stroke, thrombectomy

## eP-243

### Comparison between Postcontrast Susceptibility-Weighted Imaging and T2\* Gradient-Echo Imaging for Imaging Intracranial Arterial Clot in Patients with Acute Ischemic Stroke

Jagadeesan, B. D.<sup>1</sup>Ford, A. L.<sup>2</sup>An, H.<sup>3</sup>Lin, W.<sup>3</sup>Derdeyn, C. P.<sup>2</sup>Lee, J.<sup>2</sup>

<sup>1</sup>University of Minnesota, Minneapolis, MN,

<sup>2</sup>Washington University in St Louis, St Louis, MO,

<sup>3</sup>University of North Carolina, Chapel Hill, NC

## PURPOSE

Gradient-echo T2\* (GRE T2\*) imaging has been used to visualize intracranial arterial clot (IAC) in patients with acute ischemic stroke (AIS). Postcontrast susceptibility-weighted imaging (PCSWI) is a novel high-resolution MR imaging technique that also can be used to visualize IAC. We compared the two techniques in their ability to

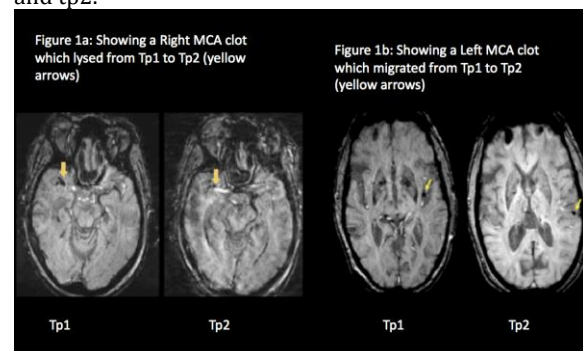
identify IAC in a series of patients with AIS who underwent serial MR imaging at two consecutive time points.

## MATERIALS & METHODS

All AIS patients underwent two MR scans: within 4.5 hours (tp1) and at 6 hours (tp2) after stroke onset. The initial MR protocol included GRE T2\* for detection of hemorrhage. After several months of scanning, the GRE T2\* was replaced by PCSWI. A board-certified neuroradiologist (BDJ) retrospectively reviewed the PCSWI and GRE T2\* scans for presence of hypointense clot in the arteries of the circle of Willis and their branches without knowledge of patient characteristics or imaging results from other sequences. Patients with GRE T2\* were placed in Group 1 and patients with PCSWI were placed in Group 2.

## RESULTS

Thirty-one AIS patients were imaged prospectively at  $2.4 \pm 0.5$  hour (tp1) and  $6.3 \pm 0.4$  hour (tp2) after symptom onset. Group 1 included 15 patients (median age = 62, median NIHSS = 14, 40% female, 87% received iv tPA, 100% MCA stroke location). Group 2 included 16 patients (age = 72, NIHSS = 12, 38% female, 81% received iv tPA, 88% MCA stroke location). There were no significant differences between the baseline characteristics in the two groups. In Group 1 GRE T2\* scans, IAC was identified in three patients (20%) at tp1 and four patients (27%) at tp2. In group 2 PCSWI scans, IAC was identified more frequently: in 13 patients (81%) at tp1 and 10 patients (62%) at tp2 ( $p = 0.001$  for tp1,  $p = 0.073$  for tp2). In Group 1, there was no change in clot appearance or location from tp1 to tp2 in any patient. However, in Group 2, PCSWI scans showed resolution of thrombus in two patients (Figure 1a) and migration of clot in one patient (Figure 1b) between tp1 and tp2.



## CONCLUSION

Likely due to its higher resolution and ability to depict the parent vessel (due to acquisition after contrast administration), PCSWI may be more sensitive than GRE T2\* for initial detection and follow-up imaging of IAC in patients with AIS.

**KEY WORDS:** Acute ischemic stroke, susceptibility-weighted imaging, thrombus imaging

## eP-244

### Utility of Diffusion-Weighted Imaging/Perfusion-Weighted Imaging-Based Combined Factor to Predict Short-Term Clinical Outcome in Stroke Patients within 4.5 Hours of Onset Due to the Carotid Artery Occlusion

Mori, T. Nakazaki, M. Iwata, T. Tajiri, H. Miyazaki, Y.

Shonan Kamakura General Hospital Stroke Center  
Kamakura, JAPAN

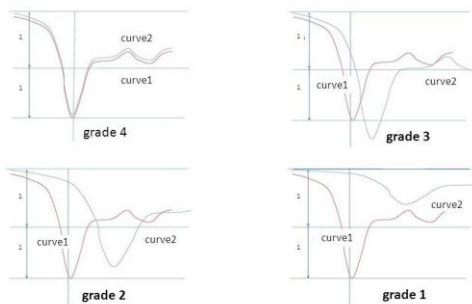
#### PURPOSE

Diffusion-weighted imaging (DWI) or perfusion-weighted imaging (PWI) is regarded as a useful tool to decide reperfusion therapy. However, it is not clear how to combine DWI/PWI results. The aim of our retrospective study was to investigate the utility of DWI/PWI-based combined factor to predict short-term clinical outcome in stroke patients admitted within 4.5 hours from sudden onset due to acute carotid artery occlusion.

#### MATERIALS & METHODS

Included for retrospective analysis were stroke patients 1) who were admitted within 4.5 hours of onset between January 2006 and January 2011, 2) who presented NIHSS score of 6 or more on admission, and 3) who underwent emergency MR imaging on admission, which suggested the affected carotid artery occlusion. We assessed baseline features, NIHSS on admission (NIHSS adm), DWI-ASPECT score, PWI-time intensity curve (TIC) grade (1 to 4), successful recanalization, NIHSS on the 7th day, and in-hospital death. Time intensity curves were generated on regions of interest set at symmetrical positions of the bilateral MCA territories, and classified into four grades according to the time to peak (TP) and the reduction value of the peak signal (PS) (Figure). DWI-ASPECT score of 5 or more and TIC grade of 2 or more were assessed as a DWI/PWI-based combined factor (A5T2).

#### Time-Intensity Curves grade



#### RESULTS

Eighty-seven patients were included for retrospective analysis. Time intensity curves were generated easily. Age was 79.3±10.3 years, NIHSS adm (median) was 20, DWI-ASPECT score (median) was 6, there were 36 in TIC grade 1, 39 in grade 2, 12 in grade 3, and 0 in grade 4, 39 patients (44.8%: 39/87) underwent reperfusion therapy (intravenous rt-PA:3 patients, endovascular

therapy: 36 patients) and successful recanalization was achieved in 18 patients (46.2%), 7-day NIHSS (median) was 20, and 29 patients died during hospitalization (in-hospital mortality rate of 33.3%: 29/87). ASPECTS of less than 5 was an independent predictor of no candidates of reperfusion therapy or in-hospital mortality ( $p<0.001$ ). Among the 46 patients with A5T2, 28 patients (60.9%) underwent reperfusion therapy and 31 patients (67.4%) obtained 7-day NIHSS improvement. Sixteen (88.9%) of 18 patients obtained 7-day NIHSS improvement. Logistic regression analysis indicated that successful recanalization ( $p<0.05$ ) and A5T2 ( $p<0.05$ ) were independent predictors for 7-day NIHSS improvement and A5T2 ( $p<0.001$ ) was an independent predictor for in-hospital survival.

#### CONCLUSION

The combined factor (A5T2) based on DWI/PWI is an independent predictor for 7-day NIHSS improvement and in-hospital survival. Successful recanalization in patients with A5T2 certainly can achieve 7-day NIHSS improvement.

**KEY WORDS:** DWI, PWI, recanalization

## eP-245

### Prediction of Long-Term Outcome of Carotid Stenting: A Practical Morphologic Scale

Pelz, D. M.

University Hospital  
London, ON, CANADA

#### PURPOSE

To determine whether carotid plaque morphology, most commonly using CTA may be predictive of the long-term Doppler ultrasound results of carotid artery stenting.

#### MATERIALS & METHODS

Over a 10-year period, 164 patients underwent carotid stenting at our institution. Mean age was 72 years (range 50-91). A calcification scale based on orthogonal neck x-ray or more commonly on CTA images was used to assess the degree of plaque calcification. This 5-point scale included: Grade 0 indicating no calcification, Grade 1 indicating involvement of <25% of vessel circumference, Grade 2 indicating 25-50% of vessel circumference, Grade 3 indicating 50-75% and Grade 4 indicating circumferentially calcified plaque. On CTA imaging, the presence or absence of soft plaque at the level of maximal stenosis also was noted. Duplex carotid (Doppler) ultrasound examinations, including mean PSV and ICA/CCA ratio measurements, were performed prior to and immediately following the procedure, within 1 week, within 4 months, at 1 year and annually thereafter. Long-term PSV outcome <200 cm/s was defined as acceptable. Univariable and multivariable analyses with logistic regression were performed to identify plaque morphologic variables associated with acceptable long-term Doppler ultrasound results.

## RESULTS

The average ultrasound follow up was 21.4 months (range 0.3 - 113 mos). Concerning plaque calcification: 18% were Grade 0, 10% were Grade 1, 18% were Grade 2, 32% were Grade 3 and 13% were Grade 4. Almost half (45%) were Grade 3 or 4. Attainment of a final PSV<200 cm/s was 25% more likely in plaques graded between 0-2 as compared to those graded at 3-4 (88% vs 63%;  $p<0.001$ ). Of the 87 cases evaluated using CTA, soft plaque was observed in 76% or 87%. Its presence led to a 44% greater chance that PSV would decrease to <200 cm/s as compared to only 36% of hard plaques (80% vs 36%;  $p = 0.005$ ). The combination of a Grade 3 or 4 calcified plaque and no soft plaque was particularly significant. A PSV<200 cm/s was attained in only 22%, vs 81% of plaques with Grade 0-2 calcium or the presence of soft plaque ( $p = 0.001$ ). Multivariable logistic regression analysis of acceptable outcome yielded: calcification (OR 0.45;  $p = 0.008$ ) and soft plaque (OR 7.42;  $p = 0.001$ ). The calcification thickness and continuity, and gradations of soft plaque from minimal to maximal, were not found to be significant.

## CONCLUSION

Long-term radiologic outcome of carotid stenting may be predicted with considerable accuracy using this simple assessment tool involving calcium grading and the observation of soft plaque on diagnostic preprocedural CTA.

**KEY WORDS:** Carotid stenting, carotid plaque morphology, CT angiography

## eP-246

### Mechanical Revascularization for Treatment of Acute Large Vessel Ischemic Stroke: Clot Disruption versus Clot Retrieval

Yoon, W.-Kim, S.-Jeong, M.-Kang, H.

Chonnam National University Hospital  
Gwangju, KOREA, REPUBLIC OF

## PURPOSE

Mechanical thrombolytic procedures are used increasingly for treatment of acute ischemic stroke. We sought to compare the therapeutic effectiveness of mechanical thrombectomy using Solitaire device versus aggressive mechanical clot disruption technique for the treatment of acute large vessel ischemic stroke.

## MATERIALS & METHODS

Between 2009 and 2011, 66 consecutive ischemic stroke patients with large vessel occlusion were treated with mechanical thrombolysis. Forty-five former patients were treated with aggressive mechanical clot disruption by using microwire or angioplasty balloon catheter (group A). Twenty-one latter patients received mechanical thrombectomy with use of the Solitaire stent device (group B). Baseline characteristics, urokinase dose, recanalization grade, duration of the procedure, symptomatic hemorrhage rate, NIHSS score at discharge, 3-month mRS were compared between the two groups. Logistic regression was used to identify

independent predictors for recanalization and good clinical outcome.

## RESULTS

Mean urokinase dose was significantly lower in group B than in group A (123,000 IU versus 35,000 IU;  $P < 0.001$ ). Successful recanalization rate (thrombolysis in cerebral ischemia grade 2b or 3) was significantly higher in group B than group A (35.6% versus 71.4%;  $P = 0.007$ ). Median NIHSS scores were lower in group B than group A at discharge (8 versus 4;  $P = 0.033$ ). Good clinical outcome (3-month mRS 0-2) was higher in group B than group A (42.2% versus 57.7%;  $P = 0.258$ ) but was not significantly different. Independent predictor for recanalization was the use of Solitaire stent device (OR, 4.53; 95% CI, 1.47-13.98;  $P = 0.009$ ). Independent prognostic factors for good clinical outcome were successful recanalization (OR, 5.25; 95% CI, 1.84-15.02;  $P = 0.002$ ) and NIHSS score at discharge (OR, 0.59; 95% CI, 0.47-0.74;  $P < 0.001$ ).

## CONCLUSION

Mechanical thrombectomy with use of the Solitaire stent device for acute large vessel ischemic stroke is associated significantly with lower urokinase dose, higher recanalization rate, and lower NIHSS score at discharge, compared with aggressive mechanical clot disruption strategy.

**KEY WORDS:** Ischemic stroke, thrombolysis, mechanical thrombectomy

## eP-247

### Mechanical Recanalization with Flow Restoration in Acute Ischemic Stroke (Reflow Study)

Papanagiotou, P.-Roth, C.-Walter, S.-Kettner, M.-Yilmaz, U.-Fassbender, K.-Reith, W.

Saarland University Hospital  
Homburg, GERMANY

## PURPOSE

The objective of this study is to collect data on the use of a stent-retriever device (Solitaire FR) for treatment of acute ischemic stroke with large artery occlusion, i.e., to investigate, whether the application of Solitaire is a safe and feasible method for interventional recanalization of large vessels with favorable patient outcome in acute stroke therapy. (ClinicalTrials.gov: NCT01210729)

## MATERIALS & METHODS

Forty patients were included in the study. Patients were included if they presented with acute ischemic stroke with occlusion of ICA, MCA, VA or BA (TICI 0 or 1 flow) within the first 6 hours. All patients were treated with a self-expandable intracranial stent (Solitaire FR), which was withdrawn in its unfolded state. Primary endpoint was the overall frequency of favorable clinical outcome (modified Rankin Scale 0 to 2), and unfavorable clinical outcome or death (modified Rankin Scale 3 to 6) after 90 days.

**RESULTS**

Twenty-three patients (57.5%) showed a favorable clinical outcome (modified Rankin Scale 0 to 2), 17 patients (42.5%) had an unfavorable clinical outcome or death (modified Rankin Scale 3 to 6) after 90 days. Fifteen patients (37.5%) showed excellent functional clinical outcome (modified Rankin Scale 0 or 1) after 90 days. The mortality rate was 12.5%.

**CONCLUSION**

Mechanical recanalization with flow restoration in acute ischemic stroke has a high rate of favorable clinical outcome.

**KEY WORDS:** Acute stroke, recanalization, Solitaire

**eP-248**

### **Intravenous Thrombolysis versus Mechanical Thrombectomy in Acute Stroke: A Single Center Observational Study**

Burns, P. A.·Flynn, P. A.·Rennie, I. M.·Smyth, G. P.·O'Leary, S. M.·McKinstry, C. S.

Royal Victoria Hospital  
Belfast, UNITED KINGDOM

**PURPOSE**

To report outcome in stroke patients receiving either intravenous thrombolysis or intraarterial mechanical thrombectomy at our institution.

**MATERIALS & METHODS**

Retrospective case review of all patients (n = 26) undergoing acute treatment for stroke over a 1-year period (January - December 2010). At our institution, intravenous thrombolysis is available as a 24/7 service. Intraarterial mechanical thrombectomy is currently only available during office hours. Neurologic outcome was assessed using the modified Rankin Score (mRS) 3 months following discharge.

**RESULTS**

Twelve patients received intravenous thrombolysis and 14 patients had intraarterial mechanical thrombectomy during this period. In the intravenous thrombolysis cohort, average age and NIHSS was 60 (range: 28-80) and 18 (range: 5-25) respectively. Average time to therapy from stroke onset was 138 minutes. Among those receiving intraarterial mechanical thrombectomy average age and NIHSS was 61 years (range: 34-85) and 18 (range: 8-25) respectively. Average time to therapy from stroke onset was 434 minutes which was significantly greater than the thrombolysis group ( $p < 0.05$ ). Of the 14 patients undergoing intraarterial mechanical thrombectomy, three had preceding intravenous thrombolysis but failed to improve. Three of 12 (25%) patients receiving intravenous thrombolysis were functionally independent (mRS  $\leq 2$ ) at 3 months. This compared to 6/14 (43%) in the mechanical thrombectomy group. This difference however was not statistically significant ( $p > 0.05$ ).

**CONCLUSION**

Despite the similar average age and baseline NIHSS, a greater proportion of patients were observed to be functionally independent at 3 months in the intraarterial mechanical thrombectomy group versus those who received intravenous thrombolysis only (43% vs 25%). Although this difference was not statistically significant, those receiving intraarterial mechanical thrombectomy had a significantly greater delay between ictus and therapy, which would be expected to negatively impact upon eventual outcome. The results of this study suggest a tendency to better outcome with intraarterial mechanical thrombectomy, which could be further improved upon with faster service delivery.

**KEY WORDS:** Stroke, thrombectomy

**eP-249**

### **Improved Outcome in Acute Stroke with the Solitaire Stent: An Emerging Paradigm Shift in Mechanical Thrombectomy**

Burns, P. A.·Flynn, P. A.·Rennie, I. M.·Smyth, G. P.·O'Leary, S. M.·McKinstry, C. S.

Royal Victoria Hospital  
Belfast, UNITED KINGDOM

**PURPOSE**

To report outcome in acute stroke using the Solitaire stent versus other mechanical thrombectomy devices at our institution.

**MATERIALS & METHODS**

Retrospective case review of all patients (n = 32) undergoing mechanical thrombectomy for acute stroke over a 3-year period. Since October 2010 the Solitaire stent (ev3 Inc) has been adopted as the device of choice in acute stroke. Prior to this, intraarterial treatment of stroke involved Merci (Concentric Medical), Penumbra (Penumbra Inc) or intraarterial thrombolysis. Revascularization was assessed using the thrombolysis in myocardial infarction score (TIMI) using standard AP and lateral angiographic projections at the end of the procedure. Neurologic outcome was assessed via the modified Rankin Score (mRS) at 3-month follow up.

**RESULTS**

Over the 3-year period (June 2008-July 2011), 13 patients were treated with the Solitaire Stent (8 anterior circulation strokes, 5 posterior circulation strokes), and 19 patients had other forms of mechanical thrombectomy (15 anterior circulation strokes, 4 posterior circulation strokes). The average age of those who were treated with the Solitaire stent was 67 years (range: 34-87) and average baseline NIHSS was 16 (range: 5-25). Among those treated with other forms of mechanical thrombectomy, average age was 60 years (17-85) and average baseline NIHSS was 19 (range: 6-26). The difference between age, NIHSS and vascular territory was not statistically significant between the two groups. Revascularization was achieved in 12/13 (92.3%) in the Solitaire stent group and in 14/19

(73.7%) with other forms of mechanical thrombectomy. This difference also was not statistically significant. However when assessing neurologic outcome, 9/13 (69.2%) of those treated with the Solitaire stent were functionally independent (mRS≤2) at 3 months compared to 6/19 (31.6%) of those treated via other forms of mechanical thrombectomy ( $p<0.05$ ). No periprocedural complications were observed with the solitaire stent. One patient had subarachnoid hemorrhage following mechanical thrombectomy with the Merci device.

#### CONCLUSION

The Solitaire stent does not significantly improve rates of vascular recanalization compared to other devices used for mechanical thrombectomy. There is however a statistically significant greater likelihood of functional independence in those patients treated with the Solitaire stent. This may reflect the nature of the retrievable stent device which achieves instant reperfusion upon deployment. Overall, the Solitaire stent is a safe and effective approach to achieve revascularization and improve functional outcome in acute stroke.

**KEY WORDS:** Stroke, thrombectomy, stent

#### eP-250

##### Endovascular Stroke Therapy in Patients with Low NIHSS and Arterial Occlusion

Raghuram, K.·Carpenter, J. S.·Domico, J. R.·Rai, A. T.  
West Virginia University

Morgantown, WV

#### PURPOSE

Endovascular treatment typically has been restricted to patients with higher NIHSS ( $\geq 6$ ) scores at presentation. However, the presence of speech impairment and basilar artery occlusion are instances where more aggressive treatment may be warranted in the presence of arterial occlusion. We reviewed our records in a retrospective manner to assess the safety of intraarterial stroke treatment in patients with low NIH stroke scales.

#### MATERIALS & METHODS

Retrospective chart review of patients that underwent intraarterial stroke therapy was conducted. Inclusion criteria were: NIHSS at presentation less than 6 and demonstration of arterial occlusion on CT angiography followed by use of endovascular stroke treatment.

#### RESULTS

Fifteen patients fit the inclusion criteria (Table 1). There were three basilar occlusions and 12 anterior circulation occlusions in the ICA, M1, M2 or M3 branches. Follow-up modified Rankin scale assessment at 90 days was available on 13 of 15 patients (86%). Three patients died (mRS = 6), (20%), (one due to cancer); eight were capable of independent living (mRS 0- 2) (53%) and two (12.5%) were severely disabled (mRS 3-5). One death was due to cancer and

was unrelated to stroke. Two patients received both intravenous (iv) and intraarterial therapy. The other candidates were excluded from iv tPA therapy based on exclusion criteria of the current national guidelines for iv tPA therapy. Intraarterial therapy varied between intraarterial tPA only (10) and intraarterial tPA plus a mechanical embolectomy device such as MERCI system or Penumbra system (5). When an anterior circulation occlusion was treated, speech impairment was among the presenting symptoms.

Table 1: Patient data

Site of Occlusion	Presenting NIHSS	NIHSS @ 24 hrs	mRS at 90 days
BASILAR ARTERY	2	24	6
L MCA	4	0	LTFU
L M2	5	1	1
R ICA	6	14	2
BASILAR ARTERY	1	1	LTFU
MCA	3	15	4
R M2	4	2	6
BASILAR	4	7	0
R M2	6	NA	6
R M2	6	0	0
L MCA, M3	2	2	0
ICA/M1	4	NA	2
M3	5	NA	1
M3	5	NA	1
M2	6	NA	3

#### CONCLUSION

In our experience of endovascular treatment for patients with low NIHSS at presentation and intraarterial thrombus, we found that the therapy had safety and results similar to those recorded in larger trials.

**KEY WORDS:** Endovascular, stroke, NIHSS

#### eP-251

##### Aneurysmal Thrombosis Postcoil Introduction in a Rat Aneurysm Model: Correlation of MR Imaging Findings with Histopathology

Elias, A. E.·Zhang, C.·Pandey, A.·Xi, G.·Thompson, B. G.·Gemmete, J. J.·Chaudhary, N.

University of Michigan  
Ann Arbor, MI

#### PURPOSE

Magnetic resonance imaging (MRI) plays a significant role in the post-embolization follow up of patients who have undergone coil embolization of cerebral aneurysms. We have utilized a rat aneurysm model to study the aneurysm healing process. Based on the



extrapolation of signal characteristics of endovascular thrombus in humans, we have determined that gradient-echo sequences (T2\* GRE-weighted images) would be the optimal method to quantify amount of endoluminal thrombus. We aim to correlate the MRI findings with histopathologic findings in this experimental rat aneurysm model.

#### MATERIALS & METHODS

This experimental aneurysm study in a rat model was approved by the University Committee on Use and Care of Animals. Male Sprague Dawley rats were anesthetized with transperitoneal injection of 50-60 mg/kg pentobarbital. In each animal an artificial aneurysm was created by permanent ligation of the rat external carotid artery (ECA) 5 mm from the carotid bifurcation (ECA blind pouch aneurysm). Subsequently a 5 mm coil segment was inserted into this aneurysm by an arteriotomy and then a ligature was placed proximal to the arteriotomy. Five rat aneurysms were treated with platinum coils and five others were treated with hydrocoils. Fourteen days posttreatment, animals underwent MRI analysis of the treated aneurysms as well as being sacrificed for histopathologic analysis. The volume of the thrombus formation was calculated by measuring the maximal area (ROI) of blooming artifact  $\times$  slice thickness (mm)/matrix (256) using NIH Image J software version 1.43U. The histologic specimens were studied under high-field microscope and thrombus formation was demarcated following staining. Measurements were performed on the MR images and histologic specimens independently in a blinded fashion. The measured values on MRI and histologic sections then were analyzed using the Pearson correlation coefficient (PCC) by SPSS version 15.0.

#### RESULTS

Our results demonstrate a significant correlation between the extent of luminal thrombus formation on histology and signal characteristics on T2\* GRE MRI sequences when the rats were treated with bare platinum coils PCC = 0.987 (P = 0.002). The hydrogel coated coils did not show MR correlation with area of thrombus formation PCC = 0.344 (P = 0.571).

#### CONCLUSION

We report the first correlation extent of luminal thrombus formation on histology with signal characteristics on T2\* GRE MRI sequences in a rat aneurysm model. Our hypothesis of direct correlation between the above-mentioned variables holds true in the bare platinum coil group and not in the hydrocoil group. Such positive correlation could allow for noninvasive evaluation of treated experimental aneurysm models.

**KEY WORDS:** Aneurysm thrombosis, coils, MR imaging

#### eP-252

#### Mechanical Thrombectomy with the Trevo Stent Device in Proximal Intracranial Arterial Occlusions of the Anterior Circulation

Majoie, C. B. L.<sup>1</sup>•Berkhemer, O.<sup>1</sup>•van den Berg, R.<sup>1</sup>•van der Kallen, B.<sup>2</sup>•Lycklama, G.<sup>2</sup>•van Zwam, W.<sup>3</sup>•Nederkoorn, P.<sup>1</sup>•Sprengers, M.<sup>1</sup>•Bot, J.<sup>1</sup>•Boiten, J.<sup>4</sup>•van Oostenbrugge, R.<sup>3</sup>•van der Lugt, A.<sup>5</sup>•Beumer, D.<sup>5</sup>•Fransen, P.<sup>5</sup>•Dippel, D.<sup>5</sup>•Roos, Y.<sup>1</sup>

<sup>1</sup>Academic Medical Center, Amsterdam, NETHERLANDS,

<sup>2</sup>MC Haaglanden, The Hague, NETHERLANDS,

<sup>3</sup>Maastricht University Medical Center, Maastricht, NETHERLANDS, <sup>4</sup>MC Haaglanden, Amsterdam, NETHERLANDS, <sup>5</sup>Erasmus Medical College, Rotterdam, NETHERLANDS

#### PURPOSE

To evaluate the safety and effectiveness of a self-expanding and fully retrievable stent (Trevo; Concentric Medical Inc, Mountain View, CA, USA) in revascularization of patients with acute ischemic stroke of the anterior circulation.

#### MATERIALS & METHODS

Retrospective analysis of 28 consecutive patients (mean age 54 years; M:F = 19:9) with an acute ischemic stroke caused by a proximal intracranial arterial occlusion of the anterior circulation treated with a fully retrievable stent within the first 8 hours from symptom onset [median National Institutes of Health Stroke Scale 19 (range 8-30)]. Thrombectomy was used as rescue therapy in patients who were refractory to, had contraindications for, or were too late for iv rtPA. The occlusion site was the MCA in 12, terminus ICA in 12, cervical ICA/MCA in four patients. Complications related to the procedure and outcome at 3-6 months were assessed.

#### RESULTS

Stent placement was feasible in all procedures and successful recanalization defined as thrombolysis in cerebral ischemia (TICI) grade 2b or 3 was achieved in 23 of 28 treated vessels (82%). The mean number of passes for maximal recanalization was two (range 1-4). The median time from groin puncture to recanalization was 79 (range 30 - 199) minutes. One significant procedural event occurred (carotid artery occlusion after stent removal). Forty-six percent of all patients had a good outcome (mRS 0 to 2), 17% a moderate outcome (mRS 3), and 37% a poor outcome (mRS 4 to 6).

#### CONCLUSION

These results suggest that with the Trevo stent device, clots can be removed safely and effectively from intracranial large vessel occlusions in acute ischemic stroke.

**KEY WORDS:** Stroke, thrombectomy, stent

## eP-253

# Dual Microcatheter Coil Embolization of Intracranial Saccular Aneurysms with a Wide Neck and Incorporated Branches: Outcomes of a Case Series of Five Patients Using a Novel Approach for Coil Sizing

Erdem, E. Akdol, M. S. Amole, A. O.

University of Arkansas for Medical Sciences  
Little Rock, AR

## PURPOSE

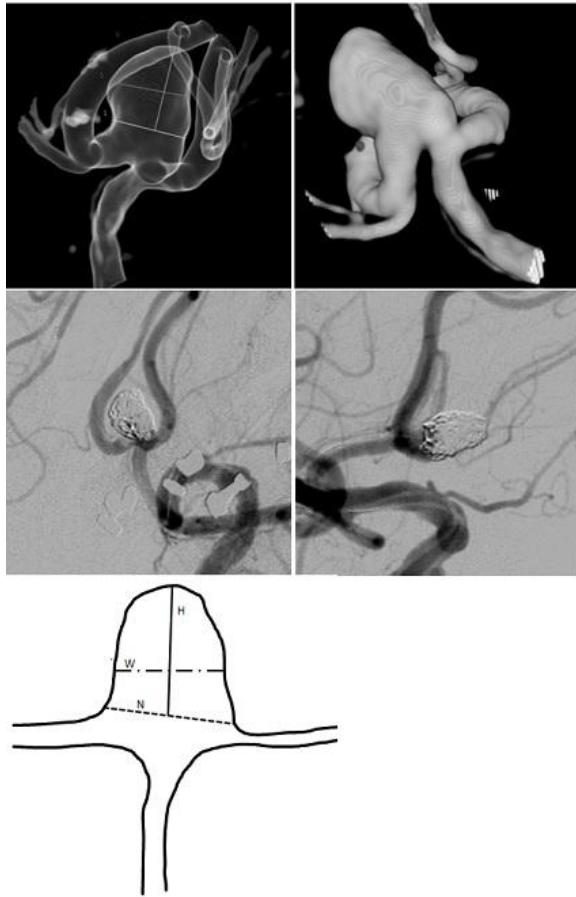
Balloon or stent-assisted neck remodification techniques now are employed widely in the treatment of endovascular occlusion of saccular aneurysms with unfavorable configuration. These techniques may not be feasible in patients presenting with subarachnoid hemorrhage and/or incorporation of an important main branch in the aneurysm sac. Though rarely used today, multimicrocatheter coil embolization is a safe and effective technique that can be used for coil embolization of these aneurysms. This report describes the method for proper sizing of the embolization coils and choice of catheter.

## MATERIALS & METHODS

Five patients, two unruptured and three ruptured intracranial aneurysms with unfavorable configuration due to incorporation of major branches in the aneurysm sac and presence of wide neck were treated between January 2010 and March 2011. All patients were poor surgical candidates and failed balloon-assisted technique. The mean dome-to-neck ratio was  $1.22 \pm 0.08$  (range, 1.08 -1.30). The maximum coil size was selected according to the height (H) of the aneurysm to avoid coil protusion into the parent or branch vessel. The second framing coil was chosen such that the sum of the diameter of the two coils is 2-3 mm greater than the maximum width (W) of the aneurysm. Table 1 summarizes the presentation, aneurysm location and morphology, choice of framing coils, catheter selection and clinical outcome.

Table 1. Endovascular embolization of complex intracranial aneurysms using dual microcatheters

Patient No/ Age/ Sex	Clinical Presentation Hunt&Hess Score	Aneurysm Location	Aneurysm Size (Depth x Width/ Neck)	Microcatheters	Framing Coil Size	Clinical Outcome
1/57 /M	SAH / 3	ACoA	6.5 x 11 / 5 mm	Echelon 10 - 45 and 90 degrees	5 mm x 10 cm, 4 mm x 8 cm	Excellent
2/79 /M	SAH/ 4	Supraclinoid ICA - PCoA	6.5 x 7 / 6 mm	Echelon 10 - 45 and 90 degrees	5 mm x 15 cm, 4 mm x 10 cm	Excellent
3/50 /F	SAH/ 4	Basilar Tip	10 x 13 / 8 mm	Prowler 14 - 45 and 90 degrees	6 mm x 15 cm, 7 mm x 21 cm	Excellent
4/81 /F	Incidental	Supraclinoid ICA	11 x 12 / 6 mm	Prowler 14 - 45 and 90 degrees	7 mm x 28 cm, 8 mm x 17 cm	Excellent
5/72 /F	Incidental	ACoA	5 x 4.5 / 4 mm	Echelon 10 - 45 and 90 degrees	4 mm x 10 cm, 3.5 mm x 9 cm	Excellent



## RESULTS

Occlusion of the body and dome of the aneurysms was achieved in all patients. Small neck residual was left in two patients at the end of the embolization intentionally to avoid side branch occlusion. No procedure-related complications were recorded and all patients had excellent clinical outcomes. No new bleeding occurred during the follow-up period.

## CONCLUSION

This small case series describes the method for proper sizing and catheter selection for dual microcatheter technique in aneurysms with unfavorable configuration.

**KEY WORDS:** Brain aneurysm, coil embolization, dual microcatheter

eP-254

## Intracranial Watershed Zone Shifting and Plasticity of the Circle of Willis: The Effects of Stenting Treatment in Carotid Steno-Occlusive Disease

Guo, W.<sup>1,2</sup>Lin, C.<sup>1</sup>Hung, A. S.<sup>1</sup>Chang, F.<sup>1</sup>Luo, C.<sup>1</sup>Chu, W.<sup>1</sup>Teng, M. M.<sup>1,2</sup>

<sup>1</sup>Taipei Veterans General Hospital, Taipei, TAIWAN,  
<sup>2</sup>National Yang-Ming University, Taipei, TAIWAN

## PURPOSE

Both corresponding and noncorresponding neurologic improvement frequently are observed in patients with

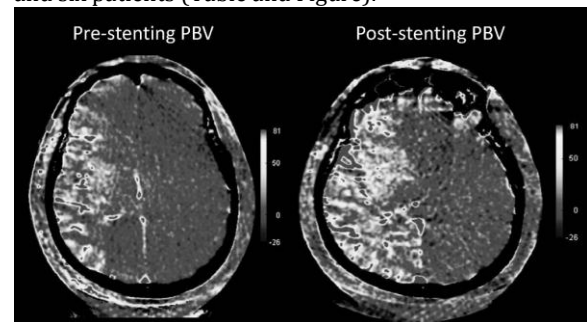
unilateral carotid stenosis after stenting. The study hypothesizes that the global improvement stems from the modulation of intracranial hemodynamics occurring longitudinally along the stenting treatment and presents as watershed zone shifting and plasticity of the circle of Willis onto the normal, in addition to the toward normalization of intracranial circulation time.

## MATERIALS & METHODS

Ten patients (9 men, 1 woman, age 71 years, 61-80) with extracranial internal carotid artery (ICA) steno-occlusive disease (>90% stenosis in 4, 70-90% in 3, and <70% in 3) and received stenting treatment for the stenotic ICA between August and October 2011 were recruited. All DSA-guided diagnostic and interventional procedures were performed on a biplane flat detector (FD) angiographic system (AXIOM-Artis®, Siemens Healthcare) in a same one angiographic session. Postprocessing software (syngo iFlow®, Siemens Healthcare) was used to color-code the DSA and quantify the intracranial circulation time. In addition to routine DSA, FDCT imaging was included for evaluating parenchyma blood volume (PBV). The FDCT imaging consisted of two rotations: an initial rotation (mask run) followed by a second rotation after appropriate contrast medium injection, selectively, through the stenotic carotid artery (fill run). The PBV evaluation was performed on a research workstation equipped with prototype software (syngo XWP, Siemens Healthcare). All imaging parameters were used to evaluate the intracranial circulation time, watershed zone of major arteries and calibers and flow directions of Willisian arteries for the plasticity of the circle of Willis.

## RESULTS

After stenting, the intracranial circulation time of all patients with >70% stenosis shifted towards normal. Watershed zone shifting and plasticity of the circle of Willis onto normal was observed, respectively, in eight and six patients (Table and Figure).



Demographic data of patients and the therapeutic effects of stenting

Patient No.	Side/% of ICA stenosis	Watershed zone shift onto normal	Plasticity of CoW onto normal
1	L/>90	+	+
2	R/<70	-	-
3	R/>90	+	+
4	L/70-90	+	+
5	R/>90	+	+

6	R/>90	+	+
7	L/<70	+	-
8	R/70-90	+	+
9	R/70-90	-	-
10	R/>90	+	-

#### CONCLUSION

The global neurologic improvement after stenting in steno-occlusive disease is evidenced by normalization of intracranial circulation time, watershed zone shifting and plasticity of the circle of Willis onto the normal. An FD angiographic system equipped with color-coded DSA and FDCT capacity provides territorial-specific imaging information within one angiographic session.

**KEY WORDS:** Steno-occlusive disease, stenting, watershed zone

#### eP-255

##### **Susceptibility-Weighted (MR) Imaging as Prognostic Indicator for Patient Selection with Endovascular Therapy of Acute Stroke**

Tsai, F. Y.<sup>1</sup>•Kao, H. W.<sup>1</sup>•Chan, W.<sup>2</sup>

<sup>1</sup>University of California, Irvine, Orange, CA, <sup>2</sup>Taipei Medical University, Taipei, TAIWAN

#### PURPOSE

To demonstrate susceptibility-weighted imaging (SWI) as a good indicator to select patients for endovascular procedures.

#### MATERIALS & METHODS

From January 2009 to December 2010, 317 patients with acute stroke were evaluated for endovascular thrombolytic therapy in our hospital. Patients who had not undergone SWI or endovascular procedure were excluded from this retrospective investigation. A total of 49 patients (24 male, 25 female; age range, 15 to 89 years; average, 56.2 years) were included. Among these, 39 (79.6%) patients underwent thrombolytic therapy with tPA and mechanical devices, including catheters, balloons, Merci and Penumbra devices, while 10 (20.4%) underwent both thrombolytic therapy and stenting. Before the endovascular procedures, all patients had CT, SWI, diffusion-weighted imaging and fluid attenuated inversion recovery MR imaging while 15 patients had MR PWI. The endovascular procedures were performed within 3.5-8.5 hours after onset of clinical symptom of stroke.

#### RESULTS

Twenty-eight patients (77.6%) recovered with either significant improving or stable clinical condition after the endovascular procedures while 21 (22.4 %) had worse outcome. On SWI, prominent hypointense cerebral vessels were present in all patients with worse outcome and eight of them (38.1%) had severe hemorrhagic complications with severe hypoplasia or atresia of ipsilateral transverse sinuses.

#### CONCLUSION

Presence of prominent hypointense cerebral vessels on SWI correlated with poor prognosis. Susceptibility-weighted imaging may be used to select acute ischemic stroke patients for endovascular therapy.

**KEY WORDS:** Stroke, thrombolysis, prognosis

#### eP-256

##### **Creation of Larger Elastase-Induced Aneurysms with Predilation of the Right Common Carotid Artery Using 3 F Fogarty Balloon before Elastase Incubation: A Retrospective Study**

Ding, Y. •Rezek, I. •Dai, D. •Kadirval, R. •Lewis, D. A. •Kallmes, D. F.

Mayo Clinic  
Rochester, MN

#### PURPOSE

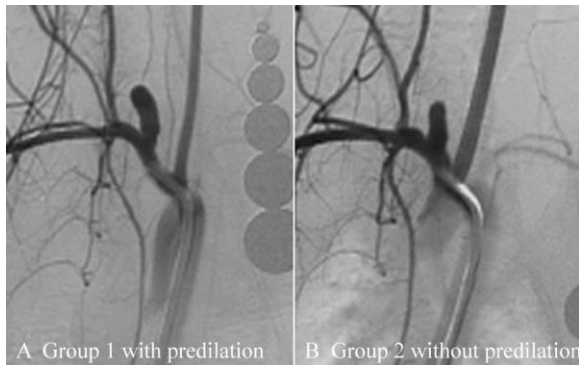
To determine whether predilation of right common carotid artery (RCCA) before elastase incubation can result in larger elastase-induced aneurysms in rabbits as compared to aneurysm creation without predilation.

#### MATERIALS & METHODS

Elastase-induced aneurysm sizes were analyzed retrospectively in 68 New Zealand white rabbits. Two groups were classified. For Group 1 (n = 34), predilation was performed by injecting contrast to a 3 F Fogarty balloon to over-expanding the RCCA for 1 minute, this procedure was repeated three times before regular elastase incubation. In Group 2 (n = 34), predilation of the RCCA was not performed, indicating no vessel dilation of RCCA before elastase incubation. Follow-up digital subtraction angiography (DSA) was performed 3 weeks after aneurysm creation. Aneurysm sizes (neck diameter, width, height) in the two groups were measured and calculated. Comparison of aneurysm sizes between the two groups was performed using the Student's t test.

#### RESULTS

The mean aneurysm neck diameter for Group 1 was not different from Group 2 ( $3.8 \pm 1.3$  mm and  $3.4 \pm .8$  mm, respectively,  $p > .05$ ) (Figure A and B). Differences in aneurysm width between the two groups were not significant ( $4.1 \pm .9$  mm and  $4.4 \pm .9$  mm, respectively,  $p > .05$ ). Mean aneurysm height for Group 1 was larger than Group 2 ( $10.5 \pm 1.9$  mm and  $9.1 \pm 2.1$  mm, respectively,  $p < .01$ ).



#### CONCLUSION

Predilation of RCCA using 3 F Fogarty balloon before elastase incubation can create larger elastase-induced aneurysms in rabbits.

**KEY WORDS:** Aneurysm, elastase-induced model, predilation

#### eP-257

#### Myth of Restenosis after Carotid Angioplasty and Stenting

Albuquerque, F. C.·Ahmed, A.·McDougall, C.

Barrow Neurological Institute, Neurosurgical Associates  
Phoenix, AZ

#### PURPOSE

Based on CREST, carotid endarterectomy (CEA) and stenting have equivalent safety and efficacy. Endarterectomy is associated with a rate of restenosis as high as 18%. In this setting, we analyzed our experience with restenosis after carotid artery stenting (CAS).

#### MATERIALS & METHODS

A retrospective chart review was conducted between 1995 and 2010. Symptomatic and asymptomatic patients were selected for stent placement based on NASCET and ACAS criteria. These patients underwent CAS with distal embolic protection. The indications, rates of technical success, intraoperative and perioperative complications, restenosis (>50%) rate, and clinical outcome were evaluated.

#### RESULTS

One hundred seventy-five patients were treated, but 24 were lost to follow up. As a result, 151 patients with 165 lesions were evaluated. Seventy-five percent of lesions were symptomatic. Indications for CAS included: poor surgical candidacy, prior endarterectomy, prior radiation, those randomized to stent placement as part of a study, acute occlusions, tandem stenosis, high bifurcation, and contralateral laryngeal nerve palsy. Procedures were technically successful in all but one case (0.6%). Intraoperative and perioperative stroke occurred in four patients (2.6%). Follow up ranged from 6 months to 10 years (mean 1 year). Fourteen arteries (8.5%) developed a restenosis greater than 50%, but moderate to severe restenosis (>70%) occurred in only

3.6%. Only four patients developed symptomatic restenosis (2.6%). The highest risk factor for developing restenosis was a prior history of neck irradiation (33%) and prior CEA (20%). In fact, of the total 14 restenoses, 13 (93%) occurred in either the prior CEA or prior radiation treatment subgroups.

#### CONCLUSION

The rate of moderate to severe restenosis after carotid stent placement is quite low (3.6%) and is likely lower than that of CEA. In addition, restenosis after stenting occurs almost exclusively in patients with a prior history of CEA or neck irradiation.

**KEY WORDS:** Carotid, angioplasty, stenting

#### eP-258

#### Endovascular Management with Coil Embolization of Intracranial Pseudoaneurysms

Agarwal, A.·Horia, M.·Kole, M.·Fourgas, E.·Sanders, W.

Henry Ford Health System  
Detroit, MI

#### PURPOSE

A pseudoaneurysm, or false aneurysm, develops in response to injury to all layers of an arterial wall, secondary to blunt or penetrating trauma, infections, or inflammatory conditions. The lack of structural integrity of the wall of a pseudoaneurysm usually leads to rapid expansion and rupture. Coil embolization of pseudoaneurysms usually is not recommended as coils will not be contained due to the lack of proper wall. Despite advances in endovascular and microsurgical techniques, these aneurysms frequently present a tremendous therapeutic challenge. Surgical trapping or endovascular occlusion of the parent artery either with or without extracranial-intracranial bypass has been the treatment of choice. However, in specific anatomical locations, the parent vessel cannot be sacrificed, and alternative treatment methods have to be selected. The purpose of our study was to describe the treatment with coil embolization of intracranial pseudoaneurysm with preservation of the parent artery.

#### MATERIALS & METHODS

Clinical and radiologic data of six cases of intracranial pseudoaneurysm treated with endovascular methods between January 2007 and September 2011 were reviewed retrospectively. All patients presented with aneurysm rupture and subarachnoid hemorrhage. Four were posttraumatic from gunshot injury, one was mycotic while one developed after surgical clipping of a true aneurysm. In three cases, the parent vessel was occluded with coils. In the rest of the cases, the pseudoaneurysms were treated with coil embolization with preservation of the parent artery.

#### RESULTS

Three pseudoaneurysms were treated successfully with coil embolization and preservation of the parent artery. The coils were undersized to the measured diameter of the aneurysm. There were no reruptures during the

coiling. There was no clinical evidence of rebleeding after embolization. In one case, there was early regrowth of the pseudoaneurysm in the follow-up angiography which was recoiled successfully.

#### CONCLUSION

Pseudoaneurysms can be treated safely and effectively by coil embolization with preservation of the parent vessel in selected cases where sacrifice of the parent vessel is not feasible. Treatment efficacy may be improved if embolization is done in the subacute period, when the wall of the pseudoaneurysm has matured and stabilized. Early follow-up to evaluate for regrowth and retreatment is advised.

**KEY WORDS:** Pseudoaneurysm, coiling, embolization

#### eP-259

##### Carotid Artery Stenting in Acute Stroke

Papanagiotou, P.·Roth, C.·Walter, S.·Reith, W.

Saarland University Hospital  
Homburg, GERMANY

#### PURPOSE

Stroke caused by acute occlusion of the internal carotid artery is associated with a significant level of morbidity and mortality. For these kinds of lesions treatment with standard iv thrombolysis alone leads to a good clinical outcome in only 17% of the cases with a death rate of up to 55%. At present there is no consensus treatment for patients with acute ischemic stroke presenting with severe clinical symptoms due to atherosclerotic occlusion of the extracranial ICA. The purpose of this study is to demonstrate the technical success of carotid artery stenting in acute extracranial internal carotid artery (ICA) occlusion as well as the benefit in clinical outcome.

#### MATERIALS & METHODS

Carotid artery stenting was performed in 34 patients with acute atherosclerotic extracranial ICA occlusion within 6 hours of stroke symptom onset. In 31 patients there was an additional intracranial occlusion; at the level of the terminal segment of the ICA (7 patients) and at the level of the middle cerebral artery (24 patients). Intracranial occlusions were treated either with the Penumbra system or the Solitaire stent-based recanalization system. Recanalization results were assessed by angiography immediately after the procedure. The neurologic status was evaluated before and after the treatment with a follow up of up to 90 days using the National Institute of Health Stroke Scale (NIHSS) and the modified Rankin Scale (mRS).

#### RESULTS

Successful revascularization of extracranial ICA with acute stent implantation was achieved in 33 patients (97%). Intracranial recanalization with TIMI 2/3 flow was achieved in 24 of the 31 patients (77%). The overall recanalization rate (extracranial and intracranial) was 27/34 (79%). Sixteen patients (47%) showed a mRS

score of 2 at 90 days. The mortality rate was 13.6% at 90 days.

#### CONCLUSION

Carotid artery stenting in acute atherosclerotic extracranial ICA occlusion with severe stroke symptoms is feasible, safe and useful within the first 6 hours after symptom onset.

**KEY WORDS:** Carotid occlusion, stenting, acute stroke

#### eP-260

##### Characterization of Neuroendovascular Devices under Fluoroscopic Conditions: A Standardized Protocol

Vedantham, S.·Gounis, M. J.·Karellas, A.·Wakhloo, A. K.

University of Massachusetts Worcester, MA

#### PURPOSE

Numerous endovascular devices are delivered under fluoroscopic guidance. However, there are no standardized methods to ensure adequate radio-opacity under clinical conditions. Inadequate device contrast may result in increased radiation dose to the patient either from prolonged fluoroscopy or from high dose-rate imaging. Clearly, lack of device contrast can lead to inaccurate positioning that could negatively impact clinical outcome. We developed a framework for theoretical optimization, and an experimental protocol for evaluating stents and flow diverters.

#### MATERIALS & METHODS

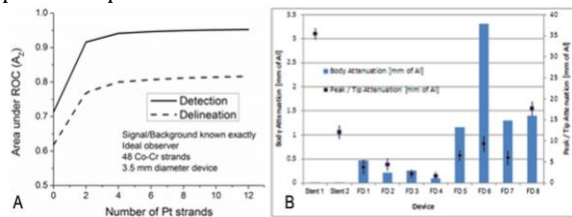
The theoretical framework is based on ICRU-recommended detectability index and consequently the area under the ROC curve (Az). Devices of 3.5 mm diameter comprising helically oriented platinum strands woven in cobalt-chromium were modeled. The Az values for detecting and delineating the device in a homogenous 16 cm water background were computed under RQA5 of IEC standards (72 kVp, 7 mm HVL) that is used for characterizing imaging systems. The experimental protocol for contrast evaluation comprises three parts: quantitative measurement of equivalent attenuation (in mm of Al) under RQA5 of IEC-standards, visual assessment of device contrast in homogenous background (water phantom) of anatomically relevant thickness, and visual assessment of the device contrast with anatomical background. All experiments were performed with ~15 cm detector field of view (0.154 mm pixel), 15 frames/second acquisition and system selected x-ray filtration of 0.4 mm Cu + 1 mm Al. Ten devices were assessed using this protocol: two FDA-cleared Nitinol stents (stent 1 and stent 2), seven cobalt-chromium alloy flow diverters (FD 1 to 7), and one Nitinol flow diverter (FD 8).

#### RESULTS

Theoretical optimization suggest that beyond four to six strands of platinum, minimal improvement in Az values were observed for detection and delineation tasks, respectively, by an ideal observer model that has exact knowledge of the signal (device) and



background (Figure 1A). Quantitative assessment of the Nitinol stents showed substantial equivalent attenuation of the marker bands, but poor attenuation characteristics of the device body (Figure 1B). The flow diverters demonstrated improved attenuation along the device body than the stents. The newer generation of flow diverters with interwoven platinum wires in the cobalt-chromium braiding demonstrated improved attenuation characteristics compared to previous generation (FD 4-6). Visual assessment under homogenous (16 cm water) phantom and anatomical background (skull phantom immersed in 16 cm water) provided qualitative confirmation.



## CONCLUSION

The proposed theoretical framework and the experimental protocol with further refinements can serve as the basis for designing and evaluating the adequacy of x-ray contrast of neuroendovascular devices that are implanted under fluoroscopic guidance.

**KEY WORDS:** Fluoroscopy, stents, flow diverters

## eP-261

### Cerebral Blood Volume Imaging by Flat Detector CT in Acute Stroke Patients: Single Center Experience in 26 Cases

Struffert, T.<sup>1</sup>•Deuerling-Zheng, Y.<sup>1</sup>•Engelhorn, T.<sup>1</sup>•Kloska, S.<sup>1</sup>•Gölit, P.<sup>1</sup>•Strother, C.<sup>2</sup>•Doerfler, A.<sup>1</sup>

<sup>1</sup>University Erlangen-Nuremberg, Erlangen, GERMANY,  
<sup>2</sup>University of Wisconsin, Madison, WI

## PURPOSE

A flat-detector CT application (syngo Neuro PBV IR) offers the possibility to perform cerebral blood volume (FD CT CBV) mapping and tissue visualization (DynaCT) within the angio suite. We report on our experience in 26 cases in comparison to multislice CT.

## MATERIALS & METHODS

In 26 patients with acute M1 or carotid artery occlusions undergoing mechanical recanalization FD CT CBV was performed directly after treatment. Volumes of lesions in FD CT CBV, pre and posttreatment CT and PCT were calculated. If available, mean CBV values of the CBV lesion were measured in FD CT CBV and PCT. DynaCT images were reviewed for signs of hemorrhage or contrast extravasation.

## RESULTS

In 13 patients we detected oligemic FD CT CBV lesions showing a high correlation of lesion volume to final infarct volume in posttreatment CT ( $r = 0.97$ ,  $p < 0.05$ ). In 11 patients we recognized hyperemic FD CT CBV lesions. Here the final infarct volume in posttreatment

CT showed a weak correlation to FD CT CBV lesion volume ( $r = 0.8$ ,  $p < 0.05$ ), but a significant correlation to the initial PCT CBV lesion volume ( $r = 0.9$ ,  $p < 0.05$ ). Comparison of FD CT CBV values to follow-up PCT CBV values showed a high correlation ( $r = 0.9$ ,  $p < 0.05$ ) in oligemic patients. Hemorrhage did not occur in our series, but contrast extravasation was recognized on DynaCT images in five of 13 oligemic and six of 11 hyperemic patients.

## CONCLUSION

The new FD CT application allows recognition of oligemic and hyperemic CBV lesions during endovascular treatment. In oligemic patients the FD CT CBV lesion volume shows a high correlation to final infarct volume and may allow prediction of final infarct size. Contrast extravasation can be recognized on DynaCT images. This application may improve monitoring and patient selection during stroke treatment.

**KEY WORDS:** Flat detector CT, perform cerebral blood volume mapping, stroke

## eP-262

### In Vivo Evaluation of the Washout Coefficient Parameter to Predict Long-Term Aneurysm Occlusion Immediately after Flow Diverter Therapy

Sadasivan, C.•Dholakia, R.•Peeling, L.•Fiorella, D. J.•Woo, H. H.•Lieber, B. B.

Stony Brook University  
Stony Brook, NY

## PURPOSE

Flow diverters currently are being used to treat a certain class of aneurysms where the devices' potential to result in aneurysm occlusion and resorption by natural thrombosis and wound-healing mechanisms offers a singular advantage. A natural progression is, however, inherently gradual and it is difficult to predict the occlusion probability of any given aneurysm after it has been treated by flow diversion. The purpose of this study is to develop a predictive index of long-term aneurysm occlusion success by quantifying alterations in the intraaneurysmal transport of angiographic contrast due to the deployed flow diverter(s), immediately after such deployment.

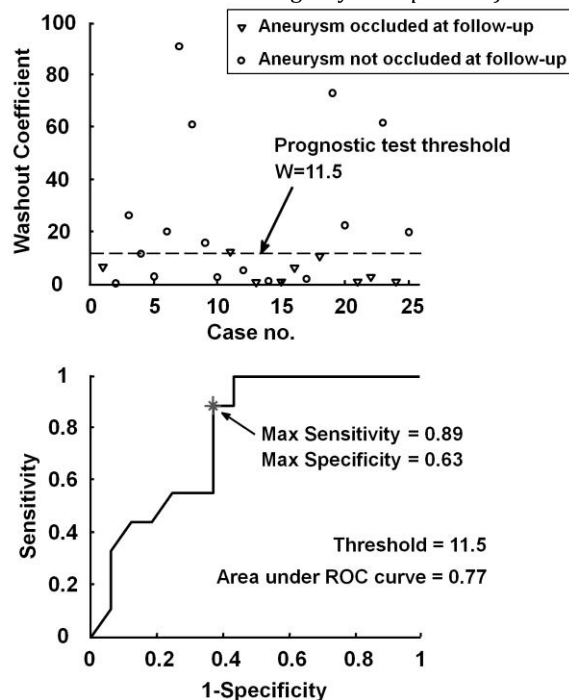
## MATERIALS & METHODS

A mathematical model that uses angiographic images acquired before and after flow diverter deployment to quantify intraaneurysmal contrast transport has been developed previously. Parent vessel-aneurysm flow exchange - recorded as aneurysmal contrast concentration-time curves - is delineated into convective and diffusive modes of transport via model fitting. A predictive index of aneurysm occlusion (called the washout coefficient,  $W$ ) is constructed as a ratio of the area under the diffusion curve after device deployment to that before device deployment. Twenty-seven rabbit elastase-induced aneurysms were treated with flow diverters of three different designs (65-70%

porosity range, 1 device per aneurysm, data attrition in 2 cases, total  $n = 25$ ). High-speed angiograms were acquired before and immediately after device deployment in each animal. Angiographic occlusion of the aneurysm was noted at either 3 month ( $n = 12$ ) or 6 month ( $n = 15$ ) follow up; any neck remnant was considered incomplete occlusion.

## RESULTS

The washout coefficient obtained immediately after device deployment (top panel) was significantly lower ( $p = 0.02$ ) for aneurysms that occluded ( $W = 4.4 \pm 4.5$ ,  $n = 9$ ) as compared to the value for aneurysms that did not occlude ( $W = 26.0 \pm 29.1$ ,  $n = 16$ ). Receiver operating characteristic curve analysis suggests that a value of  $W < 11.5$  predicts aneurysm occlusion with 89% sensitivity and 63% specificity (bottom panel, Fisher's exact test for contingency table  $p = 0.03$ ).



## CONCLUSION

Results suggest that further evaluation of angiographic data acquired during flow diverter treatment may allow the prediction of aneurysm occlusion rates over the long term immediately after device deployment. Applicability of the parameter in predicting clinical aneurysm occlusion rates is being evaluated.

**Acknowledgement:** Support: NIH R01NS045753 and Siemens.

**KEY WORDS:** Flow diversion, functional angiography

## eP-263

### Outcomes of Modern Endovascular Treatment of Vein of Galen Malformations in the Neonatal Period

Berenstein, A.<sup>1</sup>•Fifi, J.<sup>2</sup>•Niimi, Y.<sup>2</sup>•Ortiz, R.<sup>2</sup>•Molofsky, W.<sup>2</sup>

<sup>1</sup>St. Luke Roosevelt Hospital, New York, NY, <sup>2</sup>Roosevelt Hospital, New York, NY

## PURPOSE

Untreated patients with neonatal presentation of vein of Galen aneurysmal malformations (AMVG) carry almost 100% morbidity and mortality. We report our most recent patients requiring neonatal interventional endovascular treatment.

## MATERIALS & METHODS

A consecutive series of 13 neonatal patients presented with AMVG from 2005 to 2009. Nine were treated in the newborn period by transarterial liquid embolization with cyanoacrylate tissue adhesive (NBCA) targeting the fistula sites via percutaneous femoral artery access. The goal was to make their heart failure medically manageable by reducing arteriovenous shunting. Patients returned for further endovascular treatment at 6 to 9 months of age.

## RESULTS

Neonatal control of cardiac failure was achieved in eight of nine patients. One 1.5 kg premature baby expired after treatment due to diffuse intracranial hemorrhage. One patient experienced a stroke and mild hemiparesis from a microcatheter rupture. Three of nine patients demonstrated posttreatment asymptomatic intracranial hemorrhage. Angiographic cure was documented at an average age of 23 months in four of nine patients after an average of 2.5 treatments. Three of four of these patients have achieved normal milestones. One patient has a mild motor and language delay. Of the four children with planned further embolizations, the child with the neonatal microcatheter rupture has a mild hemiparesis.

## CONCLUSION

Treatment of neonatal AMVG with modern endovascular techniques in conjunction with specialized neuroanesthetic and neurointensive care results in improved outcomes with cure and normal neurologic development. Multiple stages often are necessary. These patients require care by an interdisciplinary team in specialized centers devoted to this group of diseases.

**KEY WORDS:** Vein of Galen malformations, embolization, neonates

## eP-264

### Procedural Time to Recanalization in Intraarterial Stroke Therapies: A Meta Analysis of Observational Studies Using the Merci Device, Penumbra System, and Retrievable Stents

Almekhlafi, M. A. • Menon, B. • Freiheit, E. • Demchuk, A. • Goyal, M.

University of Calgary  
Calgary, AB, CANADA

## PURPOSE

Timely and complete recanalization is one of the strongest predictors of good outcome following acute ischemic stroke. A variety of intraarterial devices are promising to achieve higher recanalization rates

compared to intravenous thrombolytics. However, their efficacy is yet to be shown in randomized trials. Until then, physicians performing intraarterial stroke therapies rely on their personal experience when choosing among the available devices. We aim to review the available literature to compare procedural time-to-recanalization, recanalization rates, and complications of the Merci device, Penumbra System (PS), and Retrievable Stents (RS) in acute ischemic stroke treatment.

#### **MATERIALS & METHODS**

We conducted a systematic review and meta-analysis of studies or abstracts published until February 2011 reporting original data on 10 patients or more and describing the time needed to achieve recanalization in ischemic stroke patients treated using the Merci device, PS, or RS. The puncture-to-recanalization time was used to define the time-to-recanalization. When this is not reported, the procedural duration was used instead.

#### **RESULTS**

We identified 16 eligible studies: four on MERCI device (N = 357), eight on PS (N = 455), and four on RS (N = 113); none had randomized treatment allocation. All studies reporting on Merci device described the procedural duration but not the puncture-to-recanalization times. Using a random effects model, mean procedural time-to-recanalization time for MERCI device was 120 minutes (CI95 105.7 to 134.2). The mean procedural duration for the PS was 64.6 minutes (CI95 44.4 to 84.8), while for RS it was 54.7 minutes (CI95 47.3 to 62.2). On average, successful recanalization (TIMI 2/3) was achieved in 63.0% of MERCI-treated patients (CI95 40.7 to 85.3) compared to 87.8% in studies using PS (CI95 82.5 to 93.1) and 92.1% in studies using RS (CI95 82.5 to 99.9). The mean incidence of symptomatic intracranial hemorrhage was 6.9% in MERCI studies (CI95 2.9 to 10.9), 5.4% (CI95 1.5 to 9.3) in PS studies and 9.6% in RS studies (CI95 6.4 to 12.8). The 3-month mortality rate was 37.8% in MERCI studies, 22.4% in PS, and 10.2% in RS studies. Functional independence (mRS $\leq$ 2) was achieved in 31.5% of studies reporting on MERCI, compared to 36.6% in PS studies and 46.9% in RS studies. Distal emboli were reported in 1.1% of MERCI studies compared to 4.4% of PS and 10.6% of RS studies.

#### **CONCLUSION**

In this meta-analysis, the use of PS and RS was associated with comparable procedural time-to-recanalization. Studies using Merci device only reported procedural duration which was relatively longer than PS and RS puncture-to-recanalization times. The use of PS and RS was associated with higher rates of successful recanalization compared to the Merci device. Studies describing RS reported the lowest mortality rates at 3 months and the best functional outcome among all devices. We could not adjust for the impact of a number of important variables including that of improved stroke care.

**KEY WORDS:** Thrombolysis, stroke, devices

#### **eP-265**

#### **Vertebroplasty Failure in AO-Magerl A2 and A3 Fractures: Is Percutaneous Augmentation with Support Better?**

Kelekis, A.·Filippiadis, D.·Oikonomopoulos, N.·Argentos, S.·Brountzos, E.·Kelekis, N.

University General Hospital "ATTIKON"  
Athens, GREECE

#### **PURPOSE**

Purpose of our study is to illustrate the efficacy and safety of percutaneous augmented vertebroplasty in cases of AO-Magerl A2 and A3 vertebral fractures.

#### **MATERIALS & METHODS**

We retrospectively studied the cases of five patients suffering from symptomatic AO-Magerl A2 and A3 vertebral fractures who were referred to our department within the last year. Two patients underwent percutaneous vertebroplasty by means of 13 G bevel-shaped needles and PMMA injection within the vertebral body. Three patients underwent percutaneous augmented vertebroplasty. Under general anesthesia and fluoroscopic control, by means of 8G trocar a biocompatible polymer (PEEK-OPTIMA) is introduced within the vertebral body and filled with PMMA. The implant functions as an internal cast which provides a mechanical support structure while potentially providing height restoration. Computed tomography (CT) scan the morning after therapy controlled the implant distribution in all five patients. Clinical evaluation included immediate and delayed follow-up studies of patient's general condition and neurologic status as well as imaging studies (x-rays and in selected cases cone-beam CT scan with 3D reconstructions). A questionnaire with NVS scale helped assessing pain relief degree, life quality and mobility improvement. Follow-up visits were performed on day 1, day 10, month 1 and month 6 post the therapeutic session with respect on each patient's general condition, pain reduction and mobility improvement.

#### **RESULTS**

Comparing the pain scores of patients who underwent augmented vertebroplasty prior (mean value 8.7 NVS units) and after (mean value 1.3 NVS units) treatment, there was a mean decrease of 7.5 NVS units on terms of pain reduction, effect upon mobility and life quality. However, in 1/3 patients who underwent augmented vertebroplasty deployment of the biocompatible polymer was not feasible (due to the high sclerotic nature of the collapsed vertebral body) resulting in a technical success rate of 66.7%. This patient underwent percutaneous vertebroplasty in the same session. No complication was observed. Comparing the pain scores of patients who underwent vertebroplasty prior (mean value 9 NVS units) and after (mean value 1.7 NVS units) treatment there was a mean decrease of 7.3 NVS units on terms of pain reduction, effect upon mobility and life quality. However, on these two patients (who underwent percutaneous vertebroplasty) a progress of the vertebral body damage was noticed with widening

of the fracture line (lines). Imaging control of the fracture line widening was performed with x-rays and cone-beam CT scan with 3D reconstructions. At 6 months there was a stabilization of the imaging findings, a factor which led to the decision of conservative therapy (brace) and observation.

#### CONCLUSION

Percutaneous augmented vertebroplasty can be proposed as initial treatment in symptomatic AO-Magerl A2 and A3 vertebral fractures. The implant functions as an internal cast which provides a mechanical support structure while potentially providing height restoration. Preliminary results report significant pain reduction and mobility improvement but further studies are required.

**KEY WORDS:** Vertebroplasty, spine, supported augmentation

#### eP-266

##### Comparison of Treatment Efficiency between the Penumbra Coil 400™ System and Conventional Coils in Cerebral Aneurysm Embolization

Kamath, A. Polykarpou, M. Patel, A. A. Parikh, S. Polanco, A. Moyle, H. Patel, A. B.

Mount Sinai School of Medicine  
New York, NY

#### PURPOSE

The Penumbra coil 400™ system (PC 400) are a new generation of softer platinum coils with a larger diameter than conventional embolic coils (Controls). The larger diameter with the inherent softness of the coils should result in a higher packing density of coils within aneurysms treated with embolization. The purpose of this study was to assess the efficiency of the PC 400's filling advantage in the treatment of cerebral aneurysms as compared to conventional coils. Particular focus was put on the comparison of packing density, embolization time and the number of coils required for aneurysm occlusion.

#### MATERIALS & METHODS

This was a single center, retrospective case-review of 95 aneurysm cases treated in 94 patients by the PC 400 (N = 16) or Controls (N = 79). The aneurysm and procedural characteristics listed below were evaluated. Aneurysm volume and packing density were calculated using AngioCalc ([www.angiocalc.com](http://www.angiocalc.com)), an open source aneurysm calculator endorsed by the manufacturers of the currently available coil systems. The data then were evaluated for statistical significance.

Results	PC 400 (N=14-16)	Controls (N=70-79)
Mean Age (yrs)	59	55
Location: ICA / P Comm. / MCA / Other (%)	50 / 31.3 / 6.3 / 12.4	41.8 / 21.5 / 8.9 / 27.8
Aneurysm Volume (mean) (cc)	204.3	187.2
Ruptured (%)	46.7	50.4

# Coils used (mean)	3.9*	6.1
Coil Length (mean) (cm)	36.3	56.9
Stent Assisted Coiling %	37.5	32.9
Procedure Time (mean)(min)	45.7*	64.1
Packing Density (mean)(%)	36.8**	28.1
Procedural Events	0	0

\*P < 0.05 \*\*P < 0.005 (Nonparametric Wilcoxon Ranked Test)

#### CONCLUSION

Aneurysm embolization with PC 400 achieved statistically significant greater packing density compared with conventional coils. This was achieved with significantly less procedure time and less total number of coils with a trend towards less total coil length for similar aneurysm volume. In addition, there were no procedure-related neurologic events. Our data confirm that when compared to conventional coils, the PC 400 is indeed more efficient in the embolization of cerebral aneurysm. Follow-up studies will be required to confirm the durability of these treatment results.

**KEY WORDS:** Coils, aneurysm, penumbra

#### eP-267

##### Feasibility, Efficacy and Safety of Transbrachial Approach for Carotid Artery Stenting

Iwata, T. Mori, T. Tajiri, H. Miyazaki, Y. Nakazaki, M.

Shonan Kamakura General Hospital  
Kamakura, JAPAN

#### PURPOSE

Transfemoral approach for carotid artery stenting (CAS) is a common technique, but patients must be bedridden for several hours following CAS. If CAS can be performed through the brachial artery route, it is less invasive for patients. The purpose of our study was to investigate the feasibility, efficacy and safety of transbrachial approach for CAS.

#### MATERIALS & METHODS

Transbrachial approach for CAS was started in October 2010 and data were collected prospectively. Included for analysis were patients who underwent transbrachial elective CAS from October 2010 to August 2011. Every CAS was started through the right brachial route with a 6Fr (ID) guiding sheath specifically designed for the brachial approach under local anesthesia. Technical success, periprocedural complications, 30-day major cardiovascular events (stroke, myocardial infarction and death) and 3-month stent restenosis were investigated.

#### RESULTS

Forty-five patients underwent transbrachial CAS. Procedures were successful through the brachial route in every case. Periprocedural complications occurred in three cases; confusion following CAS in one case, hypotension in one case and gastrointestinal hemorrhage in one case. Three patients returned to the previous state within a few days and had no neurologic

deficits. No access site-related complications occurred. Patients were free on the bed immediately after CAS even during hemostasis. Major cardiovascular events did not occur on the 30th day. Restenosis occurred in one patient only at 3 months.

#### CONCLUSION

Transbrachial CAS is feasible and safe, and has the same efficacy as transfemoral CAS.

**KEY WORDS:** Brachial artery, carotid artery stent

#### eP-268

##### Keyhole Carotid Stenting for Patients with Moderate to Severe Chronic Renal Insufficiency

Kizilkilic, O.·Kocak, B.·Korkmazer, B.·Tureci, E.·Kocer, N.·Islak, C.

Cerrahpasa Medical School  
Istanbul, TURKEY

#### PURPOSE

The carotid endarterectomy procedure might be hazardous for patients who had high risk factors because of the required general anesthesia. We describe a new carotid stenting approach for selected patients with moderate to severe chronic renal insufficiency using minimum dose of contrast media by smart mask technology as an alternative to the carotid endarterectomy.

#### MATERIALS & METHODS

Three patients with carotid artery stenosis and moderate to severe chronic renal insufficiency were included in this study. Level of the blood creatinine, ischemia-related symptoms, age and other diseases of the patients were considered in patient selection. A biplane neuroangiography suite was used to perform our technique. A biplane run which included cervical and intracranial parts of the carotid artery in a large FOV was obtained with using 6 mL contrast media at 50% dilution. Best biplane image frames of filled cervical carotid artery were selected from the run and immediately converted biplane roadmap images by smart mask technology. Placement of an embolic protection device, balloon predilatation, deployment of the stent, postdilatation and retrieving the protection device performed one by one on the same roadmap image without using any extra contrast media. The postprocedure angiography in same FOV was performed with using 6 mL contrast media at 50% dilution. The deployment of the stent and intracranial blood flow were evaluated in one biplane run. Twelve mL contrast mixture at 50% dilution (total contrast dose was 6 ml) was used during all of the procedures. The patients were followed up with considering level of the blood creatinine for 2 days.

#### RESULTS

The keyhole carotid stenting technique was performed with no technical failure and procedural (intraprocedural and postprocedural) complication in

all patients. There was no impairment of the renal function induced by this technique in the follow up.

#### CONCLUSION

The keyhole carotid stenting is a new alternative to the surgery focused on using minimal dose of contrast media without any impairment of the renal function for patients with moderate to severe chronic renal insufficiency.

**KEY WORDS:** Keyhole carotid stenting, chronic renal insufficiency

#### eP-269

##### Effect of N-Butyl 2-Cyanoacrylate/Ethiodized Oil Ratio on Injection Time and Radio-Opacity on CT and Digital Subtraction Angiography: An Experimental Flow Model Investigation

Gauvin, S.<sup>1,2</sup>·Cortes, M. D. P.<sup>1</sup>·Roncarolo, F.<sup>2</sup>·Tampieri, D.<sup>1</sup>

<sup>1</sup>Montreal Neurological Institute and Hospital, Montreal, QC, CANADA, <sup>2</sup>McGill University, Montreal, QC, CANADA

#### PURPOSE

Successful and permanent embolization of cerebral arteriovenous malformations (AVMs) requires experience and understanding of polymerization dynamics and radio-opacity properties of N-butyl 2-cyanoacrylate (NBCA) and its adjuvant, ethiodized oil. Polymerization time has been studied previously under different angles: time to acquire visual opacity, time to stop the flow and real-time analysis of binding forces. We conducted an in vitro experiment using a flow model to investigate the impact of various NBCA/ethiodized oil ratios on injection time and radio-opacity on CT and digital subtraction angiography (DSA).

#### MATERIALS & METHODS

Embolizations were performed on an in vitro flow model consisting of a graduated column filled with 0.9% NaCl solution at  $37 \pm 2^\circ\text{C}$ , a Cook side arm and plastic tubes as model vessels. Under DSA guidance, an interventional neuroradiologist injected three different mixtures of NBCA (Histoacryl®, B. Braun Medical, France) and ethiodized oil (Lipiodol® Ultra-Fluide, Guerbet LLC, USA): 25/75, 50/50 and 75/25 (%vol NBCA/ %vol ethiodized oil). The three mixtures were tested under low flow and high flow conditions ( $100 \pm 10$  ml/min and  $150 \pm 10$  ml/min). Injection time was recorded using a chronometer. A CT scan of the plastic model vessels was performed. Radio-opacity on CT and DSA was measured on Picture Archiving and Communication System (PACS) using a 0.12 square centimeter round area positioned on glue cast.

#### RESULTS

A total of 25 embolizations were performed with an average embolic material volume of 0.11 ml per injection. At low flow rate, analysis of variance (ANOVA) showed a statistically significant difference between injection times when comparing the three NBCA/ethiodized oil ratios ( $p < 0.05$ ). The

neuroradiologist took significantly more time to inject under low flow conditions than high flow conditions (Student's t-test,  $p < 0.05$ ). Radio-opacities on CT were significantly different at high flow rate only (ANOVA,  $p = 0.05$ ) although we could not establish any linear relationship. A significant difference in DSA radio-opacities was observed between 25/75 and 50/50 NBCA/ethiodized oil ratios (Student's t-test,  $p < 0.05$ ).

#### CONCLUSION

Injection time appears to vary depending on NBCA/ethiodized oil ratio and flow conditions. Embolic material radio-opacity on CT and DSA also is influenced by different NBCA/ethiodized oil ratios. These preliminary findings emphasize the importance of training and support the idea that flow models could be used in simulation centers for residents and fellows to acquire experience with the embolic material behaviors in flow and its appearance on DSA.

**KEY WORDS:** N-Butyl 2-Cyanoacrylate, polymerization, radio-opacity

#### eP-270

##### Endovascular Treatment of Acute Anterior Large Brain Vessel Occlusions with and without Preceding Intravenous Thrombolytic Bridging Therapy

Schmidt, H.·Schramm, R.·Hypa, S.·Knauth, M.·Bähr, M.·Schramm, P.

University Goettingen Medical Center  
Goettingen, GERMANY

#### PURPOSE

Without rapid recanalization, the outcome after acute large vessel occlusion of the anterior cerebral circulation is poor. Many patients develop a hemispheric infarction with life-threatening consequences. Endovascular thrombectomy can reconstitute the blood supply but outcome data on combined intravenous and intraarterial treatment for the anterior cerebral circulation are sparse.

#### MATERIALS & METHODS

We retrospectively analyzed 4 years of data of patients referred to our institution with acute occlusion of the proximal MCA or the distal ICA after mechanical thrombectomy ( $n = 94$ ,  $f = 51$ ,  $m = 43$ ) with (80%) or without (20%) concomitant rtPA therapy. Outcome was measured by the modified Rankin scale (mRS) after 3 month. A logistic regression was performed to detect independent associations with the mRS.

#### RESULTS

The in-hospital mortality (14.7%) was similar for the treatment groups (Pearson  $\chi^2$   $p = 0.82$ ) and for both the MCA and ICA occlusion groups ( $p = 0.68$ ). The median (25<sup>th</sup>/75<sup>th</sup>) outcome NIHSS at discharge was 10 (5/17), the mRS after 3 months (3/5) 4 for the group with endovascular treatment with bridging concept, and 9 (6/12) and 3 (3/5) for the group with concomitant rtPA therapy (n.s.). Logistic regression analysis revealed the important influence of age and NIHSS at admission

on the mRS ( $p = 0.02$  and  $0.007$ , resp.) but could not show differences for treatment modalities or other variables. In the univariate analysis a premedication with intravenous r-tPA did not lead to a significant better NIHSS or mRS when compared to endovascular treatment alone. Cognitive outcome measures will be reported at the meeting.

#### CONCLUSION

By reconstitution of blood supply, endovascular therapy often can prevent complete MCA or MCA/ACA infarction. The loss of neurologic functional abilities represented by a higher NIHSS at admission is a major predictive factor for the long-term result of the endovascular intervention.

**KEY WORDS:** Acute large brain vessel occlusion, endovascular treatment, intravenous thrombolytic bridging therapy

#### eP-271

##### Free-Floating Carotid Thrombus: Clinical and Imaging Findings in 17 Cases with CT Angiographic Follow Up

Carpenter, J. S.·Raghuram, K.·Rai, A.·Deberry, J.·Brown, P.

West Virginia University  
Morgantown, WV

#### PURPOSE

To investigate the clinical and imaging presentation, time course of resolution, and treatment regimens of patients presenting with free-floating thrombi at the level of the carotid bifurcation.

#### MATERIALS & METHODS

The reports of all patients within the past 10 years at a single tertiary referral hospital having undergone at least two CT angiographic studies encompassing the carotid bifurcations were reviewed. Reports denoting intraluminal defects, thrombi, or filling defects were evaluated further. All studies with free-floating clot were identified and those with at least one follow-up examination were selected for inclusion in this study. A chart and image review was performed to extract demographic information, symptoms at presentation, medical treatment regimen, degree of underlying stenosis, clot volume, stroke volume and disposition to either surgery, stenting, or medical therapy alone. Subsequent strokes during the follow-up period also were recorded.

#### RESULTS

All patients ( $n = 17$ , 14 male) presented with acute ischemic strokes (median stroke volume = 6 ml) in the perfusion territory of the floating clot (median intraluminal clot volume = 61 mm<sup>3</sup>). Resolution of the clot by either natural history or medical therapy occurred in 10 cases. In the remaining seven, either the clot remained at final imaging or was removed during endarterectomy. Median underlying stenosis was 70%. Primary medical therapy included no additional



treatment (2 cases), aspirin alone (4 cases), heparin (7 cases), t-Pa (3 cases) and dual antiplatelet therapy (1 patient). Seven patients ultimately underwent carotid endarterectomy while three received stents. The underlying degree of stenosis within the artery ranged from 30 to 92% (median = 70). Median time to documented persistence of the clot was 4 days while median documented resolution of the clot was 33 days. These varied widely with t-Pa having documented resolution of the clot at a median of 3 days (mean = 5) while aspirin therapy alone had a median documented resolution time of 90 days (mean = 89). One pathologically proven clot persisted and was removed by endarterectomy at day 99 post stroke. Three recurrent strokes occurred during the follow-up period, one of which resulted in death.

#### CONCLUSION

Free-floating thrombi at the level of the carotid bulb are uncommon (less than 0.5% of CT angiograms encompassing the neck) and present a therapeutic challenge. In this series, the finding was invariably associated with an acute stroke, although usually small (median stroke volume = 6 ml) and had an overwhelming male predominance (82%). There was wide variation in time to the resolution of the clot with the exception of those patients that had received iv t-Pa for their acute stroke. Unless the patient received t-Pa there seems to be little indication for repeat imaging before day 5 but given the wide variation in treatment and imaging intervals in this study, the optimal time to repeat imaging remains undefined.

**KEY WORDS:** Atherosclerosis, thrombus, CTA

**Monday, April 23 –  
Wednesday, April 25  
6:30 AM - 9:00 PM  
Thursday, April 26  
6:30 AM - 3:00 PM  
Americas Hall II**

**Electronic Posters  
(ePosters) 272 - 296**

**eP4 – PEDIATRICS**

**Note: A missing printed number indicates an abstract has been withdrawn.**

**eP-272**

**Brain MR Imaging Pattern Recognition in Pol III-Related Leukodystrophies**

La Piana, R.<sup>1</sup>•Tonduti, D.<sup>2</sup>•Gordish Dressman, H.<sup>3</sup>•Loewenstein, J.<sup>3</sup>•Bernard, G.<sup>4</sup>•Vanderver, A.<sup>2</sup>

<sup>1</sup>Montreal Neurological Institute, Montreal, QC, CANADA, <sup>2</sup>Children's National Medical Center, Washington, DC, <sup>3</sup>Center for Genetic Medicine Research, Washington, DC, <sup>4</sup>Montreal Children's Hospital, Montreal, QC, CANADA

#### PURPOSE

The aim of our study is to describe the neuroradiologic features of Pol III-related leukodystrophies, a spectrum of hypomyelinating disorders including tremor-ataxia with central hypomyelination (TACH), leukodystrophy with oligodontia, and hypomyelination with hypodontia and hypogonadotropic hypogonadism (4H), all caused by mutations in genes encoding the human RNA polymerase III (Pol III). The identification of a common MRI pattern of white matter involvement was crucial in considering these diseases as a continuum. In a systematic analysis of MRI findings of hypomyelinating disorders, Steenweg et al. identified a cluster of features characteristic of patients with 4H which include hypomyelination, cerebellar atrophy and T2 hypointensity of the anterolateral thalamus, the pyramidal tracts, and the dentate nuclei. The objectives of our study are 1) to test this neuroradiologic pattern in a sample of Pol III-mutation proved patients; 2) to compare the neuroradiologic findings of patients with Pol III related with those of patients with other hypomyelinating leukodystrophies.

#### MATERIALS & METHODS

The MRI exams of 14 patients with mutation-proved Pol III leukodystrophy were reviewed. The neuroradiologic findings were analyzed according to the following criteria described by Steenweg et al. as characteristic of 4H: diffuse hypomyelination, cerebellar atrophy, and T2 hypointensity of the anterolateral thalamus, the pallida, the pyramidal tracts, and the dentate nuclei. The MRI findings of 14 control subjects with other types of hypomyelinating disorders [GM1 gangliosidosis, Pelizaeus-Merzbacher disease, Pelizaeus -Merzbacher-like disease (PMLD), hypomyelination with atrophy of the basal ganglia and cerebellum (HABC), Salla disease] were reviewed for the same criteria used in the analysis of patients with Pol-III-related leukodystrophy. Logistic regression analysis was used to identify if the proposed criteria can discriminate between Pol III-related leukodystrophy and other hypomyelinating leukodystrophies.

#### RESULTS

All of the subjects with Pol III-related leukodystrophy presented diffuse hypomyelination, associated in 92.8% of cases with T2 hypointensity of the thalami, in 78.5% with T2 hypointensity of the pallida, in 64.3% with T2 hypointensity of the dentate, in 50% with T2 hypointensity of the pyramidal tracts and in 92.8% with cerebellar atrophy. In the non-Pol III hypomyelinating disorders, T2 hypointensity of thalami, pallida or dentate nuclei was found in a minority of cases (21.4%), including HABC and PMLD. Cerebellar atrophy was found in 50% of cases, including as expected HABC. The combination of the analyzed criteria can identify patients with Pol III-related leukodystrophy with a

sensitivity of 85.7%, a specificity of 92.9% and a total error rate of 10.7%.

#### CONCLUSION

Our study confirms that Pol III-related leukodystrophy is a hypomyelinating disorder characterized by diffuse hypomyelination associated in the large majority of cases with T2 hypointensity of anterolateral thalami, pallida and dentate nuclei and with cerebellar atrophy. This neuroradiologic pattern was highly sensitive and specific for Pol III-related leukodystrophy and can, thus, help in narrowing the differential diagnosis in hypomyelinating disorders.

**KEY WORDS:** White matter, hypomyelination, Pol-III related disorders

#### eP-273

#### Spinal MR Imaging Findings in Metachromatic Leukodystrophy

Alkan, O.·Erol, I.·Yildirim, T.·Altinkaya, N.·Demir, S.

Baskent University  
Adana, TURKEY

#### PURPOSE

To present spinal MR imaging findings in two patient with metachromatic leukodystrophy (MLD).

#### MATERIALS & METHODS

We present two patients (2 male, ages: 2- 4 years). Twenty-four-month-old male child presented with hypotonia, sensorimotor polineuropathy, decreased leukocyte arylsulfatase-A activity. Second case presented with hypotonia. MR images of brain and spine were examined.

#### RESULTS

Brain MR of the first case showed areas of T2 prolongation within the periventricular white matter and splenium of the corpus callosum. Brain MR of the second case revealed areas of T2 prolongation within the periventricular and deep cerebral white matter with sparing of the subcortical U fibers (Figure 1a). Imaging of the spine displayed marked contrast enhancement of nerve roots at the level of the cauda equine in all cases (Figure 1b).



## CONCLUSION

Metachromatic leukodystrophy is one of the more common leukodystrophies with well documented intracranial findings. However, spinal manifestations on MR images are being reported only recently. Lumbosacral nerve root contrast enhancement may accompany the intracranial findings of MLD, and spinal imaging may prove useful in diagnosing or differentiating the various leukodystrophies.

**KEY WORDS:** Metachromatic leukodystrophy, spinal MR imaging

## eP-274

### Pictorial Review of MR Imaging Features of Focal Cortical Dysplasias

Sahu, C. D., Jilwan, M. N.

University of Virginia  
Charlottesville, VA

## PURPOSE

Focal cortical dysplasia is a heterogeneous entity, encompassing a wide range of alterations of cortical development. It is the most common cause of refractory epilepsy in children and a very common etiology of refractory epilepsy in adults. Surgical benefits are closely related to the histopathologic subtype and extent of involvement. The purpose is to present a pictorial review of the spectrum of MRI findings in patients with focal cortical dysplasia.

## MATERIALS & METHODS

We retrospectively identified all patients who underwent surgical treatment for medically refractory epilepsy at our institution over the past 5 years. We reviewed their preoperative MRI and correlated the imaging findings with the pathologic diagnosis of focal cortical dysplasia.

## RESULTS

The International League Against Epilepsy recently has reclassified focal cortical dysplasias according to their histopathology into three types: I (abnormal cortical layering), II (including IIa: dysmorphic neurons without balloon cells and IIb: dysmorphic neurons with balloon cells), and III (abnormal cortical lamination adjacent to another lesion). Our patients' imaging is consistent with the data available in the literature. Patients with types I, IIa and type III cortical dysplasia frequently have a normal preoperative MRI, with only few patients exhibiting cortical atrophy in the region of dysplasia. Type IIb cortical dysplasia manifests by abnormal subcortical white matter signal, which tapers toward the ventricular margin (transmantle sign), blurring of the gray-white matter junction, and focal prominence of the subarachnoid space in the region of abnormality. We illustrate a wide spectrum of abnormalities ranging from subtle findings to large areas of abnormal cortical development, with an emphasis on the adequate imaging technique to identify milder cases.

## CONCLUSION

Most cases of focal cortical dysplasias identified by imaging are of the IIb subtype. Careful analysis of the preoperative MRI and knowledge of the imaging findings are crucial to identify the more subtle forms of this very prevalent disorder in patients with medically refractory epilepsy.

**KEY WORDS:** Focal cortical dysplasia

## eP-275

### Spectrum of MR Imaging Abnormalities of Focal Cortical Dysplasia Based on the Consensus Classification of the International League Against Epilepsy - 2010

Simao, G. N., Velasco, T. R., Ozaki, J. O., Cintra, M. B., Rosset, S., Sakamoto, A. C., Pittella, J. E. H., Serafim, L. N., Santos, A. C.

University of Sao Paulo, Brazil  
Ribeirao Preto, SP, BRAZIL

## PURPOSE

The purpose of this electronic education exhibit is to review the MR findings of focal cortical dysplasia (FCD) based in the 2010 ILAE consensus for FCD. Since the first description of focal cortical dysplasia (FCD) in 1971 by Taylor and colleagues, several classification schemes have been proposed. In 2010, a task force of the ILAE proposed a consensus clinicopathologic classification for focal cortical dysplasia, defining clear concepts of FCD 1 and 2, and creating the FCD type 3. The main clinical manifestation of FCD is epilepsy and unless the area of dysplasia is large, patients do not have severe neurologic deficits.

## MATERIALS & METHODS

In order to show and review the spectrum of MR appearance of FCD, the clinicopathologic and MR records of 122 patients who underwent resective epilepsy surgery at the Clinics Hospital of Ribeirao Preto Medical School from 1995 to 2010 were reviewed. This is a tertiary University Hospital of University of Sao Paulo, a national reference site for epilepsy surgery in Brazil. The pathologic analysis was based in the 2010 ILAE consensus for FCD. Milder forms of FCD classified as type Ia, Ib and Ic are characterized by abnormal radial, tangential and both respectively. MR findings in these types of malformations are used negative or sometimes characterized by reduced volumes of affected compared to the nonaffected hemisphere. Cortical dyslamination is also present in type II of FCD. The hallmark of type IIa of FCD variant is the presence of dysmorphic neurons and in type IIb is the presence of dysmorphic neurons and balloon cells, which have variable glial fibrillary acidic protein (GFAP) and neurofilament staining patterns. There is usually a reduction of myelin staining in the underlying white matter. The imaging findings in type II of FCD is variable. Blurring of the gray-white matter junction in T1-weighted images, mimicking increase of cortical thickness, increased subcortical white matter signal in T2-weighted images and T2-FLAIR images and

sometimes extending toward the ventricle (transmantle) can be seen. In type III FCD, the cortical malformation is associated with other epileptogenic lesion, such as cortical lamination abnormalities in the temporal lobe associated with hippocampal sclerosis (type IIIa), adjacent to a glial or glioneuronal tumor (type IIIb), adjacent with vascular malformation (type IIIc) and adjacent to any other lesion acquired during life, like a trauma, ischemic injury and encephalitis (type IIId).

#### RESULTS

Beside qualitative analysis, quantitative T2, magnetization transfer and DTI changes related with FCD were accessed.

#### CONCLUSION

In conclusion, FCD are classified in different types, each one characterized by some different pathologic findings and there also are some different and associated imaging findings that can characterize them.

**KEY WORDS:** Focal cortical dysplasia, epilepsy, cortical malformation

#### eP-276

##### Aberrant Course of the Cortico-Spinal Tracts in the Brainstem as Revealed by Diffusion Tensor Imaging/Tractography

Meoded, A.<sup>1</sup>•Poretti, A.<sup>1</sup>•Dzirasa, L.<sup>2</sup>•Izbudak, I.<sup>1</sup>•Huisman, T. A. G. M.<sup>1</sup>

<sup>1</sup>The John Hopkins Medical School, Baltimore, MD, <sup>2</sup>John Hopkins Odenton, Baltimore, MD

#### PURPOSE

The corticospinal tracts (CST) are major descending pathways connecting the motor cerebral cortex with the spinal cord. The middle portion of the cerebral peduncle is believed to contain the predominant portion of the CST passing through the brainstem and reach the spinal cord. Aberrant pyramidal tracts (APT) are defined as functionally intact but aberrantly located CST. The detailed course and function of the APT have not been elucidated yet. We report on the fiber tractography (FT) findings in a 1-year-old boy that presented with left side hypotonia.

#### MATERIALS & METHODS

Brain magnetic resonance imaging (MRI) was performed on a 1.5 T scanner (Avanto, Siemens Medical Systems, Erlangen, Germany). The standard departmental protocol includes a single-shot spin-echo, echo planar (EPI) axial DTI sequence. Parameters used were: balanced pairs of diffusion gradients were applied along 20 orthogonal directions; a b value of 0 s/mm<sup>2</sup> and 1000 s/mm<sup>2</sup> was used; TR = 7100 ms, TE = 84 ms, slice thickness: 2.5 mm, FOV = 192 x 192 mm; matrix = 240 x 240. Parallel imaging iPAT= 2 with GRAPPA (Generalized Auto-Calibrating Partial Parallel Acquisition reconstruction) was applied. Diffusion tensor images were postprocessed using DTI Studio software (H. Jiang & S. Mori, Johns Hopkins University). After correction for eddy currents and motion artifacts,

all images were coregistered to one another. Fiber tractography reconstruction was performed off-line using Medinria software (Asclepios Research Team, INRIA Sophia Antipolis, France).

#### RESULTS

Conventional MRI demonstrated asymmetry of the cerebral peduncles and midbrain. The right cerebral peduncle was significantly smaller than the left one. In addition, the right side of the pons was smaller than the left side. There were three foci of abnormal signal intensity: hyperintense in T2-weighted sequences, located in the periventricular white matter. The signal alteration partially extended into the deep layers of the overlying cortex. Overall, the right hemisphere appeared slightly smaller than the left one. The septum pellucidum was absent, corpus callosum was intact. Diffusion tensor imaging study revealed "absence" of the right corticospinal tract at the level of the cerebral peduncle in the midbrain, best seen on color fractional anisotropy (FA) maps. Tractography demonstrated aberrant course of the CST, which was located more posteriorly and laterally, intermixed with the medial lemniscus tracts at the level of the pons. Moreover, at the level of the right precentral gyrus the right CST appeared more dispersed.

#### CONCLUSION

Collateral pathways of the pyramidal tract have been described as APT. The radiologist who performs the MRI should be familiar with this unusual entity in order to make the correct diagnosis, especially because the APT can be misdiagnosed as absence of the pyramidal tract on conventional imaging; fiber tractography in such cases can reveal the real course of neuronal pathways and hence be an important diagnostic tool.

**KEY WORDS:** Cortico-spinal, tractography, aberrant

#### eP-277

##### Pediatric Cerebellar Tumors: Correlation between Apparent Diffusion Coefficient Values and Histology

Poretti, A. • Meoded, A. • Huisman, T. A. G.

The Johns Hopkins Medical School  
Baltimore, MD

#### PURPOSE

An accurate preoperative diagnosis is mandatory based on the different natural history, therapy strategy, and outcome of the various cerebellar tumors. Diffusion-weighted imaging (DWI) may effectively distinguish tumor types and histologic grades in tumors. High-grade tumors with high cellularity and large nuclear area should have restricted diffusion and a low apparent diffusion coefficient (ADC). The role of DWI for differentiation of cerebellar tumors has been evaluated recently. Unfortunately, the results of these studies are controversial. We aimed to evaluate the ADC values of different pediatric cerebellar tumors in our cohort of patients.

## MATERIALS & METHODS

A retrospective study was performed including patients with histologically proven cerebellar tumors evaluated presurgically between January 1, 2008 and March 31, 2011. All MRI studies were performed on 1.5 T MR units and included multiplanar T1- and T2-weighted, fluid-attenuated inversion recovery (FLAIR), postcontrast T1-weighted images, and DWI sequences. For each patient, three regions of interest (ROI) were positioned manually within the enhancing solid portion of the tumor and the mean ADC value was calculated. Additionally, control ADC values were obtained within the macroscopically normal-appearing cerebellum and in both thalami. Subsequently, a ratio between tumor and control ADC value as well as the mean value between both thalamic ADC values was calculated for each patient. The absolute ADC values and the ratios were compared with the histology grade of the tumors (high versus low grade) and with the histologic subtype.

## RESULTS

Twenty-four patients matched the inclusions criteria and included 12 females and 12 males with a median age of 10 years at the date of MRI (mean 9.05 years, range 29 days to 18.5 years). Thirteen patients had a high-grade tumor (54%, including medulloblastoma, glioblastoma, WHO grade III ependymoma, and atypical teratoid/rhabdoid tumor), 11 a low-grade tumor (juvenile pilocytic astrocytoma, WHO grade II astrocytomas and ependymoma). Absolute ADC values (mean 1.65, SD 0.51 vs  $0.63 \pm 0.18$ ), cerebellar ADC ratio ( $2.27 \pm 0.74$  vs  $0.83 \pm 0.25$ ), and thalamic ratio ( $2.21 \pm 0.75$  vs  $0.79 \pm 0.23$ ) were significantly higher in low-grade tumors than in high-grade tumors ( $P < 0.0001$ ). Additionally, absolute ADC values ( $1.63 \pm 0.4$  vs  $0.58 \pm 0.09$ ), cerebellar ADC ratio ( $2.22 \pm 0.63$  vs  $0.78 \pm 0.12$ ), and thalamic ratio ( $2.16 \pm 0.58$  vs  $0.72 \pm 0.12$ ) were significantly higher in low-grade astrocytomas ( $n = 9$ ) than in medulloblastomas ( $n = 9$ ,  $P < 0.0002$ ). Significant differences between the other histologic subgroups could not be found. Overlap was seen for WHO grade II and WHO grade III ependymomas.

## CONCLUSION

Assessment of ADC values in enhancing solid parts of cerebellar tumors generally allow to correctly differentiate high- and low-grade tumors before surgery. A cut-off ADC value of  $1.2 \times 10^3 \text{ mm}^2/\text{s}$  was found for low-grade astrocytomas. Overlap was however present for WHO grade II and WHO grade III ependymomas. Additional advanced MRI modalities may increase the presurgical differentiation of pediatric cerebellar tumors.

**KEY WORDS:** Cerebellar tumors, pediatric, diffusion-weighted imaging

## eP-278

### Rare Case of Infantile Myofibromatosis with Central Nervous System Involvement and Complete Regression

leon, j. L.·Garcia-Ferrer, L.·aliaga, r.·Pastor, R.·campos, s.

Hospital Clinico Universitario de Valencia  
Valencia, SPAIN

## PURPOSE

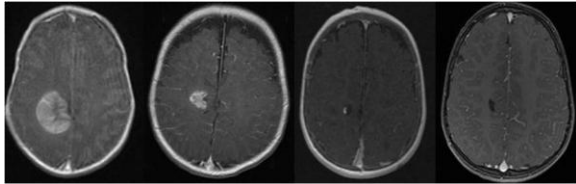
Infantile myofibromatosis is a rare infantile pathology typically characterized by lesions of skin, muscle, subcutaneous tissue, or bone. Visceral and central nervous system (CNS) is less frequent. There are two forms of disease: solitary and multicentric. The clinical evolution in the solitary form usually is a benign course with spontaneous regression. The multicentric form has a poor prognosis, especially in the patients with visceral and CNS involvement due to the progressive growing of the lesions with intestinal obstruction, lung failure or brain compression. To our knowledge, this is the first report of infantile myofibromatosis with supra and infratentorial CNS involvement described at birth and also with complete remission.

## MATERIALS & METHODS

A newborn boy was admitted to our hospital because multiple subcutaneous masses in thorax, back, pelvis, hand and also in the tongue. There were no familiar antecedents and the pregnancy had been without medical problems. An extension study was done with skeletal survey, ecocardiography, thorax and abdominal CT that demonstrated bone lesions in femur, multiple soft tissue nodules in the gluteus, left psoas, abdominal wall and retroperitoneal musculature. There was visceral involvement with multiple nodules in both lungs. A transfontanelar ultrasonography showed an echogenic nodule in the right parietal lobe, so a brain MRI was done. There were multiple supra and infratentorial nodules, hyperintense T1-weighted and hypointense T2-weighted, with a maximum measurement of 3 cm and with white matter edema surrounding the bigger lesions. After paramagnetic contrast was administered, multiple tiny lesions were evident with a number bigger than ten. Biopsy was performed on the hand lesion and was histologically diagnostic of infantile myofibromatosis.

## RESULTS

The baby had no clinical symptoms so a careful observation was decided. During the next 4 years, serial brain MRI studies showed a progressive regression of the lesions until its complete resolution. Also, the subcutaneous and lung involvement disappeared.



During four years, serial brain MRI Studies showed a progressive regression of the lesions until its complete resolution

#### CONCLUSION

Although little prevalent, it is important to know the imaging findings in order to do an appropriate diagnosis. In absence of clinical symptoms, a "look and wait" attitude could avoid aggressive interventions.

**KEY WORDS:** Myofibromatosis, CNS involvement, complete regression

#### eP-279

#### Corpus Callosum Changes in Patients with Obstructive Hydrocephalus after Ventriculoperitoneal Shunting

Alkan, O.<sup>1</sup> Kizilkilic, O.<sup>2</sup> Yildirim, T.<sup>1</sup> Sarica, F.<sup>1</sup> Demir, S.<sup>1</sup>

<sup>1</sup>Baskent University, Adana, TURKEY, <sup>2</sup>Istanbul University, Istanbul, TURKEY

#### PURPOSE

To evaluate signal abnormalities within the corpus callosum after ventricular shunting for obstructive hydrocephalus.

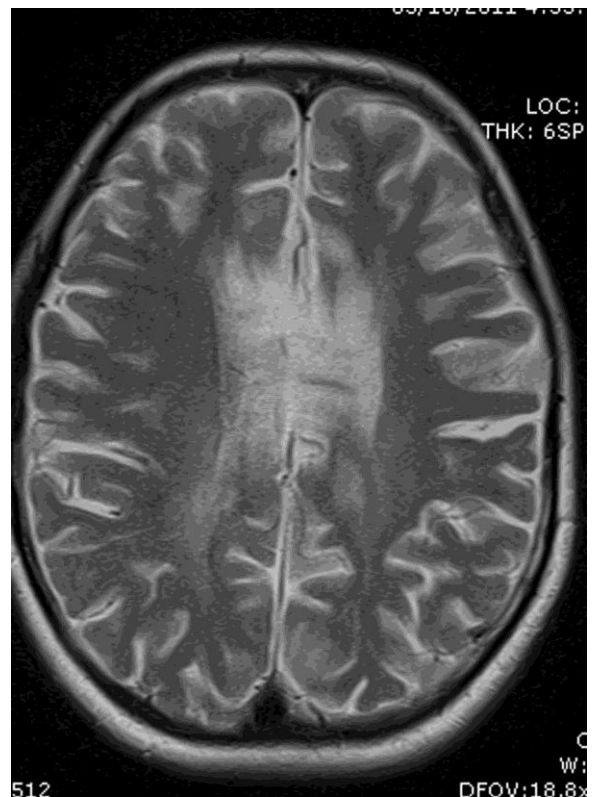
#### MATERIALS & METHODS

We present five patients (2 female, 3 male, age: 8-15 years) who underwent successful shunting for hydrocephalus. Amongst five patients with hydrocephaly; one medulloblastoma, one midbrain glioma, two aqueductal stenosis, and one traumatic hydrocephaly were identified.

#### RESULTS

MR imaging of corpus callosum before shunting was normal. All patients who underwent successful shunting for hydrocephalus subsequently developed signal changes in the corpus callosum. Brain MR showed hypointense signal on T1-weighted images and hyperintense signal on T2-weighted images within the corpus callosum. Four of the patients had signal changes in the corpus of the corpus callosum with sparing of the splenium and genu while one case had signal changes in the corpus and splenium of the corpus callosum (Figure 1a, b). Signal abnormalities within the corpus callosum after ventricular shunting for obstructive hydrocephalus are not uncommon. Lesions in the corpus callosum, both diffuse and focal, have been described in patients with long-standing hydrocephalus after shunting. The exact mechanism responsible for the production of these callosal lesions is unknown, although they may be the result of ischemia with subsequent demyelination caused by prolonged severe stretching of the corpus callosum from ventriculomegaly and subsequent rapid decompression

of the ventricles. These lesions appear hypointense on T1-weighted images and hyperintense on T2-weighted images, with sparing of the splenium. Although the changes may persist on imaging, they appear clinically silent.



#### CONCLUSION

In conclusion, this distinctive appearance should not be mistaken for significant disease. Recognition of this pattern of signal abnormality will help avoid unnecessary intervention.

**KEY WORDS:** Obstructive hydrocephalus, corpus callosum, ventriculoperitoneal shunting



## eP-280

### Acute Transverse Myelitis: Extent of T2 Intramedullary Signal and Clinical Outcome in the Pediatric Patient

Abbott, E.<sup>1</sup>Gross Kelly, T. C.<sup>1</sup>Zwienenberg-Lee, M.<sup>1</sup>Maheshwari, M. C.<sup>2</sup>Segall, H. C.<sup>2</sup>

<sup>1</sup>Wisconsin Children's Hospital, Milwaukee, WI,

<sup>2</sup>Wisconsin Children's Hospital, Brookfield, WI

#### PURPOSE

The aim of this retrospective pilot study is to evaluate whether spinal cord MR imaging features in children with acute transverse myelitis (ATM) are: (1) predictive of clinical outcome and (2) correlate with abnormal cerebrospinal fluid (CSF) and serology lab values.

#### Materials and Methods

After IRB approval was obtained and the radiologic database was searched, we preliminarily identified seven patients (age 9 months - 17 years old) who presented in the emergency room between 2007 and 2011 with a diagnosis of ATM and underwent MRI of the spine. Intramedullary spinal cord signal was evaluated by measuring maximum AP, transverse and craniocaudal dimension as well as the number of levels involved, for those lesions that were discontinuous. The Hughes scale was used to determine functional outcome.

#### RESULTS

All seven patients (100%) exhibited T2 hyperintense intramedullary cord signal. Four of seven (57%) demonstrated corresponding T1 hypointense intramedullary signal. Two patients with the least favorable clinical recovery and functional outcomes also had T2 hyperintense intramedullary lesions that were largest in craniocaudal dimension and were distributed most extensively throughout the spinal cord. On the other hand, neither the craniocaudal dimension nor extent of intramedullary T2 hyperintensity correlated with abnormal laboratory values (CSF pleocytosis and rise of protein level, serum pleocytosis or serologic evidence of a preceding infection). Additional data points will be collected to confirm our preliminary findings.



#### CONCLUSION

This preliminary retrospective pilot study suggests that the craniocaudal measurement and extent of intramedullary T2 hyperintense signal in the spinal cord of children with the diagnosis of acute transverse myelitis may be predictive of clinical outcome. However, size of the lesion did not correspond to abnormal CSF and serum laboratory values.

**KEY WORDS:** MR imaging, transverse, myelitis

## eP-281

### Evaluation of the Ischemic Penumbra with Susceptibility-Weighted Imaging in Children Affected with Arterial Ischemic Stroke

Meoded, A. Poretti, A. Tekes, A. Huisman, T. A. G. M.

The Johns Hopkins Medical School  
Baltimore, MD

#### PURPOSE

The occurrence of cerebrovascular disease is at least as common as brain cancer in children. The presenting symptoms and the clinical findings are often unspecific or misleading. Susceptibility-weighted imaging (SWI) is a new high-resolution magnetic resonance technique capable of evaluating cerebral hemodynamic and tissue viability. The goals of our study are (a) describing the clinical characteristics of children affected with ischemic stroke, (b) report the morphologic, distribution and intensity characteristics of venous structures in the ischemic region and (c) the assessment of the penumbra region by correlating SWI and diffusion-weighted imaging (DWI).

#### MATERIALS & METHODS

We retrospectively studied SWI and corresponding DWI findings in eight children who suffered from acute ischemic stroke. We also evaluated the DWI SWI mismatch in the infarcted areas. Trace of diffusion and apparent diffusion coefficient (ADC) maps were calculated from the raw diffusion tensor imaging (DTI)

data sets and were evaluated with the corresponding SWI. Signal intensity of intramedullary and sulcal veins was evaluated on SWI and was graded: 0, 1, 2 as similar, lower or significantly lower compared to noninfarcted region, respectively. In addition, the caliber (prominence) of intramedullary and sulcal veins was evaluated and graded: 0, 1, 2, 3 as normal, mildly, significantly wider or diminished, respectively. In addition, match/mismatch of DWI and SWI (DWI area less, equal or greater than SWI) areas was evaluated. Finally, SWI was inspected for additional signal abnormalities. Institutional IRB was achieved.

## RESULTS

Various patterns of normal/alterd venous drainage could be identified. Seventy-five percent (6/8) of the patient had their MRI study in the first 24 hours, 12.5% (1/8) in the first 48 hours and 12.5% (1/8) in the first 72 hours. The cause of stroke was related in: 37.5% (3/8) of patients to cardio-embolic event, in 12.5% (1/8) to inadvertent puncture of the right carotid artery, and in 12.5% (1/8) of patients to right carotid artery occlusion. In 25% (2/8) of patients no cause was identified. In 93.3% (14/15) of arterial distribution territories, there was a match between SWI and DWI images. Only in 6.7% (1/15) of regions there was a mismatch (SWI>DWI). Finally, infarcted cortex was hyperintense in the mismatch area in 13.3 % (2/15), and mildly hyperintense in 13.3 % (2/15) of the regions. In addition, in 13.3% (2/15) of regions, hemorrhagic transformation was seen.

## CONCLUSION

High quality SWI studies may provide important noninvasive data about critical brain perfusion by focusing on the venous drainage in acute cerebral ischemia. Our retrospective study corroborates the importance of SWI in the evaluation of critically perfused brain at risk for infarct progression. We would like to emphasize the importance of SWI in the diagnosis of stroke subtype and its potential role in therapeutic decision making, especially in the presence of salvageable tissue.

## eP-282

### Black Holes on Gradient-Echo MR Imaging in Pediatric Patients following Cardiac Interventions

Maller, V. G.·Choudhary, A. K.·Coulter, W.

Penn State Milton S. Hershey Medical Center  
Hershey, PA

## PURPOSE

To analyze the gradient-echo MR imaging changes in pediatric patients who underwent cardiac interventions to detect microparticle embolization.

## MATERIALS & METHODS

We reviewed the gradient MR images of 25 pediatric patients ranging from 1 month to 18 years who underwent cardiac interventions in the past 10 years at our hospital. The MR imaging findings of the patients

were reviewed to look for evidence of foci of blooming on gradient-echo sequence.

## RESULTS

We detected multiple punctuate foci of blooming on gradient images representing black holes scattered in the brain in 17/25 (68%) cases, including 12 in bilateral cerebral hemispheres. Five patients had foci of blooming in the cerebellar hemispheres.

## CONCLUSION

Multiple punctuate foci of blooming on gradient-echo images in the brain parenchyma is common in postcardiac intervention patients. These likely represent microparticle embolization during or following the intervention. The clinical significance of this finding needs to be established with further studies.

**KEY WORDS:** Black holes, cardiac, microemboli

## eP-283

### Probabilistic Diffusion Tensor Metrics and Volumetric Assessment of the Corpus Callosum at 3.0 T in Children with NF-I

Duy, L. A. N.·Watts, R.·Nickerson, J. P.·Filippi, C. G.

University of Vermont College of Medicine  
Burlington, VT

## PURPOSE

The purpose of this study was to assess the corpus callosum of children with NF-I using MR diffusion tensor imaging (DTI) at 3.0 T with probabilistic FSL and to examine cross-sectional areas of callosal segments using volumetric MR sequences.

## MATERIALS & METHODS

Seven patients with NF-I, six boys, one girls, mean age 5.3 years (range 3-17) and 11 age-matched normal controls, ten boys, one girl, mean age 5.1 years (range 3-17) had brain MR scans at 3.0 T with six direction DTI. Data were postprocessed on Mac workstation using FSL probabilistic DTI software. Fractional anisotropy, mean diffusivity, and axial and radial diffusivities (minor Eigen values) were determined for rostrum, genu, anterior and posterior body, isthmus, and splenium of the corpus callosum. Spoiled gradient volumetric isotropic T1 imaging was used to determine cross-sectional areas of the callosal segments. NF-I children with history of OPG (optic pathway glioma) or neurofibromatosis bright spots were excluded.

## RESULTS

Compared to age-matched controls, there were statistically significant decreases in fractional anisotropy in the genu, anterior body, and isthmus, but no significant differences with respect to mean diffusivity. Secondary eigen values, the radial diffusivity specifically, was elevated statistically in the anterior body and genu although major eigen value was not significantly different. Cross-sectional area showed that the children with NF-I had statistically significant larger

areas within the isthmus and posterior body of the corpus callosum.

#### CONCLUSION

There are statistically significant abnormalities in the corpus callosum of children with NF-I including reduced anisotropy in the genu, anterior body, and isthmus with no changes in mean diffusivity but elevations in the radial diffusivity, a minor eigen value that was statistically significant in the genu and anterior body. Lack of mean diffusivity changes argues against intramyelinic edema or vacuolization and may suggest other microstructural dysgenesis or architectural distortion, which will need further study.

**KEY WORDS:** Diffusion tensor MR, NF-I, probabilistic DTI

#### eP-284

##### Proton MR Spectroscopy in Acute Neonatal Focal Brain Lesions: Evidence for Metabolic Perturbations Outside of the Lesion

Wisnowski, J. L.<sup>1,2</sup>Choi, S.<sup>2</sup>Paquette, L.<sup>1</sup>Hamilton, A.<sup>1</sup>Panigrahy, A.<sup>3,1</sup>Damasio, H.<sup>2</sup>Bluml, S.<sup>1</sup>

<sup>1</sup>Children's Hospital Los Angeles, Los Angeles, CA, <sup>2</sup>University of Southern California, Los Angeles, CA, <sup>3</sup>Children's Hospital of Pittsburgh at the University of Pittsburgh Medical Center, Pittsburgh, PA

#### PURPOSE

The human brain is heavily interconnected. It remains to be determined how focal lesions in the acute epoch impact neuronal functioning in regions structurally or functionally connected to the damaged area. To address this, we retrospectively analyzed 1H MRS data from 13 neonates who presented with either an acute stroke (n=7) or focal parenchymal hemorrhage (n=6; excluding IVH) and compared those to our reference sample of 39 term neonates without evidence of brain injury, analyzing, whenever possible, both lesion voxels and our standard gray matter(sd GM) and white matter voxels(sd WM), which were outside of the lesion as demonstrated by both T2- and diffusion-weighted imaging.

#### MATERIALS & METHODS

Single-voxel 1H MR spectra were acquired as part of our clinical neonatal imaging protocol in the medial parietal-occipital gray matter(sd GM), parietal white matter(sd WM), and/or centered in the lesion (excluding blood products) using short echo time PRESS (TE=35 ms; TR=1.5 sec, 128 averages, 3 mm<sup>3</sup> voxel). All processing was performed using LCModel software (Stephen Provencher Inc., Oakville, Ontario, Canada). Absolute metabolite concentrations(in mmol/kg tissue) of N-acetylaspartate (NAA), creatine(Cr), total choline (Cho), myo-inositol(mI), glutamate (Glu), glutamine (Gln)(and also glutamate/glutamine complex, Glx), glucose(Glc), lipids(Lip) and lactate(Lac) were determined as well as ratios relative to Cr. Group differences (patients versus controls) were determined using a standard t-test.

#### RESULTS

In the lesion voxels, there was a significant decrease in Cr, mI, NAA, Cho, and an elevation in Lac and Lip, as well as a significant increase in the ratio of Glx/Cr. In the sd GM region, there was a trend toward significant elevation in Lac and in the ratio Lac/Cr. In the sd WM region, there was a significant elevation in the concentration of glucose and in the ratio of Glu/Cr.

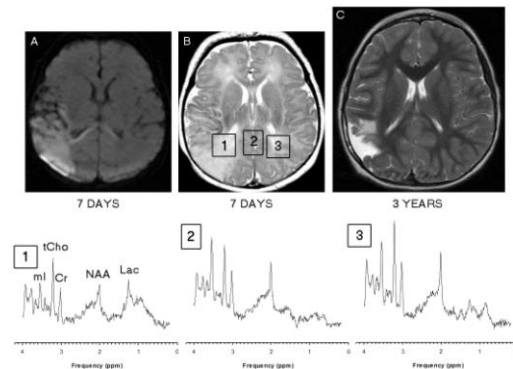


Figure. Spectra from a 7 day old infant with an acute infarct in the right parieto-temporal region. Trace DWI image (A) demonstrating diffusion restriction and T2-weighted image (B) showing voxel placement. (Note: 1 and 3 represent the middle of the 3D voxel, whereas 2 represents the lower boundary of the voxel.) Follow-up MRI at 3 years of age demonstrates chronic cavitated lesion.

#### CONCLUSION

In this study, we were able to document metabolic changes not only in the center of an acute focal brain lesion, but also in regions outside of the acute lesion. The increased lactate in the gray matter region may result from either diffusion of lactate along injured axons or altered metabolism at the cell body of neurons whose axons were damaged. The increased glucose in the nonlesioned white matter may reflect diminished neuronal activity due to less reciprocal input/output between lesioned and nonlesioned tissue. Clinically, these findings indicate that we may need to develop normal reference points for the nature and time course of MRS abnormalities in lesioned and "healthy" tissue.

**KEY WORDS:** MR spectroscopy, stroke, neonates

#### eP-285

##### Predictors of Outcome in Childhood Intracerebral Hemorrhage: A Consecutive Cohort Study

Naggara, O.<sup>1</sup>Jousset, C.<sup>2</sup>Blauwblomme, T.<sup>2</sup>Zerah, M.<sup>2</sup>Puget, S.<sup>2</sup>Sainte Rose, C.<sup>2</sup>Meder, J.<sup>1</sup>Boddaert, N.<sup>2</sup>Brunelle, F.<sup>2</sup>

<sup>1</sup>Université Descartes, Sorbonne Paris Cité, Sainte Anne Hospital, Paris, FRANCE, <sup>2</sup>Université Descartes, Sorbonne Paris Cité, Necker Hospital, Paris, FRANCE

#### PURPOSE

The purposes of this study were to describe features of children with intracerebral hemorrhage (ICH) and to determine predictors of short-term outcome in a single-center prospective consecutive cohort study.

#### MATERIALS & METHODS

All spontaneous ICH in children aged 1 to 18 years were included from January 2008 to July 2011. Exclusion

criteria were inciting trauma, intracranial tumor, isolated epidural, subdural, intraventricular, or subarachnoid hemorrhage, hemorrhagic transformation of ischemic stroke, and cerebral sinovenous thrombosis. Hospitalization records were abstracted. Follow-up assessments included outcome score using the King's Outcome Scale for Childhood Head Injury (KOSCHI). Intracerebral hemorrhage volumes and total brain volumes were measured by manual tracing.

## RESULTS

Sixty-three patients (median age  $7.9 \pm 5.2$  years; range, one day to 18.0 years) had presenting symptoms of headache in 30/63 (48%), focal deficits in 25/63 (40%), altered mental status in 22/63 (35%), and seizures in 19/63 (30%). Vascular malformations caused hemorrhage in 41/63 patients (65%) including 27 brain arteriovenous malformation (43%), six cavernoma (10%), five aneurysms (8%), one dural arteriovenous fistula (1.6%). Surgical treatment (hematoma evacuation, lesion embolization or excision) was performed at the acute phase in 47/63 patients (75%). Two patients (3.2%) died acutely. At a median follow up of 11.3 months (range, 1 to 40 months), 30/61 (49%) of survivors had neurologic deficits (KOSCHI score of 3 or 4) and 31/61 had good outcome (KOSCHI score of 5). Unfavorable clinical outcome was associated with higher initial volume hematoma ( $p = 0.01$ ), initial altered mental status ( $p = 0.006$ ). Age, gender, location, intraventricular hemorrhage, hydrocephalus did not seem to influence clinical outcome.

## CONCLUSION

Spontaneous childhood ICH was due mostly to vascular malformations. Acute surgical intervention was commonly performed. Although death was rare, 49% of survivors had persisting neurologic deficits. Higher initial volume hematoma and initial altered mental status predicted clinically significant disability.

**KEY WORDS:** Pediatrics, intracerebral hemorrhage, outcome

## eP-286

### Neuroradiologic Findings in Congenital Disorders of Glycosylation Type 1

Farage, L.<sup>1</sup>Rizzo, I. P. O.<sup>2</sup>Carvalho, D. R.<sup>2</sup>Speck-Martins, C.<sup>2</sup>Brum, J. M.<sup>2</sup>

<sup>1</sup>Brasilia University, Brasília, BRAZIL, <sup>2</sup>SARAH Hospital, Brasília, BRAZIL

## PURPOSE

Congenital disorders of glycosylation (CDG) are pan-ethnic diseases, which comprises more than 40 distinct subtypes, usually inherited as autosomal recessive trait. Glycosylation is a process that occurs in many proteins involved in cell signaling, receptor mediation and several other functions. Clinical manifestations range from organ-specific disorder to severe multisystemic disease.

## MATERIALS & METHODS

We retrospectively reviewed image studies (head CT and brain MRI) of 17 CDG type 1 patients (12 PMM2-CDG, and 5 neither-PMM2 nor-MPI-CDG).

## RESULTS

Cerebellar atrophy was found in all patients, except one (non-PMM2 non-MPI-CDG). Olivopontocerebellar atrophy was found in four patients. Ischemic changes was found in one patient.

Number	Gender, age at scan	CDG Type	Imaging	Scanner	Cerebellum	Brainstem	Supratentorial	Other abnormalities
			CT/MRI		Yermis	hemispheres	White matter	
1	M, 15	PMM2	CT	8 multislice	severe atrophy	severe atrophy		atrophy of temporal pole
2	F, 15	PMM2	MRI	1.5T	moderate atrophy	moderate atrophy		mild atrophy
3	F, 15	PMM2	MRI	0.5T	mild atrophy	mild atrophy		
4	F, 2	PMM2	MRI	0.5T	severe atrophy	moderate atrophy		
5	F, 2	PMM2	MRI	1.5T	severe atrophy	moderate atrophy		
6	M, 4	PMM2	MRI	1.5T	moderate atrophy	moderate atrophy		
7	M, 5.5	PMM2	MRI	1.5T	severe atrophy	severe atrophy	pons atrophy	
8	F, 11	PMM2	CT	non-helical	severe atrophy	severe atrophy		physiological changes enlargement
	F, 17	PMM2	MRI	1.5T	severe atrophy	severe atrophy	pons atrophy	
9	F, 16	PMM2	CT	non-helical	severe atrophy	severe atrophy	pons atrophy	
10	F, 20	PMM2	MRI	1.5T	severe atrophy	severe atrophy	pons atrophy	
11	F, 21	PMM2	MRI	1.5T	moderate atrophy	moderate atrophy		atrophy of temporal pole
12	F, 23	PMM2	MRI	1.5T	moderate atrophy	moderate atrophy		
13	M, 0.1	not PMM2	CT	64 multislice	mild atrophy	mild atrophy		incomplete myelination
14	M, 0.5	not PMM2	CT	8 multislice	normal	normal		agitated
15	M, 1	not PMM2	CT	64 multislice	severe atrophy	severe atrophy		
16	M, 1.5	not PMM2	CT	64 multislice	mild atrophy	mild atrophy		moderate atrophy
17	F, 6	not PMM2	MRI	1.5T	mild atrophy	mild atrophy	Cerebral peduncle atrophy (Vallian degeneration)	Ischemic changes in lentiform nucleus and thalamus

## CONCLUSION

Although cerebellar atrophy is not a specific finding, its presence should alert radiologists and clinicians for the possibility of CDG. Cerebellum frequently is reduced in CDG patients, just one of our 17 had normal brain and cerebellum, but he was one of the youngest in series.

**KEY WORDS:** Congenital disorders of glycosylation, cerebellum atrophy, CDG

## eP-287

### Myelination of the Fetal Midbrain on Diffusion Tensor Imaging

Woitek, R. Kasprian, G. Weber, M. Prayer, D.

Medical University of Vienna  
Vienna, AUSTRIA

## PURPOSE

In rat-pups diffusion anisotropy imaging has been shown to demonstrate postnatally increasing white matter myelination of the brainstem more sensitively than other conventional imaging modalities (Prayer D, Neuroradiology 1997). We investigated whether diffusion tensor imaging (DTI) in fetuses with normal central nervous system (CNS) development is capable of showing changes in fractional anisotropy (FA) or apparent diffusion coefficient (ADC) in the midbrain correlated with gestational age. An increasing FA would point to ongoing prenatal myelination as myelin constrains diffusion perpendicular but not parallel to fibers.

## MATERIALS & METHODS

During clinically indicated MRI (1.5 T) in 70 fetuses (17-38 GW, normal CNS development) T2W FSE sequences in three orthogonal planes of the fetal brain and an axial, single-shot, echo planar diffusion tensor sequence (32 noncollinear diffusion gradient encoding directions) perpendicular to the long axis of the fetal brainstem were acquired. After coregistering T2W FSE axial images with axial FA color-coded maps a region of interest (ROI) was drawn in the midbrain to calculate FA and ADC.

#### RESULTS

A significant positive correlation between gestational age (GA) and FA was found ( $r = .5$ ,  $p < .001$ ) and a significant negative correlation was found between GA and ADC ( $r = -.381$ ,  $p = .002$ ).

#### CONCLUSION

We could show a significant positive correlation of GA with FA and a significant negative correlation with ADC in the fetal midbrain. Increasing FA during gestation can be explained by increasing myelination. Therefore FA measurements are capable of demonstrating prenatal myelination in fetuses with normal CNS development and might serve to investigate (ab-)normal myelination or brainstem compression in hydrocephalus or Chiari II malformations.

**KEY WORDS:** Fetal MR imaging, midbrain, myelination

#### eP-288

##### Clinical Utility of Ultrashort TE Proton MR Spectroscopy in Imaging Diseases of the Pediatric Brain

Boyko, O. B. • Shiroishi, M. • Zee, C. • Law, M.

University of Southern California Keck School of Medicine  
Los Angeles, CA

#### PURPOSE

To compare the clinical utility of ultra-short TE single voxel proton MR spectroscopy (MRS) with standard short TE single voxel proton MRS using either STEAM or PRESS in imaging diseases of the pediatric brain.

#### MATERIALS & METHODS

Fifteen patients underwent single voxel MR spectroscopy at 1.5 T using either STEAM or PRESS for water and fat suppression. MR spectroscopy was acquired with ultrashort STEAM (12-15 msec) and ultrashort PRESS (20-25 msec) with standard short TE STEAM (20 msec) or standard short TE PRESS (30-35 msec). The shortest default TR allowed by the scanner was utilized.

#### RESULTS

Ultrashort TE proton MRS was acquired successfully in all patients including the supratentorium and posterior fossa. Outer saturation bands prior to shimming could only be prescribed for ultrashort TE PRESS acquisitions and not STEAM acquisitions. Peak height variability was noted between ultrashort STEAM and PRESS for

Choline. Metabolites in the 2.0-2.4 ppm range (Glx/Gln) tended to have sharper peak distinction utilizing ultrashort STEAM MRS. Myo-inositol at 4.06 ppm was highest relative to choline in imaged neonates if their supratentorial white matter, peak height varying by TE and method of water/fat suppression.

#### CONCLUSION

Ultrashort TE proton MRS using STEAM or PRESS can be acquired technically at 1.5 T. Sharper peak distinction at 2.35 ppm (Glx/Gln) can be demonstrated on both STEAM and PRESS ultrashort TE MRS compared to short TE STEAM and PRESS MRS. Brain metabolites having a short T1 can have a higher peak height signal on ultrashort TE STEAM PRESS than on standard short TE PRESS but this showed variability in the neonatal population group. Ultrashort TE STEAM should be considered for brain lesions where metabolite differentials that have short T1 metabolites are anticipated.

**KEY WORDS:** Myo-inositol, MR spectroscopy, steam

#### eP-289

##### Incidence of Forniceal Fusion and Dorsal Cysts in Lobar Holoprosencephaly

Ramirez, P. • Rouse, G. • Oyoyo, U. • Toure, S. • Harder, S. L.

Loma Linda University Medical Center  
Loma Linda, CA

#### PURPOSE

The holoprosencephalies are a complex of congenital abnormalities that are related to incomplete cleavage of the embryonic brain characterized by abnormalities of the forebrain and abnormal mid-line separation of the cerebral hemispheres and diencephalic structures. The most widely accepted classification separates this spectrum of abnormalities into three major types: alobar, semilobar, and lobar holoprosencephaly. The primary aim of the study is to measure the incidence of lobar holoprosencephaly in a high risk obstetrical population. The study also evaluated the presence of fused fornices and dorsal cyst. These features have been documented in the obstetrical literature (Pilu et al, 1994) as specific features of lobar holoprosencephaly although they are not described as well in the neuroradiology literature.

#### MATERIALS & METHODS

Cases with findings consistent with lobar holoprosencephaly were identified from prenatal ultrasounds performed from 2000 to 2011 at a high risk maternal fetal ultrasound clinic. The number of lobar holoprosencephaly cases then were compared to the total number of prenatal ultrasound cases performed during this time period to establish an incidence in this high risk population. Ultrasound and MRI examinations of these patients then were reviewed to further characterize associated findings in lobar holoprosencephaly.

## RESULTS

A total of 75 cases of holoprosencephaly were identified among a cohort of 22,455 prenatal ultrasound examinations over an 11-year period with an incidence of 1 in 299. Sixteen cases of lobar holoprosencephaly were identified for an incidence of 1 in 1,403. The following findings were identified in patients with lobar holoprosencephaly: absent septum pellucidum (100%), fused fornices (75%) and dorsal cyst (75%).

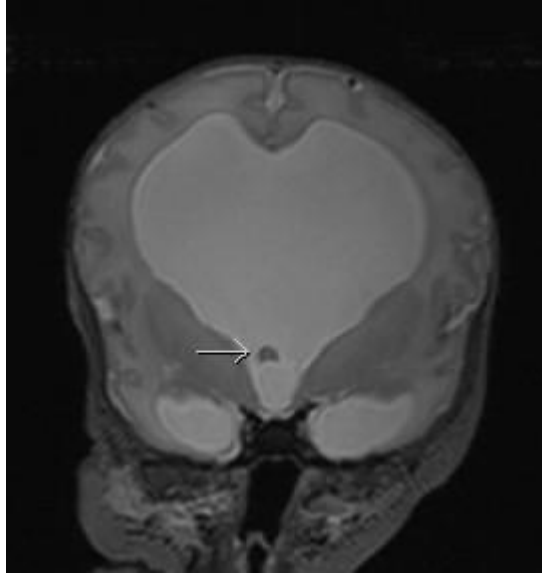


Figure 1: Lobar holoprosencephaly with a fused fornical mass (arrow) and absent septum pellucidum.

## CONCLUSION

As expected, the incidence of lobar holoprosencephaly in a high risk obstetrical population is higher than in the general population. Absence of the septum pellucidum, fusion of the fornices and a dorsal cyst are important diagnostic features because of their high incidence in patients with lobar holoprosencephaly.

**KEY WORDS:** Lobar holoprosencephaly, fusion of the fornices

## eP-290

### Nontraumatic Posterior Fossa Hemorrhage in Children

Shekdar, K. V.·Feygin, T.·Santi-Vinci, M.·Roarke-Adams, L.·Storm, P.·Zimmerman, R. A.

The Children's Hospital of Philadelphia  
Philadelphia, PA

## PURPOSE

To review imaging findings and etiologies of nontraumatic posterior fossa hemorrhage in children.

## MATERIALS & METHODS

We retrospectively reviewed 15 cases of nontraumatic posterior fossa hemorrhage in children. We excluded neonates and infants from our study. All studies included an initial CT scan evaluation followed by MR imaging. Additional MR angiography and catheter angiography was required in six cases.

## RESULTS

After excluding hemorrhage in neonates and infants, nontraumatic posterior fossa hemorrhage in children comprised a very small group. Review of imaging findings of our group of patients revealed the following: Hemorrhage in underlying mass lesion - seven cases: five - primitive neuroectodermal tumors (PNETs), one - atypical teratoid rhabdoid tumor (ATRT), one - ependymoma. Vascular malformations - five cases: two cerebellar arteriovenous malformations (AVMs), one spinal AVM, two cavernomas. Stroke -one and Indeterminate cause - two. Results based on etiology of nontraumatic posterior fossa hemorrhage:

## Results

## CONCLUSION

Nontraumatic posterior fossa hemorrhages in children are usually secondary to underlying pathologies such as primary neoplastic mass lesions, or vascular abnormalities such as arteriovenous malformations or cavernomas. Among the neoplastic lesions PNETs are the biggest group which can present with hemorrhage. Among the vascular malformations we found nearly equal incidence of cavernomas and AVMs. A search should always be made for vascular abnormality in the spine if no obvious underlying posterior fossa malformation is detected. Some uncommon cause of posterior fossa hemorrhage in children include dural venous sinus thrombosis and rarely arterial posterior circulation stroke.

: #	Etiology	#	
7	Hemorrhage in underlying mass	5	PNET
		1	ATRT
		1	Ependymoma
5	Vascular malformations	2	Cerebellar AVM
		1	Spinal AVM
		2	Cavernomas
1	Stroke	1	
2	Indeterminate cause	2	

## CONCLUSION

Nontraumatic posterior fossa hemorrhages in children are usually secondary to underlying pathologies such as primary neoplastic mass lesions, or vascular abnormalities such as arteriovenous malformations or cavernomas. Among the neoplastic lesions PNETs are the biggest group which can present with hemorrhage. Among the vascular malformations we found nearly equal incidence of cavernomas and AVMs. A search should always be made for vascular abnormality in the spine if no obvious underlying posterior fossa malformation is detected. Some uncommon cause of posterior fossa hemorrhage in children include dural venous sinus thrombosis and rarely arterial posterior circulation stroke.

**KEY WORDS:** Nontraumatic, posterior fossa, hemorrhage



## eP-291

**Feasibility of Fetal MR Imaging at 3.0 T with Parallel Transmission MR**

Filippi, C. G.<sup>1</sup> Powers, A.<sup>1</sup> Nickerson, J. P.<sup>1</sup> Sussman, B.<sup>1</sup> Watts, R.<sup>1</sup> Andrews, T.<sup>2</sup>

<sup>1</sup>University of Vermont College of Medicine, Burlington, VT, <sup>2</sup>Philips Health Care, Cleveland, OH

**PURPOSE**

To demonstrate the feasibility of fetal MR imaging at 3.0 T with the use of parallel transmission MR. Newer techniques are needed for more accurate detection of fetal brain anomalies with the hope of enhanced prognostication and may aid in research regarding fetal development.

**MATERIALS & METHODS**

Ten cases of suspected fetal anomalies on ultrasound were referred for MR imaging at 3.0 T performed with and without multitransmit MR. Oblique axial, sagittal, and coronal single shot T2-weighted turbo spin echo (TSE) images were obtained of the fetus with variable imaging parameters depending on fetal lie and maternal size: TR 2500-3500, TE 120, 4-6 NEX Philips SENSE XL Torso Coil (Best, Netherlands), FOV 200 to 250 mm, slice thickness 3-4 mm, and sequence duration less than 90 secnds. Total scan time less than 10 minutes in all cases.

**RESULTS**

Three cases of agenesis of the corpus callosum with ventricle size exceeding 15 mm. Three cases of Dandy Walker malformation in which one case had marked ventriculomegaly exceeding 20 mm with dependent material in the ventricles. One case of arachnoid cyst in left middle cranial fossa, one case normal, one case of Chiari II malformation, and one twin gestation case in which a fetus had undergone demise and the surviving fetus had severe hypoxic injury. Fetal MR cases were scanned from 20th to 32nd week of gestation. Three cases led to termination. Three cases had follow-up MR imaging after delivery confirming findings on MR in utero. In all cases image quality was better with parallel transmission MR with less dielectric shading. SAR values on all images was < 0.7W/kg with average of 0.4W/kg.

Figure 1a and 1b

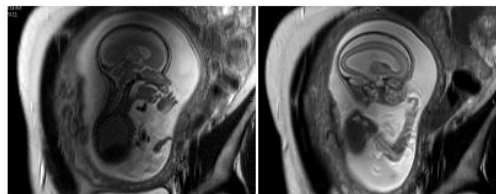


Figure on left is with conventional MR. Figure on the right is with parallel transmission MR with less dielectric shading and better uniformity of signal.

**CONCLUSION**

Fetal MR imaging at 3.0 T with parallel transmission is feasible and diagnostic.

**KEY WORDS:** fetal MR, 3.0 T, parallel transmission MR

## eP-292

**Neuroimaging Findings of Gadolinium Imaging of Pediatric Brain Disease Using Gadobenate Dimeglumine: A Higher Relaxivity Contrast Agent**

Boyko, O. B. Yan, C. & Shiroishi, M. Lerner, A. Zee, C. Law, M.

University of Southern California Keck School of Medicine  
Los Angeles, CA

**PURPOSE**

To demonstrate the clinical imaging findings at 1.5 T using a higher relaxivity contrast agent (HRCA) gadolinium contrast agent gadobenate dimeglumine (MultiHance®) in pediatric neuroimaging.

**MATERIALS & METHODS**

Fifty patients were studied with postgadolinium axial T1-weighted and coronal T1-weighted SPGR sequences as well as 10 of these patients with pre and postgadolinium T2 FLAIR imaging. Two radiologists scored enhancement intensity of FLAIR signal abnormality as none, minimal, mild and moderate. In addition five patients with perfusion calculating relative cerebral blood volume (rCBV) and dynamic contrast enhancement (DCE) vascular permeability (Ktrans) were acquired and reviewed. Quantitative regions of interest (ROI) measurements were made of normal structures (air, fat, globe, white matter, head of caudate, CSF, basal ganglia, and cortical gray matter), normal-enhancing structures (choroid plexus, pituitary stalk and cavernous sinus) and brain lesions.

**RESULTS**

The majority of enhancing lesions were scored as mild or moderate. Nonenhancing lesions such as thrombus in venous sinus were noted to be vividly conspicuous due to surrounding normal venous sinus enhancement. In addition rCBV and Ktrans could be calculated.

**CONCLUSION**

Higher relaxivity contrast agents are now available for pediatric neuroimaging and provide additional imaging characteristics of blood-brain barrier integrity and allow for successful rCBV and Ktrans calculation.

**KEY WORDS:** Gadolinium, relaxivity, brain disease

## eP-293

**A Spatio-Temporal Latent Atlas for Fetal Brain Development**

Dittrich, E.<sup>1</sup> Riklin-Raviv, T.<sup>2</sup> Kasprian, G.<sup>1</sup> Brugger, P. C.<sup>1</sup> Prayer, D.<sup>1</sup> Langs, G.<sup>1</sup>

<sup>1</sup>Medical University of Vienna, Vienna, AUSTRIA,  
<sup>2</sup>Brigham and Women's Hospital, Boston, MA

**PURPOSE**

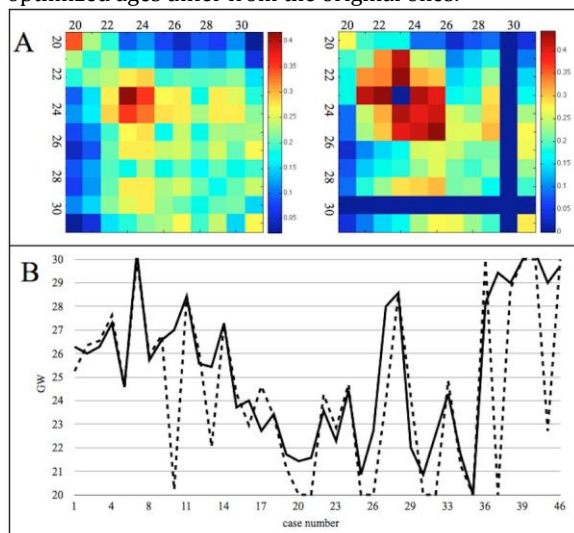
Novel imaging methods such as ultrafast magnetic resonance imaging (MRI) enable rich insights into the early human development. However, modern prenatal neuroimaging requires reference data that reflects the normal spectrum of brain development in a large series of cases. We introduce a spatio-temporal latent atlas for healthy fetuses that captures the cerebral in utero development. Based on this atlas, it is possible to segment a subcortical structure in an MRI, and afterwards re-estimate that subject's age. This opens new opportunities to a computational developmental age estimation.

## MATERIALS & METHODS

As initialization, we take advantage of only one manually annotated example in the cohort. Afterwards, we use a level-set approach to refine the segmentations in each image, and at the same time re-estimate the spatio-temporal atlas. This dynamically evolving atlas then captures the variability of the whole gestational period of interest, and the variations in between the gestational weeks. For age re-estimation, a cost function is optimized, whose minimum reveals the best-fit of the subject's age. We hypothesize that computational developmental age estimation results in an increase of coherence of cerebral morphology among equally aged subjects. Experiments with 30 manual segmentations show an improvement in the pair-wise Dice scores after the age optimization.

## RESULTS

We computed the joint histogram of the pair-wise Dice scores [binned to the gestational weeks (GW) 20 to 30] for the original age (Fig. A left) and after the optimization (Fig. A right). Consistent with the hypothesis, the joint histogram becomes narrower, which also is indicated by a drop in the entropy from 5.1583 (original age) to 4.8775 (optimized age). This demonstrates that part of the shape variability can be explained by an age shift. Fig. B shows how much the optimized ages differ from the original ones.



## CONCLUSION

A spatio-temporal latent atlas was proposed that represents healthy fetal brain development. It captures the variability of the emergence of subcortical

structures, and can be used to re-estimate a subject's gestational age. Future research will extend this atlas to segment pathologic cases.

**KEY WORDS:** Fetal brain development, atlas, segmentation

## eP-294

### Inner Ear Anatomy at 7 T MR of Prematurely Born Sheep

Postma, A. A. Smit, A. L. Schaëffer, S. M. Jellema, R. Kramer, B. W. Stokroos, R. J.

Maastricht University Medical Centre  
Maastricht, NETHERLANDS

## PURPOSE

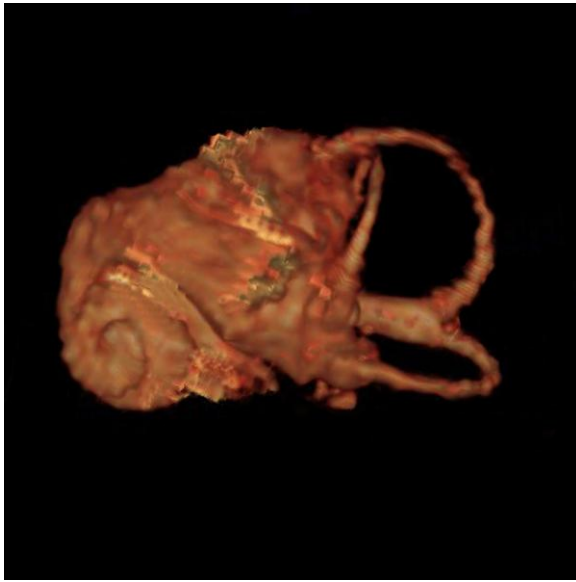
To describe normal inner ear anatomy of premature sheep at 7 T MR. Sheep models are increasingly used in ENT for otological surgery training and for research purposes. Next to anatomical similarities, the functional development of the lamb is comparable to human development. Until now one anatomical imaging study of the inner ear anatomy of adult sheep using CT has been published. No data on sheep with MR are available in the literature. To be able to study the effects of diverse insults and therapies to the normal anatomy of the inner ear radiologic imaging of the labyrinth in premature sheep is described.

## MATERIALS & METHODS

The study is part of experimental protocol for which approval of the animal ethical committee was obtained. Ex vivo the heads of 39 premature sheep (gestational age 120 days) were examined at 7 T MR. Out of these, 10 healthy premature sheep were used in this substudy. 3D T2-weighted images with whole brain and skull base coverage were performed, FOV 96 x 52 x 45 mm, matrix size: 700 x 260 x 225, voxel size 0.14 x 0.2 x 0.2 mm (Bruker Biospin USR 70/30). Images were scored visually by a neuroradiologist and measurements of the inner ear structures were performed by two ENT residents. Internal auditory canal, 7<sup>th</sup> and 8<sup>th</sup> nerve, cochlea with vestibular and tympanic scala, vestibulum, semicircular canals, round and oval windows, cochlear and vestibular aquaduct were evaluated.

## RESULTS

In all premature sheep all the inner ear structures were identified separately at both sides. The tympanic scale of the cochlea, as well as the modiolus were identified in all sheep, as well as the oval and round window. The vestibulum and three semicircular canals were present. The vestibular and cochlear aquaduct were identified. Only the 8<sup>th</sup> cranial nerve coursed through a relatively short internal auditory canal, whereas the 7<sup>th</sup> cranial nerve showed early division to the facial canal. Standardized measurements of the inner ear structures were made.



#### CONCLUSION

High-resolution MR of the inner ear of premature sheep is feasible and enhances the knowledge of the normal inner ear anatomy, which can be used in further research.

*Acknowledgement:* Financial disclosure: the study was supported by the Pediatric Fund, The NETHERLANDS

**KEY WORDS:** Inner ear, 7 T, sheep

#### eP-295

### Quantitative MR Imaging of Lower Limb Muscles in Duchenne Muscular Dystrophy: A New Approach for Monitoring the Disease Progression and Response to Therapy

Godi, C.<sup>1</sup>Gerevini, S.<sup>1</sup>Bonfiglio, S.<sup>2</sup>Lerario, A.<sup>2</sup>Napolitano, S.<sup>1</sup>Marktel, S.<sup>1</sup>Iadanza, A.<sup>1</sup>Scarlato, M.<sup>1</sup>Natali Sora, M.<sup>1</sup>Scotti, G.<sup>1</sup>Previtali, S.<sup>1</sup>Ciceri, F.<sup>1</sup>Cossu, G.<sup>1</sup>Torrente, Y.<sup>2</sup>Politi, L. S.<sup>1</sup>

<sup>1</sup>San Raffaele Scientific Institute, Milan, ITALY,

<sup>2</sup>Fondazione IRCCS Ca' Granda, Milano, ITALY

#### PURPOSE

1) To determine through magnetic resonance imaging (MRI) the pattern of lower limb involvement in Duchenne muscular dystrophy (DMD); 2) to compare quantitative MRI parameters with clinical measures in DMD patients.

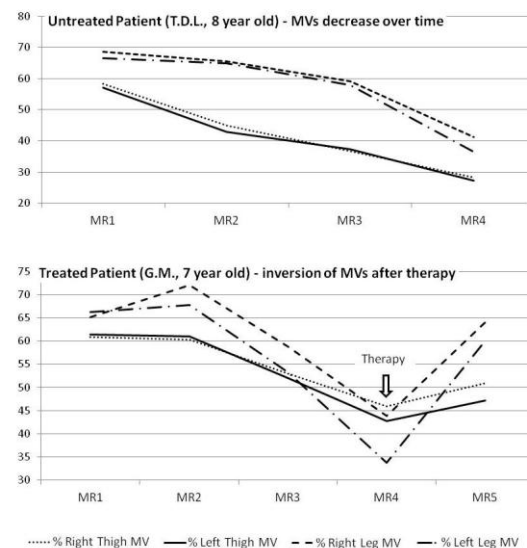
#### MATERIALS & METHODS

Twenty-six (6-12 years old) DMD patients and 4 age-matched healthy controls underwent 3 T MRI examinations of the lower limbs without sedation, at baseline and after 9 months. Axial and coronal SE T1, multi-echo T2, STIR, FSE T2-weighted and 3D THRIVE images of the legs and thighs were acquired. After threshold segmentation on T1-weighted images, the muscle volumes (MV) were measured and normalized to the entire limb volume. Muscle signal intensity derived from T1-weighted images was normalized to nearby fat intensity to obtain muscular signal intensity

ratios (SIRs) as markers of fatty degeneration. Muscle volumes and SIRs were compared with clinical measures and tests, including Gowers, 6-minute walking test, 10-meter walk time, North Star Scale and KinCom measures of isokinetic and isometric muscle strength. Three patients underwent further MRI examinations every 4 months before and after being treated with intraarterial injection of mesoangioblasts.

#### RESULTS

Fatty degeneration and atrophy were more prominent in the glutei and adductors; conversely, edema and hypertrophy were observed more frequently in the gastrocnemii, solei and tibial muscles. Duchenne muscular dystrophy patients' MV was lower than healthy subjects. Patients' SIRs (measuring fatty degeneration) were significantly higher than controls' ones, except for sartorius and gracilis. During follow up, patients showed significant thigh MV decrease and leg MV increase, while SIRs were stable or increased over time. Significant Spearman correlations between SIRs, clinical measures and thigh MV were found. In patients with suspected bad compliance, MRI disconfirmed the poor clinical results. In one patient treated with mesoangioblast transplantation, an amelioration of the above-mentioned MRI parameters and clinical test was observed.



#### CONCLUSION

MR imaging allowed an objective evaluation of muscle involvement in DMD patients; quantitative MRI provides reliable markers of muscle degeneration which correlate to neurologic/strength performances and should be employed in clinical trials as outcome measures.

**KEY WORDS:** Quantitative MR imaging, Duchenne muscular dystrophy, lower limb muscles

## eP-296

**Hemorrhagic Stroke in Term Neonates: Etiologies, Imaging Findings and Clinical Outcomes**

Klar, N.-Lin, D.

Johns Hopkins University  
Baltimore, MD**PURPOSE**

Hemorrhagic stroke in term neonates is uncommon and the causes are often unknown. In this retrospective study from a single institution we identified the etiologies behind isolated parenchymal hemorrhage in term neonates, characterized the associated imaging patterns, and correlated the results with long-term outcomes.

**MATERIALS & METHODS**

A search of our radiology database for term infants with intracranial parenchymal hematoma over 18 years (7/1992 to 3/2011) was performed. Only term infants who were 30 days old or less, and those with a predominantly parenchymal hemorrhagic pattern were included. Imaging and corresponding medical records were reviewed retrospectively and the etiology associated with the imaging findings was determined. The neonates were subdivided into five groups: nonaccidental trauma (NAT), perinatal asphyxia, infection, congenital/metabolic disorder, and unknown. The outcomes of the groups were compared.

**RESULTS**

A total of 19 cases were identified. The most common etiology of intraparenchymal hemorrhage was NAT, affecting 26.3% (5/19) of our cohort. Four (21.1%) had a difficult perinatal course with poor Apgar scores with head CT demonstrating a pattern suggestive of asphyxia. Three of these occurred in the setting of ECMO for primary cardiac or pulmonary conditions. Two (10.5%) were related to rare congenital disorders: methylmalonic academia with acute metabolic crisis that escalated to a DIC state, and incontinentia pigmenti which displayed a picture suggesting hemorrhagic necrotic encephalitis. Two (10.5%) were due to CNS infection, one presenting with an infected hematoma in the setting of *Citrobacter meningitis* and the other with hemorrhagic necrosis due to breast-feeding transmitted HSV I. Six cases (31.6%) had no identifiable risk factors or precipitating causes. These neonates were born without delivery complication and had excellent Apgar scores. Extensive workup including MRA and/or angiography for possible underlying vascular malformation, MRV, coagulopathy panel and/or genetic analysis was negative. All six who presented with spontaneous bleed of unknown etiology had excellent prognosis and were either discharged without seizure medications, or eventually were weaned off before adolescence. In contrast, those that developed parenchymal hemorrhage from known causes had significantly worse outcomes. Six out of the thirteen (46%) developed some level of developmental delay, some as severe as mental retardation and cerebral palsy. Two (15.4%) of these expired before 2 months of

age and 5 (38.5%) had no neurologic sequela. One of these was lost to follow up; however was discharged on day of life nine in good condition.

**CONCLUSION**

Although the current study population and design does not allow an estimate of the incidence of neonatal hemorrhagic stroke, our findings confirm the notion that predominantly intraparenchymal hemorrhage in full-term neonates is uncommon. There are various etiologies, some of which are rare, and others remain elusive despite extensive workup. Most patients who had unknown causes of spontaneous parenchymal hemorrhage had nevertheless excellent clinical outcome upon long-term follow up, in stark contrast to those who developed hemorrhage with known etiologies.

**KEY WORDS:** Intracranial, hemorrhage, neonatal

**Monday, April 23 -  
Wednesday, April 25**

**6:30 AM - 9:00 PM**

**Thursday, April 26**

**6:30 AM - 3:00 PM**

**Americas Hall II**

**Electronic Posters (ePosters)  
297 - 299**

**eP6 - SOCIOECONOMICS**

**Note: A missing printed number indicates an abstract has been withdrawn.**

## eP-297

**Importance of the Electronic Medical Record in Delivering High Quality Care in an Emergency Department Setting**

Franczak, M. Mark, L. P. Bergholte, J. Raslau, F. D. Klein, M. H. Ulmer, J. L.

Medical College of Wisconsin  
Milwaukee, WI

**PURPOSE**

Remote-site telemedicine is a growing phenomenon, providing increased healthcare access to patients around the world; however, remote-site telemedicine runs the risk of decreasing physician-to-physician contact, which is critical in delivering high quality care. Although electronic medical records (EMR) have been shown to optimize physician-to-physician contact, only a minority of institutions have adopted EMR. As a standard of practice at the Medical College of Wisconsin,

the EMR is accessed for all radiology examinations to search for indications beyond that entered directly by physicians, prior to rendering interpretations. This study compares the discrepancies between indications for emergency head CT scans, entered directly by emergency department (ED) physicians, with actual indications retrieved from the EMR, supported when necessary by direct verbal access to ordering physicians. Specifically, we seek to estimate the positive impact of full EMR access on patient care in the emergency department setting.

#### **MATERIALS & METHODS**

This was a prospective expert rater analysis using retrospective data from 2,000 consecutive head CT scans ordered in the emergency department of this academic Level I Trauma Center. The clinical indications entered into the electronic order directly by the ED physicians for all head CTs over a 3-month interval were compared to actual indications retrieved by practicing radiologists from the EMR, supported by direct verbal physician-to-physician contacts where necessary. Three practicing neuroradiologists independently compared the two sets of clinical indications based on the following criteria: 1) The discrepancy in *medical content* between ED physician-directed indications and actual indications retrieved through direct access to the EMR, and referring physicians where necessary. The scoring was binary; yes or no that a discrepancy existed. 2) When a discrepancy was present, each neuroradiologist determined the likelihood (very likely, possibly, or unlikely) that the discrepancy would impact their interpretation in a way that would adversely influence *medical management*.

#### **RESULTS**

A high rate of discrepancy between the physician-directed and actual EMR retrieved head CT indications was observed. On average, 49.3% of the indications showed disagreement (Figure 1, not attached). Most importantly, an average of 9.0% of the physician-entered clinical indications were rated as "very likely" to have an adverse influence on the interpretation and medical management (Figure 2, not attached). Thus, approximately 180 patients during the 3-month interval were likely to be adversely affected by the errors in physician-entered clinical indications. Additionally, 14.0% to 38.9% were rated as "possibly" having a clinically significant impact.

#### **CONCLUSION**

Due to the intense clinical demands and unique work flow requirements of ED physicians, the clinical indications entered directly by ED physicians may sometimes be incomplete or even incorrect. This study suggests that discrepancies between ED physician-directed and EMR-directed indications are "very likely" to have an adverse effect on care in nine percent of patients. Effective communication is critical between the ED physician and the interpreting radiologists, and is achieved best through direct access to the EMR, supported by direct communication between physicians. Remote-site health care organizations

should consider analogous scenarios and the serious implications of inadequate access to the full medical record.

**KEY WORDS:** EMR access, quality, telemedicine

#### **eP-298**

#### **Clinicians Perceptions of Neuroradiology Reports and What They Value Most from Radiology Interpretations**

Danaie, S. • Roudsary, B. • Kwan, A. • Anzai, Y.  
University of Washington

3Seattle, WA

#### **PURPOSE**

Clinicians in the neurosciences fields are exposed to radiology studies routinely and rely on neuroradiology reports for patient care. Their perceptions of our reports should provide valuable lessons for us as we turn our image interpretations into reports.

#### **MATERIALS & METHODS**

A nationwide survey of radiologists, emergency physicians, otolaryngologists, orthopedists, neurologists, ophthalmologists, neurosurgeons, and radiation oncologists was performed using a web-based system. The survey asked clinicians about their level of satisfaction with neuroradiology reports, their level of comfort independently interpreting MR of the brain and spine, CT of the head and temporal bone, conventional and CT angiograms of the brain. Additionally the survey asked how important the following aspects of reports are: brevity, structure, detailed description of findings, differential diagnosis, degree of confidence, and recommendation for management. Finally, the survey asked how clinicians prefer to be contacted regarding positive findings.

#### **RESULTS**

A total of 874 physicians responded to the survey, of which 39.1% were radiologists, 23.6% were emergency physicians, 9.3% were otolaryngologists, 7.7% were orthopedists, 7.1% were neurologists, 5.8% were ophthalmologists, 4.4% were neurosurgeons, 1.3% were radiation oncologists. Respondents (56.6%) identified themselves as residents, 5.9% as fellows and 37.5% as attending physicians. Overall 93.7% of respondents stated that they are moderately to very satisfied with neuroradiology reports. Clinicians stated that they are most comfortable independently interpreting noncontrast head CTs and least comfortable interpreting cerebral angiography studies. Overall the most important aspect of the radiology report according to clinicians was the degree of confidence in the final impression. Finally, most clinicians (66%) prefer a phone call when there are important positive findings.

#### **CONCLUSION**

Neuroradiology reports provide valuable information for clinicians involved in the neurosciences. According to responses from our survey, overall clinicians are

satisfied with reports, but there is much room for improvement. Although clinicians attempt to interpret neuroradiology studies, they have a variable comfort level depending on the type of study. They value many things in radiology reports, the most important of which is the degree of confidence in the final impression.

**KEY WORDS:** Survey, report, perception

## eP-299

### Determination and Communication of Critical Findings in Neuroradiology

Trotter, S. A.·Viertel, V. G.·Babiarz, L. S.·Nagy, P.·Lewin, J. S.·Yousem, D. M.

Johns Hopkins University  
Baltimore, MD

#### PURPOSE

The Joint Commission issued a National Patient Safety Goal regarding timely reporting of critical examination results. Our academic institution established a list of "critical findings" by definition requiring immediate verbal communication to the referring physician, that radiologists may encounter when reading a neuroradiologic study. As part of a practice quality initiative, we investigated the relevance of the selected items currently on the neuroradiology critical findings list. We examined the frequency with which each of the critical findings occurred. We also examined reports containing findings that, although not found on the list, resulted in immediate physician communication. Our goal was to ascertain whether the critical findings list needed modification in order to adjust to actual practice patterns and the changing incidence of disease in the patient population.

#### MATERIALS & METHODS

Every neuroradiologic report generated that contained a critical finding was analyzed over a 2-month period. The critical finding(s) were classified into one of the established critical findings (Table, List 1). When a report was flagged with a critical finding, but no finding could be categorized into one of the listed critical findings, a new entry was created for the most severe/life-threatening finding mentioned in the report. These data were refined into new categories and frequency data were calculated. The time of day/night a study was performed was analyzed for correlation with the likelihood that a critical finding macro would be used. In order to evaluate whether the severity of the findings being called varied by the time of day a study was performed, a severity index was created that ranked the critical findings into three groups. The proportion of the different grades of findings then was calculated for daytime studies and compared with the percentage of the same grade of findings being interpreted at night.

#### Neuroradiology Critical Findings, Original versus Revised List

1.	New hemorrhage (epidural, subdural, intraparenchymal, subarachnoid, intraventricular, intramedullary)	New hemorrhage (epidural, subdural, intraparenchymal, subarachnoid, intraventricular, intramedullary)
2.	New stroke	New stroke
3.	New mass, markedly enlarging mass	New mass, markedly enlarging mass
4.	New herniation	New or worsening herniation
5.	Increased intracranial pressure, brain edema	Increased intracranial pressure, brain edema
6.	New or worsening hydrocephalus	New or worsening hydrocephalus
7.	Misplaced surgical drainage catheter	Misplaced or malfunctioning surgical hardware (including fixation devices, catheters, clips, coils)
8.	Misplaced surgical hardware	Findings suggestive of meningitis, cerebritis, osteomyelitis or abscess
9.	Findings suggestive of meningitis or abscess	Findings suggestive of child abuse
10.	Incompletely clipped aneurysm	Vascular abnormality including new or enlarging aneurysm/AVM/vascular malformation, artery dissection/critical stenosis/occlusion, dural venous thrombosis
11.	Clipped normal vessel	Cord compression
12.	Findings suggestive of child abuse	Suspected cord infarction
13.	New or enlarging aneurysm or AVM	Findings of spinal instability in a trauma patient (including osseous and ligamentous injury)
14.	Cord compression	Congenital variations that may alter a surgical approach
15.	New or enlarging cord mass	Fracture
16.	Suspected cord infarction	Globe/Retina/Optic nerve compromise
17.	Spinal ligamentous injury in a trauma patient	Airway compromise
18.	Findings of spinal instability in a trauma patient	
19.	Congenital variations that may alter a surgical approach	
20.	New aneurysm, AVM or vascular malformation	

#### RESULTS

Over the time period studied, 871/12607 (6.91%) of all neuroradiology studies contained a critical finding, 69.8% of which were categorized easily into one of the 20 officially listed findings; 30.2% were not able to be categorized. Of all neuroradiology studies, 32.8% were performed at night, however most (55.1%) of the critical findings were flagged during this low volume time period. Additionally, the top ranked diagnoses varied by time of day. Finally, we found a higher frequency of low-severity findings called at night than the day.



**CONCLUSION**

We propose a revised list (Table, List 2), which covers 86.7% of all critical findings reported in our neuroradiology department. We suggest this be adopted across neuroradiology divisions at other institutions to standardize practices and elevate the level of patient care. It is important to bear in mind that physician judgment is essential for determination of the acuity of findings.

**KEY WORDS:** Critical findings, communication, reporting

**Monday, April 23 –  
Wednesday, April 25  
6:30 AM - 9:00 PM**

**Thursday, April 26  
6:30 AM - 3:00 PM  
Americas Hall II**

**Electronic Posters (ePosters)  
300 – 326**

**Ep7 – SPINE**

**Note: A missing printed number indicates an abstract has been withdrawn.**

**eP-300**

**Efficacy of 3D FIESTA for Evaluation of Lumbar Nerve Root Compression in Patients with Symptomatic Foraminal Stenosis**

Okubo, T.·Watanabe, A.·Wada, A.·Ozawa, T.·Toyone, T.·Wada, Y.

Teikyo University Chiba Medical Center  
Ichihara, JAPAN

**PURPOSE**

As MRI technique progresses, 3D MR myelography including 3D fast imaging employing steady-state acquisition (FIESTA) is widely used. 3D FIESTA creates higher resolution images of any cross-section that contributes to observation of nerve roots. The preoperative identification of lumbar nerve roots with foraminal stenosis is important because the surgical treatment is different from that for lateral recess stenosis. The purpose of this study was to compare the efficacy of 3D FIESTA with conventional MRI for evaluation of lumbar nerve root compression in patients with symptomatic foraminal stenosis.

**MATERIALS & METHODS**

Forty-seven cases of lumbar degenerative disease were examined with both conventional MRI including fast spin echo T2WI (TR/TE 4000/106.6 ms; slice thickness 5.0 mm; field of view 180 mm; matrix 320 x 256), and 3D FIESTA (TR/TE 6.0/3.0 ms; slice thickness 1.2 mm; field of view 180 mm; matrix 384 x 384). Ninety-four roots were confirmed with or without compression through operations. Two blinded observers independently evaluated the images by using conventional MRI and 3D FIESTA. After this independent evaluation was performed, discrepancies were resolved through discussion, and observations agreed on were used to analyze the data. The appearance of the nerve roots from L2-L5 was evaluated. The observers were asked to examine for the presence of abnormalities of the nerve roots in their course through the foramen and/or the presence of nerve swelling. The operative findings were compared to the imaging findings of each sequence.

**RESULTS**

Eleven compressed roots were diagnosed through operations, and clinical symptoms were improved in all cases. Ten compressed roots were depicted precisely on both 3D FIESTA and the conventional MRI. One root was falsely diagnosed as compressed on 3D FIESTA, whereas nine roots on the conventional MRI. Sensitivity and specificity were 91% and 98.8% for 3D FIESTA, 91% and 89.2% for conventional MRI, respectively. The difference of specificity was statistically significant ( $p < 0.05$ ).

**CONCLUSION**

In conventional MRI, slice widths are comparatively thicker, generating a partial volume effect which could be considered as the reason for the larger numbers of false positives. 3D FIESTA affords more specific information for the preoperative diagnosis of symptomatic foraminal stenosis. 3D FIESTA is effective for evaluation of lumbar nerve root compression with symptomatic foraminal stenosis.

**KEY WORDS:** FIESTA, nerve root, foraminal stenosis

**eP-301**

**Clinical and Radiologic Finding of Postoperative Spondylodiskitis**

Liu, W.·Lee, S.·Park, H.·Park, G.·Paeng, S.

Wooridul Spine Hospital  
Seoul, KOREA, REPUBLIC OF

**PURPOSE**

Spondylodiskitis is a serious complication of surgery, and the diagnosis frequently depends on a combination of clinical, laboratory and imaging finding. The purpose of this study was to report clinical and radiologic manifestation of 84 cases of postoperative spondylodiskitis.

## MATERIALS & METHODS

We retrospectively reviewed clinical data and imaging finding of 84 patients who were diagnosed with spondylodiskitis after surgery. They were composed of 54 men and 30 women. The average age of the patient at the time of admission was 52.7 years, ranging from 20 to 90 years. According to surgical methods, we categorized postoperative spondylodiskitis into three groups: Spondylodiskitis due 1) interbody fusion (19%), 2) open discectomy (68%), and 3) endoscopic discectomy (13%), to evaluate MR findings and clinical manifestations.

## RESULTS

Among the 84 patients of MR imaging finding, intervertebral destruction showed six of 67 (9%) cases in group 1, 51 of 67 (76%) cases in group 2, and 10 of 67 (15%) cases in group 3. Paraspinal inflammation showed four of 35 (11%) cases in group 1, 25 of 35 (71%) cases in group 2, and six of 35 (17%) cases in group 3. Of the spondylodiskitis, the pathogens included staphylococcus species in 41 (49%) and gram-negative bacilli in 11 (13%); the pathogens in the 27 remaining cases (32%) were not identified. Among the staphylococcus species, eight of 41 (20%) cases occurred in group 1, 30 of 41 (73%) cases occurred in group 2, and three of 41 (7%) cases occurred in group 3. On the gram-negative bacilli, none of 11 (0%) cases occurred in group 1, four of 11 (36%) cases occurred in group 2, and seven of 11 (64%) cases occurred in group 3.

## CONCLUSION

We delineated clinical and radiologic manifestation of postoperative spondylodiskitis. According to our results, staphylococcus species infection frequently occurs in groups 1 and 2, and gram-negative bacilli infection frequent occurs in group 3.

**KEY WORDS:** Spine, disk, MR imaging

## eP-302

### Spondylodiskitis after Percutaneous Vertebroplasty

Liu, W.·Lee, S.·Park, H.·Park, G.·Paeng, S.

Wooridul Spine Hospital  
Seoul, KOREA, REPUBLIC OF

## PURPOSE

Vertebroplasty is a well known and useful technique for the treatment of painful osteoporotic vertebral fractures. Complications, such as cord or root compression or pulmonary embolisms, are infrequent. Spondylodiskitis is extremely rare. The purpose of this study was to report 15 cases of spondylodiskitis after percutaneous vertebroplasty.

## MATERIALS & METHODS

We retrospectively reviewed clinical data and imaging finding of 15 patients who were diagnosed with spondylodiskitis after percutaneous vertebroplasty for painful compression fractures. We also evaluated preoperative MR imaging findings which could have

decreased this complication using findings of adjacent vertebral marrow edema, intervertebral disk destruction, subligamentous spread, skip lesion, paraspinal inflammation, paraspinal abscess, and epidural abscess.

## RESULTS

The infection was due to mycobacterium tuberculosis in five cases (33%) and to pyogenic bacteria in 10 patients (67%). The latter pathogens included staphylococcus species in three (20%) and gram-negative bacilli in one (7%); the pathogens in the six remained cases (40%) were not identified. Of the patients with tuberculous spondylodiskitis, three of five cases (60%) showed adjacent marrow edema, two of five cases (40%) showed paraspinal inflammation. Of the patients with pyogenic spondylodiskitis, two of 10 cases (20%) showed adjacent marrow edema, six of 10 cases (60%) showed paraspinal inflammation.

## CONCLUSION

Our study showed that 11 of 15 (73%) of the patients had preoperative MR finding abnormality in spondylodiskitis after percutaneous vertebroplasty. It is essential to have precise evaluation of MR imaging findings in patients undergoing percutaneous vertebroplasty for osteoporotic compression fracture.

**KEY WORDS:** Spine, disk, MR imaging

## eP-303

### Clinical Significance of Percutaneous Vertebroplasty for Vertebra Plana with Vacuum Cleft

Kobayashi, N.·Numaguchi, Y.·Kamo, M.·Haraguchi, M.·Shibata, E.·Akaike, G.·Saida, Y.

St' Luke's International Hospital  
Tokyo, JAPAN

## PURPOSE

The aim of this study was to determine the association between improvement of back pain and spinal alignment following percutaneous vertebroplasty (PV) for vertebra plana with vacuum cleft.

## MATERIALS & METHODS

Institutional review board approval and informed consent were obtained for this study. In 545 patients, 1214 vertebral bodies were treated during 24 months. Of these, 49 patients (38 women, 11 men; mean age, 75.8 years) underwent 51 vertebroplasties for severe osteoporotic vertebral body compression fractures. Imaging and clinical features were analyzed, including the existence of vacuum cleft, location of the involved vertebra, pattern of vertebral compression, volume of polymethylmethacrylate injected, vertebroplasty complications, spinal alignment (severity of kyphosis) and clinical outcome.

## RESULTS

Almost all patients showed good response in disability and pain and also improved spinal alignment after PV for vertebra plana with vacuum cleft.

**CONCLUSION**

Percutaneous vertebroplasty for vertebra plana with vacuum cleft is effective in terms of pain reduction and leads to improvement of spinal alignment in osteoporotic compression fracture with vacuum cleft.

**KEY WORDS:** Vertebroplasty, vertebra plana, vacuum cleft

**eP-304**

**Study on the Possibility of the Penetration Injury to the Major Neck Vessels ( Jugular Vein and Carotid Artery) during Cervical Transforaminal Epidural Steroid Injection: Comparative Study in Patients and Volunteers**

Kim, H.·Park, J.·Yoo, J.·Lee, S.

Wooridul Spine Hospital  
Seoul, KOREA, REPUBLIC OF

**PURPOSE**

There is some research in the complications of the cervical transforaminal epidural injection. But, few studies have dealt with the possibility of injury to the major neck vessels (jugular vein and carotid artery). The purpose of this study is to demonstrate the differences in the possibilities of vascular injury between patients and volunteers and to compare the possibilities of vascular injury between both.

**MATERIALS & METHODS**

From April 2005 to August 2007, we performed cervical transforaminal epidural injection in 430 patients with 594 levels (18 cases in C3-4, 62 cases in C4-5, 275 cases in C5-6, 217 cases in C6-7, and 22 cases in C7-T1). We performed MR axial scan from C3-4 to C7-T1 in bilateral neck rotation, the same position for the transforaminal epidural injection, on 30 normal individuals. The mean age of subjects was 52.2 years (range, 32 to 82) in patients and 30.9 years (range, 25 to 46) in volunteers. The imaginary line was drawn representing the path of needle from skin to the neural foramen (ventral border of the facet process) and the distance between the vessels and imaginary line was measured. We divided the subjects into three groups, "Positive" group (group P) with vessels located within the route of needle, "Negative" group (group N) with vessels within 5 mm or more far from the tract, and "Borderline" group (group B) with vessels within 0-5 mm from the tract. Group P and B were classified as risk groups in this study.

**RESULTS**

In patients, 67% (398/594) appeared as a risk group to jugular vein injury and 18.2% (108/594) to carotid artery. In volunteers, 27.7% (83/300) were the risk group to jugular vein injury and 3.3% (10/300) to carotid artery injury. There were statistically significant differences in each level comparison as well as between patients and volunteers ( $p < 0.000$ ).

**CONCLUSION**

We found that the cervical transforaminal epidural injection had a high possibility of injury on jugular

vein/carotid artery (67%/18.2% in patients, 27.7%/3.3% in volunteer with neck rotation). Therefore, CT fluoroscopy-the guidance technique is essential to check the needle path and vessels location during the procedure even after the neck of patient is contralaterally rotated in cervical transforaminal epidural injection.

**KEY WORDS:** Cervical spine, carotid artery, jugular vein

**eP-305**

**Serial Follow-Up MR Findings after Radiosurgery for Intra and Extraforaminal Nerve Sheath Tumors**

Hwang, Y.·Lee, B.·Kim, S.  
Inje University

Seoul, KOREA, REPUBLIC OF

**PURPOSE**

Stereotactic radiosurgery has been accepted as a safe and effective treatment modality in patients with acoustic schwannoma. However, there is less experience and information regarding its use for nerve sheath tumors of the spine. We analyzed the evolution of follow-up MRI findings of spinal nerve sheath tumors after radiosurgery to provide the efficacy of this treatment.

**MATERIALS & METHODS**

Between January 2004 and September 2011, 34 intra and extraforaminal nerve sheath tumors in 30 patients were treated using Novalis radiosurgery. Twelve lesions were confirmed histologically as schwannoma, but 22 lesions were regarded as nerve sheath tumor according to the typical MR findings and 11 of these lesions were associated with neurofibromatosis. MR images were reviewed to identify serial changes of tumor volume and development of intratumoral necrosis. Mean follow-up MR period was 22.1 month (12-48 months).

**RESULTS**

Changes in tumor volume were categorized into following eight patterns: 1) no changes (7/34), 2) initial no change followed by regression (1/34), 3) initial no change followed by tumor enlargement (2/34), 4) continuous enlargement (4/34), 5) initial enlargement followed by regression (6/34), 6) initial enlargement with stabilization of tumor volume (7/34), 7) regression of tumor volume (3/34), and 8) regression followed stabilization of tumor volume (4/34). Lesions in pattern 1,2,5,6,7,8 were regarded as controlled and the tumor control rate was 91.2% (31/34). Initial temporary tumor enlargements were seen in pattern 5 and 6, but regression or stabilization of tumor volume was noted on 12-month follow-up images. Intratumoral necrosis (17/34) were observed in all eight patterns, and incidence of necrosis was high in pattern 5 (4/6) and pattern 6 (6/7).

**CONCLUSION**

Dynamic changes in spinal nerve sheath tumors were seen on serial follow-up MR imagings obtained after radiosurgery. Tumor control rate was 91.2% and initial

temporary enlargement of tumor volume was regressed or stabilized on 12-month follow-up images.

**KEY WORDS:** Spine, nerve sheath tumor, radiosurgery

### eP-306

#### Is 3D Constructive Interference in Steady-State Imaging Useful for the Identification of Abnormal Vessels Associated with Spinal Dural Arteriovenous Fistula?

Uetani, H.·Hirai, T.·Kitajima, M.·Shigematsu, Y.·Yano, S.·Kai, Y.·Nakamura, H.·Kuratsu, J.·Yamashita, Y.

Graduate School of Medical Sciences Kumamoto University  
Kumamoto, JAPAN

#### PURPOSE

There are some case reports on usefulness of high-resolution T2-weighted steady-state sequences for the identification of abnormal vessels associated with spinal dural arteriovenous fistula (SDAVF), but the systematic comparison with conventional MR imaging (MRI) has not been reported. The purpose of this study was to evaluate the usefulness of three-dimensional (3D) constructive interference in steady state (CISS) imaging compared with conventional MRI at 3 T for the identification of abnormal vessels of SDAVF.

#### MATERIALS & METHODS

We enrolled six consecutive patients (5 male, 1 female; age range 58-75 years, mean 64 years) who underwent conventional MRI including sagittal and axial T1- and T2-weighted (T1WI and T2WI) and contrast-enhanced T1-weighted imaging (CET1WI) and sagittal 3D CISS imaging on a 3 T unit prior to surgery. Spinal dural arteriovenous fistula confirmation was by intraarterial digital subtraction angiography (DSA) in all patients. For 3D CISS imaging, multiplanar reconstructions were obtained for all patients. Two experienced neuroradiologists independently evaluated the presence of abnormal vessels on 3D CISS and conventional MR images using a 3-point grading system: grade 3, definitely positive; grade 2, probably positive; grade 1, equivocal or definitely negative. Final judgments of the two observers were performed by consensus. Interobserver agreement was determined by calculating the  $\kappa$  coefficient, where  $\kappa < 0.20$  = poor, 0.21-0.40 = fair, 0.41-0.60 = moderate, 0.61-0.80 = good, 0.81-0.90 = very good, and  $\kappa > 0.90$  = excellent.

#### RESULTS

On DSA, the fistula site of the SDAVF was the thoracic region in five cases and the lumbar region in one. For the presence of the abnormal vessels, all cases were judged as grade 3 for 3D CISS imaging and grade 1 for T1WI. On T2WI, grade 3 was scaled for two cases, grade 2 for three, and grade 1 for one. For CET1WI, two cases were assigned in each grade. Interobserver agreement was excellent for 3D CISS images ( $\kappa = 1.0$ ), T1-weighted images ( $\kappa = 1.0$ ) and good for T2-weighted images ( $\kappa = 0.79$ ) and contrast-enhanced T1-weighted images ( $\kappa = 0.79$ ).

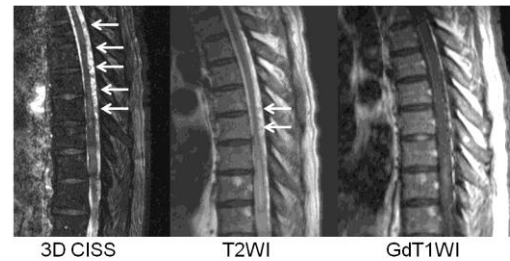


Figure 1. 75-year-old man with SDAVF

3D CISS image (left) reveals definite abnormal vessels around the spinal cord (arrows). T2WI (middle) shows probable abnormal vessels (arrows). Contrast-enhanced T1WI (right) shows equivocal findings for the abnormal vessels.

#### CONCLUSION

3D CISS imaging is useful for the identification of abnormal vessels of SDAVF. In the evaluation of SDAVF, 3D CISS imaging should be added to conventional MRI.

**KEY WORDS:** Spinal dural AVF, CISS

### eP-307

#### MR Imaging of Epidural Saline Infusions: A Pilot Study

Saindane, A. M.·Voscolopoulos, C.·Sharma, P.·Byas-Smith, M.

Emory University School of Medicine  
Atlanta, GA

#### PURPOSE

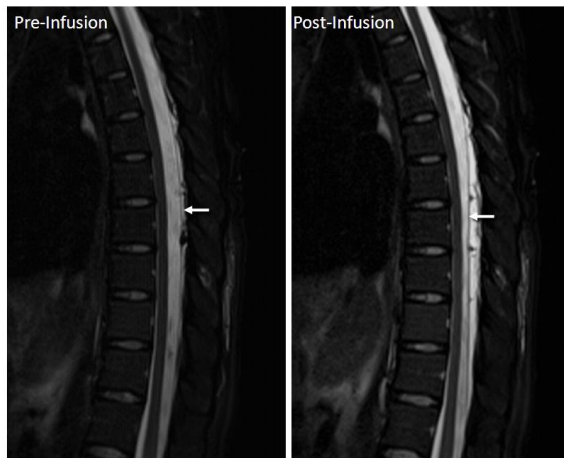
The spread of sensory blockade after epidural injection of local anesthetic (LA) differs considerably among individuals, but the factors affecting this distribution, including patient age and amount of epidural fat remain the subject of debate. This study was aimed at developing real time imaging sequences to aid in the further understanding of the distribution of LA within the epidural space during bolus dosed and continuous epidural analgesia.

#### MATERIALS & METHODS

Eight patients were imaged for this IRB-approved study (age 18.4-66.3 years). Patients underwent clinically indicated placement of thoracic epidural catheters for epidural anesthesia with continuous epidural infusions (8-12cc/h) of LA postoperatively for pain management. Catheters were maintained for 3-5 days. Prior to removal of the epidural catheter, patients underwent MRI of the spine at 3 T centered on the catheter entry site. Sagittal and axial T2-weighted fat-saturated, and sagittal T1-weighted imaging was performed prior to and immediately following bolus injection of 10-cc saline through the catheter. Subtracted images of the pre and postsaline injection datasets were generated. A dynamic mid-sagittal single 10-mm slab True-FISP sequence (TR=3.91 ms, TE=1/70 ms, 2 images/sec, 200 frames) was run during bolus saline injection. Images were evaluated for dynamic deformation of the dura and spinal cord, and extent of cranio-caudal saline migration in the spinal canal and the neural foramina following saline administration.

## RESULTS

Catheters terminated in the dorsal spinal epidural space between T5-T9. Preexisting infused local anesthetic in the spinal epidural space spanned a mean of seven vertebral segments (SD=2.6). The number of neural foramina with epidural anesthetic present ranged between 0-34. Following bolus administration of 10 cc saline, True FISP imaging demonstrated dynamic compression of the thecal sac and/or spinal cord in two patients followed by rapid redistribution. In the other six patients this dynamic change was not evident. On subtracted T2-weighted fat-saturated images, there was an average 13% (SD = 9%) decrease in thecal sac diameter following saline administration. The overall craniocaudal extent of fluid did not change in any patients, however the amount of fluid in the neural foramina increased on average 14% (SD = 12%).



## CONCLUSION

Subtraction-based MRI techniques are useful for determining the extent of epidural infusions. Dynamic True FISP-based techniques can demonstrate dynamic compression of the thecal sac and spinal cord but are not sensitive to small changes from a bolus in the presence of preexisting epidural fluid from continuous infusion.

**KEY WORDS:** Epidural space, MR imaging, dynamic imaging

## eP-308

### Effacement of the Fat in the Proximal Carpal Tunnel on MR Imaging: A Useful Indirect Indicator of Carpal Tunnel Syndrome

Thawait, S. K.<sup>1</sup>•Chalian, M.<sup>2</sup>•Thawait, G. K.<sup>2</sup>•Thakkar, R.<sup>2</sup>•Del Grande, F.<sup>2</sup>•Chhabra, A.<sup>2</sup>

<sup>1</sup>Yale University - Bridgeport Hospital, Bridgeport, CT,  
<sup>2</sup>Johns Hopkins Hospital, Baltimore, MD

## PURPOSE

The objective of this study is to determine the diagnostic utility of the effacement of fat in the proximal carpal tunnel in patients with and without carpal tunnel syndrome (CTS). The current literature evaluates several magnetic resonance imaging (MRI) features of CTS which are based on median nerve signal and

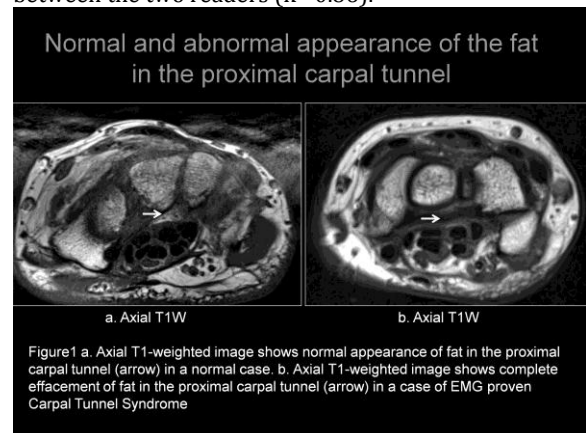
morphology characteristics. However, the utility of MRI evidence of fat pad effacement as an indirect sign of CTS has not been described.

## MATERIALS & METHODS

Institutional review board approval was obtained for this HIPAA compliant study. Informed consent was waived. The case group consisted of cases of median neuropathy at the wrist, diagnosed on MRI exams from the previous 2 years and, proven with electromyography (EMG), which was considered as the reference standard. The control group consisted of series of consecutive subjects with wrist MRIs performed for other reasons than CTS. A history of prior surgery or trauma was exclusion criteria for both groups. The presence of fat pad was evaluated on axial T1-weighted or nonfat suppressed proton density images dorsal to the tendons of flexor digitorum profundus and ventral to the carpal bones at the level of the pisotriquetral joint in the proximal carpal tunnel. One musculoskeletal fellowship-trained radiologist and one radiology resident, both blinded to the clinical findings evaluated the images independently. Sensitivity, specificity and interobserver variability was calculated.

## RESULTS

From the 16 cases of median neuropathy at the wrist proven with EMG, two cases were excluded due to history of prior carpal tunnel release and one case was excluded due to trauma. Finally, the case group consisted of 13 cases (females/male = 12/1, median  $\pm$  IQR of 49  $\pm$  37) and the control group consisted of 16 cases (females/male = 9/7, median  $\pm$  IQR of 49  $\pm$  35 years). All studies were done on 1.5 and 3 T magnets. Effacement of the fat in CTS was found in 100% (13/13) cases and in 44% (7/16) controls resulting in sensitivity, specificity, and accuracy of 100%, 56%, and 76%, respectively. There was an excellent agreement between the two readers ( $k=0.86$ ).



## CONCLUSION

The previously undescribed sign of effacement of the fat in the proximal carpal tunnel is a valuable indicator for median neuropathy. Apart from morphologic characteristics of the median nerve and T2 signal abnormality, this sign also should be reported or taken into account while suggesting a diagnosis of CTS.

**KEY WORDS:** Carpal tunnel syndrome, MR imaging, fat effacement

### eP-309

#### **Spinoplasty: Applying Vertebroplasty to the Posterior Arch**

Manfrè, L.

Minimally Invasive Spine Interventional Department AOE  
Cannizzaro  
Catania, ITALY

#### **PURPOSE**

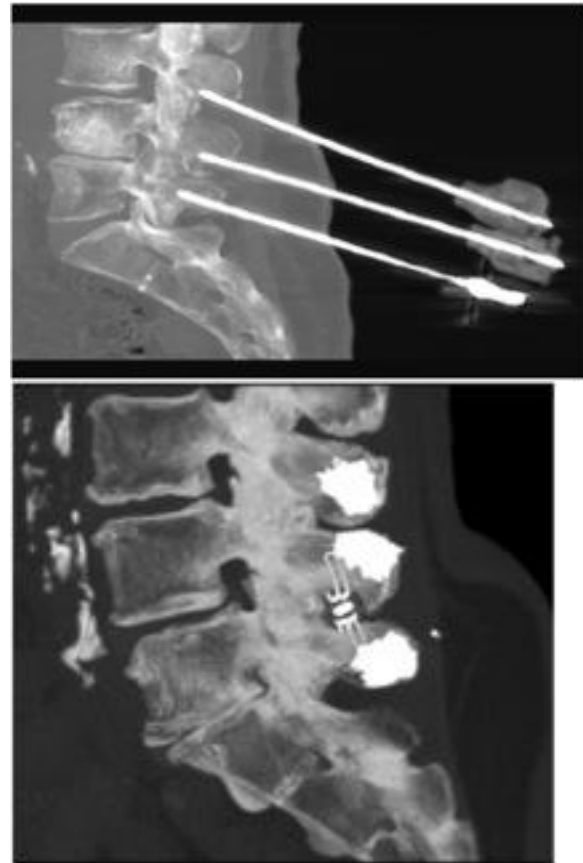
The posterior arch and the spinous processes/laminae complex can be involved in several disease. In case of severe arthrotic and/or osteoporosis contact of spinous processes related to disk degeneration can generate local chronic pain, resistant to chemical (steroid infiltration) or physical (radioablation) therapy. Moreover, osteoporosis can be responsible for laminae remodeling in patients treated with interspinous devices (ISD) because of symptomatic spinal canal stenosis. We evaluate the possibility to perform cementoplasty of the spinous processes (spinoplasty - SP) in patients affected by posterior arch painful edema and in patients affected by severe osteoporosis candidate to ISD.

#### **MATERIALS & METHODS**

Among 1244 patients undergone vertebroplasty procedures, three cases were affected by focal lumbar pain related to spinous processes edema demonstrated on MRI. Among 154 patients affected by painful lumbar spinal canal stenosis, 12 were affected by severe osteoporosis. In all the patients with painful spinous process edema, MRI revealed abnormal signal intensity inside the posterior arch of L3, L4 and L5 vertebra. In patients indicated to ISD treatment, severe spinal canal stenosis with normal appearance of the posterior arch were appreciated. Spinoplasty was performed using a CT-guided technique, 13G needles and 1 to 3cc of PMMA per level.

#### **RESULTS**

Patients affected by painful spinous processes edema became painless in 24 hours after SP and no complication was detected at 1-week to 3-months follow-up controls. Patients who had undergone prophylactic SP before ISD implant had no recurrence of pre-op symptoms nor laminae remodeling at 3, 6 and 12 months control.



#### **CONCLUSION**

Vertebroplasty of the posterior arch using CT-guided PMMA injection seems to be a powerful technique in those patients who need posterior arch augmentation.

**KEY WORDS:** Posterior arch, spinal stenosis, vertebroplasty

### eP-310

#### **Blazer Vertebral Augmentation System: A Novel Treatment for Vertebral Compression Fractures**

Hatten, H.<sup>1</sup> Miller, L. E.<sup>2</sup> Block, J. E.<sup>3</sup>

<sup>1</sup>Indian River Radiology, Vero Beach, FL, <sup>2</sup>Miller Scientific Consulting, Inc., Arden, NC, <sup>3</sup>The Jon Block Group, San Francisco, CA

#### **PURPOSE**

To describe the early experience with a novel vertebral augmentation device that creates channels in the vertebral body to allow directional cement flow for treatment of vertebral compression fracture.

#### **MATERIALS & METHODS**

This prospective, single-center, case series treated nine vertebral compression fractures in eight women (mean age: 81 years, mean collapse: 51%) using vertebral augmentation (Blazer Vertebral Augmentation System, Benvenue Medical, Inc., Santa Clara, CA). This system offers targeted circular channel creation via a unipedicular technique and controlled cement



distribution. Outcome measures included pain severity with visual analog scale, radiographically identified events including cement leak and adjacent or subsequent fracture, and clinical events including reoperation and revision at the index level. The follow-up period for all assessments was 7 days.

#### RESULTS

Clinical utility of the device was excellent. Curvilinear vertebral channels were created in each vertebra and targeted cement delivery through the bone channels was achieved easily. Mean back pain severity scores decreased from 7.2 at pretreatment to 1.1 at follow up. No clinical adverse events were reported.

#### CONCLUSION

The initial experience with the Blazer Vertebral Augmentation System suggests that this device may have particular usefulness in the treatment of vertebral compression fracture. The bone channels produced by the device allow targeted cement delivery from endplate to endplate, with potentially superior interdigitation compared to balloon-assisted systems. Larger long-term studies are needed to corroborate the findings of this early clinical experience.

**KEY WORDS:** Augmentation, fracture, vertebral

#### eP-311

##### **Safety and Effectiveness of Percutaneous Sarcoplasty: A Single Center Experience in 58 Consecutive Patients**

Pereira, L. P.·Clarençon, F.·Cormier, E.·Rose, M.·Le Jean, L.·Chiras, J.

Hôpital Pitié Salpêtrière  
Paris, FRANCE

#### PURPOSE

Percutaneous vertebroplasty has gained acceptance during the past decades for the treatment of both traumatic and metastatic vertebral compression fractures. Effectiveness and safety of sacrum cementoplasty (percutaneous sarcoplasty: PSP) however, has been reported poorly. The purpose of this study was to report our experience in percutaneous cementoplasty of metastatic tumors and insufficiency fractures of the sacrum.

#### MATERIALS & METHODS

We retrospectively reviewed the charts of 58 consecutive patients (42 women, 16 men; mean age: 62 years, range 27-88) who underwent PSP from January 2002 to July 2011 for intractable pain from sacral tumor lesions or from osteoporotic fractures. Ninety-six procedures (66% bilateral and 34% unilateral) were performed; 75% were for metastatic lesions, 15% were osteoporotic fractures and 10% for sacral primitive tumors. Twenty-six of 56 (45%) patients previously had undergone radiotherapy. Patients were treated in prone position under conscious sedation; PMMA was injected under fluoroscopic guidance. The following data were assessed: a) visual analogue scale (VAS) before and

after the procedure for global pain, b) short-term (1 month) clinical follow up using a four-grade patient satisfaction scale: worse, unchanged, mild improvement, and major improvement, c) modification in analgesics consumption at 1 month follow up, d) referred short-term walking mobility (worse, unchanged and improvement). Minor (cement leakage leading to transient neurologic deficit) and major complications (cement leakage leading to permanent neurologic deficit) were assessed systematically.

#### RESULTS

The mean VAS score was 4.7 in preprocedure and 2 in postprocedure. At 1-month follow up, 28/58 (60%) patients experienced a mild improvement; 13/58 (28%) presented a major improvement while 3/58 (6.3%) and 4/58 (8.5%) patients had unchanged or worse pain, respectively. Decreased analgesic consumption was observed in 34% (22/58) of the patients. Half of the patients had preprocedure walking limitation; 81% experienced improvement, 14% remained unchanged and 5% were worse. No procedure-related death was observed. We noted minor complications (transient neurologic deficit) in 8/58 patients (15%) and major complications (permanent neurologic deficit) in 2/58 (4%).

#### CONCLUSION

Percutaneous sarcoplasty in metastatic and osteoporotic fractures is a safe and effective technique in terms of pain relief and functional outcome. Major complication rate is acceptable (4%).

**KEY WORDS:** Sarcoplasty

#### eP-312

##### **Height Maintenance of the Augmented Vertebral Body: A Longitudinal Study of Patients Treated with Vertebral Augmentation for Painful Osteoporotic Vertebral Compression Fractures**

de Venecia, C. A.·Ortiz, O. A.

Winthrop University Hospital  
Mineola, NY

#### PURPOSE

To assess the stability of height maintenance over time in the augmented vertebral bodies of patients treated for painful osteoporotic compression fractures.

#### MATERIALS & METHODS

A series of patients who were treated with vertebral augmentation for painful osteoporotic compression fractures and who were followed for at least 6 months were included in the study. All patient imaging encounters were evaluated. An endplate to endplate cement fill pattern was observed in the treated vertebrae. The augmented vertebral body was measured and compared to a reference vertebral body from the same date of service. The measurements then were repeated for the same augmented and reference vertebrae at an imaging follow-up time point. A ratio of the augmented vertebral body height to the reference

vertebral body height was calculated and used to compare height maintenance over time. All measurements were made by a trained observer blinded to the nature of the vertebral augmentation procedure and to the patient's bone density status.

#### RESULTS

Fourteen patients, including 12 females and 2 males, were included in the study. The average patient age was 82 years, with patient ages ranging from 64 to 95 years. The mean and median length of time between date of service and follow-up imaging was 3 years and 3.4 years, respectively, ranging from 6 months to 4.3 years. The measurements demonstrated no statistically significant difference in the height of the augmented vertebral body over time.

#### CONCLUSION

There is no statistically significant change in the height of an augmented vertebral body over time. Vertebral augmentation with acrylic bone cement is a durable treatment.

**KEY WORDS:** Vertebral augmentation, compression fracture, height maintenance

#### eP-313

### 1H-MR Spectroscopy in the Evaluation of Osteoporotic and Neoplastic Vertebral Fractures Prior to Percutaneous Vertebroplasty

Massari, F.·Masala, S.·Simonetti, G.

University of Rome  
Rome, ITALY

#### PURPOSE

The detection of spongy vertebral molecular variations can be utilized to distinguish the different sources of bone pathology. The relative water intensity correlates with hematopoietic elements dominating in youth. Instead fat cells proportion increases with age resulting in a conversion of red/yellow marrow.

#### MATERIALS & METHODS

The study was performed with a 3 T magnetic resonance; we used a single voxel method (TR/TE 2000/40 msec) with point-resolved spectroscopy sequence (PRESS). We measured percent FF and lipid/water ratio (LWR) in 63 subjects with MR findings of vertebral fractures related to osteoporosis, multiple myeloma and metastasis. The control group consisted of 65 subjects with no spinal pathologies.

#### RESULTS

In accordance with the relative presence of fat and water within the vertebral body, we found that in osteoporotic vertebral fracture and in hematopoietic diseases an inversion of physiologic LWR is present. This is probably due to intraspongy edema and malignant cells infiltration with replacement of lipid-containing cells.

#### CONCLUSION

1H MR spectroscopy provides a fine evaluation of vertebral bone marrow changes due to primary or secondary pathologies and allows appreciated differences not easily assessable with conventional imaging. In the upcoming future, MR spectroscopy may be powerful in identifying physiologic as well as pathologic biochemical changes in vertebral bone. This evaluation will be useful in prevertebroplasty planning in order to evaluate vertebrae which must be treated.

**KEY WORDS:** 1HMR imaging, spine, vertebral fracture

#### eP-314

### Treatment of Osteolytic Vertebral Fractures Due to Multiple Myeloma with Radiofrequency Kyphoplasty

Pflugmacher, R.·Bornemann, R.·Karius, T.·Wirtz, D. C.

Universitätsklinikum Bonn  
Bonn, GERMANY

#### PURPOSE

The purpose of this study was to investigate the functional outcomes, safety and radiographic outcomes after the treatment of painful osteolytic vertebral fractures treated with a novel minimally invasive procedure, radiofrequency kyphoplasty (RFK).

#### MATERIALS & METHODS

Eighty-eight patients (50 females and 38 males) with 158 osteolytic vertebral fractures were treated with RFK using the StabiliT Vertebral Augmentation System (Dfine Inc, San Jose, CA). The StabiliT System provides a navigational osteotome to create a site- and size-specific cavity prior to delivering ultrahigh viscosity cement with an extended working time (done by applying radiofrequency energy to the cement immediately prior to entering the patient). Twelve months follow up in 60 patients (36 females and 24 males) with 110 treated vertebrae are reported. Pre and postoperative, 3, 6 and 12 months clinical parameters (Visual Analogue Scale, Oswestry Disability Index score), and radiologic parameters (vertebral height and kyphotic angle) were measured.

#### RESULTS

The median pain scores (VAS) ( $p < 0.001$ ) and the Oswestry Disability Score ( $p < 0.001$ ) improved significantly from pre to posttreatment and maintained at 3, 6 and 12 months follow up. Postoperative, 3, 6 and 12 months follow-up RFK restored and stabilized the vertebral height and avoided further kyphotic deformity. No symptomatic cement leaks or serious adverse events were seen in the RFK group during 3 months of follow up. In seven out of 158 vertebrae (4.4%) a cement leakage into the disk or lateral wall could be determined by radiograph postoperatively.

#### CONCLUSION

Radiofrequency kyphoplasty is a very safe and effective minimally invasive procedure for the treatment of osteolytic vertebral fractures. Radiofrequency

kyphoplasty shows excellent clinical and radiologic results in the 3 and 6 months follow up. Site-specific cavity creation and delivery of ultra-high viscosity cement in RF kyphoplasty with extended working time resulted in the added benefits of height restoration and lower cement leakages intraoperatively.

**KEY WORDS:** Multiple myeloma, osteolytic vertebral compression fractures, radiofrequency kyphoplasty

#### eP-315

##### **Treatment of Vertebral Body Fractures: Radiofrequency Kyphoplasty versus Conservative Care**

Bornemann, R. • Otten, L. • Wirtz, D. C. • Pflugmacher, R.

Universitätsklinikum Bonn  
Bonn, GERMANY

#### **PURPOSE**

There is controversy about how to treat vertebral fractures. Conservative care is the default approach, despite lack of evidence. Radiofrequency kyphoplasty (RFK) uses ultrahigh viscosity cement to restore spinal posture and stabilize the fracture. The aims of this study were to compare radiofrequency kyphoplasty to conservative care and assess the usual algorithm of starting all patients on conservative care for 6 weeks before offering surgery.

#### **MATERIALS & METHODS**

Elderly patients with painful osteoporotic vertebral compression fractures, all were treated with 6 weeks of conservative care (analgesics, bracing, and physiotherapy). They then were offered the choice of continuing conservative care or crossing over to radiofrequency kyphoplasty, at 6 and 12 weeks. Clinical success was defined as: 1) VAS pain improvement  $\geq 2$ , 2) final VAS pain  $\leq 5$ , 3) no functional worsening on ODI.

#### **RESULTS**

After the initial 6 weeks of conservative care, only one of 65 patients met the criteria for clinical success, and median VAS improvement was 0. After 12 weeks of conservative care, only five of 38 patients met the criteria for clinical success, and median VAS improvement was one. At the 6-week follow up after radiofrequency kyphoplasty, 31 of 33 surgery patients met the criteria for clinical success, and median VAS improvement was five.

#### **CONCLUSION**

For the vast majority of patients, conservative care did not provide meaningful clinical improvement. By contrast, nearly all patients who underwent radiofrequency kyphoplasty had rapid substantial improvement. Surgery was clearly much more effective than conservative care and should be offered to patients much sooner.

**KEY WORDS:** Vertebral compression fractures, kyphoplasty, conservative care

#### eP-316

##### **Pilot Study on Prophylactic Vertebroplasty for Prevention of Adjacent Segment Complications after Long Segment Posterior Spinal Fusion**

Keen, N. N. • Hess, C. P. • Chin, C. T.

University of California San Francisco  
San Francisco, CA

#### **PURPOSE**

Fractures and junctional kyphosis occur in up to 30% of patients undergoing long-segment posterior spinal fusion (PSF). Prophylactic vertebroplasty (PV) of adjacent vertebral bodies has been proposed as a method to prevent these complications. In this pilot study, we assessed the outcomes of PV in 28 patients undergoing long-segment PSF.

#### **MATERIALS & METHODS**

Medical records were queried for all patients over a 5-year period undergoing CT and fluoroscopic-guided PV of the superior adjacent vertebral body after long-segment PSF. Patients were excluded if less than 1 year of follow up was available. CT images obtained during the vertebroplasty procedure and standing radiographs obtained in follow up were reviewed. Radiographs of age and gender-matched patients undergoing long segment PSF without PV during the same time period also were reviewed. Two attending neuroradiologists performed all vertebroplasty procedures, in which either a unipedicular or bipedicular injection of polymethyl methacrylate to a volume of 1-5 mL was performed under combined CT and fluoroscopic guidance. The presence or absence of fractures and/or junctional kyphosis was assessed by consensus. The frequency of complications, length of fusion, and the presence or absence of baseline osteoporosis was compared between the two groups using Fisher's exact test.

#### **RESULTS**

A total of 28 patients undergoing PV were identified, 14 of which had follow-up imaging at 1 year (Table 1). The 14 patients who had at least 1 year of follow up were compared with 14 age- and gender-matched controls who had long segment PSF, but not PV. The average length of fusion was nine levels in both groups ( $P = 0.54$ ). Six patients (43%) developed worsening kyphosis. In the PV group, one patient developed subsequent fracture of the adjacent superior vertebral body and fracture of the surgical hardware and two patients had subsequent extension of spinal fusion for worsening proximal junctional kyphosis. In the control group, one patient developed a rod fracture, one patient had adjacent level progressive disk space narrowing, and three patients had subsequent extension of spinal fusion for worsening proximal junctional kyphosis. Although no significant difference was found in the risk of subsequent operative complication between the two groups ( $P = 0.68$ ), more patients in the PV group had clinically noted osteoporosis than the control group ( $P = 0.05$ ).

Table 1: Patient Characteristics. PV: Prophylactic Vertebroplasty.

Characteristic	All PV	PV with at least 1 year of follow-up	Control
All patients	28	14	14
Male	4	1	1
Female	24	13	13
Mean age in years (range)	70 (58-83)	67 (58-75)	69 (55-77)
Preoperative diagnosis			
Adult scoliosis	16	11	9
Posttraumatic kyphosis	5	1	1
Flat back deformity	4	2	4
Spinal stenosis	3	0	0
Length of fusion			
T7 to sacrum	1	0	0
T9 to sacrum	1	1	2
T10 to sacrum	16	9	9
T11 to sacrum	4	1	2
T12 to sacrum	5	3	1
L2 to sacrum	1	0	0

**CONCLUSION**

In this small retrospective analysis, we found no difference in the rate of functional kyphosis or fracture between patients who had PV and those who did not at 1 year. However, because more patients undergoing PV were osteoporotic, follow-up studies will be necessary to determine how bone mineral density affects the rate of fracture.

**KEY WORDS:** Vertebroplasty, adjacent segment failure, spinal fusion

**eP-317**

### Efficacy of Radiofrequency Targeted Vertebral Augmentation for Osteoporotic Vertebral Compression Fractures

Moser, F. G.·Maya, M. M.·Khiana, T.·Blaszkiwicz, L.·Pressman, B. D.

Cedars-Sinai Medical Center  
Los Angeles, CA

**PURPOSE**

Radiofrequency targeted vertebral augmentation (RF TVA) is a new method for the procedure commonly known as kyphoplasty. Radiofrequency TVA employs a novel system containing a steerable osteotome for site-specific cavity creation and radiofrequency (RF) modulation of cement viscosity delivered using a remotely controlled hydraulic delivery system. We report a prospective, post-market, IRB approved, study of patients with acute osteoporotic vertebral compression fractures (VCF) with this system.

**MATERIALS & METHODS**

Between May 2009 and January 2011, 20 patients diagnosed with 1-3 painful VCFs (confirmed by MRI and pain concordant with index level) who were to receive kyphoplasty treatment were enrolled. Inclusion criteria included age between 50-90 years, Visual Analogue Pain (VAS) score >4, a moderate (21-40%) or greater Oswestry Disability Index (ODI) score, and 20-90% vertebral compression. VAS and ODI scores were recorded preprocedure, at discharge, 1 week, 1 month, and 3 months after the procedure. Oswestry Disability Index scores were recorded at the same time points except at discharge. Each procedure was performed using this vertebral augmentation system. A trocar was placed via a unipedicular approach. A steerable osteotome was inserted and site-specific cavities were created to allow targeted delivery of cement. Using a remotely controlled delivery system RF energy was applied to warm the PMMA cement as it passed into the delivery cannula in the patient.

**RESULTS**

Average patient age was  $79.7 \pm 9.85$  years. The mean percentage of collapse was  $28 \pm 13\%$ . A majority of patients had associated diseases, the most common ones being hypertension (N = 14) and coronary artery diseases (N = 9).

All surgeries were performed within 42 days (av. 13 days) of the patient's reported date of injury. The average procedure time was  $18.6 \pm 8.95$  minutes. No procedure-related complications were encountered. No patients required bilateral procedures. The improvement in mean VAS scores from preprocedure to discharge was 3.4 (p 0.0001). After 3 months, the improvement in average scores was significant (34.14%, p < 0.0001).

**CONCLUSION**

Radiofrequency-targeted vertebral augmentation is a safe and effective method for treatment of vertebral compression fractures. The use of RF energy, to warm cement immediately prior to entering the patient, results in the unique combination of consistently high viscosity cement useable over an extended working time.

**KEY WORDS:** Kyphoplasty, compression fractures

**eP-318**

### Comparison between Three Cements with Different Viscosity and Leakage Rate during Vertebroplasty for the Treatment of Neoplastic Patients

Guarnieri, G.·Ambrosanio, G.·Izzo, R.·Diano, A.·Muto, M. Cardarelli Hospital

Naples, ITALY

**PURPOSE**

To compare three cements with different viscosity and their leakage-rate during vertebroplasty (VP) for the treatment of patients affected by secondary vertebral neoplastic lesions.

## MATERIALS & METHODS

From September 2009 to August 2011, 100 consecutive patients have been treated by VP with three different type of cement: 50 patients with Optimed® cement, 25 patients with Confidence®, 25 patients with Vertecem+®, for a total of 130 vertebral bodies affected by vertebral neoplastic lesions with this distributions: 35 patients affected by vertebral metastatic lesion from lung cancer, 25 patients by breast cancer, 30 by multiple myeloma, five by renal-cell carcinoma and five gastro intestinal carcinoma. All the patients complained of a pain syndrome resistant to continuous medical medication. An unipedicular approach has been performed in 35 vertebral bodies, while the bipedicular approach has been performed in the remaining 95. Bone biopsy was performed only in 30 cases in which there were diagnostic doubts about the histology of lesion. All procedures have been performed by local anaesthesia and neuroleptoanalgesia. Multiple levels of VP was performed in 30 cases with an average of two metamers up to six levels in one session. For all patients extravertebral vascular or diskal cement leakage, pain reduction and cement homogeneity and distribution were evaluated retrospectively. Clinical results have been evaluated with the Visual Analogue Scale (VAS) and the Oswestry Disability Index (ODI) methods.

## RESULTS

At 1-month follow up, a successful outcome has been observed in 74% of patients with a reduction (76%) or complete (24%) resolution of pain symptoms with VAS. Reduction more than 50% in 74 patients and ODI values significantly decreased to 8%, with homogeneous distribution in all three group of patients. Extravertebral vascular or diskal cement leakage have been observed in 39. Optimed-group metamer (30%), in 13 Confidence-group metamer (10%) and in eight Vertecem+-group metamer (5%). All extravertebral vascular or diskal cement leakage were asymptomatic: in three patients a pulmonary asymptomatic leakage was observed with Optimed cement. A more homogeneous cement distribution was observed in patients treated by Confidence or Vertecem+ cement compared to Optimed.

## CONCLUSION

Different cement with different characteristics and viscosity produce a different rate of extravertebral vascular or diskal cement leakage. More viscosity cement is more manageable and can be used to reduce the leakage rate.

**KEY WORDS:** Vertebroplasty, viscosity cement, leakage rate

## eP-319

### Prospective Study of Diagnostic Value of CT-Guided Injections for Spine-Related Pain

Miller, T. S.

Montefiore Medical Center  
Bronx, NY

## PURPOSE

To assess the diagnostic effectiveness of CT-guided epidural steroid injections and nerve root blocks in the management of back pain.

## MATERIALS & METHODS

Sixty-one patients referred for evaluation of CT-guided management of back pain by orthopedic surgeons, neurologists, neurosurgeons, and occupational medicine physicians in the community were studied. Treatment was determined in a routine clinical manner using standards of care based on patient information and imaging studies. Those patients scheduled for epidural steroid injections or nerve root blocks were included in this study. Baseline data were acquired from questionnaires completed by patients at their initial clinic visit. Follow-up information was gathered from patient charts. Primary analysis was based on pain reduction immediately after injection and several hours after injection. Secondary analysis was based on pain reduction given location of injection.

## RESULTS

Of the sixty-one patients in this study, the majority experienced pain relief. Overall, patients experienced an average immediate VAS pain score reduction of 4.92 and an average delayed VAS pain score reduction of 5.21. Additionally, pain relief also was assessed by injection location. Cervical spinal injections demonstrated an immediate and delayed VAS score reduction of 6.40 and 6.80, respectively. Thoracic spinal injections demonstrated an immediate and delayed VAS score reduction of 6.75 and 7.00, respectively. Lumbar spinal injections demonstrated an immediate and delayed VAS score reduction of 5.70 and 6.10, respectively. Lumbosacral spinal injections demonstrated an immediate and delayed VAS score reduction of 4.71 and 4.75, respectively. Sacral spinal injections demonstrated an immediate and delayed VAS score reduction of 3.94 and 4.50, respectively. All VAS pain score reductions were statistically significant.

Response to Treatment	Pre-Injection VAS* vs. Immediate Post-Injection VAS*			Pre-Injection VAS* vs. Delayed** Post-Injection VAS*		
	Mean Difference	95% CI	P-value	Mean Difference	95% CI	P-value
Overall (N = 61)	4.92 ± 3.55	4.01 - 5.83	< 0.001	5.21 ± 2.84	4.49 - 5.94	< 0.001
Cervical (N = 5)	6.40 ± 3.58	1.96 - 10.84	0.016	6.80 ± 2.05	4.26 - 9.34	0.002
Thoracic (N = 4)	6.75 ± 0.96	5.23 - 8.27	0.001	7.00 ± 0.82	5.70 - 8.30	< 0.001
Lumbar (N = 10)	5.70 ± 3.80	2.98 - 8.42	0.001	6.10 ± 3.14	3.85 - 8.35	< 0.001
Lumbosacral (N = 24)	4.71 ± 3.63	3.18 - 6.24	< 0.001	4.75 ± 2.75	3.59 - 5.91	< 0.001
Sacral (N = 18)	3.94 ± 3.61	2.15 - 5.74	< 0.001	4.50 ± 3.00	3.01 - 5.99	< 0.001

\* VAS pain score ranges from 0 (no pain) to 10 (worst pain possible)

\*\* Delayed several hours after injection

**CONCLUSION**

CT-guided epidural steroid injections or nerve root blocks appear to be an effective way to confirm the suspected cause of a patient's back pain.

**KEY WORDS:** CT guidance, steroid injection, prospective

**eP-320**

**Comparative Prospective Study upon Load Distribution Variation among Patients with Vertebral Fractures Treated with Percutaneous Vertebroplasty and a Control Group of Healthy Volunteers**

Kelekis, A.·Filippiadis, D.·Vergadis, C.·Papakonstantinou, O.·Brountzos, E.·Kelekis, N.

University General Hospital "ATTIKON"  
Athens, GREECE

**PURPOSE**

Through a comparison of patients with vertebral fractures and normal population we illustrate effect of percutaneous vertebroplasty (PV) upon load distribution changes (among the two feet - among rear and front of the same foot) during standing and walking.

**MATERIALS & METHODS**

Last year, we prospectively compared two groups. Vertebroplasty group (36 patients,  $75 \pm 15$  years) with osteoporotic vertebral fractures was evaluated on an electronic baropodometer. Load distribution between right and left foot during standing and walking was recorded and compared prior (Group V1) and the day after (Group V2) PV. Control group (30 patients,  $42 \pm 13$  years) with no back pain or surgery record (normal population) were evaluated on the same electronic baropodometer. The two groups were compared with related samples Wilcoxon Signed Rank test.

**RESULTS**

Mean value of load distribution variation between rear and front of the same foot for normal population was  $9.45 \pm 6.79\%$  upon standing and  $14.76 \pm 7.09\%$  upon walking. Mean value of load distribution variation between the two feet was  $6.36\%$  and  $14.6\%$  prior vertebroplasty whilst load variation was  $4.62\%$  and  $10.4\%$  postvertebroplasty upon standing and walking respectively. Mean value of load distribution between rear and front of the same foot prior to percutaneous vertebroplasty was  $16.52 \pm 11.23\%$  upon standing and  $30.91 \pm 19.26\%$  upon walking. Load distribution postvertebroplasty was  $10.08 \pm 6.26\%$  upon standing and  $14.25 \pm 7.68\%$  upon walking. Comparison of load distribution variation among Group V1 and Group V2 or Group V1 and Group B is statistically significant ( $p = 0.001$  and  $p = 0.011$  respectively). Comparison of load distribution variation among Group V2 and Group B is not statistically significant ( $p = 0.486$ ). Comparison of load distribution variation among the two feet is statistically significant during walking ( $p = + 0.005$ ) but not statistically significant during standing ( $p = 0.009$ ).

**CONCLUSION**

Comparative groups enable us to consider that PV apart from the already known pain reduction effect is efficient on equilibrium and load distribution improvement as well.

**KEY WORDS:** Vertebroplasty, baropodometry

**eP-321**

**Improved Delineation of Neural Elements in the Lumbar Spine with Commercially Available RF-Shimming at 3 T**

Dresner, M.<sup>1</sup>·Flanders, A. E.<sup>2</sup>·Talekar, K.<sup>2</sup>·Sharma, P.<sup>2</sup>

<sup>1</sup>Philips Healthcare, Springfield, PA, <sup>2</sup>Thomas Jefferson University, Philadelphia, PA

**PURPOSE**

Spine MRI provides valuable diagnostic information, but the efficacy of 3 T MRI depends on the uniformity of the static magnetic field (B0) and RF excitation (B1). Initial studies of patient-adaptive RF-shimmed (commercially "MultiTransmit") spine imaging demonstrated the acceleration enabled by increased peak B1 for shorter RF pulses and improved RF uniformity resulting in lower specific absorption rate (SAR) (Nelles, 2009). That publication demonstrated roughly 30% time savings with comparable image quality. In this work we assess the image quality of MultiTransmit (RF-shimmed) acquisitions relative to quadrature RF excitation (quad RF) for equal scan durations.

**MATERIALS & METHODS**

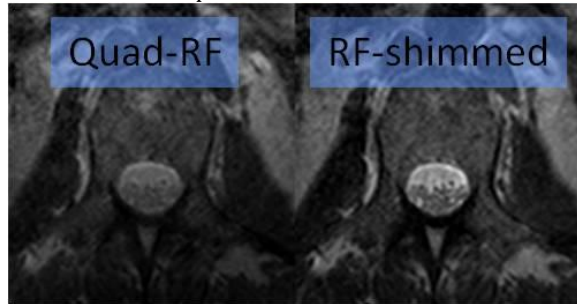
Given the scan time improvements shown by Nelles, the RF-shimmed acquisitions could improve resolution, coverage, refocusing flip angles, peak B1, saturation pulses or NSA, compared to a routine protocol which compromises these parameters to limit scan times. The use of a higher peak B1 accelerated the acquisition by shortening the duration of each refocusing pulse. As TR decreased below 3 seconds for T2-weighted axial scans, a magnetization-restoring pulse was incorporated to preserve the expected bright appearance of the cerebral spinal fluid (CSF). Adding this to the quad RF scan would require an extra minute for SAR limitations, but also did not change the CSF appearance in preliminary testing because the quad RF scan had a longer TR. To assess the reproducibility of image quality changes, ten patients referred for MRI of the lumbar spine were scanned with both the quad RF sequence (3:58) and the RF-shimmed version (3:27). Spinal canal ROIs were defined for five patients with matched quad RF and RF-shimmed axial scans. Histogram analysis was performed to distinguish whether image contrast was sufficient to delineate the cauda equina. Histograms consistent with a normal distribution signified low-contrast images, while histograms with two peaks (nerve roots and bright CSF) had a distribution statistically inconsistent with the normal distribution.

**RESULTS**

While nerve CSF contrast was adequate for most slices in both acquisitions, the figure illustrates a typical result



for the superior slices of the 32-slice stack used at our institution. Chi-squared goodness-of-fit testing on the histograms indicated that an average of 59.0% of slices had adequate contrast for quad RF scans, while 68.4% of slices were acceptable for the RF-shimmed scans.



#### CONCLUSION

RF-shimmed acquisitions can show improved image quality over conventional (quadrature RF) scans without increasing scan time. Radiologist's evaluation of these images will determine if these image quality changes translate to improved diagnostic confidence.

**KEY WORDS:** Lumbar spine, RF-shimming

#### eP-322

##### Angiographic Detection and Characterization of "Cryptic Venous Anomalies" Associated with Spinal Cord Cavernous Malformations Using Flat Panel Catheter Angiotomography

Pearl, M. S.-Chen, J. X.-Gregg, L.-San Millan, D.-Belzberg, A.-Jallo, G.-Gailloud, P.

The Johns Hopkins Hospital  
Baltimore, MD

#### PURPOSE

Spinal cord cavernous malformations (CM) are associated with two types of angiographically occult "cryptic venous anomalies", which differ in location with respect to the spinal cord. The distinction between superficial and intramedullary venous anomalies is important, as the latter heighten the risks of CM resection. We report two observations of both types of so-called "cryptic venous anomalies" associated with intramedullary CMs, documented during spinal digital subtraction angiography (SpDSA) enhanced with FPCA

#### MATERIALS & METHODS

Spinal DSA was performed in two patients with MRI documented intramedullary spinal cord CMs and prominent, nonspecific flow voids at the same levels. FPCA was performed in both patients. FPCA methodology. FPCA was obtained by selective injection of left T4 (case 1) and left T9 (case 2) using 5-French Cobra 2 catheters (Terumo, Japan) during a 20-second rotational acquisition with the patient breathing normally. Thirty milliliters of a 75%-saline and 25%-contrast solution (Omnipaque 300, GE, USA) were administered (total contrast volume, 7.5 ml). The rotational data set was reconstructed on a dedicated workstation (Leonardo, Siemens, Erlangen, Germany)

using both regular (0.4 mm voxel size) and high-resolution (0.1 mm voxel size) matrices. Case 1: 52-year-old man with a 4-year history of progressing left T10 radiculopathy. Case 2: 52-year-old man with a 7-year history of right hand weakness and new onset of finger numbness and tingling.

#### RESULTS

MRI findings: CMs at the T7 (case 1) and T1 (case 2) levels. Nonspecific prominent flow voids in both cases suggesting the possibility of a vascular malformation. SpDSA: Unremarkable in both cases. FPCA findings: Case 1: Atypical network of prominent posterior perimedullary veins at the level of the CM. Case 2: Prominent anterior-median and right posterior-lateral spinal veins, presence of two large intramedullary veins, absence of left posterior-lateral spinal veins, and radially oriented channels forming a caput medusae pattern collecting into the upper intramedullary vein.

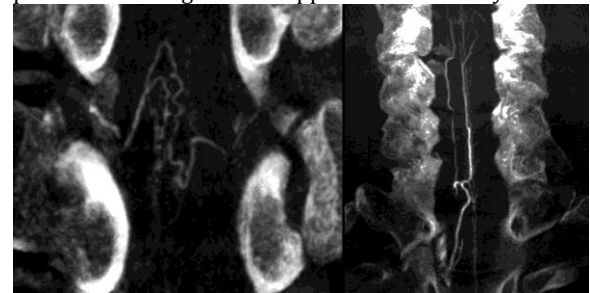


Figure 1. FPCA reconstructions of both types of "cryptic venous anomalies" associated with intramedullary CMs. A. Superficially located type. Coronal view depicts enlarged posterior perimedullary veins. B. Intramedullary type. Coronal reconstruction shows longitudinal intramedullary veins, one of which drains into anterior-median spinal vein

#### CONCLUSION

The unique ability of FPCA to image the spinal venous system enables the angiographic detection and characterization of abnormal spinal veins associated with CMs. Differentiating between the types of associated "cryptic venous malformations" may aid in surgical planning, as the intramedullary type is associated with a higher risk of surgical complication.

**KEY WORDS:** Cryptic venous anomalies, spinal cord cavernoma, angiography

#### eP-323

##### Tapering of the Spinal Canal in Patients with Chiari I

Hammersley, J. A.-Hirano, M.-Wang, Y.-Munoz Del Rio, A.-Haughton, V.

University of Wisconsin School of Medicine and Public Health  
Madison, WI

#### PURPOSE

Patients with the Chiari I malformation have abnormal cerebrospinal fluid (CSF) flow dynamics, which may have a role in the pathogenesis of syringomyelia and perhaps some neurologic symptoms. Tonsillar herniation and

small posterior fossa dimensions affect CSF flow. The possibility that cervical spinal canal anatomy in the Chiari I malformation may influence CSF flow dynamics has not received sufficient study. We studied cervical spinal canal dimensions in patients with the Chiari malformation and in control groups.

#### MATERIALS & METHODS

In one phase of the study, we selected from a registry a list of patients with Chiari I malformation. Then, in PACS, we found age- and gender-matched controls that had MR cervical spine studies reported as normal. In another phase, we reviewed MR images in scoliotic patients and classified them as having a Chiari malformation (cases) or not having Chiari I malformation (controls). For all cases and controls, we measured the AP diameter of the cervical spinal canal on sagittal T2-weighted MR images at each spinal level. Next, we fit a linear trendline by regression to the diameters and recorded the slope of that line as the taper ratio. The taper ratios of the patients with and without Chiari malformation were compared and the differences tested for significance by the Student t-test of the means.

#### RESULTS

For the first phase of the study, we obtained 21 patients with Chiari I and 21 matched controls. For the second phase, 54 scoliotic patients were identified, 22 of whom had a Chiari malformation and 32 of whom did not. In the first phase of the study, the taper ratios averaged  $-0.6 \pm 0.3$  mm/level in the Chiari cases with syrinx and  $-0.3 \pm 0.2$  mm/level in the controls. Taper ratios in cases with Chiari differed significantly from the control group ( $p = 0.003$ ). In the second phase of the study, the taper ratios averaged  $-0.9$  mm/level for the patients with a Chiari malformation and  $-0.4$  mm/level for the patients without a Chiari, significant at  $p = 0.004$ . Age differences between the two study phases explain minor differences in the taper ratios.

#### CONCLUSION

Patients with a Chiari I malformation have more severely tapered cervical spinal canals than individuals without a Chiari I.

**KEY WORDS:** Chiari I, scoliosis, spinal canal

#### eP-324

### Third Generation CT-Guided Percutaneous Interspinous Distractor in Sciatica Related to Foramina Stenosis: New Application

Manfrè, L.

Miniinvasive Spine Interventional Department AOE  
Cannizzaro  
Catania, ITALY

#### PURPOSE

Conventional surgical treatment of foraminal stenosis can be affected by several side effects. Recently, CT-guided percutaneous interspinous devices (ISD) have been used in patients affected by spinal canal stenosis

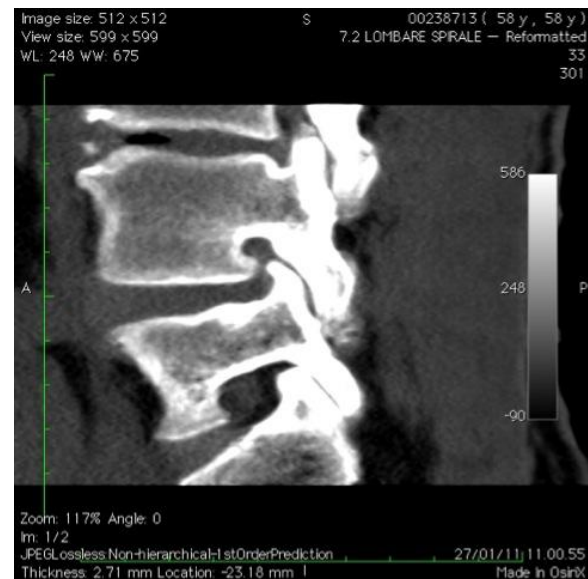
related to yellow ligaments bulging and nerve compression.

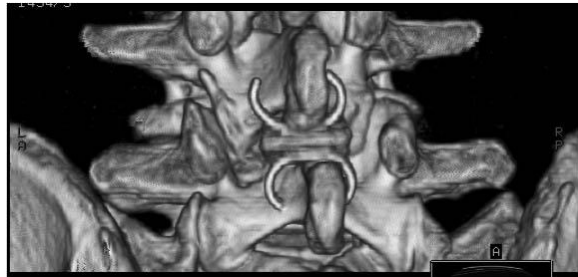
#### MATERIALS & METHODS

Among 154 patients treated from 2008 with ISD, we selected five patients with severe lateral foramina stenosis, severe selected nerve compression, positive EMG study for involvement of the nerve inside the narrowed foramen, and compatible symptoms (i.e., radicular pain, numbness, paresthesia). The width of the foramen (anteroposterior AP and caudocranial CC distance) was calculated on 2D reconstructed CT images before and after the ISD introduction. The pain of the patients was evaluated according to a VAS scale.

#### RESULTS

After the treatment, the mean width of the pathologic foramen increased 8 mm, with appreciated increase of AP and CC measurements. At 1 week and 3 months follow up, all the patients reported disappearance of previously reported monoradicular pain and, in the case with L5 dependent paresis, restitutio-ad-integrum was appreciated immediately after the decompression.





#### CONCLUSION

Percutaneous CT-guided ISD treatment seems to be useful in patients with symptomatic neural foramen stenosis related to disk degenerative disease and reduced distance between articular facets.

**KEY WORDS:** Foramina stenosis, interspinous device, sciatica

#### eP-325

#### Posterior Lumbar Interbody Fusion and Distraction Using Local Anesthesia: First Case Report Using only CT-Guided Technique

Manfrè, L.

Minimally Invasive Spine Interventional Department AOE  
Cannizzaro  
Catania, ITALY

#### PURPOSE

We performed CT-guided posterior interbody fusion (PIF) with pedicle screw fixation and vertebra distraction to treat degenerative lumbar L4-L5 spondylolisthesis with severe left sciatica.

#### MATERIALS & METHODS

The patient was suffering for L4 nerve root compression related to neural foramina stenosis. Caliber of the foramina were measured on pre and postop CT 2D reconstruction studies. As self-tapping screws were used, a progressive dilatation of the

muscular layer was performed using dedicated coaxial dilators, then Pangea screws were inserted into the pedicle, and the process was repeated for every pedicle of L4 and L5; finally a couple of 60 mm rods were applied, directly through the cannula at L5 level, moving towards the L4 screws, and a rod pusher was used to fix the rods to screws. The procedure was easy to apply with a total surgical time of 90 minutes. The neural foramina were investigated with CT scan reconstruction on sagittal plane demonstrating marked widening after the PIF application.

#### RESULTS

CT study immediately after surgery with sagittal reconstruction demonstrated reduction of L4 anterolisthesis, with relevant widening of the neural L4-L5 foramina both on the left -12 mm (AP) x 20 mm (CC), and on the right -13 mm (AP) x 20 mm (CC) side. Left leg pain immediately decreased in a few days, resolving after 2 weeks, without recurrence at 3 months follow up. CT control study at 1 and 3 months did not show any complication.



**CONCLUSION**

Chronic drug-resistant sciatica can occur in patients affected by neural foramina narrowing secondary to degenerative anterior lythesis of a lumbar vertebra. CT-guided pedicle screws fixation and distraction of vertebra could be useful in such conditions. To our knowledge, no other papers about CT-guided PIF procedure are found in the literature.

**KEY WORDS:** Posterior lumbar fusion, pedicle screw, CT

**eP-326****Concordance between MR Imaging and CT for Incidental Cervical Ribs**

Walden, M. J. • Alluwaime, F. • Viertel, V. • Patel, N. V. • Intrapromkul, J. • Yousem, D. M.

Johns Hopkins Hospital  
Baltimore, MD

**PURPOSE**

Incidental cervical ribs can be identified on 1.9% of routine cervical spine CT examinations and 1.3% of routine cervical spine MR exams. These data suggest lower sensitivity of MRI for detecting this common osseous anomaly. The purpose of our study was to determine the concordance of incidental cervical ribs on routine MR cervical spine imaging versus routine CT imaging and the rate at which they are reported on each modality.

**MATERIALS & METHODS**

We retrospectively reviewed 3,404 consecutive routine cervical spine CT examinations for the presence of cervical ribs, of which, 64 were identified with cervical ribs (1.9%). Of these patients noted to have cervical ribs, 14 also had cervical spine MR examinations. One of the MR exams did not cover the C7 level and was removed from the study. The remaining 13 exams subsequently were reviewed for the presence of cervical ribs, evidence of compression of adjacent structures, anterior termination of the ribs, laterality and if the ribs were mentioned in the radiology report. The reviewers were blinded to laterality and other characteristics of the cervical ribs identified on CT examinations.

**RESULTS**

Amongst the 13 patients with both CT and MRI imaging of the cervical spine, 11 of the MR examinations were identified as positive for the presence of cervical ribs (85% concordant). The laterality of the identified ribs on MRI was 62% concordant with CT (8/13). Evidence of compression of the adjacent brachial plexus was identified on both CT and MR in three cases. However, putative brachial plexus compression was seen only on MR in two cases and only on CT in one case. Evidence of subclavian artery compression was noted only on MR in one case and only on CT in three cases. Only 1/13 (8%) of the MRI reports mentioned cervical ribs compared to 4/13 (31%) exams reported as positive on CT.

**CONCLUSION**

Incidental cervical ribs can be identified on 11 out of 13 routine cervical spine MR examinations for patients who previously had identified cervical ribs on CT exams (86% concordance). This corresponds to prevalence data which suggest decreased sensitivity of MRI for detecting these common osseous anomalies, which in turn, may contribute to the apparent disparity in reporting cervical ribs on different modalities. Our data suggest that when cervical ribs are identified, MR is comparable to CT for evaluation of brachial plexus compression, but less sensitive than CT for evaluation of subclavian artery compression. This is likely secondary to limited field of view in routine spine MR examinations.

**KEY WORDS:** Cervical, Ribs, Anatomy

**Monday, April 23 –  
Wednesday, April 25  
6:30 AM - 9:00 PM**

**Thursday, April 26  
6:30 AM – 3:00 PM  
Rhineland**

**Education Exhibits (EdE) 1 – 37**

**EdE1 - Adult Brain**

**Note: A missing printed number indicates an abstract has been withdrawn.**

**EdE-1****CT Perfusion in Acute Stroke: Know the Mimics, Potential Pitfalls, Artifacts, and Technical Errors**

Mangla, R. • Almast, J. • Kolar, B.

University of Rochester  
Rochester, NY

**PURPOSE**

The CT perfusion imaging of brain has established as a clinically useful tool in multimodality imaging of acute stroke. CT has the advantages of being widely available and easily providing quantitative perfusion metrics. This exhibit will describe and characterize mimics, potential pitfalls, artifact and technical errors.

**APPROACH/METHODS**

There are many clinical mimics on CT perfusion and can be mistaken as acute stroke. On the other hand, there are also clinical situations when CT perfusion can be negative when patient actually had diffusion positive stroke. There are many pitfalls and artifacts in acquiring the data, calculation of maps and choosing arterial input function. . We analyze and classify all these aspects, to

allow the technician and the radiologist to know exactly what to avoid and what to choose, and we indicate when possible the way to improve the quality and of examination.

#### FINDINGS/DISCUSSION

This exhibit will describe: Technical pitfalls: AIF selection, VOI selection, Delay in arrival of bolus, Variation in P-com size, Slice selection. A few Strokes can be missed: Lacunar or microvascular stroke, borderzone infarcts, Posterior fossa infarcts, Reperfusion Phenomenon Masking Acute and Subacute Infarcts. In few conditions, you can never be sure about acute Infarct: ICA or intracranial stenosis, Vasospasm, acute on chronic infarct. Hypoperfusion without definite infarct: Post-ictal phase of epilepsy, Migraine: aura phase of migraine. Hyperperfusion leading to asymmetry and clinical mimic of acute stroke: Ictal phase of epilepsy, Migraine - during headache, Brain tumors. Hyperperfusion syndrome after carotid stenting or endarterectomy.

#### SUMMARY/CONCLUSION

This educational exhibit will describe and characterize mimics, potential pitfalls, artifact and technical errors.

**KEY WORDS:** CT perfusion, stroke, pitfalls

#### EdE-3

##### Neuroradiologic "Stroke Mimics"

Dudau, C.<sup>1</sup>Schmitt, A. J.<sup>1</sup>Pendse, D. A.<sup>1</sup>Jager, R.<sup>1</sup>Chatterjee, F.<sup>2</sup>

<sup>1</sup>University College London Hospitals NHS Foundation Trust, London, UNITED KINGDOM, <sup>2</sup>University College Hospital, London, UNITED KINGDOM

#### PURPOSE

The diagnosis of acute ischemic stroke is often straightforward but differential diagnostic problems remain because some nonvascular disorders may have clinical and radiologic pictures that appear identical to strokes.

#### APPROACH/METHODS

A retrospective analysis of data from consecutive patients at the Acute Stroke service at UCLH was performed. Each patient presented with a clinical stroke syndrome, and underwent acute NCCT brain and CT angiography at the time of presentation. Each patient later underwent stroke MRI including diffusion-weighted imaging and contrast angiography.

#### FINDINGS/DISCUSSION

In total, analysis of data from 562 patients was performed. Full data sets were available from 511 patients. We present a selection of cases, where multiparametric imaging confirmed nonvascular disorders, rather than acute stroke.

Example cases presented: abscess, hemorrhagic metastases, MS, late PRES, osmotic myelinolysis, HSE, CJD.

#### SUMMARY/CONCLUSION

Noncerebrovascular diseases may present with both acute onset and false CT/MRI signs of early ischemic stroke. The necessity for rapid administration of intravenous thrombolysis in patients with acute ischemic stroke may lead to treatment of patients with conditions mimicking stroke. This pictorial review is a reminder of conditions to be considered by the reporting radiologist when presented with an acute stroke picture.

**KEY WORDS:** Stroke, diffusion-weighted imaging

#### EdE-4

##### Spectrum of Neuroimaging Findings in Dementia Secondary to Primary Neurodegenerative Disease

Modi, J.·Mahajan, A.·Scott, J.·Molnar, C. P.·Lysack, J.  
University of Calgary

Calgary, AB, CANADA

#### PURPOSE

The purpose of this study is to describe magnetic resonance imaging (MRI) and [18]fluorodeoxyglucose positron emission tomography (FDG-PET) findings in dementia secondary to primary neurodegenerative diseases.

#### APPROACH/METHODS

This is a 2-year retrospective review of imaging of patients presenting with a clinical diagnosis of dementia suspected to be secondary to a primary neurodegenerative disease who had both MRI and FDG-PET performed.

#### FINDINGS/DISCUSSION

Out of the total 67 patients, 37 were males and 30 females with a mean age 65 years (range 45-89 years). The final diagnosis was based on clinical, MRI and FDG-PET findings. Alzheimer disease (AD) was present in 33/67 cases (49%), frontotemporal lobar degeneration (FTLD) in 17/67 (25%), dementia with Lewy body disease (DLB) in 4/67 (6%), progressive supranuclear palsy (PSP) in 2/67 (3%), and multisystem atrophy (MSA) in 1/67 (1.5%). Patients were diagnosed with mixed dementia in 6/67 (9%) and were felt to have a normal aging pattern in 4/67 (6%). Typical findings are as follows: AD: Disproportionate hippocampal atrophy and often prominent parietal lobe atrophy. Hypometabolism in the temporal, parietal, and posterior cingular regions that usually is symmetrical. In vivo amyloid imaging with Pittsburgh compound B (PIB) shows increased amyloid binding in the frontal, temporal and parietal lobes. FTLD: Three types: 1. Behavioral variant. Fronto-temporal atrophy with relative sparing of the parietal and occipital lobes, commonly bilateral, but often asymmetrical. 2. Progressive nonfluent aphasia. Asymmetric dominant (usually left) hemisphere involvement, commonly affecting the perisylvian region, particularly the inferior frontal and insular cortex. 3. Semantic dementia. Usually left greater than right temporal lobe atrophy, particularly anterior temporal lobes, with "knife-edge"



appearance. FDG-PET shows frontotemporal and anterior cingulum hypometabolism with relative sparing of the occipital and parietal, including the posterior cingular regions. DLB: Mild generalized atrophy, with no specific predilection. Hippocampal atrophy is initially mild or absent. On FDG-PET, there is diffuse hypometabolism, most marked in occipital region which is not typically involved in AD. Dopaminergic imaging is the most important marker and shows abnormal striatal uptake which is absent in AD. PSP: Midbrain and superior cerebellar peduncle atrophy giving classic "hummingbird" appearance in the midsagittal imaging plane. FDG-PET may show hypometabolism in the frontal lobes. MSA: Three types. 1. MSA-P (striatonigral degeneration). Putaminal atrophy. T2 hypointensity in the posterior putamen with a thin rim of hyperintensity at the lateral posterior putaminal rim. 2. MSA-C (olivopontocerebellar atrophy). Cerebellar and pontine atrophy. Characteristic "hot cross bun" appearance. 3. MSA-A (Shy-Drager syndrome). As in MSA-P and/or MSA-C. No specific findings on FDG-PET in MSA. CBD: Asymmetric parasagittal cortical atrophy predominantly in the parietal and temporal lobes. FDG-PET may show the asymmetric hypometabolism.

#### SUMMARY/CONCLUSION

The importance of imaging in patients suspected of dementia has extended beyond its routine role of exclusion of neurosurgical lesions. Awareness of the characteristic patterns of brain atrophy can suggest the diagnosis of a specific neurodegenerative disease. FDG-PET is more accurate than MRI in the early stages of neurodegenerative disease.

**KEY WORDS:** Neurodegenerative, MR imaging, positron emission tomography

#### EdE-5

##### Power of the Metaphor: Forty Signs on Brain Imaging

Gocmen, R.·Oguz, K. K.·Cila, A.

Hacettepe University  
Ankara, TURKEY

#### PURPOSE

The history of the medicine is full of the metaphorical descriptions. Many pathologies in particularly illustrative branches of the medicine such as radiology, dermatology, microbiology, and pathology have been described in terms of their resemblance.

#### APPROACH/METHODS

We present and illustrate the characteristic forty neuroradiologic signs of various pathologic conditions.

#### FINDINGS/DISCUSSION

Imaging Findings. A) Congenital Malformations: a. Tectal beaking sign: Chiari II malformation, b. Steer horn ventricles: Agenesis of the corpus callosum, c. Bat-wing sign: Joubert syndrome, d. Molar tooth sign: Joubert syndrome, e. Tram-track sign: Sturge-Weber

syndrome, f. Pancake sign: Holoprosencephaly, g. Corduroy sign: Lhermitte-Duclos syndrome, h. Figure eight: Lissencephaly, i. Key-hole sign: Dandy-Walker syndrome. B) Vascular/Stroke: a. Dense middle cerebral artery (MCA) sign: Acute MCA thrombosis, b. Cord sign: Cortical venous thrombosis, c. Middle cerebral artery dot sign: Acute MCA focal thrombosis, d. Caput medusa sign: Developmental venous anomaly, e. Zebra sign: Remote cerebellar hemorrhage, f. Hot nose sign: Brain death, g. Puff of smoke sign: moyamoya, h. Ivy sign: moyamoya, i. Empty delta sign: Dural sinus thrombosis, j. Popcorn sign: Cavernous malformation, k. Reversal sign or white cerebellum: Diffuse cerebral hypoxic/anoxic injury, l. Spot sign: Active bleeding within hematoma, m. Insular ribbon sign: Acute MCA infarct. C) Tumors and Tumor-like Lesions: a. Dural tail sign: Meningioma, b. Spoke-wheel sign: Meningioma, c. Ice-cream sign: Vestibular schwannoma, d. Bubbly appearance: Dysembryoblastic neuroepithelial tumor, e. Butterfly sign: Glioblastoma multiforme, lymphoma, tumefactive demyelinating lesion. D) Metabolic/Degenerative Disorders: a. The giant panda sign: Wilson's disease, b. Penguin or hummingbird sign: Progressive supranuclear palsy, c. Morning glory/Mickey Mouse sign: Progressive supranuclear palsy, d. Eye of the tiger sign: Pantothenate Kinase-associated neurodegeneration (formerly called Hallervorden-Spatz syndrome), e. Tigroid pattern or leopard skin: Metachromatic leukodystrophy, f. Hot cross bun sign: Multisystem atrophy-cerebellar type, g. Tadpole sign: Alexander disease. E) Infection and Demyelinating Disease: a. Open ring/horseshoe sign: Multiple sclerosis, b. Hockey-stick sign: Creutzfeldt-Jakob disease, c. Onion skin sign: Baló's concentric sclerosis, d. Floating membranes: Hydatid cyst. F) Miscellaneous: a. Reverse cupping sign: Raised intracranial pressure, b. En coup de sabre: Parry-Romberg syndrome/localized scleroderma.

#### SUMMARY/CONCLUSION

The signs may help characterization and memorability of certain diseases in radiology. However, the radiologists also should be aware of degree of specificity and sensitivity of the signs for each pathologic condition since the same signs can be seen in a number of other disorders.

**KEY WORDS:** Neuroradiology, images, interpretation

#### EdE-6

##### Differential Diagnosis and Research Update in Creutzfeldt-Jakob Disease

Caverzasi, E.·Hess, C. P.·Henry, R. G.·Wong,  
K.·Geschwind, M. D.

University of California San Francisco  
San Francisco, CA

#### PURPOSE

To review the imaging features, clinical phenotypes and disease course of human prion diseases and discuss the approach to the differential diagnosis between prion



disease and other nonprion rapidly progressive dementias (npRPDs).

#### APPROACH/METHODS

Cases of pathology-proved prion disease, including sporadic Creutzfeldt-Jakob disease (CJD), genetic prion disease (e.g., familial CJD and Gerstmann-Sträussler-Scheinker), and cases with npRPD were selected from a registry of patients evaluated at the UCSF Memory and Aging Center. 3 T, and some 7 T, images were reviewed together with clinical history, findings on neurologic examination, and the results of CSF sampling.

#### FINDINGS/DISCUSSION

Information is presented on the genetic susceptibility, different clinical phenotypes and various imaging appearances of different forms of prion disease and show characteristic images for both prion disease and npRPD. Recent proposed diagnostic criteria that now include imaging are presented, discussed and critiqued. MR imaging can differentiate between prion disease and npRPD with high accuracy. Critical evaluation of diffusion-weighted imaging (DWI), together with mean diffusivity maps, is more important than FLAIR in the diagnostic process. Nonprion rapidly progressive dementias, however, might present with cortical and/or deep gray matter DWI hyperintensity that sometimes might be mistaken for prion disease. As examples, reduced diffusion can be found in striatum in extrapontine myelinolysis and Wilson's disease, in the posteromesial thalamus in Wernicke's encephalopathy and in Bartonella infection. Cortical reduced diffusion can be seen in the acute phases of viral encephalitis, seizures including status epilepticus, cortical infarcts and autoimmune encephalopathy. Higher field strength and higher b-value DWI sequences might be useful for troubleshooting, as they tend to show more extensive areas of reduced mean diffusivity in the deep gray matter and other structures in sporadic CJD.

#### SUMMARY/CONCLUSION

Although prion diseases are uncommon, they are important in the differential of the patient presenting with rapidly progressive dementia. Brain diffusion MRI is crucial to the diagnosis of prion disease and recently has been included in revised diagnostic criteria. Specific patterns of involvement on MRI can be helpful for diagnosing prion disease and differentiating it from other causes of npRPD.

**KEY WORDS:** Rapid progressive dementias, diffusion-weighted imaging, Creutzfeldt-Jakob disease

#### EdE-7

#### Pathophysiology of Alzheimer Disease Explained: Towards a Better Understanding of Structural and Functional Imaging Biomarkers

Mortimer, A. M.·Bradley, M.·Likeman, M.·Lewis, T. T.

Frenchay Hospital  
Bristol, UNITED KINGDOM

#### PURPOSE

1) To describe the pathophysiologic basis for development of Alzheimer disease (AD). 2) To relate this to structural and functional imaging biomarkers that could be used in early detection of AD.

#### APPROACH/METHODS

A visual display will be provided, illustrating the development of AD with reference to initial sites of involvement and specific pathologic processes that result in secondary neurophysiologic and neuroanatomical changes. Subsequent structural and functional imaging abnormalities then will be described: a particular aim is to relate these changes to the underlying pathophysiology, stage of disease progression, and ability to differentiate from normal individuals and those with mild cognitive impairment who may or may not progress to Alzheimer disease.

#### FINDINGS/DISCUSSION

The earliest detectable microscopic changes in AD are the development of extracellular amyloid plaques and intracellular neurofibrillary tangles in the transentorhinal and entorhinal areas, before spreading to the hippocampus, and then to the association cortices and the rest of the cortex. These lesions have been targeted with various PET radiotracers including the carbon-11 Pittsburgh Compound B (PiB) which specifically to beta-amyloid deposits, and is a sensitive marker for such pathology in cognitively normal older individuals and patients with mild cognitive impairment (MCI) and Alzheimer disease. Initial data suggests that PiB-PET can accurately predict those with MCI who will go on to develop AD within 2 years and also accurately rule out the development of AD. Tau specific ligands are also under investigation. Following these changes, hippocampal atrophy, posterior cingulate and frontal glucose hypometabolism, and white-matter tract disruption are macroscopic events in Alzheimer disease. Both volumetric MRI and PET hypometabolism have been shown to predict conversion from MCI to AD, with volumetric MRI perhaps more sensitive. Whilst the chronology of these features is yet to be fully established, recent insights into the relationship of these features has been gained. An intriguing study combining PET and volumetric MRI showed that precuneus/posterior cingulate cortex hypometabolism follows medial temporal atrophy through posterior cingulum white matter degeneration. Furthermore, several studies using resting state fMRI have shown a functional disconnection between hippocampus and precuneus/posterior cingulate cortex. Indeed DTI measures of white matter degeneration, particularly in tracts connecting hippocampus with precuneus/posterior cingulate show accuracy in predicting conversion from MCI to AD comparable to macroscopic measures of hippocampal atrophy.

#### SUMMARY/CONCLUSION

Early detection of AD may be increasingly important as therapeutic advances are made. Knowledge of the pathophysiology of the condition is vital to understanding the role of potential functional and structural biomarkers of disease.

**KEY WORDS:** Alzheimer disease, dementia, functional imaging

#### EdE-8

#### **Imaging Features of Psychosurgery, Neurodegenerative Surgery, and Epilepsy Surgery**

Ginat, D. T. Schaefer, P.

Massachusetts General Hospital  
Boston, MA

#### **PURPOSE**

Medically intractable psychiatric conditions, neurodegenerative disorders, and epilepsy can be treated operatively. A wide variety of procedures and devices are available for treating and monitoring these conditions. The purpose of this exhibit is to comprehensively review the imaging features.

#### **APPROACH/METHODS**

Examples showing the typical imaging features of the following procedures and devices will be demonstrated. The utility of advanced imaging, including DTI and functional MRI, for postoperative evaluation will be discussed. In addition, selected complications will be depicted. Psychiatric - Frontal lobotomy, limbic leucotomy, cingulotomy, occipital nerve stimulators. Neurodegenerative - Deep brain stimulators, pallidotomy, GAD infusion, subcaudate tractotomy. Epilepsy - Implantable electrode grids and arrays for epileptogenic focus localization, vagus nerve stimulator, temporal lobectomy, lesionectomy, callosotomy, hemispherectomy.

#### **FINDINGS/DISCUSSION**

Some procedures no longer are performed, such as frontal lobotomy, although these patients that underwent such procedures continue to be imaged. Postoperative imaging often is requested to assess for complications, such as infection and hemorrhage, and electrode malposition in the case of deep brain stimulation. In particular, precise electrode is crucial. For example, electrodes should be positioned in the subthalamic nucleus, while these should be positioned in the ventralis caudalis for treatment of thalamic pain syndrome. Diffusion tensor imaging is useful for evaluating the degree of white matter changes after lobectomy and tractotomy. For example, fractional anisotropy decreases along the optic tracts, particularly in patients with postoperative visual deficits. Functional MRI is useful for re-resection planning for lesionectomy in patients with persistent seizures.

#### **SUMMARY/CONCLUSION**

Familiarity with the diverse types of psychosurgery, neurodegenerative surgery, and epilepsy surgery procedures is important for guiding proper management.

**KEY WORDS:** Psychosurgery, neurodegenerative surgery, epilepsy surgery

#### EdE-9

#### **Diffusional Kurtosis Imaging: Theory, Optimization of Protocol, and Clinical Applications**

Mariko, Y.<sup>1</sup>Hori, M.<sup>1</sup>Fukunaga, I.<sup>2</sup>Suzuki, M.<sup>3</sup>Kamagata, K.<sup>1</sup>Asahi, K.<sup>1</sup>Aoki, S.<sup>1</sup>Masutani, Y.<sup>4</sup>

<sup>1</sup>Juntendo University School of Medicine, Tokyo, JAPAN, <sup>2</sup>Graduate School of Health Promotion Science, Tokyo Metropolitan University, Tokyo, JAPAN, <sup>3</sup>Juntendo University School of Medicine, Chiba, JAPAN, <sup>4</sup>Graduate School of Medicine, The University of Tokyo, Tokyo, JAPAN

#### **PURPOSE**

Diffusional kurtosis imaging (DKI) is a newly highlighted technique using the non-Gaussian water diffusion analysis. Because water diffusion in the brain is restricted (non-Gaussian), DKI provides more precise diffusional information derived from microstructure of the tissue than conventional diffusion analysis such as diffusion tensor imaging (DTI, which uses Gaussian). The purpose of this exhibit is to present the basics of DKI, normal DKI atlas of the brain, and clinical application with representative cases.

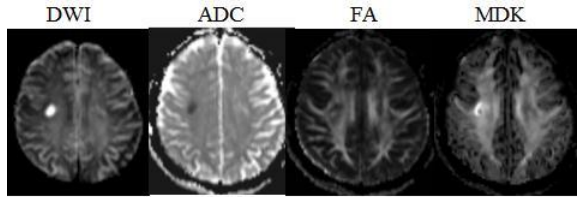
#### **APPROACH/METHODS**

Diffusional kurtosis images were acquired on a clinical 3T-MR (Philips Medical Systems) with parameters as follows: TR/TE 3000-7500/70-80 ms; slice thickness 3-5 mm; 2-3 mm resolution, 6-12 min. acquisition time; 3 or 6-*b* values (0,1000,200 or 0, 500,1000, 1500, 2000, 2500 sec/mm<sup>2</sup>) with diffusion encoding in 20-32 directions for every *b* value, large and small delta; 45.3/13.3ms. We used software to analyze DKI as well as DTI (dTV II FZR; Image Computing and Analysis Laboratory, Department of Radiology, The University of Tokyo, Japan). Diffusion tensor imaging parameters (ADC, FA, axial diffusion (i.e., Lambda 1), radial diffusion (i.e., mean of Lambda 2 and 3) and DKI parameters [diffusional kurtosis(DK), axial DK (DK along Lambda 1)], radial DK (DK perpendicular to Lambda 1) can be calculated with a combination of DTI tractography. Tract-specific DK analysis can be performed. We analyzed neurologic disorders including cerebral infarction, multiple sclerosis, normal pressure hydrocephalus and other disorders by using these techniques.

#### **FINDINGS/DISCUSSION**

1. We will explain briefly the basics of the DKI, imaging sequence, postprocessing algorithm and the factors that influence the values of diffusional kurtosis (e.g., numbers and values of *b* factor). 2. We will present DK atlas of normal brain with corresponding FA map. In general, DK shows correlation with corresponding FA because it is thought to be influenced by microstructural complexity. However, there are differences between DK and FA maps, such as at the portion of crossing fibers, where FA is decreased but DK is not. 3. We will show representative cases including cerebral infarction, multiple sclerosis and other disorders and discuss the clinical usefulness of DKI with reviewing the current publications.

## DTI and DKI of subacute infarction



### SUMMARY/CONCLUSION

Diffusional kurtosis imaging is a recently developed technique that characterizes non-Gaussian water diffusion, which are different from conventional diffusional metrics, such as FA. In some clinical situations, DKI has showed better results, compared with FA or ADC investigation. This technique has potential to provide new and additional information to conventional diffusional metrics in routine clinical study.

**KEY WORDS:** Diffusional kurtosis imaging, non-Gaussian

### EdE-10

#### Advanced Neuroimaging Pitfalls: A Pictorial Review

Aquino, C.·Mamourian, A.

Hospital of the University of Pennsylvania  
Philadelphia, PA

### PURPOSE

Advanced imaging offers a new set of tools that can be used to characterize brain disease. While the literature highlights the value of these tools, advanced imaging can at times provide misleading information. This pictorial essay will serve to demonstrate some potential pitfalls that may be encountered when using advanced imaging in neuroradiology with focus on diffusion, MR spectroscopy and MR perfusion.

### APPROACH/METHODS

The cases were selected from a weekly tumor board conference and all pathologically proven. Select examples include: • restricted diffusion with glioblastoma resembling lymphoma, • metastatic disease resembling abscess, • high relative cerebral blood flow (rCBV) and high Choline/Creatine-NAA ratio with tumefactive MS suggesting tumor (see Figure 1 below), • high rCBV with lymphoma suggesting high grade glioma, • high rCBV in benign vascular malformations mimicking high grade neoplasms, • additional rare tumor-like masses in the brain from calcifying pseudotumor and Kikuchi disease that may be mistaken from tumor.

### FINDINGS/DISCUSSION

While advanced imaging is helpful for characterization of brain masses, it is not well acknowledged in the literature that it can be misleading in some situations.

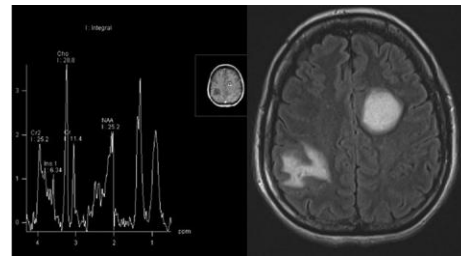


Figure 1: Multivoxel MR spectroscopy of a peripherally enhancing T2 hyperintense left frontal lobe lesion. High Cho/Cr and Cho/NAA ratio suggests high grade neoplasm; however, on pathology this was proven to be a tumefactive demyelinating lesion.

### SUMMARY/CONCLUSION

Although advanced imaging can provide additional relevant information to conventional imaging, pitfalls do exist. It is our intent with this pictorial essay to highlight some of these potential problem cases using case examples.

**KEY WORDS:** Spectroscopy, perfusion, diffusion tensor imaging

### EdE-11

#### Clinical Application of MR Perfusion and MR Spectroscopy in Brain Tumor Imaging and Its Pitfalls

Harb, J.·Patel, S.·Wang, A.·Arani, K. N.·Silbergleit,  
R.·Krishnan, A.

William Beaumont Hospital  
Royal Oak, MI

### PURPOSE

One of the most important but also most difficult tasks that face us in neuroradiology is in distinguishing tumor mimics from neoplasm and radiation necrosis from tumor recurrence. These distinctions often can not be reliably distinguished by MRI appearance, since parameters such as contrast enhancement, high T2 signal intensity and mass effect often occur in both benign and malignant entities. In addition patient symptomatology, timing of lesion presentation and even growth often overlaps (e.g., pseudo progression in postradiation inflammation). For these reasons, functional imaging is often the best noninvasive method to differentiate these lesions. This computerized exhibit will instruct radiologists on how to better distinguish tumor mimics from cerebral neoplasm and tumor recurrence from radiation necrosis using MR perfusion (MRP) and MR spectroscopy (MRS).

### APPROACH/METHODS

1. We will review normal brain values in MR spectroscopy and MR perfusion. 2. We will review characteristic patterns of MRS and MRP distinguishing brain tumors from tumoral mimics (e.g., tumefactive multiple sclerosis and brain abscess) as well as characteristic patterns distinguishing posttreatment changes (particularly radiation necrosis) from recurrent tumor. 3. We will review pitfalls of MRS and

MRP that reduce the reliability for distinguishing these entities.

#### **FINDINGS/DISCUSSION**

We will introduce viewers to a basic understanding of MRS and MRP as well as describe pitfalls in MRS and MRP imaging. In a case-based format, we will show how MRS and MRP are useful in distinguishing cerebral neoplastic processes, postradiation treatment changes (particularly radiation necrosis), and recurrence. Use of MRS and MRP in finding the best location for biopsy within a brain lesion suspicious for tumor will be described. In addition to showing multiple MRP cases using gadolinium scanning, we also will show a case of arterial spin labeling to distinguish tumor recurrence from radiation necrosis. Cases showing pitfalls using MRS and MRP imaging also will be reviewed. We will include cases showing pitfalls of sampling hemorrhagic or cystic lesions, thereby demonstrating a falsely benign appearance to the MRS and MRP as well as a pitfall of radiation necrosis mimicking tumor recurrence on MRS.

#### **SUMMARY/CONCLUSION**

After reviewing the basics of MRS and MRP as well as the potential pitfalls in a case-based format, this exhibit should give the radiologist more confidence in distinguishing tumor mimics from neoplasm and radiation necrosis from tumor recurrence.

**KEY WORDS:** MR spectroscopy, MR perfusion, brain neoplasm

#### **EdE-12**

##### **[<sup>123</sup>I] Isoflupane (DaTSCAN) SPECT Imaging: Implications for Parkinson's Disease**

Shih, J.·Solnes, L.·Osborne, J.

Weill Cornell Medical College/New York Presbyterian Hospital  
New York, NY

#### **PURPOSE**

Accurate diagnosis of Parkinsonian syndromes (PS) is necessary for initiation of appropriate therapy and accurate expectations of disease course. However, the clinical presentation of PS especially in the early stages can often mimic those of other movement disorders, most notably essential tremor (ET). Single-photon emission-computed tomography using the radiopharmaceutical Iodine 123 Isoflupane (DaTSCAN) may be helpful in the diagnostic evaluation of patients with suspected PS. [<sup>123</sup>I] labeled Isoflupane is a radiopharmaceutical that binds selectively to presynaptic striatal dopamine transporters (DaT). This property is utilized in imaging of degenerative PS as the loss of dopamine neurons in the syndromes should result in decreased striatal [<sup>123</sup>I] Isoflupane uptake. Though utilized in Europe for SPECT imaging since 2000, [<sup>123</sup>I] Isoflupane received FDA approval for use in the United States in January. The objectives of this education poster are to 1. Describe the reason and techniques for [<sup>123</sup>I] Isoflupane SPECT imaging. 2. Discuss the role of [<sup>123</sup>I] Isoflupane SPECT imaging in

clinical practice. 3. Review of the limitations of [<sup>123</sup>I] Isoflupane SPECT imaging to assist radiologists in providing relevant information to referring clinicians.

#### **APPROACH/METHODS**

This education exhibit will review the biology and mechanism for [<sup>123</sup>I] Isoflupane SPECT imaging and commonly used techniques. Multiple cases of normal and abnormal scans at our institution will illustrate the principles of image interpretation. In addition, the exhibit will review recent multicenter clinical trials which evaluate the agreeability of abnormal imaging findings to a clinical diagnosis of PS.

#### **FINDINGS/DISCUSSION**

Two recent multicenter trials have demonstrated high agreeability between abnormal findings on [<sup>123</sup>I] Isoflupane SPECT and a clinically established diagnosis of PS over a 2-3 year follow up. In patients with an equivocal diagnosis, there was initially an observed trend towards the eventual diagnosis of PS in patients with abnormal scans suggesting a possible benefit of [<sup>123</sup>I] Isoflupane SPECT in the diagnosis of early PS. The interobserver agreement with regards to the visual assessment of the study was high indicating robustness of image interpretation.

#### **SUMMARY /CONCLUSION**

[<sup>123</sup>I] Isoflupane SPECT imaging is utilized in the evaluation of patients with suspected Parkinsonian syndromes. The purpose of this poster is to improve the radiologist's understanding of the techniques, interpretation, and limitations of [<sup>123</sup>I] Isoflupane SPECT imaging to better assist referring clinicians in distinguishing PS from other movement disorders such as ET.

**KEY WORDS:** Parkinson's disease, DAT scan

#### **EdE-13**

##### **Mapping Original Thought by Functional MR Imaging, Magnetoencephalography and Diffusion Tensor Imaging**

Larson, M.<sup>1</sup>·White, M. L.<sup>2</sup>·Helvey, J. T.<sup>2</sup>·Keiper, M. D.<sup>2</sup>·Poage, D. P.<sup>2</sup>·Zhang, Y.<sup>2</sup>

<sup>1</sup>Creighton University Medical School, Omaha, NE,

<sup>2</sup>University of Nebraska, Omaha, NE

#### **PURPOSE**

Mapping the anatomical foci and networks contributing to the origination or generation of thought is potentially important. This knowledge will help to preserve these foci and networks when a subject is to undergo brain surgery, estimate potential deficits after brain injury (e.g., trauma, infection or stroke) and for potentially guiding postinjury therapy. When one is thinking originally about music, language, mathematics, images, etc. different areas or networks of the brain are engaged.

#### **APPROACH/METHODS**

A literature review was performed and analyzed concerning the origination and generation of thought and creative innovation (divergent thinking). Emphasis of the discussion is upon the anatomical regions and networks of the brain that are involved and how they have been mapped with fMRI, diffusion tensor imaging (DTI) or magnetoencephalography (MEG).

#### **FINDINGS/DISCUSSION**

This review demonstrates regions of the brain that have been associated with the origination or generation of thought (divergent thinking). Also, areas of the brain associated with creative innovation are discussed. There are numerous methodologies to try to investigate the creative brain related to the multifactorial ways that one can be creative. Not only are there numerous thought paradigms to evaluate but fMRI or MEG can be utilized to evaluate the brain activation patterns. Diffusion tensor imaging can be utilized to study the underlying neural connectivity. The evaluation of creativity by several tasks has demonstrated the frontal lobe regions to be associated with the generation of ideas and creativity. There have been associated differences of FA in frontal lobe regions associated with creativity. Also, there have been found to be task-specific effects in the parietotemporal brain areas. Alternatively, when the creative process has been evaluated by fMRI and the subjects were designing a book cover the findings differed. In this group creative generation was associated with recruitment of the medial temporal regions. This suggested the medial temporal lobe may be central to the generation of novel ideas. Musical creativity has revealed different findings. In trained pianists a network of brain regions have been found to be associated with the generation of musical improvisation. The variations found depending on the paradigm utilized are reviewed.

#### **SUMMARY/CONCLUSION**

The production of novel thought mapping in the brain is in its relatively early phases. This review demonstrates a variety of the regions of the brain involved in thought origination or generation.

**KEY WORDS:** Functional MR imaging, magnetoencephalography, diffusion tensor imaging

#### **EdE-14**

##### **Functional and Dysfunctional Anatomy of Brainstem White Matter Pathways and Nuclei**

Singh, S. Maheshwari, M. Klein, A. P. Kelly, T. G. C. Chandra, T. Tuna, I. S. Segall, H. D.

Medical College of Wisconsin  
Milwaukee, WI

#### **PURPOSE**

To illustrate and discuss the anatomy of various white matter tracts and nuclei in the brainstem. We also will discuss their functional significance and illustrate the abnormalities in various developmental and acquired disease processes.

#### **APPROACH/METHODS**

This exhibit addresses functional networks and relevant brainstem pathways, from the clinical imaging perspective. Detailed discussions about these networks will include landmarks for identification, anatomical connections, functional significance and clinical findings associated with abnormalities of these pathways. With advancement in MR scanners and imaging sequences, it is now possible to delineate a majority of these tracts with confidence. Anatomical drawings, pathway diagrams, diffusion tensor imaging (DTI) and cadaveric specimens will be utilized to illustrate anatomy, principles underlying the functions and deficits relevant to these structures.

#### **FINDINGS/DISCUSSION**

Diffusion tensor imaging of white matter networks and the functional impairments of those networks is paramount to the interpretation of DTI in clinical practice. Diffusion tensor imaging anatomy of supratentorial white matter pathways are relatively well known; however, understanding of the brainstem tracts is limited. This exhibit addresses brainstem pathways including corticospinal tract, medial/lateral lemniscus, superior, middle and inferior cerebellar peduncles, posterior columns and other regional pathways from the clinical imaging perspective.

#### **SUMMARY/CONCLUSION**

The primary goal of the exhibit is to arm neuroradiologists with an understanding of the anatomical and functional implications of brainstem pathways by utilizing a tailored perspective enabling the integration of information derived from DTI into daily radiologic practice.

**KEY WORDS:** Brainstem pathways, brainstem nuclei, DTI and functions

#### **EdE-15**

##### **Functional MR Imaging during Memory Recognition in Healthy Adults**

Panyaping, T. Panyaping, T. L. C.

Ramathibodi Hospital Mahidol University  
Bangkok, THAILAND

#### **PURPOSE**

To localize the functional cortices enrolled during abstract picture recognition task that might be a baseline study to provide Thais standard paradigm for future research.

#### **APPROACH/METHODS**

The protocol study was approved by institutional review board and local ethics committee. Informed written consent was obtained from all participants after character of the experimental study was explained fully. Twenty healthy subjects underwent functional MRI and axial T1-weighted image, the latter was anatomical reference image. Abstract picture recognition task as block paradigm was used. Statistical analysis of fMRI data were analyzed as a whole group analysis and using

sample *t* test random effect analysis model, RFX (corrected *P* value <0.01). BOLD activities on brain surface rendering images were displayed as color from red (less activity) to yellow (strong activity). The anatomical reference image was loaded to overlay the colored maps and the anatomy of the cerebral cortical lobes and gyri and hippocampal formation were defined. In addition, BOLD activities also are displayed as color overlays on axial, coronal and sagittal views of T1-weighted reference anatomical images, gradual change from dark blue (less activity) to red (most strong activity).

#### FINDINGS/DISCUSSION

Activation for abstract picture recognition was observed at the both-sided cerebellum, bilateral parietal lobes, left hippocampus, bilateral occipital lobes including calcarine cortices, left motor cortex, bilateral premotor cortices, supplementary motor area and left superior temporal gyrus (Wernicke's area). There is asymmetry of the activities in both hemispheres with left-sided predominance. Bilateral parietal and occipital lobes showed the most intense activities.

#### SUMMARY/CONCLUSION

Abstract picture recognition task showed activation in multiple areas of cortical brain, which correlates with the human memory processing.

**KEY WORDS:** Functional, memory, recognition

#### EdE-16

##### All You Ever Wanted to Know about Central Nervous System and Head and Neck Sarcoidosis (But Were Afraid to Ask)

Pereira, L. P.·Drier, A.·Leclercq, D.·Clarençon, F.·Galanau, D.·Amoura, Z.·Chiras, J.·Dormond, D.

Hôpital Pitié Salpêtrière  
Paris, FRANCE

#### PURPOSE

To review magnetic resonance imaging (MRI) features of central nervous system and head and neck lesions in patients with sarcoidosis.

#### APPROACH/METHODS

Sarcoidosis is a systemic disease of unknown cause. The diagnosis is based on clinical and laboratory findings, radiologic features and is supported by the histologic demonstration of noncaseating granulomas. Neurologic and otolaryngologic manifestations occur in approximately 5-10% of patients but involvement of the central nervous system (CNS) is present in up to 25% of patients at autopsy, implying a significant rate of subclinical disease. MR imaging is the modality of choice for the diagnosis and followup of those patients. Here we explain, describe and illustrate the spectrum of lesions encountered in patients with sarcoidosis involving central nervous system (CNS) and head and neck.

#### FINDINGS/DISCUSSION

Sarcoidosis can involve any part of the CNS and its coverings. The most characteristic MRI findings are micronodular leptomeningeal enhancement, dural thickening, hypothalamus and pituitary stalk involvement, cranial nerve enhancement and hydrocephalus. Lesions can be observed anywhere in the spine: they can be intradural extramedullary, intramedullary or extradural. Linear leptomeningeal enhancement or small nodules along spinal cord or nerve roots are the most frequent spinal cord lesions. Osteolytic lesions may occur in skull and vertebrae. Any part of the eye or orbit can be involved. Uveitis is the most frequent lesion and thickening of the uvea and the sclera with potential infiltration of the retro-ocular fat may be observed. Involvement of parotid glands is commonly bilateral with typically enlargement and enhancement of the glands, hyperintense on T2-weighted imaging. Multiple mucosal nodules of the septum and inferior turbinates also can occur. Differential diagnoses for each pattern and location of lesions are discussed.

#### SUMMARY/CONCLUSION

It is important for radiologists to recognize imaging features and patterns of sarcoidosis. This pictorial review provides a detailed description of MRI findings of CNS and head and neck lesions occurring in sarcoidosis, with emphasis on the most characteristic MRI aspects.

**KEY WORDS:** Central nervous system, head and neck, neurosarcoidosis

#### EdE-17

##### Dementia in Treated Cases of Nasopharyngeal Carcinoma: Delayed Postradiation Necrosis of the Temporal Lobes in Four Chinese Patients

Hanagandi, P. B.·Goncalves, F. G.·Torres, C. I.·Chankowsky, J.·O'Donovan, R.

McGill University  
Montreal, QC, CANADA

#### PURPOSE

To emphasize the diverse MR imaging patterns of delayed radiation-induced necrosis in the temporal lobes as well as their clinical presentation.

#### APPROACH/METHODS

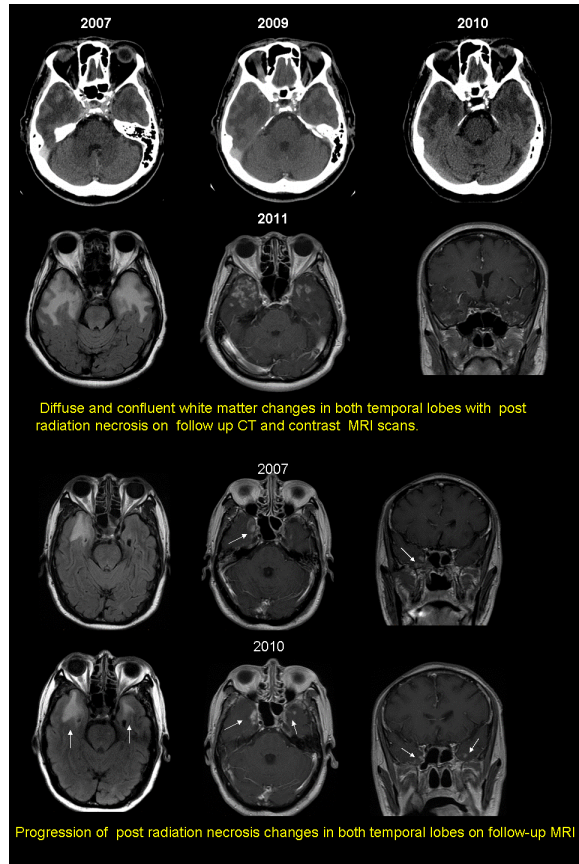
Four biopsy proven cases of nasopharyngeal carcinoma (NPC) were followed up for residual/recurrent disease on 64 slice CT scan (GE Light Speed) and 1.5 T MRI (GE Signa). Over a period of 5 years, all four patients presented with gradual onset cognitive disturbances which progressed to dementia.

#### FINDINGS/DISCUSSION

Various enhancement patterns of the anteromedial temporal lobes were seen with associated vasogenic edema and fatty marrow changes in the central skull base. We describe the CT and MR imaging appearance in four Chinese patients treated for NPC. Most complications of radiotherapy are due to lower cranial



nerve involvement but very little exists in the literature regarding dementia. Nasopharyngeal carcinoma is one of the most common malignancies in the Chinese and South East Asian populations. The primary treatment is radiotherapy, which can result in delayed neurologic complications in 10% of cases. The radiation therapy techniques vary among institutions, however, the anterior temporal lobes are invariably included in the radiation port. The incidence of postradiation necrosis in temporal lobes is approximately 3-5% and usually develops within 5-10 years of treatment. It is a potentially progressive and irreversible serious complication. Contrast-enhanced MRI is superior to CT scan in identifying these radiotherapy-induced changes in the temporal lobes. Differential diagnosis for the temporal lobe abnormalities would include local recurrence with brain invasion and hematogenous metastases.



#### SUMMARY/CONCLUSION

Dementia is an uncommon complication of radiotherapy. Given the lower incidence of NPC in Western countries, familiarity with the characteristic imaging patterns of radiation necrosis of the temporal lobes is essential in differentiating it from local tumor recurrence or metastatic disease, as these patients may benefit from steroid therapy.

**KEY WORDS:** Dementia, temporal lobes, nasopharyngeal cancer

#### EdE-18

#### Imaging Challenges during Antiangiogenic Treatment for Brain Tumors

Kim, J. P.<sup>1</sup>•Romero, J.<sup>1</sup>•Lu, J.<sup>2</sup>•Rapalino, O.<sup>1</sup>

<sup>1</sup>Massachusetts General Hospital, Boston, MA, <sup>2</sup>Peking Union Medical College Hospital, Beijing, CHINA

#### PURPOSE

1. To illustrate common imaging findings in glioblastoma patients during treatment with the antiangiogenic medication Bevacizumab. 2. To increase awareness of particular pitfalls and imaging changes during antiangiogenic treatment.

#### APPROACH/METHODS

A retrospective review of conventional and advanced MR imaging findings during antiangiogenic treatment was performed. Correlation was performed with neuropathologic slides in selected cases.

#### FINDINGS/DISCUSSION

Treatment with antiangiogenic agents significantly affect the conventional radiologic findings used for imaging follow up in high grade gliomas. Within a few days after treatment, abnormal enhancement and increased CBV/Ktrans markedly diminish due to pseudonormalization of the blood brain barrier within the tumor. Areas of edema also improve secondary to this effect. A proportion of patients treated with Bevacizumab develop areas of mineralization around the original tumoral site. Several patterns of tumoral recurrence have been described at the time of antiangiogenic treatment failure (particularly with Bevacizumab). These patterns include recurrent nodular enhancement at the original site, progressive abnormal nonenhancing signal abnormalities and restricted diffusion, and abnormal enhancement distal to the original site.

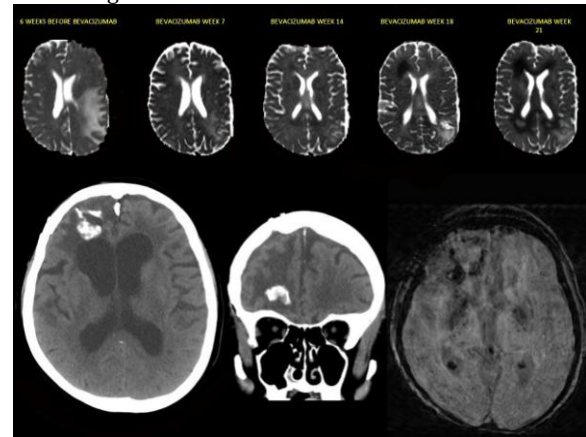


Image 1 (Top) demonstrates gradual development of new restricted diffusion (ADC hypointensity) in a patient with tumor progression, 18 weeks after initiation of Bevacizumab treatment.

Image 2 (Bottom) demonstrates development of a rim of mineralization around the tumor site, as seen on CT and MR susceptibility images obtained 610 days after initiation of Bevacizumab treatment.

**SUMMARY/CONCLUSION**

The use of antiangiogenic agents affects the classical imaging findings used for monitoring of treatment response in high grade gliomas due to their normalizing effect on the blood brain barrier. Specific patterns of recurrence have been described with antiangiogenic treatment including the development of nonenhancing signal abnormalities. Awareness of these particular imaging findings and pitfalls is important for accurate interpretation of diagnostic studies.

**KEY WORDS:** Glioblastoma, Bevacizumab, antiangiogenic treatment

**EdE-19****MR Imaging of Trochlear Nerve Schwannomas: A Rare, Often Missed Diagnosis**

Rao, N.·Sterling, M.·Moster, M.·Tartaglino, L.

Thomas Jefferson University  
Philadelphia, PA

**PURPOSE**

Disorders of the cisternal segment of the trochlear nerve are rare, subtle and often missed on imaging. The purpose of this study is to improve detection through correlation of the trochlear nerve anatomy with abnormalities detected on MR imaging (MRI).

**APPROACH/METHODS**

Six patients with varying symptoms of prolonged trochlear nerve palsies, including but not limited to vertical diplopia and ipsilateral hypertropia (stable over months to years), were referred to a neuroophthalmologist accompanied by a contrast enhanced MRI performed on a 1.5 T magnet or greater. Initial outside readings were negative in all but one case, though the initial provided history was not known. All cases then were reviewed retrospectively by two neuroradiologists independently who were aware of the clinical history and familiar with the trochlear nerve anatomy.

**FINDINGS/DISCUSSION**

Enhancing lesions of the cisternal segment of the trochlear nerve were detected in all six patients on retrospective review of MR imaging by both neuroradiologists. All of these lesions could be detected on postcontrast coronal and axial T1-weighted imaging and confirmed on higher resolution 3D imaging when available. The most common morphology was focal thickening or nodule in the cisternal segment of the trochlear nerve. Laboratory work up for inflammatory process was negative in all patients and no patients had a known primary extracranial neoplasm. Though not proved pathologically, the stable clinical signs and symptoms over months to years suggests a benign schwannoma as the likely etiology. The trochlear nerve is a purely motor nerve for the superior oblique muscle. The trochlear nerve can be divided into four segments: central, cisternal, cavernous, and orbital. Anatomy of the cisternal segment will be described in detail.

**SUMMARY/CONCLUSION**

Primary neoplasms of the trochlear nerve are uncommon but are detected more frequently than in the past due to thin-section MR imaging. These abnormalities can be confused with normal vessels and can be difficult to detect. Thorough knowledge of the anatomy of the cisternal segment of the trochlear nerve combined with appropriate history can increase detection of trochlear nerve lesions.

**KEY WORDS:** Trochlear, schwannoma

**EdE-20****Preoperative Functional Mapping and Brain Tumors: Functional MR Imaging, Magnetoencephalography and Diffusion Tensor Imaging with Correlation to Postoperative Functional Outcomes**

White, M. L.·Helvey, J. T.·Keiper, M. D.·Aizenberg, M. R.·Wilson, T. D.·Zhang, Y.

University of Nebraska  
Omaha, NE

**PURPOSE**

This exhibit reviews functional mapping in the presurgical brain tumor patient and the correlations of these findings to postoperative functional outcome. This review will focus on utilizing high resolution anatomical images, functional magnetic resonance imaging (fMRI), magnetoencephalography (MEG) and diffusion tensor imaging (DTI) tractography. It is vital to understand the strengths and weaknesses of these techniques in order to maximize their utilization.

**APPROACH/METHODS**

Cases are presented that have had preoperative mapping of language, motor, sensory and visual functions. The functional mapping was performed by MRI and MEG. These cases also have had white matter DTI tractography including the corticospinal, thalamocortical, arcuate fasciculi and optic radiations. The postoperative results are discussed.

**FINDINGS/DISCUSSION**

Secondary to the highly structured nature of the brain and the need to optimize tumor resection the precise preoperative mapping of brain function and structures can be vital. These preoperative steps help to preserve functional tissues at the time of operation. The neuroradiologist can play a critical role in this process. In order to optimize a preoperative functional mapping exam it is necessary to begin with the patient. The patient's functional deficits are a key indicator of what needs to be mapped and also will indicate potential problems that will be associated with mapping. Speaking with the requesting neurosurgeon also will help assure that functional structures of interest are mapped. High resolution 3D images obtained at the beginning of an imaging session can also change the direction of a functional mapping exam by accurately indicating what gyrus a mass is in more clearly than previously obtained imaging. The mapping of motor,

sensory, vision, auditory and language functions by fMRI are demonstrated. Correlating areas of activity detected by MEG imaging are mapped. The strengths and weaknesses of fMRI and MEG approaches are outlined. The white matter connections associated with the mentioned functional areas including the corticospinal, thalamocortical, arcuate fasciculi and optic radiations are displayed. Factors that affect the resulting postoperative functional deficits are outlined. The distance between the mass to be resected and functional tissues in question is a major factor. However, individual tumors and how they interact with the brain and the associated eloquent functions influence the margin of safety for preserving functional tissue. Neurosurgical techniques utilized also greatly affect the resection safety margin between what is mapped and resected. A major factor is utilization of intraoperative functional mapping.

#### **SUMMARY/CONCLUSION**

The utilization and benefits of preoperative functional brain mapping with fMRI, DTI tractography and MEG are demonstrated. The strengths and weaknesses of the techniques and the postoperative functional results are discussed.

**KEY WORDS:** Functional MR imaging, magnetoencephalography, diffusion tensor imaging

#### **EdE-21**

### **Nonenhancing Brain Metastases: An Important Concept in the Era of Advanced Chemotherapy**

Ravi, V.<sup>1</sup>•Haque, S. S.<sup>2</sup>

<sup>1</sup>New York Presbyterian/Weill-Cornell Medical Center, New York, NY, <sup>2</sup>Memorial Sloan-Kettering Cancer Center, New York, NY

#### **PURPOSE**

Patients with primary malignancies outside of the CNS routinely undergo brain imaging for many purposes including staging/restaging examinations as well as the new onset of neurologic symptoms. In the absence of known CNS metastases it is not uncommon for patients to be on systemic chemotherapy for their primary tumor which may alter the imaging characteristics of intracranial metastases on MRI. Of particular importance are nonenhancing metastases which may not be detected on examinations consisting of T1-postcontrast imaging only. It is important for the neuroradiologist to be aware of the potential chemotherapeutic agents which may lead to these nonenhancing metastases and the primary malignancies most likely to be treated with these agents so that imaging protocols in such situations can be tailored to optimize detection of metastases in such settings.

#### **APPROACH/METHODS**

This exhibit will review the imaging features of nonenhancing metastases on various MRI sequences which allow for detection and appropriate characterization of these masses.

#### **FINDINGS/DISCUSSION**

The effects of Bevacizumab (Avastin) on the imaging characteristics of glioblastoma are well known to neuroradiologists. Bevacizumab is an antiangiogenic agent which reduces neovascularity associated with tumors. These tumor-induced blood vessels tend to be immature vessels with incomplete endothelial layers leading to increased permeability. It is this increased permeability which leads to enhancement. Therefore, Bevacizumab therapy decreases detectable enhancement on postcontrast MR imaging of the brain. Bevacizumab also is used in the treatment of colorectal cancer, lung cancer, and breast cancer and previously unknown brain metastases in this setting may initially present without enhancement. These masses demonstrate the typical features of metastases other than enhancement such as rounded morphology, location at gray-white junction, surrounding vasogenic edema, and growth over time. Restricted diffusion also can be a helpful feature. Hypermetabolic activity on PET also can increase confidence in the diagnosis of nonenhancing metastases though this often is not detected.

#### **SUMMARY/CONCLUSION**

Although metastases classically have been thought to invariably enhance this is no longer the case. Patients being treated with Bevacizumab or its analogues can present with nonenhancing brain metastases due to its antiangiogenic effects. Furthermore, we recently have seen cases of inexplicable nonenhancing metastases in patients not on Bevacizumab with primary malignancies such as neuroblastoma or embryonal tumors. For these reasons it is imperative that neuroradiologists are aware of the possibility that metastases may not enhance as well as the scenarios in which this is most likely to occur.

**KEY WORDS:** Metastases, nonenhancing, Bevacizumab

#### **EdE-22**

### **Radiologic Diagnosis of Intracranial Hemangiopericytomas: What the (Neuro)Radiologist Needs to Know**

De Smet, K.<sup>1,2</sup>•Vanderhasselt, T.<sup>1</sup>•Dewachter, P.<sup>1</sup>•Stadnik, T.<sup>1</sup>•De Mey, J.<sup>1</sup>

<sup>1</sup>UZ Brussel, Brussels, BELGIUM, <sup>2</sup>AZ Sint-Reembert, Torhout, BELGIUM

#### **PURPOSE**

Due to similar clinical and radiologic features, the differential diagnosis between intracranial hemangiopericytomas (HPC) and malignant meningiomas in particular may be difficult. In this education exhibit, we want to highlight the CT and MRI contributions to the differential diagnosis of these entities with significantly differing therapeutic approach and prognoses.

#### **APPROACH/METHODS**

Clinicopathologic and imaging features of HPC are discussed through reviews of the literature and

illustrated by images obtained in our own institution. In particular, we evaluate the role of CT and MRI in the preoperative identification of these entities.

#### FINDINGS/DISCUSSION

Although being excellent meningioma-mimickers, HPC are rare, aggressive neoplasms with great risk of severe bleeding during surgery, high rates reported of local recurrence and having the potential to metastasize to extraneural sites as lungs, liver and bone. CT and MRI findings consist of a durally based lesion with mostly homogeneous enhancement, although it might be heterogeneous or ring-like as well. On CT, unlike meningiomas, there is an absence of tumoral calcification or adjacent hyperostosis. Instead, bony erosion often is described. On T2-weighted sequences, prominent internal flow voids are common. In contradistinction to malignant meningiomas, there is often a relative paucity of peritumoral edema.

#### SUMMARY/CONCLUSION

Hemangiopericytomas are rare neoplasms often mistakenly considered as malignant meningiomas due to similar clinical and radiological features. CT and MRI are very valuable tools in the preoperative identification of these entities, which in turn is of significant influence on therapeutic approach. Adjacent bony erosion, presence of internal signal voids and heterogeneous contrast uptake are the most useful criteria for CT/MRI differential diagnosis of between HPC and meningiomas.

**KEY WORDS:** Hemangiopericytoma, meningioma, MR imaging

#### EdE-23

##### Imaging      Neurologic      Complications      from Bronchogenic Carcinoma

Agarwal, A.·Vijay, K.·Ouyang, T.·Maller, V.

Penn State Milton S. Hershey Medical Center  
Hershey, PA

#### Purpose

To describe the clinical signs and to illustrate the imaging features of neurologic complications related to bronchogenic carcinoma at conventional radiography, CT, nuclear scan and MRI.

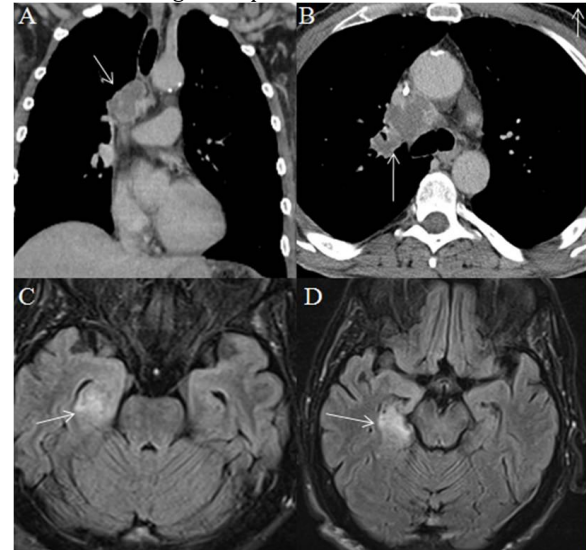
#### APPROACH/METHODS

We retrospectively selected cases from our teaching file, for patients with bronchogenic carcinoma presenting with neurologic symptoms. Set of positive cases, including radiographs and cross-sectional imaging, are show-cased through this exhibit, with an effort to cover the entire spectrum of radiologic manifestations.

#### FINDINGS/DISCUSSION

The natural history of bronchogenic carcinoma shows that 42% of patients are diagnosed with cancer-related neurologic complications either at initial presentation or at followup that can be separated in three different categories: I. Locoregional involvement of cervicothoracic nerves (recurrent laryngeal nerves,

phrenic and vagus nerves, brachial plexus and sympathetic cervical chains). II: Metastatic disease characterized by intracranial lesions (brain, meningeal, ependymal and pituitary metastases) and spinal (extradural, subarachnoid and medullary metastases) lesions. III: Paraneoplastic syndromes including limbic encephalitis (Fig1 a-d), Lambert-Eaton syndrome and paraneoplastic cerebellar degeneration. These neurologic disorders usually are associated with advanced cancer for which radical surgical management seldom is indicated. All imaging studies performed at the time of initial staging for bronchogenic carcinoma therefore should be reviewed carefully in order to detect signs that could suggest the presence of one or several neurologic complications.



#### SUMMARY/CONCLUSION

Neurologic complications of bronchial carcinomas are common and help in planning for surgical excision and guide chemotherapy or radiotherapy. Through this exhibit, the entire spectrum of neurologic complications of bronchogenic carcinoma is displayed.

**KEY WORDS:** Neurologic, bronchogenic

#### EdE-24

##### Clinical Applications of Ultrahigh-Field MR Imaging in Brain Disease

van der Kolk, A. G.<sup>1</sup>·Zwanenburg, J. J. M.<sup>1</sup>·Visser, F.<sup>1,2</sup>·Luijten, P. R.<sup>1</sup>·Hendrikse, J.<sup>1</sup>

<sup>1</sup>University Medical Center Utrecht, Utrecht, NETHERLANDS, <sup>2</sup>Philips Healthcare, Best, NETHERLANDS

#### PURPOSE

Throughout the last two decades magnetic resonance imaging (MRI) has seen a substantial evolution, not only in sequence development (functional MRI, diffusion tensor imaging, MR elastography) but also in field strength. Where a field strength of 0.5 T was practiced in the '80s, currently 1.5 T or 3.0 T provides the backbone in the clinical diagnostic process, and even higher field strengths already have emerged in the

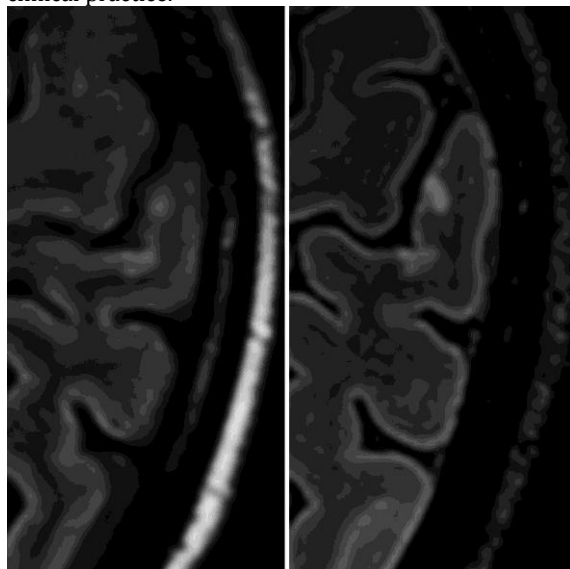
clinical research domain. The purpose of this Education Exhibit is to discuss the potential clinical applications of ultrahigh-field MRI in the brain.

#### APPROACH/METHODS

All literature regarding clinical application of ultrahigh-field MRI ( $\geq 7$  T) in the brain, including both patient studies and studies with healthy volunteers, were reviewed. Patient example data (informed consent obtained) at 7 T from our own institution were collected to further illustrate the clinical applicability of ultrahigh-field MRI.

#### FINDINGS/DISCUSSION

Several disease categories can be distinguished where ultrahigh-field MRI shows potential. In multiple sclerosis (MS), it facilitates more detailed visualization of lesions and associated intralésional vascular structures. This is also the case with cerebrovascular diseases, where it can show even very small infarcts (Figure; left, 1.5 T; right, 7 T), lenticulostriate arteries and intracranial arterial vessel walls, further elucidating underlying pathophysiology. Ultrahigh-field  $T_2^*$ -weighted imaging could prove beneficial in diagnosing several degenerative diseases, although in vivo studies are relatively lacking. It also can play a role in differentiating between low- and high-grade brain tumors, by visualizing microvasculature, and aid in the diagnosis of epileptic lesions, which would be of great value in patients with cryptogenic epilepsy. Finally, in treatment planning, ultrahigh-field shows great potential in delineating anatomical structures important for surgery, like deep brain stimulation targets. However, several caveats for ultrahigh-field MRI still exist, like inhomogeneity of the applied transmit field, causing spatial variations in signal-to-noise ratio (SNR). Furthermore, an increase in Specific Absorption Rate (SAR) limits the duty cycle of the applied sequences. Finally, there are currently extensive contraindications for patient scanning, which have to be taken into account when moving ultrahigh-field MRI to clinical practice.



#### SUMMARY/CONCLUSION

At this moment, ultrahigh-field MRI can be used only officially for clinical research purposes. When it becomes available in clinical practice, most additional value will probably be gained from high-resolution 3D sequences, and/or using contrasts currently not commonly used in clinical practice, like  $T_2^*$ -weighted imaging or phase imaging. However, several limitations, both technical and safety-associated, need to be overcome before clinical implementation will become successful.

**KEY WORDS:** Ultrahigh-field, MR imaging

#### EdE-25

##### Avoiding Pitfalls in 3D Pseudocontinuous Arterial Spin Labeling Cerebral Blood Flow Imaging: A Gallery of Common Artifacts

Yu, C.-Zaharchuk, G.

Stanford University Medical Center  
Stanford, CA

#### PURPOSE

Evaluation of brain perfusion with MRI can be performed in a noninvasive and robust manner using arterial spin labeling (ASL) technique. However, as clinical ASL becomes more common, it is important that clinicians become familiar with potential image artifacts to distinguish them from pathology. The purpose of this exhibit is to describe artifacts we have encountered in our experience with clinical 3D pseudocontinuous ASL and to suggest some possible remedies.

#### APPROACH/METHODS

We acquire approximately 1500 ASL cases per year. Cases included in this exhibit were drawn from these clinical MR examinations performed at both 1.5 and 3 T (GE Healthcare, Waukesha, WI). Pseudocontinuous ASL images were obtained with 3D spiral fast spin echo readout and background suppression. Typical parameters include TR/TE/label time/post-label delay 5500/2.5/1500/2000 ms with spatial resolution on the order of 3-6 mm, requiring between 4 and 6 minutes to acquire. Selected examples of different ASL artifacts are presented and discussed. In many cases, bolus perfusion-weighted imaging hemodynamic maps were available for comparison.

#### FINDINGS/DISCUSSION

Overall, artifacts were uncommon and could be classified as primarily originating from the labeling period or from the image acquisition. In order for the distribution of the ASL signal intensities in the brain to accurately reflect the pattern of cerebral blood flow, arterial spin labeling upstream of the imaging slices must be efficient and uniform. Two factors can contribute to poor labeling: (1) obliquity and/or tortuosity of feeding arteries in the labeling plane which can result in either multiple inversions or overall poor labeling; and (2) susceptibility changes due to the presence of metallic hardware, calcification, or blood products which can change the center frequency of the spins at the labeling plane and result in poor or no

labeling. These artifacts usually are associated with ASL signal dropout in a characteristic vascular territory. Other artifacts were associated with the readout: (1) Patient motion can give rise to misregistration of signal intensities at time of readout and inaccurate perfusion maps; in this spiral acquisition, motion often manifests as high signal intensity spiral artifacts. (2) The 3D stack-of-spirals method has significant blurring in the craniocaudal direction; high signal intensity lesions containing many tagged spins, such as giant aneurysms, can be seen to propagate in the z direction due to this effect. While not truly an artifact, if cardiac output is low, there will be significant delay between labeling of spins and their arrival in the tissue of interest; when using a fixed post-label delay, this gives rise to "arterial transit artifact," or high ASL signal in the feeding arteries with reduced signal in the brain parenchyma. Finally, it should be recognized that ASL images must be performed before the administration of intravenous contrast; contrast agents severely reduce the blood T1, leading to rapid loss of the label following tagging and nondiagnostic ASL images.

#### **SUMMARY/CONCLUSION**

Recognition of these common imaging artifacts seen using 3D pseudocontinuous ASL can help remedy potentially correctable technical challenges and avoid pitfalls in the interpretation of clinically useful ASL cerebral blood flow maps.

**KEY WORDS:** Arterial spin labeling, cerebral blood flow, artifact

#### **EdE-26**

##### **Radiation Exposure Reduction in Neuroradiology: Optimization of Lowered keV with Higher Concentration Contrast Medium**

Kuhn, M. J.<sup>1</sup>Kuhn, A. S.<sup>2</sup>

<sup>1</sup>University of Illinois, Peoria, IL, <sup>2</sup>University of Pennsylvania, Philadelphia, PA

On August 24, 2011 the Joint commission issues a sentinel event alert on the need to limit and manage radiation exposure in diagnostic imaging exams. As a specialty, neuroradiology has taken the lead in instituting training and credentialing to help reduce radiation exposure among our patients. However, low keV techniques result in loss of signal and contrast resolution which must be dealt with by adapting imaging and contrast media protocols and employing advanced reconstruction techniques such as model based iterative reconstruction. One drawback of many low keV techniques is reduced conspicuity of iodine on enhanced scans; this may be addressed by the use of a higher iodine concentration agent. Alternately, the use of dual source CT imaging with monochromatic beam generation can improve image quality and improve the detection of iodine-containing substances on low keV images leading to improved detection, characterization, and pathology and better evaluation of vascular structures. This exhibit reviews the basics of image generation and reconstruction and discusses how optimization of scanning and contrast administration

protocols can help reduce both the radiation and contrast exposure of patients.

**KEY WORDS:** Radiation, contrast-enhanced, keV

#### **EdE-27**

##### **Imaging of Neurologic Pathology in Pregnancy and the Postpartum Period: Clinical and Radiologic Features**

Mortimer, A. M.·Bradley, M.·Likeman, M.·Renowden, S. A.·Stoodley, N. G.

Frenchay Hospital  
Bristol, UNITED KINGDOM

#### **PURPOSE**

1) To provide an educational review of the range of both physiologic and pathologic processes that can be identified on neuroimaging in pregnant and postpartum patients. 2) To create an awareness of these conditions to allow swift targeting of imaging in the diagnosis of neurologic complications of pregnancy and parturition and to make appropriate suggestions for the underlying etiology of nonspecific imaging findings. 3) To illustrate neuroimaging abnormalities with an array of modalities including computed tomography (CT), magnetic resonance imaging (MRI) and catheter digital subtraction angiography (DSA). 4) To provide advice on safe imaging in pregnancy.

#### **APPROACH/METHODS**

Neuroimaging has a significant role to play in the diagnosis of pregnancy-related neurologic complications: indeed a wide array of pathology may present in pregnancy and the postpartum period. A visual display with illustrative imaging will be produced to allow the radiologist insight into the array of potential diagnoses, thus aiding selection of the appropriate imaging in order to make swift specific diagnosis or suggest the most appropriate diagnosis when imaging findings are nonspecific. Guidelines for safe imaging in pregnancy also are presented.

#### **FINDINGS/DISCUSSION**

Pregnancy predisposes to several neurologic conditions that usually require neuroimaging for definitive diagnosis. The pituitary gland demonstrates physiologic enlargement as a result of estrogen exposure: rarely there may be hemorrhage into the enlarging gland or into a preexisting adenoma (pituitary apoplexy). The pituitary also may infarct as a result of hypotension relating to obstetric hemorrhage (Sheehan's syndrome) or may be affected by a rare inflammatory condition (lymphocytic hypophysitis). The relative hypercoagulable state of pregnancy predisposes to vascular complications of ischemic stroke and cerebral venous sinus and cortical vein occlusion. Hemorrhagic stroke may result from either aneurysmal rupture by pregnancy may also predispose to nonaneurysmal subarachnoid hemorrhage. Intracerebral hemorrhage also may occur in pregnancy and a rare case of postpartum angiitis is presented. Eclampsia, defined clinically as seizure or coma as a result of pregnancy-



related hypertension demonstrates changes of posterior reversible encephalopathy on imaging studies.

#### SUMMARY/CONCLUSION

For each condition described above, imaging cases are used to illustrate characteristic radiologic features and guide the radiologist in the organization of the most appropriate imaging investigations when encountering a pregnant or postpartum patient with a neurologic presentation.

**KEY WORDS:** Pregnancy, eclampsia, neurologic complications

#### EdE-28

##### **Empty Meckel's Cave: Anatomical Variant or a Sign of Dural Pathology? A Pictorial Essay of Associated Patterns of Dural Ectasia**

Mas Bonet, A.<sup>1</sup>Quiñones Tapia, D.<sup>2</sup>Picado, M.<sup>1</sup>Vega, G.<sup>1</sup>Moll, A.<sup>1</sup>Miralbes, S.<sup>1</sup>Ibañez, J.<sup>1</sup>.

<sup>1</sup>Hospital Son Espases, Mallorca, SPAIN, <sup>2</sup>Hospital del Rosario, Madrid, SPAIN

#### PURPOSE

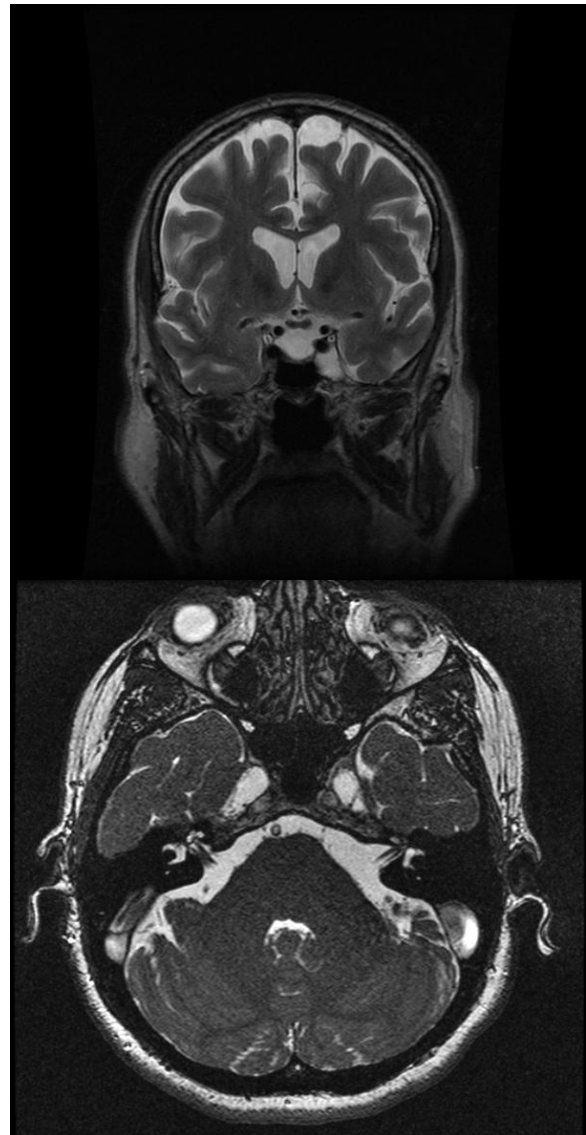
Small ectasias of Meckel's cave are not uncommon findings on routine brain MRI. Greater expansions of the Meckel's cave can produce erosions of the petrous apex and are described in the literature as "petrous apex cephaloceles". We suggest the term "Empty Meckel's Cave" (EMC) similar to "empty sella" to describe this anatomical condition. Meckel's cave and the petrous apex are occult areas to physical examination, where imaging plays a significant role in the diagnosis and approach to lesions in these areas of the skull base.

#### APPROACH/METHODS

We retrospectively reviewed 65 cases of enlarged Meckel's cave associated with bony erosion of the petrous apex. Imaging studies included MRI in all 65 patients, and CT in 45 cases. In one case intracranial pressure was monitored.

#### FINDINGS/DISCUSSION

We have encountered 5 patterns of empty Meckel's cave (EMC), most of them associated to other dural anomalies: 1) isolated EMC with erosion of the sphenoid body or clivus. 2) EMC with multiple meningoceles, or displacement of internal carotid artery in the petrous canal. 3) EMC with empty sella and optic nerve dural ectasia, mostly related to Benign Intracranial Hypertension. 4) EMC with ectatic internal auditory canals. 5) EMC with distal thecal sac dural ectasia (increased AP diameter, vertebral scalloping and perineural cysts). Associated symptoms are present in approximately 25% of cases including: trigeminal neuralgia, dizziness, tinnitus, hearing loss, CSF leak or intracranial hypertension.



#### SUMMARY/CONCLUSION

Enlargement of Meckel's cave maybe not only an anatomical variant. The frequency of other associated dural anomalies is increased, and should be observed on MRI studies. Empty Meckel's cave may be a sign of dural pathology, or reflect altered cerebro-spinal fluid dynamics.

**KEY WORDS:** Meckel's cave, dural arachnoid cysts, petrous apex cephaloceles

#### EdE-29

##### **Differential Diagnoses of Bright Lesions on Diffusion-Weighted MR Imaging**

Patel, G.·Qian, J.·Vaisfeld, J.·Young, R. J.

Memorial Sloan-Kettering Cancer Center  
New York, NY

#### PURPOSE

Different brain pathologies may cause diffusion restriction and appear bright on diffusion-weighted

imaging (DWI) and dark on corresponding apparent diffusion coefficient (ADC) maps. Diffusion-weighted imaging provides information about water diffusion that is unique from conventional imaging sequences. The purpose of this exhibit is to demonstrate the utility of DWI by reviewing the variety of brain lesions that may appear diffusion bright.

#### APPROACH/METHODS

Cases drawn from a tertiary care cancer center will be presented in an interactive quiz format. After a brief review of the physics behind DWI, a variety of brain pathologies that may appear hyperintense on DWI are illustrated. Key patterns will be identified with an emphasis on using diffusion restriction as an imaging tool to assist in narrowing the diagnosis.

#### FINDINGS/DISCUSSION

This exhibit will present a framework for approaching diffusion bright lesions in the brain, in order to narrow the differentials and lead to the correct diagnosis. A variety of cases with hyperintense brain lesions on DWI are shown. The following types of cases are included in this review: infarcts, neoplasms, demyelination, seizures, infections, hemorrhage, toxic and metabolic disorders. Each case is described in terms of the diffusion abnormality and the pathophysiology behind each finding. Other features that aid in the differentiation of diffusion bright lesions also will be described, such as location in the brain, restriction of the enhancing disease vs the cystic/necrotic nonenhancing disease, and temporal evolution.

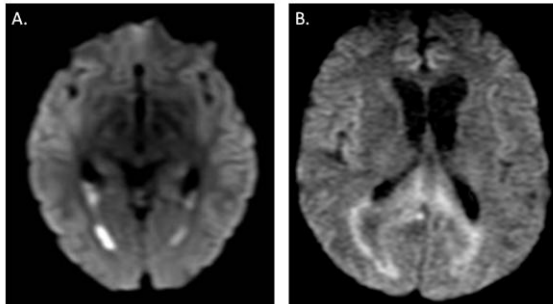


Figure. Axial DWI in two patients. (A) Diffusion restricted material is seen layering in the occipital horns of this patient status post transphenoid resection of a pituitary adenoma, whose postoperative course had been complicated by meningitis and ventriculitis. (B) Diffusion restriction and contrast enhancement (not shown) are seen along the periphery of a large posterior transcallosal bihemispheric lesion. The diffusion restriction is characteristically limited to the advancing front of active demyelination in this tumefactive demyelinating lesion.

#### SUMMARY/CONCLUSION

Diffusion-weighted imaging is an integral part of the evaluation of focal and diffuse brain pathologies. This exhibit illustrates the spectrum of diffusion abnormalities that may be encountered in a busy

clinical practice. Familiarity with the patterns of disease on DWI is useful for differential diagnosis and management options.

**KEY WORDS:** Diffusion-weighted imaging, MR imaging

#### EdE-30

##### Perihippocampal Fissures: Radiologic Importance and Potential Pitfalls

Gupta, A.Meena, M. L.Baser, S. C.

Ravindra Nath Tagore Medical College  
Udaipur,Rajasthan, INDIA

#### PURPOSE

The aim of this exhibit is to emphasize the utility of perihippocampal fissures (PHFs) in differentiating various pathologic conditions of mesial temporal lobe and to know about common interpretative pitfalls associated with it.

#### APPROACH/METHODS

We imaged a series of patients encountered in our clinical practice using 1.5 T MRI and/or 16 slice CT scan depending upon the pathology. For MRI coronal sections and axial sections parallel to the hippocampus were used. For CT scan, the imaging plane is angled 150-20° inferior to the canthomeatal line which is the plane usually used to image the brain (reverse angle CT). Intravenous contrast was used as per requirement.

#### FINDINGS/DISCUSSION

This exhibit includes: 1) Review of normal MR anatomy of the PHFs. 2) Differentiate between various conditions involving medial temporal lobes like Alzheimer disease vs normal pressure hydrocephalus, hydrocephalus vs hippocampal atrophy, intra axial vs extra axial tumor, etc., based on changes in PHFs. 3) Importance of CT scan (especially reverse angle CT) in evaluating conditions of medial temporal lobe. 4) Common pitfalls encountered in interpretation of above imaging findings like normal variants, cysts, bilateral disease, etc.

#### SUMMARY/CONCLUSION

Knowledge of normal anatomy of perihippocampal fissures can be very useful in assessing the various conditions affecting the mesial temporal lobe including the hippocampus. Although MR is the modality of choice for evaluation of PHFs, reverse angle CT scan can provide useful initial clue and aid in diagnosis.

**KEY WORDS:** Perihippocampal, fissures

#### EdE-31

##### Rehabilitation and Traumatic Brain Injury: Insights for the Neuroradiologist

Caci, D.<sup>1</sup>Gilani, S.<sup>1</sup>Macadam, B.<sup>1</sup>Nelson, K.<sup>2</sup>Singhal, R.<sup>2</sup>Chowdhry, Y.<sup>2</sup>Lev, S.<sup>1</sup>

<sup>1</sup>Nassau University Medical Center, East Meadow, NY,  
<sup>2</sup>American University of the Caribbean School of Medicine, Coral Gables, FL

**PURPOSE**

To provide the neuroradiologist with a better understanding of the challenges faced during rehabilitation by patients who have sustained severe neurologic trauma. We highlight pertinent imaging features from cases at our institution reflecting the diversity of traumatic brain discussion and discuss the implications for subsequent care.

**APPROACH/METHODS**

We present cases from our level I trauma center (CT/CTA and MR/MRA) which illustrate the broad spectrum of traumatic brain injuries. We organize injuries by location (i.e., intra or extraaxial) and type (i.e., blunt or penetrating), and discuss as well as whether the lesions are primary or secondary. We discuss which injuries have more immediate consequences and those that may be associated with a graver long-term prognosis with delayed neurologic deficits. We intend to provide insights into the unique challenges that patients face, correlating specific impairments (i.e., verbal, motor, visual, memory) to affected anatomical regions.

**FINDINGS/DISCUSSION**

The initial phase of any successful rehabilitation program is to determine the patient's neurologic deficits and specific needs. The rehabilitation doctor's assessment focuses on both the CT and MR imaging findings as well as the neurologic examination. Physical deficits including loss of balance, coordination, ambulation, and other daily activities may occur after such an injury, and requires a course of rehabilitation that can be provided based on the specific loss. These physical deficits can lead to psychological sequelae such as depression, PTSD, and anxiety. The total deficits listed can demand rehabilitation ranging from short-term acute rehab to prolonged nursing home stay. The neuroradiologist plays a crucial role by determining the anatomical extent of injury and likely long-term complications and sequelae. Primary lesions may range from subtle contusions to diffuse axonal injury, with dire consequences. In cases of penetrating trauma, secondary consequences such as vascular dissection, ischemic damage and infection may impact, in various ways, subsequent clinical course.

**SUMMARY/CONCLUSION**

Traumatic brain injury is a leading cause of morbidity and disability in patients younger than forty years old. With modern advances in medicine, survival rates have improved dramatically, increasing the need for long-term comprehensive rehabilitation services. Furthermore, hidden costs abound and socioeconomic impact on the individual and community can be staggering. We, as radiologists, can profoundly impact the course of a patient's care, and are an essential part of a multidisciplinary team aimed to improve the trauma patient's quality of life.

**KEY WORDS:** Rehabilitation

**EdE-32**

### **Variations of Vertebral Artery Origin, Duplications of the Vertebrobasilar System and Carotico-basilar Anastomoses**

An, J.-Li, S.

Baystate Medical Center  
Springfield, MA

**PURPOSE**

The purpose of this exhibit is to review the incidence and variations of the vertebral artery origin, duplications and carotico-basilar anastomoses with a discussion of their embryologic mechanisms, presenting symptoms and clinical significance.

**APPROACH/METHODS**

The literature on the incidence and variations of the vertebral arteries is reviewed. Specifically, anomalies of the origins of the vertebral arteries, duplications of the vertebrobasilar system, and persistent carotid vertebrobasilar anastomoses of the trigeminal, hypoglossal, otic and proatlantal intersegmental arteries are discussed along with their embryologic development, presenting symptoms and clinical significance. Attention will be paid to the relevant cerebrovascular anatomy and MR and CT angiography cases will be included.

**FINDINGS/DISCUSSION**

Although considerably rare, a knowledge and understanding of the variations in the vertebral artery is important as they can be associated with other intracerebral disorders. These congenital anomalies may alter cerebrovascular hemodynamics and thus increase the risk of thrombosis, aneurysm, and arterial dissection as well as contribute to atherosclerosis. Additionally, elucidation of any vertebral artery anomalies is important in the planning and approach of angiographic, endovascular and surgical procedures.

**SUMMARY/CONCLUSION**

Knowledge of the variations of the vertebral arteries with an understanding of their associated presenting symptoms and clinical significance may contribute to the detection, diagnosis and evaluation of significant cerebrovascular pathologies and facilitate the planning and approach of angiographic and surgical procedures. At the end of this presentation, the viewer will become familiar with the relevant cerebrovascular anatomy, a spectrum of vertebral artery anomalies and their embryologic mechanisms, presenting symptoms and clinical importance.

**KEY WORDS:** Vertebral artery anomalies, CNS vasculature

### EdE-33

#### **Cervical Artery Dissection: The Importance of Evaluating the Extracranial Vessels on Routine Brain MR Imaging**

Nadimpalli, S. P. R. Shah, S. Merchant, M. Vagvala, P.  
Advocate Illinois Masonic Medical Center  
Chicago, IL

##### **PURPOSE**

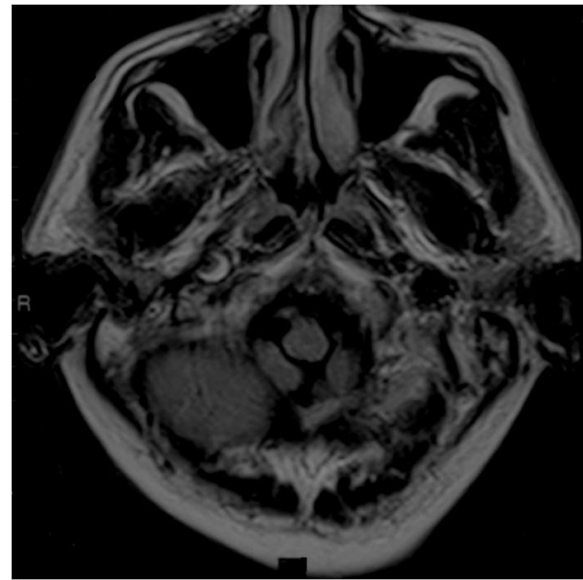
Dissection of the extracranial arteries accounts for stroke in up to one fourth of young to middle aged patients. The presenting clinical signs and symptoms can be quite variable, ranging from headache and neck pain to tinnitus and other clinically significant neuropathies. In light of the variable clinical presentation, there has been increased utilization of imaging studies such as stroke brain MR as the initial method of evaluation. Although stroke brain MR imaging provides an incomplete view of the extracranial vasculature, mural hematoma found in cervical artery dissection frequently extends into the petrous/upper cervical carotid segment or is located in the vertebral artery at the base of the skull. Therefore, systematic evaluation of the carotid and vertebral arteries at the level of the skull base on routine stroke brain MR allows for the early detection of silent cervical artery dissection (CAD), and helps in the prevention of stroke.

##### **APPROACH/METHODS**

Our radiology reporting system was queried retrospectively to identify patients with the final diagnosis of CAD. We then reviewed the multiple cases with this diagnosis. Patients who were not evaluated with stroke brain MR imaging were excluded from our review. In patients evaluated with stroke brain MR imaging, the fat-suppressed T1-weighted sequences were reviewed to identify one or more of the following criteria specific for dissection: 1) mural hematoma, 2) irregular wall contour and 3) increased external arterial wall diameter and luminal narrowing. Studies were reviewed with two neuroradiologists and the degree of agreement was recorded.

##### **SUMMARY/CONCLUSION**

The available literature outlines challenges in diagnosing CADs using various forms of imaging. O. Naggara, et al recently performed a case-control retrospective review of brain MR in patients with known diagnosis of CAD, which demonstrated that initial brain MR imaging can correctly suggest CAD in more than two-thirds of the patients reviewed. In our retrospective review, several patients showed signs which suggested CAD on initial brain MR imaging.



##### **SUMMARY/CONCLUSION**

Given the variability in patient symptoms it is important to emphasize the importance of careful evaluation of the carotid and vertebral arteries at the skull base on routine MR imaging to allow early detection of CAD. Once a suspicious lesion is noted, further diagnostic imaging can be recommended, such as CTA, MRA, or DSA, for confirmation of the diagnosis. Early diagnosis can significantly reduce the risk of stroke and associated long-term morbidity. Also patients can be identified as suitable candidates for anticoagulation or revascularization therapy.

**KEY WORDS:** Cervical artery dissection, stroke, carotid artery

### EdE-34

#### **Thunderclap Headaches: Reversible Cerebral Vasoconstriction Syndrome and Its Mimics**

Chin, M. S. Castillo, M.

University of North Carolina Chapel Hill  
Chapel Hill, NC

##### **PURPOSE**

Reversible cerebral vasoconstriction syndrome (RCVS) is an important, yet under-recognized, group of conditions characterized by severe headaches, reversible narrowing of the cerebral vasculature, and neurologic deficits. Recognition of this entity and its potential ischemic or hemorrhagic complications is important, given different management regimens. The purpose is to review the clinical, imaging manifestations (with a particular focus on its angiographic and MRI appearances), and clinical management of RCVS and its mimics.

##### **APPROACH/METHODS**

A retrospective search of imaging databases using the keywords "vasculitis" or "headache" was performed from 2001 to 2011. Clinical data and imaging, including CT, MRI, and angiography, were reviewed, with

selection of representative cases for RCVS and other mimics, such as primary angiitis of the central nervous system, aneurysmal subarachnoid hemorrhage, and intracranial arterial dissection.

#### FINDINGS/DISCUSSION

A sudden, severe headache is the presenting symptom in multiple medical conditions. Work up often includes noncontrasted computed tomography, and as needed, subsequent CT or MR angiography and/or conventional angiography. Even when multifocal segmental vasoconstriction of cerebral arteries is present, the differential remains broad, and given unfamiliarity with the entity and its associated imaging findings, RCVS may be misdiagnosed as primary angiitis or vasospasm associated with subarachnoid bleed or stroke. As shown in this series, imaging presentations are diverse and include subarachnoid hemorrhage, PRES, intracranial hemorrhage, and ischemic injury in the setting of segmental arterial narrowing. While CT and MR angiography are noninvasive, we found that segmental narrowing often is not detected on initial noninvasive vascular imaging, and review of the angiographic appearances of RCVS is important. Angiography with verapamil infusion and/or angioplasty also has been reported recently as potential therapeutic options.

#### SUMMARY/CONCLUSION

Reversible cerebral vasoconstriction syndrome is a group of conditions that has been newly described in the literature, yet continues to be under-diagnosed as a cause of thunderclap headaches with or without associated neurologic deficits. Our series reviews the various etiologies, imaging presentations, and management.

**KEY WORDS:** Reversible cerebral vasoconstriction syndrome, cerebral angiography, headache

#### EdE-35

##### **Spectrum of Imaging Findings in Reversible Cerebral Vasoconstriction Syndrome: Importance of Careful Evaluation of CT Angiography**

Mahajan, A.·Modi, J.·Bal, S.·Demchuk, A.·Goyal, M.·Eesa, M.

Foothills Medical Centre  
Calgary, AB, CANADA

#### PURPOSE

Reversible cerebral vasoconstriction syndrome (RCVS) is an under-recognized entity presenting to the emergency department. The most common patient complaint is thunderclap headache which can masquerade as aneurysmal subarachnoid hemorrhage (SAH). Initial imaging could be normal or it may reveal cortical SAH, cerebral infarcts, intracerebral hemorrhage, posterior reversible encephalopathy syndrome (PRES) and rarely intracranial dissection. The purpose of this paper is to illustrate the spectrum of imaging findings of this disease and the importance of careful evaluation of CT angiography.

#### APPROACH/METHODS

Computed tomography (CT)/CT angiography, magnetic resonance imaging (MRI) findings and MR angiography as well as catheter angiograms of patients presenting to our tertiary care center and who had imaging findings and correlated clinical features consistent with RCVS is reviewed pictorially. Selection criteria was based on reversible multifocal segmental cerebral vasoconstriction without evidence of typical patterns for aneurysmal subarachnoid hemorrhage.

#### FINDINGS/DISCUSSION

**Clinical presentation:** Most patients are young or middle aged with a female predominance. Nearly all patients report thunderclap headache at the onset. Other presentations include focal neurologic deficits or symptoms related to PRES (headache, seizures and visual symptoms) or hemorrhage. Precipitating triggers may include vasoconstrictive drugs, hypertension or recent pregnancy and are sometimes unknown. High pressure in the narrowed vessels with failure of autoregulatory mechanism could precipitate hemorrhage. **CT and MRI:** Initial imaging could be normal in up to 25% of cases. Subarachnoid hemorrhage is the most common imaging finding which is typically small and usually seen in convexity sulci. Other imaging manifestations include ischemic stroke, lobar hemorrhage and brain edema. CT may show sulcal SAH but is better seen on MRI. MR imaging also is more sensitive for ischemia and brain edema. **Vascular imaging:** Typical angiographic findings include multifocal areas of smooth or tapered arterial narrowing followed by segments of normal caliber or distended arteries. CT angiography is being increasingly used in the emergency setting and careful evaluation of distal vessels on reformatted images usually reveals multiple areas of abnormality. Catheter angiography is usually done to rule out tiny aneurysms and to confirm these findings. Follow-up vascular imaging demonstrates reversibility of these findings. An important differential diagnosis is primary angitis of CNS, which may be excluded based on CSF findings and laboratory investigations and the findings are not reversible in the absence of treatment. **Treatment and outcome:** Treatment consists of calcium channel blockers such as Nimodipine or Verapamil with or without a short course of corticosteroids.

#### SUMMARY/CONCLUSION

Reversible cerebral vasoconstriction syndrome is an important secondary cause of headache in the appropriate clinical setting. These patients can have manifestations such as SAH, ischemic stroke, cerebral hemorrhage, cerebral edema and rarely arterial dissection. CT angiography of patients with thunderclap headache with normal initial imaging should be evaluated carefully including distal vessels on reformatted images and often can aid in quickly establishing a correct diagnosis. Reversibility of findings on repeat studies usually clinches the diagnosis.

**KEY WORDS:** Reversible cerebral vasoconstriction, CT angiography

**EdE-36****Advanced Imaging Techniques of Cerebral Arteriovenous Malformations**

Mossa-Basha, M.<sup>1</sup>•Chen, J.<sup>2</sup>•Sair, H.<sup>1</sup>•Ilica, A. T.<sup>1</sup>•Gandhi, D.<sup>3</sup>

<sup>1</sup>Johns Hopkins University, Baltimore, MD, <sup>2</sup>Johns Hopkins University School of Medicine, Baltimore, MD,

<sup>3</sup>University of Maryland, Baltimore, MD

**PURPOSE**

Imaging plays a major role in the identification, grading and treatment of cerebral arteriovenous malformations (AVM). Digital subtraction angiography is the gold standard in the diagnosis and characterization of these vascular malformations, but advances in both MRI and CT, including advanced imaging techniques have provided new tools for further characterizing these lesions as well as the surrounding brain structures that may be affected, including evaluation of lesions in ways that previously could only be accomplished with digital subtraction angiography. For example, time-resolved MRA and susceptibility-weighted imaging (SWI) are helpful in the initial pretreatment characterization and planning as well as posttreatment evaluation, to assess for residual arteriovenous shunting. Techniques such as functional MRI and diffusion tensor tractography can help evaluate for eloquent cortical and white matter tract involvement.

**APPROACH/METHODS**

We will present an educational exhibit with cases of cerebral arteriovenous malformation with advanced imaging studies performed including functional MRI, diffusion tensor imaging, susceptibility-weighted imaging and time resolved MRA.

**FINDINGS/DISCUSSION**

Advanced imaging techniques provide invaluable information for the pretreatment characterization of cerebral AVM, as well as the postoperative follow up.

**SUMMARY/CONCLUSION**

Techniques such as fMRI and DTI can alter the treatment plan. Time-resolved MRA and SWI techniques provide valuable information which previously could only be evaluated on digital subtraction angiography.

**KEY WORDS:** Arteriovenous malformation, advanced MR imaging, cerebral avm

**EdE-37****Thunderclap Headache: Diagnostic Considerations in Neuroimaging**

Mortimer, A. M. •Renowden, S. A.

Frenchay Hospital  
Bristol, UNITED KINGDOM

**PURPOSE**

The aim of this presentation is to: 1) To review the potential diagnoses associated with a presentation of

thunderclap headache to aid image interpretation in the acute radiologic setting. 2) To illustrate the radiologic features of these pathologies to create a guide to imaging in this common acute presentation.

**APPROACH/METHODS**

Thunderclap headache (TCH) begins suddenly and is severe at onset but it can be caused by a range of underlying conditions. This presentation is commonly encountered by radiologists when interpreting neuroimaging. An exhibit will be designed to highlight potential diagnoses that may be encountered in the setting of thunderclap headache and to emphasize imaging features that may be encountered to make the diagnosis. We will draw attention to initial findings that can be gleaned on unenhanced CT and then those obtained using enhanced CT, MR and angiographic imaging to aid diagnostic confirmation.

**FINDINGS/DISCUSSION**

Thunderclap headache can be primary or secondary. Primary TCH is diagnosed when no underlying cause is discovered; however, imaging is crucial in distinguishing secondary causes. Subarachnoid hemorrhage (SAH) is the most common cause of secondary TCH. We will highlight cases of subtle subarachnoid blood to raise awareness of review areas as initial misdiagnosis and subsequent rebleed is associated with a worsening prognosis. While aneurysmal SAH accounts for the majority of cases, other causes include nonaneurysmal perimesencephalic hemorrhage, transmural arterial dissection, cerebral arteriovenous malformation, dural arteriovenous fistula, mycotic aneurysm, and substance abuse, examples of which will be included. Other vascular causes include cervical artery dissection, cerebral venous sinus thrombosis, ischemic stroke and reversible segmental cerebral vasoconstriction syndrome, a rare group of disorders encompassing benign angiopathy of the CNS, postpartum angiopathy, and drug-induced vasospasm. Examples will be presented using CT, MR and conventional angiography. Acute hypertensive crisis with posterior reversible leucoencephalopathy may have a similar presentation. While standard investigations of CT and lumbar puncture may be normal, MRI can show evidence of edema involving the posterior white matter and cortex, and prompt diagnosis is essential as the condition is most reversible in the early stages. Signs of spontaneous intracranial hypotension may be seen on initial CT imaging but is demonstrated reliably using MRI. Pituitary apoplexy, third ventricle colloid cyst, acute meningitis and sphenoidal sinusitis also may present with TCH.

**SUMMARY/CONCLUSION**

All patients with TCH must be assessed promptly and a range of underlying causes must be considered. Initial diagnostic studies including CT and lumbar puncture may shed light on the diagnosis but further MR and/or venographic or angiographic imaging should be performed if clinical suspicion leads to other diagnoses that may present with TCH.



**KEY WORDS:** Thunderclap headache, subarachnoid hemorrhage, neuroimaging

**Monday, April 23 –  
Wednesday, April 25  
6:30 AM - 9:00 PM**

**Thursday, April 26  
6:30 AM – 3:00 PM  
Rhinelanders**

**Education Exhibits (EdE) 1 – 37**

**EdE - Anatomy**

**Note: A missing printed number indicates an abstract has been withdrawn.**

#### **EdE-38**

##### **Anatomical Considerations for Somatotopic Organization of the Descending Motor Fibers: A Pictorial Essay**

Hamilton, J. D.<sup>1</sup>Kumar, V. A.<sup>1</sup>Prabhu, S. S.<sup>1</sup>Shah, K.<sup>1</sup>Peiffer, A.<sup>2</sup>Hayman, L. A.<sup>3</sup>Kumar, A. J.<sup>1</sup>

<sup>1</sup>M.D. Anderson Cancer Center, Houston, TX, <sup>2</sup>Wake Forest University, Winston Salem, NC, <sup>3</sup>Anatom-e Information Systems, Houston, TX

#### **PURPOSE**

To illustrate clinically important anatomical relationships of the somatotopically arranged motor fibers for the corticospinal (CST) and corticobulbar (CBT) tracts.

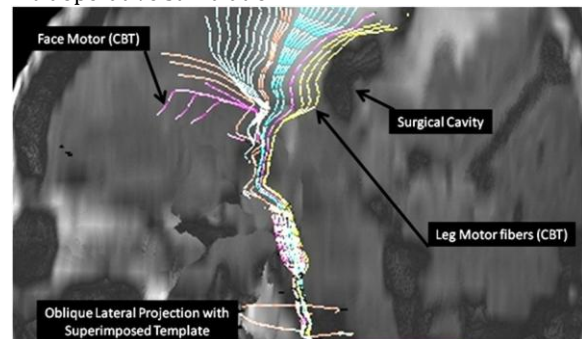
#### **APPROACH/METHODS**

We analyzed clinical cases using software that embeds annotated anatomical information into the patient's brain images (Anatom-e Information Systems, Houston, TX). This tool can create unique color-coded volume-rendered views of the motor fibers and their relationship to adjacent landmarks. The motor pathways were validated with diffusion tensor imaging (DTI). We selected cases that illustrated the important anatomical and somatotopic features of the motor fibers in the corona radiata. Clinical follow-up data were obtained from the medical records. Supporting documentation was obtained from anatomical, neurosurgical and imaging literature.

#### **FINDINGS/DISCUSSION**

Four important anatomical relationships related to the corticospinal and corticobulbar tracts are illustrated. 1) There is an anterior slant of the origin of the motor fibers moving medial from the leg to laterally for the

face. The first case illustrates a postoperative hemiparesis that resulted when this slant placed facial CBT in harm's way with an inferior frontal approach. 2) As the more medial CST fibers descend, they curve anteriorly. The second case shows paralysis of the lower limb when the leg fibers deep to the supplementary motor cortex were included in the resection cavity due to this anterior curvature. 3) The combination of the above two anatomical features creates a natural surgical approach to cingulate lesions via an entry point in the superior parietal lobule. The third case (illustration) demonstrates how this approach can avoid unplanned deficits. 4) With somatotopic organization, the CBT begins anteromedial to the CST at the level of the precentral operculum, just above the sylvian fissure. The CBT then twists to anteromedial of the CST within the middle portion of the posterior limb of the internal capsule and continues twisting through the thalamus and midbrain until posterolateral within the brainstem. The forth, fifth, and sixth cases use small ischemic strokes in the watershed zone between the lateral lenticulostriate vessels and the cortical branches of the insula to illustrate the somatotopic arrangement of the face, arm, and leg fibers. Finally, the last case shows how motor function at least can be maintained partially despite glial tumor invasion, emphasizing the need for careful preoperative planning and intraoperative stimulation.



#### **SUMMARY/CONCLUSION**

Diffusion tensor imaging, anatomical landmarks and templates are useful guides for understanding the complex, clinically important anatomical arrangement of the motor fibers in the corona radiata.

**KEY WORDS:** Corticospinal tract, diffusion tensor imaging, anatomical template

#### **EdE-39**

##### **Pediatric Cerebellum: A Pictorial Review of Normal Anatomy Using MR Imaging and Diffusion Tensor Imaging**

Tuna, I. S. Singh, S. Kelly, T. Maheshwari, M. Chandra, T. Segall, H. D.

Medical College of Wisconsin  
Wauwatosa, WI

#### **PURPOSE**

The aim of this educational exhibit is to illustrate normal anatomical and functional anatomy of the

cerebellum in the pediatric patient. The cerebellum receives sensory input from the brain and spinal cord and integrates this information to coordinate motor control. In addition, the cerebellum also plays a role in some cognitive functions such as attention and language. The first step toward understanding how cerebellar abnormalities can lead to neurologic dysfunction, is to provide a solid understanding of the neuroanatomy and functional pathways of the cerebellum. We will describe basic cerebellar embryology, the various cell types and gross anatomy using MR images as well as diffusion tensor imaging (DTI) fiber tractography.

#### APPROACH/METHODS

This exhibit will describe the microstructure, gross anatomy and functional pathways of the cerebellum through illustrations, MR images, DTI and pathologic correlation. First embryology of the cerebellum will be described, followed by MRI depiction of the developmental anatomy of the cerebellum from infancy through adolescence. Finally DTI tractography images will be used to delineate functional pathways to and from, as well as within, the cerebellum. Pathologic specimens will be photographed to further illustrate gross anatomy.

#### FINDINGS/DISCUSSION

Afferent white matter pathways travel mainly via the inferior and middle cerebellar peduncles. The main efferent cerebellar white matter pathway is through the superior cerebellar peduncle. Transverse fiber tracts are present in the vermis. There are mainly two main systems of cerebellar white matter fibers which are visualized easily with DTI color mapping; however, more anterior components of DTI tracts are intermixed with afferent white matter projections following the middle cerebellar peduncle.

#### SUMMARY/CONCLUSION

Knowledge of the precise neuroanatomy and white matter tracts of cerebellum may elucidate our ability to comprehend the clinical manifestations of cerebellar diseases in children. A solid understanding of normal cerebellar anatomy, development and functional fiber tracts in the pediatric patient can provide a baseline that may help predict the clinical outcome of various diseases or interventional procedures.

**KEY WORDS:** Cerebellum, anatomy, diffusion tensor imaging

#### EdE-40

#### Persistent Trigeminal Artery Variant: A Review and Pictorial Essay

Chen, D. C.·Chen, C. J.

Taipei Medical School, Shuang Ho Hospital  
Taipei, TAIWAN

#### PURPOSE

Persistent trigeminal artery variant (PTAV) is a rare anastomosis between the internal carotid artery (ICA)

and the cerebellar artery. We demonstrate four cases of PTAV and discuss its embryological origin, classification, and clinical implications.

#### APPROACH/METHODS

Retrospectively consecutive 395 conventional cerebral angiograms and 2861 cranial magnetic resonance angiographies (MRAs) in our hospital from Oct. 1, 2010 to Nov. 1, 2011 were evaluated for the patients with PTAV. Four patients (as listed in table one) had a PTAV. Four patients who underwent MRA had a PTAV ( $4/2861 = 0.14\%$ ). Three patients who underwent conventional angiography had a PTAV ( $3/395 = 0.75\%$ ). The PTAVs were an incidental finding in all four patients.

Case list						
Case No.	Age/Sex	Origin of PTAV	Supplying territory	Presenting symptom	Associated anomaly	Study
1	55/M	Right cavernous ICA	SCA	Seizure	Non	MRA, DSA
2	33/M	Left cavernous ICA	AICA	Thrombing headache	Non	MRA, DSA
3	72/M	Left cavernous ICA	SCA	Cerebral infarct	Non	MRA, DSA
4	35/M	Right cavernous ICA	SCA	Fainting sensation	Non	MRA, DSA

#### FINDINGS/DISCUSSION

The fetal carotid-basilar anastomoses, including primitive trigeminal, otic, hypoglossal, and proatlantal intersegmental arteries, usually regress when the posterior communicating and vertebral arteries develop. Occasionally, persistence of these vessels is noted after birth. Persistent trigeminal artery (PTA), which originates from the cavernous ICA and connects to the basilar artery, is the most common persistent carotid-basilar anastomosis. However, when PTA does not connect to the basilar artery but supplies to the cerebellar territory, it is called a PTA variant, which is a rare condition with an incidence reported to be between 0.2% and 0.76% based on MRA and conventional angiogram series. In 1959, Saltzman first grouped PTA into three types based on angiographic appearance. Some authors further include the PTAVs into Saltzman type 3 and group them by its supplying territory into Saltzman type 3a (to SCA), type 3b (to AICA) and type 3c (to PICA) (3). PTAV was reported to most often course to the AICA territory, followed by PICA and SCA. It usually has a small caliber, which makes its visualization and recognition difficult. Actually, three of the four patients underwent MRA in our series initially were misinterpreted to have an ICA aneurysm, a prominent meningo-hypophyseal trunk and was not recognized in one respectively. Furthermore, though PTAVs usually are found incidentally, they may be responsible for trigeminal neuralgia and cerebellar ischemia. A high prevalence of associated intracranial aneurysms was reported previously. However, the rate may be biased because it is based on collections of published case reports. Recent large case series with

PTAVs on MRA demonstrates that the aneurysm prevalence is no greater than the general population.

#### **SUMMARY/CONCLUSION**

Although the presence of PTAV may be clinically insignificant, neuroradiologists or neurosurgeons should be aware of the existence of PTAV for avoidance of misinterpretation on angiography and avoidance of potential risk of cerebellar hemorrhage or ischemia during a surgical approach to the parasellar region and therapeutic embolization at the carotid artery.

**KEY WORDS:** Persistent trigeminal artery, persistent trigeminal artery variant

#### **EdE-41**

##### **Rathke Cleft Cyst: from MR Imaging to Embryology**

Perazzini, C. • La Piana, R. • Melançon, D. • Tampieri, D.

Montreal Neurological Institute and Hospital, McGill University Health Centre  
Montreal, QC, CANADA

#### **PURPOSE**

The aim of this project is to review the possible localizations of the Rathke cleft cyst and to interpret them based on the embryologic development of the pituitary gland.

#### **APPROACH/METHODS**

We have reviewed all the neuroradiologic imaging of patients with confirmed Rathke cleft cysts detected at our department in the last 15 years. The cyst localization has been classified and then correlated to the different stages of the embryologic development of the pituitary gland.

#### **FINDINGS/DISCUSSION**

The neuroradiologic findings showed that the Rathke cleft cyst can have an intrasellar localization associated or not with a suprasellar extension. We correlated these findings to the embryologic development. The pituitary gland is composed of three lobes: anterior, intermediate and posterior. The anterior and intermediate lobes share the same function, while the posterior has completely different connections to the ventral hypothalamus and contains neuroglial cells called pituicytes. The anterior/intermediate and posterior lobes of the pituitary originate from two separate germinal regions. During the embryologic development, the anterior and intermediate lobes of the pituitary arise from the midline ectoderm that comes into contact with neuroectoderm of the ventral diencephalon. The oral ectoderm at the level of the roof of the stomodeum evaginates forming first a rudimentary pouch and then a definitive pouch, both known as Rathke's pouch. Subsequently, Rathke's pouch disconnects from the oral cavity following the degeneration of the connecting stalk between the pouch and the oral cavity. The Rathke's pouch is the precursor of the anterior pituitary; its formation involves the evagination of the oral ectoderm and it is regulated by cell interactions, signaling pathways and transcription factors. At the

same time, the infundibulum, originating from the neuroectoderm adjacent to the Rathke's pouch, evaginates to form the posterior lobe of the pituitary. If the Rathke's pouch fails to collapse, a cystic remnant is detectable, namely the Rathke cleft cyst. The review of the embryologic development can explain why the cysts are typically found within the gland in intrasellar localization or along the usual migration path of the pouch in sellar localization with a suprasellar extension.

#### **SUMMARY/CONCLUSION**

The Rathke cleft cysts are benign cystic lesions originating from a remnant of the Rathke's pouch. Since the Rathke's pouch is localized between the anterior and posterior lobes of pituitary gland in the region of pars intermedia, the most frequent localization of Rathke cleft cyst is intrasellar with or without suprasellar extension. In conclusion, the correlation between neuroradiologic findings and the review of the embryologic development is helpful for differential diagnosis of lesions in the sella region.

**KEY WORDS:** Rathke's pouch, Rathke cleft cyst, embryology

#### **EdE-42**

##### **Parapharyngeal Fat: The Key to Differential Diagnosis of Suprahyoid Lesions**

Mahady, K. F.<sup>1</sup> • Loney, E.<sup>2</sup>

<sup>1</sup>Carlton House, Healey Mount, Burnley, UNITED KINGDOM, <sup>2</sup>Bradford Teaching Hospitals NHS Foundation Trust, Bradford, UNITED KINGDOM

#### **PURPOSE**

The parapharyngeal space is a suprahyoid deep neck space filled by the parapharyngeal fat. It is positioned centrally within important surrounding spaces. Primary lesions of the parapharyngeal space are rare. Understanding the anatomy of its close relations and patterns of compression of the parapharyngeal fat leads to accurate differential diagnosis of suprahyoid neck lesions.

#### **APPROACH/METHODS**

We present key cross-sectional images (contrast enhanced CT and 1.5 T MRI) from a series of cases demonstrating various patterns of parapharyngeal fat compression, with histologic confirmation of diagnosis.

#### **FINDINGS/DISCUSSION**

1. Lesions arising from the pharyngeal mucosal space causing lateral compression, including cases of squamous cell carcinoma and non-Hodgkins lymphoma.
2. Lesions arising from the masticator space causing posterior compression, including primary muscle tumors (sarcoma) and perineural spread from CNV3 tumor.
3. Lesions arising from the parotid space compressing the parapharyngeal fat medially, including benign and malignant salivary gland tumors.
4. Lesions arising from the carotid space compressing the parapharyngeal fat anteriorly, including carotid body paraganglioma, jugular vein thrombus and vascular

lesions. 5. Lesions arising from the retropharyngeal space causing anterolateral compression including abscess and nodal mass. 6. Lesions completely surrounded by parapharyngeal fat, with cases of lipoma and atypical second branchial cleft cyst.

#### **SUMMARY/CONCLUSION**

A comprehensive image-based review of anatomy of deep neck spaces centered on patterns of parapharyngeal space compression provides a structured and accurate approach to differential diagnosis in suprahyoid neck lesions.

**KEY WORDS:** Parapharyngeal fat, deep space, head and neck

#### **EdE-43**

##### **Congenitally Absent Cervical Pedicle: Characteristic Radiologic Findings and Clinical Implications**

Dickinson, J. R.<sup>1</sup>Sakai, O.<sup>2</sup>Wang, J.<sup>2</sup>

<sup>1</sup>New York Medical College, Valhalla, NY, <sup>2</sup>Boston University School of Medicine, Boston, MA

#### **PURPOSE**

To examine the radiologic features of congenital absence of a cervical pedicle and educate the radiologist regarding implications of the diagnosis and current recommendations for treatment.

#### **APPROACH/METHODS**

Four recent patients with CT-confirmed congenital absence of a cervical pedicle were reviewed for clinical presentation, radiologic findings, treatment, and disposition.

#### **FINDINGS/DISCUSSION**

Four cases were diagnosed, all incidentally. Three were discovered during cervical spine evaluation in the setting of acute trauma and one during maxillofacial CT for evaluation of a mandibular cyst. Of the three cases identified during trauma evaluation, two patients initially received cervical spine radiographs which correctly diagnosed one patient; the third trauma patient was transferred from an outside hospital because their cervical spine CT had been incorrectly interpreted as fracture-dislocation. All four patients were correctly diagnosed at our facility on CT, although one preliminary resident read incorrectly diagnosed fracture/dislocation. The malformation was identified at C4-6 levels. These cases provide a background for the radiologically-based evaluation of congenital absence of pedicles in the cervical spine. As the condition is generally clinically silent and discovered in the course of trauma evaluation, it is frequently the radiologist who must decide whether the abnormality is congenital or the result of trauma, and this distinction will greatly affect subsequent patient care and outcomes. Cases have been reported in which unnecessary surgical interventions were performed, occasionally to the detriment of the patient. Thus, it is imperative that the radiologist is able to recognize this entity and clearly communicate findings to the referring physician. To this

end, we present imaging associated with these cases and highlight the characteristic findings on radiographs, CT, and MR. We also present neurologic findings, treatment, and disposition for each patient. The patients in this series who experienced trauma had only neck pain, with no other neurologic signs or symptoms. They were all treated conservatively with resolution of symptoms referable to cervical spine trauma. These cases add to evidence in the literature that with correct identification, these congenital abnormalities are stable and require no additional treatment.

#### **SUMMARY/CONCLUSION**

We examined imaging findings on four patients who were incidentally diagnosed with congenital absence of a cervical pedicle. As these congenital anomalies frequently are found in the investigation of trauma, they often are misdiagnosed as fracture-dislocation, particularly when relying on radiographs. In our series of four cases, all patients were diagnosed correctly on CT, underscoring the practicality of this modality in trauma investigation, particularly when radiographs of the cervical spine have questionable findings.

**KEY WORDS:** Congenital, spine, pedicle

**Monday, April 23 –  
Wednesday, April 25  
6:30 AM - 9:00 PM**

**Thursday, April 26  
6:30 AM – 3:00 PM  
Rhineland**

**Education Exhibits (EdE)  
44 – 66a**

**EdE3 – Head and Neck**

**Note: A missing printed number indicates an abstract has been withdrawn.**

#### **EdE-44**

##### **Imaging of the Aging Midface before and after Treatment**

Ginat, D.<sup>1</sup>Schatz, C.<sup>2</sup>

<sup>1</sup>Massachusetts General Hospital, Boston, MA, <sup>2</sup>Beverly Towers Imaging/University of Southern California, Los Angeles, CA

#### **PURPOSE**

The goal of this exhibit is to review the imaging anatomy of the midface structures, discuss the changes

that occur in this region with aging, provide an overview of the types of treatments available for midface rejuvenation, and depict the corresponding treatment changes on imaging.

#### **APPROACH/METHODS**

High-quality cross-sectional imaging, including CT and MRI, can be used to define the facial planes, mimetic muscles, and underlying osseous structures. Although radiology currently has a limited role in preoperative assessment for midfacial rejuvenation, it is sometimes indicated to evaluate patients after treatment.

#### **FINDINGS/DISCUSSION**

The midface is the portion of the face that comprises the nasal, maxillary, and zygomatic bones as well as the soft tissues covering these bones and extends from the bicanthal area to the oral commissure. With aging, a progression of characteristic changes occur in the midface, including ptosis of midfacial fat, descent of malar fat pad with separation from the suborbicularis oculi fat pad, descent of the Bichat fat pad over the upper mandible, and disproportionate hypertrophy of the superior portion of the malar fat pad. Thus, strategies to reverse the effects of aging upon the midface include volume augmentation using fillers and injectables, such as bone grafts, collagen, silicone, polytetrafluoroethylene, and hyaluronic acid. Alternatively, midface lifts can be accomplished via a variety of open surgical soft-tissue repositioning or suspension techniques (face lift) and lower lid blepharoplasty.

#### **SUMMARY/CONCLUSION**

Midface rejuvenation procedures are performed increasingly. Understanding the anatomy and mechanisms of the midfacial aging process, as well as the types of treatments and their complications is important for optimal interpretation of imaging evaluation when it is requested.

**KEY WORDS:** Midface, anatomy, facial cosmesis

#### **EdE-45**

##### **Imaging Manifestations of Histiocytic Diseases of the Head and Neck**

Abdullah, A.·Elias, A.·Hoeffner, E.·Rivas-Rodriguez, F.·Mujherji, S.

University of Michigan Health System  
Ann Arbor, MI

#### **PURPOSE**

Histiocytic diseases include a group of diverse disorders with a common primary event that begins with accumulation and infiltration of monocytes, macrophages, and dendritic cells in the affected tissues. The pathophysiology of histiocytic diseases remains poorly understood, however. Head and neck regions are common sites for a variety of histiocytic diseases. Imaging plays a crucial role in the diagnosis and evaluation of disease extent since treatment decisions are based primarily on overall extent of disease. The

goal of this presentation is to provide the reader with a case-based review of imaging features of common and rare histiocytic disorders involving the head and neck.

#### **APPROACH/METHODS**

The following points will be emphasized in this presentation: 1. The role of imaging in the initial diagnosis and management planning of histiocytic disorders of the head and neck. 2. Differential diagnosis of histiocytic diseases. 3. Role of follow-up imaging in assessment of treatment response. 4. Sample cases with pre and posttreatment imaging findings with emphasis on cross-sectional imaging.

#### **FINDINGS/DISCUSSION**

According to World Health Organization Classification, histiocytic diseases are grouped into X-type, Non X-type, malignant-type, and ungrouped histiocytosis. The X-type histiocytic disorders include Langerhans's Histiocytosis while the Non X-type includes Juvenile Xanthogranuloma, Erdheim-Chester disease, and Niemann Pick's disease. The ungrouped histiocytoses include Erdheim-Chester disease. Malignant histiocytoses include histiocytic sarcoma. Radiologically, histiocytic diseases of the head and neck often are difficult to distinguish. Clinical history and an analytical approach to imaging can aid in narrowing the differential diagnosis. Cross-sectional imaging demonstrates the exact anatomical location, extent, and involvement of adjacent structures.

#### **SUMMARY/CONCLUSION**

The diagnosis and treatment of histiocytic diseases continues to evolve to this day, and perhaps due to their relative scarcity, continue to create a diagnostic dilemma to physicians of all specialties. These diseases have manifestations in the head and neck, and many patients initially present to the radiologist with imaging studies. Imaging does not always provide a specific diagnosis of histiocytoses but should help narrow the differential diagnosis, thereby helping to guide patient treatment. Recognition of typical and atypical imaging patterns can allow radiologists to more accurately approach the correct diagnosis and aid in better clinical management of these conditions.

**KEY WORDS:** Histiocytosis, Erdheim-Chester disease, sinus histiocytosis

#### **EdE-46**

##### **Uveitis and MR Imaging**

Li, C. Q.·Mafee, M. F.·Cho, A. A.

University of California San Diego  
San Diego, CA

#### **PURPOSE**

Uveitis describes inflammation of the choroid, iris, or ciliary body, which make up the uveal tract. It can be idiopathic or associated with systemic disease which may be infectious or noninfectious. Etiology varies depending on anatomical classification, environmental or population factors. Inflammation of the uvea may be

limited to its anterior component, posterior component or the entire uveal tract. With the exception of B-scan ultrasonography, current imaging methods for diagnosing and monitoring uveitis are predominately nonradiologic. However, MRI has been shown to detect various inflammatory conditions of the ocular wall, such as posterior scleritis/uveoscleritis, choroidal effusion, and choroidal inflammation via abnormal gadolinium enhancement. MR imaging and CT findings in uveitis of varied etiology and the role of MRI in diagnosis and monitoring of uveitis are reported.

#### **APPROACH/METHODS**

Six cases of uveitis (1 ankylosing spondylitis, 1 relapsing polychondritis, 1 tuberculosis, 3 sarcoidosis) were identified from our imaging database. Key imaging characteristics and pertinent clinical findings of these cases are presented.

#### **FINDINGS/DISCUSSION**

In the six cases of clinically diagnosed uveitis, all exhibited postcontrast enhancement of various segments of the uveal tract on MRI or CT. Enhancement is thought to result from extravasation of gadolinium contrast from inflammation-induced leaky capillaries in the highly vascular uvea. Other findings included uveal tract thickening, abnormal nodular growths, calcium deposition, bright T1 and FLAIR signal, and enhancement of the optic nerve sheath and extraocular musculature. Inflammation of the choroid could be differentiated from scleral inflammation as the latter is a fibrous structure with relative hypointensity on T1- and T2-weighted images. In the case of relapsing polychondritis, diffuse thickening of the uveoscleral coat was observed in addition to a linear calcification in the posterior pole of the globe. Distorted anatomy also was visualized in the case of tuberculous panuveitis, in the form of hypointense structures attached to the ciliary body and the posterior retinal surface of the affected globe on T2-weighted MRI. Abnormal enhancement outside the globe was appreciated in one case of sarcoidosis, where gadolinium uptake was visible in the optic nerve sheath and also the extraocular muscles of the affected eye.

#### **SUMMARY/CONCLUSION**

While uveitis remains a clinical diagnosis, MRI has shown sensitivity for detecting abnormal contrast enhancement and thickening of the uveal tract. Additional findings correlated with uveitis may be useful in differentiating uveitis from multiple ocular disease entities, such as pediatric intraocular tumors, cancers/lymphomas, retinal detachment and intraocular foreign bodies. Contrast-enhanced MRI also can monitor for uveitis-related complications not apparent on ocular examination, such as calcification of the globes, internal nodular growths and spread of inflammation proximally along the optic nerve and extraocular muscles.

**KEY WORDS:** Uveitis, MR imaging, CT

#### **EdE-47**

### **Keeping an Eye Out: CT Imaging of the Postoperative Orbit**

Jaswani, V.·Kazmi, K.·Lexa, F. J.

Hahnemann University Hospital  
Philadelphia, PA

#### **PURPOSE**

This educational exhibit discusses the CT appearance of a select group of orbital and/or ophthalmologic procedures. The procedures discussed will include: scleral buckling and intraocular tamponade for the treatment of retinal tears or detachment, prosthetic lens placement for cataracts, metallic eyelid prostheses for lagophthalmos, ocular implants, glaucoma drain placement, and repair hardware related to fractures of the orbital floor.

#### **APPROACH/METHODS**

We retrospectively reviewed CTs of the head and orbits performed at our institution from 2010 to 2011 for evidence of patients with prior orbital and/or ophthalmologic surgery. For each type of procedure, we briefly review the pertinent orbital anatomy and pathophysiology, followed by a discussion of the postsurgical appearance on CT. When available, correlative MR images also will be presented.

#### **FINDINGS/DISCUSSION**

Orbital and ophthalmologic procedures exhibit characteristic appearances on CT, which allows the radiologist to generate accurate diagnoses when presented with orbital findings. Scleral buckle, whether placed with or without an associated scleral sponge, presents as a hyperattenuating or air-attenuation (solid or porous, respectively) band encircling the globe. Intraocular tamponade with gas produces an air bubble within the vitreous of the globe, not to be mistaken for gas related to globe infection or trauma. Prosthetic lens appears as thin, barely perceptible linear soft tissue density associated with absence of the native lens. Eyelid prostheses (usually composed of gold, platinum, or a platinum-iridium amalgam) are uniformly hyperdense on CT and located in the anterior orbit. These must be recognized on CTs of head trauma patients to avoid misdiagnosis of embedded foreign body. Ocular implants have distinctive appearances and should not be misconstrued for globe pathology. Valves are curvilinear hyperdensities located laterally in the orbit for fluid drainage in glaucoma patients. Finally, metallic orbital floor repair hardware can be recognized easily in the inferior orbit and proper placement also may be confirmed on CT.

#### **SUMMARY/CONCLUSION**

Knowledge of the CT appearance of the postoperative orbit and globe is crucial to the radiologist. Firstly, knowing these common appearances will enable accurate diagnosis. Equally important is the ability to differentiate the expected postoperative appearance from foreign body or gas in the setting of trauma or infection, in order to prevent misdiagnosis.



**KEY WORDS:** Orbit, postoperative

#### EdE-48

##### Imaging Features of Intraorbital Mass Lesions

Patel, G.<sup>1</sup>Qian, J.-Vaisfeld, J.-Young, R. J.

Memorial Sloan-Kettering Cancer Center  
New York, NY

##### PURPOSE

The intraorbital space may be affected by both benign and malignant masses. The purpose of this study is to review the spectrum of mass lesions that may involve the intraorbital space in adults with an emphasis on characteristic imaging features that can help in the differential diagnosis.

##### APPROACH/METHODS

Cases drawn from a tertiary care cancer center will be presented in an interactive quiz format. MR and CT images will be presented to guide the audience through a comprehensive review of common and uncommon intraorbital pathologies. Emphasis will be placed on recognizing and utilizing imaging clues to: 1) Narrow the differential diagnosis; 2) Identify patterns of spread with respect to orbital anatomy; and 3) Guide treatment and management decisions.

##### FINDINGS/DISCUSSION

Highlighted in each case are characteristic imaging findings to aid in the differential diagnosis and prognosis of these patients. Emphasis will be placed on imaging patterns such as calcification, mass effect, enhancement pattern, unilateral vs bilateral involvement, and specific location within the intraorbital space (intraconal, extraconal, muscle, nerve), as well as pertinent clinical clues such as duration of signs/symptoms and presence of pain. An in depth discussion of both common and uncommon lesions will take place. The following types of lesions are included in this review: nontumoral (vascular malformations, infection, mucocoele, sarcoid, Erdheim Chester disease, pseudotumor) and tumoral (metastasis, leukemia, lymphoma, optic nerve glioma, optic nerve sheath meningioma, lacrimal gland tumor).

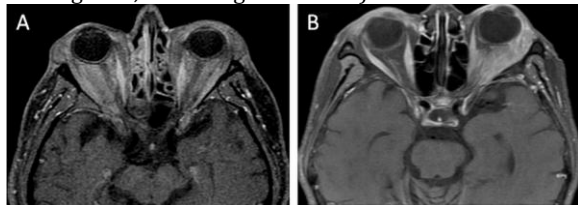


Figure. Fat saturated contrast T1-weighted images. (A) Shows bilateral ill-defined diffusely enhancing masses involving the intraconal and extraconal spaces with mild proptosis. The bilateral abnormalities suggest a systemic disease, in this case leukemic infiltration. (B) Demonstrates an ill-defined enhancing mass in the left orbit involving the extraocular muscles, intraconal and extraconal spaces with mild proptosis. This unilateral abnormality is consistent with metastatic breast cancer.

##### SUMMARY/CONCLUSION

This educational exhibit will illustrate the spectrum of intraorbital lesions on CT and MR imaging sequences. After completion of this exercise, it is expected that the reader will have a practical framework for narrowing the differential diagnosis and an understanding of the imaging findings that are essential for patient management.

**KEY WORDS:** Orbit, MR imaging

#### EdE-49

##### Benign and Malignant Odontogenic Lesions: A Pictorial Review

Mehta, P.<sup>1</sup>Maertz, N.<sup>2</sup>

<sup>1</sup>Indiana University, Indianapolis, IN, <sup>2</sup>Indiana Radiology Partners, Indianapolis, IN

##### PURPOSE

The educational exhibit will seek to provide a review of the imaging anatomy, important anatomical relationships, and pathologic entities occurring within the mandible and maxilla. Specifically, this review will focus on those lesions that involve the tissues that give rise to the teeth. Through the use of example illustrations, these entities are presented and reviewed with highlights of particular clinical importance. Histopathologic correlation is provided for select cases.

##### APPROACH/METHODS

Retrospective case review of a broad range of pathologically and clinically proven odontogenic lesions accumulated from 2001-2011 at a tertiary referral center. The anatomical relationships and major disease processes for this location are reviewed with the appropriate differential diagnostic considerations and recommended imaging approaches for common clinical presentations. High quality images illustrate the findings and complement the succinct review of disease in this location. Examples of cases discussed include but are not limited to the following: odontoma, ameloblastoma, odontogenic myxoma, odontogenic keratocyst, periapical cyst, dentigerous cyst, odontogenic keratocyst, ameloblastic odontosarcoma, ameloblastic carcinoma. Some of the cases will be accompanied by histopathologic correlation.

##### FINDINGS/DISCUSSION

The viewer of this exhibit will gain or refresh information about the anatomical relationships and disease entities involving odontogenic origin lesions for clinical practice and for preparation for certifying examinations. The images provided aid recognition with an emphasis on clinical context and differential diagnosis.

##### SUMMARY/CONCLUSION

Odontogenic lesions can present a diagnostic challenge. Extensive illustrations of the different entities and a solid understanding of the clinical presentations can aid the radiologist in arriving at the appropriate diagnosis.

**KEY WORDS:** Odontogenic, benign, malignant

## EdE-50

### **PET/CT for Head and Neck Squamous Cell Carcinoma: Who, When and Watch Out**

Pastel, D.-Lee, N.-Stensby, J. D.-Belden, C.-Guerin, S.-Seltzer, M.

Dartmouth-Hitchcock Medical Center  
Lebanon, NH

#### **PURPOSE**

Head and neck squamous cell carcinoma (HNSCC) is the sixth most common cancer worldwide. Imaging plays an important role in the detection, staging, and treatment evaluation of these tumors. Fluorine 18 fluorodeoxyglucose (FDG) positron emission tomography (PET) combined with computed tomography (CT) provides valuable information not afforded by other imaging modalities. It has improved our ability to stage tumors, monitor disease response and detect recurrent or residual disease. Knowing who and when to image with PET-CT in the setting of HNSCC and recognizing the common pitfalls is critical for accurate interpretation.

#### **APPROACH/METHODS**

This exhibit will review the role of PET-CT in the evaluation of the newly diagnosed head and neck cancer, the unknown primary, and the posttreatment neck. Limitations and common pitfalls encountered with this modality will be illustrated with examples.

#### **FINDINGS/DISCUSSION**

Positron emission tomography/CT has limited utility in assessing the primary tumor, but, compared to conventional imaging modalities, has increased sensitivity for the detection of nodal and metastatic disease. Positron emission tomography/CT can identify disease in lymph nodes that are not enlarged by size criteria. There are, however, innate limitations in camera resolution making PET insensitive for the detection of lymph nodes measuring less than 7mm. For this reason, management of patients with tumors clinically classified as lymph node negative should not rely too heavily on PET-CT to determine the need for neck dissections. Two-five per cent of patients with HNSCC presents with lymphadenopathy in the absence of an identifiable primary tumor on clinical examination and conventional imaging. In these situations, asymmetric hypermetabolic foci on PET/CT can be very valuable in directing biopsies. To minimize false positives, the radiologist must recognize the patterns of normal physiologic uptake. The posttreatment neck pose challenges to the radiologist. It can be difficult to distinguish normal posttherapy changes from residual tumor or tumor recurrence. While PET-CT has limitations, it provides important information not available by other modalities in the posttreatment setting. For example, PET-CT has a very high negative predictive value following neoadjuvant chemoradiation therapy. Many surgeons will now defer neck dissection when the post-treatment PET-CT is negative for nodal

disease. Knowing when to image following treatment is important because both sensitivity and specificity improve with time. In the early posttreatment time period, tumor cells have decreased avidity for FDG resulting in false negatives while postradiation inflammatory changes result in false positives. Early detection of residual or recurrent disease has important prognostic implications and must be balanced with the improved accuracy of PET-CT over time. Most groups will wait at least 10 weeks after treatment to image with PET-CT. Common pitfalls when imaging the head and neck include osteoradionecrosis, posttreatment inflammatory changes, reactive lymph nodes, infection, and asymmetric muscle and lymphoid uptake after surgery. This underscores the importance of close attention to the patient's treatment history when interpreting studies.

#### **SUMMARY/CONCLUSION**

Knowing who and when to image with PET/CT in the setting of HNSCC and recognizing common pitfalls allows the radiologist to provide the best imaging information possible for guiding management.

**KEY WORDS:** PET/CT, squamous cell carcinoma

## EdE-51

### **Scalp Lesions: A Hairy Situation**

Datta, V.-Almast, J.

University of Rochester  
Rochester, NY

#### **PURPOSE**

This project will aim to familiarize the exhibit viewer with the various scalp lesions which are encountered, typically incidentally, on neuroradiologic imaging.

#### **APPROACH/METHODS**

This exhibit will utilize computed tomography and magnetic resonance imaging to illustrate and help further the understanding of various scalp lesions. We will discuss the differential considerations for scalp lesions and the characteristics which facilitate accurate diagnosis.

#### **FINDINGS/DISCUSSION**

Scalp lesions are not uncommonly an incidental finding on neuroradiologic imaging; therefore, a familiarity of the different lesions is crucial. Scalp lesions, which will be discussed, include: metastasis, lymphoma, skin neoplasms (i.e., Merkel cell, pilomatrixoma, melanoma and angiosarcoma), sebaceous cysts, epidermal inclusion cysts, lipomas, fat necrosis, glomus tumors, neurofibromas and various other select lesions.

#### **SUMMARY/CONCLUSION**

Familiarity with the imaging characteristics of scalp lesions is important because they can be of clinical significance for the patient, or alternatively, they may be a benign variant and should be distinguished from more serious pathology. This exhibit will aim to familiarize the neuroradiologist with the various scalp lesions that

may be encountered, in order to facilitate accurate diagnosis.

**KEY WORDS:** Scalp

#### EdE-52

##### **Cervical Ectopic Thymus Revisited: A Common, Yet Rarely Symptomatic Pediatric Neck Mass**

Poutre, A. J.·Groom, K.·Cable, B.·Rooks, V.·Biega, T.

Tripler Army Medical Center  
Honolulu, HI

#### **PURPOSE**

Ectopic cervical thymus tissue is reported in the literature as an extremely rare entity. To date, less than 120 cases of cervical ectopic thymus have been reported, with a small fraction of these in children. Due to its purported rarity, ectopic thymus usually is not included in the differential for pediatric neck masses. Autopsy studies, however, have demonstrated that cervical thymic rests are present in up to one third of children. Given this prevalence, it is likely that the number of reported cases of ectopic cervical thymus is a significant underestimation. Imaging characteristics of cervical ectopic thymus are well described and relatively consistent throughout the literature. Radiologists should have knowledge of this entity and consider it in the diagnosis of pediatric neck masses.

#### **APPROACH/METHODS**

Four recent cases of cervical ectopic thymus reporting to our institution are presented. One patient presented with respiratory distress, while three others were detected incidentally. Imaging findings to include MRI, CT and ultrasound are presented. Treatment plan and options for follow up are discussed.

#### **FINDINGS/DISCUSSION**

It is well established that the thymus originates in the third and fourth pharyngeal pouches during the sixth week of gestation. During the seventh and eighth weeks of gestation the thymus descends into the superior mediastinum and fuses across the midline. Sequestered fragments of thymic tissue may be found anywhere along this pathway, typically extending from the angle of the mandible bilaterally to the superior mediastinum. These remnant tissues then may form a solid or cystic mass which may undergo size fluctuations or grow rapidly following precedent trauma or infection. When symptomatic, the most common presenting symptom of cervical ectopic thymus is painless fullness. Compressive symptoms of stridor or dysphagia have been reported secondary to mass effect on the trachea or esophagus. Given autopsy data, it is presumed that the vast majority of ectopic thymic rests result in no discernable symptoms and are clinically silent. Despite the well described imaging findings, surgical excision is the most common method for both diagnosis and treatment recommended in the literature. Given the benign course of this entity, relatively reliable imaging characteristics and associated surgical comorbidities, recent publications have advocated conservative

management with follow-up imaging or minimally invasive biopsy as reasonable alternative strategies.

#### **SUMMARY/CONCLUSION**

Cervical ectopic thymus is not as rare as suggested in the medical literature. Rather, it is likely a common finding which rarely produces clinical symptoms. As cross-sectional imaging of the pediatric neck increases, however, the number of cases of incidentally detected ectopic thymus will likewise increase. Radiologists and clinicians alike should be aware of this entity to avoid potentially unnecessary surgical resection. Conservative therapy should be considered as a reasonable management alternative in uncomplicated cases with classic imaging findings.

**KEY WORDS:** Thymus, ectopic, pediatric

#### EdE-53

##### **Compartmentalization of Laryngeal Cancer: Effective Imaging Guidelines in the Age of Transoral Robotic Surgery**

Rhee, S. C.·Amin, S. K.·Sadeghi, N.·Joshi, A. S.·Taheri, R.

George Washington University  
Washington, DC

#### **PURPOSE**

1. To review conventional staging and treatment strategies for supraglottic squamous cell carcinoma (SCC), including radiation and transcervical surgery. 2. To introduce the promising technology of transoral robotic surgery for partial laryngeal resection. 3. To discuss compartmentalization of laryngeal cancer in the context of radiographic interpretation.

#### **APPROACH/METHODS**

1. Patient chart review to identify imaging and laryngoscopic examples of different stages of supraglottic SCC. 2. Pictorial examples of the use of transoral robotic surgery in resection of laryngeal cancer at our institution. 3. Literature review of the long-term outcomes and complications of transoral laser microsurgery and transoral robotic surgery in resection of laryngeal cancer in comparison to the more traditional treatment options. 4. Collaboration with otorhinolaryngologists to devise a new imaging guideline that can better assist in the selection of the least invasive surgical option.

#### **FINDINGS/DISCUSSION**

In a pictorial review, we describe the imaging characteristics of T1-T4 supraglottic SCC as well as N1-N3 nodal disease. Laryngoscopic images of selected cases will be provided to better demonstrate the extent of disease. We briefly review the recommended treatment plans based on the latest AJCC guidelines. A brief review of the literature on long-term survival of patients treated with transoral approach is provided. For example, transoral laser microsurgery was reported to have an overall survival rate of 91% for T1, 88% for T2, and 81% for T3 tumors. These long-term outcomes are similar to both conventional/invasive surgical

paradigms as well as chemo-radiation therapy. However, lower complication rates are reported with transoral approach. Pictorial examples of the transoral laser microsurgery and transoral robotic equipment used for laryngeal tumor resection are presented. As the role of transoral robotic surgery expands in the resection of laryngeal tumors, it is important for radiologists to become familiar with the imaging findings that impact the surgical options offered to the patient. We introduce the concept of compartmentalization of laryngeal cancer not only as a surgical paradigm, but also as an effective approach to the image characterization of supraglottic SCC. The premise of this model is that accurate radiologic description of tumor extent becomes critical in designing the least invasive surgical approach. To maximize success, the radiologist should not only describe the three dimensional extent of the tumor, but also specifically report the degree of involvement of crucial areas. Specifically, these include the extent of tumor involvement in the preepiglottic fat, paraglottic space, suprahyoid and infrahyoid epiglottis, aryepiglottic fold, false vocal fold as well as cartilage invasion. Selected cases are provided to demonstrate involvement in these specific areas.

#### **SUMMARY/CONCLUSION**

As the role of transoral surgery expands in the management of patients with laryngeal cancer, the radiologist needs to be familiar with criteria being used by surgeons in choosing the least invasive surgical plan. This understanding would facilitate a description of the tumor in a way that will guide our colleagues in the design of an appropriate treatment strategy.

**KEY WORDS:** Supraglottic squamous cell carcinoma, transoral robotic surgery, cancer staging

#### **EdE-54**

##### **Skull Base and Cervical Spine Chordomas in Children and Adolescents: Imaging, Clinical, and Pathologic Assessment**

Wang, B.<sup>1</sup>•Weber, A. L.<sup>2</sup>•Shah, B.<sup>3</sup>•Caruso, P. A.<sup>3</sup>•Curtin, H. D.<sup>2</sup>

<sup>1</sup>M.D. Anderson Cancer Center, Houston, TX,

<sup>2</sup>Massachusetts Eye and Ear Infirmary, Boston, MA,

<sup>3</sup>Massachusetts General Hospital, Boston, MA

#### **PURPOSE**

To demonstrate the clinical, imaging, and pathologic findings of chordoma of skull base and cervical spine in children and adolescents.

#### **APPROACH/METHODS**

We analyzed a total of approximately 30 cases of chordomas in children who were referred to Massachusetts General Hospital (MGH) for proton beam therapy and MD Anderson Cancer Center (MDA). All cases were studied with CT and/or MRI, and PET-CT in some cases. Representative cases of chordomas in different head and neck locations and the cervical spine will be selected and illustrated.

#### **FINDINGS/DISCUSSION**

The imaging modalities utilized for assessment of these tumors include CT and MRI. On CT intracranial **chordomas** typically appear as centrally located, lobulated circumscribed, expansile soft-tissue masses that arise from the clivus with associated variable lytic bone destruction. In some cases the soft tissue component of the tumor may be of low attenuation secondary to abundance of mucous and myxoid tissue. MR imaging is the single best imaging modality for both pre and posttreatment evaluation. On T1-weighted MR images, intracranial **chordomas** demonstrate intermediate to low signal intensity (compared with muscle) silhouetted against the high-signal-intensity fat of the clivus. On T2-weighted MR images, they characteristically demonstrate high signal intensity, a finding likely reflecting the high fluid content of vacuolated cellular components and the myxoid stroma associated with low SI fibrous septations. Chordomas reveal moderate to marked enhancement which is commonly heterogeneous. Chordomas in children and adolescents comprise <5% of all chordomas and most frequently develop in the skull base (35%). Intracranial **chordomas** are slow growing, locally aggressive with extension into adjacent structures including sella-parasellar and suprasellar areas, sphenoid and ethmoid sinuses, middle cranial fossa, cranio-occipital junction, upper cervical spinal canal, and nasopharynx. A subgroup of chordomas has been described that arise from the intracranial dura, nasopharynx and nasal cavities with no connection to any bony structures. Metastases occur (3-10%) and most commonly involve the lymph nodes of the neck, lungs, and liver. Cervical spine chordomas cause bone destruction, widening of intervertebral foramina, displacement and compression of the cervical spinal cord and may present as a neck mass. The symptoms of children with chordoma are diverse and depend on the location of the tumor. Base of skull chordomas impact the cranial nerves (most commonly N. VI) with diplopia, palatal or tongue weakness, headache, pyramidal signs and raised intracranial pressure in while the cervical spine cause neck pain, torticollis and rarely a neck mass. Histopathologically chordomas in children are divided into conventional chordomas, chondroid chordomas and chordomas that are highly cellular and aggressive. Treatment with radical surgical resection and proton beam radiation therapy achieve the best results.

#### **CONCLUSION /SUMMARY**

We present the imaging findings of 30 cases of chordoma of head and neck and the cervical spine in children and adolescents seen at MGH and MDA. The imaging modalities consisted of CT, MRI and in some cases PET-CT. We evaluated these tumors for size, shape, margins, location, extent, bony erosion, local and distant metastases and degree of enhancement and hyper-hypometabolism on PET-CT.

**KEY WORDS:** Chordoma, head and neck, children

**EdE-55****Extralaryngeal Spread of Laryngeal Cancer: Patterns and Imaging Appearance**

Baugnon, K. L.·Hudgins, P. A.·Beitler, J. J.

Emory University  
Atlanta, GA

**PURPOSE**

The extension of laryngeal cancer beyond the confines of the larynx (extralaryngeal spread of tumor) upstages the tumor to T4a, as does cartilage penetration, as described in the most recent American Joint Committee on Cancer (AJCC), 7th edition, staging system for advanced laryngeal cancer. Old conventional teaching promoted laryngectomy for any T4a disease. However, with advances in combined modality chemotherapy and radiation protocols, now even patients with early T4a disease often are being treated with laryngeal conservation therapies, with similar oncologic and laryngeal preservation results. Thus, while in earlier years, prior diagnostic consideration focused on cartilage involvement, one of the factors which now seems to be more clinically important in determining outcomes, and ultimately initial treatment regimen (laryngeal conservation versus laryngectomy) is the extent of extralaryngeal spread of tumor. Therefore, it is very important for the neuroradiologist to become familiar with the different patterns and appearance of extralaryngeal spread of tumor on CT and MRI. This pictorial essay will highlight the imaging appearance of the different paths of extralaryngeal tumor spread.

**APPROACH/METHODS**

Staging CT, PET, and MRI scans of patients with advanced stage laryngeal cancer undergoing laryngectomy were reviewed. The normal laryngeal anatomy, along with possible routes and patterns of extralaryngeal spread of tumor are reviewed, with images demonstrating those paths. The differences between imaging modalities (particularly CT and MRI) are highlighted.

**FINDINGS/DISCUSSION**

The different routes of extralaryngeal extension of laryngeal cancer include superior extension to the base of tongue, through the thyrohyoid membrane, through the thyroid notch, direct anterior penetration through the thyroid cartilage, posterior extension through the thyroarytenoid space, or to the hypopharynx, and inferior extension through the cricothyroid membrane, or through the conus elasticus and then through the cricoid or tracheal cartilage. Extralaryngeal tumor can be seen invading the adjacent strap muscles, thyroid gland, base of tongue, hypopharynx, or deep neck soft tissues/spaces. Tumors can be extralaryngeal with or without cartilage involvement.

**SUMMARY/CONCLUSION**

With new innovations in treatment regimens for advanced laryngeal cancer, it is becoming increasingly more important to detect extralaryngeal extension of tumor. The neuroradiologist should be very familiar

with the different potential patterns of extralaryngeal extension of tumor, as well as the potential pitfalls in detection of extralaryngeal tumor. MR imaging can occasionally be helpful in the detection of extralaryngeal tumor spread.

**KEY WORDS:** Larynx, cancer, staging

**EdE-56****Desmoid Type Fibromatosis in the Head and Neck: Imaging Characteristics with Pathologic Correlation**

Kim, J.<sup>1</sup>·Park, S.<sup>2</sup>·Seo, H.<sup>3</sup>·Choi, S.<sup>1</sup>·Sohn, C.<sup>1</sup>·Yoon, T.<sup>1</sup>·Rhym, J.<sup>1</sup>

<sup>1</sup>Seoul National University Hospital, Seoul, KOREA, REPUBLIC OF, <sup>2</sup>Boramae Hospital, Seoul, KOREA, REPUBLIC OF, <sup>3</sup>Seoul National University GangNam Hospital, Seoul, KOREA, REPUBLIC OF

**PURPOSE**

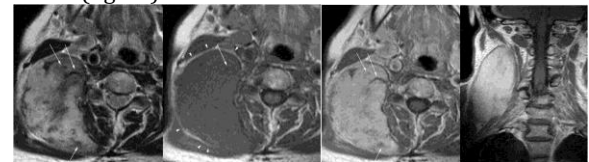
In the head and neck region, desmoid type fibromatosis is an uncommon tumor and the imaging features still have not been well described. The purpose of this study was to investigate imaging features with their pathologic correlation of desmoids type fibromatosis in this area.

**APPROACH/METHODS**

CT and MR images of 9 consecutive patients (5 women and 4 men; age range, 2-72 years; mean age, 28 years) with desmoid type fibromatosis in the head and neck were evaluated retrospectively, focusing on lesion location, size, shape, presence of split-fat sign, CT attenuation, signal intensity and enhancement characteristics on MR with their pathologic correlation.

**FINDINGS/DISCUSSION**

Desmoid type fibromatosis involved perivertebral space (n = 5) and carotid space (n = 1) in six adult patients. In three pediatric patients, it primarily involved submandibular space (n = 2) and masticator space (n = 1) with frequent invasion to the adjacent spaces (3/3). With a mean greatest dimension of 5.8 cm, elongated shape (7/9) and split-fat sign (8/9) were the common features of the desmoid type fibromatosis. They showed iso (3/7) or high (3/7) attenuation on postcontrast CT, high signal intensity (6/9) on T2-weighted image, iso signal intensity (8/9) on T1-weighted image, and strong MR enhancement (8/9). Characteristic nonenhancing low signal intensity bands (8/9) on all MR sequences were well correlated with the heavily collagenized bands (figure).

**SUMMARY/CONCLUSION**

Desmoid type fibromatosis in the head and neck frequently involves perivertebral space in adult. Along with various common imaging features, it shows

characteristic nonenhancing low signal intensity bands on MR images.

**KEY WORDS:** Fibromatosis, desmoid

#### EdE-57

### Molecular and Genetic Basis of Head and Neck Cancer

Belden, C. J.<sup>1</sup>•Andoh, H.<sup>2</sup>•Pastel, D. A.<sup>1</sup>

<sup>1</sup>Dartmouth-Hitchcock Medical Center, Lebanon, NH,

<sup>2</sup>Dartmouth Medical School, Hanover, NH

#### PURPOSE

Recent work has begun to unravel the specific molecular and genetic changes that underlie the development of squamous cell cancer of the head and neck. It is becoming more evident that head and neck cancer is a heterogeneous disease, and that different molecular and genetic changes are reflected in the varied response to treatment, prognosis, and likely imaging appearance.

#### APPROACH/METHODS

We will review the current understanding of the genetic and molecular changes that occur in squamous cell cancer of the head and neck using a pictorial approach, with a particular focus on how these changes influence biologic behavior, response to treatment, and prognosis.

#### FINDINGS/DISCUSSION

Head and neck cancer is the end result of progressive molecular and genetic changes in squamous epithelium. Exposure to environmental mutagens such as tobacco and betel nut, as well as the human papillomavirus (HPV), result in changes that create or exacerbate existing genomic instability. Common genetic alterations involve the p53 tumor suppression pathway (p16, p53), the receptor tyrosine kinase (RTK)/phosphatase and tensin homolog (PTEN)/phosphatidylinositol 3-kinase (PI3K) cell proliferation signaling pathway (EGFR, PTEN), as well as alterations in expression of genes related to angiogenesis and maintenance of the extracellular matrix. Human papillomavirus is known to disrupt the function of the p53 and retinoblastoma (Rb) tumor suppression pathways, resulting in an effect similar to p53 mutations, but different gene expression signature. Recent advances in treatment have focused on the use of drugs specifically targeted to the molecular changes in the patient's individual tumor, with some success.

#### SUMMARY/CONCLUSION

Understanding the underlying genetic and molecular changes found in head and neck cancer is becoming increasingly important as the role of these changes in the varied biologic behavior and treatment response is becoming clear.

**KEY WORDS:** Cancer, genetics, molecular

#### EdE-58

### Laryngeal Trauma: Common Findings and Imaging Pearls

Desai, H.•Lorenzo, G.•Hudgins, P.

Emory University School of Medicine

Atlanta, GA

#### PURPOSE

Laryngeal trauma is a rare injury, occurring in less than 1% of all trauma victims. Laryngeal injuries may be relatively subtle if not specifically sought. Cervical spine CT, frequently obtained in the trauma victim, includes the larynx, and laryngeal injuries can be overlooked if the neuroradiologist is not aware of range of imaging appearances. The purpose of this educational exhibit is to display the wide variety of traumatic laryngeal injuries and highlight the clinical significance with respect to acute airway management and voice function and quality.

#### APPROACH/METHODS

Computed tomographic (CT) images of laryngeal injuries were identified retrospectively and classified as cartilage fracture, cartilage dislocation, mucosal tear, submucosal hematoma, and injuries to the recurrent laryngeal nerve. Conventional CT images and 3D reformation of the airway in both adults and pediatric were reviewed and are the basis of this educational exhibit.

#### FINDINGS/DISCUSSION

The larynx is a complex, three dimensional, variably ossified structure responsible for maintaining the airway, protecting against aspiration and phonation. Availability of high spatial resolution multidetector CT scanners in emergency radiology departments has enabled rapid acquisition and multiplanar evaluation of laryngeal trauma. We identified cartilage fracture, cartilage dislocation, mucosal tear, and submucosal hematoma in our group of trauma patients.

#### SUMMARY/CONCLUSION

Larynx trauma can result in life threatening injury to the airway in the acute setting and impaired voice production if not diagnosed promptly. Accurate interpretation of laryngeal trauma CT findings can significantly affect airway management in the acute setting and can be used as a "roadmap" for planning surgical repair. The various imaging appearances of rare but critically important laryngeal injuries will be presented.

**KEY WORDS:** Trauma, larynx



**EdE-59****Dysphagia: Causes Outside of the "Food Pipe"**

Patel, S.·Patel, N.·Schmalfuss, I.

University of Florida  
Gainesville, FL

**PURPOSE**

Dysphagia is defined as the "subjective awareness of swallowing difficulty during passage of a liquid or solid bolus from the mouth to the stomach." Therefore, patients with dysphagia primarily undergo evaluation of the esophagus and upper aerodigestive tract with endoscopy, barium swallow studies and/or neck CT examinations in search for a lesion in the "food pipe". Many other disease processes that are not related directly to structural mucosal lesions of the upper aerodigestive tract and esophagus can result in dysphagia. The goal of this educational exhibit is to widen the spectrum of differential diagnostic considerations in the workup of patients with dysphagia by focusing on benign and malignant nonmucosal disease processes.

**APPROACH/METHODS**

Reflux and masses arising from the mucosa of the upper aerodigestive tract and esophagus including the gastric cardia are the most causes of dysphagia. Therefore, it is not surprising that radiologists interpreting imaging studies of patients with dysphagia primarily focus upon the "food pipe". However, lesions resulting in dysphagia can occur in a variety of places close or even remote of the "food pipe" such as the brain, skull base, spine and vasculature. A structured approach will be utilized to outline the different nonmucosal causes of dysphagia ranging from normal anatomical variations, functional abnormalities to benign and malignant lesions outside of the "food pipe" based on lesion location.

**FINDINGS/DISCUSSION**

The anatomy of the swallowing process will be discussed including functional components and neuronal contributions. Different disease processes causing dysphagia will be presented based on their location: Intracranial causes of dysphagia: e.g. brainstem masses and stroke, vascular compression of nerves, cranial nerve tumors, glomus tumors. Skull base lesions causing dysphagia: mets, lymphoma etc. Oropharyngeal causes of dysphagia: nasopharyngeal reflux secondary to insufficient closure of the nasopharynx by the soft palate, Eagle syndrome, retropharyngeal space abscess, retropharyngeal masses, Zenker's etc., goiter or other extrinsic masses. Spinal and paraspinal causes of dysphagia: diskitis, cervical osteophytes etc. Esophageal and periesophageal causes of dysphagia: vascular slings and rings, achalasia/scleroderma.

**SUMMARY/CONCLUSION**

As radiologists, we utilize modalities such as fluoroscopy and various other barium studies to evaluate the upper digestive tract, but there are a variety of both benign and malignant causes of

dysphagia that are nonmucosal in etiology. Understanding the disease process will allow radiologists to better evaluate patients with dysphagia and exclude both mucosal and nonmucosal causes.

**KEY WORDS:** Dysphagia

**EdE-60****Expected Findings and Complications of Radiotherapy in Head and Neck Imaging: A Pictorial Essay**

Agarwal, A.·Vijay, K.·Sabat, S.·Maller, V.

Penn State Milton S. Hershey Medical Center  
Hershey, PA

**PURPOSE**

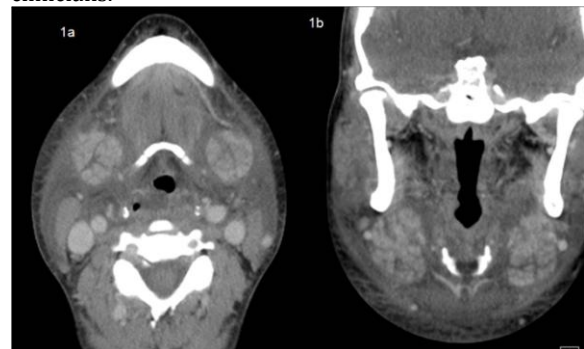
1. To review the imaging findings of expected changes and complications after radiation to the neck. 2. To discuss the imaging findings and tools helpful in demarcating tumor recurrence from posttreatment changes.

**APPROACH/METHODS**

Most common indication for neck imaging at our institution is tumor staging and followup. We retrospectively selected cases from our teaching file to review the expected postradiation changes in the neck along with the common complications, in treated patients with head and neck cancers.

**FINDINGS/DISCUSSION**

Squamous cell carcinoma of the head and neck occurs in approximately 40,000 patients annually in the United States and often is treated with radiation therapy. Radiologic studies are obtained following treatment for head and neck malignancies to assess for recurrent tumor, posttreatment changes (Fig 1 a,b), and associated complications. Radiation treatment creates a difficult clinical picture for oncologists, head and neck surgeons, neuroradiologists, and neuropathologists. As posttreatment imaging studies often are discussed at radiology/pathology working conferences, knowledge of the imaging appearance of radiation-associated changes in the head and neck and the terminology used by neuroradiologists may not only aid in interpretation of the pathologic specimen, but also assist in communications with neuroradiologists and referring clinicians.



**SUMMARY/CONCLUSION**

Understanding the normal evolution of changes in the irradiated neck facilitates evaluation of response to treatment and detection of persistent or recurrent tumor and also enables early detection of radiation complications.

**KEY WORDS:** Radiotherapy, head, neck

**EdE-61**

### **Role of Imaging in Thyroid Disease: Radiology, Nuclear Medicine, Laboratory Evaluation and Biopsy**

Hancock, S.-Alleman, A.

Oklahoma University Health Sciences Center  
Oklahoma City, OK

**PURPOSE**

Concisely summarize the current role of imaging and fine needle aspiration in the workup and management of diffuse thyroid disease and nodules.

**APPROACH/METHODS**

Discussions regarding the workup and management of thyroid disorders and nodules are widespread across several medical disciplines (Otolaryngology, Endocrinology, Oncology, etc.). Even within the radiology literature and practice, the practicing neuroradiologist may not routinely perform fine needle biopsy or interpret nuclear medicine studies or thyroid ultrasound. This exhibit is designed to concisely summarize the relevant issues and controversies in thyroid management with emphasis on the role of imaging. The exhibit is richly illustrated with radiologic images from pathologically proven clinical cases.

**FINDINGS/DISCUSSION**

Since the workup and management of thyroid disorders crosses several radiologic, medical and surgical specialties, it is easy to become lost in the diffuse body of literature, especially when the neuroradiologist may not routinely encounter all of the relevant disciplines. As guidelines have some variations and regional practice patterns result in varied approaches to thyroid disorders, it is helpful to review the commonalities in management recommendations.

**SUMMARY/CONCLUSION**

Familiarity with the full spectrum of imaging options available for thyroid disease workup and management makes the practicing neuroradiologist a valuable asset on the clinical team.

**KEY WORDS:** Thyroid

**EdE-62**

### **Juvenile Nasopharyngeal Angiofibroma: Review of Imaging Findings and Endovascular Preoperative Embolization Strategies**

Hanna, M. F.-Pride, G. L.

University of Texas Southwestern Medical Center  
Dallas, TX

**PURPOSE**

Juvenile nasopharyngeal angiofibroma (JNA) is an uncommon benign nasopharyngeal tumor arising at the superior margin of the sphenopalatine foramen that almost exclusively occurs in adolescent males. Presenting symptoms commonly include nasal obstruction and epistaxis, but approximately 20% of patients have evidence of skull base invasion at the time of diagnosis. Neuroradiologists play a crucial role in the multidisciplinary evaluation and treatment of patients with JNA. CT and MR imaging, while allowing a relatively specific noninvasive diagnosis, also assume primary importance in staging these lesions for treatment planning. Diagnostic catheter angiography defines vascular supply and potential routes of preoperative embolization, an intervention shown to significantly reduce intraoperative bleeding during surgical resection. Our purpose is to review the characteristic imaging findings in patients with JNA, discuss pertinent neurovascular anatomy and to illustrate the various endovascular approaches to preoperative embolization.

**APPROACH/METHODS**

We reviewed the imaging findings, pathology reports and hospital treatment records in 10 patients harboring JNA referred to our institution for evaluation and preoperative embolization from 2006 through the beginning of 2011. The diagnostic imaging studies reviewed included magnetic resonance imaging (MRI), computed tomography (CT) and digital subtraction catheter-based diagnostic angiographic studies. Illustrative cases are included to highlight the various diagnostic imaging findings, relevant neurovascular anatomy and to demonstrate the various endovascular strategies for preoperative embolization.

**FINDINGS/DISCUSSION**

All patients were male adolescents presenting with epistaxis and/or nasal obstruction. The tumors invariably arose within the nasal cavity or nasopharynx and involved neighboring structures. Tumor staging based on imaging demonstrated one stage IA, two stage IB, three stage IIA, two stage IIB, one stage IIC and one stage IIIA lesions. General cross-sectional imaging findings common to CT and MRI included a strongly enhancing, highly vascular nasopharyngeal soft tissue mass centered within the posterior nasopharynx in the region of the sphenopalatine foramen. Variable degrees of extension into the nasal cavity, into adjacent foramina or into the intracranial space were seen. Specific CT findings included marked contrast enhancement and widening/expansion of the sphenopalatine foramen and nearby skull base

foramina and fissures with involvement of the pterygopalatine fossa. Bony erosion of the nearby osseous structures at the base of the skull was seen. Specific MRI findings included T1 and T2 heterogeneous intermediate signal with multiple flow voids representing enlarged vessels as well as diffuse intense postcontrast enhancement. Angiographic findings included supply by branches of the internal maxillary artery (sphenopalatine and descending palatine branches) and ascending pharyngeal artery. Additional vessels were recruited with tumor spread. An early tumor blush was present during the arterial phase. Endovascular treatment involved the use of polyvinyl alcohol particles ranging from 150-500 microns in size. Significant devascularization of the tumor was accomplished in all cases with no significant complications relating to the embolization procedure. All patients underwent successful total or subtotal resection of their tumor after embolization.

#### **SUMMARY/CONCLUSION**

Juvenile nasopharyngeal angiofibromas have characteristic imaging findings on CT and MR, allowing relatively specific diagnosis and accurate pretreatment staging. Preoperative endovascular embolization is a valuable treatment adjunct.

**KEY WORDS:** Juvenile nasopharyngeal angiofibroma, preoperative, embolization

#### **EdE-63**

##### **Nasal Obstructing Lesions: Spectrum of Conditions from Congenital to Acquired**

Javed, K.-Castillo, M.

University of North Carolina at Chapel Hill  
Chapel Hill, NC

#### **PURPOSE**

Our purpose is to present the various conditions that can result in nasal obstruction with a review of their anatomy, embryology, pathology, and imaging features. We will address common and rare lesions.

#### **APPROACH/METHODS**

We searched our teaching database for cases of nasal pathology and from it all available CT and MRI studies were reviewed and those that best illustrate the findings were chosen. Clinical histories were reviewed for pertinent background information. We performed a literature review for the important clinical, therapeutic, and prognostic features of each condition.

#### **FINDINGS/DISCUSSION**

The nasal passages can be obstructed by a variety of conditions. The differential can be narrowed based on the patient's age. Congenital lesions have typical imaging characteristics and knowledge of anatomy and embryology helps in reaching a diagnosis. In the newborn, bilateral lesions (choanal atresia, pyriform aperture stenosis, bilateral nasolacrimal mucocoeles, encephaloceles) result in respiratory distress while unilateral lesions present later in life. Early and middle

age lesions include polyps and infectious or inflammatory processes such as polyposis, allergic fungal sinusitis, Wegener, sarcoid, solitary polyp, but cancers also are involved and include juvenile angiofibroma, inverted papilloma, benign mixed tumor, nerve sheath tumor, melanoma, and undifferentiated carcinoma. Later in life, tumors predominate and include inverted papilloma, non-Hodgkin's lymphoma, melanoma, squamous cell cancer, esthesioneuroblastoma, adenocarcinoma, plasmacytoma. Osseous destruction helps for further categorize the lesions.

#### **SUMMARY/CONCLUSION**

A variety of conditions can cause nasal obstruction. Taking age into consideration with an understanding of the anatomy and categorizing whether or not there is osseous destruction helps to make the diagnosis.

**KEY WORDS:** Nasal, obstruction

#### **EdE-64**

##### **Respiratory Epithelial Adenomatous Hamartomas and Sinonasal Polyposis: Significance of Olfactory Clefts Widening**

Ahmed, M.-Hawley, K.-Sindwani, R.

Cleveland Clinic Foundation  
Cleveland, OH

#### **PURPOSE**

Respiratory epithelial adenomatoid hamartoma (REAH) is a benign glandular proliferation with ciliated epithelium located in the sinonasal cavities. It was originally described in 1995 and since then has been published only as small case series. Respiratory epithelial adenomatoid hamartoma can present as an isolated polypoid lesion commonly originating from the olfactory cleft (OC), or found in association with an inflammatory process, most commonly sinonasal polyposis (SNP). It also can present adjacent to malignancy or inverted papilloma. Interestingly, Lima et al has shown OC widening as a marker of REAH. We aim to present the current understanding of REAH with emphasis on its imaging features, specifically, widening of the olfactory clefts and pseudotumoral appearance.

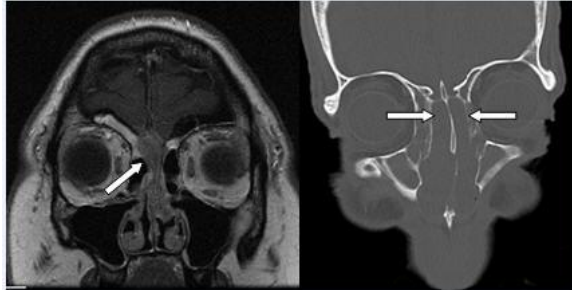
#### **APPROACH/METHODS**

Review of the limited available literature on REAH. Retrospective clinical and imaging review of all those cases in our institution with histologic evidence of REAH. We present the various radiographic findings seen with REAH. This includes CT and MRI studies performed on patients with both isolated and concurrent disease. Additionally, our study focused on the widening of opacified olfactory clefts in isolated, concurrent (with SNP) and control cases.

#### **FINDINGS/DISCUSSION**

Currently, there is an evolving understanding of REAH. The isolated cases may present as polyps or incidental pseudotumors on imaging. The concurrent cases are not identified specifically on clinical exam or imaging, as

they have been diagnosed only after pathologic review. Olfactory cleft opacification is nonspecific and sometimes a transient finding. Associated widening of the OCs suggest the diagnosis of REAH. The authors showed the correlation of OC widening to histologic diagnosis of REAH in both isolated and concurrent cases. Few cases had MRI studies, occasionally demonstrating T2 hypointense masses and even skull base erosion mimicking a neoplasm.



#### SUMMARY/CONCLUSION

Respiratory epithelial adenomatoid hamartoma is an interesting histologic diagnosis with isolated or concurrent presentations with SNP. Widening and opacification of bilateral olfactory cleft is a reliable marker of REAH.

**KEY WORDS:** Sinonasal, hamartoma, olfactory

#### EdE-65

##### Radiologic Workup of Vertigo

Massini, T. C.<sup>1</sup>Schmalfuss, I. M.<sup>2,1</sup>

<sup>1</sup>University of Florida, Gainesville, FL, <sup>2</sup>North Florida/South Georgia VA Medical Center, Gainesville, FL

#### PURPOSE

True vertigo, a whirling sensation of oneself or the surrounding environment, has numerous etiologies, and many patients undergo imaging evaluation to exclude structural pathology. Some of the most common causes include benign positional vertigo (BPV) and Meniere's disease. While BPV is a clinical diagnosis, Meniere's is often a diagnosis of exclusion. Consequently, many temporal bone CTs and posterior fossa MRIs will be negative. Since some of the disease entities manifest with subtle imaging findings, the radiologist may struggle to call a study negative with high degree of confidence. We present a structured approach for evaluation of patients with vertigo including both common and more rare conditions.

#### APPROACH/METHODS

Internal auditory canal (IAC) or cerebellopontine angle masses are the most common structural causes of vertigo and usually are recognized easily by radiologists. However, a comprehensive search pattern should include the entire vestibular system including the vestibulo-ocular and vestibulospinal pathways and their vascular supply.

#### FINDINGS/DISCUSSION

**Peripheral vestibular system:** Inner ear lesions may be primary or secondary. Primary entities include labyrinthitis, bony dehiscence of the semicircular canals, otosclerosis, and endolymphatic sac tumors. Late Paget's disease may involve the otic capsule. Most common secondary lesions are cholesteatomas and metastatic disease. Langerhan's cell histiocytosis, glomus tympanicum or jugulare and large chondrosarcomas are less likely. Otitis media may extend into the inner ear but usually is clinically suspected. **Central vestibular system:** Cisternal/canalicular portion of cranial nerve VIII: These segments are affected most commonly by schwannomas, followed by arachnoid cysts, meningiomas, epidermoid cysts, or metastatic disease. Leptomenigeal disease, hemosiderosis, and infectious neuritis are encountered less commonly. Tortuous vessels (anterior inferior cerebellar or basilar artery) can compress cranial nerve VIII at its root entry zone or in the IAC. Benign bony expansion causing compression of the canalicular segment rarely is seen. Brainstem: The most common entities are demyelinating and ischemic diseases involving the vestibulocochlear nuclei and/or fascicular fibers. Malignancies and vascular malformations including cavernous hemangiomas are less common. Neurodegenerative disorders such as mult system atrophy are less likely and typically associated with other more clinically apparent symptoms. Cerebellar: Metastases and infarctions are the most common causes, with cerebellar degeneration related to substance abuse or paraneoplastic syndrome less commonly encountered. **Vestibulospinal pathways:** Chronic "cervical vertigo", brought on by change in neck position, may be related to cord compression and lack of proprioception input to the central vestibular system. High cervical disease including os odontoideum or basilar invagination can affect this pathway. **Extra-cranial vascular system:** Subclavian steal and vertebral artery dissection are well known causes of vertigo. Vertebral artery compression related to degenerative changes, especially in the facet joints, are common but less known causes. Rarely, redirection of flow related to an arteriovenous malformation may reduce brainstem or spinal cord perfusion.

#### SUMMARY/CONCLUSION

An anatomically-based approach including the entire vestibular system from peripheral to central, the vestibulospinal pathway, and supplying vasculature should increase reporting accuracy and confidence for cross-sectional imaging of patients with vertigo.

**KEY WORDS:** Vertigo

#### EdE-66

##### MR Image Findings of Temporomandibular Joint Dysfunction

Kakimoto, N.·Tsujimoto, T.·Kataoka, M.·Tomita, S.·Shimamoto, H.·Murakami, S.·Furukawa, S.

Osaka University Graduate School of Dentistry  
Suita, Osaka, JAPAN

**PURPOSE**

The purpose of this exhibit is to illustrate MR findings of temporomandibular joint (TMJ) dysfunction and present a systematic approach for evaluating MR findings of TMJ. This area is quite familiar to the oral surgeon and the dentist but the general radiologists often feel insecure about the anatomy and terminology. This educational exhibit will present a systematic step-by-step approach to dictate TMJ MR findings.

**APPROACH/METHODS**

This exhibit is based on high quality MR imaging studies of TMJ dysfunction patients with clinical collations. Temporomandibular joint MR images included proton density and T2-weighted images in the oblique-sagittal and coronal plane in closed and opened mouth position. This exhibit illustrated disk position in closed and opened mouth position, disk shape, joint effusion, bone change, and bone edema of TMJ on MRI.

**FINDINGS/DISCUSSION**

The disk position included normal superior, partial anterior disk displacement with reduction, partial anterior disk displacement without reduction, anterior disk displacement with reduction, anterior disk displacement without reduction, medial disk displacement, and lateral disk displacement. The disk shape included biconcave, biplanar, hemiconvex, thickening of the posterior band, biconvex, and folded morphology. The joint effusion included none or minimal, moderate, marked, and extensive joint fluid in superior or inferior joint spaces. The bone change included erosion, deformity, and marginal proliferation findings as osteoarthritis. The bone edema showed in mandibular condyle. The definitions and illustrations of these findings will be presented.

**SUMMARY/CONCLUSION**

This education exhibit will illustrate how to report MR imaging of TMJ specifically related to various image findings.

**KEY WORDS:** TMJ, MR imaging, dysfunction

**EdE-066a**

### **Evaluation of the Axial versus Sagittal Diameters of the Optic Nerve and Optic Nerve Sheath Using Isovolumetric Multiplanar 3 T MR Imaging**

Riascos, R.<sup>1</sup>Chiu, A.<sup>1</sup>Kramer, L.<sup>2</sup>Sargasyan, A.<sup>3</sup>

<sup>1</sup>The University of Texas Medical Branch, Galveston, TX,

<sup>2</sup>The University of Texas Health Science Center at Houston, Houston, TX, <sup>3</sup>Wyle Laboratories, Houston, TX

**PURPOSE**

The optic nerve sheath diameter (ONSD), optic nerve diameter (OND), and ONSD/OND ratio have been used in the past to assess patients of elevated intracranial pressure (EICP). These studies have shown that perioptic cerebrospinal fluid (CSF) distention can be a sign of EICP or pseudotumor cerebri. However, no difference in sagittal versus axial measurements has been described previously in these studies. Additionally,

these studies did not use isovolumetric multiplanar 3 T MRI, which confers a higher resolution and lends to more accurate measurements. We use OND and ONSD as parameters of an EICP study and detected statistically significant inconsistencies with the measurements in the axial versus sagittal planes. This has compelled us to compare these measurements with direct coronal imaging and measurements in order to clarify the initial findings. The purpose of this exhibit is to evaluate physical dimensions of the optic nerve and the optic nerve sheath using isovolumetric multiplanar 3 T MRI. To determine optic nerve and optic nerve sheath shape in this unique patient population. The measurement of the optic nerve and optic nerve sheath is one of the parameters used to evaluate elevated intracranial pressure (EICP) in healthy patients.

**APPROACH/METHODS**

MR images are obtained with Siemens 3 T Verio MRI scanner. In total, 62 eyes scanned among 21 healthy patients (18 male, 3 female, mean age 46.9 years). Six patients (12 orbits) were scanned again to serve as a comparison. Isovolumetric T2 sagittal and axial scans were completed on all 50 orbits. Isovolumetric coronal scans were done in 22 eyes. The OND and ONSD are assessed 3 mm behind the eye fovea, perpendicular to optic nerve orientation.

**FINDINGS/DISCUSSION**

Axial and sagittal measurements of the OND and ONSD are well correlated ( $r = 0.929$ ). Optic nerve diameter and ONSD sagittal measurements are consistently greater than axial measurements in the same orbit (statistically significant by paired two tailed t-test). Average ONDs and ONSDs are longer in vertical direction than in horizontal direction by 0.2 - 0.3 mm.

**SUMMARY/CONCLUSION**

Isovolumetric multiplanar MRI demonstrates a statistically significant increase of sagittal diameters as compared to axial diameters of the optic nerve sheath. The optic nerve diameters should be measured in a different plane (i.e., coronal plane) due to a higher internal consistency in ONSD measurements as compared to OND measurements. The optic nerve sheath is not completely circular. There is more elongation along the vertical axis suggesting a misshaping of the optic nerve and sheath in this group of subjects. These differences in diameter should be taken into consideration when assessing the optic nerve sheath to optic nerve ratio for detection of elevated intracranial pressure.

**KEY WORDS:** Increased intracranial pressure, optic nerve sheath, intracranial hypertension

**Monday, April 23 –  
Wednesday, April 25  
6:30 AM - 9:00 PM**

**Thursday, April 26  
6:30 AM – 3:00 PM  
Rhineland**

**Education Exhibits (EdE) 67 – 72**

**EdE - Interventional**

**Note: A missing printed number indicates an abstract has been withdrawn.**

#### **EdE-67**

##### **Current Concepts in Endovascular Management of Posterior Circulation Aneurysm: “Moving beyond the Coil”**

Zampolin, R.·Erdfarb, A.·Farinhas, J.·Bello, J.·Brook, A.·Pasquale, D.

Montefiore Medical Center  
Bronx, NY

#### **PURPOSE**

A comprehensive review of current neurointerventional techniques and clinical management of patients with posterior circulation aneurysms.

#### **APPROACH/METHODS**

A case-based, pictorial and retrospective review of clinical experience treating 50 cases of posterior circulation aneurysms over 5 years at a tertiary referral center. A literature review is integrated to develop best practices when facing difficult management decisions in both ruptured and unruptured posterior circulation aneurysms.

#### **FINDINGS/DISCUSSION**

Aneurysms of the posterior circulation account for 5-10% of intracranial aneurysms (Peerless et al 1985). According to the most comprehensive clinical study of unruptured aneurysms (The International Study of Unruptured Intracranial Aneurysms - ISUIA, phase II 2003) the highest rupture rate was reported in patients with larger aneurysms located in the posterior circulation, and a previous history of SAH. The 5-year cumulative rupture rate for patients without a history of SAH and a posterior circulation aneurysm measuring between 7 and 12 mm was 14.5%. This is significantly higher than the reported rupture risk of anterior circulation aneurysms of 1% per year. Posterior circulation aneurysms are considered difficult to treat surgically secondary to limited surgical access to the

posterior fossa and high risk of postsurgical morbidity. While surgical treatment of posterior circulation aneurysms is limited, advances in technology and endovascular techniques drive the progress of endovascular methods. We present index cases to demonstrate and review the spectrum of posterior circulation aneurysms including: basilar terminus, vertebrobasilar junction, fusiform vertebral and basilar, PICA, AICA, and SCA aneurysms and the principle methods used to treat them endovascularly, including: coil embolization, balloon- and stent-assisted coil embolization, parent vessel sacrifice with liquid embolic agents such as precipitated polymers like Onyx and adhesive agents such as glue, flow diversion and combinations of endovascular and surgical treatment. For each case we will describe the nature of the aneurysm, evaluate the possible treatment options and explain how and why a specific technique was chosen for treatment. Finally, the pre and posttreatment clinical management strategy is discussed.

#### **SUMMARY/CONCLUSION**

Endovascular treatment of posterior circulation aneurysms is safe and efficacious, often providing a treatment option with lower risk when compared to surgical intervention, which is particularly difficult within the posterior fossa. Endovascular coil embolization remains the first choice of treatment for the majority of posterior circulation aneurysms. The ability to use detachable coils in complex and atypical aneurysms has increased with the development of balloon- and stent-assisted coil embolization techniques allowing for the treatment of previously noncoilable aneurysms. New techniques have expanded the armamentarium of the neurointerventionalist regarding the treatment of small peripheral posterior circulation aneurysm such as flow assisted liquid embolic agents like onyx and glue. Such agents allow for acute management of patients presenting with posterior fossa hemorrhage from distal AICA, PICA and SCA aneurysms (often atypical, nonsaccular aneurysms) which are beyond the reach of coils and difficult to find surgically. An interdisciplinary approach to management including the neurointerventionalist, neurosurgeon and neurointensivist is essential for optimal clinical outcome.

**KEY WORDS:** Posterior circulation aneurysm, neurointerventional, endovascular treatment

#### **EdE-68**

##### **Classification of Intracranial Aneurysms Based upon Biological Changes in Their Mural Wall and Their Treatment Options**

Muir, S.·Alvarez, H.·Castillo, M.

University of North Carolina Chapel Hill  
Chapel Hill, NC

#### **PURPOSE**

Intracranial aneurysms (IA) most often are classified according to their location and size. It is becoming evident that underlying biological mural changes may



be a better method to further an understanding of IA formation and behavior. We propose a classification of IA according to the biological changes in their walls, as reflected on imaging studies, and suggest treatment options.

#### APPROACH/METHODS

Classical descriptions group IA according to size, morphology, location and underlying aberrant hemodynamic factors. Such a classification fails to consider the arterial wall and its molecular environment as a key to understanding the primary etiologies and clinical behaviors of IA. Identification on MRI, MRA, CT, CTA and/or DSA of chronic or acute mural dissections, mural hematomas, inflammation, distal territorial infarction, and/or dysplasia provide means of constructing a new classification: A. Saccular: stable (unruptured) and prerule. B. Dissecting: giant, serpentine, fusiform, focal. C. Segmental dysplasia and dolichosegments. D. Infectious: bacteria, virus. E. Flow-related: associated to AVM and tumors.

#### FINDINGS/DISCUSSION

Saccular aneurysms correspond to traditional berry IA. Abnormal hemodynamics, smoking, alcohol consumption, aging, and familial (genetic) predisposition are factors in their formation. IA  $\leq 10$  mm in size seldom rupture (0.05%/year) thus, their treatment is of questionable value as procedural complication rates are higher than complications from spontaneous IA rupture. Inflammation (experimentally identified with iron-tagged macrophages), apoptosis, and necrosis of their walls lead to rupture. Dissecting IA result from endothelial and internal elastic lamina disruption with blood penetrating into the aneurysmal wall. Depending on their etiology and associated mural changes, intracranial dissections result in giant IA (chronic focal dissection without mural hematoma or thrombosis), fusiform IA (large segmental chronic dissection without intramural hematoma) that can be associated with immune deficiencies or atherosclerotic disease, partially thrombosed IA and serpentine IA (chronic dissecting IA with mural thrombosis and multiples mural hematomas) which grow by recurrent wall hemorrhage and inflammation, both visible on MRI and CT. Focal acute dissections, from adventitial rupture or subintimal dissection, result in IA that are frequently posterior fossa in location. Infectious IA demonstrate mural inflammation and necrosis that may be seen as edema on MRI. Flow-related IA are located in vessels supplying cerebral AVMs and are due to vascular remodeling of the IA wall in response to local high flow. Segmental dysplasias or dolichoectatic segments IA correspond to arterial dilations without atheroma changes. Thus, according to our classification, we suggest the following treatment regime: A. Saccular: stable (observation) and prerule (coil embolization, clipping). B. Dissections: coil embolization, flow diverter devices, wall stabilizing drugs, surgical resection. C. Dysplasia: observation, stents. D. Infectious: antibiotics, aneurysm or parent vessels occlusion with adhesives. E. Flow related: associated-lesion occlusion, selective embolization.

#### SUMMARY/CONCLUSION

IA are a heterogeneous group of lesions expressing different dysfunctions of varied biologic processes related to the vascular wall, i.e., remodeling, inflammation, apoptosis, and necrosis. Identification of morphologic changes in their walls allows us to recognize their different types and choose the best therapeutic approach for each type.

**KEY WORDS:** Intracranial aneurysms, aneurysm classification, aneurysm treatment

#### EdE-69

#### Effects of Hyper-Early Endovascular Treatment within 12 Hours on Clinical Outcome of Patients with Ruptured Intracranial Aneurysm

Consoli, A.·Grazzini, G.·Scarpini, G.·Renieri, L.·Nappini, S.·Mangiafico, S.

Careggi University Hospital  
Firenze, ITALY

#### PURPOSE

The ISAT study (1) provides most of the available information regarding the indications, the type of treatment and the medium and long-term clinical outcome. Although the conclusions of this study encouraging the endovascular treatment of ruptured intracranial aneurysms, only few studies focused on critical issues of this approach such as the effects of the timing of treatment on outcome. The aim of our study is to evaluate the effects of the hyper-early timing of treatment and of pretreatment and procedure-related variables on clinical outcome of patients with ruptured intracranial aneurysms.

#### APPROACH/METHODS

Five hundred ten patients (167 male, 343 female; mean age 56.45 years) with 557 ruptured intracranial aneurysms were treated at our institution from January 2000 to January 2011 immediately after their admission. Total population was divided into three groups: patients treated within 12 hours (Hyper-early, Group A), between 12-48 hours (early treatment, Group B) and after 48 hours (delayed treatment, Group C). A statistical analysis was carried out for global population. Further analyses were performed excluding patients with severe clinical grades (Hunt&Hess grades 4-5) and considering also a cut-off of 24 hours for early treatment in order to compare our series with data reported in literature.

#### FINDINGS/DISCUSSION

Two hundred thirty-four patients (46%) were included in group A, 172 (34%) in group B and 104 (20%) in group C. Pretreatment variables (Hunt&Hess and Fisher grades, older age) and procedure-related ones (ischemic/hemorrhagic complications) showed a significant correlation with worse clinical outcomes. The hyper-early treatment showed no correlation with good clinical outcomes. The incidence of periprocedural complications was not significant between the three

groups. 1.2% of pretreatment rebleedings were observed.

#### SUMMARY/CONCLUSION

Although Hyper-early endovascular treatment of ruptured intracranial aneurysm is not statistically correlated with good clinical outcomes, it may determine the reduction of incidence of pretreatment spontaneous rebleedings without being associated to a higher risk of intraprocedural complications.

**KEY WORDS:** Intracranial aneurysms, endovascular treatment, timing of treatment

#### EdE-70

#### Extracranial Head and Neck Vascular Malformations: Diagnosis and Management

Tuna, I. S. Maheshwari, M. Moe, D. Johnson, C. M. Chandra, T. Singh, S. Kelly, T. G. Segall, H. D.

Medical College of Wisconsin  
Wauwatosa, WI

#### PURPOSE

To describe and review imaging findings of various extracranial head and neck vascular malformations and discuss the interventional treatment strategies for these lesions.

#### APPROACH/METHODS

This exhibit will illustrate the characteristic imaging findings of vascular anomalies in the head and neck region. Vascular anomalies are divided into vascular tumors and vascular malformations which include slow flow malformations (capillary malformations, venous malformations, lymphatic malformations and their combinations) and high flow malformations (arteriovenous fistula and arteriovenous malformations). Complex malformations also are seen in several syndromes including Klippel-Trenaunay Syndrome, PHACE syndrome, etc. Cases from author's database will be used for illustration.

#### FINDINGS/DISCUSSION

A review of clinical manifestations, characteristic imaging findings and interventional treatment strategies in cases of head and neck vascular anomalies will be presented with pre and posttreatment imaging features. Ultrasonography and MRI are the mainstay in diagnosis of these malformations. CT scan and catheter angiography may occasionally be needed for diagnosis and treatment planning. Various imaging findings and main treatment options are listed in the attached table.

IMAGING VASCULAR LESIONS	Ultrasound		MRI		Treatment
	Gray scale	Doppler	T1, T2 and STIR	Post contrast	
Hemangioma	Hyperechoic or hypoechoic	High flow or arterial waveforms	T2 bright soft tissue mass, flow voids, no edema	Diffuse homogenous and avid enhancement.	Propranolol, Steroids, IFN, Vincristine
Kaposiform Hemangioendothelioma	Ill defined, heterogeneous soft tissue mass	High flow or arterial waveforms	Infiltrative, perilesional edema	Homogenous or heterogeneous enhancement	Steroids, Chemotherapy
Venous Malformations	Compressible, Anechoic channels with phleboliths	No flow or low velocity venous waveforms	T2 bright, septated cystic or tubular lesions with phleboliths	Delayed enhancement	Sclerotherapy
Lymphatic Malformation	Large cystic spaces with septa, echogenic debris within	No internal flow, robust vascularity in the septa	T1 shortening and fluid/fluid levels (if prior hemorrhage)	Septations may enhance	Sclerotherapy (Doxycycline / Bleomycin)
AVM/AV Fistula	Dilated vessels, nidus in AVM	High flow, arterial waveforms	Nidus in AVM, hypertrophied arteries and dilated veins	Mainly flow voids, some vascular enhancement	Embolization; AVM: Transarterial, AVF: Transvenous

#### SUMMARY/CONCLUSION

Head and neck vascular malformations are common in pediatric population. Understanding the characteristic imaging findings and clinical presentation is essential in evaluating the vascular malformations. Interventional procedures are generally the preferred treatment modality, either alone or in association with surgery in majority of these cases.

**KEY WORDS:** Vascular malformations, head and neck, interventional radiology

#### EdE-71

#### Endovascular Treatment of Carotid Cavernous Sinus Fistula: A Systematic Review

Korkmaz, B. Kocak, B. Kizilkilic, O. Kocer, N. Islak, C.

Cerrahpasa Medical School  
Istanbul, TURKEY

#### PURPOSE

The purpose of this review is to give detailed anatomical classification schemes that have described CCFs according to etiology, hemodynamic features, or the angiographic arterial architecture and endovascular treatment options.

#### APPROACH/METHODS

Several classification schemes have described CCFs according to etiology (traumatic or spontaneous), hemodynamic features (high versus low flow), or the angiographic arterial architecture (direct or indirect). The angiographic classification provides the certain angioarchitecture of the lesion on which a therapeutic strategy can be planned. The clinical features of CCF are related to their size, exact location, duration, adequacy and route of venous drainage and the presence of arterial/venous collaterals. The classic presentation for a direct, high flow CCF is the sudden development of Dandy's triad: exophthalmos, bruit, and conjunctival chemosis.

#### FINDINGS/DISCUSSION

Cerebral angiography is the gold standard for the definitive diagnosis, classification, and planning of endovascular intervention in CCFs. The treatment modalities include conservative management, which consists of medical management and manual compression therapy; surgical management; stereotactic radiosurgery and endovascular repair via transarterial or transvenous route. Recent advances in endovascular technology have made a number of different treatment options for CCFs currently available. The ocular symptoms resolve rapidly following successful treatment.

#### SUMMARY/CONCLUSION

With advances in interventional neuroendovascular techniques they have become the preferred treatment modality for carotid-cavernous fistulas and favorable long-term outcomes have been achieved. The endovascular approach should be tailored to individual cases according to the type, exact anatomy, and extent

of each fistula. With increasing knowledge about novel endovascular techniques, such as placement of covered stent-grafts, higher success rates can be achieved with preservation of the ICA even in case of urgency.

#### EdE-72

##### **Fluoroscopic Flat Panel Detectors versus Image Intensifier Technology for Neuroangiography**

Javadi, P.·Tummala, N.·Nazarian, J.·Rao, P.·Blackham, K. A.  
University Hospital Case Medical Center  
Cleveland, OH

#### **PURPOSE**

In the past decade, fluoroscopic flat panel detector technology (FPD) has been replacing the image intensifier/TV system in many neuroangiography suites. The purpose of this educational module is to discuss differences in the two modalities and underscore the advantages and potential pitfalls of FPD technology.

#### **APPROACH/METHODS**

Systemic review of literature on FPD fluoroscopy technology was performed with focus on how this modality compares to the II/TV system in terms of image quality and achieving ALARA (as low as reasonably achievable) radiation dose.

#### **FINDINGS/DISCUSSION**

The II is a large vacuum tube that captures x-ray photons transmitted through the patient and converts them into a light image of sufficient brightness to be seen on a TV camera. After entering the curved input surface of the II, x-rays interact with a layer of phosphor. The light from the phosphor then is absorbed by the photocathode layer of the II, which uses the light energy to emit electrons. The electrons then are accelerated by a high voltage and light is again produced at the output phosphor layer. These photons are directed by optical lenses to a TV camera system. The FPD consists of arrays of individual detector element (DEL) transistors in which the x-ray energy is first converted to light and then to an electronic signal. The DEL consists of a scintillation layer, which usually is composed of cesium iodide. The scintillation layer attenuates incident x-rays and produces light. The amount of light produced is related directly to the amount of x-ray flux that the DEL receives. The FPD produces a digital signal and is not coupled to a TV camera system. The FPD technology for fluoroscopy is becoming popular despite a higher cost compared to conventional II systems. The FPD provides significantly better ergonomics as it does not require a vacuum. Due to major differences in the image acquisition chain, the image quality of FPD technology is more uniform, lacking spatial distortion and less susceptible to artifact common to image intensifiers such as vignetting and flare. Limitations of FPD include degradation of spatial resolution with very large and very small fields of view. Additionally, although it has been postulated that FPD can have a potentially lower radiation dose to patients than the II/TV system, in practice it has become

increasingly evident that factory default settings for FPD may not have the proper balance of patient dose with regards to clinically acceptable image quality. This is a problem not only for FPD, but is a theme common to all digital x-ray technology. As with other digital imaging, with FPD fluoroscopy an increase in radiation dose to improve signal to noise ratio does not cause optically perceivable degradation in image quality and this creates a potential source of increased cumulative radiation dose to patients.

#### **SUMMARY/CONCLUSION**

As the FPD fluoroscopy is gradually replacing the II/TV system, an understanding of the basic physics, and advantages and potential pitfalls of this modality are important to neuroangiographers to optimize effective use and ensure ALARA goals.

**KEY WORDS:** Flat panel detector, radiation exposure, neuroangiography

**Monday, April 23 –  
Wednesday, April 25  
6:30 AM - 9:00 PM**

**Thursday, April 26  
6:30 AM – 3:00 PM  
Rhinelanders**

**Education Exhibits (EdE) 73 – 86**

**EdE 5– Pediatrics**

**Note: A missing printed number indicates an abstract has been withdrawn.**

#### EdE-73

##### **Neuroradiologic Complications of Sickle Cell Disease**

Marquez, J. C.·Medina, F. J.·Castillo, M.·Alvarez, H.  
University of North Carolina at Chapel Hill  
Chapel Hill, NC

#### **PURPOSE**

Our purpose is to present the less common neuroradiologic manifestations and complications found in patients with sickle cell disease (SSD), such as silent and overt brain and spinal cord infarctions, basilar artery ectasia, aneurysms, brain atrophy, vertebral osteomyelitis and infarcts, and extramedullary hematopoiesis, describing their clinical manifestations, pathophysiology, imaging findings, and differential diagnosis. We will emphasize the utility of advanced imaging techniques where appropriate.

**APPROACH/METHODS**

We searched our teaching database for cases of neuroradiologic complications present in patients with SSD. All available CT, MR and angiographic images were reviewed and those that better illustrate the findings were chosen. We also reviewed the available and pertinent literature and based on this, present the clinical, therapeutic, and prognostic implications of the findings.

**FINDINGS/DISCUSSION**

Sickle cell disease is a hereditary recessive autosomal multisystem disorder, which causes formation of an altered hemoglobin leading to abnormally shaped red blood cells. Nervous system complications frequently are encountered in these patients, the most common being vascular occlusive and better known as moyamoya-like disease. Less common neuroradiologic manifestations have been found in patients with sickle cell anemia. Some of these complications are directly related with vasoocclusive events, such as silent and overt brain, spinal cord, and vertebral infarctions. Other indirect secondary findings include basilar artery ectasia, aneurysms, vertebral osteomyelitis, extramedullary hematopoiesis, and ultimately, brain atrophy.

**SUMMARY/CONCLUSION**

The spectrum of neuroimaging findings of SSD is wide and includes vascular and nonvascular complications. The neuroradiologist must be familiar with possible complications present in these patients, which can have important prognostic and therapeutic consequences.

**KEY WORDS:** Sickle cell anemia, complications, diagnostic imaging

**EdE-74****From Cradle to Grave: Neuroimaging Manifestations of Cocaine Abuse**

Mirsky, D. M.<sup>1</sup>•Mohan, S.<sup>2</sup>•Srinivasan, A.<sup>3</sup>•Bello, J. A.<sup>4</sup>

<sup>1</sup>The Children's Hospital of Philadelphia, Philadelphia, PA, <sup>2</sup>Hospital of the University of Pennsylvania, Philadelphia, PA, <sup>3</sup>University of Michigan, Ann Arbor, MI, <sup>4</sup>Montefiore Medical Center, Bronx, NY

**PURPOSE**

Cocaine, an illegal recreational drug, remains in epidemic use worldwide, second only to marijuana. The United States is the world's largest consumer of cocaine, though current use in the United Kingdom and Spain has reached levels equal to that of the U.S. Many adverse central nervous system (CNS) effects as a result of cocaine use, as well as complications in the head and neck have been described in both the pediatric (neonatal) and adult populations. Knowledge of these complications and their characteristic imaging appearances is important for the practicing neuroradiologist as they may be the first to suspect underlying drug abuse. Our goal is to illustrate various CNS and head and neck pathologies associated with cocaine use from their earliest manifestation, related to

in utero exposure, to cerebrovascular complications seen in adulthood.

**APPROACH/METHODS**

Various CNS and head and neck pathologies related to cocaine abuse are reviewed, including: Pediatric/Neonatal: •Intracranial hemorrhage (Germinal matrix, intraventricular, parenchymal), •Perinatal Stroke, •Microcephaly associated with intrauterine growth restriction. Adult: •Hemorrhagic/nonhemorrhagic ischemic stroke, •Intracranial hemorrhage (Parenchymal, subarachnoid, intraventricular), •Vasculitis, •Septic emboli/mycotic aneurysms related to parenteral administration, •Nasal septal perforation.

**FINDINGS/DISCUSSION**

A spectrum of complications related to cocaine abuse is presented in both the perinatal and adult age groups. The pathophysiology underlying the imaging findings is reviewed and discussed.

**SUMMARY/CONCLUSION**

Cocaine remains a popular drug of abuse within the United States and worldwide. Knowledge of its potential complications within perinatal and adult age groups is important, as the neuroradiologist may be the first to suspect underlying drug abuse, and appropriately impact patient management.

**KEY WORDS:** Cocaine

**EdE-75****Imaging of Bithalamic Lesions in the Pediatric Brain: Demystifying a Diagnostic Conundrum**

Khanna, P.<sup>1,2</sup>•Chaturvedi, A.<sup>1,2</sup>•Chaturvedi, A.<sup>1</sup>•Iyer, R.<sup>1,2</sup>•Thapa, M.<sup>1,2</sup>•Ishak, G.<sup>1,2</sup>•Swanson, J.<sup>1,2</sup>•Ferguson, M.<sup>1,2</sup>•Shaw, D.<sup>1,2</sup>

<sup>1</sup>University of Washington School of Medicine, Seattle, WA, <sup>2</sup>Seattle Children's Hospital, Seattle, WA

**PURPOSE**

1. To review the imaging features of bilateral thalamic lesions in children. 2. To discuss differential diagnoses, including metabolic/toxic phenomena, demyelination, infection, vascular lesions and neoplastic entities. 3. To overview additional imaging sequences and techniques useful for determining the etiology of thalamic involvement.

**APPROACH/METHODS**

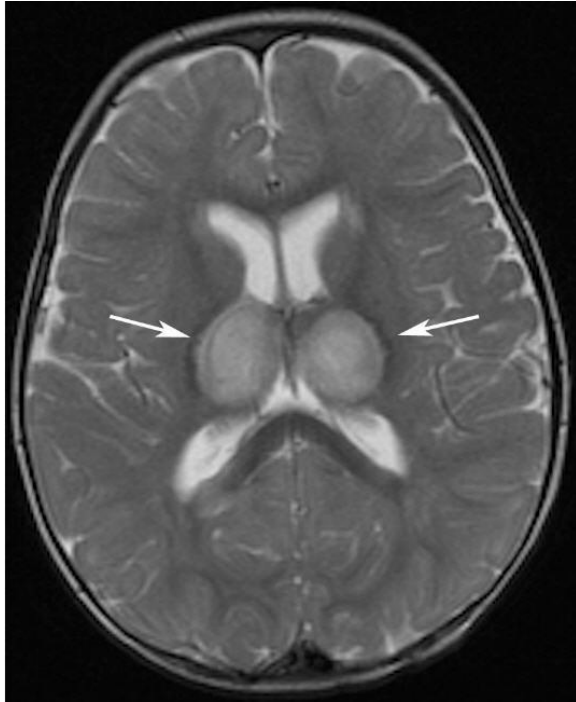
1. Description and classification of abnormal imaging appearances of the thalami. 2. Devising an approach to imaging diagnosis based on patient history, imaging appearances and presence or absence of extra-thalamic involvement. 3. Role of imaging towards formulating a management plan and in subsequent follow up. 4. Artifacts and diagnostic pitfalls were noted.

**FINDINGS/DISCUSSION**

Neuroimaging features of abnormal thalami as encountered in the pediatric population were detailed,

and wherever applicable, the relevance of additional MR imaging sequences and techniques to determine etiology was described.

While there was considerable overlap in imaging appearances, making a precise diagnosis was found to be challenging in difficult cases, and by and large, a stepwise approach was successfully formulated and used to: 1. Diagnose the more emergent conditions and to 2. Devise a management algorithm for the less acute abnormalities.



#### **SUMMARY/CONCLUSION**

Bilateral thalamic lesions occasionally are encountered in pediatric neuroimaging and have a limited differential; a good knowledge base and adequate technique are imperative to tease out the precise diagnosis and institute appropriate management.

**KEY WORDS:** Bilateral thalamic lesions, pediatric neuroimaging, MR imaging

#### **EdE-76**

##### **Congenital Cranial Nerve Abnormalities in Pediatric Patients: An Imaging Review**

Naidu, P. K. • Miller, J. H. • Curran, J. G. • Egelhoff, J. C.

Phoenix Childrens Hospital  
Phoenix, AZ

#### **PURPOSE**

Congenital anomalies of the cranial nerves (CNs) are rare and often associated with syndromes, which manifest with a broad range of clinical presentations and associations. We present the MR imaging of various congenital cranial nerve abnormalities, reviewing the relevant clinical and radiologic associations and pertinent embryology and anatomy.

#### **APPROACH/METHODS**

Our institutional imaging database was reviewed for cases of congenital cranial nerve abnormalities. Imaging from these cases was reviewed along with the medical record to obtain further clinical information.

#### **FINDINGS/DISCUSSION**

Cases of Kallman syndrome, optic nerve hypoplasia both in and outside the setting of septo-optic dysplasia, Duane retraction syndrome, facial and vestibulocochlear nerve agenesis, as well as the more obscure entity of hypoglossal nerve aplasia were identified, with pertinent images shown for each condition. Kallmann syndrome, also known as hypogonadotropic hypogonadism, is due to migration failure of olfactory and GnRH producing neurons from the olfactory placode. As a result, there is hypoplasia or aplasia of the olfactory bulbs and pituitary dysfunction. Optic nerve hypoplasia can occur in isolation but is seen most often in septo-optic dysplasia (deMorsier's syndrome), a heterogeneous group of disorders encompassing absence of the septum pellucidum, optic disk/nerve hypoplasia, and hypopituitarism. Multiple factors have been implicated in its development, from viral infection to fetal alcohol syndrome, with familial forms reported. In contrast to CN I and II, the remainder of cranial nerves have brainstem nuclei. As a consequence of close nuclei proximity, abnormalities of the mid cranial nerves (CN VI, VII, VIII) more likely are found in association. While mouse models have implicated specific genes (Kreisler and the Hoxa family) in analogous entities, other theories purport ischemic insult to the developing rhombencephalon as a potential cause of such cranial nerve abnormalities. CCDDs (congenital cranial dysinnervation disorders) refer to abnormalities of eye, eyelid, or facial musculature movement secondary to cranial nerve abnormalities. These include congenital fibrosis of the extraocular muscles (CFOEM, CN III) as well as Duane retraction syndrome (CN VI) and Moebius syndrome (CN VII).

#### **SUMMARY/CONCLUSION**

Congenital abnormalities of the cranial nerves, while rare, are intriguing entities that allow us to appreciate normal cranial nerve function and imaging appearance, anatomic factors leading to various associations, and the intricacies of neurodevelopment that still are being elucidated.

**KEY WORDS:** Cranial nerves

#### **EdE-77**

##### **Many "Faces" of Fetal Teratomas: Neuroimaging and Pathologic Correlation**

Mirsky, D. M. • Vossough, A. • Zarnow, D. M. • Kahlek, N. • Schwartz, E. S.

The Children's Hospital of Philadelphia  
Philadelphia, PA

#### **PURPOSE**

Teratomas are germ cell tumors (GCTs), the majority of which are composed of tissues derived from all three

germ layers. Theories regarding the origin of teratomas include development from misplaced primordial germ cells or abnormal development of a conjoined twin. Germ cell tumors of the nervous system typically arise in midline locations such as the sacrococcygeal region and intracranially, with GCTs of the head and neck being the exception and typically occurring off midline in the cervical region. Sacrococcygeal teratomas are the most frequently recognized fetal neoplasm with cervical being the second most common site. Over the last two decades, MRI has become a standard tool in the armamentarium of neuroradiologists in working up suspected fetal teratomas, providing a supplement to sonography in helping to guide diagnosis and treatment. Advances in fetal medicine and surgery have further solidified MRI's role in the field of prenatal imaging. Our goal is to illustrate the various presentations of teratomas in fetal life utilizing MRI and provide pathologic and postnatal *in vivo* correlates.

#### APPROACH/METHODS

Various fetal presentation of CNS and head and neck teratomas are reviewed, including: • Sacrococcygeal (Types 1-4), • Cervical, • Intracranial, • Orbital.

#### FINDINGS/DISCUSSION

A spectrum of fetal teratomas in the CNS and head and neck is illustrated utilizing MR imaging, with an emphasis on the additional detail that MRI can provide over sonography. Gross pathologic and postnatal *in vivo* correlation are provided.



#### SUMMARY/CONCLUSION

Teratoma is the most common neoplasm of fetal life, with CNS and head and neck teratomas being the most common location. MR imaging serves as a valuable supplement to sonography in the accurate depiction of fetal teratomas, helping to delineate disease extent and prognosis, and thus guide therapy.

**KEY WORDS:** Teratoma, fetal

#### EdE-78

##### Neuroimaging of Pediatric Intracranial Infections

Poretti, A.<sup>1</sup>•Nickerson, J. P.<sup>2</sup>•Richner, B.<sup>3</sup>•Santy, K.<sup>3</sup>•Lequin, M. H.<sup>4</sup>•Filippi, C. G.<sup>2</sup>•Huisman, T. A. G.<sup>1</sup>

<sup>1</sup>The Johns Hopkins Medical School, Baltimore, MD, <sup>2</sup>The University of Vermont/Fletcher Allen Healthcare, Burlington, VT, <sup>3</sup>Jayavarman VII Kantha Bopha Hospitals, Siem Reap, CAMBODIA, <sup>4</sup>Sophia Children's Hospital, Erasmus University Medical Center, Rotterdam, NETHERLANDS

#### PURPOSE

Infection of the central nervous system (CNS) in children is a relatively uncommon occurrence. However, given the rapidity with which infections of the CNS may progress and the potentially devastating short and long term neurologic sequelae of undiagnosed disease, accurate and timely diagnosis is of the utmost importance. We aim to review the imaging strategies and findings of the most frequent pediatric bacterial, viral, fungal, and parasitic infections of the CNS.

#### APPROACH/METHODS

We reviewed our pediatric MRI database searching for pediatric intracranial infections.

#### FINDINGS/DISCUSSION

We present a review with selected case histories to illustrate the neuroimaging findings of the most



common bacterial (e.g., meningitis, cerebritis, abscesses, subdural empyema, and tuberculosis infections), viral (e.g., congenital TORCH (Toxoplasmosis, Other infections, Rubella, Cyromegalovirus, Herpes simplex virus) infections as well as other viral infections such as the congenital HIV infections or the Japanese encephalitis), fungal, and parasitic infections of the pediatric CNS and discuss how both conventional and advanced MR modalities may allow to correctly diagnose the different types of infections.

#### **SUMMARY/CONCLUSION**

Antibiotics revolutionized the successful treatment of bacterial CNS infections and in many cases appropriate and early treatment may limit mortality and morbidity. Neuroimaging enhanced the noninvasive diagnosis of CNS infections and their complications. As such, early and correct recognition of the imaging findings is of crucial importance to guide treatment. While many findings may be nonspecific, a thorough understanding and familiarity of the patterns of abnormality as seen on neuroimaging in conjunction with the clinical presentation and demographic characteristics of the child may help establish or narrow the differential diagnosis and be of outmost importance to the clinicians caring for these patients. High end multimodality imaging including diffusion-weighted/tensor imaging and  $^1\text{H}$  magnetic resonance spectroscopy are essential to narrow differential diagnosis.

**KEY WORDS:** Intracranial infections, brain, pediatric

#### **EdE-79**

##### **Hypoxic-Ischemic Encephalopathy: Review of Excitotoxic Mechanisms of Injury with Neuroimaging Correlation**

Bahl, M.·Belden, C. J.·Hum, B. A.·Pastel, D. A.

Dartmouth-Hitchcock Medical Center  
Lebanon, NH

#### **PURPOSE**

Perinatal hypoxic-ischemic encephalopathy (HIE), which occurs in one to three per 1000 live full-term births, can lead to devastating and permanent neuropsychological impairment. Excitotoxicity, which refers to an excessive activation of neuronal amino acid receptors, has emerged as an important mechanism of injury in HIE. The purpose of this education exhibit is to provide a comprehensive review of these excitotoxic mechanisms and to demonstrate how familiarity with these pathways can enhance understanding of the neuroimaging findings of HIE.

#### **APPROACH/METHODS**

We will review the current literature on excitotoxic mechanisms and describe the pathways that lead to injury in HIE. Instructive magnetic resonance imaging cases of HIE that illustrate the pattern of injury based on excitatory circuitry will be discussed.

#### **FINDINGS/DISCUSSION**

During a hypoxic-ischemic event, the uptake of glutamate, the primary excitatory neurotransmitter in the central nervous system, is impaired, resulting in high levels of glutamate at the synaptic cleft and thus excitatory amino acid receptor overactivation. These receptors include N-methyl-D-aspartate (NMDA), amino-3-hydroxy-5-methyl-4 isoxazole propionate (AMPA), and kainate receptors; NMDA receptors are permeable to sodium and calcium ions, and AMPA and kainate receptors are permeable to sodium ions. The influx of sodium ions, in addition to the failure of energy-dependent enzymes such as sodium/potassium ATPase, leads to cytotoxic edema and cell death. Activation of the NMDA receptor, which results in intracellular calcium ion accumulation, and other pathways through which excitatory amino acids cause secondary calcium ion uptake also lead to cell death. Specific neuroimaging patterns of injury that are observed after a hypoxic-ischemic event can be explained largely by this excitatory circuitry. For example, a central pattern of injury to the deep gray matter and the perirolandic cortex, which contain the highest concentration of NMDA receptors, often is observed in HIE. Despite the fact that there are few synapses in white matter, receptors for glutamate also play an important role in the pathogenesis of white matter injury in the immature brain.

#### **SUMMARY/CONCLUSION**

Knowledge of the excitotoxic mechanisms that lead to injury in HIE provides a framework for the neuroradiologist to better understand and interpret the pattern of injury on magnetic resonance imaging.

**KEY WORDS:** Hypoxic-ischemic encephalopathy, excitotoxicity

#### **EdE-80**

##### **Posttransplant Lymphoproliferative Disorder in the Pediatric Head and Neck**

Mirsky, D. M.·Vossough, A.

The Children's Hospital of Philadelphia  
Philadelphia, PA

#### **PURPOSE**

Posttransplant lymphoproliferative disorders (PTLD) reflect a spectrum of abnormal lymphoid proliferation in transplant patients that range from hyperplasia to malignant lymphoid proliferation. While the frequency of PTLD is slightly higher in children than it is in adults, its overall incidence by most estimates is around 2% of transplant recipients; increased with transplants that require more immunosuppression. Within this rare cohort, head and neck involvement accounts for only 25% of affected patients. Given the low incidence of pediatric head and neck PTLD and protean clinical and imaging manifestations, a high index of suspicion for PTLD is required to make an accurate diagnosis of this disease which is universally fatal if not treated. Our goal is to illustrate our experience with the varied imaging presentations of pediatric head and neck PTLD utilizing CT and MRI. Awareness of the differing imaging

patterns in this rare but lethal diagnosis may lead to early diagnosis and potentially disease regression.

#### **APPROACH/METHODS**

Various pediatric presentations of pediatric head and neck PTLD are reviewed, including: • Cervical, • Face, • Temporal bone, • Cavernous sinus. Imaging features of these examples of PTLD will be portrayed. Differential diagnostic considerations will be reviewed. Imaging pearls and pitfalls relevant to the medical and surgical management of these lesions will be presented.

#### **FINDINGS/DISCUSSION**

A spectrum of head and neck PTLD in the pediatric population is illustrated utilizing CT and MR imaging.

#### **SUMMARY/CONCLUSION**

Posttransplant lymphoproliferative disorders are a rare but potentially lethal spectrum of diseases in chronically immunosuppressed transplant patients. Accurate diagnosis of the disease requires a high index of suspicion given the low incidence and varied clinical and imaging presentations. Awareness of the differing radiologic manifestations of pediatric head and neck PTLD may lead to early diagnosis and potentially disease regression.

**KEY WORDS:** Posttransplant lymphoproliferative disorder, pediatric, head and neck

#### **EdE-81**

##### **Pediatric Posterior Fossa Tumors: The Use of MR Imaging to Make a Specific Diagnosis**

Byott, S. • Wright, N. • Shabani, A. • Tang, V. • Stivaros, S.

Royal Manchester Children's Hospital  
Manchester, UNITED KINGDOM

#### **PURPOSE**

Posterior fossa tumors account for 54-70% of childhood brain tumors. The most common differentials include pilocytic astrocytoma, medulloblastoma and ependymoma. MR imaging is crucial to diagnosis, staging and identification of complications such as hydrocephalus and hemorrhage. Soft tissue characteristics alongside tumor location, invasion and clinical history facilitate radiologic discrimination prior to surgery. However, there is significant clinical equipoise with regards to the imaging appearances in a significant proportion of cases making definite diagnosis difficult. The aim of this study is to evaluate the radiologic findings alongside histologic findings and develop a systematic imaging model for diagnosing posterior fossa tumors.

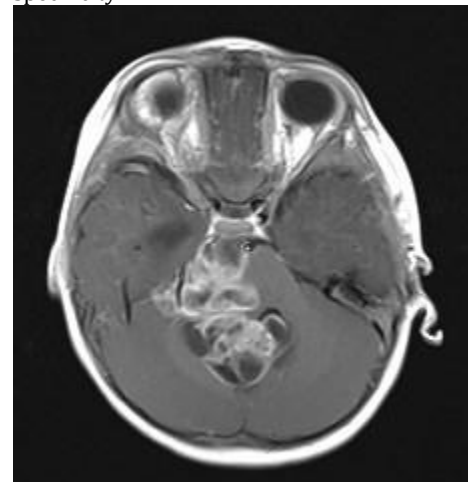
#### **APPROACH/METHODS**

We retrospectively reviewed all patients imaged at our institution over a 30-month period from January 2008 to June 2011. Thirty-six patients presented with posterior fossa tumors. They had standard tumor protocol MR scans including axial T2, coronal FLAIR, sagittal T1, T1 volume inversion recovery, diffusion imaging and postgadolinium T1-weighted in all planes.

MR reports, clinical history and histology data were collated from patient notes. MR appearances were analyzed and correlated with histology.

#### **FINDINGS/DISCUSSION**

There were 36 patients. Fifteen had pilocytic astrocytomas, 12 had medulloblastomas and 8 had ependymomas. One patient had an atypical teratoid rhabdoid tumor (ATRT). Twenty-eight patients were imaged at our institution. In 22/28 patients the radiologist correctly identified the tumor as the first differential when compared to histology findings. By tumor type it was as follows: Pilocytic astrocytoma 10/12, medulloblastoma 5/8, ependymoma 6/7 and ATRT 1/1. Six patients had discordant radiologic and histologic diagnoses. In 4 of the 6, they were mixed solid/cystic tumors and 2 medulloblastomas were felt to more closely resemble pilocytic astrocytomas, while 2 astrocytomas were felt to be cystic ependymomas/medulloblastomas. One medulloblastoma, invading the foramen of Luschka, was thought to be an ependymoma, while one brainstem ependymoma was thought to be a glioma. Traditional features alongside more advanced MR characteristics were correlated with histology, and used to build an imaging model allowing systematic discrimination of tumor types, and greater diagnostic specificity.



#### **SUMMARY/CONCLUSION**

Posterior fossa tumors have a highly variable radiologic appearance with a significant crossover between tissue types. Systematic morphologic evaluation using T1/T2 signal, cyst:solid ratio, DWI signal and contrast signal allow for an accurate diagnosis in the majority of patients. This can be used to guide treatment and aid with counselling patients and families prior to treatment.

**KEY WORDS:** Medulloblastoma, ependymoma, pilocytic astrocytoma

#### **EdE-82**

##### **Susceptibility-Weighted Imaging of the Pediatric Brain**

Poretti, A.<sup>1</sup> • Verschuuren, S.<sup>2</sup> • Meoded, A.<sup>1</sup> • Buerki, S.<sup>3</sup> • Lequin, M. H.<sup>2</sup> • Huisman, T. A.<sup>1</sup> • Huisman, T. A. G.<sup>1</sup>

<sup>1</sup>The Johns Hopkins Medical School, Baltimore, MD,  
<sup>2</sup>Sophia Children's Hospital, Erasmus University Medical Center, Rotterdam, NETHERLANDS, <sup>3</sup>University Children's Hospital of Berne, Berne, SWITZERLAND

#### **PURPOSE**

Susceptibility-weighted imaging (SWI) is a high-spatial-resolution 3D gradient-echo MR technique accentuating the magnetic properties of substances such as blood, blood products, nonheme iron, and calcifications, which disturb the magnetic field with resultant focal signal loss. To increase the signal loss caused by susceptibility effect, a mask is created by a postprocessing that enhances the phase differences between susceptibility artifacts and surrounding tissues. A minimal intensity projection (mIP) is created and facilitates differentiation between veins and micro-hemorrhages. The susceptibility difference between oxygenated and deoxygenated hemoglobin leads to a phase difference between regions with deoxygenated blood and surrounding tissues. We discuss the application of SWI in pediatric neuroradiology by demonstrating how SWI may improve the diagnosis of various frequent and less frequent pediatric neurologic disorders.

#### **APPROACH/METHODS**

We reviewed our pediatric MRI database searching for SWI studies.

#### **FINDINGS/DISCUSSION**

We present a review with selected case histories to illustrate the SWI signal characteristics and the additional value of SWI compared to other MR sequences in a variety of common and less common pediatric brain pathologies including traumatic brain injury, brain death, vascular malformations, neurocutaneous disorders, stroke, hemorrhages, sinovenous thrombosis, hemiplegic migraine, brain tumors, infections, and neurometabolic/neurodegenerative disorders. Additionally, we discuss pitfalls in the interpretation of SWI in the neonatal and pediatric age groups.

#### **SUMMARY/CONCLUSION**

The high susceptibility for blood products including iron depositions as well as for calcifications makes SWI an important additional sequence for the sensitive and specific diagnostic work up of a variety of pediatric brain pathologies. Compared to conventional MRI sequences, including 2D T2\*-weighted sequences, SWI may show lesions in better detail or with higher sensitivity. Familiarity with the pediatric SWI signal variance resulting from different levels of blood oxygenation is essential to prevent misdiagnosis.

**KEY WORDS:** Susceptibility-weighted imaging, brain, pediatric

#### **EdE-83**

#### **Pearls and Pitfalls in Pediatric Neuroimaging**

Rosa, S. D. • Mankad, K.

Great Ormond Street Hospital for Children NHS Trust  
 London, UNITED KINGDOM

#### **PURPOSE**

The interpretation of pediatric neuroradiologic imaging often induces a great deal of anxiety in those unfamiliar with it, especially the resident. This educational exhibit tackles common diagnostic pitfalls in pediatric neuroimaging that are encountered by radiology residents and considers appropriate diagnostic strategies for them. This ultimately aims to increase residents' confidence in making a diagnosis and differentiating between potentially similar imaging appearances.

#### **APPROACH/METHODS**

Common diagnostic pitfalls in pediatric neuroimaging are considered identifying specific review areas, techniques and key imaging features that help differentiate pathologies. This will be done in a succinct manner with key points (pearls) emphasized to identify differences. Focused and dynamic graphical transitions will utilize the electronic medium to highlight key points. The cases and pitfalls were predominately encountered at our institution which is a tertiary referral center for neuropediatrics in the United Kingdom and are part of our continued commitment to training.

#### **FINDINGS/DISCUSSION**

A number of diagnostic pitfalls are considered. Normal development and variants which may be confused for pathology such as the variation of the myelination pattern in under two years olds on MRI are considered. The differentiation of hydrocephalus, atrophy and subdural hemorrhages from benign enlargement of the subarachnoid spaces in infants also is considered. With radiology residents more commonly seeing elderly brain with volume loss the appearance of the pediatric and especially the adolescent brain often calls into question the issue of cerebral swelling - we consider strategies for differentiating the normal pediatric brain from the swollen brain. The basics of differentiating stroke from other pathologies that may mimic stroke [e.g., tumors and Posterior Reversible Encephalopathy Syndrome (PRES)], especially against the history of an acute neurologic deficit, are considered. The key features that may help differentiate multiple sclerosis (MS) from an acute disseminated encephalomyelitis (ADEM) are considered. Venous thrombosis often can cause much anxiety, especially out of hours, and examinations such as magnetic resonance venography are often prone to artifacts or arachnoid granulations potentially being confused for thrombus. We consider key ways to differentiate venous thrombus from potential mimics. The resident often struggles to differentiate the prominent canal from a syrinx and we consider the basic strategies for differentiating the two and the appropriate follow up. We consider the differentiation of a low cord from the tethered spinal cord syndrome and its characteristic imaging features. The diagnosis of nonaccidental injury (NAI) (both over and under diagnosis) can be a source of major anxiety for residents and the key mimics of this are considered

along with pearls on how to differentiate the mimics from NAI.

#### **SUMMARY/CONCLUSION**

Pediatric neuroimaging is initially often a daunting task for the resident. By considering common diagnostic pitfalls and associated diagnostic strategies this exhibit adds confidence to residents' diagnostic skills and helps to decrease errors.

**KEY WORDS:** Pediatrics, educational, review

#### **EdE-84**

### **Pictorial Review of Petrous Apex Lesions in the Pediatric Population**

Radhakrishnan, R.<sup>1</sup>•Son, H. J.<sup>2</sup>•Koch, B. L.<sup>2</sup>

<sup>1</sup>University of Cincinnati College of Medicine, Cincinnati, OH, <sup>2</sup>Cincinnati Children's Hospital Medical Center, Cincinnati, OH

#### **PURPOSE**

Lesions involving the petrous apex are uncommon in children, and the differential diagnosis is significantly different than lesions in a similar location in adults. The purpose of this study is to identify the varied causes of imaging abnormalities involving the petrous apex in children.

#### **APPROACH/METHODS**

Retrospective review of imaging and clinical data to find representative examples of common and uncommon lesions involving the petrous apex of the temporal bone in children.

#### **FINDINGS/DISCUSSION**

A wide spectrum of lesions may occur in the petrous apex, including benign and malignant etiologies. Similar to adults, entities include developmental variants such as asymmetric aeration of the petrous apex air cells, trapped fluid, nonaggressive inflammatory/infectious disease or more aggressive inflammatory disease such as petrous apicitis. Cholesteatoma and cholesterol granulomas isolated to the petrous apex in children are rare. Fairly unique to children are neoplastic lesions such as rhabdomyosarcoma and other sarcomas, as well as Langerhan cell histiocytosis and fibro-osseous disease.

#### **SUMMARY/CONCLUSION**

Imaging studies, especially computed tomography (CT) and magnetic resonance (MR), in association with the clinical presentation, are very important and both helpful to better characterize lesions involving the petrous apex and plan clinical management of these lesions.

**KEY WORDS:** Langerhan cell histiocytosis, rhabdomyosarcoma, fatty marrow

#### **EdE-85**

### **Pediatric Spine Disorders: Appearance on Steady-State Free Precession MR Images**

Soares, B. P.<sup>1</sup>•Barkovich, A. J.<sup>1</sup>•MacKenzie, J. D.<sup>1</sup>•Martin, K.<sup>2</sup>

<sup>1</sup>University of California San Francisco, San Francisco, CA, <sup>2</sup>Children's Hospital and Research Center, Oakland, CA

#### **PURPOSE**

The purpose of our exhibit is to demonstrate the exquisite depiction of pediatric spinal pathology using high-resolution steady-state free precession (SSFP) imaging.

#### **APPROACH/METHODS**

In this exhibit, we illustrate the utility of SSFP imaging to depict a number of pediatric spinal pathologies. The SSFP technique relies on a gradient-echo pulse sequence with small flip angles and short relaxation times to create a nonzero steady state between pulse repetitions for both the longitudinal and transverse relaxation values of the interrogated tissues. Given its characteristic strong signal in tissues that have a high T2/T1 ratio, SSFP sequences provide excellent contrast resolution between cerebrospinal fluid and soft tissues including cranial and spinal nerves and the spinal cord. Furthermore, volumetric acquisition and submillimetric spatial resolution allow reconstructions in multiple planes for high detail imaging of the pediatric neuroaxis. Steady-state free precession is a fundamental sequence in the imaging evaluation of the cranial nerves, cerebellopontine angle and inner ear structures.<sup>(2)</sup> It is also a valuable tool in the diagnostic and postoperative evaluation of hydrocephalus due to its capability of delineating the ventricular walls, detecting abnormal cystic structures and assessing the patency of ventriculostomies. Although not routinely employed in spinal imaging, SSFP has been utilized in a variety of adult spinal disorders, as well as in the preoperative evaluation of neonates with lumbosacral lipoma and myeloschisis.

#### **FINDINGS/DISCUSSION**

Steady-state free precession sequences improve the anatomical characterization and potentially increase diagnostic confidence in a wide spectrum of congenital, neoplastic and traumatic disorders of the pediatric spine including arachnoid cysts, dermoid and epidermoid tumors, tethered cord and filum terminale abnormalities, dermal sinus tracts, drop metastases and nerve root avulsions.

#### **SUMMARY/CONCLUSION**

The high spatial resolution and water/tissue contrast of SSFP imaging provides exquisite anatomical detail for depiction of subtle and complex findings. In addition to the current routine use for evaluation of cranial nerves and hydrocephalus, SSFP may be a helpful adjunct for the evaluation of complex pediatric spine pathology.

**KEY WORDS:** Pediatric spine, congenital anomalies, MR imaging

#### EdE-86

#### Image Lightly: 3DT1 Scotty Dog Reformations for Evaluation of Spondylolysis in the Child with Low Back Pain

Gross Kelly, T. C. • Tuna, I. S. • Kelly, M. • Maheshwari, M. • Walter, K. D. • Quijano, C. • Segall, H.

Wisconsin Children's Hospital  
Brookfield, WI

#### PURPOSE

The aim of this educational exhibit is to demonstrate how MRI may be used as a viable replacement for CT in the evaluation of spondylolysis.

#### APPROACH/METHODS

Sagittal 3DT1-weighted images of the lumbar spine were obtained routinely for the evaluation of children who complained of low back pain. In this exhibit we will demonstrate how 3DT1-weighted images can be reformatted in the sagittal oblique plane to create "Scotty Dog" type reformations, similar to the views constructed from lumbar spine CT studies and oblique lumbar x-ray views. We also will show how the STIR sequence can be used instead of bone scanning for detecting occult stress fractures of the pedicle. The amount of radiation exposure from the limited lower lumbar spine CT scan, lumbar spine x-ray series and nuclear medicine bone scan will be discussed.

#### FINDINGS/DISCUSSION

We have discovered that by constructing MR "Scotty Dog" reformatted images, combined with STIR imaging, we can provide the same information that CT and bone scans can provide.



#### SUMMARY/CONCLUSION

In our quest to minimize radiation to our pediatric patients, the 3DT1 "Scotty Dog" MR reformatted images provide a potentially viable alternative to CT and serial radiography.

**KEY WORDS:** Spondylolysis, Scotty, dog

**Monday, April 23 –  
Wednesday, April 25  
6:30 AM - 9:00 PM**

**Thursday, April 26  
6:30 AM – 3:00 PM  
Rhineland**

**Education Exhibits (EdE) 87 – 98**

EdE - Spine

**Note: A missing printed number indicates an abstract has been withdrawn.**

#### **EdE-87**

##### **Downward Spinal Herniation: A Potentially Dangerous Consequence of Lumbar Puncture below the Level of a Complete Spinal Subarachnoid Block**

Harri, P. A.·Lorenzo, G.·Hwang, S.

Emory University School of Medicine  
Atlanta, GA

#### **PURPOSE**

CT myelography is a critical study for patients with acute myelopathy who cannot undergo urgent MRI of the spine because of implanted defibrillators, cardiac pacers or are not candidates for MRI because of weight restrictions. While the technique and skills needed to perform lumbar puncture and CT myelography still are practiced routinely in many radiology departments throughout the country, the contraindications to performing this study in a patient with suspected complete spinal subarachnoid block are not being taught and difficult to find in the literature in an urgent situation. The purpose of this educational exhibit is to review the literature in respect to the anatomy, pathophysiology and biomechanics of removing cerebral spinal fluid (CSF) and introducing contrast below a complete spinal subarachnoid block.

#### **APPROACH/METHODS**

An extensive literature review on the subject of lumbar puncture below a complete spinal subarachnoid block was performed. The findings are summarized in this educational exhibit.

#### **FINDINGS/DISCUSSION**

When complete spinal subarachnoid block occurs, pressure differentials separate compartments above and below the block. Removal of CSF below a complete subarachnoid block in this setting allows for downward herniation whereas infusion of contrast material in a closed space further increases the pressure gradient.

The risk of neurologic deterioration after removal of CSF below the level of a complete subarachnoid block is 14% in the neurosurgical literature.

#### **SUMMARY/CONCLUSION**

Downward spinal herniation is a potentially dangerous consequence of lumbar puncture below the level of complete spinal subarachnoid block. A step-by-step approach to performing myelography in this challenging patient population is presented.

**KEY WORDS:** Emergent CT myelography, downward spinal herniation, complete spinal subarachnoid block

#### **EdE-88**

##### **Spectrum of CT Findings in Cases of Lumbar and Cervical Pseudarthrosis following Spinal Fusion**

Curnes, J. T.

Greensboro Radiology  
Greensboro, NC

#### **PURPOSE**

To assess the various CT imaging features which reliably indicate pseudarthrosis as a cause for continuing symptoms after cervical and lumbar fusion.

#### **APPROACH/METHODS**

We retrospectively reviewed the CT examinations (with or without myelography) of outpatients studied in our Outpatient Spine Imaging center over the past 12 months in whom pseudarthrosis was a clinical concern.

#### **FINDINGS/DISCUSSION**

The most common signs associated with nonunion were persistent lucency through the interspace, halo surrounding the hardware, fractured hardware, subsidence of the graft or cage, change in device position, and a previously under-recognized sign of pseudarthrosis, vacuum disk phenomenon.

#### **SUMMARY/CONCLUSION**

The exhibit's focus will be a pictorial display of the above findings, as an instructional review of this topic. Particular emphasis will be directed to the high sensitivity and specificity of vacuum disk in a previously fused level as a reliable indicator of pseudarthrosis.

**KEY WORDS:** Spine, pseudarthrosis



**EdE-89****Location, Location, Location: A Pictorial Review of Common Intraspinal Extramedullary Masses with an Emphasis on the Intraspinal Compartmental Anatomy**

Young, M. G.-Lefton, D. R.

St. Luke's-Roosevelt Hospital  
New York, NY

**PURPOSE**

The purpose of this exhibit is to review the anatomy of the intraspinal compartments and provide an imaging overview of common intraspinal extramedullary masses.

**APPROACH/METHODS**

A retrospective review of magnetic resonance (MR) imaging cases from a single institution was performed and pertinent scientific literature was reviewed. Anatomical drawings also were used to clarify the intraspinal compartmental anatomy.

**FINDINGS/DISCUSSION**

Intraspinal extramedullary masses include those found in the intradural-extramedullary and extradural compartments. Intradural-extramedullary masses typically widen the ipsilateral cerebrospinal fluid (CSF) space and narrow the contralateral CSF space. Cerebrospinal fluid usually forms acute angles with the mass and may form a meniscus or "cap" above and below the mass. Extradural masses narrow the CSF spaces on both sides of the cord by displacing the dura and cord together, away from the mass. Cerebrospinal fluid usually creates obtuse angles with the mass. Both intradural-extramedullary and extradural masses may appear to enlarge the spinal cord on either the sagittal or coronal plane but correlation with axial images will confirm their extramedullary location. After a mass has been localized correctly within an intradural-extramedullary or extradural compartment, the MR signal characteristics can be used to differentiate between masses commonly encountered in that compartment. Common masses affecting the intradural-extramedullary compartment include: meningiomas, nerve sheath tumors, arachnoid cysts, epidermoids, and drop/leptomeningeal metastases. Masses encountered in the extradural compartment include: disk material, synovial cysts, abscesses, hematomas, angioliipomas, and neoplasms that have invaded from the adjacent bone.

**SUMMARY/CONCLUSION**

When evaluating an intraspinal extramedullary mass, it is essential to first localize the mass within either the intradural-extramedullary or extradural compartment. The MR signal characteristics of the mass then can be used to further narrow the differential diagnosis.

**KEY WORDS:** Intraspinal, extramedullary, masses

**EdE-90****Time-Resolved MR Angiography of the Spine: Principle, Technique and Clinical Applications**

Datir, A.-Saindane, A.-Dion, J.

Emory University Hospital  
Atlanta, GA

**PURPOSE**

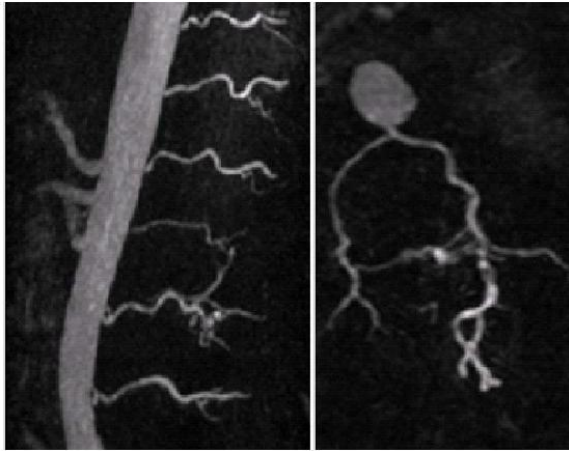
(1) To review the principle and technique of time-resolved magnetic resonance angiography (MRA) in the evaluation of the spine. (2) To discuss the important clinical applications of this technique in the evaluation of common spinal vascular pathologies.

**APPROACH/METHODS**

Noninvasive imaging of spinal vascular disease remains a challenge despite several advances in MRA technique. Conventional spinal digital subtraction angiography (DSA) is the "gold-standard" for diagnosing dural arteriovenous fistula (dAVF) and arteriovenous malformations (AVMs). This is attributed mainly to the higher temporal resolution and individual vessel assessment achieved by conventional spinal DSA. MR angiography techniques such as phase-contrast are sensitive to higher velocity lesions but are usually suboptimal for low velocity lesions. Similarly, time-of-flight MRA and single phase contrast-enhanced MRA provides static lesion anatomy, but fail to assess hemodynamic properties of vascular lesions. In this exhibit we focus on the time-resolved spinal MRA technique for evaluation of various spinal pathologies including AVM, dAVF and spinal tumors.

**FINDINGS/DISCUSSION**

Time-resolved spinal MRA technique combines a rapid multiphase dynamic MRA acquisition with parallel imaging. This technique involves very short time of repetition with partial Fourier transformation, resulting in temporal resolution of 3-6 seconds at submillimeter isotropic spatial resolution. As opposed to "unresolved" MRA techniques, time-resolved MRA allows hemodynamic assessment of the lesion vascularity, including early versus delayed vessel filling and venous drainage. A limitation of the technique is the tradeoff between increasing temporal resolution and loss of spatial resolution for a given signal-to-noise. Foreknowledge of the anatomical spinal levels involved by vascular pathology can provide valuable information preoperatively and preangiographically, potentially decreasing the time and amount of intravenous contrast required at catheter angiography, or facilitating a single stage therapeutic angiographic procedure. We utilize this technique to assess various spinal pathologies, including preangiographic planning for embolization and surgery of dAVF and vascular metastatic lesions of the spine, as well as for postsurgical surveillance for recurrence.



Sagittal maximum intensity projection and axial multiplanar reconstruction of time-resolved MRA demonstrating a spinal dAVF arising with arterial supply from the left L2 posterior radicular artery.

#### **SUMMARY/CONCLUSION**

Time-resolved MRA is an effective and practical approach to image spinal vascular pathologies, in particular spinal dAVF. It provides a definite advantage over other commonly used spinal MRA techniques, especially for the preangiographic and preoperative hemodynamic evaluation of the spinal vascular lesions.

**KEY WORDS:** Time-resolved magnetic resonance angiography, spinal arteriovenous malformation

#### **EdE-91**

##### **Sampling Perfection with Application Optimized Contrast Using Different Flip Angle Evolution Sequences in MR Neurography of the Lumbo-Sacral Plexus**

Del Grande, F.<sup>1</sup>•Thawait, G.<sup>1</sup>•Thakkar, R.<sup>1</sup>•Chalian, M.<sup>1</sup>•Thawait, S.<sup>2</sup>•Chhabra, A.<sup>1</sup>

<sup>1</sup>Johns Hopkins Hospital, Baltimore, MD, <sup>2</sup>Yale University-Bridgeport Hospital, Bridgeport, CT

#### **PURPOSE**

To illustrate the value of 3D spin echo type sequence on 3 T magnetic resonance imaging in the detection, characterization and location of lumbo-sacral (LS) plexus pathologies with relevant case examples.

#### **APPROACH/METHODS**

MR neurography is a growing technique in the diagnoses of plexus pathologies. "Sampling Perfection with Application optimized Contrast using different Flip Angle Evolution" (SPACE) sequence is a 3D isotropic spin echo type sequence with several advantages, such as it has higher signal as well as contrast to noise ratio compared to gradient echo sequences, one can cover large anatomical volume in clinically applicable acquisition time, it uses different flip angles (average 60 degree), and employ longer echo train length which reduces the specific absorption rate (SAR) deposition. Moreover 3D sequence has the advantages of the postprocessing (curved planar, multiplanar and Maximum Intensity Projection reformats), which can be

important in difficult anatomical locations such as the LS plexus due to small size of the nerves and various obliquities, they course through.

#### **FINDINGS/DISCUSSION**

In this exhibit, we will review the technical background of 3D SPACE acquisition technique of the LS plexus. We will illustrate the normal LS plexus 3D anatomy and different pathologies such as traumatic dorsal nerve root ganglia injuries, stretch injuries, branch nerve transections, tumors and tumor-like conditions, such as amyloid, perineuroma, neurocutaneous syndromes, etc.

#### **SUMMARY/CONCLUSION**

Isotropic 3D SPACE sequence is a valuable sequence to add on the standard LS plexus imaging protocol for the diagnosis of various LS pathologies.

**KEY WORDS:** MR neurography, SPACE, lumbo-sacral plexus

#### **EdE-92**

##### **Imaging Features of Sacral Lesions**

Muzzafar, S. • Bourekas, E. C. • Luttrull, M. D. • Mendel, E. • Slone, H.

Ohio State University Medical Center  
Columbus, OH

#### **PURPOSE**

The sacrum is a continuation of the spinal axis but by virtue of its anatomical location and complex embryologic development, a varied spectrum of pathology is seen. The purpose of this pictorial essay is to present the common and unusual pathologic conditions of the sacrum and highlight the pertinent findings. Cross-sectional imaging with CT, MRI and scintigraphy are indispensable in identifying and characterizing lesions in the sacrum. Postprocessing techniques further help in surgical planning when indicated.

#### **APPROACH/METHODS**

Our institutional PACS was used to search for cases with sacral lesions. CT and MRI images were reviewed. The postprocessed 3D images, plain radiographs and PET/CT images also were reviewed in cases where available.

#### **FINDINGS/DISCUSSION**

Insufficiency stress fractures, infectious processes (including osteomyelitis secondary to decubitus ulcers, tuberculosis and epidural abscesses), dural ectasia, Tarlov cysts, Paget disease and fibrous dysplasia were seen in the nonneoplastic group. Primary benign and malignant tumors of the sacrum are rare lesions and account for less than 7% of all spinal tumors. Metastases and myeloma were found to be the most common occurring neoplastic lesions in the sacrum. Other malignant tumors encountered were plasmacytoma/multiple myeloma, lymphoma and primary bone tumors such as chordoma, chondrosarcoma, giant cell tumor and Ewing tumor.

The benign neoplasms included schwannoma, ganglioneuroma and neurofibroma. CT/MRI features of benign neoplasms including the nerve sheath tumors showed smooth well-marginated contours without invasion of the surrounding structures or bony destruction. A soft tissue mass in the sacral ala with smooth sclerotic bony margins was seen in fibrous dysplasia. Thickened altered trabecular pattern involving the sacral body and the ala, with lytic and sclerotic areas were seen in Paget disease. MR imaging showed a nonspecific heterogenous signal on T1/T2-weighted sequences with no soft tissue component. An expansile soft tissue mass with adjacent bony destruction was characteristically seen in chordoma and giant cell tumor. The soft tissue component of the chordoma was predominantly presacral and hyperintense with T2-weighted imaging. Bone destruction was especially marked with the giant cell tumor. The imaging findings in lymphoma characteristically showed T2 hyperintensity with an epidural component causing thecal sac compression and hypermetabolic activity on PET/CT. A destructive lesion of the left hemisacrum with characteristic "rings and arcs" matrix was seen in chondrosarcoma. Ewing tumor showed a large ill-defined soft tissue component destroying the bone and infiltrating the paraspinal muscles, T1 hypointensity, T2 isointensity and minimal enhancement.

#### SUMMARY/CONCLUSION

A unique assortment of pathology is found within the sacrum due to the variety of tissues found in this region; including bone, cartilage at the SI joint, meninges and neural elements. CT and MRI are indispensable in the differentiation of these lesions. Scintigraphy, PET/CT and the new advances in postprocessing techniques further refine the detection, determining the extent and characterization of the lesions and their management.

**KEY WORDS:** CT, MR imaging, sacral lesions

#### EdE-93

#### Enhancing Thickened Nerve Roots of Cauda Equina: A Case-Based Illustration of Some Common and More Unusual Conditions

Mahajan, A.·Lysack, J. T.·Hu, W.·Scott, J. N.

Foot Hills Medical Centre  
Calgary, AB, CANADA

#### PURPOSE

Enhancing thickened nerve roots of the cauda equina is an imaging feature common to diverse disease categories, including inflammatory, infectious, and neoplastic etiologies. The purpose of this exhibit is to illustrate this spectrum of pathologies and ancillary radiologic features that help to narrow the differential diagnosis.

#### APPROACH/METHODS

A retrospective review was undertaken of MRI cases showing enhancement and/or thickening of the nerve

roots of the cauda equina done at our centre during the last 3 years.

#### FINDINGS/DISCUSSION

*CSF disseminated metastases* - 52-year-old female with known breast carcinoma presented with cauda equina syndrome. Imaging revealed multifocal nodular leptomeningeal enhancement along the spinal cord and cauda equina. *Guillain-Barre syndrome (Acute inflammatory demyelinating polyneuropathy)* - 5-year-old child presented with clinical features consistent with GBS. Imaging showed striking smooth pial enhancement of the lower spinal cord, conus medullaris, and ventral cauda equina nerve roots. *Miller Fischer Syndrome (Variant of GBS)* -

51-year-old male presented with ataxia, and areflexia with descending paralysis. Imaging revealed extensive diffuse smooth enhancement of cranial nerves III-VII in addition to the spinal nerves throughout the cervical and thoracic spine as well as the cauda equina. *Chronic inflammatory polyradiculopathy (CIDP)* - 47-year-old man with areflexia. EMG/NCS findings were consistent with CIDP. Imaging showed enlargement, abnormal T2 hyperintensity, and smooth enhancement of the cauda equina nerve roots. *Neurosarcoidosis* - 32-year-old male patient with diffuse leptomeningeal intracranial sarcoidosis, with abnormal enhancement of the pituitary stalk and along the undersurface of optic chiasm. Imaging revealed nodular leptomeningeal enhancement along the entire spinal cord and nerve roots of the cauda equina. *Arachnoiditis (Post-Dissectomy)* - 62-year-old female with prior disectomy. Imaging showed thickened and clumped cauda equina nerve roots. *Lymphoma* - 70-year-old male with progressive perianal numbness, lower limb paraesthesia and difficulty passing urine. Imaging revealed persistent smooth enhancement of the cauda equina nerve roots. Flow cytometry and nerve root biopsy confirmed a diagnosis of intravascular lymphoma. *Acute Myeloid Leukemia* - 54-year-old female with AML presented with fever and suspected epidural abscess. Imaging showed thickening and smooth enhancement of the cauda equina nerve roots consistent with leukemic infiltrates. *Post Radiation* - 65-year-old male with follicular lymphoma affecting the sacrum. Pos radiotherapy imaging revealed significantly reduced tumor mass but development of thickening and smooth enhancement in cauda equina. *HSV, EBV, CMV Radiculopathy* - 41-year-old female with herpes vesicles, leg weakness and urinary symptoms. Imaging shows smooth cauda equina enhancement due to HSV radiculopathy. 62-year-old male with NHL and EBV viremia with progressive leg weakness. Imaging reveals faint smooth enhancement along the conus medullaris and cauda equina nerve roots likely due to EBV polyneuropathy.

#### SUMMARY/CONCLUSION

Awareness of the spectrum of pathological conditions that can cause enhancing thickened cauda equina nerve roots is necessary to establish a useful differential diagnosis. The pattern (smooth vs. nodular) can be helpful in narrowing the differential diagnosis, but the clinical presentation and CSF analysis are critical.

Rarely, a nerve root biopsy is needed to establish a diagnosis.

#### EdE-94

##### MR Imaging Findings of Paget Disease of the Spine

Morales, H. Shivashankar, R.

University of Cincinnati  
Cincinnati, OH

##### PURPOSE

Paget's disease is the second most common bone disorder of the aging population in the United States. The most common location is the pelvis and the second most common the spine. Though it is usually polyostotic, the incidence of monostotic disease, usually involving the axial skeleton, is increasing. Our aim is to describe the most common MR findings of uncomplicated Paget's of the spine, allowing recognition of the disease particularly when no other imaging techniques are available. We also will emphasize the added diagnostic value of multiple imaging techniques including radiographs, CT and bone scintigraphy.

##### APPROACH/METHODS

Retrospective review of radiology reports containing the diagnosis of Paget's from 01-2010 to 09-2011 was performed. Sixty cases with radiologic manifestations of Paget's disease as seen on radiographs or CTs were found. Only cases with concomitant MR images were selected.

##### FINDINGS/DISCUSSION

We will review the MRI findings of seven cases of Paget's disease of the spine. We also will review the literature and previously described findings. Three patterns of bone marrow involvement have been described in Paget's. The most common is dominant increased T1 signal from "normal" fatty bone marrow, the second most common is "speckled" heterogeneous signal on T1 and T2, and the third most common is decreased signal on all sequences. They reflect the three stages of the disease: osteolytic, mixed and sclerotic phases, respectively. The lytic phase is seen uncommonly in bones with high trabecular/cortex ratio as the vertebral bodies. The most common manifestations were a coarse increased T1 signal in the center of the vertebral bodies (endosteal resorption) and decreased T1 and T2 signal of the endplates (trabecular thickening). Classic "picture in frame" appearance could be defined on sagittal images in most cases, showing decreased signal in the anterior and posterior aspect of the vertebral bodies from thickened cortical bone. All but one case had diffuse involvement of the vertebral bodies. Most cases also had involvement of the posterior elements. Expansion of the vertebral body and/or posterior elements was a frequently overlooked manifestation on MRI. Only one case had decreased bone marrow signal in all sequences and correspond to sclerosis of the posterior elements. In most cases Paget's was not included in the radiologist differential diagnosis. We believe that previously described "normal" bone marrow appearance of Paget's

is uncommon in the spine, most likely due to the unusual occurrence of the predominantly lytic phase in the vertebral bodies.

##### SUMMARY/CONCLUSION

Paget's disease of the spine can be overlooked or confused with other entities such as hemangioma or malignancy on MRI. Recognition of its imaging manifestations is important to allow appropriate management and in most cases to avoid biopsy.

**KEY WORDS:** Paget, spine, MR imaging

#### EdE-95

##### Spectrum of Intradural Intra and Extramedullary Mass Lesions: The Benign, the Malignant, and the Unusual

Pollack, E. B.<sup>1</sup>•Lis, E.<sup>2</sup>•Karimi, S.<sup>2</sup>•Krol, G.<sup>2</sup>•Young, R. J.<sup>2</sup>

<sup>1</sup>Columbia Presbyterian Hospital, New York, NY,  
<sup>2</sup>Memorial Sloan-Kettering Cancer Center, New York, NY

##### PURPOSE

To provide an approach to MRI evaluation of intradural masses, including both intramedullary and extramedullary neoplastic and nonneoplastic mass lesions. We discuss characteristic imaging features and patterns of enhancement to identify typical patterns of disease spread and relevant clinical issues, and in specific instances to develop a specific differential diagnosis.

##### APPROACH/METHODS

We present a variety of instructive cases that demonstrate typical MRI presentations of benign and malignant neoplasms and other mass lesions in the intradural space. Sample cases of extramedullary cases include leptomeningeal metastases, leptomeningeal pseudolymphoma, meningioma, nerve sheath tumor, epidermoid and arachnoid cyst. Intramedullary examples include primary CNS lesions such as astrocytoma, ependymoma, myxopapillary ependymoma, and glioblastoma, as well as secondary lesions from direct intramedullary metastases and intramedullary invasion from leptomeningeal metastases. Diagnosis is established by pathology, systemic disease and/or follow up.

##### FINDINGS/DISCUSSION

Although relatively rare, intradural spinal tumors can cause significant morbidity. Rapid and accurate diagnosis is central to patient prognosis and management. Patients commonly present with nonspecific symptoms of pain and weakness, and imaging is therefore central to the correct diagnosis. This exhibit presents an approach to the evaluation of benign and malignant intradural spinal mass lesions based on location, signal characteristics, patterns of enhancement, and patterns of spread. Classic imaging features of both extramedullary and intramedullary lesions are discussed as well as relevant clinical issues with respect to medical and surgical management.

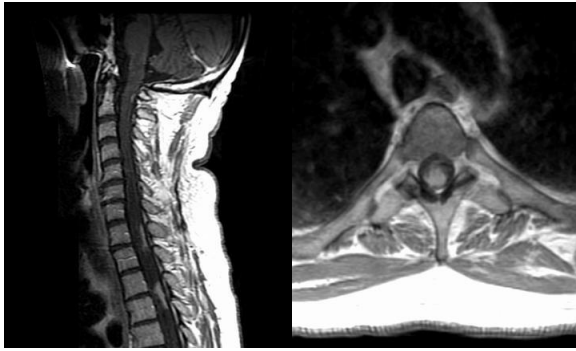


Figure: Sagittal (left) and axial (right) contrast T1-weighted images show cervical and thoracic leptomeningeal metastases from esophageal carcinoma, with frank intramedullary invasion at T3-T4 level (axial).

#### **SUMMARY/CONCLUSION**

Intradural tumors are highly associated with patient morbidity, which can be physically devastating and necessitates swift diagnosis with MRI. This exhibit will provide a review of typical imaging and clinical features of the most common extra- and intramedullary mass lesions.

**KEY WORDS:** Intradural, spinal cord, neoplasm

#### **EdE-96**

##### **What Space Am I Looking At? A Pictorial Review of Pathology Affecting the Extradural Compartments of the Spinal Canal**

Lee, N. N. • Stensby, J. D. • Pastel, D. A.

Dartmouth Hitchcock Medical Center  
Lebanon, NH

#### **PURPOSE**

To review the anatomy of the extradural compartments, the pathologic processes which can arise in these locations and the various imaging features that can help narrow the differential diagnosis.

#### **APPROACH/METHODS**

Determining the space in which an extradural lesion arises is paramount, as it can help narrow the differential diagnosis and has implications on surgical management. Through a pictorial review, we will illustrate the normal anatomy of the spinal meninges using diagrams and histologic images. We will present the imaging features of pathologic processes arising in these spaces.

#### **FINDINGS/DISCUSSION**

The imaging characteristics of pathologic processes arising from, or involving, the epidural, subdural and subarachnoid spaces will be depicted with CT and MRI. Examples include, but are not limited to: arachnoid cysts, spinal cord herniation, epidural/subdural abscesses and hematomas, cerebrospinal fluid (CSF) hypotension, arachnoiditis and intra/extradural schwannoma. Pertinent imaging pearls, clinical findings, and the importance of imaging findings upon surgical

management (such as if a lesion is epidural or subdural) will be emphasized.

#### **SUMMARY/CONCLUSION**

The approach to an extradural lesion begins with an understanding of the spinal meninges. Imaging features and location can help narrow the differential and impact management.

**KEY WORDS:** Extradural, meninges

#### **EdE-97**

##### **Spectrum of Intradural Extradural Spinal Tumors: MR Imaging and Pathologic Correlation**

Arani, K. N. • Wang, A. • Silbergleit, R.

William Beaumont Hospital  
Royal Oak, MI

**PURPOSE:** 1. To illustrate the MR spectrum of intradural extradural tumors in children and adults with pathologic correlation. 2. To discuss lesion distribution, location and contrast enhancement patterns as a way to help differentiate intradural extradural tumors. 3. To review the typical clinical history, epidemiology, and symptomatology of different intradural extradural tumors.

#### **APPROACH/METHODS**

The goal of this scientific exhibit is to provide a clear and structured approach when evaluating intradural extradural tumors. We will present a wide variety of intradural extradural tumors with characteristic MRI findings with pathologic correlation as a case series. Common Cases: Cerebrospinal fluid (CSF) seeding, neurofibroma/schwannoma, and meningioma. Uncommon Cases: Solitary fibrous tumor, paraganglioma, lobulated capillary hemangioma, dermoid cysts, and ependymoma.

#### **FINDINGS/DISCUSSION**

A wide variety of MRI findings of intradural extradural tumors will be presented in a case-based format with pathologic correlation. Characterization of intradural extradural tumors based on lesion distribution, location, and contrast enhancement pattern will be reviewed to help differentiate them.

#### **SUMMARY/CONCLUSION**

Familiarity with MRI findings of intradural extradural tumors and associated clinical history is critical for radiologists and patient care. After completing this case-based pictorial essay, the viewer should become more comfortable at diagnosing intradural extradural tumors.

**KEY WORDS:** Spinal neoplasm, intradural mass

**EdE-98****Traumatic Cervical and Thoracic Spinal Injuries in Ankylosing Spondylitis: A Comprehensive Review of Multidetector CT Findings**

Miller, A.<sup>1,2</sup>•Liu, Z.<sup>2</sup>•Doan, H.<sup>1,2</sup>

<sup>1</sup>Hahnemann University Hospital, Philadelphia, PA,

<sup>2</sup>Drexel University College of Medicine, Philadelphia, PA

**PURPOSE**

This exhibit will emphasize the critical role of multidetector CT in the evaluation of acute traumatic pathology of the cervical and thoracic spine in ankylosing spondylitis (AS).

**APPROACH/METHODS**

This exhibit will discuss multidetector CT (MDCT) findings of acute traumatic cervical and thoracic spinal pathology in AS. It will review how the disease process results in altered biomechanics that allow increased injury susceptibility. This exhibit will reinforce this information utilizing five different cases of cervical and thoracic spinal injury from the author's institution. Multidetector CT protocols and the utilization of 3D reformatted images will be discussed. A review of the literature focusing on MDCT findings and evaluation will be summarized, as well as the complementary role and limitations of MRI. The exhibit will conclude with a brief overview of further management.

**FINDINGS/DISCUSSION**

Ankylosing spondylitis (AS), also known as Marie-Strumpell arthritis or Bechterew's disease, is a commonly encountered spondyloarthropathy. The pathophysiology of AS involving enthesopathy leading to ossification of ligaments and intervertebral disks and subsequent joint fusion, significantly alters the biomechanics of the vertebral column leading to an increased susceptibility of devastating spinal injury from normally trivial mechanisms. Precise evaluation of traumatic injuries in AS is of critical importance to the radiologist to minimize patient morbidity and mortality.

**SUMMARY/CONCLUSION**

Ankylosing spondylitis leads to unique mechanisms of spinal injury. An exact description and understanding of MDCT findings in acute cervical and thoracic spinal injury in ankylosing spondylitis is of paramount importance in guiding further patient management.

**KEY WORDS:** Ankylosing spondylitis, trauma

**Monday, April 23 -  
Wednesday, April 25  
6:30 AM - 9:00 PM**

**Thursday, April 26  
6:30 AM - 3:00 PM  
Rhineland**

**Electronic Education  
Exhibits 1 - 54**

eEdE1 - Adult Brain

**Note: A missing printed number indicates an abstract has been withdrawn.**

**eEdE-1****Evidence-Based Approach to Imaging of Acute Stroke: Essentials for Stroke Management**

Abdullah, A.•Elias, A.•Hoeffner, E.•Gemmete, J.•Chaudhary, N.

University of Michigan Health System  
Ann Arbor, MI

**PURPOSE**

Stroke is the leading cause of death worldwide and one of the major causes of morbidity and mortality in the U.S. Optimal management of acute stroke patients relies on prompt clinical assessment and diagnosis followed by urgent brain imaging. It is essential for multidisciplinary stroke teams to understand the role of imaging for optimal patient selection for potential treatment. The goal of this presentation is to provide the reader with a stepwise approach to the utility of parenchymal, vascular, and perfusion imaging techniques and their limitations in acute stroke patients based on evidence-based guidelines published by the American Stroke Association in 2009.

**APPROACH/METHODS**

A case-based approach on the role of imaging in acute stroke, based on these guidelines, will be provided. Examples will be provided where imaging, in particular perfusion imaging, was critical in the diagnosis and management of stroke patients and in cases where advanced imaging may have a limited role and be of no additional benefit. We also will provide an overview of the advanced imaging techniques used at our institution for imaging of acute stroke patients.

**FINDINGS/DISCUSSION**

Optimization of acute stroke management protocols is continuous work. "Time is brain", therefore, early patient presentation and timely clinical and imaging



evaluation are essential. Advanced imaging techniques often offer complementary information, but, increasingly, protocols to extend the time to therapeutic intervention is determined by the delineation of the ischemic penumbra. Questions remain regarding which imaging modalities and criteria are most useful in expanding the therapeutic window. Nonetheless, noncontrast CT as the initial imaging test remains the reference standard across stroke centers with imaging of the extra and intracranial vasculature becoming increasingly more important.

#### SUMMARY/CONCLUSION

In summary, according to the evidence-based guidelines provided by the American Stroke Association, imaging should ideally address four essential issues in stroke management: (1) the presence of intracranial hemorrhage; (2) the presence of a potentially treatable intravascular thrombus; (3) the presence and size of an irreversibly infarcted cerebral parenchyma; and (4) the presence of ischemic penumbra. Multidisciplinary stroke teams, including neuroradiologists and neurologists, should be familiar with the strengths and limitations of various imaging techniques in acute stroke care.

**KEY WORDS:** Stroke, CT perfusion, thrombolysis

#### eEdE-2

##### Role of Diffusion Tensor Imaging in Acute Stroke Patients: When to Do It, How to Apply It, and Why to Include It in the Protocol

Puig Alcantara, J.<sup>1</sup>•Blasco, G.<sup>1</sup>•Daunis-i-Estadella, J.<sup>2</sup>•Pedraza, S.<sup>1</sup>

<sup>1</sup>Hospital Universitari Dr Josep Trueta, Girona, SPAIN,

<sup>2</sup>Universitat de Girona, Girona, SPAIN

#### PURPOSE

Diffusion tensor imaging (DTI) offers diagnostic information on the microstructural status of brain tissue by quantifying anisotropic indexes that reflect inherent biophysical properties of tissue structure and determining the direction of the anisotropic diffusion of the white matter tracts (WMT). This exhibit shows how determining the anisotropy profile in the infarcted cerebral areas and assessing the integrity of specific WMT by tractography can improve the management of acute ischemic stroke (AIS) patients.

#### APPROACH/METHODS

1. We explain DTI techniques, postprocessing, and tractography, and how to optimize the protocol for AIS. 2. We use cases of acute, subacute, and chronic strokes to address the potential role of anisotropic parameters as a biomarker of stroke age. 3. We discuss methods of analyzing quantitative and qualitative data from DTI about the integrity of functional WMT to predict clinical outcome after AIS. 4. We highlight the role of anisotropic indexes as biomarkers of stroke-related damage and the potential value of lesion mapping techniques.

#### FINDINGS/DISCUSSION

Water diffusion in brain tissue is affected by barriers to translational motion like cell membranes and white matter tracts. Anisotropic water diffusion can be specified using several indices [e.g., eigenvalues ( $\lambda_1$ ,  $\lambda_2$ ,  $\lambda_3$ ), fractional anisotropy (FA), mean diffusivity]. Stroke modifies the integrity of the tissue microstructure resulting in significant alterations in tissue anisotropy; thus, DTI provides information about the evolution of AIS that is not available from T2-weighted, FLAIR, or diffusion-weighted sequences. Evidence suggests that diffusion anisotropy increases in the first hours after AIS, indicating membrane failure that restricts transverse diffusivity in the hyperacute stage. Thus, DTI could be useful in AIS patients in whom the onset is unknown (up to 25%) and in the clinical evaluation of new treatments. Furthermore, stroke is the most common cause of disability in adults in many countries. It is difficult to predict the response to rehabilitation and outcome in AIS patients. Accurate early prediction of outcome would enable realistic goal-setting and efficient resource allocation by clinicians and patients. Predictors of outcome include location and extension of the stroke specifically within the corticospinal tract (CST) and language pathways, grade of initial deficit, and infarct volume. Damage to the posterior limb of the internal capsule is an early imaging predictor of poor motor outcome. Lower FA values on CST distal to the infarct are associated with worse motor recovery. Further research should focus on improving the accuracy of early imaging predictions of outcome after AIS.

#### SUMMARY/CONCLUSION

Diffusion tensor imaging should be incorporated into MRI protocols for AIS because it could help determine stroke age. Damage to specific WMT (e.g., CST) can help predict clinical outcome. A better understanding of predictors of outcome would help in selecting clinically meaningful outcome measures for future studies.

**KEY WORDS:** Stroke, diffusion tensor imaging

#### eEdE-3

##### Carbon Dioxide-Challenged CT Perfusion in Evaluation of the Cerebrovascular Reserve

Cheecharoen, P.

Ramathibodi Hospital, Mahidol University  
Bangkok, THAILAND

#### PURPOSE

Multiple imaging techniques utilizing acetazolamide or carbon dioxide (CO<sub>2</sub>) challenge are dedicated to assess the cerebrovascular reserve (CVR). A CVR measurement with carbon dioxide-challenged CT perfusion in patient with cerebrovascular disease is lacking.

#### APPROACH/METHODS

Four patients with cerebrovascular occlusive disease were referred for evaluation of cerebrovascular reserve. All patients underwent baseline CT perfusion. In 30 minutes later, the patients were ventilated with 5%

carbogen for 4.5 minutes, followed by post CO<sub>2</sub>-challenged CT perfusion. Cerebral blood flow, cerebral blood volume, and mean transit time values were measured in regions of interest (ROIs) encompassing the brain tissue at-risk and the normal brain tissue, defined based on the site of occlusion. Changes in PCT parameters were calculated in corresponding ROIs on baseline and post CO<sub>2</sub>-challenged PCT maps.

#### FINDINGS/DISCUSSION

The mean values of normalized rCBF and MTT were significantly different between normal and impaired CVR groups. For defining impaired CVR with percent change of normalized CBF (pcCBF), the ROC-derived threshold value of -4%, with a sensitivity, specificity, PPV, NPV and accuracy of 80.5%, 84.2%, 84.6%, 80.0% and 82.3%, respectively (the area under the ROC curves = 0.82). For defining impaired CVR with percent change of normalized MTT (pcMTT), the ROC-derived threshold value of 13%, with a sensitivity, specificity, PPV, NPV and diagnostic accuracy of 65.9%, 84.2%, 81.8%, 69.6% and 74.7% (the area under the ROC curves = 0.75). The pcCBF is the most accurate CTP parameter in defining the impaired CVR, as evidenced by the greatest area under the ROC curve.

#### SUMMARY/CONCLUSION

Carbon dioxide-challenged CT perfusion is another potential method of cerebrovascular reserve assessment. The percentage change of normalized rCBF and MTT is correlated with quantitative CVR and the pcCBF is more accurate than MTT in defining the impaired CVR. Our preliminary results in cerebrovascular occlusive patients should be validated with larger population studies.

**KEY WORDS:** Cerebrovascular reserve, CT perfusion, CO<sub>2</sub>

#### eEdE-4

##### CT Perfusion and CT Angiography in Acute Ischemic Stroke Using Dual Energy CT

Chuang, M.·Shih, Y.·Liu, Y.·Chen, Y.·Tsai, H.·Chen, C.·Lu, C.

National Cheng-Kung University  
Tainan, TAIWAN

#### PURPOSE

The CT perfusion (CTP) and CT angiography (CTA) were clinically useful tools in acute ischemic stroke for determining penumbra area and as a guidance for thrombolytic therapy. This educational exhibit will describe our procedure in clinical practice and introduce some potential pitfalls and technical errors by using DECT (dual energy CT).

#### APPROACH/METHODS

(a) Technical aspects of CTP/CTA and potential pitfall: introduce our procedures with CTA and CTP using DECT, technical errors in choosing AIF or VOF during CTP. (b) Pathologic conditions: Infarct (MCA, PCA), vasospasm, subclavian steal syndrome, vertebrobasilar

insufficiency, carotid stenosis, postcarotid stenting, postictal change. (c) Mimics of ischemic stroke: hypoglycemia, seizure, old ischemic infarct.

#### FINDINGS/DISCUSSION

Obtaining an appropriate diagnostic image is very important in dealing with acute ischemic stroke patient for thrombolytic therapy guidance. With the advent of DECT, we can obtain near whole brain perfusion with less contrast amount. CT perfusion can tell us the infarct core and penumbra region while CTA can show us the condition of carotid and vertebrobasilar arteries. We organize a practical way to understand scanning principle and procedure, to interpret various pathologic conditions and to show some stroke mimickers.

#### SUMMARY/CONCLUSION

With this knowledge, one should be able to understand the role of CTA/CTP in acute ischemic stroke.

**KEY WORDS:** CT perfusion, dual energy CT

#### eEdE-5

##### Diffusion-Weighted Imaging Findings in Intracranial Hemorrhage

Maller, V. G.·Thamburaj, K.·Sabat, S. B.·Ouyang, T. Penn State Milton S. Hershey Medical Center Hershey, PA

#### PURPOSE

To describe the diffusion-weighted imaging features of various stages of intracranial hemorrhage.

#### APPROACH/METHODS

We present a pictorial review of the diffusion imaging findings of various stages of intracranial hemorrhage and review the relevant literature.

#### FINDINGS/DISCUSSION

Stroke can be ischemic or hemorrhagic. The appearance and evaluation of intracranial hemorrhage on MRI primarily depend on the age of the hematoma and on the imaging sequence or parameters. Hyperacute bleed and intracellular stage of methemoglobin may show restricted diffusion. Diffusion of water is restricted significantly in intracranial hematomas that show MR signal intensity patterns consistent with intracellular oxyhemoglobin, intracellular deoxyhemoglobin, and intracellular methemoglobin. Understanding of temporal evolution of diffusion imaging changes after spontaneous intracerebral hemorrhage is important for accurate interpretation of MR imaging findings in stroke.

#### SUMMARY/CONCLUSION

The diffusion MR appearance of evolving intracranial hemorrhage and its underlying biophysical basis are somewhat complex. Therefore, early hematomas would be displayed as identical to the signal intensity of acute infarction on ADC maps, despite their clear differentiation on conventional MR images. This suggests that apparent diffusion coefficient (ADC) maps

always should be interpreted with conventional MR images for comparison.

**KEY WORDS:** Hemorrhage, intracerebral, diffusion

#### eEdE-6

### Radiologic Mimickers of Posterior Fossa Multiple Sclerosis Lesions

Abdullah, A.·Rivas-Rodriguez, F.·Hoeffner, E.·Dombrowski, A.

University of Michigan Health System  
Ann Arbor, MI

#### PURPOSE

Although the diagnosis of multiple sclerosis (MS) relies on the demonstration of disease dissemination in space and time, the exclusion of other neurologic disorders is also necessary. The limited specificity of abnormalities revealed by magnetic resonance imaging (MRI) may increase the likelihood of diagnosis of multiple sclerosis in patients affected by other disorders. Posterior fossa lesions, which radiologically mimic MS lesions, present with a diagnostic challenge especially in the absence of coexisting supratentorial abnormalities. The goal of this presentation is to provide the reader a systematic approach to radiologic diagnosis when faced with variety of posterior fossa lesions that mimic multiple sclerosis.

#### APPROACH/METHODS

A variety of posterior fossa pathologic conditions can mimic MS both clinically and radiologically. We will provide a radiologic review of inflammatory, vascular, neoplastic and metabolic conditions, which show features similar to those of MS on MRI. NeuroBehcet's, Lyme disease, progressive multifocal leukoencephalopathy, neurosarcoidosis, Whipple's disease, Listeria rhombencephalitis, Bickerstaff's brainstem encephalitis, systemic lupus erythematosus vasculitis, and acute disseminated encephalomyelitis (ADEM) produce inflammatory lesions radiologically and often times clinically similar to those of MS in the posterior fossa. Neoplastic diseases, in particular posterior fossa gliomas and lymphomas, can mimic MS. Vascular ischemic lesions, either due to infarction produced by occlusion of a major posterior circulation artery or due to small vessel vasculopathy, can lead to posterior fossa lesions. The MRI findings of osmotic demyelination also can mimic MS. Diffuse axonal injury, radiation and chemotherapy induce lesions that resemble MS, and however the clinical history will exclude these possibilities. We also will discuss the role of follow-up imaging for posterior fossa lesion, which present with a diagnostic challenge and cannot be separated reliably from MS lesions on clinical and radiologic grounds, based on evidence-based guidelines representing the consortium of MS centers consensus.

#### FINDINGS/DISCUSSION

The diagnosis of multiple sclerosis should not be made on basis of imaging findings alone but should take into account patient's clinical history and appropriate

laboratory findings. Due to improved MRI techniques, it has become relatively easy to exclude obvious MS mimickers such as posterior fossa tumors; however, often times it remains difficult to differentiate MS lesions from other disease processes such as neurosarcoidosis, Behcet's disease, Lyme disease, and ADEM.

#### SUMMARY/CONCLUSION

Over-diagnosis of multiple sclerosis on imaging should be avoided and the radiologist should be aware of imaging features of posterior fossa mimicker of MS lesions.

**KEY WORDS:** Multiple sclerosis, posterior fossa, neoplasm

#### eEdE-7

### Bridging the Gap: Review of Corpus Callosal Lesions

Kalra, V. B.·Gilbert, J.·Malhotra, A.

Yale University  
New Haven, CT

#### PURPOSE

The corpus callosum is the largest white matter tract in the brain and contains hundreds of millions of axonal projections. Numerous pathologic entities can occur in the corpus callosum, and it is important to recognize these for the purpose of treatment and prognostication. We present a review of callosal lesions based on etiology, presenting case examples with discussion of radiologic and pathologic features of each.

#### APPROACH/METHODS

Callosal lesions can be grouped by etiology. These groups include posttraumatic, autoimmune, neoplastic, infectious, toxic, metabolic, congenital, iatrogenic, and vascular. Examples from each group are presented with case examples and discussion of radiologic and pathologic features of each.

#### FINDINGS/DISCUSSION

Posttraumatic lesions include diffuse axonal injury and penetrating trauma. Autoimmune lesions include multiple sclerosis and acute disseminated encephalomyelitis. Neoplastic lesions include glioblastoma multiforme, lymphoma, metastases, juvenile pilocytic astrocytoma, and gliomatosis cerebri. Infectious lesions include progressive multifocal leukoencephalopathy, reversible focal splenial lesions of viral encephalitis, and toxoplasmosis. Toxic lesions include Marchiafava-Bignami disease, methotrexate, and reversible focal splenial lesions from antiepileptic drugs. Metabolic lesions include leukodystrophies and mucopolysaccharidoses. Congenital lesions include lipoma, germinoma, and agenesis/dysgenesis of the corpus callosum. Iatrogenic lesions include those from ventriculostomy, callosotomy, and radiation therapy. Vascular lesions include infarct, arteriovenous malformations, and Susac syndrome.

**SUMMARY/CONCLUSION**

Lesions of the corpus callosum can have multiple etiologies, including posttraumatic, autoimmune, neoplastic, infectious, toxic, metabolic, congenital, iatrogenic, and vascular. Awareness of these lesions is important because they can have significant treatment and prognostic implications.

**KEY WORDS:** Corpus callosum, demyelinating

**eEdE-8**

### **Encephaloceles of the Middle Cranial Fossa in Temporal Lobe Epilepsy: Radiologic/Pathologic Considerations**

Friedman, E. R. • Bhattacharjee, M. • Tandon, N.

University of Texas Houston  
Houston, TX

**PURPOSE**

To demonstrate the radiographic and pathologic manifestations of temporal meningoencephaloceles, a not uncommon, but probably underreported cause of temporal lobe epilepsy.

**APPROACH/METHODS**

MR scans of the brain acquired using a dedicated epilepsy protocol on a 3 T scanner as part of phase I epilepsy evaluation in 210 consecutive patients undergoing epilepsy surgery were evaluated for operable lesions, and the frequency of temporal meningoencephaloceles was calculated. Correlation was made with operative and pathologic findings in all surgical patients. Embryology of the sphenoid and central skull base will be reviewed.

**FINDINGS/DISCUSSION**

A spectrum of middle cranial fossa defects in patients with temporal lobe epilepsy ranges from radiographically occult meningoencephaloceles to radiographically obvious lesions. Of the 12 patients in our series, two had radiographically occult, surgically confirmed lesions that were inconspicuous on preoperative MRI. In one of these patients, additional findings of ipsilateral temporal lobe volume loss and blurring of the gray-white matter interface were present; however in the other patient, the MRI was essentially normal. Osseous defects in the radiographically obvious lesions in our series ranged from less than 5 mm to greater than 2 cm. All defects involved the floor of the middle cranial fossa either in isolation or in combination with lateral sphenoidal abnormalities. A spectrum of defects was observed in the greater sphenoid wing, ranging from areas of pitting abnormality to frank osseous dehiscence. Large infratemporal meningoencephaloceles in two cases were attributed to bony defects accessing pneumatized portions of the greater sphenoid wing. Lateral sphenoidal defects ranged from medial dural deficiencies in the middle cranial fossa to concave deformity to frank osseous defects in the lateral wall of the sphenoid sinus. Temporal meningoencephaloceles can be overlooked on neuroimaging for a number of

reasons. Their location at the anterior aspect of the middle cranial fossa may not be detectable on high resolution T2 oblique images obtained through the hippocampus, if "skin to skin" coronal imaging is not performed. Fine cut skull base CT scans with multiplanar reconstructions are also helpful in defining osseous defects associated with meningoencephaloceles. The size of meningoencephaloceles is variable, and while some lesions are truly radiographically occult and only detectable at surgery, smaller lesions require conspicuous inspection for their detection. The pathologic findings were variable, but all showed Chaslin's subpial gliosis, in addition to diffuse parenchymal gliosis. Corpora amylacea deposition was marked in two cases. The cytoarchitectural abnormalities ranged from completely disorganized neural tissue with fibrotic leptomeninges, to cortical dysplasia and nodular gray matter heterotopias. One case showed the disorganized neural tissue closely apposed to the overlying respiratory and squamous epithelium of the air sinus mucosa.

**SUMMARY/CONCLUSION**

Meningoencephaloceles of the middle cranial fossa are not an uncommon lesional etiology in patients with temporal lobe epilepsy. Neuroradiologists should be familiar with the radiographic manifestations and configure imaging protocols to optimize their detection.

**KEY WORDS:** Meningoencephalocele, epilepsy

**eEdE-9**

### **"Form Follows Function": Anatomical and Functional Localization of Eloquent Cortex**

Ho, M. • Rojas, R. • Hackney, D. B.

Beth Israel Deaconess Medical Center  
Boston, MA

**PURPOSE**

The purposes of this exhibit are: 1. Describe imaging signs of major cortical regions on conventional CT and MR, with attention to the central sulcus and surrounding anatomical landmarks. 2. Establish the validity of anatomical techniques for localizing eloquent cortex, based on correlation to functional MRI (fMRI) activation maps in selected case studies. 3. Identify scenarios in which technical, patient, and lesion factors may limit anatomical and/or functional characterization.

**APPROACH/METHODS**

Following retrospective review of all fMRI studies performed at our institution, 13 cases were selected for their particular educational value regarding patient diagnosis and imaging findings. Examinations were performed on a 3 T magnet under the supervision of a dedicated functional neuroradiologist. A standard alternating block protocol was used for identification of primary/supplementary motor and language cortex. For each study, activation areas were correlated to anatomical findings on presurgical MR examinations. Visible anatomical landmarks were identified on axial

T1 MPRAGE sequences by two neuroradiology attendings and a radiology resident (PGY-4).

#### FINDINGS/DISCUSSION

We present seven anatomical landmarks on CT and MR, as described by Naidich et al. in normal brains: 1. Superior frontal sulcus - precentral sulcus (85% sensitivity): Posterior end of SFS joins pre-CS. 2. Sigmoidal hook (89% CT, 98% MR): Posterior precentral gyrus indents CS. 3. Bifid postcentral sulcus (85% CT, 88% MR): Bifurcate post-CS encloses lateral pars marginalis. 4. Thin postcentral gyrus (98%): Post-CG is thinner than pre-CG. 5. Intraparietal sulcus - postcentral sulcus (99%): IPS intersects post-CS. 6. Midline sulcus (70%): Sulcus extending closest to midline is CS. 7. Pars bracket (96%): Paired pars marginalis on each side of interhemispheric fissure, behind CS. Next, we discuss the basic principles and techniques of fMRI. Functional MRI is used to determine the relationship between presurgical brain lesions and eloquent cortex, most importantly the primary motor and language areas. At our institution, a lesion is considered resectable at a distance of 1-1.5 cm from eloquent cortex. A location of less than 3-6 mm from eloquent cortex is considered a contraindication for gross total resection, and requires intraoperative cortical mapping (ICM) during surgery. As reported by Pujol et al., anatomical landmarks correlate well with fMRI, except when abnormalities are located close to the central sulcus. This can result in regional compression, distortion, and displacement secondary to mass effect, edema, and infiltration. We compare anatomical and fMRI findings across a variety of lesion locations and etiologies. Technical and patient-related imaging artifacts also are discussed.

#### SUMMARY/CONCLUSION

The major teaching points of this exhibit are: 1. Anatomical localization with conventional CT/MR is effective for characterizing preoperative cerebral lesions with respect to the central sulcus and surrounding anatomical landmarks. 2. Pathologic lesions may severely distort normal anatomy. In particular, when abnormalities are located close to the central sulcus, fMRI and/or intraoperative mapping may be required to more precisely determine the relationship between eloquent cortex and the lesion of interest. 3. Awareness of limiting technical/patient factors is important for performing accurate anatomical and functional localization.

**KEY WORDS:** Functional, anatomy, landmark

#### eEdE-10

##### Resting-State Functional Magnetic Resonance Imaging in the Assessment of Patients with Systemic Lupus Erythematosus

Rueda-Lopes, F. C.<sup>1,2</sup>•Pereira, D.<sup>1</sup>•Malfetano, B.<sup>1</sup>•Borges, R.<sup>1</sup>•Domingues, R.<sup>2</sup>•Gasparetto, E.<sup>1,2</sup>

<sup>1</sup>UFRJ, Rio de Janeiro, BRAZIL, <sup>2</sup>CDPI, Rio de Janeiro, BRAZIL

#### PURPOSE

Systemic lupus erythematosus (SLE) is an inflammatory disease, associated with vasculitis, causing functional neuronal disturbance. The aim of this study was to evaluate the main functional networks detected on SLE patients and also their main difference in relation to controls.

#### APPROACH/METHODS

We studied 23 women with SLE [mean age 43 years (SD +/- 8), mean disease duration of 13 years (SD +/- 8.5)] and also eight sex- and age-matched controls. All participants signed informed consent. A magnetic resonance imaging (MRI) was performed in a 1.5 T scanner with protocol that included 3D T1 GRE-weighted images. In addition, resting-state functional MRI was performed during rest. Functional MRI data were postprocessed using FMRIB's Software Library. The fMRI data set was decomposed using independent component analysis to identify large-scale patterns of functional connectivity. After that, a "dual-regression" approach was carried out allowing voxel-wise comparisons of resting functional connectivity between both groups.

#### FINDINGS/DISCUSSION

Twenty-three components were computed in the entire subject group by independent component analysis. Default-mode network, bilateral fronto-parietal, visual, auditory and language, dorsal and ventral attention, executive function and sensorio-motor networks were detected. These eight resting state networks were compared between both groups. In the default-mode network, patients showed areas of significantly higher synchronization compared to healthy controls in the medial part of the frontal lobes ( $p < 0.001$ ). If  $p$  value was increased to 0.05, multiple areas in the temporal horns also were shown. Also, the right fronto-parietal network showed increased synchronization values in the right medial frontal lobe in patients compared to controls ( $p < 0.01$ ). All other networks had no remarkable differences between patients and controls.

#### SUMMARY/CONCLUSION

Female SLE patients have an increased synchronization during rest in the frontal lobe for default-mode and fronto-parietal networks. This may be due to a mechanism of compensation that patients develop in order to keep cognition in the same level of controls.

**KEY WORDS:** Functional MR imaging, lupus, MR imaging

#### eEdE-11

##### Tract-Based Spatial Statistics in the Evaluation of Patients with Neuromyelitis Optica

Rueda-Lopes, F. C.<sup>1,2</sup>•Doring, T.<sup>1,2</sup>•Martins, C.<sup>1</sup>•Cabral, F.<sup>1</sup>•Alves-Leon, S.<sup>1</sup>•Gasparetto, E.<sup>1,2</sup>

<sup>1</sup>UFRJ, Rio de Janeiro, BRAZIL, <sup>2</sup>CDPI, Rio de Janeiro, BRAZIL

## PURPOSE

The aim of this study is to map brain white matter damage in neuromyelitis optica (NMO) patients using diffusion tensor imaging post-processed by tract-based spatial statistics (TBSS).

## APPROACH/METHODS

Seventeen patients with NMO (14 female and 3 male, mean age 45 years - SD  $\pm$  9.7) that fulfilled the revised Wingerchuck criteria of 2006. Clinical parameters evaluated were: EDSS, number of relapses and disease duration. Seventeen controls age- and sex-matched also were analyzed and signed the informed consent. The group underwent MR exams at 1.5 T scanner (Avanto, Siemens) including FLAIR and diffusion tensor imaging (DTI) within 30 directions. After eddy current correction of DTI data, voxelwise statistical analysis of fractional anisotropy (FA) data was carried out with TBSS, part of FSL (Smith 2004). Tract-based spatial statistics projects all subjects' FA data onto a mean FA tract skeleton, before applying voxelwise cross-subject statistics. After that, the radial and axial diffusivities (RD and AD) of the damaged voxels located in the corpus callosum (CC) were measured. A  $p$ -value  $\leq$  0.05 was considered statistically significant. Fractional anisotropy, RD and AD values were partially correlated with clinical parameters.

## FINDINGS/DISCUSSION

In the patient group, there was statistical significant FA value reduction ( $p < 0.05$ ) in comparison to control group in the right and left superior and anterior corona radiata, right posterior corona radiata, genu and body of the corpus callosum, bilateral posterior thalamic radiation (including optic radiation), left internal and external capsule, left cerebral peduncle, bilateral uncinate fasciculus and right sagittal striatum. The mean FA value of the voxels that showed reduction in the CC was  $0.69 \pm 0.03$  compared to  $0.75 \pm 0.02$  in the controls ( $p < 0.0001$ ). The RD ( $0.33 \pm 0.03 \times 10^{-3} \text{ mm}^2/\text{s}$  vs.  $0.39 \pm 0.04 \times 10^{-3} \text{ mm}^2/\text{s}$ ,  $p < 0.0001$ ) and AD ( $1.53 \pm 0.04 \times 10^{-3} \text{ mm}^2/\text{s}$  vs.  $1.57 \pm 0.04 \times 10^{-3} \text{ mm}^2/\text{s}$ ,  $p = 0.007$ ) values also were decreased in these voxels. A significant inverse strong correlation was found between FA and RD ( $r = -0.976$ ;  $p < 0.0001$ ). No correlation was found between clinical and DTI parameters.

## SUMMARY/CONCLUSION

The TBSS approach demonstrated extensive white matter damage in NMO patients. The corpus callosum is damaged, and the FA reduction is mainly caused by RD, suggesting demyelination as the main cause for that.

**KEY WORDS:** TBSS, NMO, MR imaging

## eEdE-12

### Clinical Potential of Diffusion Tensor Imaging and Fibertracking at 7 T

Sammet, S.<sup>1,2</sup>•Irfanoglu, M. O.<sup>2</sup>•Sammet, C. L.<sup>3</sup>•Koch, R. M.<sup>4</sup>•Yuh, W. T. C.<sup>2</sup>•Knopp, M. V.<sup>2</sup>

<sup>1</sup>University of Chicago, Chicago, IL, <sup>2</sup>The Ohio State University, Columbus, OH, <sup>3</sup>Northwestern University, Chicago, IL, <sup>4</sup>Brigham and Women's Hospital, Boston, MA

## PURPOSE

Diffusion tensor imaging (DTI) is a magnetic resonance imaging (MRI) technique that allows to measure molecular diffusion in the human brain to assess white matter fibers in vivo. At low magnetic field strengths, DTI with single excitation protocols faces limited spatial resolution and low signal-to-noise ratio (SNR). These shortcomings can be mitigated effectively by the transition to high magnetic field strengths and parallel imaging technology such as sensitivity encoding (SENSE). The purpose of this study was to evaluate quality of DTI and fibertracking of the human brain at 7 T and to assess its clinical applicability.

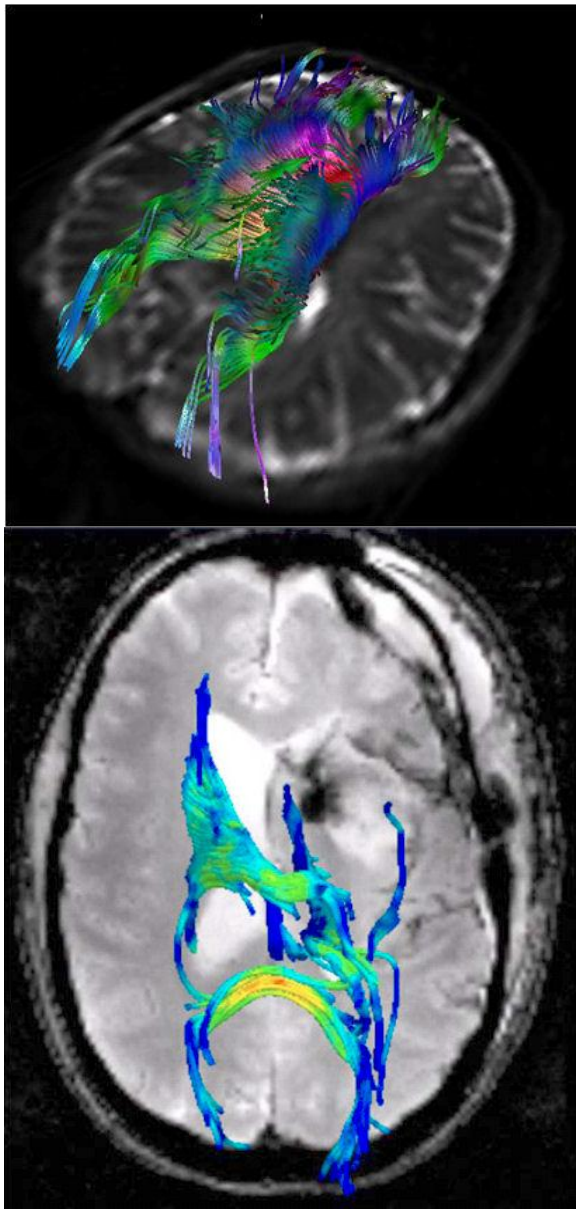
## APPROACH/METHODS

Diffusion tensor imaging of the human brain was performed in a 7 T whole body MR scanner with a 16 channel SENSE head coil on 10 volunteers to optimize the in vivo protocol. A 37-year-old female patient was scanned after the resection of a brain tumor at 7 T with the optimized DTI protocol: TR=3000 ms; TE=86 ms; FOV=230 mm<sup>2</sup>; matrix size=128x128; b=0, 1000s/mm<sup>2</sup>; slice thickness=2 mm; SENSE=4 and NSA=1. To reduce motion artifacts in the DTI images the datasets were postprocessed and tracts representing fibers were reconstructed.

## FINDINGS/DISCUSSION

Diffusion tensor imaging at 7 T allows the acquisition of diffusion-weighted images with high SNR in vivo. Sensitivity encoding mitigates susceptibility artifacts at 7 T successfully and allows the reconstruction of white-matter fiber tracts. Postoperative analysis of fractional anisotropy maps and fiber tracts in a patient after resection of a brain tumor showed the course of the remaining fibers and helped in planning a follow-up surgery.





#### SUMMARY/CONCLUSION

Advanced magnetic resonance imaging techniques such as diffusion tensor imaging at 7 T open new vistas in brain tumor research. Ultrahigh field DTI using SENSE mitigates susceptibility artifacts and can be used for neurosurgical planning.

**KEY WORDS:** MR imaging, diffusion tensor imaging, 7 T

#### eEdE-13

### MR Imaging Manifestations of Atypical Central Nervous System Infections in the Adult Brain

Nieves-Cruz, D. • Labat-Alvarez, E. J.

University of Puerto Rico School of Medicine  
San Juan, PR.

#### PURPOSE

The objective of this electronic exhibit is to review the imaging findings of atypical central nervous system (CNS) infections, including herpes encephalitis, nocardia encephalitis, neurocysticercosis and tuberculosis (TB) in the immunocompetent population as well as opportunistic infections in immunocompromised patients and their differential diagnoses.

#### APPROACH/METHODS

MRI features and presentation of atypical infectious CNS pathology cases seen at our institution will be included with the imaging differential diagnosis, and clinicopathologic correlation. Cases pertaining to atypical viral and bacterial pathogens are presented and contrasted with imaging manifestations in the immunocompromised host and respective pathogens in such population.

#### FINDINGS/DISCUSSION

Meningoencephalitis accounts for a number of visits to our Emergency Department and flourish as a complication in the inpatient setting as well. The myriad of clinical presentations combined with the lack of imaging findings in unenhanced brain CT, in many instances, poses challenges for the clinician and impedes prompt adequate treatment in certain scenarios. Recognizing the imaging manifestations in the adequate clinical scenario will entail the prompt identification or direction towards the not so common infectious pathology. Developing an algorithm when approaching these cases that includes patients immune status, age, travel history, hometown, clinical presentation and tying this together with imaging findings proves beneficial in some difficult cases.

#### SUMMARY/CONCLUSION

In the setting of an acutely ill patient with neurologic signs and symptoms it is important to recognize and remember the imaging appearances of atypical infectious nonopportunistic and opportunistic pathogens. Knowing the importance that the prompt recognition of the right diagnosis in these patients has in terms of clinical outcomes, we provide a pictorial review of MRI findings of these atypical and sometimes not so atypical infections, taking into consideration patients immunologic status. An imaging review of the manifestations of herpes encephalitis, TB, nocardiosis CNS involvement, neurocysticercosis, in combination with cases that typically afflict the immunocompromised host, is provided.

**KEY WORDS:** Encephalitis

#### eEdE-14

### Rhino-Orbito-Cerebral Mucormycosis: An Elusive Diagnosis on Imaging

Hussain, S. • Divekar, S. A. • Al Bader, F.

King Khalid University Hospital  
Riyadh, SAUDI ARABIA

#### PURPOSE

Early imaging findings and follow-up imaging in cases of rhinocerebral mucormycosis.

#### APPROACH/METHODS

Rhinocerebral mucormycosis is fulminant fungal infection often affecting patients with uncontrolled diabetes mellitus. The infection is angioinvasive and leads to multiple progressive infarctions in cerebral parenchyma. The clinical as well as imaging diagnosis often is elusive. We describe two patients with presenting symptoms sinusitis, sudden blindness and ophthalmoplegia were investigated by brain MRI, and later on followed up by CT or MRI angiography. Both the cases showed acute optic nerve infarction demonstrated on diffusion-weighted MRI, reported as earliest finding of rhino-orbito-cerebral mucormycosis. One case showed "Black Turbinate Sign" also reported to be early MR imaging feature of this condition. CT features were nonspecific. Follow up CT or MR angiographies revealed progressive occlusion of the involved arteries. Endoscopic sinus washings showed presence of fungi *Mucor* spp; however, culture was not performed.

#### FINDINGS/DISCUSSION

Despite the aggressive treatment with antifungal therapy; both the patients succumbed to the disease. We present the findings in tabular form and review of literature.

Summary of Imaging Findings		
Imaging Findings	Patient No 1	Patient No 2
Diffusion restriction in optic nerve with reduced ADC	Yes	Yes
Diffusion restriction extending to retina	Yes	No
Abnormal FLAIR signal in extra-ocular muscles with abnormal enhancement	+/-	Yes
Fat stranding around optic nerve on CT	Yes	No
Mucosal thickening in the ethmoid and sphenoid sinuses	Yes	Yes
Black turbinate sign	Yes	No
Multiple brain infarctions	Yes	Yes
Progressive occlusion of unilateral intra and extracranial internal carotid artery on CTA /MRA	Not available	Yes
Bone destruction of sinus walls	No	No

#### SUMMARY/CONCLUSION

Clinical presentation of rhino-orbito-cerebral mucormycosis is often nonspecific. CT findings are nonspecific. MRI findings of optic nerve infarction along with mucosal thickening of paranasal sinuses, black turbinate sign and progressive narrowing of internal carotid artery provide early important clues towards diagnosis.

**KEY WORDS:** Rhinocerebral, mucormycosis, diffusion

#### eEdE-15

#### Neuroimaging of Systemic Lupus Erythematosus

Lin, D.·Zessler, A.·Oh, S.

Johns Hopkins University  
Baltimore, MD

#### PURPOSE

Systemic lupus erythematosus (SLE) is an autoimmune disorder with estimated central nervous system (CNS) involvement ranging from 18 to 70% of cases. The clinical manifestations are varied, and frequently include psychiatric disturbances, memory loss, headaches, seizures, transient ischemic attack, transverse myelitis, and chorea, reflecting a wide range of pathophysiologies, some of which may be a complication of treatment rather than related to the disease itself. Since the symptoms overlap with many other diseases, diagnosis can be difficult and neuroimaging is integral in the evaluation of these patients. This presentation aims to review the neuroimaging findings in patients with SLE, and correlate with clinical course and final diagnosis.

#### APPROACH/METHODS

Patients with established diagnosis of SLE presenting for neuroimaging in the past 10 years were searched from our radiology database. Imaging and corresponding medical records were reviewed retrospectively and the etiology associated with the imaging findings was determined.

#### FINDINGS/DISCUSSION

The most frequent findings were nonspecific chronic small vessel ischemic changes. Acute findings were varied, and MRI was important in delineating large artery territory infarct, small thrombotic infarcts (with basal ganglia predilection), venous infarction, and posterior reversible encephalopathy syndrome (PRES). One case of a 17-year-old girl with lupus diagnosed since age 12 showed dense calcification involving the basal ganglia, thalami and dentate nuclei similar to Fahr's disease, a pattern that has been described in SLE with calcific deposits found in the brain parenchyma, nuclei and arterial media. Because of the immunosuppressed state often induced by medication, patients with SLE are particularly susceptible to infections, including opportunistic viral, fungal and parasitic agents with a high mortality rate. There were two cases of mycobacterial infection, including TB basilar meningitis in one patient, and multiple TB abscesses in the brain and masticator space (in addition to soft tissues in the body) in the other patient. A 19-year-old girl with severe disease on chronic immunosuppression for lupus nephritis presented with a number of complex medical complications including right atrial thrombus, vancomycin-resistant enterococcal bacteremia, candida fungemia. This patient had a rapid clinical deterioration, with development of multiple cerebral hematomas, presumably related to septicemia. Two elderly women who had longstanding disease on chronic immunosuppression therapy developed mass-like white matter lesions representing

progressive multifocal leukoencephalopathy (PML). In both patients, JC virus was documented in the cerebrospinal fluid (CSF). Finally, acute transverse myelitis affecting a long segment of the spinal cord was found in a subset of SLE patients, producing symptoms of weakness, sensory deficits and autonomic dysfunction.

#### **SUMMARY/CONCLUSION**

Neurologic diseases associated with SLE are complex and the pathogenesis is incompletely understood. Neuroimaging, particularly MRI, plays an important role of evaluation and reveals different disease patterns that can be attributable to four possible conditions leading to cerebritis: antineuronal autoantibodies, cerebral vasculitis/vasculopathy, circulatory hypercoagulation, and thromboembolism. In addition, it contributes to the diagnosis of many other conditions that are not disease-specific but rather related to systemic or metabolic abnormalities, or immunosuppressive therapy.

**KEY WORDS:** Systemic lupus erythematosus, PRES, infection

#### **eEdE-16**

#### **Genomic Imaging: Creation of a Uniformed Terminology to Describe the Morphologic MR Imaging Features of Gliomas to Augment Clinical Research in the Genomics of Cancer: A TCGA Glioma Phenotype Research Group Project**

Flanders, A. E.<sup>1</sup>•Hwang, S.<sup>2</sup>•Nicolas-Jilwan, M.<sup>3</sup>•Raghavan, P.<sup>3</sup>•Colen, R. R.<sup>4</sup>•Gutman, D.<sup>2</sup>•Jain, R.<sup>5</sup>•Holder, C. A.<sup>2</sup>•Wintermark, M.<sup>6</sup>•Kirby, J.<sup>7</sup>•Rubin, D. L.<sup>8</sup>•TCGA Glioma Phenotype Research Group

<sup>1</sup>Thomas Jefferson University Hospital, Philadelphia, PA, <sup>2</sup>Emory University, Atlanta, GA, <sup>3</sup>University of Virginia, Charlottesville, VA, <sup>4</sup>Brigham and Womens, Boston, MA, <sup>5</sup>Henry Ford Hospital, Detroit, MI, <sup>6</sup>University of Virginia, Charleston, VA, <sup>7</sup>SAIC, Bethesda, MD, <sup>8</sup>Stanford University, Palo Alto, CA

#### **PURPOSE**

Current methods for assessing brain tumors and predicting clinical course based on radiologic imaging, such as MacDonald or RECIST criteria, do not exploit the diverse features currently visible on MR imaging. The purpose of this exhibit is to introduce the VASARI MRI featureset to other neuroradiologists. This featureset has been used successfully to grade the morphologic characteristics of primary brain tumors in clinical trials. Utilization of a comprehensive and consistent set of imaging features reduces ambiguity in characterization of brain tumors. This has ramifications not only in clinical trials research but also in communicating uniform and reliable results to the clinician.

#### **APPROACH/METHODS**

The process for devising this featureset began by cataloging the various measures/criteria for grading morphologic features of primary gliomas from the peer reviewed literature. Our reporting system is made up of 30 unique MR imaging features that easily are

understood and recognizable to domain experts (neuroradiologists). We expanded on the prior work to create a comprehensive set of image assessments for reporting and a controlled subjective terminology for describing brain tumors. These features are organized into five general categories: (1)lesion location, (2)morphology of substance, (3)margin, (4)changes in vicinity of lesion, and (5)remote alterations. Moreover, each feature response is recorded using controlled terminologies, enabling interoperability with other terminological standards, such as RadLex. In this exhibit we will guide the attendee through the entire VASARI featureset using visual examples of each morphologic feature and the corresponding grading system. We also will help explain through example how consistent use of a controlled terminology in brain tumor imaging augments both clinical reporting and clinical trials research.

#### **FINDINGS/DISCUSSION**

Radiologists are trained to utilize vocabularies to describe findings and communicate results. Unfortunately, because of the idiosyncratic methods in which we report findings it is difficult to mandate consistency or to derive meaning from a temporal analysis of the status of a disease. In the context of cerebral neoplasia there is ambiguity in the use of subjective MR features such as degree of enhancement, definition of margins, infiltration, discrimination between noncontrast enhancing tumor from edema. Terminologies often are used inconsistently or incompletely. While imaging plays a key role in establishing diagnosis and assessing response in oncology, the currently devised systems (e.g., MacDonald criteria) do not exploit successfully the rich imaging features that are available with modern MRI. ACR BI-RADS is a notable exception in which use of a controlled terminology has radically changed the value added of an imaging modality (mammography) in oncology. Adaptation of a similar process to other disease processes such as primary brain tumors also has value providing that the features are comprehensive, relatively easy to use with minimal training, are reproducible and can be validated with multiple observers.

#### **SUMMARY/CONCLUSION**

Our terminology and reporting system for assessing brain tumors captures a broad spectrum of rich and detailed imaging features. These comprehensive and detailed descriptors can be quickly adapted by neuroradiologists. Moreover, consistent use of a standardized vocabulary adds value to clinical imaging as a valid biomarker for grading and treatment response.

**KEY WORDS:** Glioblastoma, terminology, controlled vocabulary

**eEdE-17****Genomic Imaging: Gliomas and Perfusion Imaging: a TCGA Glioma Phenotype Research Group Project**

Jain, R.·TCGA Glioma Phenotype Research Group

Henry Ford Health System  
Detroit, MI

**PURPOSE**

Recent developments in microarray analysis of cancer genomes have led to an additional interest in correlation of gene expression with imaging features in gliomas to better understand the physiologic basis for the imaging heterogeneity of these aggressive neoplasms. The limited number of publications on this topic have correlated the presence or absence of contrast enhancement with various gene expression pathways affecting tumor cell mitosis, migration, angiogenesis, hypoxia, edema and apoptosis. The purpose of this exhibit is to discuss glioma genomic mapping and its integration/correlation with tumor kinetics, hemodynamic and physiologic parameters with the intent of improving understanding of the molecular basis for commonly used tumor perfusion parameters (such as blood volume and permeability) and show how these imaging biomarkers perform versus various molecular subclassification systems.

**APPROACH/METHODS**

We will discuss the role The Cancer Genome Atlas (TCGA) and Repository for Molecular Brain Neoplasia (REMBRANDT), which provide extensive multidimensional datasets, are playing in presenting a unique opportunity to integrate imaging and genomic data which in turn provides a more sophisticated understanding of gliomas. The role perfusion imaging (beyond the morphologic features) can play as far as correlation with immuno-histochemical and molecular basis of gliomas and patient survival will be discussed in detail. We will present our data regarding correlation of perfusion parameters with genomic expression related to tumor angiogenesis which forms the physiologic basis of these parameters. We will discuss the correlation of perfusion parameters with specific genes, pathways and molecular subclassifications of gliomas and particularly high-grade gliomas. Additionally we will review the prognostic role of CBV (cerebral blood volume) measures versus molecular subclassification systems.

**FINDINGS/DISCUSSION**

Correlation of the perfusion parameters has shown that some of the pro-angiogenic genes (*TNFRSF1A*, *HIF1A*, *KDR*, *TIE1* and *TIE2/TEK*) have a positive correlation and some of the antiangiogenic genes (*VASH2*) have an inverse correlation with tumor perfusion parameters (CBV and PS), suggesting a molecular basis for these imaging biomarkers. In another study of glioblastomas, rCBV measures did not show any difference between different subclasses of glioblastomas using Verhaak or Phillips classification system based on genomic/molecular mapping. In fact, rCBV measures predicted patient overall survival better than the

molecular subclasses, suggesting an important role noninvasive imaging biomarkers could play in patient prognosis and survival. We also will discuss our preliminary results of our current efforts looking at IDH1 and EGFR status and correlation with perfusion parameters in high-grade gliomas and will discuss other published data on this subject.

**SUMMARY/CONCLUSION**

Integration of imaging and genomic data is critical for a better understanding of gliomas, particularly considering the increasing focus on utilization of imaging biomarkers for patient survival and treatment response. Correlation of glioma perfusion parameters can help provide a better understanding of angiogenesis, specific genes and pathways; and can provide opportunities to target those specific molecular markers/pathways for improving patient response and prognosis.

**KEY WORDS:** Genomic mapping, glioma, perfusion imaging

**eEdE-18****Methodology for Imaging Genomics of Gliomas**

Colen, R. R.<sup>1</sup>·Mahajan, B.<sup>1</sup>·Sathyan, P.<sup>2</sup>·Kovacs, A.<sup>1</sup>·Zinn, P. O.<sup>2</sup>·Jolesz, F. A.<sup>1</sup>

<sup>1</sup>Brigham and Women's Hospital, Boston, MA, <sup>2</sup>M.D. Anderson Cancer Center, Houston, TX

**PURPOSE**

To demonstrate the methodology for radiogenomic analysis by performing tumor volumetric analysis for genomic correlations and its feasibility. Radiogenomics links gene expression profiles with MRI phenotypes. The radiogenomic screen using tumor volumetrics has the potential to uncover genomic targets for subsequent development into cancer therapeutics. Here, we demonstrate the methodology and feasibility for the first comprehensive radiogenomic analysis using quantitative MRI volumetrics and large-scale gene- and microRNA expression profiling in GBM.

**APPROACH/METHODS**

Using The Cancer Genome Atlas (TCGA), we identified 78 treatment-naïve GBM patients whom had both gene- and microRNA expression profiles and pretreatment MR-neuroimaging. The 3D Slicer software 3.6 (<http://www.slicer.org>) was used for image analysis and image review was done in consensus by two neuroradiologists. Fluid-attenuated inversion recovery (FLAIR) was used for segmentation of the edema and postcontrast T1-weighted imaging (T1W1) for segmentation of enhancement (defined as tumor) and necrosis. To account for FLAIR and postcontrast T1W1 obtained with different slice parameters, angles or voxel thickness, we rigidly aligned and registered the scans to each other. In some cases where the voxel size of the FLAIR and T1W1 series varied, we resampled the FLAIR volume to the matrix of T1W1 series. Segmentation was carried out in a simple hierarchical model of anatomy, proceeding from peripheral to central. Three distinct

structures were segmented (edema/invasion, enhancing tumor, and necrosis). Subsequently, the models of edema, tumor and necrosis were generated from the previously performed segmentations, and the volumes of the same were calculated automatically. These imaging segmentations then were correlated with the genomic findings.

#### **FINDINGS/DISCUSSION**

In most scans, image registration was 100%. In those scans in which complex rotation modifications and registrations were required, registration was deemed adequate when error was 2 mm or less. The quantitative tumor volumes of edema/invasion, enhancement, and necrosis correlated highly with biologically concordant functional genomic targets.

#### **SUMMARY/CONCLUSION**

Quantitative tumor volumetry obtained from routine MRI scans can be used to predict genomic tumor composition. It can be used as a discovery tool to uncover novel genomic targets that can be used to develop targeted therapeutics. The ability to determine (uncover) genomic targets from routine clinical MRI examinations and thus subsequently if a patient is a candidate for that genomic therapy is a major step towards personalized medicine.

**KEY WORDS:** Glioblastoma, genomics, radiogenomics

#### **eEdE-19**

##### **Pseudoprogression and Pseudoresponse: MR Imaging Findings, Clinical Aspects and the Posttreatment Tumor Response Criteria**

Cruz, L. H.<sup>1</sup>Rodriguez, I.<sup>1</sup>Domingues, R.<sup>1</sup>Galheiro, D.<sup>2</sup>Fatterpekar, G.<sup>2</sup>

<sup>1</sup>IRM, Rio de Janeiro, BRAZIL, <sup>2</sup>New York University, New York, NY

#### **PURPOSE**

Though brain neoplasm treatment has improved, the characteristics and the imaging findings related to treatment have changed. This exhibit aims to illustrate the most common MRI findings related to brain neoplasm treatment, with emphasis to MRI features that can help in the differential diagnosis between residual tumor and treatment-related changes.

#### **APPROACH/METHODS**

We will review the most important imaging points of MR imaging findings related to brain neoplasm treatment. The MR findings are discussed with emphasis on feasibility, advantages and limitations over conventional and advanced MR imaging. Introduce the main MRI characteristics of pseudoprogression and pseudoresponse, discussing their pathophysiologic and clinical features as well as differential diagnosis with radionecrosis and recurrent tumor.

#### **FINDINGS/DISCUSSION**

Newly therapeutic approach to brain tumor includes drugs that cause brain parenchyma abnormalities,

mostly related to lesion enhancement and blood-brain barrier integrity. Alterations in the enhancing portion of the lesion may vary depending on the drug administered. Thus, MacDonald criteria, the mostly used criteria, are no longer able to make such difference. The differential diagnosis between posttreatment changes related to residual neoplasm is challenging, even when using advanced MR techniques. With new treatment regimen, new criteria, like RANO, could be indicated more to approach these posttreatment changes.

#### **SUMMARY/CONCLUSION**

Extensive effort in the radiology community has been expended to develop imaging methods to distinguish alterations secondary to treatment from recurrent tumor. However, none of these methods actually work. The knowledge of MRI pattern related to treatment failure and findings related to brain neoplasm treatment are of utmost importance in the patient management and prognosis. Moreover, new MRI pattern secondary to new treatment approach should be well known by radiologists.

**KEY WORDS:** Pseudoprogression, pseudoresponse

#### **eEdE-20**

##### **Albumin-Bound Blood Pool Contrast Agents and Dynamic Contrast-Enhanced Brain Tumor Imaging: Assessing Tumor Morphology and Physiology**

Chwang, W. B.<sup>1</sup>Jain, R.<sup>1</sup>Arbab, A.<sup>1</sup>Bagher-Ebadian, H.<sup>1</sup>Ewing, J.<sup>1</sup>Essig, M.<sup>2</sup>

<sup>1</sup>Henry Ford Hospital, Detroit, MI, <sup>2</sup>Heidelberg Medical School, Heidelberg, GERMANY

#### **PURPOSE**

Dynamic contrast-enhanced (DCE) T1-weighted magnetic resonance imaging is being used increasingly in clinical trials involving brain tumors. It allows characterization of the vascular microenvironment in tumors by measurement of parameters such as Ktrans (forward transfer constant), kep (reverse transfer constant), ve (volume of the extravascular extracellular space), and vp (blood plasma volume). These parameters reflect specific physiologic characteristics and relate to various aspects of tumor biology. However, currently available FDA-approved extravascular contrast agents (CAs) used for brain tumor assessment are low molecular weight (~ 0.5 kDa). Their delivery is usually flow-limited, leading to rapid extravasation from the vascular compartment into the interstitium (extravascular extracellular space), hence making them ill-suited for assessing physiologic measures. The purpose of this exhibit is to examine the pharmacokinetics of gadofosveset, an albumin-bound blood pool contrast agent, and its role in assessment of tumor morphology and tumor kinetics using DCE-T1 MR perfusion in both human as well as animal studies.

#### **APPROACH/METHODS**

Examples of human brain tumors scanned using gadofosveset (high molecular weight blood pool agent,

>64 kDa) versus Gd-DTPA (low molecular weight extravascular agent, ~ 0.5 kDa) will be shown, and the advantages and limitations of each will be discussed. Additionally, rat brain tumor model studies using gadofosveset versus Gd-DTPA will be presented, along with differences in wash-in and wash-out with each CA. Quantitative estimates of vascular physiologic measures using multicompartment pharmacokinetic modeling will be presented, and the advantages and limitations of using blood pool CAs will be detailed as will differences in treatment response assessment using the two different CAs in a rat brain tumor model after antiangiogenic treatment.

#### FINDINGS/DISCUSSION

Human brain tumors scanned with gadofosveset and Gd-DTPA demonstrated different spatial and temporal patterns of enhancement, although visual intensities and rates of tumor detection were similar. The major advantage of gadofosveset was its persistent, longer-lasting tumor enhancement relative to conventional gadolinium-based agents, achieved at roughly one third of the dose (0.03 mmol/kg of gadofosveset versus 0.1 mmol/kg of Gd-DTPA).

In the rat brain tumor model, gadofosveset intensely enhanced the margin of the tumor, while showing less enhancement of the lesion core. Gd-DTPA resulted in greater and faster diffusion of contrast in the (presumably necrotic) core regions. In addition, Gd-DTPA demonstrated faster washout of CA signal intensity over time when measured at the brightest regions of enhancement. Following antiangiogenic treatment in the rat tumor model, the differences in gadofosveset and Gd-DTPA were accentuated. At the brightest regions of enhancement, gadofosveset demonstrated significantly less extracellular extravasation, presumably due to reduced leakiness of tumor vasculature. Thus, a blood pool CA may provide a more accurate assessment of treatment response.

#### SUMMARY/CONCLUSION

Due to different pharmacokinetics (and particularly albumin-binding properties), gadofosveset and Gd-DTPA behave differently with regard to brain tumor enhancement following IV administration. The hemodynamic and physiologic parameters determined by these CAs differ significantly. Albumin-bound blood pool CAs may provide additional information about brain tumor morphology and kinetics, and hence, also may help better assess treatment response particularly after antiangiogenic therapy.

**KEY WORDS:** Blood pool, dynamic contrast-enhanced MR imaging, brain tumor

#### eEdE-21

##### Imaging Genomics: Correlation of Invasive Genomic Composition and Patient Survival Using Qualitative and Quantitative MR Imaging Parameters

Colen, R. R.<sup>1</sup>•Mahajan, B.<sup>1</sup>•Flanders, A.<sup>2</sup>•Huang, E.<sup>3</sup>•Jain, R.<sup>4</sup>•Gutman, D.<sup>5</sup>•Hwang, S.<sup>5</sup>•Kirby, J.<sup>6</sup>•Freyman, J.<sup>6</sup>•TCGA Glioma Phenotype Research Group•Jolesz, F.<sup>1</sup>•Zinn, P. O.<sup>7</sup>

<sup>1</sup>Brigham and Women's Hospital, Boston, MA, <sup>2</sup>Thomas Jefferson University Hospital, Philadelphia, PA, <sup>3</sup>National Cancer Institute, Bethesda, MD, <sup>4</sup>Henry Ford, Detroit, MI, <sup>5</sup>Emory University, Atlanta, GA, <sup>6</sup>SAIC-Frederick, Bethesda, MD, <sup>7</sup>M.D. Anderson Cancer Center, Houston, TX

#### PURPOSE

To describe and identify the invasive MRI characteristics in GBM and the implicated genes and microRNAs associated with these invasive features. Preoperative qualitative imaging data reflective of invasive tumor growth patterns have been documented. These include the presence of either T1 contrast enhancement or increase T2/FLAIR hyperintensity involving the basal ganglia, corpus callosum (unilateral, bilateral, or contralateral,) or brainstem; the presence of subependymal enhancement; the presence of pial enhancement; and a peritumoral nonenhancing FLAIR hyperintensity. Tumor volumetry of the nonenhancing FLAIR hyperintensity also has been validated to reflect increase tumor invasion.

#### APPROACH/METHODS

A total of 78 treatment-naïve GBM patients who had both gene- and microRNA expression profiles and pretreatment MR neuroimaging were analyzed. Each image (T1 axial image both before and after gadolinium contrast administration, and axial T2/FLAIR image) was assessed qualitatively by at least three independent neuroradiologists. The standardized VASARI feature set criteria was used for qualitative visual assessment of key features of invasion [presence of either T1 contrast enhancement or increase T2/FLAIR hyperintensity involving the basal ganglia, corpus callosum (unilateral, bilateral, or contralateral) or brainstem; the presence of subependymal enhancement; and the presence of pial enhancement; and a peritumoral nonenhancing FLAIR hyperintensity]. For quantitative assessment, we performed volumetric analysis using the 3D Slicer platform to quantitatively measure actual volumes of each individual region. The FLAIR-volume, contrast-enhancing region, and necrotic core were segmented independently and verified by a trained neuroradiologist (RRC, FAJ) experienced in tumor volumetry. The genes and microRNAs associated with these were elucidated and the patient survival using Kaplan Meir curves were determined.

#### FINDINGS/DISCUSSION

Invasive features of MRI as determined by both qualitative and quantitative assessment reflect tumor compositions which have genes involved in invasion and differences in patient survival. This is important as invasive phenotypes seen on MRI can help identify



patients with a certain genomic characteristic and with help predict patient survival.

#### **SUMMARY/CONCLUSION**

Invasive features identified by MRI can serve as biomarker to help predict tumor genomic compositions and patient survival.

**KEY WORDS:** Glioblastoma, imaging genomics, invasion

#### **eEdE-22**

### **Ruminating over Fat-Containing Intracranial Lesions**

Kalra, V. B.·Gilbert, J.·Malhotra, A.

Yale University  
New Haven, CT

#### **PURPOSE**

Fat-containing intracranial lesions can be recognized easily on CT and MR and often are dismissed as incidental lipomas, with their more subtle associated findings overlooked. The differential for fat-containing intracranial lesions extends beyond the common lipoma, dermoid, teratoma. We present a review of fat-containing intracranial lesions based on etiology and prevalence, discuss the various locations of lipomas and their associated findings, and present case examples of other lesions with discussion of radiologic and pathologic features.

#### **APPROACH/METHODS**

Fat-containing intracranial lesions can be grouped by etiology and prevalence. These groups include congenital, common neoplasms, rare neoplasms, and other. Examples from each group are presented with case examples and discussion of the radiologic and pathologic features of each. Lipomas, as the most prevalent fat-containing intracranial lesions, are discussed with attention to their extensive subarachnoid distribution and their associated findings.

#### **FINDINGS/DISCUSSION**

Congenital lesions include lipoma, dermoid, and epidermoid. Multiple cases of lipomas in various subarachnoid spaces are used to highlight their associated parenchymal abnormalities. Common neoplasms include germ cell neoplasms, craniopharyngioma, and primitive neuroectodermal tumor. Rare neoplasms include lipomatous transformation of meningioma, angiolipoma, hibernoma, fat-containing solitary fibrous tumor (lipomatous hemangiopericytoma), and liponeurocytoma. Other lesions include fat embolism and rupture of sacral dermoid.

#### **SUMMARY/CONCLUSION**

Fat-containing intracranial lesions have imaging features that confirm the presence of lipids. Lipoma, the most common benign fat-containing lesion, warrants close evaluation for subtle associated cortical dysplasia. Lipomas can be distinguished from other fat-containing intracranial lesions by the presence of nondisplaced intralésional vessels. Although most lesions represent

either lipoma, dermoid or teratoma, other more uncommon etiologies should be considered.

**KEY WORDS:** Lipoma, fat, neoplasms

#### **eEdE-23**

### **Imaging Glioblastoma: Neuroradiology from the Neurooncologists' Perspective**

Buckle, C.·Collins, J.·Poon, C.·Lukas, R. V.

University of Chicago Hospitals  
Chicago, IL

#### **PURPOSE**

This exhibit explores the neuroimaging of glioblastoma (GBM) by focusing on the imaging findings most important to referring neurooncologists as they evaluate and manage a patient with GBM. In doing so, we highlight the importance of close collaboration between neurooncology and neuroradiology to optimize the value of imaging in the care of the GBM patients.

#### **APPROACH/METHODS**

Using an interactive format and a case-based approach, we provide a framework for radiology reporting that specifically address neurooncologists' most important concerns. This exhibit combines the experience at our institution with the current research from the neurooncology and neuroradiology literature.

#### **Findings/Discussion**

Glioblastoma is the most common malignant brain tumor in adults, and can present with variable imaging features. Objectives of imaging include initial diagnosis, treatment planning and posttreatment follow up of patients. The exhibit will discuss each objective in three parts: 1. Diagnosis of glioblastoma. The exhibit will discuss clinical and imaging features that differentiate glioblastoma from mimics such as lymphoma and tumefactive multiple sclerosis, along with the use of imaging in the accurate localization of tumor margins and in guiding follow up with biopsy or serial imaging. 2. Treatment planning. Once diagnosed, imaging plays an important role in treatment planning. This exhibit will provide a clinical perspective on how location, size and signal characteristics of the tumor features can have implication in treatment planning. For example, the presence of hemorrhage can affect the decision of antiangiogenic therapy. 3. Posttherapy follow up: On completion of therapy, imaging is helpful to evaluate response and survey for recurrence. The exhibit will address frequency and protocols for posttherapy imaging, and discuss imaging features suggestive of recurrence and helpful in management including RANO criteria, pseudoprogression, pseudoregression and pseudoresponse.

#### **SUMMARY/CONCLUSION**

The neuroradiologist is an important member of the interdisciplinary team caring for GBM patients. Neuroimaging plays an important role at each stage of patient care and understanding the needs of the referring neurooncologist is paramount to optimizing

the use of imaging in the management of patients with GBM.

**KEY WORDS:** Glioblastoma, neurooncology, clinical

#### eEdE-24

### MR Imaging Using Blood Pool Contrast Agents for Glioblastoma: Current Status and Future Prospects

Puig Alcantara, J.<sup>1</sup>Blasco, G.<sup>1</sup>Essig, M.<sup>2</sup>Daunis-i-Estadella, J.<sup>3</sup>Bergmann, K.<sup>4</sup>Pedraza, S.<sup>1</sup>

<sup>1</sup>Hospital Universitari Dr Josep Trueta, Girona, SPAIN,

<sup>2</sup>University of Erlangen, Erlangen, GERMANY,

<sup>3</sup>Universitat de Girona, Girona, SPAIN, <sup>4</sup>GMA Diagnostic Imaging, Berlin, GERMANY

#### PURPOSE

Contrast-enhanced MRI is the modality of choice for evaluating brain tumors. Gadolinium-based agents are the most commonly used contrast agents in clinical MRI. This exhibit describes the usefulness of the protein-binding blood pool contrast agent (BPCA) gadofosveset in the pretreatment assessment of patients with glioblastoma and highlights its potential for improving the diagnostic quality of contrast-enhanced MRI in brain tumors.

#### APPROACH/METHODS

1. We explain the mechanism of action of BPCA, with particular emphasis on protein targeting and increased T1 relaxivity. 2. We explain how to optimize the use of BPCA for imaging tumors in clinical practice. 3. We use cases from our research on glioblastomas to illustrate the spectrum of tumor enhancement and findings on tumor steady-state MR angiograms obtained with BPCA and to discuss the potential clinical utility of BPCA. 4. We discuss the potential of using BPCA as a surrogate marker of tumor angiogenesis.

#### FINDINGS/DISCUSSION

Blood pool contrast agents represent a new class of contrast agents for tumor imaging. Gadofosveset binds strongly but reversibly to albumin in plasma, leading to higher relaxivity (four or five times higher) and better vascular retention resulting in longer intravascular half-life (~16 hours vs ~90 min) than extracellular contrast agents. These particular characteristics result in increased tumor enhancement, enabling better diagnostic information endpoints for high-grade glioma (more accurate delineation of tumor margins and extension that allow better planning for resection and radiation treatment) and a longer window for data acquisition. In particular, gadofosveset provides strong and persistent high intravascular enhancement, which can be exploited to acquire additional high-resolution images in the steady-state, enabling better delineation of neovessels. The ability of MRI techniques using BPCA to reveal changes in tumor microvasculature is likely to accelerate the development, testing, and monitoring of new antiangiogenic drugs. Additionally, BPCA make it possible to reduce the dose of contrast compared to extracellular gadolinium agents (0.03 mmol/kg vs 0.1-0.3 mmol/kg) without diminishing scan quality.

#### SUMMARY/CONCLUSION

Overall, the future of BPCA imaging is promising. This exhibit shows the usefulness of gadofosveset in the diagnostic workup of glioblastoma. It discusses the potential role of BPCA as a reliable noninvasive imaging technique for the in vivo assessment and monitoring of angiogenesis and the need for further studies to validate the full utility of MRI using BPCAs in the diagnosis and follow up of brain tumors.

**KEY WORDS:** Tumor, contrast agents, blood pool contrast agents

#### eEdE-26

### Central Skull Base Lesions: Pictorial Review and Diagnostic Approach

Saha, A.·Thurlow, P. C.·Fukui, M. B.·Goldberg, M. F.

West Penn Allegheny Health System  
Pittsburgh, PA

#### PURPOSE

The skull base is an anatomically complex area where a variety of pathologic processes can develop. The purpose of this exhibit is to review the computed tomography (CT) and magnetic resonance (MR) characteristics of central skull base lesions.

#### APPROACH/METHODS

This exhibit will begin with a review of skull base anatomy. The bulk of the exhibit will utilize a case-based format to discuss the imaging appearances of various lesions involving the central skull base. CT and MR are used in complementary fashion in the evaluation of skull base lesions. Specifically, CT is excellent for assessing the extent of bony involvement while MR is used primarily to more definitively characterize soft tissue components of a mass.

The reader also will learn a systematic approach to characterizing complex lesions. Emphasis will be placed on identifying 1) lesion location and extension to critical adjacent anatomy, 2) typical imaging features, 3) and imaging technique.

#### FINDINGS/DISCUSSION

The skull base is made up of five bones: paired frontal and temporal bones, unpaired ethmoid, sphenoid and occipital bones. The endocranial surface faces the brain, cisterns, cranial nerves, and intracranial vessels. Exocranial surfaces face extracranial soft tissue structures. The skull base can be divided further into the anterior skull base, central skull base, and posterior skull base; appropriate localization to one of these three locations is essential for arriving at the correct diagnosis. Within each of these locations, categories of disease to consider include: 1) skull base extension from extracranial head/neck disease, 2) non-neoplastic primary bone disease, 3) neoplastic primary bone disease, 4) metastatic disease, 5) cranial nerve neoplastic disease. Common central skull base masses to be reviewed include pituitary macroadenoma, aneurysm, arachnoid cyst, epidermoid/dermoid, craniopharyngioma, hypothalamic glioma/hamartoma,

metastasis, meningioma, and masses of the petrous apex. Rarer lesions to be discussed include chordoma/chondrosarcoma, neuroblastoma, giant cell tumor, and fungal infection, among others. Comment will be made on key diagnostic clues and pitfalls, and imaging features of particular importance for surgical planning. This review also will include "do not touch" lesion mimics, including trapped fluid within the petrous apex, asymmetric marrow/pneumatization of the petrous apex, and petrous apex cephalocele.

#### **SUMMARY/CONCLUSION**

The central skull base is host to a wide range of pathologic processes. This imaging-based educational exhibit provides a review of CT and MR characteristics of central skull base lesions as well as a systematic approach for characterizing complex lesions.

**KEY WORDS:** Skull base, neoplasm, skull anatomy

#### **eEdE-27**

##### **Response Assessment in Brain Tumor Imaging: Beyond the Morphologic Imaging**

Griffith, B.·Jain, R.

Henry Ford Hospital  
Detroit, MI

#### **PURPOSE**

Recurrent or progressive enhancing lesions following brain tumor treatment are common findings in the imaging surveillance of neuro-oncologic patients. While these lesions can represent tumor recurrence, they also may be attributed to "pseudo-progression" or treatment effects. However, differentiating these two entities based on conventional/morphologic imaging is usually difficult. The purpose of this review is to discuss a variety of functional imaging modalities/techniques that can provide information about various metabolic (MR spectroscopic imaging, PET imaging) and physiologic (DWI, perfusion imaging) aspects of the recurrent/progressive enhancing lesion to differentiate treatment effects from true tumor progression.

#### **APPROACH/METHODS**

We will show clinical examples of various entities including pseudo-progression, pseudo-response, and true tumor progression, as well as radiation necrosis. We will discuss the limited role of morphologic imaging features/conventional MRI and the importance of advanced functional imaging techniques in aiding clinical decision making. The advantages and limitations of various perfusion imaging modalities (CT perfusion, MR perfusion - DSCT2\*, DCET1) also will be discussed in detail and will be further enhanced with clinical cases from our own teaching files. We also will discuss the role of advanced functional imaging modalities, particularly perfusion imaging, in assessing treatment response and patient prognosis. We will provide data from our own research, as well as data from other published literature, to provide insight into the role of various quantitative and semiquantitative indices in

differentiating treatment effects from recurrent or progressive tumor.

#### **FINDINGS/DISCUSSION**

Most brain tumor patients undergo combination therapy regimens consisting of surgical debulking, radiation and chemotherapy. This often leads to an increase in the size of the residual enhancing lesion and/or edema in the short term, which may be misinterpreted as progression of tumor, whereas in fact, some of these changes may be attributed to "pseudo-progression". This recurrent progressive enhancing lesion may represent a combination of treatment-induced necrosis, postictal changes, postoperative infarcts, and increased vascular permeability due to tapering of steroid dose, as well as tumor growth. Similarly, patients undergoing antiangiogenic treatment may show very rapid and marked reduction in tumor enhancement even though those changes may actually reflect treatment effects rather than true response to therapy as the nonenhancing infiltrative tumor may continue to grow. This marked reduction in enhancement has been loosely referred to as "pseudo-response" and is an important consideration in evaluating response assessment. While very similar in appearance on conventional/morphologic imaging, advanced functional imaging techniques provide a potential means of differentiating these two entities and can play a vital role in patient management.

#### **SUMMARY/CONCLUSION**

Response assessment in brain tumor imaging can be quite challenging given the similar appearance of tumor progression and posttreatment change ("pseudo-progression"). As such, response assessment in the present day neurooncology practice should routinely include advanced functional imaging techniques as many decisions regarding treatment effects and treatment response require hemodynamic and/or physiologic information beyond what conventional morphologic MR imaging features can provide.

#### **eEdE-28**

##### **Tackling Pineal Region Lesions: A Case-Based Interactive Review**

Yahyavi-Firouz-Abadi, N.·Miller-Thomas, M.·Wippold, F. J.

Mallinckrodt Institute of Radiology  
St Louis, MO

#### **PURPOSE**

Accurate diagnosis of pineal region lesions is crucial given the critical anatomical location and wide spectrum of biological behavior of these lesions. This exhibit demonstrates the distinctive imaging findings of pineal region lesions using an interactive, case-based approach that emphasizes aid differential diagnosis.

#### **APPROACH/METHODS**

This presentation uses an interactive, case-based and quiz-type format. Cases include germ cell tumors (germinoma, teratoma, choriocarcinoma), primary

tumors of the pineal gland (pineocytoma, pineal parenchymal tumor of intermediate differentiation, pineoblastoma), pineal gliomas, invasion by adjacent tumors (meningioma, lymphoma), metastases, pineal cysts, and vein of Galen malformations.

#### **FINDINGS/DISCUSSION**

Pineal gland tumors display unique pathologies and behaviors and may be overlooked by the busy radiologist. Pineal masses may be discovered as incidental findings in almost 10% of brain MRIs and 40% of autopsies. Lesions may cause significant symptoms due to compression of the midbrain, aqueduct of Sylvius, and superior colliculi and may produce Parinaud syndrome or obstructive hydrocephalus. They also may cause endocrine disturbances such as precocious puberty. Masses range from benign cysts (most common) to highly malignant pineoblastomas. Despite significant overlap in the imaging features of many pineal masses, differentiation among types of malignant and benign lesions is often possible using such clues as the pattern of calcification and enhancement. Cysts are often well-circumscribed lesions with rim calcification (25%) and enhancement after contrast (60%). Germinomas often enhance and cause central calcification of the gland surrounded by tumor ("engulfed calcification"). In contrast, primary pineal parenchymal tumors may result in "exploded calcification" pattern.

#### **SUMMARY/CONCLUSION**

In summary, this exhibit reviews an approach to pineal region lesions in an interactive case-based format emphasizing distinctive imaging signs that aid in accurate diagnosis.

**KEY WORDS:** Pineal gland, mass, differential diagnosis

#### **eEdE-29**

##### **Doctor, I Need a Brain Atlas to Communicate with You**

Nowinski, W. L.·Chua, B.·Qian, G.·Johnson, A.·Drobnik-Kurzynska, P.·Aminah, B.·Nowinska, N. G.

Singapore Bioimaging Consortium  
Singapore, SINGAPORE.

#### **PURPOSE**

As the brain is the most complex living organ, explanation of its structure, function and particularly pathology by a doctor to a patient is vastly complicated. Similarly, the patient unfamiliar with neuroanatomy, pathology and terminology has great difficulty in inquiring the doctor and making decisions he/she is not prepared for. We propose to use a three-dimensional (3D), fully parcellated and labeled brain atlas along with suitable informative and simulation tools as an intelligent interface for improvement of bilateral doctor-patient communication.

#### **APPROACH/METHODS**

A 3D brain atlas was developed earlier from 3/7 T in vivo scans and a virtual cerebral model was constructed

with structure, vasculature, and white matter tracts. For our purposes, the cerebral model is extended with functional (Brodmann's) areas and cranial nerves. The cortical (Brodmann's) areas and deep nuclei also are labeled with function. A computer application is developed with: 1) atlas as an anatomy browser; 2) informative module with structure-function relationships; 3) simulator of cerebral lesions (tumors, infarcts, hematomas, aneurysms) allowing a doctor to set the location and size of a simulated lesion; 4) neurologic disorders database providing a list of disorders with symptoms and for each disorder its potential localization in the atlas; and 5) pathology module enabling a patient to study the specific simulated lesion and any other pathology from the disorders database, and to better understand structure and function involved.

#### **FINDINGS/DISCUSSION**

This atlas facilitates a doctor to explain brain pathology to a patient and its correlation to structure and function. The application helps a patient to understand doctor's explanation and study it further by correlating pathology with structure and function involved while using the brain atlas as anatomy browser. An interactive 3D brain atlas empowered with suitable tools: 1) presents pathology (such as lesion or infarct) in 3D along with structures, vessels, cranial nerves, and tracts involved; 2) teaches correlation of 3D structure with function; and 3) easily communicates pathology location and size along with the impaired functions.

#### **SUMMARY/CONCLUSION**

This exhibit illustrates a paradigm shift in doctor-patient communication by means of a 3D interactive brain atlas empowered with informative and simulation tools.

**KEY WORDS:** Brain atlas, pathology simulation, structure-function relationship

#### **eEdE-30**

##### **Web-Based Testing of Both Recognition and Interpretative Skills: Head CT Module**

Cook, T.·Aquino, C.·Mamourian, A.

Hospital of the University of Pennsylvania  
Philadelphia, PA

#### **PURPOSE**

There are countless unknown radiology cases available, both in text and online, structured as teaching files, formal presentations, or informal collections of interesting cases. Regardless, they all provide a small subset of images on which the findings of interest are conspicuous and challenge the trainee to provide the diagnosis or appropriate differential. This is a well accepted technique to teach image interpretation that has educational value and also replicates the oral boards structure. However, it does not test the trainee's observational skills. And since less than six images usually are offered for each case and all the cases are abnormal, it has little in common with daily reading

where it is not uncommon to have hundreds of images for each case. To realistically test the ability of residents and fellows to recognize abnormalities on CT scans of the brain, we have developed a web-based exam that mixes normal cases with abnormal exams. All cases are presented as scrollable image stacks, to replicate the way they would be viewed on a PACS workstation.

#### **APPROACH/METHODS**

The complete set of 5mm axial images from 20 abnormal and five normal head CT scans resides on a web server. It is available freely and trainees can create an account with which to access the system. The cases include an early infarct, meningioma, subdural, sellar mass, pineal cyst, venous occlusion, air embolus, encephalocele, and subarachnoid hemorrhage. The exam is structured as a self-test, with multiple choice questions after each case that can be viewed only after the images are reviewed. By using multiple-choice questions the test is scored automatically and trainees can see immediately how they compare with their peers. Their score is presented on a rank list without their names or program affiliations attached, and they can see how their score compares to both their peers and overall. Answers to each of the cases are provided at the conclusion of the exam, along with supporting images such as reconstructions or MR scans.

#### **FINDINGS/DISCUSSION**

We have created a test of visual perception specifically for neuroimaging using CT scans that presents the cases as they would be viewed on a PACS workstation.

#### **SUMMARY/CONCLUSION**

This demonstration image set is intended to have an educational value but this approach could be adapted easily in order to test residents' skills prior to taking call or measure progress during training.

**KEY WORDS:** Web-based teaching, interactive

#### **eEdE-31**

#### **Comparison of Free Advanced 3D Visualization Tools for CT Neuroangiography**

Blanch, R.-King, K.

University of Texas Southwestern Medical Center  
Dallas, TX

#### **PURPOSE**

As spatial resolution of CT neuroangiography continues to improve, the amount of data available for analysis increases exponentially. Postprocessing and advanced visualization tools are increasingly important in order to fully interpret, analyze, and present pertinent anatomy and pathology; 2D evaluation of cross-sectional imaging alone is often inadequate and does not utilize the full potential of volumetric datasets. Several advanced 3D visualization tools are freely available for education and research purposes that provide power, flexibility, and simplicity that can compete with similar commercial products. Although well-known and regularly utilized by some researchers,

many clinicians and educators are unfamiliar with these tools or unaware that free alternatives exist. The purpose of this education exhibit is to familiarize the reader with several free or open source 3D visualization programs useful for the analysis of CT angiography datasets of the brain. Reviews and comparisons of these tools and examples of their use in the context of education or research will be provided.

#### **APPROACH/METHODS**

The educational exhibit reviews and compares the following products: MeVisLab by MeVis Medical Solutions AG, 3D Slicer by the Slicer Community, ImageVis3D by Scientific Computing and Imaging Institute, and AmbiVu 3D Workstation by AmbiVu. Products were selected based on licensing (free for education or research) and designed use (for the display and analysis of medical datasets). For each product a brief summary of the basic features useful for visualization of CT angiography of the brain is provided, as well as a short tutorial on loading a DICOM dataset. Additionally, descriptions of licensing, advanced features, customizability, and ease of use are discussed. Comparison between the products also includes individual program size and speed, 2D and 3D rendering speed, hardware compatibility, rendering quality, and product documentation. Rendering speed compares framerates during rotation, translation, magnification, windowing, scrolling, and MPR and MIP slab thickness adjustments.

#### **FINDINGS/DISCUSSION**

MeVisLab is full-featured, flexible 2D/3D visualization software that is modular, expandable and supports large datasets (1500+ images) with GPU-enabled rendering. In addition to standard 2D/3D visualization tools, advanced features such as curved MPR and vessel tracing are provided. 3D Slicer is an open source advanced 3D visualization toolkit designed for research purposes that provides standard 2D and GPU-enabled 3D volume rendering. The program is modular and expandable with a rich set of annotation features. ImageVis3D is an open source volume rendering program designed for simplicity, scalability and interactivity that provides standard 2D/3D toolsets, allows GPU-enabled rendering, supports large datasets (terabyte+), and includes a mobile version for iOS devices. AmbiVu 3D Workstation provides 2D/3D visualization with standard 2D and 3D toolsets as well as MPR, MIP slab, and 3D volume rendering. Although less flexible and expandable than other products, AmbiVu is easy to use and provides very fast image rendering.

#### **SUMMARY/CONCLUSION**

Advanced visualization tools enhance the interpretation of CT angiograms of the brain generated by the latest generation scanners. This educational exhibit introduces the reader to some of the tools available by summarizing and comparing four freely available software packages that provide advanced 2D and 3D visualization tools.

**KEY WORDS:** CT angiography, 3D visualization, education

### eEdE-32

#### Arterial Spin Labeling Perfusion MR Imaging in Clinical Neuroradiologic Practice: A Pictorial Review

Acou, M. A. E. • Deblaere, K. • Achten, E.

Ghent University Hospital  
Ghent, BELGIUM

#### PURPOSE

To illustrate the use of arterial spin labeling (ASL) perfusion MRI in clinical neuroimaging.

#### APPROACH/METHODS

Arterial spin labeling is a noninvasive MR perfusion method capable of qualitatively and quantitatively depicting global and local states of hypo- and hyperperfusion. The ASL technique used is dynamic arterial spin labeling (dASL). We show the application of ASL perfusion in common disease entities with emphasis on neuro-oncology and cerebrovascular diseases. Correlation is made with structural MRI and dynamic susceptibility-weighted contrast-enhanced (DSC) MR imaging.

#### FINDINGS/DISCUSSION

In the setting of neurooncology, we focus on tumor grading, as well as on treatment follow up: tumor progression, tumor recurrence and radiation necrosis. Concerning cerebrovascular diseases, we show cases of acute ischemia, chronic cerebrovascular occlusive disease, arteriovenous malformations and moyamoya, as well as the possibility of testing vascular reactivity. Arterial spin labeling perfusion can be of particular interest in case of severe renal insufficiency and allergy to gadolinium-based contrast agents. Moreover, its quantitative possibilities render ASL an interesting tool in follow-up studies.

#### SUMMARY/CONCLUSION

Perfusion imaging has acquired an important role in daily neuroradiologic practice. We illustrate the role of ASL perfusion MRI as a noninvasive alternative to DSC-MR perfusion imaging, especially in tumor imaging and cerebrovascular diseases.

**KEY WORDS:** Perfusion, MR imaging, brain

### eEdE-33

#### Metallic Artifacts in MR Imaging for Dummies

Trelles de Belaunde, M.<sup>1</sup> • Ai, T.<sup>2</sup> • Goerner, F.<sup>1</sup> • Padua, A.<sup>3</sup> • Nittka, M.<sup>4</sup> • Runge, V.<sup>1</sup>

<sup>1</sup>University of Texas Medical Branch at Galveston, Galveston, TX, <sup>2</sup>Tongji Hospital, Huazhong University of Science and Technology, Wuhan, CHINA, <sup>3</sup>Siemens Healthcare, Houston, TX, <sup>4</sup>Siemens Healthcare, Erlangen, GERMANY

#### PURPOSE

To explain in a step-by-step fashion how metal affects MRI imaging by reviewing basic aspects of image acquisition and spatial localization.

#### APPROACH/METHODS

We will identify how metallic susceptibility generates: a) spin dephasing, resulting in signal voids and signal pile-up artifacts and b) inadvertent chemical shifts that cause: fat suppression to fail, geometric distortion, bending of the image, and readout and slice-direction spatial misregistration with especial emphasis on how this affects imaging in the neural axis.

#### FINDINGS/DISCUSSION

The physics of traditional methods used to reduce metallic artifacts including increasing bandwidth, increasing matrix size and reducing slice thickness also will be discussed.

#### SUMMARY/CONCLUSION

Finally, novel techniques for metallic artifact reduction will be overviewed: including view angle tilting (VAT), slice encoding metal artifact correction (SEMAC) and multiacquisition with variable resonance image combination (MAVRIC).

**KEY WORDS:** Metallic artifact, VAT

### eEdE-34

#### Susceptibility-Weighted MR Sequences: Technical Insights and Clinical Applications Focusing on Inflammatory and Infectious Diseases of the Central Nervous System

Morais, L. M. T. • Santos, G. T. • Leite, C. C. • Lucato, L. T.

Hospital das Clínicas da Faculdade de Medicina da Universidade de São Paulo  
São Paulo, BRAZIL

#### PURPOSE

To cover the major technical concepts related to acquisition of susceptibility-weighted (SW) sequences, with an emphasis in the differences among major vendors. To describe and illustrate the role of SW sequences in the evaluation of various inflammatory and infectious diseases of the central nervous system (CNS).



**APPROACH/METHODS**

Patients presenting inflammatory or infectious conditions were identified retrospectively in the teaching file database of our institution. CT and MR exams were analyzed, together with medical records; CT images were scrutinized carefully in order to depict calcifications. This database also provided SW images from selected cases in order to demonstrate concepts related to their acquisition, including vendor-related differences.

**FINDINGS/DISCUSSION**

A brief background of the physics behind SW techniques will be presented. Susceptibility-weighted techniques usually employ 3D gradient echo sequences, and especially echo-time related singularities yield slight differences among them, which can potentially impact the way they explore the magnetic susceptibility differences of tissues. Susceptibility-weighted sequences are a novel and promising neuroimaging tool. They present superb detection capacity of the well-known susceptibility differences present in various tissues (such as blood, iron and calcification); creating a unique contrast, different from that of conventional sequences. The technique superiority is based in some features: as it is a 3D sequence, the slice thickness is intrinsically thin; the images are postprocessed using minimal intensity projection (minIP), which enhances hypointense lesions; all choices of parameters are directed to increase the conspicuity of the smaller veins and other sources of susceptibility effects. Besides, the phase images, when available, have potential in differentiating between diamagnetic and paramagnetic susceptibility effects of calcium and blood, respectively. Another aim of this study is to discuss and illustrate the usefulness of this relatively new approach in the evaluation of various inflammatory and infectious diseases of the CNS, including pyogenic abscesses, fungal and other granulomatous infections, and cysticercosis. This unique MR sequence is capable of improving detection of calcification and hemorrhage in this scenario, frequently adding clinically relevant information.

**SUMMARY/CONCLUSION**

Susceptibility-weighted sequences have taken the detection of calcified and hemorrhagic lesions to a new level. They appear as a valuable tool in differentiating and characterizing diverse inflammatory and infectious conditions.

**KEY WORDS:** Brain, infection, susceptibility-weighted sequences

**eEdE-35****Dynamic Contrast-Enhanced MR Imaging: Techniques and Clinical Applications**

da Cruz, L. H.<sup>1</sup>Galheiro, D.<sup>2</sup>Fatterpekar, G.<sup>2</sup>Gasparetto, E.<sup>1</sup>de Souza, C. G.<sup>3</sup>Correa, D. G.<sup>3</sup>

<sup>1</sup>IRM, Rio de Janeiro, BRAZIL, <sup>2</sup>New York University, New York, NY, <sup>3</sup>Multi-Imagem Ressonancia, Rio de Janeiro, BRAZIL

**PURPOSE**

MR imaging permeability studies attempt to measure the degree of disruption of the blood-brain barrier (BBB) by using an analysis of dynamic contrast-enhanced imaging. This exhibit aims to illustrate the most common clinical application and imaging findings, with emphasis to MRI features that can help in the approach and management of different causes.

**APPROACH/METHODS**

We did a retrospective survey in our institutional archives, in search of different cases where MR imaging permeability were performed. We will review the different technical methods and the most important imaging points of MR imaging permeability findings. The MR imaging permeability findings are discussed with emphasis on feasibility, advantages and limitations over conventional MR imaging.

**FINDINGS/DISCUSSION**

During the recent years, tremendous progress has been made toward designing a robust method to noninvasively quantify microvascular permeability for clinical use. This parameter is typically represented by the transfer coefficient, K<sub>trans</sub>, a variable that is estimated on the basis of analysis of temporarily acquired dynamic contrast-enhanced (DCE) MR imaging data. Several recent studies have shown that quantitative estimates of microvascular permeability correlate with some clinical conditions. Can be used to characterize microvascular permeability in brain tumors including tumor grading, guiding biopsy, monitoring the efficacy of treatments, and differentiating posttreatment changes from recurring tumor. In addition, other current and potential clinical applications will be addressed like demyelinating diseases, infections, and vascular diseases.

**SUMMARY/CONCLUSION**

Dynamic contrast-enhanced (DCE) MR imaging is a new method to noninvasively quantify microvascular permeability. This MR technique can enable visualization of lesion vasculature, provides noninvasive characterization of vascular permeability and can be correlated directly with the physiopathology of different clinical conditions. Thus, DCE-MRI can be used to assess and to better understand some neurologic pathologies and changes related to their treatment, helping in the patient management.

**KEY WORDS:** Permeability

**eEdE-36****Intramyelinic Edema on Diffusion-Weighted Imaging: Is It Reversible or Irreversible?**

Moritani, T.·Capizzano, A.·Kademian, J.·Sato, Y.

University of Iowa Hospitals and Clinics  
Iowa City, IA

**PURPOSE**

To illustrate diffusion-weighted imaging (DWI) abnormalities of various central nervous system (CNS)

pathologic conditions associated with intramyelinic edema and discuss the pathology, pathophysiology, its distribution and reversibility.

#### APPROACH/METHODS

/We reviewed MRI and DWI findings in 97 patients with various white matter diseases associated with intramyelinic edema. The cases comprised five autopsy proven cases and various entities previously described in the literatures including work done with electron microscopy. Etiologies included acute cytotoxic plaque of multiple sclerosis, heroin-induced encephalopathy, delayed postanoxic leukoencephalopathy, chemotherapy-induced leukoencephalopathy, vigabatrin-associated vacuolar myelinopathy, Wallerian degeneration associated with hypoxia/ischemia, metabolic leukoencephalopathies, (phenylketonuria, Canavan disease, metachromatic leukodystrophy, etc.) and spectrum of reversible splenial lesion of corpus callosum, acute disseminated encephalomyelitis, progressive multifocal leukoencephalopathy, and diffuse white matter changes after traumatic diffuse axonal injury and cerebral fat embolism.

#### FINDINGS/DISCUSSION

Complete reversibility of restricted diffusion lesions has been reported in demyelinating disease, heroin-induced encephalopathy, phenylketonuria, vigabatrin-associated vacuolar myelinopathy, and spectrum of reversible splenial lesion of corpus callosum. Intramyelinic edema is considered one of the explanations of restricted diffusion with complete reversibility. Intramyelinic edema can occur either within the myelin sheath itself (potential intracellular space) or at the intramyelinic cleft that splits myelin at the intraperiod line (potential extracellular space). Edema of either the intra- or extracellular space causes restricted diffusion presumably due to geometric distortion of membranous structures. Complete reversibility of intramyelinic edema is thought to be related to the edema in the intramyelinic cleft. Diffuse white matter distribution pattern is seen in toxic or metabolic leukoencephalopathy. Myelin sheaths can be a target of the excitotoxic amino acids such as a glutamate. The lesion distribution presumably is related to the distribution of the receptors (glutamate, GABA etc.). Function and predominant distribution of these receptors evolve along brain maturation. Vigabatrin (antiepileptic drug) increases GABA concentration and inadvertently leads to excitotoxicity to the myelin sheath in infants associated with the characteristic distribution of intramyelinic edema. Intramyelinic edema and axonal swelling were demonstrated in Wallerian degeneration after excitotoxic insult. In an immunohistochemical study, acute multiple sclerosis plaques showed high glutamate concentration in close proximity to axonal damage that may cause peripheral intramyelinic edema. In traumatic diffuse axonal injury, a mechanism of cytotoxic edema is axonal disruption at the node of Ranvier, leading to leakage of glutamate into the extracellular space producing swelling of the surrounding myelin sheaths causing diffuse white matter distribution.

#### SUMMARY/CONCLUSION

Intramyelinic edema is considered one of the plausible explanations of complete reversibility of diffusion restricted edema in various diseases. Intramyelinic edema that causes restricted diffusion occurs either in the intracellular myelin component or at the intramyelinic cleft. We illustrate the intramyelinic edema in various pathologic conditions and discuss the pathology and pathophysiology correlated with its distribution and reversibility.

**KEY WORDS:** Intramyelinic, edema, diffusion

#### eEdE-37

#### Brain Death: What Every Radiologist Should Know

Hussain, S. Divekar, S. A. Al Bader, F.

King Khalid University Hospital  
Riyadh, SAUDI ARABIA

#### PURPOSE

1. To briefly present clinical criteria used to diagnose and document brain death. 2. To mention conditions where clinical criteria are difficult to apply or are inadequate, and hence further evaluation with imaging is warranted. 3. To describe imaging methods to diagnose brain death and the imaging findings with possible pitfalls.

#### APPROACH/METHODS

We reviewed articles describing clinical aspects of brain death diagnosis, including the various criteria used and recommended by American Academy of Neurology (AAN). We also reviewed difficulties in applying such criteria, and indications of imaging. We also reviewed published literature about imaging findings of brain death on different modalities including the gold standard catheter angiography, radionuclide scan, noncontrast head CT, CT angiography, MR angiography, diffusion-weighted MR imaging, and Doppler ultrasound, etc. We also discuss various aspects of pitfalls in imaging which every radiologist needs to be aware of.

#### FINDINGS/DISCUSSION

To declare a person as dead, the fundamental medico-legal requirement is to confirm irreversible cessation of brain function. This diagnosis needs highest level of vigilance to avoid any false/positive diagnosis. On the other hand, in this era of organ donation for transplantation, the diagnosis also needs to be made fairly quickly so as not to lose any vital organs which are still functioning. We still come across with anecdotal reports of a person declared dead only to be found alive by another person, usually a close relative. Investigations in such cases reveal lack of proper application of the clinical guidelines and failure to apply further evaluation tools. The American Academy of Neurology has put forward guidelines for diagnosis of brain death. There are also situations when the required criteria mentioned in the guidelines become very difficult to apply or results are equivocal. Well documented mimics of brain death include fulminant

Guillain-Barre syndrome, high cervical cord injury, and intoxication with organophosphates, lidocaine, baclofen and vecuronium. In these situations, various imaging techniques are indicated which can confirm or exclude the brain death. The AAN currently recommends catheter angiography, HMPAO SPECT scan or transcranial Doppler for confirmatory diagnosis. These techniques are now proven to visualize presence or otherwise of intracranial arterial circulation, the basic criteria for diagnosis of brain death. With the advances in other imaging modalities including CT angiography, perfusion CT, diffusion-weighted MR images, MR angiography and transcranial color doppler ultrasound, the intracranial arterial circulation potentially can be evaluated with the same confidence and imaging information. Several case reports have been published describing findings on individual modalities. Several other reports mentioned potential pitfalls and false/positive diagnoses in those modalities. According to our information there has not been a single publication describing all the imaging modalities, imaging findings and potential pitfalls.

#### **SUMMARY/CONCLUSION**

Every radiologist should be aware of the AAN guidelines for diagnosis of brain death, and the situations where these guidelines cannot be applied or results are equivocal. Radiologists also should be aware of the indications of imaging, available imaging techniques, various signs on these imaging studies, and potential pitfalls of individual imaging methods.

**KEY WORDS:** Brain, death, imaging

#### **eEdE-38**

##### **Neurogenetics and Imaging**

Kanekar, S.

Penn State Milton S. Hershey Medical Center and  
College of Medicine  
Hershey, PA

#### **PURPOSE**

To give an update on neurogenetics and its relevance to neuroimaging.

#### **APPROACH/METHODS**

Over the last two decades the field of neurogenetics has transformed dramatically because of technological advances in genetics and genomic analysis. This explosion in the neurogenetics has increased our understanding of various neurologic and neurosurgical disorders. In this exhibit we discuss the gene disorders in a few of the common neurologic-neurosurgical disorders and correlate them with imaging findings.

#### **FINDINGS/DISCUSSION**

For the purpose of this exhibit and for better understanding we have classified this exhibit under the following categories: neurodegenerative, CNS demyelination, neurodevelopmental, cerebrovascular syndromes, hereditary muscle disease, and hereditary peripheral neuropathies. We discuss the gene defects in

these disorders and illustrate with examples the relevant imaging findings.

#### **SUMMARY/CONCLUSION**

Neurogenetics is the fastest growing branch of neuroscience. In the next two decades we might see a major shift in the way we treat our patients (i.e., "gene targeted therapy"). It is much more important for neuroradiologist to keep updated with the relevant genetic knowledge. This exhibit on neurogenetic and imaging highlights the relevant and important breakthrough in a few of the common neurologic disorders.

**KEY WORDS:** Neurogenetics, gene targeted therapy, neuroimaging

#### **eEdE-39**

##### **Hydrocephalus and Cerebrospinal Fluid Diversion Techniques: A Pictorial Review**

Netto, J. P.·Umran Ashruf, S.·Steven, A. J.

University of Maryland  
Baltimore, MD

#### **PURPOSE**

Hydrocephalus is a potentially life-threatening condition characterized by excess volume of cerebrospinal fluid (CSF) and dilatation of the ventricular system. Cerebrospinal fluid diversion techniques are commonly utilized surgical procedures intended to reestablish CSF equilibrium by bypassing the site of obstruction and normalizing intracranial pressure. The most commonly used techniques are intraventricular catheters (IVC), ventricular shunts (VS) and endoscopic third ventriculostomies (ETV). The goal of this presentation is to discuss the causes and imaging appearance of hydrocephalus, indications for surgical intervention, various devices utilized, appearance of both early and delayed complications, and imaging evaluation and management of these patients.

#### **APPROACH/METHODS**

We present a pictorial review of cases illustrating the various aspects of the ventricular catheters and CSF diversion using conventional radiography, computed tomography (CT) and magnetic resonance imaging (MRI) from the University of Maryland Medical Center.

#### **FINDINGS/DISCUSSION**

Cerebrospinal fluid is produced within the ventricular system by the choroid plexus at a rate of approximately 500ml per day. It follows a pulsatile flow through the ventricles into the cortical and spinal subarachnoid space, ultimately being resorbed through the arachnoid granulations into the venous system. Disruption of this homeostasis can result in ventricular dilatation (hydrocephalus), which is categorized as obstructive or communicating based the level of obstruction. Obstructive (noncommunicating or intraventricular) hydrocephalus develops when there is an obstruction proximal to the ventricular outlet foramina. The less common communicating (external or extraventricular)

hydrocephalus occurs as a result of defective resorption. In an acute situation, when fast and temporary ventricular system decompression is necessary, the method of choice is the IVC. A VS is the most commonly used approach for long-term management of hydrocephalus. Endoscopic third ventriculostomies are employed with a noncommunicating hydrocephalus when the point of obstruction is at or below the cerebral aqueduct. Fenestrating the floor of the third ventricle creates a free communication between the ventricles and the subarachnoid space in the suprasellar cistern. The most common surgically related complications are intraventricular hemorrhage and pneumocephalus. Typically clinically silent, these have catastrophic potential, particularly in patients with a coagulopathy. Less common perioperative complications include misplacement, retained fragments, shunt fracture, and bowel or bladder perforation. Shunt failure is exceedingly common in long-term shunt use, with many patients requiring one or more shunt revisions. The causes of failure can be divided into infectious and noninfectious etiologies, with the former typically occurring in the first months after the procedure. Noninfectious causes of shunt failure include obstruction, mechanical failure, over drainage, loculation of the ventricles, and various abdominal complications.

#### **SUMMARY/CONCLUSION**

Surgical CSF diversion techniques commonly are employed in the management of all types of hydrocephalus. Given the widespread use of these devices and procedures, it is essential for the neuroradiologist to be familiar with the normal imaging, management, and potential complications associated with these devices.

**KEY WORDS:** Hydrocephalus, shunt, cerebrospinal fluid

#### **eEdE-40**

##### **Role of Imaging in Stereotactic Radiosurgery and Radiotherapy of Central Nervous System Lesions**

Peri, N.·Mahdevan, A.·Rojas, R.

Beth Israel Deaconess Medical Center  
Brookline, MA

#### **PURPOSE**

Stereotactic radiosurgery (SRS) and radiotherapy (SRT) are used increasingly in the treatment of various lesions of the central nervous system (CNS). The purpose of this exhibit is to discuss and illustrate the role of different imaging modalities in planning and performing SRS and SRT for various CNS lesions and follow-up assessment.

#### **APPROACH/METHODS**

This exhibit will discuss (a) the basics of stereotactic radiosurgery and radiotherapy, (b) the different techniques and equipment used, (c) the types of CNS lesions that are treated such as brain tumors, extraaxial tumors such as meningioma, acoustic schwannoma, arteriovenous malformation, etc., (d) the clinical

indications, (e) the role of different imaging modalities in planning and performing the procedures and follow up to assess response and evaluate for complications.

#### **FINDINGS/DISCUSSION**

Stereotactic radiosurgery and radiotherapy frequently are used for the treatment of various CNS lesions.

#### **SUMMARY/CONCLUSION**

This exhibit will help the viewer to understand the basics of the techniques and the role of different imaging modalities in planning the procedures, assess response to treatment and follow up of complications.

**KEY WORDS:** Imaging, stereotactic, radiosurgery

#### **eEdE-41**

##### **Neuroradiology Imaging and Management of Diseases in Pregnancy and the Puerperium**

Ekins, J. B.·Kotsenas, A. L.·Meyer, F. B.·Morris, J. M.

Mayo Clinic  
Rochester, MN

#### **PURPOSE**

Neurologic disease is common in pregnancy and the puerperium and imaging plays a frequent and important role in its evaluation. Familiarity with the distinctive types of pathology and their physiologic basis should improve correct diagnosis, imaging management, and recommendations to clinicians. Understanding of appropriate and inappropriate use of imaging and contrast with consideration for the fetus and newborn child are also essential to proper management.

#### **APPROACH/METHODS**

We present our neuroradiology experience with pregnant and post-partum patients presenting with neurologic disorders. Cases were gathered with the use of keyword searches of radiologic and pathologic databases. Our searches emphasized pathologic states directly implicated in the state of pregnancy and the post-partum state as well as those neurologic entities encountered in pregnancy whose natural history is unaltered but treatment and management options are. Clinical histories, laboratory data, and imaging data were collected and reviewed for each patient. We present representative examples of these entities. We also will review common maternal/fetal considerations including radiation exposure, and the use of imaging contrast during pregnancy and subsequent breastfeeding period.

#### **FINDINGS/DISCUSSION**

Pregnancy and the puerperium are altered physiologic states which result in a unique spectrum and natural history of diseases. This is related largely to hormonal and cardiovascular changes and their effects. This review serves to address those entities that are affected directly by pregnancy as well as those that are discovered during pregnancy but not directly influenced by the pregnancy. These entities include neoplasms

such as meningiomas and pituitary macroadenomas which are known to increase in size due to the hormonal influences of pregnancy. Vascular phenomena such as the increased rate of aneurysm rupture, increased symptomatology and hemorrhage of dural fistulas and AVM, and stability of cavernous hemangiomas are discussed. Other entities that will be presented include postpartum cerebral angiopathy (PPCA) and posterior reversible leukoencephalopathy syndrome (PRES) which are influenced by altered hemodynamics and vascular physiology. Physiologic coagulopathy will be discussed with emphasis on cerebral venous thrombosis. Complications such as post-partum pituitary hemorrhage occasionally result in pituitary infarction and subsequent hypopituitarism (Sheehan's syndrome). Complicated variations of host immunity also will be discussed including multiple sclerosis which is strongly influenced--showing decreased activity during pregnancy followed by increased activity post-partum. Lymphocytic hypophysitis is an additional autoimmune disorder almost always associated with pregnancy or the puerperium. Although ionizing radiation carries risk of untoward outcomes for the fetus, these risks are very low and usually do not change management of appropriate medical evaluations. Cases requiring examination of the abdomen may be evaluated alternatively with ultrasound or MRI, when appropriate. Iodine administration is considered safe. Due to theoretical concerns, gadolinium administration is not recommended.

#### **SUMMARY/CONCLUSION**

Radiologists must be attuned to the unique spectrum of pathology and appropriate imaging management when evaluating a pregnant or post-partum patient. Appropriate use of imaging and contrast should be directed by medical necessity and recognized, usually small, associated risks. We present the largest single review of the neuroradiographic appearances of the broad neurologic disease processes encountered in pregnancy and the immediate post-partum state.

**KEY WORDS:** Pregnancy, puerperium, fetus

#### **eEdE-42**

#### **Review of the Common, Infrequent and Unusual Lesions of the Calvarium: What the Radiologist Should Know!**

Kontolemos, M.<sup>1</sup>•Adas, R.<sup>1</sup>•Davila, J.<sup>2</sup>•Glikstein, R.<sup>1</sup>•Torres, C.<sup>1</sup>

<sup>1</sup>The Ottawa Hospital, Ottawa, ON, CANADA, <sup>2</sup>Childrens Hospital of Eastern Ontario, Ottawa, ON, CANADA

#### **PURPOSE**

This exhibit is intended to: 1. Provide a comprehensive review of the characteristic imaging findings of common and uncommon lesions affecting the bony calvarium. 2. Demonstrate examples of various calvarial pathologies affecting both adults and children, using radiographs as well as CT and MRI images. 3. Present the material in an interactive computer-based format.

#### **APPROACH/METHODS**

Images from numerous exemplary cases from our institutions were chosen and presented along with important teaching points in an interactive computer-based presentation.

#### **FINDINGS/DISCUSSION**

Lesions of various etiologies can affect the calvarium, including congenital, neoplastic, inflammatory, infectious and traumatic conditions. Many classifications have been described in the literature to facilitate an organized approach to their diagnosis. Calvarial lesions can be classified by: 1. distribution, [i.e., focal (single/ multiple) or diffuse], 2. aggressivity (i.e., benign or malignant-appearing), or 3. density (i.e., lytic or sclerotic). However, age and anatomy remain as additional important factors that strongly influence the list of differential diagnosis. Skull lesions are often incidental findings on CT and MRI, presenting a challenge for the radiologist. When symptomatic, patients usually present with a palpable mass or focal tenderness. CT is most-optimal for the evaluation of lesion nature/density (i.e., lytic or sclerotic) as well as for the presence of intralesional calcification, destructive changes in the inner or outer tables, and associated surrounding bony reaction (i.e., sclerotic margins). MR imaging is superior to CT in characterizing lesions of the diploic space, early lesions without bone destruction, or those that have an associated soft tissue component and/ or brain or meningeal involvement. Arana et al. in 1999, reviewed 185 patients with calvarial lesions and found that the most common are Langerhans cell histiocytosis (LCH) (18.9%) and osteomas (15.1%). Similarly but more recently, Garfinkle et al. reviewed the records of 141 patients and the most common lesions they encountered were osteomas (23%) and LCH (16%). Other benign lesions including hemangioma, meningioma, fibrous dysplasia, dermoid/epidermoid and lipoma were less common. Metastases constitute 10-12% of all cases and account for the majority of malignant calvarial lesions. Other malignant lesions including plasmacytoma, lymphoma/leukemia, hemangiopericytoma, and sarcoma also can be seen. Normal variants, congenital and developmental lesions as well as lesions occurring as part of systemic and metabolic illness also find themselves among those etiologies worth exploring.

#### **SUMMARY/CONCLUSION**

Both incidental and symptomatic calvarial lesions are encountered frequently on imaging, presenting a common and important challenge to radiologists. Although a wide range of pathologies can involve the calvarium, thorough knowledge of the clinical setting, skull anatomy and characteristic imaging features of calvarial lesions is key in facilitating a structured approach to their differential or definitive diagnosis.

**KEY WORDS:** Calvarium, bone, skull

**eEdE-43****"Never Judge a Book by Its Cover": Review of Various Pathologies Demonstrating Diffusion Abnormality on Brain MR imaging**

O'Connor, K. M.<sup>1</sup>•Hayashi, D.<sup>1</sup>•Moritani, T.<sup>2</sup>•Barest, G.<sup>1</sup>•Sakai, O.<sup>1</sup>•Mian, A.<sup>1</sup>

<sup>1</sup>Boston Medical Center, Boston, MA, <sup>2</sup>University of Iowa Hospitals and Clinics, Iowa City, IA

**PURPOSE**

Detection of acute infarction may be the most well known use of diffusion-weighted imaging (DWI) of the brain. There are, however, many other causes of diffusion abnormalities that are clinically significant and should be considered depending on the clinical context, distribution and associated imaging findings. The purpose of this educational exhibit is to review the pathophysiology of diffusion abnormalities and the spectrum of pathology. Examples of ischemic, neoplastic, infectious, demyelinating, toxic and metabolic, and posttraumatic abnormalities will be presented.

**APPROACH/METHODS**

Retrospective review of brain MRI examinations demonstrating diffusion abnormality was performed at a tertiary referral center. Correlative findings on other MRI sequences and CT were reviewed with clinical data to determine the underlying cause of the diffusion abnormality. We present examples to illustrate the wide spectrum of disorders that demonstrate diffusion abnormalities on brain MRI.

**FINDINGS/DISCUSSION**

Diffusion-weighted imaging signal abnormalities are nonspecific findings on brain MRI with many potential causes. Ischemic etiologies are common, including infarcts, hypoxic ischemic encephalopathy and diffuse anoxic injury. However, many other disorders may need to be considered in the differential diagnosis depending on the pattern of distribution, associated imaging findings, and clinical context. These etiologies include infection (e.g., abscess, subdural empyema, herpes encephalitis, Creutzfeldt Jakob disease), benign and malignant neoplasms (e.g., epidermoid cyst, glioblastoma multiforme, lymphoma), demyelinating diseases (e.g., multiple sclerosis), trauma (e.g., hemorrhage, diffuse axonal injury), seizures, toxic and metabolic abnormalities (e.g., methotrexate-induced leukoencephalopathy, osmotic myelinolysis) and posterior reversible encephalopathy syndrome (PRES).

**SUMMARY/CONCLUSION**

A broad spectrum of disorders may present with diffusion abnormalities on brain MRI. Determining the cause of the diffusion abnormality in a particular case requires consideration of the clinical history, pattern of distribution and associated imaging findings. Prompt recognition of ischemic as well as nonischemic causes can be critical for a positive clinical outcome.

**KEY WORDS:** Diffusion-weighted, brain, MR imaging

**eEdE-44****Review of the Pons: From Anatomy to Zoonoses**

Dupre, S. • Heran, M. K. • Graeb, D.

Vancouver General Hospital  
Vancouver, BC, CANADA

**PURPOSE**

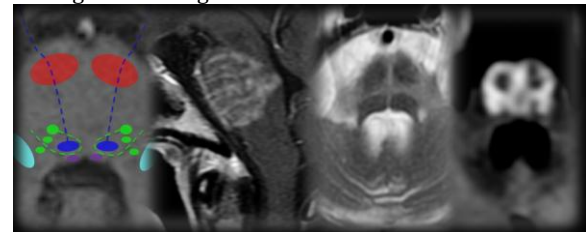
The pons is a complex structure, containing white matter tracts and cranial nerve nuclei that can be involved in a multitude of disease processes. The anatomy of the pons, and the diseases that affect it will be reviewed.

**APPROACH/METHODS**

Anatomical structures are illustrated on MRI slices through the pons. An extensive differential diagnosis of diseases affecting the pons was compiled from the literature. CT and MRI cases illustrating the majority of these entities were primarily drawn from the PACS of a quaternary hospital with the aid of a "text search" function.

**FINDINGS/DISCUSSION**

To promote active learning, both the anatomy and pathology cases are presented in a quiz format, with answers revealed after the reader has had the opportunity to review unlabelled images and relevant clinical information. The differential diagnosis of pathologies involving the pons is reviewed at the end in a categorized "surgical sieve" format.

**SUMMARY/CONCLUSION**

Upon completion of this education exhibit, the reader will have reviewed the anatomy of the pons, and the expansive list of pathologies that affect it.

**KEY WORDS:** Pons

**eEdE-45****Cognitive Errors in Neuroimaging: What They Are and How to Avoid Them**

Srinivasan, A. • Wang, P. • Bryson, T. • Bou-Assaly, W. • Hoeffner, E.

University of Michigan Health System  
Ann Arbor, MI

**PURPOSE**

To discuss different types of cognitive errors in neuroradiology with illustrated examples.

**APPROACH/METHODS**



The different cognitive errors will be presented in a quiz format where the images (with relevant history) will be presented followed by the discussion of the error in question. Some of the errors discussed include:

- satisfaction of search - Once a diagnostic finding is identified, the search stops and a potentially important finding is missed.
- capture - postcompletion error.
- alliterative error - bias from prior reports.
- ascertainment bias - personal bias towards certain characteristics.
- anchoring - early determination of diagnosis and "fitting the findings" to the diagnosis.
- gambler's fallacy.
- availability bias - recent exposure to a diagnosis increases sensitivity to that abnormality.
- framing bias.
- laterality error.

#### **SUMMARY/CONCLUSION**

Each error discussed in this presentation is common in day-to-day neuroradiology interpretations. Therefore, knowledge of these errors is the first step towards reducing their occurrence.

**KEY WORDS:** Cognitive error, alliterative error, satisfaction of search

#### **eEdE-46**

##### **Cranial Nerves Revisited**

Romano, J.

Montefiore Medical Center  
Bronx, NY

#### **PURPOSE**

This educational display presents a distinct and simplifying classification of the cranial nerves that incorporates a perspective of embryology and evolution.

#### **APPROACH/METHODS**

We demonstrate that cranial nerves V, VII, IX and X have a notably more complex character than the others and this group of cranial nerves also has a branchial arch origin. We believe that this origin is fundamental to explaining the differences between these cranial nerves and the others.

#### **SUMMARY/CONCLUSION**

We believe that the cranial nerves are understood more readily and comprehensively when additionally interpreted through the vantage point of embryology and evolution.

**KEY WORDS:** Cranial nerves, anatomy, embryology

#### **eEdE-47**

##### **Pictorial Overview of Intraaxial Temporal Lobe Lesions**

Yu, W. Choong, C. C. Liauw, L.

National Neuroscience Institute  
Singapore, SINGAPORE

#### **PURPOSE**

To provide a comprehensive overview of intraaxial lesions located in the temporal lobe.

#### **APPROACH/METHODS**

This educational exhibit explores the radiologic features of temporal lobe lesions.

#### **FINDINGS/DISCUSSION**

A wide spectrum of diseases involve the temporal lobe. This can be categorized into lesions isolated to the temporal lobe, preferentially in the temporal lobe or as part of more extensive changes. Solitary lesions involving just the temporal lobe include lesions causing temporal lobe epilepsy such as mesial temporal sclerosis, cortical dysplasia and tumors. Patients presenting with transient global amnesia may have isolated abnormality in the hippocampi. Developmental lesions such as hippocampal sulcus remnant and choroid fissure cyst should not be mistaken as pathology. Pathologies that preferentially involve the temporal lobes include infective etiologies such as herpes simplex encephalitis, neurodegenerative processes in Alzheimer disease and paraneoplastic syndromes such as limbic encephalitis and voltage gated potassium channelopathies (VGKC). Cerebral autosomal dominant arteriopathy with subcortical infarcts and leukoencephalopathy (CADASIL) is an example of a more widespread disease which involves the temporal lobes. Other pathologies which can involve the temporal lobes would include inflammatory/demyelinating disease, trauma, radionecrosis, metastatic disease and neurodegenerative conditions [frontotemporal dementia (FTD)].

#### **SUMMARY/CONCLUSION**

This exhibit presents an overview of temporal lobe lesions and their differentiating radiologic features.

**KEY WORDS:** Temporal lobe, brain, MR imaging

#### **eEdE-48**

##### **Becoming a Grandmaster: How Improving Your Chess Game Can Make You a Better Neuroradiologist**

Mirochnik, B. Lev, S.

Nassau University Medical Center  
East Meadow, NY

#### **PURPOSE**

To demonstrate how winning chess strategies can be applied to the interpretation of on-call neuroimaging studies. We highlight novice errors and provide tips and advice for an improved game.

#### **APPROACH/METHODS**

We emphasize key principles which every chess novice should follow for a better game and discuss neuroradiology parallels, such as developing an imaging strategy, implementing a targeted search pattern, formulating an accurate differential and avoiding common pitfalls. We challenge the viewer with

emergency neuroradiology (CT and MR) cases from our Level 1 trauma center to determine his or her rating. Are you a club player or on your way to grandmaster status?

#### **FINDINGS/DISCUSSION**

It is imperative to have a game plan and to think several moves ahead. In chess, avoid aimless development by moving pieces with concerted purpose. A premature attack can end in disaster without an army of supportive pieces. In neuroradiology, formulating an accurate differential diagnosis requires a systematic approach, from general to specific, and is contingent on a cast of complimentary imaging modalities. Do not let the initiative slip while trying to win irrelevant material and always make sure your opponent has no surprise checks, captures, or threats. We demonstrate a giant petrous aneurysm, a "don't touch lesion", mimicking a mass. Undue emphasis on small points, like seizing free pawns, can allow one to neglect more serious concerns, like the safety of the king. Likewise, if one focuses solely on the contusions in a trauma patient, life threatening signals may be overlooked, like effacement of the basilar cisterns presaging cerebral herniation - checkmate! In chess, avoid abandoning the center, the most important region of the board for attacking and defending. On a head CT, inspect the midline for shift and asymmetry, which can reveal a subtle lesion, like an isodense subdural hemorrhage. Continually shift perspective. Orthogonal views may uncover convexity hematomas, inconspicuous on axial images alone. Don't let your pieces become passive: Be proactive and dispatch enemy pieces expeditiously. Obtaining a CTA in severe cervical injury may reveal vertebral artery dissection, preventing subsequent stroke. Think of the way individual chess pieces, and separate imaging studies, work together as a team. We show a hyperdense lesion on CT, thought to be a contusion on-call, subsequently demonstrating the classic features of a cavernous angioma on MR. Judge every situation in context. Knowing the clinical scenario can significantly alter the differential. For example, a proper history can help distinguish an underlying mass lesion from an acute infarct, or a glioblastoma multiforme from an abscess. Finally, do not resign prematurely. Avoid "satisfaction of search" and do not neglect to identify important ancillary findings.

#### **SUMMARY/CONCLUSION**

To excel at both chess and neuroradiology, careful strategic planning is essential. Your opponent is time and morbidity. Proactive, rather than defensive thinking can help one to identify and avoid potential threats. Purposeful initiative, with an arsenal of supportive pieces can facilitate timely and accurate diagnosis.

**KEY WORDS:** Brain trauma, satisfaction of search, cerebral herniation

#### **eEdE-49**

### **Management of Intractable Bleeding in Patients with Trauma Using Neurovascular Intervention: A Pictorial Review**

Choi, J.·Roh, H.·Moon, W.

Konkuk University School of Medicine  
SEOUL, KOREA, REPUBLIC OF

#### **PURPOSE**

In this exhibit, we will illustrate our experience in neurovascular intervention in the management of trauma patients with emphasis on radiologic findings of various vascular injuries, endovascular technique including equipment and materials.

#### **APPROACH/METHODS**

The traditional interests of the radiologists in acute head and neck trauma have been to find the traumatic brain injury in brain parenchyma, extraaxial hemorrhage, fracture and vascular injury. Nowadays, the radiologists also play an important role in management of acutely traumatized patients, especially in intractable bleeding. The intractable bleeding in the head and neck area frequently is related to skull base fracture, fracture of the spine, penetrating injury, head and neck surgery including endoscopic sinus surgery, two-jaw surgery or osteoradionecrosis after radiation therapy for head and neck cancer.

#### **FINDINGS/DISCUSSION**

Various vascular injuries which can benefit from neurovascular intervention include arterial dissection, transection, pseudoaneurysm and arteriovenous fistula.

#### **SUMMARY/CONCLUSION**

Radiologists in acute trauma care setting should be aware of the role of neurointervention in traumatic emergency.

**KEY WORDS:** Trauma, bleeding, endovascular therapy

#### **eEdE-50**

### **Neuroradiology Vascular Anomaly Quiz**

Masri, D. J.·Gams, C.·Shifteh, K.·Burns, J.·Bello,  
J.·Pasquale, D.

Montefiore Medical Center  
Bronx, NY

#### **PURPOSE**

Common and rare vascular anomalies are encountered across neurovascular imaging modalities including: MR angiography, CT angiography and catheter angiography. The purpose of this exhibit is to expose the radiologist to a series of vascular anomalies involving the intracranial and extracranial circulations.

#### **APPROACH/METHODS**

Cases, presented in quiz format will include: Anomalous origin of right occipital artery from the vertebral artery. Vertebral artery arising from ECA Congenital absence of

the ICA with MCA arising from basilar tip via a large Pcom. Persistent trigeminal artery. PICA arising from ICA AICA arising from ICA Abberant ICA within the middle ear. Middle meningeal arising from ICA Azygous ACAs. Anterior temporal artery arising from ICA Retropharyngeal carotid arteries.

#### **FINDINGS/DISCUSSION**

Vascular anomalies will be encountered regularly in the interpretation of angiographic studies.

#### **SUMMARY/CONCLUSION**

Familiarity with common vascular anomalies and experience tracing aberrant vessels to the territory they supply will help the radiologist accurately identify such anomalies.

**KEY WORDS:** Vascular, anomalies, anatomy

#### **eEdE-51**

### **Imaging Central Nervous System Vasculitis and Its Mimics**

Marder, C. P. Fink, K. R. T.

University of Washington, Seattle, WA

#### **PURPOSE**

The educational objectives of this exhibit include the following: 1. Review the etiologies and relevant pathophysiology of central nervous system (CNS) vasculitis and its mimics, including reversible cerebral vasoconstriction syndrome (RCVS). 2. Highlight how clinical information such as age, past medical history, and presenting symptoms can help direct the differential diagnosis. 3. Demonstrate the utility of different imaging modalities in making the diagnosis, including CT, MRI, CT and MR angiography, and digital subtraction angiography (DSA). 4. Show the characteristic imaging findings and present an appropriate algorithm for imaging work up.

#### **APPROACH/METHODS**

This educational exhibit will utilize a case-based approach to illustrate the educational objectives. The user will review the distinguishing imaging and clinical features of CNS vasculitis and related entities by navigating an interactive, image-rich computer-based display.

#### **FINDINGS/DISCUSSION**

Central nervous system vasculitis has a variety of causes, characterized as either primary (idiopathic) or secondary. Primary CNS vasculitis also is called primary angiitis of the CNS (PACNS). Secondary causes include systemic vasculitides (e.g., polyarteritis nodosa), connective tissue diseases (e.g., systemic lupus erythematosus), drug toxicities (e.g., cocaine), and infections (e.g., HIV, VZV, and syphilis). Diagnosis of PACNS requires careful laboratory testing including cerebrospinal fluid (CSF) analysis to exclude secondary causes. Brain biopsy sometimes is used for definitive diagnosis, but false negative biopsy results remain problematic in many cases. An important mimic of CNS

vasculitis by imaging evaluation is an entity known as RCVS, previously referred to as benign angiopathy of the CNS, Call-Fleming syndrome, migrainous vasospasm and migrainous stroke. Unlike CNS vasculitis, RCVS occurs most frequently in young to middle-aged women, presents with sudden onset of severe headache with or without neurologic deficits, and resolves with removal of inciting factors. Clinical features, including the onset and time course of disease, are helpful discriminators. Both entities can present with multiple ischemic or hemorrhagic strokes, parenchymal hemorrhages, or SAH, as well as segmental vasoconstriction on angiographic studies. Central nervous system vasculitis, however, typically follows a chronic, progressive course and requires treatment with steroids. Distinguishing between CNS vasculitis and RCVS is critical, since treatments and prognoses differ markedly.

#### **SUMMARY/CONCLUSION**

Recognizing the typical imaging features, time course, and relevant clinical situations can facilitate timely and accurate diagnosis of CNS vasculitis. It is important to discriminate CNS vasculitis from its mimic, RCVS, because the evaluations, treatments, and prognoses differ between the two entities.

**KEY WORDS:** Vasculitis, RCVS, PACNS

#### **eEdE-52**

### **Anatomical Variations of the Intracranial Arterial Circulation at MR Angiography**

Docampo, J. R. Gonzalez, N. S. Delgado, E. Fernandez Mora, R. Bruno, C. H. Morales, J. C.

Fundacion Cientifica del Sur  
Ciudad de Buenos Aires, ARGENTINA

#### **PURPOSE**

To describe the imaging findings of the anatomical variations and anomalies of the intracranial arterial circulation detected on magnetic resonance angiography (MRA).

#### **APPROACH/METHODS**

We retrospectively reviewed 300 patients, 192 female and 108 male (age range 2-88 years), who underwent 3D time-of-flight (3D TOF) MRA of the circle of Willis with a 1.5 T and a 3 T MR units. The selected images were postprocessed in maximum intensity projection (MIP) and volume rendering (VR).

#### **FINDINGS/DISCUSSION**

Among total patients reviewed (n = 300), 223 patients had anatomical variations (151 of the anterior circulation, 51 of both circulations and 21 of the posterior circulation) and 77 patients showed the classic description of the circle of Willis. A total of 410 variations were identified, of these, 291 were of the anterior circulation (71%) and 119 of the posterior circulation (29%). Among the anterior circulation variations, 45% were early bifurcation of the middle cerebral artery (MCA), 20.3% early trifurcation of the

MCA, 18.2% hypoplasia of an anterior cerebral artery (ACA) A1 segment, 4.5% trifurcation of the ACA, 3.1% duplication of the MCA, 2.4% absence of an ACA A1 segment, 2.4% early bifurcation of an ACA A2 segment, 1.4% fenestration of the ACA A1 segment, 1% the presence of accessory MCA, 0.7% early MCA quadrifurcation and 0.3% were ACA quadrifurcation. One patient showed hypoplasia of the internal carotid artery (ICA) and the ACM ipsilateral arising from the posterior cerebral artery (PCA). Among the posterior circulation variations, 50% corresponded to fetal origin of the PCA, 27.1% to hypoplasia of the PCA P1 segment, 7.6% to the presence of hypoplasia of the posterior circulation, 4.2% to the origin of the posterior inferior cerebellar artery (PICA) from the basilar artery, 3.4% to the presence of a common trunk of the PCA and superior cerebellar artery (SCA), 3.4% to the origin of the SCA from the PCA, 2.5% to duplication of the SCA, 0.8% to duplication of PCA and 0.8% to basilar artery fenestration. One patient showed the presence of persistent trigeminal artery.

#### SUMMARY/CONCLUSION

MR angiography is a noninvasive imaging technique that allows structural and anatomical evaluation of the main vessels of the intracranial arteries, providing 3D anatomical images of blood vessels. In our study, the most common variations were located in the anterior circulation (71%), among them, the most common is the early branching of the ACM. The most common posterior circulation variation is the fetal origin of the PCA. Knowledge of the anatomical variations is important in the diagnosis and prognosis of vascular pathology, as well as to undergo endovascular intervention and/or surgical planning with safety.

**KEY WORDS:** Variations, MR angiography, Circle of Willis

#### eEdE-53

##### **Intracerebral Microbleeds: Aspects on MR Imaging, Differential Diagnosis and Clinical Implications**

Cruz, L. H.<sup>1</sup>•Correa, D. G.<sup>2</sup>•deSouza, C. G.<sup>2</sup>•Gasparetto, E.<sup>2</sup>

<sup>1</sup>IRM, Rio de Janeiro, BRAZIL, <sup>2</sup>Federal University of Rio de Janeiro, Rio de Janeiro, BRAZIL

#### PURPOSE

Intracerebral microbleeds are small hemorrhages in the brain that generate hemosiderin deposits, indicating cerebral small vessels disease. New imaging techniques allowed a sensitive detection of this entity on neuroimaging, allowing a better diagnosis characterization. The purpose of this study is to demonstrate the imaging appearance of intracerebral microbleeds and its clinical implications on the different causes.

#### APPROACH/METHODS

We did a retrospective survey in our institutional archives, in search of cases presenting with imaging characteristic findings of brain microbleeds on diverse causes. Also we reviewed the imaging appearance and

its different etiologies, as well as the clinical implications that these findings cause on the patient approach.

#### FINDINGS/DISCUSSION

T2\* gradient-recalled echo (GRE) and susceptibility-weighted imaging (SWI) are especially sensitive for detection of intracerebral microbleeds, generally without correspondence on others sequences. The widespread use of these techniques led to an increasing detection of this kind of bleeding. Thus, there is a growing necessity to establish the real meaning of these findings. Microbleeds may be associated or are seen more commonly with certain neurologic diseases, such as stroke, amyloid angiopathy, in cerebral autosomal dominant arteriopathy with subcortical infarcts and leukoencephalopathy, head trauma, mycotic aneurysms. The differential diagnosis of intracerebral microbleeds should be done with flow voids of pial vessels in cortical sulci, calcifications and type IV cavernous malformations.

#### SUMMARY/CONCLUSION

T2\*GRE and SWI are the sequences of choice for detecting intracerebral microbleeds, which are a frequent finding in neuroimaging. Knowledge of its different causes and clinical implications are important for correct patient management.

**KEY WORDS:** Microbleeds, SWI

#### eEdE-54

##### **Use of MIM Cloud for On Call Cases Including Acute Central Nervous System Injury on a Portable Handheld Device**

Bhatia, A. • Bhatia, V. • Raja, C. • Burke, W. • Pizarro, J.

Mount Sinai Medical Center - Miami  
Miami, FL

#### PURPOSE

The recently FDA approved mobile application MIM has improved radiologist's access to CT and MRI imaging for interpretation away from the traditional workstation. Our institution, which consists of a radiology residency program is established as an accredited comprehensive stroke center and has implemented MIM Cloud into our on-call system. We evaluated the response time, feasibility, and accuracy of using MIM Cloud in diagnosing multiple on-call cases, including CT perfusion studies, MR brain, and MRI spines on mobile devices. Hypothesis: MIM Cloud with the use of MIM application on mobile devices improves response time for on-call radiologists to interpret critical examinations when away from a traditional radiology workstation.

#### APPROACH/METHODS

Over a 6-month period, on-call cases were uploaded to MIM Cloud for access to radiologists who were on call to download onto mobile devices including the iPhone 4, iPad, or iPad 2. Parameters evaluated included the accuracy of diagnosis and response times in making the diagnosis (including upload and download times). Other

parameters will be evaluated, such as feasibility in viewing images on mobile application and downloading images via mobile MIM application. Specific evaluations of acute neurologic events were interpreted.

#### **SUMMARY/CONCLUSION**

The data, statistical analysis, and evaluations demonstrated that on-call cases (including strokes evaluation with CT perfusion and MRI of the brain) demonstrated accurate diagnoses on mobile devices and improved response time for on-call radiologists.

**KEY WORDS:** Central nervous system, injury

**Monday, April 23 –  
Wednesday, April 25  
6:30 AM - 9:00 PM**

**Thursday, April 26  
6:30 AM – 3:00 PM  
Rhineland**

**Electronic Education Exhibits  
(eEdE) 55 – 61**

**eEdE2 - Anatomy**

**Note: A missing printed number indicates an abstract has been withdrawn.**

#### **eEdE-55**

##### **Variants and Pathology of the Corpus Callosum: A Pictorial Review**

Desai, M. P.·Gray, R. I.·Slone, H. W.·Bourekas, E. C.

Ohio State University Medical Center  
Columbus, OH

#### **PURPOSE**

To illustrate imaging findings in the spectrum of diseases affecting the corpus callosum.

#### **APPROACH/METHODS**

A broad spectrum of pathologic entities--including developmental, infectious, inflammatory, neoplastic, and metabolic processes--affect the corpus callosum, some of which have distinct imaging findings. This exhibit will illustrate the neuroimaging findings of a variety of processes involving the corpus callosum and discuss the relevant differential considerations of each imaging appearance. Faculty teaching files at our institution were searched for cases of disorders involving the corpus callosum and representative images from each case are presented.

#### **FINDINGS/DISCUSSION**

After extensive review of cases at our institution, several categories of entities affecting the corpus callosum were found. Developmental processes include agenesis, dysgenesis and lipoma. Vascular etiologies include infarct and posterior reversible encephalopathy syndrome (PRES). Neoplastic processes involving the corpus callosum include glioblastoma multiforme (GBM), lymphoma, gliomatosis cerebri, and metastatic disease are depicted. Diffuse axonal injury (DAI) from severe head trauma also often affects the corpus callosum. Metabolic etiologies such as methanol toxicity, methadone overdose, cocaine, and changes of seizure medication are presented. Cases of demyelination from multiple sclerosis, acute disseminated encephalomyelitis (ADEM), Marchiafava Bignami, and progressive multifocal leukoencephalopathy (PML) also are included in this review. Infectious encephalitis from HIV, herpes zoster, and influenza also are demonstrated involving the corpus callosum. While there are overlapping imaging characteristics of many entities, certain distinctive imaging features which may aid in narrowing the differential are emphasized. In addition, the clinical scenarios in which these imaging features are most likely to be present are reviewed.

#### **SUMMARY/CONCLUSION**

Neuroimaging features of various processes involving the corpus callosum are presented. Imaging features combined with the clinical picture can be valuable in narrowing the differential diagnosis when abnormalities of the corpus callosum are identified.

**KEY WORDS:** Corpus callosum

#### **eEdE-56**

##### **Just Passing Through: A High-Resolution Guide to Brainstem Pathways**

Griffith, B.<sup>1</sup>·Jain, R.<sup>1</sup>·Naidich, T. P.<sup>2</sup>

<sup>1</sup>Henry Ford Hospital, Detroit, MI, <sup>2</sup>Mount Sinai Hospital, New York, NY

#### **PURPOSE**

The brainstem is a highly complex structure, both anatomically and functionally, which has many essential roles, one of which is as a conduit for a variety of intricate pathways connecting the brain, cerebellum, and spinal cord. Having at least a basic understanding of this complexity is essential, as it allows for more accurate diagnosis and localization of lesions. However, limitations in the resolution of our current anatomical imaging oftentimes makes lesion localization difficult. The purpose of this exhibit to use routine (1.5 or 3 T) and high-resolution (9.4 T) MR images, along with case-based examples, to define this detailed anatomy and explore the functional effects and imaging manifestations of lesions involving these pathways.

#### **APPROACH/METHODS**

Through the use of diagrams and high-resolution MR cadaveric imaging, we will explore in detail this

complex neuroanatomy with particular emphasis on the numerous pathways passing through the brainstem. In addition, we will use case-based examples from our teaching files to both define the brainstem anatomy as seen with present-day imaging techniques, as well as better delineate the functional effects and imaging manifestations of lesions involving these pathways. Examples of cases which will be shown include Wallerian degeneration of the corticospinal tract secondary to MCA infarct, hypertrophic olivary degeneration due to lesions within the dentatorubro-olivary pathway (triangle of Guillain and Mollaret), crossed cerebellar diaschisis due to functional disconnection of the contralateral cerebellar hemisphere from the cerebral cortex, disruption of afferent cerebellar pathways resulting in cerebellar atrophy, as well as others.

#### FINDINGS/DISCUSSION

The brainstem is a highly complex structure, both anatomically and functionally. While serving many essential functions, one that often goes underappreciated is its role as a conduit for the many intricate pathways “just passing through”. However, having a deeper understanding of the function and anatomy of these many pathways not only enables one to more accurately localize lesions, but also allows for the detection of subtle secondary imaging manifestations which otherwise may have gone unrecognized. Yet, due to the resolution limitations of our current imaging modalities, making these findings is oftentimes difficult without a thorough understanding of neuroanatomy. Additionally, understanding the relationship of these lesions, which oftentimes appear unrelated anatomically, is not possible without a more thorough understanding of the connections these brainstem pathways provide.

#### SUMMARY/CONCLUSION

Given its complex structure and function, brainstem anatomy and function is daunting for even the most experienced neuroradiologists. This presentation will offer a simplified and systematic approach to understanding the numerous tracts passing through the brainstem. The combination of case-based examples with high-resolution (9.4 T) MR imaging will help clarify the function and anatomy of many brainstem pathways, thereby enabling more accurate lesion detection and localization in current practice. Furthermore, as advanced imaging techniques become more widely available understanding this complex anatomy will become even more important and practical.

**KEY WORDS:** Brainstem

#### eEdE-57

##### **Diffusion Tensor Imaging Functional Anatomy: How Much Do You Know?**

Gupta, S. Klein, A. P. Ulmer, J. L. Mark, L. P. Baruah, D. Raslau, F. Goth, E.

Medical College of Wisconsin Affiliated Hospitals  
Milwaukee, WI

#### PURPOSE

An interactive electronic quiz utilizing color-coded fractional anisotropy diffusion tensor imaging (CC-FA DTI) maps tests and reinforces the user's knowledge of specific anatomical white matter tracts, structure/function relationships, and potential clinical deficits.

#### APPROACH/METHODS

Color-coded fractional anisotropy diffusion tensor imaging maps for this review were obtained with a 1.5 T system (GE Medical Systems, Milwaukee, WI) by using a dual-refocused spin-echo technique, 3 mm slice thickness, 13 gradient-encoding directions, a b-value = 900, an NEX = 2, a TE = 70 ms, and a TR min = 11 s to acquire 40 contiguous slices with a 128 x 128 matrix and 240-mm field of view. Axial, coronal, and sagittal CC-FA maps are used in an interactive quiz. Knowledge of specific white matter tracts, structure/function relationships, and proposed clinical deficits is tested and reinforced using a multiple choice format.

#### FINDINGS/DISCUSSION

This DTI quiz focuses on major white matter tracts that are encountered routinely in daily clinical practice. Familiarity with these tracts, their functions, and their proposed clinical deficits helps the neuroradiologist optimally interpret conventional MRI and CT exams as well as advanced imaging exams, such as those performed for preoperative brain mapping. Featured white matter tracts include the superior longitudinal fasciculus (including the arcuate fasciculus), uncinate fasciculus, inferior longitudinal fasciculus, fronto-occipital fasciculus, optic radiations, corona radiata, posterior limb of the internal capsule, and cingulum.

#### SUMMARY/CONCLUSION

The goal of this interactive electronic quiz is to teach and reinforce white matter structure/function concepts with DTI, an imaging modality that is becoming more and more integral to the practice of neuroradiology.

**KEY WORDS:** Diffusion tensor imaging, anatomy, tractography

#### eEdE-58

##### **Beyond an Awesome Research Resource and an Amazing Tool for Creating Colorful Images of the Brain: Diffusion Tensor Imaging, the Practical Guide for Clinical Neuroradiology**

Milch, H. S.<sup>1</sup>•Lui, Y. S.<sup>2</sup>

<sup>1</sup>Boston University School of Medicine, Boston, MA,

<sup>2</sup>New York University School of Medicine, New York, NY

#### PURPOSE

Diffusion tensor imaging (DTI) is an important tool for evaluating white matter structure and is now entering the setting of clinical practice. The purpose of this exhibit is to highlight the most clinically relevant features of DTI. Contents of the exhibit include: (1) a description of standard DTI parameters; (2) an image atlas of two clinically important tracts with clues on



how to identify them on DTI color maps; (3) a pictorial guide to creating 3D reconstruction (tractography) of specific white matter tracts using a standard and reproducible approach; and (4) a few examples of abnormal DTI.

#### APPROACH/METHODS

Data were obtained from three subjects to demonstrate normal brain anatomy and presented anonymously in a powerpoint format. Standard parameters for DTI - mean diffusivity (MD), fractional anisotropy (FA), axial diffusivity (Dax), radial diffusivity (Drad) - are reviewed with a description of the clinical relevance of these parameters. The use of anisotropy to create both color and magnitude maps is explained followed by visual examples of two clinically relevant tracts which have been shown in the literature to be reproducibly identified: the corticospinal tract (CST) and the superior longitudinal fasciculus (SLF). Series of images are shown of relevant anatomical sections in axial, sagittal, and coronal planes. Tractography images for the CST and SLF also are depicted, including a description of region of interest (ROI) selection for each tract. Both the anatomy and the functional role of these white matter tracts are reviewed. Examples of pathologic disruption of these clinically relevant tracts are shown with comparison to normal anatomy of the contralateral tract.

#### FINDINGS/DISCUSSION

Diffusion tensor imaging is a powerful research tool. As more clinical applications such as presurgical evaluation are identified, it is increasingly important for radiologists to be able to apply these methods in clinically relevant cases. The CST and SLF are two useful tracts for clinicians to recognize, as disruption of these particular tracts can cause significant neurologic impairment, and these tracts have been shown to be reproducibly identified and tracked using standard DTI protocols. The locations of white matter structures such as the SLF and CST are critical for surgeons to know preoperatively, in order to plan their approach and minimize morbidity. Diffusion tensor imaging tractography provides further detail on the integrity and location of these white matter tracts. In addition to knowing cortical anatomy, having a working knowledge of white matter anatomy also is now useful. Implementation of a standardized approach to tractography allows for reproducibility among subjects, improving both the clinical and research utility of this unique imaging tool.

#### SUMMARY/CONCLUSION

Diffusion tensor imaging has an important role in research that has now moved into clinical practice. This educational exhibit highlights the currently useful clinical applications and summarizes techniques useful in postprocessing and understanding clinical DTI. The clinical utility of DTI continues to broaden and a fundamental understanding of how to use this tool will be essential for practicing radiologists.

**KEY WORDS:** Diffusion tensor imaging, tractography, white matter anatomy

#### eEdE-59

#### Review of Methods for Localization of Eloquent Brain Structures: When Are They Helpful?

Hamilton, J. D.<sup>1</sup>•Kumar, V. A.<sup>1</sup>•Prabhu, S. S.<sup>1</sup>•Hayman, L. A.<sup>2</sup>•Jackson, E. F.<sup>1</sup>•Papanicolaou, A. C.<sup>3</sup>•Kumar, A. J.<sup>1</sup>

<sup>1</sup>M.D. Anderson Cancer Center, Houston, TX, <sup>2</sup>Anatom-e Information Systems, Ltd., Houston, TX, <sup>3</sup>University of Texas Health Science Center, Houston, TX

#### PURPOSE

A variety of methods exist to localize eloquent portions of the brain to avoid new neurologic deficits during operation. The supratentorial eloquent portions have been defined as seven cortical areas and five white matter tract related to primary sensory areas, motor and language function which cannot be resected without deficit. This presentation seeks to educate about the available imaging and intraoperative methods, their accuracies for localizing particular structures, and associated pitfalls.

#### APPROACH/METHODS

Literature searches and clinical expertise of experts in pre/perioperative localization were utilized. The noninvasive imaging techniques included anatomical cross-sectional imaging (CT and MRI), fMRI (BOLD technique), diffusion tensor imaging (DTI), magnetoencephalography (MEG) and use of superimposed anatomical and functional templates (e.g., Anatom-e Information Systems, Houston, TX). More invasive techniques included WADA testing (intracarotid amobarbital), magnetic evoked fields and surgical methods such as intraoperative ultrasound, awake electrical cortical or subcortical stimulation. Electrophysiologic recording techniques (including electroencephalogram) have a broad range of invasiveness.

#### FINDINGS/DISCUSSION

Anatomical imaging is the most commonly used and precise method for preoperative localization of structural lesions. Using certain anatomical landmarks and rules, many of the cortical areas can be localized but language dominance and location of white matter tracts (except for certain anchor points) is less accurate. Both fMRI and MEG techniques can localize cortical areas including language dominance but rarely are used as the sole technique for that purpose. Both techniques rely on assumptions for averaging over multiple time points. In a clinical population, fMRI is most robust for hand motor response. WADA testing is useful for questions of language dominance in left-handed or ambidextrous individuals. Functional MRI, WADA, and many intraoperative techniques relying on patient effort are compromised by a related neurologic deficit. Many perioperative techniques, fMRI and DTI (but not necessarily for MEG) may fail when eloquent areas are within or adjacent to tumor. Diffusion tensor imaging localizes white matter tracts but diffusion restriction on the edge of the tumor, from compression of small white matter tracts, can mimic major white matter tracts. Template-based analysis is very useful to fill in

functional detail and name structures, with limitations due to individual variance (predominately language dominance) and from a lesion's mass effect. Intraoperative ultrasound is useful for delineating vasculature and confirming intraoperative orientation in combination with other modalities. Electrophysiologic recording gains accuracy with increasing technique invasiveness and can localize the central sulcus. Electrical stimulation is considered the gold standard for identifying cortical and subcortical areas of eloquence despite failure in up to 15% of cases. It can result in seizures (improved by subcortical ultrasound stimulation) and may require the patient to be awake during testing. Unlike negative stimulation testing where there may be a question of what caused the temporary induced deficit (e.g., speech arrest from stimulation of Broca's language area or lower face motor area), technology is emerging (magnetic evoked fields, phased ultrasound) for positive stimulation testing but currently lacks necessary spatial resolution.

#### **SUMMARY/CONCLUSION**

A rational combination of the available approaches can improve efficiency and accuracy of eloquent area localization.

**KEY WORDS:** Eloquent cortex, white matter, preoperative planning

#### **eEdE-60**

### **3D Curvilinear Confocally Annotated Brain Reconstructions Improve Visualization of Anatomical Relationships of Insular Gliomas Diagnosed by 3.0 T MR Imaging**

Kumar, V. A.<sup>1</sup>Vabulas, M.<sup>2</sup>Hamilton, J.<sup>1</sup>Shah, K.<sup>1</sup>Lang, F. E.<sup>1</sup>Hayman, L.<sup>2</sup>Jackson, E. F.<sup>1</sup>Kumar, A. J.<sup>1</sup>

<sup>1</sup>M.D. Anderson Cancer Center, Houston, TX, <sup>2</sup>Anatom-e Information Systems, Houston, TX

#### **PURPOSE**

To illustrate the utility of 3D curvilinear confocal volume reconstructions of 3.0 T MRI data in the surgical planning and resection of insular gliomas.

#### **APPROACH/METHODS**

MR imaging data acquired from five patients with biopsy proven insular gliomas were analyzed retrospectively using a workstation from Anatom-e (Houston, TX), which reconstructed the DICOM images into a 3D volume set. Tools were available to independently display the data in any plane of interest including confocal curvilinear reformations, in addition to the standard views. The insular gliomas were evaluated by multiplanar reformats and volume rendered views of axial T2-FLAIR images (2 mm thick contiguous sections), axial T2-weighted fast spin-echo images (2 mm thick sections), and sagittal post-gadolinium FSPGR T1-weighted images (1.5 mm thick sections). In addition, fMRI (BOLD activation) data for language and motor mapping and source images from coronal 2D time of flight MR-Venogram studies (1.2 mm thick sections) also were incorporated in the 3D brain

reconstructions. Instead of flat sections, confocal planes of section were centered on the insula and its complex surrounding anatomical landmarks. To facilitate interpretation, a deformable template, which contained annotated structures, was superimposed on the tumor-bearing brain.

#### **FINDINGS/DISCUSSION**

The complex anatomy surrounding insular tumors was well illustrated by the tumor-induced vasogenic edema in the surrounding tracts. Confocal curvilinear reconstructions were able to capture all of the surrounding relationships, such as the relationship of insular gliomas to the surface anatomy of the sulci and gyri, venous anatomy surrounding the insular cortex, precise regional extensions of the tumor into the adjacent white matter tracts (in particular, the uncinate fasciculus), extent of deep extensions towards the basal ganglion region, and the relationship of tumor to adjacent eloquent structures (e.g., Broca's area, Wernicke's area, and sensory motor cortex). Correlation with intraoperative photographs obtained during the resection of insular gliomas also will be exhibited to further demonstrate the findings obtained by presurgical MR imaging with annotated curvilinear confocal volume reconstructions.

#### **SUMMARY/CONCLUSION**

Software which creates labeled curvilinear confocal volume reconstructions provides a new prospective of the brain anatomy. The usefulness of this technique is demonstrated in cases of insular gliomas.

**KEY WORDS:** Insular gliomas, brain atlas

#### **eEdE-61**

### **Normal Pediatric Spine: A Pictorial Review of MR Anatomy and Development in the Infant, Child and Adolescent**

Tuna, I. S. Kelly, T. G. Maheshwari, M. Singh, S. Chandra, T. Segall, H. D.

Medical College of Wisconsin  
Wauwatosa, WI

#### **PURPOSE**

Radiologic evaluation of the pediatric spine can be more challenging in children than in the adult patient due to the wide range of normal anatomical variants and synchondroses, combined with the unique effects of trauma in children. MR imaging is an excellent imaging modality for the evaluation of the pediatric spine. However, in order to provide an accurate interpretation of acute posttraumatic changes in the pediatric spine, particularly in the setting of abusive head trauma, a fundamental knowledge of normal anatomy, variants and pathology of the pediatric spine is required. The aim of this educational exhibit is to illustrate normal MRI anatomy of the spine in the infant, child and adolescent.

**APPROACH/METHODS**

This exhibit will first describe basic spinal embryology and development of the vertebra and spinal cord, followed by MRI depiction of the developmental anatomy of the spine from infancy through adolescence. The changing appearance of the spinal canal, spinal cord and vertebral bodies with age will be illustrated using normal cases from the radiology database. Sagittal and transverse diameter of vertebral bodies, thickness of the dural thecal sac, dimensions of the spinal canal, normal bone marrow signal changes, vertebral body heights, level of conus medullaris, prevertebral and paraspinal soft tissues and epidural fat thickness will be described and changes according to age will be pointed out.

**FINDINGS/DISCUSSION**

In early life, the spinal cord extends to the inferior aspect of the bony spinal column. Because the vertebral bodies grow longitudinally faster than the spinal cord does, the conus medullaris may change. Ossification of the vertebral bodies and posterior elements is nearly complete by age 10, with a resultant decrease in the spinal canal diameter. The nucleus pulposus becomes smaller after 10 years and spans approximately half the disk space in the sagittal plane. The spinal cord is elliptical in cross-section in the cervical spine and demonstrates a difference in signal between the normal gray and white matter of the spinal cord which should not be mistaken for intramedullary pathology.

**SUMMARY/CONCLUSION**

A solid understanding of normal spine anatomy and embryologic development is essential in evaluation of pediatric spine, mainly in the setting of trauma. Familiarity with normal anatomical variants is essential to provide an accurate interpretation of pathology in the pediatric spine.

**KEY WORDS:** Spine, anatomy, children

**Monday, April 23 -  
Wednesday, April 24**

**6:30 AM - 9:00 PM**

**Thursday, April 26**

**6:30 AM - 3:00 PM**

**Rhineland**

**Electronic Education Exhibits  
(eEdE) Exhibits 62 - 101**

**eEdE3 -**

**Note: A missing printed number indicates an abstract has been withdrawn.**

**eEdE-062**

**More than Meets the Eye: Imaging of Cutaneous Malignancies in the Head and Neck**

Bangiyev, L.<sup>1</sup>•Reede, D. L.<sup>1</sup>•Smoker, W.<sup>2</sup>•Ginsberg, L. E.<sup>3</sup>•Bobinski, M.<sup>4</sup>

<sup>1</sup>State University of New York Downstate Medical Center University Hospital Brooklyn at Long Island College Hospital, Brooklyn, NY, <sup>2</sup>University of Iowa Hospitals and Clinics, Iowa, IA, <sup>3</sup>M.D. Anderson Cancer Center, Houston, TX, <sup>4</sup>University of California Davis Health System, Sacramento, CA

**PURPOSE**

Review the epidemiology and clinical findings of common cutaneous malignancies. Learn key anatomy of the skin, scalp, lymphatic drainage, parotid gland and nerves that facilitates tumor spread. Understand the role of imaging in the evaluation of skin cancer, tumor spread to adjacent structures, nodes and nerves.

**APPROACH/METHODS**

This electronic exhibit module organized in quiz format reviews the epidemiology, clinical findings and key anatomical points regarding the skin, scalp, lymphatic drainage, innervation and parotid glands. Anatomy is reviewed using illustrations, cross-sectional images and animations. Cases are presented for the user to analyze that stress the importance of tumor location, involvement of adjacent structures (with special attention to the parotid), nodal metastases, and presence of perineural tumor spread.

**FINDINGS/DISCUSSION**

Lesions illustrated are organized based on structures involved to stress key points in imaging analysis. Cases shown include: basal and squamous cell carcinoma, melanoma, Kaposi's sarcoma, angiosarcoma, lymphoma (B and T cell), skin metastasis and basal cell nevus

syndrome. Abnormal findings are highlighted using animated color overlays.

#### **SUMMARY/CONCLUSION**

Cutaneous malignancies are the most common cancers with over a million new cases diagnosed per year in the U.S. Approximately 80% of these lesions occur in the head and neck region. Superficial lesions rarely are imaged; however, imaging is used in the assessment of advanced and recurrent disease. This exhibit demonstrates the role of imaging in the evaluation of cutaneous malignancies in the head and neck and aids in the development of an anatomical-based approach for imaging assessment.

**KEY WORDS:** Head and neck, cancer, skin

#### **eEdE-63**

### **Radiology of Mandibular Trauma: A Comprehensive Approach**

Byrns, K.·Penna, K.·Lev, S.

Nassau University Medical Center  
East Meadow, NY

#### **PURPOSE**

We review the broad spectrum of mandibular fractures, addressing specific patterns of injury, imaging pitfalls and clinical implications of various entities, as well as illustrating the role of MDCT in facilitating detailed analysis and surgical management.

#### **APPROACH/METHODS**

We systematically reviewed all imaging studies of patients with mandibular fractures presenting to the emergency department or surgical clinics of our community-based Level 1 trauma center, compiling a database of 488 cases representing 17 years of experience. We reviewed the surgeries performed and the use of 2D and 3D MDCT in pre and post-operative assessment. We currently employ a 320-slice MDCT for maxillofacial examinations, collimated to 0.5 mm.

#### **FINDINGS/DISCUSSION**

The current radiographic approach to mandibular injury focuses mainly upon computed tomography, less so panoramic and plain radiography, the historical gold standards. High-resolution MDCT, with detailed multiplanar 2D reformats and 3D reconstructions, has improved lesion detection significantly. MR imaging frequently is employed in suspected trauma to the temporomandibular joint to help detect occult fractures and effusions. The classification of mandibular fractures is generally done by anatomical location. Most common are condylar process fractures (36%), classified into Spiessl and Schroll Types I-VI based upon site, displacement, and dislocation. Additional sites include the body (21%), angle (20%), and symphysis (14%), with fractures involving the ramus, alveolar process, and coronoid process each comprising 3% or fewer. The mandible is classified routinely as dentulous, edentulous, or atrophic edentulous. Any single mandibular fracture should prompt careful search for

contralateral lesions, as the mandible functions as a bony "ring" to some extent, producing bilateral fractures or contralateral TMJ dislocation. Special care should be given to assess involvement of the inferior alveolar artery and nerve. The antiquated "favorable" (i.e., muscular forces drawing bony fragments together) versus "unfavorable" (distracting them) schema now is avoided, as this has little impact upon management. Modern understanding necessitates an appreciation of the complimentary and divergent forces of compression, tension, and torque at play. The surgeon must be especially sensitive to high risk regions, such as tooth roots and the mandibular canal. A minefield of potential hazards exists, one which the radiologist can help the surgeon to successfully navigate. A keen eye must be augmented with awareness of clinical implications, both immediate and long-term. Variants of condylar fractures, for example, portend complications such as avascular necrosis or, rarely, bony dislocations into the middle cranial fossa. In the setting of a shattered midface, the integrity of the ramus demands extra attention, as the vertical rami become the sole determinant of the correct facial height for the surgeon. Various long-term sequelae, including pseudoarthrosis due to fibrous nonunion of a fractured angle, must be considered on follow-up studies.

#### **SUMMARY/CONCLUSION**

In the setting of mandibular trauma it is imperative for the radiologist to consider his or her findings in a broader context. By using a structured, location-based approach in reporting and being mindful of the anatomical relationships and biophysical dynamics at play, complications, both immediate and long-term, can be avoided.

**KEY WORDS:** Mandible, trauma, MDCT

#### **eEdE-64**

### **Role of Multidetector Computed Tomography in Maxillofacial Trauma**

Feliciano, Y. Z.<sup>1</sup>·Zayas, J. O.<sup>1</sup>·Rivera, W.<sup>1</sup>·Labat, E.<sup>1</sup>·Fornaris, R.<sup>2</sup>

<sup>1</sup>RCM UPR, San Juan, PR, <sup>2</sup>RCM UPR, San Juan, PUERTO RICO

#### **PURPOSE**

- To review the relevant maxillofacial anatomy using multidetector CT (MDCT) with multiplanar reconstruction (MPR) and 3D reconstructions. - Discuss the anatomical and radiologic descriptors and terminology used in radiologic reporting of maxillofacial trauma. - Review the importance of MPR and 3D reconstructions for surgical planning.

#### **APPROACH/METHODS**

- Perform a retrospective review of maxillofacial trauma database at our PACS stations. - Present a pictorial review illustrating relevant MDCT maxillofacial anatomy. - Discuss the most common mechanisms of injury in maxillofacial trauma. - Discuss the importance of MDCT with MPR and 3D reconstruction as important

tools in the diagnosis, characterization and preoperative planning in patients with maxillofacial trauma. - Review the anatomical and radiologic descriptors and terminology in radiologic reporting including classifications.

#### **FINDINGS/DISCUSSION**

Maxillofacial trauma occurs most commonly from motor vehicle collision or assaults. Injuries range from minor soft tissue lacerations to major facial trauma with significant functional and cosmetic consequences. Although conventional radiography may demonstrate simple fractures of the nasal bone, zygomatic arch, maxilla and frontal bone, MDCT with MPR and 3D reconstruction are needed for better depiction of complex maxillofacial fractures and soft tissue complications. This project includes a pictorial review using MPR and 3D reconstruction illustrating the most common maxillofacial traumatic injuries and classifications: nasal bone fractures, naso-orbital-ethmoid fracture, frontal sinus fracture, orbital fracture, zygomatic fracture, maxillary fracture and mandibular fracture. Emphasis is placed in the advantage of complimenting MDCT with MPR and 3D reconstructions for a more complete diagnostic, evaluation and treatment planning of maxillofacial traumatic injuries.

#### **SUMMARY/CONCLUSION**

Multidetector CT with MPR and 3D reconstructions are important tools for the diagnosis, characterization and preoperative planning in patients with maxillofacial trauma. Knowledge of the appropriate standardized radiologic descriptors and terminology are key to defining imaging findings that are valuable for clinicians in the management of patients with maxillofacial trauma.

**KEY WORDS:** Maxillofacial, trauma

#### **eEdE-65**

##### **Where Do They Go?: Common Pathways of Disease Spread in the Head and Neck**

Chen, D.<sup>1</sup>Singh, V.<sup>1</sup>Guha-Thakurta, N.<sup>2</sup>Reede, D. L.<sup>1</sup>Smoker, W. R. K.<sup>3</sup>

<sup>1</sup>SUNY Downstate UHB at Long Island College Hospital, Brooklyn, NY, <sup>2</sup>MD Anderson Cancer Center, Houston, TX, <sup>3</sup>University of Iowa Hospital and Clinics, Iowa City, IA

#### **PURPOSE**

After viewing this teaching module, the user will have learned: • Key head and neck (H&N) anatomy which facilitates the spread of disease. • Common pathways of disease spread. • A systematic approach for imaging evaluation of pathology in specific locations.

#### **APPROACH/METHODS**

Cases selected from the teaching files of three major medical centers are presented in a quiz format to demonstrate common routes of disease spread. Pertinent anatomy is presented using illustrations, animations, and corresponding cross-sectional images.

#### **FINDINGS/DISCUSSION**

After a comprehensive review of the pertinent anatomy, cases are shown to demonstrate pathways of disease spread. Key anatomical structures that need to be evaluated in specific areas are emphasized. Pathology in the following areas are presented: • Scalp - lesions in the subgaleal layer with intracranial extension and lesions in the subgaleal layer limited by the aponeurosis. • Buccopharyngeal gap - spread of infection (peritonsillar abscess) and tumor (tonsillar) into the parapharyngeal space. • Buccal and masticator space communication - tumors and infection. • Pterygomandibular raphe - retromolar trigone lesion extension to the region of the maxillary tubercle to the buccal space and masticator space. • Sublingual to submandibular space - ranula, infection, and tumor. • Mylohyoid muscle - spread of dental infection in the sublingual vs submandibular or masticator space and direct extension of tumor across the muscle from the sublingual space. • Perineural - tumors spreading along the 5th and 7th cranial nerves.

#### **SUMMARY/CONCLUSION**

Head and neck anatomy is complex and often difficult to understand. Use of anatomical illustrations with corresponding cross-sectional images and animations will foster a better understanding of pertinent anatomy. An understanding of the common pathways of disease spread in the H&N is required to localize the primary site of disease as well as detect and predict spread to adjacent areas.

#### **eEdE-66**

##### **Parotid Space Lesions: An Interactive Case-Based Review**

Fletcher, B. A.·Policeni, B. A.·Smoker, W. R. K.

University of Iowa Hospitals and Clinics  
Iowa City, IA

#### **PURPOSE**

The parotid space frequently is affected by various disease processes. The purpose of this exhibit is to: 1) Review key anatomy of the parotid space; 2) Present cases that demonstrate typical imaging findings of a variety of commonly encountered parotid space pathology; 3) Illustrate imaging findings of less common pathology.

#### **APPROACH/METHODS**

We identified cases of parotid space lesions using the following inclusion criteria: 1) Imaging report was available in the radiology information system from July 2005 to September 2011; 2) Both of the terms "parotid" and "mass" were present in the report impression; 3) Cases included diagnostic quality images that were retrievable on the PACS; 4) Pathology reports were available with a definitive diagnosis. A total of 277 cases met these criteria. This exhibit provides a brief review of key parotid space anatomy followed by an interactive case-based review of a variety of these pathologically proven cases with discussion of the key imaging features. Lesions presented include: pleomorphic

adenoma (27.8%), Warthin tumor (19.9%), squamous cell carcinoma (11.2%), normal and reactive lymph nodes (5.4%), mucoepidermoid carcinoma (4%), nerve sheath tumor (1.4%), adenoid cystic carcinoma (1.4%), basal cell adenoma (1.4%), benign cysts (1%), infantile hemangiomas (1%), acinic cell carcinoma (1%), and oncocytoma (0.7%).

#### **FINDINGS/DISCUSSION**

Parotid neoplasms are statistically the most frequent parotid space lesions. However, there are other structures within the parotid space (i.e., CN VII) that can give rise to pathology. Due to significant overlap in imaging characteristics of benign and malignant parotid space lesions, tissue frequently is required for diagnosis to further guide management. It is important that the radiologist communicate the existence and nature of suspected tumors because such recognition may alter the surgical approach and influence the extent of resection.

#### **SUMMARY/CONCLUSION**

Parotid space lesions are not infrequent and neoplasms are most common. Imaging appearances may help further guide management but tissue diagnosis frequently is required. The ability to recognize key imaging features should help the radiologist manage parotid space lesions.

**KEY WORDS:** Parotid, mass, tumor

#### **eEdE-67**

##### **Orbital and Intracranial Affects of Microgravity: 3T MR Imaging**

Kramer, L. A.<sup>1</sup>•Hasan, K. M.<sup>1</sup>•Sargysan, A.<sup>2</sup>•Hamilton, D.<sup>2</sup>

<sup>1</sup>University of Texas Health Science Center Houston, Houston, TX, <sup>2</sup>Wyle Laboratories, Houston, TX

#### **PURPOSE**

Visual acuity changes in astronauts is a newly recognized phenomenon which has become more apparent with longer excursions into microgravity afforded by the international space station. On clinical exam, changes in visual acuity are associated with choroidal folds, retinal nerve fiber layer thickening, hyperopic shifts, cotton wool spots and optic disk edema. To further characterize findings seen on neuro-ophthalmologic exam and to identify potential copathologies, high resolution MR imaging of orbits and brain at 3 T were obtained in a subset of astronauts.

#### **APPROACH/METHODS**

All MRI exams were performed in normal gravity on a 3T, Philips Intera scanner utilizing a eight channel SENSE compatible head coil with a maximum slew rate of 200mT/ms/m and maximum gradient amplitude of 80mT/m. 3D axial fast spin-echo with spectral inversion recovery was obtained through the orbits (TR=2000mS, TE<sub>eff</sub>= 100mS, ETL=29, NEX=2, FOV= 10cm, ST= 0.78 mm, Matrix 128x124). 2D T2 FSE sagittal through the brain (TR= 6000mS, TE<sub>eff</sub>= 80mS, ETL=21, NEX=1, FOV= 25 cm, ST= 3 mm, Matrix 423x403). Optic

nerve sheath diameter (ONSD) and optic nerve diameter (OND) was quantified in the retrolaminar optic nerve. Optic nerve diameter and central optic nerve T2 hyperintensity was quantified at mid orbit. Qualitative analysis of optic nerve sheath redundancy, optic disk protrusion, posterior globe flattening, ventricular size and pituitary gland morphology was performed and correlated for association with intracranial evidence of hydrocephalus, vasogenic edema, central venous thrombosis or mass lesion.

#### **FINDINGS/DISCUSSION**

Some astronauts exposed to microgravity demonstrate distention of the optic nerve sheath, tortuosity of the optic nerve sheath with a kink, posterior globe flattening, optic disk protrusion and empty sella or partial concavity of the pituitary gland with posterior stalk displacement. All these imaging findings have been associated with elevated cerebrospinal fluid pressure. With increasing mission duration an increasing combination of these abnormalities are detected. With tortuosity of optic nerve sheath with a kink, congestion of the central optic nerve also has been identified.

#### **SUMMARY/CONCLUSION**

The technique of high resolution 3D MR imaging of the orbits to measure optic nerve sheath diameter and to evaluate the optic nerve will be described in detail along with a description of normal anatomy and pathologic examples. Although the exact mechanism is unknown, prolonged exposure to an environment of microgravity is associated with morphologic changes of the globe, optic nerve, optic nerve sheath and pituitary gland similar to that of idiopathic intracranial hypertension in a subset of astronauts. Further work is needed to identify those astronauts most at risk preflight and to potentially mitigate clinical symptomatology.

**KEY WORDS:** Orbit, pituitary, intracranial hypertension

#### **eEdE-68**

##### **"The Mind's Eye," Part 2: Imaging of Efferent Visual Pathways**

Ho, M.<sup>1</sup>•Moonis, G.<sup>1</sup>•Cunnane, M.<sup>2</sup>•Torun, N.<sup>1</sup>

<sup>1</sup>Beth Israel Deaconess Medical Center, Boston, MA, <sup>2</sup>Massachusetts Eye and Ear Infirmary, Boston, MA

#### **PURPOSE**

Neuro-ophthalmology is an interdisciplinary field that utilizes neurology, ophthalmology, and radiology to determine the visual implications of neurologic and systemic disorders. In this exhibit, we review the anatomy and function of the efferent visual system, which is essential for selecting appropriate imaging protocols based on a given clinical scenario. We will review the physiology of ocular motor pathways, as well as the spectrum of pathologic lesions involving these areas. Selected teaching cases will be presented, with discussion of clinical localizing signs and key ophthalmologic/radiologic findings.



### APPROACH/METHODS

Comprehensive evaluation of clinical and radiologic findings was performed in patients with selected abnormalities of the efferent visual system. Dedicated clinical examination was performed by a neuro-ophthalmology attending, including ocular alignment and motility testing, as well as video recording of eye movements in the majority of cases. Imaging findings were evaluated by two head/neck radiology attendings and a radiology resident (PGY-4).

### FINDINGS/DISCUSSION

The efferent visual system consists of the brainstem ocular motor nuclei, interconnecting fiber tracts, nerves responsible for ocular movement (cranial nerves III, IV, and VI), and sympathetic/parasympathetic fibers of the ciliary ganglion. Disease etiologies include vascular, trauma, demyelinating, infection/inflammation, degenerative, and neoplastic. Clinical examination may reveal cranial nerve palsies, ocular misalignment, pupillary changes, nystagmus, and gaze palsies. These signs help the clinician to localize anatomical regions of interest for imaging. Imaging locations of disease are classified as brainstem, fascicular, cisternal, cavernous sinus, and orbital. Specific cases to be presented include thyroid ophthalmopathy, infiltrative myopathy of extraocular muscles, third/fourth/sixth nerve palsies, skew deviation, gaze-evoked nystagmus, vertical gaze palsy, saccadic hypermetria, internuclear ophthalmoplegia, and Horner syndrome. Based on the clinical differential, a variety of imaging examinations may be utilized. Magnetic resonance (MR) imaging with gadolinium is the examination of choice for most indications. Computed tomography (CT) helps to characterize calcifications and fine osseous detail. Computed tomography also is used in the emergency setting, and when there are contraindications to MR. Ultrasonography can evaluate orbital masses, extraocular muscles, and the optic nerve. Catheter angiography is used for assessing and treating cerebrovascular lesions.

### SUMMARY/CONCLUSION

A wide variety of neurologic and systemic conditions can involve the efferent visual system. Initial evaluation should be performed by the referring clinician, with subsequent imaging based on the clinical differential. Radiologists need a detailed understanding of visual anatomy and physiology in order to relate imaging abnormalities to patient symptomatology. Accurate assessment of lesion location and etiology is crucial in determining patient diagnosis and management.

**KEY WORDS:** Visual pathways, ocular motility, efferent

### eEdE-69

#### "The Mind's Eye," Part 1: Imaging of Afferent Visual Pathways

Ho, M.<sup>1</sup>•Moonis, G.<sup>1</sup>•Cunnane, M.<sup>3</sup>•Torun, N.<sup>1</sup>

<sup>1</sup>Beth Israel Deaconess Medical Center, Boston, MA,

<sup>2</sup>Beth Israel Deaconess Medical Center, Boston, MA,

<sup>3</sup>Massachusetts Eye and Ear Infirmary, Boston, MA

### PURPOSE

Neuro-ophthalmology is an interdisciplinary field that utilizes neurology, ophthalmology, and radiology to determine the visual implications of neurologic and systemic disorders. In this exhibit, we review the anatomy and function of the afferent visual system, which is essential for selecting appropriate imaging protocols based on a given clinical scenario. We will examine the physiology of visual sensory pathways, as well as the spectrum of pathologic lesions involving these areas. Selected teaching cases will be presented, with discussion of clinical localizing signs and key ophthalmologic/radiologic findings.

### APPROACH/METHODS

Comprehensive evaluation of clinical and radiologic findings was performed in patients with selected abnormalities of the afferent visual system. Dedicated clinical examination was performed by a neuro-ophthalmology attending, including visual acuity, color vision, and visual field testing. Imaging findings were evaluated by two head/neck radiology attendings and a radiology resident (PGY-4).

### FINDINGS/DISCUSSION

The afferent visual system consists of the retinae, optic nerves, optic chiasm, optic tracts, sensory nuclei, optic radiations, and visual cortex. Disease etiologies include vascular, trauma, demyelination, infection/inflammation, neoplastic, and congenital. Clinical examination may reveal afferent pupillary defect, decreased visual acuity, and visual field deficits. These signs help the clinician to localize anatomical regions of interest for imaging. Imaging locations of disease are classified as prechiasmatic, chiasmatic, and postchiasmatic. Specific cases to be presented include optic disk drusen, optic neuritis, sphenoid wing meningioma, pituitary adenoma, cerebral infarct, and pseudotumor cerebri. Based on the clinical differential, a variety of imaging examinations may be utilized. Magnetic resonance (MR) imaging with gadolinium is the examination of choice for most indications. Computed tomography (CT) helps to characterize calcifications and fine osseous detail. Computed tomography also is used in the emergency setting, and when there are contraindications to MR. Ultrasonography can evaluate orbital masses, extraocular muscles, and the optic nerve.

### SUMMARY/CONCLUSION

A wide variety of systemic and neurologic abnormalities can involve the afferent visual system. Initial evaluation should be performed by the referring clinician, with subsequent imaging based on the clinical differential. Radiologists need a detailed understanding of visual anatomy and physiology in order to relate imaging abnormalities to patient symptomatology. Accurate assessment of lesion location and etiology is crucial in determining patient diagnosis and management.

**KEY WORDS:** Visual pathways, optic nerve, afferent

**eEdE-70****Use of MR Imaging in the Study of Glaucoma**

Cain, J. R.<sup>1</sup>·Hansen, T.<sup>1</sup>·Mercieca, K.<sup>2</sup>·Spencer, F.<sup>2</sup>·Jackson, A.<sup>1</sup>

<sup>1</sup>University of Manchester, Manchester, UNITED KINGDOM, <sup>2</sup>Central Manchester University Hospitals, Manchester, UNITED KINGDOM

**PURPOSE**

The use of advanced neuro-imaging modalities such as magnetic resonance imaging (MRI) is of increasing importance in ophthalmology, both for diagnostic and research purposes. This review will outline current state-of-the-art utilization of MRI in glaucoma covering hypotheses for glaucoma etiology and the use of MRI in glaucoma-related clinical and research situations. Recent advanced MRI techniques that could be used to further our understanding of glaucoma also will be described.

**APPROACH/METHODS**

There is a significant body of research into both primary open angle and normal tension glaucoma (optic nerve changes in the absence of high intraocular pressure) (NTG) utilizing the capability of MRI. A Medline search was conducted using search terms relating to "Glaucoma", "MRI" with additional terms including "etiology", "treatment" "research". The underlying etiology of NTG is unknown and is a target for current research. Hypotheses for NTG include neurodegeneration, ischemic changes, and cerebrospinal fluid (CSF) pressure and flow. MR imaging is the ideal methodology to investigate these hypotheses. Retinal ganglion cells (RGCs) appear to be the primary target for glaucomatous change in the eye, with degenerative changes occurring not only in glaucoma but also in conditions such as compressive optic neuropathy and arteritic anterior ischemic optic neuropathy.

**FINDINGS/DISCUSSION**

MR imaging studies also show an increased rate of intracranial lesions in patients with glaucomatous changes which could signify that glaucoma pathology originates in the optic nerve. Techniques such as manganese-enhanced MRI have been shown to be useful in monitoring glaucoma in a rat model. Clinically, MRI has been used to assess postoperative success of implanted shunts used to treat closed angle glaucoma. Diffusion tensor imaging of the optic pathways also have been shown to correlate with severity of glaucoma. Other techniques such as phase contrast measuring flow of the CSF, MR-ICP measurement, and better imaging of the optic nerve may all prove useful in future studies to determine the etiology of normal tension glaucoma.

**SUMMARY/CONCLUSION**

This educational review will provide a summary of current clinical and research uses of MRI in glaucoma and outline future directions for research in this area we also will include an overview of advanced MRI

methodologies which have applications in glaucoma research. It is intended that the reader will be in the position to undertake further research in this area.

**KEY WORDS:** Glaucoma, MR imaging, intraocular pressure

**eEdE-72****Visual Loss and MR Imaging: A Prospective Study**

Heran, F.·Watel, C.·Desxhamps, R.·Gueguen, A.·Vignal, C.  
Fondation Rothschild  
Paris, FRANCE

**PURPOSE**

MR imaging of anterior optic pathways is the imaging method needed in the etiological diagnosis of a unilateral or bilateral visual loss, once an ophthalmologic cause has been ruled out. Its technical aspect and its interpretation are often mediocre due to a poor knowledge of this pathology. The aims of our study are to propose an optimal MRI protocol, to define a simple method to analyze the images and to establish relationship between clinical data and results of this examination.

**APPROACH/METHODS**

With the collaboration of the neuro ophthalmologists and neurologists of the Fondation Ophthalmologique Rothschild, during 6 months we underwent a prospective study of 102 patients sent by their ophthalmologist, who underwent an MRI to explore a visual loss without ophthalmologic cause. The minimal MRI protocol required to include patients associated coronal T2 and T1-enhanced with fat suppression slices (focused on the anterior optic pathways from the posterior aspect of the ocular bulb to the optic tracts), axial diffusion and a brain study. Results of a careful analysis of optic nerves, optic chiasm and brain (signal and size), ophthalmologic and neurologic data (fundus, OCT, visual field, color vision...) were recorded on specific tables and statistic treatment was performed by a specialist (SAS 9.2 software, Khi2).

**FINDINGS/DISCUSSION**

Due to multiples artifacts, the results of diffusion sequence were disappointing, and this sequence was abandoned after the first 50 patients. From a technical point of view, some lesions were difficult to depict and excellent quality images were mandatory. Therefore, the radiologist had to repeat the sequences if necessary (mainly in case of blurred images due to eye movements) and had to look for small abnormalities either within or near the optic pathways. Evaluation of MRI and clinical data allowed interesting correlations. Considering the final diagnosis, in 16% of the cases, no cause has been found. In the 86 remaining patients, etiologies depicted were optic neuritis, essentially in relationship with MS (27% of cases), atrophy due to glaucoma (16% of cases), optic atrophy of other origin (Leber disease, undefined cause) (22% of cases), compression of the optic pathways (7% of cases) mainly due to meningiomas, ischemic event (6% of cases) and

initially missed ocular lesions (7% of cases). Correlations between results of MRI and final diagnosis were excellent in cases of neuritis, atrophy, compression. Normal MRI examinations, representing 28% of monocular visual loss and 32% of bilateral visual loss, were related to normal patients, ocular causes, ischemic lesions or atrophy at an initial stage.

#### **SUMMARY/CONCLUSION**

Should an ischemic or oculoretinal lesion be really ruled out, correlations between MRI and clinical data are otherwise excellent. Our MRI protocol, easy and rapid to perform on all MRI equipment and our interpretation guide associating analysis of the shape and the signal of the optic nerves and chiasm and of the surrounding structures are very helpful for the diagnosis of these visual losses. The final diagnosis remains nevertheless the result of a narrow collaboration between radiologist and clinician.

**KEY WORDS:** Optic nerve, visual loss, MR imaging

#### **eEdE-73**

##### **Ultrasound Anatomy of the Orbit: Correlation with CT and MR Imaging**

Ditta, L. C.·Cohen, H. L.·Choudhri, A. F.

University of Tennessee Health Science Center  
Memphis, TN

#### **PURPOSE**

Sonographic imaging of the orbit can provide excellent depiction of the globe, including position and differentiation of orbital and retrobulbar soft tissues, as well as characterize neoplastic and inflammatory orbital disorders, mass lesions, and vascular malformations. Despite these possible benefits, this technique is not commonly performed at most institutions. CT and MRI remain the most common modalities in orbital imaging. We review normal sonographic anatomy of the globe and orbit and common ocular and orbital pathology, as well techniques for performing orbital ultrasound.

#### **APPROACH/METHODS**

We will present annotated ultrasound images of the globe and orbit with correlative images from CT and MR. Images will be provided from a normal orbit, as well as patients with orbital disorders, masses and vascular malformations. Images also will be provided showing scanning techniques and parameters for safely performing orbital sonography.

#### **FINDINGS/DISCUSSION**

Sonography of the orbit is an underutilized technique that can provide high resolution evaluation of the globe including position and differentiation of orbital and retrobulbar soft tissues. Doppler imaging can provide a noninvasive dynamic assessment of orbital masses and suspected vascular lesions.

#### **SUMMARY/CONCLUSION**

With knowledge of CT and MR anatomy of the orbit, as well as a general understanding of ultrasound techniques, orbital sonography can be offered as an adjunct tool for further characterizing orbital pathology. This tool may have a specific role in lesions that are indeterminate on CT or MR, in particular masses and vascular lesions.

**KEY WORDS:** Orbit, ultrasound, anatomy

#### **eEdE-74**

##### **Classification of Soft Tissue Vascular Anomalies in the Head and Neck in Children: MR Evaluation Using Dynamic Contrast-Enhanced MR Angiography and Blood Pool Contrast Agent**

Bonekamp, D.·Huisman, T. A.·Mitchell, S.·Pryde, S.·Tekes, A.

Johns Hopkins Hospital  
Baltimore, MD

#### **PURPOSE**

The purpose is to discuss and illustrate the advantages of radiation-free high-quality diagnostic imaging of soft tissue vascular anomalies (VA) of the head and neck in children using gadofosveset trisodium in combination with high temporal resolution dynamic three-dimensional contrast-enhanced MRA (TWIST).

#### **APPROACH/METHODS**

Children with suspected diagnosis of VA in the head and neck were imaged using a dedicated VA protocol including a triplanar T2 with fat saturation, precontrast axial T1, triplanar T1-weighted imaging with fat saturation. Time resolved dynamic contrast-enhanced MRA (TWIST) was performed using gadofosveset trisodium.

#### **FINDINGS/DISCUSSION**

Contrast-enhanced MRA (TWIST) offers high temporal resolution in the order of seconds, allowing acquisition of multiphase studies, with post-hoc selection of optimal arterial, venous and delayed venous phases. Gadofosveset trisodium reversibly binds to serum albumin with high affinity with a binding fraction of approximately 90%. Therefore, it is strongly restricted to the blood pool in which it remains for a prolonged period of time with only minimal tissue enhancement and extravasation. Multiple advantages include higher achievable contrast to noise and signal to noise ratios, use of approximately 3-fold lower contrast doses allowing shorter bolus and more compact bolus injection, and enhanced temporal discrimination and separation of the various contrast phases. These improvements are useful especially for the imaging of small children, as they can account for differences in pediatric hemodynamics such as a significant faster circulation time, slower injection rates, larger bolus dispersion and smaller contrast doses. Contrast enhancement dynamics are key decision criteria in the evaluation of vascular anomalies of the pediatric craniofacial region and excellently depicted with DCE-

MRA. We review key MR imaging characteristics of infantile hemangiomas, venous malformations, and lymphatic malformations using conventional MRI sequences with specific discussion of the importance of timing of contrast enhancement in accurate classification of these complex anomalies.

#### **SUMMARY/CONCLUSION**

High-quality diagnostic imaging for the characterization of vascular anomalies of the head and neck in children using blood pool MR contrast agents and TWIST has high potential as an alternative to CT angiography (CTA) and digital subtraction angiography (DSA), while providing unique advantages especially for imaging in the pediatric population. High temporal resolution imaging with prolonged vascular phase aids in determination of the exact enhancement pattern (arterial, venous or no enhancement) of vascular anomalies as a decisive factor in their diagnosis.

**KEY WORDS:** Vascular anomalies, time-resolved contrast-enhanced dynamic MRA, blood pool contrast agent

#### **eEdE-75**

### **MR Imaging of the Temporomandibular Joint: Pearls, Pitfalls, and What the Surgeon Needs to Know**

Talbott, S.·Aiken, A.·Bouloux, G.·Hudgins, P. A.

Emory University  
Atlanta, GA

#### **PURPOSE**

The purpose of this exhibit is to use a case-based review to illustrate the pertinent MR imaging findings a surgeon needs to know for treatment and surgical planning of the temporomandibular joint (TMJ). Both common and rare diagnoses of the TMJ will be displayed. Many MR images have surgical confirmation.

#### **APPROACH/METHODS**

We retrospectively reviewed our experience of performing and interpreting 101 TMJ MR studies over the past 2 years. In collaboration with a maxillofacial surgical colleague who specializes in TMJ arthroscopy and surgery, we determined the five most important findings a surgeon will need to know to determine treatment. Potential pitfalls of interpretation were determined. A literature review of the entities affecting the TMJ, including internal derangement, osteoarthritis and rarer diagnoses, also was performed. Our MRI TMJ protocol consists of axial and coronal T1-weighted images, first and second echo T2-weighted sagittal oblique images through both TMJs in open and closed mouth positions, and dynamic cine T2-weighted images during opening and closing on a 1.5 T unit.

#### **FINDINGS/DISCUSSION**

Painful disorders affecting the TMJ are common, with a prevalence ranging from 16-59%. In patients undergoing MR imaging of the TMJ at our institution, the average age is 42 with 92% being female.

Approximately 63% of these patients proceeded to surgery. The majority of patients presenting with TMJ pain or trismus demonstrate internal derangement upon MR imaging, with anterior disk displacement with or without recapture. This can lead to osteoarthritis including abnormal morphology of the mandibular head, osteophytosis, and articular erosion. The position of a degenerated disk can be difficult to identify on static images, and in approximately 75% of these cases the cine dynamic sequence has been valuable to identify the disk. A scanning angle parallel to the angle of the mandible in the sagittal oblique position is ideal for imaging the mandibular condyle and glenoid fossa. A large field of view of 16cm and 18cm on the coronal and axial T1-weighted images respectively is helpful to detect masses such as osteochondromas arising from the TMJ. From the surgeon's perspective, every interpretation should include the position of the disk in the open and closed mouth positions, the morphology of the disc, morphology of the mandibular condyle and glenoid fossa, and exclusion of other pathologies that could occur in the masticator space. We also explore other non-degenerative etiologies of pain and trismus in this pictorial review, including rheumatoid arthritis, synovial chondromatosis, idiopathic resorption of the condylar head and septic arthritis. Squamous cell carcinoma including direct spread from the external auditory canal or perineural spread along the auriculotemporal nerve also can result in TMJ dysfunction which can be seen at the time of imaging.

#### **SUMMARY/CONCLUSION**

By integrating the technical and interpretative pearls and pitfalls of TMJ imaging, recognizing which MR findings are important to the surgeon for treatment planning, and being able to identify the nondegenerative etiologies of TMJ dysfunction, the radiologist can be more confident in his or her interpretation of an MRI of the TMJ.

**KEY WORDS:** Temporomandibular joint, MR imaging

#### **eEdE-76**

### **High Resolution 3 T Magnetic Resonance Neurography Evaluation of Neurogenic Thoracic Outlet Syndrome**

Thawait, G. K.<sup>1</sup>·Thawait, S. K.<sup>2</sup>·Chalian, M.<sup>1</sup>·Thakkar, R. S.<sup>1</sup>·Del grande, F.<sup>1</sup>·Chhabra, A.<sup>1</sup>

<sup>1</sup>Johns Hopkins University School of Medicine, Baltimore, MD, <sup>2</sup>Yale University-Bridgeport Hospital, Bridgeport, CT

#### **PURPOSE**

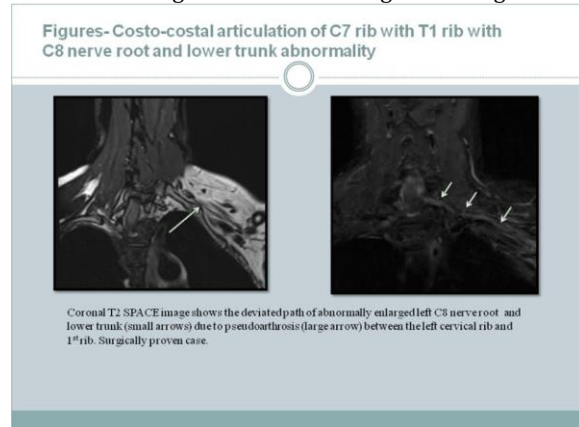
1. Gain knowledge of spectrum of pathologies causing neurogenic thoracic outlet syndrome (TOS). 2. Learn the high resolution 3 T magnetic resonance neurography (MRN) technique and optimal use of 3D sequences employed for evaluation of neurogenic TOS. 3. Familiarize the readers with the typical MRN findings of the pathologies contributing to the neurogenic TOS.

### APPROACH/METHODS

Following a discussion of spectrum of pathologies causing neurogenic TOS, their imaging evaluation using 3 T MRN technique will be presented with relevant cases proven on EMG and/or surgery. High resolution 2D and 3D MRN images depicting segmental brachial plexus involvement will be shown in representative cases of cervical ribs, aberrant vessels, focal fibrosis, narrowing of scalene triangle with hypertrophied muscle, intramuscular course of nerves, failed surgical procedures and mass lesions.

### FINDINGS/DISCUSSION

This exhibit highlights the importance of high resolution 3 T MRN in evaluating the neurogenic TOS proven by cases correlating with clinical or surgical findings.



### SUMMARY/CONCLUSION

3 T high resolution MRN is an excellent modality for evaluation of neurogenic TOS in both preoperative and postoperative setting.

**KEY WORDS:** Thoracic outlet syndrome, MR neurography, peripheral neuropathy

### eEdE-77

#### Review of Posttherapeutic Imaging in Head and Neck Cancer: Conventional and Advanced Biologic Modalities

Lober, P., Srinivasan, A., Shah, G., Mukherji, S. K.

University of Michigan Health System  
Ann Arbor, MI

### PURPOSE

To comprehensively review the literature on post-therapeutic imaging in head and neck cancer with special emphasis on the current role of advanced biologic imaging techniques including MR spectroscopy, CT perfusion, MR diffusion-weighted imaging, perfusion-weighted MRI, and 18F-FDG-PET.

### APPROACH/METHODS

This exhibit is divided into the following sections: A. Postsurgical neck - Appearances of the neck after various surgeries including radical neck dissection, modified radical neck dissection, selective neck dissection. B. Postradiation neck - expected changes on

CT and MRI. C. Imaging of complications after surgery or chemoradiation. D. Role of advanced imaging in posttreatment neck evaluation - i. Detection of tumor recurrence, ii. Evaluation of lymph nodal metastases, iii. Prediction and monitoring of therapy.

### FINDINGS/DISCUSSION

Knowledge of the surgical procedures in the neck and their expected postoperative appearances is key to avoid false/positive interpretations. While conventional CT and MRI often are adequate for differentiation of expected posttherapeutic changes from tumor recurrence in treated head and neck cancer, an array of advanced biologic imaging techniques may prove useful in this regard, looking beyond size, morphologic, and enhancement criteria to focus on molecular level differences between active tumor and benign tissue.

### SUMMARY/CONCLUSION

This exhibit provides a quick overview of expected postsurgical and postradiation appearances in the neck and elaborates on the role of conventional and advanced imaging modalities in posttherapeutic neck evaluation using illustrated examples.

**KEY WORDS:** Head and neck cancer, posttherapy, advanced imaging

### eEdE-79

#### "Cat Got Your Tongue?": Imaging Anatomy and Pathology of the Tongue

Pantol, G.<sup>1</sup>, Frankenthaler, R. A.<sup>1</sup>, Juliano, A.<sup>2</sup>, Moonis, G.<sup>1</sup>

<sup>1</sup>Beth Israel Deaconess Medical Center - Harvard Medical School, Boston, MA, <sup>2</sup>Massachusetts Eye and Ear - Harvard Medical School, Boston, MA

### PURPOSE

The anatomy and pathologic conditions of the tongue are complex and can pose a diagnostic challenge for the radiologist. The goal of this exhibit is to review the imaging anatomy of the tongue and its relationship to the floor of the mouth and to present selected teaching cases with common and uncommon pathologic processes and their corresponding clinical findings.

### APPROACH/METHODS

Comprehensive evaluation of clinical and radiologic findings was performed in 15 pediatric and adult patients with different tongue abnormalities. Dedicated clinical examination was performed by an otolaryngologist. Cross-sectional imaging findings using CT and MRI were evaluated by a head/neck radiology attending and a neuroradiology fellow (PGY-6). Clinico-radiologic correlation was performed during multidisciplinary head and neck conferences.

### FINDINGS/DISCUSSION

We describe in detail the imaging anatomy of the tongue on both MRI and CT imaging and emphasize landmarks to demarcate different morphologic parts of the tongue including the root of tongue. Representative cases depicting the various pathologies of the different

portions of the tongue are discussed with emphasis on imaging findings relatively specific for these entities. The following lesions of the tongue are included: malignancies - squamous cell carcinoma, ewing's sarcoma, rhabdomyosarcoma, melanoma, abscess - both bacterial and fungal, congenital lesions like thyroglossal duct cyst remnants, ectopic thyroid, foregut duplication cysts, ranulas, vascular lesions like venolymphatic malformations and AVMs, hemangiomas, lipomas, dermoid and epidermoid cysts. The tongue is a muscular organ situated in the mouth cavity and in the oropharynx with the function of swallowing, taste, touch and speech. It is composed chiefly of a skeletal muscle partly covered by mucous membrane. The tongue can be morphologically divided in four parts: the root, the apex (which rest against the incisor teeth), the dorsum which includes the presulcal part (oral anterior 2/3) and the postsulcal part (pharyngeal posterior 1/3); and the inferior surface. The root of the tongue rests on the floor of the mouth and is formed by the genioglossus and geniohyoid muscle attached to the mandible and hyoid bone. The nerves, vessels, and extrinsic muscles enter or leave the tongue through its root. On imaging it may be difficult to differentiate between the root of tongue and floor of mouth and often time lesions can involve both spaces. Abnormalities of the tongue can be classified on the basis of congenital, inflammatory, infectious, vascular and neoplastic disorders and imaging plays an important role in generating a differential in conjunction with clinical information. We have described clinico-radiologic correlative findings in common and uncommon tongue lesions.

#### **SUMMARY/CONCLUSION**

Imaging plays an important role in evaluating a wide variety of tongue masses and the radiologist's role is crucial in determining the patient diagnosis, prognosis and management.

**KEY WORDS:** Tongue

#### **eEdE-80**

### **Role and Utility of Diffusion-Weighted Imaging in Assessing Head and Neck Cancer: A Pictorial Review**

Sol, Y.-Kim, H.-Lee, T.

Pusan National University School of Medicine and Medical Research  
Busan, KOREA, REPUBLIC OF

#### **PURPOSE**

Although conventional MRI and CT are the imaging modalities of choice in evaluating head and neck cancer, sometimes both diagnostic tools yield low sensitivity and accuracy in making the diagnosis, staging, and assessing the posttreatment response. This exhibition will review the role and utility of DWI in assessing head and neck cancer.

#### **APPROACH/METHODS**

I. Biological concept of DWI in head and neck cancer. II. Utility of DWI in head and neck cancer. 1.

Characterization and differential diagnosis of head and neck cancer. 2. Evaluation of pathologic lymph nodes. 3. Differentiation between viable and necrotic lesion in malignant tumor. 4. Differentiation between tumor recurrence and posttreatment changes. 5. Assessment of treatment response. III. Technical limitations of DWI. IV. Future perspectives.

#### **FINDINGS/DISCUSSION**

The biophysical mechanism of DWI is based on the microscopic random translational motion of water molecules in biological tissues. Diffusion in biologic systems is affected by water exchange between intracellular and extracellular compartments and the tortuosity of the extracellular space (which in turn is affected by cell sizes, organization, and packing density). Apparent diffusion coefficient (ADC) value of malignant tumor is significantly lower than those of benign. The histopathologic characteristics of malignant tumor, such as enlarged nuclear/cytoplasm ratio, hyperchromatism, and hypercellularity, reduces the ratio of extracellular and intracellular volume and diffusion space for water molecules. Several studies have reported the ability of DWI to discriminate malignant from benign LNs in the neck delineation of viable and necrotic parts of a tumor is essential for determining the biopsy site and for diagnosis and treatment planning. The mean ADC value of viable tumors was reported to be significantly lower than that for necrotic parts. On conventional MR imaging, residual or recurrent lesions and treatment-induced changes show similar imaging characteristics and often are difficult to distinguish. Residual or recurrent lesions exhibits lower ADC values compared to posttreatment change. Changes in DWI may be an effective early biomarker for treatment outcome. In most malignant tumors, successful treatment is reflected by increases in ADC values.

#### **SUMMARY/CONCLUSION**

Diffusion-weighted imaging is a technique which analyzes the structures of biological tissue at a microscopic level. Apparent diffusion coefficient value, determined from DWI, can help detect the differences in the microstructures of tumor tissue and nontumor tissue. Therefore, DWI is a useful technique in a clinical practice, which provides informations of histopathologic characterization, differential diagnosis, and stage of head and neck cancer and assessment of treatment response.

**KEY WORDS:** Diffusion-weighted image, head and neck cancer, ADC value

#### **eEdE-81**

### **CT and MR Imaging Features of Articular and Periarticular Temporomandibular Joint Lesions: A Pictorial Review of Common and Uncommon Pathology**

Fourgas, E.-Corrigan, J.-Agarwal, A.-Patel, S.

Henry Ford Hospital  
Detroit, MI



## PURPOSE

Temporomandibular joint (TMJ) is affected by common and uncommon pathologic processes which often present a radiographic diagnostic challenge. The purpose of this exhibit is three-fold. First we review the embryology and normal anatomy of this anatomical structure. Second, imaging techniques for evaluation of TMJ dysfunction and common pathologies that result in derangement of this joint are presented. Finally, we review the CT and MR imaging characteristics of numerous common and rare lesions arising from or near the TMJ.

## APPROACH/METHODS

Representative MR images of normal TMJ examinations emphasizing the intricate anatomy are provided. The MR imaging signs of TMJ dysfunction are discussed and illustrated. We retrospectively reviewed cases of TMJ pathology from our institution over the past 10 years. We present the CT and MR imaging features of these lesions in pictorial format and emphasize distinguishing characteristics that aid in accurate diagnosis.

## FINDINGS/DISCUSSION

Cases demonstrating common TMJ derangements including meniscal and temporomandibular dislocations, fractures, and osteoarthritis are presented. Tumors of cartilaginous and synovial origin such as chondroblastoma, osteochondromatosis, PVNS and tenosynovial giant cell tumor are described. Involvement of the TMJ by a mandibular Ewing's sarcoma and squamous cell carcinoma of the EAC are illustrated. Examples of multiple myeloma and osseous metastasis also are included. Auriculo-temporal nerve involvement by a plexiform neurofibroma and by secondary perineural spread of tumor are presented. Inflammatory arthropathies such as rheumatoid arthritis and CPPD involving the TMJ are illustrated. Extension of local infections to involve the TMJ including cases of tooth extraction abscess and aggressive necrotizing otitis externa are discussed. Examples of surgical reconstruction of the mandibular body and condyles will be provided. Cases illustrating involvement of the TMJ by syndromes such as Goldenhar, Pierre Robin and EAC atresia are presented. Finally, other entities rarely involving the TMJ such as fibrous dysplasia, osteopetrosis, ameloblastoma and synovial cysts also are illustrated.

## SUMMARY/CONCLUSION

This exhibit presents a practical approach to the evaluation of the TMJ addressing normal anatomy and MR techniques. The diagnostic challenge of approaching the evaluation of the various pathologies in this articular and periarticular location is aided by presenting a pictorial review of a wide spectrum of such lesions.

**KEY WORDS:** Temporomandibular joint, TMJ

## eEdE-82

### Radiologic Evaluation of the Dental Implant Candidates

Ozgen, B.<sup>1</sup> Aktas, A.<sup>2</sup> Cila, A.<sup>1</sup>

<sup>1</sup>Hacettepe University, Faculty of Medicine, Ankara, TURKEY, <sup>2</sup>Hacettepe University, Faculty of Dentistry, Ankara, TURKEY

## PURPOSE

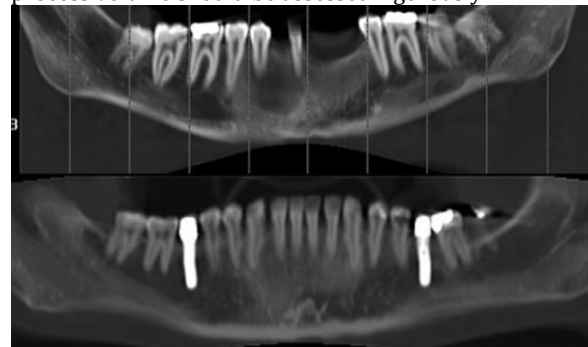
This exhibit will review the techniques used and the important aspects of imaging in the evaluation of the patients before dental implantation. The radiographic anatomy of the tooth and the dental alveolus will be reviewed. The different types and components of the dental implant devices; standard surgical techniques of implantation and augmentation also will be described briefly to familiarize the reader with this treatment method.

## APPROACH/METHODS

The conventional radiographs and CT imaging of the jaw, before and after implantation, will be used to illustrate the pertinent radiologic findings.

## FINDINGS/DISCUSSION

Preoperative evaluation should include a general assessment of the jaw, describing edentulous regions and the appearance of the residual teeth. The evaluation should include measurements of the height - thickness of the alveolar processes in edentulous regions and the bone quality in those regions also should be reported. The assessment should detect entities that may increase the degree of surgical difficulty such as maxillary sinus septations, variations in the inferior alveolar nerve course. The potential sites of complication such as maxillary sinus disease, residual endodontic disease, prior root canal procedures, retained roots and congenital anomalies also should be noticed and conveyed to the referring physician. Contraindications for the implantation including insufficient alveolar process volume should be assessed rigorously.



## SUMMARY/CONCLUSION

For the evaluation of the patients before dental implantation, the radiologists should be familiar with the surgical techniques and be able to identify clinically and surgically relevant findings that may contraindicate the implantation or alter the surgical methods.

**KEY WORDS:** Dental, implants, CT

### eEdE-83

#### CT Perfusion of Head and Neck: Current Status and Future Prospective

Abdel Razek, A.·Tawfik, A.·Elsorogy, L.·Soliman, N.

Mansoura University Hospital  
Mansoura, EGYPT

##### PURPOSE

CT perfusion of head and neck can detect vascular changes and angiogenesis of head and neck cancer. Performance of CT perfusion of head and neck is technically difficult with great challenge. Recent advances in postprocessing techniques improve the results of CT perfusion of head and neck.

##### APPROACH/METHODS

1) To illustrative basic background for angiogenesis. 2) To describe technique of CT perfusion of head and neck. 3) To review perfusion maps and their role. 4) To illustrate the application of CT perfusion in patients with head and neck tumors. 5) To review the role of CT perfusion in monitoring patients after radio and or chemotherapy. 6) To describe the merits and limitations of this method. 7) To discuss the recent advance and future directions of this technique.

##### FINDINGS/DISCUSSION

CT perfusion has been used for differentiation of malignant head and neck tumors from benign lesions as well as it can differentiate squamous cell carcinoma from normal muscles. It helps in characterization of cervical lymph nodes. Also, it can be used for prediction of treatment outcome, differentiation of recurrent squamous cell carcinoma and lymphoma from posttreatment changes and monitoring patient after treatment.

##### SUMMARY/CONCLUSION

CT perfusion of head and neck has important role in management of patients with head and neck cancer helps in differentiation malignant head and neck tumors from benign lesions, characterization of cervical lymphadenopathy and monitoring patients with malignancy after therapy.

**KEY WORDS:** CT perfusion, head and neck, cancer

### eEdE-84

#### Pediatric Skull Lesions

Kalra, V. B.·Gilbert, J.·Malhotra, A.  
Yale University  
New Haven, CT

##### PURPOSE

Skull lesions in the pediatric population represent a large array of congenital, neoplastic, and inflammatory etiologies and are concerning for parents, patients, and physicians alike, given their close proximity to the

brain. We present a review of pediatric skull lesions based on etiology, presenting case examples with a discussion of the radiologic and pathologic features of each.

##### APPROACH/METHODS

Pediatric skull lesions can be grouped by etiology. These groups include congenital, developmental, traumatic, primary neoplastic, metastatic, and vascular. Examples from each group are presented with case examples and discussion of radiologic and pathologic features of each.

##### FINDINGS/DISCUSSION

Congenital lesions include dermoid, epidermoid, and encephalocele. Developmental lesions include fibrous dysplasia. Traumatic lesions include caput succedaneum, cephalohematoma, and leptomenigeal cyst. Primary neoplastic lesions include Langerhans Cell Histiocytosis, osteoblastoma, infantile myofibroma, cranial fasciitis, and intradiploic meningioma. Metastatic lesions include neuroblastoma, rhabdomyosarcoma, lymphoma, fibrosarcoma, angiosarcoma, PNET, and Ewing's sarcoma. Vascular lesions include sinus pericranii and intraosseous hemangioma.

##### SUMMARY/CONCLUSION

Pediatric skull lesions can be a diagnostic challenge to the radiologist as they can arise from a large array of etiologies including congenital, developmental, traumatic, primary neoplastic, metastatic, and vascular. We present a review of pediatric skull lesions with examples from each etiologic group.

**KEY WORDS:** Skull, calvarial, calvarium

### eEdE-85

#### Getting to Know Aunt Minnie's and Their Head and Neck Relatives: A Collection of Head and Neck Lesions and Their Mimics

Sara, R.·Ledermann, E.·Reede, D. L.

SUNY Downstate UHB at Long Island College Hospital  
Brooklyn, NY

##### PURPOSE

• Review a selection of common "Aunt Minnie" head and neck lesions, with an emphasis on imaging findings. • Learn imaging features that help distinguish them from similar appearing lesions (close relatives). • Review pertinent anatomy and clinical features of these primary entities presented.

##### APPROACH/METHODS

Cases are presented in a quiz format and the user is asked to choose the correct answer from a selection of cases based on information provided. A review of the pertinent imaging characteristic of the "Aunt Minnie" cases will be made along with the distinguishing features from the mimics "Close Relatives".

##### FINDINGS/DISCUSSION

The following cases will be presented and discussed using illustrations and animations: • TDC vs anterior cervical space lipoma, sebaceous cyst and superficial cervical space abscess. • Ranula vs FOM lipoma, dilated submandibular duct and lymphangioma. • Anterior ethmoid sinus mucocele vs dacryocystitis, dacryocystocele and nasoalveolar cyst. • 2<sup>nd</sup> Branchial cleft cyst vs lymphangioma, ranula and metastatic node. • Carotid body tumor vs vagal schwannoma, resolving IJ thrombosis and fenestrated IJ vein. • Ectopic thyroid vs enlarged pyramidal lobe and dilated anterior jugular vein and necrotic node. • Antrochoanal polyp vs dentigerous cyst and maxillary sinus mucocele. • Inverting papilloma vs esthesioneuroblastoma, sinonasal sarcoid and juvenile angiofibroma. • Benign lymphoepithelial lesions vs Sjögren's syndrome, nodes associated with Rosai Dorfman syndrome and Warthin's tumor.

#### **SUMMARY/CONCLUSION**

Radiologist must be cognizant of specific imaging findings for entities such as those presented. This will enhance imaging interpretation.

**KEY WORDS:** Aunt Minnie, head and neck, thyroglossal duct cyst

#### **eEdE-86**

#### **Pediatric Head and Neck Nonrhabdomyosarcomatous Sarcomas: Imaging, Clinical and Pathologic Assessment**

Wang, B.<sup>1</sup>•Weber, A.<sup>2</sup>•Caruso, P.<sup>3</sup>•Shah, B.<sup>3</sup>•Curtin, H.<sup>2</sup>

<sup>1</sup>M.D. Anderson Cancer Center, Houston, TX,

<sup>2</sup>Massachusetts Eye and Ear Infirmary, Boston, MA,

<sup>3</sup>Massachusetts General Hospital, Boston, MA

#### **PURPOSE**

To demonstrate the clinical, imaging, and pathologic findings of different head and neck nonrhabdomyosarcomatous sarcomas in children and adolescents.

#### **APPROACH/METHODS**

We evaluated 20 cases of nonrhabdomyosarcomatous sarcomas in 2-20 year old patients from the Massachusetts General Hospital (MGH), the Massachusetts Eye and Ear Infirmary (MEEI), and MD Anderson Cancer Center (MDA). All cases were studied with CT and/or MRI, and PET-CT that was available in some patients. Representative cases of different types of sarcomas were evaluated including osteosarcomas (3), chondrosarcomas (2), synovial sarcomas (3), the Ewing's sarcoma family of tumors (4), spindle cell sarcomas (undifferentiated) (2), alveolar soft part sarcomas (1), fibrosarcomas (2), and neurofibrosarcomas (4). We analyzed the location, size, extent and local and distant metastatic disease. Pertinent differential diagnosis of imaging findings will be presented with the illustrated cases.

#### **FINDINGS/DISCUSSION**

On CT the densities were homogeneous showing variable enhancement but usually low to medium. Calcification was encountered in osteosarcomas, chondrosarcomas, and in some large tumors with necrosis. The MRI findings revealed low signal intensities relative to muscle on T1-WI, variable increased signal intensities on T2-WI, and slight to moderate enhancement on post-gadolinium images. Tumor necrosis was related to size of tumor and was observed in large tumors. Local lymph node metastases are less common than in carcinomas of the head and neck. PET-CT was helpful to assess the activity of residual or recurrent tumor after therapy along with assessment of local and distant metastases. PET-CT was also useful in monitoring response to chemotherapy, radiation therapy, and radiofrequency ablation.

#### **SUMMARY/CONCLUSION**

Nonrhabdomyosarcomatous sarcomas represent a large variety of different histopathologic tumors that may obtain a large size before diagnosis. Osteosarcomas and chondrosarcomas arise from cartilage and bone and frequently reveal calcifications. Osteosarcomas occur most commonly in the mandible while chondrosarcoma arises from bony structures of the face especially the maxillary bone. They frequently include the nasal cavity and maxillary sinuses. Synovial sarcoma originates most commonly in the neck including parapharyngeal space. Neurofibrosarcoma is associated with neurofibromatosis type I in 50% of cases. Most soft tissue sarcomas have no distinctive features on imaging with CT, MRI and PET-CT. The patients with nonrhabdomyosarcomatous sarcomas are treated with a combination of surgery, chemotherapy and radiation. We present the imaging findings of 20 cases of nonrhabdomyosarcomatous sarcomas in children and adolescents that were seen at MGH, MEEI, and MDA. The imaging modalities consisted of CT, MRI and in some cases PET-CT. We evaluated these tumors for size, shape, margins, location, extent, bony erosion, multiplicity and local and distant metastases. In addition, we characterized the tumor matrix as to pattern and degree of enhancement, necrosis, signal intensities on MRI, and hyper-hypometabolism on PET-CT

**KEY WORDS:** Sarcoma, head and neck, pediatric

#### **eEdE-87**

#### **Diffuse Neck Swelling: Beyond Cellulitis**

Siddiqui, A. •Lyons, T. •Shatzkes, D.

eth Israel Medical Center  
New York, NY

#### **PURPOSE**

Diffuse neck swelling can be caused by a broad spectrum of pathology, which may present with overlapping clinical and imaging findings. In many cases, imaging guides clinical management. The purpose of this educational exhibit is to illustrate imaging manifestations of both common and uncommon causes of diffuse neck swelling on computerized tomography

(CT), magnetic resonance imaging (MRI) and positron emission tomography/computerized tomography (PET/CT).

#### **APPROACH/METHODS**

In addition to a comprehensive review of the causes and imaging findings of cervical cellulitis, additional entities discussed include necrotizing fasciitis, Ludwig's angina, angioedema, internal jugular vein thrombosis, Madelung's disease and lymphadenopathy. Key imaging features are illustrated with the use of diagnostic images and diagrams, and findings important in differential diagnosis are emphasized. Relevant clinical concepts are presented, as well.

#### **FINDINGS/DISCUSSION**

Cervical cellulitis is an extremely common presenting symptom in the emergency department and may result from odontogenic, salivary, skin and pharyngeal infections. Polymicrobial odontogenic infections can lead to a very aggressive cervical necrotizing fasciitis, where mortality is high and early diagnosis is essential to patient survival. Ludwig's angina is a life-threatening cellulitis of the floor of the mouth that may result in laryngeal edema and airway compromise. Angioedema can present with swelling in both the neck and aerodigestive tract and may be due to allergy, medications (particularly ACE inhibitors), heat or even emotional stress. Clinical manifestations of internal jugular vein thrombosis (IJVT) are based on infectious (complicated) versus noninfectious (uncomplicated) etiologies. Complicated IJVT can progress to Lemierre syndrome, a rare condition characterized by septic thrombophlebitis with subsequent septicemia, septic embolization and metastatic abscesses. Madelung's neck, or benign symmetric lipomatosis, is a rare disease of unknown origin that is characterized by painless symmetric large fat deposits in the head and neck region as well as shoulders and upper extremity. Bulky cervical lymphadenopathy common in lymphoma may present with findings of diffuse neck swelling rather than discrete palpable nodal masses. Burkitt's lymphoma is a rare subtype, but important because it is one of the fastest growing tumors known and may mimic cervical infection on both history and imaging.

#### **SUMMARY/CONCLUSION**

A wide variety of entities may result in the common clinical presentation of diffuse neck swelling. Combining key clinical concepts with imaging findings is essential to forming a focused approach and reaching the correct diagnosis.

**KEY WORDS:** Cervical cellulitis, angioedema, cervical fasciitis

#### **eEdE-88**

##### **Imaging of Posttreatment Neck**

Kanekar, S.

Penn State Milton S Hershey Medical Center and College of Medicine  
Hershey, PA

#### **PURPOSE**

1. To familiarize with illustrations the various postoperative neck changes on imaging. 2. To highlight the postchemo and radiotherapy changes on CT, MR and PET scan. 3. To illustrate the various posttreatment complications. We retrospectively studied 214 patients from our oncology data which formed the basis for this exhibit. All patients had undergone surgical procedures for their head and neck cancer. One hundred sixty-three patients also had received RT while 51 patients had received RT and CT combination.

#### **APPROACH/METHODS**

For better understanding of posttreatment changes we have categorized this exhibit into: 1) Neck dissections (ND): a) radical ND, b) modified ND, c) selective ND, d) extended ND. 2) Reconstructive surgery: appearances of various types of myocutaneous flaps, infection and recurrence, 3) Radio and chemotherapy changes, 4) Treatment related complications: vascular: thrombosis, pseudoaneurysm, vessel wall injury; osseous: infection, necrosis; chylous fistula; postsurgical neuroma; skin metastasis; and flap infection.

#### **SUMMARY/CONCLUSION**

1. Knowledge of postsurgical procedures is essential for evaluation of posttreated neck follow up and surveillance. 2. Distinguishing early recurrence verses expected postsurgical changes are important to avoid unnecessary surgical biopsies. 3. This exhibit is core learning tool for imaging of posttreatment neck.

**KEY WORDS:** Posttreatment neck, postchemo and radiotherapy changes, posttreatment complications

#### **eEdE-89**

##### **Transoral Robotic Surgery: Technical Review and Postoperative Imaging Findings**

Kim, J.-Lee, Y.-Ahn, S.-Shin, N.-Kim, S.

Yonsei University College of Medicine, Severance Hospital  
Seoul, KOREA, REPUBLIC OF

#### **PURPOSE**

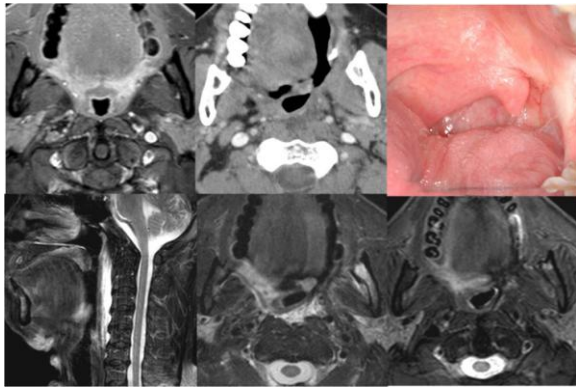
To introduce transoral robotic surgery (TORS) for head and neck cancer, including its advantages, operation procedure, and indications, and to describe various postoperative imaging findings after TORS.

#### **APPROACH/METHODS**

Transoral robotic surgery has been actively performed on approximately 100 human patients with head and neck cancers in our institution since 2008, and postoperative imaging findings after TORS were reviewed.

#### **FINDINGS/DISCUSSION**

Transoral robotic surgery has many advantages based on improved optics and wristed instrumentation. Postoperative imaging findings of TORS are different from those of conventional approaches for head and neck cancer.



#### SUMMARY/CONCLUSION

Understanding of this new technique will be helpful to head and neck surgeons and radiologists for the accurate evaluation of postoperative imaging studies in patients with head and neck cancer.

#### eEdE-90

##### From Cord to Cords: Spectrum of Brachial Plexus Pathologies from Proximal to Distal

Bryson, T. C. • Shah, G. V. • Srinivasan, A.

University of Michigan Health System  
Ann Arbor, MI

#### PURPOSE

1. To review the spectrum of brachial plexus pathologies from their origin in the spinal cord to the final division into the peripheral cords with review of the imaging anatomy and appearance of common pathologies. 2. To review the different imaging techniques used in evaluation of the various segments of the brachial plexus.

#### APPROACH/METHODS

A. Normal imaging anatomy. B. Review of common pathologies: i. Evaluation of the supraclavicular brachial plexus (roots and trunks), including Erb-Duchenne and Dejerine-Klumpke palsies, primary nerve sheath neoplasms and entrapment syndromes, such as thoracic outlet syndrome, and cervical rib syndrome. ii. Evaluation of the retroclavicular brachial plexus (divisions), including pancoast tumor and metastatic disease (infiltration or lymphadenopathy). iii. Evaluation of the infraclavicular plexus (cords), including postradiation plexopathy, desmoid tumor/fibromatosis, and vascular pathologies. C. Discussion of imaging techniques including US, CT, CT myelogram, MRI, CISS MRI, MR neurography, DTI.

#### SUMMARY/CONCLUSION

The brachial plexus is a complex structure which is difficult to image in its entirety using one modality or protocol. Therefore, using an anatomical approach and understanding the spectrum of disease is essential for choosing the correct imaging study and arriving at an accurate diagnosis of the patient with a brachial plexopathy.

**KEY WORDS:** Brachial plexus, anatomy

#### eEdE-91

##### "Losing your Voice": Etiologies and Imaging Features of Vocal Cord Paralysis

Vachha, B. A.<sup>1</sup> • Cunnane, M.<sup>2</sup> • Moonis, G.<sup>1</sup>

<sup>1</sup>Beth Israel Deaconess Medical Center, Boston, MA,

<sup>2</sup>Massachusetts Eye and Ear Infirmary, Boston, MA

#### PURPOSE

Neurogenic compromise of vocal cord function exists along a continuum encompassing vocal cord hypomobility (paresis) to vocal cord immobility (paralysis) with varying degrees and patterns of reinnervation. The intrinsic muscles of the vocal cord are supplied by the recurrent laryngeal nerve which is a branch of the vagus nerve. Vocal cord paralysis (VCP) may result from injury to the vagus or the recurrent laryngeal nerves anywhere along their course from the brainstem to the larynx. In this educational exhibit, we review the anatomy of the vagus and recurrent laryngeal nerves and examine the various etiologies of VCP. Selected teaching cases will be presented with discussion of key imaging features of VCP including radiologic findings specific to central vagal neuropathy and peripheral recurrent nerve paralysis.

#### APPROACH/METHODS

Comprehensive evaluation of radiologic findings was performed in 15 adult patients with a clinical diagnosis of VCP. In this pictorial survey we highlight the characteristic CT and MR imaging findings of VCP. Representative cases depicting the various pathologies along the course of the vagus and recurrent laryngeal nerves resulting in VCP will be shown and discussed. Imaging differentiation of central vagal neuropathy from purely recurrent laryngeal nerve (peripheral) neuropathy will be illustrated.

#### FINDINGS/DISCUSSION

Disease etiologies implicated in vagal or recurrent laryngeal nerve injury can be classified as vascular insults, viral/bacterial infections, neurotoxic drugs, tumors and trauma. In at least 50% of patients with VCP, no causative lesion is identified on imaging studies and either an idiopathic or toxic cause is diagnosed. Pathology at various locations along the course of the vagus and recurrent laryngeal nerves contribute to either central (less common) or peripheral (more common) VCP. Lesions along the course of the vagus nerve within the medulla oblongata, skull base/jugular foramen or carotid sheath result in a more central vagal neuropathy. Mediastinal diseases such as lung cancer, thyroid tumors in the trachea-esophageal groove, lymphoma/lymphadenopathy and aortic aneurysms are all potential causes of injury to the recurrent laryngeal nerve. The left recurrent laryngeal nerve is more susceptible to injury than the right due to its longer course through the mediastinum. Imaging findings associated with vocal cord paralysis include ipsilateral pyriform sinus dilation, medial positioning and thickening of the ipsilateral aryepiglottic fold and ipsilateral laryngeal ventricle dilation. Presence of ipsilateral pharyngeal constrictor muscle atrophy

suggests a more central vagal neuropathy. Atrophy of the posterior cricoarytenoid muscle on both CT and MRI imaging is a useful confirmatory imaging finding of recurrent laryngeal nerve palsy as a cause of vocal cord paralysis.

#### **SUMMARY/CONCLUSION**

Our exhibit illustrates the different causes of VCP and highlights imaging findings to help localize the lesion level. Radiologists need a detailed understanding of the anatomy of the head, neck and chest, as well as the course of the vagal and recurrent laryngeal nerves in order to relate imaging abnormalities to patient symptomatology. Accurate localization of etiologies causing VCP is crucial in determining specific management and in predicting recovery.

**KEY WORDS:** Vocal cord paralysis, larynx

#### **eEdE-92**

### **Head and Neck Manifestations of Endocrine Disorders**

Chapman, M. N.<sup>1</sup>Nadgir, R. N.<sup>1</sup>Saito, N.<sup>2</sup>Fujita, A.<sup>3</sup>Sakai, O.<sup>1</sup>

<sup>1</sup>Boston Medical Center, Boston, MA, <sup>2</sup>Saitama International Medical Center, Saitama Medical University, Hidaka, Saitama, JAPAN, <sup>3</sup>Jichi Medical Center, Shimotsuke, Tochigi, JAPAN

#### **PURPOSE**

Patients with established endocrine disorders may present with a wide range of neurologic signs and symptoms. Physical manifestations may directly relate to poorly controlled disease or may represent sequelae of chronic disease. In some cases, the treatment itself may be the cause of neurologic symptoms, as in the case of bisphosphonate-related osteonecrosis. Endocrine disorders can cause hormonal or metabolic dysfunction that may result in secondary soft tissue or osseous changes, which may be the first sign of the disease or condition. Imaging often is performed when symptoms are present, and early recognition of the radiologic manifestations of various endocrine disorders that affect the head and neck is important in decreasing patient morbidity and mortality.

#### **APPROACH/METHODS**

We will review the head and neck imaging findings of endocrine disease, including disorders of calcium, glucose metabolism, as well as thyroid and parathyroid disease, using a multimodality case-based approach. A review of the pathophysiology responsible for imaging findings, as well as treatments aimed at reducing symptoms, morbidity, and mortality will be performed.

#### **FINDINGS/DISCUSSION**

Imaging findings will be organized into sub-categories including: I. Thyroid disease: a. Thyroiditis, i. Acute - infectious, ii. Subacute - de Quervain's thyroiditis, iii. Chronic - Hashimoto's thyroiditis, iv. Granulomatous disease. b. Graves' disease: i. Glandular changes, ii. Orbital changes. c. Neoplasm: i. Benign tumors - 1.

Adenoma, 2. Plummer disease, ii. Malignant tumors - 1. Thyroid Carcinoma (Papillary, Follicular, Medullary, Anaplastic), 2. Lymphoma. II. Parathyroid disease: a. Hyperparathyroidism, i. Primary (parathyroid adenoma) vs secondary hyperparathyroidism, ii. Osseous manifestations in head and neck - 1. Brown tumor, 2. Renal osteodystrophy, 3. Dural calcifications. b. Neoplasms, i. Parathyroid cyst, ii. Parathyroid carcinoma: c. Syndromic associations (MEN). III. Other disorders of calcium metabolism: a. Osteoporosis, b. Bisphosphonate changes, c. Calcium pyrophosphate deposition disorder (pseudogout). IV. Pituitary disease: a. Adenoma - prolactinoma, GHoma, etc., i. Adenoma local invasion, ii. Gigantism/acromegaly - calvarial hyperostosis, prognathism, paranasal sinuses changes, b. Hypophysitis, c. Diabetes insipidus, d. Apoplexy. V. Neuroendocrine neoplasm: a. Paraganglioma. VI. Disorder of glucose metabolism: a. Vascular calcifications in head and neck, b. Trochlear calcifications.

#### **SUMMARY/CONCLUSION**

Endocrine disorders are common and may present with a wide range of neurologic symptoms and signs. Recognition of the imaging manifestations of endocrine disease in the head and neck is essential to differentiate from more ominous processes such as malignancy and to reduce patient morbidity and mortality.

**KEY WORDS:** Endocrine, metabolic dysfunction

#### **eEdE-93**

### **Many Faces of Fungal Disease in Paranasal Sinuses: CT and MR Imaging Findings**

Ilica, A.<sup>1</sup>Mossa-Basha, M.<sup>2</sup>Maluf, F.<sup>2</sup>Aygun, N.<sup>2</sup>

<sup>1</sup>Gulhane Military Medical Academy, Ankara, TURKEY, <sup>2</sup>Johns Hopkins Hospital, Baltimore, MD

#### **PURPOSE**

This review is aimed to highlight different CT and MRI manifestations of fungal disease of paranasal sinuses (FDPNS ), and to correlate those with clinical and histopathologic findings and classifications.

#### **APPROACH/METHODS**

We retrospectively reviewed 31 cases with cross-sectional imaging of the paranasal sinuses performed between 2002 and 2011, in which there was a diagnosis of a form of fungal sinusitis. The imaging studies including noncontrast and contrast-enhanced maxillofacial CTs and MRIs and in some cases advanced MR techniques. MRA and DSA exams were reviewed and correlated with clinical and histopathologic findings.

#### **FINDINGS/DISCUSSION**

Four clinically and radiologically distinct forms of FDPNS were identified. 1) In acute invasive FDPNS, unilateral ethmoid and/or sphenoid sinus and nasal cavity soft tissue thickening as well as bone destruction and rapid intracranial, intraorbital, intracavernous extension was observed sometimes even with intact bony walls. 2) In chronic invasive FDPNS mass-like



hyperattenuating soft tissue lesions with or without bony destruction were seen on CT. Soft tissue changes were hypointense on T1W and markedly hypointense on T2 W MR images. Anterior and posterior periantral soft tissue thickening was observed in both forms of invasive disease. Cerebral, vascular, orbital complications due to extension outside the sinonasal fossa was observed in both chronic and acute invasive forms but mostly in the chronic form. Differentiation of chronic FDPNS from sinus malignancy was sometimes impossible on imaging. 3) In allergic FDPND, hyperattenuating soft tissue opacities causing expansion of the paranasal sinuses and nasal cavity were seen on CT and corresponded to allergic mucin seen during surgery. Paranasal soft tissue signal showed variable T1 signal and prominent T2 hypointensity. Some patients presented with a distinctly unilateral involvement while others with a pattern of diffuse bilateral involvement. 4) Mycetoma (fungus ball) presented as an intrasinus hyperattenuating lesion sometimes with punctate or coarse calcifications. These lesions were hypointense on T1- and T2-weighted images with no enhancement other than peripheral mucosal enhancement. Illustrative cases were selected to visually demonstrate the differences between these entities, review the spectrum of potential complications and highlight the differences in clinical features including patient's immune status. A differential diagnosis table was provided for each case.

#### SUMMARY/CONCLUSION

Radiologists should be familiar with the different radiologic and clinical manifestations of FDPNS on CT and MRI to provide an accurate and timely diagnosis.

**KEY WORDS:** Paranasal sinuses, fungal disease, CT and MR imaging

#### eEdE-95

##### Wegener's Granulomatosis: What Is It Anyway?

Berg, A. D.<sup>1</sup>•Policeni, B. A.<sup>1</sup>•Smoker, W. R. K.<sup>1</sup>•Sato, Y.<sup>1</sup>•Gentry, L. R.<sup>2</sup>

<sup>1</sup>University of Iowa, Iowa City, IA, <sup>2</sup>University of Wisconsin, Madison, WI

#### PURPOSE

Wegener's Granulomatosis (WG) is a systemic disease characterized by necrotizing granulomatous inflammation and antineutrophil cytoplasmic antibody (ANCA) associated small vessel vasculitis. Its etiology is unknown. It is a relatively rare disorder with a varied presentation, ranging from localized granulomatous manifestations involving the upper and lower respiratory tract, to a systemic necrotizing vasculitis resulting in multiorgan dysfunction and death. Many patients with WG develop disease manifestations in the head and neck (73-99%). Sites of involvement include the sinuses and nasal cavity, orbits, temporal bone, skull base, cranial nerves, and multiple intracranial sites. Symptoms are often nonspecific which makes clinical diagnosis difficult. The purpose of this exhibit is to review common and uncommon manifestations of WG

in the head and neck. This knowledge will allow the radiologist to suggest the diagnosis, resulting in earlier treatment and decreased patient morbidity.

#### APPROACH/METHODS

1) Review clinical criteria for WG diagnosis, pathologic findings, and pathophysiologic mechanisms of head and neck involvement. 2) Present imaging findings of head and neck WG involvement emphasizing imaging findings that alter therapy. 3) Provide a differential diagnosis for WG.

#### FINDINGS/DISCUSSION

CT and MR are the primary modalities for imaging WG and its complications. Key imaging findings in the head and neck include: Sinonasal: Mucosal thickening involving the maxillary sinuses and nasal cavity, with varying degrees of opacification, nasal septal perforation, bone destruction, and osteoneogenesis. Laryngotracheal: Subglottic tracheal and bronchial wall thickening with focal or multifocal segments of stenosis. Orbital: infiltrative soft tissue masses involving the intraconal and/or extraconal space. Temporal Bone: Granulomatous inflammation that can result in bone destruction, nonspecific opacification of the middle ear and mastoid air cells, inner ear involvement with enhancement. Intracranial: Diffuse pachymeningitis, vasculitis manifestations (including nonspecific T2/FLAIR hyperintensities, infarction, intracerebral and subarachnoid hemorrhage, and generalized cerebral volume loss), and pituitary involvement from extension of skull base inflammation.

#### SUMMARY/CONCLUSION

Wegener's Granulomatosis frequently involves the head and neck. Knowledge of common and uncommon imaging findings enables the radiologist to suggest the diagnosis early, resulting in earlier treatment and decreased patient morbidity.

**KEY WORDS:** Wegener's, granulomatosis

#### eEdE-96

##### Head and Neck Involvement in ANCA-Associated Small-Vessel Vasculitis: Imaging Findings

Cassafieres, S.<sup>1</sup>•Savatovsky, J.<sup>2</sup>•Drier, A.<sup>3</sup>•Martin-Duverneuil, N.<sup>3</sup>•Heran, F.<sup>2</sup>•Bonafe, A.<sup>1,4</sup>•Menjot de Champfleury, N.<sup>1,4</sup>

<sup>1</sup>Guidé Chaucic Hospital, Montpellier, FRANCE, <sup>2</sup>Fondation Rothschild, Paris, FRANCE, <sup>3</sup>Groupe Hospitalier Pitié-Salpêtrière, Paris, FRANCE, <sup>4</sup>Institut of Neurosciences of Montpellier, Saint Eloi Hospital, Montpellier, FRANCE

#### PURPOSE

The purpose of this study was to define patterns of head and neck involvement in Wegener's granulomatosis (WG) and Churg and Strauss syndrome (CSS).

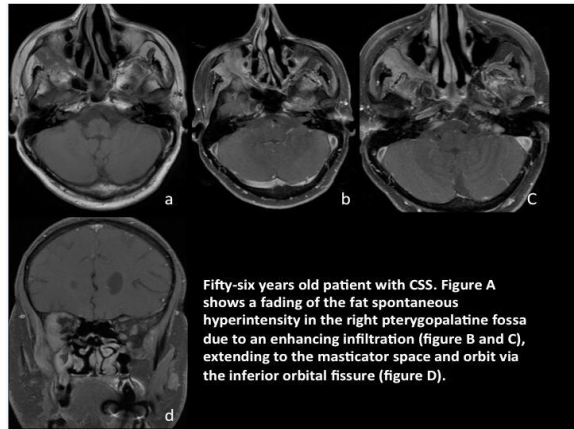
#### APPROACH/METHODS

We evaluated the skull base of 91 patients (78 WG and 13 CSS) with both CT and MR in 46 patients, CT only (40

patients), or MR only (5 patients). Lesions' topography, extension to the orbits and brain, sinus involvement, bone erosion, and nerves compression were assessed retrospectively in each patient. MR images were analyzed for signal characteristics and enhancement patterns.

#### FINDINGS/DISCUSSION

In 12 patients (13%), orbital and sinus diseases coexisted. Orbital disease without sinus disease was seen in two patients (2%). Cavernous sinus involvement was found in seven patients (8%) and pterygopalatine fossa in nine patients (10%). An extension to the foramen rotundum and the Meckel's cave was present in five patients (5%). The foramen ovale was involved in one case.



#### SUMMARY/CONCLUSION

Head and neck involvement in ANCA-associated small vessel vasculitis is not uncommon, especially as it can be due to the local extension of a sinonasal involvement.

**KEY WORDS:** Wegener's granulomatosis, Churg and Strauss syndrome, head and neck

#### eEdE-97

##### Paranasal Sinuses: Multidetector Computed Tomography Preoperative Evaluation

Feliciano, Y. Z.<sup>1</sup>Zayas, J. O.<sup>1</sup>Rivera, W.<sup>1</sup>Labat, E.<sup>1</sup>Santacana, G.<sup>2</sup>

<sup>1</sup>RCM UPR, San Juan, PR, <sup>2</sup>RCM UPR, San Juan, PUERTO RICO

#### PURPOSE

- To review the relevant paranasal sinuses anatomy using MDCT with multiplanar reconstruction (MPR). - Discuss the most common paranasal sinus anatomical landmarks as well as anatomical variations and their relevance for preoperative evaluation. - Discuss the anatomical and radiologic descriptors and terminology used in radiologic reporting for paranasal sinus surgical guidance. - Review the importance of MPR and 3D reconstructions for surgical planning.

#### APPROACH/METHODS

- Perform a retrospective review of paranasal sinus MDCT imaging database at PACS stations. - Present a

pictorial review illustrating relevant paranasal sinus anatomy and the most common anatomical variations and its relevance during surgery. - Discuss the relevance of MPR and 3D reconstruction as important tools in the diagnosis, characterization and preoperative planning in patients with paranasal sinus disease. - Review the anatomical and radiological descriptors and terminology in reporting paranasal sinuses for preoperative work up.

#### FINDINGS/DISCUSSION

Multidetector CT is the optimal radiographic modality to evaluate the paranasal sinuses and represents a fundamental tool for preoperative planning. The success of paranasal sinus surgery is based in part upon the proper identification of normal anatomical landmarks and variants and their relation to paranasal disease. Multiplanar reconstruction examination of paranasal sinuses provides an anatomical road map, establishing the anatomical relationships of the key structures, the extent of disease, and relevant anatomical variations. Multiplanar reconstruction and endoscopy are complementary in the diagnosis and treatment of paranasal sinus disease, with the end goal of reducing surgical morbidity and complications.

#### SUMMARY/CONCLUSION

Multidetector CT with MPR are important tools for the diagnosis and preoperative planning in patients with paranasal sinus disease. Radiologist must provide precise guidance including the identification of critical anatomical landmarks and variants used for preoperative planning.

**KEY WORDS:** Sinuses, paranasal, MDCT

#### eEdE-98

##### Case Cluster@: Complications of Sinusitis

Peddi, S.<sup>1</sup>Wippold, F. J.  
Mallinckrodt Institute of Radiology  
St. Louis, MO

#### PURPOSE

1. Present the imaging findings of the most common complications of sinusitis.

#### APPROACH/METHODS

1. Review the anatomy and pathophysiology pertinent to the complications of sinusitis. 2. Discuss imaging features of the following: - Frontal sinusitis with subgaleal abscess; - Intracranial abscess; - Osteomyelitis; - Postseptal orbital cellulitis; - Sagittal sinus thrombosis; - Silent sinus syndrome; - Sphenoid sinusitis with cavernous sinus thrombosis; - Subdural empyema; - Subperiosteal abscess. 3. Present a case-based quiz designed to reinforce key concepts.

#### FINDINGS/DISCUSSION

About 14% of all adults will have an episode of rhinosinusitis each year and approximately 1-2% of viral rhinosinusitis cases are complicated by bacterial superinfection. While complications are not common, they can have high morbidity, even leading to death.

**SUMMARY/CONCLUSION**

Being familiar with the imaging appearance of the complications is important in detecting them early and minimizing morbidity.

**KEY WORDS:** Sinusitis, complications

**eEdE-99****Approach to Temporomandibular Joint**

Morales, H.·Fischer, I.·Cornelius, R.

University of Cincinnati  
Cincinnati, OH

**PURPOSE**

To provide a systematic approach for interpretation of temporomandibular joint (TMJ) imaging. To show key imaging characteristics in common and less common TMJ disorders.

**APPROACH/METHODS**

Retrospective review of 50 cases of TMJ's MR images performed in our institution during 2008-2011. Review of state-of-the-art literature about TMJ imaging and clinical management.

**FINDINGS/DISCUSSION**

Internal derangement is the most common TMJ disorder. Osteoarthritis and trauma are next in frequency. Less common pathology includes rheumatoid arthritis (RA), synovial chondromatosis (SC), calcium pyrophosphate dihydrate deposition disease (CPPD), pigmented villonodular synovitis (PVNS), tumors and osteonecrosis. We provide a systematic approach to facilitate interpretation based in three major structures: disk, condyle and joint space. Visualization of the disk position, shape and changes with open mouth-reduction are paramount in the evaluation of internal derangements. Evaluation of the cortical bone, bone marrow and shape of the condyle can help in the diagnosis of osteoarthritis, RA, osteonecrosis and tumors. The joint space evaluation includes presence of effusion, loose bodies/calcifications and abnormal synovium; keeping in mind less common disorders such as SC, CPPD and PVNS. Relevant imaging and graphic anatomy and dynamics of the TMJ also are discussed.

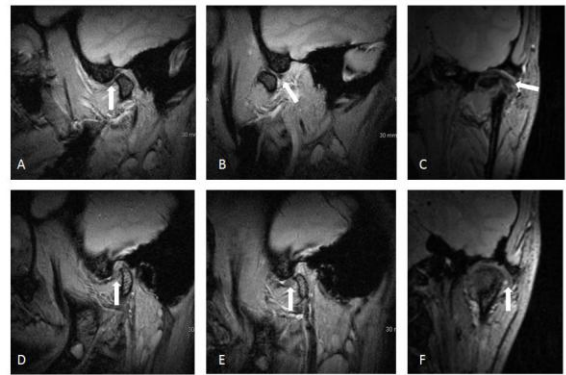


**Fig. 1.** Gradient-echo MR images of the TMJs from two patients. Oblique sagittal with closed mouth (A, D), open mouth (B, E) and coronal views (C, F). A, B and C, images from the same patient show normal signal, morphology and location of the disc (arrows). The posterior band is located within 10° of the 12 o'clock position in closed mouth and move to a position between the condyle and articular eminence in open mouth. D, E, and F, images show anterior and lateral displacement of the disc (arrows). The disc has lost its normal bowtie appearance, it is desiccated, deformed and the posterior band is displaced more than 10° anteriorly to the 12 o'clock position on sagittal views (there is persistent malposition in open mouth, which is regarded as poorer clinical prognosis as compared with dislocations that recapture).

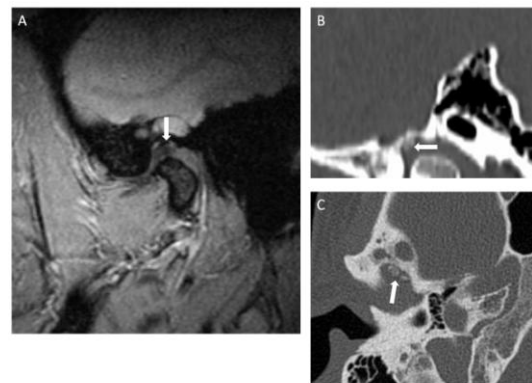


**Fig. 2.** (A) Gradient-echo MR images of the TMJ with closed mouth shows normal position of the disc. However, there is a subtle small GRE susceptibility artifact / calcification in the most superior aspect of the joint (arrow). (B, C) Sagittal reformat and axial CT images better depict ossified loose bodies (arrows) in the superior aspect of the joint. This is a typical location and most consistent appearance of synovial chondromatosis.

**SUMMARY/CONCLUSION**

Disorders of the disk are the most common findings on TMJ imaging. Discussed systematic approach also can help in the diagnosis of less common but important pathology of the TMJ.

**KEY WORDS:** Temporomandibular, joint, MR imaging

**eEdE-100****Decoding the Audiogram: An Illustrative Guide for the Radiologist**

Kennedy, T. A.·Gailushas, S.·Gentry, L. R.·Hartman, M. J.·Gubbels, S.

University of Wisconsin Madison  
Madison, WI

**PURPOSE**

Audiometry is used to determine the functional status of an individual's hearing and often is the primary testing performed in patients presenting with hearing loss. A radiologist reviewing MRI and CT examinations for hearing loss should have an understanding of the components of an audiogram and how the information is used to guide differential diagnosis and subsequent imaging. The purpose of this exhibit is to review the components of an audiogram with an interactive case-based review with radiology-audiometry correlation.

### APPROACH/METHODS

The components of an audiogram will be discussed. Subsequently, the audiograms and imaging studies of patients with known acquired conditions and developmental anomalies of the external, middle and inner ear will be reviewed and deciphered with a practical approach.

### FINDINGS/DISCUSSION

Audiometry consists of a battery of tests including pure tone testing, word recognition, stapedial reflex testing, auditory brainstem response evaluation and tympanometry. Many processes that result in conductive and sensorineural hearing loss will exhibit characteristic patterns on an audiogram or other audiometric tests. For example, otosclerosis often presents with a conductive or mixed loss with a depression in sensorineural levels at 2000 Hz and absence of stapedial reflexes on the affected side. A vestibular schwannoma, on the other hand, is characterized by asymmetrical sensorineural hearing loss with diminished word recognition scores. These types of characteristic findings on audiometric evaluation often guide the selection and interpretation of subsequent imaging tests.

### SUMMARY/CONCLUSION

An understanding of the components of audiometry testing will enable a radiologist to more effectively interpret imaging of patients with hearing loss and guide decision-making for subsequent evaluation and treatment.

**KEY WORDS:** Audiogram, hearing loss

### eEdE-101

#### High-Resolution Computed Tomography of the Isolated Stapes Congenital Anomalies

Gentric, J.<sup>1</sup>•Rousset, J.<sup>2</sup>•Ben Salem, D.<sup>1</sup>•Garetier, M.<sup>1,2</sup>•Meriot, P.<sup>1</sup>

<sup>1</sup>Brest University Hospital, Brest, FRANCE, <sup>2</sup>Clermont-Tonnerre Hospital, Brest, FRANCE

### PURPOSE

The stapes grows at the cranial end of the second branchial arch and dissection works showed that the stapes presents considerable morphologic variations. Because of the small size of stapes and its components, imaging this ossicle remains a challenge. The enhanced multiplanar performance of current multisection CT allows morphologic and morphometric analysis of the stapes superstructure. Isolated congenital anomalies of the stapes are infrequent but highly variable. The goal of this study is to present the numerous observed anomalies based on a large number of cases, and to describe anatomical variations and malformations of the stapes using high-resolution computed tomography (CT), after proper reorientation in the "axial stapes" plane.

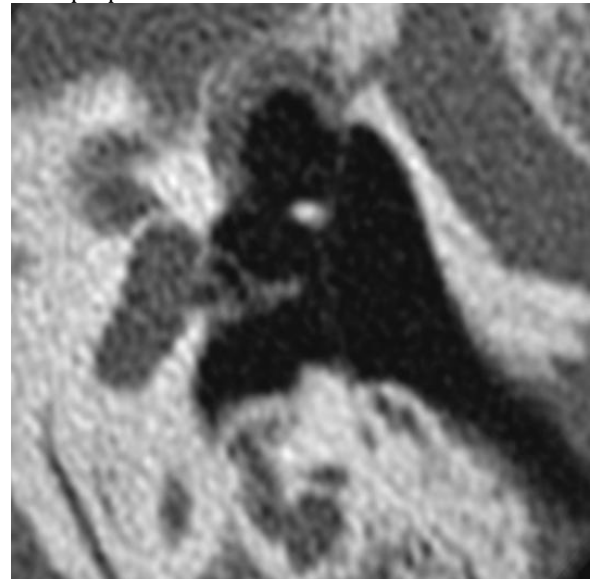
### APPROACH/METHODS

The 1805 CT of temporal bones performed in our institution for various indications between January

2005 and April 2011 have been studied retrospectively. Standardized acquisition protocol was used on two multislices CT scans. All acquisitions were made in the axial plane. After reconstructing the images in the stapes axial plane, the ears presenting a congenital anomaly of the stapes were included. All the ears with acquired lesions were excluded. The anomalies have been sorted according to the affected part of the stapes: the superstructure, the footplate or the obturator foramen. Two neuroradiologists classified the anomalies as either anatomical variation, malformation, or undetermined.

### FINDINGS/DISCUSSION

Sixty-one stapes in 47 patients were found to have one or more congenitally abnormal shapes. Bilateral anomalies were found in 14 of these patients. The abnormal part of the stapes was the superstructure in 17 cases, the footplate in 13 cases, the obturator foramen in 19 cases (with a high frequency of "double stapes" shape) while in 12 cases multiple parts were affected.



### SUMMARY/CONCLUSION

The use of ossicle reconstructions in the "axial stapes" plane with current multislice CT allows analyzing even minor congenital anomalies of the stapes. The boundaries between normal variations and malformations are sometimes difficult to set, especially when anomalies are minor. Malformations are diagnosed more easily when multiple parts of the stapes are affected. In this study, 19 abnormal congenital patterns of the obturator foramen were observed. Most of abnormal patterns noticed are the presence of a linear hyperdensity within the obturator foramen lying between the superstructure and the footplate. Concerning the pathologic significance of this anomaly, the literature is poor and these radiologic findings raise the question of whether this abnormality is a normal variation or a malformation.

**KEY WORDS:** Computed tomography, stapes, middle ear

**Monday, April 23 –  
Wednesday, April 25**

**6:30 AM – 9:00 PM**

**Thursday, April 26**

**6:30 AM – 3:00 PM**

**Rhineland**

**Electronic Education Exhibits  
(eEdE) 102 – 106**

**eEdE4 – Interventional**

**Note: A missing printed number indicates an abstract has been withdrawn.**

#### **eEdE-102**

##### **Endovascular Repair of Small Intracranial Aneurysms, Tips and Tricks**

Jindal, G.·Fortes, M.·Zahra, K.·Aldrich, F.·Simard, M.·Gandhi, D.

University of Maryland  
Baltimore, MD

#### **PURPOSE**

Endovascular treatment of intracranial aneurysms has evolved rapidly over the last two decades and has become the preferred method of intracranial aneurysm repair in many cases. The endovascular treatment of small intracranial aneurysms has been shown to be associated with higher levels of technical difficulty and complications in comparison to similar treatment of medium and large size aneurysms. Newer endovascular devices and flow diversion methods now are making it possible to treat small intracranial aneurysms with high success rates and relatively low morbidity.

#### **APPROACH/METHODS**

We prospectively collected an interventional neuroradiology database on the embolization of aneurysms at our institution from January 2007 to November 2011. Small aneurysms were defined as being less than 4 mm in greatest dimension. The size, neck, location, branch vessels, treatment methods, coils and/or stents used, complications, and follow-up results were recorded in addition to the demographic data.

#### **FINDINGS/DISCUSSION**

A total of 408 aneurysms were treated at our institution via endovascular therapy from January 2007 to November 2011. Eighty-two (20%) of these aneurysms were under 4 mm in greatest dimension at presentation. Endovascular repair was successful at aneurysm obliteration in the majority of these cases

with a low rate of technical failure. Treatment methods included coil embolization with or without a stent as well as use of single or multiple stents alone without coils. The approach and technical aspects involved in treating these difficult lesions are highlighted in this exhibit. New distal access devices, including softer and more flexible sheaths and guiding catheters were used to provide the necessary support to optimize microcatheter trackability and stability. Very small aneurysms often were coiled from the microcatheter tip placed at the aneurysm neck. Introduction of new, very small complex coils by many vendors facilitated the framing, filling, and finishing of small aneurysms. Side-wall blister aneurysms were treated with the use of stents alone via alteration in local flow hemodynamics.



#### **SUMMARY/CONCLUSION**

Endovascular treatment of small intracranial aneurysms as defined as less than 4 mm in greatest dimension can be safe and effective. The ongoing introduction of new endovascular devices (distal access catheters, softer long sheaths, more trackable microcatheters, stents, and new, small complex coils) has helped to facilitate treatment of these lesions. As the endovascular treatment of these small lesions continues to evolve, long-term data on these newer techniques will be required to better assess their safety and efficacy.

**KEY WORDS:** Endovascular, aneurysm, coil

#### **eEdE-103**

##### **Endovascular Repair of Traumatic Vascular Lesions in the Head and Neck: Recent Experiences from a Large Level I Trauma Hospital**

Jindal, G.·Fortes, M.·Gandhi, D.

University of Maryland  
Baltimore, MD

#### **PURPOSE**

Endovascular treatment of traumatic vascular lesions in the head and neck is a rapidly evolving discipline with

great potential benefit via minimally invasive techniques. These lesions are recognized increasingly in the setting of trauma as both awareness of these lesions and utilization of cross-sectional imaging for screening continue to evolve. We present our recent endovascular experience treating these lesions in the head and neck with an emphasis on novel approaches and new concepts to consider.

#### **APPROACH/METHODS**

Traumatic admissions to a single center, large, university-based, level I trauma center were calculated from January 2007 to November 2011. Cases of endovascular repair of traumatic head and neck lesions during this time were collected via retrospective search of the picture archiving and communicating system. Type and location of lesions treated, Biffi grading of lesions, techniques and devices used for repair, complications, and follow-up clinical outcomes when available are presented in a case-based format.

#### **FINDINGS/DISCUSSION**

Over 35,000 patients were admitted to our trauma center from January 2007 to November 2011. The overall incidence of traumatic vascular lesions in the head and neck has been estimated to be 1.1-1.6% in recent large studies. A total of 42 of these lesions were treated via an endovascular approach during this time period. Endovascular repair was performed using both deconstructive and reconstructive methods. Complications occurred infrequently and included groin hematoma, arterial dissection, and stroke. Open surgical repair rarely was required. Treated lesions in the head and neck included arterial dissection, pseudoaneurysm, arteriovenous fistulae, and arterial transection. Decision-making in regards to when and how to treat these lesions is discussed. Case presentations highlight novel approaches and new devices used in treating these lesions, including several cases of endovascular repair using covered stent-grafts.

#### **SUMMARY/CONCLUSION**

Endovascular repair of traumatic vascular lesions in the head and neck is increasingly utilized as these lesions are becoming increasingly recognized. These minimally invasive treatment options can be safely and successfully performed. The ongoing introduction of new endovascular devices has facilitated the treatment of these lesions. Continued investigation will be required to assess the long-term safety and efficacy of these treatment strategies.

**KEY WORDS:** Endovascular, trauma, head and neck

#### **eEdE-104**

##### **Morphologic and Functional Anatomy of the Ophthalmic Artery in the Pediatric Age**

Romano, D.·Cesaretti, K.·Bracco, S.·Cioni, S.·Gennari, P.·Sanna, A.·Cerase, A.·Venturi, C.

Aous Siena  
Siena, ITALY

#### **PURPOSE**

Intraarterial superselective infusion of chemotherapy in the ophthalmic artery recently has been proposed in the hope of salvaging more of the eyes with retinoblastoma. The purpose of this education exhibit is to describe the morphologic and functional anatomy observed during the endovascular neuroangiographic procedure.

#### **APPROACH/METHODS**

From June 2008 to October 2011, a consecutive series of 53 patients (25 females, 28 males; age range at first treatment, 7 months to 22 years) with 60 eyes with retinoblastoma have been scheduled for a total of 190 procedures of superselective ophthalmic artery infusion of melphalan (181 procedures), or melphalan and topotecan (9 procedures) for intraocular retinoblastoma.

#### **FINDINGS/DISCUSSION**

The treatment has been feasible, repeatable and safe. No permanent procedure-related complications occurred. One hundred forty-nine procedures have been performed by navigation of the internal carotid artery. Forty-one procedures have been performed by the external carotid artery via the middle meningeal artery (n:39), anterior branch of the superficial temporal artery (n:1), and infraorbital branch of the maxillary artery (n:1).

#### **SUMMARY/CONCLUSION**

Embryology, anatomical variations including extracranial-intracranial anastomoses, and dynamic functional vascular anatomy concept explain our findings. Modern guidewires and microcatheters allow a safe intraarterial navigation into the vessels originating from the external carotid artery also in the pediatric age. This results in a larger number of treatments of eyes with retinoblastoma. A thorough knowledge of morphology and functional vascular anatomy concept of the ophthalmic artery in the pediatric age is mandatory when dealing with superselective intraarterial chemotherapy for retinoblastoma.

**KEY WORDS:** Ophthalmic artery, anatomy, angiography

#### **eEdE-105**

##### **MR-Guided Perineural Injection: Pelvic Pain Syndromes**

Chhabra, A.

Johns Hopkins University Hospital  
Baltimore, MD

#### **PURPOSE**

To depict MR-guided perineural injections for pelvic pain syndromes.

#### **APPROACH/METHODS**

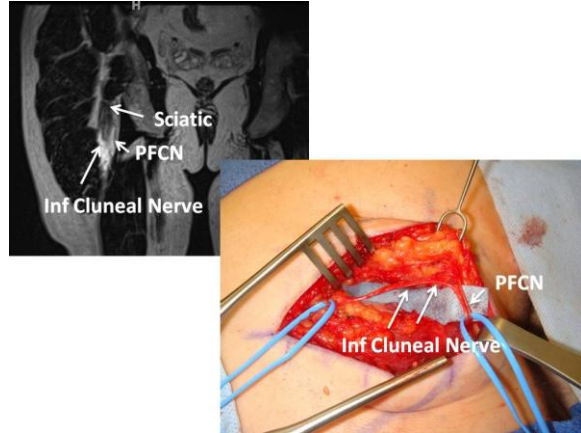
Ten cases of 1.5 T MR-guided injections of various pelvic nerves [sciatic, posterior femoral cutaneous nerve (PFCN), lateral femoral cutaneous nerve (LFCN), perineal branch of PFCN, pudendal, obturator and femoral, inferior cluneal nerve], as well as



intramuscular botox (scalene, piriformis) are demonstrated. MR-guided technique, advantages and limitations are highlighted.

#### FINDINGS/DISCUSSION

Good diagnostic identification of small pelvic nerves is possible with current MR techniques. MR-guided injections are safe, radiation free and effective for therapeutic purposes.



#### SUMMARY/CONCLUSION

MR-guided perineural injections are ideal for deeply situated small peripheral nerves with various advantages.

**KEY WORDS:** MR imaging, perineural, block

#### eEdE-106

#### Development of Workflow Task Analysis during Cerebral Endovascular Procedures: Analysis and Comparison of Junior and Senior Competencies

Gentric, J.<sup>1</sup>Jannin, P.<sup>2</sup>Threlu, B.<sup>2</sup>Riffaud, L.<sup>3</sup>Ferré, J.<sup>3</sup>Gauvrit, J.<sup>3</sup>

<sup>1</sup>Brest University Hospital, Brest, FRANCE, <sup>2</sup>INRIA, VisAGeS Unit/Project, Rennes, FRANCE, <sup>3</sup>Rennes University Hospital, Rennes, FRANCE

#### PURPOSE

Objective assessment of interventional or surgical procedures usually is based on simulation systems, such as bench models, live animals, cadavers, or virtual simulators. These systems focus on competency outside the operating room (OR) and cannot reliably assess the operator due to the lack of clinical realism and evaluation directly in the OR. We developed a workflow task analysis approach to evaluate neuroradiologists' competencies in the radiology operating room (OR) while performing cerebral endovascular procedures.

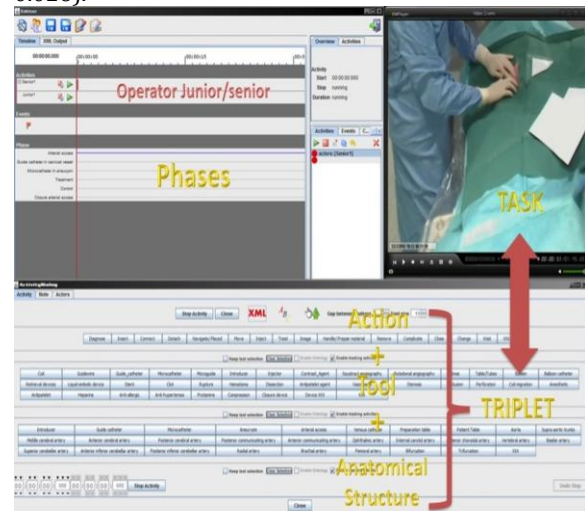
#### APPROACH/METHODS

We analyzed 16 cerebral angiography procedures: eight performed by a senior neuroradiologist and eight performed by a junior with the supervision and aid of a senior. Dedicated software with specific terminology was used to record the operator's tasks in the OR. Procedures were subdivided into three phases (i.e., arterial access, navigation, and closure of the access),

each comprising multiple tasks. Each task was defined as a triplet, associating an action, an instrument, and an anatomical structure. The duration of each task was the principal metric. The total duration of the procedure, the duration per task, and the number of times a task was repeated, were isolated. Moreover, we focused on the tasks using fluoroscopy or moving the x-ray system. We recorded 373 tasks performed by junior neuroradiologists and 609 by senior neuroradiologists.

#### FINDINGS/DISCUSSION

The total duration of tasks of the entire procedure was longer for juniors than for seniors ( $p = 0.012$ ). The mean duration per task was 86 seconds for the junior group and 43 seconds for the senior group ( $p = 0.002$ ). The total and mean durations of tasks involving use of fluoroscopy were longer in the junior group ( $p = 0.002$  and  $p = 0.033$ ). Concerning the tasks involving table and tube the total and mean durations of tasks are longer in the junior group ( $p = 0.019$  and  $p = 0.082$ ). Concerning the tasks involving table and tube before imaging cerebral vessels, the total and mean durations of tasks are shorter in the senior group ( $p = 0.019$  and  $p = 0.026$ ).



Snapshot of the interface on the laptop PC where the observer each task by a triplet (Action+ Tool+ Anatomical Structure) and select the appropriate phase and the operator

#### SUMMARY/CONCLUSION

This approach allows for reliable skills assessment in the radiology OR and for comparison of junior and senior competencies during cerebral endovascular procedures. This new tool could improve the quality and safety of procedures, and facilitate the learning process of neuroradiologists.

**KEY WORDS:** Workflow, interventional radiology, safety management

**Monday, April 23 –  
Wednesday, April 25**

**6:30 AM – 9:00 PM**

**Thursday, April 26**

**6:30 AM – 3:00 PM**

**Rhineland**

**Electronic Education Exhibits  
(eEdE) 107 – 136**

**eEdE - 5 – Pediatrics**

**Note: A missing printed number indicates an abstract has been withdrawn.**

#### **eEdE-107**

##### **Nonaccidental Head Injury in the Pediatric Patient: A Pictorial Essay**

Koerber, A. J. • Challa, H.

University of Kentucky Hospital  
Lexington, KY

#### **PURPOSE**

Traumatic injury to the central nervous system in pediatric population results in about 100,000 emergencies annually and about 50% of the total number of deaths from infancy through puberty in the United States, which makes it reportedly the leading cause of morbidity and mortality in the pediatric population. Most of the cases of traumatic injury are accidental, but nonaccidental trauma (NAT) is responsible for about 9% to 14% of pediatric head injuries each year. Nonaccidental trauma to the head is responsible for approximately 80% of the deaths from traumatic CNS injuries in patients younger than 2 years old. Kentucky has the unfortunate distinction as being the number one state in terms of deaths from NAT. It is sometimes difficult to distinguish NAT head injuries from accidental injuries or other “mimickers”; therefore, it is important for the radiologist to have a good working knowledge of some of the types of injuries seen in NAT to the head. The purpose of this exhibit is to illustrate by pictorial review, the spectrum of neuroimaging findings seen in NAT to the head; as well as, some of the common mimickers.

#### **APPROACH/METHODS**

A retrospective review of multiple MRI and CT examinations in patients with the diagnosis of nonaccidental trauma to the head was performed at Kentucky Children’s Hospital. Multiple examples of classical imaging findings were compiled and placed into a pictorial review. Select cases of mimickers of NAT also were compiled and placed into the pictorial review.

#### **FINDINGS/DISCUSSION**

Nonaccidental trauma to the head in the pediatric population can present with a variety of different imaging findings. The most “specific” signs of NAT to the head are subdural hematoma and subarachnoid hematoma. Epidural hematomas are much less likely to occur in patients with NAT. The other main category of injury that can occur in NAT is an injury to the brain itself, which usually presents in one of three ways: sheering, contusion, and edema.

Radiologists can play an important role in the forensic aspect of NAT cases by estimating when the injuries took place by using clues on CT and MRI studies. Sometimes it is very difficult to tell whether the image findings are from nonaccidental trauma or from some other cause. The list of differential diagnosis is long, and includes: accidental trauma, traumatic delivery, developmental anomalies, genetic disorders, metabolic disorders, coagulopathies, infectious processes, oncological disease, or toxins.

#### **SUMMARY/CONCLUSION**

Nonaccidental trauma to the head is unfortunately a significant source of pediatric morbidity and mortality. There are some imaging findings that are highly suggestive of NAT, but even so, it is difficult to determine whether or not the injury is nonaccidental based on imaging findings alone versus from one of the other numerous differential diagnoses. This determination can only be made by careful consideration of all of the details of each particular case. By being familiar with the classic findings in NAT and those seen in some of the more common mimickers, the radiologist will be better prepared to help make the diagnosis of NAT.

**KEY WORDS:** Nonaccidental, trauma, pediatrics

#### **eEdE-108**

##### **Spectrum of Pediatric Diffusion Abnormalities: A Neuroimaging Pictorial Review**

Ozsvath, J. A.<sup>1</sup> • Hanhan, S.<sup>2</sup> • Milla, S.<sup>1</sup>

<sup>1</sup>New York University Langone Medical Center, New York, NY, <sup>2</sup>Jersey Shore University Medical Center, Jersey Shore, NJ

#### **PURPOSE**

In the pediatric population, a group who lack traditional adult risk factors for “stroke”, diffusion abnormalities can present a challenge as their etiologies and appearances are wide and varied. It is our goal to review the neuroimaging findings of pediatric diffusion abnormalities, as well as illustrate less common entities that typically present during or preferentially affect the pediatric age range [e.g., mitochondrial encephalomyelopathy, lactic acidosis (MELAS), moyamoya disease, and child abuse].

#### **APPROACH/METHODS**

We will review the current literature on pediatric diffusion abnormalities and present a case-based illustration of the MRI findings that best exemplify

many of the different etiologies and accentuate imaging findings that may help aid in the differential diagnosis.

#### **FINDINGS/DISCUSSION**

We will discuss the epidemiology, risk factors and morbidity/mortality of pediatric diffusion abnormalities as they relate to vascular and nonvascular etiologies. We will discuss briefly the role of MRI and other advanced imaging techniques in evaluating this age group. We will review the pathophysiology of different etiologies of pediatric diffusion abnormalities and demonstrate how they relate to imaging findings. Sample cases will be presented to demonstrate and discuss the classic imaging appearances of each pediatric diffusion abnormality entity.

#### **SUMMARY/CONCLUSION**

Pediatric diffusion abnormalities can be seen in many varied etiologies and can have a spectrum of imaging appearances. As pediatric patients lack the traditional adult-type risk factors for "stroke", understanding and reviewing the gamut of these abnormalities is imperative. Our pictorial review will provide case-based illustrations and discussions of the various etiologies causing diffusion abnormalities to elucidate patterns and neuroimaging findings to help reach the correct diagnosis.

**KEY WORDS:** Diffusion, abnormalities

#### **eEdE-109**

### **Many Disguises of Mitochondrial Disease in Children: Pictorial Essay**

Bonfante, E.<sup>1</sup>•Koenig, M. K.<sup>1</sup>•Riascos, R.<sup>2</sup>•Supsupin, E. P.<sup>1</sup>

<sup>1</sup>University of Texas Health Sciences Center Houston, Houston, TX, <sup>2</sup>University of Texas Medical Branch, Galveston, TX

#### **PURPOSE**

To illustrate the variable clinical and radiologic presentations of central nervous system involvement in patients with mitochondrial disease.

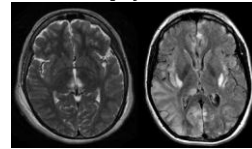
#### **APPROACH/METHODS**

Using a case-based format we present a group of patients with diagnosis of probable or definite mitochondrial disease based on Walker criteria, and discuss the clinical presentation, imaging and genetic findings. We discuss the differential diagnosis from the neurologic and radiologic perspective.

#### **FINDINGS/DISCUSSION**

Mitochondrial disease is a heterogeneous group of multisystem disorders resulting from dysfunction or depletion of mitochondria, secondary to either mutations in the maternally inherited mitochondrial genome, or nuclear DNA mutations. The clinical presentation of patients with mitochondrial disease is variable, with nonspecific symptoms related to involvement of multiple organs. The nervous system is the most commonly involved system. Some of the

symptoms of nervous system dysfunction in mitochondrial disorders include muscle weakness; hypotonia; peripheral neuropathy; ataxia; ptosis; ophthalmoplegia; bulbar signs; spasticity; stroke-like episodes; migraine headaches; movement disorders such as tremor, chorea, and ballismus; dystonia; seizures; and myoclonus. Symptoms related to multiple other organ systems isolated or in combination often are present. Brain MRI of patients with mitochondrial disorders frequently may be normal, at least in some stages of their evolution. Other findings include brain atrophy, stroke in atypical distribution, and lesions in the basal ganglia, brainstem and cerebellum. Since both the clinical presentation and imaging findings of mitochondrial disorders are nonspecific, additional diagnosis that are considered during the assessment of these patients include hypoxic ischemic injury, toxic insults, ADEM, encephalitis, vasculitis, brainstem tumor and leukodystrophies. Additional investigations in these patients include laboratory and biochemical analysis, tissue biopsy, and DNA studies.



#### **SUMMARY/CONCLUSION**

The diagnosis of mitochondrial disease in children is challenging due to the variability of clinical presentations, imaging findings and genetic abnormalities. This diagnosis should be considered in patients with multisystem involvement or single-system involvement without a clear explanation.

**KEY WORDS:** Mitochondrial, cytopathy, genetic

#### **eEdE-110**

### **Central Nervous System Toxicity in Children: Review**

Sanchez-Montanez, A.<sup>1</sup>•Armario, D.<sup>2</sup>•Delgado, I.<sup>2</sup>•Raspall, M.<sup>2</sup>•Gros, L.<sup>2</sup>•Vazquez, E.<sup>2</sup>

<sup>1</sup>IDI Hospital Universitari Vall d'Hebron, Barcelona, SPAIN, <sup>2</sup>ICS Hospital Universitari Vall d'Hebron, Barcelona, SPAIN

#### **PURPOSE**

- To review different radiologic findings in pediatric central nervous system (CNS) due to endogenous, both by excess and by default, and exogenous substances and make a differential diagnosis. - To highlight the importance of establishing an early diagnosis of drug-related toxicity to minimize side effects and propose possible alternative treatments.

#### **APPROACH/METHODS**

Imaging findings, particularly by MRI, in some cases of pediatric CNS toxicity seen at our center in recent years are presented in a didactic manner. Endogenous factors that may give rise to a clinical-radiologic picture include glucose deficiency, and ammonia, manganese or copper accumulation. Metabolic diseases are etiologies to be

considered in any differential diagnosis, particularly when clinically suspected. Some cases of carbon monoxide or methanol poisoning also are included. Many pharmacologic agents, such as methotrexate, vigabatrin, etanercept, tacrolimus, radiation therapy, vincristine, L-asparaginase, cyclosporine, metronidazole or benzodiazepines are used in oncology, infections, metabolic disorders, granulomatous diseases and epilepsy. We should be able to recognize their possible side effects when children being treated begin to present neurologic symptoms.

#### **FINDINGS/DISCUSSION**

The most common conditions that have an impact on the CNS in childhood related to the use of different standard therapies in clinical practice, as well as some resulting from the deficiency of a substance are shown.

#### **SUMMARY/CONCLUSION**

MR imaging is a highly useful tool for evaluating neurologic manifestations caused by an excess or lack of some toxic substances in children. These entities should be taken into account when assessing a pediatric patient with onset of neurologic symptoms in the emergency room department. As they often go underdiagnosed, it is therefore a great challenge for radiologists to know how to recognize them early for then to be treated and future complications prevented.

**KEY WORDS:** Side effects, second neoplasms

#### **eEdE-111**

#### **Diagnostic Clues to Differentiate White Matter Disease in Children**

Craven, I. J.<sup>1</sup>Griffiths, P. D.<sup>2</sup>Warren, D. J.<sup>3</sup>Currie, S.<sup>1</sup>Connolly, D. J. A.<sup>1</sup>

<sup>1</sup>Royal Hallamshire Hospital, Sheffield, UNITED KINGDOM, <sup>2</sup>Academic Department of Radiology, Sheffield, UNITED KINGDOM, <sup>3</sup>Leeds General Infirmary, Leeds, UNITED KINGDOM

#### **PURPOSE**

The diagnosis of white matter disease in pediatrics is often very complicated due to the wide range of pathologies that occur and the relative infrequency that they are encountered. There are specific MR patterns to many of the disorders which if identified correctly can provide a prompt accurate diagnosis.

#### **APPROACH/METHODS**

The MRI patterns of normal terminal myelination will be compared to typical findings in hypomyelination and dysmyelination. For the latter two, many of the common pathologies encountered in the pediatric setting will be discussed. Illustrative examples will include Alexander disease, Canavan disease, Krabbe disease, Acute disseminated encephalomyelitis (ADEM), X-Linked adrenoleukodystrophy, L-2-hydroxyglutaric aciduria, Kearns Sayer syndrome and pediatric multiple sclerosis.

#### **FINDINGS/DISCUSSION**

The salient findings of each group of disorders will be discussed including the pattern of white matter findings. This will include confluent vs multifocal changes and the geographic distribution of abnormality seen. The use of advanced MR sequences (e.g., MR spectroscopy) also will be discussed as a possible discriminator between the differential pathologies.

#### **SUMMARY/CONCLUSION**

The electronic educational format is ideally suited for this methodical approach to white matter disease. The use of many textbook examples will aid comprehension of this often complex subject.

**KEY WORDS:** White matter disease, leukodystrophy

#### **eEdE-112**

#### **Acquired Pediatric Leukoencephalopathy**

Orrin, S.<sup>1</sup>Collins, J.<sup>1</sup>Burrowes, D.<sup>2</sup>

<sup>1</sup>University of Chicago, Chicago, IL, <sup>2</sup>Northwestern University, Chicago, IL

#### **PURPOSE**

Pediatric white matter disease or the leukoencephalopathies often can present a diagnostic challenge, especially in the previously developmentally normal patient. We intend to present an extensive sampling of the combined institution's experience of Children's Northwestern Memorial and University of Chicago Hospitals with a spectrum of acquired white matter disease, with MRI modalities, and supporting clinical data in cases where this distinction could not be made on the basis of conventional MRI.

#### **APPROACH/METHODS**

We will present a selection of patients, all of whom demonstrated concerning white matter changes on MR imaging. For each case, the following will be provided: a brief history of disease, all pertinent imaging, and a final diagnosis (on the basis of genetic, laboratory analysis, tissue pathology or definitive findings on subsequent clinical or radiologic follow up).

#### **FINDINGS/DISCUSSION**

The utility of MRI in the detection of leukoencephalopathies is accepted widely. While there are two accepted broad categories including heritable and acquired diseases we will focus on acquired myelin disorders which will include infectious, inflammatory, toxic-metabolic, hypoxic-ischemic and posttraumatic. Additionally wherever applicable, we will supply the initial imaging modalities including CT and US, outlining the contribution which these modalities may have made toward acquiring additional MR imaging leading to a definitive diagnosis.

#### **SUMMARY/CONCLUSION**

The accurate differentiation of acquired white matter disease is difficult; however, certain imaging pattern distinctions may direct the clinical differential and significantly aid in the diagnosis when used in

conjunction with conventional history, physical and laboratory data.

**KEY WORDS:** Leukoencephalopathy, pediatric, acquired

#### eEdE-113

### **Diffusion Tensor Imaging as an Adjunct to Conventional MR Imaging in Brainstem Malformations**

Rollins, N. K. • Koral, K. • Veltkamp, D. • Morriss, M. C. • Booth, T.

Childrens Medical Center  
Dallas, TX

#### **PURPOSE**

To depict brainstem malformations using diffusion tensor imaging (DTI).

#### **APPROACH/METHODS**

Institutional PACs was queried for brainstem malformations which were identified using conventional MRI (cMRI) and classified as per Barkovich. Directionally encoded color maps and diffusion tractography of the pons and midbrain were evaluated for integrity and location of dorsal and ventral transverse pontine fibers (TPF), medial-lateral lemniscus, and decussation of the superior cerebellar peduncles (SCP).

#### **FINDINGS/DISCUSSION**

Brainstem malformations in Group I (malformations resulting from defects in early differentiation of the neural tube) were associated with variable pontine and cerebellar hypoplasia. By DTI, there was hypoplasia or absence of the dorsal TPF with variable hypoplasia of the ventral TPF and preservation of medial-lateral lemniscus fibers and decussation of the superior cerebellar peduncles (SCP). In the most severe Chiari II malformations, there was complete absence of TPF. Group II malformations, which were associated with malformations of the cerebrum and/or cerebellum, included Type I lissencephaly, congenital muscular dystrophies with CNS involvement (cobblestone lissencephaly), variable malformations of cortical development, and callosal agenesis/dysgenesis. The appearance of the brainstem by DTI in Group II was variable and included a single midline cortico-spinal tract with preservation of TPF, and absence or ectopia of dorsal TPF with thickening of the ventral TPF, and intact medial-lateral lemnisci and decussation of the SCP. Group III were localized brainstem malformations with or without cerebellar involvement. Group III included Joubert syndrome and related disorders (JSRD) and were the most variable in appearance of all the groups by cMRI and DTI. The decussation of the SCP was not consistently absent in this group. In some patients with JSRD, there were ectopic transversely oriented fibers in the pons and pontomedullary junction. Rhomboencephalosynapsis and Dandy-Walker continuum were associated with normal brainstem by DTI.

#### **SUMMARY/CONCLUSION**

Diffusion tensor imaging is a useful adjunct to cMRI in delineation of aberrant projection fibers in the brainstem of patients with a myriad of congenital brain malformations in addition to those in which the brainstem malformation is the dominant feature. Diffusion tensor imaging provides information about aberrant axonal migration not possible with cMRI.

**KEY WORDS:** Brainstem malformations, diffusion tensor imaging, pediatrics

#### eEdE-114

### **Cortical Developmental Abnormalities in Pediatric Seizure Patients**

Tuna, I. S. • Maheshwari, M. • Singh, S. • Chandra, T. • Kelly, T. G. • Segall, H. D.

Medical College of Wisconsin  
Wauwatosa, WI

#### **PURPOSE**

To describe various cortical malformations with illustrative examples. We also will discuss briefly the embryology, genetic basis, classification schemes and characteristic imaging findings.

#### **APPROACH/METHODS**

This exhibit will illustrate three main categories of cortical malformations: neuronal proliferation, migration and organization. Understanding of this complex topic would be facilitated by brief discussion on the embryologic basis and proposed genetic causes of some of these cortical malformations. Classification schemes on embryology and imaging will be discussed. Characteristic imaging findings of these malformations will be discussed and examples from the authors database will be shown.

#### **FINDINGS/DISCUSSION**

Neuroimaging in pediatric seizures is challenging. MR imaging is considered the imaging modality of choice because of superior soft tissue contrast and better ability to characterize the pathologic process. We also will discuss the dedicated seizure protocol which is used in our institute. Positron emission tomography (PET)-CT imaging also provides additional information in cases where MRI is negative, inconclusive or does not correlate with EEG/clinical findings. Brief discussion on advanced imaging techniques also will be presented. Malformations frequently are detected in infancy. However, if the initial MRI scan performed in infancy is negative, a repeat scan after 2 years of age may be helpful.

#### **SUMMARY/CONCLUSION**

Evaluation of cortical malformation in seizure patients still remains a challenging area of pediatric neuroimaging. Reviewing of the embryologic basis, classification schemes and characteristic imaging findings would improve the understanding of the cortical malformations and interpreting the images.

**KEY WORDS:** Seizure, cortical malformations, embryology

#### eEdE-115

##### Posterior Fossa Abnormalities in Children

Gupta, A.<sup>1</sup>•Chandra, T.<sup>2</sup>•Meena, M. L.<sup>1</sup>•Baser, S. C.<sup>1</sup>

<sup>1</sup>Ravindra Nath Tagore Medical College, Udaipur, Rajasthan, INDIA, <sup>2</sup>Childrens Hospital of Wisconsin, Milwaukee, WI

##### PURPOSE

The aim of this exhibit is to demonstrate various conditions involving the posterior fossa in children with emphasis on importance of embryologic development of cerebellum in reaching a correct diagnosis.

##### APPROACH/METHODS

This pictographic presentation displays the imaging features of cases encountered in our clinical practice on 1.5 T magnetic resonance (MR) imaging.

##### FINDINGS/DISCUSSION

With the advent of MR imaging, there has been a revolution in identification and characterization of malformations of the brain. This is especially true in posterior fossa, where the sensitivity and specificity of MR imaging with its multidimensional imaging capability are far superior to those of computed tomography (CT) in the detection of subtle morphologic abnormalities. However, there is still a great deal of confusion regarding their classification, terminology, and spectrum of expression and this is where neuroembryology is of great help. This exhibit demonstrates : 1) Review of embryology and normal anatomy of cerebellum. 2) MR appearance of spectrum of conditions involving posterior fossa in children which includes developmental abnormalities (Dandy-Walker complex, Arnold Chiari malformations, cerebellar dysplasia/hypoplasia, Joubert's syndrome, etc.), cysts (arachnoid cyst, giant cisterna magna, etc.), tumors (medulloblastoma, ependymoma, hemangioblastoma, etc.) and miscellaneous conditions.

##### SUMMARY/CONCLUSION

Abnormalities of the posterior fossa often are difficult to differentiate solely on the basis of their radiologic appearances alone. However, an accurate diagnosis is essential for proper treatment planning and genetic counselling. Therefore it is imperative for radiologists to be well versed with the normal anatomy and development of cerebellum so as to correctly diagnose the various posterior fossa abnormalities.

**KEY WORDS:** Posterior fossa, cerebellum

#### eEdE-116

##### Epilepsy Surgery Demystified: Goals of Structural Imaging and Utility of Diffusion Tensor Imaging Tractography

Allmendinger, A.<sup>1,2</sup>•Rohatgi, S.<sup>1,2</sup>•Prabhu, S.<sup>3,2</sup>

<sup>1</sup>Brigham and Women's Hospital, Boston, MA, <sup>2</sup>Harvard Medical School, Boston, MA, <sup>3</sup>Children's Hospital Boston, Boston, MA

##### PURPOSE

To review various surgical procedures used for management of intractable pediatric epilepsy. To review the presurgical work up, goals of structural imaging with an emphasis on the role of advanced imaging techniques like DTI, MEG and fMRI. To review the findings of diffusion tractography in presurgical mapping, intraoperative assessment, and detecting postprocedural complications and assessment of completeness of resection.

##### APPROACH/METHODS

Imaging studies obtained for pediatric patients with intractable epilepsy presented at the weekly multidisciplinary surgical procedures at our institution over a 4-year period (2007 -2011). MR images were obtained on 3 T, 32 channel coil magnet. We identified salient features of abnormalities seen in these cases and the corresponding surgical procedure chosen for treatment. We illustrate the diagnostic workup with emphasis on the utility of DTI, MEG, SPECT and fMRI data. We describe innovative ways used to visualize data for surgical planning, including multimodality overlays and use of 4D data sets.

##### FINDINGS/DISCUSSION

A variety of surgical procedures are available for the treatment of patients with intractable epilepsy ranging from anterior temporal lobectomy, subpial resections and lesionectomy to nonlesional cortical resection and hemispherectomy. Surgical treatment is influenced greatly by imaging studies. Key points that the epilepsy team is looking for include; 1) extent and nature of lesion 2) functionally abnormal regions, 3) relationship to eloquent brain areas 4) white matter tract connections - both important functional and aberrant tracts that need to be resected and 4) vascular landmarks. Examples of underlying lesions (hippocampal sclerosis, malformations of cortical development, neoplastic and vascular lesions) of focal epilepsy, and common pitfalls in diagnosis will be discussed. We emphasize with case examples our experience in the utility of DTI tractography in all three phases of epilepsy surgery, namely, presurgical workup, intraoperative MRI assessment and postprocedure surveillance. Finally, there will be a focused discussion on the role of DTI tractography in decision making and surgical planning, but also we will discuss it's role in intraoperative assessment, and the role of DTI in postoperative surveillance.

##### SUMMARY/CONCLUSION

This review illustrates the presurgical workup of intractable epilepsy, including ways to maximize the information available from structural and functional imaging studies and emphasizes the increasing role of advanced imaging techniques (DTI, MEG and fMRI). We highlight imaging findings following numerous epileptic surgical procedures including a focused review of DWI and diffusion tractography in surgical mapping,



intraoperative assessment, and in postprocedural complications and surveillance.

**KEY WORDS:** Epilepsy surgery, DTI tractography, diffusion tensor imaging

#### eEdE-117

### MR Imaging with a 32-Channel Head Coil at 3 T in the Evaluation of Focal Epilepsies: Experience at Childrens Hospital Boston

Ellika, S. K. Grant, E. Paldino, M.

Childrens Hospital Boston  
Boston, MA

#### PURPOSE

Unlike in adults, developmental lesions predominate as the source of seizures in children; in particular, focal cortical dysplasia (FCD) is the most common anatomical substrate for intractable epilepsy in the pediatric population. Pre-operative identification and complete excision of a localized structural lesion are the most important prognostic factors in the surgical management of medically refractory partial epilepsy. Although great progress has been made on these fronts, many FCDs are not detected prior to surgery. One reason for lack of detection is the lack of recognition of the spectrum of imaging features. A second reason for lack of detection is the use of suboptimal imaging protocols and equipment. In this exhibit, we aim to demonstrate the spectrum of imaging features of FCD and highlight the added utility of MR imaging with a 32-channel head coil at 3 T in a subset of pediatric patients undergoing evaluation for focal epilepsy.

#### APPROACH/METHODS

A general review of the classification of malformations of cortical development (MCD) and the MR features of FCD will be depicted with case examples. Imaging at 1.5 with a 12-channel head coil and 3 T with a 32-channel head coil will be compared in representative cases of patients with FCD. The importance of high-resolution volumetric imaging, optimized image contrast as well as the potential role for diffusion tractography and arterial spin labeling will be illustrated.

#### FINDINGS/DISCUSSION

Advances in MR technology, including higher field strength and improved phased array coils, dramatically increase the signal-to-noise ratio (SNR). Higher SNR then can be leveraged for imaging speed and spatial resolution and, therefore, offers the potential for improved detection of subtle epileptogenic lesions when the imaging features of FCD are known. Although the FCD are detected better with these technical improvements, further studies are necessary to determine the ability of imaging to accurately detect the margins of the FCD and the full extent of the lesion that needs to be resected for seizure freedom.

#### SUMMARY/CONCLUSION

Current guidelines recommend that all patients with epilepsy should be investigated with MRI. In our

experience at Children's Hospital Boston, MR imaging with a 32-channel head coil at 3 T is superior to 12-channel head coil studies performed at 1.5 T and constitutes our standard for all patients with focal seizures. In addition optimized protocols with high resolution and high contrast are needed. Arterial spin labeling and tractography offer potential future advances. Familiarity with the radiologic findings of malformations of cortical development at 3 T, especially focal cortical dysplasia, should aid in prompt and accurate diagnosis and significant improvement in patient outcomes.

**KEY WORDS:** 3 T, 32-channel head coil, pediatric epilepsy

#### eEdE-118

### Diffusion Tensor Imaging in Language Delay and Autistic Disorders: A Primer and Roadmap for the Future

Rohatgi, S.<sup>1</sup>Allmendinger, A. M.<sup>1</sup>Prabhu, S.<sup>2</sup>

<sup>1</sup>Brigham and Women's Hospital, Boston, MA,

<sup>2</sup>Children's Hospital, Boston, MA

#### PURPOSE

1. To define normal anatomy of language pathways using current literature with a clinical perspective. 2. To illustrate examples of normal appearances of the language pathway and variations with age and between subjects on diffusion tractography. 3. To illustrate with examples, DTI tractography findings in patients with autism in correlation with genetic findings in selected cases.

#### APPROACH/METHODS

We processed tractography data obtained on a 3 T MRI scanner from patients with autism and language delay imaged over a 3-year period at Children's Hospital Boston. A number of normal subjects with documented normal language development also were processed. These data were evaluated in conjunction with conventional MRI and assessed by a pediatric neuroradiologist and quantified using standard visualization software analysis package (Trackvis). The superior and inferior longitudinal fasciculus (ILF), uncinate fasciculus, cingulate and arcuate fasciculus were analyzed and ADC and fractional anisotropy were calculated.

#### FINDINGS/DISCUSSION

Language is a highly complex function with multiple interconnected pathways. Language dysfunction is now believed in part to have a genetic basis appearing more often in cluster of families. Conventional MR imaging is insufficient to detect structural abnormalities in this subset of patients. Diffusion tensor imaging (DTI) has provided us with the ability to analyze various white matter tracts and provide structural information and integrity about neural networks. Normal language pathways predominantly include the superior longitudinal fasciculus, its subparts and the arcuate fasciculus. On tractography, the differences between

normal and a subset of autistic patients with language delay was striking, with absent arcuate fasciculus on one or both sides in some and in others, there was asymmetry that was more marked than age-matched samples. Autism and language disorder now is thought to be related to dysfunction of neural networks. Diffusion tensor imaging in patients with autistic features and language delay have demonstrated abnormalities in white matter tracts in diffusion, fiber length and distribution associated with language tracts especially the arcuate fasciculus. We found genetic abnormalities in a small proportion of these patients which correlated with the tractography abnormalities.

#### **SUMMARY/CONCLUSION**

We have summarized normal and abnormal appearances of the language pathways in children. Using case examples, we show the potential utility of DTI in stratifying this diverse group of children who are considered autistic. We illustrate the potential to identify a subset of patients with specific language pathway abnormalities and identifying a genotype-phenotype correlation using DTI.

**KEY WORDS:** Diffusion tensor imaging, language, autism

#### **eEdE-119**

#### **Diffusion Tensor Imaging: Fractional Anisotropy and Tractography in Pediatric Cortical Abnormalities Evaluation with Tract-Based Spatial Statistics Analysis**

Fonda, C.·Ciccarone, A.·Esposito, M.·Mortilla, M.

Meyer Children's University Hospital  
Firenze, ITALY

#### **PURPOSE**

The microstructure of tissues and white matter tracts in vivo may be studied with diffusion tensor imaging (DTI). Alterations of cortical design and structure are associated to an altered subcortical white matter tract with frequent different pattern of organization and often with different fractional anisotropy (FA) on DTI. The alterations involving the cerebral cortex associated in various degree with subcortical white matter abnormalities often affect the projection white matter tracts. The white matter in cortical brain abnormalities are evaluated with DTI and tract-based spatial statistics (TBSS).

#### **APPROACH/METHODS**

Fifty-eight patients (1-14 year range, 32 males, 26 females) with different pattern of cortical alterations, diffuse (9) and focal (49) were studied with MR imaging at 3T magnet (Achieva, Philips Medical System, Best, Netherlands) and a 8-channel head coil. 3D T1-weighted images, conventional T1 and T2 multiplanar acquisitions and White matter/gray matter suppression acquisitions were collected in all patients. Diffusion tensor imaging acquisitions were performed in all patients on axial plane. The DTI data were processed in FSL. For each DTI exam, brain extraction only of images with b value equal to zero was performed and a mask of entire brain was created. We built 7 templates for

coregistering different sizes of the pediatric brain. Our templates were built taking into account the age of patients. We chose seven age ranges: 0-6 months; 6 months,1 day -12 months; 1 year,1 day - 3 years; 3 years,1 day - 5 years; 5 years,1 day -10 years; 10 years,1 day -13 years; 13 years,1 day -16 years. Viewing the movie of DTI acquisition a slight mismatch among different directions of diffusion gradients was observed. It is due to eddy current interferences. Artifact movements and eddy current distortions were removed and all diffusion images of DTI to the first one with b value equal to zero, were coregistered. Mean diffusivity (MD) and fractional anisotropy (FA) were quantified together to the three principal directions of diffusion (eigenvectors) with their own eigenvalues (tensor diagonalization). Analysis of single fiber orientation for each voxel with a bayesian algorithm was executed. Two-fiber analysis output also was performed for each patient. Probabilistic approach means that for each voxel there is an estimated proportion of the diffusion signal that can be accounted for by the first fiber orientation (and second orientation). We make use of target masks to inform tractography. Voxelwise statistical analysis of the FA, MD, radial diffusivity and axial diffusivity data were carried out using TBSS (two-sample unpaired T-tests, statistical threshold  $t > 3$ ,  $P < 0.05$ , corrected for multiple comparisons with threshold-free cluster enhancement between focal cortical abnormalities sites and the contralateral normal ones.

#### **FINDINGS/DISCUSSION**

Different patterns of cortical organization and white matter projections are evidenced depending on lesional load and extension, site and age. In focal cortical abnormalities the TBSS analysis revealed significant differences ( $p < .05$ ) between the affected cortical sites and the contralateral normal ones.

#### **SUMMARY/CONCLUSION**

Different FA data were collected. The reductions of FA, the associated elevation of diffusivity (D) in altered contiguous or distal area are evidenced.

**KEY WORDS:** Diffusion tensor imaging, brain abnormalities, fractional anisotropy

#### **eEdE-120**

#### **Tractography of the Pediatric Corpus Callosum in Health and Disease: A Comprehensive Review**

Ellika, S. K.·Prabhu, S.

Childrens Hospital Boston  
Boston, MA

#### **PURPOSE**

Anomalies of the corpus callosum (CC) may be better characterized with diffusion tensor imaging (DTI) and fiber tractography (FT) than with conventional magnetic resonance (MR) imaging. The purpose of our exhibit is to describe various abnormalities of the corpus callosum with emphasis on congenital malformations, DTI imaging protocol used at our

institute and its use along with fiber tractography, to further understand fiber connectivity.

#### **APPROACH/METHODS**

A review of the various anomalies and diseases affecting the corpus callosum with use of DTI and FT will be depicted with illustrative images.

#### **FINDINGS/DISCUSSION**

The corpus callosum is the largest white matter tract that crosses the two cerebral hemispheres. Various types of lesions can occur within this structure such as congenital anomalies, toxic and metabolic diseases, ischemic-hypoxic disease, demyelinating diseases, tumors, trauma and transient signal changes. Ultrasonography (US), computed tomography (CT) and magnetic resonance imaging (MRI) can be used in the assessment of CC. However, MRI is the modality of choice for the evaluation of this structure. Diffusion tensor imaging and FT are emerging tools for mapping white matter tracts and to better assess the presence, location and organization of white matter tracts.

#### **SUMMARY/CONCLUSION**

In conclusion, DTI and FA may be useful for studying disease processes affecting the corpus callosum, for understanding fiber connectivity, and to better assess presence, location and organization of white matter tracts.

**KEY WORDS:** Corpus callosum, diffusion tensor imaging, fiber tracking

#### **eEdE-121**

##### **Pictorial Essay of Multimodal Neuroimaging in Pediatric Epilepsy**

Elлика, S. K. Poduri, A. Paldino, M.

Childrens Hospital Boston  
Boston, MA

#### **PURPOSE**

Preoperative identification and complete excision of a localized structural lesion are the most important prognostic factors in the surgical management of medically refractory partial epilepsy. Although great progress has been made on these fronts, many malformations of cortical development (MCDs) are not detected prior to surgery. Advances in neuroimaging, including MRI, nuclear medicine, and magnetoencephalography, not only have the potential to improve lesion detection but also now occupy a major role in preoperative planning. The purpose of this exhibit is to demonstrate the spectrum of abnormalities which underlie focal epilepsies in children and to highlight the role of multimodal imaging in the evaluation of this challenging patient population.

#### **APPROACH/METHODS**

In this exhibit, we will review various epileptogenic pathologies, highlighting the role of multimodal imaging with illustrative examples. Focal cortical dysplasia in particular will be discussed in detail, with specific

attention to imaging features; representative examples will be shown.

#### **FINDINGS/DISCUSSION**

The causes of pediatric focal epilepsy are diverse, and include malformations of cortical development, neurocutaneous syndromes (predominantly tuberous sclerosis and Sturge Weber syndrome), mesial temporal sclerosis, neoplasms, encephalitis and stroke. Teaching cases depicting various pathologies will be illustrated along with the work up of these patients with multimodal imaging.

#### **SUMMARY/CONCLUSION**

Multimodality neuroimaging plays an essential role in the work up and management of pediatric patients with medically refractory seizures.

**KEY WORDS:** Pediatric epilepsy, multimodal imaging

#### **eEdE-122**

##### **Differential Diagnosis of Pathologic Pediatric Intracranial Calcifications: A Multimodality Approach Pictorial Essay**

Nakamura, O. K. Wosny, C. Barbosa, A. A. Sameshima, Y. T. Carmignani, M. Funari, M. B. G.

Albert Einstein Israelite Hospital  
Sao Paulo, BRAZIL

#### **PURPOSE**

To review and demonstrate differential diagnosis of pathologic pediatric intracranial calcifications, discussing imaging findings based on a multimodality approach (brain transfontanellar sonography, CT and MRI).

#### **APPROACH/METHODS**

Systematic review and demonstration of imaging findings of different pediatric intracranial calcifications, such as congenital (tuberous sclerosis, Sturge-Weber syndrome and lipoma), infectious (congenital Cytomegalovirus and toxoplasmosis, neurocysticercosis), endocrine and metabolic (mitochondriopathy and diabetes insipidus), neoplastic (choroid plexus carcinoma and medulloblastoma), and vascular (arteriovenous malformation) calcifications in pediatric patients.

#### **FINDINGS/DISCUSSION**

Pediatric intracranial calcifications are related to many causes. They can be classified into physiologic, congenital, infectious, endocrine and metabolic, vascular, and neoplastic. Intracranial physiologic calcifications are uncommon in pediatric patients younger than 9 years old, but can occur in the pineal gland and choroid plexus. Congenital calcifications can be observed in intracranial lipoma, tuberous sclerosis, Sturge-Weber syndrome, and less commonly in other syndromes, such as neurofibromatosis, Cockayne and Gorlin syndromes. Infectious calcifications are associated with a large number of congenital infections, most commonly with TORCH agents (toxoplasmosis,

rubella, Cytomegalovirus (CMV), Herpes simplex virus (HSV)). Other infections can cause calcifications, such as cysticercosis, tuberculosis, HIV, and cryptococcosis. Hormonal and metabolic-related calcifications occur in Fahr disease, parathyroid hormone disorders, and less commonly in mitochondriopathy and diabetes insipidus. Neoplastic calcifications are associated with some types of cancer such as oligodendroglioma, craniopharyngioma, germ cell neoplasms, pineal neoplasms, and others. Vascular calcifications in pediatrics are uncommon, but they can occur in aneurysms, arteriovenous and cavernous malformations.

#### **SUMMARY**

Pediatric intracranial calcifications are present in physiologic and pathologic situations. Regarding pathologic causes, they can be classified into congenital, infectious, endocrine and metabolic, vascular, and neoplastic calcifications. These imaging findings must be correlated with age and clinical presentation. Some calcifications present typical morphology and distribution, which can lead to more precise differential diagnosis.

**KEY WORDS:** Calcification, brain, pediatrics

#### **eEdE-123**

##### **Complicated Perinatal Central Nervous System Infection: Spectrum of Findings and Prognostic Implications**

Rebollo Polo, M.<sup>1</sup>·Muchart Lopez, J.<sup>1</sup>·Miller, E.<sup>2</sup>·Davila, J.<sup>2</sup>·Cusi, V.<sup>3</sup>·Agut, T.<sup>3</sup>·Hurteau-Miller, J.<sup>2</sup>

<sup>1</sup>Hospital Sant Joan de Deu, Esplugues de Llobregat, SPAIN, <sup>2</sup>Children's Hospital of Eastern Ontario, Ottawa, ON, CANADA, <sup>3</sup>Hospital Sant Joan de Deu, Barcelona, SPAIN, <sup>4</sup>Hospital Sant Joan de Deu, Barcelona, SPAIN

#### **PURPOSE**

Perinatal central nervous system (CNS) infections, whether acquired in utero or postnatal remain an important cause of acute and long-term neurologic morbidity. Neuroimaging plays a crucial role in the early depiction of complications and has a prognostic value regarding late neurologic sequelae. The purpose of this exhibit is to illustrate the common and uncommon imaging findings in complicated perinatal CNS infections. We will emphasize the different complications regarding the etiology of the infection and the timing of the insult (prenatal versus postnatal).

#### **APPROACH/METHODS**

Through an interactive approach we will conduct a comprehensive overview of the different imaging patterns of brain injury (in fetal and neonatal MR and US) in complicated perinatal CNS infections, depending on the timing of the infection and the etiological agent. We present a systematic imaging approach depending on the different clinical scenarios. Moreover, we discuss the imaging follow up and the correlation of prognostic imaging findings with late neurologic sequelae.

#### **FINDINGS/DISCUSSION**

In our exhibit we discuss these main following points: Main etiological agents in neonatal brain infection. Different microorganisms (viruses, bacteria, parasites) act through diverse pathophysiologic mechanisms to produce brain injury. Discussion of the imaging protocol and approach in this setting. Fetal MRI is most useful to identify potential CNS complications of in utero infections. Doppler US is the initial modality of choice to image the neonatal brain. However, MRI is more sensitive for the detection of complications. Diffusion-weighted imaging, diffusion tensor-imaging and angiographic TOF sequences allow the detection of complications minimizing the use of intravenous contrast. Spectrum of complications in perinatal CNS infections: - Regarding the timing of the infection. Early intrautero infections may produce migration anomalies, severe encephaloclastic effects etc. - Common complications: hydrocephalus, effusions, empyemas. - Vascular complications: vasculitis, thrombosis. - Parenchymal complications: cerebritis, infarction, abscess, myelination delay. - Severe complications: massive brain edema, diffuse necrosis. Late neurologic sequelae. Perinatal CNS infections often disturb cerebral maturation and result in severe neurodevelopmental delay. Neuroimaging has a prognostic value regarding late neurologic sequelae.

#### **SUMMARY/CONCLUSION**

After reading this exhibit the visitor will be able to recognize the most common patterns of brain injury in complicated perinatal CNS infections and the frequent and unusual complications.

**KEY WORDS:** Perinatal, infection, complication

#### **eEdE-124**

##### **Fetal MR Imaging: Brain, Head and Neck Malformations: A Pictorial Essay**

Singh, S.·Maheshwari, M.·Kelly, T. G. C.·Johnson, C. M.·Chandra, T.·Tuna, I. S.·Segall, H. D.

Medical College of Wisconsin  
Milwaukee, WI

#### **PURPOSE**

The purpose of the exhibit is to illustrate various brain, head and neck masses/vascular anomalies on fetal MRI. We also will discuss the briefly normal fetal brain anatomy as seen on fetal MRI.

#### **APPROACH/METHODS**

Major indications for fetal MRI include evaluation of inconclusive sonographic findings in cases of central nervous system (CNS) malformations. In our institute patients are scanned on 1.5 T MR scanner. A body surface six-channel phased array coil is used to maximize signal to noise. All the scans are checked by a neuroradiologist to make sure adequate three plane imaging of the brain or other lesion in question were performed. Three plane scanning of the fetal body also is performed for the laterality determination of the lesion and also screen for other congenital anomalies.

**FINDINGS/DISCUSSION**

Prenatal USG is frequently inconclusive for evaluation of complex fetal brain and head and neck anomalies. Most studies suggest that MRI after first trimester is safe. In addition, advent of rapid MRI sequences like single shot fast spin echo (ssFSE) have helped in reducing scan time and motion artifacts leading to availability of diagnostic quality images. These have led to increasing use of MRI as supplemental tool to further investigate inconclusive fetal sonographic findings. MR imaging provides better anatomical delineation of these complex abnormalities. It helps in making appropriate diagnosis with high confidence and aids in appropriate obstetric and prenatal/neonatal surgical planning or intervention. This educational exhibit will illustrate few common fetal anomalies. These will include agenesis of corpus callosum, malformation of cortical development, posterior fossa malformations, ventriculomegaly, in utero stroke, orbital abnormalities and some fetal neck masses/vascular anomalies. Correlation and confirmation with the postnatal MRI also will be provided for some cases.

**SUMMARY/CONCLUSION**

Technical and therapeutic advances have driven the development of fetal MRI. It is an important adjunctive tool for prenatal imaging in those instances in which a complex anomaly is suspected by sonography, when fetal surgery is contemplated, or when a definitive diagnosis cannot be determined. It has prognostic implications and may help in optimal and timely obstetric and neonatal management.

**KEY WORDS:** Fetal MR imaging, congenital brain malformations, congenital head and neck malformations

**eEdE-125****Brain MR Imaging in Neonatology: Why, When and How**

Nakamura, O. K. •Wosny, C. •Barbosa, A. A. •Sameshima, Y. T. •Carmignani, M. •Funari, M. B. G.  
Albert Einstein Israelite Hospital  
Sao Paulo, BRAZIL

**PURPOSE**

To demonstrate clinical indications of brain MRI in neonatology, discussing technical issues, advantages and contraindications involving this method.

**APPROACH/METHODS**

Systematic review and clinical correlation of the most common and important indications of brain MRI in neonatology, demonstrating normal aspects and findings in periventricular leukomalacia, intracranial hemorrhage, venous thrombosis, basal nuclei infarcts, acute stroke, acute meningoencephalitis, hypoxic-ischemic injury and head trauma.

**FINDINGS/DISCUSSION**

Brain MRI in neonatology is indicated in the evaluation of the extremely preterm infant; anoxia, regardless of

gestational age; seizures assessment; congenital infections; brain malformation screening; and prognostic value of motor sequelae. Neonatal brain MRI has important advantages compared to transfontanellar sonography, such as the whole brain evaluation, with sulcation and anatomy details, early diagnosis of white matter lesions, details of the posterior fossa, evaluation of myelination and the posterior limb of internal capsule (PLIC) and greater interobserver concordance. Abnormal MRI signal in the PLIC, the topography of the corticospinal tract, can predict poor neurologic outcome in infants after hypoxic-ischemic encephalopathy, when performed during the first week after birth. Diffusion-weighted imaging is very important and can detect acute ischemic injuries and early Wallerian degeneration. Most neonatal brain MRI exams should be performed either in the first week after birth or around term equivalent age for those preterm neonates. Nevertheless, neonatal brain MRI has some disadvantages, such as necessity of transportation to MRI examining room, sedation, equipment adaptations, monitoring, high cost, involves potential risks, difficulty of serial evaluation, requirement of training and expertise of radiologists and support staff. New MR compatible incubators have been developed and are commercially available, allowing neonatal intensive care unit patients to perform the exam with proper monitoring and care.

**SUMMARY/CONCLUSION**

Brain MRI has been used increasingly to evaluate neonates, providing whole brain scan and more detailed anatomy, compared to transfontanellar sonography. This technique should be performed in a proper moment, considering clinical indications, advantages and potential risks. New sequences and equipment have been developed, improving the quality and safety of the exam.

**KEY WORDS:** Brain MR imaging, neonatology, hypoxic-ischemic injury

**eEdE-126****Germinal Matrix Hemorrhage in Preterm Infants: A Comprehensive Ultrasound and MR Imaging Review**

Lopez-Alvarez, Y. •Rivera-Morell, M. •Echevarria, M. G. •Melendez, M. •Labat, E.

University of Puerto Rico School of Medicine  
San Juan, PR.

**PURPOSE**

Review the anatomy and normal sonographic appearance of the neonatal brain. Discuss the intracranial hemorrhage (ICH) grading system. Review the differential diagnosis of ICH in preterm infants as well as normal variants and pitfalls. Discuss the importance of sonographic evaluation in preterm infants suspected to have intracranial pathology. Discuss the role of MRI in the evaluation of ICH in preterm infants.

**APPROACH/METHODS**

Perform a retrospective review at our PACS workstation of normal preterm infant brains on both US and MRI. Perform a retrospective review at our PACS database of intracranial hemorrhage in preterm newborns seen by both ultrasonography and MRI. A pictorial review with both normal subjects and preterm newborns with ICH, correlated with the current ICH classification scheme, as well as pitfalls to avoid will be presented.

### FINDINGS/DISCUSSION

Germinal matrix hemorrhage (GMH) is most common in preterm and low birth weight infants in the first week of life. Currently, the grading system is based on the extent of involvement of hemorrhage to adjacent structures. Due to its high specificity, sensitivity, accessibility and ease of use, ultrasonography is the most commonly used modality for diagnosis. In many instances, MRI can be utilized as a complementary study to us. We will compose a pictorial review showing the gamma of findings in patients with GMH on US and MRI, as well as pitfalls to avoid.

### SUMMARY/CONCLUSION

Review the normal anatomy and sonographic/MRI appearance of the neonatal brain. Review the classification of intracranial hemorrhage (ICH) in preterm infants providing an imaging/pictorial representation from our PACS database. Compare ICH findings on both ultrasonography and MRI. Present normal variants and important pitfalls to avoid when evaluating patients with ICH.

**KEY WORDS:** Hemorrhage

### eEdE-127

#### Approaching Pediatric Spinal Neoplasms: An Interactive Tutorial

Illoreta, S. F.<sup>1</sup>·Haverkamp, B.<sup>1</sup>·Jarmakani, M.<sup>2</sup>·Lowe, L.<sup>1</sup>·Gibson, S.<sup>3</sup>

<sup>1</sup>University of Missouri Kansas City, Kansas City, MO,

<sup>2</sup>Kansas City University of Medicine and Biosciences, Kansas City, MO, <sup>3</sup>Children's Mercy Hospital, Kansas City, MO

### PURPOSE

The objective of this educational electronic exhibit is to provide the radiologist with an approach to spinal neoplasms in the pediatric population.

### APPROACH/METHODS

The exhibit format will include a case-based review of various pediatric spinal neoplasms. Several cases will include radiologic-pathologic correlation. There also will be a brief discussion of imaging findings useful in guiding surgical management. Emphasis will be placed on narrowing the differential diagnosis using a combination of lesion location, characteristic imaging findings, and relevant clinical history. An interactive self-assessment exam will be presented at the end of the exhibit.

### FINDINGS/DISCUSSION

Pediatric Spinal Neoplasms: Location, Key Imaging Features, and other comments			
Location	Neoplasm	Key imaging features	Age, associations and treatment
IM	Astrocytoma	Cervical most common	10 years of age
		Tend to be eccentric within cord +/- syrinx	Rx - surgical debulking +/- chemotherapy & radiation
	Ependymoma	Tend to be central within cord, cervical most common	13-14 years of age
		Hemosiderin cap on T2 weighted MRI	If multiple lesions, consider neurofibromatosis, type 2
	Ganglioglioma	Drop metastases	Rx - surgery +/- radiation & chemotherapy
		Similar appearance to ependymoma	7 years; Associated with NF-2; Rx - Surgical resection
	Hemangioblastoma	Cystic lesion with enhancing mural nodule	Associated with von-Hippel Lindau disease
		Flow voids	Rx - surgery
EM	Leptomeningeal metastasis	Lumbosacral involvement	Common with ependymomas, medulloblastoma, higher-grade astrocytomas & atypical teratoid rhabdoid tumor
		Variable in size and number of lesions	Rx - depends on primary lesion
	Nerve sheath tumor (schwannoma/neurofibroma)	Expansion of intervertebral foramina, posterior vertebral body scalloping, target sign	Associated with NF-1 and NF-2
			Rx - Typically conservative & rarely debulking
	Meningioma	Isointense on noncontrast imaging	Teenagers: Multiple lesions in setting of NF-2
		Homogeneous, vigorous enhancement	Rx - surgical resection
	Primary osseous lesions		
ED	Osteoblastoma	Posterior element, solid, expansile, enhancing mass	10-30 years; 40% occur in spine; Rx-surgical resection
	Aneurysmal bone cyst	Posterior element, expansile, multicystic, fluid-fluid levels	10-30 years; 20% occur in spine
			Treatment - Embolization, surgical curettage & packing
	Osteoid osteoma	Posterior element lucent nidus with marked surrounding enhancement +/- central calcification	90% < 25 years age; 10% occur in spine
			Rx - Radiofrequency ablation
	Lymphoma	Vertebral body lesion with little or no loss of height; Single > multiple	Spinal involvement with systemic disease; Rarely primary lesion; Rx - chemotherapy
	Leukemia	Vertebral body lesion with slight loss of height; Multiple > single	Spinal involvement with systemic disease
			Rx - chemotherapy
	Langerhans cell histiocytosis	Vertebral body lesion(s) with severe loss of height (vertebra plana) & soft tissue mass; Single > multiple	Ranges from single osseous lesion to systemic disease; Rx - usually chemotherapy
	Sacrococcygeal teratoma	Paraspinal (adrenal is most common) mass encasing vessels with calcifications	1-5 years of age
			Rx - Chemotherapy and surgery

Rx = treatment

### SUMMARY/CONCLUSION

After viewing this exhibit, the learner will be able to: a. Recognize the clinical, imaging, and pathologic characteristics of pediatric spinal neoplasms. b. Systematically approach a case using lesion location, key imaging findings, and characteristic clinical associations. c. Identify relevant imaging findings pertinent to further surgical management. d. Test their understanding of the presented material through an interactive self-assessment.

**KEY WORDS:** Pediatrics, spine, neoplasms

### eEdE-128

#### Medulloblastoma: Spectrum of Imaging Appearances with Focus on Atypical Findings

Bricker, A. A. O.·Ahmed, M.

Cleveland Clinic Foundation  
Cleveland, OH

### PURPOSE

Although medulloblastoma or posterior fossa primitive neuroectodermal tumor (PNET) is the most common pediatric central nervous system malignancy and the most common primary tumor of the posterior fossa in children, its imaging appearances can be quite varied. Familiarity with both the classic and diverse imaging



presentations of this common tumor is important given its highly aggressive nature and improved clinical outcomes with early surgical resection and chemoradiation therapy.

#### **APPROACH/METHODS**

MR and CT images from several patients with biopsy proven medulloblastoma are presented. Both characteristic and somewhat atypical imaging features are demonstrated with short discussion of key differential considerations. Cases with varying sites of tumor origin, diverse tumor-cystic-enhancement patterns, as well as cases with differing patterns of tumor spread and leptomeningeal disease are presented, with emphasis on common mimics such as pilocytic astrocytomas, ependymomas and atypical teratoid rhabdoid tumors.

#### **FINDINGS/DISCUSSION**

Ranging from solid to predominantly cystic, avidly enhancing to non-enhancing, well circumscribed to infiltrative tumor - we present imaging features on structural CT and MR imaging from several different cases of biopsy proven medulloblastoma collected from the database at our institution. Even recurrent intracranial disease can have a variety of presentations, such as nonenhancing subependymal leptomeningeal nodules or a large meningioma-like dural metastases.

#### **SUMMARY/CONCLUSION**

Familiarity with both the classic and atypical appearances of this common pediatric tumor is important given its predilection for early drop metastasis and improved clinical outcomes with early diagnosis and treatment. It is also of practical importance to be aware of the variant presentations of this common pathology, as these can be a potential diagnostic confusion in day-to-day imaging.

**KEY WORDS:** Medulloblastoma, posterior fossa primitive neuroectodermal tumor, pediatric neoplasms

#### **eEdE-129**

##### **Inner Ear Malformations: Classification System and Embryologic Basis**

Singh, S.<sup>1</sup>•Maheshwari, M.<sup>1</sup>•Kelly, T. G. C.<sup>1</sup>•Chun, R. H.<sup>2</sup>•Chandra, T.<sup>1</sup>•Tuna, I. S.<sup>1</sup>•Segall, H. D.<sup>1</sup>

<sup>1</sup>Medical College of Wisconsin, Milwaukee, WI,

<sup>2</sup>Children's Hospital of Wisconsin, Milwaukee, WI

#### **PURPOSE**

The purpose of the exhibit is to discuss spectrum of inner ear malformations with illustrative examples. We also would discuss the new classification system of cochleovestibular malformations and their embryologic basis.

#### **APPROACH/METHODS**

High resolution CT scan and MRI are mainstay of diagnosis and assessment in patients with sensorineural hearing loss. In this exhibit we will present a pictorial review of CT scan and MRI images of

various causes of sensorineural hearing loss which are seen on imaging. Reviewing the embryologic basis of these anomalies would enable better understanding of this complex subject.

#### **FINDINGS/DISCUSSION**

The new system classifies these malformations according to descending order of severity into complete labyrinthine aplasia, cochlear aplasia, common cavity, cystic cochleovestibular malformation or incomplete partition - I (IP-I), cochleovestibular hypoplasia, and incomplete partition - II (IP- II). There is a lot of confusion in literature especially pertaining to Mondini deformity. The new classification divides incomplete partition into IP- I representing cystic cochleovestibular malformation and IP-II representing the classic Mondini deformity with three components (cystic cochlear apex, dilated vestibule, and large vestibular aqueduct). Recently a subclassification of IP-I and IP-II has been proposed (subdividing into typical and atypical subtypes). This will be discussed briefly. Isolated large vestibular aqueduct without associated cochlear abnormalities also will be discussed. We will discuss the relevant embryology with correlations of malformations to the timing of embryologic insult. We will discuss briefly the relevant embryology with correlations of malformations to the timing of embryologic insult. We also will present other causes of sensorineural hearing loss like hypoplastic internal auditory canal or narrow cochlear aperture. These frequently are associated with cochlear nerve hypoplasia or absence.

#### **SUMMARY/CONCLUSION**

The new classification system provides uniformity in description of inner ear malformation. This also helps in providing a uniform scale for comparison of effectiveness of different treatment strategies (including cochlear implant) for different malformations.

**KEY WORDS:** Cochleovestibular malformations, new classifications with recent modifications, embryologic basis

#### **eEdE-130**

##### **Pictorial Review of Causes of Sensorineural Hearing Loss in Children**

Greenblatt, K.•Grimm, J. P.•Nelson, M. D.

Childrens Hospital Los Angeles  
Los Angeles, CA

#### **PURPOSE**

The purpose of this exhibit is to review both common and uncommon causes of sensorineural hearing loss (SNHL) in children, and their specific imaging characteristics.

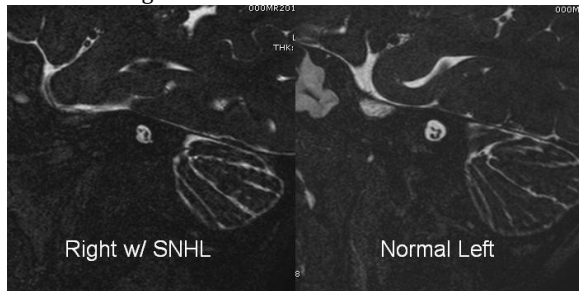
#### **APPROACH/METHODS**

Common and uncommon causes of SNHL will be reviewed, along with the preferred imaging modalities and protocols. Cases of various causes of SNHL will be

presented and specific imaging findings and developmental and/or pathologic considerations will be discussed with each case.

#### FINDINGS/DISCUSSION

Sensorineural hearing loss is a common manifestation of multiple different disease processes. Underlying etiologies can be developmental, inflammatory/infectious, posttraumatic and neoplastic. Those reviewed in this exhibit will include: cochlear malformations, enlarged vestibular aqueduct syndrome, labyrinthine ossification, otosclerosis, semicircular canal dehiscence, congenital cochlear nerve deficiency, acquired cochlear nerve deficiency, primary masses in the internal auditory canal (e.g., schwannoma), and leptomeningeal metastatic disease to the internal auditory canal. Many of these abnormalities can be detected by CT or MRI, but can be very subtle. With a thorough knowledge of the causes of SNHL and their specific imaging characteristics, an algorithmic approach to image interpretation often can direct the radiologist to a subtle yet specific finding, leading to a definitive diagnosis.



#### SUMMARY/CONCLUSION

Sensorineural hearing loss is a frequently encountered problem in children for which imaging plays a significant role in diagnosis. It is important that radiologists have a familiarity with both the common and uncommon causes of SNHL, as well as their imaging characteristics, in order to develop an algorithmic approach to image interpretation and to provide a definitive diagnosis.

**KEY WORDS:** Temporal bone, hearing loss, pediatric

#### eEdE-131

##### Regional Differences in Brain Maturation Using Fast T2-Weighted Images and Diffusion-Weighted Imaging in Fetal MR Imaging

Wilson, N. • Hurteau-Miller, J. • Davila-Acosta, J. • Miller, E.

Children Hospital of Eastern Ontario  
Ottawa, ON, CANADA

#### PURPOSE

Normal fetal brain maturation can be studied through in vivo magnetic resonance imaging and relying primarily on fast T2-weighted sequences. These maturational changes must be interpreted with knowledge of the histologic background and the course of the respective developmental steps. Signal changes associated with maturational processes can be ascribed mainly to the

changes in tissue composition and organization, which occur at the histologic level. The purpose of this exhibit is to describe the regional differences in fetal T2-weighted and diffusion-weighted imaging (DWI) images as well as their evolution with gestational age to reflect differences in brain maturation.

#### APPROACH/METHODS

This exhibit is intended to give a comprehensive review of the use of Fast T2-weighted sequences and DWI at b value of 1000. We will describe the regional difference in brain maturation of various essential brain structures including: supratentorial cortex, germinal zone, white matter, temporal lobes, cerebellum and brainstem.

#### FINDINGS/DISCUSSION

MR imaging currently is used to evaluate the fetal brain, particularly when a fetus is at increased risk for neurodevelopmental disabilities or when an abnormality has been detected on a prenatal ultrasound. Since its introduction, studies have consistently shown that fetal MRI can detect abnormalities that are not apparent on prenatal sonography. Moreover, the identification of abnormalities by fetal MRI can influence decisions made about pregnancy management and delivery. Studies on DWI in infants and children clearly have demonstrated a progressive decline in water diffusivity in the brain, which parallels known histologic and functional data about brain development. Increasing interest in fetal therapy, combined with the rising incidence of premature births has resulted in an increasing need to understand normal brain maturation before term and in utero.

#### SUMMARY/CONCLUSION

We believe that a firm knowledge of the MRI appearances of fetal brain maturation is mandatory to be able to recognize impairment of fetal brain development. It also offers insight into developmental anomalies that may be imaged at a later stage.

**KEY WORDS:** Fetal MR imaging, normal development, brain

#### eEdE-132

##### How Brain Maturation Affects Imaging Characteristics of Different Brain Pathologies at Varying Ages in Children

Davila-Acosta, J. H.<sup>1,2</sup> • Lopez-Bueno, J.<sup>1,2</sup> • Torres, C.<sup>3,2</sup> • Rebollo-Polo, M.<sup>4</sup> • Miller, E.<sup>1,2</sup>

<sup>1</sup>Children Hospital of Eastern Ontario, Ottawa, ON, CANADA, <sup>2</sup>University of Ottawa, Ottawa, ON, CANADA, <sup>3</sup>The Ottawa Hospital, Ottawa, ON, CANADA, <sup>4</sup>Hospital Sant Joan de Déu de Barcelona, Barcelona, SPAIN

#### PURPOSE

Normal brain maturation is characterized by changes in brain morphology and composition, which includes myelination changes over time. Major changes can be detected by different MRI pulse sequences, including morphologic sequences (T1WI and T2WI), and

functional DWI, DTI and MRS sequences. Brain maturation begins around the second trimester of gestation and progresses to reach adult-like pattern by 2 years; however, this continues until early adulthood. The brain maturation process is responsible for different windows of brain vulnerability and therefore varying disease patterns that present in fetuses, neonates, infants and older children. This exhibit will describe how brain maturation can affect the imaging characteristics of brain pathology depending on the child's age at presentation.

#### Approach Methods

The objective of this exhibit is to use MR imaging to give a comprehensive review of normal brain maturation and compare how similar brain pathology can show different imaging patterns at varying ages. We will describe and compare the changes in ischemic and infectious processes, metabolic diseases, cortical development malformations, phakomatosis, tumors and genetic disorders affecting children of different ages.

#### FINDINGS/DISCUSSION

The maturation process involves morphologic and brain composition changes. Morphologic changes include a decrease in the size of extra axial and ventricular spaces, and increased brain volume. These changes can be seen easily with ultrasound and MRI. Brain composition changes include changes in cellular density, increase in complex lipid content (myelination process), decrease in free fluid white matter water content, developing white matter and cortical fiber networks and neurotransmitters, and neurotransmitters-receptors interactions. Brain composition changes result in a progressive shortening of T1WI and T2WI sequences and changes in MRS curves. These changes can be seen early with DWI and DTI. As a result of these changes, MR protocols and parameters of acquisition are varied depending on the patient's age. Another important element that occurs during brain maturation is caused by the immature oligodendrocytes. These are actively reproducing and forming myelin, but they have a poor reparative function in younger ages. This factor can explain how similar brain pathology can have different characteristics at various ages. Brain maturation can affect the appearance of a disease and this can be noted clearly in ischemic and infectious process, metabolic disease, cortical development malformations, phakomatosis, tumors and genetic disorders when comparing their appearance over time.

#### SUMMARY/CONCLUSION

A comprehensive understanding of normal brain maturation is vital for recognizing and understanding the multiple patterns of brain disease at varying ages in children. This knowledge is essential for creating accurate MRI brain protocols which are dependent on a patient's age.

**KEY WORDS:** Brain maturation, MR imaging, myelination

#### eEdE-133

#### Imaging of Nontraumatic Pediatric Brain Emergencies

Campeau, N. G.·Patton, A.

Mayo Clinic  
Rochester, MN

#### PURPOSE

Hypoxic ischemic encephalopathy, neoplasms, and metabolic disorders are common conditions leading to urgent or emergent pediatric imaging. The goal of this electronic exhibit is to illustrate the clinical and imaging features of various additional nontraumatic urgent and emergent conditions affecting children who present with symptoms of coma, altered mental status, seizures, sensory motor dysfunction, increased head circumference, and focal neurologic deficit.

#### APPROACH/METHODS

A retrospective study with review of the clinical history and imaging findings of children who presented to the radiology department without known recent trauma requesting urgent imaging of the brain was performed.

#### FINDINGS/DISCUSSION

The relevant CT and MRI imaging findings of these conditions will be presented: venous cerebral infarction, inflammatory processes, and demyelinating disease including acute disseminated encephalomyelitis and multiple sclerosis. Migraine headaches and moyamoya which may mimic stroke also will be illustrated. Intracranial infection which may present with fever and seizures also will be discussed. Finally, the clinical and potential imaging abnormalities associated with the sequelae of tacrolimus, cyclosporine and methotrexate "neurotoxicity" will be described. Such patients may present with nonspecific symptoms of decrease level of consciousness, hypertension and motor dysfunction.

#### SUMMARY/CONCLUSION

Knowledge of the clinical and imaging findings of some of these described potentially life-threatening nontraumatic urgent and emergent conditions is essential for timely accurate diagnosis and prompt initiation of appropriate treatment to these children.

**KEY WORDS:** Pediatrics, brain, emergency

#### eEdE-134

#### Pediatric Spinal Ultrasound: Pearls and Pitfalls

Chandra, T.·Maheshwari, M.·Gross Kelly, T. C.·Singh, S.·Tuna, I. S.·Segall, H. D.

Medical College of Wisconsin  
Milwaukee, WI

#### PURPOSE

The purpose of this exhibit is to review the technique, indications and limitations of neonatal spinal

ultrasound with emphasis on normal variants and imaging pitfalls that may mimic disease processes.

#### **APPROACH/METHODS**

In this exhibit, we will illustrate ultrasound anatomy of the neonatal spinal cord. Discussion of the normal anatomical variants and pathologic conditions of the spinal cord will be provided. Representative images of a variety of common and uncommon pathologic conditions of the spine will be presented to illustrate teaching points. In abnormal cases, follow-up MRI images also will be illustrated for comparison.

#### **FINDINGS/DISCUSSION**

Ultrasound is a robust screening modality for evaluation of the lumbosacral spine in neonates. It is cheaper, readily available, safer first line imaging modality in neonates suspected to have spinal malformations. Under able and well trained operator, diagnostic accuracy of spinal ultrasound approaches MRI. However, MRI remains the gold standard for imaging evaluation of spine. Normal variants that simulate disease processes like ventriculus terminalis, prominent filum terminale and central echo complex will be presented. Congenital malformations of the cord such as tethered cord, hydromyelia, lipoma, diastematomyelia, myelomeningocele, lateral meningocele and presacral masses also will be discussed.

#### **SUMMARY/CONCLUSION**

Ultrasound is a very useful screening technique for evaluation of pathologic conditions of lumbosacral spine in neonates. This review would improve the understanding of utility and limitations of ultrasound in evaluation of neonatal spinal malformations.

**KEY WORDS:** Pediatric, spinal, ultrasound

#### **eEdE-135**

##### **Imaging of Nontraumatic Urgent and Emergent Conditions in the Pediatric Spine**

Patton, A. Campeau, N. G.

Mayo Clinic  
Rochester, MN

#### **PURPOSE**

The goal of this electronic exhibit is to provide an imaging overview of a wide variety of nontraumatic conditions afflicting children presenting with suspected urgent or emergent spine pathology.

#### **APPROACH/METHODS**

A retrospective review of the clinical history and imaging findings of children who presented to the radiology department with a request of urgent imaging of the spinal axis was performed.

#### **FINDINGS/DISCUSSION**

The essential clinical and imaging features of the following congenital, infectious, inflammatory, neoplastic and metabolic conditions will be presented:

spinal dysraphism, sacrococcygeal teratoma, dermal sinus, diskitis, osteomyelitis and epidural abscess, nontraumatic vertebral subluxation, osseous and parenchymal neoplastic processes such as aneurysmal bone cyst, osteoblastoma, astrocytoma, ganglioglioma, ependymoma and metastasis will be illustrated. Additional conditions such as acute disseminated encephalomyelitis, transverse myelitis and sequelae of methotrexate neurotoxicity also will be discussed.

#### **SUMMARY/CONCLUSION**

Awareness and familiarity of the typical clinical and imaging features of these spinal "emergencies" in the pediatric population is essential to avoid delayed or misdiagnosis of these potentially perilous conditions leading to inherently significant associated morbidity and mortality.

**KEY WORDS:** Pediatrics, spine, emergent

#### **eEdE-136**

##### **Pediatric Spinal Cord Tumors: A Pictorial Overview**

Chandra, T. Maheshwari, M. Gross Kelly, T. C. Singh, S. Tuna, I. S. Segall, H. D.

Medical College of Wisconsin  
Milwaukee, WI

#### **PURPOSE**

The aim of this educational exhibit is to provide a comprehensive review of imaging features, classification and management of pediatric spinal cord tumors. We also aim to elicit the differences between pediatric spinal cord tumors and their adult counterparts. We will summarize the differences between the individual tumors based on histologic cell types and the pertinent implications on management and outcome.

#### **APPROACH/METHODS**

This exhibit will provide an overview of the common as well as uncommon tumors of the pediatric spinal cord. Various classification systems for these tumors - anatomical as well as histologic will be discussed. We will illustrate the relevant imaging findings that can help in differentiating these tumors.

#### **FINDINGS/DISCUSSION**

Pediatric spinal cord tumors account for 1% to 10% of all pediatric central nervous system tumors. MR imaging is the mainstay for the initial diagnosis as well as the postsurgical evaluation and surveillance of these tumors. Pediatric and adult spinal cord tumors differ both in terms of anatomical location as well as histology. The disease and treatment related morbidities are also different in children as compared to adults. Astrocytomas, ependymomas, glioneural tumors and cerebrospinal fluid (CSF) metastasis represent the vast majority of cord neoplasms in the pediatric age group. Some of cord tumors also may be associated with inherited syndromes (like Neurofibromatosis type 2) or may have genetic predisposition. These also will be discussed. We will

also illustrate and discuss common nonneoplastic spinal masses that may mimic tumors.

#### SUMMARY/CONCLUSION

Pediatric spinal cord tumors have varied clinical presentations, imaging appearance and outcome. This review would improve the understanding of these tumors thereby helping in diagnosis, management and follow up of these uncommon neoplasms.

**KEY WORDS:** Pediatric spinal cord, tumors

**Monday, April 23 –  
Wednesday, April 24  
6:30 AM – 9:00 PM  
Thursday, April 26  
6:30 AM – 3:00 PM  
Rhinelander**

**Electronic Education Exhibits  
(eEdE) 137 – 154**

eEdE7 – Spine

**Note: A missing printed number indicates an abstract has been withdrawn.**

#### eEdE-137

##### **High-Resolution MR Imaging Anatomy of the Lumbar Spine: The Anatomy You May Not Know**

Nicholson, A. D. • Kitajima, H. D. • Saindane, A. M.

Emory Healthcare  
Atlanta, GA

#### PURPOSE

Although the gross anatomy of the intervertebral disks, facet joints, spinal canal, and intervertebral foramina generally is well known to the neuroradiologist, an improved appreciation of the detailed muscular, ligamentous, nervous, ganglionic, and vascular anatomy of the lumbar spine is beneficial for gaining a better understanding of the derangements of the lumbar spine and the various potential etiologies of lower back pain.

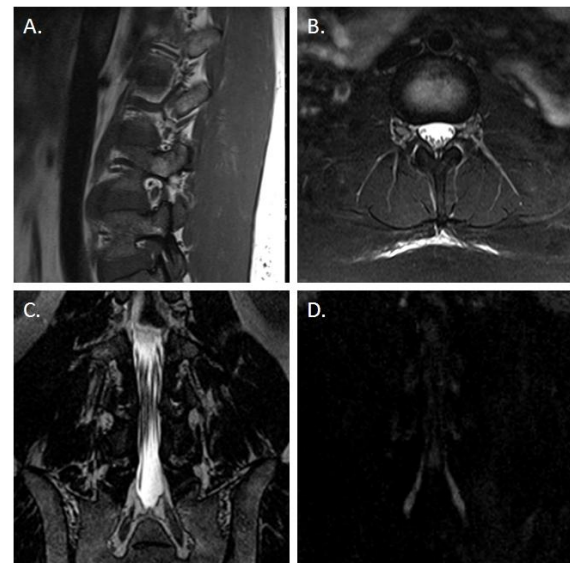
#### APPROACH/METHODS

Utilizing high-resolution MR imaging sequences at 3T we have been able to image and highlight detailed lumbar spinal anatomy that is underappreciated and not commonly taught. Specifically, multiplanar T1- and T2-weighted, diffusion-weighted imaging (DWI), MR neurography, and time-resolved MR angiography sequences were utilized in normal controls and in patients presenting with lower back pain. Detailed correlation with anatomical atlases was performed with

illustrative MR images and corresponding diagrams to clearly depict important portions of the anatomy of the lumbar spine. The figure demonstrates representative A. Sagittal T1-weighted, B. Axial T2-weighted fat-saturated, C. Coronal T2-weighted, and D. Coronal DWI images of the lumbar spine.

#### FINDINGS/DISCUSSION

High-resolution anatomical T1- and T2-weighted images clearly demonstrated the individual posterior paraspinal muscles, the spinal and iliolumbar ligaments, and ventral dorsomedian septum. MR neurographic and DWI sequences added to depiction of the nerve roots and branches, dorsal root ganglia, and sympathetic ganglia. High-resolution T1- and T2-weighted sequences and time-resolved MR angiographic images demonstrated the segmental, radicular, and muscular arteries, as well as the epidural and basivertebral plexus and intervertebral veins. Key anatomy in this exhibit is highlighted with correlative anatomical illustrations



#### SUMMARY/CONCLUSION

High-resolution anatomical imaging along with MR neurography, DWI, and time-resolved MRA clearly identify the important anatomy of the lumbar spine, in particular the less well known elements of the muscular, ligamentous, nervous, ganglionic, and vascular anatomy.

**KEY WORDS:** Anatomy, high-resolution, MR imaging

#### eEdE-138

##### **Focusing on the L5 Nerve Root**

Gomez, F.<sup>1</sup> • Gomez, A. M.<sup>2</sup> • Anaya, C.<sup>3</sup> • Gomez, J. F.<sup>4</sup>

<sup>1</sup>Clinica Neurocardiovascular DIME, Cali, COLOMBIA, <sup>2</sup>Ronald Reagan University of California Los Angeles, Los Angeles, CA, <sup>3</sup>Cedars Sinai Hospital, Los Angeles, CA, <sup>4</sup>Johns Hopkins, Baltimore, MD

#### PURPOSE

Provide a thorough description of the L5 nerve root anatomy as it emerges from the thecal sac, and its course along the spinal canal, lateral recess, lateral canal, neural foramen, and extraforaminal-lateral region. Demonstrate the most common pathologic conditions which affect the nerve roots along their pathway.

#### **APPROACH/METHODS**

This focused anatomical and pathologic review is demonstrated through cross-sectional imaging of the lumbar spine utilizing a multislice 64 dual source CT scan, a 3.0 T MRI, 3D reconstructions and graphics: Nerve roots: An anatomical description is performed on the nerve roots and their branches: recurrent meningeal nerve, ventral nerve root, dorsal nerve root, dorsal root ganglion, and the spinal nerve. Anatomical Landmarks: These include: 1) The L4-L5 intervertebral disk and the L5 origin (at the disk - superior end plate junction). 2) The boundaries and relationships that the L5 nerve root has within the spinal canal, lateral recess, lateral canal, neural foramina and extra foraminal region. At the L5-S1 level, illustrations demonstrate how the L5 superior articular facets, ligament flavum and osteophytes cause L5-S1 foraminal stenosis and secondary L5 nerve root impingement. Pathology: L5 nerve root compression is caused by a variety of pathologic conditions affecting the L4-L5 intervertebral disk space, lateral canal, neural foramen and extraforaminal-lateral region. These include: • Intervertebral disk pathologies such as bulgings, protrusions, and herniations which can be central, paramedian, foraminal or extraforaminal in location (with extrusion or migration). Trans-osseous disk herniation due to avulsion of the apophyseal rim of the L5 vertebral endplate. • Secondary nerve root compression by different types of foraminal stenosis which include: caudo-cephalic stenosis, antero-posterior stenosis, and pinhole stenosis. • Spinal degenerative instability at the L4-L5 level (with anterolisthesis or retrolisthesis), and the mechanism by which compression of the thecal sac and L5 nerve roots occur. • Spondylolisthesis with spondylolysis at L5-S1 with secondary entrapment of L5 nerve root. • Double compression for L5 nerve root (at the L4-L5 nerve root origin, and as the nerve exits at the L5-S1 level).

#### **FINDINGS/DISCUSSION**

The purpose of evaluating the origin and entire course of the L5 nerve roots is not to find causes of discogenic pain or pain secondary to a degenerated disk. The real purpose is to accurately identify the lesions that cause L5 radicular pain. This approach will ultimately lead to an adequate patient care and will provide the exact information that the surgeons need to know.

#### **SUMMARY/CONCLUSION**

This anatomical review facilitates the identification of L5 nerve root compression along the entire L5 nerve root pathway, independently of the pathologic cause. This knowledge allows an effective and reliable method for the diagnosis of lumbar spine pathology, which ultimately results in a more precise diagnosis and a decrease in the number of failed back surgeries.

**KEY WORDS:** Lumbar spine, nerve roots

#### **eEdE-139**

### **Brachial Plexopathy: A Primer to Diagnosis of Uncommon Nontraumatic and Nonneoplastic Etiologies**

Noujaim, S. • Goldin, D.

William Beaumont Hospital  
Royal Oak, MI

#### **PURPOSE**

MR imaging has become the modality of choice for evaluation of many pathologic conditions affecting the brachial plexus. The purpose of this work is to present less common pathologies other than tumors and traumatic lesions, encountered in the practice of neuroradiology.

#### **APPROACH/METHODS**

A brief review of the brachial plexus anatomy will be followed by presentation of a number of nontraumatic and nonneoplastic brachial plexopathies encountered in a busy major tertiary care medical center. Selected MR images of each condition along with a brief patient history will be used for presentation followed by differential diagnosis and discussion of each condition.

#### **FINDINGS/DISCUSSION**

Most radiologists interpreting MRI of the brachial plexus are familiar with the diagnosis of traumatic and neoplastic lesions encountered in their practice. Primary and secondary tumors are the most common nontraumatic causes of brachial plexopathy, after radiation fibrosis. For this presentation the authors selected a spectrum of idiopathic, viral, immune-mediated and postradiation etiologies resulting in brachial plexopathy which were diagnosed in their practice. Cases presented include, but are not limited to, acute brachial plexitis (Parsonage-Turner syndrome), Charcot-Marie-Tooth plexitis, and postradiation plexitis and its differential diagnoses with plexitis caused by tumors.

#### **SUMMARY/CONCLUSION**

A number of nontraumatic and nonneoplastic conditions affecting the brachial plexus will be presented and discussed in this review. The readers should feel familiarized and comfortable with interpretation of brachial plexitis after reading this work.

**KEY WORDS:** Brachial plexus, brachial plexitis

#### **eEdE-140**

### **Percutaneous Image-Guided C-Spine Procedures**

Massari, F.<sup>1</sup> • Rumboldt, Z.<sup>2</sup> • Vandergrift, A. W.<sup>2</sup> • Bonaldi, G.<sup>3</sup> • Cianfoni, A.<sup>2</sup>

<sup>1</sup>University of Rome "Tor Vergata", Rome, ITALY,

<sup>2</sup>Medical University of South Carolina, Charleston, SC,

<sup>3</sup>Riuniti Hospitals, Bergamo, ITALY



**PURPOSE**

Aim of this educational exhibit is to offer an overview on neuroradiologic armamentarium in the minimally invasive percutaneous image-guided procedures on the cervical spine.

**APPROACH/METHODS**

Spinal neurointerventional radiology, through the use of fluoroscopic and/or CT imaging guidance offers a wide variety of percutaneous procedures on the cervical spine, for tissue diagnosis, drainage of fluid collections, pain management, diagnostic and therapeutic blocks, radiofrequency ablations, disk procedures, osteoporotic and neoplastic vertebral fractures treatment. Procedures under fluoroscopy and/or CT guidance, with different approaches (anterior, lateral, posterior, transmaxillary, and trans-oral), will be shown, and indications, relevant anatomy, procedural techniques will be outlined. -Anterior approach: Under fluoroscopic or CT guidance, it is used to access: Disk spaces: for biopsy, diskography, percutaneous disk decompression. Vertebral bodies: from C4 to C7, for biopsy, cement vertebral augmentation, percutaneous tumor ablation. Stellate ganglion: for diagnostic, prognostic and therapeutic blocks in painful and nonpainful conditions related to sympathetic dysfunctions of head, neck and upper extremities. -Lateral approach: Under fluoroscopic or CT guidance, it is used to access: Central canal at C1-C2 for CSF collection or myelography, Neuroforamina C3-C8: for diagnostic, prognostic and therapeutic blocks in radicular pain. Zygoapophyseal joints: for diagnostic, prognostic and therapeutic blocks in facet-related pain. Median branch nerves: for diagnostic and prognostic blocks in facet-related pain. -Posterior approach: Under fluoroscopic or CT guidance, it is used to access: Interlaminar space: for epidural blocks, posterior bony elements: for bone biopsies and cementoplasty, C1 lateral masses: for bone biopsies and cementoplasty, C1 and C2 neuroforamina: for diagnostic, prognostic and therapeutic blocks in radicular pain, C1-C2 joint: for diagnostic, prognostic and therapeutic blocks, Zygoapophyseal joints: for diagnostic, prognostic and therapeutic blocks in facet-related pain, radiofrequency median branch denervation: for pain management of facet-related pain radiofrequency transverse occipital nerve denervation: for pain management of occipital neuralgia. -Transmaxillary approach: Under CT guidance, it is used to access: C1 and C2 anterior bony elements: for biopsy, cement vertebral augmentation, percutaneous tumor ablation. -Transoral approach: Under fluoroscopic guidance, it is used to access: C1-C3 anterior bony elements: for biopsy, cement vertebral augmentation, percutaneous tumor ablation.

**FINDINGS/DISCUSSION**

A wide variety of image-guided cervical spine procedures are illustrated, with their different approaches. Fluoroscopic or CT guidance can be chosen on the basis of personal preference, anatomical features, type of approach, and specific procedure to be performed. Percutaneous image-guided procedures on the cervical spine require thorough knowledge of loco-regional anatomy, precise and reliable imaging

guidance, and rigorous technique, due to the complex, delicate, and vital anatomical environment, to avoid serious complications. Elements of relevant fluoroscopic and cross-sectional anatomy, as well as procedural technique elements are discussed and displayed.

**SUMMARY/CONCLUSION**

This educational exhibit illustrates a wide variety of percutaneous image-guided accesses to the cervical spine, utilized for diagnostic and therapeutic purposes, their indications, the anatomy and the techniques, under fluoroscopy or CT guidance.

**KEY WORDS:** Spine intervention, neurointerventional radiology, vertebral fracture

**eEdE-141****Image-Guided Sympathetic Blocks**

Massari, F.<sup>1</sup> Tsai, N. T.<sup>2</sup> Rumboldt, Z.<sup>2</sup> Pedicelli, A.<sup>3</sup> Bonaldi, G.<sup>4</sup> Cianfoni, A.<sup>2</sup>

<sup>1</sup>University of Rome "Tor Vergata", Rome, ITALY,

<sup>2</sup>Medical University of South Carolina, Charleston, SC,

<sup>3</sup>Catholic University of Rome, A.Gemelli Hospital, Rome, ITALY, <sup>4</sup>Riuniti Hospitals, Bergamo, ITALY

**PURPOSE**

Aim of this education exhibit is to offer an overview on image guided sympathetic blocks, focusing on specific indications and techniques, through the use of Fluoroscopy and/or CT imaging guidance, at each level of blockade.

**APPROACH/METHODS**

Sympathetic blocks are used for diagnostic, prognostic and therapeutic purposes for painful and other conditions associated with sympathetic system dysfunctions.

Main indications for sympathetic blockade are: Complex regional pain syndrome (CRPS), phantom limb pain, central pain, hyperhydrosis, acute pancreatitis, and abdominal viscera cancer pain.

Stellate ganglion blocks are utilized for painful and non-painful conditions related to sympathetic dysfunctions of head, neck and upper extremities.

Thoracic sympathetic blocks are utilized for CRPS, postoperative analgesia, pain from fractured ribs, therapeutic control of hyperhydrosis of the upper limbs and torso, liver capsule pain after blunt trauma, acute postherpetic neuralgia, and premature ventricular contractions (PVCs).

Coeliac plexus blocks are utilized in pain due to intra-abdominal cancer, stemming from organs innervated by coeliac plexus.

Lumbar sympathetic blocks are utilized for CPRS of the lower extremities, herpes zoster, amputation stump pain and inoperable peripheral vascular vasospastic diseases of the lower limb.

Superior hypogastric blocks are utilized for pelvic pain, and pelvic organs cancer pain (uterus, cervix, bladder, prostate, urethra, testes and ovaries).

Impar ganglion blocks are utilized in coccydynia.

**FINDINGS/DISCUSSION**

The sympathetic nervous system has been implicated in numerous pain syndromes including neuropathic, vascular and visceral pain. In relation to this, in order to determine the sympathetic role in the transmission of pain and to manage these algic syndromes, sympathetic ganglia are targeted for local anesthetic blocks, for diagnostic, prognostic, and therapeutic purposes, balanced in a more complex pain treatment strategy, in the treatment of CRPS and other pain conditions. Safe and precise performance of these blocks requires knowledge of the loco-regional anatomy, accurate imaging guidance, and rigorous technique. Elements of relevant fluoroscopic and cross sectional anatomy, as well as procedural technique elements are discussed and displayed.

**SUMMARY/CONCLUSION**

This educational exhibit summarizes the indications, the anatomy and the techniques, under Fluoroscopy or CT guidance, for the sympathetic blocks.

**KEY WORDS:** Sympathetic blocks, spine interventional, interventional neuroradiology

**eEdE-142****Percutaneous, Image-Guided Spinal Infiltrations: From Alpha to Omega**

Kelekis, A.·Filippiadis, D.·Mazioti, A.·Malagari, A.·Alexopoulou, E.·Brountzos, E.·Kelekis, N.

University General Hospital "ATTIKON"  
Athens, GREECE

**PURPOSE**

Purpose of our study is to demonstrate the various current techniques of percutaneous spinal infiltrations. In addition we will address indications and contraindications as well as possible approaches and the various imaging guidance systems. Finally we will illustrate advantages and disadvantages for each approach and each image guiding system.

**APPROACH/METHODS**

Spinal infiltrations are minimally invasive, therapeutic or diagnostic procedures involving injection of a long acting steroid with or without local anesthetic. They constitute a symptomatic treatment for back pain and radiculalgia refractory to conservative medical therapy. In addition, they can clarify whether certain pathology could be the source of pain. However, the main purpose of this technique is to control painful symptoms during the acute phase until natural recovery occurs.

**FINDINGS/DISCUSSION**

Spinal infiltrations are performed under minimal or no anesthesia. Percutaneous spinal infiltrations include epidural (general) nerve blocks, transforaminal (selective) nerve blocks, caudal infiltrations, as well as facet and sacroiliac joint infiltrations. Image-guided percutaneous spinal steroid infiltrations are more effective concerning pain reduction and mobility improvement than placebo, local anesthetic alone or

bed rest. Within an average of 6-13 days post the infiltration session, 65% of patients experience at least 50% pain reduction, an improvement that lasts for an average of 15 months.

**SUMMARY/CONCLUSION**

IR allows minimally invasive percutaneous treatment of radiculalgia and back pain. Percutaneous spinal infiltrations are safe and cost-effective techniques with significant and long lasting results concerning pain reduction and mobility improvement. They can be proposed as diagnostic tests, initial treatment or attractive supplements to conservative therapy.

**KEY WORDS:** Spine, infiltrations, pain

**eEdE-143****Radiologic-Pathologic Correlation of Image-Guided Percutaneous Spine and Paraspinal Soft Tissue Biopsies**

Wu, R.·Tseng, Y.·Drexler, S.·Ortiz, O.

Winthrop-University Hospital  
Mineola, NY

**PURPOSE**

To review a series of consecutive image-guided percutaneous spine and paraspinal soft tissue biopsies with radiologic-pathologic correlation and present suggestions regarding sample acquisition in order to optimize pathologic evaluation.

**APPROACH/METHODS**

A retrospective review of image-guided percutaneous spine and paraspinal soft tissue biopsies from two-year period by a single operator at our institution was performed. A total of 89 cases were reviewed along with their respective procedure, pathology and microbiology reports. Preprocedure imaging examinations were reviewed carefully prior to each biopsy procedure. Coaxial technique was used to facilitate multiple lesion sampling and to increase specimen yield for pathologic diagnosis.

**FINDINGS/DISCUSSION**

Eighty-six patients underwent biopsy procedures. All patients were adults with the exception of one adolescent. Seventy-three of the 89 biopsies reviewed were performed with an indication of evaluating for malignancy or metastatic disease and 16 biopsies were performed for a concern of infection. Of the 73 biopsies performed for evaluation of malignancy or metastatic disease, 36 were positive for malignancy on pathology (49.3%). The majority (27) of these positive cases was indicative of metastatic disease. Of the 16 procedures performed for an indication of possible infection, 25% were proven to be positive based on pathology and/or microbiology results. Four patients out of a total of 16 (25%) were already on antibiotic therapy at the time of their biopsy.

**SUMMARY/CONCLUSION**

Image-guided percutaneous biopsies are an attractive alternative to open biopsy for tissue diagnosis of bony spinal and paraspinal soft tissue lesions for a variety of reasons. While percutaneous biopsies do minimize morbidity, these procedures are not without inherent risks. A significant degree of planning is required for each procedure and must be tailored to the patient's needs and conditions. Since many patients undergoing such procedures are older with multiple comorbidities, procedure planning should take into account the patient's ability to tolerate certain positions. Ensuring patient comfort is essential to maximizing cooperation such that adequate specimens can be obtained for pathologic diagnosis. Also, the potential need for repeat biopsies, whether percutaneous or open, should be stressed. As in the operating room, image-guided percutaneous spine and paraspinal soft tissue biopsies require successful collaboration between multiple parties: the patient, the pathologist, and the radiologist.

**KEY WORDS:** Percutaneous spine biopsy, coaxial technique

#### **eEdE-144**

##### **Intradural Lesions of the Cauda Equina and Conus: A Myriad of Conditions**

Krishnan, A.·Zaki, M.·Harb, J.·Silbergleit, R.·Wang, A.

William Beaumont Hospital  
Royal Oak, MI

##### **PURPOSE**

To present and discuss the spectrum of intradural extramedullary mass and mass-like conditions of the lumbar spine and differentiate them using a combination of imaging features.

##### **APPROACH/METHODS**

Intradural masses of the lumbar spine include common conditions such as nerve sheath tumors, meningiomas, ependymomas, and metastases. However less common masses including paragangliomas, hemangiomas, vascular malformations, granulomatous diseases, infections, and syndromic conditions also can present in this location. We shall systematically display and discuss a variety of conditions and assess their salient features. An attempt will be made to use features such as the presence of flow voids, distribution of lesions, associated findings in the rest of the spine, among others to separate them and facilitate diagnoses. An interactive case-based medium also will be used to aid in the learning process.

##### **FINDINGS/DISCUSSION**

Intradural masses of the lumbar spine can be clumped into categories based on their imaging features.

##### **SUMMARY/CONCLUSION**

Our hope is to provide a framework to facilitate interpretation of these conditions.

**KEY WORDS:** Intradural, lumbar, conus

#### **eEdE-145**

##### **Iterative Decomposition of Water and Fat with Echo Asymmetric and Least-Squares Estimation: Is It Really Ideal for Detecting Spinal Lesions?**

Vachha, B. A.·Sarkar, S.·Greenman, R.·Hackney, D.

Beth Israel Deaconess Medical Center  
Boston, MA

##### **PURPOSE**

Iterative decomposition of water and fat with echo asymmetric and least-squares estimation (IDEAL) is a chemical shift-based technique that has gained recent attention in MRI spine applications. The availability of both water-only and fat-only images allows direct image-based water and fat characterization and quantification. The goal of this presentation is to provide an overview of the underlying principles and highlight the uses of IDEAL in a spectrum of common spine lesions. We discuss the role of IDEAL in lesion detection and characterization, overall anatomical sharpness, common technical and interpretative challenges, and quantitative techniques to facilitate the incorporation of IDEAL into routine clinical practice.

##### **APPROACH/METHODS**

We routinely perform IDEAL to evaluate spine lesions. Here we review our institutional results with IDEAL imaging of a large number of patients encompassing the spectrum of common spine pathology including osteomyelitis, primary and secondary tumors, focal fat and degenerative changes. In this pictorial survey we present our findings along with the imaging correlates. Representative cases depicting the advantage of fat-only and water-only IDEAL images over more conventional MRI imaging will be presented and discussed. Images demonstrating the technical and interpretive challenges will be illustrated.

##### **FINDINGS/DISCUSSION**

Reliable fat suppression is particularly important in MRI sequences such as fast-spin echo (FSE) imaging where bright signal from fat may obscure underlying pathology. Conventional fat suppression techniques such as STIR provide homogenous fat suppression at the cost of reduced signal-to-noise ratio (SNR) and T1-dependent mixed contrast effects. Chemical shift dependent fat suppression with saturation pulses can suffer from low SNR and inhomogeneous suppression across the imaging volume. IDEAL is a novel technique that can be used for robust separation of fat and water by compensating for the effects of field inhomogeneity, while maintaining a high SNR. Although STIR has proven helpful for identifying increased vertebral water content, earlier work with inversion recovery methods have suggested that loss of high signal fat may provide excellent contrast for common vertebral lesions. We have found high SNR and excellent contrast between lesion and normal vertebral bodies on both fat and water IDEAL images. We will illustrate these applications and describe our optimized IDEAL imaging parameters.

**SUMMARY/CONCLUSION**

Our review indicates that IDEAL can replace STIR imaging, produce both fat and water images in a single acquisition, and increase sensitivity for lesion detection. This is now part of our routine clinical spine protocol.

**KEY WORDS:** IDEAL, spine, MR imaging

**eEdE-146****Imaging of the Anterior Spinal Artery for Aortic Surgery Planning**

Johnson, M. H. • Eleftheriades, J. E. • Mojibian, H. R.

Yale University School of Medicine  
New Haven, CT

**PURPOSE**

To review standard imaging techniques used to visualize the anterior spinal artery with attention to the clinical needs of surgeons and interventionalists.

**APPROACH/METHODS**

Collected teaching file and clinical cases are utilized to demonstrate the traditional imaging modality of spinal catheter angiography and newer techniques such as magnetic resonance angiography, CT angiography and CT angiography using dual energy techniques.

**FINDINGS/DISCUSSION**

Spinal catheter angiography has been the traditional method of evaluating the anterior spinal artery prior to aortic surgery, as up to 17 percent of patients may suffer spinal ischemia secondary to inadvertent compromise of the anterior spinal artery. In more recent years magnetic resonance angiography and CT angiography have begun to replace this more invasive procedure. In this exhibit we demonstrate each technique with attention to the clinical needs of the surgeons. The protocols, pitfalls and limitations of each technique are highlighted with illustrative case material. In addition, we present an innovative protocol for dual energy CT angiography of the anterior spinal artery in 15 patients with surgical correlation.

**SUMMARY/CONCLUSION**

Imaging algorithms for evaluation of the anterior spinal artery prior to aortic surgery and intervention can be optimized with knowledge of the available techniques. Dual energy CT angiography may afford a uniquely sensitive method for evaluating the artery prior to surgery.

**KEY WORDS:** Anterior spinal artery, spinal angiography, dual energy spinal CTA

**eEdE-147****High Resolution Magnetic Resonance Neurography Findings in Diabetic Neuropathy**

Thakkar, R. S. • Chhabra, A.

Johns Hopkins University  
Baltimore, MD

**PURPOSE**

Diabetic neuropathy (DN) is the most common cause of neuropathy and is associated with a wide range of clinical manifestations. The most common form of diabetic neuropathy is the distal symmetrical form of the disorder. Focal diabetic neuropathy although less common, clinically manifests with a confusing picture or as an entrapment neuropathy. The goal of this abstract is to depict the spectrum of imaging abnormalities in diabetic subjects on MR neurography as well as discuss relevant differential diagnosis.

**APPROACH/METHODS**

A case series of subjects with various manifestations of DN and related differential diagnoses (entrapment neuropathy, multifocal motor neuropathy, chronic inflammatory demyelinating neuropathy, hereditary motor-sensory polyneuropathy). The spectrum of imaging abnormalities of DN on high resolution 3 T MR neurography will be depicted.

**FINDINGS/DISCUSSION**

Imaging abnormalities in diabetic subjects vary from abnormal T2 hyperintensity and fascicular enlargement in acute-subacute stages to atrophic-appearing fascicles with intraepineural fat deposition in chronic stage of neuropathy. Nerve enlargement may be seen in all stages of neuropathy. Associated regional muscle denervation changes (edema-like T2 signal abnormality in acute-subacute stages and fatty replacement with or without atrophy in subacute-chronic stages of the disease) are helpful findings to confirm the diagnosis of neuropathy. Other key roles of imaging to exclude mass lesions or entrapment neuropathy and differentiate from above-mentioned polyneuropathy conditions will be highlighted.

**SUMMARY/CONCLUSION**

A spectrum of imaging abnormalities of diabetic neuropathy is depicted on high resolution 3T MR neurography, which also aids in its differential diagnosis.

**KEY WORDS:** Diabetic neuropathy, MR neurography, fascicles

**eEdE-148****Spinal Vascular Malformations: A Review of Classification, Clinical Presentation, and Imaging Findings**

Harshman, B. • Davis, D. J. • Malhotra, A. .

Yale University School of Medicine  
New Haven, CT

**PURPOSE**

Our purpose is to review the evolution of classification systems for spinal vascular malformations (SVM), their typical clinical presentation, and pertinent imaging findings.

**APPROACH/METHODS**

An electronic search of the scientific literature for SVM classification generated publications from the 1860s through present day. There has been an evolution of classification systems from a purely histologic approach in the early stages to a more pathophysiologic basis for the vascular malformations. Our focus is on the most recent classification system proposed by Spetzler in 2002, a revision of his earlier work with Anson in 1992. The clinical presentations are well documented and vary depending on location, lesion type, and other systemic factors. We provide case examples from our institution of the various spinal vascular malformations as depicted on conventional angiogram, computed tomography (CT), and magnetic resonance (MR) imaging.

#### FINDINGS/DISCUSSION

Rudolph Virchow provided the earliest classification of spinal vascular malformations from autopsy specimens in 1864. He described them in two categories, angioma racemosum and angioma cavernosum, based on the presence or absence of intervening parenchyma in the vascular mass. Since that time, classification systems have been proposed continuously and revised by several groups internationally. In tracking the progress from a purely histologic approach to a pathophysiologic nomenclature in SVM classification, we see the gradual progression to a four-category approach as described by Spetzler and Anson in 1992. Spetzler later revised this classification in 2002, keeping the four-category system, but adjusting the groups to account for vessel origin, anatomical location, and treatment requirements. Despite the introduction of this progressive scheme, the older Type 1 to 4 classification persists in radiology literature/parlance. Small spinal vascular malformations may go undetected for years. Larger vascular malformations progress with venous engorgement, mass effect, myelopathy, and less frequently hemorrhage or arterial steal. Traditionally, imaging of spinal vascular malformations was limited to conventional angiography. With the advent of cross-sectional imaging, imaging of spinal vascular malformations in multiple planes became possible. New techniques of dynamic and three-dimensional MR flow imaging are being developed for noninvasive evaluation with DSA angiography remaining the gold standard modality.

#### SUMMARY/CONCLUSION

The classifications of spinal vascular malformations have evolved continuously from histologic descriptions to a pathophysiologic approach that accounts for vessel origin, anatomical location, and treatment needs. The clinical presentations are well documented in the literature, varying based on location, lesion, and extent. Advances in radiologic imaging now provide an accurate, noninvasive, multiplanar evaluation of spinal vascular malformations beyond conventional angiography.

**KEY WORDS:** Spine, vascular, arteriovenous

#### eEdE-149

### MR Imaging Diagnosis of Spinal Cord Lesions with Emphasis on Diffusion-Weighted Imaging: Characteristic Findings, Differential Diagnoses and Imaging Pitfalls

Sibai, S. Moritani, T. Kim, J. Capizzano, A. Kademian, J. Sato, Y.

University of Iowa  
Iowa City, IA

#### PURPOSE

Acute paraplegia can result from ischemia/infarction, spinal cord compression, inflammation, infection, or tumor. The poor prognosis of spinal cord lesions often is related to treatment delay, so that early diagnosis is essential. Diffusion-weighted imaging (DWI) techniques can help in making these diagnoses. Here we demonstrate characteristic findings and differential diagnoses of spinal cord lesions using DWI, focusing on imaging pitfalls and limitations of this technique.

#### APPROACH/METHODS

We reviewed conventional MRI and DWI findings in 76 patients with spinal cord lesions, which included spinal cord ischemia/infarction (arterial and venous), demyelinating diseases (multiple sclerosis, ADEM), transverse myelitis, sarcoidosis, viral myelitis, acute cord injury, cord contusion, spinal cord hemorrhage, compression myelopathy/myelomalacia, syrinx, presyrinx state, subacute combined degeneration, spinal cord abscess, and various neoplasms. In our institution, DWI has been performed in routine spine MRI sequences on 1.5 and 3 T scanners from 2006. Spin-echo type echo-planar DWI with parallel imaging and the ADC maps ( $b=0$ , 1000 sec/mm<sup>2</sup>) was used. In some cases, RESOLVE (readout segmentation of long echo-trains) or HASTE (half-Fourier acquisition single-shot turbo spin echo) DWI were used as a comparison.

#### FINDINGS/DISCUSSION

Diffusion-weighted imaging hyperintensities associated with decreased ADC values were observed in spinal cord ischemia/infarction, acute demyelination, acute cord injury, spinal cord abscess/pus collection, and hypercellular neoplasm. Diffusion-weighted imaging iso or hyperintensities with various increased ADC values were observed in compression myelopathy/myelomalacia, syrinx, presyrinx state, subacute or chronic demyelination, idiopathic transverse myelitis, sarcoidosis, viral myelitis, and subacute combined degeneration. Diffusion-weighted imaging signals of hemorrhage were variable depending on the age of hemorrhage. We observed that RESOLVE DWI can help reduce the image distortion, especially with the 3 T scanners, often by improving spatial resolution.

#### SUMMARY/CONCLUSION

Diffusion-weighted imaging is useful in the differential diagnosis of spinal cord lesions. Specific DWI intensity and ADC values are associated with particular disease

processes and allow the radiologist to narrow the differential diagnosis of spinal cord lesions.

**KEY WORDS:** Diffusion-weighted images, spinal cord lesions, spinal infarction

#### eEdE-150

### **Cervical Spinal Cord Normal-Appearing White Matter in Multiple Sclerosis and Neuromyelitis Optica: The Columns that Really Matter**

Miraldi, F.·Rueda Lopes, F.·Alves Leon, S.·Gasparetto, E.

Federal University of Rio de Janeiro  
Rio de Janeiro, BRAZIL

#### **PURPOSE**

The aim of this study is to evaluate NASC damage pattern in neuromyelitis optica (NMO) and in multiple sclerosis (MS) patients in different regions of the cervical spinal cord using diffusion tensor MRI.

#### **APPROACH/METHODS**

We studied 32 patients with relapsing-remitting MS (20 female and 12 male, mean age 38.9 years old) and eight patients with NMO (7 female and 1 male, mean age 47.6 years old). In addition, 12 healthy volunteers (9 female and 3 male, mean age 37.4 years old) without any known spinal disease or neurologic disorder were included. MR imaging of the cervical spinal cord was conducted on a 1.5 MR scanner (Siemens, Avanto), including T2\*-WI, STIR-WI and diffusion tensor imaging (DTI) images. Fractional anisotropy (FA), axial diffusivity (AD), radial diffusivity (RD) and mean diffusivity (MD) were calculated within regions of interest (ROIs) in the C2 and C7 levels. The ROIs were drawn in the anterior, posterior and both lateral columns of the spinal cord. A ROI with any lesion detected on T2\*-WI was excluded. We applied Student's t-test to compare the parameters between the groups. A p-value of 0.05 was considered statistically significant.

#### **FINDINGS/DISCUSSION**

The results in the anterior column were: in the C2 level, the FA value was decreased ( $p = 0.04$ ) in NMO (0.46) in comparison to MS (0.58); the difference between FA values at C2 was also statistically significant ( $p = 0.02$ ) in NMO (0.46) and controls (0.63). DR value in the C2 level showed significant increase ( $p = 0.03$ ) in NMO (1.03) in contrast to MS (0.76), as well as statistically significant increase ( $p = 0.008$ ) between NMO (1.03) and controls (0.67). The left lateral column analysis did not reveal any significant result. The FA value of the posterior column was decreased ( $p = 0.04$ ) in the C2 level in NMO (0.55) in comparison to controls (0.76). The right column demonstrated in the C7 level significant increase ( $p = 0.04$ ) in the MD values in NMO (1.40) compared to MS (1.19), and higher increase ( $p = 0.02$ ) between NMO (1.40) and controls (0.99).

#### **SUMMARY/CONCLUSION**

Fractional anisotropy and RD are hallmarks for NASC damage in NMO patients compared to MS and controls in peripheral different regions of the cervical spinal

cord. Radial diffusivity increase in the anterior column suggests the occurrence of demyelination in that region. Besides, AD and MD values must be considered in the evaluation of NMO compared to MS and controls, once both parameters did show NASC peripheral damage. Continuing studies are necessary to establish a better correlation between DTI parameters and histopathologic aspects.

**KEY WORDS:** Normal-appearing white matter, multiple sclerosis, neuromyelitis optica

#### eEdE-151

### **Practical Approach in the Evaluation of T2-Weighted Hyperintense Spinal Cord Lesions: An Overview of their Differentiating Radiologic and Clinical Features**

Liauw, L.·Tan, K.·Yu, W.

National Neuroscience Institute  
Singapore, SINGAPORE

#### **PURPOSE**

This educational exhibit gives an approach to assessing intramedullary lesions exhibiting T2-weighted hyperintensity.

#### **APPROACH/METHODS**

The list of potential differential diagnoses of T2-weighted hyperintense spinal cord lesions is large and may be nonspecific. Additional radiologic findings and clinical information are important to arrive at the correct diagnosis. A systematic approach is provided to help narrow the differential diagnoses.

#### **FINDINGS/DISCUSSION**

The segmental length of the lesion and whether it is in the anterior, central or posterior aspect of the spinal cord should be determined. Multiple sclerosis (MS) lesions typically involve a shorter segment compared to neuromyelitis optica (NMO) lesions. Infarction occurs anteriorly whereas pathology due to subacute combined degeneration/vitamin B12 deficiency is seen in the posterior part of the spinal cord. Transverse myelitis typically is seen centrally (central dot sign). Multifocality and location in the cervical, thoracic cord or conus will help to further narrow the differential diagnosis. Presence of cysts, necrosis and hemorrhagic areas will suggest tumors such as astrocytoma and ependymoma. A search for flow voids, in arteriovenous malformations (AVM) and dural arteriovenous fistulas (DAVF), should be made and distinguished from CSF pulsation artifacts. Enhancement patterns are important and also will be discussed. One must never forget to assess other included areas such as the brain when reading a spine study.

#### **SUMMARY/CONCLUSION**

The differentiating radiologic features of T2-weighted hyperintense cord lesions are discussed and the importance of relevant clinical information also is highlighted.



**KEY WORDS:** Spinal cord, MR imaging

#### eEdE-152

### Intradural Extramedullary Spinal Lesions: An Interactive Case-Based Approach

Yahyavi-Firouz-Abadi, N. • Miller-Thomas, M. • Wippold, F. J.

Mallinckrodt Institute of Radiology  
St Louis, MO

#### PURPOSE

Defining the compartmental location of a spinal lesion comprises the first and foremost step in generating reasonable differential diagnoses. Intradural extramedullary lesions account for almost 40% of spinal masses and include a wide spectrum of conditions. This exhibit shows the distinctive imaging features that aid in distinguishing these lesions.

#### APPROACH/METHODS

This presentation employs an interactive, case-based and quiz-type format. Cases include nerve sheath tumors as the most common lesions (neurofibromas, schwannomas), meningiomas as the second most common entity, metastases (medulloblastoma, ependymoma, glioma), benign tumors (lipoma, dermoid, epidermoid), inflammatory diseases (arachnoiditis, sarcoidosis), vascular lesions (arteriovenous fistula, intradural hematoma), and cystic lesions (perineural or Tarlov cysts).

#### FINDINGS/DISCUSSION

Intradural extramedullary spinal lesions usually are recognized readily on imaging. These masses are located in the subarachnoid space and originate within the dura but external to the spinal cord. They may displace the spinal cord, expand the thecal sac, and create the "meniscus sign". Neoplasms are the most common and range from benign to highly malignant. Identifying the lesion's location, distribution in the spine, and distinctive imaging characteristics may aid in differentiating the identity of the lesion and subsequently the patient's management.

#### SUMMARY/CONCLUSION

This exhibit reviews an approach to intradural extramedullary lesions in an interactive case-based format emphasizing the distinctive imaging characteristics that aid in accurate diagnosis.

**KEY WORDS:** Intradural extramedullary, spine, differential diagnosis

#### eEdE-153

### I've Lost My Head! Craniocervical Dissociation: Imaging Diagnosis and Additive Value of MR Imaging

Gupta, S. • Lehnert, B. E. • Fink, J. R. • Fink, K. R.

University of Washington  
Seattle, WA

#### PURPOSE

- Review the anatomy of the craniocervical junction, with emphasis on ligamentous structures.
- Review the imaging findings of craniocervical dissociation (CCD) including atlanto-occipital and atlanto-axial dissociation on radiography, CT and MRI with particular attention to the utility of each modality in the evaluation of this injury.
- Highlight the diagnostic criteria of MRI for injury to the atlanto-occipital and atlanto-axial joints in CCD.
- Discuss potential pitfalls on imaging, including normal and nonspecific findings.

#### APPROACH/METHODS

Using a case-based interactive approach, this exhibit will illustrate the imaging evaluation and characteristics of CCD. Key anatomical structures for the stability of the craniocervical junction will be reviewed with side-by-side comparison of normal and injured tissues. Findings of CCD on radiography, CT and MRI will be illustrated, with particular attention to the utility of MRI for the evaluation of this injury. A discussion of the complications of CCD including epidural hematoma, spinal cord injury and associated injuries will be discussed.

#### FINDINGS/DISCUSSION

Craniocervical dissociation can be a difficult diagnosis to make both clinically and radiologically. Neurologic examination may be limited in intubated and sedated patient, and neurologic signs may be subtle or absent. The diagnosis may be missed if the correct imaging modality or sequences are not used, or if the radiologist is simply not actively searching for such an injury. Radiographs and CT remain the mainstay for diagnosis, which depends on recognition of an abnormal craniocervical relationship. Secondary signs such as prevertebral soft tissue swelling can be misleading, as these patients usually have endotracheal or nasogastric tubes in place. Evaluation of CCD by CT and radiographs relies on widening at the C0-C1 and C1-2 joints using osseous landmarks. While joint-space widening also may be visualized by MRI, the ability to directly evaluate the integrity of the craniocervical junction ligaments, including the apical, alar, and transverse ligaments; the tectorial membrane; the ligamentum flavum; and the facet joint capsules, may enable more complete assessment of the nature of the injury, as well as allow diagnosis of less severe forms of CCD. In addition, MRI can evaluate for additional acute spinal soft tissue injuries, including epidural hematoma and injury of the spinal cord.

#### SUMMARY/CONCLUSION

Craniocervical dissociation is a potentially devastating traumatic injury that has in the past been almost uniformly lethal. With increasing access to rapid medical care and advances in medical technology, patients are surviving the initial injury and presenting for further evaluation and care. Radiographic and CT diagnostic criteria of CCD rely mainly on osseous widening. MR imaging allows direct evaluation of the craniocervical ligaments, and may enable more complete assessment of the injury and enable diagnosis of less severe forms of CCD. Radiologists play a key role

in diagnosis of this entity, and knowledge of the various imaging findings is important in early diagnosis and improving patient outcomes.

**KEY WORDS:** Craniocervical dissociation, Spine trauma, Spine ligamentous injury

---

**eEdE-154****2012 Case of the Week**

Fatterpekar, G. M.

Mt Sinai Medical Center  
New York, NY

### Index of Program Participants

Numbers refer to session and presentation numbers, *not to page numbers*.

Index Key: O = Scientific Paper (Oral Presentation); EE = (Electronic) Excerpta Extraordinaire;

P = Scientific Poster (Print Format); eP = Electronic Scientific Poster (ePoster);

EdE = Education Exhibit (Print Format); eEdE = Electronic Education Exhibit

<b>A</b>			
Aagaard-Kienitz, B.	eP-214, eP-225, eP-236	Ahn, K-J.	eP-122, eP-161, eP-98
Abanou, A.	O-60	Ahn, Sung Soo S.	EdE-89, eP-49, P-70, P-72
Abbott, E	eP-280	Ai, T.	eEdE-33, O-117
Abdel Mottalib, A.	eP-33, O-242	Aiken, A.	eEdE-75
Abdel Razek A.	eEdE-83	Aisen, P.	O-125
Abdullah, A.	EE-62, eEdE-1, eEdE-6, EdE-45, eP-172, eP-180	Aisen, P. S.	eP-67, O-500
Abe, K.	P-41, P-36	Aiyagari, V.	eP-60
Abe, T.	P-36	Aizenberg, M. R	EdE-20
Abramovitch R.	P-55	Aizenstein O.	P-55
Abruzzo, T. A.	eP-202	Akaike, G.	eP-303
Aceves, M.	P-93	Akashi, T.	eP-28, eP-35, eP-48, eP-117
Achten, E	eEdE-32	Akdede, B. B.	P-60
Acou, M. A. E.	eEdE-32	Akdol, M. S	eP-253, P-87
Acu, B.	O-73, O-394	Akgün, B.	P-60
Ada, E.	P-60	Akin, E. A.	eP-179
Adachi, Y.	P-11	Akin, S.	eP-44
Adamek, E	O-416	Akpınar, B.	EE-101
Adams, A.	eP-46	Akpınar, H. S.	O-433
Adams, M.	eP-88	Aksoy, M.	eP-164
Adams, R.	O-30	Aktas, A.	eEdE-82
Adappa, N. D.	eP-191	Akvardar, Y.	P-60
Adas, R.	eEdE-42	Al Azri, F.	eP-172
Adas, R. A. A.	eP-149, O-153	Al Bader, F.	eEdE-14, eEdE-37
Adisetiyo, V.	O-52	Alıcıoğlu, B.	O-433
Aesse, F.	P-76	Alahmadi, K. O A	eP-114
Agarwal, A.	EdE-23, EdE-60, EE-5, EE-57, EE-58, EE-89, EE-102, eEdE-81, eP-127, eP-258, O-063a, O-298	Al-Ali, F.	O-486
Agarwal, R.	eP-179, P-82, P-83	Albayram, S.	EE-15, EE-77
Agarwal, V.	O-195, O-410	Albers, G. W.	eP-115, O-20
Aghaebrahim A.	eP-4, P-2	Albes, G.	O-533, O-583
Agid, R.	EE-66	Albino, Sr. P.	EE-16
Agildere, M.	EE-92, EE-101, O-409	Albuquerque, F. C.	eP-257
Agosta, F.	O-472	Alderliesten, T.	O-174
Agostinis, C.	P-34, P-85	Aldrich, F.	eEdE-102
Aguilar Perez, M.	O-317, O-518, O-572	Alexander, A.	O-566
Aguilera, A.	O-227	Alexander, M.	O-557
Aguilera, A. L.	P-44	Alexander, M. J.	O-22, O-561
Agut, T.	eEdE-123	Alexandrou, M.	O-569
Ahlhelm, F. J.	eP-105, eP-107	Alexopoulou, E	eEdE-142
Ahmad, I.	P-81	Alfayate, E	eP-71
Ahmed, A.	eP-121, eP-257	Ali, S.	O-48
Ahmed, A. T.	P-1	Aliaga, R.	eP-23, eP-278
Ahmed, M.	EdE-64, eEdE-128, O-326	Al-Ibraheemi, A. K.	P-79
Ahmed, M. E.	O-062	Al-Jabri, S.	eP-172
Ahmed, S.	eP-142, eP-184, O-328	Alkan, O.	eP-44, eP-273, eP-279
Ahmed, T. F.	eP-11	Al-Khalili, R.	eP-87
Ahn, J. S.	eP-219	Alleman, A.	EdE-61, P-124
		Allmendinger, A.	eEdE-116
		Allmendinger, A. M	eEdE-118
		Alluwaimi, F.	eP-326, P-122, P-123
		Almast, J.	EdE-1, EdE-51
		Almekhlafi, M. A.	eP-224, eP-264, O-571
		Almekhlafi, M.	P-74
		Al-Mukhtar, A.	O-135
		Al-Riyami, A.	eP-172
		Al-Senaidi, K.	eP-172
		Altankus, A.	O-394
		Altinkaya, N.	eP-273, eP-44
		Altinok, D.	O-298
		Altintas, A.	EE-15
		Altmeyer, W.	eP-37
		Altschul, D.	eP-126
		Alvarado, B.	O-399
		Alvarez, H.	EdE-68, EdE-73
		Álvarez-Linera, J.	eP-71
		Álvarez-Linera, J. Mato	O-123
		Alves Leon, S.	eEdE-150, eEdE-11
		Al-Waily, A.	eP-172
		Al-Zuhibi, S.	eP-172
		Amans, M. R	eP-55
		Ambrosanio, G.	eP-318
		Ambrosi, A.	O-250
		Amezcu, L.	O-509
		Amin, S. K.	EdE-53
		Aminah, B.	eEdE-29
		Amin-Hanjani S.	O-566
		Amole, A. O.	eP-253
		Amole, A.	P-87
		Amoura, Z.	EdE-16
		Amundson, P.	P-103
		An, H.	eP-121, eP-243
		An, J.	EdE-32
		Anantaram, G.	eP-24
		Anaya, C.	eEdE-138
		Anderson, J. S	O-612
		Anderson, R. E.	EE-65,
			eP-216, O-421, O-422
		Ando, K.	EE-82, O-103, P-42
		Andoh, H.	EdE-57
		Andoh, H. M	O-444
		Andrade, C. S	O-226, O-229
		Andre, J.	O-208
		Andrews, S.	P-66
		Andrews, T.	eP-291, O-596
		Angermaier, A.	O-634
		Anghel, T.	eP-45
		Anik, Y.	eP-131, eP-133, O-603
		Ansari, S. A.	EE-63, EE-70,
			EE-93, eP-104, eP-129, eP-148, O-111, O-237, O-520, O-522, O-560, O-576
		Ansari Gilani, K.	EE-84
		Antar, O.	O-243
		Antoun, N. M	O-26
		Anumula, N.	O-31

### Index of Program Participants

Numbers refer to session and presentation numbers, *not to page numbers*.

Index Key: O = Scientific Paper (Oral Presentation); EE = (Electronic) Excerpta Extraordinaire;

P = Scientific Poster (Print Format); eP = Electronic Scientific Poster (ePoster);

EdE = Education Exhibit (Print Format); eEdE = Electronic Education Exhibit

Anumula, N. S.	eP-160, eP-61	Babiarz, L. S.	eP-299, O-438	Baser, S. C.	EdE-30, eEdE-115
Anzai, Y.	eP-298	Babic, D.	O-310	Bashir, M.	O-113
Anzalone, N.	eP-77, O-442	Badie, B.	eP-22	Bashir, U.	eP-170
Aoki, S.	EdE-9, eP-21, P-14	Badoud, S.	eP-132	Bastianello, S.	eP-77
Aoyama, H.	eP-19	Baek, H. J.	O-293	Batchelor, T.	O-101
Aquino, C.	EdE-10, eEdE-30	Baek, J. H.	O-329	Batchelor, T. T.	O-211, O-5, O-640
Arab, A. F.	O-62	Bagepally, B. Shankara	O-503	Batjer, H.	EE-70, eP-129, O-520
Arabi, M.	EE-55	Bagher-Ebadian, H.	eEdE-20	Batjer, H. H.	EE-63, eP-104
Arani, K. N.	EdE-11, EdE-97,	Bahl, M.	EdE-79, eP-231	Battisti-Charbonney, A.	O-564
Arani, K. A.	EE-103	Bähr, M.	eP-270	Batty, R.	P-64
Arbab, A.	eEdE-20	Bai, D. H.	P-74	Bauer, J.	O-570
Arbelaez, A.	O-189	Baird, S. H.	P-124	Bauer, Z.	O-591
Archer-Arroyo, K.	O-164	Baker, J. N.	O-549	Baugnon, K.	O-321
Argentos, S.	eP-265	Bal, S.	EdE-35, eP-224	Baugnon, K. L.	EdE-55
Arita, N.	EE-82, O-103	Balériaux, D.	O-218	Bäumer, P.	eP-86, eP-95
Armario, D.	eEdE-110	Balkman, J.	O-444	Baxi, N.	eP-126
Armstrong, G. T.	EE-59	Ballon, D. J.	eP-199	Bäzner, H.	O-317, O-533, O-572,
Arneja, A. K.	eP-59	Baltzer, P. A. T.	O-67		O-583
Aronin, N.	eP-227	Bammer, R.	eP-115, eP-116,	Bäzner, H. J.	O-518
Arquizan, C.	O-575		eP-164, O-20, O-37, O-79,	Beards, S.	O-228
Arrighi, H. M.	O-501		O-179, O-208, O-307	Beauchamp, N.	O-637
Arsava, E M.	O-562	Bangiyev, L.	eEdE-062	Beckmann, C.	O-537
Arsilan, H.	O-148	Baptista, T.	eP-242	Beckwith, T.	O-506, O-507
Arslankoz, S.	eP-27	Bapuraj, J. R.	O-131	Behpour, A. M.	O-176
Artzi, M.	P-55	Bapuraj, R.	EE-62	Beitler, J. J.	EdE-55
Arya, R.	eP-52	Barajas, R. F.	O-100	Belden, C.	EdE-50
Arya, S.	eEdE-78	Barajas, Jr. R. F.	O-292	Belden, C. J.	EdE-57, EdE-79,
Asahi, K.	EdE-9	Barakat, N.	O-180, O-181		O-444
Asdaghi, N.	O-27, O-29	Baranton, K.	O-609	Bello, J.	EdE-67, eEdE-50
Ashoori, I.	O-608	Barbe, C.	eP-218	Bello, J. A.	EdE-74, eP-63, O-299,
Asik, M.	EE-15, EE-77	Barbisan, F.	P-102		O-449
Aslan, A.	EE-67	Barbosa, Jr. A. A.	eEdE-122,	Belzberg, A.	eP-322
Aslan, H.	EE-92		eEdE-125	Ben Bashat, D.	P-55, P-104,
Aslan Dundar, T.	O-431	Barest, G.	eEdE-43		eEdE-101
Asselin, M-C.	eP-81	Bargallo, N.	O-535	Benayoun, M.	eP-54, O-397
Atamer, A.	O-610	Barker, P. B.	O-332, O-462, O-78	Ben-Bashat, D.	P-110
Atkinson, I. C.	O-566	Barkhof, F.	O-469, O-501, O-510	Bender, F.	O-416
Aubry, S.	O-50, O-590	Barkovich, A. J.	EdE-85, O-9,	Benders, M.	O-174
Auger, C.	eP-70, O-128, O-510		O-137, O-259, O-263	Bendfeldt, K.	eP-130
Aulino, J.	EE-23	Barkovich, J. A.	P-109	Bendok, B. R.	EE-63, EE-70,
Aurora, T.	P-39	Barnaure, I.	O-492		eP-104, eP-129, O-520, O-576
Avins, A. L.	O-591	Barnaure-Nachbar, I.	eP-132	Bendszus, M.	eP-86, eP-95
Aviv, R. I.	eP-114, O-25, O-61	Barnes, P.	O-179	Benedict, A.	O-442
Aw, J.	eP-124, O-44	Barnes, P. D.	O-256, O-257, O-45,	Benndorf, G.	P-90, P-120
Awai, K.	eP-68		O-551	Bennett, M.	O-224
Ay, H.	O-562	Baron, J-C.	O-28	Bennink, E.	O-398, O-636
Aygun, N.	eEdE-93, O-324	Barr, D.	O-611	Ben-Sira, L.	P-104, -110
Aykol, S.	eP-38	Barr, R. M.	O-201	Bent, R. S.	O-550
Aylward, S.	eP-156	Barraza, L.	O-22, O-561	Benzinger, T.	eP-153
Azzam, R. I.	eP-101	Bartleson, J. D.	O-145	Benzinger, T. L S.	O-120
		Bartolini, B.	O-310	Berenstein, A.	eP-232, eP-263,
		Bartolini, B. M.	O-517		O-355
		Bartuli, A.	EE-78	Berenstein, Sr. A.	O-311
		Bartynski, W. S.	O-445, O-523	Berg, A. D.	eEdE-95
		Baruah, D.	eEdE-57, P-71	Berger, I.	P-110
<b>B</b>					
Babb, J.	eP-113, O-127				
Babb, J. S.	O-34				
Babcock, E.	O-262				

### Index of Program Participants

Numbers refer to session and presentation numbers, *not to page numbers*.

Index Key: O = Scientific Paper (Oral Presentation); EE = (Electronic) Excerpta Extraordinaire;

P = Scientific Poster (Print Format); eP = Electronic Scientific Poster (ePoster);

EdE = Education Exhibit (Print Format); eEdE = Electronic Education Exhibit

Berger, R.	O-49	Blanc, R.	eP-220, O-517	Bowden, D. W.	O-40
Bergès, O.	O-249	Blanc, R. P B	O-310	Bowerson, M.	P-59
Bergholte, J.	eP-297	Blanch, R.	eEdE-31	Bowes, J.	O-399
Bergman, R.	eP-136	Blasco, G.	eEdE-2, eEdE-24, eP-64, O-563, O-593	Boxerman, J. L.	eP-158, eP-75, eP-82
Bergmann, K.	eEdE-24	Blasco, J.	O-511, O-568	Boyko, O.	EE-72, eP-137, eP-288, eP-292
Berkefeld, J.	O-514	Blaser, S. I.	EE-81, O-134, O-138, O-154	Boylan, E. E.	O-44
Berkhemer O.	eP-252	Blaszkiwicz, L.	eP-317	Bozkurt, P.	O-603
Berkhemer O. A.	O-584	Blauwblomme, T.	eP-285	Bozzao, A.	eP-102, eP-230, O-287
Bernard, G.	eP-272	Blazun, J. M.	EE-36	Bracco, S.	eEdE-104, eP-200
Bernardi, B.	EE-78, EE-80	Bleicher, MD A. G.	O-194	Bradley, M.	EdE-27, EdE-7, eP-124, P-100
Bernhardt, A.	eP-222	Bleise, C.	eP-221, O-413, O-415	Braham Chaouch, R.	EE-29
Bert, R. J.	O-33	Blennow, K.	O-500	Brahler, T.	eP-52
Bert, R.	O-393	Block, J. E.	eP-310	Branch, C. A.	O-55, O-618, P-65
Bertini, E. Silvio	EE-80	Bluml, S.	eP-284, O-254, O-255, O-553, O-608	Branera, J.	O-568
Bertrand, A.	eP-162, O-249	Boada, I.	O-563	Brans, B.	eP-181
Besachio, D. A.	O-236	Bobinski, M.	eEdE-062	Branson, H.	O-138
Betensky, R.	O-638	Bobra, S. J.	eP-166	Branson, H. M.	EE-81
Bettelheim, D.	O-429	Boddaert, N.	eP-285	Branstetter, IV B. F.	O-346
Betz, R.	O-181	Boeckh-Behrens, T.	O-570	Brant-Zawadzki, M.	O-557
Beumer, D.	eP-252	Boes, J.	eP-146	Brashear, H. Robert	O-501
Beydoun, A.	O-540	Boiten, J.	eP-252, O-584	Braun, C.	eP-96
Bezerra, R.	O-562	Bolacchi, F.	eP-173	Braz, A.	EE-44
Bhadelia, R.	eP-183	Boltshauser, E.	O-142	Bredow, S.	O-406, O-601, O-602
Bhadelia, R. A.	O-374, O-594	Bonafé, A.	eEdE-96, eP-169, eP-213, O-575, O-581	Brennan, N.	O-219, O-221, P-21
Bhan, V.	eP-135	Bonaldi, G.	eEdE-140, eEdE-141	Bresnahan, B. W.	O-591
Bhanusali, N.	P-90	Bonaldi, G.	P-34, P-85	Bresson, D.	O-309
Bhatia, A.	eEdE-54	Bonamini, M.	eP-102	Brewer, J.	O-125
Bhatia, R.	EE-98	Bonekamp, D.	eEdE-74	Brewer, J. B.	eP-67, O-500
Bhatia, V.	eEdE-54	Bonfante, E.	eEdE-109	Brian, S.	O-411
Bhattacharjee, M.	eEdE-8	Bonfiglio, S.	eP-295	Bricker, A. A. O.	eEdE-128
Bianchi, S.	O-250	Bonilha, L.	O-30	Brisigotti, M.	P-102
Bickin, H.	eP-131, eP-133	Boogaarts, J.	eP-223, O-484	Brisson, M.	eP-88
Bidari, S. S.	P-84	Boop, F.	O-400	Britton, J. W.	eP-13
Biega, T.	EdE-52	Boop, F. A.	O-46	Brizel, D. D.	O-327
Biessels, G. J.	O-579, O-635	Boosararuxapong, K.	P-48	Broadwater, G.	O-327
Bigger, J.	O-440	Booth, T.	eEdE-113	Brodle, J.	O-611
Bigler, E. D.	O-617	Booth, T. N.	O-3	Brodoefel, H.	O-390
Bilello, M.	O-567	Borges, M. T.	O-33	Brody, J.	eP-17
Bilir, E.	eP-14	Borges, R.	eEdE-10	Broniscer, A.	EE-91, O-549
Billon-Grand, C.	O-521, O-541	Bornemann, R.	eP-314, eP-315, O-531	Brook, A.	EdE-67, eP-126, O-527, O-528
Billsky, M.	O-490, O-546, O-597	Boronat, S.	O-139	Brook, A. L.	eP-63, O-623
Bilsky, M. H.	eP-226, eP-240, O-545	Bose, A.	O-22, O-556, O-557, O-561	Brountzos, E.	eEdE-142, eP-265 eP-320
Bink, A.	O-514	Bot, J.	eP-252, O-584	Browaey, P.	O-240
Biondi, A.	O-50, O-483, O-521, O-541	Bou Ayache, J.	O-540	Brown, A. D.	EE-52
Biousse, V.	O-238	Bou-Assaly, W.	eEdE-45	Brown, K.	O-440
Birchall, D.	P-117	Boulanger, T.	O-581	Brown, P.	eP-271
Birchansky, S. B.	EE-94	Bouloux, G.	eEdE-75	Bruce, B. B.	O-238
Bisdas, S.	eP-85, eP-96, eP-167	Bourekas, E. C.	EdE-92, EE-20, EE-25, EE-37, eEdE-55	Brückmann, H.	O-600
Biswal, B. B.	P-4				
Bitter, T.	O-67				
Black, D. F.	eP-120, O-145				
Blackham, K. A.	EdE-72, EE-84				
Blair, P. S.	EE-71				

### Index of Program Participants

Numbers refer to session and presentation numbers, *not to page numbers*.

Index Key: O = Scientific Paper (Oral Presentation); EE = (Electronic) Excerpta Extraordinaire;

P = Scientific Poster (Print Format); eP = Electronic Scientific Poster (ePoster);

EdE = Education Exhibit (Print Format); eEdE = Electronic Education Exhibit

Brugger, P. C.	eP-293, O-252, O-261, O-429	Campeau, N.	EE-35	Cerase, A.	eEdE-104, eP-200
Brum, J. M.	eP-286	Campeau, N. G.	eEdE-133, eEdE-135, eP-120	Ceratto, R.	eP-221, O-413, O-415
Brun, C. C.	eP-103	Campen, C. J.	O-551	Cervantes, A.	P-3
Brunelle, F.	eP-285, O-197	Campodonico, D.	O-568	Cesaretti, K.	eEdE-104
Bruno, C. H.	eEdE-52	Campos, S.	eP-23 eP-278	Ceschin, R.	O-254, O-255
Bruyere, J.	O-98	Candy, S. E.	O-408	Cha, J.	O-323
Bryan, N.	O-567	Cannatà, V.	EE-78, EE-80	Cha, S.	eP-233, O-100, O-277, O-292
Bryan, R. N.	O-354	Cano, P.	O-139	Cha, S-H.	eP-128
Bryson, T.	eEdE-45	Capela, C.	EE-44	Chai, B.	O-395
Bryson, T. C.	eEdE-90	Capizzano, A.	eEdE-36, eEdE-149	Chai, J. W.	P-18, P-57
Buckle, C.	eEdE-23, O-147	Capraz, G.	eP-14	Chakrabarti, S.	eP-124
Buerki, S.	EdE-82	Carbone, J.	P-103	Chakraborty, A. K.	EE-51
Buetow, K. H.	O-102	Carducci, F.	eP-102	Chakraborty, S.	eP-149, O-153
Buglione di Monale, M.	O-286	Carelsen, B.	eP-209	Chalak, L.	O-175
Bulakbaşı, N.	O-433	Carling, T.	O-424	Chalian, M.	EdE-91, eEdE-76, EE-50, eP-308, O-75
Bulas, D.	O-256	Carmignani, M.	eEdE-122 eEdE-125	Chaljub, G.	EE-68
Bulic, S.	P-9			Challa, H.	EE-86, EE-95 eEdE-107
Bulters, D. O.	O-231	Carniato, S. L.	eP-217	Chamorro, A.	O-568
Burke, W.	eEdE-54	Carpenter, J. S.	eP-250, eP-271	Chan, C. M.	O-485
Burkhard, P.	eP-132	Carpenter-Bailey, K.	O-404	Chan, H.	EE-40
Burmeister, H. P.	O-67	Carr, C. M.	O-505	Chan, M. D.	O-224
Burns, J.	eEdE-50, eP-63	Carr, J.	O-520	Chan, S.	O-299
Burns, P. A.	EE-38, EE-83, eP-248, eP-249, P-91	Carreno, M.	O-535	Chan, W. P.	eP-123
Burrowes, D.	eEdE-112, O-44	Carriero, A.	EE-99	Chan, W.	eP-255
Busselberg, P. D.	O-643	Carroll, T.	O-111	Chandra, T.	EdE-14, EdE-39 EdE-70, eEdE-114, eEdE-115, eEdE-124, eEdE-129, eEdE-134, eEdE-136, eEdE-61
Butcher, K. S.	O-27, O-29	Carroll, T. J.	eP-104, eP-129, eP-148, O-237, O-520, O-560	Chang, C-D.	P-33, P-38
Butler, J.	O-594	Caruso, P.	eEdE-8, O-258	Chang, C-I.	P-57
Butler, P.	eP-198	Caruso, P. A.	EdE-54, O-302	Chang, C-Y.	eP-143
Butman, J. A.	O-295, O-319	Carvalho, D. Rocha	eP-286	Chang, F-C.	eP-143, eP-254
Byas-Smith, M.	eP-307	Caseiro, A. R.	eP-32	Chang, G.	O-408
Byington, K. E.	eP-144	Casey, B. J.	P-31	Chang, H. W.	EE-19, O-72
Byott, S.	EdE-81	Casey, K. L.	EE-68	Chang, J. P.	EE-9
Byrne, J. V.	O-582	Cassafieres, S.	eEdE-96	Chang, K-H.	P-80
Byrns, K.	eEdE-63, eP-59	Castanho, P.	EE-22, EE-56	Chankowsky, J.	EdE-17
		Castanho, P. R.	EE-60	Chapman, M. N.	eEdE-92
<b>C</b>		Castellanos, M.	eP-64, -563	Chapuy, S.	O-50
Cable, B.	EdE-52	Castillo, M.	EdE-34, EdE-63, EdE-68, EdE-73, EE-18, EE-42, eP-34, eP-139, O-294, O-434, P-28	Chareewit, S.	P-5
Cabral, F.	eEdE-11			Chatterjee, F.	EdE-3
Caçador, N.	EE-44	Castro, L. H. M.	O-229	Chaturvedi, A.	EdE-75, EdE-75
Caci, D.	EdE-31	Catana, C.	O-640	Chaturvedi, N.	O-637
Cadavid, D.	P-32	Cattin, F.	O-50, O-483, O-521, O-541	Chaudhary, N.	eEdE-1, eP-251
Cadel, G.	O-590			Chaudhary, S.	eP-204
Cahill, D. P.	eP-142	Caverzasi, E.	EdE-6	Chaudhry, Z.	eP-65
Cai, P.	eP-8	Cavusoglu, I. G.	eP-15	Chaudhry, Z. A.	O-22, O-556, O-561, O-577
Cain, J. R.	EE-29, EE-106, eEdE-70, O-228, R P-69	Cebeci, H.	eP-26	Chauvet, D.	O-310
Cairns, B.	O-399	Cecil, K. M.	O-304, O-506, O-507	Chawalparit, O.	eP-7, P-5, P-15, P-48
Cakir, O.	eP-133	Cekirge, S.	EE-67	Chawda, S.	eP-53
Calabria, L. F.	O-287	Çelikyay, F.	O-394		
Camargo Faye, E.	P-3	Cen, Y.	eP-137, eP-140, P-44		
Cambron, S. C.	O-526	Centonze, D.	O-508		
Cammarata, G.	O-250				
Campbell, R.	O-31				



### Index of Program Participants

Numbers refer to session and presentation numbers, *not to page numbers*.

Index Key: O = Scientific Paper (Oral Presentation); EE = (Electronic) Excerpta Extraordinaire;

P = Scientific Poster (Print Format); eP = Electronic Scientific Poster (ePoster);

EdE = Education Exhibit (Print Format); eEdE = Electronic Education Exhibit

Cheecharoen, P.	eEdE-3	Cho, Y. D.	eP-193, O-513	Clark, D.	EE-47
Chen, B. T.	eP-137, P-22	Choi, B. S.	eP-50	Clark, J. F.	O-304
Chen, C.-C.	P-56	Choi, C. G.	O-605	Clark, M. R. J.	O-150, O-225
Chen, C. C. C.	P-18, P-57	Choi, C-W.	O-126	Clarke, A.	O-412
Chen, C. J.	EdE-40	Choi, H. S.	eP-122, eP-161, eP-98	Clarke, D.	O-300
Chen, C-W.	eEdE-4	Choi, J. W.	eEdE-49, O-323	Clemm, C.	P-30
Chen, D. C.	EdE-40	Choi, S.	eP-284, O-608	Clifford, R.	O-289
Chen, D.	eEdE-65	Choi, S. H.	EdE-56, P-80	Cloft, H.	O-144
Chen, H-L.	P-17, P-27, P-33, P-38, P-56	Choi, S. S.	P-95	Cloran, F. J.	P-54
Chen, H-M.	P-57	Choi, W. S.	eP-211	Cloughesy, T. F.	O-290, O-291, O-97
Chen, J.	O-405	Chonde, D. B.	O-640	Coban, G.	EE-92
Chen, J.	EdE-36	Chong, B.	O-557	Cohen, B. A.	O-100
Chen, J. X	eP-238, eP-322, O-308	Choong, C. C.	eEdE-47	Cohen, H. L.	eEdE-73
Chen, J. Y	EE-32	Chou, D.	O-547	Colafati, G. Stefania	EE-80
Chen, K.	eP-8	Chou, J.	O-258	Colantoni, III W.	O-33
Chen, L.	P-7, P-26	Chou, K-H.	P-27, P-38, P-56	Colen, R.	P-39
Chen, M-H.	P-17, P-27, P-33	Choudhary, A. K.	EE-89, eP-282	Colen, R. R.	eEdE-16, eEdE-18, eEdE-21, eP-79, eP-94, eP-141, O-98, O-99, O-289
Chen, P-C.	P-27, P-38	Choudhri, A. F.	eEdE-3, O-46	Coley, S.	O-412
Chen, R.	O-57	Chow, D. S	O-212, -214	Collins, J.	eEdE-23, eEdE-112
Chen, S-Y.	P-57	Chow, M.	O-420	Colombo, B.	EE-2
Chen, T. C.	eP-137	Chowdhry, Y.	EdE-31	Colonne, C.	eP-212
Chen, W.	eP-143, eP-145, eP-147	Christen, T.	O-37	Colosimo, C.	eP-77
Chen, Y-C.	eEdE-4	Christian, S.	eP-137, P-44	Combs, J. T	P-63
Chen, Y-F.	P-96	Christoforidis, G.	EE-64, EE-66, eP-54, O-397, O-522	Combs, S. E.	O-442
Chen, Z.	O-177	Chu, S.	O-597	Commins, D. L	eP-137
Chenevert, T.	O-131	Chu, W-F.	eP-254	Comparelli, A.	eP-102
Chenevert, T. L.	eP-146	Chua, B. C.	eEdE-29	Comstock, B. A.	O-591
Cheng, H.	O-256	Chuang, M-T.	eEdE-4	Comunale, J.	eP-61, eP-160, O-118, O-565
Cheng, J. F.	eP-174	Chudyk, J.	eP-221, -413, O-415	Comunale, J. P.	P-6
heng, K. M	O-485	Chueh, J.	eP-217	Conklin, C.	O-607
Cheung, Y. Y	O-444	Chui, H.	O-227	Connolly, D.	P-64
Cheung, Y. L	O-485	Chun, J-E.	P-80	Connolly, D. J. A.	eEdE-111
Chhabra, A.	EdE-91	Chun, R. H.	eEdE-129	Consigny, D.	eP-236
Chhabra, A.	EE-50, eEdE-105, eEdE-147, eEdE-76, eP-308, O-75	Chundru, R.	eP-76	Consoli, A.	EdE-69
Chi, T. L.	P-79	Chung, G-H.	eP-205	Constantini, S.	P-104
Chiang, C. M.	P-18	Chung, H. W	eP-123	Conway, A. E.	O-549
Chihara, C.	eP-39	Chung, W-J.	eP-99	Cook, Sr. M.	O-536
Chin, B. M	eP-155, O-151, O-182	Chwang, W. B.	EE-54, eEdE-20	Cook, T.	eEdE-30, O-371
Chin, C. T.	eP-316, O-411, O-547	Ciacchi, J. D.	EE-32	Cooper, S.	O-56, O-57
Chin, E M	O-46	Cianfoni, A.	eEdE-140, eEdE-141	Copen, W. A.	O-562
Chin, M. S.	EdE-34	Ciccarone, A.	eEdE-119	Cormier, E	eP-311
Chinnadurai, P.	eP-207	Ciceri, F.	eP-295	Cornelius, R.	eEdE-99
Chintalapani, G.	eP-207	Cicuendez, M.	eP-47	Cornwell, B.	P-124
Chiras, J.	EdE-16, eP-212, eP-311	Cila, A.	EdE-5, eEdE-82, eP-182, O-432	Corral, J. F.	eP-70, O-128
Chitayat, D.	O-134	Cini, Sr. F.	EE-16	Correa, D. G.	eEdE-35, eEdE-53
Chiu, A.	EdE-066a	Cintra, M. B.	eP-275	Corrigan, J.	eEdE-81
Chiu, F-Y.	eP-143	Cioni, S.	eEdE-104, eP-200	Cortes, M. D. P.	eP-269
Cho, A.	O-613	Citterio, A.	eP-77	Cossu, G.	eP-295
Cho, A. A.	EdE-46	Civelli, V.	O-515	Costalat, V.	eP-213, O-519, O-575
		Claassen, J.	P-16		
		Clarençon, F.	EdE-16, eP-212, eP-311, O-309, O-483, O-521		

### Index of Program Participants

Numbers refer to session and presentation numbers, *not to page numbers*.

Index Key: O = Scientific Paper (Oral Presentation); EE = (Electronic) Excerpta Extraordinaire;

P = Scientific Poster (Print Format); eP = Electronic Scientific Poster (ePoster);

EdE = Education Exhibit (Print Format); eEdE = Electronic Education Exhibit

Couldwell, W. T.	O-151	Daram, S. P	eP-184	Delgado Almandoz, J. E.	EE-65,
Coulter, J. I.	O-27, O-29	Darkhabani, Z.	P-71		P-216, O-421, O-422
Coulter, W.	eP-282	Das, A.	O-256, O-257	Delman, B.	O-42, O-592
Coutts, S. B.	O-27, O-29, O-558	Das, S.	O-327	Delman, B. N	O-407
Crandall, B.	O-557	Das, T.	O-231, O-26	Demchuk, A.	EdE-35, eP-224,
Crandall, B. M.	EE-65, eP-216,	Date, S.	eP-68		eP-264, O-556, O-571
	O-21, O-422	Datir, A.	EdE-90	Demchuk, A. M	O-235, O-27,
Craven, I. J.	eEdE-111, O-105,	Datta, V.	EdE-51		O-29, O-558
	O-150, O-225	Daunis-i-Estadella, J.	eEdE-2,	Demir, S.	eP-273, eP-279, eP-44
Crawley, A. P	O-564		eEdE-24, eP-64, O-	Demirci, A.	eP-131, eP-133,
Creasy, J. L	O-130	Davatzikos, C.	O-567		O-603
Cross, III D. T	O-456	David, C.	EE-64	Deml, M.	O-531
Croul, S.	EE-66	Davidson, H. C.	eP-187	den Hollander, J.	O-217
Crowley, T.	O-146	Davies, P.	O-54	Derakhshan, J. J.	O-251
Cruz, J. P.	O-420	Davila, J.	eEdE-42, eEdE-123	Derakhshani, S.	eP-53, eP-198
Cruz, Jr. L. C. H.	eEdE-19,	Davila-Acosta, J.	eEdE-131	Derdeyn, C.	eP-60
	eEdE-53	Davila-Acosta, J. H.	eEdE-132	Derdeyn, C. P	eP-243, O-614
Cruz, L. C. H.	O-599	Davis, A.	EE-7, O-441	Derman, A. Y	EE-39
Crystal, R. G.	eP-199	Davis, B.	eP-225, O-587, O-589	Desai, H.	EdE-58, O-102, O-289
Cunnane, M. B	eEdE-68,	Davis, D. J.	eEdE-148	Desai, M. P	EE-37, eEdE-55
	eEdE-69	Davis, M. A.	eP-34	Desai, N.	O-177
Cunnane, M. E.	eEdE-91, O-184	Davis, P.	eP-60	Desikan, R. S	eP-67, O-125,
Cupino, A.	O-604	De Araujo, D. B.	P-23		O-500, O-502
Curnes, J. T	EdE-88	De Jesus, R.	P-84	deSouza, C. G.	eEdE-53
Curran, J. G.	EdE-76, EE-88,	de Jong, H.	eP-151	Desxhamps, R.	eEdE-72
	EE-90, EE-96, O-552	de Jong, H. W A	O-398, -636	Detterich, J. A.	O-255
Currie, S.	eEdE-111, O-105,	De Keyzer, F.	O-209	Deuerling-Zheng, Y.	eP-230,
	O-150, O-225	de Macedo Rodrigues, K.	O-260		eP-239, eP-261, 582
Curtin, H.	eEdE-86	De Mey, J.	EdE-22	Devlin, T. G.	O-22, O-561
Curtin, H. D.	EdE-54	De Smet, K.	EdE-22	Devuyst, F.	O-218
Curtis, S. L	eP-124	de Souza, C. G.	eEdE-35	Dewachter, P.	EdE-22
Cusi, V.	eEdE-123	de Venecia, C. A.	eP-312	DeWitte, O.	O-218
Cutalo, M. J.	O-427	De Vis, J. B.	O-174	Deyo, R. A.	O-591
Cuvinciuc, V.	O-492	de Vries, J.	eP-223, O-484, O-580	Dholakia, R.	eP-262
		de Vries, L. S	O-174	Diano, A. A.	eP-318
<b>D</b>		Deberry, J.	eP-271	Diaz, K.	P-9
D' Ambrosio, F.	O-246	Deblaere, K.	eEdE-32	Dickinson, J. R	EdE-43
da Cruz, Jr. L. C. H.	eEdE-35	Debnam, J. M	EE-24, P-50, P-52,	Diehn, F.	O-43
Daams, M.	O-501		P-53	Diehn, F. E.	O-241, O401, P-1
Dahlgren, R. M	O-559	Dehkharghani, S.	EE-27, eP-215,	Dietrich, K. N	O-506, O-507
Dai, D.	eP-256		eP-57	Dietzel, M.	O-67
Dairong, C.	eP-188	DeHoff, III G. W	P-63	Dikici, A. Suleyman	EE-15
Dake, M. D.	O-427	Del Carpio-O'Donovan, R.	eP-45	Dillon, W. P	eP-110, O-38,
Dale, A. M.	eP-67, O-192, O-500,	Del Castillo, S.	O-255		O-411, P-116
	O-502	Del Giudice, C.	eP-241	DiMarco, A.	O-607
Dale, B.	eP-138	Del Grande, F.	EdE-91, EE-50,	DiMaria, F.	eP-212
Dalwani, M.	O-146		eEdE-76, eP-308, O-75	Ding, X.	P-7, P-26
Daly, B.	O-39	del Pilar Cortes, M.	O-516	Ding, Y.	eP-256
Damasio, H.	eP-284	del Prado, G.	eP-93	Diniz, P. P R	eP-16
Danaie, S.	eP-298	Delaney, H.	O-118, O-565, P-6	Dion, J.	EdE-90, eP-215
Daniel, B.	O-285	Delapaz, R. L	O-212, P-16	DiPatri, A. J.	EE-93
Dankbaar, J. W	O-23, O-234,	Delfyett, W. T	O-410, O-436,	Dipetrillo, T.	eP-75, eP-82
	O-635		O-643	Dippel, D.	eP-252, O-584
Danz, S.	O-390	Delgado, E	eEdE-52	Ditta, L. C.	eEdE-73
Dar, S.	O-487	Delgado, I.	eEdE-110, O-139	Dittrich, E	eP-293

### Index of Program Participants

Numbers refer to session and presentation numbers, *not to page numbers*.

Index Key: O = Scientific Paper (Oral Presentation); EE = (Electronic) Excerpta Extraordinaire;

P = Scientific Poster (Print Format); eP = Electronic Scientific Poster (ePoster);

EdE = Education Exhibit (Print Format); eEdE = Electronic Education Exhibit

Divekar, S. A. eEdE-37, eEdE-14  
 Diwan, I. O-562  
 Djalilvand, A. O-25  
 Do, L. eP-222  
 Doan, H. EdE-98  
 Docampo, J. R. eEdE-52  
 Dodge, J. EE-11  
 Dodrill, L. K. EE-46  
 Doerfler, A. eP-230, eP-261,  
 O-416  
 Doerschner, K. eP-12, O-305  
 Dolatowski, K. eP-159  
 Dolgun, A. eP-182, O-432  
 Dombrowski, A. EE-62, eEdE-6  
 Domico, J. R. eP-250  
 Domingues, R. eEdE-10, eEdE-19  
 Don, S. O-543  
 Donaire, A. O-535  
 Doneda, C. O-133, O-140  
 Donmez, F. Y. O-409, EE-101,  
 EE -92  
 Donovan, W. D. O-450  
 Doring, T. eEdE-11  
 Dormond, D. EdE-16  
 Dorne, H. L. O-365  
 Dort, J. C. O-443  
 Doshi, P. M. eP-73  
 Dowd, C. F. eP-233, O-316, O-578  
 Downer, J. O-582  
 Downs, Sr. R. K. O-113  
 Dremmen, M. H. G. O-325  
 Dresner, M. A. eP-321  
 Drexler, S. eEdE-143  
 Dreyer, S. EE-84  
 Dreyfuss, P. O-466  
 Drier, A. EdE-16, eEdE-96  
 Drobnik-Kurzynska, P. eEdE-29  
 Druzgal, J. eP-134, O-585, O-612  
 du Mesnil de Rochemont, R. O-514  
 Dubow, J. eP-2  
 DuBray, M. B. O-612  
 Duckwiler, G. O-573  
 Dudau, C. EdE-3  
 Dulay, M. O-534  
 Dumeer, S. EE-45, EE-85  
 Dundamadappa, S. eP-41  
 Dunning, A. P-6  
 Dupre, S. eEdE-44  
 Dupuy-Bonafé, I. eP-169  
 Duy, L. A. N. eP-283  
 Duzgol, C. eP-131  
 Dzirasa, L. eP-276

**E**  
 Ealing, J. EE-106  
 Eastwood, J. D. eP-185  
 Echevarria, M. G. eEdE-126  
 Ecin, G. eP-38  
 Eckbo, R. P-30  
 Eckel, L. J. EE-35, O-241, O-401,  
 O-43, P-1  
 Eckert, B. O-149  
 Edasery, D. P-3  
 Edelstein, W. eP-237  
 Edwards, M. S B O-551  
 Eesa, M. EdE-35  
 Efendi, H. eP-131, eP-133  
 Egelhoff, J. C. EdE-76, EE-88,  
 EE-90, EE-96, O-552  
 Eggebrecht, H. O-392  
 Ehtiati, T. eP-237, O-511  
 Eichler, F. S. O-302  
 Eilaghi, A. O-25  
 Eisenman, D. EE-61  
 Ekholm, S. eP-100, eP-83, O-223  
 Ekins, J. B. eEdE-41  
 Ekorkmaz, U. O-394  
 Ekram, T. O-210  
 Elefteriades, J. E. eEdE-146  
 Elias, A. EdE-45, eEdE-1  
 Elias, A. E. eP-251  
 Elias, W. O-585  
 Elias, W. J. O-604  
 Elinazano, H. D. eP-75  
 Elinzano, H. D. eP-82  
 Elison, A. eP-1  
 Elkins, C. J. O-427  
 Ellika, S. K. eEdE-117, eEdE-120,  
 eEdE-121  
 Ellingson, B. M. eP-75, eP-82,  
 O-290, O-291, O-97  
 Ellis, T. L. O-224  
 Ellison, D. EE-91  
 Ellison, D. W. EE-33  
 Elman, L. B. eP-103  
 El-Nisr, M. O-243  
 El-Sharkawy, A-M. eP-237  
 Elsorogy, L. eEdE-83  
 Emblem, K. O-211  
 Engeler, S. O-514  
 Engelhorn, T. eP-230, eP-261  
 English, J. D. eP-233, O-316, O-578  
 Enokizono, M. P-67  
 Enterline, D. O-442  
 Enterline, D. S. eP-42  
 Ercan, K. O-148  
 Erdem, E. eP-253, P-87

Erdemli, H. E. EE-77  
 Erdfarb, A. EdE-67  
 Erer, B. EE-15  
 Erkorkmaz, U. O-73  
 Ernemann, U. eP-96, O-390  
 Erol, I. eP-273  
 Ertl-Wagner, B. B. O-320  
 Eryurt, B. eP-14  
 Escada, P. P-25  
 Escobar, W. eP-234, eP-235, O-315  
 Esenkaya, A. O-48  
 Eshetu, T. eP-62  
 Eskey, C. J. eP-231, O-351  
 Eskreis-Winkler, S. O-114  
 Esposito, M. eEdE-119  
 Essig, M. eEdE-20, eEdE-24  
 Essig, M. O-442  
 Ethiat, T. eP-238  
 Eubig, J. A. O-34  
 Evans, G. EE-29  
 Evans, L. eP-222  
 Ewing, J. eEdE-20

**F**  
 Faber, J. E. eP-156  
 Fabiano, S. O-508  
 Faghfoury, H. EE-8  
 Fakhro, S. A. O-211  
 Falini, A. EE-2, O-250  
 Fallatah, S. M. eP-88  
 Famini, P. eP-101  
 Fanou, E M. O-297  
 Fantozzi, L. M. eP-102, O-287  
 Farage, L. eP-286  
 Farb, R. EE-66  
 Fardanesh, M. O-32  
 Fardanesh, R. M. O-39  
 Farid, N. EE-17  
 Farinhas, J. EdE-67, eP-126  
 Farinhas, J. M. eP-63  
 Farkas, J. O-557  
 Farmer, D. O-132  
 Faro, S. O-181  
 Faro, S. H. O-180, O-607  
 Faruqui, Z. eP-170  
 Fasel, J. H. D. O-405  
 Fassbender, K. eP-247  
 Fatterpekar, G. EE-7, EE-39,  
 eEdE-19, eEdE-35, O-246  
 Fatterpekar, G. M. eEdE-154, O-599  
 Fazekas, F. O-510  
 Fease, J. L. EE-65, eP-216, O-421,  
 O-422  
 Federau, C. O-240  
 Feldmann, M. eP-81

### Index of Program Participants

Numbers refer to session and presentation numbers, *not to page numbers*.

Index Key: O = Scientific Paper (Oral Presentation); EE = (Electronic) Excerpta Extraordinaire;

P = Scientific Poster (Print Format); eP = Electronic Scientific Poster (ePoster);

EdE = Education Exhibit (Print Format); eEdE = Electronic Education Exhibit

Feliciano, Y. Z	eEdE-64, eEdE-97	Flatz, W. H.	O-320	Fukunaga, I.	EdE-9
Feng, W.	O-30	Fletcher, B. A.	eEdE-66	Fukunaga, I.	P-14
Ferguson, M.	EdE-75	Fletcher, G. P	O-489	Fukusumi, A.	eP-48
Fernandez Mora, R.	eEdE-52	Floris, R.	eP-173, O-508	Fullerton, H. J.	O-316
Ferrara, M.	O-286	Flower, E N	eP-192	Funari, M. B. G.	eEdE-122, eEdE-125
Ferrario, A.	eP-221, O-413, O-415	Flynn, P.	EE-71	Fung, S. H.	O-534
Ferre, J.	P-44	Flynn, P. A.	EE-38, EE-83, eP-248, eP-249, P-91	Furtner, J.	O-215
Ferré, J.-C.	eEdE-106, eP-140	Foerschler, A.	O-217	Furukawa, S.	EdE-66
Ferreira, H.	P-20	Foley, C. P	eP-199	Furukawa, S.	P-86
Ferreira, Sr. R. M	EE-16, EE-76	Fonda, C.	eEdE-119		
Ferriero, D. M	P-109	Fons Estupina, M. D.	O-260	<b>G</b>	
Ferrone, A.	O-31	Forbes, K.	eP-3	Gabriel, G. E.	EE-95
Feygin, T.	eP-290	Ford, A. L eP-121,	eP-243	Gad, K.	O-243
Fiehler, J.	EE-10, -149	Foreman, B.	EE-3	Gaddikeri, S.	P-63
Field, A.	O-109, O-112, O-220	Fornari, M.	O-508	Gaetz, W. C.	O-347
Fieremans, E	O-52	Fornaris, R.	eEdE-64	Gafton, A. R	O-424
Fieselmann, A.	eP-239	Förschler, A.	O-570	Gahramanov, S.	eP-20, eP-93
Fifi, J.	eP-263	Fortes, M.	eEdE-102, eEdE-103, O-488	Gailloud, P. E.	EE-49
Fifi, Jr. J.	O-311	Foster, J.	eP-3	Gailloud, P.	eP-237, eP-238, eP-322, O-314, O-405, O-511, O-512, O-74, P-73
Figà Talamanca, L.	EE-80	Fourgas, E	eEdE-81, eP-258	Gailushas, S.	eEdE-100
Figueiredo, P.	eP-106	Fox, A.	O-412	Gajjar, A.	O-400, O-548, O-554, O-555
Figuerras, J.	eP-64	Fox, A. J.	eP-114	Galanaud, D.	EdE-16
Filippi, C. G.	EdE-78, eP-283, eP-291, O-596, P-108	Fox, J.	O-611	Galban, C. J.	eP-146
Filippi, M.	O-510, P-32	Fragata, I.	EE-22, EE-44, EE-56, EE-60	Galban, S.	eP-146
Filippiadis, D.	eEdE-142, eP-265, eP-320	Fragata, I. R e	P-242	Galheigo, D.	O-246, O-599
Filizzolo, M.	O-515	Franceschi, A. M	O-233, O-577	Galheiro, D.	eEdE-19, eEdE-35
Findikoglu, A. S	O-148	Franciscatto, A. C.	EE-41, P-92	Gallizioli, G.	P-85
Finer, N.	O-256	Franczak, M.	eP-297	Galluzzi, P.	eP-200
Fink, J. R.	eEdE-153	Frank, A.	eP-71, O-23	Galtelli, C.	P-85
Fink, K. R.	eEdE-153	Frank, L. M	O-299	Gams, C.	eEdE-50
Fink, K. R T	eEdE-51	Frankenthaler, R. A.	eEdE-79	Gamss, C.	eP-63
Finlay, J. L	O-553	Fransen, P.	eP-252	Gan, C. L	O-121
Finocchi, V.	O-287	Frary, A. J.	O-216	Gan, Jr. S-M.	O-536
Finsterbusch, J.	O-180, O-181	Frederick, M. J.	O-328	Gan, Y.	O-544
Fiorella, D. J.	eP-262, O-22, O-337, O-420, O-561	Frei, D.	O-557	Gandhe, A.	EE-20
Fiori, R.	O-529	Frei, D. F.	O-22, O-561	Gandhi, D.	EdE-36
Firat, M. M.	O-394, O-73	Frei, Jr D. F.	O-364	Gandhi, D.	eEdE-102, -103, O-308, O-488
Fischbein, N.	eP-164, O-427	Freiheit, E	eP-264	Gandini, R.	eP-241
Fischer, I.	EE-97, eEdE-99	Freyman, J.	eEdE-21, eP-141	Ganesh, A.	eP-172
Fischer, K. C.	P-111	Freyman, J.	O-289	Gao, G.	eP-227
Fischer, S.	O-317, O-518, O-572, O-583	Friedly, J.	O-591	Gao, W.	O-253, O-296
Fisher, J. A.	O-564	Friedman, E R	eEdE-8	Garaci, F. G.	eP-173, O-508
Fisher, P. G.	O-551	Froeber, R.	O-67	Garcia, A.	O-399
Fitzgerald, R. T	O-523	Froelich, A.	eP-159	García-Álvarez, R.	O-123
Fitzsimmons, B-F.	P-71	Froehlich, A. L	O-612	Garcia-Ferrer, L.	eP-23, eP-278
Fladt, J.	eP-95	Frölich, A. M J	O-24	Garcia-Polo, P.	eP-71
Flamm, E	eP-126	Fu, J. C.	P-18	Gardin, T. M	O-53, O-54
Flanders, A.	eEdE-21, eP-141, O-063a, O-102, O-285, O-289, P-39	Fugate, J. E.	P-1	Garetier, M.	eEdE-101
Flanders, A. E.	eEdE-16, eP-321	Fujimura, M.	O-318	Garg, N.	eP-54, O-397
		Fujita, A.	eEdE-92	Garg, P.	O-562
		Fujita, S.	EE-82		
		Fukui, M. B.	eEdE-26		

### Index of Program Participants

Numbers refer to session and presentation numbers, *not to page numbers*.

Index Key: O = Scientific Paper (Oral Presentation); EE = (Electronic) Excerpta Extraordinaire;

P = Scientific Poster (Print Format); eP = Electronic Scientific Poster (ePoster);

EdE = Education Exhibit (Print Format); eEdE = Electronic Education Exhibit

Garibotto, V.	eP-132	Glastonbury, C. M.	O-272	Goth, E	eEdE-57
Garlick, C.	EE-104	Glenn, O. A.	O-132	Gould, R.	O-38
Gascou, G.	O-581	Glikstein, R.	eEdE-42	Gounis, M. J.	eP-209, eP-, eP-227, eP-228, eP-260, O-586
Gasparetto, E.	eEdE-10, eEdE-11, eEdE-35, eEdE-53, eEdE-150	Go, J. L.	eP-137, O-509	Goyal, K.	EE-104
Gasparetto, E. L.	O-86	Gobin, P.	O-490	Goyal, M.	EdE-35, eP-, eP-264, O-22, O-27, O-29, O-556, O-558, O-561, O-571, P-74
Gasparotti, R.	O-286	Gobin, Y. P.	eP-197, eP-199, eP-226, eP-240, O-417, O-418	Graber, J. J.	O-207
Gass, A.	P-32	Gocmen, R.	EdE-5, eP-27, O-305	Graeb, D.	eEdE-44
Gaughan, J.	O-181	Godi, C.	EE-2, eP-295, O-250	Graham, Jr. J. M.	O-429
Gauvin, S.	eP-269	Goel, A.	O-571	Grant, E.	eEdE-117
Gauvrit, J.-Y.	eEdE-106	Goericke, S.	O-392	Grant, Sr. G. P.	EE-76
Ge, Y.	O-129, O-58	Goerner, F.	eEdE-33, O-117	Grant, P. E.	O-258, O-260, O-301, O-542, O-8
Gedroyc, W.	O-637	Gohel, S.	P-4	Gray, J.	O-548
Gee, J. C.	eP-103	Gokce, E.	O-73, O-394	Gray, R. I.	eEdE-55
Gemmete, J.	eEdE-1	Golan, S. S.	O-36	Grazzini, G.	EdE-69
Gemmete, J. J.	eP-251, O-522	Golay, X.	eP-88	Greenberg, E.	eP-2, eP-197, O-118, O-417
Genc, A.	O-431	Golby, A.	P-29	Greenblatt, K.	eEdE-130, O-553, O-608
Gencurk, M.	eP-133, O-603	Golby, A. J.	O-222	Greenman, R.	eEdE-145, O-598
Gennari, P.	eEdE-104	Gold, R.	eP-160	Greenstein, M.	O-220
Genovese, E.	EE-80	Goldberg, M. F.	eEdE-26	Gregg, L.	eP-322
Gentric, J. C.	eEdE-101, eEdE-106	Goldin, D.	eEdE-139	Gregson, B.	P-117
Gentry, L. R.	eEdE-95, eEdE-100	Goldman, M.	eP-75, eP-82	Griffith, B.	eEdE-27, eEdE-56, O-439
George, A.	O-599	Goldmann, S.	O-218	Griffiths, P.	O-297
George, A. E.	eP-66, O-34, O-504	Goldsberry, G.	O-400	Griffiths, P. D.	eEdE-111, O-105, O-150, O-225
Georgy, B.	O-527, O-528, O-530	Goldsher, D.	eP-136	Grilli, C. J.	eP-144
Gerevini, S.	eP-295	Goldstein, S.	EE-86	Grimm, J. P.	eEdE-130, O-553, O-608
Gerloff, C.	EE-10, O-149	Gölitiz, P.	eP-230, eP-261	Grinband, J.	O-212
Gerstner, E. R.	O-101, O-211, O-640	Golland, P.	O-222	Grisanti, S.	O-286
Geschwind, M. D.	EdE-6	Golomb, J. B.	eP-66, O-34, O-504	Griswold, M. A.	O-251
Geva, R.	P-110	Golshan, A.	O-573	Gritti, P.	P-34
Gezmis, E.	O-409	Golshani, B.	P-71	Groenendaal, F.	O-174
Ghajar, J.	O-56	Gomes, W. A.	O-299	Groneman, M.	O-68
Ghanem, T.	EE-54	Gomez, A. M.	eEdE-138	Groom, K.	EdE-52
Ghitis, J.	O-559	Gomez, F.	eEdE-138, eP-234	Gros, L.	eEdE-110
Ghodke, B. V.	O-22, O-561	Gomez, J. F.	eEdE-138	Gross Kelly, T. C.	EdE-86, eEdE-134, eEdE-136, eP-280
Ghosh, K.	EE-106	Gomyo, M.	eP-6, eP-43, O-110	Grosshans, D.	O-406
Gibson, S.	eEdE-127	Goncalves, F. G.	EdE-17	Grossman, R.	eP-113
Gidwani, G.	EE-100	Gonçalves Pereira, P. M.	eP-32, P-25	Grossman, R. I.	O-58, O-129, O-358
Giglio, P.	O-639	Gonen, O.	eP-113, eP-66, O-127, O-504	Grossman, R. G.	O-534
Gilani, S.	EdE-31, eP-59			Gros-Tsur, V.	P-110
Gilbert, IV J.	eEdE-22, eEdE-7, eEdE-84	Gonyea, J. V.	O-596	Grüner, R.	O-71
Gilbertson, J.	EE-35	Gonzales, R. G.	O-391	Grutters, J. P. C.	eP-157
Giles, B. P.	O-524	Gonzalez, A.	P-103	Guarnieri, G.	eP-318
Gillard, J. H.	O-231	Gonzalez, G.	O-137	Gubbels, S.	eEdE-100
Gilles, F. H.	O-255	Gonzalez, N. S.	eEdE-52	Gubitz, G.	eP-135
Gilloon, B.	O-220	Gonzalez, R. G.	O-185, O-22, O-230, O-556, O-561		
Gilmore, J.	O-253	Gonzalez-Martinez, J.	O-538		
Ginat, D.	EdE-44	Goodgold, A.	O-599		
Ginat, D. T.	EdE-8, O-423	Gordish Dressman, H.	eP-272		
Ginsberg, L. E.	eEdE-062, eP-184, O-328, O-361, P-78	Gorelick, J.	EE-30		
Girardi, P.	eP-102	Gorelik, N.	O-516		
Glass, J. O.	EE-91, O-549, O-555	Gory, B.	O-309		
Glastonbury, C.	eP-155, eP-76	Gorynski, E.	O-127		
		Goss, J.	P-46		

### Index of Program Participants

Numbers refer to session and presentation numbers, *not to page numbers*.

Index Key: O = Scientific Paper (Oral Presentation); EE = (Electronic) Excerpta Extraordinaire;

P = Scientific Poster (Print Format); eP = Electronic Scientific Poster (ePoster);

EdE = Education Exhibit (Print Format); eEdE = Electronic Education Exhibit

Gudziol, H.	O-67	Hamilton, J. D.	O-68, O-328	Heiland, S.	eP-86, eP-95
Gueguen, A.	eEdE-72			Heiler, P. M.	O-67
Guergue, C.	O-593	Hamilton, Jr. J. D.	eP-184, EdE-38,	Heilman, C.	O-594
Guerin, S.	EdE-50, O-526		eEdE-59	Heit, J. J.	O-230
Guha-Thakurta, N.	EE-24, eEdE-65,	Hamilton, M.	eP-124	Hellinger, II F. R.	O-22, O-561
	P-50, P-52, P-53	Hammersley, J. A.	eP-323	Helpern, J. A.	O-30
Guida, P.	EE-30	Hammoud, D.	O-289	Helton, K.	EE-91
Guitard, J.	O-535	Han, J. S.	O-564\	Helton, K. J.	EE-74, EE-75, O555
Gulko, E. O-55,	P-65	Han, M-H.	eP-193, O-513, P-80	Helvey, J.	EE-1, EE-51
Gunbey, H. P.	O-148	Hanagandi, P. B.	EdE-17	Helvey, J. T.	EdE-13, EdE-20
Guntinas-Lichius, O.	O-67	Hancock, S. B.	EdE-61	Henderson, J. B.	EE-43
Guo, W-Y.	eP-143, eP-254	Hanhan, S.	eEdE-108	Hendler, T.	P-55
Gupta, A.	EdE-30, eEdE-115,	Hanna, M. F.	EdE-62	Hendrikse, J.	EdE-24, O-174,
	O-565, P6	Hansen, T.	eEdE-70, P-69		O-275
Gupta, N.	O-132, O-316	Hanson, T. J.	O-173	Henkes, H.	O-317, O-518, O-533,
Gupta, R.	eP-65, O-14	Haque, S. S.	EdE-21		O-572, O-583
Gupta, S.	eEdE-153, eEdE-57	Haraguchi, M.	eP-303	Henkin, R.	P-82, P-83
Gupta, V.	O-489	Harb, J. EdE-11,	eEdE-144	Hennekam, R. C. M.	O-142
Güresir, E.	O-514	Harder, D.	eP-107	Henry, R. G.	EdE-6
Gurkov, R.	O-320	Harder, S. L.	eP-289	Heo, J.	eP-206
Gutman, D.	eEdE-16, eEdE-21,	Harikrishna, B.	eP-172	Heran, F.	eEdE-72, eEdE-96,
	eP-141, O-285	Harnsberger, H. R.	EE-61, eP-187,		eP-162
Gutman, D. A.	O-102, P-39		O-321, O-430, O-458	Heran, M. K.	eEdE-44
		Harnsberger, R.	O-428	Héran, F.	O-249
<b>H</b>		Harper, J.	O-60	Herbert, J.	O-127, O-129
Ha, E. J.	O-329	Harreld, J. H.	EE-33, EE-59, EE-75,	Herman, M.	eP-77
Habba, M.	O-243		EE-91, O-400, O-548, O-554, O-555	Hernandez, R. J.	EE-48
Habib, A.	eP-148, O-111, O-237,	Harri, P. A.	EdE-87, O-177	Hernández-Tamames, J. A.	eP-71,
	O-560, O-576	Harrigan, M. R.	O-22, O-561		O-123
Hacein-Bey, L.	EE-36, EE-40, EE-46	Harshman, B.	eEdE-148	Herrmann, C.	O-118
Hacker, C.	O-213, O-598	Harter, D.	EE-7	Hervo, P.	O-28
Hackney, D.	eEdE-145	Hartl, R.	eP-226	Herwadkar, A.	eP-154, O-313
Hackney, D. B.	eEdE-9, O-1, O-359,	Hartman, M. J.	eEdE-100	Hesdorffer, D. C.	O-299
	O-369	Hartmann, M.	O-580	Hess, A.	O-28
Hadjistilianou, T.	eP-200	Hasan, K. M.	eEdE-67, eP-17, eP-18	Hess, C.	O-292
Hadjivassiliou, M.	O-150, O-225	Hasiloglu, Z. I.	EE-15, EE-77	Hess, C. P.	EdE-6, eP-316, eP-67,
Hagmann, P.	O-240	Hatten, Jr. H. P.	eP-310		O-100, O-259, O-38, P-116
Hainfellner, J.	O-215	Haughton, V.	eP-323, O-403, O-544	Hetts, S. W.	eP-222, eP-233, eP-55,
Hainfellner, J. A.	O-261	Haverkamp, B.	eEdE-127		O-316, O-578
Hajjar, I.	O-227	Hawley, K.	EdE-64, O-326	Hiai, Y.	O-115
Hakyemez, B.	eP-15, eP-26	Hayakawa, M.	eP-1, O-557	Hidaka, S.	eP-28
Halbach, V. V.	eP-233, O-316,	Hayashi, D.	eEdE-43	Higashida, R.	O-578
	O-578	Hayashi, K.	P-67	Higashida, R. T.	eP-233, O-316
Halidpur, A.	O-49	Hayman, L. A.	EdE-38, -59,	Higgins, R.	O-256, -257
Hallam, D. K.	O-475		eEdE-60, O-68	Hilario, A.	eP-47
Haller, S.	eP-132, O-492	He, M.	eP-119	Hildebolt, C.	O-543
Halm, K.	O-434	He, X.	P-16	Hildenbrand, P. G.	EE-61
Halpin, S.	O-121	He, Y.	O-544	Hildreth, K.	O-393
Hamberg, L. M.	O-423	Heagerty, P. J.	O-591	Hilibrand, A. S.	O-446
Hamed, M.	O-243	Heasman, J.	O-637	Hill, J. A.	EE-23
Hamilton, A.	eP-284	Heck, D.	EE-69, O-557	Hill, M. D.	O-27, O-29, O-558
Hamilton, B. E.	eP-20, eP-93, O-321	Heck, D. V.	O-22, O-561, O-615	Himmelreich, U.	O-209
Hamilton, D.	eEdE-67	Hedges, K.	O-542	Hintz, S.	O-256, O-257
Hamilton, J.	eEdE-, eP-142	Heffernan, A.	O-56	Hipko, S. G.	O-596
		Heidenreich, J.	O-113		



### Index of Program Participants

Numbers refer to session and presentation numbers, *not to page numbers*.

Index Key: O = Scientific Paper (Oral Presentation); EE = (Electronic) Excerpta Extraordinaire;

P = Scientific Poster (Print Format); eP = Electronic Scientific Poster (ePoster);

EdE = Education Exhibit (Print Format); eEdE = Electronic Education Exhibit

Hirai, T.	eP-90, eP-92, eP-306, O-115, P-40	House, P.	eP-155	Huynh, T.	O-61
Hirano, M.	eP-323	Howard, P.	eP-114	Hwang, J.	eP-164a
Hiratsuka, Y.	eP-165, eP-5	Howe, D.	O-297	Hwang, S.	EdE-87, eEdE-16, eEdE-21, eP-141, P-39
Hirota, S.	EE-82, O-103, P-42	Hoy, M.	O-443	Hwang, S. N.	eP-57, EE-27, O-102, O-289
Hirsch, J. A.	O-230, O-577	Hreib, K.	EE-64	Hwang, Y. J.	eP-305
Hirsch, N.	O-217	Hsiao, A.	O-427	Hyman, B. T.	eP-67, O-500
Hise, J. H.	EE-43	Hsu, D.	O-487	Hypa, S.	eP-270
Hiwatashi, A.	P-41	Hsu, D. P.	O-251		
Hmaimess, G.	O-540	Hsu, N-W.	P-27, P-33, P-38		
Ho, M.	eEdE-68, eEdE-69, eEdE-9	Hsu, T-W.	P-12		
Hoang, A.	eP-61	Hu, L. S.	O-489	<b>I</b>	
Hoang, B. H.	P-118	Hu, W.	EdE-93	Iadanza, A.	eP-295
Hoang, J. K.	eP-185, O-327, O-532	Huan, X.	O-544	Ibañez, J.	EdE-28
Hobbs, G.	eP-186	Huang, D. Y.	eP-156	Ideguchi, R.	P-67
Hoeberigs, M. C.	EE-4, eP-189	Huang, E.	eEdE-21, eP-141, O-289, P-39	Ifthikharuddin, S.	eP-11
Hoeffner, E.	EdE-45, eEdE-1, eEdE-45, eEdE-6	Huang, H.	O-262	Igarashi, Y.	EE-82, P-42
Hoelscher, A.	O-118	Huang, J.	O-511	Ihn, Y-K.	P-10
Hof, J. R.	O-325	Huang, R.	O-395	li, Y.	eP-10
Hoffman, B.	eP-69	Huang, W.	O-544	Ikeda, H.	P-47, eP-86
Hofman, P. A. M.	O-325	Huckman, M. S.	O-352	Alıcıoğlu, A. T.	O-433
Hogg, J.	eP-186	Hudgins, P.	EdE-58, O-321	Ilica, A. T.	EdE-36, eEdE-93
Hoggard, N.	O-105, O-150, O-225	Hudgins, P. A.	EdE-55, eEdE-75, O-356	Illoreta, S. F.	eEdE-127
Holder, C.	eP-141, P-39			Imai, M.	eP-6, O-110
Holder, C. A.	eEdE-16, O-102, O-289	Hudon, M. E.	O-443	Imbesi, S. G.	EE-32
Holdsworth, R.	O-220	Huerga, E.	O-128	Inecikli, F.	eP-26
Holdsworth, S. J.	eP-116, O-179, O-307	Huerta, T.	O-585	Inecikli, M. F.	eP-15
Holland, D.	eP-67, O-125, O-500, O-502	Hughes, A.	O-637	Inoue, M.	eP-116, O-20
Holodny, A.	O-219	Hui, E.	O-30	Intrapiromkul, J.	eP-326, O-324, P-122, P-123
Holodny, A. I.	eP-80, 207, O-221, O-372, O-597, P-21, P-51	Hui, F.	O-557	Iosif, C.	eP-212
Holsapple, J.	P-3	Hui, F. K.	O-22, O-561	Iqbal, A.	P-117
Holshouser, B.	O-262	Huisman, T. A. G.	EdE-78, EdE-82, EdE-82, eEdE-74, eP-276, eP-277, eP-281, O-142	Irfanoglu, M. Okan e	EdE-12
Honce, J.	O-606	Hunca Memis, C.	eP-31	Irintchev, A.	O-67
Honda, H.	P-41	Hung, A. S-C	eP-254	Isaac, M. L.	P-23
Honeyfield, L.	O-537	Hunt, C.	O-43, O-505	Klsalberti, M.	O-515
Hopf, N.	O-518, O-533	Hunt, C. H.	eP-120, O-144, O-241, O-401, O-437, P-1	Ishak, G.	EdE-75
Horenstein, C. I.	O-212, O-214	Hunter, G. J.	O-423	Ishigame, K.	eP-9
Hori, M.	EdE-9, EE-6, P-14	Hunter, L.	O-181	Ishikura, R.	EE-82, O-103, P-42
Horia, M.	eP-258	Hunter, L. N.	O-180	Ishimaru, H.	eP-51, P-89
Horie, N.	P-67	Hurley, M. C.	EE-63, EE-70, EE-93, eP-104, eP-129, eP-148, O111, O-237, O-520, O-560, O-576	Isidro, R. A.	eP-20
Horowitz, K.	O-567			Islak, C.	EdE-71, eP-229, eP-268, O-414
Horsburgh, A.	P-61, P-68, P-75	Hurteau-Miller, J.	eEdE-123, eEdE-131	Islam, O.	O-399
Horsch, A.	O-579			Ivan, C.	eP-60
Horsch, A. D.	O-635	Huson, S. M.	EE-106	Iwamura, A.	eP-48
Horsley, W.	EE-1, O-435	Huss, D.	O-220	Iwashita, K.	eP-90, P-40
Horvath-Rizea, D.	O-317, O-533	Huss, D. S.	O-585	Iwata, T.	eP-108, eP-244, eP-26 P-8, P-97, P-99
Hosten, N.	O-634	Hussain, A.	eP-83	Iyer, R.	EdE-75
Hou, P.	O-68, P-79	Hussain, S.	eEdE-14, eEdE-37	Izadi, K.	P-44
Hou, S. Y e	P-209	Hussein, M. A.	O-62	Izbudak, I.	eP-276
Houdart, E.	eP-196	Huston, J. M.	O-109, O-112	Izzo, R.	eP-318
Hourani, R.	O-540	Hutner, A.	EE-105		

### Index of Program Participants

Numbers refer to session and presentation numbers, *not to page numbers*.

Index Key: O = Scientific Paper (Oral Presentation); EE = (Electronic) Excerpta Extraordinaire;

P = Scientific Poster (Print Format); eP = Electronic Scientific Poster (ePoster);

EdE = Education Exhibit (Print Format); eEdE = Electronic Education Exhibit

<b>J</b>			
Jaba, I. M	O-424	Jimenez, L.	eP-202
Jabehdar Maralani, P.	eP-78	Jindal, G.	eEdE-102, eEdE-103, O-488
Jackson, A.	eEdE-70, eP-81, eP-84, O-228, O-69, O-70, P-69	Jirari, M.	O-483, O-521
Jackson, E. F.	eEdE-59, eEdE-60, O-68	Jitpratoom, P.	eP-7, P-15
Jackson, R. F.	EE-36	Jocson, V. D.	EE-12
Jacobs, T. P. S	Y-020	Johnson, A.	eEdE-29
Jafar, J. J.	EE-39	Johnson, A. J.	O-224, O-345
Jaffe, C.	O-285	Johnson, C.	eP-160, eP-61, O-565
Jagadeesan, B. D.	eP-243	Johnson, C. M	EdE-70, eEdE-124
Jager, R.	EdE-3	Johnson, C. E.	P-6
Jäger, H.	eP-88, O-129	Johnson, G.	O-34
Jahng, G.	O-126	Johnson, J. M	O-233, O-258
Jain, R.	EE-54, EE-54, eEdE-16, eEdE-17, eEdE-20, eEdE-21, eEdE-27, eEdE-56, eP-141, O-063, O-210, O-285, O-289, O-322, O-439	Johnson, K.	O-108, O-112
Jakobovic, R.	O-61, O-25	Johnson, M. H.	eEdE-146
Jallo, G.	eP-322	Johnson, T. D.	eP-146
Jambawalikar, S.	O-212, O-214	Jolesz, F.	eEdE-21, O-99
James, K. T	O-591	Jolesz, F. A.	eP-141, eEdE-18, eP-94, eP-141, O-98, P-39
Janjua, N.	O-557, P-9	Jolesz, F. O	eP-79
Jannin, P.	eEdE-106	Jones, C. A.	O-344
Janse van Rensburg, P.	O-430	Jones, J. G.	eP-140
Jansen, O.	eP-56	Jones, J. G. A.	EE-72, eP-91
Janssen, H.	eP-89	Jones, S. E.	O-538
Jara, H.	eP-174, eP-33, eP-52, O-244, O-245	Jones, W.	EE-1
Jarmakani, M.	eEdE-127	Jordan, J. E.	O-200
Jarso, S.	P-24	Joshi, A. S.	EdE-53
Jarvik, J. G.	O-178, O-447, O-591	Joskowicz, L.	P-104
Jasinski, T. H.	O-136	Jou, L-D.	eP-208
Jaswani, V.	EdE-47	Jousset, C.	eP-285
Jatt, M.	O-391	Jovin, T.	eP-4, P-2
Javadi, P.	EdE-72, EE-84	Jovin, T. G.	O-22, O-561
Javed, K.	EdE-63	Joy, H.	O-297
Jayaraman, M. V	eP-158, O-350	Juliano, A.	eEdE-79
Jea, A.	EE-94	Juluru, K.	O-118
Jellema, R.	eP-294	Jun, Sung Woo W.	O-72
Jellinek, D. A.	O-105	Jung, C.	eP-50
Jenabi, M.	eP-80, O-221	Jung, H-K.	P-80
Jenkins, J. J.	EE-59	Jung, S-L.	eP-98, eP-122, eP-161
Jennings, D. L	O-101, 211, O-640	Jung, W. S.	P-10
Jensen, J.	O-30, O-52	Juvekar, S.	eEdE-78
Jeon, S. J.	P-95	<b>K</b>	
Jeong, M. Y.	eP-246, P-45	Karakach, T. K.	P-22
Jeyapalan, S.	eP-75, eP-82	K. Oguz, K.	eP-182
Ji, R.	O-562	Kabir, K.	O-531
Jiang, J.	eP-214, O-419	Kaddoum, R. N	O-554, O-555
Jilwan, M. N	eP-274	Kademian, J.	eEdE-36, eEdE-149
Jilwan-Nicolas, M.	O-102	Kadirval, R.	eP-256
		Kadkhodayan, Y.	eP-216, O-421, O-422
		Kadziolka, K.	eP-218, O-419
		Kagetsu, N.	P-113
		Kahlek, N.	EdE-77
		Kahlert, P.	O-392
		Kai, Y.	eP-306
		Kaichi, Y.	eP-68
		Kaiser, W. A.	O-67
		Kaji, T.	eP-25
		Kajiwara, Y.	eP-30, P-43
		Kakeda, S.	eP-39, eP-68, O-115
		Kakimoto, N.	EdE-66, P-86
		Kalapos, P.	O-440
		Kalkanis, S.	O-210
		Kallmes, D. F.	eP-256, O-144, P-1
		Kalmmes, D. F.	O-437
		Kalra, V.	EE-105
		Kalra, V. B.	eEdE-7, eEdE-22, eEdE-84
		Kamagata, K.	EdE-9
		Kamagata, K.	P-14
		Kamali, A.	eP-17, eP-18
		Kamalian, S.	eP-58, eP-59, O-21, O-577, O-638
		Kamaly, I.	EE-29
		Kamath, A.	eP-266
		Kamholz, J.	O-303
		Kaminou, T.	eP-195
		Kamo, M.	eP-194, eP-303
		Kamran, M.	O-582
		Kan, I.	O-573
		KAN, I.	P-36
		Kanagal Shamanna, R.	EE-14
		Kanal, E	O-11
		Kaneda, T.	eP-171, eP-192, O-242
		Kanekar, S.	EE-5, EE-57, eEdE-38, eEdE-88, eP-127
		Kang, H. K.	eP-246, P-45
		Kang, H-S.	eP-193, O-513
		Kannu, P.	O-138
		Kao, H. W	eP-255
		Kao, Y-H.	eP-143
		Kapinos, G.	eP-61
		Kaplitt, M.	O-114
		Kappelle, J.	O-579
		Kappelle, L. J.	O-635
		Kappos, L.	eP-130
		Kara, B.	O-610
		Karaman, B.	EE-67
		Karaoglanoglu, M.	O-148
		Karellas, A.	eP-260
		Karimi, S.	EdE-95, O-207, O-545, O-546, O-597, P-51
		Karius, T.	eP-314
		Karmonik, C.	O-534
		Karunasaagar, K.	P-64
		Karwacki, G.	eP-105
		Kashgari, A.	P-22
		Kasprian, G.	eP-287, eP-293, O-215, O-252, O-261

### Index of Program Participants

Numbers refer to session and presentation numbers, *not to page numbers*.

Index Key: O = Scientific Paper (Oral Presentation); EE = (Electronic) Excerpta Extraordinaire;

P = Scientific Poster (Print Format); eP = Electronic Scientific Poster (ePoster);

EdE = Education Exhibit (Print Format); eEdE = Electronic Education Exhibit

Kassell, N.	O-585	Khaw, A. V	O-634	King, R. M	eP-217
Kassner, A.	O-176	Khiana, T.	eP-317	Kini, Sr. J.	EE-76
Kastler, A.	O-50, O-590	Khawaja, O.	O-260	Kinoshita, T.	P-30
Kastler, B.	O-50, O-590	Kichikawa, K.	eP-28, eP-35, eP-48, eP-117, eP-201, O-574	Kirby, J.	eEdE-16, eEdE-21, eP-141, O-102
Kataoka, M.	EdE-66, P-86	Kido, D.	O-65	Kirollos, R. W	P-61, P-75
Kathuria, S.	O-308	Kikinis, Z.	P-30	Kirov, I.	eP-113, eP-66, O-127, O-504
Katsuura, T.	EE-82, O-103, P-42	Kikuchi, K.	eP-5, eP-165, P-41	Kirsch, C.	EE-31, O-426
Katz, Z.	O-511	Kilic, O.	EE-77	Kirsch, M.	O-634
Katz, Z. M	EE-49	Killeen, R. P	O-565	Kister, I.	O-129
Katzman, G.	O-402, P-101	Killeen, R. P.	P-6	Kitajima, H. D.	eEdE-137
Kaufmann, T. J.	O-401	Kim, B. M.	eP-49, eP-206	Kitajima, M.	eP-306, eP-90, eP-92
Kayahan Ulu, E M	eP-31	Kim, B-S.	eP-98, eP-122, eP-161	Kitajima, M.	P-40
Kazmi, K.	EdE-47	Kim, D. I.	eP-49, eP-206	Kitchin, D.	O-543
Keating, G.	O-43	Kim, D. J.	eP-49, eP-206	Kiura, Y.	P-88
Keen, N. N	eP-316	Kim, E-H.	eP-50	Kizilkilic, O.	EdE-71, eP-229
Keiper, M. D.	EdE-13, EdE-20, EE-1	Kim, E.S. J.	eP-211		eP-268, eP-279, O-414
Keiper, M.	EE-51	Kim, E Y	P-116, P-70, P-72	Klar, N.	eP-296
Keiper, M. D.	O-435	Kim, H. J.	eEdE-80, eP-177, eP-178, eP-304	Klein, A. P	EdE-14, eEdE-57
Kelahan, L.	P-83	Kim, H. I.	O-323	Klein, M. H.	eP-297
Kelekis, A.	eEdE-142, eP-265	Kim, H. J.	O-290, O-319, O-605, O-323	Kleindorfer, D.	eP-202
Kelekis, A.	eP-320	Kim, H. S.	eP-97	Kleinschmidt-DeMasters, B. K.O-151	
Kelekis, N.	eEdE-142, eP-265, eP-320	Kim, Ho Kyun K.	eP-118, P-125	Klimo, P.	EE-33, EE-91, O-46
Kelly, H. R	O-423	Kim, Ho Sung S.	O-293, O-605	Klimo, Jr. P.	EE-59
Kelly, M.	EdE-86, O-439	Kim, J.	EE-104	Kloska, S.	eP-230, eP-261
Kelly, T.	EdE-39	Kim, J.	eEdE-149	Klostranec, J.	eP-237
Kelly, T. G.	EdE-70, eEdE-114, eEdE-61	Kim, J.	eEdE-89	Klostranec, J. M	O-74
Kelly, T. G. C.	EdE-14, eEdE-124, EdE-129	Kim, J. H.	eP-50, O-247	Klotz, E	eP-159
Kemmling, A.	eP-58, O-21	Kim, J-H.	EdE-56, eP-177, eP-178, P-80	Klotz, E	O-24
Kemmling, A.	O-638	Kim, J. K.	O-329	Klucznik, R.	O-557, eP-159, eP-270, O-24, O-35, P-93, P-98
Kennedy, T. A.	eEdE-100	Kim, J. P	EdE-18	Knopp, M. V	eEdE-12
Kersbergen, K.	O-174	Kim, M. J.	EE-19, O-126, O-72, P-44	Kobayashi, M.	EE-6, eP-303
Keshari, K.	O-107, O-41	Kim, M-C.	EE-66	Kocak, B.	EdE-71, eP-229, eP-268, O-414
Keshishian, M. D.	O-84	Kim, N.	O-53, O-54, O-55, O-605, P-65	Kocer, N.	EdE-71, EE-77, eP-229 eP-268, O-414
Kessler, C.	O-634	Kim, P. E.	eP-137, O-509, P-44	Koch, B. L	EdE-84
Kessler, L. G.	O-591	Kim, R. H.	O-573	Koch, R. Maria	eEdE-12
Kessler, M. M	eP-153, O-543	Kim, S-H.	eEdE-89	Koçuk, N.	P-60
Ketonen, L. M	EE-87	Kim, S. J.	O-293, O-605	Kodera, J.	EE-6
Ketonen, L.	P-50, P-52, P-52	Kim, S. K.	eP-246, P-45	Koeller, K. K.	P-62
Kettner, M.	eP-247	Kim, S. Y.	eP-305	Koenig, M. Kay	eEdE-109
Keyak, J. H.	P-118	Kim, Sun Mi M.	O-126	Koepp, M.	eP-81
Khaled, M. A.	O-585	Kim, Sung Tae T.	O-323	Koerber, A. J.	EE-86, eEdE-107
Khaleel, Z.	O-428	Kim, T.	O-247	Koerte, I.	P-30
Khaleel, Z. L	O-288	Kim, Y. H.	EE-19	Koh, J. S.	eP-211
Khamaysi, Z.	eP-136	Kim, Y. D.	eP-206	Kolar, B.	EdE-1
Khan, M. N -	P-22	Kimberly, W. T	O-562	Kole, M.	eP-258
Khan, S.	eP-54, O-397	Kimura, F.	O-248	Kontolemos, M.	eEdE-42
Khan, U.	eP-202	Kimura, H.	eP-29	Kontzialis, M.	eP-54, O-426
Khankan, A. A.	O-62	Kimura, M. C. G.	eP-139, O-294	Kooijman, H.	O-217
Khanna, G.	P-111	King, K.	eEdE-31	Koonce, J. D.	EE-69
Khanna, P.	EdE-75	King, K. S	O-64	Koppeinigg, D.	eP-164
Khashper, A.	eP-45				

### Index of Program Participants

Numbers refer to session and presentation numbers, *not to page numbers*.

Index Key: O = Scientific Paper (Oral Presentation); EE = (Electronic) Excerpta Extraordinaire;

P = Scientific Poster (Print Format); eP = Electronic Scientific Poster (ePoster);

EdE = Education Exhibit (Print Format); eEdE = Electronic Education Exhibit

Koral, K.	eEdE-113	Kuo, J.	O-220	Law, M.	EE-72-, eP-137, eP-140,
Korkmazer, B.	EdE-71, eP-229,	Kuo, J. V	P-118		eP-288, eP-292, eP-91, O-161,
	eP-268, O-414	Kural, F.	EE-101, EE-92, O-409		O-227, O-370, O-442, O-509, P-44
Korn, A.	O-390	Kuratsu, J-I.	eP-306, eP-90, P-40	Lawhn- Heath, C.	O-147
Körner, H.	O-569	Kurhanewicz, J.	O-41	Laws, P. M	EE-106
Korogi, Y.	eP-39, eP-68, O-115	Kurusu, K.	eP-, P-43, P-88	Layton, K. F.	EE-43
Kortman, K.	O-527, O-528	Kurokawa, S.	O-574	Lazar, R. M	O-567
Korutz, A.	eP-148, O-237, O-249	Kurre, W.	O-572	Lazzaro, M.	A. P-71
Kosuda, S.	eP-25	Kurt, G.	eP-14	Le Jean, L.	eP-212, eP-311
Kotsenas, A.	O-505	Kussman, S.	O-244, O-245	Leake, D. R	EE-13
Kotsenas, A. L	eEdE-41, O-489	Kusumawidjaja, D.	eP-3	Learned, K. O	eP-191
Kouo, T.	O-32	Kwak, H. H-S.	eP-205	Lebel, R. M	eP-137, eP-140
Kouo, T. C.	O-39	Kwak, J. H.	eP-219	Lecler, A.	eP-210
Kovacs, A.	eEdE-18, O-99	Kwan, A.	eP-298	Leclercq, D.	EdE-16
Kowarschik, M.	eP-225, O-416,	Kwon, D. H.	eP-219	Ledermann, E	eEdE-85
	O-587, O-589	Kwon, M.	EE-14	Lee, B. H.	eP-305
Koyfman, F.	P-3	Kwun, B. D.	eP-219	Lee, C.	O-605
Kramer, B. W.	eP-294			Lee, C-W.	P-96
Kramer, L.	EdE-066a	<b>L</b>		Lee, D.	eP-219
Kramer, L. A.	eEdE-67	La Piana, R.	EdE-41, eP-272, O-516	Lee, H.	O-132, O-56
Kramp, L.	eP-86	Labat, E	eEdE-126, eEdE-64,	Lee, H. B.	O-323
Kranz, P. G.	O-491, O-532		eEdE-97	Lee, H. J.	eP-87, eP-118, eP-125
Krecke, K.	O-505	Labat-Alvarez, E J.	eEdE-13	Lee, H. Y.	O-293
Krecke, K. N	eP-13, O-145	Labeyrie, M-A.	O-28	Lee, I.	O-210
Kreiser, K.	O-570	Lachance, D. H.	O-145	Lee, J.	eP-118, eP-60
Kreth, F. W.	eP-89	Lafitte, F.	O-249	Lee, J. H.	O-329
Krings, T.	EE-8	Lagares, A.	eP-47	Lee, J-M.	eP-121, eP-243
Krishna, V.	O-611	Lagemann, G. M	O-547	Lee, J. S.	O-425
Krishnamoorthy, K.	O-258	Lahiji, K.	O-39	Lee, J. Y K	eP-191
Krishnamurthy, B.	eP-134	LaHue, S.	O-56, O-57	Lee, M.	O-213
Krishnan, A.	EdE-11, eEdE-144,	Lai, A.	O-97, O-290, O-291	Lee, N.	EdE-50
	eP-88, O-231	Lainhart, J. E.	O-612	Lee, N. J.	O-247
Krisht, K.	O-151	Lake, Jr. J. R	P-124	Lee, N. N	EdE-96
Krmpotich, T.	O-116, O-146	Lanaghan, K.	eP-3	Lee, P. N	P-109
Krol, G.	EdE-95	Lane, J. I.	O-457	Lee, R.	eP-139, O-613
Krumm, R.	eP-58, O-21	Laner, Sr. C.	EE-76	Lee, R. R	EE-32
Krupinski, E. A.	O-331	Lang, F. E.	eEdE-60	Lee, R. Yueh	O-294
Krupp, S.	O-439	Langford, L. A.	EE-24, P-53	Lee, S. J.	O-513
Kubicki, M.	P-30	Langner, S.	O-634	Lee, S. Y.	eP-128, O-425
Kuhn, A. Luisa	eP-228	Langs, G.	eP-293, O-222	Lee, Sang Rae R.	eP-128
Kuhn, A. S.	EdE-26	Langtangen, H. Petter	O-403	Lee, S-H.	eP-301, eP-302, eP-304
Kuhn, M. J.	EdE-26	Lansberg, M.	O-20	Lee, S-K.	EE-64, EE-66, P-57
Kuklisova-Murgasova, M.	O-51	LaPlante, J.	eP-187	Lee, T.	eEdE-80, O-395
Kumar, A. J.	EdE-38, eEdE-59,	Laptook, A.	O-257	Lee, T. Yim	O-25
	eEdE-60, O-328, O-68	Larsen, J.	O-105	Lee, Y.	eP-190, O-247
Kumar, G.	eP-121	Larson, M.	EdE-13	Lee, Y. H.	eEdE-89, P-95
Kumar, S.	O-063a	Larvie, M.	O-59	Lee, Y-J.	eP-175, eP-203
Kumar, V. A.	EdE-38, eEdE-59,	Lasater, O. E.	EE-59	Lee, Y. Z	eP-156
	eEdE-60, O-68	Lashkari, D.	O-222	Leech, R.	O-537
Kummer, S.	eP-105	Laufer, I.	eP-240	Lefton, D. R	EdE-89
Kumpe, D. A.	O-366	Laughlin, S.	EE-81	Lehman, V. T	O-489
Kun, L.	O-549	Laukka, J. J.	O-303	Lehnert, B. E.	eEdE-153
Kun, L. E.	EE-33	Launer, L. J.	O-567	Leigh, R.	eP-62, O-511
Kunimatsu, A.	eP-21	Laurans, M. S H	EE-105	Leite, C. C.	eEdE-34, O-226, O-229
Kunitomi, Y.	O-232			Leite, J. P	eP-16

### Index of Program Participants

Numbers refer to session and presentation numbers, *not to page numbers*.

Index Key: O = Scientific Paper (Oral Presentation); EE = (Electronic) Excerpta Extraordinaire;

P = Scientific Poster (Print Format); eP = Electronic Scientific Poster (ePoster);

EdE = Education Exhibit (Print Format); eEdE = Electronic Education Exhibit

Leitner, Y.	P-110	Lin, W.-C.	P-12, P-17, P-27, P-33,	Lu, H.	O-268
Leiva Salinas, C.	P-2		P-38, P-56	Lu, J. J.	EdE-18
Lemasson, B.	eP-146	Lindell, E. P.	O-145	Lucarelli, R. T.	O-64
Lemmers, P. Ma	O-174	Linden, C.	P-9	Lucato, L. T.	eEdE-34
Leng, L. Z.	eP-226, eP-240, O-417,	Lindquist, D. M.	O-304	Ludwig, B. J.	eP-185
	O-418	Linetsky, M.	O-396	Luetmer, M. T.	O-437
Leon, J. Luis e	P-23, eP-278	Linglong, K.	O-296	Luetmer, P. H.	O-489
Lequin, M. H.	EdE-78, EdE-82	Linn, J.	eP-89	Lui, C.-C.	P-17
Lerario, A.	eP-295	Linn, J.	O-600	Lui, Y.	eP-164a
Lerner, A.	EE-72, eP-137, eP-292,	Linscott, L.	O-543	Lui, Y. S.	eEdE-58
	O-509	Lipshutz, G.	EE-11	Lui, Y. W.	O-58
LeRoux, L.	O-406, O-601	Lipton, M. L.	O-53, O-54, O-55,	Luijten, P. R.	EdE-24
LeRoux, L. G.	O-602		O-196, O-620, P-65	Luitse, M.	O-579
Lesser, G. J.	O-224	Lipton, R. B.	O-53, O-54, O-55, P-65	Lukas, R. V.	eEdE-23
Letourneau-Guillon, L.	O-61	Lis, E.	EdE-95, O-490, O-546, O-597	Lummel, N.	O-600
Leung, J.	O-176	Lisserre, R.	O-286	Lundquist, J.	eP-221, O-413, O-415
Leuthardt, E.	O-213	Litt, A. W.	O-82	Luo, C.	eP-8
Lev, M. H.	eP-58, eP-59, O-21,	Litt, H. I.	O-13	Luo, C.-B.	eP-254
	O-577, O-638	Liu, C. Y.	eP-137	Lupson, V. C.	O-216
Lev, S.	EdE-31, eEdE-48, eEdE-63,	Liu, H.	O-301	Luttrull, M. D.	EE-25, EdE-92
	eP-59	Liu, H.-M.	P-96	Lutz, J.	eP-89, O-600
Levi, A. D.	EE-52	Liu, T.	eP-145, -147, O-114	Lutz, K.	eP-95
Levy, E. I.	O-22, O-561	Liu, W.-C.	eP-301, eP-302	Lycklama, G.	eP-252
Levy, L. M.	P-82, P-83	Liu, X.	eP-83, eP-100, eP-144	Lycklama, G. J.	O-584
Lewin, J. S.	eP-299, O-251, 438	Liu, Y.	eP-119, O-118	Lylyk, P.	eP-221, eP-223, O-413,
Lewis, D. A.	eP-256	Liu, Y.-S.	eEdE-4		O-415, O-484, O-580
Lewis, D. V.	O-299	Liu, Z.	EdE-98	Lyo, J.	O-219, O-597
Lewis, T. T.	EdE-7	Lo, E.	eP-166	Lyons, T.	eEdE-87
Lexa, F. J.	EdE-47	Lo, S. S. M.	O-485	Lyra, K. P.	O-229
Lexa, VII F. J.	O-83	Löbel, U.	EE-10, O-149	Lysack, J.	EdE-4
Li, C. Q.	EdE-46	Lobert, P.	eEdE-77	Lysack, J. T.	EdE-93, O-443
Li, S.	EdE-32	Lobotesis, K.	O-575		
Li, Y.	O-400, O-549	Loeckner, C. Patrick	O-439	<b>M</b>	
Li, Y.-O.	O-57, -31	Loes, D. J.	O-302	Macadam, B.	EdE-31
Li, Z.	P-21	Loevner, L. A.	eP-191, O-89	Macchiaiolo, M.	EE-78
Liao, J. H.	O-244, O-245	Loewenstein, J.	eP-272	MacFall, J.	O-299
Liauw, L.	eEdE-47, eEdE-151	Loftus, M. L.	O-152	Machi, P.	eP-213, O-575, O-581
Lieb, J. M.	eP-107	Loh, J.	EE-7	Macho, J.	O-568
Lieber, B. B.	eP-262	Londy, F. J.	O-131	Macingwane, N.	O-408
Liem, J.	EE-104	Loney, E.	EdE-42	MacKenzie, J. D.	EdE-85
Lignelli, A.	EE-21, EE-45, EE-85	Longo, D.	EE-78	Madan, N.	O-136, O-594
Likeman, M.	EdE-7, EdE-27, P-100	Lonser, R. R.	O-319	Madison, M. T.	O-22, O-561
Lim, H. K.	O-329	Loomba, J. J.	O-585	Madsen, J. R.	O-301
Lim, J. W.	eP-193	Lopez Rueda, A.	O-568	Maeda, M.	eP-10, P-7
Lima, P. F.	P-23	Lopez-Alvarez, Y.	eEdE-126	Maeder, P.	O-240
Limperopoulos, C.	O-10	Lopez-Bueno, J.	eEdE-132	Maertz, N.	EdE-49
Lin, C.-J.	eP-254	Lopez-Gonzalez, R.	eP-3	Mafee, M. F.	EdE-46
Lin, C.-P.	P-27, P-28, P-35, P-38, P-4,	Lorenzo, G.	EdE-58, EdE-87	Maggialetti, A.	eP-40
	P-5	Lotz, J. C.	O-367	Magnus, T.	EE-10, O-149
Lin, D.	eEdE-15, eP-296	Lovato, J.	O-567	Mahadevan, A.	eP-183
Lin, D. D.	O-314, P-73	Lovblad, K.-O.	eP-132, O-492	Mahady, K. F.	EdE-42, O-595
Lin, E.	P-113	Love, Z.	O-487	Mahajan, A.	EdE-4, EdE-35,
Lin, T.-T.	P-12	Low, S. B. L.	eP-53, eP-198		EdE-93, P-142, -424
Lin, W.	eP-121, eP-243, O-253,	Lowe, L.	eEdE-127	Mahajan, B.	eEdE-18, eEdE-21,
	O-296	Lu, C.-H.	eEdE-4, P-27, P-33, P-38		eP-79, O-98, O-99

### Index of Program Participants

Numbers refer to session and presentation numbers, *not to page numbers*.

Index Key: O = Scientific Paper (Oral Presentation); EE = (Electronic) Excerpta Extraordinaire;

P = Scientific Poster (Print Format); eP = Electronic Scientific Poster (ePoster);

EdE = Education Exhibit (Print Format); eEdE = Electronic Education Exhibit

Mahdevan, A.	eEdE-40	Manzoni, P.	O-50	Mazioti, A.	eEdE-142
Maher, C.	O-131	Manzoor, M. U	eP-170, O-639	Mazura, J.	O-418
Maheshwari, M.	EdE-14, EdE-39, EdE-70, EdE-86, eEdE-61, eEdE-114, eEdE-124, eEdE-129, eEdE-134, eEdE-136	Marano, G.	eP-186	Mazura, J. C.	O-545
Maheshwari, M. C.	eP-280	Mardal, K. A.	O-403	Mazzola, A.	P-76
Maier, A.	eP-207	Marden, F. A.	EE-63	McAleer, M. F.	eP-142
Maizeroi-Eugène, F.	O-309	Marder, C. P	eEdE-51	McCluskey, L. F.	eP-103
Majeed, Y.	eP-170	Mariko, Y.	EdE-9	McCollom, V. E.	O-22, O-561
Majoie, C. B. L.	eP-252, O-584	Marini, B.	P-85	McDermott, M.	eP-233
Majumder, S.	eP-141	Mark, L. P	eEdE-57, eP-297	McDonald, S.	O-257
Makino, K.	eP-90, P-40	Markl, M.	eP-129, O-520	McDougall, C.	eP-257
Malagari, A.	eEdE-142	Marktel, S.	eP-295	McDougall, C. G.	O-338
Malba, V.	eP-222	Marom, R.	P-110	McEvoy, L.	O-125
Maldjian, J. A.	eP-150, O-104, O-40, O-63, O-66, O-77, P-19	Marotta, B.	O-420	McEvoy, L. K.	eP-67, O-500, O-502
Maldonado, I. L.	eP-169, eP-213, O-575	Marotta, T. R	O-420	McGinty, G.	O-451
Malek, R.	O-557	Marquez, J. C.	EdE-73	McGregor, A.	O-300
Malfetano, B.	eEdE-10	Marrone, A. C. H.	P-76	McHugh, J.	EE-54
Malhotra, A.	EE-105, eEdE-7, eEdE-22, eEdE-22, eEdE-148	Martin, A. J.	eP-222, eP-233	McIntosh, E	O-562
Mali, W.	eP-151	Martin, B. A.	O-131	McIntyre, J. J.	O-526
Mali, W.	O-579	Martin, K.	EdE-85	McKenzie, G. A.	O-144
Malisch, T.	O-557	Martin, R.	eP-124	McKevitt, F.	O-105
Malisch, T. W	O-22, O-561	Martin-Duverneuil, N.	eEdE-96	McKinney, A.	O-173
Maller, V.	EdE-23, EdE-60, EE-5, EE-57, EE-58, eP-127	Martinelli, V.	EE-2	McKinney, A. M	eP-69
Maller, V. G.	EE-89, EE-102, eEdE-5, eP-282	Martinez, M.	P-44, P-49	McKinstry, C. S	EE-38, EE-83, eP-248, eP-249, P-91
Maloney, W.	eP-152	Martins, C.	eEdE-11	McKinstry, R. C.	O-543
Malter Cohen, M.	P-31	Martucci, A.	eP-173	McLean, A.	O-260
Maluf, F.	eEdE-93	Maruoka, Y.	P-41	McMahon, A.	eP-81
Maluste, N.	O-316	Marziali, S.	eP-173, O-508	McNally, S.	eP-187
Maly Sundgren, P.	O-131	Mas, J-L.	O-28	McTaggart, R. A.	O-427
Mamourian, A.	EdE-10, eEdE-30, O-12	Mas Bonet, A.	EdE-28	Mead, L.	O-435
Mamourian, A. C.	P-54	Masala, S.	eP-313, O-529	Meagher, S.	O-341, O-557
Manaças, R.	eP-32, 25	Masi, P.	O-31	Mechl, M.	eP-77
Manara, O.	P-34	Mason, G. F.	O-349	Medeiros de Bustos, E	O-541
Manconi, F. M.	P-114	Masri, D. J.	eEdE-50	Meder, J-F.	eP-210, eP-285, O-28
Mancuso, A. A.	P-84	Masrur, S.	O-638	Medina, F. J.	EdE-73
Mandel, A.	EE-3	Massager, N.	O-218	Meena, M. Lal	EdE-30, eEdE-115
Mandelin, P.	eP-91	Massari, F.	eEdE-140, eEdE-141, eP-241, eP-313, O-529	Mehdizade, A.	O-492
Mandell, D. M	eP-163, O-239, O-564	Massini, T. C.	EdE-65	Mehra, M.	O-586
Manfrè, L.	eP-309, P-324, eP-325, P-119, 121	Massoud, T. F.	P-61, P-68, P-75	Mehta, D.	O-39
Mangat, H.	eP-61	Masutani, Y.	EdE-9, P-14	Mehta, P.	EdE-49
Mangiafico, S. E	dE-69	Matheus, G.	eP-156	Mehta, Z.	O-412
Mangla, R.	EdE-1, O-223	Mathis, C. A.	O-191	Meier-Cillien, M.	O-149
Manhart, M.	eP-239	Mathis, J.	O-527, O-528	Melançon, D.	EdE-41
Mankad, K.	EdE-83, eP-46	Mato Abad, V.	O-123	Melendez, M.	eEdE-126
Manley, G.	O-56, O-57	Matouk, C. C.	O-239	Melford, C.	O-60
		Matsumoto, J.	O-404	Melhem, E R	eP-103, eP-78
		Matsumoto, M.	P-36	Melis, M.	eP-173, O-508
		Matsuoka, Y.	eP-51, P-89	Meltzer, C. C.	O-276, O-452
		Matsushige, T.	P-88	Mendel, E	EdE-92
		Matsushima, N.	P-37	Mendelsohn, D.	P-106
		Matte, U. S	P-92	Mendelsohn, D. B.	P-46, P-66
		Mawad, M.	eP-207, eP-208	Menjot de Champfleure, N.	eEdE-96
		Maxwell, A. W. P.	P-108	Menon, B.	eP- eP-264, O-571
		Maya, M. M.	eP-101, eP-317	Menon, B. K.	O-235, P-74
		Mayank, D.	O-235	Menon, N.	O-595



### Index of Program Participants

Numbers refer to session and presentation numbers, *not to page numbers*.

Index Key: O = Scientific Paper (Oral Presentation); EE = (Electronic) Excerpta Extraordinaire;

P = Scientific Poster (Print Format); eP = Electronic Scientific Poster (ePoster);

EdE = Education Exhibit (Print Format); eEdE = Electronic Education Exhibit

Menon, P.	O-132	Miller-Thomas, M.	eEdE-152,	Montanera, W.	O-420
Meoded, A.	EdE-82, eP-276,		eEdE-28	Monteith, S.	O-585
	eP-277, eP-281	Mills, S.	EE-29	Moody, E. A.	O-40
Merchant, M.	EdE-33	Mills, S. J.	eP-84	Moon, W-J.	eEdE-49
Merchant, T. M	O-548	Milwid, R.	O-61	Moonis, G.	eEdE-68, eEdE-69,
Mercieca, K.	eEdE-70, P-69	Minja, F. J.	EE-48		eEdE-79, eEdE-91, O-183, O-390
Meriot, P.	eEdE-101	Minkowitz, S.	O-152	Moore, H.	O-182
Mernes, R.	O-575	Minniti, G.	O-287	Moore, K. R	O-182
Meschini, A.	O-508	Mintzer, J.	O-124, O-143	Moquete, E	eP-196
Messina, S. A.	O-511	Miralbes, S.	EdE-28	Morais, L. M T	eEdE-34
Metherall, P.	O-105	Miraldi, F.	eEdE-150	Morales, H.	EdE-94, eEdE-99
Mettenburg, J. M	O-120	Mirochnik, B.	eEdE-48	Morales, J. C.	eEdE-52
Meuli, R.	O-240	Mirsadraei, L.	O-290	Morales, R. E.	EE-61
Meyer, F. B.	eEdE-41	Mirsky, D. M	EdE-74, EdE-77,	Morales, R.	O-39
Meyerand, E	O-220		EdE-80, EE-73	Moran, C. J.	O-616
Mian, A.	eEdE-43, P-3	Mirza, N.	O-420-389	Moreau, K.	O-393
Miayazaki, Y.	P-97, P-99	Mishra, A.	EE-47	Moreno, A.	O-581
Michals, E	eP-166	Miskolczi, L.	O-557	Morgan, P.	O-639
Michel, M. A.	O-334	Mistretta, C.	eP-225, O-587, O-589	Mori, H.	eP-21
Middleton, D. M	O-180	Mitchell, L. A.	O-551	Mori, K.	O-103
Mihlon, IV F.	O-393	Mitchell, S.	eEdE-74, O-48	Mori, M.	P-42
Miki, H.	eP-165	Mitjana, R.	eP-70, O-128, O-510	Mori, S.	eP-9, eP-171
Mikkelsen, T.	O-063, O-285, P-39,	Mitra, A.	O-213	Mori, T.	eP-108, eP-244, eP-267,
	eP-146	Mitter, C. S	O-261		P-8, P-97, P-99
Mikulich-Gilbert, S.	O-146	Miyasaka, T.	eP-28, eP-35, eP-48,	Morikawa, M.	P-67
Mikulis, D.	eP-163		eP-108, eP-117, eP-244, eP-267	Moritani, T.	eEdE-36, eEdE-43,
Mikulis, D. J.	O-176, O-239, O-274,	Miyazaki, Y.	P-8		eEdE-149, eP-1
	O-564	Mizoguchi, M.	P-41	Moritz, C.	O-220
Milani, S.	O-133	Mizumura, S.	EE-6	Moriya, J.	eP-68
Milch, H.	eP-164a, eP-66, O-504	Mlynash, M.	O-20	Morón, F.	P-90
Milch, H. S	eEdE-58	Mochizuki, T.	eP-5, eP-165	Morozova, L. V.	EE-79
Milhaud, D.	O-575	Mocking, S.	O-562	Morris, J. M.	eEdE-41, eP-120,
Milla, S.	eEdE-108, eP-164a, O-52	Modi, J.	EdE-35, EdE-4, O-235,		O-145
Millan-Juncos, J. M.	eP-47		O-27, O-29, O-558, O-571, P-74	Morris, K.	O-501
Millar, W. S	EE-21, EE-3, EE-45,	Modic, M. T	O-464	Morris, P.	EE-69
	EE-85	Moe, D.	EdE-70	Morris, S.	O-297
Miller, A.	EdE-98	Moen, G.	O-71	Morriss, M. C.	eEdE-113, O-175
Miller, C. Ryan	eP-139, O-294	Mohtakhar, P.	O-578	Morsi, H.	eP-207, eP-208
Miller, D.	O-116	Mohamed, F.	O-181	Mortilla, M.	eEdE-119, EdE-7
Miller, D.	O-146	Mohamed, F. B.	O-180, O-607	Mortimer, A. M	eP-124, P-100
Miller, E	EdE-123, eEdE-131,	Mohamed, M. A.	P-115	Moseley, M. E.	O-37
	eEdE-132	Mohammed, N.	O-400	Mosen, L. A.	O-216
Miller, G. M	eP-120	Mohan, S.	EdE-74, eP-78	Moser, F. G.	eP-101, eP-317
Miller, J. H.	EdE-76	Mohr, A.	P-93	Moser, R. P	eP-227
Miller, J. H.	EE-88, EE-90,	Mohr, J. P	eP-196	Moshe, S. L	O-299
	EE-96, O-552	Mohsin, H.	P-22	Mosier, K. M	P-81
Miller, J. W	O-576	Mojibian, H. R	eEdE-146	Moskowitz, A. J.	eP-196
Miller, L. E.	eP-310	Molina, X.	O-593	Mossa-Basha, M.	EdE-36, eEdE-93,
Miller, M. I.	eP-9	Moll, A.	EdE-28		O-314, P-73
Miller, M. E.	O-567	Molnar, C. P.	EdE-4	Moster, M.	EdE-19
Miller, P.	O-70	Molofsky, W.	eP-263	Motos, N.	O-593
Miller, S. L.	O-524	Molofsky, Sr. W.	O-311	Motta, S.	P-92
Miller, T.	O-527, O-528	Molyneux, A. J.	O-339, O-412	Mouannes-Srour, J.	eP-104
Miller, T. S	eP-63, eP-126, eP-319	Mong, S.	O-290	Moulin, T.	O-541
		Montalban, X.	eP-70, O-128, O-510	Mounayer, C.	eP-220, O-309

### Index of Program Participants

Numbers refer to session and presentation numbers, *not to page numbers*.

Index Key: O = Scientific Paper (Oral Presentation); EE = (Electronic) Excerpta Extraordinaire;

P = Scientific Poster (Print Format); eP = Electronic Scientific Poster (ePoster);

EdE = Education Exhibit (Print Format); eEdE = Electronic Education Exhibit

Mouri, M.	EE-82, O-103	Nagornaya, N.	O-559	Netto, J. P	eEdE-39
Moy, C. S	eP-196	Nagot, N.	O-575	Neuwelt, E	eP-93
Moyle, H.	eP-266	Nagpal, S.	O-208	Neuwelt, E. A.	eP-20, O-267
Mualem, E	O-556, O-557	Nagy, P.	eP-299, O-438	Newman, J.	eP-191
Muchart Lopez, J.	eEdE-123	Nahser, H. C.	P-91	Newman, N. J.	O-238
Mueller-Lenke, N.	eP-130	Naidich, T. P	eEdE-56, O-368,	Newman, S. A.	eP-103
Mugikura, S.	O-318		O-407	Newton, H. B.	EE-20
Muir, S.	EdE-68	Naidu, P. K.	EdE-76, EE-88,	Ng, S. A.	O-36
Mujherji, S.	EdE-45		EE-90, EE-96	Ng, S-H.	P-28
Mukherjee, P.	O-56, O-57, O-619,	Naidu, P. K.	O-552	Ngamsombat, C.	P-15
	P-31	Nair, D.	O-538	Nghiemphu, P. L	O-97, O-290,
Mukherjee, S.	O-404	Nair, S.	eP-226, eP-240		O-291
Mukherji, S. K.	EE-62, eEdE-77,	Nair, V.	O-220	Nguyen, D.	EE-58, eP-132
	eP-180, eP-190, O-278, O-340,	Najm, I.	O-538	Nguyen, D. T	EE-89, EE-102
	O-360, O-453	Nakagawa, H.	eP-117, eP-201,	Nguyen, R.	eP-187
Mukundan, G.	EE-40, EE-46		O-574	Nguyen, T.	O-442, P-3
Mukundan, S.	P-29	Nakahira, M.	O-248	Nguyen, T. H.	O-609, P-118
Mukundan, Jr S.	O-16	Nakai, MD K.	eP-25	Ni, W.	O-37
Mulcahey, M. J.	O-180, O-181	Nakajima, Y.	EE-26	Nicholson, A. D.	eEdE-137
Muldoon, L. L	eP-20	Nakamura, H.	EE-26, eP-306, eP-90,	Nickerson, J. P.	EdE-78, eP-283,
Mullins, M. E.	O-177		P-40		eP-291, O-596
Munoz Del Rio, A.	eP-323	Nakamura, L.	EE-68	Nickols, H. H.	EE-23
Muradyan, N.	eP-22, eP-137,	Nakamura, O. K.	eEdE-122,	Nicolas-Jilwan, M.	eEdE-16
	eP-140		eEdE-125	Niemann, D.	eP-225, eP-236
Murakami, S.	EdE-66, P-86	Nakashima, K.	eP-, P-89	Niessen, J.	eP-151, O-579
Muraszko, K.	O-131	Nakashima, R.	eP-90, P-40	Niessen, J. M	O-635
Murata, T.	O-318	Nakazaki, M.	eP-108, eP-244,	Nieves-Cruz, D.	eEdE-13
Murayama, Y.	O-573		eP-267, P-8, P-97, P-99	Niimi, Y.	eP-232, eP-263
Murph, D.	EE-68	Nakoneshny, S. C.	O-443	Niimi, Sr. Y.	O-311
Murphy, R.	O-435	Nam, H. S.	eP-206	Nishimura, J.	eP-39
Murray, A.	O-567	Nandiraju, D.	O-607	Nishimura, S.	eP-90, P-40
Mutlu, A.	O-610	Napolitano, A.	EE-78	Nishizawa, M.	O-232
Muto, M.	eP-318	Napolitano, S.	eP-295	Nitatori, T.	eP-43, eP-6, O-110
Muzard, E	O-541	Nappini, S.	EdE-69	Nittka, M.	eEdE-33, O-117
Muzzafar, S.	EdE-92, EE-25	Narang, J.	O-063a, O-285	Noorian, A. R	eP-57
Myers, J. N	eP-184, O-328	Narayan, A.	EE-54, O-439	Nordli, D.	O-299
Myochin, K.	eP-117	Narayanan, S.	P-94	Norenberg, M. D.	EE-52
Myouchin, K.	eP-201, O-574	Nasreddine, W.	O-540	Northam, M. C.	O-434
<b>N</b>		Natali Sora, M. G.	eP-295	Nosaka, R.	eP-30, P-43
Nada, E	P-115	Nawashiro, H.	eP-25	Noujaim, S.	eEdE-139
Nadgir, R.	eP-52, eP-174, O-248	Nazarian, J.	EdE-72	Nour, S. G.	O-251
Nadgir, R. N	eEdE-92, eP-33	Neal, M.	EE-69	Novais, G.	EE-22, EE-56, EE-60
	eP-192, O-242, O-244, O-245	Nedeljkovic, S. S	O-591	Novakovic, R. L.	O-524
Nadimpalli, S.	EE-100	Nederkoorn, P.	eP-252	Nowinska, N. G.	eEdE-29
Nadimpalli, S. P. R.	EdE-33	Nederkoorn, P. J.	O-584	Nowinski, W. L	eEdE-29
Naegelin, Y.	eP-130	Neimann, D.	eP-214	Nucci, C.	eP-173
Naeini, R. M	O-411	Nella, R.	eP-221, O-415	Numaguchi, Y.	eP-303
Nael, K.	O-396	Nella Castro, R.	O-413	<b>O</b>	
Nagarwala, J.	O-439	Nelson, K.	EdE-31	Oakes, T. R	O-60
Nagasunder, A. C.	O-175, O-255	Nelson, Jr. M. D.	eEdE-130, O-553,	Obach, V.	O-568
Nagata, I.	P-67		O-608	Oberstar, E	eP-225, O-587, O-589
Nägele, T.	eP-96	Nemec, S. F.	O-429	O'Brien, K.	O-240
Naggara, O.	eP-210, eP-285	Nemec, U.	O-429	Ochi, T.	eP-117, eP-28, eP-35,
Nagornaya, N.	eP-73	Nerenz, D. R	O-591		eP-48
		Neto d'Almeida, G.	P-25		

### Index of Program Participants

Numbers refer to session and presentation numbers, *not to page numbers*.

Index Key: O = Scientific Paper (Oral Presentation); EE = (Electronic) Excerpta Extraordinaire;

P = Scientific Poster (Print Format); eP = Electronic Scientific Poster (ePoster);

EdE = Education Exhibit (Print Format); eEdE = Electronic Education Exhibit

O'Connor, K. M	eEdE-43	Owens, S.	EE-55	Park, H. S.	eP-301, eP-302
Oda, S.	eP-165, eP-5	Oygar, A. E.	EE-32	Park, J-H.	eP-304
Odawara, S.	EE-82, O-103, P-42	Oyoyo, U.	eP-289, O-65	Park, K. Y.	eP-206
O'Donovan, R.	EdE-17	Ozaki, J. O.	eP-275	Park, S-W.	EdE-56, eP-177,
Ogawa, T.	eP-195	Ozawa, T.	eP-300		eP-178, P-80
Oguz, K. K.	EdE-5, eP-12, eP-27,	Ozen, O.	EE-92, EE-101	Park, T. C.	EE-46
	O-305	Ozgen, B.	eEdE-82, -182, O-431	Parker, G. J. M.	eP-84, O-70
Oh, S. J.	eEdE-15		O-432	Parker, R.	O-124, O-143
Ohara, A.	eP-6, eP-43	Ozhand, A.	eP-137	Parker, R. O.	O-122
Ohara, A.	O-110	Ozsvath, J.	EE-39	Parker, S.	EE-31
Ohnari, N.	eP-39, eP-68, O-115	Ozsvath, J. A.	eEdE-108, O-441	Parkes, L. M	O-228
Oikonomopoulos, N.	eP-265			Parlak, M.	eP-26
Oishi, K.	eP-9	<b>P</b>		Parmar, H. A.	eP-111
Okada, Y.	EE-6	Padua, A.	eEdE-33, O-117	Parra, P. A.	O-139
Okazaki, T.	P-88	Paeng, Sung Suk S.	eP-301, eP-302	Parsons, M.	P-59
O'Kelly, C.	O-420	Pagani, J.	O-68	Pasowicz, M.	eP-77
Okubo, T.	eP-300	Pagnini, P.	eP-137	Pasquale, D.	EdE-67, eEdE-50,
Okuchi, K.	eP-48	Pajares, G.	eP-71		eP-126
Oleaga, L.	O-535	Pakbaz, R.	O-613	Pastel, D.	EdE-50, O-526
O'Leary, S.	EE-71	Pal, P. Kumar	O-503	Pastel, D. A.	EdE-57, EdE-79,
O'Leary, S. M	EE-38, EE-83	Palacios, E	O-187		EdE-96
	eP-248, eP-249, P-91	Palasis, S.	O-199	Pasternak, O.	P-30
Oliveira, A. R.	EE-56	Paldino, M.	eEdE-117, eEdE-121,	Pastor, R.	eP-278
Olson, R.	EE-9, EE-103		O-260	Patay, Z.	EE-33, EE-74, EE-91,
Omodon, M.	O-210	Paldino, M. J.	O-542, O-80		O-300, O-400, O-548, O-549,
Omojola, M.	EE-1, EE-51	Palmer, J. N	eP-191		O-554, O-555
Omuro, A. Mp	O-207	Pamathy, S.	EE-20	Patel, A. A.	eP-266
Onat, L.	O-610	Pampana, E	eP-241	Patel, A. B.	eP-266
Oner, A. Y.	eP-14, eP-38	Pamplona, J.	EE-44	Patel, G.	EdE-29, EdE-48, eP-80,
Onodera, S.	eP-19	Pan, J. J.	O-302		P-21
Ooi, M.	eP-164	Pandey, A.	eP-251, eP-284, O-254,	Patel, G. V	P-51
Opatowsky, M. J.	EE-43		O-255, O-262, O-49, O-608	Patel, N.	EdE-59
Oppenheim, C.	eP-210, O-28	Pantol, G.	eEdE-79	Patel, N. V	EE-49, eP-326, P-122,
Orbach, D. B.	O-81	Panyaping, T. Lojana Tuntiyatorn			P-123
Orlandi, R.	eP-187	Chakrit Sugying	EdE-15	Patel, R.	O-488, P-106, P-46
Orlandi, R. R.	O-644	Panyaping, T.	EdE-15	Patel, S.	EdE-11, EdE-59, eEdE-81
Orrin, S.	eEdE-112	Paolucci, A.	O-515	Patel, S. K.	O-558
Ortiz, A. O.	eP-22, O-527, O-528	Papakonstantinou, O.	eP-320	Pathmanaban, O.	eP-81
Ortiz, O.	eEdE-143, O-525	Papanagiotou, P.	eP-247, eP-259,	Patricio, M.	EE-44
Ortiz, O. A.	eP-312		O-569	Patrick, K.	O-122, O-124, O-143
Ortiz, R.	eP-263, O-557	Papanicolaou, A. C.	eEdE-59	Patrie, J.	O-604
Ortiz, Jr. R.	O-311	Paquette, L.	eP-284, O-255	Patrie, J. T	P-2
Osborn, A. G.	O-151, O-353	Paramveer, S.	eP-24	Patsalides, A.	eP-197, eP-2,
Osborn, D.	O-322	Paraniak-Gieszczyk, B.	eP-77		eP-226, eP-240, O-417, O-418,
Osborne, J.	EdE-12	Parazzini, C.	O-133, O-140		O-490, O-545
O'Sullivan, M.	O-121	Pardo, C.	O-405	Patton, A.	eEdE-133, EdE-135
Oswood, M. C.	EE-28	Pareto, D.	eP-70	Patz, S.	O-594
Otaduy, M. C. G.	O-226, O-229	Parides, M. J.	eP-196	Pauliah, M.	O-545
Otero, A. V	P-77	Parikh, A.	eP-65	Paulsson, A. K.	O-224
Otsuka, T.	P-30	Parikh, G.	eP-61, P-16	Pawha, P. S	EE-53
Ott, S.	O-416	Parikh, S.	eP-266	Pawha, P.	O-42, O-389, O-592
Otten, L.	eP-315	Parish, M. E.	O-554, O-555	Pawha, P. S	O-407
Ouyang, T.	EdE-23, eEdE-5	Park, E. S.	eP-219	Payabvash, S.	O-21, O-638
Ow, T. J.	eP-184	Park, E. J.	O-226, O-229	Paydar, A.	O-52
Owen, J.	P-31	Park, G. Y.	eP-301, eP-302	Paz, D.	EE-34

### Index of Program Participants

Numbers refer to session and presentation numbers, *not to page numbers*.

Index Key: O = Scientific Paper (Oral Presentation); EE = (Electronic) Excerpta Extraordinaire;

P = Scientific Poster (Print Format); eP = Electronic Scientific Poster (ePoster);

EdE = Education Exhibit (Print Format); eEdE = Electronic Education Exhibit

Pearl, M.	eP-237, O-314, P-73	Piotin, M.	eP-220, O-640, O-310,	Prajapati, H. J.	EE-27
Pearl, M. S.	eP-322, O-511, O-512		O-517, O-581	Prasad, C.	O-588
Peatfield, R.	O-537	Pirastehfar, M.	O-396	Prasad, V. R.	O-38
Peck, K.	O-546	Pistocchi, S.	O-310 O-517	Prats, A.	O-563
Peck, K. K.	eP-80, O-219, O-221,	Pittella, J. E. H.	eP-275	Prayer, D.	eP-287, eP-293, O-215,
	O-545, O-597, P-21, P-51	Pizarro, J.	eEdE-54		O-252, O-261, O-429
Peddi, S.	eEdE-98	Pla, J.	eP-70	Prayoonwiwat, N.	eP-7, P-15
Pedicelli, A.	eEdE-141	Plebani, M.	O-133	Precel, R.	P-104
Pedraza, S.	eEdE-2, eEdE-24,	Poage, D.	EE-1, EE-51	Preibisch, C.	O-217
	eP-64, O-563, O-593	Poage, D. P.	EdE-13	Pressman, B. D.	eP-101, eP-317
Pedroza, A.	eP-235, -315	Podda, A.	eP-73	Preusser, M.	O-215
Peeling, L.	eP-262	Poduri, A.	eEdE-121	Previtali, S.	eP-295
Peeters, R. R.	O-209	Poisson, L.	O-285	Price, S. J.	O-216
Pehrs-Jurvillier, A. C.	eP-130	Polanco, A.	eP-266	Pride, Jr. G. L.	EdE-62
Peiffer, A.	EdE-38	Polaskova, P.	O-101, O-211	Prokop, M.	O-23
Pelletier, D.	P-32	Poliani, P. L.	O-286	Prologo, J.	O-487
Pellock, J.	O-299	Policeni, B. A.	eEdE-66, eEdE-95	Prothmann, S.	O-570
Peltz, M. T.	P-114	Politi, L. S.	EE-2, O-250	Provenzale, J.	O-442
Pelz, D. M.	eP-245	Politi, L. Salvatore	eP-295	Provenzale, J. M.	O-90
Pendse, D. A.	EdE-3	Pollack, E. B.	EdE-95	Pruetz, J. D.	O-255
Penna, K.	eEdE-63	Pollice, S.	eP-40	Pryde, S.	eEdE-74
Perandreu, J.	O-568	Pollock, J. M.	EE-11, EE-79, O-104	Psychogios, M.	O-35
Perazzini, C.	EdE-41	Polman, C.	O-510	Pucci, O.	O-564
Perchinunno, M.	EE-99	Polykarpou, M.	eP-266	Puget, S.	eP-285
Pereira, D.	eEdE-10	Pomerantz, S. R.	O-15	Puig Alcantara, J.	eEdE-2, eEdE-24
Pereira, L. P.	EdE-16, eP-311	Ponisio, M. R.	P-111	Puig Alcantara, J.	eP-64, O-563,
Pereira Loureiro, J.	O-123	Ponti, A.	O-405		O-593
Peri, N.	eEdE-40, EP-183	Poon, C.	eEdE-23	Pulfer, K.	eP-236, eP-239
Perkins, F. F.	O-300	Pope, W.	O-290	Purdy, P. D.	O-524
Perko, R.	EE-75	Pope, W. B.	eP-75, eP-82, O-6, O-97,	Pyne-Geithman, G. J.	O-304
Pervez, M. A.	O-638		O-291		
Petersen, E. T.	O-174	Poplawski, M. M.	O-407	<b>Q</b>	
Peterson, B. L.	O-327	Popovic, P.	eP-167	Qazi, A.	O-27, O-29
Peterson, B. S.	P-16	Poppert, H.	O-570	Qian, G.	eEdE-29
Petrella, J. R.	O-76	Popy, K. A.	eP-19	Qian, Sr. G.	O-536
Pezzulo, M.	O-218	Poretti, A.	EdE-78, EdE-82,	Qian, J.	EdE-29, EdE-48, eP-80
Pflugmacher, R.	eP-314, eP-315,		eP-276, eP-277, eP-281, O-142	Qian, R.	eP-104, eP-148
	O-531	Port, J. D.	O-159, P-62	Qian, R.	O-111
Phan, C.	eP-65	Portelo, A.	eP-106	Qiu, D.	O-37, O-45
Phillips, C. D.	O-270	Portnow, J.	eP-22	Quaghebeur, G.	O-51
Phillips, J.	O-292	Post, J. D.	eP-73	Quayle, K.	O-543
Phillips, M.	O-538	Post, M. J. D.	EE-98, O-85	Quencer, R.	eP-73
Philpott, C.	O-134, O-138	Postma, A. A.	EE-4, eP-294, O-325	Quencer, R. M.	O-621
Picado, M. J.	EdE-28	Potigailo, V.	O-402	Quigley, E.	eP-187
Pickering, C. R.	O-328	Poublanc, J.	O-564	Quigley, III E. P.	O-236, P O-288
Picot, M.-C.	eP-169	Poutre, A. J.	EdE-52	Quijano, C.	EdE-86
Pienpuck, W.	eP-7, -15	Powell, D. K.	P-113	Quinet, S.	O-544
Pierot, L.	eP-218, O-419	Powers, A.	eP-291	Quiñones Tapia, D.	EdE-28
Pierpaoli, C.	O-550	Powers, A. K.	O-63	Quint, D. J.	O-131
Pile-Spellman, J.	eP-196	Prabhakaran, S.	eP-60	Qureshi, A. I.	eP-204
Pillai, J. J.	P-24	Prabhakaran, V.	O-220		
Pinarbasili, T.	O-73	Prabhu, S.	eEdE-116, eEdE-118,		
Pinheiro, C. P.	P-76		eEdE-120		
Pinho, M. C.	O-101, O-211	Prabhu, S. S.	EdE-38, eEdE-59,		
			O-68		

### Index of Program Participants

Numbers refer to session and presentation numbers, *not to page numbers*.

Index Key: O = Scientific Paper (Oral Presentation); EE = (Electronic) Excerpta Extraordinaire;

P = Scientific Poster (Print Format); eP = Electronic Scientific Poster (ePoster);

EdE = Education Exhibit (Print Format); eEdE = Electronic Education Exhibit

## R

R, A.	O-588	Raymond, J.	eP-210	Riordan, A. J.	O-398, O-636
Radbruch, A.	eP-86, eP-95	Raz, E.	EE-7, O-246, O-599	Rios, A.	EE-44
Radhakrishnan, R.	EdE-84	Re, T. J.	O-133, O-140	Riquelme, C.	O-575
Radu, A.	eP-45	Reale, C. A.	eP-241	Ritz, R.	eP-96
Raduazo, P. A.	eP-185	Reardon, M. A.	O-404	Rivas-Rodriguez, F.	EdE-45, eEdE-6, eP-180
Radue, E. Wilhelm	eP-130	Reasonda, L. G.	eP-142	Rivera, W.	eEdE-64, eEdE-97
Radue, E-W.	P-32	Reaume, J.	O-58	Rivera-Morell, M.	eEdE-126
Radvany, M. G.	eP-237, O-511	Rebollo Polo, M.	eEdE-123, eEdE-132	Rives, A. F.	eP-174
Raghavan, N.	EE-46	Recht, L.	O-208	Rizzi, M.	P-34
Raghavan, P.	eEdE-16, O-102, O-404, O-604	Reddick, G. W.	EE-91, O-549, O-555	Rizzo, I-M. Pinto Oliveira	eP-286
Raghuram, K.	eP-250, eP-271	Ree, A.	O-606	Roarke-Adams, L.	eP-290
Rahman, F. N.	EE-18	Ree, A. A.	P-77	Roberson, G.	P-63
Rahmanuddin, S.	EE-72, eP-137, eP-140, P-44	Reede, D. L.	eEdE-062, eEdE-65, eEdE-85	Roberts, D.	O-300
Rahme, R.	eP-202	Reeves, M. J.	O-297	Roberts, D. R.	O-611
Rahme, R. J.	eP-129	Rehemtulla, A.	eP-146	Roberts, T.	eP-186
Rai, A.	eP-271, O-118	Reichenbach, J. R.	O-67	Roberts, T. P. L.	O-330
Rai, A. T.	eP-250	Reis, J.	EE-44	Robertson, R. L.	O-198
Raja, C.	eEdE-54	Reis, J. L.	eP-242	Robson, C. D.	O-156
Rajamohan, A.	EE-72	Reis, J.	P-20	Roca, P.	O-28
Rajaram, V.	EE-93	Reiser, M. F.	O-320	Rocca, M. A.	O-510
Rajderkar, D.	P-111	Reith, W.	eP-247, eP-259, O-569	Rock, J.	O-210
Rajpal, G.	eP-218	Renieri, L.	EdE-69, EE-71	Rockette, H. E.	O-448
Raju, R. C.	P-58	Rennie, I. M.	EE-38, EE-83, eP-248, eP-249, P-91	Roddey, C.	eP-67, O-500
Raju, S.	P-58	Renowden, S. A.	EdE-27, EdE-37, P-100	Rodegher, M.	EE-2
Raju, S. C.	P-58	Renshaw, P. F.	O-157	Rodrigues, K. M.	O-542
Ramachandra, T. R.	EE-23	Rezek, I.	eP-256	Rodriguez, F. R.	eP-190
Ramalho, J.	P-20	Reznikov, B.	eP-144	Rodriguez, I.	eEdE-19
Ramirez, P.	eP-289	Rhee, H. Y.	O-126	Rodriguez, P.	eP-37
Ramos, A.	eP-47, O-123	Rhee, S. C.	EdE-53	Rogers, G. F.	O-155
Ranawat, N. S.	eP-204	Rhym, J. H.	EdE-56	Rogg, J. M.	eP-158
Randisi, F.	EE-80	Riascos, R.	EdE-066, eEdE-109, O-391	Roh, H. G.	eEdE-49
Rankine, J.	O-595	Ribeiro, C.	eP-242	Rohatgi, S.	eEdE-116, eEdE-118
Rao, G.	eP-142	Richert, N.	P-32	Rojas, D.	O-116, O-146
Rao, N.	EdE-19	Richner, B.	EdE-78	Rojas, R.	eEdE-40, eEdE-9
Rao, P.	EdE-72	Riedel, C. H.	eP-56	Rollins, N. K.	eEdE-, O-175, O-262
Rao, S.	P-90, P-120	Riedy, G.	O-60	Romano, A.	eP-102, O-287
Rapalino, O.	EdE-18	Riegel, M. S.	O-524	Romano, D. G.	eEdE-104, eP-200
Rarey, K.	EE-79	Riffaud, L.	eEdE-106	Romano, J.	eEdE-46
Raslan, O.	eP-41	Riggeal, B. D.	O-238	Romanowski, C.	P-64
Raslau, F.	eEdE-57, P-71	Righini, A.	O-133, O-140	Romanowski, C. A.	O-105
Raslau, F. D.	eP-297	Rigolo, L.	O-222, P-29	Romero, J.	EdE-18, eP-65, O-391
Raspall, M.	eEdE-110	Rigucci, S.	eP-102	Romero, J. M.	O-230, O-233
Rassner, U.	O-288	Riina, H. A.	eP-197, O-418	Roncaroli, F.	O-106
Ratai, E.	O-258	Riklin-Raviv, T.	eP-293	Roncarolo, F.	eP-269
Rathi, Y.	P-30	Riley, K. O.	P-63	Rondinoni, C.	P-105
Rauch, R.	EE-94	Rimoin, D. L.	O-429	Rooks, V.	EdE-52
Ravi, V.	EdE-21	Ringel, F.	O-217	Roos, I.	O-584
Rawal, S.	EE-8	Ringer, A. J.	eP-202	Roos, Y.	eP-252
Raybaud, C.	EE-81, O-138	Rink, C.	eP-54	Roppongi, T.	P-30
Ray-Chaudhury, A.	EE-20	Riordan, A.	eP-151, O-234	Rosa, S. D.	EdE-83
Rayes, M.	P-94			Rose, M.	eP-311
				Rosebrock, R. E.	eP-13
				Rosen, B. R.	O-357
				Rosenbaum, D. G.	O-152

### Index of Program Participants

Numbers refer to session and presentation numbers, *not to page numbers*.

Index Key: O = Scientific Paper (Oral Presentation); EE = (Electronic) Excerpta Extraordinaire;

P = Scientific Poster (Print Format); eP = Electronic Scientific Poster (ePoster);

EdE = Education Exhibit (Print Format); eEdE = Electronic Education Exhibit

Rosenbaum, S. B.	O-53, O-54	Sabbag, D. J.	O-391	Salzman, K. L.	eP-155, O-151,
Rosenberg, J.	O-427	Sabbagh, S.	O-540		O-236
Rosenblum, M.	O-210	Sabbharwal, P. S	O-588	Sam, K.	O-564
Rosengart, A.	eP-61	Sabby, T. L	eP-120	Samdani, A.	O-180, O-181
Roser, H. W	eP-107	Sabel, B.	eP-65	Sameshima, Y. T	eEdE-122,
Ross, B. D.	eP-146	Sabin, N.	EE-91		eEdE-125
Ross, J. S.	O-463	Sabin, N. D.	EE-33, O-548, O-554	Sammet, C. L	eEdE-12
Rosset, S.	eP-16, eP-275 P-105,	Sablauer, A.	EE-91, O-400, O-549	Sammet, C.	eP-104
	P-23	Sadasivan, C.	eP-262	Sammet, S.	eEdE-12
Rossi, A.	O-264, O-470	Sadeghi, N.	EdE-53	Sampat, M.	O-56
Rossi Espagnet, M. C.	eP-102	Saeed, M.	eP-222	San Millan, D.	eP-322
Roth, C.	eP-247, eP-259, O-569	Safder, S.	EE-42	San Roman, L.	O-568
Roth, S.	O-522	Safran, H.	eP-75, eP-82	Sanchez-Montanez, A.	eEdE-110,
Röther, J.	O-149	Safriel, Y.	eP-138		O-139
Rottoli, M. R.	P-34	Sagar, J. R	eP-60	Sanders, D. S	O-150
Roudsari, B.	O-178	Saginoya, T.	P-47	Sanders, W.	eP-258
Roudsary, B.	eP-298	Saha, A.	eEdE-26	Sandhu, G. S	O-251
Rouse, G.	eP-289	Sahu, C. D.	eP-274	Sandulache, V. C.	eP-184
Rousset, J.	eEdE-101	Said, N.	O-604	Sanelli, P.	eP-61, O-31, O-118,
Roux, P.	eP-162	Saida, Y.	eP-303		O-152, O-163, O-473, O-565
Rovira, A.	eP-70, O-128, O-188,	Saigal, G.	eP-73	Sanelli, P. C.	eP-160, P-6
	O-442, O-510	Sailer, A. M H	eP-157	Sanford, R.	O-400
Rowland, L. M	O-348	Saindane, A.	EdE-90	Sangruchi, T.	P-48
Rowley, H. A.	O-17, O-461	Saindane, A. M	eEdE-137, eP-215,	Sanna, A.	eEdE-104
Royalty, K.	eP-214, eP-225, eP-236,		307, O-238	Sansgiri, R.	O-555
	eP-239, O-587, O-589	Saini, J.	O-503, O-588	Santacana, G.	eEdE-97
Rua, S.	O-31	Sainil, J.	eP-24	Santillan, A.	eP-197 eP-199,
Rubenstein, J.	O-107	Sainte Rose, C.	eP-285		O-417, O-418, O-545
Rubi, S.	O-535	Sair, H.	EdE-36, O-269	Santi-Vinci, M.	eP-290
Rubin, D. L	eEdE-16	Saito, K.	eP-68	Santos, A. C.	eP-16, eP-275, P-105,
Rubin, D. G.	eP-199	Saito, N.	eEdE-92, eP-33, eP-52,		P-23
Rubinstein, D.	P-77		O-248	Santos, G. T	eEdE-34
Rueda Lopes, F.	eEdE-150	Saito, Y.	P-30	Santy, K.	EdE-78
Rueda-Lopes, F. C.	eEdE-10,	Sakaguchi, H.	eP-28	Sanverdi, E	eP-182, O-305, O-432
	eEdE-11	Sakai, J.	O-146	Sanverdi, E S.	eP-12
Ruijters, D.	eP-209	Sakai, O.	EdE-43, eEdE-43,	Sara, R.	eEdE-85
Rumboldt, Z.	eEdE-140, EdE-141,		eEdE-92, eP-33, eP-52, eP-171,	Saraf Lavi, E	EE-52, O-559
	O-122, O-124, O-143, O-639, O-87		eP-174, eP-192, O-242, O-244,	Sargasyan, A.	EdE-066a
Runge, V. M.	eEdE-33, O-117		O-245, O-248, P-3	Sargysan, A.	eEdE-67
Ruscalleda, J.	eP-77	Sakaie, K.	O-538	Sarica, F. B.	eP-279
Rusinak, D.	O-108	Sakamoto, A.	P-36	Sarikaya, B.	O-173
Rusine, H.	eP-66, O-504	Sakamoto, A. C.	eP-16, eP-275	Sarkar, S.	eEdE-145, O-598
Russell, P. T	EE-23	Sakamoto, M.	eP-195, eP-201,	Sarlls, J.	O-550
Russell, S.	O-297		eP-28, eP-35, eP-48, O-574	Sasaki, Y.	eP-171
Ryan, G.	O-134	Sakamoto, S.	P-88	Sastre-Garriga, J.	O-128
Rydberg, C. H.	P-62	Salamon, E	eP-2	Sathyakumar, V. D.	P-78
Rykken, J. B.	O-401	Salamon, N.	O-396	Sathyan, P.	eEdE-18, eP-14,
Ryu, C-W.	eP-211, O-126	Salinas, C. Leiva	eP-4		eP-94
		Salloway, S.	O-190	Sathyan, P.	O-98
<b>S</b>		Salmon, C. E. G.	eP-16, P-105	Sato, K.	eP-9
Saad, M.	O-607	Saloner, D.	eP-233	Sato, N.	P-11
Saadeh, T.	P-120	Saltz, J.	O-102, P-39	Sato, T.	O-115
Sabat, S.	EdE-60, O-440	Salvador, E	eP-47	Sato, Y.	eEdE-36, eEdE-95, eEdE
Sabat, S. B.	eEdE-5	Salvaggio, K.	eP-197		149, eP-1
Sabbag, D.	O-230			Sauer, R. N	O-224



### Index of Program Participants

Numbers refer to session and presentation numbers, *not to page numbers*.

Index Key: O = Scientific Paper (Oral Presentation); EE = (Electronic) Excerpta Extraordinaire;

P = Scientific Poster (Print Format); eP = Electronic Scientific Poster (ePoster);

EdE = Education Exhibit (Print Format); eEdE = Electronic Education Exhibit

Sauvageau, E	EE-37	Scoffings, D. J.	O-231, O-26	Shaibani, A.	EE-63, EE-70, EE-93,
Savatovsky, J.	eEdE-96, eP-162,	Scott, B.	eP-11		eP-148, O-111, O-22, O-237,
	O-310	Scott, J.	EdE-4		O-560, O-561, O-576
Savino, M. R.	O-436	Scott, Sr. J. N.	EdE-93	Shaltoni, H.	eP-207, eP-208
Scarabino, T.	eP-40	Scotti, G.	eP-295	Shankar, J.	eP-135
Scarlato, M.	eP-295	Scrivano, E	eP-221, O-413, O-415	Shankar, J. J. S.	EE-47, eP-152
Scarpace, L.	O-210, P-39	Sedlacik, J.	EE-10, O-149	Shankaran, S.	O-257
Scarpini, G.	EdE-69	Sedrak, P.	P-50	Shannon, P.	O-134
Schad, L. R.	O-67	Segall, H.	EdE-8	Shapiro, M. D.	eP-72
Schaefer, P.	EdE-8	Segall, H. D.	EdE-14, EdE-39,	Sharma, A.	O-363, P-59
Schaefer, P. W	O-230, O-373,		EdE-70, eEdE-114, eEdE-124,	Sharma, P.	eP-307, eP-321
	O-562, O-651		eEdE-129, eEdE-134, eEdE-136,	Sharma, R.	O-165
Schaëffer, S. M.	eP-294		eEdE-61, eP-280	Sharma, S.	P-82, P-83
Schallert, E. K.	EE-52	Seidenwurm, D. J.	O-204, O-342	Sharp, D. J.	O-537
Schatz, C.	EdE-44	Seidl, Z.	eP-77	Sharples, P.	P-100
Schauburger, J. S.	O-532	Seidman, M.	EE-54, O-322	Shatzkes, D.	eEdE-87
Schellingerhout, D.	O-406, O-601,	Sekhon, A. K.	EE-46	Shatzkes, D. R	O-333
	O-602	Sekiya, K.	eP-192, eP-33, O-242,	Shaw, D.	EdE-75
			O-244, O-245	Sheikh-Bahaei, N.	O-231
Scheltens, P.	O-501	Selcuk, H.	O-610	Shekdar, K. V	eP-290
Schiffman, J. S.	P-79	Seltzer, M.	EdE-50	Sheline, Y. I.	O-120
Schlamann, M. U	O-392	Sen, C.	eP-54	Shen, C-Y.	eP-168
Schlegel, J.	O-217	Sena-Estevés, M.	eP-227	Shen, D.	O-296
Schmalfluss, I.	EdE-59	Senage, T.	eP-162	Shen, P. Y	O-259
Schmalfluss, I. M	EdE-65, O-362	Seneviratne, Sr. U.	O-536	Shenton, M.	O-158, P-30
Schmid, E	O-518, O-572, O-583	Sennaroglu, L.	O-431	Shepherd, T. M	O-38
Schmidt, H.	eP-270	Seo, H.	eP-177, eP-178	Sheth, H.	O-52
Schmidt, P.	eP-35	Seo, H. B.	EdE-56, P-80	Shetty, C.	P-31
Schmiedeskamp, H.	O-37, O-208	Seo, H. S.	O-247	Shi, F.	O-296
Schmitt, A. J.	EdE-3	Seo, Y.	O-175	Shibata, D. K.	O-637
Schnabel, J. A.	O-51	Seol, H. Y.	O-247	Shibata, E	eP-303
Schneider, D.	eP-89	Sepulcre, J.	O-301	Shifteh, K.	eEdE-50, eP-63, eP-90
Schneider, F. L	P-76	Serafim, L. N	eP-275	Shigematsu, Y.	eP-92, eP-306, P-40
Schneider, G.	eP-77	Serena, J.	eP-64, O-563	Shih, J.	EdE-12, O-118, O-152
Schnell, O.	eP-89	Seri, I.	O-255	Shih, Y. Y	eP-123
Schnell, S.	O-520	Seris, C.	eP-213	Shih, Y-H.	eEdE-4
Schoeneman, S. E.	O-44	Serulle, Y.	eP-66, O-504	Shim, H.	O-160
Schoepf, V.	O-215	Sethi, I.	P-82, P-83	Shimamoto, H.	EdE-66, P-86
Scholz, J. M	EE-65, eP-216, O-421,	Setoain, X.	O-535	Shimoji, K.	eP-21
	O-422	Settecase, F.	eP-222	Shimony, J.	eP-60, P-103
Schöpf, V.	O-252	Seyedmehdi, P.	eP-58	Shimony, J. S	O-120, O-213, P-107
Schrader, D.	O-24	Shabani, A.	EdE-81	Shin, B.	O-31
Schramm, P.	eP-159, eP-270, O-24	Shaff, D.	O-557	Shin, N-Y.	eEdE-89, P-72
	P-93, P-98	Shah, A. D.	P-51	Shinagawa, K.	P-88
Schramm, R.	eP-159, eP-270, O-24,	Shah, B.	EdE-54, eEdE-86, eP-52	Shinnar, R. C.	O-299
	P-93, P-98	Shah, G.	EE-55, EE-62, eEdE-77	Shinnar, S.	O-299
Schrauben, E	O-112	Shah, G. V	eEdE-90	Shinohara, Y.	eP-195
Schultz, L.	O-063a	Shah, K.	EdE-38, eEdE-60	Shiraga, N.	EE-6
Schumacher, M.	O-580	Shah, K.	O-328, O-428	Shiraishi, S.	eP-90, P-40
Schwamm, L. H.	O-577, O-638	Shah, L. M	O-236, O-288	Shiran, S.	P-104, P-110
Schwarm, F.	O-99	Shah, P.	O-180, O-181, O-322	Shirato, H.	eP-19
Schwartz, E S	EdE-77	Shah, P. D.	EE-37	Shiroishi, M.	eP-288, eP-292,
Schwartz, K.	O-43	Shah, Q. A.	O-22, O-561		eP-91
Schwartz, K. M	O-241, O-401, P-1	Shah, S.	EdE-33, EE-14, P-50	Shiroishi, M. S	O-509, P-44
Schweitzer, A.	O-207	Shahi, K.	EE-40	Shivashankar, R.	EdE-94, eP-202
Sciubba, J.	O-243				

### Index of Program Participants

Numbers refer to session and presentation numbers, *not to page numbers*.

Index Key: O = Scientific Paper (Oral Presentation); EE = (Electronic) Excerpta Extraordinaire;

P = Scientific Poster (Print Format); eP = Electronic Scientific Poster (ePoster);

EdE = Education Exhibit (Print Format); eEdE = Electronic Education Exhibit

Shofty, B.	P-104	Soares, B. P	EdE-85	Stecco, A.	EE-99
Shreiber, R.	eP-136	Sodickson, D. K.	O-460	Steeple, L.	P-69
Shushrutha Hedna, V.	P-84	Sohn, C-H.	EE-29, EE-106,	Stefanatos, G.	O-607
Sibai, S.	eEdE-149		eP-84, EdE-56	Stefanini, M.	O-508
Sidani, C.	EE-98, O-559	Sohn, Sung Il I.	O-235	Stefani, M. A.	EE-41, P-76, P-92
Siddiqui, A.	eEdE-87	Sol, Y. L.	eEdE-80	Steffen-Smith, E. A.	O-550
Siegel, E.	O-32	Soliman, N.	eEdE-83	Stein, E. G.	O-36
Sijbers, J.	O-209	Solnes, L.	EdE-12	Stemkens, B.	O-640
Silbergleit, R.	EdE-11, EdE-97,	Soltanolkotabi, M.	EE-63, EE-93	Stensby, J. D.	EdE-50, EdE-96
	EE-103, eEdE-144		O-576	Stephenson, C.	eP-224
Silva, C. F.	eP-217	Som, P. M.	EE-53, O-246	Sterbis, K.	O-32
Silver, B.	eP-158	Soman, S.	O-45	Sterling, M.	EdE-19
Silver, F. L.	O-239	Son, C-H.	P-80	Steven, A.	O-39
Simao, G. N.	eP-275	Son, H. J.	EdE-84	Steven, A. J.	eEdE-39
Simard, M.	eEdE-102	Sondhi, D.	eP-199	Stewart, E.	eP-224
Simonetti, G.	eP-173, eP-241,	Sonne, D. C.	O-203	Stewart, M. G.	O-343
	eP-313, O-508, O-529	Sorensen, A. G.	O-101, O-211	Stewart, R.	O-637
Sindwani, R.	EdE-64, O-326	Sorenson, E. J.	O-489	Stewart, W.	O-55, P-65
Singal, M.	O-566	Soria, G.	O-563	Stieg, P. E.	eP-197, O-417
Singh, M.	EE-72, eP-91, O-227	Soriano, C. J.	eP-153	Stievenart, J. L.	O-609
Singh, S.	EdE-EdE-39, EdE-70,	Soun, J. E.	O-104	Stilwill, S. E.	O-644
	eEdE-114, eEdE-124, eEdE-129,	Sourour, N.	eP-212, eP-220, O-309	Stippich, C.	eP-105, eP-107,
	eEdE-134, eEdE-136, eEdE-61,	Sousa, I.	eP-106		eP-130
	eP-141	Sousa, P.	eP-32	Stitzel, J. D.	O-63, O-66
Singh, V.	eEdE-65	Souza, L.	eP-58, O-21	Stivaros, S.	EdE-81
Singhal, A. B.	O-562	Souza-Oliveira, C.	P-105	Stockley, H. M.	O-313
Singhal, R.	EdE-31	Sowiak, S.	P-117	Stokroos, R. J.	eP-181, eP-189,
Sintini, M.	P-102	Soylemezoglu, F.	eP-27		eP-294, O-325
Siripurapu, R.	eP-154	Sozzer, A. R.	O-576	Stone, J. A.	O-467
Siritho, S.	eP-7, P-15			Stoodley, N. G.	EdE-27, P-100
Sit, S. P.	O-22, O-556, O-557, O-561	Spampinato, M. V.	eP-170, O-122,	Storm, P.	eP-290
Skare, S.	eP-116, O-179		O-124, O-143, O-639	Stout, A.	EE-79
Skarpathiotakis, M.	eP-163	Spandorfer, R.	O-31	Støverud, K. H.	O-403
Skinner, H. D.	eP-184	Spano, V. R.	O-564	Straka, M.	eP-115, eP-116, O-20
Slezak, M.	O-439	Spears, J.	O-420	Straus, C.	O-147
Slone, H. W.	EdE-92, EE-25, EE-37,	Speck-Martins, C. E.	eP-286	Strojan, P.	eP-167
	eEdE-55	Spencer, F.	eEdE-70, P-69	Stroman, P.	O-399
Slone, W. H.	EE-20	Sperb, F.	P-92	Strother, C.	eP-214, eP-225,
Slovic, T.	O-256	Sperling, R.	O-125		eP-239, eP-261, O-589
Smit, A. L.	eP-294	Sperling, R. A.	eP-67	Strother, C. M.	eP-236, O-419,
Smit, E. J.	O-23, O-234	Spilberg, G.	eP-209, eP-217,		O-587
Smith, C. B.	P-63		eP-228	Struffert, T.	eP-230, eP-261, O-416
Smith, E. A.	O-119	Spilberg, G. Z.	eP-41	Stuart, G. A.	eP-124
Smith, E. E.	O-235	Sprenger, T.	eP-130	Stufflebeam, S. M.	O-301
Smith, J. K.	eP-156	Sprengers, M.	eP-252	Subramanian, M.	eP-174
Smith, J. Keith	O-296	Sprengers, M. E.	O-584	Succar, E.	O-322
Smoker, W.	eEdE-062	Squires, J.	O-49	Sugiyama, K.	eP-30
Smoker, W. R. K.	eEdE-65, eEdE-66,	Srinivasan, A.	EdE-74, EE-55,	Sugiyama, K.	P-43
	eEdE-95		eEdE-45, eEdE-77, eEdE-90	Suh, C. H.	eP-97
Smolak, A.	P-9	Stadler, A. A. R.	eP-189	Suh, S. H.	eP-49
Smyth, G. P.	EE-38, EE-83, eP-248,	Stadnik, T.	EdE-22	Suh, S-I.	O-247
	eP-249, P-91	Staib, L.	O-424	Suk, E. H.	eP-219
Sneade, M.	O-412	Standring, R.	O-322	Sukerkar, A.	EE-100
Snyder, A.	eP-60, O-213	Stapf, C.	eP-196	Sukumar, S.	O-107
Snyder, A. Z.	O-120	Starkey, L. J.	eP-1	Sullivan, S. D.	O-591

### Index of Program Participants

Numbers refer to session and presentation numbers, *not to page numbers*.

Index Key: O = Scientific Paper (Oral Presentation); EE = (Electronic) Excerpta Extraordinaire;

P = Scientific Poster (Print Format); eP = Electronic Scientific Poster (ePoster);

EdE = Education Exhibit (Print Format); eEdE = Electronic Education Exhibit

Sun, K.	P-100	Tanaka, Y.	EE-26, eP-68	Thomas, R.	O-208
Sun, S.	O-299	Tandon, N.	eEdE-8	Thompson, B. G.	eP-251
Sunaert, S.	O-209	Tanenbaum, L.	O-389	Thompson, G.	eP-81, eP-84, O-228, O-69, O-70
Sundgren, P. Maly	O-4	Tanenbaum, L. N	eP-36, O-36, O-407, O-42, O-592	Thompson, L.	O-146
Sung, J. Y.	O-329	Tang, K. W	O-485	Thompson, W.	O-125
Sunshine, J. L	O-251	Tang, V.	EdE-81	Thompson, W. K.	eP-67, O-500
Supsupin, E P	eEdE-109	Tanner, C. E.	O-136	Threlu, B.	eEdE-106
Surlan Popovic, K.	eP-167, eP-85	Tantillo, G.	O-219	Thulborn, K. R	O-566
Sussman, B.	eP-291	Tantiwongkosi, B.	eP-37	Thurlow, P. C.	eEdE-26
Suzuki, H.	EE-6	Tao, Y.	eP-237	Thurnher, M. M.	O-471
Suzuki, K.	EE-6	Taoka, T.	eP-117, eP-201, eP-28, eP-35, eP-48, O-574, P-25	Tian, W.	eP-100, eP-83
Suzuki, M.	EdE-9	Tardie, N.	O-391	Tie, Y.	O-222, P-29
Suzuki, M.	P-14	Tarr, R.	O-557	Tillin, T.	O-637
Swan, B.	O-220	Tartaglino, L.	EdE-19	Timothy, K.	O-505, eP-70, O-510
Swanson, J.	EdE-75	Tateishi, H.	eP-43, eP-6, O-110	Tishkoff, N.	EE-30
Swartz, J. D.	O-459	Tatsugami, F.	eP-68	Togao, O.	P-41
Swartz, R.	O-273a	Tatter, S. B.	O-224	Toh, C. H.	P-28, P-35
Swartz, R. H.	eP-163, O-239, O-25	Tavanti, F.	O-287	Tokgoz, N.	eP-38
Sweet, A.	O-222	Tavaré, J. C.	O-255	Tomasello, A.	O-568
Sweriduk, S. T	O-202	Tawfik, A.	eEdE-83	Tomimoto, H.	eP-10, P-37
Swischuk, L.	EE-68	TCGA Glioma Phenotype Research Group	P-39, eEdE-16, eEdE-17, eEdE-21, eP-141, O-102, O-285, O-289	Tomita, S.	EdE-66, P-86
Symons, S. P	eP-114	Tejada, J. G.	O-315	Tomita, T.	EE-93
Szatmary, Z.	eP-212	Tekchandani, L.	O-492a, O-525	Tomiyama, N.	O-232
Szczykutowicz, T.	eP-225, O-589	Tekes, A.	eEdE-74, eP-281, O-48	Tomlinson, G.	eP-163
Sze, G.	O-424	Teknos, T.	O-426	Tomsick, T.	EE-97
Sze, G. K.	O-91	Teng, M. M H	eP-143	Tomura, N.	P-47
<b>T</b>		Teng, M. Mu-Huo	eP-254	Tonduti, D.	eP-272
Tabesh, A.	O-30, O-639	Terae, S.	eP-19	Tong, D.	P-26, P-7
Taheri, M. R.	eP-179	Tessitore, E	O-492	Tong, F.	eP-215
Taheri, R.	EdE-53	Tha, K. K.	eP-19	Tong, F. C.	O-19
Tajiri, H.	eP-108, eP-244, eP-267, P-8, P-97, P-99	Thakkar, R.	EdE-91, eP-308	Topiwala, P.	O-639
Tajlil, A. T	EE-40	Thakkar, R. S	EE-50, eEdE-147, eEdE-76	Torrente, Y.	eP-295
Takada, Y.	O-103	Thamburaj, K.	EE-57, eEdE-5, eP-127	Torres, C. I.	EdE-17
Takahashi, S.	O-318	Thapa, M.	EdE-75	Torres, C.	eEdE-132, eEdE-42
Takahata, H.	eP-51, P-89	Thawait, G.	EdE-91, EE-50	Torun, N.	eEdE-68, eEdE-69
Takayama, K.	eP-117, eP-201, O-574	Thawait, G. K.	eEdE-76, eP-308, O-75	Tosun, O.	O-433
Takayasu, T.	eP-30, P-43	Thawait, S.	EdE-91, EE-50	Toth, V.	O-217
Takeuchi, H.	eP-195, P-29	Thawait, S. K.	eEdE-76, eP-308, O-75	Toure, S.	eP-289
Takhtani, D.	eP-41	The FEBSTAT Study Team,	O-299	Touzé, E	O-28
Tal, A.	eP-113, O-127	The PICS Investigators,	O-557	Towle, V. Leo	O-522
Talbott, S.	eEdE-75	The START Investigators,	O-22, O-561	Toyone, T.	eP-300
Talekar, K.	eP-321	Theyel, B.	eP-54, O-397	Tranvinh, E	eP-37
Tali, E T.	O-88	Thielen, K. R	O-144	Trelles de Belaunde, M	eEdE-33, O-117
Tali, T.	eP-14, eP-38	Thomas, J.	P-124	Trimble, C. R	EE-61
Tamargo, R. J.	O-511	Thomas, O.M.	O-216, O-231, O-26	Triplett, B. M.	EE-74
Tampieri, D.	EdE-41, eP-269, O-516			Tritrakarn, S.	P-48.
Tan, J. C.	eP-110			Triulzi, F. Maria	O-133, O-140, O-515
Tan, K.	eEdE-151			Trobe, J.	eP-111
Tanabe, J. L.	O-116, O-146			Trotter, S.	O-438
Tanaka, H.	O-232			Trotter, S. A.	eP-299
Tanaka, N.	O-301			Truitt, K. A.	eP-13
				Truwit, C. L	eP-69, O-173

### Index of Program Participants

Numbers refer to session and presentation numbers, *not to page numbers*.

Index Key: O = Scientific Paper (Oral Presentation); EE = (Electronic) Excerpta Extraordinaire;

P = Scientific Poster (Print Format); eP = Electronic Scientific Poster (ePoster);

EdE = Education Exhibit (Print Format); eEdE = Electronic Education Exhibit

Tsagakis, K.	O-392	University of São Paulo,	P-105	Vanderver, A.	eP-272
Tsai, F. Y.	eP-123, eP-255	Uno, T.	eP-195	Vandorpe, R.	eP-152
Tsai, H-M.	eEdE-4	Unsöld, R.	O-317	Vargas, M. I.	O-492
Tsai, N. Trevanian	eEdE-141	Unver, O.	EE-77	Vattoth, S.	P-63
Tsai, P. H.	eP-123	Updahyay, N.	O-106	Vavro, H.	O-122, O-124, O-143
Tsai, Y-H.	P-4	Urban, J.	O-63	Vazquez, E	eEdE-110
Tsay, J.	O-410, O-436, O-643	Urban, J. E.	O-66	Vazquez, E	O-139
Tseng, Y-A.	eEdE-143	Urkin, M.	eP-232	Vedantham, S.	eP-260
Tsiouris, A.	eP-160, eP-61, eP-147	Useche, N.	O-315	Vedolin, L.	O-137
Tsiouris, A. J.	O-114, O-565, P-6	Uyeda, J. W	eP-171	Veerasarn, V.	P-48
Tsuchiya, K.	eP-21, eP-43, eP-6, O-110			Vega, E	O-441
		<b>V</b>		Velasco, T.	eP-16
Tsujimoto, T.	EdE-66, P-86	Vabulas, M.	eEdE-60, O-68	Velasco, T. R	eP-275
Tsukabe, A.	O-232	Vachha, B. A.	eEdE-145, eEdE-91, O-598	Velioglu, M.	O-414
Tsunemi, M. H.	O-226			Velthuis, B.	eP-151, O-23, O-398, O-579
Tsunoo, M.	EE-6	Vagvala, P.	EdE-33		
Tubman, D. E.	EE-65, eP-216, O-421, O-422	Vaisfeld, J.	EdE-29, EdE-48, eP-80, O-207	Velthuis, B. K.	O-635
				Veltkamp, D.	eEdE-113
Tumkur, S. M	EE-95	Vaisfeld, J. A.	P-51	Vendrell, J-F.	O-575, eP-200
Tummala, N.	EdE-72	Vajda, Z.	O-518, O-572, O-583	Venugopal, S.	O-56
Tumminelli, T.	eP-105, eP-107	Vakil, P.	eP-104, eP-129, eP-148, O-111, O-237, O-520, O-560	Veraart, J.	O-209
Tuna, I. S	EdE-14, EdE-39, EdE-70, EdE-86, eEdE-114 eEdE-124 eEdE-129, eEdE-134, eEdE-136, eEdE-61	Valadao, M. N	P-23	Verdolotti, T.	EE-78
Turc, G.	O-28	Valente, E M.	O-142	Verdoorn, J. T	O-437
Tureci, E	eP-229, eP-268, O-414	Valente, K. D. R.	O-226	Vergadis, C.	eP-320
Turk, III A. S	O-22, O-561	Valente, M.	P-112	Verma, A.	O-534
Turk, S.	eP-12, O-305	Vallee, P.	O-439	Verschuuren, S.	EdE-82
Turk III, A.	O-557	Vallinga, M.	eP-181	Vezina, G.	O-2
Turner, J. A.	O-591	Valvassori, G.	eP-166	Viana, M.	EE-99
Turner, M.	eP-124	Van, A. T	O-307	Vicaud, E	eP-196
Turski, P.	O-108	Van Cauter, S.	O-209	Viera, J.	O-569
Tustison, N. J.	O-604	van de Haar, P.	eP-209	Viertel, V.	eP-326, P-122, P-123
Tutton, S.	O-527, O-528	van den Berg, R.	eP-252, O-584	Viertel, V. G.	eP-299, O-438
Tyan, Y-S.	eP-168	van der Bom, I. M J	eP-209, eP-227, eP-228, O-586	Viets, R. B.	P-59
Tyndall, A. J.	eP-105	van der Graaf, Y.	O-579, O-635	Vigen, K.	O-109
		van der Kallen, B.	eP-252	Vignal, C.	eEdE-72, eP-162, O-249
		van der Kallen, B. F. w.	O-584	Vijay, K.	EdE-23, EdE-60, EE-5, EE-58
		van der Kolk, A. G.	EdE-24		
U, H. Sang	EE-32	van der Lugt, A.	eP-252, -584	Vilela, P.	eP-106
Ucar, M.	eP-14, eP-38	van der Schaaf, I.	eP-151, O-579	Villablanca, P. J.	O-396
Uchiada, M.	EE-26	Van Der Schaaf, I. C.	O-23, O-635	Vincentelli, C.	EE-27
Uchikoshi, M.	eP-35	van Doorn, M. M	O-584	Vinters MD, H. V	O-573
Uchino, A.	O-248	Van Ginneken, B.	O-23	Vinuela, F.	O-186, O-573
UdDin, N.	eP-170	Van Goethem, J. W	O-622	Visser, F.	EdE-24
Uemura, A.	eP-194	Van Gool, S.	O-209	Vitiello, G.	O-142
Uetani, H.	eP-306, eP-90, eP-92, P-40, P-67	van Oostenbrugge, R.	eP-252	Vittori, J.	EE-30
		van Oostenbrugge, R. J.	O-584	Vivoda, M.	EE-2
Ugurel, M. S	EE-67	Van Poppel, K.	O-300	Vo, K. D.	eP-121, O-454, O-474
Uliel, S.	P-110	van Seeters, T.	O-23, O-579, O-635	Volokhina, Y.	O-65
Ulmer, J. L	eEdE-57, eP-297	Van Stavern, G.	P-59	Voloschin, A.	EE-27
Ulmer, S.	eP-105, eP-107	van Zwam, W.	eP-252, O-584	Voluck, M.	eP-78
Ulusoy, L.	O-610	van Zwam, W. H.	eP-157	von Kummer, R.	O-580
Umino, M.	eP-10, P-37	Vandergrift, A. W	eEdE-140	von Morze, C.	O-100, O-259, O-292
Umran Ashruf, S.	eEdE-39	Vanderhasselt, T.	EdE-22	von Ritschl, R.	EE-68
				Vonken, E-J. J.	O-23
				Vos, P. C.	O-234

### Index of Program Participants

Numbers refer to session and presentation numbers, *not to page numbers*.

Index Key: O = Scientific Paper (Oral Presentation); EE = (Electronic) Excerpta Extraordinaire;

P = Scientific Poster (Print Format); eP = Electronic Scientific Poster (ePoster);

EdE = Education Exhibit (Print Format); eEdE = Electronic Education Exhibit

Voscolopoulos, C.	eP-307	Watanabe, T.	eP-195	Williams, III D. W	O-335
Voss, J.	O-220	Watanabe, Y.	eP-30, O-232, P-43	Williams, M. D.	P-50
Vossough, A.	EdE-77, EdE-80, EE-73, O-306, O-47	Wattel, C.	eEdE-72	Williams, R. G.	O-255
Vranic, J.	O-111	Waters, M. F.	P-84	Williams, T.	O-313
Vranic, J. E.	EE-70, eP-148, O-237, O-560	Waterval, J. J.	eP-181, eP-189	Williamson, J.	O-567
Vu, T.	eP-142	Watson, A.	eP-3	Willy, R.	EE-34
Vuillier, F.	O-483	Watson, Jr. R. E.	P-62	Wilson, D. M.	O-107, O-41
Vymazal, J.	eP-77	Wattjes, M. P.	O-501	Wilson, J.	EE-69
		Watts, R.	eP-283, eP-291, O-596	Wilson, M. W	eP-222
		Watts, R. P.	P-108	Wilson, N.	eEdE-131
		Weatherall, M.	O-537	Wilson, T. D.	EdE-20
		Weber, A.	eEdE-86	Wintermark, M.	eEdE-16, eP-141, eP-4, O-289, O-585 O-604, P-2
		Weber, A. L.	EdE-54	Wippold, F. J.	eP-153
		Weber, C.	O-509	Wippold, II F. J.	eEdE-152, eEdE-28, eEdE-98
		Weber, M.	eP-287, O-215, O-429	Wirtz, D. C.	eP-314, eP-315, O-531
		Wei, C.-C.	eP-168	Wisnowski, J.	O-254, O-255
		Wei, K.-C.	P-28, P-35	Wisnowski, J. L	eP-284
		Weininger, M.	O-122, P-110	Witsell, D. L	eP-185
		Weinstein, P. R	O-547	Witthiwei, T.	P-48
		Weiss, C.	O-48	Woitek, R.	eP-287
		Weiss, I.	eP-232	Wolfbreg, A.	O-136
		Weizman, L.	P-104	Wolford, J.	O-49
		Welker, K.	O-43	Wolfowitz, R.	O-60
		Wen, P. Y	O-7	Wolfsberger, S.	O-215
		Wen, Y.	P-16	Woltjer, R.	eP-20
		Weng, H.	O-533	Wong, D. F.	O-266
		Weng, H.-H.	P-4	Wong, G. K. C	O-642
		Werhun, E	EE-100	Wong, H.-F.	P-28, P-35
		Wesemann, T.	O-600	Wong, K.	EdE-6
		West, D.	O-537	Wong, W. H. M.	O-468
		Westcott, G.	P-19	Wongsripuemtet, J.	P-15, P-48
		Wetjen, N.	O-43	Woo, H. H.	eP-26
		Whalen, M.	O-59	Woo, J. H.	eP-103
		Wheless, J.	O-300	Wood, C.	O-505
		White, E	P-29	Wood, C. P	O-144, O-401, O-437
		White, M. L	EdE-13, EdE-20	Worrell, G. A.	O-145
		White, M.	EE-1, EE-51	Wosny, C.	eEdE-122
		Whitehead, M. T	O-46	Wrage, L.	O-256
		Whitlow, C. T	eP-150, O-019a, O-104, O-224, O-40 O-63, O-66 P-19	Wright, K. D.	EE-75, O-548
		Wick, W.	eP-86, eP-95	Wright, N.	EdE-81
		Widhalm, G.	O-215	Wu, C.	eP-119
		Widjaja, E	O-138, O-539	Wu, H.	O-108
		Wieben, O.	O-112	Wu, L.	EE-11
		Wiestler, B.	eP-86, eP-95	Wu, M.-C.	eP-168
		Wiggins, R.	eP-187	Wu, O.	O-562
		Wiggins, III R.	O-428	Wu, R.	eEdE-143
		Wiggins, R. H.	O-644	Wu, Y.	O-108
		Wiggins, III R. H.	O-271, O-430	Wu, Y. Y.	P-18
		Wigginton, T.	O-612	Wycliffe, N. D.	O-65
		Wilde, P.	eP-124	Wylie, J. D.	O-491
		Wilkinson, I. D.	O-105, O-150, O-225		
Wada, A.	eP-300				
Wada, T.	eP-117, eP-201, eP-35, O-574				
Wada, Y.	eP-300				
Wagle, N.	eP-137				
Wagner, J. S	O-224				
Wakata, Y.	EE-82, O-103, P-42				
Wakely, Jr. P.	O-426				
Wakhloo, A.	eP-223, O-484, O-580				
Wakhloo, A. K.	eP-209, eP-217, P-228, eP-260, O-336, O-586				
Walden, M.	P-122, P-123				
Walden, M. J.	eP-326				
Waldman, A. D.	O-106, O-537				
Waldron, N.	O-391				
Walker, L.	O-550				
Walter, K. D.	EdE-86				
Walter, S.	eP-247, eP-259				
Wang, A.-M.	EdE-11, EdE-97, EE-103, EE-9, eEdE-144				
Wang, B.	EdE-54, EE-87, eEdE-86				
Wang, G.	eP-237				
Wang, J.	EdE-43				
Wang, J.	eP-8, P-26, P-52, P-7				
Wang, L.	O-296				
Wang, P.	eEdE-45				
Wang, S.	eP-103, eP-147, eP-78, eP-81				
Wang, Y.	eP-145, eP-147, eP-323, O-114, O-544				
Wang, Y.-H.	P-96				
Wang, Z.	O-175, O-262				
Warren, A. L.	O-151				
Warren, D. J.	eEdE-111				
Warren, D.	O-595				
Warren, K. E.	O-550				
Wasserman, B. A.	O-273				
Watanabe, A.	eP-300				
Watanabe, A. T.	O-465				
Watanabe, H.	eP-5				
Watanabe, M.	eP-192, eP-33, O-244, O-245				

### Index of Program Participants

Numbers refer to session and presentation numbers, *not to page numbers*.

Index Key: O = Scientific Paper (Oral Presentation); EE = (Electronic) Excerpta Extraordinaire;

P = Scientific Poster (Print Format); eP = Electronic Scientific Poster (ePoster);

EdE = Education Exhibit (Print Format); eEdE = Electronic Education Exhibit

## X

Xi, C. eP-188  
Xi, G. eP-251  
Xu, D. O-132, P-109, P-16

## Y

Yadav, R. O-503  
Yahyavi-Firouz-Abadi, N.  
eEdE-152, EdE-28, P-107  
Yakes, W. F. O-312  
Yamada, J. O-490, O-546  
Yamada, Y. O-597  
Yamamoto, T. eP-29  
Yamano, T. O-103  
Yamasaki, F. eP-30, P-43  
Yamasaki, M. EE-82, O-103  
Yamashita, K. P-41  
Yamashita, Y. eP-306, eP-90,  
eP-92, P-40  
Yan, C. eP-292  
Yang, E. P-101  
Yang, I-H. P-17  
Yang, Z. O-39  
Yano, S. eP-306, eP-92  
Yasue, M. P-36  
Yavagal, D. O-557, O-559  
Yazbek, S. eP-36  
Yemen, B. eP-77  
Yen, P. eP-135  
Yeom, K. O-179, O-45  
Yeom, K. W. O-551  
Yetkin, Z. F. P-106, P-46, P-66  
Yeung, R. eP-114, eP-77  
Yildirim, O. eP-26  
Yildirim, T. eP-273, eP-279, eP-44  
Yilmaz, U. eP-247, O-569  
Yin, N. O-573  
Ying, L. eP-188  
Ying, S. eP-9  
Yokoyama, K. P-14  
Yonash, T. P-104  
Yong, W. H. O-290  
Yoo, A. eP-65, O-557  
Yoo, A. J. O-22, O-233, O-556,  
O-561, O-577  
Yoo, D. O-327  
Yoo, J-Y. eP-304  
Yoo, W-J. eP-175, eP-203  
Yoon, T. EdE-56  
Yoon, W. eP-246, P-45  
Yorgason, J. G. O-430, O-116  
York, P. O-146  
Yoshida, M. O-609, P-14  
Yoshida, Y. EE-26  
Yoshimoto, K. P-41

Yoshiura, T. P-41  
Yoshiya, K. O-232  
You, C. eP-119  
Youn, Sung won W. eP-118, eP-125  
Young, A. M H O-216  
Young, K. H. EE-14  
Young, M. G. EdE-89  
Young, R. J. EdE-29, EdE-48,  
EdE-95, eP-80, O-207, O-221,  
P-21, P-51  
Young, V. E. O-231  
Young, W. L. eP-196, O-316  
Yousem, D. O-243  
Yousem, D. M. eP-299, eP-326,  
eP-62, O-279, O-324, O-438,  
P-122, P-123  
Yousry, T. A. P-32  
Yu, C. EdE-25  
Yu, J. O-176  
Yu, J. P. O-292  
Yu, J-P. J. O-100  
Yu, M. H. O-513  
Yu, W-Y. eEdE-151, eEdE-47  
Yue, J. O-56, O-57  
Yuh, W. T C eEdE-12  
Yuki, I. O-573  
Yushkevich, P. A. eP-103

## Z

Zacá, D. P-24  
Zada, G. EE-72, eP-137  
Zagzag, D. EE-39  
Zahaczewsky, M. L. O-546  
Zaharchuk, G. EdE-25, O-20, O-37,  
O-427, O-551  
Zahra, K. eEdE-102  
Zaharchuk, G. G. O-18  
Zaidat, O. O. O-22  
Zaidat, O. O-557  
Zaidat, O. O. O-561, P-71  
Zaitout, Z. P-64  
Zaki, M. eEdE-144  
Zampolin, R. EdE-67  
Zan, E. O-148  
Zanni, G. EE-80  
Zarghouni, M. EE-43  
Zarnow, D. M. EdE-77  
Zaterka-Baxter, K. O-257  
Zauner, A. O-557  
Zaw, T. M. O-290  
Zaw, T. O-97  
Zayas, J. O. eEdE-64, eEdE-97  
Zazulia, A. eP-60  
Zee, C. eP-288, eP-292  
Zeiler, S. R. O-511

Zeilefsky, M. O-546  
Zeng, H. O-544  
Zerah, M. eP-285  
Zessler, A. eEdE-15  
Zhang, C. eP-251  
Zhang, D. O-213  
Zhang, J. eP-8  
Zhang, J. Q. EE-21  
Zhang, M. O-538  
Zhang, Y. EdE-13, EdE-20  
Zhao, S. eP-84, O-70  
Zhao, Y. O-594  
Zhao, Z. eP-119  
Zheming, F. eP-188  
Zhou, Y. O-129, O-58  
Zhu, F. O-397, P-101  
Zhu, G. eP-4, P-2  
Zhu, H. O-296  
Zhu, W. eP-145  
Ziai, P. O-306, O-47  
Ziegler, K. O-569  
Zimmer, C. O-217, O-570  
Zimmerman, M. O-54, O-55, P-65  
Zimmerman, M. E. O-53  
Zimmerman, R. A. EE-73, eP-290,  
O-306  
Zinn, P. O. eEdE-18, eEdE-21,  
eP-141, eP-79, eP-94, O-98, O-99  
Zipfel, G. eP-60, O-455  
Zuccoli, G. O-49  
Zwanenburg, J. J. M. EdE-24  
Zwienenberg-Lee, M. eP-280  
Zylak, C. O-557